38th EPS

European Peptide Symposium

PROCEEDINGS

6– 11 September 2026

Vienna, Austria



http://doi.org/10.17952/38EPS

Proceedings of the 38th European Peptide Symposium

Vienna, Austria, 6-11 September 2026

Edited by:

Michal Lebl

Spyder Institute Prague, Czech Republic

Copyright ©2026 European Peptide Society
All rights reserved. No part of the material protected by this copyright notice may be reproduced or utilized in any form or by any means, electronic or mechanical, including photocopying, recording or by any information storage and retrieval system, without written permission from the copyright owner.

Introduction

The 38th European Peptide Symposium was held in Vienna, Austria, 6-11 September 2026, and its success was made possible by the contributions of 993 registered participants from 45 countries, alongside the generous support of over 35 sponsors and exhibitors. With a rich program featuring 70 oral presentations, 12 young scientist communications, and 566 posters, the symposium stood out as a significant milestone in advancing the dynamic field of peptide science.

The International Scientific Advisory Board played a key role in shaping the program, ensuring a comprehensive blend of traditional and innovative topics. These included advancements in peptide chemistry, cutting-edge industry technologies, emerging peptide-based applications, bioactive and therapeutic peptides, antimicrobial and antiviral peptides, peptide structural studies, computational approaches to peptide discovery, delivery systems, peptide materials, and the intersection of peptides with chemical biology. This diversity provided opportunities for both seasoned researchers and early-career investigators, with special emphasis on young scientists.

The 2026 symposium introduced several exciting new features to enhance engagement and accessibility. For the first time, the program included a dedicated Career Development Workshop, as well as a session on translational peptide drug development featuring speakers from industry and small biotech companies, including university spin-offs, followed by a panel discussion.

The impact and breadth of the symposium are reflected in this Proceedings book. Thanks to the new format, which incorporates PDF contributions of lectures and posters, this collection showcases 280 poster contributions and 10 lectures, capturing the wide range of topics addressed during the symposium.

We extend our heartfelt gratitude to all participants, invited speakers, the International Scientific Advisory Board, the Local Organizing Committee, including the Local Helper Team, the University of Vienna event team and our sponsors and exhibitors. Your invaluable contributions have made this symposium a truly memorable and impactful event.

Christian Gruber & Christian Becker

Editor's Comments

This proceedings format follows the test from the last symposium in Italy. Since many Symposium participants were experiencing this type of meeting for the first time, many of them had no idea that the production of symposium proceedings has a long tradition, starting with the first peptide symposium in Prague in 1958, organized by Professors Rudinger and Šorm. Every word presented at that meeting, including the discussion after each lecture, was transcribed and published in the special issue of Collection of Czechoslovak Chemical Communication, which became the first book of proceedings. Nowadays not everything can be included in the book of proceedings, but since everything is available in the electronic form, we can try to compile most of the materials presented at the time of the meeting in this Collection.

So, the format of the proceedings book is based on the following principles:

• Every lecture or poster is available in electronic form – usually as PowerPoint presentation or pdf file.

• Once the lecture or poster is presented at the symposium, everything in it is legally public knowledge.

• Presentation at the meeting is considered preliminary publication and should not prevent publication of the full version of the particular paper in Science or Nature or anywhere else.

• Every presentation receives the doi identifier once it is included in The Proceedings.

• Authors did not have to do anything else in addition to preparing their lecture or poster. Just submit their pdf through The Proceedings web site.

In this way the original idea of the founders utilizing the technologies which were not available at their time is revitalized. (Personally, I believe that Prof. Rudinger would approve of this without hesitation.)

Some observations from this year's book production. We still did not achieve the goal of including everything what was presented in this symposium, especially the lectures. Only 12% were submitted. Poster's situation is much better – 280 posters are included in the proceedings – about 50% of all posters were captured and provided with DOI numbers. Out of all submitted pdfs only 8 (1.2%) were created as the classical proceedings papers.

Let us hope that the next European Peptide Symposium will have even higher success in capturing all new ideas presented there!

Michal Lebl

Organization

Co-Chairs

Christian Gruber & Christian Becker

Scientific Advisory Board

Fernando Albericio
Jane Aldrich
Gregor Anderluh
Jan Bakos
Steven Ballet
Claudia Bello
Vanderlan Bolzani
Ashraf Brik
Florine Cavelier
Gong Chen
Ratmir Derda
Ingrid Dijkgraaf
Fernando Formaggio
Shiroh Futaki
Paula Gomes
Rosario González-muñiz
Yuji Ito
Knud Jensen
Daniela Kalafatovic
Annie Kan
Beate Koksch
Beata Kolesińska
William Lubell
Nermina Malanovic
Istvan Mandity
Goran Mauša
Norman Metanis
Markus Muttenthaler
Ines Neundorf
Thomas E. Nielsen
Anna Maria Papini
Timothy Reichart
Sam Robinson
Johan Rosengren
Paolo Rovero
Joel Schneider
Oliver Seitz
Norbert Sewald
Roderich Süssmuth
Alesia Tietze
Jan Tytgat
Andreas Tzakos
Wilfred van der Donk
John Wade

Local organizing team

Anne Conibear
Tim Baldensperger
Roland Hellinger
Nina Stuppacher
Hannah Back
Boglárka Blanka Bata
Jonas Bußmann
Elena Becker
Martina Bosic
Michaela Cherrier
Claudia Cobos
Stepan Denisov
Jonathan Dieringer
Manuel Felkl
Andreas Fraunhofer
Tobias Gökler
Anna Hampel
Simon Hasinger
Julius Hermes
Kirtikumar Jadhav
Ludmila Kassihina
Rumsha Khan
Yanying Li
Lilly Lindner
Julia Lisa Molina
Olubunmi Mada
Anna Mädge
Gerhard Niederacher
Isabell Ober
Maria Orfanoudaki
Peter Palánkai
Monika Perisic Boehm
Miriam Preissler
Konstantin Raabe
Justina Reis
Semir Sahmanovic
Sabrina Schmied
Medine Soydan
Moritz Urschbach
Natasha Wanko
Herwig Weißinger
Dominik Windisch
Pamina M. Winkler

EPS Officers

Knud JENSEN – Chairman
Beata KOLESINSKA – Secretary
Fernando FORMAGGIO - Treasurer
Florine CAVELIER – Scientific Affairs Officer
Beate KOKSCH – Communications Officer

EPS National Representatives

Austria	>	Anne CONIBEAR	✉
Belgium	>	José MARTINS	✉
Bulgaria	>	Dancho DANALEV	✉
Croatia	>	Ruža FRKANEC	✉
Czech Republic	>	Jiří JIRÁČEK	✉
Denmark	>	Thomas Eiland NIELSEN	✉
France	>	Oleg MELNYK	✉
Germany	>	Roderich SÜßMUTH	✉
Greece	>	Andreas TZAKOS	✉
Hungary	>	Gábor TÓTH	✉
Ireland	>	Eoin SCANLAN	✉
Israel	>	Muhammad JBARA	✉
Italy	>	Daniela MARASCO	✉
The Netherlands	>	Ingrid DIJKGRAAF	✉
Poland	>	Rafał LATAJKA	✉
Portugal	>	Paula GOMES	✉
Slovakia	>	Jana OSACKÁ	✉
Slovenia	>	Tomaž BRATKOVIČ	✉
Spain	>	Carles MAS-MORUNO	✉
Sweden	>	Alesia TIETZE	✉
Switzerland	>	Nathalie GROB	✉
United Kingdom	>	Louise WALPORT	✉

Awards

Josef Rudinger Memorial Award

Sponsored by PolyPeptide Group

The Josef Rudinger Memorial Lecture Award is presented "in commemoration of Josef Rudinger's role in the foundation of the European Peptide Symposia and of diverse contributions he made to peptide chemistry".

Awardee: Norbert Sewald, University of Bielefeld, Germany



Leonidas Zervas Award

The Leonidas Zervas Award is presented in commemoration of his outstanding contributions to peptide science. The award is given to the scientist who has made the most outstanding contributions to the chemistry, biochemistry and/or biology of peptides in the five years preceding the date of selection and is sponsored by the donation of **Dr. Rao Makineni**.

Awardee: Steven Ballett, Free University of Brussels, Belgium



Miklós Bodanszky Award

Sponsored by BCN Peptides

The Miklos Bodanszky Award is presented in commemoration of Miklos Bodanszky's contributions to peptide research, to a young scientist who has in the opinion of the General Assembly of the Society made the most outstanding contribution to peptide research in the period of maximum ten years after obtaining the PhD degree.

Awardee: Anne Conibear, Technical University of Vienna, Austria



Invited speakers

Paramjit Arora
Gaurav Bhardwaj
Jeffrey Bode
Florence Brunel
Jayanta Chatterjee
Irene Coin
Paul Alan Cox
Bobo Dang
Phil Dawson
Marta De Zotti
Maurice Elphick
Nicolas Gilles
Ranganath Gopalakrishnan
Tom N. Grossmann
Nina Hartrampf
Alexander Hauser
Christian Heinis
Sonia Henriques
Kata Horvati
Yasuhiro Kajihara
Daniela Kalafatovic
Roland Kersten
Xuechen Li
Hyun-Suk Lim
Lei Liu
Morten Meldal
Oleg Melnyk
Anaïs Noisier
Benjamí Oller-Salvia
Monika Raj
Sylwia Rodziewicz-Motowidło
Helena Safavi
Ali Tavassoli
Meritxell Teixido
Dirk Trauner
Olalla Vázquez
Louise Walport
Dek Woolfson

Plenary lectures were given by:

Richard Payne (University of Sydney)

Hiroaki Suga (University of Tokyo)

Tom Muir (Princeton University)

David Baker (University of Washington)

Jens Juul Holst (University of Copenhagen)

Big Thanks to our Sponsors

Platinum Sponsor

GYROS PROTEIN Technologies

Gold Sponsors

CEM

Biotage

Silver Sponsors

Agilent

aapptec Complete Peptide Product Source

WuXi TIDES

Bronze Sponsors

Iris Biotech

ZEALAND PHARMA

CAT Chromatography and Analysis

RAPP POLYMERE

BCN peptides

CSBio INSTRUMENTATION

BACHEM

BioDuro

PolyPeptide

PharmaBlock

AstraZeneca

JPT WE MAKE PEPTIDES

Exhibitors

HIGHFINE

polypure

ALMAC

Space Peptides Peptide CRDMO Services at Premium Speed & Quality

Luxembourg Bio Technologies

CIPPS Centre for Innovations in Peptide and Protein Science

CPC scientific Tides Partner. Concept to Commercial.

SENN

JYMed Peptide

PEPTISYSTEMS SCALABILITY · FLOWTHROUGH · AUTOMATION

GLS

CHRISTOF SENN LABORATORIES AG

HECHENG

Sai

Sponsor & Media Partner

novo nordisk®

Chem Bio Chem | Chem Med Chem | Chemistry Europe

Company profiles

AAPPTec

AAPPTec delivers **complete peptide synthesis solutions—from chemistry and instrumentation to custom peptide production**. With decades of peptide expertise, we support pharmaceutical, biotechnology, academic, and peptide manufacturing laboratories worldwide.

Our portfolio combines **automated peptide synthesizers, amino acids, resins, reagents, custom peptides, and scale-up equipment**, giving customers a single partner for peptide development from discovery through production.

From high-throughput research to larger-scale synthesis, AAPPTec provides the **equipment, chemistry, applications expertise, and technical support** needed to improve productivity, accelerate development, and simplify peptide workflows.

One partner. Complete peptide solutions. www.peptide.com

Agilent

Agilent, a global leader in analytical laboratory technologies, provides trusted answers that help our customers solve their most ambitious scientific challenges, increase laboratory performance, and advance quality of life. Our solutions for pharma and biopharma—from research and drug discovery, to development, manufacturing, and quality control—help to optimize pharma small molecule and biotherapeutic characterization methods, to get products to market faster.

Explore further: https://www.agilent.com/en/solutions/biopharma-pharma

---

Bachem

Bachem is a leading, innovation-driven company specializing in the development and manufacture of peptides and oligonucleotides.

The company, which has over 50 years of experience and expertise, provides products for research, clinical development, and commercial application to pharmaceutical and biotechnology companies worldwide and offers a comprehensive range of services.

Bachem operates internationally with headquarters in Switzerland and locations in Europe and the US.

BioDuro

BioDuro, an Advent International portfolio company, is a global CRDMO with 30 years of experience supporting biotech and pharmaceutical innovators. With 2,000+ scientists across 8 global sites, we provide integrated peptide discovery and development services spanning chemistry, biology, DMPK and CMC. Our peptide capabilities include AI-enabled design, Peptide DEL, Direct-to-Biology, and oral peptide development, supporting programs from early discovery through development and scale-up. Our integrated approach brings scientific disciplines together to address key challenges in peptide design, optimization, bioavailability and developability. With broad capabilities and flexible, tailored programs, BioDuro helps partners accelerate development, reduce risk and advance promising peptide therapeutics toward the clinic.

Biotage

Biotage is a global supplier and solutions partner to a wide range of customers within drug discovery and development and analytical testing. With strong expertise in separation and purification technologies, and a focus on leveraging intelligent workflow solutions, we aim to efficiently support the advancement and protection of human health. Learn more at www.biotage.com

---

C.A.T.

We offer chromatographic analyses as a service to our customers, specializing in the analyses of peptides, amino acid derivatives and other chiral substances. We are inspected by FDA as well as German Authorities.

We offer:

→ Reliable determination of enantiomeric purity via GC-MS using deuterated reagents and amino acid analysis.
→ Peptide sequencing and determination of the monoisotopic masses of peptides by high resolution mass spectrometry.
→ Determination of water content, solvent residues (OVI analysis) and counter ions with minimal sample consumption.
→ All methods are generically validated. Validation reports can be issued for specific substances.
→ Fulfillment of the FMP requirements has always been of prime concern in our company.

CEM

CEM Corporation is a global leader in peptide synthesis technology, providing innovative solutions for research, discovery, and peptide production. From automated microwave peptide synthesis to high-throughput and parallel platforms, CEM systems are designed to accelerate workflows, improve peptide quality, and simplify complex synthesis. CEM also supports manufacturing-scale peptide synthesis with the Liberty PRO, enabling efficient scale-up from development to production. Trusted by leading academic, pharmaceutical, biotechnology, and CRO laboratories worldwide, CEM continues to advance peptide science through intelligent instrumentation, innovative chemistry, and dedicated application support.

CSBio

CSBio is a leading manufacturer of fully automated peptide and oligonucleotide synthesizers, proudly serving the life sciences industry for over 30 years. Our systems have been refined into the flexible, reliable, and cost-effective solutions trusted by researchers and manufacturers worldwide. From research scale to commercial-scale production, CSBio synthesizers are used in top universities, biotech, and pharmaceutical labs across the globe. Today, CSBio is the world's leading provider of pilot and commercial-scale peptide synthesizers, with more systems in operation than any other manufacturer.

Gyros Protein Technologies

Gyros Protein Technologies has built instruments for automated peptide synthesis since 1985, when it began in Tucson, Arizona.
The PurePep® portfolio runs from method development to clinical material: PurePep® Chorus for modular R&D synthesis, Symphony® X for parallel synthesis with per-channel protocol control, PurePep® Sonata®+ for pilot scale to 200 mmol, and PurePep® EasyClean (PEC™) for purification where HPLC reaches its limits.
Progress depends on synthesis you can trust.
Find us in The Forum, our room on the first floor: a session each day Monday to Wednesday, forty years of the PurePep story, and good coffee. #forpeptidescientists
Gyros Protein Technologies is part of the Biopharmaceutical Development Division of Mesa Laboratories, Inc. (Nasdaq: MLAB).

Iris Biotech

Iris Biotech is providing high quality products for the fields peptide synthesis, linkerology®, drug delivery, and life sciences in flexible quantities from research scale to commercial production, for academia as well as industry.
Besides our broad portfolio from standard to exotic, we have the know-how and facilities to manufacture your compound of choice based on a Custom Synthesis.
We are in continuous exchange with scientists all around the world to gather ideas and be ahead regarding technologies and innovations true to our slogan Empowering Peptide Innovation.
All our services are rounded off by a strong and competent personnel customer support.

JPT

For more than 20 years, JPT Peptide Technologies has supported peptide research from discovery to clinical research with high-quality custom solutions manufactured in Berlin under an ISO 9001:2015-certified quality management system. Our expertise spans linear, cyclic, stapled and highly modified peptides, peptide libraries, conjugation-ready and site-specifically functionalized peptides, as well as light and heavy labelled standards. From hit discovery, macrocycle and peptide-drug conjugate development to screening, bioanalysis and preclinical studies, JPT combines flexible synthesis, advanced modifications and application-focused support. Meet us at EPS 2026 in Vienna to discuss your next peptide challenge.

PharmaBlock

Empowering next-generation therapies with green and intelligent chemistry

PharmaBlock was officially operated in 2008 as a provider of drug-like small molecule building blocks and has since evolved into a fully integrated CRDMO partner following its IPO in 2017 (Stock Code: 300725.SZSE). Today, the company offers end-to-end solutions spanning from early-stage discovery to commercial manufacturing, with expanding capabilities in emerging modalities such as oligonucleotides, peptides, and complex conjugates. PharmaBlock's strategy is anchored in advancing sustainability through innovation in green and intelligent chemistry to empower next-generation therapies. In discovery, the company has advanced its building blocks into "PharmaChips" for next generation therapies including novel and high-purity short peptides, amidites and conjugate linkers. Leveraging three distinctive libraries: a DNA-encoded library, a fragment library, and an ultra-large, synthetically accessible virtual library and AI technologies, it enables customers to accelerate hit discovery and lead optimization.
In development, drawing on extensive experience in the production of thousands of building blocks, PharmaBlock has built a strong green and intelligent technology platform for both development and manufacturing. This platform includes flow chemistry, process modeling, computational fluid dynamics (CFD), bio-/metal catalysis, high-throughput experimentation (HTE), process analytical technology (PAT), and digitalization, as well as advanced capabilities in Liquid Phase Peptide Synthesis (LPPS). These capabilities allow the company to address complex chemistry challenges, reduce development risks, and minimize environmental impact.
Committed to green and intelligent chemistry, PharmaBlock combines speed with sustainability. Its global "region-for-region" model ensures fast turnaround, reliable supply, and consistent quality for partners worldwide.

PolyPeptide

PolyPeptide Group is a specialized Contract Development & Manufacturing Organization (CDMO) for peptide-based active pharmaceutical ingredients. By supporting its customers mainly in pharma and biotech, it contributes to the health of millions of patients across the world. PolyPeptide serves a fast-growing market, offering products and services from pre-clinical through to commercial stages. Its broad portfolio reflects the opportunities in drug therapies across areas and with a large exposure to metabolic diseases, including GLP-1. Dating back to 1952, PolyPeptide today runs a global network of six GMP-certified facilities in Europe, the U.S. and India. PolyPeptide's shares (SIX: PPGN) are listed on SIX Swiss Exchange.

Rapp Polymere GmbH

Rapp Polymere is a world leader for high quality polymer supports. We offer a broad range of novel supports. based on **T**enta**G**el® or polystyrene. They are used in solid phase chemistry, combinatorial chemistry, as polymer supported reagents, for library generation, peptide and oligonucleotide synthesis, as well as for diagnostic applications. The exceptional properties of the highly swellable TentaGel® XV make this resin the first choice for the synthesis of large peptides and difficult-to-make peptides.

A second line are reagents for **PEG´ylation**. Our portfolio comprises hundreds of high sophisticated derivatives from Methoxy PEG´s, homofunctional PEG´s to hetero-bifunctional PEG´s. We also offer custom synthesized PEG derivatives and resins.

http://www.rapp-polymere.com

WuXi TIDES

WuXi TIDES, part of WuXi AppTec, Inc., is an industry-leading, integrated pharmaceutical technology and capability platform, serving the life sciences industry with operations across North America, Europe, and Asia. As an innovative Contract Research, Development and Manufacturing Organization (CRDMO), we provide efficient, flexible, high-quality solutions for our partners worldwide – from discovery to development and commercial supply for oligonucleotides, peptides, and related conjugates.
tides.wuxiapptec.com

Zealand Pharma

Zealand Pharma is a biotechnology company focused on advancing medicines for obesity and metabolic health. Combining more than 25 years of peptide R&D expertise with a proprietary data platform that leverages advanced data-driven and AI/ML approaches, Zealand Pharma aims to lead a new era in obesity and metabolic health. To date, more than ten Zealand Pharma-invented drug candidates have entered clinical development, of which two products have reached the market and three candidates are in late-stage development. The Company has collaborations with global pharmaceutical and biotechnology partners for research, development, and commercialization. Founded in 1998, Zealand Pharma is headquartered in Denmark, with a U.S. presence in Massachusetts. Learn more at www.zealandpharma.com.

Proceedings of the 38th European Peptide Symposium

The books of older symposia available for all EPS members can be found at https://www.eurpepsoc.com/category/archive/proceeding/

The final full proceedings pdf is available now. However, the full pdf file is rather large (573 MB), so we recommend to use this page, which in addition contains full res files.

For finding anything in this pdf use Ctrl + F

About the 38th EPS

List of Lectures

O08 Practical Green Aqueous Solid-Phase Peptide Synthesis (ASPPS) Using Nanoassemblies of Fmoc-Amino Acids: A DMF-Free Approach
Keiko Hojo, Ayumi Nonaka, Yuki Manabe, Cedric Rentier, Amit Mehrotra, Kazuhito Hioki, Munetaka Kunishima

O12 Neurotensin(8-13) Analogs Targeting NTS1 and NTS2 Receptors: A Comparative In vitro and Molecular Modeling Study
Nikolay T. Tzvetkov, Kiril Kirilov, Maya G. Georgieva, Aneliya A. Balacheva, Tamara I. Pajpanova, Toni Kühl, Harald Hübner, Peter Gmeiner, Diana Imhof

O32 Peptide Nucleic Acid Probes for Affinity-Based Targeted Cancer Therapy
Amelie Eriksson Karlström

O37 Sequence-driven modulation of the multistage self-assembly process in lamellin-type β-peptides
Imola Cs. Szigyártó, K. Ferentzi, András Wacha, Kamal el Battioui, Olivér Pavela, Tünde Juhász, Judith Mihály, István Mándity, Viktor Farkas, Tamás Beke-Somfai

O46 Total synthesis of the proposed structure of threoglucin A
Natalia Cano-Sampaio, Juan Del Valle

O49 Cyclopeptide-Based Fluorescent Conjugates for Monitoring Prefibrillar Aβ42 Nanostructures
Steven Panek, Anne Cécile Van Baelen, Norbert Sewald, Nicolo Tonali

O51 Synthesising Libraries of a,d-Foldamers using Solid Phase Peptide Synthesis
Si Zhe Wang, Andre Cobb

O53 Retro-Inverted Host Defense Peptides as Inhalable Antitubercular Therapies
Diptomit Biswas, Hugh D. Glossop, Gebremichal Gebretsadik, Sabiha Sultana, Nathan

A. Schacht, Neela H. Yennawar, Muzafar Ahmad Rather, Anthony D. Baughn, Scott H. Medina

O55 Searching for Nanostructured or pOre fOrming Peptides for therapY COST Action
Daniela Kalafatovic

O60 Computational/Experimental Symbiosis to Design Functional Supramolecular Peptide Assemblies
Ivan R Sasselli

O63 Discovery of novel peptide-GPCR signalling systems across evolutionary domains
Luuk R. H. Dijkhof, Teemu K.E. Rönkkö, Marin Matic, Alexander S. Hauser

List of Posters

P001 Diastereoselective Ugi Reactions via Biocatalytic Desymmetrization: A Modular Route to Collagen Mimetic peptides
Felix M.J. Boerman, Jannes Wagemakers, Alessia Bubula, Daniele Castagnolo, Romano V.A. Orru, Jordy M. Saya

P002 Diagnostic 7-Mer Model Peptide for Rapid Evaluation of Cysteine Racemization in Solid-Phase Peptide Synthesis
Saundra Mason, Wesley Grenier, Dario Slavazza, Hanson Chang

P005 Tag-Assisted Peptide Synthesis (TAPS) Enabling Efficient and Sustainable Peptide Synthesis and Purification
Raimund Maier, Karin Rustler, Haixiang Zhang, Thomas Bruckdorfer, Kai Holland-Nell, Jacqueline Dalski, Stephan Pritz

P008 Total Chemical Synthesis of RNF4 by Sequential Native Chemical Ligation: C-To-N Versus N-To-C Strategies
Saed Bisher, Rajesh Pallava, Ashraf Brik

P010 C-Glycosyl a-Amino Acids as Structural Encoders of Peptide Conformation
Ivanka Jeric, Barbara Bogovic, Ivana Nikšic-Franjic

P013 Scalable PEC Purification Enables API-Grade Semaglutide with Minimal HPLC Intervention
Stephan Lüdtke, Lucrezia Sforza, Manoj Muthyala, Robert Zitterbart, Dominik Sarma, Paolo Rovero, Anna Maria Papini

P014 Synthesis, Radiolabelling and Preliminary Characterization of an EGFR-Targeting DOTA-Conjugated Peptide for Cancer Imaging
Aline De Souza, Leonardo Carvalheira, Marycel Barboza, Fernanda Mendonca, Leonardo Fuscaldi, Luciana Malavolta

P019 Pyridium-p Interaction Preserves the N,S-benzylidene Thioacetals (NTDs) in Acidolysis Enabling Efficient Protein Chemical Synthesis
Zhenquan Sun, Yaoyue Zhang, Xueqian Zhao, Yisa Xiao, Zhixiang Zhong, Hongxiang Wu. Xuechen Li

P020 Development of a Generalized Platform for Hydrophobic Peptide Synthesis by

Utilizing WuXi TIDES-Solubilizing Tag
Qingqing Zhou, Xiaosheng Luo, Yazhou Li, Xiao Zhang, Yvonne Angell, Li Wang, Haiying He

P023 Towards peptide libraries: HPLC-based flow peptide synthesis and combinatorial chemistry
Viktor Farkas, Kristóf Ferentzi, András Perczel

P025 High-Loading Seplife Fmoc-RinkAmide-PS-PEG Resin: A Robust Solid Support for the Synthesis of Complex Peptides and Tirzepatide
A. Kumar, P.K. Kabwe, M. Alhassan, W. Hou, C. Wang, C. Zhang, Y. Li, XK. Kou, A. Basso, A. Sharma, BG. De La Torre, F. Albericio

P027 Accelerating peptide discovery via high throughput plate-based synthesis
An Nguyen, Siddique Amin, Caroline Morris, Christina Dumitriu Jackson, Hannah Bolt, Jefferson Revell

P028 A Novel Metal Catalyzed Peptide Ligation Method
Nathalie Ollivier, Remi Desmet, Oleg Melnyk

P029 Catalytic peptide-based coacervates for enhanced function through structural organization and substrate specificity
David Reis, Sara Pereira, Ana Ramos, Pedro Pereira, Leonor Morgado, Joana Calvário, Ana Pina

P032 Peptide functionalization of hybrid polyoxometalates
Teresa Bell, Nadiia Gumerova, Annette Rompel

P033 Accelerated Linker-Free Solid-Supported Native Chemical Ligation
Océane Bonningue, Vincent Diemer, Oleg Melnyk

P034 From Monomers to Dendrimers: Novel Synthetic Strategies for Highly Branched Peptide Nanostructures for Next-Generation Drug Delivery
Tom Götze-Ebert, Frida Fritzsche, Christina Lamers

P038 Induction heating solid-phase strategy to improve the total chemical synthesis of ester insulin
Silvia Bracci, Michael Quagliata, Paolo Rovero, Stephen B.H. Kent, Anna Maria Papini

P039 Engineering nucleophilic catalysis coupled to tandem electrostatic assistance enables native chemical ligation at nanomolar concentrations
Julie Di Adamo, Vincent Diemer, Oleg Melnyk

P042 Direction-Switching One-Pot Peptide Ligation with Orthogonal Cysteinyl Protection
Koki Nakatsu, Fumika Yoshitomi, Hiroki Onoda, Reia Shikimachi, Kyohei Arita, Akimitsu Okamoto, Hiroshi Murakami, Gosuke Hayashi

P044 Methionine Oxidation Effect on GLP-2 Synthesis and Amyloid Kinetics
Szebasztián Szaniszló, Dániel Horváth, Kata Geszti, Anna J. Kiss-Szemán, Dóra K. Menyhárd, András Perczel

P045 Thiol-yne Mediated Peptide Macrocyclisation and Derivatisation Strategies

Conor Williams, Dearbhla Tully, Konstantin Raabe, Dominik Windisch, James O'Brien, Cristina Trujillo, Joanna F. McGouran, Markus Muttenthaler, Eoin M. Scanlan

P047 Affinity-driven transfer of a mass tag for the direct profiling of matrix metalloproteases in complex biological matrices
Lomane Berthy, Ugo Pasco, Mylene Sejalon-Cipolla, Monika Kaminska, Carole Malgorn, Fabrice Beau, Metka Novak, Barbara Breznik, Dimitris Georgiadis, Isabelle Correia,Olivier Lequin, Sarah Bregant, Robert Thai, Gilles Subra, Sonia Cantel, Laurent Devel

P048 Clustered antigen architectures enhance monoclonal antibody adhesion: insights from biomimetic surfaces
Océane Ricloux, Laure Bar, Quentin Laurent, Liliane Guerente, Didier Boturyn

P052 Engineering a snake toxin as a positron emission tomography agent for diagnosing metastatic renal carcinoma
Goran Stanajic Petrovic, Charles Truillet

P055 New therapeutic option in autoimmune diseases to prevent the release of soluble CD95L
Marie Launay, Sarah Huot-Marchand, Farah Kotaich, Patrick Blanco, Patrick Legembre, Laurent Devel

P058 Modulating Integrin and Growth Factor Signaling with Synthetic Peptides: a New Paradigm in Regenerative Medicine
Carlos Mas-Moruno

P062 Olfactory Inspired Peptides as Tuneable Platforms for Selective Detection of Explosives
Adriana Rathner, Prabhat Prakash, Julian Widhalm, Malina Mairhofer, Vera Podrabska, William III Goddard

P067 Small Molecules, Big Impact: Quantifying the Influence of Amino Acids on Protein Interactions
Pamina M. Winkler, Christian F.W. Becker

P070 Stapled Peptide Inhibitors Targeting pre-miR-155 to Suppress miRNA Maturation
Heejoo Roh, Jinseo Heo, Yeongju Lee

P072 Screening of Algae Processing Technology for Easily Digestible Bioactive Hydrolysates
Ladislav Bim, Miloš Jelinek, Lubomir šánek, Veronika Matušu, Pavla švestková, Jiri Pecha

P073 Development of PNA-Based Antisense Oligonucleotides Targeting XIAP mRNA for Sensitizing TRAIL-Resistant Cancer Cells
Hyein Jung, Yeongju Lee

P074 Role Of Metal Nanoparticles As Artificial Chaperones In Modulating The Aggregation Propensity Of ?-Amyloid (Aβ40) Polypeptide
Harshit Kalra, Suman Jha

P076 Characterizing the cell-permeability, stability and toxicity of high affinity foldamer targeting the histone chaperone ASF1
Emma Maillard, B. Li, M. Perrin, A. Vitard, G. Moal, J. Mbianda, C. André, M. Teixerira-Nunes, M. Vandamme, G. Pinna, C. Douat, E. Thinon, R. Guerois, P. Legrand, F. Ochsenbein

P081 Rapid Assessment of Size, Shape, and Chemical Complementarity of Ligands for Computational Protein Design
Rokas Petrenas, Katarzyna Ozga, Joel J. Chubb, Andrey V. Romanyuk, Jennifer J. McManus, Graham J. Leggett, Nigel S. Scrutton, Thomas A. A. Oliver, Derek N. Woolfson

P086 A (poly)Pro tip for preserving native disulfide connectivity during thiol-maleimide bioconjugation of disulfide-rich peptides
Lylia Azzoug, Ana Novak, Hervé Meudal, Jean-Baptiste Madinier, Stéphane Charpentier, Karine Loth, Séverine Morisset-Lopez, Carlo Pifferi, Vincent Aucagne

P091 Random versus site-specific conjugation: impact on ADME properties of biologics with different format
Georgina Ilieska, Robert Thai, Carole Malgorn, Steven Dubois, Melissa De Souza, Camille Le Drezen, Justyne Vetel, Mathilde Keck, Antoine Sallustrau,Stephane Hua, Herve Nozach, Nicolas Joubert,Caroline Denevault-Sabourin,Laurent Devel

P095 Redox-Responsive Peptide Dimers to Stabilize and Release Therapeutic dsRNA
Marvin A. Albers, Niall M. McLoughlin, Zainab M. Rashid, David Dulin, Tom N. Grossmann

P097 Post-translational modifications regulate a synuclein aggregate structure and propagation properties
Yan-Mei Li

P100 Engineering Softness: How Molecular Tweeks in Coiled Coil Shape Hydrogel Behavior
Annelie Puhlmann, Cihan Baydaroglu, Merten Strehlau, Santiago Andres Ardila Fernandez, Boris Schade, Michael Gradzielski, Beate Koksch

P108 From inhibitor to affinity probe: Pepstatin A derivates enable AfBPP of plant aspartic proteases
Pierre Bena, Paula Dewes, Alexander Ciattoni, Leonardo González Ceballos, Bernhard Westermann, Pitter Huesgen, Mariana Schuster

P111 Conformational reprogramming of c-Myc via intracellular cyclisation
Rachel A. Johnson, Jody M. Mason

P116 Investigating the Synergistic Effect of Acetylation and Phosphorylation on Alpha-Synuclein Function Using Bioorthogonal Chemistry
Bernard Abakah, Marie Shimogawa, Grace Shin Hye Park, Elizabeth Rhoades, E. James Petersson

P120 Novel melanogenesis-modulating peptides for dermocosmetic applications
Carmen Gallo, Fosca Errante, Cristina Luceri, Paolo Rovero

P121 Peptide Therapeutics Targeting Drp1-Mid51 Protein-Protein Interactions to Preserve Mitochondrial Dynamics in Cardiovascular Disease
Rajkumar Khubiram, Liron Davis, Nir Qvit

P122 Electronic Reprogramming of Amylin Self-Assembly via Single-Residue Aromatic Tuning
Artem Pavlov, Hossein Batebi, Nicklas österlund, Kevin Pagel, Mario Schubert, Roland Netz, Beate Koksch

P123 Macrocyclic Molecular Glues for the 14-3-3/ChREBP Interaction; Affinity and Cooperativity in an Inverse Relationship
Merel van den Bosch, Marloes Pennings, Ansgar Oberheide, Carlo Verhoef, Christian Ottmann, Albert Markvoort, Galen Miley, Luc Brunsveld

P127 Lys acetylation and Ser phosphorylation crosstalk in the nucleosome binding domain of HMGN1
Medine Soydan, Anne C. Conibear

P128 Deciphering the Role of Posttranslational Modifications on the DNA-Binding Activity of Max Transcription Factor Using Chemical Protein Synthesis
Nithun Raj V, Yumi Minyi Yao, Omer Harel, Shada Khoury, Shaimaa Habiballah, Xiaoxi Lin, Ariel Afek, Muhammad Jbara

P130 Miniaturized HOXB13 Mimetics Are Sequence-Specific, Methyl-Sensitive DNA Binders
Claire Wong, Shiao.Y. Chow

P131 Enhancing Affinity of Peptide and Peptoid Ligands Using Boronic Acid-Catechol Reversible Dimerization
Elizabeth Bredice, Madeline Swanson,Thomas Kodadek, Skander Abboud

P132 Azapeptide Assembly Using Resonant Acoustic Mixing
William D. Lubell, Michael Quagliata, Justin Desjardins-Michaud, Nassim Maarouf-Mesli, Ida Boccino, Zahra Bigdeli, Felix Polyak

P133 Smart Amino Acid-based Nanovectors for RNA Anti-viral Therapeutics: Design, Synthesis and Physicochemical / Biological Characterization
Luisa do Vale, Sandra Silva, Pedro Cardoso, Isabel Oliveira, Eduardo Marques

P135 Synthesis of novel chiral peptoid-based metal chelators
Ludovica Dei, Bethany L Hardman, Gary J Sharples, Gaetano Angelici, Gennaro Pescitelli

P136 Downsizing The Histone H3-H4 Quaternary Structure Into Foldamer Mimetics Yields High-Affinity And Cell-Permeable Ligands Of Asf1
G. Guichard, B. Li, M. Perrin, E. Maillard, A. Vitard, G. Moal, J. Mbianda, C. André, M. T. Nunes, M. Vandamme, G. Pinna, C. Douat, E. Thinon, R. Guerois, P. Legrand, F. Ochsenbein

P138 Target-Directed Stapled Peptides through Dynamic Combinatorial Chemistry
Ashmi Rodrigues, Jose Garcia Coll, Delphine Ravault, Benjamin Zagiel, Ludovic Carlier, Lou Rocard, Roba Moumné

P139 Toward True avβ8 Selectivity: Cyclopeptide Ligands that Discriminate Homologous Integrins
Chiara Savian, Michela Spirelli, Andrea Sartori, Pietro Delcanale, Cristiano Viappiani, Monica Civera, Francesca Vasile, Laura Belvisi, Franca Zanardi, Lucia Battistini

P141 Design and synthesis of novel antibacterial oligourea foldamers
Kinga Chaniewicz, Paulina Bachurska-Szpala, Renata Kurek, Katarzyna Kozak, Karolina Pulka-Ziach

P144 Amino-acid based amphiphiles as chemical permeation enhancers, for transdermal drug delivery: Synthesis and In vitro permeation activity
Barbara Sampaio, Maria L.C. do Vale

P146 Development of a G protein mimetic toolbox to conformationally lock G protein coupled receptors (GPCRs) in the active state
Thijs Vynckier, Morgane Mannes, Morgane Rivoal, Charlotte Martin, Christel Menet, Toon Laeremans, Jean-Louis Baneres, Steven Ballet

P147 ?/a-Foldamers: Helical Constructs for asymmetric Catalysis
Junyan Xu, Dr. Saidul Islam, Prof. Andre Cobb

P148 Engineering Robust and Photoswitchable β-turns Through Hydrazide Incorporation
Samprete Bhattacharyya, Kalpita Baruah, Bani Kanta Sarma

P149 Comparison of conformational propensities of peptide backbones containing 1,5- or 1,4- disubstituted [1,2,3] triazoles
Francesco Brenzini Biagioni, Karine Porte, Pierre-Yves Renard, Anna Maria Papini

P152 Scalable Cyclic Peptide Synthesis Featuring Copper-Catalyzed Aldehyde-Alkyne-Amine Chemistry
Nassim Maarouf-Mesli, Felix Polyak, William D. Lubell

P154 Structure-Guided Synthesis of Triazole-Stabilized Peptidomimetics as Inhibitors of New Delhi Metallo-β-Lactamase-1
Msanif Msanif, M. Jewginski, F. Nuti, P. Rovero, A. M. Papini, R. Latajka

P156 Full Circle Chemistry: Expanding Macrocyclic Peptidomimetics
Jacob Simms, Oscar Shepperson, Michael Malone, Andrew Reid, Maxime Rouah, David Battersby, Andrew Jamieson

P157 Structure-Based Design Leads to uPA Loop Mimetic that Accumulates in uPAR-expressing Tumors in Mice
E. Vangeloven, S. Pollenus, M. Hosseini, T. Dal Maso, W. Versées, S. Ballet

P161 Controlling Nanonet Morphology via Residue-Specific Modulation of β-hairpin Peptide for Enhanced Bacterial Trapping
Wei Meng Chen, Dhanya Mahalakshmi Murali, Nhan Dai Thien Tram, Peiyan Yu, Daniel Tianyu Wang, Pui Lai Rachel Ee

P162 Trade-offs in Antimicrobial Peptide Activity: Faster Is not Always Better
Alessio Fragasso, Tatjana Schlechtweg, Wei-Hsiang Lin, Annelise Barron, Christine Jacobs-Wagner

P163 NMR-based Structure-Activity Relationship Studies of Antimicrobial Peptides
Michael Quagliata, Sonja Bazhenova, Joshua Grabeck, Philipp Holz, Anna Maria Papini, Paolo Rovero, Ines Neundorf, Daniel Friedrich

P165 Cyclo-(His-Phe) Complexes with Copper and Zinc Nanoparticles Have Targeted Anticancer Potential Against Osteosarcoma Cells
Anna Mitraki, Chrysanthi Pinelopi Apostolidou, Georgios Charalambidis, Aikaterini Gialouri, Maria Chatzinikolaidou

P166 SAR Study of Antimicrobial Peptide with Cross-Kingdom Activity
Aparna Palakkurussi Rathessan, Fereshteh Ghazisaeedi, Krithika Unmesh, Pascal-Kolja Bingül, Johannes Kupke, Suvrat Chowdhary, Dennis Hanke, Maria Andrea Mroginski, Marcus Fulde, Beate Koksch

P169 Mining bacteriophage endolysin structures for novel membrane-active antibacterial peptides
Monika Wojciechowska, Mateusz Wdowiak, Emil Stefanczyk, Joanna Trylska

P172 Development of an inhibitor of plasminogen activator inhibitor (PAI-1) for the treatment of inflammatory and fibrotic disorders
Eszter Erdei, Nikolett Varró Kormosné, Boldizsár Jójárt, Petra Pallagi, József Maléth, István Mándity

P180 Identification of novel peptide binders targeting TPP riboswitch in E. coli
Jinseo Park, Yujin Jung, Dasom Song, Jung Kim, Hong Gi Kim

P183 Antibacterial Activity of Novel Oncocin-Peptoid Hybrids
Jacopo Bucchioni, Bee Ha Gan, Markus Orsi, Robert Rauscher, Norbert Polacek, Jean-Louis Reymond

P184 Peptide-Daunomycin Conjugates Targeting Glioblastoma Cells
Levente Endre Dókus, Lili Szokolai, Viktor Farkas, Szilvia Bosze, Gábor Mezo

P185 Synthesis And Characterization Of Ferrocene-Peptide Conjugates With Antimicrobial Activity
Martina Rotondo, Annalisa Bisello, Saverio Santi, Fernando Formaggio, Simona Oancea, Teodora Calin, Anna Mkrtchyan, Liana Hayriyan, Tatevik Sargsyan, Cristina Peggion, Barbara Biondi

P188 Deciphering the Role of Citrulline and Cyclization in the Rational Design of Antimicrobial Peptides Derived from Equinin B
Andreja Jakas, Mariele Staropoli, Lea Pašalic, Anna Marin, Jasmina Tuzlak, Nermina Malanovic

P191 Stability and Antimicrobial Activity of Synthetic Peptides Derived from Lactoferricin B20-30
Tamara I. Pajpanova, Ivan P. Bogdanov, Momtchil Lambev, Georgi I. Ivanov, Silvia Mihaylova, Victor Sándor, Kveta Kalikova, Nikolay T. Tzvetkov, Ferenc Kilar

P192 Discovery Of An Antiviral Protease Inhibitor From Cytosorb Desorbate (Identification of SPINK1 from CytoSorb Desorbateas a Novel Antiviral TMPRSS2

Inhibitor)
Armando A. Rodriguez Alfonso, Jan Lawrenz, Nico Preising, Ludger Standker, Sebastian Wiese, Eberhard Barth, Frank Kirchhoff, Jan Münch

P193 ARHLFW: More than a cosmetic peptide
Y. Sarigiannis, A. Miliotou, T. Panayi, Ch. Petrou, P. Rodosthenous, P. Kaloumenos, C.M. Samiotou, M.V. Fronimou, C.M. Mikelis

P198 Discovery and membrane-selective bactericidal activity of Spat1, a novel cyclotide from Spigelia anthelmia L. (Loganiaceae)
Toluwanimi E. Akinleye, Latifat Sidiq, Alfred F. Attah, Roland Hellinger, Lisa Pabi, Nermina Malanovic, Omonike O. Ogbole, Christian W. Gruber

P202 An N-capping asparagine-lysine-proline (NKP) motif contributes to a hybrid flexible/stable multifunctional peptide scaffold
Joao P.F. Pimentel, Lai Y. Chan, E.S. Candido, D.F. Buccini, Samilla B. Rezende, Marcelo D. T. Torres, Karen G. N. Oshiro, Itala C. Silva, Sonia Goncalves, T.K. Lu, Nuno C. Santos, Cesar de la Fuente-Nunez, David J. Craik, O.L. Franco, M.H. Cardoso

P203 New peptide-based vaccines to target melioidosis
Krisztina Kiss, Julen Tomás-Cortázar, Siobhán McClean, Viktor Farkas, Kata Horvati

P207 Functional and Bioinformatic Analysis of Antimicrobial Peptide Derived from Lactic Acid Bacteria
Sylwia Nawrot, Natalia Czarnecka, Magdalena Jankowska, Agnieszka Jablonska-Wawrzycka, Patrycja Rogala, Grzegorz Czerwonka

P208 Mapping the G-Quadruplex Binding Determinants of a Vimentin-Derived Peptide by Alanine Scanning
Martina Rotondo, Nicola Dal Ponte, Marta Cozzaglio, Riccardo Rigo, Barbara Biondi, Claudia Sissi

P209 Design, Synthesis, and Biological Evaluation of Triazolyl-Bridged Antiviral Peptides Against Arboviruses
Shima Siadohoni, Michael Quagliata, Silvia Bracci, Rosaria Arvia, Simone Giannecchini, Anna Maria Papini, Paolo Rovero

P212 New antimicrobial peptides on the horizon: comprehensive investigation of bioactive peptaibols for future practical application
Dóra Balázs, ákos Rozsnyói, Henriett Hunkár, Gergo Terna, Fanni Kovács, András Szekeres, Mónika Varga, Csaba Vágvölgyi, Tamás Papp, Tamás Marik, Chetna Tyagi, László Kredics

P214 Synthesis and Antimicrobial Activity of Cyclic Temporin L Analogues via Non-Conventional Guanidinium-Based Functionalization
Ida Boccino, Rosa Bellavita, Bruno Casciaro, Paolo Grieco, Maria Luisa Mangoni, Francesco Merlino

P215 Design and characterization of monoclonal antibody peptide mimics
Lais Callo, Océane Ricloux, Quentin Laurent, Liliane Guerente, Véronique Frachet, Didier Boturyn

P216 Concentration-Dependent Mechanisms of Melittin-Induced Membrane Destabilization: an Interdisciplinary Approach
A. Chacón Calderón, P. Zelenovskii, M. Soares, E. C. Wrobel, O. N. Oliveira Jr., D. Pereira, M. Sardo, L. Mafra, I. Marin Montesinos, A. Barros-Timmons

P217 Guiding Peptide Nanonet Formation and Antibacterial Activity via Hydrophobic Aromatic Ring Engineering for Sepsis Control
Wei Meng Chen, Haoting Shi, Jun Hao Chiew, Ho Ying Low, Jan Kazimierz Marzinek, Din Bao Nguyen, Khai Shuen Heidi Lek, Zhi Wen Tay, Peter John Bond, Pui Lai Rachel Ee

P220 Broad-spectrum antiviral activity of Ranalexin-1G against respiratory viruses
Laura Di Clemente, Carla Zannella, Francesca Palma, Roberta Della Marca, Marina Acunzo, Carla Capasso, Annalisa Chianese, Rosa Giugliano, Anna De Filippis, Massimiliano Galdiero

P221 Rational structure-based design of potent antimicrobial peptides using artificial intelligence
Brigitte Fernández Garcia, Jordi Gómez Borrego, Roberto Bello Madruga, Marc Torrent Burgas

P224 Chemical Engineering of Transcription Factors Uncovers Cell-Permeable uMax Modulators
Omer Harel, Ferran Nadal-Bufi, Raj V. Nithun, Yumi M. Yao, Ariel Afek, Marc Vendrell, Muhammad Jbara

P225 In vivo evaluation using C. elegans, on the bioactive potential of synthesized dipeptides previously identified in Spanish dry-cured ham.
Noelia Hernandez Correas, Luis Tejada, Adela Abellan, Andrea M. Liceaga.

P226 Stereochemistry vs Linker: Exploration of Ring C Analogues of Antimicrobial Peptide Nisin
Fiona L. Kinnis, William T.P. Darling, Mate Erdelyi, Alethea B. Tabor

P227 Zwitterionic lipid head group influence on the adsorption of antimicrobial peptide to the model lipid membrane
Vedrana Krajnovic, Andreja Jakas, Danijela Bakaric

P228 Bioactive Skin Peptides from Caudate Amphibians: Structural and Functional Insights
Lorena Kröner, Jutta Meier, Marie-T. Hopp

P230 Development of new peptide-based antimicrobial agents targeting trans-translation in bacteria
Flore Miomandre, Andrés Corral Lugo, Olivier Delalande, Emmanuel Guidice, Sophie Chat, Francois-Hugues Porée,Charlene Gadais, Reynald Gillet

P232 Shortened Aurelin-Derived Peptides: The Role of Derivatization in Modulating Antimicrobial Efficacy
Lea Pašalic, Anna Marin, Jasmina Tuzlak, Nermina Malanovic, Andreja Jakas

P233 Multifunctional Short Chimeric Peptides: Potential Antimicrobial Activity and Enhanced Cell Proliferation for Tissue Healing
Naiara Maia Pereira, Reinaldo Marchetto

P234 Synthesis, Characterization and Microencapsulation of the Antimicrobial Peptide Ctx(Ile21)-Ha for Necrotic Enteritis Control in Broiler Chickens
Rayssa Piton Rijo Costa, Andrea B. Meneguin, Mariana Q. Nascimento, Cesar A. Roque-Borda, Silvio R. Teixeira, Marcus Chorilli, Eduardo Festozo Vicente

P235 Targeting the SARS-CoV-2 fusion mechanism: potent peptide inhibitors of the IFP-MPER interaction
Michael Quagliata, Maria Alfreda Stincarelli, Andrea Di Santo, Rosaria Arvia, Shima Siadohoni, Sonja Bazhenova, Feliciana Real-Fernandez, Daniel Friedrich, Simone Giannecchini, Anna Maria Papini, Paolo Rovero

P236 OBOC libraries targeting the SIRPa/CD47 axis: from combinatorial diversity to checkpoint modulation
Paula Quesada-Martinez, Macarena Sanchez Navarro

P237 Targeting beta-PIX SH3 domain-mediated protein-protein interactions in breast cancer using peptide inhibitors
Srijon Sen, Soumya De

P238 Rational Design of Melittin-Derived Peptides for Enhanced Biological Activity
M. Sleziak, J.J. Panek, T. Janek, A. Jezierska, K. Cieslik-Boczula, M. Kijewska

P239 Rational design and synthesis of bioactive miPEP205-derived fragments as modulators of Wnt/β-catenin signaling in triple-negative breast cancer
Francesco Tammaro, Carlo Irace, Maria Grazia Ferraro, Marialuisa Piccolo, Stefania Galdiero, Rosa Bellavita, Paolo Grieco

P245 Hydrophilic-Interaction-Chromatography (HILIC) as a Go-To Alternative for Synthetic Peptide Analysis and Purification
Yiping Wu, Daniel Tietze, Annika L. Weinmann, Linda Thunberg

P246 Bioassay-guided peptidomic characterization of antioxidant peptides generated from corn gluten meal using SSF-produced subtilisin BPN
N. Drulovic, M. Pavlovic, M. Ristovic, A. Leonardi, I. Krizaj, S. Orhanovic, B. Dojnov, M. šokarda Slavic

P247 Comprehensive Chromatographic and Mass Spectrometric Approaches for in Vitro Analysis of Site-Specific Antibody-Peptide Conjugates
Niklas van den Bergh, Eric Mühlberg, Barbara Roether, Walter Mier

P248 Engineering the MALDI interface for in situ detection of modified peptides in synovial fluids : application to osteoarthritis diagnosis
Ugo Pasco, Lomane Berthy, Emeline Groult, Robert Thai, Fabrice Beau, Daniele Noel, Laurent Devel, Gilles Subra, Sonia Cantel

P250 Transfer Learning for Prediction of Liquid-Liquid Phase Separation
Karlo Barjaktaric, Patrik Paunovic, Leonard Lecic, Erik Otovic, Joana Calvário, Ana Sofia Pina, Yoshimasa Kawaguchi, Daniela Kalafatovic, Goran Mauša

P251 Computational approaches for analysis and design of peptides containing non-canonical amino acids
Rodrigo Ochoa

P252 AI-driven generative peptide design targeting GC-C dimer for Parkinson's
Elpiniki Paspali, Lars van der Heide, Ioana M. Ilie

P256 PeptiDesCalculator 2.0: a next-generation descriptor platform for peptide informatics, sequence analysis, and QSAR modeling
Laureano E. Carpio, Rafael Gozalbes, Eva Serrano-Candelas

P257 Beyond natural amino acids: extending immunogenicity risk assessment to non-canonical peptide drugs through chemical feature encoding
Maria Cairoli, Catherine Betts, Morten Nielsen, Olga Obrezanova, Leonardo De Maria

P261 An Integrated Ai-Guided Pipeline For Antimicrobial Peptide Discovery And Optimization
Maryam Nawaz, Ma Tianyue, Fahad Akhtar, Liu Hongyu, Amna Farooq, Heng Zheng

P263 Decoding Pentapeptide Self-Assembly Using Molecular Dynamics: From Aggregation To Architecture
Shimanto Roy, Camille Bilodeau, Kyle Lampe

P264 Active Learning-Driven Surrogate Modeling for the Generative Discovery of Self-Assembling Peptides
Denis Ibiši, Daniela Kalafatovic, Goran Mauša

P266 Peptides involved in interaction with heavy metals for environmental remediation, an in silico approach.
Ximena Carolina Pulido, Hector Fabio Cortes Hernandez, Cesar Jaramillo-Páez

P267 Adaptive Evolutionary Optimization for the Discovery of Self-Assembling Peptides
Milica Injac, Ena Drazic, Marko Njirjak, Gordana Rakic, Daniela Kalafatovic, Goran Mausa

P268 Machine Learning-driven Prediction of Circular Dichroism Spectra for Peptides through Multi-scale Structural Descriptors
Michele Casoria, Marina Macchiagodena, Paolo Rovero, Claudia Andreini, Anna Maria Papini, Marco Pagliai

P269 Inverse folding improves structure prediction for confidence-aware peptide deorphanization
Alexis Dougha, Samuel Murail, Jerome Leprince, Pierre Tuffery

P270 Can we Confidently Sequence the Peptide Dark Matter? Reaching a Consensus for De Novo Peptide Sequencing
Sebastian Johannes Eder, Manuela Schmidt, David Gomez-Varela

P274 AI-driven discovery of cross-kingdom peptide ligands
Marin Matic, Alexander S. Hauser

P275 TFA-Free Cleavage and Deprotection in Solid-Phase Peptide Synthesis: Advantages and Drawbacks of Formic Acid
Maria Leko, Polina Filippova, Sergey Anisimov, Andrey Murko, Sergey Burov

P276 Application of an Automated System for Flow Solid Phase Peptide Synthesis
Manish Kumar, Łukasz Berlicki

P277 Green Liquid-Phase Peptide Synthesis (LPPS) Methodology for the Sustainable Production of Therapeutic Peptides
Naoki Nishizawa, Haruka Machida, Ryo Hatakochi, Yuji Mimori, Akihiro Nagaya, Michiharu Handa

P278 Tag-Assisted Peptide Synthesis (TAPS) - Development of a continuous liquid-phase process
Stefan Peters, Tim Kramer, Mareike Helmdach, Fabian Hogenkamp, Andreas Heindl

P280 Racemization-Free Peptide Synthesis In Water Under Batch And Flow Conditions
Sri Hari Anandhi Rajendran, Sándor B. ötvös, C. Oliver Kappe, Wilfried M. Braje, Matthew Burns

P283 Reusable Photoredox Catalysts for Sustainable Peptide Synthesis
Kelly Materna, Duilio Bacigalupo

P284 TBDC Salts: Advanced Coupling Reagents For Liquid Phase Peptide Synthesis (Lpps)
Nicola Patrian, Dario Corbisiero, Riccardo Grigolato, Alessandra Tiberti, Leonardo Rapisarda, Lucia Ferrazzano, Alessandra Tolomelli, Walter Cabri

P286 ?-Valerolactone-sulfuric acid: a sustainable alternative to TFA for efficient peptide cleavage and global deprotection
M.C. Scala, M. Rega, M. Landi, P.Campiglia, M.Sala

P289 Chemo-Selective Catch-and-Release Purification: An Orthogonal Alternative When Chromatography Fails
Robert Zitterbart, Dominik Sarma

P290 Towards Greener Solid-Phase Peptide Synthesis: Combining a Novel Support with Eco-Friendly Solvents
Luana Lastella, Marco Zecca, Paolo Centomo, Karel Jerabek, Fernando Formaggio, Ivan Guryanov, Marco Macis, Antonio Ricci, Barbara Biondi

P293 Enantioselective synthesis of antiplasmodial cyclic tetrapeptide Koshidacin A
Preeti Kapri, Devki Nandan, Ramesh Ramapanicker

P295 Fishing for Function: From Predicted Binding to Functional Block by a Cone Snail Peptide
Izhar Karbat, Sapir Nutkewitz, Daria Adam Steinberg, Maital Katz, Eitan Reuveny

P296 Efficient TEV tag-assisted one-pot protein semisynthesis
Benoit Snella, Magalie Sénéchal, Jérome Vicogne, Vangelis Agouridas, Oleg Melnyk

P297 Beyond SMCC: Uniform Isothiocyanate-Peptide Bioconjugates
Barbara Roether, Eric Mühlberg, Niklas van den Bergh, Uwe Haberkorn, Walter Mier

P299 Glycerol-derived drop-in solvents for sustainable and more efficient peptide synthesis
Vincent Freiburghaus, Tom Nelis, Jeremy Luterbacher, Nina Hartrampf

P300 Towards the improvement of non-canonical amino acid incorporation via Decoupled Synthesis of Ribosomes (DeSyR)
Benedikt Golisch, Anton Meier, Martin Weissenborn

P302 Eco-Friendly SPPS: overcoming challenges in cosmetic Argireline production
Lucrezia Sforzi, Fosca Errante, Robert Zitterbart, Manoj Kumar Muthyala, Stephan Lüdtke, Dominik Sarma, Anna Maria Papini, Paolo Rovero

P303 Selective peptide bond formation via side chain reactivity and self-assembly of abiotic phosphates
Arti Sharma, Kun Dai, Charalampos G. Pappas

P304 Analogs of [D-Phe4]CJ-15,208 with modifications to improve kappa opioid receptor antagonist potency in the CNS as potential treatments for substance abuse
Jane Aldrich, Jeremy Coleman, Moustafa Hamaad, Brian Knapp, Ryosuke Shinouchi, Megan Quinones, Andrew Watson, Shainnel Eans, Jean Bidlack, Jay McLaughlin

P305 Decoding Heme-Gai Protein Crosstalk with Peptide Tools
Sabriye Aydogdu, Sonali M. Vaidya, Diana Imhof

P307 Discovery and Optimization of an mRNA Display Cyclic Peptide inhibitor of the IL1b/IL1R Interaction
Stefania Colarusso, Francesca Pavone, Elisabetta Bianchi, Roberto Iaccarino, Emanuela Mandic, Emanuela Nizi, Willy Costantini, Martina di Geronimo, Faben Cruz, Dennis Feng, Yan Guo, Jennifer Hanisak, Charles Jayne, Ahmet Kekec, Angelea Kerekes, Victor Mak, Michael Lo, Jennifer Hickey, Christopher Plummer

P312 Discovery of Potent RSV Peptides Antivirals
Origene Nyanguile, Nadege Pidoux, Stéphane Duquerroy, Mathilde Keck, Thibaut Larcher, Marie Galloux

P313 Developability screening of pharmaceutical peptides
Marie Pedersen, Rodrigo Ochoa, Mathias Norrman, Christian Tornoe, Sebastian Swanson, Jacob Larsen, Stephanie Hansen, Alexander Büll

P314 Two New Orbitides, [1-10-NaC]-croheorbs A1 and A2, Isolated from the Latex of Croton heliotropiifolius
Suzana A. S. Queiroz, Ana Leticia P. Dos Santos, Paula Rezende-Teixeira, Leticia Costa-Lotufo, Vanderlan S. Bolzani

P315 Chemical synthesis and evaluation of insulins derived from a venom insulin of the cone snail Conus geographus

Nicholas Schumann, Amber Vogel, Reza Moosavi, Zildjian Acyatan, Christopher Hill, Helena Safavi-Hemami

P317 Targeting Neurodegenerative Diseases with Priavoid's Peptide Drug Development Platform
Mathias Wendt, Marc Sevenich, Kira Allmeroth, Gina Hartmann, Karolina Korostov, Antje Willuweit, Dieter Willbold

P319 A cardiolipin-targeting a-helical bundle peptide stabilizes inner membrane of mitochondria, down-regulating ALCAT1 to shut down pathogenic remodeling in oxidative stress condition
Yoonhwa Choi, Tae Yeon Kim, Hyeong Woon Choe, Gwangsu Shin, Seung Hee Yang, Hyo Youl Moon, Jaehoon Yu

P325 Mirror-Image Random Nonstandard Peptides Integrated Discovery (MI-RaPID) Technology Yields Highly Stable and Selective Macrocyclic Peptide Inhibitors for Matrix Metallopeptidase 7
Hiba Ghareeb, Choi Yi Li, Anjana Shenoy, Naama Rotenberg, Julia M. Shifman, Takayuki Katoh, Irit Sagi, Hiroaki Suga, Norman Metanis

P327 A PCSK9 Vignette: From mRNA Display to Passively Permeable Macrocycles
Yuhua Huang

P328 Preparation of peptides and their inhibitory activity effects against BACE1
Shinji Katsuoka, Daisuke Nakashinn, Taeko Kakizawa

P330 Novltex: A New Class Of Antibiotics With Potent Activity Against Multidrug Resistant Bacterial Pathogens
Esra Malkawi, Anish Parmar, Ishwar Singh

P331 Optimization and Selection of ASF1-Binding Peptides with optimized quantitative bacterial two-hybrid Using qB2H
Francoise Ochsenbein, Antoine Guyot, Emma Maillard, Kelly Ferreira-Pinto, Laure Plancon-Arnould, Aravindan A. Nadaradjane, Raphael Guerois, Loic Martin, Oscar H.P. Ramos

P333 Unlocking Macrocycles at Scale with nGen: Integrated High-Throughput Synthesis and Generative AI
Herve Siendt, Mischa Schüttel, Zander Harteveld, Sevan Habeshian, Chiara Toniolo, Sara Cristinelli

P334 Amide-to-Chloroalkene Substitution as Peptide Backbone Modification for Enhancement of Membrane Permeability
Sayuri Takeo, Mio Takeda, Chihiro Iio, Ai Sakakibara, Showmitra Saha, Natsuki Shibata, Yuki Yamazaki, Takahiro Fujii, Ryuhei Harada, Kohei Sato, Nobuyuki Mase, Mizuki Watanabe, Takanori Oyoshi, Tetsuo Narumi

P336 Mapping and Linking Druggable Sites on Rad6 Using Proteomimetic Fragments and AI-assisted Design
E. Wéber, F. Bogár, B. Nagymihály, M. R. F. Mohamed, é. Bartus, A. Tököli, Z. Kupihár, G. M. Keseru, T.A. Martinek

P337 RaPID Selection of Nonstandard Thioisoindole-Bridged Bicyclic (TiB) Peptides Targeting TNIK
Yue Zhang, Hiroaki Suga

P339 Affibody-mediated Peptide Nucleic Acid Pretargeting Using Dual Hybridization Sequences for Increased Therapeutic Potential
Jacob Clinton, Kristina Westerlund, Amelie Eriksson Karlström

P344 New Positive Allosteric Modulators for u Opioid Receptor from Oxytocin
Takaaki Mizuguchi, Kanako Miyano, Ami Yamazaki, Hideki Takahashi, Risa Yamauchi, Yuki Yoshida, Haruka Ono, Miku Inagaki, Miki Nonaka, Yasuhito Uezono, Hideaki Fujii

P346 Design And Synthesis Of Novel Desmuramyl Peptide Glycoconjugates
Vesna Petrovic Perokovic, Zeljka Car, Jelena Pavic, Luka Sumic, Rosana Ribic

P347 PDGF-Derived Peptides: From Receptor Binding To Cellular Signaling In Wound Healing
Krzysztof Polaczek, Przemyslaw Karpowicz, Malgorzata Zawrzykraj, Milena Deptula, Michal Pikula, Emilia Ilowska, Rafal Slusarz, Emilia Sikorska

P354 Targeting HER2-Positive Breast Cancer With a New Affibody-Nanodrug System
Ewa Wieczerzak, Milena Czeszejko, Patrycja Rachubik, Daria Sowik, Justyna Sawicka, Kamila Kitowska, Rafal Sadej, Sylwia Rodziewicz-Motowidlo

P356 Synthesis And Characterization Of Thermo-responsive Magnetic Molecularly Imprinted Polymers For Selective Recognition Of Peptide-drug Conjugates
Sima Alvani Alamdari, Justyna Fraczyk, Sebastian Schwaminger

P357 Synthesis of PLGA Nanoparticles Encapsulated with Immunodominant MOG35-55 Peptide Analogues for the Treatment of Multiple Sclerosis
Georgia Biniari, Iro Triantafyllakou, Carmen Simal, Spyridon Mourtas, Theodore Tselios

P364 Novel macrocyclic peptide-based uPAR-targeting fluorescent probes for intraoperative fluorescence imaging
Tuule Treiberg, Nadia Hajib, Kasper Kildegaard Sorensen, Mikkel Boas Thygesen, Karina Straede, Knud Jorgen Jensen, Andreas Kjaer

P368 From small molecules investigated as Factor XIIIa Inhibitors to biological target diversity
Ivan P. Bogdanov, Nikolay T. Tzvetkov

P369 A Cardiolipin-Targeting a-Helical Bundle Peptide forms Self Assembled Trimer to Facilitate Cell Penetration and Stabilizes Inner Membrane to Rejuvenate Mitochondrial Dysfunction
Hyeong Woon Choe, Yan Lee, Jaehoon Yu

P370 Design And Development Of Novel Low-Molecular-Weight Carboxamides As Dual Modulators Of Mao-B And ?-Synuclein
Georgi I. Ivanov, Nikolay T. Tzvetkov

P371 Harnessing nature's defences to treat gut biofilms
Bernhard Jandl, Michaela Lang, Athanasios Makristathis, Christoph Gasche, Markus

Muttenthaler

P373 Multifunctional Bone-Targeting Peptides for Inhibition of the RANK-TRAF6 Interaction
Sofia Martins, Catia Rosa, Marco Cavaco, Rita Melo, David Andreu, Javier Valle, Vera Neves, Miguel Castanho, Sandra Casimiro; Joao Correia

P376 Development of PNA-Peptide Chimeras targeting G-quadruplex structures
Matilde Rossi, Paola Gratteri, Ines Neundorf, Carla Bazzicalupi, Daniel Friedrich, Anna Maria Papini

P377 Antidiabetic Effects of Cyclotide-Rich Extracts from Selected Nigerian Medicinal Plants: An Ethnopharmacological Approach
Latifat O. Sidiq, Abraham O. Nkumah, Omonike O. Ogbole

P378 Targeting GLP-1 Receptor and DPP-4 Enzyme for Diabetes Drug Discovery
Aditi Singh, Soumendra Rana

P379 Mechanistic Insights into Antimicrobial Peptide-Extracellular Vesicle Interactions and Therapeutic Applications in Sepsis
Tasvilla Sonallya, Tünde Juhász, Imola Cs. Szigyártó, Kinga Ilyes, Kata Horvati, Yumi Kumagai, Zoltán Varga, Tamás Beke-Somfai

P381 Non-destructive quantification of peptide trifluoroacetates
Charity D. Yongo-Luwawa, Nassim Maarouf-Mesli, Ida Boccino, Karen C. Waldron, William D. Lubell

P384 A Nanometric Platform for Live Cell Multiplex Screening of Non-natural Peptides
Sinyal Abu-Rabia, Danit Zagiel, Coral Yohay, Gila Kazimirsky, Gerardo Byk

P386 Innovative phage display libraries for precision protein targeting
Cristina Diaz-Perlas, Benjami Oller-Salvia, Christian Heinis

P388 Assessing the Efficacy of Peptides on Acute Coronary Syndrome In-vivo
Offir Ertracht, Rani Wainer Shlomo, Mulate Zerihun, Shulamit Fluss Ben-Uliel, Shmuel Silitsky, Samar Gani, Liron Davis, Mona Shehadeh, Tali Reuveni, Shaul Atar, Nir Qvit

P389 Microfluidics-Driven Assembly of Sonoresponsive Peptidic Nanoparticles for Ultrasound-Mediated Gene Delivery
Guy Gouarin, Vicentiu Moraru, Samir Cherkaoui

P393 Application of Antibody Site-Specific Modification Method tCAP to Brain-Penetrating Antibody-Oligonucleotide Conjugate
Yuji Ito, Abdur Rafique, Hiroko Kawakami, Taku Yoshiya

P394 Engineered Peptide-Based Nanosystemsfor Improving Therapeutic and Diagnostic Potential of Anticancer agents
Prashant Mishra, Ritu Bhardwaj

P399 Multifunctional Bioactive Cotton: Synergistic Antimicrobial and Regenerative Properties through Chemoselective Peptide Conjugation
Francesca Albini, Adriana Di Stasi, Mario Mardirossian, Barbara Biondi, Cristina Peggion

P400 Hybrid Peptide Functionalized Nanoparticles For Breast Cancer Therapeutics
Priyanshu Priya, Peter M Moyle, Zyta M Ziora, Prashant Mishra

P401 Making new PALs: A Directed Evolution Platform for Rapid Peptide Asparaginyl Ligase Engineering
Simon Tang, James Leech, Zihao Song, Louis Luk, Jody Mason

P403 Development of pH-Responsive Peptide Systems for mRNA-Mediated Antimicrobial Peptide Delivery
Hala Alnasif Alhadi, Tam T. Bui, Jenny Lam, Vincenzo Abbate, A. James Mason

P404 Peptide Stability in GMP-Manufacturing: Minimizing Risk to Peptide Drugs from Single-Use Assemblies
Stephanie Bellmaine, Sarah Parsons

P405 A Multifunctional Thermoresponsive Micellar Hydrogel System for Targeted Skin Depigmentation, Enhanced Dermal Penetration, and Extracellular Matrix Stimulation
Yajima Campos Mora, Luis Javier Cruz, Yaimara Solis, Julio Cesar Aguilar, Gerard Esteruelas, Elena Sanchez, Marta Espina

P408 Engineering Anticancer Peptides To Improve Oral Bioavailability Via Lipidation
Giuseppina Guida, Aurelie Benfield, Nicole Lawrence, Sonia T. Henriques

P411 Peptide-Based Surface Engineering of Biomimetic Liposomes for Biomedical Applications
Giulia Lodigiani, Roberto Frigerio, Alessandro Gori, Francesca Baldelli Bombelli, Greta Bergamaschi

P412 The development of topical formulations of liposomal micrococcin P1 for wound infections
Bezael Gurmessa, Colin Charnock, Kirill Ovchinnikov, Tage Thorstensen, Sanko Nguyen

P413 Preliminary evaluation of the stability of a liposomal formulation of OmegaCalm based on active peptides for cosmetic applications
Y. Solis, Yaima Campos, Julio Cesar Aguilar, Gerad Esteruelas, Elena E. Sánchez, Luis Javier Cruz

P419 Peptidoglycan-Based Biomimetic Nanomaterials Reveal Lectin Recognition In Dap-Type Bacteria: Toward Rational Design Of Antimicrobial Therapeutics
R. Frkanec, Marcela šišic, Anne Imberty, Antonija Tomic, Andrea Usenik, Vladislav Tomišic, Leo Frkanec

P420 Peptide Microarray Platform For High Throughput Discovery And Optimization Of Protein-Binding Peptides
Sravanthi Guggilapu, Ryan Clark, Geoff Eddinger, Ken Lo, Sarah Fahlberg, Eric Sullivan, Lauren Goodrich

P422 Phage display validation of lysosomal targeting receptors for the treatment of lung cancer
Vanesa Nozal, Petar Petrov, Juan Sebastián Ruiz, Benjami Oller-Salvia, Cristina Diaz-Perlas

P424 Characterization of a Novel Thiazole-Installing RiPP Maturase from Acidobacteriota
Dora Racunica, Daniel Richter, Anda Pop, Jörn Piel

P425 Transcending Amino Acid Limitations: Enzymatic Halogenation for Phage Display Diversification
Richard Schreiter, Leonard Kaysser, Christina Lamers

P426 ADMET of peptides: Are we there yet?
Canay Yildiz, Nicola Köhler, Amy Park, Toni Kühl, Diana Imhof

P429 Rational Design of Fc-Binding Peptide Ligands as Next-Generation Alternatives to Protein A for Antibody Purification
Tuba Polat, Alp Ertunga Eyupoglu, Ahmet Can Timucin, Batu Erman, Tanil Kocagoz, Ozge Can

P430 Bifunctional de novo peptides to tackle antimicrobial resistance
Lucie Bastien, Emna Ben El-Hadj Salem, Pauline Samper, Mehavi Mehavarnan, Eric Pardoux, Arnaud Buhot, Muriel Jourdan, Didier Boturyn, Sandrine Boisset, Yoann Roupioz

P435 Design of smart peptide-based nanoparticles for siRNA delivery in gastrointestinal stromal tumors (GIST)
Thania Hammoum, Jules Vastra, Julien Fabre, Karidia Konate, Eric Vives, Sandrine Faure, Pascal de Santa Barbara, Sébastien Ulrich, Prisca Boisguerin

P438 Self-assembly control with hydrophobicity gradients in short peptide sequences
Irene Toledo, Natalia Baranova, Ivan Sasselli

P439 Nuclear Delivery of Antibodies for the Modulation of TDP-43 Liquid-Liquid Phase Separation
Daisuke Yamasaki, Yoshimasa Kawaguchi, Miki Imanishi, Shiroh Futaki

P440 Synthesis of MUC1 Tn/Sialyl-Tn Glycopeptides and Combinatorial Libraries for Lectin Binding Studies
Mare Cudic, Ivet Boneva, Ramya Ayyalasomayajula, Donella Beckwith, YashoNandini Singh, Sabine Andre, Herbert Kaltner

P442 Impact of glycoclustering on the structure of mucin peptides
Oliver Seitz, Arseniy Galashov, Elisabetta di Gregorio, Polina Ponomareva, Marc Safferthal, Ekaterina Kazakova, Leila Bechtella, Kevin Pagel, Marina Pigaleva, Benesh Joseph, Kim Greis, Lyna Bourehill, Renato Zenobi

P443 Target, Capture, Treat -Peptide Nucleic Acid (PNA)-Guided Pretargeting for HER2-Targeted Antibody-Mediated Radionuclide Therapy
Kristina Westerlund, Mohamed Altai, Wahed Zedan, Jacob Clinton, Susanne Geres, David Ulmert, Amelie Eriksson Karlström

P444 Parallel-Stranded Design of Peptide Nucleic Acids for Efficient Recognition of Double-Stranded DNA
Yuichiro Aiba, Masanari Shibata, Hiroshi Sugimoto, Osami Shoji

P446 Biosynthetic Peptide Screening Platform for various Drug Discovery and Delivery
Shin Izuta, Taishi Fuda, Hiroki Takahashi, Koo Suzuki, Nao Yamazaki, Anri Nishiguchi, Tomoki Ota, Ryo Ukekawa, Yukiko Ishii

P447 Structural characterization of fatty acid modifications in ribosomally encoded N-acylated lipopeptides
Julien König, Johannes Eckert, Ian Yunus, Gabriel Cervera Arriaga, Anna Vagstad

P449 Radiolabelling in the New Age of Peptide Therapeutics
Cian Reid, Roger Glanville, Yukuang Guo, Eric Ballard, Sean Zhu

P453 Peptide-Oligonucleotide Conjugates: Effect on Endosomal Escape?
Fie Davidsen, Kolfinna Hjálmarsdóttir, Adrian Hernandez, Ewa Sitarska, Anand Saminathan, Tom Kirchhausen, Knud J. Jensen

P454 Investigation of the interactions between mannosylated desmuramyl peptides and mannose-binding proteins
Marija Paurevic, Vesna Petrovic Perokovic, Zeljka Car, Rosana Ribic

P455 Synthesis and FRET-Based Cleavage Study of an aVβ6-Targeting Peptide Drug Conjugate
Caroline Brinkmann, Andreas Brockhinke, Norbert Sewald

P457 Photocatalytic Proximity Labelling to Probe Cell Surface Glycan Interactomes
Jerrard Hayes, Mia Huang, Eoin Scanlan

P458 Engineering antimicrobial peptides through nanocarrier surface design and intracellular targeting for tuberculosis therapy
Cesar Augusto Roque-Borda, Laura MDG Primo, Christian S.C. Canales, Eduardo F. Vicente, Joao Perdigao, Beatriz G. de la Torre, Fernando Albericio, Henrik Franzyk, Paul Robert Hansen, Fernando R. Pavan

P459 De novo Design and AI-supported Flow Synthesis of Catalytic Miniproteins
Manish Kumar, Ewa Rudzinska-Szostak, Anna Szczepanska, Lukasz Berlicki

P461 Deciphering the Fluorous Effect in Protein Quaternary Assembly
David Reiter, Jacob S. Jordan, Javier Camargo Diaz, Malkeet Singh, Moritz Engl, Kevin Pagel, Beate Paulus, Mario Schubert, Christian Roth, Beate Koksch

P464 Exploring the Design Space of 310-helical Bundles using Non-canonical Amino Acid
Xiyue Leng, Jonathan Clayden, Derek N. Woolfson

P466 Uncovering the structural logic of Cnn autoinhibition: an integrative NMR, SAXS, and AlphaFold approach
Arthur Vitard, Abir Elfarkouchi, Nicolas Joly, L. Mammri, Sébastien Brier, Lola Tanneur, Cécile Hu, Aurélien Thureau, Nicolas Joly, Francoise Ochsenbein, Paul Conduit

P469 Evolutionarily Conserved Amyloid Architecture in the PACAP–Glucagon Peptide Superfamily
Dániel Horváth, Zsolt Dürvanger, Szebasztián Szaniszló, Anna Kiss-Szemán, Duong Kim Hoang Yen, Michael Hons, Meytal Landau, András Perczel

P470 Twist in the Tail: Capping Turns Modulates Collagen Thermal Stability
Aritra Naha, Amar Ghosh, Bani Kanta Sarma

P474 NMR - Restrained Structural Elucidation of Mitoxantrone Conjugates with GnRH Peptide Analogues
Carmen Simal, Georgia Biniari, Haralambos Tzoupis, Nikitas Georgiou, Thomas Mavromoustakos, Theodore Tselios

P475 Stabilization of Helical Structures in Oligopeptides Through Modification of Phenylalanine Residues
Vikrant Vini, Jisna T., Prema G. Vasudev, Ramesh Ramapanicker

P476 Conformational complexity of the disordered N-terminal region in biological function of tumor suppressor p53 protein
Elena Zindovic, Moath Yousef, Edwige Voisset, Vladimir Torbeev

P478 Conformational Effects of Fluorinated Aminocyclopropane Carboxylic Acids Incorporation in Peptides
Eliott Roy, Zoé Weber, Baptiste Legrand, Thomas Poisson, Ludovic Maillard, Philippe Jubault, Florine Cavelier

P479 Turning Peptides with Cyrene-Derived Amino Acid Residues
Kajumee Bora Bhowal, William D. Lubell

P483 Dual Peptide Strategy for Enhanced Rescue of Mutated CFTR Channel Function in Cystic Fibrosis
Prisca Boisguérin, Clémentine Teko-Agbo, Chloé Felgerolle, Maha Sinane, Karine Delétang, éric Vives, Magali Taulan Cadars

P484 Cyclic Peptide-Based Platform for Targeted Delivery to the Brain
Predrag Cudic, Harrison Hutchings, Aleksandra Nedovic, Lucas Costa

P487 A helical peptide antagonist of the human growth hormone receptor
Justin M. Holub, Khairun Nahar, Reetobrata Basu, Arshad Ahmad, Joseph A. Pettis, Udani Gamage, John J. Kopchick

P493 Evolution Did Not Eliminate Aggregation: Functional Amyloids Enable Hormone Storage and Signaling
Dániel Horvátha, Zsolt Dürvanger, Szebasztián Szaniszló, Anna Kiss-Szemán, Duong Kim Hoang Yen, Michael Hons, Meytal Landau, András Perczel

P494 Molecular Mimicry by Venom Peptides
Samuel D. Robinson

P500 Pullulan-Based Microcondensates with Cationic Peptides for Efficient Cytosolic IgG Delivery

J. Michibata, Y. Kawaguchi, S. Futaki

P501 Photoisomerization-Dependent Glycan Binding of Engineered Lectin-like Peptides: Toward Light-Controlled Bioactivity of Lectins
Serhii Kharchenko, I. Semchuk, A. Cherednichenko,V. Hryhorieva, S. Afonin, I. V. Komarov, Anne S. Ulrich

P502 Design and synthesis of therapeutic peptides with anti-inflammatory and regenerative properties for use in the treatment of equine gastric ulcer syndrome (EGUS)
Kinga Marszalek, Ewa Wieczerzak, Krzysztof Marycz, Sylwia Rodziewicz-Motowidlo

P506 A Modular Neuropilin-Hsv Derived Rf-Tuftsin Platform For Targeted Delivery: Validated In Spheroids And Epithelial Barrier Models
K. Uray, M. Krátky, E.L. Méhes, F. Sebák, A. Bodor, F. Zsila, T. Visnovitz, T. Bárkai, F.K. Grébecz, K. Fodor, L. Lakatos, R. Oláhné Szabó, J. Horcic, J. Vinšová, S.E. Bosze

P511 Selection, synthesis and interaction of hACE2 peptide fragments towards spike protein of the SARS-CoV-2 virus
Aleksandra Czerchawy, Manoj Muthyala, Feliciana Real-Fernandez, Francesca Nuti, Paolo Rovero, Anna Maria Papini, Beata Kolesinska

P512 An opioid-neurotensin hybrid outperforms morphin in acute and chronic pain models
L. Durand-Baudet, J. De Neve, E. Breault, S. Gonzalez, V. Utard, E. Vangeloven, F. Simonin, P. Sarret, S. Ballet

P516 Rational Design and Structure-Activity Relationship of Spider- and Snake-Venom-Derived Peptides Targeting Acid-Sensing Ion Channels
Nataliia Petlovana, Serhii Kharchenko, Tessa Sussek, Vladyslava Hryhorieva, Fabian Hoffmann, Illia Hutskalov, Iryna Semchuk, Sergiy Afonin, Jan Tytgat, Anne Ulrich

P517 Design of biased GPCR modulators by combining artificial intelligence and molecular simulation
Alaa Reguei, Samuel Murail, Serge Luquet, Franck Oury, Pierre Tuffery

P519 Targeted Inhibition of Fis1/Mfn1 Protein-Protein Interactions with Peptides Promotes Cardioprotection
Ayetenew Abita, Hellena Shumaff, Liron Davis, Nir Qvit

P521 Enhancer-driven changes in Peptide Permeability on In Vitro models
Josip Mihalac, Astrid Milic, Daniela Kalafatovic

P522 A multimodal molecular toolbox for in vitro and in vivo studies of the oxytocin receptor
Monika Perisic Böhm, Predrag Kalaba, Erik Keimpema, Rachel S. Gormal, Frédéric A. Meunier, Thierry Langer, Karine Mardon, Christian W. Gruber, Markus Muttenthaler

P523 AI-Guided Discovery of Anti-Inflammatory Peptides from Edible Rhizomes and Root Vegetables
Kruttika Purohit, Mitchell Low, Fabien Plisson, Evan Hayes, Anwar Sunna

P524 Evaluation of Different Photocaging Strategies to Develop Next-Generation Photoprobes
Konstantin Raabe, Predrag Kalaba, Hilary Yong, Greta Crudeli, Sarah Melzer, Victor Anggono, Erik Keimpema, Markus Muttenthaler

P526 Dynamic PEGylation of Peptide-based Nanoparticles for siRNA Delivery
Jules Vastra, Thania Hammoum, Prisca Boisguérin, Sébastien Ulrich

P528 Graphene Oxide-Peptide Nanofibers As Platforms For Cell Bioactive Responses
C. Garcia Delgado, A. Sánchez-Temprano, I. Obregón-Gómez, MV. Sulleiro, A. Criado, E. Pazos

P529 Hydrogel Formation Via Base-Triggered Conversion Of A Peptide Progelator
Ana M. Garcia, Yasmina Berruga, Polina Topalska, Pilar Prieto, Daniel Iglesias

P530 Peptide-functionalized Nanocoatings for Prevention of Biofouling and Device-Associated Infections
Shubhi Joshi, Avneet Saini

P532 Sequence-Programmed Control of Coacervate Stabilisation Mechanisms Using Modular Peptides
Roi Lopez-Blanco, Willem van den Hout, Sander Huisman, Jan C. M. van Hest

P533 Data-Driven Mapping of Interfacial Properties of Pure and Multicomponent Peptide Amphiphiles
Justin Houx, Marco Kong, Octavia Tao, Pim Dankloff, Gijs Martens, Joost Hoeksel, William Robinson, Wilhelm Huck, Mathijs Mabesoone

P535 A peptide interface for collection and functional analysis of migrasomes
Mina Okochi, Shogo Saito

P538 Optically switched transient amyloid-like fibrils for antibiotic degradation
Shubhra Kanti Bhaumik, Sisira Mambram Kunnath, Elad Arad, Einat Nativ-Roth, Arunavo Chatterjee, Albert Batushansky, Nitzan Shauloff, Hanna Rapaport, Raz Jelinek

P539 Catalytic DNA Degradation by Pancreatic β-cell Peptide Hormone: A New Pathway Towards Amylin Pathology
Arunavo Chatterjee, Uri Ben Nun, Neha Singh, Itamar Kass, Shubhra Kanti Bhaumik, Sisira Mambram Kunnath, Raz Jelinek

P540 An Artificial Light-Harvesting System Built from a Peptide-Based Triaxial Weave
Tatiana Da Silva-Ferreira, Helma Wennemers

P541 Fullerenol-Based Mimicry of LarE-Type Sulfur Insertase Activity
Volkan Dolgun, Antoine Marion, Salih özcubukcu

P543 Computational Exploration of Nanoscale Chemical Patterning Using Short Peptides
Md Jakir Hossen, Adel Nematipour, Camille Bilodeau

P545 Cytoskeleton Stabilized Artificial Cells and their Dynamic Behaviour
Victoria Remacha, Lars Paffen, Andoni Rodriguez, Angshuman Dasm Roi Lopez, Jan van Hest

P548 Amino acid-based hydrogels for electrochemical applications
Sandro Amador, Felipe Conzuelo, Ana C. Baptista, Leonor Morgado, Ana S. Pina

P550 Multifunctional amphicharged and bolaamphiphilic surfactants derived from amino acids: The effect of pH and temperature on their interactions with bovine serum albumin (BSA) and lysozyme (LYZ)
Sumedha Gupta, Neelakshi, Nikita Jain, Ramesh Ramapanicker

P551 Amplifying Magnetic Responsiveness of Self-Assembled Peptide Nanostructures via Synergy of MNP-Helix and Rod-Coil Building Blocks
Seong-Jae Han, Zhihao Zhang, Shouqin Feng, Jeongsu Park, Yong-Beom Lim

P552 From Thermodynamic Stability to Hemocompatibility: Self-Assembling Peptide Nanotubes for mRNA Delivery
Jungyeon Ryu, Hyeonsuk Hwang, Kyuwon Hwang, Taehyun Kim, Yongbeom Lim

P554 From Self-Assembly to Function: Tunable Peptide Fibrils as Nanocarriers
Milena Czeszejko, Justyna Sawicka, Ewa Wieczerzak, Daria Sowik, Patrycja Rachubik, Tomasz Kulesza, Kamila Kitowska, Rafal Sadej, Zuzanna Pietralik-Molinska, Maciej Kozak, Olena Ivashchenko, Sylwia Rodziewicz-Motowidlo

P555 Self-Assembling Peptides Forming Anti-Parallel beta-sheet Nanostructures Cross-Linked with Genipin
Quentin Chenin, N. Follain, Claudia Bello, Luca Rosi, Paolo Rovero, Anna Maria Papini

P556 Peptide Self-assembly Beyond Known Design Principles: Sequence and Context Interplay
Ena Drazic, Helena S. Azevedo, Daniela Kalafatovic

P557 Integrating semiconducting organic polymers with biological systems
Chao Lyu, Bob Schroeder, Alethea Tabor

P558 Allosteric amyloid catalysis by coiled coil fibrils
Sisira Mambram Kunnath, Elad Arad, Elinor Slavsky, Lonia Friedlander, Hanna Rapaport, Raz Jelinek

P559 Self-Assembled Peptide-Au Nanoparticle Hybrid Systems for Catalytic Applications
Vanessa Quattrociocchi, Claudia Pigliacelli, Elena Pazos

P561 Toward Next-Generation ADC Platform tCAP for Site-Specific IgG Modification
Hiroko Kawakami, Abdur Rafique, Shugo Tsuda, Taku Yoshiya, Yuji Ito

P563 Edman degradation beyond standard
Toni Kühl, Alexander Terekhov, Diana Imhof

P564 The antimicrobial peptide Esc(1-21) potentiates CFTR channel via direct targeting of the nucleotide binding domains
Maria Luisa Mangoni, Loretta Ferrera, Giacomo Cappella, Mario Passalacqua, Mattia Mori, Debora Baroni

P616 Screening Cyclised Peptides Inside Cells Identifies a Short Helical Inhibitor of

Alpha-Synuclein Aggregation
Scott G. Allen, Richard M. Meade, Amy J. Lopez, Christopher Williams, Iona Thomas-Wright, Bangfu Zhu, Mara Carey-Wood, Julia E. Sero, Vicky L. Hunt, Andrew Brennan, Richard Wade-Martins, Robert J. Williams, Matthew P. Crump, Jody M, Mason

P633 Creating Antibiofilm and Antibacterial Endotracheal Tubes Using Antimicrobial Peptides and Antibiotics
Elizabeth Ogunfeibo, Sam Boateng, Doug Fraser-Pitt, Ying Yang, Wen-Wu Li

LECTURES

EPS 2026 | O08

Green, DMF-Free ASPPS

Beyond Dissolution

Nanoassembly-Enabled Aqueous Solid-Phase Peptide Synthesis

K. Hojo, A. Nonaka, Y. Manabe, M. Kishimoto, A. Nagai, C. Rentier, A. Mehrotra, K. Hioki, M. Kunishima

Faculty of Pharmaceutical Sciences, Kobe Gakuin University · Biotage

https://doi.org/10.17952/38EPS.2026.O08

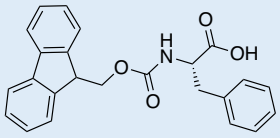
The idea

***Beyond Dissolution**: the substrate builds the reaction field*

We discovered that in-water mixing of Fmoc-amino acids, bases, and coupling reagents produces nanoassemblies.

Amphiphilic Fmoc-amino acids

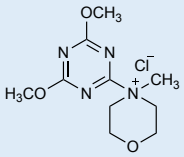
Hydrophobic Fmoc group & hydrophilic COOH
Surfactant-like structure



Organic Base



Water soluble coupling reagents



① Mix two components in water to obtain a clear solution
② Add the water-soluble coupling reagent

Three-component

Nanoassembly

Self-assembled dynamic reaction field

The standard Fmoc-AA-OH toolbox can be used in water

We thought that a reaction field might have been formed inside.
If this is the case, the reaction should be accelerated in water.

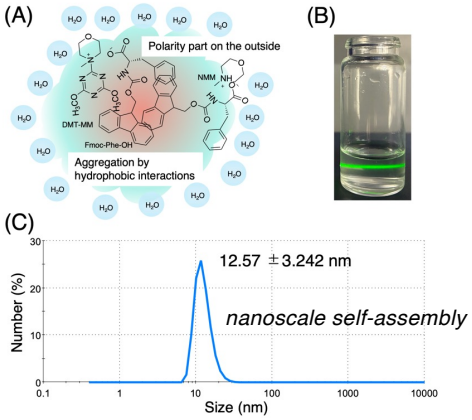


Fig. 1 Aqueous three-component nanoassemblies of Fmoc-Phe-OH with DMT-MM and NMM.
(A) Schematic diagram of nanoassemblies;
(B) (B) Tyndall effects by nanoassemblies;
(C) Particle size distribution for nanoassemblies

PDI is consistently high across amino acids — indicating that a range of assembly sizes coexist, rather than a single defined structure. The measured size itself is not the determinant of reactivity; DLS instead confirms that hydrophobic self-assembly is occurring.

RSC Adv. 2026, **16**, 18073. Patents: JP2022-208765; WO2024-143052.

Proof of concept

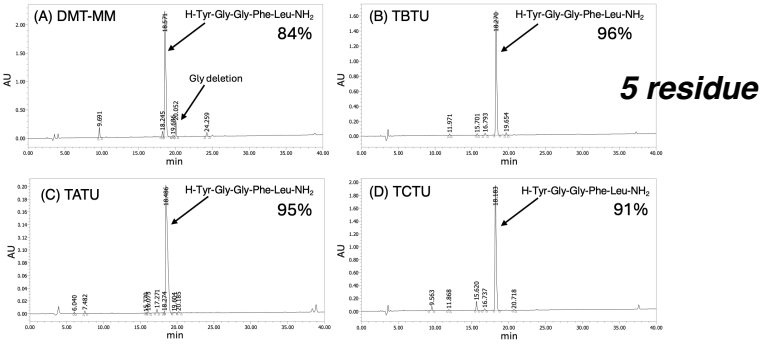
Nanoassembly-enabled ASPPS

We next applied this chemistry to peptide synthesis.

Table 3. The protocols for ASPPS using nanoassemblies of Fmoc amino acids.

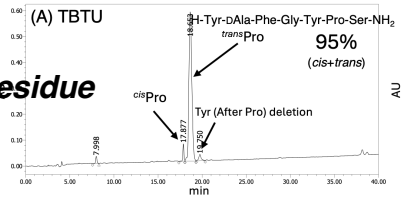
SP Wave
Biotage® Initiator+

Step	Reagents	Volume (ml)	Temp (°C)	Time
Wash	Water	5	25	3 min × 5
Coupling reaction	Nanoassemblies of Fmoc-amino acids with coupling agent and base	6	75	10 min
Wash	Water	5	25	3 min × 5
Wash	EtOAc	5	25	3 min × 3
Deprotection	20% pip-EtOAc	5	25	20 min
Wash	EtOAc	5	25	3 min × 3



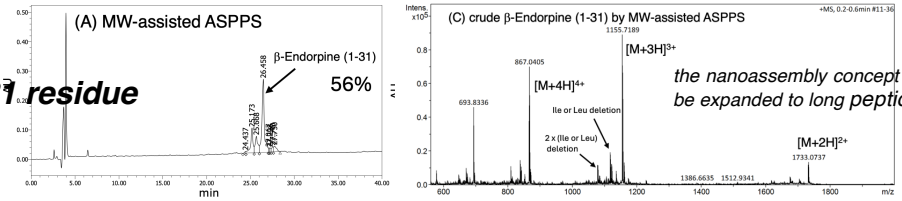
5 residue

Fig. 2 HPLC profiles of crude Leu-enkephalin amide by ASPPS using nanoassemblies Fmoc-amino acids with (A) DMT-MM and NMM; (B) TBTU and DIEA; (C) TATU and DIEA; (D) TCTU



7 residue

Fig. 3 HPLC profiles of crude dermorphin by ASPPS using nanoassemblies Fmoc-amino acids with TBTU and DIEA.



31 residue

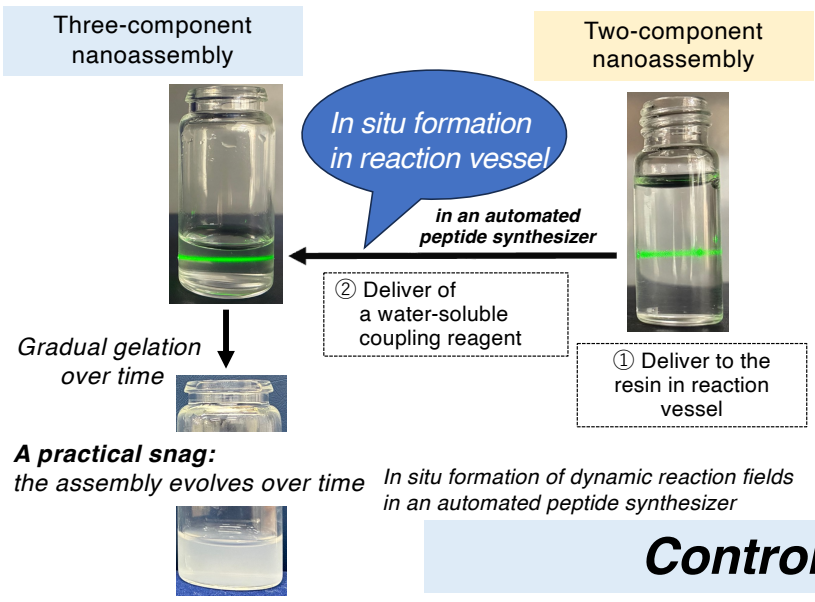
the nanoassembly concept could be expanded to long peptides.

Fig. 4 HPLC profiles of crude b-Endorphin (1-31) obtained by ASPPS employing nanoassemblies. (C) ESI-MS (TOF) spectra of crude b-Endorphin (1-31) obtained by ASPPS.

The next problem and solution

Controlled nanoassembly for automation

Although the chemistry worked well, we encountered a practical problem for automation.



In situ formation of dynamic reaction fields in an automated peptide synthesizer

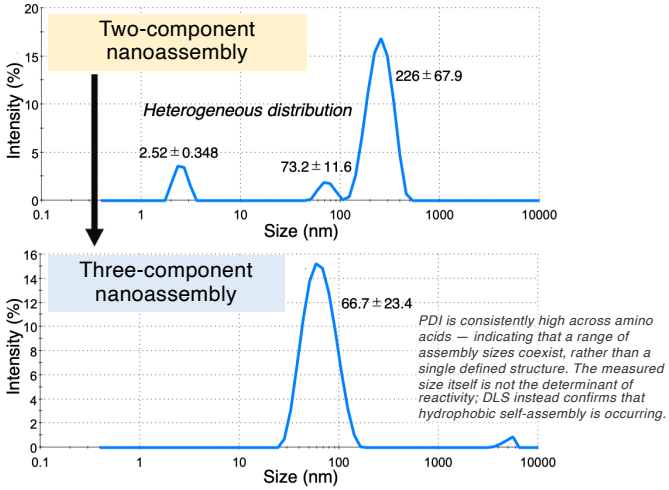


Fig. 5 DLS of two- and three-component nanoassemblies.

Controlled nanoassembly

The reaction field is not stored — it is generated on demand through controlled nanoassembly.

RSC Adv. 2026, **16**, *in press.* Patents: WO2024-143052; JP2025-143052

Fully automated ASPPS enabled by nanoassemblies

We then evaluated this ASPPS automated program.

Even at this level, aqueous peptide synthesis remained feasible.

5 residues

Leu-enkephalin amide

11 residues

Substance P

37 residues

GLP-1 (1-37)

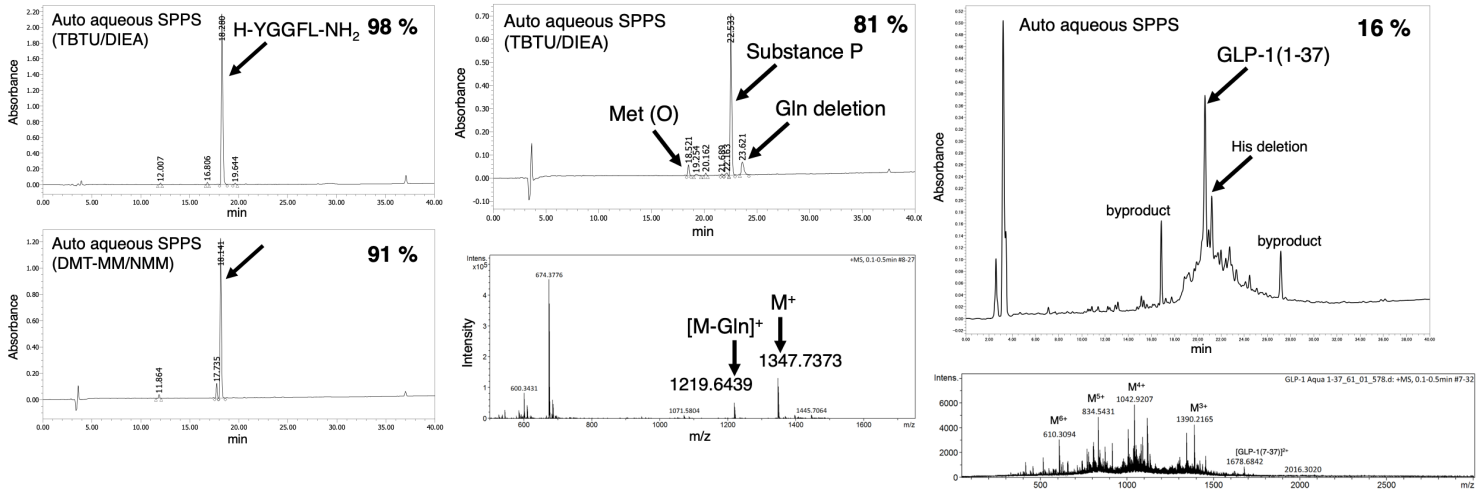


Fig. 6. Product analysis of Leu-enkephalin amide, substance P, and GLP-1 (1-37) synthesized by fully automated ASPPS.

Overall, controlled nanoassemblies really do work for fully automated aqueous SPPS.

CONCLUSION

Beyond Dissolution: water, the architect of the reaction field

We set out to replace DMF with water. What we found was something more fundamental — Water is not simply a replacement solvent.

Through self-assembly of substrates, water builds a reaction field. It concentrates the substrates within a hydrophobic microenvironment, creating conditions that favor coupling.

DMF-free | Fully automated | Beyond 30 residues | Green by design

Neurotensin(8-13) Analogs Targeting NTS1 and NTS2 Receptors: A Comparative *In vitro* and Molecular Modeling Study

N.T. Tzvetkov[1], K. Kirilov[1], M.G. Georgieva[1], A.A. Balacheva[1], T.I. Pajpanova[1], T. Kühl[2], H. Hübner[3], P. Gmeiner[3] & D. Imhof[2]

[1]*Department of Biochemical Pharmacology and Drug Design, Institute of Molecular Biology "Roumen Tsanev", Bulgarian Academy of Sciences, Acad. G. Bonchev Str., bl. 21, 1113 Sofia Bulgaria*

[2]*Pharmaceutical Biochemistry and Bioanalytics, Pharmaceutical Institute, University of Bonn, An der Immenburg 4, D-53121 Bonn, Germany*

[3]*Department of Chemistry and Pharmacy, Medicinal Chemistry, Friedrich-Alexander-Universität Erlangen-Nürnberg, Nikolaus-Fiebiger-Str. 10, D-91058 Erlangen, Germany*

Email: ntzvetkov@bio21.bas.bg.

https://doi.org/10.17952/38EPS.2026.O12

The simultaneous activation of both neurotensin type 1 and 2 receptors (NTS1R and NTS2R) through the neuronal peptide neurotensin (NT), activating the dopamine (DA) release and DA signaling within the dopaminergic system in the brain, suggest that NTS1R/NTS2R dual-specific NT analogs may represent an attractive tool in the treatment of Parkinson's disease (PD) and/or other related conditions.[1,2] Herein, we report *in silico* exploration of NTS1R and NTS2R driven by *in vitro* pharmacological evaluation of the linear hexapeptide NT analogs **3** (sequence Lys^{8}-Cav^{9}-Pro^{10}-Tyr^{11}-Ile^{12}-Leu^{13}) and **6** (Arg^{8}-Cav^{9}-Pro^{10}-Tyr^{11}-Ile^{12}-Leu^{13}), both active towards the human NTS1R and NTS2R. Compared to the parent peptide NT(8-13), compounds **3** and **6** showed improved *in vitro* human plasma stability and BBB permeability (Figure 1). Moreover, *in silico* ADMET evaluation indicated that both NT-analogs have strong pharmacological properties combined with good safety profiles, highlighting their potential for further structural improvements. Furthermore, we applied an AI-based approach to generate the homology models of hNTS1R and hNTS2R, followed by MD simulations of their ligand-free state and molecular docking in order to estimate the most probable protein–ligand complexes of peptides **3** and **6**. Binding interaction/affinity analysis of the best-ranked docking modes, obtained with selected time-frames from the respective MD trajectories, suggest that the receptor activation occurs via a ligand-receptor binding into the initial "entry" conformation of hNTS1R and hNTS2R (Figure 2). This assumption is supported by additional HYDE analysis confirming the binding affinities of peptides **3** and **6** towards hNTS1R and hNTS2R obtained by radioligand binding experiments (Figure 3).[3] The reported study may serve as a ready-to-use *in silico* approach for further development of therapeutic options against PD and potentially other neurological disorders.

		NT(8-13)	Lys[8]-Cav[9]-Pro[10]-Tyr[11]-Ile[12]-Leu[13] (3)	Arg[8]-Cav[9]-Pro[10]-Tyr[11]-Ile[12]-Leu[13] (6)
Binding Affinity Data				
EXPERIMENT K_i binding (nM)	**hNTS1R**	0.68 ± 0.04 (K_d)	**6.9 ± 0.59**	**5.5 ± 1.7**
	hNTS2R	1.8 ± 0.17 (K_d)	**6.5 ± 0.63**	**5.6 ± 1.0**
Selectivity K_i (hNTS1R) / K_i hNTS2R)		0.38	1.06	0.98
PREDICTION $K_{i\ HYDE}$ range (nM)	**hNTS1R**	0.13–12.6	**0.43–43.2** (MD, „entry" pose 1)	**2.95–293** (MD, „entry" pose 1)
	hNTS2R	4.28–42.5	**6.13–609** (MD, „entry" poase 1)	**1.16–115** (MD, „entry" pose 1)
ADME Data				
Peptide stability (@50 µM)				
% remaining @24 h, pH 2.0/7.4		100 / 100	100 / 100	100 / 100
% remaining >30 d, pH 2.0/7.4		> 97 / 100	> 97 / 100	> 94 / > 95
Plasma stability (@30 min, after 5 min @37°C)				
% remaining @100 µM		0.02	0.65	0.22
$t_{1/2}$ (min) @100 µM		< 2.5	< 7.3	< 3.7
PAMPA permeability				
P_e (×10^{-6} cm/s) @pH 7.4		0.64 ± 0.20	**2.81 ± 0.45**	0.89 ± 0.10
–logP_e		6.12 ± 0.13	**5.55 ± 0.07**	6.05 ± 0.03

Figure 1. *In vitro* data for NT(8-13) and selected peptides **3** and **6**.[2,3]

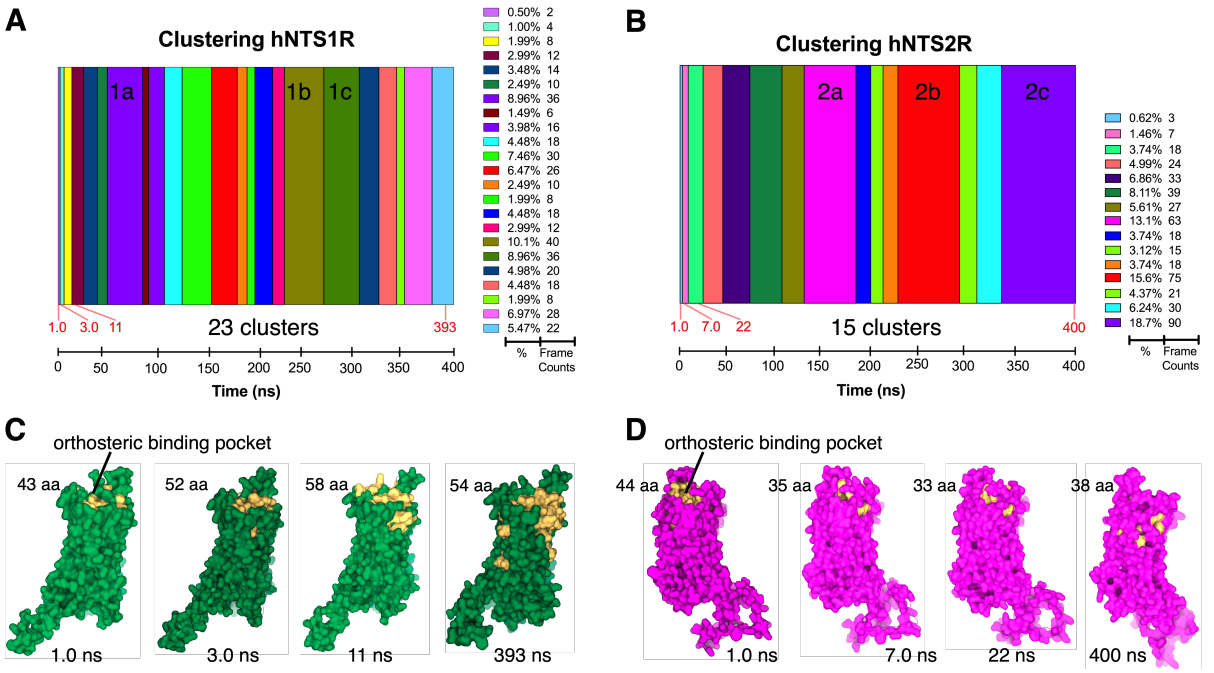


Figure 2. Molecular dynamic simulations with apo-state of hNTSRs showing the most distributed clusters (**1a–1c**) for hNTS1R (**A**) and (**2a–2c)** for hNTS2R (**B**). Flexible *vs.* more "closed" conformational extracellular changes of the actives site from 43 to 54 aa for hNTS1R (**C**) and from 44 to 38 for hNTS2R (**D**), respectively.[3]

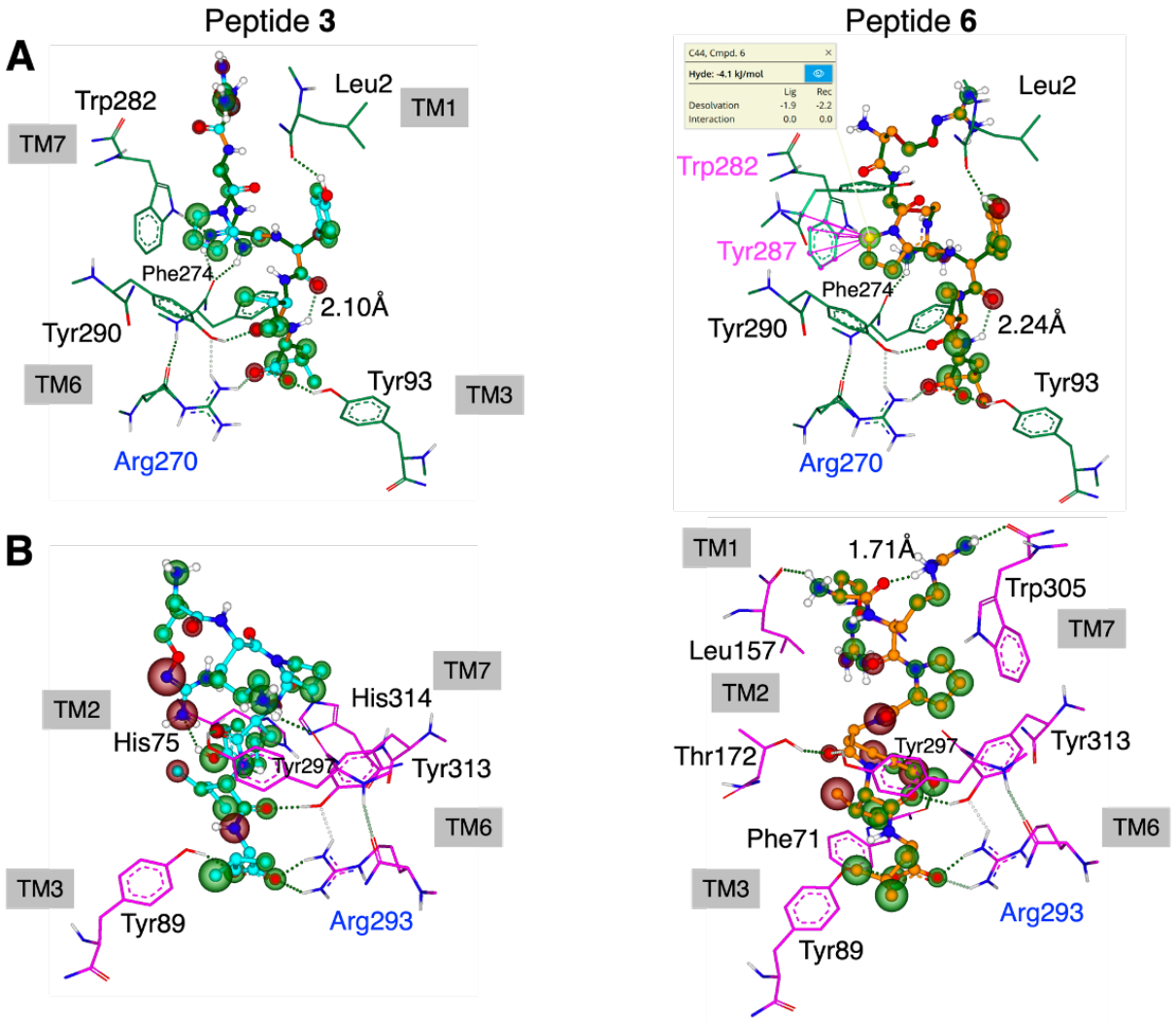


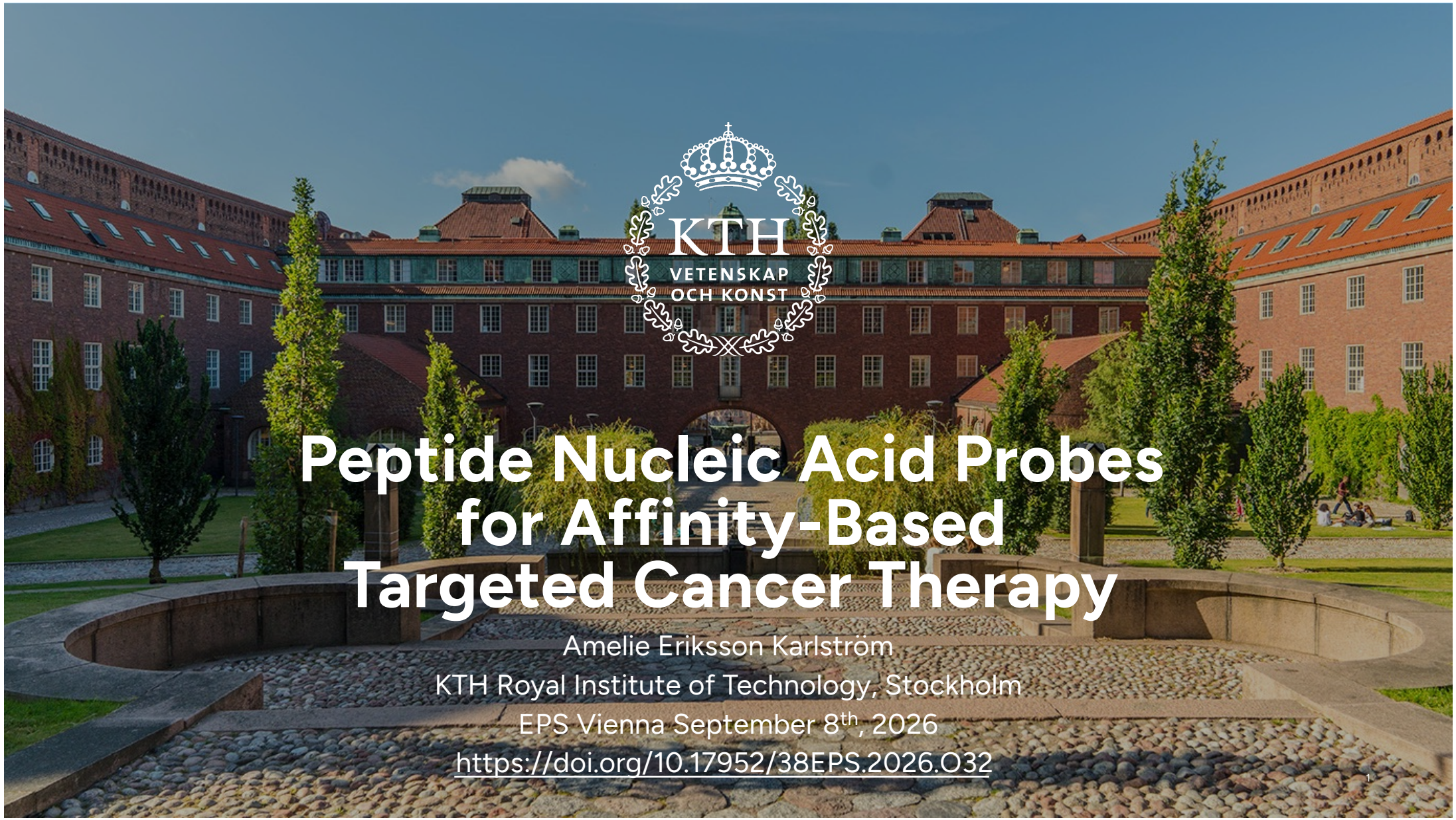
Figure 3. Docking models for the best-ranked poses of peptides **3** and **6** using ”entry” conformations at 1.0 ns MD with hNTS1R (**A**) and hNTS2R (**B**).

Acknowledgements

The author gratefully acknowledges the financial support provided by the Scientific Exchange Programme between Bulgaria and Switzerland (SCIEX) under the Swiss National Science Foundation (SNF) Project No: IZSF-0_235779**.**

References

1. A. W. K. Yeung, M. G. Georgieva, K. Kirilov, A. A. Balacheva, M. I. Peeva, O. K. Horbañczuk, J. O. Horbañczuk, M. Lucarini, A. Durazzo, A: Santini, E. B. Souto, T. I. Pajpanova, L. Milella, A: G. Atanasov, N. T. Tzvetkov, *Future Med. Chem.* **2020**, *12*, 19, 1779-1803.
2. T. Kühl, M. G. Georgieva, H. Hübner, M. Lazarova, M. Vogel, B. Haas, M. I. Peeva, A. A. Balacheva, I. P. Bogdanov, L. Milella, M. Ponticelli, T. Garev, I. Faraone, R: Detcheva, B. Minchev, P. Petkova-Kirova, L. Tancheva, R: Kalfin, A. G. Atanasov, L. Antonov, T. I. Pajpanova, K. Kirilov, M. Gastreich, P. Gmeiner, D. Imhof, N. T. Tzvetkov, *Eur. J. Med. Chem.* **2023**, *254*, 115386.
3. K. Kirilov, M. Ponticelli, T. Kühl, H. Hübner, T. I. Pajpanova, M. G. Georgieva, M. Vogel, A. A. Balacheva, B. Haas, T. I. Pajpanova, M. Matin, L. Milella, P. Gmeiner, D. Imhof, N. T. Tzvetkov, *Curr. Res. Biotechnol.* **2025**, *9*, 100298.



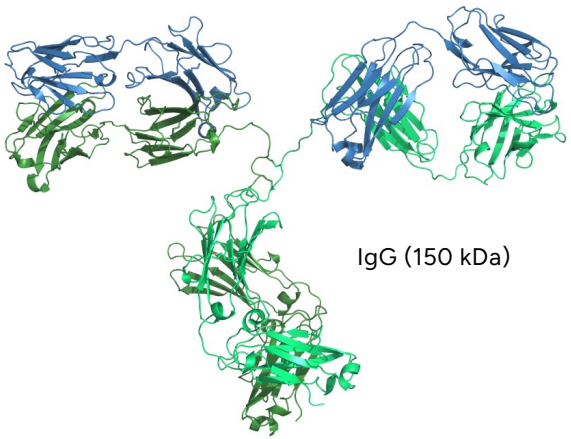
Peptide Nucleic Acid Probes for Affinity-Based Targeted Cancer Therapy

Amelie Eriksson Karlström
KTH Royal Institute of Technology, Stockholm

EPS Vienna September 8th, 2026
https://doi.org/10.17952/38EPS.2026.O32

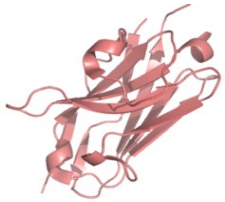
Tumor-targeting affinity proteins for cancer therapy

Monoclonal antibodies

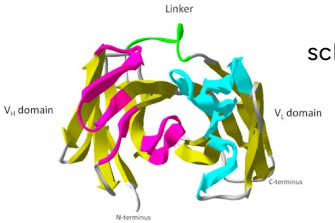


IgG (150 kDa)

Antibody fragments

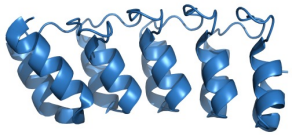


Nanobody/VHH domain (~27 kDa)

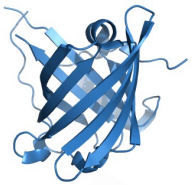


scFv (~27 kDa)

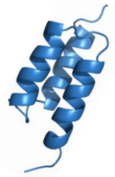
Engineered scaffold proteins



DARPin (14-21 kDa)



Anticalin (20 kDa)



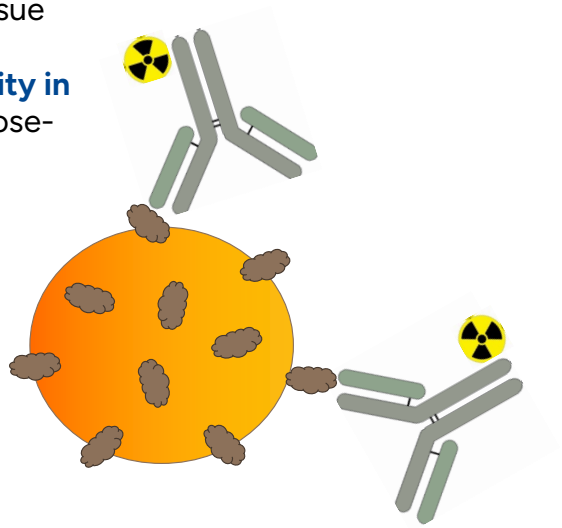
Affibody molecules (6-7 kDa)

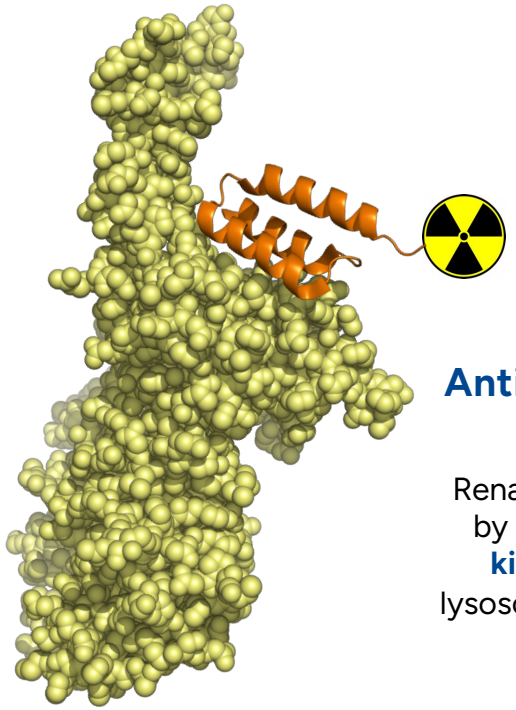
- Proteins binding tumor-associated antigens, typically cell surface receptors
- Can be used for delivery of cytotoxic payloads, e.g. antibody-drug conjugate (ADC) or radioimmunotherapy (RIT)

Targeted radionuclide therapy

Monoclonal antibodies

Long half-life and slow tissue penetration, leading to **accumulation of radioactivity in bone marrow** leading to dose-limiting toxicity



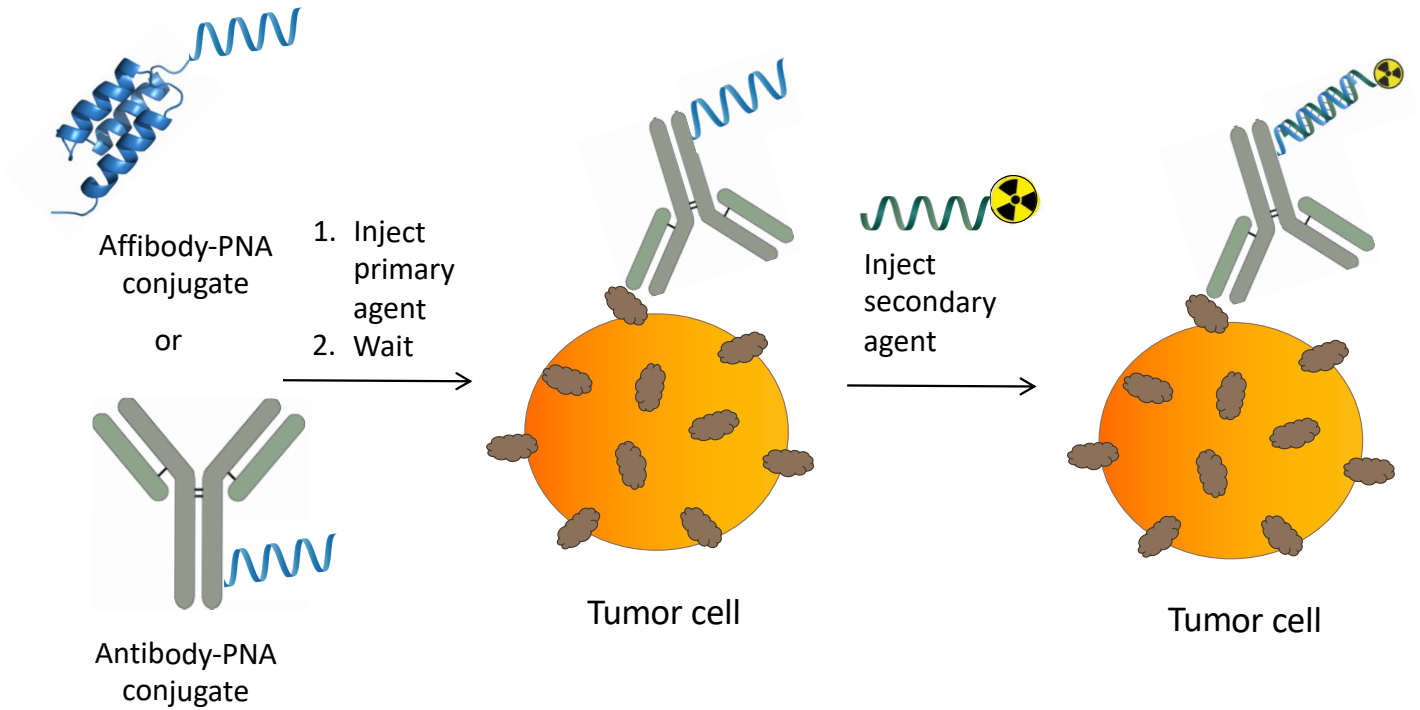


Antibody fragments and small scaffold proteins

Renal clearance typically accompanied by **accumulation of radioactivity in kidneys** because of reabsorption, lysosomal digestion, and retention in the proximal tubule cells

➢ **Difficult to reach therapeutic efficiency because of insufficient tumor-to-nontumor ratio**

Pretargeting strategy for targeted radionuclide therapy



The secondary agent should have:

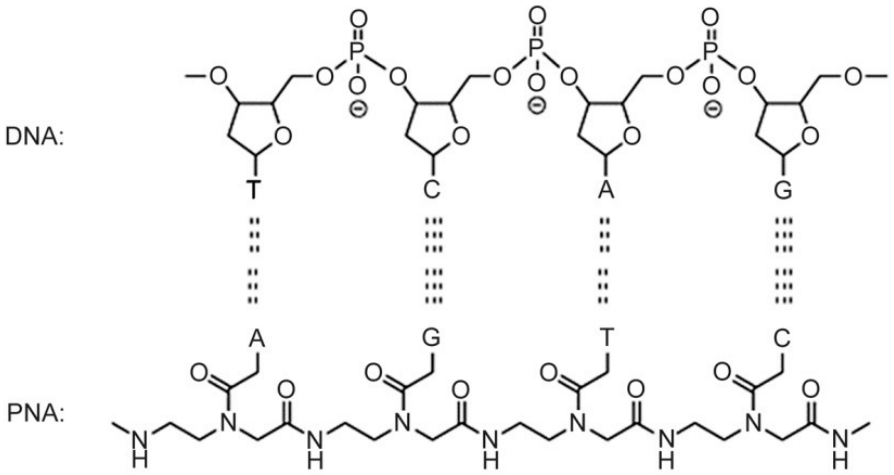
- fast clearance
- low accumulation in nontumor tissue
- high-affinity binding or bioorthogonal covalent reaction with the primary agent

➢ **Delivery of the tumor-targeting protein is separated from delivery of the cytotoxic radionuclide**

Peptide nucleic acid (PNA) probes for pretargeting

Hybridizing PNA probes:

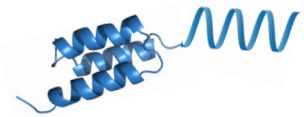
- No reported **immunogenicity** or **toxicity**
- High *in vivo* **stability**
- High specificity
- Easily tunable binding strength
- Synthesis fully compatible with peptide synthesis:
  - standard SPPS protocols
  - possible automation
  - GMP synthesis
  - flexible and modular combination with different chelators and radionuclides



➢ **Pseudo-peptide backbone fully compatible with standard solid phase peptide synthesis (SPPS) protocols**

Proof-of-concept: PNA-based pretargeting with tumor-targeting affibody molecules

Primary agent:

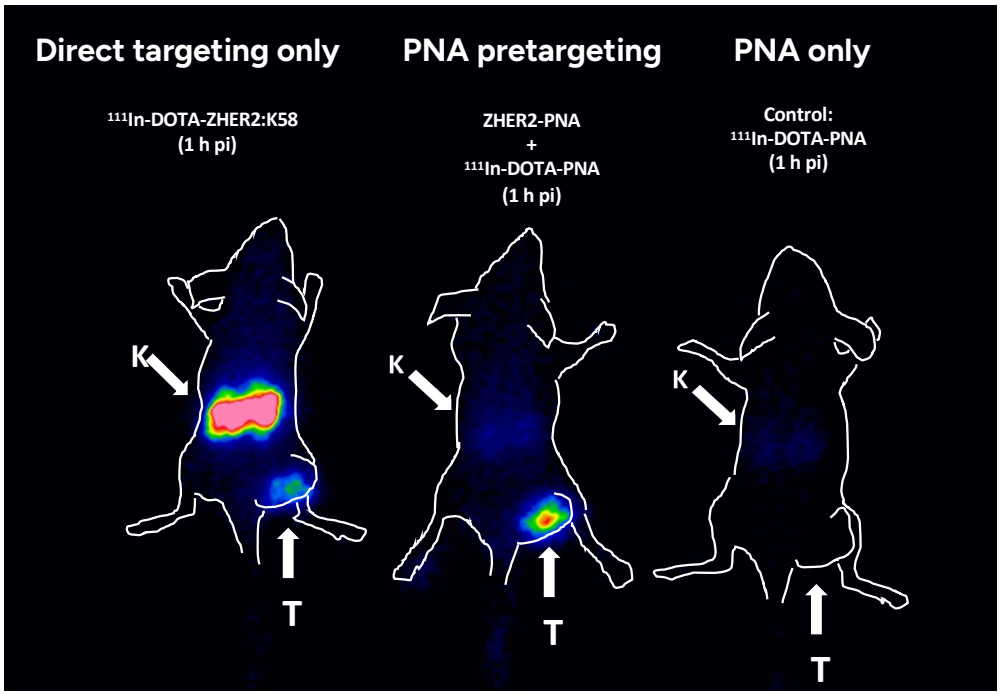


HER2-binding affibody molecule enzymatically conjugated to a synthetic PNA probe

Secondary agent:



Radiolabeled complementary PNA probe



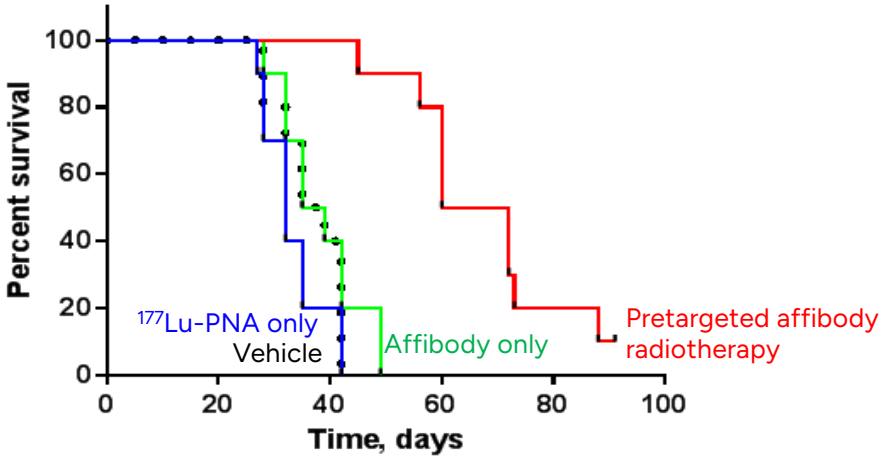
- SKOV3 (HER2+) xenograft tumors in mice
- Anti-HER2 affibody
- Secondary PNA probe labeled with indium-111
- 4 h interval between injections

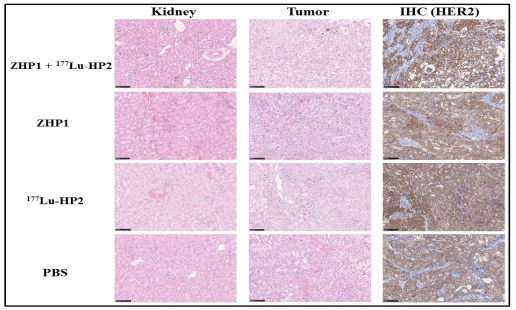
➢ **Affibody-based PNA-mediated pretargeting provides specific delivery of radiometals to tumors with higher radiometal concentration in tumors (T) than in kidneys (K)**

Westerlund *et al, Bioconjug. Chem.*, 2015, 26, 1724; Honarvar *et al, Theranostics,* 2016, 6, 93.

Affibody-based PNA-mediated pretargeted radionuclide therapy for treatment of HER2-expressing cancer

- SKOV3 (HER2+) xenograft tumors in mice
- Anti-HER2 affibody
- Secondary PNA probe labeled with lutetium-177
- Injections once/week for 6 weeks
- 16 h interval between injections





Hematoxylin and eosin staining of kidneys (left column) and tumor (middle column), IHC of HER2-expression in tumor (right column)

➢ **Pretargeted therapy increases median survival with no signs of toxic impact to kidneys**

Westerlund, et al (2018) *J. Nucl. Med.*, 59, 1092.

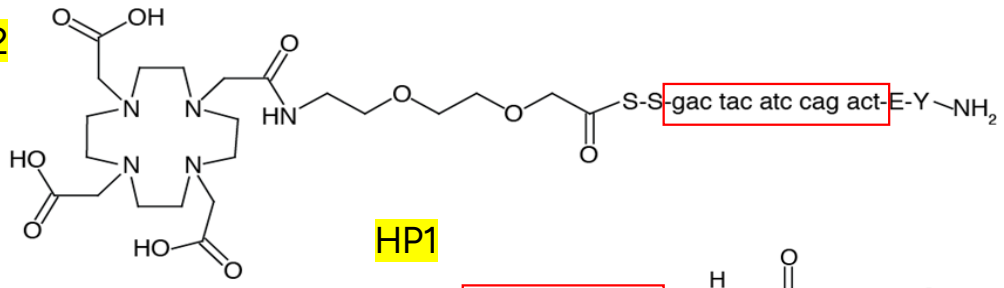
PNA probe engineering

Could shorter PNA probes be used for pretargeting?

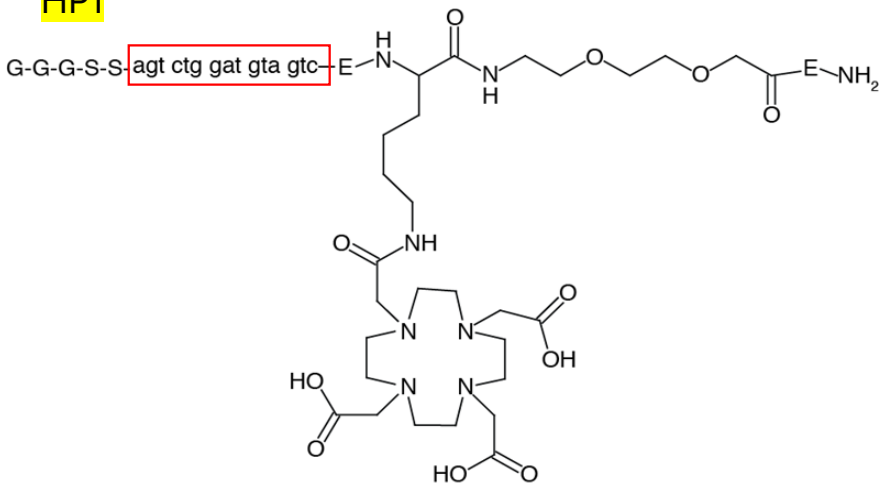
HP1:HP2 hybridization probes

PNA length:	15-mer
MW: approx.	5 kDa
T_m of hybrid:	86 °C

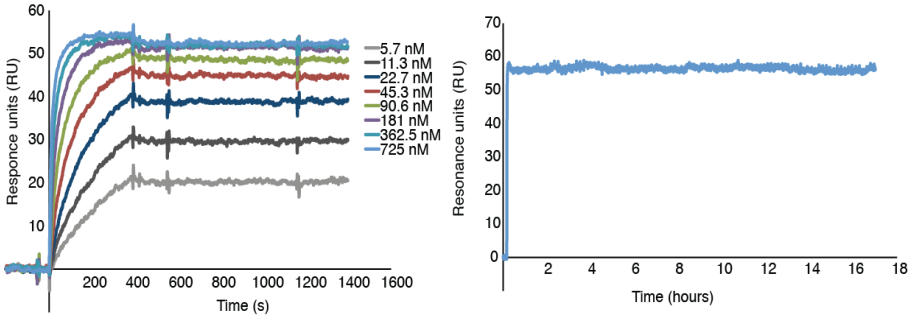
HP2



HP1



SPR sensorgrams of *HP2* binding to immobilized $Z_{HER2:342}$-SR-*HP1* show very slow dissociation:



Evaluation of new shorter secondary PNA probes

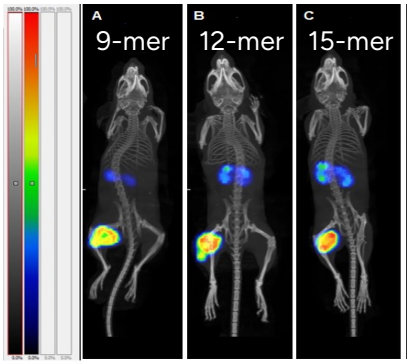
A new primary probe (15-mer):

HP15 GSS-cctggtgttgatgat-EK(DOTA)-AEEA-E-NH_2

Three new secondary probes (15-mer, 12-mer, 9-mer):

HP18 DOTA-AEEA-SS-atcatcaacaccagg-EEY-NH_2
HP17 DOTA-AEEA-SS-atcaacaccagg-EEY-NH_2
HP16 DOTA-AEEA-SS-aacaccagg-EEY-NH_2

Estimated dosimetry to tumor and kidney in mice bearing HER2-expressing SKOV3 xenografts:



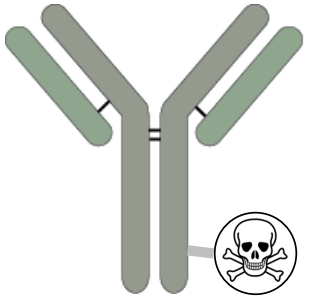
Secondary probe	PNA length	Tumor-to-kidney AUC ratio
[^{177}Lu]Lu-HP16	9-mer	3.8
[^{177}Lu]Lu-HP17	12-mer	2.8
[^{177}Lu]Lu-HP18	15-mer	2.0

The new secondary probes were evaluated in combination with a new 15-mer primary probe

- **The new 9-mer secondary probe HP16 provides the highest tumor-to-kidney AUC ratio**
- **Shorter probes provide better biodistribution, higher solubility and more cost-efficient production**

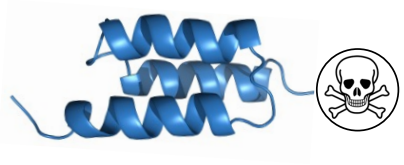
Tano *et al*, *Cancers*, **2021**,

Targeted delivery of cytotoxic drugs



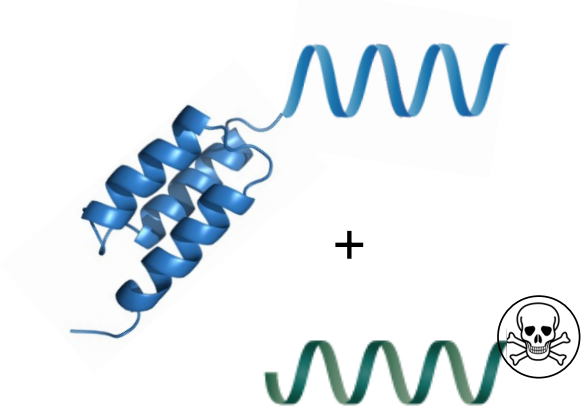
Antibody-drug conjugate (ADC)

- Hydrophobic payloads in ADCs can lead to
  - aggregation
  - rapid clearance
  - hepatotoxicity



Affibody-drug conjugate (AffiDC)

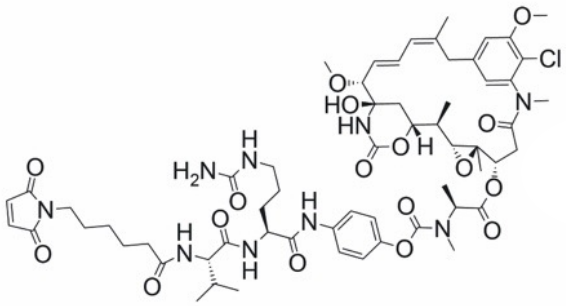
Alternative approach:



PNA-pretargeted delivery of cytotoxic drug

Design of DM1-conjugated secondary PNA probes

SP1	EC(DM1)-K($COCH_3$)-PEG_8-EE-acaccagg-EK(DOTA)-Y-NH_2
SP2	EC(DM1)-K(EE)-EE-acaccagg-EK(DOTA)-Y-NH_2
SP3	EC(DM1)-K($COCH_3$)-EEEE-acaccagg-EK(DOTA)-Y-NH_2
SP4	EC(DM1)-K(EE)-EEEE-acaccagg-EK(DOTA)-Y-NH_2
SP5	EC(DM1)-K(PEG_8)-EE-acaccagg-EK(DOTA)-Y-NH_2
SPc	EC(DM1)-K($COCH_3$)-EE-acaccagg-EK(DOTA)-Y-NH_2

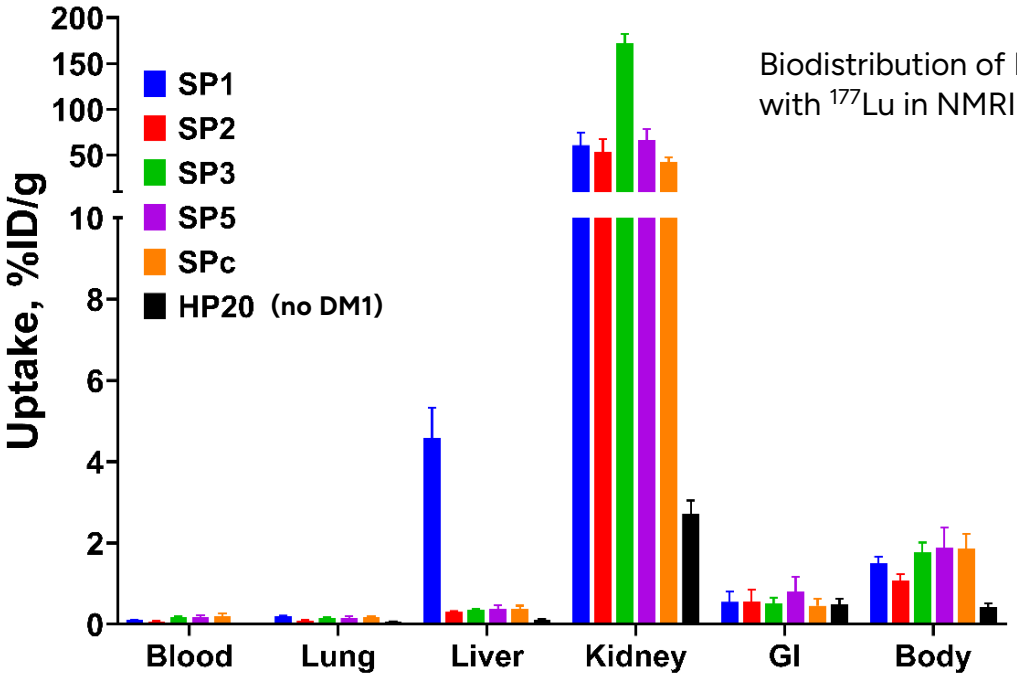


Mal-VC-PAB-DM1

- PNA-drug conjugates based on the 8-mer HP20 probe
- Hydrophilic modifications in backbone or side chain:
  - **Glutamate residues**
  - **PEG8 linkers**
- Maytansine drug DM1 attached via cathepsin-cleavable maleimide-valine-citrulline-*p*-aminobenzylcarbamate (Mal-VC-PAB) linker

Clinton *et al, Bioconjug. Chem, .*, **2026**, 37:1562

Biodistribution of DM1-conjugated PNA probes



Biodistribution of DM1-PNA probes labeled with ^{177}Lu in NMRI mice 4 h after injection.

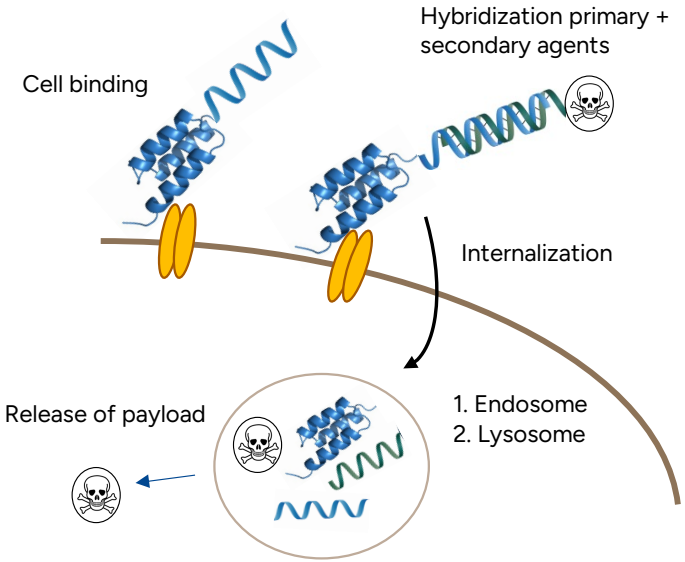
SP1 EC(DM1)-K($COCH_3$)-PEG_8-EE-acaccagg-EK(DOTA)-Y-NH_2
SP2 EC(DM1)-K(EE)-EE-acaccagg-EK(DOTA)-Y-NH_2
SP3 EC(DM1)-K($COCH_3$)-EEEE-acaccagg-EK(DOTA)-Y-NH_2
SP4 EC(DM1)-K(EE)-EEEE-acaccagg-EK(DOTA)-Y-NH_2
SP5 EC(DM1)-K(PEG_8)-EE-acaccagg-EK(DOTA)-Y-NH_2
SPc EC(DM1)-K($COCH_3$)-EE-acaccagg-EK(DOTA)-Y-NH_2

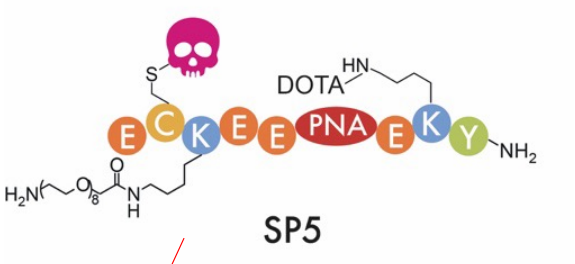
HP20 DOTA-PEG_2-SS-acaccagg-EEY-NH_2

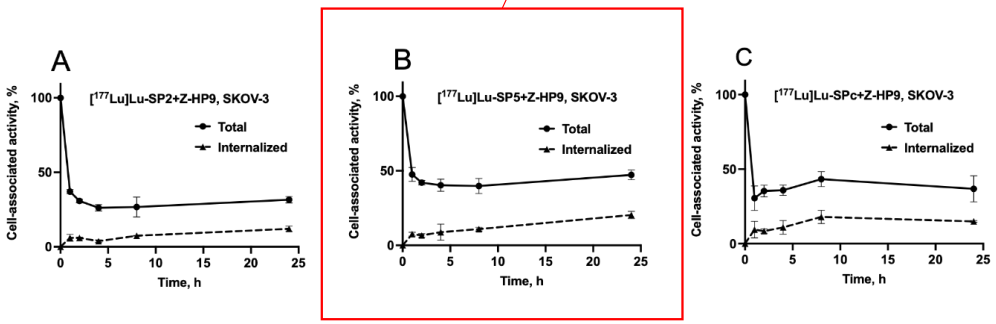
- Significant differences in liver and kidney uptake
- SP2, SP5 and SPc show favorable biodistribution patterns

Clinton *et al, Bioconjug. Chem, .*, **2026**, 37:1562

Cell binding and internalization





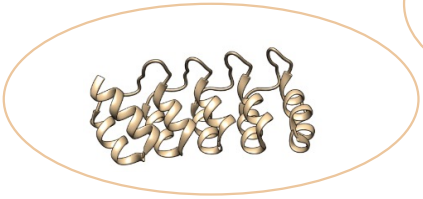


Retention and internalization of (**A**) [^{177}Lu]Lu-SP2, (**B**) [^{177}Lu]Lu-SP5, and (**C**) [^{177}Lu]Lu-SPc pretreated with Z-HP9 (1 h) on SKOV-3 cells after interrupted incubation.

- **SP5 shows favorable biodistribution, cell binding, and internalization**
- **SP5 is a promising candidate for *in vivo* tumor targeting**

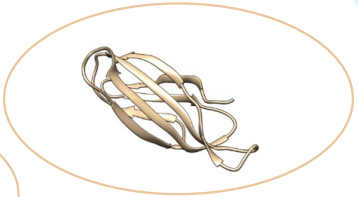
Clinton *et al, Bioconjug. Chem*, ., **2026**, 37:1562

PNA-based pretargeting is a versatile platform technology

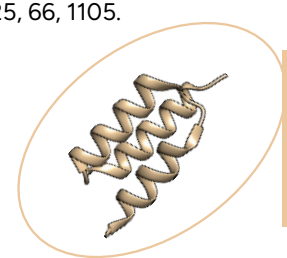


DARPin

- Oroujeni, M., *J. Nucl. Med.*, 2025, 66, 1105.

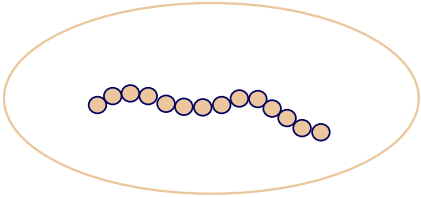


Nanobody



Affibody

- Westerlund, K. *ACS Pharmacol. Transl. Sci.*, 2024, 7, 1595
- Oroujeni, M. *J. Nucl. Med.,* 2022, 63, 1046
- Tano, H. *Cancers,* 2021, 13, 500
- Westerlund, K. *J. Nucl. Med.,* 2018, 59, 1092
- Vorobyeva, A. *Sci. Rep.,* 2019, 8, 9643
- Altai, M. *Nucl. Med. Biol.,* 2017, 54, 1
- Honarvar, H. *Theranostics,* 2016, 6, 93
- Westerlund, K. *Bioconjug. Chem.*, 2015, 26, 1724



Peptide

Tumor-targeting agents



Antibody

- Altai, M. *J. Control. Release,* 2025, 381, 113551
- Myrhammar, A. *Sci. Rep.,* 2020, 10, 20777
- Westerlund, K. *Biomaterials,* 2019, 203, 73

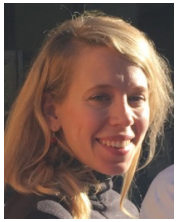
Short half-life
Renal clearance
Kidney toxicity

Long half-life
Slow tissue penetration
Bone marrow toxicity

Acknowledgments

KTH team:


Kristina Westerlund


Hanna Tano


Maxime Gestin


Anders Myrhammar


Ábel Nagy


Jacob Clinton


Pauline Granit


Astrid Haraldsson


Alexander van Deventer


Ebba Nordén


Linnéa Wiklund

Uppsala University:

- Vladimir Tolmachev
- Anna Orlova
- Maryam Oroujeni
- Anzhelika Vorobyeva
- Hadis Honarvar

Lund University:

- Mohamed Altai

Funding:

POSTERS at 38th EPS:

- **Kristina Westerlund: Poster #443**

"Peptide Nucleic Acid (PNA)-Guided Pretargeting for HER2-Targeted Antibody-Mediated Radionuclide Therapy"

- **Jacob Clinton: Poster #339**

"Affibody-mediated Peptide Nucleic Acid Pretargeting Using Dual Hybridization Sequences for Increased Therapeutic Potential"

Sequence-driven modulation of the multistage self-assembly process in lamellin-type β-peptides

Imola Cs. Szigyártó[1], K. Ferentzi[2], András Wacha[1], Kamal el Battioui[1], Olivér Pavela[1], Tünde Juhász[1], Judith Mihály[1], István Mándity[1], Viktor Farkas[2], Tamás Beke-Somfai[1]

[1]*HUN-REN Research Centre for Natural Sciences, Institute of Materials and Environmental Chemistry, Budapest, Hungary;* [2]*HUN-REN - ELTE Protein Modeling Research Group, Eötvös Loránd University, Institute of Chemistry, Budapest, Hungary*
https://doi.org/10.17952/38EPS.2026.O37

Introduction

Self-assembling peptides serve as useful building blocks of functional supramolecular materials and have gained increasing attention in nanotechnology, drug delivery, and molecular biology. Among these systems, non-natural β-peptides are particularly promising due to their high chemical and conformational diversity, increased resistance to proteolytic degradation, and ability to form stable intermolecular interactions that support higher-order assembly. The side-chain chirality pattern of β-peptides plays a crucial role in the formation of higher-order structural elements. To explore new directions in β-peptide supramolecular assembly, and inspired by the extended strand conformation of natural peptides, in which alternating side-chain positions can facilitate intermolecular interactions between neighbouring molecules, we designed a series of short, acyclic β³-peptide sequences with alternating side-chain chirality.

Results and Discussion

We previously designed [1] a charge-neutral β³-hexapeptide comprising a Leu-rich hydrophobic region together with Glu and Lys residues, in which alternating side-chain chirality favours an extended, non-helical zig-zag backbone conformation. MD simulations revealed that this amphiphilic arrangement promotes the formation of finite oligomeric bundles consisting of two nearly parallel layers held together by a hydrophobic Leu-rich core in aqueous solution (Figure 1). The resulting hydrophobic interior can host fluorescent probes and hydrophobic guest molecules.

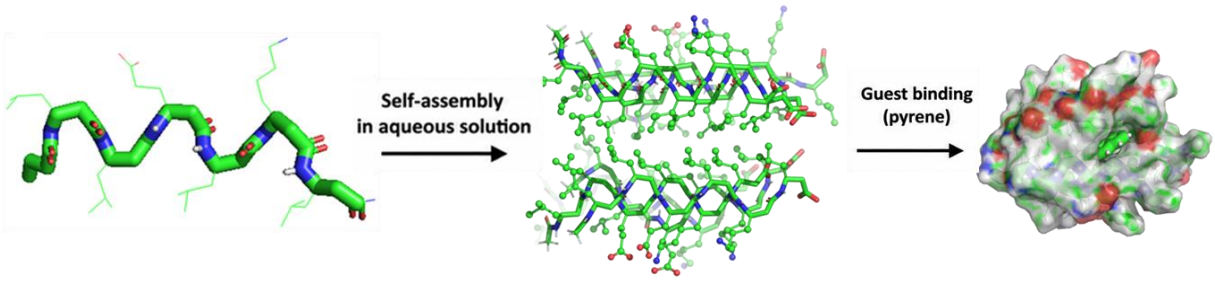


Figure 1. Self-assembly of an acyclic β³-hexapeptide with alternating side-chain chirality into nanometer-sized oligomeric bundles with a hydrophobic Leu-rich core, enabling the encapsulation of small hydrophobic guest molecules.

Based on this initial design concept, subsequent sequence modifications were used to control higher-order assembly and to develop environmentally responsive lamellar structures with membrane-active and antimicrobial properties.

Increasing the cationic character of the peptides transforms this adaptable scaffold into an environment-responsive antibacterial system [2, 3]. Some of these sequences with alternating chirality self-assemble into characteristic striped lamellae, which were termed lamellins. While the 2K and 3K sequences predominantly adopt a random-coil structure in water, inorganic phosphate (e.g., in PBS) and bacterial cell-wall components (e.g., LPS) trigger their organization into extended lamellar structures (Figure 2). Molecular dynamics simulations, electron microscopy, and bacterial assays demonstrated that this phosphate-induced self-assembly leads to the formation of ordered, striped lamellae capable of incising the cell envelope of Gram-negative bacteria, thereby exerting antibacterial activity.

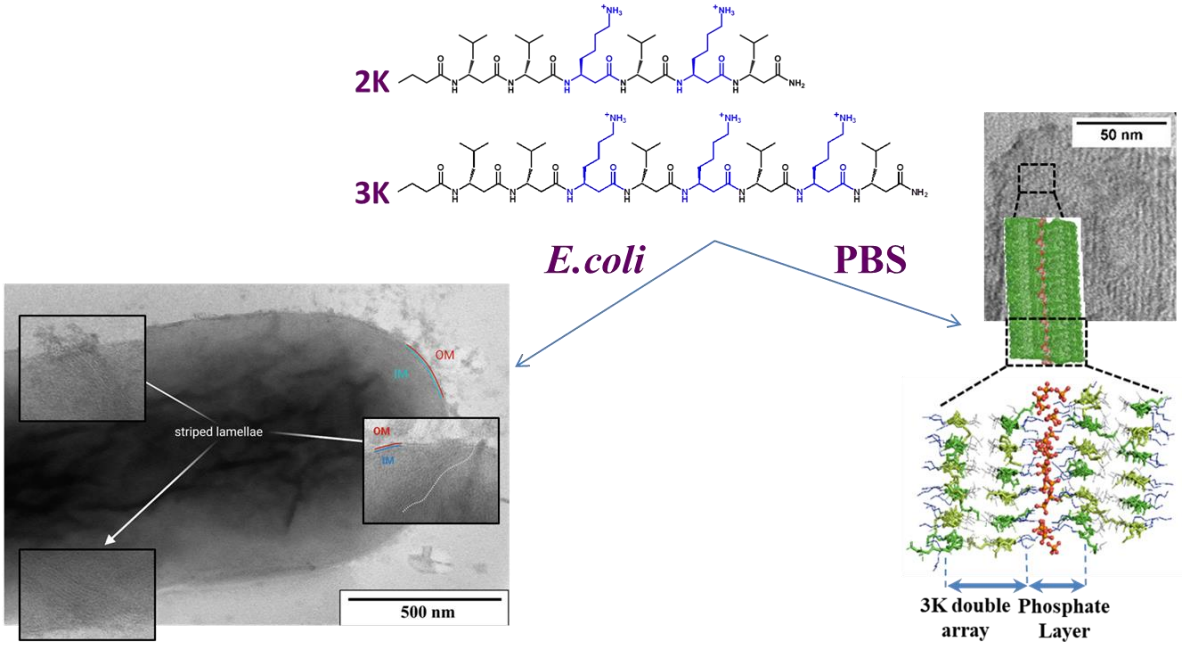


Figure 2. Environment-responsive self-assembly of cationic lamellin-2K and lamellin-3K in the presence of PBS and E.coli.

To gain a more comprehensive understanding of β-peptide assembly behaviour, we investigated systems with an overall neutral charge, in which supramolecular organization could be modulated in a controlled manner. We systematically replaced [4] β^3 -homoleucines (Leu) with β^3 -homoalanines (Ala) and changed the hydrophobic N-terminal butyryl protecting group (But) to the more water-soluble acetyl group (Ac) (Figure 3) to examine how changes in hydrophobic core formation influence the assembly process and the resulting morphology. MD simulations confirmed that all investigated peptides predominantly adopt a zig-zag conformation, facilitating their association into sandwich-type oligomers. Peptides containing an N-terminal acetyl group and homoleucine at the second position preferentially formed twisted structures, whereas the combination of an N-terminal butyryl group and homoalanine favoured more ordered assemblies with reduced internal twisting. Based on the combined experimental (cryo-EM, NS-TEM and molecular biophysics data) and

computational (MD simulations) observations five distinct structural stages of self-assembly process were identified (Figure 3), from small oligomers, twisted strands to extended flat lamellae, which can assemble to lamellar bundles, and finally to macroscopic lamellar clusters.

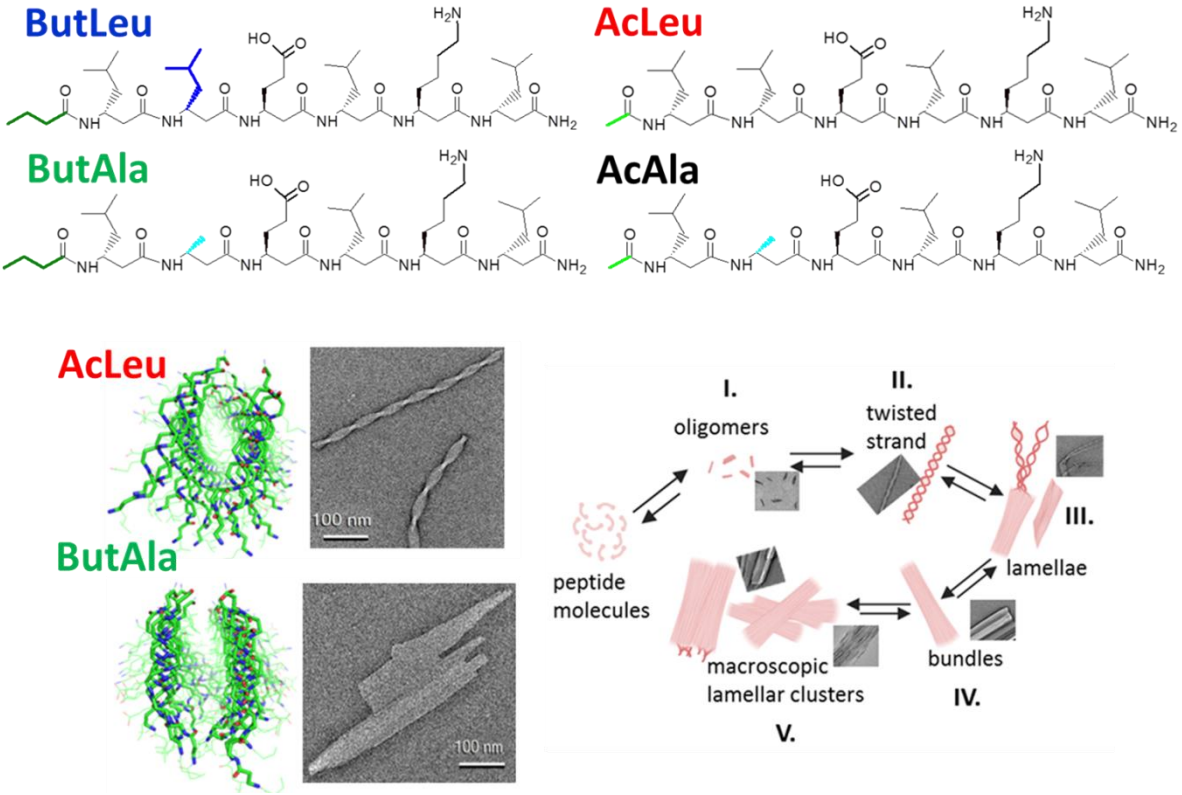


Figure 3. Selected chemical structures of β³-hexapeptides with representative twisting and packing of the formed morphologies in view of EM images and MD simulations for the two extremes, AcLeu and ButAla. Schematic representation of assembly formation with the five identified stages based on morphological investigations.

Acknowledgements

These works was funded by the National Research, Development and Innovation Office, Hungary (TKP2021-EGA-31, 2020--1.1.2-PIACI-KFI-2020-00021, KKP_22 (144180) and FK-146081). Support from Eötvös Loránd Research Network (SA-87/2021 and KEP-5/2021) are also acknowledged. The authors acknowledge Cryo- electron microscopy and tomography core facility CEITEC MUof CIISB, Instruct-CZ Centre, supported by MEYS CR (LM2023042) and European- Regional Development Fund-Project "Innovation of Czech Infrastructure forIntegrative Structural Biology"(No. CZ.02.01.01/00/23_015/0008175).

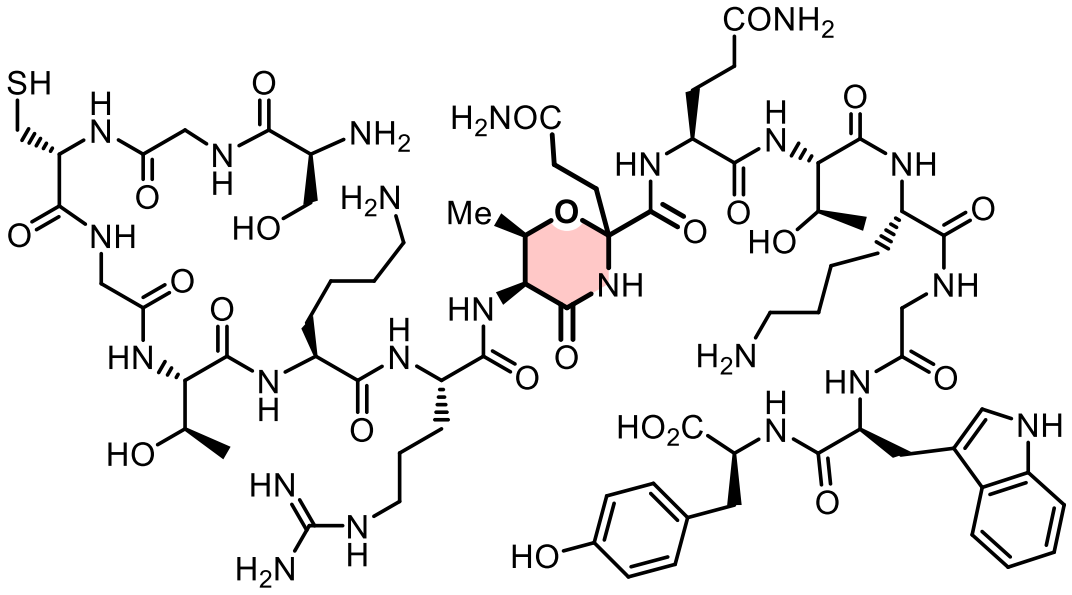
References

[1] I. Cs. Szigyártó, J. Mihály, A. Wacha, et al., “Membrane active Janus-oligomers of β³-peptides,” Chemical Science 11 (2020) 6868–6881. doi:10.1039/D0SC01344G.
[2] K. el Battioui, S. Chakraborty, A. Wacha, et al., “In situ captured antibacterial action of membrane-incising peptide lamellae,” Nature Communications 15 (2024) 3424. doi:10.1038/s41467-024-47708-4.
[3] S. Chakraborty, K. el Battioui, T. Sonallya, I. Cs. Szigyártó, et al., “Charge and length dependent build-up of environment sensitive lamellin β-peptides,” Physical Chemistry Chemical Physics 27, 8540–8551 (2025). doi:10.1039/D4CP04561K.
[4] I. Cs. Szigyártó, K. Ferentzi, A. Wacha, et al., “Sequence-Driven Modulation of the Multistage Self-Assembly Process in Lamellin-Type β-Peptides,” Aggregate 7 (2026) e70282. doi:10.1002/agt2.70282.

https://doi.org/10.17952/38EPS.2026.O46

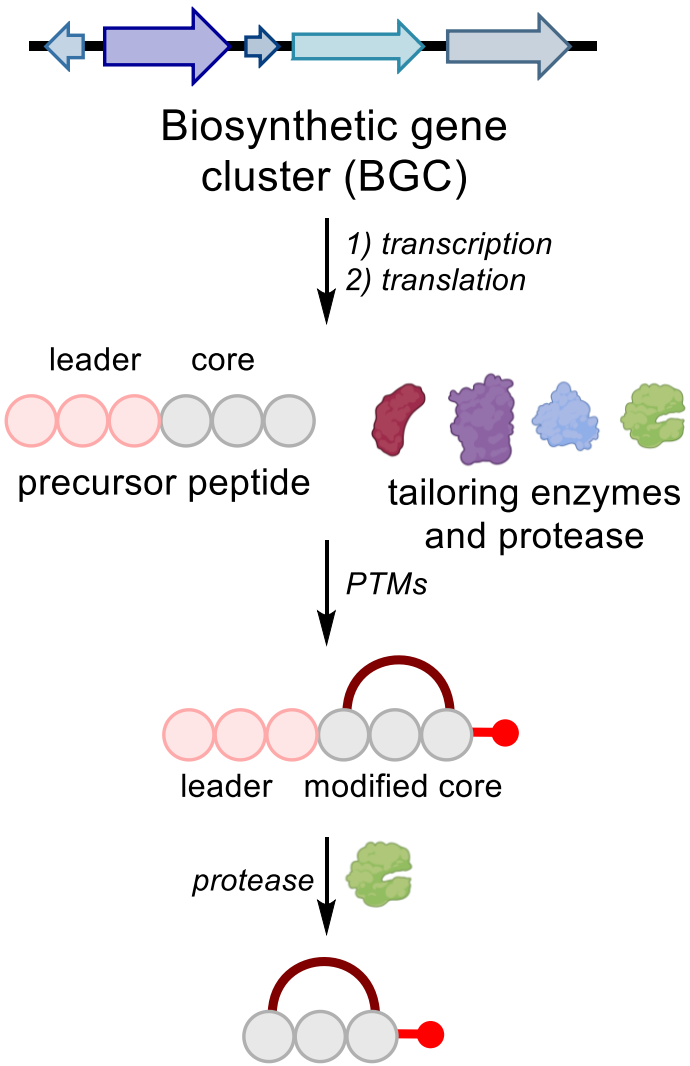
Total synthesis of the proposed structure of threoglucin A

Natalia Cano-Sampaio

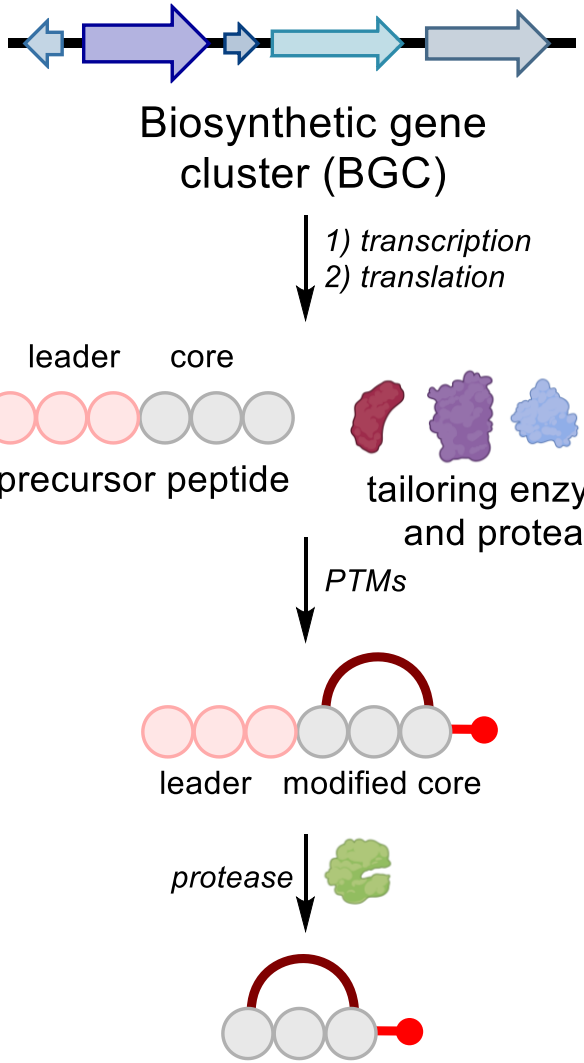


Del Valle Lab
University of Notre Dame
Department of Chemistry and Biochemistry

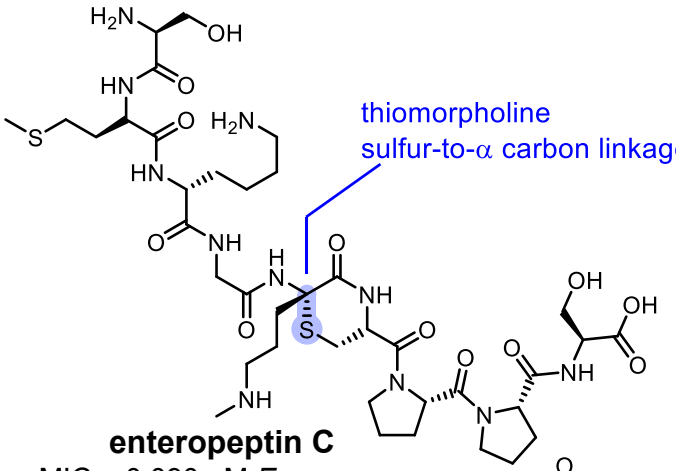
RiPP natural products biosynthesis and examples



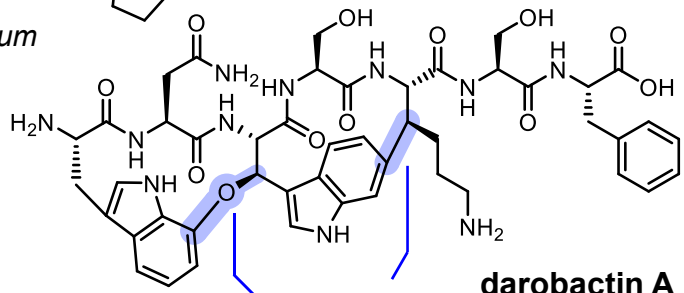
RiPP natural products biosynthesis and examples



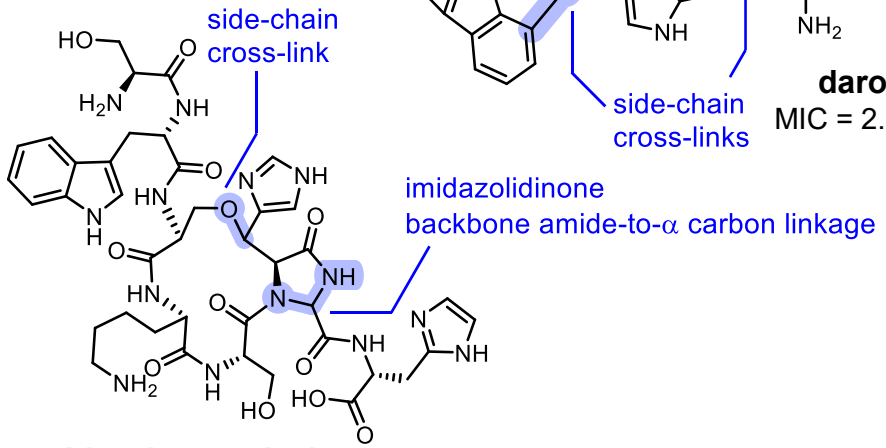
antimicrobial RiPPs



enteropeptin C
MIC = 0.090 μM *E. cecorum*

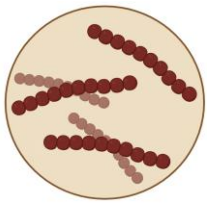


darobactin A
MIC = 2.07 μM *E. coli*

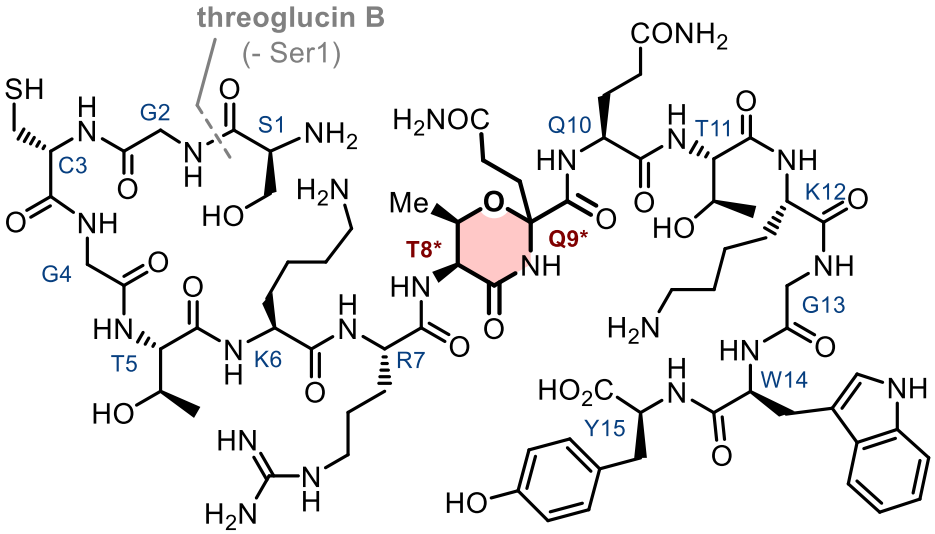


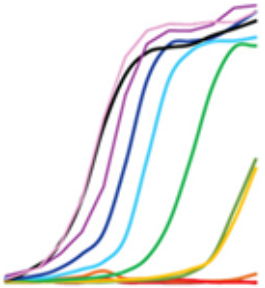
bicyclostreptin A
MIC = 0.27 μM *S. thermophilus*

Threoglucins: oxazinane-containing family of RiPPs



S. suis
(gram +)





bacteriostatic activity

Family of 22 congeners
(threoglucins A–R, *oxo*-variants A–D)

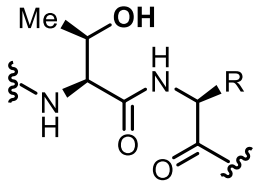
High selectivity against *S. suis (ThrA/B)*

Yield: 3.2 mg of an **inseparable** mixture of ThrA/B (from 10 L fermentation)

Non-toxic to human cells

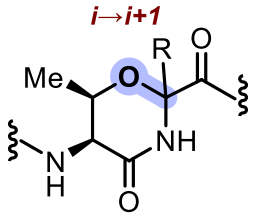
Unassigned Q9 Cα configuration

Cα amidoketal critical for biological activity



SPPS-derived
unmodified product

MIC > 30 µM *S.suis*



enzymatic
proposed product

MIC = 0.5 µM *S.suis* (ThrA/B)

Chemical synthesis required for structural validation and SAR studies

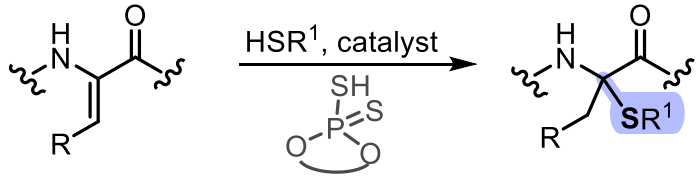
Synthetic approaches to heteroatom-to-α-carbon linkage

previous approaches

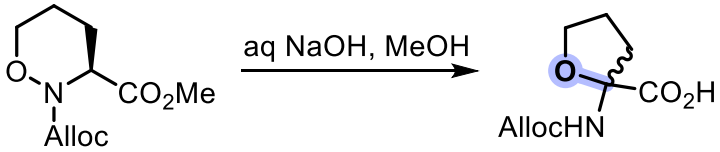
Waser, J. *et al.* (2024)



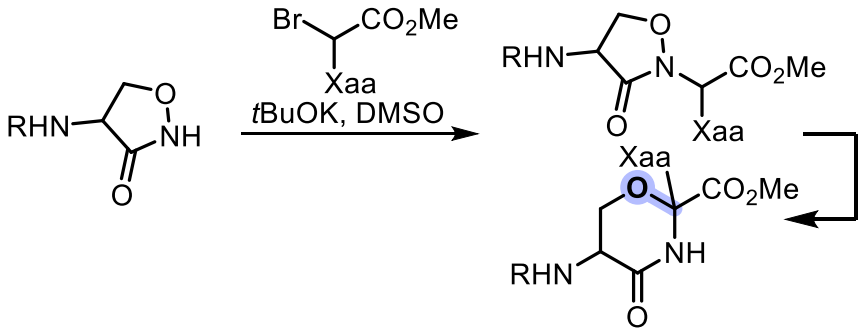
Ting, C. *et al.* (2025)

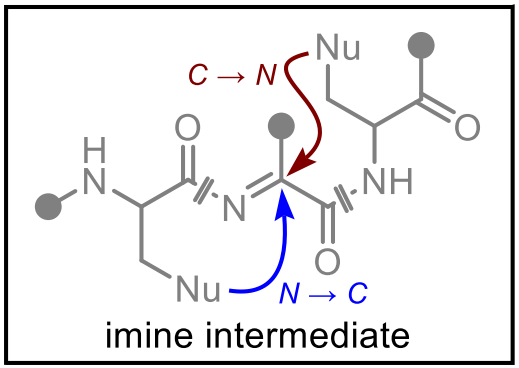


Del Valle, J. R. *et al.* (2020)



Gordon, E.M. *et al.* (1974)

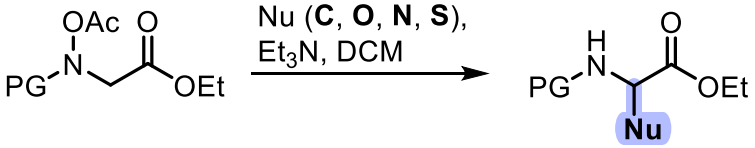




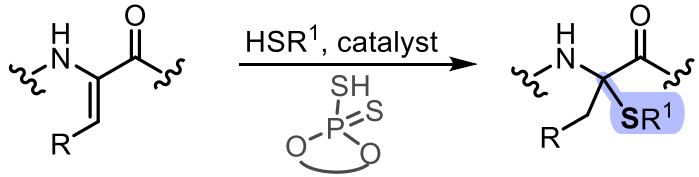
Synthetic approaches to heteroatom-to-α-carbon linkage

previous approaches

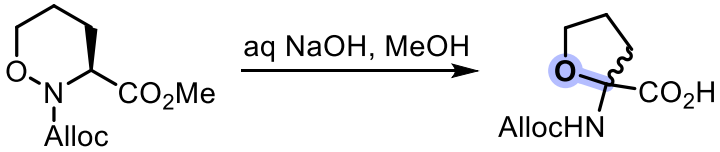
Waser, J. *et al.* (2024)



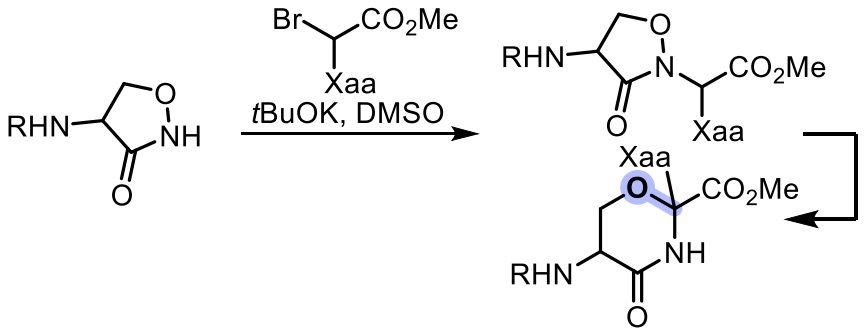
Ting, C. *et al.* (2025)

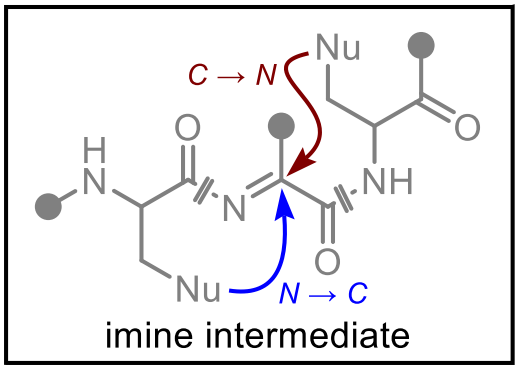


Del Valle, J. R. *et al.* (2020)

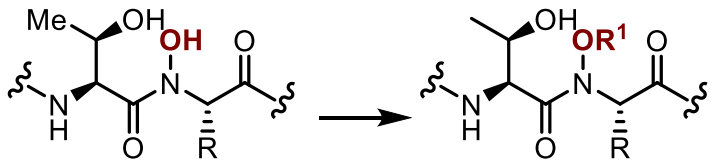


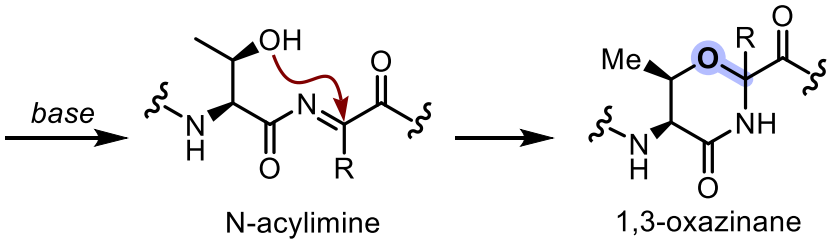
Gordon, E.M. *et al.* (1974)



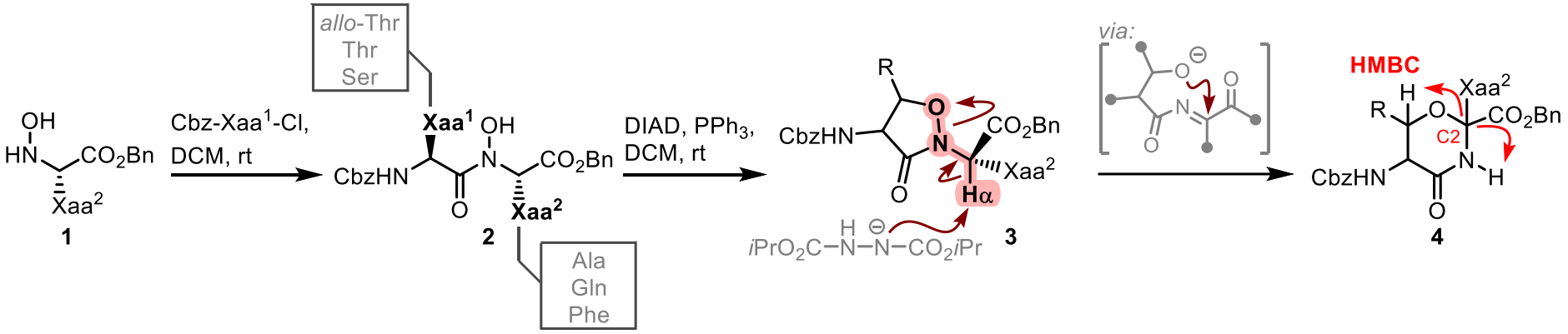


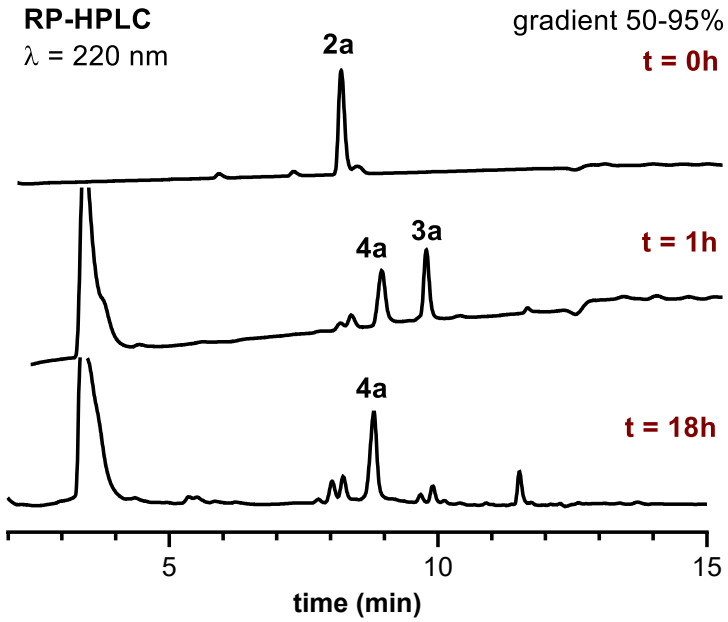
this work





Synthesis of 1,3-oxazinanes via cyclothreonine rearrangement

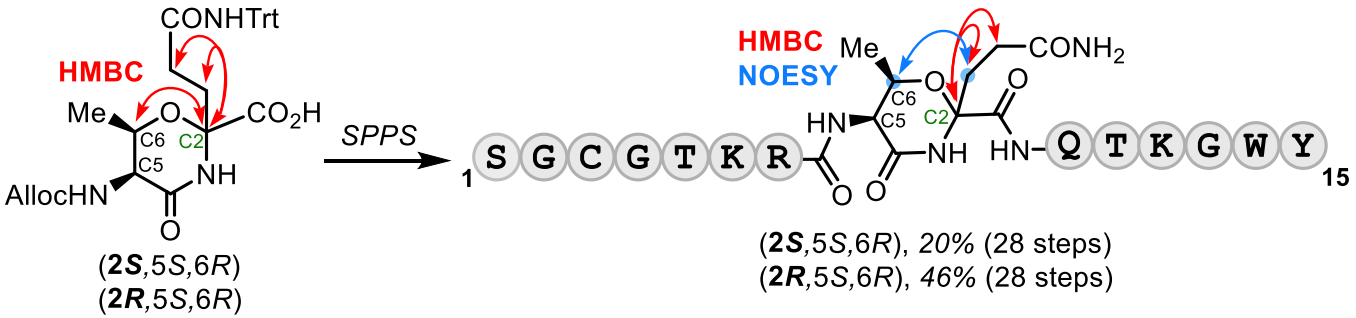




SM	Xaa^1	Xaa^2	time	product	yield	dr
2a	*allo*-Thr	Gln	18 h	**4a**	81%	60:40
2b	*allo*-Thr	Ala	18 h	**4b**	70%	75:25
2c	Thr	Gln	1 h	**4c**	99%	63:37
2d	Thr	Ala	1 h	**4d**	62%	88:12
2e	Thr	Phe	1 h	**4e**	82%	55:45
2f	Ser	Gln	18 h	**4f**	91%	53:47
2g	Ser	Ala	18 h	**4g**	88%	70:30
2h	Ser	Phe	1 h	**4h**	90%	50:50

Overall yields and dr values were determined based on ^{1}H NMR peak integration of Ser/Thr α/β ^{1}H signals relative to internal standard.

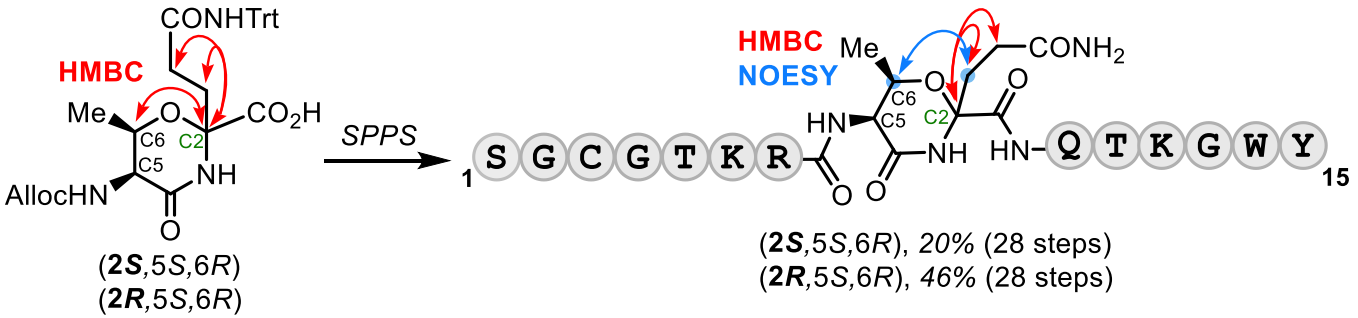
Synthesis of the proposed structure of threoglucin A and diastereomers



(**2*S***,5*S*,6*R*)
(**2*R***,5*S*,6*R*)

(**2*S***,5*S*,6*R*), *20%* (28 steps)
(**2*R***,5*S*,6*R*), *46%* (28 steps)

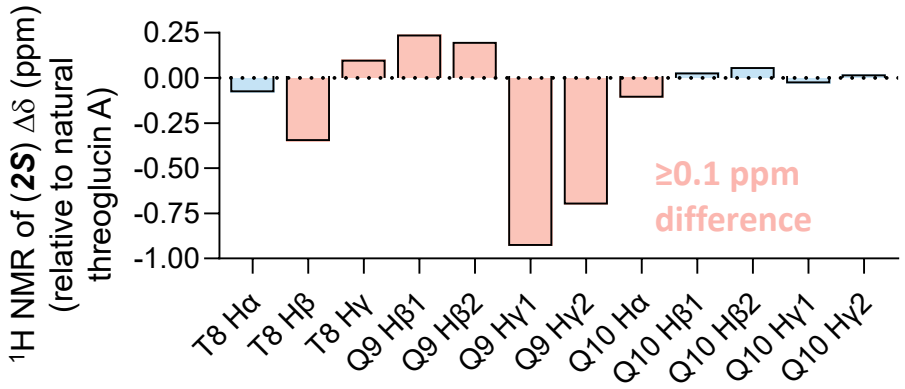
Synthesis of the proposed structure of threoglucin A and diastereomers

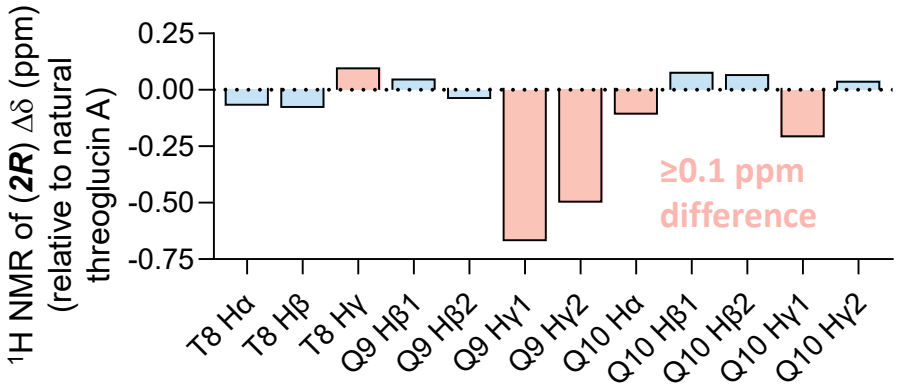


(**2*S***,5*S*,6*R*)
(**2*R***,5*S*,6*R*)

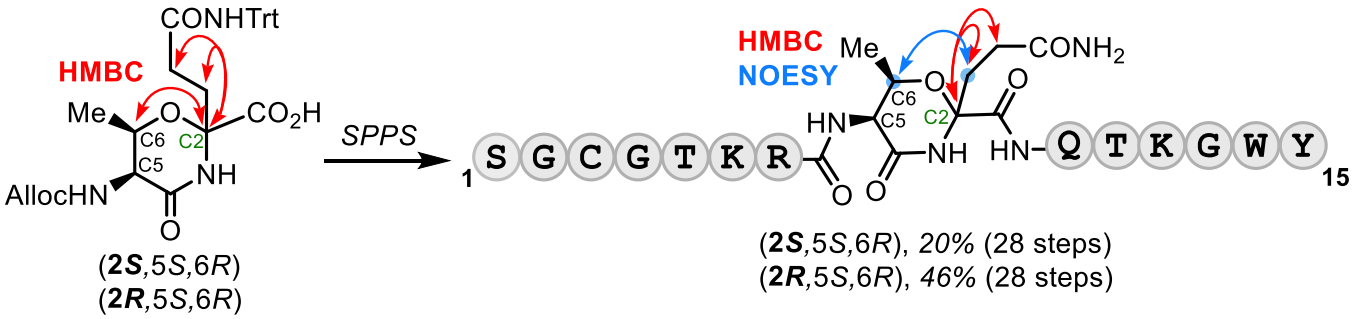
(**2*S***,5*S*,6*R*), *20%* (28 steps)
(**2*R***,5*S*,6*R*), *46%* (28 steps)

^{1}H NMR chemical shift deviations for synthetic products relative to natural product

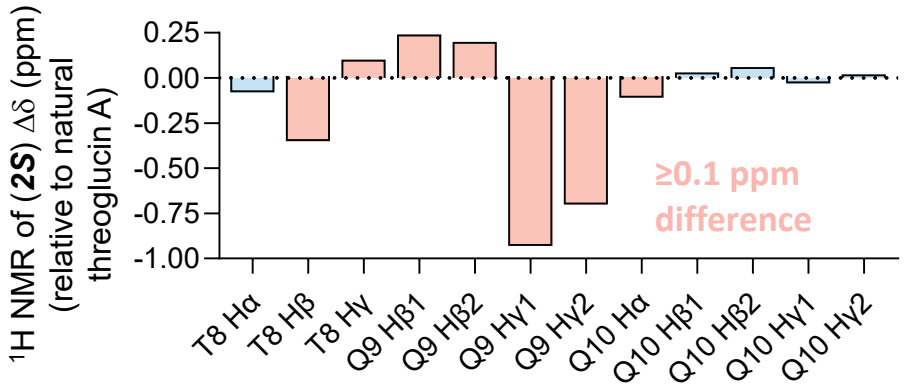


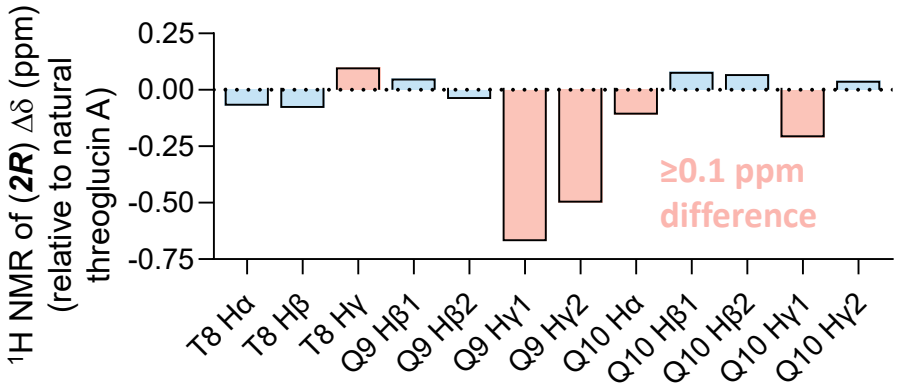


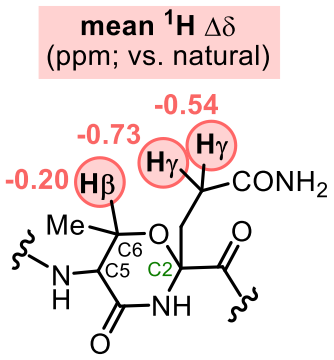
Synthesis of the proposed structure of threoglucin A and diastereomers



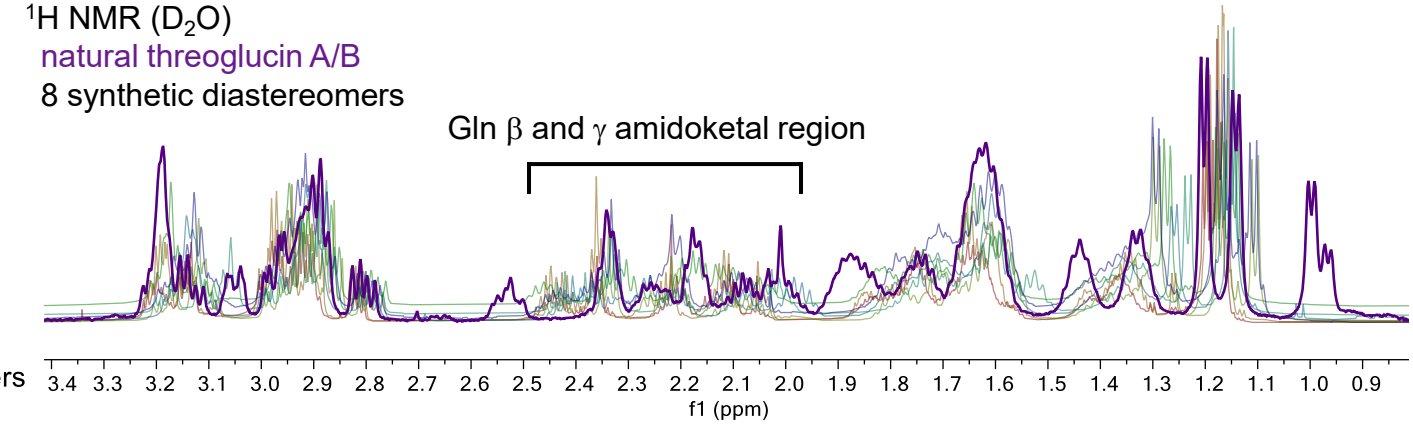
^{1}H NMR chemical shift deviations for synthetic products relative to natural product





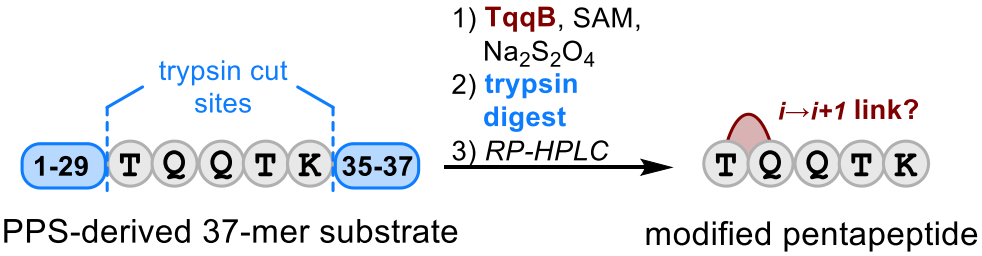


6 remaining oxazinane diastereomers



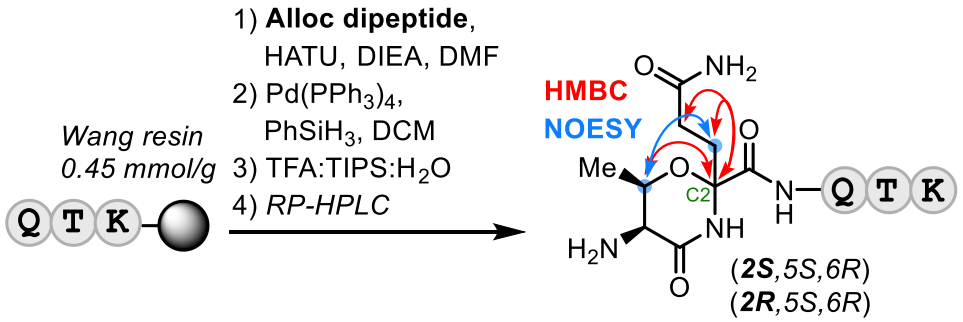
Synthesis of the proposed pentapeptides of the TqqB reaction

enzymatic synthesis



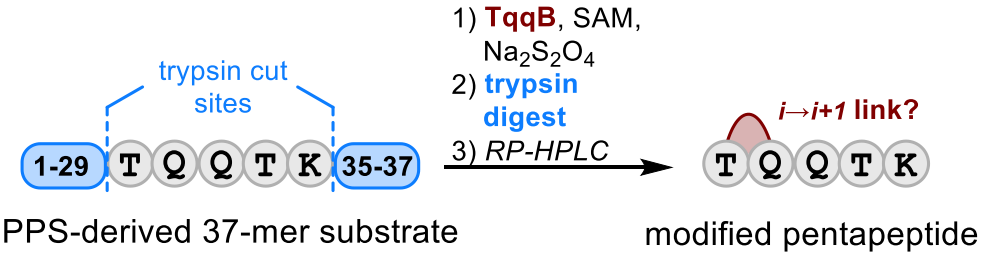
Clark, K. A.; Bushin, L. B.; Seyedsayamdost, M. R. (2019) *JACS. 141,* 27.

chemical synthesis



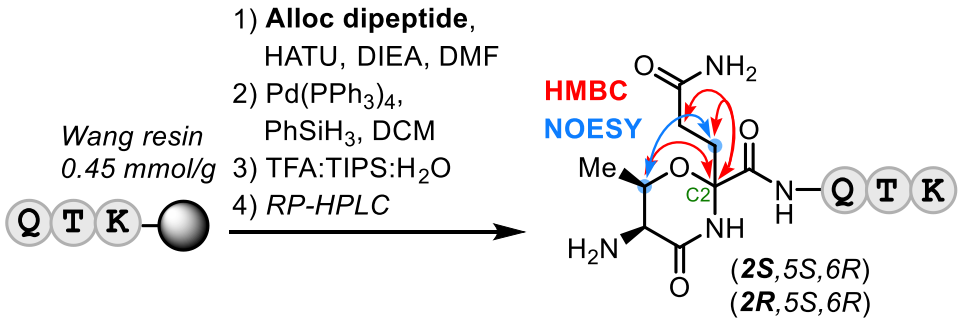
Synthesis of the proposed pentapeptides of the TqqB reaction

enzymatic synthesis

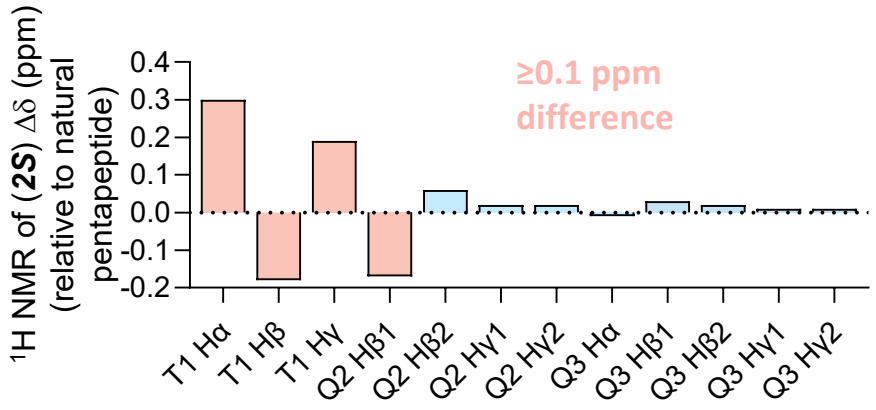


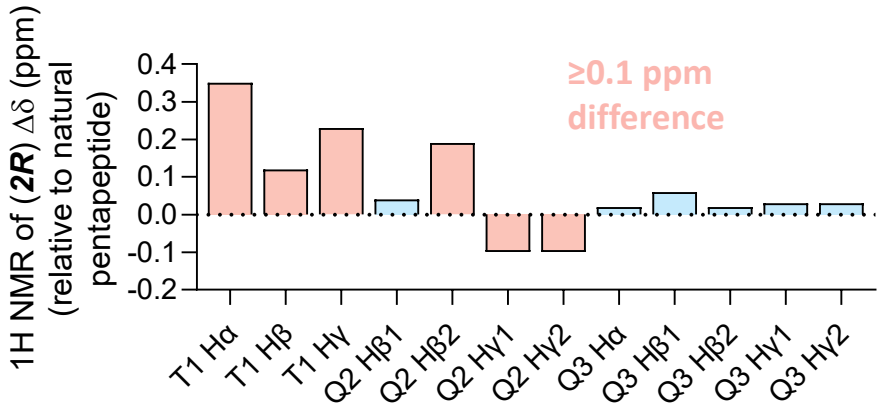
Clark, K. A.; Bushin, L. B.; Seyedsayamdost, M. R. (2019) *JACS. 141,* 27.

chemical synthesis

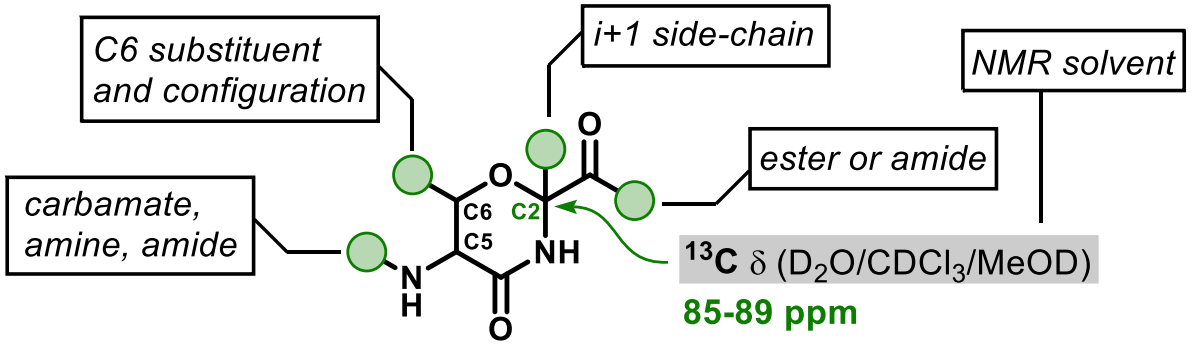


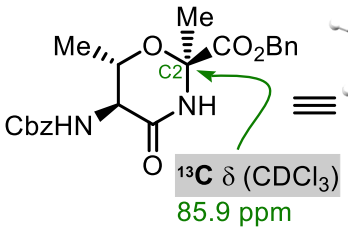
^{1}H NMR chemical shift deviations for synthetic products relative to enzymatic

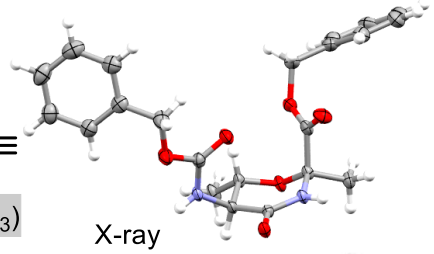


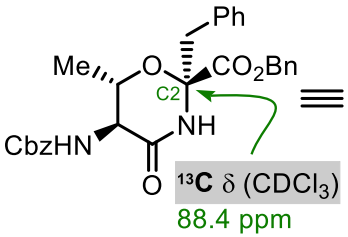


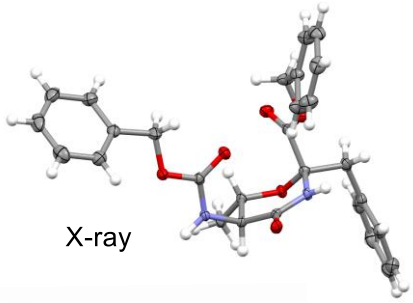
Diagnostic ^{13}C chemical shift in oxazinane amidoketals

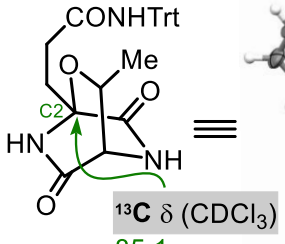


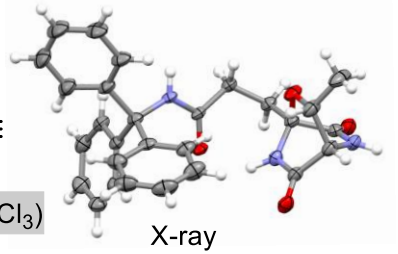


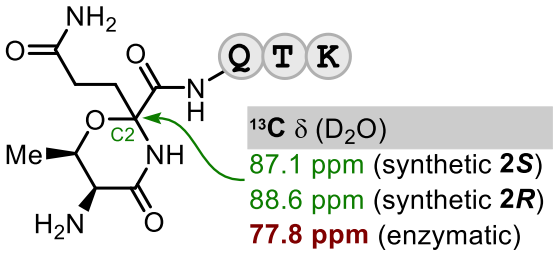


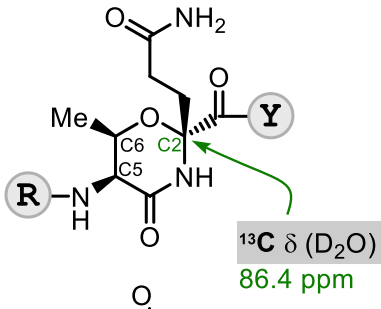


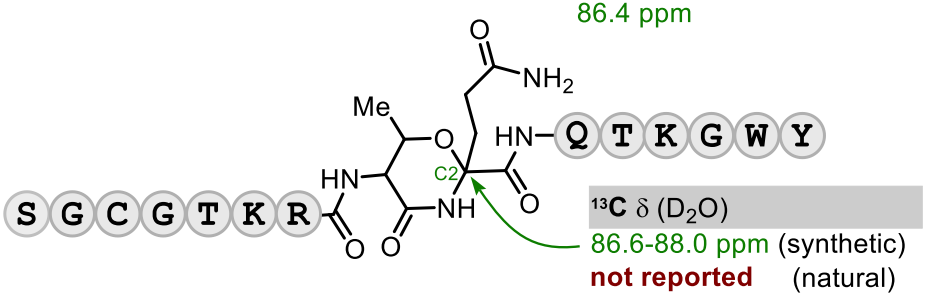




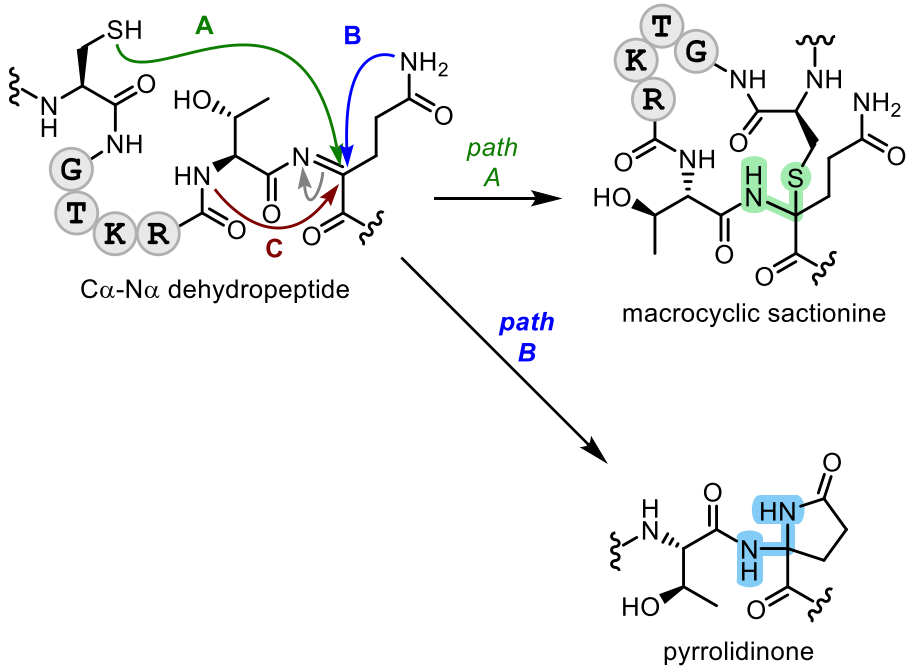


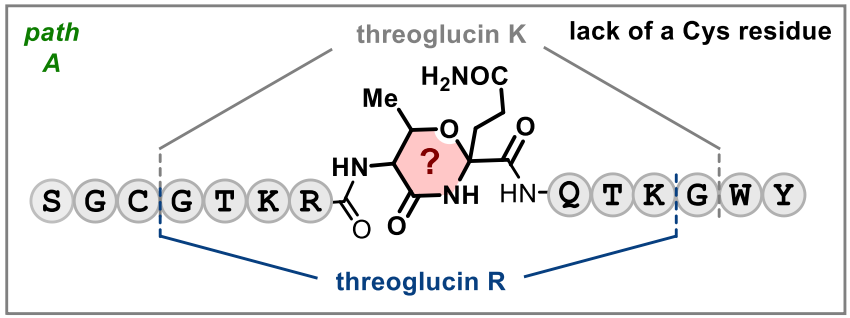


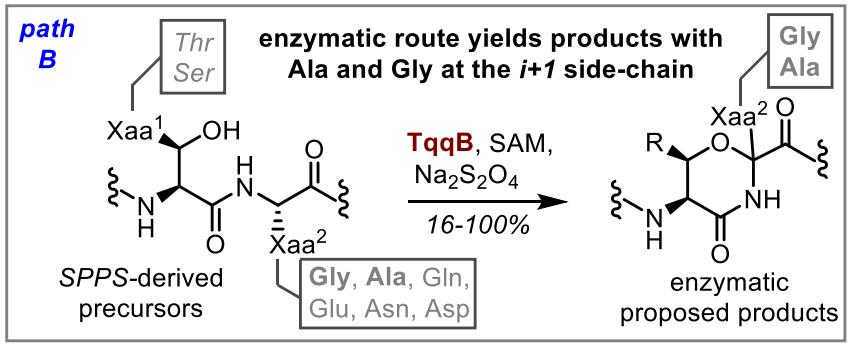




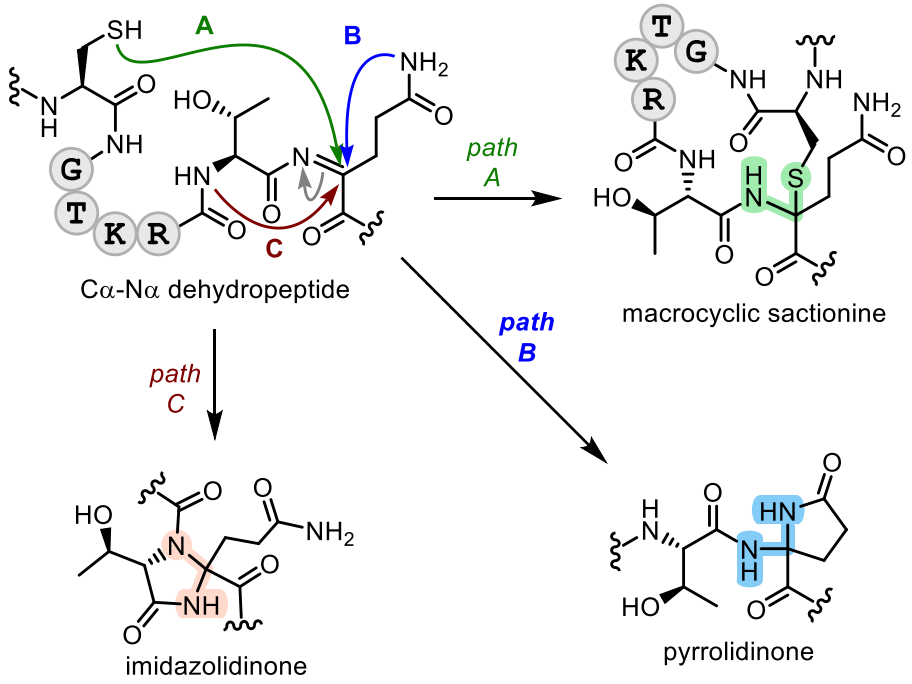
Potential connectivities in natural threoglucin A

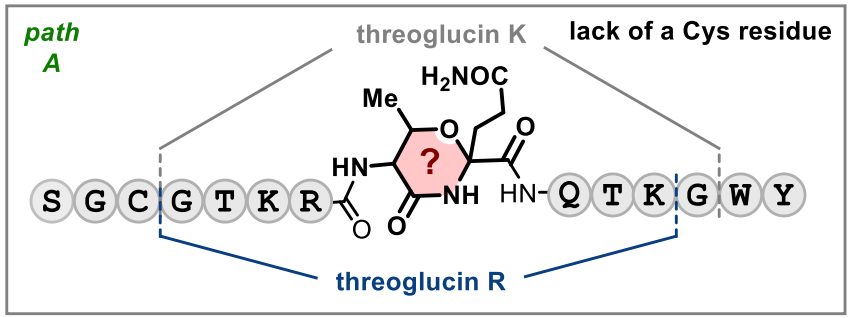


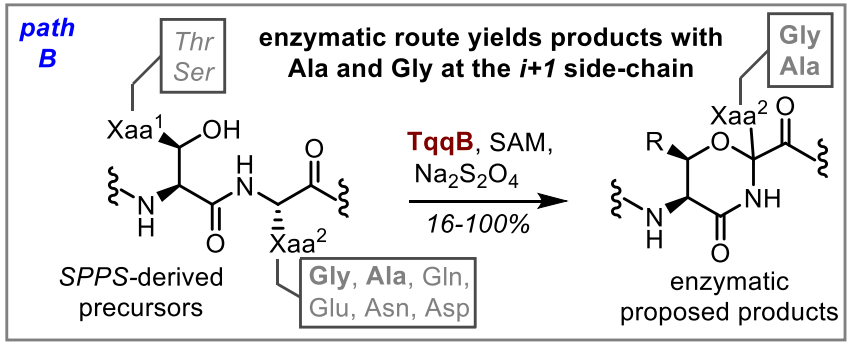


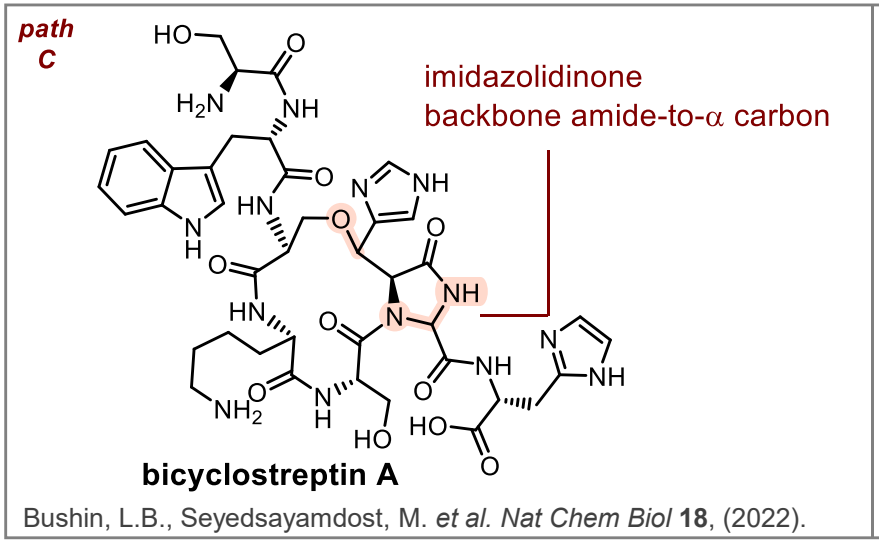


Potential connectivities in natural threoglucin A

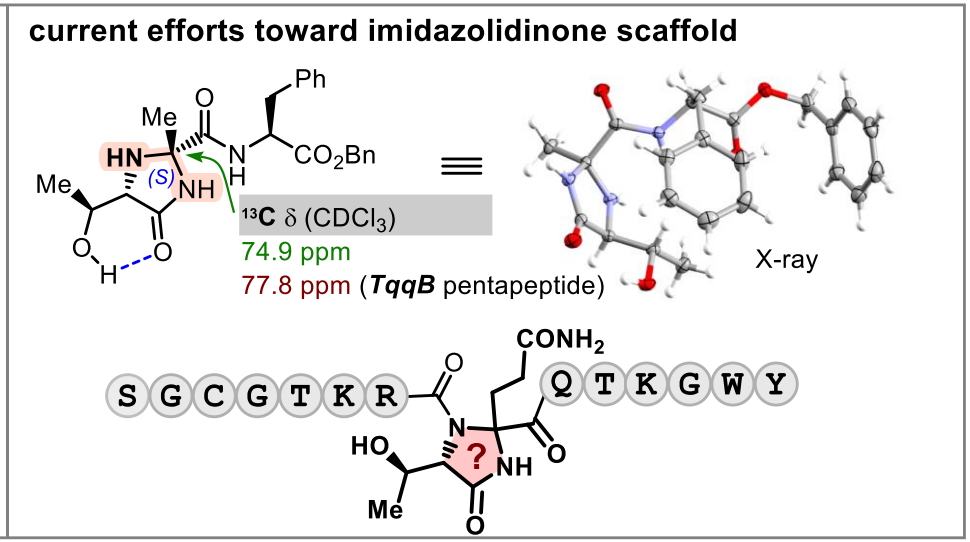








Bushin, L.B., Seyedsayamdost, M. *et al. Nat Chem Biol* **18**, (2022).



Acknowledgments

Committee members
Prof. Juan Del Valle
Prof. Shahriar Mobashery
Prof. Brittany Morgan
Dr. Syrah Starnes
Dr. Avraz Anwar
Dr. Isaac Angera
Dr. Madison Wright

Lab members
Dr. Abha Dangi
Dr. Krishna Shivakumar
Alexandre Renon
Ana-Teresa Mendoza
Laura Hession
Quinton Perry
Emma Litzelman
Kathleen George
Nick Grande

Core facility members
Dr. Evgueni Kovrigin (NMR)
Dr. Allen Oliver (XRD)

Former Lab Members
Theodore Stathopoulos
Dr. Alejandro Yeste Vázquez
Dr. Taylor Gerrein
Dr. Sebastian Pardo-Tamayo

UNIVERSITY OF NOTRE DAME

EPS NSF (CHE2109008)





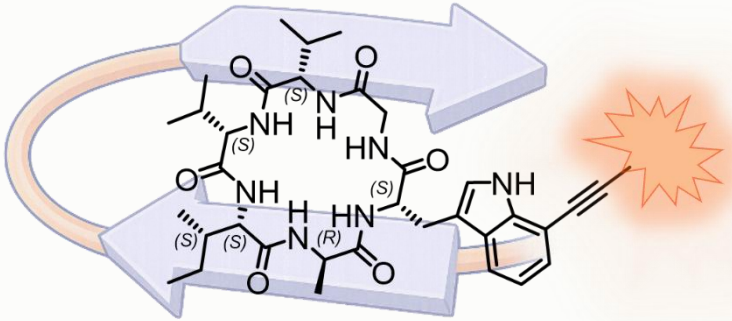
Cyclopeptide-Based Fluorescent Probes for Monitoring Prefibrillar Aβ42 Nanostructures

Steven Panek

PhD Candidate

Bielefeld University, Germany · Université Paris-Saclay, France

https://doi.org/10.17952/38EPS.2026.O49



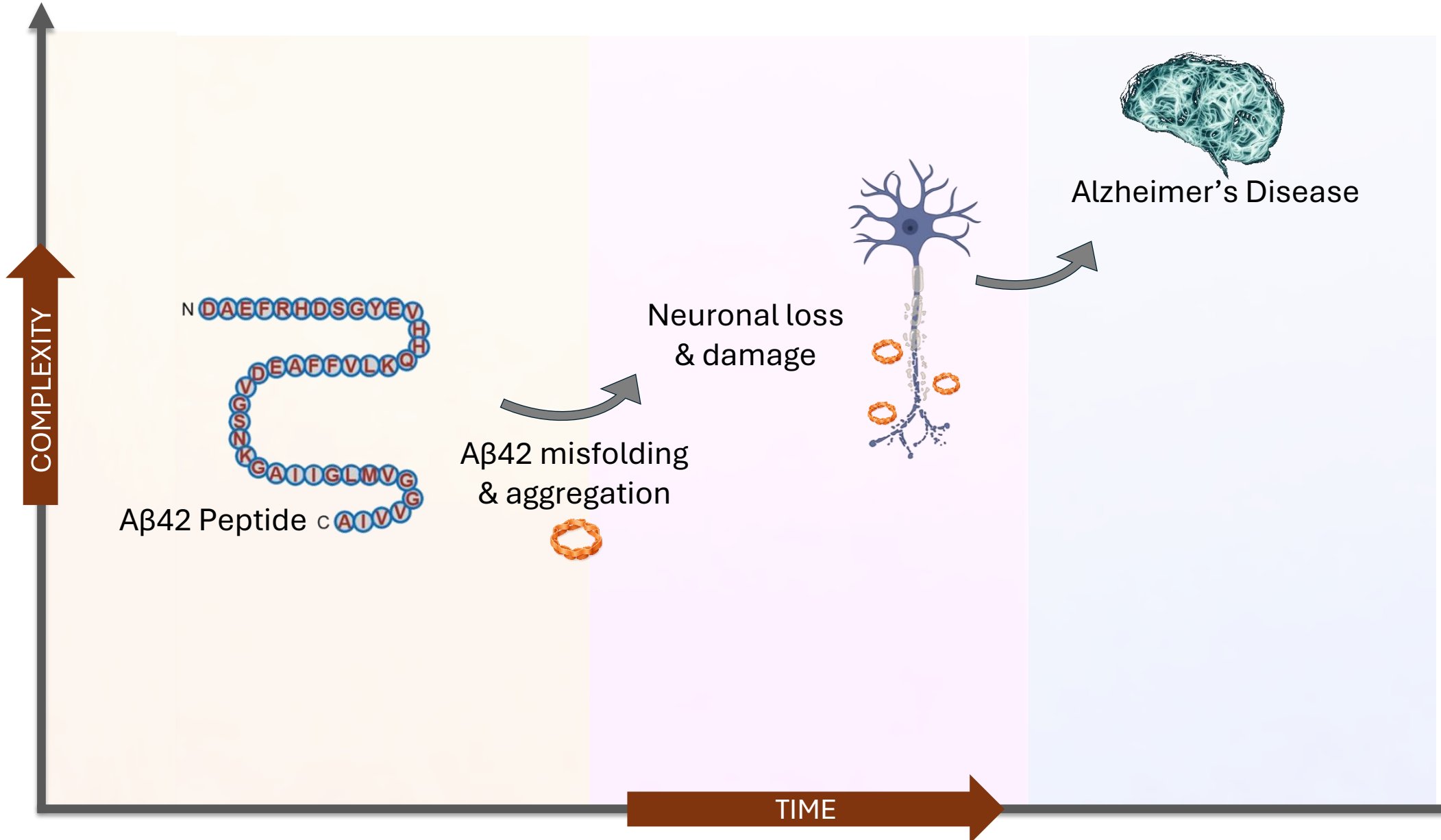
Research conducted in

Norbert Sewald Group
Bielefeld University

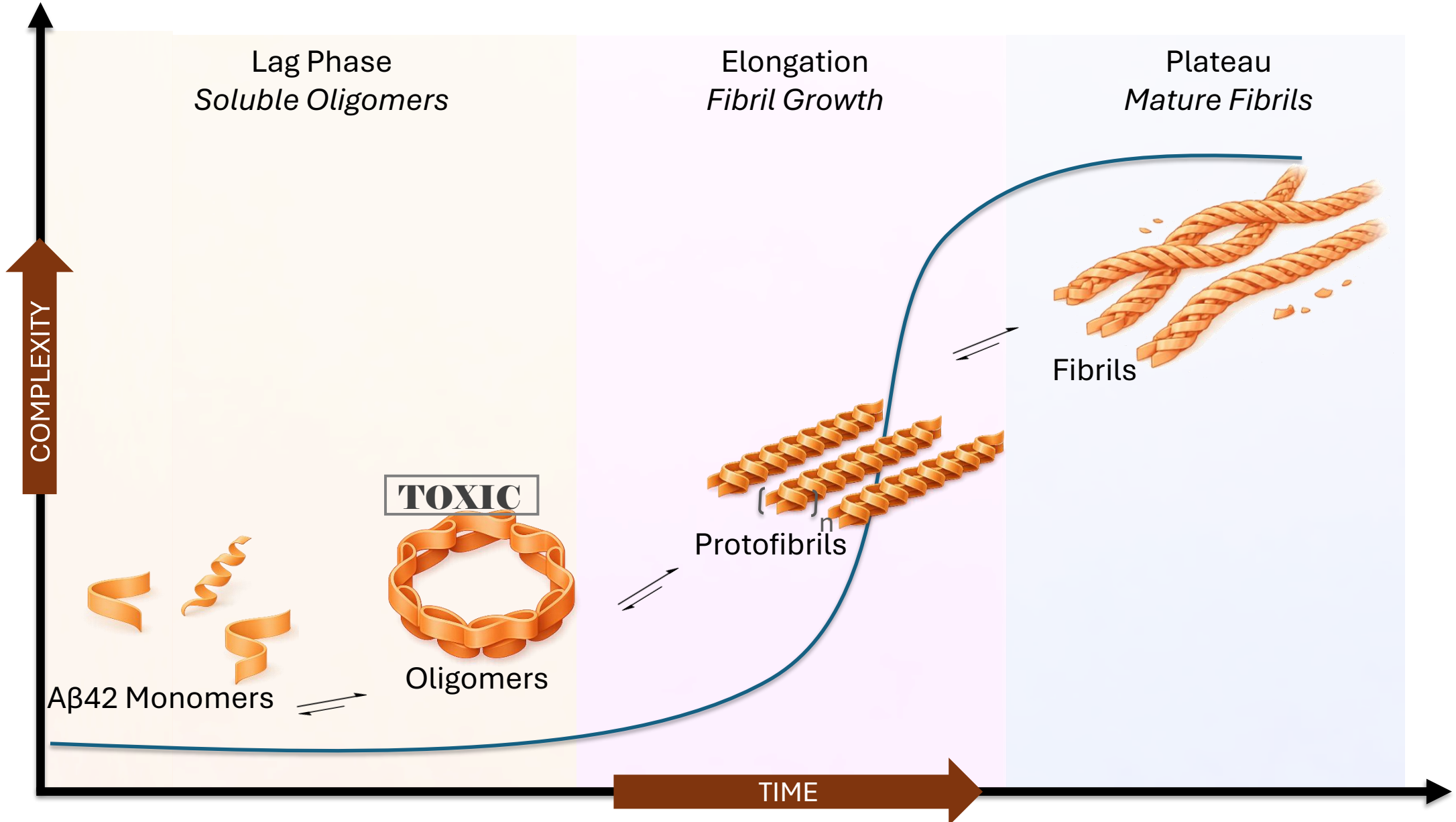
Nicolò Tonali Group
CEA Paris-Saclay

38th European Peptide Symposium
Vienna, Austria · September 9, 2026

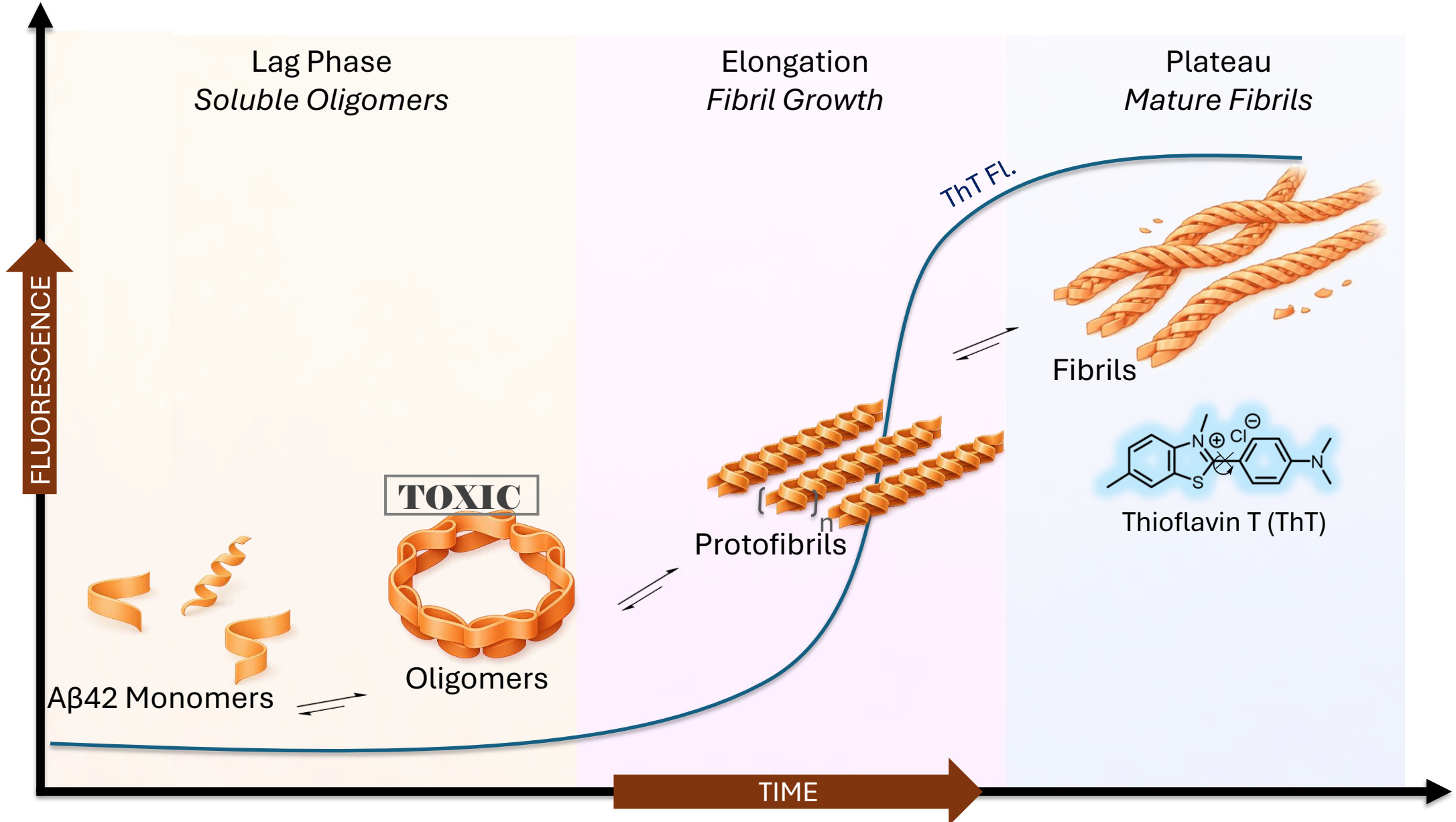
Aβ42 Misfolding in Alzheimer's Disease



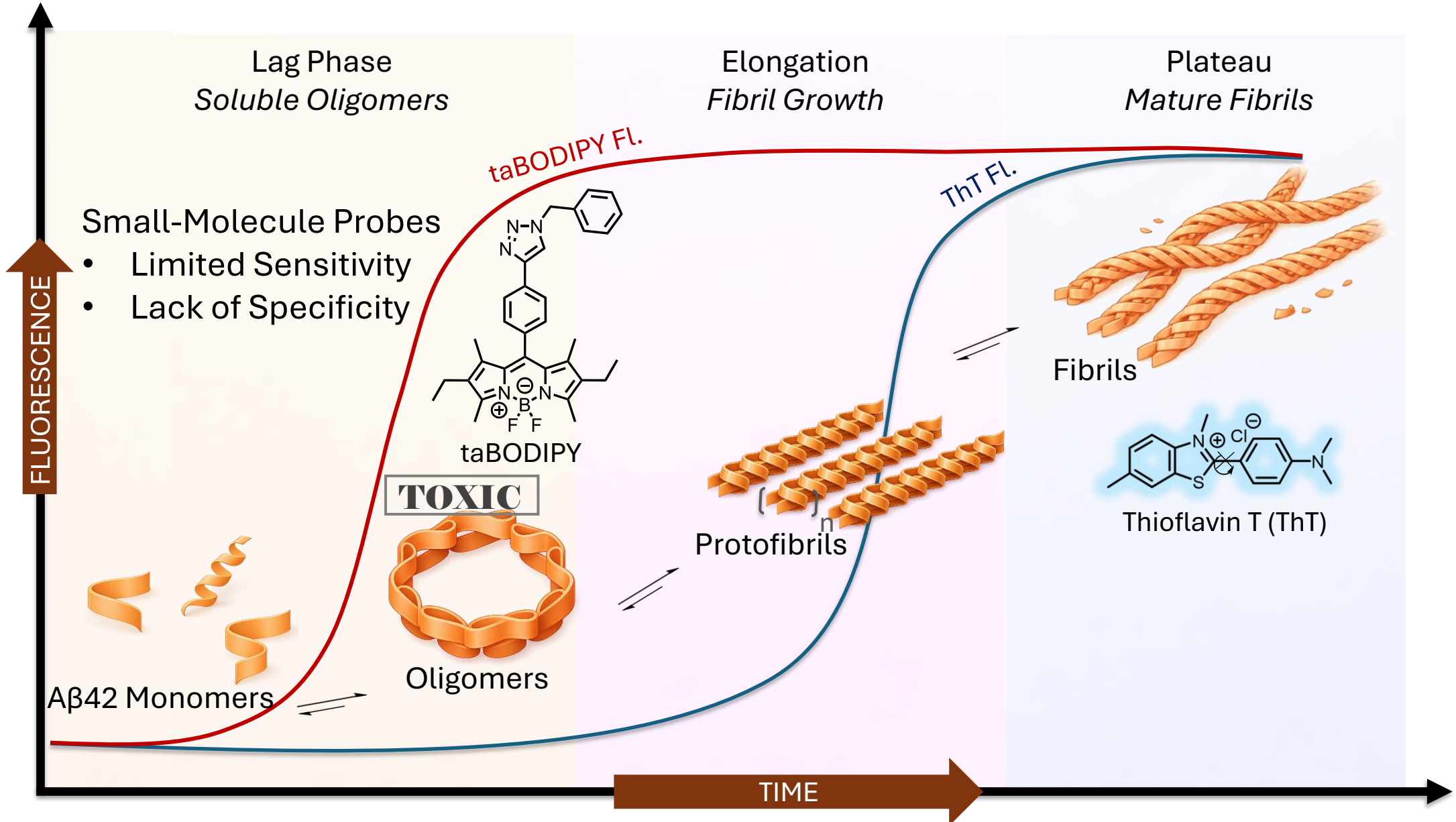
Aβ42 Aggregation Pathway



Aβ42 Aggregation Pathway

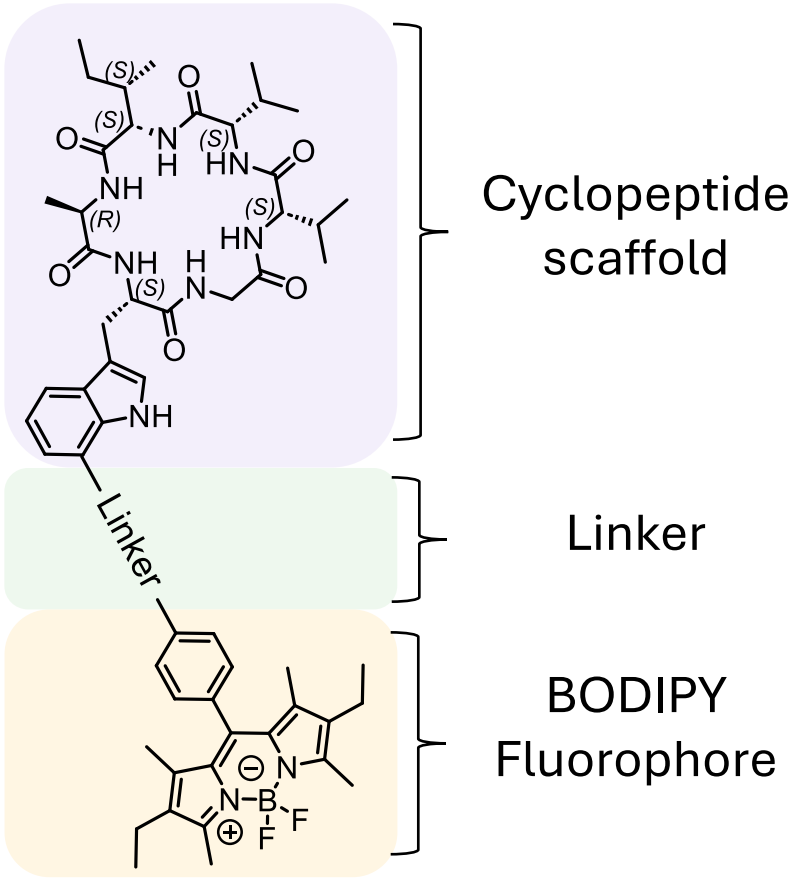


Aβ42 Aggregation Pathway



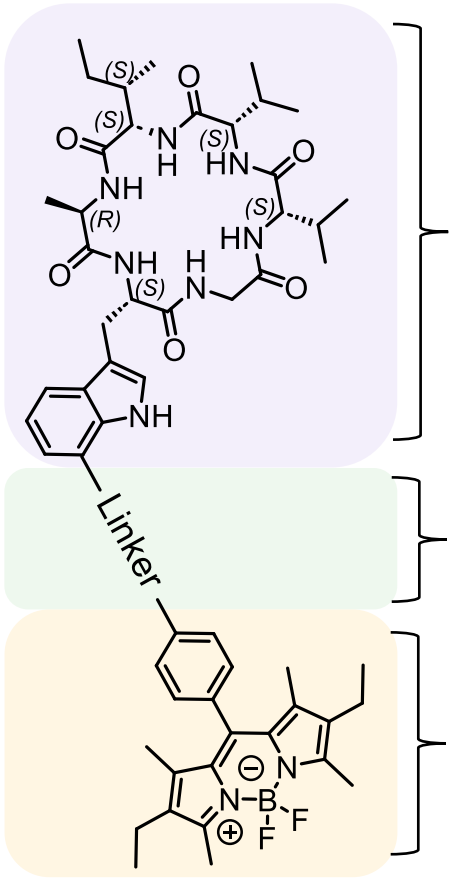
Design of Peptide-Fluorophor-Conjugate

Probe Architecture



Hypothesis: Aβ42 Oligomer Detection

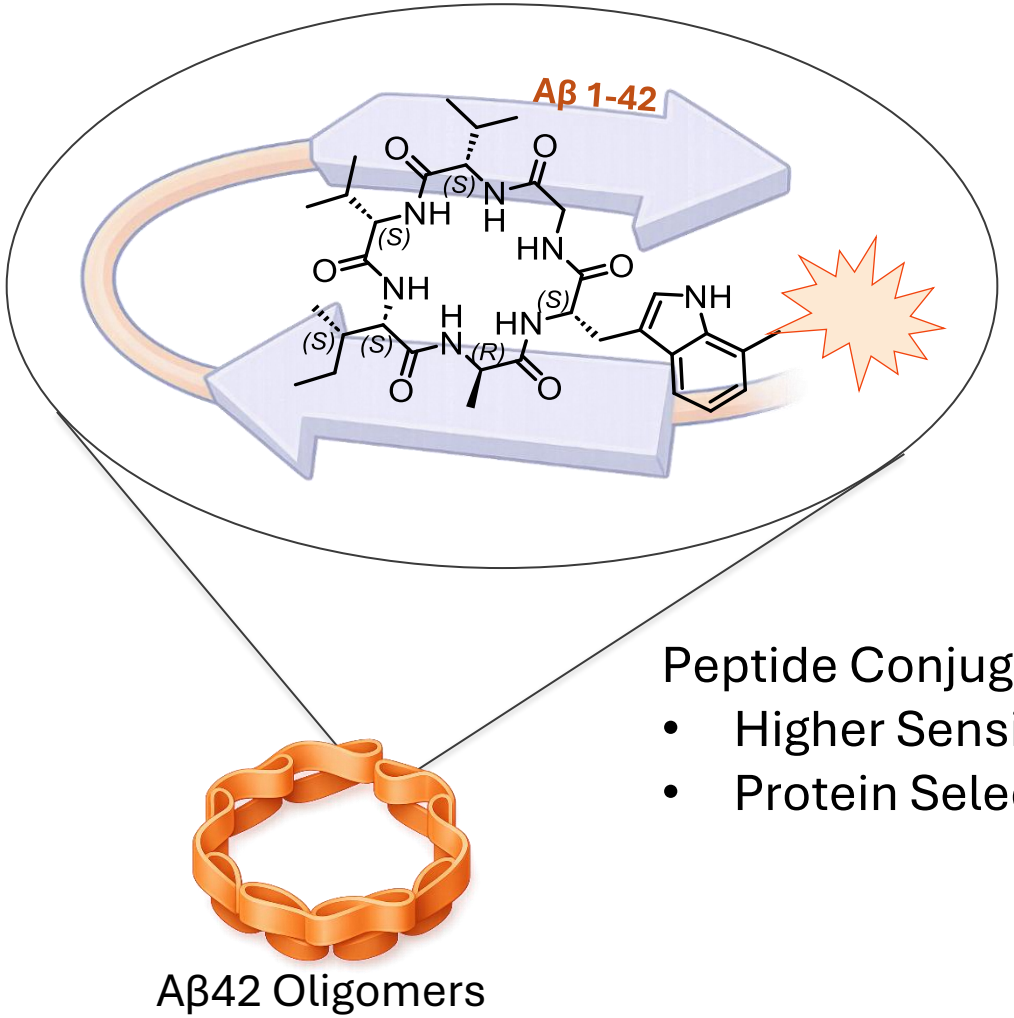
Probe Architecture



Cyclopeptide scaffold

Linker

BODIPY Fluorophore



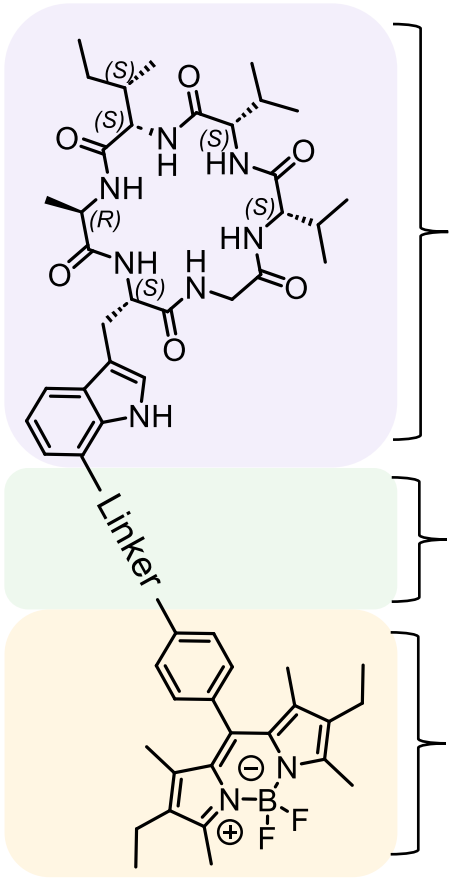
Aβ42 Oligomers

Peptide Conjugate Probes:

- Higher Sensitivity?
- Protein Selectivity?

Hypothesis: Aβ42 Oligomer Detection

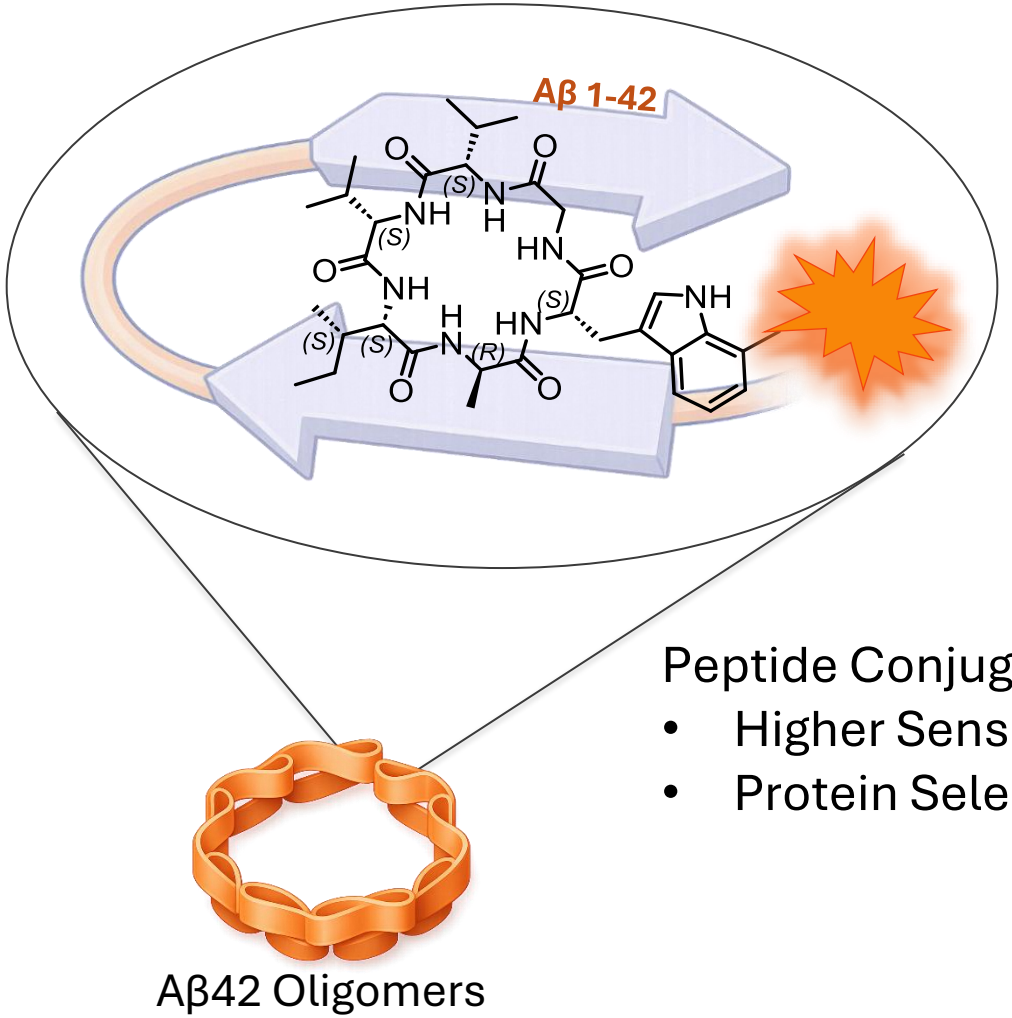
Probe Architecture



Cyclopeptide scaffold

Linker

BODIPY Fluorophore



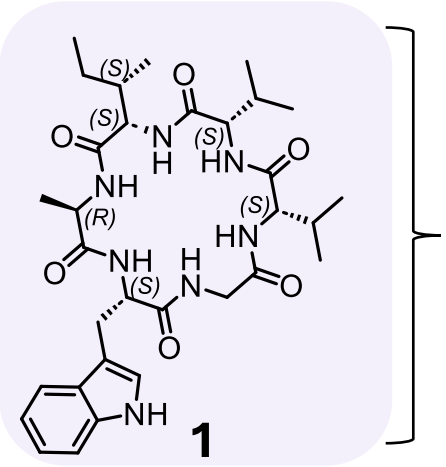
Aβ42 Oligomers

Peptide Conjugate Probes:

- Higher Sensitivity?
- Protein Selectivity?

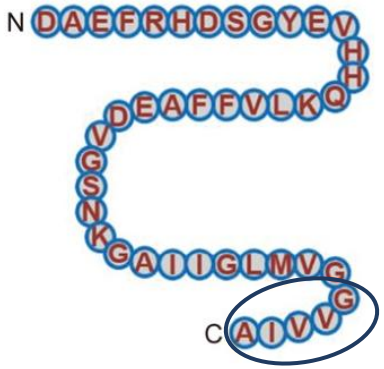
Cyclopeptide Design & Characterization

Probe Architecture



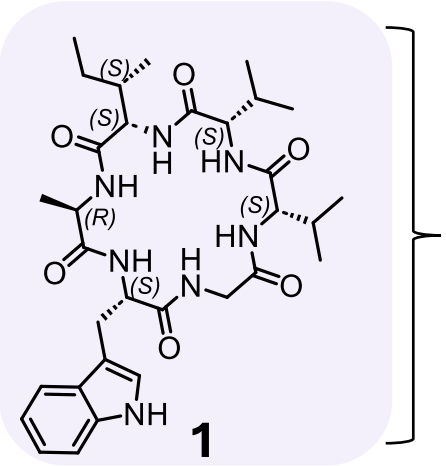
c(G[38]VVIa[42]W)

Aβ1-42 Sequence



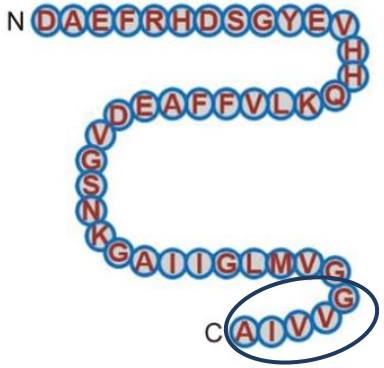
Cyclopeptide Design & Characterization

Probe Architecture

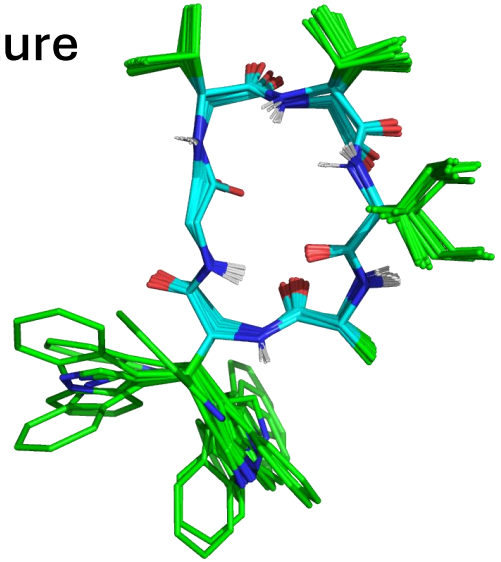


c(G[38]VVIa[42]W)

Aβ1-42 Sequence



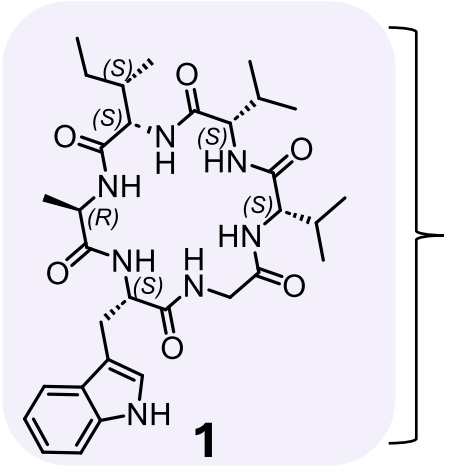
NMR Structure



- Well-Defined Confromation

Cyclopeptide Design & Characterization

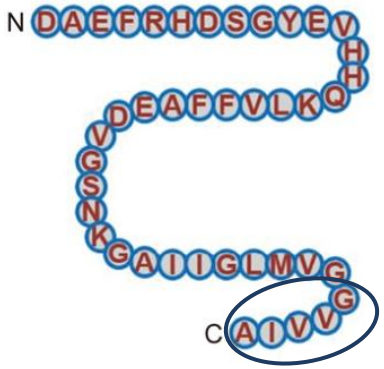
Probe Architecture



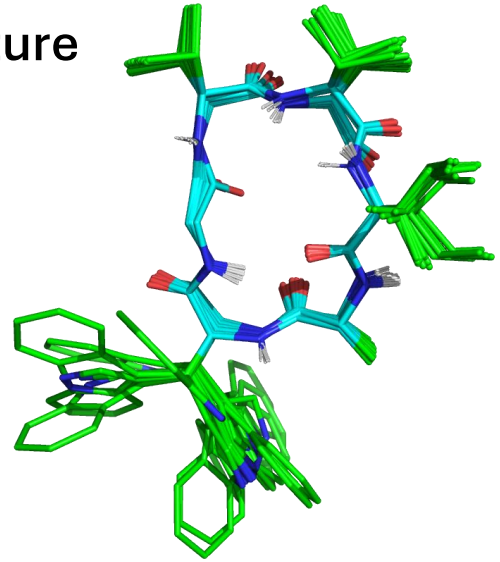
c(G^{38}VVIa^{42}W)

- Well-Defined Confromation
- No Interference with Aβ Aggregation

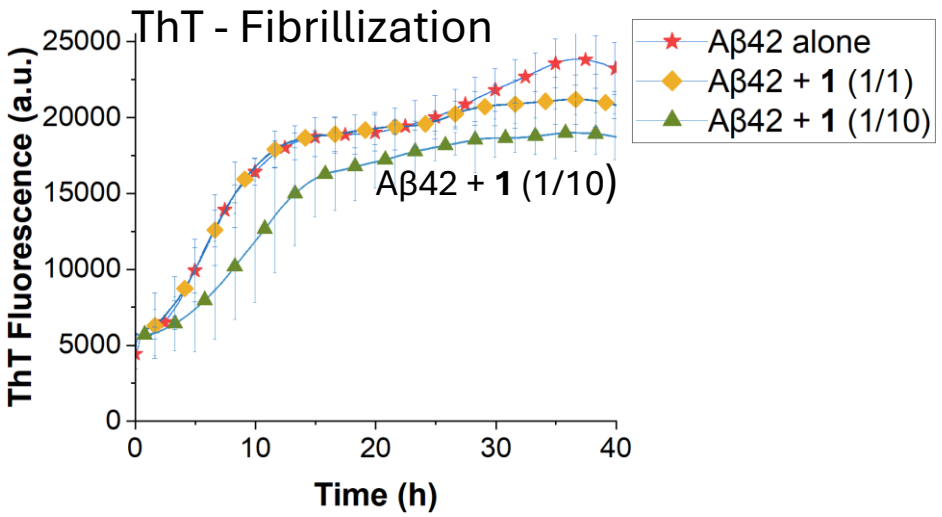
Aβ1-42 Sequence

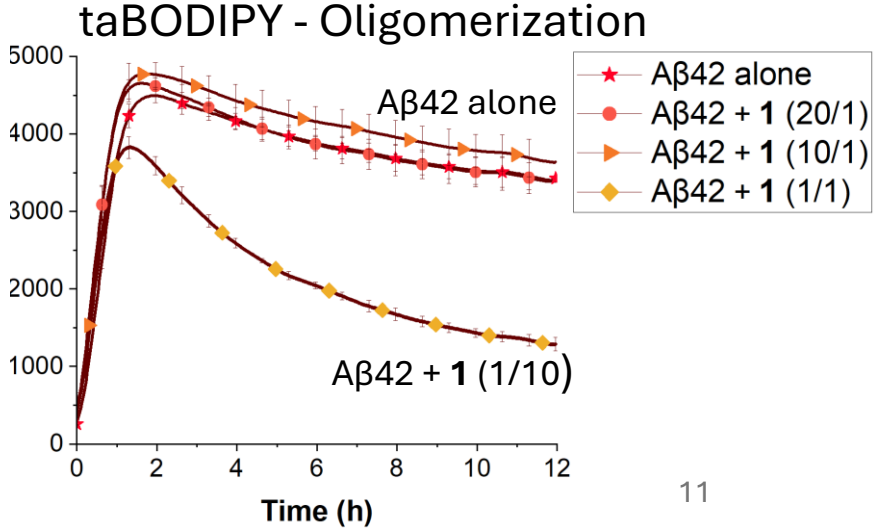


NMR Structure



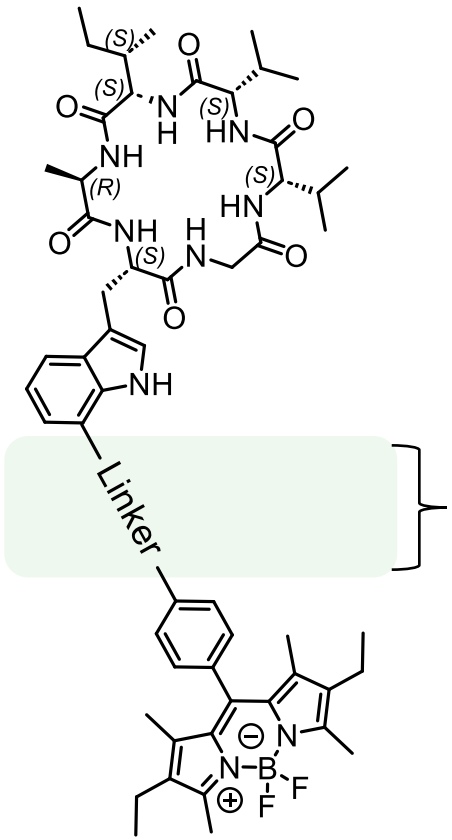
Effect on Aβ42 Aggregation



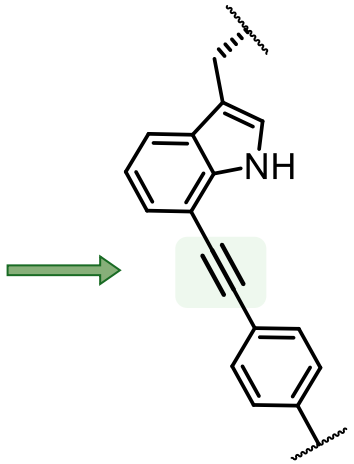


Design of Peptide-Fluorophor-Conjugate

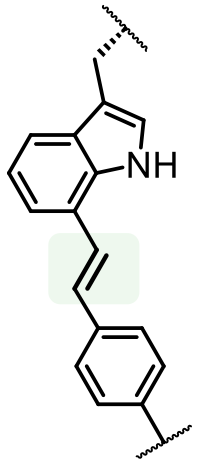
Probe Architecture



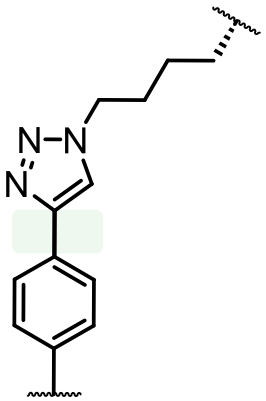
Linker



Rigid



Semi-flexible

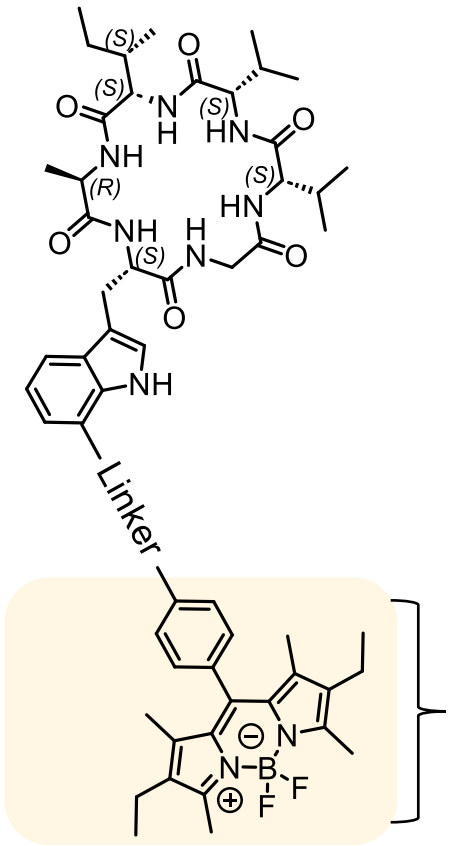


Flexible

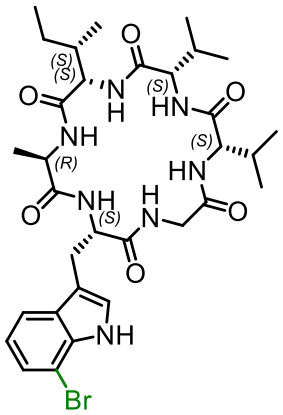
Increasing Linker Flexibility

Design of Peptide-Fluorophor-Conjugate

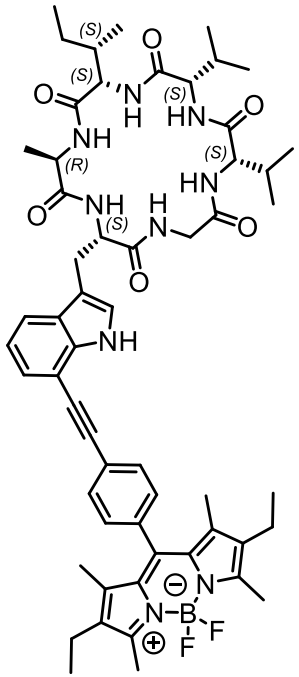
Probe Architecture



BODIPY
Fluorophore



Cross Coupling

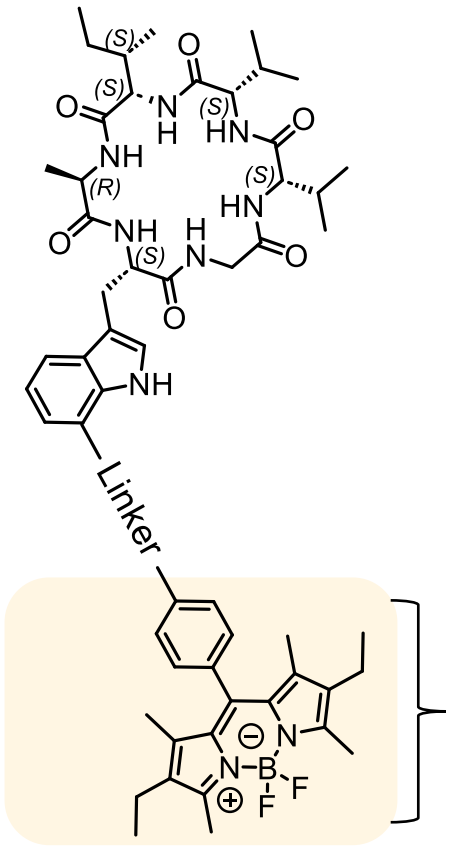


2

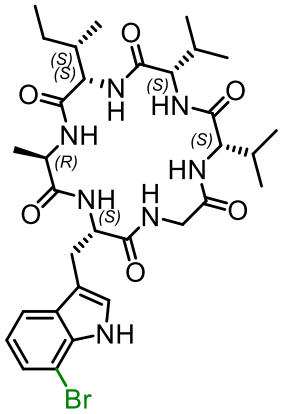
18%

Design of Peptide-Fluorophor-Conjugate

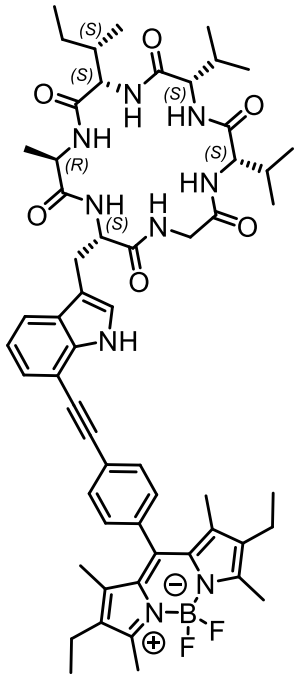
Probe Architecture



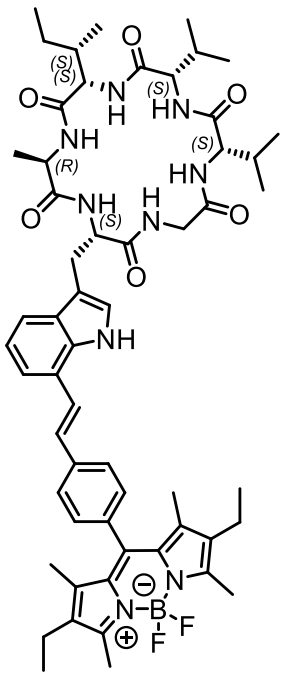
BODIPY
Fluorophore



Cross Coupling

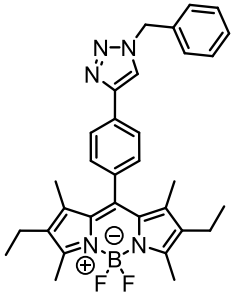


2
18%

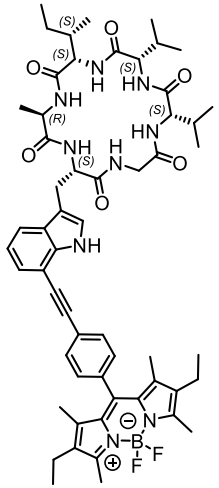


3
22%

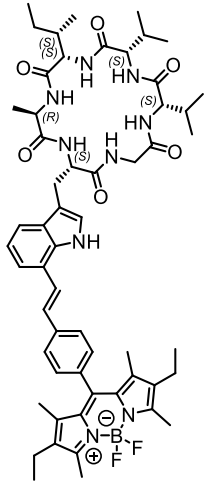
Probe–Linker Architectures



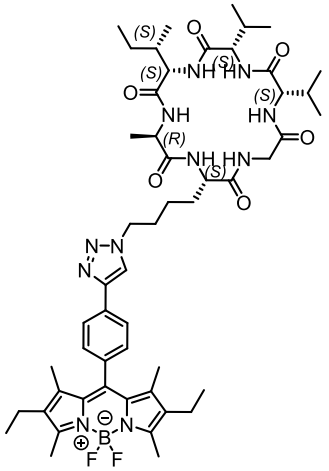
taBODIPY
Reference probe



2

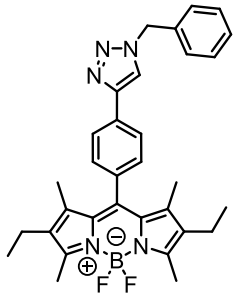


3

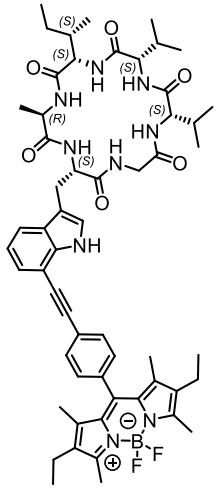


4

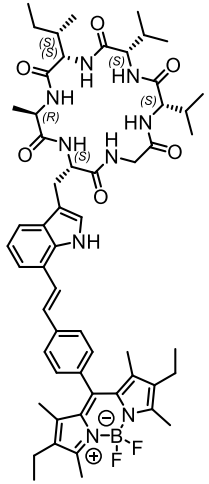
Aβ42 Detection



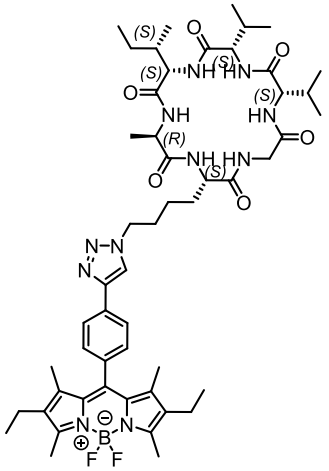
taBODIPY
Reference probe



2

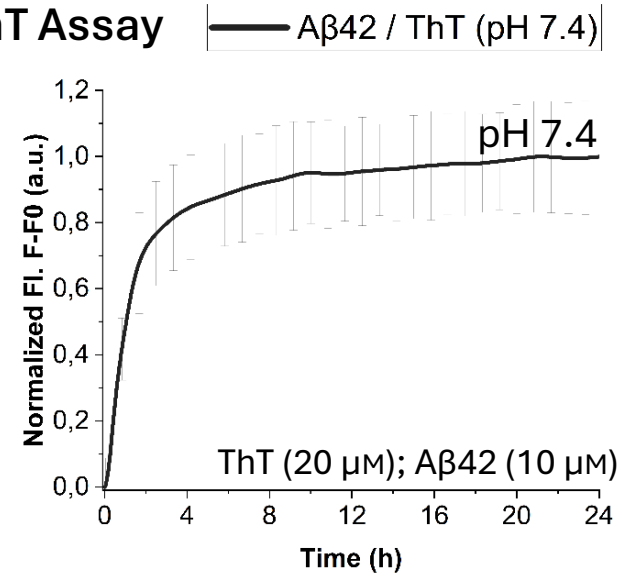


3

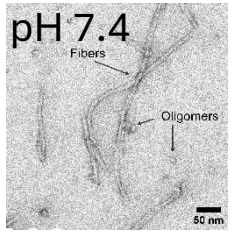


4

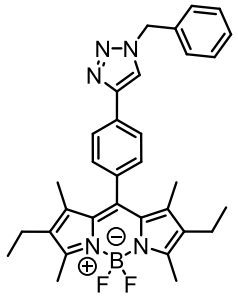
ThT Assay



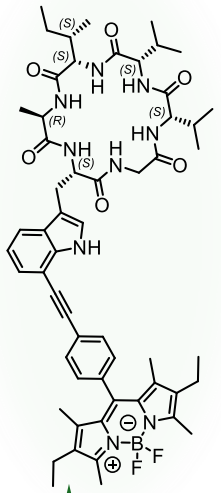
TEM, 24h



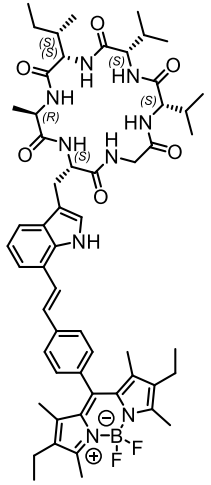
Aβ42 Detection



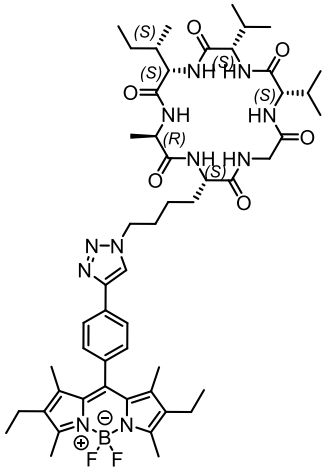
taBODIPY
Reference probe



★2

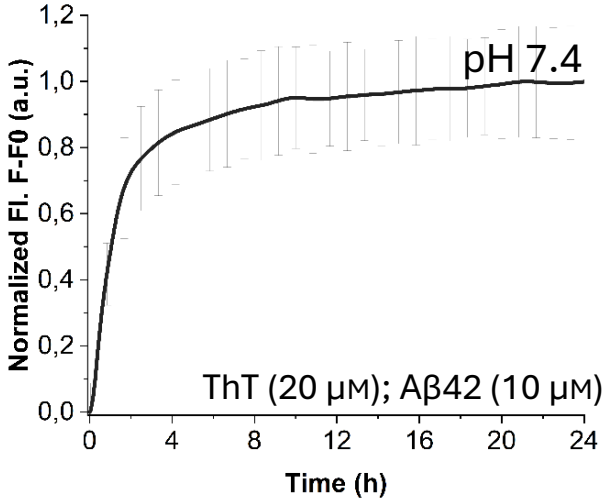


3

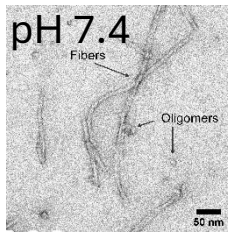


4

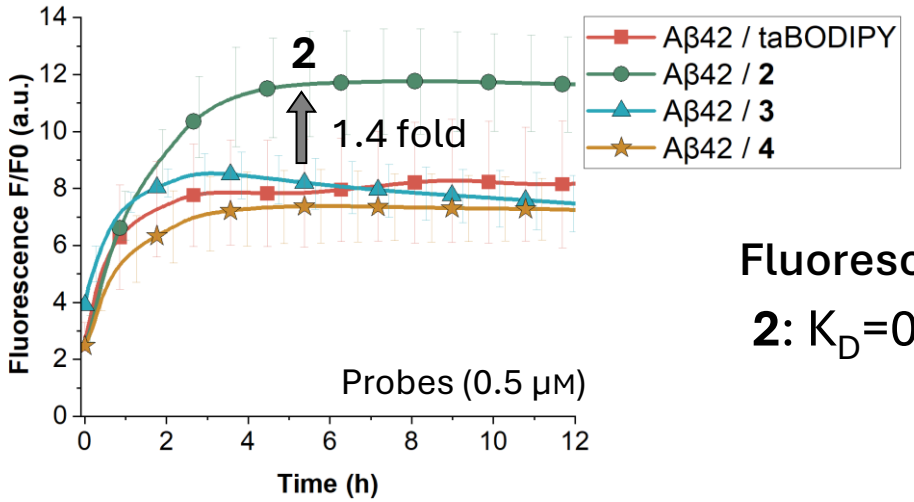
ThT Assay — Aβ42 / ThT (pH 7.4)



TEM, 24h



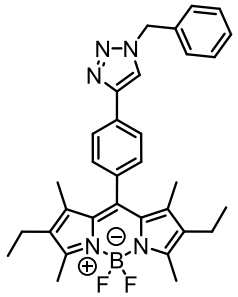
Probe Assay (pH 7.4)



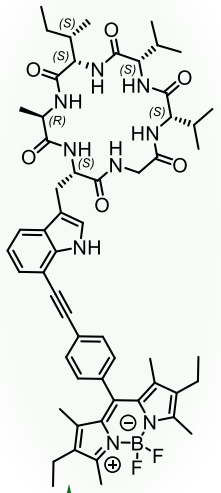
Fluorescence Titration

2: K_D=0.07 ± 0.04 μM

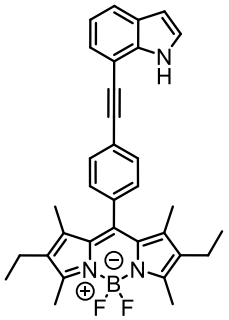
Aβ42 Oligomer Detection



taBODIPY
Reference probe



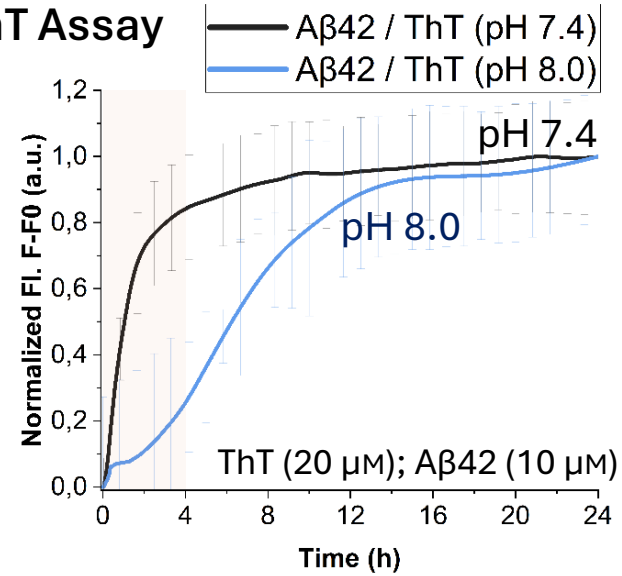
★2



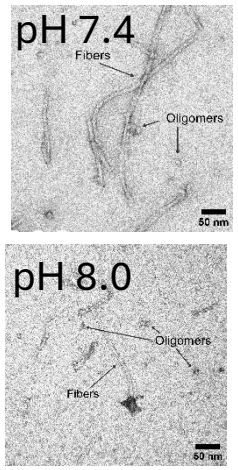
control (**5**)

- Sensitive Detection of Aβ1–42 Oligomers

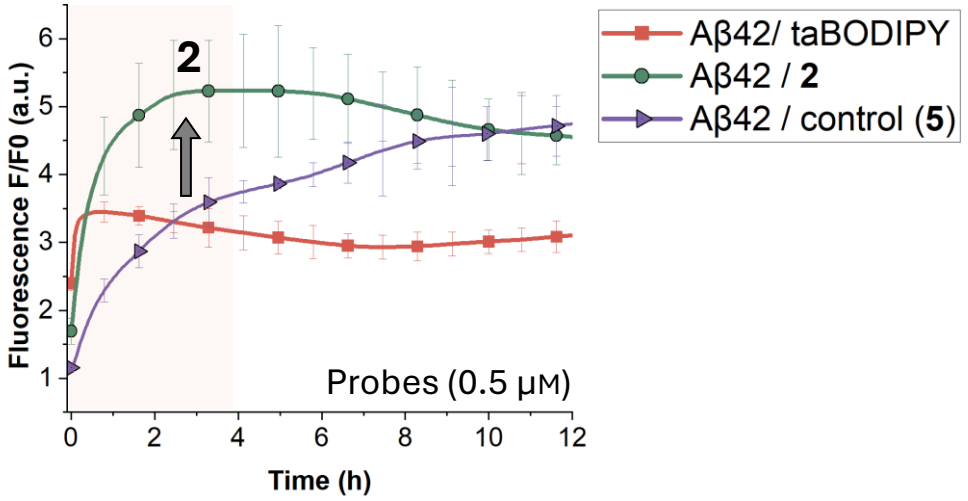
ThT Assay



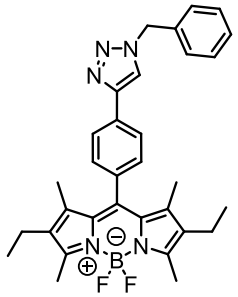
TEM, 24h



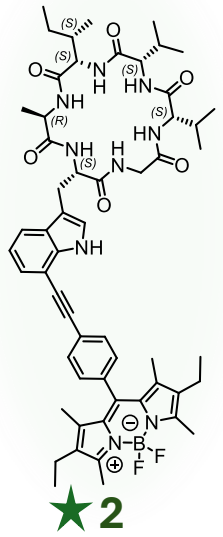
Probe Assay (pH 8.0)



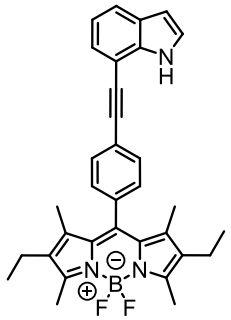
Selective Aβ42 Detection over IAPP



taBODIPY
Reference probe



★2



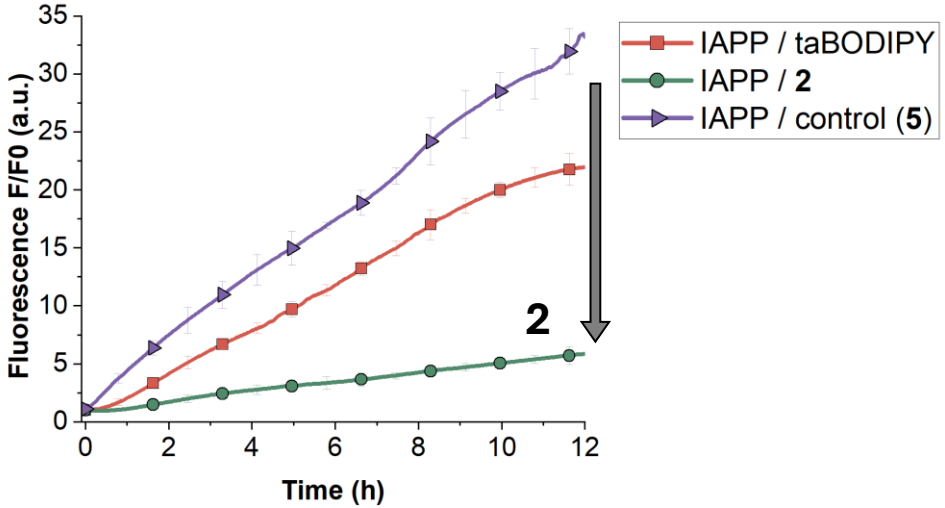
control (**5**)

- Sensitive Detection of Aβ1–42 Oligomers
- Aβ42 Selectivity over IAPP

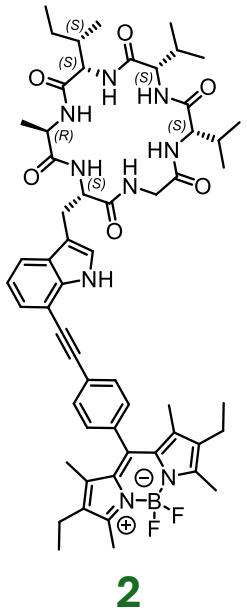
IAPP (Amylin)

- 37-Residue Amyloidogenic Peptide
- Linked with Diabetes Type 2

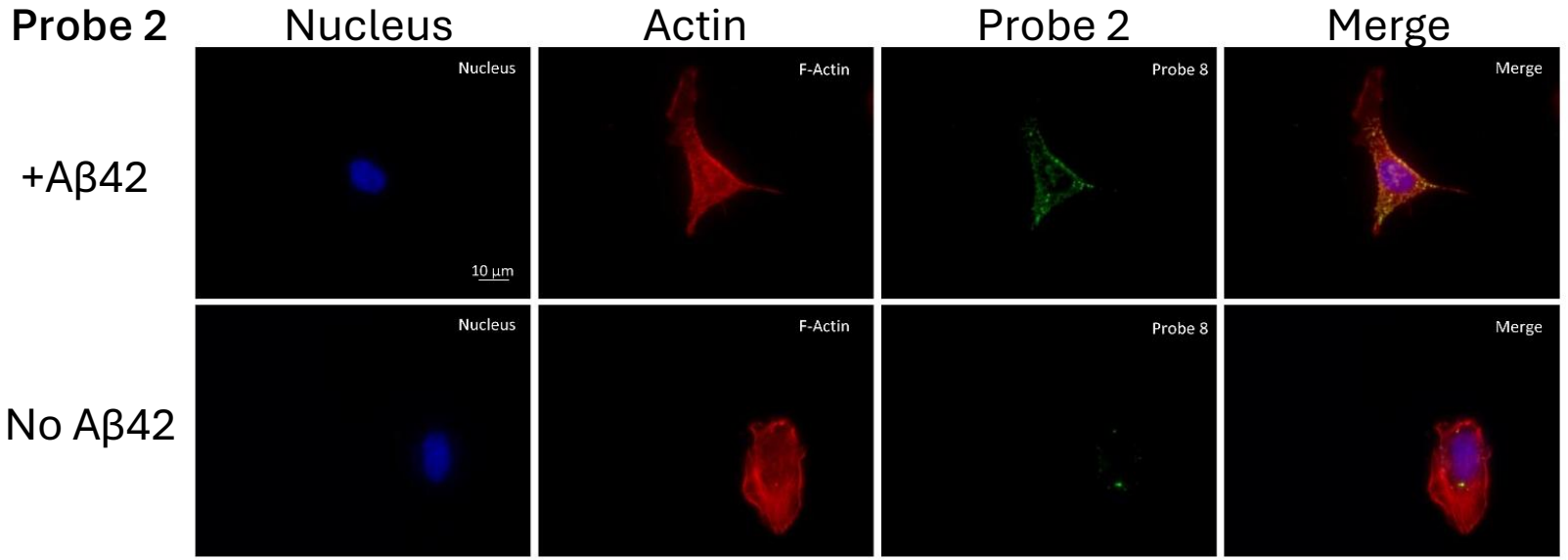
IAPP Assay



Cellular Aβ42 Oligomer

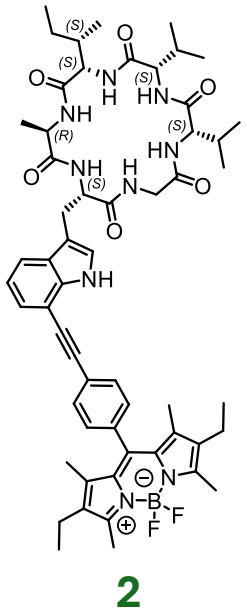


2

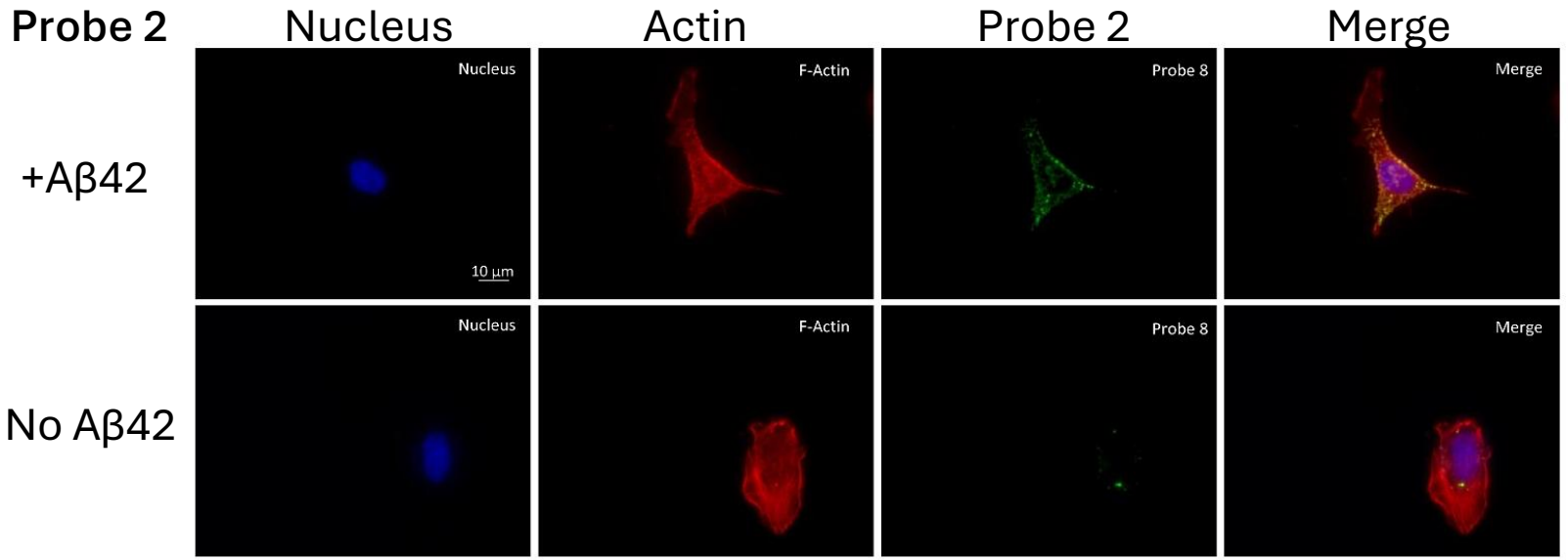


S. Panek et al., J. Med. Chem. 2026; 69 (6): 7377-7392.

Summary



2



Take-Home Message:
Peptide-based probes enable sensitive and selective detection of Aβ42 oligomerization.

S. Panek et al., J. Med. Chem. 2026; 69 (6): 7377-7392.

THANK YOU!

for your support & collaboration

Prof. Norbert SEWALD
& OCIII Group
Bielefeld University



Dr. Nicolo TONALI
& SIMoS Group
CEA Paris-Saclay



Collaborators
Dr. Anne Cécile VAN BAELEN
Prof. Aphrodite KAPURNIOTU
Dr. Denis SERVENT
Dr. Veronica DODERO
Prof. Olivier LEQUIN
Prof. Maria Luisa MANGONI
Dr. Macarena SANCHÉZ-NAVARRO
Dr. Maud LARREGOLA

Interested in a post-doc collaboration..?

Funding & Support

AGENCE NATIONALE DE LA RECHERCHE ANR DFG Deutsche Forschungsgemeinschaft

SNOOPY Searching for Nanostructured or pOre fOrming Peptides for therapY

université PARIS-SACLAY

EPS

GYROS PROTEIN Technologies

https://doi.org/10.17952/38EPS.2026.O51

Synthesising Libraries of α,δ-Foldamers using Solid Phase Peptide Synthesis

Si Zhe Wang, Department of Chemistry, King's College London

Supervisor: Prof. Andre Cobb

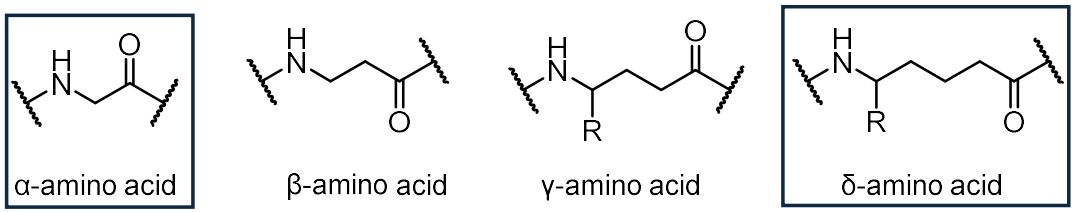
EPS 2026 YIMS Oral Presentation · Vienna · 9th September 2026

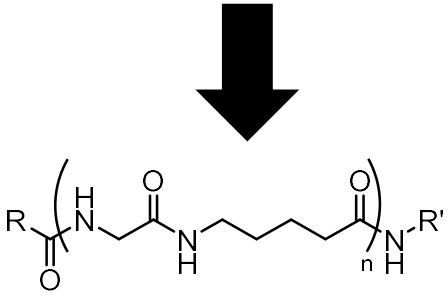
Introduction to Foldamers

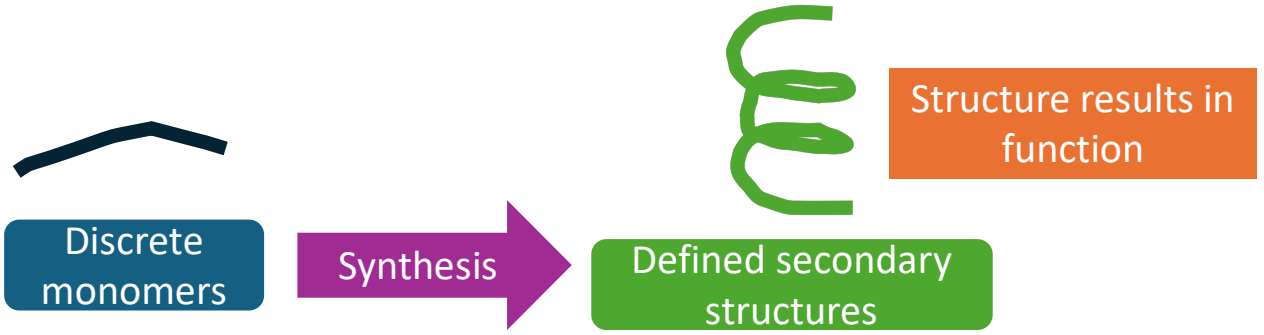
- Foldamer – oligomers that fold due to noncovalent interactions from non-adjacent units.

- Key subunits:
  - Amino acids
  - Ureas
  - Aromatic groups
  - Carbohydrates

- Applications:
  - Therapeutics
  - Materials
  - Catalysis



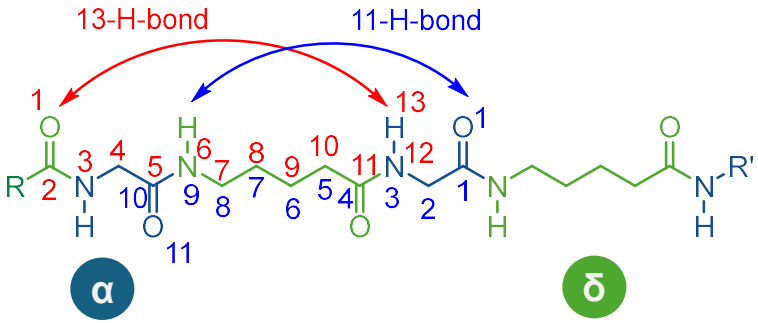


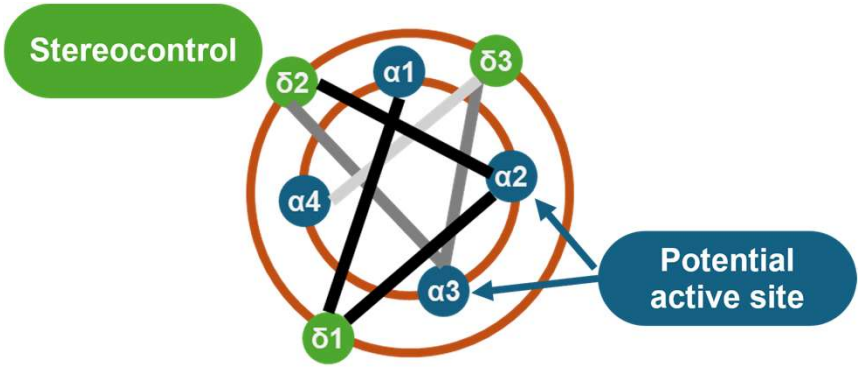


S. H. Gellman, *Acc. Chem. Res.,*1998, **31**, 173–180; D. J. Hill *et al.*, *Chem. Rev.,* 2001, **101**, 3893 – 4012;
R. Gopalakrishnan *et al.*, *J. Med. Chem.*, 2016, **59**, 9599–9621; Z. C. Girvin and S. H. Gellman, *J. Am. Chem. Soc.,* 2020, **142**, 17211–17223.

Hybrid α,δ-Foldamers

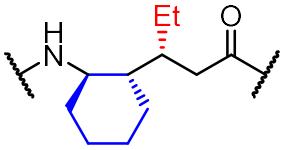
- Hybrid α,δ-foldamers form predictable 13/11 helix
  - δ-residues form a binding pocket + exposed α-residues – sites of interests
  - Potential catalyst scaffold



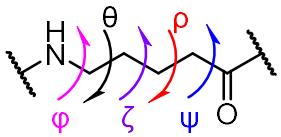


- Our δ-amino acid (AchPA) shows similar dihedral angles computed by Hofmann

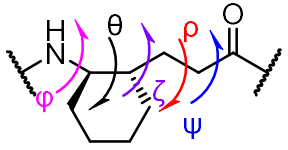
Stabilises helix through noncovalent interactions



Responsible for chiral environment during folding



Dihedral angles



AchPA

Dihedral angles	ϕ	θ	ζ	ρ	ψ
Predicted angles of 13/11 helix by Hofmann	137	-79	64	57	-143
Low energy conformation of AchPA	111	-64	73	49	-125

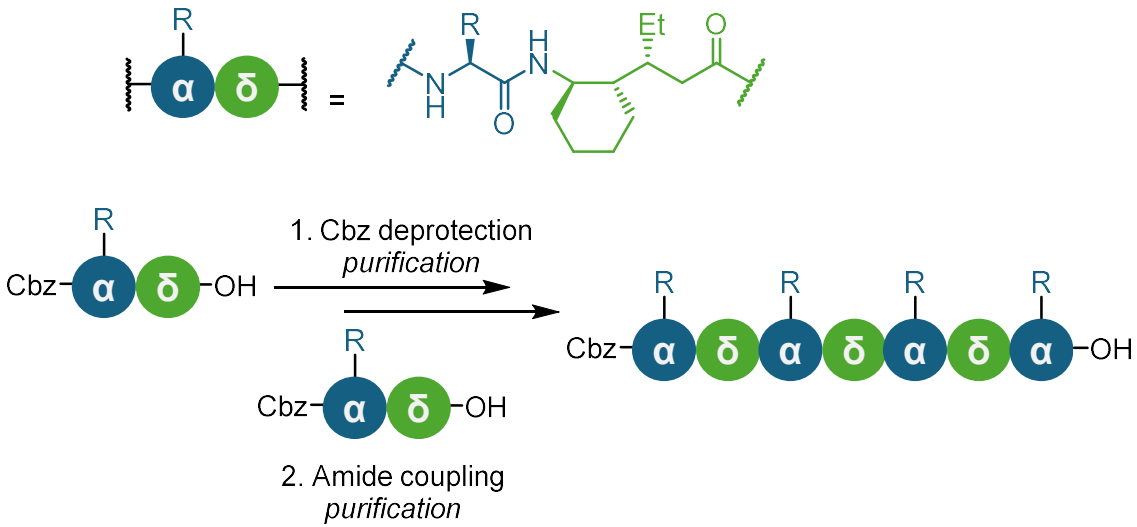
Q. Lin *et al.*, *Angew. Chem Int. Ed.*, 2023, **62**, e202305326. G. V. M. Sharma *et al.*, *Chemistry – A European Journal,* 2009, **15**, 5552–5566

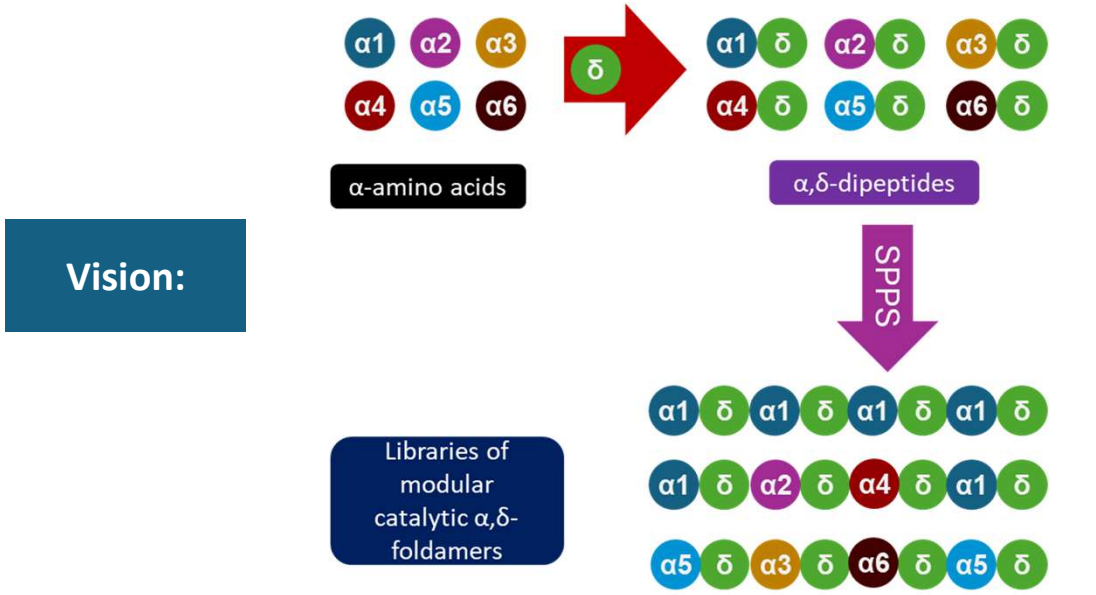
Aims and Objectives

- 1:1 α,δ-Foldamers synthesised by solution phase peptide synthesis
  - <50 mg produced after 20 steps

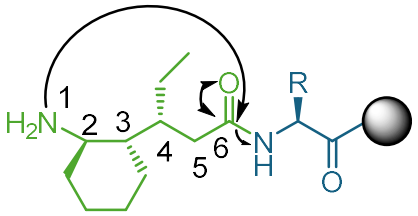
- SPPS methodologies for faster syntheses of diverse foldamers.
  - Libraries could be developed for catalytic studies

Solution phase synthesis developed by Cobb group (2023)

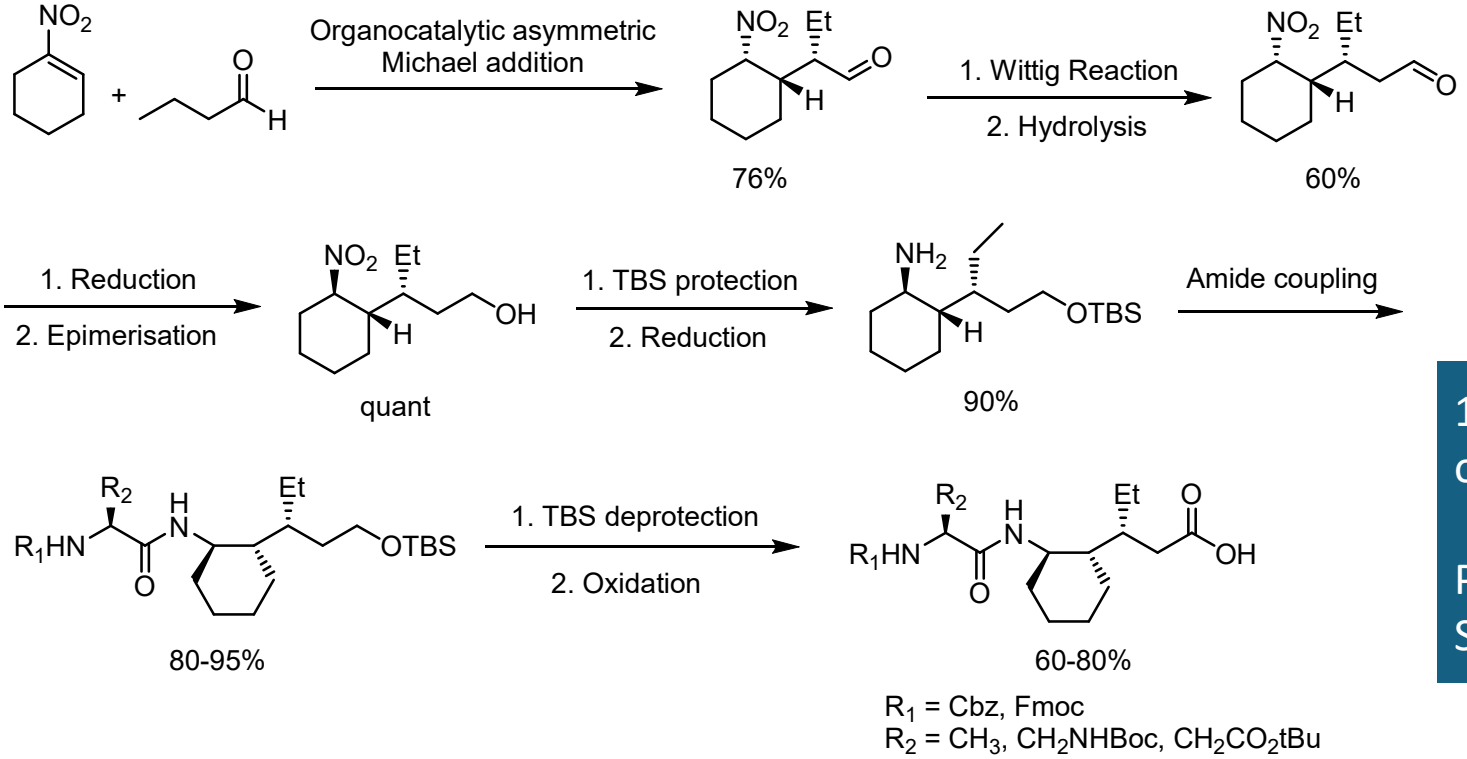




Synthesis of Dipeptide Building Blocks



Loading AchPA impossible -> 6-exo-trig cleavage

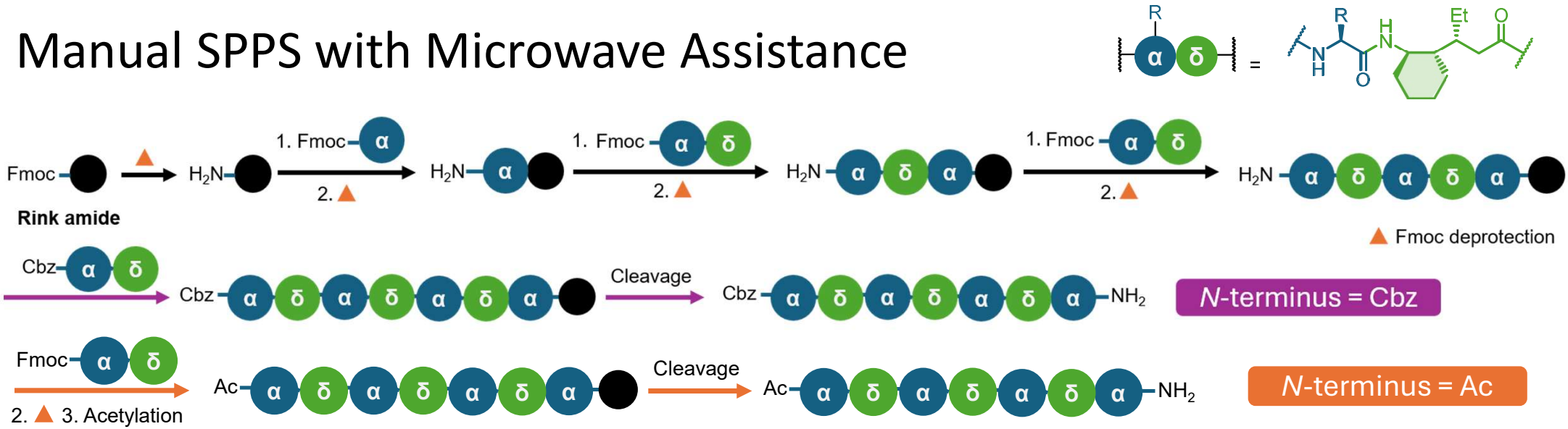


R_1 = Cbz, Fmoc
R_2 = CH_3, CH_2NHBoc, CH_2CO_2tBu

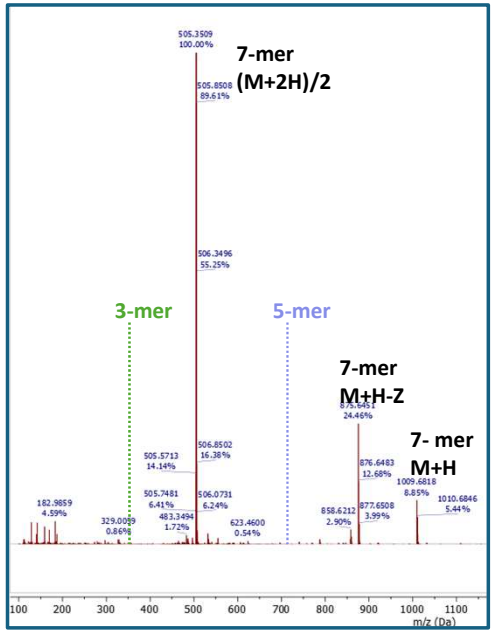
1-2 g scale of dipeptide from 3 mL of 1-nitro-cyclohexene SM

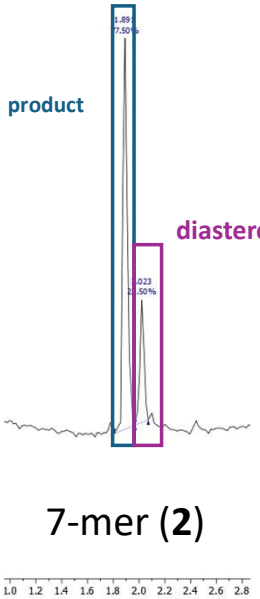
Purity assessed by HPLC before SPPS

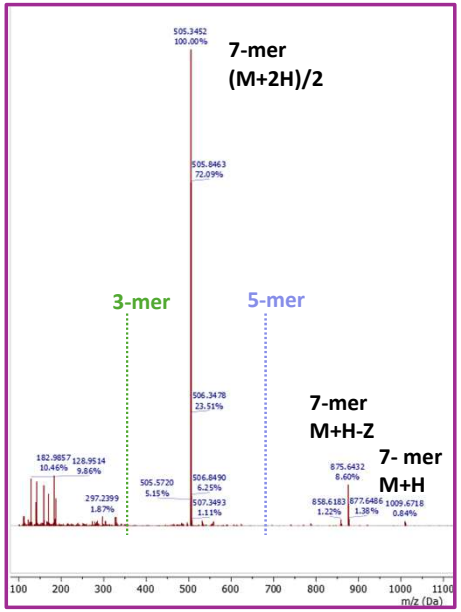
Manual SPPS with Microwave Assistance



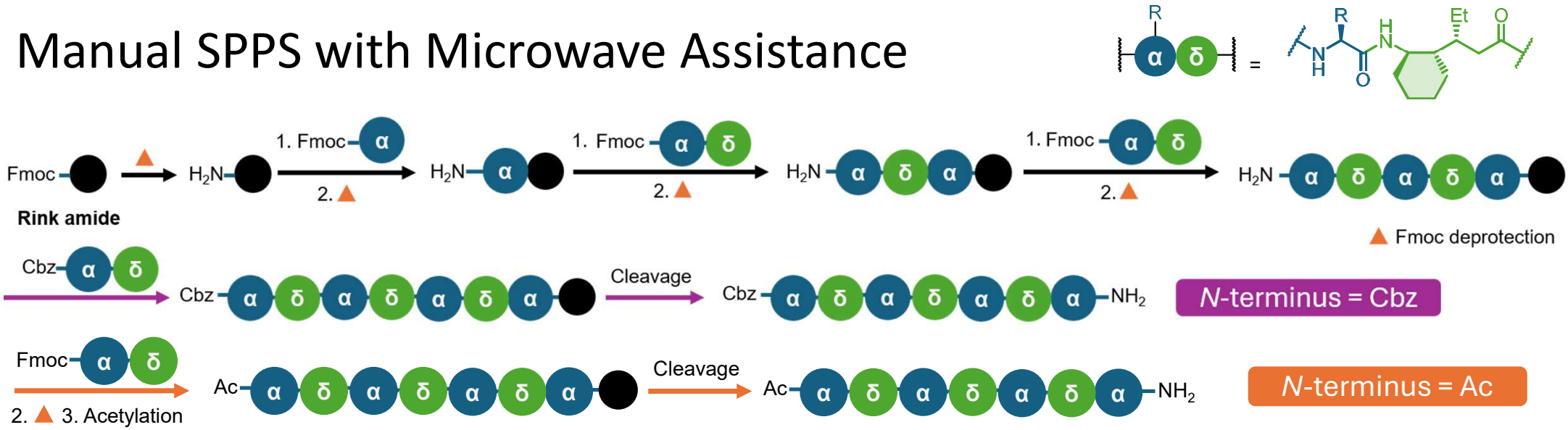
- 2.0 equiv. of dipeptide needed
- 15 min, 65 °C in microwave synthesiser
- High coupling efficiency – no capping required

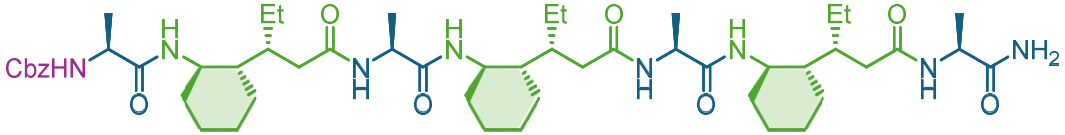




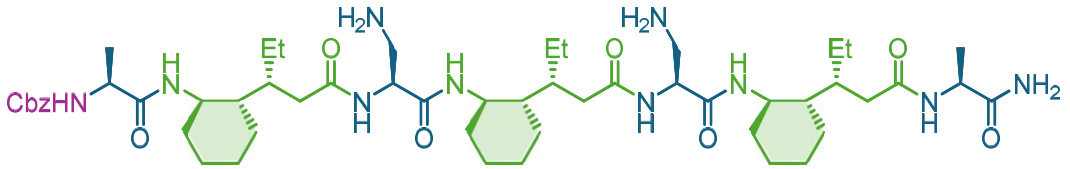


Manual SPPS with Microwave Assistance

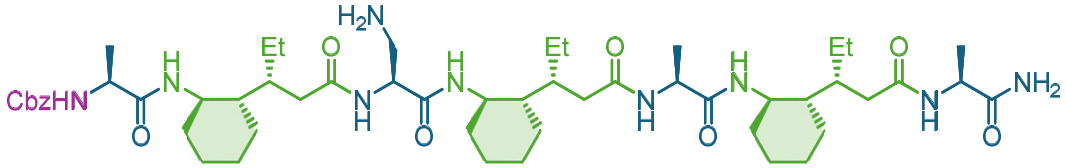




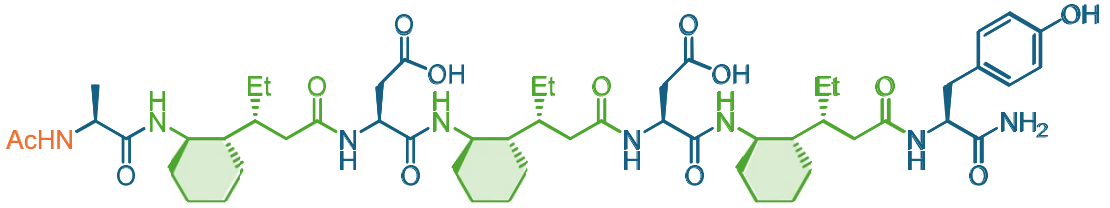
Z-Ala-AchPA-Ala-AchPA-Ala-AchPA-Ala-NH_2 (**1**), 70 mg (36% yield)



Z-Ala-AchPA-Dap(NH_2)-AchPA-Dap(NH_2)-AchPA-Ala-NH_2 (**2**), 68 mg (34% yield)

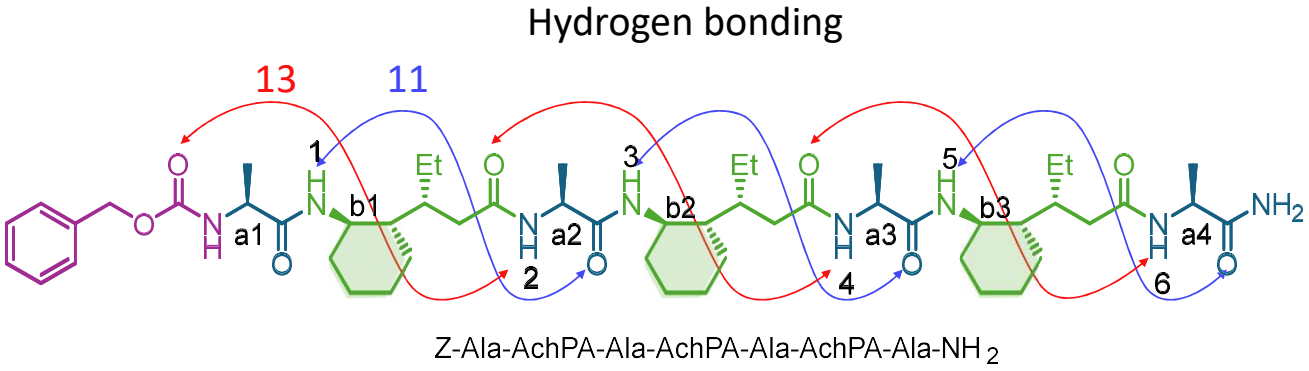


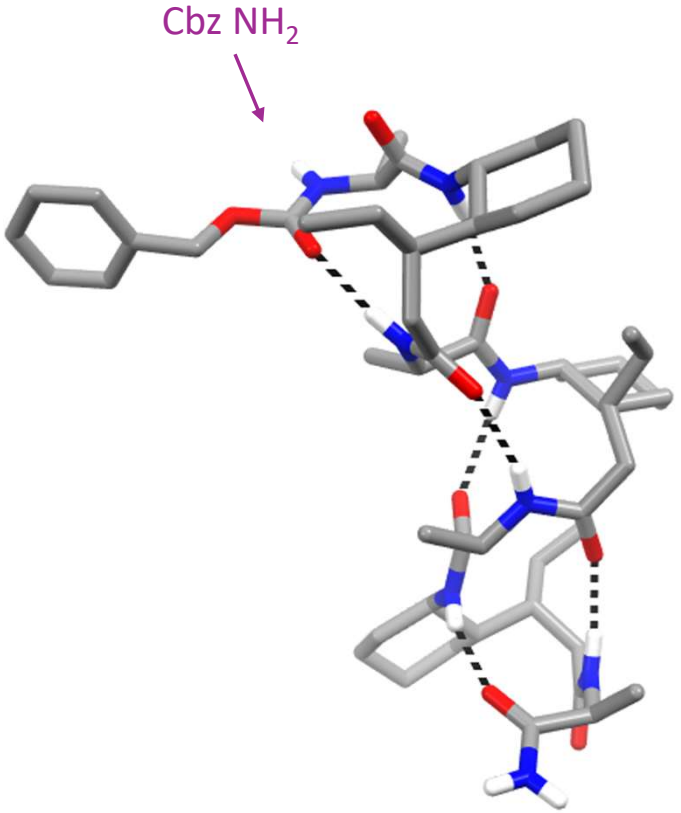
Z-Ala-AchPA-Dap(NH_2)-AchPA-Ala-AchPA-Ala-NH_2 (**3**), 173 mg (87% yield)



Ac-Ala-Asp(OH)-AchPA-Asp(OH)-AchPA-Tyr(OH)-NH_2 (**4**), 75 mg (35% yield)

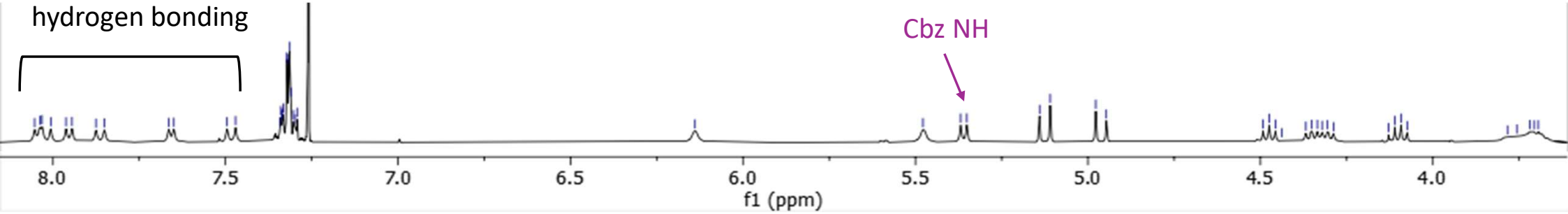
Do the SPPS Foldamers Fold?



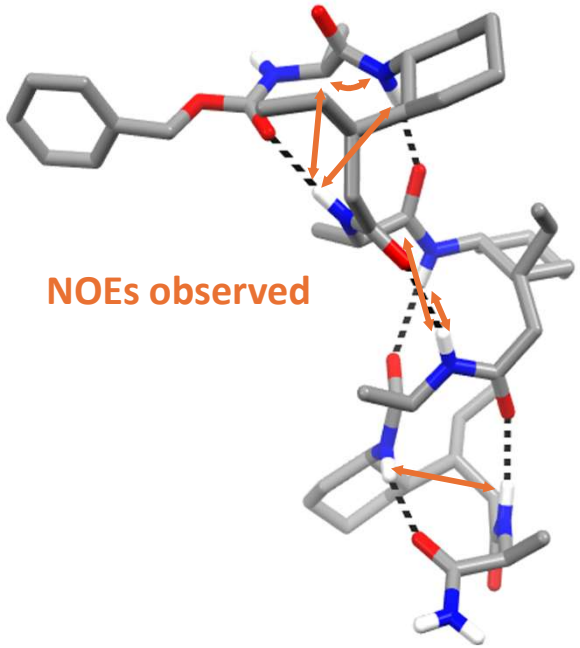


400 MHz, $CDCl_3$

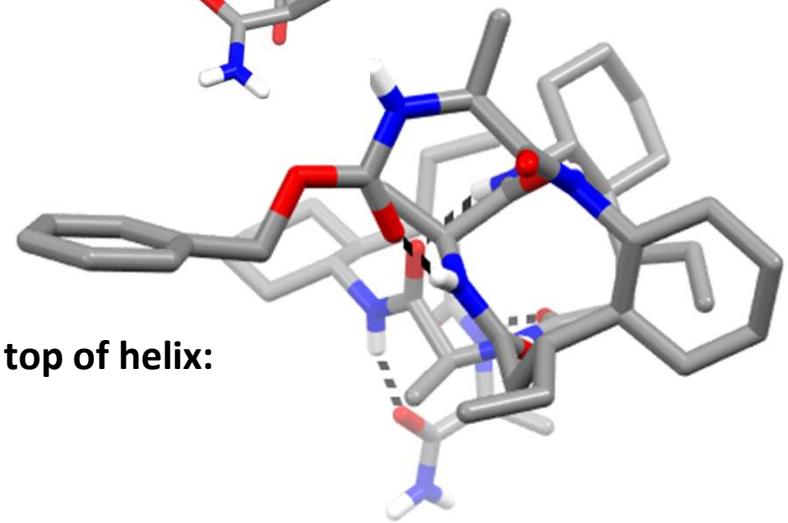
6 × NH involved in hydrogen bonding



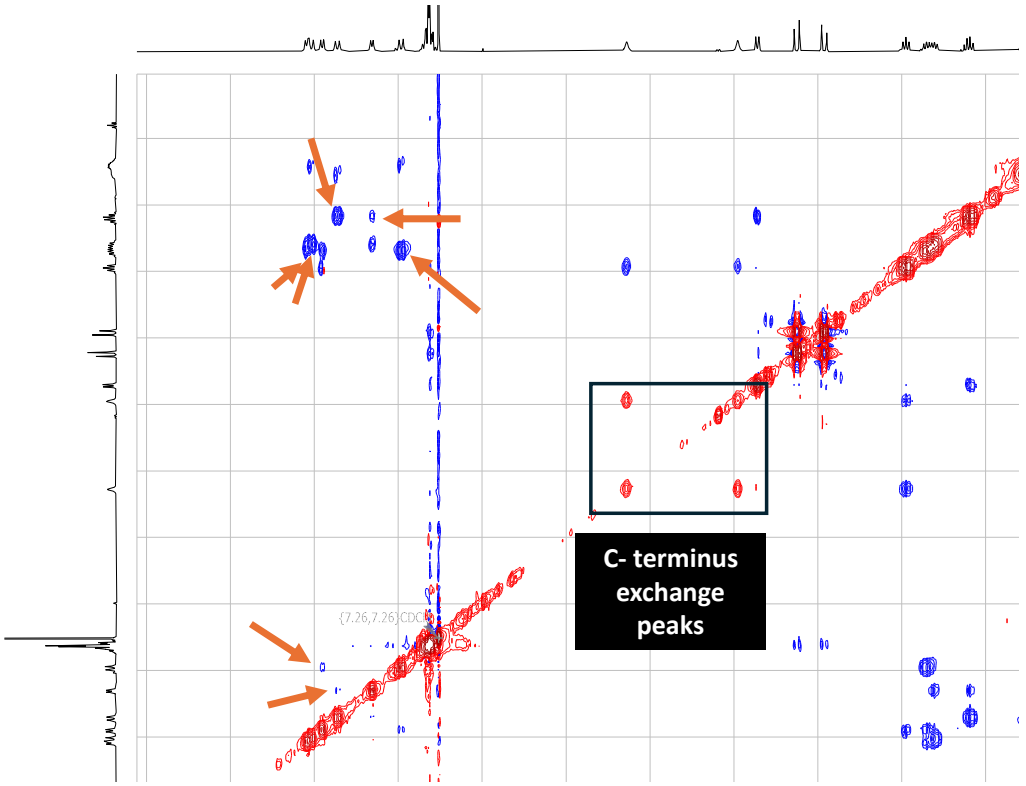
Structure in Solid vs Solution



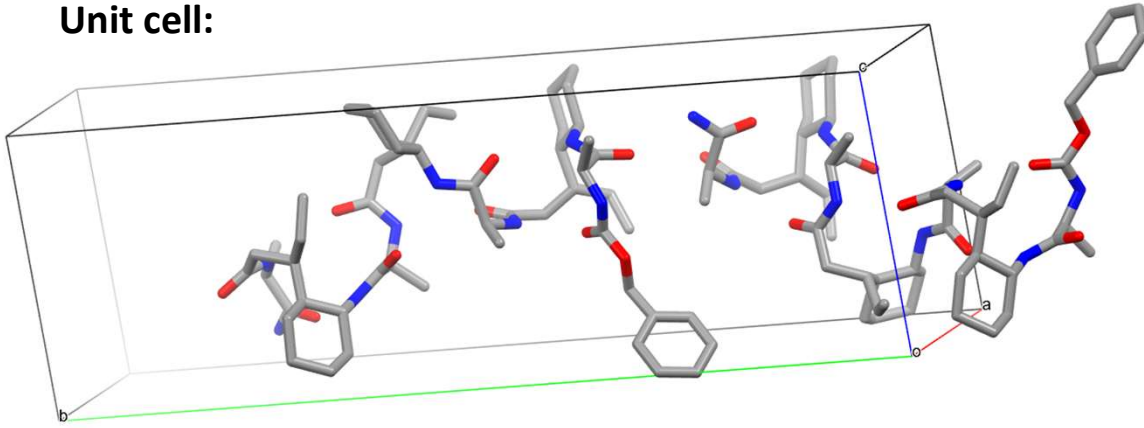
NOEs observed



View from top of helix:



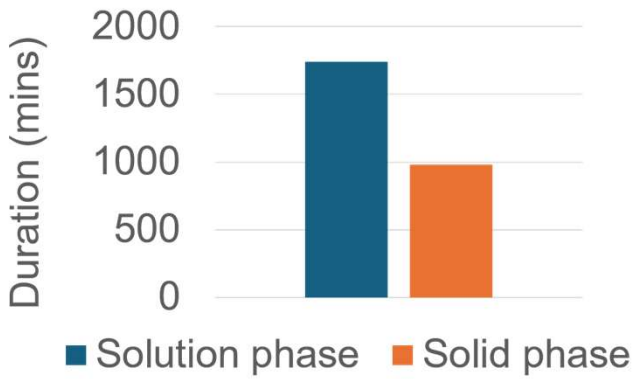
Unit cell:



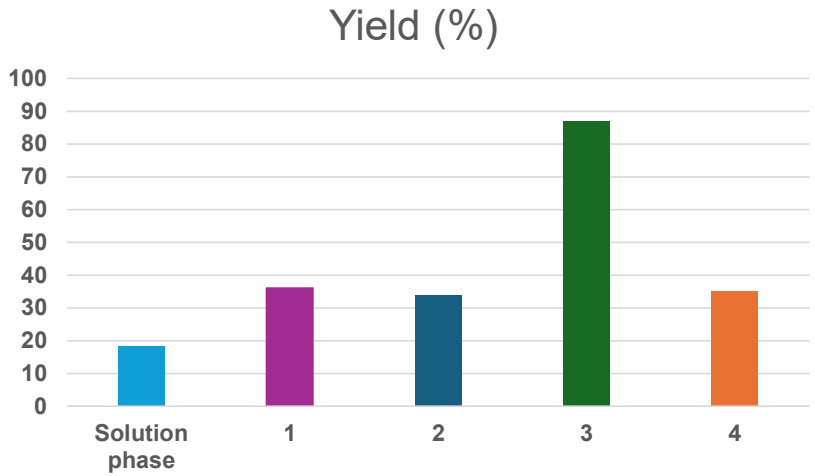
Conclusion

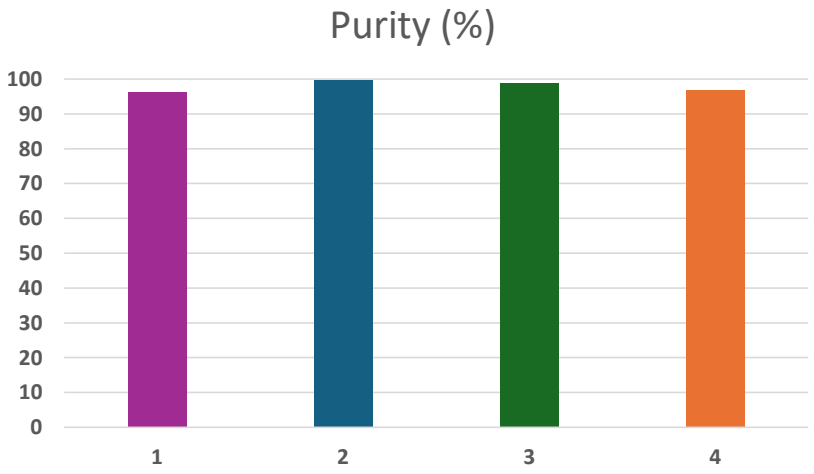
- Heteromers with different functionalities synthesised and characterised
- Solution (NMR) structure matches solid state structure (X-ray)

- Duration for synthesis of heteromers reduced



- Yield improved vs solution phase with good purities

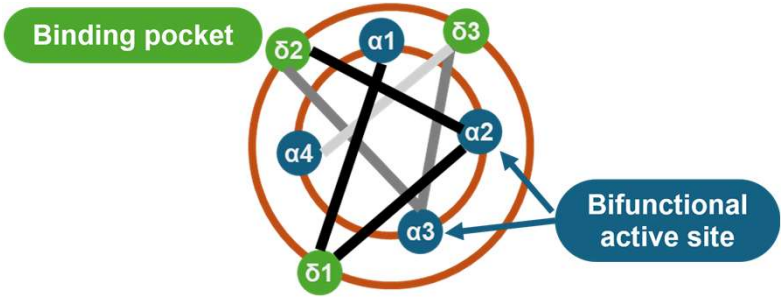




Outlook and Acknowledgement

Future work:

- Investigate synthesising libraries with new functional groups
  - Bifunctional catalytic active sites
- Synthesise longer chains of heteromers
- Greener SPPS methods.







Cobb group, KCL

Prof. Andre Cobb
Seungwon Lee
Lewis Picken
Junyan Xu
An-Jie Ler
Beth Clent
Inés Cruz Blanco

Müller Lab, KCL
Dr Manuel Müller
Lewis Picken

KCL NMES Faculty Studentship

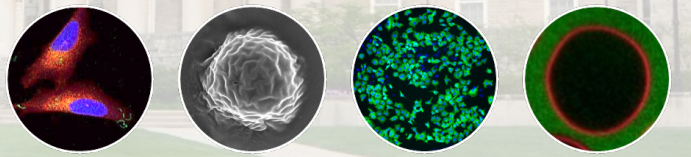
38th EPS European Peptide Symposium
6-11 September 2026, Vienna, Austria

https://doi.org/10.17952/38EPS.2026.O53

Retro-Inverted Host Defense Peptides as Inhalable Antitubercular Therapies

Diptomit Biswas,
Ph.D. Student
Sep. 9th, 2026

the Medina Group
Precision Therapeutics and Bioresponsive Materials Lab

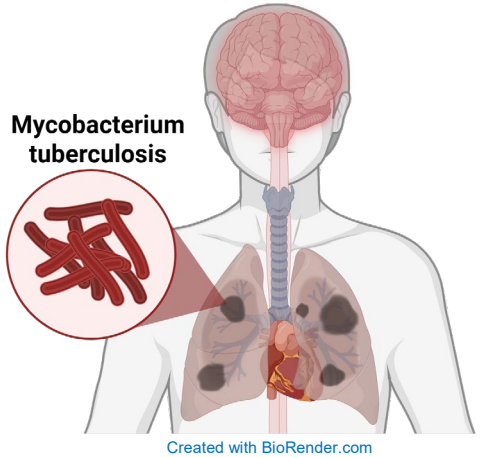


PennState Huck Institutes of the Life Sciences

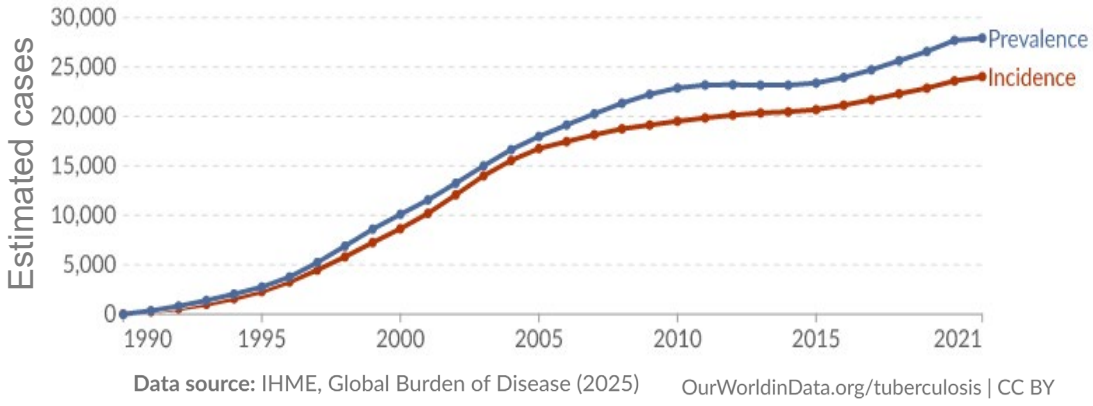
Dr. Scott Medina, Associate Professor,
Department of Biomedical Engineering, PSU

PennState College of Engineering

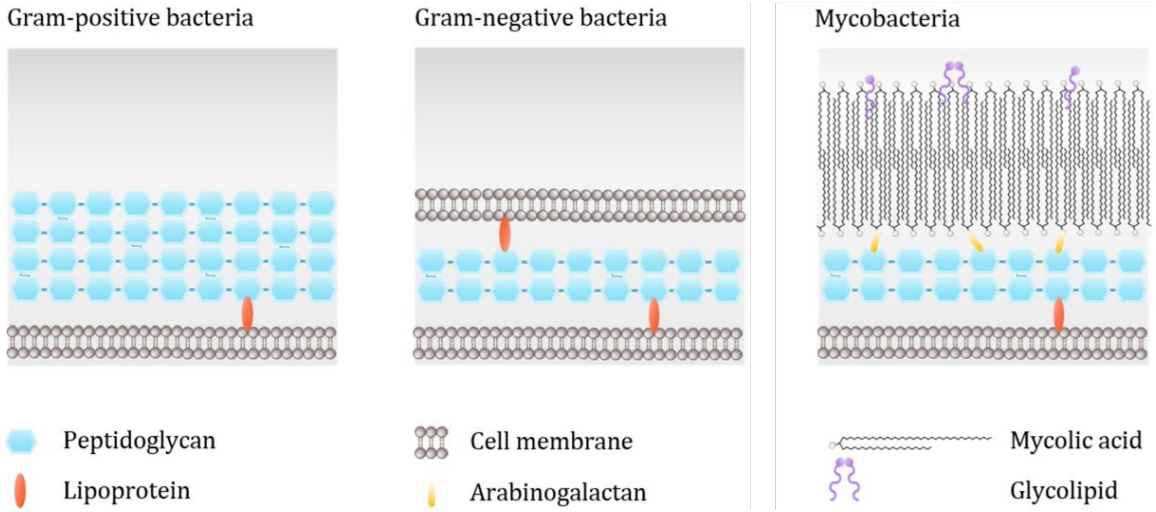
Drug Resistant Tuberculosis (TB) remains a serious global health concern



Despite modern diagnostic and therapeutic successes, drug-resistant TB cases continue to emerge and spread across the world.



1. Thick hydrophobic Outer Membrane



2. Residence inside Macrophages within Granulomas

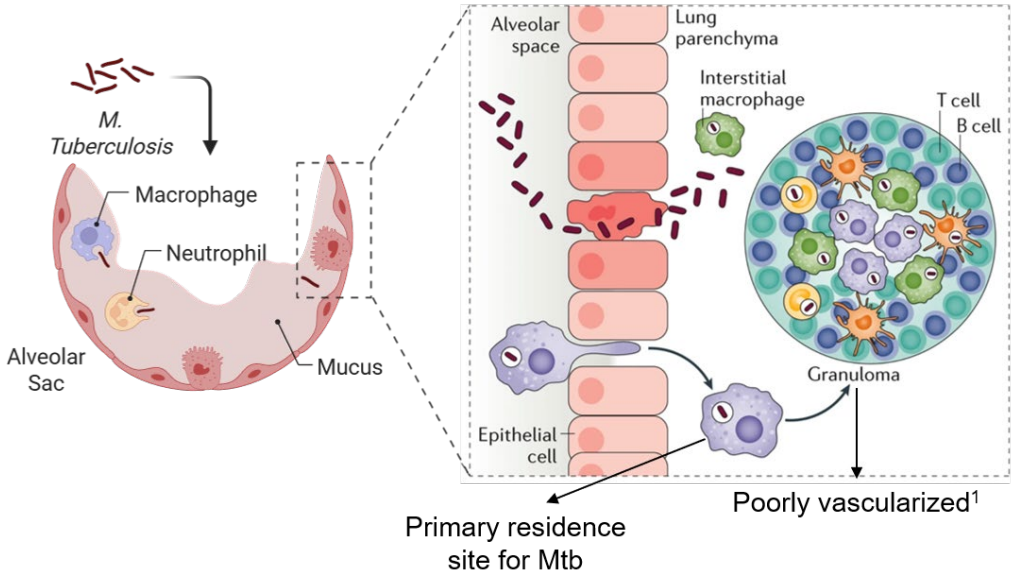


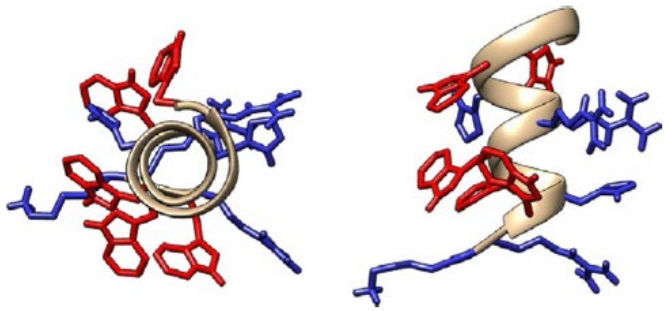
Fig. (bottom left) Djik J.H.M.V, et al. *Chem. Rec.*, 2021.; (bottom right) Pai M, et al. *Nat Rev Dis Primers*, 2016.; (1) Polena H, et al. Sci Rep, 2016

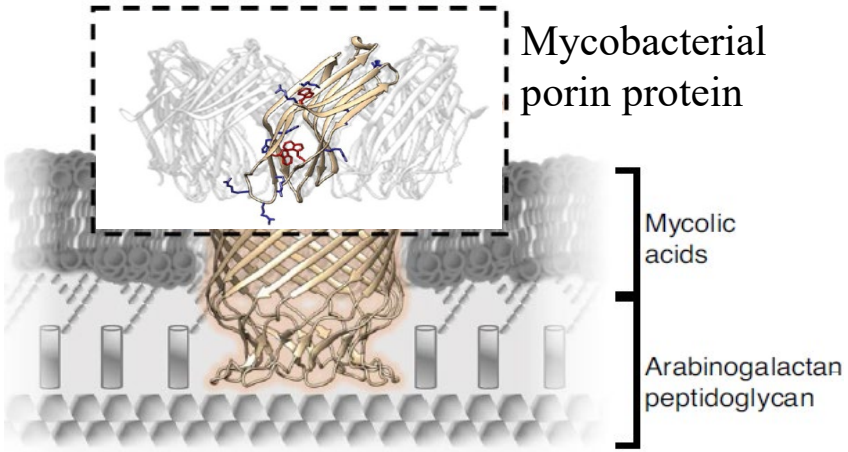
De novo synthetic host defense peptide showed specific inhibitory activity against Mycobacteria

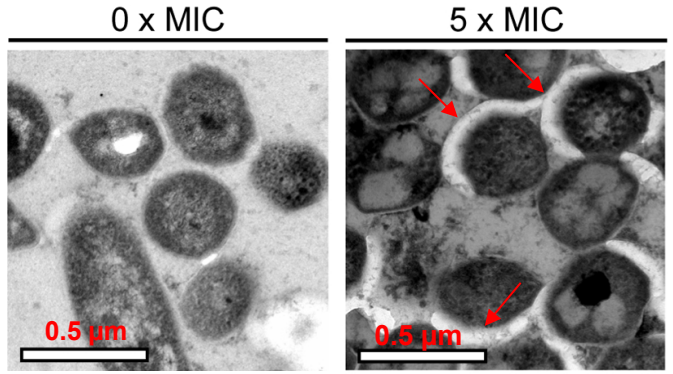
Previous Work from our Lab

(Simonson AW, et al. *Nat Biomed Eng*, 2021)

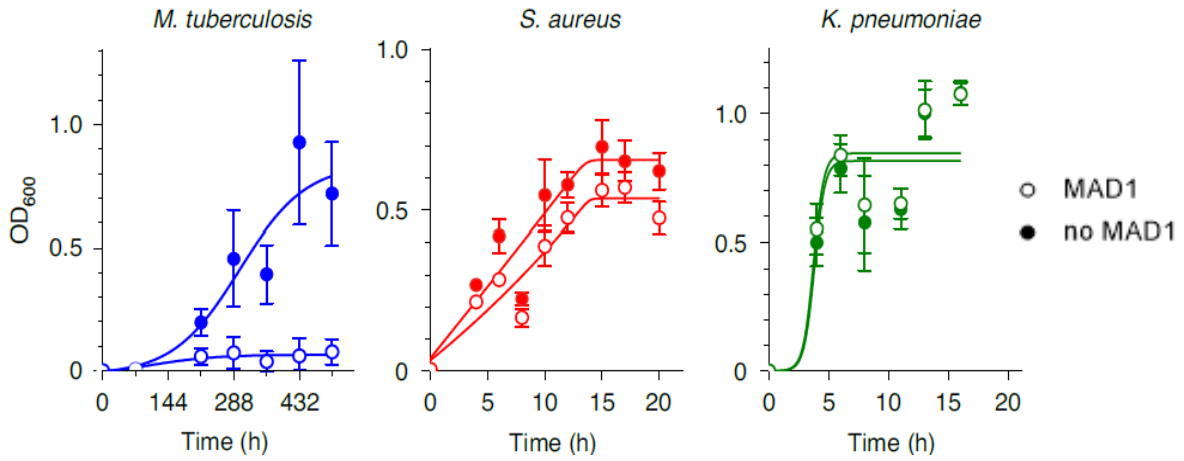
MAD1 peptide
(KRWHWWRRHWVVW-CONH$_2$)

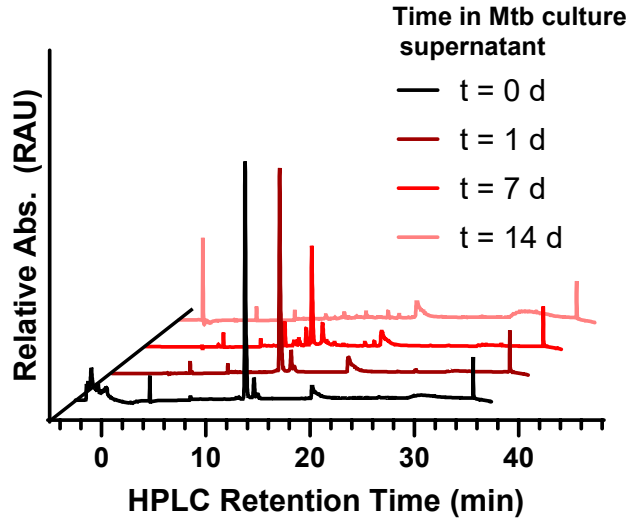






TEM Images showing MAD1-driven membrane effects



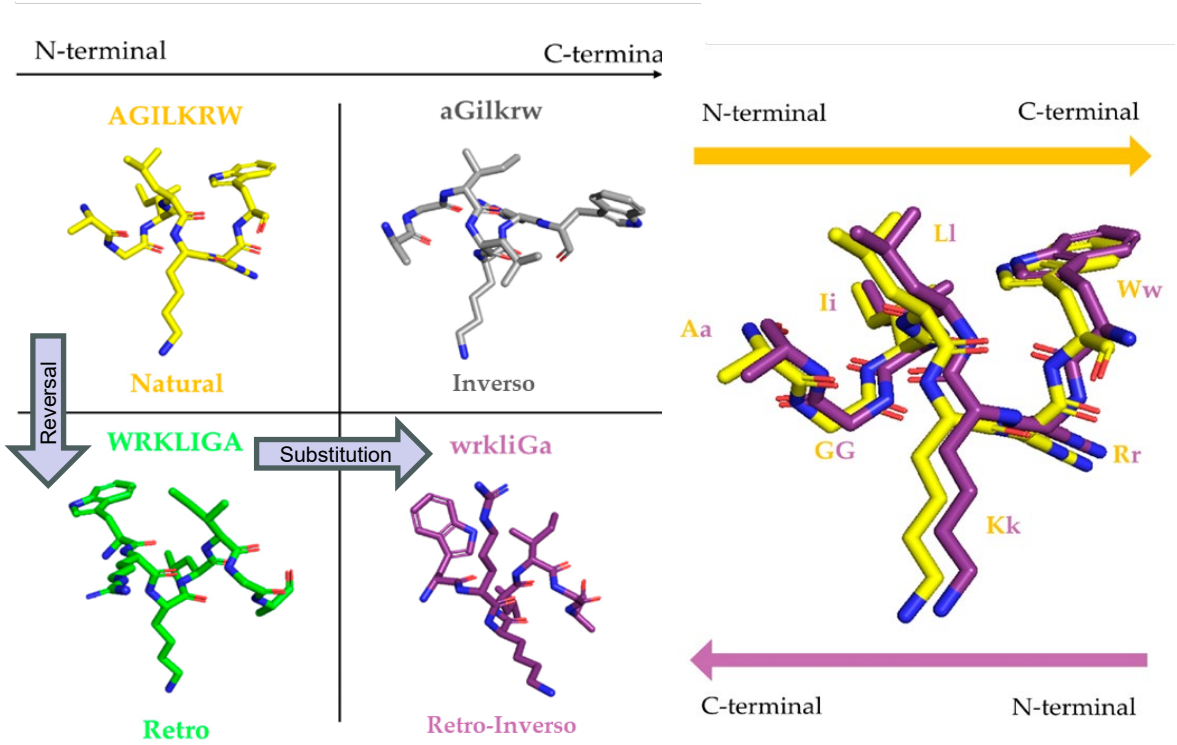


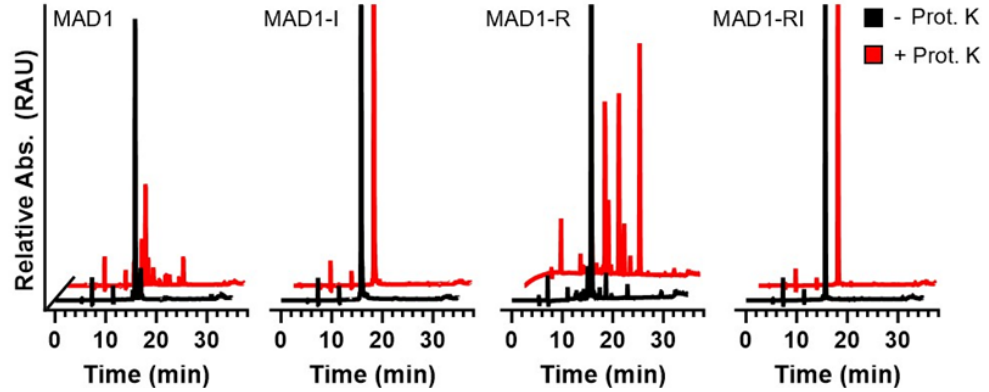
However, proteolytic instability makes them clinically unfeasible.

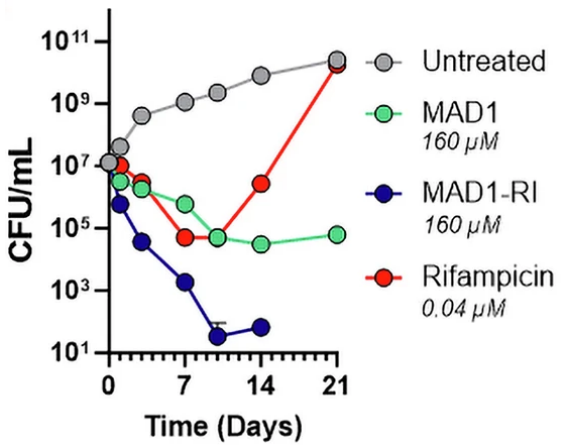
Fig. (bottom right) Glossop H.D, et al. *Nat. Comms.*, 2025.

MAD1 Retro-inversion improved proteolytic stability, enhanced anti-TB potency while retaining synergistic activity with second line TB antibiotic Moxifloxacin

Retro-inversion flips the peptide backbone but preserves the spatial orientation of amino acids as shown below with this example-







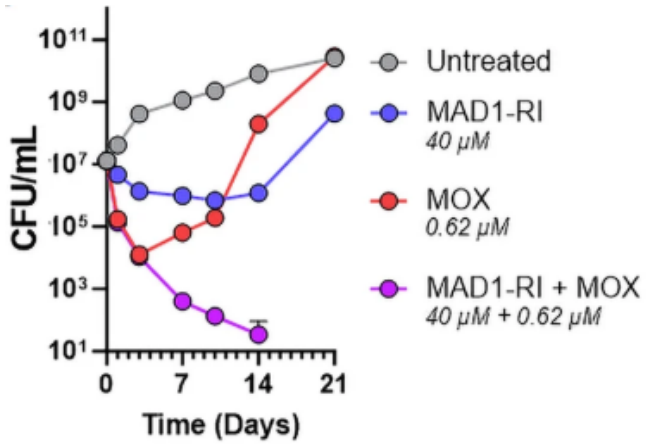
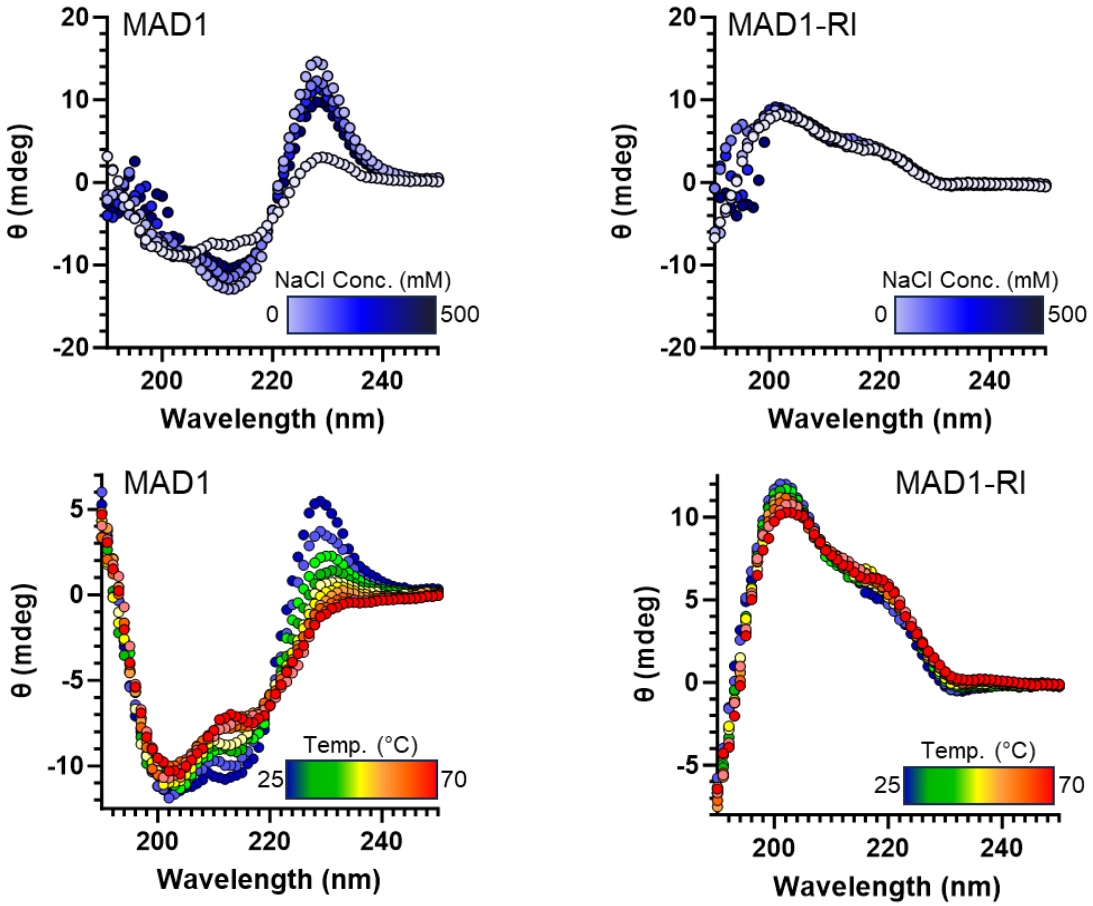


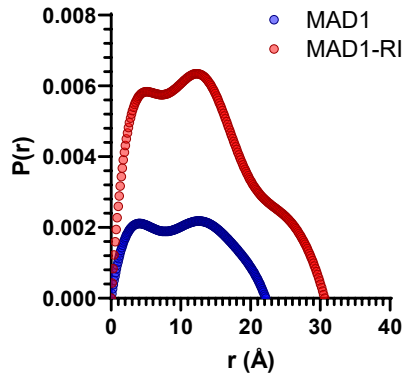
Fig. (Left) Carrera-Aubesart A, et al. *Pharmaceutics*, 2023.; Fig. (Right top and bottom) Glossop H.D, et al. *Nat. Comms.*, 2025.

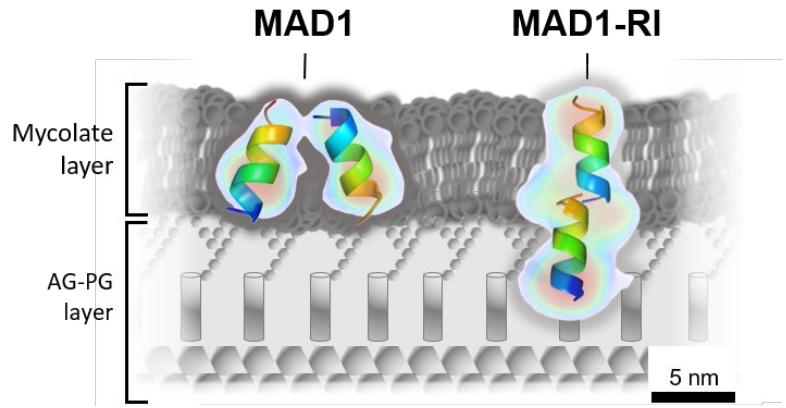
Retro-inverted MAD1 adopts a more elongated conformationally rigid assembly relative to MAD1

Circular Dichroism studies



Small-Angle X-ray Scattering-Analytical Ultracentrifugation studies





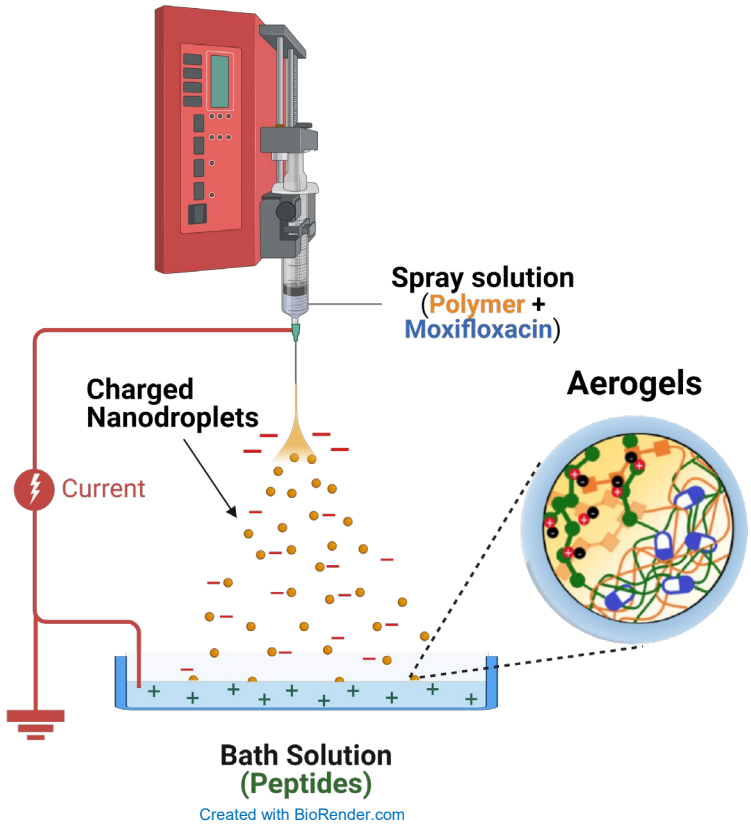
These features potentially lower the entropic barrier for interpolation and assembly of MAD1-RI within the mycomembrane, further contributing to improved anti-TB potency

All figures: Glossop H.D, et al. *Nat. Comms.*, 2025.

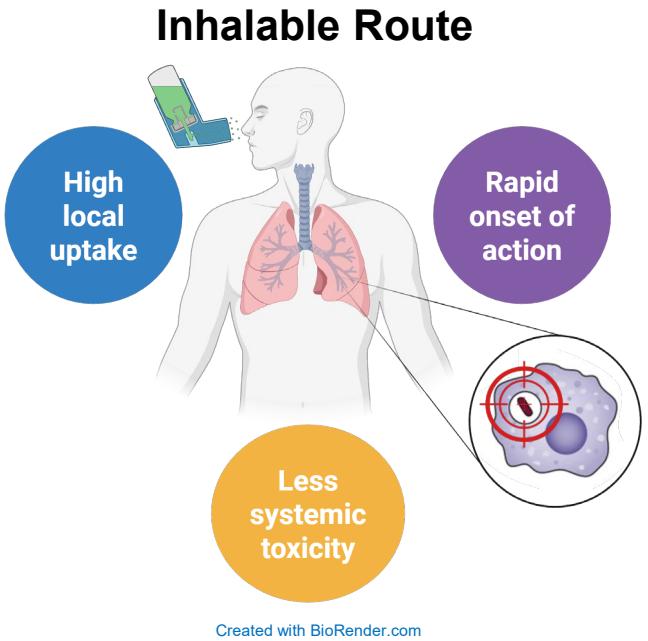
Targeting anti-TB drugs to infected lung macrophages using biocompatible anionic polymers

Previous Work from our Lab

(Simonson AW, et al. *Biomaterials*, 2021)



Anionic carbohydrate-based polymers can be complexed with cationic peptides like MAD1 to form nano-sized aerosolizable particles loaded with moxifloxacin.





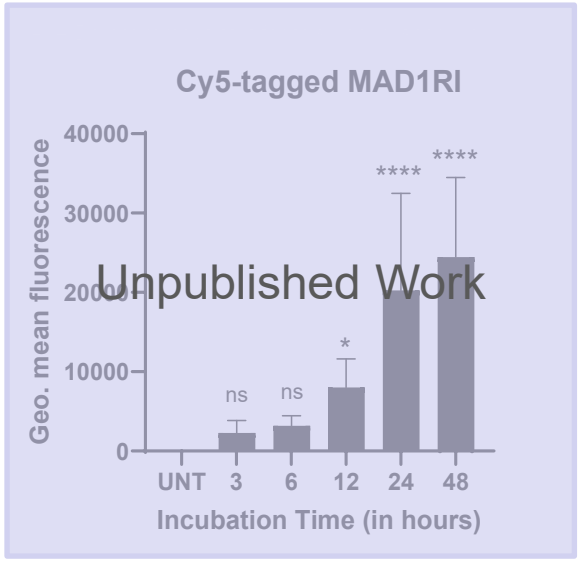
Different ratios of polymers and peptides were tested to optimize size of aerogels and ensure maximal loading of therapeutics

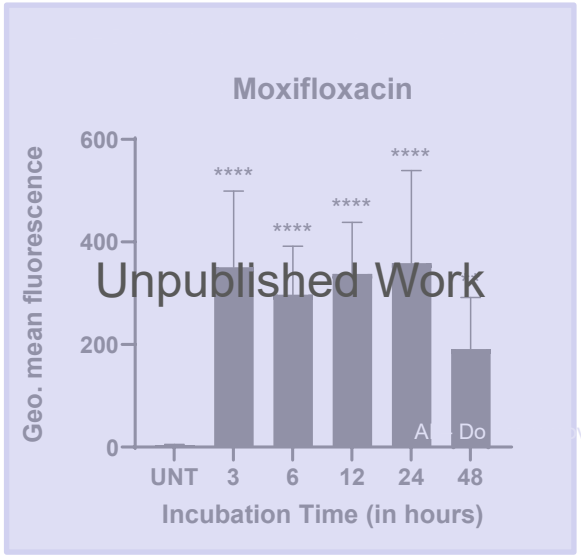


Figs. (right) *Unpublished work*

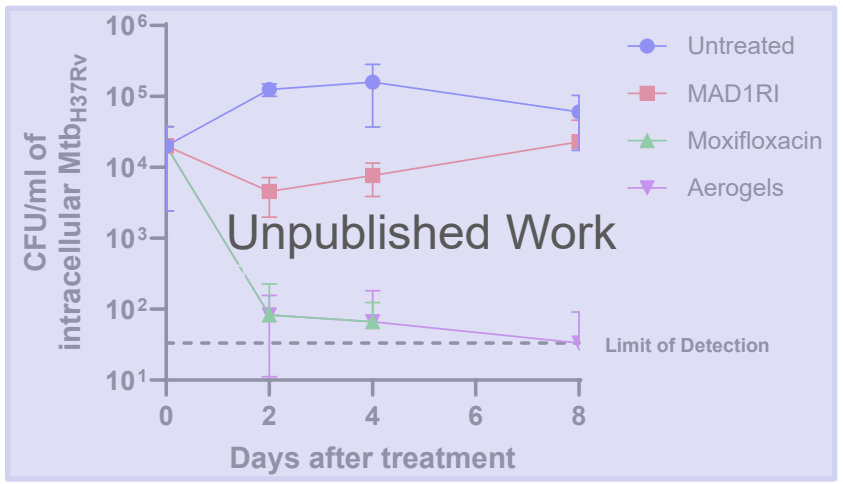
Aerogels efficiently deliver therapeutics to Macrophages to clear TB persisters

Uptake, Localization and Effect of Aerogel Cargo on THP1 macrophages



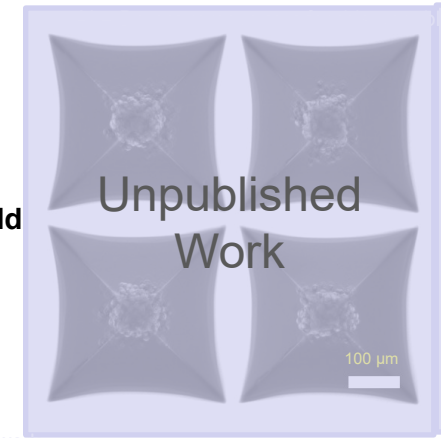


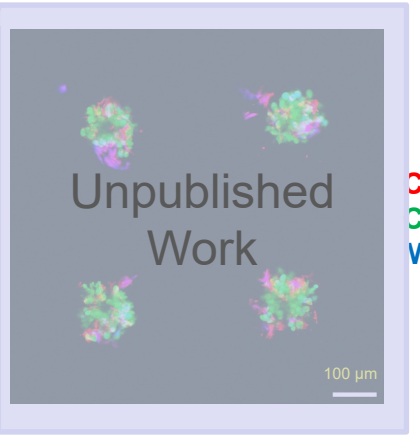




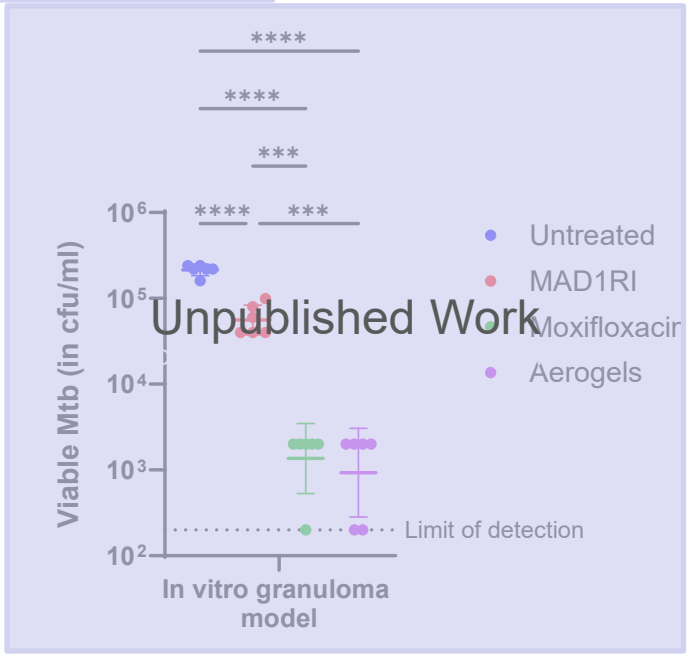
Penetration of Aerogel Cargo into in vitro THP1 spheroids and clearance of intracellular Mtb

Brightfield



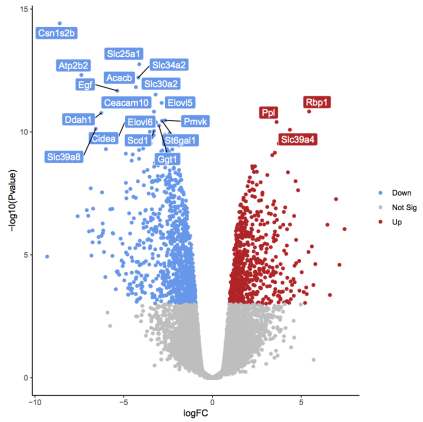


Cy5-MAD1-RI,
Calcein AM,
Moxifloxacin

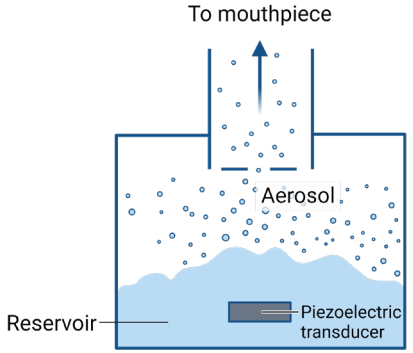


Ongoing and Future Experiments

- Gene expression analysis of uninfected macrophages treated with different polymer-based aerogels loaded with MAD1-RI.



- Post-Aerosolization size and stability of aerogels.

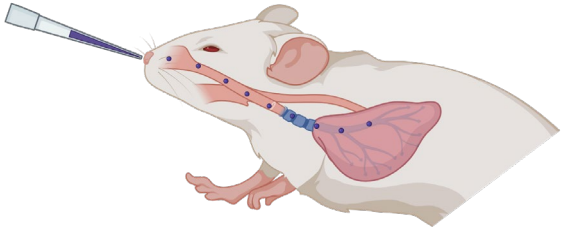


Ultrasonic nebulizer



Microspray aerosolizer

- *In vivo* efficacy and biocompatibility of MAD1-RI and Moxifloxacin-loaded aerogels in mice models of TB infection.



Acknowledgements



Dr. Hugh Glossop,
Research Fellow,
DFCI



Sabiha Sultana,
PhD Student,
PSU



Dr. Gebremichal Gebretsadik,
Post Doctoral Fellow,
CWRU



Dr. Scott Medina,
Associate Professor,
PSU



Dr. Anthony D. Baughn,
Professor,
UMN



Other contributors: Nathan A. Schacht, Neela H. Yennawar, Muzafar Ahmad Rather, as well as other members of the Medina Lab.

PennState Huck Institutes of the Life Sciences

NIH National Institutes of Health

PennState College of Engineering

To know more about this work and other ongoing research in our lab, please visit -

Hugh D. Glossop, et al. Retro-inversion imparts antimycobacterial specificity to host defense peptides, *Nature Communications*, **2025**, 17, 469, doi:10.1038/s41467-025-67162-0.

Lab Website: https://sites.psu.edu/medinalabgroup/

Email Address: dzb5866@psu.edu

Thank you for your attention!

Questions?

Searching for Nanostructured or pOre fOrming Peptides for therapY COST Action

Daniela Kalafatovic[1]

[1]*Faculty of Engineering, University of Rijeka, Croatia*
https://doi.org/10.17952/38EPS.2026.O55

Introduction

Peptide science increasingly relies on the integration of design, synthesis, characterization, biological evaluation, and computational prediction within unified research workflows [1,2]. Functional peptides, including self-assembling, antimicrobial, and pore-forming systems, are of particular interest because of their potential in biomedical and materials-related applications [2,3]. The field is highly interdisciplinary, reflecting the structural diversity of peptides and the wide range of available experimental methods, computational tools and application contexts. At the same time, this diversity can hamper progress by making it more difficult to integrate approaches, compare results, and establish common workflows.

COST Action CA23111, *Searching for Nanostructured or pOre fOrming Peptides for therapY* (SNOOPY), running from 2024 to 2028, was established to address these challenges through a coordinated international network bringing together researchers from institutions across Europe and beyond. The Action is chaired by Daniela Kalafatovic, University of Rijeka, Faculty of Engineering, and co-chaired by Paula Gomes, Faculty of Sciences, University of Porto, and currently comprises more than 600 participants from 48 countries. The network brings together researchers, innovators, stakeholders, and industry representatives, with the aim of connecting fundamental peptide research with real-world applications.

COST Actions are designed as European networking frameworks supporting collaboration among researchers and innovators. Their main role is to create international networks, facilitate knowledge exchange and training, connect academic, industrial, and societal stakeholders, and promote collaborative approaches to common scientific challenges. Within this framework, SNOOPY aims to strengthen interactions across peptide-related disciplines while creating opportunities for mobility, knowledge transfer, career development, and wider scientific and societal impact.

Structure of the SNOOPY network and goals

SNOOPY is organized into interconnected Working Groups (WGs), each addressing a complementary aspect of the peptide research pipeline (Figure 1): computational approaches (WG1), synthesis and characterization (WG2), biological applications (WG3), and WG4, fully dedicated to dissemination.

WG1 focuses on computational approaches for understanding, predicting and designing bioactive peptides and peptide nanostructures. Its activities encompass *in silico* prediction and design, molecular dynamics (MD) simulations, data mining and database development, machine learning (ML) and deep learning (DL), and the integration and sharing of computational data. Emphasis is placed on linking peptide sequence, structure, dynamics and function, while developing computational resources, workflows and recommended practices that support reproducibility and accelerate peptide discovery.

A central challenge is the enormous size of peptide sequence and structural search spaces, making computational approaches increasingly important for prioritizing candidates before experimental validation [4, 5, 6, 7]. An emerging WG1 contribution, entitled *Solving the Computational Peptide Design Puzzle: Challenges and Opportunities* under consideration in *ACS Omega*, considers peptide discovery as an interconnected process involving artificial intelligence (AI), MD simulations, experiments, and automation. Each approach provides complementary information: AI identifies patterns in data, MD provides

microscopic insight, experiments provide macroscopic validation, and automation creates opportunities for autonomous experimental workflows [8]. A key objective is to improve integration across these components and, ultimately, enable closed-loop peptide design.



Figure 1. Overview of the CA23111 COST Action generated using OpenAI ChatGPT's image-generation tool, based on the input form the MoU and information available on the Action website (https://cost-snoopy.eu/).

WG2 focuses on the production and characterization of bioactive peptides and peptide-based nanostructures. Its activities encompass synthetic strategies, with interest in development of greener approaches, purification and quality control, optimization of production efficiency and sustainability, and the application of advanced analytical and automated characterization methods. In addition, WG2 focuses on design, formation and characterization of self-assembled peptide nanostructures, including nanofibrils, nanoparticles, and nanotubes, as well as on understanding how the self-assembly process can be controlled through sequence design and experimental conditions.

A major WG2 initiative, *From Community Experience to Best Practices,* aims to convert community experience into guidelines for peptide synthesis and characterization. The initiative is based on a survey involving more than 100 participants and includes respondents from academia and industry. The survey captures current approaches, challenges, and priorities across key areas including synthetic strategies, purification, quality control, characterization methods, and common limitations. By analyzing the responses, WG2 aims to assess the current state of the field, identify key challenges and sources of variability, and use these insights to guide the development of practical, community-driven recommendations and best practices. This is especially important in peptide science, where variations in synthesis, purification, sample preparation, and characterization can strongly influence reproducibility.

WG3 focuses on the biological evaluation and application of bioactive peptides and peptide-based nanostructures, with emphasis on their therapeutic potential and translation toward clinical applications. Its activities encompass peptide bioactivity and mechanisms of action, interactions with biological membranes and other biomolecular targets, antimicrobial and antiviral activity, drug delivery and cellular transport, as well as amyloid-related systems and emerging therapeutic and diagnostic applications. A central aim of WG3 is to connect molecular and materials-level properties with biologically relevant function and performance. In this way, WG3 complements the computational design activities of WG1 and the production and characterization efforts of WG2 by evaluating how peptide properties translate into activity in increasingly complex biological systems. A major WG3 contribution will be the *Roadmap on the Biological Applications of Peptides and Peptide Nanostructures*, which will assess the current landscape of biomedical applications, identify key scientific and translational challenges, and define priorities and opportunities for future development.

WG4 supports the activities of WG1, WG2 and WG3 through dissemination, scientific communication, career development, inclusiveness, and engagement with industry and wider society. It promotes knowledge exchange across the network through initiatives that strengthen skills, visibility, collaboration, and career development, particularly for young researchers.

From innovation to standardization and best practices

Methodological innovation is particularly challenging in peptide research because of the broad diversity of scientific questions, experimental and computational techniques, disciplinary expertise, and application areas that must be integrated across the field. SNOOPY promotes integration of computational and experimental approaches with the long-term goal to establish closed-loop peptide discovery systems in which design, synthesis, testing, and model refinement become progressively interconnected. Such approaches could substantially accelerate the discovery of peptides with desired structural, functional, or therapeutic properties.

In parallel with methodological innovation, SNOOPY recognizes that progress in peptide science requires reproducible and transferable experimental procedures. The WG2 community survey therefore represents an important effort to collect practical experience from peptide researchers and transform it into shared recommendations. By developing such resources collectively, SNOOPY seeks to improve reliability and comparability between laboratories. This network-driven approach also enables expertise from different countries, institutions, and research environments to contribute to the development of common standards.

Scientific dissemination is supported through meetings, publications, joint activities, and dedicated journal collections. Two SNOOPY-associated special issues highlight this effort: a WG2 collection in *Materials Advances (RSC)* on supramolecular peptide and protein systems, and a WG1 special issue in *Journal of Peptide Science* (Wiley) on computational approaches for the assessment of peptides and peptide nanostructures. Together, these collections provide focused platforms for sharing advances across design, synthesis, characterization, computation, and applications.

Networking, Mobility, and Capacity Building

A defining feature of SNOOPY is its emphasis on researcher mobility and international network building. The Action supports Short-Term Scientific Missions, conference participation, meetings, workshops, and training schools. These mobility mechanisms allow researchers to visit partner laboratories, acquire new experimental or computational skills, access complementary infrastructure, initiate collaborations, and present results at international conferences. To date, SNOOPY has approved 70 grant applications. The number of approved grants increased from 20 in 2025 to 50 in 2026, reflecting growing participation and connections within the network. SNOOPY also promotes industry engagement to strengthen knowledge

transfer, connect academic research with practical challenges, and support the translation of peptide technologies toward real-world applications.

SNOOPY has also developed a dedicated “Find the Partner” platform (https://cost-snoopy.eu/find-the-partner/), enabling researchers to identify collaborators by research topic, technique, country, WG, or individual expertise. The tool reflects the Action’s broader objective of making scientific capabilities visible across the network and facilitating the formation of new collaborations.

WG meetings and training activities form another major component of the network. Activities highlighted include a WG1 meeting in Cres, Croatia (2025), a WG2 meeting in Nottingham, UK (2026), an upcoming WG3 meeting in Granada (2027), and training activities in Porto (2026) and Lyon (2027). These events are designed not only to present scientific results, but also to encourage methodological exchange and strengthen interactions between researchers at different career stages.

Conclusions

COST Action CA23111 SNOOPY provides an interdisciplinary framework for advancing research on peptides through coordinated European collaboration with connections across continents. SNOOPY combines complementary areas: computational design, synthesis and characterization and biological applications. Beyond its scientific goals, SNOOPY is designed as a community-building platform. Through researcher mobility, training schools, WG meetings, conference grants, partner-search tools, surveys, journal collections, and industry participation, the network aims to create a sustainable collaborative ecosystem for peptide science. At the same time, the development of shared experimental guidelines and standards should improve reproducibility and facilitate translation between laboratories. SNOOPY represents not only a coordinated scientific effort in peptide research, but also an infrastructure for knowledge exchange, inclusiveness, training, and long-term European and global collaboration.

Acknowledgements

This work is based upon activities of COST Action CA23111 SNOOPY – Searching for Nanostructured or pOre fOrming Peptides for therapY, supported by COST (European Cooperation in Science and Technology). The author acknowledges all members of the SNOOPY network for contributing to meetings, training schools, short-term scientific missions, surveys, and dissemination activities. The author gratefully acknowledges the EPS organizers for hosting a dedicated Special Session for SNOOPY – COST Action CA23111. The figure was generated with the assistance of OpenAI ChatGPT’s image-generation tool based on content and instructions provided by the author.

References

[1] P. W. J. M. Frederix, et al., Nature Chemistry 2015, **7**, 30–37, 10.1038/nchem.2122
[2] E. Dražić et al., ACS Nano, 2025, **19**, 20295–20320, 10.1021/acsnano.5c00670
[3] R. Deb et al., Nature Chemical Biology 2026, 10.1038/s41589-026-02269-z
[4] M. Njirjak et al., Nature Machine Intelligence, 2024, **6**, 1487–1500, 10.1038/s42256-024-00928-1
[5] G. Mausa, D. Kalafatovic, Nature Machine Intelligence 2026, 10.1038/s42256-026-01258-0
[6] T. K. Piskorz et al., ACS Omega 2024, **9**, 31254–31273, 10.1021/acsomega.4c02628
[7] M. Babić et al., ACS applied materials & interfaces 2026, **18**, 12353–12367, 10.1021/acsami.5c14754
[8] D. Kalafatovic et al., ACS Omega, under revision

https://doi.org/10.17952/38EPS.2026.O60

Computational/Experimental Symbiosis to Design Functional Supramolecular Peptide Assemblies





38th EPS

European Peptide Symposium



Ivan R. Sasselli

Materials Physics Center (CFM), CSIC-EHU

Donostia-San Sebastián, Spain

i.sasselli@csic.es

2026/09/10

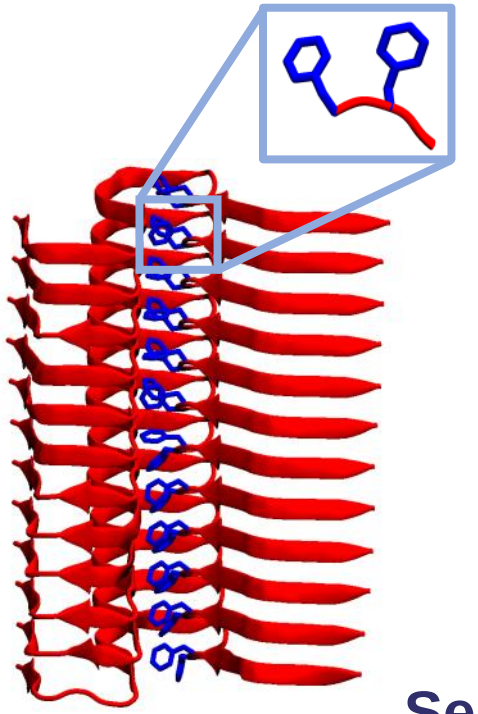

Bordeaux
Donostia / San Sebastián
A Coruña
Gijón
Oviedo
Toulouse
Bilbao
Carcassonne
Santiago de Compostela
Lugo
Vitoria-Gasteiz
Pamplona
León
Perpignan
Andorra
Burgos
Girona
Madri
Toledo
Spain
Eivissa
Centro de Física de Materiales
Materialen Fisika Zentroa
CSIC
CFM

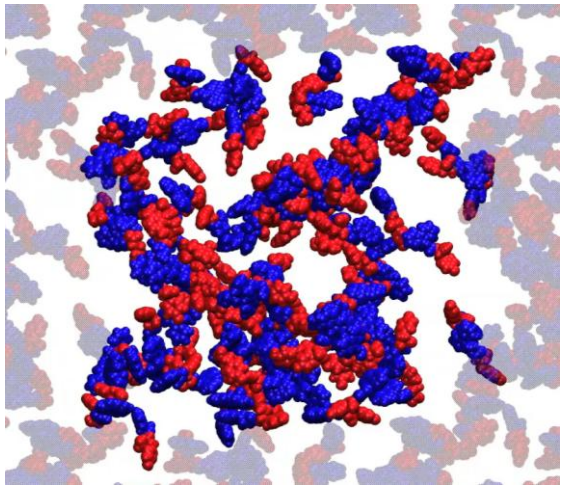
Supramolecular Peptide Assemblies (SPAs)

Inspired by Highly ordered Protein Sections

Short Peptide (n ≤ 10) ► self-assemble

►nanostructures

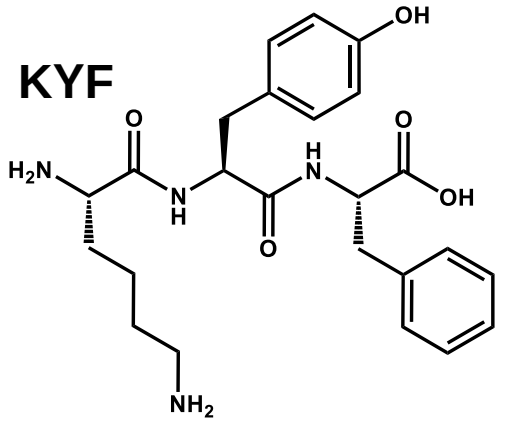




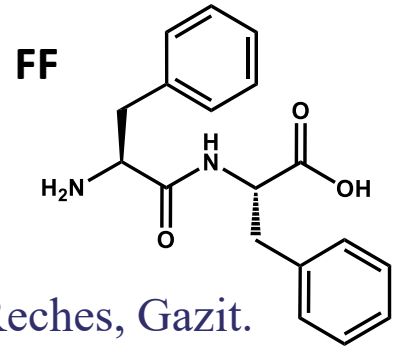
Self-assembly

Spontaneous formation of

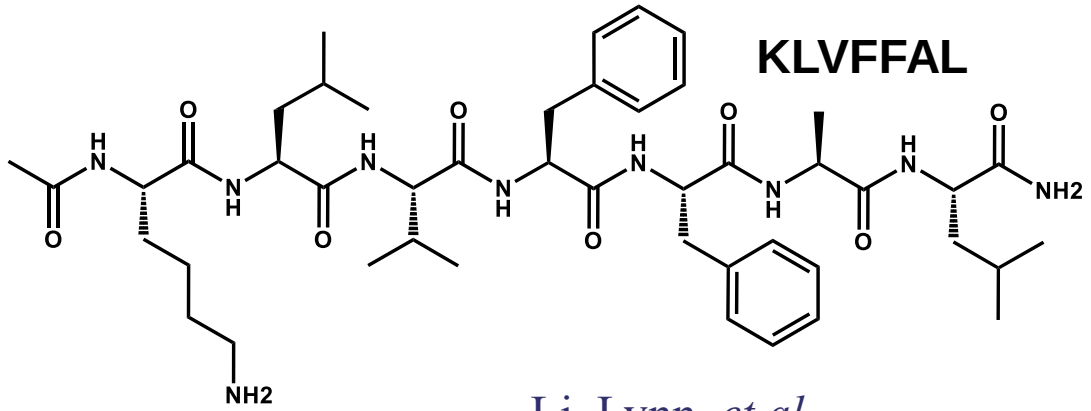
highly ordered nanostructures in solution



Frederix, Tuttle, *et al.*
Nat. Chem. **2015,** *7*, 30

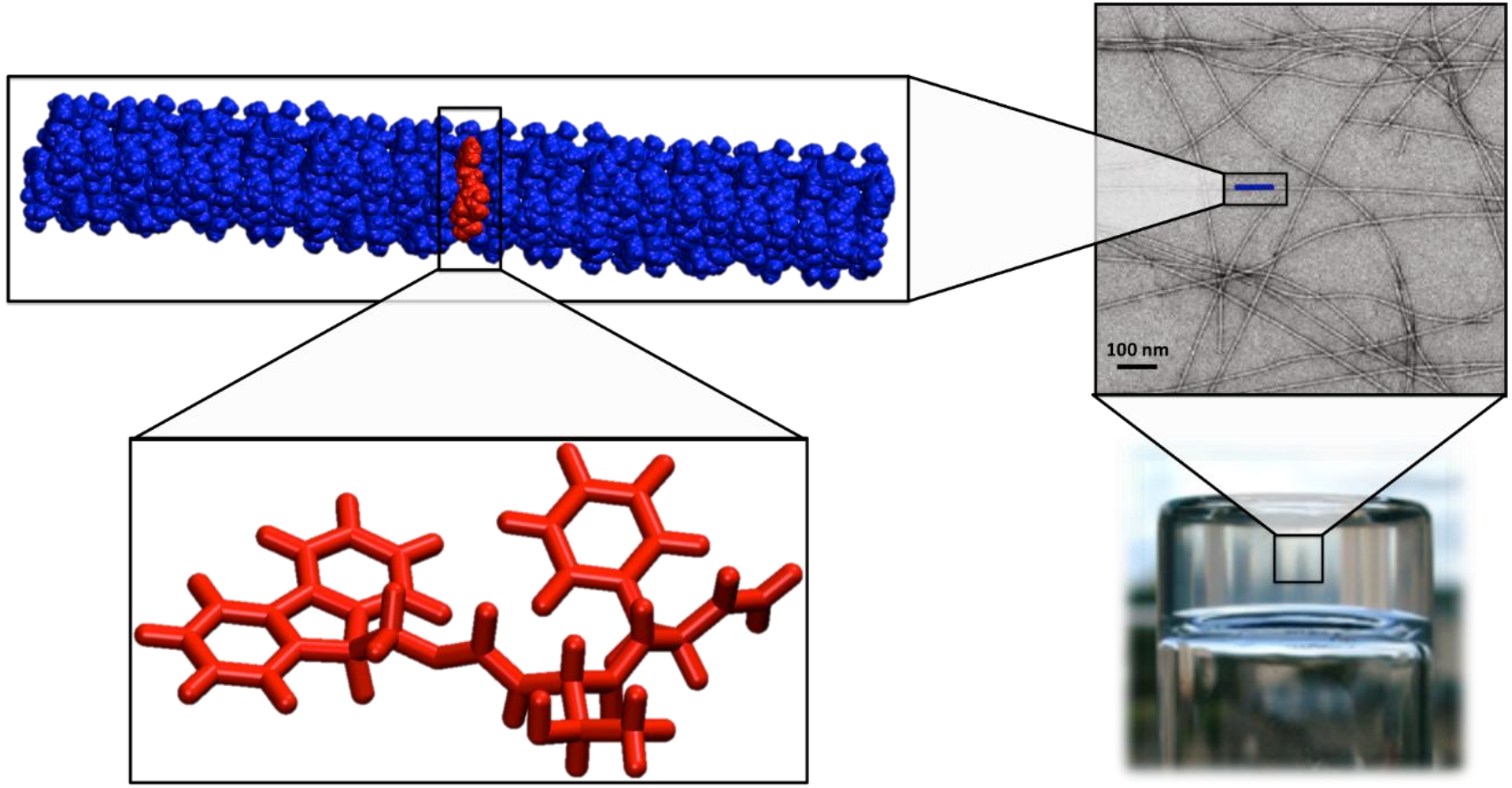


Reches, Gazit.
Science **2003**, *300*, 625



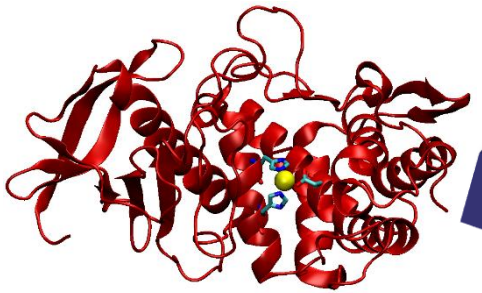
Li, Lynn, *et al.*
J. Am. Chem. Soc. **2016**, *138*, 3579

Supramolecular Peptide Assemblies (SPAs)

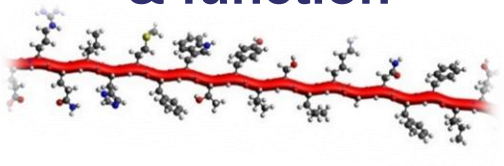


Small Simple Molecules → **Complex Biomaterials**

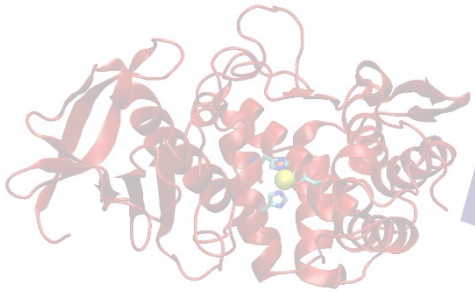
Chemical/Structural/Functional Diversity



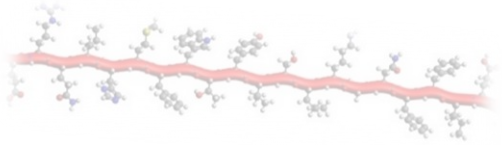
Sequence encodes structure, properties, & function



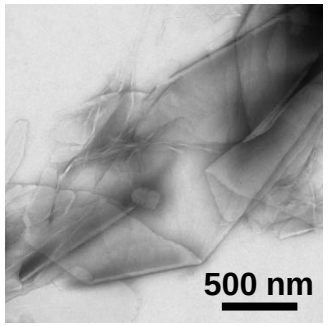
Chemical/Structural/Functional Diversity

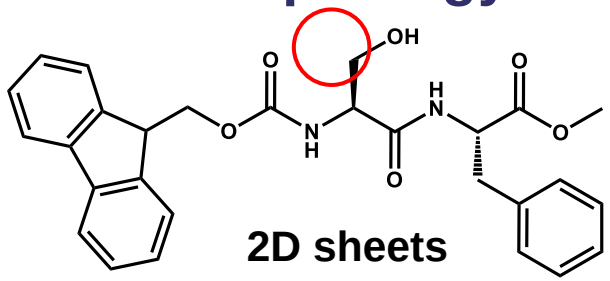


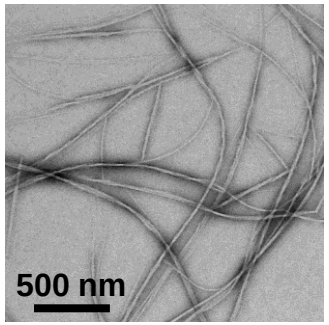
Sequence encodes structure, properties, & function

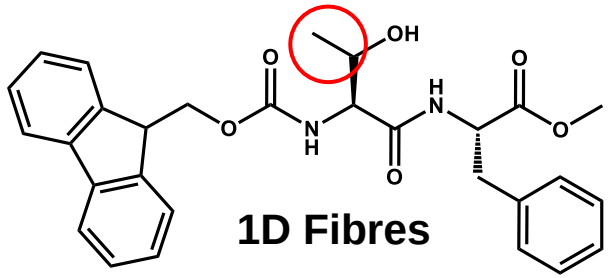


Sequence ↔ Morphology



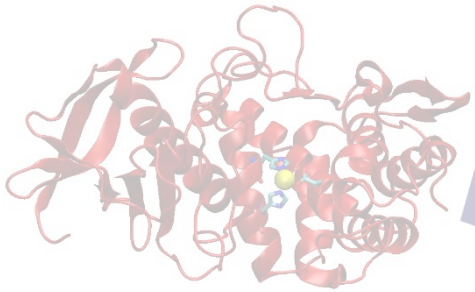




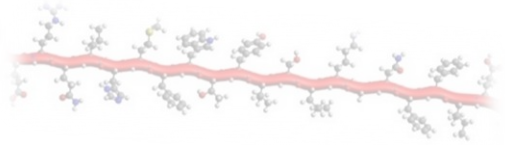


Hughes, Ulijn, *et al. Soft Matter*, **2012**, *8*, 5595

Chemical/Structural/Functional Diversity

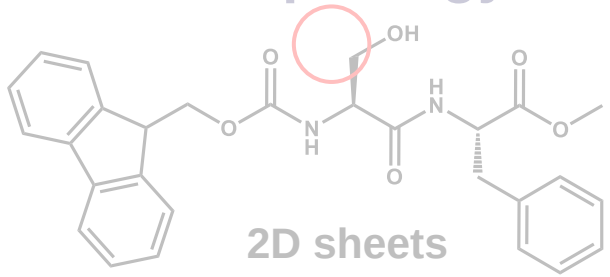


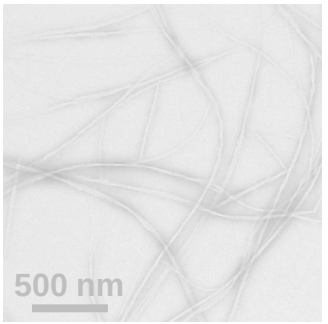
Sequence encodes structure, properties, & function

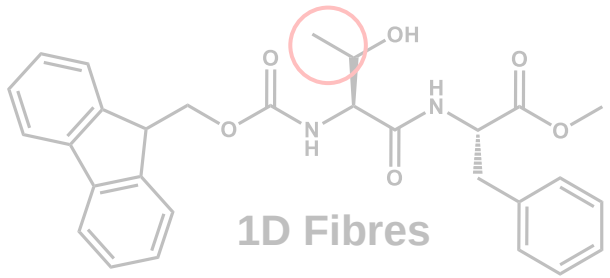


Sequence ↔ Morphology



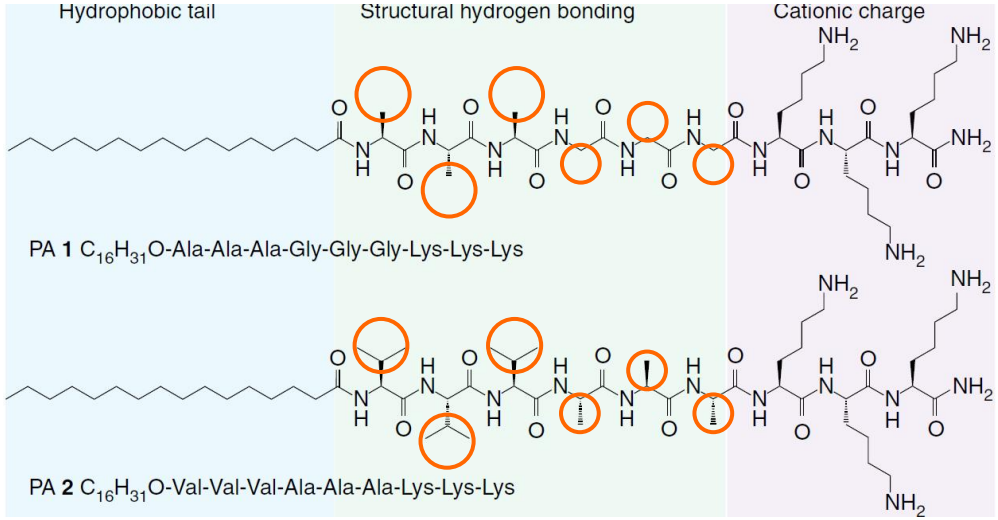


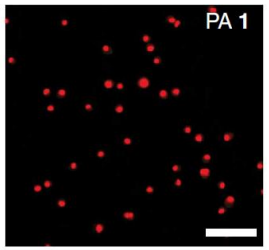


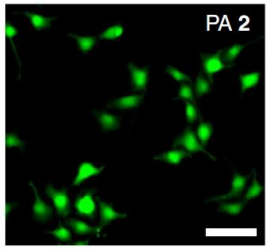


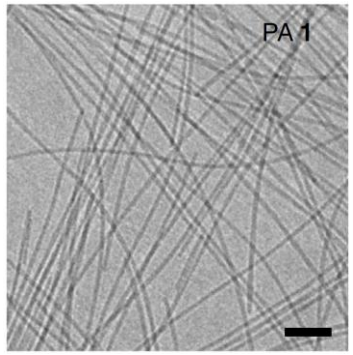
Hughes, Ulijn, *et al. Soft Matter*, **2012**, *8*, 5595

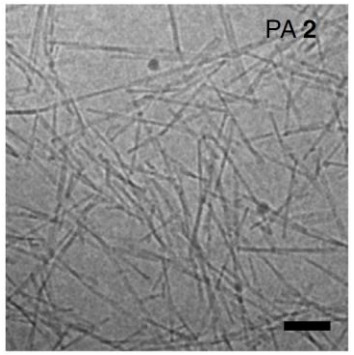
Sequence ↔ Crystallinity ↔ Biocompatibility

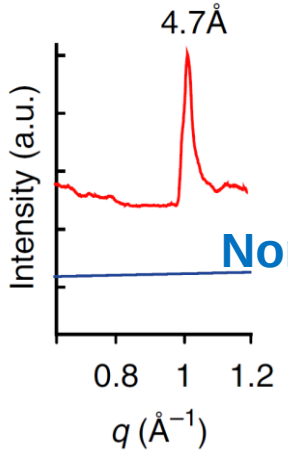












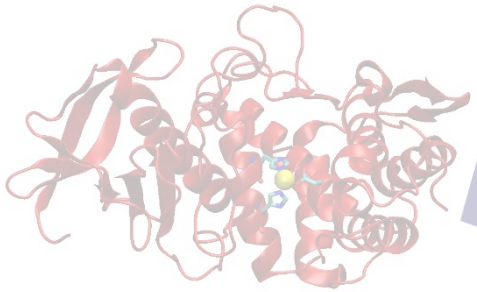
Crystalline

vs

Non-crystalline

Newcomb, Stupp, *et al. Nat. Commun.*, **2014,** *5*, 3321

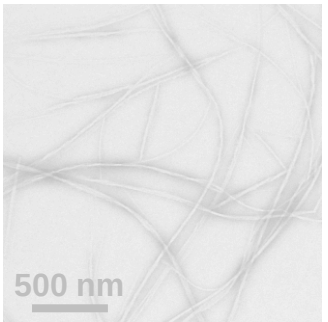
Chemical/Structural/Functional Diversity

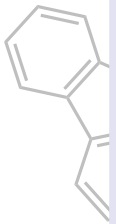


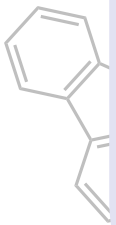
Sequence encodes structure, properties,

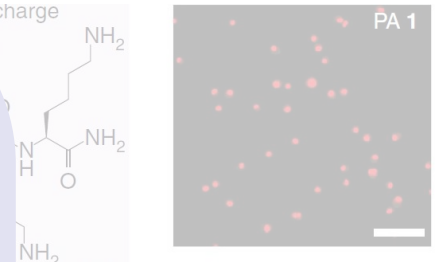
Sequence ↔ Crystallinity ↔ Biocompatibility

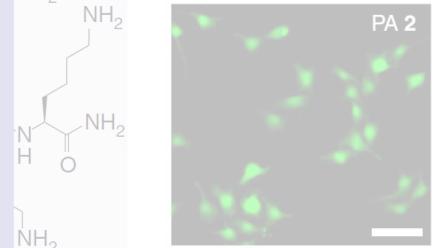


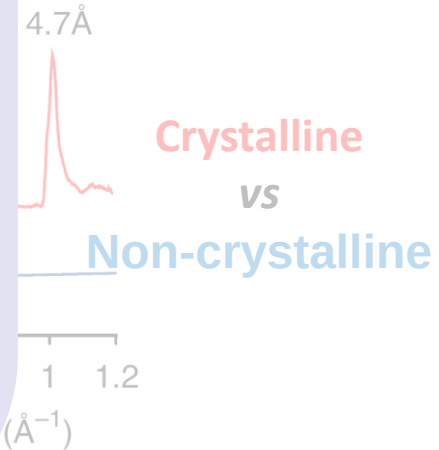








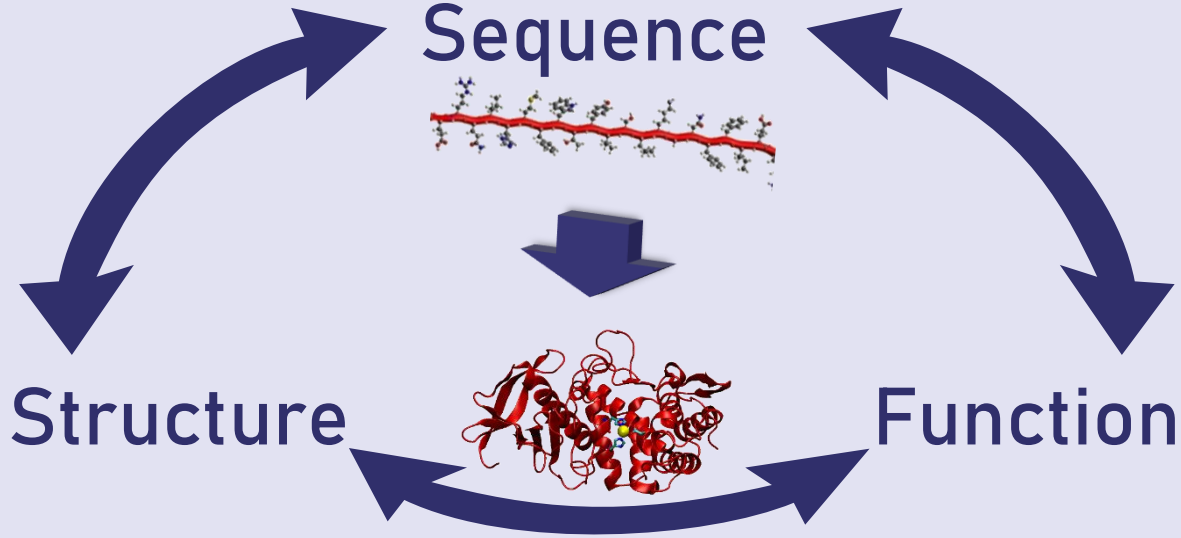




Crystalline

vs

Non-crystalline



Understood?

- ¬ Proteins ☑
- ¬ SPAs ☒

Hughes, Ulijn, *et al. Soft* … *nmun.*, **2014**, *5*, 3321

Experimental Challenges in SPAs

Characterization techniques from Proteins

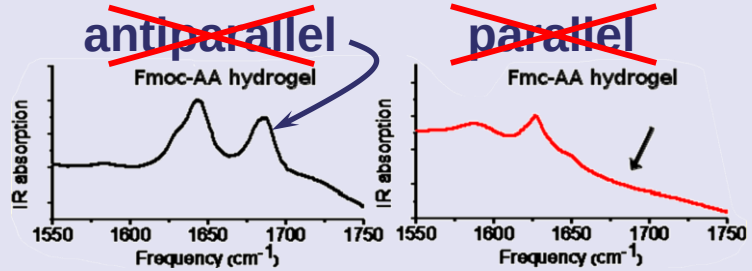
- Same techniques (chemically identical)
- Different interpretation

FT-IR

- Different interpretation

β-sheet:

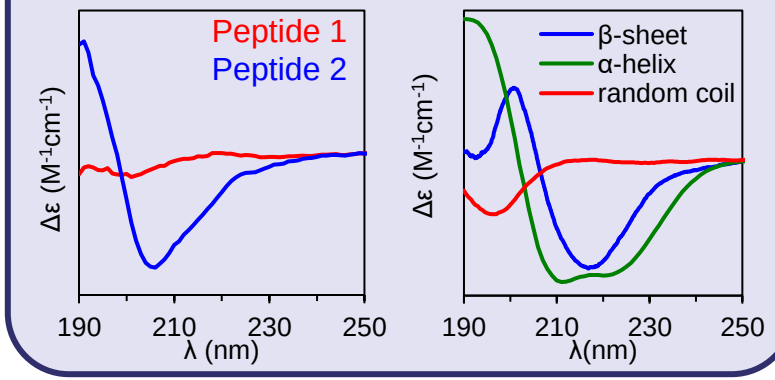
~~antiparallel~~ ~~parallel~~



Sasselli *et al*. *Langmuir*, **2013**, *29*, 9510

Circular Dichroism (CD)

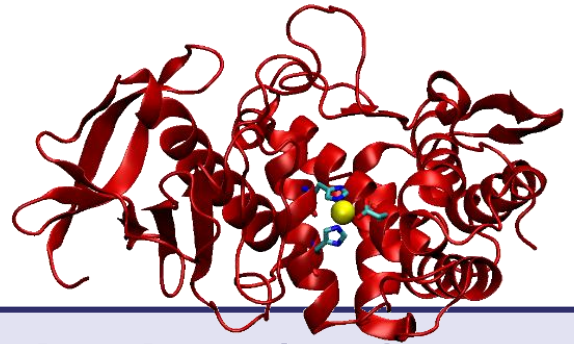
- Non-perfect 2^{ary} structures
- No orientation information

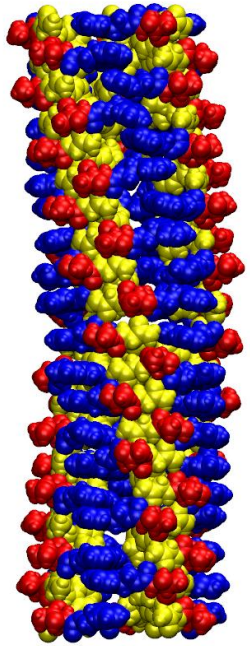


Experimental Challenges in SPAs

Characterization techniques from Proteins

- Same techniques (chemically identical)
- Different interpretation
- *Cannot resolve structure*



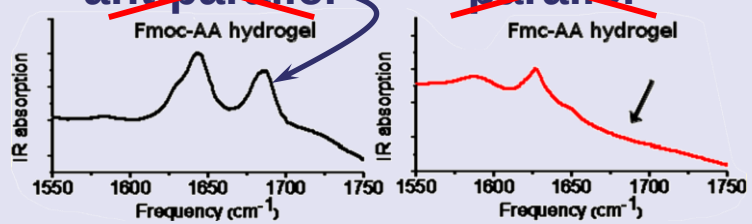


FT-IR

- Different interpretation

β-sheet:

~~antiparallel~~ ~~parallel~~

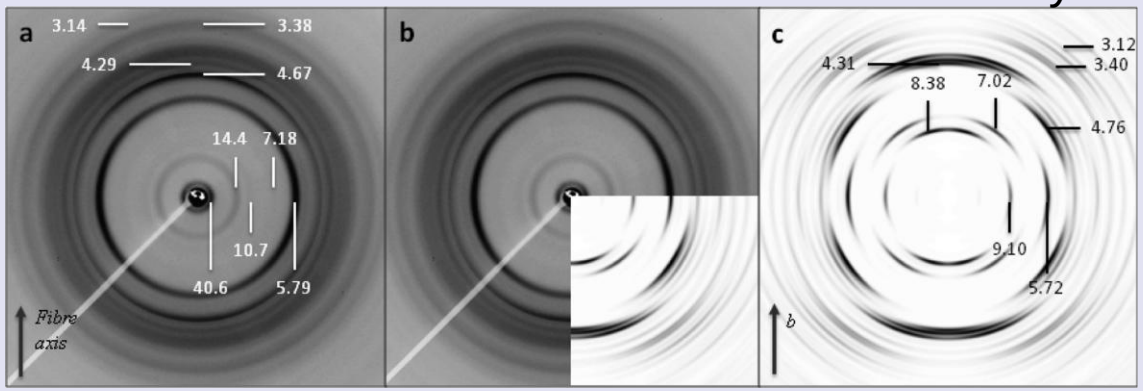


Sasselli *et al. Langmuir*, **2013**, *29*, 9510

Assemblies (1-2D) ≠ Crystals (3D)

Fiber diffraction

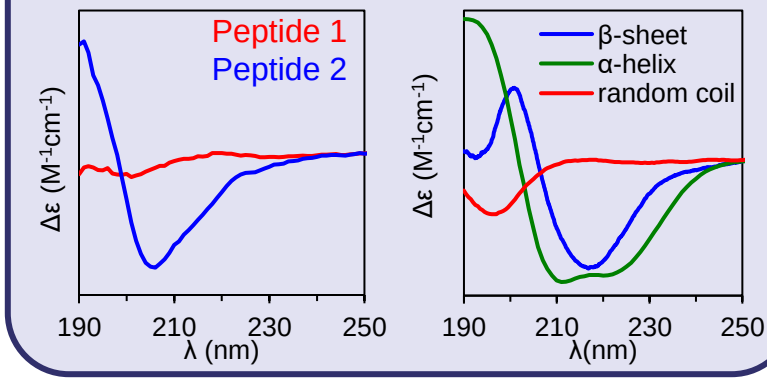
Model from crystal



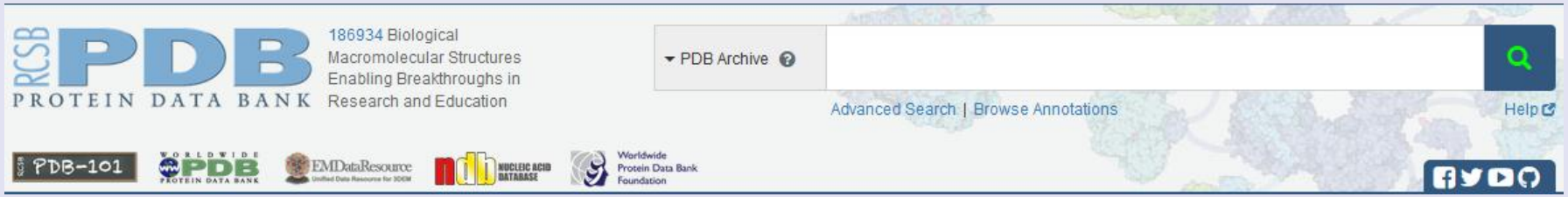
Houton, Adams, *et al. Langmuir*, **2012**, *28*, 9797

Circular Dichroism (CD)

- Non-perfect 2^{ary} structures
- No orientation information

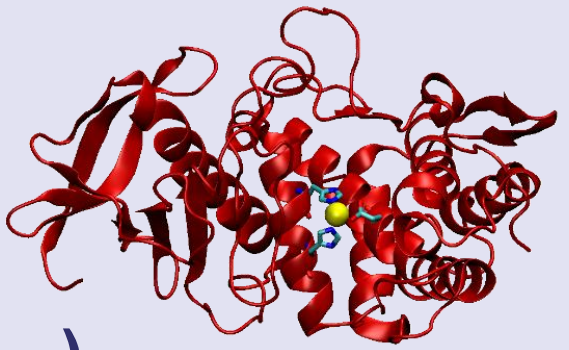


Experimental Challenges in SPAs

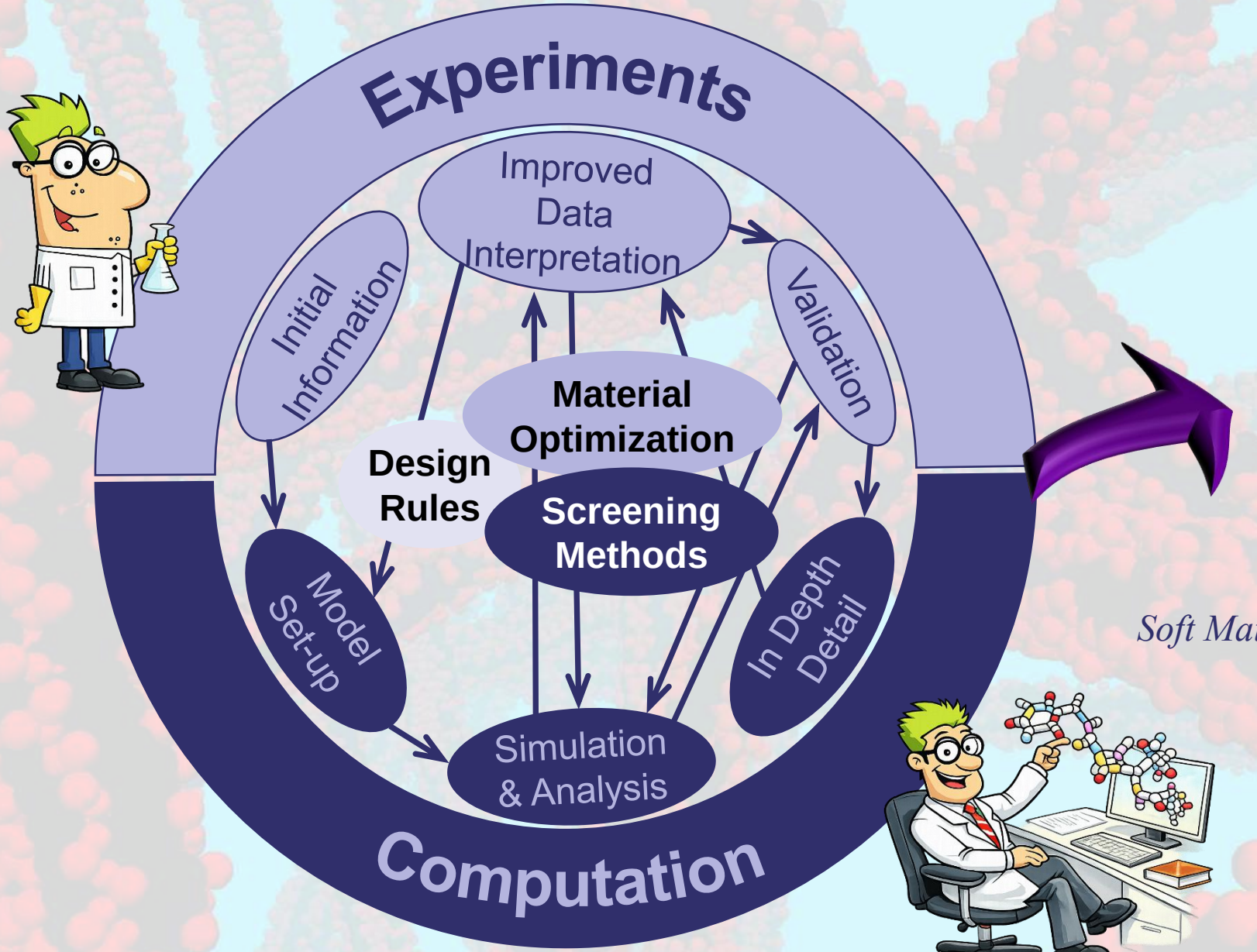


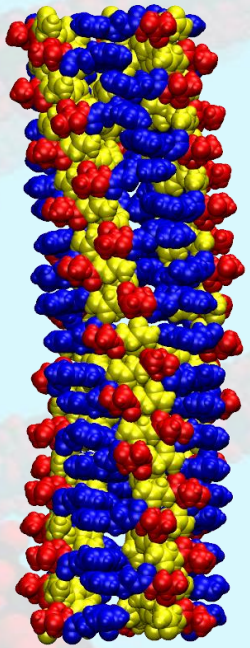
Huge Protein Crystals Databases:

- Structure → resolved with Å resolution
- Benchmarking of:
  - Characterization techniques
  - Computational methods (MD, α-fold…)



Computational/Experimental Symbiosis



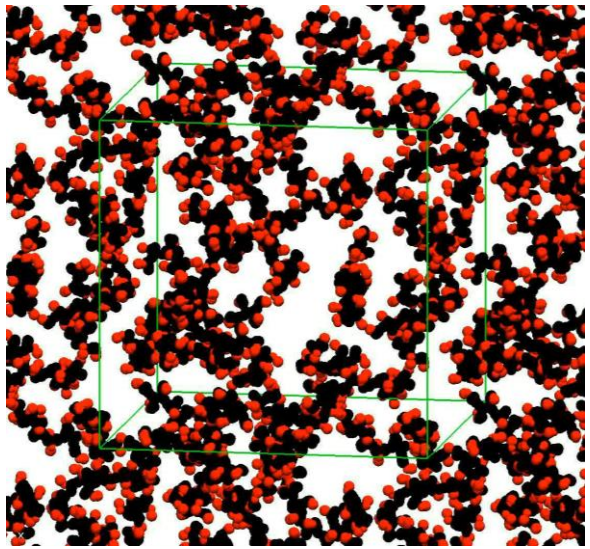


Sasselli, *et al.*
Soft Matter, **2016**, *12*, 8307

CG Self-Assembly Simulation

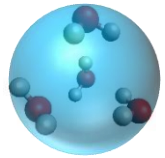
Martini

Reproduce/Predict: Self-assembly from scratch

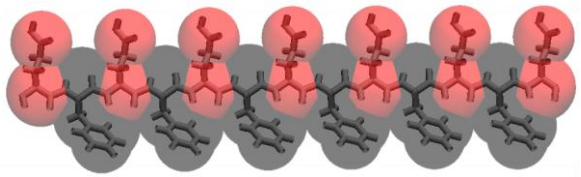


From solution (No input needed)

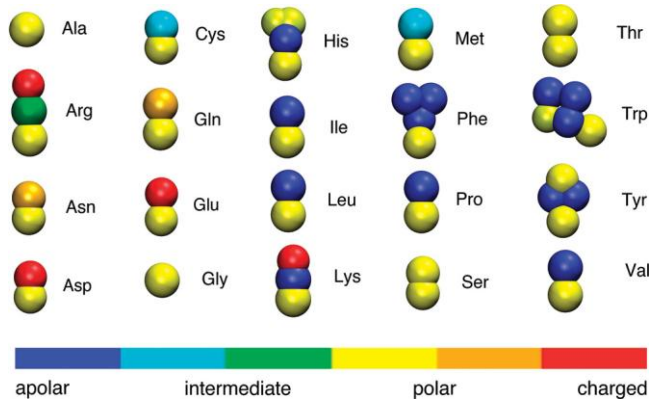
1-4 (1-2) Mapping



1 bead → 12 atoms

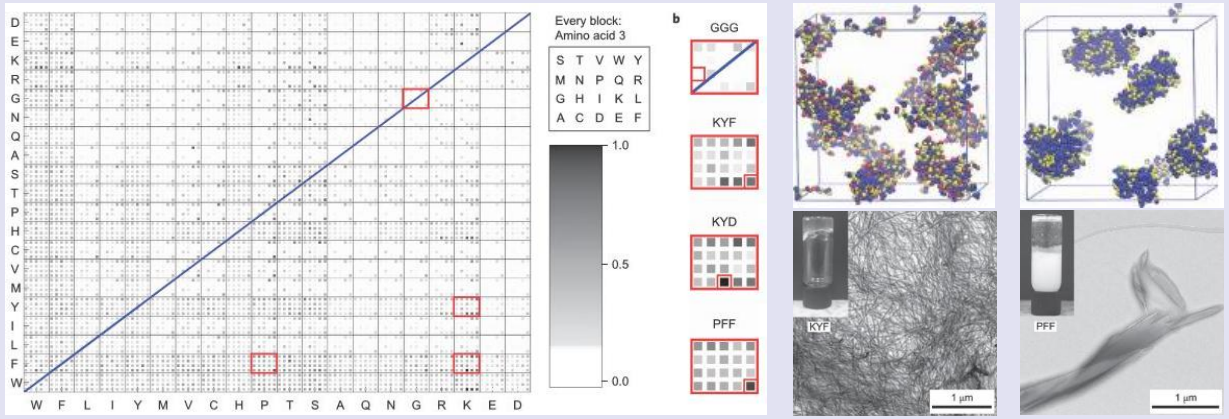


38 beads → 235 atoms



Monticelli, Marrink, *et al. J. Chem. Theory Comput.* **2008**, *4*, 819

Screening of 8000 Tripeptides

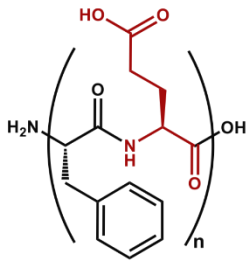


Frederix, Tuttle, *et al. Nature Chem.* **2014**, *7*, 30

Self-assembling Peptide Design

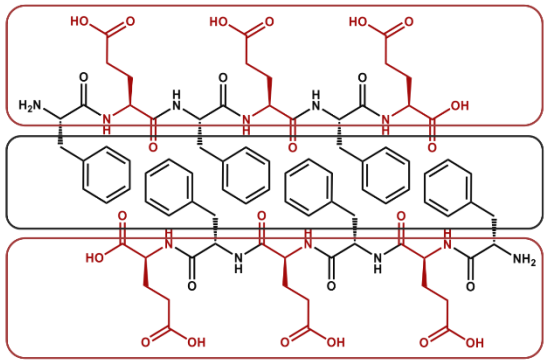


Glutamic acid



Phenylalanine

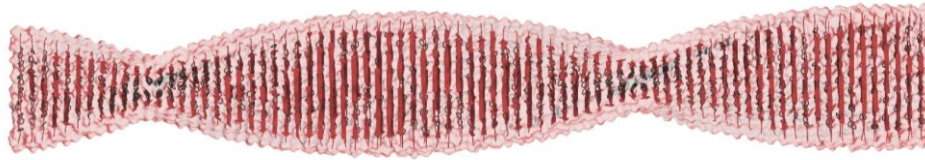
n repetitions

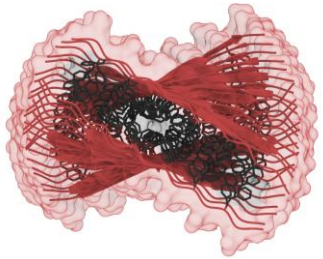


Hydrophilic surface

Hydrophobic core

Hydrophilic surface

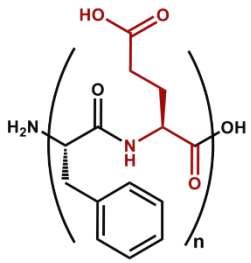




Self-assembling Peptide Design

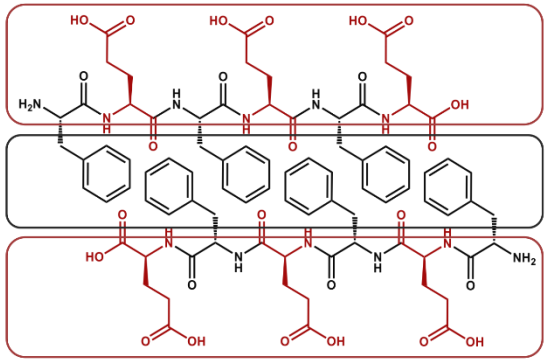


Glutamic acid



Phenylalanine

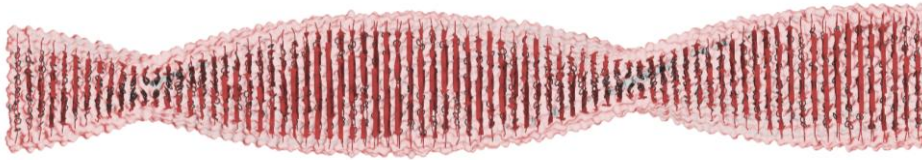
n repetitions

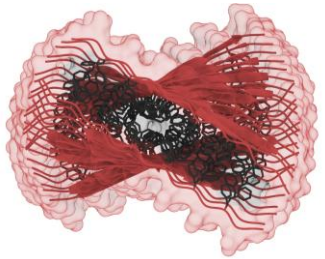


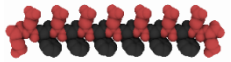
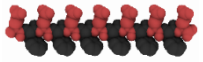
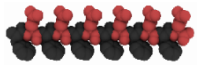
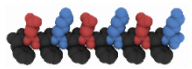
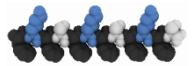
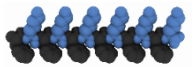
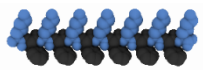
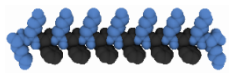
Hydrophilic surface

Hydrophobic core

Hydrophilic surface



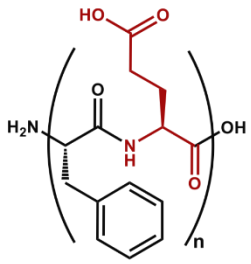


	q	n
	-9	1
	-7	2
	-6	3
	-3	4
	0	5
	+3	6
	+6	7
	+7	8
	+9	

Self-assembling Peptide Design

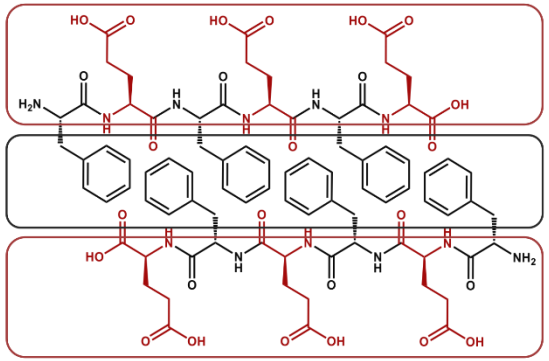


Glutamic acid



Phenylalanine

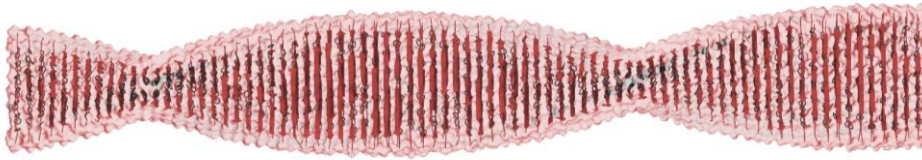
n repetitions

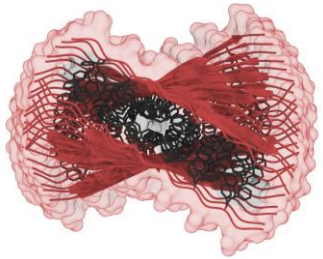


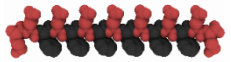
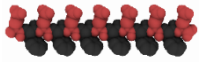
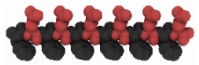
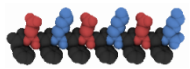
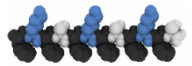
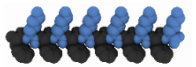
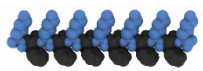
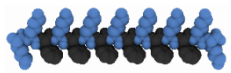
Hydrophilic surface

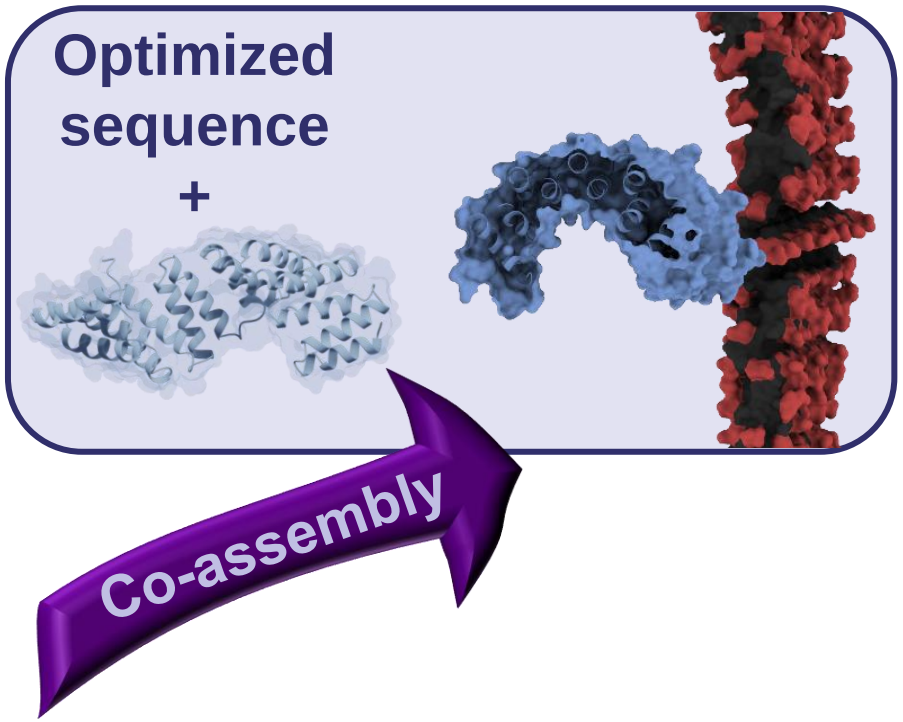
Hydrophobic core

Hydrophilic surface





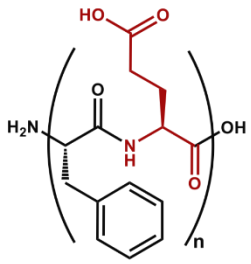
	q	n
	-9	1
	-7	2
	-6	3
	-3	4
	0	5
	+3	6
	+6	7
	+7	8
	+9	



Self-assembling Peptide Design

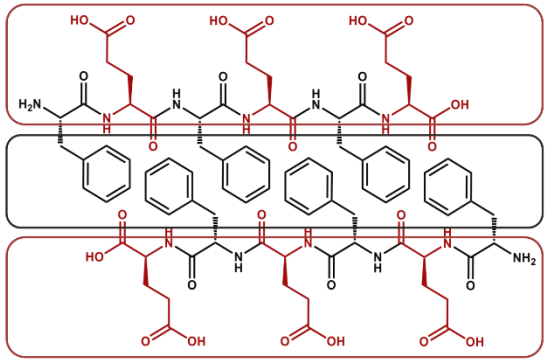


Glutamic acid



Phenylalanine

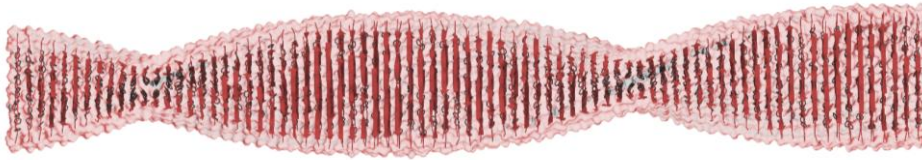
n repetitions

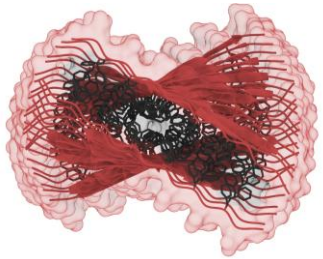


Hydrophilic surface

Hydrophobic core

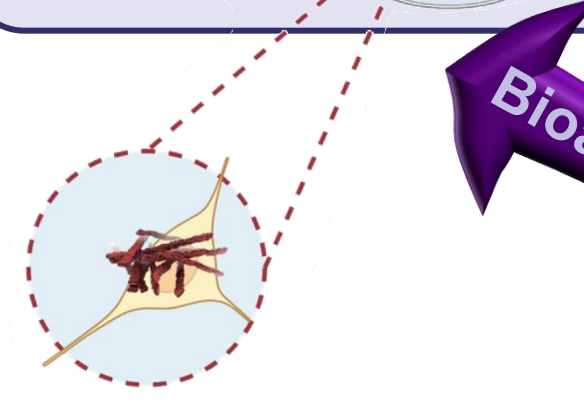
Hydrophilic surface







Library:
-q ⇔ +q

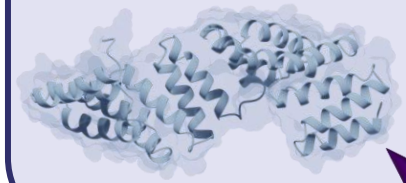


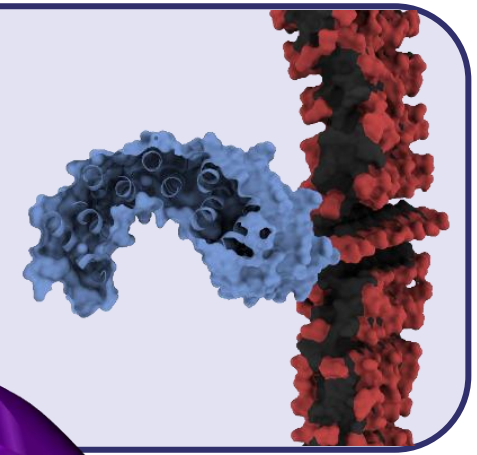
Bioactivity=f(q)

q	n
-9	1
-7	2
-6	3
-3	4
0	5
+3	6
+6	7
+7	8
+9	

Optimized sequence

+



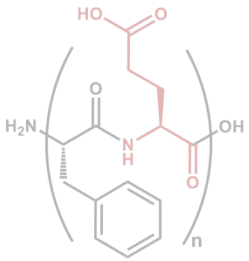


Co-assembly

Self-assembling Peptide Design

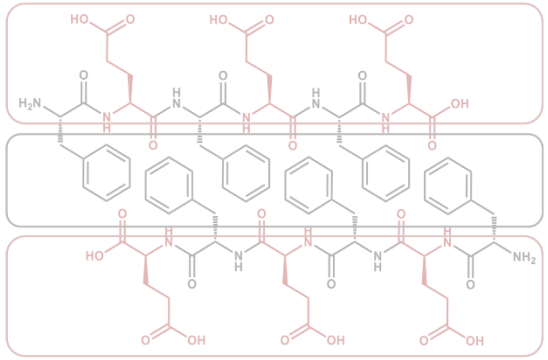


Glutamic acid



Phenylalanine

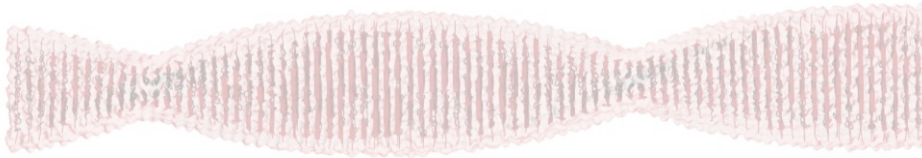
n repetitions

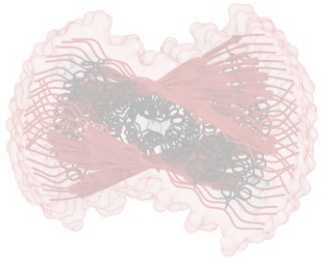


Hydrophilic surface

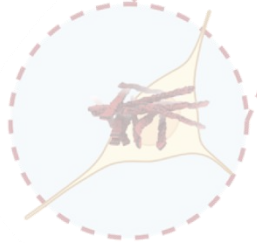
Hydrophobic core

Hydrophilic surface









Bioactivity=f(q)

q	n
-9	1
-7	2
-6	3
-3	4
0	5
+3	6
+6	7
+7	8
+9	



Co-assembly

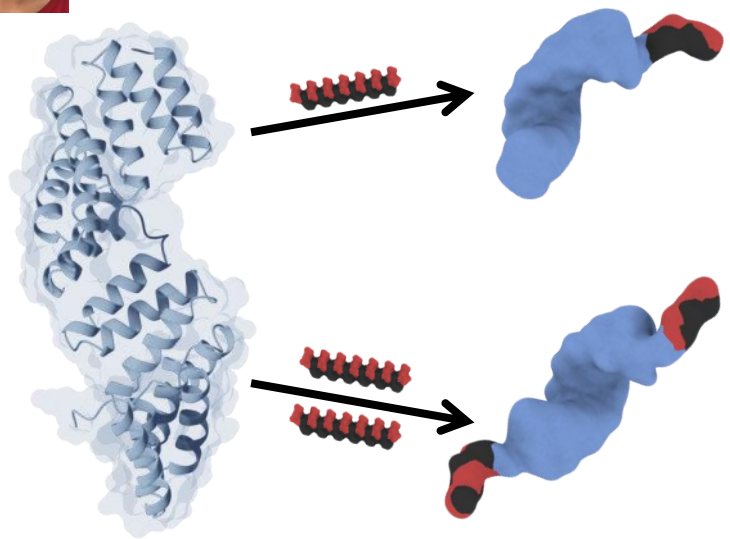
Protein-Peptide Co-assemblies

- **Peptide Assembly:**



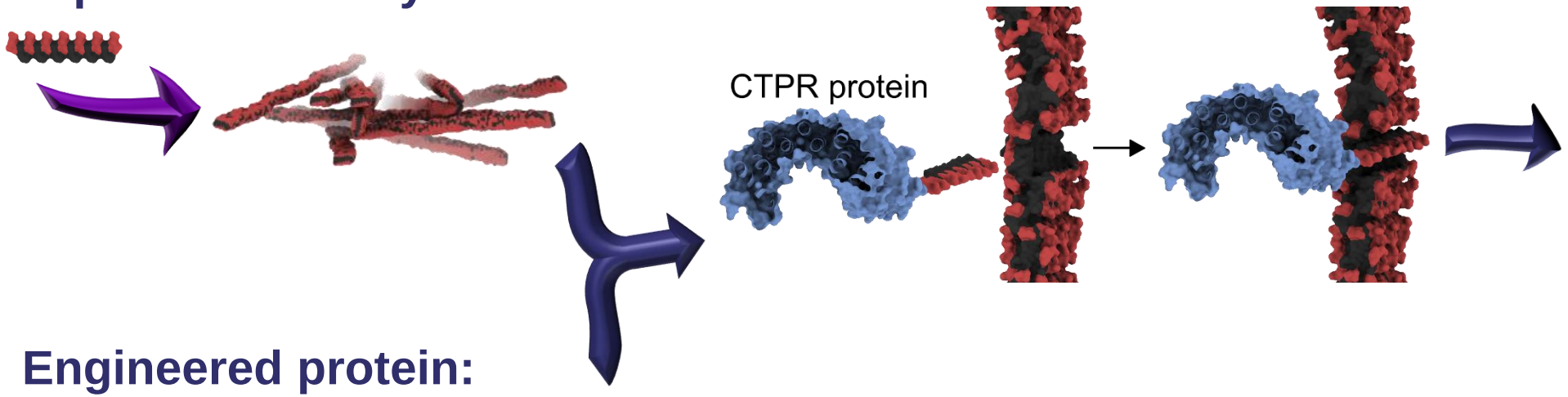
- **Engineered protein:**
  - **CTPR + 1-2 Peptides**
  - **Aitziber L. Cortajarena**

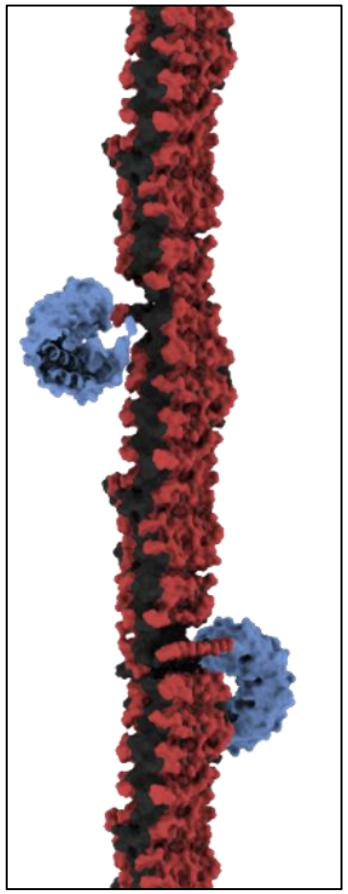




Protein-Peptide Co-assemblies

- **Peptide Assembly:**

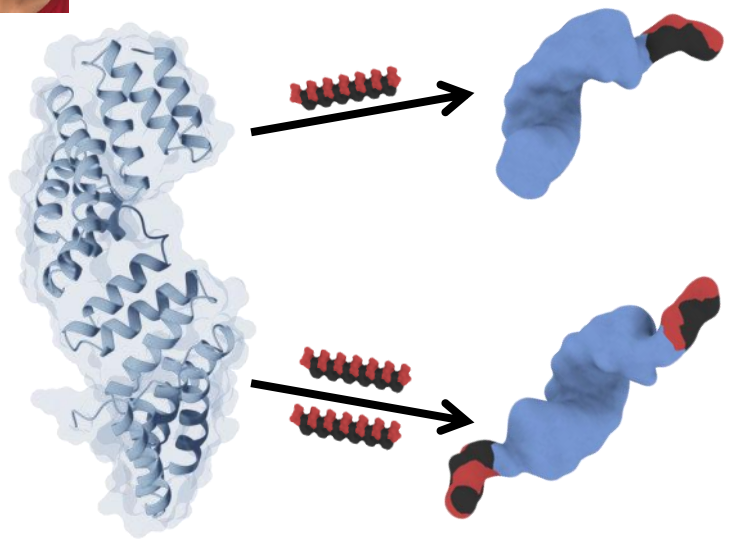




CTPR decorated assemblies

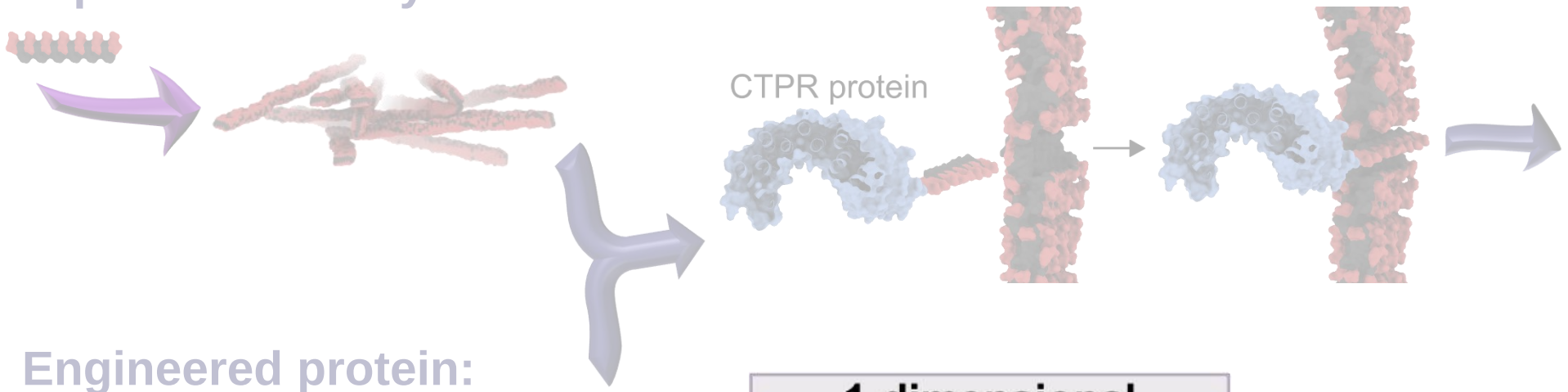
- **Engineered protein:**
  - **CTPR + 1-2 Peptides**
  - **Aitziber L. Cortajarena**





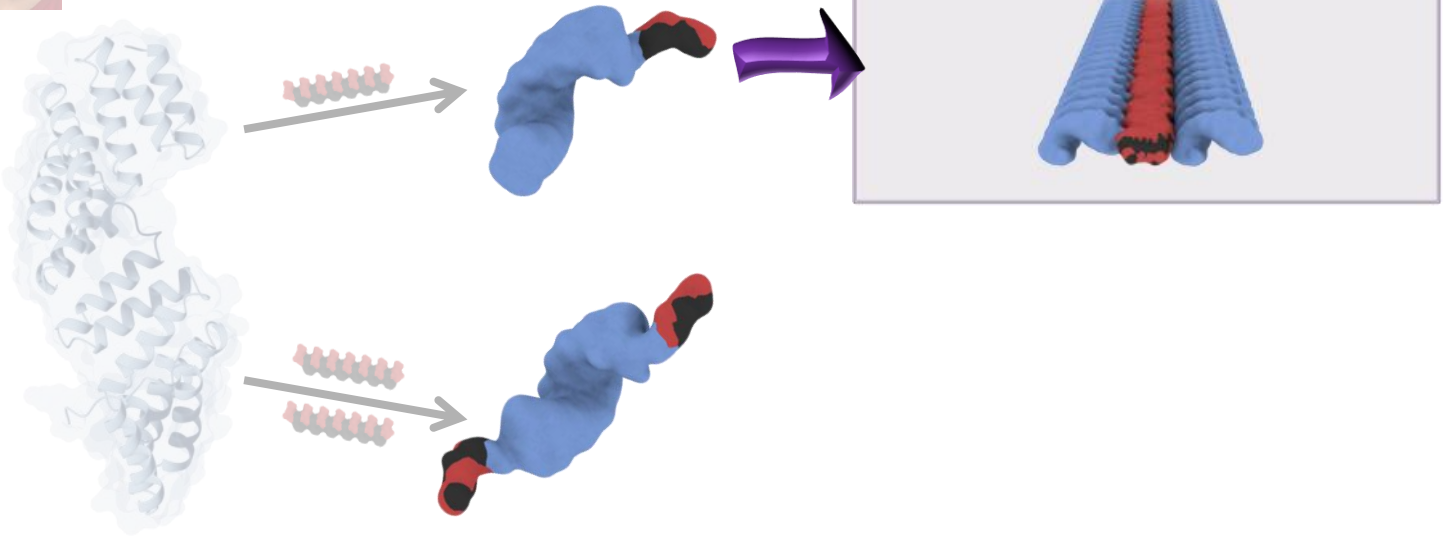
Protein-Peptide Co-assemblies

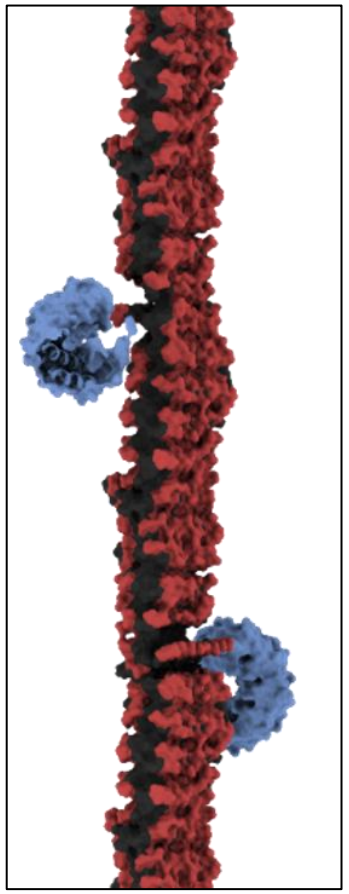
- Peptide Assembly:



- Engineered protein:
  - CTPR + 1-2 Peptides
  - Aitziber L. Cortajarena

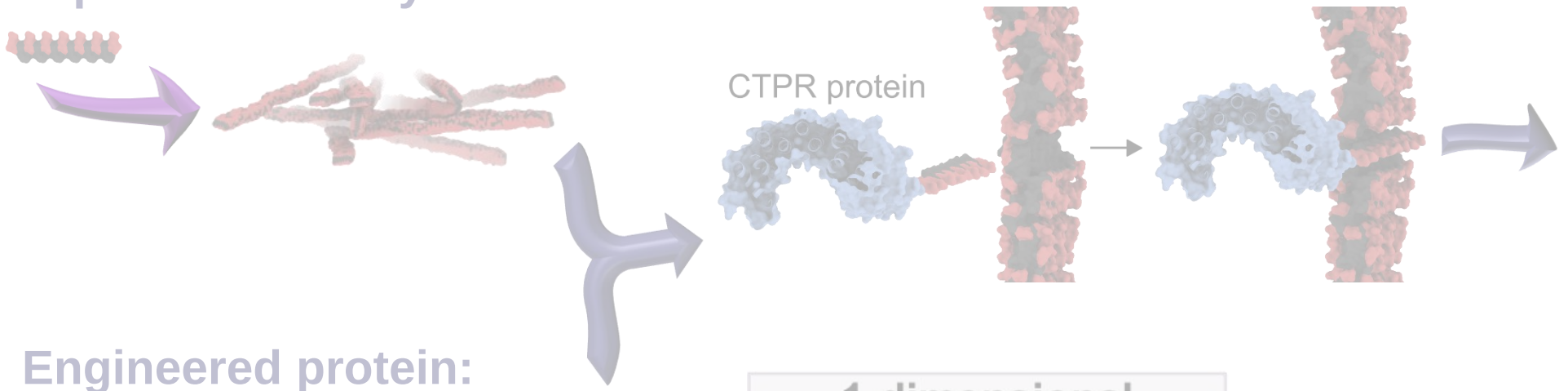


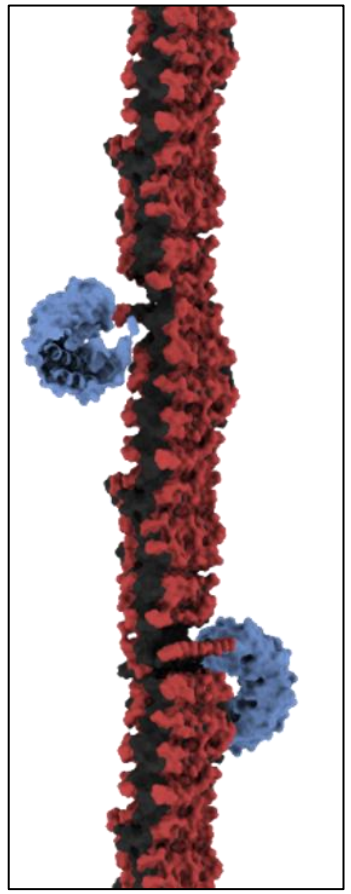




Protein-Peptide Co-assemblies

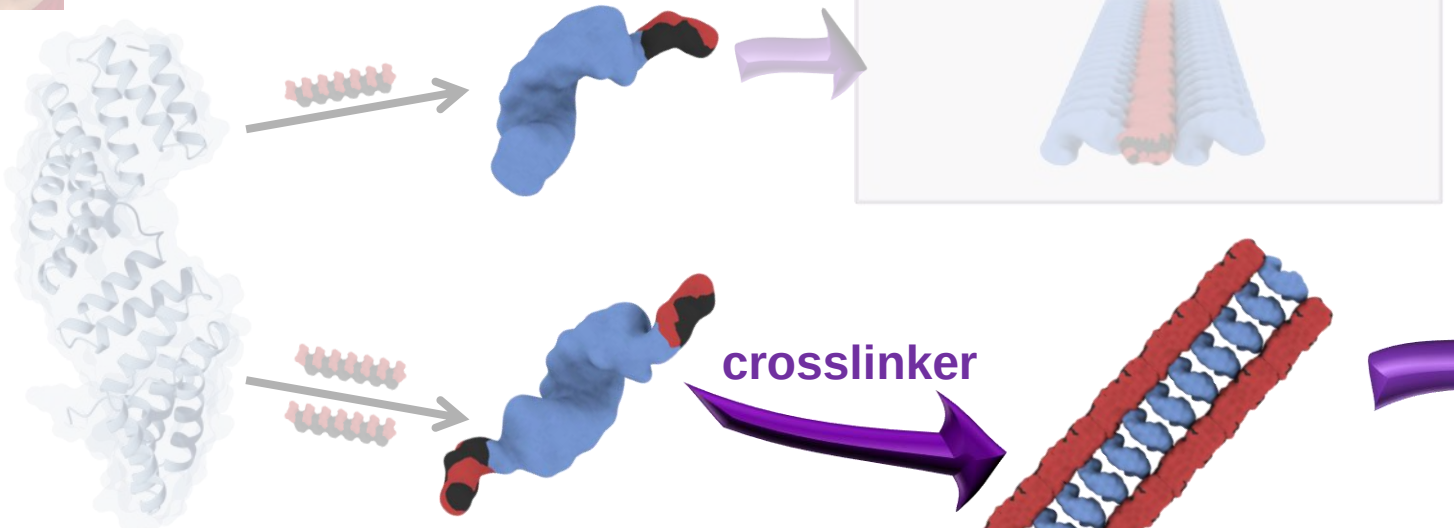
- Peptide Assembly:





- Engineered protein:
  - CTPR + 1-2 Peptides
  - Aitziber L. Cortajarena

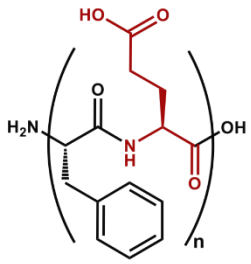




Peptide Self-assembly Optimization

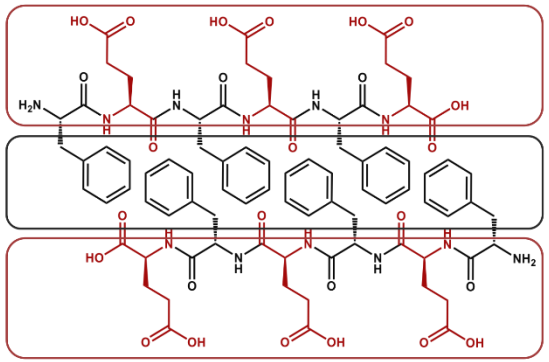


Glutamic acid



Phenylalanine

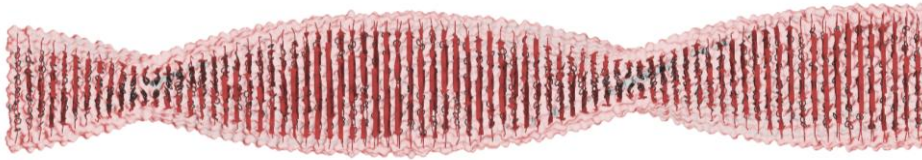
n repetitions

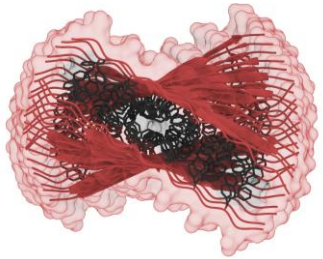


Hydrophilic surface

Hydrophobic core

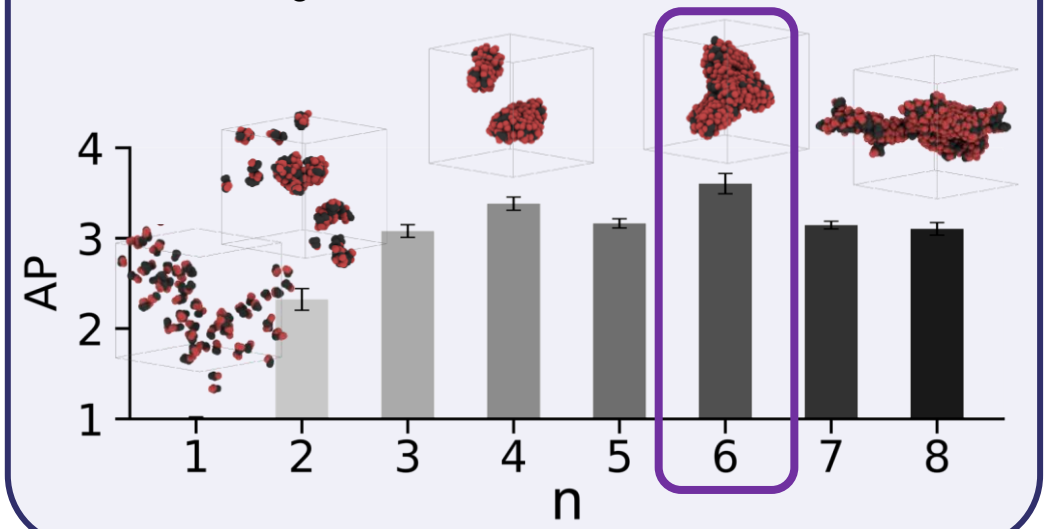
Hydrophilic surface





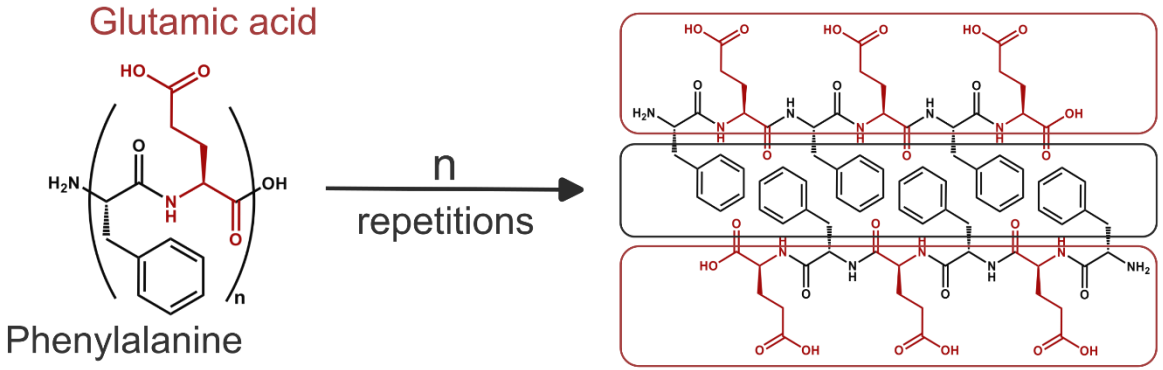
Peptide length optimization:

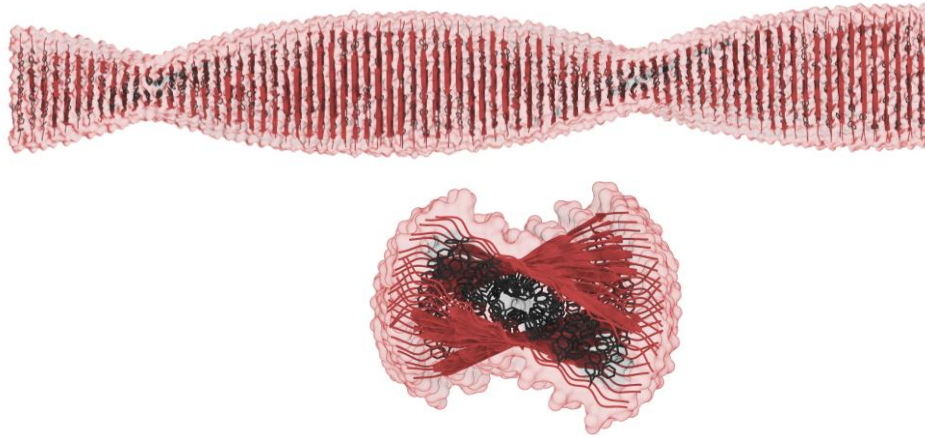
¬ $(FE)_6$



Peptide Self-assembly Optimization

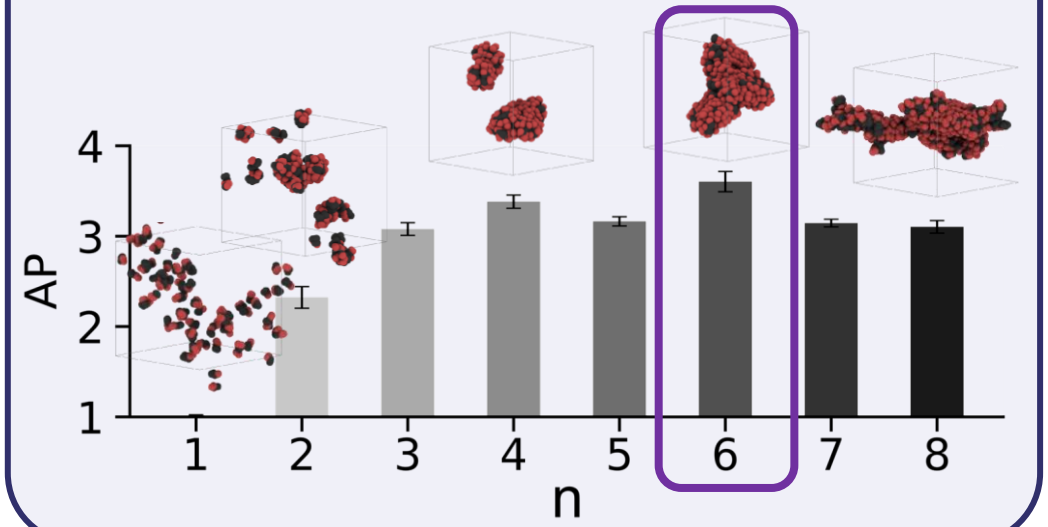
Cortajarena, Sasselli, *et al.*
ACS Nano **2025**, *19*, 16500.





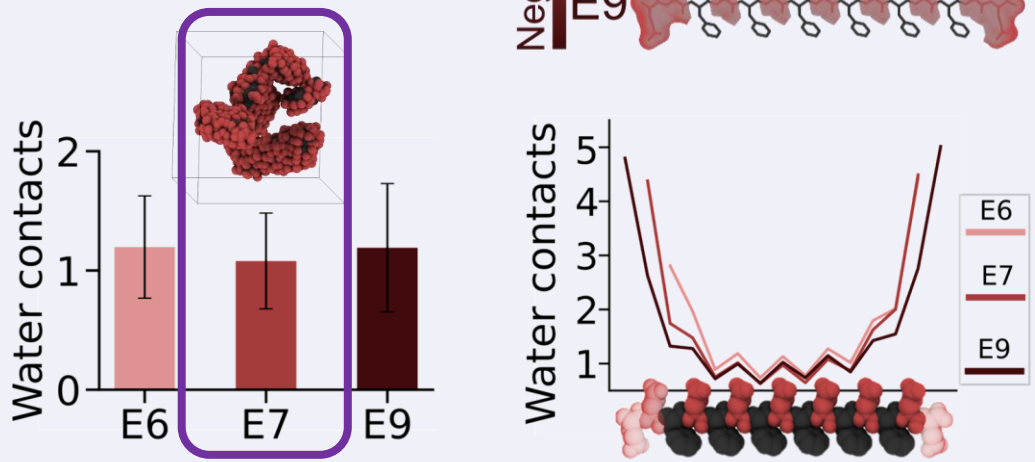
Peptide length optimization:

¬ $(FE)_6$



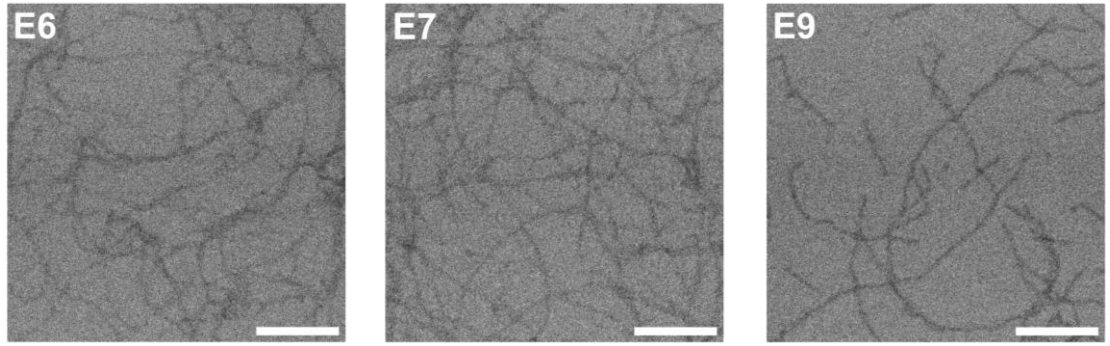
Charge/peptide optimization:

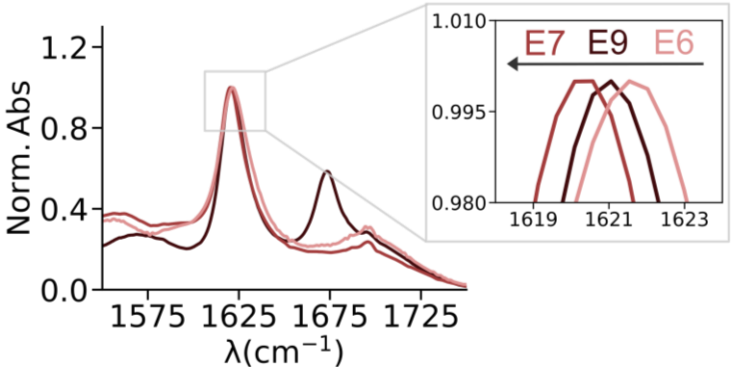
¬ E7 ≡ $E(FE)_6$



Experimental Validation – E7 Selected

Cortajarena, Sasselli, *et al.*
ACS Nano **2025**, *19*, 16500.



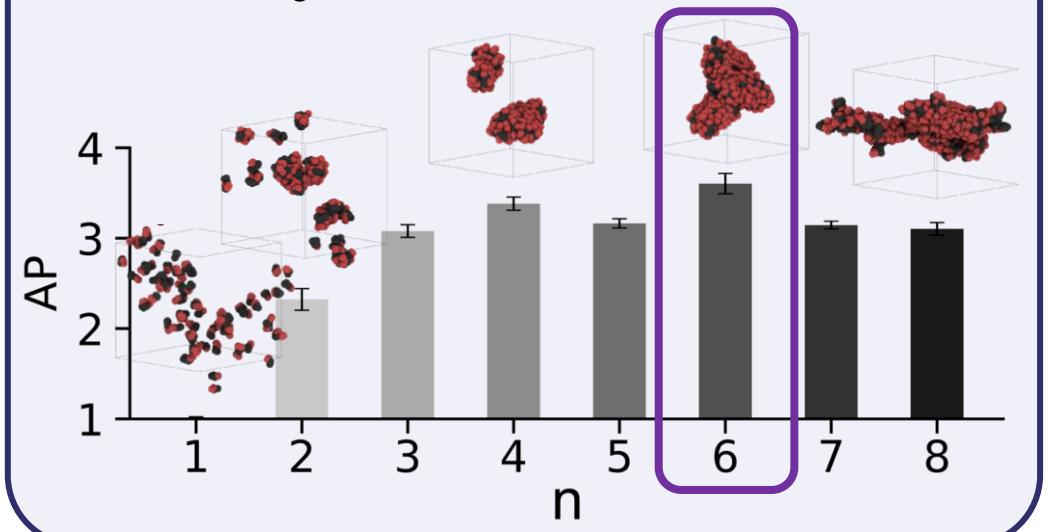


Experimentally:

- ¬ Fiber formation
- ¬ β-sheet:
  E7 > E9 > E6

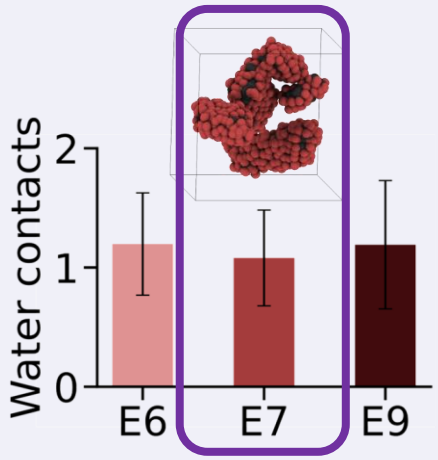
Peptide length optimization:

- ¬ **$(FE)_6$**

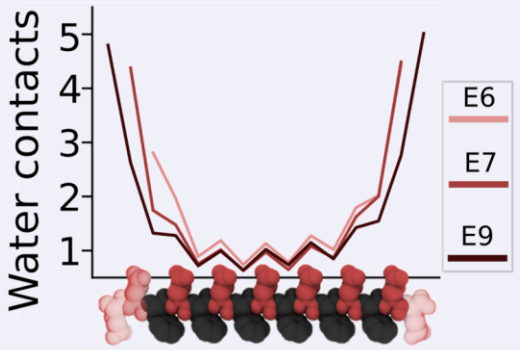


Charge/peptide optimization:

- ¬ **E7 ≡ $E(FE)_6$**

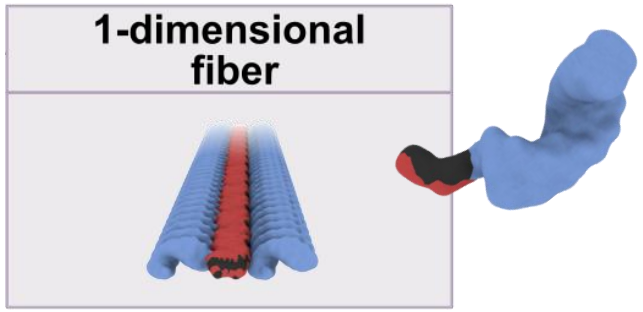




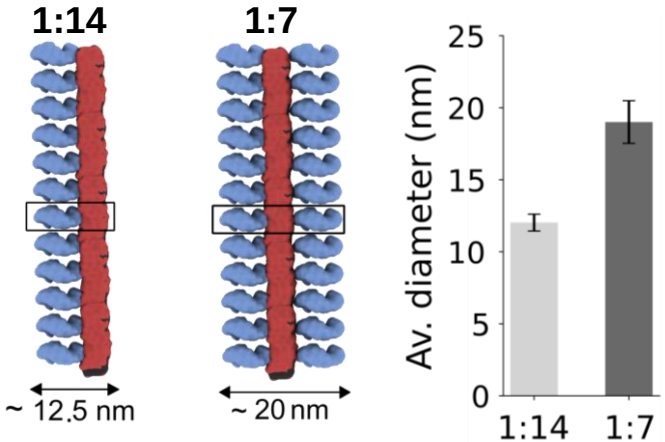


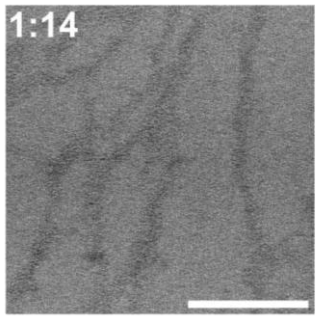
Protein-Peptide Co-assemblies

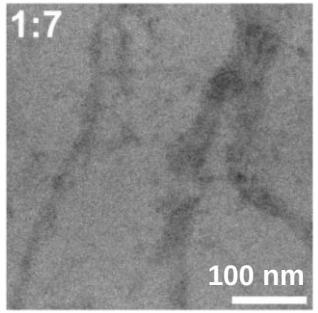
Cortajarena, Sasselli, *et al.*
ACS Nano **2025**, *19*, 16500.



protein:peptide ratio

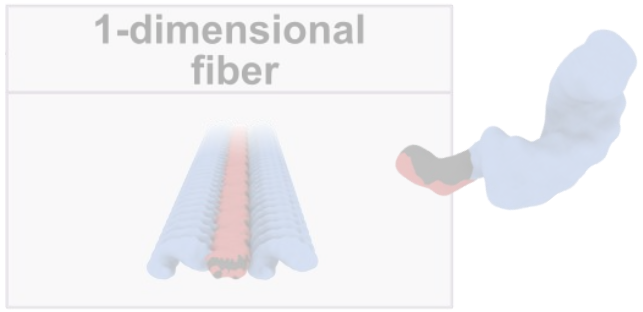


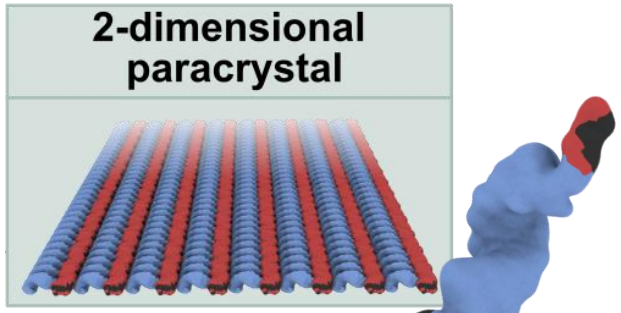


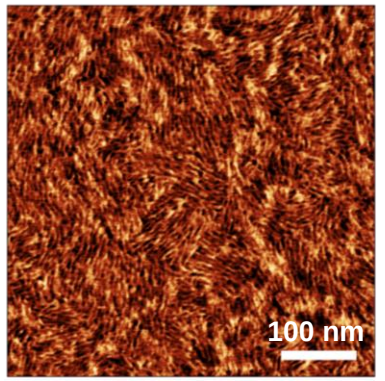


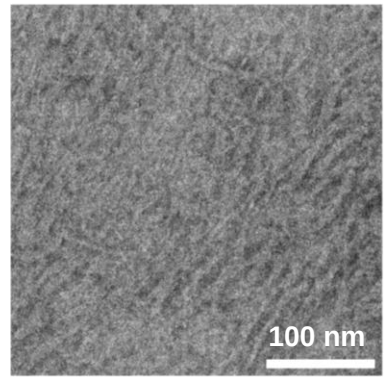
Protein-Peptide Co-assemblies

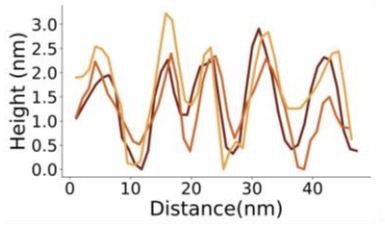
Cortajarena, Sasselli, *et al.*
ACS Nano **2025**, *19*, 16500.

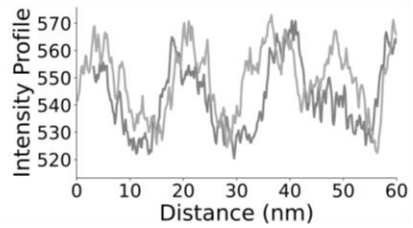




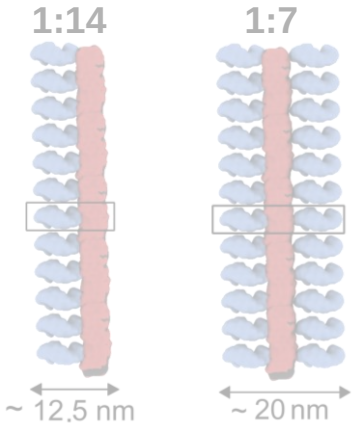


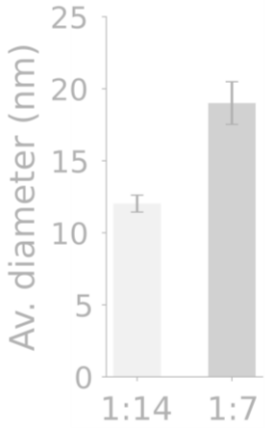


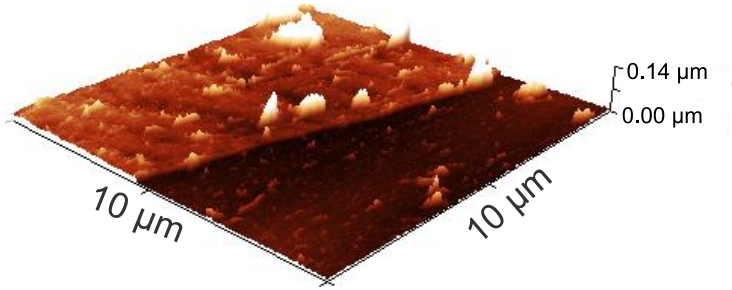


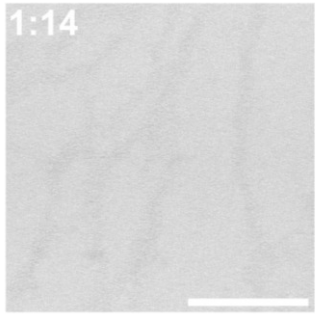


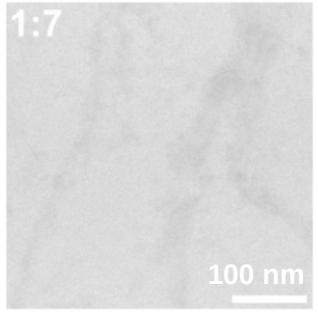
protein:peptide ratio



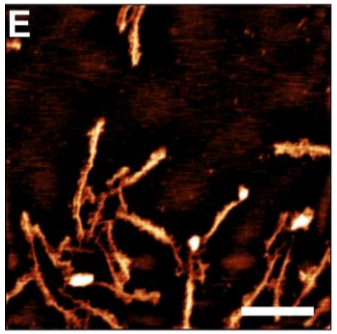






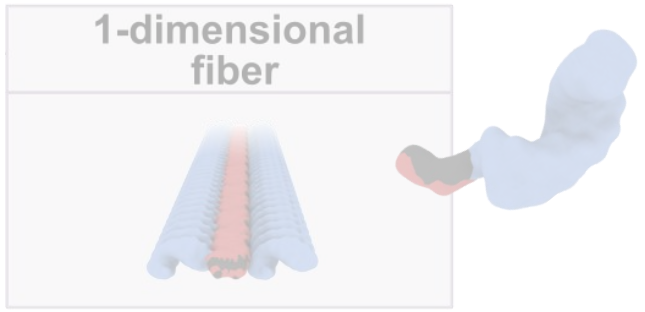


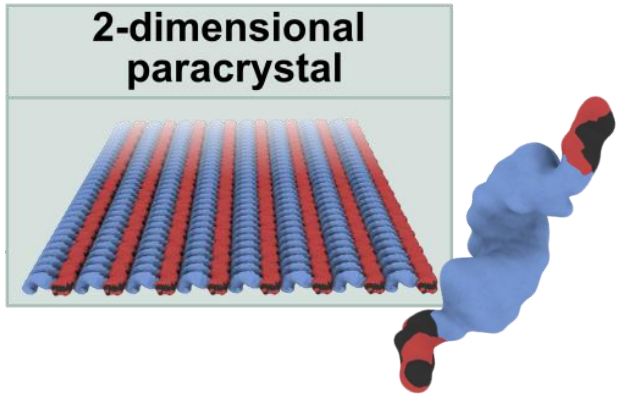
Disassembled control

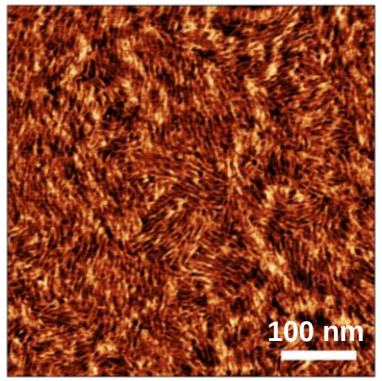


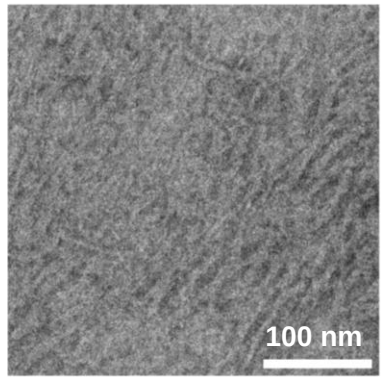
Protein-Peptide Co-assemblies

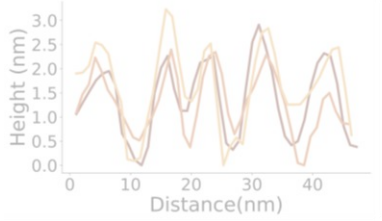
Cortajarena, Sasselli, *et al.*
ACS Nano **2025**, *19*, 16500.

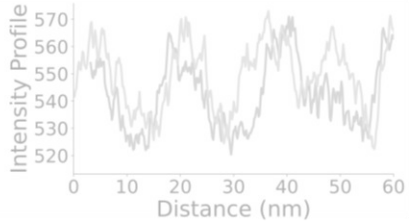




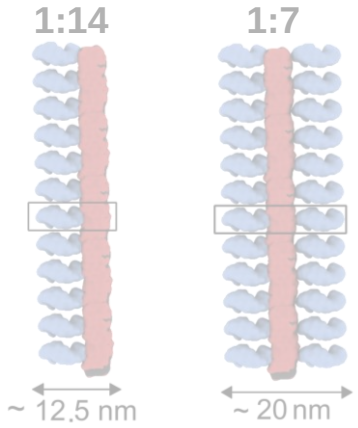


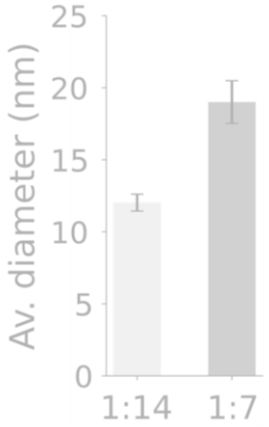


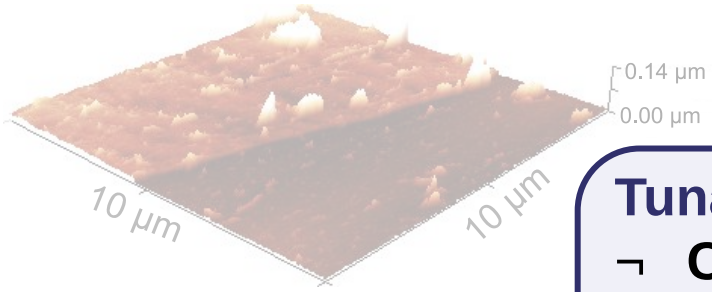


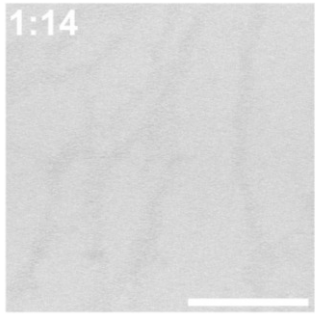


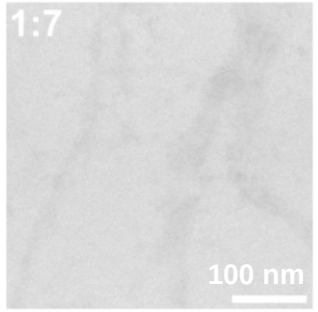
protein:peptide ratio



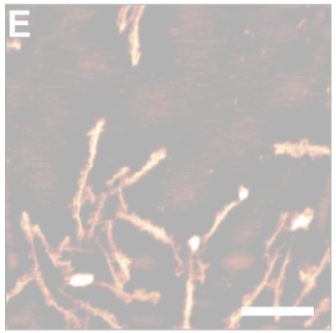






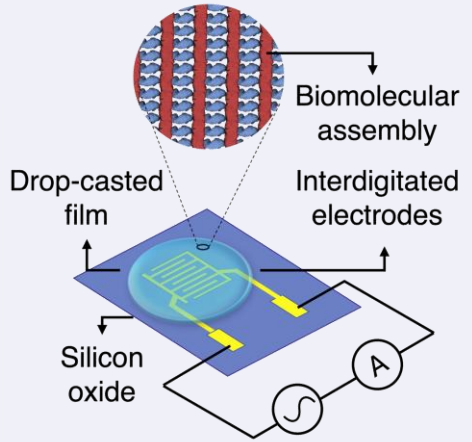


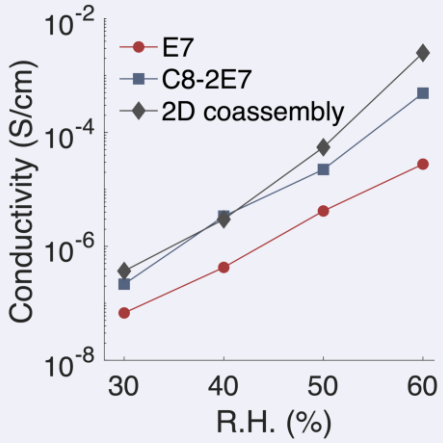
Disassembled control



Tunable 2D materials

¬ **Controlled thickness & morphology**

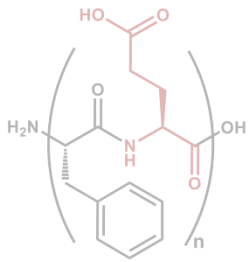




Self-assembling Peptide Design

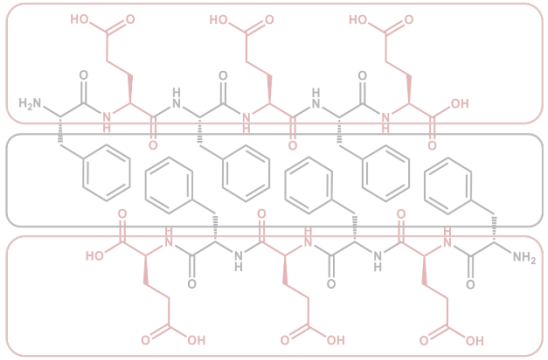


Glutamic acid



Phenylalanine

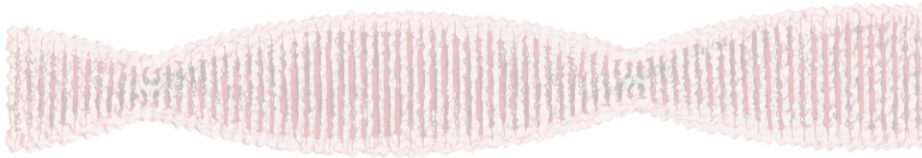
n repetitions

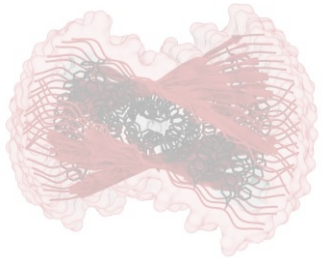


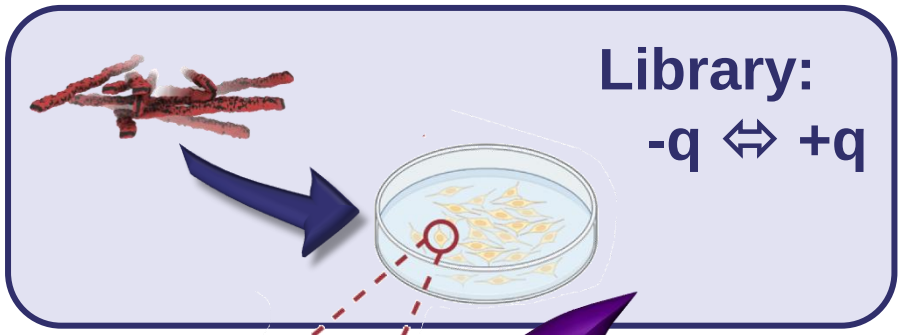
Hydrophilic surface

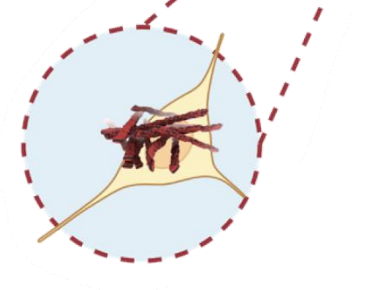
Hydrophobic core

Hydrophilic surface



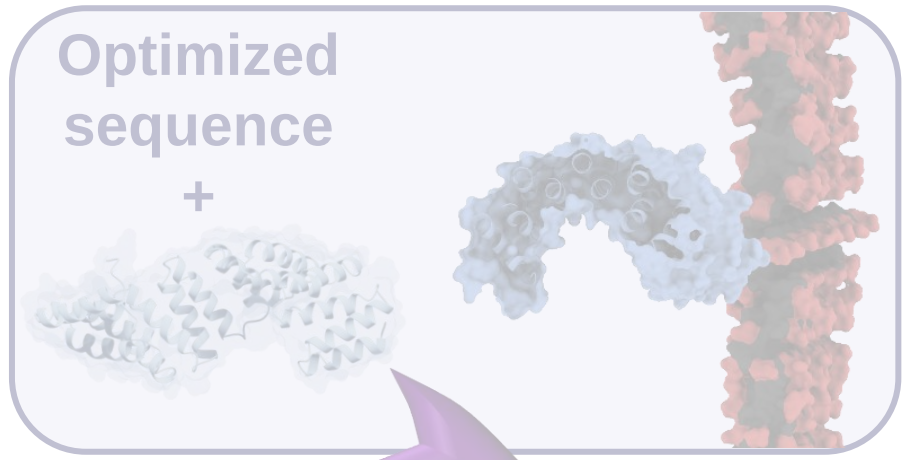






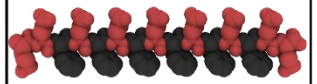
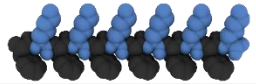
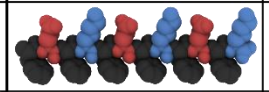
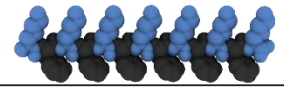
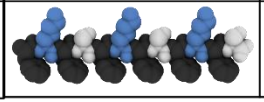
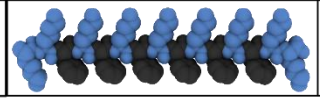
Bioactivity=f(q)

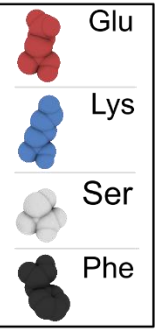
q	n
-9	1
-7	2
-6	3
-3	4
0	5
+3	6
+6	7
+7	8
+9	



Co-assembly

SPA Library with Charges: -9 – +9

Peptide	Charge	Name	Peptide	Charge	Name	Peptide	Charge	Name
	- 9	E9		- 3	E3		+ 6	K6
	- 7	E7		0	EK		+ 7	K7
	- 6	E6		+ 3	K3		+ 9	K9



Negative

Positive

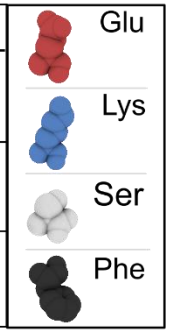
Polar

Hydrophobic

Sasselli, Alvarez, Cortajarena, *et al. Adv. Sci.* **2026**, *13*, e07946

SPA Library Screening using CG-MD

Peptide	Charge	Name	Peptide	Charge	Name	Peptide	Charge	Name
	- 9	E9		- 3	E3		+ 6	K6
	- 7	E7		0	EK		+ 7	K7
	- 6	E6		+ 3	K3		+ 9	K9

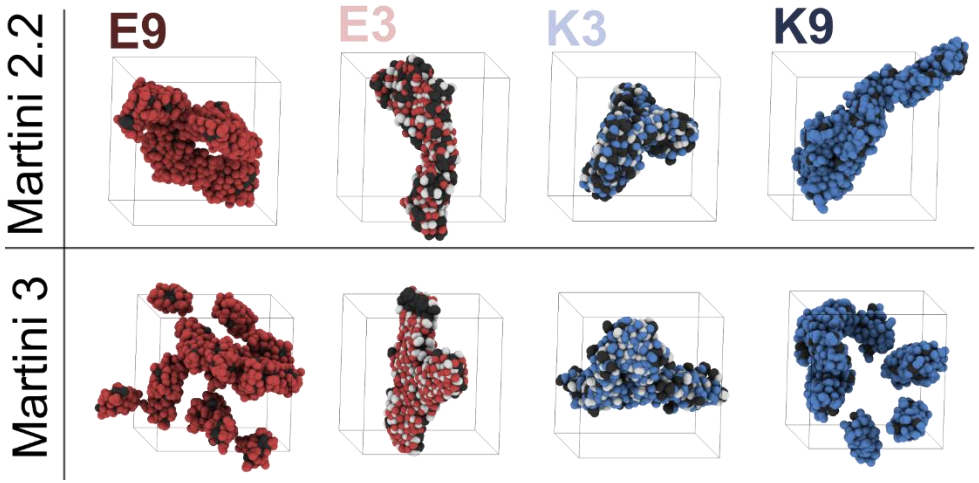


Negative

Positive

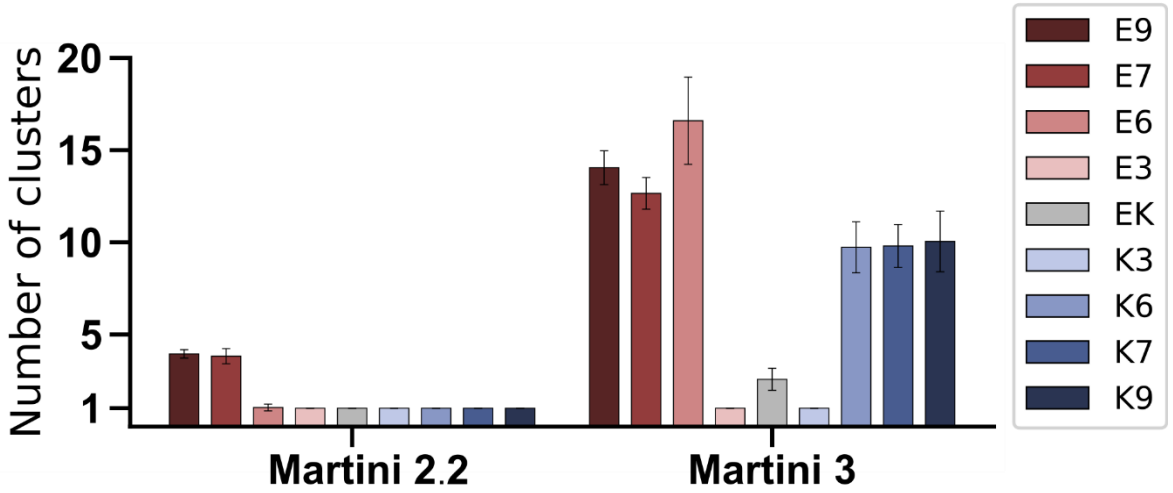
Polar

Hydrophobic



MARTINI 2.2 vs MARTINI 3 screening

- MARTINI 2.2: all SPAs self-assemble
- MARTINI 3: discrepancies at q ↑ (±6-9)



SPA Library Screening using CG-MD

Peptide	Charge	Name	Peptide	Charge	Name	Peptide	Charge	Name
	- 9	E9		- 3	E3		+ 6	K6
	- 7	E7		0	EK		+ 7	K7
	- 6	E6		+ 3	K3		+ 9	K9

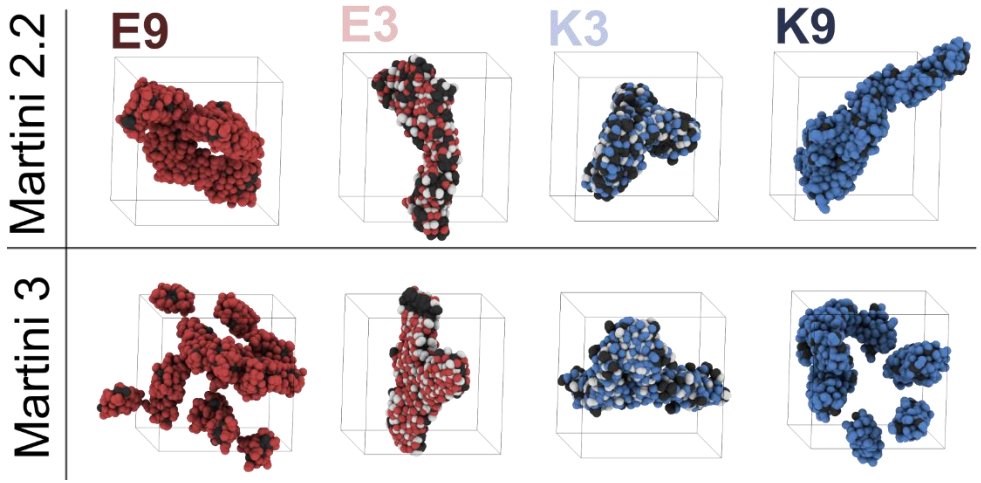
Glu
Lys
Ser
Phe

Negative

Positive

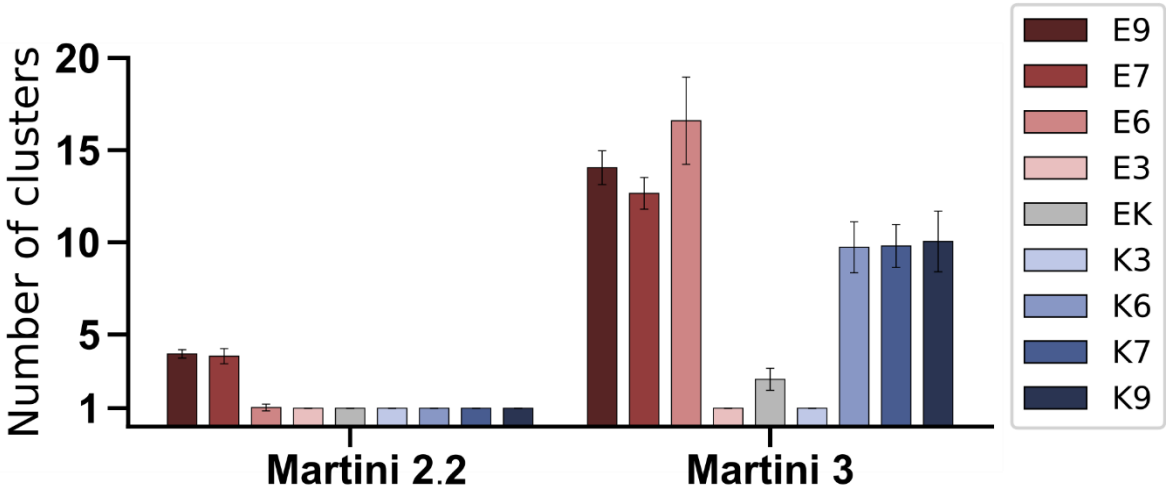
Polar

Hydrophobic



MARTINI 2.2 vs MARTINI 3 screening

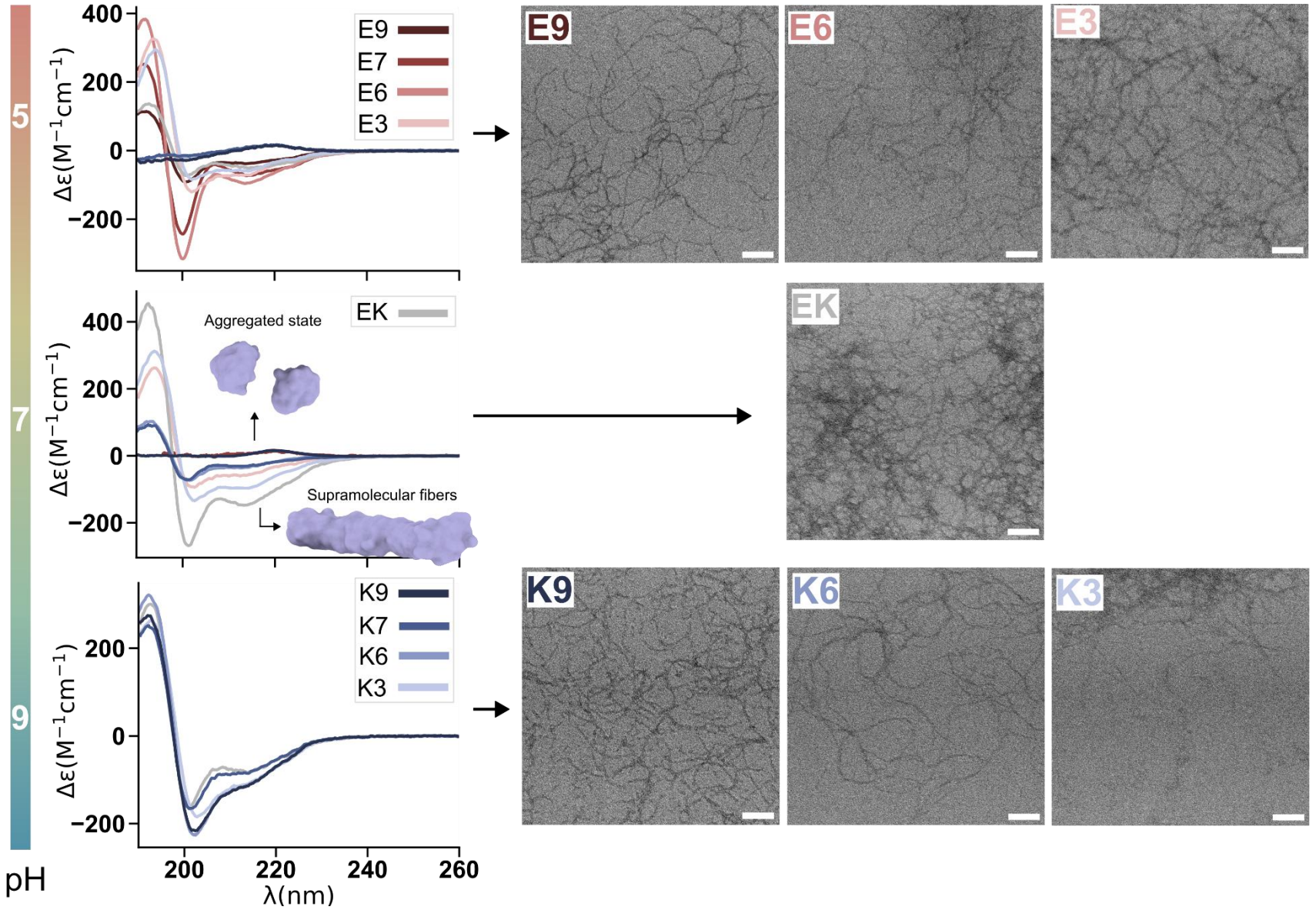
- MARTINI 2.2: all SPAs self-assemble
- MARTINI 3: discrepancies at q ↑ (±6-9)



***q* = ±6-9 → electrostatic repulsion @ pH 7**

- K (pk_a=10.53) → pH 9
- E (pk_a=4.25) → pH 5

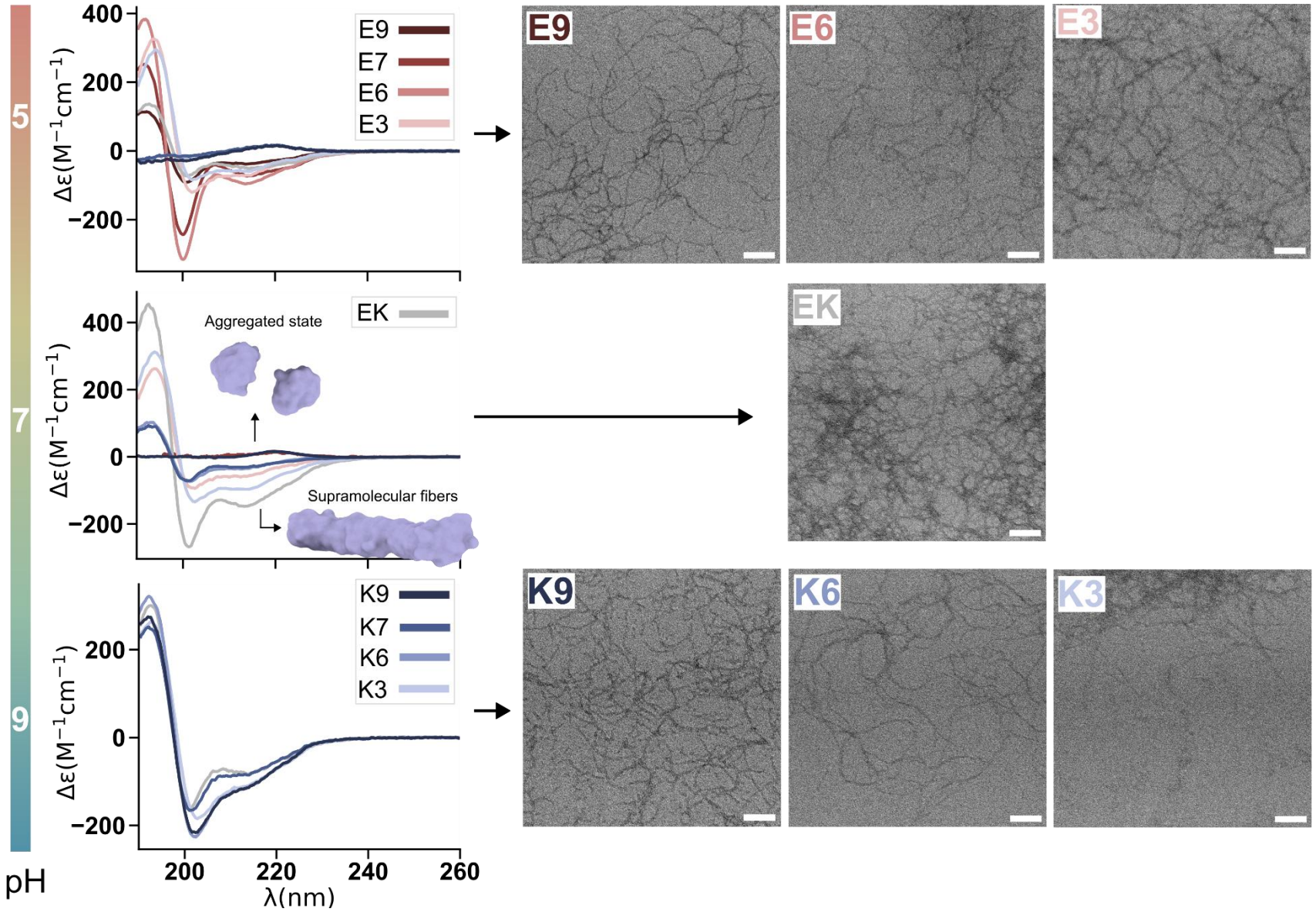
SPA Library – Experimental Characterization



All peptides form fibers:

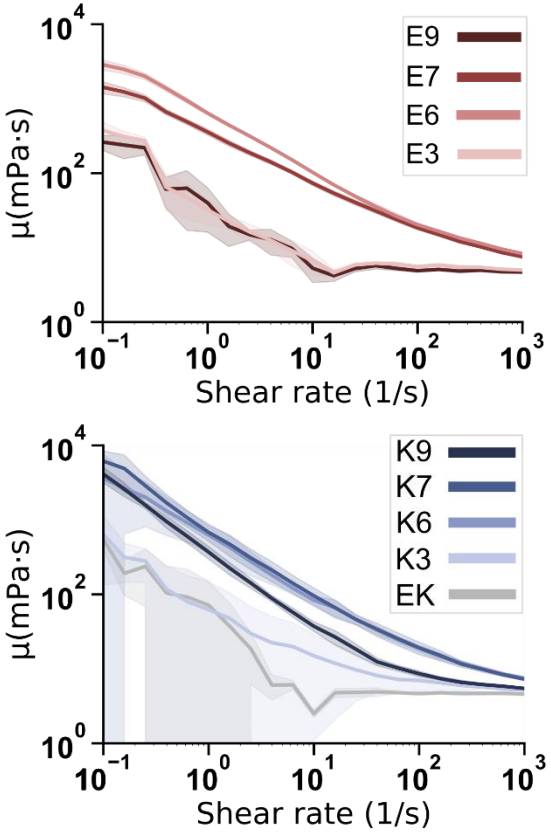
- ≈ size
- ≈ morphology
- ≈ intermolecular order

SPA Library – Experimental Characterization

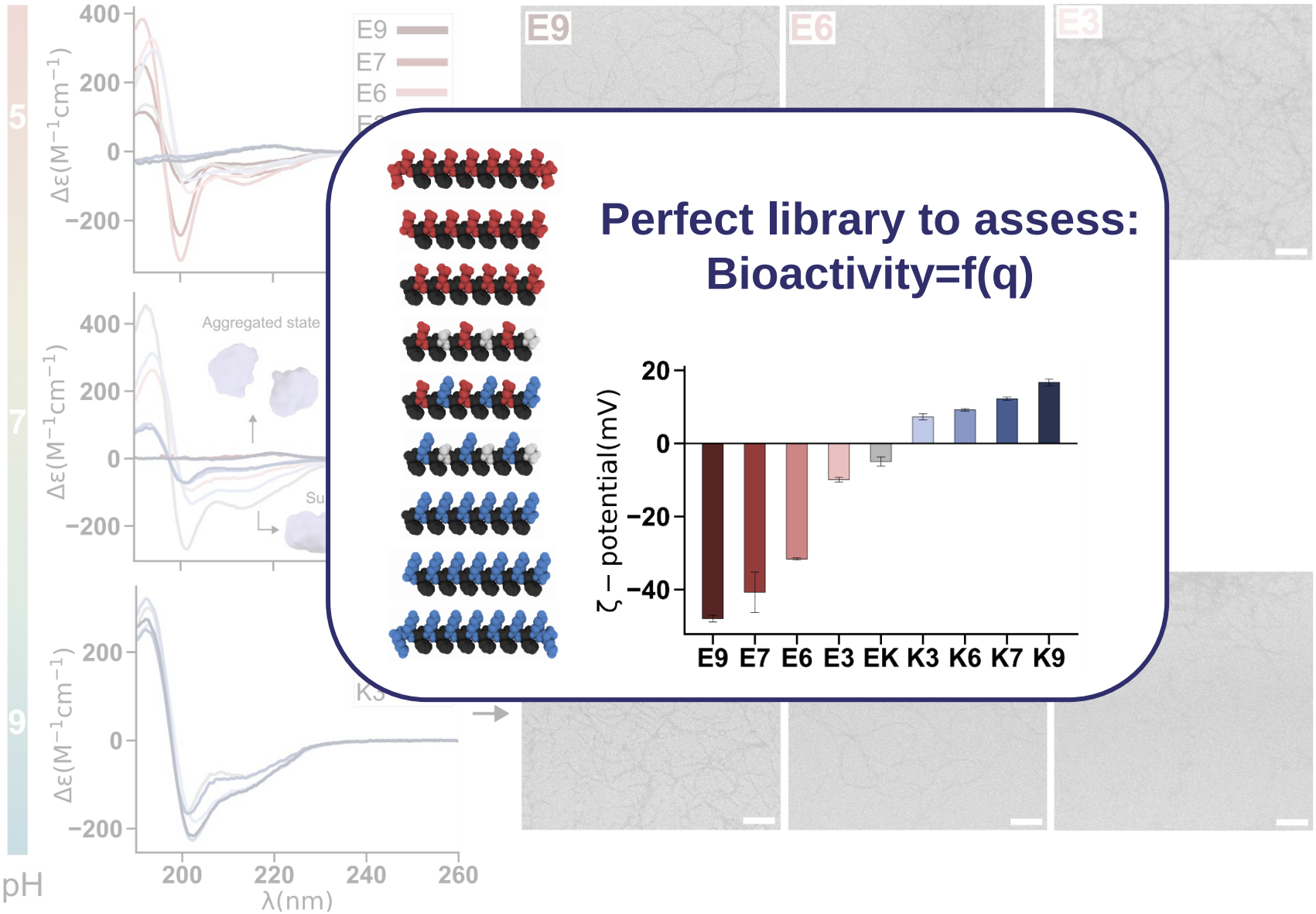


All peptides form fibers:

- ≈ size
- ≈ morphology
- ≈ intermolecular order
- ≈ mechanical properties



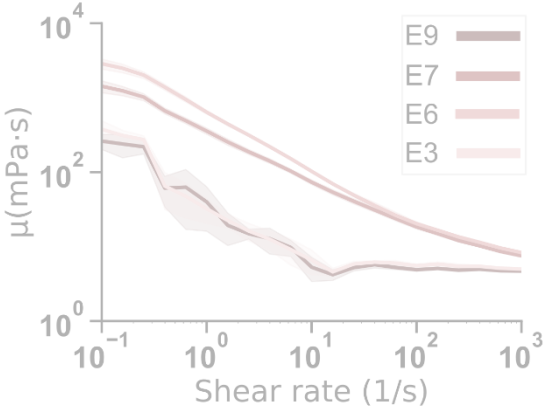
SPA Library – Experimental Characterization

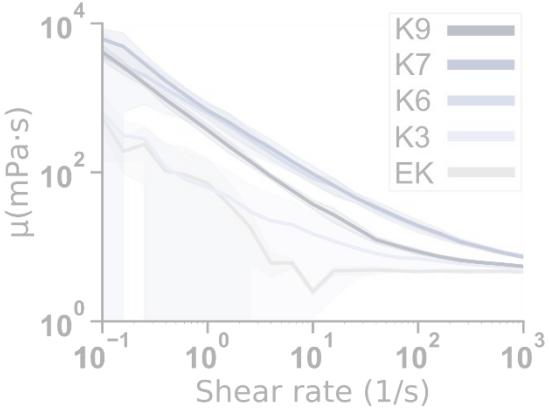


Perfect library to assess:
Bioactivity=f(q)

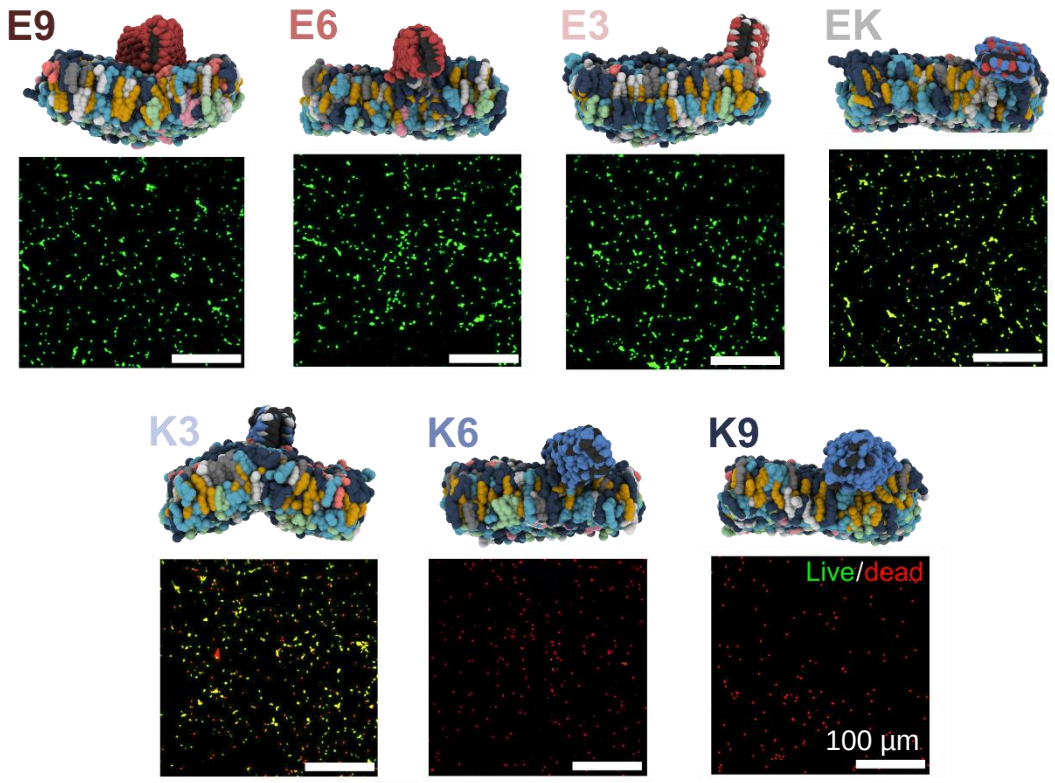
All peptides form fibers:

- ≈ size
- ≈ morphology
- ≈ intermolecular order
- ≈ mechanical properties



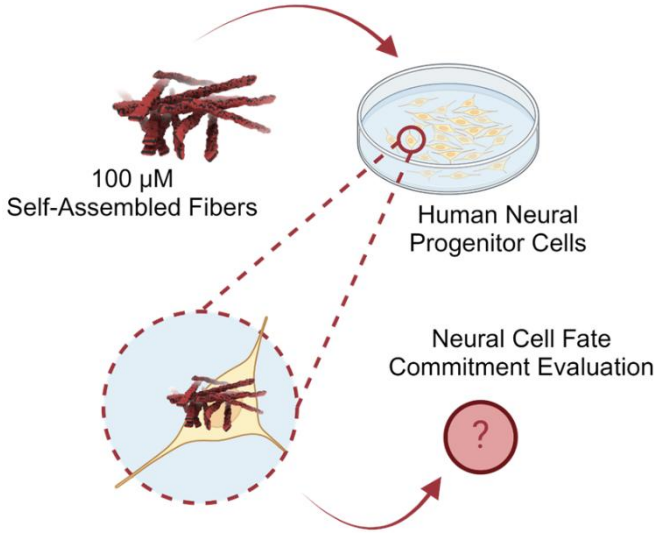


Electrostatics Modulates Cytotoxicity



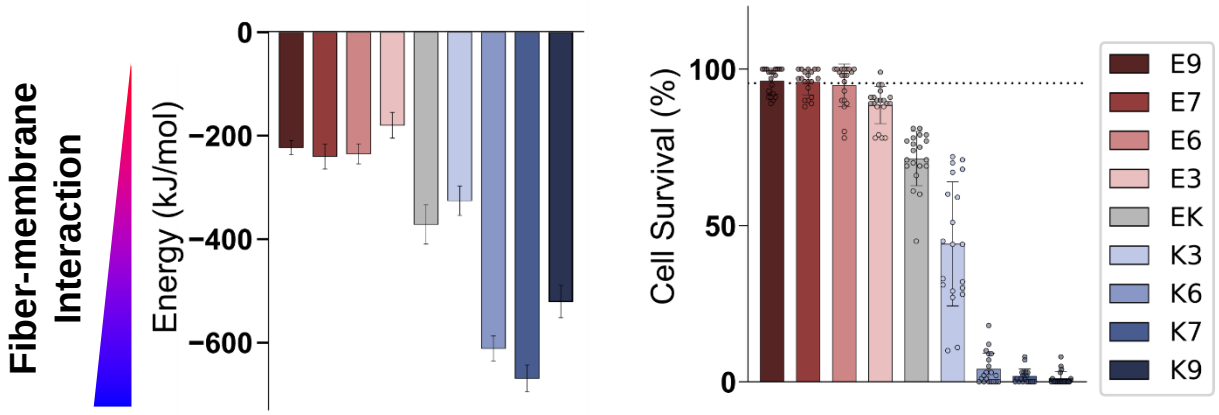


Zaida Alvarez



Charge affects survival:

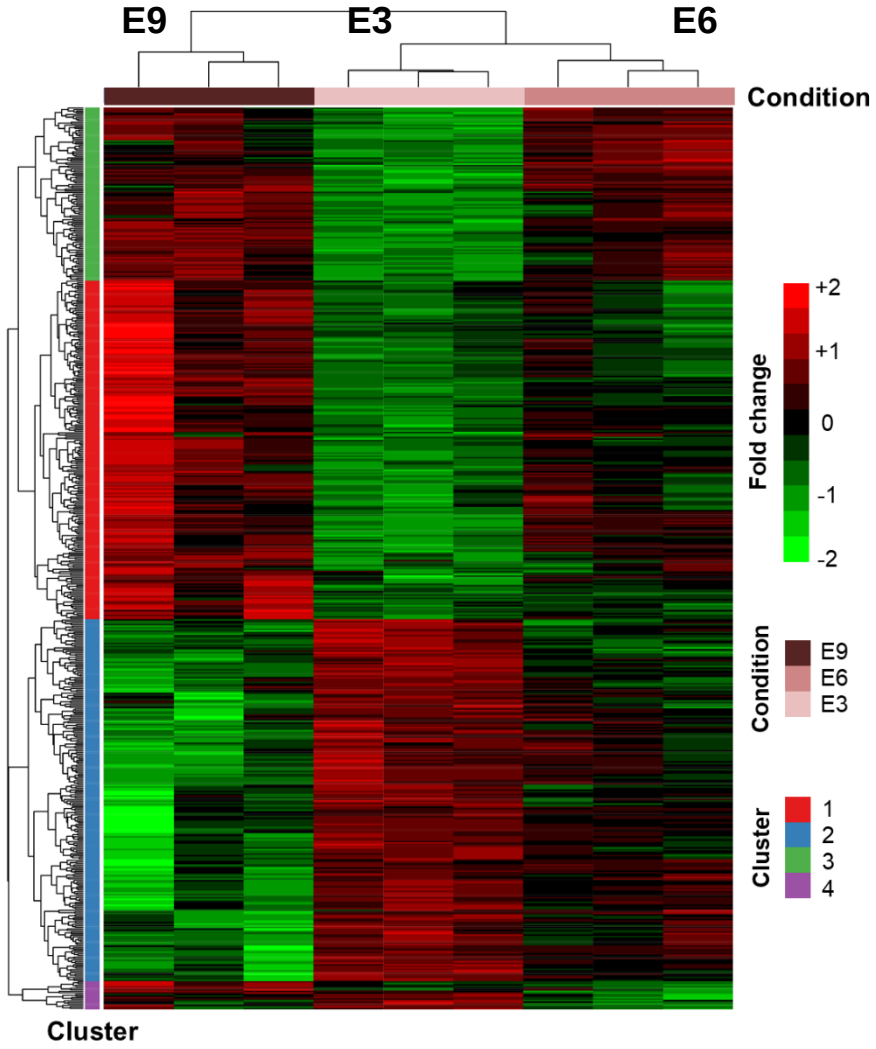
- Negative charges:
  - ↑ survival
- Positive charges:
  - ↑ interaction with membrane
  - ↑ cytotoxicity



Sasselli, Alvarez, Cortajarena, *et al. Adv. Sci.* **2026**, *13*, e07946

Electrostatics Modulates Bioactivity

Hierarchical clustering heatmap of differentially abundant proteins:

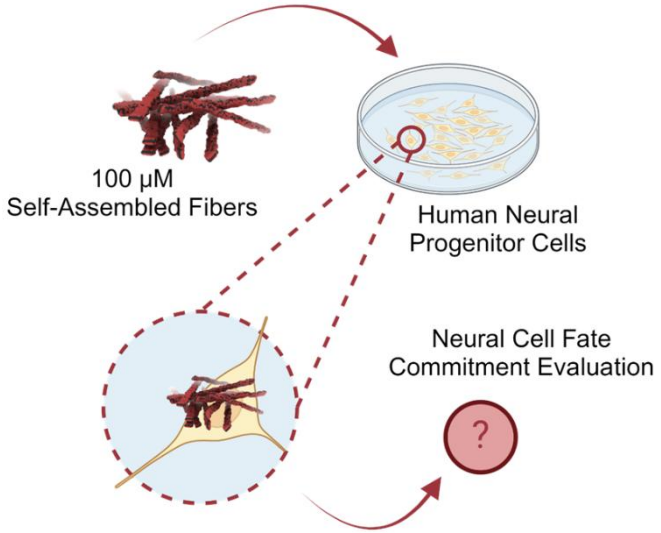


E3:

- ↑ metabolic adaptations
- ↑ stress responses

E9:

- ↑ cell-cell adhesion
- ↑ cell-substrate adhesion
- ↑ neuron projection development
- ↑ positive regulation of the MAPK cascade



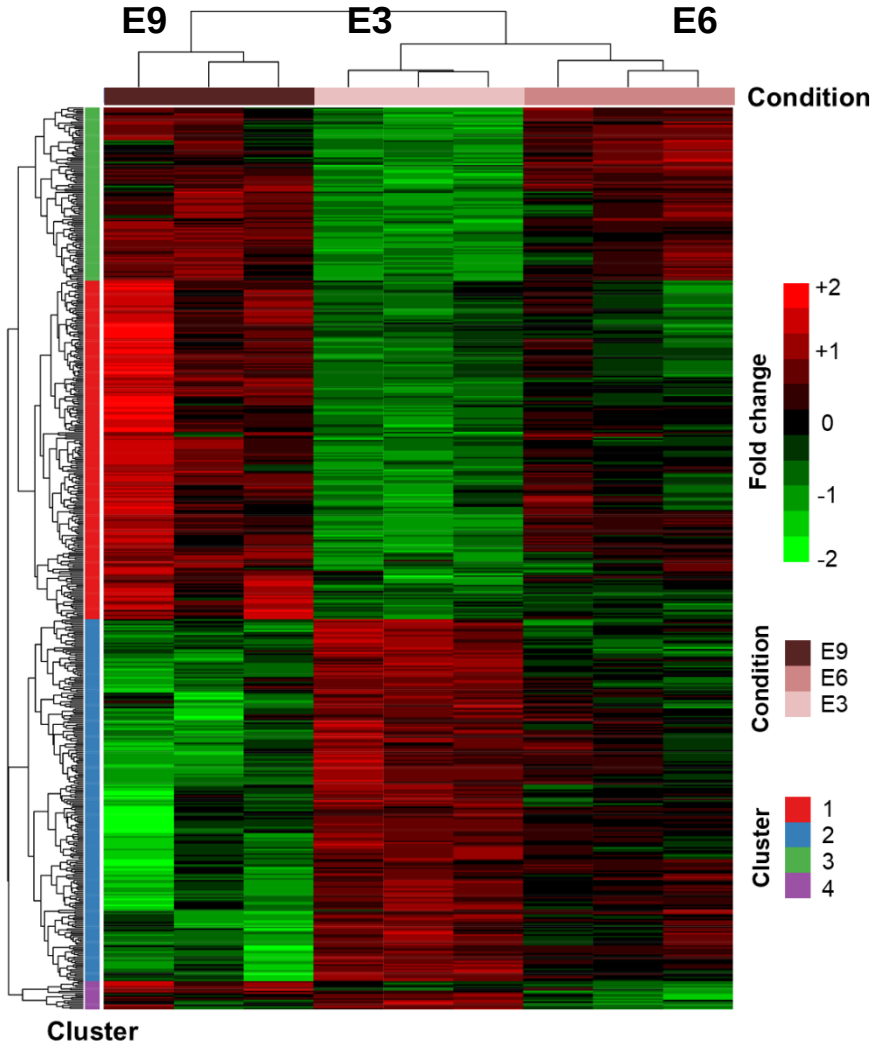


Zaida Alvarez

Sasselli, Alvarez, Cortajarena, *et al. Adv. Sci.* **2026**, *13*, e07946

Electrostatics Modulates Bioactivity

Hierarchical clustering heatmap of differentially abundant proteins:

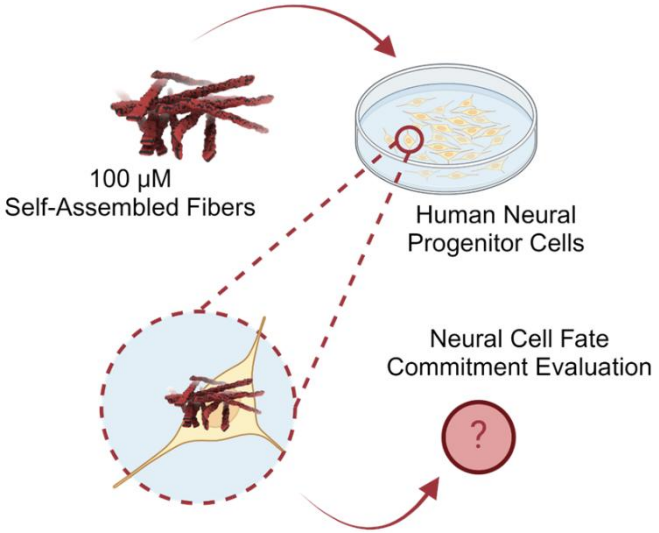


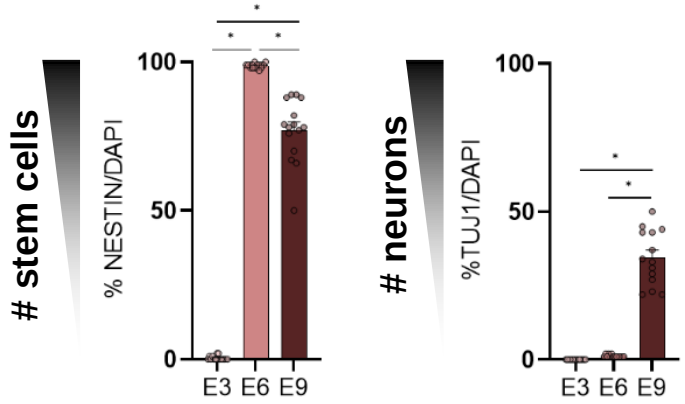
E3:

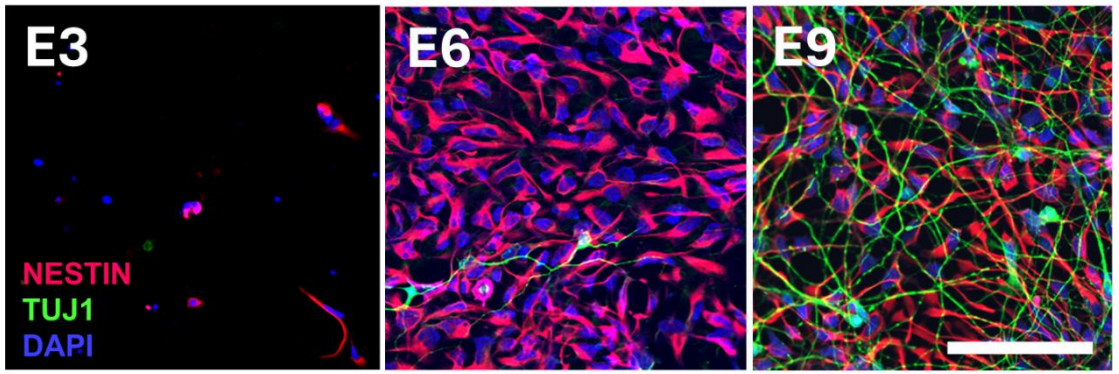
- ↑ metabolic adaptations
- ↑ stress responses

E9:

- ↑ cell-cell adhesion
- ↑ cell-substrate adhesion
- ↑ neuron projection development
- ↑ positive regulation of the MAPK cascade

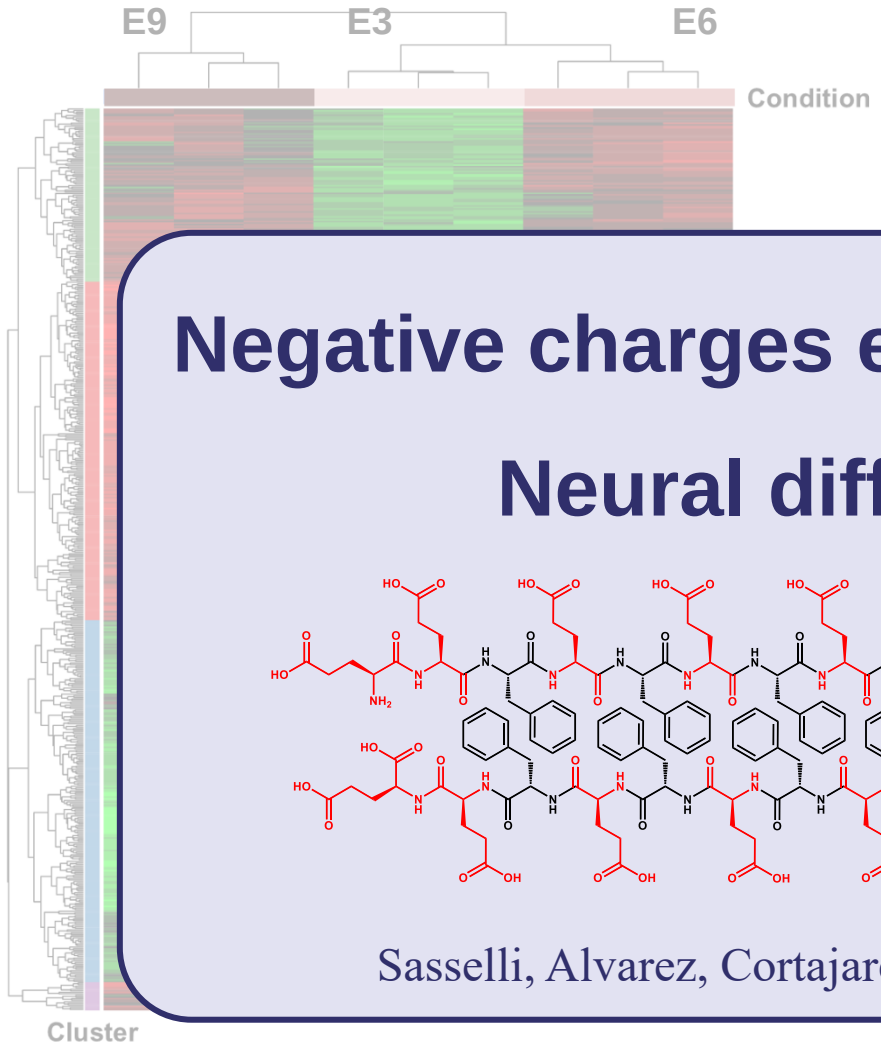






Electrostatics Modulates Bioactivity

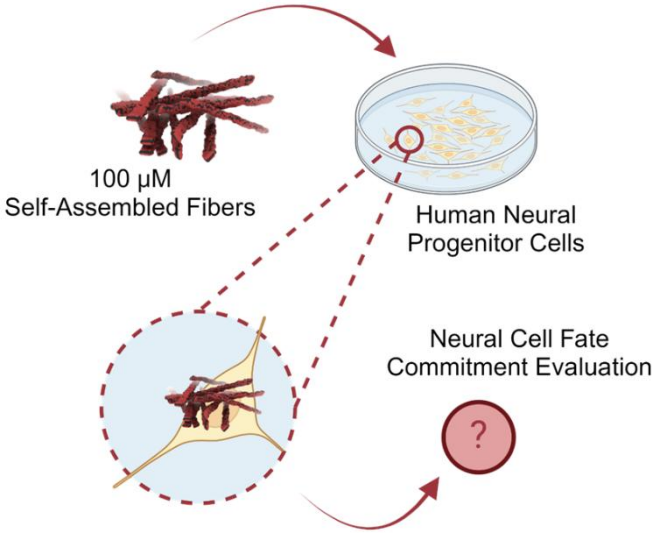
Hierarchical clustering heatmap of differentially abundant proteins:



E3:

- ↑ metabolic adaptations
- ↑ stress responses

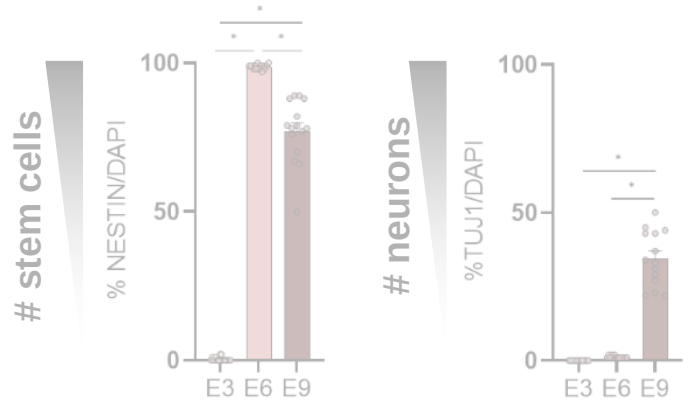
E9:

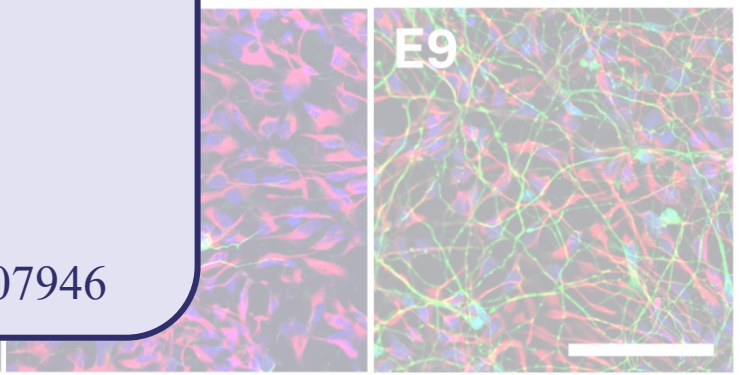


Negative charges enhance bioactivity:

Neural differentiation

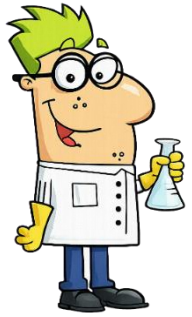
Sasselli, Alvarez, Cortajarena, *et al. Adv. Sci.* **2026**, *13*, e07946



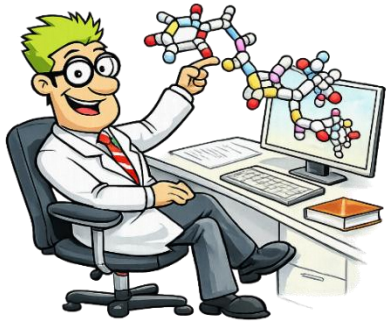


Take Home Messages

Ivan R. Sasselli
i.sasselli@csic.es

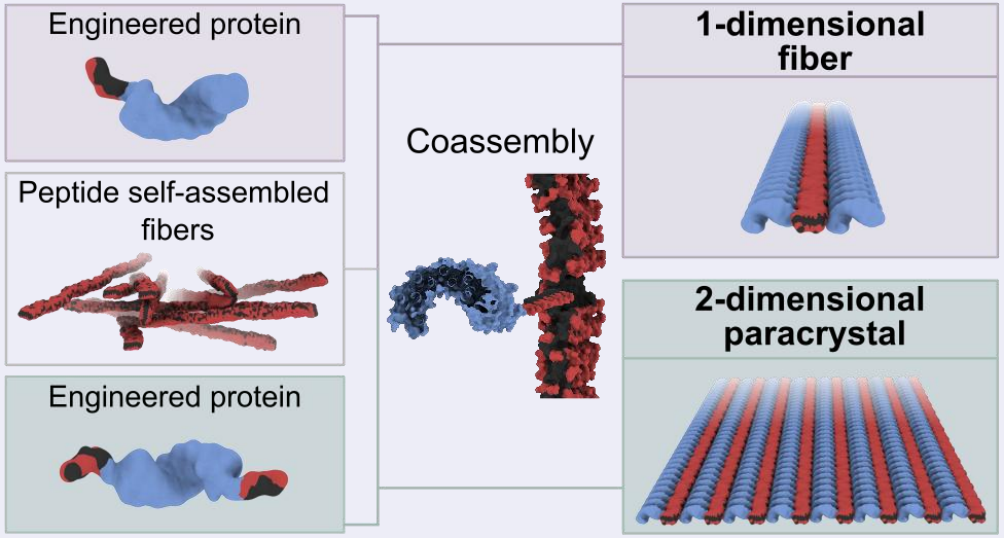


Computational/Experimental Symbiosis:



Design of Complex Architectures

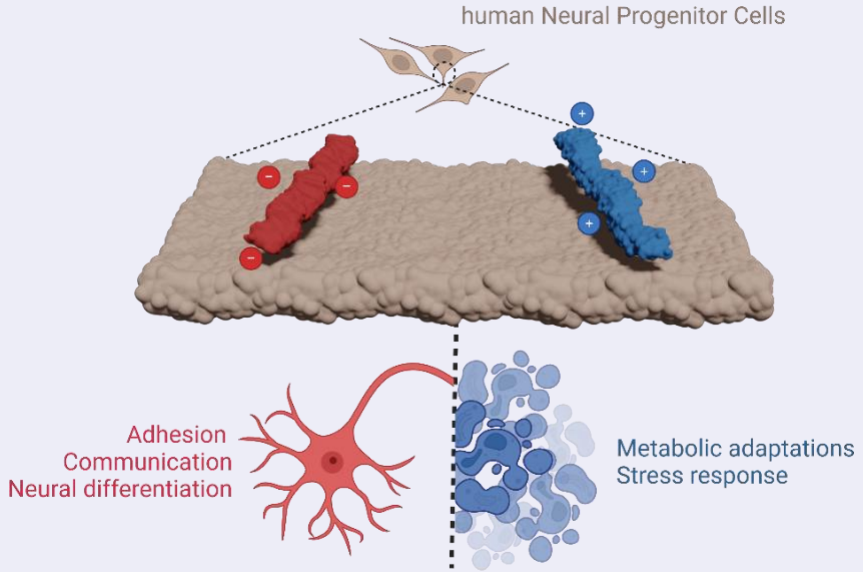
→ 2D Protein-Peptide Co-assemblies



Cortajarena, Sasselli, *et al.*
ACS Nano **2025**, *19*, 16500.

Library of peptides (q= -9 – +9):

→ Electrostatics Effect in Bioactivity



Sasselli, Alvarez, Cortajarena,
et al. Adv. Sci. **2026**, *13*, e07946



The Team:

- **Sebastian Jimenez Millan**
- **Irene Carbajo de la Guerra**
- **Irene Toledo Alday**

Alumni:

- **Laura Perez-Chirinos Lallana**

Materials Physics Center
Centro de Física de Materiales

CSIC
Consejo Superior de Investigaciones Científicas

MINISTERIO DE CIENCIA, INNOVACIÓN Y UNIVERSIDADES

AGENCIA ESTATAL DE INVESTIGACIÓN

Gipuzkoako Foru Aldundia
Diputación Foral de Gipuzkoa

CNS2025-166365
2025-IZEN-000015-01
PID2022-136392NA-I00
RYC2021-033294-I
2019-FELL-000017-01

cost
EUROPEAN COOPERATION IN SCIENCE & TECHNOLOGY

SNOOPY

www.cost-snoopy.eu

CA23111

Collaborators

Zaida Alvarez Pinto	**IBEC**
Aitziber L. Cortajarena	**CIC biomaGUNE**
Siewert Marrink	**University of Groningen**
Daniela Kalafatovic	**University of Rijeka**
Ana M. Garcia	**UCLM**
Elena Pazos	**CICA**
Carolina Horta Andrade	**Univ. Federal de Goias**
Oliver Dumele	**University of Koln**
Alberto Ortega	**University of Barcelona**
Goran Mausa	**University of Rijeka**
Fouzia Boulmedais	**ICS – CNRS**
Jennifer Rodon	**ICS – CNRS**

Ivan R. Sasselli
i.sasselli@csic.es

Discovery of novel peptide-GPCR signalling systems across evolutionary domains

Luuk R. H. Dijkhof[1], Teemu K.E. Rönkkö[1], Marin Matic[1], & Alexander S. Hauser[1]

https://doi.org/10.17952/38EPS.2026.O63

Department of Drug Design and Pharmacology, Center for Pharmaceutical Data Science Education, University of Copenhagen, 2100 Copenhagen, Denmark

Oral contribution to the EPS 2026 Conference Proceedings

Abstract. Peptide signalling through G protein-coupled receptors (GPCRs) underlies fundamental physiological processes and has repeatedly provided starting points for therapeutic innovation. Yet the canonical set of human peptide hormones represents only a small fraction of the sequence space capable of engaging GPCRs. Here, I summarize a strategy for expanding peptide–receptor discovery beyond annotated human hormones by combining evolutionary and metagenomic sequence mining, structure-aware prediction, benchmarking, and experimental pharmacology. A receptor-aware benchmark shows that modern structure-prediction approaches can discriminate cognate peptide–GPCR pairs from challenging decoys, and that rescoring local receptor–peptide interfaces can further improve classification. Applying related concepts to the human gut microbiome identifies candidate molecular mimics of endogenous peptide hormones, including a microbial peptide with agonist activity at melanocortin receptors. Together, these studies illustrate how evolutionary diversity, computational prioritization and scalable pharmacology can be integrated to uncover previously hidden peptide signalling systems.

Introduction

G protein-coupled receptors (GPCRs) form one of the largest families of cell-surface receptors and translate a remarkable diversity of extracellular signals into intracellular responses. Approximately 800 GPCRs are encoded by the human genome, with hundreds of approved medicines acting on this receptor family. Peptides are particularly important GPCR ligands: they combine high potency and selectivity with a vast, evolutionarily diversified chemical and sequence space. Classic examples also show that useful peptide pharmacology need not originate from humans. Exendin-4 from Gila monster saliva helped establish the therapeutic potential of GLP-1 receptor agonism, salmon calcitonin has been used clinically, and microbial or venom-derived peptides can engage human receptors with striking specificity.[1–3]

At the same time, peptide discovery is undergoing a change in scale. Genome and transcriptome sequencing, metagenomics, peptidomics and improved annotation of small open reading frames are revealing large numbers of secreted or potentially bioactive peptides that are absent from canonical hormone catalogues. Recent work has demonstrated that precursor-first and genome-first discovery can uncover peptides with strong physiological effects even before their cognate receptor is known. The emerging bottleneck is therefore increasingly not whether candidate peptides exist, but how to identify their receptor targets and signalling profiles efficiently.[4–6]

Our approach treats this as a peptide–receptor pairing problem, where computational models can prioritize receptor pairs for experimental testing. A central requirement is rigorous benchmarking: models must distinguish genuine interactions not only from obviously unrelated peptides, but also from biologically plausible alternatives that resemble true ligands or target related binding pockets.

Results and Discussion

Benchmarking peptide–GPCR interaction prediction

A useful benchmark must reflect the many-to-many architecture of peptide signalling: individual peptides may activate multiple receptors, while individual receptors may respond to more than one endogenous ligand. We assembled a benchmark centred on 124 known positive peptide–GPCR interactions. For each receptor, negative examples were selected in two deliberately different regimes. Five dissimilar decoys were sampled from principal agonists of GPCRs with less than 35% sequence similarity, whereas five challenging decoys were drawn from principal agonists of receptors with the most similar binding pockets. The resulting dissimilar and similar decoys had mean binding-pocket similarities of approximately 20% and 62%, respectively. This design asks models to solve both an easier interaction-recognition problem and a more pharmacologically meaningful discrimination problem among related receptor environments.

We compared sequence- and structure-based approaches using model-appropriate confidence or interaction scores, including AlphaFold-derived complex confidence, ESMFold/NeuralPLexer confidence, D-SCRIPT interaction probability and structure-based error metrics. The benchmark highlighted strong discriminatory power from approaches that exploit evolutionary information and showed that performance depends substantially on the difficulty of the decoy set. This is important for prospective discovery: a model that separates a cognate ligand from random peptides may still fail when confronted with related peptide systems.[7]

We therefore asked whether the predicted complex could be evaluated at the local receptor–peptide interface rather than by global confidence alone. Rescoring strategies based on local interaction scores, energetic terms and graph-neural-network representations improved the ability to surface true binders from decoys. In the presented benchmark, interface-focused rescoring improved ROC performance by about 0.11. These results support a practical two-stage strategy in which co-folding proposes plausible complexes and local interface models provide an additional filter before experimental testing. The broader implication is that structural prediction is most useful when embedded in a benchmarked ranking framework rather than interpreted as a binary claim of binding.

Microbial peptide mimics as an emerging signalling space

Evolution has repeatedly generated peptides that interact with conserved human receptor architectures, including peptides from animals, plants, microorganisms, venoms, and population variability (**Figure 1**). This motivates systematic searches across biodiversity for sequence or structural motifs compatible with human GPCRs. Candidate-generation strategies can combine profile hidden Markov models, sequence similarity, structural searches, secretion signals and precursor context before moving to receptor co-folding and experimental pharmacology. For disulfide-rich venom peptides such as conotoxins, cysteine connectivity and topology provide an additional layer of information that can be incorporated into prediction. Here we employ structure-aware models because peptide sequence similarity alone can be weak even when receptor engagement is conserved.[2,3]

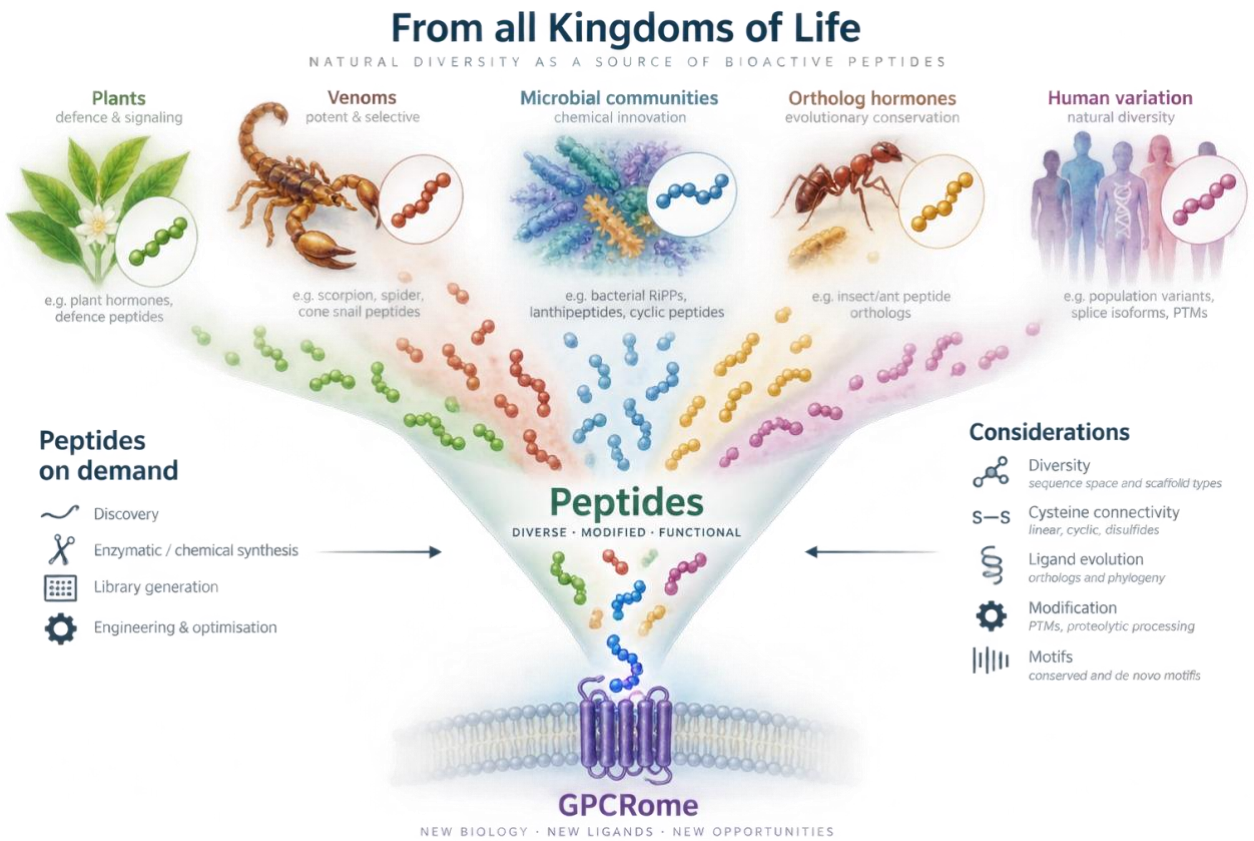


Figure 1: Nature-derived diversity as a source of bioactive peptides targeting GPCRs. Peptide candidates from plants, venoms, microbial communities, evolutionary hormone orthologs and human variation provide diverse sequence and structural space for discovery, engineering and experimental screening against the GPCRome.

The human gut microbiome provides a particularly compelling test case because microbial molecules are continuously produced in close proximity to the host. Gut bacteria are already known to generate small molecules and peptides that resemble or modulate human signalling systems. We therefore developed an in silico workflow that starts from shotgun metagenomic sequence data, translates the microbial sequence space into candidate proteins and searches for peptide segments that mimic endogenous human ligands. In the presented analysis, approximately 150 million gut microbial proteins were searched using endogenous human peptides as reference signals, followed by AlphaFold 3-based co-folding, local rescoring, and prioritization against candidate GPCR targets.[8,9]

This procedure yielded 89 tentative microbial peptide candidates spanning 11 GPCR families. These candidates are hypotheses rather than established endogenous microbial ligands, but they demonstrate the scale of the accessible search space. Initial experimental testing provided a first proof of principle: one gut microbial peptide showed agonist activity at melanocortin receptors in cell-based dose–response experiments. The observation is notable because melanocortin signalling participates in processes ranging from inflammatory regulation to energy homeostasis. Whether such microbial peptides reach relevant concentrations, compartments, and receptors *in vivo* remains unresolved and will require additional physiological experiments.

This example is therefore a demonstration of a discovery route that may lead to the discovery of novel microbiome-to-host physiology. Metagenomic sequence space can be reduced from hundreds of millions of proteins to a tractable set of structurally plausible receptor–peptide pairs, which can then be tested experimentally. Similar workflows can be extended to other microbial communities and to biodiversity-derived peptide libraries from different domains of life.

Perspective

Taken together, these studies suggest a general framework for peptide discovery. Evolution supplies candidate ligands far beyond the canonical human hormone set. Benchmarked computational models narrow the receptor pairs worth testing and local interface scoring can add resolution when related receptors or ligands create difficult decoys. Experimental validation remains essential, particularly because structural confidence does not establish receptor activation, potency, efficacy or physiological exposure. The most productive role of current AI and structure-prediction methods is therefore as prioritization engines coupled tightly to pharmacology. As sequence databases, metagenomic cohorts and structural models continue to expand, this integration should make it increasingly feasible to map previously inaccessible regions of the peptide–GPCR signalling landscape.

Acknowledgements

This research was funded by Biodiversa+, the European Biodiversity Partnership, in the context of the ‘Biodiversity2Drugs’ project under the 2023-2024 BiodivNBS joint call and the Innovation Fund Denmark. We also acknowledge support by the Carlsberg Foundation (grant CF20-0248). We also acknowledge collaborators and partners across the peptide-discovery network, including Christian Gruber, Markus Muttenthaler, Dominik J. Windisch. We thank the EPS 2026 organizers for the invitation and discussion.

References

1. Sánchez Lorente, J. et al. GPCR drug discovery: new agents, targets and indications. Nat. Rev. Drug Discov. 24, 458–479 (2025).
2. Hermes, J. et al. Peptide ligand discovery of G protein-coupled receptors. Nat. Rev. Methods Primers 6, 52 (2026).
3. Gruber, C. W. et al. Biodiversity2Drugs—Renaissance of exploring nature-derived peptides for GPCR ligand discovery. Br. J. Pharmacol. 182, 3691–3694 (2025).
4. Foster, S. R. et al. Discovery of human signaling systems: pairing peptides to G protein-coupled receptors. Cell 179, 895–908.e21 (2019).
5. Coassolo, L. et al. Prohormone cleavage prediction uncovers a non-incretin anti-obesity peptide. Nature 641, 192–201 (2025).
6. Deutsch, E. W. et al. Expanding the human proteome with microproteins and peptideins. Nature 654, 813–825 (2026).
7. Hoegen Dijkhof, L. R., Rönkkö, T. K. E., von Vegesack, H. C., Lenzing, J. & Hauser, A. S. Deep learning in GPCR drug discovery: benchmarking the path to accurate peptide binding. Brief. Bioinform. 26, bbaf186 (2025).
8. Cohen, L. J. et al. Commensal bacteria make GPCR ligands that mimic human signalling molecules. Nature 549, 48–53 (2017).
9. Fan, Y. et al. Polypeptides synthesized by common bacteria in the human gut improve rodent metabolism. Nat. Microbiol. 10, 1918–1939 (2025).

POSTERS

Parallel-Stranded Design of Peptide Nucleic Acids for Efficient Recognition of Double-Stranded DNA

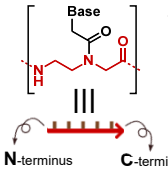
○**Yuichiro Aiba**,[1,*] Masanari Shibata,[2] Hiroshi Sugimoto,[3] Osami Shoji[1,*]

[1)] Graduate School of Science, Nagoya University, [2)] Research Center for Materials Science, Nagoya University, [3)] RIKEN SPring-8 Center

https://doi.org/10.17952/38EPS.2026.P444

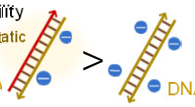
1. Introduction

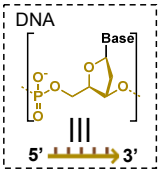
❑ Peptide Nucleic Acid (PNA) [1]



- electrostatically-neutral backbone
- stable duplex formation with DNA [2]

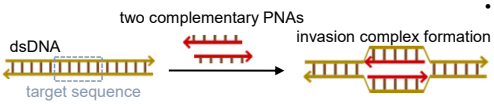
Thermal stability





Ref: [1] P. E. Nielsen *et al.*, *Science* **1991**, *254*, 1497. [2] M. Egholm *et al.*, Nature **1993**, *365*, 566.

❑ Double-duplex invasion by PNAs



PNAs can directly recognize target sequences in dsDNA.

This PNA invasion is expected to be a powerful tool for controlling dsDNA functions.

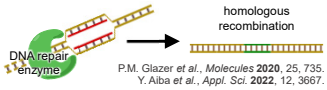
Applications

- Control of gene expression



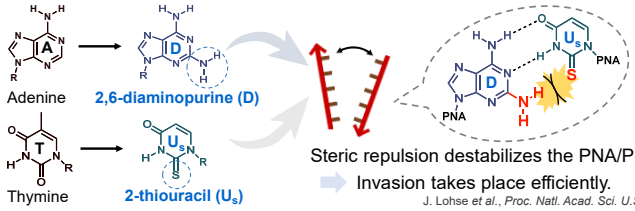
J. Lohse *et al.*, *Proc. Natl. Acad. Sci. USA.* **1999**, *96*, 11804..

- Genome editing



P.M. Glazer *et al.*, *Molecules* **2020**, *25*, 735.
Y. Aiba *et al.*, *Appl. Sci.* **2022**, *12*, 3667.

❑ Use of modified nucleobases (pseudo-complementary PNAs)



Steric repulsion destabilizes the PNA/PNA duplex.

Invasion takes place efficiently.

J. Lohse *et al.*, *Proc. Natl. Acad. Sci. U.S.A.* **1999**, *96*, 11804.
M. Komiyama, Y. Aiba *et al.*, *Nat. Protoc.* **2008**, *3*, 646,

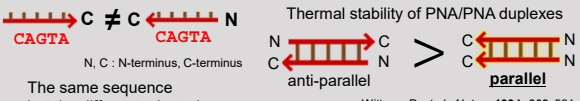
Problems

- Oligomer synthesis requires PNA monomers specially modified with unique nucleobases
  ➡ **Synthetic techniques are required**
- Not applicable to automatic synthesizers, limited to manual synthesis (Boc-protection)
  ➡ **Time-consuming and laborious**

Research aim: Development of a simple and accessible PNA invasion method (**using PNAs with natural nucleobases**)

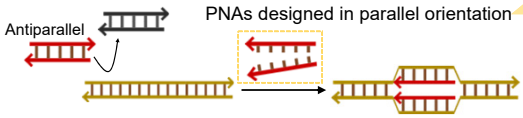
2. Strategy

Suppression of self-duplex formation by changing the orientation of nucleic acids



Wittung, P. *et al.*, *Nature* **1994**, *368*, 561.

▪ Approach in this study



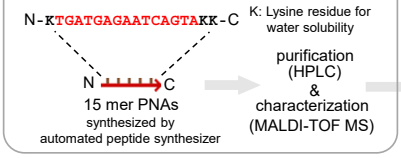
This approach does not require the modified nucleobases (pcPNAs).

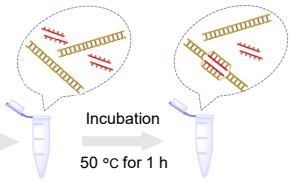
M. Shibata, **Y. Aiba** *et al.*, *RSC Chem. Biol.*, **2025**, *6*, 1566.

3. Results and Discussion

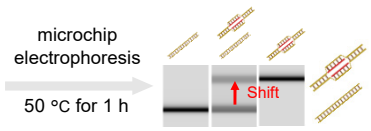
❑ Outline of invasion experiments

Synthesis of PNA oligomer
(Fmoc solid-phase peptide synthesis)



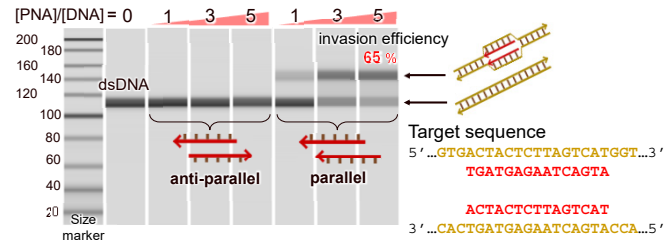


Conditions:
[DNA (119 bp)] = 100 nM
[each PNAs] = 100 - 500 nM
[HEPES (pH = 7.0)] = 5 mM



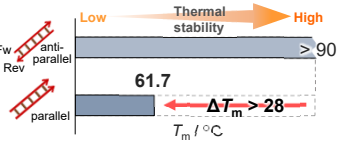
The formation of invasion complex was evaluated by EMSA.

❑ Evaluation of the invasion complex formation

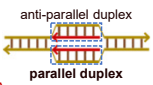


This result is the first reported instance of successful double-duplex invasion without the use of any modified nucleobases.

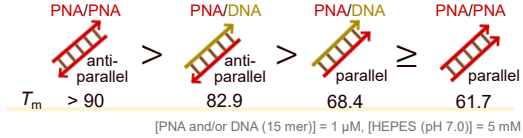
❑ Melting temperature analysis of PNA/PNA duplex



sequences of PNAs (15 bp)
Fw: ACTACTCTTAGTCAT
Rev: TGATGAGAATCAGTA



Thermal stability of PNA/PNA and PNA/DNA duplexes

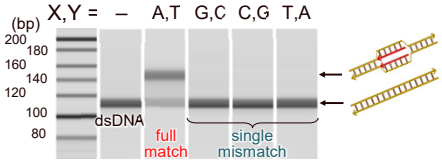


[PNA and/or DNA (15 mer)] = 1 μM, [HEPES (pH 7.0)] = 5 mM

The suppression of PNA/PNA duplex formation was effectively achieved as designed in parallel orientation.

❑ Mismatch sequence discrimination

Conditions: [DNA (119 bp)] = 100 nM, [each PNA] = 500 nM, [HEPES (pH = 7.0)] = 5 mM at 50 °C for 1 h.



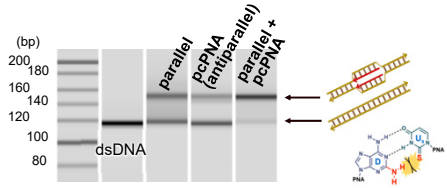
Single mismatch was introduced at the center of the target sequence.

5'...GTGACTACTCTAGTCATGGT...3'
TGATGACXATCAGTA
ACTACTCYAGTCAT
3'...CACTGATGACATCAGTACCA...5'

PNAs containing a single mismatch did not form an invasion complex.

➡ Parallel-stranded PNAs recognize dsDNA with high sequence selectivity.

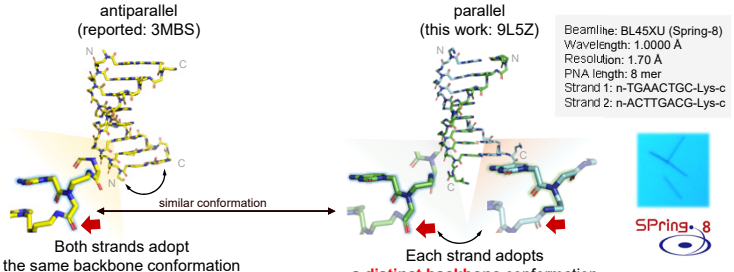
❑ Parallel design + pseudo-complementary nucleobases



Sequences of PNAs
parallel
C-TGATGAGAATCAGTA-N
C-ACTACTCTTAGTCAT-N
pcPNA (antiparallel)
N-TGATGD GAAUSCAGTA-C
C-ACTACUSCTTD GTCAT-N
parallel + pcPNA
C-TGATGD GAAUSCAGTA-N
C-ACTACUSCTTD GTCAT-N

Parallel invasion is effective even when combined with modified nucleobases.

❑ X-ray crystal structure of parallel PNA/PNA duplex



➡ The first crystal structure of parallel-stranded PNA/PNA was reported, revealing distinct structural differences compared to its antiparallel counterpart.

4. Summary

- ✓ Parallel-stranded PNAs form the invasion complex with dsDNA.
- ✓ High sequence specificity enables single mismatch discrimination of target sequences.
- ✓ The first crystal structure of a parallel-stranded PNA/PNA duplex was determined, revealing structural differences from its antiparallel counterpart.

M. Shibata, H. Sugimoto, M. Hibino, O. Shoji*, **Y. Aiba***, *RSC Chem. Biol.*, **2025**, *6*, 1566 (***outside back cover***).

Analogs of [D-Phe^4]CJ-15,208 with Modifications to Improve Kappa Opioid Receptor Antagonist Potency in the CNS as Potential Treatments for Substance Abuse

Jane V. Aldrich[1], Jeremy S. Coleman[1], Moustafa Hamaad[1], Brian I. Knapp[3], Ryosuke Shinouchi[2], Megan B. Quinones[2], Andrew Watson[2], Shainnel O. Eans[2], Jean M. Bidlack[3] & Jay P. McLaughlin[2]

Departments of [1]Medicinal Chemistry and [2]Cellular and Systems Pharmacology, College of Pharmacy, University of Florida, Gainesville, FL, 32610, U.S.A.; [3]Department of Pharmacology and Physiology, University of Rochester, School of Medicine and Dentistry, Rochester, NY, 14642, U.S.A.

https://doi.org/10.17952/38EPS.2026.P304

Introduction

- We are exploring cyclic peptides with kappa opioid receptor (KOR) antagonist activity as potential treatments for relapse to substance abuse, specifically cocaine abuse.
  - Stress is a potent cause of relapse to drug-seeking behavior in abstinent individuals with substance use disorder. Stress exposure increases the levels of dynorphins, the endogenous KOR agonists.
  - KOR antagonists block KOR activation by the dynorphins and prevent stress-induced reinstatement of cocaine-seeking behavior in rodent models of cocaine use disorder (CUD).
- The macrocyclic tetrapeptide [D-Trp]CJ-15,208 is an orally active kappa opioid kappa opioid receptor (KOR) antagonist.[1]
  - Macrocyclic peptides are promising compounds for potential therapeutic development because they are stable to proteolytic degradation and can cross biological barriers.
  - Exploration of the structure-activity relationships (SAR) of [D-Trp]CJ-15,208 led to the identification of **[D-Phe^4]CJ-15,208** (*cyclo*[Phe^1-D-Pro-Phe-D-Phe^4]) as a 2nd-generation lead compound that is 6-fold more potent than [D-Trp]CJ-15,208 in a mouse model of CUD.[2]
  - Like [D-Trp]Cj-15,208 [D-Phe^4]CJ-15,208 undergoes rapid metabolism by human and mouse liver microsomes.[2]
- We are exploring the SAR of [D-Phe^4]CJ-15,208 to further improve its potency in the CNS after oral administration and improve its ADME properties.
  - Here we report the effects of amino acid substitution in position 1 on KOR affinity, metabolic stability and *in vivo* activity.

Methods

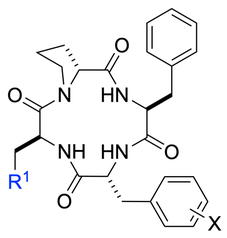
- **Synthesis.** Peptides were synthesized by a combination of solid phase peptide synthesis of the linear precursor peptides, followed by cyclization in solution as previously described and purified by normal phase flash chromatography plus reversed phase flash chromatography when needed.[2]
- **Metabolism**. The metabolic stability of the peptides (1 µM) was determined in human (HLM) and mouse liver microsomes (MLM; 1 mg/mL protein) by Curia Global, Buffalo, NY.
- ***In vitro* pharmacological evaluation.** KOR and mu opioid receptor (MOR) affinities and KOR antagonist activity in the cAMP assay were determined as previously described.[2] IC_{50} values represent antagonism of an IC_{80} concentration of U50,488 (10 nM) calculated from nonlinear regression analysis from 3-4 experiments, each performed in triplicate.
- ***In vivo* pharmacological testing.** Peptides were evaluated following oral (*per os*, p.o.) administration in a solution of 10%DMSO/10% Solutol/80% saline (0.9%) in the mouse 55 ºC warm water tail withdrawal (WWTW) assay as previously described.[2] KOR antagonism by the peptides was assessed against U50,488 administered either peripherally (10 mg/kg, i.p., -2.5 h) or centrally (30 nmol i.c.v. (intracerebroventricular), -2.5 h). To determine opioid receptor antagonist selectivity of the test peptides the mu or delta opioid receptor agonists morphine (10 mg/kg i.p.) and SNC-80 (100 nmol, i.c.v.) were administered in place of U50,488 and activity assessed.

  One peptide was evaluated for its ability to prevent reinstatement of stress-induced reinstatement of cocaine conditioned place preference (CPP) as previously described.[2]

  Statistical analysis as appropriate was performed with Prism 10.5 software by Student's t-test or one- or two-way ANOVA and further analyzed with appropriate post hoc tests.

Results

- We incorporated both aromatic and aliphatic amino acids in place of Phe^1 in [D-Phe^4]CJ-15,208 analog since Ala substitution of Phe^1 is tolerated in [D-Trp]CJ-15,208.[3]



Analogs of [D-Phe^4]CJ-15,208 with a substitution for Phe^1

- **KOR affinity, selectivity and antagonism**
  - Analogs containing an aromatic amino acid in position 1
    - Out of the more than 45 analogs >70% had a KOR affinity comparable to or higher than [D-Phe^4]Cj-15,208 ($K_i \leq 30$ nM) (Fig. 1)
    - KOR selectivity over mu opioid receptors (MOR) was generally modest (K_i (MOR)/K_i (KOR) $\leq$10)
      - Three analogs with high KOR affinity (K_i = 1-3 nM) exhibited much higher KOR selectivity (K_i ratio = 35-62) than [D-Phe^4]CJ-15,208 (K_i ratio = 11)
      - These are comparable or better than the KOR selectivity of the small molecule KOR antagonists aticaprant and navacaprant (19 and 40, respectively) that were in clinical trials for major depression
  - Analogs containing an aliphatic amino acid in position 1
    - 60% of the 18 analogs also have a KOR affinity comparable or higher than [D-Phe^4]Cj-15,208 (Fig. 1)
    - Seven analogs also exhibited high KOR selectivity (K_i ratio > 40)
  - KOR antagonist potency varied substantially. Most analogs were more potent than [D-Phe^4]CJ-15,208 (IC_{50} = 460 nM); half a dozen analogs were more potent than navacaprant (IC_{50} = 69 nM)

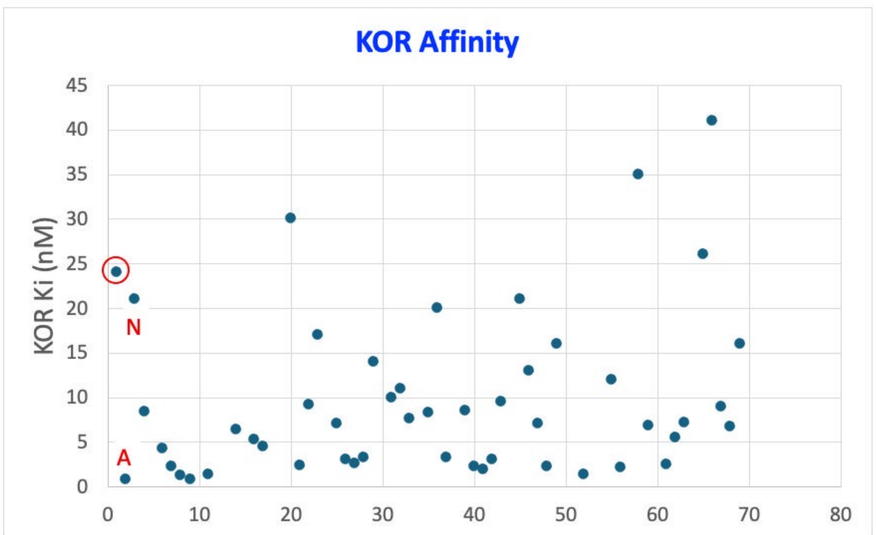


Fig. 1. KOR affinities of analogs containing an aromatic amino acid (peptides 4-49) or an aliphatic amino acid (peptides 52-69) in position 1 compared to [D-Phe^4]CJ-15,208 (circled) and the small molecule KOR antagonists aticaprant (A) and navacaprant (N). Analogs with K_i > 60 nM are not shown.

- **Metabolic stability**
  - [D-Phe^4]CJ-15,208 is metabolized rapidly by both human (HLM; $t_{1/2}$ = 4.2 min) and mouse liver microsomes (MLM; $t_{1/2}$ = 1.6 min)[2]
    - Seven analogs containing an aromatic amino acid in position 1 had half-lives in HLM of >20 minutes (Cl_{int} < 35 µg/min/mg protein)
    - Only one analog with an aliphatic amino acid in this position had a half-life in HLM >20 minutes
- ***In vivo* activity**
  - Analogs were screened after oral administration at 30 mg/kg, p.o.
    - None of the analogs tested exhibited substantial antinociception (agonist activity) in the 55º WWTW assay
  - Among the analogs containing an aromatic amino acid in position 1 screened to date
    - Seven out of 10 analogs screened antagonized i.p. U50,488
    - Two analogs antagonized centrally administered (i.c.v.) U50,488 (Fig. 2)

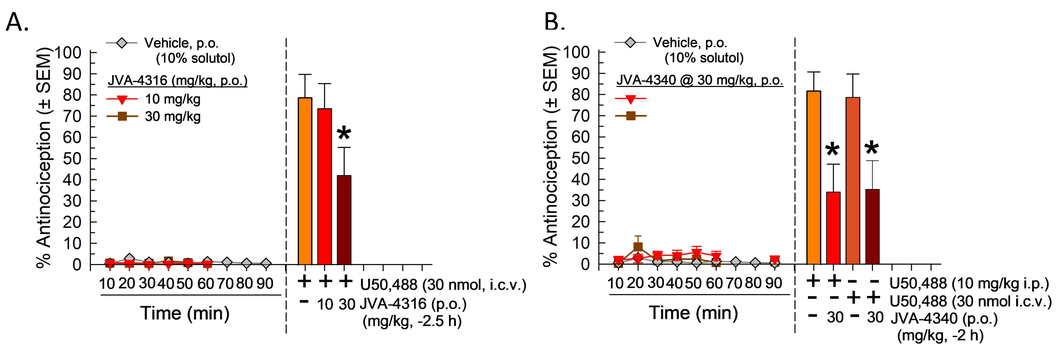


Fig. 2. Antagonism of U50,488 (30 nmol, i.c.v.) by A. JVA-4316 and B. JVA-4340. *p < 0.05 compared to vehicle treated mice

- Among the analogs containing an aliphatic amino acid screened to date
  - Three of the five analogs screened antagonized i.c.v. U50,488 (Fig. 3)

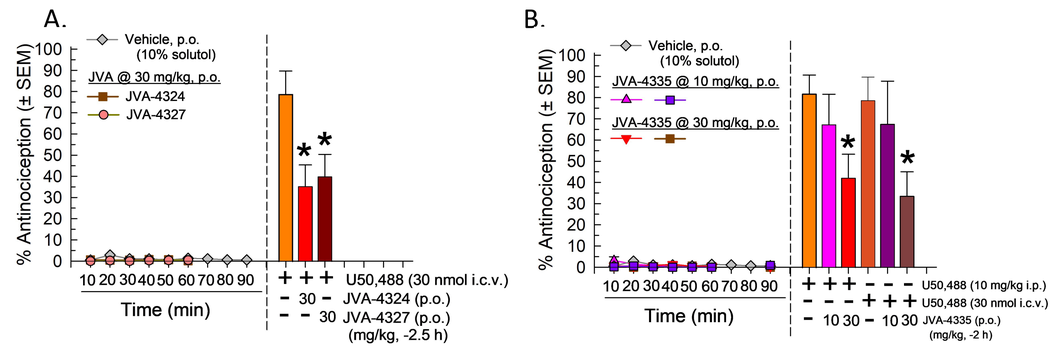


Fig. 3. Antagonism of U50,488 (30 nmol, i.c.v.) by A. JVA-4324, JVA-4327 and B. JVA-4335. *p < 0.05 compared to vehicle treated mice

- Analog JVA-4316
  - Selectively antagonized U50,488, but not the mu opioid receptor preferring agonist morphine or the delta opioid receptor selective agonist SNC-80
  - Antagonized U50,488 (i.p.) when administered 2.5 hours, but not 6 hours, prior to testing, similar to [D-Trp]- and [D-Phe^4]CJ-15,208.[1,2]
  - **Prevented stress-induced reinstatement of cocaine CPP at a dose of 10 mg/kg, p.o.** (Fig. 4A), which is comparable to [D-Phe^{4}CJ-15,208 [2] and navacaprant (Fig. 4B)

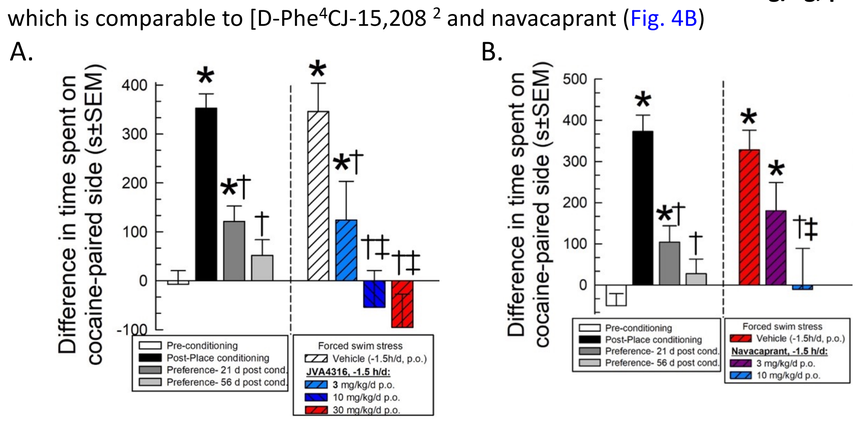


Fig. 4. A. JVA-4316 and B. the small molecule KOR antagonist navacaprant significantly decreased stress-induced reinstatement of cocaine CPP at a dose of 10, but not 3, mg/kg p.o. *, †, and ‡= sig. different (p < 0.05) from preconditioning, postconditioning and reinstated response, respectively

- Did not significantly decrease respiration, in contrast to morphine. It also did not result in hyperlocomotion (data not shown).

Conclusions

- A variety of aromatic and aliphatic amino acids are tolerated by KOR in position 1 of [D-Phe^4]Cj-15,208 analogs
  - Analogs with increased selectivity for KOR over MOR were identified
- The majority of the analogs underwent oxidative metabolism in liver microsomes with Cl_{int} > 35 µg/mL/mg protein
- Four analogs were identified that significantly antagonized centrally administered (i.c.v..) U50,488, consistent with central KOR antagonism
- JVA-4316 is a promising new lead peptide that significantly reduced stress-induced reinstatement of cocaine CPP in mice after pretreatment with 10 mg/kg, p.o., demonstrating comparable potency to the small molecule KOR antagonist navacaprant that was in clinical trials for major depression

Acknowledgements. This work was supported by National Institutes of Health grants UG3 NS132600 and UH3 NS132600.

References

1. S. O. Eans *et al.*, *Br. J. Pharmacol.* 2013, *169*, 426-436.
2. J. V. Aldrich *et al.*, *Molecules* 2025, *30*, 3993.
3. J. V. Aldrich *et al.*, *Br. J. Pharmacol.* 2014, *171*, 3212-3222.

Screening Cyclised Peptides Inside Cells Identifies a Short Helical Inhibitor of Alpha-Synuclein Aggregation

Scott G. Allen[1], Richard M. Meade[1], Amy J. Lopez[2], Christopher Williams[2], Iona Thomas-Wright[3], Bangfu Zhu[1], Mara Carey-Wood[1], Julia E. Sero[1], Vicky L. Hunt[1], Andrew Brennan[1], Richard Wade-Martins[3], Robert J. Williams[1], Matthew P. Crump[2], Jody M. Mason[1]

[1] Department of Life Sciences, University of Bath, Bath, UK. [2] School of Chemistry, University of Bristol, Bristol, UK. [3]Department of Physiology, Anatomy and Genetics, University of Oxford, Oxford, UK.

sga46@bath.ac.uk
j.mason@bath.ac.uk

Connect:

https://doi.org/10.17952/38EPS.2026.P616

1. Introduction

- Alpha-Synuclein (αSyn) aggregation is a hallmark of Parkinson's disease (PD), resulting in toxic oligomers and fibrils that drive neuronal death (Fig. 1a)[1].
- Lipid interactions induce an α-helical conformation in αSyn, essential for its synaptic role, with key residues in the N-terminal region (Fig. 1b, purple)[2]. Lipid interactions are also known to accelerate αSyn aggregation.

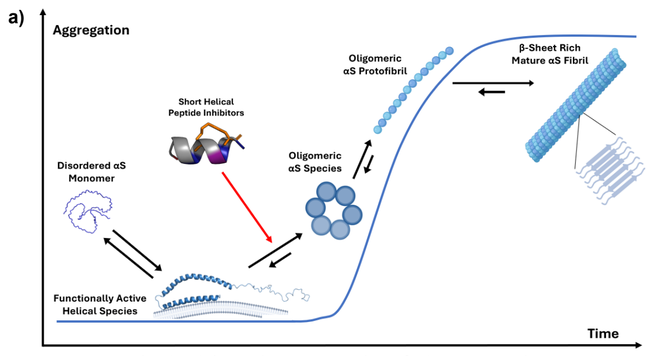


Fig. 1a) Schematic representation of αSyn aggregation.

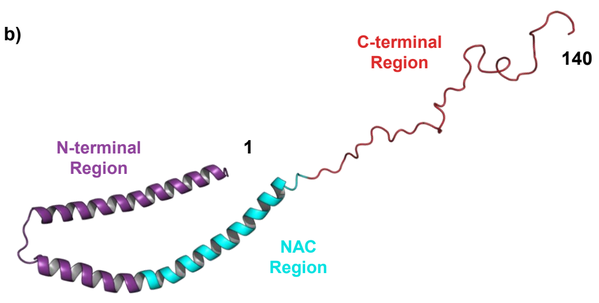


Fig. 1b) Domain organisation of αSyn: N-terminal region (purple), NAC region (blue), and C-terminal region (red)

- Short peptides can inhibit αSyn aggregation and toxicity[3,4]. We recently reported $\alpha S_{2\text{-}12}$(L6), an N-terminal-derived, α-helical peptide inhibitor of αSyn aggregation[5] (Fig. 1c-d).
- Here, we employ a novel intracellular cyclisation screening approach to improve upon $\alpha S_{2\text{-}12}$(L6) and identify a more potent inhibitor, $\alpha S_{2\text{-}12}$W.

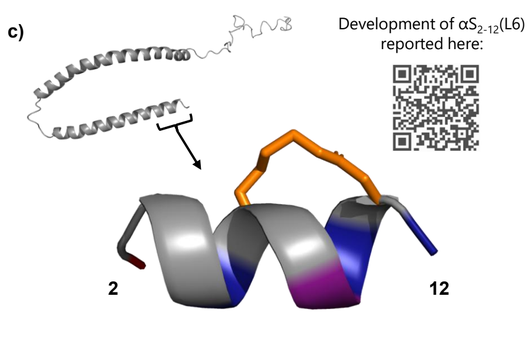


Fig. 1c) Solution NMR structure of $\alpha S_{2\text{-}12}$(L6) (PDB: 8OL8)

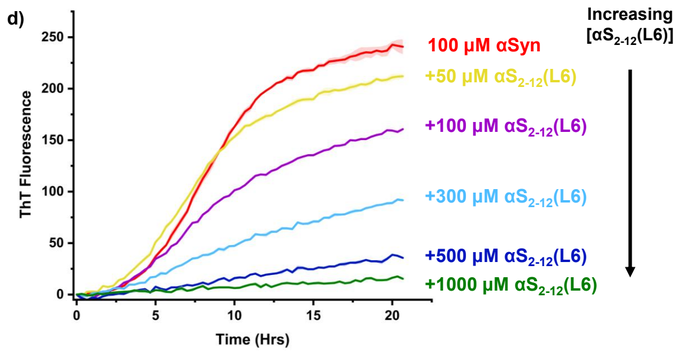


Fig. 1d) ThT fluorescence assay demonstrating dose-dependent inhibition of αSyn aggregation by increasing concentrations of $\alpha S_{2\text{-}12}$(L6).

2. Peptide Screening: Protein-fragment Complementation Assay

- We screened a peptide library using a Protein-fragment Complementation Assay (PCA), in the presence of cell-penetrant bis-alkylating agents[6], selecting peptides that bind to αSyn by enabling bacterial survival in the presence of the antibiotic, trimethoprim (TMP) (Fig. 2).
- TMP inhibits bacterial dihydrofolate reductase (DHFR), but survival is restored when a split exogenous murine DHFR (mDHFR) is reformed via a peptide–αSyn interaction.
- The strongest peptide binder is identified as the fastest-growing colony during liquid passaging.

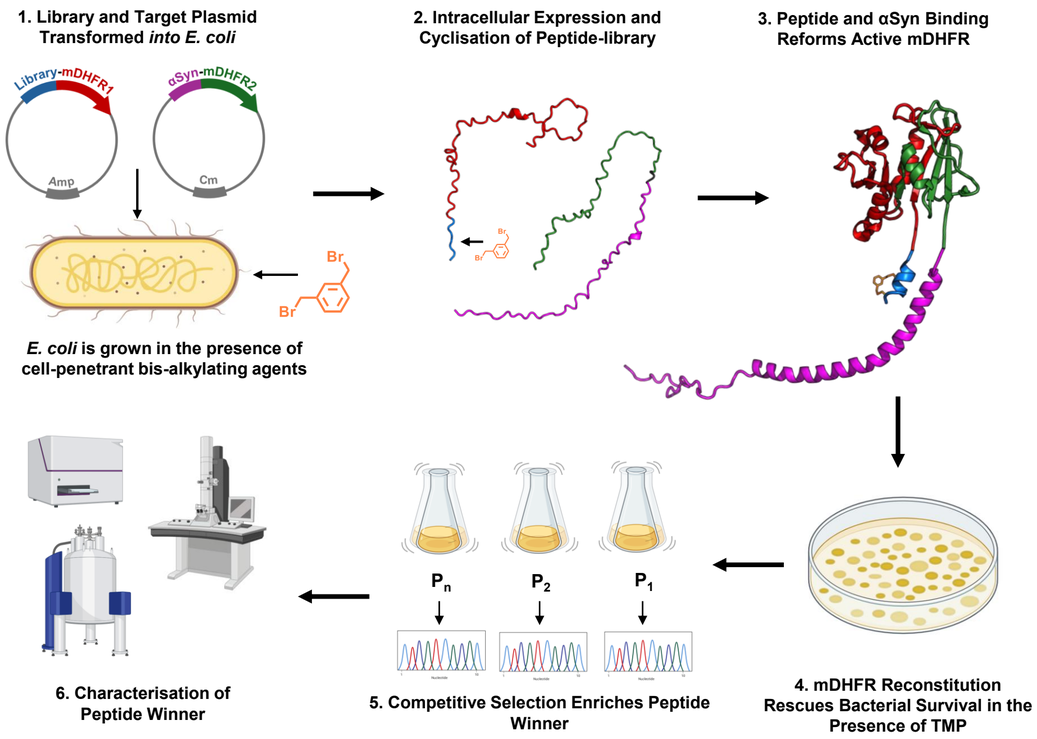


Fig. 2) Protein-fragment Complementation Assay used to screen the peptide library.

3. Library Design and Selection of $\alpha S_{2\text{-}12}$W

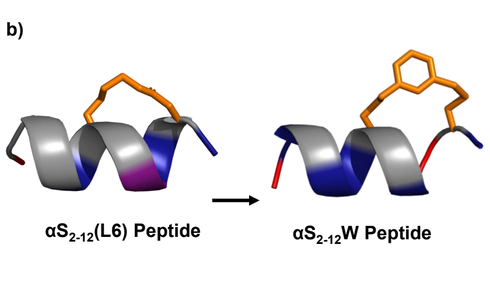
- A 20-million-member library based on $\alpha S_{2\text{-}12}$(L6) was designed with charged, polar, and hydrophobic residues at each position (Fig. 3a).
- The design enabled intracellular *i→i+4* cyclisation, locking peptides into an α-helical conformation using a cell-penetrating bis-alkylating agent.

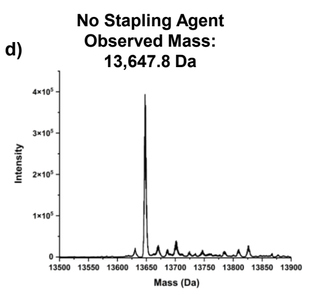
a)

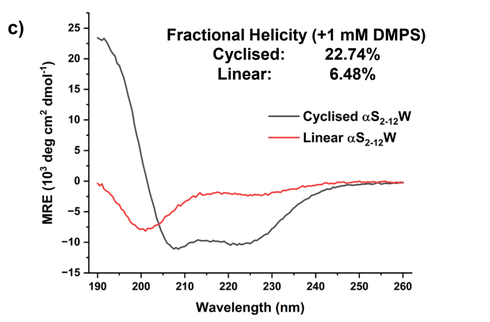
	2	3	4	5	6	7	8	9	10	11	12
Native $\alpha S_{2\text{-}12}$ Sequence	D	V	F	M	K	G	L	S	K	A	K
$\alpha S_{2\text{-}12}$(L6) Sequence	D	V	F	M	K	K	L	S	K	D	K
Library Options	D	V	F	M	K	C	L	S	K	C	K
	V	I	L	V	I		V	I	I		I
	I	G	V	G	G		M	L	G		G
	N	E	Y	E	V		Q	V	V		V
	E	K	D	R	E		E	G	E		E
	K	R	H	K	R		K	N	R		R
								D			
								R			
								H			
								K			
								E			
								Q			

Fig. 3a) Peptide library design

- Screening identified the hit peptide, $\alpha S_{2\text{-}12}$W (Fig. 3b).
- Circular Dichroism (CD) confirmed that cyclisation induced helicity in $\alpha S_{2\text{-}12}$W (Fig. 3c), while mass spectrometry verified successful intracellular cyclisation of the purified SUMO-fused peptide (Fig. 3d).







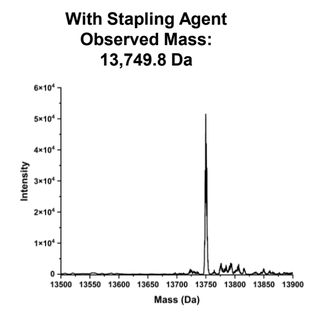


Fig. 3b) Solution NMR structures of $\alpha S_{2\text{-}12}$(L6) (PDB: 8OL8) and $\alpha S_{2\text{-}12}$W (PDB: 9SG1). **3c)** CD spectra showing helical induction of $\alpha S_{2\text{-}12}$W by addition of stapling agent in the presence of lipid (DMPS). **3d)** MS spectra showing mass increase of 102 Da for purified $\alpha S_{2\text{-}12}$W-SUMO fusion when expressed in the presence of the stapling agent, confirming intracellular cyclisation.

4. $\alpha S_{2\text{-}12}$W Inhibits αSyn Aggregation

- ThT fluorescence assays demonstrated that $\alpha S_{2\text{-}12}$W inhibits αSyn aggregation at substoichiometric concentrations, indicating greater inhibitory potency than $\alpha S_{2\text{-}12}$(L6) (Fig. 4a).
- Removal of the stapling agent reduced the level of inhibition (Fig. 4a).

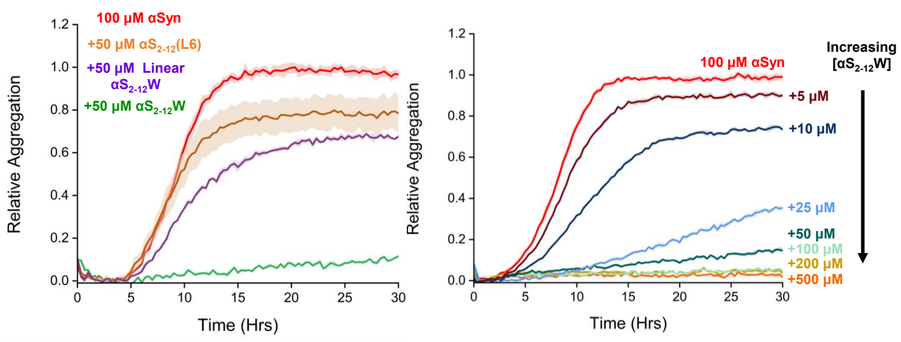


Fig. 4a) (Left) ThT fluorescence assay showing inhibition of αSyn aggregation by the $\alpha S_{2\text{-}12}$W peptide compared to the initial $\alpha S_{2\text{-}12}$(L6) peptide and linear, unstapled version. **(Right)** $\alpha S_{2\text{-}12}$W induces a strong concentration-response.

- TEM confirmed that $\alpha S_{2\text{-}12}$W significantly reduced αSyn fibril formation (Fig. 4b).

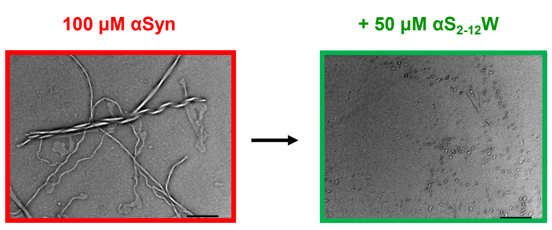


Fig. 4b) TEM micrographs of endpoint ThT assay samples, showing no αSyn fibril formation with $\alpha S_{2\text{-}12}$W addition.

5. $\alpha S_{2\text{-}12}$W Binds the C-terminal Region of αSyn

- αSyn chemical shift perturbations were tracked in the presence of increasing concentrations of $\alpha S_{2\text{-}12}$W (Fig. 5a).

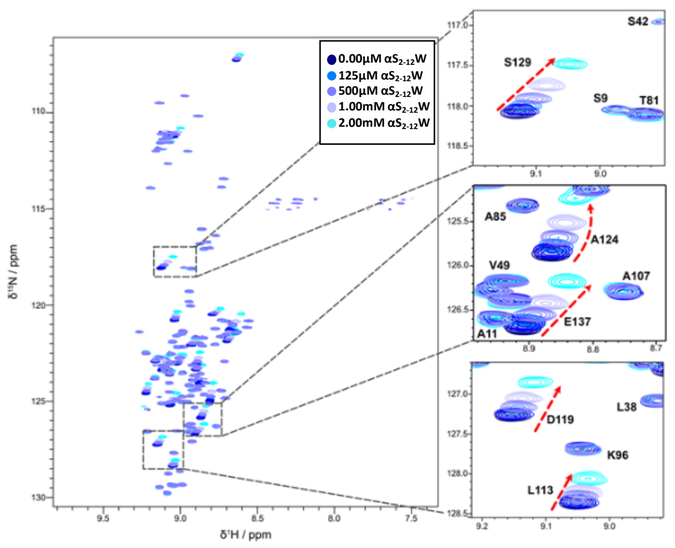


Fig. 5a) ^{1}H-^{15}N HSQC spectra of αSyn in the presence of $\alpha S_{2\text{-}12}$W at increasing concentrations. Residues in the C-terminal region show the largest chemical shift perturbations.

- The $\alpha S_{2\text{-}12}$W peptide interacts with the C-terminal region of αSyn based on CSP analysis (Fig. 5b).

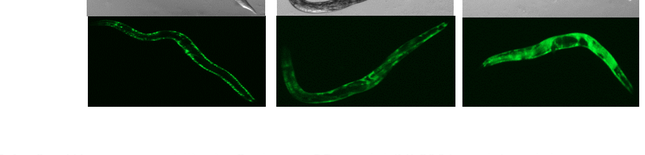


Fig. 5b) The chemical shift perturbation per residue at 2 mM $\alpha S_{2\text{-}12}$W.

6. $\alpha S_{2\text{-}12}$W is Cell-Penetrant and Non-Toxic

- Rhodamine B-labelled $\alpha S_{2\text{-}12}$W shows strong dose-dependent uptake in SH-SY5Y neuronal cells versus $\alpha S_{2\text{-}12}$ and $\alpha S_{2\text{-}12}$(L6) (Fig. 6a-b).
- $\alpha S_{2\text{-}12}$W is also non-toxic at concentrations tested (Fig. 6c-d)

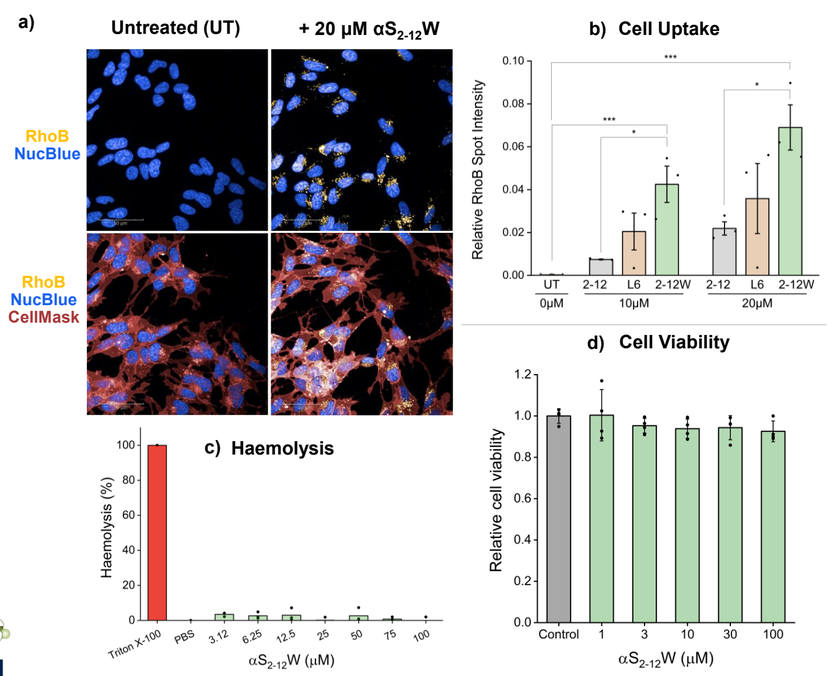


Fig. 6a) RhoB-$\alpha S_{2\text{-}12}$W (Yellow) uptake into SH-SY5Y cells. 6b) Quantitative comparison of uptake between native $\alpha S_{2\text{-}12}$ sequence, $\alpha S_{2\text{-}12}$(L6) and $\alpha S_{2\text{-}12}$W. 6c-d) Cell viability and haemolysis not impaired by $\alpha S_{2\text{-}12}$W up to 100 μM.

7. $\alpha S_{2\text{-}12}$W Rescues Mobility in *C. elegans* PD Model

- $\alpha S_{2\text{-}12}$W rescues thrashing (bending) in αSyn-mobility impaired *C. elegans* model (Fig. 7a).
- $\alpha S_{2\text{-}12}$W reduces αSyn inclusions in YFP-αSyn overexpressing worm (Fig. 7b-c).

Fig. 7a) $\alpha S_{2\text{-}12}$W rescues mobility in *C. elegans* PD model (NLS901 strain) and does not impact control strain. 7b-c) $\alpha S_{2\text{-}12}$W treatment reduces αSyn inclusion formation in *C. elegans* PD model.

References and Acknowledgments

1. Meade, R.M., *et al.* (2019). Alpha-synuclein structure and Parkinson's disease – lessons and emerging principles. *Molecular Neurodegeneration,* 14(29).
2. Bartels, T., *et al.* (2011). Alpha-synuclein occurs physiologically as a helically folded tetramer that resists aggregation. *Nature* 477, 107–110.
3. Meade, R.M., Allen, S.G., *et al.* (2023). An N-terminal alpha-synuclein fragment binds lipid vesicles to modulate lipid-induced aggregation. *Cell Reports Physical Science,* 4(9), 101563.
4. Allen, S.G., Meade, R.M., *et al.* (2023). Peptide-based approaches to directly target alpha-synuclein in Parkinson's disease. *Molecular Neurodegeneration*, 18(80).
5. Meade, R.M., Allen, S.G., *et al.* (2025). Stabilising a native fold of alpha-synuclein with short helix-constrained peptides. *JACS Au*, 5(9), 4321-4336.
6. Brennan, A., *et al.* (2026). Intracellular cyclization-coupled peptide library screening yields potent transcription factor antagonists. *Cell Chemical Biology*, 33, 409-423.e7.

BIOCHEMICAL SOCIETY
ALZHEIMER'S RESEARCH UK FOR A CURE
SWBio DTP
University of BRISTOL
EPS
Biotechnology and Biological Sciences Research Council
UNIVERSITY OF OXFORD

38th EPS European Peptide Symposium

Synthesis And Characterization Of Thermo-responsive Magnetic Molecularly Imprinted Polymers For Selective Recognition Of Peptide–drug Conjugates

Sima Alvani Alamdari[1], Justyna Frączyk[1], Sebastian Schwaminger[2]

[1]Institute of Organic Chemistry, Faculty of Chemistry, Lodz University of Technology, Zeromskiego 114, 90-543 Lodz, Poland.
[2]Medical University of Graz, Division of Medicinal Chemistry, Neue Stiftingtalstraße 6, 8010, Graz, Austria.

Email: sima.alvani-alamdari@dokt.p.lodz.pl

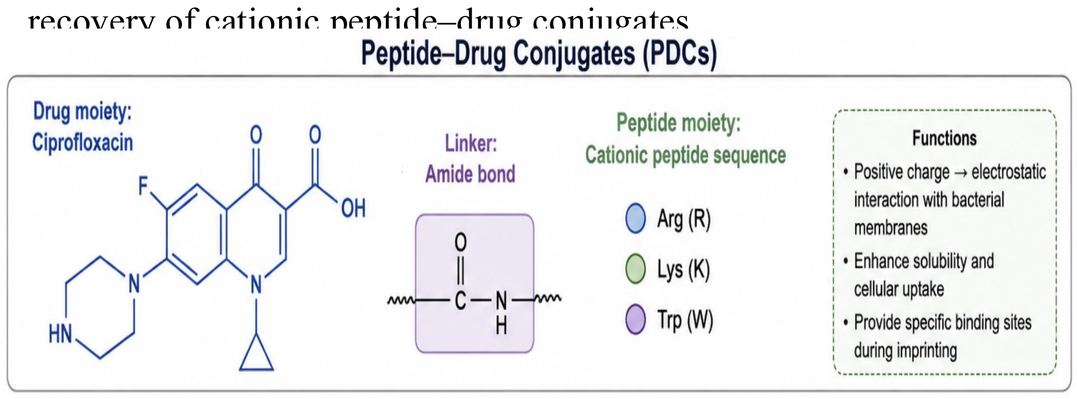
https://doi.org/10.17952/38EPS.2026.P356

Instytut Chemii Organicznej Politechniki Łódzkiej

Introduction

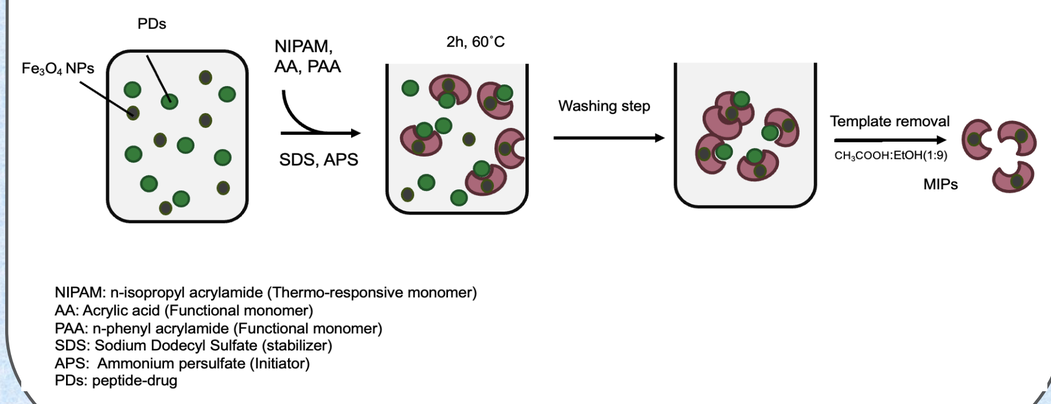
Peptide–drug conjugates (PDCs) are promising antimicrobial systems that combine the therapeutic activity of antibiotics with the targeting, membrane interaction, and cellular uptake properties of peptides. Incorporation of cationic amino acids such as arginine and lysine can enhance electrostatic interactions with negatively charged biological interfaces and provide additional hydrogen-bonding sites, potentially influencing the biological and physicochemical properties of the conjugates. In this study, two ciprofloxacin-based conjugates, Ciprofloxacin–Arg–Lys–Arg and Ciprofloxacin–Arg–Trp–Arg, were used as template molecules to develop thermo-responsive magnetic molecularly imprinted polymers (MMIPs).

The MMIPs were designed to provide selective recognition, temperature-controlled binding/release, and magnetic separation of the peptide–drug conjugates. The materials were characterized using FT-IR, TEM, and DLS, followed by adsorption and selectivity studies to evaluate their recognition performance.
This work explores thermo-responsive MMIPs as promising platforms for the selective extraction, separation, and controlled recovery of cationic peptide–drug conjugates.



Experimental

In this research, Fe_3O_4@poly(AA-*co*-PAA-*co*-NIPAM) MMIPs were synthesized via bulk polymerization in the presence of functional monomers capable of hydrogen bonding and ionic interactions. The integration of thermo-responsive polymer NIPAM with MMIP technology allows reversible modulation of polymer affinity around its lower critical solution temperature (LCST), enabling temperature-controlled binding and release of targets, while the magnetic core facilitates rapid separation under an external magnetic field.
Peptide-drug conjugates were prepared by solid-phase peptide synthesis (SPPS) with Fmoc/tBu strategy using triazine coupling reagent (4-(4,6-dimethoxy-1,3,5-triazin-2-yl)-4-methylmorpholinium toluene-4-sulfonate (DMT/NMM/$TosO^-$)).
In the last step, we characterized prepared nanoparticles by FT-IR, DLS, and TEM. Additionally, peptide-drug fragments were characterized by mass spectrometry techniques.



NIPAM: n-isopropyl acrylamide (Thermo-responsive monomer)
AA: Acrylic acid (Functional monomer)
PAA: n-phenyl acrylamide (Functional monomer)
SDS: Sodium Dodecyl Sulfate (stabilizer)
APS: Ammonium persulfate (Initiator)
PDs: peptide-drug

Results and discussion

Table 1.Results of peptide synthesis (LC-Mass analysis):

No.	Conjugate	Molecular Formula	Monoisotopic Mass (g/mol)	$[M+H]^+$ (m/z)	Purity %
1	Ciprofloxacin–Arg–Lys–Arg	$C_{35}H_{54}FN_{13}O_6$	771.4304	772.4377	96
2	Ciprofloxacin–Arg–Trp–Arg	$C_{40}H_{52}FN_{13}O_6$	829.4148	830.4220	94

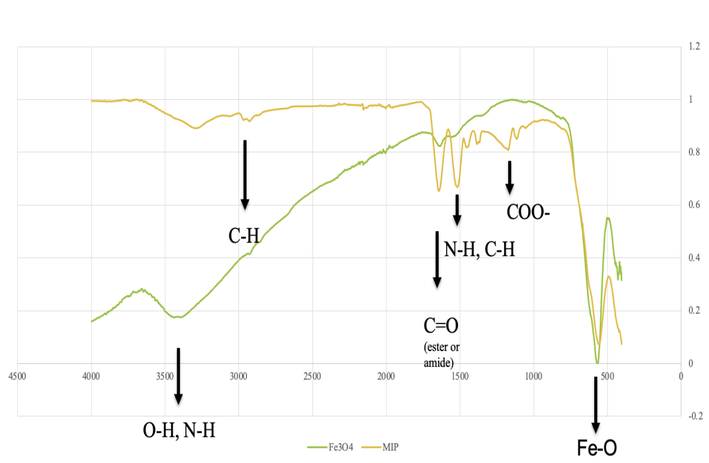
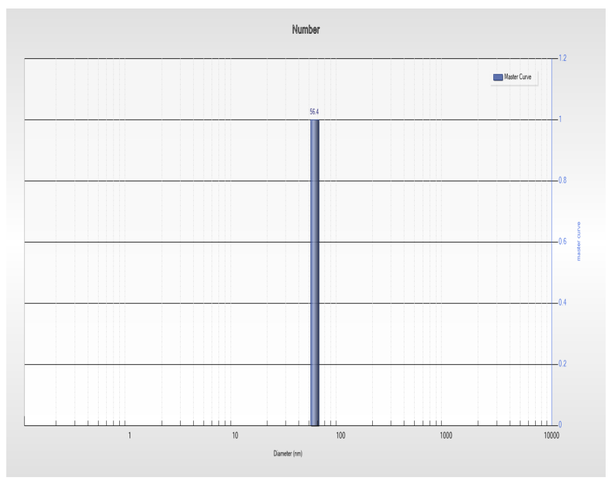


Fig 1. FTIR Spectra of MMIPs



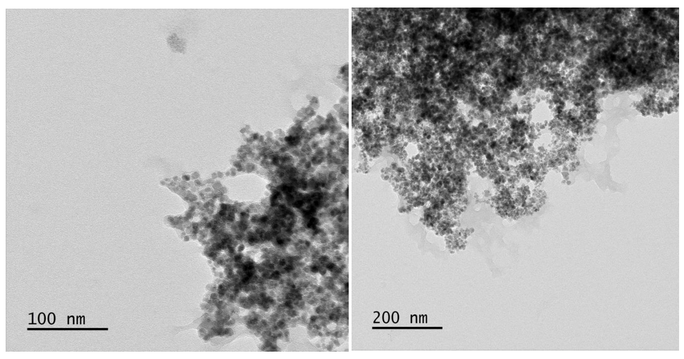


Fig 2. TEM images of MMIPs

Parameter	Mean ± SD
Z-Average (nm)	56.4 ± 0.02
PDI	0.23 ± 0.05

Fig 3. DLS result of MMIPs

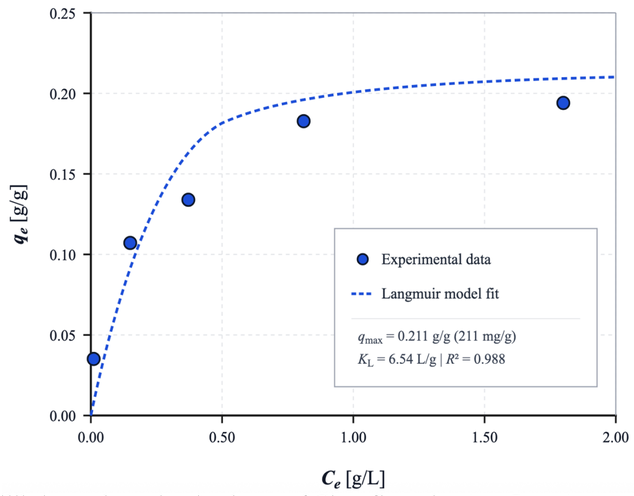


Fig 4. Equilibrium adsorption isotherm of Ciprofloxacin–Arg–Lys–Arg on MMIPs fitted with the Langmuir model

Conclusions

Core-shell thermo-responsive MMIPs (Fe_3O_4@poly(AA−*co*−PAA−*co*−NIPAM)) with a mean hydrodynamic size of 56.4 nm were successfully prepared. The material demonstrated high binding affinity toward Ciprofloxacin–Arg–Lys–Arg, conforming to the Langmuir isotherm ($R^2 = 0.988$) with a maximum capacity of 211 mg/g, highlighting its strong potential for selective magnetic separation of cationic peptide–drug conjugates.

Acknowledgment

‘This research was created as part of participation in the project entitled “IMPROVE – International Mission for the Promotion of Research and Optimal Values in Education” under the National Agency for Academic Exchange STER program – Internationalization of Doctoral Schools – Call for Applications 2024.’

POLISH NATIONAL AGENCY FOR ACADEMIC EXCHANGE

References

[1] N. Ptaszyńska, K. Gucwa, K. Olkiewicz, A. Łęgowska, J. Okońska, J. Ruczyński, A. Gitlin-Domagalska, D. Dębowski, S. Milewski, K. Rolka, ACS Chem. Biol. 2019, 14, 2233–2242.
[2] L. Xu, J. Pan, J. Dai, X. Li, H. Hang, Z. Cao, Y. Yan, J. Hazard. Mater. 2012, 233, 48–56.
[3] J. Li, Y. Wang, X. Yu, Front. Chem. 2021, 9, 706311.

Amino acid-based hydrogels for electrochemical applications

Sandro Amador [a,b*], **Felipe Conzuelo** [a], **Ana C. Baptista** [b], **Leonor Morgado** [c,d], **Ana S. Pina** [a]

a. Instituto de Tecnologia Química e Biológica António Xavier (ITQB), Universidade NOVA de Lisboa, Av. da República, 2780-157, Oeiras, Portugal
b. CENIMAT/I3N, Department of Materials Science, NOVA School of Science and Technology, Universidade NOVA de Lisboa, 2829-516 Caparica, Portugal
c. UCIBIO – Applied Molecular Biosciences Unit, Department of Chemistry, NOVA School of Science and Technology, Universidade NOVA de Lisboa, 2829-516 Caparica, Portugal
d. Associate Laboratory i4HB - Institute for Health and Bioeconomy, NOVA School of Science and Technology, Universidade NOVA de Lisboa, 2829-516 Caparica, Portugal

*** Presenting Author: sandro.amador@itqb.unl.pt**

https://doi.org/10.17952/38EPS.2026.P548

INSTITUTO DE TECNOLOGIA QUÍMICA E BIOLÓGICA ANTÓNIO XAVIER | ITQB.UNL.PT

INTRODUCTION

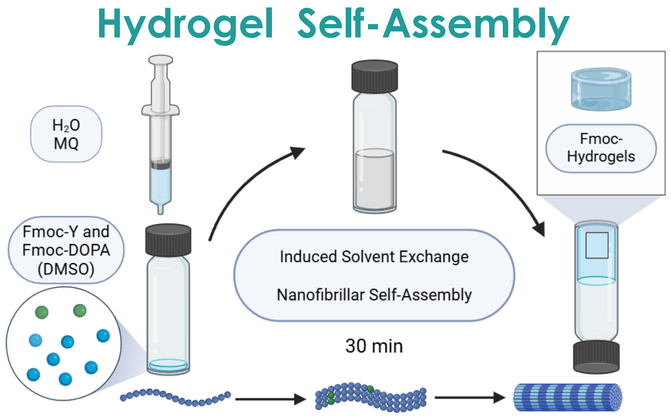
Soft bioelectronics require electrolyte materials that are biocompatible, flexible, ionically conductive, electrically isolating, and electrochemically stable. Conventional liquid electrolytes can suffer from leakage and poor mechanical integration, motivating the development of solid-state alternatives [1].

Fmoc-protected amino acids are promising low-molecular-weight building blocks because they self-assemble into hydrated supramolecular networks through aromatic π–π stacking and side-chain interactions [2,3]. Compared with larger protein-based biomaterials, these systems offer simpler molecular design, easier processing, and tunable functionality [4].

In this work, Fmoc-Tyrosine (Fmoc-Y) and Fmoc-Tyrosine:DOPA (Fmoc-YD) hydrogels were explored as supramolecular amino acid-based electrolyte matrices for soft bioelectronic applications. By comparing their self-assembly behavior, structural features, and electrochemical performance, this study aims to assess whether these low-molecular-weight hydrogels can function as simple and tunable solid-state electrolyte candidates.

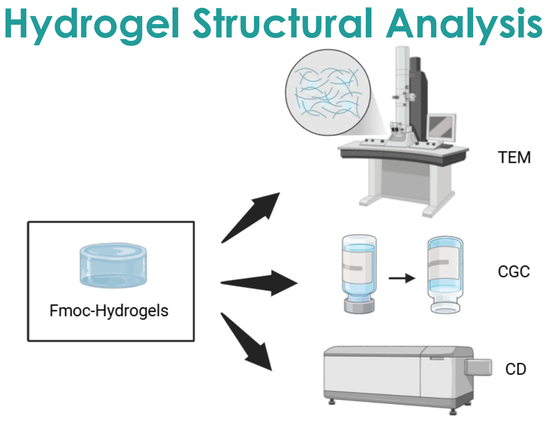
MATERIALS AND METHODS

Hydrogel Self-Assembly



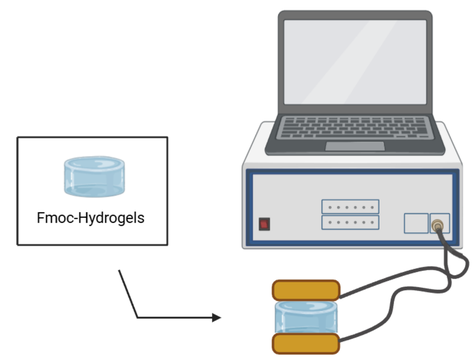
Fmoc-Y and Fmoc-YD (3:1 ratio) ranging from 2 to 10 mg/mL. Solvent exchange-triggered self-assembly using MiliQ water. Samples left to stand for 30 min to gelate.

Hydrogel Structural Analysis



Fmoc-hydrogels' structural analysis comprised Transmission Electron Microscopy (TEM), Circular Dichroism (CD) and Critical Gelation Concentration (CGC) assays.

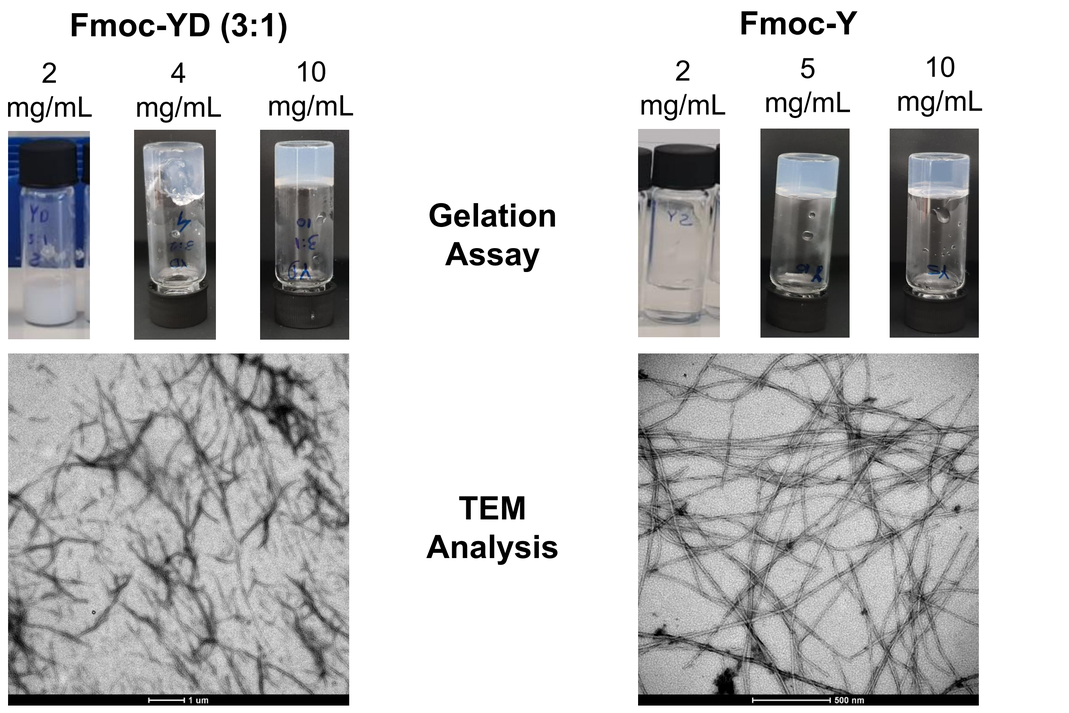
Solid-state Electrochemical Analysis



Solid-state electrochemical analysis was performed using a two-electrode (Gold) sandwich setup inside a Faraday cage. Open circuit potential (OCP), Impedance spectroscopy (EIS) and Voltammetry assays were conducted (CV; LSV).

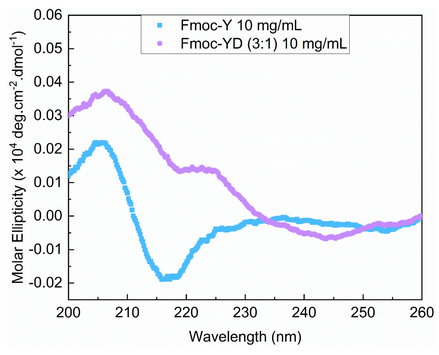
RESULTS

Fmoc Hydrogels Structural Characterization



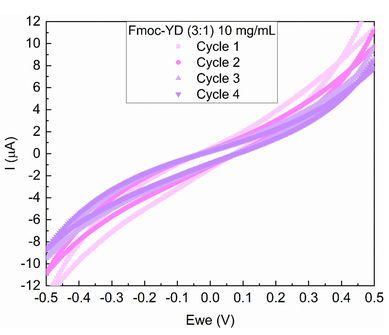
Dispersed fiber network (10 mg/mL)

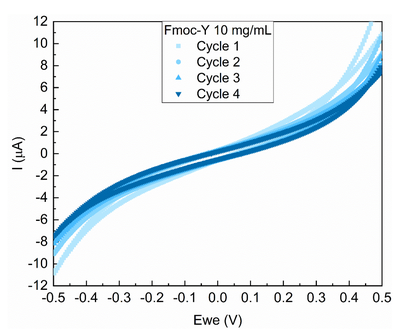
Densely packed fiber network (10 mg/mL)

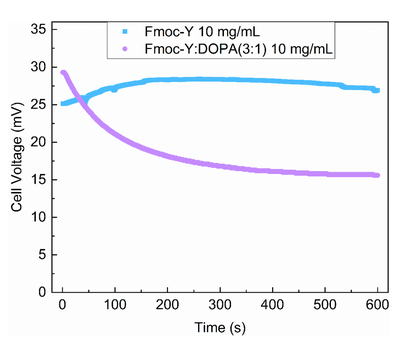


Evidence of β-sheet supramolecular configuration, more pronounced in Fmoc-Y with a minimum at ~215 nm.

Fmoc Hydrogels Solid-state Electrochemical Analysis

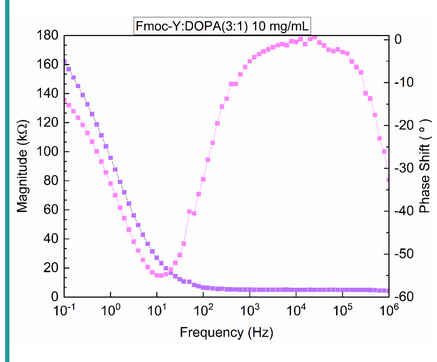


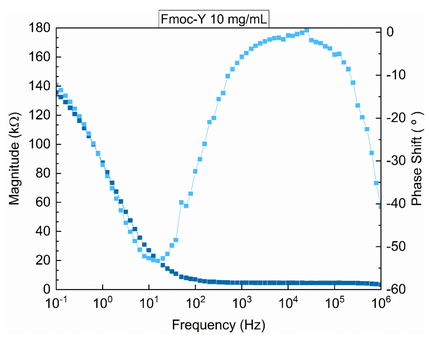




Absence of distinct redox peaks suggests ion-mediated interfacial response

Both materials reach a stable electrochemical response over time





- Ion-conducting behavior
- Phase shift → Bulk ionic conduction to electrode polarization
- High Hz plateau → Bulk resistance
- Low Hz → Electrode Polarization

System	Method	Source of conductivity (σ)	σ (S/cm)
Fmoc-Y 10 mg/mL	LSV (DC)	Apparent	4.5E-06
	EIS (AC)	Bulk	9.0E-05
Fmoc-YD (3:1) 10 mg/mL	LSV (DC)	Apparent	4.9E-06
	EIS (AC)	Bulk	8.3E-05

Both hydrogels show measurable ionic conductivity; EIS provides bulk conductivity, while LSV reflects apparent DC conductivity influenced by polarization, supporting their potential as soft electrolyte materials.

MAIN CONCLUSIONS AND FUTURE WORK

- ✓ Fmoc-hydrogels form fibrillar networks with β-sheet supramolecular organization and stable ion-conducting behavior with conductivities of 10^{-5} S/cm.
- ✓ Fmoc-Y appears as the more promising system, with higher conductivity and structural stability.
- ✓ Fmoc-hydrogels appear as electrolyte-like ion-conducting matrices promising for low-current electrochemical applications.
- Future work will include the structural and electrochemical evaluation of other Fmoc-protected amino acids.

REFERENCES

[1] Q. Liu, C. Xia, C. He, W. Guo, Z. P. Wu, Z. Li, Q. Zhao and B. Y. Xia, Angew. Chemie, 2022, 134, e202210567.
[2] N. Balasco, D. Altamura, P. L. Scognamiglio, T. Sibillano, C. Giannini, G. Morelli, L. Vitagliano, A. Accardo and C. Diaferia, Langmuir, 2024, 40, 1470–1486.
[3] G. Fichman, T. Guterman, L. Adler-Abramovich and E. Gazit, CrystEngComm, 2015, 17, 8105–8112
[4] Y. Huo, J. Hu, Y. Yin, P. Liu, K. Cai and W. Ji, ChemBioChem, 2023, 24, e202200582.

ACKNOWLEDGEMENTS

A. S. P. and F.C. acknowledge the support from Fundação para a Ciência e Tecnologia (FCT), through MOSTMICRO-ITQB R&D Unit (UIDB/040612/2020, UIDP/04612/2020), LS4FUTURE Associated Laboratory (LA/P/0087/2020). A.S.P., L.M. and F.C. are grateful to FCT for the researcher contracts under the Scientific Employment Stimulus–Individual Calls 2021 and 2022, specifically 2021. 01283.CEECIND/CP1657/CT0004 for A.S.P., 2021.02185.CEECIND/CP1657/CT0008 for L.M. and 2022.05842.CEECIND/CP1725/CT0001 for F.C. L.M. also acknowledge the support from FCT for the projects (i) UIDP/04378/2020 and UIDB/04378/2020 (Research Unit on Applied Molecular Biosciences—UCIBIO) and (ii) LA/P/0140/2020 (Associate Laboratory Institute for Health and Bioeconomy—i4HB). A. C. B. acknowledge the funding by national funds from FCT - Fundação para a Ciência e a Tecnologia, I.P., in the scope of the projects UID/50025/2025 and LA/0037/2020 of the Associate Laboratory Institute of Nanostructures, Nanomodelling and Nanofabrication – i3N. The consortium acknowledges the funding from "la Caixa" Foundation under the grant agreement (LCF/TR/CI23/56000027), and the InnOValley Proof of Concept under the grant agreement IOVPoC-2022-07 funded by Oeiras Municipality and co-funded by MOSTMICRO-ITQB.

https://doi.org/10.17952/38EPS.2026.P280
European Peptide Symposium, 6th – 11th September 2026, Vienna, Austria

RACEMIZATION-FREE PEPTIDE SYNTHESIS IN WATER UNDER BATCH AND FLOW CONDITIONS

Sri Hari Anandhi Rajendran[a,b], Sándor B. Ötvös[a,b], C. Oliver Kappe[a,b], Wilfried M. Braje[c], Matthew Burns[d]

[a] Research Center Pharmaceutical Engineering GmbH (RCPE), Inffeldgasse 13, A-8010 Graz, Austria
[b] Institute of Chemistry, University of Graz, NAWI Graz, Heinrichstrasse 28, A-8010 Graz, Austria
[c] *AbbVie Deutschland GmbH & Co. KG, 67061 Ludwigshafen, Germany*
[d] *Chemical Development, Pharmaceutical Technology & Development, Operations, AstraZeneca, Macclesfield SK10 2NA, United Kingdom*

hari.rajendran@rcpe.at | www.goflow.at

INTRODUCTION

Established technology — Reactions in Organic Solvents

- ✓ Excellent solubility for organic compounds
- ✓ Well-understood, well-established protocols
- ✓ Readily scalable



- ✗ Harmful and toxic: **DMF, NMP, DCM, MTBE**
- ✗ Make up most of the waste generated
- ✗ Expensive, and restricted by legislation

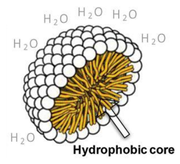


'New' approach — Reactions in Water

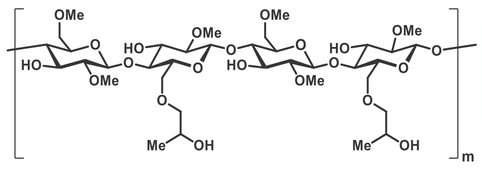
- ✓ Non-toxic, not flammable
- ✓ Inexpensive and readily available
- ✓ Mild conditions, Rate enhancement



- ✗ Poor solubility of organic compounds
- ✗ Enablers, e.g. surfactants are needed
- ✗ Designer surfactants are expensive!

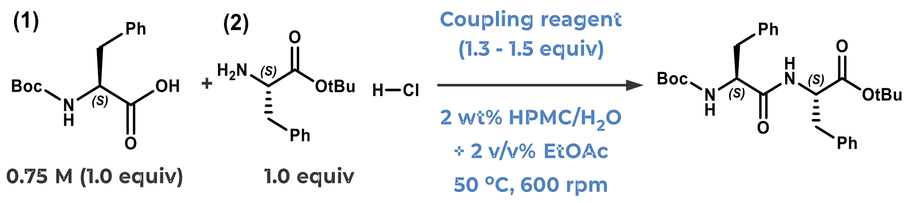


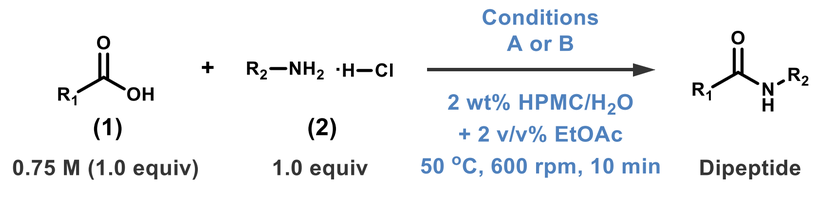
This work — Why HPMC?



- ✓ **Bulk commodity**, not a designer surfactant
- ✓ Pharma excipient (E464) — cheap, non-toxic
- ✓ **Hydrophobic pockets** concentrate the reagents

BATCH OPTIMIZATION & SUBSTRATE SCOPE





Screening coupling reagents

Reagent	Base	t [min]	Conv [%]	Sel [%]	d.r
COMU	2,6-Lutidine	60	94	93	>99 : 1
EDC·HCl	Pyridine	60	80	94	—
CDI	—	10	60	95	—
EEDQ	**none***	**≤10**	**>99**	**97**	**>99 : 1**

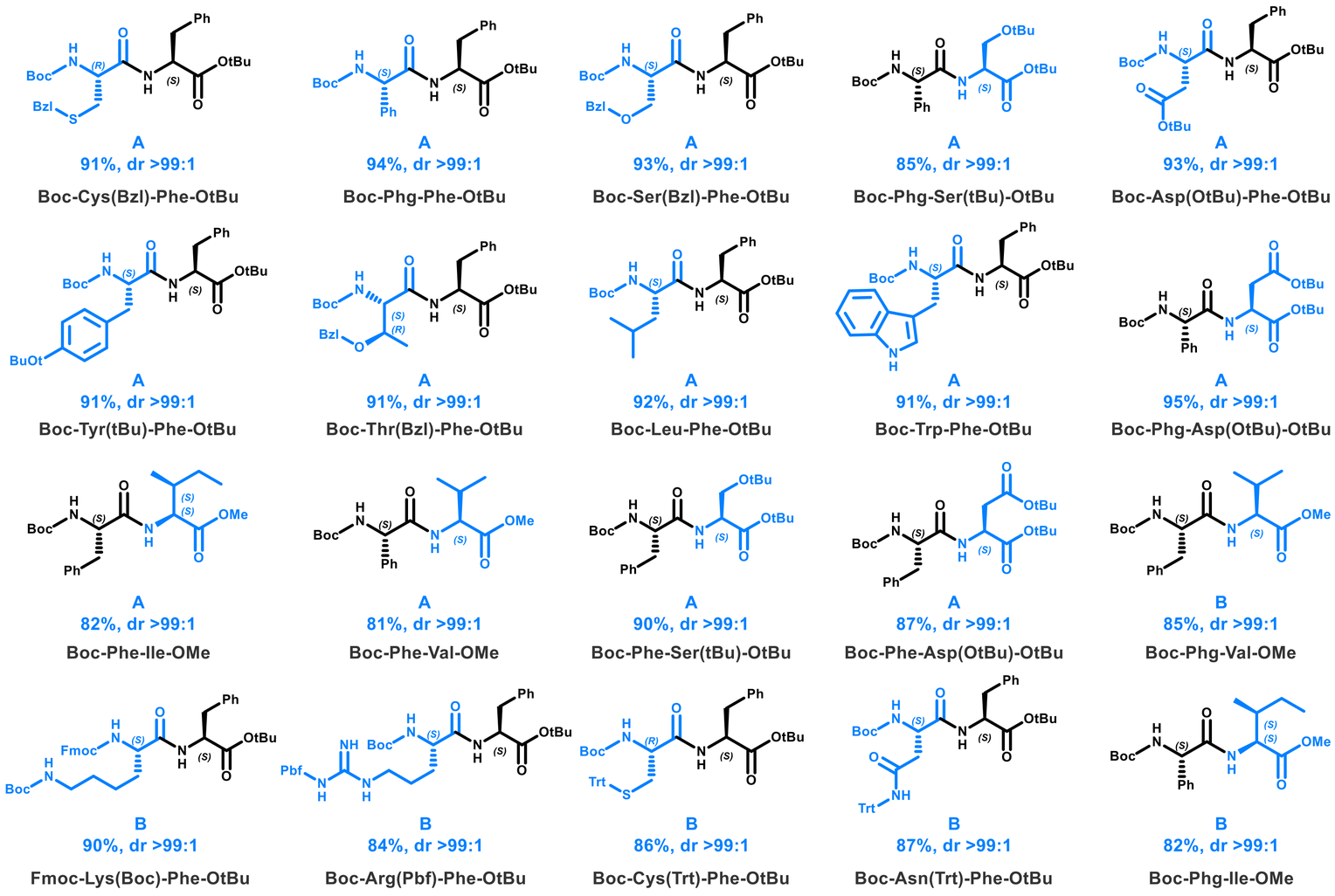
Advantages of EEDQ

- ✓ **Racemization-free** - d.r >99 : 1
- ✓ **No external base** - quinoline in situ
- ✓ **Easy and simple work-up**
- ✓ **Fast** - ≤10 min
- ✓ **Improved atom economy**
- ✓ **Low cost per mole**

Scale-up

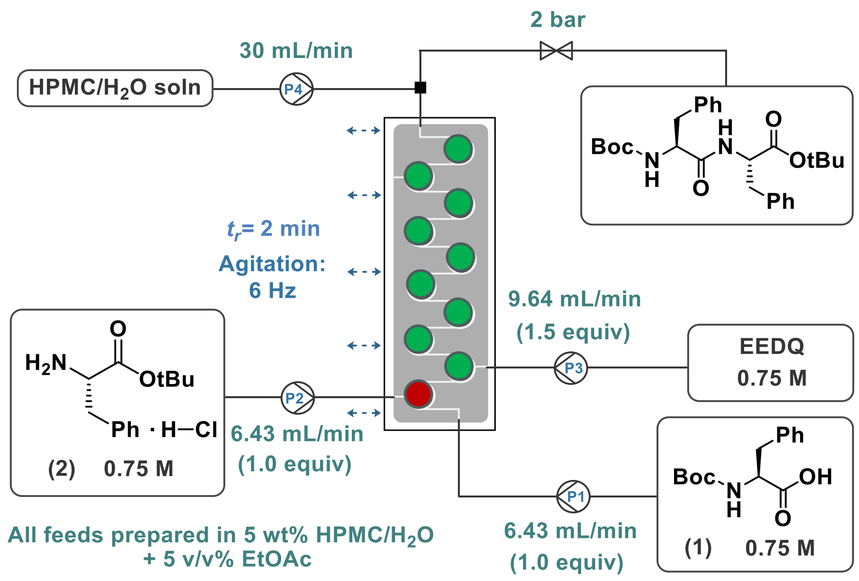
Volume	Isolated yield	d.r
5 mL	89 %	>99 : 1
100 mL	91 % (32 g)	>99 : 1
500 mL	92 % (163 g)	>99 : 1

Chemistry scales well in batch but CO_2 evolution becomes significant at higher volumes, making flow chemistry an attractive approach!



plus 13 additional substrates...

PEPTIDE COUPLINGS IN FLOW



PREPARATIVE RUN (2 h)
248 g
91.5 % yield · 124 g/h · ≈ 3 kg/day

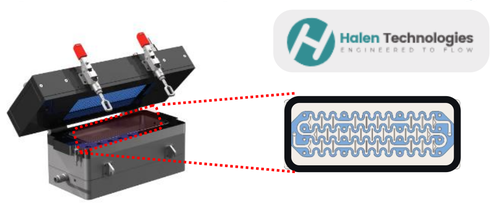
E-factor : 2.1

PMI : 3.1

Halen XFR 200

Serpentine design, oscillatory mixing, 11.6 mL

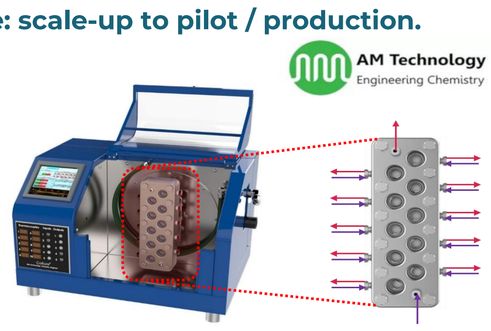
Role: process development & screening.



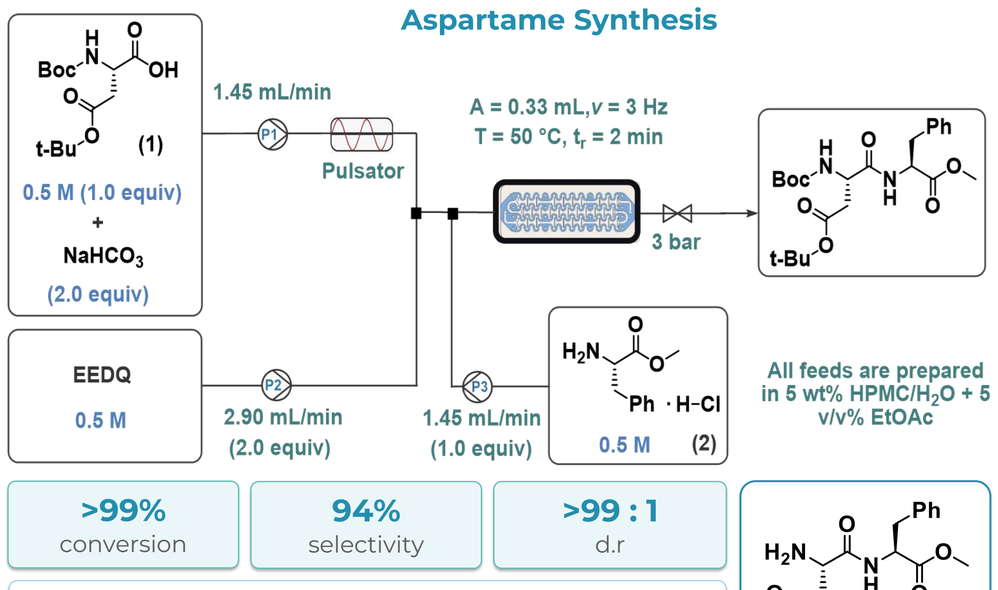
Coflore ACR

10 CSTRs in series, lateral agitation, 30–90 mL

Role: scale-up to pilot / production.



Aspartame Synthesis



>99% conversion	94% selectivity	>99 : 1 d.r

1. **Flow coupling** — steady state in < 5 min
2. **Boc/OtBu removal** — TFA/DCM, rt, 30 min
3. **Anti-solvent wash** — by-products removed

82%
isolated yield

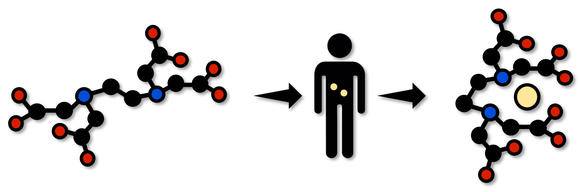
This project is supported by the Innovative Health Initiative Joint Undertaking (IHI JU) under grant agreement No 101165889. The JU receives support from the European Union's Horizon Europe research and innovation programme and COCIR, EFPIA, Europa Bio, MedTech Europe, and Vaccines Europe.

Federal Ministry Republic of Austria Climate Action, Environment, Energy, Mobility, Innovation and Technology
Federal Ministry Republic of Austria Labour and Economy
FFG Promoting Innovation.
Das Land Steiermark Wirtschaft, Tourismus, Regionen, Wissenschaft und Forschung
SFG NEUES DENKEN. NEUES FÖRDERN.

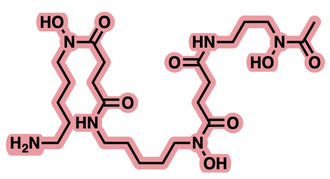
Synthesis of novel chiral peptoid-based metal chelators

Ludovica Dei[1], Bethany L Hardman[2], Gary J Sharples[2], Gaetano Angelici[1], Gennaro Pescitelli[1]
[1]*Dipartimento di Chimica e Chimica Industriale, Università di Pisa, Pisa 56124, Italy*
[2]*Department of Biosciences, Department of Chemistry, Science Site, Durham DH1 3LE, United Kingdom*
https://doi.org/10.17952/38EPS.2026.P135
ludovica.dei@phd.unipi.it

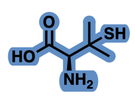
Introduction



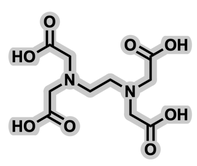
Chelation therapy involves administering a chemical agent, known as a **«chelator»**, to remove toxic exogenous metals from the body and reduce excess levels of essential metals in cases of overload disorders linked to various pathologies. The therapy works by binding metal ions into **high-affinity complexes**, which are then **excreted through the liver or kidneys** [1,2].



Desferal®
Iron chelator
Used for long-term iron chelation in beta-thalassemia



Pemine®
Copper chelator
Used for reduction of copper levels in Wilson's disease



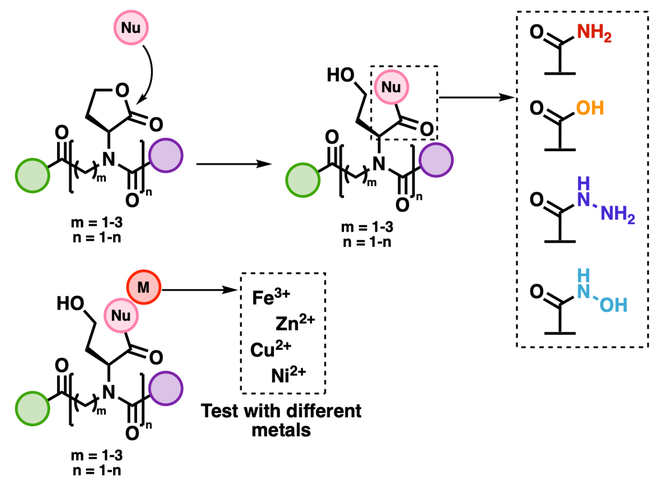
EDTA
Heavy metals chelator
Used for the treatment of acute heavy metal poisoning



✗ **Poor selectivity**, which leads to the depletion of essential metals
✗ The possible **biological activity** of the resulting metal complex

Aim of the work

Developing a class of peptoid-based chelators derived from L-homoserine lactone (L-HSL) with high selectivity for treating metal-related diseases

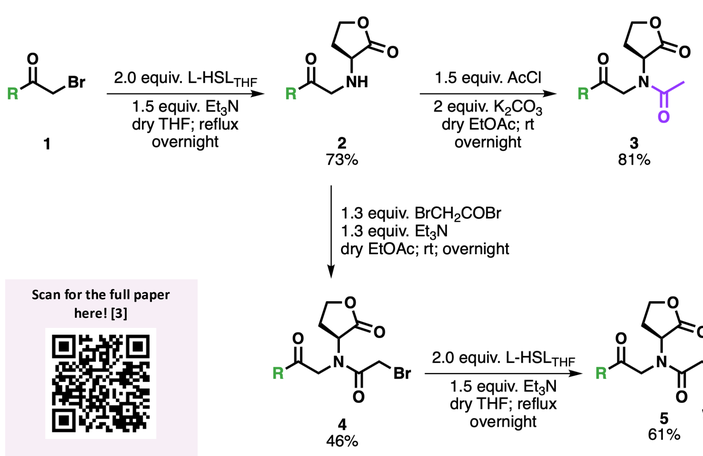


✔ Highly functionalizable peptoids
✔ Modular, divergent and side-chain protecting-group-free synthetic processes
✔ Promising biocompatible molecules
✔ Good bioavailability

The aim of this work is to optimize a solution-phase synthetic strategy for the preparation of chiral peptoid oligomers bearing L-homoserine lactone-derived side chains and their subsequent diversification via nucleophilic ring opening. Furthermore, this study evaluates the antibacterial activity of these potential chelating peptoids against antibiotic-resistant Gram-positive bacteria (*S. aureus)* and Gram-negative bacteria (*E. coli*).

Optimization of the solution synthetic protocol

Peptoid synthesis via Zuckermann Submonomerich Approach



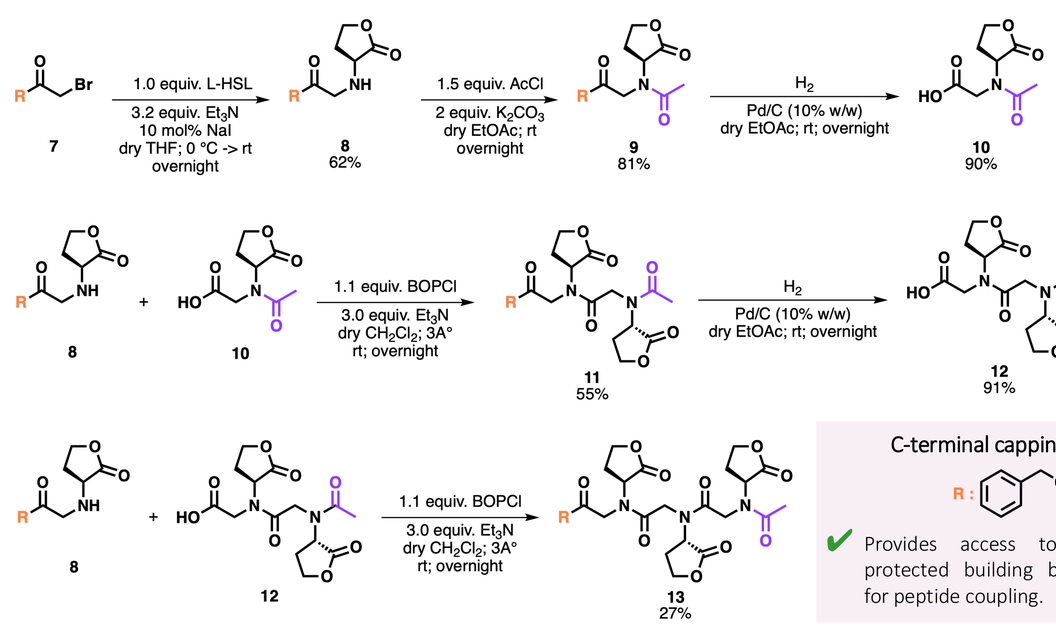
C-terminal capping group



✔ Simmetrical amide that simplifies NMR spectra interpretation
✔ It prevents the diketopiperazine formation

Scan for the full paper here! [3]

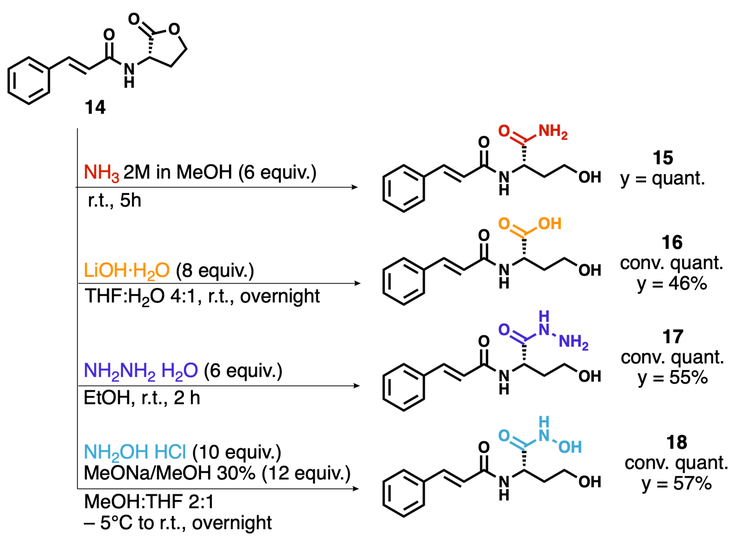
Peptoid synthesis via Peptide Coupling Approach



C-terminal capping group

✔ Provides access to orthogonally protected building blocks, suitable for peptide coupling.

Optimization of the ring-opening reaction on the model molecule 14



Highlights

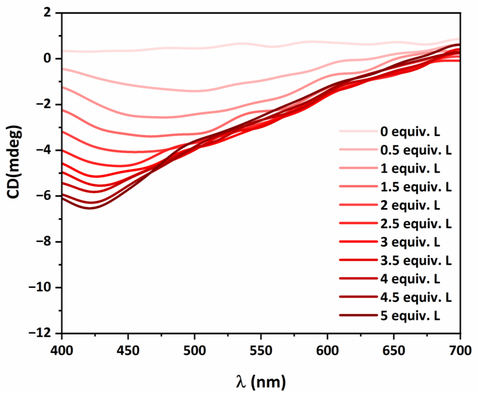
✔ Complete conversion under mild reaction conditions
✗ High product water-solubility limits purification yield
✔ Model molecule bearing a chromophoric moiety for ECD chelation studies

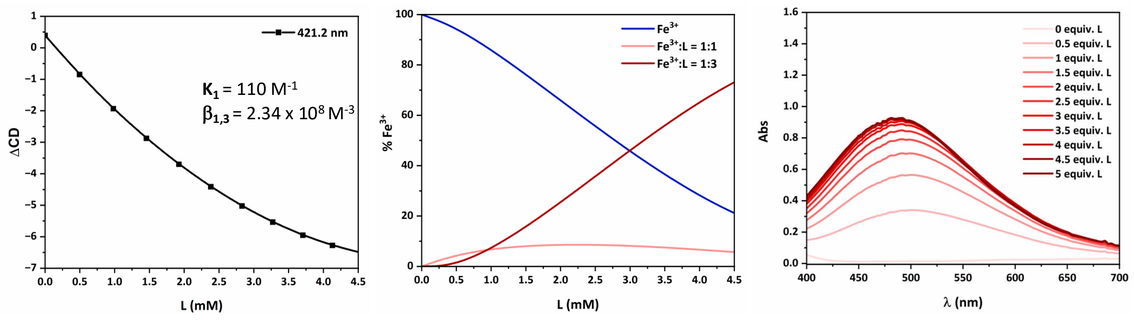
Conclusions

We have developed a **modular**, **side-chain protecting-group-free** strategy to access **chiral** peptoids bearing L-homoserine lactone-derived side chains, which can be easily functionalized via nucleophilic ring opening to yield **carboxylic acids**, **amides**, **hydrazides**, and **hydroxamic acids**. This late-stage diversification strategy expands peptoid chemical space, bypassing protecting-group manipulations that typically burden the synthesis of peptidomimetic systems containing natural chiral amino acid-derived motifs. Preliminary metal binding and antibacterial activity screening studies provide a strong basis for synthesizing novel derivatives with enhanced chelating properties and boosted biological efficacy.

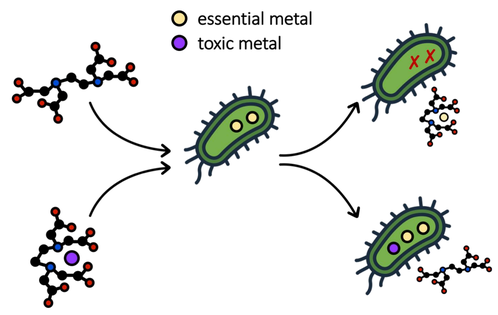
Metal binding pre-screening studies

A competition ECD titration was carried out on a multi-element mixture (Fe^{3+}, Ca^{2+}, Mg^{2+}, Mn^{2+}, Zn^{2+}, Cu^{2+} at 1 mM) in HCl/KCl (pH=2) with **hydroxamic acid** 18 (up to 5 equiv.). The induced ECD band supports the formation of a new ferric complex, while the spectral evolution suggests the involvement of two species. The best fit was obtained by considering a 1:1 transient complex followed by the formation of a more stable 1:3 complex. This complex retains a high affinity ($\beta_{1,3}$ = 2.34 x 10^8 M^{-3}) despite competition, compared to the single-metal Fe^{3+} titration ($\beta_{1,3}$ = 1.84 x 10^{10} M^{-3}), confirming high Fe^{3+} selectivity over competing metal ions.



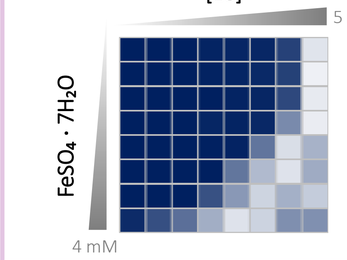


Antibacterial activity evaluation

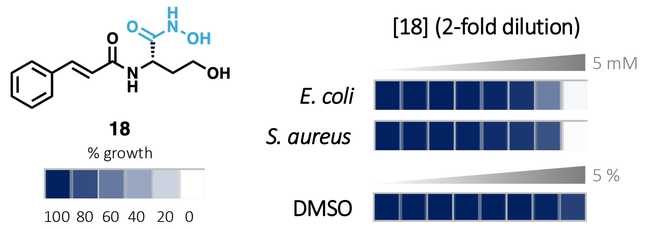


Targeting **bacterial metal homeostasis** [4,5] offers several biological advantages over conventional antibiotics. Antibacterial activity can occur through two main mechanisms of action:
→Sequestering essential metal ions
→Causing a metal overload from either intrinsically toxic metals or an excess of essential metals

Chequerboard assay: 18-Fe combination against *S.aureus* [18]

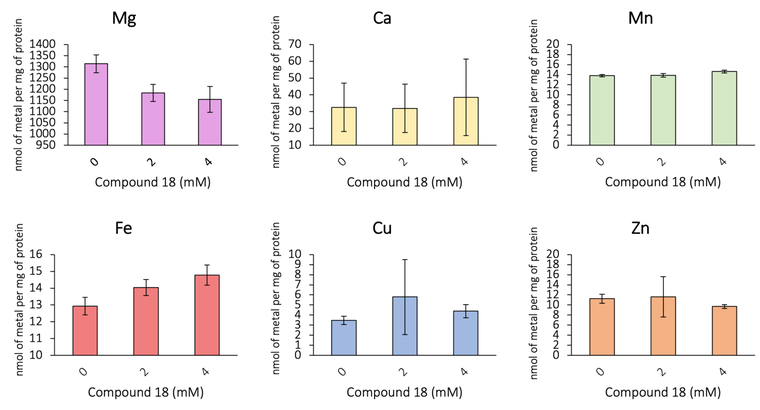


MIC determination of 18 against E. coli and S. aureus using the broth microdilution method [4,6]



Hydroxamic acid 18 showed a MIC of 5 mM against both *E. coli* and *S. aureus,* regardless of their distinct biological barriers. An increase in cellular Fe levels was observed only in S. aureus upon treatment with 18. Coupled with the observed synergistic effect with Fe, it suggests that the compound may facilitate cellular iron uptake, leading to iron overload and subsequent toxicity.

Cellular metal content of *S. aureus* after the treatment with 18 using ICP-MS



References

[1] K. Franz, *Curr. Opin. Chem. Biol.* **17**, 143–149 (2013). **[2]** E. Vigna et al. *Eur J Haematol.* **110,** 490–497 (2023). **[3]** L. Dei et al. *Org, Biomol. Chem* 10.1039.D6OB00951D (2026) **[4]** C. C. Murdoch et al. *Nat. Rev. Microbiol.* **20**, 657–670 (2022). **[5]** J. R. Paterson et al. *J. Appl. Microbiol.* **136**, lxaf258 (2025).

https://doi.org/10.17952/38EPS.2026.P008

Total Chemical Synthesis of RNF4 by Sequential Native Chemical Ligation: C-To-N Versus N-To-C Strategies

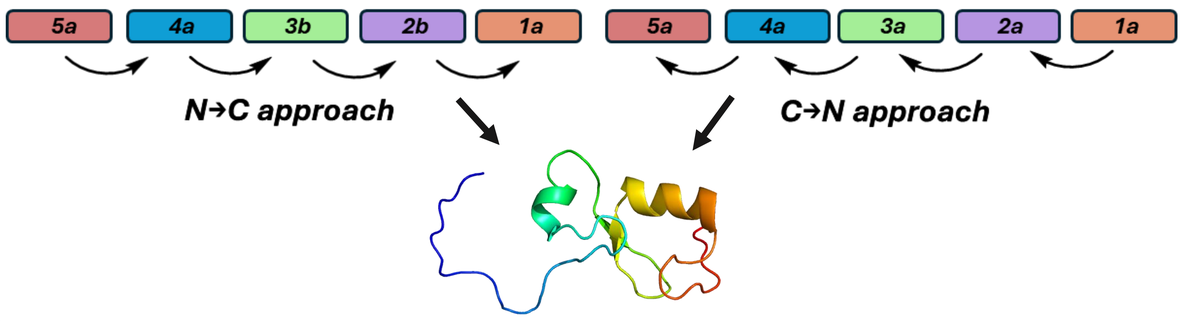
Saed Bisher [#1], Rajesh Pallava[#1], **Ashraf Brik**[1*]

[1]Schulich Faculty of Chemistry, Technion-Israel Institute of Technology, Haifa, 3200008, Israel.
[#]Contributed equally

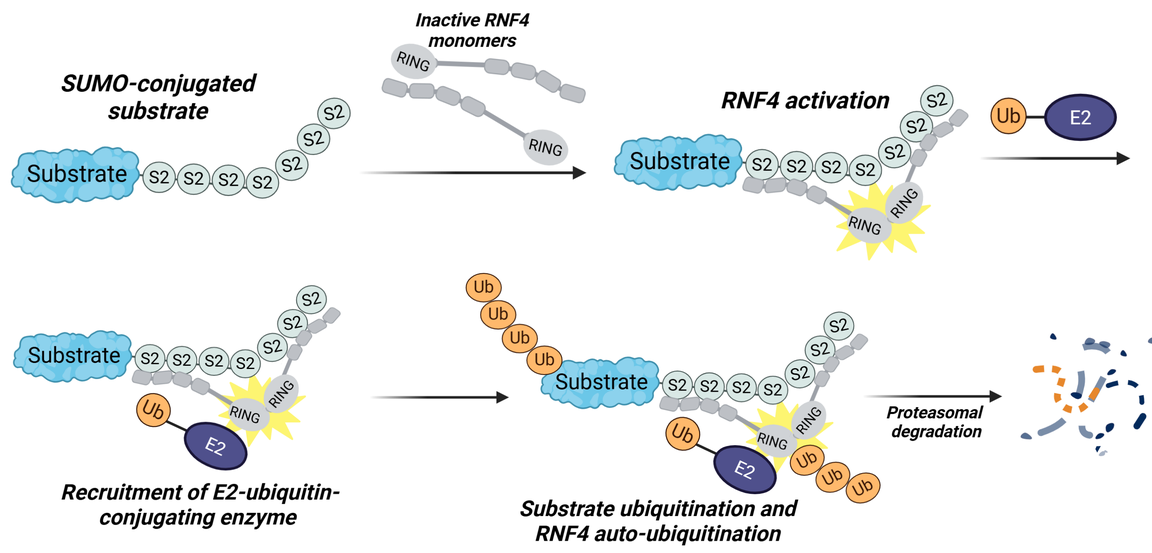
Email: Saed.bisher@campus.technion.ac.il

1 Abstract

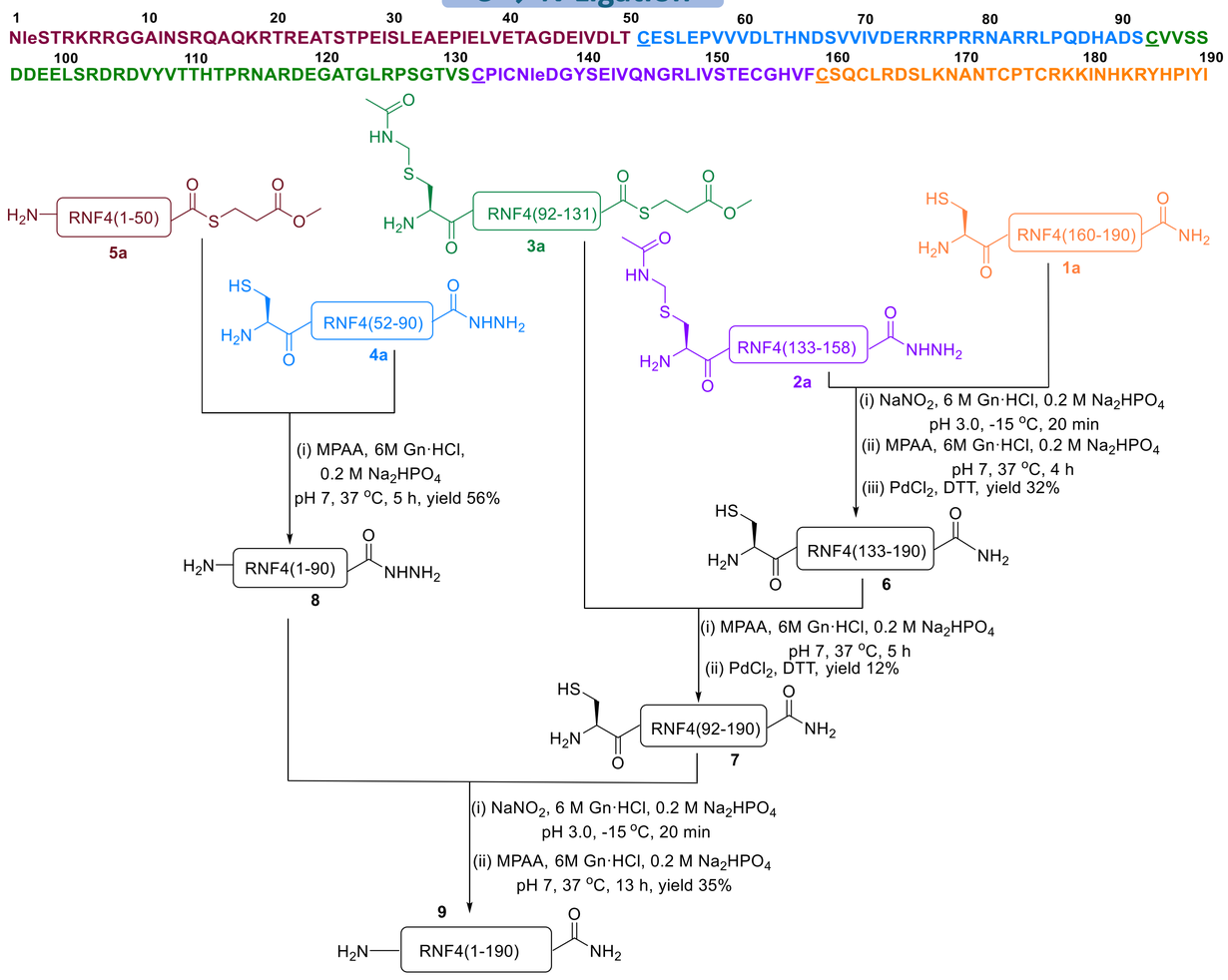
RNF4 is a RING-type E3 ubiquitin ligase. It targets polySUMOylated proteins for ubiquitination and subsequent proteasomal degradation. Chemical synthesis of RNF4 provides new opportunities to study its structure. It also enables deeper investigation of its biological function, including its role in degrading the oncoprotein PML-RARα in acute promyelocytic leukemia (APL). Importantly, this synthetic access allows the generation of site-specifically modified RNF4 variants bearing defined post-translational modifications (PTMs). To achieve this, we performed a total chemical synthesis of RNF4 via sequential native chemical ligation (NCL). Since RNF4 contains nine cysteine residues, we assembled it stepwise from five peptide fragments. Two synthetic strategies were explored: a convergent C → N ligation approach and a linear N → C ligation. The C → N strategy required Acm protection of cysteine residues, which increased deprotection and purification steps, whereas the N → C approach avoided cysteine protection, and further simplified the workflow. Overall, this work provides a reliable synthetic platform for RNF4 and enables future preparation of PTM-defined RNF4 variants for future biological studies.



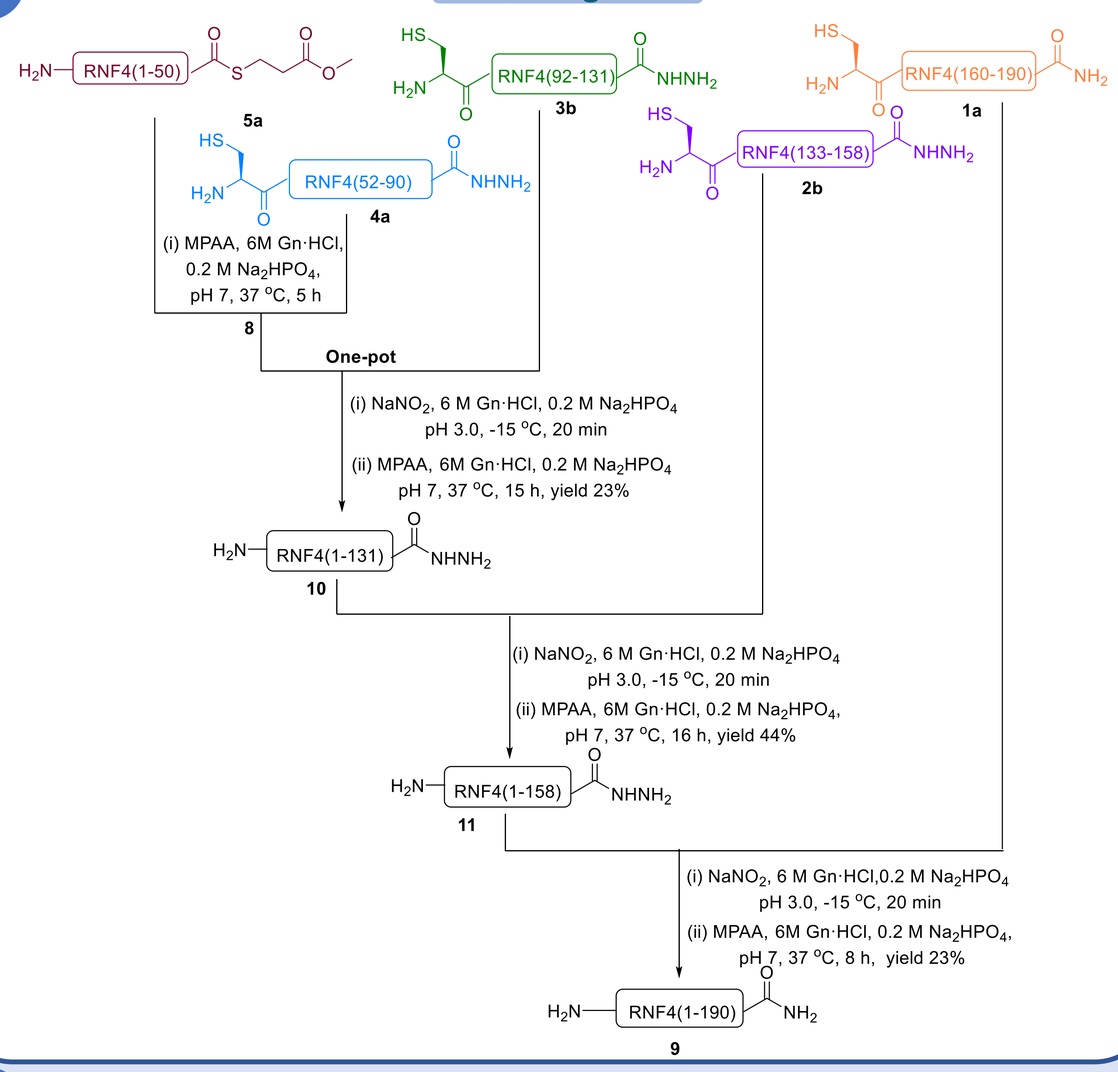
2 RNF4 SUMO-Targeted Ubiquitin Ligase



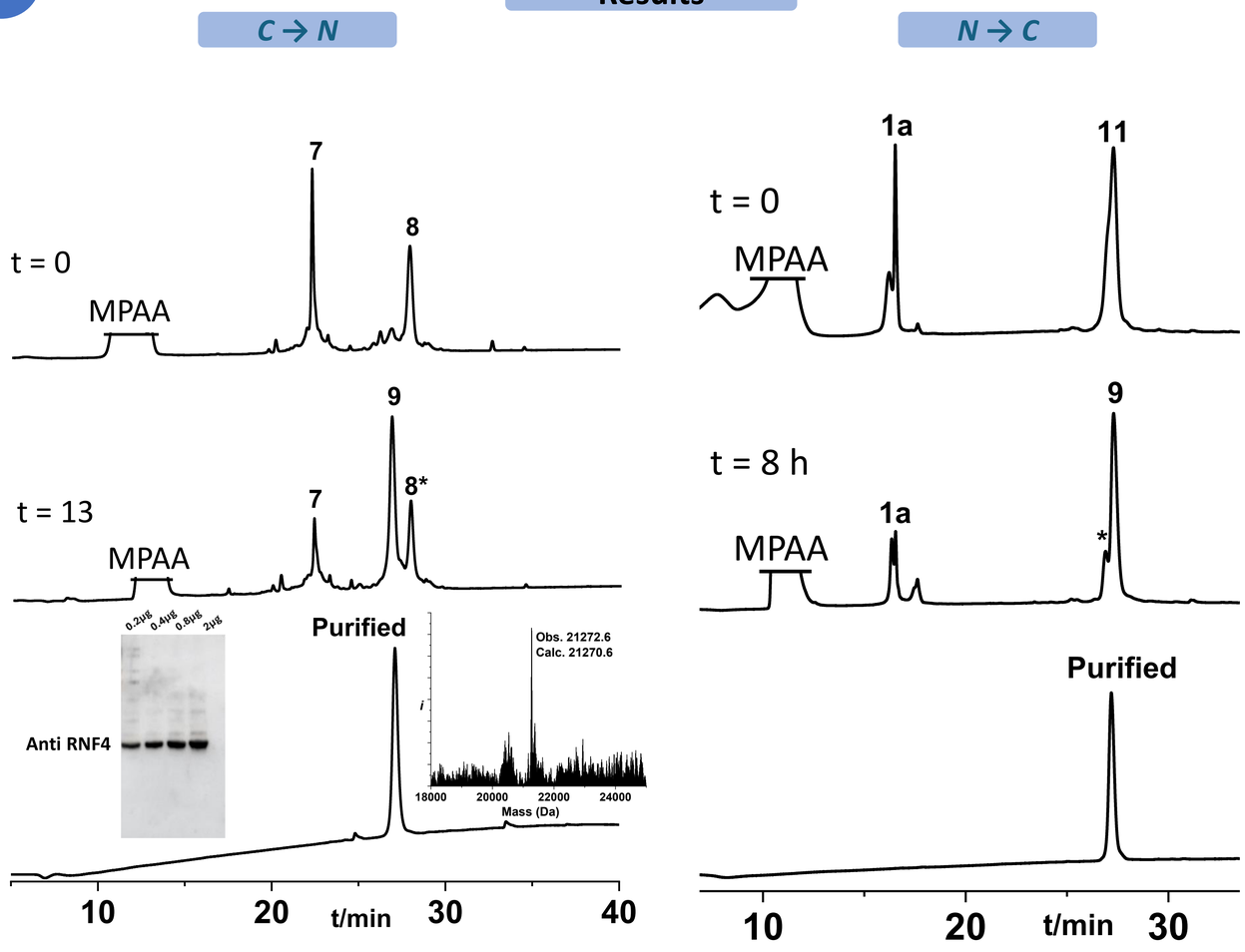
3 C → N Ligation



4 N → C Ligation



5 Results



6 Conclusion

1. We successfully achieved the **total chemical synthesis of full-length RNF4** via **native chemical ligation (NCL)**.
2. The C→N approach required cysteine protection/deprotection, additional purification steps, and a longer time - 3 weeks.
3. The N→C approach proceeded without cysteine protection, involved no purification steps a shorter workflow - 2 weeks.
4. The N→C ligation strategy not only enables efficient chemical synthesis of RNF4 but also provides a robust platform for the site-specific incorporation of future post-translational modifications, allowing systematic investigation of how defined PTMs regulate RNF4 activity, interactions, and cellular function.

7 Reference

1. Pallava, R.; **Bisher, S**.; Brik, A. *Total Chemical Synthesis of RNF4 by Sequential Native Chemical Ligation: C-to-N versus N-to-C Strategies.* J. Org. Chem. 2026

For further reading :

2. Tatham, M. H. et al. RNF4 is a poly-SUMO-specific E3 ubiquitin ligase required for arsenic-induced PML degradation. Nat. Cell Biol. 10, 538–546 (2008).
3. Seenaiah, M.; Jbara, M.; Mali, S. M.; Brik, A. "Convergent Versus Sequential Protein Synthesis: The Case of Ubiquitinated and Glycosylated H2B." *Angewandte Chemie International Edition* **2015**, *54*, 12374–12378.

For more scientific publications please visit our website:

https://doi.org/10.17952/38EPS.2026.P086

A (poly)Pro tip for preserving native disulfide connectivity during thiol-maleimide bioconjugation of disulfide-rich peptides

Lylia Azzoug, Ana Novak, Hervé Meudal, Jean-Baptiste Madinier, Stéphane Charpentier, Karine Loth, Séverine Morisset-Lopez, Carlo Pifferi* and Vincent Aucagne*

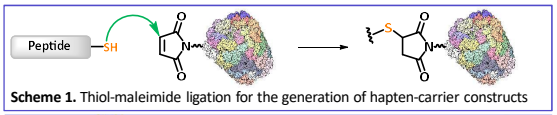
Centre de Biophysique Moléculaire – UPR CNRS 4301 – Rue Charles Sadron 45071 Orléans Cedex 2, France - carlo.pifferi@cnrs-orleans.fr vincent.aucagne@cnrs-orleans.fr

38th EPS European Peptide Symposium

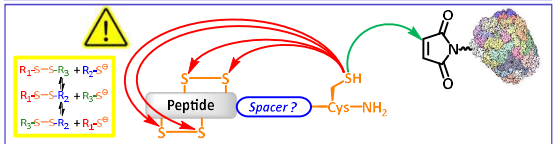
Background and project's aim

Generating specific antibodies against weakly immunogenic peptides requires their covalent conjugation to large protein carriers, such as keyhole limpet hemocyanin (KLH). This "hapten-carrier" approach exploits the carrier protein in two ways: (i) it provides, upon processing by antigen-presenting cells (APCs), CD4+ peptide epitopes essential for helper T-cell activation; and (ii) it displays multiple hapten copies, promoting B-cell receptor-mediated uptake and antibody production.

Most hapten-carrier approaches exploit highly efficient thiol-maleimide ligation, which enables the attachment of multiple copies of cysteine-containing peptides to commercial maleimide-functionalized carriers. Besides its fast kinetics and simple setup, this benchmark reaction proceeds under mild conditions (aqueous buffers, near-neutral pH, room temperature), compatible with a wide range of biomolecules (Scheme 1). While widely used for linear peptides by introducing a spare thiol (e.g., an extra cysteine), **thiol-maleimide conjugation of disulfide-containing haptens has an inherent limitation: the free thiol can attack disulfide bonds, disrupting the native hapten pattern and generating incorrectly folded, disulfide-scrambled structures** (Scheme 2). To address this issue, Katayama et al. [1,2] introduced **a long spacer between the thiol and disulfide-containing hapten to reduce the effective molarity of the thiol/disulfide reaction and slow it down**. While conceptually convincing, their approach was validated only by demonstrating the generation of native disulfide-rich hapten-specific antibodies, which was not possible using classical approaches. However, the possibility and extent of disulfide scrambling under conjugation conditions were not investigated, prompting us to explore this issue and develop a potentially more general strategy. Here, **we aimed to develop a general strategy for synthesizing disulfide-containing peptide conjugates while preserving their native disulfide pattern under thiol-maleimide coupling conditions**. We selected the well-structured N-terminal region of LINGO-1 as a model: a 20-mer containing two disulfide bridges. This peptide was coupled to a small set of thiol-containing spacers, and disulfide scrambling was rigorously monitored under maleimide conjugation conditions.



Scheme 1. Thiol-maleimide ligation for the generation of hapten-carrier constructs

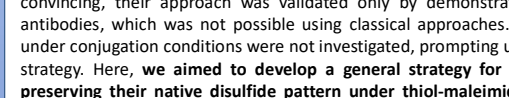


Scheme 2. Introducing **an additional thiol group** into a disulfide-containing hapten may **compromise its native disulfide connectivity** through an undesired intramolecular thiolate attack on disulfide bonds, competing with the intended thiol–maleimide conjugation. Incorporating an appropriate **spacer between the free thiol and the disulfide-rich core could suppress this side reaction** by decreasing the effective molarity of the reactive thiol near the disulfide bonds.

Spacers aimed to reduce disulfide scrambling

Previous work: the advent of the concept

Absence of disulfide pattern disruption during thiol / maleimide conjugation to a carrier protein was expected, but not checked. Indirect proof through the production of selective antibodies.

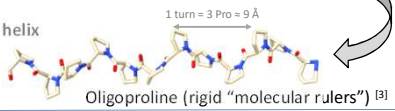


This work: validating and generalizing the approach

Peptide-based spacers, readily synthesized through SPPS

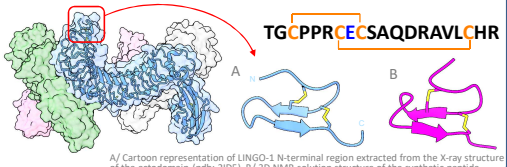
Flexible spacers:
- $(GGGGS)_2GGC(SH)$ ≡ 54 atoms
- $(GGGGS)_4GGGGC(SH)$ ≡ 90 atoms
- $(GGGGS)_8GC(SH)$ ≡ 141 atoms

Rigid spacers:
- $P_6C(SH)$ ≡ 36 atoms
- $P_{12}C(SH)$ ≡ 54 atoms



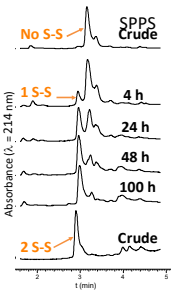
A model disulfide-rich peptide: LINGO-1[1-20]

Small disulfide-constrained peptide mimicking the 3D structure of the extracellular N-terminal part of LINGO-1, a trans-membrane protein involved in neurodegenerative diseases. Valuable model because **super sensitive to disulfide scrambling.**



A/ Cartoon representation of LINGO-1 N-terminal region extracted from the X-ray structure of the ectodomain (pdb: 2ID5). B/ 3D NMR solution structure of the synthetic peptide.

1. Synthesis of an azide derivative of LINGO-1[1-20]



H-TGC(Acm)PPRCEC(Acm)SAQDRAVLCHRGK(N_3)-NH_2

380 µM peptide
10% aq. DMSO,
RT, 100 h [*then lyophilization*]

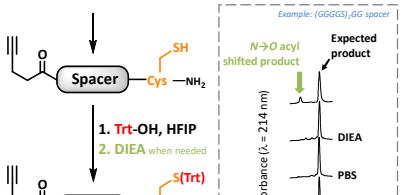
H-TGC(Acm)PPRCEC(Acm)SAQDRAVLCHRGK(N_3)-NH_2

1 mM peptide, 10 mM I_2
6.25% aq. HCl (160 mM) in AcOH, RT, 2 h
[*then precipitation with* Et_2O]

H-TGCPPRCECSAQDRAVLCHRGK(N_3)-NH_2

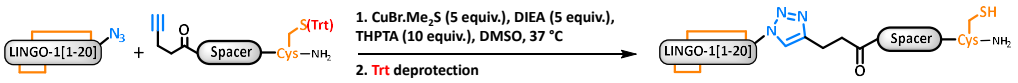
Overall yield after HPLC purification = 20%

2. Synthesis of spacers



- ***S*-Trityl** protection to prevent thiolate and thus disulfide scrambling during CuAAC
- **DIEA** treatment to reverse serine *N→O* shift (occurring upon TFA cleavage, for GGGGS-containing spacers).

3. Assembly through copper-catalyzed azide/alkyne Cycloaddition (CuAAC)



Spacer	Isolated yield (%)
$(GGGGS)_2GG$	43
$(GGGGS)_4GGGG$	35
$(GGGGS)_8G$	43
P_6	78
P_{12}	42

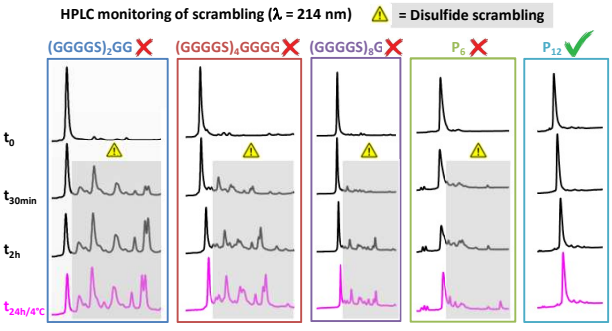
Yields not optimized.

- One single HPLC purification after step 1 (CuAAC).
- Non-standard CuAAC conditions because low water solubility of GGGGS linkers.
- ***S*-trityl** deprotection with TFA/H_2O/phenol/DODT/iPr_3SiH : 83/5/5/5/2 followed by precipitation in cold Et_2O. Very clean, quantitative reactions.
- LINGO-1[1-20]-SPACER-SH crude conjugates used for scrambling monitoring, and for KLH conjugation.

Evaluation of disulfide scrambling under thiol-maleimide conjugation conditions

Incubation of the LINGO-1[1-20]-SPACER-SH constructs under standard thiol-maleimide conjugation conditions: 20 mM phosphate buffer pH 6.6, 30 mM EDTA and 150 mM NaCl.

➢ HPLC and LC-MS monitoring at t = 0 and up to t = 2 h at RT and at t = 24 h at 4 °C (recommended conditions for conjugation to maleimide activated proteins).

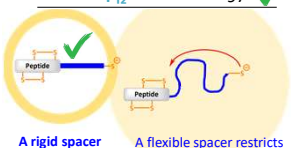


All solutions were thoroughly degassed and flushed with Ar to avoid SS dimer formation that would compromise the chromatograms (confirmed by MS).

The RIGID $(Pro)_{12}$ spacer very efficiently prevents disulfide scrambling

% of intact construct after incubation at 4 °C for 24 h

Spacer	% intact
$(GGGGS)_2GG$	11
$(GGGGS)_4GGGG$	18
$(GGGGS)_8G$	30
P_6	45
P_{12}	97 ✓

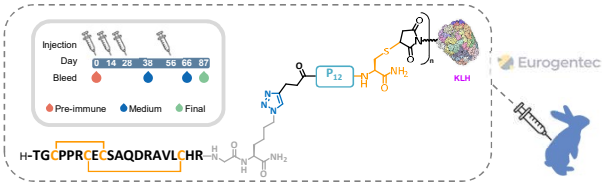


A rigid spacer restricts the accessible space for the thiolate to a sphere surface. => NO SS ATTACK (if spacer long enough)

A flexible spacer restricts the accessible space for the thiolate to a sphere volume => longer spacers slow down but do not abolish the SS attacks. Plus potential preferential folding issues.

Biological validation of the synthetic methodology

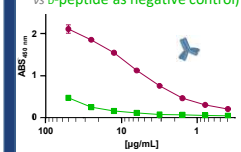
Immunization of a rabbit with the Lingo-1[1-20]-P_{12}-KLH conjugate



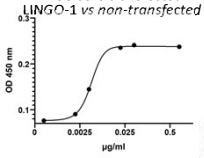
Immuno-ELISA and Western Blot assays of obtained polyclonal IgGs

Purification of IgGs from serum through protein-A affinity chromatography – similar results obtained using non-purified serum

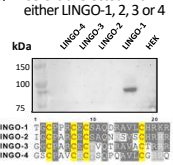
ELISA : *coating* = LINGO-1[1-20]-GK(N_3) *vs* D-peptide as negative control)



Live cells ELISA : HEK293 cells transfected with LINGO-1 *vs non-transfected*



Western blot : Cells transfected with either LINGO-1, 2, 3 or 4



WB shown = standard SDS PAGE, 1/5000 Ab dilution. Behaves equally well under (unboiled) native conditions.

=> Obtention of specific LINGO-1 antibodies

Validated for ELISA assays, cell assays and Western blot (either denaturating or not SDS-PAGE)
Large amounts (418 mg from the immunisation of only one animal)
Much superior than the best commercially available Ab against LINGO-1 (470$ for 100 µg !)

Conclusions and perspectives

Small disulfide-rich peptides (DRPs) require conjugation to large carrier proteins to elicit an effective immune response because of their low immunogenicity. Thiol–maleimide chemistry is widely used for such peptide–protein conjugates, facilitated by commercial maleimide-functionalized carriers such as KLH. However, introducing a spare thiol into a DRP can disrupt its native disulfide pattern, generating heterogeneous immunogens that fail to accurately mimic the intended epitope. Here, **we established a robust strategy for the late-stage introduction of thiol-containing linkers onto DRPs, generating "DRP–spacer–thiol" constructs that preserve their native disulfide pattern under thiol–maleimide coupling conditions** and enable conjugation to protein carriers. Using LINGO-1[1–20] as a model DRP, whose solvent-exposed disulfides are particularly prone to nucleophilic attack, we generated an immunogen that elicited an IgG response following standard immunization. ELISA showed that protein A-purified polyclonal IgG selectively bound LINGO-1 on transfected cells. Western blot analysis demonstrated superior sensitivity to a commercial IgG and strong specificity for LINGO-1 over homologs LINGO-2, -3, and -4, which share the same cysteine pattern and 45–75% sequence similarity. Overall, our results establish a robust strategy for generating DRP-specific antibodies while preserving native disulfide patterns, readily adaptable to diverse DRPs.

Check out for the full story ! link to the published article:

References: [1] Katayama, H. and Mita, M. Bioorg. Med. Chem., **2016**, *24*, 3596. [2] Katayama, H.; Mizuno, R. and Mita, M. *Biosci. Biotechnol. Biochem.*, **2019**, *83*, 1791. [3] Wilhelm, P.; Lewandowski, B.; Trapp, N.; Wennemers, H. *J. Am. Chem. Soc.*, **2014**, *136*, 15829.

New antimicrobial peptides on the horizon: comprehensive investigation of bioactive peptaibols for future practical application

Dóra Balázs, Ákos Rozsnyói, Henriett Hunkár, Gergő Terna, Fanni Kovács, András Szekeres, Mónika Varga, Csaba Vágvölgyi, Tamás Papp, Tamás Marik, Chetna Tyagi & László Kredics

Department of Biotechnology and Microbiology, Faculty of Science and Informatics
University of Szeged, Szeged, Hungary
dora.balazs91@gmail.com
https://doi.org/10.17952/38EPS.2026.P212

PEPTAIBOL

Peptide, rich in special non-proteinogenic amino acids, like α-aminoisobutyric acid (**Aib**), and containing **aminoalcohol** group at C-terminal.

WHY ARE PEPTAIBOLS IMPORTANT?

Peptaibols are **bioactive, small peptides** produced by the filamentous fungal *Trichoderma* species. Peptaibols aggregate and **form ion channels** in the cell membrane and exert **strong antibiotic effect** on other microorganisms. In the future, they may play an **important role in agriculture**, biological plant protection, and we are exploring further areas of possible benefits. Their **comprehensive investigation** is essential for their future practical application.

DETERMINATION OF PEPTAIBIOM

- Each *Trichoderma* strain produces a characteristic **mixture of peptaibiotics** - compound of short and long peptaibols or lipopeptaibols
- **Peptaibiome** → total peptaibol production of a *Trichoderma* strain
- Preparation of the peptaibol extracts and determination of the total peptaibiom by **mass spectrometry (HPLC-MS)** (*Figure 1*)
- **Comprehensive investigation** of their characteristic properties is fundamentally important to facilitate their future application in agriculture and biotechnology

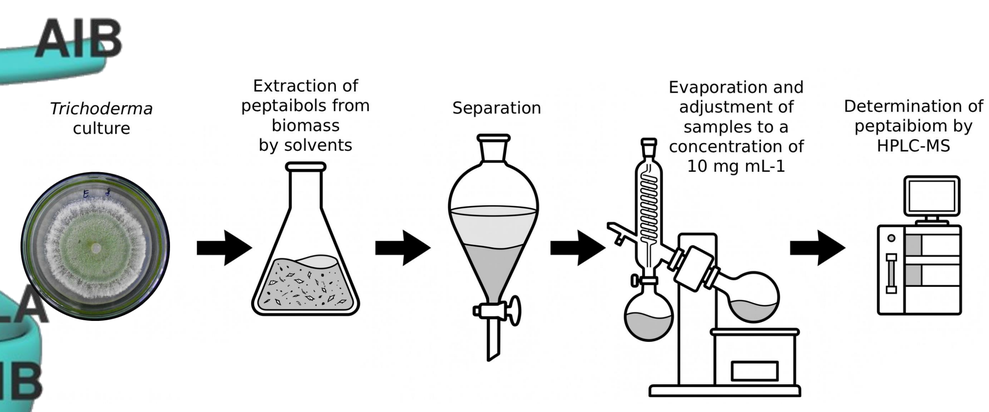


Figure 1. The process of the extraction and determination of peptaibiome

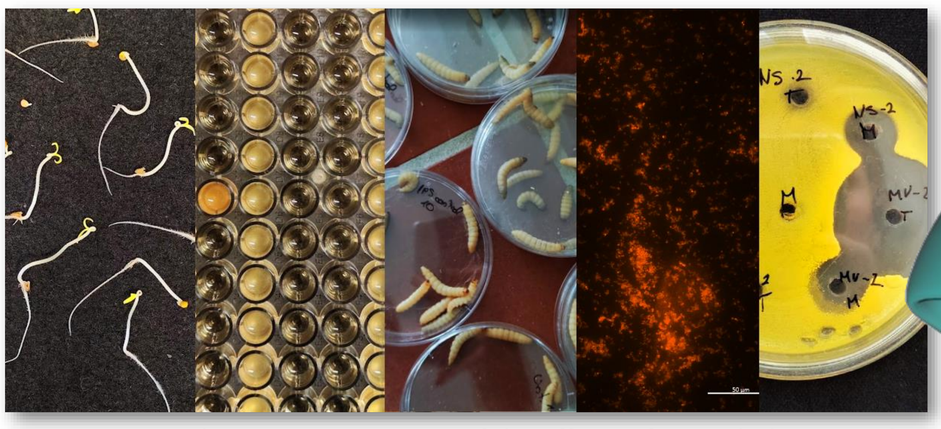


Figure 2. Comprehensive investigation of the effects of peptaibol extracts from various perspectives

COMPREHENSIVE STUDY OF BIOACTIVITY

- Exploring their biological effects against Gram-positive and -negative bacterial and fungal species
  - ➢ Most of the investigated peptaibol extracts inhibit Gram-positive, and several Gram-negative bacterial and phytopathogenic fungal species **between the concentration of 10 and 0.156 mg ml^{-1}**
  - ➢ Further studies on **plants, model organisms, biofilm-forming bacteria**, and **ecotoxicological studies** for safe and effective practical application (*Figure 2*)

COMPUTATIONAL SIMULATIONS

- For **computational investigations** of the most produced peptaibol sequences 1 microsecond long **accelerated molecular dynamics (aMD)** simulations were performed
- Dihedral-angle based principal component analysis (dPCA) method was used to cluster the trajectory based on their **internal motions and obtain lowest energy representative structures** (*Figure 3*)
- The various structural properties and folding characteristics have been summarized

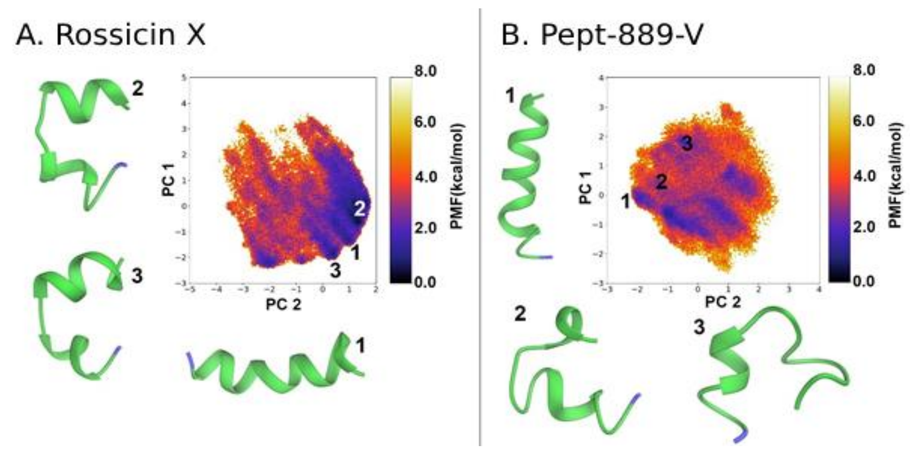


Figure 3. dPCA performed with the selected, most produced peptaibol sequences

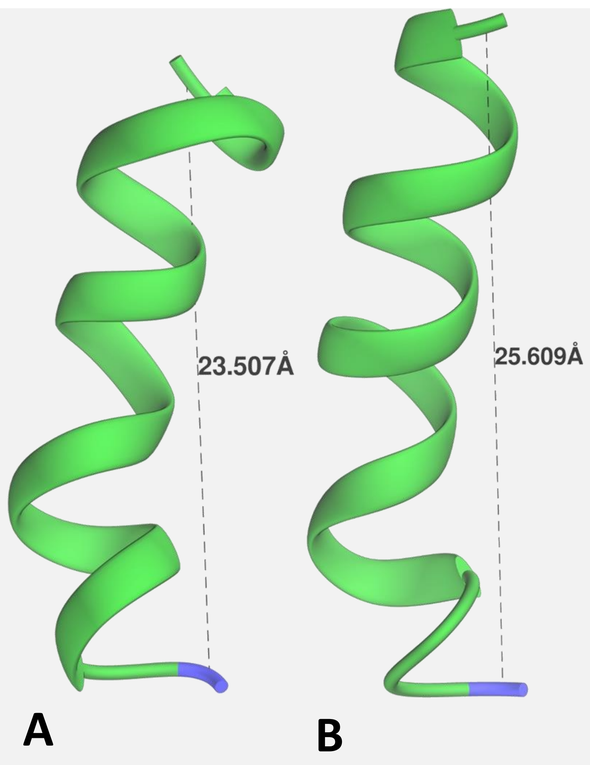


Figure 4. The length of Rossicin X (A) and Pept-889-V (B)

STRUCTURE-ACTIVITY RELATIONSHIPS

The search for connections between the amino acid compositions, structural dynamics changes and characteristics and their exerted bioactivites

➢ AMINO ACID MOTIFS

- Characteristic motif allows more defined folding process and less stable states, which provides the forming of ion channels.

➢ AMINO ACID CONTENT

- The sequences with more Aib form 3^{10} helix structure more often, which allows the tighter incorporation of amino acids with larger side chains. This process leads to the elongation of peptaibol chains.

➢ LENGTH OF PEPTAIBOLS

- Based on the results of bioactivity tests, the longer peptaibols (with 19-and 20-residue sequences) are more active against microorganisms (*Figure 4*).

➢ HYDROPHOBIC AND HYDROPHILIC REGIONS

- The different hydrophobic and hydrophilic regions cluster on the same side of the peptaibols. The position of regions may affect their bioactivity (*Figure 5*).

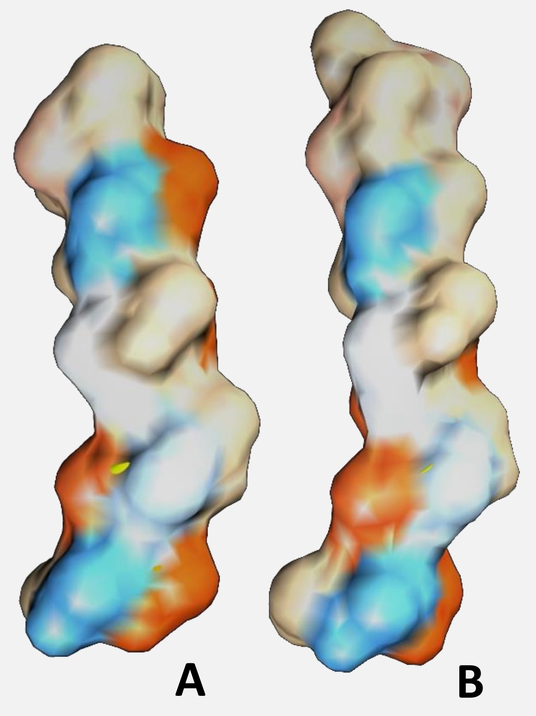


Figure 5. The hydrophobic and hydrophilic regions of Rossicin X (A) and Pept-889-V (B)

THIS WORK WAS SUPPORTED BY THE HUNGARY–SERBIA IPA CROSS-BORDER CO-OPERATION PROGRAMME (PROJECT FERTILEAVES, HUSRB/23S/11/027) AND BY THE SCHOLARSHIP PROGRAM OF THE MINISTRY OF CULTURE AND INNOVATION, FINANCED FROM THE NATIONAL RESEARCH, DEVELOPMENT AND INNOVATION FUND (EKÖP-24-4SZTE-629 AND EKÖP-24-4-SZTE-605).

Development of a G protein mimetic toolbox to conformationally lock G protein-coupled receptors (GPCRs) in the active state

Thijs Vynckier,[a] Morgane Mannes,[a] Morgane Rivoal,[a] Charlotte Martin,[a] Christel Menet,[b] Toon Laeremans,[b] Jean-Louis Banères,[c] and Steven Ballet[a]

[a]*Research Group of Organic Chemistry (ORGC), Department of Chemistry and Bioengineering Sciences, Vrije Universiteit Brussel, Brussels, Belgium.*

[b]*Confo Therapeutics, Ghent, Belgium.*

[c]*Institut des Biomolécules Max Mousseron (IBMM), Université de Montpellier, CNRS, ENSCM, Montpellier, France*

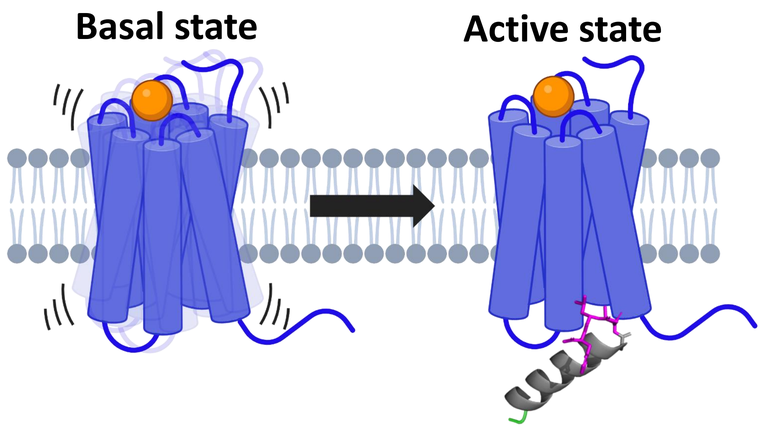
https://doi.org/10.17952/38EPS.2026.P146

thijs.vynckier@vub.be

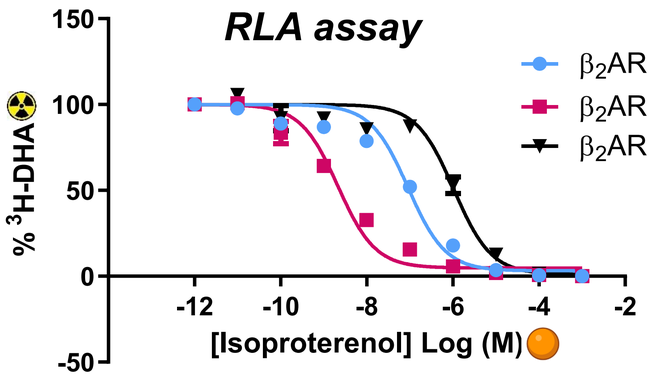
INTRODUCTION

G protein-coupled receptors (GPCRs) are membrane-spanning proteins and are targeted by over 30% of prescribed drugs on the market. Despite their central role in modern medicine, they are therapeutically underexplored because of their intrinsic dynamic behavior, which makes them difficult to study. Stabilizing defined receptor states has therefore become essential for functional and structural investigations.[1] Our group is developing generic **G protein-mimicking peptides** capable of **locking GPCRs in their active signaling state**.[2-5] The optimized G protein mimetics are **generic** and successfully lock several **Gαs-** & **Gαq-controlled GPCRs** in their active signaling state (β2AR, D1R, GHSR & M1R). Our tool compounds were proven useful in **reverse pharmacology screening** approaches (β2AR, D1R) and in examining GPCR signaling (GHSR).

OBJECTIVE

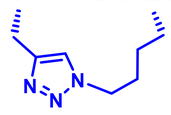


ALLOSTERIC STABILIZATION



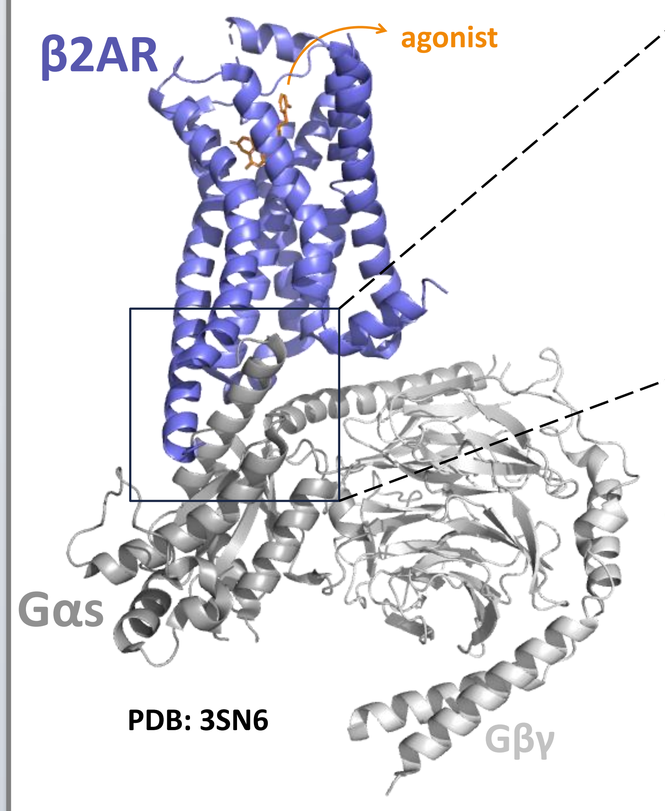
SBL-CM-51

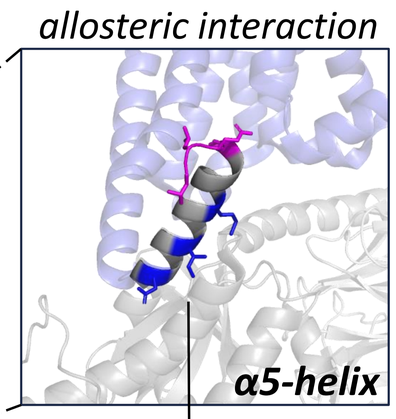
Ac-**KKK**FN**Pra**CRD**Azk**IQRMHLRQYE**Cha**L-OH

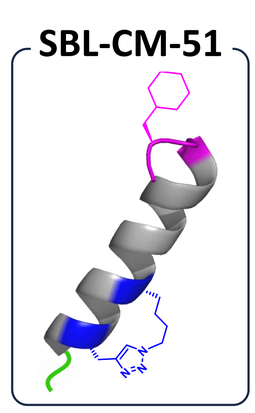


→ Also locks **D1R**

Gαs PEPTIDOMIMETIC DESIGN



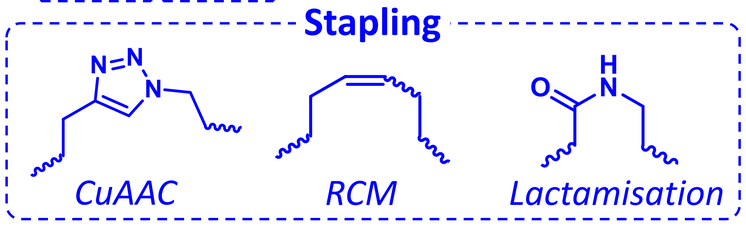




Point modifications

Ac-KKK-FN**D**CRD**I**IQR**M**HLRQ**YELL**-OH

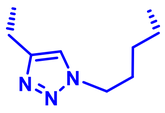
Stapling



Other G protein subfamilies? [3, 5]

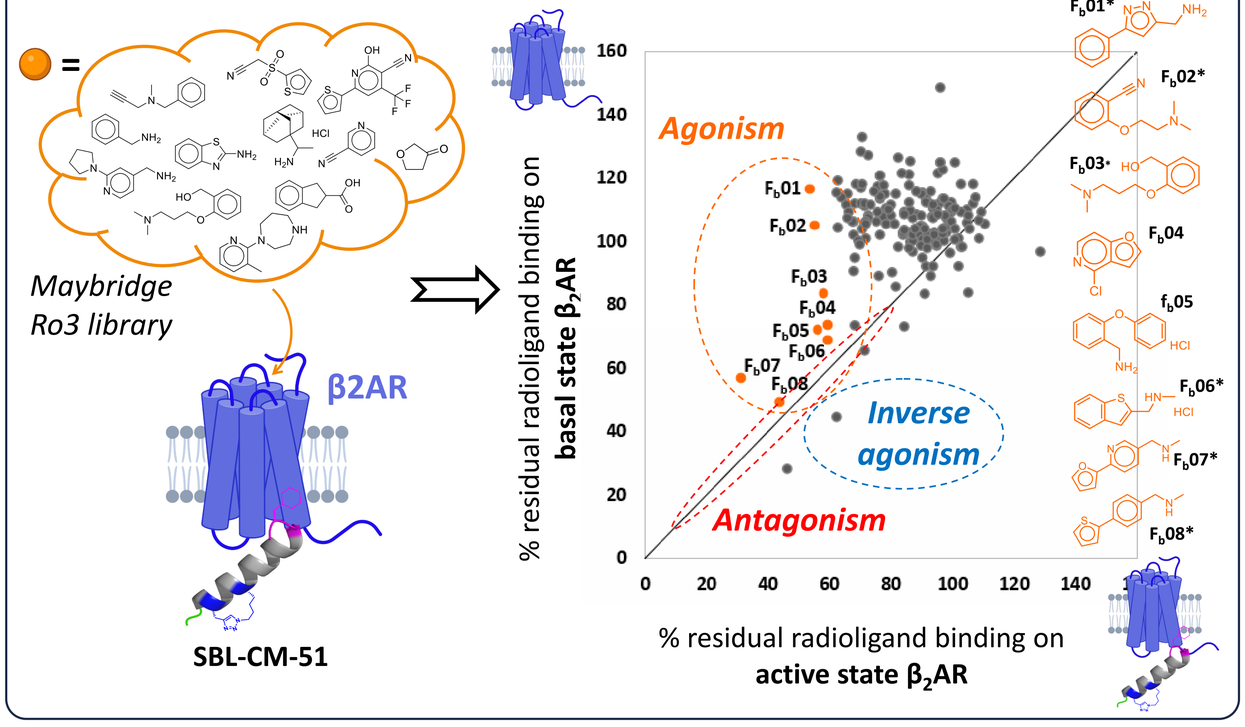
SBL-Gq-05

Ac-**KKK**FA**[Pra**VKD**Azk]**ILQLNLKEYNLV-OH ⟶ Locks the Gq-controlled Ghrelin- **(GHSR)** & Muscarinic-1- **(M1R)** receptor in the active state

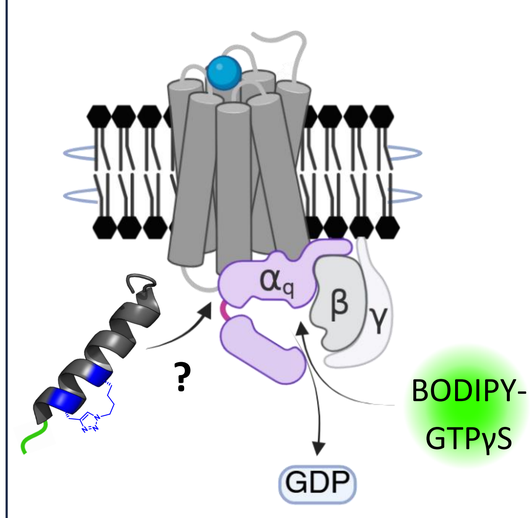


APPLICATIONS

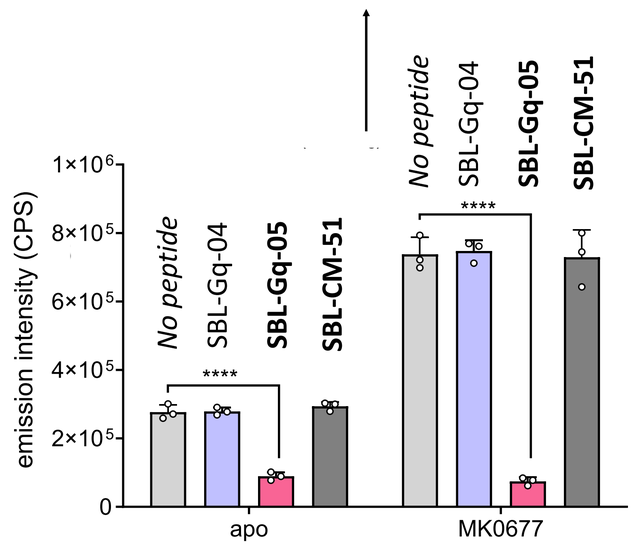
Fragment-based drug screens [2]



GPCR signaling studies [3]

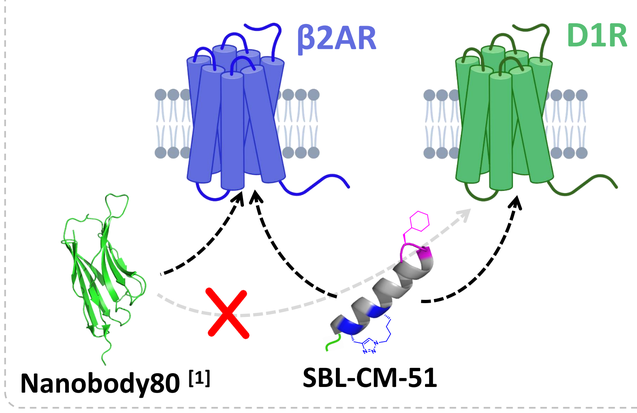


***SBL-Gq-05 competes** with Gq protein binding, while SBL-CM-51 does not*

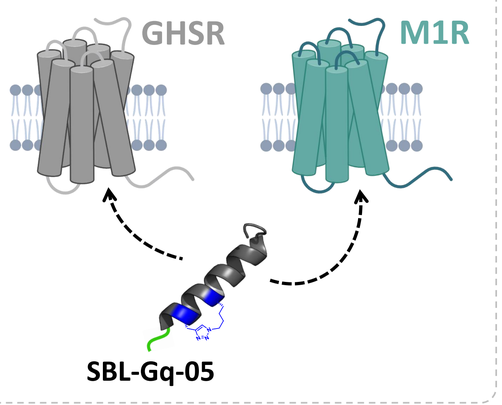


GENERICITY OF THE TOOLS

Gs-controlled GPCRs [2, 4]



Gq-controlled GPCRs [3, 5]



CONCLUSIONS & PERSPECTIVES

SBL-CM-51 stabilizes **Gs**-controlled GPCRs in the active state

SBL-Gq-05 stabilizes **Gq**-controlled GPCRs in the active state

→ **Tool compounds** for use in **FBDS, GPCR signalling studies,…**

Acknowledgments

1SA8226N & OZR3939

SRP95

References

[1] E. Pardon, *Angew. Chem. Int. Ed.* **2018**, *57*, 5292
[2] M. Mannes, *Angew. Chem. Int. Ed.* **2021**, *60*, 10247
[3] M. Mannes, *Sci. Signal.* **2025**, *18*, 7692
[4] M. Mannes, WO/2022/129630
[5] M. Mannes, WO/2023/247717

Structure-Based Design Leads to uPA Loop Mimetic that Accumulates in uPAR-expressing Tumors in Mice

E. Vangeloven,[1,3,4] S. Pollenus,[4] M. Hosseini,[1,3] T. Dal Maso,[2,3] S. Hernot,[4] W. Versées,[2,3] S. Ballet[1]

[1]Research Group of Organic Chemistry, Vrije Universiteit Brussel, Pleinlaan 2, 1050 Brussels, Belgium; [2]VIB-VUB Center for Structural Biolc Pleinlaan 2, 1050 Brussels, Belgium; [3]Structural Biology Brussels, Vrije Universiteit Brussel, Pleinlaan 2, 1050 Brussels, Belgium; [4]Laboratory for In-vivo Cellular and Molecular Imaging, Vrije Universiteit Brussel, Brussels, Belgium.

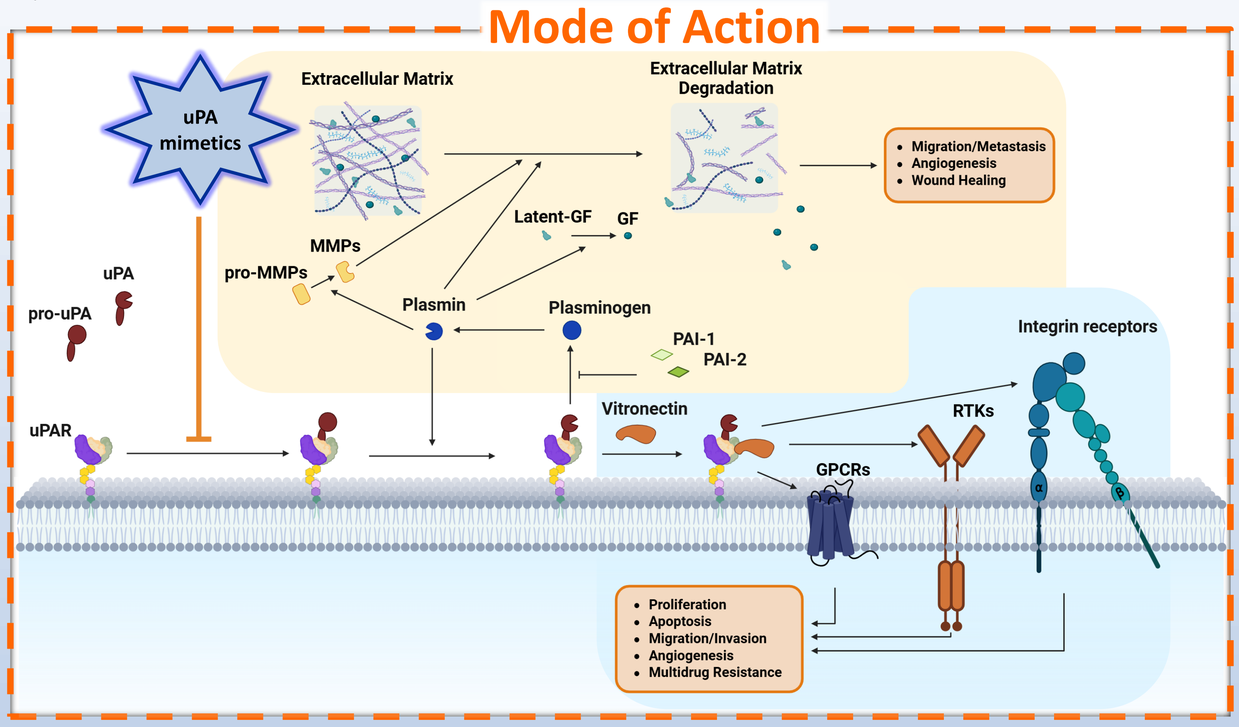
esau.vangeloven@vub.be

https://doi.org/10.17952/38EPS.2026.P157

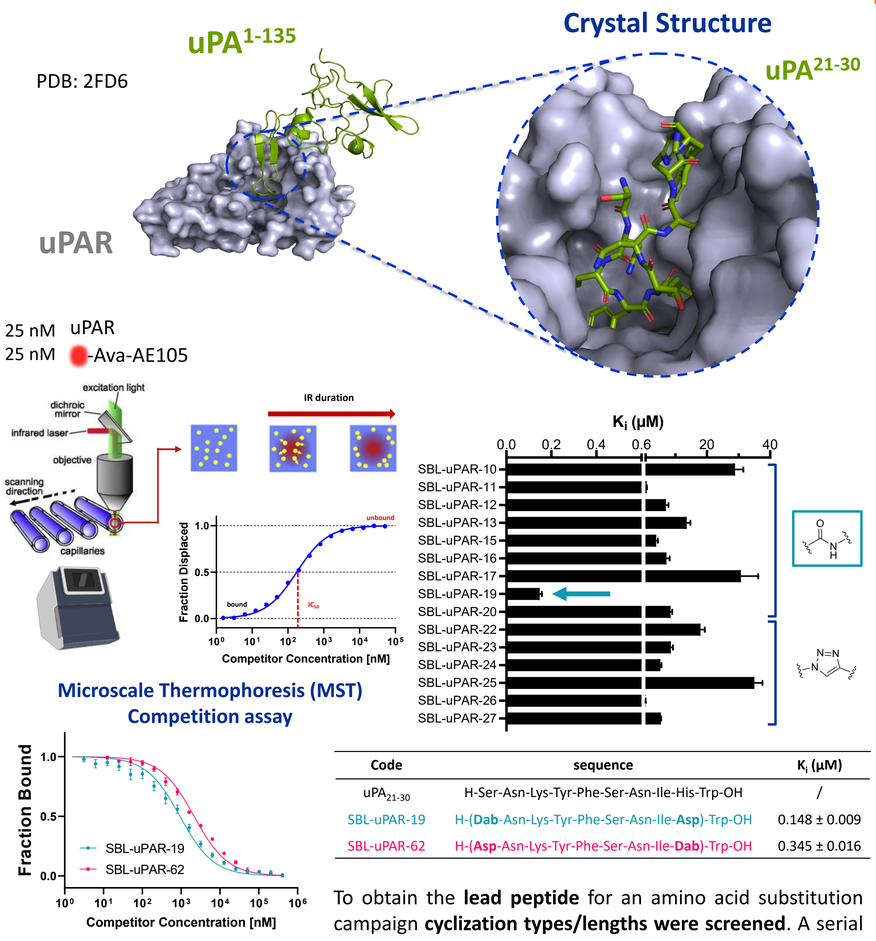
INTRODUCTION

The urokinase-type plasminogen activator receptor (**uPAR**) is a membrane-anchored glycoprotein expressed at low levels during physiological processes such as tissue remodeling and inflammation. However, in many human **cancers** elevated uPAR expression is associated with **poor prognosis**.[1] **In addition to** being a compelling target for **cancer therapy**, uPAR represents a promising **generic imaging target**.[2] Universal uPAR **probes** could **facilitate** the emergence of **fluorescence-guided surgery**, a technique shown to improve tumor-free survival following resective surgery.[3] The loop region uPA$^{21-30}$ of the endogenous ligand uPA interacts within the confined central cavity of uPAR and is responsible for the majority of the binding interactions.[1] Through systematic **structure-based design**, we developed a **high affinity** uPAR **ligand** based on uPA$^{21-30}$, that accumulates in colorectal cancer in mice.

Mode of Action

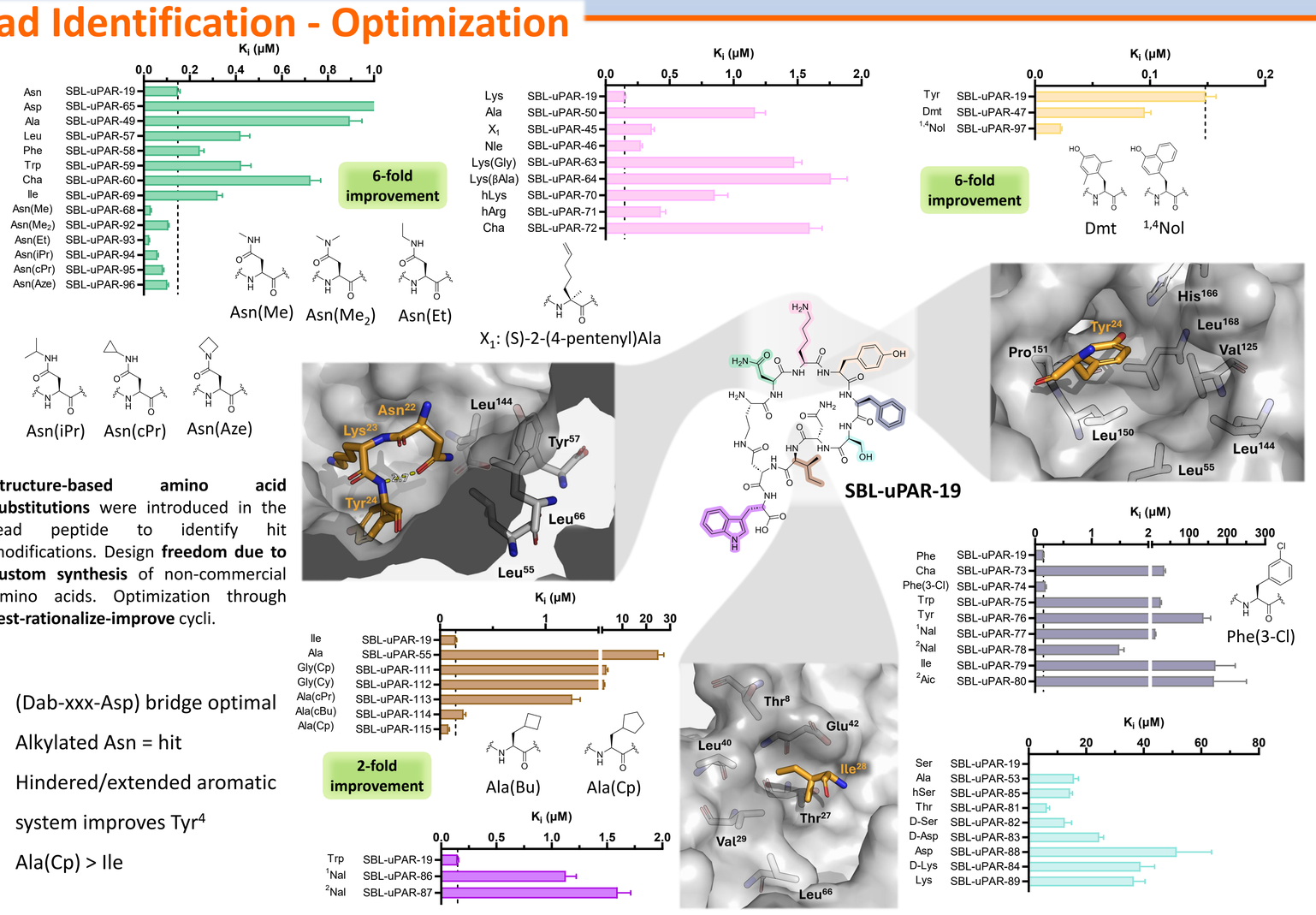


Lead Identification - Optimization



Code	sequence	K_i (μM)
uPA$_{21-30}$	H-Ser-Asn-Lys-Tyr-Phe-Ser-Asn-Ile-His-Trp-OH	/
SBL-uPAR-19	H-(**Dab**-Asn-Lys-Tyr-Phe-Ser-Asn-Ile-**Asp**)-Trp-OH	0.148 ± 0.009
SBL-uPAR-62	H-(**Asp**-Asn-Lys-Tyr-Phe-Ser-Asn-Ile-**Dab**)-Trp-OH	0.345 ± 0.016

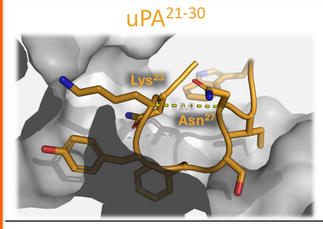
To obtain the **lead peptide** for an amino acid substitution campaign **cyclization types/lengths were screened**. A serial dilution of the competitor was incubated with constant concentration of uPAR and labeled reference peptide AE105. After incubation for 5 minutes, the **thermophoresis** was measured on a Nanotemper Monolith.

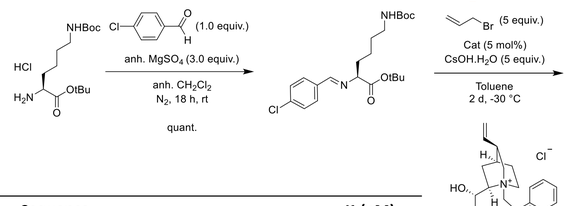


Structure-based amino acid substitutions were introduced in the lead peptide to identify hit modifications. Design **freedom due to custom synthesis** of non-commercial amino acids. Optimization through **test-rationalize-improve** cycli.

- (Dab-xxx-Asp) bridge optimal
- Alkylated Asn = hit
- Hindered/extended aromatic system improves Tyr^4
- Ala(Cp) > Ile

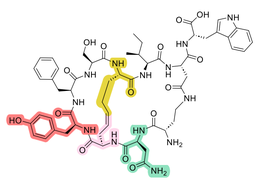
Custom Bicycles – NMR Sructure – High-Affinity Labeled Analogs





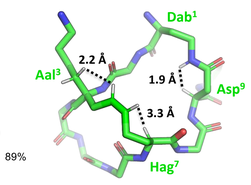
code	Sequence	K_i (nM)
SBL-uPAR-19	Dab Asn Lys Tyr Phe Ser Asn Ile Asp Trp	148 ± 9
SBL-uPAR-50	Ala	1 167 ± 81
SBL-uPAR-66	Dab D-Gly(Allyl) Hag Asp	196 ± 10
SBL-uPAR-91	Dab Aal Hag Asp	11.2 ± 0.3
SBL-uPAR-99	Dab Aal Dmt Hag Asp	0.66 ± 0.06
SBL-uPAR-100	Dab Asn(Et) Aal Hag Asp	0.35 ± 0.04
SBL-uPAR-101	Dab Asn(Et) Aal Dmt Hag Asp	0.17 ± 0.04

Hag: homoallyl glycine

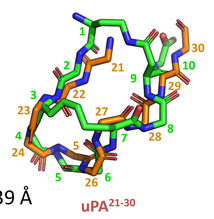


SBL-uPAR-66

NMR Structure



SBL-uPAR-100



SBL-uPAR-110

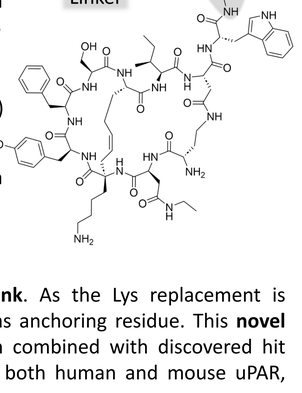
MST direct binding ← TAMRA — K_d = 1.3 ± 0.2 nM (Human); K_d = 0.21 ± 0.15 nM (Mouse)

SBL-uPAR-107

Near-infrared fluorescence imaging ← s775z — K_d = 4.7 ± 0.8 nM (Cells (HT-29))

SBL-uPAR-104

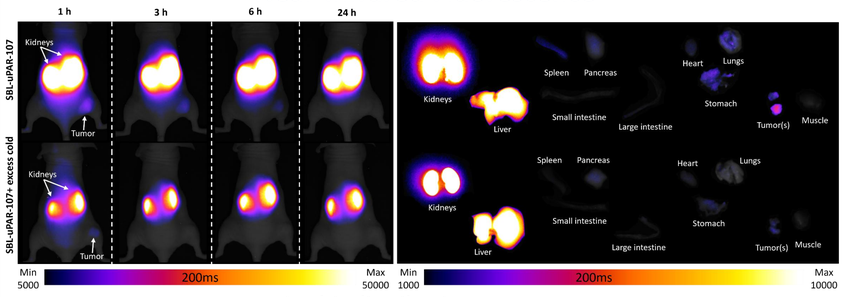
^{111}In chelation SPECT ← DOTA — K_i = 3.3 ± 0.3 nM (Human)



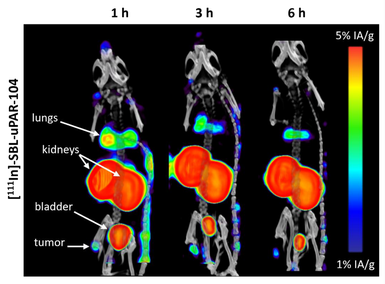
The lead peptide was regidified with a **second crosslink**. As the Lys replacement is detrimental for binding, **Aal was synthesized** and used as anchoring residue. This **novel constrain architecture** resulted in **sub-nM ligands** when combined with discovered hit modifications. The TAMRA-labeled **SBL-uPAR-110** bound both human and mouse uPAR, indicating **species cross-reactivity**.

In Vivo Imaging

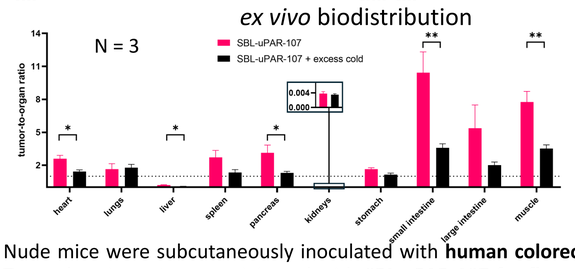
Near-Infrared Fluorescence



SPECT/CT



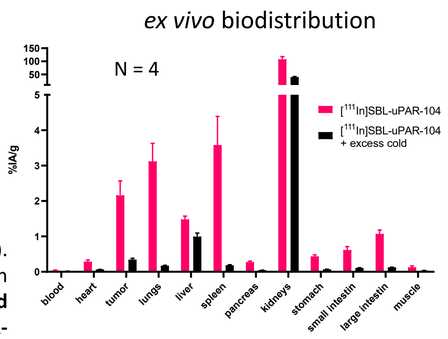
ex vivo biodistribution



dosage
Fluorescence:
SBL-uPAR-107
2 nmol

SPECT:
[^{111}In]**SBL-uPAR-104**
7.45 ± 0.53 MBq
0.5 nmol

ex vivo biodistribution



Nude mice were subcutaneously inoculated with **human colorectal cancer** cells (HT-29). Tumor-bearing mice were injected with **SBL-uPAR-107** for **fluorescence** imaging or with [^{111}In]**SBL-uPAR-104** for **SPECT** imaging, either with or without a 60-fold **excess of cold ligand** (**SBL-uPAR-100**). Images were acquired at 1, 3, 6, 24 h post injection. Clear **uPAR-specific tumoc accumulation** was observed in both imaging modalities.

Conclusions

- ❖ Development sub-nM **uPA mimetic**
- ★ **Approaching K_d uPA** (0.1-0.5 nM)
- ❖ Striking **backbone mimicry**
- ❖ Human-mouse **species cross-reactivity**
- ❖ *In vivo* **imaging contrast** from **1 h p. i.**

Perspective

- ❑ **Combine** hit modifications in **monocycle**
- ❑ Combine ^{1,4}**Nol** & **Ala(Cp)** in **bicycles**
- ❑ Investigate **targeted therapies**
- ❑ **Expand design** for other PPI's

References

1. Smith H. W. & Marshall C. J. *Nat Rev Mol Cell Biol* **2010**, 11, 23–36.
2. Masucci M. T. *et al. Cancers* ***2022***, 14(3), 498
3. Hernot S. *et al. Lancet Oncol* **2019**, 20(7), e354-367
4. Ploug M. *et al. Biochem* **2001**, 40, 12157-12168
5. Mateusiak Ł. *et al. Adv. Sci.* **2024**, 11(30), 2400700

Acknowledgments

SRP95

MOLECULAR IMAGING & THERAPY RESEARCH GROUP
ORGANIC CHEMISTRY RESEARCH GROUP
VIB-VUB CENTER FOR STRUCTURAL BIOLOGY

An opioid-neurotensin hybrid peptide outperforms morphine in acute and chronic pain models

L. Durand-Baudet,[a] J. De Neve,[a] É. Breault,[b] S. Gonzalez,[a] V. Utard,[c] E. Vangeloven,[a] F. Simonin,[c] P. Sarret[b] & S. Ballet[a]

[a]Research Group of Organic Chemistry, Departments of Engineering and Bioengineering Sciences, Vrije Universiteit Brussel, Brussels, Belgium
[b]Institut de Pharmacologie de Sherbrooke, Department of Pharmacology and Physiology, Faculty of Medicine and Health Sciences, Université de Sherbrooke, Sherbrooke, Canada
[c]Biotechnologie et Signalisation Cellulaire, Centre National de la Recherche Scientifique, Université de Strasbourg, Illkirch, France

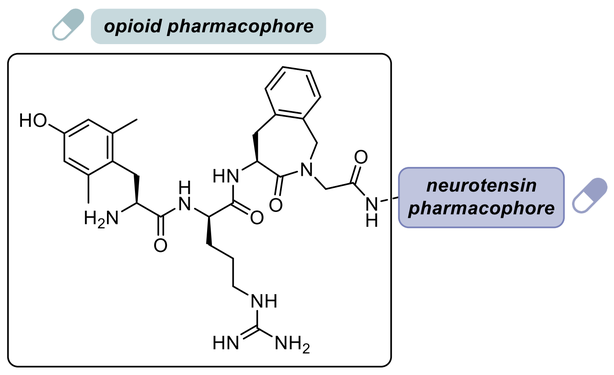
https://doi.org/10.17952/38EPS.2026.P512

Abstract

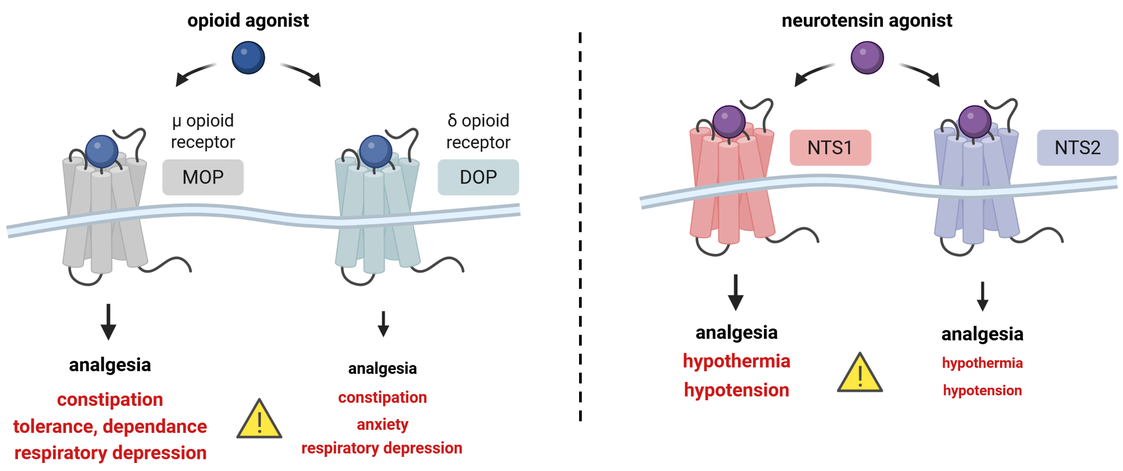
Best of both worlds:

- ***More potent than morphine***
  in acute & chronic pain models
- ***Prolonged effect***
- ***Reduced side effects***

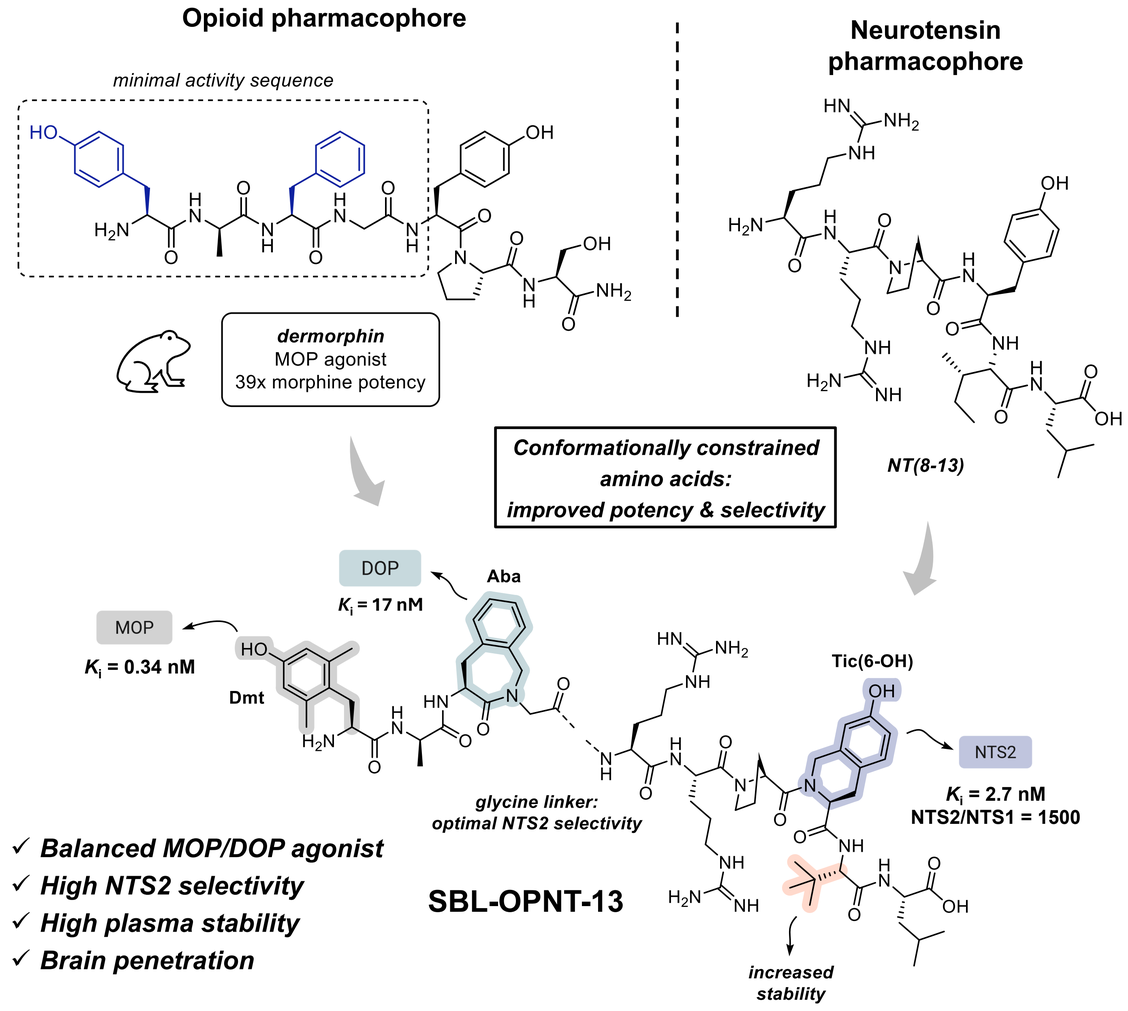
⇒ **Safer analgesic profile**



Opioid and neurotensin receptors[1]

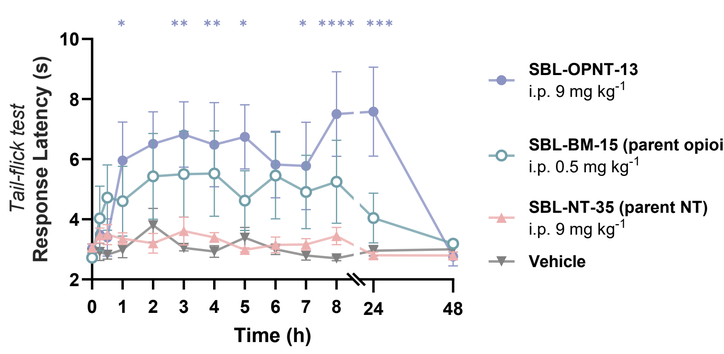


Lead peptide design[2,3]



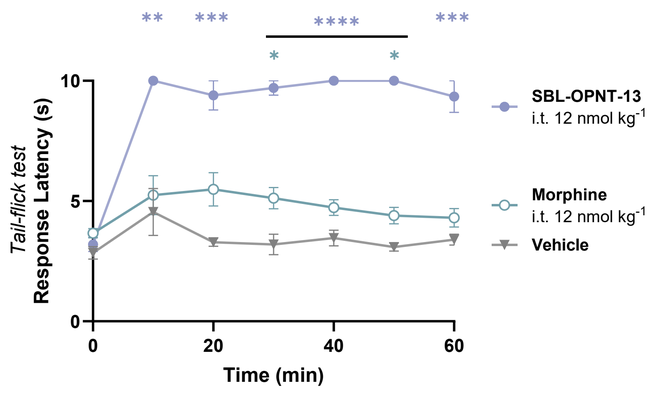
Preclinical efficacy[4]

The hybrid peptide outperforms the parent moieities



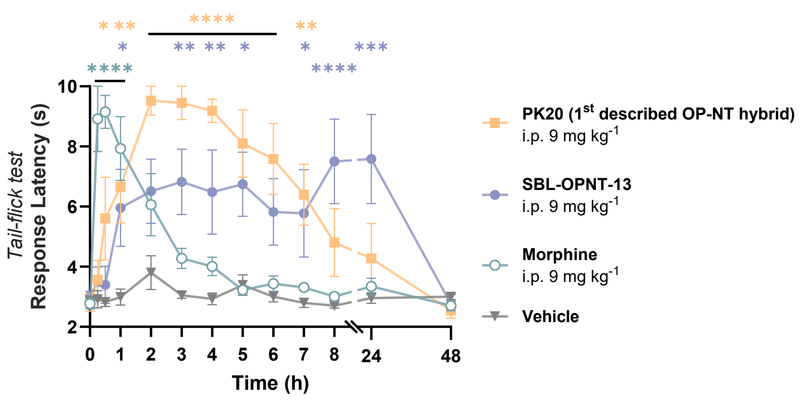
n = 5-6

Efficacy in acute pain model



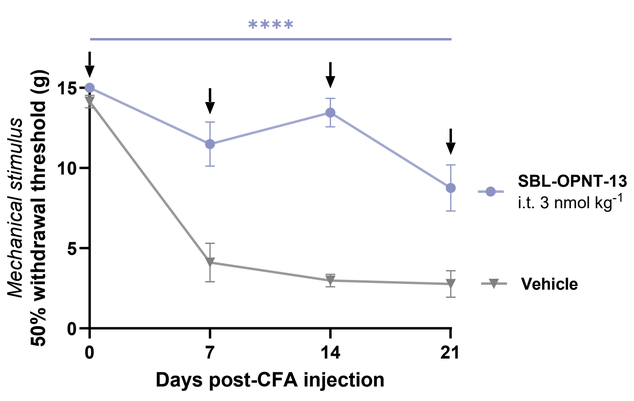
n = 6

Sustained analgesia >24 hours



n = 5-6

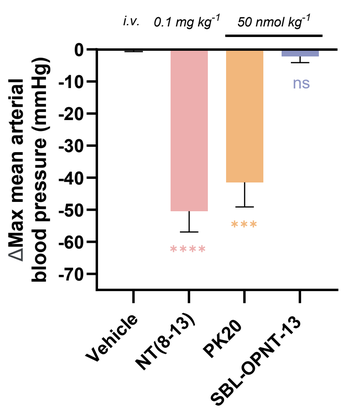
Efficacy in chronic pain model



n = 6

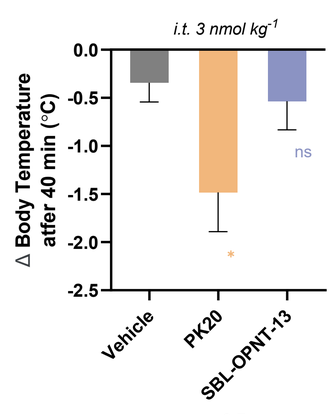
Adverse effects[4]

Hypotension



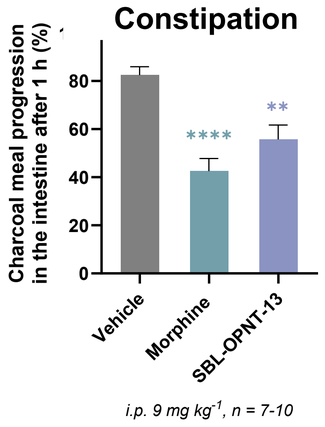
n = 6

Hypothermia



n = 6-7

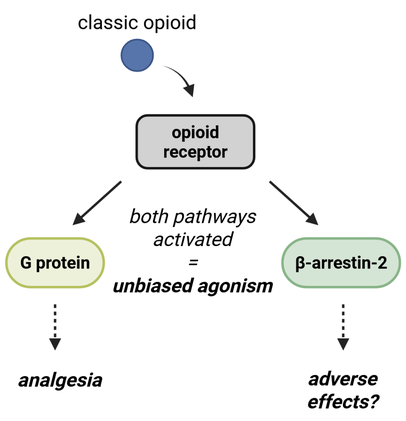
Constipation

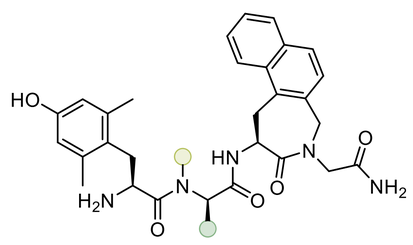


i.p. 9 mg kg-1, n = 7-10

- ✓ ***No NTS1-related hypotension***
- ✓ ***No NTS1-related hypothermia***
- × ***Opioid-related constipation still observed***
- × ***Opioid tolerance still observed***

Perspectives: biased opioid agonism[5]





Mechanistic studies & therapeutic perspectives

Charge vs. no charge	*N*-Sustitution	β-Arrestin-2 max. efficacy
D-Ala	H	94 ± 6%
D-Arg	H	50 ± 3 %
D-Arg	Me	25 ± 1 %
D-Arg	Pr	7 ± 4 %

Conclusions

- **SBL-OPNT-13** is potent in preclinical acute and chronic pain models
- High NTS2 selectivity prevented neurotensin-related side effects
- Opioid-related side effects remain challenging to understand and address

References

1. Breault *et al.*, *Pharmacol. Res.* **2024**, *209*, 107408.
2. Gonzalez *et al.*, *J. Med. Chem.* **2020**, *63* (21), 12929–12941.
3. De Neve *et al.*, *ACS Pharmacol. Transl. Sci.* **2024**, *7* (9), 2784–2798.
4. Breault *et al.*, *Biomed. Pharmacother.* **2026**, *199*, 119488.
5. De Neve *et al.*, unpublished data.

More information

Acknowledgements

VRIJE UNIVERSITEIT BRUSSEL · fwo · Université de Sherbrooke · Université de Strasbourg

P430: BIFUNCTIONAL *DE NOVO* PEPTIDES TO TACKLE ANTIMICROBIAL RESISTANCE

Lucie BASTIEN [a,b,c,*], **Emna BEN EL-HADJ SALEM** [a], **Pauline SAMPER** [a, b], **Mehavi MEHAVARNAN** [c], **Eric PARDOUX** [a,b], **Arnaud BUHOT** [a], **Muriel JOURDAN** [b], **Didier BOTURYN** [b], **Sandrine BOISSET** [c] **and Yoann ROUPIOZ** [a]

[a] *Univ. Grenoble Alpes, CEA, CNRS, Grenoble INP, IRIG, UMR 5819, SyMMES, 38000 Grenoble, France;*

[b] *Univ. Grenoble Alpes, CNRS, UMR 5250, DCM, 38000 Grenoble, France;*

[c] *Univ. Grenoble Alpes, CHU Grenoble Alpes, CNRS, CEA, UMR5075, IBS, 38000 Grenoble, France.*

https://doi.org/10.17952/38EPS.2026.P430

*lucie.bastien@univ-grenoble-alpes.fr

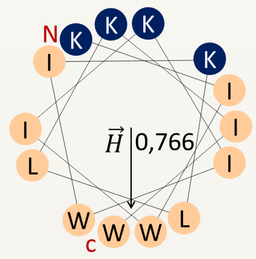
Context

Nearly 5 **million deaths** were associated to **antimicrobial resistance** worldwide in 2021, driving the urgent need for both new antimicrobial **therapeutics** and rapid **diagnostic** tools to reduce antibiotic misuse and improve patient outcomes.

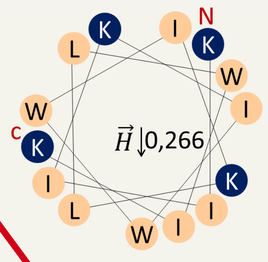
In this context, we designed ***de novo* peptides,** PACHA01 and PACHA02 with the dual aim of developing **new antimicrobial therapeutics** and bacterial **detection probes**. PACHAs were produced by solid-phase peptide synthesis with identical amino acid compositions but different primary sequences:

Peptide design and characterisation

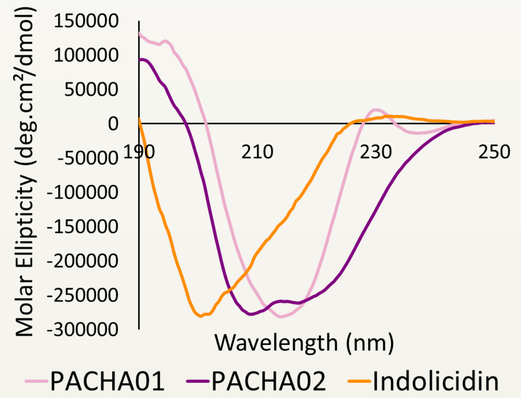
PACHA01 :



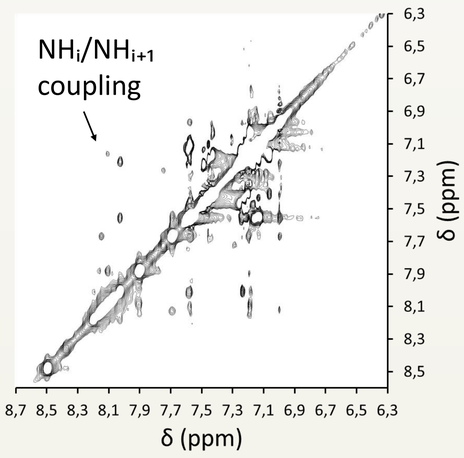
PACHA02 :



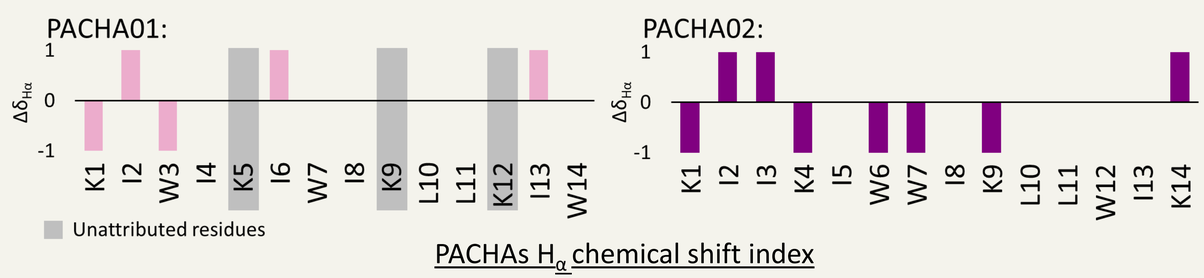
PACHAs ...



Circular dichroism of PACHAs compared with indolicidin



PACHA02 NOESY experiment, 600 MHz NMR

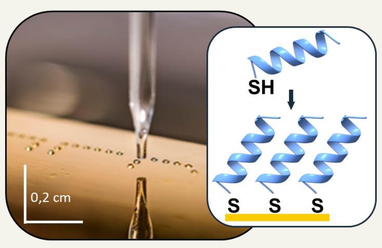


PACHAs H_α chemical shift index

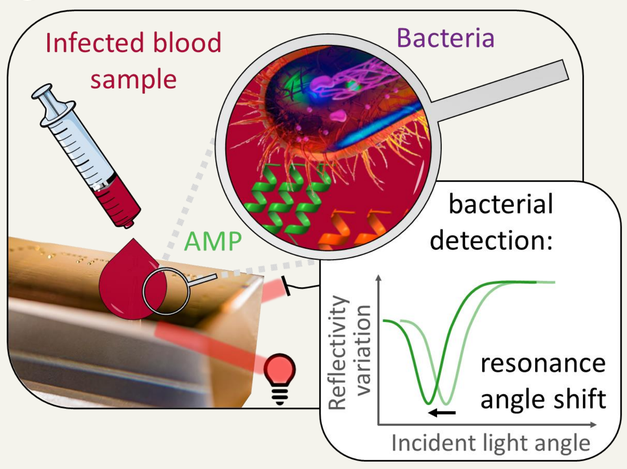
➥ PACH01 is less structure than PACH02 which folds into a partial α-helix at pH 7.

Biosensor development

① Peptide arraying

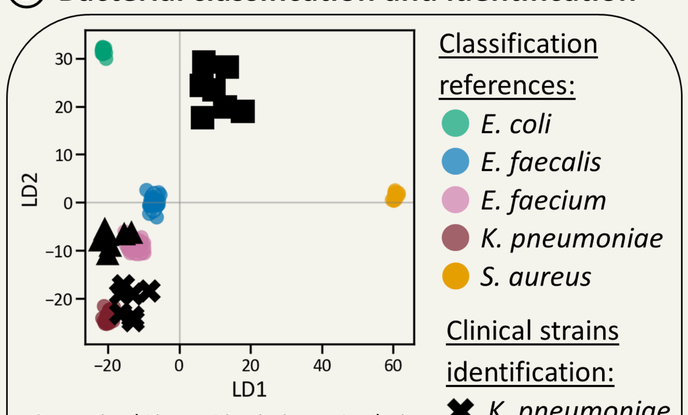


② SPRi monitoring : bacterial detection



... as probes for biosensor

③ Bacterial classification and identification



Supervised Linear Discriminant Analysis (3 replicates per specie microarray with 7 replicates per probe)

Accuracy : 93,3 ± 25,8%

➥ The method enables bacterial detection under 15 hours.

➥ The selected AMP panel generates distinct affinity profiles for each bacterial species. It enables species discrimination within the same genus with few experiments.

➥ The LDA model enable bacterial identification of clinical strains with limits.

Therapeutic development

... as antimicrobial agent

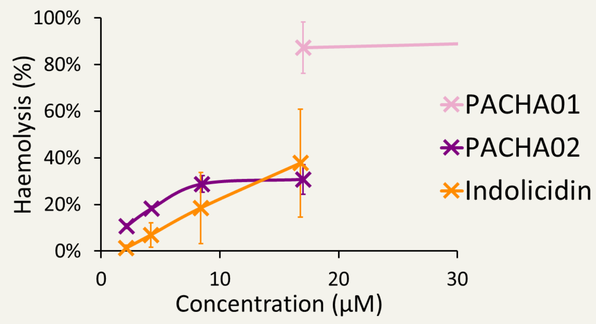
Antimicrobial activity:

MIC (mg/L / µM)	PACHA01	PACHA02	Indolicidin
S. aureus	4 2	4 2	8 4
E. coli	64 34	16 4	8 4
A. baumannii	N. D.	8 4	4 2
P. aeruginosa	N. D.	4 2	4 2
K. pneumoniae	N. D.	2 to 128 1 to 68	8 4

➥ Despite identical amino acid composition PACHA01 is less active than PACHA02 against *E. coli.*

➥ The antimicrobial activity of PACHA02 against a broad spectrum of bacterial species is comparable to that of a well-established AMP.

Toxicity:



Hemolytic ratio on human erythrocytes

IC_{50} (mg/L / µM)	PACHA01	PACHA02	Indolicidin
A-549	P	>256 >136	>64 >34
THP-1	P	>128 >68	>32 >17

P: precipitation prevents reading

Cytotoxicity toward epithelial and circulating cells

➥ PACHA02 is non-toxic to tested cells, except for RBCs, where it shows toxicity similar to Indolicidin but nearly 3-fold lower than PACHA01.

Optimisation:

		KIIKIAAIKLLAIK	KIIKIAAIKLLWIK	KIIKIWAIKLLAIK	KIIKIAWIKLLAIK
MIC (mg/L / µM)	*E. coli*	4 2	4 2	4 2	4 2
	S. aureus	4 2	4 2	4 2	4 2
IC_{50} (mg/L / µM)	A-549	>256 >167	>256 >155	>256 >155	>256 >155
	THP-1	>256 >167	>256 >155	>256 >155	>256 >155

➥ Reducing the tryptophan proportion of PACH02 sequence does not affect its antimicrobial activity and toxicity.

Conclusion & Perspectives

➥ PACHA02 is as promising an antimicrobial candidate as Indolicidin.

➥ Ongoing optimization shows highly encouraging results.

➥ AMP micro-array enables rapid bacterial detection and identification.

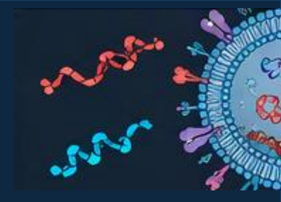
- Further optimization of PACHA02, including additional toxicity testing.
- Dataset expansion and enhanced data analysis.
- Method validation using relevant clinical samples, such as blood cultures.

New !

Check our last accepted results: É. Pardoux, L. Bastien, R. Mathey, A. Buhot, S. Boisset, D. Boturyn, Y. Roupioz, **Rapid classification of live bacteria in blood using antimicrobial peptides micro-arrays** *J. Mater. Chem. B*

New !

MECHANISTIC INSIGHTS INTO ANTIMICROBIAL PEPTIDE-EXTRACELLULAR VESICLE INTERACTIONS & THERAPEUTIC APPLICATIONS IN SEPSIS



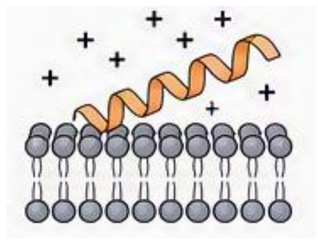
Tasvilla Sonallya, Tünde Juhász, Imola Cs. Szigyártó, Kinga Ilyes, Kata Horvati, Yumi Kumagai,Zoltán Varga, Tamás Beke-Somfai

[1]*Institute of Materials and Environmental Chemistry, Research Centre for Natural Sciences, Budapest, Hungary*

[2]*Department of Biochemistry and Systems Biomedicine, Juntendo University Graduate School of Medicine, Tokyo, Japan*

tasvilla.sonallya@ttk.hu https://doi.org/10.17952/38EPS.2026.P379

INTRODUCITON



Membrane Active Peptides (MAPs)

- **High affinity towards lipid bilayers**
- **Disrupting cell membranes**
- **Modulating the innate immune response**

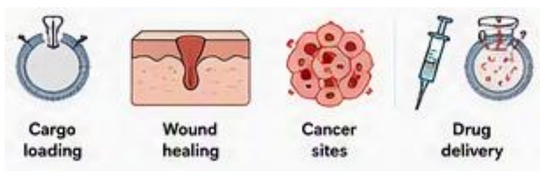
Two major classes of MAP

- **Antimicrobial peptides (AMPs)**
- **Cell-penetrating peptides (CPPs)**

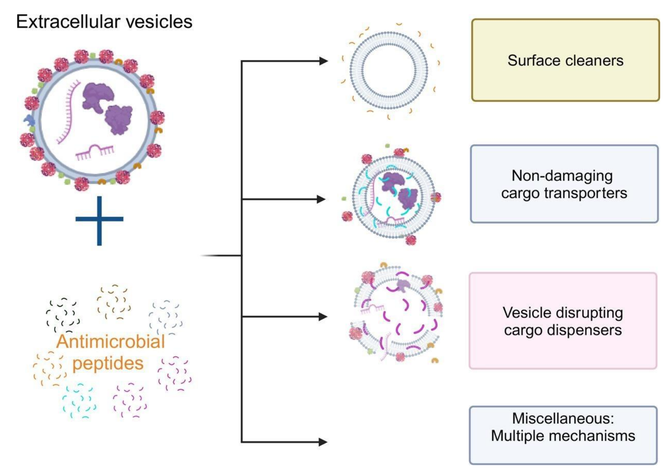
Extracellular vesicles (EVs)

- **Membrane-enclosed nanostructures**
- **Cargo carriers and cellular communication**
- **Present in biofluids: blood, urine, saliva, cerebrospinal fluid**
- **Phospholipid bilayer**
- **Protein corona on the surface: dynamic and reflects the immediate**

APPLICATIONS OF MAPS-EV SYSTEMS

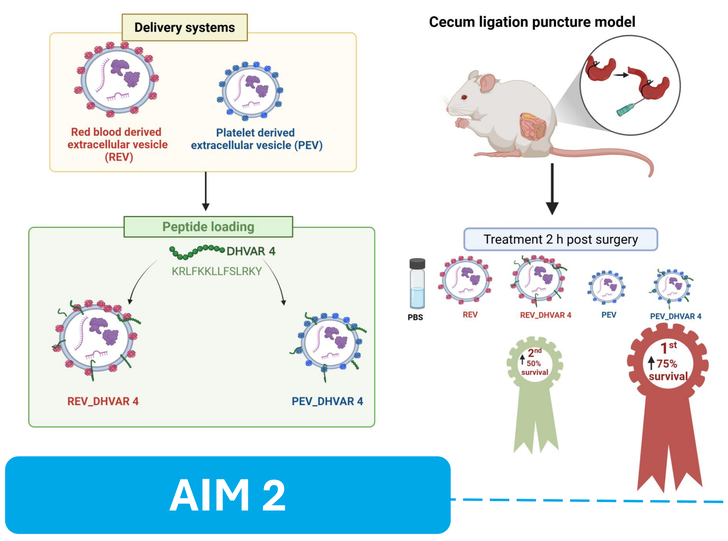


GRAPHICAL ABSTRACT



AIM 1

Characterize interactions between **26 membrane – active peptides(MAPs) and red blood cell-derived extracellular vesicles (REVs)**



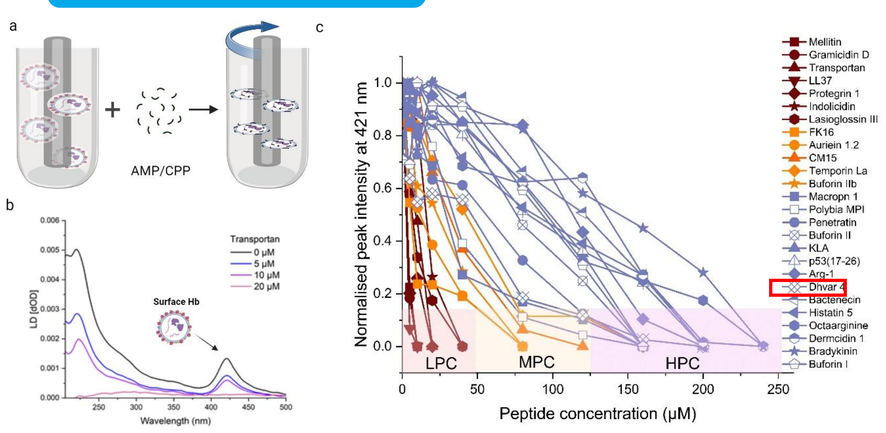
AIM 2

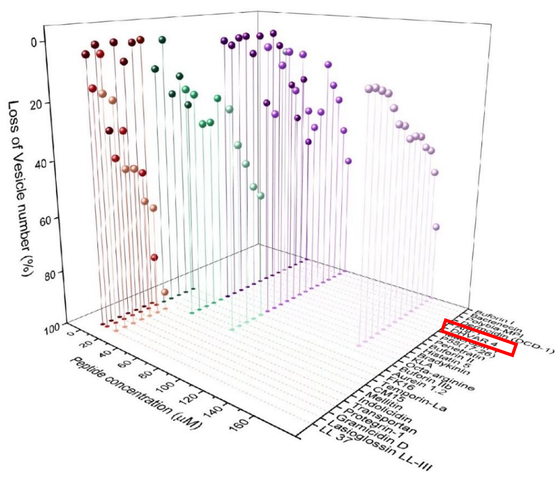
Evaluate the therapeutic efficacy of REV-DHVAR 4 and PEV-DHVAR 4 in **a cecum ligation puncture sepsis model**

RESULTS

1. MAP- EV interactions

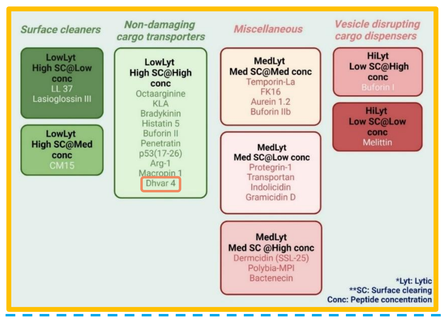
Peptide name	Sequence	Net charge*	Length	Origin	Known mechanism, active conformation
Arg-1	RQWRRWWQR	+4	9		AMP
Aurein 1.2	GLFDIIKKIAESF	+1	13	Litoria frog skin secretions	AMP, helical
Bactenecin	RLCRIVVIRVCR	+5	12	bovine neutrophils	AMP
Bradykinin	RPPGFSPFR	+2	9	Produced during inflammation	Membrane active peptide
Buforin I	AGRGKQGGKVRAKAKTRSSRAGLQFPVGRVHRLLRKGNY	+13	39	Stomach tissue of the Asian toad bufo bufo gargarizans	AMP/CPP, helical
Buforin II	TRSSRAGLQFPVGRVHRLLRK	+6	17	Derived from Buforin I	AMP/CPP, helical
Buforin IIb	RAGLQFPVGRLLRRLLRRLLR	+7	21	Derived from Buforin II	AMP/CPP, helical
CM15	KWKLFKKIGAVLKVL	+6	15	Cecropin-melittin derivative	AMP, carpet, helical
Dermcidin (SSL-25)	SSLLEKGLDGAKKAVGGLGKLGKDA	+3	25	Human sweat	AMP-Pore and ion channel formation, helical
Dhvar 4	**KRLFKKLLFSLRKY**	**+7**	**14**	**Oral host defence peptides**	**AMP, helical**
FK16	FKRIVQRIKD FLRNLV	+5	16	Derived from LL37	AMP, carpet, helical
Gramicidin	Mix of A ,B ,C			Bacillus aneurinolyticus	AMP
Histatin 5	DSHAKRHHGYKRKFHEKHHSHRGY	+4	24	Saliva	AMP, helical
Indolicidin	ILPWKWPWWPWRR	+4	13	Cattle, granules of bovine neutrophil	AMP-oxidised lipid targeting,
KLA	KLAKLAKKLAKLAK	+6	14	Synthetic	AMP, helical
Lasioglossin III (LL-III)	VNWKKILGKIIKVVK	+6	16	Venom, eusocial bee Lasioglossum laticeps	AMP, membrane permeabilization, helical
LL37	LLGDFFRKSKEKIGKEFKRIVQRIKDFLRNLVPRTES	+7	37	Homo sapiens, skin, and intestine	AMP, carpet, helical
Macropin 1	GFGMALKLLKKVL	+4	15	skin secretions of the frog species Litoria genimaculata	AMP/CPP, membrane disruption
Melittin	GIGAVLKVLTTGLPALISWIKRKRQQ	+6	26	Honey bee venom	AMP,toroidal pore, helical
Octa-arginine	RRRRRRRR	+9	8	Arginine derivative	CPP
Penetratin	RQIKIWFQNRRMKWKK	+7	16	Drosophila Antennapedia homeodomain	**CPP α-helical/β-sheet conformations depend on phospholipid composition and peptide–lipid ratio**
Polybia-MPI	IDWKKLLDAAKQIL	+1	14	Social wasp venom	AMP,pore formation, helical
Protegrin-1	RGGRLCYCRRRFCVCVGR	+6	18	Pigs	AMP-Pore formation, sheet
p53 (17-26)	ETFSDLWKLL	0	10		ACP
Temporin-La	LLRHVVKILEKYL	+3	13	Anuran skin, Rana Temporia	AMP helical
Transportan	GWTLNSAGYLLGKINLKALAALAKKIL	+4	27	Galanin-mastoparan Conjugatem linked by lysine	CPP , helical





Characterization of surface protein by Linearly polarized light spectroscopy (LD)

- Peptides classified into **low (LPC), medium (MPC), and high (HPC)** groups based on the effective peptide concentration (**ec_{max}**) required for complete signal loss.
- These groups were used to assess **protein corona removal efficiency**.



Correlative flow cytometry analysis of lytic trends in REVs at various peptide concentrations

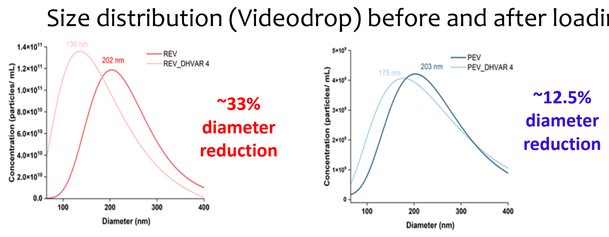
- Vesicle counts measured at three EC_{max} levels.
- Color gradient = increasing concentration.
- Lower vesicle count = higher lytic activity.

DHVAR 4, selected for therapeutic efficacy evaluation with REV and PEV

T. Sonallya et al., *Journal of Colloid and Interface Science*, Feb 2025

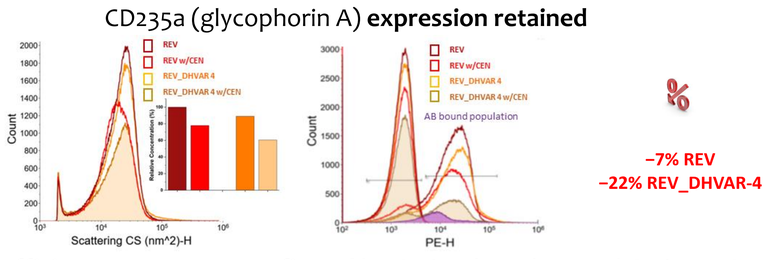
2. Effects of DHVAR 4 loading and washing on EV properties

Size distribution (Videodrop) before and after loading



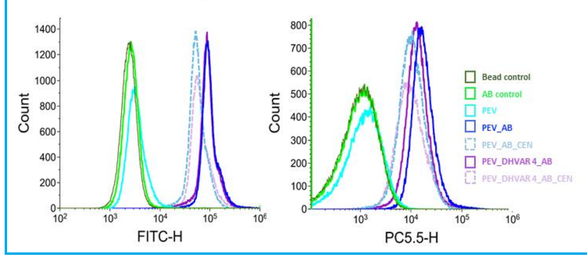
Overall vesicle integrity retained

CD235a (glycophorin A) **expression retained**



−7% REV
−22% REV_DHVAR-4

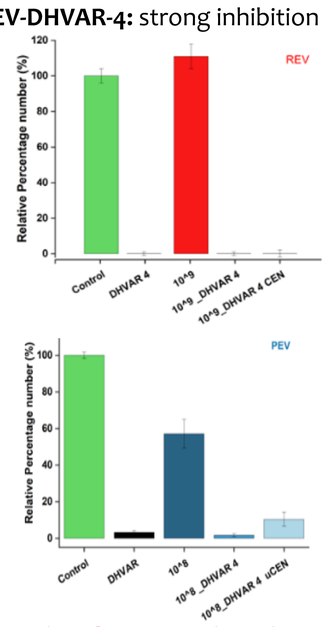
Efficient PEV capture confirmed by CD63-AlexaFluor and CD61-PerCy5.5 -positive fluorescence



	CD63	CD61
PEV %	23%	32%
PEV_DHVAR 4 %	45%	37%

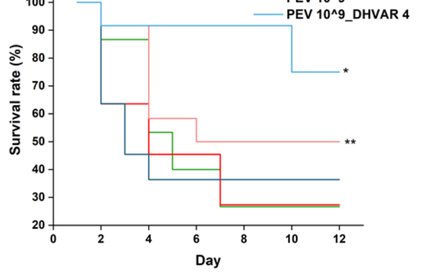
3. Antimicrobial activity against *E.coli*

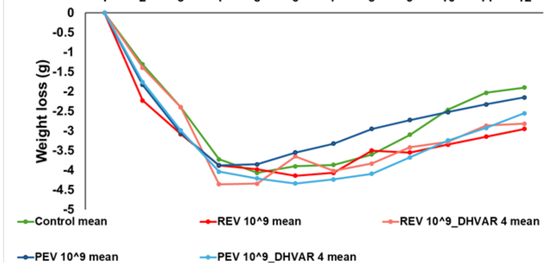
EVs alone: no inhibition of *E. coli*
REV-DHVAR-4: complete inhibition at low bacterial load
PEV-DHVAR-4: strong inhibition



EV-associated DHVAR-4 is active even after centrifugation

4. Therapeutic evaluation of treatment on the CLP sepsis model





PEV_DHVAR 4 ACHIEVES 75% SURVIVAL RATE

CONCLUSIONS

- Eight distinct MAP-EV interaction mechanism identified
- REVs and PEVs retain structural integrity and surface markers
- EV-loaded DHVAR 4 shows potent antimicrobial activity with minimal toxicity
- **Platelet derived EV (PEV)** DHVAR 4 are promising platform for targeted AMP delivery and sepsis therapy.

ACKNOWLEDGEMENT

This work was funded by the Ministry of Innovation and Technology of Hungary from the National Research, Development and Innovation Fund (TKP2021-EGA-31, 2020-1-1-2-PIACI-KFI_2020-00021, and KKP_22 144180). **HUN-REN Mobilitási pályázat II**

Peptide functionalization of hybrid polyoxometalates

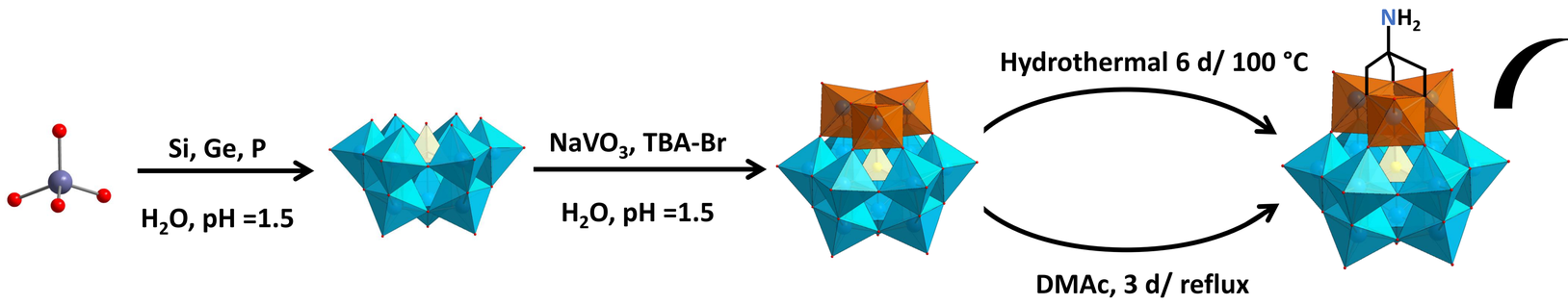
Teresa Bell[1,2,3] Nadiia Gumerova[1] Annette Rompel[1,2]

1) Universität Wien, Fakultät für Chemie, Institut für Biophysikalische Chemie, Josef-Holaubek-Platz 2, 1090 Wien, Austria; https://www.bpc.univie.ac.at,
2) Universität Wien, Fakultät für Chemie, Vienna Doctoral School in Chemistry (DoSChem), Währingerstraße 42, 1090 Wien, Austria,
3) https://doi.org/10.17952/38EPS.2026.P032

Introduction

Polyoxometalates (POMs) are discrete, water soluble, predominantly anionic polynuclear metal-oxo coordination compounds. They are constructed of an ionic core comprising corner- and edge-sharing pseudo-octahedral $\{MO_6\}$ units with early transition metals from group V or VI (M = $V^{IV/V}$, $Mo^{V/VI}$, $W^{V/VI}$).[1] The modification to organic-inorganic hybrid-POMs represents a growing area of interest. Organic molecules can be attached through ionic interactions (Class I) or bound covalently/ iono-covalently (Class II) to the inorganic core.[2] The combination of inorganic and organic physical properties can enhance the bioactivity and biospecificity[3], improve the stability[2], and expand the potential applications in biomedicine[4].
Hereby we concentrate on the synthesis of the hybrid POMs with amino- and carboxy-functions based on the two archetypes **Keggin** ($[XM_{12}O_{40}]^{n-}$), and **Wells-Dawson** ($[X_2M_{18}O_{62}]^{n-}$), where X = Al, Ge, SI, P; M = Mo, W, V; n = 3, 6.[5]

Keggin



^{51}V NMR: δ = -565 ppm.

^{51}V NMR: δ = -559 ppm.

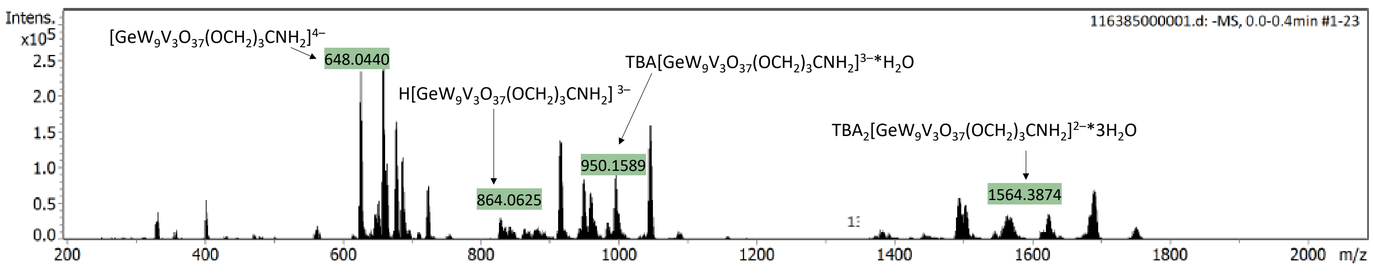
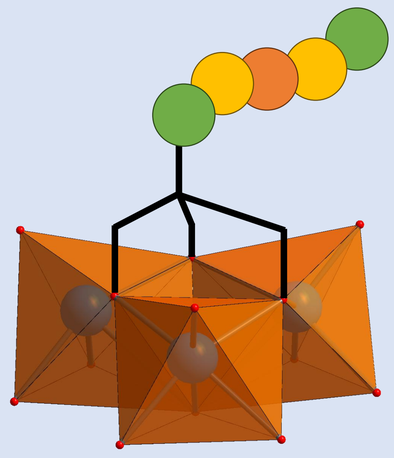


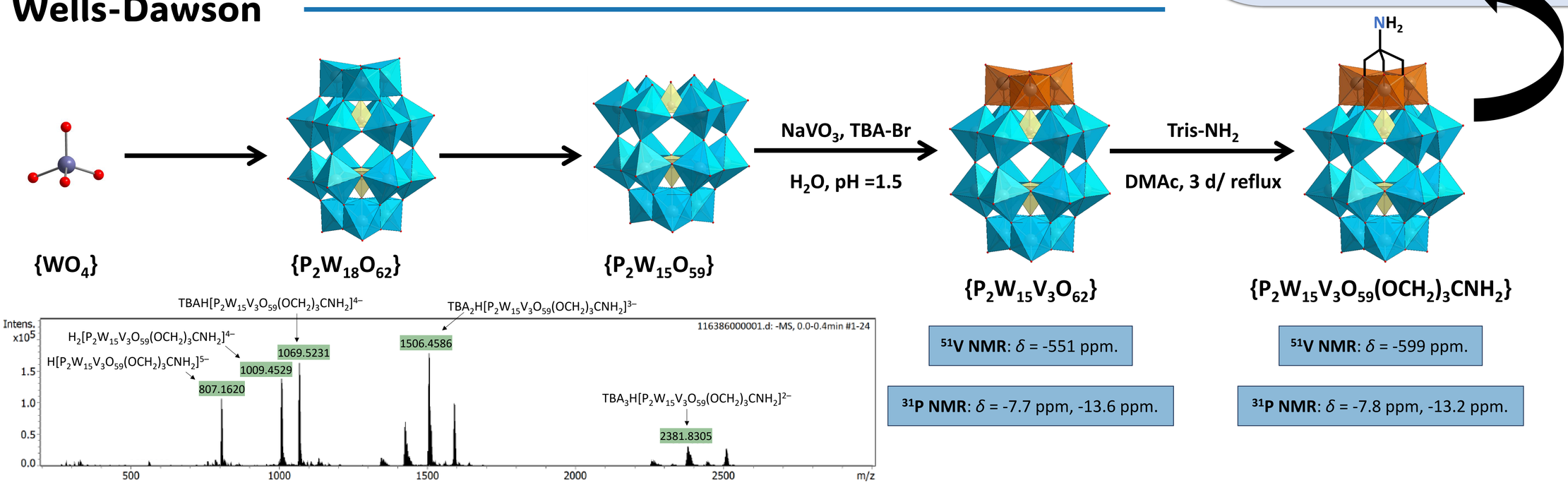
Fig.1 ESI-MS spectra of **$[GeW_9V_3O_{37}(OCH_2)_3CNH_2]^{4-}$**. Color code: blue – W, orange – V, yellow – P/Si/Ge.

The heteropolyanionic mixed-metal W/V POMs with different hetero atoms (Ge, Si, P) are synthesized by a step-by-step procedure from simple $[WO_4]^{2-}$ building blocks in an acidified aqueous solution through self-assembly in condensation reaction.[6][7]
The organic functionalization can be achieved through reaction under argon atmosphere and in the dark or through hydrothermal reaction (thermodynamic favored pathway).[8]
The Keggin and Wells-Dawson structures were analyzed with ^{1}H, ^{31}P, and ^{51}V nuclear magnetic resonance spectroscopy (NMR), infrared spectroscopy (IR) and Electrospray Ionization Mass Spectrometry (ESI-MS).[9]



The advantages of hybrid POMs over traditional POMs lies in their enhanced functional properties, which result from combining POM attributes (e. g. redox capabilities) with organic framework characteristics, (e. g. high surface area, organized structure). The organic component of the hybrid POMs can be subjected to chemical modification either through pre-functionalization or post-functionalization.[2]
Therefore hybrid POMs can be used as "inorganic" amino acids in peptide synthesis.[4]

Wells-Dawson



^{51}V NMR: δ = -551 ppm.

^{31}P NMR: δ = -7.7 ppm, -13.6 ppm.

^{51}V NMR: δ = -599 ppm.

^{31}P NMR: δ = -7.8 ppm, -13.2 ppm.

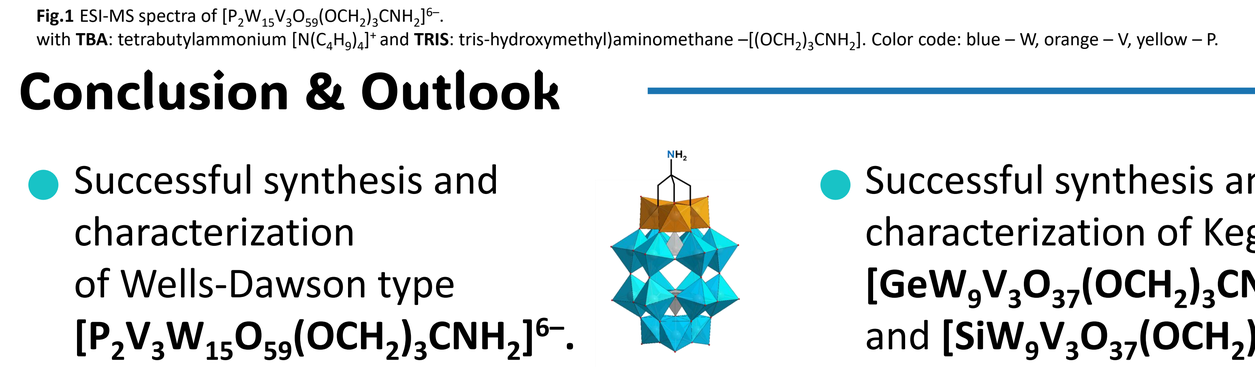


Fig.1 ESI-MS spectra of $[P_2W_{15}V_3O_{59}(OCH_2)_3CNH_2]^{6-}$.
with **TBA**: tetrabutylammonium $[N(C_4H_9)_4]^+$ and **TRIS**: tris-hydroxymethyl)aminomethane $-[(OCH_2)_3CNH_2]$. Color code: blue – W, orange – V, yellow – P.

Conclusion & Outlook

- Successful synthesis and characterization of Wells-Dawson type **$[P_2V_3W_{15}O_{59}(OCH_2)_3CNH_2]^{6-}$.**

- Successful synthesis and characterization of Keggin type **$[GeW_9V_3O_{37}(OCH_2)_3CNH_2]^{4-}$** and **$[SiW_9V_3O_{37}(OCH_2)_3CNH_2]^{4-}$.**



- Side-chain functionalization of amino acids with TRIS-functionalized Hybrid-POMs.

References
[1] Yang, H.-K. *et al.*, *Colloids Surf. Physicochem. Eng. Asp.* **538**, 711–719 (2018). **DOI**: 10.1016/j.colsurfa.2017.11.039.
[2] Anyushin, A. *et al., Chem. Soc. Rev.* **49**, 382–432 (2020). **DOI**: 10.1039/c8cs00854j.
[3] Fu, L. *et al., Small* **11**, 2938– 2945 (2015). **DOI**: 10.1002/smll.201500232.
[4] Fani, M. & Maecke, H. R., *Eur. J. Nucl. Med. Mol. Imaging* **39**, 11–30 (2012). DOI: 10.1007/s00259-011-2001-z.
[5] Gumerova, N. I. & Rompel, A., *Nat. Rev. Chem.* **2**, 0112 (2018). **DOI**: 10.1038/s41570-018-0112.
[6] Pradeep, C. P. *et al., Angewandte Chemie International Edition* ***47*** (23), 4388–4391 (2008). **DOI**: 10.1002/anie.200800431.
[7] Karimian, D. *et al., Microporous and Mesoporous Materials* **247**, 23–30 (2017). **DOI**: 10.1016/j.micromeso.2017.03.048.
[8] Gao B., *et al., Journal of Solid State Chemistry* **179** ,1681–1689, (2006). **DOI**: 10.1016/j.jssc.2006.02.033
[9] Hasenknopf, B., Delmont, R., Herson, P. & Gouzerh, P., *Eur. J. Inorg. Chem.* 1081-1087 (2002).
DOI: 10.1002/1099-0682(200205)2002:5<1081::AID-EJIC1081>3.0.CO;2-W.

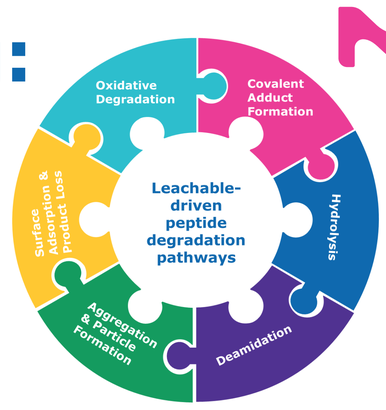
Acknowledgment
We thank colleagues from the NMR center (University of Vienna, Austria) for their great support. This research was funded by the Austrian Science Fund (FWF) [**DOI** 10.55776/PAT4299925 (to AR) and **DOI**: 10.55776/PAT2849824 (to NG)].

teresa.bell@univie.ac.at
LinkedIn\Teresa Bell

annette.rompel@univie.ac.at
LinkedIn\Rompel Group



Peptide Stability in GMP-Manufacturing: Minimizing Risk to Peptide Drugs from Single-Use Assemblies



Stephanie Bellmaine, Sarah Parsons
Process Solutions, Merck Life Science KGaA, Darmstadt, Germany
https://doi.org/10.17952/38EPS.2026.P404

Risk mitigation in peptide therapeutic manufacturing

Peptides as therapeutics have undergone a rapid acceleration in recent years, due largely to the GLP-1 receptor agonist class (e.g., semaglutide, liraglutide, tirzepatide), however pipelines also encompass metabolic disease, oncology, infectious disease, and rare conditions. Peptides are an attractive therapeutic class due to their high target specificity, strong biological potency, and lower off-target toxicity compared with small molecules. Today, over 100 peptide therapeutics are on the market, with 150+ in clinical trials and 400–600 in preclinical research.

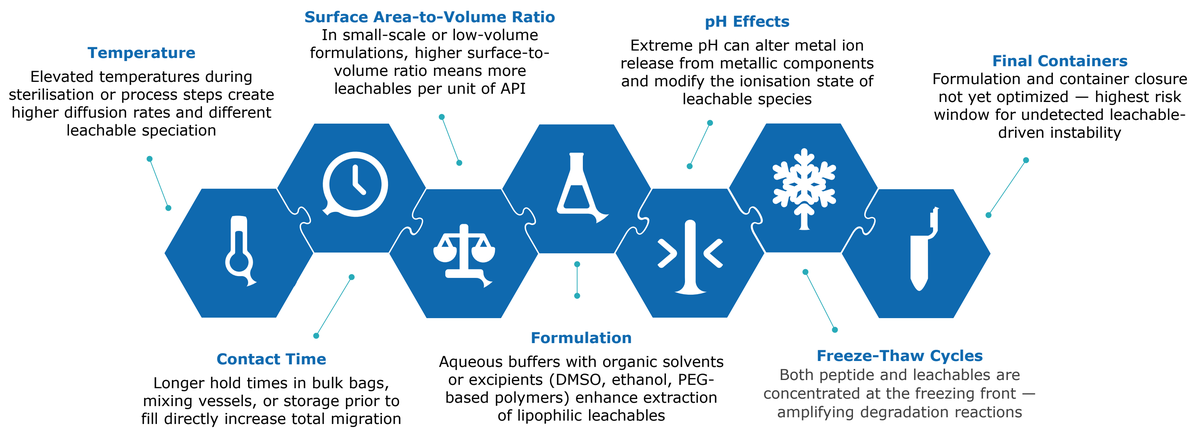
Due to the rapid growth and evolution of the peptide therapeutic market, risk mitigation in peptide therapeutic manufacturing has yet to be fully established and peptide-specific risk guidance is largely absent from the literature. Inexperienced manufacturers may be tempted to treat peptides like smaller mAbs, however, peptides are inherently more sensitive and have smaller, more exposed reactive residues with no structural redundancy to absorb process-related stresses.

One critical consideration in risk management for peptide therapeutic manufacturing is the adoption of single-use (SU) systems. While these systems are being increasingly used for their flexibility, contamination control and speed of changeover between products, they bring the known risk of chemical contaminants known as extractables and leachables (E&L). E&L are not as well characterized for peptides as for mAbs and regulators (e.g. FDA, EMA) are tightening E&L scrutiny, underscoring the need for peptide-focused frameworks.

What are extractables & leachables?

Extractables are compounds that migrate from a material under aggressive or exaggerated laboratory conditions (e.g. elevated temperatures, organic solvents) and they are used for worst-case risk screening. Identification of these compounds allows predictions of what could potentially leach.[1]

Leachables are the compounds that actually migrate under normal processing conditions, i.e., the actual temperature, formulation and contact time used in the manufacturing process. These are the primary risks, and they are the species most likely to carry across from the SU assembly into the final drug product.[1]



Leachables are influenced by temperature, contact time, surface area-to-volume ratio, formulation composition, and pH extremes. Compared with a typical mAb scenario, peptide processes can incur a disproportionate leachable burden due to low API concentrations, complex organic formulations, and extended hold times. In a single-use process train, every component contributes a unique leachable fingerprint—from PVC tubing to polyolefin bags, connectors, adhesives, and filters. Understanding each material's chemistry is essential for a science-driven risk assessment and patient safety.

Primary leachable contributors across a SU process train

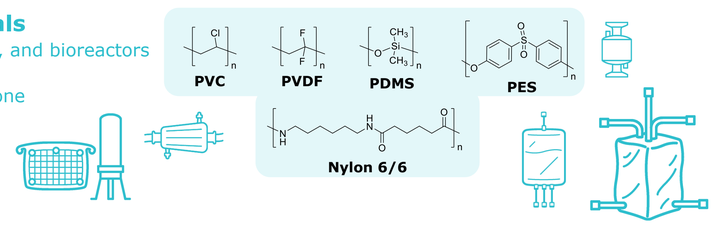
During the drug production process, leachables coming from a device used in one process step can be carried into the next process step. It has been demonstrated that these PERLs (process equipment-related leachables) usually decrease over the course of a process during the purification steps (e.g. tangential flow filtration, chromatography), as they are removed via the waste stream. As a result, most literature focuses on the leachables coming from the final fill assemblies and the direct pharmaceutical packaging (e.g. syringes).[2,3]

While PERLs may be most likely removed to a non-hazardous level during processing, for the duration in which they are in contact with the peptide, any reactivity they have toward the peptide will result in degradation of the drug product during processing.[4] For this reason, understanding the PERLs coming from SU systems and their ability to degrade the peptide during processing is critical.

SU process trains contain multiple components made from a variety of materials, opening peptides up to hazards from a wide range of chemical species. The most common base materials are organic or silicone-based polymers and metals, and these SU assemblies often also contain additives such as plasticizers, stabilizers, lubricants, antioxidants and colorants.[5] The risk is not only from the leachables that can react directly with the peptides, but also any degradation products from these leachables that may arise as a result of process steps applied during preparation or running of the process.[6]

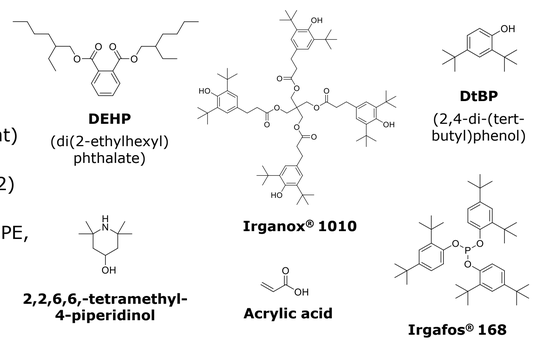
Common SU components and base materials

- Single-use bags and liners for storage, mixing systems, and bioreactors (nylon, LDPE)
- Tubing and connectors (thermoplastic elastomers, silicone (polydimethylsiloxane), PVC)
- Chromatography resins
- Filters and filtration assemblies (PES, PVDF)
- Filling needles and fluid transfer components



Common leachables and their material origin

- DEHP (plasticizer, e.g. in PVC tubing and bags)
- Irganox® 1010 (antioxidant, e.g. in mixing bags)
- Organotin compounds (heat stabilizers in PVC materials)
- Acrylic acid (degradant from acrylic adhesives, e.g. for needle attachment)
- DtBP (degradant from antioxidant Irgafos® 168)
- 2,2,6,6-tetramethyl-4-piperidinol (degradant from stabilizer Tinuvin® 622)
- Aldehydes/Ketones (degradation of many base material polymers)
- Short chain hydrocarbon acids (degradants from polyolefins e.g. PVC, LDPE, PP)
- Cyclic siloxanes (degradant from silicone tubing)



Peptide degradation pathways originating from leachables

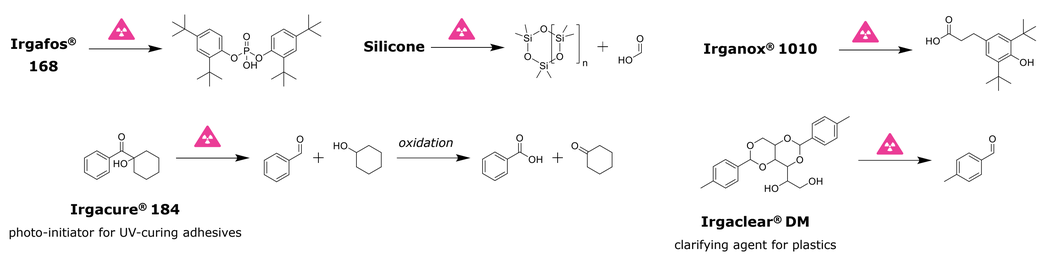
A large part of the risk that leachables and their degradants pose to peptide products is their ability to degrade the therapeutic during processing and storage.[4,7,8] Small molecule therapeutics and mAbs are not as easily degraded by contaminants as peptides; peptides have more reactive functional groups than small molecules, are less protected from their environment by tertiary structure than mAbs, and have a higher risk of potency loss due to modification of a single amino acid residue compared to mAbs.

	Key Leachables	Most Affected Residues	Impact – Product & Patient
Oxidative Degradation	Peroxides from antioxidant autoxidation; phenolic degradation products; Fe^{2+}/Fe^{3+}, Cu^{2+} from metallic fittings	Methionine > tryptophan > cysteine > histidine > tyrosine	Altered bioactivity, potency loss, immunogenicity, aggregation
Covalent Adduct Formation	Aldehydes and ketones; acrylic acid and other acrylates; acids -> all form covalent bonds with amines	Lysine, histidine, arginine, N-terminal amines	Altered bioactivity, potency loss, immunogenicity, aggregation
Peptide bond hydrolysis	Acidic or alkaline leachables altering local pH; transition metals	Asparagine-proline bonds; residues adjacent to bulky/charged groups	Fragment formation > altered bioactivity, potency loss, immunogenicity, aggregation
Deamidation	Acidic or alkaline leachables altering local pH	Asparagine, glutamine (at susceptible sequence positions), C-terminal amide	Potency reduction (10–80%); pharmacokinetic shifts; charge variant accumulation
Aggregation & Particulate Formation	Surface-active leachables form nucleation sites for aggregation, e.g. silicone oligomers, surfactant residues, plasticizers; Metal ions catalyse oxidative cross-linking	Hydrophobic/cationic peptides; e.g. methionine, cysteine, histidine, tryptophan, tyrosine	Fails particle limits; reduces effective dose; direct injection safety risk; immunogenicity
Surface Adsorption	Surface-active leachables can alter polymer surface hydrophobicity; hydrophobic plasticizer residues	Short, hydrophobic, cationic peptides at <0.1 mg/mL, lipidated analogues	Under-dosing; dose variability; aggregation seeding; increased injection-site reactions

Sterilization method of SU-systems as peptide risk

An undervalued risk that SU assemblies pose to peptide therapeutics stems from the common use of radiation to sterilize the SU equipment. Gamma irradiation (typically at 25–45 kGy using ^{60}Co sources) is the dominant sterilisation method primarily because of its deep penetration and established regulatory acceptance.[9] While suitable for mAbs, this method may significantly increase the leachable profile, which could pose a greater risk to the more sensitive peptide structures. This risk can be mitigated by using autoclaving as the sterilization method. Autoclaving uses saturated steam at 121 °C, approximately 15 psi, 15-20 minutes — a purely thermal and physical sterilisation process. While there might be a marginal increase in the pre-sterilization leachables due to the temperature increase, this still offers a much lower risk to the peptide product with the significant decrease in highly reactive degradants.

	Irradiation	Autoclave
1 **Radical Generation**	Carbon- and oxygen-centered **radicals persist** post-irradiation — ongoing **oxidative burden** during storage and drug contact	No ionising radiation → **no radical** generation in polymer matrix
2 **Antioxidant Consumption**	Irradiation consumes polymer antioxidants → antioxidant **products** become **leachables**	Stabiliser package remains intact — no consumption, **no degradation** products
3 **Polymer Chain Scission**	Chain scission produces aldehydes, ketones, carboxylic acids —**degradation catalysts** for deamidation, hydrolysis, covalent adduct formation	**No new chemical species created** — extractables profile is qualitatively and quantitatively equivalent to non-sterilised material
4 **New Leachable Species**	**Novel species** generated that do not exist in the un-irradiated material. **Pre-irradiation** extractables data is therefore **not applicable.**	**No new species** — predictable, stable, characterisable from material composition alone



Summary

- Peptides have greater structural sensitivity than mAbs, whereby trace levels of leachables from SU materials can drive degradation at typical process concentrations.
- The industry lacks peptide specific risk guidance and needs a higher level of science-led education to minimize process risks from E&L in peptide manufacturing.
- Elimination of the radiation-generated leachable burden from SU materials by preferencing autoclaved systems is the highest-leverage risk reduction available before formulation or process controls are considered.
- Sterilisation is not just a processing step—it can fundamentally change the chemistry of single-use materials and therefore directly impact peptide product quality and patient safety.

Key References

1. Draft ICH Q3E guideline for extractables and leachables, EMA/CHMP/ICH/236669/2025
2. Kuzmič, S., Zlobec, T., Dolenc, M.S., Roškar, R. and Lušin, T.T., (2026). *Toxics*, *14*(1), 92.
3. Li, K., *et al.*, (2015). *PDA J. Pharm Sci Technol.*, *69 (5)* 590-619.
4. Christensen, S., Moeller, E.H., Bonde, C., Lilleoere, A.-M. (2007). *66,* 366-371
5. Hahladakis, J. N., Velis C. A., Weberb R., Iacovidoua E., Purnella P., (2018). *J. Hazard. Mater., 344,* 179-199
6. Baderdin, S., Janousek, J., Brandstaetter, H., Morley, N., Weber, L., & Sobańtka, A. (2023 *Int. J. Pharm.*, *634*, 122664.
7. Cuadros-Rodríguez, L., Lazúen-Muros, M., Ruiz-Samblás, C., Navas-Iglesias, N., (2020). *Int. J. Pharm., 583,* 119332.
8. Erckes, V., Rendueles, L. C., Misiek, A., Steuer, C., (2026). *RSC Med. Chem., 17(2)*, 1144-1154.
9. Menzel, R., Pahl, I., Dorey, S., Maier, T., Hauk, A., (2023). *Int. J. Pharm., 634,* 122677.

The Life Science business of Merck operates as MilliporeSigma in the U.S. and Canada.

SigmaAldrich.com

© 2026 Merck KGaA, Darmstadt, Germany and/or its affiliates. All Rights Reserved. Merck, Millipore, and the vibrant M are trademarks of Merck KGaA, Darmstadt, Germany or its affiliates. All other trademarks are the property of their respective owners. Detailed information on trademarks is available via publicly accessible resources. Lit. No. MK_PS14587EN

Millipore®
Expert Pharm/BioPharm Products & CTDMO Services

https://doi.org/10.17952/38EPS.2026.P459

De novo Design and AI-supported Flow Synthesis of Catalytic Miniproteins

Manish Kumar, Ewa Rudzińska-Szostak, Anna Szczepańska, Łukasz Berlicki

Department of Bioorganic Chemistry, Wroclaw University of Science and Technology, Wybrzeże Wyspiańskiego 27, 50-370 Wrocław, Poland

Introduction

Miniproteins are bridging the gap between peptides and proteins. The combination of a stable tertiary structure with the feasibility of synthesizing miniproteins provides a significant advantage for the development of demanding functions.[1,2] Recent significant progress in the computational design of proteins has also impacted the field of miniproteins, opening the way to create structures of any desired geometry and size. Several examples of *de novo*-designed miniproteins have been published.[3,4] These also included miniproteins incorporating non-canonical amino acids, in particular backbone-modifying ones. Moreover, it has been shown that miniproteins constitute a unique scaffold for the construction of biologically active molecules. Published examples confirm their usefulness for creating binders of difficult molecular targets, as numerous well-defined intermolecular interactions can be feasibly designed.[5] In particular, inhibitors of various protein-protein interactions were developed using miniproteins. However, constructing miniproteins with catalytic activity remains challenging, and only a few examples have been reported to date.[6]

The goal

Development of rational methodology of catalytic miniprotein construction.

Results

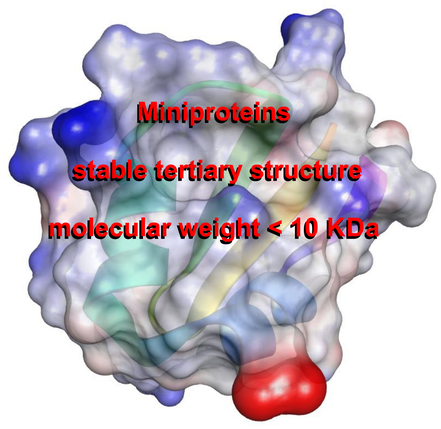
Using the FastDesign protocol from the Rosetta software suite, new miniproteins with cavities were designed. The improved conformational stability was achieved by incorporating conformationally constrained β-amino acids. To efficiently synthesize miniproteins with long and difficult sequences, we have developed a fully automated flow peptide synthesizer. Online control of synthesis progress using a UV detector enabled direct, fully automatic adjustment of several synthesis parameters. In particular, the optimal coupling time is determined using an AI model trained on numerous experimental datasets. The cavity-containing miniproteins were used for the construction of various enzyme-like catalysts. Several catalytic miniproteins that act according to Michaelis-Menten kinetics and significantly increase reaction rates were developed.

Synthesis

Poster 276

Application of an Automated System for Flow Solid Phase Peptide Synthesis

Manish Kumar



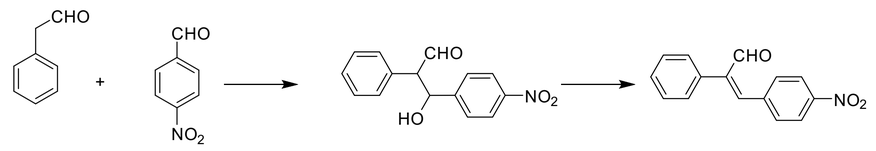
Structure

Poster 472

The NMR Structures of De Novo-designed Novel Miniproteins Containing 2-Aminocyclopentane-carboxylic Acid Residues

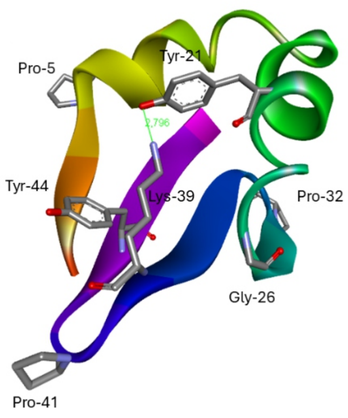
Ewa Rudzińska-Szostak

Catalysis

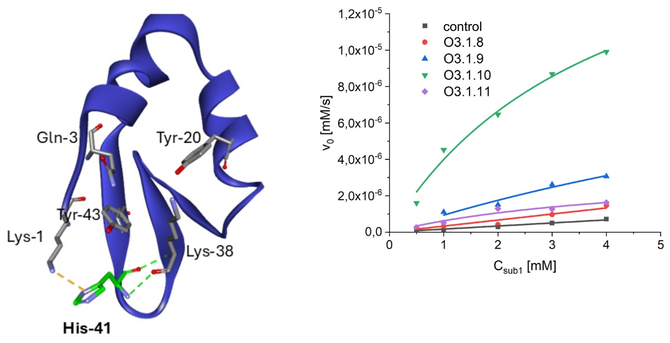


De novo-designed scaffold with active motiff

HHEEE

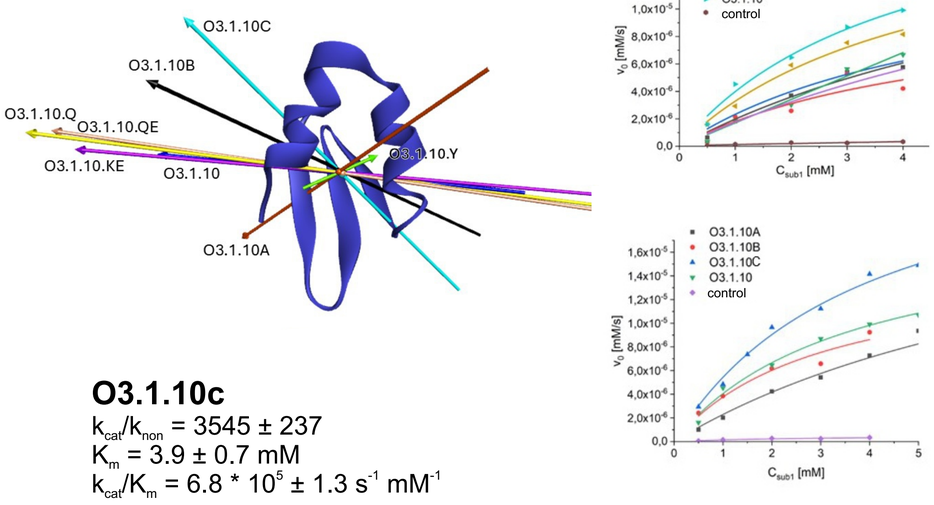


Optimisation of first sphere of interactions



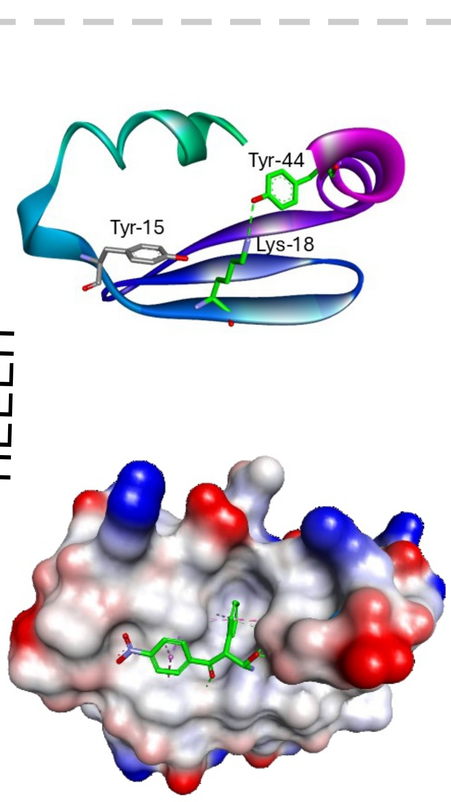
O3.1.10
k_{cat}/k_{non} = 2765 ± 291
K_m = 4.4 ± 1.9 mM
k_{cat}/K_m = 4.8 * 10^5 ± 2.1 s^{-1} mM^{-1}

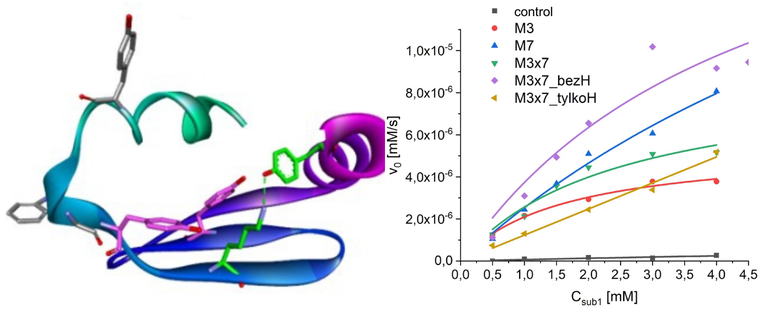
Global dipol moment-based optimisation



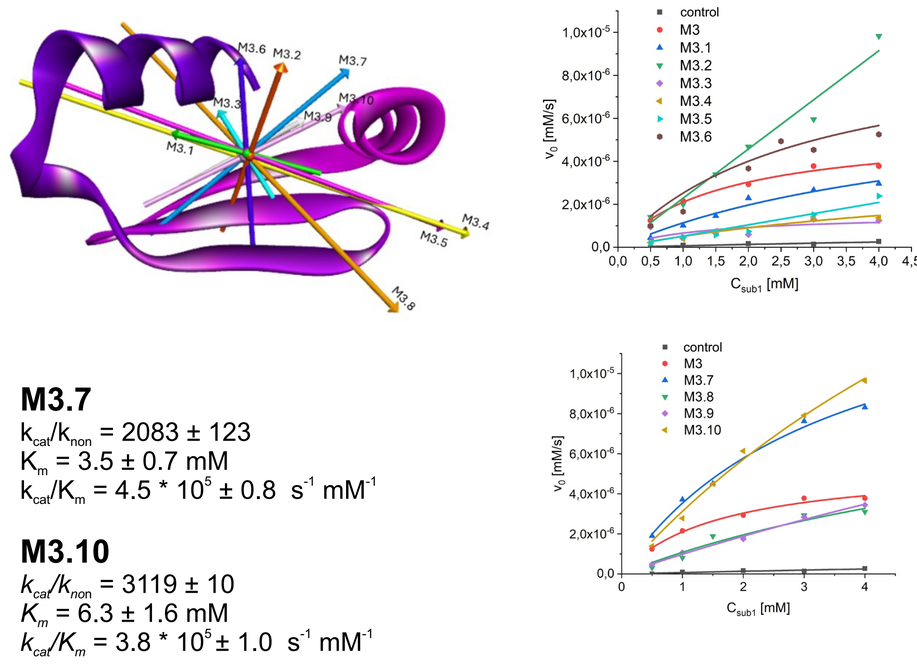
O3.1.10c
k_{cat}/k_{non} = 3545 ± 237
K_m = 3.9 ± 0.7 mM
k_{cat}/K_m = 6.8 * 10^5 ± 1.3 s^{-1} mM^{-1}

HEEEH





M3x7_bezH
k_{cat}/k_{non} = 2581 ± 157
K_m = 4,4 ± 2,6 mM
k_{cat}/K_m = 4,6 * 10^5 ± 1,9 s^{-1} mM^{-1}



M3.7
k_{cat}/k_{non} = 2083 ± 123
K_m = 3.5 ± 0.7 mM
k_{cat}/K_m = 4.5 * 10^5 ± 0.8 s^{-1} mM^{-1}

M3.10
k_{cat}/k_{non} = 3119 ± 10
K_m = 6.3 ± 1.6 mM
k_{cat}/K_m = 3.8 * 10^5 ± 1.0 s^{-1} mM^{-1}

References

[1] K. Ożga, Ł. Berlicki, "Design and Engineering of Miniproteins" ACS Bio & Med Chem Au 2022, 2, 316–327.
[2] E. Rudzińska-Szostak, Ł. Berlicki, "Towards filling the gap between organocatalysis and biocatalysis — catalysis by folded peptides and miniproteins" Tetrahedron Chem 2026, 18, 100161.
[3] M. Bejger, P. Fortuna, M. Drewniak-Świtalska, J. Plewka, W. Rypniewski, Ł. Berlicki, "A computationally designed β-amino acid-containing miniprotein" Chemical Communications 2021, 57, 6015–6018.
[4] M. Drewniak-Świtalska, B. Barycza, E. Rudzińska-Szostak, P. Morawiak, Ł. Berlicki, "Constrained beta-amino acid-containing miniproteins" Org. Biomol. Chem. 2021, 19, 4272–4278.
[5] A. Ciesiołkiewicz, J. Lizandra Perez, L. Skalniak, P. Noceń, Ł. Berlicki, "Miniprotein engineering for inhibition of PD‐1/PD‐L1 interaction" Protein Science 2024, 33, e5106.
[6] K. Ożga, Ł. Berlicki, "Miniprotein-Based Artificial Retroaldolase" ACS Catal. 2022, 12, 15424–15430.

Poster n°047

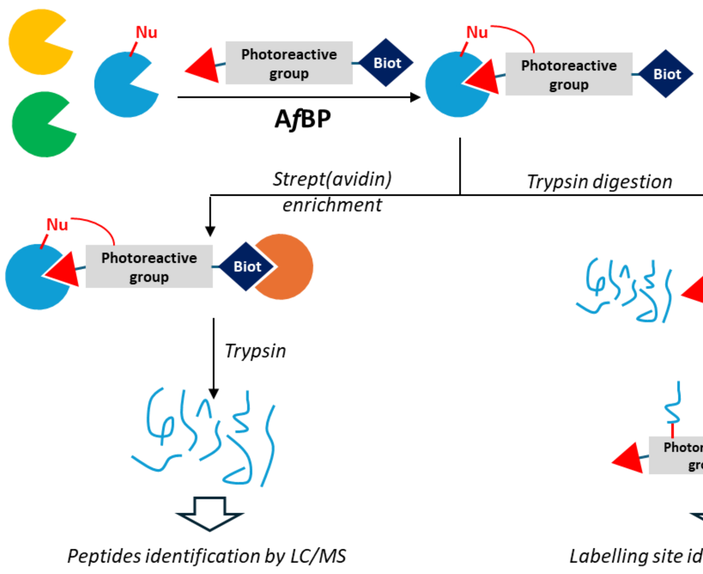
Affinity-driven transfer of a mass tag for the direct profiling of matrix metalloproteases in complex biological matrices

Lomane Berthy[a#], Ugo Pasco[b#], Mylene Sejalon-Cipolla[b#], Pierrick Bruyat[a], Monika Kaminska[a], Carole Malgorn[a], Fabrice Beau[a], Manca Osolin[c], Metka Novak[c],Barbara Breznik[c], Dimitris Georgiadis[d], Isabelle Correia[e], Olivier Lequin[e], Sarah Bregant[a], Robert Thai[a], Gilles Subra[b], Sonia Cantel[b], and Laurent Devel[a]*

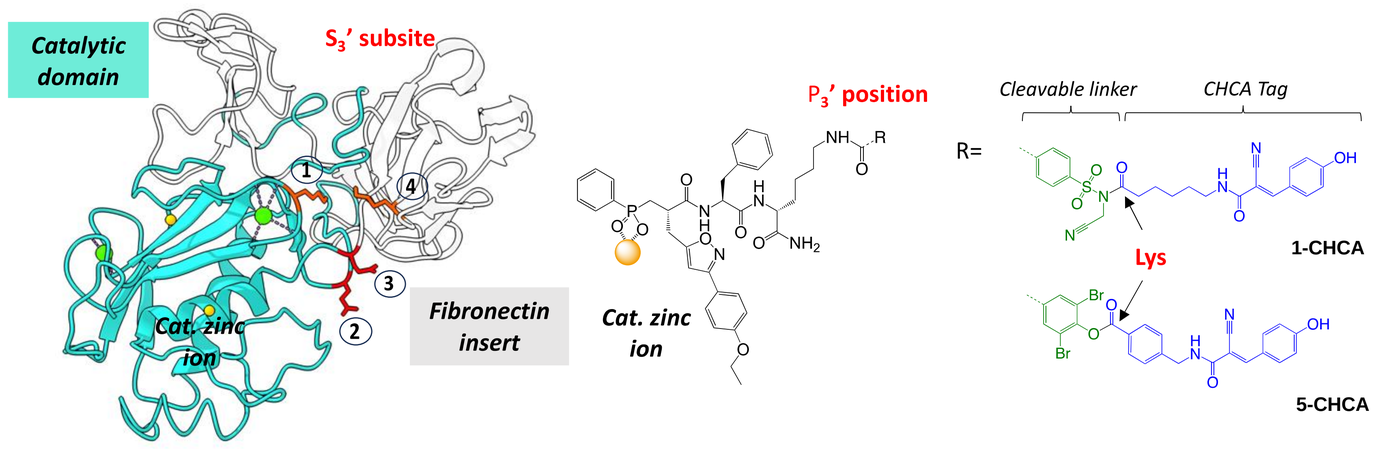
[a]CEA, INRAE, Médicaments et Technologies pour la Santé (MTS), SIMoS, Université Paris-Saclay, 91191, Gif-sur-Yvette, (France), https://doi.org/10.17952/38EPS.2026.P047 [b]IBMM, Univ. Montpellier, ENSCM, CNRS, Montpellier, (France)., [c] National Institute of Biology, Department of Genetic Toxicology and Cancer Biology, 121 Večna pot, 1000 Ljubljana, (Slovenia). [d] Department of Chemistry, Laboratory of Organic Chemistry, University of Athens, Panepistimiopolis, Zografou, 15771, Athens (Greece). [e]Sorbonne Université, Ecole Normale Supérieure, PSL University, CNRS, Laboratoire des Biomolécules, LBM, 75005 Paris, (France).

Among the diverse family of proteases, matrix metalloproteinases (MMPs) are a notable subset of 23 zinc-dependent endopeptidases. MMPs play essential roles in numerous physiological and pathological processes[1]. These enzymes are initially synthesized as inactive zymogens and require activation in the pericellular or extracellular environment. Activated MMPs process a broad spectrum of substrates, including components of the extracellular matrix (ECM) and non-ECM molecules, influencing tissue architecture and cellular functions. Under normal physiological conditions, MMP activity is tightly regulated by endogenous inhibitors; however, this balance is often disrupted in disease states. MMPs also initiate complex proteolytic cascades, activating other MMPs and generating novel substrates[2]. Detecting the activation profile of MMPs in specific pathological contexts is crucial for elucidating their precise functions and confirming their potential pathological roles, which remain unclear in many diseases where these proteases are overexpressed.

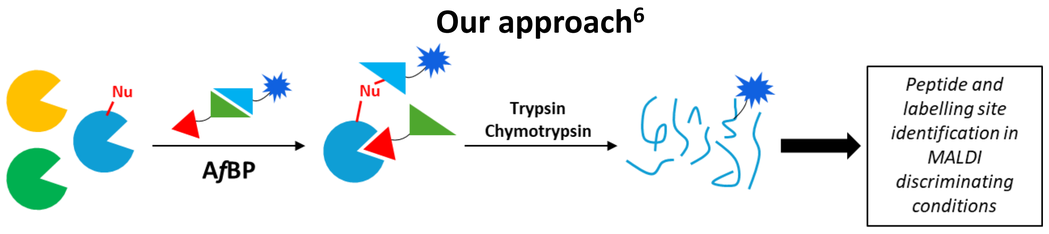
Traditional approaches for the profiling of metalloproteases



Structural context and design of the probes



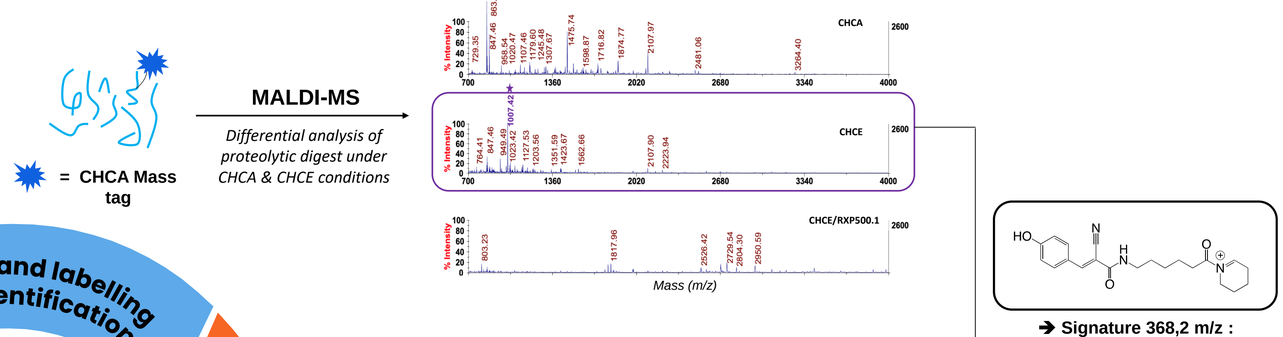
Our approach[6]

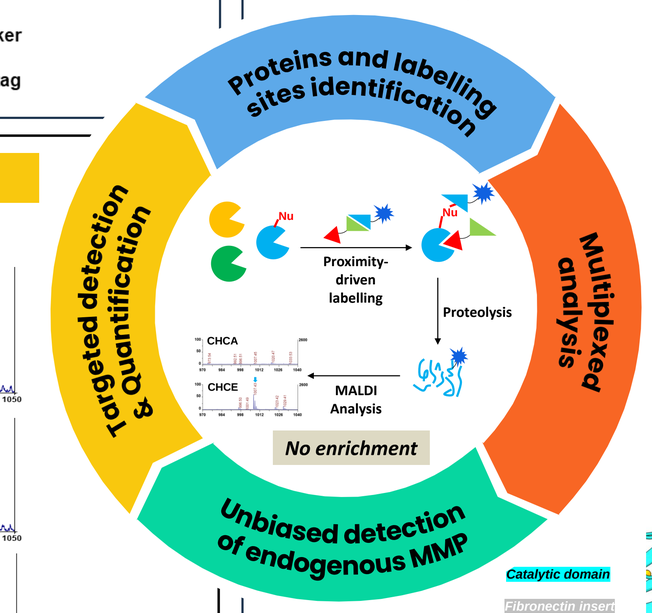


- ✓ No enrichment step required
- ✓ Qualitative & Quantitative profiling
- ✓ Photoactivation-free process of labelling[3, 4, 5]

= Recognition motif
= Cleavable linker
= CHCA Mass tag

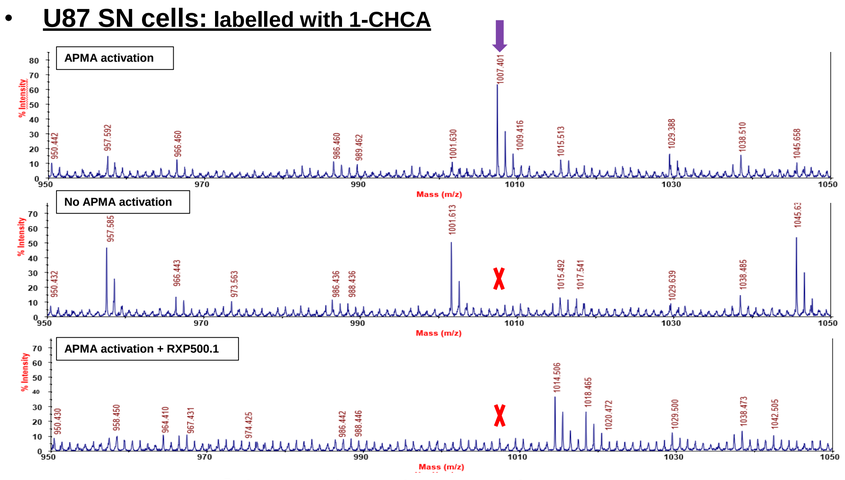
Labelled MMPs are associated to characteristic signature peptides





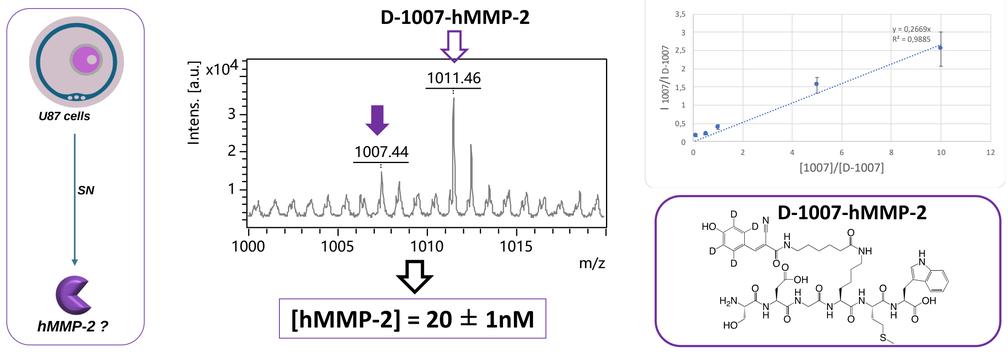
hMMP2 in U87 cells supernatant

- **U87 SN cells: labelled with 1-CHCA**



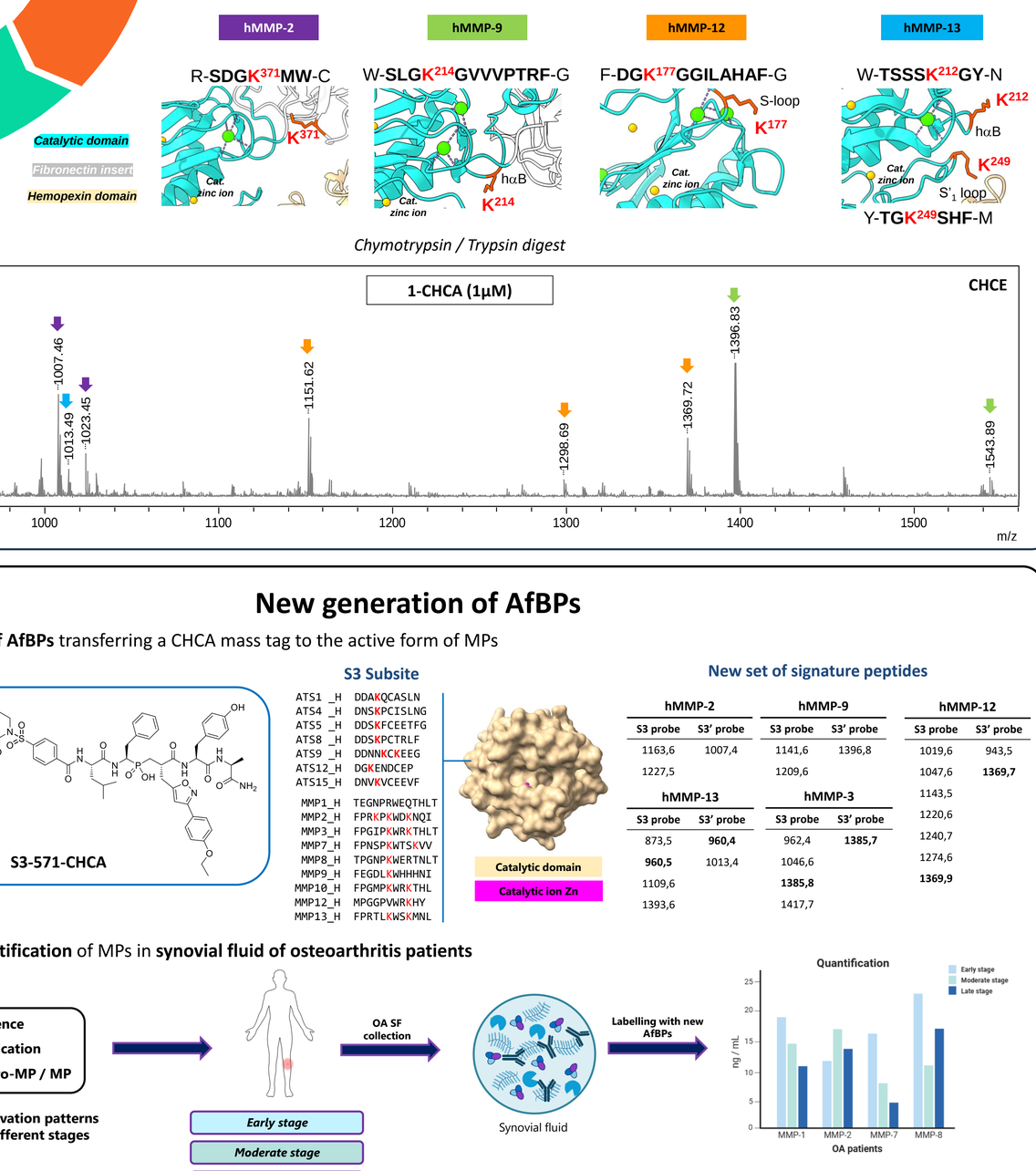
➔ hMMP-2 detected in U87 SN after APMA activation

- **Quantitative profiling**



hMMP3 in chondrocytes supernatant

Multiplexed detection of MMP-2, -9, -12 & -13



New generation of AfBPs

- **New generation of AfBPs** transferring a CHCA mass tag to the active form of MPs

S3 Subsite

ATS1 _H	DDAKQCASLN
ATS4 _H	DNSKPCISLNG
ATS5 _H	DDSKFCEETFG
ATS8 _H	DDSKPCTRLF
ATS9 _H	DDNNKCKEEG
ATS12_H	DGKENDCEP
ATS15_H	DNVKVCEEVF
MMP1_H	TEGNPRWEQTHLT
MMP2_H	FPRKPKWDKNQI
MMP3_H	FPGIPKWRKTHLT
MMP7_H	FPNSPKWTSKVV
MMP8_H	TPGNPKWERTNLT
MMP9_H	FEGDLKWHHHNI
MMP10_H	FPGMPKWRKTHL
MMP12_H	MPGGPVWRKHY
MMP13_H	FPRTLKWSKMNL

New set of signature peptides

hMMP-2		hMMP-9		hMMP-12	
S3 probe	S3' probe	S3 probe	S3' probe	S3 probe	S3' probe
1163,6	1007,4	1141,6	1396,8	1019,6	943,5
1227,5		1209,6		1047,6	**1369,7**
hMMP-13		**hMMP-3**		1143,5	
S3 probe	S3' probe	S3 probe	S3' probe	1220,6	
873,5	**960,4**	962,4	**1385,7**	1240,7	
960,5	1013,4	1046,6		1274,6	
1109,6		**1385,8**		**1369,9**	
1393,6		1417,7			

- **Detection** & **Quantification** of MPs in **synovial fluid of osteoarthritis patients**

Conclusion & Perspectives

- **New generation of AfBPs** transferring a CHCA mass tag to the active form of MMPs.
- Identification of CHCA-labelled MMPs & determination of their labelling sites within **a single workflow**.
- New ABPP to characterize the complete **activation pattern of MMPs** in a specific pathological context.
- This approach could be expanded for **probe-based target deconvolution** within **a single workflow**.
- Significant potential for the **rapid analysis of multiple proteins** in complex proteomes.
- By leveraging the MALDI-TOF format, our approach could be applied to multiple pathological fluids, ultimately serving as a **robust diagnostic platform.**

[1]De Almeida, L. G. N. *et al. Pharmacological Reviews* **74**, 714–720 (2022). [2]Kollet, O., Das, A., Karamanos, N., Auf Dem Keller, U. & Sagi, I. *Trends in Molecular Medicine* **30**, 147–163 (2024). [3]Kaminska, M. *et al. Angew Chem Int Ed* **60**, 18272–18279 (2021). [4]Malgorn, C. *et al. Proteases and Cancer* (ed. Santamaria, S.) vol. 2747 29–39 (Springer US, New York, NY, 2024). [5]Devel, L. *et al. ChemBioChem* **25**, e202400441 (2024). [6]Berthy, L., Pasco U. *et al. Angew Chem Int Ed* **65**, e23132 (2026).

Decoding Pentapeptide Self-Assembly Using Molecular Dynamics: from Aggregation to Architecture

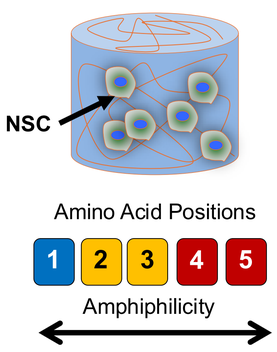
https://doi.org/10.17952/38EPS.2026.P263

Shimanto Roy, Camille L. Bilodeau, Kyle J. Lampe

Department of Chemical Engineering, University of Virginia, Charlottesville, VA 22903, United States

Background

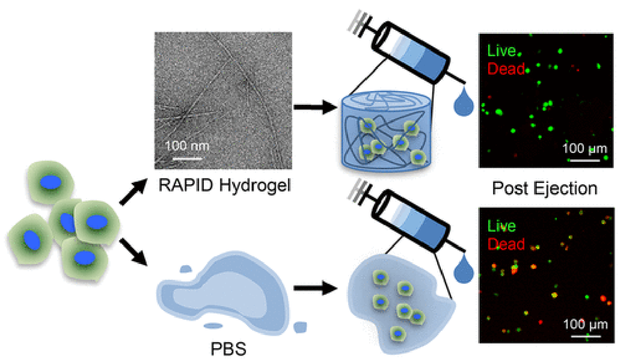
Injectable hydrogels are promising for neural stem cell (NSC) delivery and tissue engineering, requiring shear-thinning and self-healing properties.



- **Pentapeptides** can **self-assemble** into RAPID hydrogels, **mimicking** the **extracellular matrix** to support cell growth and differentiation.
- Understanding **peptide sequence effects** on self-assembly **permits designer gelation** and **mechanical properties** for biomedical applications.

Computational modeling provides insights into **peptide self-assembly**, guiding experimental peptide design.

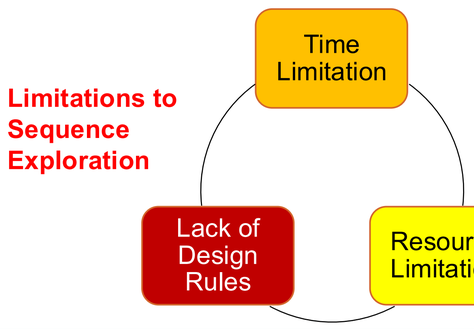
Experimental Motivation



Tang et al.[1]

Using RAPID hydrogel increases cell viability significantly.

(Rapidly Assembling Pentapeptides for Injectable Delivery)

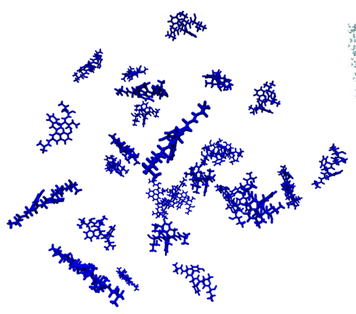


Limitations to Sequence Exploration

Even for a peptide with five amino acids
The total number of sequences possible is
3,200,000

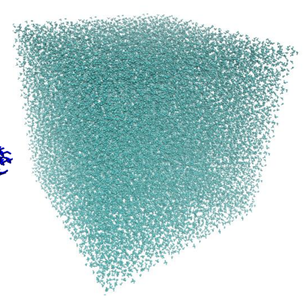
Molecular Dynamics Setup

30 Peptides



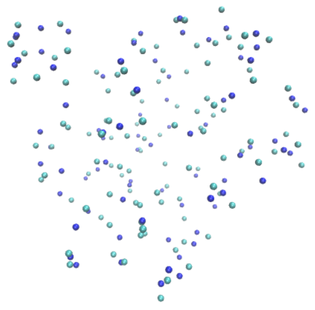
Protein Force Field
FF19SB

Water Box

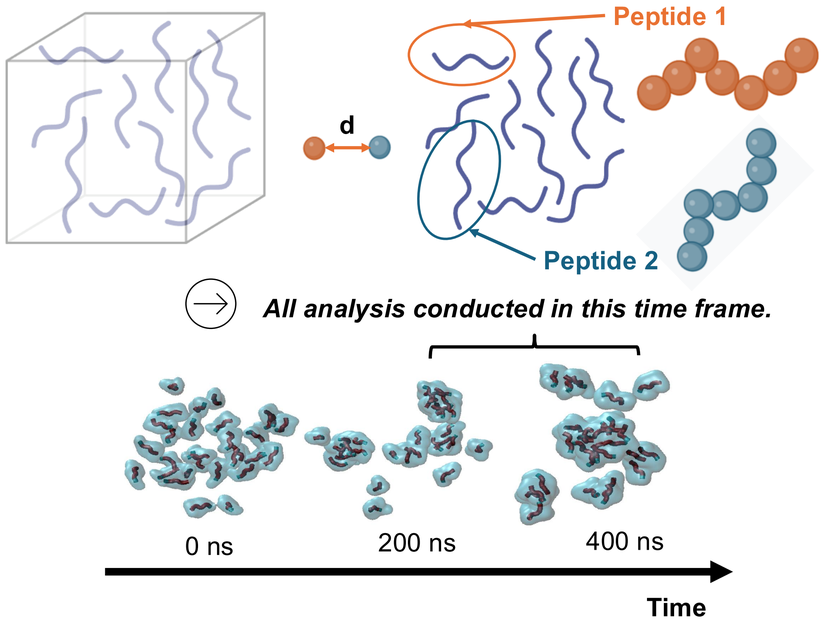


Water Force Field
Optimal Point Charge (OPC)

150 mM Salt



Additional ions were added to neutralize the system



All analysis conducted in this time frame.

Acknowledgments

Lampe Biomaterials Group

Bilodeau Group

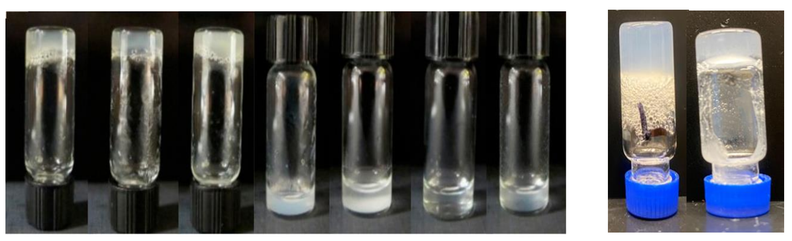
RESEARCH COMPUTING

NSF

Molecular Dynamics Outcome Matches Experimental Results

KYFIL
- **A**YFIL / K**A**FIL / KY**A**IL / KYF**A**L/
- KYFI**A** / KYFI**V**/ KFFFL / KYYYL

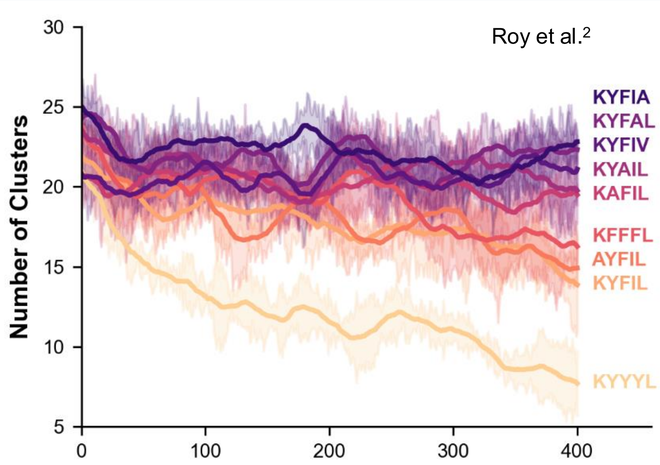
Test Sequence



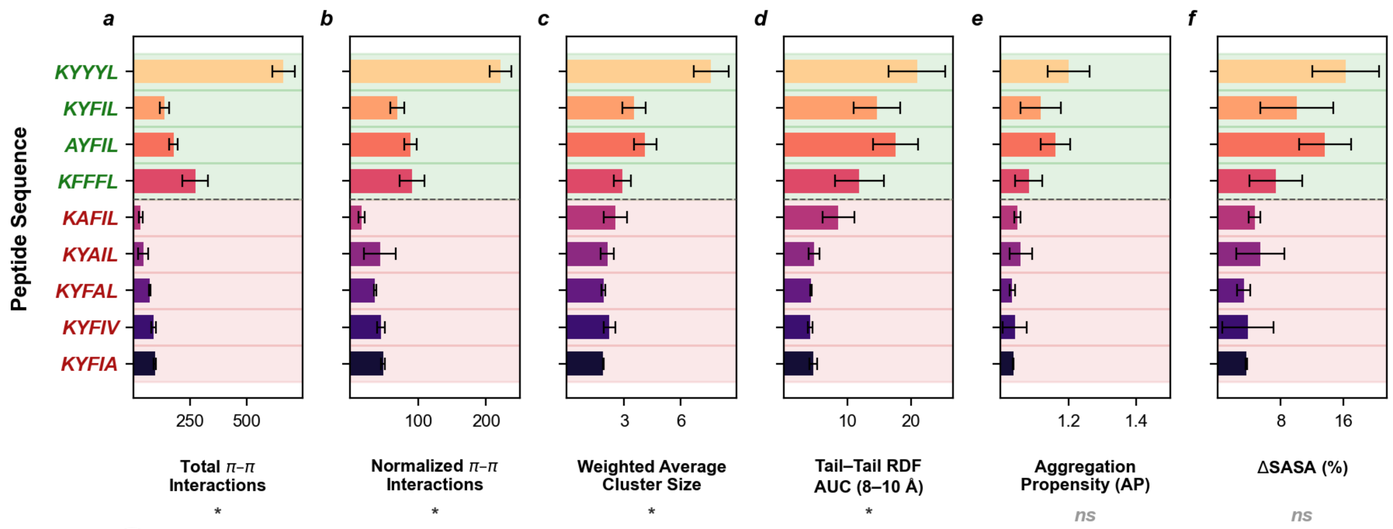
KYFIL AYFIL KYFAL KYFIV KYFIA KAFIL KYAIL

KFFFL KYYYL

Gelling → Non-Gelling



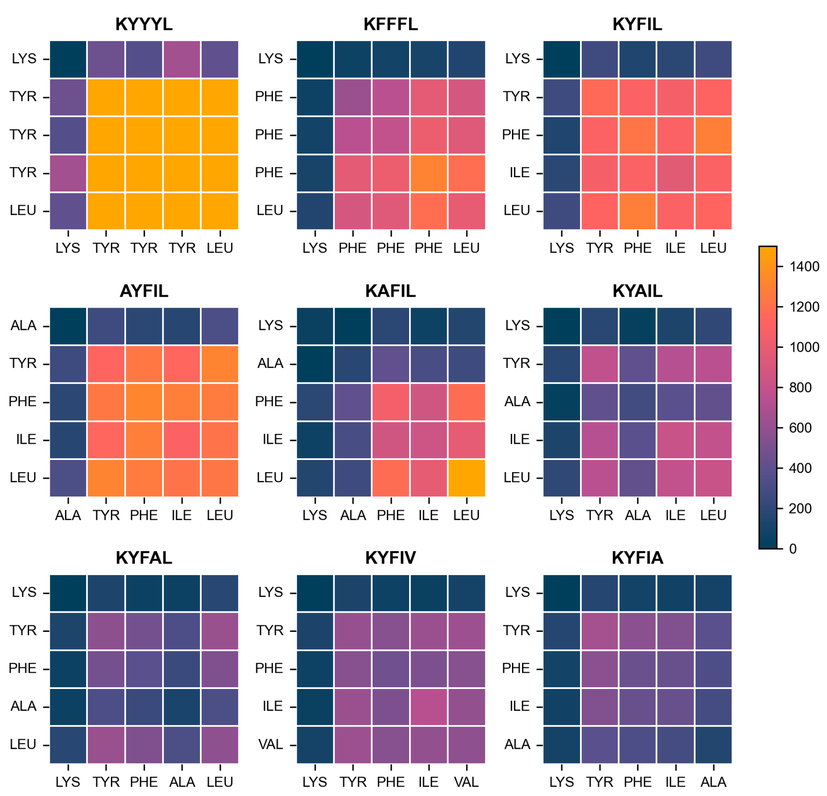
Lower number of clusters indicate higher assembly of peptides.



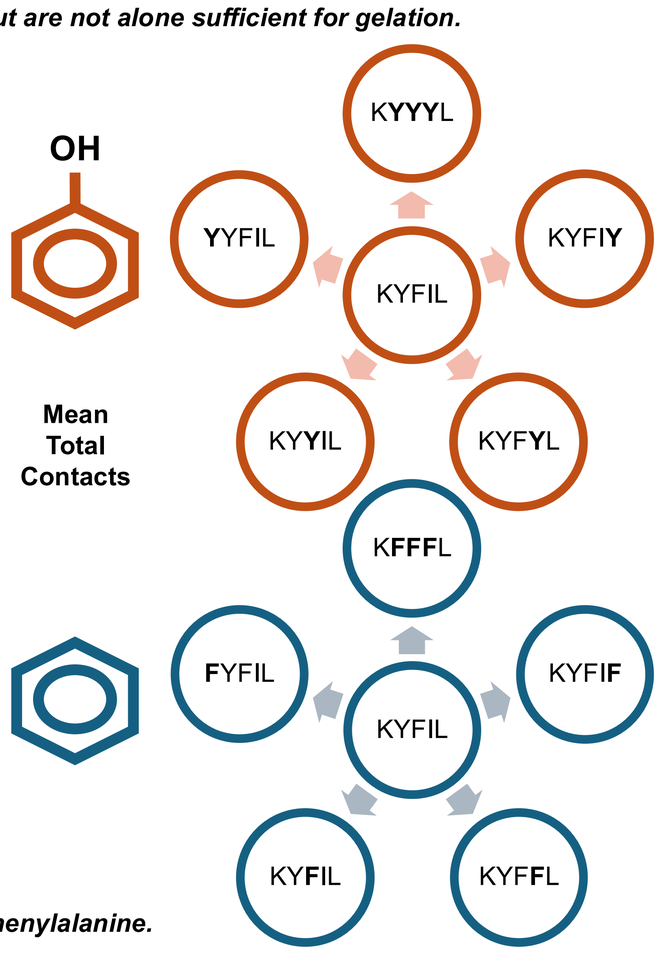
Order Parameters derived from MD simulation can differentiate Self-Assembly.

Aromatic-biased Contact Pattern

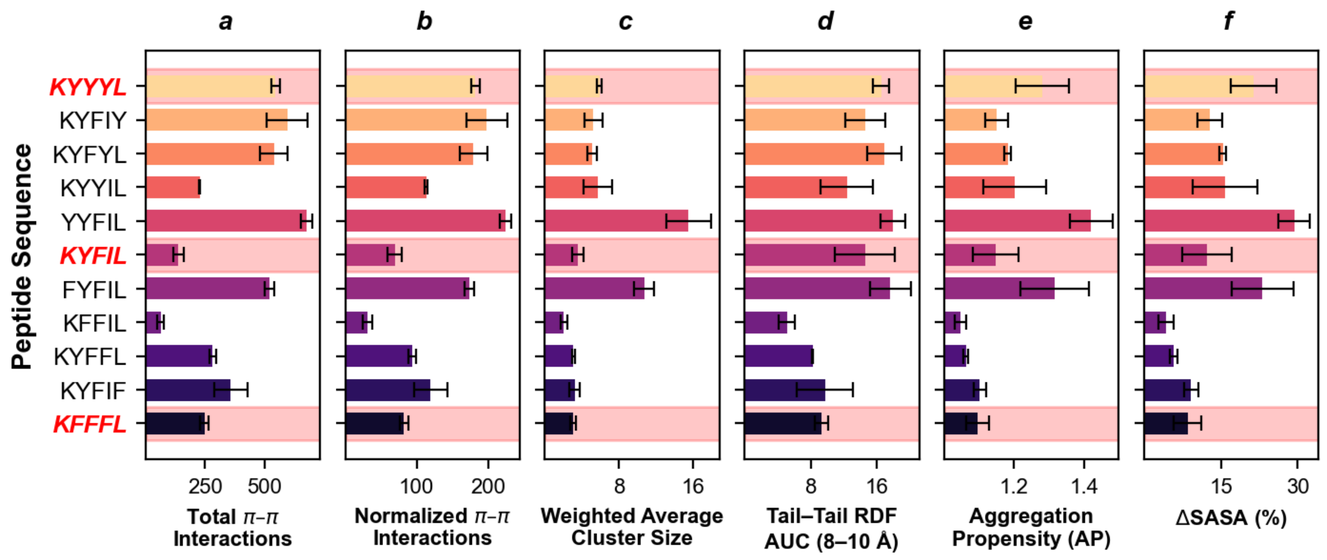
Aromatic residues play crucial role in self-assembly but are not alone sufficient for gelation.



Mean Total Contacts



Tyrosine has a greater influence on self-assembly than Phenylalanine.



References

1. Tang, J. D.; Mura, C.; Lampe, K. J. (2019). A Stimuli-Responsive, Pentapeptide, Nanofiber Hydrogel for Tissue Engineering. Journal of American Chemical Society.
2. Roy, S., Hur, R. K., McAllister, L. C., Lampe, K. J., & Bilodeau, C. L. (2026). A methodological approach to relate pentapeptide sequence, Atomistic Self-Assembly, and gelation behavior. ACS Biomaterials Science & Engineering.

https://doi.org/10.17952/38EPS.2026.P543

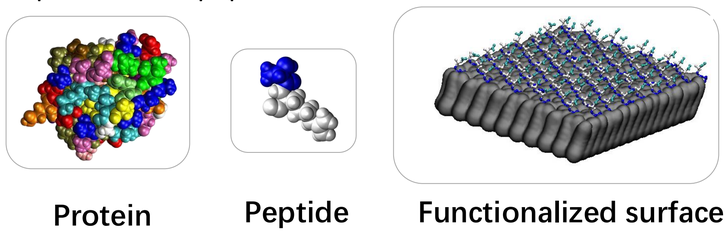
Computational Exploration of Nanoscale Chemical Patterning Using Short Peptides

Md Jakir Hossen [1], Adel Nematipour [1], and Camille Bilodeau [1]

[1]Department of Chemical Engineering, University of Virginia

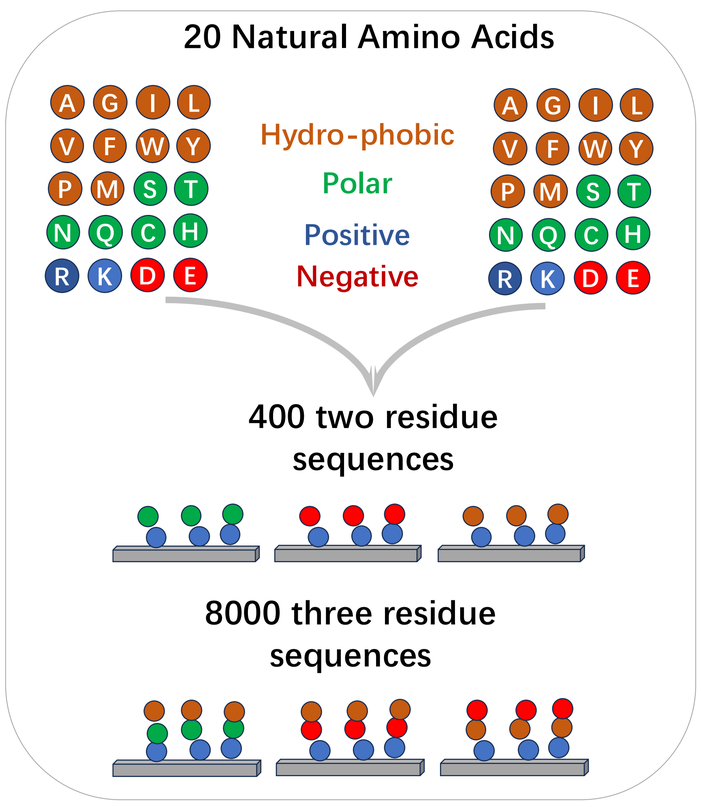
Overview

- Chemically patterned surfaces refers to the surfaces that are chemically and structurally diverse such as proteins and peptides.



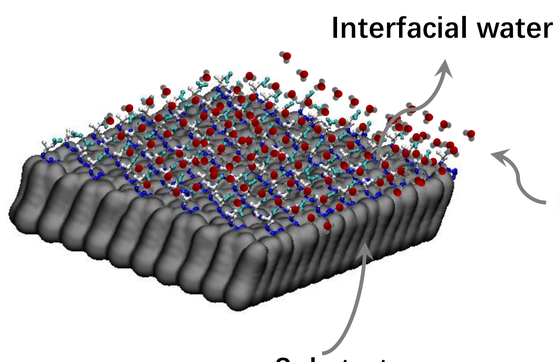
Protein | Peptide | Functionalized surface

- **Applications:** Enable selective nanoparticle binding, antifouling materials, and separation membranes.
- Peptides offer a versatile platform for surface functionalization due to their broad chemical and structural diversity.



- Assuming fixed substrate and grafting density, peptides can efficiently be modeled using computational approaches.

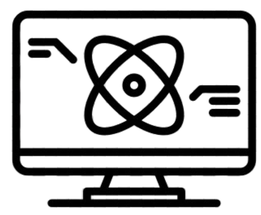
Background



Water at interface controls stickiness, i.e., adsorption property[1]

Polymeric materials such as peptides provide chemical and structural diversity[2]

Substrate mostly controls peptide assembly on surface[3]



This study: Computationally explores a **dipeptide library** at a fixed grafting density for wetting properties using MD simulation and predictive models.

System and Simulation

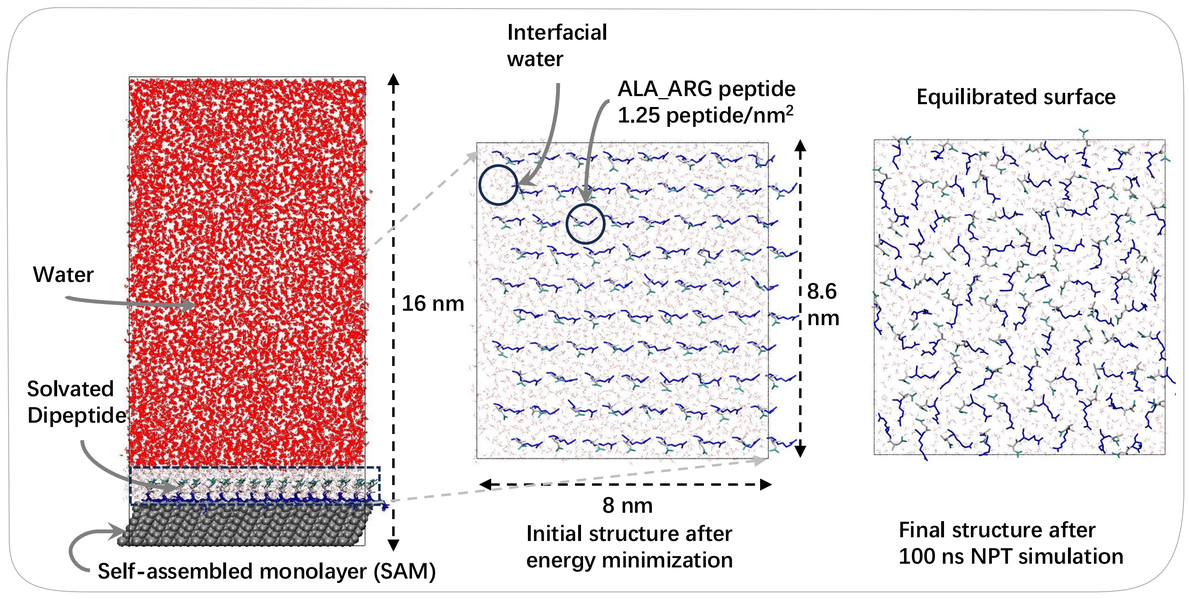
Step 1: *Avorgadro* — Create Single SAM strand and Functionalized SAM strand

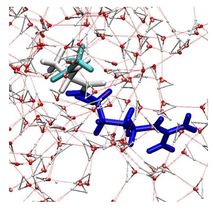
Step 2: *Python* — Build peptide-functionalized surface by repeating strands in xy plane to match 1.25 peptide/nm^2

Step 3: *AMBER* — Force field parameters SAM: GAFF2 Peptides: FF19SB Water Model: OPC (4 point)

Step 4: *VMD* — Visualize using visual molecular dynamics (VMD)

MD Simulation of 289 Dipeptides (Cys, Met, Pro excluded) Immobilized on SAM Surfaces to Probe Peptide–Water Interface Hydrophobicity



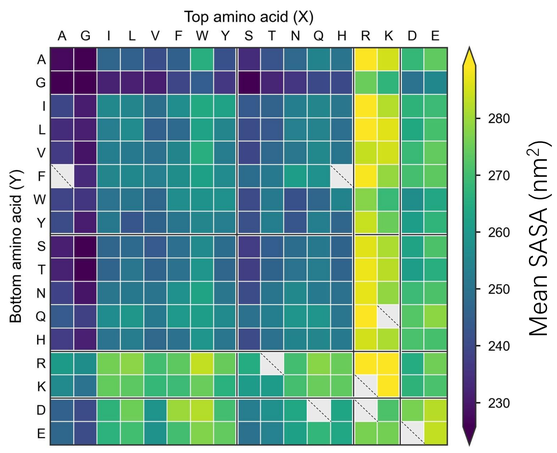


Surface Properties

- **SASA: Solvent accessible surface area**
  Calculated by rolling 0.14 nm probe sphere across the Van der Waals surface of the molecule
- **Peptide-water hydrogen bond:** calculated by Luzar-Chandler[4] geometric criteria
- **Mean Free OH fraction:** Calculated by defining hydration shell around 0.6 nm of peptide heavy atoms and getting the fraction that does not contribute to any hydrogen bond

Results

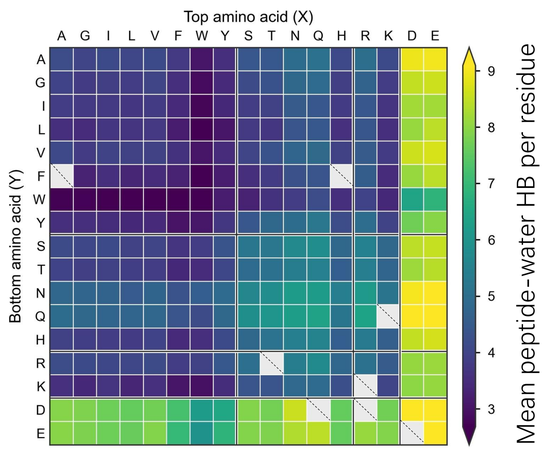
Solvent Accessible Surface Area (SASA)



*Gray boxes refer to missing data

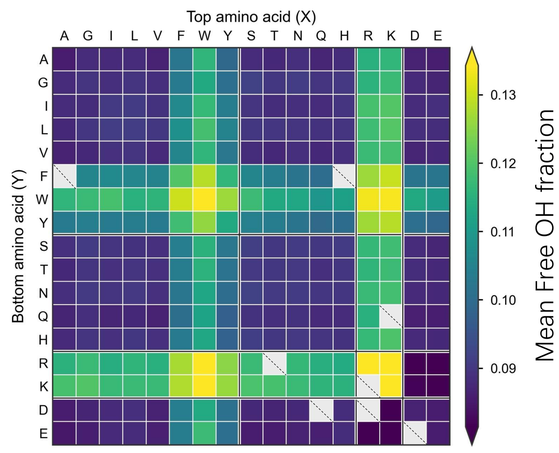
Long, flexible basic residues (R, K) consistently maximize total SASA (~ 280−311 nm^2)

Peptide-water hydrogen bonding

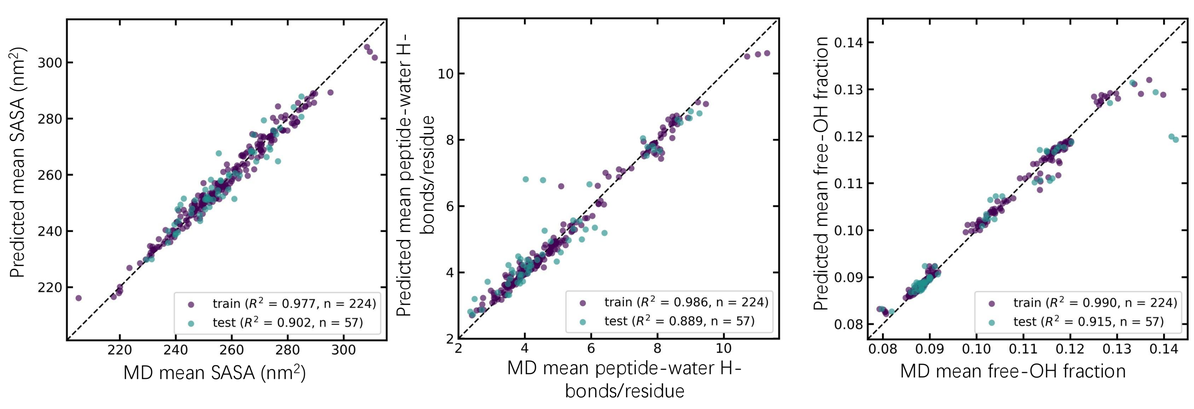


Anionic carboxylates (D, E) dominate hydrogen bonding across all sequences, reaching up to ~11.3 H-bonds per dipeptide

Local water network disruption



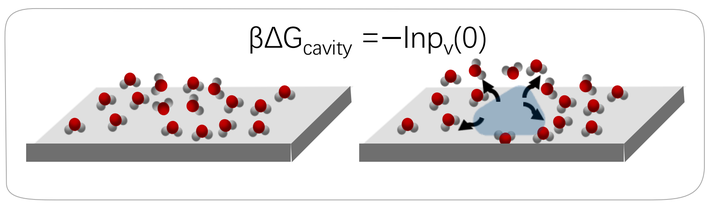
Pairing basic residues (R, K) with aromatic residues (W, F) produces the highest free-OH fraction (~0.13-0.143)



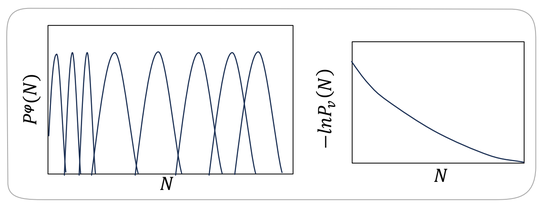
- The models provide a rapid and reasonable approximation of interfacial properties, making them useful for initial screening
- While the models capture general trends well, some scatter in the test data suggests they are approximations rather than exact replacements for detailed MD simulations

Future work

Prepare hydrophobicity dataset

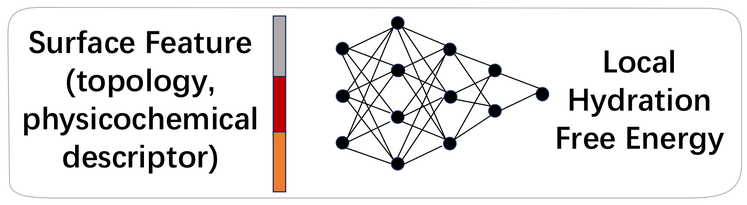


- **Free energy** of cavity formation at interface provides direct quantification of hydrophobicity at molecular scale



- **INDUS** (Indirect Umbrella sampling) quantifies the free energy

Generate Surface Feature and model to predict



- We expect to build a model that predicts local hydrophobicity of peptide functionalized surfaces at nanoscale

Acknowledgements

NSF | Research Computing | BG

References

1. Garde, S. Sticky when dry. *Nat. Chem.* **2020**, *12* (7), 587–588.
2. Fang, Z.; Chen, J.; Zhu, Y.; Hu, G.; Xin, H.; Guo, K.; Li, Q.; Xie, L.; Wang, L.; Shi, X.; et al. High-throughput screening and rational design of biofunctionalized surfaces with optimized biocompatibility and antimicrobial activity. *Nat. Commun.* **2021**, *12* (1), 3757.
3. Rahmani, R.; Lyubartsev, A. P. Uncovering sequence effects in titanium binding peptides adsorption on TiO_2: A molecular dynamics study. *Sci. Rep.* **2025**, *15* (1), 26885.
4. Luzar, A.; Chandler, D. *J. Chem. Phys.* **1993**, *98*, 8160–8173

Towards Greener Solid-Phase Peptide Synthesis: Combining a Novel Support with Eco-Friendly Solvents

Luana Lastella[1], Marco Zecca[1], Paolo Centomo[1], Karel Jeřabek[2], Fernando Formaggio[1,3], Ivan Guryanov[4], Marco Macis[4], Antonio Ricci[4] and Barbara Biondi[3]

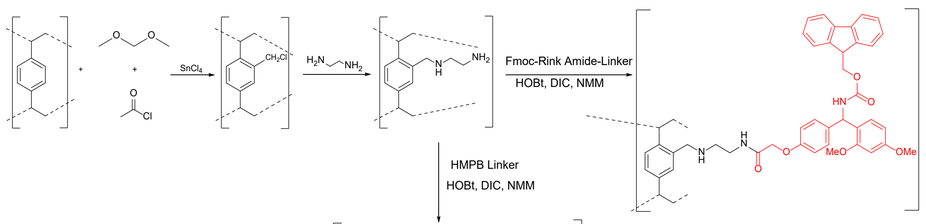
[1]Department of Chemical Sciences, University of Padova, 35131 Padova, Italy [2]Institute of Chemical Process Fundamentals of the CAS, v.v.i., 16502 Prague 6, Czech Republic
[3]Institute of Biomolecular Chemistry, Padova Unit, 35131 Padova, Italy [4]Fresenius Kabi Ipsum, 45010 Villadose, Rovigo, Italy
https://doi.org/10.17952/38EPS.2026.P290

Introduction

Peptides are attracting increasing investment across multiple sectors, particularly in the pharmaceutical industry, where they represent a highly important class of active pharmaceutical ingredients (APIs). Over the past decade, a growing number of peptide-based therapeutics have received regulatory approval, further highlighting their clinical and commercial relevance.
Peptide synthesis is predominantly performed using solid-phase peptide synthesis (SPPS). Despite significant advances in protecting group strategies, coupling reagents, and optimized reaction protocols, SPPS remains a costly process. This is largely due to the substantial excess of amino acids and coupling reagents required to drive reactions to completion, which necessitate the use of large volumes of solvents to remove the excess materials and washing steps. Additionally, downstream purification significantly contributes to overall waste generation, representing a major concern from both economic and industrial sustainability perspectives.
A further challenge is associated with the toxicity and environmental impact of commonly used solvents in peptide synthesis, such as N,N-dimethylformamide (DMF), dichloromethane (DCM), and N-methyl-2-pyrrolidone (NMP).[1]
To address these limitations, we recently introduced a novel mesoporous polymeric support for SPPS based on poly(divinylbenzene) (pDVB).[2] Owing to its unique morphology, this material exhibits minimal solvent-dependent swelling behavior, making it largely unaffected by the nature of the solvents employed during synthesis. Using this support, we successfully synthesized model peptides in alternative solvent systems, including acetonitrile (ACN) and isopropanol/dimethyl sulfoxide (IPA/DMSO) mixture. Here, we extend our evaluation to the synthesis of APIs., Degarelix and fragment (1-14) of Tirzepatide.

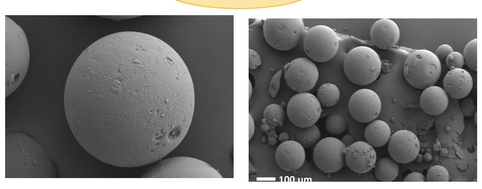
New solid support

The novel **polymeric mesoporous support** (pDVB) was modified with the two different linkers and used for SPPS

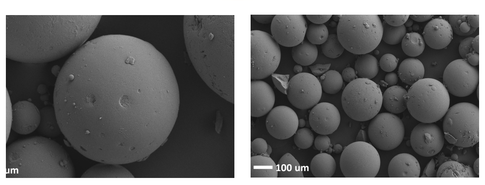


An important feature of this new support is the **reduced dependence** on swelling capacity, which allows the use of a **wider range of solvents**.

pDVB-Cl resin



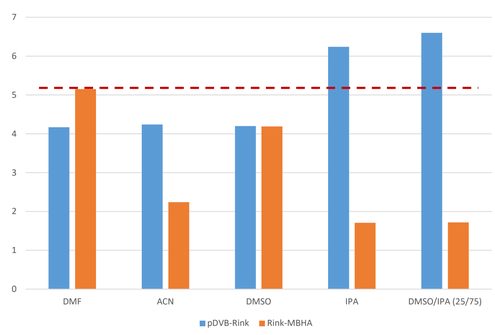
pDVB-Rink resin

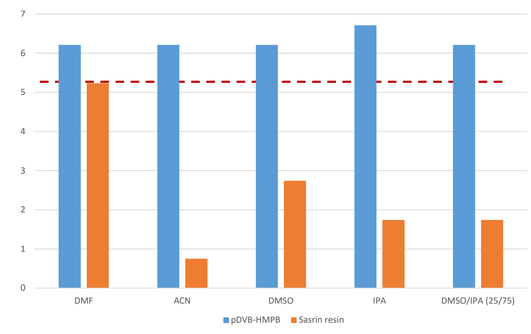


SEM performed with a Zeiss Sigma HD microscope. The samples were deposited on carbon tape and sputter coated with 15 nm of gold.

Swelling Test

The degree of swelling in pure and mixed solvents of pDVB supports was evaluated in comparison with the corresponding commercial resins.



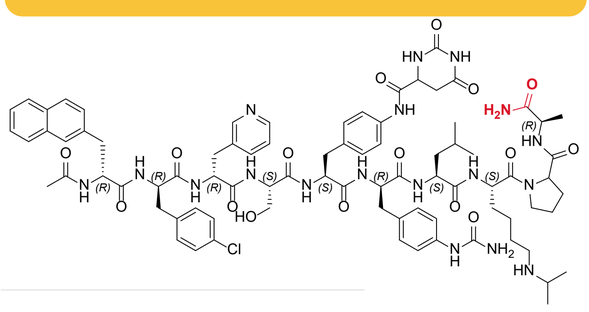


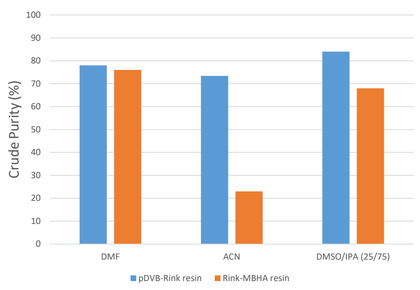
While the swelling properties for gel-type resins are highly dependent on the solvent used, the swelling degree values for the pDVB resins are almost the same in most solvents.

$$\text{Degree of swelling } (mL \cdot g^{-1}) = \frac{(V_{swollen\ resin} - V_{filter})\ (mL)}{m_{resin}\ (g)}$$

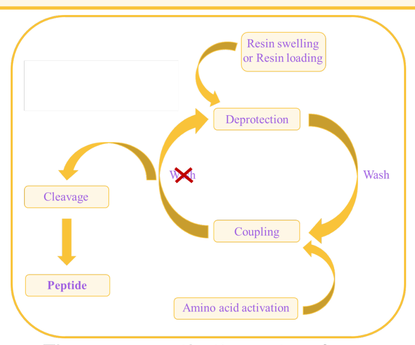
The minimal effect of solvent type on swelling, combined with the generally high swelling degrees, supports the conclusion that the pDVB resins allow for a broader range of solvents to be used in SPPS, potentially improving the environmental sustainability of the process.

Degarelix



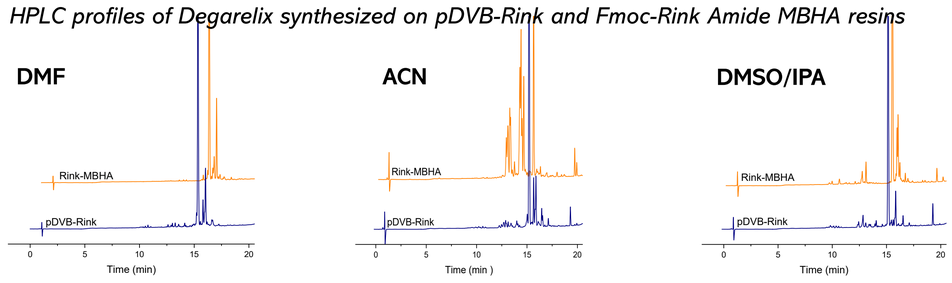


Although most of the amino acids are unconventional and have bulky side chains, **pDVB Rink outperformed the classical gel-type Rink Amide MBHA** resin in ACN and DMSO/IPA mixture

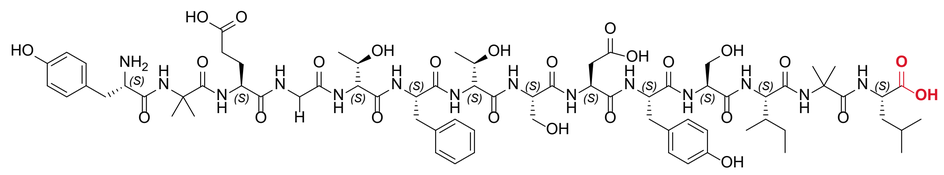


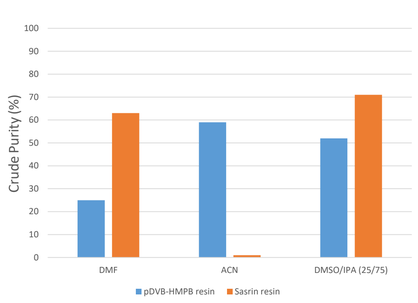
The same synthetic protocol was applied to obtain the two peptides, **no sequence-based optimization** was carried out.

HPLC profiles of Degarelix synthesized on pDVB-Rink and Fmoc-Rink Amide MBHA resins



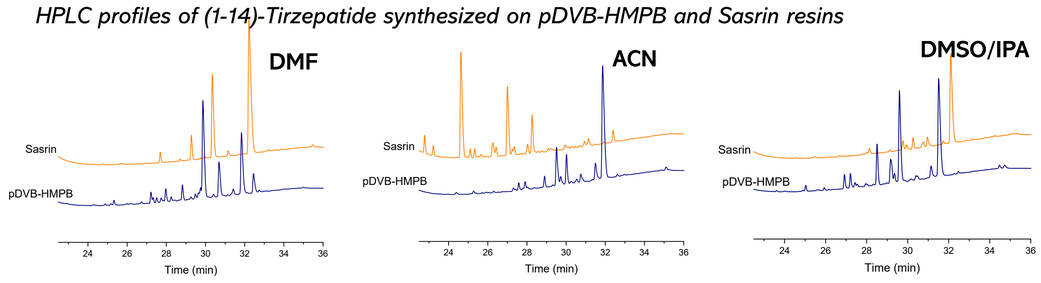
(1-14)-Tirzepatide





pDVB HMPB resin outperformed the classical gel-type Sasrin in ACN while also the conventional resin produces good results in DMSO/IPA mixture

HPLC profiles of (1-14)-Tirzepatide synthesized on pDVB-HMPB and Sasrin resins



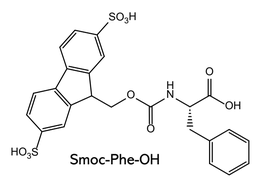
Conclusions

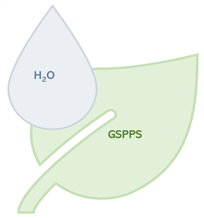
- Functionalization of pDVB support with Rink-Amide and HMPB linkers
- Identification of a support with reduced dependency on swelling properties
- Possibility of using a wider range of solvents other than DMF
- Relevant results using ACN and the promising mixture DMSO/IPA
- Synthesis of peptides of pharmaceutical interest with good results using more sustainable solvents
- Development of a greener process for peptide synthesis

Perspectives

Optimization and scale–up of the synyhetic process using pDVB resins

Development of in-water procedure using Smoc-AA-OH





References

[1] Green Chemistry 2016, 18, 3879–3890.
[2] J. Pept. Sci. 2025; 31:e70038

barbara.biondi@cnr.it
fernando.formaggio@unipd.it
luanalastellalu@gmail.com

Synthesis and Antimicrobial Activity of Cyclic Temporin L Analogues via Non-Conventional Guanidinium-Based Functionalization

I. Boccino[1], R. Bellavita[1], B. Casciaro[2], P. Grieco[1], M.L. Mangoni[2], F. Merlino[1]

[1]*Department of Pharmacy, University of Naples Federico II, Naples, Italy.*

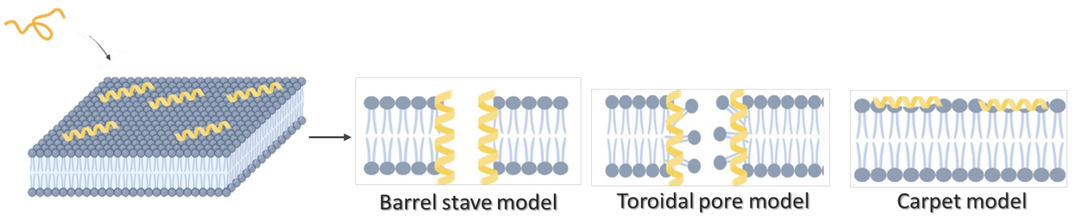
[2]*Department of Biochemical Sciences, Laboratory affiliated to Istituto Pasteur Italia-Fondazione Cenci Bolognetti, Sapienza University of Rome, Rome, Italy.*

ida.boccino@unina.it

38th European Peptide Symposium

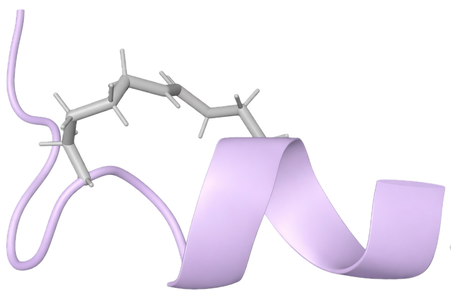
Background

Antimicrobial peptides (**AMPs**) represent versatile scaffolds for the development of novel antimicrobial agents, owing to the following properties: *i)* short sequence length, *ii)* activity against a wide range of pathogens, *iii)* additional chemotactic activity and immunomodulatory effects.[1]



Aim & Novel Design

Temporin L (TL) has undergone site-specific modifications, stereoinversion, and different cyclization strategies to optimize its biological profile.[2,3] Building on these findings, a new library of **cyclic TL derivatives** was designed and synthesized by introducing a **guanidino group** at selected positions along the peptide sequence.



F V P W F K K F *l* E R I L **(1)**

Peptide **12** in Bellavita et al, *J.Med.Chem.*, **2021**

Stereoinversion of cyclizing aa:

FVPWF[KKFl**e**]RIL **(2)**

PENDANT guanidino group:

$(H_2N)_2C$=N-FVPWF[KKFl**e**]RIL **(3)**

$(H_2N)_2C$=N-βAla-FVPWF[KKFl**e**]RIL **(4)**

$(H_2N)_2C$=N-GABA-FVPWF[KKFl**e**]RIL **(5)**

F[***p*-NHC(=NH)NH_2]**VPWF[KKFl**e**]RIL **(6)**

FV**P[4-NHC(=NH)NH_2]**WF[KKFl**e**]RIL **(7)**

FVPW**F[*p*-NHC(=NH)NH_2]**[KKFl**e**]RIL **(8)**

FVPWF[K**R**Fl**e**]RIL **(9)**

FVPW F[KK**F[*p*-NHC(=NH)NH_2]**l**e**]RIL **(10)**

BRIDGED guanidino group:

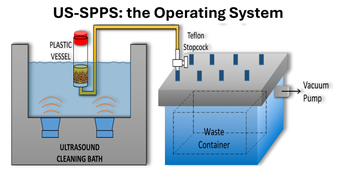
FVPWF[**K**KFl**K**]RIL **(11)**

FVPWF[**K**KFl**k**]RIL **(12)**

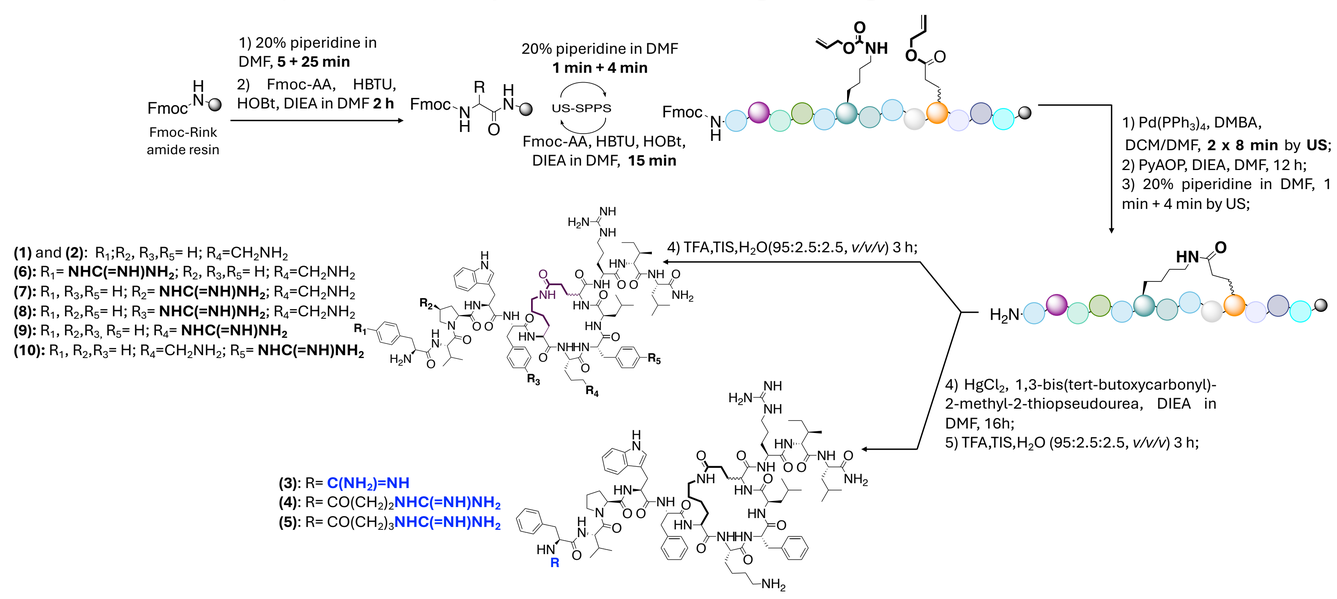
FVPWF[**Orn**KFl**Orn**]RIL **(13)**

PEPTIDE SYNTHESIS

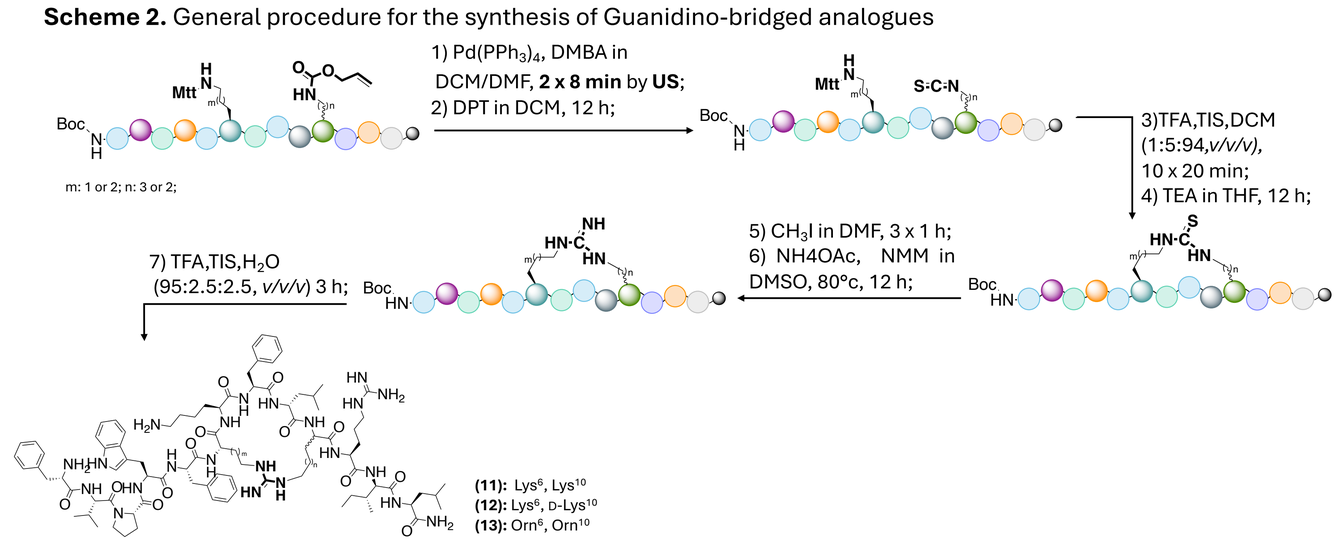
Linear peptides were assembled by ultrasonic-assisted solid-phase peptide synthesis (**US-SPPS**).[4] Peptides **1-10** were cyclized through lactam bridge formation using an orthogonal protection strategy (Scheme **1**), while peptide **11-13** underwent *side chain-to-side chain* cyclization according to Scheme **2**.



Scheme 1. General procedure for the synthesis of Lactam-bridged analogues



Scheme 2. General procedure for the synthesis of Guanidino-bridged analogues



RESULTS

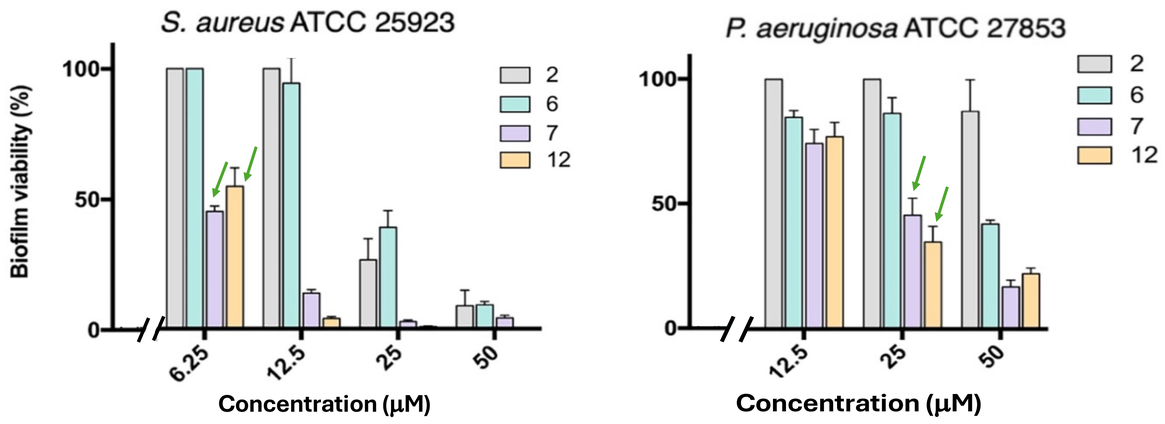
☑ Antimicrobial & AntiBiofilm Activity

Biological evaluation highlighted a favorable structure-activity relationship, particularly against Gram-negative bacteria when the **guanidino group** was located in the *N*-terminal region or incorporated into the cyclization bridge.

MIC (μM)

Peptides	Gram-positive			Gram-negative		
	S. aureus ATCC 25923	*S. epidermidis* ATCC 12228	*Bac.megaterium* Bm11	*E. coli* ATCC 25922	*P. aeruginosa* ATCC 27853	*Ac. baumannii* ATCC 19606
(1)	3.12	3.12	1.56	25	100	3.12
(2)	12.5	3.12	0.78	6.25	50	6.25
(6)	25	3.12	0.78	6.25	25	3.12
(7)	6.25	3.12	0.78	3.12	12.5	3.12
(12)	6.25	1.56	0.39	6.25	12.5	1.56

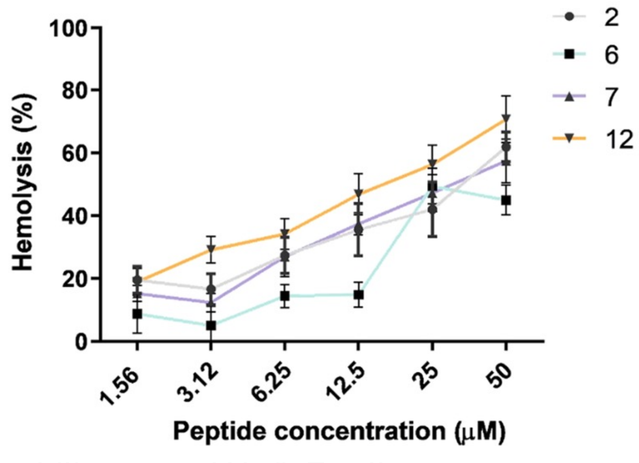
Peptides **7** and **12** emerged as the most active antibiofilm derivatives, reducing *S. aureus* biofilm viability by 50% at 6.25 μM and *P. aeruginosa* biofilm viability by >50% at 25-50 μM.



☑ Cytotoxicity

vs red blood cells

Lactam-bridged peptide **6** retained the most favorable hemolytic profile, showing limited hemolysis up to 25 μM. In contrast, guanidino-bridged peptide **12** displayed increased hemolytic activity from 12.5 μM.

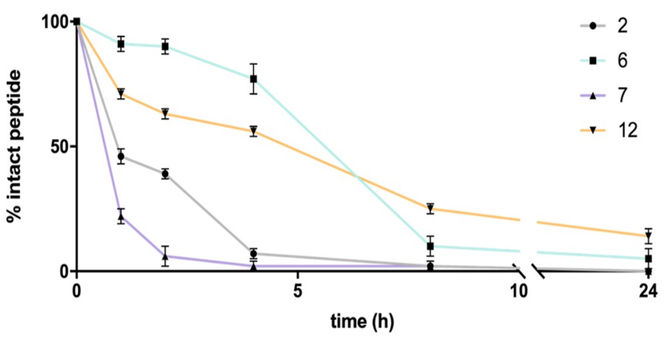


vs human keratinocytes (HaCaT)

All tested peptides maintained good tolerability toward HaCaT cells up to 12.5 μM, with peptide **6** showing the most favorable cytotoxicity profile and peptide **12** the lowest tolerability.

☑ Human Serum Stability

Peptides **6** and **12** showed the highest serum stability, retaining a high percentage of intact peptide over 4-8 h.



Conclusions & Future Outlook

These findings identify **guanidinium incorporation** into the cyclic peptide as a promising strategy to enhance TL antimicrobial activity. This structure-activity insight will guide the design of next-generation cyclic TL analogues toward an improved **activity-cytotoxicity balance**.

References: 1. I.Boccino et al., *ChemMedChem*. **2026**, *21*, e70397; 2. R. Bellavita et al., *J.Med.Chem*. **2021**, *64*, 11675-11694; 3. R. Bellavita, I. Boccino et al., *J.Med.Chem*. **2025**, *68*, 25038-25060; 4. F. Merlino et al., *Org. Lett*. **2019**, *21*, 6378–6382.

Development of visceral smooth muscle

PHYSIOLOGIE & MEDECINE EXPERIMENTALE COEUR MUSCLES MONTPELLIER

38th EPS European Peptide Symposium — 6 - 11th of September 2026 — Vienna, Austria

Dual Peptide Strategy for Enhanced Rescue of Mutated CFTR Channel Function in Cystic Fibrosis

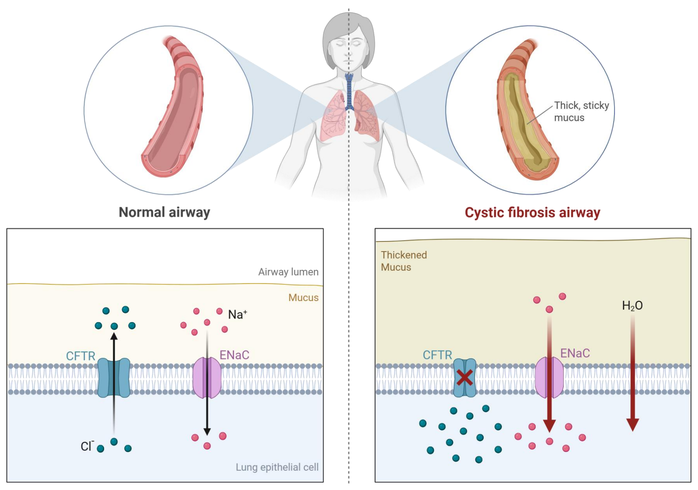
Prisca Boisguérin[1, 2], Clémentine Teko-Agbo[1], Chloé Felgerolle[1], Maha Sinane[1], Karine Delétang[1], Éric Vivès[1], Magali Taulan Cadars[1,2]

(1) PhyMedExp, University of Montpellier, INSERM U1046, CNRS UMR 9214, Montpellier, France
(2) Aceso Therapeutics, Montpellier, France

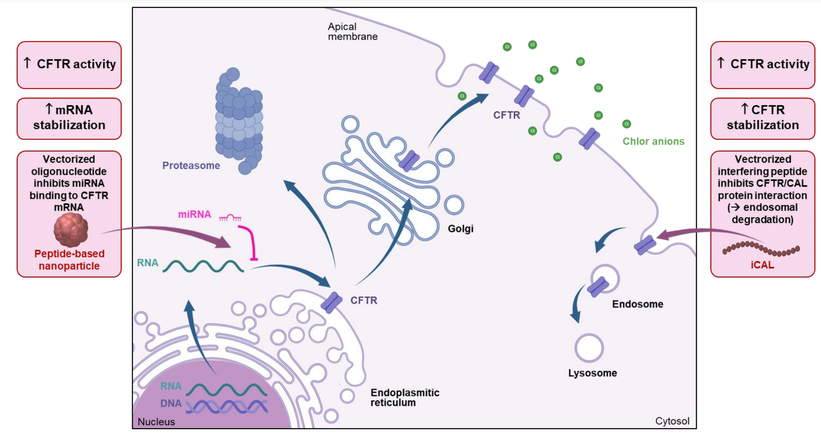
prisca.boisguerin@inserm.fr

https://doi.org/10.17952/38EPS.2026.P483

Introduction



Cystic fibrosis (CF) is a life-limiting genetic disorder affecting approximately 160,000 individuals worldwide and is most frequently associated with the p.Phe508del mutation, which is the most common CF-causing variant [1]. Although CFTR modulators (Trikafta = ETI) have revolutionized CF treatment, restoration of CFTR function remains incomplete, creating a need for complementary strategies to further enhance mutant CFTR rescue and stability [2].
The disease is characterized by the accumulation of thick mucus, leading to chronic lung infections, ongoing inflammation, substantial treatment burden, and reduced survival.



Complementary strategies to enhance p.Phe508del-CFTR activity: an oligonucleotide [3] encapsulated in peptide-based nanoparticles [4] increases CFTR mRNA stability by preventing miRNA binding, while an interfering peptide [5] blocks CFTR degradation and promotes its stabilization at the cell membrane.

Take–home message: complementary strategies to enhance CFTR activity

- Stable peptide nanoparticles for ACT-101 delivery
- Improved reproducibility of CFTR rescue
- Efficient lung targeting with 5% P-W1:ACT-101
- TRI-iCALp9 acts on CFTR amount without VX pre-incubation
- TRI as a suitable vector for iCAL36 and iCALp9 delivery
- TRI-iCALp9+VX with enhanced CFTR function in CF epithelia

I — Peptide–based nanoparticles to deliver ACT–101 oligonucleotide and increase CFTR activity

To improve p.Phe508del-CFTR function, we developed peptide-based nanoparticles able to efficiently deliver the ACT-101 oligonucleotide into airway epithelial cells. ACT-101 promotes CFTR expression by protecting CFTR mRNA from miRNA-mediated regulation, ultimately enhancing channel activity.

FIGURE 1

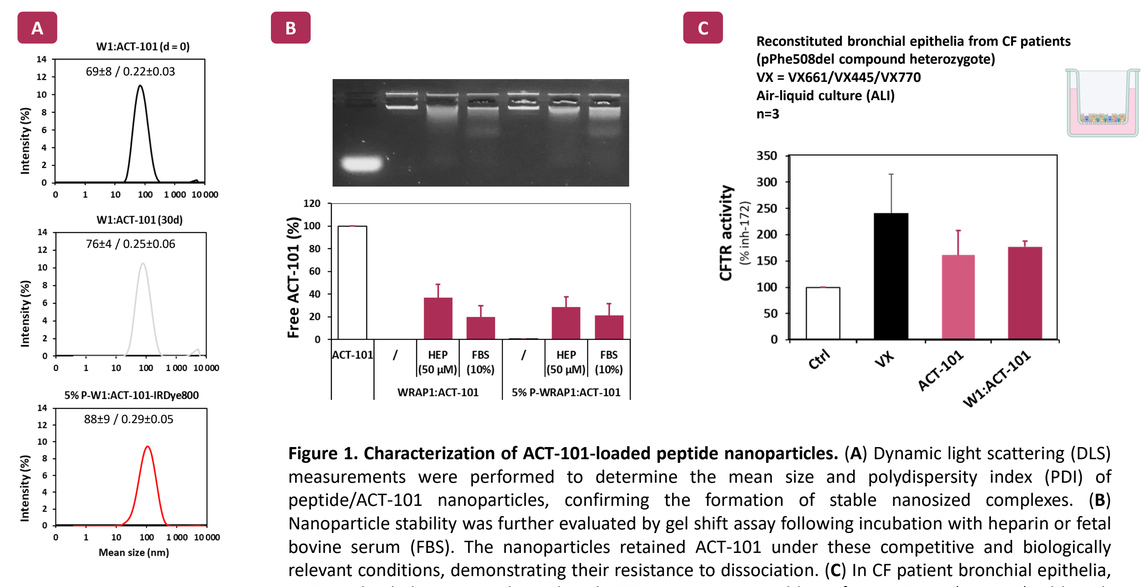


Figure 1. Characterization of ACT-101-loaded peptide nanoparticles. (**A**) Dynamic light scattering (DLS) measurements were performed to determine the mean size and polydispersity index (PDI) of peptide/ACT-101 nanoparticles, confirming the formation of stable nanosized complexes. (**B**) Nanoparticle stability was further evaluated by gel shift assay following incubation with heparin or fetal bovine serum (FBS). The nanoparticles retained ACT-101 under these competitive and biologically relevant conditions, demonstrating their resistance to dissociation. (**C**) In CF patient bronchial epithelia, ACT-101-loaded nanoparticles induced CFTR activity comparable to free ACT-101 (100 nM), although both treatments remained less effective than the VX modulators (ETI).

II — TRI–iCAL to stabilize the CFTR at the apical membrane and increase its activity

TRI-iCAL36 is a peptide composed of an interfering peptide (iCAL36) and a cell-penetrating peptide (TRI = Tat retro-inverso) previously shown to stabilize p.Phe508del-CFTR by disrupting its interaction with the CAL protein. To improve this strategy, the iCAL36 sequence was optimized using SPOT synthesis, leading to the identification of the peptide iCALp9, which contains several non-natural amino acids (confidential sequence).

FIGURE 3

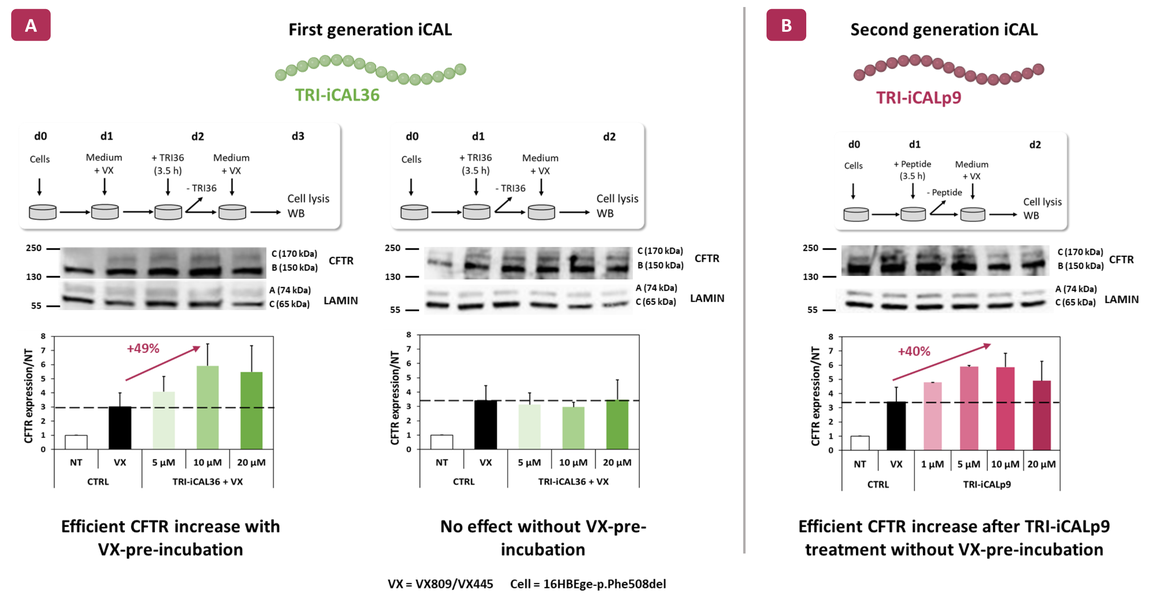


Figure 3. Optimization of the iCAL interfering peptide enhances CFTR accumulation. (**A**) Western blot analysis of p.Phe508del-CFTR in 16HBEge cells treated with the first-generation peptide TRI-iCAL36. No significant increase in CFTR expression was observed in the absence of VX-809/VX-445 pre-incubation, whereas pre-treatment with the corrector combination enabled a marked increase in CFTR levels (+49%). (**B**) Second-generation peptide TRI-iCALp9 increased CFTR expression (+40%) without prior VX-809/VX-445 pre-incubation, demonstrating improved activity of the optimized peptide.

FIGURE 2

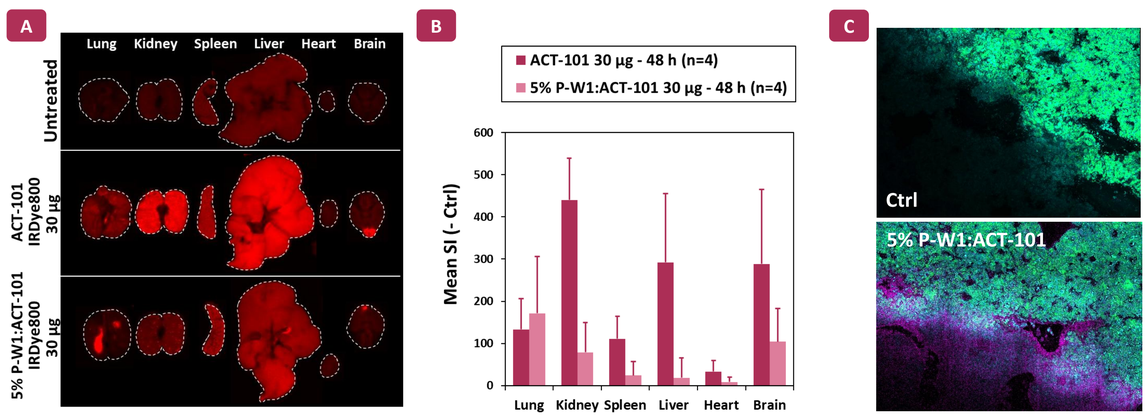


Figure 2. In vivo biodistribution and lung endothelial cell localization of ACT-101-loaded nanoparticles. The tissue distribution of fluorescently labeled ACT-101, delivered alone or by peptide-based nanoparticles, was compared 48 h after a single intranasal administration (30 µg) in mice. Ex vivo imaging (**A**) and fluorescence quantification (**B**) were performed in harvested organs. Microscopic examination (**C**) of lung sections revealed the localization of ACT-101 within lung epithelial cells, confirming successful delivery of the oligonucleotide to the lungs and its internalization within lung endothelial cells (green = actin, blue = nuclei, magenta = 5% PEG-WRAP1:ACT-101-IRdye800).

FIGURE 4

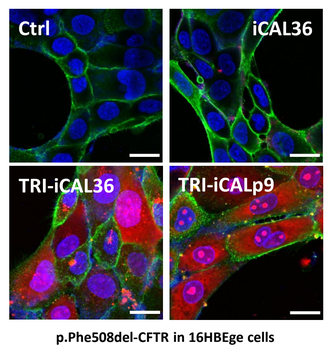


Figure 4. Internalization of fluorescently labeled iCAL peptides in 16HBEge-p.Phe508del cells. Representative fluorescence microscopy images show limited uptake of iCAL36 and efficient intracellular delivery of TRI-iCAL36 and TRI-iCALp9 (magenta, 1 µM), demonstrating that the optimized peptide retains the cell-penetrating properties conferred by the TRI sequence.

FIGURE 5

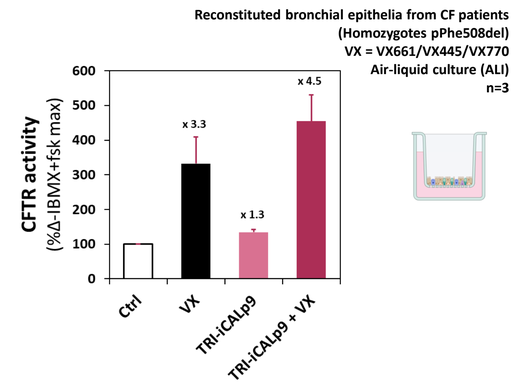


Figure 5. **Functional activity of TRI-iCALp9 in patient-derived CF bronchial epithelia.** CFTR activity was evaluated in reconstituted bronchial epithelia from homozygous p.Phe508del patients cultured at the air-liquid interface (ALI). Treatment with TRI-iCALp9 alone (10 µM) resulted in limited CFTR rescue. However, the combination of TRI-iCALp9 with ETI produced a greater restoration of CFTR function than ETI alone.

References

[1] Kerem et al., Science, 245, 1073 (1989). - [2] Scotet et al. Genes 2020. - [3] Viart V et al. Eur Respir J. 2015. - [4] Konate et al., Bioconjug Chem, 30(3), 592 (2019). - [5] Seisel et al., Pharmaceutics, 14(4), 808 (2022).

Financial support

ACESO THERAPEUTICS — VAINCRE LA MUCOVISCIDOSE — MYOccitanie — AFMTÉLÉTHON INNOVER POUR GUERIR — anr agence nationale de la recherche AU SERVICE DE LA SCIENCE

Accelerated Linker-Free Solid-Supported Native Chemical Ligation

https://doi.org/10.17952/38EPS.2026.P033

Océane Bonningue, Vincent Diemer, Oleg Melnyk

Univ. Lille, CNRS, Inserm, CHU Lille, Institut Pasteur de Lille, U1019 – UMR 9017 – CIIL – Center for Infection and Immunity of Lille, F-59000, Lille, France

Introduction

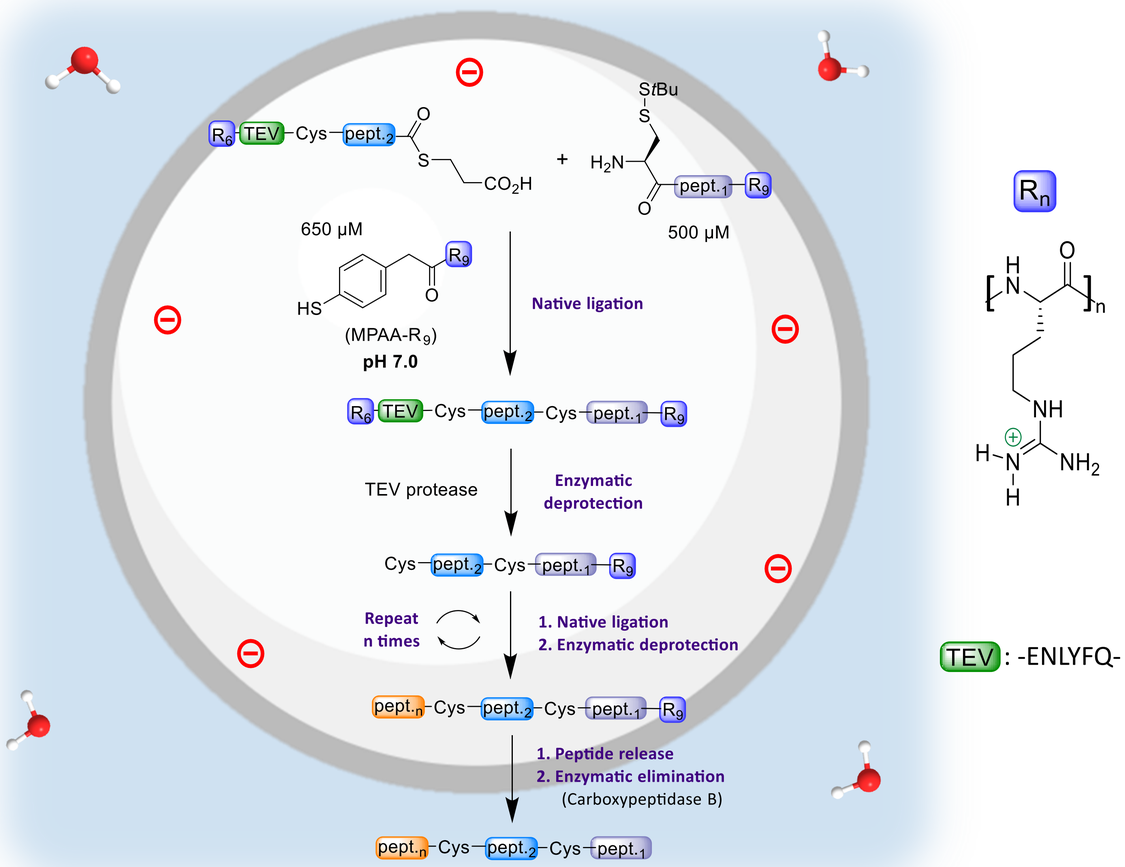
Native chemical ligation (NCL) involves the reaction of a C-terminal thioester peptide with a N-terminal cysteinyl peptide to form a native peptide bond in water. This reaction enables the assembly of unprotected peptide segments either in solution or on a solid support. Combined with the solid phase peptide synthesis (SPPS), NCL allows the synthesis of longer peptide sequences in greater quantities[1,2].

However, chemical protein synthesis by chemoselective concatenation of unprotected peptide segments remains limited. Major challenges include the poor solubility of certain peptides and intermediates in aqueous environments, the need for intermediate purification steps, and the relatively slow kinetics of ligation reactions. To overcome these limits, the solid-phase chemical ligation (SPCL) was developed, but this approach often requires the attachment of the growing peptide chain to the solid support. SPCL methods also face several challenges, including the need for specific attachment chemistry, difficulties to monitor the reaction and slow diffusion which can lead to reduced yields[3].

In this study, we present an alternative strategy to existing SPCL approaches, based on the incorporation of the species into the solid support through electrostatic interactions.

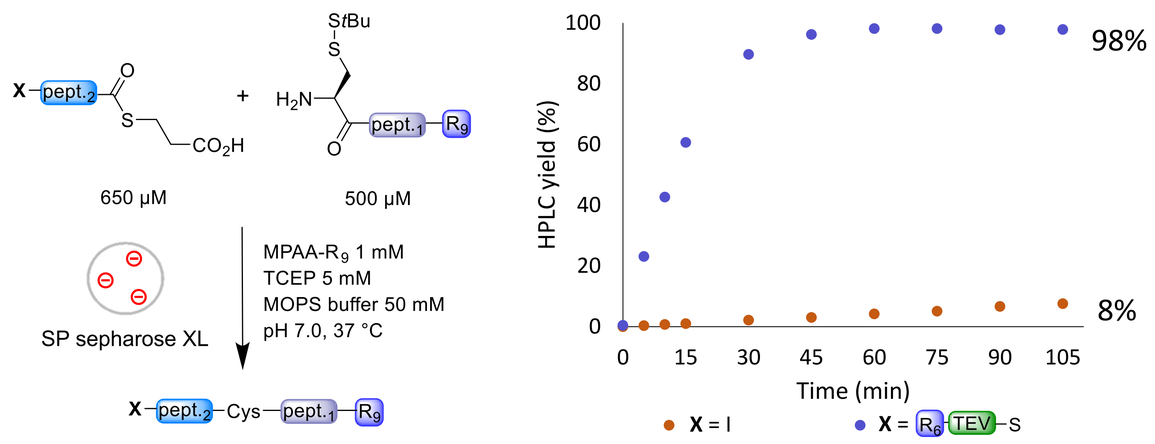
1. Electrostatically-assisted ligation with reversible peptide binding

The SPCL process we develop takes place in an anionic solid support (SP Sepharose XL), enabling the peptide segments and the catalyst (MPAA-R_9) tagged with poly-Arg to be incorporated into the solid support and retained within it at the working pH. Through these interactions, the catalyst only needs to be added once, remains throughout the process and can be recycled at the end.



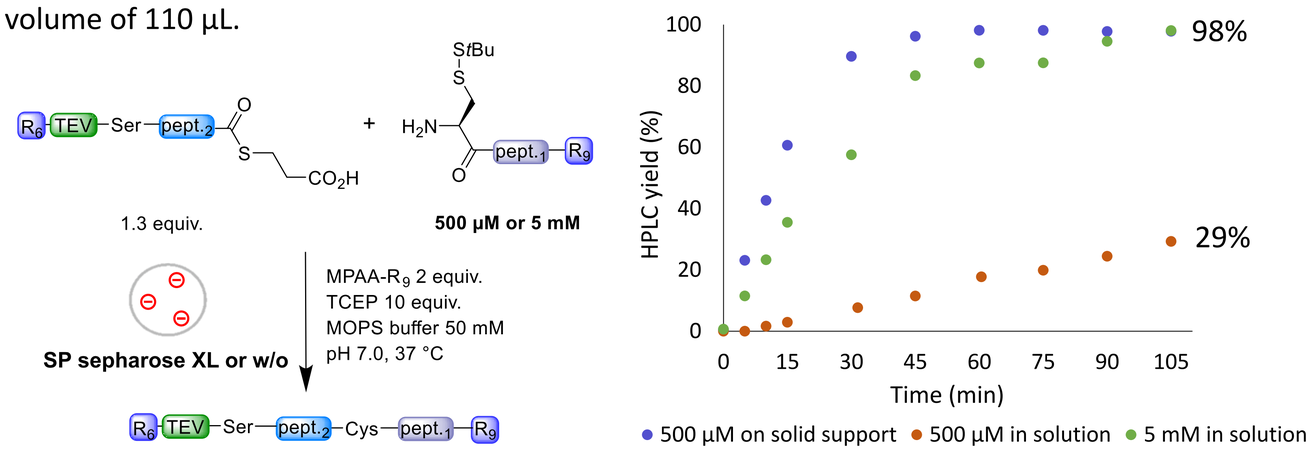
The thioester peptide carries a TEV tag at the N-terminal position, which can be removed by TEV protease. The resulting free cysteine then reacts with another thioester peptide to form a new native peptide bond. Finally, the poly-Arg tag is enzymatically cleaved by carboxypeptidase B after release into solution.

2. Exploring the impact of key parameters on ligation efficiency



The presence of the poly-Arg tag is essential to allow the concentration of all species into the support and enable the acceleration of ligation rate.

The experiment with SP sepharose XL was performed with 10 µL of beads for a total reaction volume of 110 µL.



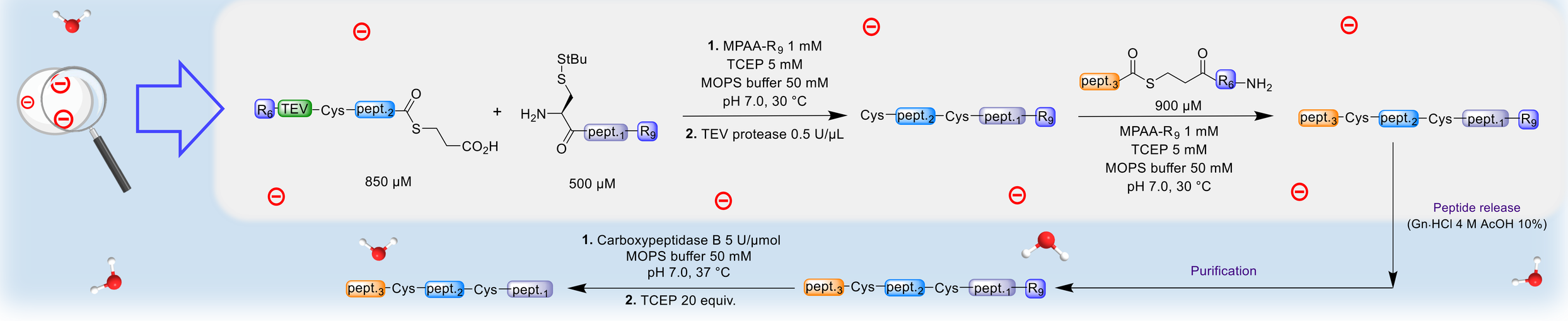
In the absence of the solid support, the reaction is significantly slower despite identical species concentrations (500 µM). Even with tenfold higher concentrations (5 mM) in solution to mimic those within the support, the reaction remains slower than on the solid support. This suggests that mechanisms beyond the concentration effect contribute to the SPCL reaction.

pept.1 : -ILKEPVHGAW- pept.2 : -LKEPVHGA- TEV : -ENLYFQ- R_9 : -RRRRRRRRR R_6 : RRRRRR-

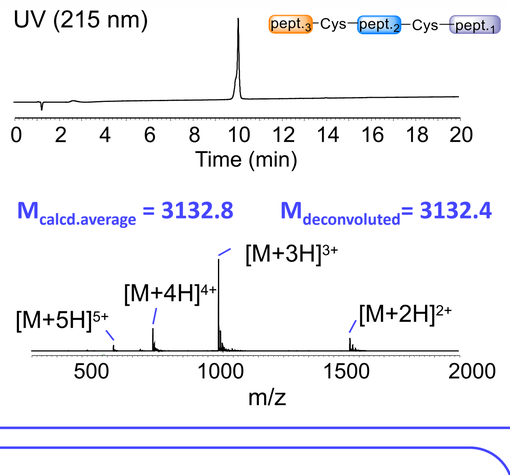
3. Synthetic pathway toward a native polypeptide

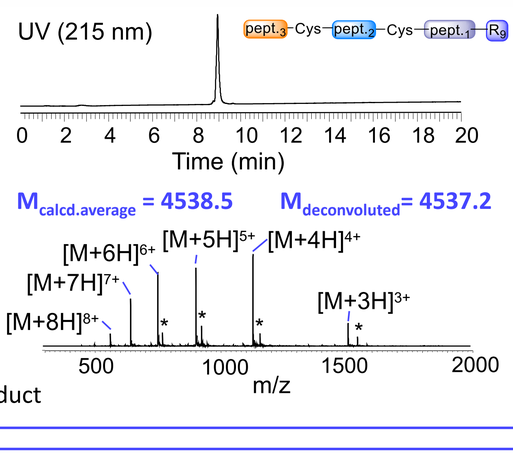
First, the peptide segments and catalyst accumulate within the support, allowing the ligation reactions to take place into it. Electrostatic binding to the support enables rapid release upon increasing the ionic strength, allowing the reaction to be easily monitored at any stage.

pept.1 : -ILKEPVHGAW- TEV : -ENLYFQ-
pept.2 : -LKEPVHGA- R_6 : RRRRRR-
pept.3 : ILKEPVHGA- R_9 : -RRRRRRRRR

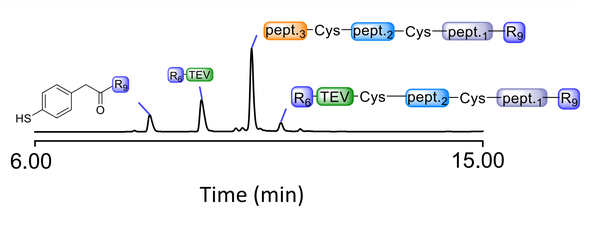


Finally, the R_9-tag was removed in solution to form the native peptide sequence in presence of carboxypeptidase B. The native polypeptide was obtained with a yield of 67%.





* : TFA adduct



Once all ligation steps were completed, the R_9-tagged polypeptide was released from the support and isolated with a yield of 65%.

Conclusion

Electrostatic interactions between the negatively charged solid support and the positively charged poly-Arg tags on the peptide segments and catalyst enhance the ligation rate. The reaction proceeds significantly faster on the solid support than in solution, even at tenfold higher concentrations. Combined with enzymatic deprotection and C-terminal poly-Arg tag removal, this strategy enabled the successful synthesis of a native polypeptide from three peptide segments.

The next objective is to extend this strategy to the synthesis of a full-length protein in its native form.

References

(1) Dawson, P. E.; Muir, T. W.; Clark-Lewis I.; Kent, S. B. H. *Science* **1994**, *266*, 766-779.
(2) Agouridas, V.; El Mahdi, O.; Diemer, V.; Cargoet, M.; Monbaliu, J.-C.; Melnyk, O. *Chem. Rev.* **2019**, *12*, 7328-7443.
(3) Agouridas, V., Ollivier, N. ; Vicogne, J. ; Diemer, V. ; Melnyk, O. *Acc. Chem. Res.* **2022**, *55*, 2685-97.

Acknowledgments

This work is supported by ANR under grant #ANR-23-CE07-0016-01. We gratefully acknowledge the EPS for funding my conference registration.

38th EPS European Peptide Symposium

Clustered antigen architectures enhance monoclonal antibody adhesion: insights from biomimetic surfaces

Océane Ricloux [1], Laure Bar [1], Quentin Laurent [1], Liliane Guerente [1] and Didier Boturyn [1]

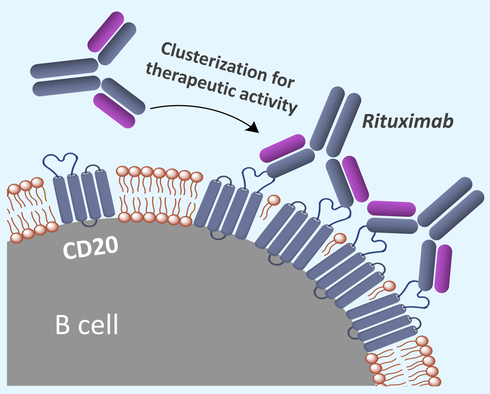
[1] *University Grenoble-Alpes, CNRS, DCM UMR 5250, 38058 Grenoble Cedex 9, France*

didier.boturyn@univ-grenoble-alpes.fr ; https://doi.org/10.17952/38EPS.2026.P048

Introduction

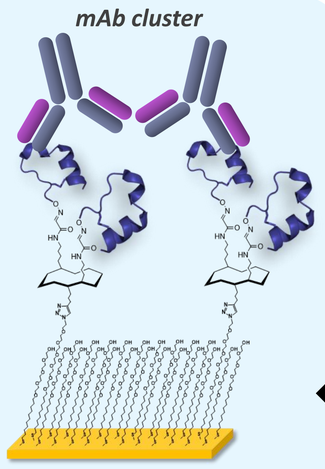
Since the 90s, **monoclonal antibodies** (mAb) have emerged as a promising class of pharmaceuticals. **Understanding antigen–antibody interactions is important to many applications** including diagnostics and treatment of diseases. The **CD20 antigen expressed by B cells has received significant attention** as it is a target for immunotherapy of B cell-related cancers but also autoimmune diseases. The CD20 antigen is the target of several therapeutic mAbs including rituximab. It is well-known that antigen-binding activity of mAbs, and associated biological efficacy, depends on several factors such as antigen density, association, and dissociation rates. It was shown that the **levels of CD20 expression at the cell surface may determine antibody-mediated cell death**.[1] We and others reported an optimal inter-CD20 spacing of nearly 2 nm on surfaces for efficient interaction with RTX.[2-4] To systematically study the effect of CD20 density on antibody recognition**, we designed self-assembled monolayer (SAM) functionalized gold surfaces that display tunable CD20 epitope densities**.[2-5] Quartz crystal microbalance with dissipation monitoring (QCM-D) and surface plasmon resonance (SPR) techniques were chosen to analyze the binding of the mAb rituximab.

Design of clustered CD20 surfaces

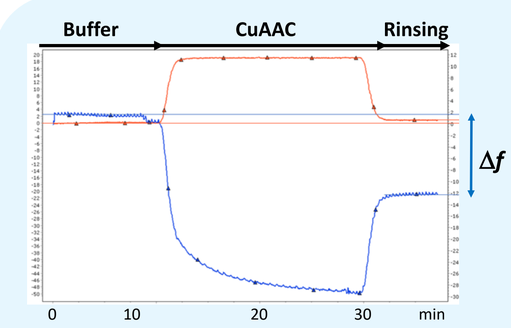


Biological context: CD20 antigen forms clusters at the cell surface upon interaction with mAbs which is essential for therapeutic activity

Highly biomimetic surface

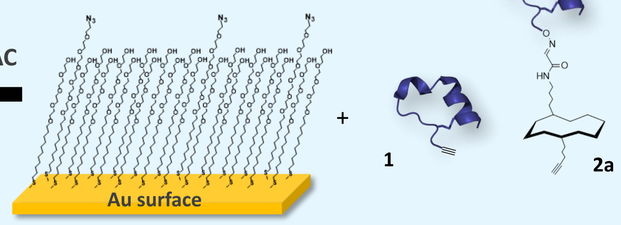


Characterizing Biomolecular Interactions *via* Label-Free QCM-D and SPR

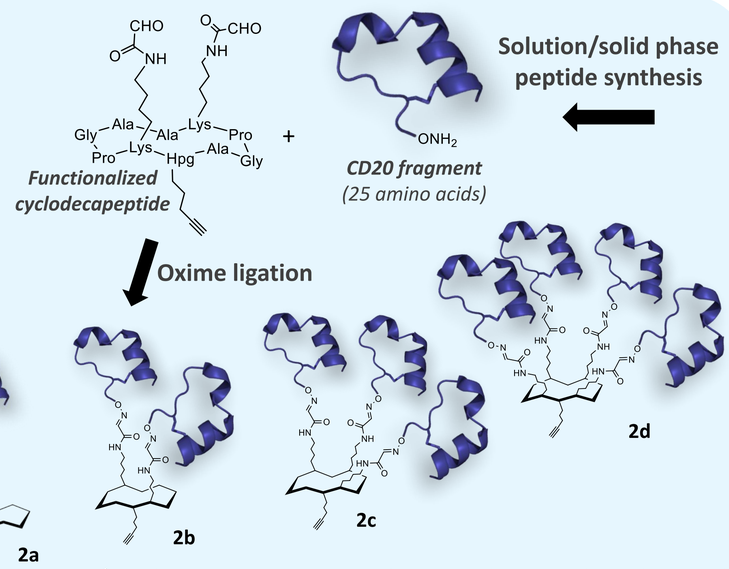


Real-time QCM-D monitoring of conjugate **2b** immobilization on alkane-thiol SAM

CuAAC



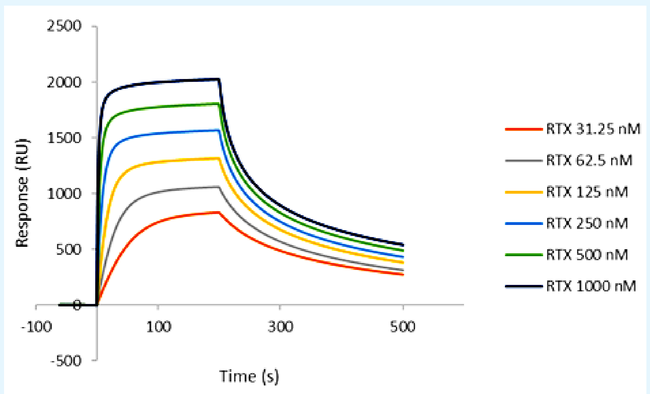
✓ **Determination of CD20 density** by using the Sauerbrey equation: $m_{QCM} = -C\Delta f$ and additional spectroscopic ellipsometry experiments (*data not shown*).



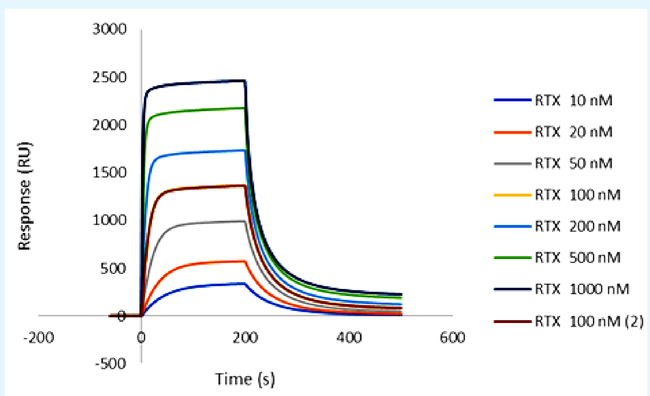
✓ **Cyclodecapepides were functionalized with orthogonal chemoselective functions**. Aldehyde functions were introduced for grafting the CD20 epitope, while alkyne functions allowed surface attachment through copper(I)-catalyzed alkyne–azide cycloaddition (CuAAC).

Impact of clustered CD20 on RTX adhesion

➢ SPR sensorgrams recorded on surfaces functionalized with CD20 derivatives

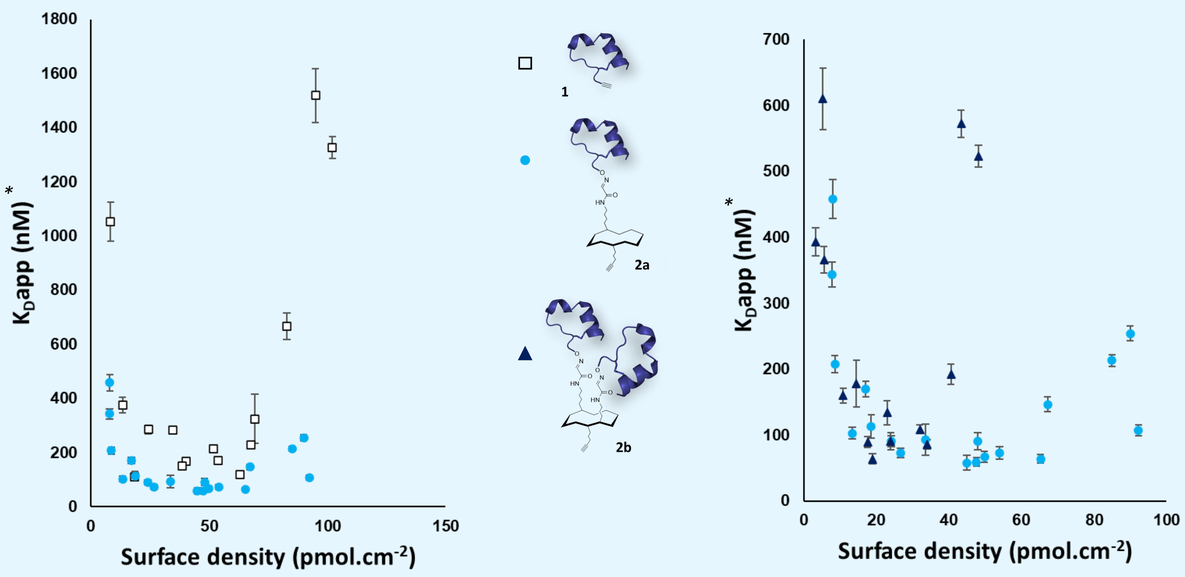


SPR binding profiles of 2a with RTX. Sensorgram was recorded on a surface functionalized with **CD20 monomer 2a** at 26.3 pmol.cm^{-2}. The RTX concentrations were 31.25, 62.5, 125, 250, 500, 1000 nM.



SPR binding profiles of 2b with RTX. Sensorgram was recorded on a surface functionalized with **CD20 dimer 2b** at 37.5 pmol.cm^{-2}. The RTX concentrations were 10, 20, 50, 100, 200, 500, 1000 nM.

➢ Impact of epitope surface density and clustering on RTX/CD20 affinity



** K_{Dapp} values were determined using a steady-state model based on the equilibrium response of the sensorgrams*

✓ The presence of **the cyclodecapeptide scaffold in monomer 2a enhances RTX recognition** at comparable surface densities: 60 nM compared to ~150 nM for surfaces modified respectively with **2a** or **1** at 50 pmol·cm^{-2}.

✓ Introducing the cyclodecapeptide spacer improves epitope accessibility and promotes antibody binding.

✓ Surfaces functionalized with **CD20 monomer 2a and dimer 2b exhibited similar minimum K_{Dapp} values**, with slightly enhanced affinity for the dimer at their respective optimal surface densities (50 and 20 pmol·cm^{-2}).

✓ The minimum K_{Dapp} values for trimer **2c** and tetramer **2d** (~120 nM) were higher than that of the dimer. This reduced affinity is the result of increased steric hindrance and conformational rigidity imposed by packing multiple CD20 units onto a single cyclodecapeptide scaffold.

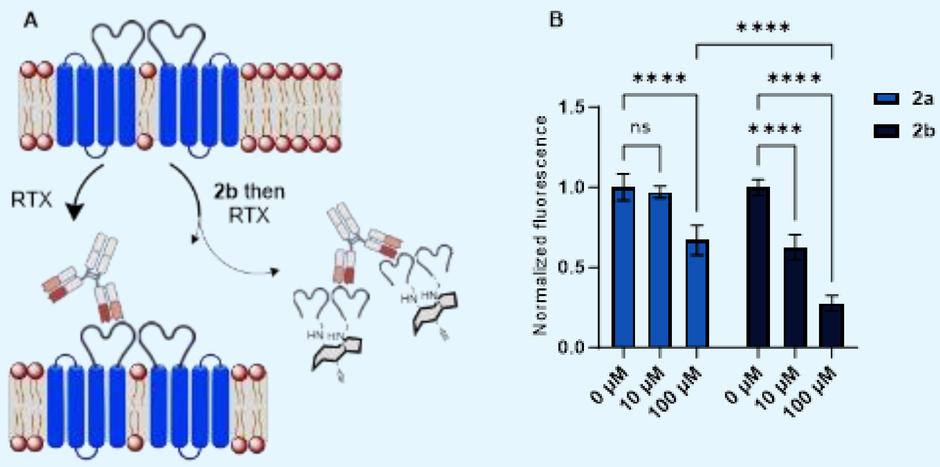
➢ Apparent dissociation constants of anti-CD20 mAbs on mono- and dimeric CD20-functionalized surfaces

mAb	Compound 2a (K_{Dapp} nM)	Compound 2b (K_{Dapp} nM)
RTX	86 ± 16	45 ± 3
MEM-97 **	41 ± 6	311 ± 19
L26 ***	ND	ND

*** MEM-97 binds a different extracellular epitope from RTX*
**** L26 recognizes an intracellular epitope and was used as a negative control*

✓ **Formation of a more favorable interaction between RTX and CD20 dimer 2b**, which faithfully mimics the prerequisite 2 nm distance between two CD20 proteins at the cell surface.

➢ Inhibition of cell–antibody interaction with multivalent CD20 constructs



(A) Schematic of the competition assay between Raji cells and synthetic CD20 dimer **2b**. (B) Flow cytometry analysis of competition between Raji cells and synthetic CD20 dimer **2b**. Raji cells were co-incubated for 30 min at 4 °C with increasing concentrations of **2b** and RTX, followed by incubation with fluorescent secondary antibody for 30 min at 4 °C.

*Statistical significance was assessed using a two-way ANOVA test (comparison across concentrations). ****: $p < 0.0001$ and ns: $p > 0.123$*

✓ **The results indicate enhanced competition for dimeric constructs 2a**, supporting their relevance to CD20 organization and binding stoichiometry at the cell surface.

✓ The synthesized CD20 constructs appear to be **promising candidates for the affinity-based selection of RTX mimics**.

Conclusion & Outlooks

❖ Conclusion

- We designed and characterized **biomimetic surfaces** displaying clustered multivalent CD20 architectures based on cyclodecapeptide scaffolds.
- We demonstrated that both the **spatial organization and valency of CD20** epitopes strongly **influence RTX binding affinity and specificity**.
- Dimeric CD20 constructs offers the best compromise between epitope accessibility and multivalent interaction.

❖ And now ?

- Design of **clustered CD20 on lipid bilayer surface**.
- Impact of the lateral mobility on rituximab adhesion.
- **Screening of mAb mimics** on CD20 biomimetic surfaces.

References

1. K. B. Melhus et al, *Cancer Biother. Radiopharm.* **2007**, *22*, 469 – 479.
2. L. Bar et al, *Anal. Chem.* **2020**, *92*, 5396 – 5403.
3. L. Rougé et al, *Science* **2020**, *367*, 1224 – 1230.
4. A. Kumar et al, *Science* **2020**, *369*, 793 – 799.
5. O. Ricloux et al, *Anal. Chem.* **2026**, *98*, 19418 – 19426.

Induction heating solid-phase strategy to improve the total chemical synthesis of ester insulin

S. Bracci[1,2], M. Quagliata[1,3], P. Rovero[1,3], S. B. H. Kent[4], A. M. Papini[1,2]

[1]*Interdepartmental Research Unit of Peptide and Protein Chemistry and Biology - PeptLab, University of Florence, 50019 Sesto Fiorentino, Italy*
[2]*Department of Chemistry "Ugo Schiff", University of Florence, 50019 Sesto Fiorentino, Italy*
[3]*Department of Neurosciences, Psychology, Drug Research, and Child Health, University of Florence, 50019 Sesto Fiorentino, Italy*
[4]*University of Chicago, IL, USA*

Email: silvia.bracci@unifi.it

38th EPS European Peptide Symposium

Introduction

From insulin, the first therapeutic peptide, to today's increasingly complex peptide therapeutics, advances in peptide chemistry have enabled the development of modified analogues with improved properties and clinical performance. This evolution, exemplified by insulin analogues and GLP-1 receptor agonists, highlights the growing need for efficient synthetic strategies capable of accessing complex peptide architectures.

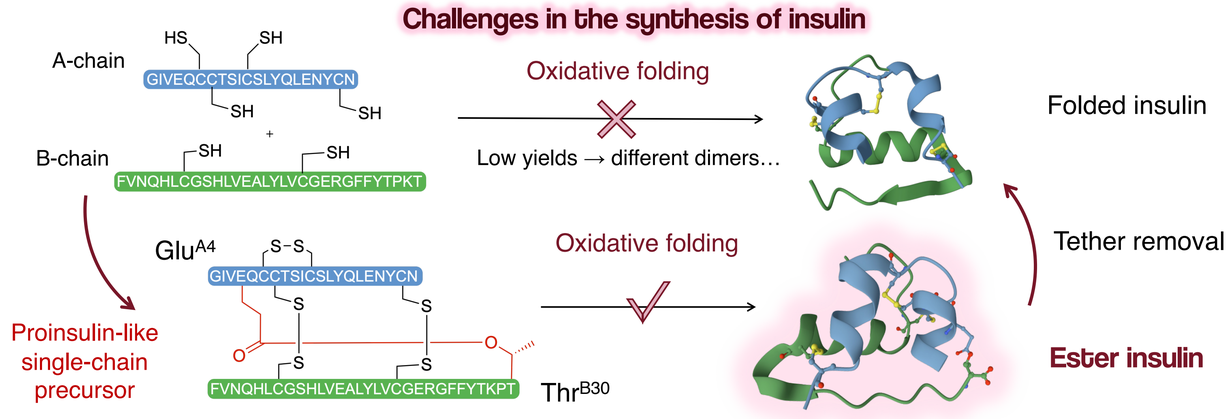
Recombinant production vs. Chemical synthesis

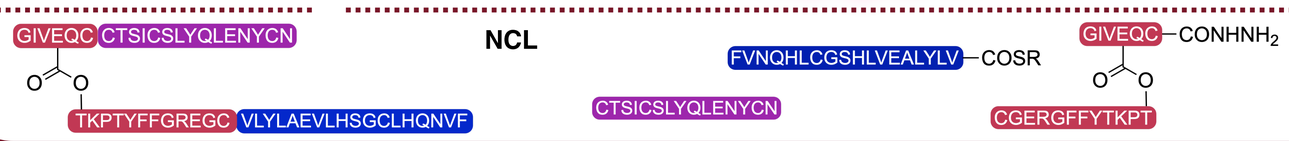
- Large scale production
- High purity
- Cost-effective
- Limitation to the twenty encoded amino acids

- Introduction of non-natural amino acids (e.g. Aib, D-amino acids, …)
- Introduction of chemical modifications (e.g. PEGylation, palmitoylation, …)

→ **Synthesis of new complex peptide therapeutics to improve**

Challenges in the synthesis of insulin





Induction – Assisted SPPS of peptide fragments



- Rapid and controlled temperature increase
- Significant reduction in synhesis time
- Enhanced reaction rates

Ester insulin as a demanding case study

- Accelerate and further optimize peptide fragment synthesis through **induction-assisted high-temperature solid-phase peptide synthesis**, using the PurePep® Chorus instrument.
- Refine the synthetic procedure and expand the understanding of the synthetic process, ultimately establishing more efficient and reproducible conditions.

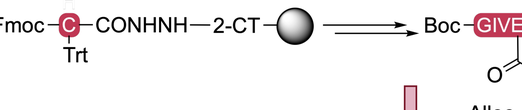
The increasing complexity of therapeutic peptides calls for more efficient and reliable synthetic strategies. Using ester insulin as a challenging case study, this work explores induction-assisted HT-SPPS to accelerate and optimize peptide synthesis, with the broader aim of developing approaches applicable to complex peptide therapeutics such as GLP-1 receptor agonists.

Beyond improving synthetic efficiency, this study also aims to understand an unwanted O-to-N acyl shift observed during synthesis, highlighting the importance of using a good model to optimize a synthetic process.

Induction - Assisted SPPS of peptide fragments

CTSICSLYQLENYCN

Induction Heating SPPS

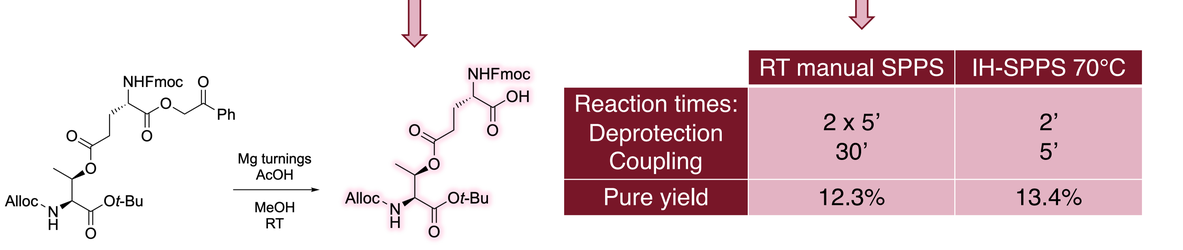


	RT manual SPPS	IH-SPPS 90°C
Reaction times: Deprotection / Coupling	2 x 5' / 30'	1' / 2'
Pure yield	18,7%	15.4%

>90% reduction in synthesis time!

FVNQHLCGSHLVEALYLV—COSR

$NaNO_2$ oxidation to MESNa thioester



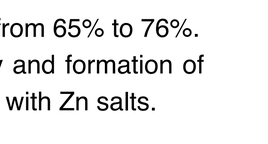
Induction Heating SPPS

	RT manual SPPS	IH-SPPS 70°C
Reaction times: Deprotection / Coupling	2 x 5' / 30'	2' / 5'
Pure yield	12.3%	13.4%

78% reduction in synthesis time!

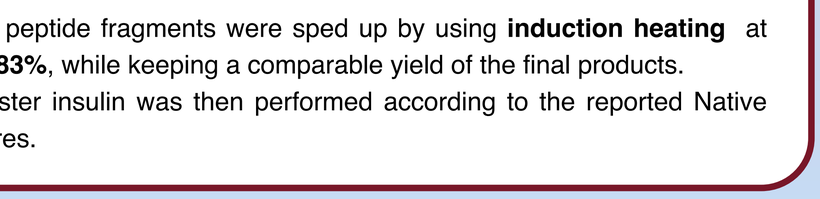
FVNQHLCGSHLVEALYLV

Fmoc-Leu-OH
Fmoc-Val-OH
Double couplings



Gly-Ser pseudoproline

GIVEQC CONHNH2
CGERGFFYTKPT





	RT manual SPPS	IH-SPPS 70°C
Reaction times: Deprotection / Coupling	2 x 5' / 30'	2' / 5'
Pure yield	12.3%	13.4%

80% reduction in synthesis time!

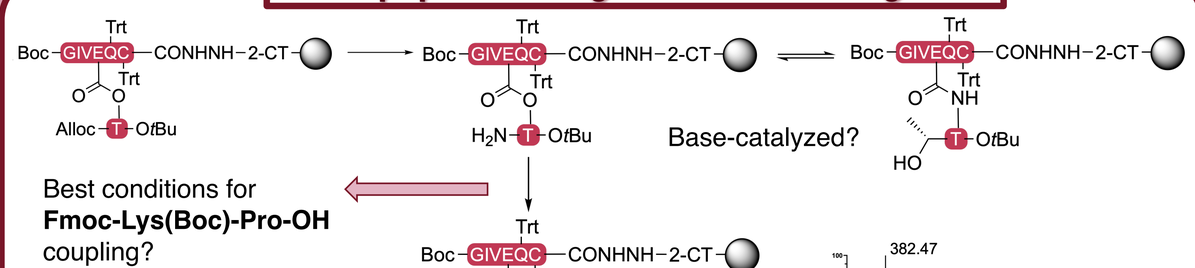
Zn → Mg for OPac ester removal

- From 78% to quantitative yield, bringing the total 5 step synthesis yield from 65% to 76%.
- Improved performance of Mg attributed to its higher reducing reactivity and formation of soluble Mg salts, avoiding stirring issues and ester cleavage associated with Zn salts.

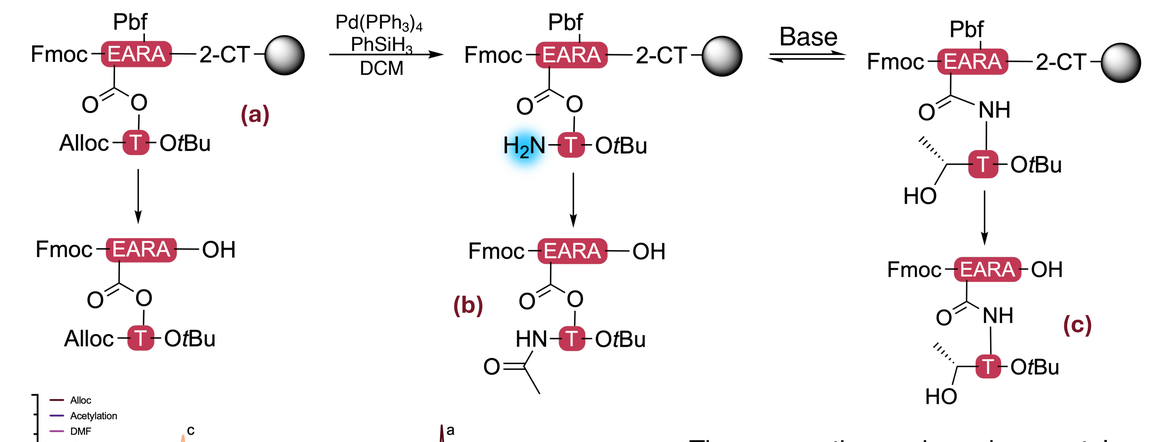
Conclusions

- The synthesis of the three peptide fragments were sped up by using **induction heating** at 70-90°C overall by around **83%**, while keeping a comparable yield of the final products.
- The synthesis of the full ester insulin was then performed according to the reported Native Chemical Ligation procedures.

Model peptide study of the O-to-N acyl shift



Model peptide



- The reaction is base-catalyzed (NMM > DIPEA), but also occurs in the absence of one.
- In the absence of a proper base, the catalyst of the shift is the α-amino group of neighboring O-linked Thr residues within the same solvent-swollen resin bead.
- When swelled, the collision frequency between peptide chains on the resin is comparable to that observed in solution.

Conclusions

Best conditions for **Fmoc-Lys(Boc)-Pro-OH** coupling:

- DIC and OxymaPure instead of HATU/HOBt and DIPEA
- Green binary mixture of EtOAc/DMSO 4:1 as solvent instead of DMF (traces of amine impurities)
- No wait time or drying after Alloc deprotection

References

B. Dhayalan *et al.*, *Chemistry – A European Journal*. **23**, 1709–1716 (2017).

Y. Sohma, Q.-X. Hua, J. Whittaker, M. A. Weiss, S. B. H. Kent, *Angewandte Chemie International Edition*. **49**, 5489–5493 (2010).

L. Moroder, H.-J. Musiol, *Angewandte Chemie International Edition*. **56**, 10656–10669 (2017).

Acknowledgements

For Silvia Bracci's travel grant.

For providing access to the PurePep® Chorus peptide synthesizer and for technical support.

This project was funded in part by EUniWell: 5th seed funding call for the TTPep project and 3rd Well-Being Research Incubator Call for the project "Sustainable and green upscaling processes for peptide(-based) in vitro diagnostics and cosmeceuticals" and the Champion program "Peptides4Wellness".

Enhancing Affinity of Peptide and Peptoid Ligands Using Boronic Acid-Catechol Reversible Dimerization

Elizabeth Bredice,[1] Madeline Swanson,[1] Thomas Kodadek,[2] Skander Abboud [1,2]

[1]Department of Chemistry and Biochemistry, University of North Carolina Wilmington, 601 College Rd, Wilmington, NC 28403, USA

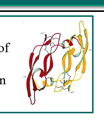
[2] Department of Chemistry, UF Scripps Institute for Biomedical Innovation & Technology, 120 Scripps Way, Jupiter, FL 33458, USA

The Abboud Lab

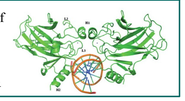
Overview

Dimerization of small peptides and peptoids enhances drug design by improving binding affinity and specificity, particularly for homodimeric drug targets. Bivalent ligands can simultaneously engage two binding sites, boosting efficacy, selectivity, and reducing side effects. Traditional dimerization often relies on irreversible reactions, increasing molecular weight and limiting bioavailability. In contrast, reversible dimerization uses chemoselective reactions to dynamically assemble monomers into dimers under specific conditions. This preserves pharmacokinetic properties like solubility and bioavailability while achieving high binding affinity and specificity at the target site

Dimer ribbon representation of the receptor-binding domain of VEGF

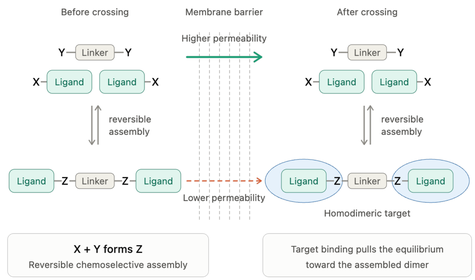


The structure of the p53 core domain in dimeric form bound to DNA



Reversible Chemistry for Increased Dimer Permeability

To exploit these benefits, we have developed a novel strategy for generating dimers using reversible chemoselective reactions. Our approach centers on a streamlined synthetic design: a single monomer is functionalized with a chemoselective handle, which then reacts with a symmetrical, difunctionalized linker to form the dimer. This modular assembly minimizes synthetic steps, avoids the need to prepare two different peptide arms, and allows for easy tuning of dimer geometry and spacing.



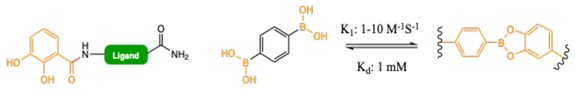
Why Boronic Acid–Catechol Chemistry?

Reversible Covalent Bonding:
Forms boronate esters through dynamic covalent interactions that remain reversible under physiological (pH 7) conditions due to equilibrium between free and bound states.

Highly Chemoselective:
Boronic acids are selective for catechol over natural amino acid side chains, enabling clean conjugation in complex mixtures.

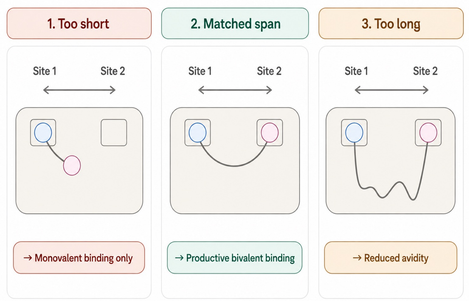
No Catalyst Required:
Proceeds efficiently in aqueous solution without the need for metal catalysts.

Arylboronic Acid Diol Complexation



Chem. Sci. **2021**, 12 (5), 1585–1599.

Why Linker Design Matters

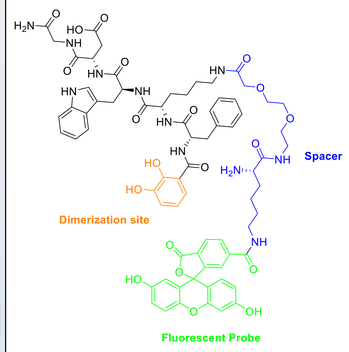


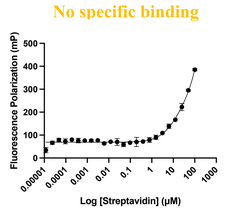
Bivalent binding depends on matching linker length and flexibility to the spacing between target binding sites. Matched linkers favor productive bivalent engagement, whereas poorly matched linkers can limit avidity.

Streptavidin – Proof of Concept

Streptavidin (SA), from *Streptomyces avidinii*, has an exceptionally high affinity for biotin (K_d ~10^{-15} M), making it a key tool in biotechnology and diagnostics. Beyond biotin, streptavidin can bind peptides with the GDWXF-like motif, which mimics biotin's structure. The motif interacts with streptavidin's binding pocket through hydrophobic/π–π contacts; binding is specific but weak, with Kd typically in the tens–hundreds of μM (sometimes up to mM)

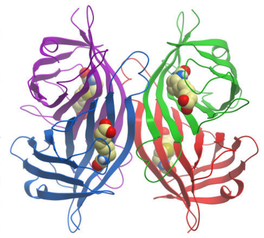
Monomer SA Binding Peptide





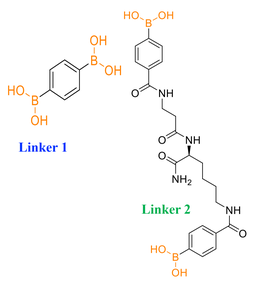
Binding isotherm of the monomer peptide against SA derived from fluorescence polarization experiments

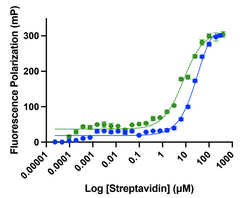
SA is a tetrameric protein with four binding sites, allowing it to interact with multiple ligands simultaneously. To enhance the binding strength of the monomer, a promising strategy is to dimerize the peptide, enabling it to engage two binding sites on the streptavidin tetramer simultaneously. However, the success of this approach depends on factors like spacing and flexibility of the linker between the two monomers. The linker must be designed to allow both monomers to access streptavidin's binding sites without steric hindrance, ensuring optimal binding efficiency.



Ligand bound Streptavidin homotetramer showing each unit binding to individual biotin molecules

Reversibly Dimerized SA Binding Peptide





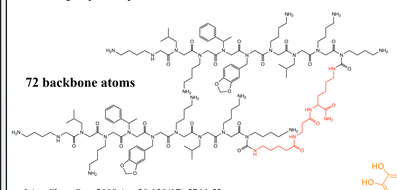
Binding isotherm of the reversibly dimerized peptide with linker 1 and linker 2 against SA derived from fluorescence polarization experiments

Dimerization enhances apparent affinity via avidity; linker length shifts the curve

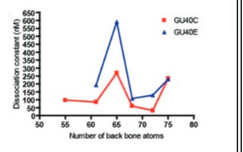
Successful application of this strategy to a SA binding peptide, demonstrating the feasibility and effectiveness of our approach.

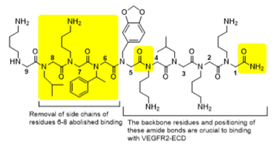
VEGFR2 / GU40C – Affinity Enhancement + Cellular Validation

The Kodadek group identified a peptoid (GU40C) antagonist of the cell surface Vascular Endothelial Growth Factor Receptor 2 (VEGFR2) with extremely high selectivity for this receptor, but modest affinity. To get a higher affinity, they took advantage of the fact that VEGFR2 functions as a dimer and synthesized dimers of the peptoid which resulted in an improvement of about 90-fold potency relative to the monomeric parent compound. Homodimerization was achieved irreversibly with a central Lys linker from which branch additional linker arms would separate the N-termini of each monomeric unit by approximately 45–85 Å. The best binding affinity was displayed by GU40C4 72 backbone atoms.

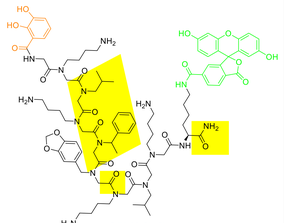


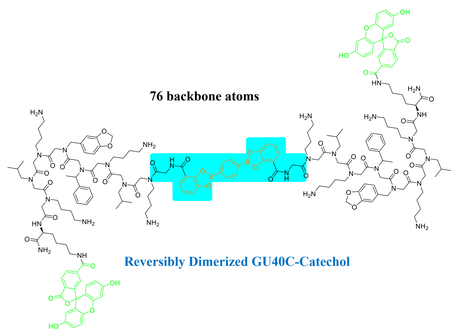
J Am Chem Soc. 2008 Apr 30;130(17):5744-52.



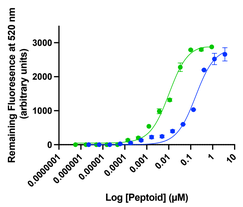


Bioorg Med Chem Lett. 2008 Nov 15; 18(22): 5892–5894.



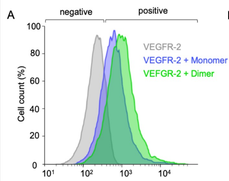


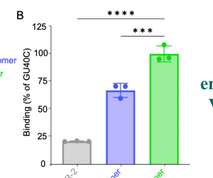
Binding Isotherm of GU40C Peptoids Against VEGFR2, Derived from ELISA-Like Experiments



≈ 100-fold increase in binding between monomer and dimer

Flow Cytometry Analysis of GU40C Cellular Uptake and Binding in VEGFR2 Expressing Cells



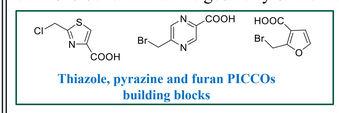


Reversible dimerization enhances GU40C binding to VEGFR2 expressing cells

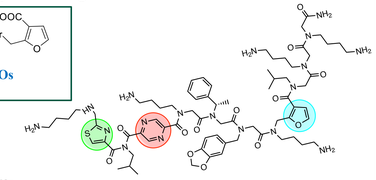
Inserm
La science pour la santé
From science to health

VEGFR2 / GU40C-Th9Py8-Fr4 – SAR-Guided Optimization

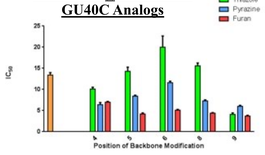
Peptoids generally lack conformational constraints due to their homogenous backbone. To enhance potency, we systematically altered backbone positions 4-9 with more rigid, structurally distinct analogs, also called PICCOs (Peptoid-Inspired Conformationally Constrained Oligomers). These substitutions increased spacing, with the aim of overcoming the conformational disorder of peptoids and enabling side chains to better match the geometry of the target.



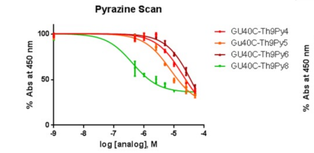
UF UNIVERSITY of FLORIDA Scripps Research

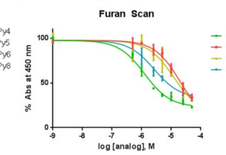


Relative IC_{50} of Modified GU40C Analogs

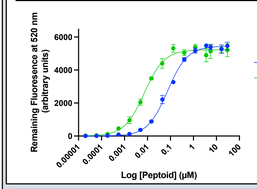


Thiazole is ineffective at positions 4–8 but improves potency at position 9, suggesting it should be used only there. In contrast, furan and pyrazine shows stronger activity across multiple positions, making them better suited for further optimization.





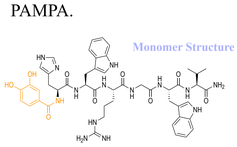
Binding Isotherm of GU40C Peptoids Against VEGFR2, Derived from ELISA-Like Experiments

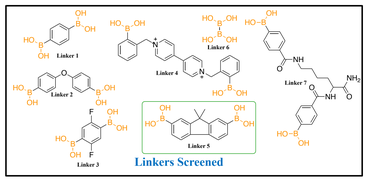


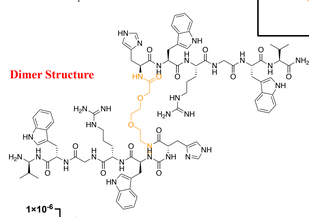
≈ 12-fold increase in binding between monomer and dimer

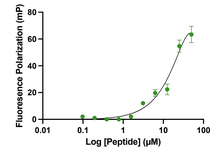
IgG1-Fc / HWRGWV – Linker Screening + Permeability

We extended this strategy to HWRGWV, a hexapeptide that binds human IgG1-Fc with ~10 μM affinity. Diboronic acid linkers were screened by FP, and a selected reversible system was compared with the monomer and irreversible dimer by PAMPA.

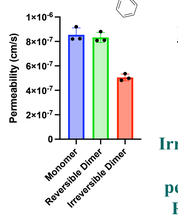






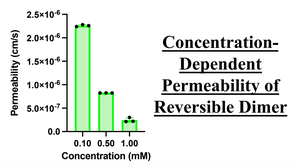


Binding isotherm of the reversibly dimerized peptide with linker 5 against IgG1-Fc derived from fluorescence polarization experiments



Reversible vs. Irreversible Dimer Permeability

Irreversible Dimer is about 38% less permeable than the Reversible Dimer



Concentration-Dependent Permeability of Reversible Dimer

https://doi.org/10.17952/38EPS.2026.P149

Comparison of conformational propensities of peptide backbones containing 1,5- or 1,4- disubstituted [1,2,3] triazoles

Francesco Brenzini Biagioni[1,2,3], Karine Porte[3], Pierre-Yves Renard[3], Anna Maria Papini[1,2]

[1]*Interdepartmental Research Unit of Peptide and Protein Chemistry and Biology, University of Florence, Sesto Fiorentino (FI), Italy.*

[2]*Department of Chemistry "Ugo Schiff", University of Florence, Sesto Fiorentino (FI), Italy.*

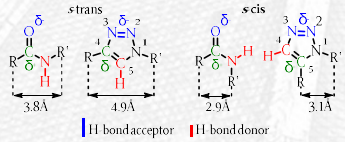
[3]*Normandie Univ, UNIROUEN, INSA Rouen, CNRS, CARMEN (UMR 6014) IRCOF, Mont-Saint-Aignan Cedex, France.*

Project code: RF-2021-12374177

1. Introduction

We previously obtained promising results using the side chain-to-side chain triazolyl bridge to stabilize specific conformation. These include the α-helical conformations of ACE2(24-42), the minimal peptide fragment containing all the residues involved in RBD binding to the SARS-CoV-2 spike glycoprotein,[1] and hPTHrP(11-19), fragment of antagonist of parathyroid hormone-related peptide.[2] We also demonstrated the stabilization of the β-turn in the melanocotin agonist MT-II[3] and oxytocin.[4]

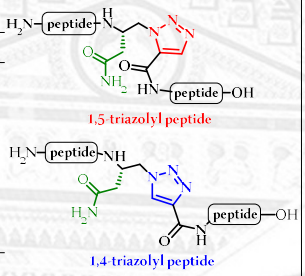
This project aims to evaluate the effects of **1,4- and 1,5-disubstituted [1,2,3]triazoles**, incorporated into the peptide backbone of model peptides, exploiting their ability to act as rigid, metabolically stable and structurally compatible amide bioisosteres.[5,6]



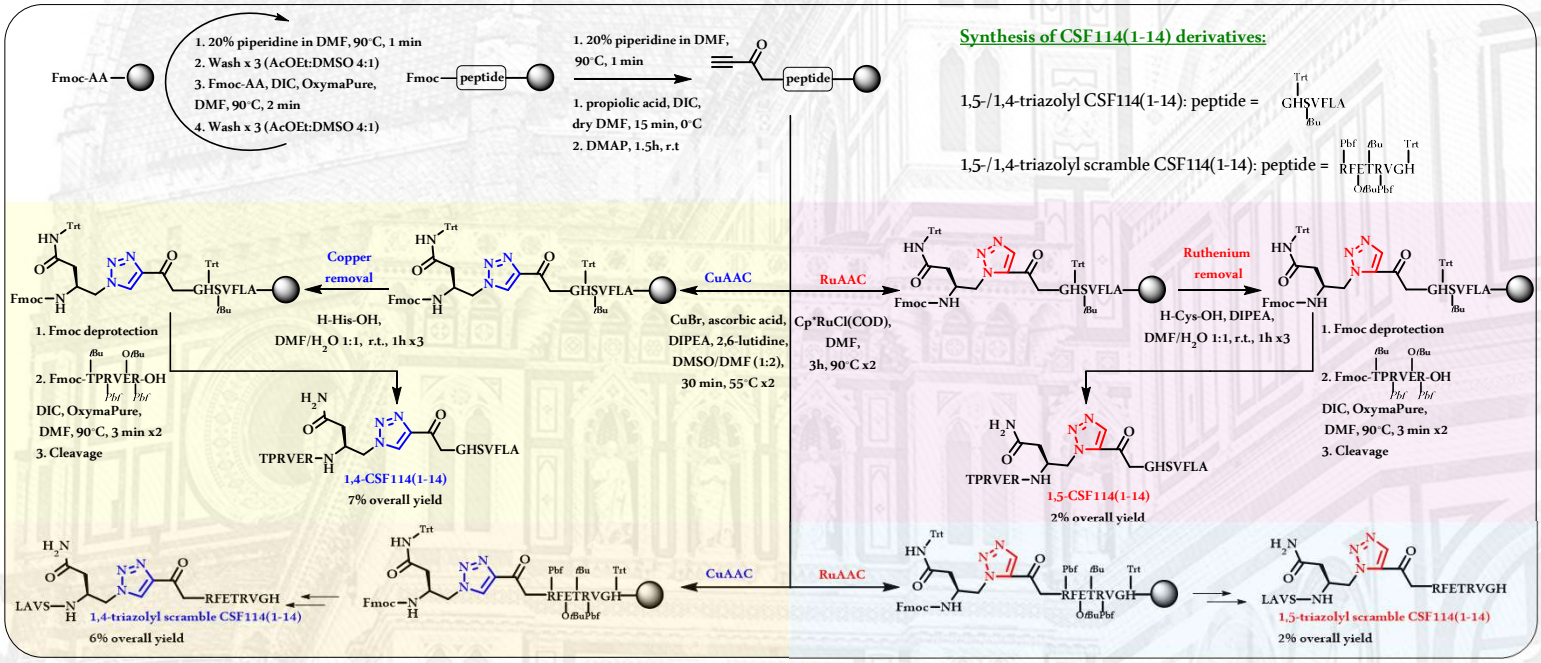
2. Objectives

The selected model peptides are: **CSF114**, a structure-based designed **β-turn** peptide and its scramble sequence, which does not induce a β-turn.[3,4] CSF114 presents a type I' β-turn, best exposing an asparagine residue at position 7.

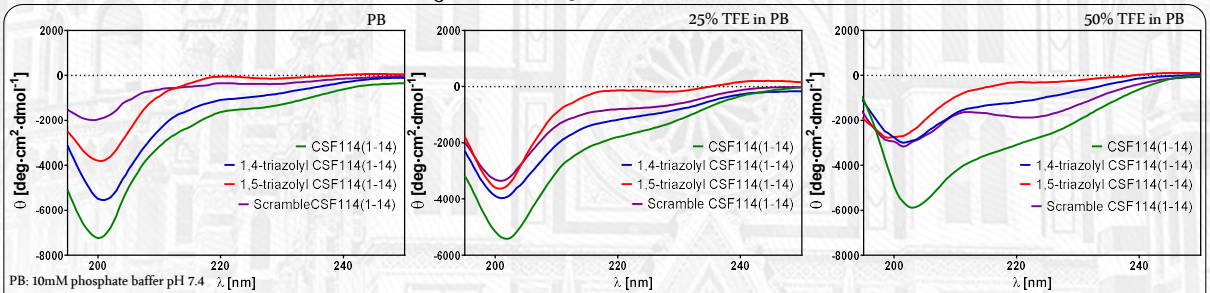
Peptide sequences	
CSF114(1-14)	TPRVERNGHSVFLA
Scramble CSF114(1-14)	PLAVSNRFETRVGH
1,5-triazolyl CSF114(1-14)	TPRVERN-1,5-Triazole-GHSVFLA
1,4-triazolyl CSF114(1-14)	TPRVERN-1,4-Triazole-GHSVFLA
1,5-triazolyl scrambleCSF114(1-14)	PLAVSN-1,5-Triazole-RFETRVGH
1,4-triazolyl scrambleCSF114(1-14)	PLAVSN-1,4-Triazole-RFETRVGH



3. Research and development



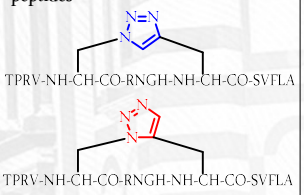
4. Results and Conclusion



➢ Both 1,5- and 1,4-disubstituted triazole replaced amide bond at positions i+1(Asn[7])-i+2 (Gly[8]) on the tip of the β-turn result β-turn disruptors in CSF114(1-14)

Future Perspectives

➢ Comparison with side chain-to-side chain 1,5- and 1,4-triazolyl bridged peptides



Acknowledgments

This project was funded in part by EUniWell: 5th seed funding call for the TTPep project and 3rd Well-Being Research Incubator Call for the project "Sustainable and green upscaling processes for peptide(-based) in vitro diagnostics and cosmeceuticals" and the Champion program "Peptides4Wellness".

Thanks to the European Peptide Society for the Registration fee to attend 38th EPS.

The author, Francesco Brenzini Biagioni, gratefully acknowledges the Italian Ministry of Health for funding the "borsa di ricerca" under project code DF-2021-12374177.

1. Quagliata M. *et al ACS Omega* **2023**, 8 ,22665-22672. 2. Cantel S. *et al J. Org. Chem.* **2008**, 73, 5663–5674. 3. Testa C. *et al J. Med. Chem.* **2014**, 57, 9424-9434. 4. Nuti F. *et al journal of enzyme inhibition and medicinal chemistry* **2023**, 38, 1, 2254019 . 5. Tornøe C.W., *et al J. Org. Chem.* **2002**, *67*, 3057-3064. 6. Tam A, *J. AM. CHEM. SOC.* **2007**, 129, 12670-12671. 7. Carotenuto A *et al J. Med. Chem.* **2001**, 44, 2378-23813. 8. Lolli F. *et al PNAS* **2005**, 102, 10273-10278.

https://doi.org/10.17952/38EPS.2026.P455

Faculty of Chemistry - Organic and Bioorganic Chemistry - OCIII

UNIVERSITÄT BIELEFELD

Synthesis and FRET-Based Cleavage Study of an $\alpha_V\beta_6$-Targeting Peptide Drug Conjugate

Caroline Brinkmann[1], Andreas Brockhinke[2] and Norbert Sewald[1]

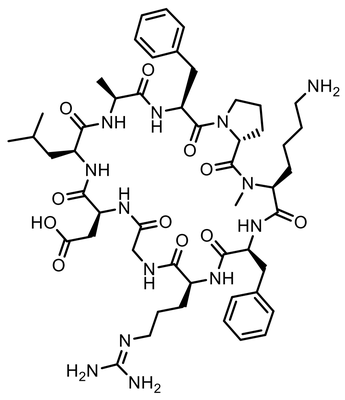
[1] Organic and Bioorganic Chemistry, Faculty of Chemistry, Bielefeld University, Germany.
[2] Physical und Biophysical Chemistry, Faculty of Chemistry, Bielefeld University, Germany

caroline.brinkmann@uni-bielefeld.de

$\alpha_V\beta_6$-Targeting Peptide

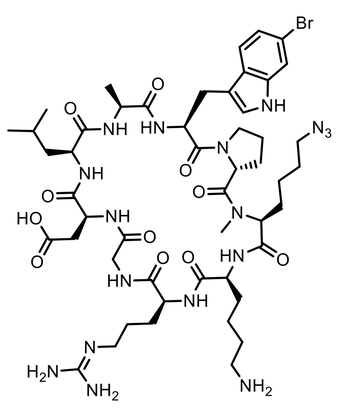
- Integrins are heterodimeric transmembrane receptors, whose functions can be exploited by tumor cells to support their survival.[1,2]
- Integrin $\alpha_V\beta_6$ is involved in breast and colon cancer. [3]
- RGD peptides can specifically bind to these integrins.[4]
- Incorporation of 6-Br-Trp at *i+3* relative to the RGD sequence improves the binding affinity.[5]

Maltsev *et al.*[6]



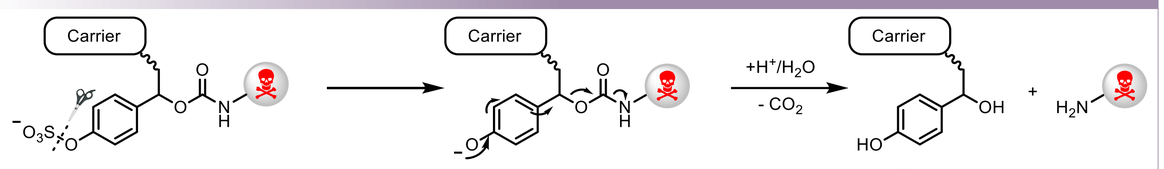
c(FRGDLAFp(*N*Me)K)
IC_{50} = 0.26 nM

This work



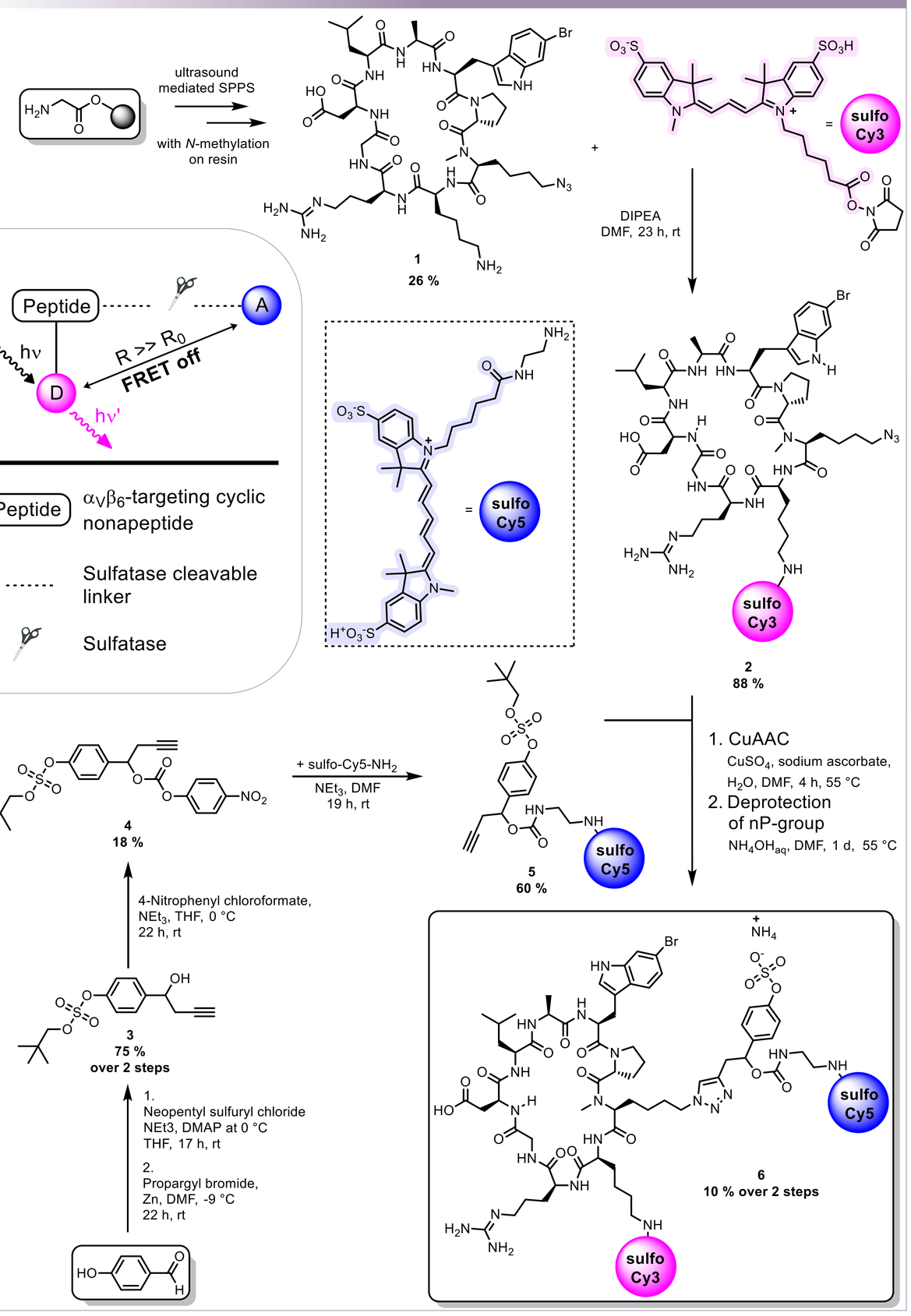
c(KRGDLA(6-Br)Wp(*N*Me)K(N_3))
IC_{50} = 0.12 ± 0.09 nM

Sulfatase Cleavable Linkers

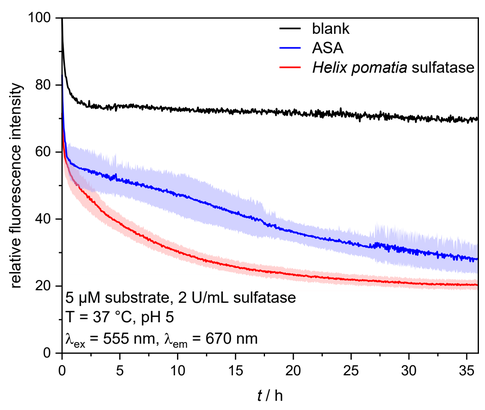


- Arylsulfatases (E.C.3.1.6.1.) catalyze the hydrolysis of aromatic sulfate esters.[7]
- It was found that sulfatase levels were twice as high in breast cancer tissue as in normal tissue.[7]
- Benefits of sulfatase cleavable linkers are stability in mouse and human plasma and their simple synthesis.[8]

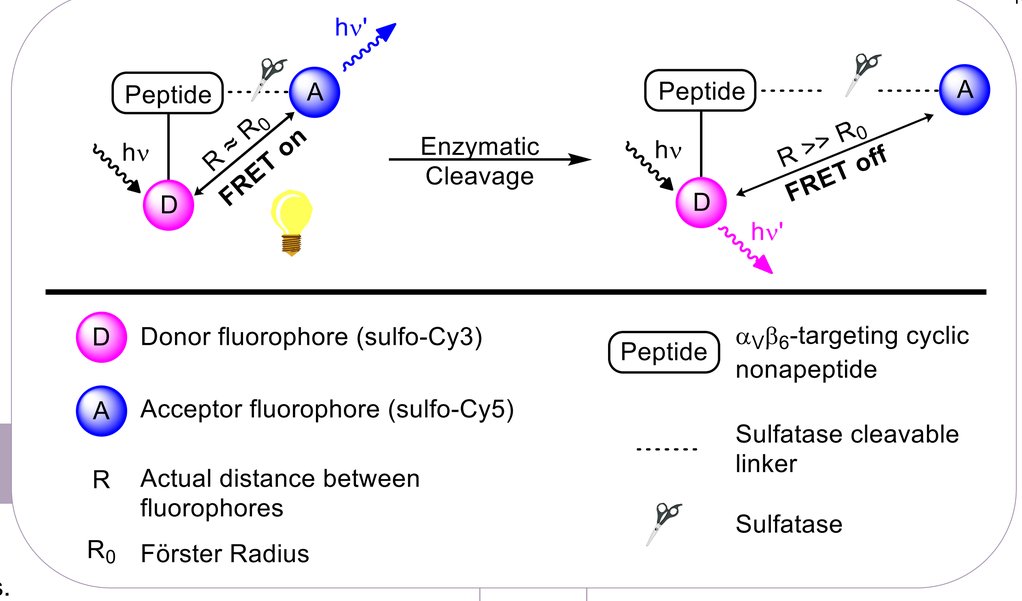
Synthesis



Cleavage Assay

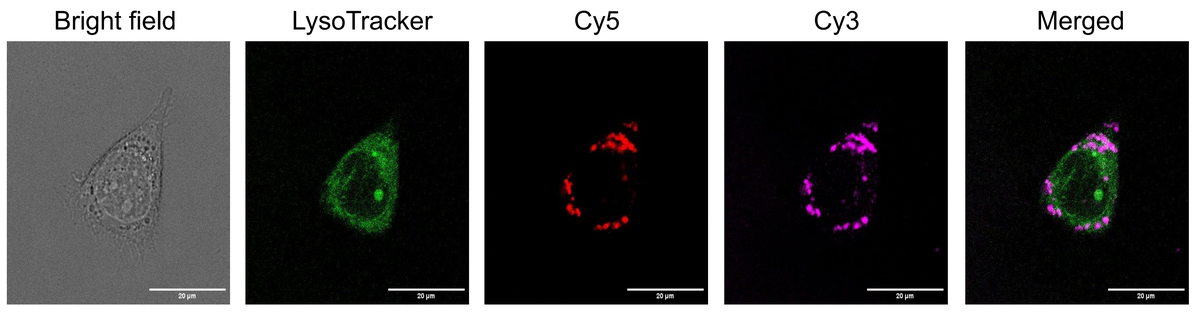


The cleavage of conjugate **6** can be detected via the decrease of acceptor fluorescence over time. It was carried out with two different sulfatases.



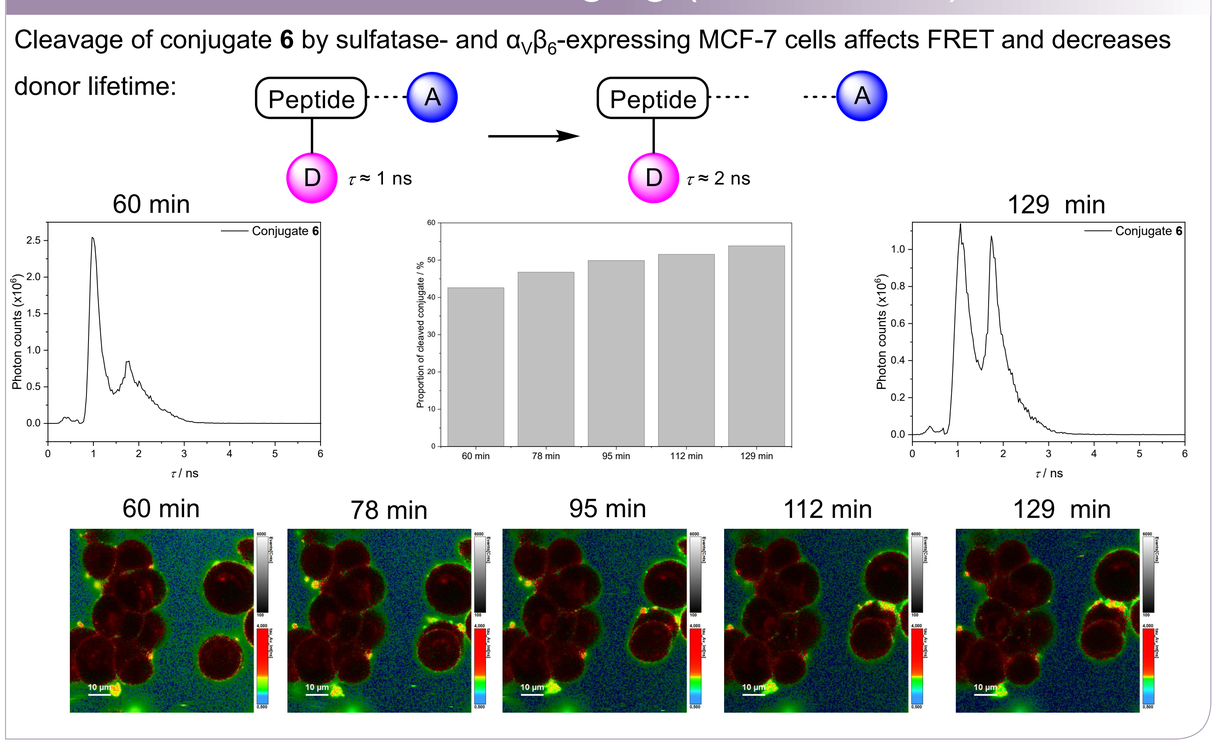
Internalization into MCF-7 cells

Conjugate **6** was incubated with $\alpha_V\beta_6$-expressing MCF-7 cells. LysoTracker Green was used to stain acidic cell compartments.



Fluorescence Lifetime Imaging (FLIM-FRET)

Cleavage of conjugate **6** by sulfatase- and $\alpha_V\beta_6$-expressing MCF-7 cells affects FRET and decreases donor lifetime:



Summary

- Conjugate **6** with sulfo-Cy3 as the FRET donor at the lysine side chain and sulfo-Cy5 as the FRET acceptor instead of a toxophore was synthesized.
- Both the human arylsulfatase A and the sulfatase from *Helix pomatia* cleave the conjugate **6**, which can be detected by the loss of FRET.
- Conjugate **6** is internalized by sulfatase- and $\alpha_V\beta_6$-expressing MCF-7 cells and its cleavage can be detected via FLIM-FRET.

References

[1] R. O. Hynes, *Cell* **2002**, *110*, 673. [2] J. Xiong, L. Yan, C. Zou, *et al. J. Hematol. Oncol.* **2021**, *14*, 177. [3] J. Paulus, N. Sewald, *J. Pept. Sci.* **2024**, *30*, e3561. [4] T. Inoue, P. G. Cavanaugh, P. A. Steck, N. Brünner, G. L. Nicolson, *J. Cell. Physiol.* **1993**, *156*, 212. [5] B. Nachtigall, C. Brinkmann, J. Langosch, A. Nieß, and N. Sewald, *Chem. – Eur. J.*, **2026**, e71559. [6] O. V. Maltsev, U. K. Marelli, T. G. Kapp et al., *Angew. Chem. Int. Ed.* **2016**, *55*, 1535. [7] S. Türkmen, P. Oner, F. Cinar, H. Koçak, G. Güvenen, H. Altun, Y. Eryavuz, *Cancer Letters* **2001**, *166*, 95. [8] J. D. Bargh, S. J. Walsh, A. Isidro-Llobet, S. Omarjee, J. S. Carroll, D. R. Spring, *Chem. Sci.* **2020**, *11*, 2375.

38th EPS
European Peptide Symposium



6 - 11th of September 2026
Vienna, Austria

www.sewaldlab.de

https://doi.org/10.17952/38EPS.2026.P183

“Antibacterial Activity of Novel Oncocin-Peptoid Hybrids”

Jacopo Bucchioni, Bee Ha Gan, Markus Orsi, Robert Rauscher, Norbert Polacek and Jean-Louis Reymond*

Department of Chemistry, Biochemistry and Pharmaceutical Sciences, University of Bern, Freiestrasse 3, CH-3012 Bern, Switzerland
Emails: jacopo.bucchioni@unibe.ch, jean-louis.reymond@unibe.ch

European Research Council
Established by the European Commission

Swiss National Science Foundation

b UNIVERSITÄT BERN

Introduction

The escalating prevalence of multidrug-resistant Gram-negative bacterial infections necessitates the exploration of novel antimicrobial agents. Proline-rich antimicrobial peptides (PrAMPs) have emerged as promising candidates due to their unique mechanisms of action. Among them, Oncocin (VDKPPYLPRPRPPRRIYNR-NH_2), a synthetic derivative inspired by peptides from the milkweed bug Oncopeltus *fasciatus*, has demonstrated potent antibacterial activity against *K. pneumoniae* and *E. coli* by inhibiting bacterial ribosome (Figure 1).[1,2]

We have recently demonstrated that stereorandomization is compatible with target binding peptides to the C-terminal region of Oncocin. It preserved ribosome binding and antibacterial effects including activities against drug-resistant bacteria and protected against serum degradation.[3] Following up on this progress, we focus on the modification of the last 9 C-terminal residues by incorporating mixed peptide/peptoid chains, along with random chirality alterations.

Structure Oncocin

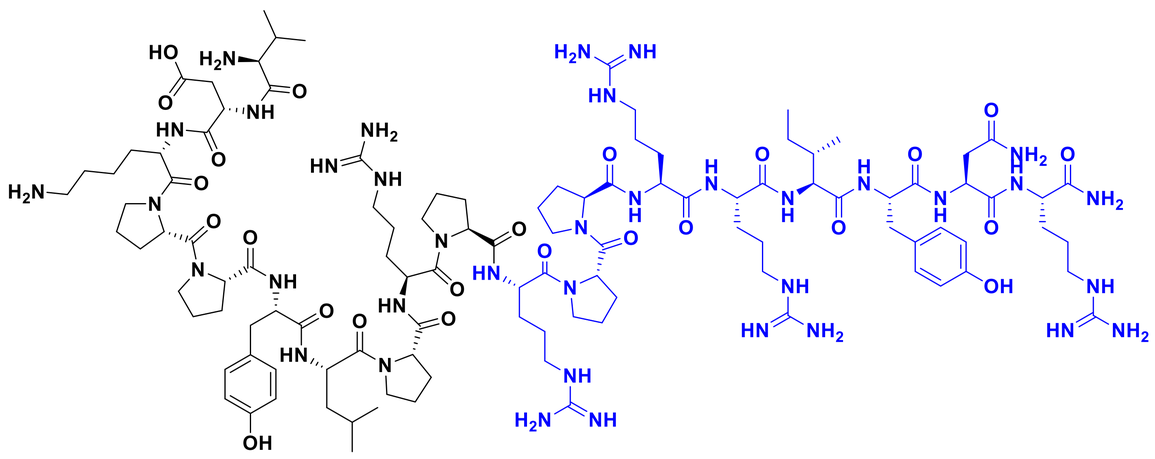


Figure 1. Chemical structure of L-Oncocin. The different parts are indicated through colours: BLACK - fixed part; BLUE – modifiable part.

Oncocin analogs visualization

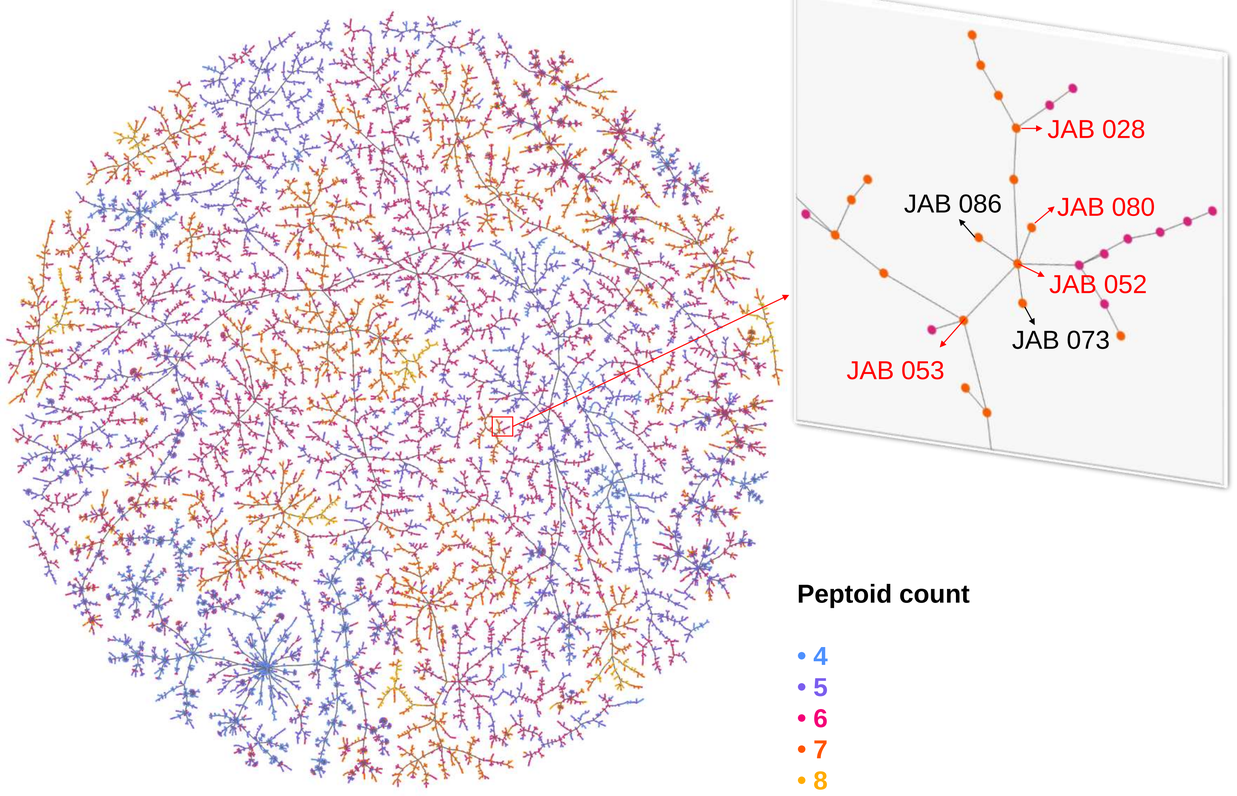
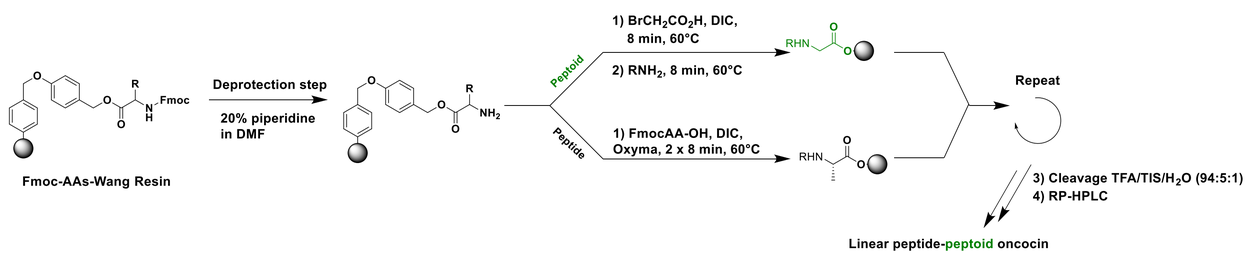


Figure 2. TMAP (Tree map) visualization of the virtual library of oncocin peptoid analogs, color-coded by the number of peptoid residues in the sequence. Each dot represents a different sequence; neighbouring dots are structurally related

Synthesis of mixed peptide-peptoid oncocin



Scheme 1. General procedure for the synthesis of linear peptide-peptoid oncocin analogs

Contact

SCAN ME

MIC and MHC

Compound	Sequence [a]	MHC [b]	MIC [c]		
			A. baumannii ATCC 19606	*K. pneumoniae NCTC 418*	*E. coli W 3110*
JAB 019	VDKPPYLPRP R p P r B_{75}I Y N R	>2000	8	32	32
JAB 020	VDKPPYLPRP R P p R R I B_{83}n R	>2000	8	64	>64
JAB 021	VDKPPYLPRP n p B_{73}R R V Y B_{57}R	>2000	8	32	32
JAB 022	VDKPPYLPRP R B_{57}P R R I y B_{52}R	>2000	8	16	32
JAB 028	VDKPPYLPRP R p P r B_{75}I Y n R	>2000	8	32	32
JAB 043	VDKPPYLPRP P p P B_{52}R V Y r R	>2000	4	32	32
JAB 051	VDKPPYLPRP R p B_{53}r R I y B_{73}R	>2000	8	8	32
JAB 052	VDKPPYLPRP R P P r B_{75}I y n R	>2000	4	16	8
JAB 053	VDKPPYLPRP R P P r B_{52}I y n R	>2000	8	32	16
JAB 055	VDKPPYLPRP n p P R R B_{61}Y B_{57}R	>2000	4	32	64
JAB 075	VDKPPYLPRP n p P R R B_{52}Y B_{57}R	>2000	4	16	32
JAB 080	VDKPPYLPRP R P P R B_{75}I y n R	>2000	4	16	8
JAB 089	VDKPPYLPRP R p P B_{63}R V Y r R	>2000	8	32	16
JAB 092	VDKPPYLPRP R p P r R B_{61}Y N R	>2000	>64	64	64
JAB 094	VDKPPYLPRP R p P r R I B_{86}n R	>2000	8	32	64
L-Onc	VDKPPYLPRP R P P R R I Y N R	>2000	64	16	16
Onc 112	VDKPPYLPRP R P P R r I Y N r	>2000	64	8	16

[a] One letter code for aminoacids. The L-amino acids are denoted with BLACK capital letters, D-amino acids with RED lower-case letters and N-substituted residues are indicated in GREEN in Italics; [b] Minimum hemolytic concentration (MHC) measured on human red blood cells (hRBC) in 10 mM phosphate buffer, 150 mM NaCl, pH 7.4, 25 °C, 4 h. [c] Minimum inhibitory concentration (MIC) in μg mL^{-1}, was determined on bacteria in Mueller-Hinton (MH) broth at pH 7.4 after incubation for 16-20 hours at 37 °C. Values two different duplicate MIC determinations.

Preliminary ribosome foot-printing assay

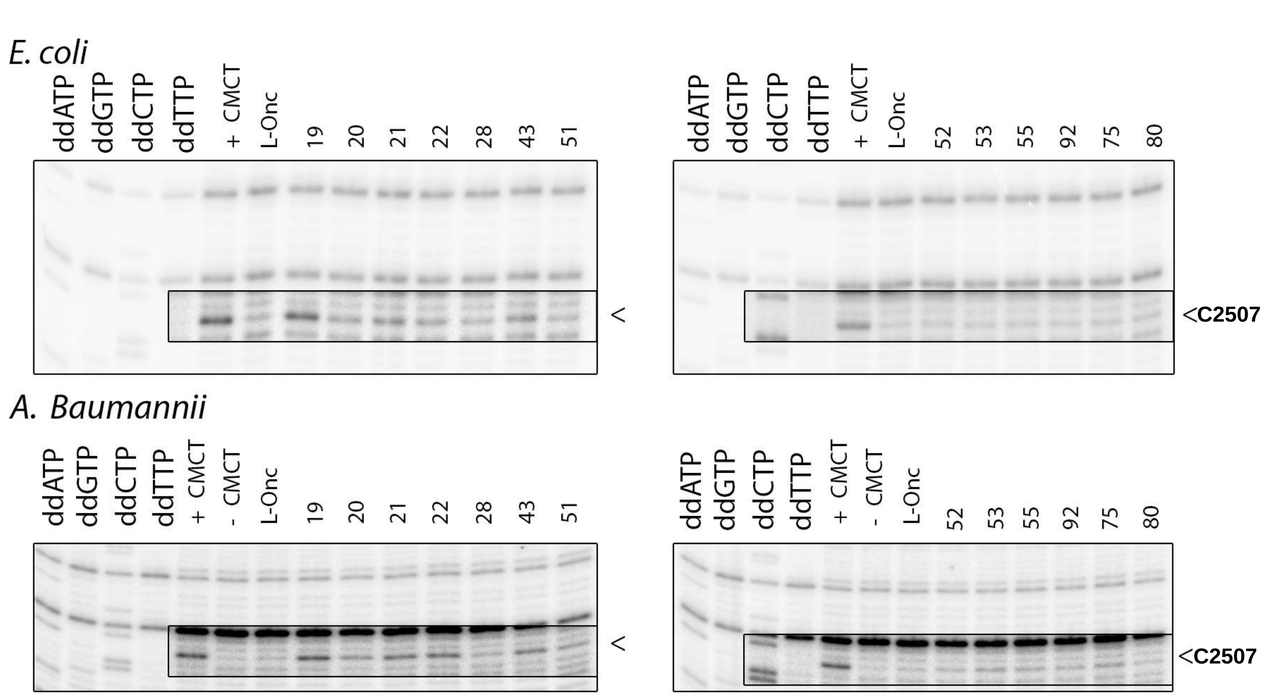


Figure 3. Ribosome foot printing experiment: The arrows indicate the position C2507 on the sequencing gel of the 23S Ribosomal RNA (*E. coli* W 3110 and *A. Baumannii ATCC 19606*). The more intense bands result from the U2506 CMCT modification in absence of peptide binding. The CMCT modifies U2506 and produces a visible band at the position C2507, in absence of CMCT there is no modification of U2506. No bands are observable with **L-Onc**, **JAB 020**, **028**, **051**, **052**, **053**, **055**, **075**, **080** and **092** compared to background (*A. Baumannii ATCC 19606)*; revealing the interaction of the peptide with U2506. [3]

Conclusion and Outlook

Our research started from the idea of modifying the last 9 C-terminal residues to create a mixed peptide-peptoid oncocin derivatives. This approach led to an increase in antibacterial activity, as shown by the MIC values of the tested compounds. Notably, **JAB 055** and **JAB 094** appear to be selectively active against *A. baumannii* and inactive against *K. pneumoniae* and *E. coli* in preliminary analyses.

These promising initial results prompted us to further investigate whether the new oncocin derivatives retain the same ribosomal binding site, and to explore the role of bacterial membrane uptake in enhancing antibacterial activity and selectivity.

Acknowledgement

This work was supported by the Swiss National Science Foundation and the European Research Council .

References

(1) Seefeldt, A. C., *et al*. The proline-rich antimicrobial peptide Onc112 inhibits translation by blocking and destabilizing the initiation complex. *Nat. Struct. Mol. Biol.*, **2015**, *22*, 470–475.

(2) Roy, R. N., *et al*. The mechanism of inhibition of protein synthesis by the proline-rich peptide oncocin. *Nat. Struct. Mol. Biol.*, **2015**, *22*, 466–469

(3) Gan, B. H., *et al. Stereorandomized Oncocins with Preserved Ribosome Binding and Antibacterial Activity. J. Med. Chem.* ***2024****, 67, 19448-19459.*

TFA-Free Cleavage and Deprotection in Solid-Phase Peptide Synthesis: Advantages and Drawbacks of Formic Acid

Maria Leko[1,2], Polina Filippova[1], Sergey Anisimov[1], Andrey Murko[1] and Sergey Burov[1,2]

[1]Cytomed JSC, Peptide synthesis laboratory, St-Petersburg, Russia

[2]Luxembourg Bio Technologies Ltd., Nes Ziona 7403631, Israel

https://doi.org/10.17952/38EPS.2026.P275

Introduction

Solid-phase synthesis is one of the main techniques for the production of peptides applied in the pharmaceutical and cosmetic industries. However, the synthetic process relies on the application of trifluoroacetic acid (TFA) at the stage of global peptide deprotection and cleavage from the polymeric support. Beyond its health and environmental hazards, TFA increases operational costs by requiring strict safety measures, waste disposal, and counterion conversion into pharmaceutically acceptable acetate or hydrochloride forms.

Due to growing evidence of accumulation in surface waters and resistance to biodegradation, TFA use faces imminent regulatory restrictions by the European Chemicals Agency. Nevertheless, its application remains unavoidable for industrial-scale peptide production via SPPS.

Herein, we present a PFAS-free cleavage and deprotection protocol* based on *in situ* generation of HCl in formic acid, yielding the final product in a pharmaceutically acceptable salt form.

* Patent-pending technology

Results and Discussion

Analysis of the literature suggests the utility of formic acid (FA) as the primary component of deprotection systems. Owing to its acidity (pK_a 3.75), it can be applied in peptide chemistry for the removal of Boc and *t*Bu protecting groups[1,2].

Our preliminary experiments demonstrated that neat FA enables the removal of Trt protecting groups from Gln, Asn, and His (**Table 1**). However, achieving complete deprotection requires heating the reaction mixture to 40-50 ^{0}C, depending on the peptide structure.

These results prompted us to reinvestigate the utility of HCl/FA for peptide deprotection and cleavage from the solid support. Therefore, subsequent experiments were performed on the most challenging models: Pbf removal from Arg and the cleavage of Fmoc-Phe-OH from Wang resin.

It was shown that deprotection efficiency strongly depends on the water content in the reaction mixture (**Table 2**). The best results were obtained by generating HCl *in situ* through mixing of anhydrous FA with TMSCl or related reagents (**Tables 1 and 3**).

The practical utility of this approach was tested on a number of peptides for both pharmaceutical and cosmetic applications. It was shown that using of the TMSCl/FA mixture significantly reduced Met alkylation compared to the standard TFA treatment (**Fig. 1**).

While peptide deprotection is accompanied by partial Ser, Thr, Tyr, and Trp formylation, the desired product is easily recovered by treatment with nucleophilic agents (**Fig. 2 and 3A**). Lys residue formylation via formyl group transfer from the adjacent hydroxy acid can be suppressed using an appropriate nucleophile (**Fig. 3B and Table 4**).

Deprotection of some Trp-containing peptides was accompanied by an unexpected side reaction: C-2 alkylation of Trp with the bulky Trt cation. However, the side-product formation can be efficiently suppressed by adding TIS to the reaction mixture (**Fig. 5**).

It was shown that the purity and yield of the model peptides after TMSCl/FA deprotection were at least comparable to those obtained via the standard TFA procedure **(Table 5**).

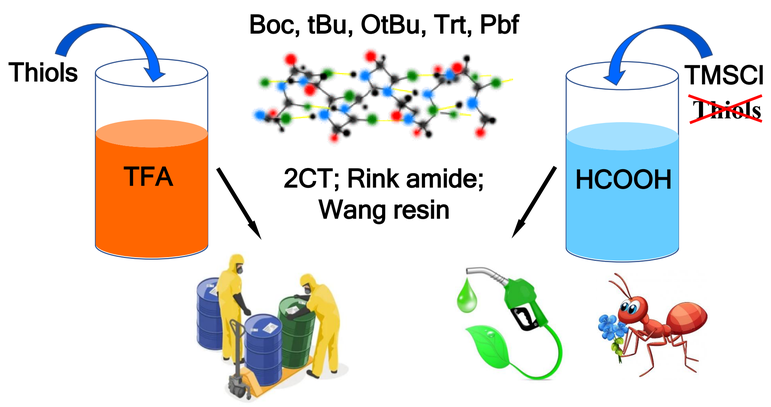


Table 2. Influence of water content on Arg(Pbf) deprotection

Deprotection conditions	HCOOH (%)	Fmoc-Arg(Pbf)-OH (%)		
		30 min	1 h	2 h
1 M HCl(aq)/FA	85	98	94	88
1 M HCl(aq)/FA	90	92	81	69
1 M HCl(aq)/FA	98	45	6	0.4
1 M TMSCl/FA	98	7	0.6	0.1

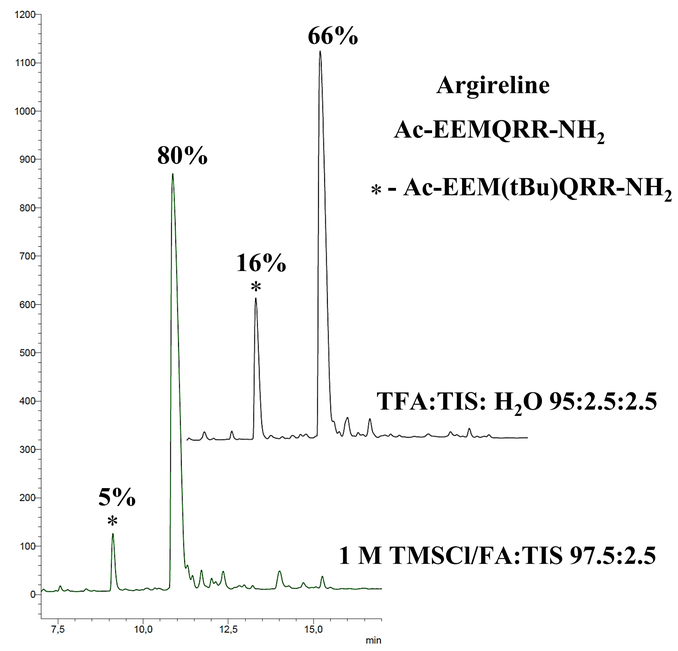


Fig. 1. Peptide deprotection in FA reduces Met alkylation.

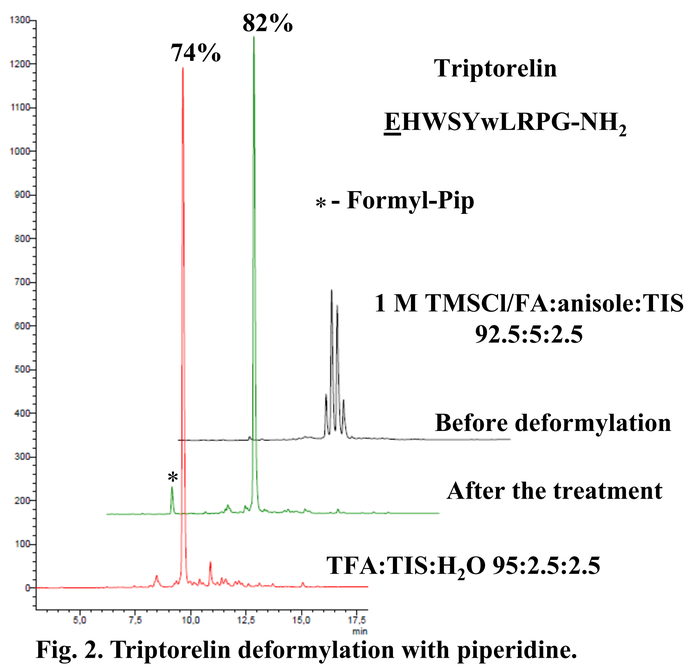


Fig. 2. Triptorelin deformylation with piperidine.

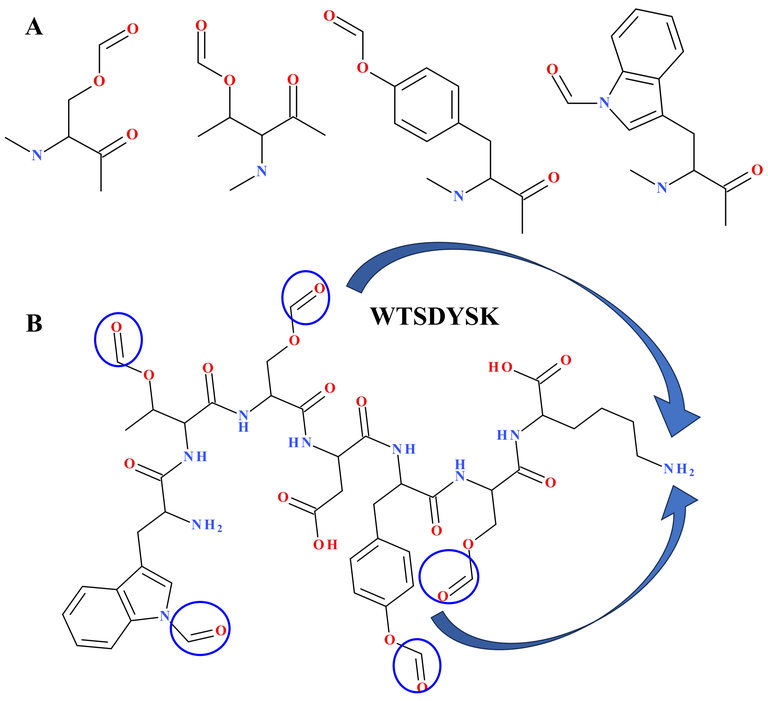


Fig. 3. Formation of primary (A) and secondary (B) side products.

Table 4. Recovery of the final product

Reagent	Lys formylation (%)
Piperidine	**18.6**
Piperazine	**8.5**
Morpholine	**3.7**
Substance "H"	**0.3**

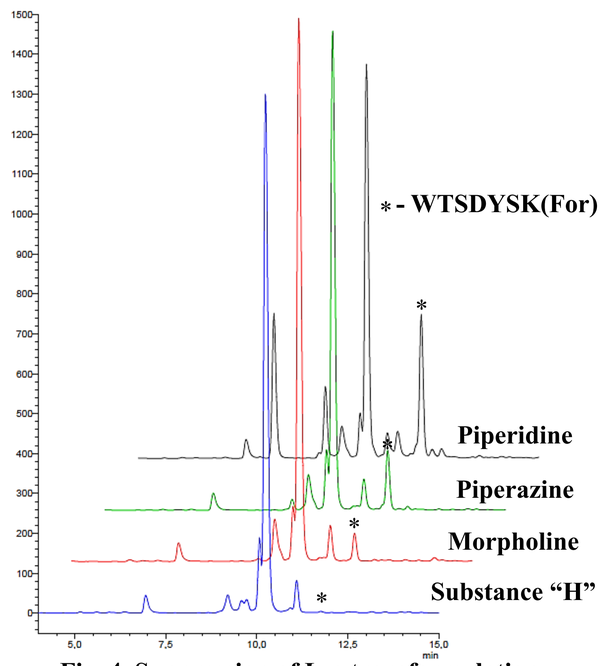


Fig. 4. Suppression of Lys transformylation.

Table 1. Removal of side-chain protecting groups

Protecting group	Amino acids	Deprotection conditions	
		FA	TMSCl/FA
^{t}Bu	Ser, Thr	30 min, RT	<30 min, RT
	Tyr	30 min, RT	30 min, RT
O^{t}Bu	Glu, Asp	30 min, RT	30 min, RT
BOC	Lys, Orn	1 h, RT	30 min, RT
	Trp	30 min, RT	30 min, RT
Trt	His	3 h, 50 ^{0}C	3 h, 40 ^{0}C
	Gln, Asn	2 h, 50 ^{0}C	1 h, RT
	Cys	Stable	2 h, RT (5% TIS)
Pbf	Arg	Stable	2 h, RT

Table 3. Cleavage yields (%) from Fmoc-Phe-resin after 2 h

Cleavage cocktail	Rink amide AM resin	Wang resin	
	RT	RT	40 ^{0}C
95% TFA/H_2O	78	41	92
1 M HCl(aq)/FA	63	15	89
1 M TMSCl/FA	84	79	93
1 M TMSBr/FA	93	96	95

TMSCl/FA vs. TFA deprotection

Entry	TFA	TMSCl/FA
Cleavage efficiency	✓ High	✓ High
Aspartimide formation	✓Low	Moderate
Reagents cost	High	✓ Moderate
Waste management	Costly	✓Cheap
Environmental hazard	High	✓ Moderate
Toxicity	High	✓Moderate
Counterion	TFA	✓HCl

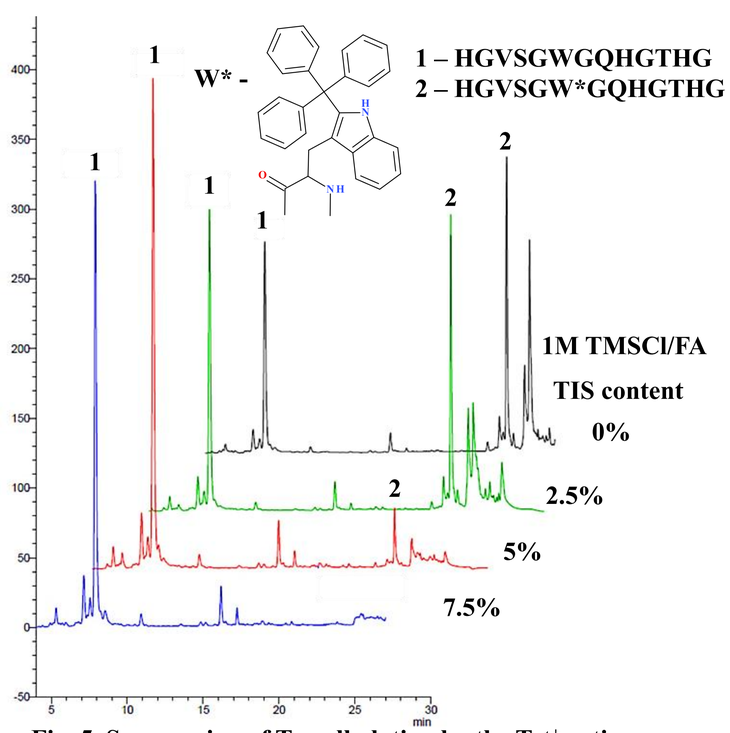


Fig. 5. Suppression of Trp alkylation by the Trt$^+$ cation.

Table 5. Deprotection of the model peptides

Peptide sequence	Brand name	Resin	Purity (%)[a]	
			A	B
Pal-HfR-NH_2	Neutrazen	Rink amide AM	91	91
Pal-HfRW-NH_2	Greyverse	Rink amide AM	77	84
GLYYF-NH_2	P5N	Rink amide AM	90	89
Ac-EEMQRR-NH_2	Argireline	Rink amide AM	86	89
deamino-CYFQNCPrG-NH_2[b]	Desmopressin	Rink amide AM	40	55
EHWSYwLRPG-NH_2	Triptorelin	Rink amide AM	74	82
HGVSGWGQHGTHG	Allostatin	2CT	69	76
		Wang	59	71
PKKKRKV$_\beta$AHAIYPRH-NH_2	–	Rink amide AM	84	86
YLQDQARLNSWGCAFRQVC-NH_2[c]	HIV-2-19	Rink amide AM	34	34

[a] Purity of the crude product after deformylation. [b] Linear precursor.
[c] Acm protected (synthesis was not optimized). A – TFA cleavage protocol; B – 1 M TMSCl/FA.

Conclusions

- **The proposed PFAS-free procedure, based on *in situ* generation of HCl in formic acid, enables global peptide deprotection and cleavage from Rink amide and Wang resins.**
- **This synthetic protocol utilizes inexpensive, readily available reagents and simplifies hazardous waste disposal.**

References

1. Kinoshita, H.; Kotake H. *Chemistry Letters*., **1974**, *3*, 631–634.
2. Toonstra, C.; Amin, M. N.; Wang L.-X. *J Org Chem*. **2016**, *81*, 6176–6185.

A Nanometric Platform for Live Cell Multiplex Screening of Non-natural Peptides

Sinyal Abu-Rabia, Danit Zagiel, Coral Yohay, Gila Kazimirsky and Gerardo Byk

Bar Ilan University, Department of Chemistry, Laboratory of Nano-Biotechnology Ramat Gan - 52900, Israel.

https://doi.org/10.17952/38EPS.2026.P384

Abstract

The unique available *in vivo* high throughput screening system was proposed by Ruoshlati and Pasqualini [1]. The system is based on the use of a library of filamentous phages expressing at their surface a high number of degenerated peptide sequences. Each individual phage expresses only one peptide sequence. The selection and identification of peptide sequences on phages associated with a tumor or other tissue after IV administration of the library, permits identification of novel tumor/tissue targeted peptide sequences. However, this approach is intrinsically limited to peptides. The aim of our work is to develop a new chemistry-based technology to overcome the limitation of phage libraries, thus extending the scope of *live cell*/in *vivo* biological panning to non-natural peptides using a synthetic multiplex "phage-like" system. In this presentation we have developed a nanometric monodispersed system substituted with a panel of fluorescent probes and candidate D-peptides both tethered using click chemistry. As a first prove of concept we have synthesized a library of all-D peptides that were conjugated and screened using flowcytometry, in a variety of cancer cell lines. A positive peptide has been further validated directly using FACS and microscopy analysis.

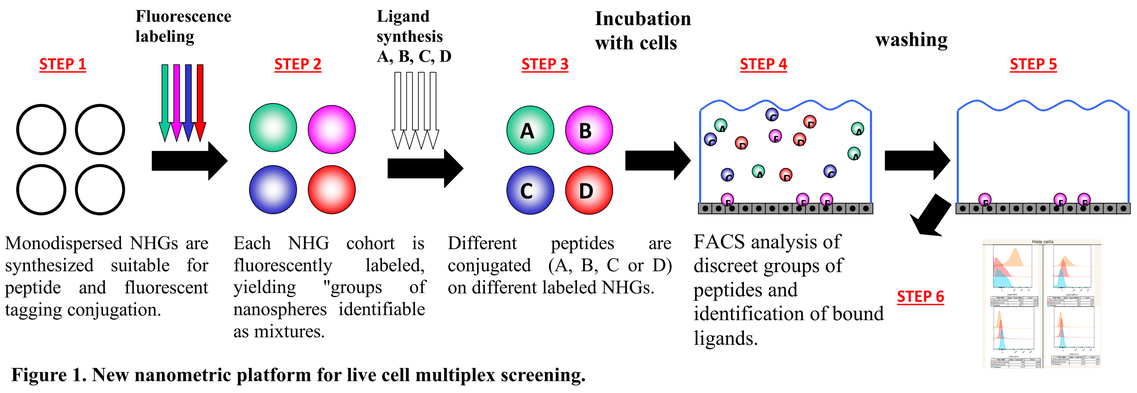


Figure 1. New nanometric platform for live cell multiplex screening.

Results and Discussion

For our system, we used monodispersed NHGs of 400 nm [2]. The NHGs possess free amino groups that are modified with propiolic acid amide. Candidate D-peptides are synthesized on a peptide synthesizer and an azido tail is placed at their N-terminus. Azido peptides and Azido probes are mixed and clicked onto the NHGs (figure 2). As a proof of concept, we have synthesized a library of 16 D-peptides that were conjugated with 4 different fluorescent probes to result in 4 multiplexed groups of 4 peptides. The groups were screened in a panel of cancer cell lines using flow-cytometry. Positive hits are defined as cells displaced into the fluorescent quadrant of the histogram at a given emission wavelength.

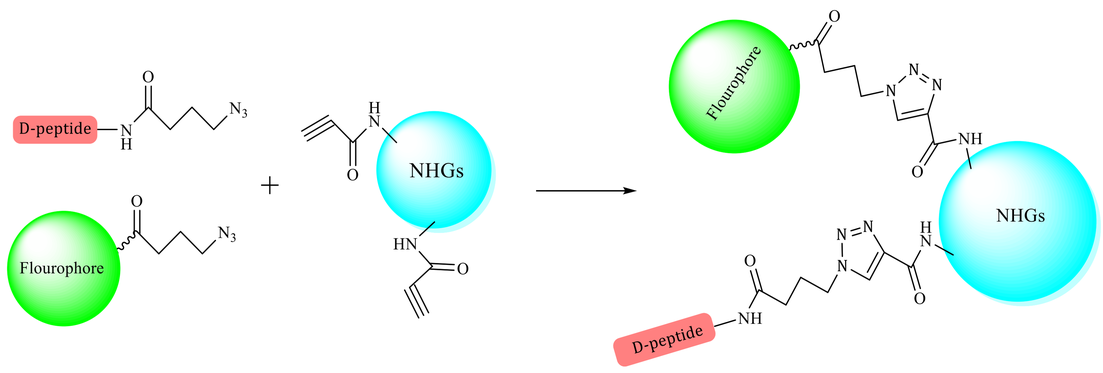
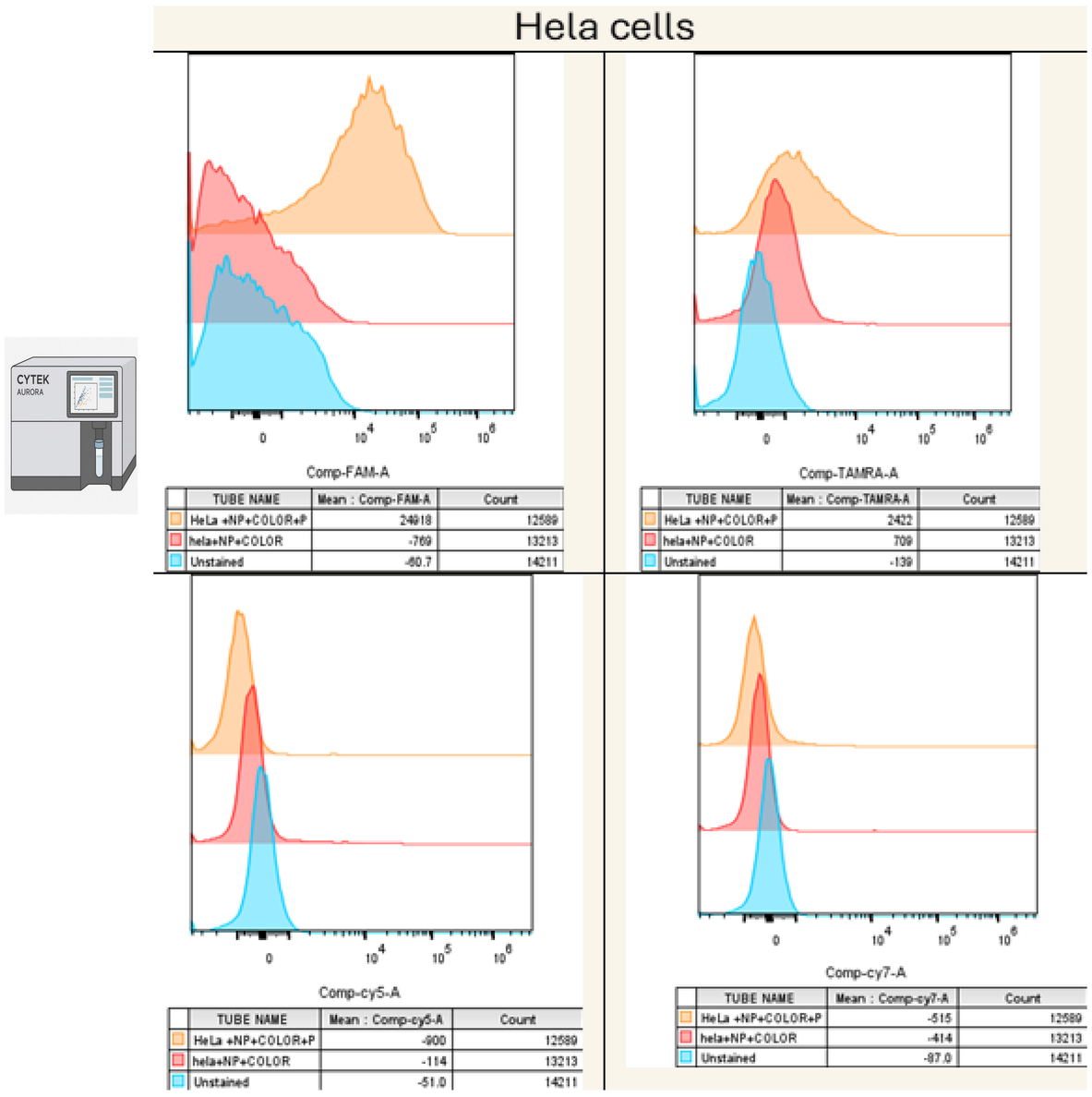


Figure 2. Strategy for conjugation to nanohydrogels using click chemistry

Peptide #	Probe on NHG	Sequence on NHG
9	FAM	n-t-a-s-y-d-w-NH_2
10	FAM	v-l-p-k-w-s-a-NH_2
11	FAM	m-p-k-e-s-q-f-NH_2
12	FAM	w-g-k-d-t-f-v-NH_2
5	TAMRA	l-t-v-a-p-w-y-NH_2
8	TAMRA	l-t-v-s-p-w-a-NH_2
13	TAMRA	f-t-k-m-r-g-d-y-a-l-h-g-NH_2
14	TAMRA	g-h-l-a-y-d-g-r-m-k-t-f-NH_2
1	*Sulfo Cy-5*	l-t-v-s-p-w-y-NH_2
4	*Sulfo Cy-5*	l-t-a-s-p-w-y-NH_2
6	*Sulfo Cy-5*	l-t-v-s-a-w-y-NH_2
15	*Sulfo Cy-5*	v-y-t-e-h-p-r-f-a-t-k-g-NH_2
2	*Sulfo Cy-7*	a-t-v-s-p-w-y-NH_2
3	*Sulfo Cy-7*	l-a-v-s-p-w-y-NH_2
7	*Sulfo Cy-7*	l-t-v-s-p-a-y-NH_2
16	*Sulfo Cy-7*	g-k-t-a-f-r-p-h-e-t-y-v-NH_2

Figure 3. Peptide/probes conjugated to nanohydrogels used in this study.



TUBE NAME	Mean : Comp-FAM-A	Count
HeLa +NP+COLOR+P	24918	12589
hela+NP+COLOR	-769	13213
Unstained	-80.7	14211

TUBE NAME	Mean : Comp-TAMRA-A	Count
HeLa +NP+COLOR+P	2422	12589
hela+NP+COLOR	709	13213
Unstained	-139	14211

TUBE NAME	Mean : Comp-cy5-A	Count
HeLa +NP+COLOR+P	-900	12589
hela+NP+COLOR	-114	13213
Unstained	-51.0	14211

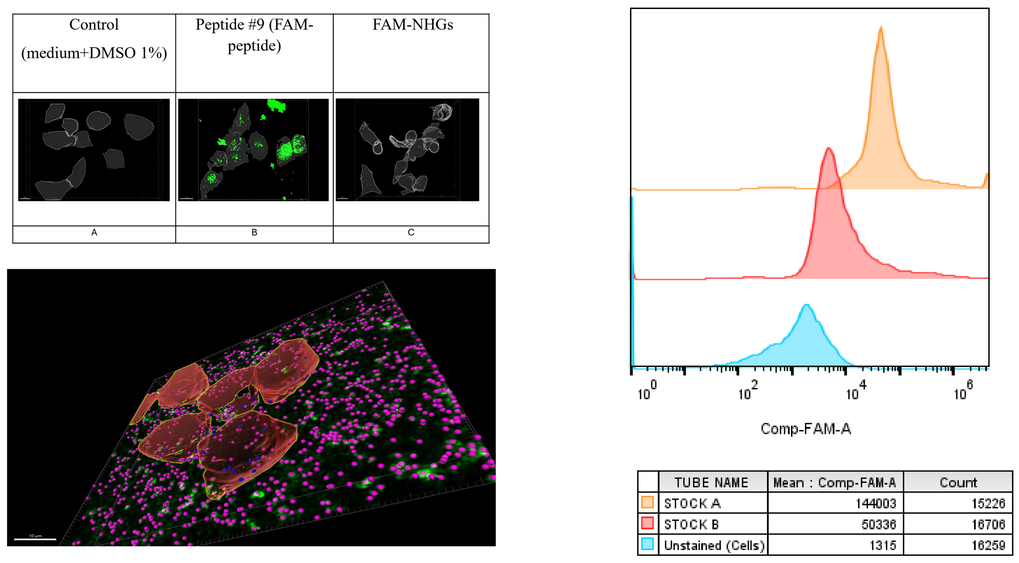
TUBE NAME	Mean : Comp-cy7-A	Count
HeLa +NP+COLOR+P	-515	12589
hela+NP+COLOR	-414	13213
Unstained	-87.0	14211

Figure 4. Example of multiplex screening using Cytek flow cytometer: peptide #9 co-labeled with 5-FAM, peptide #14 co-labeled with 5-TAMRA, peptide #4 co-labeled with Sulfo-Cy5 and peptide #2 co-labeled with Sulfo-Cy7. Blue= non labelled NHGs, Red= NHGs labelled only with probe, Orange= NHG co-labeled with peptide and probe.

Peptide #	Sequence	HeLa cells	PC-3 cells	MCF-7 cells
1 (S1-3)	l-t-v-s-p-w-y-NH_2	-	-	-
2 (S7-9)	a-t-v-s-p-w-y-NH_2	-	-	-
3 (S1-3)	l-a-v-s-p-w-y-NH_2	-	-	-
4 (S7-9)	l-t-a-s-p-w-y-NH_2	-	-	-
5 (S1-3)	l-t-v-a-p-w-y-NH_2	-	-	-
6 (S10-12)	**l-t-v-s-a-w-y-NH_2**	**-**	**+**	**+**
7 (S10-12)	l-t-v-s-p-a-y-NH_2	-	-	-
8 (S10-12)	l-t-v-s-p-w-a-NH_2	-	-	-
9 (S7-9)	**n-t-a-s-y-d-w-NH_2**	**+**	**-**	**-**
10 (S1-3)	v-l-p-k-w-s-a-NH_2	-	-	-
11 (S4-6)	m-p-k-e-s-q-f-NH_2	-	-	-
12 (S10-12)	w-g-k-d-t-f-v-NH_2	-	-	-
13 (S4-6)	f-t-k-m-r-g-d-y-a-l-h-g-NH_2	-	-	-
14 (S7-9)	**g-h-l-a-y-d-g-r-m-k-t-f-NH_2**	**+**	**-**	**-**
15 (S4-6)	v-y-t-e-h-p-r-f-a-t-k-g-NH_2	-	-	-
16 (S4-6)	g-k-t-a-f-r-p-h-e-t-y-v-NH_2	-	-	-

Figure 5. Multiplex screening of 16 peptides conjugated to NHGs on three cancer cell lines. Screening results were confirmed by two separate experiments.

Direct validation of peptide 9#



TUBE NAME	Mean : Comp-FAM-A	Count
STOCK A	144003	15226
STOCK B	50336	16706
Unstained (Cells)	1315	16259

Figure 6. Validation of FAM-peptide #9 incubated with HeLa cells during 1 h. Left Upper panel: Internal stack of confocal microscopy (A) Control cells, (B) FAM#9 100 µM, (C) FAM-NHGs (no peptide). Left lower panel: 3D illustration of fluorescence using Imaris: pink dots=extracellular peptide, blue dots= intracellular peptide. All pictures were taken in the FAM channel using the same sensitivity parameters. Right panel: FACS analysis of FAM-labeled peptide 9 at 10 (red) and 100 (orange) µM.

Conclusion

We have developed a new technique for simultaneous screening of a number of small ligands. The technique is based on the establishment of a phage –like synthetic system composed of an inert biocompatible nanohydrogel (400nm), a panel of fluorescent tags and the ligands to be tested. The technique is suitable for the detection using flow-cytometry. By this method we could identify several peptides with spefic affinity for certain cancer cell lines. Here we present the validation of peptide 9# that was directly labelled and studied under confocal microscopy and flowcytometry. We have clearly shown that a cell-based combinatorial (multiplex) screening can be performed using a mixture of different small molecules and/or peptides linked to appropriately tagged nanohydrogels. Since the hydrogels are biocompatible, the next step would be to use them directly in vivo.

Acknowledgements

We are indebted to the Israel Science Foundation Grant number1482/22 and to the Marcus Center for Medicinal Chemistry for supporting this research.

References

1. Pasqualini, R. Koivunen, E. and Ruoshlati, E. Nature Biotech. 15, 542-515(1997)
2. Khandadash, R.; Machtey, V.; Sheiner, I.; Gotilied, H.; Gothilf, A.; Ebenstein Y.; Weiss A. and Byk G. Novel biocompatible hydrogel nanoparticles: Generation and size-tuning of nanoparticles by the formation of micelle templates obtained from thermo-responsive monomers mixtures. Journal of Nanoparticle Research (2014) 16(12), 1-18.

Concentration-Dependent Mechanisms of Melittin-Induced Membrane Destabilization: an Interdisciplinary Approach

A. Chacón Calderón*[1], P. Zelenovskii[2], M. Soares[1], E. C. Wrobel[3], O. N. Oliveira Jr.[3], D. Pereira[1], M. Sardo[1], L. Mafra[1], I. Marín Montesinos[1], A. Barros-Timmons[1].

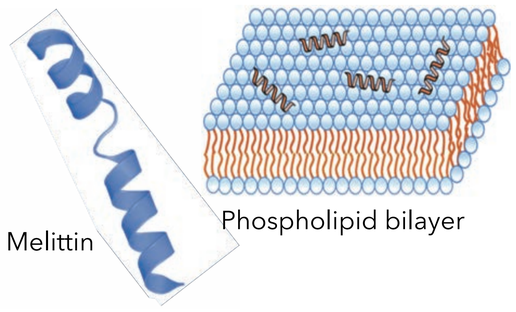
[1] Aveiro Institute of Materials (CICECO), Department of Chemistry, University of Aveiro, Aveiro, Portugal.
[1] Aveiro Institute of Materials (CICECO), Department of Physics, University of Aveiro, Aveiro, Portugal
[3] Sao Carlos Institute of Physics, University of São Paulo, São Carlos, Brazil.

*a.chacon@ua.pt

https://doi.org/10.17952/38EPS.2026.P216

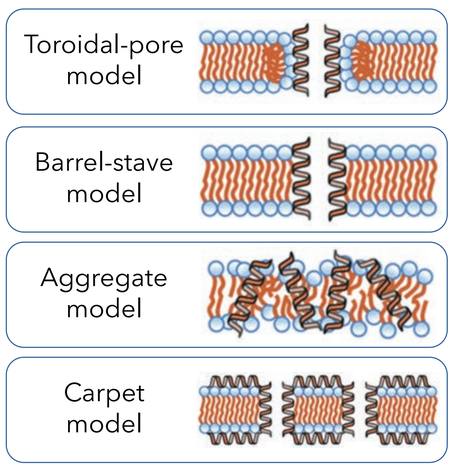
Introduction

Peptide – cell membrane interaction

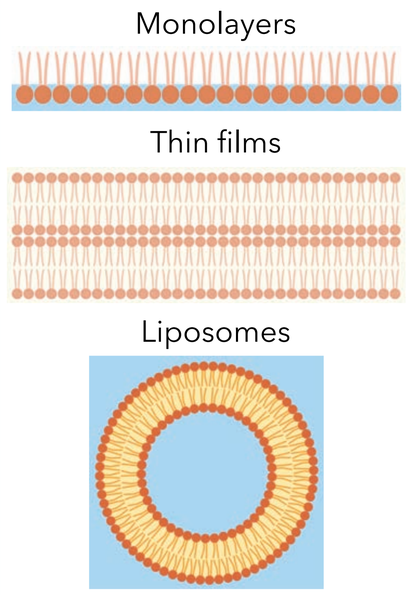


Antimicrobial peptides (AMPs) are promising alternatives to conventional antibiotics with different mechanisms of action

Possible mechanisms of action



Methods

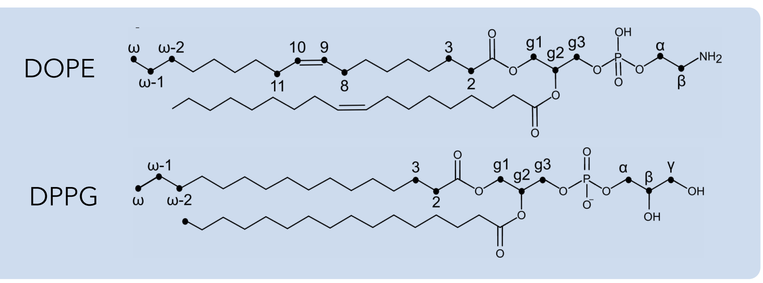


Complementary techniques that allow to obtain a full view of the mechanism of action of a peptide

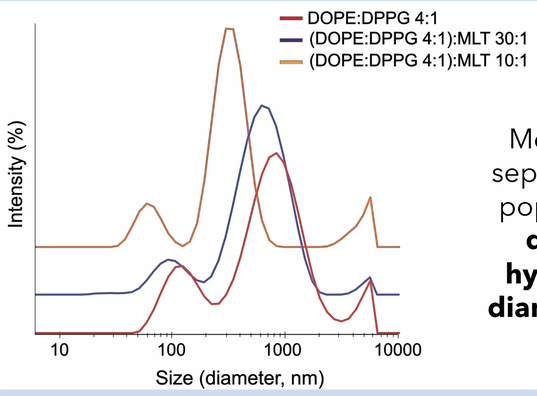
- Micro level: Langmuir-Blodgett (BAM, PM-IRRAS); DLS
- Nano level: AFM
- Atomic level: ss-NMR

Results

DOI: 10.1021/acs.langmuir.6c02887



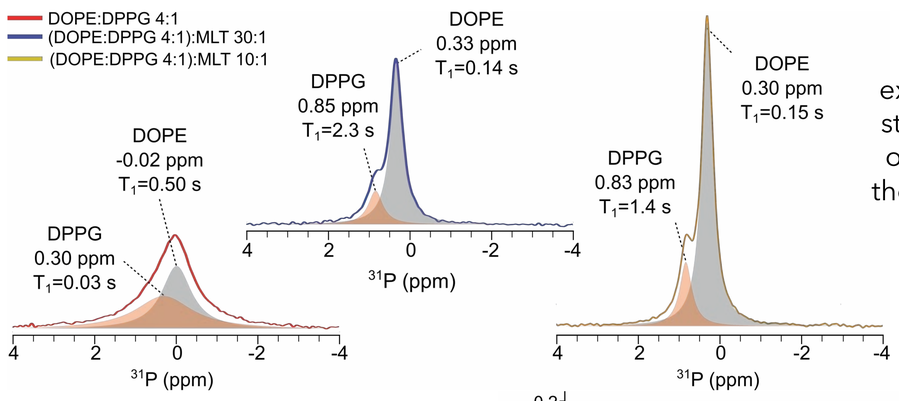
Dynamic light scattering (DLS)



Melittin causes separation of size populations and **decrease in hydrodynamic diameter** of MLVs

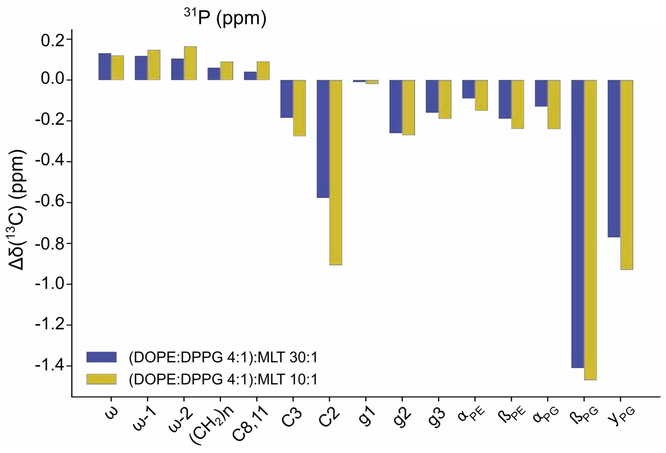
Solid-state NMR (ssNMR)

^{31}P @ MAS freq. of 10 kHz on a 700 MHz spectrometer



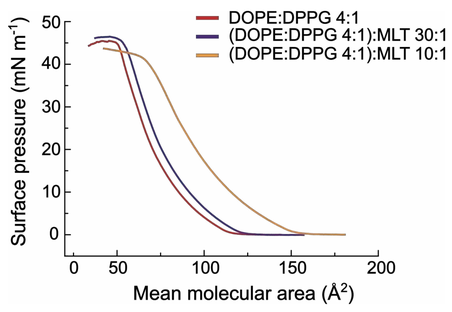
The ^{31}P-NMR experiments show a stronger interaction of the peptide with the **anionic group** of DPPG

The change in ^{13}C chemical shifts when melittin is introduced shows a favored interaction with the **C=O and DPPG headgroups**

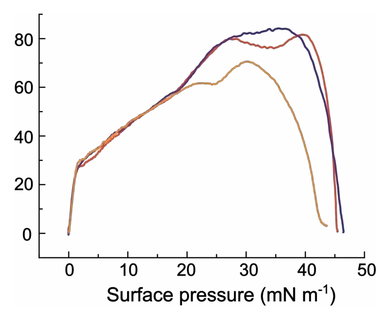


Langmuir-Blodgett (LB) technique

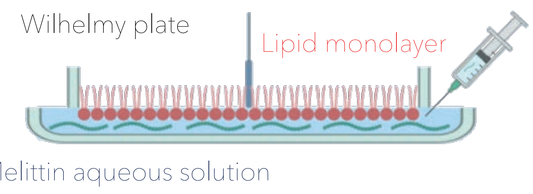
LB confirms the expansion of the lipid monolayer when melittin is present, as well as a decrease in the overall rigidity of the system



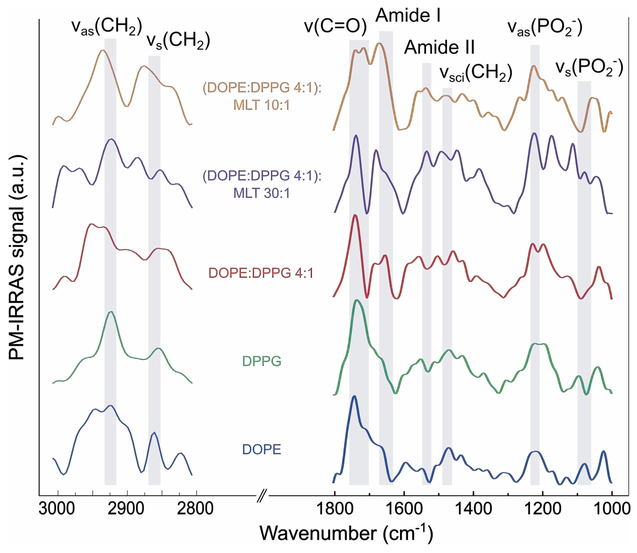
Surface pressure – Area isotherms



Compressibility modulus



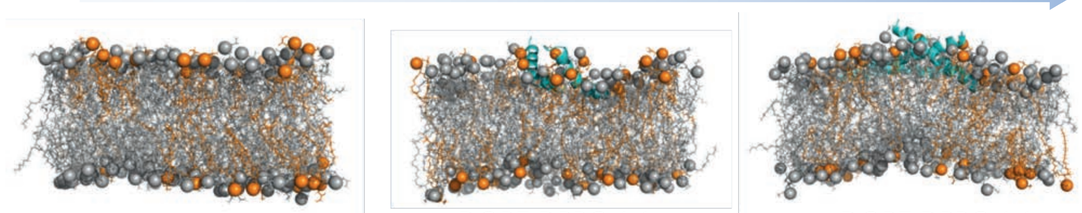
PM-IRRAS shows an increase in the **disorder of the acyl chains** proportional to the melittin concentration, as well as **higher hydration of the C=O and PO_2^- groups**



The position of melittin's amide I and amide II bands confirms its **α-helical** conformation when in contact with the lipid monolayer

Molecular Dynamics

Melittin concentration



DOPE:DPPG 4:1

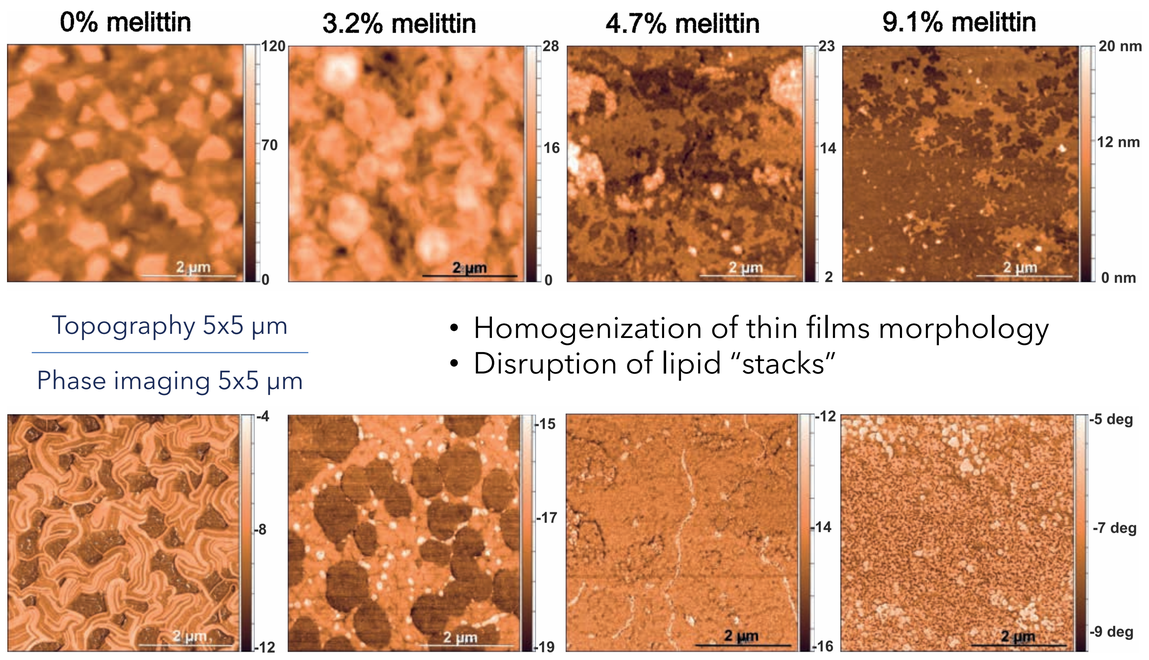
DOPE:DPPG 4:1
2 melittin chains

DOPE:DPPG 4:1
4 melittin chains

Membrane thickness - Order parameters

Area per lipid - Diffusion coefficient

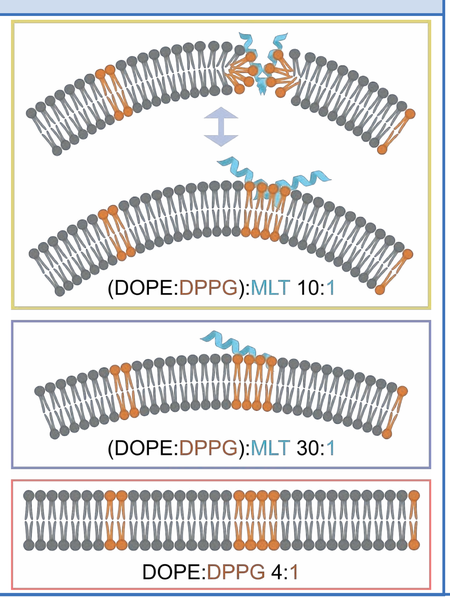
Atomic force microscopy (AFM)



- Homogenization of thin films morphology
- Disruption of lipid "stacks"

Conclusions

- Increase in melittin content increases **acyl chain disorder and water penetration.**
- Predominant interaction with the **carbonyl groups** of phospholipid bilayer.
- Predominant interaction with the **anionic phosphate group.**
- Melittin causes acts via a **concentration-dependent mechanism**: nonspecific permeabilization at low concentrations, and kinetic defects at higher concentrations.



This work was developed within the scope of the project CICECO-Aveiro Institute of Materials, UIDB/50011/2020 (DOI 10.54499/UIDB/50011/2020), UIDP/50011/2020 (DOI 10.54499/UIDP/50011/2020), and LA/P/0006/2020 (DOI 10.54499/LA/P/0006/2020) financed by national funds through the FCT/MEC (PIDDAC). The NMR spectrometers are part of the National NMR Network (PTNMR) and are partially supported by the Infrastructure Project 022161 (cofinanced by FEDER through COMPETE 2020, POCI and PORL and FCT through PIDDAC). This work has received funding from the European Research Council (ERC) under the European Union's Horizon 2020 research and innovation program (Grant Agreement 865974), and from CNPq and FAPESP (2025/27044-5 and 2020/15571-7) (Brazil). This poster is based upon work from COST Action CA23111, supported by COST (European Cooperation in Science and Technology).

Design and characterization of monoclonal antibody peptide mimics

Laïs CALLO[1,2], Océane RICLOUX[1], Quentin LAURENT[1], Liliane GUERENTE[1], Véronique FRACHET[2] & Didier BOTURYN[1]

[1] *University Grenoble-Alpes, CNRS, DCM UMR 5250, 38058 Grenoble Cedex 9, France*

[2] *Institute for Advanced Biosciences, Grenoble, France*

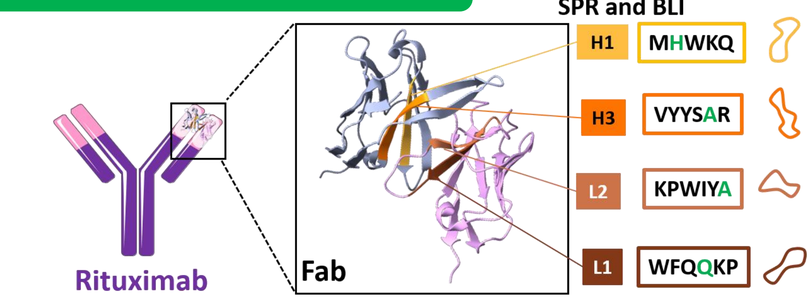
lais.callo@univ-grenoble-alpes.fr

https://doi.org/10.17952/38EPS.2026.P215

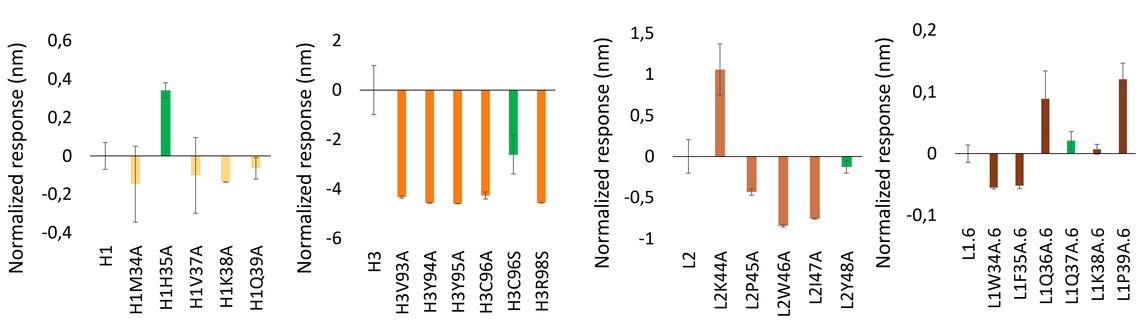
Introduction

Since their introduction in the 1990s, **monoclonal antibodies** (mAbs) have emerged as **essential therapeutic agents**, although their clinical use can be limited by factors such as restricted tissue penetration and immunogenicity. To address these challenges, we are developing **peptide-based mimics of Rituximab** designed to target the CD20 antigen, a key marker in immunotherapy. These mimics consist of **selected peptide sequences** assembled onto a **multivalent scaffold** to enhance target recognition. Their binding to CD20 is characterized using sensitive biophysical techniques, including **BLI** and **SPR**, while their specificity is further assessed through **biological assays**.

Study of RTX/CD20 interaction



- **Identification of key residues** involved in the RTX/CD20 interaction by ***ala-scan***



***Ala-scan* results obtained on a BLI biosensor.** Normalized responses were calculated by subtracting the R_{max} of the *wt* peptide. R_{max} values were determined using the Steady State model.

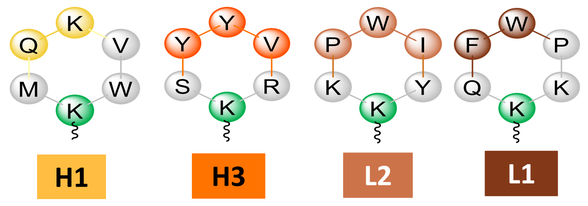
- **Aromatic** (W, F, Y) and **basic** residues (K, R) are critical for binding

	Essential amino acids
Heavy chain	K^{38}, V^{93}, Y^{94}, Y^{95}, C^{96}, R^{98}
Light chain	W^{34}, F^{35}, P^{45}, W^{46}, I^{47}, Y^{48}

Design of RTX mimics

Recognition Elements:

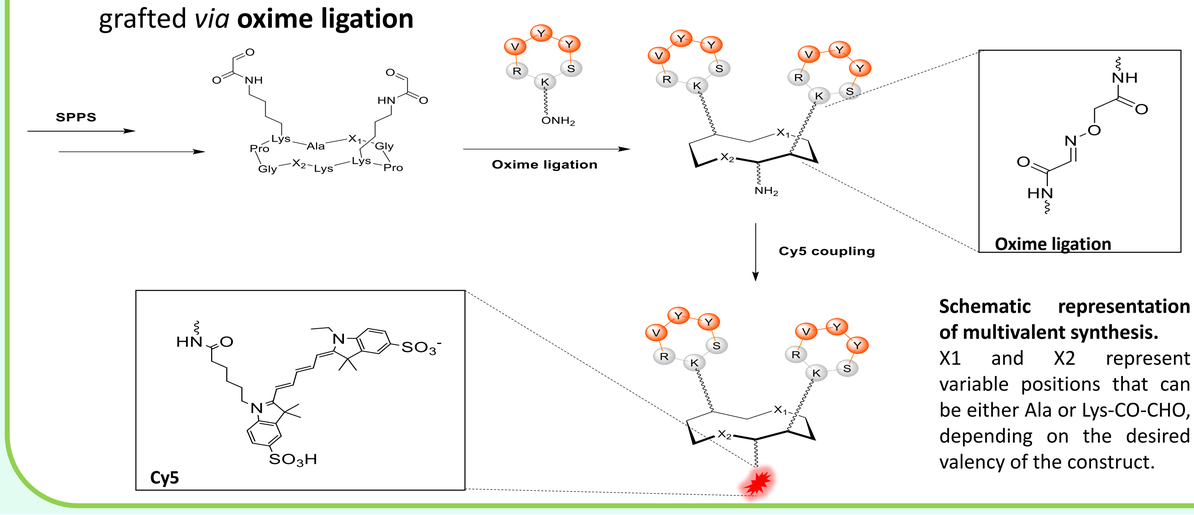
- **Selected cyclohexapeptides** synthesized *via* **SPPS**
- **Non-essential residue** were replaced by a **modified lysine for anchoring** to multivalent scaffolds



Recognition peptide derived from the RTX paratope, engineered for grafting onto a peptidic scaffold. Modified lysines are shown in green. Other colored amino acids highlight the most critical side chains for CD20 binding.

Multivalent Constructs:

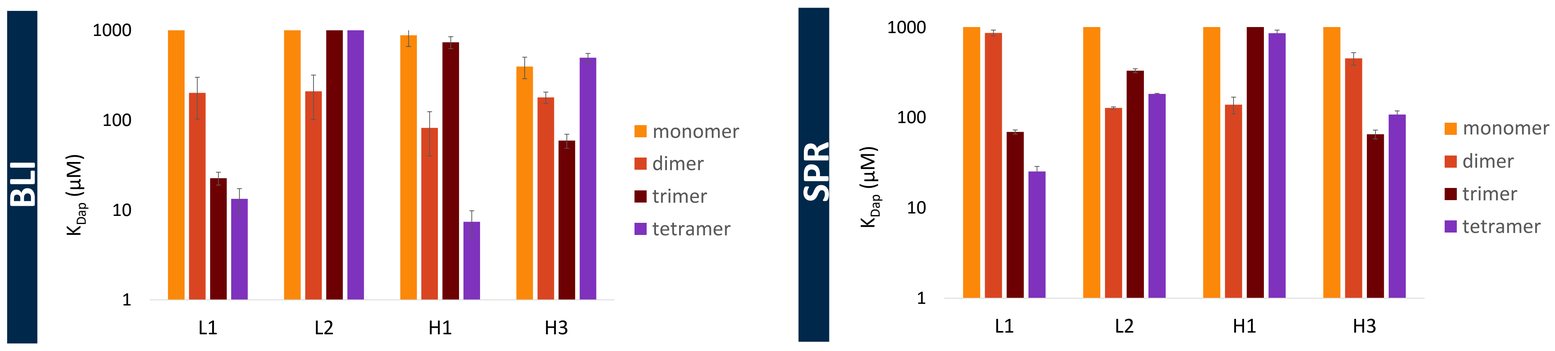
- **Decapeptide scaffolds** synthesized by **SPPS**
- Cyclopeptides mimicking RTX paratope were grafted *via* **oxime ligation**
- Multivalent mimics contain **2 to 4 copies of the same motif**



Schematic representation of multivalent synthesis. X1 and X2 represent variable positions that can be either Ala or Lys-CO-CHO, depending on the desired valency of the construct.

Evaluation of RTX mimics *in vitro*

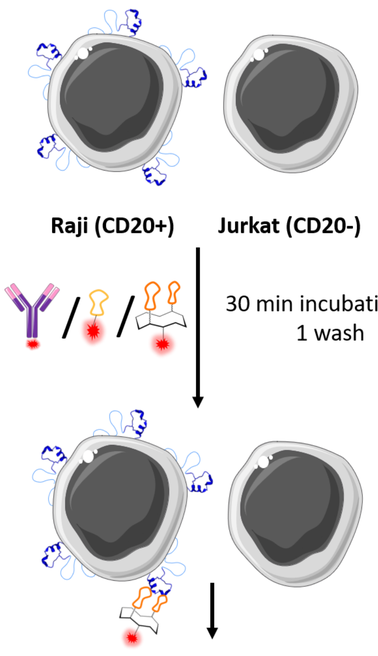
- **BLI** and **SPR** assays on biomimetic surfaces developed in the laboratory [1,2]
- **Dimerization** significantly **increased** binding affinity (statistical rebinding)
- **L1** displayed a **synergic effect** upon multimerization
- Tri- and tetrameric forms of L2, H1, and H3 exhibited limited improvement, likely due to intramolecular constraints



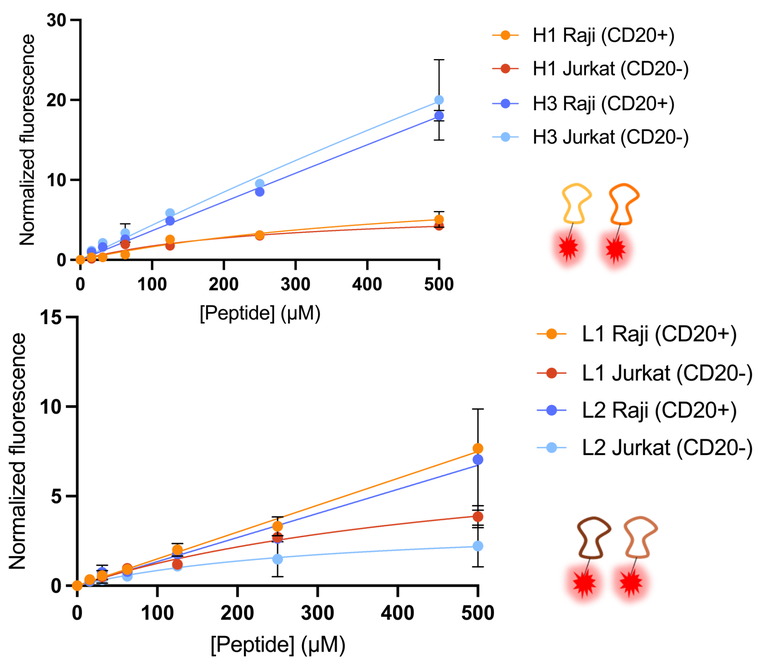
Evaluation of mimic affinity by Biolayer Interferometry and Surface Plasmon Resonance. The K_{Dapp} were determined *via* the Steady State (SS) model. n = 3

Evaluation of RTX mimics *in cellulo*

- **Flow cytometry performed** on Raji (CD20+) and Jurkat (CD20-) cell lines



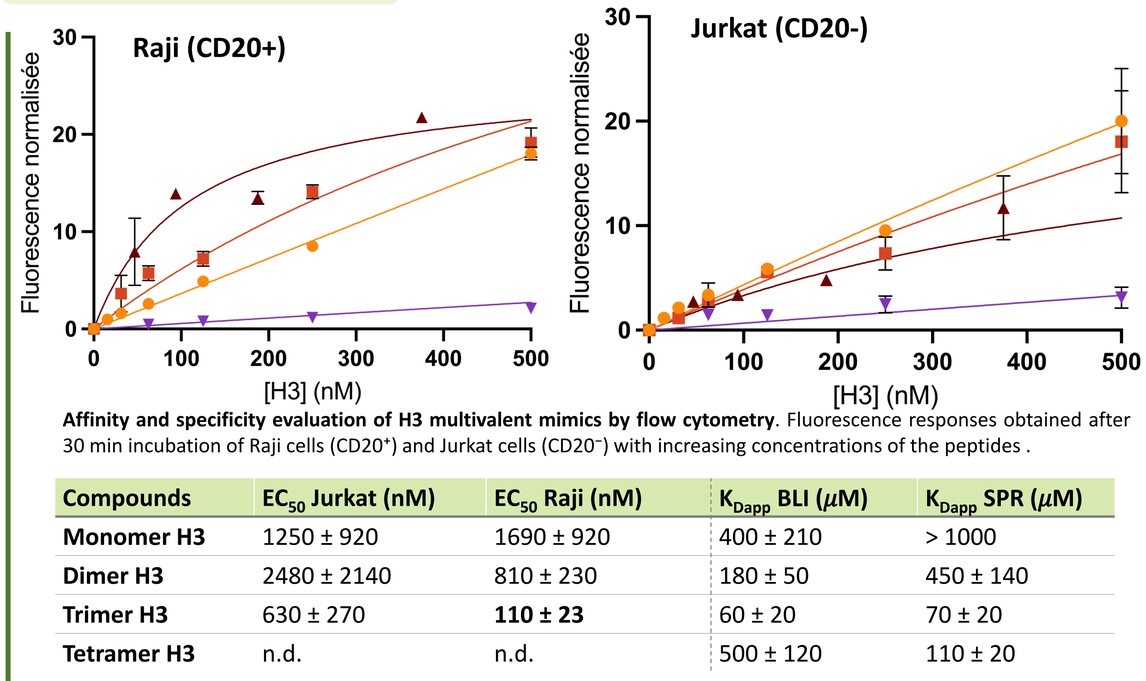
Monomers



Evaluation of monomer affinity and specificity by flow cytometry. Fluorescence responses obtained after 30 min incubation of Raji cells (CD20+) and Jurkat cells (CD20-) with increasing concentrations of the peptides .

- The **H3** cyclopeptide exhibits the **strongest response**
- H1 and H3 display non-specific binding
- **L1** and **L2** show **specificity toward CD20**

H3 multivalent mimics



Affinity and specificity evaluation of H3 multivalent mimics by flow cytometry. Fluorescence responses obtained after 30 min incubation of Raji cells ($CD20^+$) and Jurkat cells ($CD20^-$) with increasing concentrations of the peptides .

Compounds	EC_{50} Jurkat (nM)	EC_{50} Raji (nM)	K_{Dapp} BLI (µM)	K_{Dapp} SPR (µM)
Monomer H3	1250 ± 920	1690 ± 920	400 ± 210	> 1000
Dimer H3	2480 ± 2140	810 ± 230	180 ± 50	450 ± 140
Trimer H3	630 ± 270	**110 ± 23**	60 ± 20	70 ± 20
Tetramer H3	n.d.	n.d.	500 ± 120	110 ± 20

Comparison of cellular interaction parameters (EC_{50}) derived from flow cytometry experiments and apparent dissociation constants (K_{Dapp}) obtained by BLI and SPR. EC_{50} values were determined using a specific binding model (n = 2), whereas K_{Dapp} values were determined using the Steady-State (SS) model (n = 3).

- **Similar responses** observed by **BLI** and **SPR** experiments
- Monomer and tetramer show non-specific binding
- **Specific binding** observed with the **dimer**, and particularly with the **trimer**
- **Multimerization improves binding affinity and specificity**

Conclusion

1. **Rational identification of Rituximab paratope mimics :** four **key peptide sequences** were identified through an **Ala-scan**, highlighting the critical contribution of **some residues** to **CD20 binding**.
2. **Multimerization** resulted in a **significant increase in binding affinity**. It also **improved CD20 specificity especially for H3**, as demonstrated by **flow cytometry**.
3. **Promising cell specificity :** the **L1** and **L2** mimics showed **selective binding to CD20+ cells (Raji)**, with minimal interaction with CD20- cells (Jurkat), validated by **flow cytometry.**

Nexts steps

- **Perform biological assays on the L1 series to confirm the synergistic effect.**
- **Develop a Dynamic Combinatorial Library (DCL)** to identify the best-performing **heteromultimers**.

References

1. L. Bar et al, *Anal. Chem.* **2020**, *92*, 5396 – 5403.
2. O. Ricloux et al, *Anal. Chem.* **2026**, *98*, 19418 – 19426.

A Multifunctional Thermoresponsive Micellar Hydrogel System for Targeted Skin Depigmentation, Enhanced Dermal Penetration, and Extracellular Matrix Stimulation

Campos, Y. [1,2]; Cruz, L. J. [1]; Solís, Y. [1,2]; Aguilar, J.C. [1,2]; Esteruelas, G. [2]; Sanchez, E. [2] and Espina, M. [2].

[1]*Peptidepharma Nova S.L, Barcelona, Spain*

[2]*Department of Pharmacy, Pharmaceutical Technology and Physical Chemistry, Faculty of Pharmacy and Food Sciences of the University of Barcelona, Barcelona, Spain*

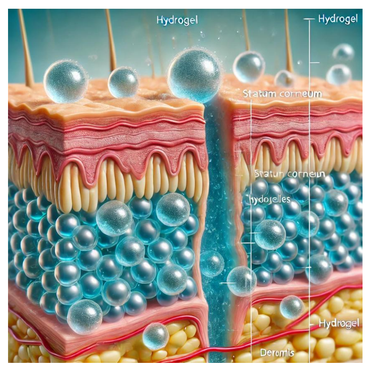
https://doi.org/10.17952/38EPS.2026.P405

Email: y.campos.mora@gmail.com

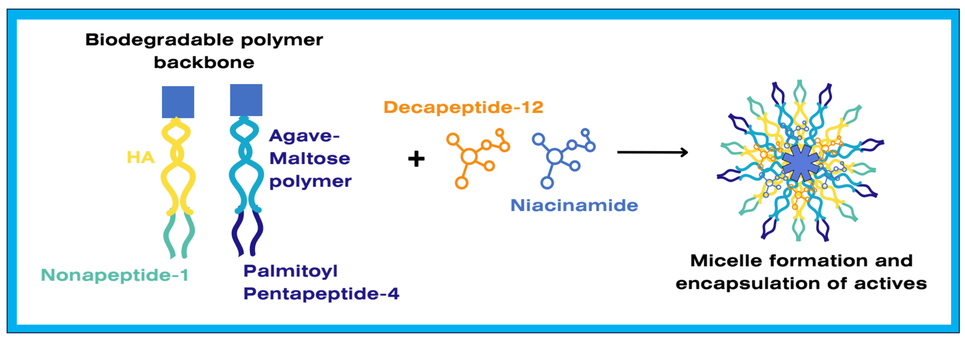
INTRODUCTION

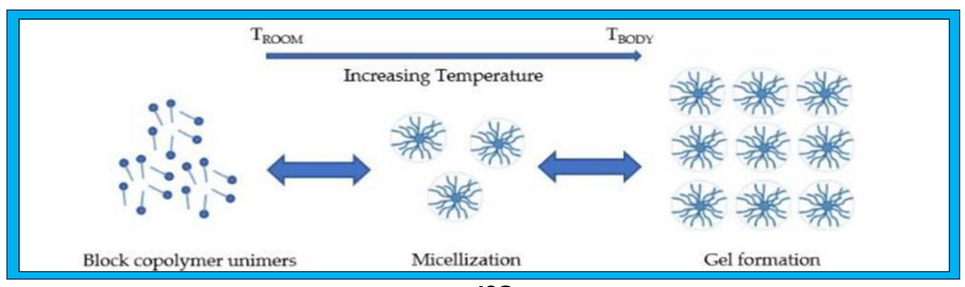
Skin hyperpigmentation and aging are closely associated with increased melanin production and degradation of the extracellular matrix. Advanced delivery systems are required to improve penetration, stability, and sustained release of active compounds.

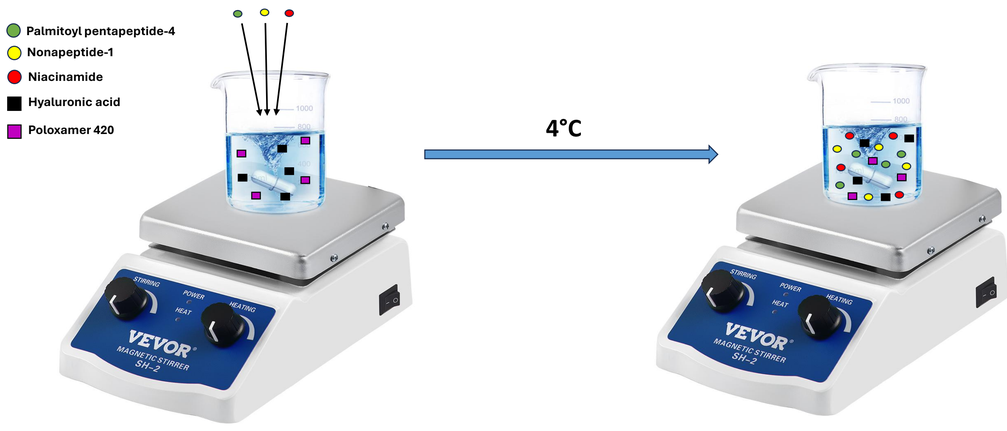
This study describes the development and evaluation of a thermoresponsive micellar hydrogel designed to enhance dermal delivery while providing combined depigmenting and anti-aging effects. The formulation is based on a micelle-forming polymeric system containing hyaluronic acid, niacinamide, and biomimetic peptides.

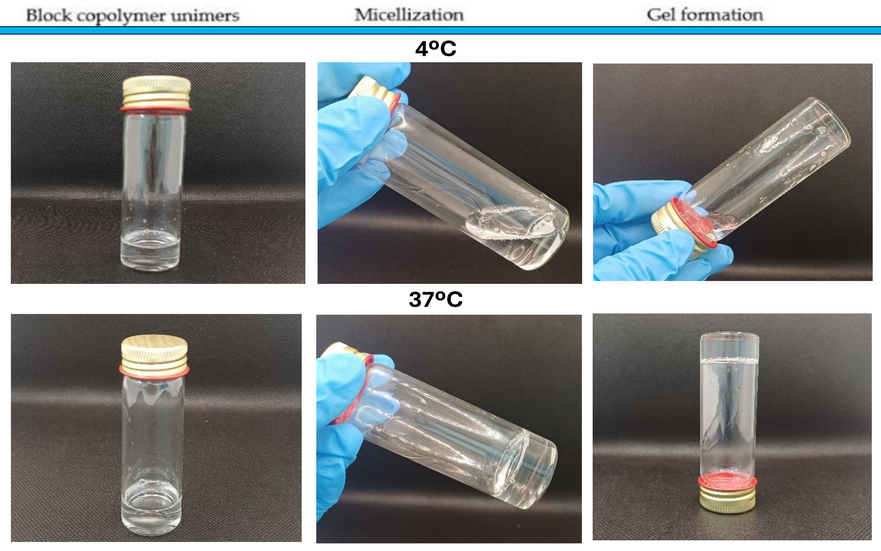


METHODS



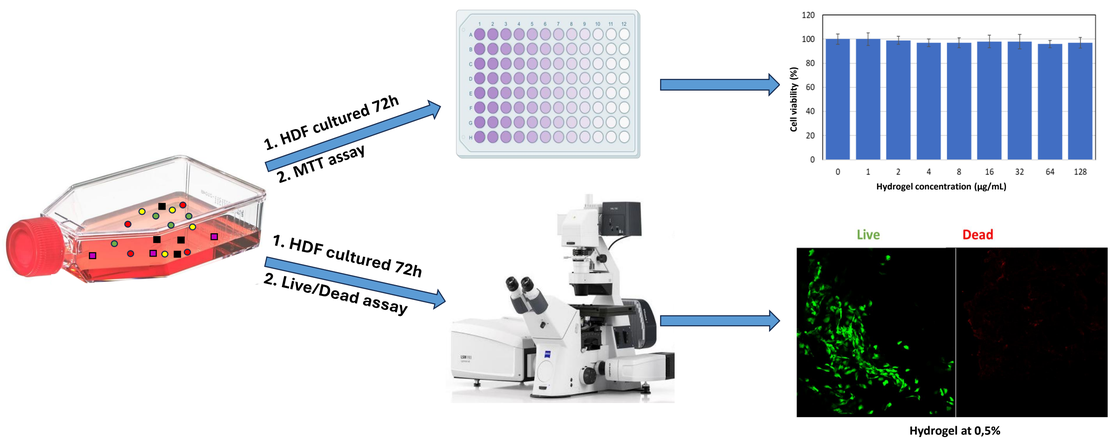




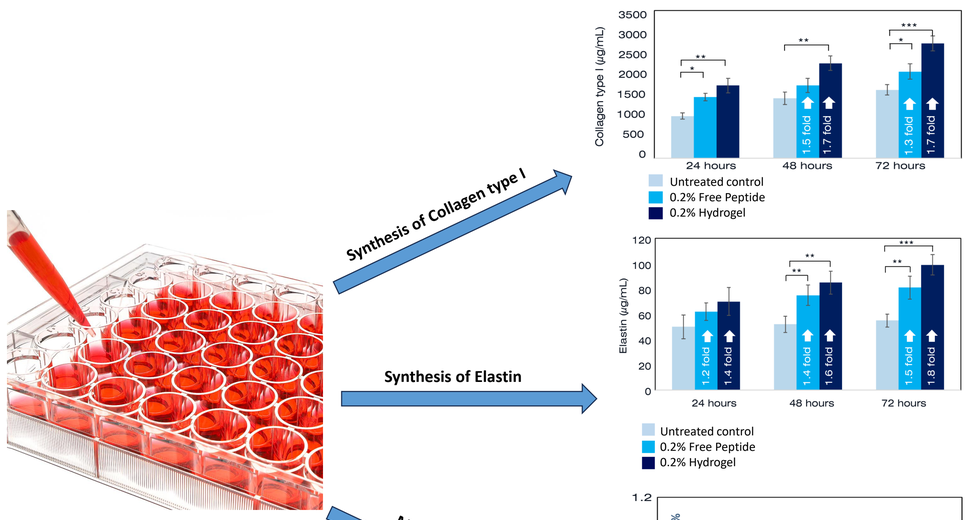


RESULTS

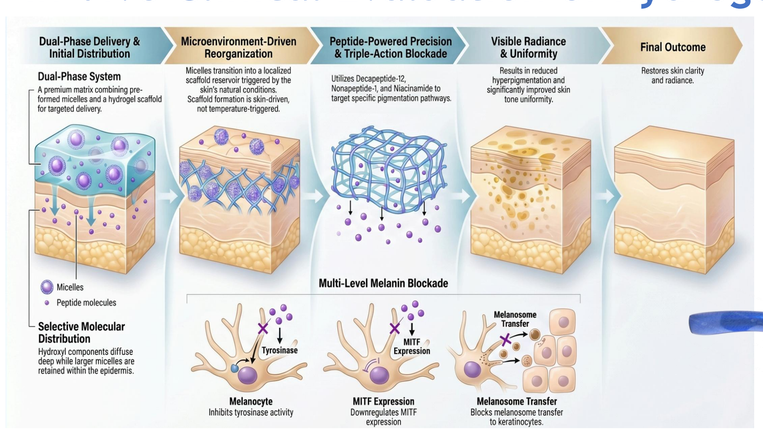
In vitro studies: Cytotoxicity and cell viability

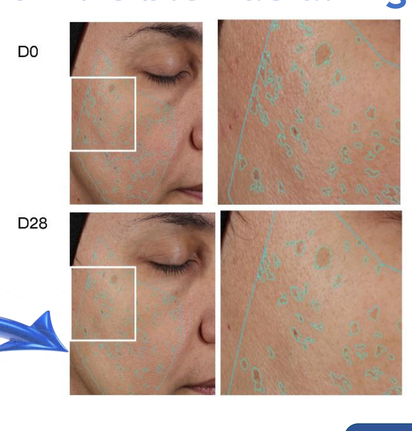


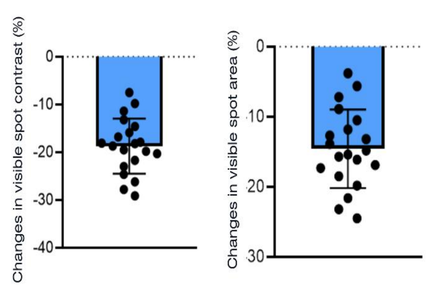
Extracellular matrix production



In Vivo Clinical Evaluation of hydrogel on Visible Facial Pigmentation







CONCLUSION

This thermoresponsive micellar hydrogel represents a promising multifunctional platform for skin depigmentation and anti-aging applications, combining efficient dermal delivery, sustained bioactive release, and clinically validated efficacy.

Acknowledgement

This work was supported by University of Barcelona granted from the Agency for Management of University and Research Aid (AGAUR) number 2024 DI 00117

Engineering the MALDI interface for in situ detection of modified peptides in synovial fluids : application to osteoarthritis diagnosis

U. PASCO[1], L. BERTHY[2], E. GROULT,[3] R. THAI[2], F. BEAU[2], D. NOEL,[3] L. DEVEL[2], G. SUBRA[1], S. CANTEL[1*]

[1] IBMM, Univ. Montpellier, ENSCM, CNRS, Montpellier, France; [2] CEA, INRAE, MTS, SIMoS, Université Paris-Saclay, Gif-sur-Yvette, France ;[3] IRMB, University of Montpellier, INSERM, CHU, Montpellier, France

ugo.pasco@umontpellier.fr ; sonia.cantel@umontpellier.fr ;

https://doi.org/10.17952/38EPS.2026.P248

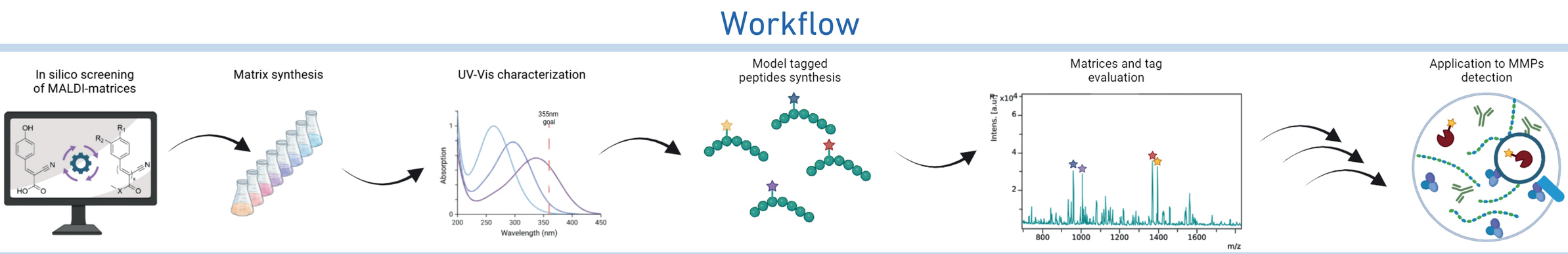
IBMM Institut des Biomolécules Max Mousseron

Introduction

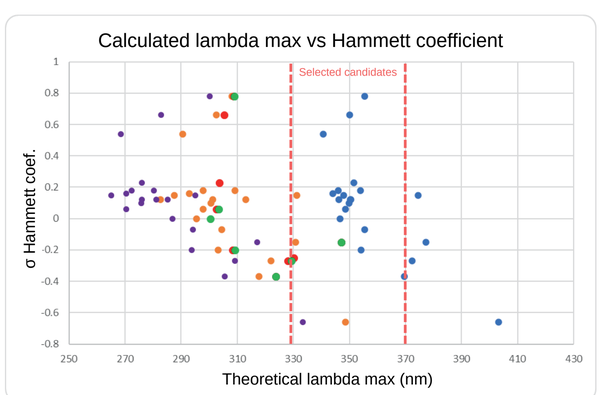
Osteoarthritis is one of the most common joint diseases, but its **treatment remains limited**, largely due to late diagnosis. It is usually detected only when pain appears, by which point significant tissue damage has already occurred.[1] This degradation is attributed to increased concentration of **active matrix metalloproteinases** (MMPs), making them promising **early biomarkers**, but their detection remains challenging because of their low abundance and the coexistence of inactive forms and active forms.[2,3]

Here, we present a sensitive and selective **MALDI-MS based approach** to detect active MMPs in synovial fluid. The method relies rational design of **aprotic MALDI matrices** combined with specific **mass-tag probes**, allowing selective **detection of active enzymes down to the nanomolar range**.[4] This approach highlights the potential of tailored MALDI-MS strategies for early OA biomarker detection.

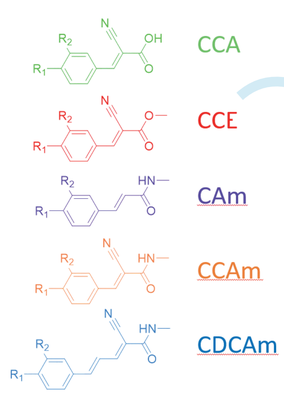
Workflow



Screening of five classes of molecules (n=79)

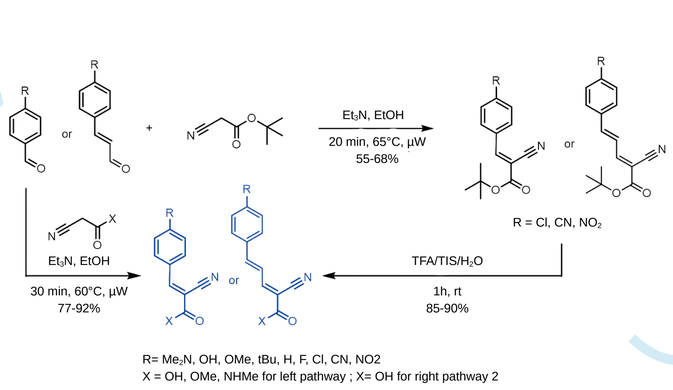


Graph showing predicted lambda max of 79 molécules over Hammett coef.[5] DFT used for geometry optimization and TD-DFT for excited states energies and lambda max calculation using B3LYP/def2-SVG as functional and basis



R1 = NH_2, OH, OMe, tBu, CH_3, H, F, $SiCH_3$, CH_2Cl, SH, CH_2CN, I, Cl, CF_3, CN, NO_2
R2 = OMe, OH, SCH_3, CH_2CN

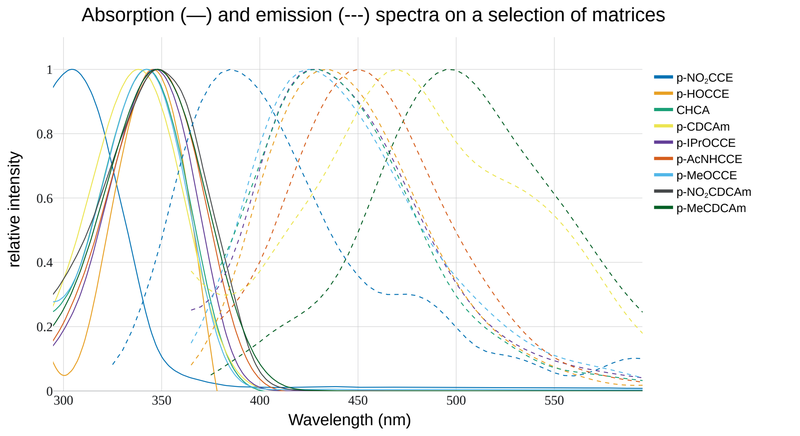
Synthesis of selected candidates (n=30)



R= Me_2N, OH, OMe, tBu, H, F, Cl, CN, NO2
X = OH, OMe, NHMe for left pathway ; X= OH for right pathway 2

Synthetic pathways of selected matrices and tags. For acidic matrices and tags with strong para-EWG, protection was necessary to prevent decarboxylation.

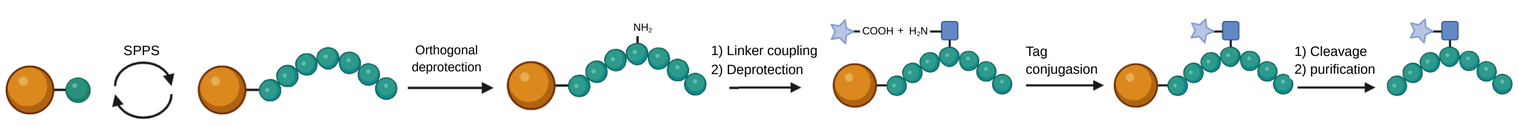
UV-Visible characterization (n=16)



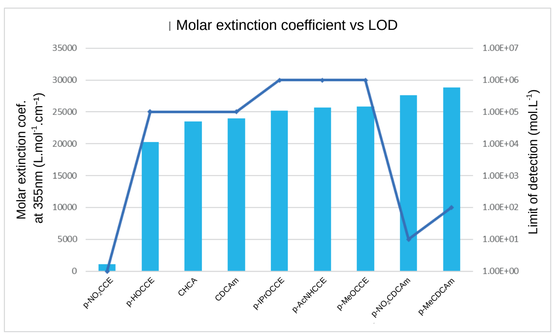
Emission spectra were recorded from 200 to 800 nm and normalized to the maximum absorption of each compound. The emission scans were collected from λmax +30 nm to 800 nm, using an excitation wavelength set to each compound's maximum absorption wavelength.

Matrices and tags evaluation (n=9)

Model peptides synthesis



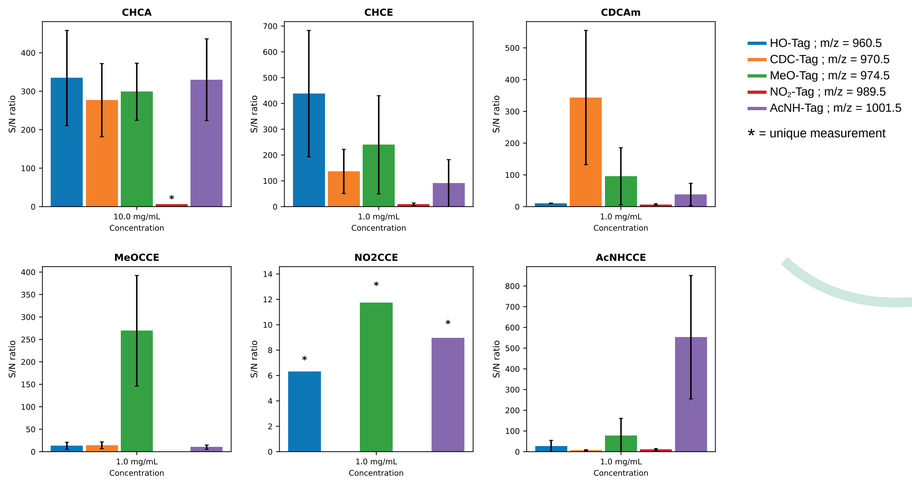
LODs measurement



Molar extinction coefficients were measured at 355 nm from 5-point calibration curves (n=3 per point). Limits of detection (LOD) were determined by serial dilution of the pure peptide (10^{-7}-10^{-14} M) analyzed on CHCA (10 mg/mL) and the corresponding para-substituted matrix (1 mg/mL). Results are expressed as fold-increase in sensitivity relative to CHCA

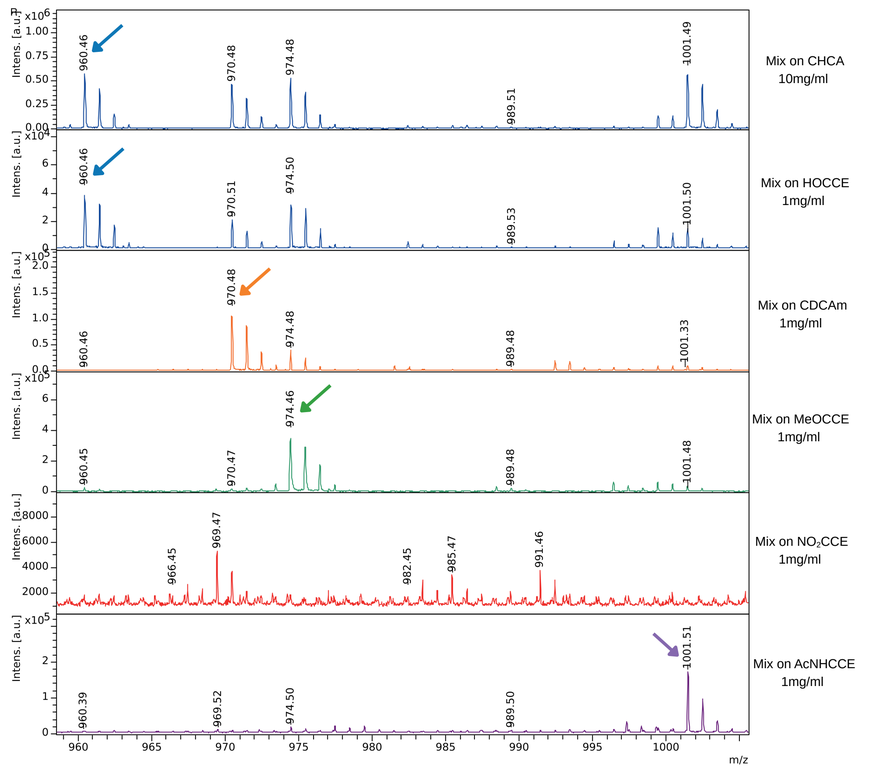
A higher molar extinction coefficient initially results in a higher limit of detection. However, above 27000 L·mol⁻¹·cm⁻¹, the limit of detection decreases, potentially due to matrix effects and/or photodegradation of the mass tag.

Ionisation selectivity



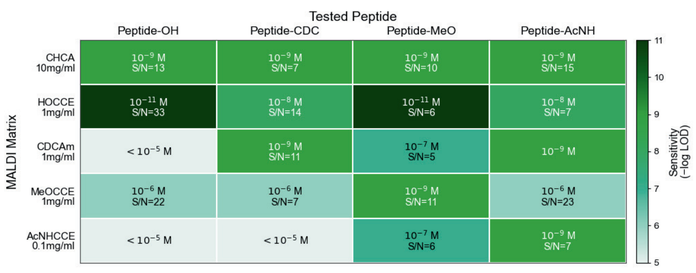
S/N ratios for each tagged peptide were extracted from MALDI spectra. An equimolar peptide mix at 10^{-7}M was analyzed on 6 different matrices : CHCA 10mg/ml and engineered ones at 1 mg/mL, using the same substitutions as the tags (3 replicates per condition). Bars represent individual tags; boxes represent matrices.

MALDI-MS spectra

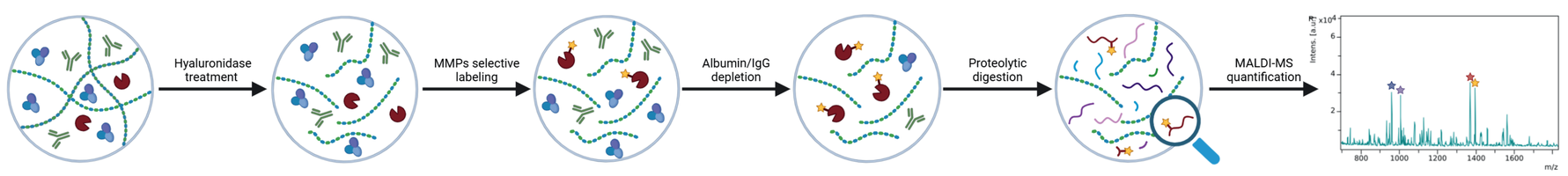


Application to MMPs detection in OA (n=4)

Heatmap of peptide's LODs in synovial fluid



Treatment of synovial fluid for MALDI-MS analysis



Synthetic synovial fluid was purchased to optimize our treatment pipeline. Viscosity was first reduced from 0.1 to 0.01 Pa·s using hyaluronidase (1 µg/ml). Tailored affinity-based probes[5] (AfBPs) were then used for selective labeling of hMMPs (37°C, 1 µM, 4h), followed by immunodepletion of albumin and gamma globulins to simplify the medium (from 0.7 g/l to 10 µg/ml). Samples were then digested with trypsin (1:16 enzyme/protein ratio, 2h, 50°C) followed by chymotrypsin (1:32, 2h, 50°C). Samples are then desalted on zip-tip column and analysed in MALDI mass spectrometry.

Take home messages

Matrix design

Among 79 screened structures, 30 were synthesized and 9 selected for MALDI-MS evaluation. Lamdba max were predicted with a mean error of 10nm.

Matrix and tag interplay

High molar extinction coefficients did not systematically translate into improved MALDI performance, with optimal performance observed around 25,000 L·mol⁻¹·cm⁻¹.

Biological application

A synovial-fluid treatment pipeline was established, enabling LOD determination of peptides bearing the four best-performing tags.

Perspectives

Validation in human synovial fluid samples and extension of the approach to active MMP profiling for early osteoarthritis detection.

References

[1] Mobasheri, A. et al. Biomarkers for osteoarthritis: Current status and future prospects. Best Practice & Research Clinical Rheumatology 37, 101852 (2023). **[2]** Stamenkovic, I. Extracellular matrix remodelling: the role of matrix metalloproteinases. The Journal of Pathology 200, 448–464 (2003). **[3]** Almeida, L. G. N. de et al. Matrix Metalloproteinases: From Molecular Mechanisms to Physiology, Pathophysiology, and Pharmacology. Pharmacological Reviews 74, 714–770 (2022). **[4]** Berthy, L. et al. Proximity-Induced Transfer of a Mass Tag Enables Direct Profiling of Active Matrix Metalloproteases. Angewandte Chemie International Edition 65, e23132 (2026). **[5]** Hansch, Corwin., Leo, A. & Taft, R. W. A survey of Hammett substituent constants and resonance and field parameters. Chem. Rev. 91, 165–195 (2002).

https://doi.org/10.17952/38EPS.2026.P058

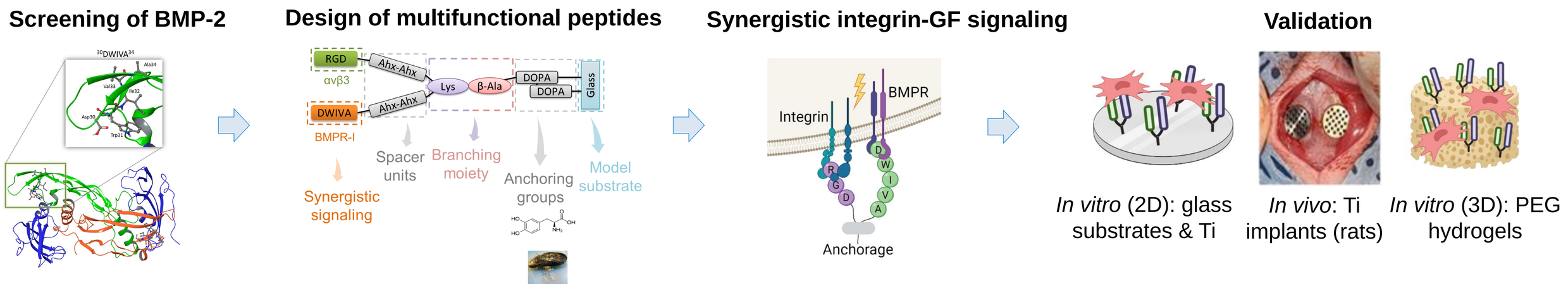
Modulating Integrin and Growth Factor Signaling with Synthetic Peptides: a New Paradigm in Regenerative Medicine

Carlos Mas-Moruno[1,2,3*]

[1]Biomaterials, Biomechanics and Tissue Engineering Group, Department of Materials Science and Engineering, and Institute for Research and Innovation in Health (IRIS), Universitat Politècnica de Catalunya (UPC), Barcelona, Spain; [2]Barcelona Research Center in Multiscale Science and Engineering, UPC, Barcelona, Spain; [3]Centro de Investigación Biomédica en Red, CIBER-BBN, Madrid, Spain

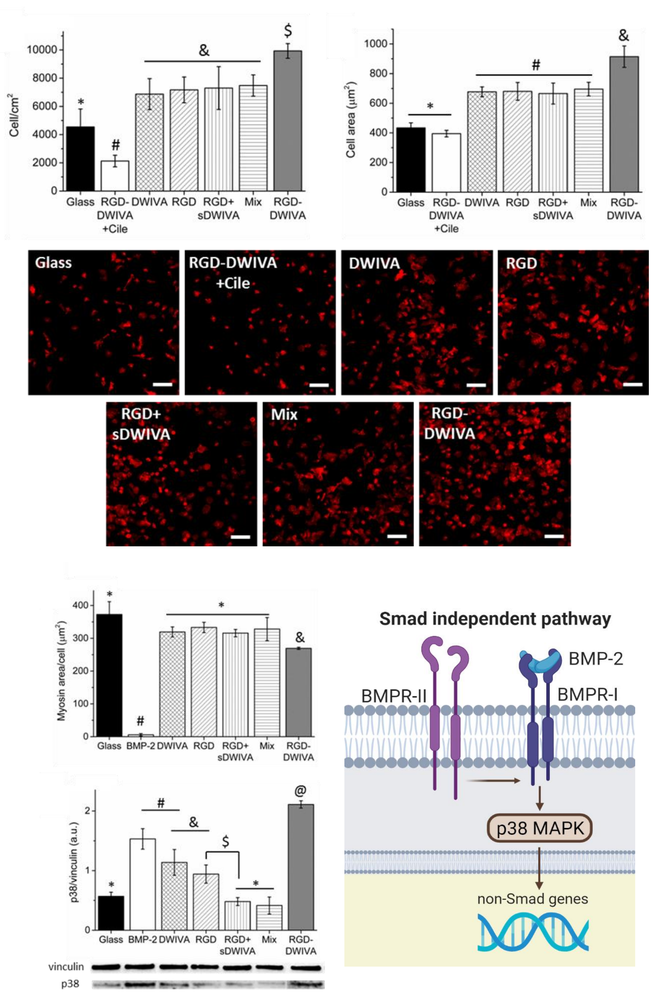
* email: carles.mas.moruno@upc.edu

Background & Aim: Recreating the cellular microenvironment that promotes integrin and growth factor (GF) signaling is a major goal to trigger bone regeneration.[1] However, the use of GFs, such as bone morphogenetic protein 2 (BMP-2), entails clinical risks. Thus, the aim of this study was to combine integrin-binding ligands together with osteogenic peptides derived from BMP-2 to recapitulate the healing microenvironment of bone and foster its regeneration.



Results & Discussion:

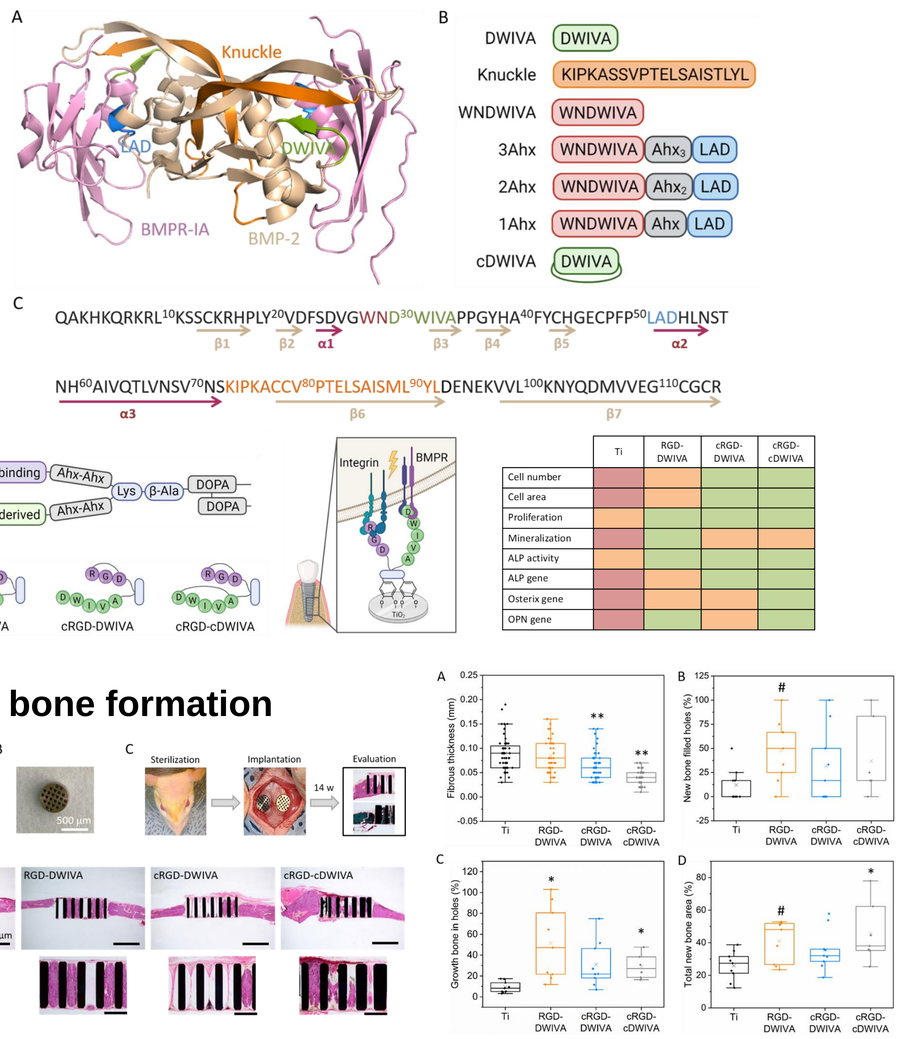
Model glass substrates (C2C12 cells)[2]



✓ **Synergistic signaling (geometry)**

✓ **αvβ3-mediated & P38-mediated**

Ti: *in vitro* (MSCs) & *in vivo* (rat calvarial defect)[3]

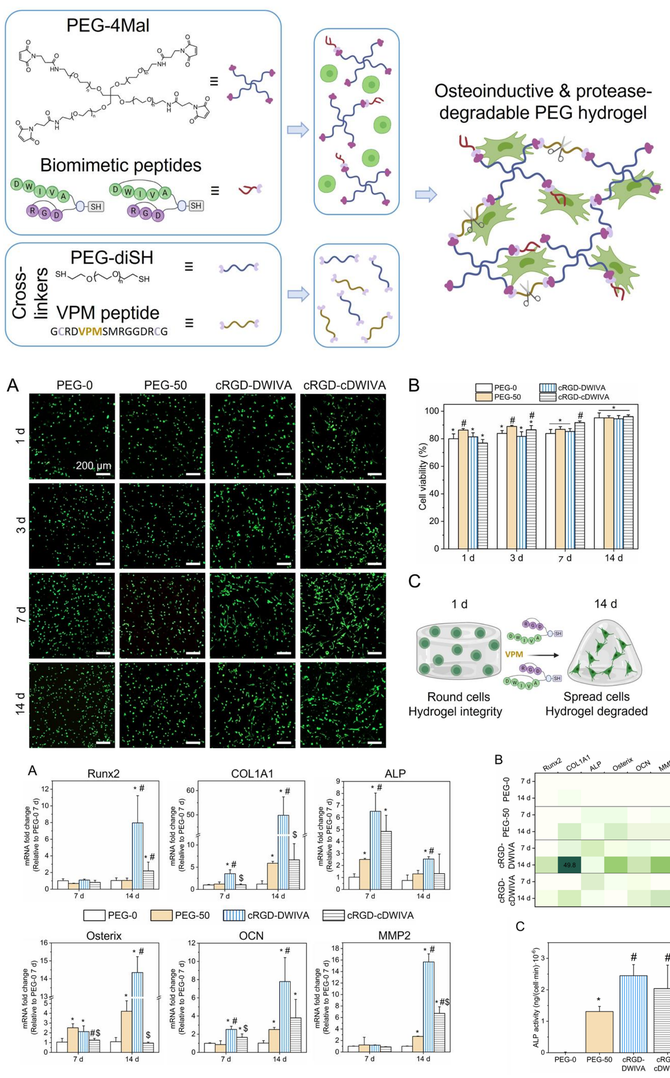


In vivo bone formation

✓ **Improved osteodifferentiation**

✓ **Enhanced new bone formation *in vivo***

Protease-degradable PEG hydrogels[4]



✓ **Improved cell adhesion & differentiation (stimuli-responsive)**

Conclusions: These results prove the biological potential of recreating the ECM and engaging in integrin and GF crosstalk via synthetic peptides. This biomimetic strategy holds promise in bone tissue engineering, without the need for exogenous GFs.

References:

[1] *Adv. Sci.* **2026**, 14782; [2] *Adv. Healthcare Mater.* **2021**, *10*, 2001757; [3] *Adv. Healthcare Mater.* **2022**, *11*, 2201339; [4] *Front. Bioeng. Biotechnol.* **2023**, *11*, 1192436.

Acknowledgements: This work was supported by the European Union's Horizon 2020 (grant Agreement No. 872869) and the Agencia Estatal de Investigación (MICIU/AEI/10.13039/501100011033) through grant PID2023-148538OB-I00 and the Maria de Maeztu Units of Excellence Programme CEX2023-001300-M.

38th EPS European Peptide Symposium
6 - 11th of September 2026
Vienna, Austria

Novel melanogenesis-modulating peptides for dermocosmetic applications

Carmen Gallo[a,b], Fosca Errante[a,b], Cristina Luceri [b], and Paolo Rovero[a,b]

[a] *Interdepartmental Research Unit of Peptide and Protein Chemistry and Biology, University of Florence, Via Ugo Shiff, 6 -Sesto Fiorentino (FI), Italy.*
[b] *Department of Neuroscience, Psychology, Drug Research and Child Health (NEUROFARBA), University of Florence, Viale Pieraccini, 6 - Firenze (FI), Italy.*

E-mail: carmen.gallo@unifi.it

https://doi.org/10.17952/38EPS.2026. P120

Background

Melanogenesis is the process by which melanin is synthesized in melanocytes and transferred to keratinocytes, contributing to skin color and UV protection. Altered melanogenesis can lead to **hyper-** or **hypopigmentation disorders**, often associated with psychological distress. Current pigmentation-modulating agents frequently show poor bioavailability or cytotoxicity, highlighting the need for safer alternatives. **Peptides** represent **promising dermocosmetic ingredients** due to their tunable stability, specificity, and safety. **AIMP1** (Aminoacyl-tRNA synthetase complex-interacting multifunctional protein 1) is a multifunctional protein with distinct biological domains.[1] A peptide corresponding to residues **6–46** of AIMP1 (AdP) was reported to **reduce melanin content and tyrosinase activity in melanocytes**.[2] However, AdP may also promote fibroblast proliferation, an undesirable effect in cosmetic applications.

Aim of the project

This PhD project aims to **identify minimal AIMP1-derived peptide sequences that modulate melanogenesis while avoiding fibroblast-proliferative activity,** enabling the development of safe and effective dermocosmetic peptides.

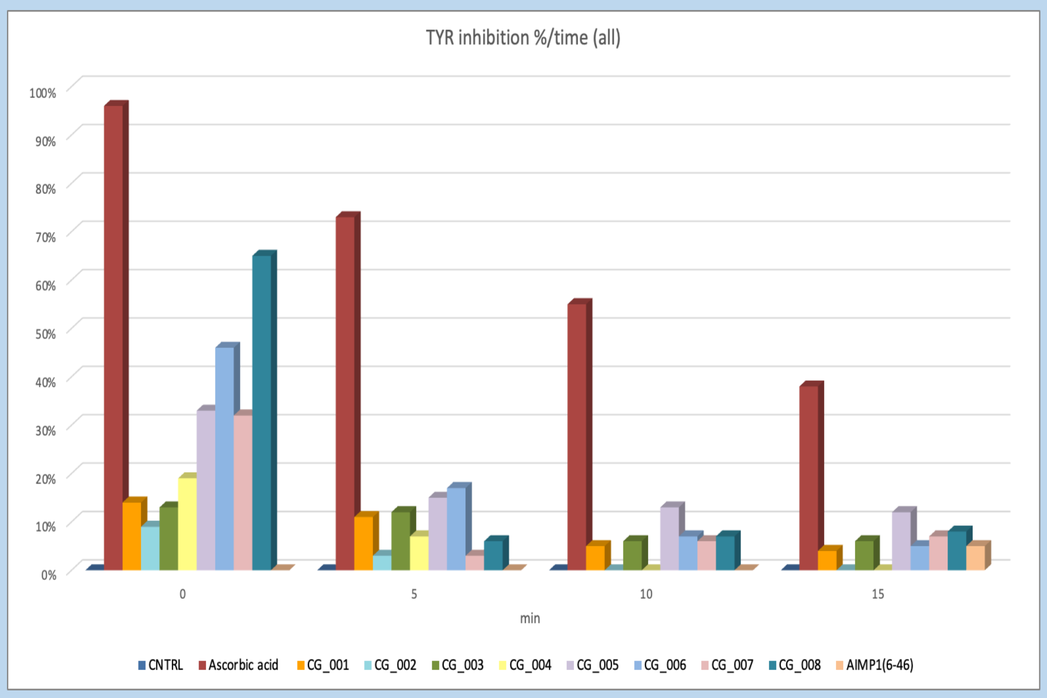
Peptides Design and Synthesis

Eight overlapping peptides spanning the AIMP1(6–46) region were designed to map melanogenesis-regulating domains. Peptides were synthesized by **solid-phase peptide synthesis** (SPPS), purified by RP-HPLC or flash chromatography, and characterized by RP-HPLC and mass spectrometry, achieving purities >95%.

Tyrosinase Inhibition Assay

Peptides were initially screened using a mushroom tyrosinase assay with L-DOPA as substrate.[3] Enzyme activity was monitored spectrophotometrically at 475 nm. **Ascorbic acid** was used as a **positive control**.

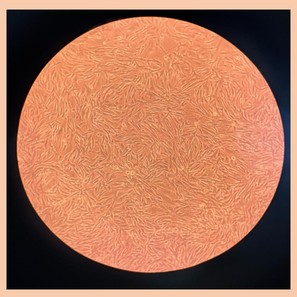
Key finding: **None of the peptides**, including AIMP1(6–46), **showed significant tyrosinase inhibition**, suggesting that melanogenesis modulation may occur through indirect or non-enzymatic mechanisms.



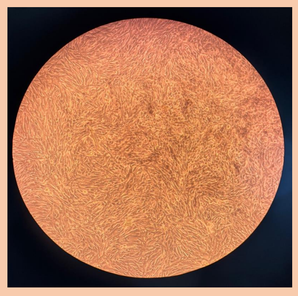
Melanin Content Assay

B16F10 mouse melanoma cells were used to evaluate melanogenesis-related effects. Cells were treated with peptides or **α-MSH** as a **positive control**. Melanin content was quantified spectrophotometrically at 405 nm.

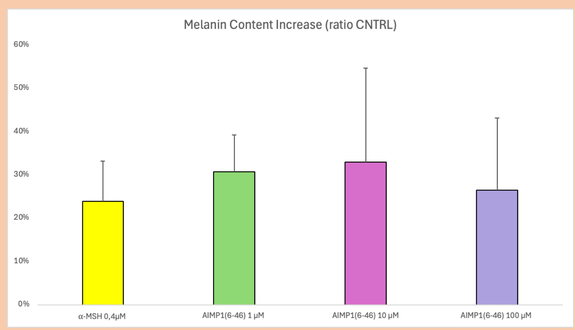
Key Findings: Parent **AIMP1(6–46)** peptide significantly **stimulated melanin content** at 10 μM. Interestingly, **screening of the eight overlapping peptides revealed divergent biological activities**. Certain fragments induced a strong, decrease in melanin production, whereas others stimulated synthesis.

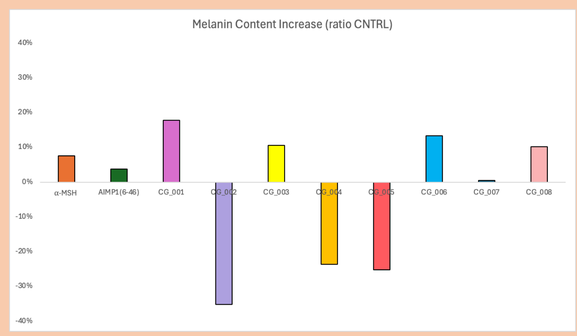


CNTRL



TRT





Conclusions

Our results showed that **AIMP1-derived peptides do not directly inhibit mushroom tyrosinase**, suggesting that their effects on melanogenesis may involve **cell-mediated mechanisms** rather than direct enzyme inhibition. Interestingly, the screening of the **overlapping peptides revealed opposite effects on melanin production**, with different fragments showing either stimulatory or inhibitory activities. These findings highlight the potential of AIMP1-derived sequences as **melanogenesis modulators** and provide a basis for further investigation of the mechanisms underlying their distinct biological effects.

References

[1]J. M. Han et al., *Biochem. Biophys. Res. Commun.* **2006**, *342(1)*, 113–118.
[2] J. Kim et al., *J Cosmet Dermatol.* **2019**; *18(1)*, 251-257.
[3] Y.Y. Liu et al., *Fish Physiol Biochem.* **2017**; *43(2)*, 517-525.

Acknowledgements

Carmen Gallo is the recipient of a PhD fellowship D.M. 630/2024 "Sviluppo di nuovi peptidi modulatori della melanogenesi per applicazioni dermocosmetiche", XL Cycle in Area del Farmaco e Trattamenti Innovativi, supported in part by Istituto Ganassini S.p.A. di Ricerche Biochimiche, Milano, Italy.

PeptiDesCalculator 2.0: a next-generation descriptor platform for peptide informatics, sequence analysis, and QSAR modeling

Laureano E. Carpio[1], Rafael Gozalbes[1,2] & Eva Serrano-Candelas[2]

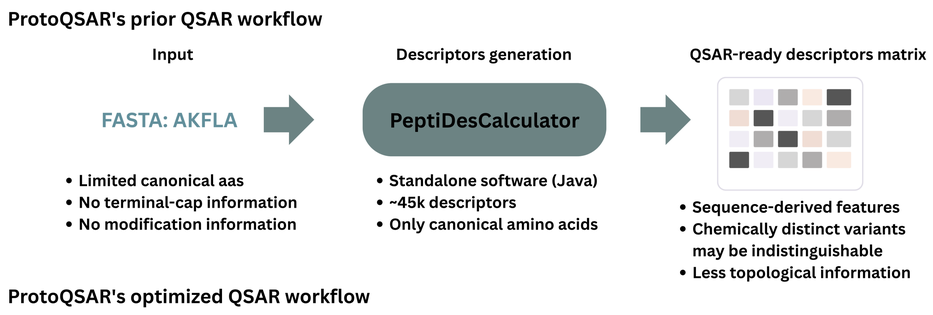
[1]*MolDrug AI Systems, Technological Park of Valencia, Spain*
[2]*ProtoQSAR, Technological Park of Valencia, Spain*

Email: lcarpio@moldrug.com

https://doi.org/10.17952/38EPS.2026.P256

Introduction

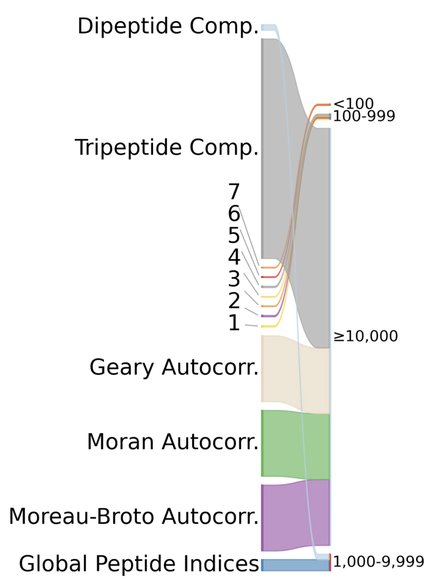
Peptides are increasingly relevant therapeutic modalities due to their high selectivity, structural diversity and broad biological applicability[1]. However, their computational representation for Quantitative Structure-Activity Relationships (QSAR) modelling and predictive purposes remains challenging because peptide properties depend not only on amino acid composition, but also on sequence order, residue-level physicochemical patterns, stereochemistry and chemical modifications. Conventional molecular descriptors do not explicitly capture many of these peptide-specific features, while existing sequence-based tools are frequently restricted to canonical amino acids[2,3]. Therefore, extensible and peptide-centered descriptor frameworks are required to support sequence analysis, chemical interpretation and machine learning-driven discovery.



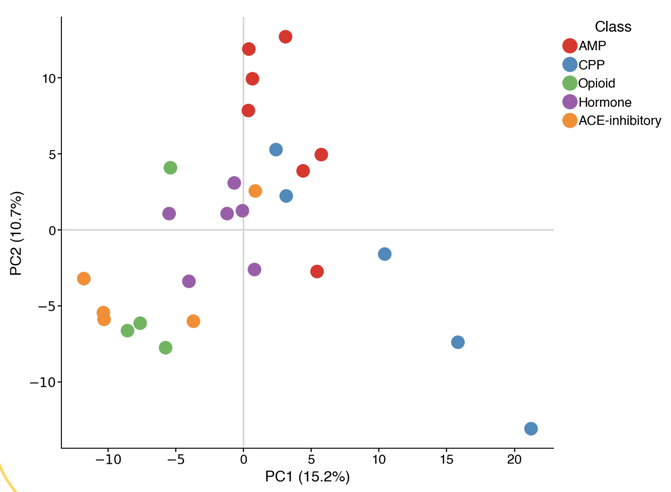
Results

1. PeptiDesCalculator 2.0 provides a modular universe of 127,840 descriptors

The Java engine was reimplemented in Python as a modular framework comprising **13 descriptor families and up to 127,840 variables**. Tripeptide composition and sequence autocorrelations account for most of the descriptor universe, while smaller families provide complementary information.



2. Multi-family descriptors capture chemically meaningful peptide diversity



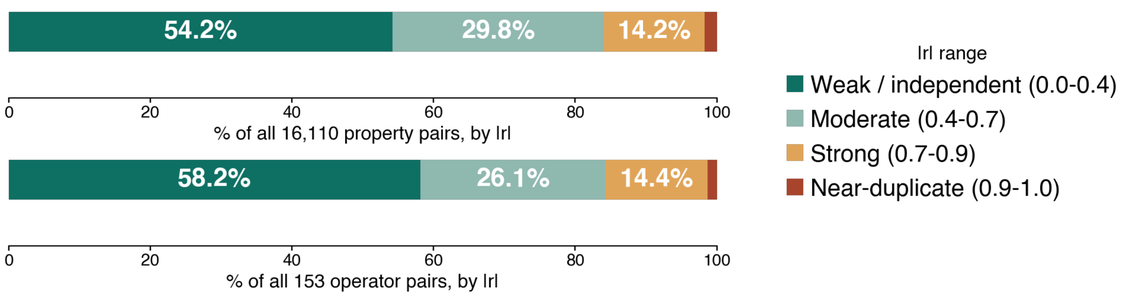
An unsupervised PCA was performed using 375 non-constant descriptors calculated using PeptiDesCalculator v2.0 for 27 published peptides from five functional classes. Patterns emerged without supervision, demonstrating that the descriptors capture peptide information and effectively represent differences among peptide classes.

3. Descriptor families respond predictably to D-residue substitutions

Descriptor group	Achatini	Deltorphin I	Dermorphin	Fulicin
Composition: AA / di / tri	Changed	Changed	Changed	Changed
CTD / Conjoint / autocorr. / GPI	Preserved	Preserved	Preserved	Preserved
PSAC / APSAC / QSO	Partial N/A	N/A	N/A	Partial N/A
Global descriptors	Partial N/A	Partial N/A	Partial N/A	Partial N/A

Across four natural D-peptides, identity-based descriptors detected the D/L substitution, physicochemical families remained invariant, and unsupported formulations returned explicit missing values.

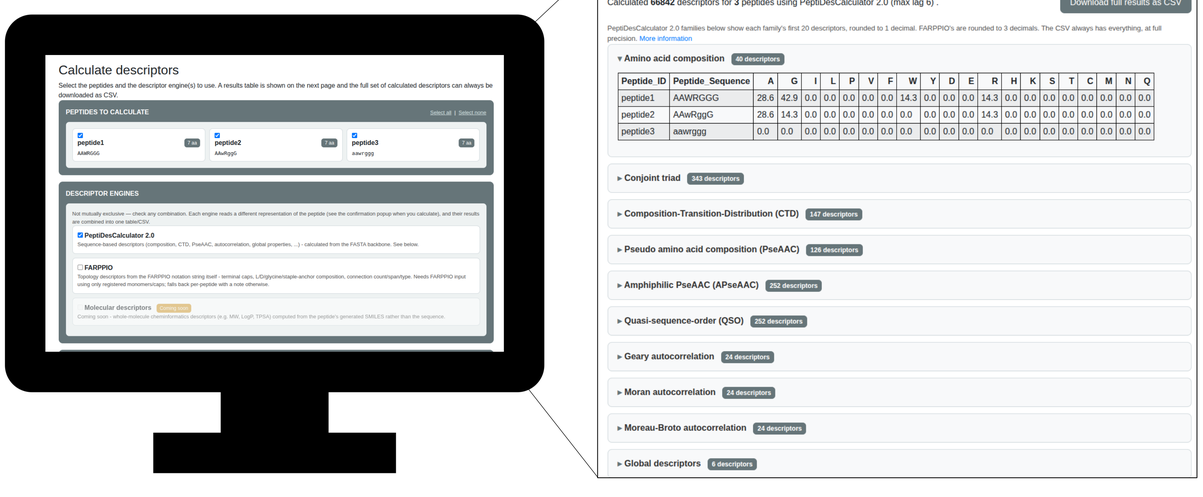
4. AAindex scales and aggregation operators show limited pairwise redundancy



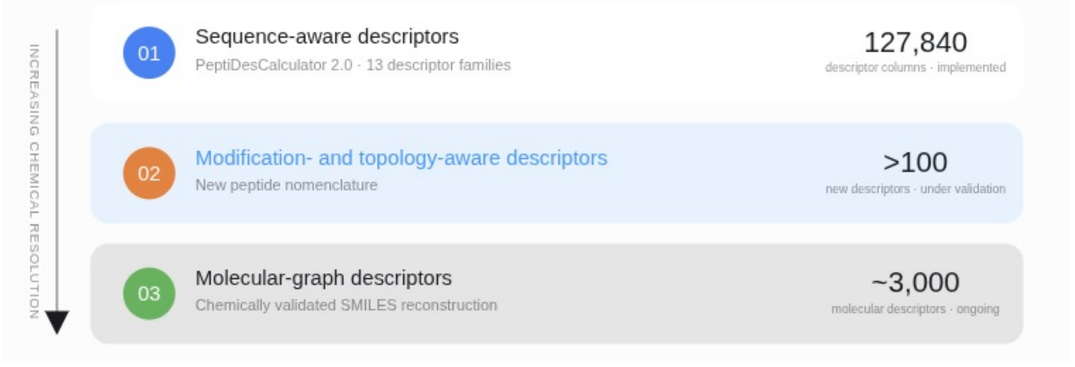
Only approximately 16% of AAindex-scale and operator pairs showed strong or near-duplicate correlations. This supports retaining broad descriptor coverage during calculation, while dataset-specific feature selection is performed later within each QSAR workflow.

Web server ProtoPEP

PeptiDesCalculator 2.0 is integrated into **ProtoPEP**, a web-based platform that calculates the selected peptide descriptors and exports the resulting machine learning ready matrix as a downloadable CSV file.



Ongoing work & conclusions



- PeptiDesCalculator 2.0 offers 13 modular descriptor families and ML-ready CSV export.
- Combined descriptors capture meaningful peptide-class variation.
- D/L and correlation analyses confirm predictable, complementary behavior.
- The new nomenclature adds modification-, topology- and SMILES-based molecular descriptors that can be employed for QSAR modelling.

References

1. L. Wang, N. Wang, W. Zhang, X. Cheng, Z. Yan, Y. Shao, G. Wang, X. Wang, R. Fu, P. Liu, Y. Wang, Q. Lei, Z. Guo and C. Fu, Signal Transduct. Target. Ther. 2022, 7, 48.
2. B. Zheng, Y. Chen, J. Li, H. Zhang and X. Liu, Int. J. Mol. Sci. 2025, 26, 5123-5148.
3. S. J. Barigye, S. Gómez-Ganau, E. Serrano-Candelas and R. Gozalbes, Proteins 2021, 89, 174-184.

Design and synthesis of novel antibacterial oligourea foldamers

Kinga Chaniewicz[1], Paulina Bachurska-Szpala[1], Renata Kurek[2], Katarzyna Kozak[2], Karolina Pułka-Ziach[1]

[1]University of Warsaw, Faculty of Chemistry, Pasteura 1, 02-093, Warsaw, Poland; *k.chaniewicz@uw.edu.pl, **https://doi.org/10.17952/38EPS.2026.P141**

[2]Łukasiewicz – Industrial Chemistry Institute, Pharmacy, Cosmetic Chemistry and Biotechnology, Genetic Engineering and Biosynthesis Section; Rydygiera 8, 01-793 Warsaw, Poland

https://doi.org/10.17952/38EPS.2026.P141

Introduction

In recent years, the rapid spread of bacterial strains resistant to conventional antibiotics has become one of the most serious global health threats. This growing challenge highlights the urgent need to develop alternative antimicrobial strategies that are both effective and less prone to inducing resistance.

One of the most promising approaches involves antimicrobial peptides (AMPs), which are naturally occurring in living organisms and exhibit a broad spectrum of activity against various pathogens.[1] Natural AMPs are limited by enzymatic degradation and low stability. Peptidomimetics, particularly **oligourea foldamers**, overcome these limitations by mimicking AMP activity while providing enhanced stability and well-defined secondary structures.

This project focused on the design, synthesis, and biological evaluation of analogues of a compound with known antibacterial activity.[2] The analogues differed in the length of their basic side chains to investigate the influence of this structural modification on polarity, conformation and antibacterial properties.

Biological test and results

Five lipooligourea with antibacterial activity were successfully obtained. All compounds exhibited great activity against bacteria, indicating a distinct preference for Gram-positive bacterial cells. MBC assays confirmed that their activity is bactericidal, demonstrating that the compounds not only inhibit bacterial growth but also effectively eliminate bacterial cells.

CD spectroscopy indicated a well-defined helical structure. Concentration-dependent CD measurements showed that the value of molar ellipticity, which varies with concentration, indicates a strong tendency towards higher-order lipooligoureas assemblies in solution.[3]

Further studies will focus on aromatic derivatives and the effect of N-terminal chain length on biological activity.

Synthesis of building blocks

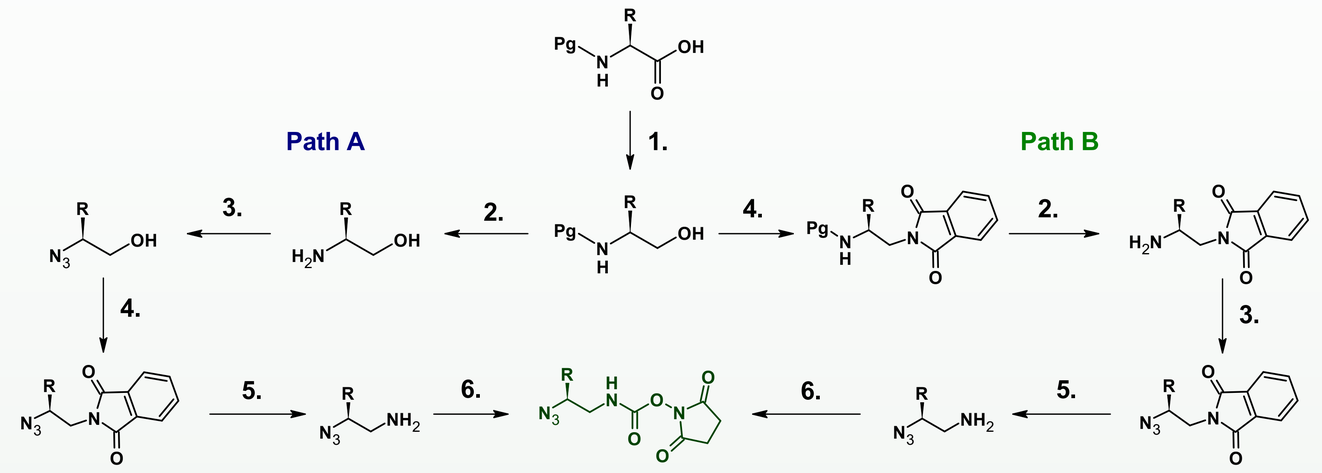


Fig. 1. Schematic diagram of building block synthesis.[4] Final building block structure is marked in **green**. Reagents used: **(1)** IBCF, NMM; $NaBH_4$; **(2)** PG-deprotection; **(3)** $ImSO_2N_3$. HCl, $CuSO_4$. $5H_2O$, K_2CO_3; **(4)** PhthNH, PPh_3, DIAD; **(5)** N_2H_4 . H_2O; **(6)** DSC;

BB obtained* via path A and total yields	
N_3-Dap(Boc)-OSu	52 %
N_3-Dab(Boc)-OSu	50 %
N_3-Orn(Boc)-OSu	50 %
N_3-Lys(Boc)-OSu	23 %
N_3-Arg(Pbf)-OSu	48 %
BB obtained via path B and total yields**	
N_3-Leu-OSu	49 %
N_3-Phe-OSu	52 %

*obtained from Fmoc-AA(Pg)-OH
**obtained from Boc-AA-OH

Synthesis of oligoureas

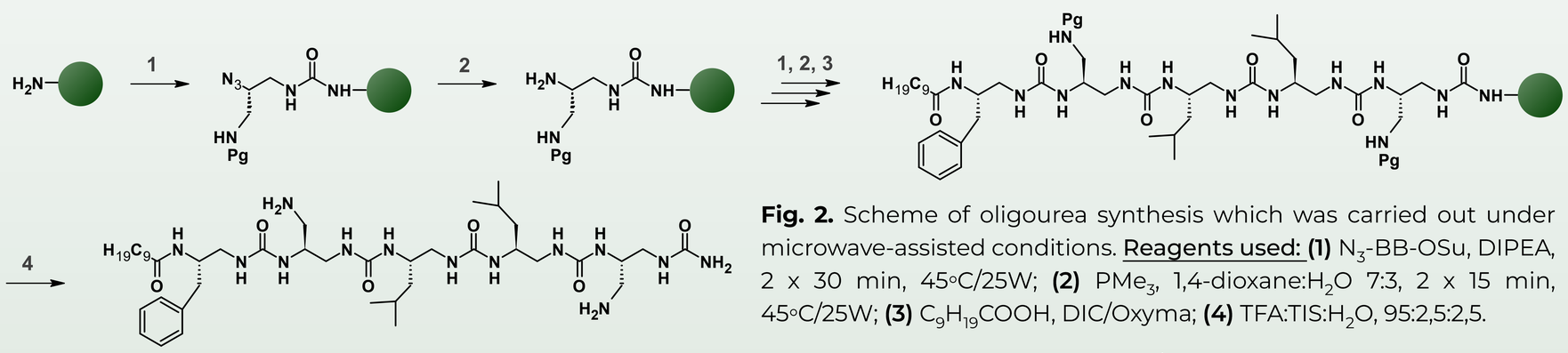


Fig. 2. Scheme of oligourea synthesis which was carried out under microwave-assisted conditions. Reagents used: **(1)** N_3-BB-OSu, DIPEA, 2 x 30 min, 45°C/25W; **(2)** PMe_3, 1,4-dioxane:H_2O 7:3, 2 x 15 min, 45°C/25W; **(3)** $C_9H_{19}COOH$, DIC/Oxyma; **(4)** TFA:TIS:H_2O, 95:2,5:2,5.

Total yields* of oligoureas synthesis		
1.	C_9H_{19}CO-Phe^{u}Dap^{u}Leu^{u}Leu^{u}Dap^u	10 %
2.	C_9H_{19}CO-Phe^{u}Dab^{u}Leu^{u}Leu^{u}Dab^u	16 %
3.	C_9H_{19}CO-Phe^{u}Orn^{u}Leu^{u}Leu^{u}Orn^u	34 %
4.	C_9H_{19}CO-Phe^{u}Lys^{u}Leu^{u}Leu^{u}Lys^u	28 %
5.	C_9H_{19}CO-Phe^{u}Arg^{u}Leu^{u}Leu^{u}Arg^u	38 %

*after purification, ^{u} means urea bond

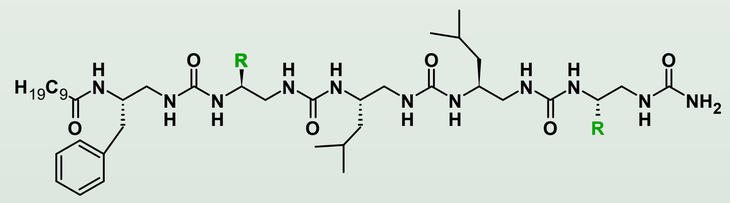
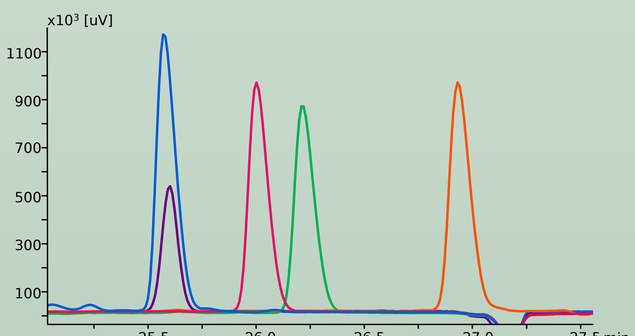


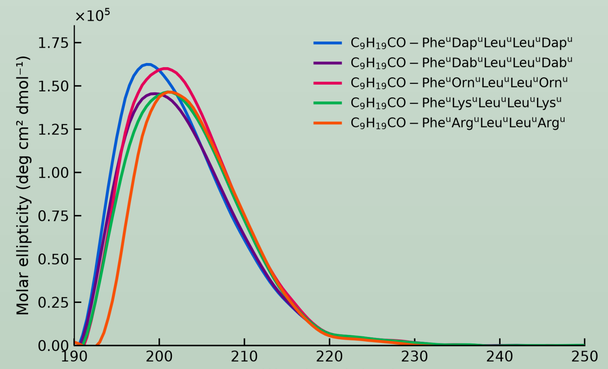
Fig. 3. The general sequence of oligoureas. **R** represents different basic residues showed in the table.

Analitycal characterisation of obtained compunds

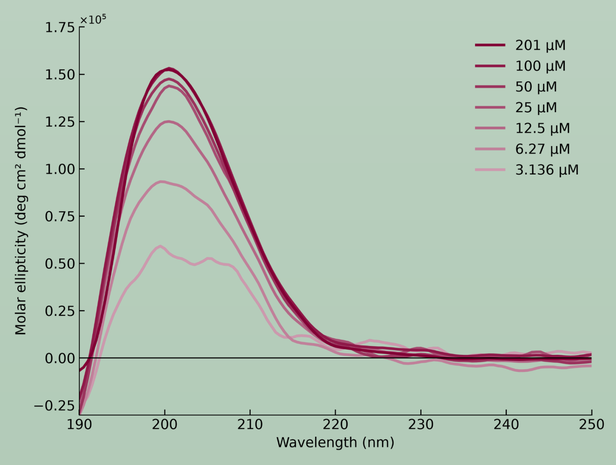
Fig. 4. HPLC chromatograms and CD spectra of oligoureas: **1.** C_9H_{19}CO-Phe^{u}Dap^{u}Leu^{u}Leu^{u}Dap^u, **2.** C_9H_{19}CO-Phe^{u}Dab^{u}Leu^{u}Leu^{u}Dab^u, **3.** C_9H_{19}CO-Phe^{u}Orn^{u}Leu^{u}Leu^{u}Orn^u, **4.** C_9H_{19}CO-Phe^{u}Lys^{u}Leu^{u}Leu^{u}Lys^u, **5.** C_9H_{19}CO-Phe^{u}Arg^{u}Leu^{u}Leu^{u}Arg^u. The synthesized compounds exhibit differences in polarity due to side chains length.



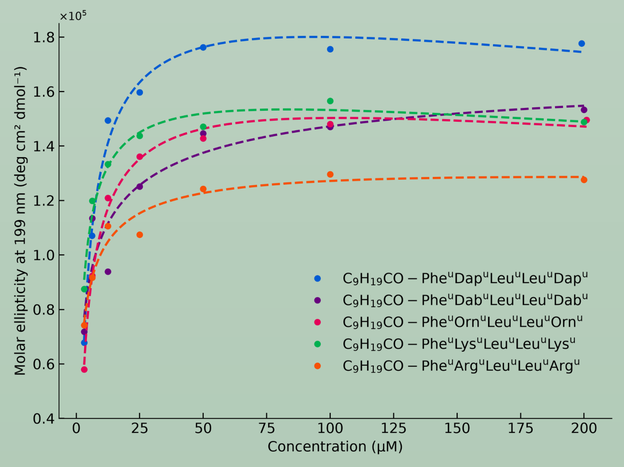
RP-HPLC: Jupiter Proteo (C12) 250 x 4,6 mm. Eluents: (A): 0.1 % TFA in H_2O and (B): 0.1 % TFA in acetonitrile; gradient 10-97 % B for 2.5-33 min. with flow 1 ml/min, λ = 200 nm.



CD: CD spectra of the compounds in Milli-Q water at 200 µM, showing a band characteristic for the helix around 200–203 nm.



Representative **concentration-dependent CD** spectra of compound 3. with ornithine side chain.



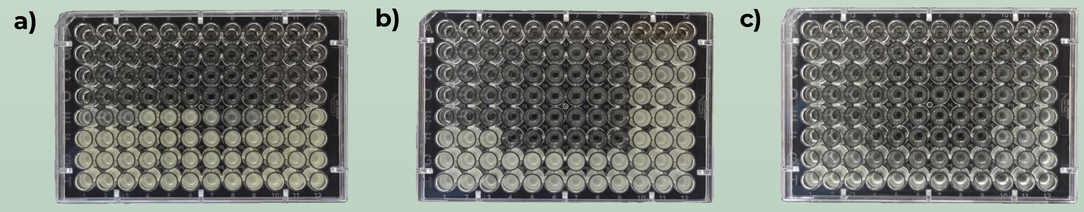
Concentration dependence of molar ellipticity at λ = 199 nm for all investigated compounds.

Biological studies

Fig. 5. Minimum inhibitory concentrations (MIC) were determined by the broth microdilution method using 96-well plates in LB medium. The compounds were tested against Gram-negative bacteria (e.g. *E. coli, K. pneumoniae, P. aeruginosa*), Gram-positive bacteria (e.g. *S. aureus, S. epidermidis*), and the yeast *C. albicans*.

MIC assay for **a)** *S. aureus* (5-0.5 µg/ml); **b)** *K. pneumoniae* (50-5 µg/ml); **c)** *C. albicans* (50-5 µg/ml).
First row (A) – negative control; last row (H) – positive control; columns 1–3, 4–6, and 7–9 correspond to oligourea **4. Lys**, **1. Dap** and **2. Dab**, respectively; columns 10-12 correspond to daptomycin (5-0.5 µg/ml).

MBC assay for *S. epidermidis* at **d)** 3 µg/ml and **e)** 2 µg/ml. At concentration 2 µg/ml bacteria growth was observed. In contrast, no bacterial growth was observed at concentration 3 µg/ml, indicating the absence of viable bacteria.



	MBC/MFC value		
Oligourea:	1. Dap	2. Dab	4. Lys
E.coli	20	20	20
S. epidermidis	3	4	-
C. albicans	10	10	30

Oligourea	1. Dap	2. Dab	3. Orn	4. Lys	5. Arg
Gram-negative bacteria (MIC values in µg/ml)					
E. coli	20	20	20	20	n.d.
K. pneumoniae	10	10	10	20	n.d.
P. aeruginosa	10	10	20	20	n.d.
Gram-positive bacteria (MIC values in µg/ml)					
S. aureus	3	3	2	3	2
S. epidermidis	2	3	1	2	3
L. plantarum	20	20	20	30	5
Yeast (MIC values in µg/ml)					
C. albicans	10	10	10	20	n.d.

References

[1] Spring D. R., et. al., Chemical Society reviews, 50(13), 7820–7880, **2021**
[2] Bachurska-Szpala P., et. al. European Journal of Medicinal Chemistry, Vol. 259, 115700, **2023**
[3] Collie, G., Pulka-Ziach, K., Lombardo, C. et al. Nature Chem 7, 871–878, **2015**
[4] Douat-Casassus, Céline et al. Organic letters vol. 14, No. 12; 3130-3133 **2012**

Acknowledgements

Financial support for participation in EPS 2026 was provided through a travel grant „**IDUB IV.4.1**" and a registration fee waiver sponsored by the **European Peptide Society.** Reaserch: **NCN OPUS 29**, grant number **2025/57/B/ST5/02281**, led by dr hab. Karolina Pułka-Ziach.
The author thanks **Łukasiewicz – Industrial Chemistry Institute – Genetic Engineering and Biosynthesis Section** for enabling the biological studies.

Self-Assembling Peptides Forming Anti-Parallel β-sheet Nanostructures Cross-Linked with Genipin

Self-Assembled Peptide-Coated Fibers: Bilayer Materials for Sustainable Textile and Packaging Applications

Q. CHENIN[1,2], N. FOLLAIN[1], C. BELLO[2], L. ROSI[3], P. ROVERO[4], A.M. PAPINI[2]

[1] *Université de Rouen Normandie, INSA Rouen Normandie, Polymères Biopolymères Surface (PBS) UMR 6270 CNRS, 76000 Rouen, France*
[2] *Interdepartmental research Unit of Peptide and Protein Chemistry and Biology, University of Florence, 50019-Sesto Fiorentino (FI), Italy*
[3] *Department of Chemistry "Ugo Schiff", University of Florence, 50019-Sesto Fiorentino (FI), Italy*
[4] *Department of Neurosciences, Psychology, Drug Research and Child Health, University of Florence, 50019-Sesto Fiorentino (FI), Italy*
https://doi.org/10.17952/38EPS.2026.P555
Quentin Chenin e-mail *: quentin.chenin@unifi.it*

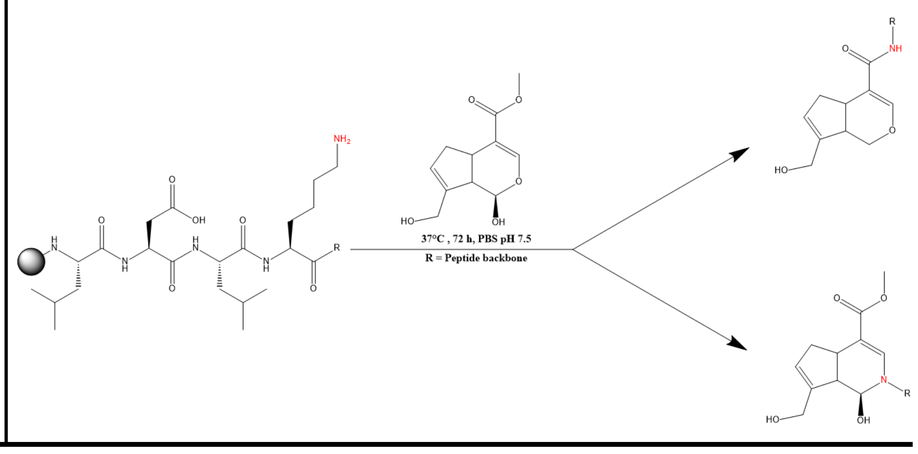
Self-assembling peptides are versatile biomolecular building blocks for hydrogel scaffolds in biomedical and technological applications. However, their limited mechanical stability often requires reinforcement. Here, two peptide sequences were designed from a parent sequence (1) identified in the N-terminal region of the *Helicobacter pylori* MutS2 protein and conserved among related *ε-proteobacteria* [1]. Peptides were synthesized by induction heating-assisted Solid-Phase Peptide Synthesis and used for hydrogel formation without chromatographic purification, reducing processing requirements while enabling mechanically reinforced ***materials for sustainable packaging and biomaterial applications***. The project leverages EUniWell's "infrastructure without walls," combining the University of Florence's expertise in sustainable peptide-based materials with the University of Rouen Normandie's advanced polymer characterization capabilities.

Peptide design, synthesis and characterization

Peptide	Mw (g/mol)	GRAVY score[2]	Isoelectric point	Average hydrophilicity	HPLC purity^{bp} (%)	HPLC purity^{ap} (%)	[M + H]+ calcd/found	Minimally processed yield (%)
LDLKLDLKLDLK-NH_2 (1)	1425.90	0.8375	9.68	0.6	77	88	1425.90/ 1427.58	84
DDLKLDLKLDLK-NH_2 (2)	1427.85	0.4917	7	1	68	83	1428.81/ 1427.85	80
LDLKLDLKLDLKFF-NH_2 (3)	1720.04	1.1179	9.68	0.16	70	88	1721.83/ 1720.04	52

bp : before purification; ap : after purification

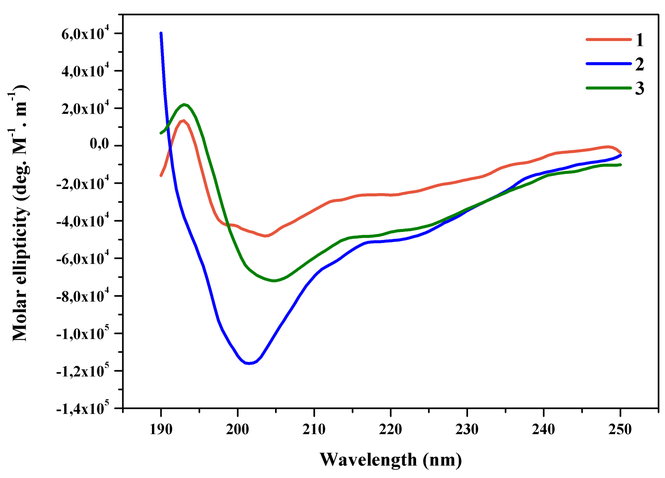
Genipin cross-linking



To enhance network stability, Genipin was investigated as a naturally derived cross-linker forming covalent networks through amino functionalities [3]. Genipin treatment improved the mechanical and thermal properties of hydrogels, increasing the storage modulus from 9 to 21 kPa and the residual mass from 1% to 26%. Notably, minimally processed peptides exhibited hydrogel-forming behavior comparable to purified materials, highlighting a more streamlined, cost-effective, and sustainable approach to peptide-based hydrogels.

Peptide morphology

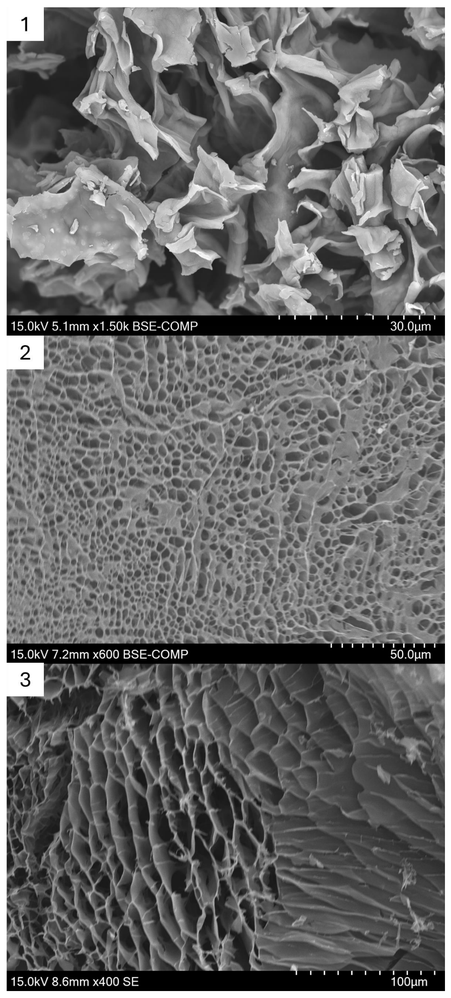
Circular dichroism



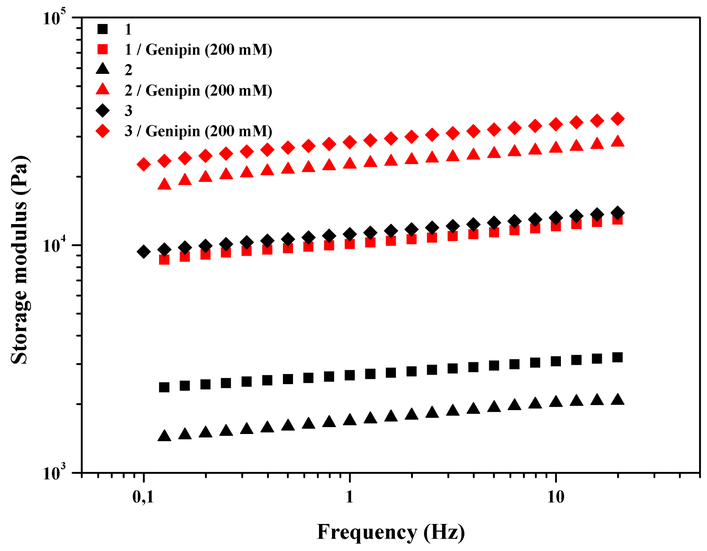
Secondary structures (%)	1	2	3
α-helix	0,8	6,4	2,3
β-sheets	0	3,1	1,7
Anti β-sheets	34,8	22,5	27,2
β-turns	16,1	14,2	15,3
Random coils	48,3	53,9	53,5

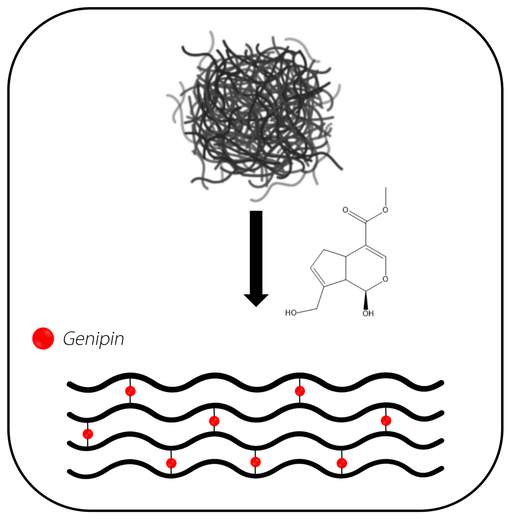
- ***Majority of anti-parallel β-sheets and random coil structures by CD measurements for all peptides.***
- ***Hydrogels showed a porous structure as made in evidence by scanning electron microscopy analysis.***

Scanning electron microscopy



Hydrogel rheology and peptide cross-linking





Conditions
0,1 – 100 Hz frequency – sweep at 25 °C, 1% strain,20 mm serrated parallel plate geometry

Improvement in the storage modulus G' after Genipin cross-linking (increase of G' up to 20-times).

- G' > G" for all tests, proving that the materials **exhibit solid-like viscoelastic behavior.**
- Peptide 3 shows higher initial storage modulus before cross-linking, as it binds less to water through hydrogen bonds, relying more on ***hydrophobic interactions.***
- Cross-linked hydrogels: storage modulus (G') ranging between 9-21 kPa.
- Unreacted hydrogels: G' values ranging between 1-10 kPa.

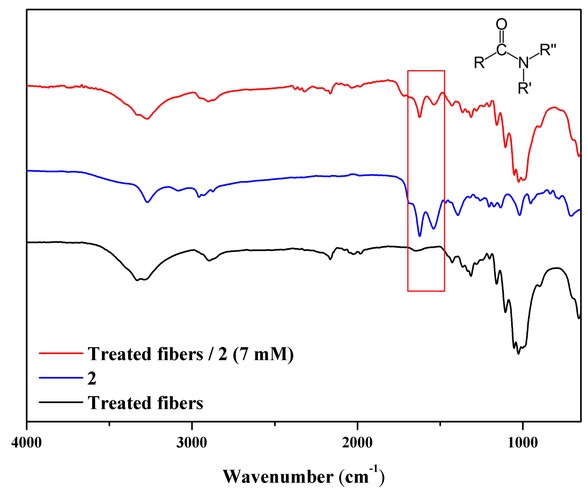
Conclusions and ongoing researches

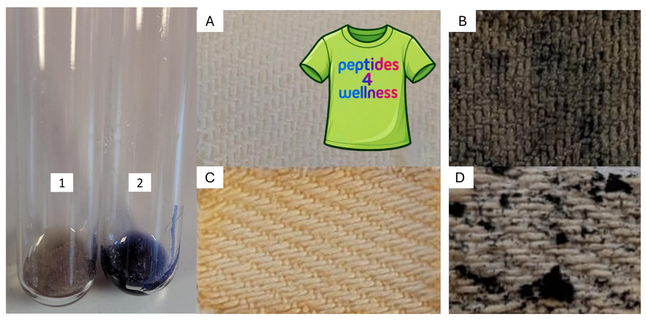
- ***Minimally processed peptides*** were obtained, employed for hydrogel formation, and subsequently cross-linked with Genipin.
- ***Thermal, mechanical and self-assembling properties*** of all peptides (1-3) in solution revealed chemical cross-linking with Genipin in the hydrogels.
- ***Grafting peptide DDLKLDLKLDLK-NH_2 (2) onto cellulose fibers*** paves the way for the development of stronger, environmentally friendly and ***biodegradable materials*** in textiles.

- Grafting ***RYamide*** onto fabrics could activate ***NPYLR7 signaling*** in mosquitoes, potentially inducing satiety and reducing biting behavior [4].
- Antiviral peptide-functionalized fibers could pave the way for next-generation protective masks designed to inhibit SARS-CoV-2 and reduce viral transmission.

Self-assembled peptide-fibers bilayer material

FTIR-ATR





(1) Kaiser test of raw cotton treated with peptide. (2) Kaiser test of oxidized cotton treated with peptide. (A) Untreated cotton fibers. (B) Oxidized cotton fibers treated with a Genipin solution, showing a homogeneous cross-linking distribution. (C) Oxidized cotton fibers treated with oxidized hyaluronic acid. (D) Unoxidized cotton fibers treated with a Genipin solution, showing a heterogenous cross-linking distribution.

Following oxidative treatment of textile cellulose fibers, a bilayer cellulose–peptide matrix is obtained through **Schiff base formation**. This complex can undergo further cross-linking with molecules such as Genipin via the amino groups of lysine residues.

Acknowledgments

This work is financially supported by XL-CHEM, PBS, PeptLab and the Italian Ministry of Health for funding the "borsa di ricerca" under project code RF-2021-12374177.
This project was funded in part by EUniWell: 5th seed funding call for the TTPep project and 3rd Well-Being Research Incubator Call for the project "Sustainable and green upscaling processes for peptide(-based) in vitro diagnostics and cosmeceuticals" and the Champion program "Peptides4Wellness".
Quentin Chenin gratefully acknowledges the European Peptide Society for the registration grant to attend the 38th European Peptide Symposium.

[1] P. P. Damke, R. Dhanaraju, S. Marsin, J. P. Radicella and D. N. Rao, Molecular Microbiology, 2015, 96, 1240–1256.
[2] J. Kyte and R. F. Doolittle, Journal of Molecular Biology, 1982, 157, 105–132.
[3] M. F. Butler, Y. Ng and P. D. A. Pudney, J. Polym. Sci. A Polym. Chem., 2003, 41, 3941–3953.
[4] C. Greppi, K. Frank, V. Saltz and L. B. Duvall, *Current Biology*, 2026, **36**, 1702-1715.e6.

Miniaturized HOXB13 Mimetics Are Sequence-Specific, Methyl-Sensitive DNA Binders

University of Strathclyde Science

Claire Wong, Shiao Chow

claire.wong@strath.ac.uk
www.thebotcatalysts-lab.com/

Department of Pure and Applied Chemistry, Thomas Graham Building, 295 Cathedral Street, G1 1XL, Glasgow, UK

https://doi.org/10.17952/38EPS.2026.P130

[1]. INTRODUCTION

Cancer-associated DNA methylation is difficult to target selectively.

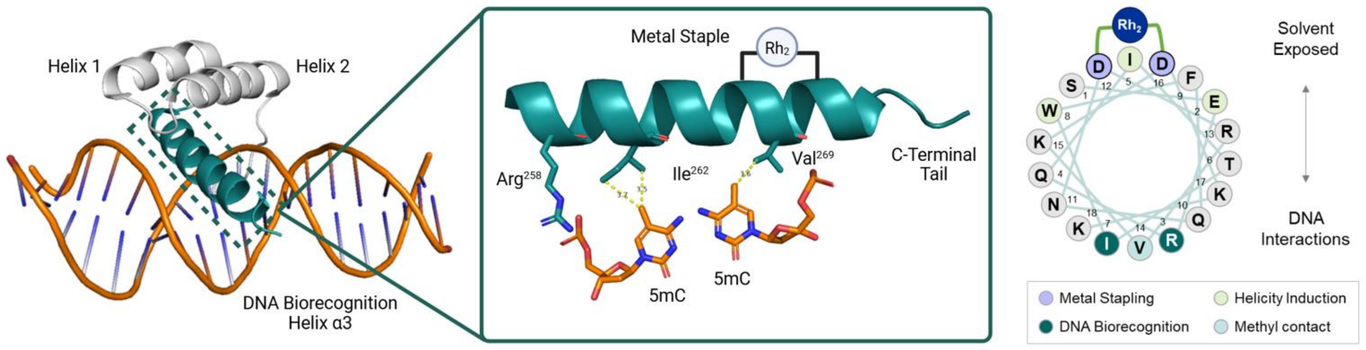
Targeting modification sites is an effective strategy to study these epigenetic changes. The homeobox protein **Hox-B13 (HOXB13)** is an **oncogenic transcription factor** known to bind to regions of high DNA methylation.[1,2]

PROBLEM: HOXB13 recognises specific methylated DNA motifs but is too large to use as a molecular tool.

SOLUTION: Miniaturising transcription factors can be used to create synthetic tools to study transcription factor-DNA interactions and binding preferences.

[2]. MINIATURISATION STRATEGY

HOXB13 Transcription Factor [284 residue] >90% Size Reduction **α3 Stapled Mimetic** [18 residue]



Methylated DNA : 5′-GGACCT**mCG**TAAAACACAA-3′

[3]. METHODS

1. METALLOPEPTIDE SYNTHESIS

[P1] Ac-SERQITIWFQNRRVKEKK-NH_2

[P2] Ac-SERQITIWFQNDRVKDKK-NH_2

$Rh_2(OAc)_2(TFA)_2$
MES buffer, pH 4.5
50^0C

[MP2] Ac-SERQITIWFQNDRVKDKK-NH_2 = Rh_2

P1 (wild type) and **P2 (Asp/Asp modified)** synthesised *via* standard SPPS.

MP2 (metal-stapled) synthesized *via* direct metal chelation.

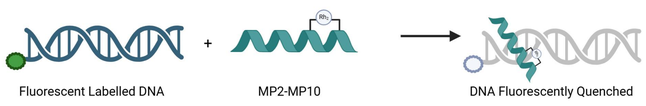
MP2 was systematically modified to investigate influence of **structural rigidity (MP3-5), methyl-recognition (MP6-8) and truncation (MP9-10)** on DNA binding and methyl sensitivity.

Entry	Peptide Sequence	fH	$\Theta_{222}/\theta_{208}$
P1	Ac-SERQITIWFQNRRVKEKK-NH_2	0.07	0.46
MP2	Ac-SERQITIWFQN**D**RVK**D**KK-NH_2	0.15	1.05
MP3	Ac-SERQ**B**TIWFQN**D**RVK**D**KK-NH_2	0.22	1.47
MP4	Ac-S**B**RQITIWFQN**D**RVK**D**KK-NH_2	0.28	1.00
MP5	Ac-SERQIT**B**FQN**D**RVK**D**KK-NH_2	0.24	0.95
MP6	Ac-SERQITIWFQN**D**R**L**K**D**KK-NH_2	0.22	0.97
MP7	Ac-SERQITIWFQN**D**R**T**K**D**KK-NH_2	0.15	1.01
MP8	Ac-SERQITIWFQN**D**R**F**K**D**KK-NH_2	0.20	1.02
MP9	Ac-RQITIWFQN**D**RVK**D**-NH_2	0.26	0.90
MP10	Ac-RQITIWFQN**D**RVK**D**KK-NH_2	0.23	0.83

*B = aminoisobutyric acid (AIB), helical inducing amino acid.

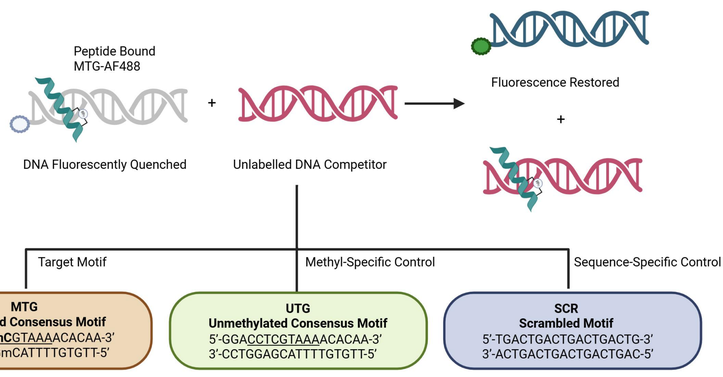
2. DNA BINDING ASSSESSMENT

Direct Peptide-DNA Binding: Fluorescence Quenching Assay



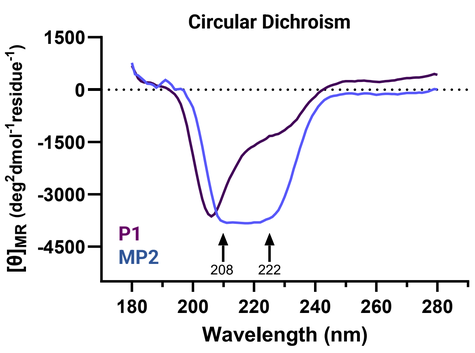
Methylated DNA Tracer **(MTG-AF488)**
5′-GGACCTmCGTAAAACACAA-3′
3′-[AF488]-CCTGGAGmCATTTTGTGTT-5′

Binding Specificity through Competitive Displacement: Fluorescence Restoration Assay

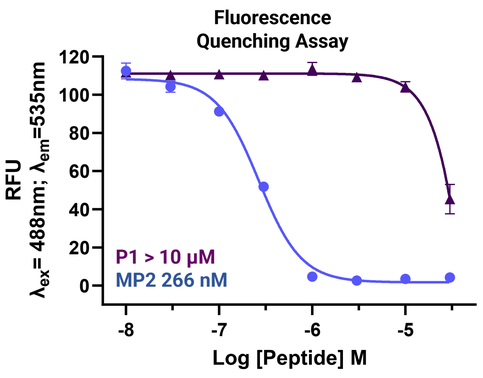


[4]. RESULTS

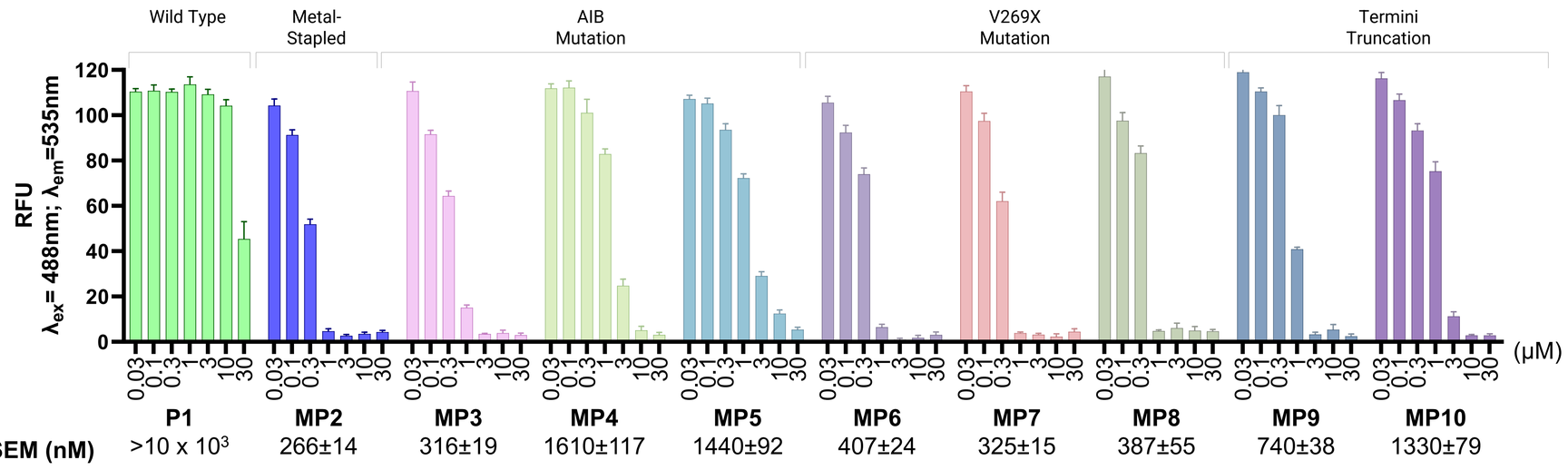
STAPLING INDUCES HELICITY



HELICITY RESTORES DNA BINDING

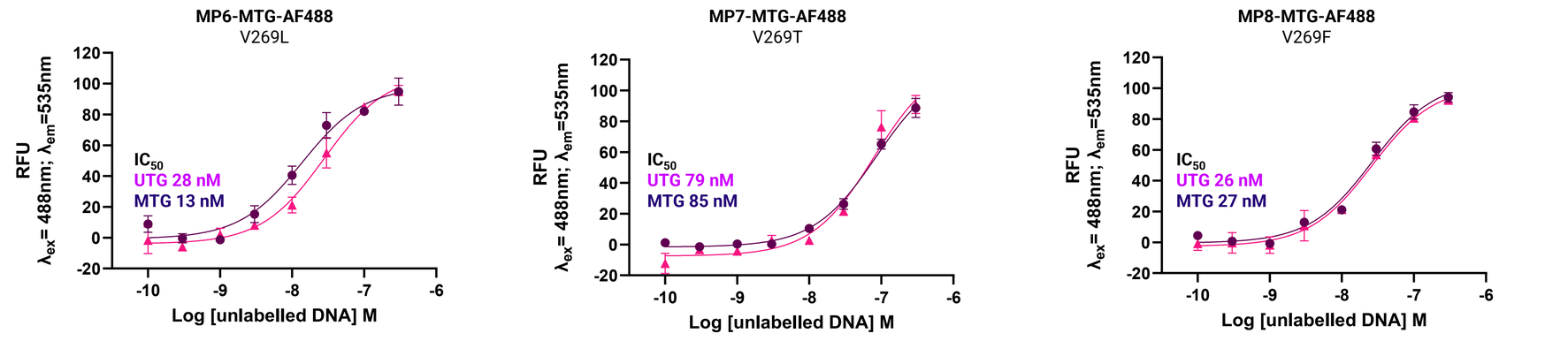


PEPTIDE DESIGN OPTIMISATION

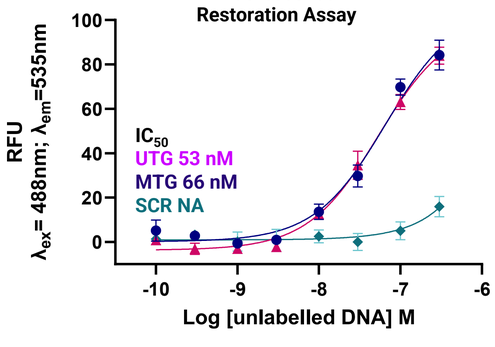


K_D ± SEM (nM)	P1	MP2	MP3	MP4	MP5	MP6	MP7	MP8	MP9	MP10
	>10 x 10^3	266±14	316±19	1610±117	1440±92	407±24	325±15	387±55	740±38	1330±79

ANALYSIS OF METHYL-SENSITIVITY USING V269X MUTANTS



MP2 IS SEQUENCE-SPECIFIC



$IC_{50}^{UTG}/IC_{50}^{MTG}$	2.15	>	0.93	≈	0.96

V269L (MP6) introduces **methyl-sensitivity,** favouring methylated DNA by **2.15-fold. MP7** and **MP8** show no preference.

Metal-stapled HOXB13 mimetics provide compact, sequence-specific tools for interrogating disease-associated DNA methylation.

C. Wong, S. Y. Chow, *J. Am. Chem. Soc.*, 2026, **148**, 30785–30792.

[5]. CONCLUSION

KEY FINDINGS

- ✓ Miniaturisation of HOXB13 DNA binding domain to an 18-residue stapled peptide retains DNA recognition despite >90% size reduction.
- ✓ V269L mutation (MP6) generates a 2.15-fold preference for methylated DNA.
- ✓ MP2 recognises the HOXB13 consensus sequence but not scrambled DNA.

References

1. W. D. Dupont, J. P. Breyer, S. H. Johnson, W. D. Plummer and J. R. Smith, *Scientific Reports 2021 11:1*, 2021, **11**, 1–10.
2. Y. Yin, E. Morgunova, A. Jolma, E. Kaasinen, B. Sahu, S. Khund-Sayeed, P. K. Das, T. Kivioja, K. Dave, F. Zhong, K. R. Nitta, M. Taipale, A. Popov, P. A. Ginno, S. Domcke, J. Yan, D. Schübeler, C. Vinson and J. Taipale, *Science*, 2017, **356**, eaaj2239

Funding Acknowledgements
Conference attendance was supported by the RSC Biological and Medicinal Chemistry (RSC-BMCS) International Travel Grant.

Explore the full story behind our HOXB13 mimetics, recently published in JACs.

Affibody-mediated Peptide Nucleic Acid Pretargeting Using Dual Hybridization Sequences for Increased Therapeutic Potential

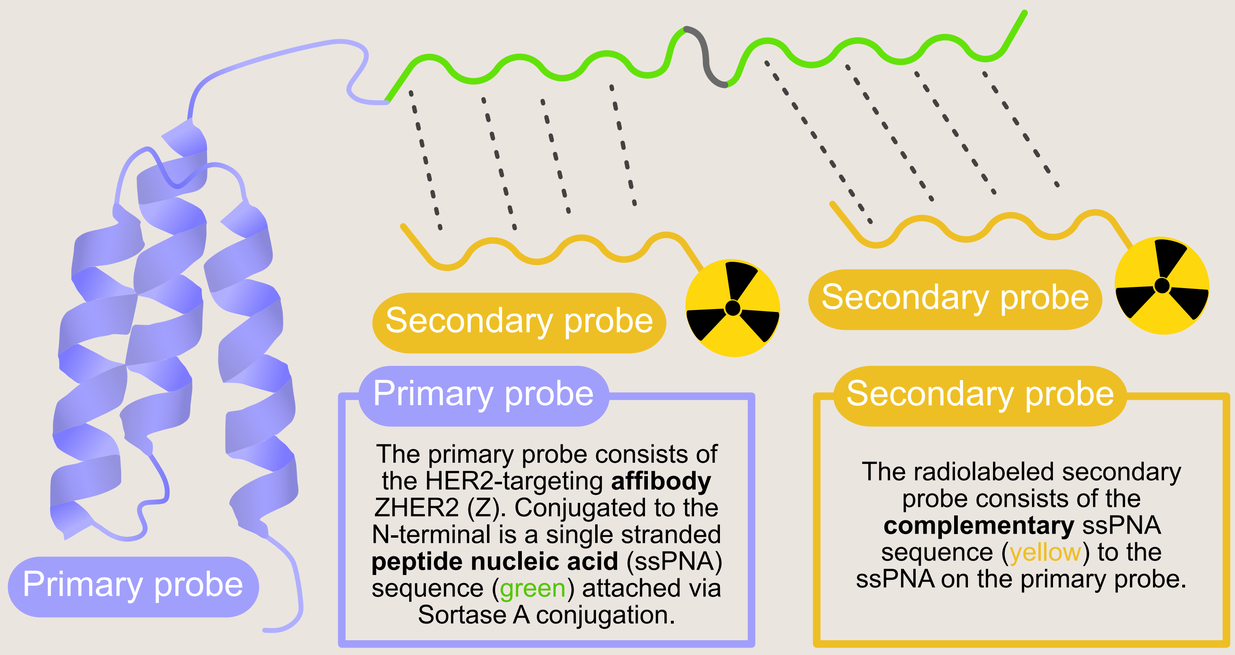
Jacob Clinton[1], Kristina Westerlund[1], and Amelie Eriksson Karlström[1]

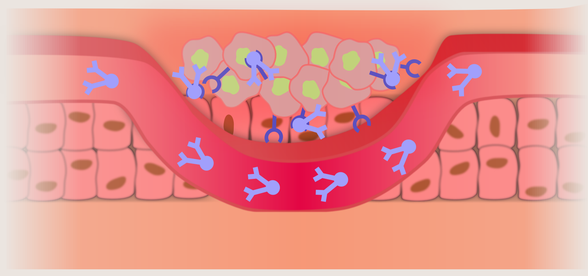
[1] Department of Protein Science, School of Enigneering Sciences in Chemistry, Biotechnology and Health, KTH Royal Institute of Technology, Stockholm 106 91, Sweden

https://doi.org/10.17952/38EPS.2026.P339

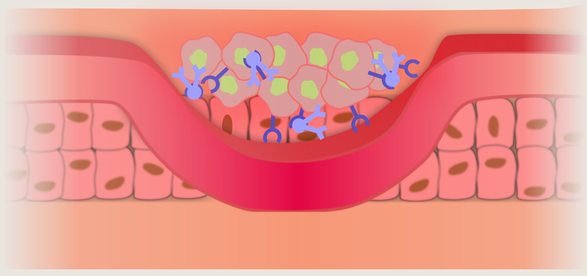
Key concepts

- **Pretargeted radioimmunotherapy** is the concept of separating the tumor targeting agent from the radioactive cell-killing agent in order to reduce toxic radiation exposure to healthy tissues.
- First, a **primary tumor-targeting probe** is injected followed by a waiting time where any unbound probe is **cleared** from circulation and healthy organs.
- Secondly, a **fast clearing radiolabeled probe** is injected with high affinity and specificity to the primary probe.
- This results in higher tumor-to-healthy tissue ratios and opens up for potential treatments with higher doses of radioactivity.

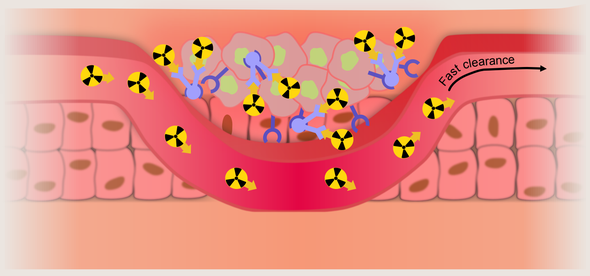




1 Tumor targeting with **primary probe**



2 **Clearance** of unbound primary probe



3 Injection of fast clearing **radiolabeled secondary probe**

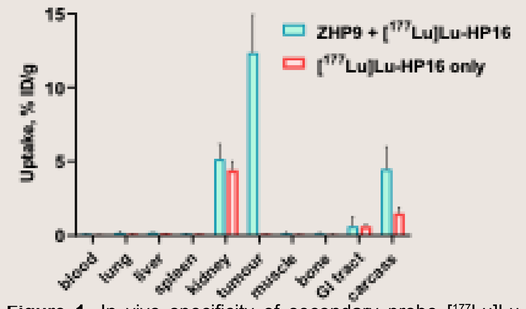


Figure 1. In vivo specificity of secondary probe [^{177}Lu]Lu-HP16 in BALB/C nu/nu mice bearing SKOV3 xenografts at 4h p.i. with and without pre-injection of primary probe, Z-HP9. Data are presented as an average of %ID/g ± SD, n = 4.

Aim

- So far affibody-meditated PNA pretargeting has only been explored in a 1:1 ratio of primary probe (**Z-HP9**) to secondary probe (**HP16**). Results show successful delivery of radioactivity to tumors with favorable tumor to healthy tissue ratio.
- To further develop the **therapeutic potential** of pretargeting we now aim to increase the amount of delivered radioactivity to tumors without increasing radioactivity to healthy tissues.
- By **redesigning the PNA** of the **primary probe** to be able to bind **two secondary probes** simultaneously we hope to further **increase tumor irradiation** without increasing kidney toxicity.
- A new primary probe (**Z-HP9x2**) was produced, consisting of a longer PNA part, namely two **HP9** sequences connected by a short PEG-linker.

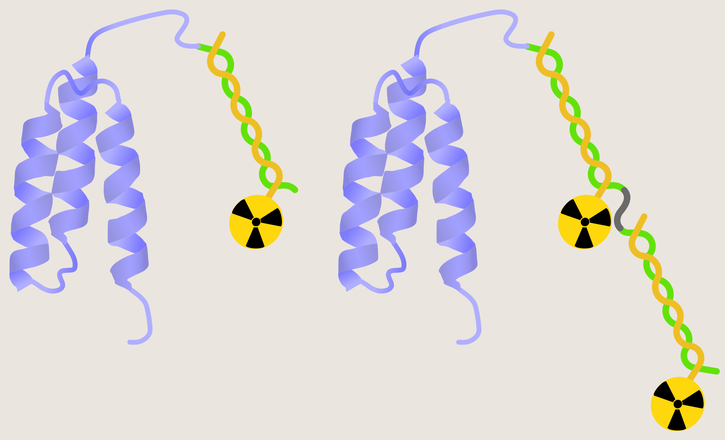


Figure 2. Depiction of primary and secondary probes hybridized through PNA hybridization. **Left**: affibody **ZHER2** (purple) conjugated to the old **HP9** (green) probe with a single secondary probe **HP16** (yellow) hybridized. **Right**: affibody **ZHER2** (purple) conjugated to the new **HP9x2** (green and gray) probe with two **HP16** (yellow) probes hybridized.

HP9x2 DOTA
Gly-Gly-Gly-Ser-Ser-cctggtgtt-AEEA-cctggtgtt-Glu-Lys-AEEA-Glu

HP9 DOTA
Gly-Gly-Gly-Ser-Ser-cctggtgtt-Glu-Lys-AEEA-Glu

HP16
DOTA-AEEA-Ser-Ser-aacaccagg-Glu-Glu-Tyr

Figure 3. Sequence of **new** primary PNA probe **HP9x2** (top), **old** primary PNA probe **HP9** (middle) and secondary probe **HP16** (bottom). PNA bases in red, DOTA chelator in blue, amino acids in black and AEEA (PEG_2) molecule in green.

Results

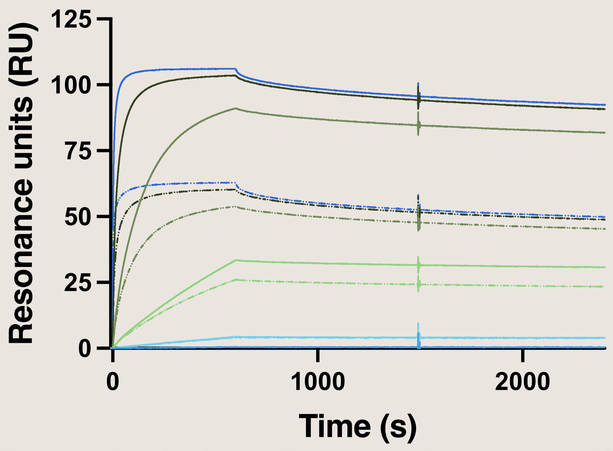


Figure 4. Surface Plasmon Resonance (SPR) sensorgrams of **HP16** as analyte at concentrations ranging from 0.05 nM (light blue) - 5000 nM (dark blue) over surfaces immobilized with **equimolar** amounts of either **Z-HP9** (dotted lines) or **Z-HP9x2** (full lines).

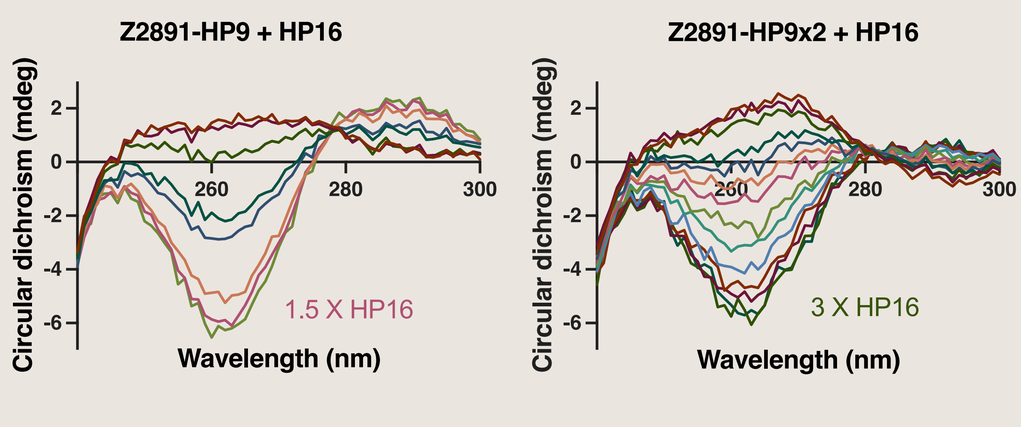


Figure 5. Circular dichroism (CD) data plots showing induced structural changes from PNA-PNA hybridization of Z-HP9 (left) and Z-HP9x2 (right) by adding increasing amounts of HP16. **Left**: Molar ratios of Z-HP9:HP16 ranging from 1:0.25 (brown) to 1:2 (light green). **Right**: Molar ratios of Z-HP9x2:HP16 ranging from 1:0.25 (brown) to 1:3.25 (dark green).

Conclusions

- The aim of this study is to further **increase the tumor-to-healthy tissue ratio** of radioactivity for pretargeted radioimmunotherapy with affibodies.
- By increasing the **length if the primary PNA probe** to have the capacity to hybridize with **two radiolabeled secondary probes**, instead of one, we hope to increase tumor irradiation without increasing irradiation of healthy tissues.
- Initial characterization of the **new, longer Z-HP9x2** primary tumor binding probe shows good potential as both SPR and CD results indicate that hybridization of twice the amount of HP16 secondary probe at higher concentrations is indeed possible compared to the **older primary probe Z-HP9**.

CANCERFONDEN

Presenting author:
Jacob Clinton, Ph.D student
jclinton@kth.se

γ/α-Foldamers: Helical Constructs for asymmetric Catalysis

Junyan Xu, Dr. Saidul Islam, Prof. Andre Cobb*

Department of Chemistry, King's College London, Britannia House, 7 Trinity Street, London, SE1 1DB

junyan.xu@kcl.ac.uk

https://doi.org/10.17952/38EPS.2026.P147

1. Introduction

- Foldamers are designed peptides in which α-amino acids alternate with unnatural cyclic γ-amino acids residues. In solution, these backbones adopt defined helical architectures stabilized by noncovalent interactions.[1]
- Helical foldamers enable asymmetric catalysis by creating well-defined three-dimensional chiral environments that promote selective substrate recognition and enantioinduction.[2]
- Compared to small-molecule catalysts, the well-defined and repetitive structures of hybrid γ/α-peptide backbone offer superior modularity for the incorporation of functional groups.[3]

Aims and objectives

- To optimize the synthesis of γ-cyclic amino acid monomers.
- To synthesize the γ/α helix with potential catalytic property.
- To explore the application of a new and stable peptide helix.

Related techniques

- XRD (X-Ray Diffraction): characterization of foldamer crystals.
- NMR (NOESY, ROESY): validation of folding behavior.
- Chiral HPLC: *ee* test for asymmetric synthesis.
- CD (Circular dichroism), SPPS (Solid-phase peptide synthesis), etc.

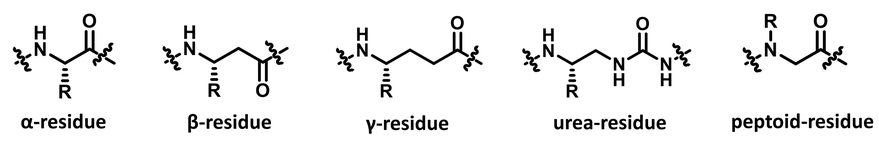
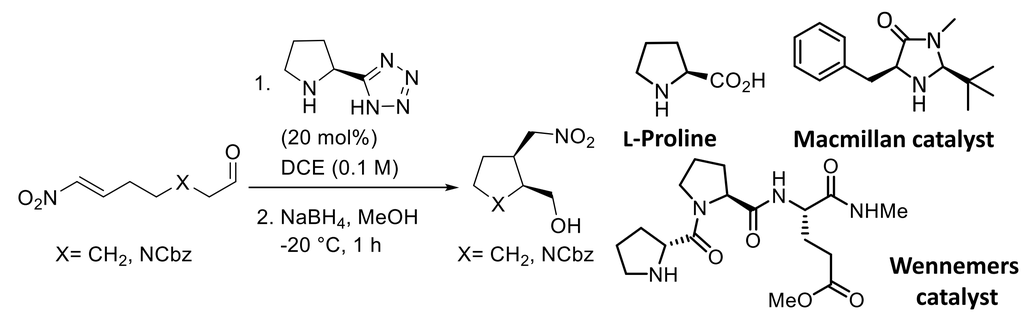


Figure 1 Selected natural and non-natural subunits found in foldamer backbones. R = generic side-chain group.[1]



Scheme 1 Asymmetric synthesis of γ-cyclic amino acid precursors.[2]

Figure 2 small-molecule catalysts.

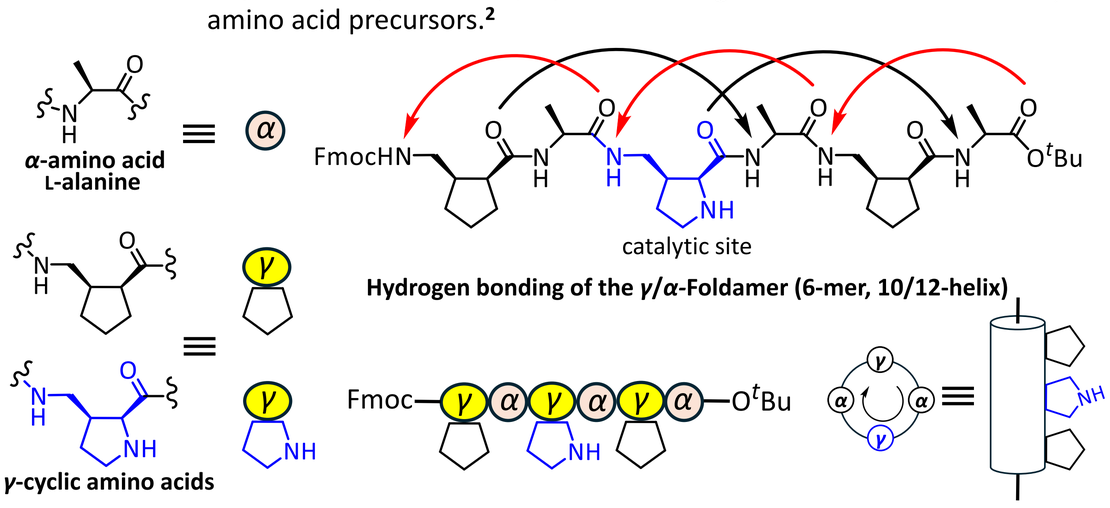
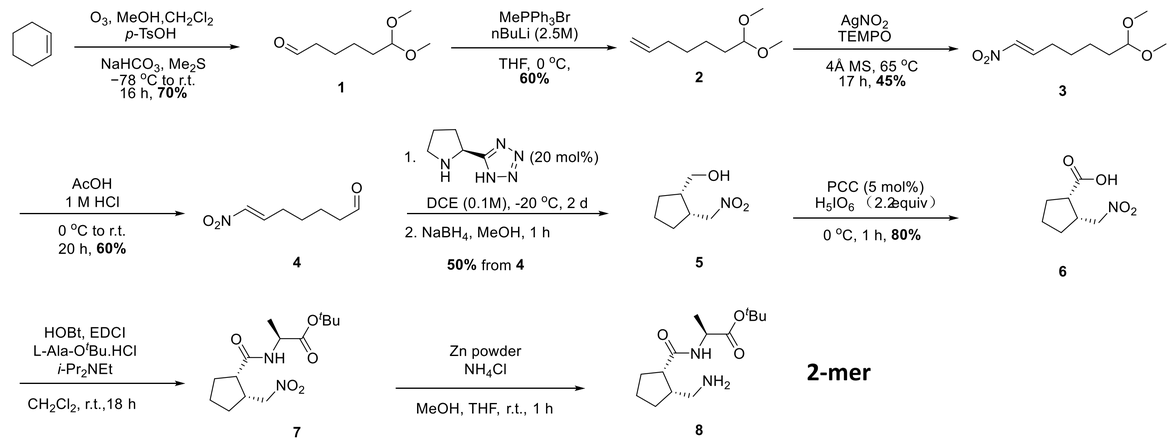
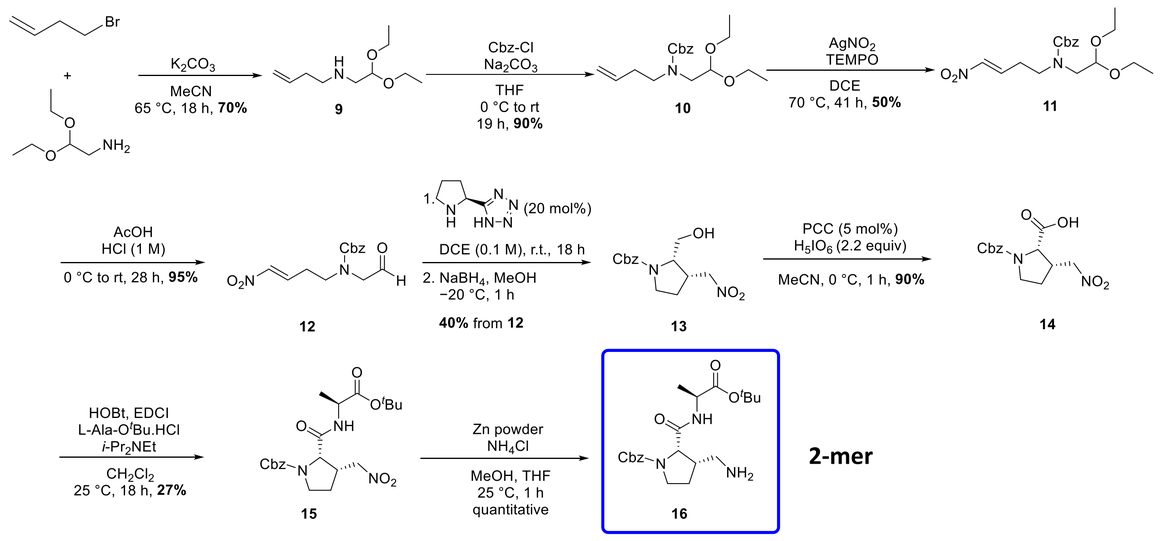


Figure 3 α- and γ-cyclic amino acid monomers and molecular design.

2. Synthesis of γ-cyclic amino acids

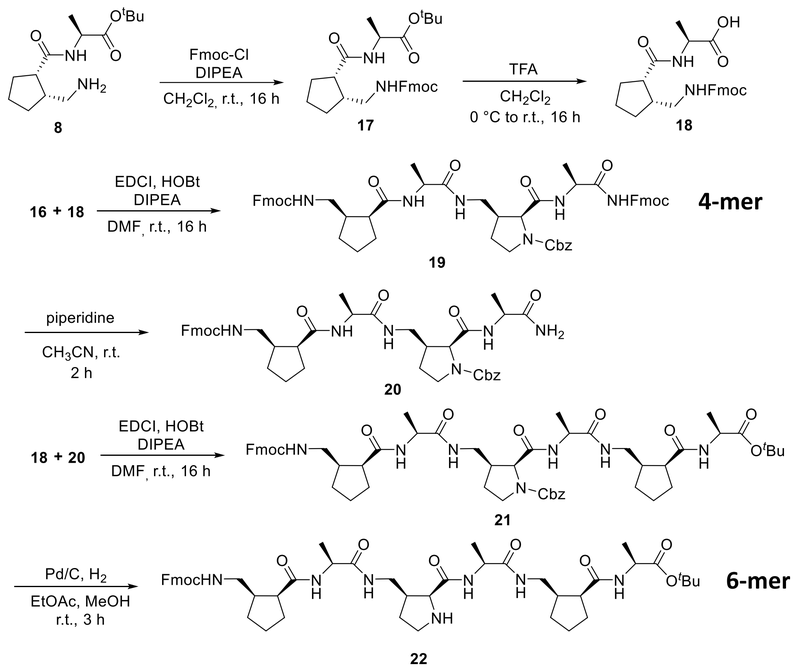


Scheme 2 The Synthesis of cyclopentane-based nitro olefin.



Scheme 3 The Synthesis of Cbz-protected pyrrolidine-based nitro olefin.

3. Amide coupling



Scheme 4 Peptide synthesis employing an orthogonal protecting group strategy.

- Single crystals of the foldamer will be grown and its structure elucidated by X-ray diffraction (XRD).
- The structural insights will enable a preliminary evaluation of the monofunctional model's catalytic potential and guide the future design of bifunctional systems.

4. Results

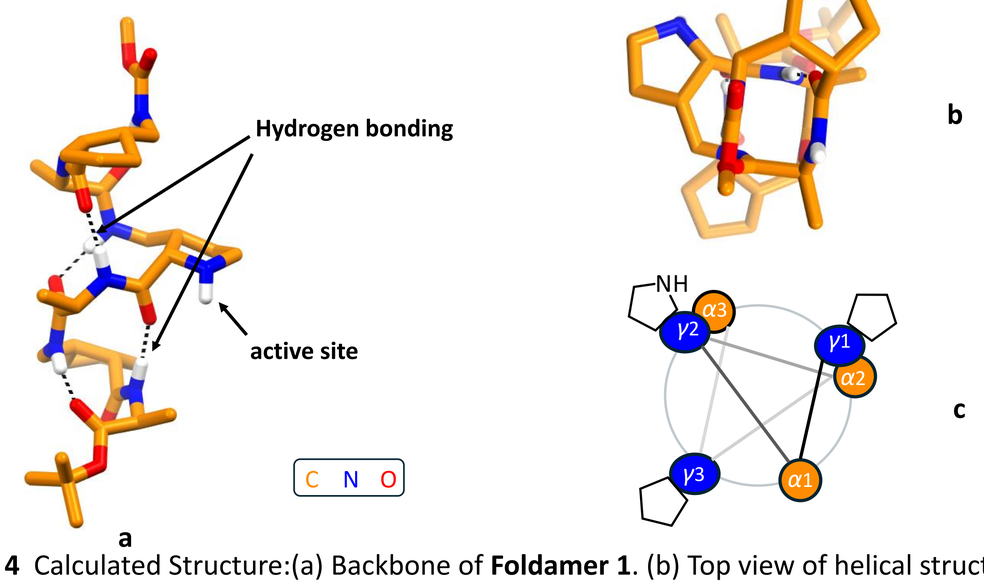


Fig 4 Calculated Structure:(a) Backbone of **Foldamer 1**. (b) Top view of helical structure (c) The corresponding wheel diagram of simplicity.

5. Future work

- Obtain single crystals of the foldamer and elucidate its solid-state structure by X-ray diffraction (XRD).
- Use the resolved structure to guide the design of suitable substrates and reaction types, enabling evaluation of the foldamer's catalytic activity.

6. Reference

1. Girvin, Z. C. & Gellman, S. H. Foldamer Catalysis. *J. Am. Chem. Soc.* **142**, 17211–17223 (2020).

2. Girvin, Z. C., Andrews, M. K., Liu, X. & Gellman, S. H. Foldamer-templated catalysis of macrocycle formation. Science 366, 1528–1531 (2019).

3. Fanelli, R. *et al.* Organocatalytic Access to a *cis* -Cyclopentyl-γ-amino Acid: An Intriguing Model of Selectivity and Formation of a Stable 10/12-Helix from the Corresponding γ/α-Peptide. *J. Am. Chem. Soc.* **142**, 1382–1393 (2020).

4. Lin, Q. et al. Crystal Structure and NMR of an α,δ-Peptide Foldamer Helix Shows Side-Chains are Well Placed for Bifunctional Catalysis: Application as a Minimalist Aldolase Mimic**. Angew. Chem. 135, e202305326 (2023).

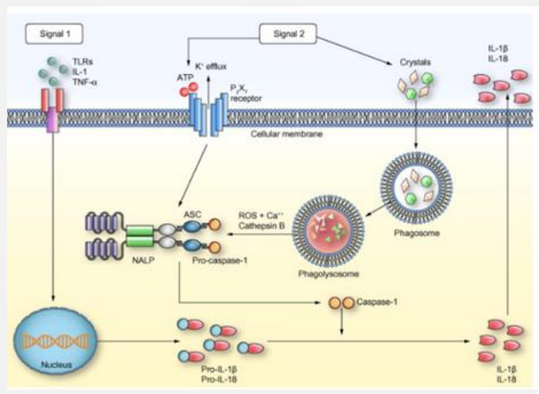
Discovery and Optimization of an mRNA Display Cyclic Peptide inhibitor of the IL1β/IL1R Interaction

Stefania Colarusso[1], Francesca Pavone[1], Elisabetta Bianchi[1], Roberto Iaccarino[1], Emanuela Mandic'[1], Emanuela Nizi[1], Willy Costantini[1], Martina di Geronimo[1], Faben Cruz[2], Dennis Feng[2], Yan Guo[2], Jennifer Hanisak[2], Charles Jayne[2], Ahmet Kekec[2], Angelea Kerekes[2], Victor Mak[2], Michael Lo[2], Jennifer Hickey[2] & Christopher Plummer[2]

[1]Peptides and Small Molecules R&D Department, IRBM Spa, Via Pontina km 30.600, 00071 Pomezia (RM), Italy.
[2]Merck & Co., Inc., Rahway, New Jersey 07065, United States.
https://doi.org/10.17952/38EPS.2026.P307

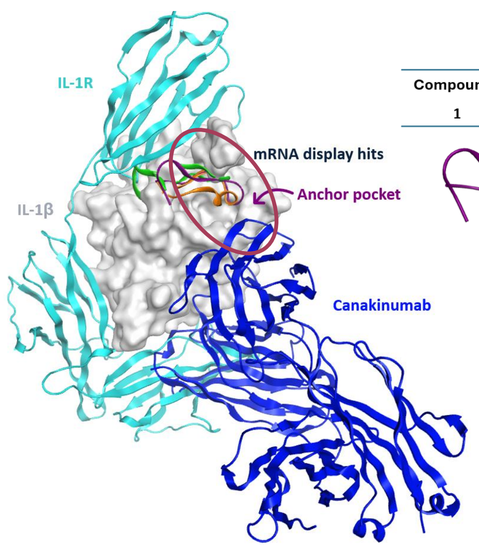
INTRODUCTION

Interleukin-1β (IL-1β), a member of the IL1 family of cytokines, is a key mediator of the inflammatory response[1]. Dysregulated IL-1β signaling plays a critical role in the pathogenesis of numerous diseases, including autoimmune, autoinflammatory, infectious, and degenerative disorders[2]. IL-1β is also involved as target in cardiovascular (CV) diseases, since inflammation drives the progression of atherosclerosis. Lowering inflammation through IL-1β pathway, provides atheroprotection, independent of lipid levels[3]. IL-1β activity can be inhibited by blocking the protein-protein interaction (**PPI**) between IL-1β and its cell-surface receptor IL1R. Clinically, IL-1β inhibition has been achieved using injectable anti-IL-1β monoclonal antibodies[3,4]. However, monoclonal antibody-based therapies are limited by challenges in fine-tuning cytokine modulation and achieving an optimal risk–benefit profile.

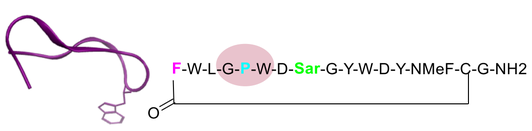


Macrocyclic Peptides Targeting IL-1β

- Macrocyclic peptides (**MCPs**) represent an innovative therapeutic modality for diseases involving protein-protein interactions (**PPI**)
- They offer potential advantages compared to large biological agents, such as increased tissue penetration and possibility for oral administration.
- mRNA display performed by Merck using PeptiDream platform identified a peptide hit (**Compound 1**) interfering with IL-1β signaling having a binding epitope distinct from mAB Canakinumab (about 450 Å^2 overlap)
- The peptide was binding close to the floppy N-terminal and C-terminal regions of IL1β.



Compound#	Biochem IC_{50} (nM)	Cell IC_{50} (nM)	Chymotrypsin $T_{1/2}$ (min)
1	324	1084	9



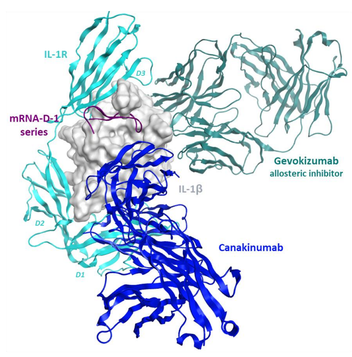
Assays → Disruption of IL-1β/IL-1R interaction

Biochemical: AlphaLISA assay

Cell: MRC-5 (human fibroblasts); measuring effect on downstream IL-6 release

Fig. 1 Initial Lead from mRNA Display

mRNA display hit (**Compound 1**) recapitulates Canakinumab pharmacology, inhibiting IL-6 expression induced by human IL-1β in fibroblast cells



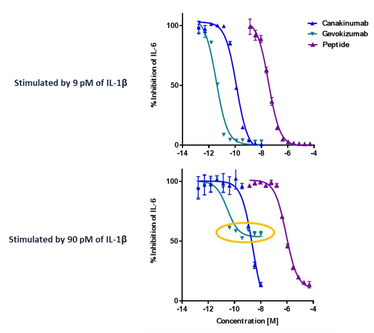
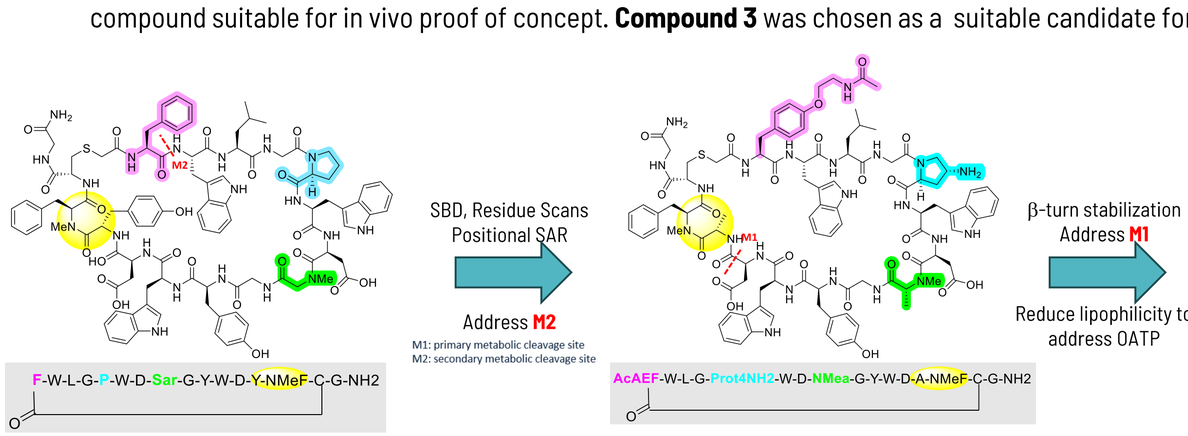


Fig. 2 Pharmacology of Lead from mRNA Display

RESULTS AND DISCUSSION

SAR Evolution

- Residue scanning and structure-based initial design allowed the evolution of **Compound 1** through potency improvement due to target engagement and conformational stabilization
- Further SAR studies helped addressing GI tract instability and OATP transporter issues achieving sufficient potency to develop a compound suitable for in vivo proof of concept. **Compound 3** was chosen as a suitable candidate for in vivo PK/PD study



Compound 1
Biochem IC_{50}: 324 nM
Cell IC_{50}: 1084 nM
Chymotrypsin $T_{1/2}$: 9 min
ALogP98: -1.05; OATP IC_{50}: 100 nM

Compound 2
Biochem IC_{50}: 30 nM
Cell IC_{50}: 75 nM
Chymotrypsin $T_{1/2}$: 106 min

Compound 3
Biochem IC_{50}: 46 nM
Cell IC_{50}: 211 nM
Chymotrypsin $T_{1/2}$: >12 h
ALogP98: -7.02; OATP IC_{50}: >10 μM

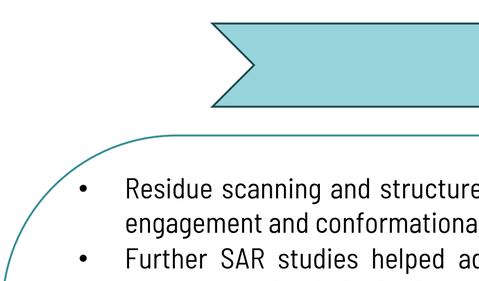
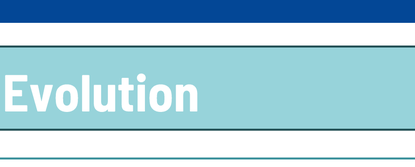


Fig.3 X-ray co-crystal of IL-1β and **Compound 1**

Residue scans
- Alanine
- D-amino acid
- *N*-methylation
- Identify which residues are essential and which are amenable to change



AA1	Biochemical (nM)	Cell (nM)
F (**Cpd 1**)	324	1084
ChA	676	2017
YCH2COOH	304	83
AcAEF	42	249

AA5	Biochemical (nM)	Cell (nM)
P (**Cpd 1**)	324	1084
4RNH2Pro	28	848
4F2Pro	193	1179
aMeP	na	Na

AA13	AA14	Biochemical (nM)	Cell (nM)
Y(**Cpd 1**)	NMeF(**Cpd 1**)	324	1084
A	NMeF	36	102
Aib	G	314	4517
Aib	Sar	332	2169

Fig.4 Scan results and examples of relevant single point positional SAR on Compound 1

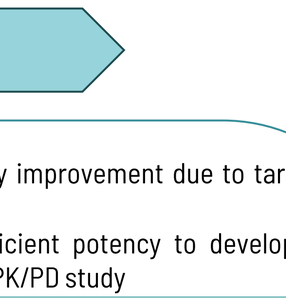
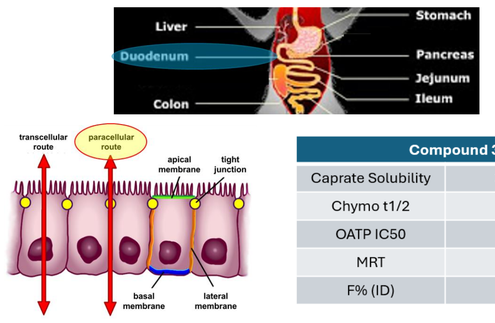


Fig.5 Crystal of **Compound 3** illustrates extension from F1 into space occupied by Arg4

In Vivo data

✓ **Compound 3** demonstrated oral bioavailability when administered to intraduodenally cannulated rats in the presence of 30% Na Caprate as permeation enhancer



Compound 3	
Caprate Solubility	>4 mg/mL
Chymo t1/2	>750 min
OATP IC50	>10 uM
MRT	0.4 h
F% (ID)	24 %; 4 %

✓ **Compound 3** was used to benchmark the MCP modality with Cana and test the specificity of cyclic peptides with IL-1RKO mice in air pouch model

✓ It demonstrated in vivo reduction in IL-6 in air pouch model with a MOA similar to Canakinumab

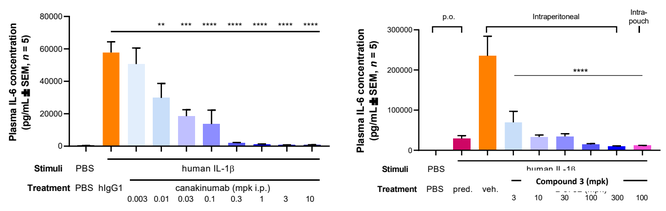


Fig.5 **Compound 3** blocks IL-6 induced by human IL-1b in the mouse air pouch modelIL1R

CONCLUSIONS

✓ An mRNA Display macrocyclic peptide lead inhibiting IL1β/IL1R PPI was evolved through structure-based design and data-driven multi-parameter optimization to a proof-of-concept molecule demonstrating formulation-enabled oral exposure (>2% F) in rodent ID PK study with a permeation enhancer (30% Na Caprate) and PD effect in in vivo with a profile which compares favorably with benchmark antibody Canakinumab and retains a similar MOA

✓ This work demonstrated the tractability of macrocyclic peptides as alternative chemical modality to efficiently tackle the PPI between IL1β and IL1R, and opens the path to future development of peptide-based oral therapies for diseases involving this pathway

REFERENCES
1. Garlanda, C. *Cellular & Molecular Immunology* **2025**, *22*, 1345
2. Dinarello, C.A. *Nature Reviews Drug Discovery* **2012**, *11*, *633*
3. CANTOS trial; NEJM **2017**; 377:1119-1131
4. Fields, J. *Cell Reports* **2024**, *43*, 114099
5. Peacock, H. *Trends in Pharmacological Sciences* **2021**, *42*(5),385

http://doi.org/10.17952/38EPS.2026.P127

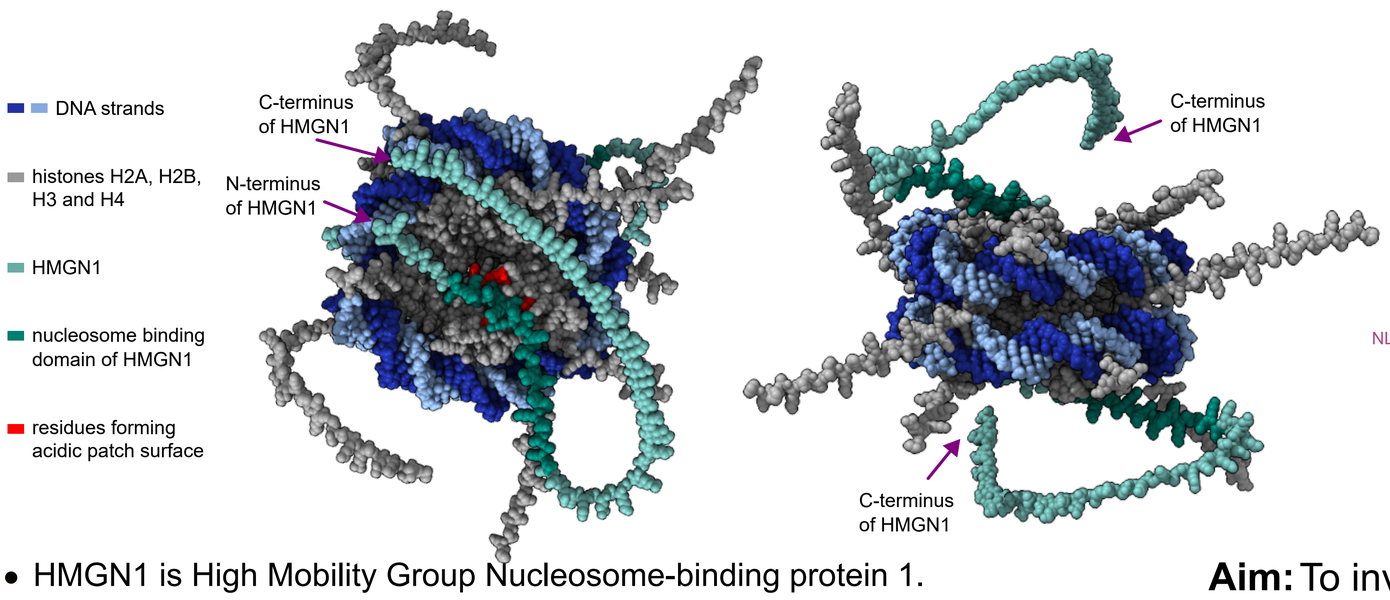
Lys acetylation and Ser phosphorylation crosstalk in the nucleosome binding domain of HMGN1

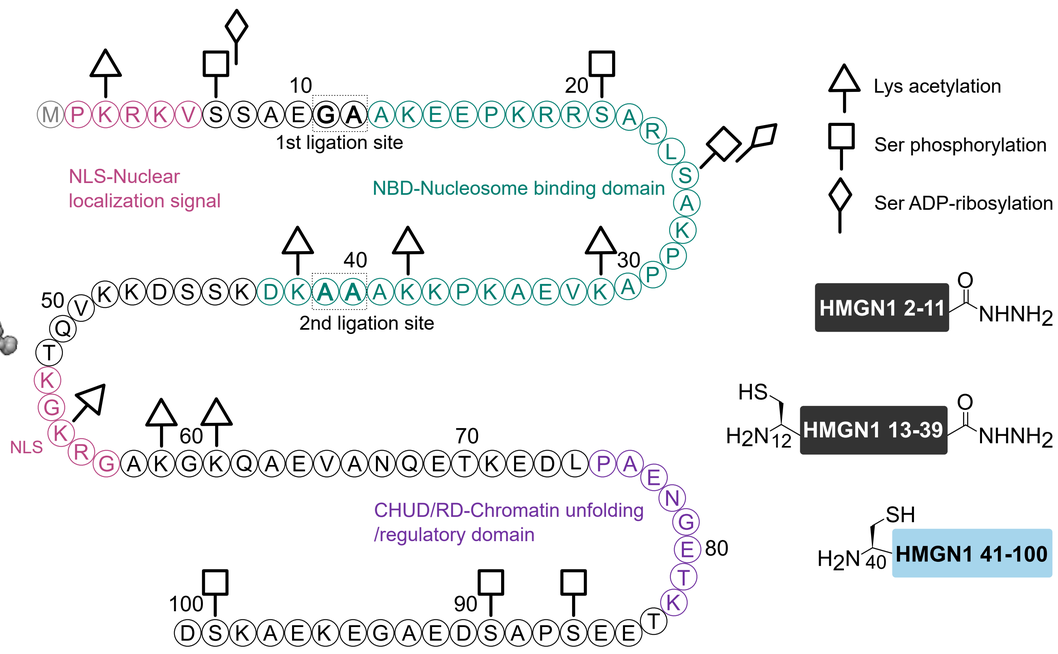
Medine Soydan, Anne C. Conibear

Institute of Applied Synthetic Chemistry, TU Wien, Vienna, Austria
E-mail: medine.soydan@tuwien.ac.at

Background

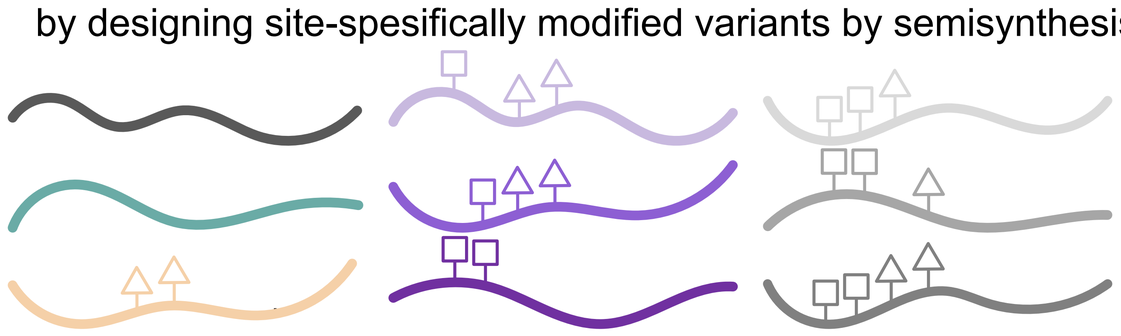
- Alphafold3 prediction of interactions between 2 molecules HMGN1 and nucleosome





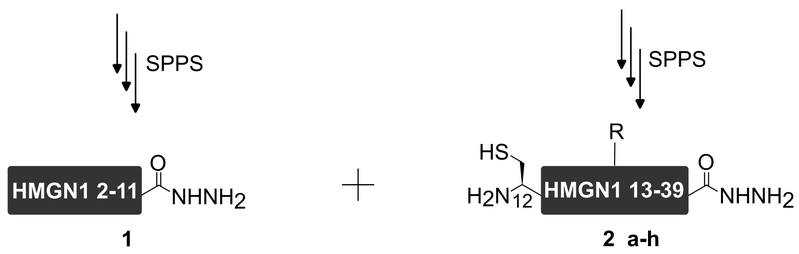
- HMGN1 is High Mobility Group Nucleosome-binding protein 1.
- HMGN1 is non-histone nucleosome binding protein interacting through the acidic patch surface.
- Acidic patch surface is Glu rich surface between H2A-H2B.
- HMGN1 is intrinsically disordered.
- HMGN1 undergoes extensive post-translational modifications (PTMs).

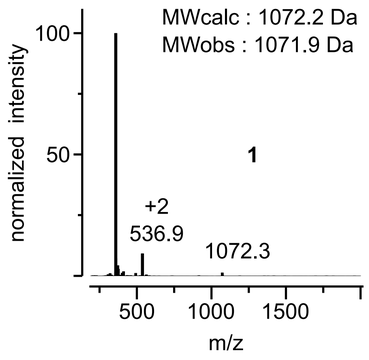
Aim: To investigate crosstalk between Lys acetylation and Ser phosphorylation in NBD of HMGN1 in nucleosome binding by designing site-spesifically modified variants by semisynthesis.



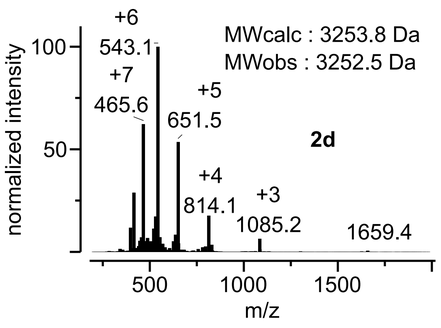
Synthesis

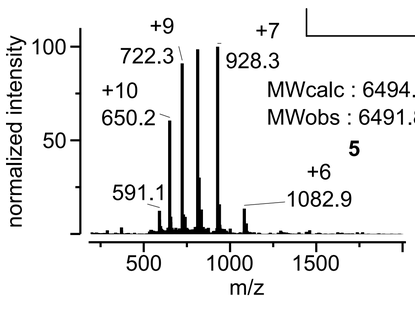
- 3 steps semisynthesis in N-to-C direction
- Ala to Cys mutation at Ala12 and Ala40



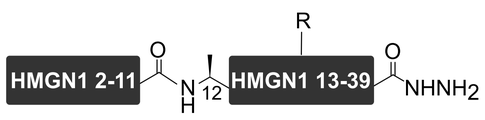


2a R=unmodified
2b R=acK31acK38
2c R=pS21acK31acK38
2d R=pS25acK31acK38
2e R=pS21pS25
2f R=pS21pS25acK31
2g R=pS21pS25acK38
2h R=pS21pS25acK31acK38



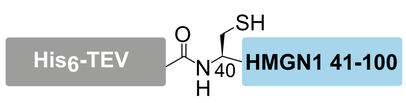


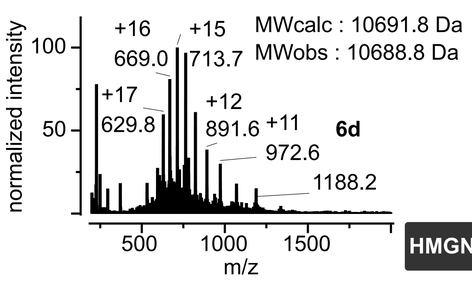
1i. Oxidation
1ii. Thiolysis
1iii. Ligation
1iv. Desulfurization



Ni-NTA affinity chromatography

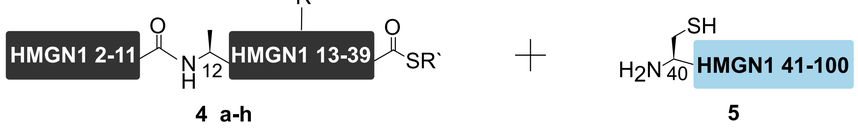
Recombinant expression in *E. coli*

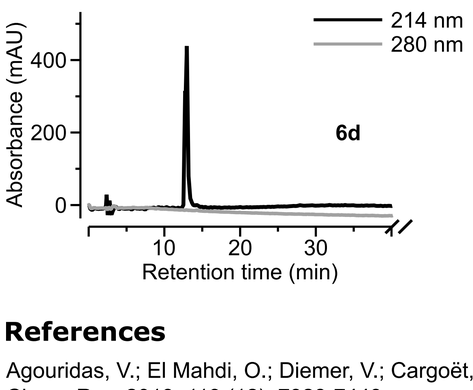




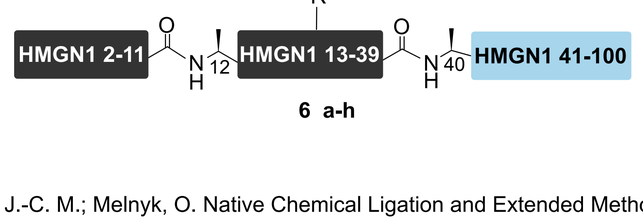
2i. Oxidation
2ii. Thiolysis

protease cleavage



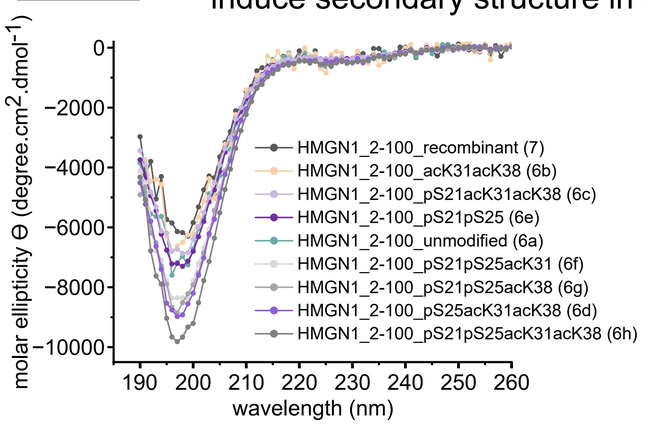


3i. Ligation
3ii. Desulfurization



Analysis

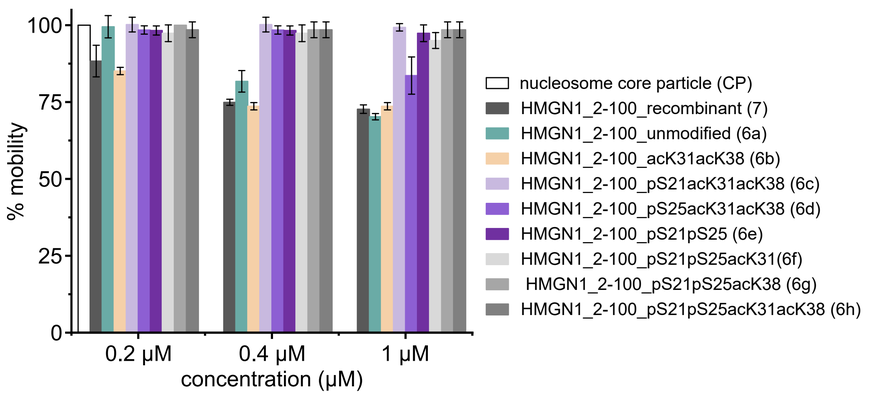
- Circular dichroism shows that modifications did not induce secondary structure in whole protein.



- All variants are random coil.
- Phosphorylation of Ser21 and/or Ser25 abolishes nucleosome binding, regardless of Lys31 and/or Lys38 acetylation.
- >1.2× TBE buffer (1× TBE: 89 mM Tris, 89 mM borate, 1 mM EDTA, pH 8.4) → cooperative binding (i.e., 2 molecules HMGN1/nucleosome) → 2× TBE buffer was used

A representative native gel

- 3 experimental replicates of EMSA gels were performed.
- 20 R R S A R L S A — core conserved sequence of NBD in HMGN family
- Partial recovery of binding in 6d with 5 equiv. implies the critical role of Ser21 in nucleosome binding.
- As Ser phosphorylation has a dominating effect in abolishing the binding affinity, a crosstalk effect between Ser phosphorylation and Lys acetylation was not observed



References

Agouridas, V.; El Mahdi, O.; Diemer, V.; Cargoët, M.; Monbaliu, J.-C. M.; Melnyk, O. Native Chemical Ligation and Extended Methods: Mechanisms, Catalysis, Scope, and Limitations. Chem. Rev. 2019, 119 (12), 7328-7443.
Postnikov, Y. V.; Bustin, M. Functional Interplay between Histone H1 and Hmg Proteins in Chromatin. Biochim. Biophys. Acta Gene Regul. Mech. 2016, 1859 (3), 462-467.
Niederacher, G.; Urwin, D.; Dijkwel, Y.; Tremethick, D. J.; Rosengren, K. J.; Becker, C. F. W.; Conibear, A. C. Site-Specific Modification and Segmental Isotope Labelling of Hmgn1 Reveals Long-Range Conformational Perturbations Caused by Posttranslational Modifications. RSC Chem. Biol. 2021, 2 (2), 537-550.

Acknowledgements

Lydia Jane Barber, Julia Leitgeb, Mohamed Elshazly, Sascha Gumprecht, Tobias Gökler

FWF Austrian Science Fund
Project no. P36101-B

https://doi.org/10.17952/38EPS.2026.P440

Synthesis of MUC1 Tn/Sialyl-Tn Glycopeptides and Combinatorial Libraries for Lectin Binding Studies

Maré Cudic[1], Ivet Boneva[1], Ramya Ayyalasomayajula[1], Donella Beckwith[1], YashoNandini Singh[1], Sabine André[2] and Herbert Kaltner[2]

[1]Department of Chemistry and Biochemistry, Florida Atlantic University, 777 Glades Road, Boca Raton, Florida 33431
[2]*Ludwig-Maximilians-Universität München, Department of Veterinary Sciences, Physiological Chemistry, Lena-Christ-Str. 48, 82152, Planegg-Martinsried, Germany*

Introduction

Mucin 1 (MUC1) is a heavily glycosylated transmembrane protein, altered in both expression and glycosylation pattern in human carcinomas of the epithelium. The incomplete or truncated glycan structures, often capped by sialic acid are overexpressed in premalignant and malignant tissue.[1,2]

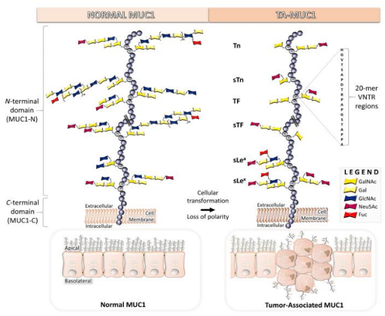


Fig 1: Structural differences between normal and tumor- associated MUC1.

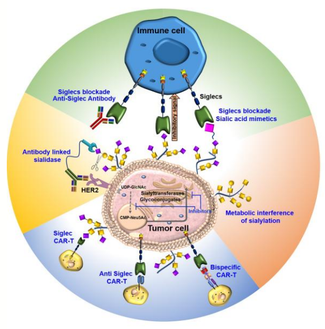


Fig 2: Strategies to target Siglec-sialylated MUC1 immune axis in cancer.

Interactions between the tumor-associated carbohydrate antigens (TACAs) of MUC1 and the carbohydrate-binding proteins, lectins, often lead to the creation of a pro-tumor microenvironment favoring tumor initiation, progression, metastasis, and immune evasion.

Macrophage galactose binding lectin (MGL) is a C-type lectin receptor found on antigen-presenting cells that facilitates the uptake of carbohydrate antigens for antigen presentation, modulating the immune response homeostasis, autoimmunity, and cancer.

The specific aim of this research is to synthesize mono and multiple glycosylated MUC1 glycopeptide models carrying the Tn or sTn (sialyl Tn), that allow for the control of the complexity of the chemical space of the multivalent ligands.[3,5] In addition, we use Positional Scanning Synthetic Glycopeptide Combinatorial Libraries (PS-SGCLs) as a tool to model the diversity in the type and positions of *O*-glycans on MUC1.[4] This focused combinatorial library with defined structural complexity allow us to evaluate the effect of neighboring residue glycosylation, glycan density, and/or the presence of unique patterns of *O*-glycan clusters on binding to lectins, thus helping us understand the multivalent carbohydrate–lectin recognition processes at the molecular level.

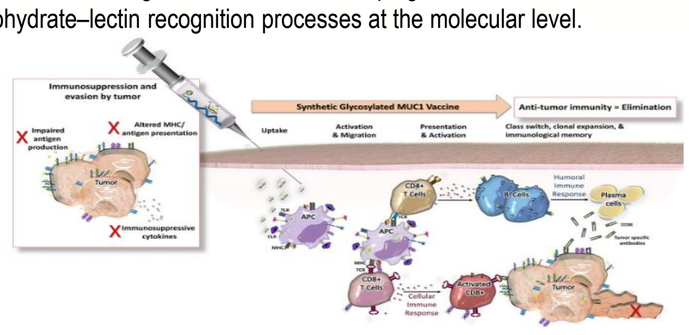
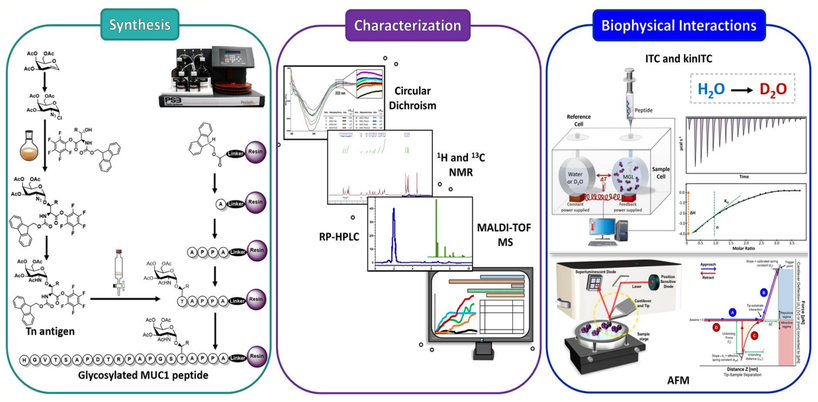


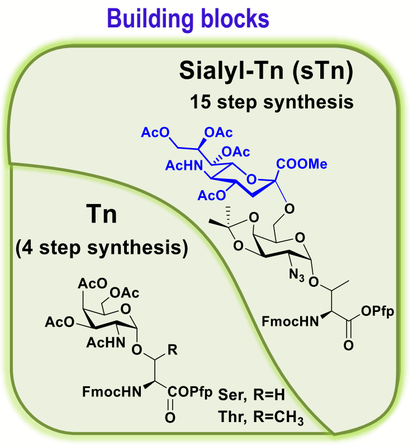
Fig3: Cancer vaccines either aim to prevent precancerous tumors from shifting into a microenvironment that favors regulatory and immunosuppressive mechanisms (preventive) or to restore immunosurveillance (therapeutic).

Considering the crucial role of tumor-associated forms of MUC1 with MGL in tumor immunology, a thorough understanding of this interaction is essential for it to be exploited for cancer vaccine strategies.

Methodology



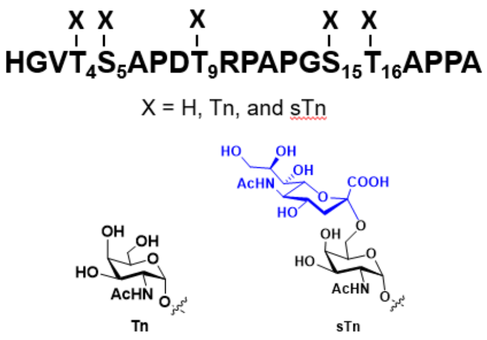
Building blocks



The Tn antigen building block was prepared via one-pot azidochlorination to generate the glycosyl donor, followed by a modified Koenigs–Knorr reaction to incorporate the Fmoc-protected Thr acceptor.[3] For the sTn analog, orthogonal protections enabled selective C6 glycosylation using a phenylthiosialoside donor activated by NIS/TMSOTf.[5]

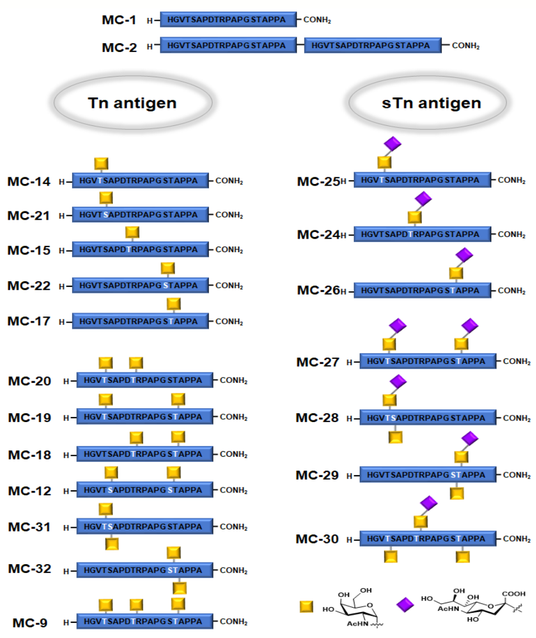
Positional Scanning Synthetic Glycopeptide Combinatorial Library (PS-SGCL)

A PS-SGCL was constructed using the "tea bag" method and standard Fmoc solid-phase peptide synthesis (SPPS). In each positional sublibrary one position on either Thr or Ser is fixed while the remaining glycosylation sites were incorporated as the isokinetic mixtures.

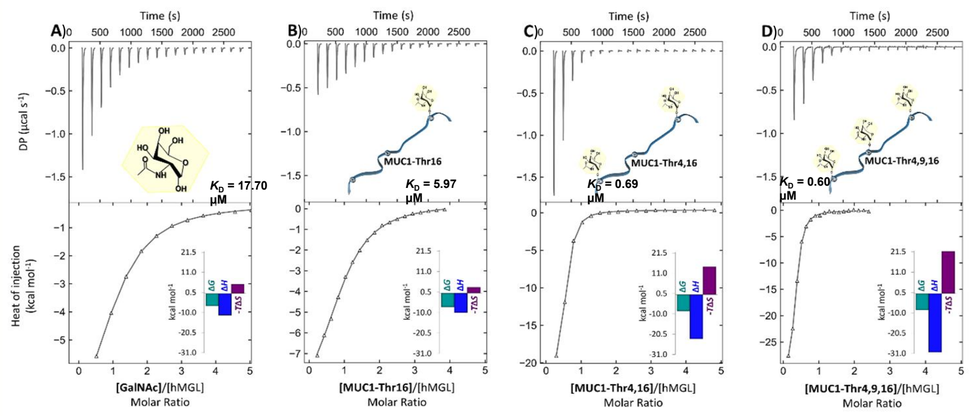


Results

MUC1 Glycopeptide models



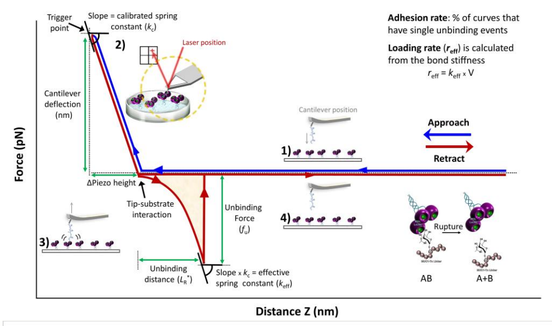
Thermodynamics of hMGL binding to GalNAc and MUC1 Glycopeptides



Selected ITC binding curves including thermographic profiles for interaction between (A) Gal*N*Ac (1.50 mM) with hMGL (29.6 μM), (B) MUC1-Thr^{16}(Tn) (0.50 mM) with hMGL (22 μM), (C) MUC1-Thr^{4,16}(Tn) (0.50 mM) with hMGL (20 μM), and (D) MUC1-Thr^{4,9,16}(Tn) (0.25 mM) with hMGL (20 μM) in buffered H_2O determined by ITC. Isotherms and thermograms were reproduced in GUSSI v.1.4.2 from data generated by MicroCal PEAQ-ITC software.

Kinetics of hMGL binding to GalNAc and MUC1 Glycopeptides

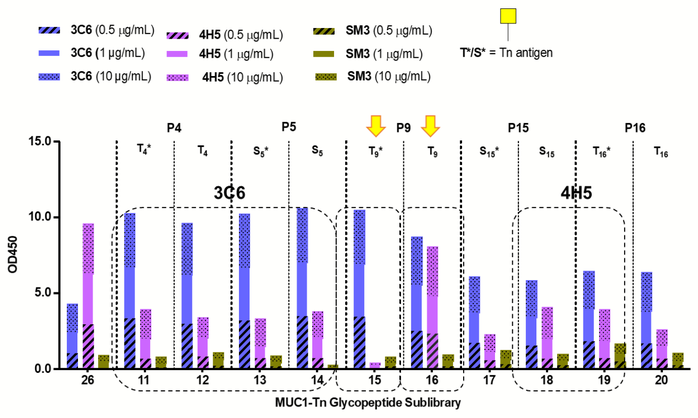
Force-Distance Rupture Curve



Parameters for the Energy Landscape of Immobilized Ligand: Receptor	MUC1-Thr^4(Tn): hMGL	MUC1-Thr^9(Tn): hMGL	MUC1-Thr^{16}(Tn): hMGL
Most Probable Force, F^* (pN)	54	34	33
Width of the energy barrier, x_β (nm)	0.353	0.807	0.733
Off-rate, k_{off} (s^{-1})	1.823	0.0789	1.159
Lifetime, τ_0 (s)	0.548	12.672	0.862

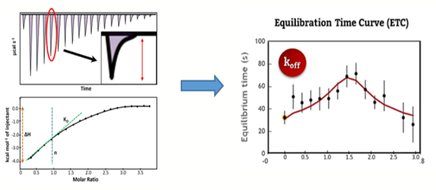
Screening and deconvolution of MUC1-Tn PS-SGCL by ELISA assay

Anti-MUC1 mAbs



- **Sublibrary 16** showed a strong preference for a non-glycosylated Thr^9 in the PDTR epitope of MUC1 for **4H5** anti-MUC1 mAb.

Kinetic parameters and lifetime calculated from experimental ITC data using AFFINImeter KinITC software

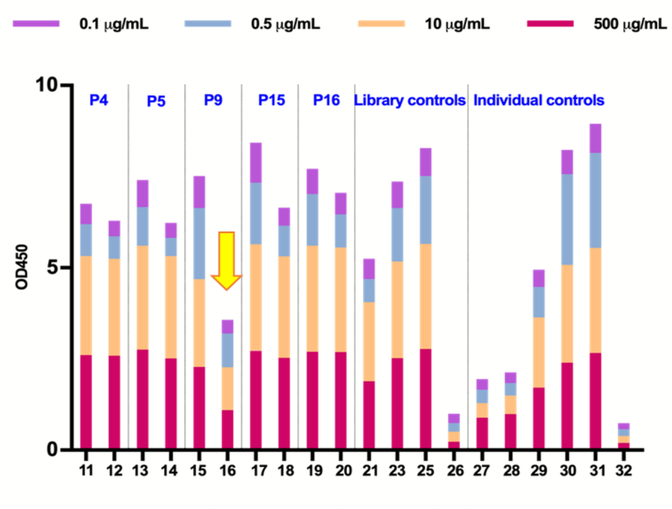


Ligands	k_{on} $x\ 10^6\ M^{-1}\ s^{-1}$	k_{off} s^{-1}	τ s
GalNAc	-	-	-
MUC1-Thr^4(Tn)	-	-	-
MUC1-Thr^9(Tn)	-	-	-
MUC1-Thr^{16}(Tn)	0.096	0.60	1.67
MUC1-Thr^{9,16}(Tn	0.032	0.049	20.41
MUC1-Thr^{4,16}(Tn)	0.058	0.051	19.61
MUC1-Thr^{4,9}(Tn)	0.016	0.060	16.67
MUC1-Thr^{4,9,16}(Tn)	0.026	0.019	52.63

- KinITC analysis revealed a prolonged lifetime of the lectin–glycan complex with increasing glycan valency.

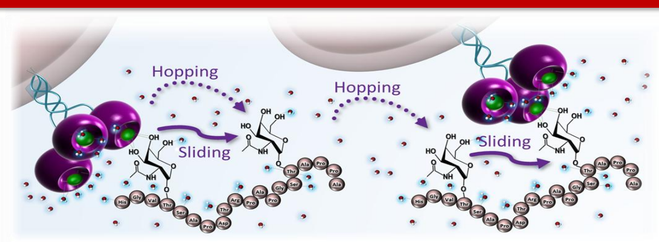
Screening and deconvolution of MUC1-Tn PS-SGCL by ELLA assay

Glycine max soybean agglutinin (SBA)



- **Sublibrary 16** showed a major loss in affinity when Thr^9 is non-glycosylated while other positions are mixtures.

Conclusion



- Glycan density, as well as the topology in the vicinity of the glycan site of attachment in the MUC1 epitope impact lectin affinity differently and can be used to manipulate thermodynamic and kinetic signatures of binding.
- "Bind and jump" mechanism is evident, from the additive –ΔH, non-additive -ΔS, and increasing lifetimes as the glycan density increases.
- The success of vaccine strategies is also dependent on a better understanding of the role of the tumor microenvironment (TME) in cancer progression.

References

1. Donella M. Beckwith and Maré Cudic, Seminars in Immunology, https://doi.org/10.1016/j.smim.2020.101389
2. R. Ayyalasomayajula, M. Cudic, *Cancers (Basel)* **2024**, *16*, 1334. https://doi.org/10.3390/cancers16071334
3. D. M. Beckwith, F. G. FitzGerald, M. C. Rodriguez Benavente, E. R. Mercer, A.-K. Ludwig, M. Michalak, H. Kaltner, J. Kopitz, H.-J. Gabius, M. Cudic, *Biochemistry* **2021**, *60*, 547–558. https://doi.org/10.1021/acs.biochem.0c00942
4. Y. Singh, M. C. Rodriguez Benavente, M. H. Al-Huniti, D. Beckwith, R. Ayyalasomayajula, E. Patino, W. S. Miranda, A. Wade, M. Cudic, J. Org. Chem. 2020, 85, 1434–1445. https://doi.org/10.1021/acs.joc.9b02396
5. R. Ayyalasomayajula, I. Boneva, D. Ormaza, A. Whyte, K. Farook, Z. Gorlin, E. Yancey, S. André, H. Kaltner, M. Cudic, *ChemBioChem* **2024**, https://doi.org/10.1002/cbic.202400391

Acknowledgments

Support for this study was provided by the National Institute of Health to Dr. M. Cudic (R15 grant CA178754).

Cyclic Peptide–Based Platform for Targeted Delivery to the Brain

Predrag Cudic, Harrison Hutchings, Aleksandra Nedovic, Lucas Costa

Department of Chemistry and Biochemistry, Florida Atlantic University, Boca Raton, FL 33431, USA.

Email: pcudic@fau.edu

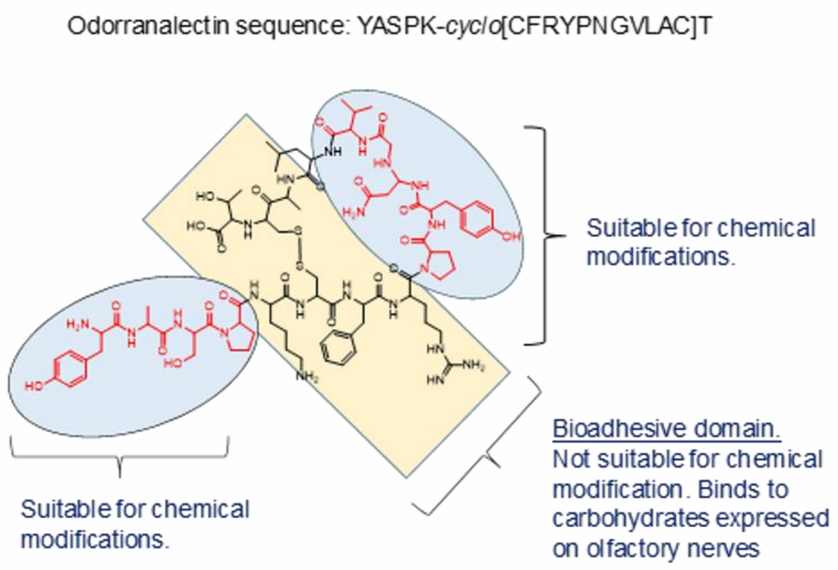
https://doi.org/10.17952/38EPS.2026.P484

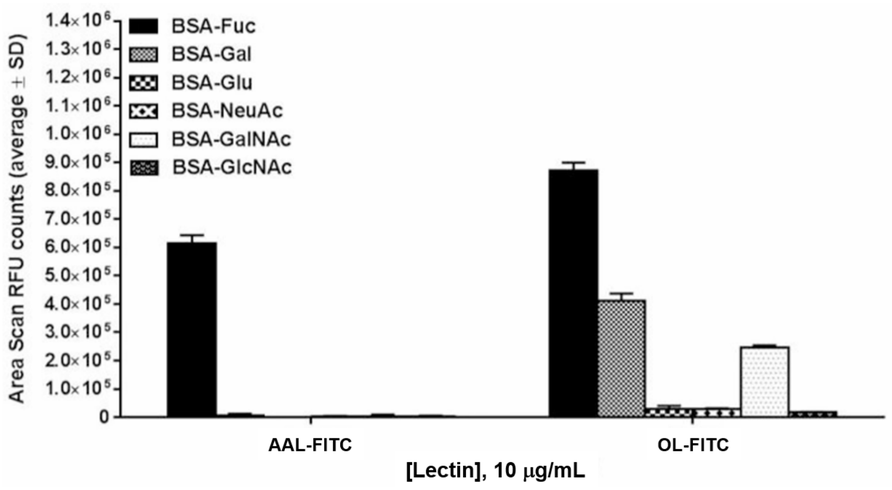
Introduction

Brain and central nervous system diseases are leading causes of disability worldwide, contributing substantially to hospitalization and long-term care. Peptides and small interfering RNA (siRNA) molecules offer significant therapeutic potential because of their ability to selectively target disease-associated proteins and genes. However, conventional delivery routes, such as oral and intravenous administration, are largely ineffective for transporting these molecules into the brain because of the restrictive nature of blood-brain barrier (BBB) and blood-cerebrospinal fluid barrier (BCB). Alternatively, intranasal (i.n.) delivery offers an attractive alternative that enables direct nose-to-brain delivery, bypassing these barriers while reducing systemic exposure and minimizing hepatic and renal clearance related toxicity.

Lectinomimic approach

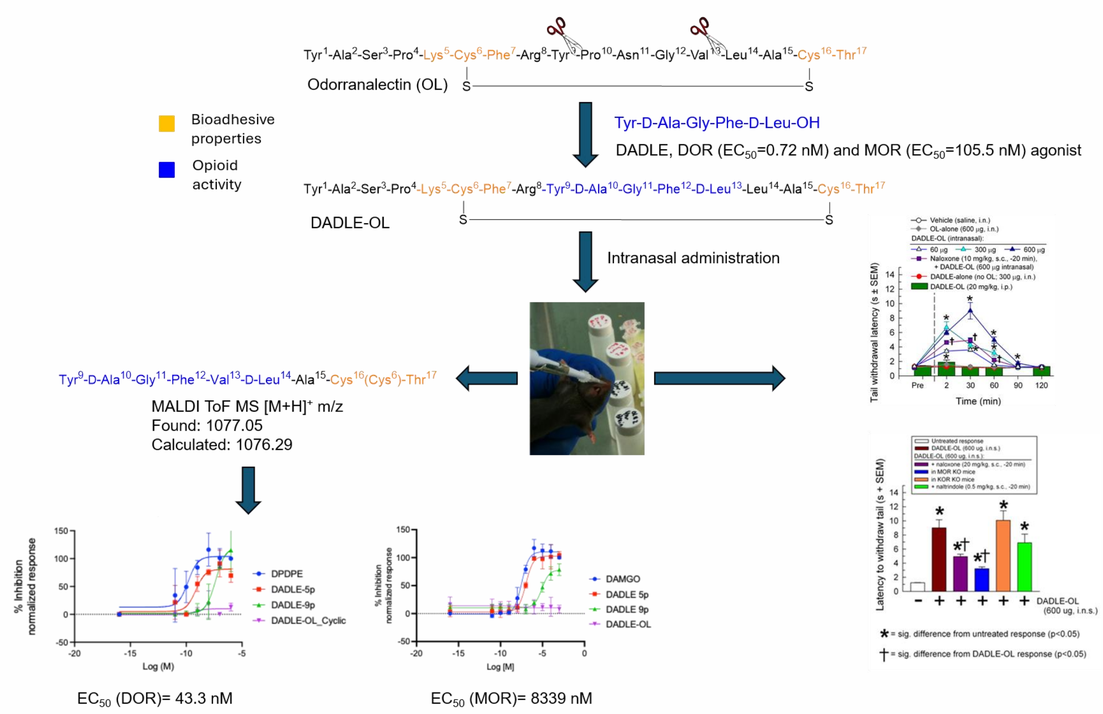
To enhance intranasal (i.n.) delivery of therapeutic peptides to the brain, we developed a novel strategy based on grafting a bioactive amino acid sequence onto the scaffold of the cyclic peptide odorranalectin (OL), which exhibits lectin-like properties. OL binds preferentially to L-fucose (Fuc) and, to a lesser extent, to D-galactose (Gal) and N-acetyl-D-galactosamine (GalNAc), carbohydrates that are widely distributed on the olfactory epithelium of the nasal mucosa. This binding profile suggests that OL may prolong residence time within the nasal cavity, thereby increasing mucosal retention and enhancing peptide absorption across the olfactory epithelium.





Binding of AAL-FITC and OL-FAM to BSA-monosaccharides.

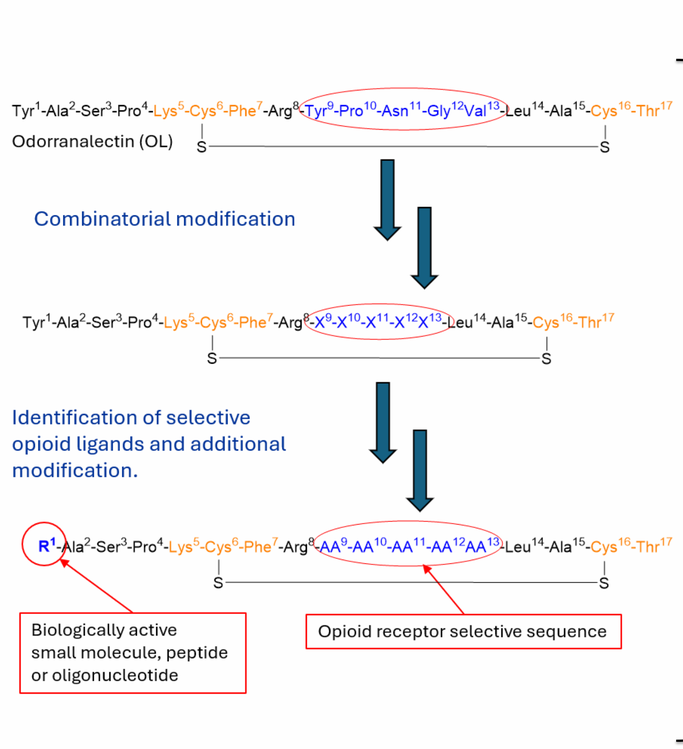
DADLE sequence grafting: proof of principle



Antinociceptive effects observed 2 min after i.n. administration. No effects observed after i.p. administration.

In vivo selectivity demonstrated by antinociception in wild-type, MOR-KO, KOR-KO, and in mice pre-dosed with naloxone and naltrindole.

OL-based KOR-selective ligand

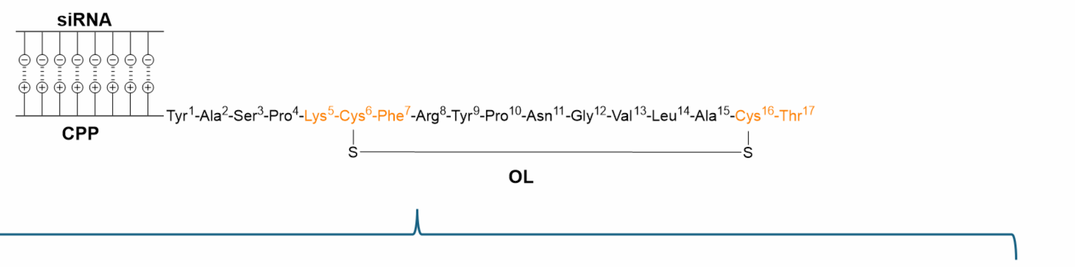


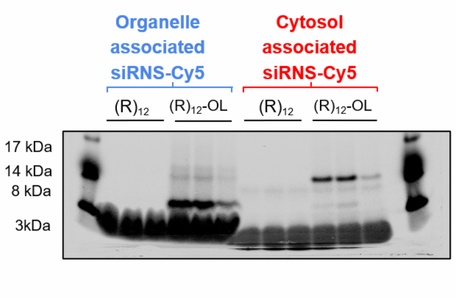
Improved *in vivo* selectivity.

More potent and longer lasting antiallodynic effects observed in the mouse chronic constriction injury (CCI) model of neuropathic pain compared to morphine.

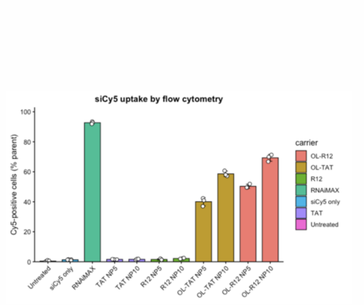
Effects on mice respiration.

OL-mediated cellular uptake of siRNA

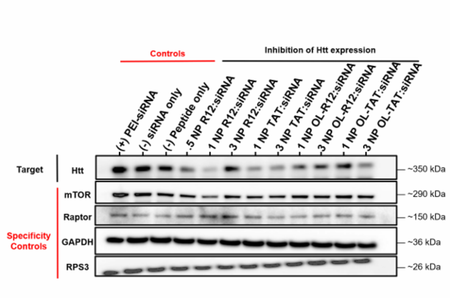




The size of the siRNA-Cy5 is conserved in the cytosolic fraction



siRNA-Cy5 uptake by flow cytometry (4h incubation)



Suppression of Huntingtin (htt) protein expression upon siRNA internalization in Q7 cells

Acknowledgment

This research was partially supported by the National Institute of Health (NIH) Grant 1R15DA061114-01 awarded to P.C.

FLORIDA ATLANTIC

SELECTION, SYNTHESIS AND INTERACTION OF hACE2 PEPTIDE FRAGMENTS TOWARDS SPIKE PROTEIN OF THE SARS-COV-2 VIRUS

A. Czerchawy[1,2*], M. K. Muthyala[3], F. Real-Fernandez[4], F. Nuti[2], P. Rovero[5], A. M. Papini[2], B. Kolesińska[1]

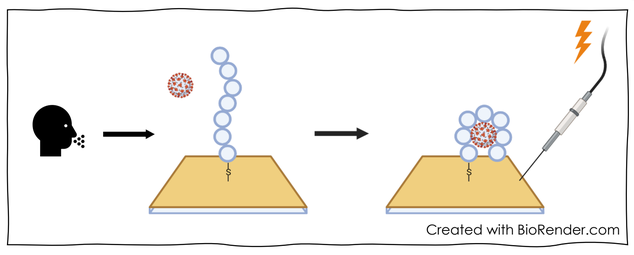
ola.czerchawy@gmail.com

https://doi.org/10.17952/38EPS.2026.P511

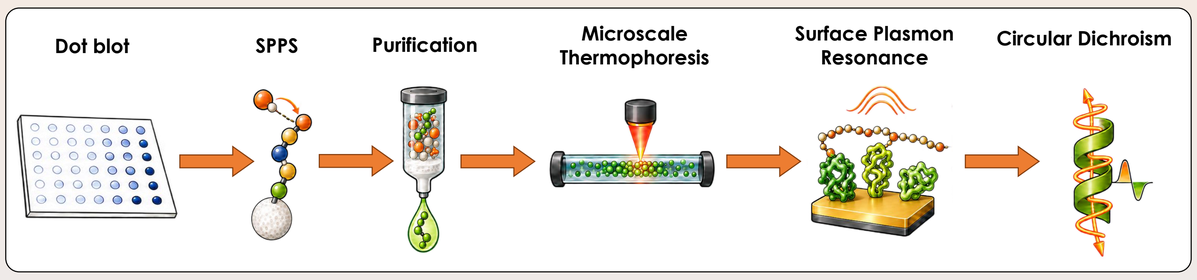
1) *Institute of Organic Chemistry, Faculty of Chemistry, Lodz University of Technology, Lodz, Poland*
2) *Interdepartmental Research Unit of Peptide and Protein Chemistry and Biology, Department of Chemistry "Ugo Schiff", University of Florence, Sesto Fiorentino, Italy*
3) *Gyros Protein Technologies AB, Teltow, Germany*
4) *4CNR - Istituto di Chimica dei Composti Organometallici (CNR-ICCOM), Sesto Fiorentino, Italy*
5) *Interdepartmental Research Unit of Peptide and Protein Chemistry and Biology, Department of Neurosciences, Psychology, Drug Research and Child Health, University of Florence, Sesto Fiorentino, Italy*

AIM OF THE STUDY

To identify hACE2 peptide fragments capable of recognising the SARS-CoV-2 spike protein and to evaluate their potential as biorecognition elements for detecting virus in exhaled air and indor environmental samples

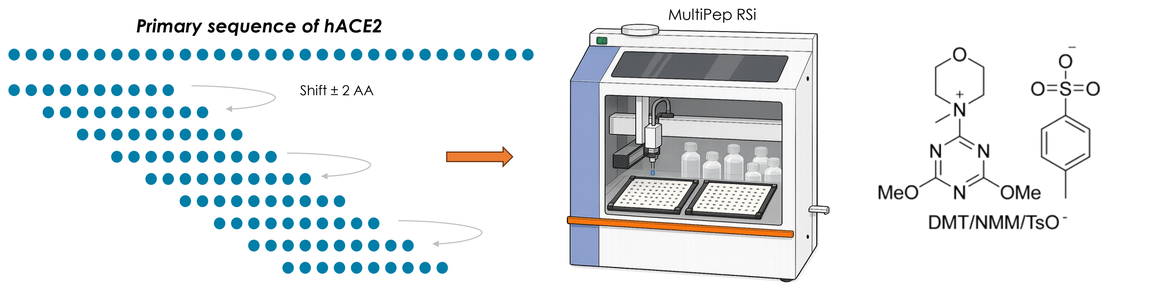


METHODS



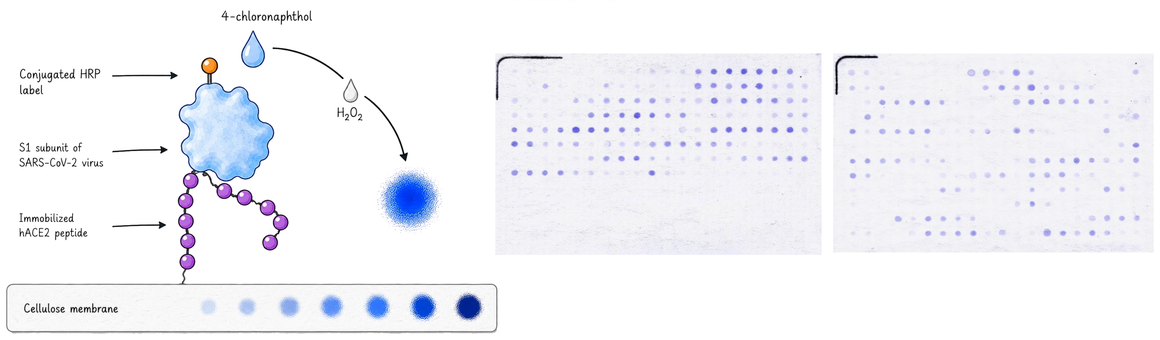
RESULTS

SPOT SYNTHESIS



Frączyk J., Walczak M., Kamiński Z.J. J. Pept. Sci. 2018, 24, e3063.

SELECTION

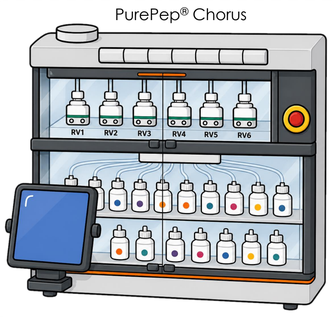


Fragments strongly interacting with the S1 subunit of the SARS-CoV-2 virus

No.	Locant	AA	Peptide fragment
1.	505-526	22	H-HVSNDYSFIRYYTRTLYQFQFQ-OH
2.	667-692	26	H-EEDVRVANLKPRISFNFFVTAPKNVS-OH
3.	545-562	18	H-SNSTEAGQKLFNMLRLGK-OH
4.	641-666	26	H-YLFRSSVAYAMRQYFLKVKNQMILFG-OH
5.	611-632	22	H-SPYADQSIKVRISLKSALGDKA-OH
6.	587-606	20	H-YFEPLFTWLKDQNKNSFVGW-OH
7.	755-776	22	H-VGIVILIFTGIRDRKKKNKARS-OH
8.	699-718	20	H-EVEKAIRMSRSRINDAFRLN-OH
9.	265-282	18	H-HLLGDMWGRFWTNLYSLT-OH
10.	103-122	20	H-NGSSVLSEDKSKRLNTILNT-OH

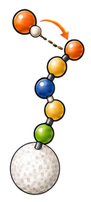
Kolesińska B. et al. *Engineering of Biomaterials* **2018**,*148*, 41.

INDUCTION-HEATED SPPS



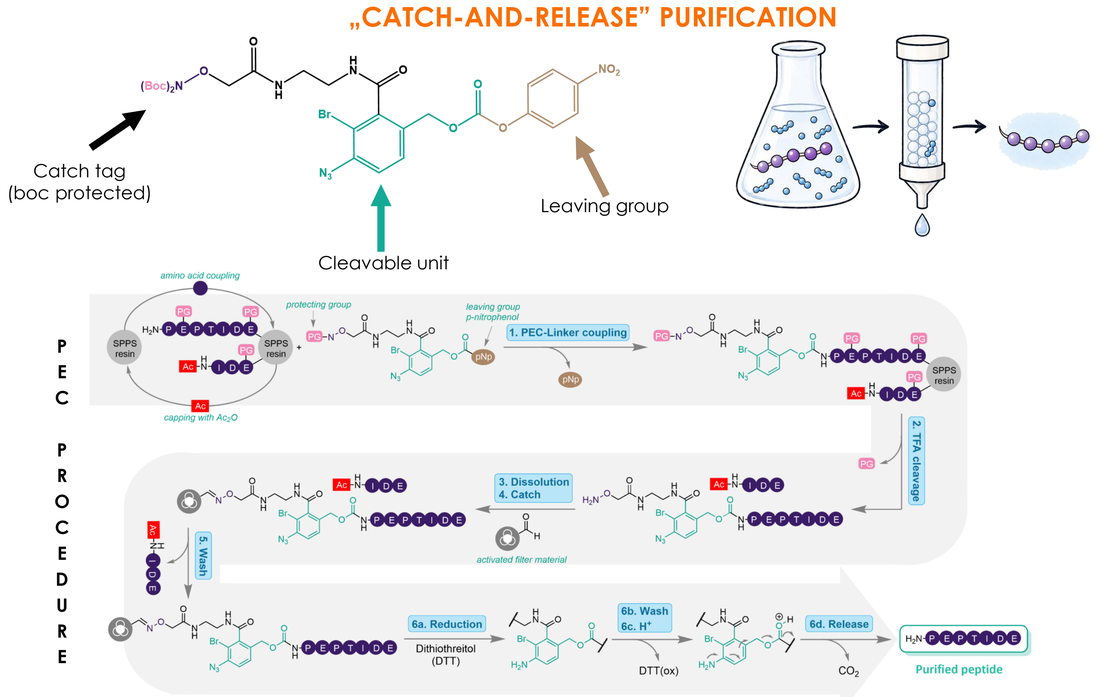
IH-SPPS conditions

- Fmoc/tBu strategy
- 50-200 µmol scale
- Preloaded Wang or TCP resin
- HCTU/DIPEA or DIC/OxymaPure coupling reagents
- RT, 60 or 90 °C



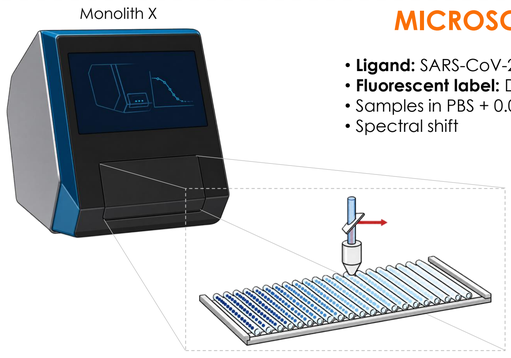
The synthesis conditions were adjusted individually according to peptide length, hydrophobicity and aggregation tendency

„CATCH-AND-RELEASE" PURIFICATION



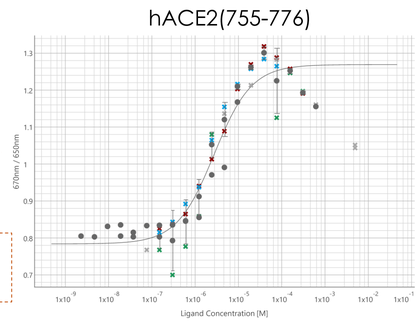
Zitterbart R., Berger N., Reimann O., Noble G.T., Lüdtke S., Sarma D., Seitz O. Chem. Sci. **2021**, 12, 2389.

MICROSCALE THERMOPHORESIS

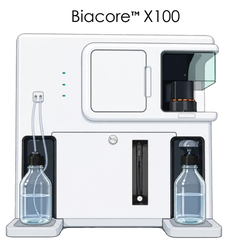


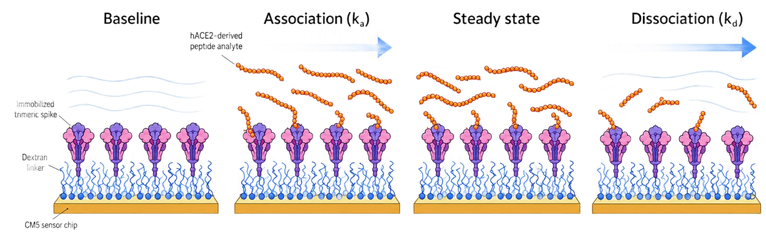
- **Ligand:** SARS-CoV-2 hFc with His tag
- **Fluorescent label:** Dye 2nd Gen (MST)
- Samples in PBS + 0.05% Tween-20
- Spectral shift

$K_D \approx 2.74$ µM (confidence interval 1.86-4.02 µM)



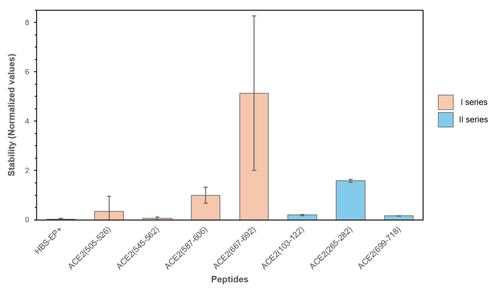
SURFACE PLASMON RESONANCE





- **Ligand:** trimeric SARS-CoV-2 spike protein
- **Analyte:** selected hACE2 peptides
- **Sensor:** CM5
- **Buffer**: HBS-EP+

Ligand was immobilised on a sensor chip by amine coupling. Selected hACE2 peptides were injected as analytes and their binding responses were monitored in real time

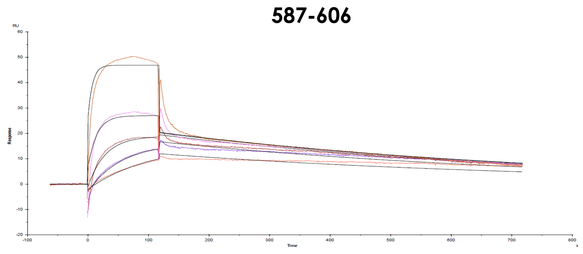


Key observations

- hACE2(587–606) produced a reproducible binding response.
- hACE2(265–282) also showed reproducible interaction with the immobilised spike protein.
- Responses obtained for hACE2(641–666) and hACE2(667–692) were not fully reproducible.
- hACE2(755–776) produced a complex response that could not be reliably interpreted using the applied SPR conditions.

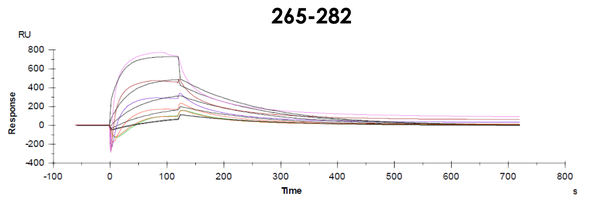
Kinetic studies

587-606



Model	k_{a1} [M^{-1} s^{-1}]	k_{d1} [s^{-1}]	Apparent K_D [µM]	R_{max} [RU]	Chi^2 [RU^2]	U-value
1:1	2669	0.001506	0.564	20.77	2.77	5

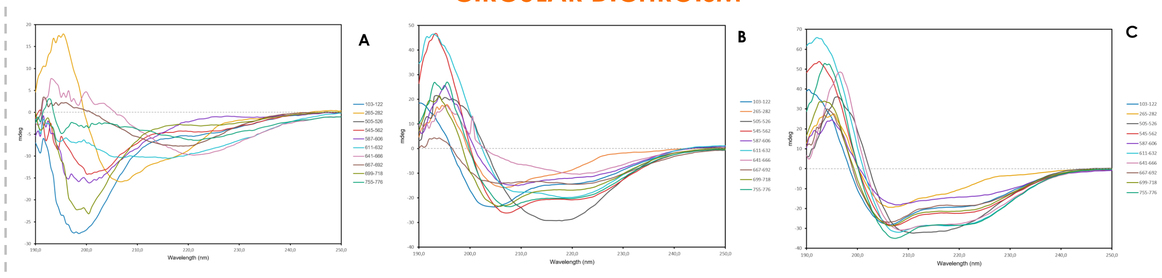
265-282



Model	k_{a1} [M^{-1} s^{-1}]	k_{d1} [s^{-1}]	Apparent K_D [µM]	R_{max} [RU]	Chi^2 [RU^2]	U-value
1:1	454.4	0.006918	15.2	584.3	1520	5

M. Quagliata et al. *ACS Omega* **2023**, *8*, 25, 22665-22672.

CIRCULAR DICHROISM



A – phosphate buffer (PB); **B** – 25% TFE in PB; C – 50% TFE in PB

TFE promoted a-helical structure formation in the selected hACE2 fragments, revealing their intrinsic conformational propensity. **The highest a-helical content was observed for hACE2(755–776).**

TAKE-HOME MESSAGE

- Dot-blot screening enabled the selection of ten hACE2-derived sequences for further investigation.
- The selected peptides were successfully produced using individually optimised SPPS and purification strategies.
- MST and SPR identified hACE2 fragments capable of interacting with SARS-CoV-2 spike constructs, although the observed behaviour depended on the applied method.
- CD analysis revealed pronounced environment-dependent conformational changes, with hACE2(755–776) showing the highest a-helical propensity
- **Combining complementary biophysical methods is essential for the reliable evaluation of peptide–spike interactions.**

ACKNOWLEDGEMENTS

MST measurements were performed at the Centre of Molecular and Macromolecular Studies, Polish Academy of Sciences (CMMS PAS), Lodz, Poland with the assistance of Agnieszka Krakowiak, DSc.

Peptide synthesis and purification using PEC technology were performed in collaboration with Gyros Protein Technologies, Teltow, Germany, with the support of Dr. Manoj Muthyala

Peptide synthesis and purification, surface plasmon resonance measurements, and circular dichroism spectroscopy were carried out in collaboration with PeptLab, University of Florence, Italy

Participation in the conference was supported by the European Peptide Society (EPS) and the SNOOPY COST Action (CA23111)

LET'S CONNECT!



ALEKSANDRA CZERCHAWY, MSc.
PhD candidate in Chemical Sciences
Peptide Chemistry • Interaction studies

LET'S TALK ABOUT

- Peptide-based biorecognition
- Spike-peptide interactions
- Detection of viral markers

Open to scientific collaborations in peptide chemistry, biochemistry and related research areas

Scan to explore my research and connect

https://doi.org/10.17952/38EPS.2026.P554

From Self-Assembly to Function: Tunable Peptide Fibrils as Nanocarriers

Milena Czeszejko[1], Justyna Sawicka[1], Ewa Wieczerzak[1], Daria Sowik[2], Patrycja Rachubik[3], Tomasz Kulesza[3], Kamila Kitowska[4], Rafał Sądej[4], Zuzanna Pietralik-Molińska[5], Maciej Kozak[5], Olena Ivashchenko[6], Sylwia Rodziewicz-Motowidło[1]

[1]Department of Biomedical Chemistry, Faculty of Chemistry, University of Gdańsk, Gdańsk, Poland [2]Department of Food Chemistry and Biotechnology, Faculty of Chemistry, Gdańsk University of Technology, Gdańsk, Poland [3]Mirosław Mossakowski Medical Research Institute, Polish Academy of Sciences, Laboratory of Molecular and Cellular Nephrology, Gdańsk, Poland [4]Intercollegiate Faculty of Biotechnology of the University of Gdańsk and the Medical University of Gdańsk, Gdańsk, Poland [5]Department of Macromolecular Physics, Institute of Physics, Adam Mickiewicz University, Poznań, Poland [6] NanoBioMedical Centre, Adam Mickiewicz University in Poznań, Poznań, Poland

milena.czeszejko@phdstud.ug.edu.pl

38th EPS

Uniwersytet Gdański

Katedra Chemii Biomedycznej

Chemia UG

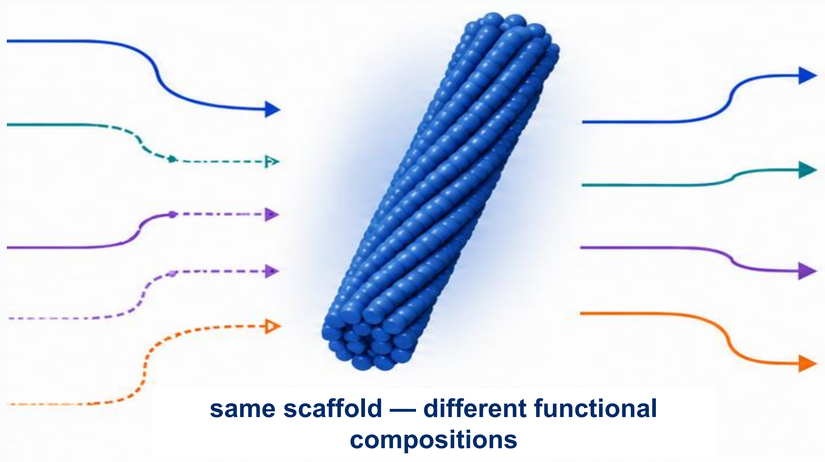
1 MODULAR DESIGN OF THE S7 FIBRIL PLATFORM

One fibrillogenic sequence enables multiple structurally and functionally distinct fibril systems.

Molecular building blocks

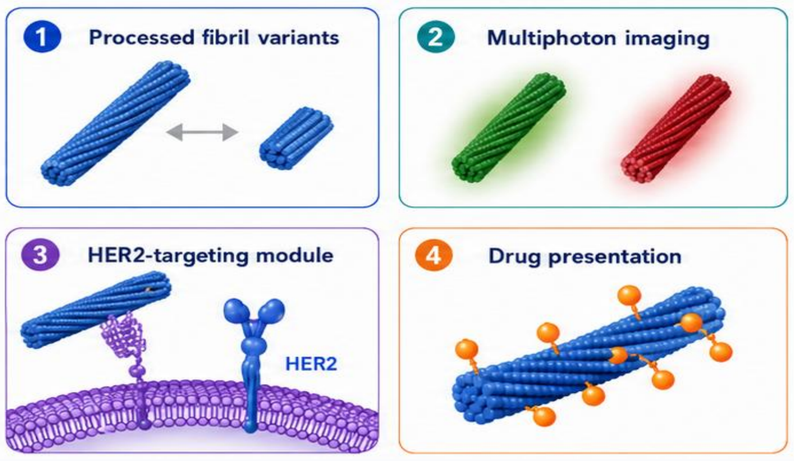
1. **fibrillogenic scaffold** s7: GQAGIVV
2. **Fluorescently labeled** S7 variants — PyTAP, BODIPY
3. **Targeting module** Af-PEG-s7, Af-SS-Cys-s7, (Cys-s7) = s8
4. **Therapeutic module** s7-MMAE

Ratio-controlled co-assembly



same scaffold — different functional compositions

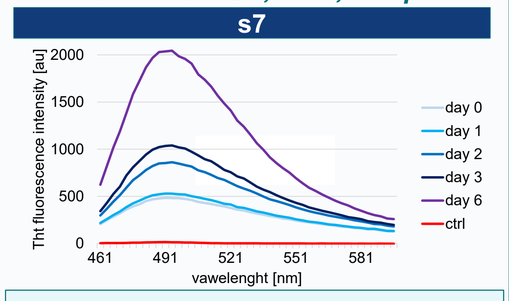
Tunable functional outputs



2 FIBRILLIZATION KINETICS

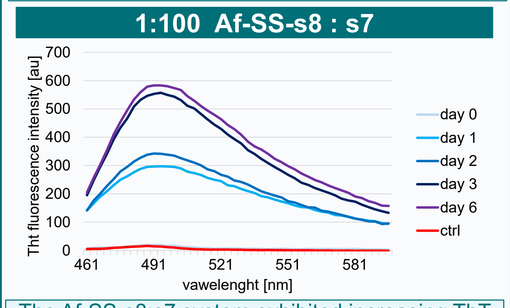
Time-resolved ThT fluorescence was used to monitor the formation of β-sheet-rich assemblies during 6 days of incubation in PBS, 37°C, 300rpm.

s7



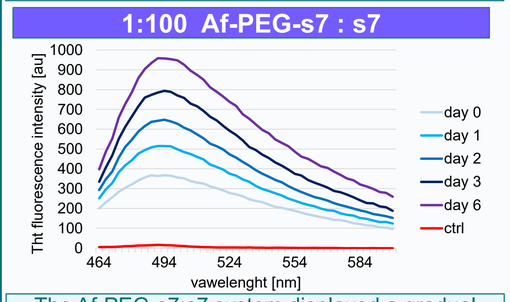
s7 showed a pronounced time-dependent increase in ThT fluorescence, with the highest signal observed on day 6, indicating progressive formation and maturation of ThT-binding fibrillar structures.

1:100 Af-SS-s8 : s7



The Af-SS-s8:s7 system exhibited increasing ThT fluorescence up to day 3, followed by only a minor change on day 6, suggesting that the ThT response reached an apparent plateau earlier than for s7 alone.

1:100 Af-PEG-s7 : s7

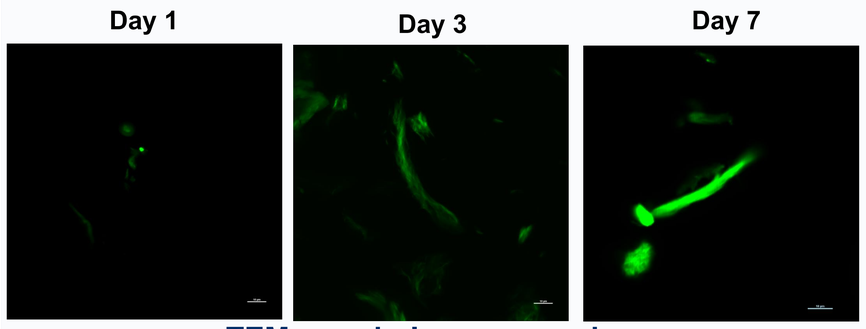


The Af-PEG-s7:s7 system displayed a gradual increase in ThT fluorescence throughout the incubation period. The final signal remained lower than for s7 alone but higher than for the Af-SS-s8-containing system.

3 FLUORESCENT TRACKING OF s7 FIBRILLIZATION

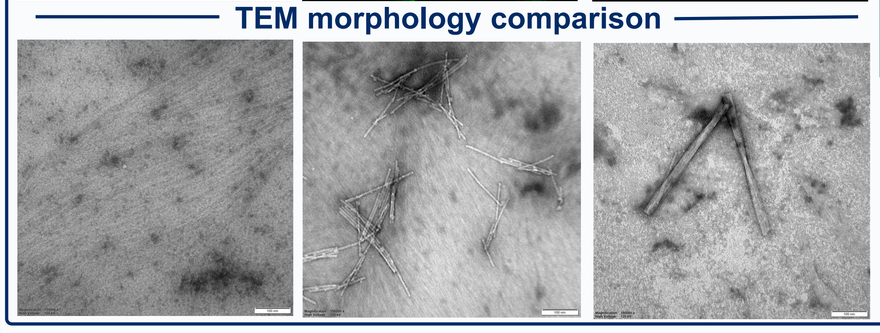
Fluorescently labelled s7 variants enable time-resolved and multichannel visualization of fibril formation.

A. Time-resolved fibrillization of BODIPY-s7



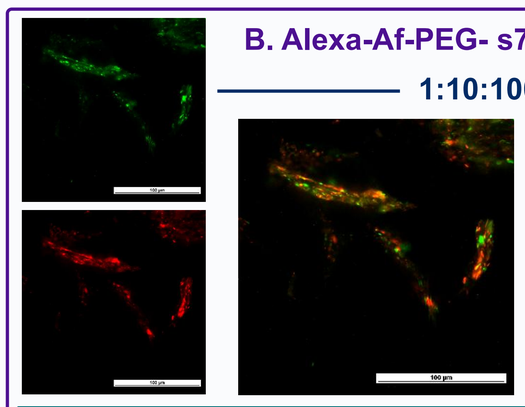
BODIPY-labelled s7 was monitored by confocal microscopy after 1, 3, and 7 days of fibrillization. A progressive increase in fluorescence intensity along fibrillar structures was observed over time, indicating ongoing fibril formation and maturation.

TEM morphology comparison



TEM imaging confirmed that the fluorescent structures corresponded to peptide fibrils.

B. Alexa-Af-PEG- s7 : PyTAP-s7 : s7 mixed systems



Mixed fibrillar systems composed of AlexaFluor-s7, PyTAP-s7, and unlabelled s7 were analysed after 7 days of fibrillization. Among the tested compositions, the 1:10:1000 ratio provided the most effective confocal imaging, with numerous well-defined fibrils visible in both fluorescence channels. The signal pattern was consistent with the co-presence of both labelled peptide variants within the fibrillar network.

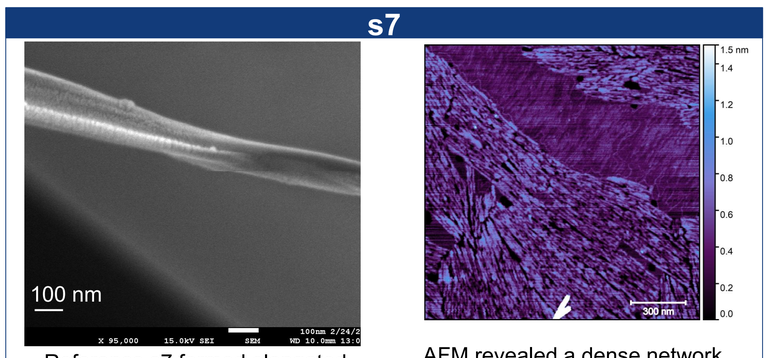
TEM analysis showed that fibril morphology depended on the proportion of unlabelled s7. At the 1:10:1000 ratio, the fibrils were shorter (approximately 200 nm), whereas at the 1:10:5000 ratio, longer fibrils (approximately 1 µm) were observed. In both cases, the fibril thickness remained comparable.

4 NANOSCALE MORPHOLOGY OF FUNCTIONALIZED FIBRILS

Affibody-containing systems retain fibrillar morphology while exhibiting linker-dependent structural organization.

A. cryo-SEM B. AFM

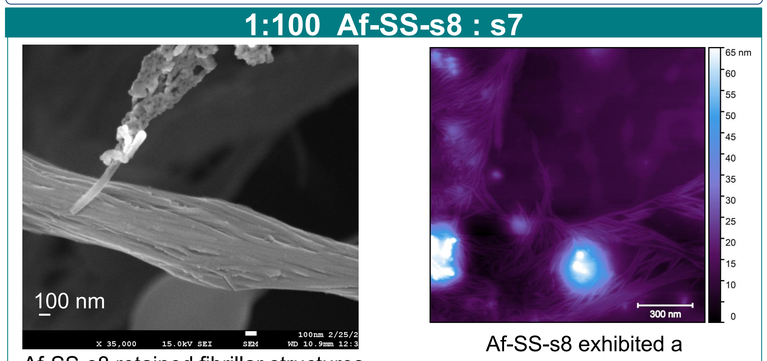
s7



Reference s7 formed elongated, continuous fibrillar structures.

AFM revealed a dense network of elongated reference fibrils.

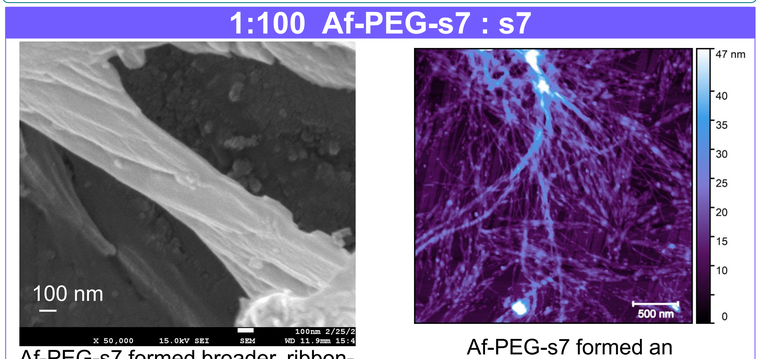
1:100 Af-SS-s8 : s7



Af-SS-s8 retained fibrillar structures with increased morphological heterogeneity.

Af-SS-s8 exhibited a heterogeneous surface distribution of fibrillar structures.

1:100 Af-PEG-s7 : s7



Af-PEG-s7 formed broader, ribbon-like fibrils with a pronounced tendency to bundle.

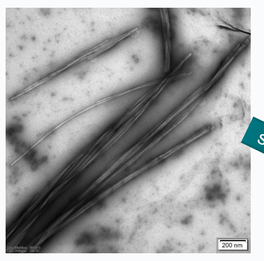
Af-PEG-s7 formed an interconnected fibrillar network with pronounced lateral association.

Cryo-SEM and AFM were used as complementary techniques to compare the nanoscale morphology of reference s7 fibrils and affibody-functionalized s8 systems. Both affibody-functionalized systems retained fibrillar morphology. The disulfide-linked conjugate was more heterogeneous, whereas the PEG-linked system showed pronounced ribbon formation and bundling.

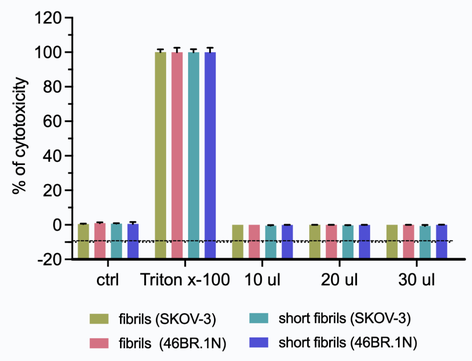
5 BIOLOGICAL READOUTS OF THE s7 PLATFORM

Sonicated s7 fibrils remained cytocompatible, while the mode of MMAE presentation influenced the morphology of BT-474 spheroids.

A. Cytocompatibility of sonicated fibrils

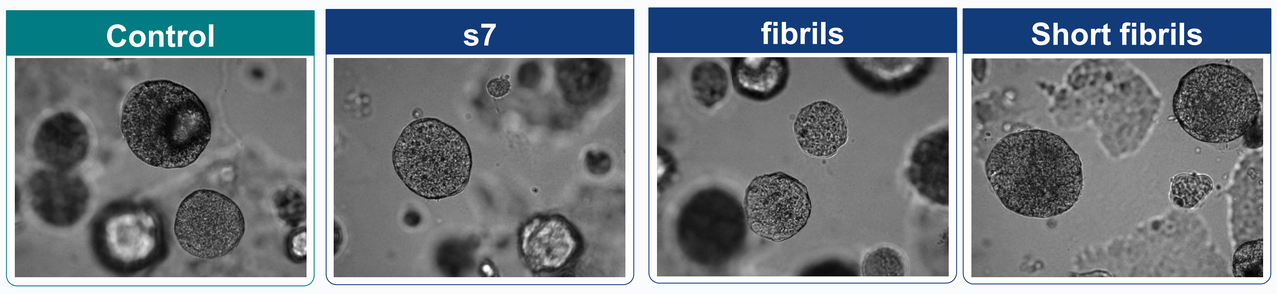


Amplitude = 40%, pulse cycle 2/3s on/off, 2 x 7,5 min



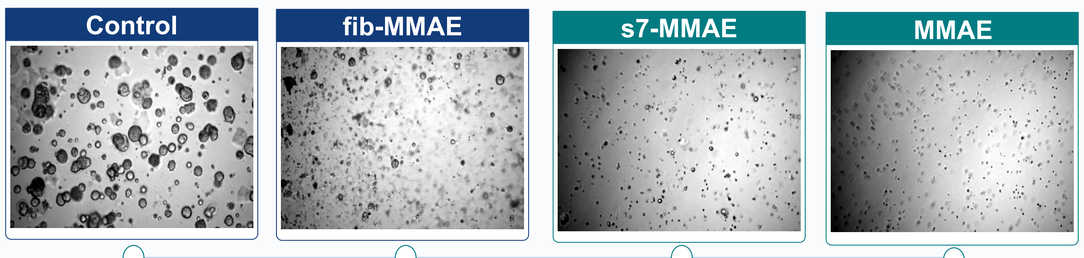
SKOV-3 cells and 46BR.1N human fibroblasts were incubated with non-sonicated and sonicated s7 fibrils. Cytotoxicity was assessed using an LDH-release assay. Neither fibril preparation caused a substantial reduction in cell viability under the tested conditions, indicating that sonication-induced fragmentation did not increase cytotoxicity.

B. Effect of the Investigated Systems on BT-474 Spheroid Morphology



BT-474 spheroids were cultured in Matrigel and treated with 10 µM s7, long s7 fibrils, or short s7 fibrils for 19 days. Neither s7 nor its fibrillar forms induced marked morphological changes compared with the control.

C. MMAE presentation in BT-474 spheroids



BT-474 spheroids were exposed to free MMAE, monomeric s7-MMAE, or fibrillar MMAE-containing systems and analysed by bright-field microscopy. The extent of spheroid disruption depended on the mode of drug presentation. Free MMAE produced the strongest morphological effect, whereas peptide-associated MMAE showed a reduced response, consistent with lower immediate drug accessibility.

6 KEY FINDINGS AND OUTLOOK

Summary of the modular s7 fibril platform and next experimental steps

KEY FINDINGS

1. **s7 scaffold** — Forms structurally defined fibrillar assemblies suitable for modular functionaization
2. **Affibody system** — Retain fibrillar morphology, while linker chemistry influence supramolecular organization
3. **Fluorescent modules** — Eneble time-resolved and multichannel visualization of s7 fibrils
4. **Sonication** — Remain cytocompatible with SKOV-3 cells and 46BR.1N fibroblasts.
5. **Biological performance** — s7 fibrils did not markedly alter BT-474 spheroid morphology, whereas MMAE presentation influenced the spheroid response.

OUTLOOK

- **Integrate functional modules** — Combine targeting, imaging, and therapeutic modules within a single fibrillar construct.
- **Optimize module composition** — Define optimal module ratios and linker chemistry for controlled fibril organization.
- **Assess nanocarrier performance** — Evaluate stability, drug accessibility, and biological activity of the complete nanocarrier.

This work is funded by a grant from the National Science Centre 2022/45/B/NZ7/03889 and by the University of Gdansk BMN no. 539-T070-B264-26.

Beyond natural amino acids: extending immunogenicity risk assessment to non-canonical peptide drugs through chemical feature encoding

Maria Cairoli[1], Catherine Betts[2], Morten Nielsen[3], Olga Obrezanova[4], **Leonardo De Maria**[1]

1 Hit Discovery, Discovery Computation & AI, Discovery Sciences, Biopharmaceuticals R&D, AstraZeneca, Gothenburg, Sweden
2 Immune Safety, Clinical Pharmacology and Safety Sciences, Biopharmaceuticals R&D, AstraZeneca, Cambridge, UK
3 Department of Health Technology, Technical University of Denmark, Lyngby, Denmark
4 Biologics Engineering, Oncology R&D, AstraZeneca, Cambridge UK

https://doi.org/10.17952/38EPS.2026.P257

Abstract

Peptide therapeutics increasingly incorporate non-natural amino acids (NNAAs) to improve their properties, yet current in silico MHC class II binding predictors, central to immunogenicity risk assessment, do not account for their chemical diversity. We present a machine learning framework combining chemical fingerprints with sequence information to predict MHC-II binding for peptides containing both natural (NAA) and non-natural amino acids. Evaluating 31 molecular representations, we show that peptide-level fingerprints fail due to loss of positional information, while residue-level fingerprints (direct-encoding and similarity-based) match BLOSUM62 and one-hot encodings and correctly recover binding cores and canonical motifs. In a citrullination case study, we observed similar linear correlation across encoding strategies, with residue-level fingerprints showing marginal improvements in quantitative accuracy. This is consistent with citrulline rarely occupying anchor positions. The framework is compatible with pan-allele architectures (NNAlign / NetMHCIIpan) and extensible to diverse synthetic modifications, supporting immunogenicity risk assessment for emerging peptide therapeutics.

Introduction

Therapeutic peptides incorporate NNAAs to improve half-life, permeability, and stability. Yet the impact of NNAAs on immunogenicity, driven largely by peptide–MHC class II (pMHC-II) binding and downstream T-cell activation, remains poorly characterized. Current *in silico* pMHC-II predictors are trained almost exclusively on the 20 natural amino acids. Existing NNAA extensions use sparse encodings or neutral placeholders (e.g., 'X'), which cannot represent the chemical diversity of synthetic residues used in modern peptide design.

Gap: No framework simultaneously (i) encodes chemically diverse NNAAs, (ii) preserves the positional information needed for binding core identification, and (iii) is compatible with existing pan-allele architectures.

Objective

Evaluate if chemical fingerprints, combined with sequence positional information, provide effective molecular representations for MHC-II binding prediction across peptides containing both natural and non-natural amino acids.

Methods

Data

- MHC-II binding affinity (IEDB): 14 HLA-DR alleles
- Citrullinated peptides: 225 (DRB1*01:01) and 283 (DRB1*04:01).
- MHC-I benchmark: 5 HLA-A/B alleles, 9-mers.
- Human proteome sampling (UNIPROT) for motif validation.
- Hobohm clustering to minimize train/test redundancy.

Molecular Representations (31)

- **Sequence-based:** BLOSUM62, one-hot, NNAAIndex.
- **Peptide-level fingerprints:** ECFP4/16, FCFP, RDKit, AVALON, TT, AP, MACCS, MAPC, PepFuNN, AmorProt.
- **Direct-encoding residue fingerprints (F):** per-residue chemical fingerprint matrices.
- **Similarity-based residue fingerprints (S):** pairwise Tanimoto matrices, BLOSUM-like.

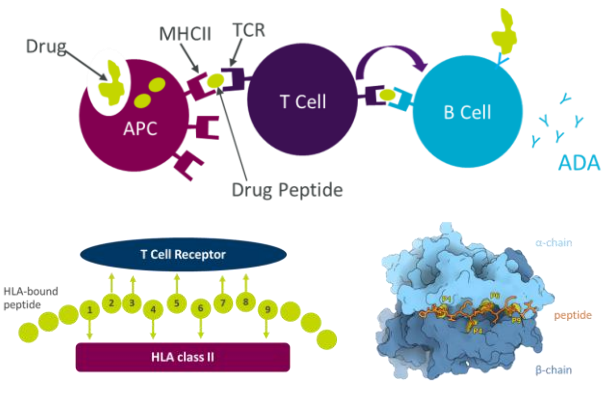
Model

NNAlign-based MLP, with nested 5-fold CV, Optuna hyperparameter tuning, 15-epoch hydrophobic-anchor burn-in and ensembling.

Evaluation

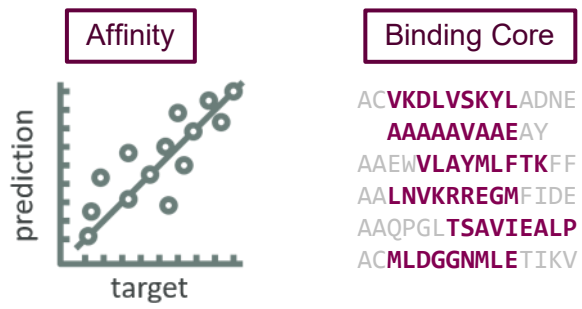
- Out-of-fold PCC, R^2, RMSE;
- paired Wilcoxon vs. BLOSUM62 with Benjamini-Hochberg FDR correction;
- bootstrap 95% CIs;
- binding-core validation against 15 HLA-DR peptides with PDB-derived cores;
- sequence logos via Seq2Logo.

The Immune Response



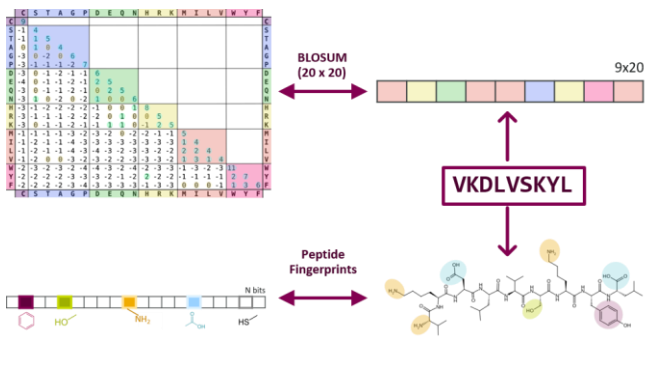
Schematics of Anti-Drug Antibodies (ADAs) generation. A stretch of nine amino acids drives peptide-MHC II presentation that can lead to helper T cells activation, generating ADAs.

In-silico predictions

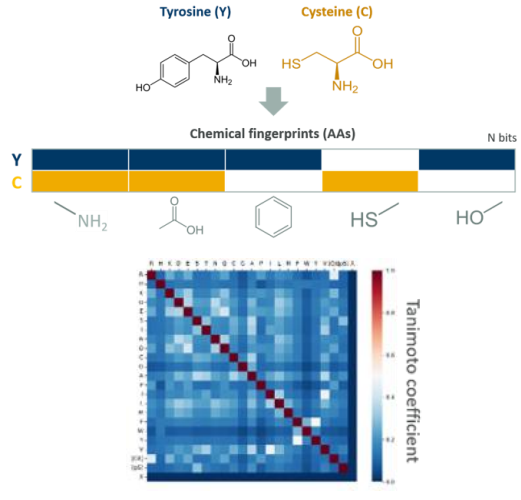


MHC II binding prediction methods should be able to predict *both* the peptide binding affinity and its binding core.

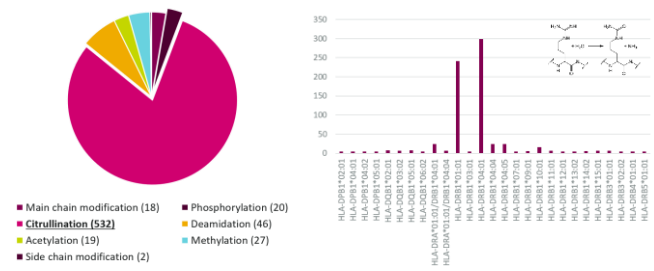
Encodings for Model Building



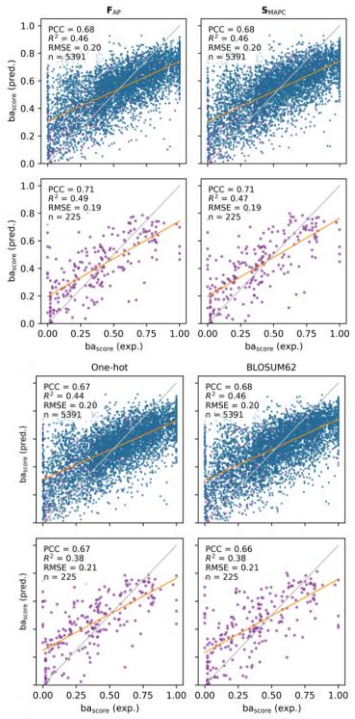
Sequence-based encodings capture AA-level peptide information using substitution scores such as BLOSUM but are limited mainly to the 20 natural amino acids and a few non-natural amino acids. SMILES-based encodings add chemical, structural, and compositional information, but initially lose positional information. This can be fixed with residue-level fingerprints and similarity (Tanimoto).



Results: citrullination case study



Citrullination provided the largest dataset for model building as per data availability in IEDB.



Prediction performance Binding affinity predictions for DRB1*01:01 and using models trained using both NAA-based (blue) and citrullinated (purple) peptides. In each subplot, the first row shows out-of-fold predictions on both NAA-based and citrullinated peptides, while the second row shows predictions on citrullinated peptides only. Blue dots: NAA-based peptides; purple dots: citrullinated peptides. Yellow line: fitted regression; gray line: identity line.

Conclusions

Novel framework: A machine learning approach combining chemical fingerprints with sequence encodings for MHCII binding prediction, where residue-level fingerprints match traditional encodings (BLOSUM62, one-hot) and accurately identify binding cores.

Promising for NNAAs: Chemical encoding offered only marginal improvements for citrullinated peptides but is expected to be more valuable for non-natural amino acids without natural analogues, though data scarcity limits full evaluation.

Extensible and application-ready: Compatible with pan-allele architectures, this framework could support early-stage immunogenicity risk assessment for therapeutic peptides, vaccines, and antibody-drug conjugates as more NNAAs data becomes available.

References

Cellular Immunology. 2015. 295: 118-126
Frontiers in Immunology. 2023. 14: 1285899
Annu. Rev. Biomed. Data Sci. 2020. 3:191–215

Acknowledgements

Maria Cairoli is supported by the AstraZeneca Postdoc Programme. The authors thank W. Czechtizky, C. Tyrchan, E. Nittinger, G. Geylan, and A. Tibo for helpful discussions.
Data & code: Training data available at *Zenodo: 10.5281/zenodo.19692117* upon publication.

38th EPS
European Peptide Symposium

6 - 11th of September 2026
Vienna, Austria

SYNTHESIS, RADIOLABELING AND PRELIMINARY CHARACTERIZATION OF AN EGFR-TARGETING DOTA-CONJUGATED PEPTIDE FOR CANCER IMAGING

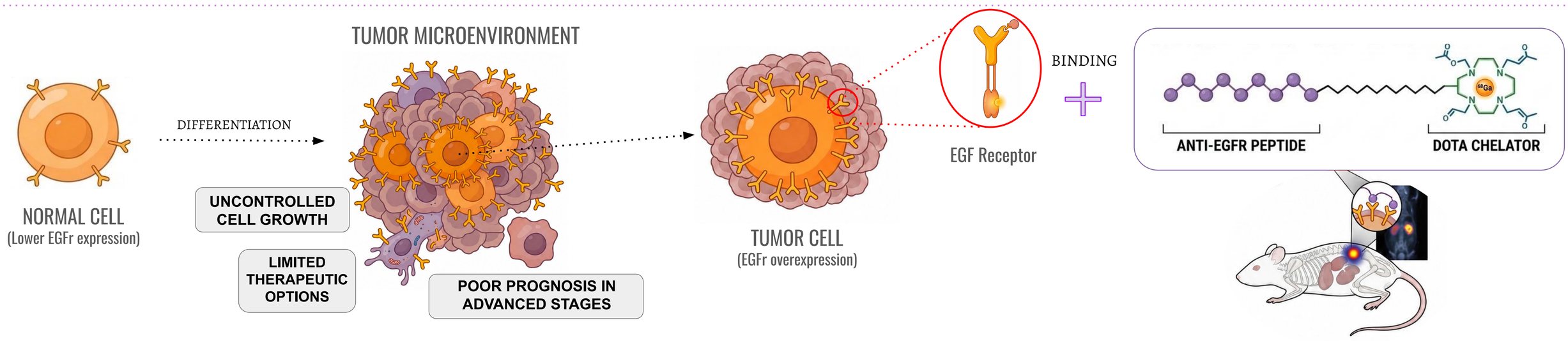
Souza, A.M.[1a], Carvalheira, L.Y.[1], Barboza, M.R.F.F.[2], Mendonça, F. F.[1], Fuscaldi, L.L.[1] & Malavolta, L.[1]

[1]*Santa Casa de São Paulo School of Medical Sciences, Department of Physiology, Sao Paulo, Brazil*
[2]*Hospital Israelita Albert Einstein, Department of Nuclear Medicine, Sao Paulo, Brazil*

[a]*https://doi.org/10.17952/38EPS.2026.P014*

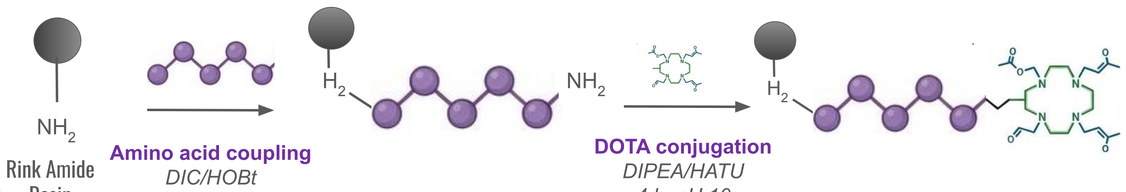
aline.morais.ms@gmail.com

INTRODUCTION

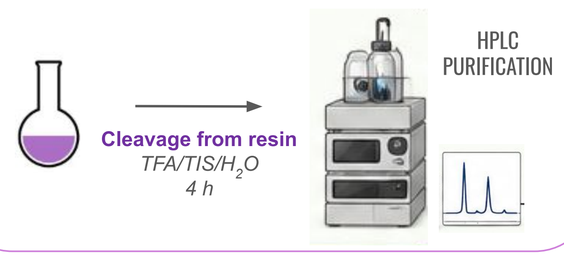


METHODOLOGY

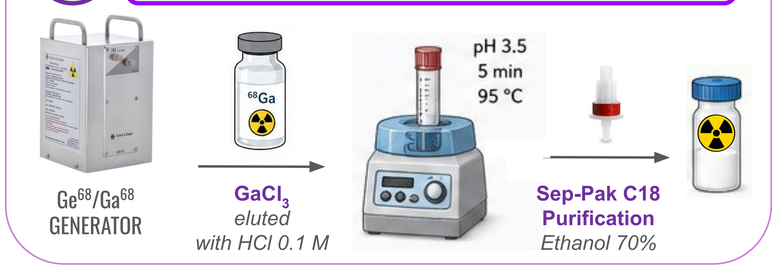
1 PEPTIDE SYNTHESIS (Fmoc SPPS)



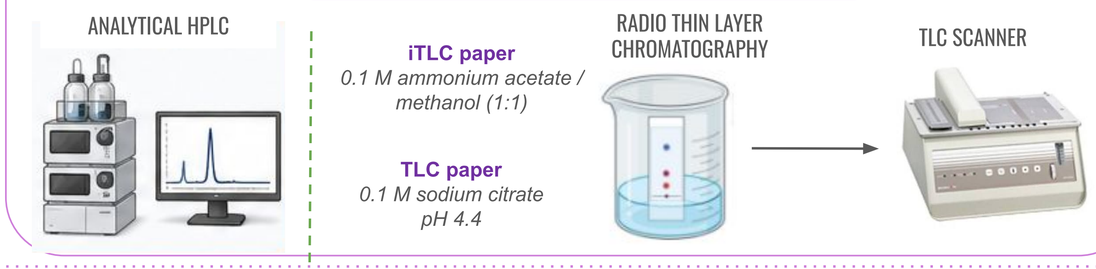
2 CLEAVAGE AND PURIFICATION



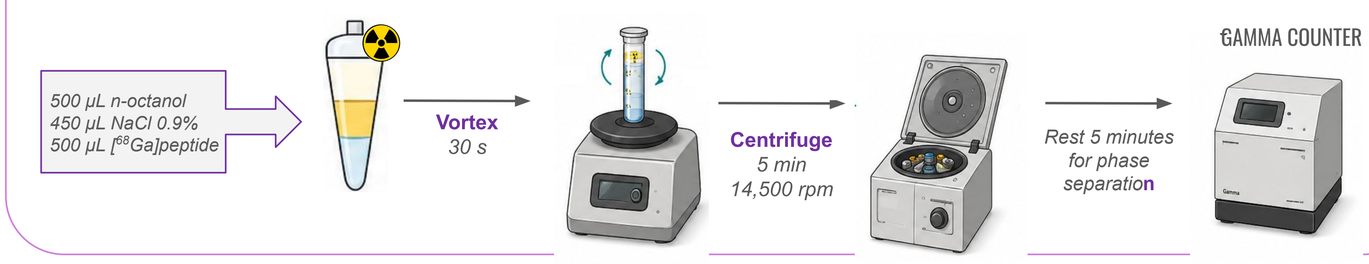
3 RADIOLABELING



4 QUALITY CONTROL



5 PARTITION COEFFICIENT (LogP)



RESULTS

PEPTIDE SYNTHESIS OVERALL YIELD

30%

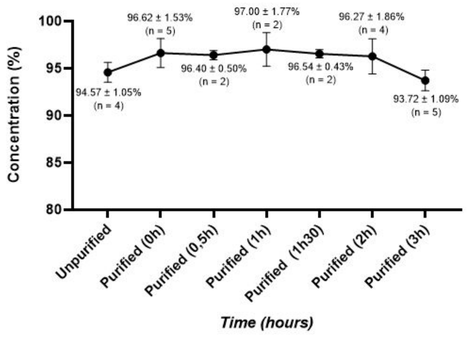
Peptide synthesis resulted in an overall yield of **30%**.

RADIOSYNTHESIS OVERALL YIELD

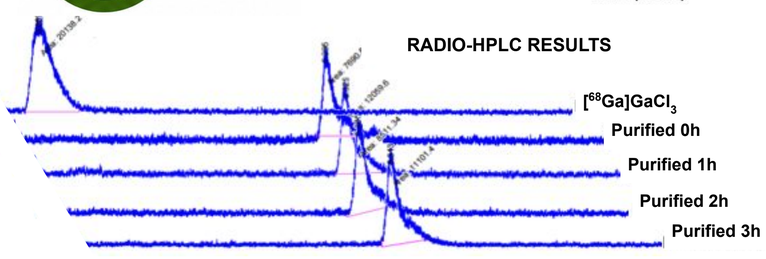
≥77%

Radiolabeling showed yield above **77%**.

RADIOCHEMICAL PURITY AND STABILITY



RADIO-HPLC RESULTS



~95% radiochemical purity (HPLC)

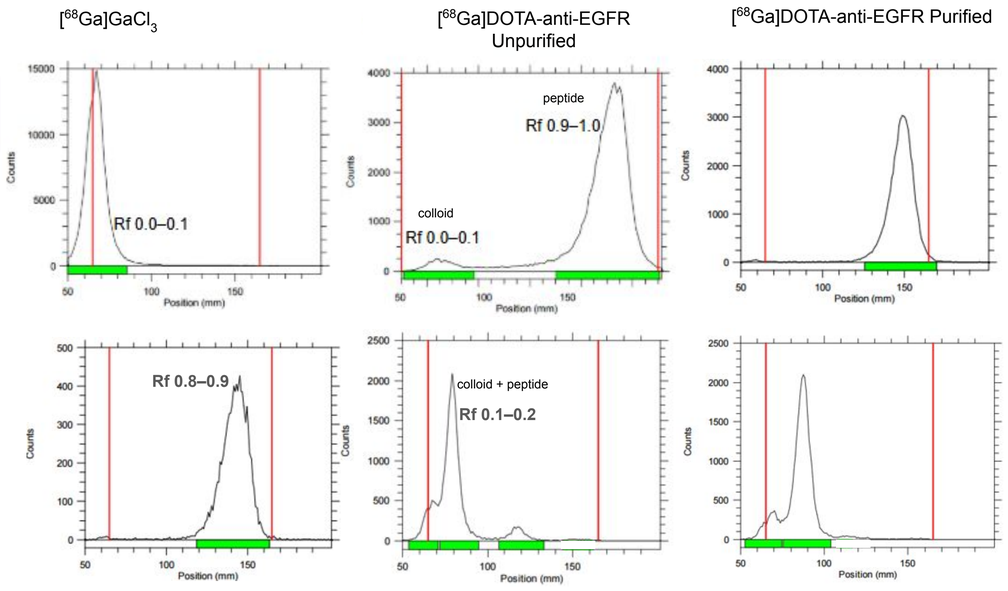
~95% radiochemical purity (iTLC)

0.1 M ammonium acetate / methanol (1:1)

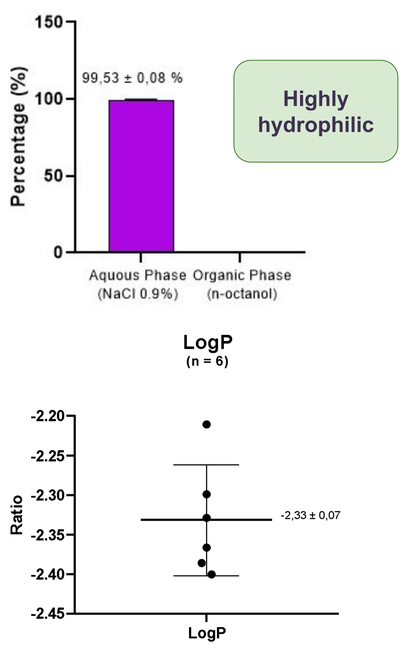
TLC method optimization

0.1 M sodium citrate pH 4.4

iTLC AND TLC RESULTS



PARTITION COEFFICIENT



CONCLUSION

This preliminary study demonstrates the successful synthesis and radiolabeling of a promising EGFR-targeting radiopeptide for cancer imaging, highlighting important parameters for further optimization and biological validation.

Acknowledgements: This work was supported by FAPESP grants #2025/12735-2 and #2021/10265-8, Cancer Theranostics Innovation Center (CancerThera)/CEPID. Chamada CNPq/MCTI/FNDCT nº 22/2024 - Programa Conhecimento Brasil - Apoio a Projetos em Rede com Pesquisadores Brasileiros no Exterior (CNPq): grant number 444492/2024-0.

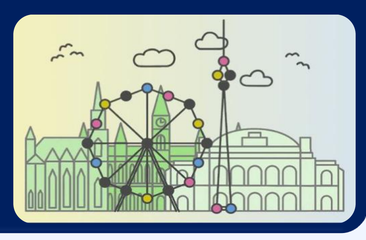
TARGETING β-PIX SH3 DOMAIN-MEDIATED PROTEIN-PROTEIN INTERACTIONS IN BREAST CANCER USING PEPTIDE INHIBITORS

Srijon Sen and Soumya De

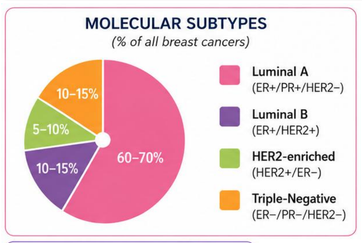
Department of Bioscience and Biotechnology, IIT Kharagpur, WB, 721302, India

https://doi.org/10.17952/38EPS.2026.P237

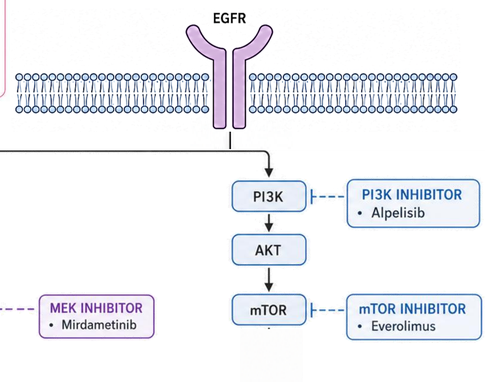




BREAST CANCER STATISTICS AND CURRENT TREATMENT STRATEGIES

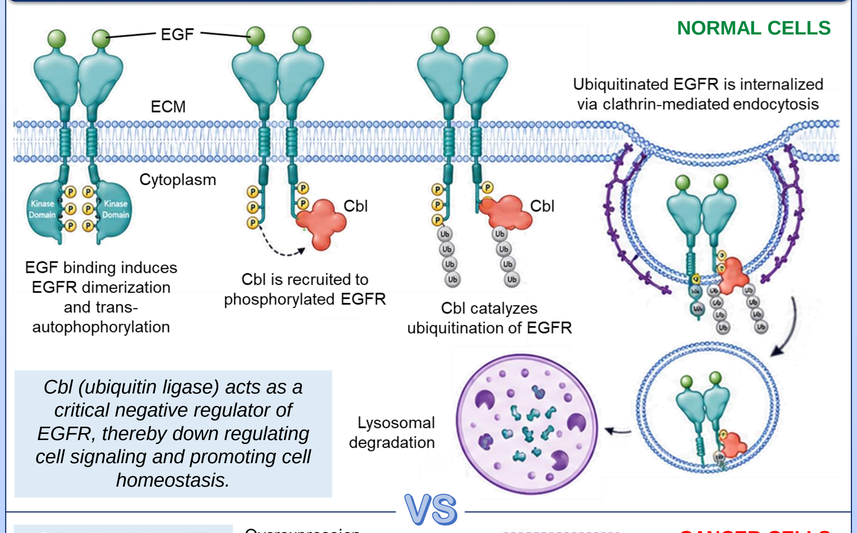


Breast cancer is the largest cancer burden women face worldwide. Conventional therapies target the EGFR kinase directly – drugs like the tyrosine kinase inhibitors. This approach fails due to mutations, and reactivation of the kinase domain.



Where EGFR kinase inhibitors have failed, can disrupting the protein-protein interactions that sustain oncogenic signaling provide a novel therapeutic strategy in breast cancer?

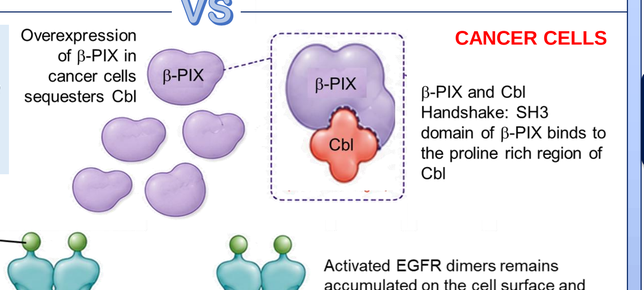
EGFR SIGNALING:FROM NORMAL REGULATION TO ONCOGENIC DYSREGULATION

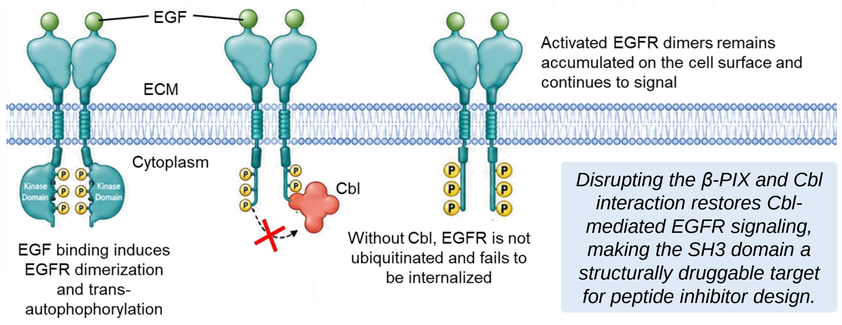


Cbl (ubiquitin ligase) acts as a critical negative regulator of EGFR, thereby down regulating cell signaling and promoting cell homeostasis.

VS

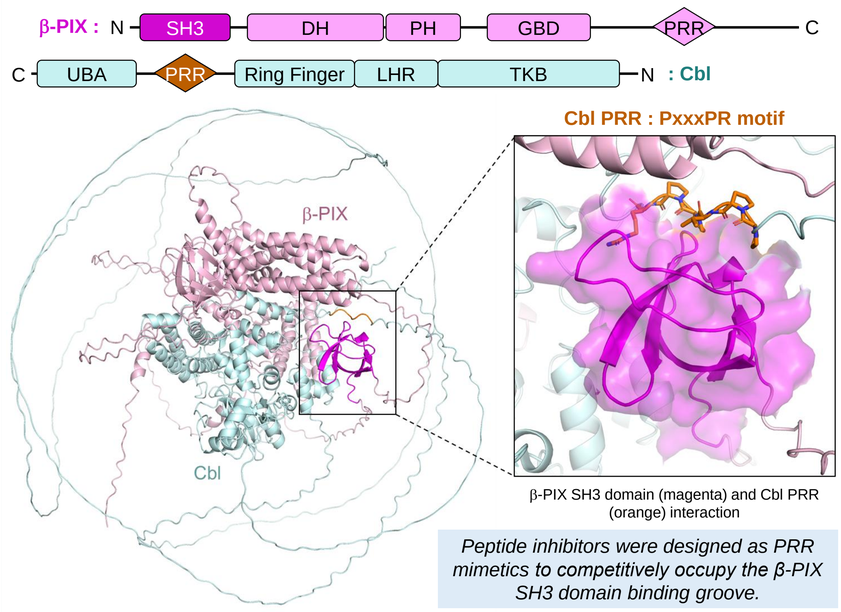
β-PIX is a Rho-GEF that activates Rac1/Cdc42 to mediate enhanced migration/ invasion and drives metastasis.





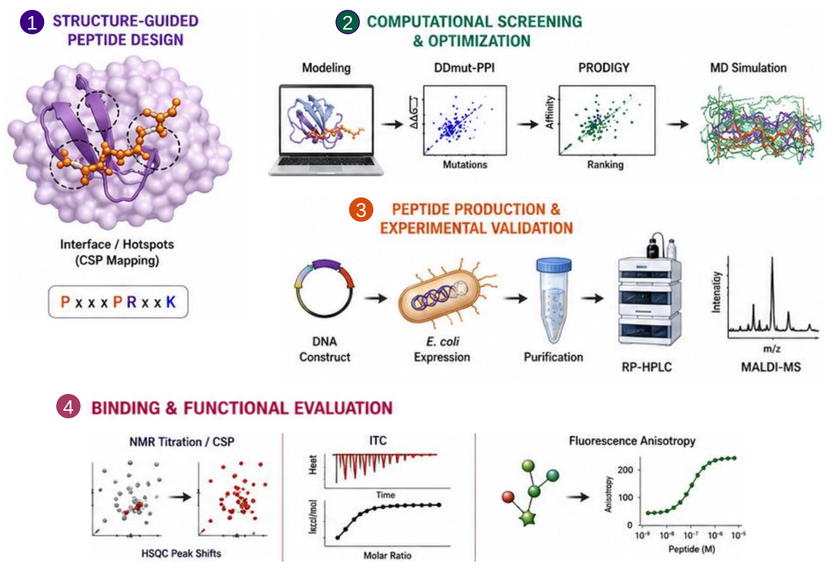
Disrupting the β-PIX and Cbl interaction restores Cbl-mediated EGFR signaling, making the SH3 domain a structurally druggable target for peptide inhibitor design.

INTERACTION BETWEEN β-PIX SH3 DOMAIN AND PROLINE RICH REGION (PRR) OF CBL

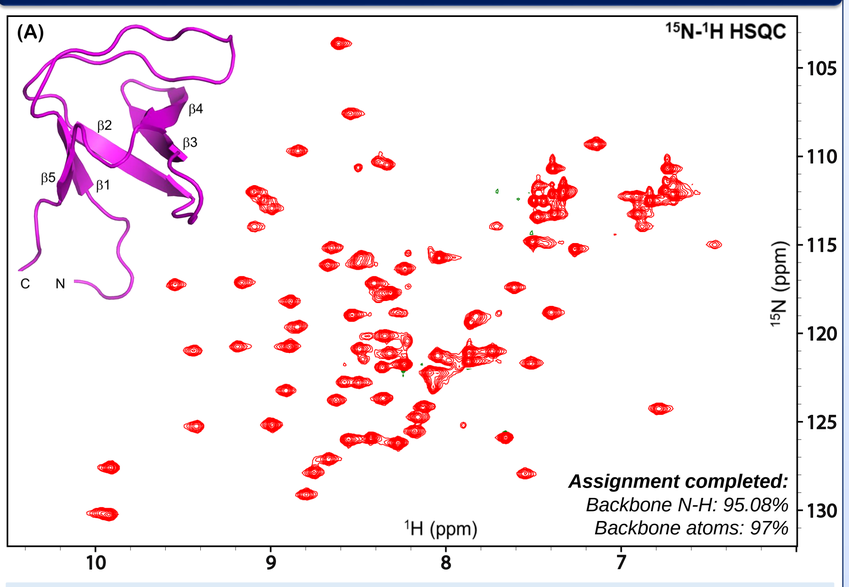


Peptide inhibitors were designed as PRR mimetics to competitively occupy the β-PIX SH3 domain binding groove.

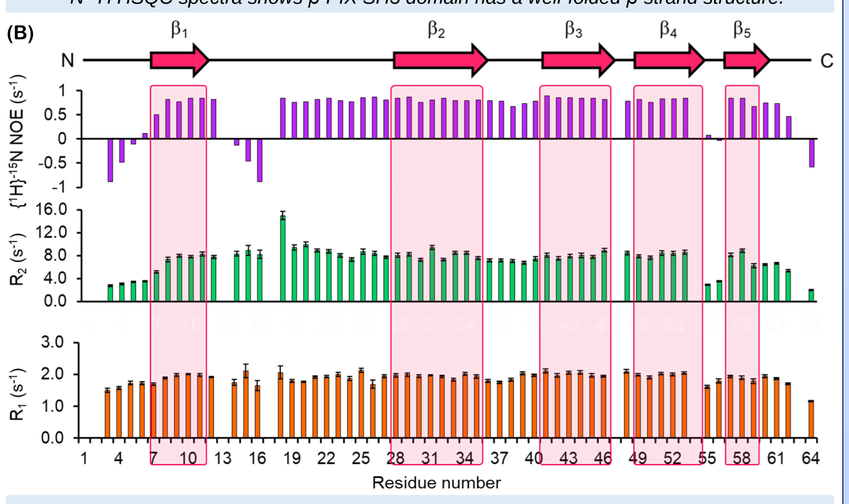
METHODOLOGICAL WORKFLOW



CHARACTERIZATION OF β-PIX SH3 DOMAIN FOR STRUCTURE-GUIDED PEPTIDE DESIGN



^{15}N-^{1}H HSQC spectra shows β-PIX SH3 domain has a well-folded β-strand structure.



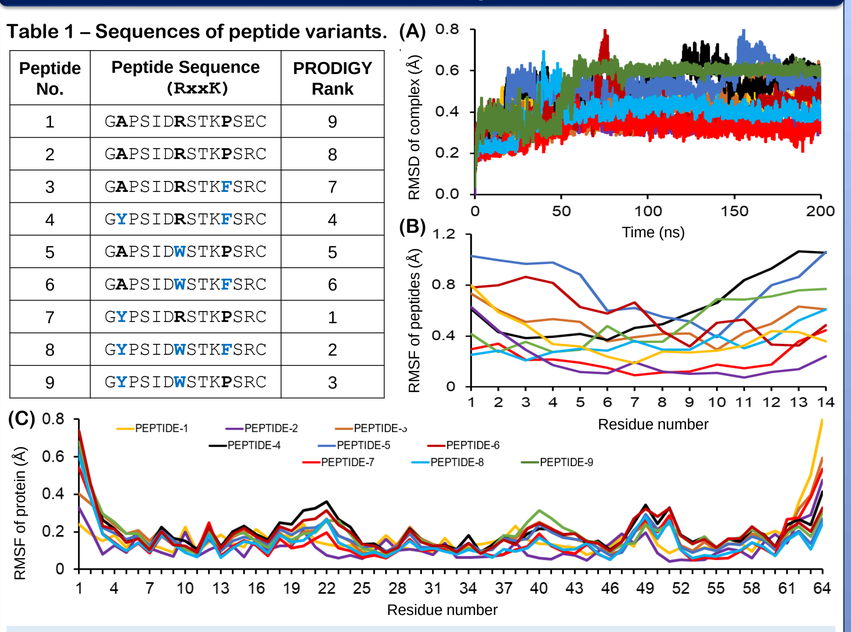
^{15}N relaxation analysis of ps-ns timescale motions show uniform NOE values for each residue, indicating the domain having rigid folds. Decreased NOE values between β1 and β2 suggest local flexibility. T18 has significantly higher transverse relaxation (R_2) value, which suggests μs-ms conformation exchange.

Figure 1 – (A) ^{15}N-^{1}H HSQC spectra and solution NMR structure of β-PIX SH3 domain. (B) Fast-timescale (ps–ns) dynamics of backbone amides in the β-PIX SH3 domain.

DESIGN AND SCREENING OF PEPTIDE INHIBITORS TARGETING β-PIX SH3 DOMAIN

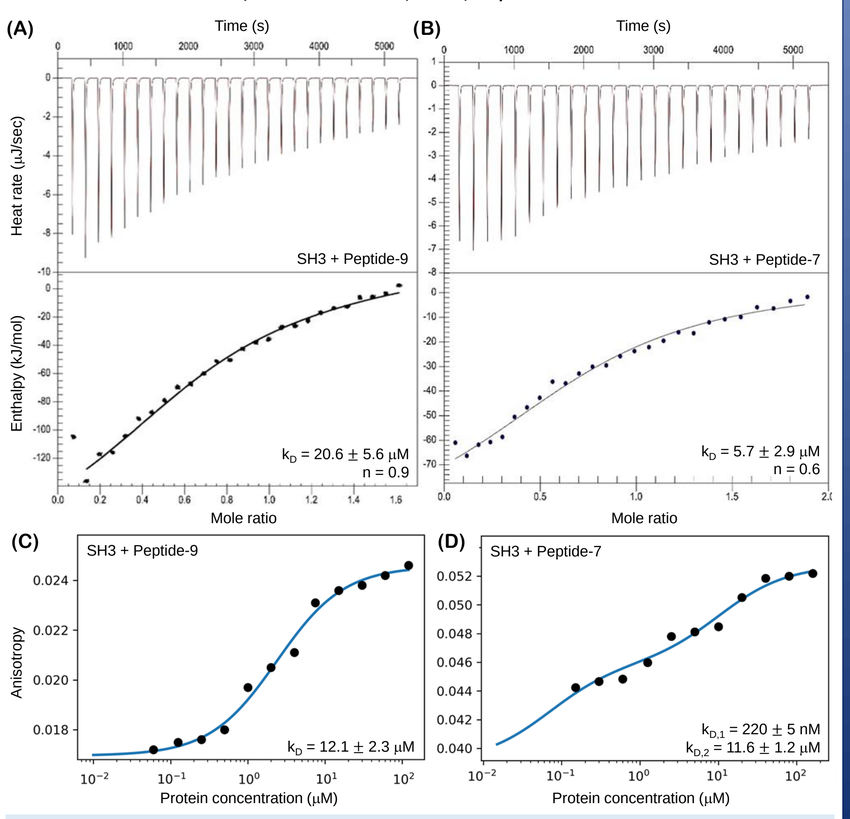
Table 1 – Sequences of peptide variants.

Peptide No.	Peptide Sequence (RxxK)	PRODIGY Rank
1	GAPSIDRSTKPSEC	9
2	GAPSIDRSTKPSRC	8
3	GAPSIDRSTKFSRC	7
4	GYPSIDRSTKFSRC	4
5	GAPSIDWSTKPSRC	5
6	GAPSIDWSTKFSRC	6
7	GYPSIDRSTKPSRC	1
8	GYPSIDWSTKFSRC	2
9	GYPSIDWSTKPSRC	3



9 peptide variants were generated using DDmut-PPI and ranked by predicted binding affinity using PRODIGY. Following MD simulations, 5 variants were selected, purified, characterized, binding affinity was evaluated by ITC, fluorescence anisotropy, and NMR.

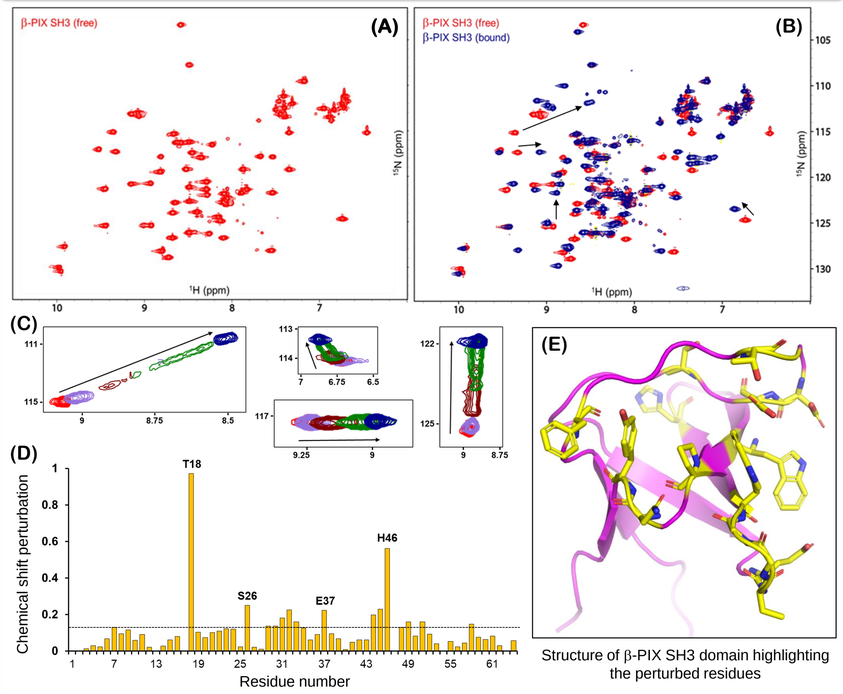
Figure 2 – (A) Root mean square deviation (RMSD) of peptide bound β-PIX SH3 domain from 200 ns simulation. (B) Root mean square fluctuation (RMSF) of peptides. (C) Root mean square fluctuation (RMSF) of β-PIX SH3 domain.



Peptide-7 demonstrated enhanced binding to the β-PIX SH3 domain with 2:1 SH3:peptide binding stoichiometry. R→W mutation in Peptide-9 weakened SH3 binding and shifted the stoichiometry to 1:1, highlighting the role of Arg in the RxxK motif.

Figure 3 – ITC heat responses from titrating (A) Peptide-9 and (B) Peptide-7 into β-PIX SH3 domain. Anisotropy changes upon titrating β-PIX SH3 into fluorescently labelled (C) Peptide-9 and (D) Peptide-7

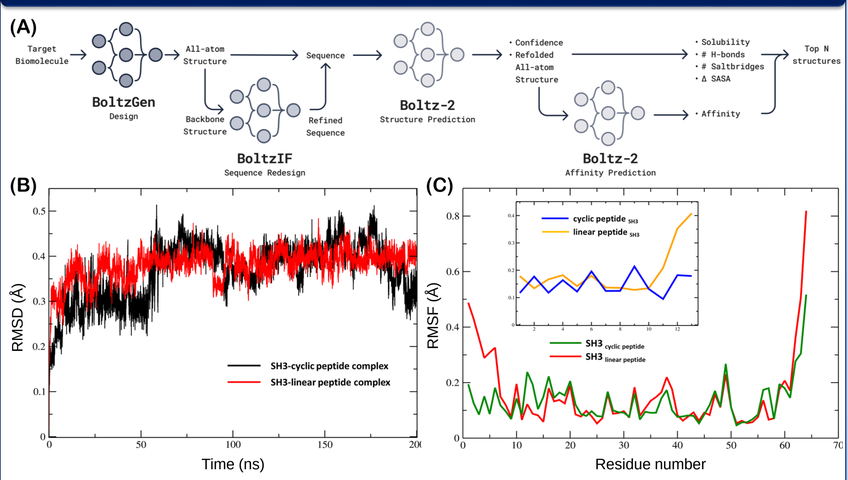
STRUCTURAL MAPPING OF β-PIX SH3 DOMAIN AND PEPTIDE-7 INTERACTION

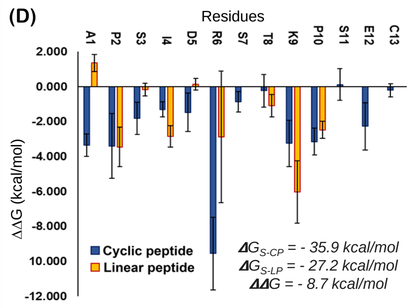


NMR-based titration experiments demonstrate that Peptide-7 directly binds the β-PIX SH3 domain, inducing distinct residue-specific chemical shift perturbations that map the molecular recognition interface.

Figure 4 – ^{15}N-^{1}H HSQC spectra of (A) apo and (B) overlay of free peptide-bound β-PIX SH3 domain. (C) Representative perturbed residues. (D) Chemical shift perturbations quantification and analysis. (E) Mapping of perturbed residues onto β-PIX SH3 domain.

AI-GUIDED DESIGN OF CYCLIC PEPTIDES





Experimental validation of cyclic peptide binding via Spl DnaX split intein mediated cyclization is ongoing!

Cyclic peptide achieves lower average RMSD and RMSF values compared to the linear peptide. Lower RMSD values suggests a more favorable and consistent binding interaction of cyclic peptide with SH3. Cyclic peptide shows tighter binding from Molecular Mechanics/Generalized Born Surface Area (MMGBSA) calculations.

Figure 5 - (A) Cyclic peptide design using BoltzGen for structure prediction. (B) MD simulations showing the RMSD profiles of β-PIX SH3 complexes with cyclic (red) and linear (black) peptides. (C) Per-residue RMSF analysis and comparative residue fluctuations, with the inset showing peptide backbone RMSF. (D) Per-residue binding free-energy contributions (MMGBSA) comparing cyclic and linear peptides.

EVALUATION OF PEPTIDES USING CELL STUDY

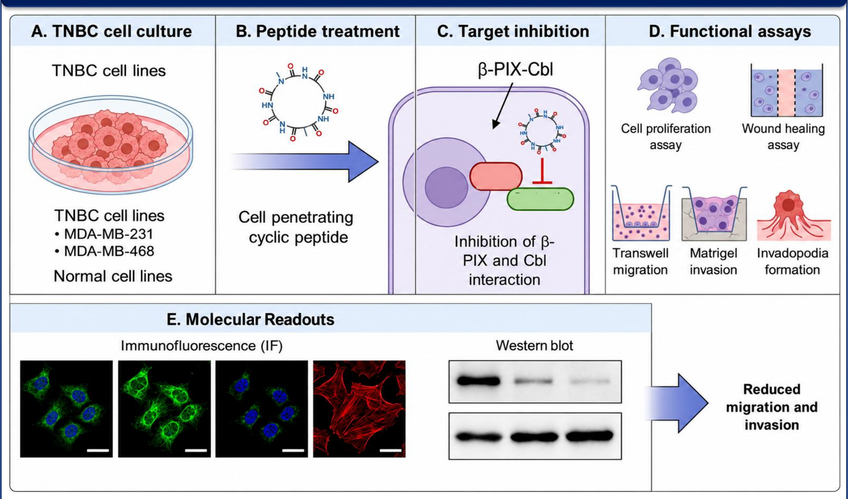


Figure 6 - (A) Cell culture using TNBC cell lines (MDA-MB-231 and MDA-MB-468) and normal cell lines. (B) Treatment with a cell-penetrating peptides. (C) Inhibition of the β-PIX & Cbl interaction (D) Functional assays assessing proliferation, migration, invasion, and invadopodia formation. (E) Readouts by immunofluorescence and western blot.

CONCLUSION

- Disrupting the β-PIX-Cbl PPI offers a structurally tractable alternative to EGFR kinase inhibition, which has failed clinically due to resistance mutations and pathway reactivation.
- Solution NMR structural characterization of the apo β-PIX SH3 domain provided the structure-guided template for rational peptide inhibitor design against this target.
- An integrated computational-to-experimental pipeline identified Peptide-7 as a novel lead binder, with NMR chemical shift perturbation mapping confirming its interaction interface.
- The Arg of the RxxK motif in peptides is functionally essential for high affinity with 2:1 SH3:peptide binding – Mutating it to Trp weakens binding and shifts the stoichiometry to 1:1.
- Synthesis of the optimized cyclic peptide using split *Spl* DnaX intein is underway, with TNBC cell-based assays planned to assess functional inhibition of β-PIX-Cbl signaling.

REFERENCES

1. D. Nagpal, *Journal of Drug Delivery Science and Technology* **2023**, 89, 105049.
2. W. Wu, *Cell* **2003**, 114(6), 715-725.
3. A. Hoelz, *Journal of Molecular Biology* **2006**, 358(2), 509-522.
4. M. Fatima, *Drug Discovery Today* **2022**, 27(11), 103353.

FUNDING AND ACKNOWLEDGEMENT

जैवप्रौद्योगिकी विभाग DEPARTMENT OF BIOTECHNOLOGY
PMRF Prime Minister's Research Fellowship
IIT Kharagpur PLATINUM JUBILEE
SERB DIA

The Azrieli Faculty of Medicine
Bar-Ilan University

38th EPS European Peptide Symposium — 6 - 11th of September 2026 — Vienna, Austria

QVIT LAB

Targeted Inhibition of Fis1/Mfn1 Protein-Protein Interactions with Peptides Promotes Cardioprotection

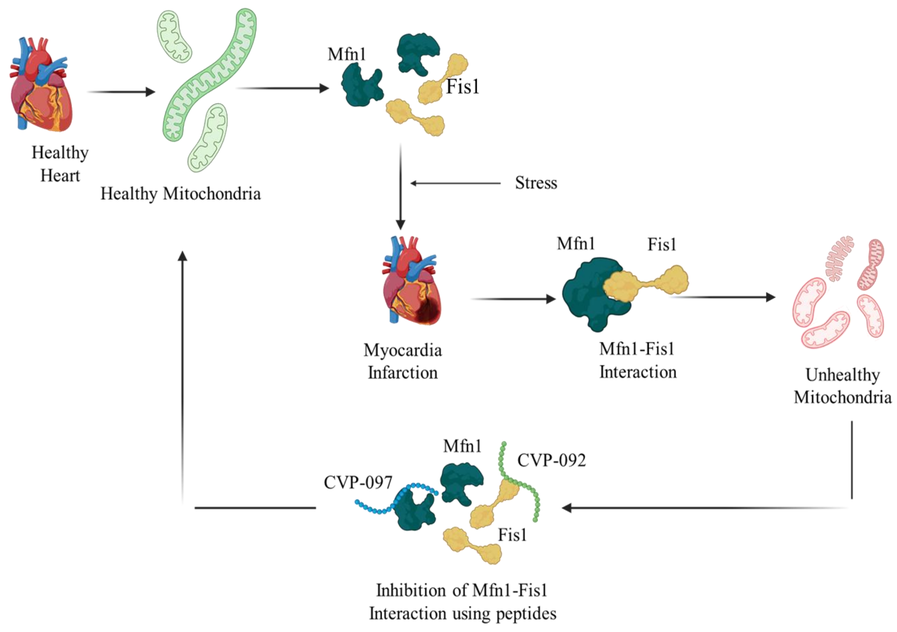
Ayetenew Abita[1], Hellena Shumaff[1], Liron Davis[1], Nir Qvit[1]*

[1]The Azrieli Faculty of Medicine in the Galilee, Bar-Ilan University, Safed 1311502, Israel

https://doi.org/10.17952/38EPS.2026.P519

Scientific Rationale

Pathological stress is proposed to favor Fis1-Mfn1 binding and suppress Mfn1-mediated mitochondrial fusion. CVP-097 was designed to bind Fis1; CVP-092 was designed to bind Mfn1.

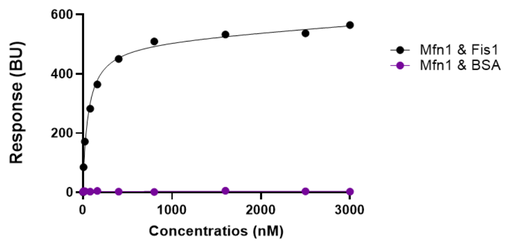


Question: Does selective inhibition of this protein-protein interaction preserve mitochondrial function during cellular stress?

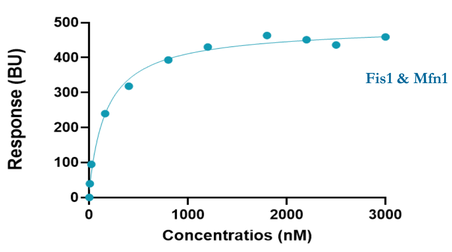
Results

Fis1-Mfn1 Interaction and Target Binding Confirmed

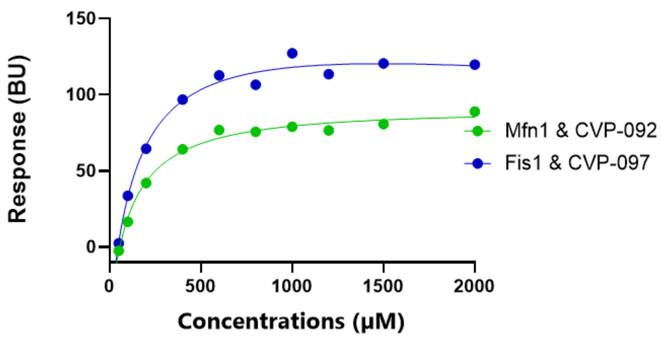
Mfn1 & Fis1 Interaction Mfn1 on Chip



Fis1 & Mfn1 Interaction Fis1 On Chip



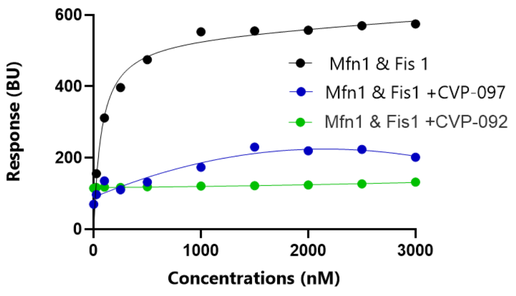
Peptide Protein Interaction



PPI	K_D (μM)
Mfn1 & Fis1 (Mfn1 on Chip)	0.060 ± 0.002
Fis1 & Mfn1 (Fis1 on Chip)	0.058±0.003
Mfn1 & BSA	undetectable binding
Fis1 & CVP-097	197± 16
Mfn1 & CVP-092	237±29

Experimental studies confirmed both Fis1-Mfn1 complex formation and the specific binding of CVP-092 and CVP-097 to their intended protein targets.

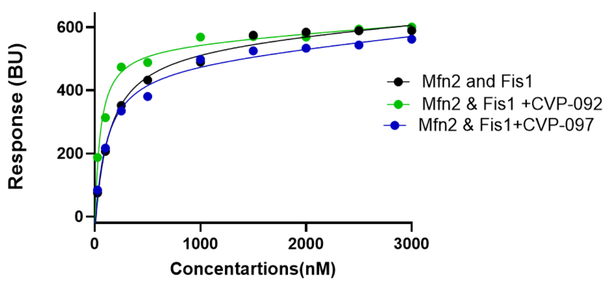
CVP-092 & CVP-097 Specifically Inhibit the Fis1-Mfn1 Interaction

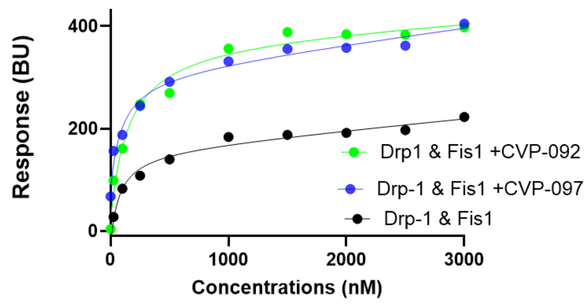


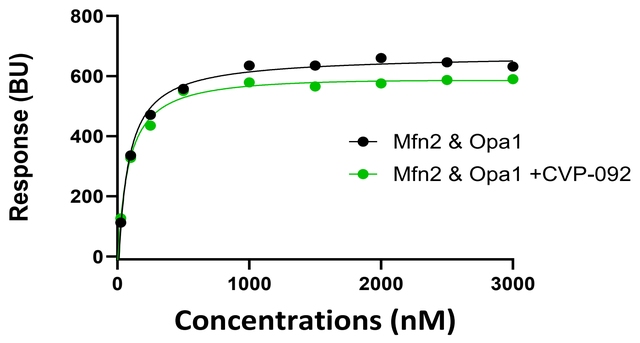
Competitive (PPI)	K_D (μM)
Mfn1 & Fis1	0.06 ± 0.002
Mfn1 & Fis1 + CVP-097	9.178 ± 0.18
Mfn1 & Fis1 + CVP-092	2.819 ± 0.26

Both CVP-092 and CVP-097 disrupted the Fis1-Mfn1 interaction, with CVP-097 producing a larger increase in K_D than CVP-092 (153-fold versus 47-fold, respectively).

Peptide Selectivity Study





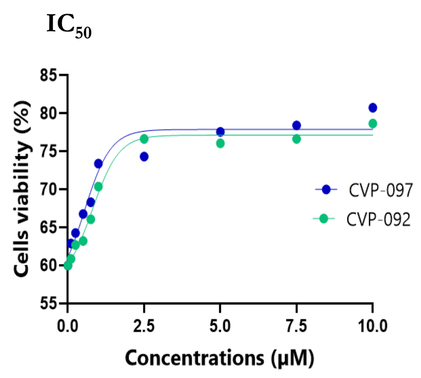


Competitive (PPI)	K_D (μM)
Mfn2 & Fis1	0.103 ± 0.002
Mfn2 & Fis1 + CVP-097	0.130± 0.024
Mfn2 & Fis1 + CVP-092	0.102 ± 0.032
Drp1 & Fis 1	0.072 ±0.010
Drp1 & Fis1 + CVP-097	0.095 ±0.020
Drp1 & Fis1 + CVP-092	0.153±0.018
Mfn2 & Opa1	0.068 ± 0.008
Fis1 & Opa1 + CVP-092	0.078 ± 0.010

CVP-092 and CVP-097 selectively disrupted the Fis1-Mfn1 interaction without affecting the other mitochondrial protein interactions tested.

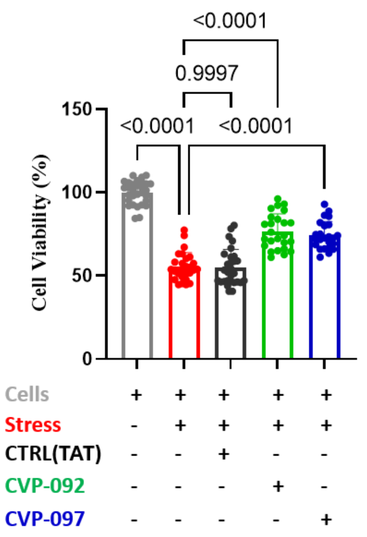
Peptides Protect H9c2 Cardiomyoblasts Under Chemical Ischemia Mimicry

IC_{50}

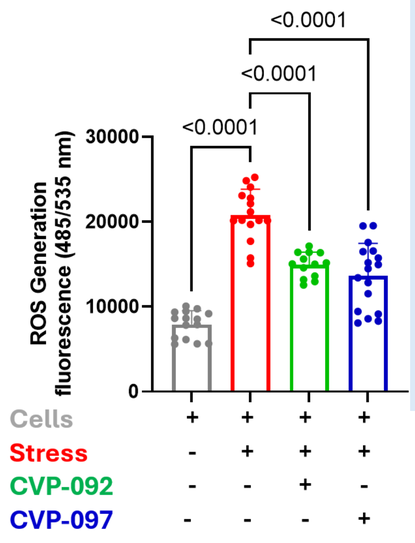


Peptides	IC_{50} (μM)
CVP-097	3.42± 0.60
CVP-092	3.76±0.49

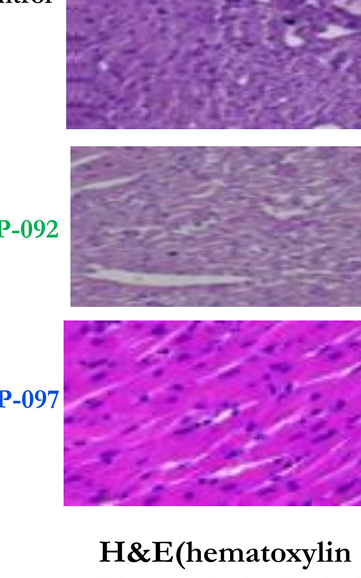
Cell Viability



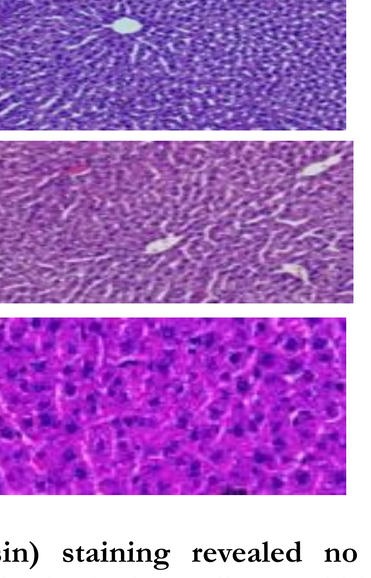
Reactive Oxygen Species



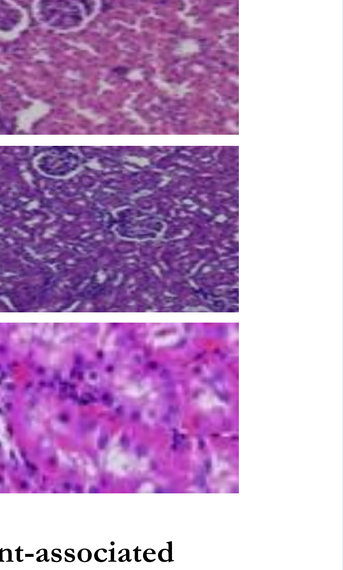
Mitochondrial Membrane Potential



LDH



ATP Level



CVP-092 and CVP-097 improved H9c2 cell viability and reduced stress-induced mitochondrial and cellular injury.

Peptides Show No Detectable Organ Toxicity

H&E(hematoxylin and eosin) staining revealed no treatment-associated histopathological abnormalities in the heart, liver, or kidney.

Take Home Message

1) CVP-097 and CVP-092 selectively weakened Fis1-Mfn1 binding, producing approximately 153-fold and 47-fold increases in apparent (KD), respectively.

2) Both peptides attenuated stress-induced H9c2 cell injury by improving viability, mitochondrial membrane potential, and ATP while reducing ROS and LDH release.

3) These findings support the Fis1-Mfn1 interface as a candidate therapeutic target; intracellular target engagement and in vivo cardioprotective efficacy remain to be established.

For more information: Ayetenew Abita; ayetenew.abita@gmail.com,
Prof. Nir Qvit: nir.qvit@biu.ac.il

Engineering nucleophilic catalysis coupled to tandem electrostatic assistance enables native chemical ligation at nanomolar concentrations

Julie Di Adamo[a], Vincent Diemer[a], Oleg Melnyk[a]

[a] Univ. Lille, CNRS, Inserm, CHU Lille, Institut Pasteur de Lille, U1019 - UMR 9017 - CIIL - Center for Infection and Immunity of Lille, Lille, France

https://doi.org/10.17952/38EPS.2026.P039

Introduction

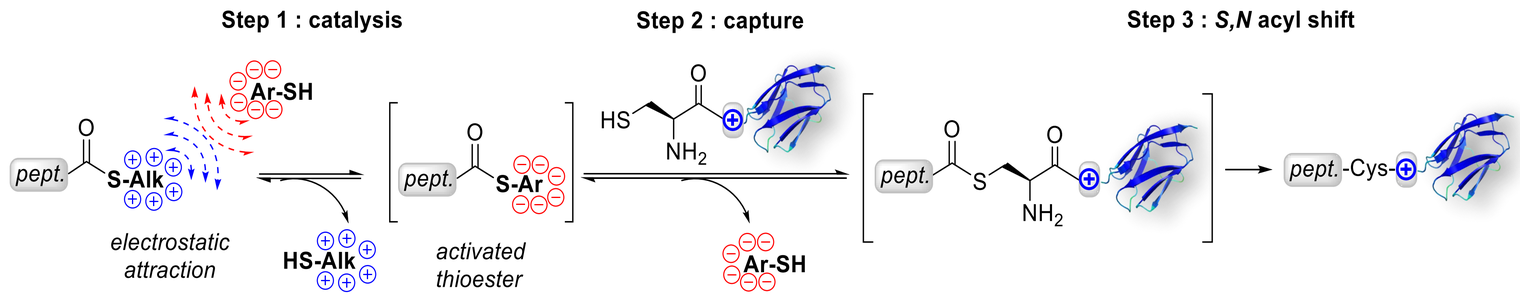
Native chemical ligation (NCL)[1] couples a C-terminal peptide thioester with an N-terminal cysteinyl peptide to form a native peptide bond. This strategy has greatly expanded access to proteins through **semi- or total synthesis**, enabling numerous applications. When **peptide alkyl thioesters**[2] are used, the reaction begins with **nucleophilic catalysis**: a thiol-thioester exchange with an aryl thiol catalyst converts the alkyl thioester into a more reactive aryl thioester. In a subsequent **capture step**, this intermediate reacts with the cysteinyl peptide to generate the native peptide bond.

Despite requiring a **large excess of catalyst**, the reaction exhibits only **moderate rate** constants at millimolar peptide concentrations (~50 M^{-1} s^{-1})[3], promoting side reactions and limiting efficiency at lower concentrations. Considerable efforts have therefore been devoted to **accelerate this reaction** through a variety of strategies.[4] Among them, preliminary work from our laboratory demonstrated that **incorporating charged motifs** into peptide sequences to promote **electrostatic interactions** can significantly **enhance NCL kinetics**.[5]

Objective and Method

Building on this approach, we aimed to retain the kinetic benefits of **electrostatic assistance** while **minimizing or avoiding** charged residues in the final product.

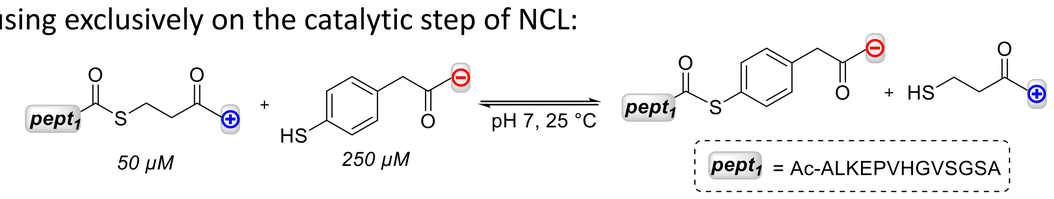
To achieve this, we developed a **tandem electrostatic assistance strategy** that accelerates both key steps of the NCL reaction, **catalysis** and **capture**, as depicted in the scheme on the right.



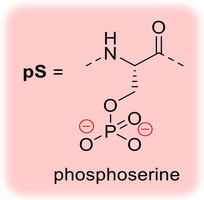
Tandem electrostatic assistance of aryl thiol-catalysed NCL between an alkyl thioester and a cysteinyl protein

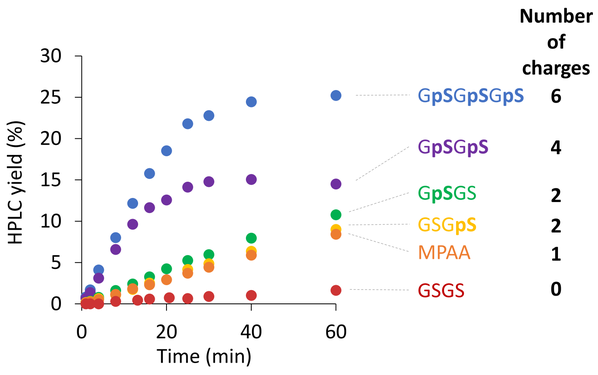
1. Nucleophilic catalysis

First, we sought to identify the **optimal charged moieties** for electrostatic assistance by focusing exclusively on the catalytic step of NCL:



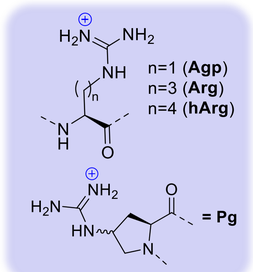
- How does the **catalyst's charge** affect the thiol-thioester exchange rate with Arg_6 thioester?

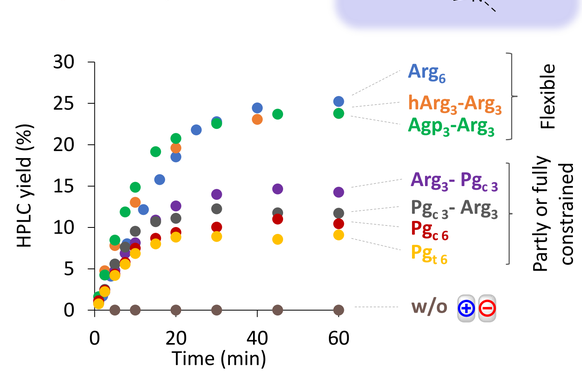




The reaction rate **increases** with the catalyst's charge

- How does **thioester charge pre-organization** affect the thiol-thioester exchange rate with **3pS** catalyst?



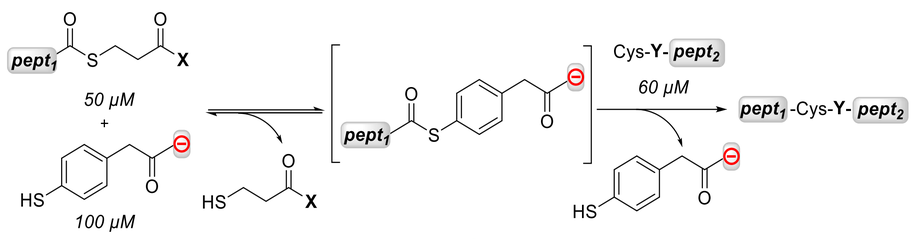


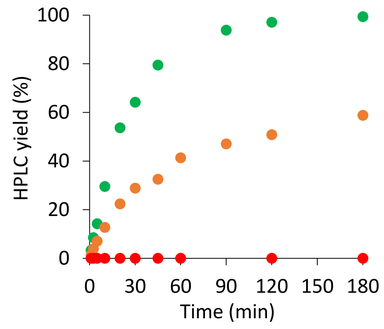
Introducing conformational constraints **decreases** the reaction rate

Combination of Arg_6 **thioester** and **3pS catalyst** enable to achieve the fastest rate

2. Tandem NCL

Next, we demonstrated the **feasibility and efficiency** of the tandem NCL strategy using **3pS catalyst** :





Tandem assistance → **X = Y = Arg_6**
No aryl thioester accumulation
Significant rate enhancement

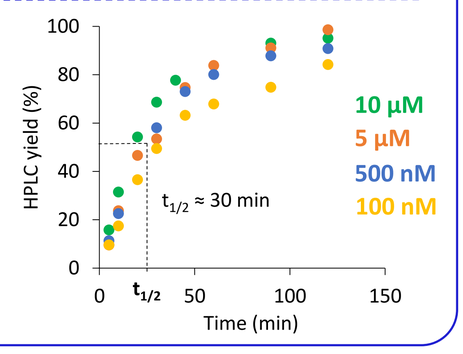
Catalysis assistance → **X = Arg_6 and Y = GSGSGS**
Aryl thioester accumulation

w/o assistance → **X = OH and Y = GSGSGS**
No ligation product

The **potential** of this approach at low concentrations was determined with ligations from **10 µM to 100 nM** between:

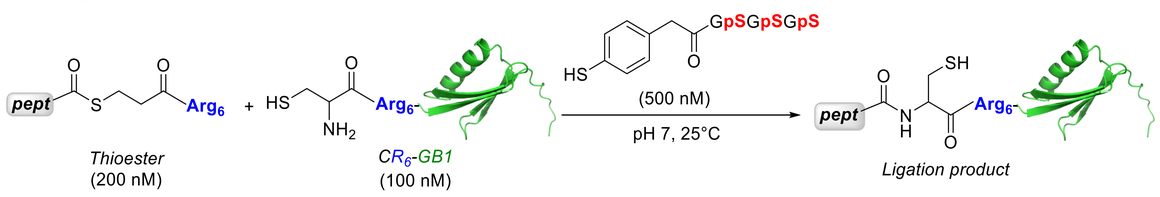
Arg_6 thioester (1 equiv.)
3pS catalyst (5 equiv.)
Arg_6 cysteinyl peptide (1.2 equiv.)

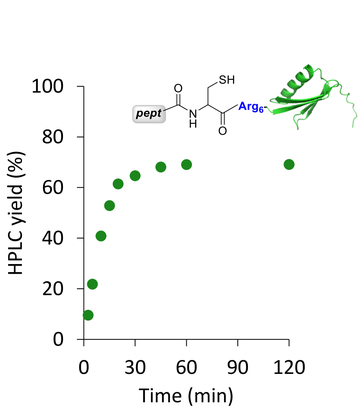
Kinetic profile almost **unchanged** upon 100-fold dilution

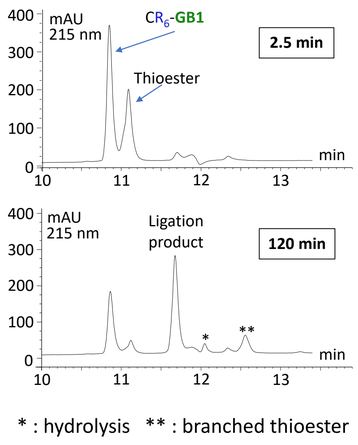


3. Protein modification

After demonstrating its efficiency on model peptides at low concentrations, we applied this tandem strategy to **protein modification** at 100 nM with only submicromolar catalyst loadings (500 nM):







pept = Ac-ALKEK(dnp)VHGVSGSA

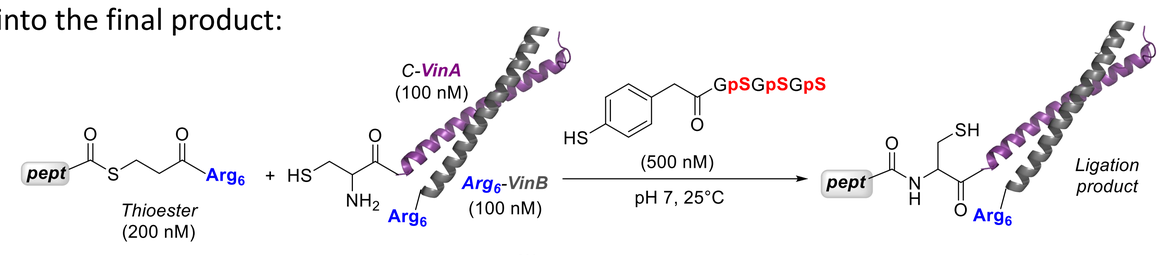
GB1 = GSTYKLILNGKTLKGETTTEAVDA ATAEKVFKQYANDNGVDGEWTY DDATKTFTVTEGSGSHHHHHH

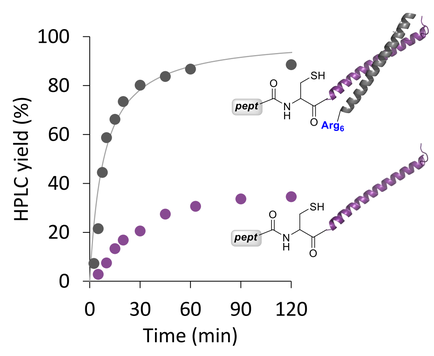
CR_6-GB1 was produced by recombinant expression

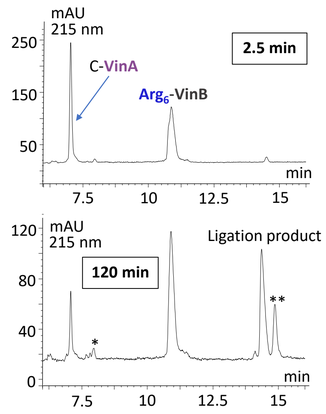
* : hydrolysis ** : branched thioester

4. Protein modification in trans

Unlike the previous approach, introducing the charged module ***in trans*** brings the charged group **close to**, but not directly next to, the cysteine, avoiding its incorporation into the final product:







Theoretical kinetic profile of a second-order reaction (k = 2 10^4 M^{-1} s^{-1})

pept = Ac-ALKEK(dnp)VHGVSGSA

VinA = LEIEAAFLERENTALETRVAELRQRV QRLRNRVSQYRTRYGPLGGGK$_{biot}$

VinB = LEIRAAFLRQRNTALRTEVAELEQE VQRLENEVSQYETRYGPLGGGK

* : hydrolysis ** : branched thioester

Conclusion

Overall, **tandem electrostatic assistance** of the NCL reaction offers an **efficient** and **catalyst-sparing** approach for protein modification under dilute conditions, with reaction rates reaching ~ 10^4 M^{-1} s^{-1}.

Building on these promising results, the ***in trans*** approach could ultimately enable **fast** and **traceless** protein modification.

References:

[1] P. E. Dawson, T. W. Muir, I. Clark-Lewis, S. B. H. Kent, *Science* **1994**, 266, 776–779

[2] J. Di Adamo, N. Ollivier, S. Cantel, V. Diemer, O. Melnyk, *J. Org. Chem.* **2024**, *89* (18), 13719–13724

[3] J. Di Adamo, V. Agouridas, V. Diemer, O. Melnyk, *Org. Lett*. **2025**, 27, 13991–13996

[4] V. Agouridas, O. El Mahdi, V. Diemer, M. Cargoët, J.-C. M. Monbaliu, O. Melnyk, *Chem. Rev.* **2019**, *119*, 7328–7443

[5] N. Ollivier, M. Sénéchal, R. Desmet, B. Snella, V. Agouridas, O. Melnyk, *Nat. Commun.* **2022**, *13*, 6667

Acknowledgements to:

Agence de la Recerche Nationale (ANR-23-CE07-0016, TURBO project)
Jean ZAY supercomputer (IDRIS,CNRS) AD010816084R1
European Peptide Society (EPS) for providing a registration fee waiver

Innovative phage display libraries for precision protein targeting

Cristina Díaz-Perlas[1,2], Benjamí Oller-Salvia[1] & Christian Heinis[2]

[1] Institut Químic de Sarrià (IQS), Universitat Ramon Llull, 08017 Barcelona, Spain
[2] École Polytechnique Fédérale de Lausanne (EPFL), CH-1015 Lausanne, Switzerland
https://doi.org/10.17952/38EPS.2026.P386

Highly diverse peptide and sdAb phage display libraries

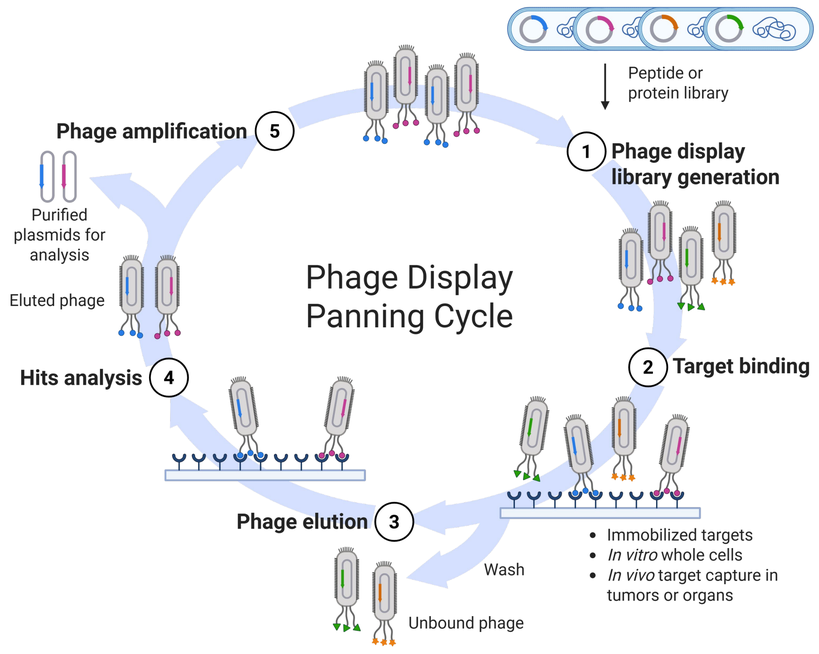
Phage display is a robust molecular display technology widely used to generate and screen peptide, antibody fragment, and single-domain antibody (sdAb) libraries.

We are developing **peptide phage display libraries**:

- **Linear and cyclic** peptide formats, including single- and double-disulfide-constrained scaffolds

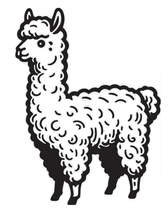


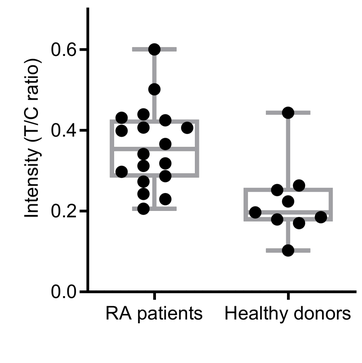
- High diversity, ranging from **10^9 to 10^{11} independent variants**, confirmed by NGS and Sanger sequencing
- Validated across **multiple targets**, yielding peptide binders with nanomolar affinities



We are constructing **sdAb phage display libraries**:

- **Naïve libraries** derived from 10 alpacas, preserving natural sequence diversity throughout the sdAb framework and CDR regions.
- **Semi-synthetic libraries** based on stable sdAb scaffolds with targeted CDR diversification.
- High diversity, ranging from 2 to **5×10^8 independent variants**



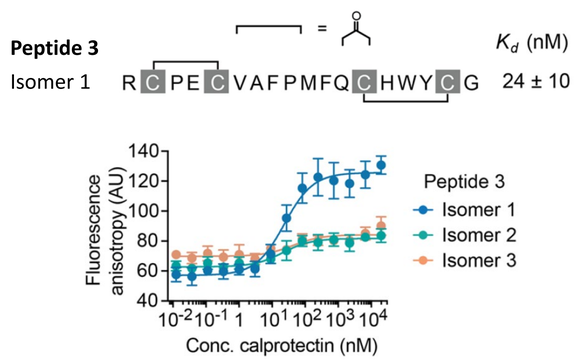


Nanomolar Peptide Binder for Calprotectin Detection

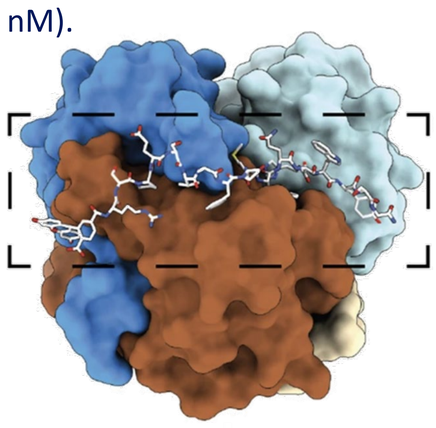
Calprotectin is an important biomarker for inflammatory diseases, and its concentration can be used to monitor inflammatory bowel disease, rheumatoid arthritis (RA) or sepsis.

We screened our peptide libraries, synthesized and cyclized selected peptides, and measured the binding to calprotectin by fluorescence polarization (FP).

Peptide 3 showed the highest affinity, with both the cyclic and linear forms binding calprotectin in the nanomolar range (24 nM).



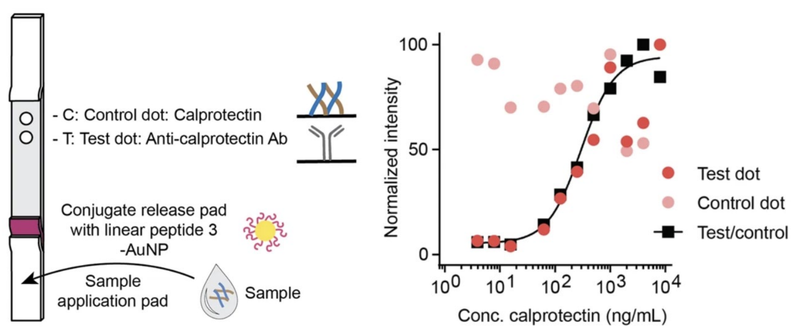
FP measurements of binding of peptide 3 isomers to calprotectin



X-ray crystal structure of linear peptide 3 bound to calprotectin

We developed a **lateral flow assay (LFA) using linear peptide 3**, demonstrating a linear response to calprotectin concentrations ranging from 50 to 2000 ng/mL.

The assay was applied to quantify calprotectin in serum samples from patients with rheumatoid arthritis. Clear signal bands obtained from both serum and whole blood samples demonstrated the **robustness and applicability of the peptide-based LFA**.

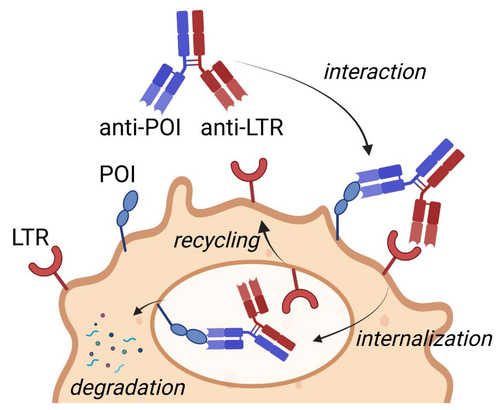


Lateral flow assay using peptide 3 conjugated to gold nanoparticles (AuNP) as the detection reagent, showing the assay schematic and corresponding calibration curve

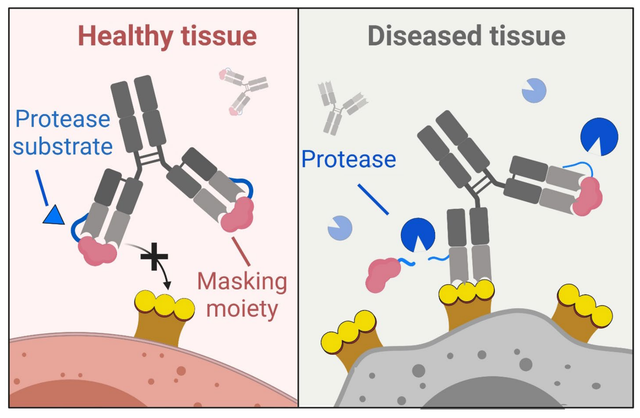
Analysis of serum samples from 18 rheumatoid arthritis and 9 healthy donors

Development of biotherapeutics

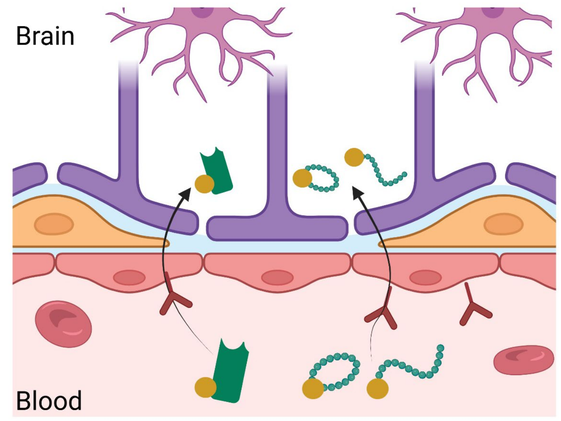
Our phage display libraries are being leveraged to develop smart protein degraders capable of crossing the blood-brain barrier for the treatment of brain tumors.



In targeted protein degradation (TPD), an antibody conjugate binds both the protein of interest (POI) and a lysosome-targeting receptor (LTR), facilitating the internalization and lysosomal degradation of the POI. **We are developing novel antibody derivatives and peptides targeting both known and newly identified LTRs.**



The presence of the therapeutic target in both diseased and healthy tissues leads to dose-limiting side effects. Conditionally active antibodies allow selective activation at the desired site. **We are engineering novel, highly transferable reversible masking strategies for antibody derivatives based on chemogenetic approaches.**



Biotherapeutics often fail to reach the brain in sufficient amounts due to the restrictive nature of the blood-brain barrier (BBB). Using endogenous transport mechanisms provides a non-invasive way to deliver drugs to the brain. **We are developing new peptide and sdAb brain shuttles capable of transporting other therapeutics across the BBB.**

References

Oller-Salvia, et al. *Chem Soc Rev*. **2016**, 45, 4631
Kale, et al. *Nat Chem.* **2018**, 10, 715
Lucchi, et al. *ACS Cent. Sci*. **2021**, 7, 724
Díaz-Perlas, et al. *Nat Commun.* **2023**, 14, 2774
Lucana, et al. *RSC Chem Biol.* **2024**, *5*, 7
Escobar-Rosales, Montaner, et al. *JACS*. **2025**, 147, 45495

www.chemsynbio@iqs.edu

e-mail: cristina.diaz@iqs.url.edu
LinkedIn: cristina-díaz-perlas-2259774a

Acknowledgments

This work was supported by an Innosuisse grant (28020.1 IP-LS) and from MICIU/AEI/10.13039/501100011033 and FEDER, EU (PID2023-151988OB-I00). C.D.-P held a MSCA-PF (101063066) during this time. The project that gave rise to these results also received the support of fellowships from the "la Caixa" Foundation (ID 100010434). The fellowship code from the Postdoctoral Junior Leaders programs to C.D-P is LCF/BQ/PR25/12110008. Some images in this poster have been created with BioRender.com

Peptide-Daunomycin Conjugates Targeting Glioblastoma Cells

Levente Endre Dókus[a *], Lili Szokolai[b], Viktor Farakas[c], Szilvia Bősze[d], Gábor Mező[a,b]

https://doi.org/10.17952/38EPS.2026.P184

[a]*HUN-REN-ELTE Research Group of Peptide Chemistry, Budapest, Hungary.*
[b]*Eötvös Loránd University, Faculty of Science, Institute of Chemistry, Budapest, Hungary*
[c]*HUN-REN-ELTE Protein Modelling Research Group ELTE, Budapest, Hungary*
[d]*Department of Genetics, Cell- and Immunobiology, Faculty of Medicine, Semmelweis University, Budapest, Hungary*
E-mail: endre.dokus@ttk.elte.hu

INTRODUCTION

Cancer is the second most prevalent cause of death worldwide. Glioblastoma is one of the most aggressive fast growing primary brain cancer types presented in 50% of all brain tumors which results in 8 months median survival[1]. Treating cancer runs into a lot of difficulties, but the case of glioblastoma is even more difficult due to the heterogeneity and the blood-brain barrier (BBB) [2].

Fortunately, the Cadhedryn 2 transmembrane receptor was identified as an overexpressed surface protein on glioblastoma (stem) cells which may be good target for tumor targeting. Furthermore, their substrate peptide (AWEFYFP) has been already identified by phage-display technique [3].

Here we report the development of peptide - drug conjugates which contain daunomycin as anticancer agent attached to different variants of AWEFYFP **(1)** homing peptide *via* oxime bound – a linkage that could be suitable for targeted tumor therapy[4].

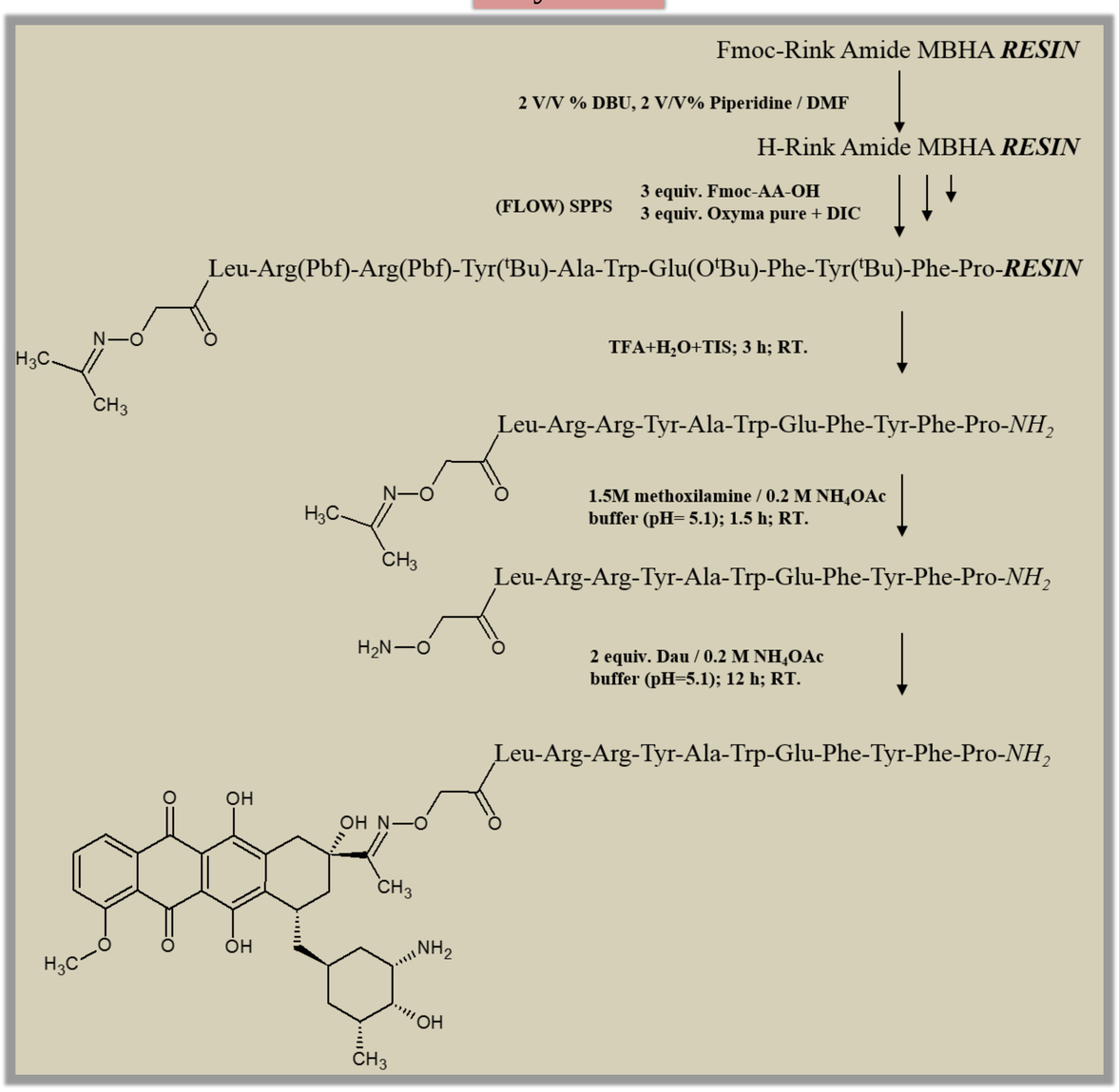
Four different daunomycin - peptide conjugates were prepared by combination of change of aromatic amino acids in position 2 and 5 resulted in AWEF**W**FP **(2)** A**Y**EFYFP **(3)**, A**Y**EF**W**FP **(4)** derivatives of the original sequence. A cathepsin B enzyme labile spacer LRRY was built into the sequences between the homing and the aminooxyacetyl moieties that may enhance the intracellular degradation and the release of the active drug-metabolite(s).

The peptides were synthetized by flow-peptide synthesis using Fmoc/^{t}Bu strategy[5]. The aminooxyacetyl moiety was attached manually to the N-terminus of peptide chains. Finally, the Dau-conjugation was carried out in solution.

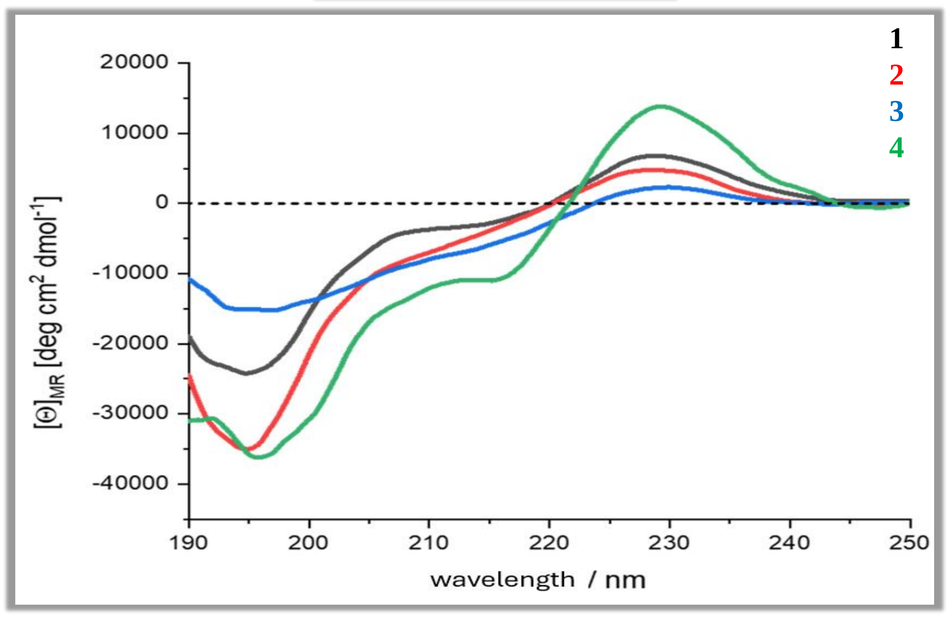
Biological activity of conjugates was characterized by MTT-test on U87 (glioblastoma) and Vero E6 (monkey kidney epithelial cells) as a healthy control cell line. Finally, CD measurement was carried out to identify the structural character of the peptide derivatives for lay down structure- activity relationships.

RESULTS

I. Synthesis



CD measurements



From the graph prepared for the sequences suitable for the study it can be observed that the positive band around ~228 nm indicates the presence of aromatic side chains, typically tyrosine or tryptophan.

The low intensity negative bands around ~215-220 nm may indicate a partial bend structure or even the formation of a temporary β-sheet structure. The negative band pairs observed at ~195 nm indicate the disordered appearance of the amide groups, i.e. very dynamic and mobile, but without a characteristic structure. In the case of conjugate **2**, a negative band can be observed around ~215 nm, which may be a sign of a β-sheet structure or an interaction between the aromatic side chains.

Compared to the other peptides, a slightly more ordered structure was formed in the case of this sequence.

However, we can say that the structure of the new derivatives is significantly different from the conjugate containing the original sequence (conjugate **1**).

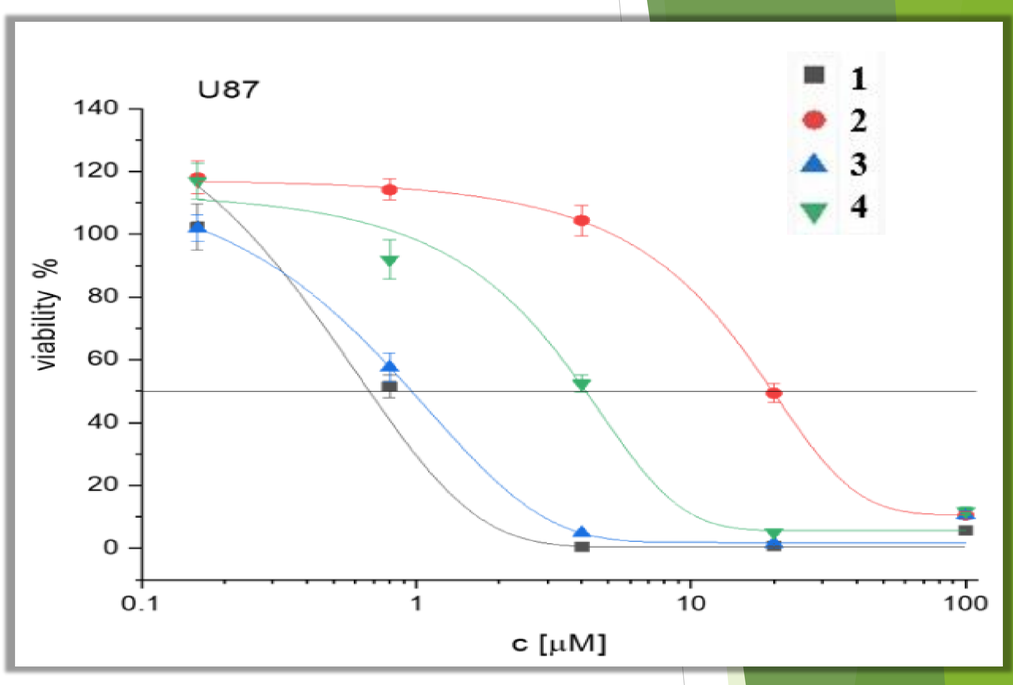
Characterization of biological activity

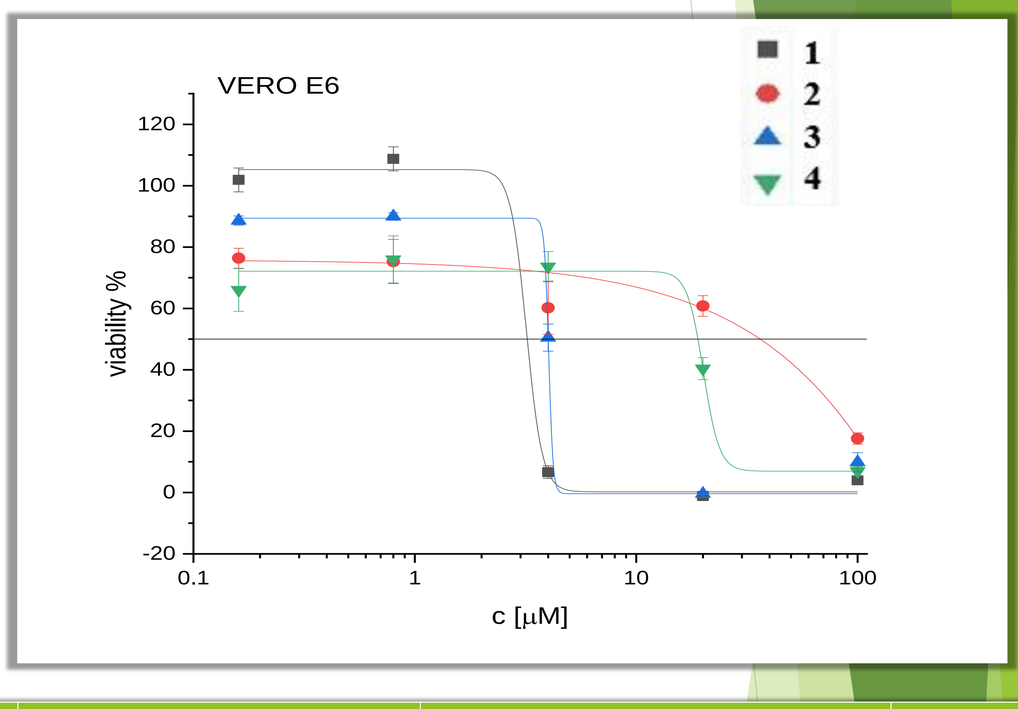
The conjugates were tested in vitro on two cell lines:

U87 glioblastoma cell line as a tumor model, and
Vero E6, a monkey kidney epithelial cell line,

the latter is a model of non-tumorous, healthy cells, as a control.

The cytostatic activity of the conjugates was tested on the former, while the selectivity of the conjugates was tested on the latter one. The results are summarized in the table below and illustrated by the two graphs presented.





CODE	SEQUENCE	IC_{50} (μM)		SELECTIVITY INDEX
		U87	Vero E6	IC_{50} (Vero E6/U87)
1	*Dau=Aoa*-LRRY-AWEFYFP-NH_2	0.67	3.23	4.85
2	*Dau=Aoa*-LRRY-AWEFWFP-NH_2	19.58	35.49	1.78
3	*Dau=Aoa*-LRRY-AYEFYFP-NH_2	0.96	4.02	4.38
4	*Dau=Aoa*-LRRY-AYEFWFP-NH_2	4.09	19.04	4.66

CONCLUSIONS

- The studies showed that the AWEFWFP (**2**) based conjugate has a slightly more ordered structure compared to the others.
- In contrast, the others indicate very dynamic and mobile disordered structures without a characteristic structures, but they also showed a partial bend structure or even the formation of a temporary β-sheet structure.
- Based on the results of the MTT test we can conclude that the biological activity of the variants were not better than the original targeting peptide, but the conjugate **3** with two Tyr showed similar activity with additional advantages such as easier to synthesize due to the absence of tryptophan, and better solubility that might be important point of view in drug development.
- Based on the biological expeiments, it can be concluded that the new conjugates are not better or more selective than the original one, but the results directly highlight that the position of the tyrosine in the sequence is important, as it influenced the efficacy of the conjugate the most.
- Tryptophan is not preferred in the 5th position of the sequence (counting from the left, excluding the spacer), therefore tyrosine substitution is not allowed in this position;
- Replacing the tryptophan in the 2nd position of the sequence with tyrosine does not cause a significant deterioration in the cytostatic effect;
- However, it does not perform better than the sequence taken from the original article, but it significantly reduces the hydrophobicity of the conjugate and can be conjugated to daunomycin *via* an oxime bond more easily than conjugates with more tryptophans
- These properties make it more advantageous for drug development.

ACKNOWLEDGEMENTS

This work was supported the OTKA Grant No. 146039 under grant. L.E. Dókus thanks the Foundation for the Hungarian Peptide and Protein Research for its travel support.

REFERENCES

[1]:R. Stupp, et al. *N Engl J Med*. **2005**, 352(10), 987-996.
[2] L. Pethő, et al. *Int. J. Mol. Sci.* **2023**, 24, 3016.
[3] J.M. Kim, et al. *Stem Cells.* **2023,** 41, 762–774.
[4] G. Mező, et al. *Int. J. Mol. Sci.* **2024,** 25(3) 1864.
[5] V Farkas, et al. *Org. Process Res. Dev.* **2021**. 25, 182−191.

FULLERENOL-BASED MIMICRY OF LarE-TYPE SULFUR INSERTASE ACTIVITY

V. Dolgun[1] · A. Marion[2] · S. Özçubukçu[1]

[1]Department of Chemistry, Middle East Technical University, Ankara, Türkiye
[2]Meddenovo Drug Design, Lyon, France
dvolkan@metu.edu.tr

https://doi.org/10.17952/38EPS.2026.P541

38th European Peptide Symposium · Vienna · 6–11 September 2026

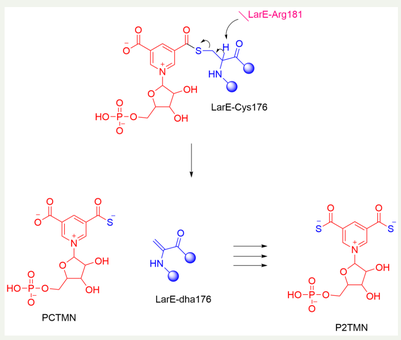
38th EPS
European Peptide Symposium

P541

INTRODUCTION

The development of synthetic systems capable of reproducing complex enzymatic transformations remains a central challenge in biomimetic catalysis. Enzymatic activity commonly depends not only on individual catalytic functional groups, but also on their precise spatial organization within a cooperative microenvironment.[1] LarE provides a particularly unusual model for such studies. It is a sacrificial sulfur insertase involved in the biosynthesis of the nickel-pincer cofactor of lactate racemase.[2] During sulfur insertion, an active-site cysteine residue acts as the sulfur donor and is subsequently converted into dehydroalanine (Dha), resulting in irreversible enzyme inactivation.[3] Thus, unlike conventional enzymes that undergo repeated catalytic turnover, LarE is consumed during the transformation it promotes. Reproducing this distinctive reactivity using a simplified synthetic platform would provide a useful model for investigating enzyme-inspired sulfur chemistry. Building on fullerene-based enzyme mimics ("fullerenzymes"), originally developed for hydrolase-like activity,[4] we therefore extended this concept to a non-enzymatic model of LarE-type reactivity.

Herein, arginine-functionalized fullerenol (F-Arg) was employed as a multifunctional and multivalent catalytic platform. The arginine-derived guanidinium groups distributed around the water-compatible fullerenol scaffold were expected to create a localized basic environment and facilitate cooperative interactions with the reacting substrates. The aim was to promote dehydroalanine formation from cysteine-derived substrates under mild, biologically relevant aqueous conditions. A series of cysteine derivatives was evaluated to establish a thioester-mediated biomimetic pathway in which thioester formation was followed by conversion of the cysteine residue into the corresponding Dha derivative. Among the investigated substrates, N-acetyl-L-cysteine-N′-benzylamide enabled productive conversion in the presence of F-Arg. The catalytic system was also compared with free arginine to examine the importance of presenting multiple arginine groups on the fullerenol scaffold. Reaction progress and product identity were evaluated by HPLC and LC–MS analysis, respectively.

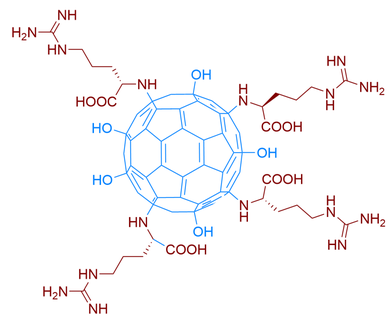


Native LarE: sulfur donation converts the active-site cysteine into dehydroalanine (Dha) and irreversibly inactivates the enzyme.

Our aim is to reproduce LarE-type sulfur chemistry with a cooperative F-Arg platform

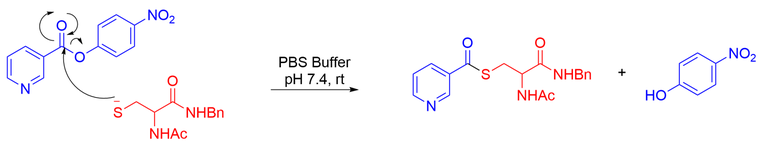
BIOMIMETIC DESIGN

F-Arg presents multiple guanidinium groups around a fullerenol core, creating a cooperative catalytic microenvironment.



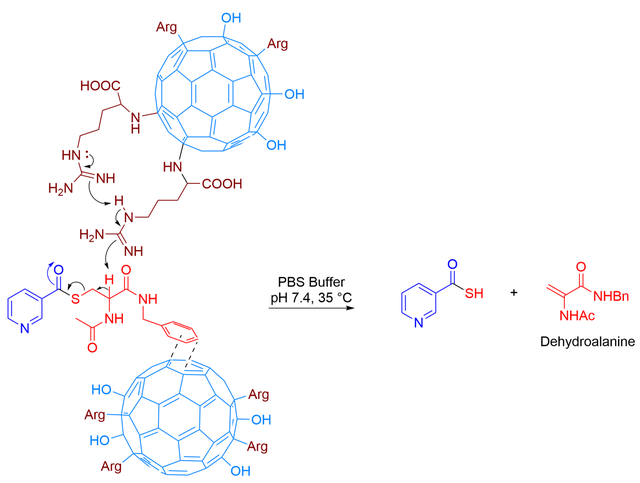
Arginine Functionalized Fullerenol
Arginine-functionalized fullerenol (F-Arg)

THIOESTER-MEDIATED PATHWAY



Substrate system: *p*-Nitrophenyl nicotinate was used as an activated nicotinic-acid-derived substrate analogue, while *N*-acetyl-L-cysteine-*N*′-benzylamide (2d) was selected as the cysteine-derived substrate. The corresponding dehydroalanine derivative is denoted 5d in the analytical data.

PROPOSED CATALYTIC MODEL



*Proposed **F**-Arg-assisted conversion of the thioester intermediate to the Dehydroalanine (Dha) product.*

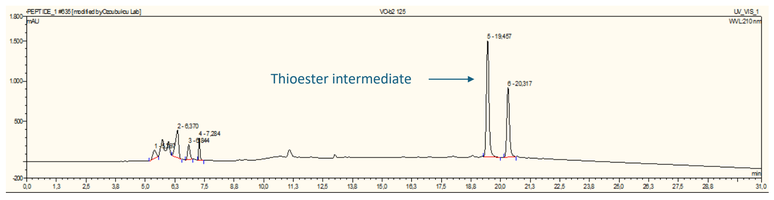
OPTIMIZED SEQUENCE

1. Pre-form the thioester in PBS (pH 7.4) for 1 h at room temperature.
2. Add F-Arg and incubate the reaction at 35 °C.
3. Withdraw timed aliquots and quench by acidification.
4. Quantify Dha formation by HPLC and confirm product identity by LC–MS.

RESULTS · HPLC AND LC–MS

STEP 1 Thioester Preformation

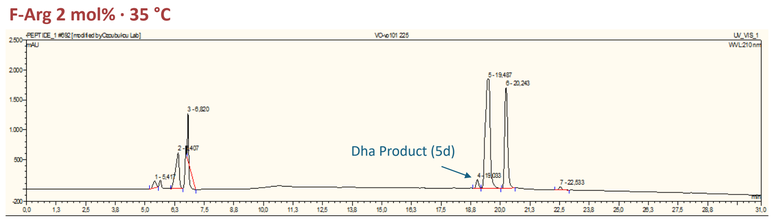
PBS, pH 7.4 · room temperature · 1 h · before F-Arg addition



Thioester formation was observed, with no detectable Dha product.

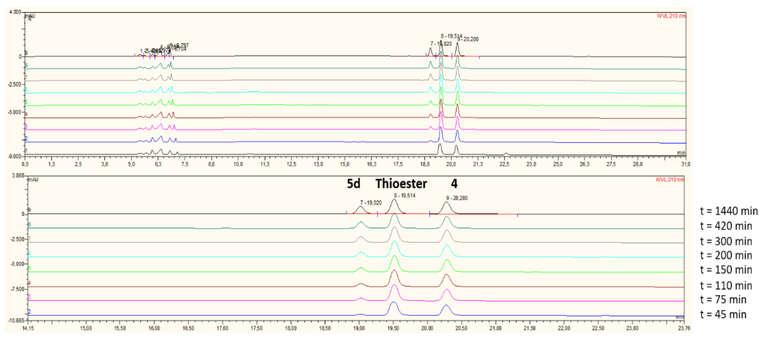
STEP 2 F-Arg-mediated Dha formation

F-Arg 2 mol% · 35 °C



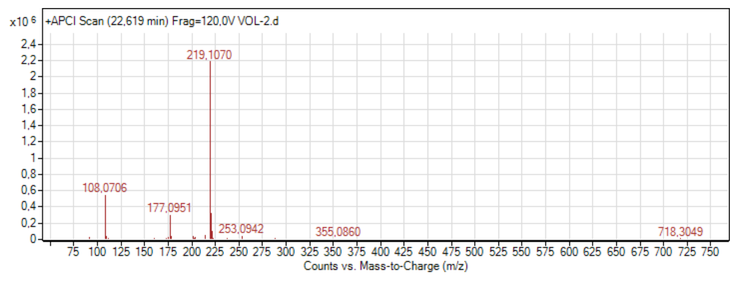
*A new peak assigned to Dha product 5d appeared after **F**-Arg addition.*

TIME-DEPENDENT PRODUCT FORMATION



The peak assigned to 5d increased progressively with reaction time.

LC–MS PRODUCT CONFIRMATION



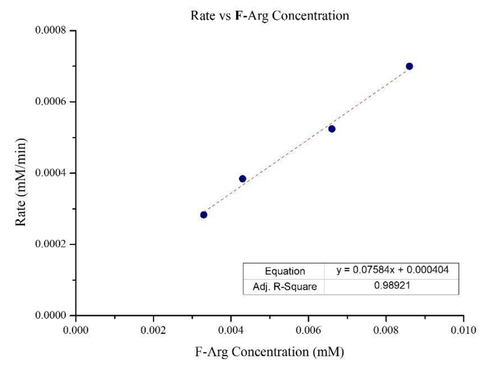
Dha product 5d: observed m/z 219.1070; calculated m/z 219.1089 for $[M+H]^+$.

CONTROLS ESTABLISH CATALYTIC ACTIVITY

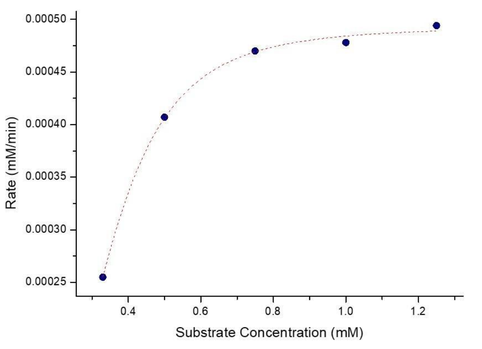
No F-Arg	**No Dha**
Free Arg · catalytic loading	**No Dha**
Free Arg · stoichiometric	**Dha formed**
F-Arg · catalytic loading	**Dha formed**

F-Arg promotes Dha formation at catalytic loading, whereas free arginine requires a stoichiometric amount. The controls support a cooperative effect of the multivalent F-Arg platform.

KINETIC CHARACTERIZATION



Linear catalyst dependence (R^2 = 0.989)



Substrate saturation is consistent with Michaelis–Menten-like behavior.

k_{cat} :	K_M:	k_{cat}/K_M:
0.0758 min^{-1}	0.33 mM	0.2297 $mM^{-1}\,min^{-1}$

K_M is a preliminary estimate; additional low-substrate points would improve precision.

CONCLUSIONS

- Screening of cysteine derivatives identified *N*-acetyl-L-cysteine-*N*′-benzylamide as a suitable substrate for the thioester-mediated formation of the corresponding Dha derivative.
- Under the optimized conditions (PBS, pH 7.4, 35 °C), Dha formation was observed by HPLC and the product identity was confirmed by LC–MS. No detectable Dha formation occurred in the absence of F-Arg.
- Free arginine required a stoichiometric amount to induce conversion, whereas F-Arg promoted Dha formation at catalytic loading. This difference supports a cooperative effect arising from the multivalent **F**-Arg platform.
- Reaction rate increased linearly with **F**-Arg concentration, giving k_{cat} = 0.0758 min^{-1}. Substrate-concentration analysis showed Michaelis–Menten-like saturation behavior and provided a preliminary K_M estimate of 0.33 mM.

KEY FINDING

The multivalent F-Arg platform provides a cooperative catalytic microenvironment that promotes LarE-inspired dehydroalanine formation under mild aqueous conditions. This study extends the fullerenzyme concept beyond hydrolase mimicry to sulfur-transfer chemistry.

ACKNOWLEDGEMENT

Supported by TÜBİTAK under grant no. 118Z921.

REFERENCES

1. Yin, Y.; Dong, Z.; Luo, Q.; Liu, J. *Prog. Polym. Sci.* **2012**, *37*, 1476–1509.
2. Desguin, B.; Soumillion, P.; Hols, P.; Hausinger, R. P. *Proc. Natl. Acad. Sci. U.S.A.* **2016**, *113*, 5598–5603.
3. Fellner, M.; Desguin, B.; Hausinger, R. P.; Hu, J. *Proc. Natl. Acad. Sci. U.S.A.* **2017**, *114*, 9074–9079.
4. Gülseren, G.; Saylam, A.; Marion, A.; Özçubukçu, S. *ACS Appl. Mater. Interfaces* **2021**, *13*, 45854–45863.

Peptide Self-assembly Beyond Known Design Principles: Sequence and Context Interplay

Ena Dražić,[a] Helena S. Azevedo,[b] Daniela Kalafatović,[a,*]

[a] *University of Rijeka, Faculty of Engineering, Rijeka, Croatia*

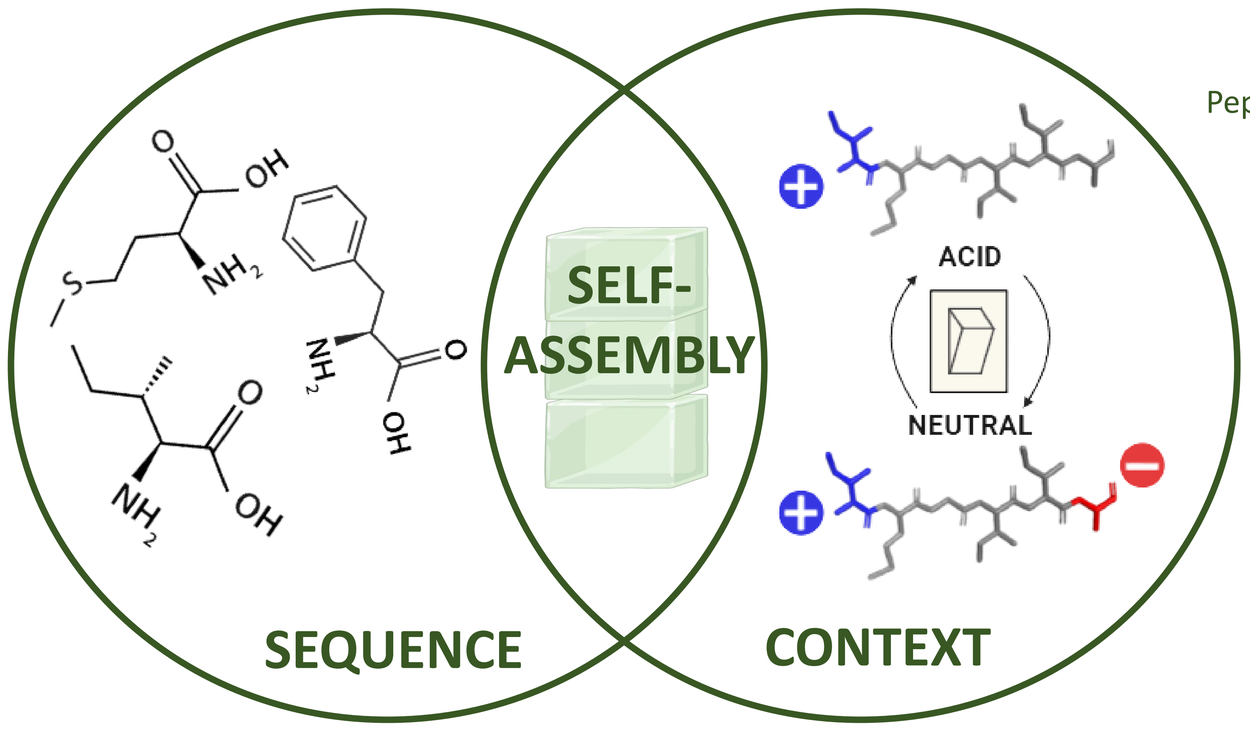
[b] *Institute for Research and Innovation in Health, Porto, Portugal*

ena.drazic@uniri.hr

https://doi.org/10.17952/38EPS.2026.P556

AI generated hexapeptides with increasing aromaticity were assessed for their self-assembly propensity.[1]

Can sequence-assembly relationship in AI-generated hexapeptides reveal new design principles?



Peptides can form supramolecular assemblies guided by **sequence** and **experimental context.**[2]

Is self-assembly determined by sequence alone or changing conditions can redirect the outcome?

Sequence Matters: Self-Assembly of an Unconventional Hydrophobic Peptide

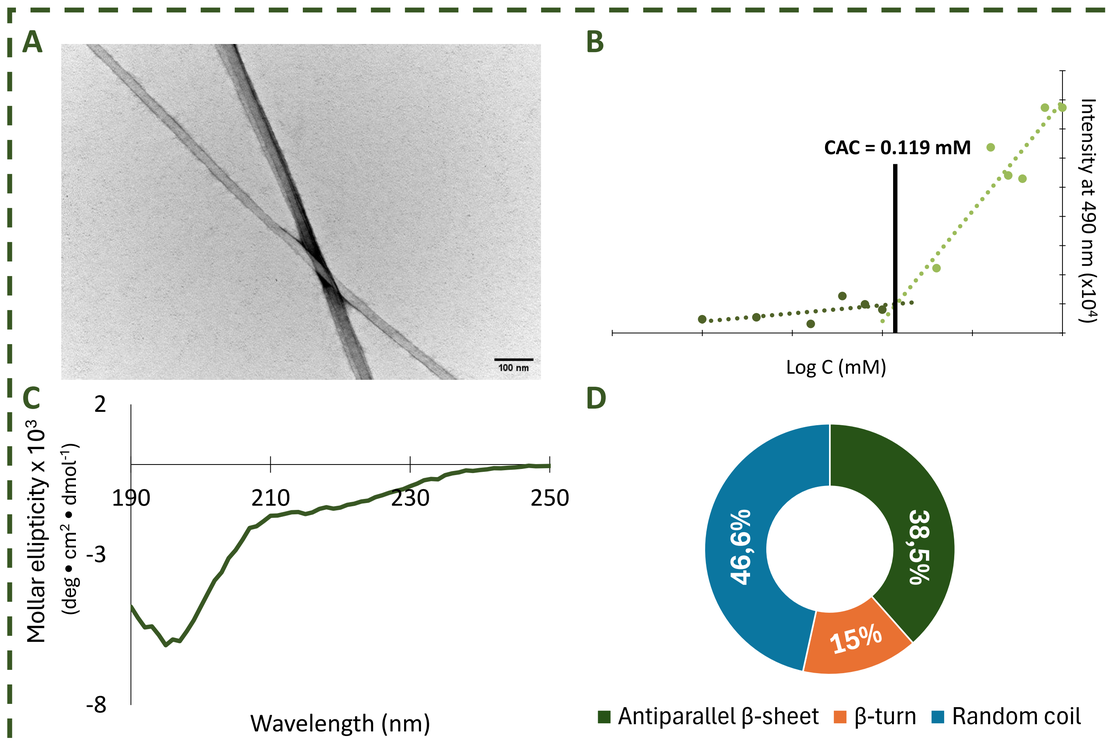


Figure 1. Despite lacking typical amphiphilic design, IMGIIA self-assembles into elongated fibrillar structures **(A)**. Concentration-dependent increase in ThT fluorescence indicates β-sheet-like assembly propensity **(B)**, while CD shows an overall random-coil-like organization **(C)**. BeStSel analysis shows a mix of random coil and antiparallel β-sheet content **(D)**, suggesting the mixed supramolecular organization of IMGIIA.

More Aromatic, More Ordered: Aromaticity Drives Assembly Toward β-sheet-like Organization

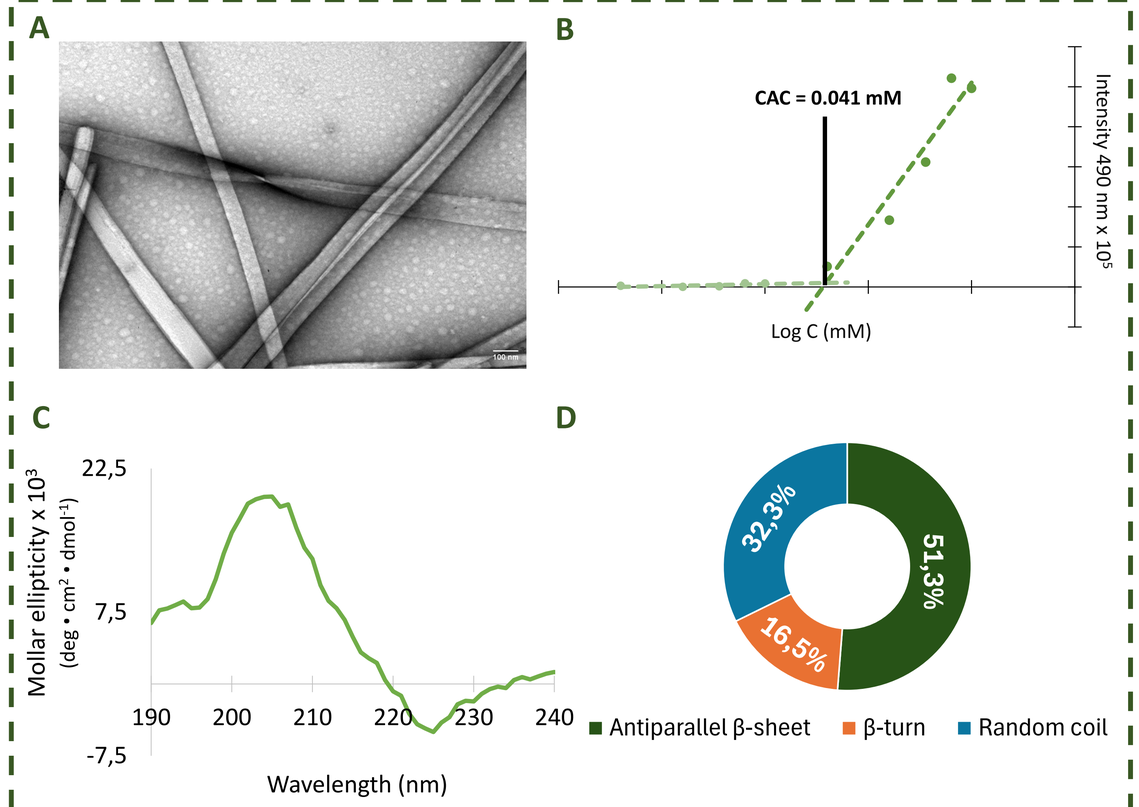


Figure 2. Introducing aromaticity by replacing the terminal I and A residues with F in FMGIIF changes the assembly behavior toward supramolecular order **(A)**. ThT fluorescence suggests the formation of fibrillar assemblies with CAC of 0.041 mM **(B)**, while CD confirms β-sheet-rich organization **(C)**, with antiparallel β-sheet content increasing from 38.5% in IMGIIA (Fig. 1) to 51.3% in FMGIIF **(D)**.

SELF-ASSEMBLY IS DRIVEN BY MORE THAN SEQUENCE ALONE: pH AND CONCENTRATION SHAPE THE SUPRAMOLECULAR OUTCOME

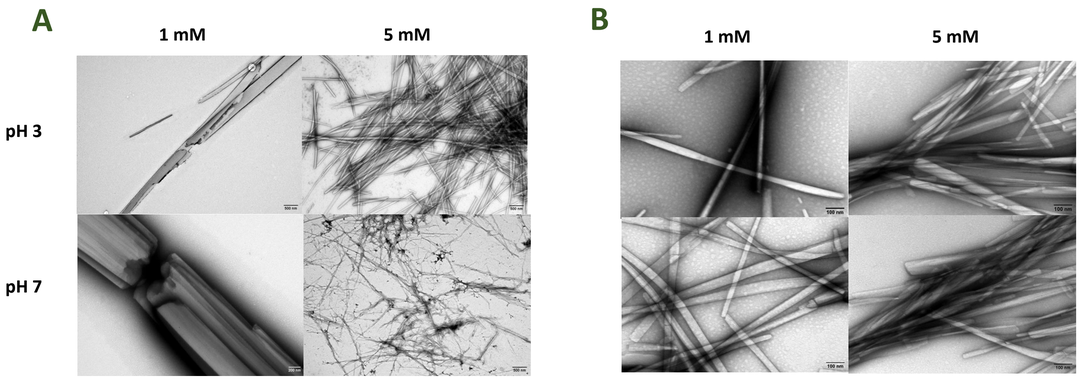


Figure 3. Both peptides self-assemble at pH 3 and pH 7, with fibrillar morphology influenced by concentration. **(A)** IMGIIA forms denser fiber networks at higher concentration at both pH values. **(B)** FMGIIF shows similar fibrillar assemblies at 5 mM at both pH values, while at 1 mM a denser fibril network is observed at pH 7. These results indicate that pH and concentration act together in defining the assembly outcome.

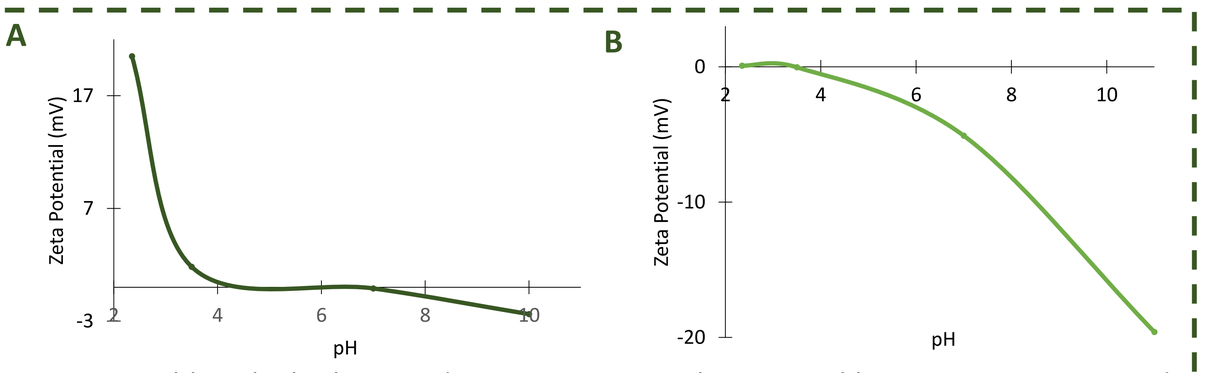


Figure 4. Although both peptides contain equivalent ionizable termini, amino acid substitutions at the N- and C-terminal positions may alter supramolecular packing and the surface exposure of these groups, explaining different pH-dependent zeta-potential profiles. **(A)** IMGIIA rapidly loses its positive surface charge between pH 2 and 4 and remains near neutral at higher pH. **(B)** FMGIIF gradually shifts toward a more negative surface charge with increasing pH.

SEQUENCE-CONTEXT INTERPLAY IS A KEY:
Sequence and experimental conditions (pH and concentration) together shape the self-assembly of IMGIIA and FMGIIF.

REFERENCES

[1] M. Njirjak, L. Žužić, M. Babić, P. Janković, E. Otović, D. Kalafatovic and G. Mauša, Nat. Mach. Intell., 2024, 6, 1487–1500

[2] E. Dražić, D. Jelušić, P. Janković Bevandić, G. Mauša and D. Kalafatovic, ACS Nano, 2025, 19, 20295–20320

[grant no. CA23111]

[grant no. IP-2025-02-3357]
[grant no. DOK-NPOO- 2023–10-8638]

[grant no. uniri-mzi-25-2]

Controlling Nanonet Morphology via Residue-Specific Modulation of β-hairpin Peptide for Enhanced Bacterial Trapping

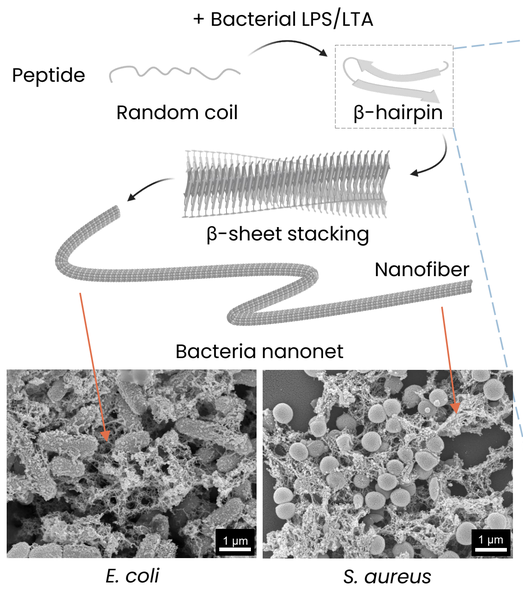
Wei Meng Chen[a], Dhanya Mahalakshmi Murali[a], Nhan Dai Thien Tram[a], Peiyan Yu[a], Daniel Tianyu Wang[b], and Pui Lai Rachel Ee[a,*]

[a] *Department of Pharmacy and Pharmaceutical Sciences, National University of Singapore,*

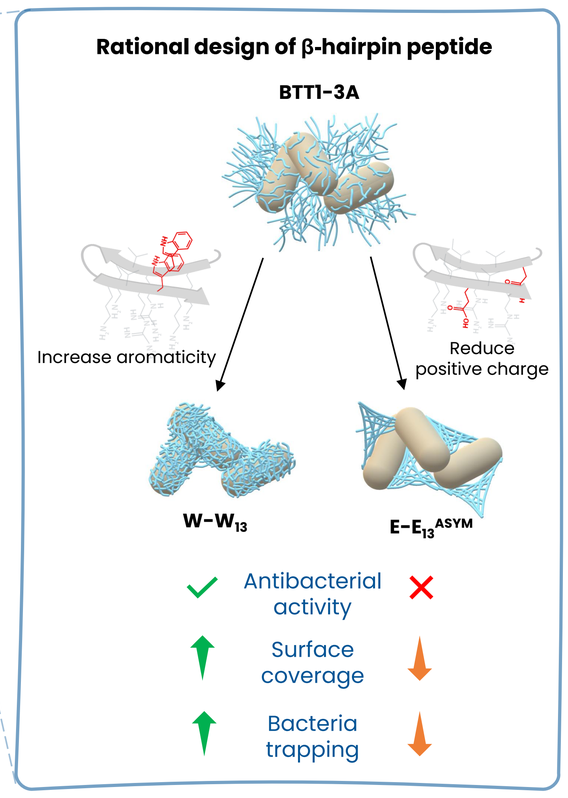
[b] *Department of Anthropology & Forensic Science Program, University of Toronto, Canada*

https://doi.org/10.17952/38EPS.2026.P161

Introduction



- **Self-assembling peptides** can form nanonets to control bacterial infections and combat antibiotic resistance.
- Our previously designed synthetic peptide, **BTT1-3A**, forms nanonets that trap-and-kill bacteria [1], but its **loose** architecture may limit trapping efficiency.
- In this work, we demonstrate that rational peptide design can **modulate nanonet morphology** and enhance antibacterial and trapping activity [2].



Design Rationale

Aromatic residues may promote membrane interaction to form **tight** trap-and-kill nanonets.

Reduced net positive charge may result in **loosely** trapping nanonets without effective killing.

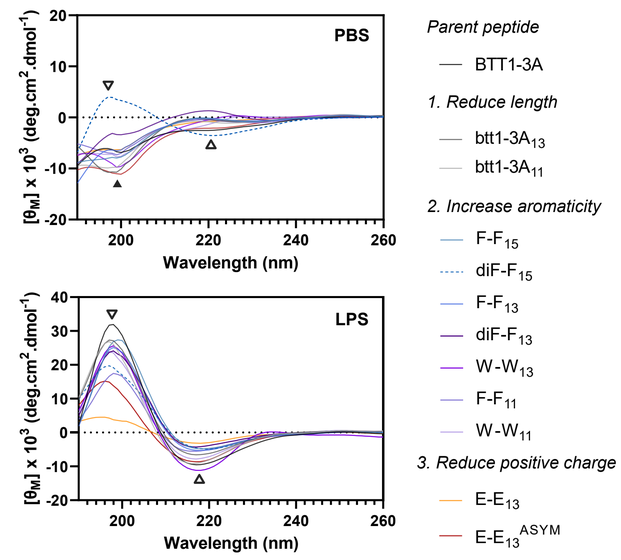
Peptide Designs

Peptide	Sequence	Length	Charge
BTT1-3A	LKLKLKLTAKLKLKL	15	7
1. Reduce length			
btt1-3A$_{13}$	KLKLKLTAKLKLK	13	7
btt1-3A$_{11}$	LKLKLTAKLKL	11	5
2. Increase aromaticity			
F-F$_{15}$	LK**F**RVKLTAKVR**F**KL	15	7
diF-F$_{15}$	LK**F**R**F**KLTAK**F**R**F**KL	15	7
F-F$_{13}$	K**F**RVKLTAKVR**F**K	13	7
diF-F$_{13}$	K**F**R**F**KLTAK**F**R**F**K	13	7
W-W$_{13}$	K**W**RVKLTAKVR**W**K	13	7
F-F$_{11}$	**F**RVKLTAKVR**F**	11	5
W-W$_{11}$	**W**RVKLTAKVR**W**	11	5
3. Reduce positive charge			
E-E$_{13}$	**E**VRIKLTAKIRV**E**	13	3
E-E$_{13}^{ASYM}$	EVRIKLTAKI**E**VR	13	3

Acronym: lipopolysaccharide (LPS), lipoteichoic acid (LTA), phosphate buffer saline (PBS)

1 Bacteria-induced peptide folding

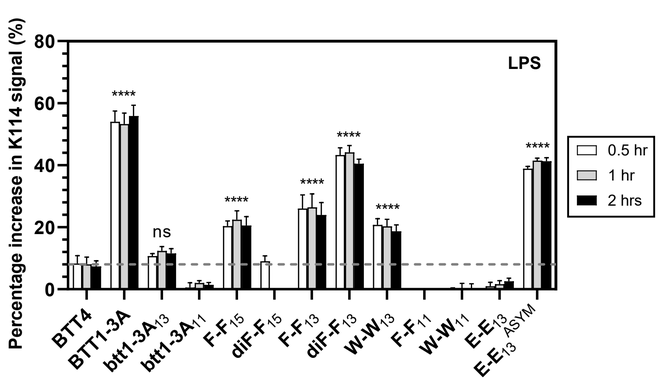
Circular dichroism spectroscopy



- All peptides remained as random coils (▲) in PBS, except diF-F$_{15}$, which adopted a β-sheet structure (△).
- All peptides folded into **β-sheets** upon binding to bacterial LPS, indicating their **responsiveness to bacterial presence.**
- This bacteria-triggered folding enables **targeted self-assembly** only at infection sites.

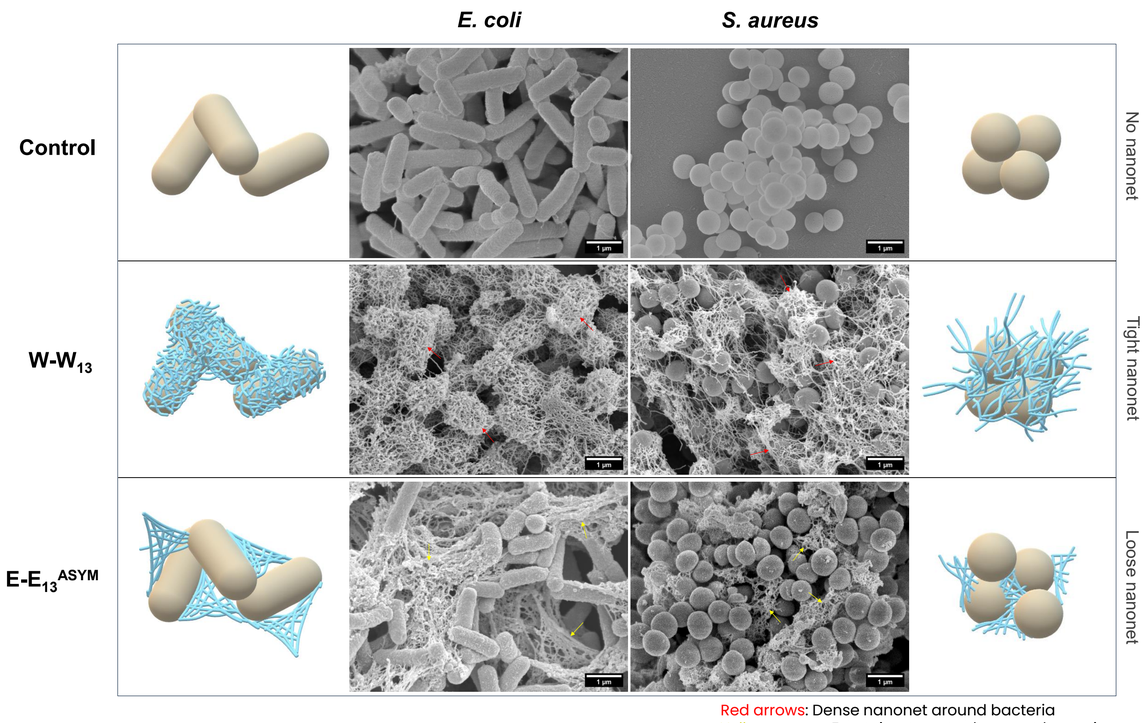
2 Bacteria-responsive nanonet formation

K114 fluorescence assay



- K114 dye bind specifically to **cross β-sheet** structure and fluoresces, confirming self-assembly upon binding to bacterial LPS.
- BTT1-3A, F-F$_{15}$, F-F$_{13}$, diF-F$_{13}$, W-W$_{13}$ and E-E$_{13}^{ASYM}$ **rapidly self-assemble** after binding to LPS within 30min.
- **π–π stacking** and **electrostatic interactions** can stabilize the β-hairpin and promote self-assembly in the shorter 13-mer peptide.

Scanning electron microscopy

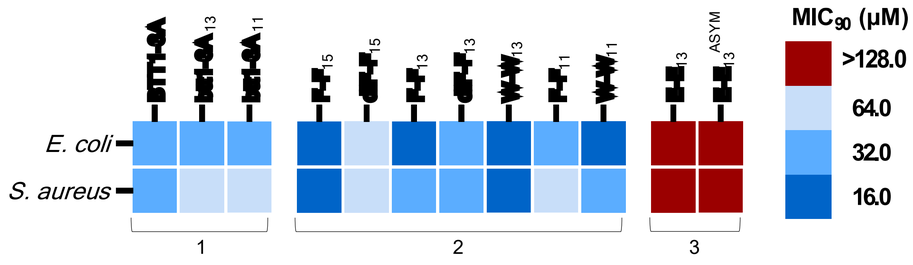


Red arrows: Dense nanonet around bacteria
Yellow arrows: Extensive nanonet between bacteria

- W-W$_{13}$ forms **dense, interwoven nanofibers** on individual *E. coli* surface, forming **tight nanonets** that fully encage the bacteria, but shows lower surface coverage on *S. aureus*.
- E-E$_{13}^{ASYM}$'s nanofibers tend to **self-interweave** into extensive nanonets, with **minimal surface coverage** on *E. coli* and *S. aureus*, resulting in **loose** bacterial trapping.

3 Bacterial trapping efficacy

Minimum inhibitory concentration (MIC) assay

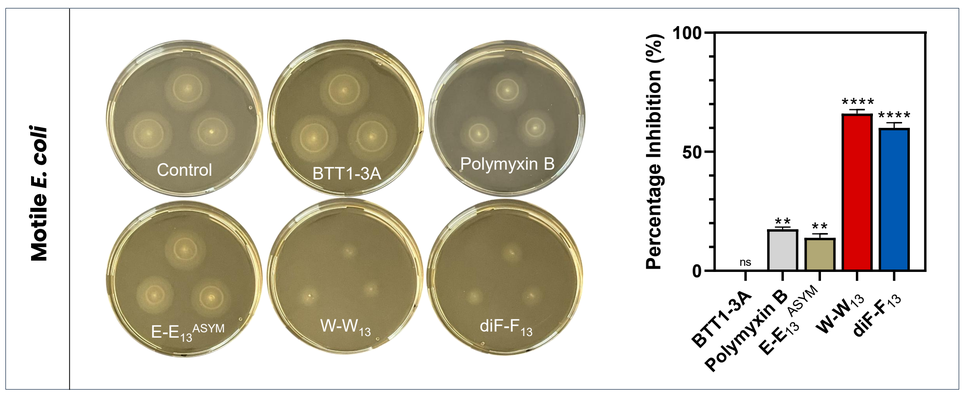


MIC$_{90}$: Lowest concentration of peptide that kill 90% of the bacteria

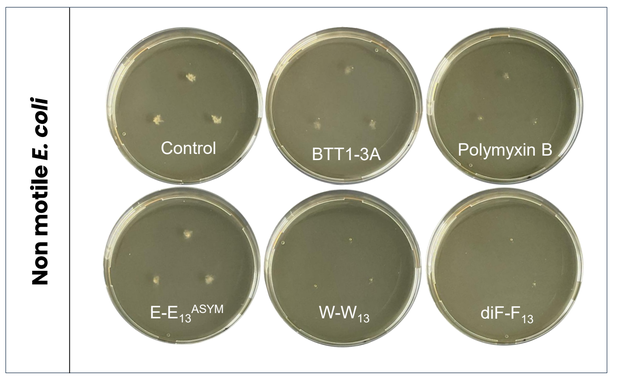
- W-W$_{13}$ and F-F$_{15}$ showed 2-fold **improved killing** of *E. coli* and *S. aureus* while retaining nanonet formation.
- Reducing net positive charge in E-E$_{13}^{ASYM}$ **abolished antibacterial activity** despite preserved nanonet formation.
- High positive charge and aromaticity are critical for balancing nanonet formation and antibacterial function of β-hairpin peptides.

Soft agar motility assay

Nanonet-trapped bacteria were seeded in soft agar to assess post-entrapment escape



- Motile *E. coli* move freely and proliferate in soft agar, forming a clear motility halo.
- Kill-only antibiotic (Polymyxin B): *E. coli* survive by **escaping** from high-concentration zones.
- Loose trap-and-kill nanonet (BTT1-3A): Kills bacteria but **ineffective trapping** allows escape.
- Tight trap-and-kill nanonet (W-W$_{13}$ & diF-F$_{13}$): Effectively trap and **inhibit bacteria spread**.
- Loose trap-only nanonet (E-E$_{13}^{ASYM}$): Slows movement only but fails to kill bacteria.



- Non-motile *E. coli* (ΔflhD mutant) were **more susceptible** to polymyxin B and loose BTT1-3A nanonets due to impaired escape.
- W-W$_{13}$ and diF-F$_{13}$ effectively blocked the growth of non-motile bacteria.
- Without antibacterial activity, E-E$_{13}^{ASYM}$ nanonets failed to prevent bacterial outgrowth and potential spread.

Key takeaways

- **Design-Driven Assembly:** Rational modification of β-hairpin side strands controls nanonet morphology through amino acid side chain chemistry.
- **Tight vs. Loose Nanonets:** W-W$_{13}$ forms dense, surface-bound nanonets that effectively limit bacterial spread, while E-E$_{13}^{ASYM}$ forms loose trap-only nanonet.
- **Motility Matters:** Bacterial motility reduces antibiotic effectiveness; tight nanonets that encage and restrict motile bacteria offer a promising alternative strategy.

References:
1. Tram, N. D. T., et. al., Bacteria-Responsive Self-Assembly of Antimicrobial Peptide Nanonets for Trap-and-Kill of Antibiotic-Resistant Strains. *Adv. Funct. Mater.* 2023, 33, 2210858.
2. Chen. W. M., et, al., Controlling Nanonet Morphology via Residue-Specific Modulation of β-Hairpin Peptide for Enhanced Bacterial Trapping. *Small* 2025, 2505823.

LinkedIn

Contact Information
Wei Meng CHEN
Email: E1101893@u.nus.edu

LinkedIn

Contact Information
A/Prof: Pui Lai Rachel EE
Email: phaeplr@nus.edu.sg

Guiding Peptide Nanonet Formation and Antibacterial Activity via Hydrophobic Aromatic Ring Engineering for Sepsis Control

Wei Meng Chen[a], Haoting Shi[a], Jun Hao Chiew[a], Ho Ying Low[a], Jan Kazimierz Marzinek[b], Din Bao Nguyen[b], Khai Shuen Heidi Lek[b], Zhi Wen Tay[a], Peter John Bond[b] & Pui Lai Rachel Ee[a,*]

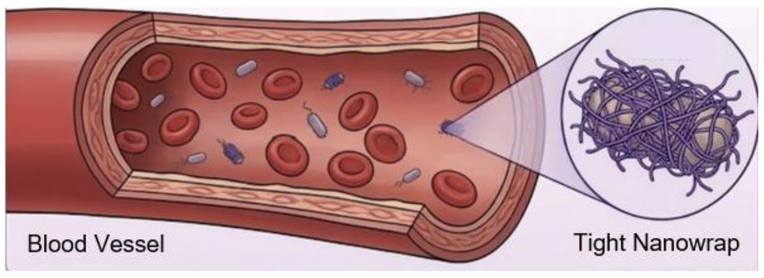
[a] *Department of Pharmacy and Pharmaceutical Sciences, National University of Singapore,*

[b] *Bioinformatics Institute, Agency of Science, Technology and Research (A*STAR), Singapore*

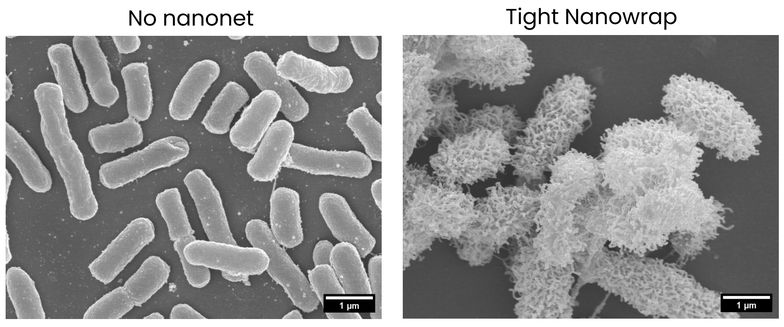
https://doi.org/10.17952/38EPS.2026.P217

National University of Singapore

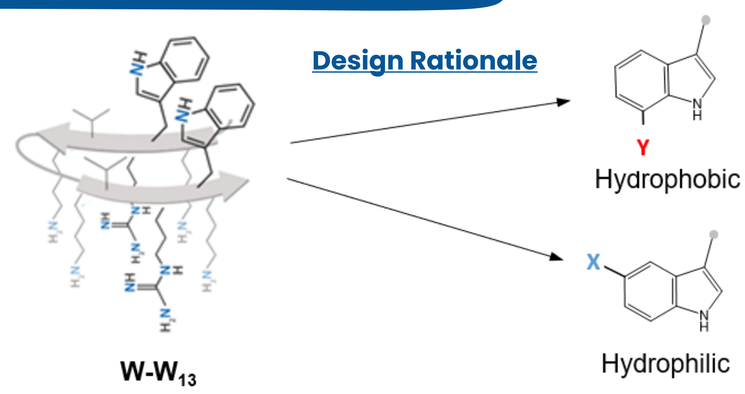
Introduction



Precise bacterial capture by Tight Nanowraps:
A potential new strategy against bacteremia and fatal sepsis.



P. aeruginosa PAO1 — **W-W$_{13}$**



- **Bacteria-responsive self-assembly:** β-hairpin peptides can self-assemble upon binding to bacterial surface components to form trap-and-kill nanonets [1].
- Tight Nanowrap: **Aromatic ring**-containing β-hairpin peptide **W-W$_{13}$** forms dense nanofibers that tightly encapsulate individual bacteria [2].

Research Questions:

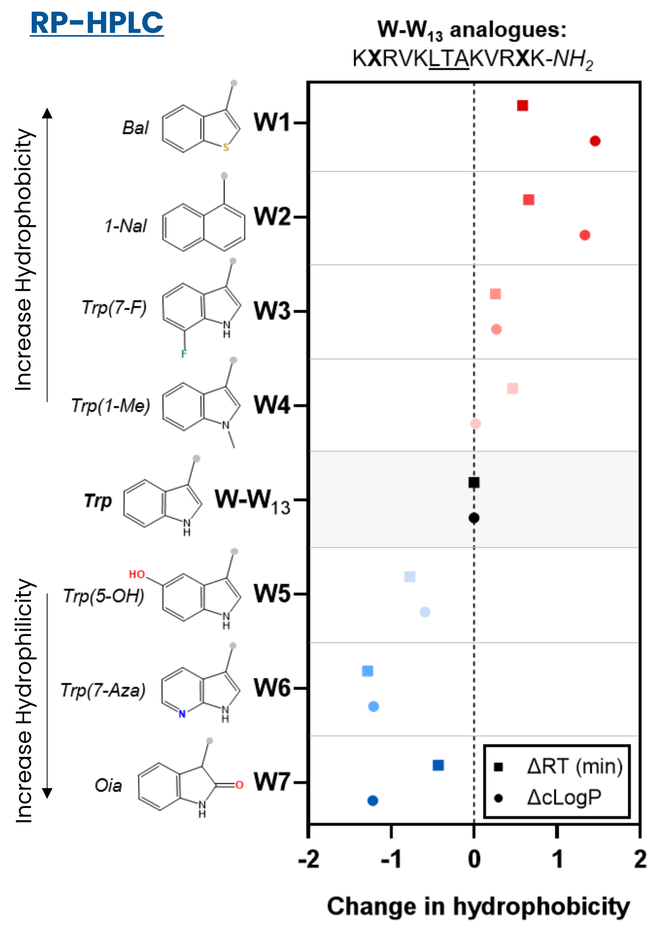
Aromatic ring as a scaffold: How chemical modification of the aromatic ring tunes nanonet morphology and activity remains unknown.

Increase hydrophilicity — Hydrogen bonding opportunity to stabilize nanofiber?

W-W$_{13}$

Increase hydrophobicity — Enhanced self-assembly and denser nanofibers?

Peptide Design

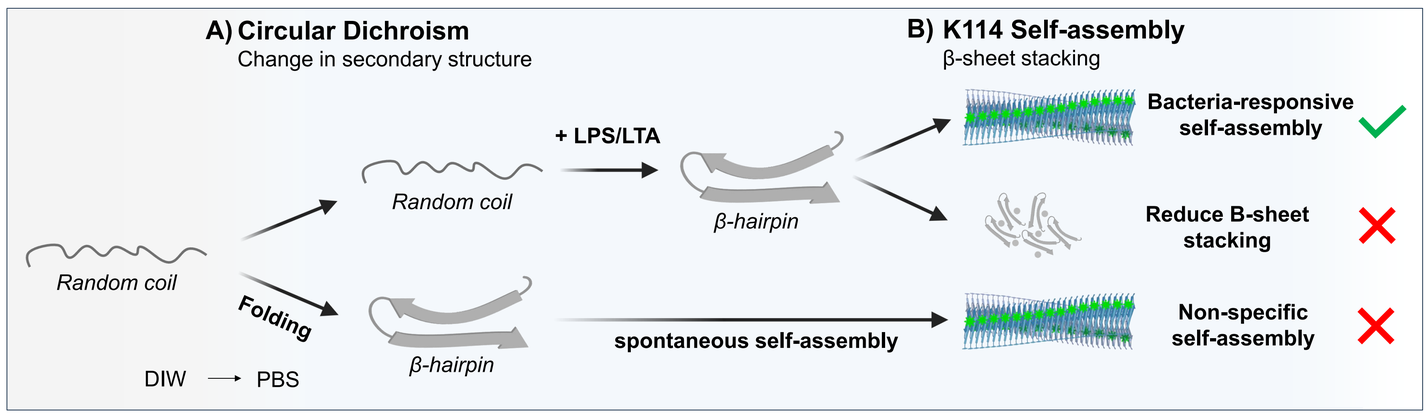


Small changes to the aromatic ring **alter peptide lipophilicity**, as measured by RP-HPLC and correlated with cLogP.

Aromatic Lipophilicity Impacts Self-Assembly and Activity

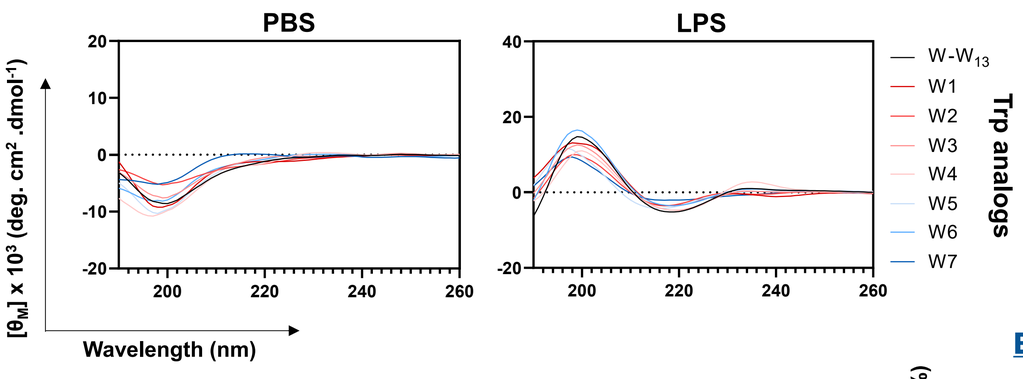
Cell-free Peptide Self-assembly Screening Workflow

*Only peptide candidates that **specifically** form nanofibers upon binding to bacterial LPS/LTA were selected for evaluation.



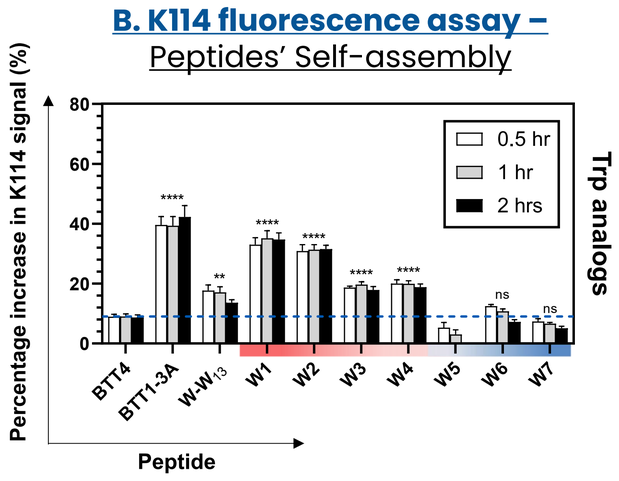
Legend: Fluorescent K114 / Quenched K114
LPS=Lipopolysaccharide
LTA=Lipoteichoic acid

A. Circular Dichroism - Peptides Secondary Structure



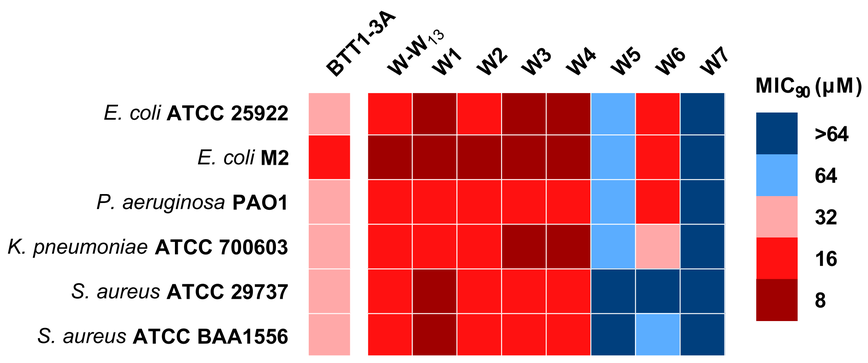
- Lipophilicity does not affect peptide secondary structure formation.
- Peptides remain as soluble random coils and fold into **β-hairpins** only upon binding to LPS specifically.

B. K114 fluorescence assay – Peptides' Self-assembly



- **Only hydrophobic aromatic Trp analogues** self-assemble in response to bacterial LPS.
- W3 and W4 show **similar self-assembly to W-W$_{13}$** (similar cLogP), while W1 and W2 with **higher hydrophobicity enhance nanofiber formation.**
- In contrast, **hydrophilic aromatic analogues significantly impair nanofiber formation.**

C. MIC Screening Assay– Antibacterial Activity



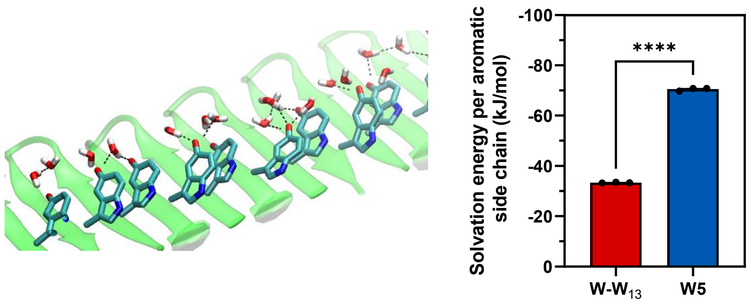
- Hydrophobic aromatic Trp analogues exhibit **broad-spectrum antibacterial activity.**
- W1, W3, and W4 showed a **2-fold increase** in bacterial killing.
- Hydrophilic aromatic Trp analogues **impaired antibacterial activity.**

Molecular Basis of Nanonet Formation

Scanning Electron Microscopy – Nanonet's Morphology

- Hydrophilic aromatic analogues (W5) **abolish nanonet formation.**
- W3 and W4 **maintain tight nanowrap** formation, similar to W-W$_{13}$.
- W1 and W2 nanofibers tend to self-assemble away from the bacterial surface.

Molecular Simulation – Mechanistic Studies



Weak π–π interactions and **strong water solvation** disfavor the intermolecular assembly of hydrophilic aromatic analogues (W5) into nanofibers.

Key Takeaways

- Hydrophobic aromatic analogues are critical for maintaining nanofiber assembly and antibacterial activity.
- Fine-tuning aromatic hydrophobicity modulates nanonet morphology and activity, with an optimal range for tight nanowrap formation.
- Hydrophilic aromatic modifications disfavor self-assembly due to weaker π–π stacking and strong water solvation.

References:
1. Tram, N. D. T., et. al., Bacteria-Responsive Self-Assembly of Antimicrobial Peptide Nanonets for Trap-and-Kill of Antibiotic-Resistant Strains. *Adv. Funct. Mater.* 2023, 33, 2210858.
2. Chen. W. M., et, al., Controlling Nanonet Morphology via Residue-Specific Modulation of β-Hairpin Peptide for Enhanced Bacterial Trapping. *Small* 2025, 2505823.

LinkedIn

Contact Information
Wei Meng CHEN
Email: E1101893@u.nus.edu

DEVELOPMENT OF AN INHIBITOR OF PLASMINOGEN ACTIVATOR INHIBITOR-1 (PAI-1) FOR THE TREATMENT OF INFLAMMATORY AND FIBROTIC DISORDERS

Eszter Erdei[1,2], Nikolett Varró Kormosné[1], Boldizsár Jójárt[3], Petra Pallagi[3], József Maléth[3], István Mándity[1,2]

[1]HUN-REN Research Centre for Natural Sciences, Artificial Transporters Research Group
[2]Department of Organic Chemistry, Semmelweis University, Faculty of Pharmacy
[3]MTA-SZTE Momentum Epithelial Cell Signalling and Secretion Research Group
https://doi.org/10.17952/38EPS.2026.P172

INTRODUCTION

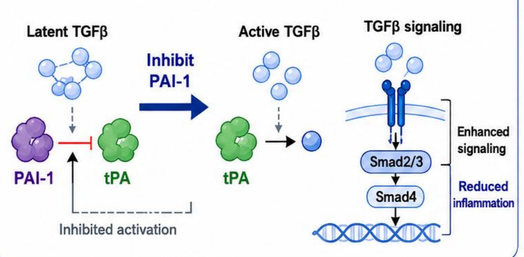
Inflammatory bowel disease (IBD), including Crohn's disease and ulcerative colitis, is a chronic relapsing inflammatory disorder that affects millions of people worldwide and often requires lifelong treatment.[1] **Persistent inflammation** can drive **intestinal fibrosis**, resulting in **excessive fibroblast activation** and **extracellular matrix deposition.**[2] **Plasminogene activator inhibitor (PAI-1) is a key mediator** that links chronic inflammation to intestinal fibrosis by decreasing the concentration of TGF-β from the latent complex and promoting extracellular matrix accumulation.[3]

AIMS

PAI-1 – tissue-type plasminogen activator (tPA) inhibition represents a promising strategy for the treatment of IBD and IBD-associated fibrosis.

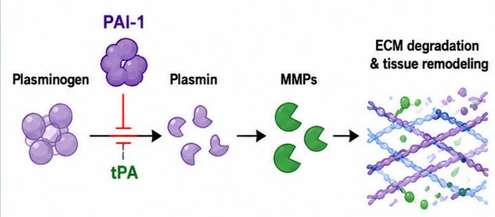
TGFβ signaling is impaired in IBD

- **Inhibition of PAI-1** increases the local concentration of mature TGFβ,
- enhances TGFβ signaling and **suppresses inflammation**.



Regulation of tissue fibrosis

- The inhibition of PAI-1 is promising strategy to **inhibit the tissue fibrosis**
- Inhibiting the activity of PAI-1 and therefore allows tPA to convert plasminogen into active plasmin, which **activates MMPs**.

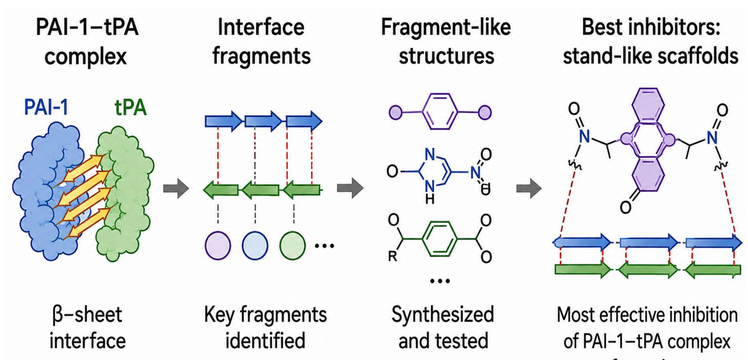


Develop a synthetic peptide-based inhibitor for PAI-1, which

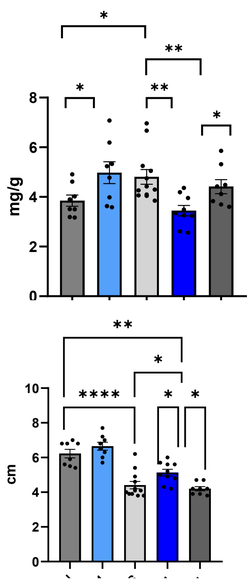
- can increase the local active concentration of TGFβ
- can promote the degradation of the extracellular matrix and tissue remodeling

CHEMICAL BACKGROUND

The PAI-1 – tPA complex is stabilized by a **ß-sheet interface**. Fragment-based screening identified **stand-like scaffolds** as the most effective inhibitors of complex formation.



EXPERIMENTAL RESULTS - IBD



Spleen weight

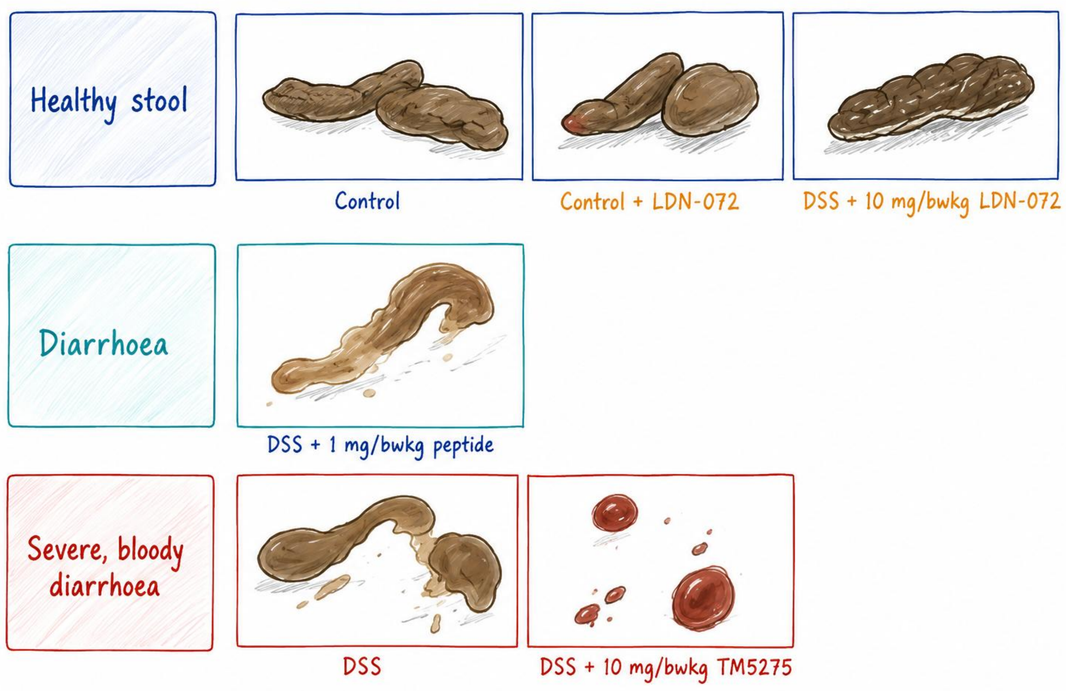
In dextran sulfate sodium (DSS) induced colitis, increased spleen weight reflects inflammation, while **peptide** (LDN-072) **treatment reduces spleen weight.**

Colon length

DSS-induced inflammation causes colon shortening, while **peptide treatment increases colon length.**

Grey: control, light blue: control + peptide , light grey: DSS , dark blue: DSS + petide , dark grey: DSS + TM5275 (PAI-1 inhibitor)

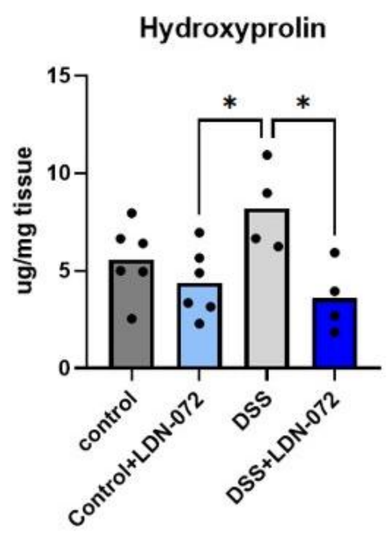
EXPERIMENTAL RESULTS - IBD



The peptide treatment **ameliorates DSS-induced colitis** and **prevents bloody diarrhoea.** In contrast to untreated DSS mice, peptide-treated mice exhibit **improved stool consistency** and **reduced signs of intestinal bleeding.**

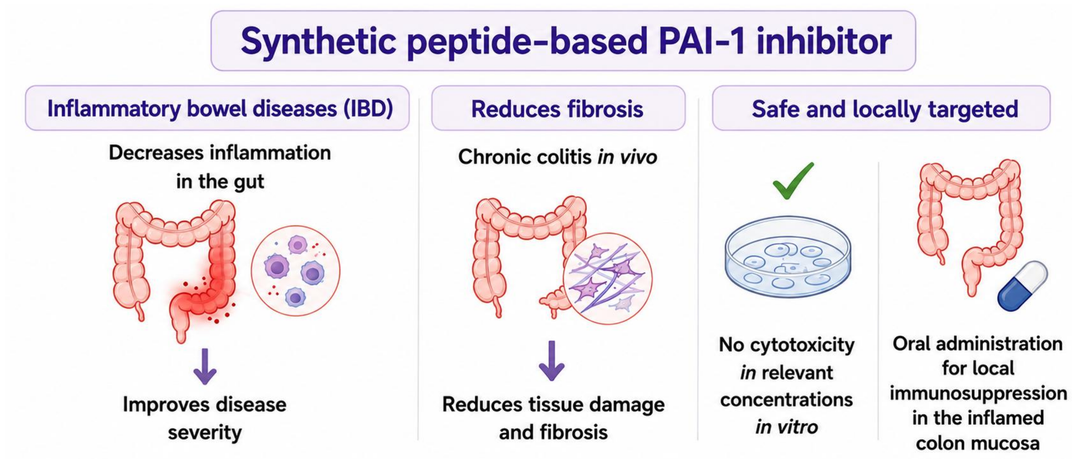
CHRONIC FIBROSIS

Chronic DSS administration induces **severe transmural inflammation, epithelial damage, loss of crypt architecture**, and **extensive fibrosis** in the colon. Treatment with **10 mg/kg peptide significantly reduces inflammation, epithelial erosion**, and **fibrosis**, indicating a protective effect against chronic DSS-induced colonic damage.



CONCLUSION

The developed synthetic peptide-based PAI-1 inhibitor **effectively ameliorates disease-associated inflammation and fibrosis**, improving key outcomes in experimental colitis and chronic pancreatitis. **Oral peptide treatment** reduces tissue damage and fibrosis without cytotoxicity at relevant concentrations, supporting its potential as a **local therapeutic strategy for inflammatory and fibrotic diseases.**



References:
1. Sands, B. E. Inflammatory bowel disease: past, present, and future. J. Gastroenterol. 42, 16–25 (2007).
2. Wang, X. et al. Plasminogen Activator Inhibitor-1 Potentiates Neutrophil Infiltration and Tissue Injury in Colitis. Int. J. Biol. Sci. 19, 2132–2149 (2023).
3. Jójárt, B. et al. Plasminogen Activator Inhibitor 1 Is a Novel Faecal Biomarker for Monitoring Disease Activity and Therapeutic Response in Inflammatory Bowel Diseases. J. Crohns Colitis 18, 392–405 (2024).
Ackwonledgements: This work was supported by the NRDIO Hungary under the grant Advanced 152725.

https://doi.org/10.17952/38EPS.2026.P388

Assessing the Efficacy of Peptides on Acute Coronary Syndrome *In-vivo*

Offir Ertracht[1], Rani Wainer Shlomo[1,4,5], Mulate Zerihun[4], Shulamit Fluss Ben-Uliel[4], Shmuel Silitsky[4], Samar Gani[4], Liron Davis[4], Mona Shehadeh[3], Tali Reuveni[1], Shaul Atar[1,2,4], Nir Qvit[4]

[1]*The cardiovascular research laboratory,* [2]*Department of cardiology,* [3]*Clinical Laboratories Division, Galilee Medical Center, Naharyia,* [4]*The Azrieli Faculty of Medicine in the Galilee, Bar-Ilan university, Safed,* [5]*Cardiac rehabilitation, the Cardiovascular Department, Tzafon Medical Center, Poriya, Israel*

Introduction

- Cardiovascular disease (CVD), mainly myocardial infarction (MI) lead cause of morbidity and mortality worldwide.
- MI followed by reperfusion (ischemia/reperfusion – I/R) induces severe mitochondrial stress, characterized by calcium and reactive oxygen species overload, mitochondrial dysregulation - excessive fission, and attenuated fusion.
- All contributing the cardiomyocytes dysfunction, cardiac remodeling and death.
- Peptides are highly clinically relevant class of therapeutics in CVD.
- They offer high target specificity, favorable safety profiles, and the ability to modulate complex biological pathways.

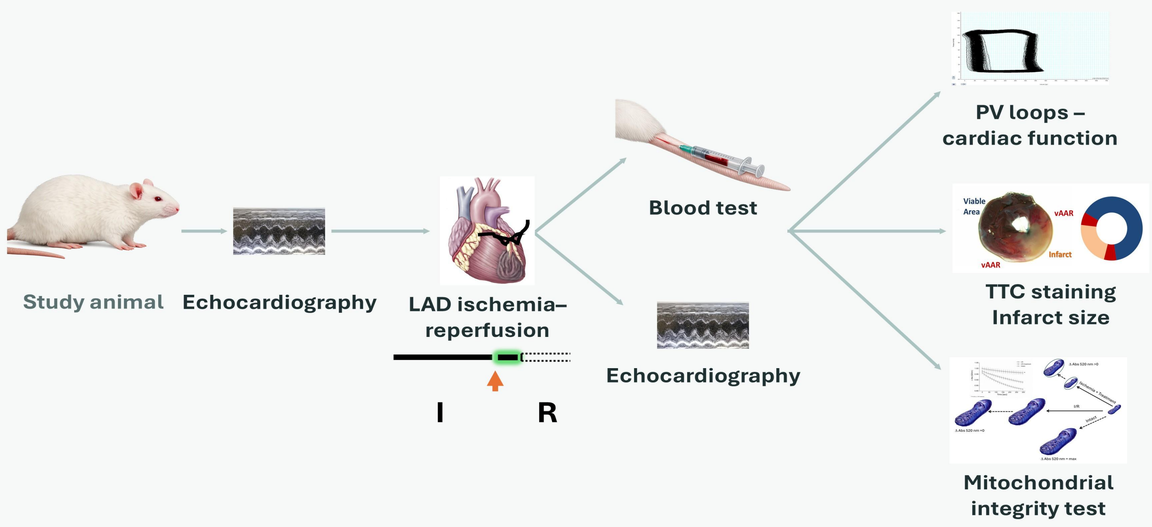
Hypothesis and aims

We hypothesized that CVP-350, a macrocyclic peptide specifically designed to inhibit the Drp1/Fis1 interaction, would preserve mitochondrial integrity and improve cardiac outcome following ischemia-reperfusion injury.

Methods

- Animal experiments were conducted according to ethical committee guidelines.
- A rat model of left anterior descending (LAD) coronary artery occlusion for 30 min, followed by reperfusion was applied. Five min prior to reperfusion, CVP-350 (2 mg/kg), was administered i.v. Infarct size was determined by triphenyl-tetrazolium chloride (TTC) staining, cardiac injury was evaluated using hematological biomarkers, and cardiac structure and function were assessed by echocardiography. Mitochondrial integrity was assessed by Ca^{2+}-induced swelling assay.

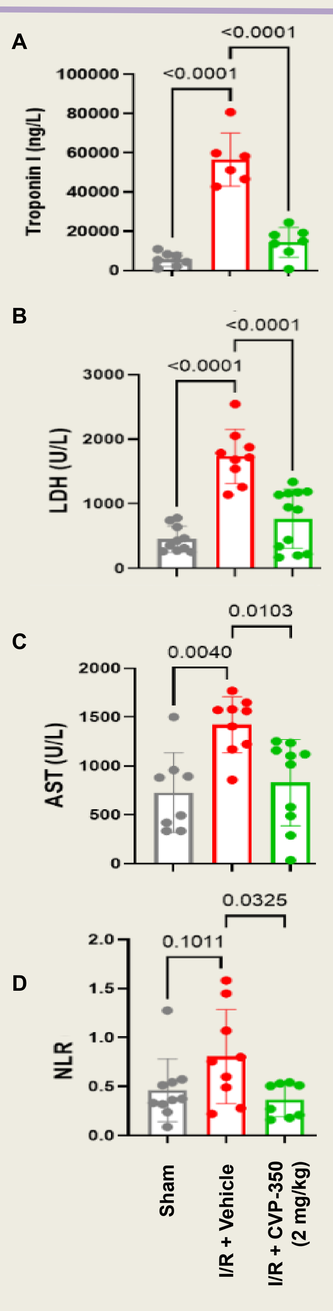
Rat LAD ischemia–reperfusion study design:

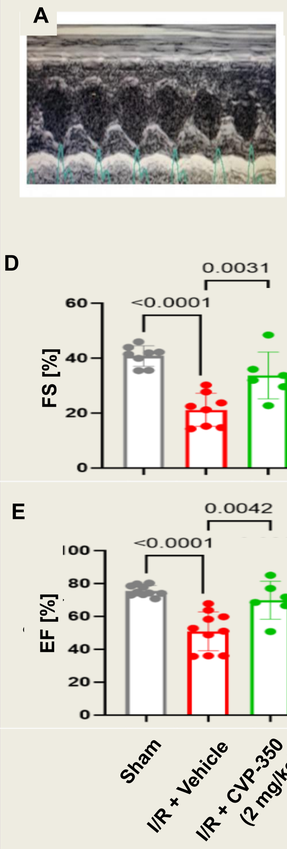


Results:

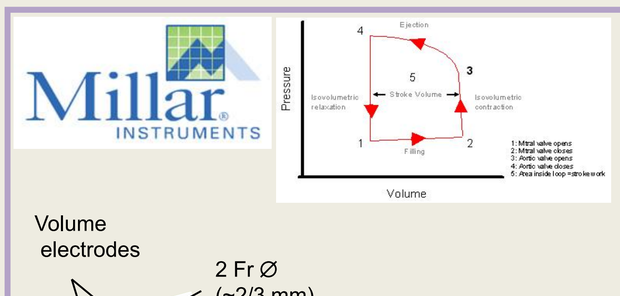
Blood samples results characterizing cardiac damage: **A.** Cardiac Troponin I, **B.** Lactate Dehydrogenase, **C.** Aminotransferase (AST), and **D.** Neutrophiles to Leucocytes ratio (NLR).

Results: Cardiac Troponin I show dramatic increase of over 50,000 ng/L, LDH increases to ~2000 u/l, AST and NLR to ~ 0.8, 24 hrs after I/R. ***CVP-350 decreases all these parameters significantly back to control (sham) level, indicating its cardiac protective efficacy.***

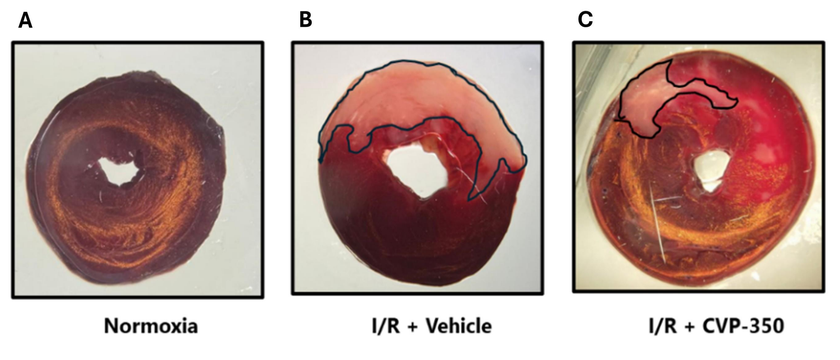




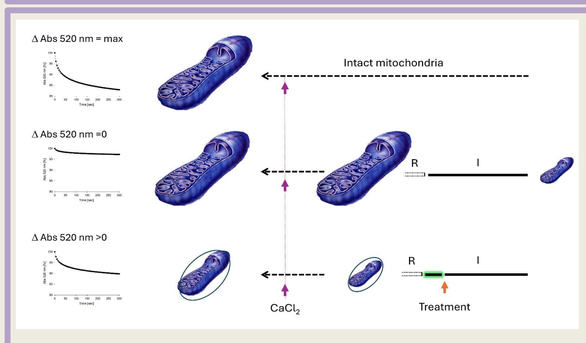
Echocardiography M-mode cines of: **A.** Sham **B.** I/R + Vehicle **C.** I/R + CVP-350 treatment. I/R attenuated wall motion seen as lack of waves in the upper side of the cine (**B**) preservation of function is seen in (**C**).
D. FS, and **E.** EF show summary of functional parameters.
CVP-350 efficacy is seen as preservation of FS and EF.

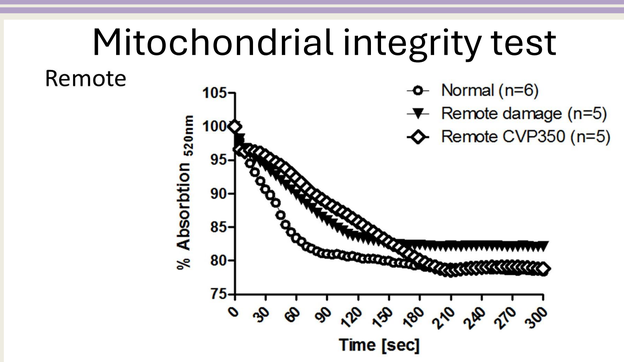


I/R decreases loop's size, i.e. attenuates SV, CO, SW and EF, further it moderates contraction and relaxation rates dp/dt_{max} and $_{min}$, respectively, and increases τ (relaxation time). ***CVP-350 treatment, preserved SV, CO, SW, EF and dp/dt_{max} and dp/dt_{min}.***

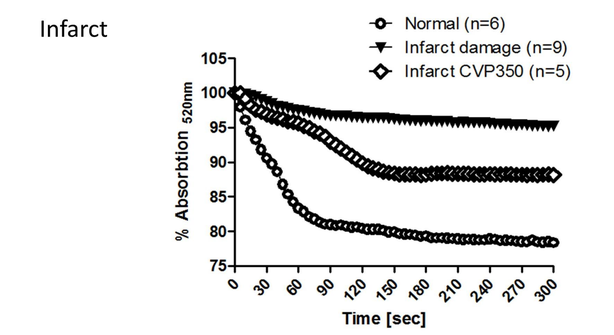


A-C representative mid cardiac level slices stained with TTC, for the **A.** sham operated rats (normoxia), **B.** I/R, and **C.** I/R + CVP-350, respectively. Infarct size assessments **D.** ***shows >50% reduction of infarct following CVP-350 administration.***





Mitochondria extracted from intact hearts or 4 h after I/R or 4 h after I/R + CVP-350 treatment were exposed to high (200 µM $CaCl_2$) calcium level, followed by 5 min of 520 nm inner mitochondrial cristae absorbance reading.



Ca^{2+} entrance to the mitochondria brings also water, causing membrane swelling, flattening of the cristae and reducing absorbance. As ***CVP-350 lowers the rate of 520 nm absorbance reduction, it possibly protects the mitochondria, preserving its ability to swell, during the ischemia period.***

Conclusions: ***CVP-350 prevents cardiac deterioration post I/R. It preserve mitochondrial integrity, reduced infarct size I/R, attenuates cardiac dysfunction seen by both echocardiography and direct cardiac performance measurements (PV-loop assessment). CVP-350 has the potential to become an adjacent treatment in a clinical scenario of MI and percutaneous intervention.***

DEVELOPMENT OF AN INHIBITOR OF PLASMINOGEN ACTIVATOR INHIBITOR-1 (PAI-1) FOR THE TREATMENT OF INFLAMMATORY AND FIBROTIC DISORDERS

Eszter Erdei[1,2], Nikolett Varró Kormosné[1], Boldizsár Jójárt[3], Petra Pallagi[3], József Maléth[3], István Mándity[1,2]

[1]HUN-REN Research Centre for Natural Sciences, Artificial Transporters Research Group
[2]Department of Organic Chemistry, Semmelweis University, Faculty of Pharmacy
[3]MTA-SZTE Momentum Epithelial Cell Signalling and Secretion Research Group

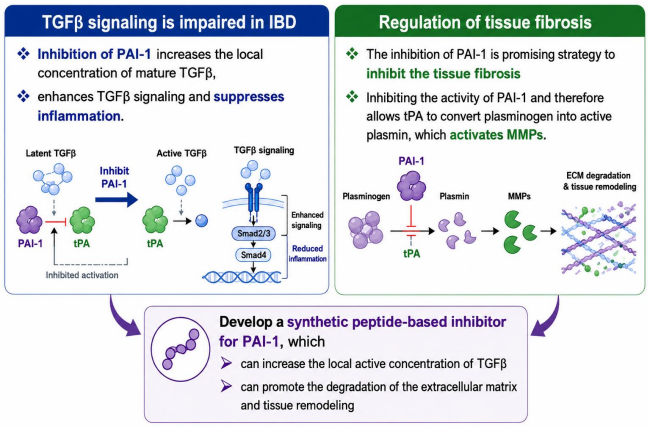
https://doi.org/10.17952/38EPS.2026.P172

INTRODUCTION

Inflammatory bowel disease (IBD), including Crohn's disease and ulcerative colitis, is a chronic relapsing inflammatory disorder that affects millions of people worldwide and often requires lifelong treatment.[1] **Persistent inflammation** can drive **intestinal fibrosis**, resulting in **excessive fibroblast activation** and **extracellular matrix deposition.**[2] **Plasminogene activator inhibitor (PAI-1) is a key mediator** that links chronic inflammation to intestinal fibrosis by decreasing the concentration of TGF-ß from the latent complex and promoting extracellular matrix accumulation.[3]

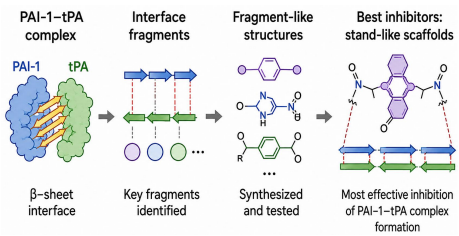
AIMS

PAI-1 – tissue-type plasminogen activator (tPA) inhibition represents a promising strategy for the treatment of IBD and IBD-associated fibrosis.

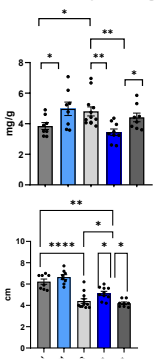


CHEMICAL BACKGROUND

The PAI-1 – tPA complex is stabilized by a **ß-sheet interface**. Fragment-based screening identified **stand-like scaffolds** as the most effective inhibitors of complex formation.



EXPERIMENTAL RESULTS - IBD



Spleen weight

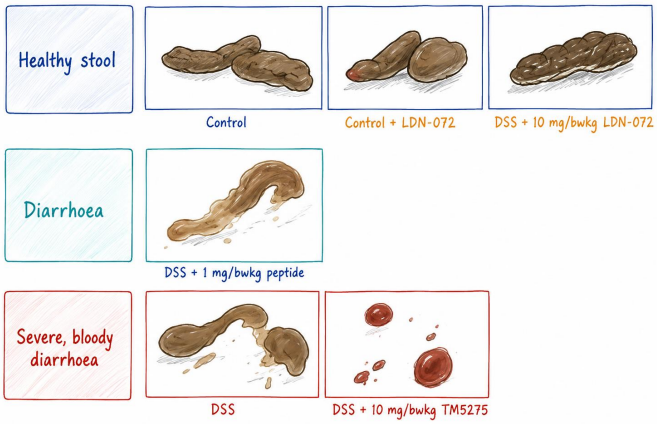
In dextran sulfate sodium (DSS) induced colitis, increased spleen weight reflects inflammation, while **peptide** (LDN-072) **treatment reduces spleen weight.**

Colon length

DSS-induced inflammation causes colon shortening, while **peptide treatment increases colon length.**

Grey: control, light blue: control + peptide , light grey: DSS , dark blue: DSS + petide , dark grey: DSS + TM5275 (PAI-1 inhibitor)

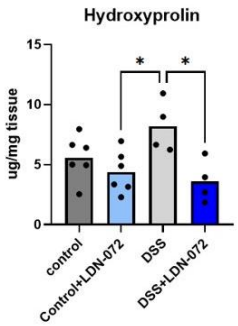
EXPERIMENTAL RESULTS - IBD



The peptide treatment **ameliorates DSS-induced colitis** and **prevents bloody diarrhoea.** In contrast to untreated DSS mice, peptide-treated mice exhibit **improved stool consistency** and **reduced signs of intestinal bleeding.**

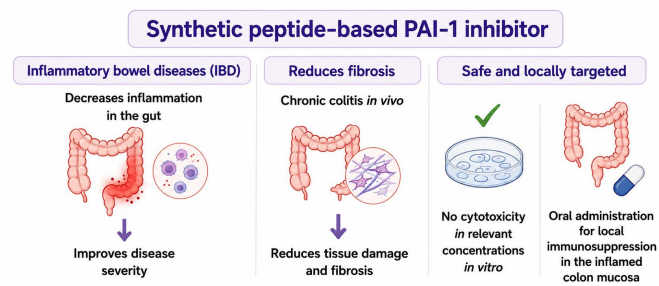
CHRONIC FIBROSIS

Chronic DSS administration induces **severe transmural inflammation, epithelial damage, loss of crypt architecture**, and **extensive fibrosis** in the colon. Treatment with **10 mg/kg peptide significantly reduces inflammation, epithelial erosion**, and **fibrosis**, indicating a protective effect against chronic DSS-induced colonic damage.



CONCLUSION

The developed synthetic peptide-based PAI-1 inhibitor **effectively ameliorates disease-associated inflammation and fibrosis**, improving key outcomes in experimental colitis and chronic pancreatitis. **Oral peptide treatment** reduces tissue damage and fibrosis without cytotoxicity at relevant concentrations, supporting its potential as a **local therapeutic strategy for inflammatory and fibrotic diseases.**



References:
1. Sands, B. E. Inflammatory bowel disease: past, present, and future. J. Gastroenterol. 42, 16-25 (2007).
2. Wang, X. et al. Plasminogen Activator Inhibitor-1 Potentiates Neutrophil Infiltration and Tissue Injury in Colitis. Int. J. Biol. Sci. 19, 2132-2149 (2023).
3. Jójárt, B. et al. Plasminogen Activator Inhibitor 1 Is a Novel Faecal Biomarker for Monitoring Disease Activity and Therapeutic Response in Inflammatory Bowel Diseases. J. Crohns Colitis 18, 392-405 (2024).
Ackwonledgements: This work was supported by the NRDIO Hungary under the grant Advanced 152725.

Towards peptide libraries: HPLC-based flow peptide synthesis and combinatorial chemistry

Viktor Farkas, Kristóf Ferentzi, András Perczel

HUN-REN – ELTE Protein Modelling Research Group
Laboratory of Structural Chemistry and Biology, Institute of Chemistry

e-mail: farkas.viktor@ttk.elte.hu
web: http://prot.chem.elte.hu/en/

Eötvös Loránd University, Pázmány P. s. 1/A, H-1117 Budapest, **Hungary**

https://doi.org/10.17952/38EPS.2026.P023

Introduction

Solid-phase peptide synthesis (SPPS) is one of the most widely used methods to produce peptide drug molecules, but in its current form it poses a significant environmental burden and faces several efficiency limitations. The synthesis of so-called “difficult sequences” is particularly challenging, since under the synthesis conditions the growing polymer chains aggregate in an undesirable manner to form β-pleated sheets, which impairs the predictability and efficiency of the process. The recent emergence of more efficient and tightly controlled synthesis methods creates an opportunity to optimize the peptide synthesis process to be faster, cheaper and more environmentally friendly.
With a focus on keeping costs as low as possible and making amino acid coupling increasingly environmentally friendly, we are continuously improving our applied methods. We call this approach Smart Peptide Chemistry in Flow, or SPF for short. This strategy considers the size of the environmental footprint, as well as the synthesis time, reagent volume, and solvent type, all of which are optimized simultaneously. In our previous articles, we have shown that flow chemistry can significantly reduce solvent waste.

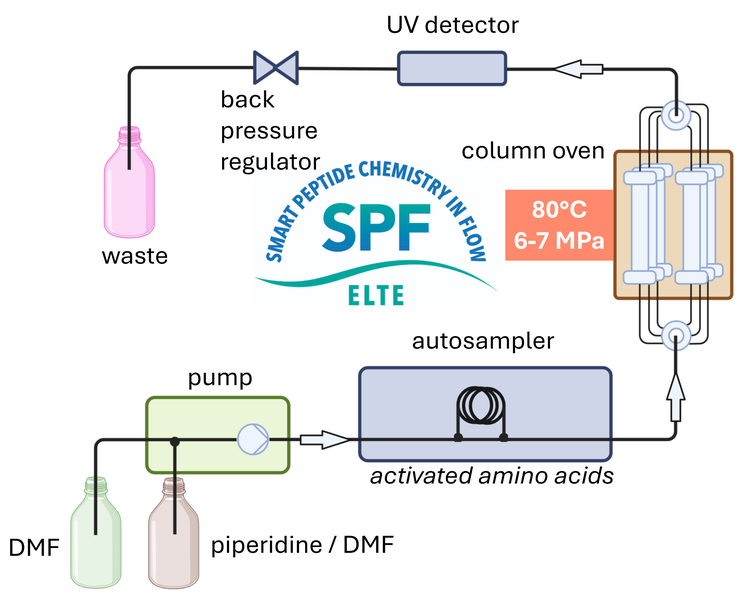
Goal

In this new project, we are interested in whether it is possible to produce **multiple peptides simultaneously in the same synthesis time** by trying to attach multiple amino acids to a given site in the sequence. If we succeed in producing multiple peptides, is this method suitable for producing peptide derivatives that **we can then purify**? Additional questions arise when trying to attach multiple amino acids at once, such as how much they "compete" for the given site.

Aim

Our next research direction is to investigate the efficiency of coupling reactions under flow conditions. Our goal is to analyze the different reaction rates of individual activated reagents in amino acid mixtures. Different amino acid derivatives participate in coupling reactions in different ways, so we need to understand this thoroughly to design effective experiments.
As a long-term goal, we are investigating the possibility of creating peptide libraries that can be used to study the simultaneous synthesis of large numbers of molecules in a single pot.

Schematic diagram of our system





Our system consists of **standard JASCO HPLC modules**, a PU4180 pump with RCY-4000 unit, AS4150L autosampler, UV4075 UV detector, CO4060 column oven. It is a commercially available flow peptide instrument (HPPS-4000, METALON Ltd., Hungary). The ChromNAV2 software ensures a fully automated process.

Residence time:

coupling:	3.30 min. (1.00 ml activated amino acid / NMP)
washing #1:	4.70 min. (1.41 ml DMF)
Fmoc-cleavage:	1.40 min. (1.05 ml 20% piperidine / DMF)
washing #2:	2.60 min. (2.43 ml DMF)
Cycle time:	**12 min.**

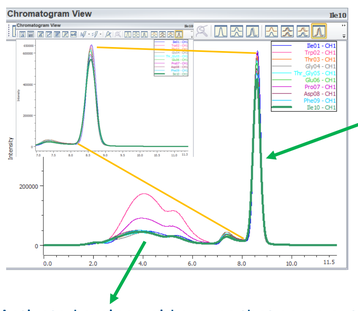
Synthesis of10-mer peptide in resin: less than 2.5 hours

We selected two sequences: one easy and one difficult to synthesize:

fkp1:
H-IFDPETGTWI-NH_2

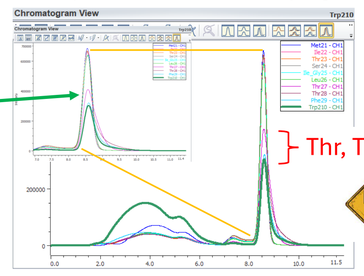
JR10:
H-WFTTLISTIM-NH_2

UV spectra of amino acids coupling



FMOC cleavage

UV spectra of amino acids coupling



Thr, Thr, Phe, Trp

DANGER ZONE



Activated amino acid excess that came out of the column.

Note: At the peak of Fmoc cleavage, it can be seen that after the first Thr coupling, the free amino group becomes difficult to access and the efficiency of coupling the remaining amino acids is greatly reduced.

In the case of the **easy sequence**, we were interested in:
- at what position the coupling of multiple amino acids could be applied so that it could be purified;
- whether the individual amino acids compete with glycine, that is, they couple better or worse if we inject them at the same time.

In the case of the difficult sequence, we will investigate how glycine competes with the original amino acid as we approach the DANGER ZONE and and how this influences overall synthesis.

fkp1 IFDPETGTWI	JR10 WFTTLISTIM
$\frac{A}{G}$FDPETGTWI	WFTTL$\frac{I}{G}$STIM
Ac-$\frac{A}{G}$FDPETGTWI	WFTT$\frac{L}{G}$ISTIM
IFDPE$\frac{A}{G}$GTWI	WFT$\frac{T}{G}$LISTIM
IFDPE$\frac{R}{G}$GTWI	all peptides have an amidated C-terminus
IFDPE$\frac{T}{G}$GTWI	
IFDPE$\frac{I}{G}$GTWI	
IFDPE$\frac{V}{G}$GTWI	

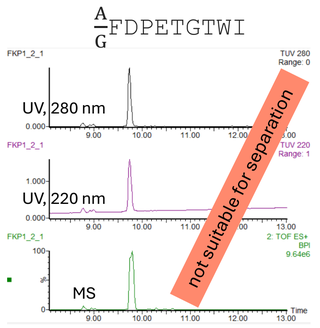
Synthesis:

150 mg of TentaGel resin with a capacity of 0.24 mmol/g
Coupling: AA/OxymaPure/DIC – 3/3/6
Cleavage: 95%TFA/2.5% TIS/2.5% H_2O

Results

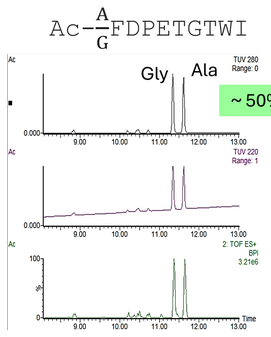
The cleaved products of syntheses were analyzed by UPLC-MS on an ACQUITY UPLCR BEH T3 1.8µm column (Waters, 100 mm × 2.1 mm, 100 A) using a gradient elution consisting of 0.1% TFA in water (eluent A) and 0.1% TFA in MeCN (eluent B) with a gradient from 25% to 65% B over 8 min and the column temperature set at 45 ◦C. The flow rate was set to 0.20 mL/min, and the absorbance was detected at λ = 220 and 280 nm. MS: Waters ACQUITY RDa Detector and on UPLC: Waters ACQUITY UPLC H-Class PLUS System using UNIFI 1.9.13.9 (Waters Corporation, Milford, UK)

$\frac{A}{G}$FDPETGTWI

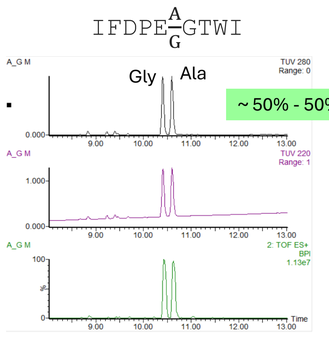


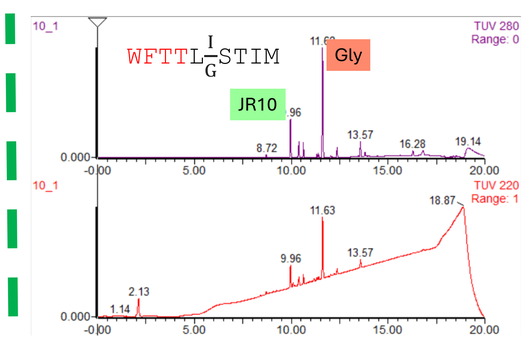
+Ac

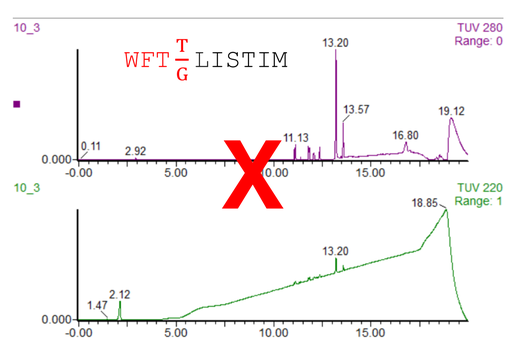
Ac-$\frac{A}{G}$FDPETGTWI

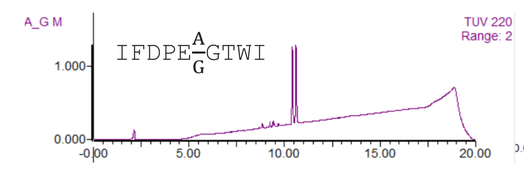


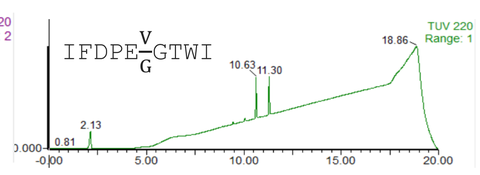
IFDPE$\frac{A}{G}$GTWI

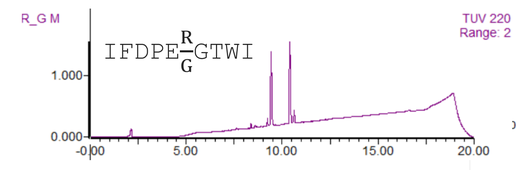


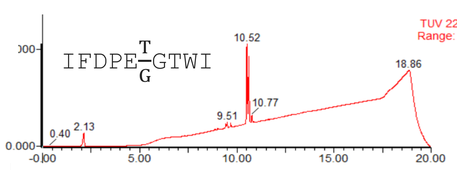


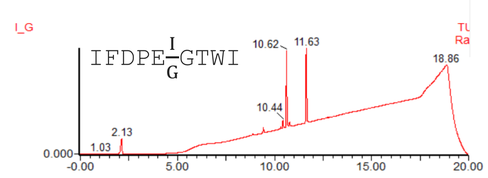




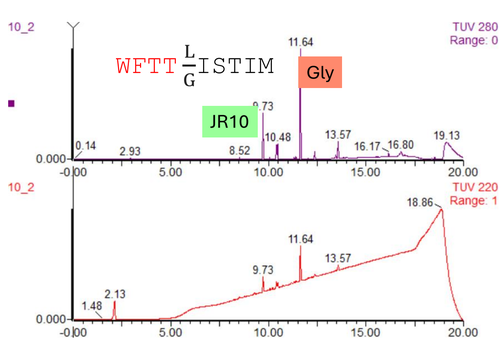








Based on the results of the easy sequence, we can say that if we want to produce several peptides during one synthesis time, then the successful production may be position-dependent. This mainly affects the purification step. It may happen that the applied chromatography method after cleavage is not suitable for separation. In our case, in the 5th position of the **fkp1** peptide, there seems to be no "competition" between glycine and the amino acids tested so far.



In the case of the difficult sequence, the result was not 50-50%, but the glycine-containing peptide was formed in a higher proportion. In the section most exposed to aggregation, we were unable to synthesize any detectable amount of peptide. Neither JR10 nor any glycine-containing molecule.

During synthesis, if one amino acid reacts at a higher rate than the other, then more of that amino acid remains and could be used to synthesize another peptide by attaching a modular column.

Modular column assembly in use, designed by Kristóf.



ReactChemEng **2024**, *9*: 58
OPRD **2023**, *27*: 1053
IJMS **2024**, *25*: 4150
OPRD **2021**, *25*: 182
ChemEurJ **2025**, *31*: e02335

Acknowledgement Project no. RRF-2.3.1-21-2022-00015 has been implemented with the support provided by the European Union. Project no. 2025-3.1.1-ED-2025-00013 has been implemented with the support provided from the National Research, Development and Innovation Fund of Hungary, financed under the 2025-3.1.1-ED-NKP funding scheme.

Rational structure-based design of potent antimicrobial peptides using artificial intelligence

Brigitte Fernández García‡, Jordi Gómez Borrego‡, Roberto Bello Madruga and Marc Torrent Burgas*
The Systems Biology of Infection Laboratory, Department of Biochemistry and Molecular Biology, Biosciences Faculty, Universitat Autònoma de Barcelona, 08193, Cerdanyola del Vallès, Spain.
brigitte.fernandez@uab.cat, marc.torrent@uab.cat, https://doi.org/10.17952/38EPS.2026.P221

Abstract

Antimicrobial peptides (AMPs), key components of the innate immune system, represent promising alternatives to conventional antibiotics. However, their therapeutic application against multidrug-resistant pathogens remains limited due to cytotoxicity, poor stability, and insufficient selectivity. Here, we present an integrated artificial intelligence (AI)-guided strategy combining computational peptide design with experimental validation to generate highly active AMPs with reduced toxicity. We developed a computational pipeline based on machine learning models capable of generatively designing short peptide sequences and identifying prototype–analog pairs with optimized antimicrobial activity, selectivity, and predicted stability. To validate the pipeline, selected peptides were synthesized and evaluated in vitro against clinically relevant multidrug-resistant pathogens, including *Escherichia coli*, *Acinetobacter baumannii*, *Pseudomonas aeruginosa*, *Staphylococcus aureus*, *Enterococcus faecium*, and *Listeria monocytogenes*, using minimum inhibitory concentration assays. Nearly 90% of the tested peptides displayed broad-spectrum antimicrobial activity at low micromolar concentrations. Safety profiles were assessed through hemolysis assays and cytotoxicity studies in human HepG2 and MRC-5 cell lines, revealing several peptides with minimal cytotoxicity at therapeutically relevant concentrations. Mechanistic analyses suggested a predominantly membrane-disruptive mode of action, particularly against Gram-negative bacteria. In addition, serum stability assays demonstrated favorable stability under physiological conditions. Finally, selected peptide candidates were evaluated in vivo in a murine model of *A. baumannii* infection, where treatment resulted in reduced bacterial burden in infected organs, supporting their anti-infective potential and further development as therapeutic candidates.

Pipeline

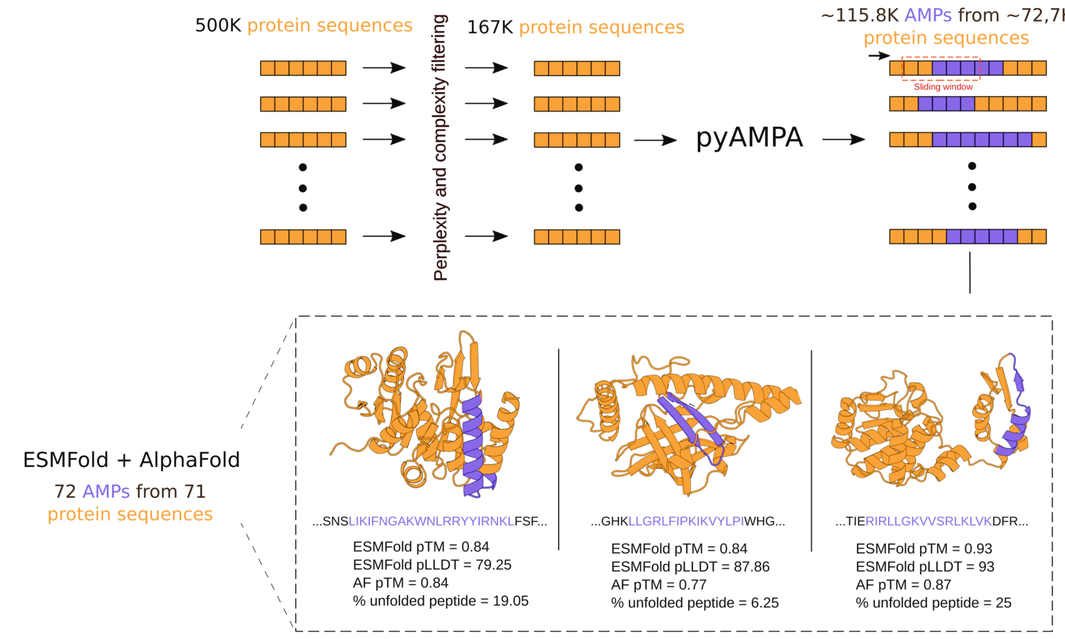


Figure 1. Proposed AI-guided workflow for the discovery of antimicrobial peptide candidates. Protein sequences are computationally processed to identify potential antimicrobial regions, which are subsequently evaluated based on their predicted properties and structural characteristics. The resulting candidates are prioritized for experimental characterization and validation

Structural Characterization

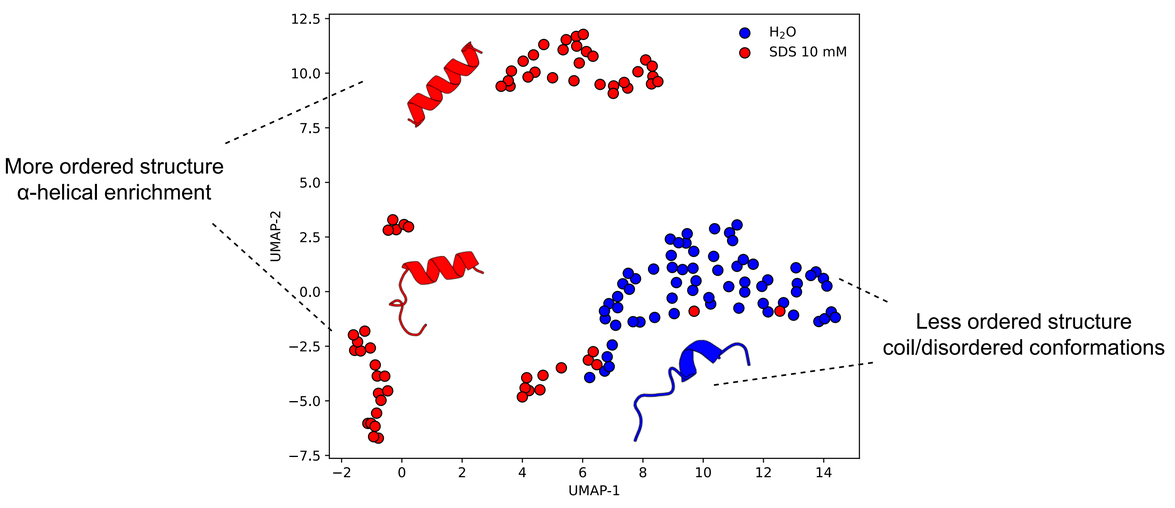


Figure 2. UMAP projection of circular dichroism spectra obtained for 66 experimentally validated AMPs in H_2O and SDS 10 mM. Peptides in aqueous solution clustered separately from those in SDS, indicating a pronounced environment-dependent conformational transition. The spectral shift observed in SDS suggests the acquisition of more ordered secondary structures, consistent with membrane-induced folding, likely toward α-helical conformations.

Antimicrobial activity

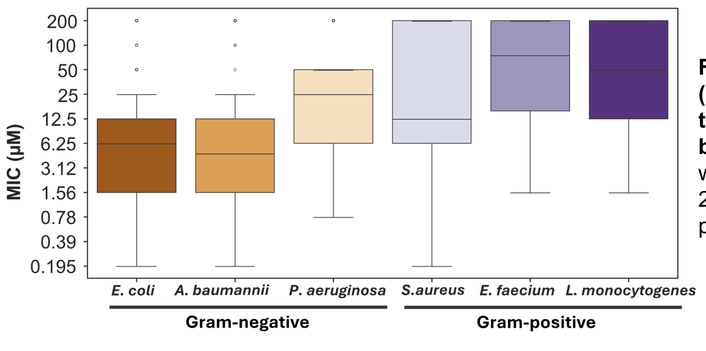


Figure 3. Minimum inhibitory concentrations (MICs) of 66 experimentally validated AMPs tested against six clinically relevant bacterial strains. 88% percent of peptides were active against at least one strain (MIC <= 25 μM). Overall, peptides displayed greater potency against Gram-negative species.

Biocompatibility and Cytotoxicity

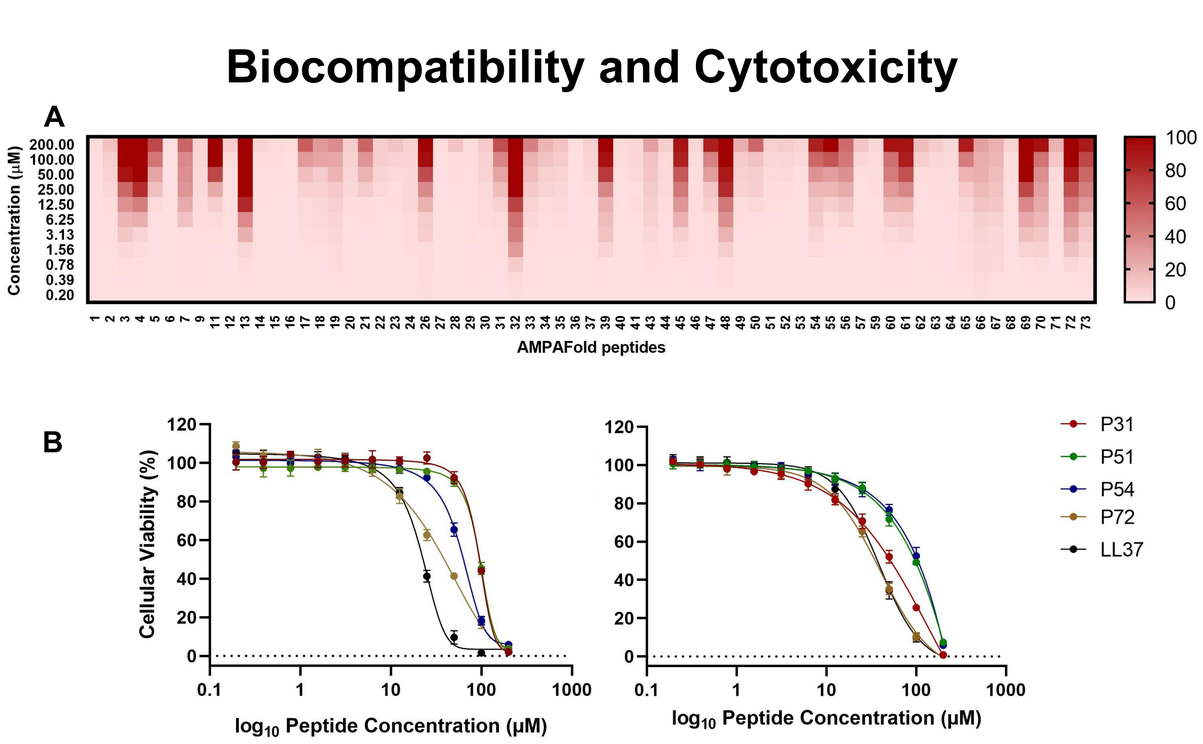


Figure 4. Biocompatibility and cytotoxicity evaluation of AI-designed antimicrobial peptides. (A) Heatmap showing the hemolytic activity of designed peptides in horse blood across increasing peptide concentrations. Color intensity represents the percentage of hemolysis, with darker red indicating higher hemolytic activity. (B) Dose–response cytotoxicity assays performed in MRC-5 human lung fibroblasts (left) and HepG2 human hepatocellular carcinoma cells (right), showing cellular viability as a function of peptide concentration. Several peptide candidates displayed low cytotoxicity and favorable biocompatibility profiles at therapeutically relevant concentrations. Data are presented as mean ± standard deviation.

Membrane Interaction and Stability Characterization

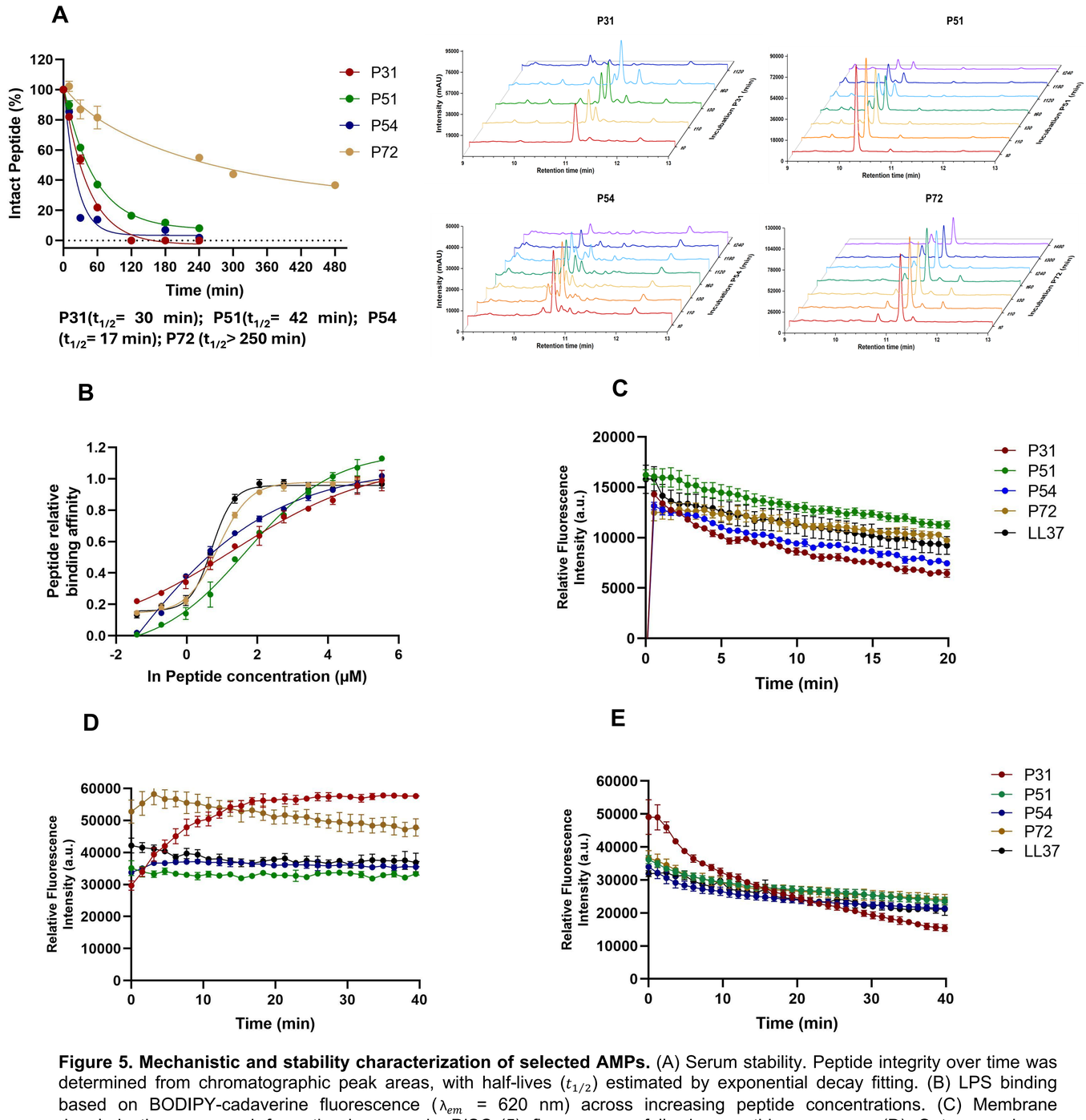


Figure 5. Mechanistic and stability characterization of selected AMPs. (A) Serum stability. Peptide integrity over time was determined from chromatographic peak areas, with half-lives ($t_{1/2}$) estimated by exponential decay fitting. (B) LPS binding based on BODIPY-cadaverine fluorescence (λ_{em} = 620 nm) across increasing peptide concentrations. (C) Membrane depolarization assessed from the increase in $DiSC_3(5)$ fluorescence following peptide exposure. (D) Outer membrane permeabilization and (E) Inner membrane permeabilization, determined by 1-N-phenylnaphthylamine (NPN) and propidium iodide (PI) fluorescence, respectively. Assays (B–E) were performed against *E. coli* ATCC 11775. LL-37 served as a positive control for all assays (B–E). Data are presented as mean ± standard deviation.

In vivo Validation

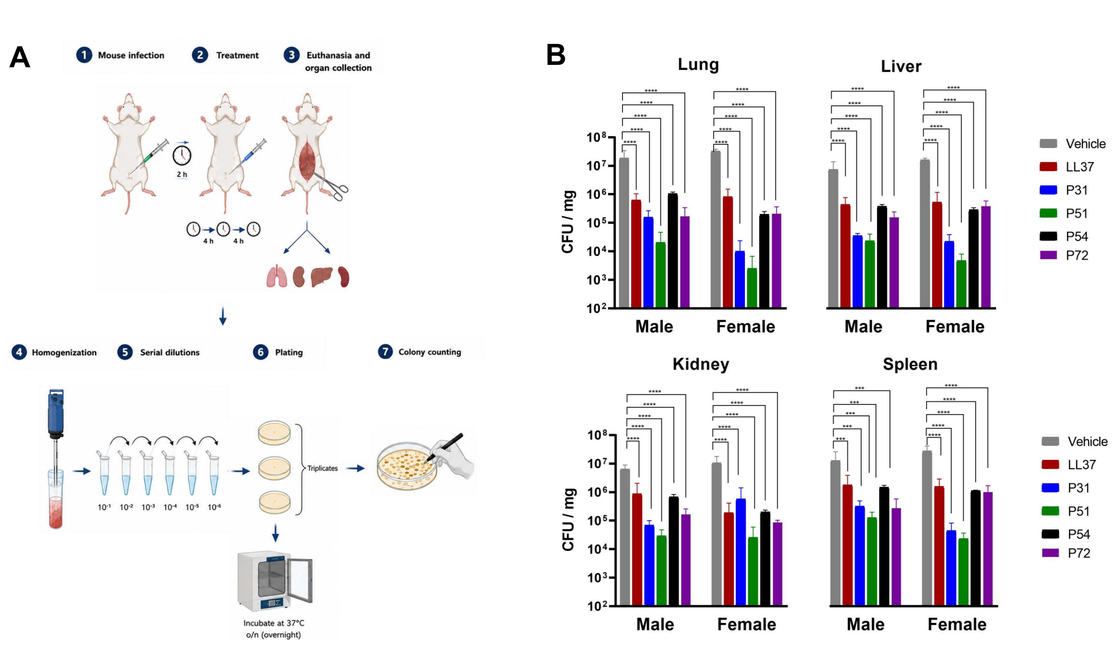


Figure 6. Anti-infective activity of peptides in an animal model. (A) Schematic of the sepsis mouse model used to assess AMPs (n = 6) against *A. baumannii* ATCC 15308. (B) Average CFU/mg in organs after 12 h treatment. Statistical significance compared to vehicle was determined using two-way ANOVA followed by Dunnett's test (denoted as ****P < 0.0001).

Conclusions

- An integrated AI-guided pipeline for the rational design of antimicrobial peptides was successfully developed and experimentally validated.
- The designed peptide candidates exhibited broad-spectrum antimicrobial activity against clinically relevant multidrug-resistant pathogens at low micromolar concentrations.
- Several peptides demonstrated low hemolytic activity, limited cytotoxicity in human cell lines, and favorable serum stability, supporting their potential therapeutic applicability.
- Mechanistic studies indicated membrane disruption as the predominant mode of antimicrobial action, particularly against Gram-negative bacteria.
- *In vivo* validation demonstrated significant reductions in bacterial burden for selected AMPs in infected organs, providing preclinical evidence of their anti-infective activity against *A. baumannii*.

References

1. Huan, Y.; Kong, Q.; Mou, H.; Yi, H. Antimicrobial Peptides: Classification, Design, Application and Research Progress in Multiple Fields. Front Microbiol 2020, 11, 582779. https://doi.org/10.3389/fmicb.2020.582779.
2. Ferruz, N., Schmidt, S. & Höcker, B. ProtGPT2 is a deep unsupervised language model for protein design. Nat Commun **13,** 4348 (2022).
3. Ramos-Llorens, M., Bello-Madruga, R., Valle, J., Andreu, D. & Torrent, M. PyAMPA: a high-throughput prediction and optimization tool for antimicrobial peptides. *mSystems* **9**, e01358-23 (2024).
4. Lin, Z. *et al.* Evolutionary-scale prediction of atomic-level protein structure with a language model. *Science* **379**, 1123–1130 (2023).

Agència de Gestió d'Ajuts Universitaris i de Recerca AGAUR
Generalitat de Catalunya Departament de Recerca i Universitats
Cofinanciado por la Unión Europea
Gobierno de España Ministerio de Ciencia e Innovación

Peptide-Based Stimuli-Responsive Antibacterial Hydrogels for Bone Tissue Engineering

Ferrandi G.[1], Bautista-Cases M.[1], Godoy-Gallardo M.[1,2,3], Mas-Moruno C.[1,2,3]

[1]*Materials Science and Engineering Dpt. & Barcelona Research Centre in Multiscale Science and Engineering (CCEM), Universitat Politècnica de Catalunya-BarcelonaTech (UPC), Barcelona, Spain*

[2]*Institute for Research and Innovation in Health (IRIS), Universitat Politècnica de Catalunya – BarcelonaTech (UPC), Barcelona, Spain*

[3]*Centro de Investigación Biomédica en Red de Bioingeniería, Biomateriales y Nanomedicina, ISCIII, Madrid, Spain*

https://doi.org/10.17952/ 38EPS.2026.P222



giovanni.ferrandi@upc.edu

Aim & Background

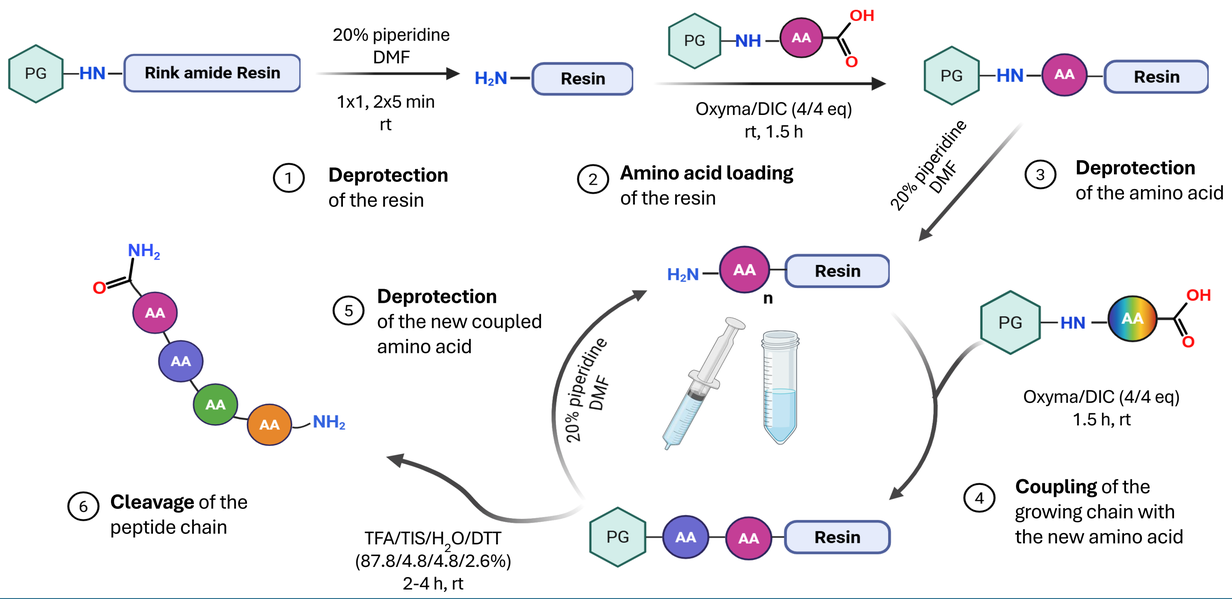
Bone implant-associated infections remain one of the leading causes of **implant failure**, highlighting the need for biomaterials that combine antibacterial activity with regenerative potential.[1] The goal of our research is to develop an infection-responsive **hydrogel** capable of releasing **antimicrobial peptides (AMPs)** only in the presence of bacterial infections. As a first step, cleavable peptide linkers responsive to bacterial proteases were identified and characterized. The most promising linkers were subsequently conjugated to AMPs and immobilized onto titanium substrates as a proof of concept for the future development of **peptide-based stimuli-responsive biomaterials**.[2]

Peptide Linker Design

Peptide sequence	Target protease	Source	Infection stage
GPLG | VL	MMP-2/9	Host	Inflammation
AAPV | AAPV	hNE	Host	Inflammation
AAG | LA	LasB	*P. aeruginosa*	Infection
WELQ | GS	SplB	*S. aureus*	Infection

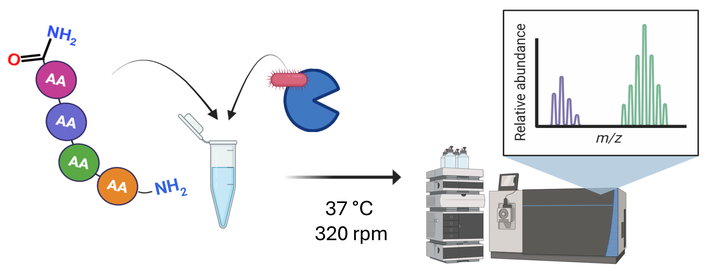
Peptide linkers were selected based on their susceptibility to the most abundant bacterial and host proteases associated with bone implant infections. The table summarizes the target enzymes and the corresponding peptide sequences, where the vertical bar (|) denotes the expected proteolytic cleavage site.

Solid-Phase Peptide Synthesis



Preliminary peptide cleavage screening

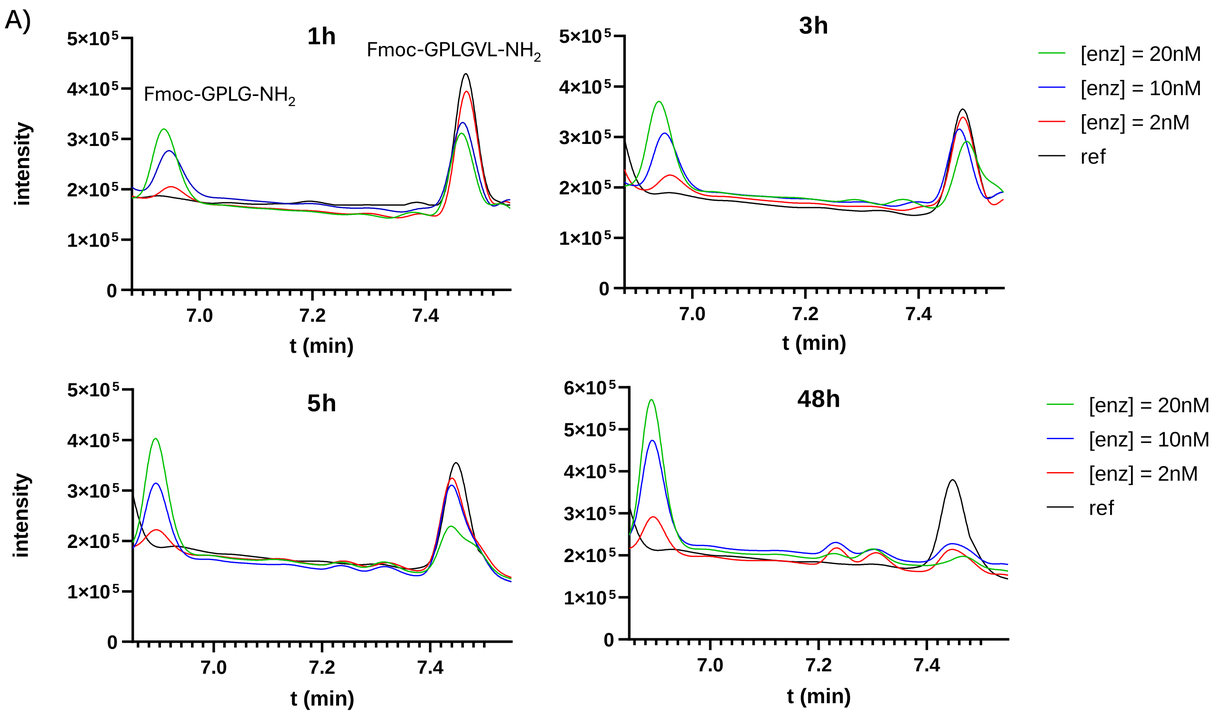
Peptide	Enzyme	Result
Fmoc-AAPVAAPV-NH_2	hNE	✓
Fmoc-WELQGS-NH_2	SplB	✗
H-WELQGS-NH_2		
H-SGWELQGS-NH_2		
Fmoc-GPLGVL-NH_2	MMP-2/9	✓
Fmoc-AAGLA-NH_2	LasB	✗
H-AAGLA-NH_2		
H-AGLAGLA-NH_2		



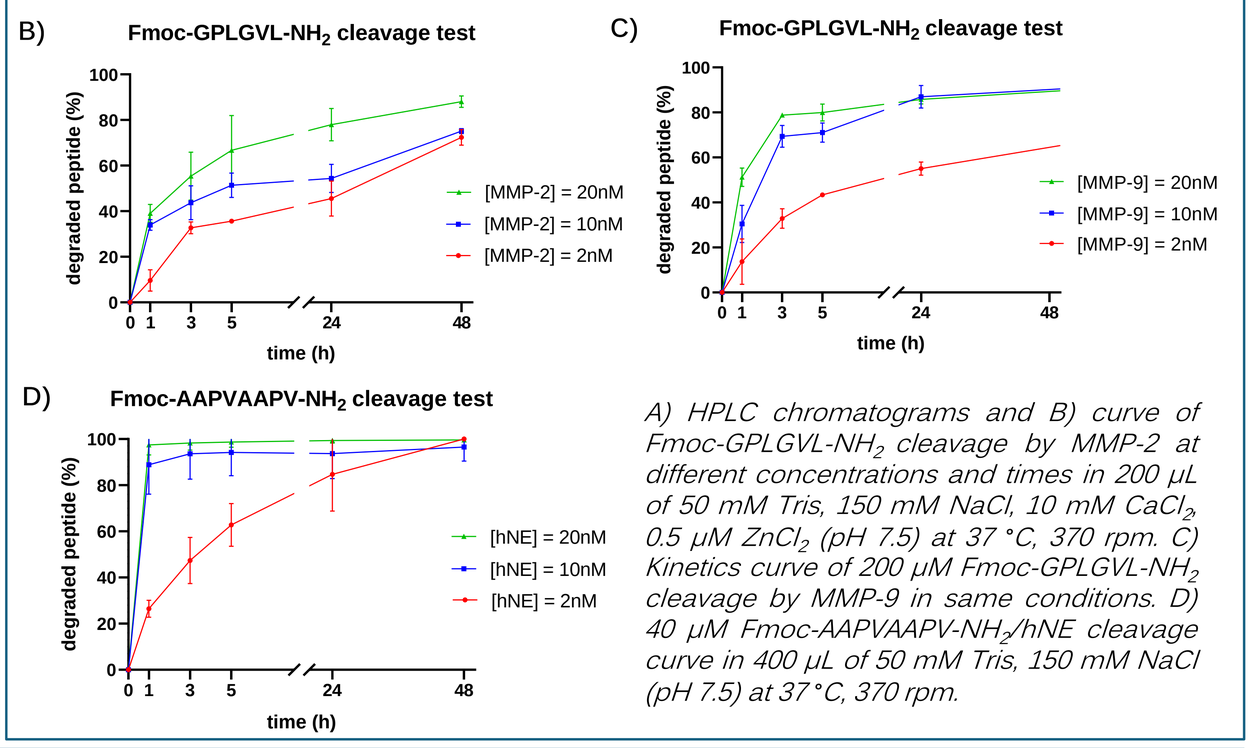
The elected peptides were synthesized by SPPS and purified by HPLC. Each peptide was solubilized in Tris solution at 200 µM and a 0.2 µM solution of the corrisponding bacterial enzyme was added and shaken. At different time points, aliquotes of the mixtures were neutilized by 0.5% TFA solution and injected in HPLC-MS.

Kinetics studies

Kinetics studies were carried out just with peptides that showed positive results in the preliminary cleavage studies. After the injection in HPLC-MS, the areas of the cleavable peptide at different times were compared with its starting area to generate kinetics curves.



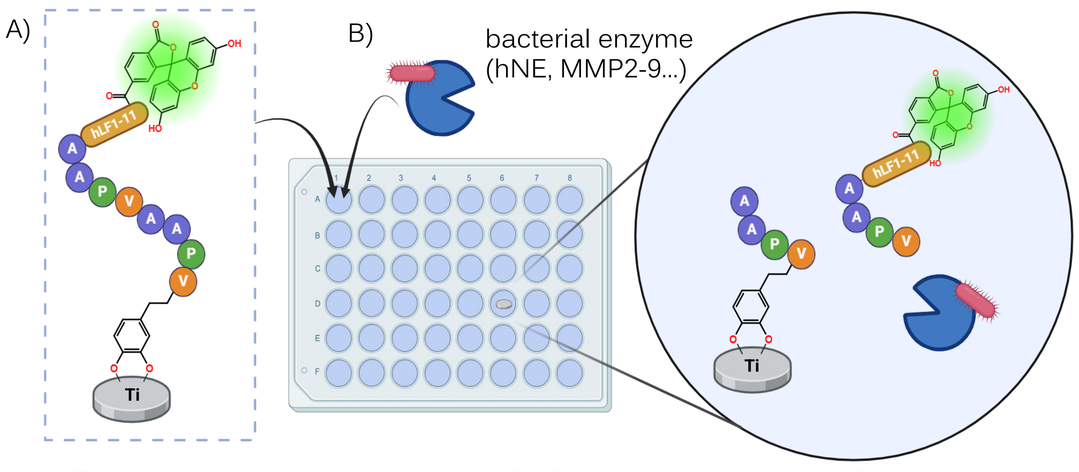
Kinetics curves



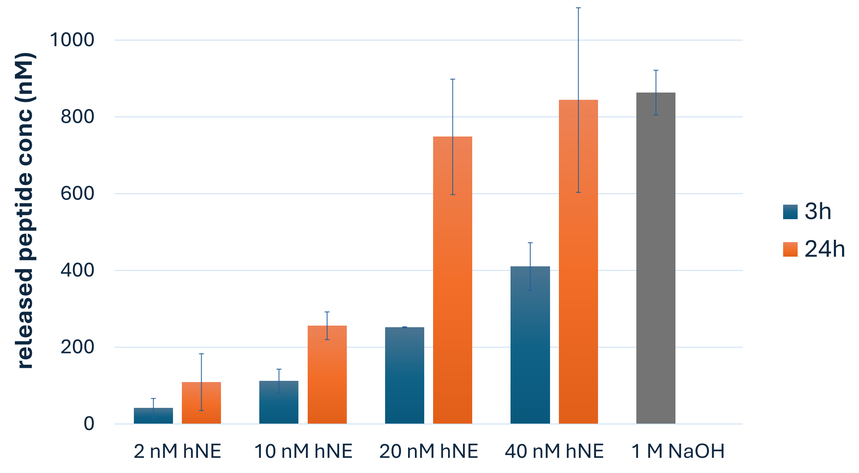
A) HPLC chromatograms and B) curve of Fmoc-GPLGVL-NH_2 cleavage by MMP-2 at different concentrations and times in 200 µL of 50 mM Tris, 150 mM NaCl, 10 mM $CaCl_2$, 0.5 µM $ZnCl_2$ (pH 7.5) at 37 °C, 370 rpm. C) Kinetics curve of 200 µM Fmoc-GPLGVL-NH_2 cleavage by MMP-9 in same conditions. D) 40 µM Fmoc-AAPVAAPV-NH_2/hNE cleavage curve in 400 µL of 50 mM Tris, 150 mM NaCl (pH 7.5) at 37 °C, 370 rpm.

Proof of concept: AMP-linkers on Ti surfaces

Synthesis of FAM-hLF1-11-AAPVAAPV-$DOPA_2$-NH_2 and functionalization of Ti surfaces



Ti-AMP release assay results



A) The peptide was dissolved in 10% DMF/distilled water at pH 6.5 at 100 µM and 20 µL of the solution were deposited onto the Ti samples overnight at rt. Samples were then gently washed with distilled water and dried with nitrogen. B) 250 µL of 2/10/20/40 µM of hNE solution in 50 mM Tris, 150 mM NaCl (pH 7.5) were added to the functionalized Ti discs and left at 37 °C, 320 rpm. The total release is conducted using 250 µL of 1M NaOH solution at 70 °C for 30 min at 320 rpm. C) After 3/24 h, 100 µL of solution were taken and their fluorescence signals were analyzed by microplate reader.

Conclusion and future perspectives

This work demonstrates the feasibility of using protease-cleavable peptide linkers to achieve **infection-responsive antimicrobial peptide release**. The validated linker-AMP platform will be integrated into multifunctional **PEG-based hydrogels** to develop smart biomaterials that combine **infection control** with **bone tissue regeneration**.

References

1. Neumann, M., **2023**, Macromolecules, 56, 8377;
2. López-Gómez P., **2026**, Biomater Adv, 180, 214553;
3. Böhner D.A., **2025**, Materials Today Bio, 33, 101958.

Acknowledgements

Authors acknowledge the project PID2023-148538OB-I00, funded by MICIU/AEI/10.13039/501100011033 and by FEDER, UE and the Spanish Ministry of Universities for the support received through the Ramon y Cajal Program (RYC2022-038428-I).

SCAN ME

https://doi.org/10.17952/38EPS.2026.P185

SYNTHESIS AND CHARACTERIZATION OF FERROCENE-PEPTIDE CONJUGATES WITH ANTIMICROBIAL ACTIVITY

Martina Rotondo,[a] Annalisa Bisello,[a] Saverio Santi,[a,b] Fernando Formaggio[a,b] Simona Oancea,[c] Teodora Călin,[d,e] Anna Mkrtchyan,[f,g] Liana Hayriyan,[f,g] Tatevik Sargsyan,[f,g] Cristina Peggion,[a] and Barbara Biondi[b]

[a]*Department of Chemistry, University of Padua, Padua, Italy;* [b]*Institute of Biomolecular Chemistry, CNR, Padua, Italy;*
[c]*Department of Agricultural Sciences and Food Engineering, University of Sibiu, Sibiu, Romania;* [d]*Faculty of Medicine, University of Sibiu, Sibiu, Romania*
[e]*Laboratory of Diagnostic and Investigation, Directorate of Public Health, Sibiu, Romania;*
[f]*Scientific and Production Center "Armbiotechnology" of NAS RA, Yerevan, Armenia;* [g]*Institute of Pharmacy, Yerevan State University, Yerevan, Armenia*

INTRODUCTION

Over the past five years we have synthesized a variety of ferrocene (Fc)-peptide conjugates with the aim of studying how the peptide backbone affects charge/electron transfer, Fc being an easy-to-handle electrochemical probe.[1] In addition, Fc is also able to promote the generation of reactive oxygen species (ROS) under physiological conditions. High levels of ROS are associated with cytotoxic effects. Therefore, Fc-peptide conjugates were designed to create new anticancer drugs.[2]

AIM

Here, we extended the same approach to the antibacterial field. We selected a set of ultrashort, antimicrobial lipopeptides, characterized by the presence of a non-coded His structural isomer (Figure 1), which we recently published.[3] We connected an Fc moiety to them via spacers of different lengths to evaluate whether Fc is able to enhance the antibacterial action, as reported in the literature.[4] A representative example is reported in Figure 1. In addition, we planned to explore the role of His* chirality as in our previous report the two His* of each lipopeptide were of the same configuration. The amino acid sequences of the six newly synthesized lipopeptides and of two reference compounds, previously published,[3] are reported in Table 1.

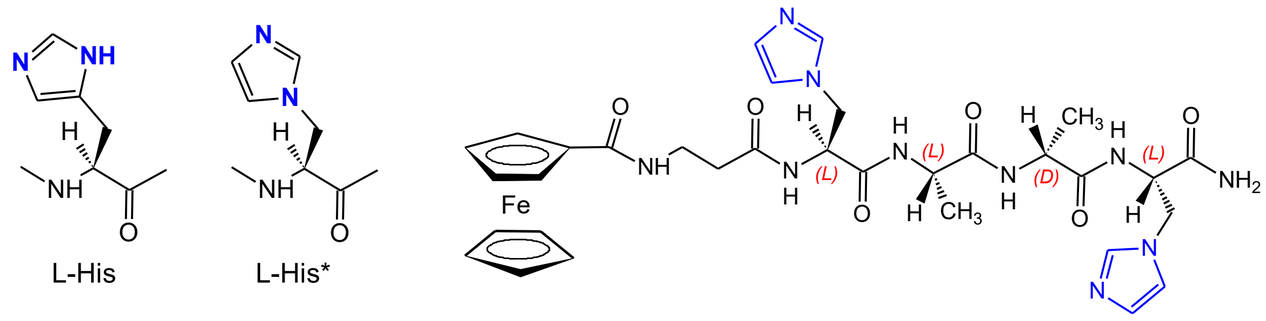


Figure 1. Molecular structures of His and its structural isomer His* and of Fc-βAla-His*-Ala-D-Ala-His*-NH_2.

Table 1. Amino acid sequences of the peptides discussed. Ahx, 6-aminohexanoyl; Laur, Lauroyl (dodecanoyl).

Code	Peptide sequence	Reference
1	Fc-CO-βAla-^{L}His*-Ala-^{D}Ala-^{L}His*-NH_2	This work
2	Fc-CO-βAla-^{D}His*-Ala-^{D}Ala-^{D}His*-NH_2	This work
3	Fc-CO-Ahx-^{L}His*-Ala-^{D}Ala-^{L}His*-NH_2	This work
4	Fc-CO-Ahx-^{D}His*-Ala-^{D}Ala-^{D}His*-NH_2	This work
5	Laur-^{L}His*-Ala-^{D}Ala-^{D}His*-NH_2	This work
6	Laur-^{D}His*-Ala-^{D}Ala-^{L}His*-NH_2	This work
7	Laur-^{L}His*-Ala-^{D}Ala-^{L}His*-NH_2	Ref. 3
8	Laur-^{D}His*-Ala-^{D}Ala-^{D}His*-NH_2	Ref. 3

Table 2. Bacteria growth inhibition after 20 hours from peptide incubation at 37 °C. The values are the diameters of inhibition in millimeters, the higher the better.

	Microorganism strain	Peptide							
		1	2	3	4	5	6	7[a]	8[a]
Gram-positive	Staphylococcus aureus ATCC 25923	-	-	-	-	-	-	9	12
	Streptococcus pyogenes ATCC 19615	-	-	-	-	-	-	-	17
	Enterococcus faecalis ATCC 29212	-	-	-	-	-	-	12	9
	Bacillus subtilis ATCC 6633	-	-	-	-	8	12	11	12
	Vancomycin-resistant enterococcus ATCC 51299	-	-	-	-	-	-	b	b
Gram-negative	Escherichia coli ATCC 25922	-	-	-	-	-	-	9	7
	Pseudomonas aeruginosa ATCC 27853	-	-	-	-	-	-	8	8
	Acinetobacter Baumannii ATCC 19606	-	-	-	-	-	-	-	-
	Proteus mirabilis ATCC 25933	-	-	-	-	-	-	b	b
	Klebsiella pneumoniae ATCC 13883	-	-	-	-	-	-	b	b

[a]Data from ref. 2. [b] Strain not investigated in ref. 2

DATA INTERPRETATION

The action of the six new peptides (Table 2) does not correspond to expectations, contrary to what happened with literature Lys-rich hexapeptides.[4] Insertion of Fc did not enhance the antibacterial activity of our lead tetrapeptide, but actually eliminated it. Perhaps, the too bulky Fc prevents the peptide from interacting properly with the membrane. We are therefore planning the synthesis of an analog with a longer spacer, so that the peptide can first bind to the membrane and then possibly drag Fc inside. Compounds **5** and **6** with the two His* of opposite configurations are active only against *bacillus subtilis*. The mechanism of action might involve membrane insertion of the lauroyl group and a subsequent electrostatic interaction of the positively charged His* with the negatively charged bacterial membranes. Then, the different behavior could result from a less productive alignment of the positive charges that disadvantages interaction with membranes.

CONCLUSIONS

- Replacement of lauroyl with Fc in an antimicrobial lipopeptide abolished the activity. This outcome is ascribable to the too close proximity of Fc to the peptide. We are now planning the synthesis of analogsa with a longer spacer between Fc and the peptide.
- Chirality plays an important role in the potency of our lead, antibacterial lipopeptide.3
- Chirality could, however, be exploited to design antimicrobial peptides capable of selectively targeting specific bacterial strains.

REFERENCES

1. A. Bisello, B. Biondi, R. Cardena, R. Schiesari, M. Crisma, F. Formaggio, S. Santi. *Inorganics* **2023**, 11, art. N. 482.
2. B. S. Ludwig, S. Tomassi, S. Di Maro, F. S. Di Leva, A. Benge, F. Reichart, M. Nieberler, F. E. Kühn, H. Kessler, L. Marinelli, U. Reuning, S. Kossatz. *Biomaterials* **2021**, 271, art. N.120754.
3. C. Peggion, A. Schivo, M. Rotondo, S. Oancea, L.-F. Popovici, T. Călin, A. Mkrtchyan, A. Saghyan, L. Hayriyan, E. Khachatryan, F. Formaggio, B. Biondi. *J. Pept. Sci.* **2025**, 31, art. N. e70021.
4. J. Gómez, D. Sierra, C. Ojeda, S. Thavalingam, R. Miller, F. Guzmán, N. Metzler-Nolte. *J. Biol. Inorg. Chem.* **2021**, 26, 599-615.

ACKNOWLEDGEMENTS

✓ This work was supported by a Joint Bilateral Agreement between CNR (Italy) and MESRA (Armenia).

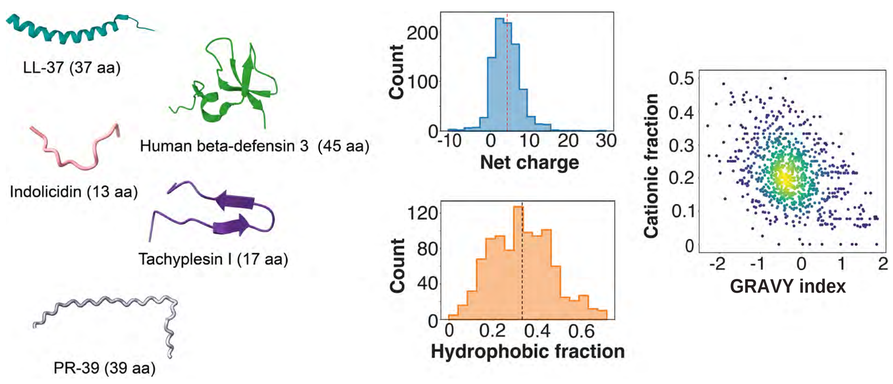
Trade-offs in Antimicrobial Peptide Activity: Faster Isn't Always Better

Alessio Fragasso[1,2,3], Tatjana Schlechtweg[1,3], Wei-Hsiang Lin[1,3], Annelise Barron[4], Christine Jacobs-Wagner[1,2,3,5]

1. Sarafan ChEM-H Institute, Stanford University, CA, USA; 2. Department of Biology, Stanford University, CA, USA; 3. Howard Hughes Medical Institute, Stanford University, CA, USA;
4. Department of Bioengineering, Stanford University, CA, USA; 5. Department of Microbiology and Immunology, Stanford School of Medicine, CA, USA; https://doi.org/10.17952/38EPS.2026.P162.

Antimicrobial peptides (AMPs)

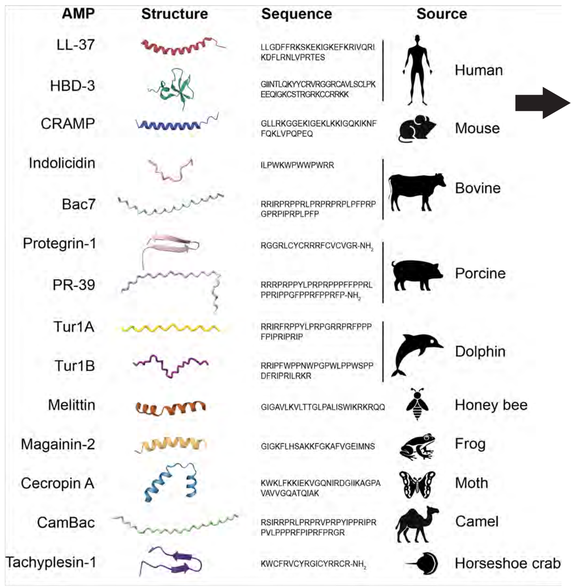
- Part of the innate immune system, first line of defense against pathogens (bacteria, viruses, fungi, etc).
- Produced by virtually all living organisms. In humans: by neutrophils, macrophages, epithelial cells, NK cells, neurons, and more...
- Typically cationic (+2 to +9) and amphiphilic (~1/3 hydrophobic), AMPs exhibit broad-spectrum activity against bacteria and viruses and have a low propensity to induce resistance, making them promising antibiotic candidates.
- Positive charge: thought to allow AMPs to selectively target bacteria, viruses, fungi, cancer cells, vs (zwitterionic) host cells.
- Hydrophobic character: thought to enable membrane partitioning and translocation, destabilization, permeabilization



Lack of general principles, unifying framework, sequence-function relation
Single-cell approaches are powerful but currently limited to few isolated studies

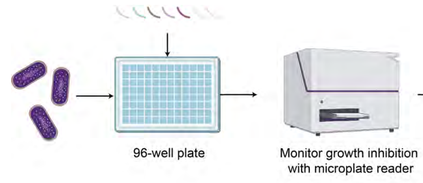
Approach

1. Select a representative subset of AMPs with diverse sequence, structure, origin, physicochemical properties



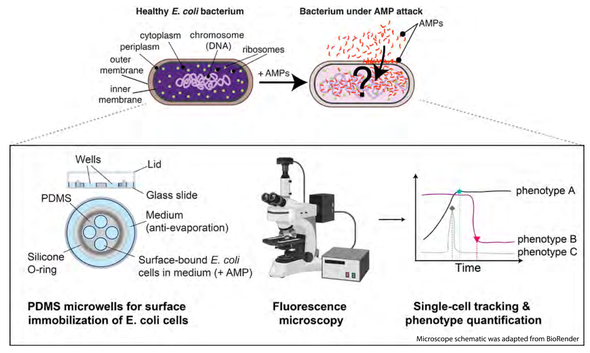
Animal schematics were adapted from https://thenounproject.com/. Structures were downloaded and adapted from PDB and AlphaFold.

2. Characterize their minimum inhibitory concentration (MIC) against our *E. coli* strain by measuring growth rate (inhibition) using a microplate reader.



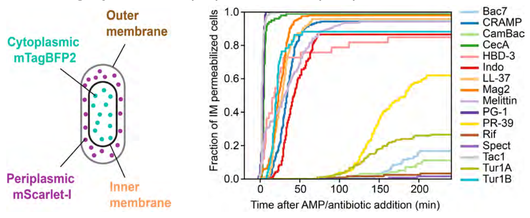
Name (abbreviation)	MIC (μM)
Bactenecin-7 (Bac7)	0.6
CamBac	0.5
Cecropin A (CecA)	0.5
CRAMP	4
Human β-defensin 3 (HBD-3)	20
Indolicidin (Indo)	12.5
LL-37	1
Magainin-2 (Mag2)	40
Melittin (Mitt)	4
Protegrin-1 (PG-1)	1
PR-39	2
Tachyplesin-1 (Tac1)	0.6
Tur1A	1
Tur1B	8

3. Monitor AMP-induced phenotype in real time with single-cell microscopy



Kinetics of membrane permeabilization

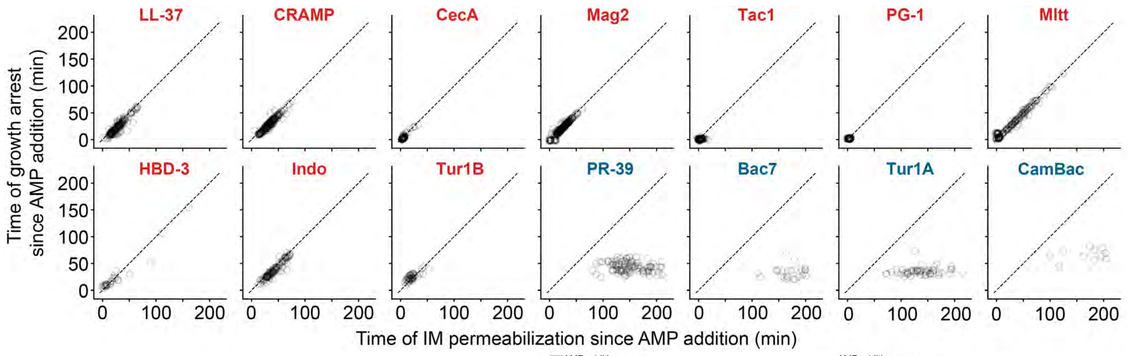
E. coli strain was engineered with free periplasmic (mScarlet) and cytoplasmic (mTagBFP2) fluorescent proteins to independently probe integrity of inner (IM) and outer (OM) membrane.



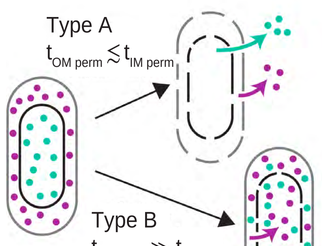
1. **All selected AMPs exhibit some degree of IM permeabilization** during the course of the experiment, higher than control antibiotics Rifampicin and Spectinomycin.

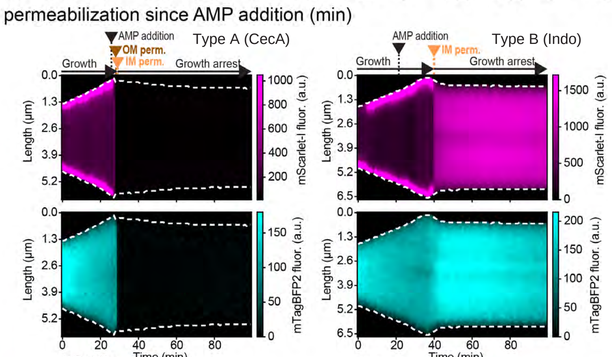
2. What differs is the **timing of IM permeabilization** *vs* **growth arrest**, which forms two classes.

Class I: Associated
Class II: Not associated



3. Class I AMPs feature two **sub-types A/B**, depending on the timing of IM vs OM perm.

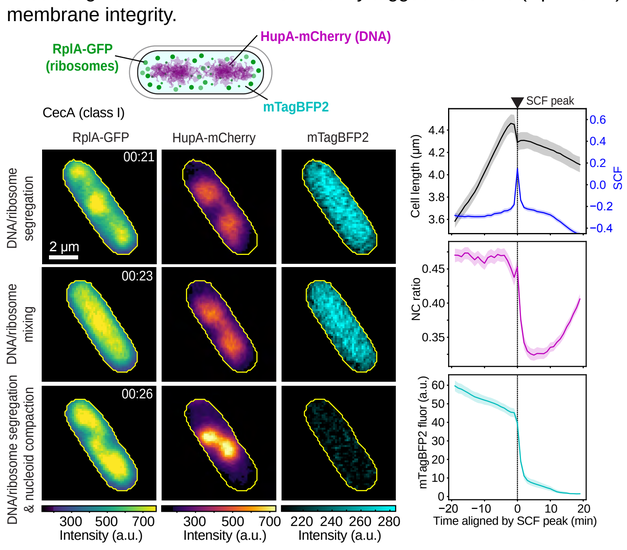




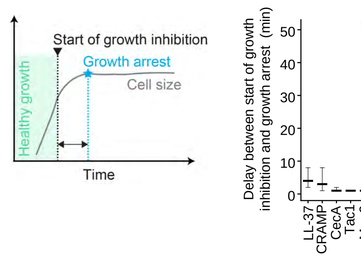
CecA — Scan to view timelapse movies of membrane permeabilization kinetics. — Indo

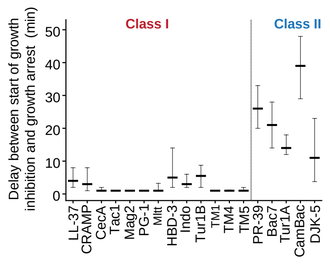
Intracellular perturbations

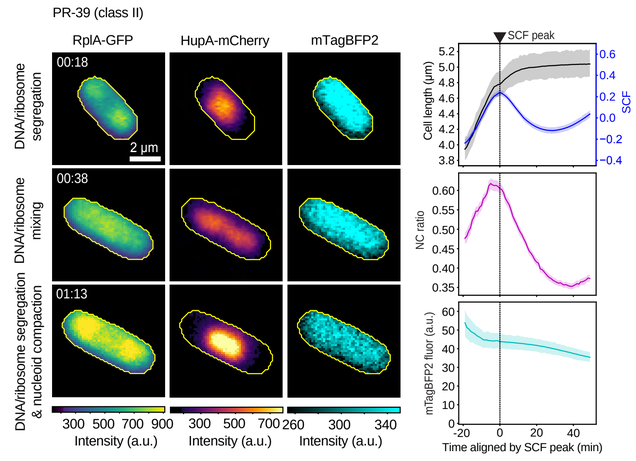
E. coli engineered strain with fluorescently tagged ribosome (RplA-GFP) and DNA (HupA-mCherry), plus free cytoplasmic mTagBFP2 to monitor membrane integrity.



CecA — Scan to view timelapse movies of AMP-induced intracellular effects. — PR-39







1. Class I AMPs induce rapid **ribosome/DNA mixing at the time of growth arrest**, followed by demixing and nucleoid compaction.

2. Ribosome/DNA mixing, which indicated halting of protein synthesis, seems to occur slightly before the loss of cytoplasmic mTagBFP, suggesting **intracellular effects may occur prior to membrane permeabilization** to proteins.

3. Class II exhibit **similar but slower rearrangements** of the ribosome and DNA, likely a result of absent or delayed IM permeabilization

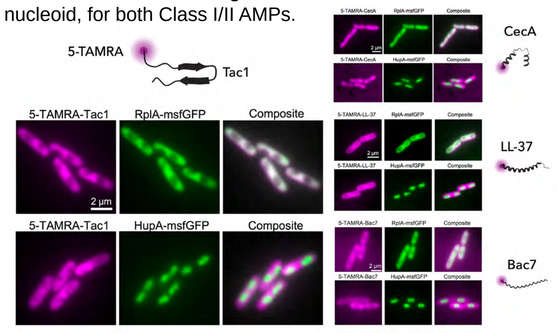
4. Consistent with the speed of intracellular effects, **class I induce more abrupt growth inhibition than class II**

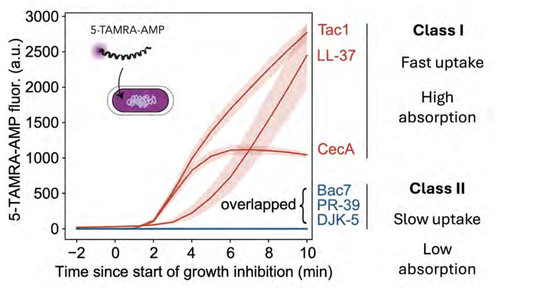
Acknowledgements

This work was supported in part by the Netherlands Organization for Scientific Research (Rubicon 2022-2 Science programme, 019.222EN.001804 to A.F.). A.E.B. acknowledges work at the Molecular Foundry supported by the OSice of Science, OSice of Basic Energy Sciences, of the U.S. Department of Energy under Contract No. DE-AC02-05CH11231. C.J.W. is an investigator of the Howard Hughes Medical Institute.

Localization & enrichment

1. Fluorescently labelled AMPs show **colocalization with ribosomes/DNA-free regions** and exclusion from the nucleoid, for both Class I/II AMPs.

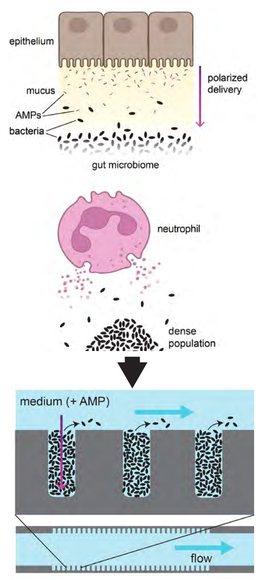




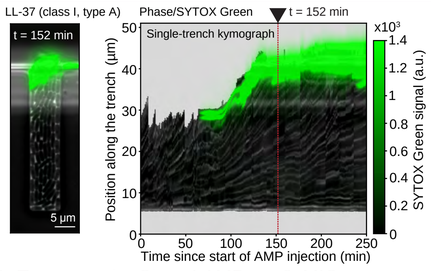
2. Class I act fast, but are also **rapidly absorbed intracellularly**, whereas class II are slow-acting and feature **low absorption.**
→ Will this lead to trade-offs?

AMPs *vs* high cell densities using wide-trench microfluidics

In real physiological systems, **local cell density can be very high** or AMPs can be asymmetrically delivered.

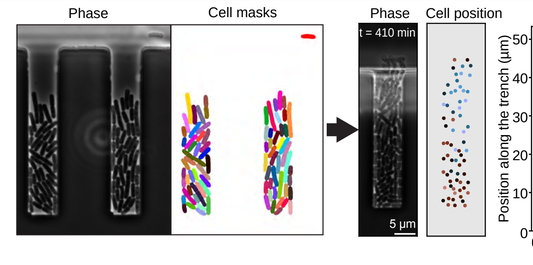


We devised wide-trench microfluidics to **confine cells at high density** while flowing AMPs in the feeding channel.



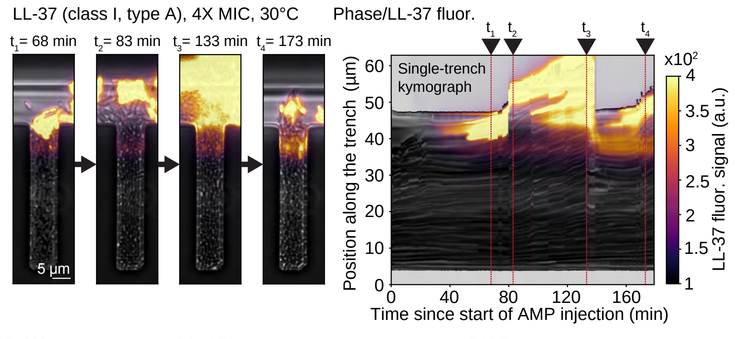
1. Treatment by Class I AMPs at 2xMIC causes **only top cells to become SYTOX Green positive**.

Scan to view timelapse movie of wide-trench under LL-37 treatment + SYTOX Green.



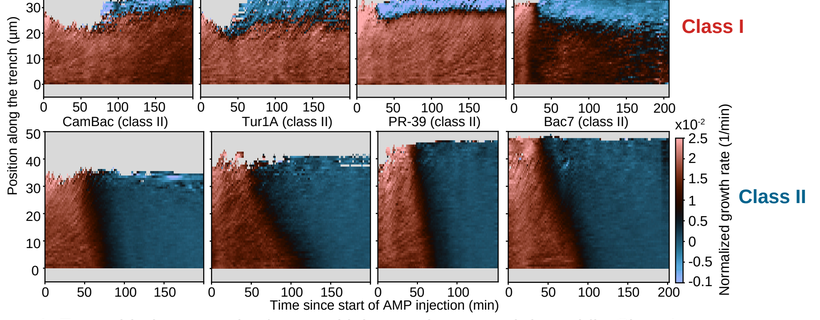
Tac1 — PR-39 — Scan to view timelapse movies of single-cell growth tracking in wide trenches.

3. To **quantify growth at the single-cell level**, we retrained Omnipose (PMID: 36253643) deep neural network to segment and **track individual cells** in the wide trenches, which quantitatively shows that Class I Tac1 only manages to inhibit growth of the first exposed cells, at the top of the trench (blue color), whereas the cells deeper in the trench keep growing (brown color).



2. We found natural LL-37 to be weakly fluorescent at 30°C and used this to show that **LL-37 (4xMIC) only accumulates into the top exposed cells**, consistent with the SYTOX data.

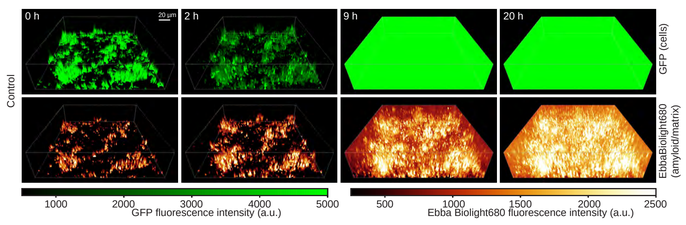
Scan to view timelapse movie of wide-trench under LL-37 treatment.

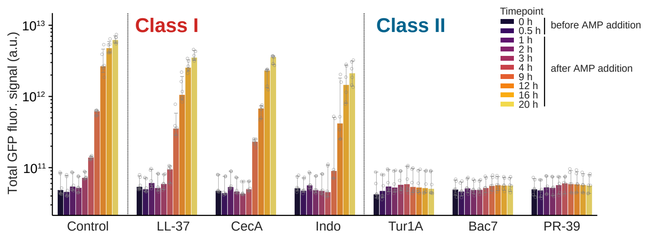


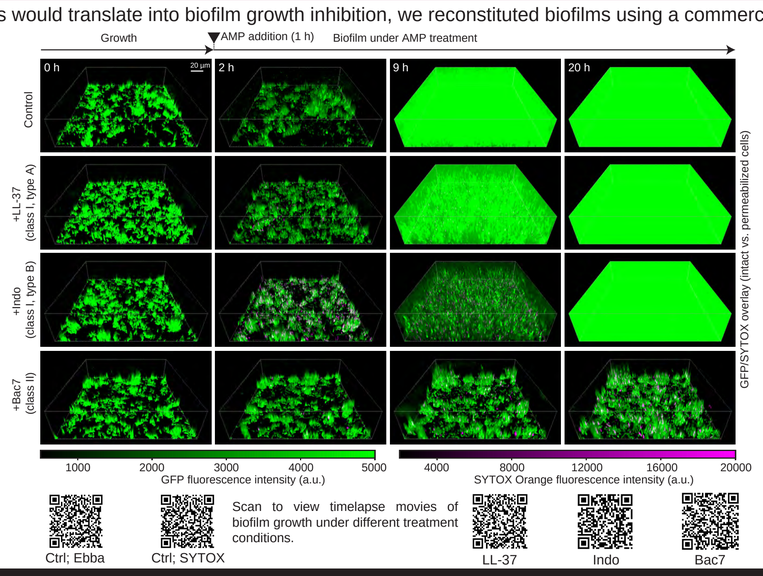
4. Ensemble kymographs from multiple trenches reveal that while Class I act poorly against high cell densities, **Class II can effectively and uniformly arrest the growth of the entire bacterial population.**

AMPs *vs* growing *E. coli* biofilms & final remarks

To assess whether the differential efficacy of class I/II against high cell densities would translate into biofilm growth inhibition, we reconstituted biofilms using a commercially available GFP-expressing *E. coli* strain (ATCC 25922GFP) that is known to form biofilms.







Ctrl; Ebba — Ctrl; SYTOX — Scan to view timelapse movies of biofilm growth under different treatment conditions. — LL-37 — Indo — Bac7

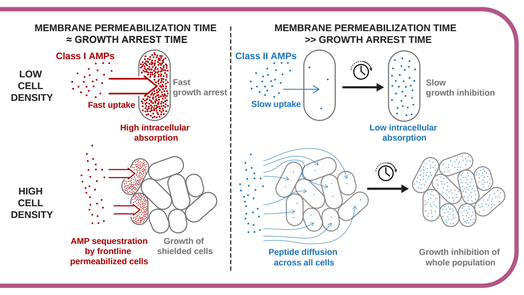
1. Using widefield fluorescence microscopy and deconvolution **we could monitor biofilm growth**, by imaging both cells (GFP), extracellular matrix (amyloid-staining EbbaBiolight680), and SYTOX orange to assess cell membrane permeabilization.

2. Adding **Class I AMPs** at 2X MIC (e.g. LL-37) to biofilms caused only some detectable permeabilization by SYTOX, with some growth delay depending on the AMP, but **no sustained growth inhibition**.

3. On the contrary, **all Class II AMPs** at 2X MIC (e.g. Bac7), **strongly inhibited biofilm growth** as soon as they were injected, accompanied by increasing SYTOX Orange fluorescence.

Together, this work reveals a fundamental **trade-off: class I** peptides are **fast-acting** against sparse bacteria but become **rapidly sequestered** at high cell densities.
On the contrary, **class II act slower** but retain activity under **high-density** and **biofilm conditions**, pointing to distinct, complementary roles in host defense for the two classes.

bioRxiv — THE PREPRINT SERVER FOR BIOLOGY



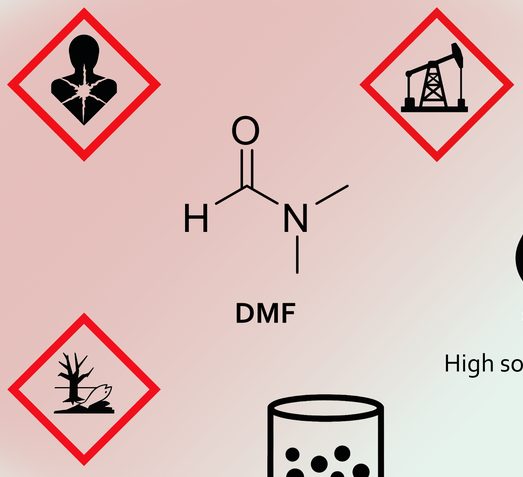
Glycerol-derived drop-in solvents for sustainable and more efficient peptide synthesis

Vincent Freiburghaus[a], Tom Nelis[b], Jeremy Luterbacher[b], Nina Hartrampf[a]

a Department of Chemistry, University of Zurich, Switzerland, https://doi.org/10.17952/38EPS.2026.P299

b Laboratory of Sustainable and Catalytic Processing (LPDC), École Polytechnique Fédérale de Lausanne (EPFL), Switzerland

Background



- The growing demand for therapeutic peptides[1] calls for more **sustainable** synthetic approaches. **Solid-phase peptide synthesis** (SPPS) remains the method of choice due to its reliability and versatility.[2]
- *N,N*-Dimethylformamide (DMF), the most commonly used solvent, is classified as a substance of very high concern (SVHC) under REACH, emphasizing the **urgent need for greener, safer alternatives** in peptide manufacturing.[3]

Preliminary SPPS compatibility studies

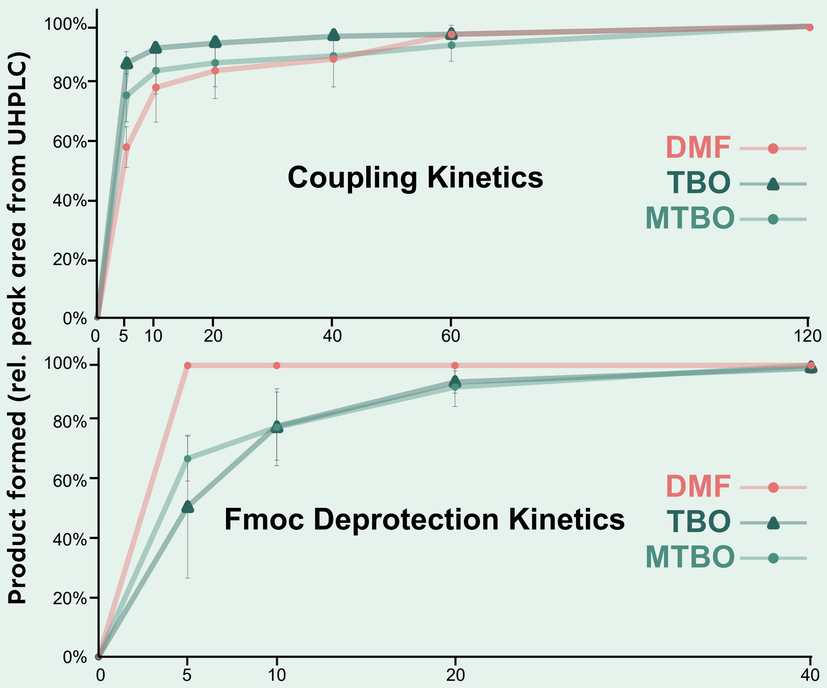
Reagent Solubility

20 canonical Fmoc amino acids (0.4 M)
Fmoc Rink Amide linker (0.2 M)
PyAOP (0.4 M)
HCTU (0.4 M)
DIC (1 M)
Oxyma (1 M)
Piperidine (20% *v/v*)
Pyrrolidine (20% *v/v*)

Resin Swelling

Polystyrene aminomethyl-RAM
Polystyrene-2CTC
TentaGel-RAM
TentaGel-PHB
NovaPEG-RAM
Li-RAM

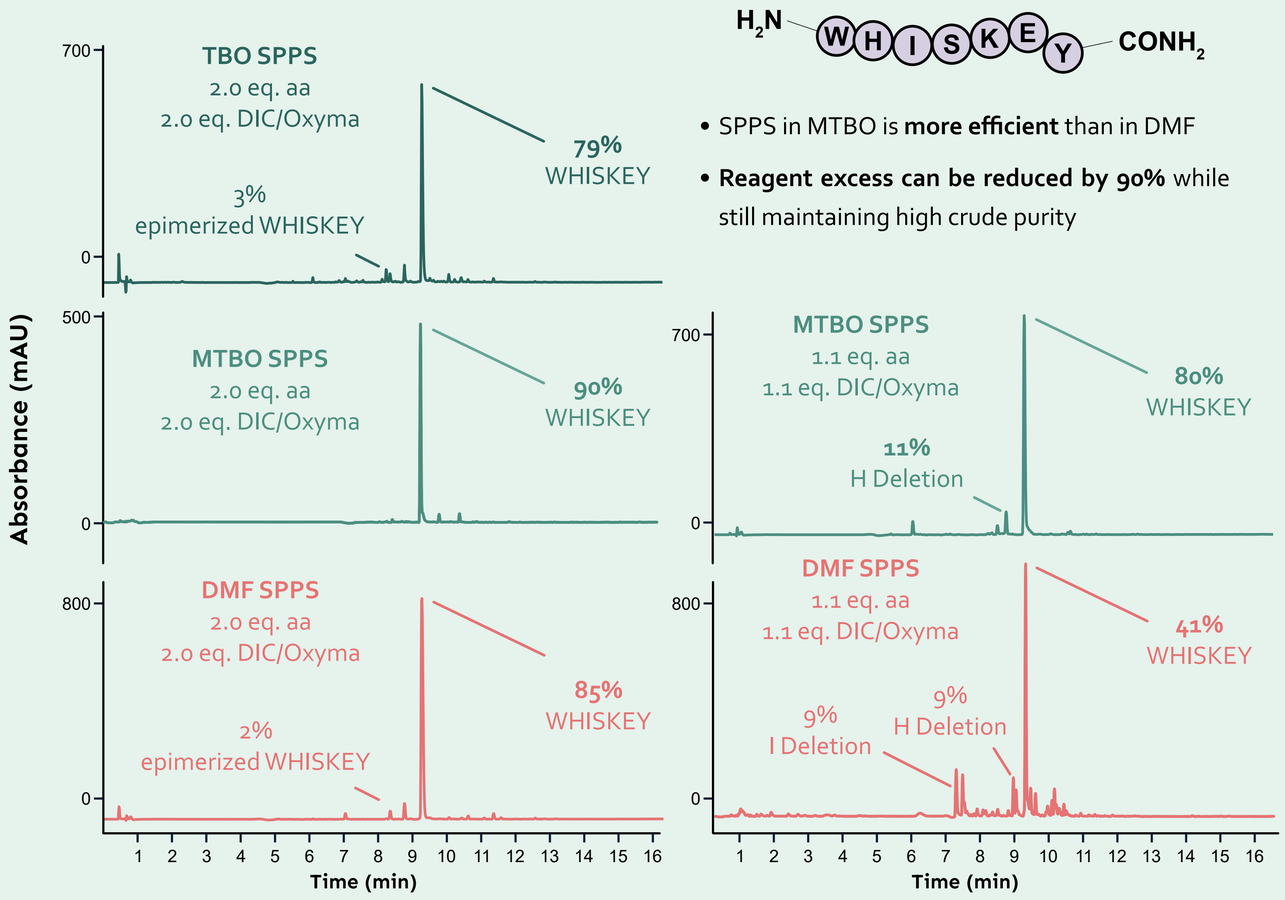
Reaction kinetics: Coupling and Fmoc deprotection



- Slightly **faster in (M)TBO** compared to DMF
- Standard protocol of 1 h per coupling remains unchanged

- Slower in (M)TBO compared to DMF
- Standard protocol of 2 x 5 min incubation for deprotection changed to **3 x 10 min**

SPPS with low reagent excess: MTBO outperforms DMF

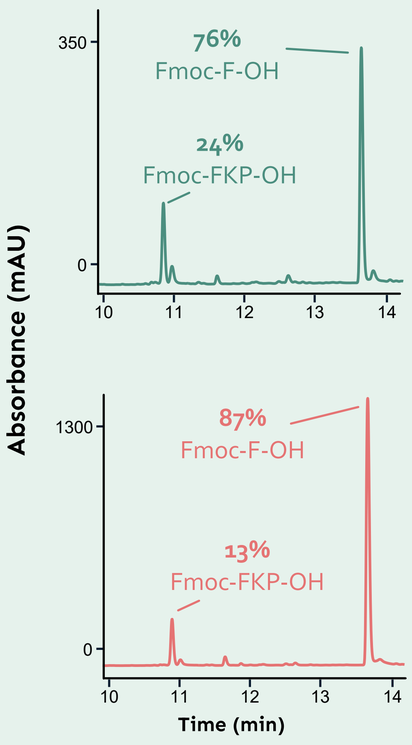


- SPPS in MTBO is **more efficient** than in DMF
- **Reagent excess can be reduced by 90%** while still maintaining high crude purity

Diketopiperazine formation

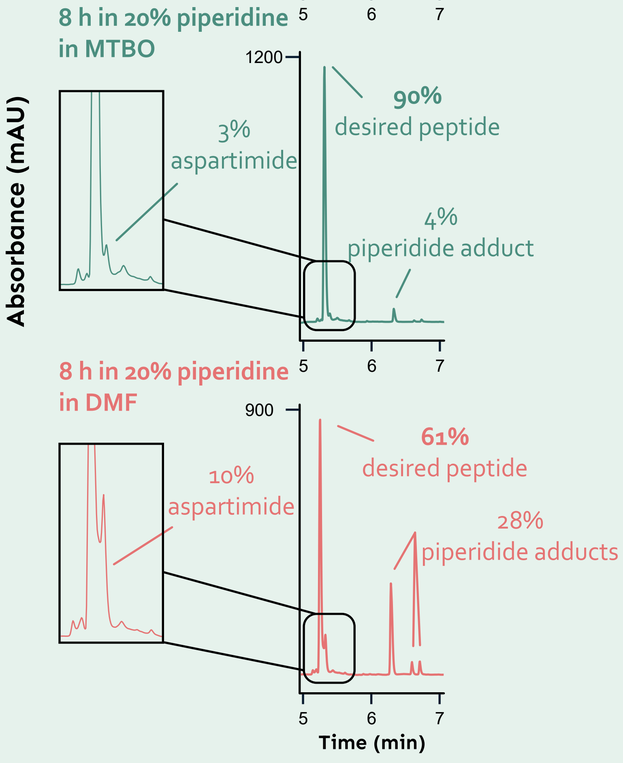


- Synthesis of **DKP prone motif** (Lys-Pro) on **TentaGel-PHB** resin
- Ratio of recovered full peptide (Fmoc-Phe-Lys-Pro) vs. liberated resin sites esterified with Fmoc-Phe for quantification

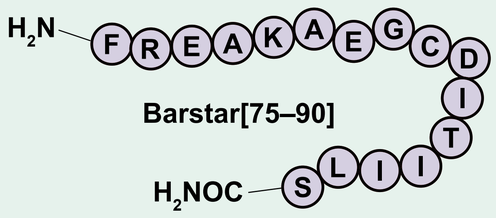


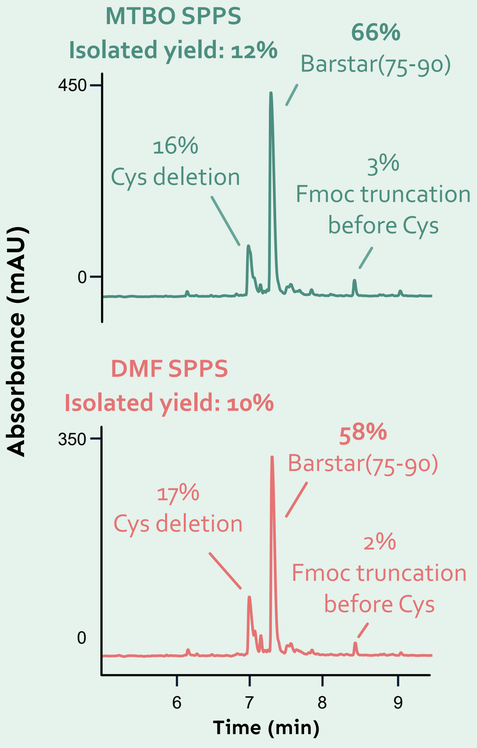
Aspartimide formation



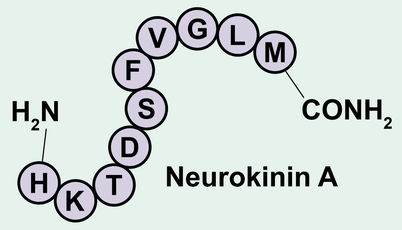


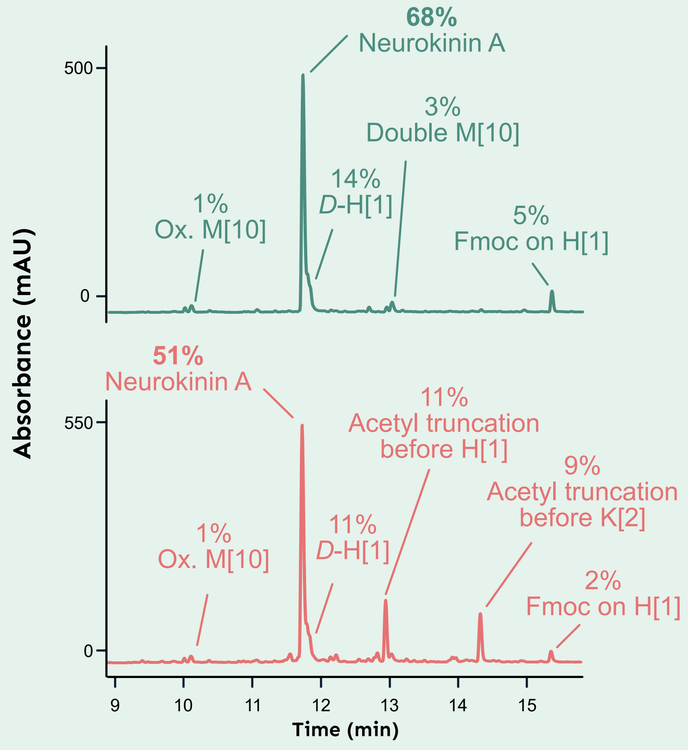
SPPS of a longer, aggregating peptide





Fully automated flow SPPS on PeptiPilot system





1 Topouzis, S *et al.*, *Br. J. Pharmacol.*, **2025,** 182, 1416–1445.

2 Merrifield, B., *J. Am. Chem. Soc.*, **1963**, 85 (14), 2149–2154.

3 Sherwood, J.; Albericio, F.; de la Torre, B. G. , *ChemSusChem*, **2024**, 17 (8).

Schweizerischer Nationalfonds

Conclusions

- Novel, bio-based & sustainable glycerol-derived solvents **compatible with SPPS**
- Ultra efficient coupling reaction enables **reduction of reagent excess**
- **Supression of notorious SPPS side-reactions** improves crude purity
- **MTBO outperforms DMF** in the synthesis of aggregating sequences & is **fully compatible with automated peptide synthesizers**

See the paper here

NMR-based Structure-Activity Relationship Studies of Antimicrobial Peptides

Visit our lab here

Michael Quagliata[1], Sonja Bazhenova[2,3], Joshua Grabeck[2], Philipp Holz[2], Anna Maria Papini[1], Paolo Rovero[1], Ines Neundorf[2] and Daniel Friedrich[3]

[1] Interdepartmental Research Unit of Peptide and Protein Chemistry and Biology, Department of Chemistry "Ugo Schiff", University of Florence, Italy;
[2] Institute of Biochemistry, University of Cologne, Germany; [3] Department of Chemistry and Biochemistry, University of Cologne, Germany; https://doi.org/10.17952/38EPS.2026.P163

A triazolyl bridge enhances antimicrobial activity, while Arg3, Arg7 and Asn11 are key determinants of activity.

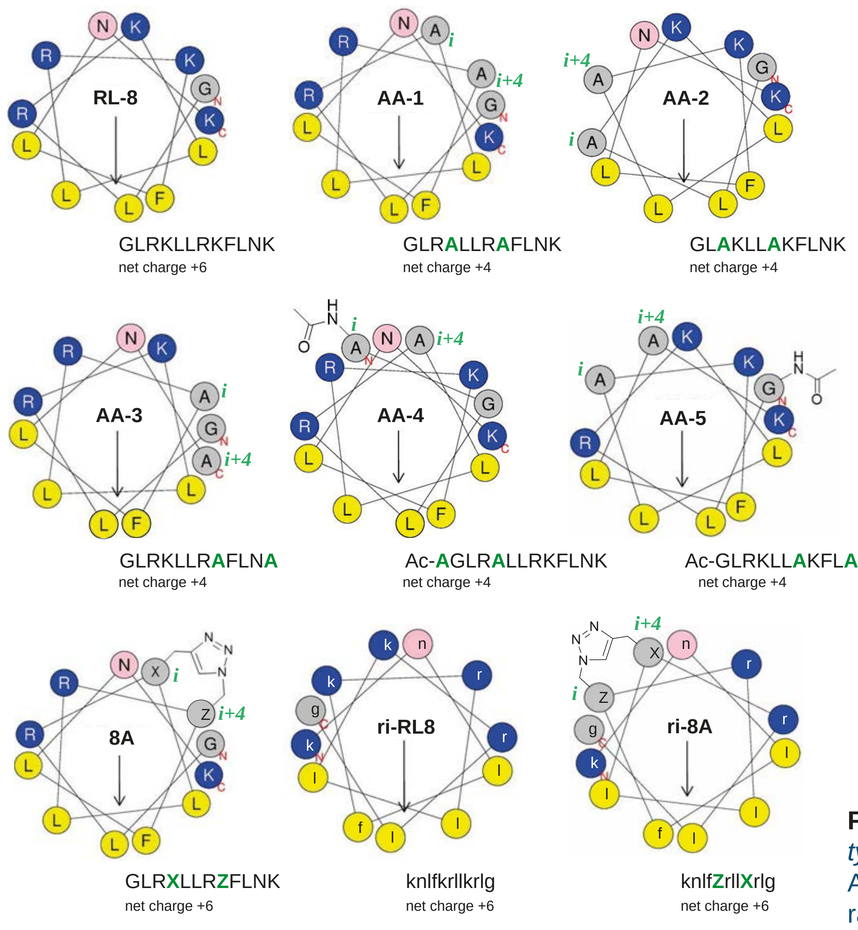


Figure 1. Helical-wheel projections of the designed and analysed peptides.
The N- and C-termini are indicated by red upper-case letters. Amino acids are labelled using the one-letter code, with lower-case letters used for the retro-inverso peptides ri-RL8 and ri-8A. Positively charged residues are highlighted in blue, Asn11 (Asn2 in the retro-inverso peptides) in pink, hydrophobic residues in yellow and all other residues in grey. Acetylation and the triazolyl bridge are shown by their chemical structures. L-Propargylglycine and L-ε-azido-norleucine are denoted X and Z, respectively. Modified residues at positions i and i + 4 are highlighted in green to indicate their spacing within the peptide sequence.

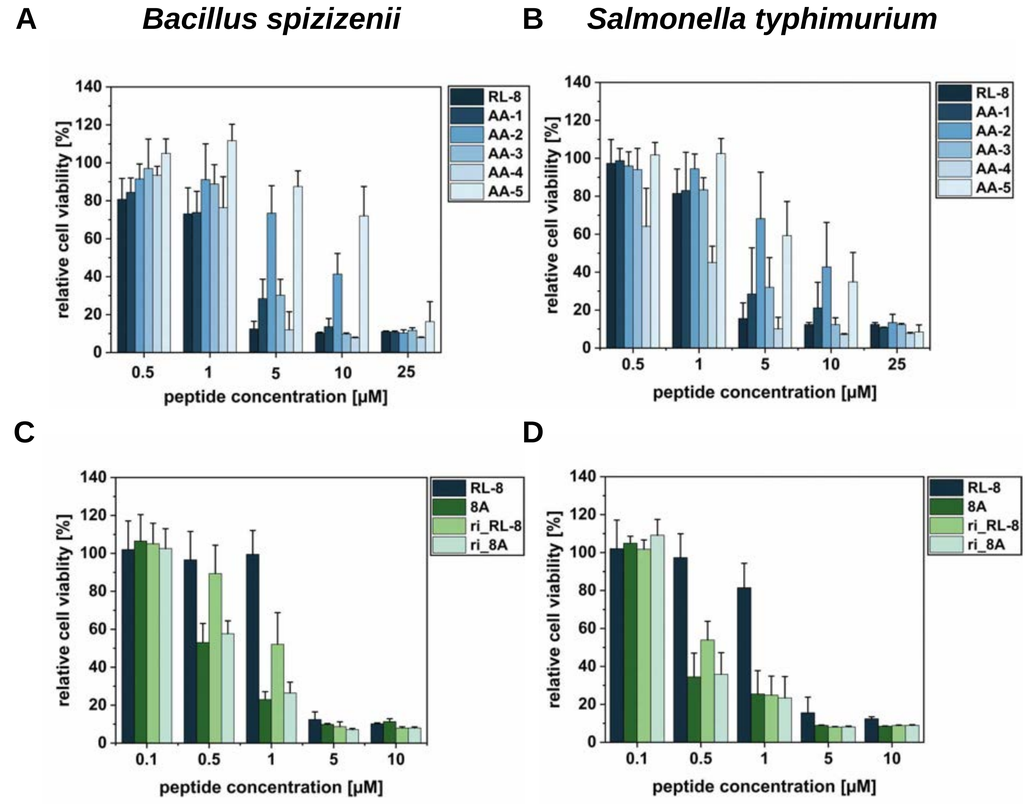


Figure 2. Antimicrobial activity of the analysed peptides. Relative cell viability of *B. spizizenii* (**A**, **C**) and *S. typhimurium* (**B**, **D**) was determined at increasing peptide concentrations. Panels **A–B** show RL-8 and AA-1 to AA-5, whereas panels **C–D** compare RL-8, 8A, ri-RL-8 and ri-8A. Note the different peptide concentration ranges used in the two sets of experiments.

The molecular surface of peptide 8A presents favourable features for membrane interaction.

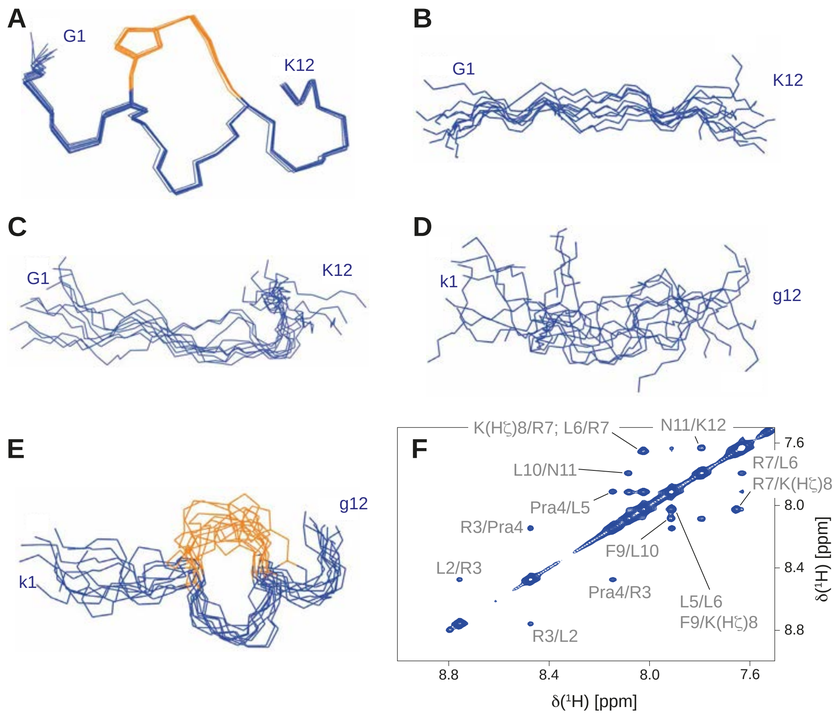


Figure 3. NMR-derived structures of the analysed peptides.
A–E Conformational ensembles of the ten lowest-energy structures of 8A (**A**), RL-8 (**B**), AA-2 (**C**), ri-RL-8 (**D**) and ri-8A (**E**). Peptide backbones are shown in blue and triazolyl bridges in orange. N- and C-termini are labelled by residue and position.
F Amide–amide region of the 2D $^{1}H,^{1}H$-NOESY spectrum of 8A. Amino acids are labelled using the one-letter code; Pra, L-propargylglycine.

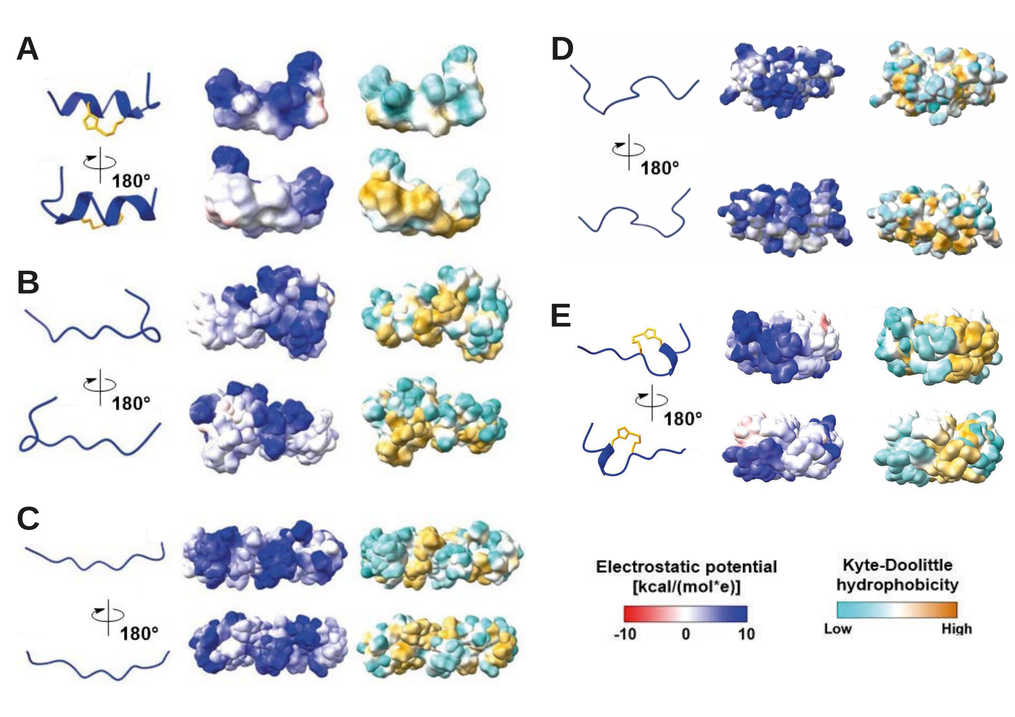


Figure 4. Surface properties of the NMR-derived peptide structures.
A–E Electrostatic surface potential and Kyte–Doolittle hydrophobicity of 8A (**A**), AA-2 (**B**), RL-8 (**C**), ri-RL-8 (**D**) and ri-8A (**E**). Surface orientations correspond to the representative structures shown on the left; colour scales are indicated at the bottom right.

CD validates the NMR-derived structures, while chemical modification improves serum stability and micelle binding promotes α-helicity.

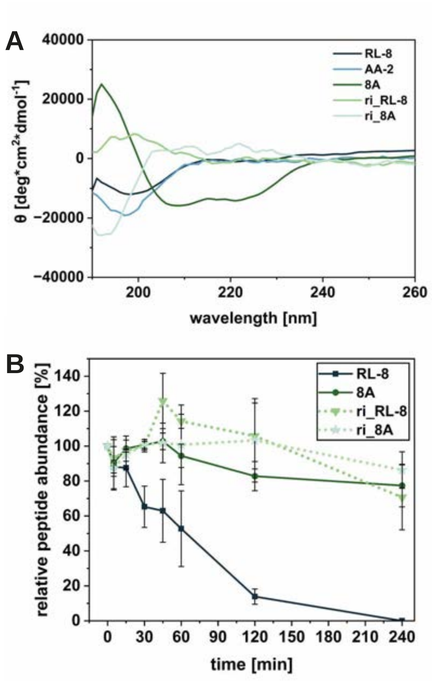


Figure 5. CD spectroscopy and serum stability of the analysed peptides.
A CD spectra of the indicated peptides recorded in H_2O.
B Stability of RL-8, 8A, ri-RL-8 and ri-8A in human serum.

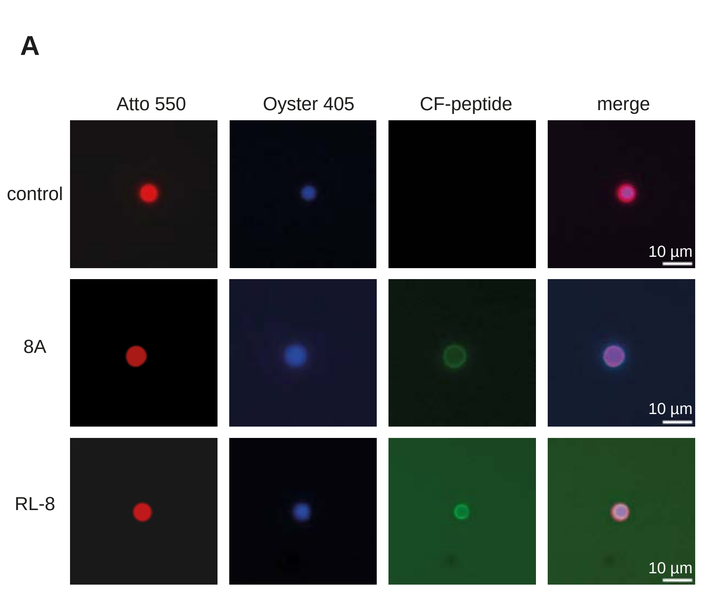
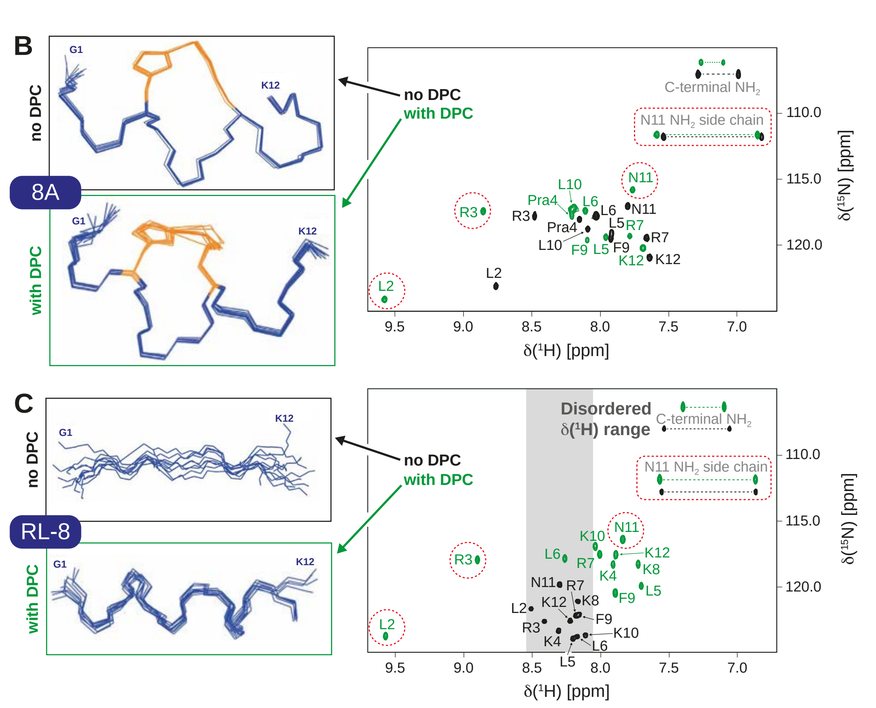


Figure 6. Membrane interactions of peptides 8A and RL-8.
A Fluorescence microscopy images of GUVs without peptide (control, top row), with 8A (middle row) and with RL-8 (bottom row).
B–C NMR-derived structures and $^{1}H,^{15}N$-HSQC spectra of 8A (**B**) and RL-8 (**C**) in H_2O in the absence and presence of DPC micelles.



Department of Chemistry and Biochemistry
University of Cologne
DFG Deutsche Forschungsgemeinschaft German Research Foundation
FULBRIGHT Germany
EMBO
HFSP International Human Frontier Science Program Organization

PEPTIDOGLYCAN-BASED BIOMIMETIC NANOMATERIALS REVEAL LECTIN RECOGNITION IN DAP-TYPE BACTERIA: TOWARD RATIONAL DESIGN OF ANTIMICROBIAL THERAPEUTICS

R. Frkanec[1], M. Šišić[1], A. Imberty[2], A. Tomić[3], A. Usenik[4], V. Tomišić[4] & L. Frkanec[3]

[1]University of Zagreb, Centre for Research and Knowledge Transfer in Biotechnology, Croatia • [2]CERMAV–CNRS, Grenoble, France • [3]Ruđer Bošković Institute, Zagreb, Croatia • [4]Faculty of Science, University of Zagreb, Croatia

https://doi.org/10.17952/38EPS.2026.P419

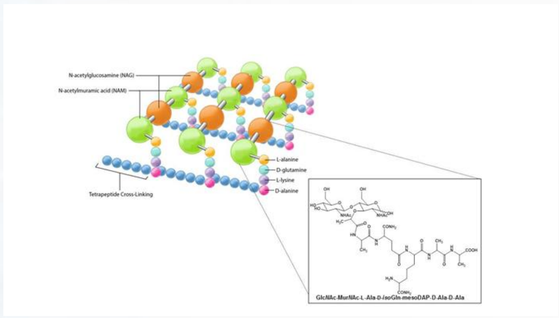
INTRODUCTION

Biomimetic nanomaterials mimic biological systems and offer versatile platforms for biomedical applications, including targeted drug delivery and personalized medicine. Peptidoglycan (PG), an essential component of bacterial cell walls, supports bacterial viability and activates host innate immunity. Building on the known recognition of PG fragments by WGA, this study quantitatively and mechanistically links soluble PGM binding and peptide-stem contributions with the effects of multivalent presentation. We designed PGM-functionalized biomimetic nanomaterials and investigated their interactions with selected lectins to elucidate glycan recognition relevant to host–pathogen interactions.

BACKGROUND & OBJECTIVE

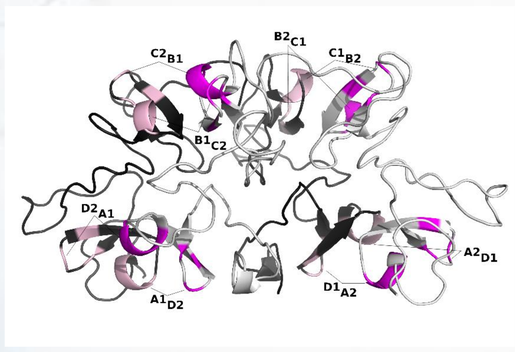
PGM is a chemically defined minimal fragment of DAP-type bacterial cell walls that combines a GlcNAc–MurNAc recognition motif with a native peptide stem.

This study investigates how WGA recognizes soluble PGM and how multivalent presentation influences binding.



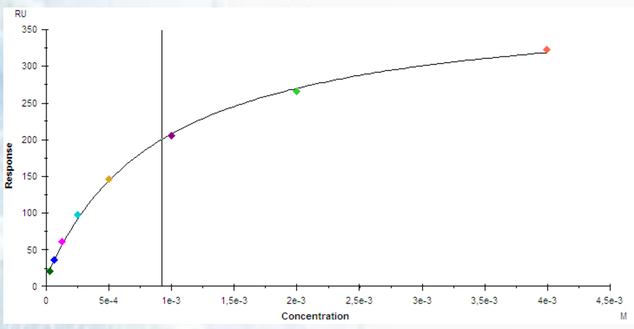
MULTISCALE APPROACH

SPR • ITC • fluorescence spectroscopy
Molecular modelling & 1 µs MD simulations
PGM-functionalized AuNPs and liposomes
DLS and TEM agglutination readouts



Multiple WGA binding sites enable molecular recognition and multivalent crosslinking.

MOLECULAR BINDING

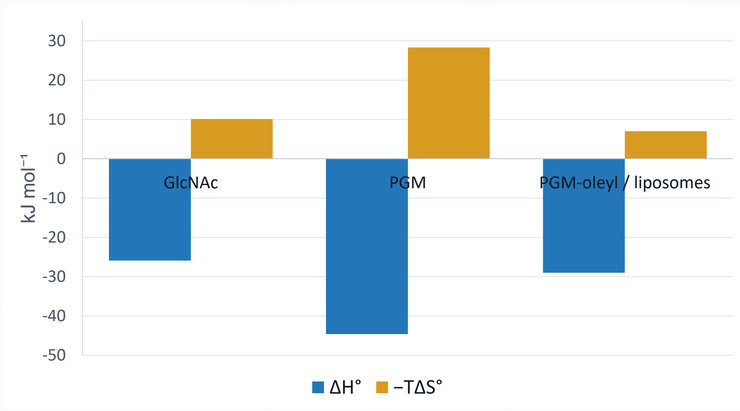


SPR apparent K$_D$ **9.3×10^{-4} M**

Rapid association/dissociation; equilibrium response fitted with a 1:1 steady-state model.

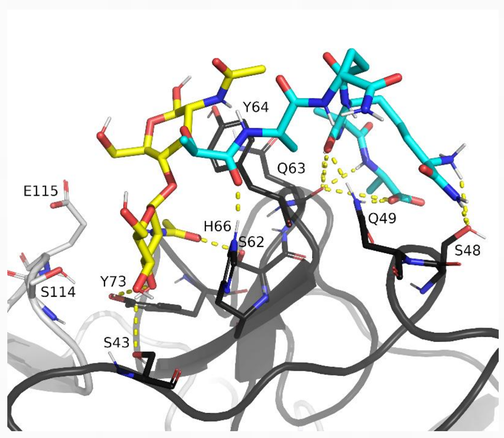
THERMODYNAMIC SIGNATURE

PGM and GlcNAc show similar millimolar affinity, but PGM binding is more exothermic and carries a larger entropic penalty.



Intrinsic K$_D$ (ITC)
GlcNAc 1.68 mM • PGM 1.44 mM

STRUCTURAL INTERPRETATION



The GlcNAc–MurNAc head group remains anchored in canonical WGA sites. The peptide stem samples multiple orientations and forms transient protein contacts.

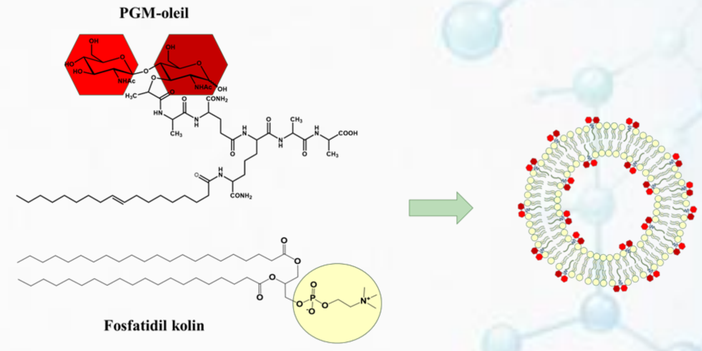
MECHANISTIC INSIGHT

The peptide stem modulates the energetic and conformational signature—without substantially increasing monovalent affinity.

LECTIN SELECTIVITY

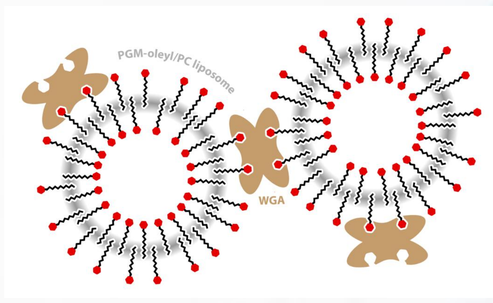
WGA showed reproducible PGM recognition. UEA-II and GS-II did not show comparable SPR responses: GlcNAc content alone does not predict PGM binding.

MULTIVALENT AMPLIFICATION ON BIOMIMETIC NANOSYSTEMS

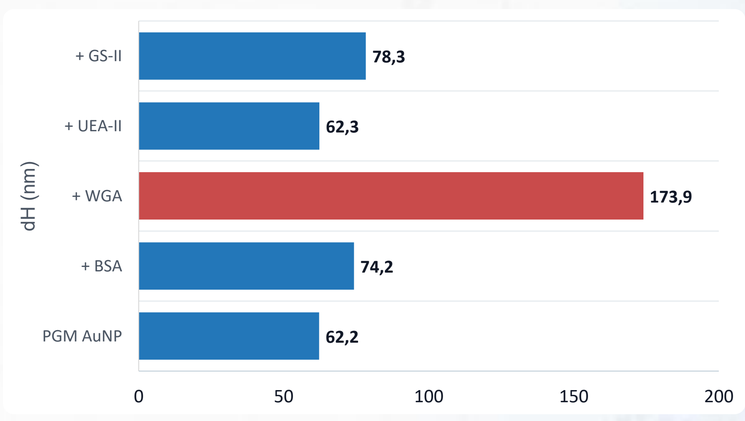


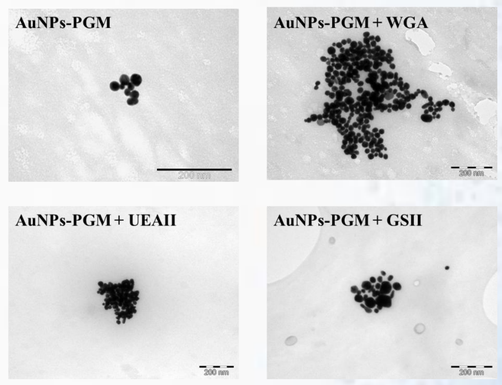
~10× higher apparent affinity
K$_D$ = 0.14 mM for PGM-oleyl/PC liposomes

Surface preorganization lowers the entropic cost and enables WGA-mediated bridging between lipid assemblies.



WGA DRIVES AuNP–PGM AGGREGATION





DLS and TEM confirm pronounced, time-dependent aggregation in the WGA–AuNP–PGM system.

CONCLUSIONS

- WGA primarily recognizes the GlcNAc–MurNAc head group, while the peptide stem forms heterogeneous, transient contacts that modulate the bound state.
- Peptide-stem interactions provide favorable enthalpy but impose an entropic penalty, resulting in an affinity comparable to GlcNAc yet a distinct thermodynamic and conformational response.
- Multivalent PGM presentation on liposomes and gold nanoparticles enhances functional avidity, crosslinking and agglutination.
- These findings provide a mechanistic bridge between molecular binding and recognition at complex biological interfaces and establish a foundation for the rational design of glyco-biomimetic materials and more biologically relevant models of lectin–bacterial cell-wall interactions.

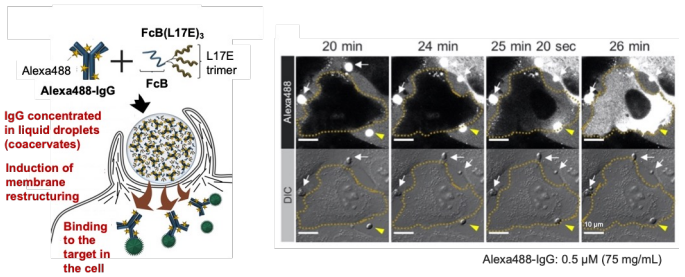
CONTACT • rfrkanec@unizg.hr

38th European Peptide Symposium
6-11th of September 2026, Vienna, Austria

Pullulan-Based Microcondensates with Cationic Peptides for Efficient Cytosolic IgG Delivery

J. Michibata[1], Y. Kawaguchi[1] & S. Futaki[2]
[1]Institute for Chemical Research and [2]Graduate School of Pharmaceutical Sciences, Kyoto University

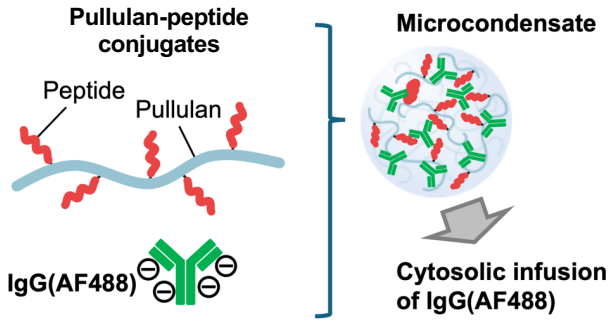
Introduction | Microcondensate-mediated delivery using L17E



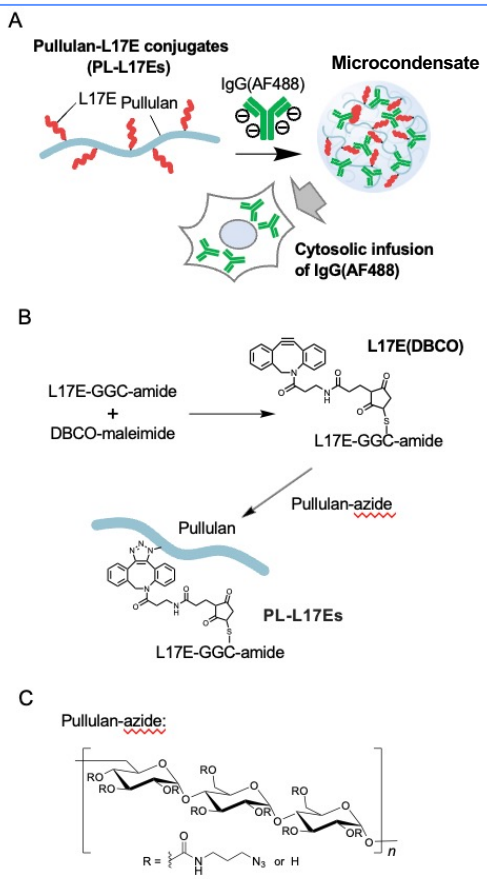
Alexa488-IgG: 0.5 μM (75 mg/mL)

L17E: IWLTALKFLGKHAAKHEAKQQLSKL-amide (Akishiba *et al. Nat. Chem.* **2017**, *9*, 751)
FcB: HWRGWV (Yang *et al. J. Pept. Res.* **2005**, *66*, 120)

Objective | To demonstrate the versatility of the approach

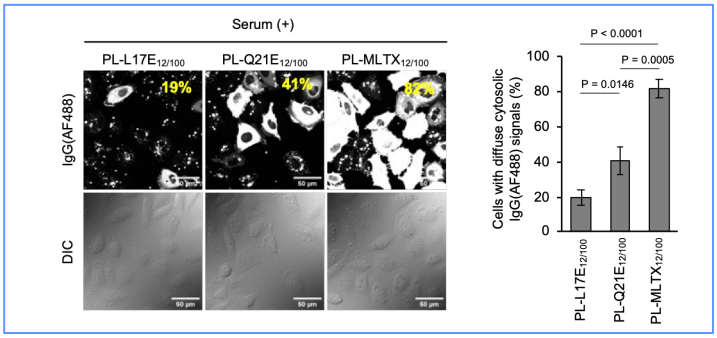


Results 1 | Preparation of the pullulan-peptide conjugates

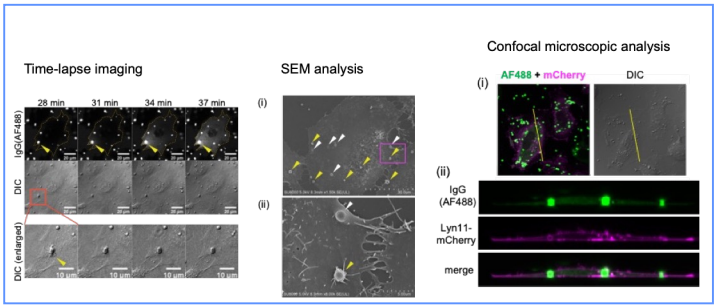


Membrane-permeabilizing peptides:
L17E: IWLTALKFLGKHAAKHEAKQQLSKL-amide
Q21E: IWLTALKFLGKHAAKHLAKQELSKL-amide
MLTX: IWLTALKFLGKHAAKHLAKQQLSKL-amide
MLTXRn: IWLTALKFLGKHAAKHLAKQQLSKL-R_n-amide (n=2~8)

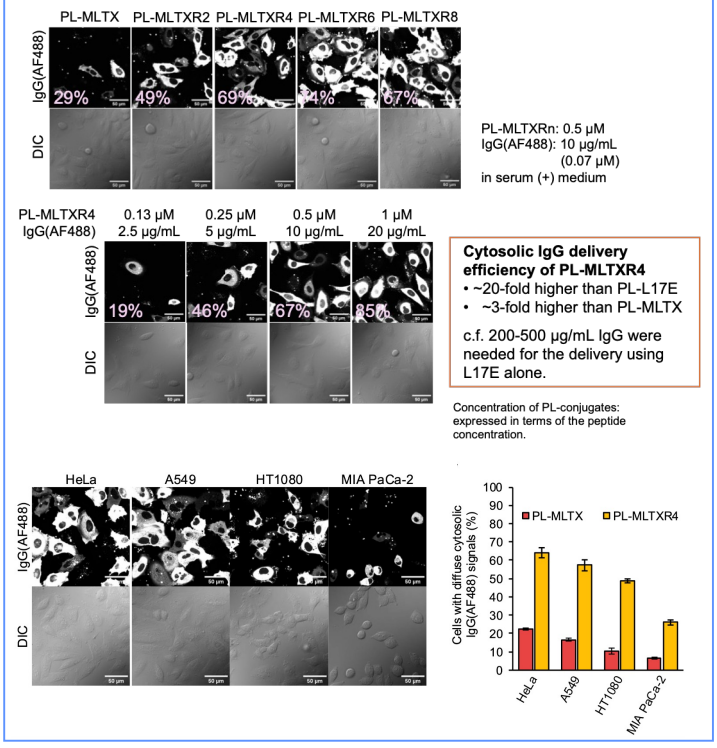
Results 2 | Evaluation of delivery efficiency



Results 3 | Modes of cellular uptake



Results 3 | PL-MLTXR4 exhibits the highest delivery activity



Summary

- Micrometer-sized coacervates (microcondensates) were formed simply by mixing PL-L17E with IgG labeled with IgG(AF488). These microcondensates exhibited efficient cytosolic infusion of IgG.
- Dynamic structural alterations of the cell membrane that entrapped the microcondensates, leading to cytosolic IgG infusion, were captured by confocal and electron microscopy.
- Replacement of L17E with M-lycotoxin (MLTX) or tetra-arginine-tagged MLTX (MLTXR4) further enhanced IgG delivery efficiency, reducing the required amounts of both IgG and the pullulan–peptide conjugate.

1) Michibata et al. *Bioconjug. Chem.* **2024**, *35*, 1888
2) Michibata et al. *Bioconjug. Chem.* **2025**, *36*, 1494
This work was supported by JSPS KAKENHI JP24H00051.

38th EPS
European Peptide Symposium
6 - 11th of September 2026
Vienna, Austria

Broad-spectrum antiviral activity of Ranalexin-1G against respiratory viruses.

Università degli Studi della Campania Luigi Vanvitelli

Laura Di Clemente[1], Carla Zannella[1,2], Francesca Palma[1], Roberta Della Marca[1], Marina Acunzo[1], Carla Capasso[1], Annalisa Chianese[1,3], Rosa Giugliano[1,4], Anna De Filippis[1,2], Massimiliano Galdiero[1,2]

[1]Department of Woman, Child and General and Specialized Surgery, University of Campania Luigi Vanvitelli, 80138 Naples, Italy
[2]UOC Virology and Microbiology, University Hospital "Luigi Vanvitelli", 80138 Naples, Italy
[3]Department of Life Sciences, Health and Health Professions, Link Campus University, 00165 Rome, Italy
[4]Department of Veterinary Medicine and Animal Production, University of Naples Federico II, 80137, Naples, Italy

https://doi.org/10.17952/38EPS.2026.P220

Email: laura.diclemente@unicampania.it

Introduction:

Respiratory viral infections represent a major global health burden, particularly in infants, older adults, immunocompromised individuals, and patients with underlying conditions. Despite their clinical impact and the continuous emergence of respiratory viruses, effective broad-spectrum antiviral strategies remain limited. Antimicrobial peptides (AMPs) are emerging as promising antiviral candidates due to their ability to interfere with multiple stages of the viral life cycle. Amphibian skin secretions are particularly rich in AMPs, which contribute to the natural defense of these animals against diverse pathogens. Several amphibian-derived peptides have already demonstrated antiviral activity against clinically relevant respiratory viruses.Ranalexin-1G is a cationic 20-amino-acid peptide belonging to the ranalexin family, previously characterized mainly for its antibacterial and antifungal properties. However, its antiviral potential remains largely unexplored. In this study, we investigated the antiviral activity of ranalexin-1G against a panel of clinically relevant respiratory viruses, including human coronavirus 229E (HCoV-229E), respiratory syncytial virus (RSV), human parainfluenza virus type 3 (HPIV-3), and measles virus (MeV).

Materials and Methods:

Cytotoxicity of ranalexin-1G was evaluated in Vero76, Vero/hSLAM, and human bronchial epithelial BEAS-2B cells by MTT assay and in human erythrocytes by hemolysis assays. Its antiviral activity was assessed against HCoV-229E and MeV by plaque reduction assay, and against RSV, poliovirus type 1 (PV-1), and HPIV-3 using tissue culture infectious dose ($TCID_{50}$) assay. Experiments included both simultaneous treatment of cells with virus and peptide (co-treatment) and pre-incubation of virus with the peptide (virus pre-treatment), with viral inhibition quantified as the reduction in plaque numbers or cytopathic effects relative to untreated infected cells. In addition, HCoV-229E replication was quantified by real-time quantitative PCR targeting the S and RdRp genes, to confirm the antiviral activity at the molecular level.

Results:

Ranalexin-1G showed selective antiviral activity against enveloped respiratory viruses, with minimal cytotoxicity and no significant hemolytic activity, indicating a favorable in vitro safety profile (Fig. 1). Strong inhibition was observed against HCoV-229E and MeV (Figs. 2-3), while the peptide was inactive against the non-enveloped PV-1 (Fig. 4), suggesting a role for direct interactions with the viral envelope. RSV showed moderate susceptibility, with the strongest activity at the two highest concentrations tested (50 and 25 µM) in the pre-virus assay, while in the co-treatment assay activity was mainly observed at 50 µM. HPIV-3 was only affected at 50 µM in both assays (Fig. 5). Notably, qPCR confirmed a significant reduction in HCoV-229E viral RNA, supporting inhibition of viral replication (Fig. 2).

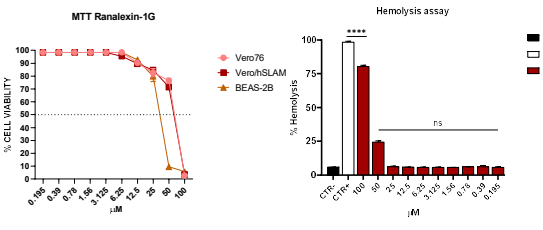


Figure 1. MTT assay on Vero76, Vero/hSLAM, and BEAS-2B cells and hemolysis assay of ranalexin-1G. Triton X-100 (20%) was used as the positive control (CTRL+), while untreated erythrocytes served as the negative control (CTRL−).

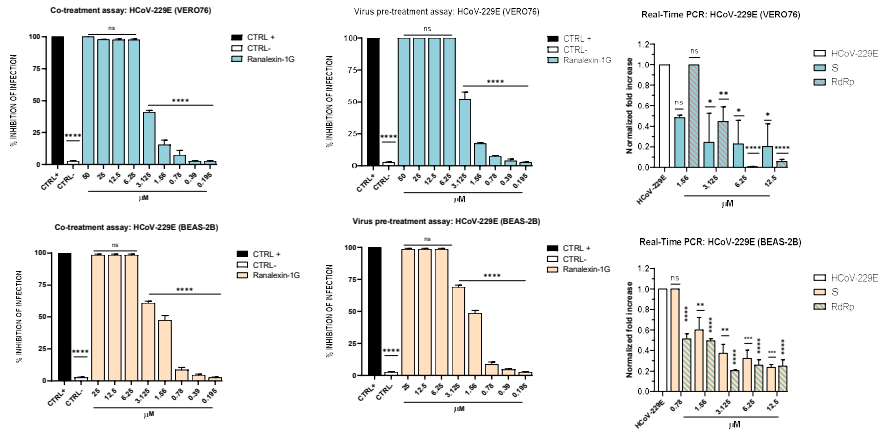


Figure 2. *Antiviral activity of ranalexin-1G against HCoV-229E in Vero76 and BEAS-2B cells, assessed by plaque reduction assay under co-treatment and virus pre-treatment conditions, and confirmed by RT-qPCR targeting the S and RdRp genes. Hylin-a1 (25 µM) was used as the positive control (CTRL+), while uninfected cells served as the negative control (CTRL−).*

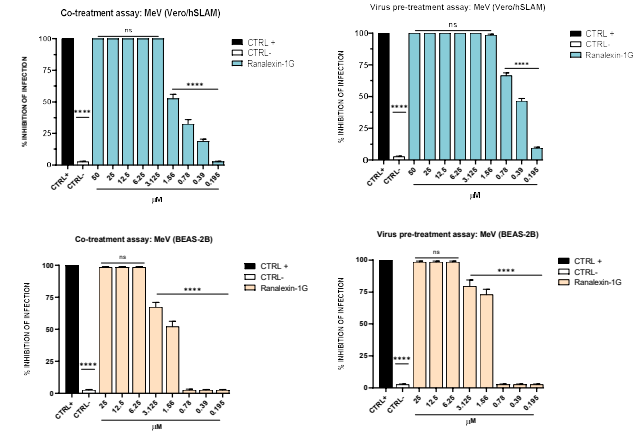


Figure 3. *Antiviral activity of ranalexin-1G against MeV in Vero76 and BEAS-2B cells, assessed by plaque reduction assay under co-treatment and virus pre-treatment conditions. Hylin-a1 (25 µM) was used as the positive control (CTRL+), while uninfected cells served as the negative control (CTRL−).*

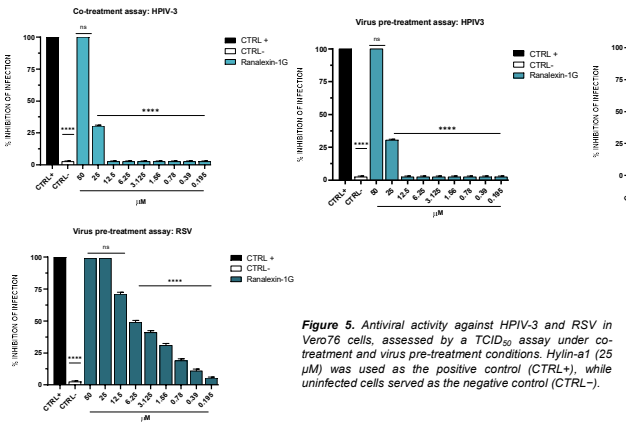


Figure 5. *Antiviral activity against HPIV-3 and RSV in Vero76 cells, assessed by a $TCID_{50}$ assay under co-treatment and virus pre-treatment conditions. Hylin-a1 (25 µM) was used as the positive control (CTRL+), while uninfected cells served as the negative control (CTRL−).*

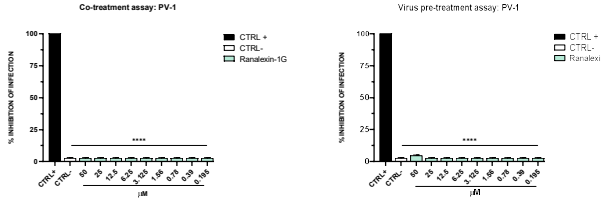


Figure 4. *Antiviral activity against a non-enveloped virus in Vero76 cells, assessed by a $TCID_{50}$ assay under co-treatment and virus pre-treatment conditions. The data showed that the peptide did not inhibit viral replication in either treatment. Pleconaril (2 µg/mL) was used as the positive control (CTRL+), while uninfected cells served as the negative control (CTRL−).*

Discussion and Conclusion.

Ranalexin-1G exhibits a selective, virus-dependent antiviral profile. Its strong activity against HCoV-229E and MeV, coupled with inactivity against non-enveloped PV-1, supports a role for direct interactions with the viral envelope. The reduction of HCoV-229E RNA confirms inhibition of viral replication, while the limited activity against RSV and HPIV-3 highlights virus-specific susceptibility. Together with its favorable safety profile, these findings support ranalexin-1G as a promising antiviral peptide candidate. Further studies will evaluate its activity in BEAS-2B cells against RSV and HPIV-3, while efforts will focus on identifying ranalexin-1G analogues or modified peptides with improved cytotoxicity and antiviral activity.

GRAPHENE OXIDE-PEPTIDE NANOFIBERS AS PLATFORMS FOR CELL BIOACTIVE RESPONSES

C. García Delgado[1], A. Sánchez-Temprano[1], I. Obregón-Gómez[1], MV. Sulleiro[1], A. Criado. [1], E. Pazos[1,2]

[1] CICA-Centro Interdisciplinar de Química e Bioloxía and Departamento de Química, Facultade de Ciencias, Universidade da Coruña, As Carballeiras s/n 15008, A Coruña, Spain.
[2] Oportunius, Axencia Galega de Innovación, 15702 Santiago de Compostela, Spain.

38th European Peptide Symposium • EPS 2026
https://doi.org/10.17952/38EPS.2026.P528

UNIVERSIDADE DA CORUÑA

CICA CENTRO INTERDISCIPLINAR DE QUÍMICA E BIOLOXÍA

1 BACKGROUND

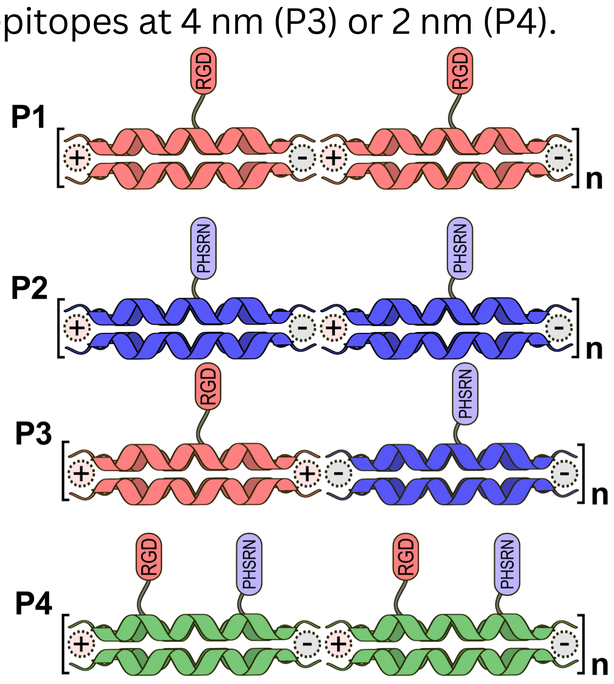
Cellular adhesion to the extracellular matrix (ECM) regulates essential processes, including proliferation, migration, and differentiation. Several studies have focused on mimicking the characteristics of the ECM by developing and modifying biomaterial surfaces, optimizing protein adsorption to promote early cell attachment and spreading. (1) Cellular interactions with the scaffold can be coordinated through peptide functionalization with the canonical RGD motif and its synergistic partner, PHSRN, two key fibronectin-derived epitopes that promote integrin-mediated cell adhesion. (2)

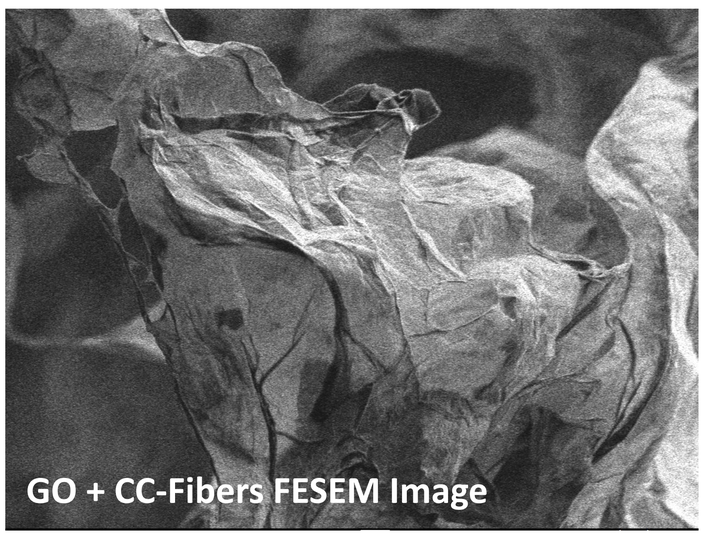
β-sheet peptides are commonly used as biomimetic scaffolds in tissue engineering owing to their ability to form nanofibrous hydrogels that mimic the ECM. However, their self-assembly mechanism offers limited control over the relative positioning of multiple functional domains, such as RGD and PHSRN. (3)

Coiled-coil (CC) peptides, in contrast, rely on a predictable heptad-repeat architecture that allows functional domains to be placed at defined, controllable distances, while also self-assembling into nanofibrous structures. (3,4) This combination of structural predictability and nanostructure formation makes coiled-coil scaffolds particularly well suited to reproducing the RGD–PHSRN synergy that drives integrin-mediated adhesion.

2 SCAFFOLD DESIGN AND CHARACTERIZATION

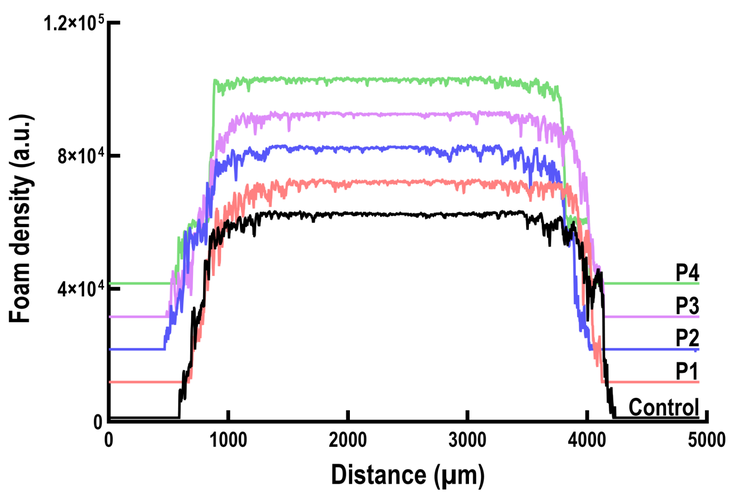
In this study, we designed a biomimetic scaffold based on coiled-coil tetramers that self-assemble into long nanofibers via electrostatic interactions and are functionalized only with RGDS (P1) or PHSRN (P2) epitopes, or with both epitopes at 4 nm (P3) or 2 nm (P4).





To evaluate cellular response, these nanostructures were integrated into graphene oxide (GO) foams, which were chosen as the supporting scaffold owing to their superior surface area, mechanical resilience, and biocompatibility. (5)

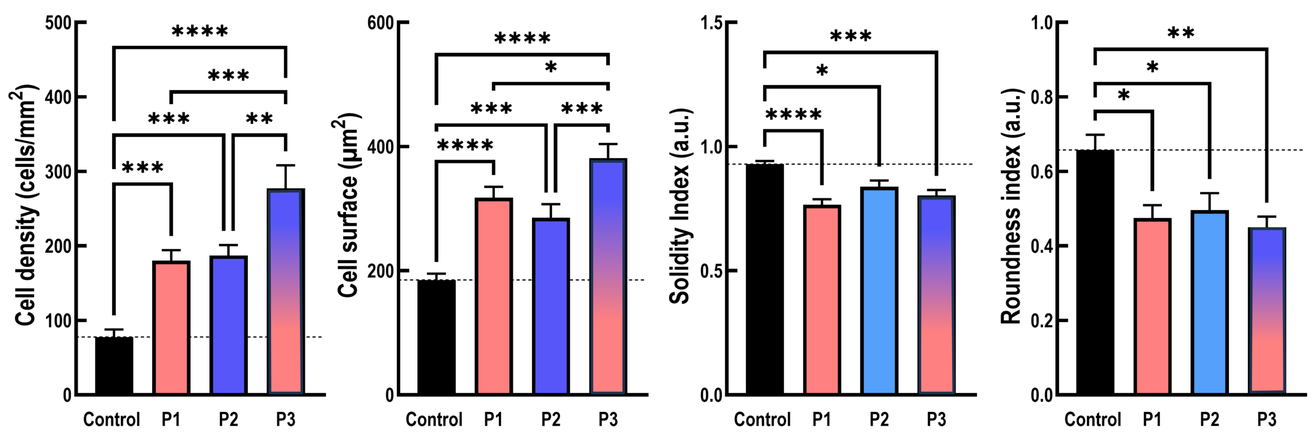
Hybrid and control GO foams had equivalent optical densities, confirming that the integration of peptide fibers does not alter the density or structural homogeneity of the foam, thus providing a consistent physical substrate for subsequent cell studies.

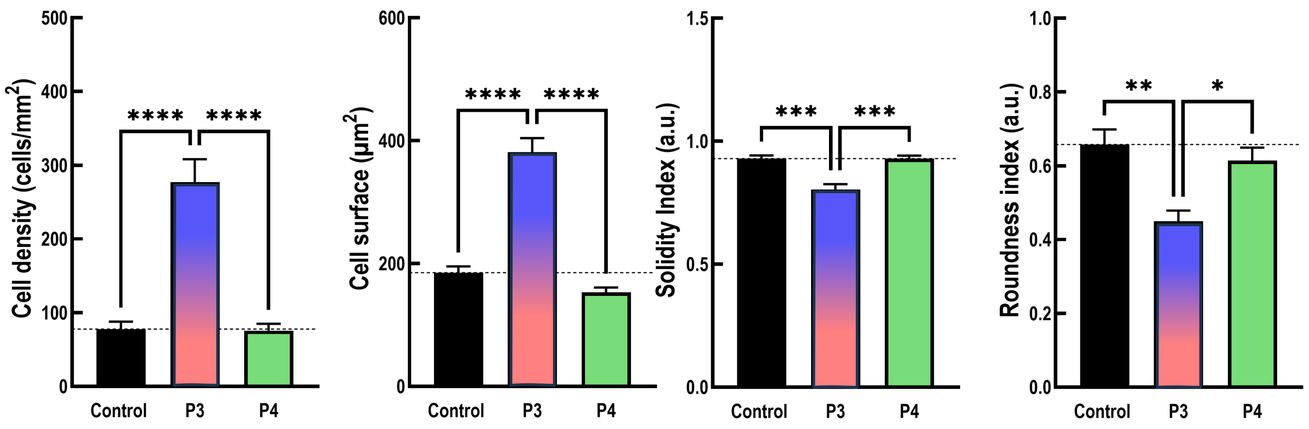


3 BIOACTIVITY OF THE HYBRID SCAFFOLDS

Spatial disposition determines the bioactivity of the scaffold: while functionalization with either the RGDS (P1) or PHSRN (P2) motifs increased the cell adhesion and spreading of SH-SY5Y cells compared to the control, the combination of both motifs at a distance of 4 nm (P3) resulted in a synergistic improvement.

In contrast, reducing the distance between RGDS and PHSRN to 2 nm (P4) severely compromised scaffold bioactivity, decreasing SH-SY5Y cell density and spreading to levels even lower than the control.





4 CONCLUSIONS

- Monofunctionalized RGDS or PHSRN peptide fibers significantly improved SH-SY5Y cell adhesion and spreading compared to the control.
- A precise 4 nm epitope spacing is essential for SH-SY5Y adhesion and spreading on GO scaffolds, whereas shorter distances compromise bioactivity.
- These functionalized GO scaffolds represent a highly tunable platform for advanced biomedical applications.

1. L. V. Tapia-López, M. A. Luna-Velasco, E. K. Beaven, A. S. Conejo-Dávila, M. Nurunnabi, and J. S. Castro, *ACS Biomater. Sci. Eng.,* 2023, **9**, 5270–5278.
2. F. Javed, S. S. A. Zaidi, S. F. Zaidi, A. R. Rauf, M. U. Munir and H. A. Santos, *J. Controlled Release*, 2024, **365**, 532–552
3. M. Rad-Malekshahi, L. Lempsink, M. Amidi, W. E. Hennink and E. Mastrobattista, *Bioconjugate Chem.*, 2016, **27**, 3–18.
4. M. D. Jorgensen and J. Chmielewski, Chem. Commun., 2022, 58, 11625–11636
5. P. Laaksonen and O. Ikkala, *Nanoscale*, 2020, **12**, 13214–13233.

Rede CIGUS
Centros de investigación do Sistema Universitario de Galicia

MINISTERIO DE CIENCIA E INNOVACIÓN
UNIÓN EUROPEA
FONDO EUROPEO DE DESARROLLO REGIONAL
AGENCIA ESTATAL DE INVESTIGACIÓN

erc
European Research Council
Established by the European Commission

CICA, as a center accredited for excellence within the Galician University System and a member of the CIGUS Network, receives subsidies from the Department of Education, Science, Universities, and Vocational Training of the Xunta de Galicia. Additionally, it is co-financed by the EU through the FEDER Galicia 2021-27 operational program (Ref. ED431G 2023/09)

Hydrogel formation via base-triggered conversion of a peptide progelator

ANA M. GARCIA,[1] Y. BERRUGA,[1] P. TOPALSKA,[1] P. PRIETO,[1] D. IGLESIAS[1]

https://doi.org/10.17952/38EPS.2026.P529

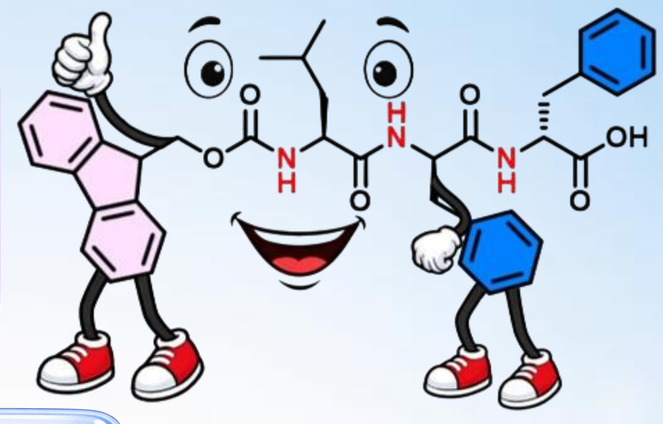
[1]Department of Inorganic, Organic and Biochemistry, Faculty of Chemical Sciences and Technologies, IRICA, University of Castilla La Mancha, 13071 Ciudad Real, Spain.

Email: **AnaM.Garcia@uclm.es**

INTRODUCTION

Short peptides are promising low molecular weight gelators (LMWGs) due to their biocompatibility and structural versatility, although controlling their gelation remains challenging. [1] Here, we present a chemically activated supramolecular hydrogel based on a heterochiral [2] tripeptide progelator (**Fmoc-L-Leu-D-Phe-D-Phe**), enabling spatiotemporal control over gel formation and generating architectures different from conventional pH-triggered systems. [3]

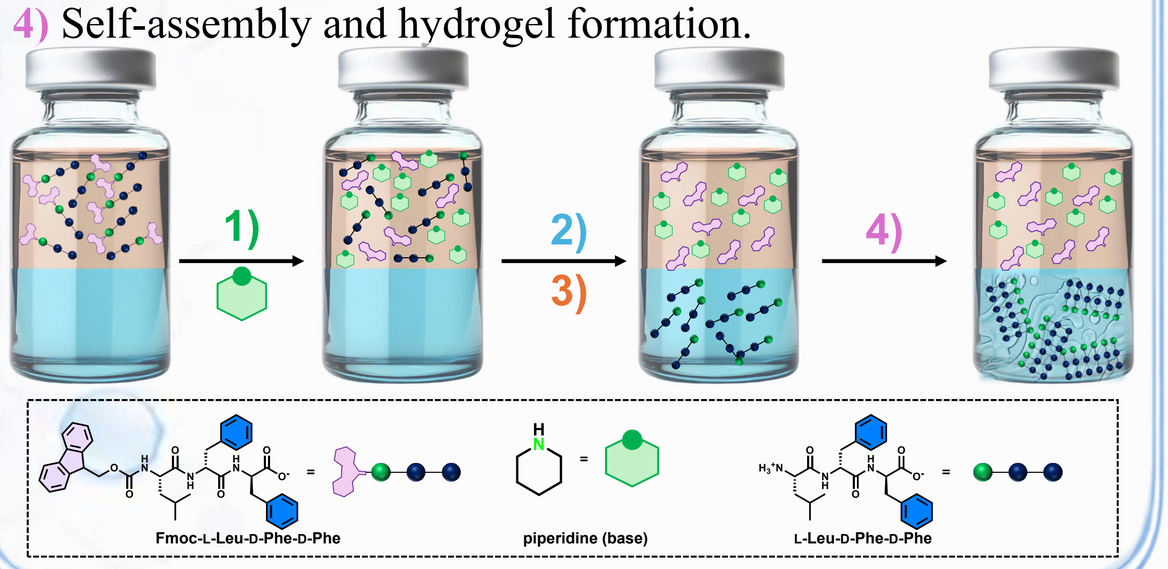
Fmoc-L-Leu-D-Phe-D-Phe



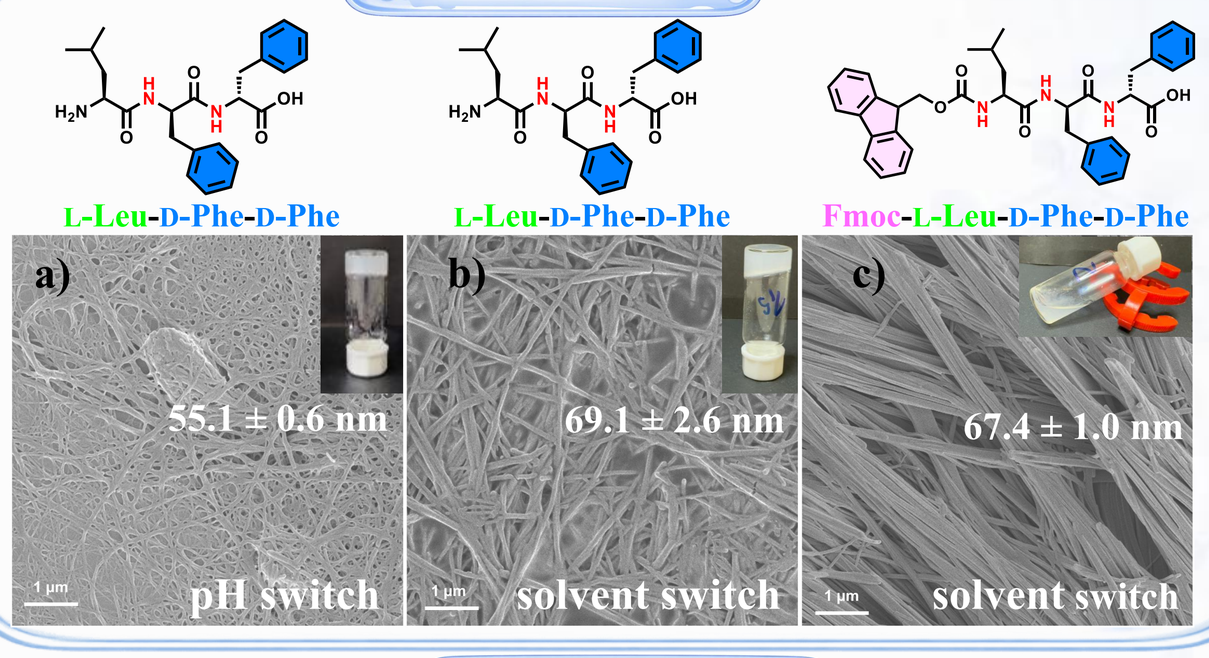
RESULTS AND DISCUSSION

Experimental setup

1) Biphasic system: ethyl acetate / phosphate buffer (pH 7.4).
2) Addition of piperidine triggers Fmoc removal, generating **L-Leu-D-Phe-D-Phe**.
3) Migration of **L-Leu-D-Phe-D-Phe** to the buffer layer.
4) Self-assembly and hydrogel formation.



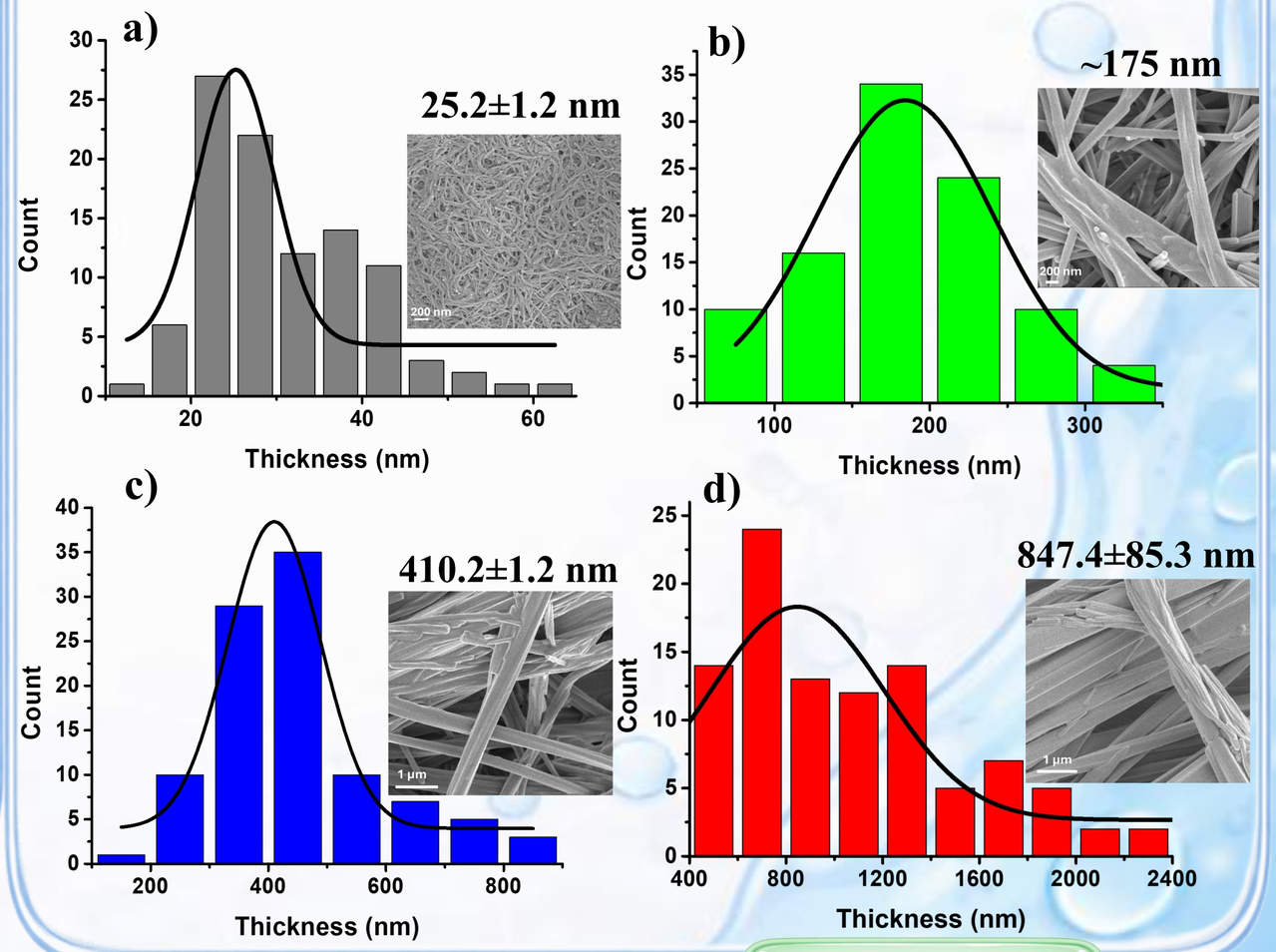
Gelation behavior



Gels morphology

- ❑ **Control (a)** ⇨ curved fibrils typical of peptide organogel.
- ❑ **1 eqs. (b)** ⇨ thicker fibrils than (**a**), due to partial Fmoc removal.
- ❑ **5 eqs. (c)** ⇨ thicker and more bundled fibrils than in (**b**).
- ❑ **10 equiv. (d)** ⇨ further increase in fiber diameter, more hetereogeneity than in (**c**).

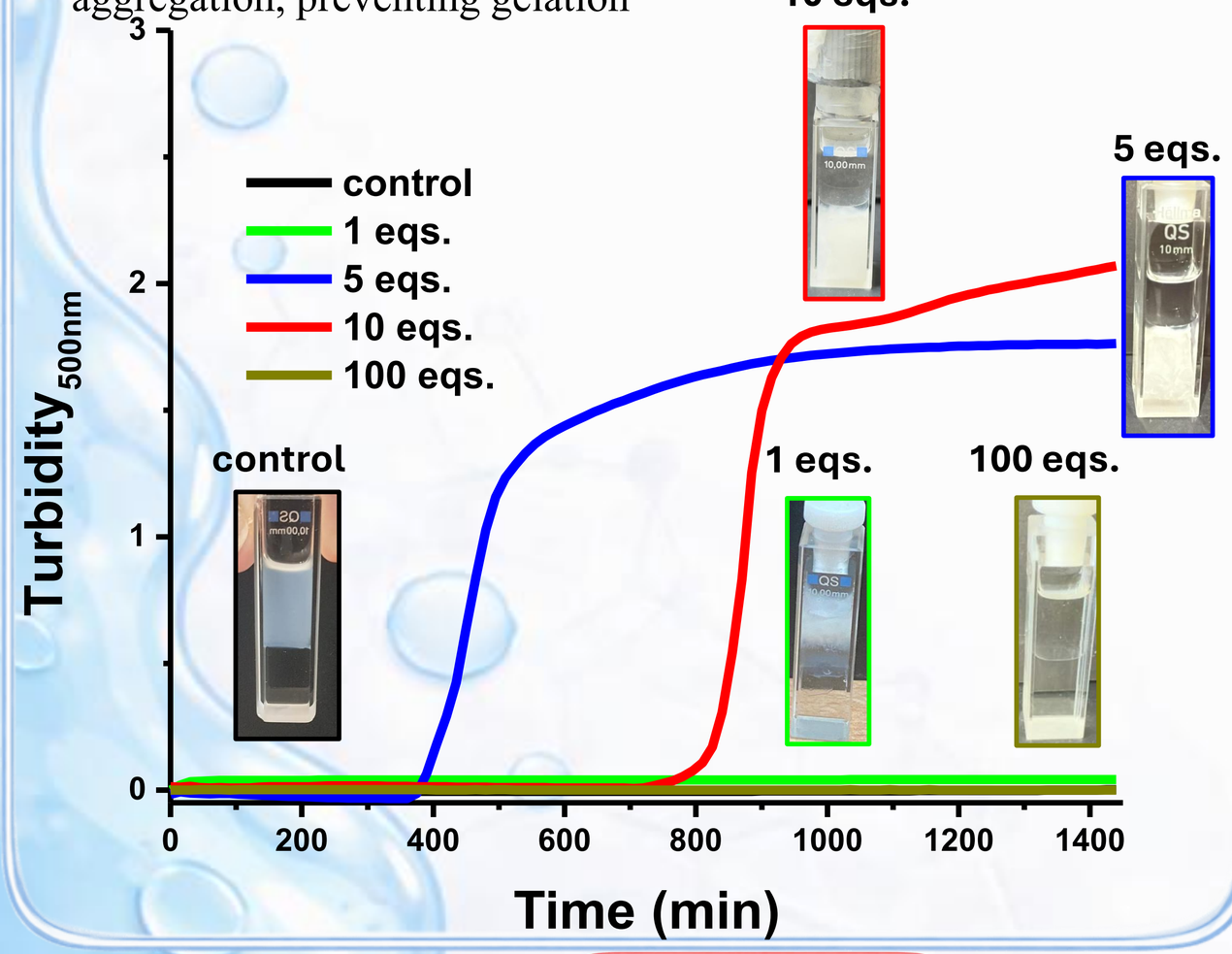
❑ **Biphasic ethyl acetate/phosphate buffer system yields significantly thicker fibrils than pH-switch assembly.**



UV-Vis kinetic studies

❑ **Turbidity** was monitored over time ⇨ evaluation of hydrogel formation with different equivalents of piperidine.

- ❑ **0–1 equivalents** ⇨ organogel formation
- ❑ **5–10 equivalents** ⇨ hydrogel formation
- ❑ **100 equivalents** ⇨ high aqueous pH suppresses peptide aggregation, preventing gelation



CONCLUSIONS

- Reaction-driven biphasic activation enables spatiotemporal control over peptide hydrogelation via in situ gelator generation.
- Hydrogelation occurs after base-mediated deprotection and peptide transport into the aqueous phase within a narrow operational window defined by kinetics, transport, and local pH.
- Distinct fibrillar morphologies reveal reaction-controlled supramolecular organization.

REFERENCES

[1] Draper, E. R.; Adams, *D. J. Chem,* **2017**, *3*, 390–410.
[2] Marchesan, S. ; *et al. Nanoscale* **2012**, *4*, 6752–6760.
[3] *10.26434/chemrxiv.15005985/v1*

Mirror-Image Random Nonstandard Peptides Integrated Discovery (MI-RaPID) Technology Yields Highly Stable and Selective Macrocyclic Peptide Inhibitors for Matrix Metallopeptidase 7

https://doi.org/10.17952/38EPS.2026.P325

Hiba Ghareeb*, Choi Yi Li*, Anjana Shenoy, Naama Rotenberg, Julia M. Shifman, Takayuki Katoh, Irit Sagi, Hiroaki Suga, Norman Metanis

Institute of Chemistry, Hebrew University of Jerusalem · University of Tokyo · Weizmann Institute of Science

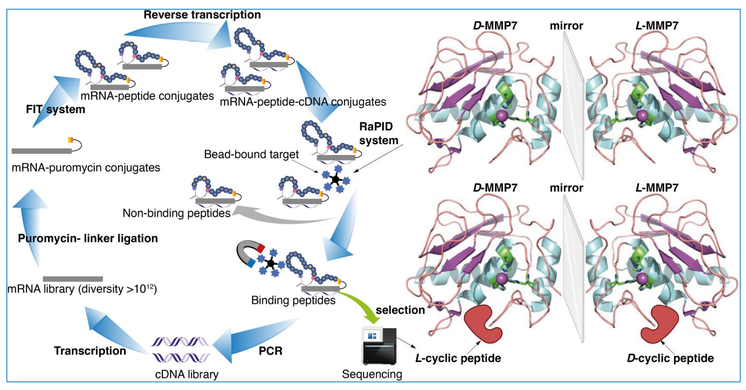
BACKGROUND & RATIONALE

MMP7 (matrilysin) is the smallest MMP, overexpressed in colorectal, gastric, pancreatic and lung cancers and associated with tumor metastasis and poor survival.

Key challenge: Conservation of active sites across 23 MMPs makes selective inhibition very difficult.

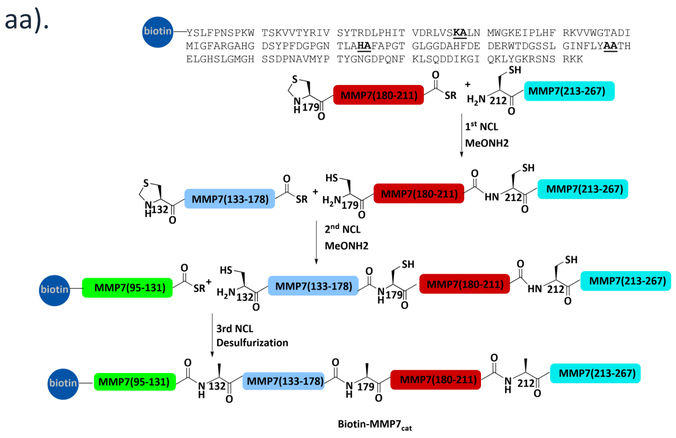
Existing MMP7 inhibitors: moderate selectivity, limited stability — no viable clinical candidate.

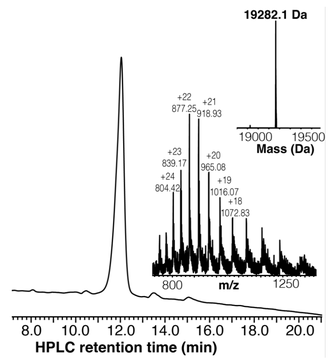
Our approach: Exploit *D*-amino acid chemistry to create innately protease-resistant macrocyclic peptide inhibitors with high selectivity.

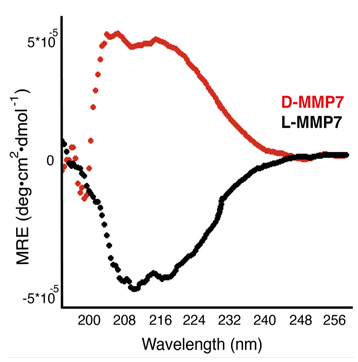


CHEMICAL SYNTHESIS OF L- and *D*-MMP7

Chemically synthesize MMP7 (mirror-image protein) via Native Chemical Ligation + desulfurization (4 segments, 173 aa).





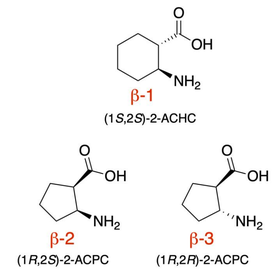


SELECTION & HIT ID

6 rounds of RaPID affinity selection against both *L*- and *D*-MMP7 immobilized on streptavidin-coated magnetic beads.

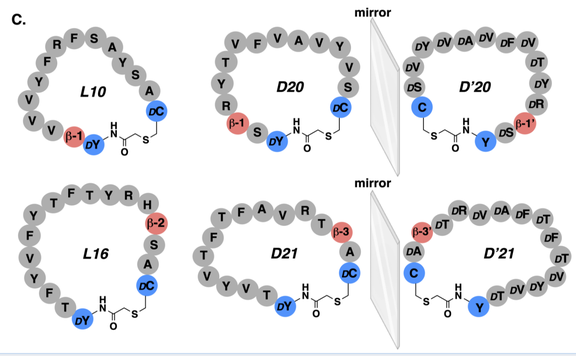
a.

1st	2nd U	2nd C	2nd A	2nd G	3rd
U	Phe	Ser	Tyr	β-3	U
	Leu	Ser	Stop	D-Cys	C
					A
					G
C	β-2	Pro	His	Arg	U
	Leu	Pro		Arg	C
					A
					G
A	β-1	Thr	Asn	Ser	U
	ClAcD-Tyr	Thr	Lys	Arg	C
					A
					G
G	Val	Ala	Asp	Gly	U
	Val	Ala		Gly	C
					A
					G



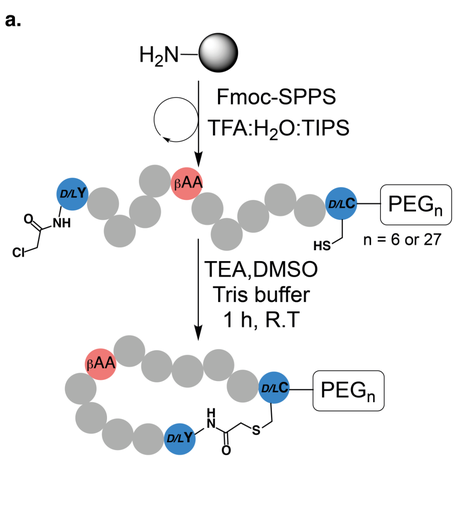
Top hits selected for synthesis:

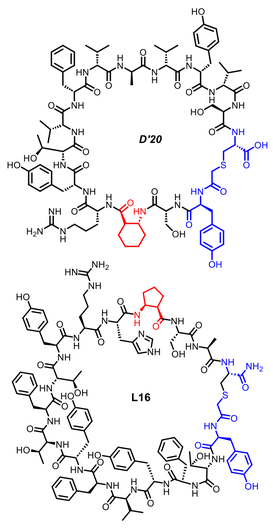
- L10, L16 (L-MMP7 selection)
- D20, D21 (D-MMP7 selection) → mirror-image forms *D'20, D'21*

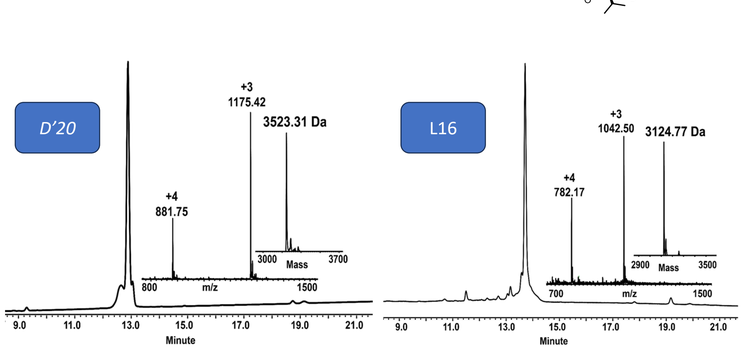


LEAD COMPOUND SYNTHESIS

a.

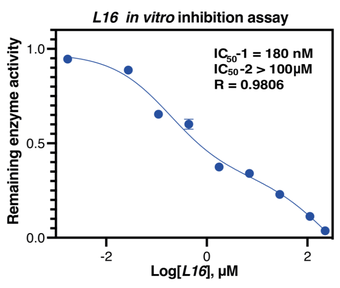




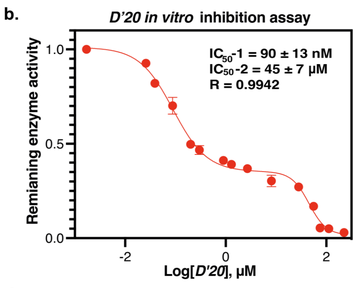


LEAD COMPOUND: *D'20*

IC_{50} = 90 nM vs MMP7

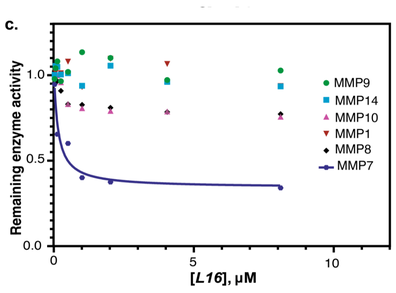


b.

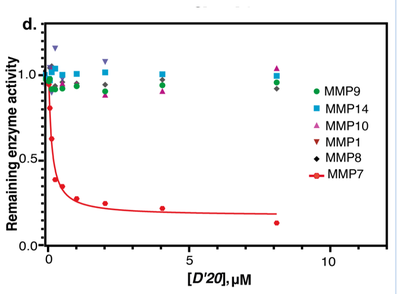


D`20 >60× selectivity over MMP1/8/9/10/14

c.



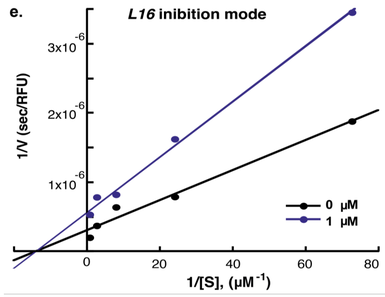
d.



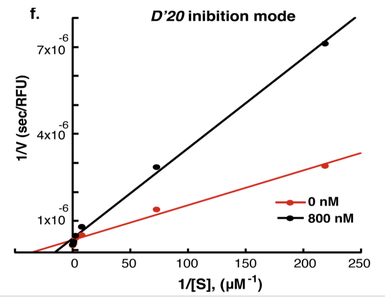
LEAD COMPOUND: *D'20*

Competitive inhibition mode

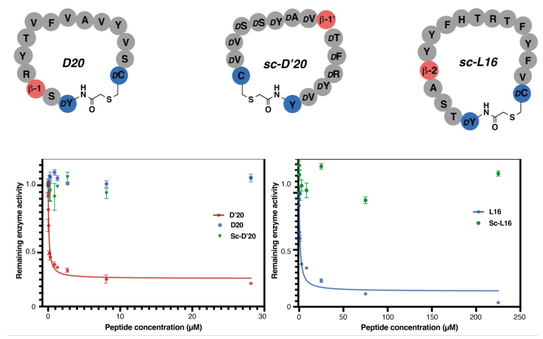
e.



f.



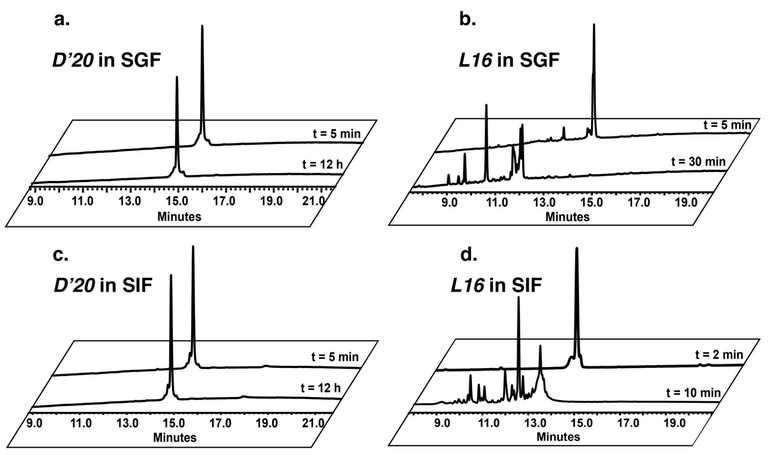
Sequence and Stereospecific



STABILITY — SERUM & GI

Human serum: Both *D'20* and L16 are stable for >24 h.

Condition	*D'20*	L16
Simulated Gastric Fluid (SGF, pH 1.3, pepsin)	>12 h ✓	<30 min ✗
Simulated Intestinal Fluid (SIF, pH 6.8, pancreatin)	>12 h ✓	<10 min ✗



CELL MIGRATION INHIBITION

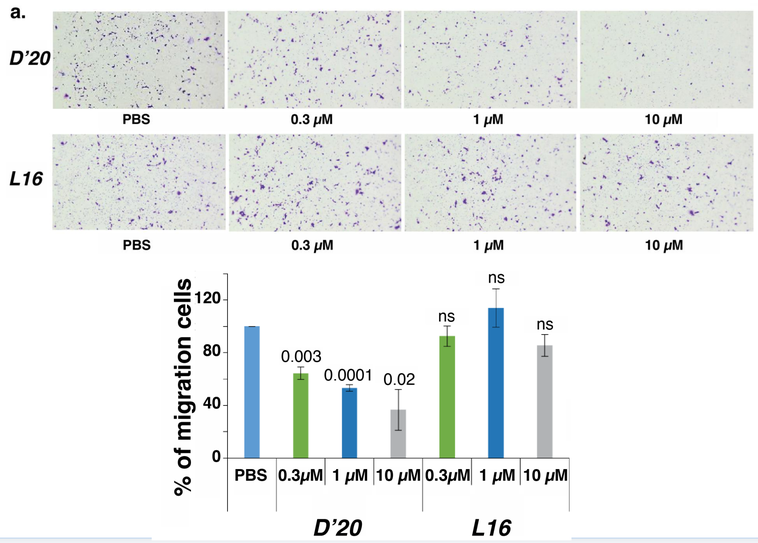
Pancreatic cancer cell line CFPAC-1 (endogenous MMP7 expression). Transwell migration assay with FBS chemoattractant (18 h).

D'20 migration IC_{50} ≈ 1 μM

Comparable to GSM-192, a highly selective anti-MMP7 monoclonal antibody (IC_{50} = 132 nM enzymatic inhibition).

No effect on cell proliferation or viability at tested concentrations — *D'20* specifically targets migration.

a.



CONCLUSIONS

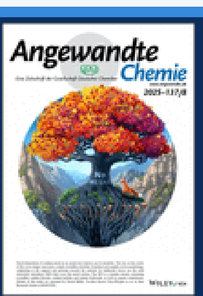
▶ MI-RaPID enables de novo discovery of fully D-amino acid macrocyclic inhibitors — bypassing the D-amino acid incorporation limit of standard RaPID.

▶ *D'20* is potent (IC_{50} 90 nM), selective (>60× over related MMPs), stereospecific, and sequence-specific.

▶ Exceptional stability in human serum and GI fluids (>12 h) makes *D'20,* a key advantage over L-peptide comparators.

▶ *D'20* inhibits pancreatic cancer cell migration (IC_{50} ~1 μM) without affecting proliferation or viability.

▶ MI-RaPID is a broadly applicable platform — not limited to MMPs — for any overexpressed disease target.



Ghareeb, Hiba, Choi Yi Li, Anjana Shenoy, Naama Rotenberg, Julia M. Shifman, Takayuki Katoh, Irit Sagi, Hiroaki Suga, and Norman Metanis. "Mirror-image random nonstandard peptides integrated discovery (MI-RaPID) technology yields highly stable and selective macrocyclic peptide inhibitors for matrix metallopeptidase 7." *Angewandte Chemie* 137, no. 8 (2025): e202414256.

PCT/IL2025/050321

Dreaming. Creating. Innovating. Since 1925

THE HEBREW UNIVERSITY OF JERUSALEM

P270

https://doi.org/10.17952/38EPS.2026.P270

universität wien
Vienna Doctoral School of Pharmaceutical, Nutritional and Sport Sciences

Vienna Doctoral Schools

Can we Confidently Sequence the „Peptide Dark Matter“? Reaching a Consensus for De Novo Peptide Sequencing

Sebastian Johannes Eder[1,2,3], Manuela Schmidt[1,2], David Gomez-Varela[1,2]

1. University of Vienna, Division of Pharmacology and Toxicology,
2. University of Vienna, Bruker Daltonics Center of Excellence for Metaproteomics

Overview

Database search controls error by target-decoy competition. De novo sequencing has none, so it returns model-specific confidence scores rather than an error rate, and those scores are not calibrated. Any threshold placed on them is arbitrary, which leaves the unidentified majority of a run unquantifiable. Here I present QUORUM, a model to effectively increase accuracy and FDR control for de novo sequencing

How it works

CasaNovo[1], InstaNovo[2] and PrimeNovo[3] sequence the same spectrum independently. A gradient-boosted model scores every aligned residue from what all three proposed there together with the peak evidence supporting it and assembles fourth candidate. All four are described by one identical feature set, dominated by the ion evidence class at each boundary and by agreement between observed and predicted retention time. A selector, based on a logistic regression, selects the best one and assigns a probability score.

The consensus beats every model that built it

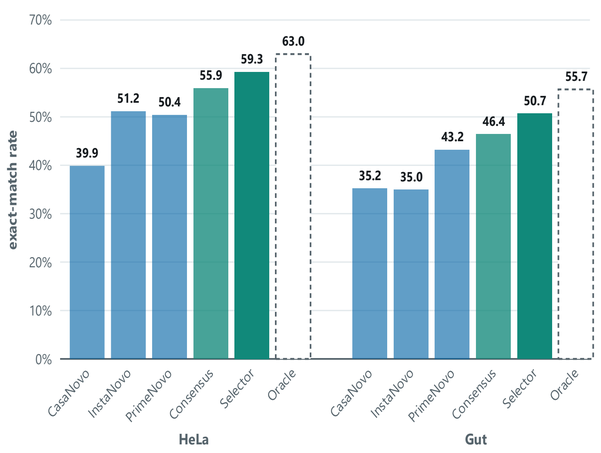


Fig. 1: Model accuracy against database-search-derived peptides. Measured on a HeLa lysis sample and a Gut fecal metaproteome fraction. Consensus refers to the assembled candidate. Oracle refers to the maximum possible percent, where at least 1 of the models predicted the correct peptide.

Calibration is conservative off training

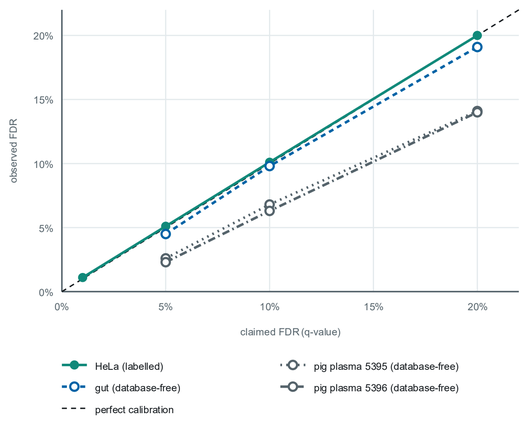
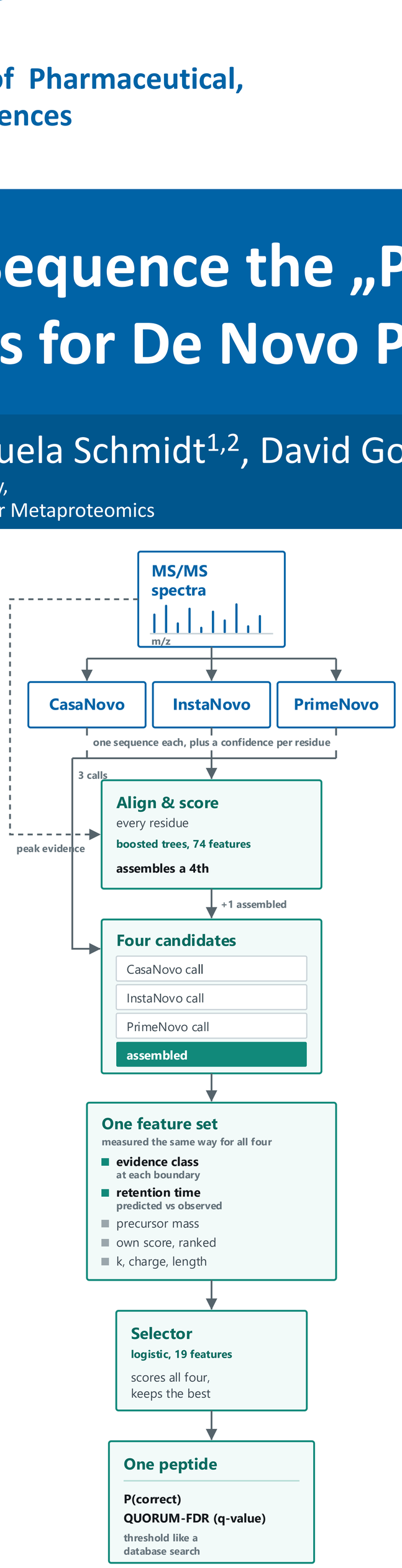


Fig. 2: Claimed against delivered false discovery rate. Within a dataset a nominal 5% delivers 5.1%. Transferred truth-free to a dataset the selector had never seen (pig plasma and gut metaproteomics) it delivers 3.7% - 4.9%, conservative at every cut, because nothing is refitted there except the base rate, by an estimator known to under-shoot.



More peptides at a controlled error rate

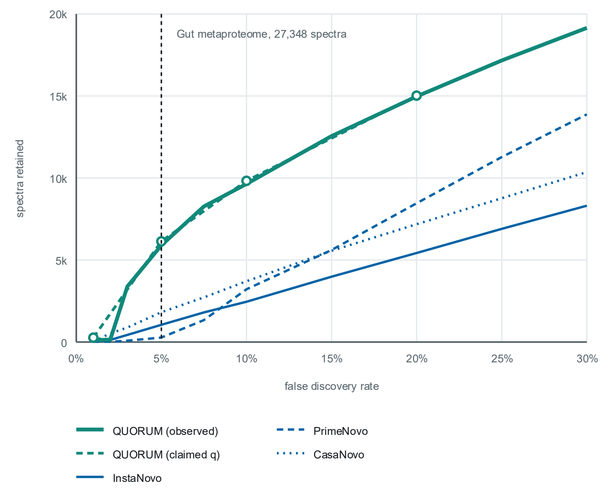


Fig. 3: Spectra retained against delivered false discovery rate. At a 5% delivered error rate QUORUM returns 5,893 gut spectra where the best model returns 1,814. The model curves use a threshold derived from ground truth, which is unavailable in practice without a database, so they flatter the models rather than quorum.

Benchmark FDR against Winnow

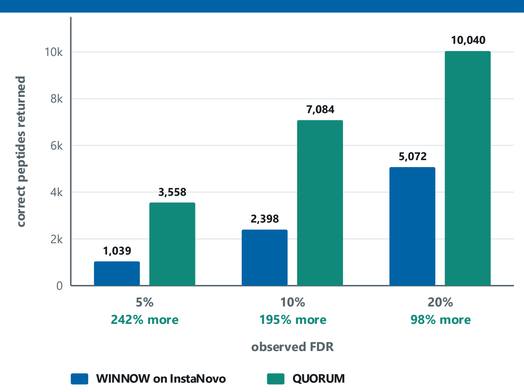


Fig. 4: Correct peptides at a matched error rate. Gut sample. Both tools run without a database, then graded on the 18,756 spectra both scored. Winnow[4], another FDR-rescorer, rescores InstaNovo, the only one of our three models whose output it can, and both score the same peptides. Both models deliver a conservative FDR, but QUORUM delivers over 240% more peptides.

Confirmation of QUORUM predicted peptides not found by FragPipe database search

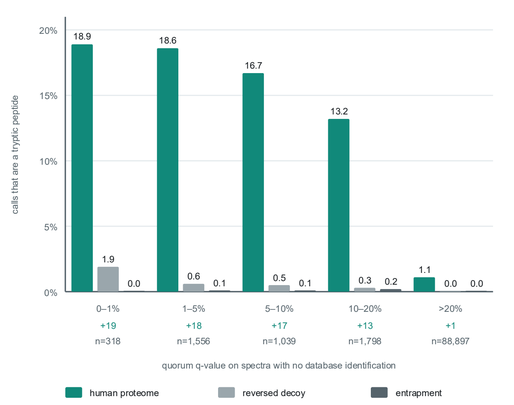


Fig. 5: Tryptic entrapment validation of calls on spectra no database search identified. HeLa, 38,039 spectra the database search never identified. Each call is looked up as a tryptic peptide in the human database and in two nulls: the reversed decoy half, and Arabidopsis plus yeast with every human-shared peptide removed. All three matched at 2,369,611 peptides.

Conclusion

QUORUM follows the approach PostNovo[5] introduced in 2018, combining several de novo models under FDR control. What differs is the evidence it runs on: the ion evidence class at each boundary and retention time, neither of which PostNovo used, and a full-length candidate assembled residue by residue rather than a consensus subsequence.

With no database and no PSM table at any stage, the pipeline reaches 50.7% exact matches on unseen gut metaproteomics, and 52.6% on a pig plasma sample from a species absent from training. Validation stands at two sample types. A synthetic community of known composition is the next test and would make the currently unmeasurable fraction gradable.

University of Vienna
Vienna Doctoral School of Pharmaceutical, Nutritional and Sport Sciences
Department of Pharmaceutical Sciences

Sebastian Johannes Eder:
sebastian.johannes.eder@univie.ac.at

References:

1. **Yilmaz M et al. Casanovo. Nat Commun 2024 (orig. ICML 2022)**
2. **Eloff K et al. InstaNovo. Nat Mach Intell 2025**
3. **Zhang et al. N-PrimeNovo. Nat Commun 2025**
4. **Mabona A et al. Winnow, arXiv 2025**
5. **Miller SE et al. PostNovo. J Proteome Res 2018**

UNIVERSITÄT LEIPZIG
Medizinische Fakultät

Tom Götze-Ebert
Institute for Drug Discovery
Brüderstr. 34, 04103 Leipzig
+49 341 97 11817
tom.goetze@medizin.uni-leipzig.de



From Monomers to Dendrimers: Novel Synthetic Strategies for Highly Branched Peptide Nanostructures for Next-Generation Drug Delivery

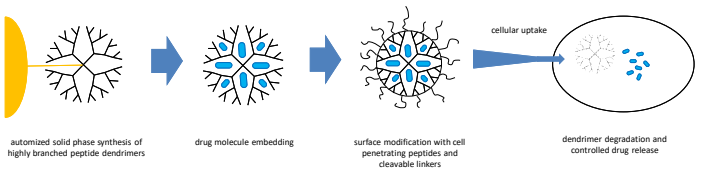
Tom Götze-Ebert[1], Frida Fritzsche[1], Christina Lamers[1]
[1] Institute for Drug Discovery, Faculty of Medicine, University Leipzig
https://doi.org/10.17952/38EPS.2026.P034

MOTIVATION

DENDRITIC PEPTIDES ARE PROMISING DRUG DELIVERY SYSTEMS

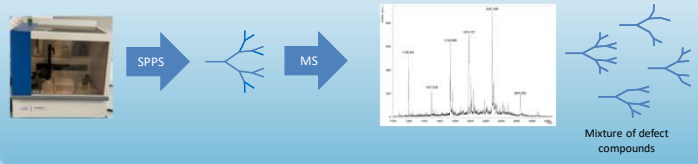
- readily available and inexpensive starting materials
- easy access through automated solid-phase peptide synthesis
- customizable structural design through selection of amino acids
- degradable into non-toxic metabolites through endogenous enzymes

PROJECT OUTLINE



CHALLENGE

Standard SPPS for peptide dendrimers bears high risk of structural defects



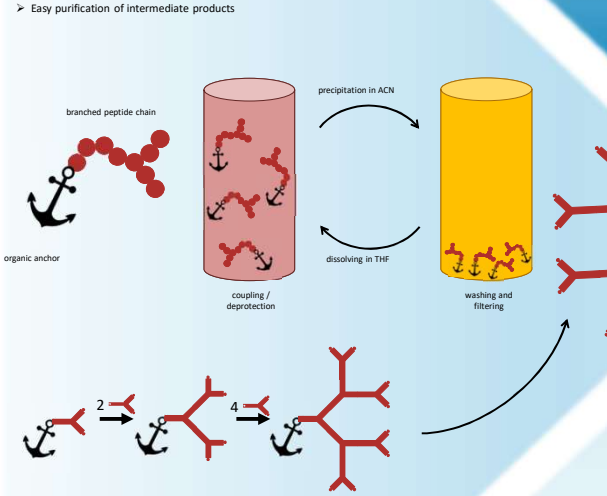
NEW APPROACH

Double-Stage Convergent Growth

- Batch Synthesis of branched Monomers in large scale
- Reduced coupling steps
- Easy purification of intermediate products

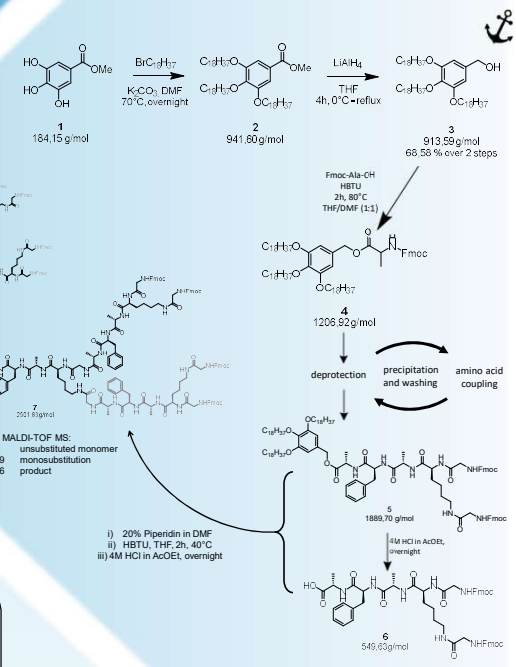
Key Findings

- 1st Generation dendrimers are built reliably
- Weakspots near branching centres
- Defect probability increased with higher degree of branching



SYNTHETIC WORK

Tag-assisted LPPS was applied for the synthesis of peptide dendrimers

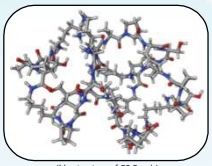


Benefits

- Less coupling steps minimize risk of structural defects
- High dilution prevents intermolecular agglomeration during coupling steps
- On-line reaction control is possible through mass spectrometry or TLC

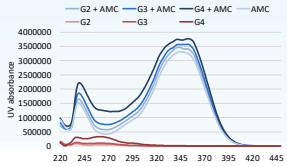
APPLICATION

Embedding of small organic molecules


possible structure of G2 Dendrimer

AMC: 7-Amino-4-methylcoumarin
G2: $((KSAP)_2KSAP)_2KSAP$
G3: $(((KSAP)_2KSAP)_2KSAP)_2KSAP$
G4: $((((KSAP)_2KSAP)_2KSAP)_2KSAP)_2KSAP$

Sample preparation:
1. 10 µmol AMC in DMF
2. 2 µmol dendrimer in EtOH
3. 1:8 dilution with water
4. Centrifugation
5. Analyze supernatant



Key Findings

- Presence of a dendrimer increases UV absorbance at 345 nm up to 13% with a 4th generation dendrimer
- UV absorbance increases with dendrimer generation

Key Findings

- Tag-assisted LPPS works for the synthesis of branched peptides.
- High temperatures promote reaction conversion.
- Still incomplete coupling ocurring.

SUMMARY

- ✓ Synthesis of branched peptide monomers through automated solid phase synthesis leads to deletions
- ✓ Double-stage Convergent Growth as an alternative method for peptide dendrimer synthesis
- ✓ Tag-assisted LPPS has been applied successfully for peptide dendrimer synthesis
- ✓ Peptide dendrimers were able to stabilize AMC in an aqueous solution

REFERENCES

1. P. Milla, F. Dosio, L. Cattel, Curr Drug Metab. 2012, 13(1), 105-19
2. R. V. Cardoso, P. R. Pereira, C. S. Freitas, V. M. F. Paschoalin, Pharmaceutics 2022, 14(12), 2808
3. M. Liu, X. Fang, Y. Yang, C. Wang, Front Bioeng Biotechnol. 2021, 9, 701504
4. J. P. Tam, F. Zavala, J Immunol Methods 1989, 124(1), 53-61
5. T. M. El-Dine, M. Lavayssiere, ChemistryEurope 2024, 2, e202300007
6. Y. Okada, H. Suzuki, J. Org. Chem. 2013, 78, 2, 320 – 327
7. N. Chevrollier, A. Dougha, C. Ye et al., Nucleic Acids Research 2026, W287-W294

Microfluidics-Driven Assembly of Sonoresponsive Peptidic Nanoparticles for Ultrasound-Mediated Gene Delivery

Guy GOUARIN*, Vicentiu MORARU and Samir CHERKAOUI

BRACCO SUISSE SA, Plan-les-Ouates, Switzerland
https://doi.org/10.17952/38EPS.2026.P389
guy,.gouarin@bracco.com

BRACCO
LIFE FROM INSIDE

INTRODUCTION

Context – Building on S. Medina work,[1] Bracco previously explored nanopeptisomes, a novel class of peptide-based phase-change nanodroplets formulated with high-boiling-point perfluorocarbons (PFCs) for ultrasound-mediated gene delivery.[2,3]

Problematic – Extending this platform to low-boiling-point PFCs, which offer improved acoustic responsiveness allowing sonoporation at reduced acoustic pressure , remains challenging due to their high volatility and the need to preserve nanoparticle integrity during formulation.

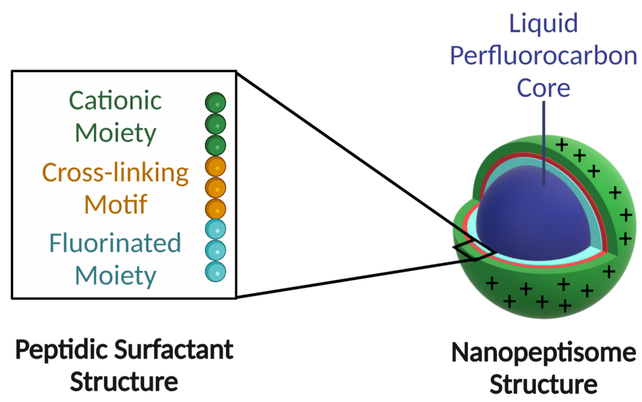
Solution – By combining **microfluidic assembly** with a **disulfiram-based** (DSF) **peptide cross-linking strategy**,[4] we successfully formulated stable low-boiling-point PFC Nanopeptisomes, overcoming the volatility-associated formulation challenges while maintaining ultrasound responsiveness.[5]

NANOPEPTISOME DESIGN

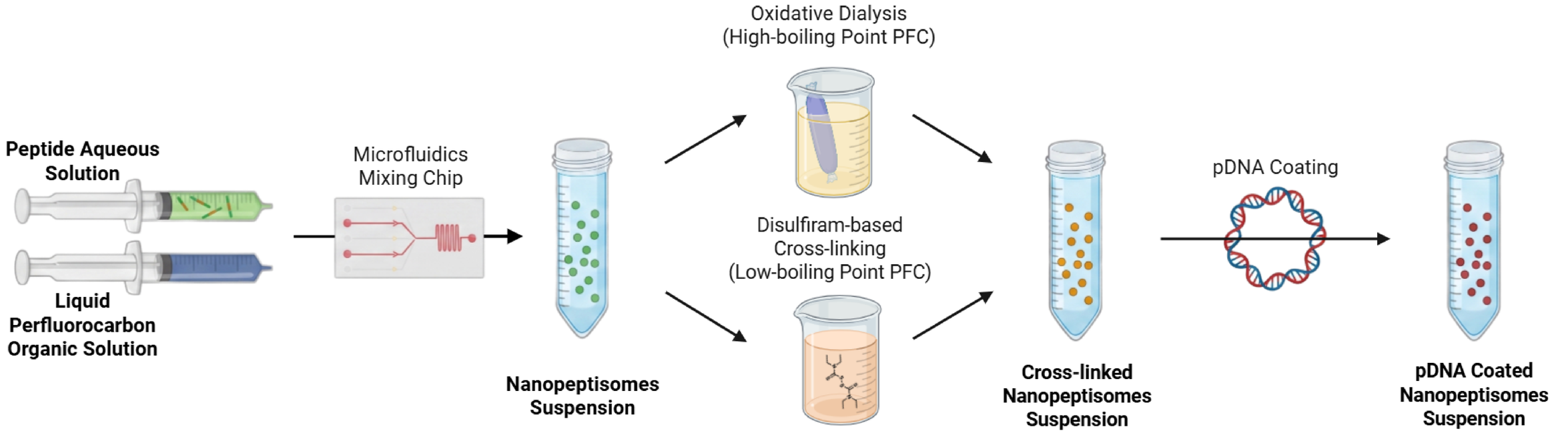
Hydrophilic cationic moiety using either Cell Penetrating Peptide (CPP) or Nuclear Localization Sequence (NLS) to bind anionic payload such as genetic material

Cross-linking region to enhance the NPP stability.

Hydrophobic fluorinated tail stabilize the PFC liquid core.



NANOPEPTISOME PREPARATION



Formulation

- Shell: Peptidic Surfactants
- Core:
  - C_6F_{14} Perfluorohexane PFH (b.p. 56°C)
  - C_5F_{12} Perfluoropentane PFP (b.p. 29°C)
  - C_4F_{10} Perfluorobutane PBP (b.p. - 2°C)

Microfluidics Process Settings

- **Flow Rate Ratio (FRR):** Volumetric ratio of the aqueous & organic phases → 2:1 (aqueous : organic)
- **Total Flow Rate (TFR):** Total speed at which both fluid streams are injected → 10 mL/min

Cross-linking

- **Oxydative Dialysis:**
  - Oxidation: Aqueous DMSO (2.5% v/v),
  - Purification: 5% Glucose dialysis
- **Disulfiram-based:**
  - Oxidation: 5% Glucose, 5 eq DSF, 4°C
  - Purification: Centrifugation

pDNA Coating

- **Plasmid:** pCPG-hCMVSCEP-LucSH
- **Solvent:** 5% Glucose
- **Incubation:** 15 min, r.t.
- **NPP Concentration:** 10^9 p/mL
- **pDNA Concentration:** 10 µg/mL

RESULTS

Optimization of Disulfiram-based cross-linking for Nanopeptisomes

Influence of Peptide/PFC molar ratio

Peptide/PFC Molar Ratio	Size (nm)	Polydispersity Index (PDI)	ζ-Potential (mV)	Conc. (p/mL)
0.08	847 ± 499	0.80 ± 0.18	1 ± 0.6	$4.9 \pm 0.1 \times 10^8$
0.02	**566 ± 38**	**0.58 ± 0.17**	**1 ± 2.5**	**$3.9 \pm 0.3 \times 10^8$**

- A **lower** peptide/PFC **molar ratio** (0.02) **reduced** particle **size** and **polydispersity**.

Influence of aqueous formulation phase

Aqueous Phase	Size (nm)	Polydispersity Index	ζ-Potential (mV)	Conc. (p/mL)
6M Gu.HCl	566 ± 38	0.58 ± 0.17	1 ± 2.5	$3.9 \pm 0.3 \times 10^8$
25 mM HEPES (pH 7.4)	> 1000	1	5.4 ± 1.3	$< 1 \times 10^8$
mQ H2O (pH 6.3)	492 ± 34	0.22 ± 0.04	18.4 ± 1.4	$1.2 \pm 0.1 \times 10^9$
Glucose 5% (pH 4.3)	**424 ± 4**	**0.25 ± 0.03**	**38.6 ± 1.6**	**$1.5 \pm 0.01 \times 10^9$**

- **5 eq. DSF** provided the **best overall compromise**, improving nanopeptisome monodispersity while maintaining a high particle concentration.

Influence of disulfiram stoechiometry

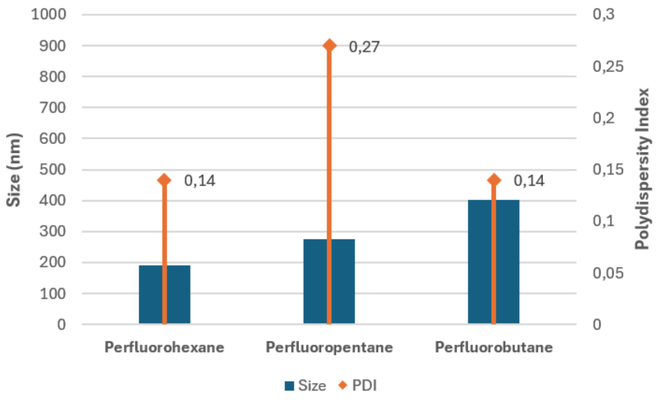
Stoechiometry (eq. DSF)	Size (nm)	Polydispersity Index	ζ-Potential (mV)	Conc. (p/mL)
0.5	431 ± 8	0.09 ± 0.03	48.2 ± 2.3	$4.5 \pm 0.4 \times 10^9$
2.5	403 ± 10	0.17 ± 0.04	42.6 ± 0.7	$2.4 \pm 0.2 \times 10^9$
5	**401 ± 10**	**0.14 ± 0.04**	**39.9 ± 2.5**	**$3.9 \pm 0.1 \times 10^9$**
7.5	398 ± 15	0.18 ± 0.03	30.8 ± 5.6	$2.2 \pm 0.1 \times 10^9$
10	424 ± 4	0.25 ± 0.03	38.6 ± 1.9	$1.5 \pm 0.01 \times 10^9$

- A **low-pH 5% glucose** aqueous phase **improved particle size**, monodispersity, concentration and ζ-potential, **suggesting enhanced colloidal stability**.

Mechanistic Hypothesis: Optimized pH and DSF stoichiometry may limit DDTC-anion accumulation and the associated destabilizing neutralization of the nanopeptisomes surface charge.

Influence of the Perfluorocarbon Core on Nanopeptisome Properties

Physico-Chemical Properties

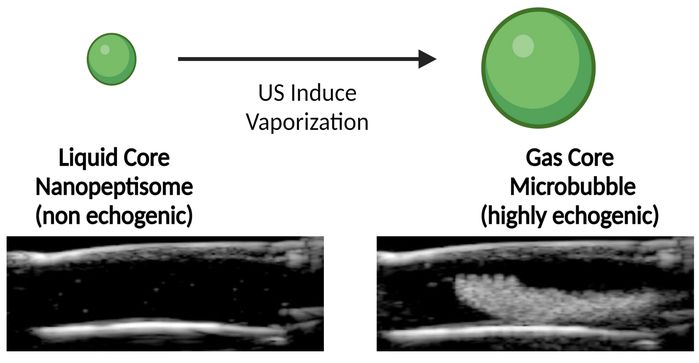


PFH and PFP Nanopeptisomes were prepared by oxidative dialysis, whereas PFB required the newly developed disulfiram cross-linking strategy.

- Nanopeptisome size increase with decreasing PFC boiling point.
- PDI seems uncorrelated to PFC.
- All formulations achieved concentration > 1×10^9 p/mL.

Trend likely to reflects a combined influence of **PFC** physicochemical **properties** and **peptide-shell organization**, which together **determine interfacial stabilization** during assembly.

Acoustic Response



Gas	ADV Threshold (MPa)	Mechanical Index
C_6F_{14}	~ 10,20	~ 4,16
C_5F_{12}	~ 7,64	~ 3,13
C_4F_{10}	~ 4,14	~ 1,69

- **Acoustic properties mainly driven** by the **perfluorocarbon liquid core**.
- **Lowering the boiling point** led to **reduced mechanical index (MI).**
- **Mechanical Index** suitable **only** for **therapeutic applications**.

CONCLUSIONS

- An optimized **disulfiram-mediated cross-linking strategy enabled the stable formulation of low-boiling-point nanopeptisomes**, overcoming a key limitation of previous nanopeptisome formulations.
- **Expanding** the **nanopeptisome** platform to both high- and low-boiling-point PFCs **increases** formulation **tunability**, notably low-boiling-point cores enable NPP activation at lower acoustic pressures, potentially reducing sonoporation-induced cellular stress.
- The **optimized** low-boiling-point **nanopeptisome platform** is **compatible** with our **previously** established **genetic** cargo **loading** strategy.

REFERENCES

1. Medina *et al.*, Fluorous Phase-Directed Peptide Assembly Affords Nano-Peptisomes Capable of Ultrasound-Triggered Cellular Delivery, *Angew. Chem. Int. Ed. Engl.*, **2017**, 56 (38), 11404–11408
2. Microfluidic preparation of fluorocarbon cross-linked vesicles – WO2023/084048
3. Cationic Cross-Linked Vesicles - WO2024/133892
4. Laps, S. et al., A. General Synthetic Strategy for Regioselective Ultrafast Formation of Disulfide Bonds in Peptides and Proteins. *Nat. Commun.* **2021**, 12 (1), 870
5. Cross-linked Vesicles with Low-boiling Point Fluorinated Compound - WO2024261165

38th EPS European Peptide Symposium · 6 - 11th of September 2026 · Vienna, Austria

Discovery and membrane-selective bactericidal activity of Spat1, a novel cyclotide from *Spigelia anthelmia* L. (Loganiaceae)

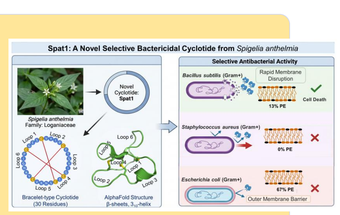
Toluwanimi E. Akinleye[1,3,4], Latifat Sidiq[1], Alfred F. Attah[2], Roland Hellinger[3], Lisa Pabi[4], Nermina Malanovic[4], Omonike O. Ogbole[1], Christian W. Gruber[3]

[1] Department of Pharmacognosy and Herbal Medicine, Faculty of Pharmaceutical Sciences, University of Ibadan, Nigeria · [2] University of Ilorin, Nigeria · [3] Centre for Physiology and Pharmacology, Medical University of Vienna, Austria · [4] Institute of Molecular Biosciences, University of Graz, Austria

https://doi.org/10.17952/38EPS.2026.P198

Key finding

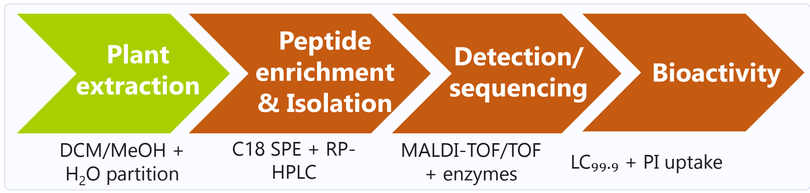
Spat1 is a new 30-residue bracelet cyclotide from Spigelia anthelmia that rapidly kills *Bacillus subtilis* by membrane permeabilization, while showing no detectable activity against *Staphylococcus aureus* or *Escherichia coli* up to 400 μM.



Background & aim

Cyclotides are plant-derived circular mini-proteins stabilized by a cyclic cystine-knot motif. Their exceptional stability and membrane-active properties make them attractive antimicrobial scaffolds. However, they exhibit a remarkably restricted phylogenetic distribution, occurring in only ~1% of angiosperm families (Rubiaceae, Violaceae, Cucurbitaceae, Fabaceae, Poaceae, and Solanaceae). This work asked whether an unexplored Loganiaceae medicinal plant contains novel cyclotides and whether these peptides possess selective bactericidal activity.

Experimental workflow



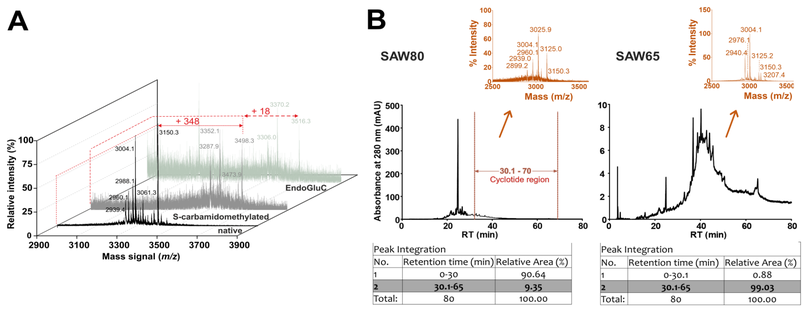
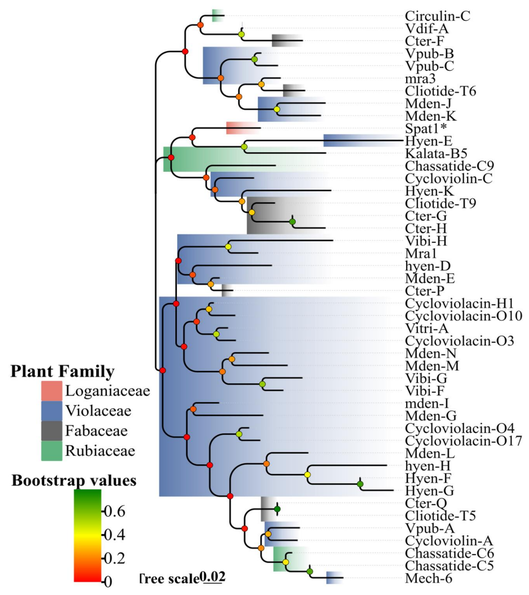


Fig. 1. MALDI-TOF detection and enrichment of the cyclotide-containing fraction from *S. anthelmia*.
Detection of cyclotides in Spigelia anthelmia whole plant. (A) MALDI MS spectra showing a +348 Da shift were observed after carbamidomethylation and an additional +18 Da shift (+366 total) following EndoGluC proteinase digestion, which implies a hydrolytic cleavage of Glutamic acid that is usually conserved in cyclotides, leading to the circular opening of the cyclotides. (B) Analytical HPLC chromatogram showing peptide enrichment to improve solid-phase peptide extraction toward large-scale extraction and isolation after a 10% buffer B wash and 80% buffer B elution, 30% buffer B wash, and 65% elution.

Spat1 sequence & Phylogenetic relationship

***cyclo*-GIPCGESCVYIPCFTSVIGCSCSNKVCYKN**

30 residues · bracelet-type cyclotide · m/z 3150.1 · net charge +1



Phylogenetic relationship of Spat1 with other RefSeq cyclotides (≤86% similarity) from the UniProt BLAST interface.

Purification-guided bactericidal activity

Bioassay-guided fractionation localized bactericidal activity to fraction G, which yielded purified Spat1.

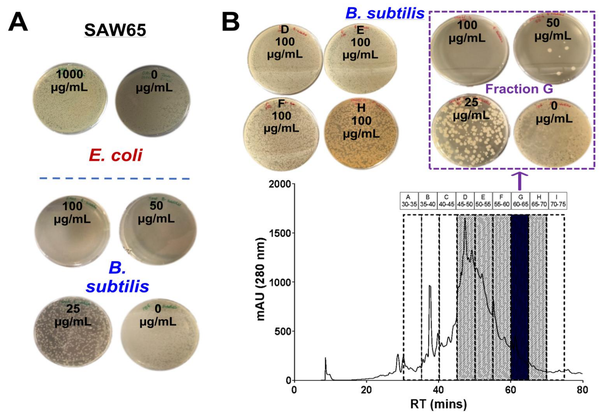


Figure 2: Bactericidal effect of SAW65 peptide extract (A) and HPLC fractions (C) on Gram-negative *E. coli* and Gram-positive bacteria *B. subtilis* after 1 h incubation. Fraction G (highlighted in lilac; B) maintained the bactericidal effect observed in the SAW65 peptide extract.

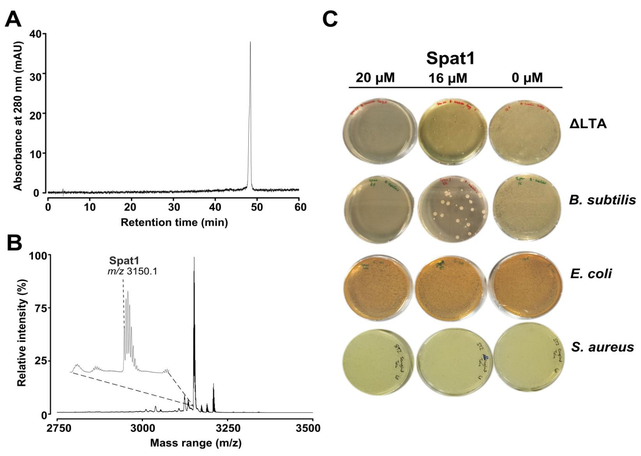


Figure 3: After 1 h incubation with bacterial cells, pure Spat1 (≥95% purity) demonstrated $LC_{99.9}$ at 20 µM against B. subtilis and LTA-deficient B. subtilis but no effect against Gram-negative E. coli and Gram-positive *S. aureus*.

Activity profile

● ***Bacillus subtilis***	$LC_{99.9}$ = 20 µM within 1 h
● **ΔLTA B. *subtilis***	$LC_{99.9}$ = 20 µM
● ***Staphylococcus aureus***	No activity up to 400 µM
● ***Escherichia coli***	No activity up to 400 µM

Interpretation: Activity does not require lipoteichoic acid and is consistent with direct engagement of cytoplasmic membrane phospholipids.

Membrane permeabilization

Propidium iodide influx occurred rapidly at bactericidal concentrations, matching the lethal concentration range.

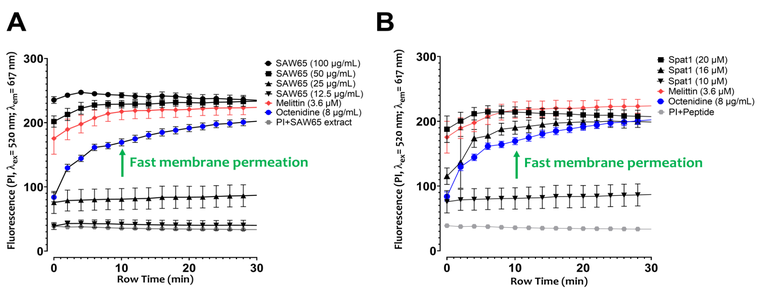


Figure 4: Permeabilization of bacterial membranes by peptide cocktails (A) and Spat1 (B).

Structural and mechanistic insight

- AlphaFold-based modelling supports a canonical cyclic cystine-knot fold with amphipathic surface topology.
- Spat1 has a low net positive charge (+1), which may limit penetration of the Gram-negative outer membrane.
- Low LTA affinity and preserved activity in ΔLTA B. subtilis support a membrane-phospholipid-driven mechanism.

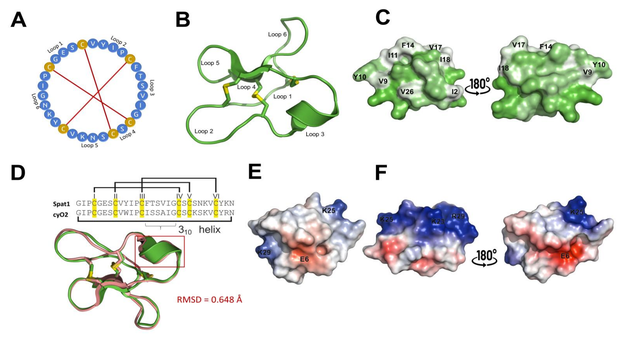


Figure 5: Primary sequence (A), cartoon (B) representations displaying the two antiparallel β-sheets, the 3_{10}-helix, and three disulfide linkages (yellow); intercysteine loops are indicated. Surface representation showing the hydrophobicity (C) of Spat1 using the Eisenberg hydrophobicity scale; hydrophobic residues are displayed in green, whereas hydrophilic residues are displayed in white. Structural alignment of Spat1 (green) and another bracelet cyclotide, cycloviolacin O2 (salmon), at RMSD = 0.648 Å (D); Electrostatic potential of Spat1 (E) and cyO2 (F), outlining negatively charged residues in red and positively charged residues in blue.

De novo sequencing evidence

Reduction/alkylation, EndoGluC, trypsin, and chymotrypsin fragments supported full sequence assignment.

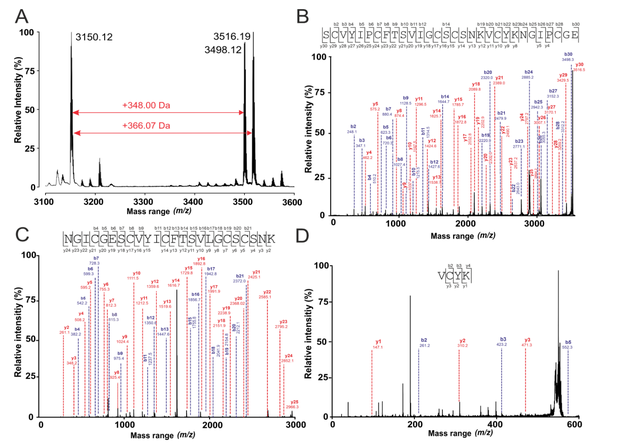


Figure 6: MALDI-TOF MS/MS de novo annotation. (A) Ring opening of the native peptide m/z 3150.12 to a linear product m/z 3516.19 was observed in a digestion experiment with endopeptidase GluC. The m/z 3496.12 corresponds to the cyclic reduced and S-acetamidated intermediate. (B). The peptide m/z 3516.19 was used for an MS/MS fragmentation experiment, and the b- and y-ions of the resulting fragmentation spectrum were de novo annotated, providing the full-length amino acid sequence of Spat1. Similarly, a trypsin digestion experiment was carried out, and two tryptic fragments, m/z 2966.3 (C) and m/z 570.3 (D), were observed.

Conclusions

- Spat1 expands the known phylogenetic distribution of cyclotides to Loganiaceae.
- It shows narrow-spectrum, rapid bactericidal activity against B. subtilis.
- Membrane permeabilization is the dominant measurable killing event.
- Net charge and surface topology appear to tune bacterial specificity and should guide SAR design.

Future direction

Engineer Spat1 analogues with tuned basic residues and hydrophobic patch orientation to test whether Gram-negative penetration and spectrum can be rationally improved without losing selectivity.

Proposed membrane-selective model

1 Spat1 scaffold — Cyclic cystine-knot peptide; 30 aa · bracelet type · +1 charge

→ **2 Selective engagement** — PE-containing Bacillus membrane; minimal dependence on LTA

→ **3 Rapid permeabilization** — PI influx within minutes; $LC_{99.9}$ = 20 µM in 1 h

→ **4 Narrow spectrum** — No detectable killing of *S. aureus* or *E. coli* up to 400 µM

Overall interpretation: Spat1 activity is best explained by direct engagement with the PE-containing cytoplasmic membrane rather than by teichoic acid binding. Species specificity likely reflects a combination of membrane lipid composition, outer-membrane barrier effects, net charge, and hydrophobic surface topology.

Selected references

[1] Craik et al. J Mol Biol 1999;294:1327–1336.
[2] Daly et al. Adv Drug Deliv Rev 2009;61:918–930.
[3] Akinleye et al. J Nat Prod 2026; doi:10.1021/acs.jnatprod.5c01216.
[4] Henriques et al. J Biol Chem 2011;286:24231–24241.
[5] Henriques et al. J Biol Chem 2012;287:33629–33643.

Acknowledgment

2026 EPS Young Investigator Award; OeAD's Ernst Mach Grant (weltweit, MPC-2021-00037); Coimbra Group scholarship at the University of Graz.

PEPTIDE MICROARRAY PLATFORM FOR HIGH-THROUGHPUT DISCOVERY AND OPTIMIZATION OF PROTEIN-BINDING PEPTIDES

P420

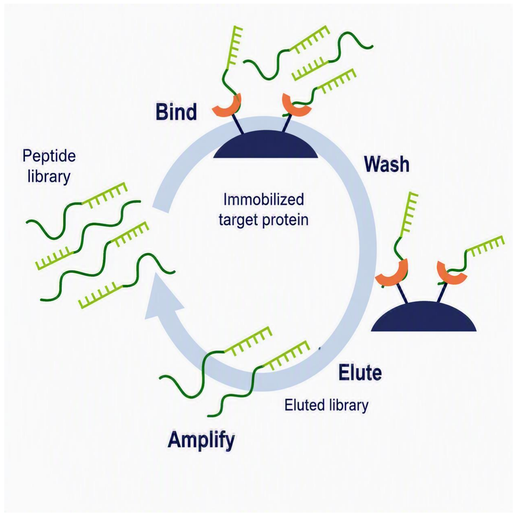
Sravanthi Guggilapu[1] • Ryan Clark • Geoff Eddinger • Ken Lo • Sarah Fahlberg • Eric Sullivan • Lauren Goodrich

[1] Madison Peptide Therapeutics, SMTPT, AbbVie, Madison, Wisconsin, United States

doi.org/10.17952/38EPS.2026.P420

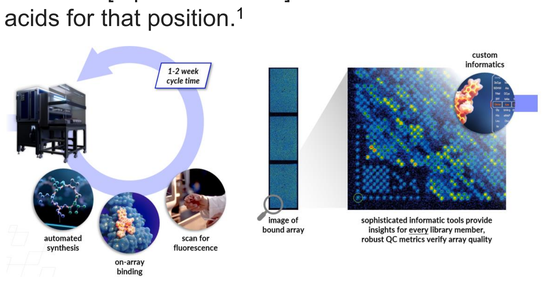
DISPLAY

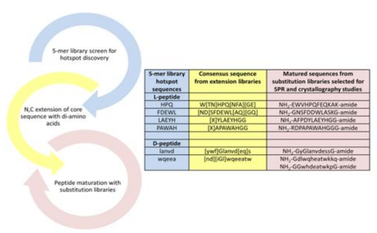
- Both phage and mRNA display facilitate the screening of highly diverse peptide libraries (from 10^9 to 10^{13} peptides) to identify peptides that bind to a target protein of interest.
- Through multiple rounds of iterative binding, washing, and amplification, high-affinity peptides are enriched.



RATIONAL PEPTIDE ARRAY DESIGN

- A schematic representation of the combined stepwise evolution and rational peptide array design approach.
- The table shows L- and D-peptide sequences (shown in uppercase and lowercase, respectively) selected at different steps of streptavidin binder evolution by using 5-mer, extension, and substitution libraries. Residues shown in [square brackets] are alternative amino acids for that position.[1]

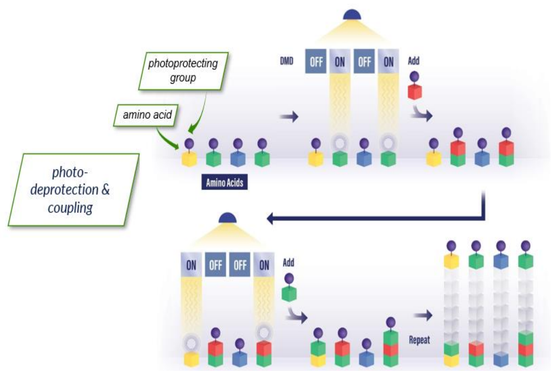




5-mer library hotspot sequences	Consensus sequence from extension libraries	Matured sequences from substitution libraries selected for SPR and crystallography studies
L-peptide		
HPQ	WITN[HPQ]NFA[EGE]	NH$_2$-EWVHPQFEQKAK-amide
FDEWL	IND[SYDEWL]AQ[GSD]	NH$_2$-GNDFDDWLASKG-amide
LAEYH	[KTYLAEYHGG	NH$_2$-AFPDYLAEYHGG-amide
PWAAH	[KJAPAWAHGG]	NH$_2$-RDPAPAWAHGGG-amide
D-peptide		
lamvd	[ywfiSGlamvd[eq]s	NH$_2$-GyGlamvdessG-amide
wqeea	[nd][Gf]wqeeatw	NH$_2$-GdwgheatwkkG-amide
		NH$_2$-GGwhdeatwkyG-amide

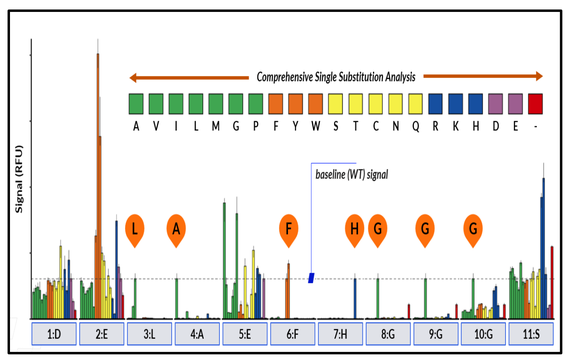
PEPTIDE MICROARRAYS

- Peptide microarray platform enables the synthesis of millions of user-defined peptides on a glass slide using patterned UV light and amino acids with photo-protecting groups.
- After on-array binding of fluorescently labelled protein, the slide is scanned for fluorescent signal, and the intensities are mapped to the identity of peptide synthesized in each feature.

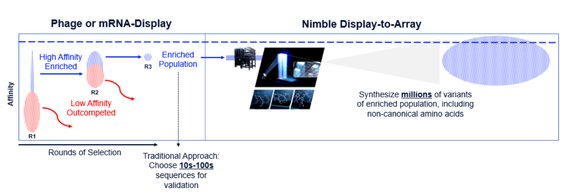


ARRAY DATA READOUT & ANALYSIS

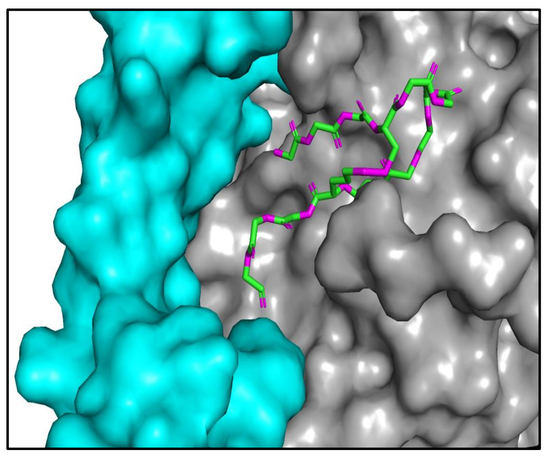
- Comprehensive amino acid mutational scanning on the array is used for high-throughput validation of potential peptide binders from display selections.
- The baseline fluorescent signal is used to identify peptides that bind the target protein while the signal of the single amino acid mutants pinpoints residues critical for protein binding.



TOGETHER: DISPLAY AND ARRAY



One such optimized peptide identified via phage display has been matured with non-natural incorporation of amino acids on array for Protein X, to identify 8 nM binder. The image below depicts peptide co-crystallized with ligand (Grey) followed by overlay on ligand-receptor (Grey-Cyan) structure. Peptide side chains are removed from this image to not disclose the sequence identity of the peptide.



EXAMPLE OF A WORKFLOW

DISPLAY

Find enriched binders

↓

ARRAY

Validate and map sequence determinants

↓

CHEMISTRY

Introduce non-natural residues or cyclization

↓

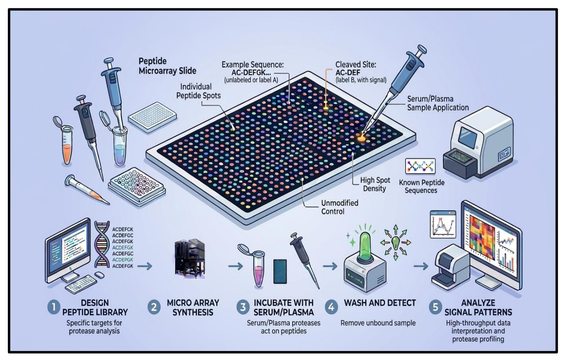
MEASURE

Track affinity, specificity and stability

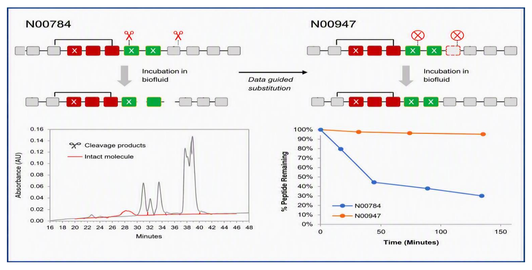
Integrated iteration accelerates progression from hit identification to optimized peptide properties.

PEPTIDE STABILITY STUDIES

The image below is generated using go/AI tool in AbbVie. The Step1 to 5 are Design Peptide Library, Make Microarrays, Incubate Biofluids, Detect, Analyze. [2]



P001 is the reference sequence that has 2 cut sites. Arrays are deployed to identify mutations in P001 that tolerated the biofluid cut sites. This resulted in identifying P002. The stability improvement is visually depicted below where % Peptide Remaining is measured against Time.



AI/ML DISCOVERY HITS ON ARRAY

Peptide sequences designed using AI/ML tools are explored on array to identify streptavidin binders.

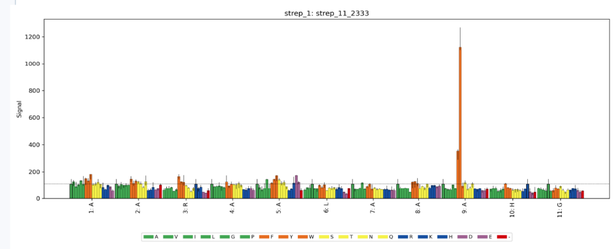


Fig 1: Initial ML-designed peptide displayed mild specificity for wild-type sequence

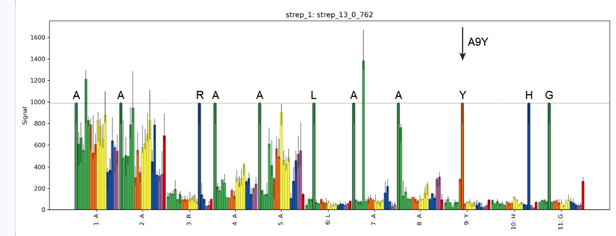


Fig 2: A single array-suggested point mutation drastically improved peptide binding signal and specificity for wild-type sequence

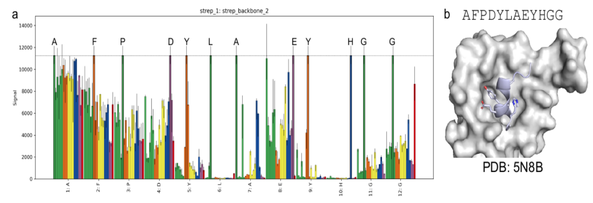
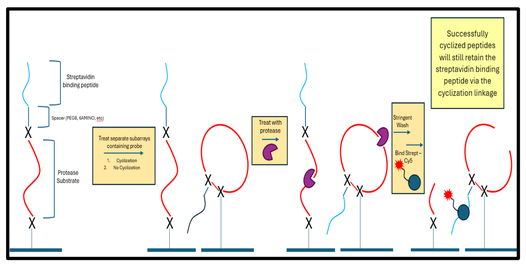


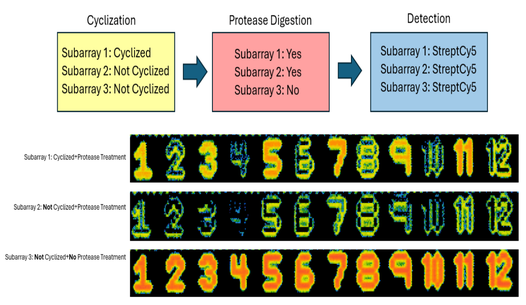
Fig 3: a) Mutation scan plot of known streptavidin binder, AFPDYLAEYHGG b) The ML-designed peptide overlaps well sequence- and specificity-wise with known helical streptavidin binder

METHOD DEVELOPMENT: MACROCYCLIZATION

The macrocyclization on the array is tested using Streptavidin binding peptide and known protease substrate where X represents the cyclization monomers in odd-numbered sub-arrays and non-cyclization monomers in even-numbered sub-arrays.



Example Data:
Numbers 1,3,5,7,9,11 → protease substrates flanked with cyclization monomers ("**can** be cyclized")
Numbers 2,4,6,8,10,12 → paired linear protease substrate controls in which the cyclization monomers are replaced with non-cyclizing monomers ("**cannot** be cyclized")



TAKE-HOME MESSAGE

Display finds hits. Arrays explain, optimize and de-risk them

- **Expanded validation across thousands of sequences**
- **Single-residue resolution for affinity and specificity**
- **Rapid testing of non-natural amino acids and cyclization**
- **Direct integration with AI/ML-designed peptide libraries**
- **Parallel optimization of binding and stability**

Display hit → Array optimization → 8 nM binder

CONCLUSIONS

1. **Peptide microarrays substantially expand post-display validation depth.**
2. **The same platform supports affinity maturation, specificity mapping, stability optimization and chemistry development.**
3. **Array-guided point mutations can produce large improvements in binding signal and specificity.**
4. **AI/ML-designed peptides can be tested and refined experimentally at scale.**
5. **Display and array technologies form a complementary discovery and optimization engine.**

High-throughput arrays turn sequence-level experimental data into clear next-design decisions.

ACKNOWLEDGEMENTS & REFERENCES

Acknowledgements



All authors are employees of AbbVie. The design, study conduct and financial support were provided by AbbVie. AbbVie participated in data interpretation, review and approval of the publication. No honoraria or payments were made for authorship.

References

1. Lyamichev V, Goodrich L, Sullivan E, et al. Stepwise Evolution Improves Identification of Diverse Peptides Binding to a Protein Target. Scientific Reports. 2017;7:12116.

2. Salisbury CM, Maly DJ, Ellman JA. Peptide microarrays for the determination of protease substrate specificity. Journal of the American Chemical Society. 2002;124(50):14868–14870.

Corresponding author: Sravi Guggilapu

DOWNSIZING THE HISTONE H3–H4 QUATERNARY STRUCTURE INTO FOLDAMER MIMETICS YIELDS HIGH-AFFINITY AND CELL-PERMEABLE LIGANDS OF ASF1

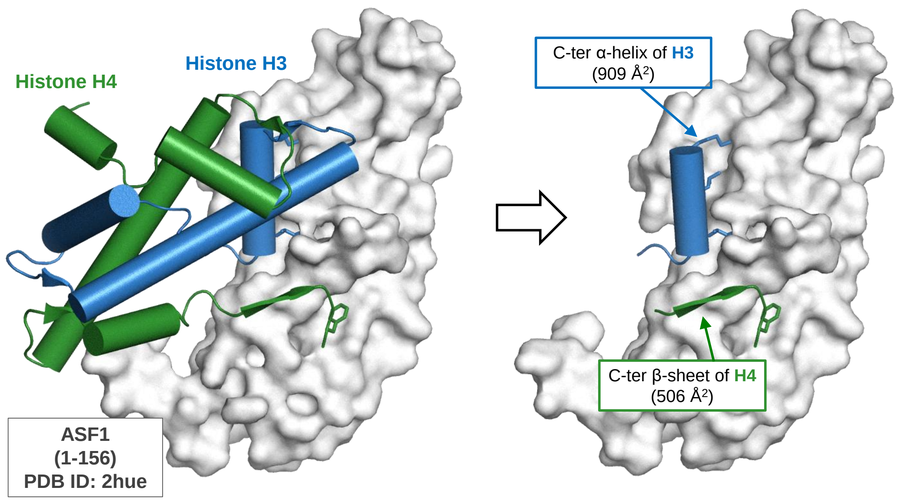
Gilles Guichard[1], Bo Li[1], Marie Perrin[2], Emma Maillard[2], Arthur Vitard[2], Gwenaëlle Moal[2], Johanne Mbianda[1], Christophe André,[1] Magda Teixeira Nunes[3], Marie Vandamme[4], Guillaume Pinna[4], Céline Douat[5], Emmanuelle Thinon[1], Raphaël Guerois[2], Pierre Legrand[3], Françoise Ochsenbein[2]

[1]Univ. Bordeaux, CNRS, Bordeaux INP, CBMN, UMR 5248, Institut Européen de Chimie et Biologie, Pessac, France, [2]Institute for Integrative Biology of the Cell (I2BC), Université Paris-Saclay/CEA/CNRS, Gif sur Yvette, France, [3]Synchrotron SOLEIL, HelioBio group, l'Orme des Merisiers, Saint-Aubin, France, [4]Université Paris Cité, Université Paris-Saclay, Inserm, CEA, PARi facility, iRCM/IBFJ, Stabilité Génétique Cellules Souches et Radiations, Fontenay-aux-Roses, France, [5]Department Pharmazie, Ludwig-Maximilians-Universität München, München Germany

https://doi.org/10.17952/38EPS.2026.P136

Introduction

Histone chaperones, such as Anti-Silencing Function 1 (ASF1A and ASF1B) regulate the dynamics of histones within chromatin and contribute to the establishment of numerous epigenetic markers.[1,2] Their dysfunction is associated with a number of pathologies including aging-related diseases, pathogen infections, or cancer.

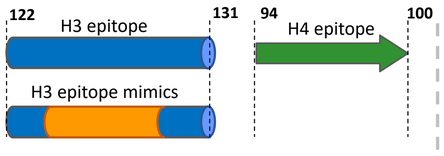


Designing effective ASF1 inhibitors is challenging due to its intracellular localization, a binding affinity for the H3-H4 dimer in the low nM range, and a rather flat and extensive binding interface (1,415 Å²) with two shallow interaction pockets 26 Å apart.[3]

We recently introduced an approach based on **oligourea helical foldamers to reduce the peptide character of PPI inhibitors**,[4] and reported a rationally designed H3 helix mimetic that binds both ASF1A and ASF1B with a K_D in the low µM range and shows improved stability in the human plasma.[5] Capitalizing on this early work, we now report a general workflow that led to the discovery of **cell-permeable, medium-size (M_w < 2.5 kDa) H3-H4 quaternary structure mimetics with high affinity for ASF1.**[6]

[1] F. Mousson et al. *Chromosoma* **2007**, *116*, 79-93
[2] Z. A. Gurard-Levin et al. *Annu. Rev. Biochem.* **2014**, *83*, 487-517
[3] F. Mousson et al. *Proc. Nat. Acad. Sci. U.S.A.* **2005**, *102*, 5975-5980
[4] L. Cussol, et al. *Angew. Chem. Int. Ed.* **2021**, *60*, 2296-2303
[5] J. Mbianda et al., *Science Adv.* **2021**, *7*, eabd9153
[6] B. Li et al. *Angew. Chem. Int. Ed.* **2026**, e4112426

Foldamer Quaternary Structure Mimetics with Optimal Linker Display Enhanced ASF1 Binding Affinity



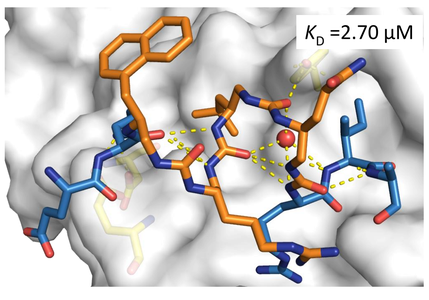
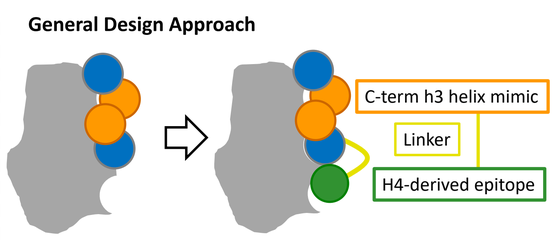


Figure 2: X-ray structure of **C2** in complex with ASF1[5]



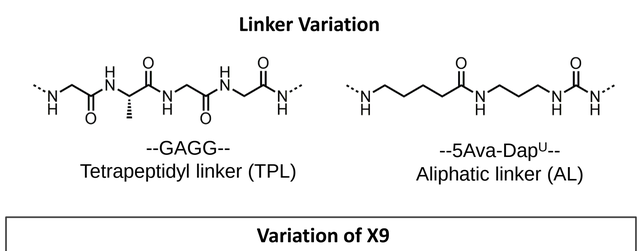
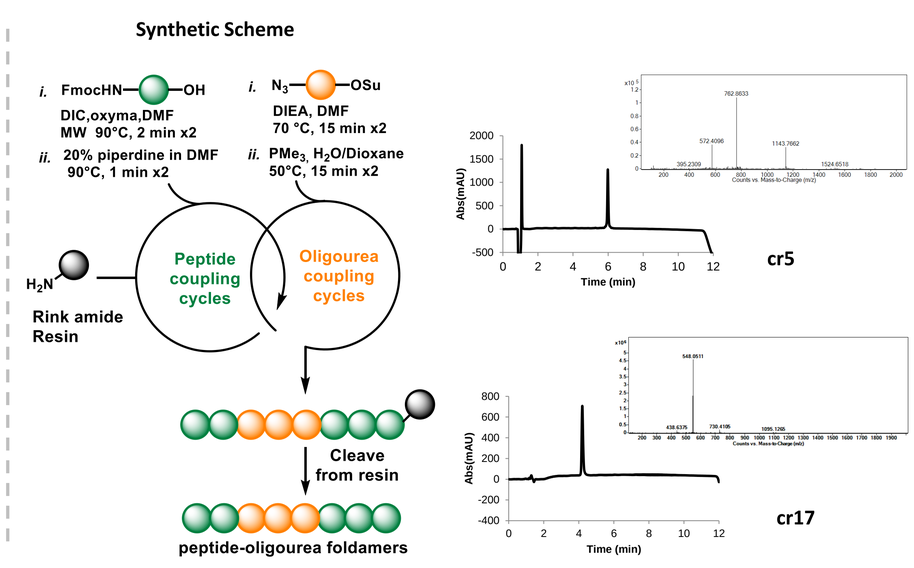
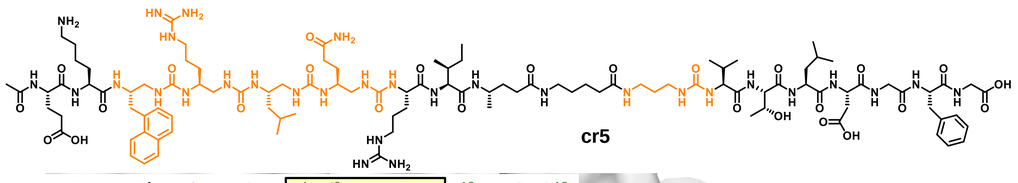


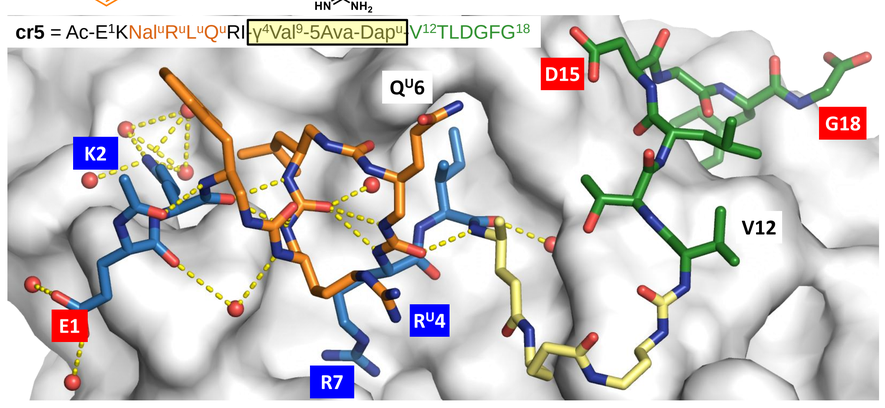
Table 1: Dissociation constants of urea-peptide chimeras as measured by ITC

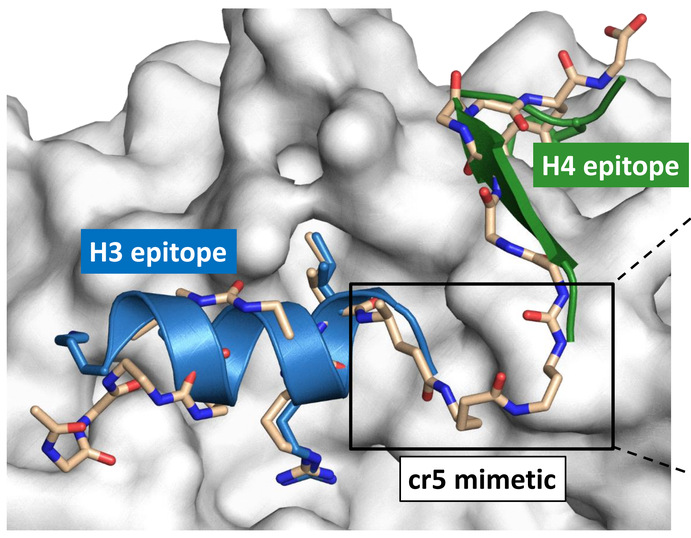
Cmpd	X9+Linker	K_D (µM)
C2		2.70 ± 0.60
cr1	Ala+TPL	1.16 ± 0.06
cr2	Ala+AL	0.69 ± 0.02
cr3	βAla+AL	1.24 ± 0.11
cr4	Ala^U+AL	0.42 ± 0.05
cr5	γ^{4}Ala+AL	**0.14 ± 0.03**
cr6	δ^{5}Ala+AL	0.52 ±0.12



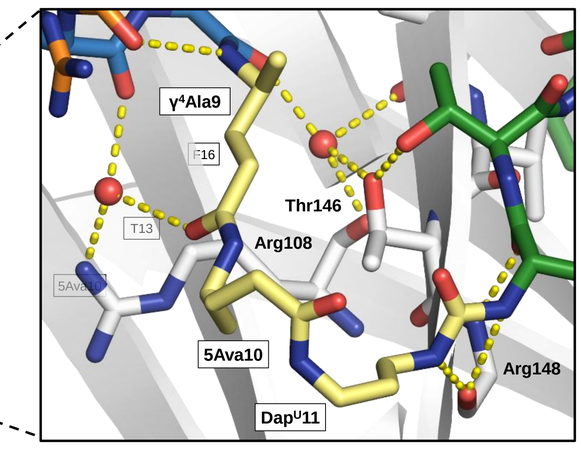
Crystal Structure of the Complex Between ASF1 and cr5







Figures 3 – 5 : X-ray structure of the complex between **cr5** and ASF1. Superimposition with H3 and H4 epitopes at the surface of ASF1 and details of representative H-bond interactions between the linker of **cr5** and ASF1



cr5 Charge Optimization

Table 2: Formal charges and K_D values measured by ITC

		cr5	cr7	cr8
Residue	1	E	R	R
	6	Q^U	K^U	K^U
	11	V	V	R
	C-ter	OH	NH_2	NH_2
Formal charge		0	+4	+5
K_D (nM)		135 ± 29	**38 ± 3.1**	165 ± 10

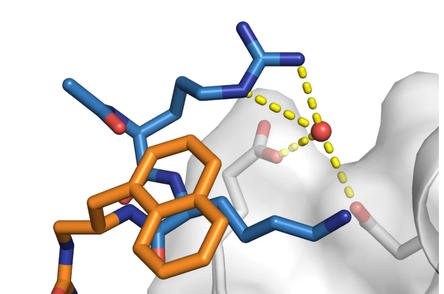
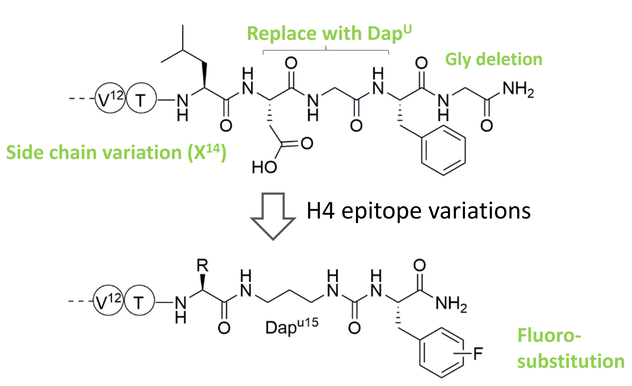
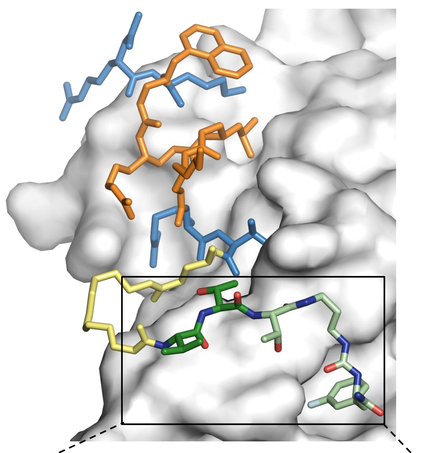


Figure 6 : Crystal structure of **cr7** with ASF1 and details of the H-bond network involving R1

H4 β-strand Mimicry & Backbone *N*-methylation





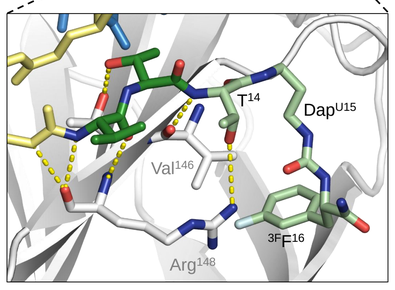


Figure 7: Crystal structure of **cr17** with ASF1 and details of the interactions with H4 mimetic

Table 3 : H4 epitope simplication and optimization strategy with binding affinities as measured by ITC

	X^{14}	Dap^U	Fluorinated Phe	Gly Deletion	K_D (nM)
cr7	L	-	-	-	38 ± 4
cr9	L	yes	-	yes	33 ± 6
cr10	G	yes	-	yes	60 ± 2
cr11	A	yes	-	yes	43 ± 8
cr12	V	yes	-	yes	22 ± 3
cr13	T	yes	-	yes	10 ± 2
cr14	L	-	4-F	-	70 ± 7
cr15	G	yes	4-F	yes	89 ± 3
cr16	L	yes	3-F	yes	22 ± 3
cr17	T	yes	3-F	yes	**6 ± 1**

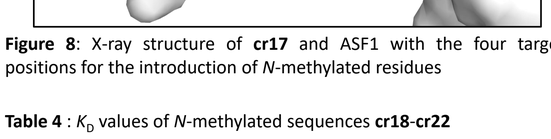


Figure 8: X-ray structure of **cr17** and ASF1 with the four targeted positions for the introduction of *N*-methylated residues

Table 4 : K_D values of *N*-methylated sequences **cr18-cr22**

	N-Methylation	K_D (nM)
cr18[a]	*N*-Me-R1	146 ± 16
cr19[a]	*N*-Me-5Ava10	59 ± 5
cr20[a]	*N*-Me-T13	531 ± 122
cr21[b]	*N*-Me-5Ava10	38 ± 6
cr22[c]	*N*-Me-5Ava10	27 ± 3

[a] **cr18**-**cr20** are **cr10** analogues
[b] **cr21** is a **cr9** analogue
[c] **cr22** is a **cr17** analogue

❑ Conclusions (B. Li et al. *Angew. Chem. Int. Ed.* **2026**, e4112426):

For Biological Results see Poster 76

- **A general workflow to downsize and mimic the quaternary structure of the histone H3-H4 dimer using a combination of structure-guided design, foldamer chemistry, amino acid substitutions for positive charge optimization & backbone *N*-methylation**
- **Discovery of medium-sized (≈ 2 kDa) high-affinity binders for the histone chaperone ASF1**
- **As revealed by X-ray structures, the peptide-oligourea ligands recapitulate the binding mode of the natural protein heterodimer**

https://doi.org/10.17952/38EPS.2026.P408

REENGINEERING ANTICANCER PEPTIDES VIA LIPID CONJUGATION

GIUSEPPINA GUIDA[1,2], AURÉLIE BENFIELD[1,2], NICOLE LAWRENCE[2,3], SÓNIA T. HENRIQUES[1,2]

[1]School of Biomedical Sciences, Translational Research Institute, Queensland University of Technology, QLD, Australia;
[2]ARC Centre of Excellence for Innovations in Peptide and Protein Science, Brisbane, QLD, Australia;
[3]Institute for Molecular Bioscience, The University of Queensland, Brisbane, Queensland, 4072, Australia

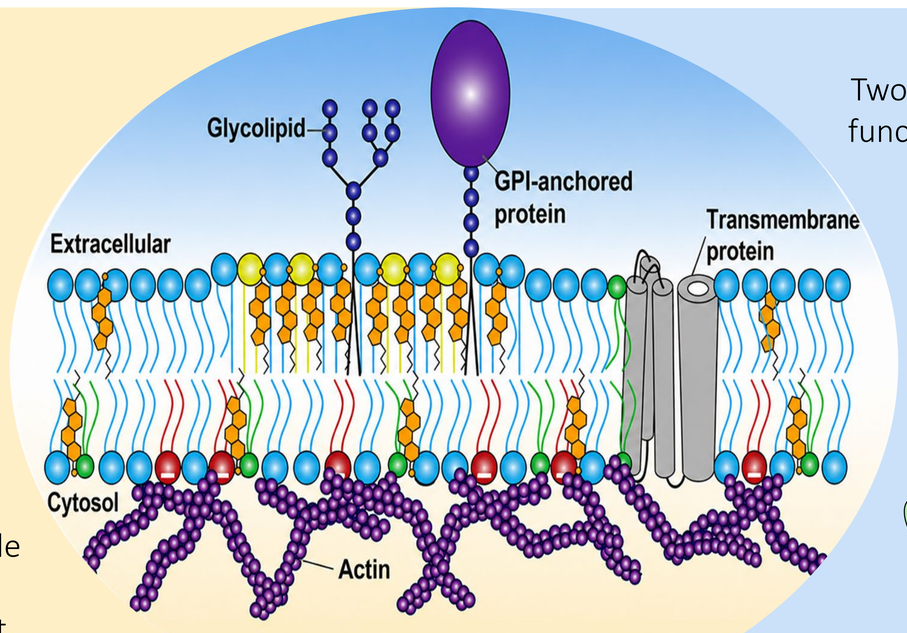
g.guida@qut.edu.au

INTRODUCTION

Peptides are emerging as a powerful therapeutic modality, combining the high specificity of biologics with the versatility of small molecules. However, their clinical translation remains limited by poor oral bioavailability due to rapid degradation, fast systemic clearance, and inefficient transport across epithelial barriers in the gastrointestinal tract.

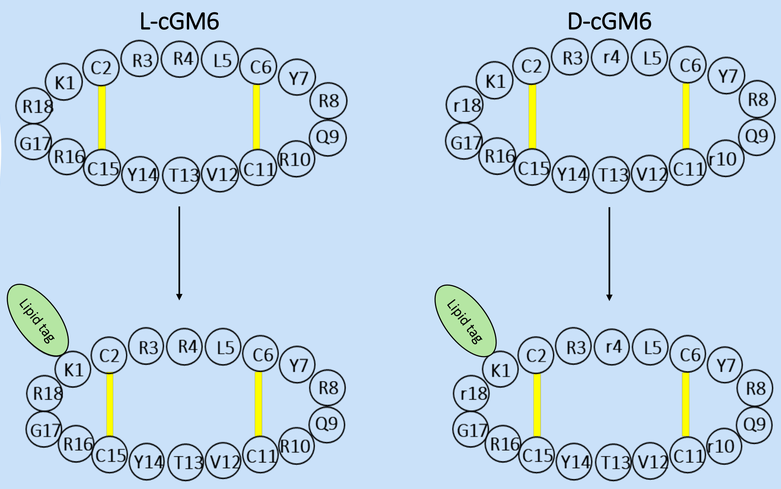
Lipidation, a clinically proven post-translational modification, has recently emerged as a promising strategy to overcome these limitations, as exemplified by therapeutics like semaglutide (Ozempic).

This study investigates how lipidation influences peptide membrane interactions in a set of gomesin-derived peptide analogues, aiming to support the development of orally bioavailable peptide therapeutics.



RESEARCH STRATEGY

Two cyclic gomesin derivatives (L-cGM6 and D-cGM6) were functionalised via conjugation with lipid chains at the lysine residue in position 1.



METHODS & RESULTS

Peptide Cytotoxicity: Comparison of cytotoxicity of cGm6 analogues against WM164 (human melanoma), HEK293 (human embryonic kidney), Caco-2 (human colon epithelium) and HIEC6 (human small intestinal epithelium) cell lines. Cell viability following 24 h peptide treatment was assessed using a resazurin-based assay, while haemolytic activity was evaluated in red blood cells (RBCs). Data represent the mean of three biological replicates (n = 3), with error bars indicating the standard error of the mean (SEM). Estimated half-maximal cytotoxic concentrations (CC_{50}) are listed in table 1.

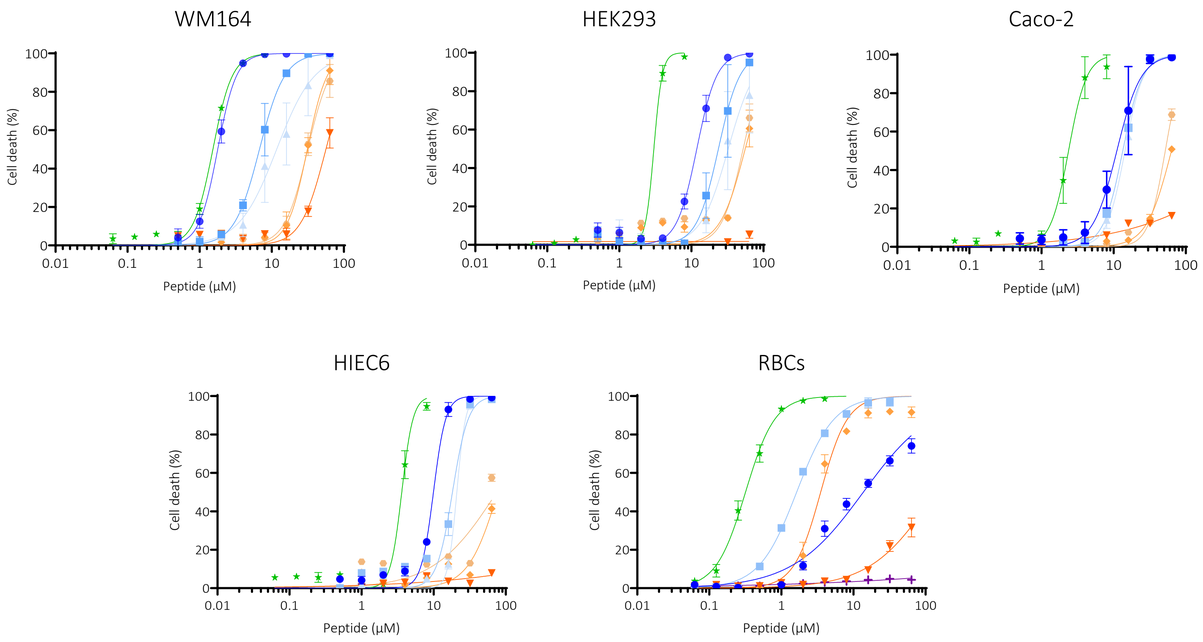
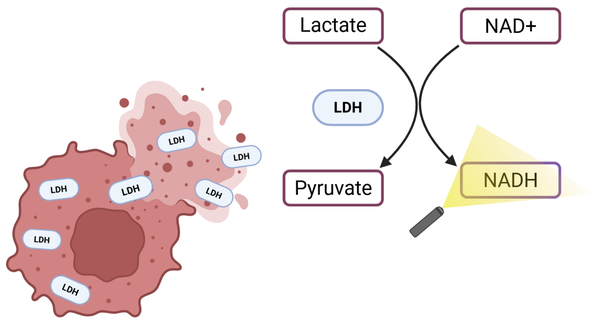
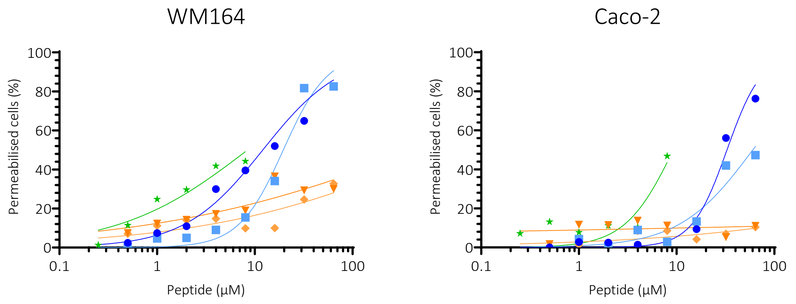


Table 1. Estimated half-maximal cytotoxic concentrations (CC_{50})

	CC_{50} (μM)				
Peptide	**WM164**	**Caco-2**	**HEK293**	**HIEC6**	**RBCs**
L-cGm6	1.8 ± 3.3	11.8 ± 2.6	12.0 ± 3.1	9.9 ± 0.3	13.2 ± 0.9
L-cGm6 (Palm)	6.8 ± 2.5	13.4 ± 3.1	23.7 ± 2.9	18.2 ± 0.9	1.3 ± 2.3
L-cGm6 (Stearic)	11.7 ± 1.7	14.4 ± 3.4	32.4 ± 2.2	20.1 ± 0.8	N/A
D-cGm6	56.4 ± 2.5	>64	>64	>64	>64
D-cGm6 (Palm)	31.1 ± 3.1	>64	55.8 ± 2.5	>64	2.9 ± 3.4
D-cGm6 (Stearic)	31.6 ± 2.7	52.0 ± 3.7	52.3 ± 2.9	>64	N/A
Semaglutide	N/A	N/A	N/A	N/A	>64
Melittin	1.5 ± 3.2	2.4 ± 3.4	3.0 ± 4.8	3.6 ± 0.1	0.3 ± 0.1

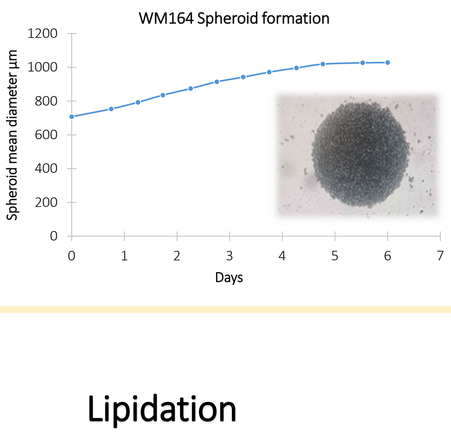
Enzymatic activity of cytosolic lactate dehydrogenase (LDH): Membrane disruption of WM164 and Caco-2 cells was quantified by measuring the enzymatic activity of the cytosolic lactate dehydrogenase released from damaged cells after treatment with peptide for 2 h at 37°C. Peptide concentration required to permeabilise 50% of cells (LC_{50}) was determined by fitting dose-response curves using binding with Hill slope equation.

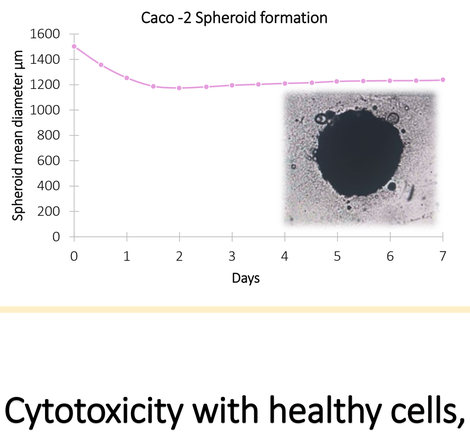


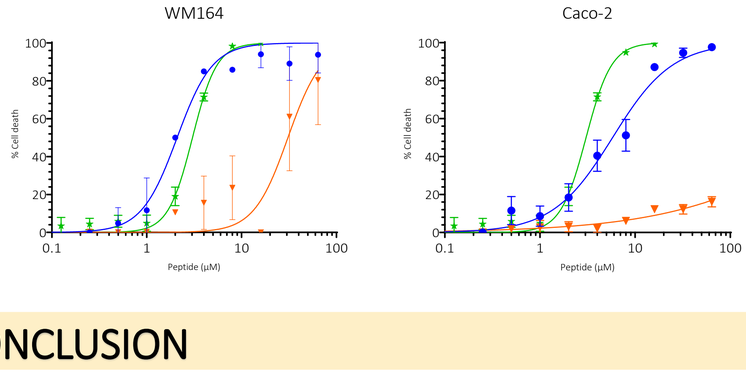


	LC_{50} (μM)	
Peptide	**WM164**	**Caco-2**
L-cGm6	12.0 ± 1.0	32.7 ± 2.4
L-cGm6 (Palm)	19.5 ± 1.9	41.8 ± 1.2
D-cGm6	> 64	>64
D-cGm6 (Palm)	> 64	>64
Melittin	8.4 ± 0.6	9.2 ± 1.7

Development of cancer spheroids to evaluate cytotoxic response to anticancer peptide: WM164 and Caco-2 spheroids were generated using the liquid overlay technique. Spheroid cell metabolic activity was evaluated daily over 6 days by measuring the fluorescent emission of resorufin with microplate reader. After spheroid formation, cells were treated with increasing peptide concentration up to 6 days in culturing condition.



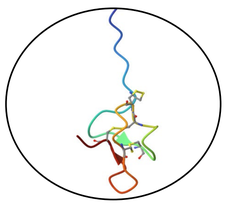




	CC_{50} (μM)	
Peptide	**WM164**	**Caco-2**
L-cGm6	1.7 ± 1.5	4.9 ± 1.2
D-cGm6	23.2 ± 0.9	>64
Melittin	2.8 ± 2.9	2.9 ± 2.0

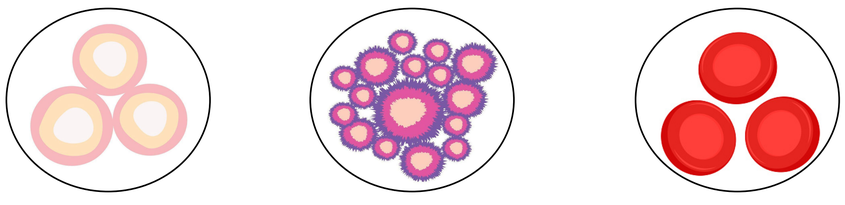
CONCLUSION

Lipidation



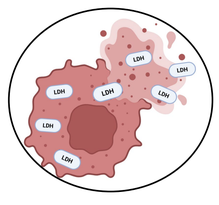
- L-cGm6 (Palm)
- D-cGm6 (Palm)

Cytotoxicity with healthy cells, cancer cells and RBCs



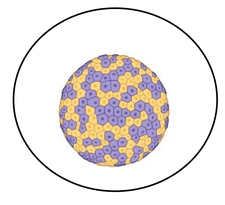
- L-cGm6
- L-cGm6 (Palm)
- L-cGm6 (Stearic)
- L-cGm6 (Palm)
- L-cGm6 (Stearic)

Membrane disruption



- L-cGm6 (Palm)

Spheroids development



- L-cGm6
- D-cGm6

Design of smart peptide-based nanoparticles for siRNA delivery in gastrointestinal stromal tumors (GIST)

Thania Hammoum[1], Jules Vastra[2], Julien Fabre[1], Karidia Konate[1], Eric Vivès[1], Sandrine Faure[1], Pascal de Santa Barbara[1], Sébastien Ulrich[2], Prisca Boisguerin[1]

[1]PhyMedExp, University of Montpellier, INSERM, CNRS, Montpellier, France; [2]IBMM, Institut des Biomolécules Max Mousseron, University of Montpellier, CNRS, ENSCM, Montpellier, France

thania.hammoum@inserm.fr

https://doi.org/10.17952/38EPS.2026.P435

1. Gastrointestinal Stromal Tumor (GIST)

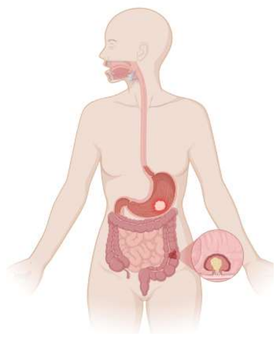
FIGURE 1

Epidemiology
- ➤ **10-15** per million/year (FR) (1)
- ➤ Most common gastrointestinal sarcomas

Molecular Basis
- ➤ Primary KIT or PDGFRA mutations in **85%** (2)

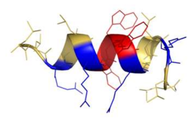
First-Line Treatment
- ➤ Imatinib (IM)

Resistance Mechanism
- ➤ **~90%** develop IM resistance
- ➤ Due to secondary KIT mutations



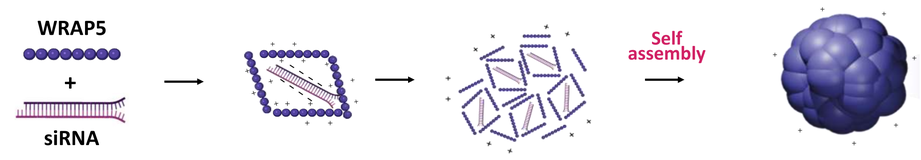
2. WRAP-based nanoparticles for delivery

FIGURE 2



WRAP5 (W5):
- 15 amino acids
- Rich in : **Tryptophan (W)** and **Arginine (R)**
- Amphipathic peptide

ID	Sequences	AA	Charges	Leucine (L)	Tryptophan (W)	Arginine (R)
W5	LLRLLRWWWRLLRLL	15	5	8	3	4



- Stable nanoparticles
- ~60-150 nm
- Fast cellular internalization
- Direct translocation

3. pH-sensitive PEG-WRAP5 nanoparticles

FIGURE 3

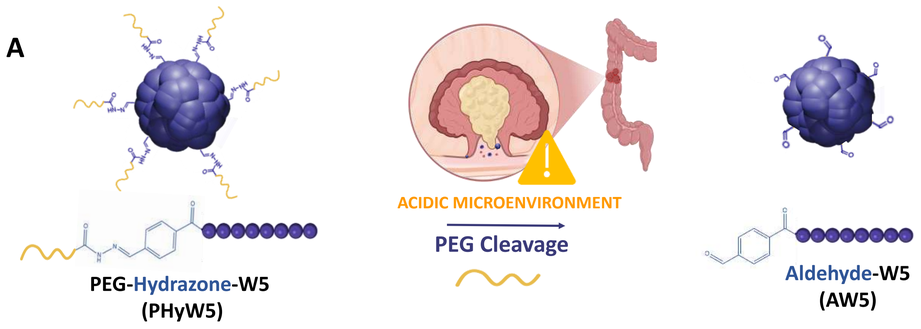
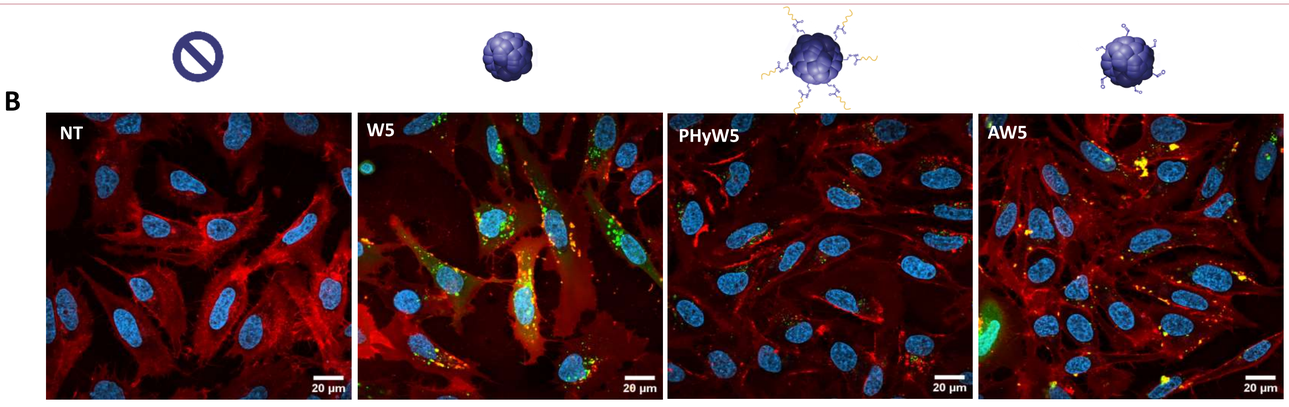


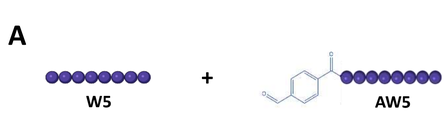
Figure 3. The use of pH-sensitive PHyW5 nanoparticles to target GIST.
(A) Principle of the pH-dependent cleavage reaction of PEG-Hydrazone-W5 (PHyW5) in the acidic environment of a GIST tumor. Hydrazone linker cleavage generates a W5 peptide carrying a 4-carboxybenzaldehyde group at its N-terminus, referred to as aldehyde-W5 (AW5).



(B) Visualization of **siCDK4-Alexa488 (green)** internalization in GIST-T1 cells after 2 h transfection with W5, PHyW5, or AW5 nanoparticles, compared to NT cells (Live Cell Confocal Microscopy). **Nuclei stained with Hoechst (cyan),** membranes with **DeepRed CellMask (red).** Efficient cytoplasmic internalization of siCDK4 using W5 nanoparticles, nearly no detectable siCDK4 internalization with PHyW5 nanoparticles, and membrane colocalization of siCDK4 with the AW5 nanoparticles.

4. Impact of AW5 on nanoparticle activity in GIST cells

FIGURE 4



PBN:siCDK4 (40 nM)			Size [d.nm]	PdI
W5	PHyW5	AW5		
100%	0%	0%	70.6 ± 9.9	0.218 ± 0.035
0%	0%	100%	90.9 ± 24.7	0.258 ± 0.191
25%	0%	75%	84.9 ± 42.8	0.239 ± 0.048
50%	0%	50%	61.2 ± 3.1	0.207 ± 0.036
80%	0%	20%	79.5 ± 9.8	0.192 ± 0.026
95%	0%	5%	85.1 ± nd	0.253 ± nd
0%	100%	0%	66.0 ± 7.9	0.324 ± 0.052

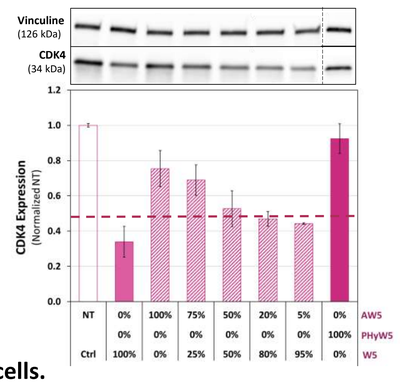
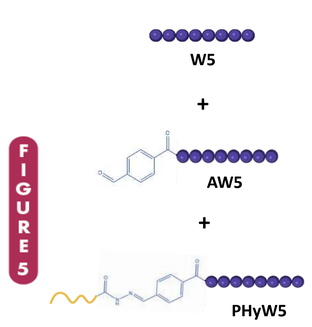


Figure 4. Evaluation of the AW5 nanoparticle activity in GIST cells.
(A) DLS characterization of siCDK4-loaded nanoparticles with variation in W5/AW5 ratios. Measurements revealed sizes of ~65 – 91 nm and PdI values of ~0.25. **(B)** Quantification of CDK4 protein levels in GIST-T1 cells transfected for 48 h with siCDK4-loaded nanoparticles with variation in W5/AW5 ratios. Data are expressed as mean ± SD. (n = 2-3). CDK4 silencing ≥50% was observed only with nanoparticles composed of less than 70% AW5.

5. Optimizing [W5/PHyW5/AW5] ratio for protection and internalization

FIGURE 5



PBN:siCDK4 (40 nM)			Size [d.nm]	PdI
W5	PHyW5	AW5		
100%	0%	0%	70.6 ± 9.9	0.218 ± 0.035
0%	0%	100%	90.9 ± 24.7	0.258 ± 0.191
0%	100%	0%	66.0 ± 7.9	0.324 ± 0.052
30%	70%	0%	193.9 ± nd	0.288 ± nd
	50%	20%	70.6 ± 2.4	0.189 ± 0.025
	40%	30%	92.2 ± 20.7	0.196 ± 0.003
	30%	40%	72.9 ± 1.3	0.184 ± 0.021
	20%	50%	63.3 ± 12.7	0.215 ± 0.023
	10%	60%	62.9 ± 2.4	0.237 ± 0.019
	0%	75%	84.9 ± 42.8	0.239 ± 0.048
50%	50%	0%	63.5 ± 3.8	0.221 ± 0.032
	40%	10%	62.4 ± 6.9	0.206 ± 0.021
	30%	20%	66.3 ± 3.5	0.185 ± 0.023
	20%	30%	65.3 ± 8.9	0.220 ± 0.02
	10%	40%	87.4 ± 34.6	0.231 ± 0.006
	0%	50%	61.2 ± 3.1	0.207 ± 0.036

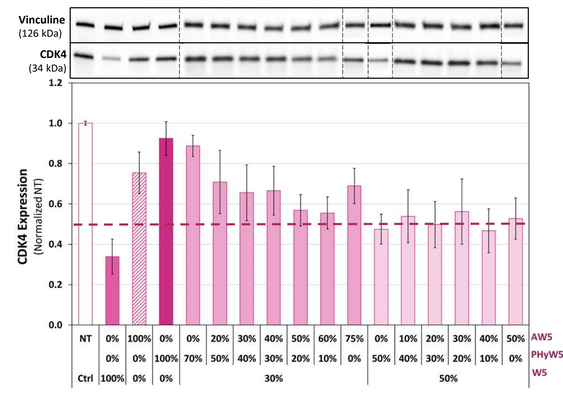


Figure 5. Evaluation of the three-peptide co-formulation activity in GIST cells.
(A) DLS characterization of co-formulated PBNs with variation in [W5/PHyW5/AW5] ratios and encapsulated siCDK4. Measurements revealed sizes of ~60- 193 nm and PdI values of ~0.20. **(B)** Quantification of CDK4 protein levels in GIST-T1 cells transfected for 48 h with the co-formulated nanoparticles. Data are expressed as mean ± SD. (n = 2-3). A knockdown of ~50% was observed for all nanoparticles containing 50% W5, as well as for those with ratios of [30%W5/20%PHyW5/50%AW5] or [30%W5/10%PHyW5/60%AW5].

Conclusion

WRAP5-Based Nanoparticle Optimization

- **WRAP5 nanoparticles are effective carriers for siRNA delivery in GIST.**
- **AW5 alters nanoparticle-cell interactions and limits silencing when used alone.**
- **Maintaining ≥30% W5 restores efficient intracellular delivery.**

➤ **The W5/PHyW5/AW5 strategy combines pH responsiveness with preserved biological activity.**

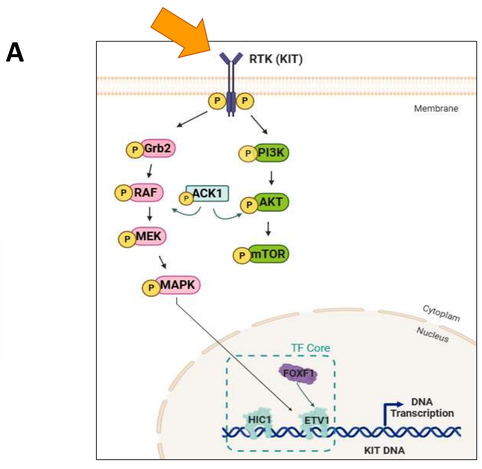
Choice of the Target and siRNA Design

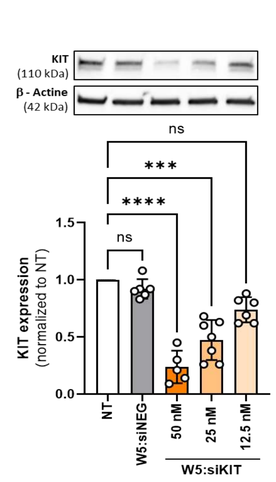
- **W5 nanoparticles efficiently deliver siRNA and achieve ~75% KIT silencing in GIST cells.**
- **More than 80% of proliferation inhibition with W5:siKIT**

➤ **Potent therapeutic tools.**

6. Targeting KIT-dependent proliferation pathways in GIST cells

FIGURE 6





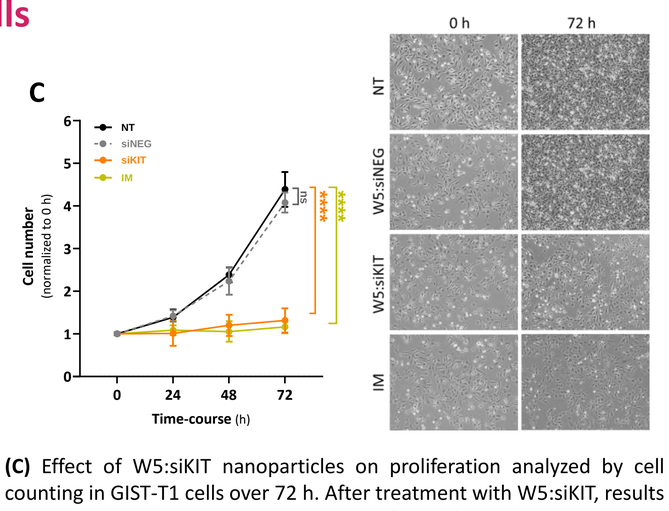
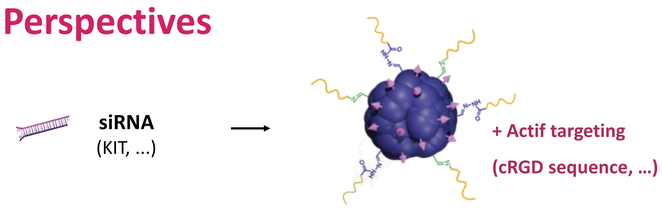


Figure 6. Impact of KIT Receptor Silencing on Cell Proliferation in GIST .
(A) Schematic overview of KIT signaling in GIST, showing MAPK and PI3K/AKT/mTOR pathway activation and regulation of core transcription factors: ETV1, FOXF1, HIC1. **(B)** Quantification of KIT protein levels in GIST-T1 cells transfected with increasing concentrations of W5-based nanoparticles encapsulating siKIT. Results were compared with untreated cells (NT) and W5:siNEG-treated cells. Data are expressed as mean ± SD. (n = 5-6) After 24 h of transfection, W5:siKIT showed ~75% protein silencing with an siRNA concentration of 50 nM.

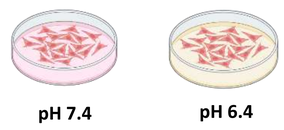
(C) Effect of W5:siKIT nanoparticles on proliferation analyzed by cell counting in GIST-T1 cells over 72 h. After treatment with W5:siKIT, results were normalized to the initial cell density (t = 0 h), then, compared with untreated cells (NT), 50 nM imatinib-treated cells (IM), and W5:siNEG-treated cells. The W5:siKIT conditions induced a significant inhibition of cell proliferation, comparable to that achieved with imatinib (IM).
Data are expressed as mean ± SD (n = 4). Statistical significance was evaluated by ANOVA (ns: not significant; ****: p < 0.0001 compared to the untreated group).

7. Perspectives

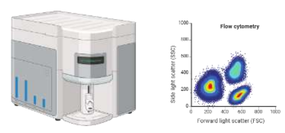


***In vitro* studies**

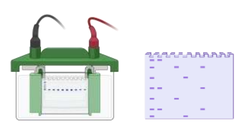
- Incubation condition



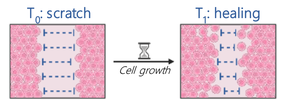
- Apoptosis induction



- Protein-silencing efficiency



- Inhibition of cell migration



References

(1) Landi B et al., Dig Liver Dis. 2019;51(9):1223-1231.

(2) Schaefer IM et al., Am Soc Clin Oncol Educ Book. 2022;42:1-15.

https://doi.org/10.17952/38EPS.2026.P274

38th European Peptide Symposium
Vienna · 6-11 September 2026

AI-driven discovery of cross-kingdom peptide ligands

CysTopoFold Exact probabilistic disulfide-topology prediction for cysteine-rich peptides

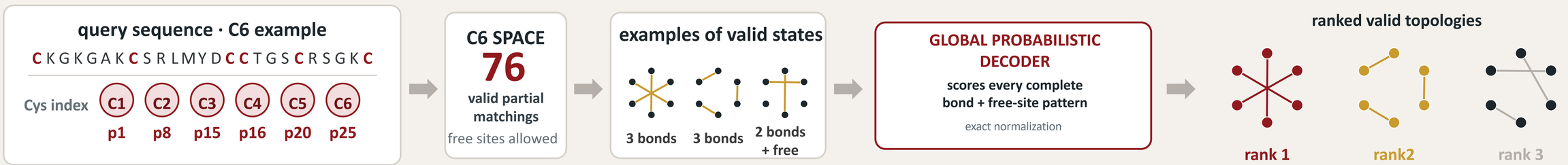
Marin Matic[1,2] · Alexander S. Hauser[1,2]

[1] Department of Drug Design and Pharmacology, University of Copenhagen, Denmark
[2] Center for Pharmaceutical Data Science Education (CPDSE)

BACKGROUND & CHALLENGE

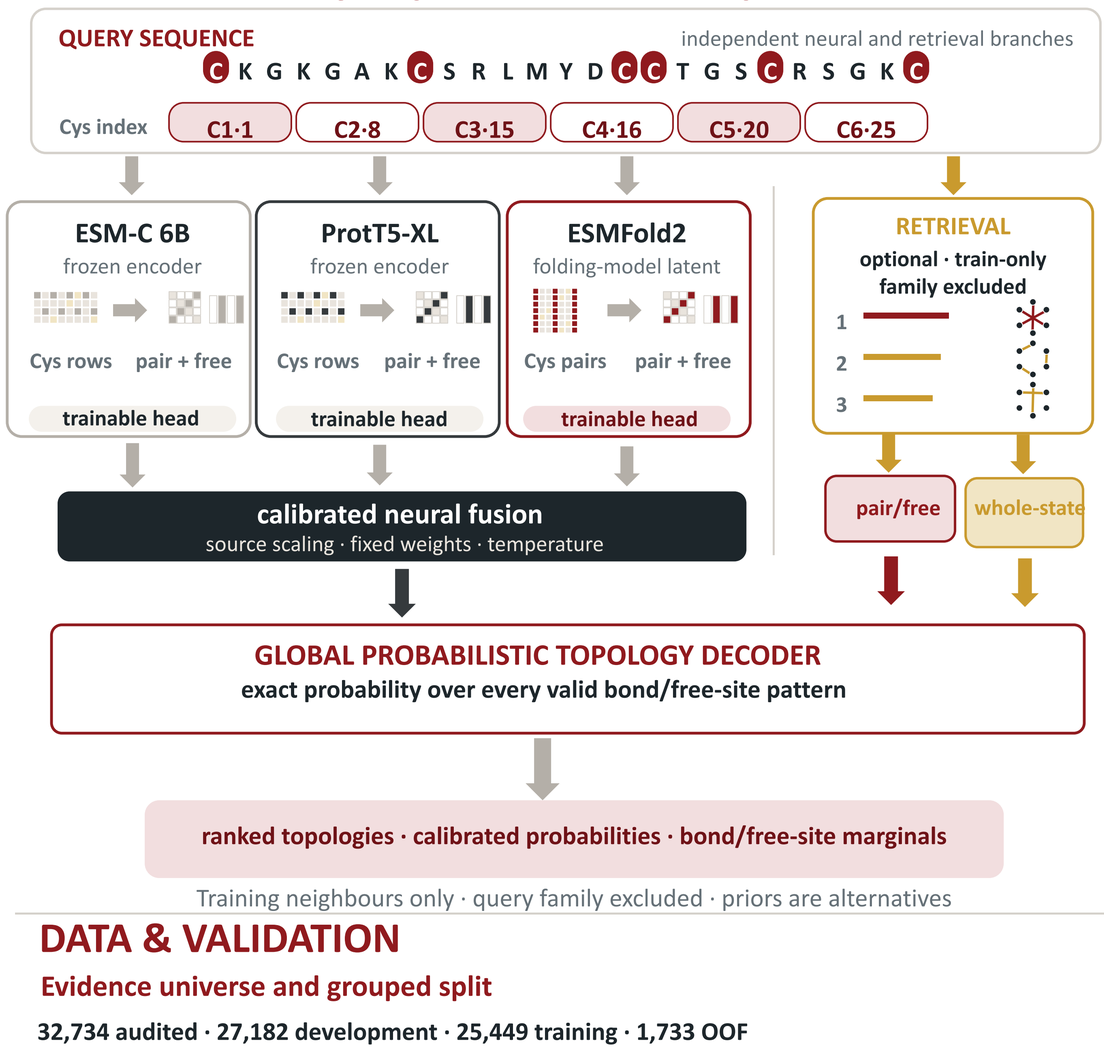
One peptide sequence can encode many valid disulfide connectivities

Connectivity determines peptide fold and stability. One sequence can admit many valid bond patterns, including free cysteines and odd cysteine counts.



Output: ranked topologies · calibrated probabilities · bond/free-site marginals · bond-count uncertainty

METHOD · How CysTopoFold learns and predicts

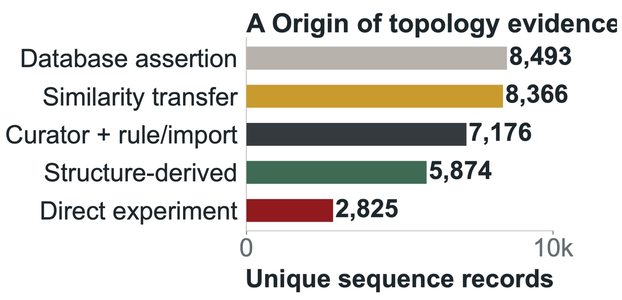


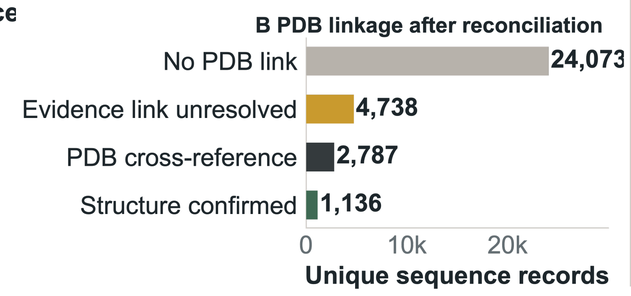
Training neighbours only · query family excluded · priors are alternatives

DATA & VALIDATION

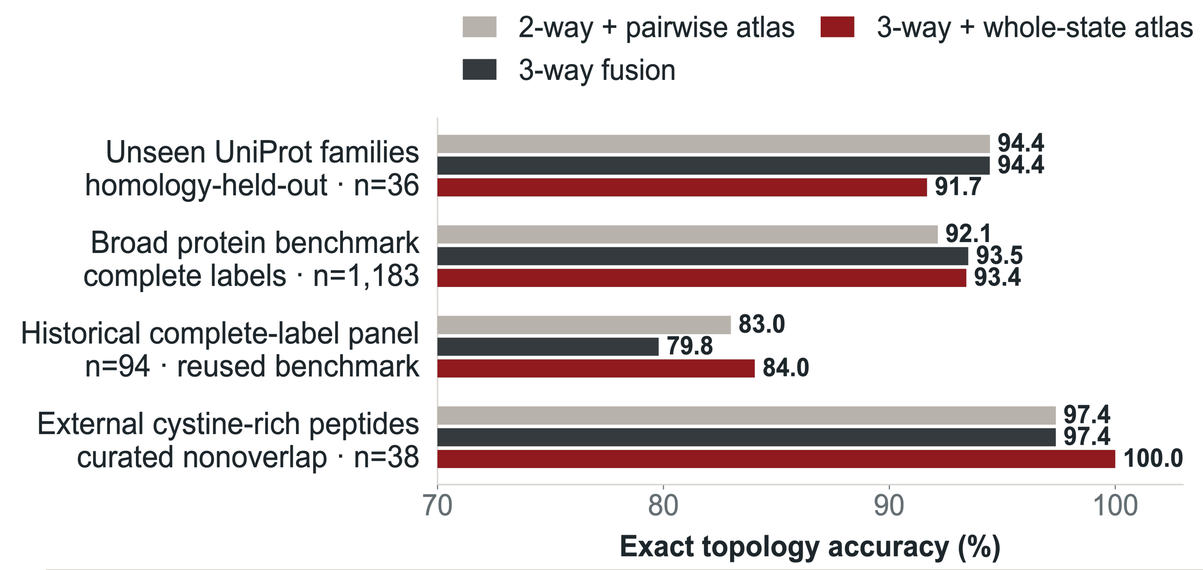
Evidence universe and grouped split

32,734 audited · 27,182 development · 25,449 training · 1,733 OOF

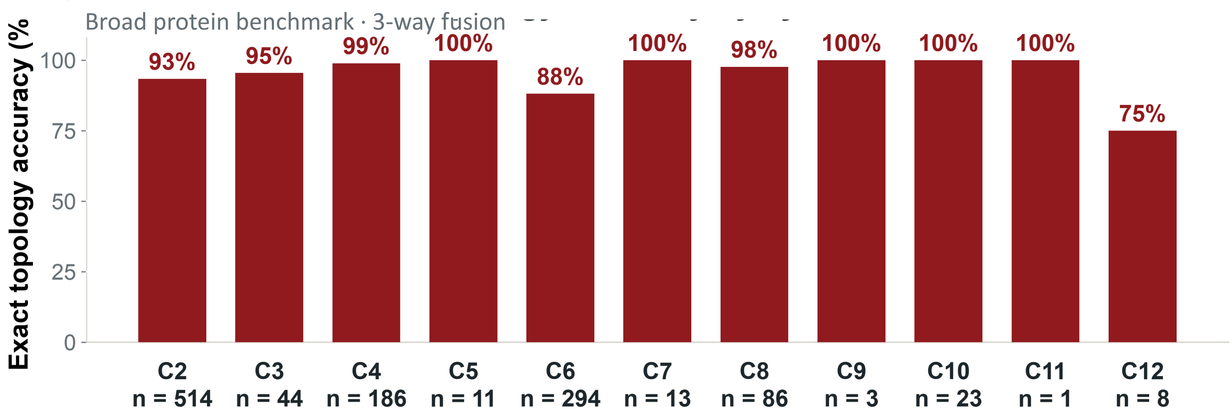




RESULTS · Performance across complementary cohorts

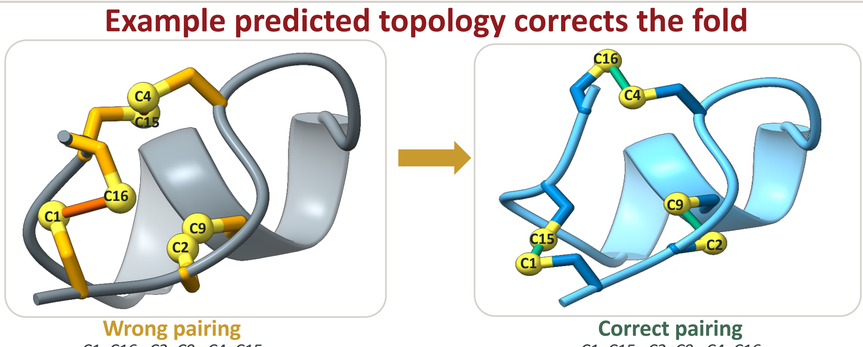


Cysteine-count audit



All C2-C12 groups shown · C9 (n=3) and C11 (n=1) are descriptive

Example predicted topology corrects the fold

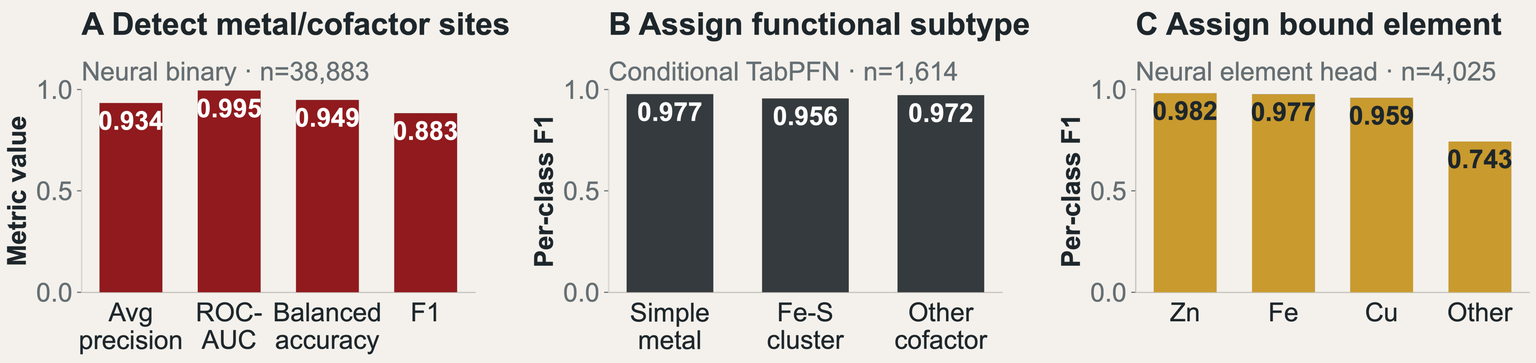


Wrong pairing
C1–C16 · C2–C9 · C4–C15

Correct pairing
C1–C15 · C2–C9 · C4–C16

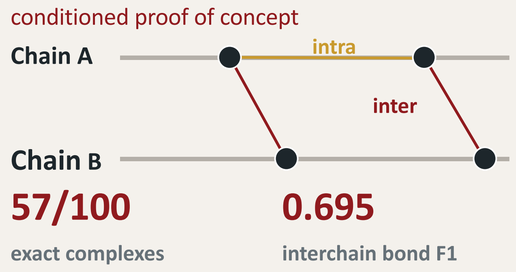
ADDITIONAL PREDICTIONS · Metal and interchain

Cysteine metal roles · three separate predictors



Interchain disulfides

conditioned proof of concept



57/100 exact complexes

0.695 interchain bond F1

Input: two sequences, eligible cysteines, bond count.
Exact: every typed bond correct.

CONCLUSIONS

Global decoding yields valid topologies and calibrated uncertainty.

Neural and retrieval evidence improve robustness across evaluation cohorts.

Next: prospective validation and joint endpoint discovery for interchain disulfides.


Marin Matic
Postdoctoral researcher


Alexander Hauser
Associate Professor

Supported by the Lundbeck Foundation

Department of Drug Design and Pharmacology · University of Copenhagen

Pharmacoinformatics group

Research group · University of Copenhagen

drug.ku.dk/research-sections/pharmaceutical-informatics/pharmacoinformatics/

Related work: Hermes J, Matic M, et al. Peptide ligand discovery of G protein-coupled receptors. Nat Rev Methods Primers 6, 52 (2026). doi:10.1038/s43586-026-00503-5

For Center for Pharmaceutical Data Science Education check cpdse.dk

Scan for group website

Connect with Marin on LinkedIn

linkedin.com/in/marin-matic-7401329a

Marin Matic · marin.matic@sund.ku.dk

Project questions, collaboration and updates

Scan to connect

38th EPS
European Peptide Symposium
6 - 11th of September 2026
Vienna, Austria

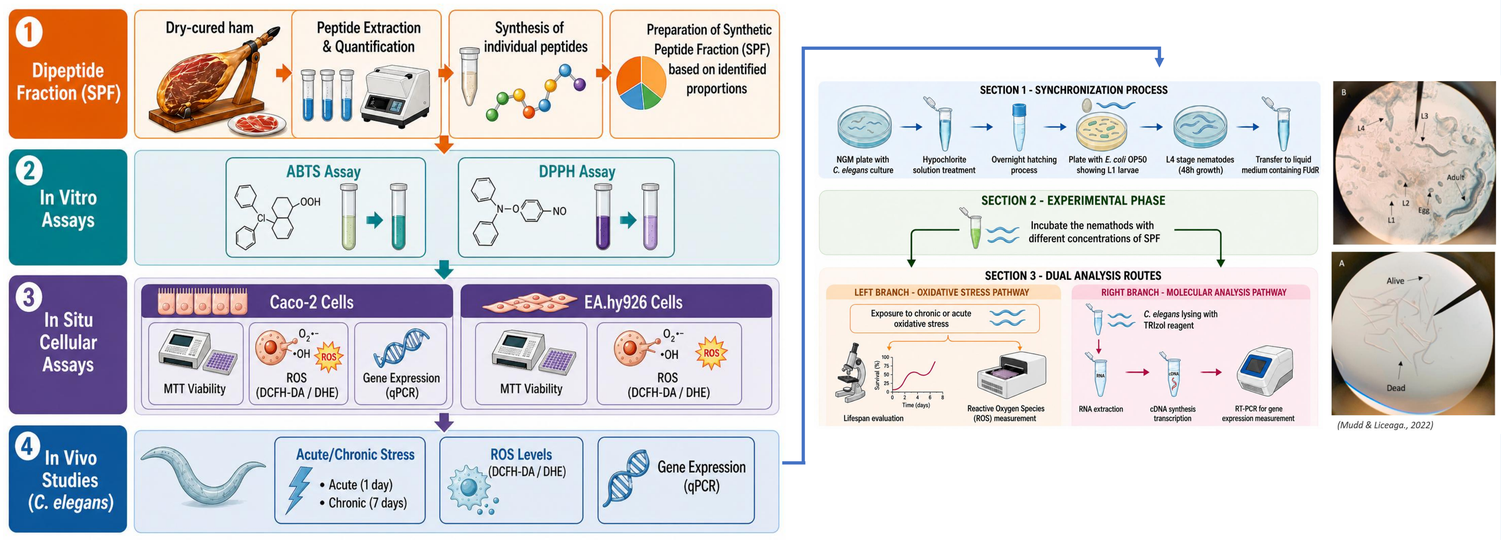
In vivo evaluation using *C. elegans*, of the bioactive potential of synthesized dipeptides previously identified in Spanish dry-cured ham.

H.C. Noelia[1], T. Luis[2], A. Adela[2] & L. Andrea M[1]
[1]*Protein Chemistry and Bioactive Peptides Laboratory, Department of Food Science, Purdue University, West Lafayette, IN, USA.*
[2]*Faculty of Pharmacy and Nutrition, Universidad Católica de Murcia – UCAM, Campus de los Jerónimos, 30107, Murcia, Spain.*
Email: herna923@purdue.edu, aliceaga@purdue.edu

INTRODUCTION

Oxidative stress causes cellular damage and contributes to chronic diseases. Food-bioactive peptides (BAP) are gaining interest as potential antioxidant compounds. Our previous work identified BAP from Spanish dry-cured ham, but their specific contribution to antioxidant activity remains poorly understood. In this study, ten dipeptides previously identified in digested Spanish dry-cured ham were synthetized according to their relative abundance and evaluated for their antioxidant activity using chemical, cellular and *in vivo* methods.

METHODS



(Mudd & Liceaga., 2022)

RESULTS & CONCLUSIONS

Table 1. In vitro antioxidant activity of digested ham peptide fraction (HDP) and a reconstructed synthetic peptide fraction (SPF) determined by DPPH and ABTS radical scavenging assays, measured as IC_{50} (mg/mL) ± SEM*.

	DPPH	ABTS
Sample code[1]	IC_{50} (mg/mL)	
HDP	$0.431^{a} \pm 0.092$	$0.279^{a} \pm 0.019$
SPF	$0.722^{b} \pm 0.108$	$0.322^{a} \pm 0.082$
Control	-	-

HDP: Ham digested peptide fraction
SPF: Synthetized dry-cured ham peptide fraction
Control: Distilled water. «-»: not detected / not applicable.
**SEM: standard error of the mean.*

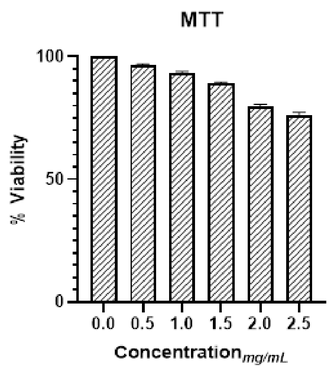


Fig. 1. Effect of ham synthetized peptide fraction (SPF) on the viability of Caco-2 cells, reported as Cell Viability % using the MTT assay.

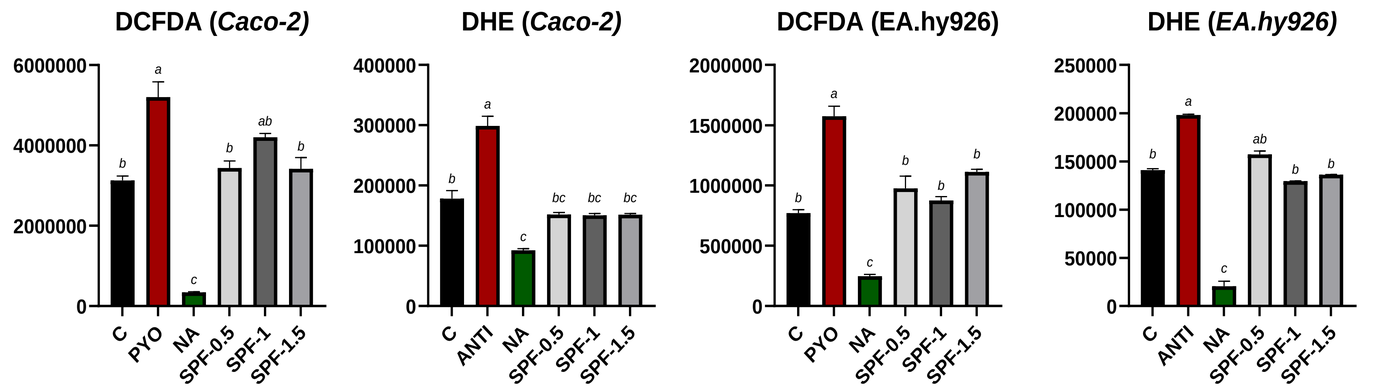


Fig. 2. Cellular antioxidant activity in Caco-2 & EA.hy926 cells, reported as ROS generation in the DCFDA & DHE assays, for synthetized Spanish dry-cured ham peptide fraction (SPF) at different concentrations (0.5, 1 and 1.5 mg/ mL). Values represent the mean of three replicates ± SEM. Trials that do not share the same letter (a, b, c) are significantly different (P<0.05).

The synthetic dry-cured ham peptide fraction (SPF) showed antioxidant activity in both DPPH and ABTS assays (**Table 1**), with activity comparable to the digested ham fraction (HDP) in ABTS. SPF showed no relevant cytotoxicity in Caco-2 cells (**Fig.1**), maintaining approximately 80% viability up to 2.0 mg/mL. In both Caco-2 and EA.hy926 cells (**Fig.2**), SPF significantly (*P<0.05*) decreased intracellular ROS generation compared with the oxidated control (PYO). No significant differences (*P>0.05*) were observed among the SPF concentrations tested (0.5–1.5 mg/mL), confirming its cellular antioxidant activity.

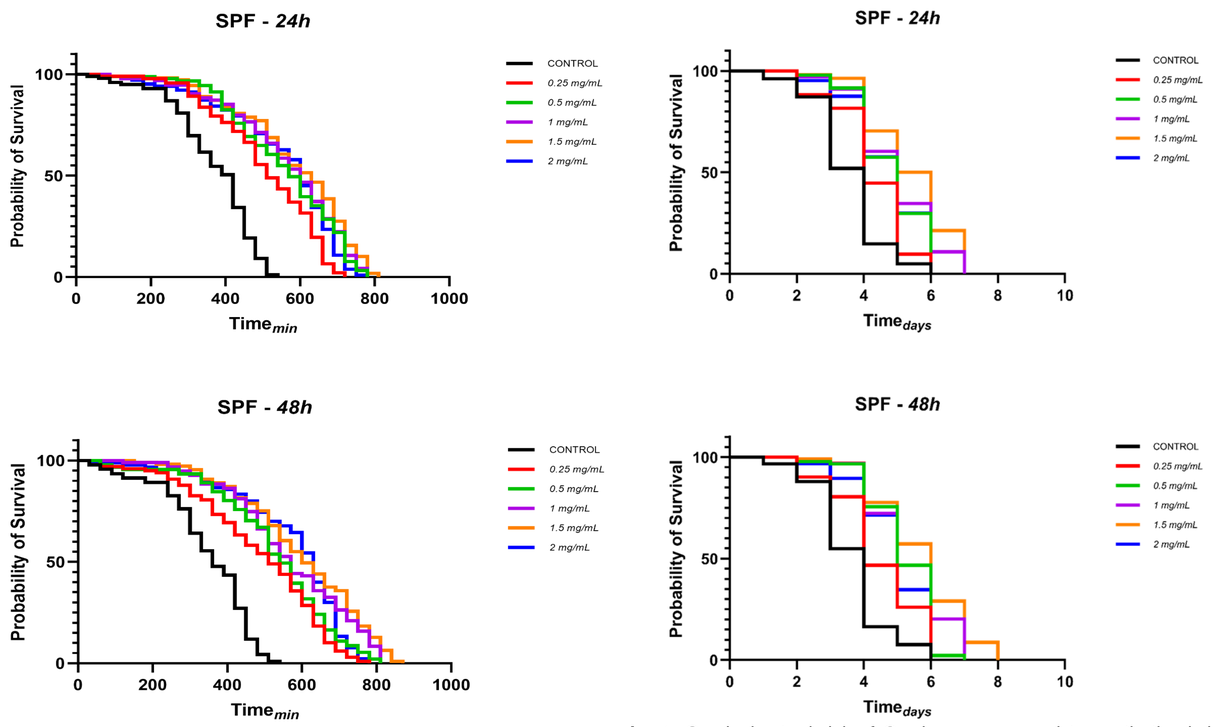


Fig. 3. Survival rate (min) of C. elegans exposed to synthetized dry-cured ham peptide fraction (SPF) at 0.25 to 2.0 mg/mL for 24 and 48 h, followed by acute oxidative stress conditions in the presence of 5mM t-BOOH.

Fig. 4. Survival rate (min) of C. elegans exposed to synthetized dry-cured ham peptide fraction (SPF) at 0.25 to 2.0 mg/mL for 24 and 48 h, followed by chronic oxidative stress conditions in the presence of 25mM paraquat.

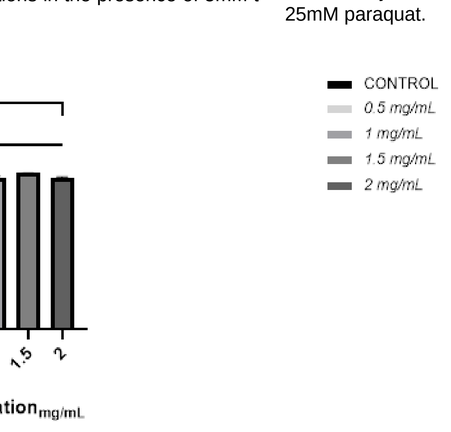


Fig. 5. Reactive oxygen species (ROS) levels in *C. elegans* pretreated with different concentrations of synthetized dry-cured ham peptide fraction (SPF) at different concentrations and then exposed to paraquat (PQ) for 48 h. Results are expressed as mean ± SEM from three independent biological experiments.

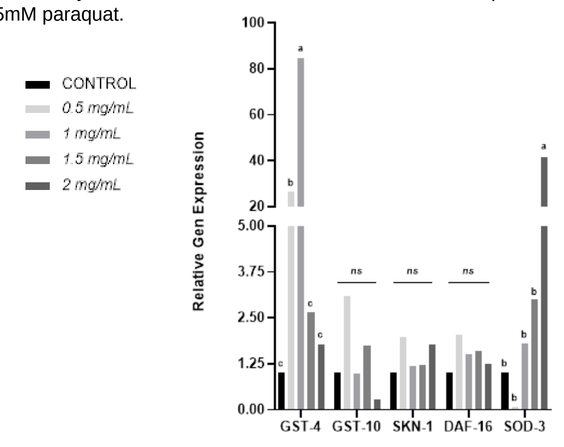


Fig. 6. Effect of synthetized dry-cured ham peptide fraction (SPF) on antioxidant gene expression in *C. elegans*. Trials for each gene that do not share the same letter (a, b, c) are significantly different (P<0.05); ns, not significant.

SPF pretreatment significantly increased *C. elegans* survival to acute oxidative stress (**Fig. 3**) conditions induced by t-BOOH (*P<0.05),* with the strongest protective effect observed at 1.0 and 1.5 mg/mL. Survival reached approximately 600–650 min compared with ~350 min in the control group. Under chronic oxidative stress (**Fig.4**) induced by paraquat, SPF also significantly increased nematode longevity *(P<0.001),* with 1.0 mg/mL increasing mean survival rate from approximately 3 to 5 days. Overall, SPF enhanced survival of *C. elegans* to both acute and chronic oxidative stress conditions.

SPF pretreatment significantly decreased intracellular ROS accumulation in *C. elegans* (**Fig. 5**) exposed to paraquat (48 h), with all tested concentrations showing lower ROS levels than the oxidant control *(P<0.05)*. ROS levels approached those of the untreated control, while no significant differences *(P>0.05)* were observed among SPF concentrations. SPF treatment modulated the expression of antioxidant defense genes (**Fig. 6**), showing an upregulation of GST-4 and SOD-3, although the response varied depending on the SPF concentration used. These findings support the antioxidant and protective effects of SPF against oxidative stress in *C. elegans*.

In **conclusion**, the synthetic dry-cured ham peptide fraction (SPF) showed consistent antioxidant activity across chemical, cellular, and *in vivo* (*C. elegans*) studies, decreasing ROS levels and enhancing resistance to acute and chronic oxidative stress. Overall, these results support the potential of the identified Spanish dry-cured ham dipeptides as bioactive antioxidant compounds.

BIBLIOGRAPHY
1. *Hernández-Correas N, Liceaga-Gesualdo AM, Abellán A, Noguera-Navarro C, Montoro-García S, Tejada L. In Vivo Evidence of Antioxidant Activity from Dipeptides Synthesized from Spanish Dry-Cured Ham. Int J Pept Res Ther 2026;32:70. https://doi.org/10.1007/s10989-026-10850-2.*
2. *Mudd N, Liceaga AM. Caenorhabditis elegans as an in vivo model for food bioactives: A review. Curr Res Food Sci 2022;5:845–56. https://doi.org/10.1016/j.crfs.2022.05.001.*

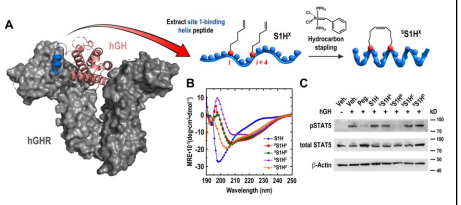
https://doi.org/10.17952/38EPS.2026.P225

https://doi.org/10.17952/38EPS.2026.P487

A Helical Peptide Antagonist of the Human Growth Hormone Receptor

J. M. Holub*, K. Nahar, R. Basu, A. Ahmad, J. A. Pettis, U. Gamage and J. J. Kopchick
Department of Chemistry and Biochemistry, Ohio University
133 University Terrace, Athens, OH 45701 United States

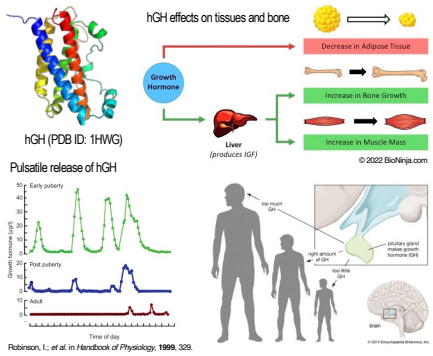
Abstract



The binding of human growth hormone (hGH) to the human growth hormone receptor (hGHR) is a key endocrinological process that controls critical aspects of cell growth, proliferation and differentiation. This sequential, asymmetric binding event involves the interaction between a single hGH molecule and distinct sites (site 1 and site 2) on the extracellular domain of a preformed hGHR homodimer. Our group recently identified S1H, a rationally-designed peptide sequence mimetic of the hGH site 1-binding helix that disrupts the hGH-hGHR interaction and inhibits hGH-mediated STAT5 phosphorylation in cultured hGHR-positive cell lines. Structure-activity relationship studies revealed a strong correlation between helical propensity and inhibitory potency of the S1H peptide, prompting the design of structurally "stabilized" S1H variants (SS1H) with improved helicity (Figure A). Here, we used hydrocarbon stapling to generate a series of ^{S}S1H peptides that proved to be more helical, proteolytically stable and biologically active compared to linear (unstructured) S1H (Figures B and C). Notably, one ^{S}S1H derivative, ^{S}S1H^{B}, inhibited hGH-induced STAT5 phosphorylation in hGHR-positive bladder cancer cells more effectively than pegvisomant, the only hGHR antagonist currently approved by the FDA. Collectively, our results demonstrated that hydrocarbon stapling improves the antagonistic effects of S1H peptides and elevates their potential as chemical probes to study the molecular mechanisms of hGH signaling. It is also anticipated that ^{S}S1H peptides will serve as potent lead compounds for developing next-generation therapeutics designed to treat endocrine disorders that manifest along the hGH-hGHR signaling axis.

1

Biology of the Human Growth Hormone (hGH)



Robinson, I.; *et al. in Handbook of Physiology*, **1999**, 329.

Growth Hormone Actions in Humans

Normal Physiology

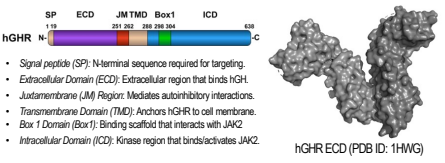
- **Promotes bone and muscle growth**
- **Supports insulin resistance**
- **Stimulates lipolysis in adipose tissue**

Disease and Medicine

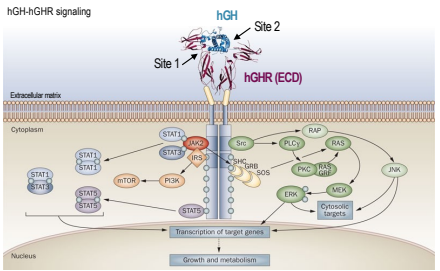
- **Excess growth hormone can lead to gigantism or acromegaly**
- **Growth hormone deficiency (GHD)**
- **Used to increase muscle mass, reduce body fat, and aid recovery**

2

The Human Growth Hormone Receptor (hGHR)



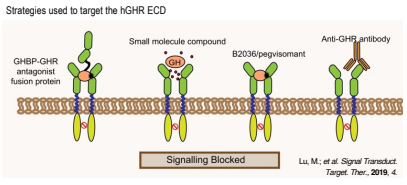
- *Signal peptide (SP)*: N-terminal sequence required for targeting.
- *Extracellular Domain (ECD)*: Extracellular region that binds hGH.
- *Juxtamembrane (JM) Region*: Mediates autoinhibitory interactions.
- *Transmembrane Domain (TMD)*: Anchors hGHR to cell membrane.
- *Box 1 Domain (Box1)*: Binding scaffold that interacts with JAK2
- *Intracellular Domain (ICD)*: Kinase region that binds/activates JAK2.

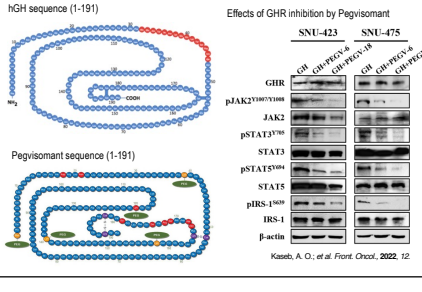


Brooks, A.; *et al. Nat. Rev. Endocrinol.* **2010**, *6*, 515.

3

Inhibiting the hGH-hGHR Signaling Axis

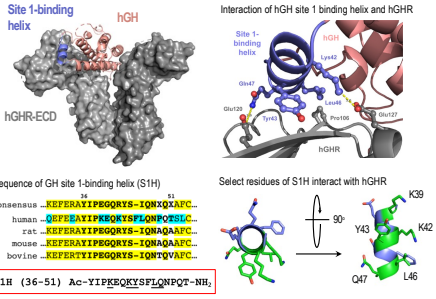




Kaseb, A. O.; *et al. Front. Oncol.*, **2022**, *12*.

4

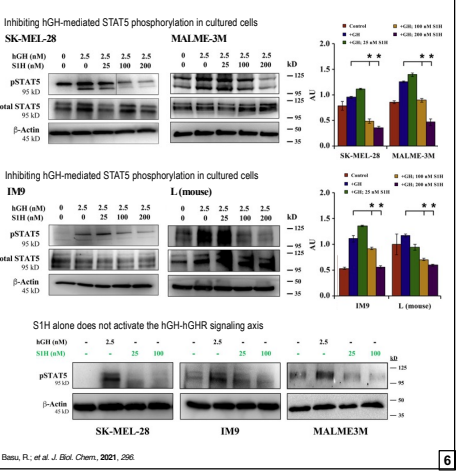
Design and Characterization of S1H Peptide



Basu, R.; *et al. J. Biol. Chem.*, **2021**, *296*.

5

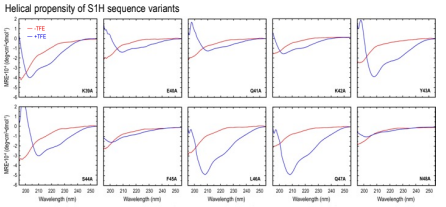
S1H Inhibits hGH-mediated STAT5 Phosphorylation

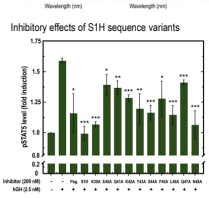


Basu, R.; *et al. J. Biol. Chem.*, **2021**, *296*.

6

Correlating Helicity and Inhibitory Activity





Structural and inhibitory data of S1H sequence variants

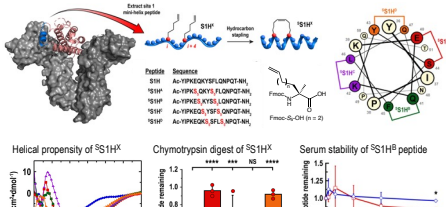
Peptide	Sequence	% helical peptide - TFE	% helical peptide + TFE	Percent inhibition
S1H (36-51)	^{36}YIPKEQKYSFLQNPQT-NH2	1.1	48.2	93.3
S1H (K36A)	^{36}YIPAEQKYSFLQNPQT-NH2	23.4	67.1	88.5
S1H (E40A)	^{36}YIPKAQKYSFLQNPQT-NH2	5.7	28.6	93.4
S1H (Q41A)	^{36}YIPKEAKYSFLQNPQT-NH2	8.3	25.4	97.4
S1H (K42A)	^{36}YIPKEQAYSFLQNPQT-NH2	2.4	24.4	91.7
S1H (Y43A)	^{36}YIPKEQKASFLQNPQT-NH2	11.2	68.8	66.6
S1H (S44A)	^{36}YIPKEQKYAFLQNPQT-NH2	15.7	63.5	72.3
S1H (F45A)	^{36}YIPKEQKYSALQNPQT-NH2	11.1	21.4	92.5
S1H (L46A)	^{36}YIPKEQKYSFAQNPQT-NH2	7.0	66.3	79.1
S1H (Q47A)	^{36}YIPKEQKYSFLANPQT-NH2	8.2	66.2	90.1
S1H (N48A)	^{36}YIPKEQKYSFLQAPQT-NH2	6.7	12.2	89.1

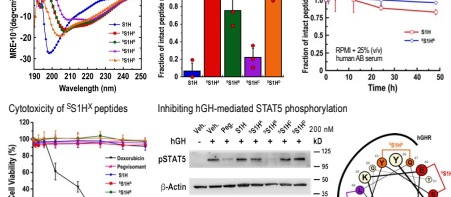
- Helical propensity for each variant was determined in the presence of TFE, a structure-inducing co-solvent.
- Inhibitory activity was evaluated by co-treating SK-MEL-28 cells with peptides and hGH and quantifying pSTAT5.
- Results showed a strong correlation between helical propensity and inhibitory function, *structured S1H variants?*

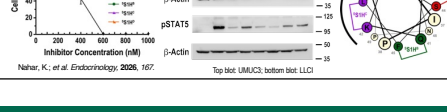
Basu, R.; *et al. J. Biol. Chem.*, **2021**, *296*.

7

Characterization of ^{S}S1H^{X} Peptides







Nahar, K.; *et al. Endocrinology*, **2026**, *167*.

Top blot: UMUC3; bottom blot: LLC1

8

Conclusions and Future Directions

What have we learned?

- We developed a novel peptide-based antagonist (S1H) of the human growth hormone receptor.
- S1H was derived from the hGH site 1-binding helix; inhibits hGH-mediated STAT5 phosphorylation.
- SAR studies revealed a strong correlation between helical propensity and inhibitory function.
- Select stapled S1H derivatives show enhanced helicity, proteolytic stability, and biological activity.

…and where can we go from here?

- Purify recombinant hGHR from bacteria for *in vitro* binding assays; map S1H-hGHR interaction.
- Testing the activity of ^{S}S1H^{B} *in vivo* (*e.g.* lowering hGH-mediated IGF-1 levels in mice).
- Develop scyllatoxin-based S1H derivatives; more stable structure and genetically encodable.
- Develop S1H derivatives as *agonists* of the hGHR; linked peptides for hGHR dimerization.

9

Funding and Support

NIH 1R21AG081962-01
NSF MRI2018802
OHIO UNIVERSITY 1804
OHIO UNIVERSITY Heritage College of Osteopathic Medicine

38th EPS European Peptide Symposium
6 - 11th of September 2026
Vienna, Austria

10

https://doi.org/10.17952/38EPS.2026.P228

38th EPS
European Peptide Symposium
6 - 11th of September 2026
Vienna, Austria

Lorena Kröner[1], Jutta Meier[2], Marie-T. Hopp[1]

Bioactive Skin Peptides from Caudate Amphibians: Structural and Functional Insights

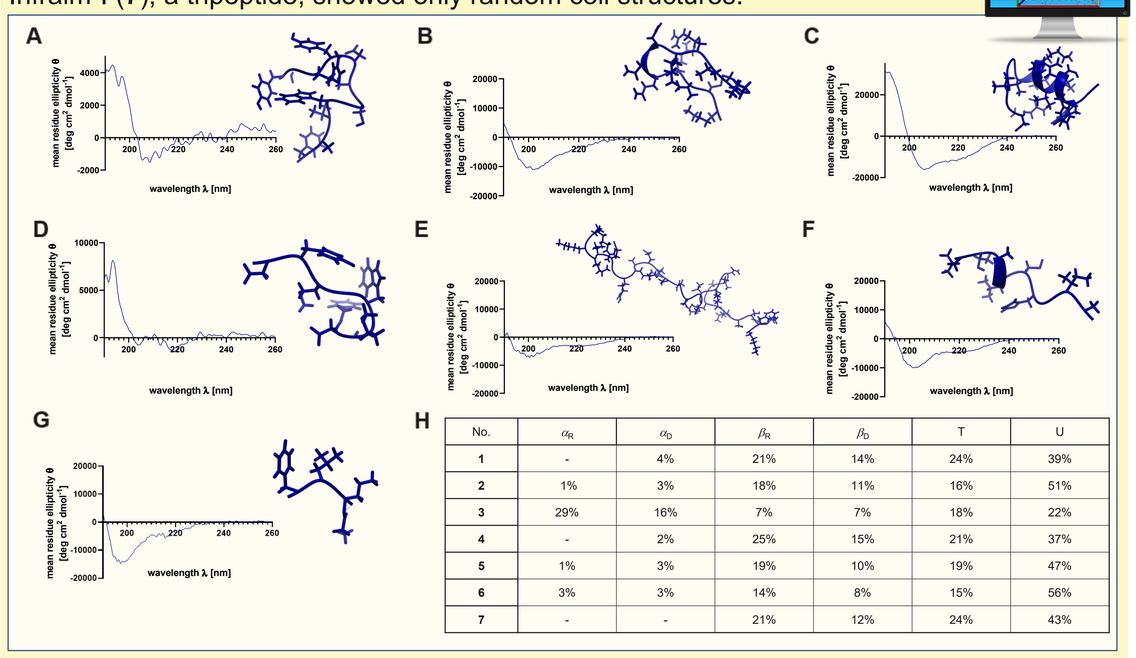
Background

Bioactive peptides from amphibian skin comprise a spectrum of molecules that are highly diverse in terms of both their structure and function, resulting in their essential role in the discovery and development of **novel therapeutic agents**. While skin peptides from Anura (i.e., frogs and toads) have been extensively studied over the past decades, the order Caudata (i.e., salamanders and newts) remains comparatively underexplored, although previous studies of caudate amphibian skin peptides reported promising bioactivities, like antimicrobial, wound-healing, and antiinflammatory effects.[1,2] To address this gap, seven currently known **caudate amphibian skin peptides** (3-34 mer) were synthesized and systematically compared.[3] Peptide synthesis was performed via standard Fmoc-based solid-phase peptide synthesis, incorporating native post-translational modifications, like C-terminal amidation, disulfide bond formation, and N-ethylation.[3] Analytical characterization was conducted by means of RP-HPLC, thin layer chromatography, and mass spectrometry.[3]

Results

Secondary structure analysis based on *in silico* studies and electronic circular dichroism (ECD) spectroscopy

Secondary structures of salamandrin-I (**1**), tylotoin (**2**), and andricin-I (**5**) unfolded during the course of the molecular dynamics (MD) simulation.[3] These **observations are coherent with the ECD analysis**: salamandrin-I (**1**) showed highest proportion in disordered regions, the β-sheet of tylotoin (**2**) is proportionally considerably lower than predicted (~29%), and in case of andricin-I (**5**) only a small proportion of helical elements (~4%) was observed (**Fig. 1**).[3] Ramosin (**3**) showed **highest proportions of α-helix**, which was substantiated by ECD spectroscopy (~45%) and MD simulation (~41%). Infraim-I (**7**), a tripeptide, showed only random coil structures.[3]



H

No.	α_R	α_D	β_R	β_D	T	U
1	-	4%	21%	14%	24%	39%
2	1%	3%	18%	11%	16%	51%
3	29%	16%	7%	7%	18%	22%
4	-	2%	25%	15%	21%	37%
5	1%	3%	19%	10%	19%	47%
6	3%	3%	14%	8%	15%	56%
7	-	-	21%	12%	24%	43%

Fig. 1. Secondary structure elements of caudate amphibian skin peptides. ECD spectra and structures after 100 ns MD simulation of peptide **1** (**A**), peptide **2** (**B**), peptide **3** (**C**), peptide **4** (**D**), peptide **5** (**E**), peptide **6** (**F**), and peptide **7** (**G**) are represented.[3] Secondary structure proportions based on deconvolution analysis of peptide **1-7** are displayed (**H**).[3] ECD spectra were recorded in 50% TFE in 10 mM phosphate buffer (pH 7.4).[3] α_R, regular α-helix; α_D, distorted α-helix; β_R, regular β-sheet; β_D, distorted β-sheet; T, turns; U, unordered.[3]

Determination of antioxidant capacity

The **ABTS$^{\bullet+}$ radical scavenging assay**, based on the decolorization of the radical, was used to assess the antioxidant capacities (**Fig. 2**).[3] Peptides and reduced glutathione (GSH; as a positive control) were tested in the range of 1 nM to 100 μM.[3] The **strongest antioxidant activity** was exhibited by salamandrin-I (**1**) and CCK-TV (**4**) with EC_{50} of ~4.07 μM and ~4.94 μM, while GSH achieved an EC_{50} of ~11.43 μM.[3] Ramosin (**3**) showed an antioxidant effect with an EC_{50} of ~6.39 μM, followed by andricin-I (**5**) with an EC_{50} of ~25.14 μM.[3] Weak or no antioxidant effects were observed for tylotoin (**2**), Ad-Cath (**6**), and infraim-I (**7**).[3]

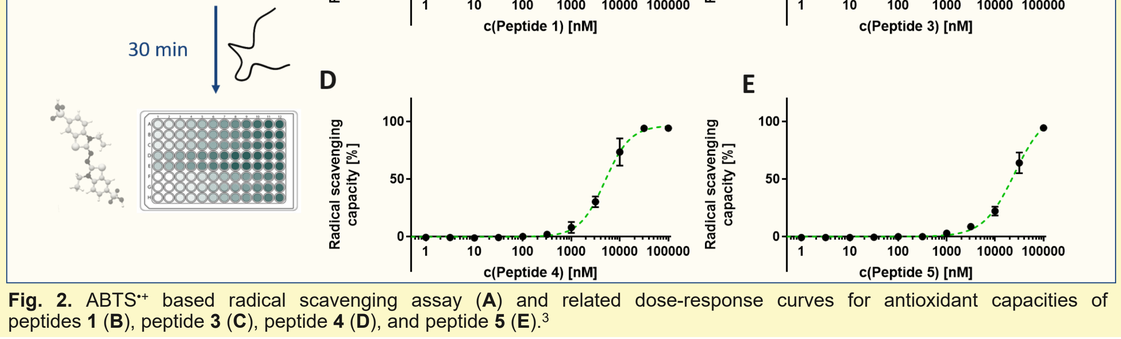


Fig. 2. ABTS$^{\bullet+}$ based radical scavenging assay (**A**) and related dose-response curves for antioxidant capacities of peptides **1** (**B**), peptide **3** (**C**), peptide **4** (**D**), and peptide **5** (**E**).[3]

Evaluation of antimicrobial properties

Antimicrobial properties of caudate amphibian skin peptides were determined by optical density growth measurements testing against two **Gram-positive** (*B. spizizenii*, *E. durans*) and two **Gram-negative bacterial strains** (*E. coli*, *P. fluorescens*) as well as yeast (*S. cerevisiae*) as a **fungal representative**.[3] Applied peptide concentrations varied from 100 nM up to 100 μM.[3] Salamandrin-I (**1**) affected the growth of both Gram-positive and Gram-negative bacteria as well as yeast.[3] Tylotoin (**2**) showed no antibacterial effect, but inhibited the growth of *S. cerevisiae*, leading to a prolonged lag phase at highest concentration tested.[3] Ramosin (**3**) has shown the **most potent antimicrobial properties against all selected microorganisms**, which was characterized by declining growth rates (e.g., starting at 10 μM for *E. durans* and 31.6 μM for *P. fluorescens*) or elongating lag phases at higher concentrations (**Fig. 3**).[3] In contrast, CCK-TV (**4**) lead to an increase of the growth rate and the lag phase of *S. cerevisiae* at 316 nM.[3] Andricin-I (**5**), Ad-Cath (**6**), and infraim-I (**7**) did not exhibit any inhibitory effect on the growth of the selected microorganisms.[3]

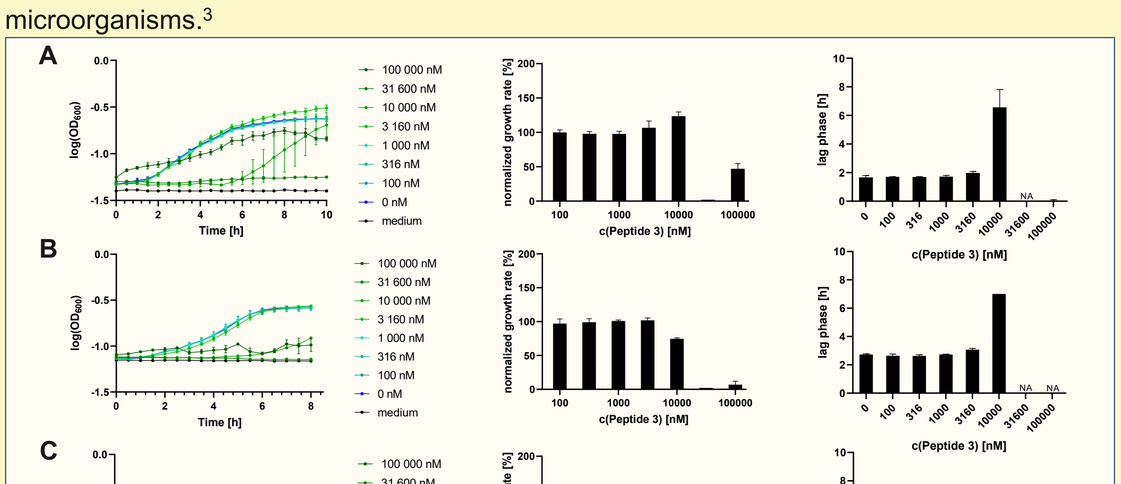


Fig. 3. Dose-dependent growth curves, normalized growth rates, and lag phases of representative bacteria and yeast in presence of selected peptides: Gram-positive *Bacillus spizizenii* DSM 618 in presence of peptide **3** (**A**) and Gram-positive *Enterococcus durans* ATCC 11576 in presence of peptide **3** (**B**).[3] Gram-negative *Escherichia coli* DSM 498 in presence of peptide **3** (**C**) and Gram-negative *Pseudomonas fluorescens* DSM 4358 in presence of peptide **3** (**D**).[3] Fungus *Saccharomyces cerevisiae* DSM 70449 in presence of peptide **1** (**E**) and in presence of peptide **3** (**F**).[3]

Conclusions

Peptides isolated from caudate amphibian skin secretions were synthesized and thoroughly characterized. ⊕ Four peptides exhibit strong antioxidant activity, while another four display distinct antimicrobial effects. ⊕ A correlation between the structural features of these peptides and their respective antimicrobial properties was substantiated. ⊕ The selective antimicrobial properties and antioxidant activities underscore their potential as scaffolds for peptide-based drug development. ⊕ Moreover, ADMET assessments are necessary to support their safe and effective progression toward pharmacological applications.

Contact
Prof. Dr. Marie-T. Hopp, Bioorganic Chemistry, Institute for Integrated Natural Sciences, University of Koblenz, Universitätsstraße 1, D-56070 Koblenz, +49 261 287 2259, mhopp@uni-koblenz.de

References
1 Xu, X. and Lai, R., Chem. Rev. **2015**, 115, 1760-1846.
2 Kröner, L. et al., Biol. Chem. **2024**, 405(9-19): 641-660.
3 Kröner, L. et al., J. Nat. Prod. **2026**, 89(5), 1426-1439.

Affiliations
[1] Bioorganic Chemistry, Institute for Integrated Natural Sciences, University of Koblenz, Koblenz, Germany
[2] Microbiology, Institute for Integrated Natural Sciences, University of Koblenz, Koblenz, Germany

Acknowledgement
This work is supported by the Joachim Herz Foundation. Financial support by the CZS STEM-Forum for interdisciplinary dialogue and material allowances by the Funds of the Chemical Industry are gratefully acknowledged. Conference grant (registration fee waiver) by the European Peptide Society is acknowledged as well.

EVOLUTIONARILY CONSERVED AMYLOID ARCHITECTURE IN THE PACAP–GLUCAGON PEPTIDE SUPERFAMILY

Dániel Horváth[a,b]*
Zsolt Dürvanger[a,b]
Szebasztián Szaniszló[a,b]
Anna Kiss-Szemán[b]
Duong Kim Hoang Yen[b],
Michael Hons[c],
Meytal Landau[c],
András Perczel[a,b]

[a] HUN-REN-ELTE Protein Modeling Research Group ELTE Eötvös Loránd University, Budapest, Hungary
[b] Laboratory of Structural Chemistry and Biology ELTE Eötvös Loránd University, Budapest, Hungary
[c] CSSB Centre for Structural Systems Biology, Hamburg, Germany

*daniel.horvath@ttk.elte.hu

https://doi.org/10.17952/38EPS.2026.P469

P469

HUN-REN Hungarian Research Network | CSSB Centre for Structural Systems Biology | ELTE FACULTY OF SCIENCE | INSTITUTE OF CHEMISTRY

AIM OF THE STUDY

To characterize the structural basis of amyloid formation within the human PACAP–glucagon peptide hormone superfamily.

WHY IS THIS IMPORTANT?

Members of the human PACAP–glucagon peptide hormone superfamily act through class B G protein-coupled receptors (GPCRs) to regulate diverse metabolic, neural, endocrine, and developmental functions. Their synthetic analogues have major therapeutic potential, exemplified by the current rise of GLP-1-based therapies.

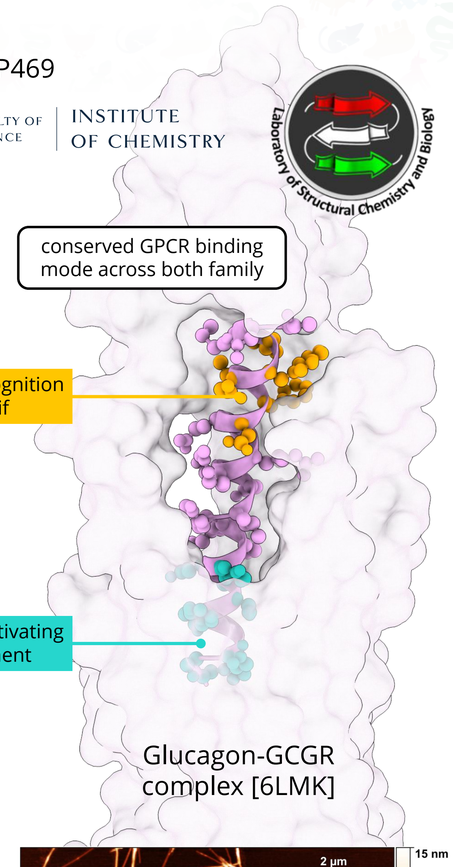
However, their efficient synthesis and formulation are challenged by their intrinsic aggregation propensity, which is linked to their physiological storage as amyloid assemblies (R1) at high concentrations in acidic secretory vesicles (R2) prior to release into the bloodstream.

Unlike pathological amyloids, these assemblies represent a functional and reversible state. Understanding their structural basis may therefore provide a basis for novel peptide formulation strategies.

GCG – glucagon; **GLP-1/2** - glucagon-like peptide-1/2; **GIP** - glucose-dependent insulinotropic polypeptide; **PACAP** - pituitary adenylate cyclase activating polypeptide; **PRP** – PACAP-related polypeptide; SCT – secretin; **GHRH** - growth hormone–releasing hormone; **VIP** - vasoactive intestinal peptide; **PHM/I** - peptide histidine methionine/isoleucine

GLUCAGON-FAMILY SEQUENCES	
GCG	HSQGTFTSDY SKYLDSRRAQ DFVQWLMNT
GLP-1	HAEGTFTSDV SSYLEGQAAK EFIAWLVKGR-NH_2
GLP-2	HADGSFSDEM NTILDNLAAR DFINWLIQTK ITD
GIP	YAEGTFISDY SIAMDKIHQQ DFVNWLLAQK GKKNDWKHNI TQ

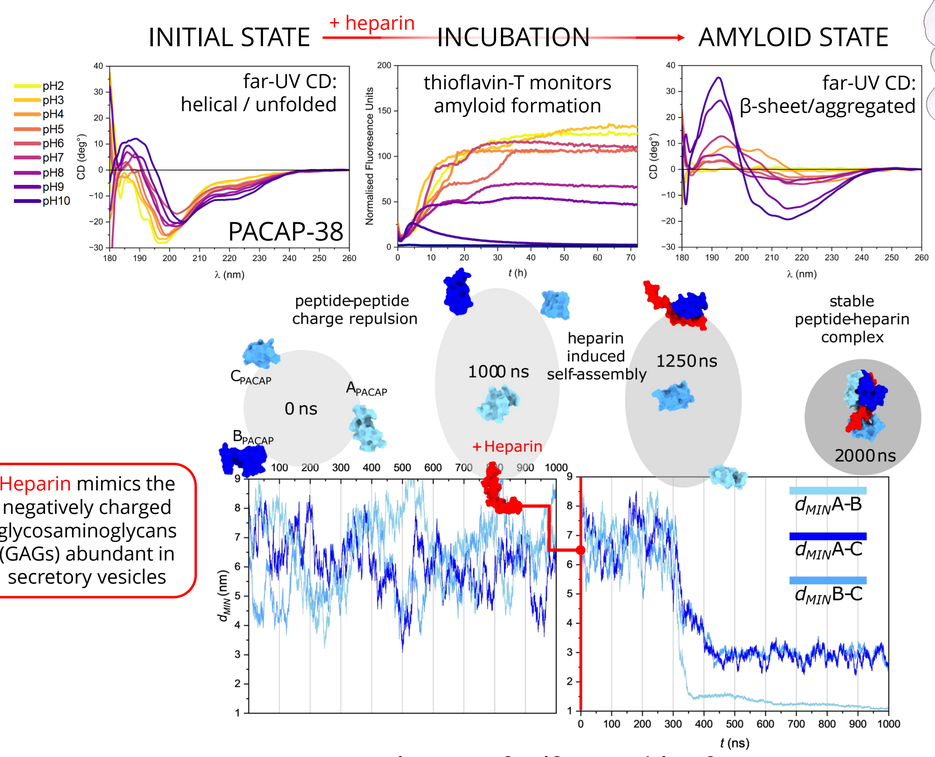
PACAP-FAMILY SEQUENCES	
PACAP-38	HSDGIFTDSY SRYRKQMAVK KYLAAVLGKR YKQRVKNK-NH_2
VIP	HSDAVFTDNY TRLRKQMAVK KYLNSILN-NH_2
PRP	DVAHGILNEAY RKVLDQLSAG KHLQSLVARG VGGSLGGGAGDDAEPLS
PHI	HADGVFTSDF SKLLGQLSAK KYLESLI
SCT	HSDGTFTSEL SRLREGARLQ RLLQGLV-NH_2
GHRH	YADAIFTNSY RKVLGQLSAR KLLQDIMSRQ QGESNQERGARARL-NH_2



WHAT DID WE FIND?

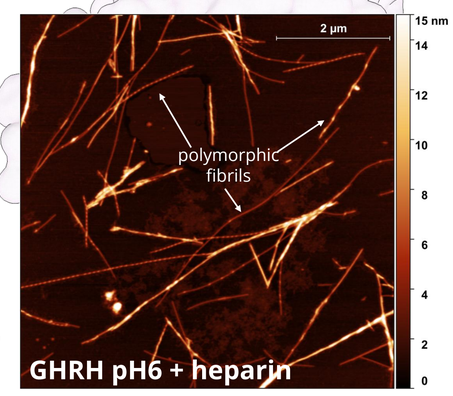
1. Glucagon-family peptides aggregate independently of heparin, whereas PACAP-family peptides require heparin for aggregation.

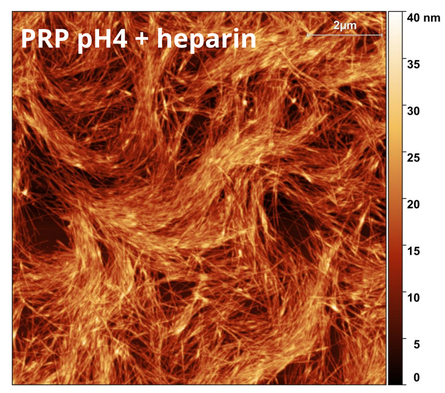
- 9/10 human hormones formed nanofibrillar amyloids at pH 4–6, close to secretory-granule conditions; secretin was the exception.
- Aggregation extended beyond this pH range, being generally favored at lower pH (pH < 5) but dependent on peptide charge distribution at higher pH (pH > 5).
- PACAP-family peptides required heparin for amyloid formation.
- MD simulations suggest that heparin recruits peptide monomers through electrostatic interactions, increasing their local concentration and promoting seed formation.
- Amyloid polymorphism occurred even within individual samples.



Heparin mimics the negatively charged glycosaminoglycans (GAGs) abundant in secretory vesicles

MD simulations of self-assembly of PACAP27



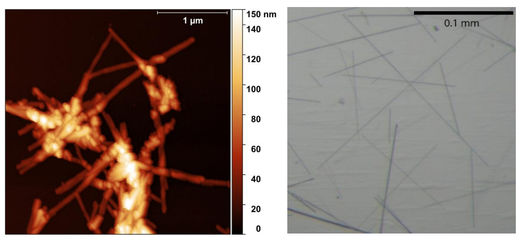


Atomic force microscopy micrographs of the amyloid fibrils

2. Amyloid formation is driven by sequence regions that also mediate receptor binding and activation.

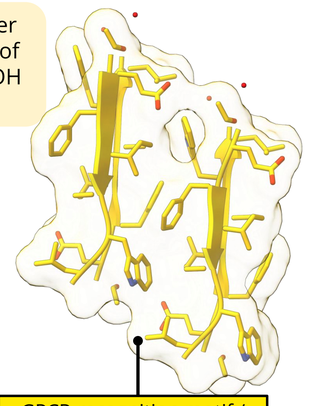
- Aggregation-prone hexapeptide regions (APRs) at conserved positions drive self-assembly and overlap with sequences involved in GPCR **binding** and **activation**.
- These hexapeptide segments form β-sheet-rich nano- and microcrystals with amyloid-like architecture revealed by X-ray crystallography.
- Aggregation propensity varies substantially between APRs:

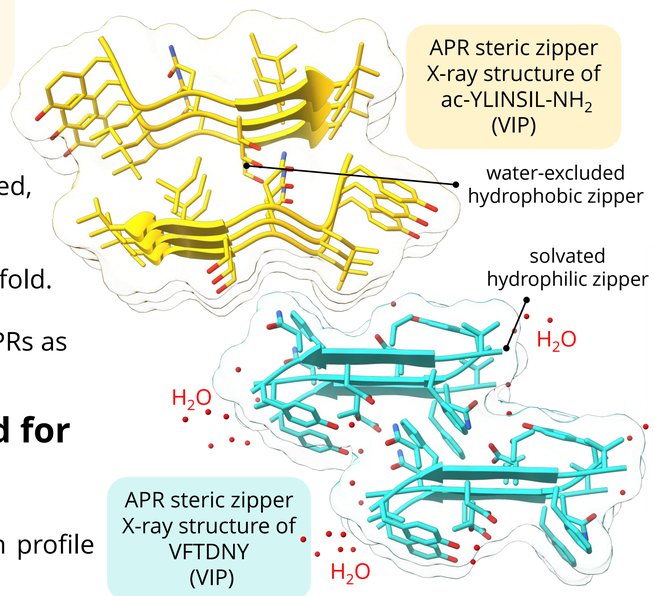
N-proximal APRs	**C-proximal APRs**
More polar	More hydrophobic
Similar sequence features across both families	Distinct sequence patterns between the two families
Weak aggregation propensity	Stronger aggregation propensity
Poorly predictedable	Well predictedable by aggregation predictors
Aggregate with protected APR termini	Glucagon family aggregate with free termini

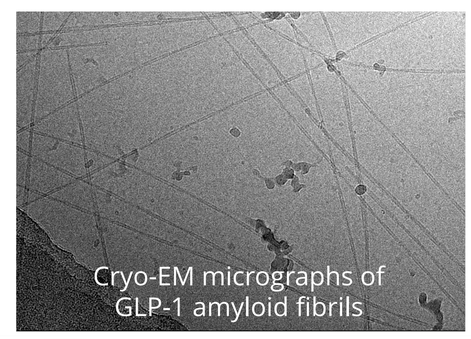


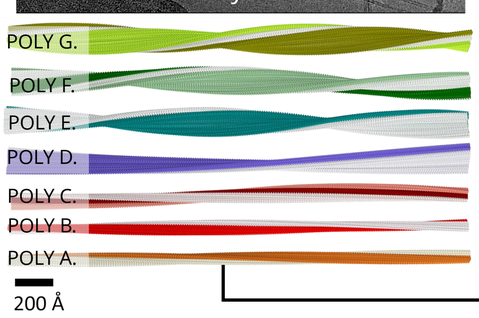
Nano- and microcrystals of hexapeptide ac-YLINSIL-NH_2 (VIP)

PDB-deposited APRs: 8ANJ; 8ANK; 8ONQ; 8ANN; 8ANL; 8ANH; 8ANM; 8ANI; 8ANG; 29VU; 29WR; 29VT; 29VS; 29VR; 29VQ; 29VP; 29VO

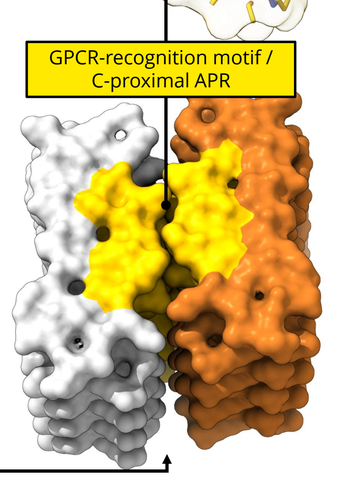








GLP-1 amyloid polymorphs



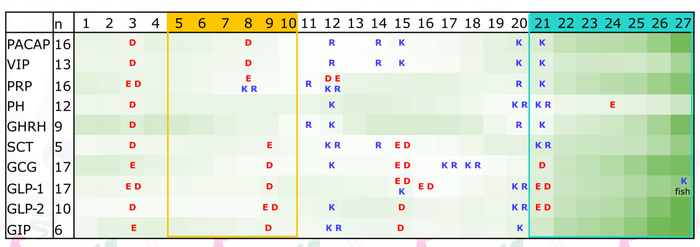
Cryo-EM structure of GLP-1 polymorph A (PDB deposited, not yet released)

- Aggregation is favored when amyloid gatekeeper Asp/Glu side chains are protonated, removing their negative charge.
- Tight steric zippers formed by diverse side-chain interactions stabilize the amyloid fold.
- Cryo-EM reveals pronounced GLP-1 polymorphism at two pH values, supporting APRs as key drivers of self-assembly.

3. The aggregation pattern of the family has been conserved for ~600 million years.

- Despite extensive evolution of receptor–ligand interactions (R3), the aggregation profile remained remarkably conserved across vertebrate evolution.
- PACAP–glucagon-related peptides from the extant protochordate *Chelyosoma productum* (R4), which diverged from the vertebrate lineage ~600 million years ago, retained this aggregation property.
- Early evolutionary divergence gave rise to distinct PACAP and glucagon families with chemically different amyloid gatekeeper patterns adjacent to the APRs.

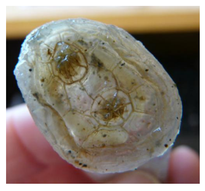
Gatekeepers in PACAP family	**Gatekeepers in glucagon family**
Lys/Arg dominance	Glu/Asp dominance
Positive charges limit self-assembly	Negative charges limit self-assembly
Less sensitive to pH changes	Protonation removes charge: →pH-sensitive aggregation
Heparin is required to neutralize these charges	Less sensitive to heparin



0 — Aggregation propensity — 1

Mean position-specific aggregation propensity across ***n*** species. Coloured residues indicate amyloid gatekeepers.

THE TAKE-HOME MESSAGE



Chelyosoma productum

- Our structural and genomic analyses reveal that amyloid formation is a more deeply conserved property of the PACAP–glucagon family than receptor specificity.
- Although this intrinsic aggregation propensity is often considered a “bug” in peptide synthesis and formulation, its remarkable evolutionary conservation suggests that it may in fact be a conserved biological feature.
- Understanding this functional, reversible amyloid state may therefore inspire novel strategies for peptide drug formulation.

OUR PAPERS

R1 R2 R3 R4

Research funded by:

National Research, Development and Innovation Office Hungary — PROJECT FINANCED FROM THE NRDI FUND
Project NO. STARTING 150597

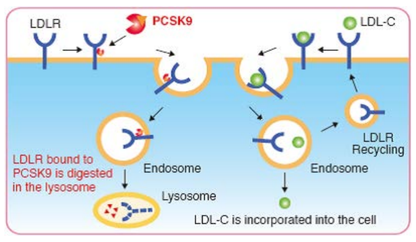
HUNGARIAN ACADEMY OF SCIENCES

https://doi.org/10.17952/38EPS.2026.P327

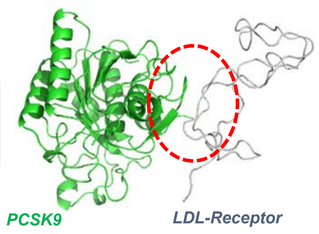
A PCSK9 Vignette: From mRNA Display to Passively Permeable Macrocycles

Yuhua Huang
on behalf of the PCSK9 team
Merck & Co., Inc., Rahway, NJ, USA

Proprotein Convertase Subtilisin-Kexin type 9 (PCSK9) as a therapeutic target



Blocking PCSK9:LDL-R increases clearance of LDL particles (↓LDL-C)



- **PCSK9 binds to LDL-R: blockade of PCSK9 relieves inhibition of LDL-R, permitting LDL particle clearance**
- **Large and flat interface of PCSK9:LDL-R amenable to mAb and peptide modalities. No SM leads**
- **Repatha® and Praluent® approved mABs PCSK9 inhibitors, sub-Q, 75-300 mg/2-4 weeks, costly**
- **Patients and prescribers prefer oral delivery; oral agents remain a significant unmet need**

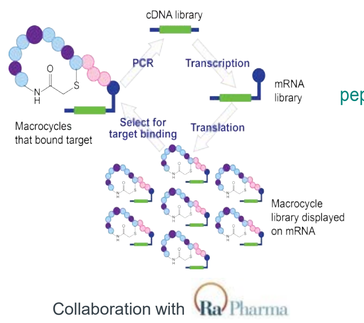
Formulation enabled oral (FEO)

Intrinsic passive permeability (IPP)

mRNA Display libraries as "hit" finding platform

Macrocyclic peptides can bind large, flat surfaces and can be more stable than linear peptides

mRNA Display screen

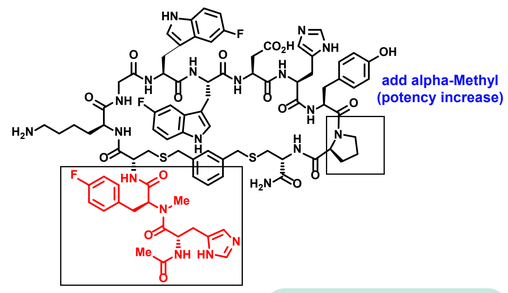


Collaboration with Ra Pharma

A trillion barcoded peptides in an eppendorf tube



Massive diversity

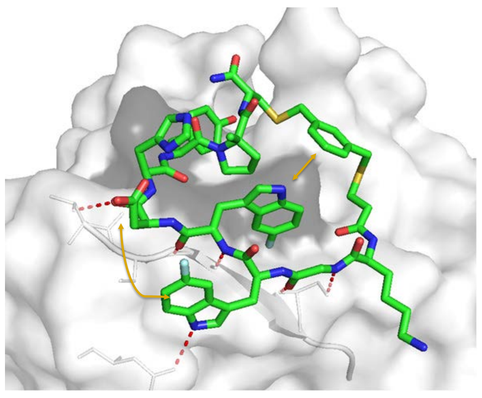


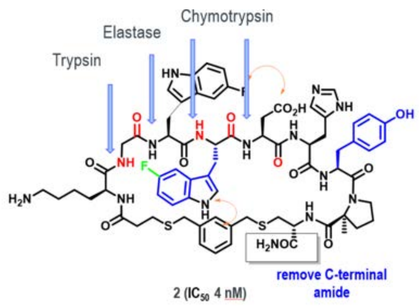
Lead A / compound 1
MW = 1889; 10-13 AA
TR-FRET IC_{50} = 483 nM

- Good potency
- Poor metabolic stability
- Poor physical properties
- No structural enablement
- No cellular permeability

J. Med. Chem. **2020**, 63, 13796; *J. Med. Chem.* **2021**, 64, 16770; *J. Biol. Chem.* **2013**, 289, 942; *Nat. Struct. Mol. Biol.* **2017**, 24, 848; Angew. *Chem. Int. Ed.* **2015**, 54, 8896.

Structure based drug design drives optimization of SAR



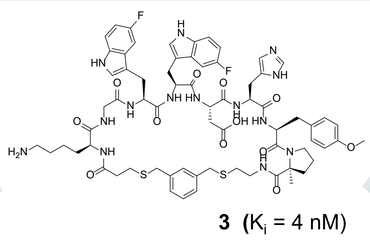


- Doughnut-like, flat contact surface (~190 Å²)
- 5 H-bonds with beta-sheet
- Key hydrophobic interactions
- 5F-TRP in center is a key interaction
- Potential areas for cross linking
- Sites prone to protease cleavage identified early

J. Med. Chem. **2020**, 63, 13796.

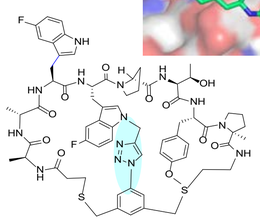
Cross-linking results in improvement in potency and protease stability

Top cross-link

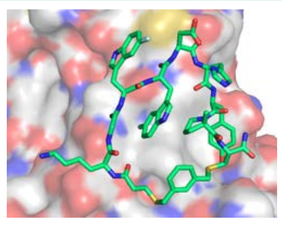


3 (K_i = 4 nM)

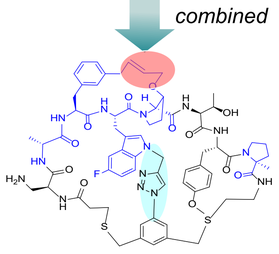
Middle cross-link



5 (K_i = 1.36 nM)



combined



4 (K_i = 0.3 nM)

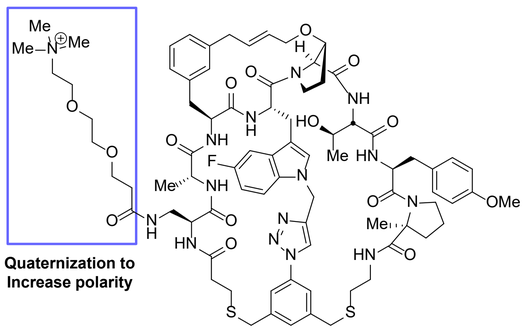
6 (K_i = 0.006 nM, protease stable PK improvement needed)

- 5 of the 8 amino acids are unnatural
- 3 of the unnatural amino acids are not commercially available

J. Med. Chem. **2020**, 63, 13796; *J. Med. Chem.,* **2021**, 64, 16770.

Optimize lead cyclic peptide

Chemistry tactics improved PK and stability



7 (K_i = 0.002 nM)

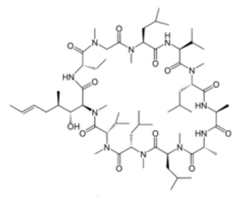
Pharmacokinetic Profile		
7	**Cyno**	**Rat**
CL (mL/min/kg)	**1.4**	**4**
$t_{1/2}$ (hr)	**7.6**	**4.6**
PPB (% bound)	**74**	**75**
Clu (mL/min/kg)	**6**	**15**
%F (30% Labrasol/PBS)	**2.9***	**1.4***

- ✓ Clean – MK499, CYP, ion channels
- ✓ PanLabs – no hits
- ✓ Oral delivery (enabled formulation)

*Dosed at 1 mpk PO gavage in cyno; 5 mpk ID (catheter) in rats.

Fully protease stable and not an OATP substrate.
Further Developed into MK-0616 (Elicitide) and approved as Lipfendra.

Inspired by precedence for bRo5, bioavailable macrocycles

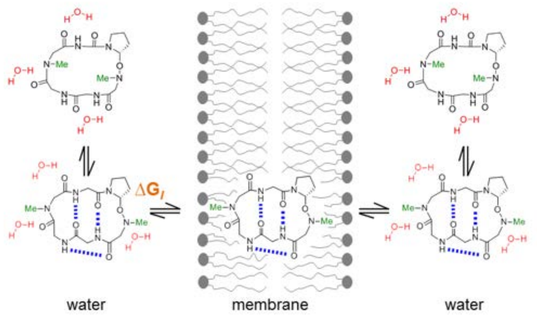


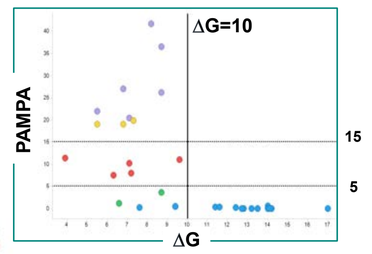
Cyclosporin A



HBD = 4
HBA =12
EPSA = 70
MW = 1215
Aromatic ring count = 0
ΔG = 5
F%: 10-89%

Build in chameleon-like properties driven by ΔG - incorporation of IMHBs





For PCSK9: *Predicted ΔG of <10 correlates well with passive permeability*

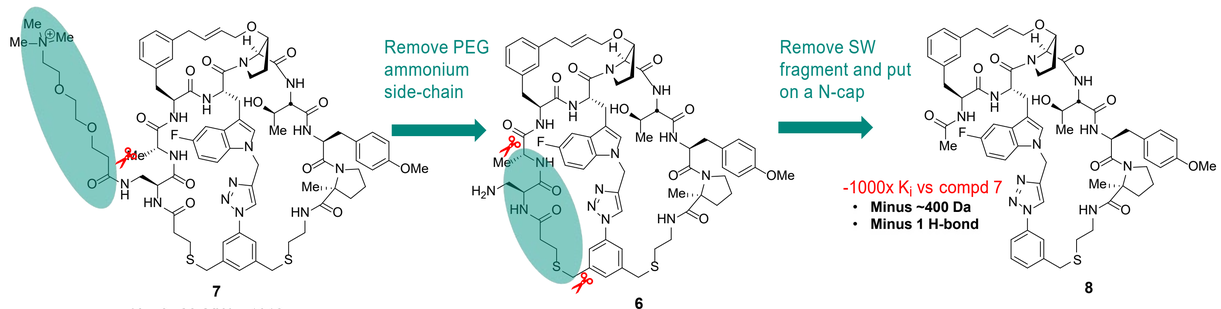
Guidelines for passive permeability:
EPSA <80; ΔG <15; HBD <4; MW <1000
Pampa >15; Papp >10;
Stable to stomach/gut enzymes

Passive transport

- *ΔG_I the free energy for transferring the LDC (low dielectric conformer) from water to the low-dielectric environment;* ***most informative for predicting passive permeability***
- Peptides in H_2O - adopt multiple, rapidly inter-converting conformations.
- The low dielectric of the membrane promotes the formation of intramolecular H-bonds (IMHBs)

Identification of minimum pharmacophore(s) is crucial in path to optimization

Reducing MW by removing PEG Ammonium side-chain and SW fragment



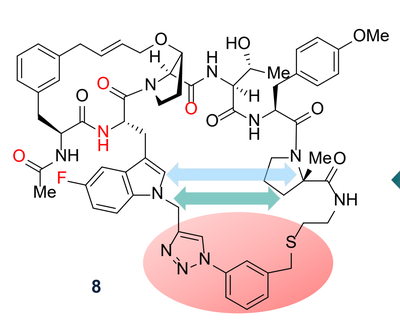
7
K_i = 2 pM; MW = 1612

6
K_i <6 pM; MW = 1408

8
K_i = 2.1 nM; MW = 1194
EPSA = 132; HBD = 6; ΔG = 13
Pe = **0**; Papp = 0.59
Rat Cl = 56 (OATP substrate)

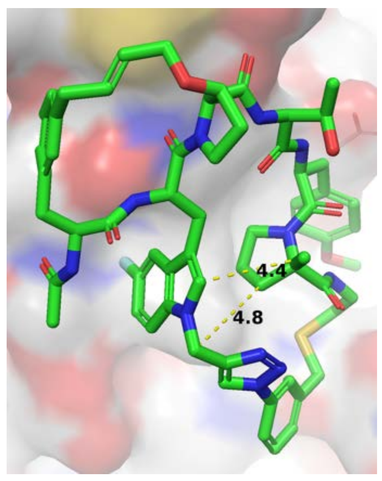
- Potent (single digit nM); 4 critical HBD retained with MW reduced by one third
- Few compds have Pe = 5-10; Papp – poor (compd stickiness)
- Poor physicochemical properties (very poor solubility)
- No oral BA
- ΔG = 13

Insight from structure suggests opportunity for new design



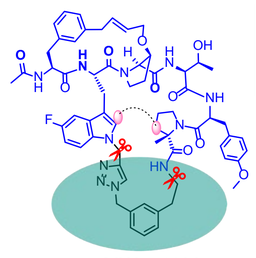
8

Structure guided truncation cross-link



As designed the truncated molecule ***retains the critical C=O/N-H*** that make contacts with the protein. The distances highlighted by the arrows are within ***4-5 Å, ideal for new crosslinks*** comprising of around 4 atoms. These new crosslinks can then replace the portion of the molecule highlighted in teal and still maintain the overall rigidity of the peptide.

Assess C2 connectivity

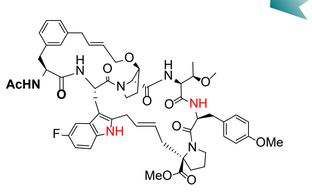


9 (K_i = 0.4 nM)

MW = 1162
Pe = 0
EPSA= 132

- **Permeability enhancement through N-methylation**
- Capping of N-terminal H-bond donor led to additional ***gains in permeability***

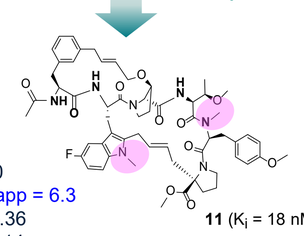
Truncate southern linker
Connect at C-2



10 (K_i = 35 nM)

MW = 1032
Pe = 16 , Papp = 2.0
EPSA = 102.5
PSA = 210.0

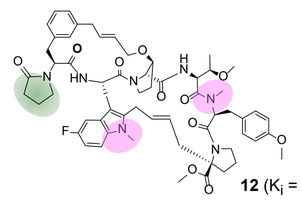
N-Methylation



11 (K_i = 18 nM)

MW = 1060
Pe = 38, Papp = 6.3
EPSA = 95.36
PSA = 177.14
ΔG = 8.3, F% = 0.3 (Rat PK)

Capping of N-terminal



12 (K_i = 164 nM)

MW = 1086
Pe = 21.85, Papp = 9.7
EPSA = 96.23
PSA = 183.4
ΔG = 6.8; F% = 2 (Rat PO)

Rat IV PK
CL = 32 mL/min/kg
Vss = 3.34 L/kg
MRT = 1.7 hr

Rat PO PK
%F = 2.2%
%F = 9.7% + pgp inhibitor
%F = 28.0% + pgp & CYP inhibitor

Conclusions

Translating permeability into oral absorption — balancing the potency trade-off

✓ C-2 linked series SAR validates medicinal chemistry strategy to maintain PCSK9 binding affinity and achieve moderate passive permeability in MDCKII cells

✓ **First moderately potent IPP molecule to have F >1% without any permeation enhancer**

- Additional in vivo studies suggest significant first pass metabolism and transporter activity
- Met ID studies suggest benzylic, olefin and N-methyl oxidative metabolism
- What is the impact of metabolism and transporter activity on bioavailability?

Presented at American Medical Women's Association (AMWA); November 4-7, 2026; Washington, DC, USA.

Copyright © 2026 Merck & Co., Inc., Rahway, NJ, USA and its affiliates. All rights reserved.

Random versus site-specific conjugation: impact on ADME properties of biologics with different format

Georgina Ilieska[1], Robert Thai[1],Carole Malgorn[1], Steven Dubois[1], Melissa De Souza[1], Camille Le Drezen[1], Justyne Vetel[1], Mathilde Keck[1], Antoine Sallustrau[2],Stephane Hua[1], Hervé Nozach[1], Nicolas Joubert[3],Caroline Denevault-Sabourin[3],Laurent Devel[1]

[1]Université Paris-Saclay/CEA/DRF/DMTS/SIMoS; F91191, Gif-sur-Yvette, France. [2] Université Paris-Saclay/CEA/DMTS/Service de Chimie Bio-organique et Marquage F91191, Gif-sur-Yvette, France. [3] UMR 1100/CEPR/University of Tours/ Proteolytic enzymes and their pharmacological targeting in lung diseases

georgina.ilieska@cea.fr

https://doi.org/10.17952/38EPS.2026.P091

ABSTRACT

Antibody format and conjugation strategy can strongly influence the properties and performance of antibody–drug conjugates. Here, we compare lysine-based and site-selective cysteine conjugation across anti-HER2 formats (IgG, Fab, VHH, and VHH-Fc) to determine how antibody size and conjugation affect stability, affinity, and in vivo behaviour. ^{3}H radiolabelling was performed by lysine acylation or disulfide rebridging followed by click chemistry [2]. Conjugates were characterized by SDS-PAGE, β-imaging, mass spectrometry, and BLI, with in vivo biodistribution assessed by β-imaging, ^{3}H quantification [3], and autoradiography. **Aim: Assess how antibody size and conjugation influence overall biological performance.**

1 Conjugation strategy

Protein size

Small protein (~15-25kDa) — VHH

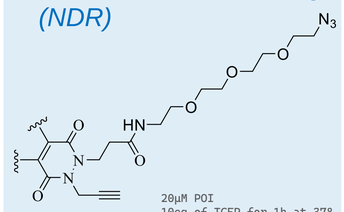
Medium protein (~50-90kDa) — Fab, VHH-Fc

Large protein (~150kDa) — IgG

HER2+ antigen binding site

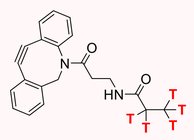
Site-specific conjugation

Step 1 — *Native disulfide rebriding (NDR)*



20µM POI
10eq of TCEP for 1h at 37°
40eq of TAG for 2h at 37°C

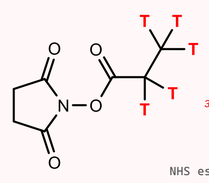
Step 2 — *SPAAC*



20µM of POI
20eq of DBCO-X for 5h at 4°C

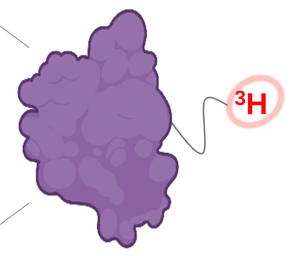
Random conjugation

Step 1 — *Lysine Acylation*

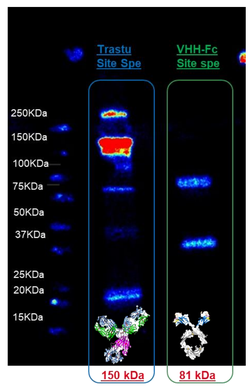


NHS ester chemistry

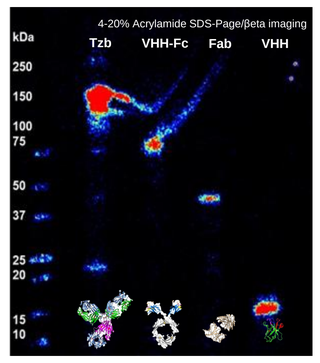
Radiolabelled conjugate



*protein size **x** conjugation strategy comparison*



N° of disulfide bridges:
- IgG → 4
- VHH-Fc → 2
- Fab → 1
- VHH → 1



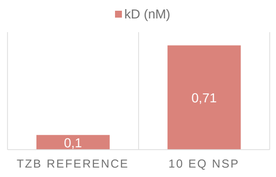
N° of lysines:
- IgG → 45 x 2 = 90
- VHH-Fc → 23 x 2 = 46
- Fab → 26
- VHH → 4

2 *In-vitro* characterization

Binding Affinity
Bio-Layer Interferometry (BLI)

Site specific vs *Random*

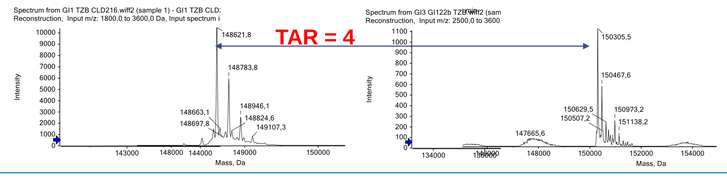
	Ref	NDR	SPAAC
IgG	0,1 nM	0,30 nM	0,33 nM
VHH-Fc	0,62 nM	0,63 nM	0,60 nM



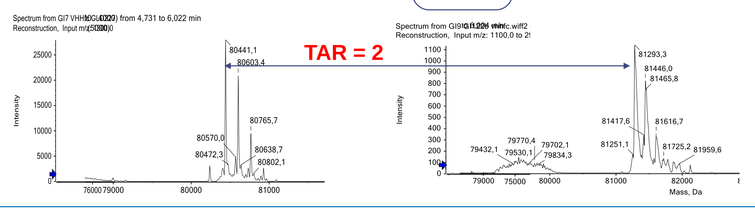
- No evident change of affinity
- Evident change of affinity

TAG to format ratio
HRMS (ZenoTOF) analysis

1) Trastuzumab



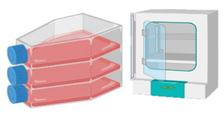
2) VHH-Fc

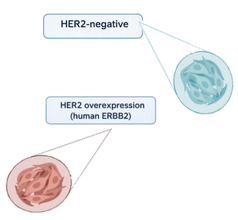


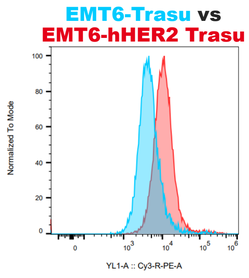
3 *In-vivo / Ex-vivo* characterization

Identification of HER2+ cells
Flow cytometry assay

EMT6/HER2-EMT6 mouse breast cell line culture

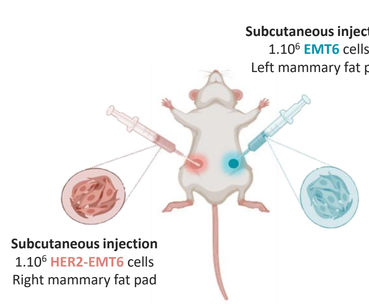






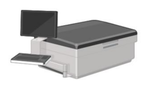
100k cells → 100pmol of protein

IV dose administration

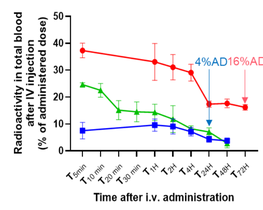


Syngeneic orthotopic mouse model

Pharmacokinetic results



[³H] Quantification by liquid scintillation



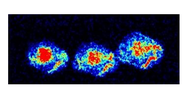
BioDistribution data



Beta imager



whole body imaging



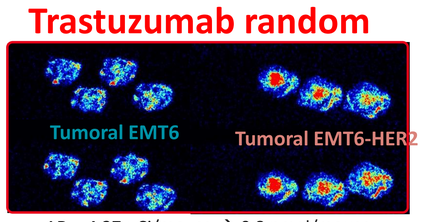
Tumoral sections imaging

3 *In-vivo / Ex-vivo* characterization

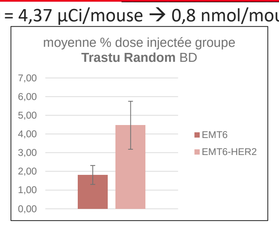
Biodistribution on tumor sections



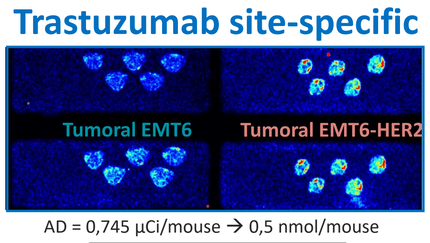
Trastuzumab random



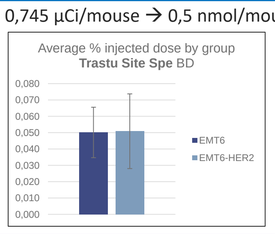
AD = 4,37 µCi/mouse → 0,8 nmol/mouse



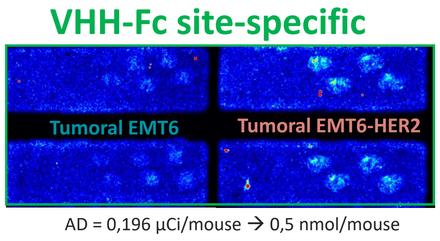
Trastuzumab site-specific



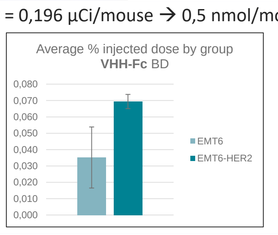
AD = 0,745 µCi/mouse → 0,5 nmol/mouse



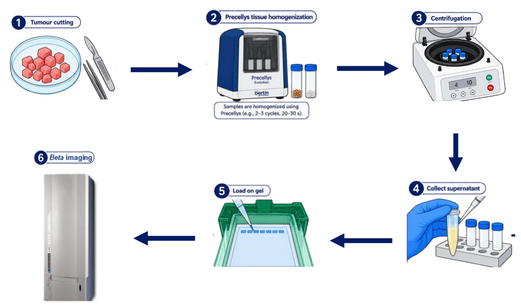
VHH-Fc site-specific

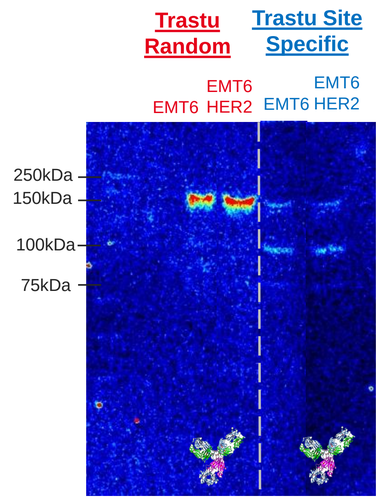


AD = 0,196 µCi/mouse → 0,5 nmol/mouse



Tumor tissue homogenization





Recovery of ^{3}H-labelled biomolecules with the tumor

CONCLUSION

- ✓ **Two bioconjugation strategies were validated**
- ✓ **Determination of TAR of site-specific modification**
- ✓ **Confirmation of HER2 expression**
- ✓ **Affinity tests**
- ✓ **Validation of overall workflow**

✓ ***Next steps:***

The workflow be applied to all of the formats
- **Tissular distribution** : ADME studies and Autoradiography (enables spatial discrimination between the tumor core and peripheral regions)
- **Cellular distribution**: Micropatterning

Our aim with this study is determine the optimal balance between exposure, tumor delivery, stability and safety

[1] N. C. Yoder, C. Bai, D. Tavares, W. C. Widdison, K. R. Whiteman, A. Wilhelm, S. D. Wilhelm, M. A. McShea, E. K. Maloney, O. Ab, L. Wang, S. Jin, H. aeK. Erickson, T. A. Keating, and J. M. Lamber *Mol. Pharmaceutics* **2019**, *16*, 3926−3937.

[2] C. Bahou, D. A. Richards, A. Maruani, E. A. Love, F. Javaid, S. Caddick, J. R. Baker and V. Chudasama *Org. Biomol. Chem.,* **2018**, *16*, 1359

[3] Cahuzac, H.; Sallustrau, A.; Malgorn, C.; Beau, F.; Barbe, P.; Babin, V.; Dubois, S.; Palazzolo, A.; Thai, R.; Correia, I.; Lee, K. B.; Garcia-Argote, S.; Leguin, O.; Keck, M.; Nozach, H.; Feuillastre, S.; Ge, X.; Pieters, G.; Audisio, D.; Devel, L. J. Med. Chem. 2022, 65, 6953–6968.

https://doi.org/10.17952/38EPS.2026.P563

EDMAN DEGRADATION BEYOND STANDARD

Toni Kühl,[1] Alexander Terekhov,[1] and Diana Imhof[1]*

[1]*Pharmaceutical Biochemistry and Bioanalytics, Pharmaceutical Institute, University of Bonn, Bonn, Germany*

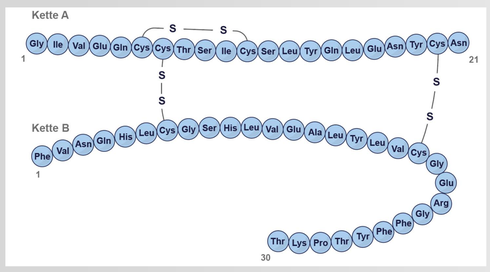
→ BACKGROUND

This study has been published recently in the *Journal of Peptide Science* [1]. Detection and annotation of disulfide bridges in multiply bridged peptides and proteins is complicated and requires careful evaluation of multiple data sets. We studied the elucidation of the cysteine connectivity by relaunching Edman sequencing to solve this specific structural feature [1,2]. Here, we demonstrate the identification of **diPTH-cystine** and **PTH-cysteine** for comparison with **PTH-Cys(Cam)** [2] during Edman sequencing when a disulfide bond is detected in a peptide. In addition, Edman sequencing was applied to selected peptides containing two or three disulfide bridges [1]. The study provides further insight into the differentiation of cysteines that form a disulfide bridge for half-cystines both in the same cycle and in separated cycles enabling correct disulfide bond assignment of cysteine-rich peptides.

→ AIM OF STUDY

To solve the problem of cysteine and disulfide bridge detection in automated Edman sequencing of multiple disulfide-bonded peptides and proteins.

Insulin

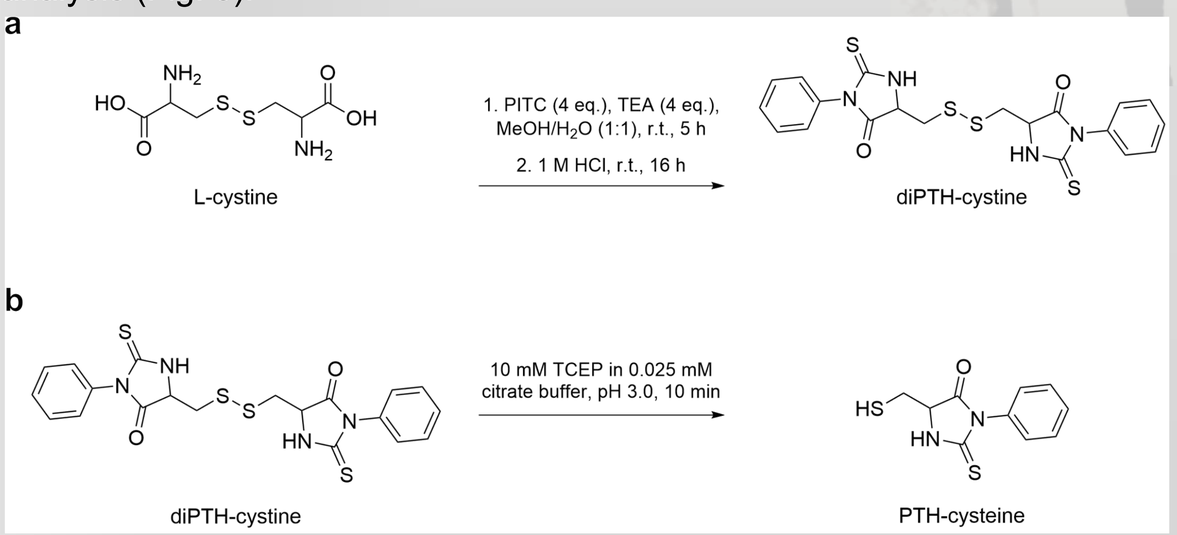


→ MATERIALS AND METHODS

Synthesis of diPTH-cystine:
L-Cystine was reacted with triethylamine, methanol, and PITC under argon. DiPTH-cystine was obtained after acidification and drying (Fig. 1a). Crude product: 95%; purified: 31%. Purification was done via C18-HPLC (Shimadzu) and identity confirmed by LC-ESI MS and $^{1}H/^{13}C$-NMR. MS: m/z 475.04 $[M+H]^+$; HPLC retention time: 28.2 min.

Synthesis of PTH-cysteine:
DiPTH-cystine was reduced with 10 mM TCEP in citrate buffer (pH 3) for 10 min (Fig. 1b). Conversion was >95%. MS: m/z 239.03 $[M+H]^+$; retention time: 22.2 min.

Automated Edman sequencing was performed using a Shimadzu PPSQ-53A. The new PTH-amino acids were separated chromatographically and identified using standards (Fig. 2). DiPTH-cystine and PTH-cysteine served as references for Cys-rich peptide analysis (Fig. 3).



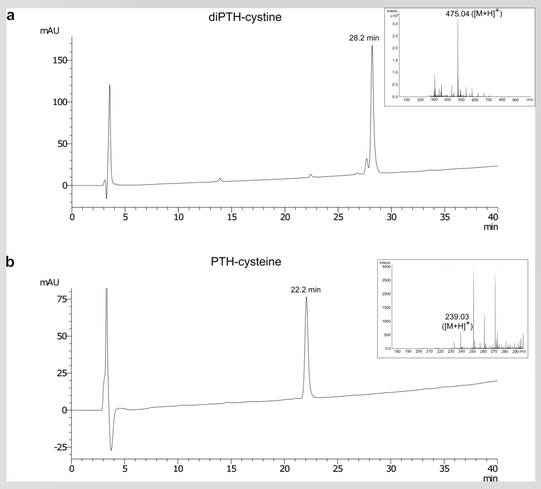


Fig. 1 (above)
Synthesis scheme for the generation of (a) diPTH-cystine and (b) PTH-cysteine by solution synthesis.

Fig. 1 (left)
Analytical characterization by RP-HPLC and mass spectrometry (inset) of diPTH-cystine (gradient: 20-60% acetonitrile containing 0.1% TFA (eluent B) in water containing 0.1% TFA (eluent A) in 40 min; calculated molecular weight: 474.03 g/mol) (a) and PTH-cysteine (gradient: 10-50% eluent B in eluent A in 40 min; calculated molecular weight: 238.02 g/mol) (b).

→ RESULTS

Edman sequencing was performed on human insulin, conotoxin μ-KIIIA, and the tridegin analogue $B_{[C19S,C25S]}$ under the manufacturer's recommended reducing conditions. In the case of the insulin C7(A)–C7(B) disulfide bridge, where both half-cystines are released in the same cycle, a distinct peak was observed in cycle 7. Based on retention time and DTT-mediated reduction of diPTH-cystine, this peak was unequivocally identified as PTH-cysteine. The results indicate that direct detection of disulfide bridges via Edman degradation is feasible primarily when both half-cystines appear in the same cycle.

„The following quotation reflects on the importance Pehr Edman placed on the discovery of his sequence method. Pehr Edman's mother, … in 1962, tells the following: ‚One day Pehr came home to me and asked me to sit down with him because he had something interesting to tell me. He then told me that **he had discovered a way to analyze proteins which had not been possible before and that this discovery would certainly be of great importance for biochemistry in the future**.'"

Selected Topics in the History of Biochemistry: Personal Recollections VII
Edited by G. Semenza, A.J. Turner, Elsevier, 2003

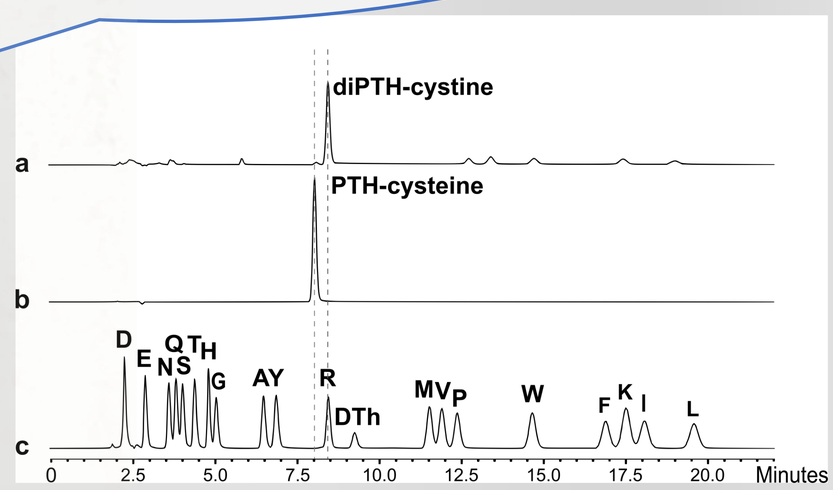


Fig. 2. Direct Edman degradation runs of (a) diPTH-cystine, (b) PTH-cysteine, and (c) PTH-amino acids standard mixture in 37% acetonitrile.[29]

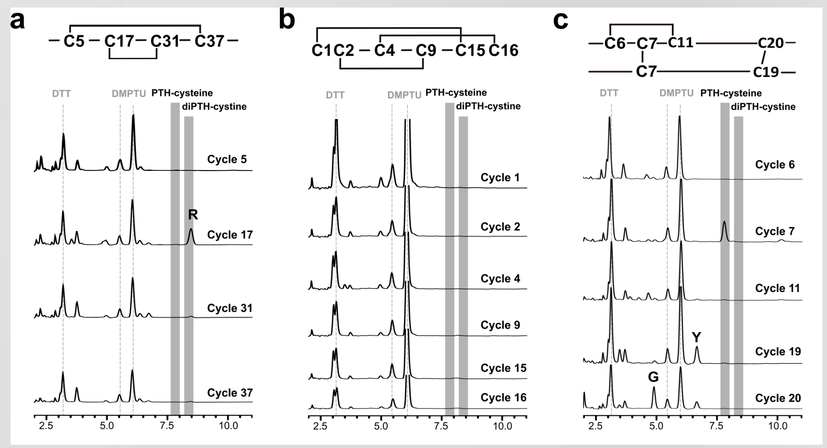


Fig. 3. Chromatograms of cycles covering cysteine positions in (a) tridegin, (b) μ-KIIIA, and (c) insulin. Frames indicate the retention times of PTH-cysteine and diPTH-cystine. DTT, dithiothreitol; DMPTU, (2,6-dimethylphenyl)thiourea.

→ CONCLUSIONS

While Edman sequencing has been used to elucidate disulfide bonds, this approach has largely been replaced by mass spectrometry. However, thorough MS analysis can be time-consuming, and some protein and peptide structures cannot be resolved by MS alone. Combining Edman sequencing with MS/MS enables faster and easier analysis of disulfide connectivity in complex peptides and proteins. It also addresses MS limitations, such as low fragment-ion intensities near disulfide-linked cysteines.

In this study, diPTH-cystine and PTH-cysteine were provided and characterized for Edman sequencing and evaluated as standards for the PPSQ sequencing device. These compounds are particularly valuable when multiple disulfide bridges occur in the same sequencing cycle, as frequently observed in nature, e.g., in antibodies.

We therefore introduce a workflow [1] to elucidate disulfide connectivity: Edman sequencing serves as the starting point for detecting disulfide bridges, followed by complementary MS and Edman analyses, potentially supported by partial reduction. Early identification or exclusion of specific disulfide bridges significantly simplifies the subsequent analysis.

References

1) Kühl T, Elsayed YY, Terekhov A, Imhof D., J. Pept. Sci. 2025, (10):e70053.
2) Elsayed YY, Kühl T, Imhof D., Anal Chem. 2024, 96(10):4057-4066.

Acknowledgments

Financial support by the University of Bonn and the GDCh is gratefully acknowledged. The authors like to thank Yomnah Y. Elsayed for fruitful discussions and Dirk Menche (University of Bonn) for access to the NMR spectrometer.

Check Imhof Lab

Adaptive Evolutionary Optimization for the Discovery of Self-Assembling Peptides

Milica Injac[1] , Ena Dražić[2], Marko Njirjak[2], Gordana Rakić[3], Daniela Kalafatovic[2], Goran Mauša[2]

1 - University of Novi Sad, Faculty of Technical Science, Serbia, 2 - University of Rijeka, Faculty of Engineering, Croatia, 3 - University of Novi Sad, Faculty of Science, Serbia

https://doi.org/10.17952/38EPS.2026.P267

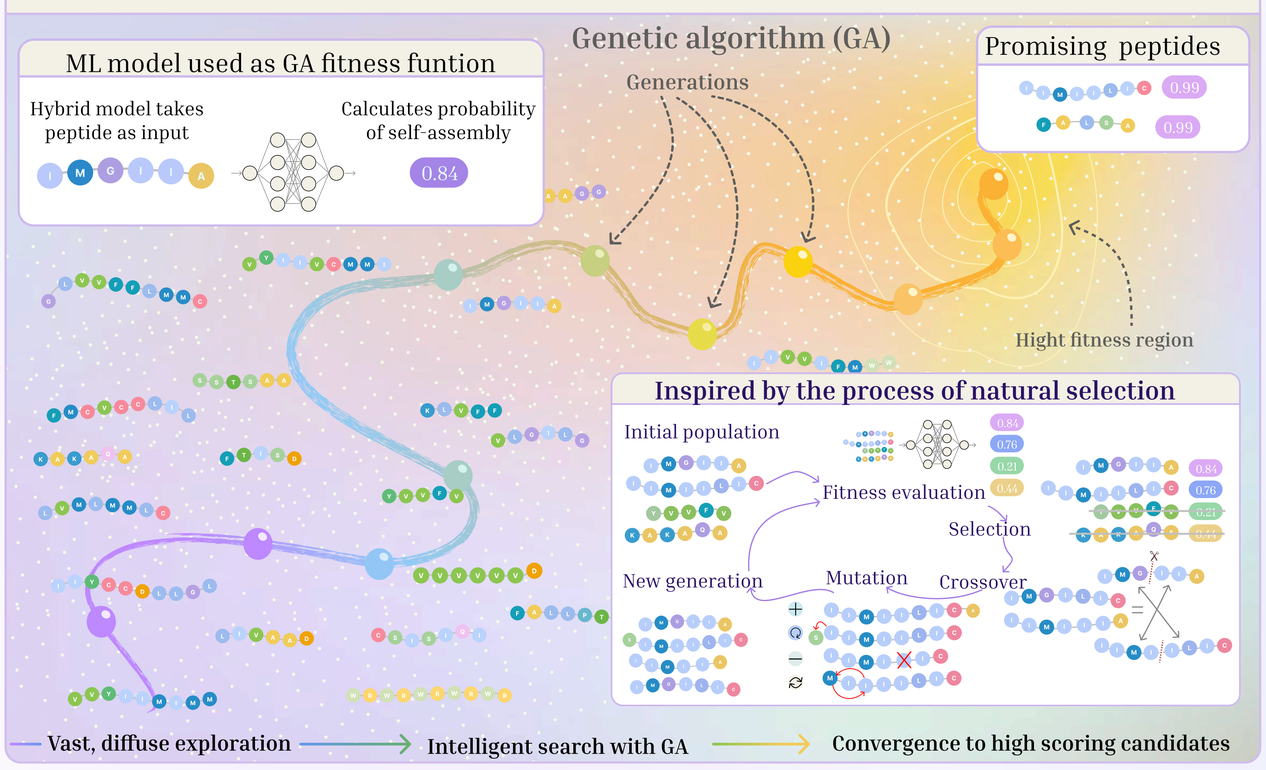
milica.injac@uns.ac.rs

RQ1 Does ML-driven GA find unique promising self-assembling peptides (high quality candidates) while exploring the global space?

RQ2 What does the GA reveal about the ML self-assembly predictor?

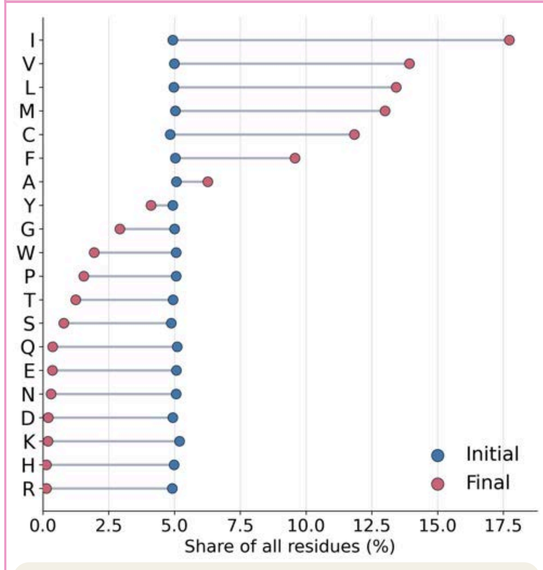
RQ3 How do GA-generated peptides compare to peptides from the experimental dataset?

Exploration of Large Peptide Space Guided by GA Driven ML



Analysis of GA-Generated Peptides Collected Over 200 Independent GA Runs

GA selection reshaped aa composition



Selection enriched I/V/L/M/C/F and strongly depleted charged residues, revealing the compositional region favored by generative model. This computational preference does not establish that individual residues cause self-assembly.

What do mutations tell us about the predictive model?

Delete Removes aa | Substitute Replaces aa | Insert Adds aa | Swap Exchanges aa

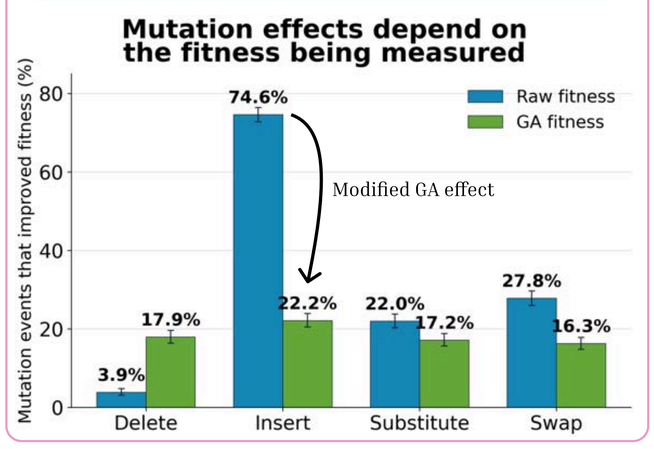
8,761 mutation events

89,6% of them happened on high-scoring peptides

GA used mutation mainly to probe local variants within the predictor's high-score region.

Length-associated preference

Adding one residue usually **increased** the predicted score, whereas **deletion** rarely did.



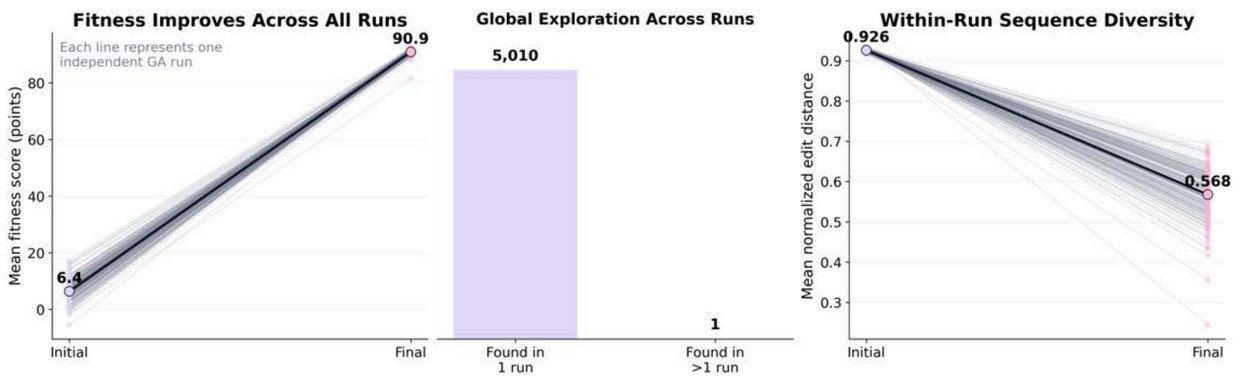
Global Exploration and Local Exploitation

200 independent GA runs | GA guided by Retrained prediction model | **5011** suggested peptides where **5010** are unique sequences

Within each run, the GA focused the population on a smaller set of high-fitness peptides.

Different runs produced different results: 99.9% of final sequences were not found in any other run

Within a single run, peptides converge to a place and are more similar than starting population.



RQ1 Thousands unique, high scoring candidates; runs converged locally, but explored different sequence neighborhoods. This reflects **local exploitation within each run**, while the lack of overlap between runs indicates **global exploration** of different sequence solutions. Median fitness in final populations is 90.9 which means while exploring the global space **solutions are high scoring**.

Experimental setup

4 experimental conditions x200 GA runs

Larger and more balanced dataset

[1] dataset: 256 SA, 112 NSA + [2] dataset: 91 SA, 117 NSA = Combined dataset: 334 SA, 276 NSA

368 → 610 peptides total

Retrained model accuracy: 77.1%

[1] Mauša et al., Reshaping the discovery of self-assembling peptides with generative AI guided by hybrid deep learning. Nat Mach Intell. 6. (2024). 10.1038/s42256-024-00928-1.
[2] Batra et al., Discovery of unconventional and nonintuitive self-assembling peptide materials using experiment-driven machine learning. Sci. Adv. 11. (2025). 10.1126/sciadv.adt9466

RQ2 GA search exposed predictor preferences for hydrophobicity, charge, and peptide length

Strategies to dampen length bias

	Original GA	Modified GA
Original ML model	5251	5016
Retrained ML model	3870	4270

number of peptides

Modifying GA with:
→ Fitness penalty favoring length diversity,
→ Initial populations with shorter peptides

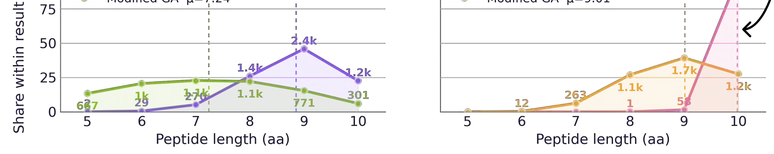
Modification of initial population strategy

Original GA: 100% peptides with 3-24 aa (3 aa – 24 aa)

Modified GA: 90% peptides with 3-6 aa (3 aa – 24 aa)

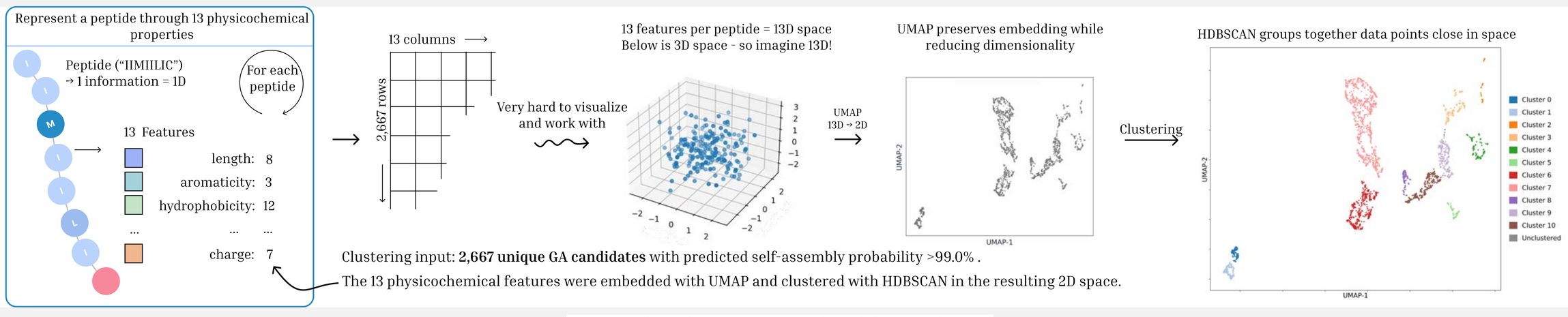
Peptide length distributions

98.5% peptides length 10



Clustering GA-Generated Peptides: Where Do Experimental Peptides Map?

What is clustering? → grouping similar data points based on defined measure of similarity. For example: HDBSCAN →Groups together data points that are tightly packed, leaving out points in sparse areas as outliers.



Clustering input: **2,667 unique GA candidates** with predicted self-assembly probability >99.0% .

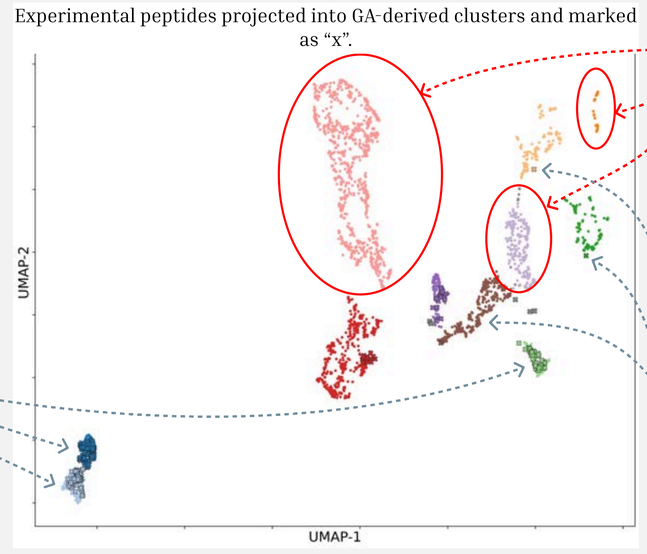
The 13 physicochemical features were embedded with UMAP and clustered with HDBSCAN in the resulting 2D space.

3.9% peptides from the dataset map to unclustered regions

0 GA candidates match sequences from the dataset

0.887 median HDBSCAN membership strength

Experimental peptides projected into GA-derived clusters and marked as "x".



3 GA-derived clusters contain no peptides from the experimental dataset

0 experimental peptides map to the largest cluster, which contains 32.4% of GA candidates

84.7% SA peptides from the dataset concentrate in those 3 clusters

3 GA clusters

13.4% generated SA peptides occupy those clusters

84.7% peptides from the dataset maps to 3 small clusters, in which 13.4% GA generated peptides is located

3 clusters contain only one experimental peptide each

RQ3 Despite the limited search space coverage by the dataset, GA explores new peptide-property regions

2,667 candidates · 11 clusters · 0.5% unclustered · largest family 32.4% · bootstrap stability: ARI 0.76 ± 0.16

TAKE HOME MESSAGE: ML-guided GA explored diverse search space neighbourhoods and identified thousands of high scoring self assembling peptide candidates, including regions not covered by the experimental dataset. The search also revealed model preferences for hydrophobicity, charge, and peptide length providing candidates for experimental testing.

Acknowledgements: This work was carried out within COST Action CA23111 – SNOOPY "Searching for Nanostructured or pOre fOrming Peptides for therapY", supported by COST (European Cooperation in Science and Technology). In addition, the authors were supported by European Union – NextGenerationEU [PepNanoDisco, grant no. uniri-mzi-25-2], Croatian Science Foundation [Super DeShPet 2.0, grant no. IP-2025-02-3357], Ministry of Science, Technological Development and Innovation (Contract No. 451-03-34/2026-03/200156) and the Faculty of Technical Sciences, University of Novi Sad through project "Scientific and Artistic Research Work of Researchers in Teaching and Associate Positions at the Faculty of Technical Sciences, University of Novi Sad 2026" (No. 01-3609/1).

P-393

Application of Antibody Site-Specific Modification Method tCAP to Brain-Penetrating Antibody-Oligonucleotide Conjugate

○Yuji Ito[1], Abdur Rafique[1], Hiroko Kawakami[1,2], Taku Yoshiya[2,3]

[1] Graduate School of Science and Engineering, Kagoshima University, Kagoshima, Japan
[2] Peptide Institute, Inc., Osaka, Japan.
[3] Institute for Protein Research, The University of Osaka, Osaka, Japan
Email: yito@sci.kagoshima-u.ac.jp, https://doi.org/10.17952/38EPS.2026.P393

Abstract

We developed a site-specific IgG modification method, tCAP, which employs an Fc-binding affinity peptide to induce proximity-driven introduction of an azide group at Lys248 on the Fc region.[1,2] Site-specific modification is achieved simply by mixing native antibodies with the tCAP reagent. Here, we report the preparation of antibody–oligonucleotide conjugates (AOCs) using this method and their brain delivery in mice.

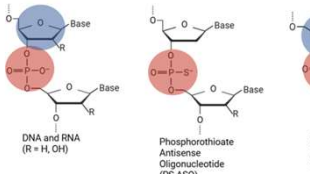
An anti-TfR VHH-Fc antibody with BBB-penetrating capability and reaching to neuronal cells[3] was modified with an azide group using tCAP, followed by click conjugation with IR-800-labeled DBCO-oligonucleotides (PS or PMO types) added at threefold molar excess. LC–MS analysis confirmed a bivalent AOC (DAR = 2.0) with approximately 95% purity.

After intravenous administration in mice, brain fluorescence imaging and microscopy at 24, 48, and 96 h demonstrated that PMO-modified AOCs achieved ~70% of the brain uptake of the unconjugated antibody and reached neuronal cells in the brain parenchyma. In contrast, PS-modified AOCs showed <3% uptake, and monovalent PS-AOCs did not improve brain penetration.

These findings indicate that the physicochemical properties of oligonucleotides, particularly charge characteristics, critically affect AOC transport from blood to brain. Further optimization, including linker design, will be required to enhance BBB penetration of PS-modified AOCs.

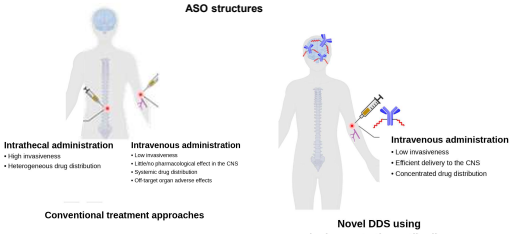
Background

• Antisense Oligonucleotide (ASO)

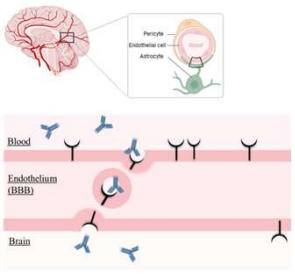


Modification	Backbone / charge	Key advantages	Main limitations
PS ASO	• Phosphorothioate backbone • Negatively charged	• High nuclease resistance • High membrane permeability	• Potential cytotoxicity
PMO	• Morpholine ring + phosphorodiamidate linkage • Charge-neutral	• High nuclease resistance • Low cytotoxicity	• Low membrane permeability

ASO structures



• Blood–Brain Barrier (BBB)



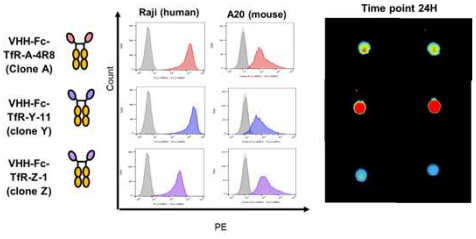
The blood–brain barrier (BBB) separates the blood from the brain and restricts the entry of substances into the brain.

Antibody therapeutics and many other drugs cannot efficiently reach the brain.

Brain delivery using anti-TfR antibodies targeting the transferrin receptor (TfR) expressed at the BBB.

TfR-mediated antibody transport across the BBB

• Isolation of anti-TfR VHH antibodies



TfR-mediated antibody transport across the BBB

• Fc site-specific modification: tCAP

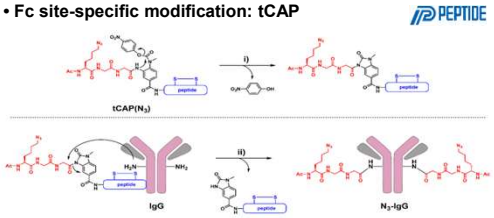


Fig. tCAP method

The tCAP method is an Fc site-specific antibody modification technology developed in our laboratory using a human IgG-affinity peptide. In the tCAP reagent, an azide group is linked to an Fc-specific antibody-affinity peptide through an activated acyl-donor moiety, enabling introduction of two azide groups into the Fc region of IgG. The introduced azide groups can subsequently be coupled to diverse molecules, including fluorescent probes and oligonucleotide therapeutics, by click chemistry with DBCO groups.

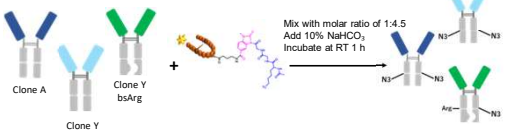
Methods

• Preparation of antibody–ASO conjugates (AOCs)

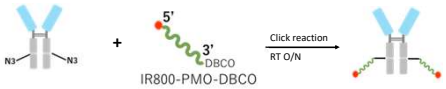
1. DBCO and IR800 labeling of PMO and ASO



2. VHH-TfR (Clone A, Y, bsArg) hFcm + tCAP reagent



3. VHH-TfR(Clone A, Clone Y) tCAP(N3) + DBCO-PMO-IR800



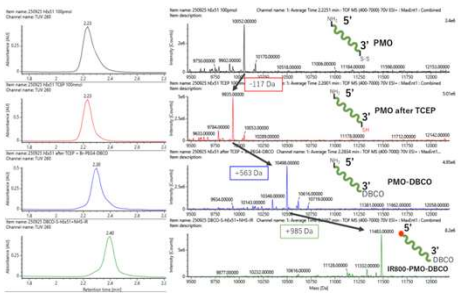
4. VHH-TfR(Clone Y bsArg) tCAP(N3) + DBCO-PS ASO-IR800



Results & Discussion

• Preparation of antibody–ASO conjugates (AOCs)

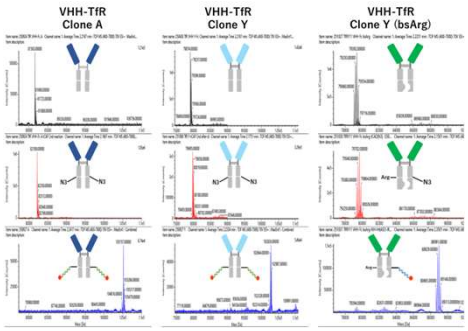
1. DBCO and IR800 labeling of PMO



Confirmation of DBCO and IR800 labeling of PMO by Waters BioAccord LC-MS

PMO was reacted with TCEP·HCl at a 1:10 molar ratio and purified using a Sephadex G-25 column. Br-PEG4-DBCO was then reacted at pH 8.9. After confirming the reaction, NHS-IR800 was added, and the product was purified using a Sephadex G-25 column.

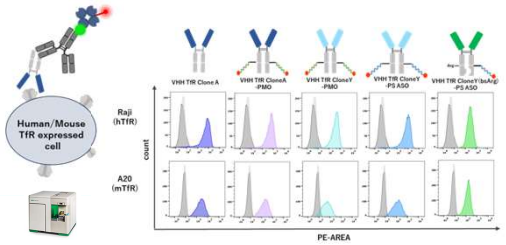
2. Preparation and characterization of AOCs using the tCAP method



Various ASO conjugates prepared by the tCAP method

Anti-TfR antibodies bearing azide groups introduced by the tCAP method were mixed at a 1:3.5 molar ratio with DBCO/IR800-labeled ASO and conjugated by click chemistry.
Unreacted ASO was removed using a Sephadex G-75 column. TOF-MS analysis confirmed formation of the desired AOCs with either bivalent or monovalent ASO conjugation.

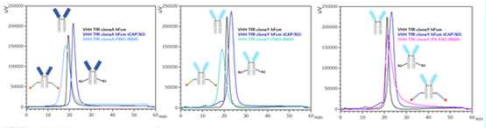
• TfR-binding activity by flow cytometry



Binding activity of AOCs assessed by flow cytometry

The binding activity of the prepared AOCs was evaluated using human and mouse TfR-expressing cells. Reduced binding was observed for VHH TfR clone Y-PMO and VHH TfR clone Y-PS ASO.

• rFcRn binding activity

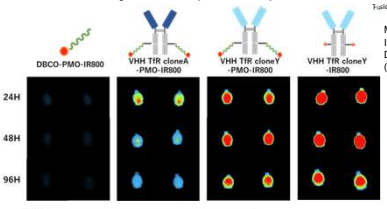


Evaluation of rFcRn binding using an rFcRn affinity column

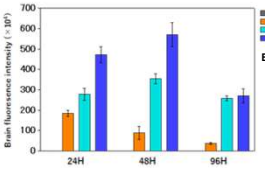
To evaluate FcRn binding of the prepared AOCs, we used a column (TOSOH) immobilized with recombinant FcRn.
For all antibodies, tCAP modification resulted in stronger binding than the unmodified antibody. All AOCs showed binding comparable to the corresponding unmodified antibodies, indicating that FcRn binding activity was retained after AOC formation.



• Brain delivery of AOC (Ab–PMO)



Mouse: male ICR
Injection: tail vein
Dose: 50 nmol/kg (PMO: 100 nmol/kg)

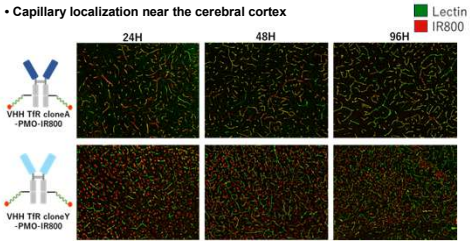


Brain delivery evaluation of AOC (PMO)

AOCs were prepared by conjugating PMO to VHH TfR clone A or clone Y, and brain delivery was evaluated.
Clone Y AOC showed higher brain fluorescence than clone A AOC. At 24 and 48 h, the fluorescence intensity of clone Y AOC was approximately 60% of that of clone Y alone.

• Brain localization of AOC (Ab–PMO)

• Capillary localization near the cerebral cortex



Localization of AOC (Ab–PMO) evaluated using Lectin488

At each time point for VHH TfR clone A-PMO and clone Y-PMO, brain capillaries were stained with Lectin488 and compared with IR800 fluorescence. In the clone A-PMO group, IR800 fluorescence was localized mainly to capillaries.
In contrast, clone Y-PMO showed a different distribution, with IR800 fluorescence located away from capillaries.

• Neuronal localization near the cerebral cortex

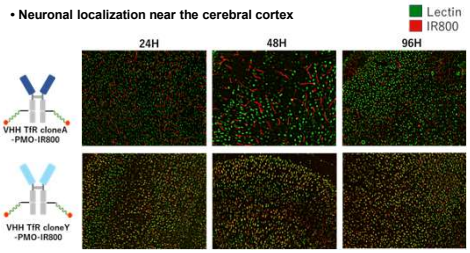
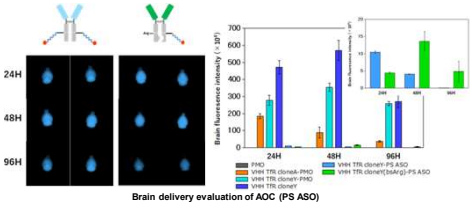


Fig. Localization of AOC (Ab–PMO) evaluated by NeuN staining

At each time point, neurons were stained with an anti-NeuN antibody and a secondary antibody and compared with IR800 fluorescence. For VHH TfR clone Y-PMO, IR800 fluorescence overlapped with NeuN-positive signals, indicating that PMO could cross the BBB and reach neurons.

• Brain delivery of AOC (Ab–PS ASO)



Brain delivery evaluation of AOC (PS ASO)

Mouse: male ICR (7–8 weeks)
Injection: tail vein
Dose: 50 nmol/kg
(bsArg AOC: 100 nmol/kg to normalize IR800 valency)
Time points: 24, 48, 96 h

Brain delivery of bivalently and monovalently conjugated AOC (PS ASO) was evaluated. Neither showed appreciable brain delivery compared with the PMO-conjugated AOCs.

Summary

Two anti-TfR VHH antibodies (clone A and clone Y) were conjugated with PMO or PS ASO to generate AOCs, and their brain delivery and localization were evaluated. The VHH TfR clone Y-PMO conjugate showed high brain delivery and was detected in neurons. In contrast, PS ASO-conjugated VHH TfR clone Y showed little brain delivery compared with the PMO conjugate; however, monovalent PS ASO conjugation tended to provide greater brain delivery than bivalent conjugation.
These results suggest that brain-penetrating antibodies can serve as carriers for CNS delivery of oligonucleotide therapeutics.

References

1. H. Kawakami, T. Yoshiya, Y. Ito et al., Chem. Eur. J., 2026, 32, e03144. DOI: 10.1002/chem.202503144.
2. K. Tsuji, Y. Ito, T. Yoshiya, H. Tamamura et al., ChemMedChem, 2026, 21, e202500820. DOI: 10.1002/cmdc.202500820.
3. F. Jatnika, A. Nagashima, W. Miyahara, A. Rafique, Y. Ito, *under submission.*

Biosynthetic Peptide Screening Platform for various Drug Discovery and Delivery

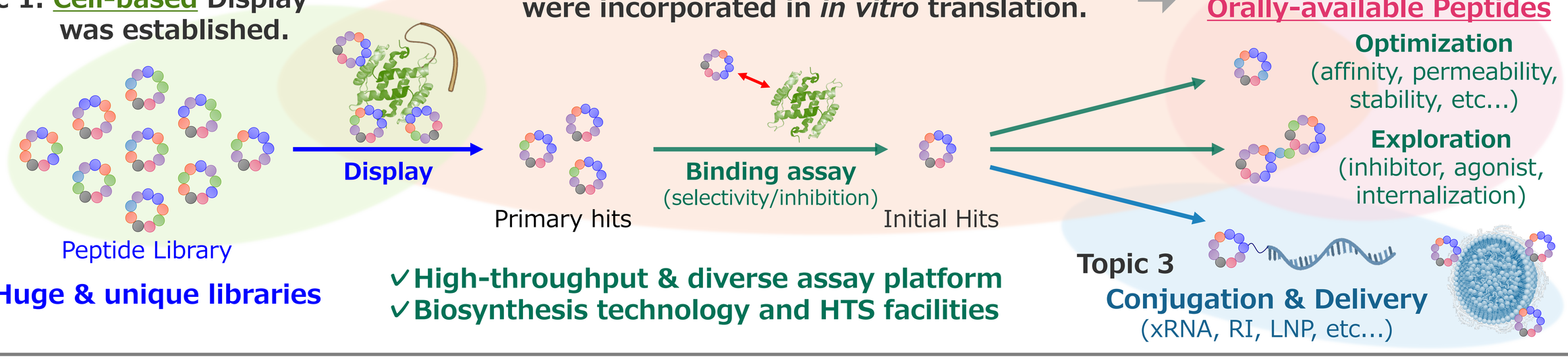
Shin Izuta, Taishi Fuda, Hiroki Takahashi, Koo Suzuki, Nao Yamazaki,
Anri Nishiguchi, Tomoki Ota, Ryo Ukekawa, Yukiko Ishii (FUJIFILM Corporation)

FUJIFILM
Value from Innovation

Partners for *Life*™
collaborated with PURE*frex*® Reconstituted cell-free protein synthesis kit

Peptide screening platform

A representative screening workflow is shown below. Successful examples related to three challenges in peptide discovery; (1) targets that are difficult to isolate, (2) oral abministration, and (3) conjugation for deliverly, were obtained in this report.

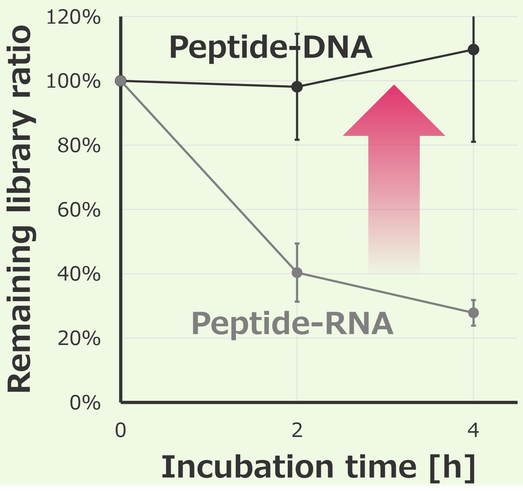


Topic 1. Cell-based Display from Stable Library

The stability of the library has been improved, enabling display screening using cells. Novel peptide binders were successfully identified for FGFR and three GPCR targets; CaSR, FZD5, and GHSR.

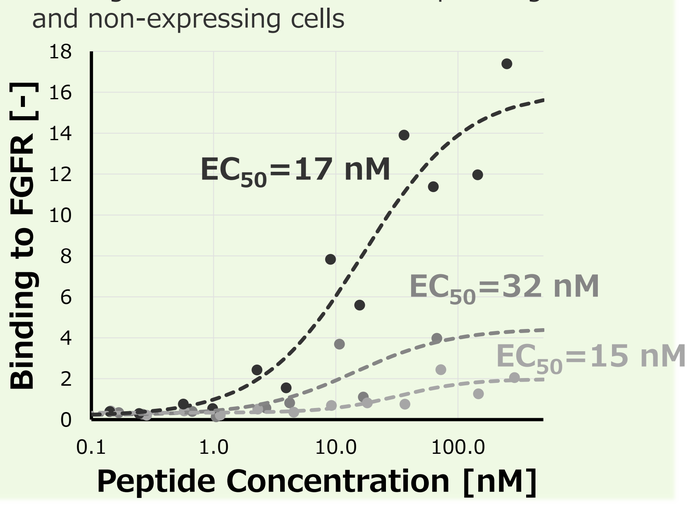
Stability of the Library

···Covalent conjugation of peptides to DNA substantially improved their stability in cell culture supernatants.



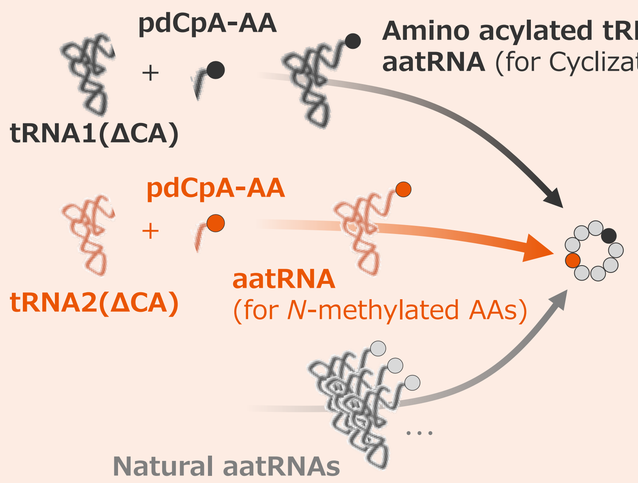
Affinity of the discovered Hits

···A highly target-specific binding signal was observed, as evidenced by the difference in binding levels between FGFR-expressing cells and non-expressing cells

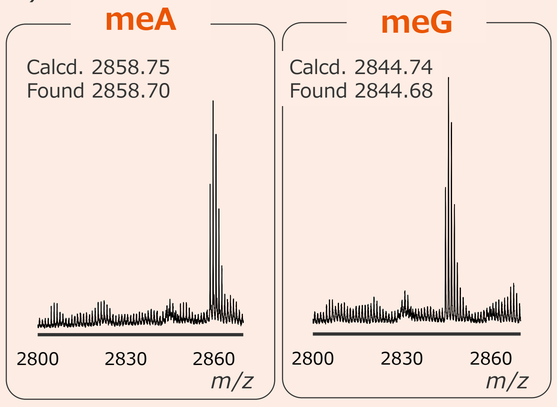


Topic 2a. *N*-methylated AAs in *in vitro* translation system

The combination of the improved pdCpA method and PURE system enabled the efficient incorporation of *N*-methyl alanine (meA) and *N*-methyl glycine(meG) into peptides via *in vitro* translation system.

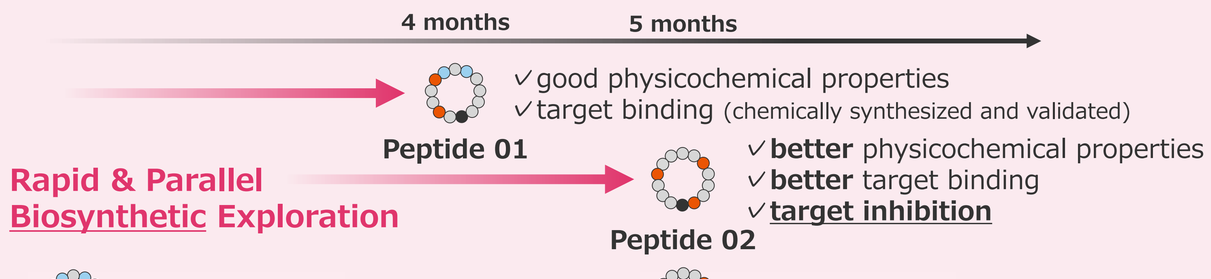


MALDI-MS identification



Topic 2b. Potentially Orally-available Peptides

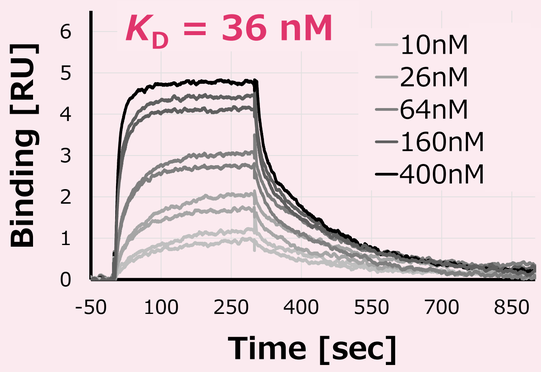
A rapid screening and optimization are being demonstrated with famous IL inhibitor. Within five months, peptides with favorable physicochemical properties, binding, and inhibitory activity were identified, and *in vivo* oral absorption PKs are currently underway.



Peptide 01

- 13 aa ring
- **2 *N*-alkylated residues**
- 2 charged residues

SPR binding validation

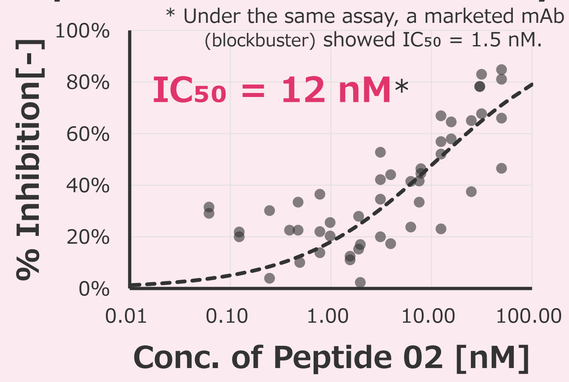


Peptide 02

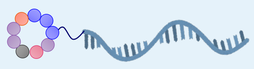
- 14 aa ring
- **3 *N*-alkylated residues**
- **0 charged residues**

Alpha-screen inhibition assay

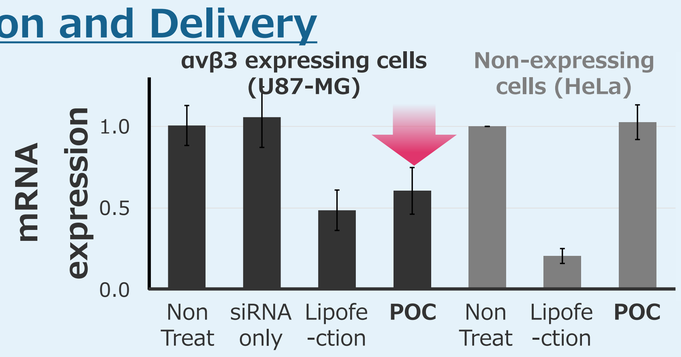
* Under the same assay, a marketed mAb (blockbuster) showed IC50 = 1.5 nM.



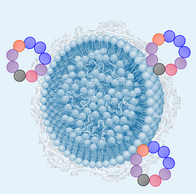
Topic 3. Conjugation and Delivery



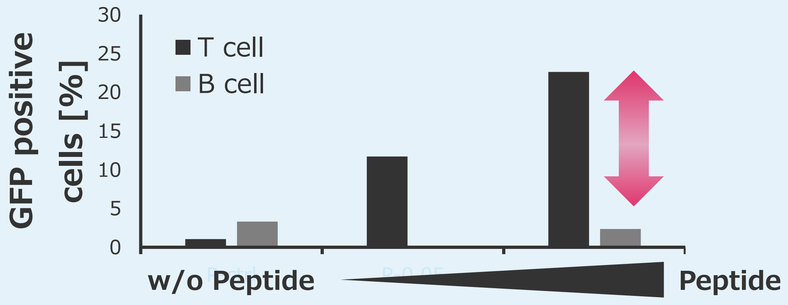
Peptide - siRNA conjugate (POC)



A Integrin-binding peptide was conjugated to a model siRNA. The resulting peptide-siRNA conjugates exhibited selective knockdown activity in cells expressing Integrin at 40 nM.



Peptide – LNP (lipid) conjugate



A CD7-binding peptide was chemically conjugated with a lipid, and peptide-LNP were formed without any additional process. This LNPs enabled T cell-selective mRNA(GFP) delivery in PBMC.

Peptide Discovery Service in FUJIFILM

contact: shin.izuta@fujifilm.com

USEFUL

- **No milestones and no royalty obligations**.
- **No intellectual property claims** on discovered peptides.
- **Rapid discovery** (4Ms for initial hits, +2Ms for SAR).

POWERFUL

- **Huge libraries** (≧10^{13} varieties) with **unique peptides**.
- **High-throughput activity-based screening/optimization** with biosynthetic tech.

→ **High affinity** (K_D: 0.1~50 nM) and **Wide variety** in hits.

Hit peptides have been obtained toward >30 targets with our platform.

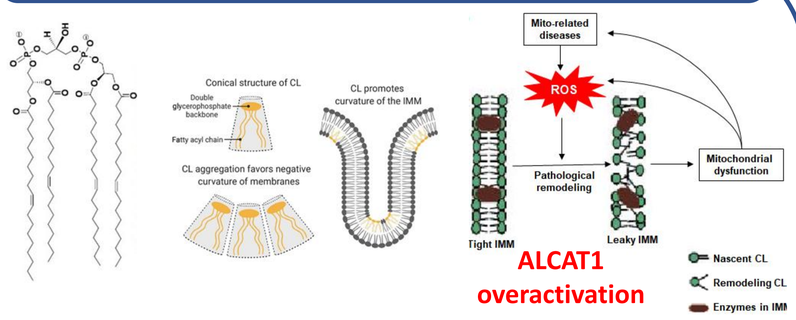
A cardiolipin-targeting α-helical bundle peptide stabilizes inner membrane of mitochondria, down-regulating ALCAT1 to shut down pathogenic remodeling in oxidative stress condition

Yoonhwa Choi[1,#], Tae Yeon Kim[2,#], Hyeong Woon Choe[1], Gwangsu Shin[1], Seung Hee Yang*[3], Hyo Youl Moon*[2], Jaehoon Yu*[1]

[1]CAMP Therapeutics Co., Ltd. Seoul, Korea, [2]Department of Physical Education, Seoul National University, Seoul, Korea, [3]Kidney Research Institute, Seoul National University Hospital, Seoul, Korea

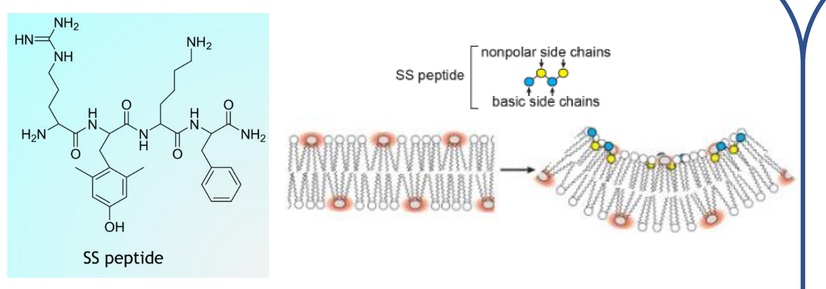
https://doi.org/10.17952/38EPS.2026.P319

Background: ROS-driven pathological cardiolipin (CL) remodeling destabilizes the IMM



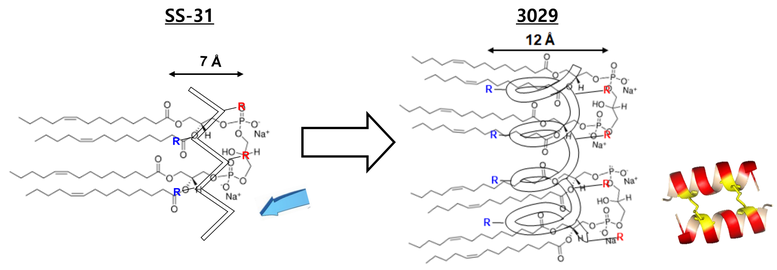
- **Essential role of CL:** Maintains IMM negative curvature and cristae stability via its unique conical structure.
- **ALCAT1 overactivation:** Oxidative stress (ROS) up-regulates ALCAT1, driving pathological CL remodeling.
- **IMM destabilization:** Altered CL composition transforms a healthy, "tight" IMM into a "leaky" membrane.
- **The vicious cycle:** Leaky IMM disrupts the electron transport chain (ETC), amplifying ROS production and mitochondrial diseases.

Proof of concept: SS-31 as a first-in-class CL-targeting peptide



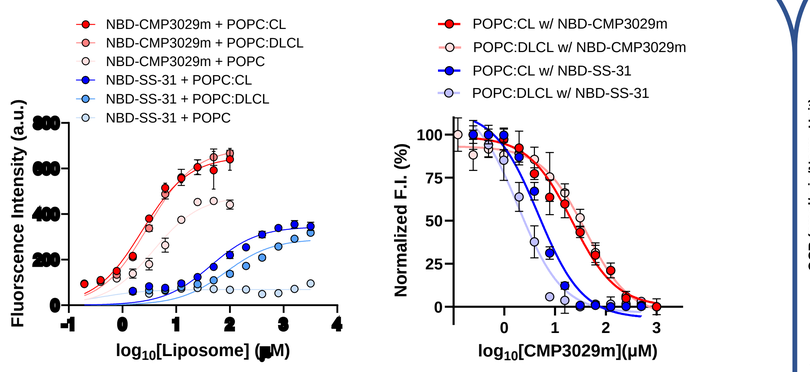
- **Selective CL binding:** SS-31 is a representative tetrapeptide that specifically binds to CL via alternating electrostatic and hydrophobic interactions.
- **Curvature protection:** It localizes to the IMM surface, maintaining structural curvature and preventing ROS-induced CL degradation.
- **Validation of target:** The established efficacy of SS-31 proves that stabilizing CL is a highly viable approach to treating mitochondrial dysfunction.

3029 vs. SS-31: α-Helical structure makes strong interaction w/ multiple CL binding



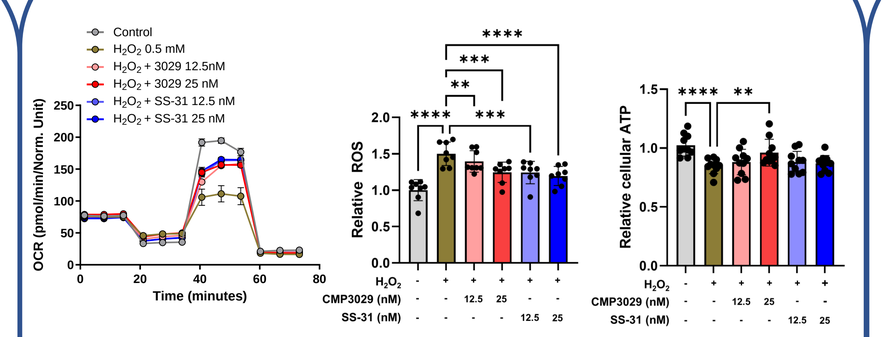
- **Broader interface:** α-helical **3029** provides a wider binding surface (~12 Å) than the short, β-sheet-like **SS-31** (~7 Å).
- **Multiplexed binding:** 3029 optimally arrays multiple Arginine (R) residues to cross-link multiple CL molecules simultaneously.
- **Superior stabilization:** This multi-point electrostatic binding offers significantly stronger IMM structural support compared to SS-31.

In vitro validation: 3029 exhibits stronger CL binding than SS-31



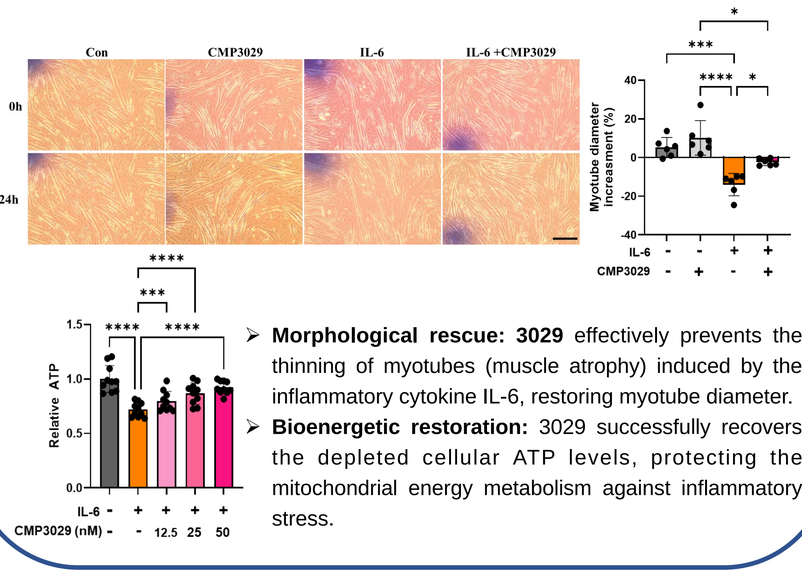
- **Enhanced affinity: 3029** demonstrates significantly stronger binding to CL/DLCL-containing liposomes compared to the benchmark **SS-31**.
- **Higher capacity:** The drastically elevated fluorescence intensity indicates a maximized insertion and interaction of 3029 into CL-rich membranes.
- **Tighter interaction:** Displacement assays confirm that 3029 forms a highly stable and robust complex with CL, slower dissociation than SS-31.

3029 vs. SS-31: Protection against oxidative stress



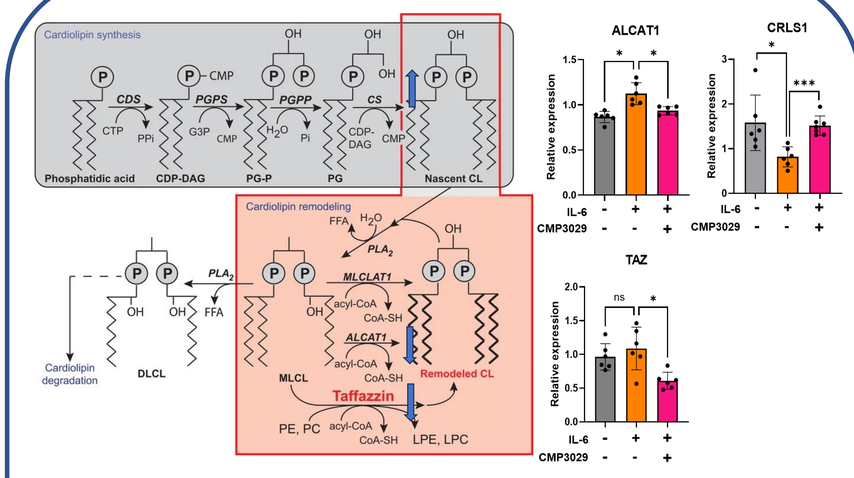
- **Respiration recovery: 3029** efficiently restores the Oxygen Consumption Rate (OCR) against H_2O_2-induced oxidative stress.
- **ROS suppression:** While **SS-31 exhibits a slightly stronger direct ROS scavenging effect**, 3029 still significantly reduces intracellular ROS accumulation.
- **Superior ATP recovery:** Notably, despite moderate ROS quenching, **3029 (25 nM) achieves better ATP restoration than SS-31**. This highlights that its robust structural IMM stabilization ultimately translates to superior bioenergetic protection.

3029 prevents IL-6-Induced muscle atrophy in C2C12 myotubes



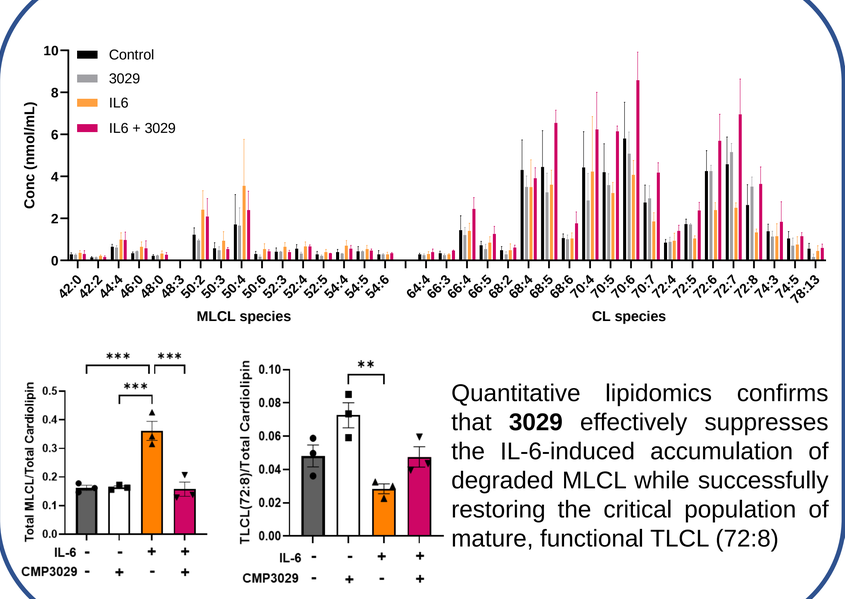
- **Morphological rescue: 3029** effectively prevents the thinning of myotubes (muscle atrophy) induced by the inflammatory cytokine IL-6, restoring myotube diameter.
- **Bioenergetic restoration:** 3029 successfully recovers the depleted cellular ATP levels, protecting the mitochondrial energy metabolism against inflammatory stress.

Mechanism of action: 3029 shuts down pathological CL remodeling



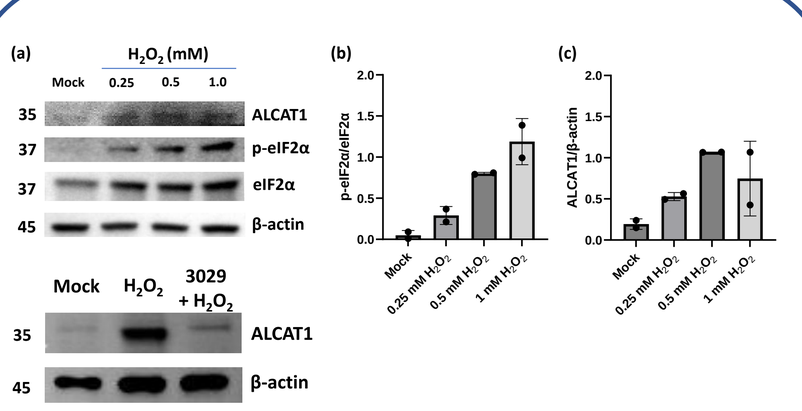
- Mechanistically, **3029** preserves mitochondrial integrity by simultaneously down-regulating the pathological remodeling enzyme **ALCAT1** and restoring the healthy nascent CL synthase **CRLS1** against IL-6-induced stress.

Lipidomic validation: 3029 restores healthy cardiolipin composition in C2C12 myotubes



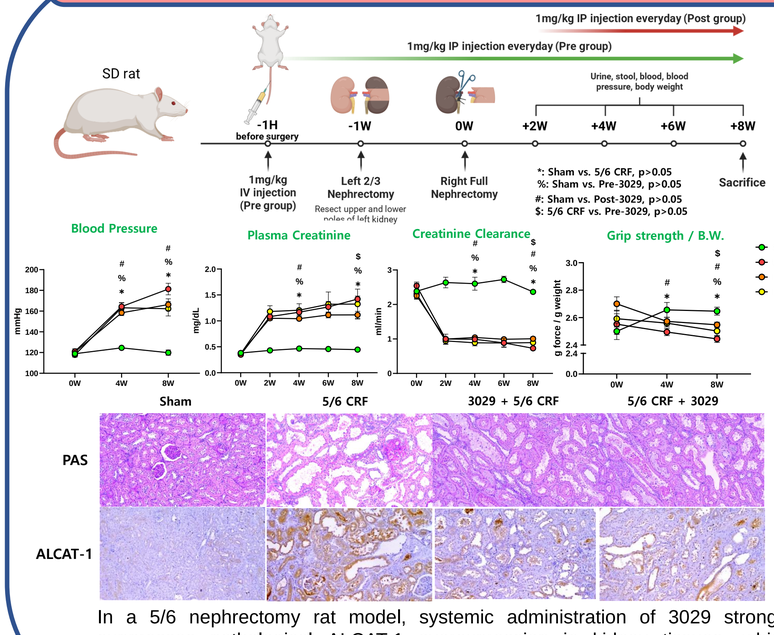
Quantitative lipidomics confirms that **3029** effectively suppresses the IL-6-induced accumulation of degraded MLCL while successfully restoring the critical population of mature, functional TLCL (72:8)

Inhibitory effect of 3029 on H_2O_2-induced ER Stress and ALCAT1 expression in HK-2 cells



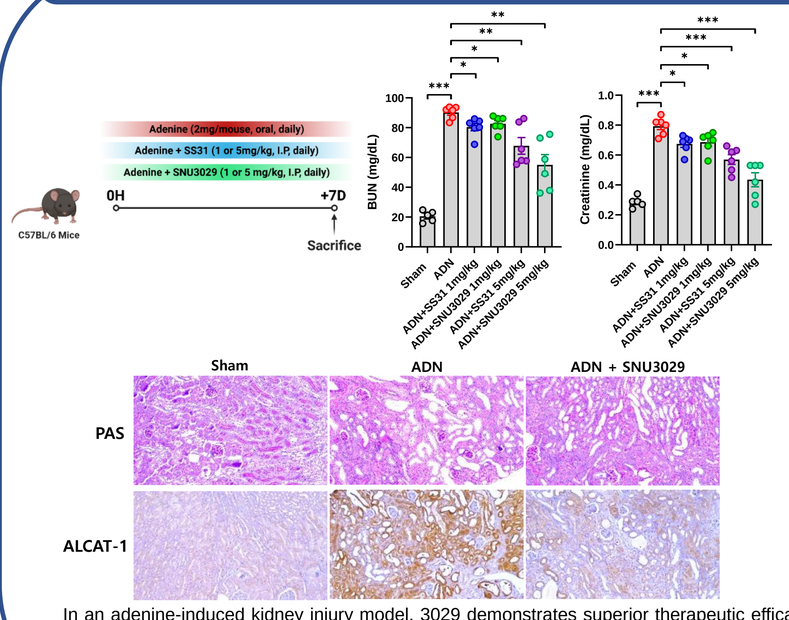
- Upregulation of ALCAT1 by H_2O_2: Concurrently with the elevation of p-eIF2α, ALCAT1 expression level also markedly increased in proportion to the H_2O_2 concentration.
- Inhibitory efficacy of 3029: Compared to the group treated with H_2O_2 alone, co-treatment with 3029 effectively suppressed the H_2O_2-induced abnormal overexpression of ALCAT1.

In vivo validation: 3029 ameliorates renal failure by suppressing ALCAT-1 in 5/6 CRF model rat



In a 5/6 nephrectomy rat model, systemic administration of 3029 strongly suppresses pathological ALCAT-1 overexpression in kidney tissues, which directly translates to mitigated renal dysfunction, normalized blood pressure, and prevention of muscle weakness.

Comparative *in vivo* efficacy: 3029 exhibits superior protection over SS-31 in adn-induced model mouse



In an adenine-induced kidney injury model, 3029 demonstrates superior therapeutic efficacy compared to SS-31 by more robustly suppressing structural tissue damage (PAS) and pathological ALCAT-1 overexpression, leading to a significantly greater reduction in renal dysfunction markers (BUN and Creatinine).

Conclusion: 3029 overcomes pathological CL remodeling

- **Structural superiority:** The optimized α-helical structure of 3029 enables multiplexed and maximized cardiolipin (CL) binding, providing fundamentally stronger inner mitochondrial membrane (IMM) stabilization than SS-31.
- **Pathological reversal:** 3029 successfully restores mitochondrial bioenergetics and healthy lipid profiles by effectively shutting down the ALCAT1-mediated pathological CL remodeling pathway.
- **Next-generation efficacy:** Demonstrating superior therapeutic outcomes over the benchmark SS-31 in treating *in vivo* renal failure and muscle atrophy, 3029 emerges as a highly promising next-generation candidate for mitochondria-targeted diseases.

References

1) Shin, G., Hyun, S., Kim, D., Choi, Y., Kim, K. H., Kim, D., ... & Yu, J. (2023). Cyclohexylalanine-containing α-helical amphipathic peptide targets cardiolipin, rescuing mitochondrial dysfunction in kidney injury. Journal of Medicinal Chemistry, 67(5), 3385-3399.

A Cardiolipin-Targeting α-Helical Bundle Peptide forms Self-Assembled Trimer to Facilitate Cell Penetration and Stabilizes Inner Membrane to Rejuvenate Mitochondrial Dysfunction

Hyeong Woon Choe[1,2], Yan Lee[1*], Jaehoon Yu[2,3*]

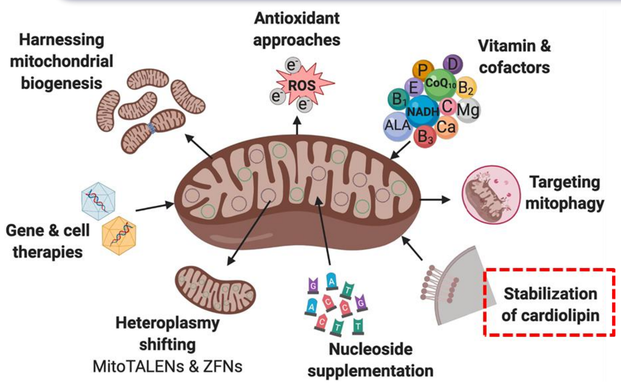
[1]Department of Chemistry, Seoul National University, Seoul, Republic of Korea

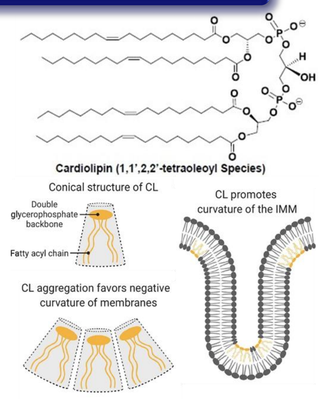
[2]CAMP Therapeutics, Seoul, Republic of Korea

[3]Department of Chemistry & Education, Seoul National University, Seoul, Republic of Korea

https://doi.org/10.17952/38EPS.2026.P369

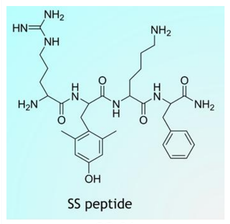
Cardiolipin as a Therapeutic Target in Mitochondria



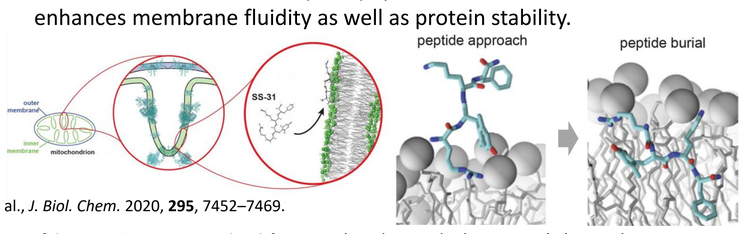


Rahman et al., *Epilepsy Behav.* 2019, **101B**, 106546.

Falabella M et al., *Trends in Endocrinology & Metabolism*, 2021; **32**, 224-237



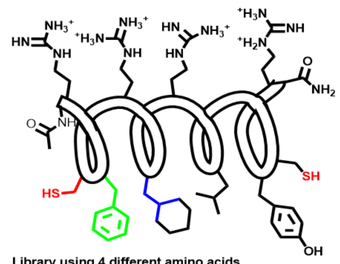
- **Cardiolipin** accounts for approximately 20% of the lipids in the **inner mitochondrial membrane (IMM),** promotes membrane curvature, and enhances membrane fluidity as well as protein stability.



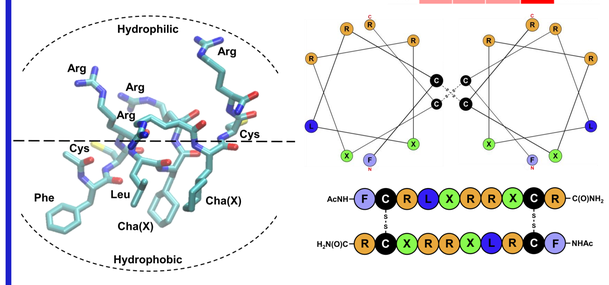
Mitchell et al., *J. Biol. Chem.* 2020, **295**, 7452–7469.

- **SS-31 was first reported in 2005 as an antioxidant**, It binds cardiolipin, stabilizes the IMM, and suppresses pathological remodeling. **Approved by the FDA for Barth Syndrome in September 2025**, **SS-31 is the first-in-class mitochondria-targeting peptide therapeutic.**

Discovery of 3029 Peptide

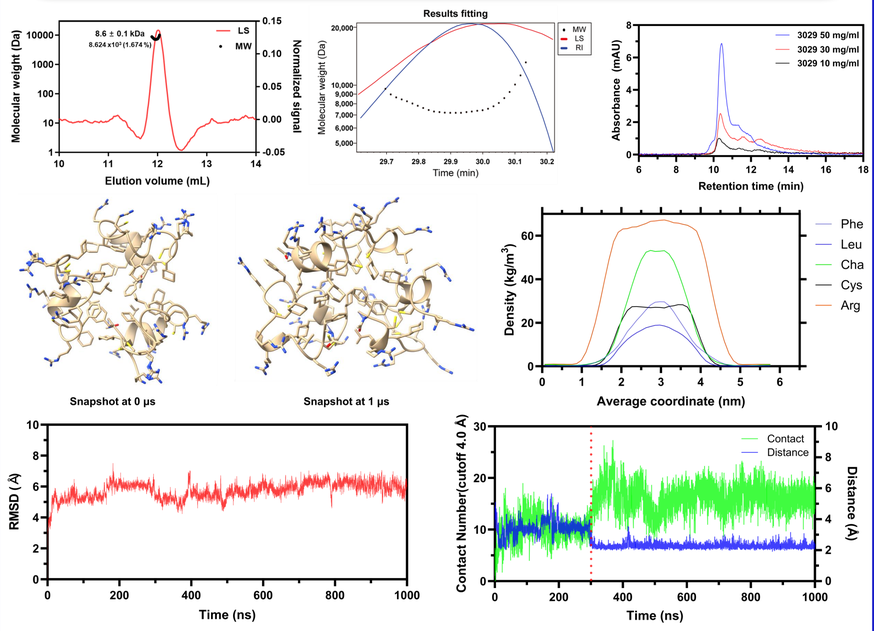


N-	hdf1	hdf2	hdf3	hdf4	-C
Ac-	Phe	Hdf	Hdf	Hdf	-amide
Ac-	Leu	Hdf	Hdf	Hdf	-amide
Ac-	Tyr	Hdf	Hdf	Hdf	-amide
Ac-	Cha	Hdf	Hdf	Hdf	-amide
Ac-	Hdf	Phe	Hdf	Hdf	-amide
Ac-	Hdf	Leu	Hdf	Hdf	-amide
Ac-	Hdf	Tyr	Hdf	Hdf	-amide
Ac-	Hdf	Cha	Hdf	Hdf	-amide
Ac-	Hdf	Hdf	Phe	Hdf	-amide
Ac-	Hdf	Hdf	Leu	Hdf	-amide
Ac-	Hdf	Hdf	Tyr	Hdf	-amide
Ac-	Hdf	Hdf	Cha	Hdf	-amide
Ac-	Hdf	Hdf	Hdf	Phe	-amide
Ac-	Hdf	Hdf	Hdf	Leu	-amide
Ac-	Hdf	Hdf	Hdf	Tyr	-amide
Ac-	Hdf	Hdf	Hdf	Cha	-amide



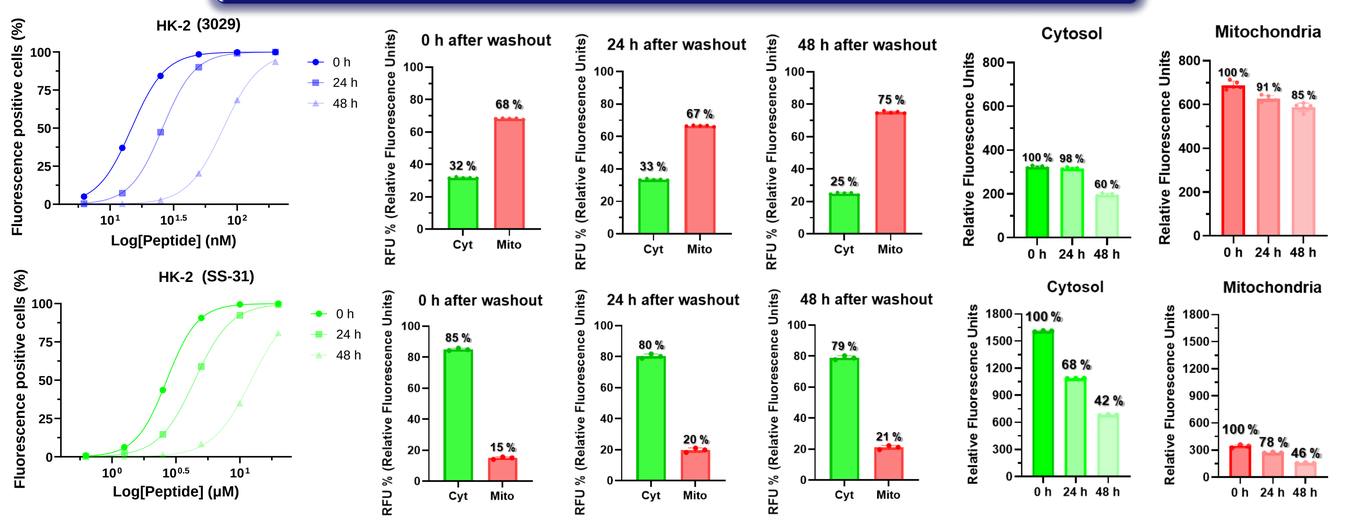
- Using a mixture of known **mitochondrial specific hydrophobic AA** (Phe, Leu, Tyr & Cha), **Each hydrophobic AA was position-scanned** to make 16 sub-libraries (each sub-library contains 64 kinds, total 1,024 kinds of peptides).
- 16 sub-libraries were screened for **the inhibition of ROS production, 3029 was selected.**

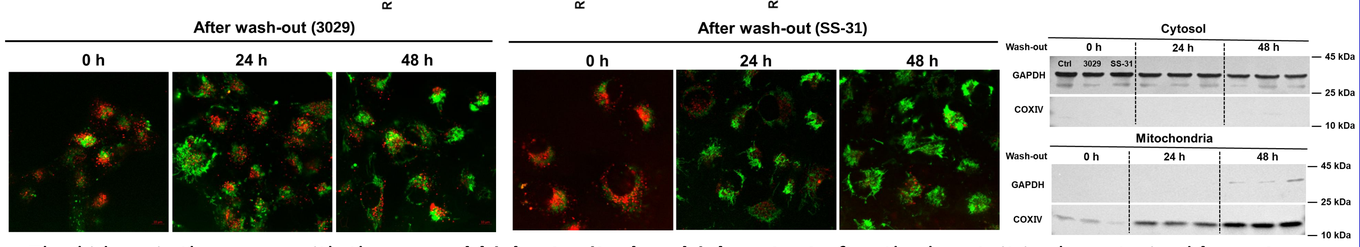
Trimerization of 3029 Confirmed by SEC-MALS and MD



- **Cyclohexylalanine (Cha) residues** are preferentially located in inter-region of 3029, **forming oligomeric status with compact hydrophobic core.**
- 3029 is **self-assembled into a discrete trimer,** The measured molecular wight (8,624 g/mol ±1.674 %) **corresponded to a trimeric assembly** (8,729 g/mol) of the cyclic peptide. MD simulations of the trimeric assembly further supported its **structural stability**, since the trimer maintains a compact bundle structure over 1 μs timescale.

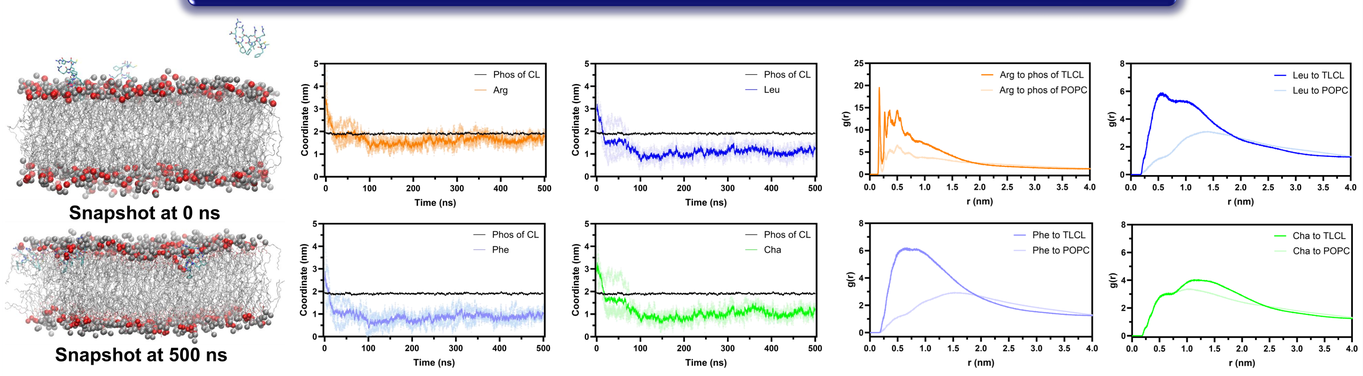
3029 Persists in Cells and Accumulates in Mitochondria





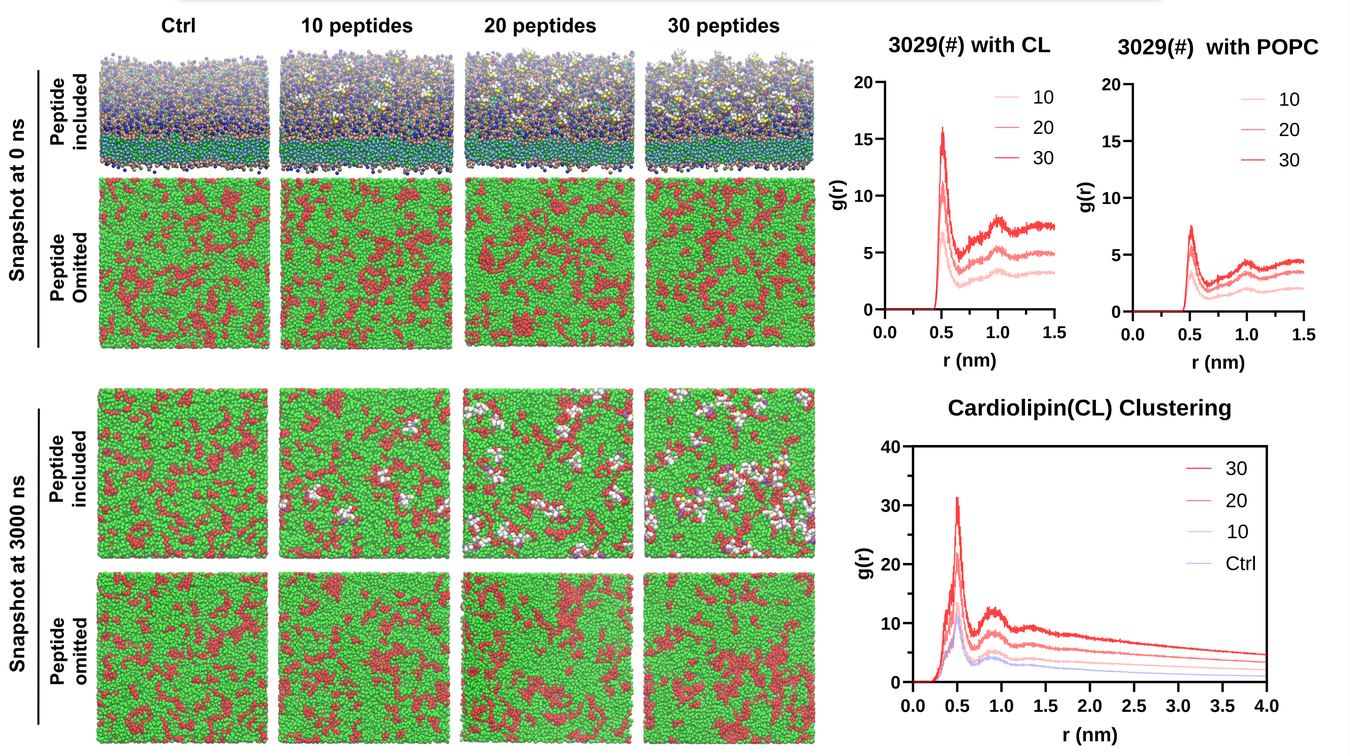
- The kidney is the organ with the **second-highest mitochondrial content** after the heart. it is characterized **by a strong dependence on mitochondria for ATP production.**
- The intracellular EC_{50} at 48 h was 78 nM, indicating that 3029 persistently are **within cells at nanomolar scales even after 48 h**.
- These results suggest that **the preferential accumulation of 3029 in mitochondria** after cell penetration lasts for long period of time.
- **3029 is preferentially going to mitochondria, remaining there**. In contrast, small portion of 3029 in cytosol is removed from cell.

All-Atom MD Reveals Cardiolipin-Selective Membrane Insertion



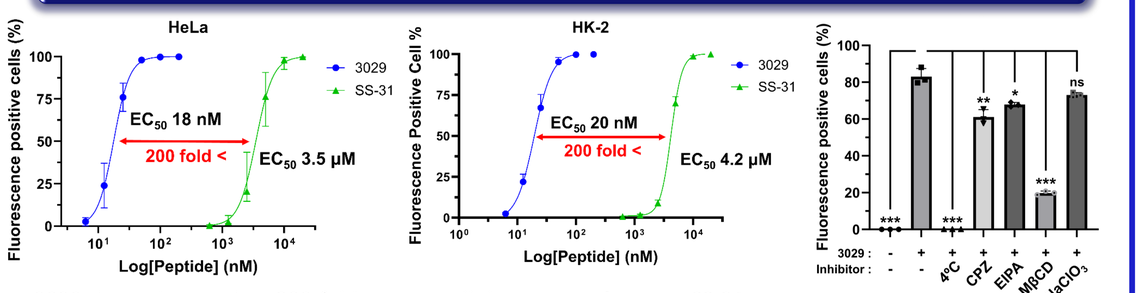
- **MD simulations in a 20% cardiolipin (CL)-containing IMM model** demonstrate that 3029 initially binds to TLCL phosphate groups before flipping its hydrophobic residues into the membrane interior for structural stabilization.
- The radial distribution function (RDF) analysis of key residues—Arg, Cha, Leu, and Phe—further confirms the high selectivity of 3029 for TLCL over POPC, **demonstrating its specific anchoring mechanism within the mitochondrial inner membrane.**

3029-Induced Cardiolipin Clustering in Martini CG Simulations



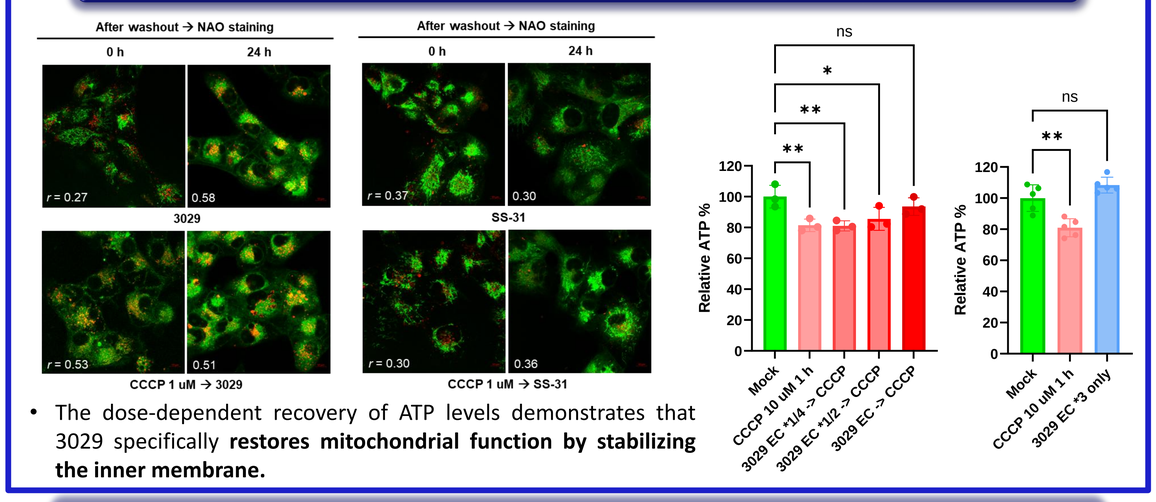
- Martini CG MD simulations reveal that **3029 induces concentration-dependent clustering of cardiolipin (CL),** with RDF analysis confirming its superior selectivity for CL over POPC. These results highlight **the critical role of 3029 in restoring mitochondrial structural and functional integrity. Curvature structural stability of the inner mitochondrial membrane (IMM)**, in which cardiolipin (CL) is a major phospholipid, is **essential for the recovery of mitochondrial dysfunction.**

3029 Efficiently Penetrates Cells via Endocytosis Compared with SS-31



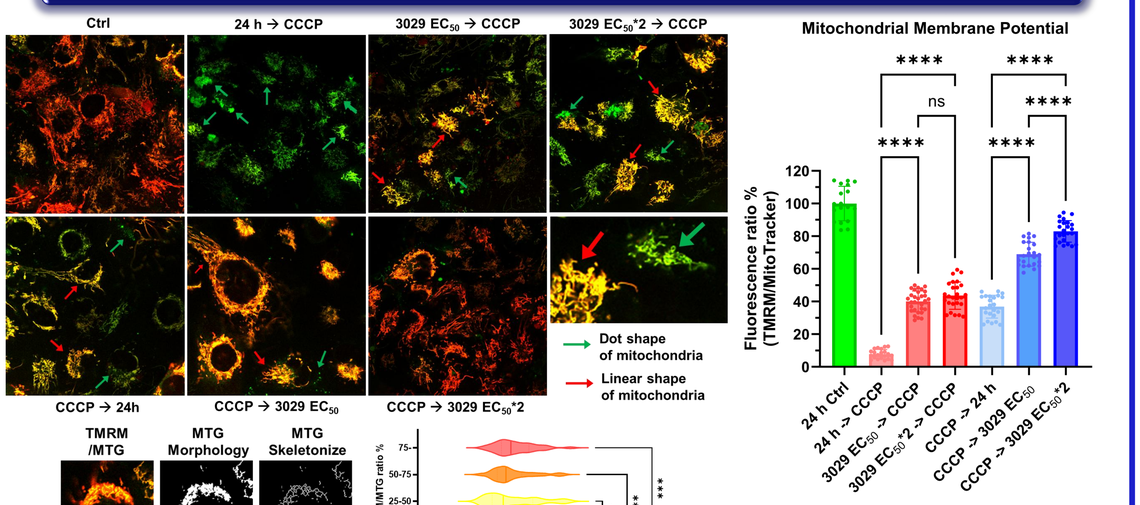
- 3029 showed more than **200-fold greater cellular penetration** than SS-31.
- TAMRA-labeled 3029 penetrates into HeLa and HK-2 cells in 3 h, at EC_{50} **values as 18 nM and 20 nM**, respectively. 3029 penetrates into cells through a clearly defined **energy- and cholesterol-dependent endocytosis mechanism.**

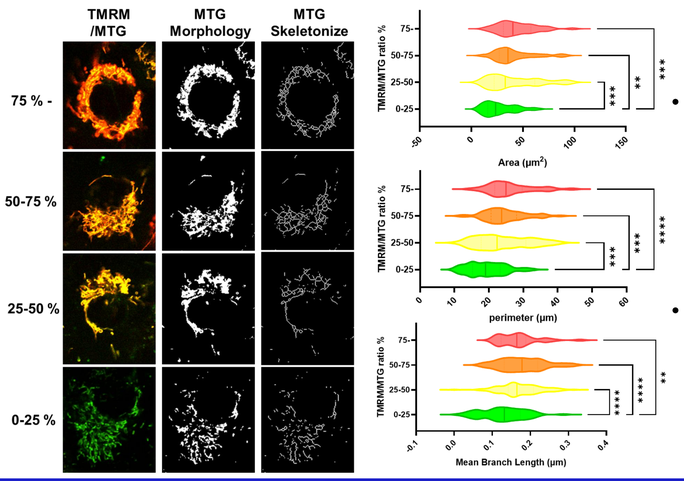
3029 Restores Mitochondrial Function by Targeting Cardiolipin



- The dose-dependent recovery of ATP levels demonstrates that 3029 specifically **restores mitochondrial function by stabilizing the inner membrane.**

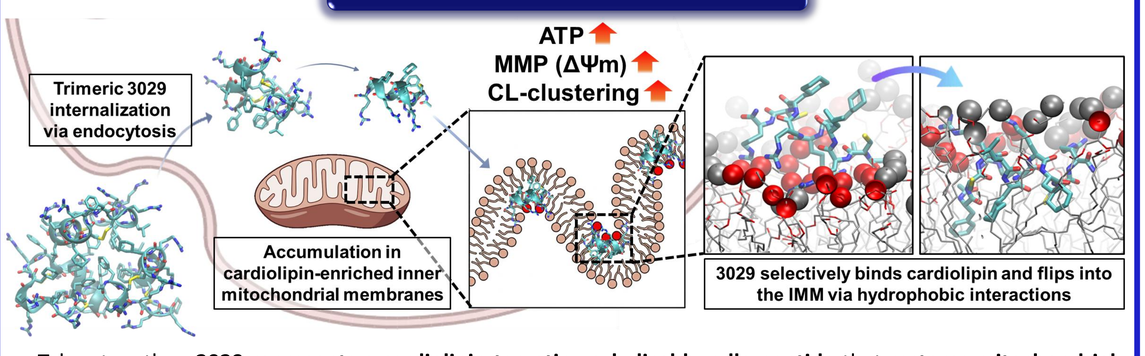
3029 Rejuvenates Mitochondrial Membrane Potential and Morphology





- Indicating **sustained association of the 3029 with cardiolipin-rich regions under oxidative stress conditions.** In contrast to the gradual increase observed in CCCP untreated cells, these results suggest that **mitochondrial dysfunction triggers rapid targeting of 3029 to cardiolipin**.
- MMP and Morphological analysis reveals that while **CCCP induces dysfunctional 'dot-shaped' mitochondria**, 3029 treatment maintains or **rejuvenates the healthy 'linear-shape' structure**, indicating its protective and therapeutic potential.

Conclusion



- Taken together, **3029 represents a cardiolipin-targeting α-helical bundle peptide** that **restores mitochondrial function** through **selective membrane interaction and lipid reorganizatio**n. This strategy provides a promising framework for the **development of mitochondria-targeted therapeutics.**

38th EPS
European Peptide Symposium
6 - 11th of September 2026
Vienna, Austria

Deciphering the Role of Citrulline and Cyclization in the Rational Design of Antimicrobial Peptides Derived from Equinin B

Andreja Jakas [1], Mariele Staropoli[1,2], Lea Pašalić[1], Anna Marin[3] , Jasmina Tuzlak[3] & Nermina Malanović[3]

[1]Rudjer Bošković Institute, Division of Organic Chemistry and Biochemistry, Zagreb, Croatia; [2]University of Palermo, Department of Earth and Marine Sciences, Zagreb, Croatia;
[3]University of Graz, Institute of Molecular Bioscience, Graz, Austria

https://doi.org/10.17952/38EPS.2026.P188

andreja.jakas@irb.hr

Introduction: Equinin B is an antimicrobial peptide (AMP) isolated from the cnidarian *Actinia equina* (Linnaeus, 1758), an anthozoan coelenterate of the family Actiniidae distributed from the Indo-Pacific to the Mediterranean and the Atlantic. The amino acid sequence of equinin B, GQCQRKCLGHCSKKCPKHPQCRKRCIRRCFGYCL, consists of 34 amino acids and shows 37.78% similarity to another AMP, aurelin, isolated from jellyfish.[1] We prepared truncated peptides from equinin B to identify the smallest fragment that still retains antimicrobial activity.[2] Subsequently, we prepared derivatives of these three fragments. First, we substituted Lys with Arg (**EB1-K**, **EB2-K**), then we substituted Cys with Arg (**EB1-C**, **EB2-C**), and after that all Cys were substituted with Cit (**EB1-Cit, EB2-Cit, EB3-Cit**). Finally, cyclization was achieved with disulfide bridges[3] (**EB1-Cyc, EB2-Cyc, EB3-Cyc**) and by inserting bipyridine-dicarboxylic acid (**EB3-Py**) (Table 1).

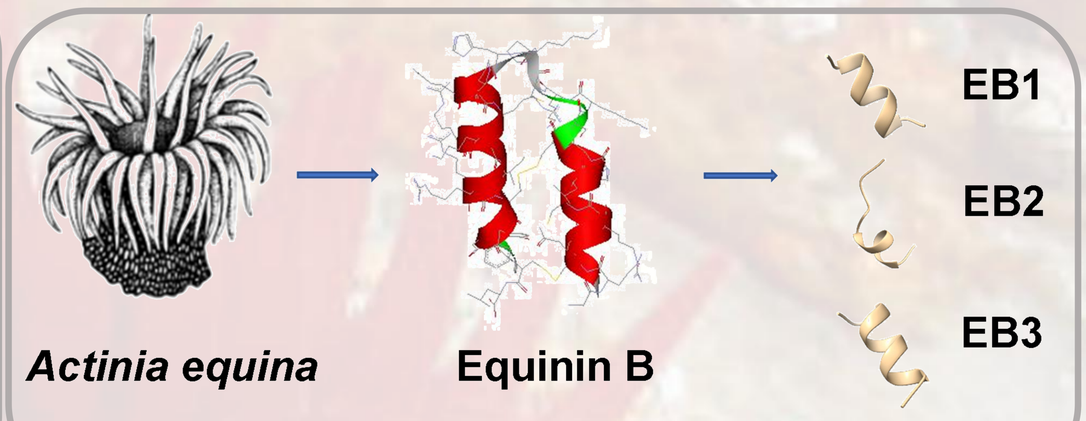


Table 1. Basic characteristics of the peptides used in the study

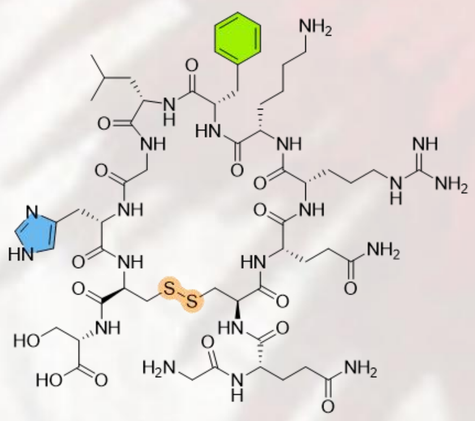
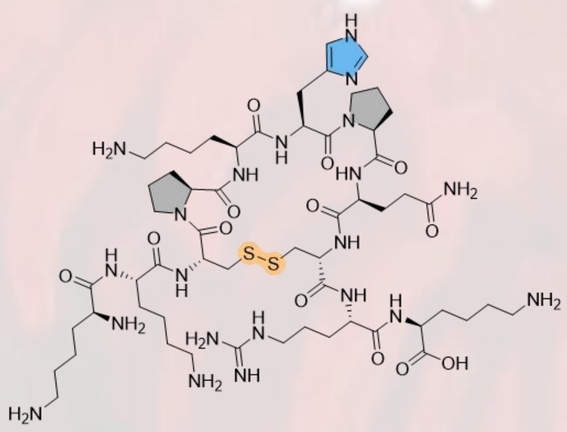
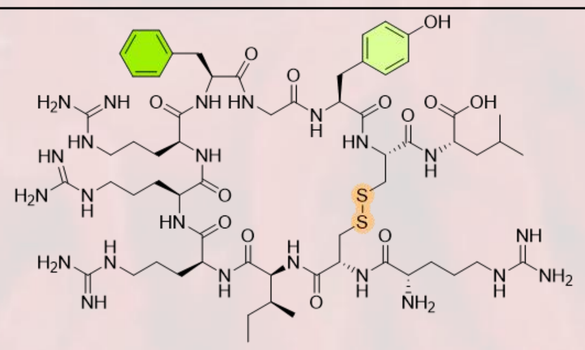
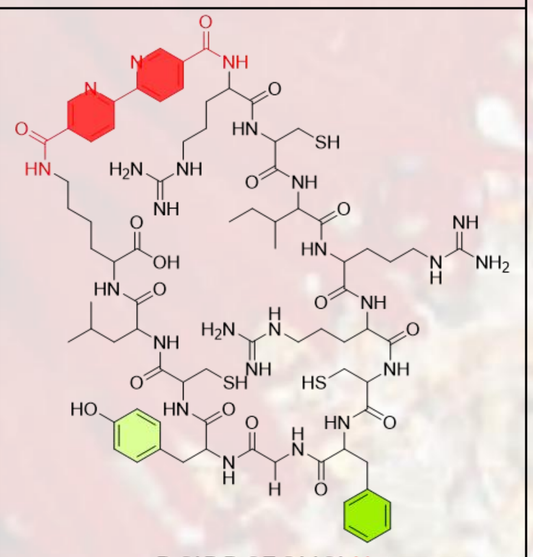
GQCQRKCLGHCSKKCPKHPQCRKRCIRRCFGYCL **Equinin B**		
Fragment 1	**Fragment 2**	**Fragment 3**
GQCQRKCLGHCS **EB1**	KKCPKHPQCRK **EB2**	RCIRRCFGYCL **EB3** ANTIMICROBIAL, CYTOTOXIC
Equinin B derivatives		
GQCQRRCLGHCS **EB1-K** ANTIFUNGAL (BF)	RRCPRHPQCRR **EB2-K** ANTIFUNGAL (BF)	
GQRQRKRLGHRS **EB1-C**	KKRPKHPQRRK **EB2-C** ANTIFUNGAL (BF)	RRIRRRFGYRL **EB3-C** ANTIBACTERIAL, NON-CYTOTOXIC
GQCitQRKCitLGHCitS **EB1-Cit**	KKCitPKHPQCitRK **EB2-Cit**	RCitIRRCitFGYCitL **EB3-Cit** INACTIVE
 GQCQRKCLGHCS **EB1-Cyc**	 KKCPKHPQCRK **EB2-Cyc**	 RCIRRCFGYCL **EB3-Cyc** INSOLUBLE
		 RCIRRCFGYCLK **EB3-Cyc-Py** INSOLUBLE

Table 2. Antimicrobial activity

Comp.	*E.coli*		*S.epidermidis*		*S. aureus*		*E. faecalis*		*P.aeruginosa*		*C. albicans*	
	MIC	IBF	MIC	IBF	MIC	IBF	MIC	IBF	MIC	IBF	MIC	IBF
EB1	>400	>400	>100		>400	>400	>400	>400	>400	>400	>400	>400
EB2	>400	>400	>100		>400	>400	>400	>400	>400	>400	>400	>400
EB3	200	>400	25		>400	200	>400	200	>400	>400	200	150
EB1-K	>400	>400	>100		>400	200	>400	>400	>400	>400	>400	200
EB2-K	>400	>400	>100		>400	>400	>400	>400	>400	>400	>400	100
EB1-C	>100		>100									
EB2-C	>100		>100									
EB3-C	>100		25-50									
EB1-Cit	>1200		>1200									
EB2-Cit	>1200		>1200									
EB3-Cit	>1200		>1200									
EB1-Cyc	>1200		>1200									
EB2-Cyc	>1200		>1200									

MIC = minimum inhibitory concentration (μg/mL)
IBF = inhibition of biofilm formation (μg/mL)

Conclusion:

- Truncated peptides of equinin B, a 34 amino acid peptide, were synthesized by Fmoc solid phase peptide synthesis (SPPS)
- Cyclization was acheved either via a disulfide bridge or with bipyridine-dicarboxylic acid
- The main AM activity was observed in the third part of the peptide, EB3
- Citrullinated EB3-Cit lost the activity observed in EB3 and EB3-C
- Cyclic derivatives obtained either with a disulfide bridge or with a bipyridine bridge were not soluble and could not be used
- Interesting results were obtained with compounds EB1-K and EB2-K, which exhibited activity against biofilm formation (Table 2)
- Further investigation of compounds for biofilm activity should be carried out with other synthesized compounds, especially the cyclic ones

References:

[1]C. La Corte et al., *Mar. Drugs* 2024, 22, 172. https://doi.org/10.3390/md22040172
[2]M. Staropoli et al., *Mar. Drugs* 2026, *24*, 46. https://doi.org/10.3390/md24010046
[3]T. M. Postma and F. Albericio, *Eur. J. Org. Chem*. 2014, 3519–3530. https://doi.org/10.1002/ejoc.201402149

Acknowledgement:

This work was supported by Croatian Science Foundation under grant HRZZ IP-2024-05-1216 and Croatian Government and the European Union, Program (KK.01.1.1.01), under the project Sustainable Bioprospecting of Organisms from the Adriatic Sea for Innovative Natural Products (KK.1.1.10.0001)— BioProCro, granted to the Center of Research Excellence for Marine Bioprospecting.

Harnessing Nature's Defences to Treat Gut Biofilms

Bernhard Jandl[1,2,3], Michaela Lang[4,5], Athanasios Makristathis[6], Christoph Gasche[4,7] and Markus Muttenthaler[1,3]

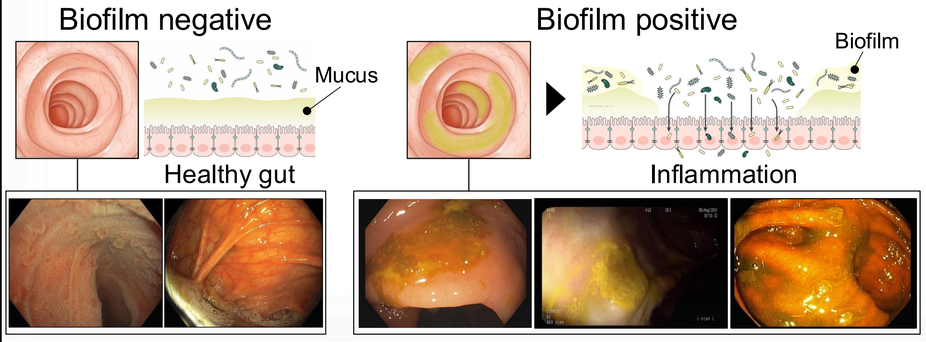
[1]Institute of Biological Chemistry, Faculty of Chemistry, University of Vienna, Vienna, Austria.
[2]Vienna Doctoral School in Chemistry (DoSChem), University of Vienna, Vienna, Austria.
[3]Institute for Molecular Bioscience, The University of Queensland, Brisbane, Queensland, Australia.
[4]Division of Gastroenterology and Hepatology, Department of Internal Medicine 3, Medical University of Vienna, Vienna, Austria.
[5]Centre for Microbiology and Environmental Systems Science, Department of Microbiology and Ecosystem Science, University of Vienna, Vienna, Austria.
[6]Division of Clinical Microbiology, Department of Laboratory Medicine, Medical University of Vienna, Vienna, Austria.
[7]Loha for Life, Center for Gastroenterology and Iron Deficiency, Vienna, Austria.

https://doi.org/10.17952/38EPS.2026.P371

Email: bernhard.jandl@univie.ac.at; markus.muttenthaler@univie.ac.at

Gut Biofilms – A New Drug Target

Irritable bowel syndrome (IBS) and **inflammatory bowel diseases** (IBD, including **Crohn's disease** (CD) and **ulcerative colitis** (UC)) are increasingly prevalent chronic gastrointestinal disorders **affecting over 10% of the global population**.[1,2] These gastrointestinal disorders can lead to severe complications (i.e., chronic inflammation, abdominal pain, intestinal bleeding, anaemia) with annual associated costs at €115 billion in Europe, $75 billion in the USA and €1.5 billion in Austria.[1] In a recent clinical study with over 1,100 participants, we observed that gut biofilms are macroscopically visible and highly prevalent in **IBS (57%)**, **UC (34%)** and **CD (22%)** patients but less in **healthy individuals (6%)**, indicating that gut biofilms could be a new drug target for the treatment IBS and IBD.[1,2,3]

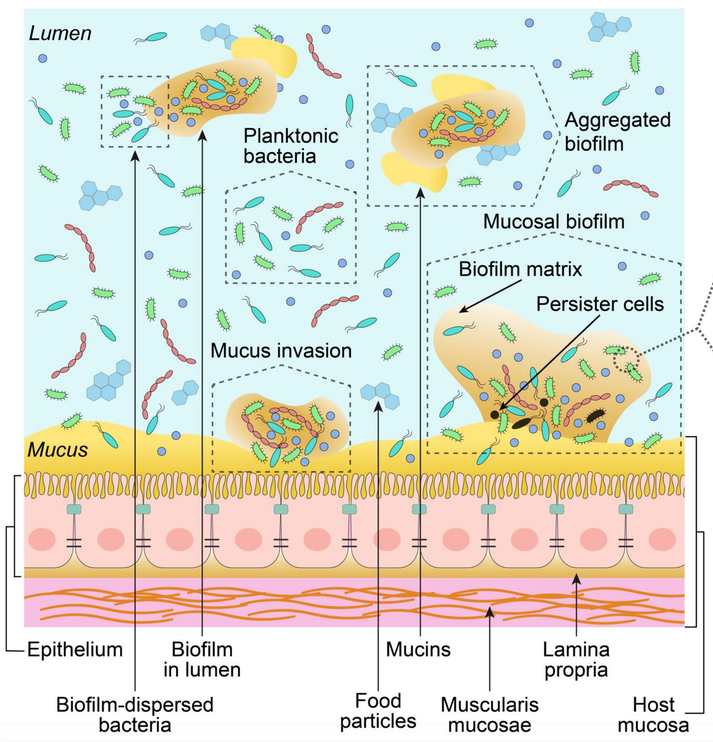


Biofilm occurrence

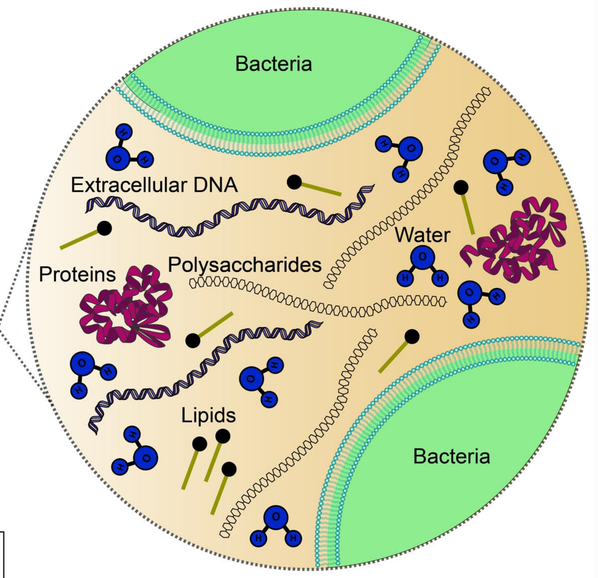
57% in IBS
34% in UC
22% in CD



Gut bacteria arrangement



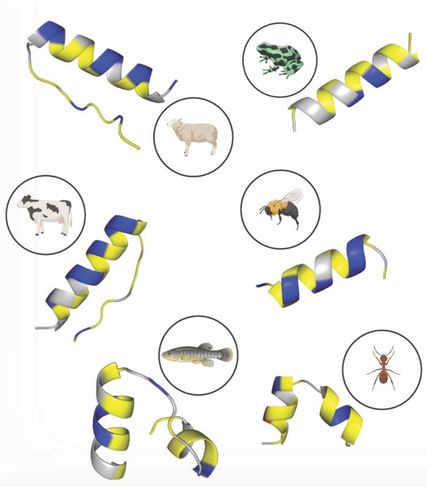
The biofilm matrix



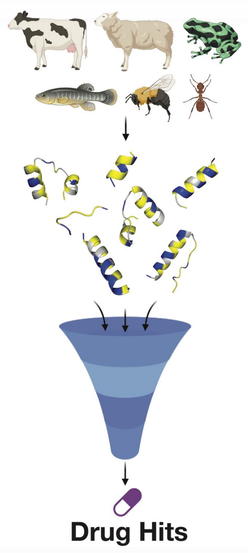
Components	Regulatory systems
Extracellular DNA	Quorum sensing
Polysaccharides	Stringent response
Proteins	Second messengers
Water	

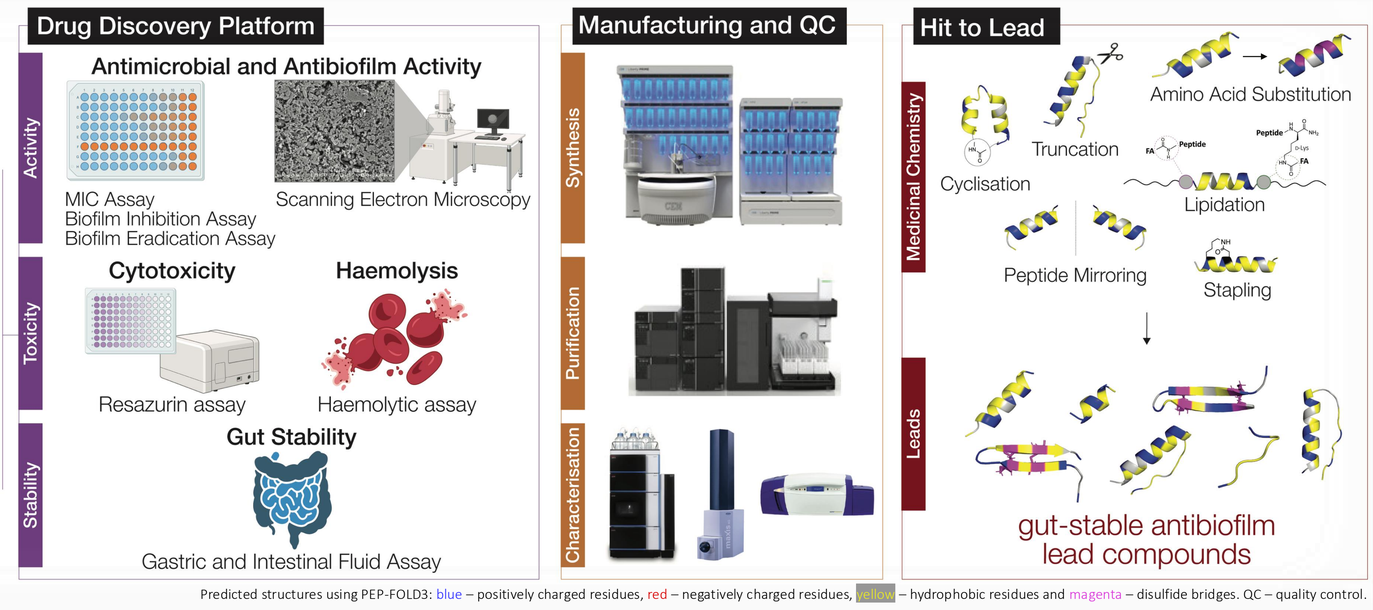
Drug Discovery and Development Platform

Nature's molecular defences



Our drug discovery strategy builds on nature's molecular defences by focusing on animals that routinely encounter biofilms, including ants, bees, cows, fish, frogs, pigs, sea urchins, sheep, and wasps. Building on this concept, we established the first gut-biofilm-targeted drug discovery and development platform that harnesses nature-derived antimicrobial peptides (AMPs) and integrates clinical biofilm samples from IBS patients, aiming to develop highly stable oral antibiofilm therapeutics.





Predicted structures using PEP-FOLD3: blue – positively charged residues, red – negatively charged residues, yellow – hydrophobic residues and magenta – disulfide bridges. QC – quality control.

Highly-stable Antibiofilm Peptides

Hit screen. We synthesised 31 AMPs *via* Fmoc-solid-phase peptide synthesis and evaluated their inhibition of planktonic and biofilm growth, eradication of mature biofilms and cytotoxicity against HEK-293 cells (**Figure 1**). This screen used two clinical isolates from biofilm-positive IBS patients and two biofilm-forming control strains.

Hit-to-lead development. MMBJ018 and MMBJ020 were identified as hit compounds due to their broad-spectrum antimicrobial and antibiofilm activity. Both AMPs underwent hit-to-lead optimisation using state-of-the-art medicinal chemistry guided by structure-stability-activity relationship data which produced D-MMBJ055 and D-MMBJ059 as highly stable antibiofilm leads (**Figure 2**). We also applied circular dichroism to analyse the peptides' secondary structure and scanning electron microscopy to evaluate antibiofilm activity and biofilm penetration capacity.

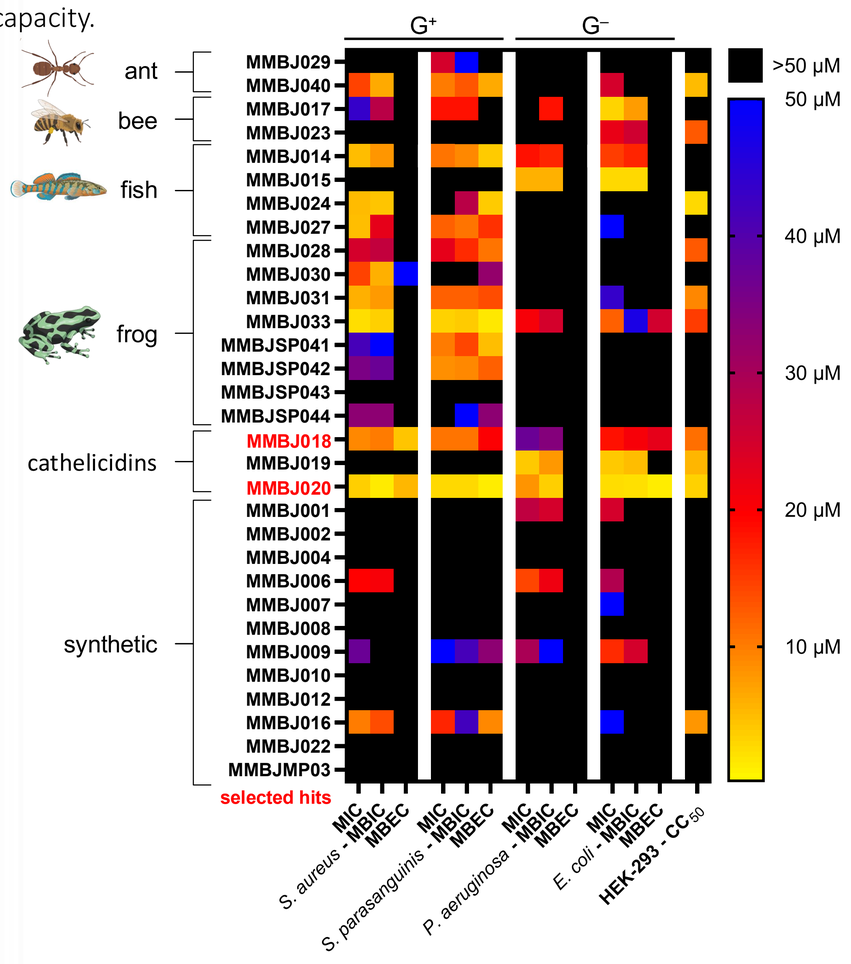


Figure 1. Heat map displaying the results of the antimicrobial, antibiofilm and cytotoxicity screen. MIC – minimum inhibition concentration; MBIC – minimum biofilm inhibition concentration; MBEC – minimum biofilm eradication concentration; CC_{50} – half-maximal cytotoxic concentration; G^+ – Gram-positive; G^- – Gram-negative.

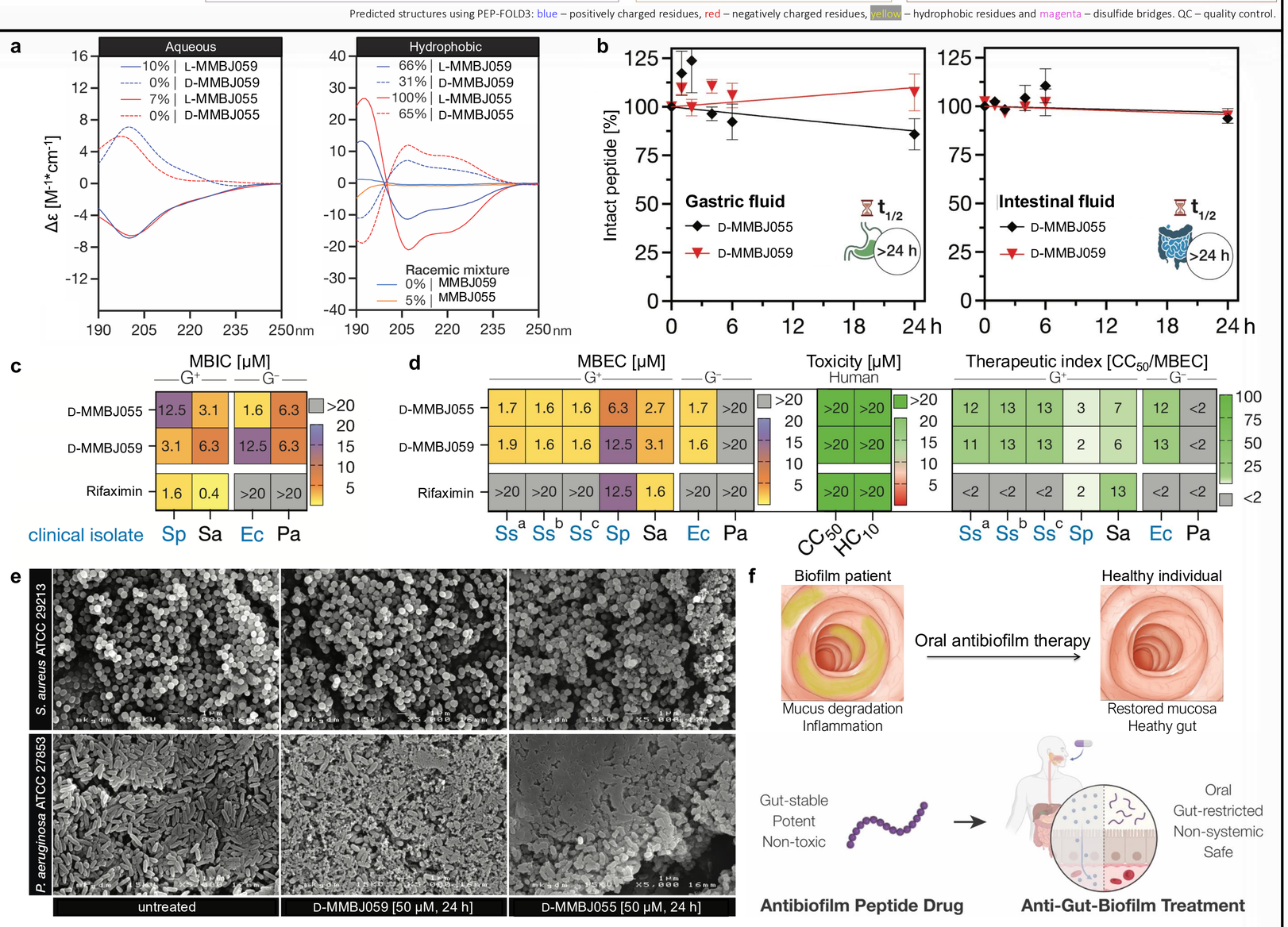


Figure 2. Hit-to-lead development. a) Circular dichroism analysis. b) Stability in gastric and intestinal fluid. c) Biofilm inhibition activity. d) Biofilm eradication activity, cytotoxicity, haemolytic activity and therapeutic indices. e) Scanning electron microscopy images of mature biofilms. f) Therapeutic strategy. Ss, *Streptococcus salivarius* [a] – R22-K2¶ / [b] – R22-K3¶ / [c] – R30-K3¶; Sp, *Streptococcus parasanguinis* 102-K3/3¶; Sa, *Staphylococcus aureus*; Ec, *Escherichia coli*; Pa, *Pseudomonas aeruginosa;* ¶ – in-house patient ID; CC_{50}, half-maximal cytotoxic concentration; HC_{10}, 10% of maximal haemolytic concentration; G^+ – Gram-positive; G^- – Gram-negative.

Conclusion

We present a novel antibiofilm peptide drug discovery platform for the development of gut-specific oral therapeutics for patients with gut biofilms. Nature proved to be a rich source of potent antibiofilm compounds, evolved to penetrate and eradicate mature biofilms, including patient-derived isolates. Our approach resulted in two strong drug leads, D-MMBJ055 and D-MMBJ059, for gut-biofilm-targeted therapy. Both peptides are fully gut stable and have potent biofilm eradication activity (MBEC=1.6–12.5 µM) with favourable therapeutic indices (TI_{MBEC}=2–13) against clinical biofilm isolates. This work established the first nature-inspired drug discovery platform and delivered an initial set of highly stable antibiofilm drug leads for further development as oral treatments for patients with gut-biofilm-associated chronic gut disorders.

Reference

(1) Intestinal biofilms – Pathophysiological relevance, host defence and therapeutic opportunities. Jandl B et at., *Clinical Microbiology Reviews* 2024.
(2) Gastrointestinal biofilms – Endoscopic detection, disease relevance and therapeutic strategies. Jandl B et al., *Gastroenterology* 2024.
(3) Mucosal biofilms are an endoscopic feature of irritable bowel syndrome and ulcerative colitis. Baumgartner M et. al., *Gastroenterology* 2021.

Funding

Deciphering the Role of Posttranslational Modifications on the DNA-Binding Activity of Max Transcription Factor Using Chemical Protein Synthesis

Nithun Raj V,[1] Yumi Minyi Yao,[2] Omer Harel,[1] Shada Khoury,[1] Shaimaa Habiballah,[1] Xiaoxi Lin,[1] Ariel Afek,[2] Muhammad Jbara[1]

[1]*School of Chemistry, Raymond and Beverly Sackler Faculty of Exact Sciences, Tel Aviv University*

[2]*Department of Chemical and Structural Biology, Weizmann Institute of Science*

Email: jbaram@tauex.tau.ac.il

https://doi.org/10.17952/38EPS.2026.P128

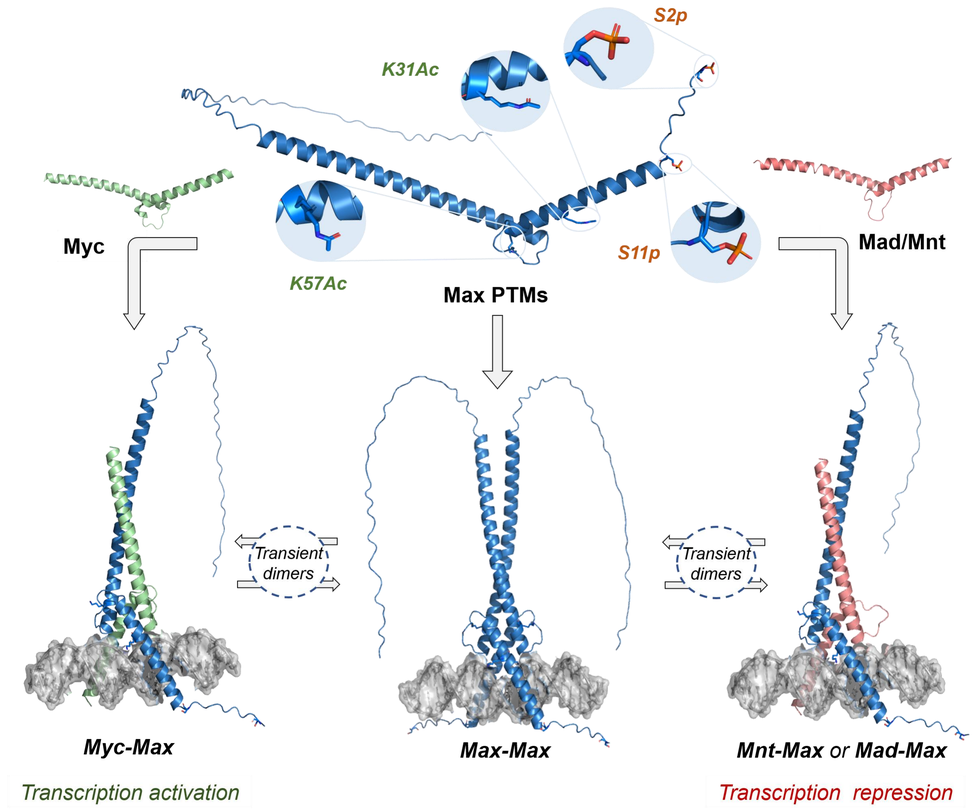
TEL AVIV UNIVERSITY

Jbara Lab
Chemical Biology & Drug Discovery

Abstract

Transcription factors (TFs) are proteins that regulate gene transcription through sequence-specific DNA binding, and their activities are tightly controlled by dynamic post-translational modifications (PTMs). The Myc–Max–Mad TF network plays a pivotal role in regulating the expression of approximately 15% of the human genome, and its dysregulation is implicated in nearly 70% of human cancers. Within this network, the selective dimerization of Max with its binding partners, including Myc, Mad, and Mnt, is central to transcriptional regulation. Max activity is regulated by PTMs, with Ser-phosphorylation and Lys-acetylation considered key regulatory mechanisms. However, the precise molecular mechanisms by which these PTMs regulate Max oligomerization and DNA binding remain elusive. In this study, we developed a practical synthetic strategy for the preparation of homogeneous full-length Max, enabling the systematic investigation of site-specific PTM effects on its DNA-binding activity. Using this approach, we generated a focused library of Max variants incorporating defined phosphorylation, acetylation, and fluorescent modifications. Comprehensive DNA-binding analyses revealed that both phosphorylation and acetylation significantly inhibit Max DNA binding activity. Notably, our results further show that PTMs, e.g. Lys-acetylation, can alter the binding specificities of Max towards certain sequences flanking its consensus binding sites. Furthermore, the total synthesis of site-specifically labelled Myc, Mnt, and Mad TF analogs enabled the combinatorial assembly of 24 distinct Max heterodimeric complexes, allowing systematic characterization of dimerization and DNA-binding properties across the network. Our work provides insights into the hidden molecular code of PTM-dependent regulation of TF-DNA interactions, paving the way to interpret gene expression regulation programs and engineering bioactive TFs.

Regulation of the Myc–Max–Mad Transcription Factor Network by Posttranslational Modifications

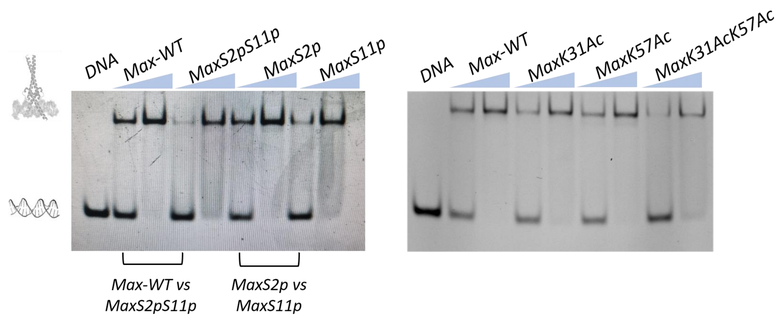


- Controls the expression of ≈15% of the entire genome
- Implicated in over 70% of all human cancers
- Challenging drug target

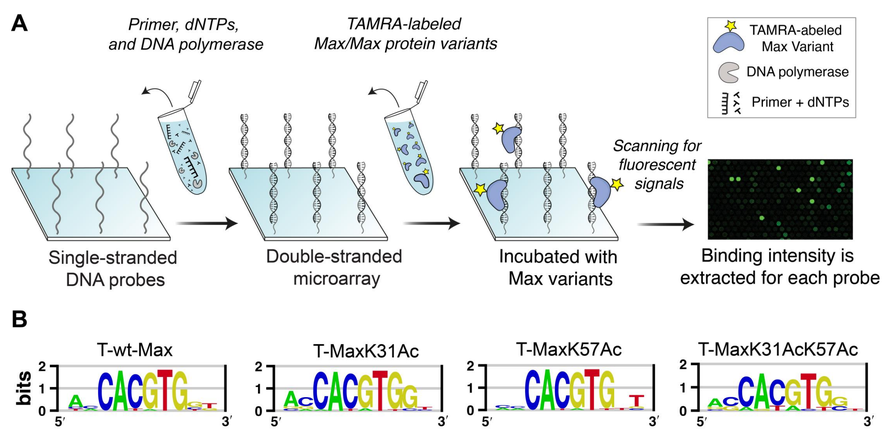
- Max is Essential for heterodimerization & activity
- Endogenous inhibitor for Myc (*homodimerization*)
- Potential synthetic regulator

DNA Binding Activity of Site-specifically Modified Max Analogs

Electrophoretic Mobility-Shift Assay (EMSA)



In Vitro High-Throughput Analysis Using a Protein Binding Microarray



Biolayer Interferometry Assay (BLI)

Protein	K_D (E-box)
Max-WT	15.3 ± 0.3 nM
MaxS2pS11p	54.4 ± 0.6 nM
MaxS2p	23.9 ± 0.4 nM
MaxS11p	41.9 ± 1.1 nM
MaxK31AcK57Ac	294.3 ± 3.0 nM
MaxK31Ac	134.0 ± 13.9 nM
MaxK57Ac	51.8 ± 6.8 nM
MaxS2pS11pK31AcK57Ac	1100.0 ± 30.0 nM

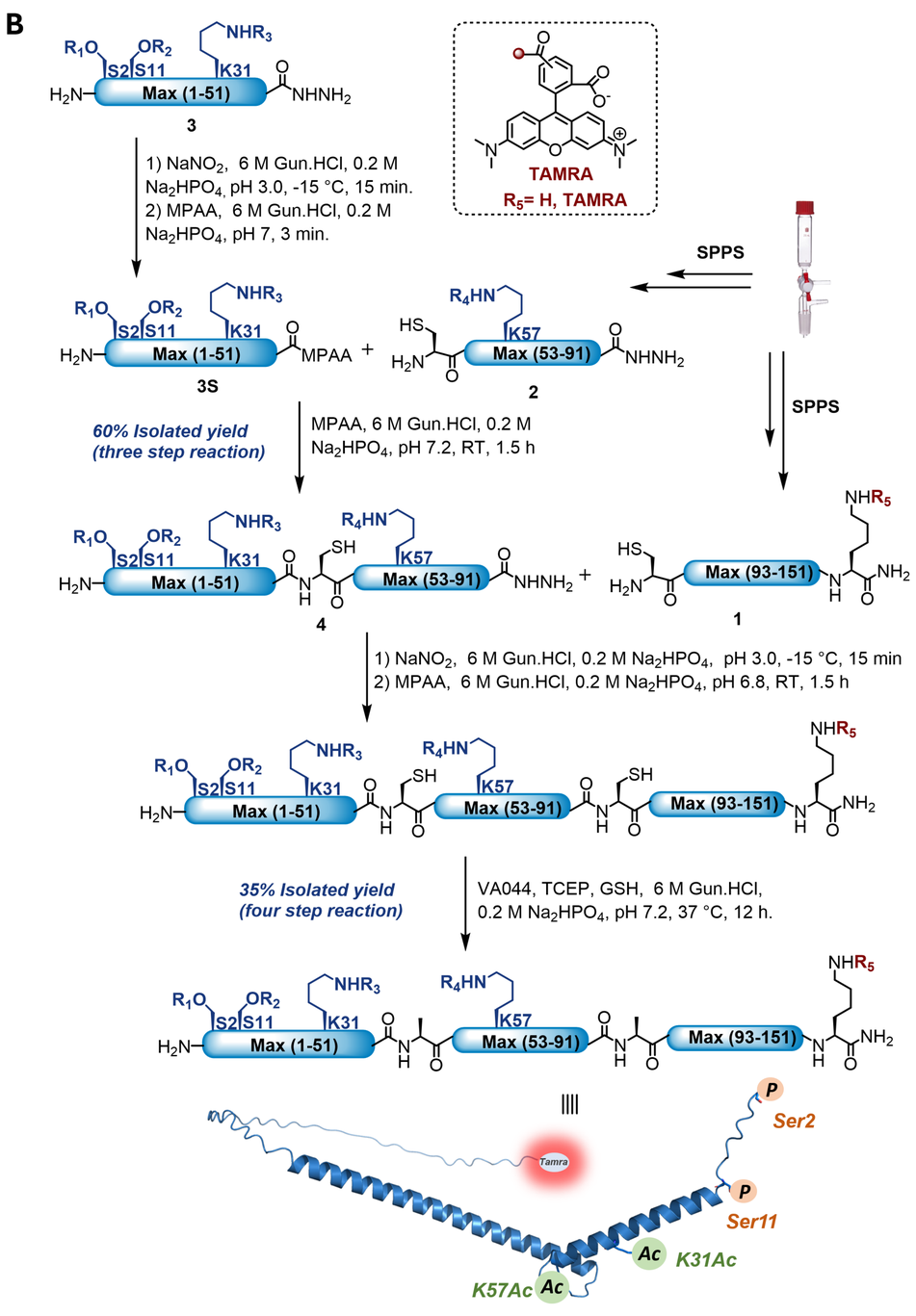
- ***Ser-phosphorylation and Lys-acetylation significantly inhibit the DNA binding activity of Max TF***
- ***PTM marks do not significantly impact Max's binding specificity to the core E-box sequence (CACGTG)***
- ***Doubly acetylated variant displays a robust preference for DNA sequences with 'GG' at positions +3 and +4.***

Design and Chemical Synthesis of Site-specifically Modified Max Transcription Factor Analogs

A

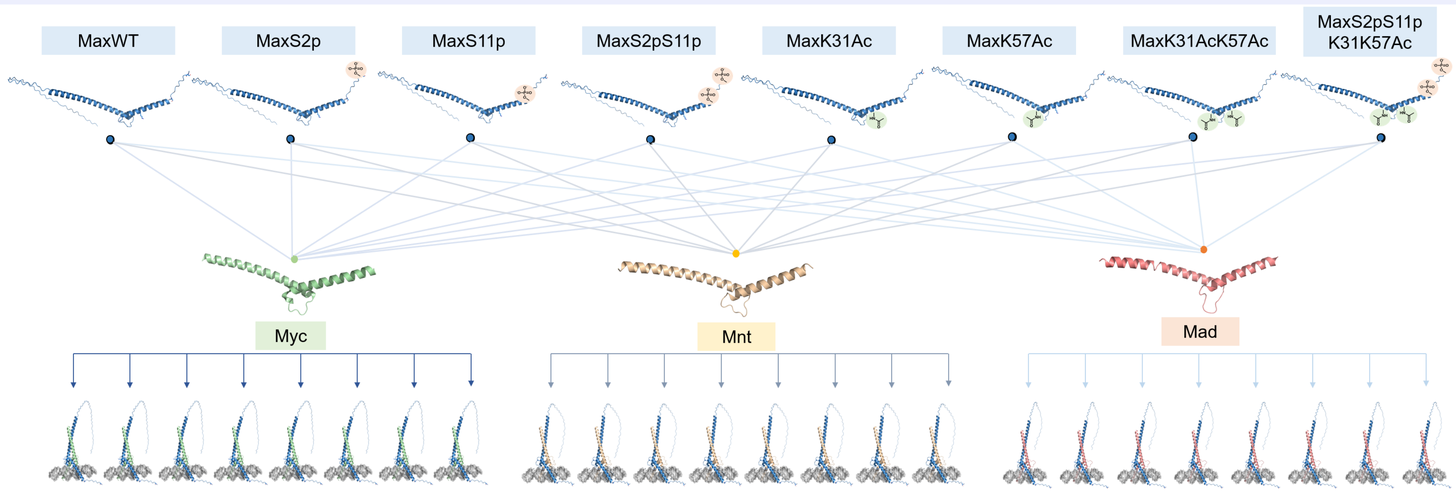
MS[2]DNDDIEVES[11]DADKRAHHNALERKRRDHIK[31]DSFHSLRDSVPSLQGEKASRA
QILDK[57]ATEYIQYMRRKNHTHQQDIDDLKRQNALLEQQVRALEKARSSAQLQTNY
PSSDNSLYTNAKGSTISAFDGGSDSSSESEPEEP QSRKKLRMEAS

B



- ***Developed a practical synthetic strategy to prepare homogeneous full-length Max transcription factor for the first time and generated a focused library of 15 distinct analogs with defined modification patterns, including site-specific phosphorylation, acetylation, and fluorescent tagging.***

The Myc–Max–Mad Oligomerizations and DNA Binding Activity are Modulated by Both Specific PTM Pattern and Transcription Factor Partner

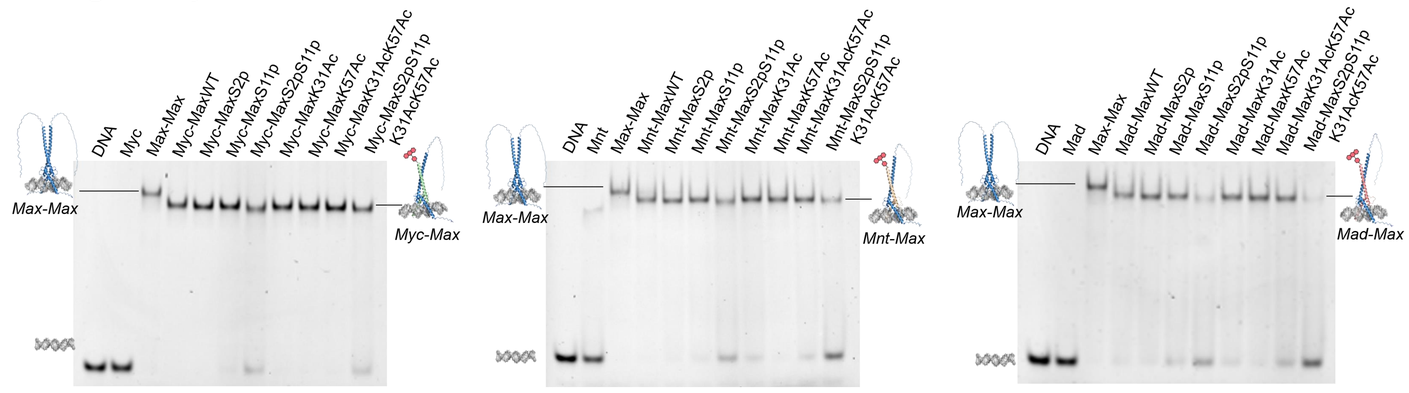


Myc-Max-Mad Interactions via BLI Assay

Myc-Max interaction	K_D (nM)	Mnt-Max interaction	K_D (nM)	Mad-Max interaction	K_D (nM)
Myc-MaxWT	74.6	Mnt-MaxWT	214.8	Mad-MaxWT	208.7
Myc-MaxS2pS11p	58.8	Mnt-MaxS2pS11p	142.4	Mad-MaxS2pS11p	143.1
Myc-MaxK31AcK57Ac	79.1	Mnt-MaxK31AcK57Ac	139.7	Mad-MaxK31AcK57Ac	196.0
Myc-MaxS2pS11pK31AcK57Ac	74.3	Mnt-MaxS2pS11pK31AcK57Ac	73.6	Mad-MaxS2pS11pK31AcK57Ac	95.1

- ***Ser-phosphorylation in combination with Lys-acetylation selectively enhances Max heterodimerization with Mnt and Mad, but not with Myc***

DNA Binding Activity of Max Heterodimers via EMSA



- ***PTMs markedly reduce DNA binding in Mnt–Max and Mad–Max complexes, whereas they are largely tolerated in Myc–Max complexes***
- ***Our work provides insight into the molecular code of PTM-TFs and DNA interactions, paving the way to interpret gene expression regulation programs***

Find these articles on LinkedIn

References

1. R. V. Nithun, Y. M. Yao, X. Lin, S. Habiballah, A. Afek, M. Jbara, *Angew. Chem. In. Ed.* **2023**, *62*, e202310913
2. R. V. Nithun, Y. M. Yao, O. Harel, S. Habiballah, A. Afek, M. Jbara, *ACS Cent. Sci.* **2024**, 10, 1295–1303.
3. R. V. Nithun, S. Khoury, M. Jbara, *Org Lett.* **2025**, 27, 3760–3764.
4. R. V. Nithun, S. Khoury, M. Jbara, *Bioconjug. Chem.* **2026,** 37, 332–340.
5. O. Harel, F. Nadal-Bufi, R. V. Nithun, Y. M. Yao, A. Afek, M. Vendrell, M. Jbara, *J Am Chem Soc.* **2025**, 147, 42647–42658

DOI: https://doi.org/10.17952/38EPS.2026.P224

Chemical Engineering of Transcription Factors Uncovers Cell-Permeable µMax Modulators

Omer Harel,[1] Ferran Nadal-Bufí,[2] Raj V. Nithun,[1] Yumi M. Yao,[3] Ariel Afek,[3] Marc Vendrell,[2] Muhammad Jbara[1]

[1] School of Chemistry, Raymond & Beverly Sackler Faculty of Exact Sciences, Tel Aviv University · [2] Centre for Inflammation Research & IRR Chemistry Hub, The University of Edinburgh · [3] Department of Chemical & Structural Biology, Weizmann Institute of Science · jbaram@tauex.tau.ac.il



Jbara Lab
Chemical Biology & Drug Discovery

TEL AVIV UNIVERSITY אוניברסיטת תל אביב

Read the paper

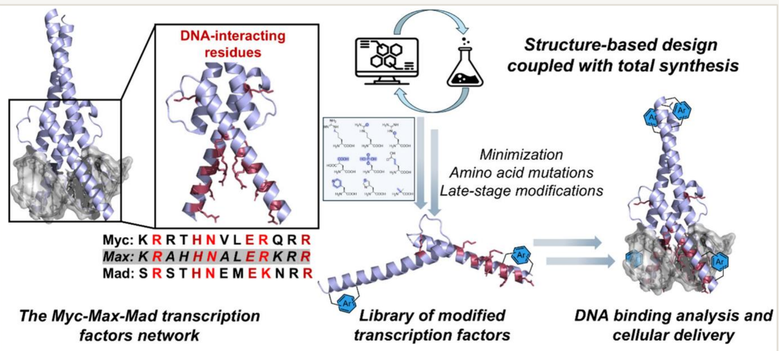
LinkedIn

The Result **Non-natural modifications of Max transcription factor reveal $2S_b$-µMax20 – a stapled, intrinsically cell-permeable, and bioactive engineered transcription factor capable of inhibiting cancer cell proliferation.**

01 Design of Abiotic Transcription Factors

The Myc–Max–Mad network controls ~15% of the human genome and is dysregulated in ~50% of tumors. Synthetic transcription factor (TF) mimetics exist but remain largely constrained to native sequences and structures.

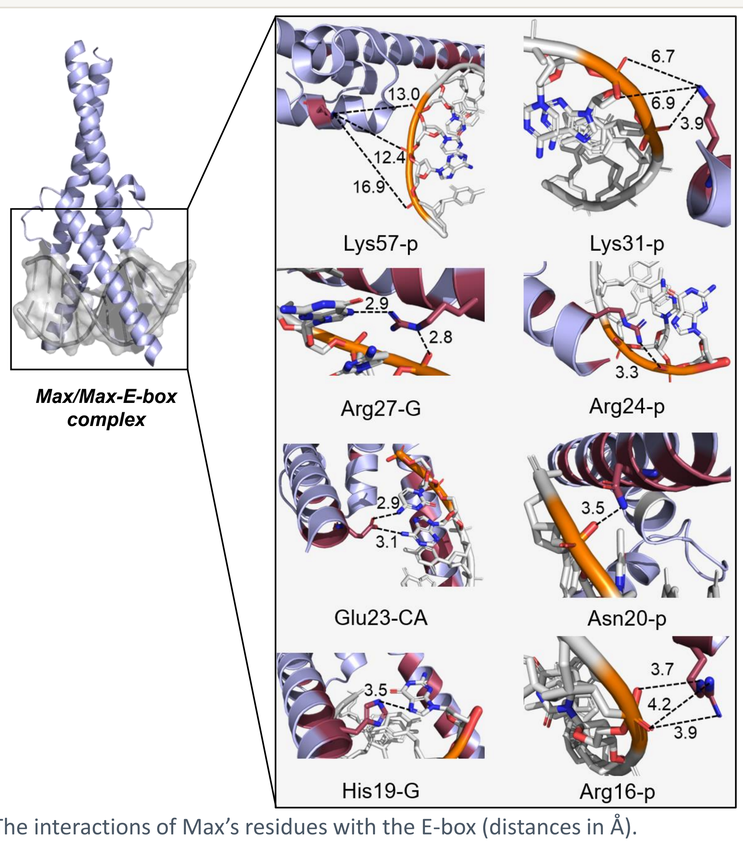
Our approach: Combining rational design with total synthesis to engineer novel abiotic transcription factors with enhanced stability and cell permeability, derived from the DNA-binding domain of Max to suppress Myc-driven gene expression.



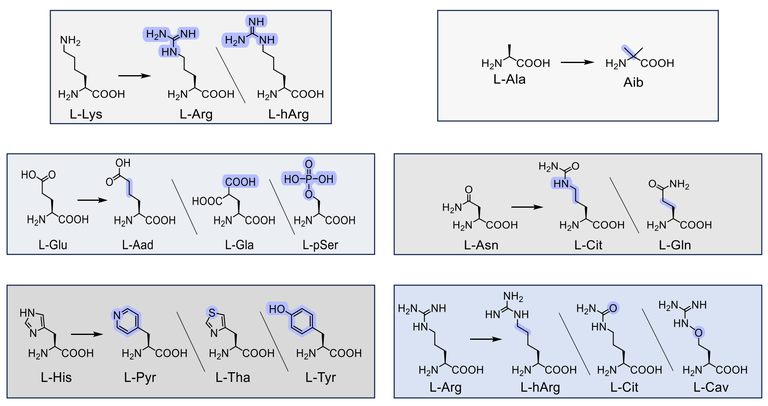
Structure-based design coupled to total synthesis: minimization, strategic mutation, late-stage modification (PDB 1HLO).

02 Engineering of µMax Abiotic Transcription Factors

10 strategic sites, 12 novel residues of which 9 non-proteinogenic. Six residues contact the E-box directly; Lys31 and Lys57 contact the DNA phosphate backbone.



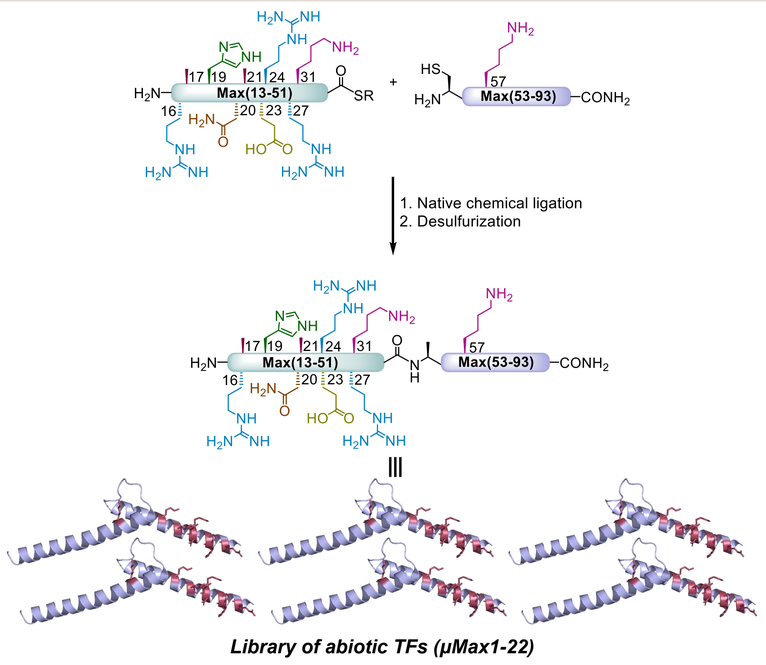
The interactions of Max's residues with the E-box (distances in Å).



The repertoire of canonical and noncanonical amino acids used in this study to replace native amino acids.

03 Chemical Synthesis of µMax Modulators

Two Fmoc-SPPS segments joined by **one-pot native chemical ligation and desulfurization**. Ala52 was temporarily mutated to Cys for ligation.



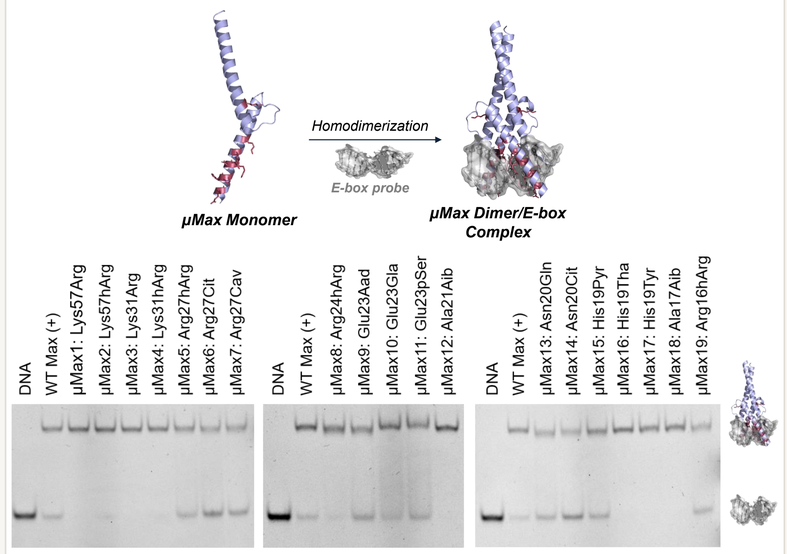
One-pot ligation-desulfurization delivers homogenous, site-specifically modified transcription factors.

30 Abiotic TF analogs

Up to **6** Mutations per chain

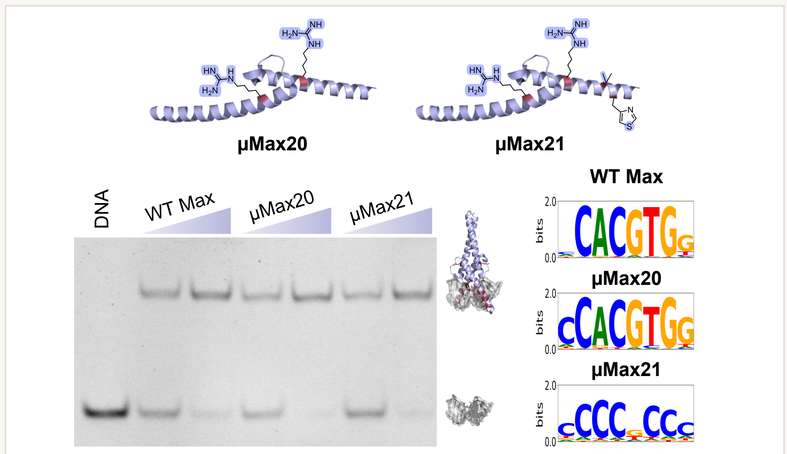
04 Potent DNA-binding Activity and Sequence Specificity

Synthetic **µMax** analogs are functional and capable of binding to the canonical E-box DNA sequence. hArg at Lys31/Lys57 and Aib at Ala17/Ala21 enhance DNA-binding activity.



EMSA analysis of µMax1-19 analogs.

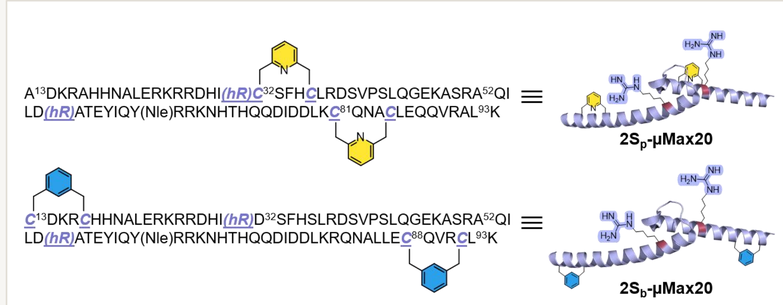
Multi-mutated **µMax** analogs show potent E-box binding: **µMax20** retains wild-type specificity, whereas **µMax21** does not.



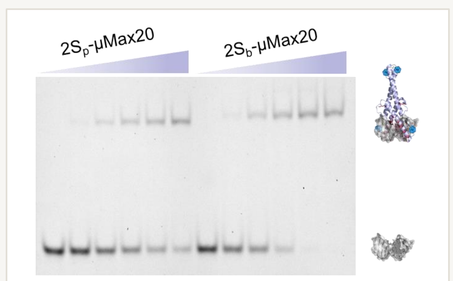
EMSA and PWM analyses of multi-site mutated µMax20-21 analogs.

05 Late-stage editing of µMax Modulators

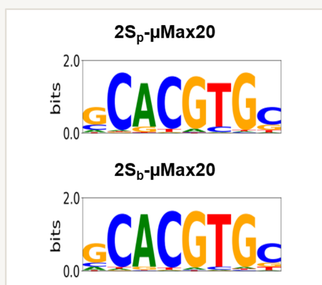
Dual aromatic staples on Cys pairs of **µMax20** give **$2S_p$-** and **$2S_b$-µMax20** yielding analogs with ~2.5-fold higher proteolytic stability, while maintaining E-box binding activity and specificity.



Staples installed by late-stage Cys alkylation with bis(bromomethyl)pyridine /benzene.



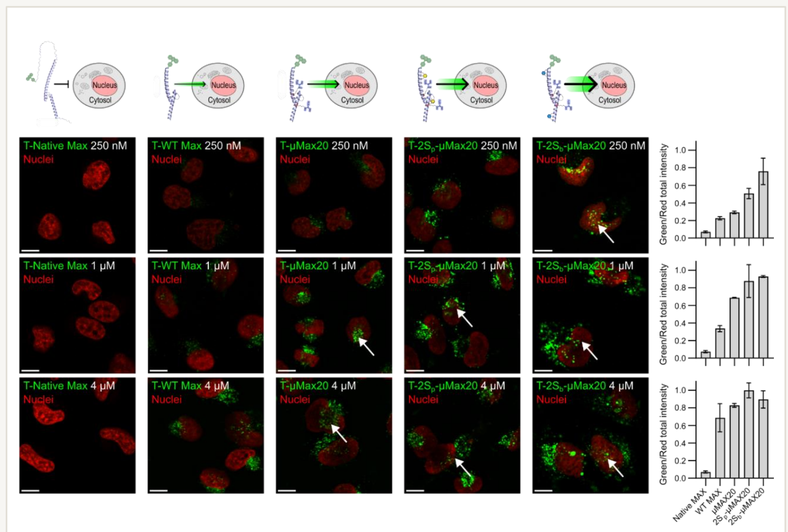
Dose-response EMSA of stapled analogs.



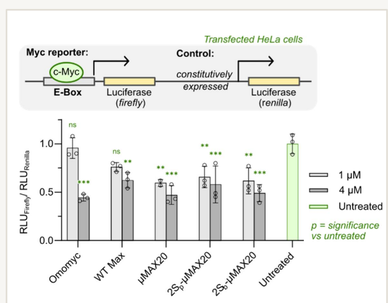
PWM of top-scoring probes.

06 Cell Permeable µMax Inhibits Myc-driven Gene Expression and Cell Proliferation

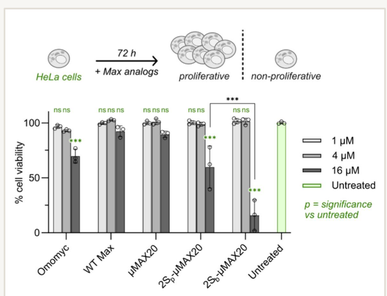
µMax stapled analogs internalize at **250 nM** with nuclear accumulation — without delivery vehicle or cell-penetrating tag.



TAMRA (green) / Hoechst (red) in HeLa; 250 nM, 1 µM, 4 µM. Arrows: nuclear accumulation. Scale bars 10 µm.



Myc reporter suppressed below 1 µM – outperforming clinically trialed Omomyc.



$2S_b$-µMax20 cuts HeLa viability to 16% at 16 µM.

MiTMAB endocytosis inhibitor only partly blocks uptake – the stapled analogs also translocate directly across the membrane.

Conclusions

- Chemical protein synthesis expands the chemical space of transcription factors: 30 abiotic Max analogs with non-proteinogenic residues and aromatic staples capable of binding the DNA target site and inhibit gene expression.
- **µMax20** binds the core E-box with nanomolar affinity while retaining wild-type specificity and α-helical fold.
- **$2S_b$-µMax20** is intrinsically cell-permeable at submicromolar concentration and suppresses Myc-driven transcription and proliferation.

REFERENCES

1. **O. Harel**, M. Jbara, Angew. Chem. Int. Ed. **2023**, 62, e202217716.
2. X. Lin, R. V. Nithun, R. Samanta, **O. Harel**, M. Jbara, Org. Lett. **2023**, 25, 4715–4719.
3. **O. Harel**, F. Nadal-Bufí, R. V. Nithun, Y. M. Yao, A. Afek, M. Vendrell, M. Jbara, J. Am. Chem. Soc. **2025**, 147, 46, 42647–42658.
4. X. Lin, **O. Harel**, M. Jbara, Angew. Chem. Int. Ed. **2024**, 63 (5), e202317511.

ACKNOWLEDGEMENTS

Israel Science Foundation 493/23 · Ministry of Innovation, Science and Technology 0007031 · Neubauer Foundation (M.J.) · EPSRC EP/X525819/1 and ERC Consolidator Grant 771443 (M.V.).

Screening of Algae Processing Technology for Easily Digestible Bioactive Hydrolysates

L. Bím[1], M. Jelínek[1], L. Šánek[2], V. Matůšů[2], P. Švestková[2] & J. Pecha[2]

[1]KORTAN, spol. s r.o., Hrádek nad Nisou – Loučná, Czech Republic

[2]Faculty of Applied Informatics, Tomas Bata University in Zlín, Zlín, Czech Republic

kortanh@seznam.cz

Tomas Bata University in Zlín
Faculty of Applied Informatics

https://doi.org/10.17952/38EPS.2026.P072

Introduction

Microalgae are a prospective alternative source of proteins and bioactive compounds in human and animal nutrition.[1] However, their utilisation is often limited by low digestibility due to robust cell walls.[2] Protein extracts in the form of protein hydrolysates can improve digestibility. These hydrolysates possess promising bioactive properties and may act as antioxidants or ACE inhibitors.[2,3]

Challenge: The processing method significantly influences the final hydrolysate's properties, bioactivity, purity, and overall production costs.



Figure 1 Spirulina (left) and Chlorella (right) algae tested

Research Objective

Comprehensive analysis of protein extraction from microalgae *Chlorella* and *Spirulina,* comparing:

- Enzymatic hydrolysis with different enzymes
- Subcritical water extraction (SWE)
- Alkaline and aqueous extraction
- Combined two-step procedures

Methods Tested

All experiments: 5% algae dry matter in reaction mixture

1. Aqueous Extraction

Water extraction at elevated temperatures (60-100°C) for 3 hours with constant stirring. Used as control method.

2. Alkaline Extraction

0.2-0.4 M NaOH at room temperature or boiling, 5-17 hours.

3. Enzymatic Hydrolysis

Alcalase: pH 8.5-9.0, 62.5°C, 2-4h
PROMOD 295L: pH 8.4, 60°C, 6h
Pancreatin: pH 7.5, 40°C, 6h

4. Subcritical Water Extraction (SWE)

Hydrothermal extraction in PARR pressure reactor at 140-180°C, 40-300 min under inert atmosphere.

5. Two-Step Procedures

A) Enzymatic (Alcalase) → SWE (180°C, 40 min)
B) SWE (180°C, 40 min) → Enzymatic (Alcalase)
C) Alkaline extraction (0,4M NaOH) → Enzymatic (Promod 295L)

Analytical Methods:

- Dry matter yield and nitrogen content (Flash2000, Thermo Scientific)
- Antioxidant activity: DPPH radical scavenging and FRAP (ferric reducing power)
- All separations by centrifugation (6000 rpm, 20 min) or vacuum filtration

Results and discussion

Enzymatic Hydrolysis

Enzyme	Microalgae	Protein yield [%]
PROMOD 295L	***Spirulina***	**83.5**
	Chlorella	64.5
Pancreatin	*Spirulina*	80.3
	Chlorella	**69.0**
Alcalase	*Spirulina*	66.2
	Chlorella	62.0

Two-Step Extraction

Procedure	Microalgae	Protein yield [%]		Increase
		Step 1	Step 2	
Enzymatic → SWE	*Spirulina*	62.3	71.4	+9.1
Enzymatic → SWE	*Chlorella*	**47.3**	**66.8**	**+19.5**
SWE → Enzymatic	*Spirulina*	65.3	70.0	+4.7
SWE → Enzymatic	*Chlorella*	59.5	62.2	+2.7
Alkali → Enzymatic	*Spirulina*	50.4	61.6	+11.2

Observation: *A two-step hydrolysis significantly enhanced nitrogen extraction. Enzymatic pretreatment cleaves proteins and disrupts cell structures, increasing the accessibility of intracellular compounds for the subsequent SWE step, which likely further disrupts residual polysaccharide layers and mobilises remaining intracellular substances. The synergistic effect was particularly pronounced for Chlorella (+20 percentage points), despite the enzymatic treatment lasting only 2 hours.*

Antioxidant Activity

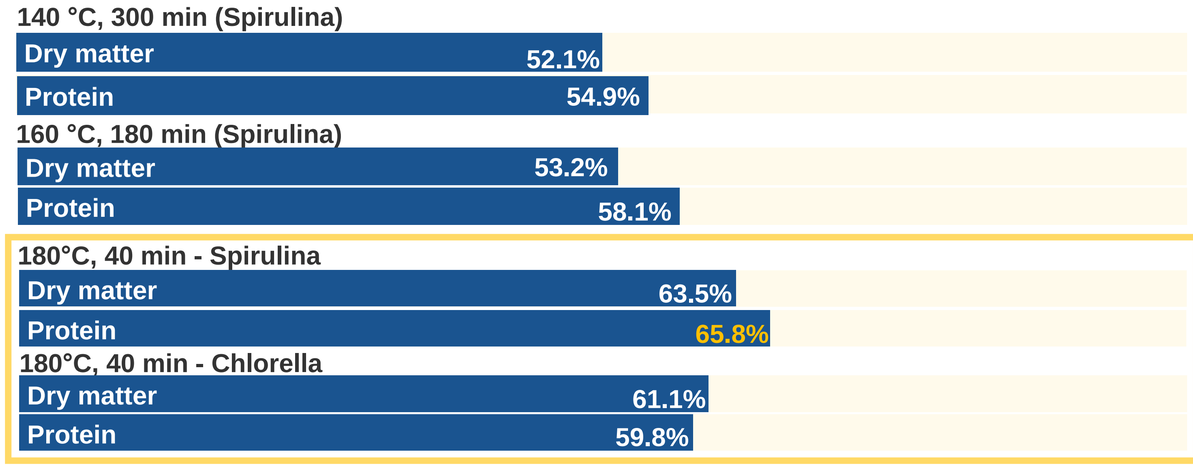
Method	FRAP (µM/g)	DPPH (µM/g)	Microalgae
Two-step (Enzyme+SWE)	**439**	**373**	*Spirulina*
SWE 180°C, 60 min	403	352	*Spirulina*
SWE 180°C, 30 min	402	367	*Chlorella*
SWE 180°C, 40 min	318	301	*Spirulina*
PROMOD 295L	193	74	*Spirulina*
Alcalase	190	111	*Spirulina*
Pancreatin	169	81	*Spirulina*
Aqueous (boiling point)	157	180	*Spirulina*

Values expressed as Trolox equivalents per gram dry matter



Figure 2 Protein hydrolysate from Chlorella – Enzymatic (Pancreatin)

Subcritical Water Extraction



Key Findings

- Spirulina showed better processability than Chlorella due to a less robust cell wall structure.
- Enzymatic hydrolysis proved the most effective: **PROMOD 295L** achieved 79% dry matter and **83.5% protein yield** for Spirulina.
- In the case of Chlorella, the most effective enzyme was **pancreatin → 69 % protein yield**.
- Temperature, not prolonged time, determines **SWE efficiency**; the highest Spirulina protein yield (65.8%) occurred **at 180 °C for 40 min**.
- Two-step extraction of Spirulina combining enzymatic (Alcalase) and SWE processing yielded of 66.6 % of dry matter and 71.4 % of protein
  - Combination of enzymatic and SWE showed the highest antioxidant activity (>350 µM Trolox equiv./g).

Conclusions

Most Effective Method:

- *Spirulina:* Enzymatic hydrolysis with **PROMOD 295L** achieved **83.5% protein yield and 79% dry matter**
  - Thin peptidoglycan layer enables superior enzyme penetration; all methods showed **10-20% higher protein yields vs. *Chlorella***
- *Chlorella*: Robust cellulosic wall requires more aggressive processing; **pancreatin** (broad enzyme spectrum) was the most effective, achieving a **69% protein yield**

Highest Bioactivity:

- Subcritical water extraction consistently yielded high antioxidant activity (>300 µM Trolox/g in both the FRAP and DPPH assays).

Two-step Extraction Synergy:

- Combining enzymatic pretreatment with SWE significantly enhanced nitrogen recovery and antioxidant activity
  - Spirulina: FRAP 439 µM Trolox/g; DPPH 373 µM Trolox/g
  - Further optimisation of reaction time and enzyme selection may improve overall extraction efficiency.

Overall Impact: This comprehensive screening demonstrates that substantial yields of bioactive protein hydrolysates can be obtained from microalgae using straightforward, industrially viable methods. Method selection should be optimised based on target algae species, desired product properties (protein content vs antioxidant activity), and available processing infrastructure.

Acknowledgements: This work was supported by Technology Agency of the Czech Republic under project TN02000122 RETEMED (REcombinant TEchnologies for MEDicine).

References:

1. S. Weber, P. M. Grande, L. M. Blank, H. Klose, PLoS ONE. 2022, 17(1): e0262500 https://doi.org/10.1371/journal.pone.0262500
2. E. Aurino, L. Mora, A. Marzocchella, C. M. Kuchendorf, B. Ackermann, M. Hayes, Mar. Drugs. 2025, 23, 53. https://doi.org/10.3390/md23020053
3. M. Mohammadi, M. Soltanzadeh, A. R. Ebrahimi, H. Hamishehkar, Algal Res. 2022, 65, 102739 https://doi.org/10.1016/j.algal.2022.102739



Optically switched transient amyloid-like fibrils for antibiotic degradation

Shubhra Kanti Bhaumik, Sisira Mambram Kunnath, Elad Arad, Einat Nativ-Roth, Arunavo Chatterjee, Albert Batushansky, Nitzan Shauloff, Hanna Rapaport, and **Raz Jelinek***

Department of Chemistry, Ben Gurion University of the Negev, Beer Sheva 8410501, Israel

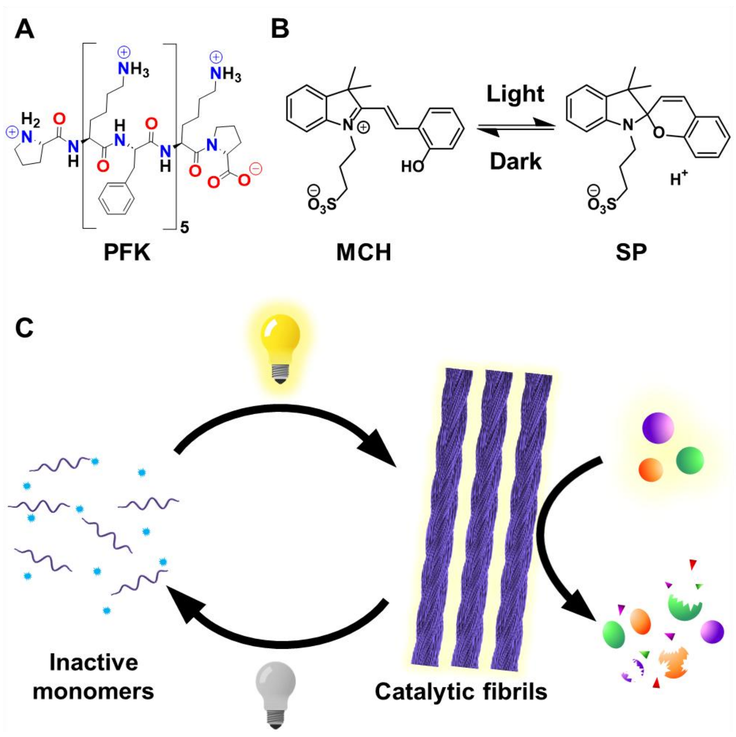
https://doi.org/10.17952/38EPS.2026.P538

Abstract

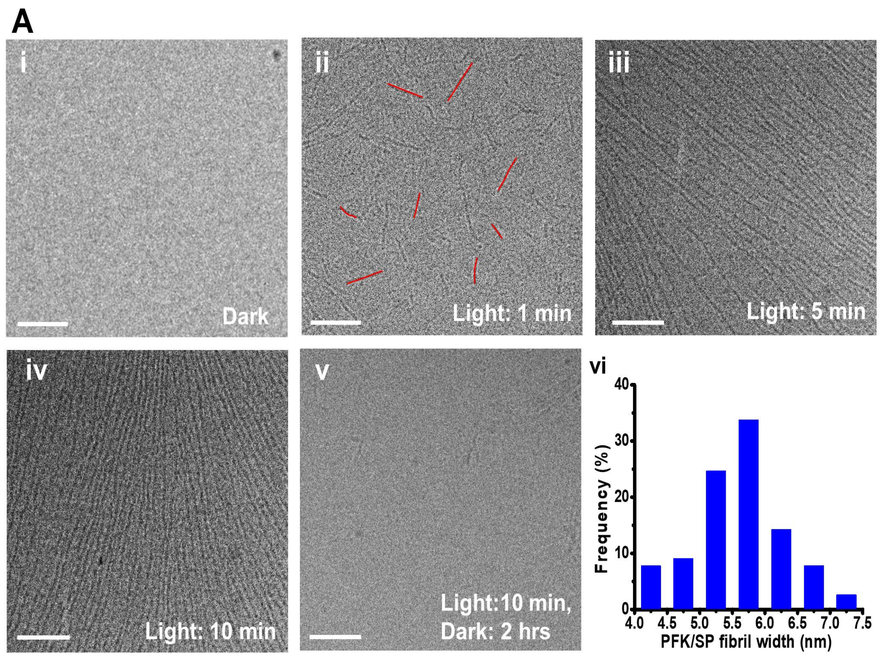
Light-mediated, nematic liquid-crystalline ordered amyloid-like fibrils form in water from a short peptide, PFK, and the photoacid **MCH**. The fibrils with an **anti-parallel ß-sheet structure** are formed **exclusively under light** due to the transformation of **MCH** to **SP, which** interacts with PFK to form fibrils. Such light-mediated fibrils are highly **catalytic towards ß-lactam ring opening** of common antibiotics, offering a platform for light-mediated degradation of antibiotic pollutants in water, a major health and environmental hazard.

Overview

- Optically-switched **nematic liquid-crystal-like** arrangement of fibrils
- Photo-switchable **anti-parallel ß-sheet** like transient amyloid assembly
- Efficient catalytic activity towards **hydrolysis of ß-lactam antibiotics**

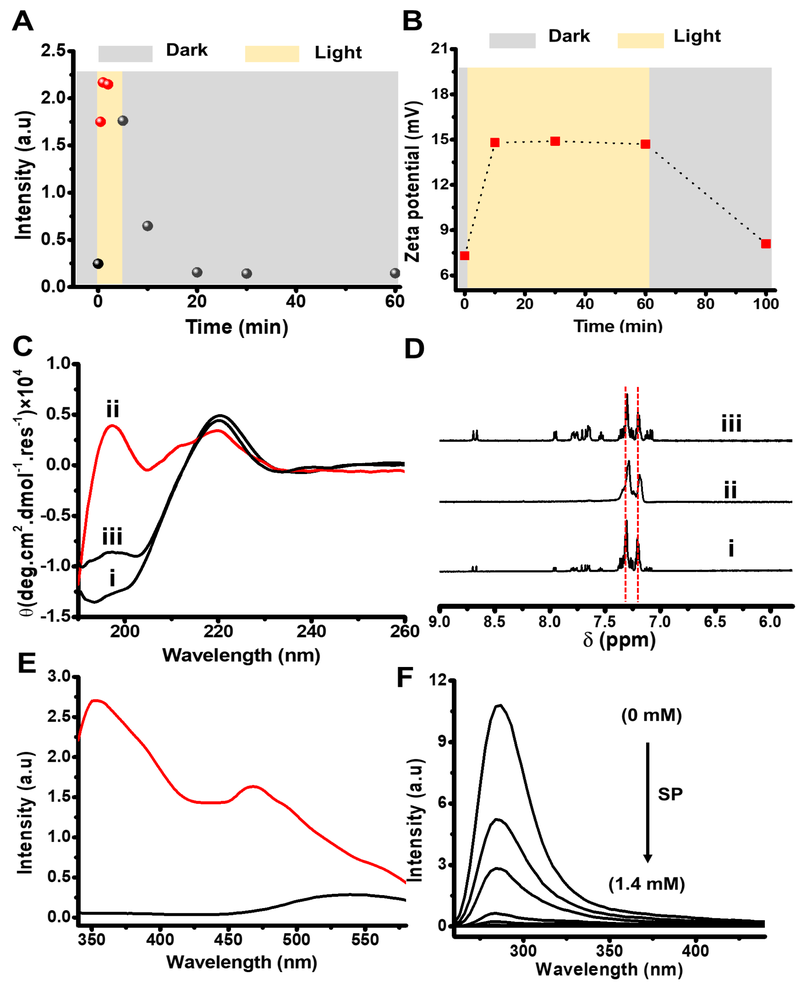


Microscopic analyses



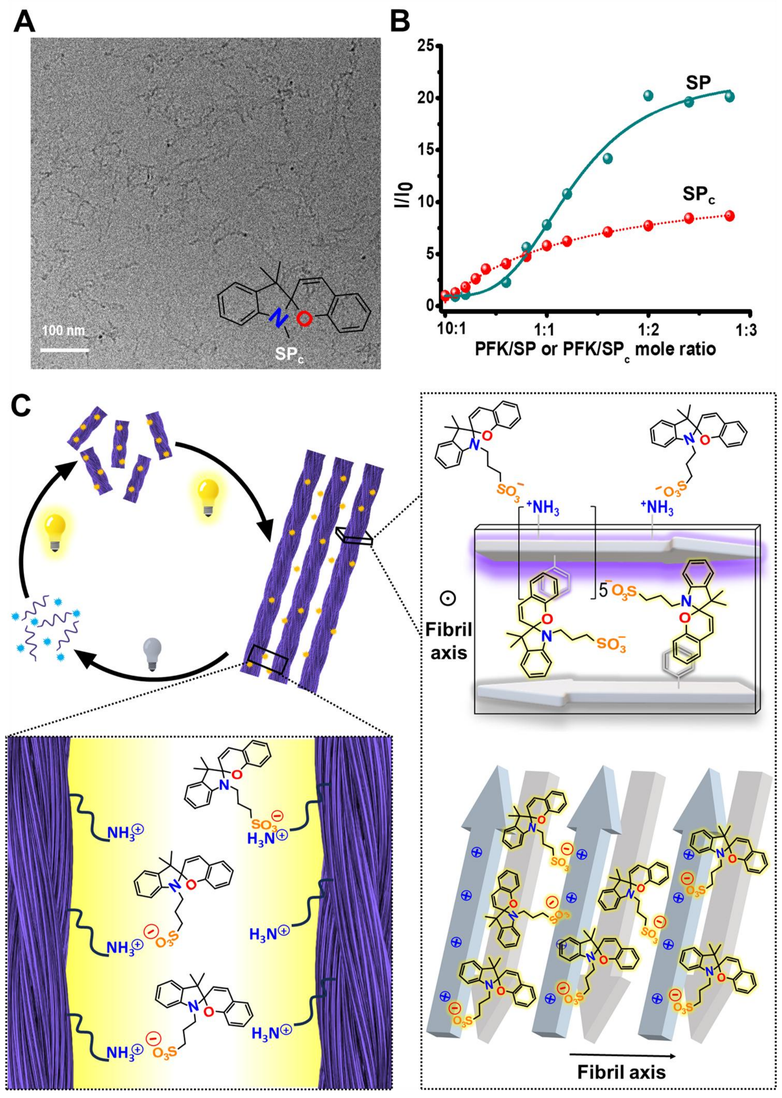
- Light-mediated reversible and highly **ordered** fibril formation
- Time- and **MCH-concentration-dependent** fibrillation

Spectroscopic analyses



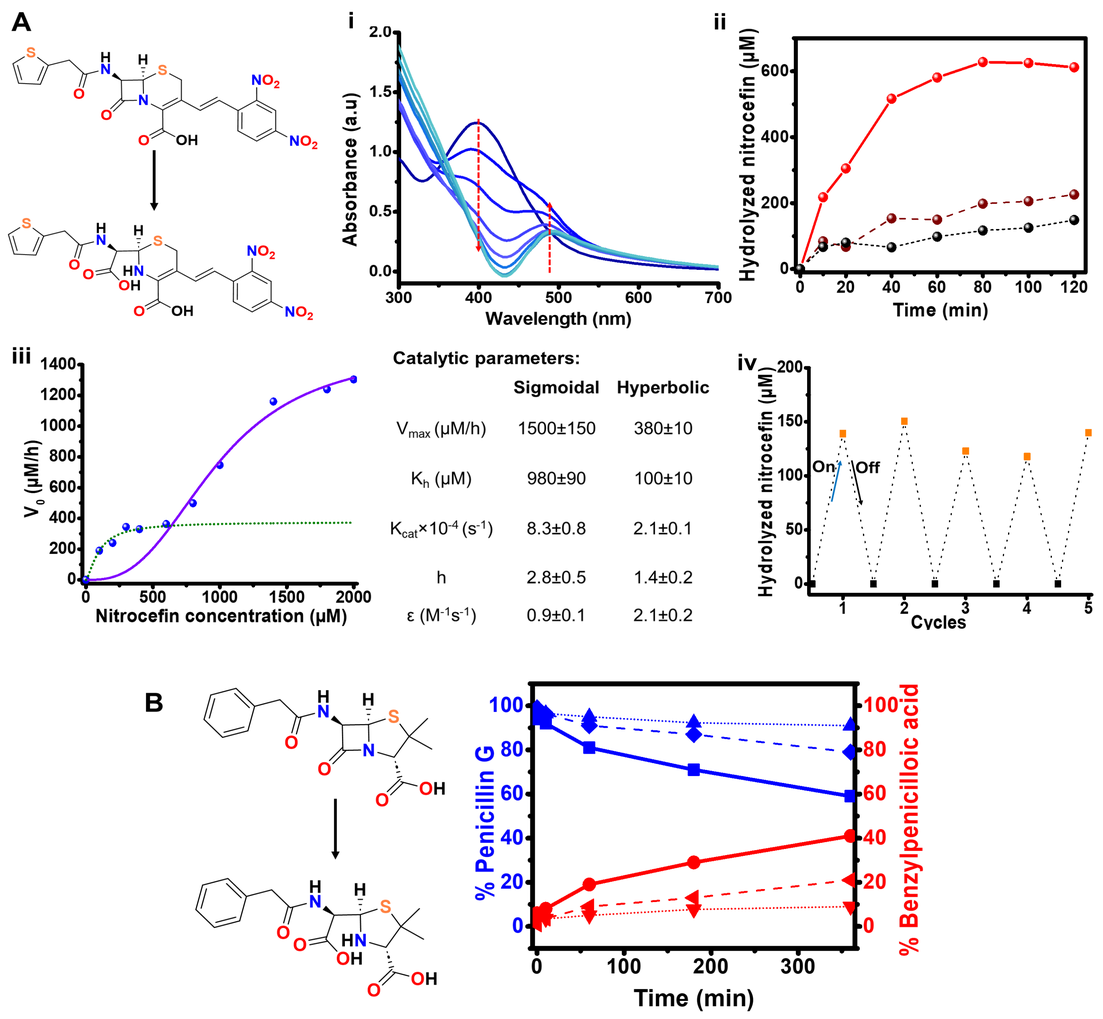
- Amyloids with anti-parallel ß-sheet structure with positively charged surfaces
- **Polar MCH to non-polar SP transformation** is responsible for such fibrillation under light

Structural Insight



- **SP_c** also induced **fibrillation of PFK**
- SP-induced fibrillation follows a sigmoidal isotherm
- **π-π interactions** drive **PFK fibrillation**, whereas **electrostatic interactions** govern the fibril arrangement

Hydrolysis of Antibiotics



- Enzyme-like **ß-lactam ring hydrolysis** of **nitrocefin** and **penicillin G** by light-mediated **catalytic amyloids**

Conclusion

- Light-induced **reversible amyloid** formation
- Photoinduced **long-range amyloid assembly** (fibril alignment)
- Photo-regulated **amyloid functionality** (catalysis)

Bibliography

- E. Arad *et al.*, *Nat. Commun.* **2023**, *14*, 8198
- S. M. Kunnath *et al.*, *Nat. Commun.* **2025**, *16*, 5071
- Bhaumik *et al.*, *Small*, **2026** (early view)

Contact

- **Prof. Raz Jelinek**, Email: razj@bgu.ac.il
- **Dr. Shubhra Kanti Bhaumik**, Email: bhaumiks@post.bgu.ac.il



Catalytic DNA Degradation by Pancreatic β-cell Peptide Hormone: A New Pathway Towards Amylin Pathology

Arunavo Chatterjee, Uri Ben Nun, Neha Singh, Itamar Kass, Shubhra Kanti Bhaumik, Sisira Mambram Kunnath and **Raz Jelinek***

Department of Chemistry, Ben Gurion University of the Negev, Beer Sheva 8410501, Israel. https://doi.org/10.17952/38EPS.2026.P539

Email: arunavo@post.bgu.ac.il; razj@bgu.ac.il.

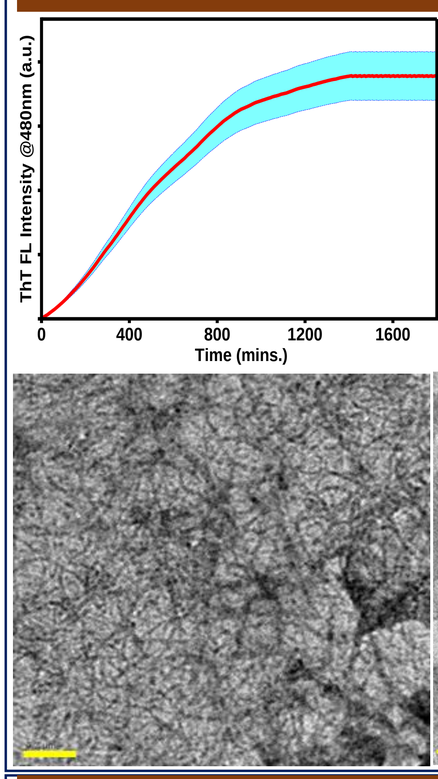
Motivation

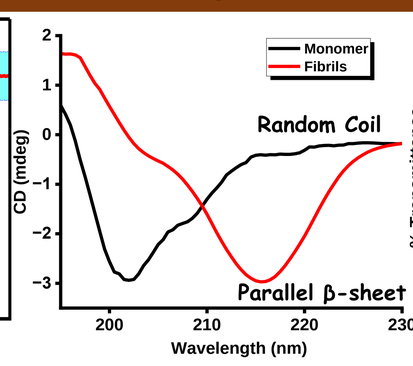
- Amylin or human islet amyloid polypeptide (hIAPP) is a 37 amino acid residue amyloidogenic hormone, co-secreted with Insulin from the β-cells of pancreas.
- Aggregation of Amylin to toxic amyloids is central to ~90% cases of T2DM causing β-cell death and consequent disease progression.
- DNA damage drives the dysfunction of pancreatic β-cells, senescence and deaths, in T1DM and T2DM.
- Important to envisage on the DNA damage ability of the Amylin fibrils as a possible mechanism of β-cell death and subsequent T2DM progression.

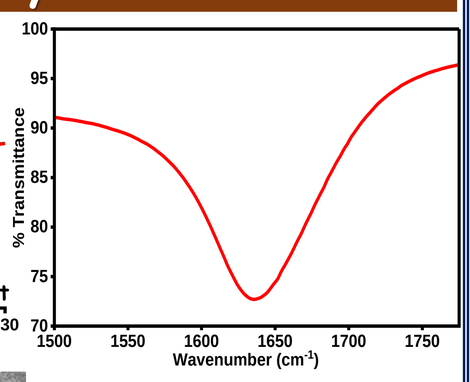
Objectives

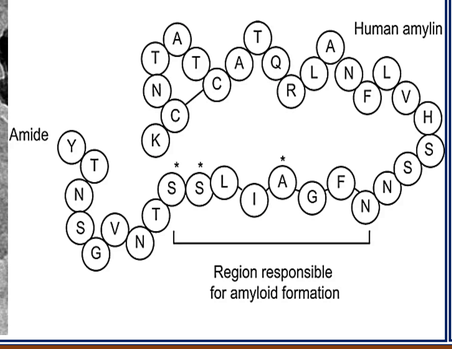
- Catalytic phosphodiester hydrolysis of the DNA model substrate bis(p-nitrophenyl) phosphate (BNPP) in diabetic mimic conditions (33mM glucose) by Amylin fibrils.
- Catalytic DNA degradation of a model single stranded DNA (ssDNA) and a model double stranded DNA (dsDNA) by Amylin fibrils.
- Theoretical validation of the binding and degradation by MD Simulation.
- The ability of the Amylin fibrils to induce replication slowdown in yeast cells using a CFP-tagged hIAPP overexpressed yeast plasmid (IAPP-CFP).

Characterization of the Amylin Fibrils

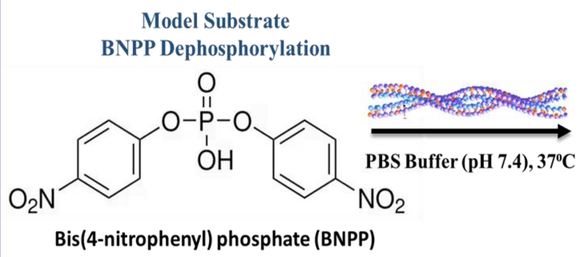


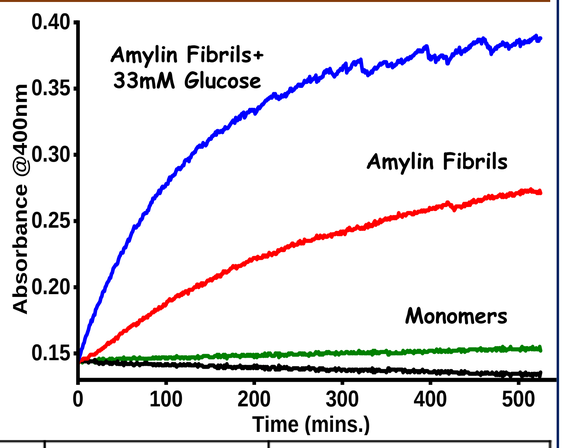


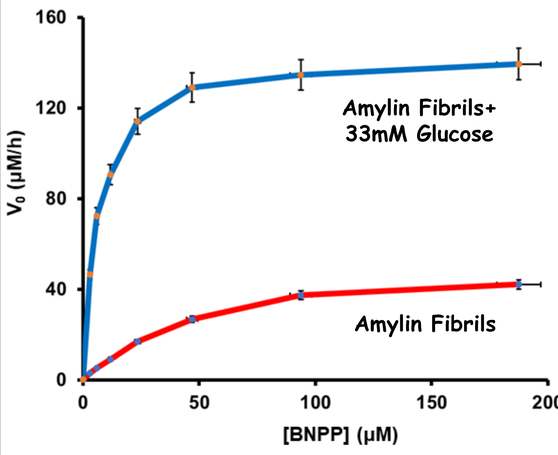




Phosphodiester Hydrolysis (DNAse mimic)





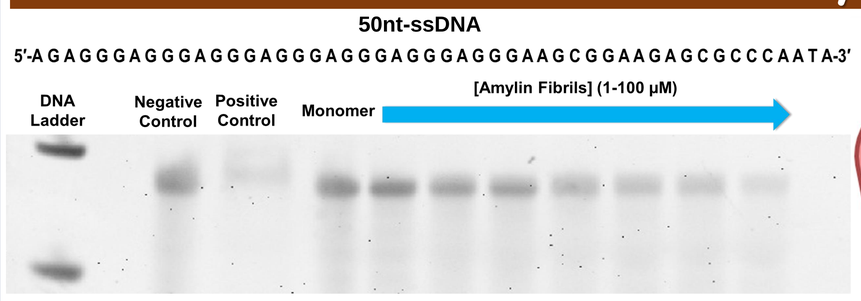


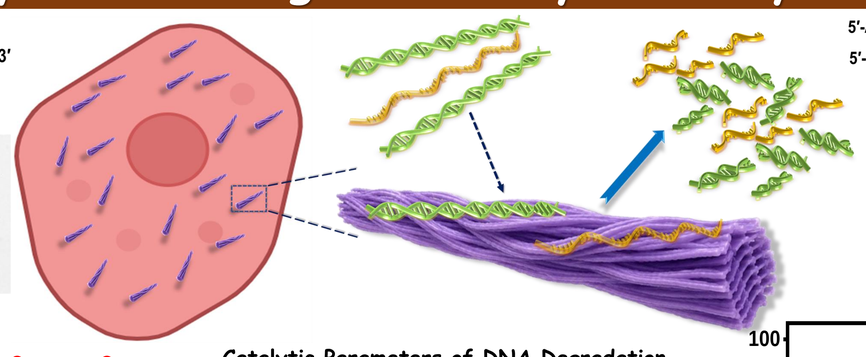
	– Glucose	+ Glucose
V_{max} (μM/h)	55 ± 2	144 ± 0.8
k_M (μM)	50 ± 5	6 ± 0.3
k_{cat} (s^{-1})	$9x10^{-4}$ ± $3x10^{-5}$	$3x10^{-3}$ ± $1x10^{-5}$
ε (Mol^{-1} s^{-1})	18 ± 0.7	502 ± 4

Catalytic DNA Degradation by the Amylin Fibrils

50nt-ssDNA

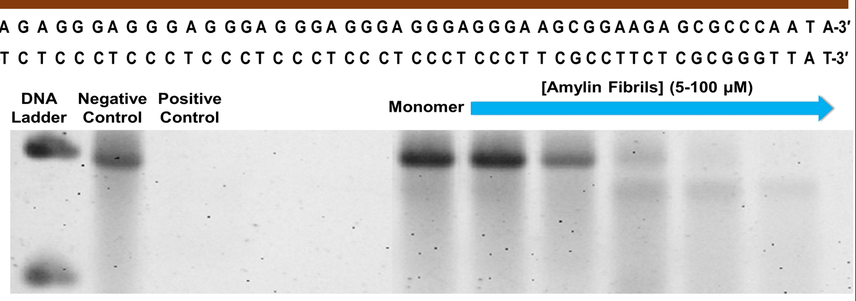
5′-A G A G G G A G G G A G G G A G G G A G G G A G G G A G G G A A G C G G A A G A G C G C C C A A T A-3′

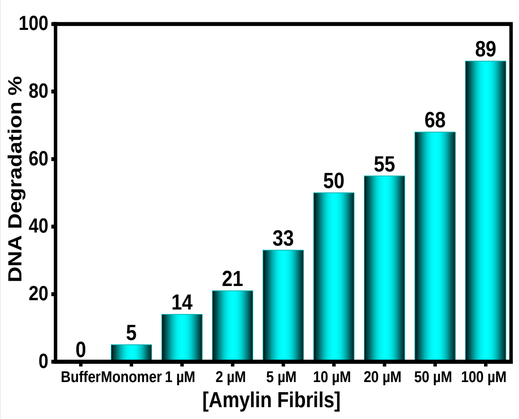


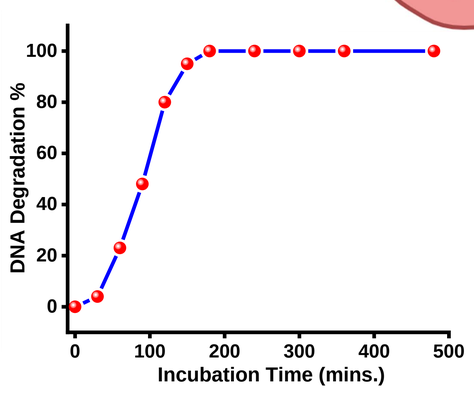


5′-A G A GG GA G G G A G GGA G GGA GGGA GGGAGGGA A GCGGAAGA GCGCCCA A T A-3′

5′-T C T C C CT C C C T C C CT C C CT CC CT CCCT CCCT T CGCCTTCT CGCGGGT T A T-3′

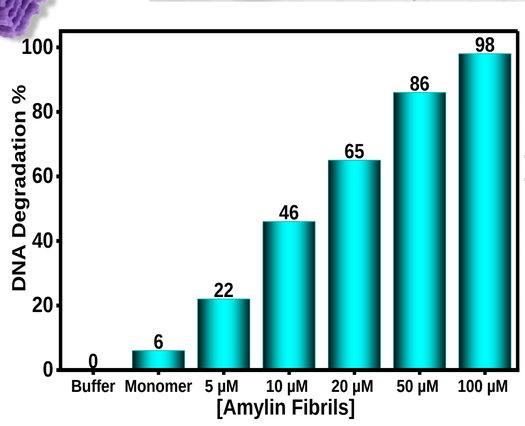


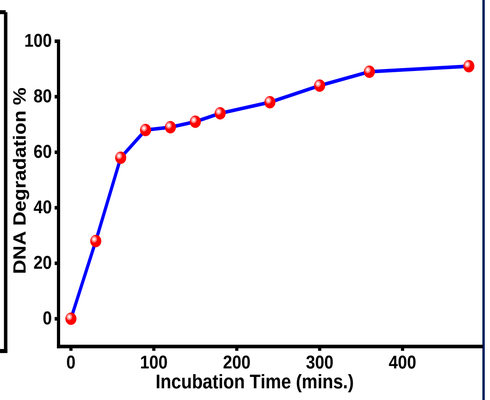




Catalytic Parameters of DNA Degradation
(Pseudo-first order MM kinetics)

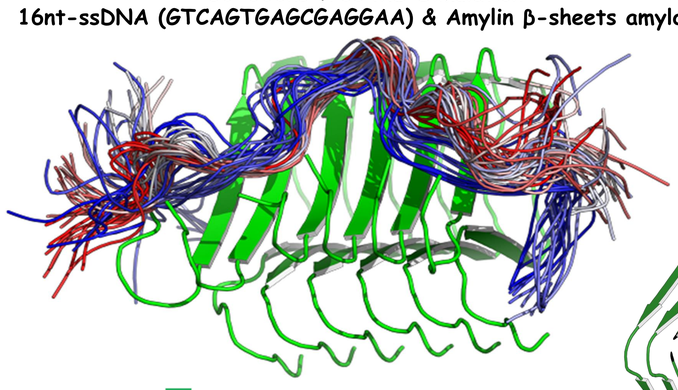
	ssDNA	dsDNA
K_M (μM)	71 ± 5	16 ± 4
K_{cat} (h^{-1})	$3x10^{-1}$ ± $2x10^{-5}$	$7x10^{-1}$ ± $3x10^{-5}$
ε (Mol^{-1} s^{-1})	13 ± 0.7	12 ± 0.4

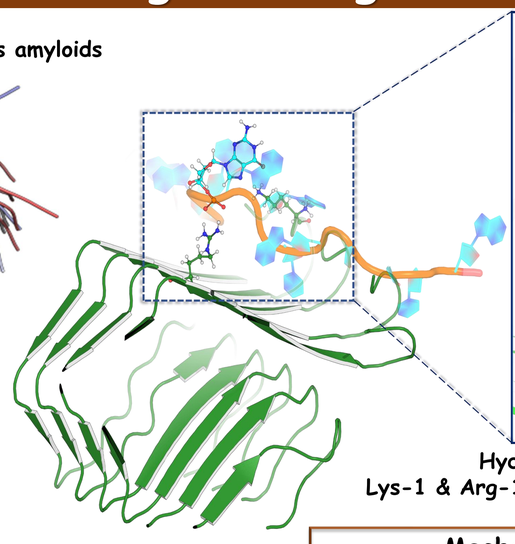


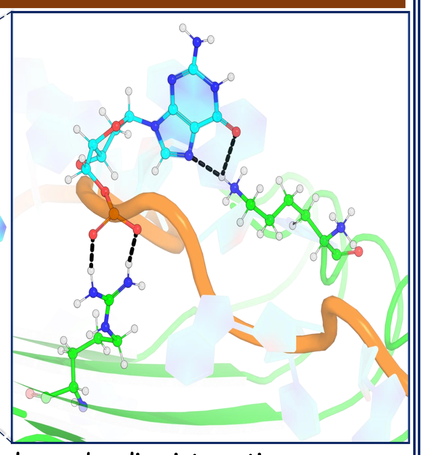


Validation of Binding and Degradation

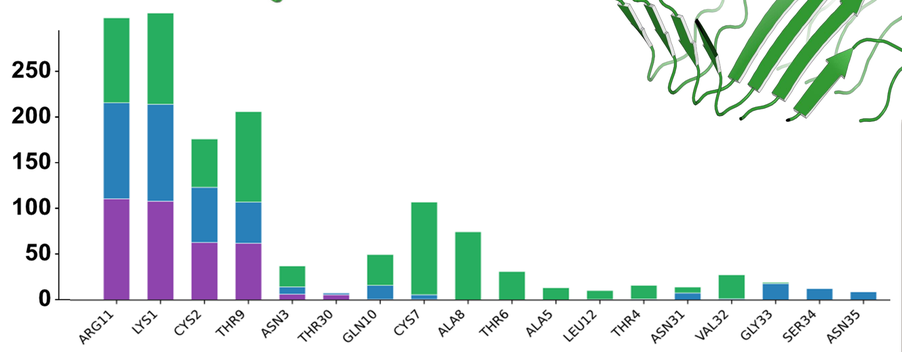
50-300ns free MD Simulation
16nt-ssDNA (GTCAGTGAGCGAGGAA) & Amylin β-sheets amyloids







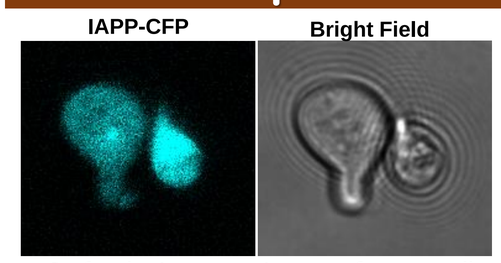
Hydrogen bonding interaction
Lys-1 & Arg-11 with phosphate backbone of DNA



Mechanism of Degradation

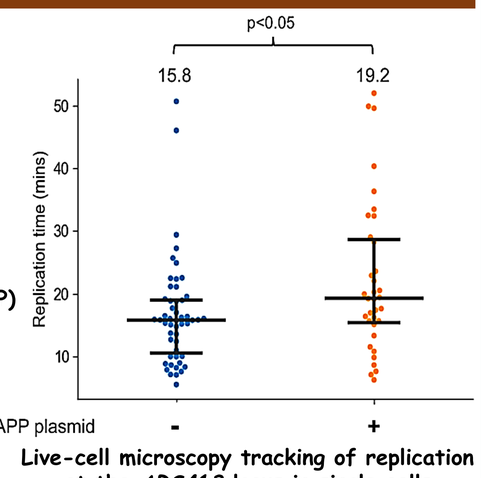
- The guanidinium group (of ARG11) binds and polarizes the negatively charged DNA phosphate
- A water molecule initiates a nucleophilic attack on the phosphate
- Resulting in DNA cleavage

DNA Replication Slowdown in Yeast



Confocal microscopy images of yeast cells expressing human IAPP fused to CFP (IAPP-CFP)

- Replication fork progression is monitored by quantifying the duplication of *lacOx128* and *tetOx160* arrays, located downstream of *ARS413*
- Replication time represents the time delay between the duplication of the lacO and tetO arrays



Live-cell microscopy tracking of replication at the *ARS413* locus in single cells expressing IAPP (+) and in control cells (–)

Conclusions:

- Toxic Amylin amyloid fibrils can catalyze BNPP hydrolysis.
- Catalytic activity is enhanced in diabetic mimic condition.
- They can catalytically damage DNA.
- Due to H-bonding of Arg 11 & Lys1 residues with DNA.
- Amylin fibrils can slowdown DNA replication in yeast cells.
- Catalytic DNA degradation by Amylin fibrils is a new pathway towards Amylin pathology

Acknowledgement:

SCAN ME!

Allosteric amyloid catalysis by coiled coil fibrils

Sisira Mambram Kunnath[1,2], Elad Arad[1,2], Itamer Kass[1], Ran Zalk[1], Anat Shahar[1], Albert Batushansky[1] Hanna Rapaport[1,3] and Raz Jelinek[1,2*]

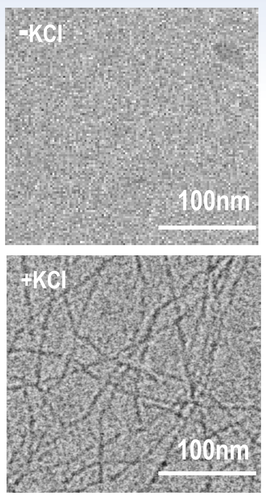
1. Ilse Katz Institute for Nanoscale Science and Technology (IKI), 2. Department of Chemistry, 3. Avram and Stella Goldstein-Goren Department of Biotechnology Engineering, Ben-Gurion University of the Negev, Be'er Sheva 84105, Israel,

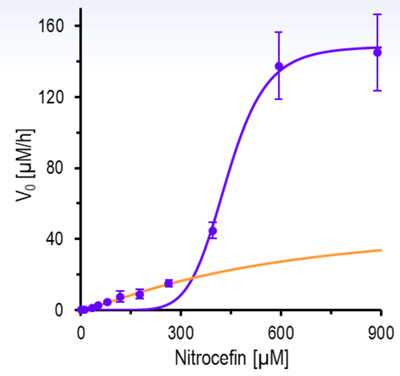
https://doi.org/10.17952/38EPS.2026.P558

Abstract

Amyloid fibrils formed from alternating lysine/phenylalanine β-sheet peptides catalyze the hydrolysis of β-lactam antibiotics, a major contaminant in wastewater linked to antibiotic resistance. Peptide variant analysis, MD simulations, and cryo-EM show that β-lactams dock to fibril surfaces via lysine sidechains, and hydrolysis occurs through an allosteric mechanism in a coiled double-fibril structure that embeds the substrates and enables nucleophilic attack. When displayed on silica beads in a column setup, these catalytic fibrils efficiently degrade and remove β-lactams from water, offering a promising strategy to mitigate antibiotic pollution.

Fibrillation and catalytic activity

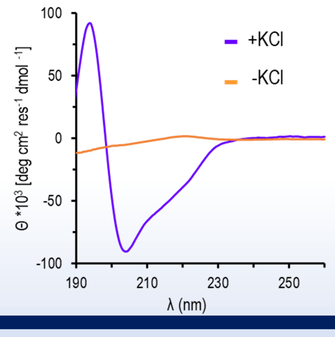




Catalytic parameters

	Sigmoidal	Hyperbolic
$V_{max.}$ [μM/h]	150 [20]	52.213 [0.005]
$K_{cat.}$ *10^{-4} [s^{-1}]	2.5 [0.2]	0.9 [6*10^{-5}]*
K_h [μM]	440 [40]	600 [300]
h	7 [4]	1.2 [0.2]
ε [$M^{-1}s^{-1}$]	0.56 [0.04]	0.14 [0.01]

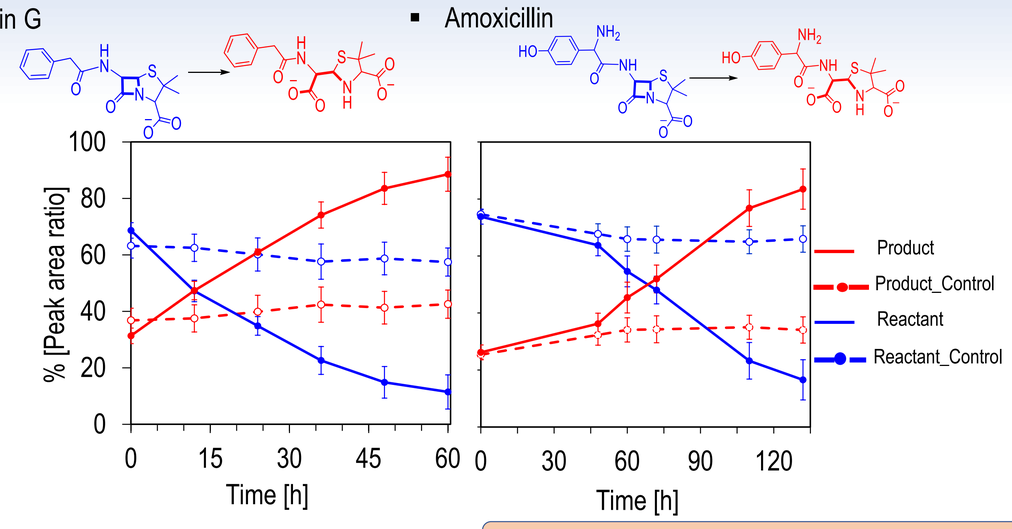
The sigmoidal purple curve corresponds to fitting to the Hill equation. The orange line corresponds to the fitting of only the low nitrocefin concentrations (<300 μM), showing a hyperbolic pattern.



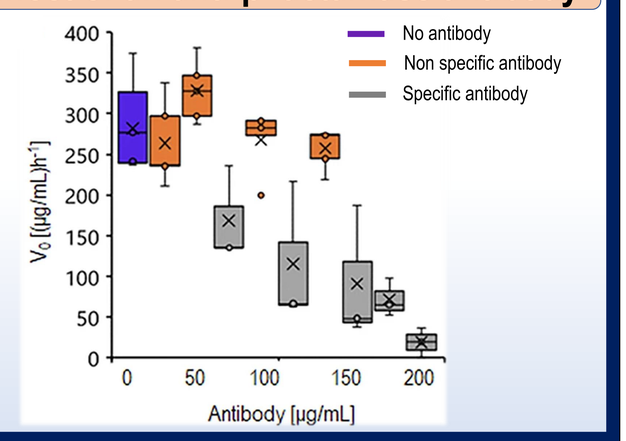
PFK monomers were dissolved in 5 mM Hepes buffer (pH 7.4) with and without added KCl (0.3 M).

The catalytic activity towards clinical antibiotics

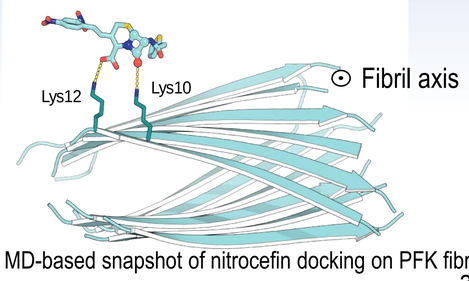
- Penicillin G
- Amoxicillin



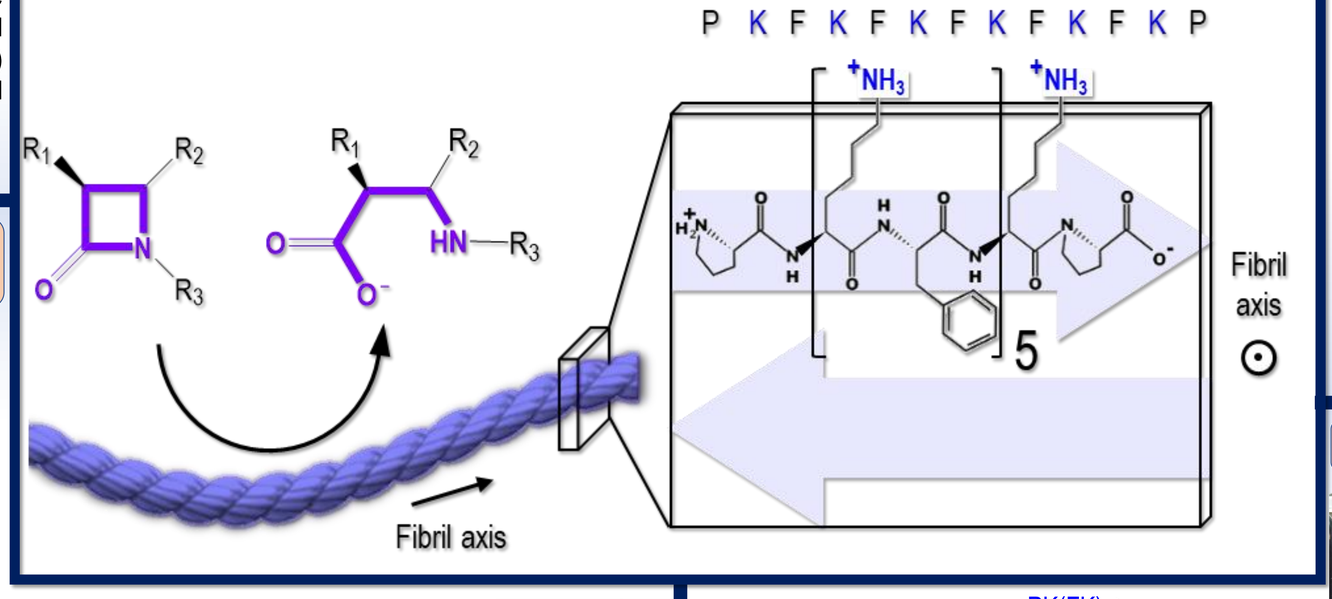
Effect of an anti-β-lactamase antibody

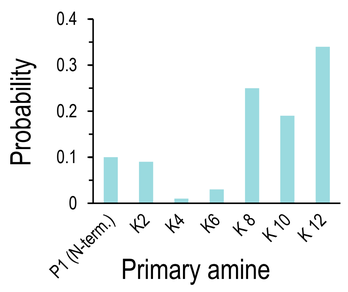


Structural analysis of the PFK fibril-nitrocefin assembly.

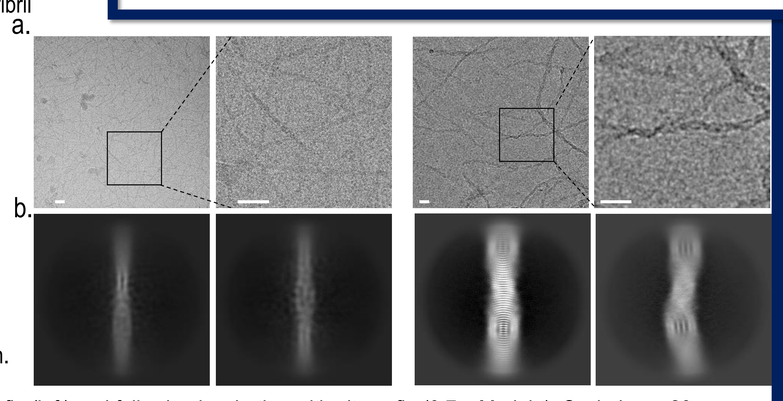


MD-based snapshot of nitrocefin docking on PFK fibril

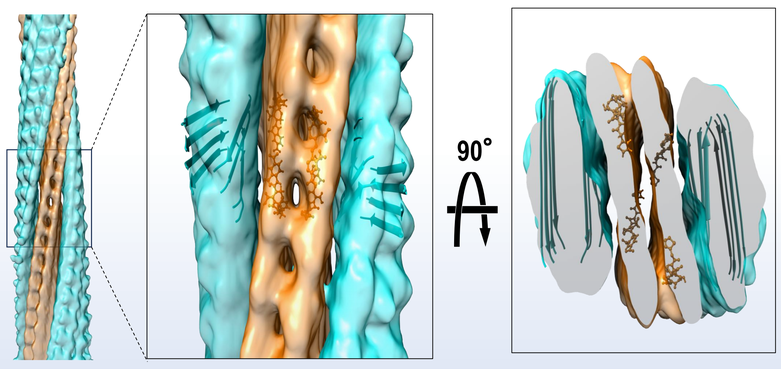




Relative probabilities of lysine binding to Nitrocefin.



a. Cryo-EM micrographs of PFK fibrils without nitrocefin (left) and following incubation with nitrocefin (0.7 mM; right). Scale bars -20 nm.
b. Representative 2D class averages of PFK amyloid fibrils without (two left images) and after incubation with nitrocefin (right images). Scale bars -5 nm.

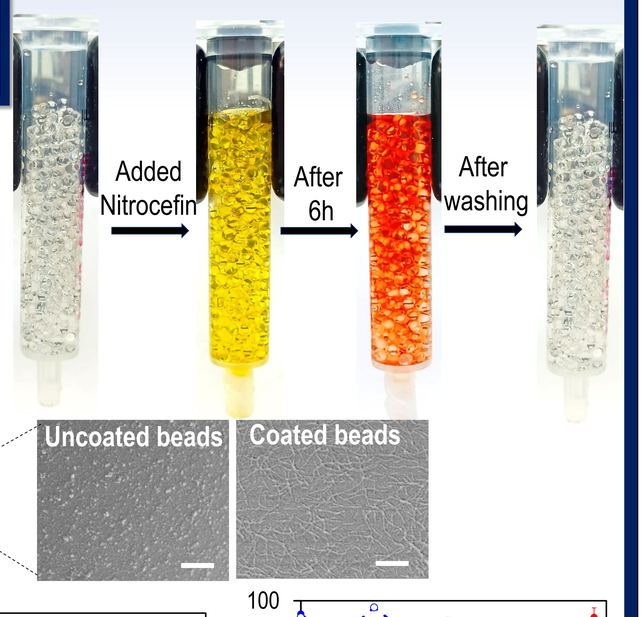


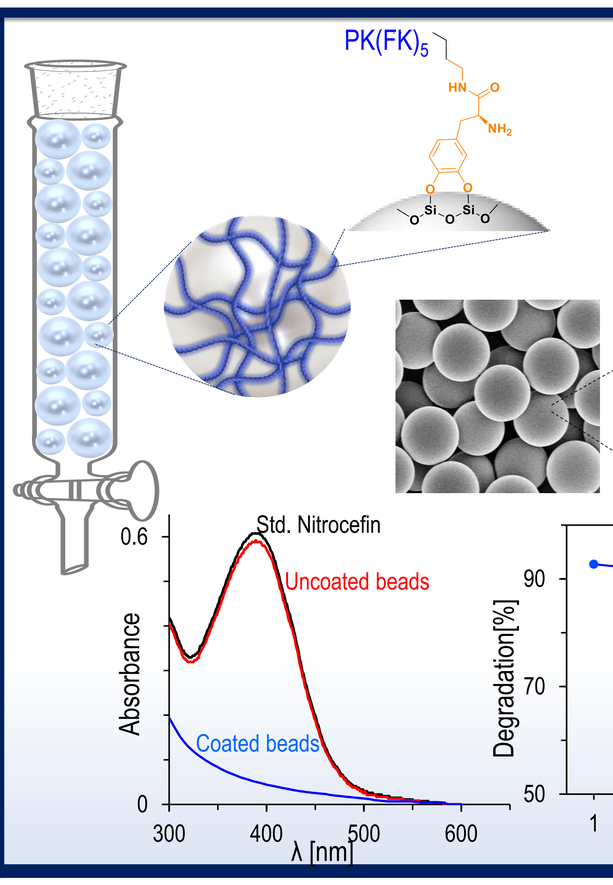
3D cryo-EM map of PFK fibrils incubated with nitrocefin.

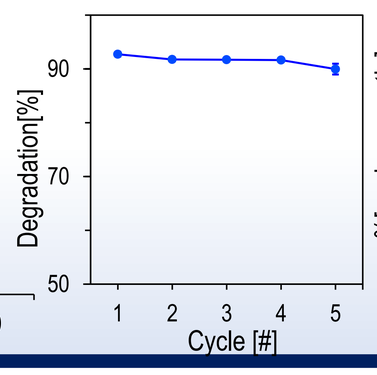
Zoomed-in are the side (center) and radial (right)

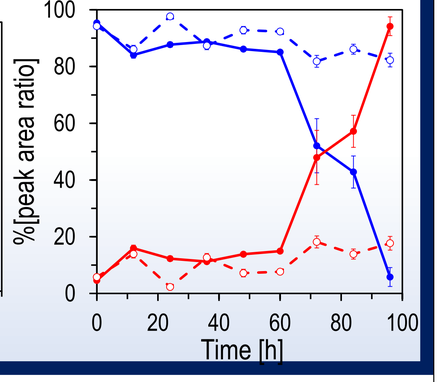
Views of a manually fitted MD-based model to the 3D cryo-EM map.

PFK fibrils on beads









Conclusion

- PFK fibrils form at low concentration with salt.
- Catalytically degrade β-lactam antibiotics.
- Activity via a unique allosteric coiled double fiber mechanism.
- Lysine residues enable nucleophilic attack on β-lactams.
- Active against Penicillin G and Amoxicillin.
- Bead-attached fibrils usable in filtration for antibiotic removal.

References

- Kunnath, Sisira Mambram, et al. "Allosteric amyloid catalysis by coiled coil fibrils." *Nature Communications* 16.1 (2025): 5071.
- Arad, Elad, et al. "Staphylococcus aureus functional amyloids catalyze degradation of β-lactam antibiotics." *Nature Communications* 14.1 (2023): 8198.

UNIVERSITY OF COPENHAGEN
DEPARTMENT OF CHEMISTRY

Peptide-Oligonucleotide Conjugates
Effect on Endosomal Escape?

Fie Davidsen[1], Kolfinna Hjálmarsdóttir[1], Adrian Hernandez[1],
Ewa Sitarska[2], Anand Saminathan[2], Tom Kirchhausen[2] , Knud J. Jensen[1]

[1]University of Copenhagen, Department of Chemistry, Thorvaldsensvej 40, 1871 Frederiksberg C, Denmark,
[2]Department of Cell Biology, Harvard Medical School, Boston Children's Hospital, 200 Longwood Ave, Boston, MA 02115, USA

https://doi.org/10.17952/38EPS.2026.P453

Abstract

RNA- and DNA-based oligonucleotide (ON) therapeutics are transforming disease treatment due to their high specificity and clinical efficacy. However, their therapeutic potential remains limited by inefficient intracellular delivery.[1] Following cellular uptake, most of the ONs are entrapped in endosomal compartments and undergo lysosomal degradation. Only a small fraction (estimated < 4%) of internalized RNA successfully escapes into the cytosol to reach their target. [2] Although several mechanisms of endosomal escape have been proposed, their molecular basis remains incompletely understood. Peptide-based ONs strategies have been explored to enhance endosomal escape, yet efficiency-toxicity trade-offs persist.[2]

This project aims to systematically investigate the mechanisms governing endosomal escape through the design of multifunctional peptide-oligonucleotide conjugates. This will be supported by real-time single particle molecular microscopy of labelled oligonucleotide-peptide conjugates in living cells, isolated endosomes and membrane models. This approach reveals how individual conjugates interact with membranes, move through cells and escape from endosomes, providing mechanistic insight into the factors governing efficient intracellular delivery and functional release

1. Intracellular Uptake of Oligonucleotides

Following cellular uptake by endocytosis, ONs are transported from early endosomes (pH 6.0-6.5) to late endosomes (pH 5.0-6.0) and lysosomes (pH 4.5-5.0). The increasing acidification and changes in membrane composition promote cargo sorting and degradation of the ONs.[2]

Peptide conjugation may enhance uptake and interact with endosomal membranes to promote endosomal escape into the cytosol. These include cell-penetrating peptides (CPPs), hydrophobic endosomal escape domain peptides (EEDs), and pH-responsive peptides. However, identifying peptides that selectively disrupt endosomal membranes without causing toxicity remains a challenge.

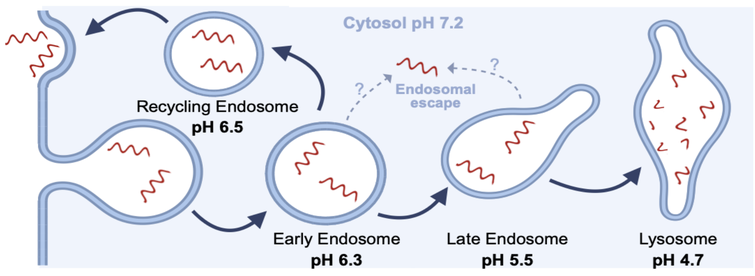


Figure 1 The intracellular pathway and trafficking of ONs and the great endosomal escape

2. Fluorophore Labelling of Antisense Oligonucleotides

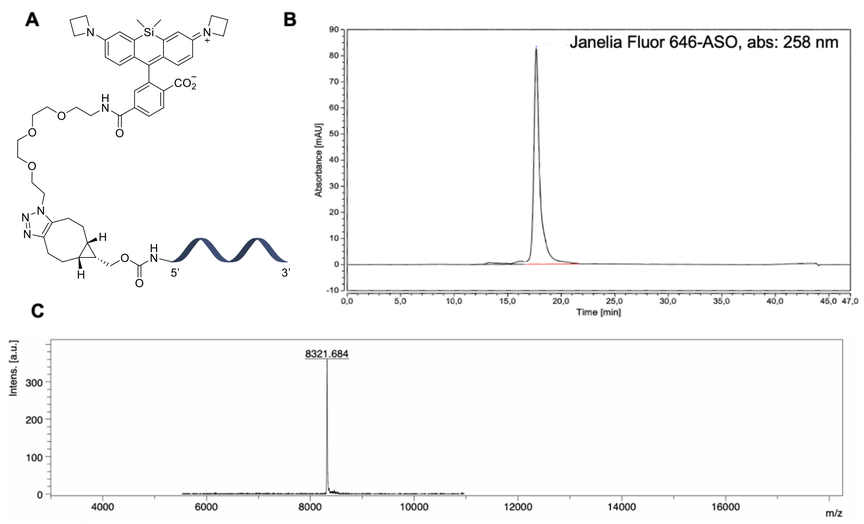


Figure 2 **Janelia Fluor 646 – MALAT1_ASO (A)** Structure of Janelia Fluor 646 – MALAT1_ASO **(B)** HPLC chromatogram (258 nm) of Janelia Fluor 646-MALAT1_ASO, obtained on Vanquish UHPLC equipped with a C18 column (250 x 10 mm from Phenomenex) at 60 °C. **(C)** MALDI-TOF MS obtained on Bruker Mircroflex calcd. [M+H⁺] 8318.8; m/z found 8321.684.

3. Fluorophore Labelled Antisense Oligonucleotides are Heterogeneously Distributed and Sequestered Within the Endolysosomal Lumen [6]

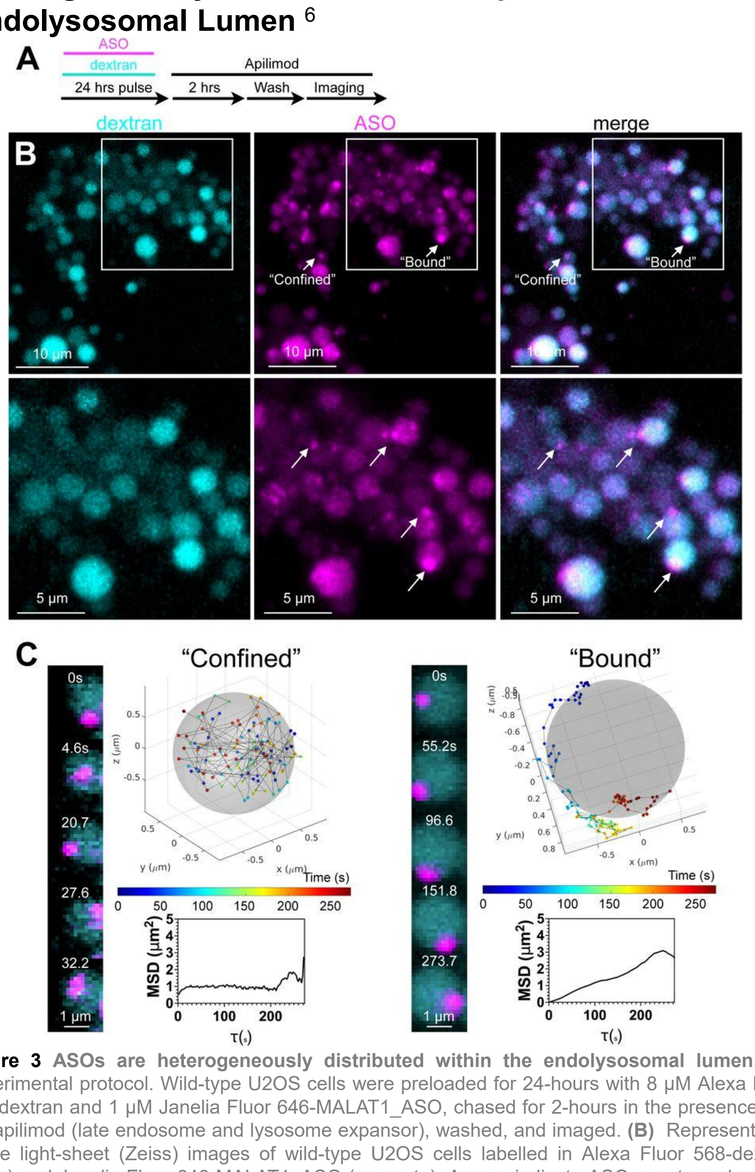
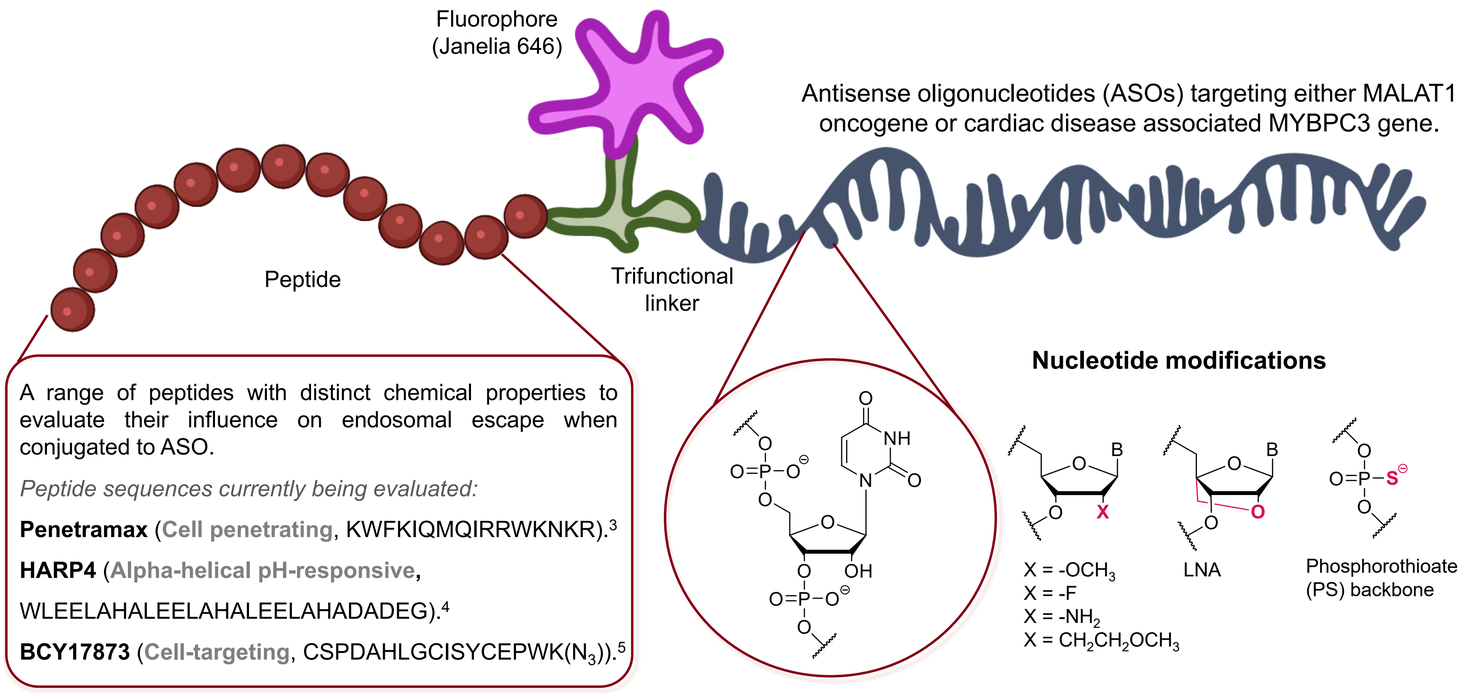


Figure 3 **ASOs are heterogeneously distributed within the endolysosomal lumen. (A)** Experimental protocol. Wild-type U2OS cells were preloaded for 24-hours with 8 µM Alexa Fluor 568-dextran and 1 µM Janelia Fluor 646-MALAT1_ASO, chased for 2-hours in the presence of 5 µM apilimod (late endosome and lysosome expansor), washed, and imaged. **(B)** Representative lattice light-sheet (Zeiss) images of wild-type U2OS cells labelled in Alexa Fluor 568-dextran (cyan) and Janelia Fluor 646-MALAT1_ASO (magenta). Arrows indicate ASO puncta undergoing confined and bound motion. **(C)** Representative real time three-dimensional trajectories of individual ASO particles exhibiting confined or bound motion within endolysosomal compartments. Mean squared displacement (MSD) plots are shown for each trajectory. Data are representative from one of three independent experiments.

4. Design of Oligonucleotide Conjugates for Evaluation of Endosomal Escape



A range of peptides with distinct chemical properties to evaluate their influence on endosomal escape when conjugated to ASO.

Peptide sequences currently being evaluated:

Penetramax (**Cell penetrating**, KWFKIQMQIRRWKNKR).[3]

HARP4 (**Alpha-helical pH-responsive,**

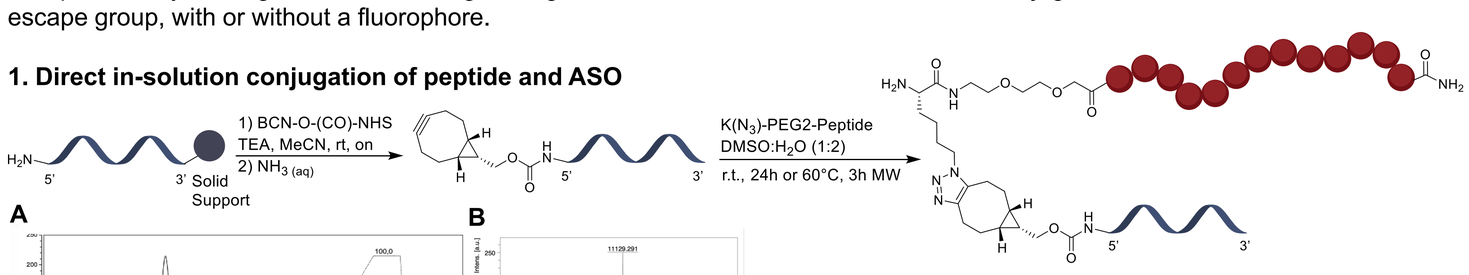
WLEELAHALEELAHALEELAHADADEG).[4]

BCY17873 (**Cell-targeting**, CSPDAHLGCISYCEPWK(N_3)).[5]

5. Peptide-Oligonucleotide Conjugation: Our Synthetic Strategies

Complementary strategies for introducing orthogonal chemical handles to enable the conjugation of an ASO to an endosomal escape group, with or without a fluorophore.

1. Direct in-solution conjugation of peptide and ASO



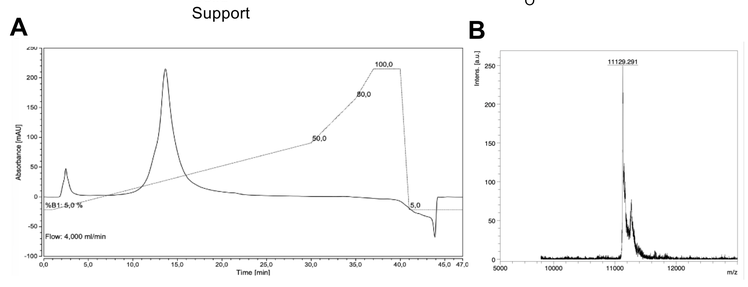
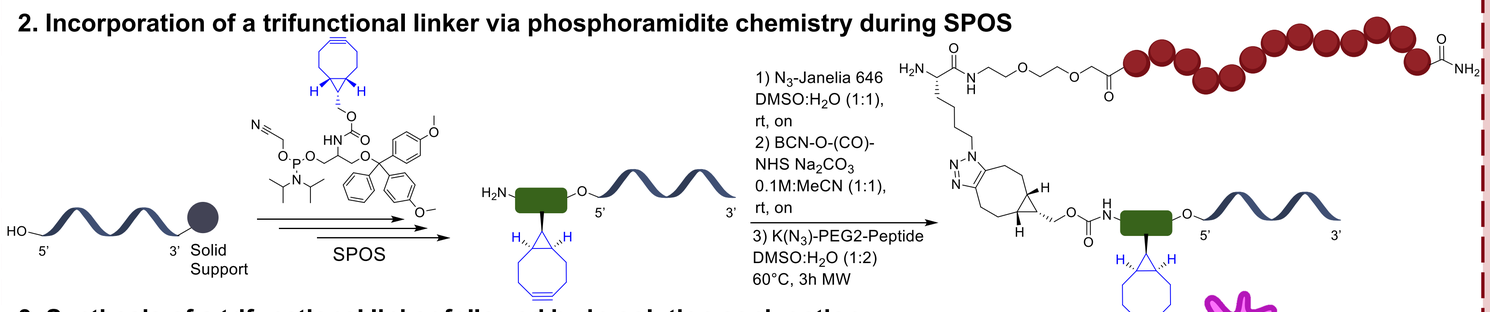
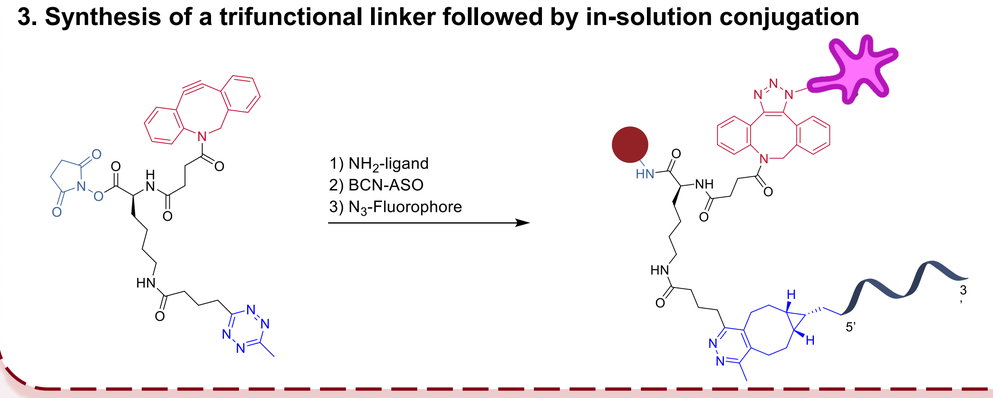


Figure 4 **(A)** HPLC chromatogram (258 nm) of Penetramax-ASO, obtained on Vanquish UHPLC equipped with a C18 column (250 x 10 mm from Phenomenex) at 60 °C. **(B)** MALDI-TOF mass spectrometry of Penetramax-ASO, obtained on Bruker Mircroflex calcd. [M+H⁺] 11130.01; m/z found 11129.291.

2. Incorporation of a trifunctional linker via phosphoramidite chemistry during SPOS



3. Synthesis of a trifunctional linker followed by in-solution conjugation



6. Concluding Remarks

- We have established different synthetic routes for peptide-ASO conjugates, both via direct in-solution conjugation and through a trifunctional linker enabling an additional conjugation group.
- Successful conjugation of three distinct peptides to ASO; CPP (Penetramax), pH-responsive membrane targeting (HARP4), and cell-targeting (BCY17873), confirmed by HPLC and MALDI-TOF MS and are being evaluated for their effects on endosomal escape.
- ASOs were successfully detected within the endosomes
- Live-cell imaging reveals heterogeneous ASO distribution within the endolysosomal lumen, with particles exhibiting both confined and bound motion.
- Future work will focus on evaluating endosomal escape efficiency across peptide-ASO conjugates

Acknowledgement: This work is supported by the Novo Nordisk Foundation through the Center for Optimized Oligo Escape and Control of Disease (COE)

References: **(1)** S. Azari et al., *Int. J. Pharm.* **2026**, 687, 126393, **(2)** S. F. Dowdy, *RNA.* **2023**, 29, 396–401, **(3)** R. G. Diedrichsen et al., *J. Control. Release.* **2025**, 380, 1031–1042, **(4)** H. Sakurai et al., *ACS Appl. Bio Mater.* **2021**, 4, 2442–2452. **(5)** M. E. Østergaard et al., *Nucleic Acids Res.* **2025**, 5 **(6)** E. Sitarska et al., bioRxiv **2026**, 2026.05.11.724403. **(7)** C. Lou, et al., *Chem. Eur. J.* **2020**, 26, 5676–5684.

COE

C-Glycosyl α-Amino Acids as Structural Encoders of Peptide Conformation

Ivanka Jerić, Barbara Bogović, Ivana Nikšić-Franjić

Ruđer Bošković Institute, Division of Organic Chemistry and Biochemistry, Bijenička cesta 54, 10000 Zagreb, Croatia

https://doi.org/10.17952/38EPS.2026.P010; ijeric@irb.hr

INTRODUCTION

Inspired by Nature's own biopolymers, where folding unlocks function, and by expanding the pool of 20 amino acids with non-canonical ones, numerous synthetic oligomers have been shaped to carry on different functions. Non-canonical amino acids have become not just tools, but keystones of modern science; they are indispensable in drug discovery, impart useful functional properties to catalysts and materials, and provide diverse hinges for bioconjugation reactions. *C*-glycosyl amino acids represent a privileged class of non-canonical amino acids; they occur in nature as products of bacterial metabolism and display wide spectrum of biological activities.

The *C*-glycoside linkage is inherently resistant to acidic, basic and enzymatic hydrolysis; therefore *C*-glycosylation is a well-established strategy for improving the pharmacokinetic properties of peptides. However, the influence of chiral *C*-glycosyl amino acid incorporation on peptide conformation remains insufficiently explored. Most existing synthetic approaches restrict *C*-glycosyl amino acid placement to the N-terminus, C-terminus, or specific residues containing pre-installed reactive groups.[1,2] Here, we present a more versatile strategy based on the design and synthesis of customized C-glycosyl amino acids (Figure 1).[3]

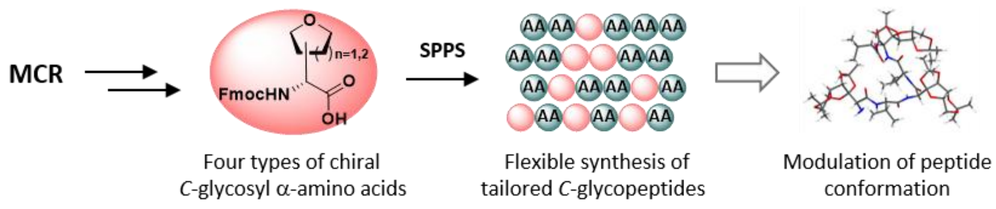
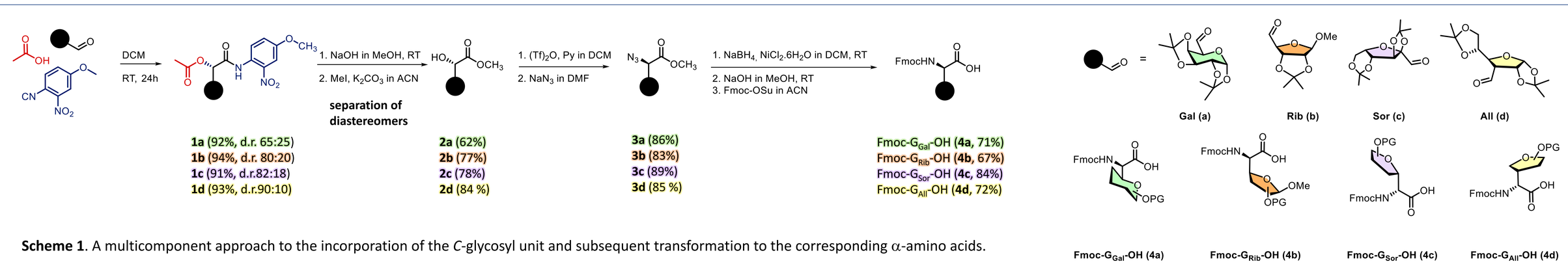


Figure 1. General approach to customized *C*-glycosyl α-amino acids for a flexible *C*-glycopeptide synthesis.

RESULTS

Four α-amino acids bearing protected galactopyranose, ribofuranose, sorbofuranose, or allofuranose side chains were synthesized by modification of multicomponent reaction (MCR) products (Scheme 1), and incorporated into peptides using a solid-phase methodology, enabling substitution at diverse sequence positions (Figure 2). Solid-phase synthesis was carried out with 2-chlorotrityl chloride resin, which can be cleaved under mild acidic conditions that leave isopropylidene groups in place. Thus, protected peptides were obtained after cleavage from the resin and purified by a combination of precipitation and RP-HPLC.



Scheme 1. A multicomponent approach to the incorporation of the *C*-glycosyl unit and subsequent transformation to the corresponding α-amino acids.

Conformational analysis of the model peptide **5** and *C*-glycopeptides was done by combination of NMR spectroscopy (in DMSO) and geometry optimization based on the collected NOE distance restraints from the 2D 1H–1H NOESY spectra. Typically, 7-15 NOEs were identified and used for constrained geometry optimizations. All calculations were performed in Gaussian 16 program package, Revision C.01. Detailed NMR analyses revealed that each *C*-glycosyl α-amino acid promotes distinct conformational preferences, primarily stabilized by hydrogen-bonding networks between backbone amides and carbohydrate side chains (Figure 3).[3]

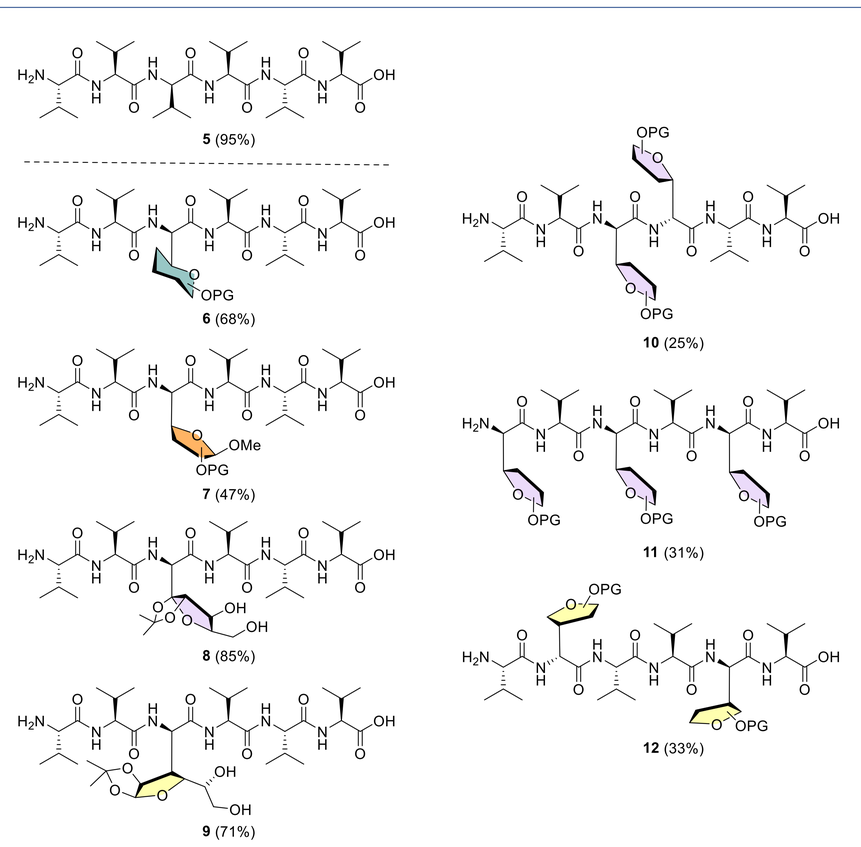


Figure 2. Model peptide **5** and *C*-glycopeptides obtained by SPPS

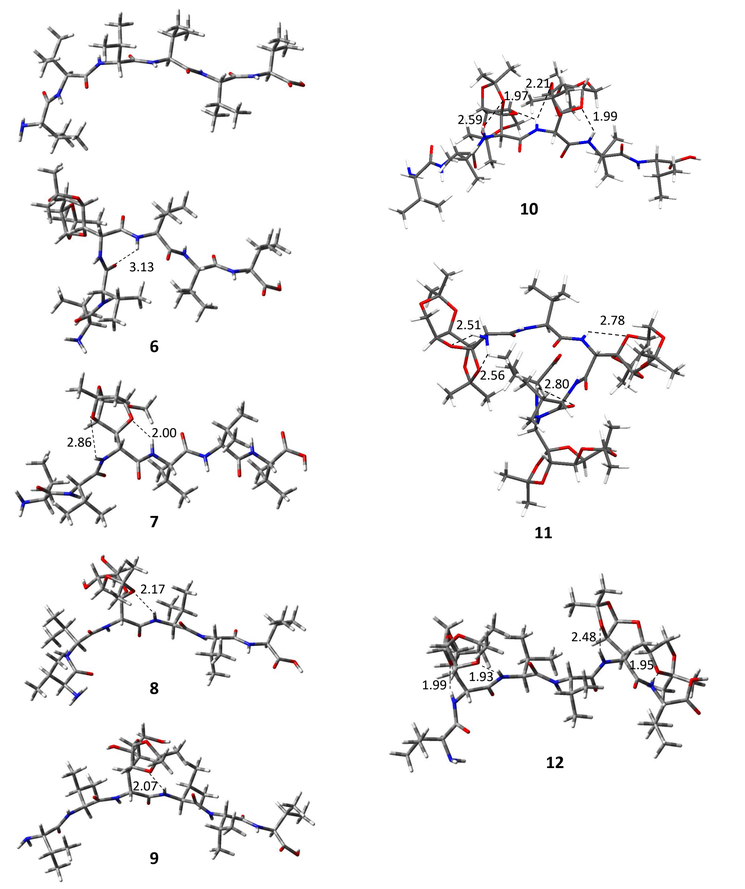


Figure 3. Conformational analysis of selected *C*-glycopeptides

CONCLUSIONS

While *C*-glycosylation represents a powerful strategy to overcome the limitations of *O*-glycosides and peptides in the drug discovery process, exploiting *C*-glycosyl amino acids as structural modulators is impeded by limited knowledge of the influence of carbohydrate ring size, stereochemistry, and substituents on the conformational preferences of peptides. We demonstrated that a flexible strategy comprising customized *C*-glycosyl α-amino acids enables synthesis of tailored *C*-glycopeptides with site-specific, consecutive or alternating positioning of these non-canonical amino acids.[3] NMR analysis uncover conformational information encoded within four non-canonical *C*-glycosyl α -amino acids, offering new molecular tools for catalysis, materials development and drug discovery.

References:

1. A. Chen, S. Zhao, Y. Han, Z. Zhou, B. Yang, L. G. Xie, M. A. Walczak, F. Zhu, *Chem. Sci.* **14** (2023) 7569–7580
2. M. Wang, C. Wang, X. Xie, D. Pan, L. Liu, Q. Chen, Z. Li, Q. Zhang, Z. Xu, *Chem. Commun*. **59** (2023) 3305–3308
3. B. Bogović, I. Colić, I. Nikšić-Franjić, V. Smrečki, I. Jerić, *Angew. Chem. Int. Ed*. **65** (2026) e22704

This work was supported by the Croatian Science Foundation Grant Number 9617.

https://doi.org/10.17952/38EPS.2026.P530

Peptide-functionalized Nanocoatings for Prevention of Biofouling and Device-Associated Infections

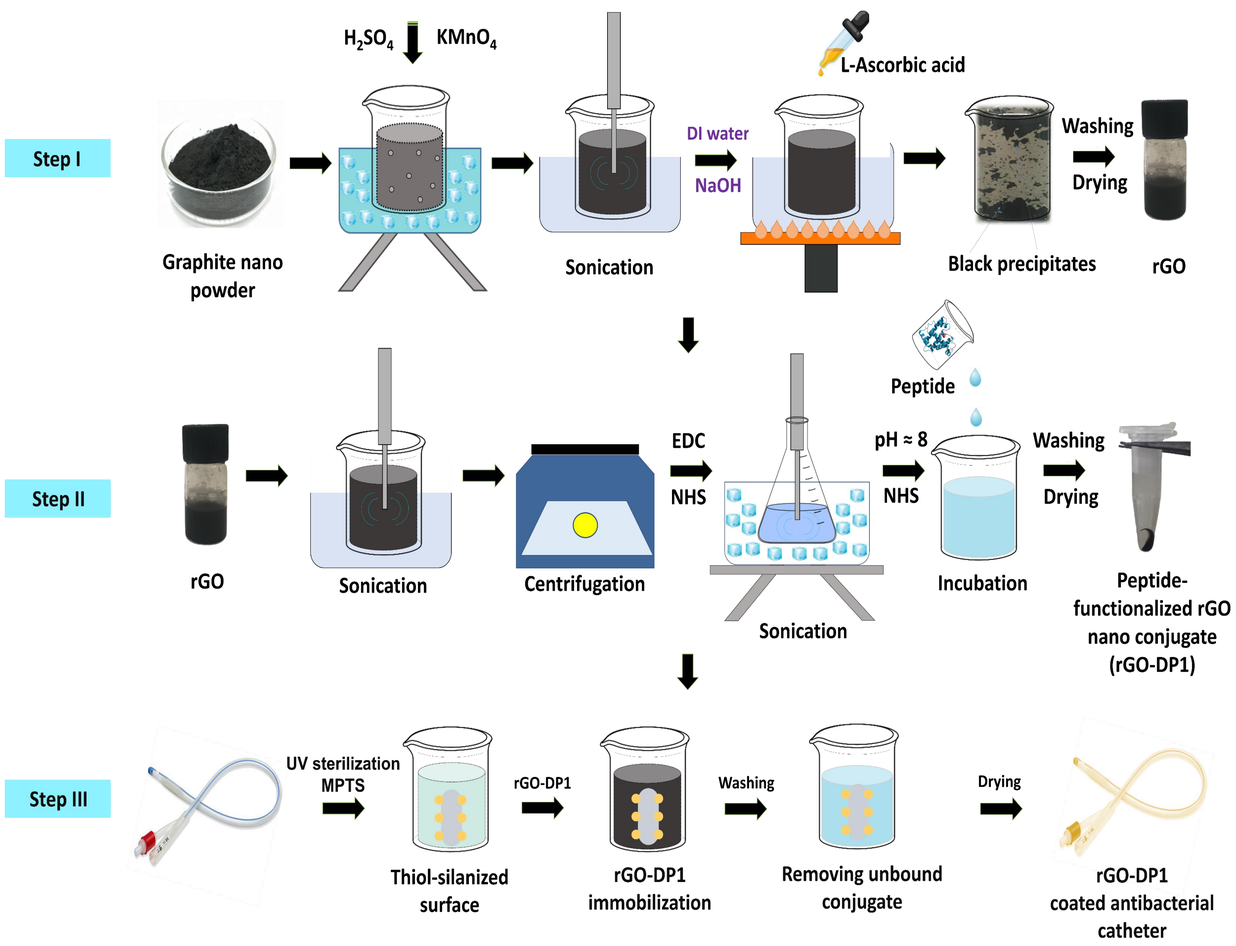
Shubhi Joshi[1,2] & Avneet Saini[1*]
[1]Department of Biophysics, Panjab University, Sector 25, Chandigarh, India
[2]University School of Allied Health Sciences, Rayat Bahra University, Mohali, Punjab, 140103, India
Email correspondence at shubhijoshi@pu.ac.in & avneet@pu.ac.in

38th European Peptide Symposium
Vienna, Austria-2026

Background

- Indwelling medical devices are highly susceptible to microbial colonization, with bacterial adhesion and subsequent biofilm formation contributing to device-associated infections.
- Catheter-associated urinary tract infections (CAUTIs) account for a substantial proportion of healthcare-associated infections, with approximately 75% of hospital-acquired UTIs associated with urinary catheters[1].
- Biofilm formation on device surfaces promotes persistent bacterial colonization and increases tolerance to antimicrobial treatment.
- Antimicrobial peptides (AMPs) are short, cationic and amphipathic biomolecules that exhibit potent antimicrobial activity through interactions with bacterial membranes. However, properties such as proteolytic instability, rapid clearance, structural degradation and concentration-dependent cytotoxicity reduces their biomedical applicability.
- Conjugation of peptides with nanomaterials results in the formation of peptide-functionalized nanoconjugates that combine the bioactivity of peptides with the physicochemical properties of nanomaterials, offering enhanced stability, surface association and biocompatibility for biomedical applications[2].
- **In this study, a novel synthetic antimicrobial peptide DP1 (RFGRFLRKILRFLKK)[3] was covalently conjugated with reduced graphene oxide (rGO) to develop a peptide-functionalized nano conjugate (rGO-DP1)[4], which was further developed as an antimicrobial and antibiofilm nanocoating for medical-device surfaces[5].**

Experimental design



Results

Synthesis and characterization of peptide-functionalized nanocoating

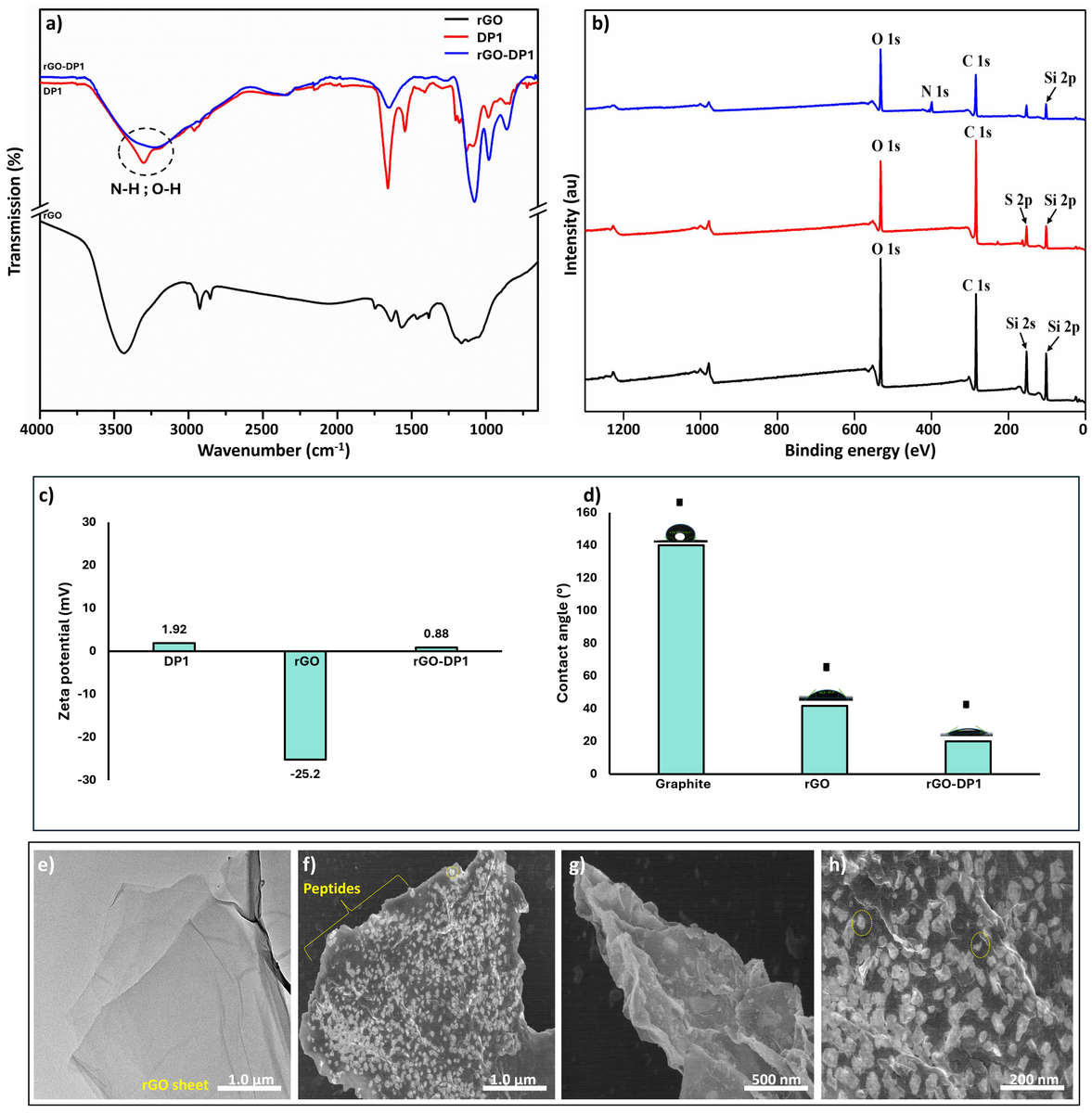


Fig. 1: Characterization of peptide functionalized nano conjugate by fourier-transform infrared spectroscopy (a), X-ray photoelectron spectroscopy (b), zeta potential (c), water contact angle (d) and High-Resolution Transmission Electron Microscopy images of rGO (e) and peptide functionalized nano conjugate (rGO-DP1) (f-h).

In vitro evaluation of peptide-functionalized nanocoating

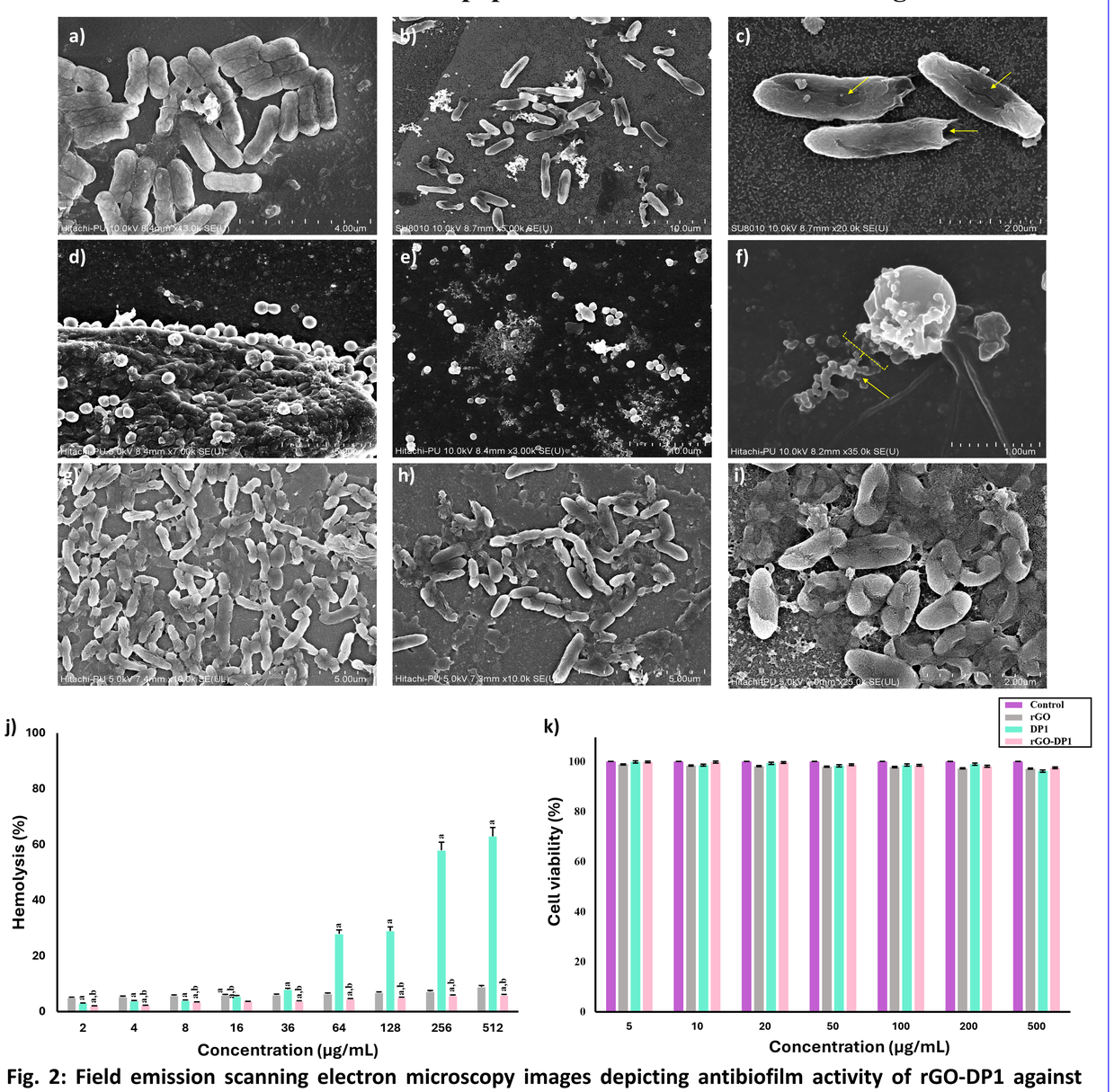


Fig. 2: Field emission scanning electron microscopy images depicting antibiofilm activity of rGO-DP1 against *Escherichia coli* (a-c), *Staphylococcus aureus* (d-f) and *Pseudomonas aeruginosa* (g-i). Percent hemolysis towards erythrocytes (J) and cell viability (%) of 3T3-L1 cells after incubation with rGO, DP1 and rGO-DP1 (k). Values are expressed as mean ± SD (n = 6).

Conclusion

- **Covalent conjugation of the novel synthetic antimicrobial peptide DP1 (RFGRFLRKILRFLKK) with reduced graphene oxide (rGO) resulted in the synthesis of peptide-functionalized nano conjugate (rGO-DP1).**
- **Biophysical and spectroscopic characterization confirmed peptide functionalization with retention of structural integrity and enhanced stability of the nano conjugate.**
- **rGO-DP1 exhibited broad-spectrum antibacterial and antibiofilm activity with enhanced membrane permeabilization and inhibition of early-stage bacterial adhesion.**
- **rGO-DP1 demonstrated minimal hemolytic activity and high mammalian cell viability, indicating good hemocompatibility and cytocompatibility.**
- **These findings establish immobilization of rGO-DP1 onto medical-device surfaces as an effective strategy to reduce bacterial attachment and biofilm maturation under simulated physiological conditions, supporting its application as a peptide-functionalized antimicrobial and antifouling nanocoating for medical devices.**

References

1. Centers for Disease Control and Prevention. (2025, June 27). *Catheter-associated urinary tract infection (CAUTI) basics*. https://www.cdc.gov/uti/about/cauti-basics.html
2. Joshi, S., Barman, P., Maan, M., Goyal, H., Sharma, S., Kumar, R., Verma, G., & Saini, A. (2024). Development of a two-dimensional peptide functionalized-reduced graphene oxide biomaterial for wound care applications. *Nanoscale, 16*(45), 20986–21001. https://doi.org/10.1039/D4NR02233E
3. Sharma, P., Sharma, S., Joshi, S., Barman, P., Bhatt, A., Maan, M., Singla, N., Rishi, P., Ali, M. E., Preet, S., & Saini, A. (2022). Design, characterization and structure–function analysis of novel antimicrobial peptides based on the N-terminal CATH-2 fragment. *Scientific Reports, 12*, 12058. https://doi.org/10.1038/s41598-022-16303-2
4. Joshi, S., Siddiqui, R., Sharma, P., Kumar, R., Verma, G., & Saini, A. (2020). Green synthesis of peptide functionalized reduced graphene oxide (rGO) nano bioconjugate with enhanced antibacterial activity. *Scientific Reports, 10*, 9441. https://doi.org/10.1038/s41598-020-66230-3
5. Joshi, S., Chadha, J., Harjai, K., Verma, G., & Saini, A. (2024). Synthetic peptide (DP1) functionalized graphene oxide: A biocompatible nanoformulation with broad-spectrum antibacterial and antibiofilm activity. *FlatChem, 44*, 100626. https://doi.org/10.1016/j.flatc.2024.100626

Acknowledgement

S. Joshi and A. Saini acknowledge Indian Council of Medical Research (ICMR) - Department of Health Research (DHR), India for granting Women Scientist fellowship. Authors would also like to like to express gratitude to the Sophisticated Analytical Instrumentation Facility (SAIF) and Central Instrumentation Lab (CIL), Panjab University, Chandigarh, India for providing instrumentation facilities.

https://doi.org/10.17952/38EPS.2026.P328

Preparation of peptides and their inhibitory activity effects against BACE1

Shinji Katsuoka[1], Daisuke Nakashinn[2], and Taeko Kakizawa[1,2]
[1]*Graduate School of Materials and Life Sciences, Kanto Gakuin University, Kanagawa, Japan;*
[2]*College of Science and Engineering, Kanto Gakuin University, Kanagawa, Japan*

Introduction

β-Site amyloid precursor protein cleaving enzyme 1 (BACE1) is an enzyme targeted for drug development in Alzheimer's disease (AD) [1]. BACE1 produces amyloid β-peptides, which may contribute to the onset of AD. We examined BACE1-cleavage peptide sequences through the digestion of synthetic peptides, including part of the Swedish (SW) mutant amyloid precursor protein sequence, using recombinant BACE1 [2, 3]. The results enabled us to design substrate-based enzyme inhibitors. Several sequences were identified for BACE1-targeted drug development. In this study, we synthesized peptide-based inhibitors using predetermined sequences, and their inhibitory effects against recombinant BACE1 were determined.

Results and Discussion

The synthetic scheme and structure of peptide **1** are shown in Figure 1. The design H-Glu-Ile-Thi-Sta-Nva-OH (**1**, Thi: 3-(2-thienyl)-L-alanine, Nva: L-norvaline) was based on the previously determined sequence H-Ser-Glu-Ile-Thi-Thi ↓ Nva-Ala-Glu-Phe-Arg-OH (↓ indicates the cleavage site targeted by BACE1). Peptide **1** was prepared as a pentapeptide with positions P_4–$P_{1'}$. At the P_1 position, statine (Sta: (3S,4S)-4-amino-3-hydroxy-6-methylheptanoic acid), which is a common unnatural amino acid used in protease inhibitors, was introduced. Similarly, several peptides, H-Glu-Ile-Thi-Xaa-Nva-OH, which included statine-related amino acids (Xaa) at the P_1 position, were synthesized. The SW mutant-based peptide H-Glu-Val-Asn-Sta-Asp-OH was also prepared. The peptides were synthesized by solid-phase peptide synthesis. Typically, Fmoc-amino acids were coupled to a resin in the presence of *N*,*N*'-diisopropylcarbodiimide and 1-hydroxybenzotriazole monohydrate in *N*,*N*-dimethylformamide. Piperidine was used to remove the protecting group. After elongating the whole peptide chain, cleavage from the resin was achieved using a cocktail containing trifluoroacetic acid. The resulting crude products were purified by high-performance liquid chromatography (HPLC).

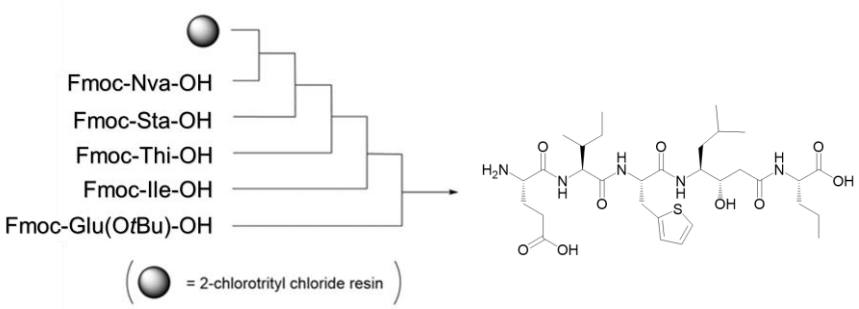


*Figure 1. Synthesis of H-Glu-Ile-Thi-Sta-Nva-OH (**1**). Synthesis was achieved based on a standard solid-phase synthesis method. Piperidine was used to remove the protecting group. Coupling reactions were conducted in the presence of N,N'-diisopropylcarbodiimide and 1-hydroxybenzotriazole monohydrate in N,N-dimethylformamide. The products were purified by high-performance liquid chromatography.*

Inhibitory activity was evaluated using previously described methods with slight modifications [2, 3]. The inhibitors were incubated at 37°C in the presence of recombinant BACE1 (R & D Systems, 931-AS-050) and a fluorescence-quenching substrate (Peptide Institute Inc., code 3212-v) in acetate buffer (pH 4.0) for 1 h. The reaction mixture was subjected to HPLC, and the cleaved fragments were identified by mass spectrometry. The peak areas from the chromatogram were used to evaluate the inhibitory activity. Peptide **1** exhibited activity against BACE1, and its inhibition was higher than that of the SW-based peptide. We subjected the (3R,4S)-derivative of statine to peptide synthesis to generate H-Glu-Ile-Thi-(3R,4S)Sta-Nva-OH. Consistent with previous findings, peptide **1,** including statine, showed higher inhibitory activity compared with the peptide that included the (3R,4S)-derivative at the P_1 position [1]. Peptides containing phenylnorstatine (Pns; (2R, 3S)-3-amino-2-hydroxy-4-phenylbutyric acid) and its stereoisomer allophenylnorstatine (Apns; (2S, 3S)-3-amino-2-hydroxy-4-phenylbutyric acid) were also synthesized. The Pns in the P_1 position showed higher efficiency compared with Apns [4]. Overall, several peptides were prepared based on the BACE1 superior-cleavage sequence, and their inhibitory activities were evaluated. Some peptides showed inhibitory activity against BACE1. A detailed evaluation of inhibitory activity is currently underway.

Acknowledgments

This work was financially supported in part by the Society of Science and Engineering/Architecture and Environmental Design, Kanto Gakuin University in 2025. We thank Mr. Koyo Yamamoto for his technical support.

References

1. Sinha, S.; Anderson, J. P.; Barbour, R.; Basi, G. S.; Caccavello, R.; Davis, D.; Doan, M.; Dovey, H. F.; Frigon, N.; Hong, J.; Jacobson-Croak, K.; Jewett, N.; Keim, P.; Knops, J.; Lieberburg, I.; Power, M.; Tan, H.; Tatsuno, G.; Tung, J.; Schenk, D.; Seubert, P.; Suomensaari, S. M.; Wang, S.; Walker, D.; Zhao, J.; McConlogue, L.; John, V. *Nature*. **1999**, *402*, 537-540.
2. Kakizawa, T.; Sanjoh, A.; Kobayashi, A.; Hattori, Y.; Teruya, K.; Akaji, K. *Bioorg. Med. Chem*. **2011,** *19*, 2785-2789.
3. Katsuoka, S.; Watanabe, R.; Uchida, Y.; Midorikawa, M.; Yamada, R.; Kakizawa, T. *Bioorg. Med. Chem. Lett*. **2025**, *127*, 130290.
4. Kakizawa, T.; Hidaka, K.; Hamada, D.; Yamaguchi, R.; Uemura, T.; Kitamura, H.; Tagad, H. D.; Hamada, T.; Ziora, Z.; Hamada, Y.; Kimura, T.; Kiso, Y. *J. Pept. Sci.* **2010**, *16*, 257-262.

ROLE OF METAL NANOPARTICLES AS ARTIFICIAL CHAPERONES IN MODULATING THE AGGREGATION PROPENSITY OF β-AMYLOID (Aβ40) POLYPEPTIDE

Harshit Kalra# & Suman Jha

Department of Life Science, National Institute of Technology Rourkela, Rourkela-769008, Odisha, India

#Email: 521ls6012@nitrkl.ac.in (+91 8447915255)

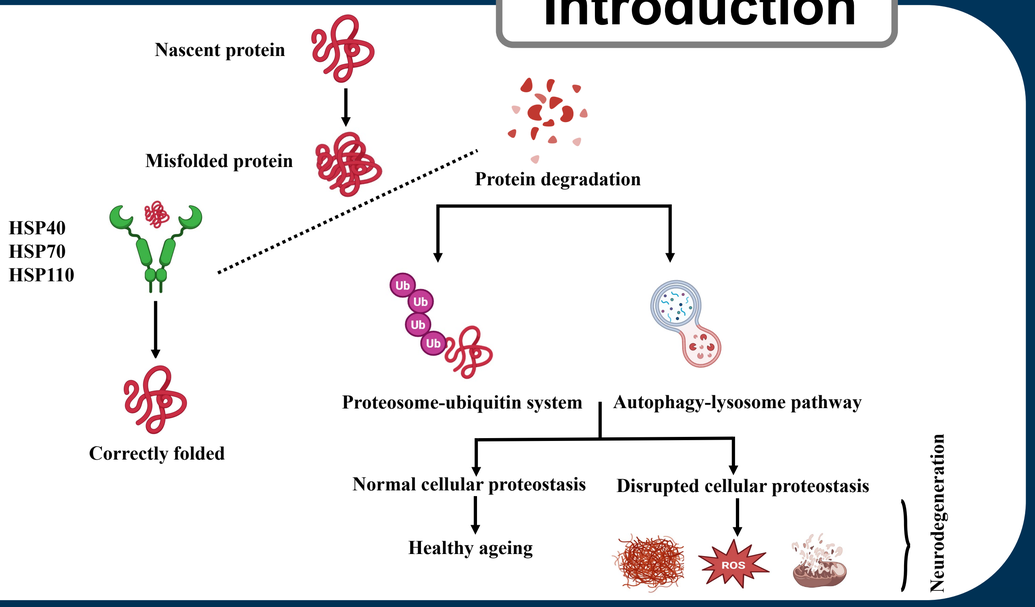
38th European Peptide Symposium
Poster No: 74

https://doi.org/10.17952/38EPS.2026.P074

Abstract

The abnormal cleavage of Amyloid Precursor Protein (APP), and the subsequent aggregation of the cleaved fragments, i.e. beta-Amyloid Polypeptides (Aβ40/42), are linked to the pathogenesis of Alzheimer's disease (AD)(1). Although molecular chaperones of the proteostasis network look after the fragments and consequent aggregates, they become inefficient with age and stress that result in the accumulation of Aβ40/42 peptides(2,3). Herein, by combining different techniques, we report the impact of metal nanoparticles (MNPs), including Zinc Oxide (ZnO), Cerium Oxide (CeO), and Gold (Au), as artificial Chaperones to modulate the aggregation propensity of Aβ40, the relatively abundant fragment found in the AD patients(4). The binding analysis revealed that the Aβ40 enthalpically binds with ZnONP and CeONP, whereas no binding is observed with AuNP. The binding resulted in flocculation of the complex, trapping Aβ40 monomers into non-amyloid aggregates with the native-like random coil conformation, compared to Aβ40 alone or with AuNP where the peptide adopted fibrillary morphology, which was also confirmed using amyloid-specific thioflavin T fluorescent dye. In conclusion, our results highlight the efficacy of the ZnONP interface in sequestering Aβ40 monomers and preventing their pathological self-assembly, underscoring its potential as a platform to modulate amyloid aggregation.

Introduction



Results

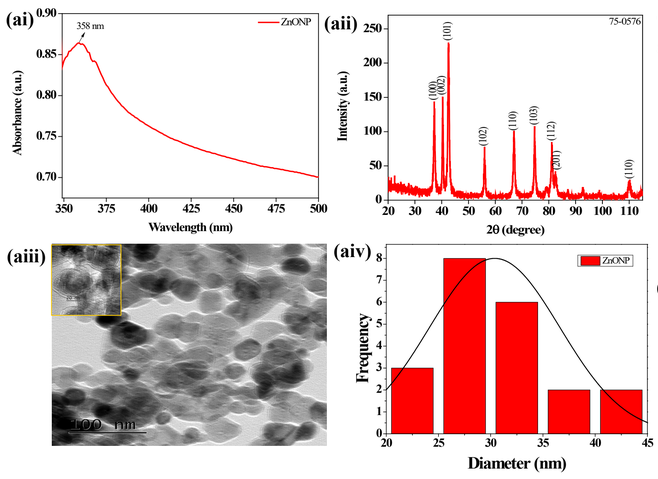


Table: Zeta potential of different NPs by Zeta analyzer.

Nanoparticles	Zeta (mV) ± S.D.
ZnONP	36.6 ± 4.14
CeONP	39.4 ± 6.32
AuNP	-24.8 ± 6.98

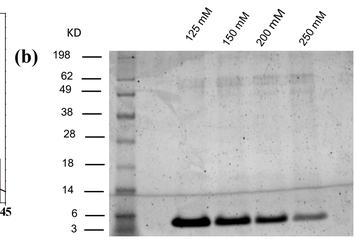


Fig.: (a) Characterization of ZnONP using (ai) UV-Visible spectra, (aii) XRD spectra, (aiii) TEM micrographs in 100 nm range and HRTEM insets, and (aiv) Size distribution. (b) A 15% SDS gel showing the bands of Aβ40 eluted in gradient NaCl eluents.

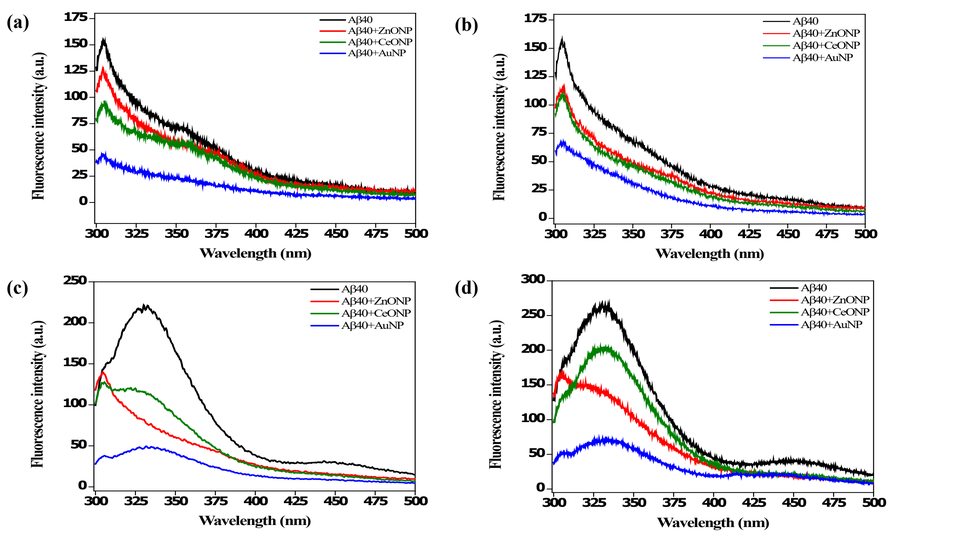
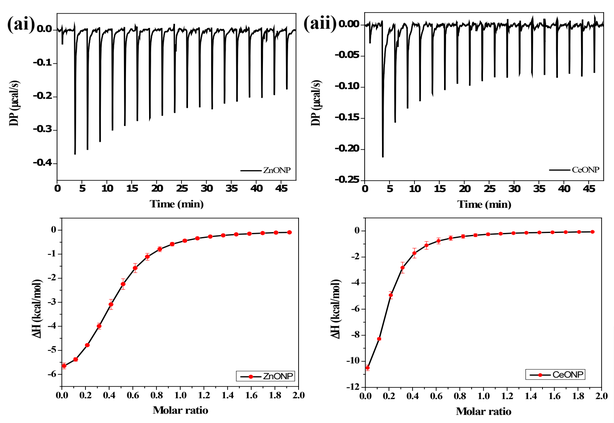
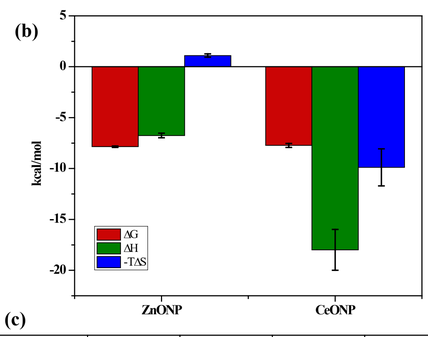


Fig.: Time-dependent intrinsic fluorescence spectra of 25 µM Aβ40 incubated at 37 °C with 50 µg/mL of ZnONP, CeONP, AuNP at (a) 0 h, (b) 24 h, (c) 48 h, and (d) 72 h.





(c)

25 µM Aβ40 and 50 µg/mL of nanoparticles	Dissociation constant (K_D), µM	Enthalpy change (ΔH), Kcal/mol	Entropy change (TΔS), Kcal/mol	Free energy change (ΔG) Kcal/mol
ZnONP	1.77 ± 0.44	-6.75 ± 0.23	1.103 ± 0.15	-7.85 ± 0.07
CeONP	2.31 ± 0.70	-17 ± 2	-9.88 ± 1.81	-7.72 ± 0.19

Fig.: (a) Thermograms showing isothermal titration curves for 25 µM Aβ40 titrated with 50 µg/mL (ai) ZnONP, and (aii) CeONP at 25 °C in water. (b) Signature plot calculated by applying 1:1 binding model. (c) Calculated thermodynamics parameters.

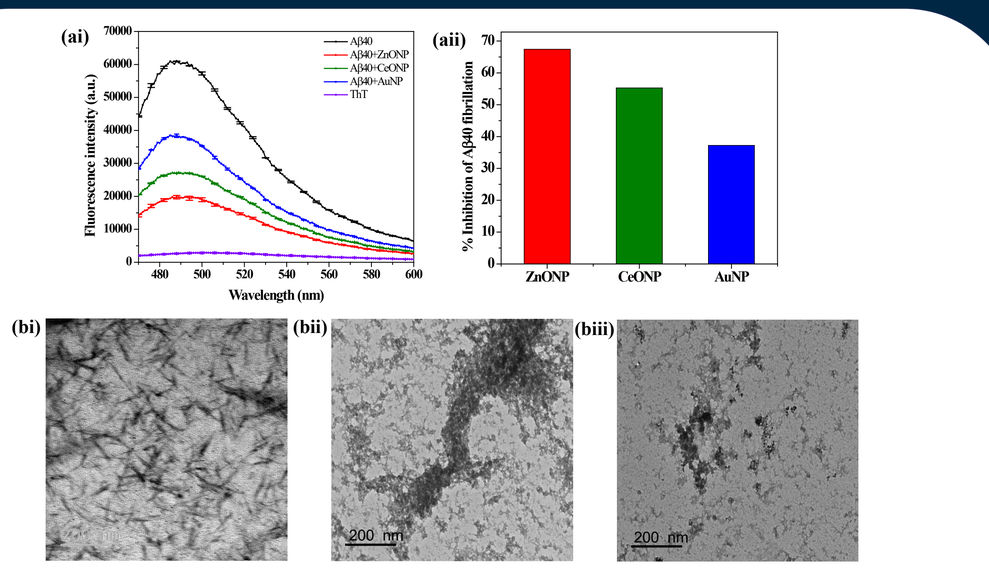


Fig.: (ai) Thioflavin T spectral scan upon excitation at 440 nm, and emission in the range of 470-600 nm, recorded for 25 µM Aβ40 incubated at 37 °C with 50 µg/mL of ZnONP, CeONP, and AuNP at 72 h. (aii) % inhibition of Aβ40 fibrillation in the presence of NPs bar graph. (b) TEM micrograph of (bi) 25 µM Aβ40 only (bii) 25 µM Aβ40 in presence of 50 µg/mL ZnONP (biii) 25 µM Aβ40 in presence of 50 µg/mL CeONP.

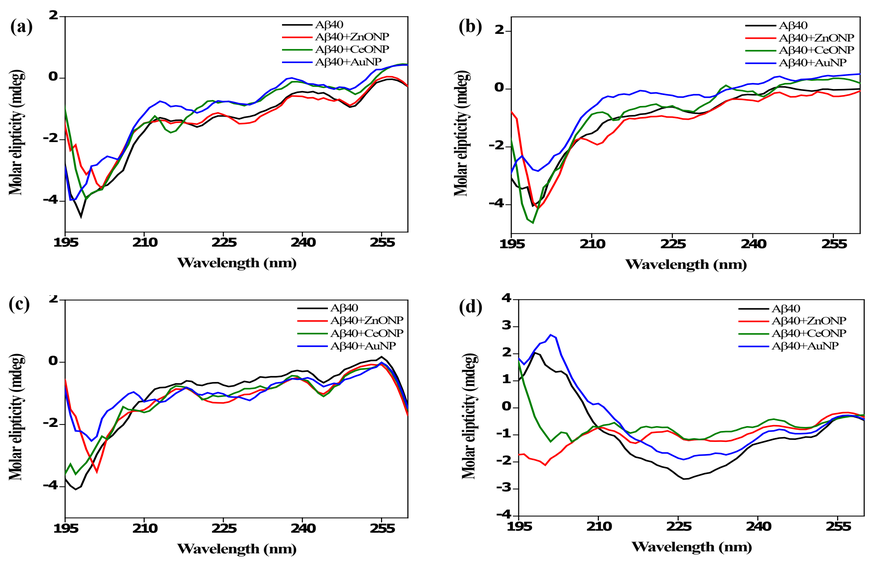


Fig.: Far-UV spectra of 25 µM Aβ40 incubated at 37 °C with 50 µg/mL of ZnONP, CeONP, AuNP at (a) 0 h, (b) 24 h, (c) 48 h, and (d) 72 h.

Conclusion

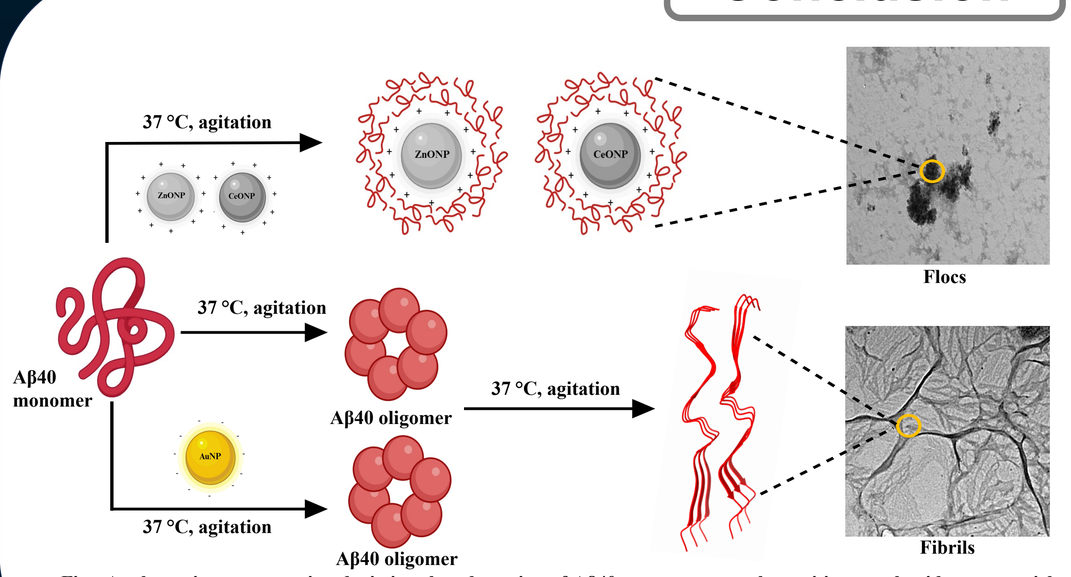


Fig.: A schematic representation depicting the adsorption of Aβ40 monomer onto the positive metal oxide nanoparticles interface leading to the formation of thermodynamically stable amorphous aggregates (flocs) instead of the amyloid fibril.

References

1. Chen, G. F., Xu, T. H., Yan, Y., Zhou, Y. R., Jiang, Y., Melcher, K., & Xu, H. E. (2017). Amyloid beta: structure, biology and structure-based therapeutic development. Acta pharmacologica sinica, 38(9), 1205-1235.

2. Maiti, P., Manna, J., Veleri, S., & Frautschy, S. (2014). Molecular chaperone dysfunction in neurodegenerative diseases and effects of curcumin. BioMed research international, 2014(1), 495091.

3. Sherman, M. Y., & Goldberg, A. L. (2001). Cellular defenses against unfolded proteins: a cell biologist thinks about neurodegenerative diseases. Neuron, 29(1), 15-32.

4. Seubert, P., Vigo-Pelfrey, C., Esch, F., Lee, M., Dovey, H., Davis, D., ... & Schenk, D. (1992). Isolation and quantification of soluble Alzheimer's β-peptide from biological fluids. Nature, 359(6393), 325-327.

Acknowledgment

The author acknowledge the financial support from Indian Council of Medical Research, Govt. of India, India, under the grant 35/05/2020-Nano/BMS. Additionally, we are very thankful to the Central Research Facility of N.I.T. Rourkela.

Fishing for Function: From Predicted Binding to Functional Block by a Cone Snail Peptide

Karbat I., Nutkewitz S, Adam Steinberg D, Katz M. and Reuveny E.

WEIZMANN INSTITUTE OF SCIENCE

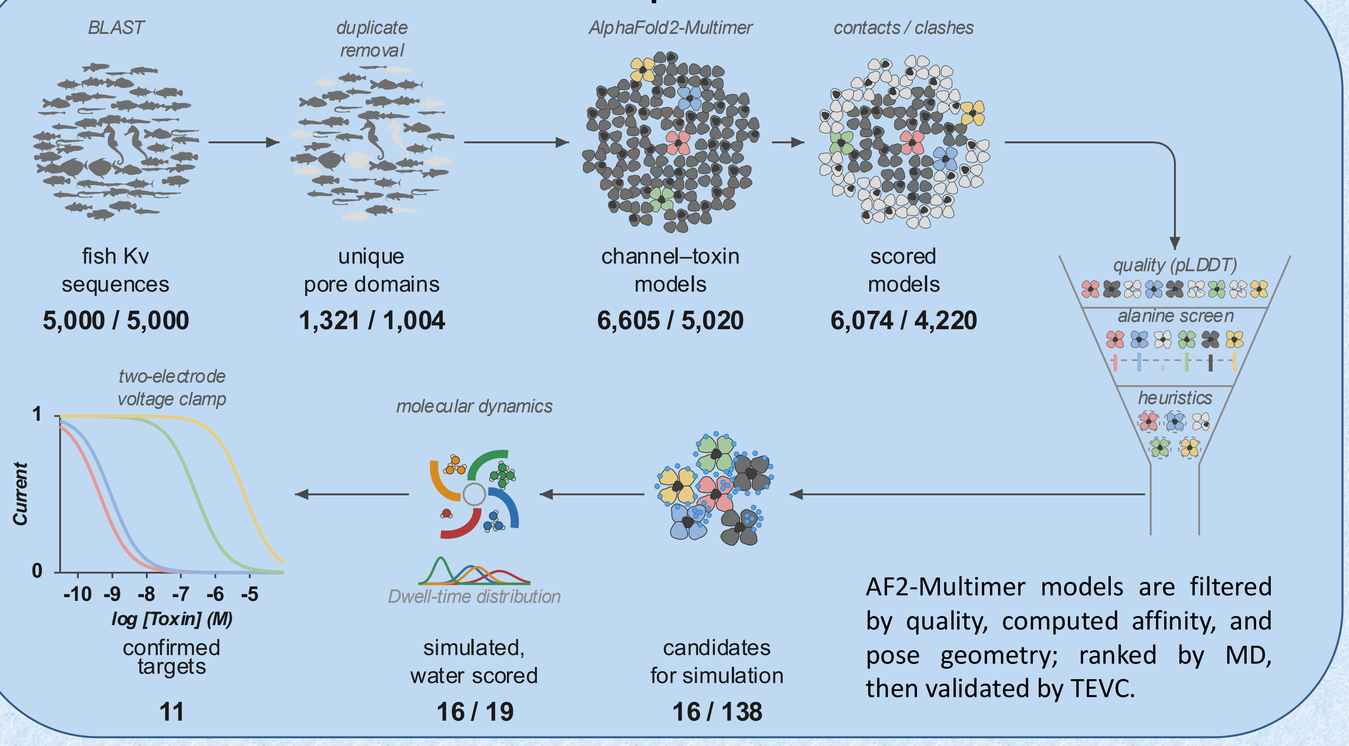
izhar.karbat@weizmann.ac.il
https://doi.org/10.17952/38EPS.2026.P295



Abstract

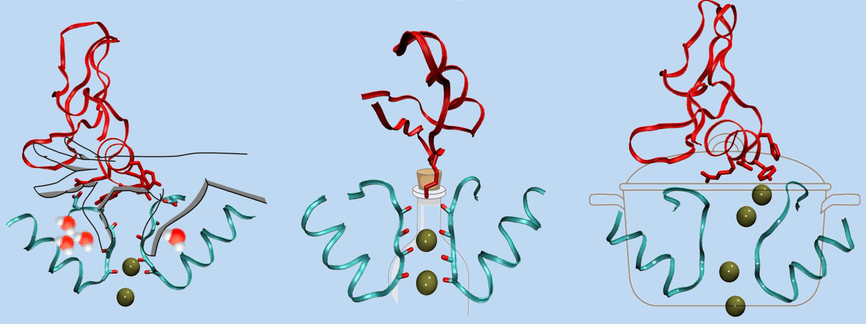
Pore-modulating peptide toxins block K^+ channels by perturbing water dynamics around the selectivity filter (SF). The cone-snail toxin Conkunitzin-S1 (Cs1), the first identified toxin of this class, was initially characterized on the Drosophila Shaker channel, but its natural targets remained elusive. Initial screening with conventional ML-based methods yielded numerous false positives. We therefore asked whether molecular dynamics, informed by the toxin's mode of action, could pinpoint the true targets. To test this, we combined AlphaFold2-Multimer structure prediction with automated molecular dynamics screening and an Equivariant Transformer (ET3) trained to classify the water network surrounding the SF. Screening over 2,300 unique fish K^+ channel sequences for toxin-induced water asymmetry identified eleven previously unknown high-affinity Cs1 targets, validated electrophysiologically (EC_{50} 0.9–8.7 nM). Crucially, resistant channels bound Cs1 in the same pose and remained stably associated throughout, showing that neither structural compatibility nor binding stability predicts peptide activity. Instead, sensitivity depended on the channel's intrinsic water dynamics: a single residue, Shaker 449, determines whether the asymmetry Cs1 induces becomes sustained and structured. Our computational framework showcases the power of integrating structure prediction, machine learning, and mechanism-aware molecular dynamics to decode toxin-channel interactions, opening new possibilities for in silico ecological research and drug interaction studies.

The Pipeline



AF2-Multimer models are filtered by quality, computed affinity, and pose geometry; ranked by MD, then validated by TEVC.

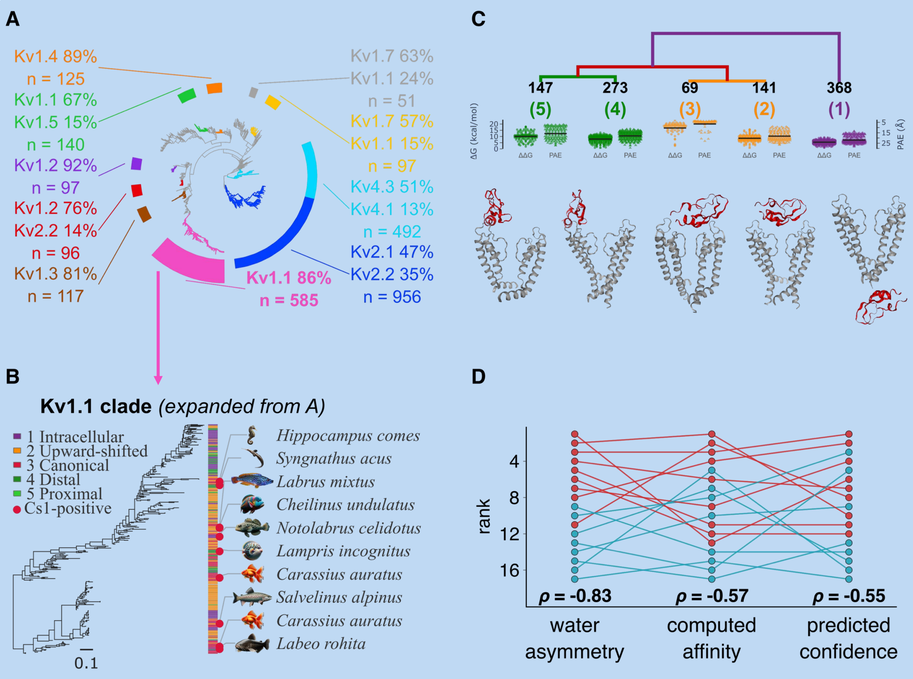
K^+ Pore-Blockers : Modes of action



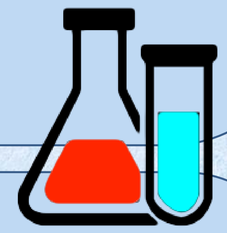
Voltage-gated potassium channels (K_vs) mediate the flow of potassium ions in and out of cells, playing a crucial role in cell signaling and regulation. These channels are targeted by multiple animal toxins which block ion conduction, leading to toxic outcomes. Classical scorpion K_v blockers physically occlude the ion permeation pathway by inserting a charged Lysine residue into the pore, akin to a “Cork” or a “Plug”. Recently , we described two alternative modes of action for K_v channel blockers [1,2]. The first is the “Pinch” mechanism, in which the toxin modifies the permeation of water molecules into protein cavities surrounding the channel pore, creating highly asymmetric water distributions at these regions and trigger a local collapse of the channel pore, analogous to slow inactivation. The second is the “Molecular Lid” block mechanism, in which K^+ ions are diverted and trapped in ectopic binding sites formed at the channel-toxin interface.

1. Saikia, C. *et al.* A Molecular Lid Mechanism of K+ Channel Blocker Action Revealed by a Cone Peptide. *J. Mol. Biol.* 166957 (2021) doi:10.1016/j.jmb.2021.166957.
2. Karbat, I. *et al.* Pore-modulating toxins exploit inherent slow inactivation to block K^+ channels. *Proc. Natl. Acad. Sci.* **116**, 18700–18709 (2019).

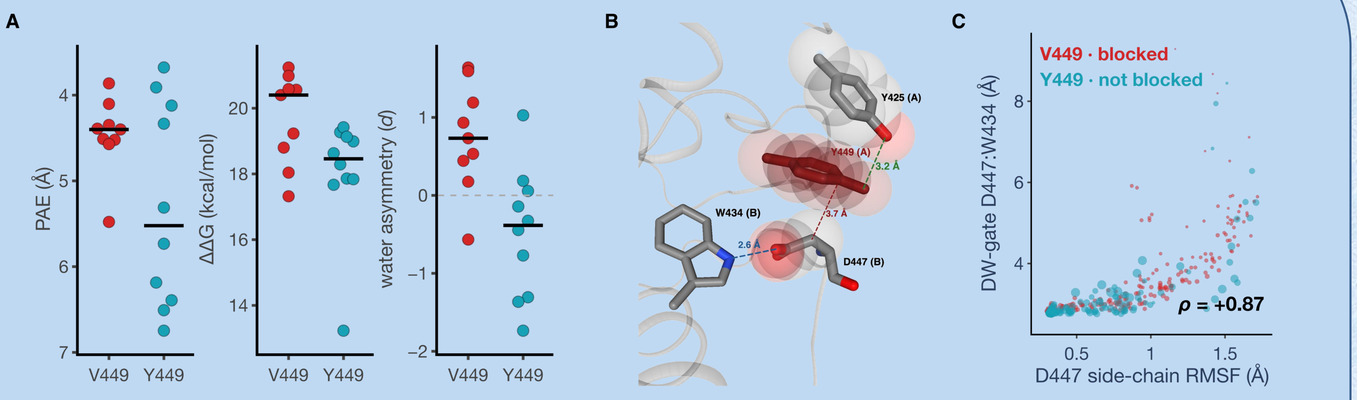
Results



All confirmed targets map exclusively to the $Kv_{1.1}$ clade (585 sequences; **A, B**) and universally adopt the tightest predicted binding pose (canonical, 69 models, 1.0 ± 0.4 Å; **C**). Among complexes adopting this pose, static affinity and interface confidence are blind to functional outcomes, falsely ranking inert binders alongside active targets (ρ = −0.57 and −0.55; **D**). Dynamic ET3 - assigned water asymmetry resolves this computational blind spot, successfully tracking actual the measured toxicity (ρ = −0.83).

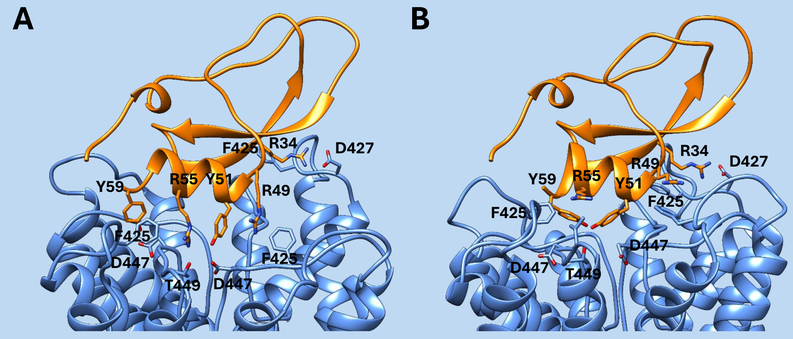


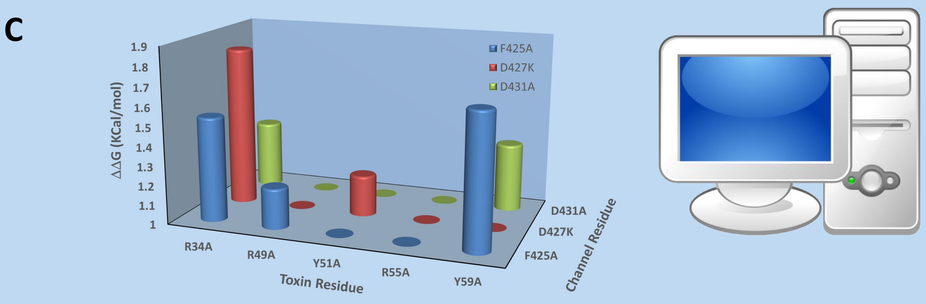
The Mechanism



A single substitution cleanly sorts the functional outcomes: Cs1 blocks channels with valine but not tyrosine at position 449. Both variants form a similar interface with the toxin, and static ML metrics rank them equally (A). The functional divergence traces to the channel’s intrinsic mechanics. To establish asymmetric water flow, Cs1 must trap the D447-W434 gate open. A tyrosine at 449 prevents this by packing against F/Y425; the resulting rigid ring restrains the adjacent subunit's D447, firmly stabilizing the closed state (B). Gate opening strictly depends on this baseline D447 mobility (C). Lacking this aromatic lock, V449 leaves D447 highly mobile, providing the flexibility the toxin requires to trap the gate open.

AlphaFold multimer model of Cs1-Shaker





AlphaFold (B) Vs Experimental (A) complex between Conkunitzin-S1 and dmK_v1.1. Experimental restraints derived from double-mutant cycle analysis and used for model validation are displayed in (**C**).

Conclusion

Distinguishing mere binding from a functional consequence remains a fundamental challenge in computational protein-peptide interaction screening. By anchoring a simulated dynamic rate to a macroscopic functional measurement, we established a generalizable strategy to separate active targets from inert binders.

- **Prospective Discovery**: Yielded 11 novel targets, all confirmed in vitro (EC_{50} 0.9–8.7 nM).
- **The Static Blind Spot:** Affinity filters failed; unresponsive channels held the toxin in the identical canonical pose throughout 200 ns simulations, forming perfectly stable but functionally inert complexes.
- **The Dynamic Solution**: The rate of asymmetric water exchange behind the filter successfully resolved the cohorts, tracking the macroscopic slow-inactivation time constant across a position 449 mutant series.

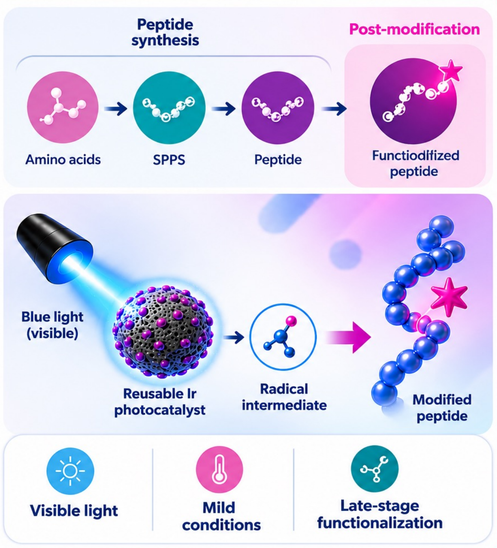
38th EPS
European Peptide Symposium
Vienna, 2026

https://doi.org/10.17952/38EPS.2026.P283

Reusable Photoredox Catalysts for Sustainable Peptide Synthesis

Dr. Kelly L. Materna • Duilio Bacigalupo | Ouralia, Stockholm, Sweden

INTRODUCTION: PHOTOREDOX CATALYSIS + PEPTIDE POST-MODIFICATION



Peptides are a fast-growing class of therapeutics, and late-stage modification adds non-natural functionality without rebuilding the sequence. Visible-light photoredox catalysis excels here: it drives selective radical chemistry under mild conditions using room temperature and simple LED light (Figure 1); it has already been used to modify amino acids, peptides, and proteins.[1–3] But the most capable photocatalysts are precious-metal complexes used homogeneously and lost after one use, motivating recoverable, reusable catalysts that keep this reactivity.

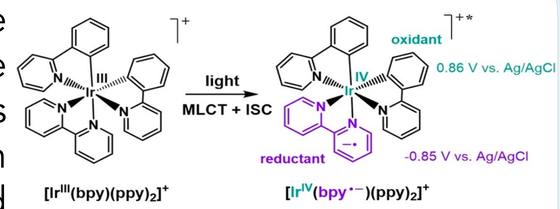


Figure 1. Iridium photoredox catalyst activation under illumination. Upon illumination, the catalyst reaches an excited state, which can act as either a strong oxidant or a strong reductant, allowing a variety of chemical transformations to be performed.

OUR MISSION

Enabling recoverable photoredox catalysis for more sustainable pharmaceutical manufacturing.

Performance • Recovery • Reuse

Ouralia

LIGHT-DRIVEN CHEMISTRY · REUSABLE BY DESIGN

OUR MOTIVATION

Ouralia keeps the molecular performance of photoredox catalysts while making them recoverable, reusable, and circular, cutting waste of one of the world's scarcest precious metals without compromising the chemistry.

THE SCIENCE BEHIND OURALIA

Homogeneous control meets heterogeneous recovery: the molecular Ir catalyst is covalently anchored to a metal-oxide support (Fig. 2), so it filters off and is reusable.[4] Catalysts have been anchored to Al_2O_3, ZrO_2, or ITO as nanopowder or film; the fastest Al_2O_3 system runs the model reaction in 15 min at ≥1000 turnovers.[4]

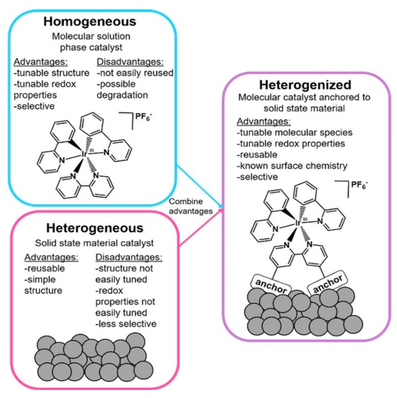


Figure 2. Heterogenized catalysts combine the advantages of homogeneous and heterogeneous catalysis.

Expanded across **five mechanistically distinct reactions** (Fig. 3) at loadings as low as **0.01 mol% Ir**, the heterogenized catalyst runs **faster** than the homogeneous catalyst (Fig. 4) and is reusable ≥5×.[5]

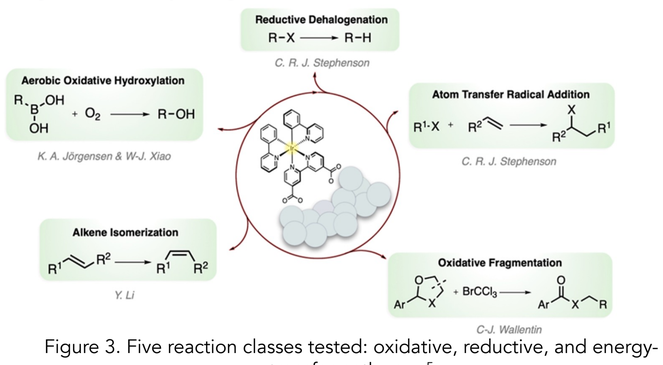


Figure 3. Five reaction classes tested: oxidative, reductive, and energy-transfer pathways.[5]

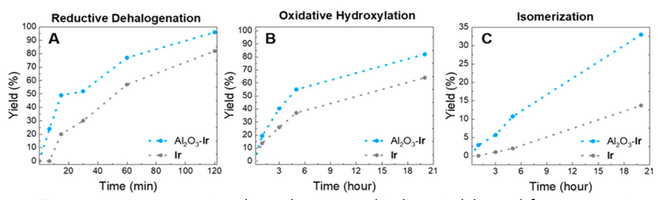


Figure 4. Heterogenized catalysts give higher yields and faster reaction times than homogeneous version.[5]

0.01 mol% lowest Ir loading · **≥1000** turnovers · **5×** catalyst reuse · **99%** gram-scale yield

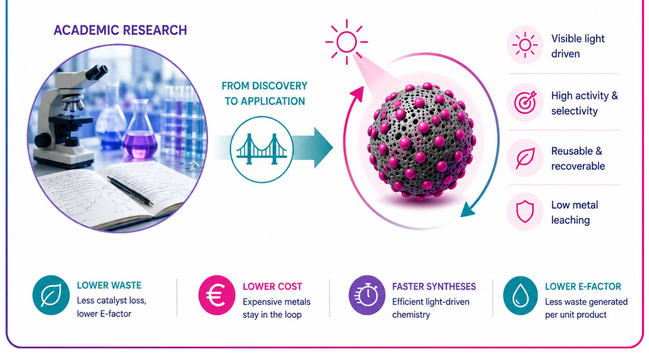
FROM ACADEMIC RESEARCH TO OURALIA

Ouralia builds on the published platform, expanding our catalyst portfolio for peptide post-modification. We achieve reusability and maintain selectivity while keeping a robust catalyst structure.[4,5] The solid catalyst is easily separated from the reaction solution either via filtration (nanopowder) or mechanical extraction (thin film) and can be reused. The catalyst structure can be adapted to your needs and tuned to the desired reactor.

We bring deep expertise, practical know-how, and the agility to accelerate catalyst development.

FROM ACADEMIA TO APPLICATION

Translating academic innovation into a reusable catalyst platform



KEEP THE PERFORMANCE. RECOVER THE CATALYST. REUSE THE PRECIOUS METAL.

APPLICATIONS TOWARD PEPTIDE POST-MODIFICATION

Ouralia's five demonstrated reaction classes map onto high-value peptide transformations. Each card links an established mechanism[5] to a target modification:

THIOL–ENE LIGATION
ATRA / radical addition
ATRA is the closest precedent for radical addition across C=C.[5,6]

DISULFIDE FORMATION / REDUCTION
Oxidative + reductive SET
Both quenching regimes accessible; photoredox cysteine coupling is precedented (oxytocin).[5,1]

DECARBOXYLATIVE C–C
Reductive SET + C-radical chemistry
Reductive activation of Asp/Glu NHPI esters → carbon radical → C–C bond.[5,7,8]

SIDE-CHAIN MODIFICATION
SET / radical diversification
Broad oxidative/reductive radical reactivity for late-stage side-chain edits.[5]

α-AMINO C–H FUNCTIONALIZATION
HAT + radical intermediates
HAT to an **α**-oxy radical models functionalization **α** to nitrogen.[5]

TYROSINE / TRYPTOPHAN MODIFICATION
Oxidative SET / arene functionalization
Oxidative SET → tyrosyl-radical bioconjugation and dityrosine cross-linking.[5,2]

COLLABORATION OPPORTUNITIES

GEN 1 CATALYSTS — AVAILABLE FOR TESTING

Our published reusable Ir photoredox catalysts are available to researchers and companies interested in evaluating the platform in their own chemistry.

JOINT DEVELOPMENT

We are seeking industry partners to jointly develop and validate reusable photoredox catalysts for peptide post-modification and other high-value synthetic applications.

INTERESTED IN TESTING OUR CATALYSTS OR DEVELOPING AN APPLICATION TOGETHER? LET'S TALK.

CONCLUSIONS

Ouralia is turning a published, reusable Ir-photoredox platform into robust catalysts for peptide post-modification and seeking partners to co-develop and validate applications.[4,5]

CONTACT US!

Duilio Bacigalupo, CEO & Co-Founder, duilio@ouralia.se

Dr. Kelly Materna, CTO & Co-Founder, kelly@ouralia.se

Ouralia, Stockholm, Sweden, info@ouralia.se

REFERENCES

1. C. Bottecchia, T. Noël, Chem. Eur. J. 2019, 25, 26–42. DOI: 10.1002/chem.201803074.
2. J. C. Lee, J. D. Cuthbertson, N. J. Mitchell, Org. Lett. 2023, 25, 5459–5464. DOI: 10.1021/acs.orglett.3c01795.
3. N. Kaplaneris, M. Akdeniz, M. Fillols, F. Arrighi, F. Raymenants, G. Sanil, D. T. Gryko, T. Noël, Angew. Chem. Int. Ed. 2024, 63, e202403271. DOI: 10.1002/anie.202403271.
4. K. L. Materna, L. Hammarström, Chem. Eur. J. 2021, 27, 16966–16977. DOI: 10.1002/chem.202101651.
5. R. Lindroth, K. L. Materna, L. Hammarström, C.-J. Wallentin, ACS Org. Inorg. Au 2022, 2, 427–432. DOI: 10.1021/acsorginorgau.2c00024.
6. M. Ahangarpour, I. Kavianinia, P. W. R. Harris, M. A. Brimble, Chem. Soc. Rev. 2021, 50, 898–944. DOI: 10.1039/D0CS00354A.
7. S. Pal, J. Openy, A. Krzyzanowski, A. Noisier, P. 't Hart, Org. Lett. 2024, 26, 2795–2799. DOI: 10.1021/acs.orglett.3c03070.
8. S. J. McCarver, J. X. Qiao, J. Carpenter, R. M. Borzilleri, M. A. Poss, M. D. Eastgate, M. Miller, and D.W. C. MacMillan Angew. Chem. Int. Ed. 2016, 55, 1 – 6. DOI: 10.1002/anie.201608207

Redox-Responsive Peptide Dimers to Stabilize and Release Therapeutic dsRNA

Jannik Keyser Paulus[a], Marvin A. Albers[b], Niall M. McLoughlin[b], Zainab M. Rashid[b], David Dulin[b] and Tom N. Grossmann[a]

a Institute of Organic and Biomolecular Chemistry, Faculty of Chemistry, Georg-August Universität Göttingen, Germany
b Department of Chemistry and Pharmaceutical Sciences and AIMMS, VU Amsterdam, The Netherlands
https://doi.org/10.17952/38EPS.2026.P095

GEORG-AUGUST-UNIVERSITÄT GÖTTINGEN

IN PUBLICA COMMODA

Motivation: Double-stranded RNA (dsRNA) is a key scaffold in antiviral defence, gene regulation, and emerging RNA therapeutics.[1] Moreover, dsRNA-based approaches can access biological targets that are otherwise difficult to modulate.

Problem: Its clinical translation is limited by rapid degradation, low uptake, and immunogenicity.[2] Current stabilization strategies offer only partial solutions and lack a broadly applicable mechanism combining protection with controlled intracellular release.

Our Solution: Natural RNA-binding proteins such as TAV2b[3] provide a structural blueprint for synthetic ligands capable of recognizing dsRNA in a sequence-independent manner. Redox-responsive peptide dimers build on this principle, offering modular RNA binders that not only engage dsRNA but can also modulate its structural and mechanical properties, including twist and flexibility, features increasingly recognized as relevant for stability and delivery. Their redox-sensitive architecture further enables environment-triggered release under intracellular reducing conditions, opening new avenues for stabilizing and deploying therapeutic dsRNA across diverse biomedical applications.

1 Design of RNA Binding Peptides

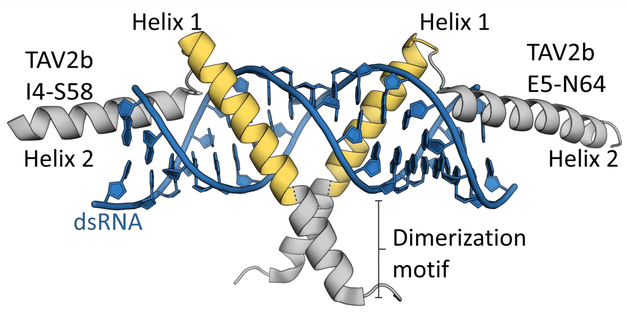


Figure 1 Crystal structure (pdb: 2zi0) of two TAV2b subunits (I4-S58 and E5-N64) bound to dsRNA (blue). Dimerization motif and helices 1 and 2 are indicated. The minimal binding motif is indicated in yellow as also shown in Figure 2A.

- TAV2b is a viral gene-silencing suppressor that binds dsRNA as a non-covalent dimer
- Starting from the native sequence, truncation and peptide stapling strategies were applied to enhance RNA binding and improve dsRNA-stabilizing properties

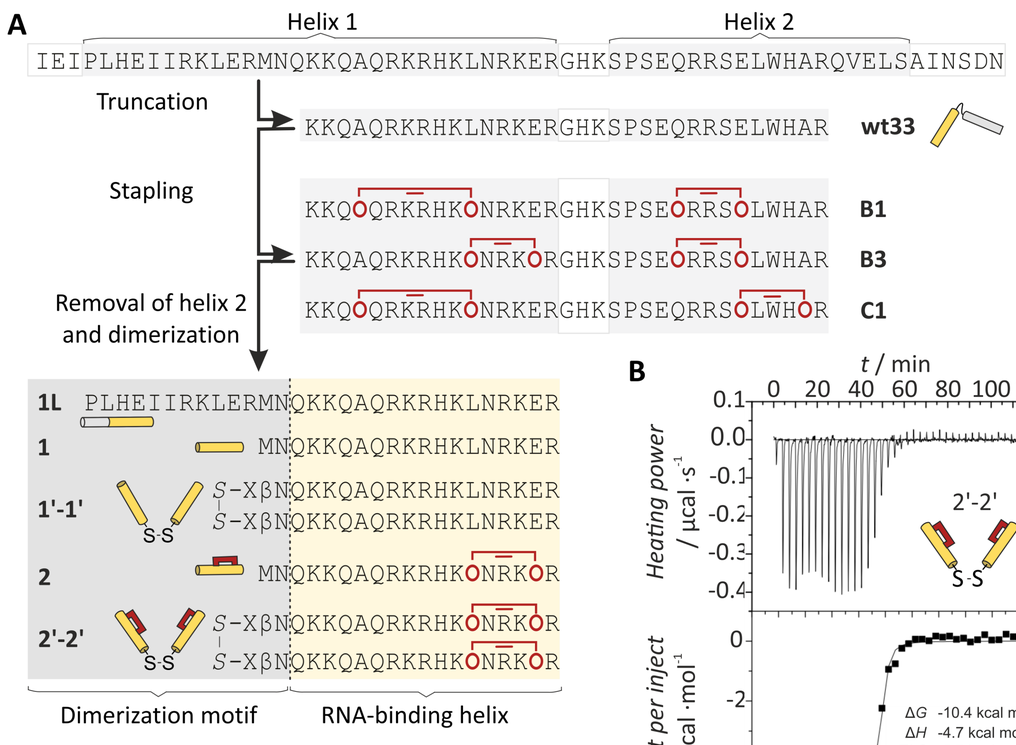


Figure 2 A) Schematic representation of the development process peptide dimer **2′-2′** starting from the native TAV2b crystal structure sequence via truncation studies and stapling of helices 1 and 2. Red O´s indicate staples. B) ITC of **2'-2'** (c= 305 µM) with miR-21 (c= 15 µM) at 30 °C in PBS. C) EMSA of miRNA-21 (c = 3 µM) incubated with **1**, **1'-1'**, **2**, **2'-2'**, **1L** and **wt33** (c= 6 µM), native PAGE, TAE-buffer, SYBR gold stain.

- **B1**, **B3**, and **C1** represent the strongest binders among a panel of 11 stapled peptides and effectively protect dsRNA from degradation[4]
- ITC measurements show that **2′-2′** binds dsRNA with high affinity (K_d = 31.7 nM), exhibiting a 10-fold stronger interaction than **wt33** (K_d = 328 nM)
- Thermal denaturation experiments reveal increased melting temperatures for RNA-peptide complexes formed by **1′-1′** and **2′-2′** compared to their monomers
- **2′-2′** binds dsRNA in a sequence-independent manner and extends the lifetime of miRNA-21 in FBS, preventing degradation for up to 6 hours in 27.5 % FBS at rt[5]

4 References

[1] K. Paunovska *et al.*, *Nat. Rev. Genet*. **2022**, 23, 265
[2] J. N. Shukla *et al.*, *RNA Biol*. **2016**, 13, 656
[3] H.-Y. Chen *et al.*, *EMBO Rep*. **2008**, 9, 754
[4] A. Kuepper *et al.*, *NAR* **2021**, 49, 22, 12622
[5] N. McLoughlin, M. A. Albers *et al.*, *Angew. Chem. Int. Ed.* **2023**, 62, e202308028
[6] Z. M. Rashid *et al.*, *JACS* **2026**, 148(8), 8298

2 RNA Uptake and Release

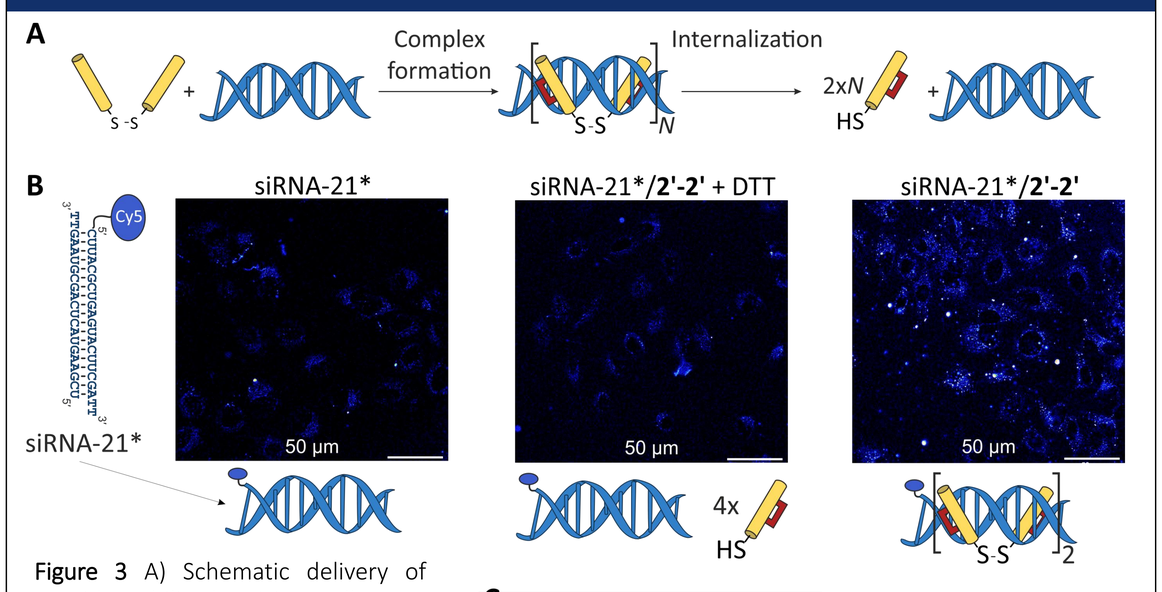
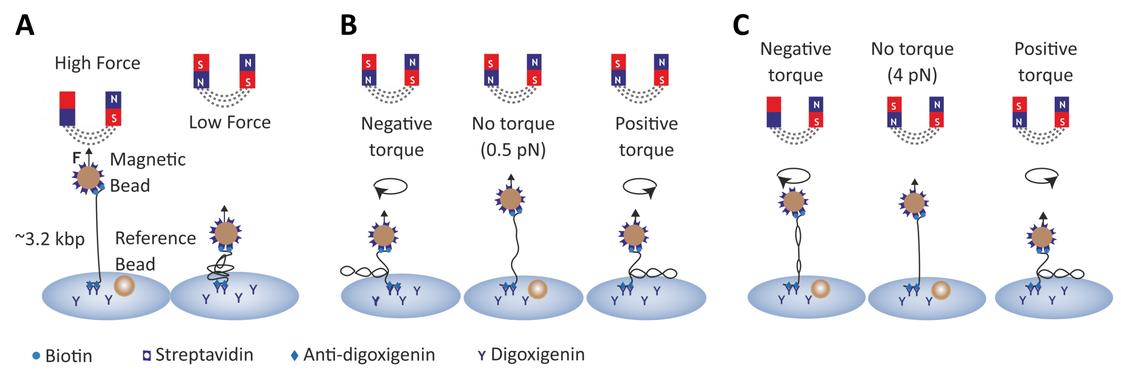


Figure 3 A) Schematic delivery of peptide stabilized RNA into cells. B) Confocal Microscopy of HEK293 cells after incubation with siRNA-21* (c=1 µM) for 1h. Only siRNA-21* (left); siRNA-21* and peptide **2′-2′**pre-treated with DTT (middle); siRNA-21* with **2′-2′** (right). C) LC-MS glutathione cleavage assay. Incubation of peptide **2′-2′** alone (left) or in complex with miRNA-21 (right) together with glutathione (5 mM).

- Cy5 labeled siRNA-21* alone showed low intracellular signal – low uptake
- Increased cellular uptake with **2'-2'**, **1′-1′** revealed similar effect on siRNA uptake
- Prior DTT treatment lowers uptake, similar behavior as shown for siRNA-21* alone
- Disulfide is cleaved under physiological glutathione concentration within 5 min
- EMSA of miRNA-21 co-incubated with peptide dimers **1′-1′** and **2′-2′**and reducing agent TCEP (c= 6, 60 and 600 µM) results in loss of binding[5]

3 Mechanical Modulation of dsRNA



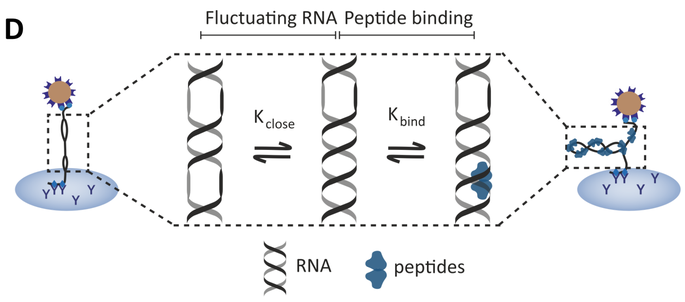


Figure 4 Schematics of magnetic tweezer assay experiments: A) force-extension; B) and C) rotation-extension experiments. D) Schematic of the two-step reaction model in which the RNA fluctuates between double-stranded and melted conformations, followed by peptide binding, which results in plectoneme formation.

- Peptide binding underwinds and elongates dsRNA, with **wt33** and **1′-1′** both increasing contour length and reducing helical twist
- **wt33** softens dsRNA, lowering persistence length and stretch modulus, and stabilizing underwound states = a flexibilizing, dynamic binder
- **1′-1′** induces dsRNA condensation at low forces, remains tightly bound, and releases only under reducing conditions = a compact, redox-controlled binder[6]

➢ Peptide dimers ideal for delivery strategies, offering high-affinity binding, compaction, and controlled cytosolic release

Karlsruhe Institute of Technology

Institute of Biological Interfaces (IBG-2), Department of Molecular Biophysics
Institute of Organic Chemistry (IOC), Department of Biochemistry

https://doi.org/10.17952/38EPS.2026.P501

Photoisomerization-Dependent Glycan Binding of Engineered Lectin-like Peptides: Toward Light-Controlled Bioactivity of Lectins.

Serhii Kharchenko[1], I. Semchuk[2,3], A. Cherednichenko[4],V. Hryhorieva[2,3], S. Afonin[1], I. V. Komarov[3,4,5], Anne S. Ulrich[1,6]

[1]*Karlsruhe Institute of Technology, Institute of Biological Interfaces 2, Karlsruhe, Germany*
[2]*Nonprofit Organization "National Cancer Institute," Kyiv, Ukraine*
[3]*Taras Shevchenko National University of Kyiv, Kyiv, Ukraine.*
[4]*Enamine Ltd., Kyiv, Ukraine*
[5]*Lumobiotics, Karlsruhe, Germany*
[6]*Karlsruhe Institute of Technology, Institute of Organic Chemistry, Karlsruhe, Germany*

Aim

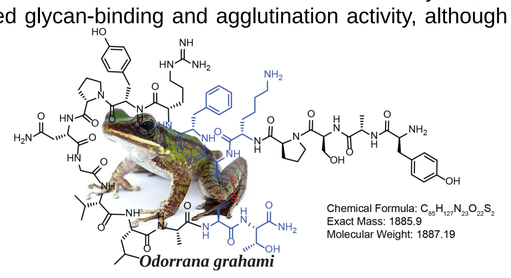
To uncover the molecular and conformational principles that govern glycan recognition by lectin-like peptides, with Odorranalectin serving as a model scaffold, and to determine how backbone preorganization, rigidity, and macrocycle topology shape biological activity. These structure-activity relationships were further exploited to guide the rational design of photoresponsive diarylethene-containing macrocycles, aiming to achieve reversible, light-controlled modulation of peptide conformation and glycan-binding function.

Odorranalectin

Odorranalectin [1] represents a compact lectin-like peptide scaffold for studying structure-dependent glycan recognition. Our systematic re-evaluation showed that, although several previously reported glycan interactions could not be reproduced, native Odorranalectin retained binding to selected glycans and displayed additional interactions with serum proteins. Structural studies further indicated a preference for a rigid β-turn-like conformation rather than a classical lectin fold, suggesting that conformational preorganization is an important determinant of its molecular recognition properties. This concept was further supported by a series of Odorranalectin-derived macrocycles, in which increased structural rigidity was associated with enhanced glycan-binding and agglutination activity, although excessive activity also introduced safety-related effects.

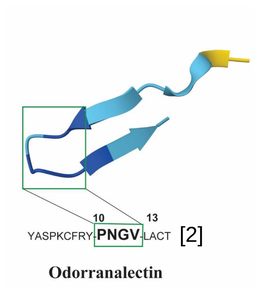
The main literature data are given below:

- Odorranalectin is a 17-residue disulfide-constrained peptide (YASPKCFRYPNGVLACT) from *Odorrana grahami*.
- NMR shows a β-turn structure stabilized by a S6-S16 bond.
- It is plasma-stable, low toxicity / low cytotoxicity.
- Binding specificity was tested by hemgglutination-inhibition and SPR assays.
- Only L-fucose inhibited agglutination [1].



Chemical Formula: $C_{85}H_{127}N_{23}O_{22}S_2$
Exact Mass: 1885.9
Molecular Weight: 1887.19

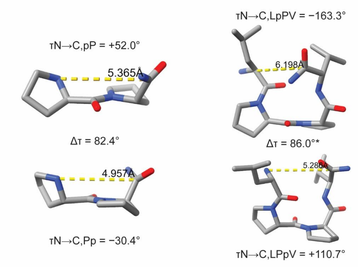
Derivatives of Odorranalectin



№	Sequence	Modification	K_D, ASF
1	**YASPKCFRYPNGVLACT**	native	356μM
2	YASPKC**f**RYPNGVLACT	f	973μM
3	TCALVGNPYRFCKPSAY	revers	n/a
4	YASPKCFRY**pP**GVLACT	pP	417μM
5	YASPKCFRY**Pp**GVLACT	Pp	840μM
6	YASPKCFRYPNG**pP**ACT	pP	3.14mM
7	YASPKCFRYPNG**Pp**ACT	Pp	3.75mM
8	YASPKCFRY**LpPV**GVLACT	LpPV	1.37mM
9	YASPKCFRY**LPpV**GVLACT	LpPV	126μM
10	YASPKCFRYPNG**LpPV**ACT	LPpV	594μM
11	YASPKCFRYPNG**LPpV**ACT	LPpV	3.75mM
12	YASPKCFRY**LpPV**LACT	LPpV	1.97mM
13	YASPKCFRY**LPpV**LACT	LPpV	611μM
14	YASPKCFR**LpPV**GVLACT	LPpV	1.40mM
15	YASPKCFR**LPpV**GVLACT	LPpV	539μM

P = L-Pro; p = D-Pro; f-D-Phe

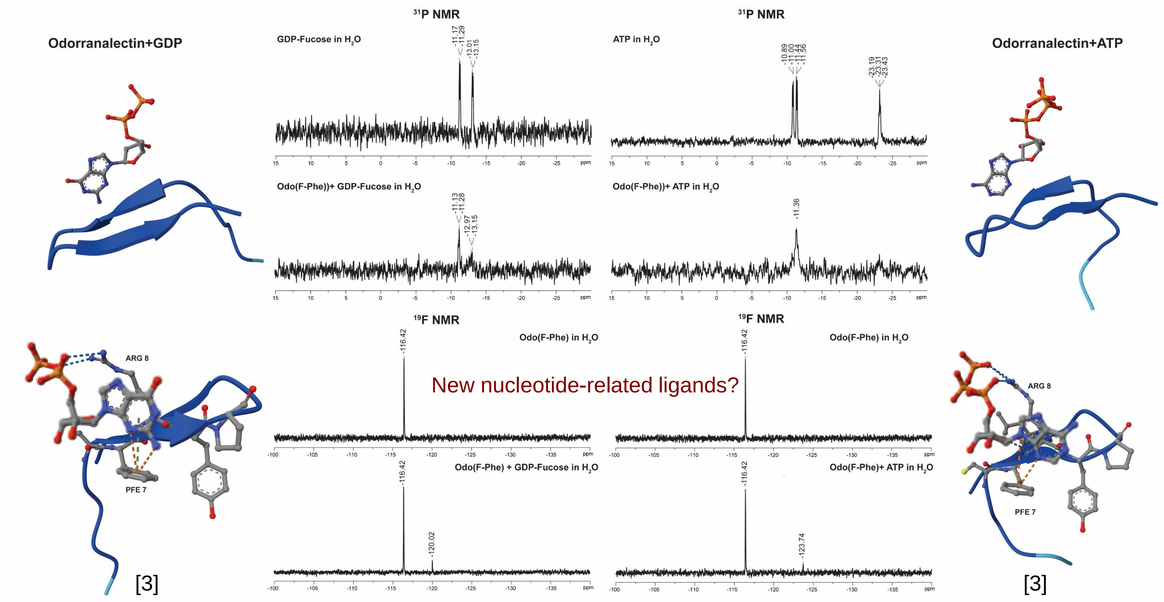
Model based on pseudo-dihedral angle



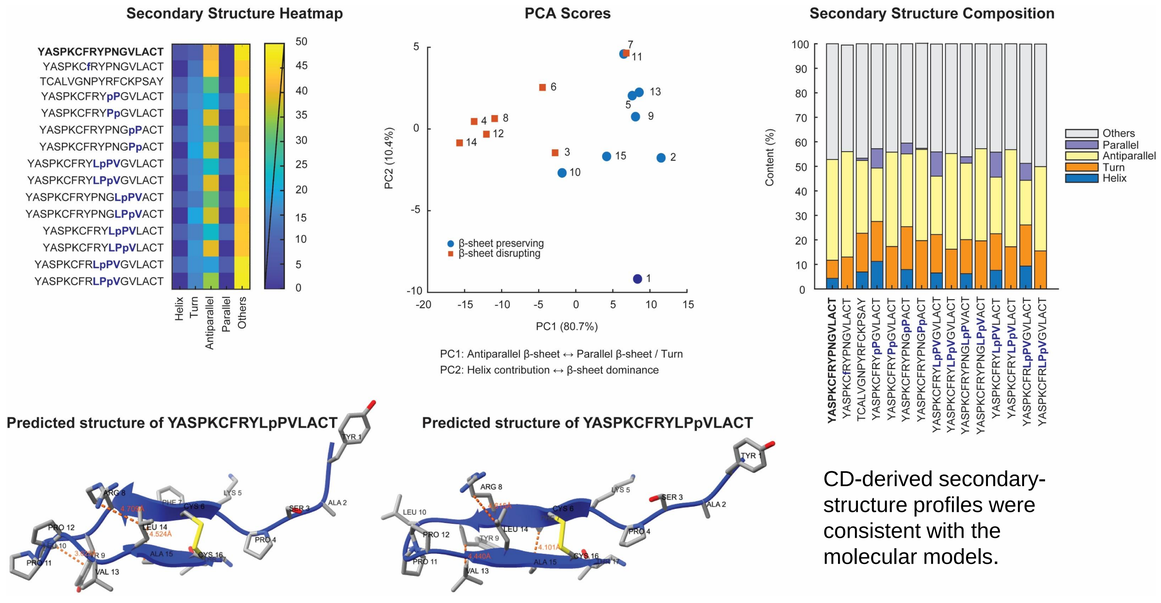
*For τN→C, the shortest angular difference was used because dihedral angles are periodic.

We established a conformational model library of Odorranalectin analogues incorporating pP/Pp and LpPV/LPpV motifs to determine how peptide preorganization influences biological activity. We then used the resulting structure–activity relationships as a predictive framework for diarylethene-containing derivatives, enabling prediction of activity from their light-dependent conformational state, backbone geometry, and degree of structural preorganization.

Nucleotide-related ligand interactions

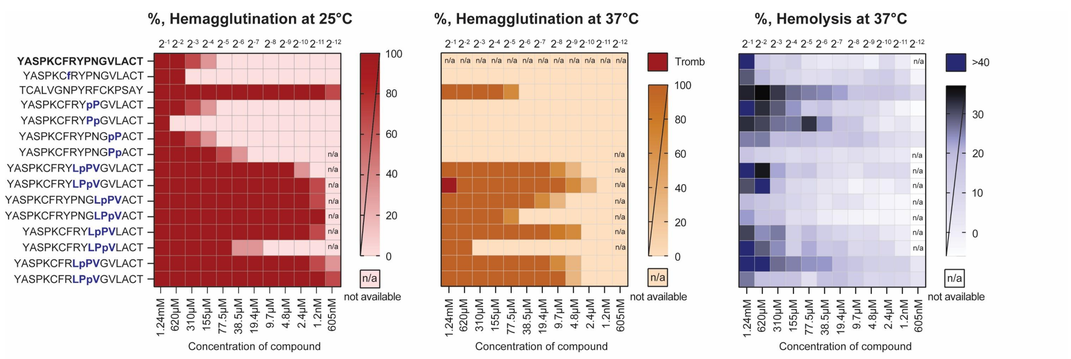


Secondary structure



CD-derived secondary-structure profiles were consistent with the molecular models.

Hemagglutination, hemolysis, toxicity



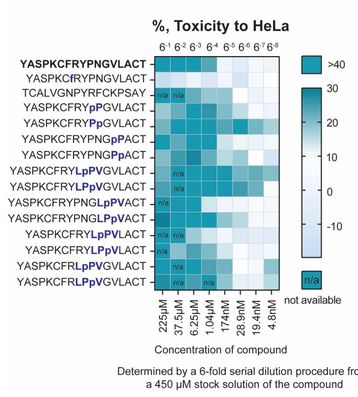


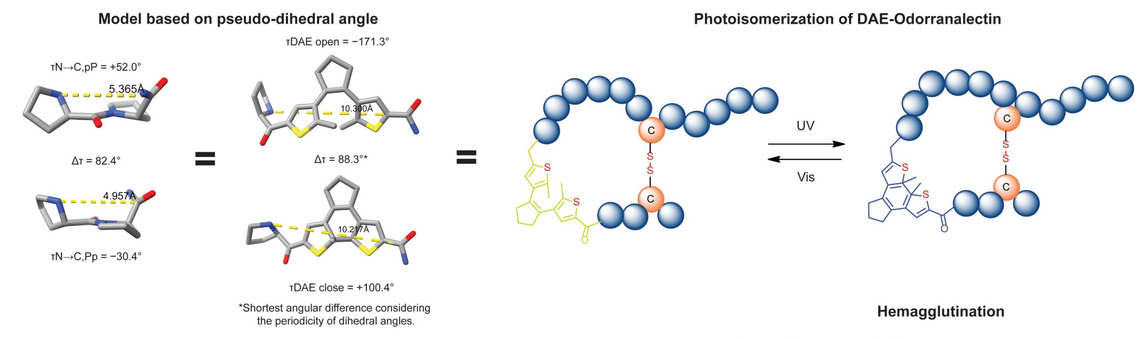
Table Inhibition of hemagglutination by monosaccharides, ATP, Inosytol

№	Sequence	Modification	L-Fuc, mM	D-Fuc, mM	L-Gal, mM	D-Gal, mM	ATP, mM	Inosytol, mM
1	**YASPKCFRYPNGVLACT**	native	+ n/a +/- n/a	+ n/a +/- n/a	+ n/a n/a n/a	n/a n/a n/a n/a	+ +/- +/- n/a	+/- n/a +/- n/a
6	YASPKCFRYPNG**Pp**ACT	pP	+ + + +	+ + + +	n/a n/a n/a n/a	n/a n/a n/a n/a	+ + + +	n/a n/a n/a n/a
7	YASPKCFRYPNG**PP**ACT	Pp	+ + + +	+ + + +	+ + + +	+ + + +	+ + + +	+ + + +
12	YASPKCFRY**LpPV**LACT	LPpV	+ + + +	+ + + +	+ + + +	+ + + +	+ + + +	+ + + +
13	YASPKCFRY**LPpV**LACT	LpPV	+ + + +	+ + + +	+ + + +	+ + + +	+ + + +	+ + + +
14	YASPKCFR**LpPV**GVLACT	LPpV	- - - -	- - - -	- - - -	- - - -	+ + + -	+ - - -
15	YASPKCFR**LPpV**GVLACT	LpPV	- - - -	- - - -	- - - -	- - - -	+ + - -	- - - -

+ Hemagglutination inhibition
- None hemagglutination inhibition
+/- Partial Inhibition of Hemagglutination
n/a not available

The library-derived analogues did not discriminate between the tested sugar enantiomers.

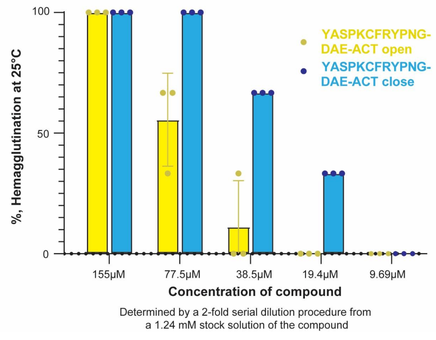
DAE-Odorranalectin



Conclusion and Outlook

The conformational model successfully reproduced the activity trends observed for the diarylethene-containing derivatives, supporting its use as a predictive framework for photoresponsive peptide design. Sugar-inhibition studies will be performed to further validate the glycan-recognition mechanism, while future work will extend this approach to larger lectin systems, including UEA-I (*Ulex europaeus agglutinin I*). Importantly, the concept will not be limited to diarylethene photoswitches, but will be expanded toward alternative photoresponsive scaffolds to enable broader and more versatile light-controlled modulation of lectin–glycan interactions.

Hemagglutination



References:

1. Li, J.X., et al., *Odorranalectin Is a Small Peptide Lectin with Potential for Drug Delivery and Targeting.* Plos One, 2008. **3**(6).
2. The UniProt Consortium , UniProt: the Universal Protein Knowledgebase in 2025, *Nucleic Acids Research*, Volume 53, Issue D1, 6 January 2025, Pages D609–D617.
3. Jumper, J., Evans, R., Pritzel, A. *et al.* Highly accurate protein structure prediction with AlphaFold. *Nature* **596**, 583–589 (2021).

Acknowledgements and contact information

Prof. Dr. Anne S. Ulrich, Dr. Birgid Langer, Dr. Tamta Turdzeladze, Dr. Torsten Walther, Anton Cherednichenko, Iryna Semchuk, Nataliia Petlovana, Dr. Sergiy Afonin, Prof. I. V. Komarov, All members of AK Ulrich

Funded by the European Union

MSCA 4 UKRAINE

Alexander von HUMBOLDT STIFTUNG

This project has received funding through the MSCA4Ukraine project, which is funded by the European Union. Views and opinions expressed are however those of the author(s) only and do not necessarily reflect those of the European Union, the European Research Executive Agency or the MSCA4Ukraine Consortium. Neither the European Union nor the European Research Executive Agency, nor the MSCA4Ukraine Consortium as a whole nor any individual member institutions of the MSCA4Ukraine Consortium can be held responsible for them.

Contact information:

Stereochemistry vs Linker: Exploration of Ring C Analogues of Antimicrobial Peptide Nisin

Fiona L. Kinnis,[1] William T. P. Darling,[2] Máté Erdélyi,[2] Alethea B. Tabor.[1]

[1]Department of Chemistry, University College London, London, WC1H 0AJ, U.K. [2]Department of Chemistry–BMC, Uppsala University, Uppsala, 751 23, Sweden.

https://doi.org/10.17952/38EPS.2026.P226

Introduction

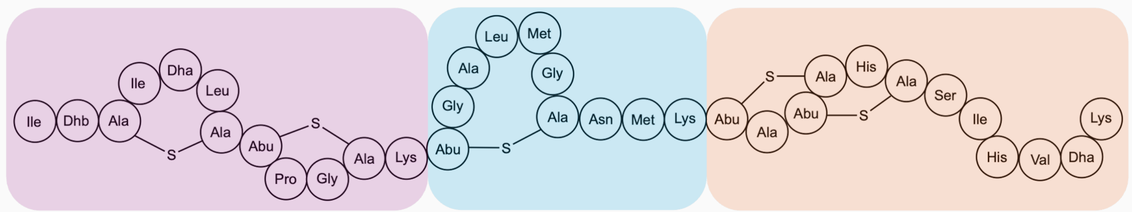
- Due to the rapidly increasing rate of resistance emerging against conventional antibiotics, which vastly exceeds the rate of novel therapeutic development, humanity is approaching a "post-antibiotic era".[1]
- Membrane-active macrocyclic peptides are a potential class of antimicrobial agents to address this gap in the antimicrobial development space.
- The lantibiotic nisin is a polycyclic peptide with broad-spectrum activity against Gram-positive bacteria, targeting lipid II to form stable pores composed of eight nisin and four lipid II molecules.[2]
- The complex structure of nisin is distinguished by five thioether-bridged rings, A–E, which are formed from the bis-amino acids lanthionine and methyllanthionine.

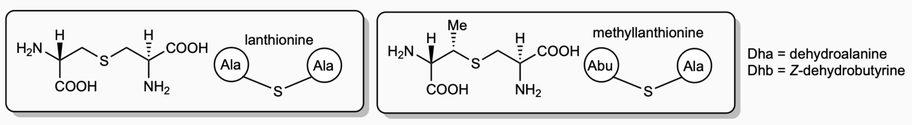
Aims

- Does ring C undergo a conformational change when entering the non-polar membrane environment?[4]
- Is the mode of action of nisin partly a function of the conformation(s) of ring C in the membrane?
- Do alterations of nisin's structure in the membrane environment facilitate its interaction with lipid II?

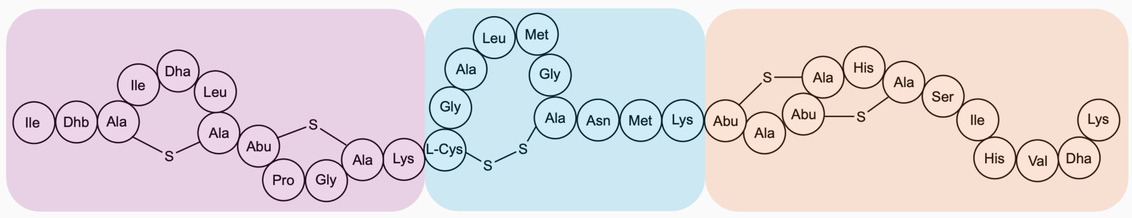
Analogues

Wild-type nisin

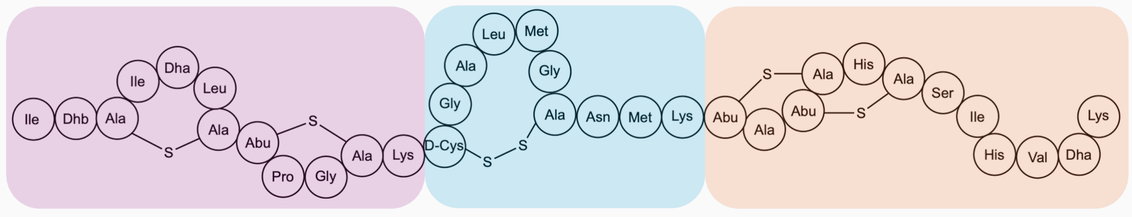


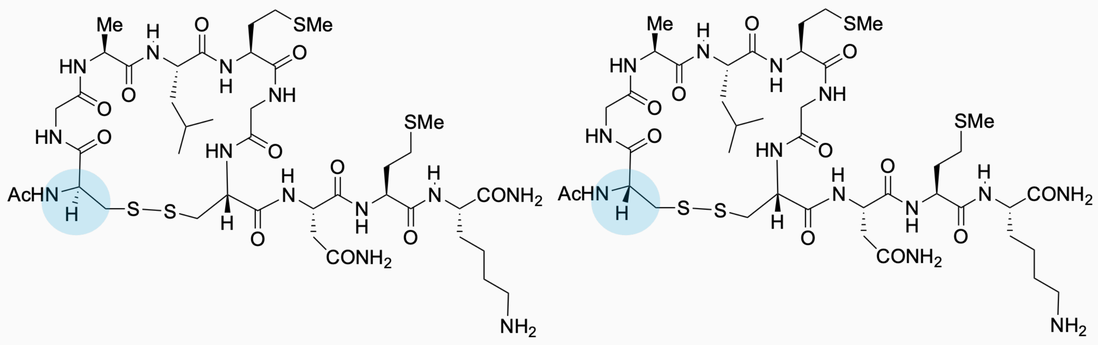


Disulfide mutant with inverted stereochemistry – inactive[3]



Disulfide mutant with native stereochemistry – active?

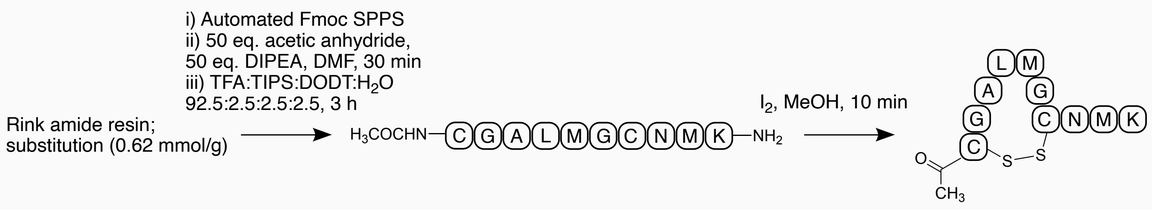




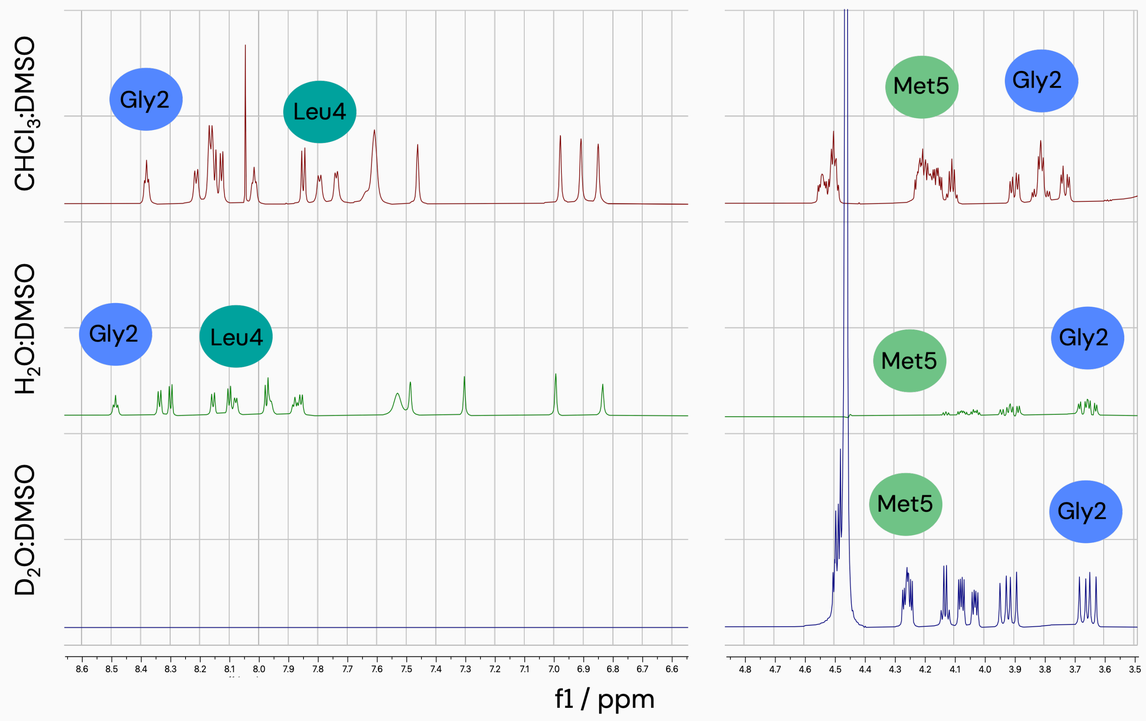
Analogue 1
(D,L)-Cys residues

Analogue 2
(L,L)-Cys residues

Synthesis of Analogues 1 and 2



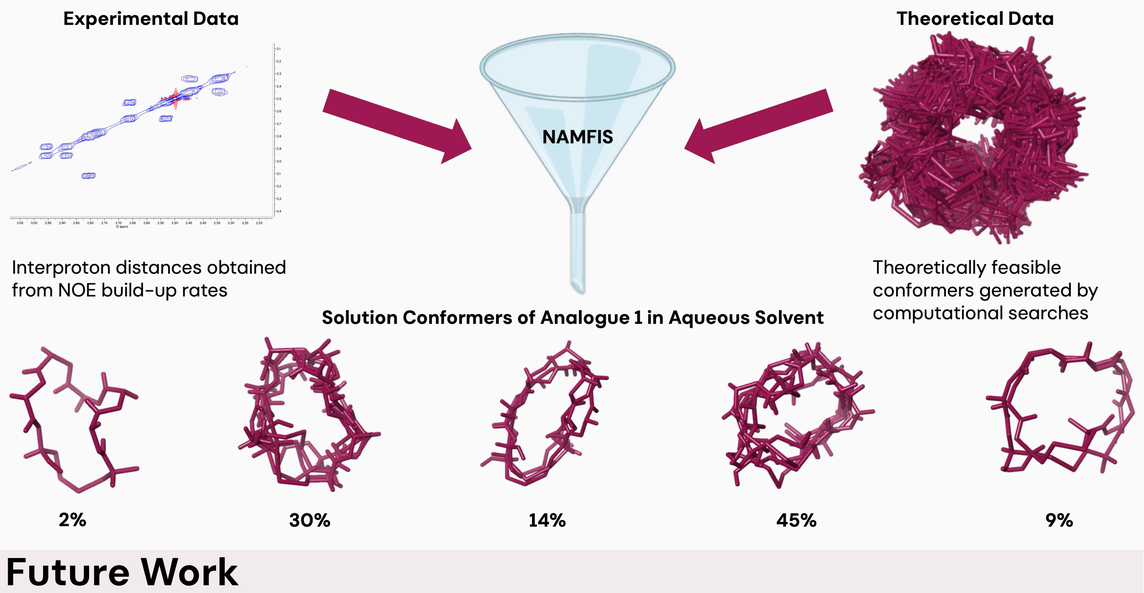
Chemical Shift Perturbations of Analogue 1 in Membrane-Like and Aqueous Solvents



Results

- Chemical shift perturbations in the 1D proton spectra between solvent systems indicate that Analogue 1 may be adopting different conformations depending on its environment.
- Solution ensembles determined by the NMR Analysis of Molecular Flexibility in Solution (NAMFIS)[5] algorithm suggest that Analogue 1 is a partial molecular chameleon.

NAMFIS Workflow



Future Work

- Develop semi-synthetic full-length hybrid nisin analogues to investigate if the disulfide mutants retain native activity levels against Gram-positive bacteria.
- Inform the development of subsequent analogues which retain the native, cyclic structure of the peptide family whilst increasing their antimicrobial activity.

1. World Health Organisation. Antimicrobial resistance: global report on surveillance. 2014. 2. E. Breukink and B. de Kruijff, *Nat. Rev. Drug. Discov.* 2006, 5, 321–323. 3. C. van Kraaij *et al. Eur. J. Biochem.* 2000, 267, 901–909. 4. J. Medeiros-Silva *et al. Nat. Commum.* 2018, 9, 3963. 5. L.H.E. Wieske *et al. Nat. Rev. Chem.* 2023, 7, 511–524.

Supported by the BBSRC and the RSC.

https://doi.org/10.17952/38EPS.2026.P203

NEW PEPTIDE-BASED VACCINES TO TARGET MELIOIDOSIS

Krisztina Kiss[1], Julen Tomás-Cortázar[2], Siobhán McClean[2], Viktor Farkas[3], Kata Horvati[1]

[1]MTA-HUN-REN TTK "Momentum" Peptide-Based Vaccines Research Group, Institute of Materials and Environmental Chemistry, Research Centre for Natural Sciences, Budapest, Hungary
[2]UCD Conway Institute, University College Dublin, Belfield, Dublin, Ireland
[3]HUN-REN - ELTE Protein Modeling Research Group, Eötvös Loránd University, Budapest, Hungary

MTA–HUN-REN TTK Momentum Peptide-Based Vaccines Research Group

Introduction

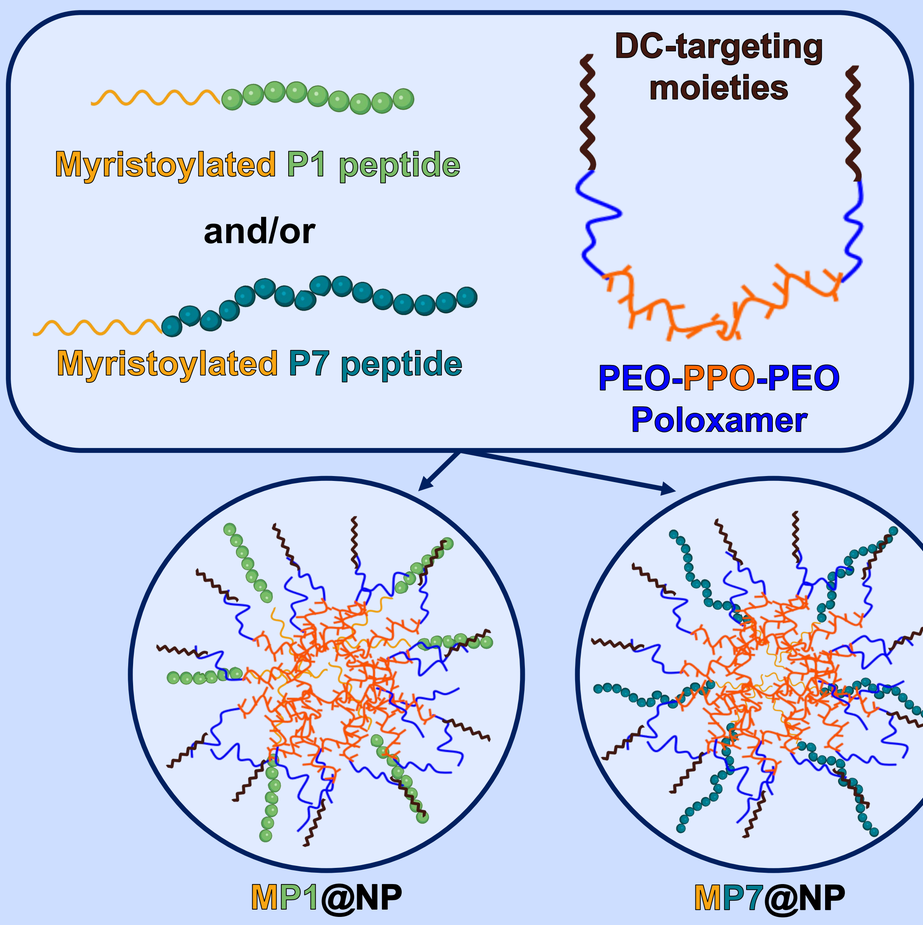
Melioidosis, which is caused by *Burkholderia pseudomallei*, was originally considered as a relatively rare human disease, however recent studies estimate approximately 165.000 cases per year, with up to 45% fatality rate. To make matters worse, comorbidities, like diabetes – which increases the risk factor by 12-fold – or climate change and severe weather events – which promotes the spread of *B. pseudomallei* geographically beyond the tropical and subtropical regions where it is endemic – increase future outbreaks. Due to these factors, over the next decade, the number of cases will increase globally, and *B. pseudomallei* will spread from the original Asian region even to Europe.[1]

Recently, two new proteins have been discovered, the protective BpOmpW[2] and BpPhbB, which are promising in vaccine research, because they stimulate relevant immune responses to combat melioidosis infection[3]. Epitope peptides were subsequently identified from the above-mentioned proteins (**P1** and **P7**), that can trigger IFN-γ responses in CD4+, CD8+ and NKT cells. Compared to expressed proteins, peptides have several advantages for vaccine antigens, as they can elicit a more precise immune response, thus making them safer with wider applicability, and they can be produced more efficiently without potential bio-contamination and do not require refrigerated transport.

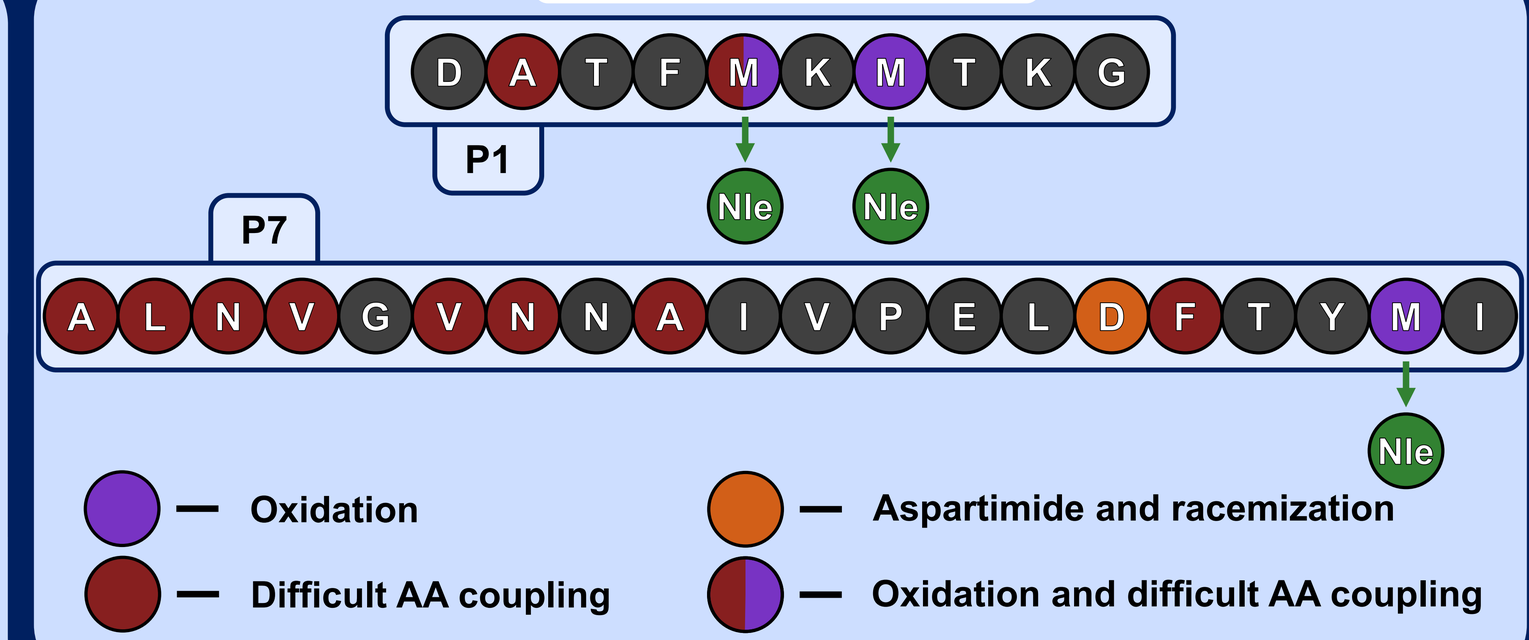
Aims

Develop vaccine candidates from P1 (DATFMKMTKG) and P7 (ALNVGVNNAIVPELDFTYMI) peptides

Apply nanovaccine design strategies[4]



Synthetic challenges

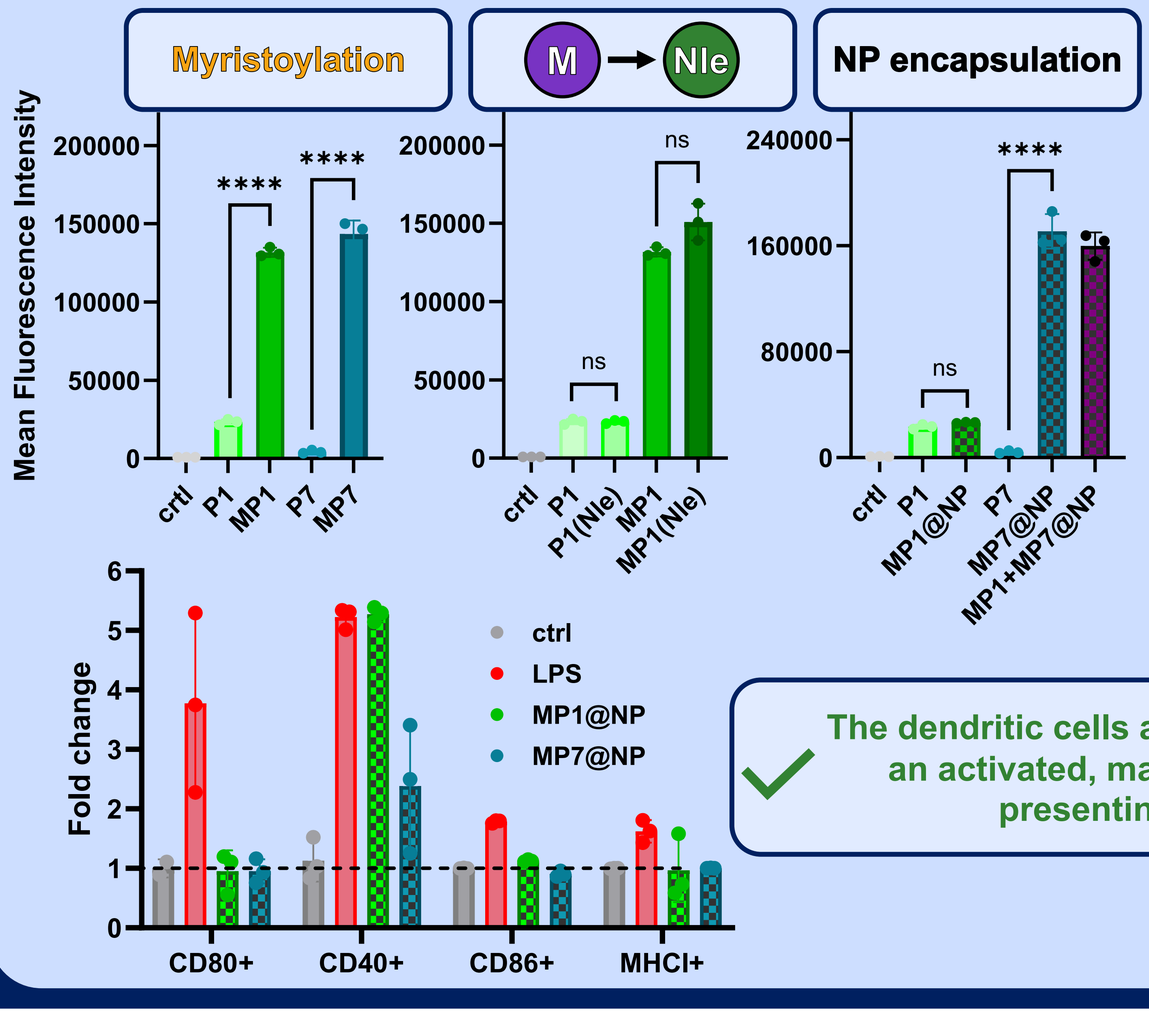


Synthetic solutions – P7 peptide

Classical „batch" type SPPS automated synthesizer - RevoPSy[5]	Continuous flow SPPS synthesizer[6]
Difficult AA coupling	Difficult AA coupling
✓ Double coupling	✓ Heat assisted single coupling
Aspartimide and racemization	Aspartimide and racemization
✓ 0.1M HOBt 2-2% DBU-pip Fmoc deprotection, RT 3x5 min	✓ Fmoc-Asp(OBno)-OH and Fmoc-(Dmb)Gly-OH
40.3% crude purity	58.5% crude purity

However, same desired product amount / mg crude peptide!!!

Nanovaccine design - step by step improvements



✓ **Improved cellular uptake**

✓ **The dendritic cells are shifted toward an activated, mature, antigen-presenting state**

Summary

We have demonstrated that the selected peptides can be produced with good purity using improved synthetic methods both with classical „batch" and with continuous flow SPPS.

From the perspective of cell recognition, the replacement of Met with a non-oxidizable Nle is permitted.

Moreover, we have shown that myristoylation provides a self-adjuvating property, and the DC-targeting poloxamer (PEO-PPO-PEO) encapsulation further improved the *in vitro* efficacy of the modified peptides.

Acknowledgement:
This work was supported by the Lendület (Momentum) Programme of the Hungarian Academy of Sciences (LP2021-28), NKFIH, 2024-1.2.9-NETWORKING-2024-00005 and the COST Action CA2311-SNOOPY 'Searching for Nanostructured or pOre fOrming Peptides for therapY' and VALIDATE Pump-Priming Grant (March 2019) led by Julen Tomás-Cortázar.

https://doi.org/10.17952/38EPS.2026.P364

NOVEL MACROCYCLIC PEPTIDE-BASED UPAR-TARGETING FLUORESCENT PROBES FOR INTRAOPERATIVE FLUORESCENCE IMAGING

T. Treiberg[1,2], N. Hajib[1], K. K. Sørensen[2], M. B. Thygesen[2], K. Stræde[1], K. J. Jensen[2] & A. Kjaer[1]

[1]Department of Clinical Physiology and Nuclear Medicine & Cluster for Molecular Imaging, Copenhagen University Hospital – Rigshospitalet & Department of Biomedical Sciences, University of Copenhagen, Denmark
[2]Department of Chemistry, University of Copenhagen, Denmark

INTRODUCTION

- Intraoperative fluorescence imaging is a promising approach for real-time visualization of malignant tissue during surgery through the use of targeted fluorescent probes[1].
- The urokinase-type plasminogen activator receptor (uPAR) exhibits a desirable expression pattern on the surface of several tumor types and tumor-associated tissue, making it an attractive target for intraoperative fluorescence imaging[2].
- The development of uPAR-targeting peptides with high potency towards the receptor could facilitate the construction of peptide-based fluorescent probes and expand the imaging toolbox.
- Aim: Develop novel macrocyclic peptide-based uPAR-targeting fluorescent probes based on a known uPAR-targeting peptide AE344[3].

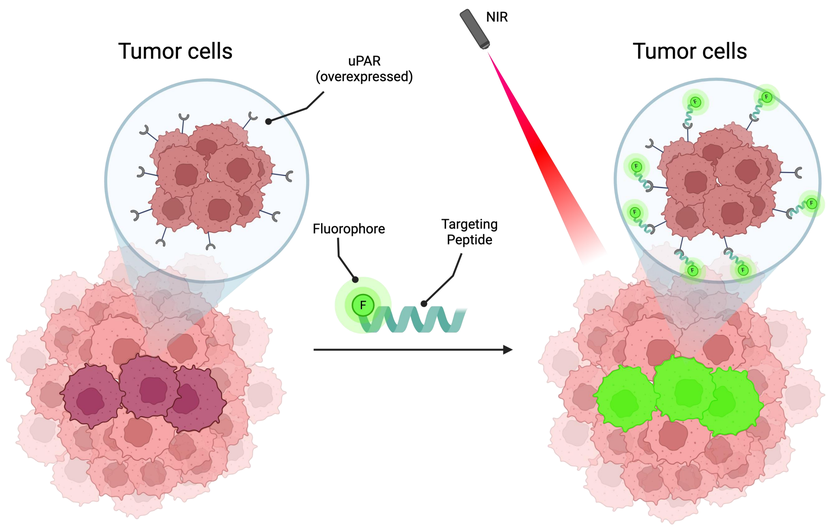


Figure 1. Illustration of intraoperative fluorescence imaging.

RESULTS

- We designed and synthesized a series of bis-thioether-linked macrocyclic uPAR-targeting peptides using cysteine cross-linking. Systematic variation of amino acid composition of AE344 and linker structures yielded 36 new uPAR-targeting peptides.
- The used linker structures were bis-electrophiles, like dibromoxylenes and dibromoketones.
- The direct binding of the peptides towards uPAR was thereafter evaluated in real time using surface plasmon resonance (SPR). The data revealed a favorable position for the macrocyclisations, and the most suitable linker structure.

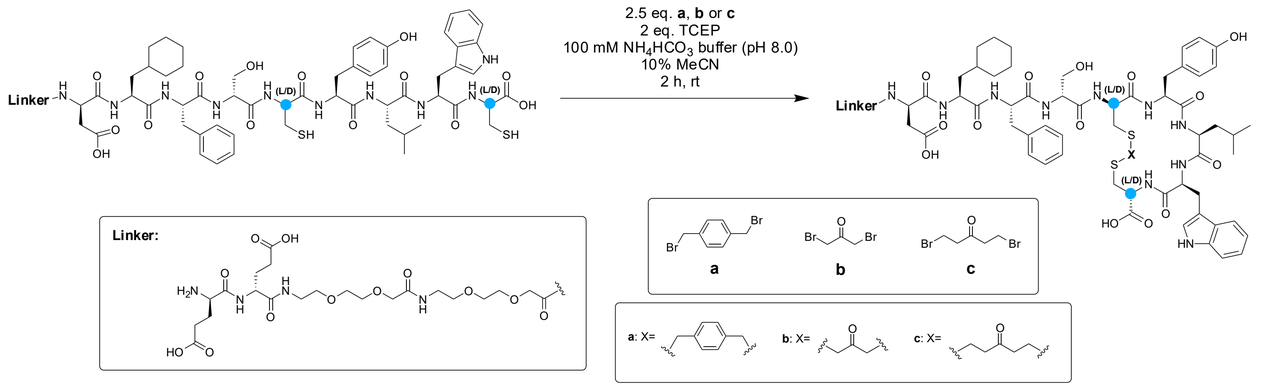


Figure 2. Reaction scheme of cysteine bis-alkylation of AE344 derivatives in solution. The blue dot represents the position of varying cysteine chirality. The left box represents a solubility linker, the upper right box the used dibromo reagents a, b and c. The lower right box represents the introduced linkage corresponding to the used reagent.

Table 1. Representation of a selection of macrocyclic uPAR-targeting peptides with a bis-thioether-linkage between positions 9 and 13[a] and kinetic parameters of peptide-uPAR interactions[b]

Peptide	Sequence	K_D (nM)	k_a (±SE) (10^5 $M^{-1}s^{-1}$)	k_d (±SE) (10^{-3} s^{-1})
AE344	E-E-O2Oc-O2Oc-D-Cha-F-s-r-Y-L-W-S	132	2.22±0.15	29.3±1.9
5b	E-E-O2Oc-O2Oc-D-Cha-F-s-C(O)-Y-L-W-C	70	3.04±0.06	21.2±0.22
6b	E-E-O2Oc-O2Oc-D-Cha-F-s-C(O)-Y-L-W-c	61	2.27±0.09	13.9±0.26
7b	E-E-O2Oc-O2Oc-D-Cha-F-s-C(O)-Y-L-W-C	75	3.70±0.09	27.9±0.36
8b	E-E-O2Oc-O2Oc-D-Cha-F-s-C(O)-Y-L-W-c	97	2.33±0.08	22.6±0.39

[a] All peptides are C-terminal acids. [b] Direct binding kinetics of all peptides were determined by SPR. The equilibrium dissociation constant (K_D) and the association (k_a) and dissociation (k_d) rates were determined from sensorgram fitting to a 1:1 interaction model. Standard errors (SE) are obtained from the fitting procedure.

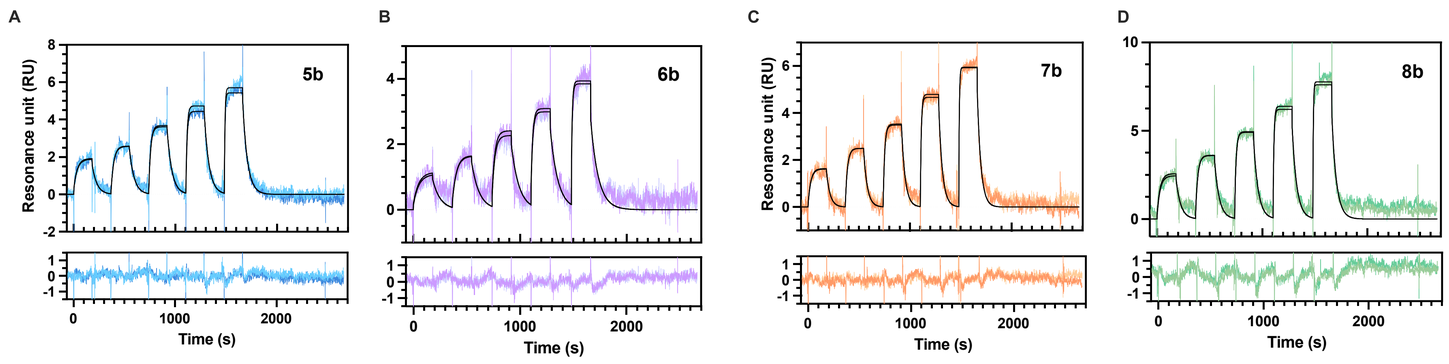


Figure 3. Direct binding kinetics of peptide-uPAR interactions analyzed by SPR. The single-cycle injections represent five consecutive injections of each analyte 5b-8b in varying concentrations. The analysis is performed in duplicates, the curve fitting to a simple 1:1 interaction model is marked with a black line. The residuals are shown in the graphs below each sensorgram.

- Selected high affinity peptides **5b** and **7b** were fluorescently labelled with a near-infrared dye IRDye800CW, yielding two novel fluorescent probes.

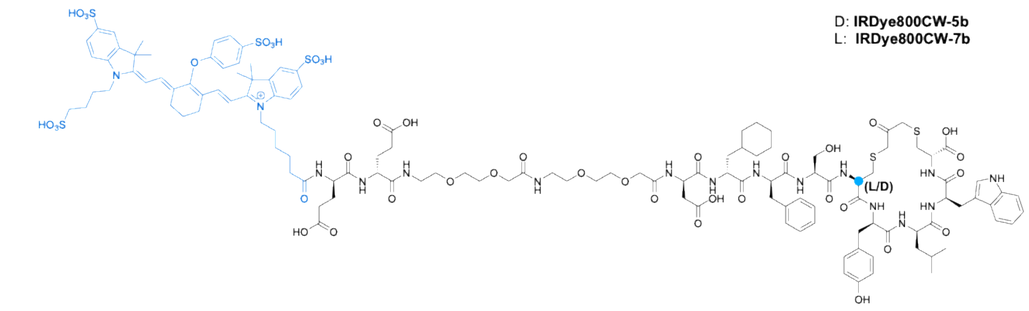


Figure 4. Structures of novel fluorescent probes IRDye800CW-5b and IRDye800CW-7b. IRDye800CW is indicated in blue.

- Exposure of the novel probes to chymotrypsin demonstrated enhanced proteolytic stability compared to a linear control probe.

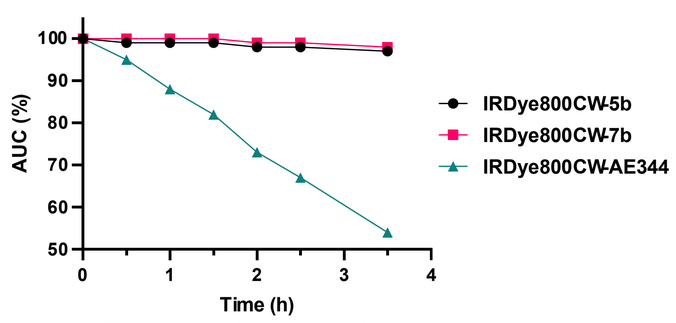


Figure 5. Fluorescent probe stability against chymotrypsin over time.

- Evaluation of the efficacy of the novel fluorescent probes in an *in vivo* fluorescence imaging study in a subcutaneous human glioblastoma xenograft tumor mouse model showed evident accumulation of the probes in uPAR-expressing tumors *in vivo* and *ex vivo*.

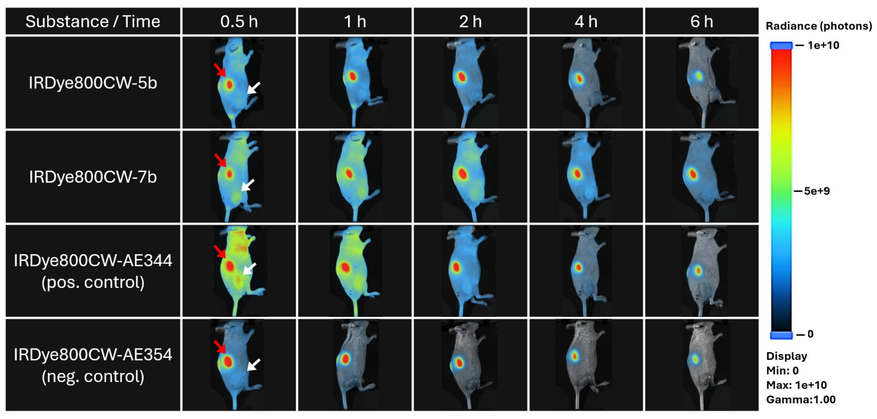


Figure 6. Dynamic *in vivo* images of tumor-bearing mice. Uptake in kidneys is indicated by a red arrow, while uptake in the flank tumor is indicated by a white arrow.

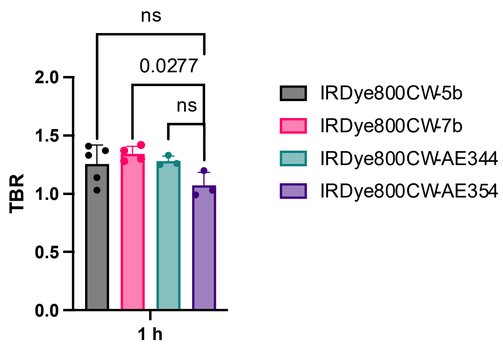


Figure 7. Tumor-to-background ratios (TBR) derived from *in vivo* fluorescent images. TBR calculations are based on the mean (ph/s/cm²/sr) for the signal and background.

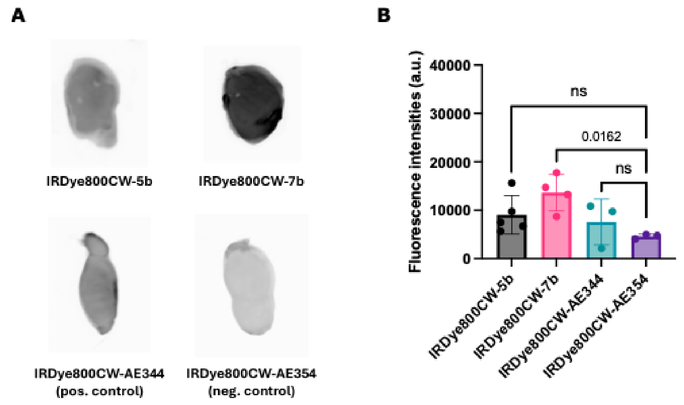


Figure 8. *Ex vivo* images of dissected tumors (A) and comparison of their mean fluorescence intensities (B).

CONCLUSION

- We designed and synthesized a series of macrocyclic uPAR-targeting peptides. Evaluation of peptide-uPAR interactions revealed a favorable position in the peptide sequence for macrocyclisations, and the most suitable linker structure.
- Two macrocyclic peptides with improved binding affinities were labelled with a near-infrared fluorophore IRDye800CW.
- Exposure of the novel probes to chymotrypsin demonstrated enhanced proteolytic stability compared to a linear control probe.
- Both developed probes showed evident accumulation in uPAR-expressing tumors *in vivo* and *ex vivo*.
- We anticipate that the developed fluorescent probes represent promising candidates for clinical translation.
- Further studies investigating probe pharmacokinetics and biodistribution in a more complex tumor model could substantiate their translational potential.

References:
1. Stewart, H. L. & Birch, D. J. S. Fluorescence Guided Surgery. *Methods Appl Fluoresc* **9**, (2021).
2. Zhai, B. T. *et al.* Urokinase-type plasminogen activator receptor (uPAR) as a therapeutic target in cancer. *J Transl Med* **20**, (2022).
3. Kurbegovic, S. *et al.* IRDye800CW labeled uPAR-targeting peptide for fluorescence-guided glioblastoma surgery: Preclinical studies in orthotopic xenografts. *Theranostics* **11**, 7159–7174 (2021).

Engineering Softness: How Molecular Tweaks in Coiled Coils Shape Hydrogel Behavior

Annelie Puhlmann[1a)], Cihan Baydaroglu[2], Merten Strehlau[2], Santiago Andres Ardila Fernandez[1a)], Boris Schade[1b)], Michael Gradzielski[2] and Beate Koksch[1a)]

1a) Institute of Chemistry and Biochemistry, Freie Universität Berlin, Arnimallee 20, 14195 Berlin, Germany
b) Research Center of Electron Microscopy, Freie Universität Berlin, Arnimallee 20-22, 14195 Berlin, Germany
2 Stranski-Laboratorium für Physikalische und Theoretische Chemie, Institut für Chemie, Technische Universität Berlin, Straße des 17. Juni 124, 10623 Berlin, Germany

https://doi.org/10.17952/38EPS.2026.P100

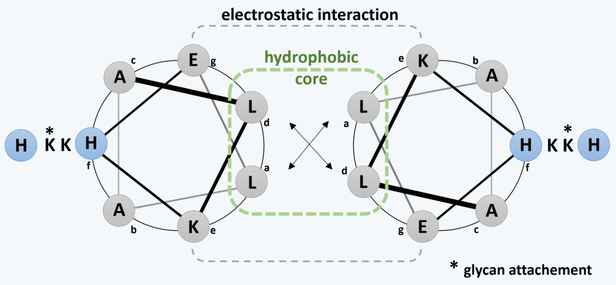
Introduction

Hydrogels are three-dimensional polymer networks that retain large amounts of water. The networks themselves are held together by different types of cross-linkages that are fine-tuned by chemical modification and external stimuli, e.g., heat, ions, or pH.[1] Hydrogels have been used in numerous biomedical and bioengineering applications, like drug-delivery systems or as soft contact lenses. [2]

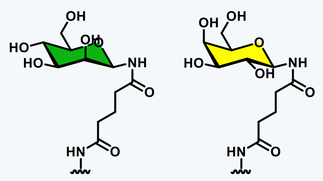
Aim

- tuning viscoelastic properties of mucin-inspired peptide hydrogels
- synthesis of a peptide scaffold suitable for metal-ion coordination
- investigating structural and viscoelastic property changes in modified peptide hydrogels

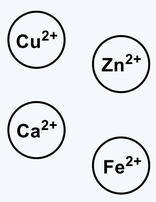
Metal-induced cross-linking



glycan attachement



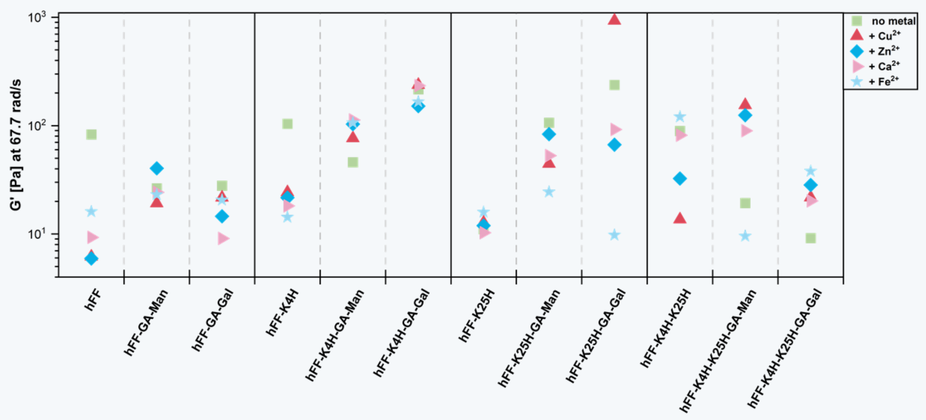
bivalent metal-ions



name	sequence
hFF-K4H	[2]-Abz-LK**H**ELAALKKELAALK**K***ELAALKKEL
hFF-K25H	[2]-Abz-LKKELAALKKELAALK**K***ELAALK**H**EL
hFF-K4H-K25H	[2]-Abz-LK**H**ELAALKKELAALK**K***ELAALK**H**EL

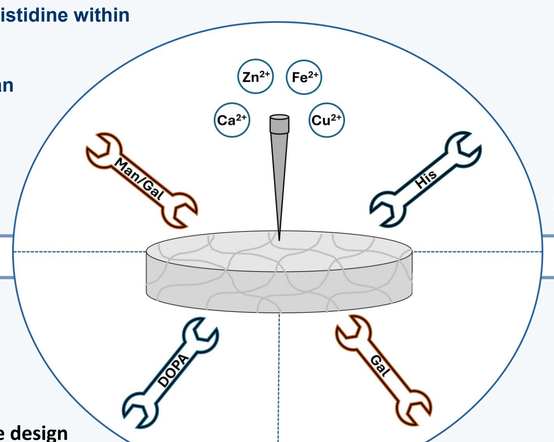
Rheological properties

conditions: c = 0.5 wt%; pH 7.4 [(glyco)-peptide: hFF-K4H-K25H at pH 7]; water; T = 37° C



Key factors:

- position of histidine within the peptide
- type of glycan
- metal(II)-ion

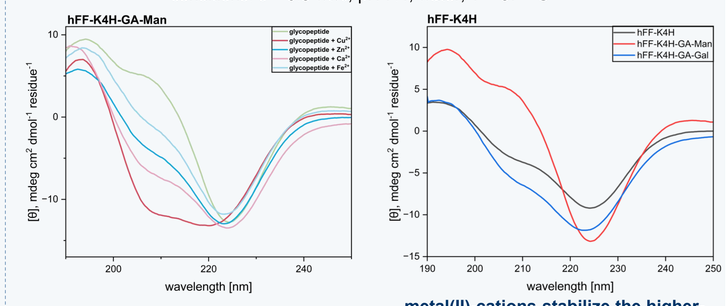


Full publication:[3]

DOI: 10.1002/psc.70059

Circular dichroism (CD)

conditions: c = 0.5 wt%; pH 7.4; water; T = 37° C

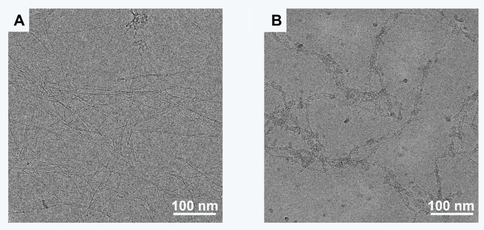


mannose-functionalized peptide adopts a higher-order structure

metal(II)-cations stabilize the higher-order structure of the non-glycosylated peptide, inducing an α-helical conformation

Cryo-TEM

conditions: c = 0.1 mM; pH 7.4; water



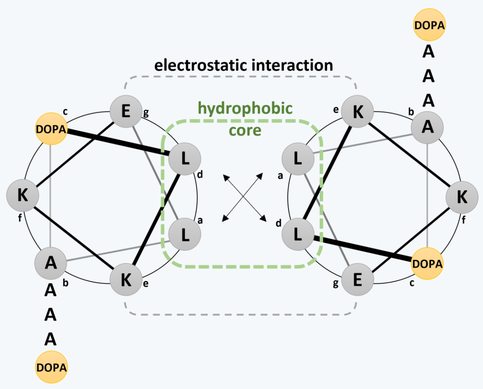
hFF03-K4H-GA-Gal

hFF03-K4H-GA-Gal + 0.25 eq. Cu2+

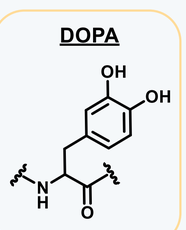
formation of long fibres without copper ions

densely packed fibre bundels after addition of 0.25 eq. copper ions

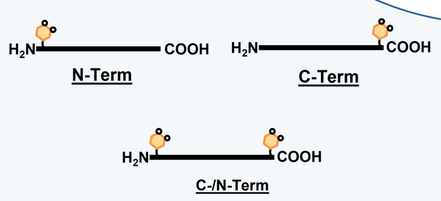
C-/N-Modifications: DOPA



DOPA



Peptide design

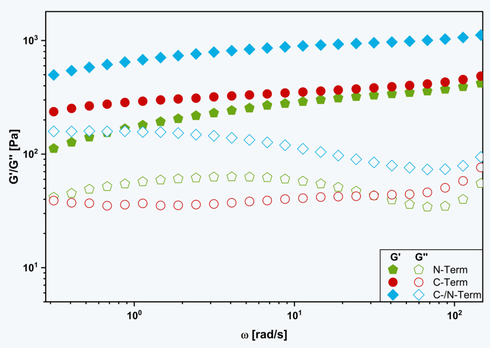


sequence:

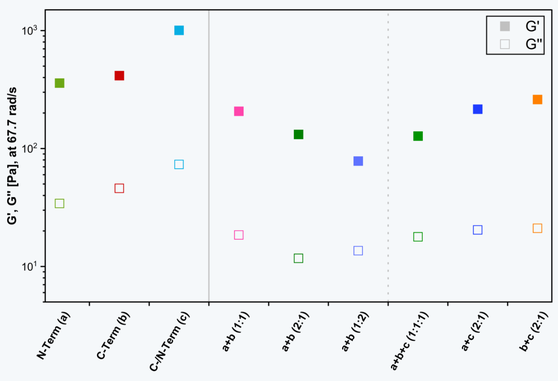
H_2N-DOPA-LKKELAALKKELAALKKELAALKKEL-DOPA-OH

Rheological properties

conditions: c = 0.5 wt%; pH 7.4; PBS ; T = 37° C



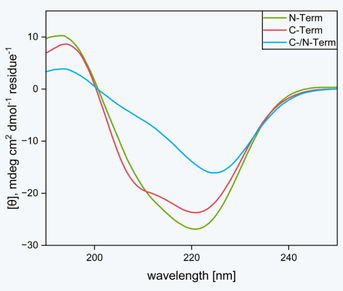
C- and N-Term DOPA-functionalized peptides show similar viscoelastic properties, whereas dual-terminal DOPA modification results in a stiffer hydrogel



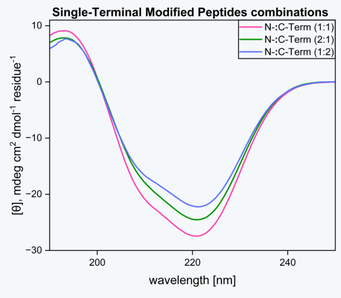
mixtures of the different DOPA-modified peptides form less stiff hydrogels compared to the pure samples

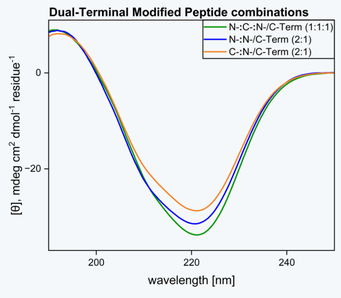
Circular dichroism (CD)

conditions: c = 0.5 wt%; pH 7.4; PBS; T = 37° C



formation of higher ordered structures from N-Term and C-/N-Term, while C-Term forms α-helix

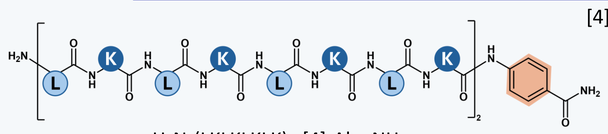




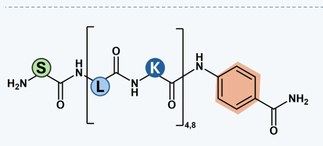
regardless of the specific mixtures, C- and N-terminal modifications of hFF03 lead to the formation of higher ordered structures

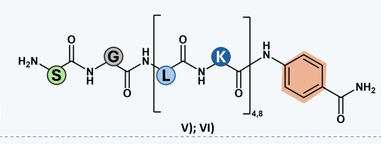
N-terminal glycosylation

[4]

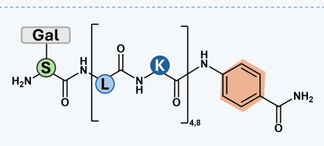


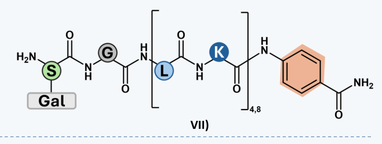
H_2N-(LKLKLKLK)$_2$-[4]-Abz-NH_2





Sequence extension

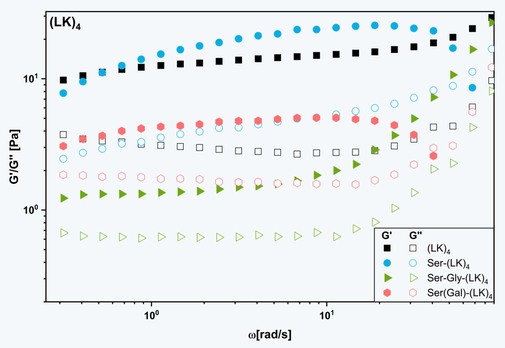




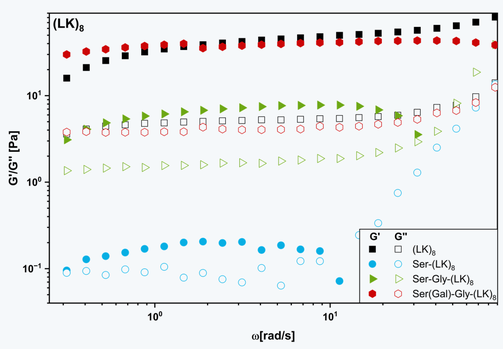
Glycosylation

Rheological properties

conditions: c = 0.5 wt%; pH 7.4; 50 mM bis-tris propane + 150 mM NaCl; T = 37° C



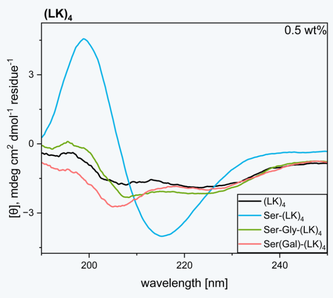
$(LK)_4$ shows minimal change with the addition of one amino acid, while two reduce viscoelastic properties. Glycosylated peptide exhibits stable hydrogel properties.



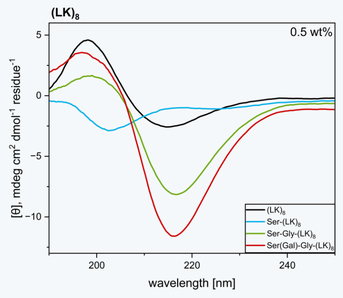
Adding one amino acid drastically reduces $(LK)_8$ viscoelastic properties, while elongation by two forms a stable hydrogel. Glycosylation with a glycine spacer retains viscoelastic properties similar to the unmodified peptide.

Circular dichroism (CD)

conditions: pH 7.4; 50 mM bis-tris propane + 150 mM NaCl; T = 37° C



$Ser-(LK)_4$ adopts beta-structure, whereas the other peptides exihibit likely alpha-helical conformation



Least viscous peptide (Ser-(LK)8) exhibits random coil structure; others adapt beta-sheet confirmation

Outlook

- no-linker glycosylation
- multiple glycosylation
- Glycan in sequence: LK-series
- other cross-linkers

References:

[1] Q. Wang, Y. Zhang, Y. Ma, *Materials Today Bio*, 20 (**2023**), p. 100640; V. Kudryavtseva, M. Otero, J. Zhang, A. Bukatin, D. Gould, G. B. Sukhorukov, *ACS Nanoscience Au*, 3.3 (**2023**), pp. 256–265; T. Tseng, L. Tao, F. Hsieh, Y. Wie, I. Chiu, S. Hsu, *Advanced Materials*, 27.23 (**2015**), pp. 3518–24.
[2] R. García-Sobrino, I. Ruiz-Blas, C. García, H. Reinecke, C. Elvira, J. Radríguez-Hernández, E. Martínez-Campos, A. Gallardo, *Biomaterials Advances*, 159 (**2024**), p. 213826.
[3] A. Puhlmann, C. Baydaroglu, B. Schade, M. Gradzielski, B. Koksch, *Journal of Peptide Science*, 31.11 (**2025**), p. e70059.
[4] S. Chowdhary-Fouquet, R. F. Schmidt, A. K. Sahoo, T. Hohmann, B. Schade, K. Brademann-Jock, A. F. Thünemann, R. R. Netz, M. Gradzielski, B. Koksch, *Nanoscale*, 14(28) (**2022**), p. 10176-10189.

Funded by the Deutsche Forschungsgemeinschaft (DFG, German Research Foundation) through the CRC 1449 *Dynamic Hydrogels at Biointerfaces* (ID 431232613). The authors acknowledge the assistance of the core facility BioSupraMol supported by the DFG.



Contact:
a.puhlmann@fu-berlin.de
LinkedIn: Annelie Puhlmann

Zwitterionic lipid head group influence on the adsorption of antimicrobial peptide to the model lipid membrane

Vedrana Krajnović, Andreja Jakas, Danijela Bakarić

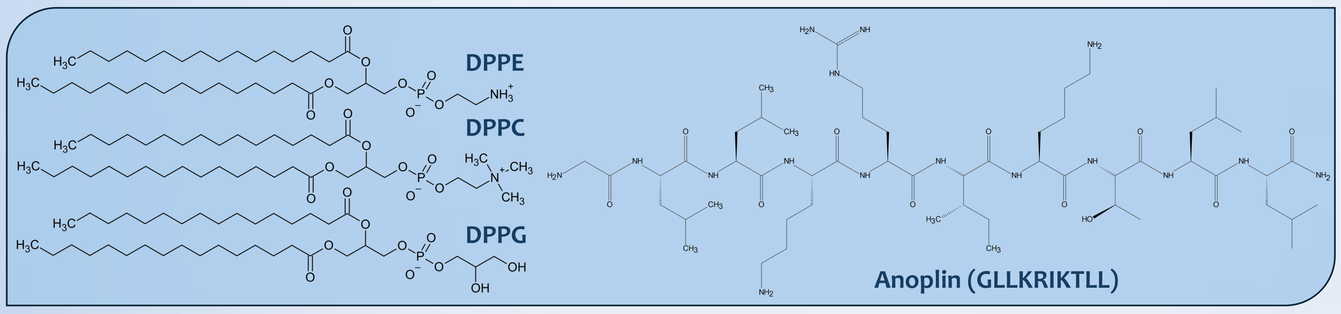
Ruđer Bošković Institute, Department of organic chemistry and biochemistry, University of Zagreb, Zagreb, Croatia

https://doi.org/10.17952/38EPS.2026.P227

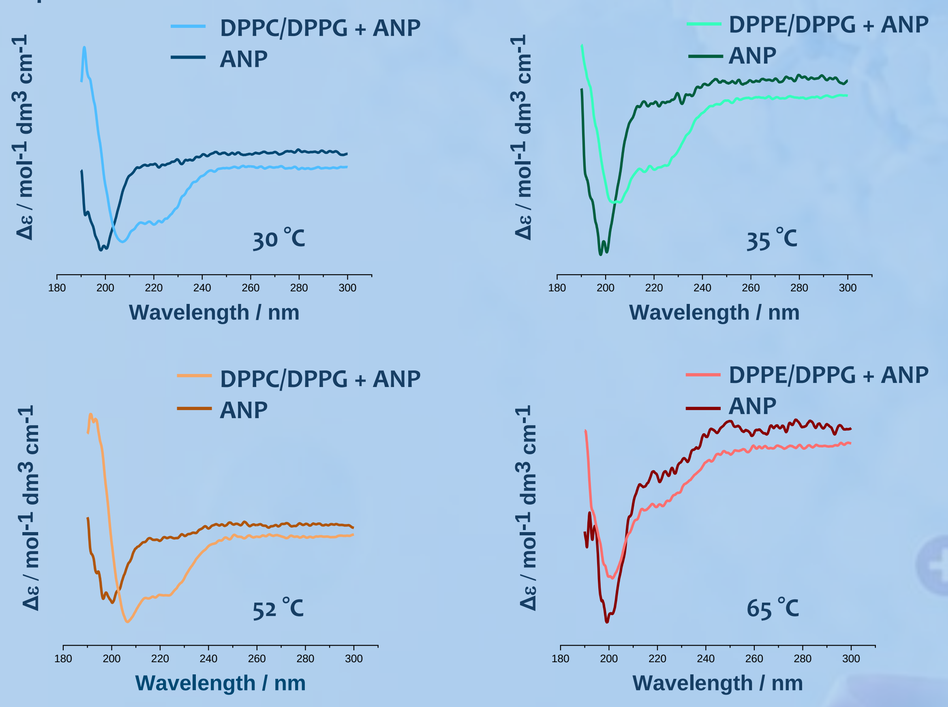
* vedrana.krajnovic@irb.hr

Introduction: The increasing prevalence of bacterial resistance to conventional antibiotics has driven the search for alternative antimicrobial agents, including antimicrobial peptides (AMPs) [1]. Anoplin (ANP), a 10-residue AMP from wasp venom, possesses an amidated C-terminus essential for maintaining its positive charge, amphipathicity, and biological activity [2]. Previous studies have shown that ANP adopts different conformations depending on the lipid environment and that its membrane interactions are concentration-dependent, suggesting the formation of distinct equilibrium helical states [3]. As cationic and amphipathic molecules, AMPs are initially attracted to negatively charged bacterial membranes through electrostatic interactions, followed by membrane insertion and destabilization. Consequently, anionic membranes generally promote stronger peptide binding and permeabilization than zwitterionic membranes, contributing to AMP selectivity toward bacterial cells [4]. Beyond membrane charge, lipid composition and organization also play an important role. PE-containing membranes are more ordered than PC-containing membranes due to differences in headgroup size and interlipid hydrogen bonding. Increased lipid chain order can reduce AMP-induced membrane perturbation and thereby affect pore formation, independently of peptide folding [5].

Aim: To investigate the events preceding membrane leakage, we examined how ANP influences the lateral segregation of anionic lipids in mixed membranes with different zwitterionic lipid headgroups. Mixed membranes composed of fully saturated DPPC/DPPG or DPPE/DPPG (3:1) were characterized using differential scanning calorimetry (DSC) and spectroscopic methods (UV–Vis and CD) at temperatures corresponding to the gel and fluid phases. CD spectroscopy was used to assess changes in the secondary structure of ANP upon membrane phase transitions and to determine how these changes depend on the zwitterionic lipid headgroup (DPPC vs. DPPE).



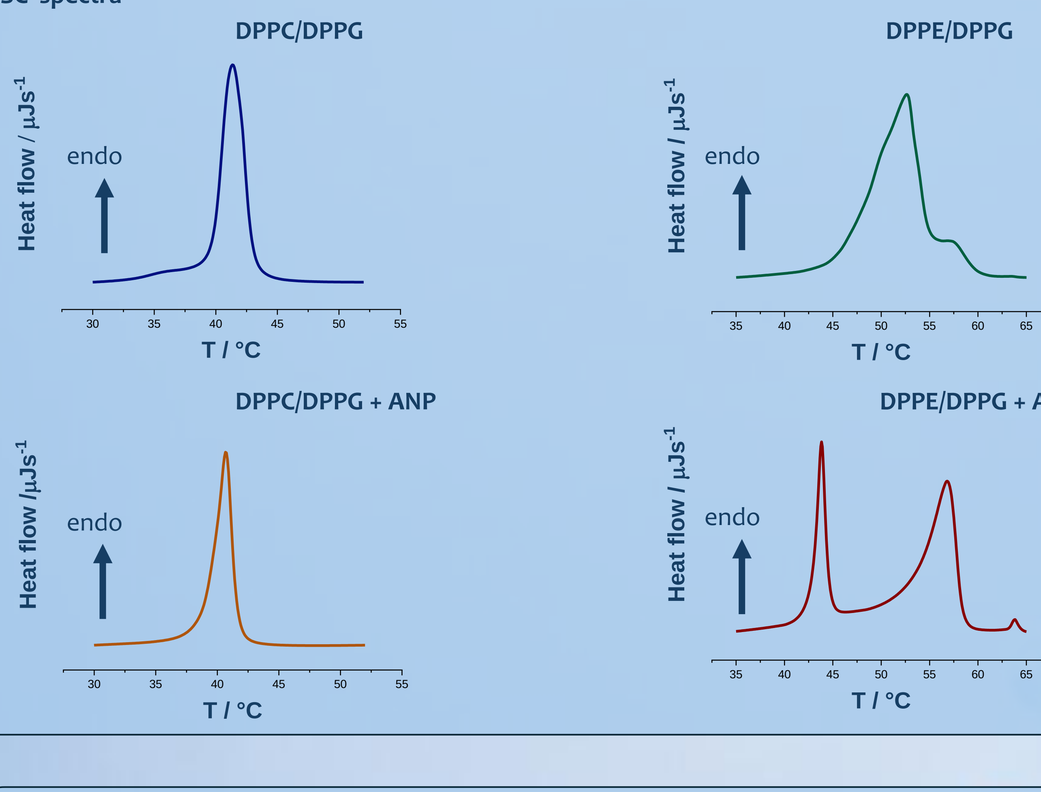
CD spectra



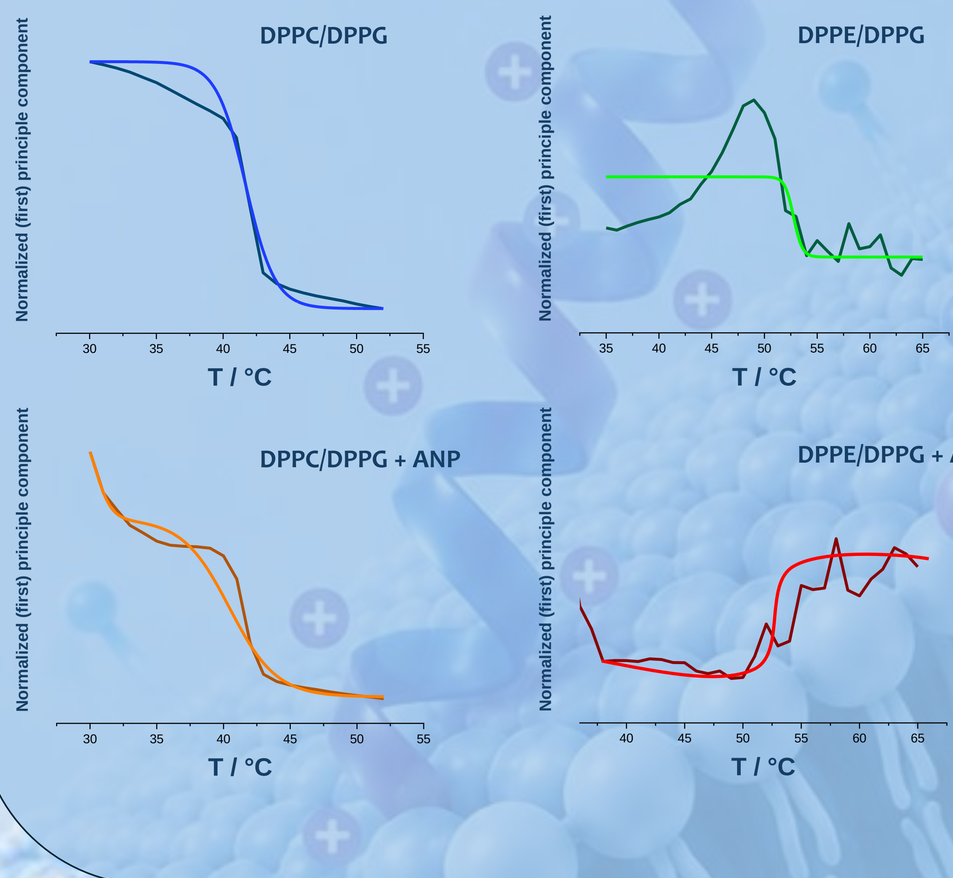
system		α-helix / %	β-sheet / % antiparallel/parallel	β-turn / %	Other / %
DPPC/DPPG + ANP	30 °C	34 ± 0.3	8 ± 2	9 ± 5	48 ± 5
	52 °C	39.5 ± 0.3	5 ± 5% / 8 ± 4	14.5 ± 0.5	47.5 ± 0.5
DPPE/DPPG + ANP	35 °C	13.6 ± 0.6	13.9 ± 0.8%/ 4 ± 3	14 ± 0.5	54 ± 2
	65 °C	7 ± 3	4 ± 3% / 5.5 ± 0.3	14.2 ± 0.1	52.3 ± 0.5

[6]

DSC spectra



UV-Vis spectra



system	T_{pt}s[a] DSC[b] T_p	$T_{m,1}$	$T_{m,2}$	$T_{m,3}$	UV-Vis $T_{m,1}$	$T_{m,2}$
DPPC/DPPG	35.8 ± 0.1	41.4 ± 0.1	-	-	39.3 ± 0.1	41.9 ± 0.1
DPPC/DPPG + ANP	-	40.7 ± 0.1	-	-	~30 ± 7	40.5 ± 0.8
DPPE/DPPG	-	57.3 ± 0.1	52.9 ± 0.4	-	~45.3	~52.0
DPPE/DPPG + ANP	-	43.8 ± 0.1	56.8 ± 0.1	63.8 ± 0.1	-	54.4 ± 0.4

[a] In °C; [b] The uncertainty is ± 0.1 °C; ~ refers to the estimation of the inflection point.

Literature: [1] K. A. Brogden et al., Nat Rev Microbiol 3 (2005) 238–250.
[2] M. P. D. S. Cabrera et al., J. Pept. Sci. 14 (2008) 661–669.
[3] M. Wojciechowska et al., Int. J. Mol. Sci. 21 (2020) 9672, (24)
[4] N. Malanovic et al., BBA - Biomembranes 1862 (2020) 183275, (14)
[5] A. J. Mason et al., Biophys. J. 93 (2007) 4289–4299.
[6] B. Hungary BeStSelTM (2014-2023) – ELTE Eötvös Loránd University, BeStSel, (n.d.).

Conclusion: The presented experimental data demonstrate that ANP–induced segregation of anionic lipids in mixed lipid bilayers is strongly dependent on the identity of the zwitterionic lipid. This dependence is particularly evident in the thermotropic properties of the membranes, as observed by both DSC and UV–Vis spectroscopy. Moreover, the secondary structure adopted by ANP differs between the two membrane environments, with DPPC-containing membranes favoring a higher proportion of α-helical conformations, whereas DPPE-containing membranes promote a greater contribution of β-sheet structures. Since both structures are present in each system, these differences likely reflect shifts in their relative populations rather than the exclusive formation of a single conformation. In particular, the increased β-sheet content observed in DPPE-containing membranes may indicate an enhanced tendency for peptide aggregation in the presence of negatively curved membrane surfaces associated with DPPE.

Acknowledgements: This work was supported by HRZZ under grant UIP-2020-02-7669 and IP-2024-05-1216.

https://doi.org/10.17952/38EPS.2026.P276

Application of an Automated System for Flow Solid Phase Peptide Synthesis

Manish Kumar and Łukasz Berlicki

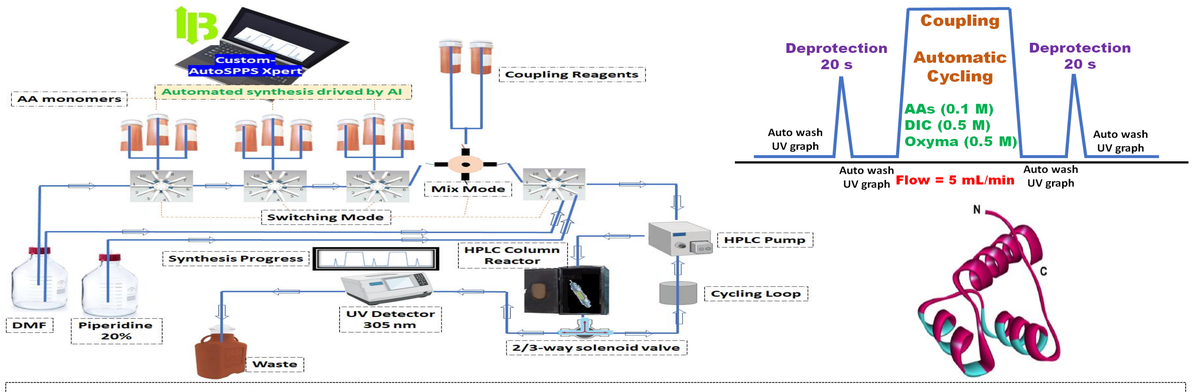
Department of Bioorganic Chemistry, Faculty of Chemistry, Wrocław University of Science and Technology, Wrocław, Poland

manish.kumar@pwr.edu.pl

Introduction

Over the past 60 years, significant advancements have been made in SPPS technologies, including flow-based SPPS.[1,2] In particular, the overall progress of batch SPPS is limited, and ligation chemistry for longer peptides/proteins is highly time-consuming, laborious, leading to undesired side-products, and relatively low yields. Nowadays, flow-based SPPS is gaining momentum due to its advantageous features—for example, control over physical parameters and greatly reduced formation of side products. Recently, it has been demonstrated that the automatic fast-flow peptide synthesis (AFPS) technology is highly effective, however, produces substantial amount of waste due to uses of high amount of reagents and DMF.[3] Therefore, a single-shot and effective SPPS for large and complex proteins with a low amount of waste production remains a challenge. Nowadays, the chemical synthesis of miniproteins/proteins has been of great interest due to their broad applications from basic research to the manufacture of clinically approved therapies, but it is far from being a fail-safe method for all.[2,4-7] To overcome all these challenges in SPPS, we describe the development of a custom-build fully automated flow SPPS technology and its optimizations for the synthesis of peptides, miniproteins, and proteins, yielding high-purity crude products with less production of waste.

Results and Discussion



Schematic Setup for Automatic Flow SPPS, Operation, and Studied Miniprotein (PDB ID 1ENH)

No.	Peptide	Coupling (AA/DIC/Oxyma)	Time of Deprotection (s)	Crude amount (mg)	Crude Purity
1	ENH	3/3/3	60	120	NA
2	ENH	4/4/4	40	132	10%
3	ENH	4/6/4	30	130	12%
4	ENH	4/8/4	25	134	11%
5	ENH	5/5/5	25	135	45%
6	ENH	6/6/6	20	142	70%
7	ENH	8/8/8	25 sec	139	45%
8	ENH	10/10/10	25 sec	153	42%

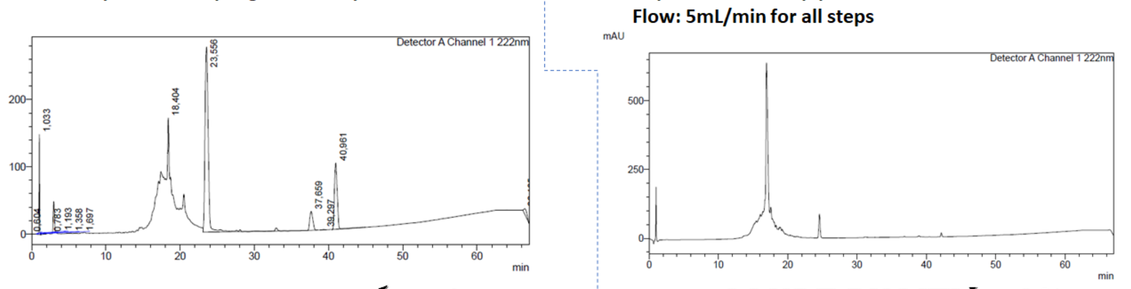
Optimization conditions for the Flow SPPS of ENH miniprotein

INITIAL CONDITIONS:

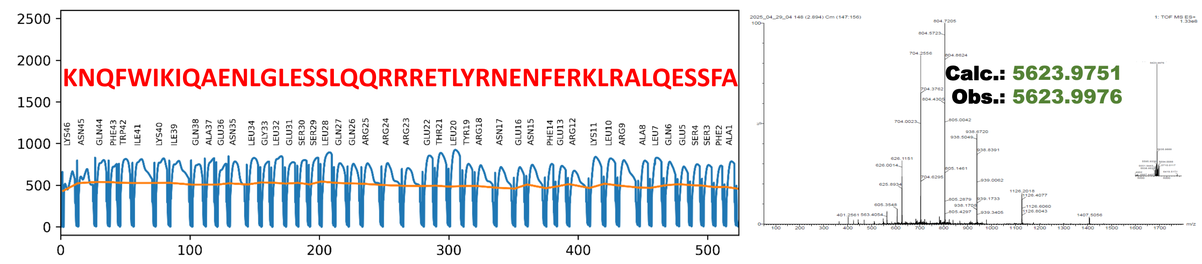
Temperature: 85-70 °C
Coupling step: 0.1 M amino acids stock solution in DMF
0.5 M oxyma stock solution in DMF
0.5 M DIC stock solution in DMF
Deprotection step: 20% piperidine solution in DMF
Flow: 1 mL/min for coupling and 2.5mL/min for wash

FINAL CONDITIONS:

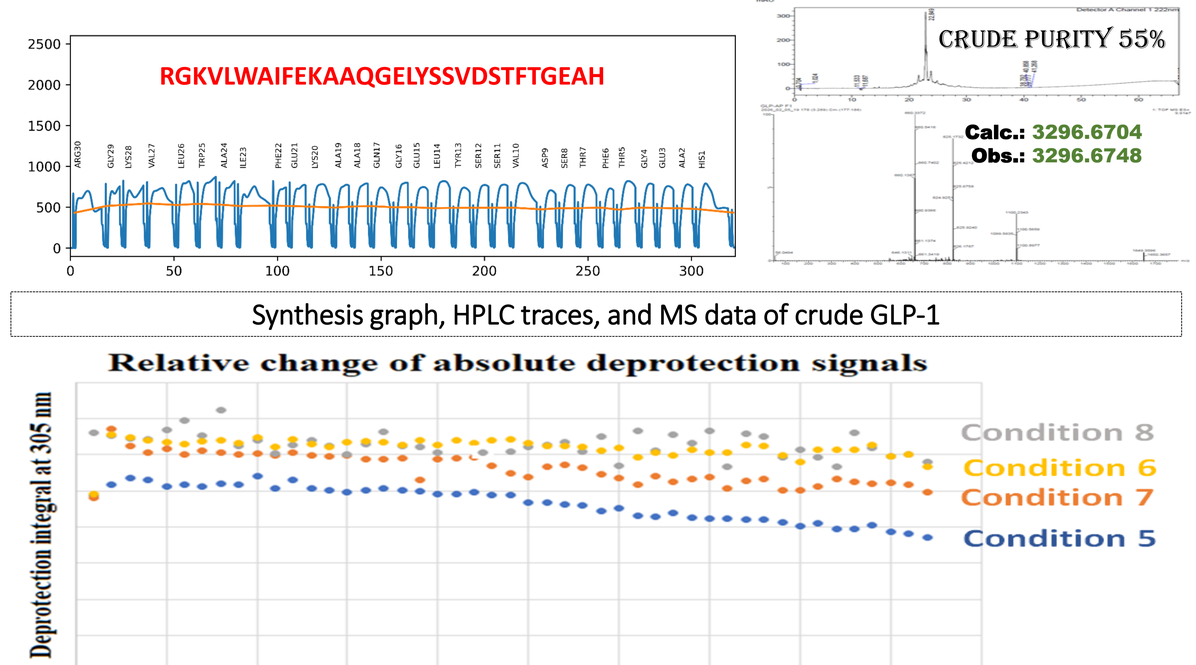
Temperature: 70 °C
Coupling step: 0.1 M amino acids stock solution in NMP
0.5 M oxyma stock solution in NMP
0.5 M DIC stock solution in NMP
Automatic Cycling fully AI based
Deprotection: 20% piperidine solution in DMF
Flow: 5mL/min for all steps



HPLC traces of ENH miniprotein before and after optimized conditions



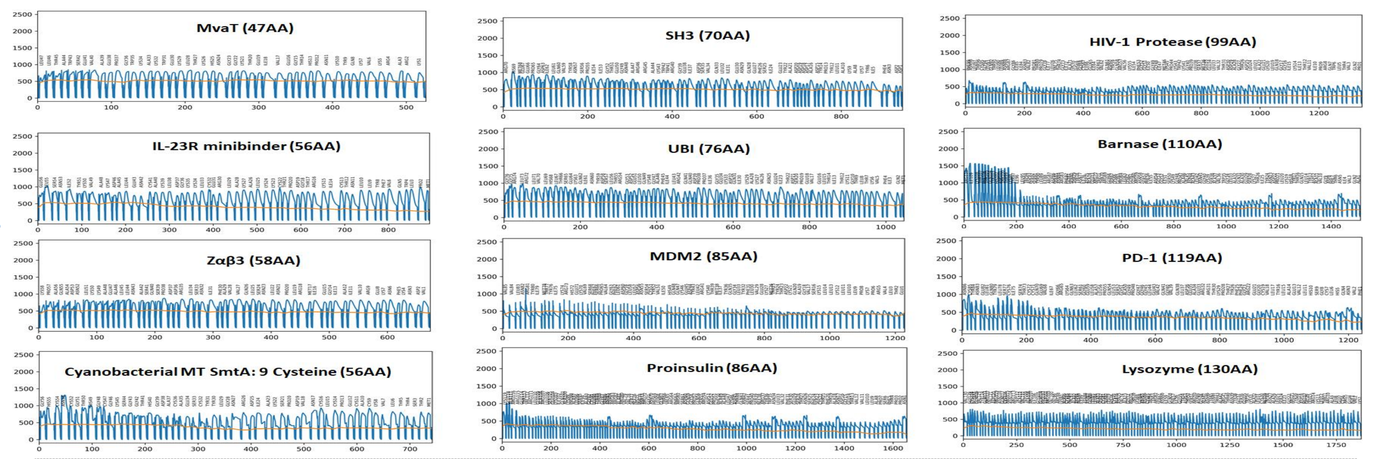
Synthesis graph and MS data of crude ENH miniprotein



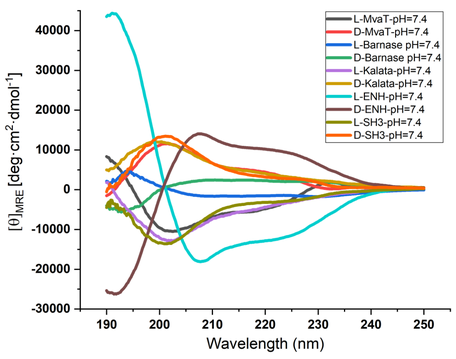
Synthesis graph, HPLC traces, and MS data of crude GLP-1

SPPS	Sequence	Length
EETII	GCPRILMRCKQDSDCLAGCVCGPNGFCG	28
NN92	RVVVGEHNLSQNDGTEQYVNVQKIVSHPY	29
Kalata B1	CGETCVGGTCNTPGCTCSWPVCTRNGLPV	29
D-Kalata B1	CGETCVGGTCNTPGCTCSWPVCTRNGLPV	29
GLP-1	HAEGTFTSDVSSYLEGQAAKEFIAWLVKGR	30
5JI4	APCECDVNGETYTVSSSEECERLCRKLGVTNCRVHCG	37
Amyloid β	DAEFRHDSGYEVHHQKLVFFAEDVGSNKGAIIGLMVGGVVIA	42
ENH	AFSSEQLARLKREFNENRYLTERRQQLSSELGLNEAQIKIWFQNK	46
D-ENH	AFSSEQLARLKREFNENRYLTERRQQLSSELGLNEAQIKIWFQNK	46
MvaT	KRARKVKQYKNPHTGEVIETKGGNHKTLKEWKAKWGPEAVESWATLL	47
D-MvaT	KRARKVKQYKNPHTGEVIETKGGNHKTLKEWKAKWGPEAVESWATLL	47
IL-23R	MPLWQVFYLLNTCIKRTGDPTCKKLAKALRECLKKGDLKACNELADKAVKYINSLE	56
MT SmtA	MTSTTLVKCACEPCLCNVDPSKAIDRNGLYYCSEACADGHTGGSKGCGHTGCNCHG	56
BPTI	RPAFCLEPPYAGPGKARIIRYFYNAAAGAAQAFVYGGVRAKRNNFASAADALAACAAA	58
Z(αβ3)	VDNKFNKERVIAIGEIMRLPNLNSLQVVAFINSLRDDPSQSANLLAEAKKLNDAQAPK	58
DHFR	VFPSNATFGMGDRVRKKSGAAWQGQIVGWYCTNLTPEGYAVESEAHPGSVQIYPVAALERIN	62
SH3	DDNFIYKAKALYPYDADDDDAYEISFEQNEILQVSDIEGRWWKARRANGETGIIPSNYVQLIDGPEEMHR	70
D-SH3	DDNFIYKAKALYPYDADDDDAYEISFEQNEILQVSDIEGRWWKARRANGETGIIPSNYVQLIDGPEEMHR	70
UBI	MQIFVKTLTGKTITLEVEPSDTIENVKAKIQDKEGIPPDQQRLIFAGKQLEDGRTLSDYNI QKESTLHLVLRLRGG	76
MYC[1-84]	MPLNVSFTNRNYDLDYDSVQPYFYCDEEENFYQQQQQSELQPPAPSEDIWKKFELLPTPPLSPSRRSGLCSPSYVAVTPFSLRG	84
MDM2	ETLVRPKPLLLKLLKSVGAQKDTYTMKEVLFYLGQYIMTKRLYDEKQQHIVYCSNDLLGDLFGVPSFSVKEHRKIYTMIYRNLVV	85
D-MDM2	ETLVRPKPLLLKLLKSVGAQKDTYTMKEVLFYLGQYIMTKRLYDEKQQHIVYCSNDLLGDLFGVPSFSVKEHRKIYTMIYRNLVV	85
Proinsulin	FVNQHLCGSHLVEALYLVCGERGFFYTPKTRREAEDLQVGQVELGGGPGAGSLQPLALEGSLQKRGIVEQCCTSICSLYQLENYCN	86
Barstar	KKAVINGEQIRSISDLHQTLKKELALPEYYGENLDALWDCLTGWVEYPLVLEWRQFEQSKQLTENGAESVLQVFREAKAEGCDITIILS	89
ERG	MEEKHMPPPNMTTNERRVIVPADPTLWSTDHVRQWLEWAVKEYGLPDVNILLFQNIDGKELCKMTKDDFQRLTPSYNADILLSHLHYLRETPLP	94
BCL11A	RSDTCEYCGKVFKNCSNLTVHRRSHTGERPYKCELCNYACAQSSKLTRHMKTHGQVGKDVYKCEICKMPFSVYSTLEKHMKKWHSDRVLNNDIKTE	96
HIV-Protease-1	PQVTLWQRPIVTIKIGGQLKEALLDTGADDTVLEEMSLPGKWKPKMIGGIGGFIKVRQYDQVSIEICGHKAIGTVLIGPTPVNIIGRNLLTQLGCTLNF	99
HIV-Kent type	PQITLWKRPLVTIRIGGQLKEALLDTGADDTVIEEXNLPGKWKPKXIGGIGGFIKVRQYDQIPVEIZGHKAIGTVLVGPTPVNIIGRNLLTQIGATLNF X = norleucine, Z = aminobutyric acid	99
Collagen	GLPGAKGLAGAPGAPGPDZKAGPPGPAGQDCpsRPGPPGPPGARGQAGPPGFPGPKGAAGEPGKAGERGVPGPPGAVGPAGKDCpsEAGAQG PPGPAGPAGER Z = Fmoc-(Dmb)Gly-OH building blocks)	99
TRX-1	SDKIIHLTDDSFDTDVLKADGAILVDFWAEWCGPCKMIAPILDEIADEYQGKLTVAKLNIDQNPGTAPKYGIRGIPTLLLFKNGEVAATKVGALSKGQL KEFLDANLA	108
Barnase	AQVINTFDGVADYLQTYHKLPDNYITKSEAQALGWVASKGNLADVAPGKSIGGDIFSNREGKLPGKSGRTWREADINYTSGFRNSDRILYSSDWLIY KTTDHYQTFTKIR	110
D-Barnase	AQVINTFDGVADYLQTYHKLPDNYITKSEAQALGWVASKGNLADVAPGKSIGGDIFSNREGKLPGKSGRTWREADINYTSGFRNSDRILYSSDWLIY KTTDHYQTFTKIR	110
Barnase[R110FBr]	AQVINTFDGVADYLQTYHKLPDNYITKSEAQALGWVASKGNLADVAPGKSIGGDIFSNREGKLPGKSGRTWREADINYTSGFRNSDRILYSSDWLIY KTTDHYQTFTKIX X = (p-Br-Phe)	110
PD-L1[18-133]	AFTVTVPKDLYVVEYGSNXTIECKFPVEKQLDLAALIVYWEXEDKNIIQFVHGEEDLKVQHSSYRQRARLLKDQLSLGNAALQITDVKLQDAGVYRCX ISYGGADYKRITVKVNAPK X= norleucine	117
STIP1	MEQVNELKEKGNKALSVGNIDDALQCYSEAIKLDPHNHVLYSNRSAAYAKKGDYQKAYEDGCKTVDLKPDWGKGYSRKAAALEFLNRFEEAKRTYE EGLKHEANNPQLKEGLQNMEAR	118
PD-1[33-150]	NPPTFSPALLVVTEGDNATFTCSFSNTSESFVLNWYRXSPSNQTDKLAAFPEDRSQPGQDSRFRVTQLPNGRDFHXSVVRARRNDSGTYLCGAISLA PKAQIKESLRAELRVTERRAEK X= norleucine	119
Ribonuclease A	KETAAAKFERQHMDSSTSAASSSNYCNQMMKSRNLTKDRCKPVNTFVHESLADVQAVCSQKNVACKNGQTNCYQSYSTMSITDCRETGSSKYPN CAYKTTQANKHIIVACEGNPYVPVHFDASV	124
MDM2[1-118]	MHHHHHHGSMCNTNMSVPTDGAVTTSQIPASEQETLVRPKPLLLKLLKSVGAQKDTYTMKEVLFYLGQYIMTKRLYDEKQQHIVYCSNDL LGDLFGVPSFSVKEHRKIYTMIYRNLVVVNQQESSDS	127
Lysozyme	VFERCELARTLKRLGMDGYRGISLANWMCLAKWESGYNTRATNYNAGDRSTDYGIFQINSRYWCNDGKTPGAVNACHLSCSALLQDNIA DAVACAKRVVRDPQGIRAWVAWRNRCQNRDVRQYVQGCGV	130

List of AI- supported cost-effective flow-SPPS of proteins in this work



Some Examples of Protein Syntheses With Our AI-Model Approach



CD-spectra measurement for L- and D-conformation of selected proteins

Conclusions

- AI-supported efficient fully automated flow technology has been developed for SPPS.
- The initial optimization of synthesis parameters such as flow, pressure, temperature, and duration of individual steps leads to a AI-supported methodology that allows peptides and miniproteins/proteins synthesis up to 100 residues in a routine manner.
- The low usage of solvents and reagents provided the high purity crude products is another advantage of this approach. ***Our AI-supported flow SPPS technology also provides the access to D-conformation proteins with high crude purity validated by MS, analytical HPLC, and CD results.***

References

[1] Merrifield, R. B. *J. Am. Chem. Soc.* **1963**, 85, 2149–2154.
[2] Gates, Z. P.; Hartrampf, N. *Pept. Sci.* **2020**, 112, e24198.
[3] Hartrampf, N. *et al. Science* **2020**, 368, 980–987.
[4] Ciesiołkiewicz, A. *et al. Protein Sci.* **2024**, 33, e5104.
[5] Baker, E. G. *et al. Acc. Chem. Res.* **2017**, 50, 2085–2092.
[6] Ożga, K.; Berlicki, Ł. *ACS Bio Med Chem Au* **2022**, 2, 316–327.
[7] Ferentzi, K.; Nagy-Fazekas, D. *et. al., React. Chem. Eng.* **2024**, 9, 58–69.

Project financed by: De novo design of cavity-incorporating mini-proteins and their application in catalysis, OPUS, NCN, 2021/43/B/ST4/01837

Poster No.55

New therapeutic option in autoimmune diseases to prevent the release of soluble CD95L

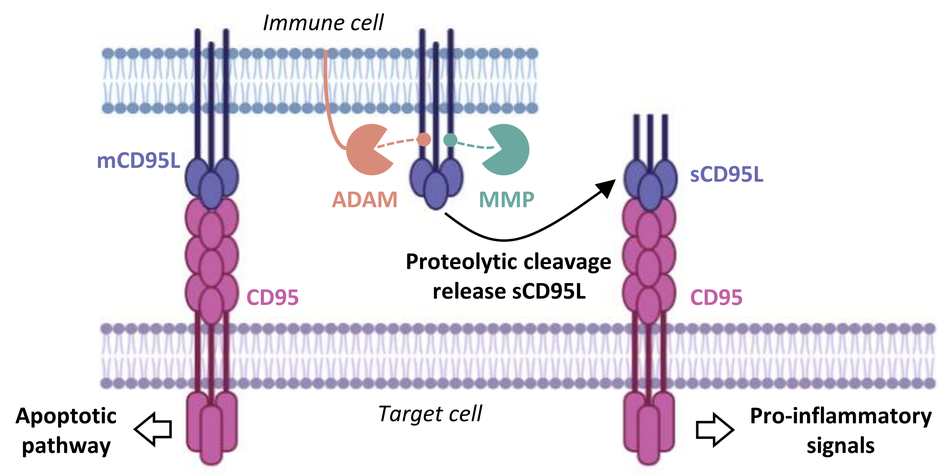
LAUNAY Marie[1], HUOT-MARCHAND Sarah[2], KOTAICH Farah[3], BLANCO Patrick[2], LEGEMBRE Patrick[3], DEVEL Laurent[1]

[1]**Université Paris-Saclay**, *CEA, INRAE, Médicaments et Technologies pour la Santé (MTS), SIMoS, France.* [2]**ImmunoConcept**, *CNRS UMR 5164, Université de Bordeaux, France.* [3]**UMR CNRS 7276,** INSERM U1262, CRIBL, *Université Limoges, France*

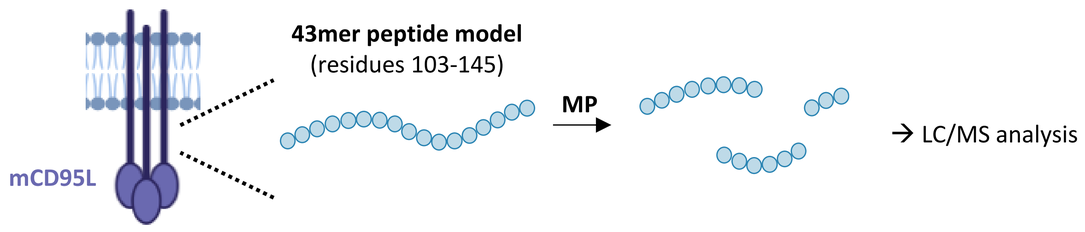
https://doi.org/10.17952/38EPS.2026.P055

1 Pathological context

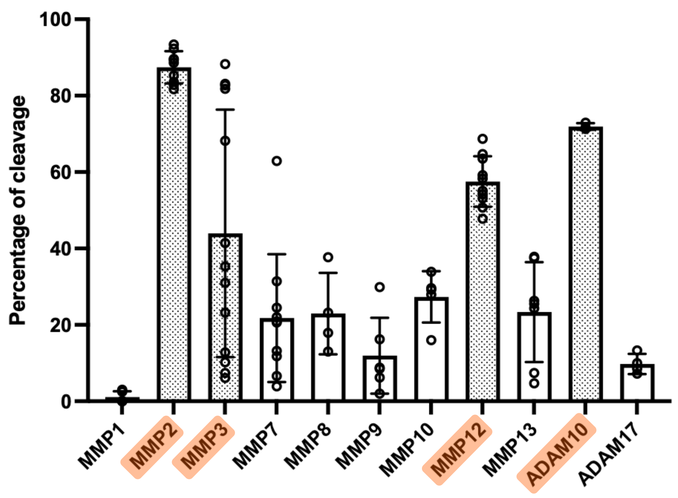
Autoimmune diseases affect approximately 10% of the population, with elevated levels of soluble CD95L (sCD95L) notably observed in systemic lupus erythematosus (SLE). While membrane-bound CD95L (mCD95L) induces apoptosis and contributes to immune regulation, its proteolytic cleavage by metalloproteases (MPs) generates sCD95L, shifting signaling toward a pro-inflammatory response. The mechanisms and precise cleavage sites involved in MP-mediated CD95L processing remain unclear. To investigate this process, we designed a peptide model corresponding to the CD95L cleavage region. This study aims to identify the cleavage sites and characterize the role of MPs in CD95L processing. In addition, we evaluate an antibody-based strategy to prevent CD95L cleavage, in order to preserve its apoptotic function and limit inflammatory signaling.



2 MPs identification & cleavage sites



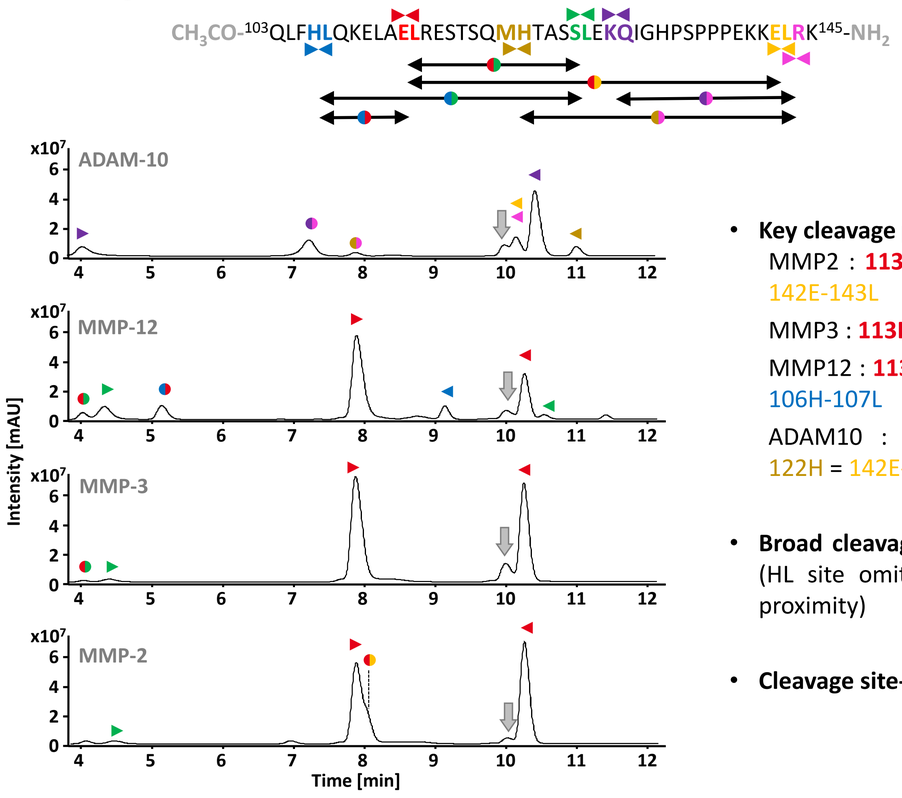
- **Most active MPs in peptide processing**



Metalloprotease families involved:

- **Matrix Metalloproteases (MMPs):** conserved cleavage sites within the family (**113E–114L** & **126S–127L**).
- **A Disintegrin And Metalloproteases (ADAM):** preferential cleavage at a distinct **129K–130Q** site.

- **Cleavage site identification**

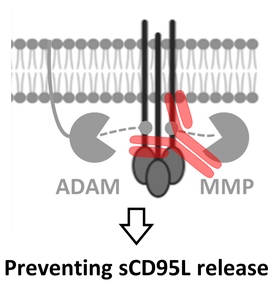


- **Key cleavage position :**
  MMP2 : **113E–114L** >> **126S–127L** > 142E-143L
  MMP3 : **113E–114L** >> **126S–127L**
  MMP12 : **113E–114L** >> **126S–127L** = 106H-107L
  ADAM10 : **129K–130Q** >> 121M-122H = 142E-143L = 143L-144R

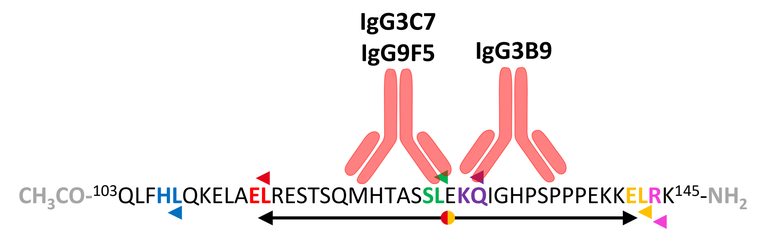
- **Broad cleavage diversity for MMP12** (HL site omitted due to membrane proximity)

- **Cleavage site-rich region**

3 New strategy to block sCD95L release

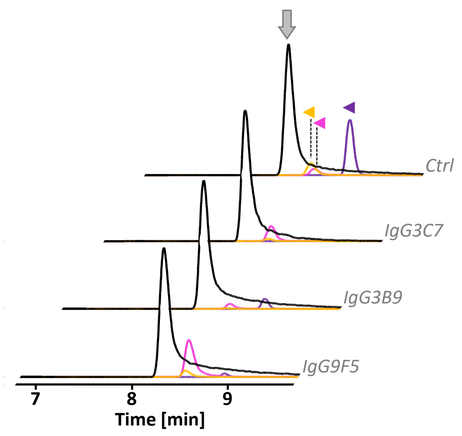


→ **Screening of three antibodies (IgG)**



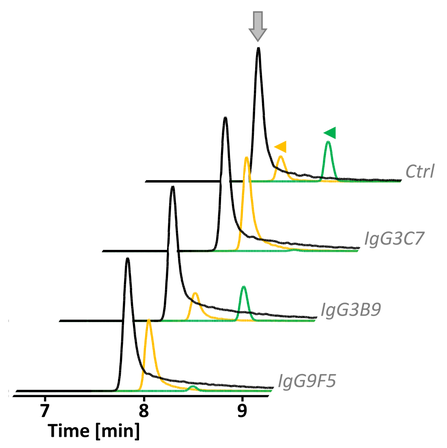
For MMPs, cleavage at 113E–114L masked protection at the 126S–127L epitope. The 113E–114L → GG mutant was used to assess protection at this site

- **Against rhADAM-10 processing (n=3)**



✓ **IgG3C7** and **IgG9F5** provide stronger protection against cleavage at **129K–130Q** site

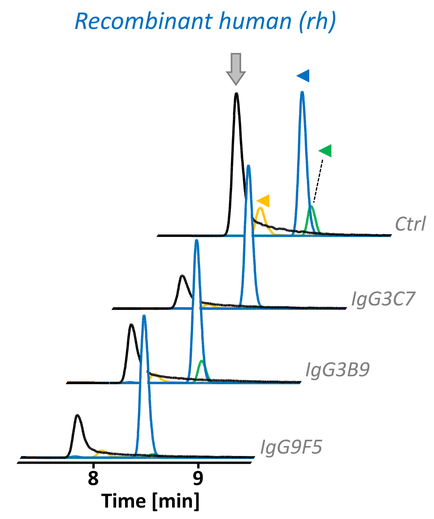
- **Against rhMM-2 processing (n=3)**



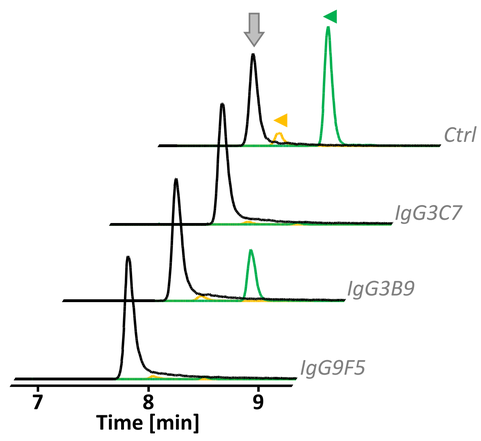
✓ **IgG3C7** provides stronger protection of the **126S–127L** site.

- **Against MMP-12 processing (n=3)**

Recombinant human (rh)

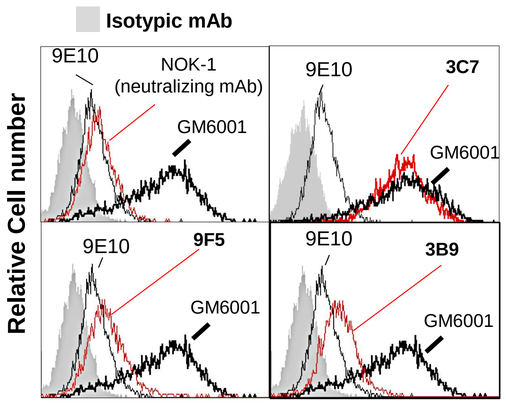


Recombinant mouse (rm)



✓ **Differential processing** between rhMMP-12 and rmMMP-12, consistent with **low homology (61%)**
✓ **IgG3C7** provides stronger protection of the **126S–127L** site.

- **Evaluation on cell**



- Assessment mCD95L expression levels in cells (increasing towards the right)
- GM6001, a broad-spectrum metalloprotease inhibitor, blocks mCD95L cleavage
- IgG3B9 and IgG9F5 show low mCD95L expression compared to GM6001
- **IgG3C7**: increased mCD95L levels, comparable to GM6001

4 Future perspectives

✓ **IgG3C7 :**
- Emerged as the **best candidate for preventing cleavage** within the cleavage site-rich region
- Has shown a **protective effect in cell-based assays**
- Currently **being tested in murine models** of autoimmune disease to prevent mCD95L cleavage

→ **Evaluate protection against rmADAM-10 (96% homology with rhADAM-10)**

→ **Identifying MPs in murine models of autoimmune disease:**
- Use a broad-spectrum substrate to identify metalloproteolytic activity
- ELISA assays to **quantify** MMP2, MMP3, MMP12, and ADAM10 **levels across** different disease stages
- **Activity-based probes** used to capture and identify **active metalloproteases** at different pathological stages.

Collaborations

SIMoS · MTS Médicaments et Technologies pour la Santé · anr agence nationale de la recherche ANR-24-CE18-2934 · ImmunoConcEpT · cnrs

[1]Legembre P, Blanco P, Jean M. WO2023161412. 31 août 2023.
[2]Devel L et al. Role of metalloproteases in the CD95 signaling pathways. Frontiers in Immunology. 05 dec 2022;13:1074099.

https://doi.org/10.17952/38EPS.2026.P070

Stapled Peptide Inhibitors Targeting pre-miR-155 to Suppress miRNA Maturation

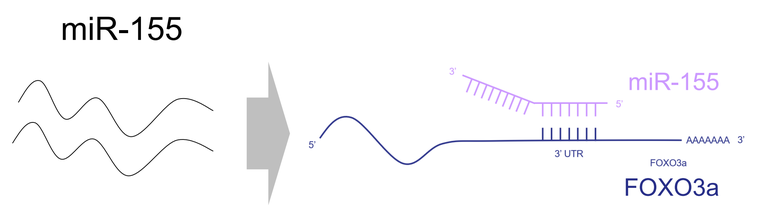
Heejoo Roh, Jinseo Heo, Yeongju Lee*
Department of Chemistry, Pusan National University

Abstract

MicroRNA-155 (miR-155) is a well-established oncogenic microRNA, and inhibition of its maturation from precursor miR-155 (pre-miR-155) offers a potential strategy for modulating miR-155-driven signaling. Because pre-miR-155 contains a structured hairpin region involved in Dicer-mediated processing, it represents an attractive target for RNA-directed ligands. In this study, we investigated hydrocarbon-stapled peptides as modulators of pre-miR-155 maturation. Stapled analogues were designed from a previously reported pre-miR-155-binding peptide by introducing i, i + 4 hydrocarbon staples at selected positions predicted to avoid the RNA-recognition interface. Among the analogues, **S1** retained strong pre-miR-155 binding, inhibited Dicer-mediated cleavage, and showed improved serum stability and cellular uptake relative to the parent linear peptide. In cells, **S1** decreased mature miR-155 levels, increased pre-miR-155 accumulation, restored expression of the miR-155 target protein SOCS1, and reduced cell viability. These findings indicate that hydrocarbon stapling can improve the functional properties of RNA-targeting peptides when the staple is positioned to preserve the RNA-recognition interface. Overall, this work highlights stapled peptides as a promising modality for targeting structured RNA motifs involved in microRNA processing.

Introduction

How miR-155 Drives Tumor Progression



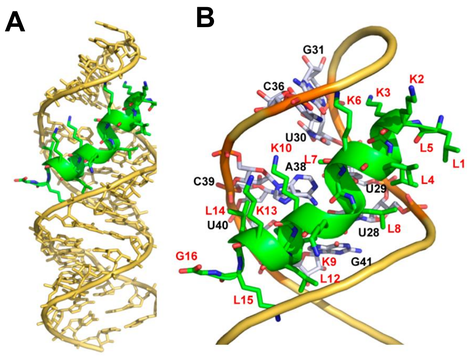
Overexpressed in cancer cell → Suppress tumor suppressor genes → Inhibit apoptosis → Tumor progression

Structure Basis for Targeting pre-miR-155

N-terminal **C-terminal**

159: LKKLLKLLKKWLK

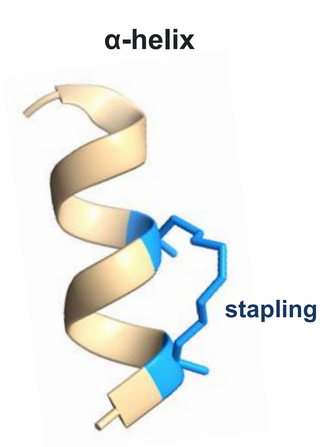
A B



"Peptide 159, a pre-miR-155 Dicer cleavage site-binding peptide, was used as a template for inhibitor development."

J. Am. Chem. Soc. **2016**, *138*, 857–867.

Advantage of stapled peptide



Stablize α-helix structure → Binding affinity↑ → Cell Penetration↑ → Protease resistance↑ → Drug property↑

Fig. 1. Molecular model of peptide 159 bound to pre-miR-155. (A) Overall structure of the peptide 159–pre-miR-155 complex. (B) Close-up view showing peptide binding within the major groove of the apical stem-loop.

Binding assay

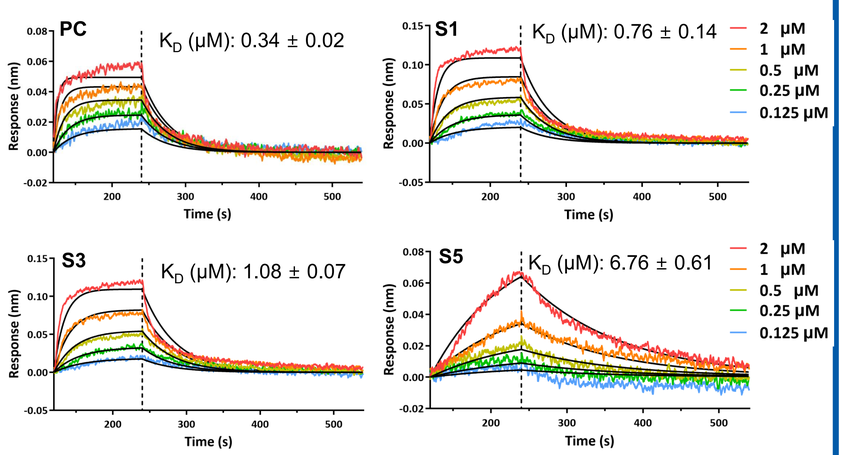
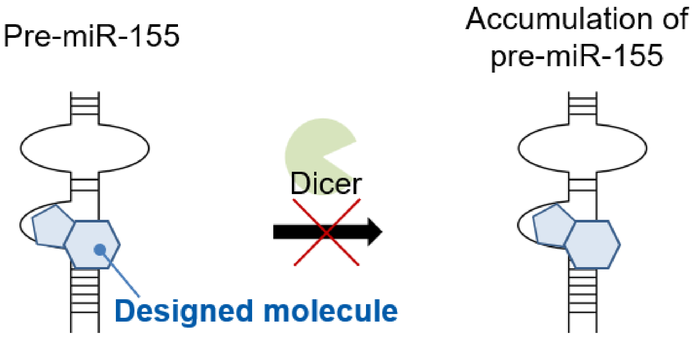


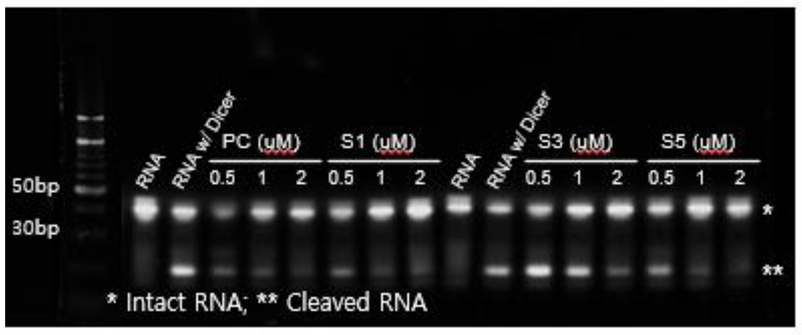
Fig. 3. BLI binding curves of fluorescein-labeled peptide 159 and its stapled analogs (S1, S3, and S5) with pre-miR-155. K_D values were determined from the binding curves.

Dicer Inhibition Assay

A. Experimental Design



B.



C.

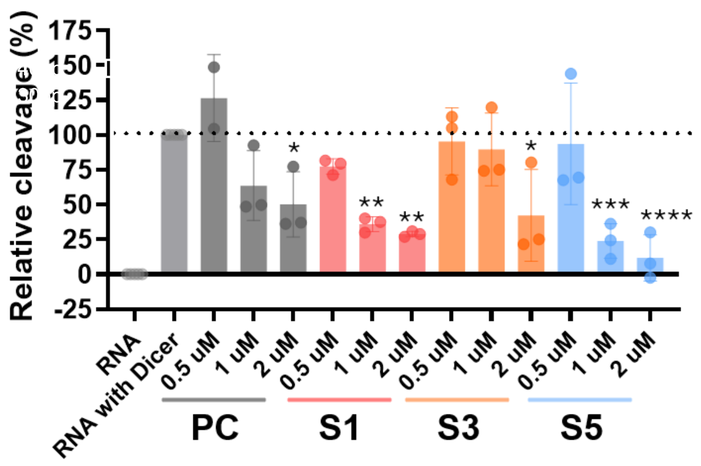


Fig. 4. (A) Experimental design of dicer inhibition assay. (B) Fluorescence-labeled pre-miR-155 was treated with peptide **159** (positive control) and synthesized peptides **S1**, **S3**, and **S5** at concentration 1μM. After incubation with Dicer at 37 °C for 2 hours, samples were analyzed by 8% PAGE. (C) Quantification of Dicer-mediated pre-miR-155 cleavage relative to the RNA with Dicer control (100%).

Cell Penetration Efficiency

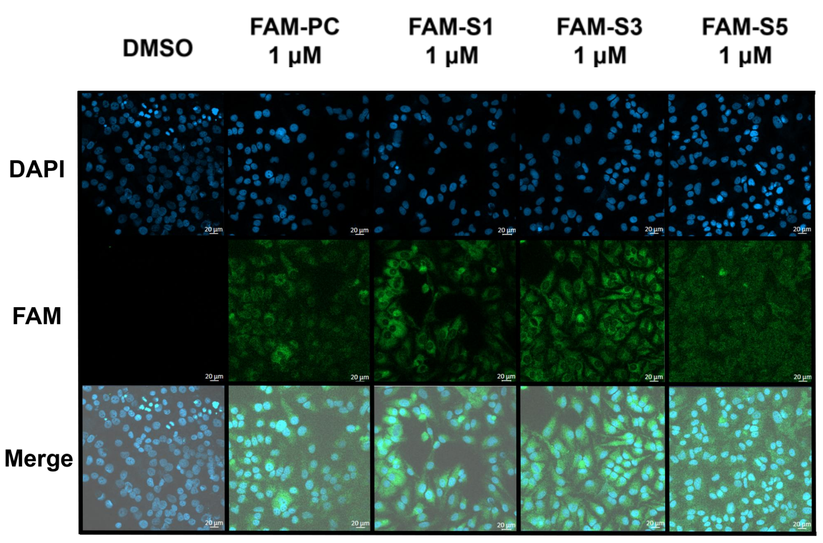


Fig. 5. Cellular uptake of FAM-labeled peptide 159 (PC) and its stapled analogs (S1, S3, and S5) in HeLa cells. Cells were treated with each peptide at 1 μM for 12 h, and cellular uptake was visualized by confocal microscopy.

RT-qPCR & Western Blot

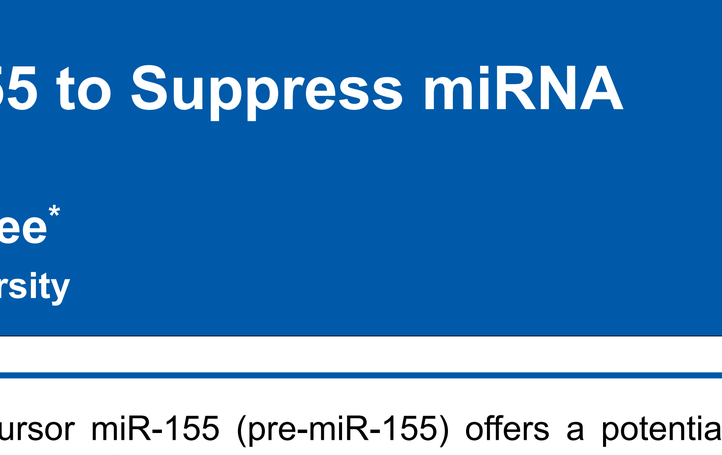


Fig. 6. (A) RT-qPCR analysis of relative miR-155 levels normalized to GAPDH for respectively.
(B) Representative Western blots and corresponding quantification of SOCS1 protein levels normalized to α - actinin. Data are presented as mean ± SD (n = 3).

Effect of Dicer inhibitor in Apoptosis

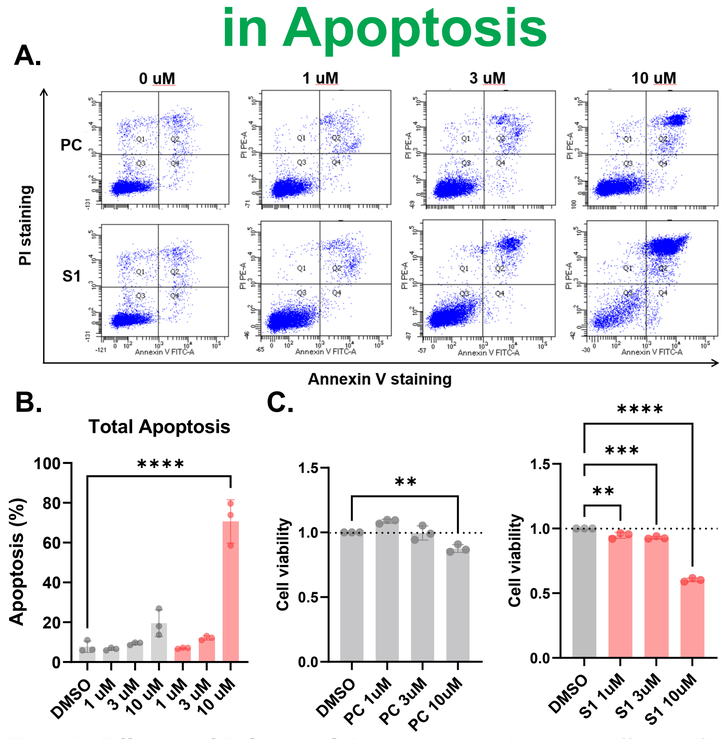


Fig. 7. Effects of PC and S1 on apoptosis and cell viability. (A) Annexin V/PI analysis following treatment with PC or S1. (B) Quantification of total apoptosis. (C) Cell viability at the indicated peptide concentrations.

Conclusions

Stapling of peptide **159** generated conformationally constrained analogs with distinct RNA-binding and cellular properties. Among the stapled peptides, S1 and S3 showed favorable binding to pre-miR-155 and efficient cellular uptake, whereas S5 exhibited relatively weak binding and uptake. The stapled peptides modulated Dicer-mediated pre-miR-155 processing, resulting in increased pre-miR-155 accumulation and reduced mature miR-155 levels in cells. In particular, S1 induced dose-dependent apoptosis accompanied by reduced cell viability. Collectively, these results demonstrate that peptide stapling can enhance the functional properties of RNA-targeting peptides, supporting their potential as a strategy for modulating miRNA maturation.

Reference

[1] J Pai et al., "Screening of pre-miRNA-155 Binding Peptides for Apoptosis-Inducing Activity Using Peptide Microarrays", J. Am. Chem. Soc. **2016**, *138*, 857–867.

Contact information
Web: https://dldudwn11111.wixsite.com/lee-group
Prof. Yeongju Lee. lyj0308@pusan.ac.kr +82-51-510-2868
Jinseo Heo. jsheo1031@pusan.ac.kr

https://doi.org/10.17952/38EPS.2026.P073

Development of PNA-Based Antisense Oligonucleotides Targeting XIAP mRNA for Sensitizing TRAIL-Resistant Cancer Cells

Hyein Jung, and Yeongju Lee*

Department of Chemistry, Pusan National University

Abstract

Peptide nucleic acids (PNAs) offer a chemically stable antisense platform for sequence-specific regulation of disease-associated RNA targets. Owing to their neutral pseudopeptide backbone, PNAs exhibit strong hybridization to complementary RNA sequences and high resistance to nuclease-mediated degradation. These properties make PNAs particularly suitable for targeting regulatory RNA elements that control the expression of disease-relevant proteins.

X-linked inhibitor of apoptosis protein (XIAP) is an anti-apoptotic factor frequently overexpressed in cancer and a key mediator of resistance to TRAIL-induced apoptosis, where it suppresses caspase activation downstream of death receptor signaling. XIAP translation is sustained under cellular stress through an internal ribosome entry site (IRES), making this regulatory RNA element an attractive target for selective downregulation of XIAP in apoptosis-resistant cancer cells.

Here, we developed cell-penetrating peptide (CPP)-conjugated PNAs directed against the XIAP IRES to enable both sequence-specific translational repression and efficient intracellular delivery. The XIAP-targeting CPP-PNAs effectively reduced XIAP protein levels in multiple cancer cell lines, including TRAIL-resistant cells. In the TRAIL-resistant context, co-treatment of the CPP-PNAs with TRAIL produced a synergistic effect that restored caspase activation and substantially enhanced apoptotic cell death compared with either treatment alone. These findings demonstrate that PNA-based antisense targeting of the XIAP IRES can overcome XIAP-mediated apoptosis resistance by re-engaging the caspase cascade, and highlight CPP-conjugated PNAs as a promising modality for RNA-directed regulation of oncogenic survival pathways.

Introduction

1. XIAP/XIAP IRES

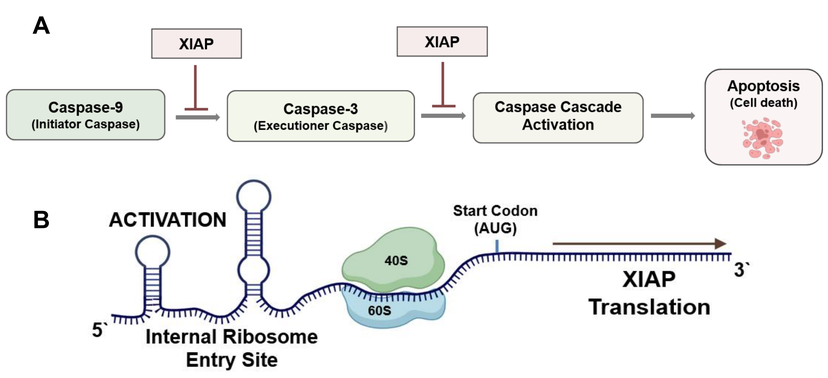


Fig. 1 A. XIAP regulates caspase process **B.** Translation controlled by IRES

2. TRAIL/XIAP Signaling

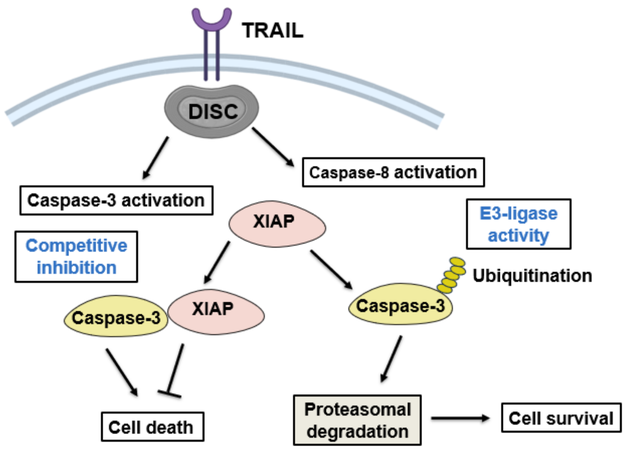


Fig. 2 Molecular mechanism of TRAIL, caspase, and XIAP

3. Types of ASO(Antisense Oligonucleotide) in project

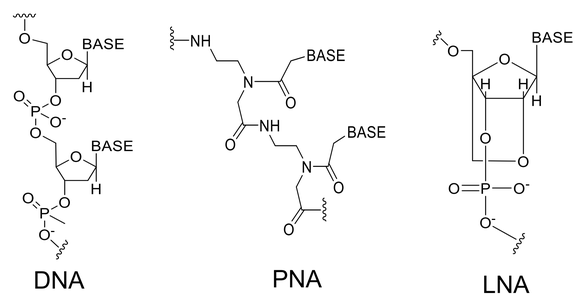


Fig. 3 The structure of DNA, PNA, and LNA

Identification of the Targeting Site of XIAP IRES

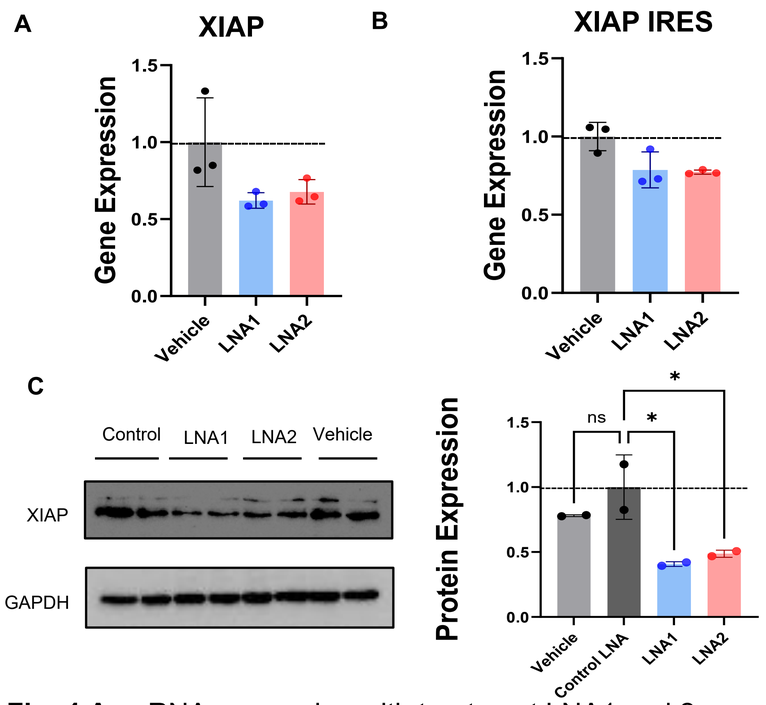
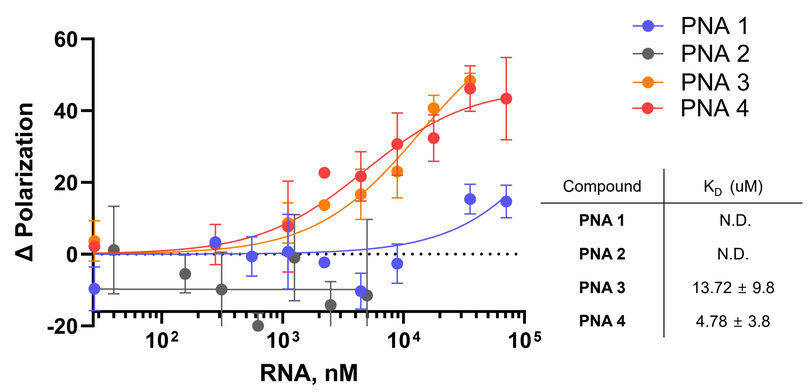


Fig. 4 A. mRNA expression with treatment LNA1 and 2 targeting XIAP **B.** mRNA expression with treatment LNA1 and 2 targeting XIAP IRES **C.** Western blot analysis of treatment Control LNA, LNA1, and 2 in HeLa cells

Binding Assay



Compound	K_D (uM)
PNA 1	N.D.
PNA 2	N.D.
PNA 3	13.72 ± 9.8
PNA 4	4.78 ± 3.8

Fig. 5 Fluorescence polarization assay result. N.D. Not detected.

Reporter Assay

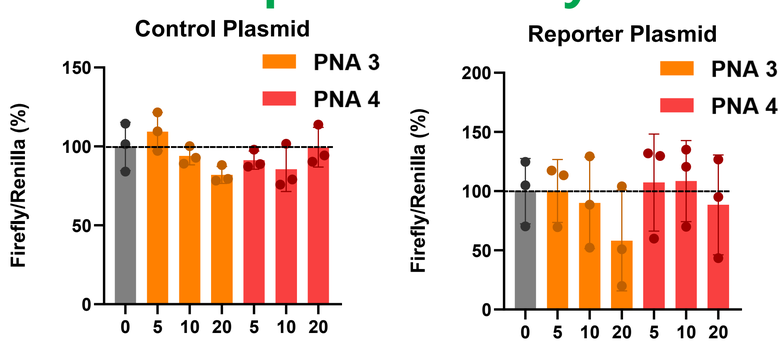


Fig. 6 Reporter assay result with treatment **PNA 3** and **4**

Western Blot Analysis

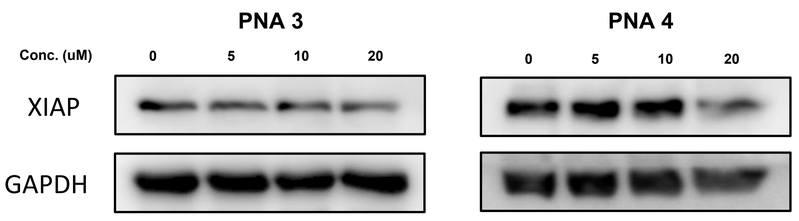


Fig. 7 Western blot analysis of treatment **PNA 3** and **4** in HeLa cells using XIAP Antibody

Effect of PNA Inhibitors in Apoptosis

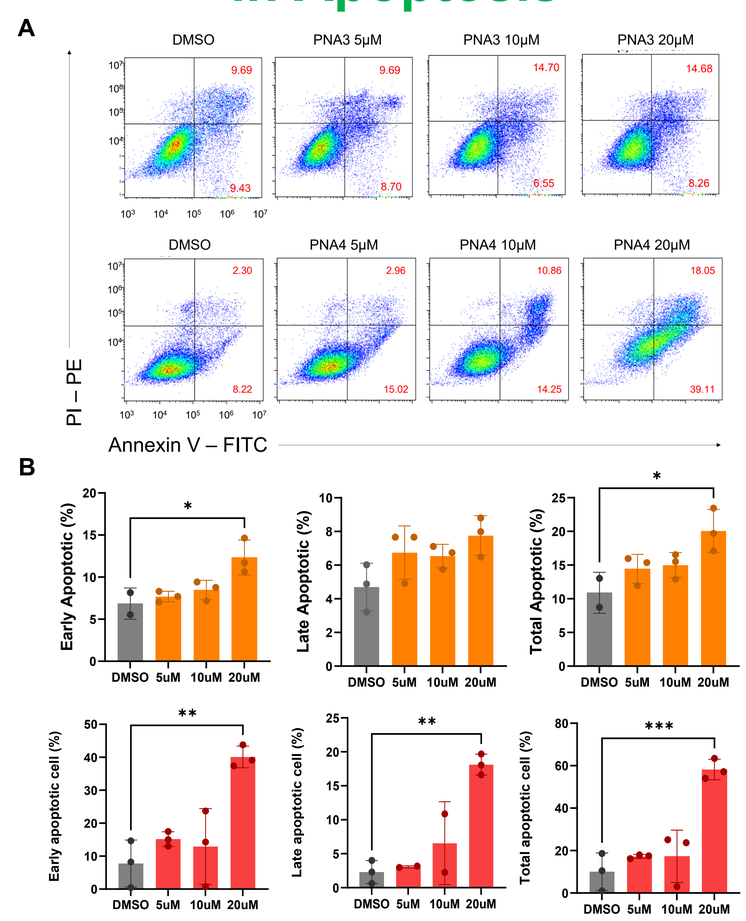


Fig. 8 A. FACS analysis with treatment **PNA 3** and **4** **B.** Apoptotic cell quantification graph with treatment **PNA 3** and **4**

Combination Treatment

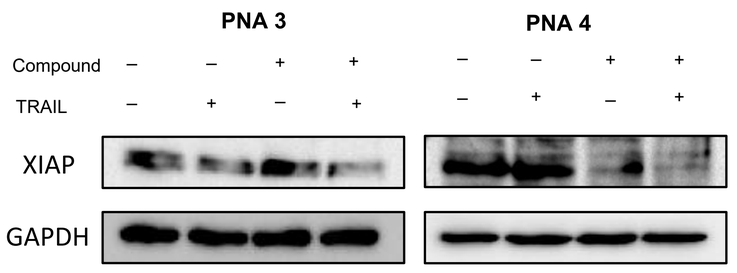


Fig. 10 Western blot analysis of combination treatment **PNA 3** or **4** with TRAIL in AsPC-1 cells

Caspase Activation

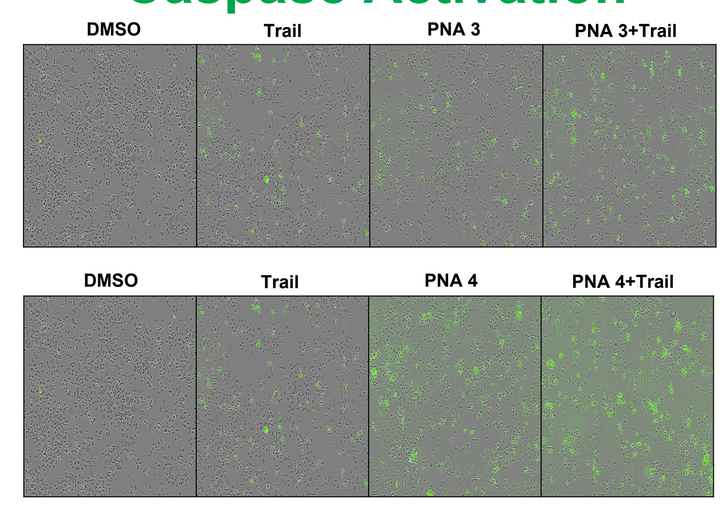


Fig. 9 Caspase activation analysis of combination treatment **PNA 3** or **4** with TRAIL in AsPC-1 cells

Synergetic Effect of TRAIL and PNA Inhibitor

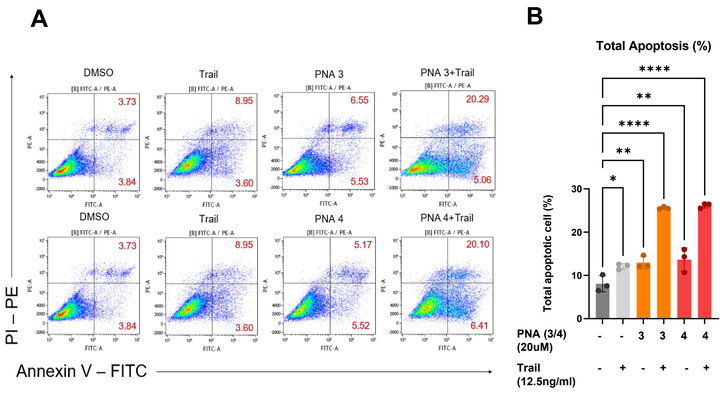


Fig. 11 A. FACS analysis with treatment **PNA 3** and **4** **B.** Apoptotic cell quantification graph with treatment **PNA 3** and **4**

Conclusions

We developed PNA compounds specifically targeting the XIAP IRES and confirmed theirz strong RNA binding affinity and effective suppression of XIAP expression at both mRNA and protein levels. In TRAIL-resistant AsPC-1 cells, co-treatment with TRAIL significantly enhanced apoptotic cell death, demonstrating that XIAP IRES-targeting PNAs can sensitize resistant cancer cells to TRAIL. These findings suggest that PNAs targeting XIAP IRES represent a promising strategy to overcome apoptosis resistance and may serve as potent candidates for combination cancer therapy against TRAIL-resistant cancers.

Contact information

Web: https://dldudwn11111.wixsite.com/lee-group

Prof. Yeongju Lee. lyj0308@pusan.ac.kr **+82-51-510-2868**

Hyein Jung. haein7052@pusan.ac.kr

Exploring the Design Space of 3_{10}-helical Bundles using Non-canonical Amino Acid

Xiyue Leng[1], Jonathan Clayden[1], and Derek N. Woolfson[1,2,3,4]

[1]School of Chemistry, [2]School of Biochemistry, and [3]Max Plack-Bristol Centre for Minimal Biology, University of Bristol, Bristol, UK; [4]Novo Nordisk Foundation Center for Protein Design, Department of Biology and Department of Drug Design and Pharmacology, University of Copenhagen, DK. 10.17952/38EPS.2026.P464 Presenting author: xiyue.leng@bristol.ac.uk

Overview Peptides and proteins based on α-amino acids predominantly adopt α-helical and β-strand structures, while extended assemblies of the noncanonical 3_{10} helix remain rare. We previously designed the *de novo* peptide $(\mathtt{ELUULK})_4$, which forms a hexameric 3_{10}-helical bundle in which Aib promotes 3_{10}-helix formation, Leu forms the hydrophobic core, and Glu/Lys define the solvent-exposed surface.[1] Here, we investigate the sequence requirements underlying this noncanonical fold and explore routes to its functionalisation. Surface substitutions are well tolerated, whereas the Aib flanking positions show substantially greater constraints. Core positions are more restrictive, with Leu uniquely supporting bundle formation among proteinogenic hydrophobic residues. Extending to seven hexad repeats enables substitution of two central core Leu residues with Ala or Gly while retaining stable, hexameric 3_{10}-helical assemblies. These substitutions generate hydrophobic cavities capable of binding environment-sensitive dyes. Together, these results define sequence constraints governing the stability of *de novo* 3_{10}-helical bundles and demonstrate how controlled core modification can alter these otherwise highly constrained assemblies.

1. Why design 3_{10} helices?

Extended 3_{10} helices occupy a narrow backbone-conformational region, and are rare as stand-alone higher-order assemblies in Nature.

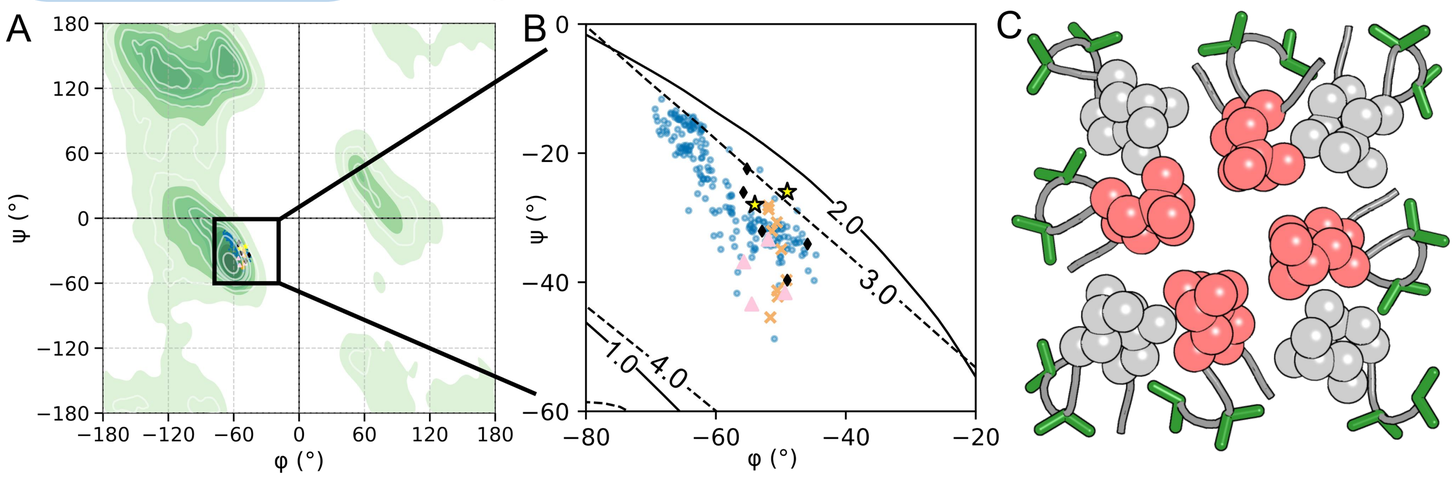


Fig. 1 Backbone geometry and design rationale of the 3_{10}-helical bundle. (**A**) Ramachandran distribution for residues in the Top8000 dataset overlayed with backbone dihedral angles (φ, ψ) from the representative 3_{10} helices extracted using the AMPAL library.[2-3] The experimental 3_{10} points occupy a restricted region adjacent to the α-helical basin; the green contour represents structural occurrence. (**B**) Expanded view of the region where φ is within (-80, -20) and ψ is within (-60,0) overlaid with helix parameters, rise per residue (Å) (solid line) and residues per turn (dotted line). The idealised 3_{10} helical geometry (3 residues per turn and 2.0 Å rise per residue) defines a narrow ridge, sampled by the experimental structures. (C) Top view of the X-ray crystal structure of *de novo* 3_{10}-helical bundle (PDB ID: 7qdi). The hydrophobic seam consisting of Leu side chains shown as spheres, featuring an inner (pink) and outer (grey) ring of helices.

2. A positional hierarchy of mutability

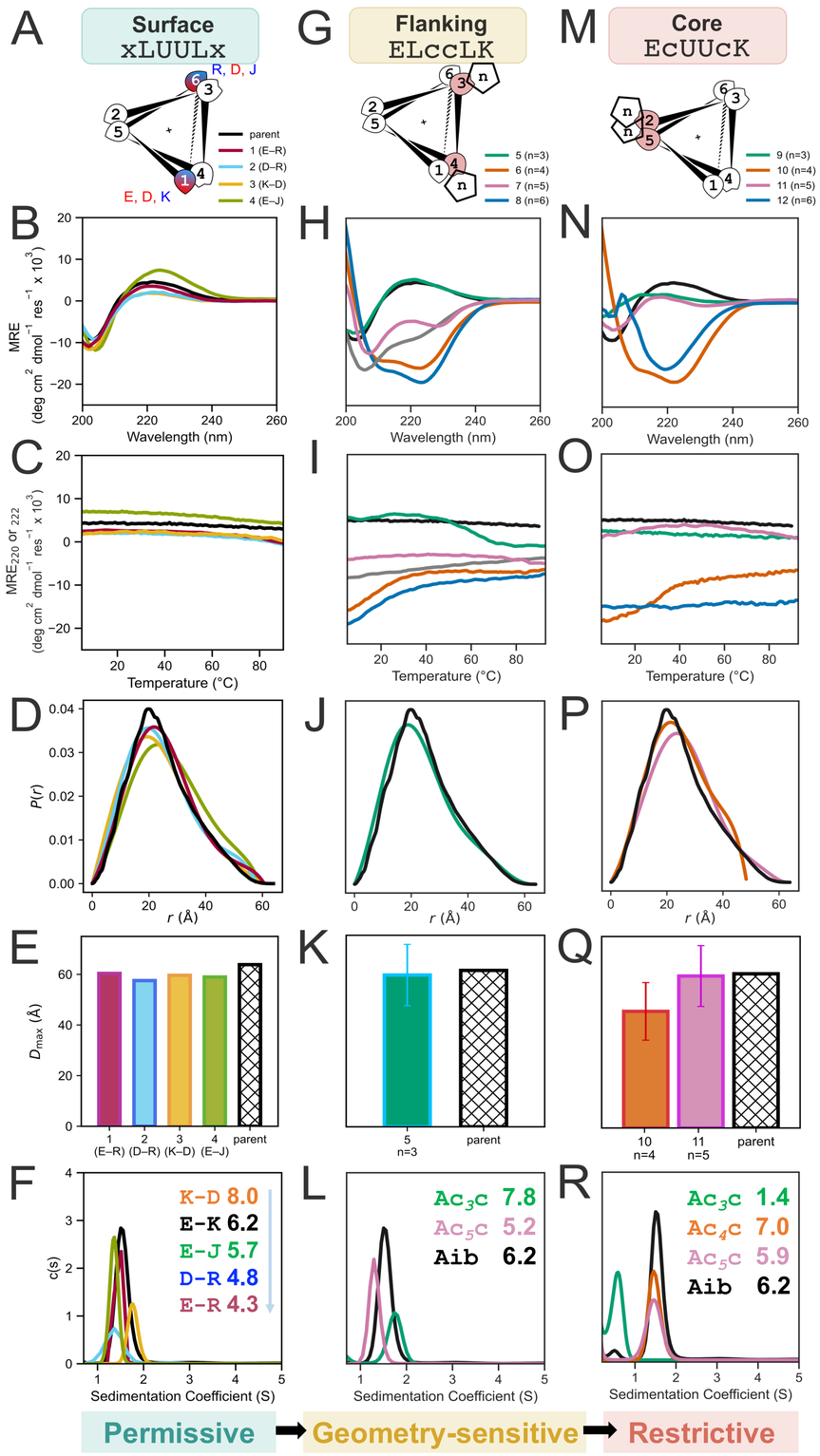


Fig. 2 Biophysical characterisation of surface (**1–4**), flanking (**5–8**), and core (**9–12**) variants, with the parent 3_{10}HD peptide as reference. (**A,G,M**) Helical-wheel representations and sequence motifs highlighting the substituted positions. (**B,H,N**) CD spectra at 5 °C. (**C,I,O**) Thermal unfolding monitored by CD at 220 or 222 nm (5–95 °C, 1 °C min⁻¹). (**D,J,P**) SAXS P(r) distributions and (**E,K,Q**) corresponding maximum particle dimensions. (**F,L,R**) Sedimentation-velocity AUC profiles showing the oligomeric states adopted in solution.

3. Residue energetics explain α ↔ 3_{10} switching

Dipeptide torsional free-energy surfaces provide residue-level context for the experimental switches.

Ac_3c shows the smallest energetic separation between α- and 3_{10}-helical basins, consistent with its greater compatibility with the noncanonical fold.

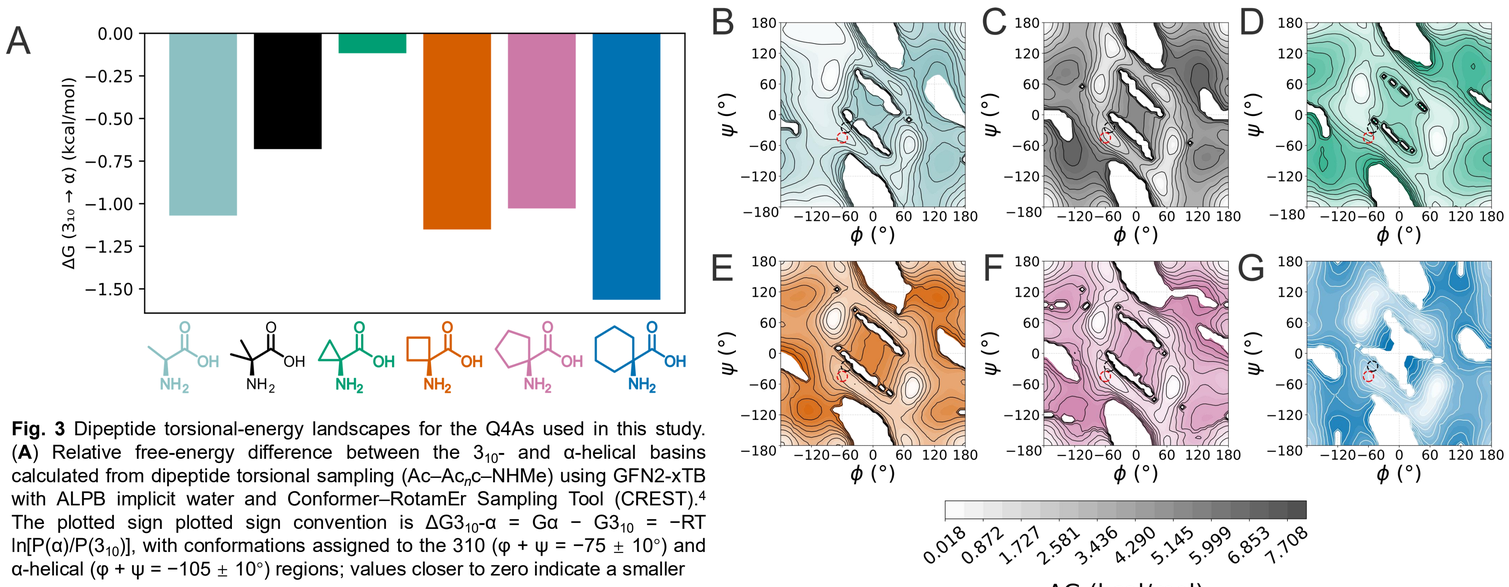


Fig. 3 Dipeptide torsional-energy landscapes for the Q4As used in this study. (**A**) Relative free-energy difference between the 3_{10}- and α-helical basins calculated from dipeptide torsional sampling (Ac–Ac_nc–NHMe) using GFN2-xTB with ALPB implicit water and Conformer–RotamEr Sampling Tool (CREST).[4] The plotted sign plotted sign convention is $\Delta G3_{10}$-α = Gα − $G3_{10}$ = −RT ln[P(α)/P(3_{10})], with conformations assigned to the 310 (φ + ψ = −75 ± 10°) and α-helical (φ + ψ = −105 ± 10°) regions; values closer to zero indicate a smaller energetic preference for α over 3_{10}. (**B–G**) Ramachandran free-energy distributions of Ala, Aib, and the larger cyclic Q4As show pronounced low-energy minima in the α-helical region, whereas Ac_3c gives the smallest separation between the two helical basins.

4. First demonstration of a functional 3_{10}-assembly

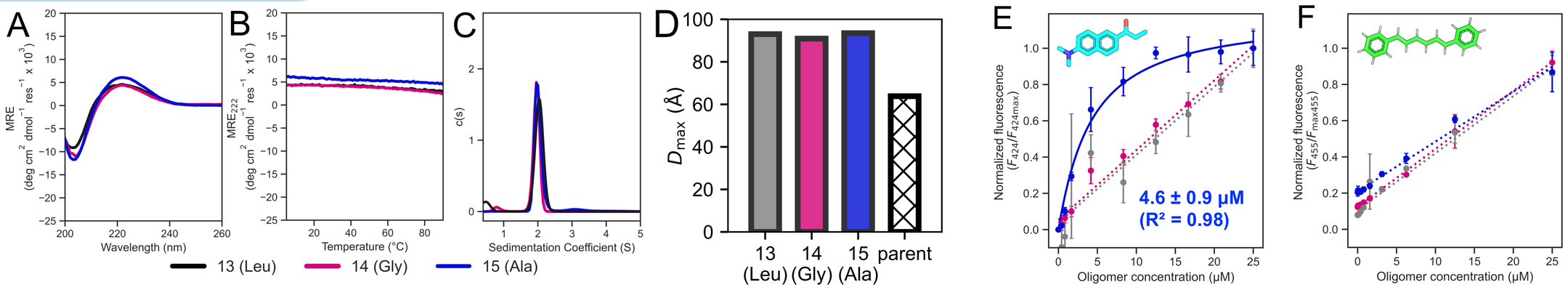


Fig. 4 Ligand recognition within extended 3_{10}-helical peptide assemblies **13–15**. Environment-sensitive dyes, 6-propionyl-2-dimethylaminonaphthalene (prodan) and 1,6-diphenylhexa-1.3,5-triene (DPH), have been assayed by us and others to probe for channels and cavities in *de novo* designed α-helical bundles and barrels.[5] Fluorescence-based binding assays only showed saturation binding for **15** with prodan, giving a dissociation constant (K_d) of 4.6 ± 0.9 μM (R^2 = 0.98). No saturation was observed for DPH binding under these conditions. Measurements were performed over 0–30 μM peptide oligomer with 1 μM dye in the final sample (5% v/v DMSO) at pH 7.4, upon incubation at 20 °C. Each dataset was normalised to its observed maximum fluorescence, and error bars represent the standard deviation of four replicate measurements.

Discussion and Conclusion The $(\mathtt{ELUULK})_4$ 3_{10}-helical bundle displays strongly position-dependent mutational tolerance. Surface residues can be readily substituted while preserving the 3_{10} architecture, whereas the interfacial Aib positions and hydrophobic core impose much tighter geometric constraints. Computational analysis indicates that successful 3_{10}-bundle formation requires both compatible backbone conformational preferences and precise side-chain geometry, explaining why small changes can redirect folding towards α-helical conformations or disrupt assembly entirely. Despite these constraints, extending the scaffold to seven hexad repeats enables controlled modification of the central hydrophobic core. Substitution of two Leu residues with Ala or Gly generates stable hexameric 3_{10}-helical bundles containing hydrophobic cavities that bind small environment-sensitive dyes in the μM range. This demonstrates that sequence extension can overcome local packing constraints and provides a route to functionalising 3_{10}-helical scaffolds through selective removal of methylene groups. Together, these results establish a sequence–structure framework for *de novo* 3_{10}-helical bundle design and show that, although more constrained than canonical α-helical assemblies, 3_{10} helices can serve as programmable scaffolds for tuning oligomerisation and creating defined molecular-recognition sites.

References

(1) Kumar, P.; Paterson, N. G.; Clayden, J.; Woolfson, D. N. *Nature* 2022, 607 (7918), 387–392. DOI: 10.1038/s41586-022-04868-x. (2) Hintze, B. J.; Lewis, S. M.; Richardson, J. S.; Richardson, D. C. *Proteins* 2016, 84 (9), 1177–1189. DOI: 10.1002/prot.25039. (3) Wood, C. W.; Heal, J. W.; Thomson, A. R.; Bartlett, G. J.; Ibarra, A. Å.; Brady, R. L.; Sessions, R. B.; Woolfson, D. N. *Bioinformatics* 2017, 33 (19), 3043–3050. DOI: 10.1093/bioinformatics/btx352 (acccessed 2024-08-08T13:56:36). (4) Pracht, P.; Grimme, S.; Bannwarth, C.; Bohle, F.; Ehlert, S.; Feldmann, G.; Gorges, J.; Müller, M.; Neudecker, T.; Plett, C.; et al. *J. Chem. Phys.* 2024, 160 (11). DOI: 10.1063/5.0197592 (5) Thomas, F.; Dawson, W. M.; Lang, E. J. M.; Burton, A. J.; Bartlett, G. J.; Rhys, G. G.; Mulholland, A. J.; Woolfson, D. N. *ACS Synth. Biol.* **2018**, 7 (7), 1808–1816. DOI: 10.1021/acssynbio.8b00225.

Amplifying Magnetic Responsiveness of Self-Assembled Peptide Nanostructures via Synergy of MNP-Helix and Rod-Coil Building Blocks

Self-Assembled Biomaterials Lab

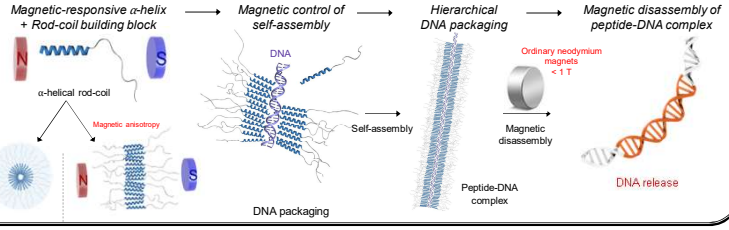
SJ.Han, ZH.Zhang, SQ.Feng, JS.Park and YB.Lim

Department of Materials Science and Engineering, Yonsei University, Seoul 03722, Republic of Korea

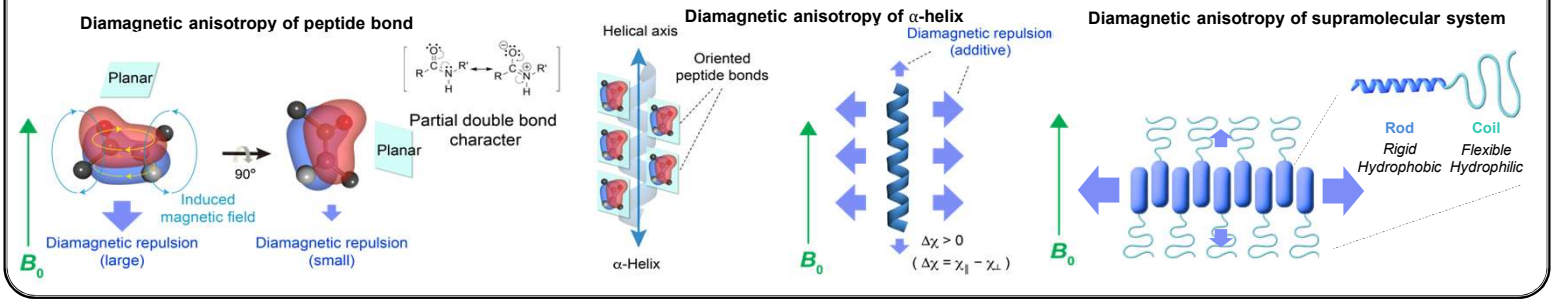
https://doi.org/10.17952/38EPS.2026.P551

Introduction

Organic molecules and materials are generally insensitive to magnetic fields due to their weak diamagnetism, typically requiring extremely strong fields to influence their behavior. This study presents a novel strategy to significantly amplify the magnetic responsiveness of self-assembled peptide nanostructures by leveraging the synergistic combination of perfect α-helices and rod-coil supramolecular building blocks. The core innovation involves the development of a monomeric, nonpolar, and perfect α-helix (MNP-helix) that maintains its helical conformation in the monomeric state, serving as an effective hydrophobic rod block in rod-coil amphiphiles. The design leverages the constructive addition of diamagnetic anisotropy from peptide bonds oriented parallel to the helical axis, which dramatically amplifies the overall diamagnetism of the α-helix. By utilizing the MNP-helix within rod-coil amphiphiles, we demonstrate that self-assembly processes can be controlled using relatively weak magnetic fields (0.07–0.25 T) provided by ordinary neodymium magnets. This practical magnetic field directly influences the morphology of the assemblies, leading to the formation of unique anisotropic nanostructures without the need for specialized high-field equipment. Furthermore, the study explores the integration of positively charged rod-coils that cooperatively assemble with DNA to form hierarchically ordered "artificial chromosomes." These rationally designed complexes effectively package and protect DNA from enzymatic degradation. Importantly, the packaged DNA can be released on demand through magnetically induced disassembly using a rotating magnetic field (RMF). Because magnetic fields are noninvasive and safe for humans, these magnetically responsive organic assemblies hold significant potential for advanced biological and medical applications. This work paves the way for future developments in responsive self-assembled structures, particularly highlighting their promise for DNA data storage and smart drug delivery systems.

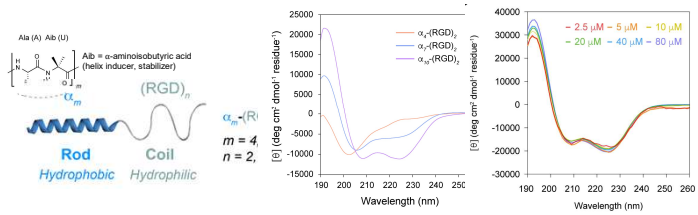


Magnetic anisotropy in organic molecules

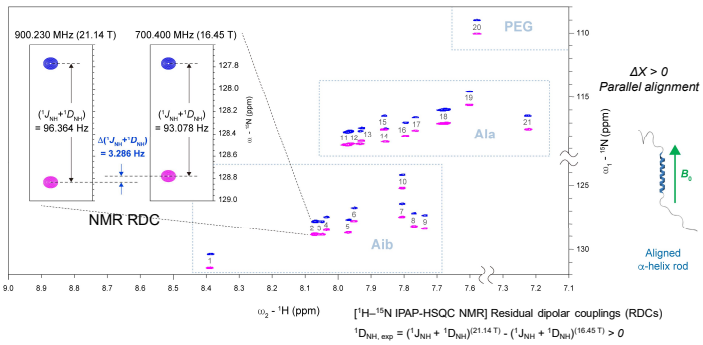


Magnetic-responsive self-assembly of α-helical rod-coils

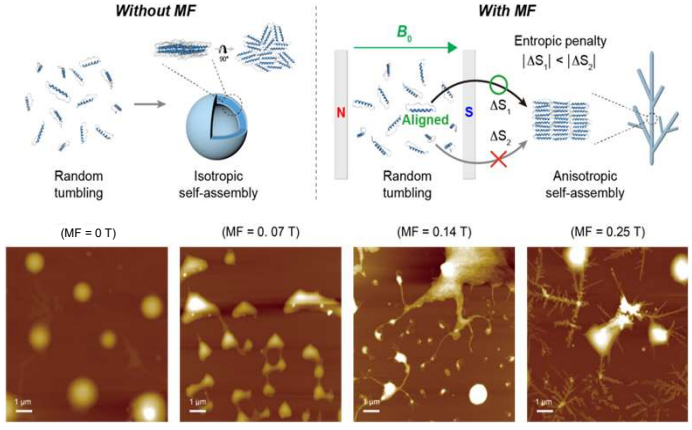
Monomeric, Nonpolar, Perfect α-helix (MNP-helix)



Magnetic alignment of MNP-helix (α_{10})

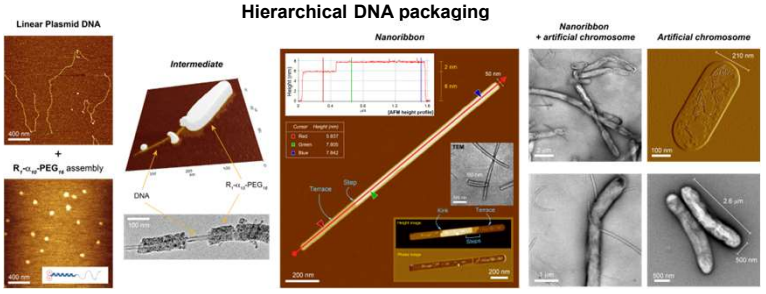


Effect of magnetic field strength on self-assembly

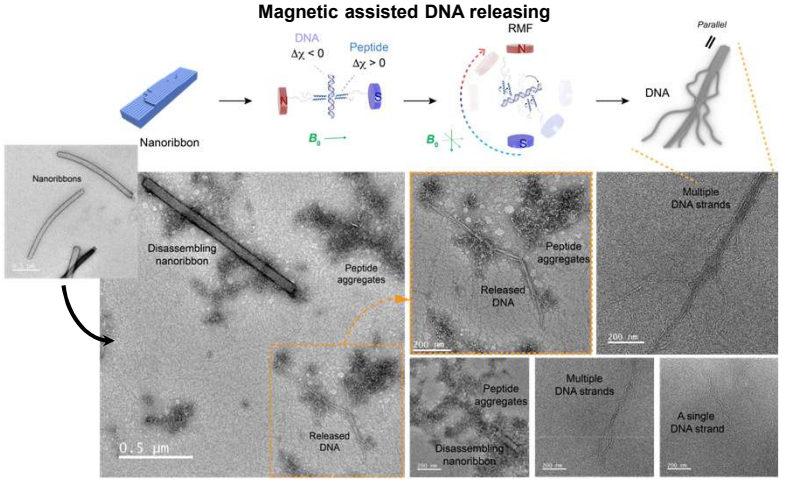


Magnetic control of self-assembly and disassembly

Hierarchical DNA packaging



Magnetic assisted DNA releasing



Reference

· "Magnetic control of self-assembly and disassembly in organic materials." ***Nature Communications,*** 14 (2023): 3081.

Pyridium-π Interaction Preserves the *N,S*-benzylidene Thioacetals (NTDs) in Acidolysis Enabling Efficient Protein Chemical Synthesis

Zhenquan Sun,[1] Yaoyue Zhang,[1] Xueqian Zhao,[2] Yisa Xiao,[1] Zhixiang Zhong,[1] Hongxiang Wu[1,3] & Xuechen Li[1,4]

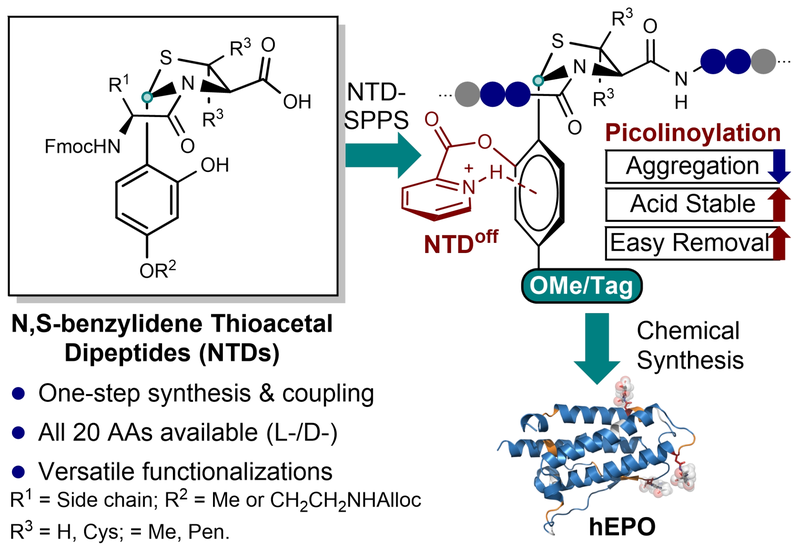
[1] *Department of Chemistry, State Key Laboratory of Synthetic Chemistry, The University of Hong Kong, Hong Kong, China.*
[2] *Department of Applied Biology and Chemical Technology, The Hong Kong Polytechnic University, Hong Kong, China.*
[3] *Zhongshan Institute for Drug Discovery, Shanghai Institute of Materia Medica, Chinese Academy of Sciences, Zhongshan, China.*
[4] *Laboratory for Marine Drugs and Bioproducts, Qingdao Marine Science and Technology Center, School of Medicine and Pharmacy, Ocean University of China, Qingdao,China.*

E-mail: xuechenl@hku.hk

https://doi.org/10.17952/38EPS.2026.P019

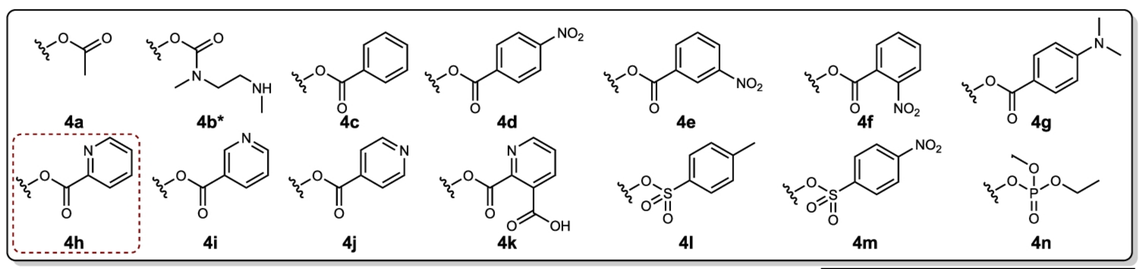
Introduction

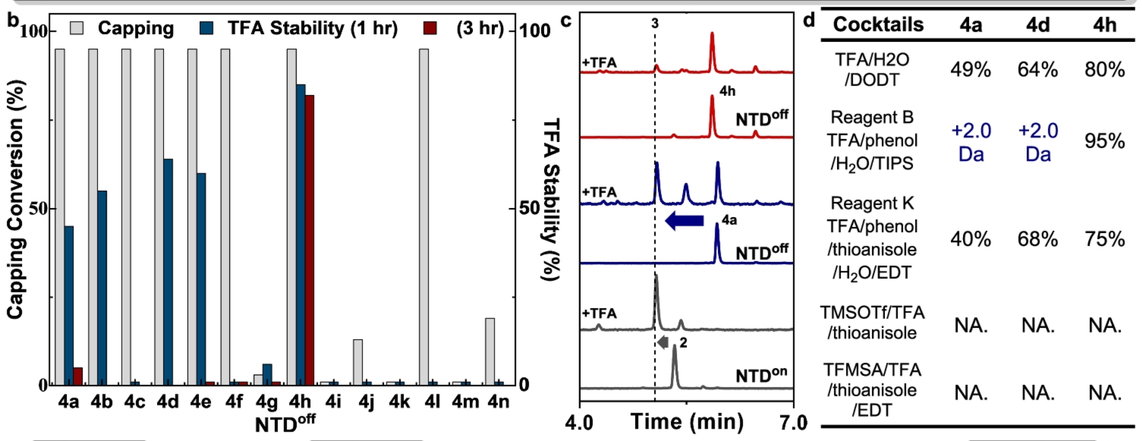
Li et al. reported the chemoselective serine/threonine ligation (STL) and cysteine/penicillamine ligation (CPL) where a C-terminal salicylaldehyde (SAL) esters of an unprotected peptide fragment is ligated with the N-terminal Ser/Thr/Cys/Pen residue of the other peptide fragment. The resulting ligation intermediates, *N,O/S*-benzylidene (thio)acetal, could serve as aggregation disruptors.[1] While such moieties could be introduced by ligation,[2,3] here, we report the synthesis and installation of *N,S*-benzylidene thioacetal dipeptides (NTDs) via standard SPPS. Moreover, we discovered a picolinoylation-based strategy to retain the NTD scaffold during global deprotection. This approach effectively suppresses aggregation both on-resin and in-solution. As a demonstration, we achieve the chemical synthesis of hEPO via a convergent route with NCL and STL incorporating the NTD chemistry.[4]



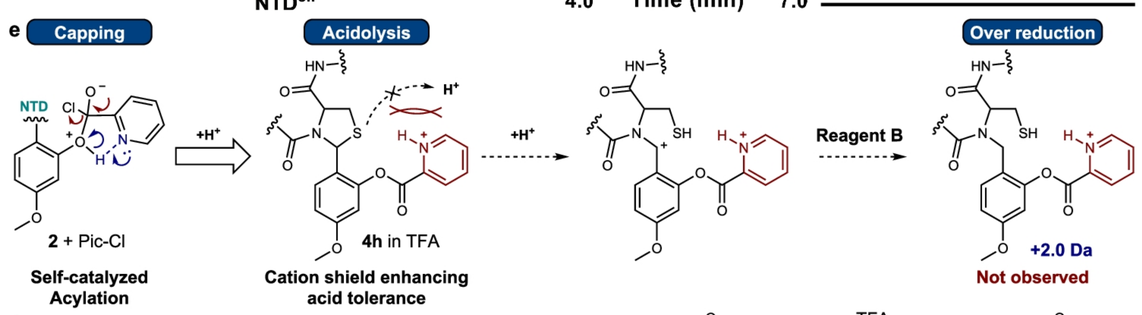
Picolinoylation enhances NTD stability in acidolysis

We incorporate an NTD scaffold in our model peptide. When the phenol group of NTD was capped by a series of acylation reagents (NTD^{off}), it will hopefully be retained during acidolysis. We found that picolinoyl-capped peptide showed superior acid-resistance, and a pyridinium-π coordination was proposed.





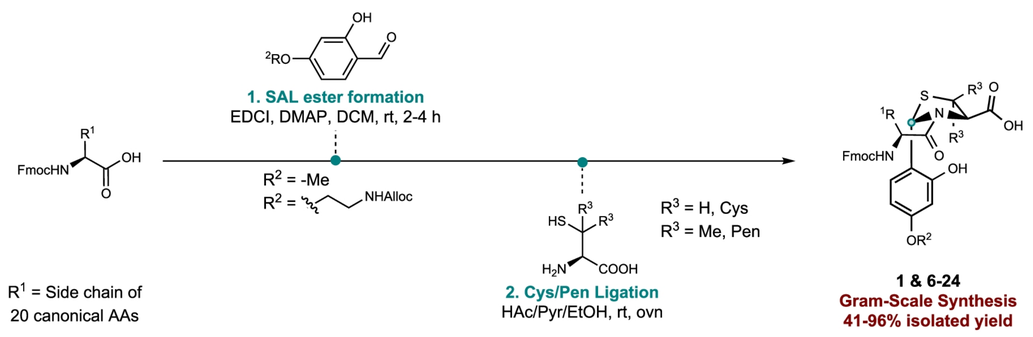
Cocktails	4a	4d	4h
TFA/H2O /DODT	49%	64%	80%
Reagent B TFA/phenol /H_2O/TIPS	+2.0 Da	+2.0 Da	95%
Reagent K TFA/phenol /thioanisole /H_2O/EDT	40%	68%	75%
TMSOTf/TFA /thioanisole	NA.	NA.	NA.
TFMSA/TFA /thioanisole /EDT	NA.	NA.	NA.



Peptide Sequence	Capping group	Conversion
Ac-AFA-IS(NBD^{off})- -APDTRPAPG-OH	Ac- (**5a**)	58%
	Pic- (**5b**)	89%
AcYGV-YT(NBD^{off})- -APDTRPAPG-OH	Ac- (**5c**)	42%
	Pic- (**5d**)	71%
AcG-VS(NBD^{off})-TAPPA- -YGVTSAPDTRPAPG-OH	Ac- (**5e**)	70%
	Pic- (**5f**)	87%
Fmoc-TT(NBD)^{off}- -APPA-OH	Ac- (**5g**)	0%
	Pic- (**5h**)	0%

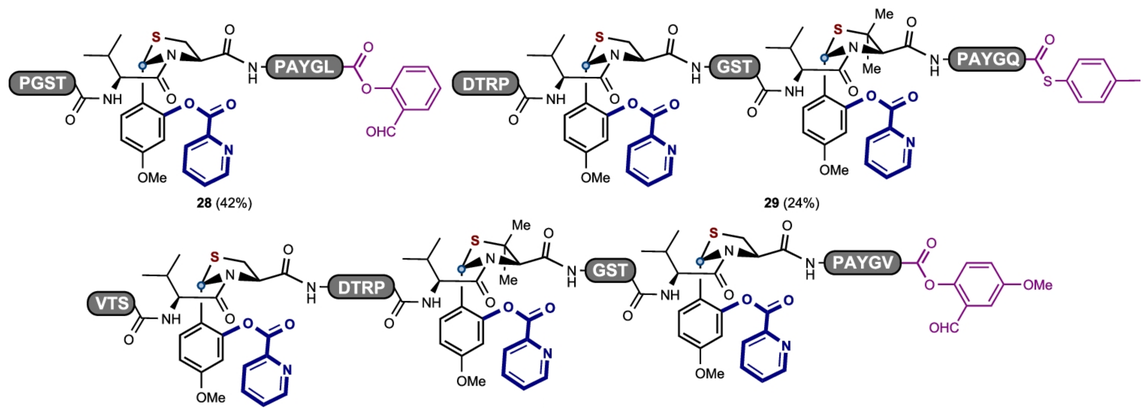
Preparation and installation of NTDs

NTD could be synthesized in a one-pot manner with satisfying isolated yields.



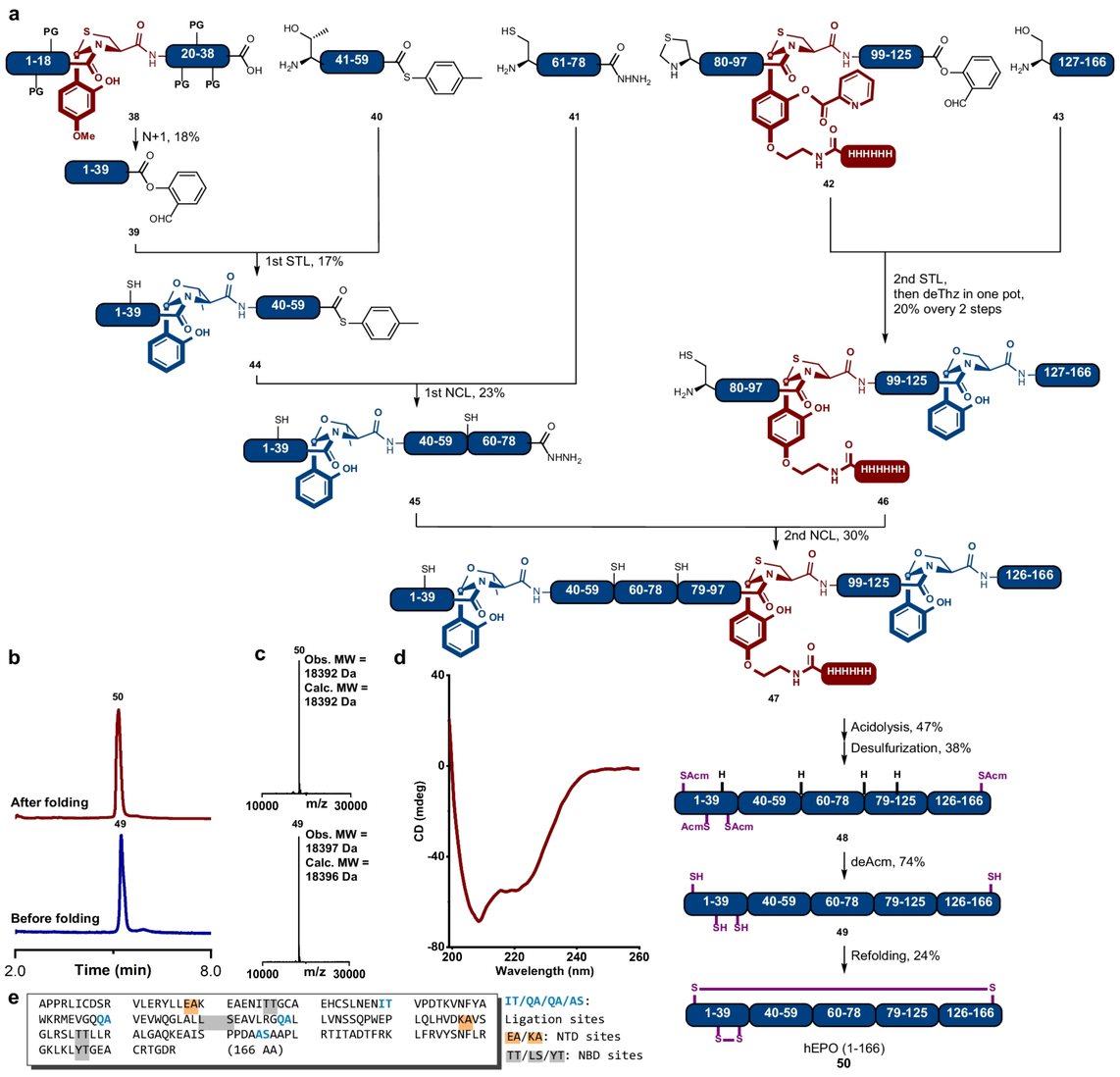
NTD can be efficiently incorporated into Fmoc-SPPS approximating other normal amino acid building blocks.

After completion of the whole peptide sequence, the NTDs are switched off by picolinoyl capping. Then the peptide undergoes either globally deprotection by TFA cocktails or soft cleavage with side-chain protected and then coupled to amino acid bearing SAL ester or thioester through N+1 strategy.[5]



Chemical synthesis of hEPO using NTD chemistry

hEPO is an important therapeutic hormone protein containing 166 amino acid residues and complicated glycosylation modification. We divided it into five fragments for a convergent synthesis adopting two NCL and two STL.



References

[1] Liu, H.; Li, X. *Acc. Chem. Res.* **2018**, *51*, 1643-1655.
[2] Wu, H.; Wei, T.; Ngai, W. L.; Zhou, H.; Li, X. *J. Am. Chem. Soc*. **2022**, *144*, 32, 14748-14757.
[3] Wu, H.; Tan, Y.; Ngai, W. L.; Li, X. *Chem. Sci.* **2023**, *14*, 1582.
[4] Sun, Z.; Zhang, Y.; Zhao, X.; Xiao, Y.; Zhong, Z.; Wu, H.; Li, X. *Nat Commun*, **2026**, *17*, 7105.
[5] Lee, C. L.; Liu, H.; Wong, C. T. T.; Chow, H. Y.; Li, X. *J. Am. Chem. Soc*. **2016**, *138*, 10477-10484.

Acknowledgements The work was supported by the Research Grants Council of Hong Kong (17312022, 17303424, T11-104/22-R, SRFS2324-7S01), Morningside professorship in chemical biology, Laboratory for Synthetic Chemistry and Chemical Biology under the Health@InnoHK Program by the Innovation and Technology Commission, Natural Science Foundation of Shanghai (25ZR1402555) and Zhongshan Science and Technology Bureau (CXTD2024006).

https://doi.org/10.17952/38EPS.2026.P097

清華大學
Key Laboratory of Bioorganic Phosphorus Chemistry
& Chemical Biology (Tsinghua University), Ministry of Education

Post-translational modifications regulate α-synuclein aggregate structure and propagation properties

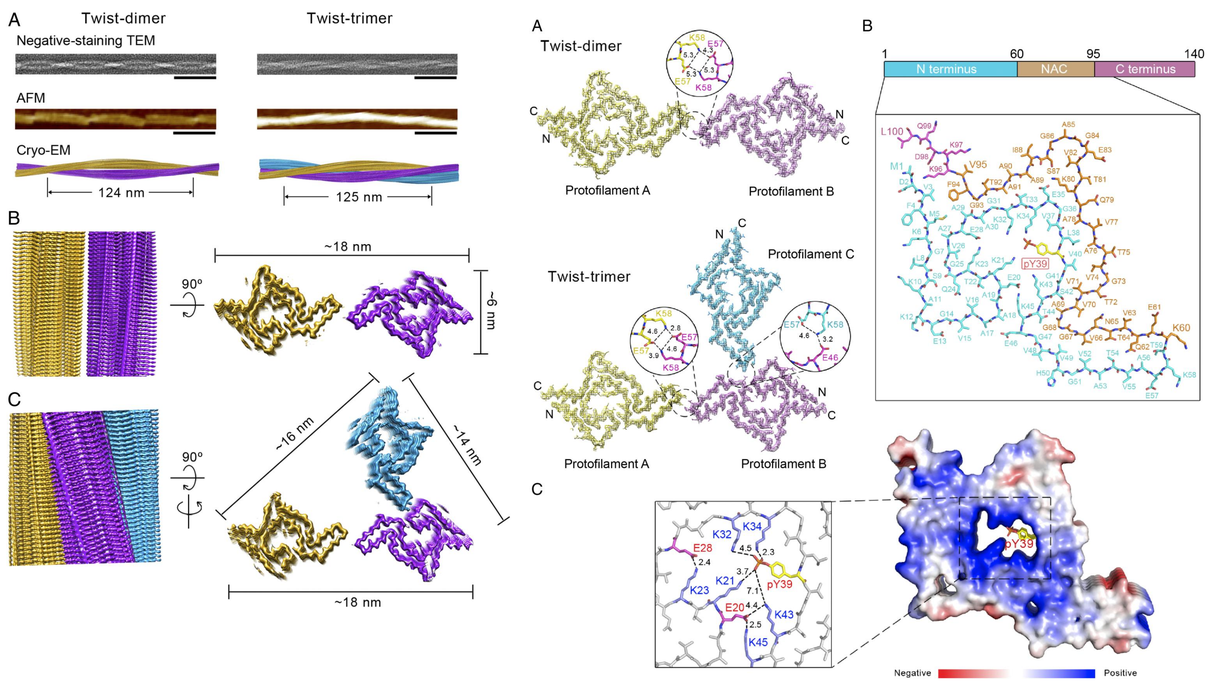
Yan-Mei Li[a]*

[a] *Department of Chemistry, Key Lab of Bioorganic Phosphorus Chemistry & Chemical Biology (Ministry of Education), Tsinghua University, Beijing, 100084, P.R. China.*
Email: liym@mail.tsinghua.edu.cn

One pathological hallmark of Parkinson's disease (PD) is α-synuclein (α-syn) forming pathological fibrils that propagate between neurons. Post-translational modifications (PTMs) critically regulate amyloid aggregation and fibril structure.

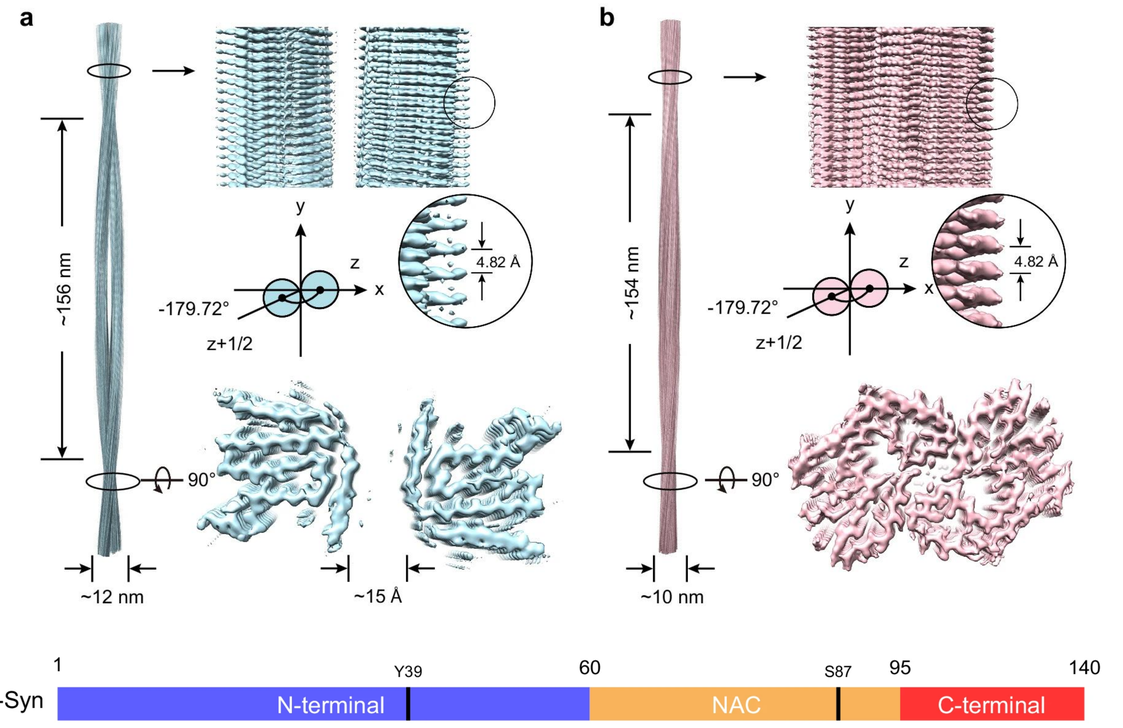
We determined the cryo-EM structure of α-syn fibrils phosphorylated at tyrosine 39 (pY39), revealing that phosphorylation acts as a "structural switch" driving pathogenic conformations. We further demonstrated that distinct PTMs at the same residue produce structural heterogeneity: Ser87 phosphorylation (pS87) and O-GlcNAc glycosylation (gS87) generate completely different fibril cores with distinct propagation properties.Mechanistically, we identified lymphocyte-activation gene 3 (LAG3) as a key receptor mediating pathological α-syn fibril endocytosis. The LAG3 D1 domain recognizes fibril β-sheet grooves through hydrophobic interactions, essential for transcellular transmission.

pY39 rearranges α-synuclein amyloid fibril structure

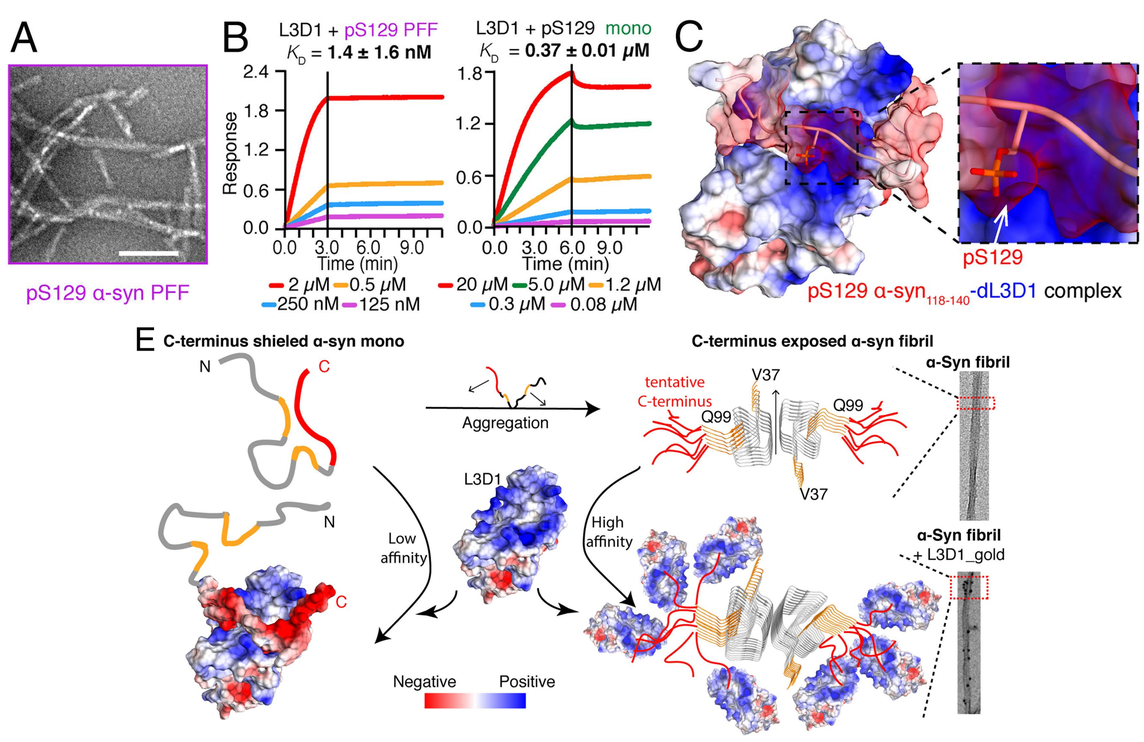


Cryo-EM polymorphs and fibril structure of pY39 α-syn (Proc. Natl. Acad. Sci. USA, 2020)

PTMs at the same site generate distinct fibril structures



pS129 enhances the binding of α-Syn fibril to LAG3



Mechanism of the preferential binding of L3D1 with α-syn fibrils (Proc. Natl. Acad. Sci. USA, 2021)

Comparison of α-syn fibril structures with different modifications (Nat. Commun., 2024)

Reference:

[1] Zhao, K.[#], Lim, Y.-J.[#], Liu, Z.[#], Long, H., Sun, Y., Hu, J.-J., Zhao, C., Tao, Y., Zhang, X., Li, D., **Li, Y.-M.*,** Liu, C.*, *Proc. Natl. Acad. Sci. USA*, **2020**, 117, 20305.

[2] Zhang, S.[#], Liu, Y.-Q.[#], Jia, C.[#], Lim, Y.-J.[#], Feng, G.[#], Xu, E., Long, H., Kimura, Y., Tao, Y., Zhao C., Wang C., Liu Z., Hu, J.-J., Ma, M.-R., Wang, R., Dawson, V. L., Dawson, T. M.*, **Li, Y.-M.*,** Mao, X.*, Liu, C.*, *Proc. Natl. Acad. Sci. USA*, **2021**, 118(26), e2011196118.

[3] Hu, J.[#], Xia, W.[#], Zeng, S.[#], Lim, Y.-J.[#], Tao, Y., Sun Y., Zhao, L., Wang, H., Le, W., Li, D., Zhang, S., Liu, C.*, **Li, Y.-M.*,** *Nat. Commun.*, **2024**, 15, 2677.

Acknowledge:

This work was supported by the National Natural Science Foundation of China (92053108 and 92353302), the National Key R&D Program of China (2018YFA0507600 and 2019YFA0904200).

Creating Antibiofilm and Antibacterial Endotracheal Tubes Using Antimicrobial Peptides and Antibiotics

Elizabeth Ogunfeibo, Sam Boateng, Doug Fraser-Pitt, Ying Yang, Wen-Wu Li

School of Life Sciences, Keele University, UK

https://doi.org/10.17952/38EPS.2026.P633

Keele UNIVERSITY

Introduction

- Endotracheal tubes are a major site of microbial contamination, where bacteria rapidly adhere to PVC surfaces and initiate biofilm formation, contributing to airway infections during mechanical ventilation.
- Biofilms on PVC medical devices significantly reduce antibiotic effectiveness, enabling pathogens to survive, spread, and contribute to antimicrobial resistance in critical-care settings.
- Surface modification of PVC offers a promising strategy to prevent bacterial attachment, using chemical grafting methods (e.g., dopamine, diazonium chemistry) to introduce reactive groups for antimicrobial attachment.
- Antimicrobial peptides and antibiotics[1] can be immobilised onto modified PVC surfaces, creating coatings with potential antibiofilm and antibacterial activity while maintaining material integrity.

➢ Aims and Objectives

This study aimed to develop a surface-based strategy to reduce biofilm-associated antimicrobial resistance by attaching antimicrobial peptides and antibiotics to modified PVC endotracheal tube materials, and to determine surface modifications that influence antibiofilm efficacy against *Staphylococcus aureus* and *Pseudomonas aeruginosa*.

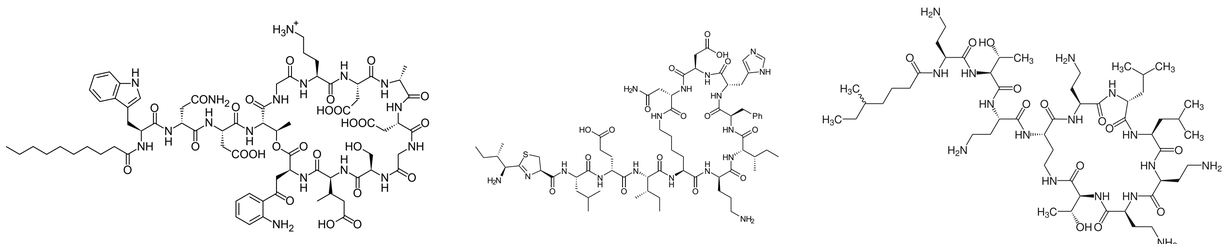


Figure 1: Chemical structures of the peptide antibiotics used in this study, including Daptomycin, Bacitracin, and Colistin.

Methods

a) **Samples & Pretreatment**: PVC discs (8 × 8 mm; 1 mm thick) were cut from medical-grade sheets, sonicated in dH_2O (3 × 5 min, 37 kHz), air-dried, and placed in sterile 24-well plates**.**

b) **Surface Modifications: i)** Polydopamine introduced amine groups. **ii)** Triple polydopamine (PDA) assembly (3 cycles of PDA), and **iii)** Diazonium chemistry: 4-carboxybenzenediazonium tetrafluoroborate was reduced with H_3PO_2/HBF_4 to graft aryl radicals, followed by NHS/EDC activation.

c) **Peptide & Antibiotic Attachment:** Ciprofloxacin was prepared at 10 mg·mL^{-1} in acetone: H_2O with HCl, and peptide solutions (Daptomycin, Bacitracin, Colistin) were prepared at 40 µg·mL^{-1}. Modified discs were immersed in peptide and antibiotic solutions for 24 h, rinsed, and dried.

d) **Surface Analysis: XPS and FT-IR** were used to confirm the introduction of functional groups and antimicrobial attachment. **Contact angle:** The sessile drop method was used to assess wettability**. Antimicrobial Assays:** Biofilm activity (TTC extraction) and planktonic growth (OD_{600}) were measured using a modified BOAT assay to assess antimicrobial efficacy.[2]

e) **Data Processing: Contact angle**: Welch's ANOVA with Dunnett's T3 post-hoc test (n = 9; α = 0.05). **Fold-change (OD_{600}):** One-way ANOVA with Dunnett's T3 post-hoc test (n = 3; α = 0.05).

Results and Discussion

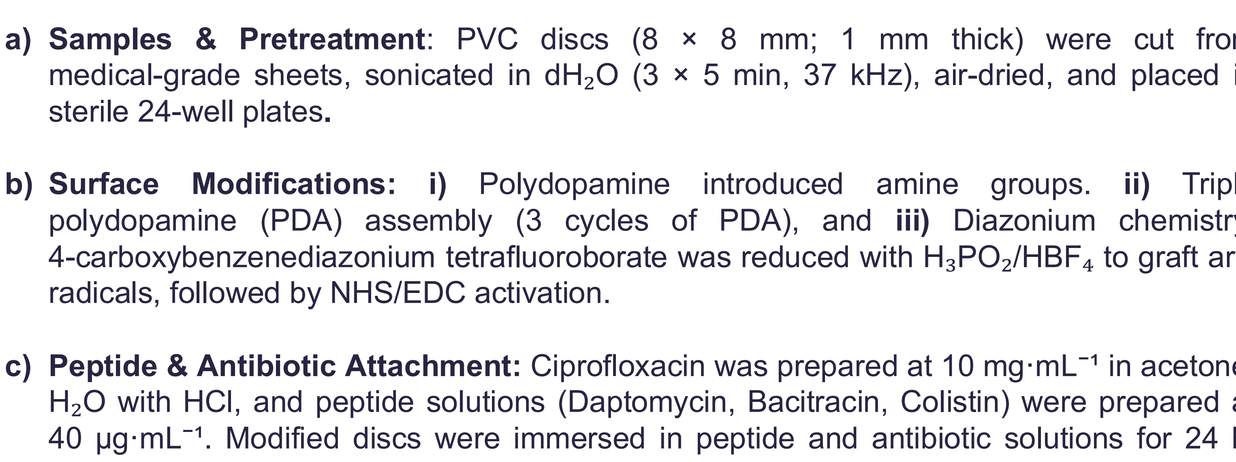


Figure 2: FTIR spectra of chemically modified PVC surfaces. (A) Dopamine-treated PVC: dopamine introduces aromatic and O–H/N–H features, while daptomycin adds amide I/II bands confirming peptide attachment. **(B) Diazonium-modified PVC**: diazonium grafting introduces new aromatic peaks, and subsequent daptomycin coupling produces characteristic amide bands, indicating successful peptide attachment.

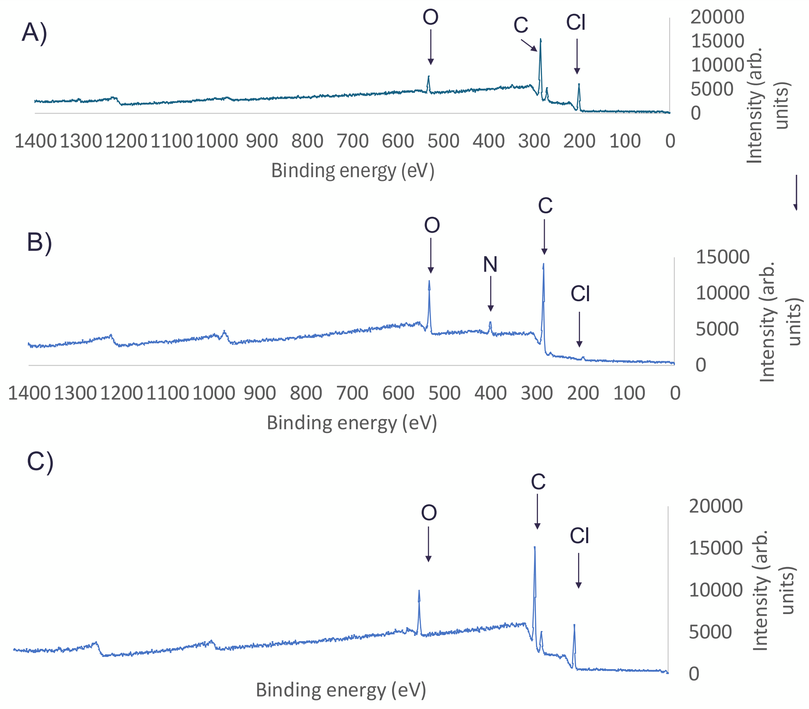


Figure 3: XPS survey spectra of PVC surfaces. A) Uncoated PVC showing characteristic carbon (C), oxygen (O), and Chlorine (Cl) peaks of the native polymer surface. **B) Polydopamine-coated PVC** displaying C, O, Cl, and an additional nitrogen (N) peak, confirming successful PDA deposition. **C) Diazonium-modified PVC** retaining the core PVC peaks: O, C and Cl.

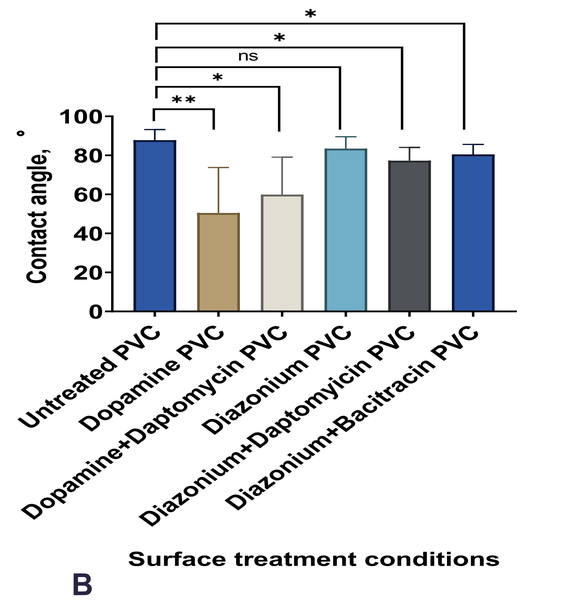


Figure 4: Contact angle measurements of PVC surfaces under different chemical treatments. Mean contact angles (n = 9) for untreated PVC, dopamine PVC, dopamine + daptomycin PVC, diazonium PVC, diazonium + daptomycin PVC, and diazonium + bacitracin PVC. Statistical analysis was performed using Welch's ANOVA with Dunnett's T3 post-hoc test (α = 0.05). * indicates significant differences compared with untreated PVC; "ns" denotes non-significant differences.

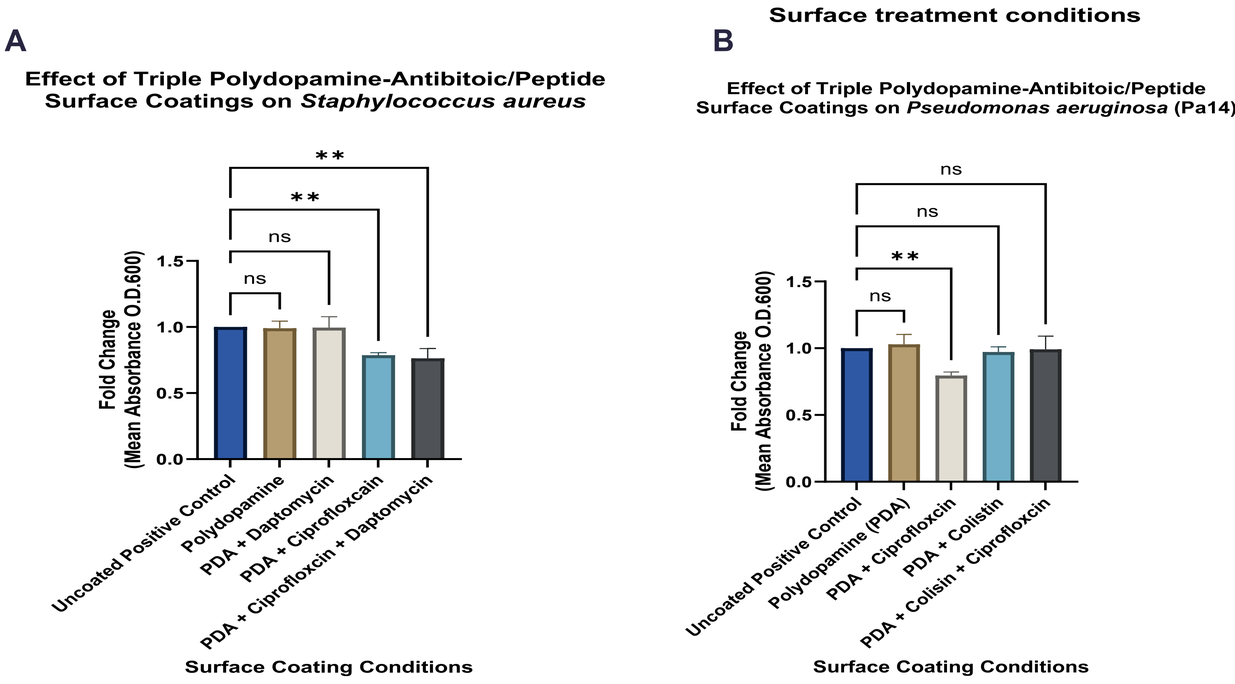


Figure 5: Effect of 3-fold polydopamine (PDA) coatings with antibiotics on biofilm formation. **(A)** ***S. aureus***: PDA + ciprofloxacin and PDA + ciprofloxacin + daptomycin significantly reduced biofilm biomass (OD_{600}) compared with uncoated PVC (One-way ANOVA, $p < 0.0001$). **(B)** ***P. aeruginosa*** **(Pa14):** PDA + ciprofloxacin significantly reduced biofilm biomass relative to uncoated controls (One-way ANOVA, $p = 0.0047$; $p < 0.01$).

Conclusion

- PVC surfaces were successfully functionalised using polydopamine and diazonium chemistry, as confirmed by XPS and FTIR analysis.
- Surface modification altered PVC surface wettability, indicating changes in surface energy necessary for antimicrobial attachment.
- PDA + ciprofloxacin and PDA + ciprofloxacin + daptomycin coatings produced a significant reduction in *S. aureus* biofilm biomass.
- PDA + ciprofloxacin also reduced *P. aeruginosa* biofilm formation, demonstrating strong Gram-positive and moderate Gram-negative antibiofilm activity.
- These findings show that combining surface chemistry with antimicrobial loading can create effective antibiofilm PVC surfaces suitable for improving endotracheal tube safety.
- Further optimisation of coating stability and peptide–antibiotic combinations could enhance performance and broaden clinical applicability.

References:

1. Raheem, N. and Straus, S.K. (2019). Mechanisms of Action for Antimicrobial Peptides With Antibacterial and Antibiofilm Functions. Frontiers in Microbiology, 10. doi:https://doi.org/10.3389/fmicb.2019.02866.
2. Revdiwala, S., Rajdev, B.M. and Mulla, S. (2012). Characterization of Bacterial Etiologic Agents of Biofilm Formation in Medical Devices in Critical Care Setup. Critical Care Research and Practice, 2012, pp.1–6. doi:https://doi.org/10.1155/2012/945805.

THIS IS KEELE

Peptide-Based Surface Engineering of Biomimetic Liposomes for Biomedical Applications

Giulia Lodigiani,[1,2] Roberto Frigerio,[1] Alessandro Gori,[1] Francesca Baldelli Bombelli,[2] Greta Bergamaschi.[1]

[1] Consiglio Nazionale delle Ricerche, Istituto di Scienze e Tecnologie Chimiche "Giulio Natta" (SCITEC), Milano, Italy.

[2] Dipartimento di Chimica, Materiali e Ingegneria Chimica "Giulio Natta", Politecnico di Milano, Milano, Italy.

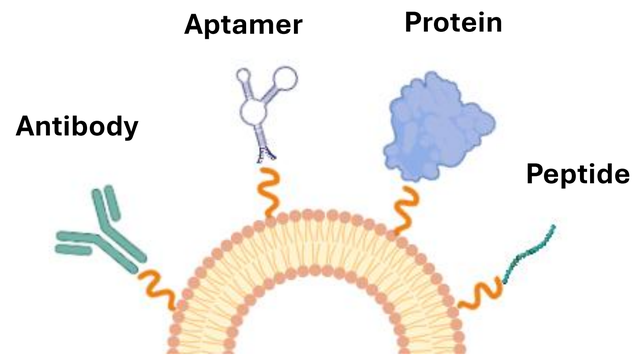
giulia.lodigiani@polimi.it

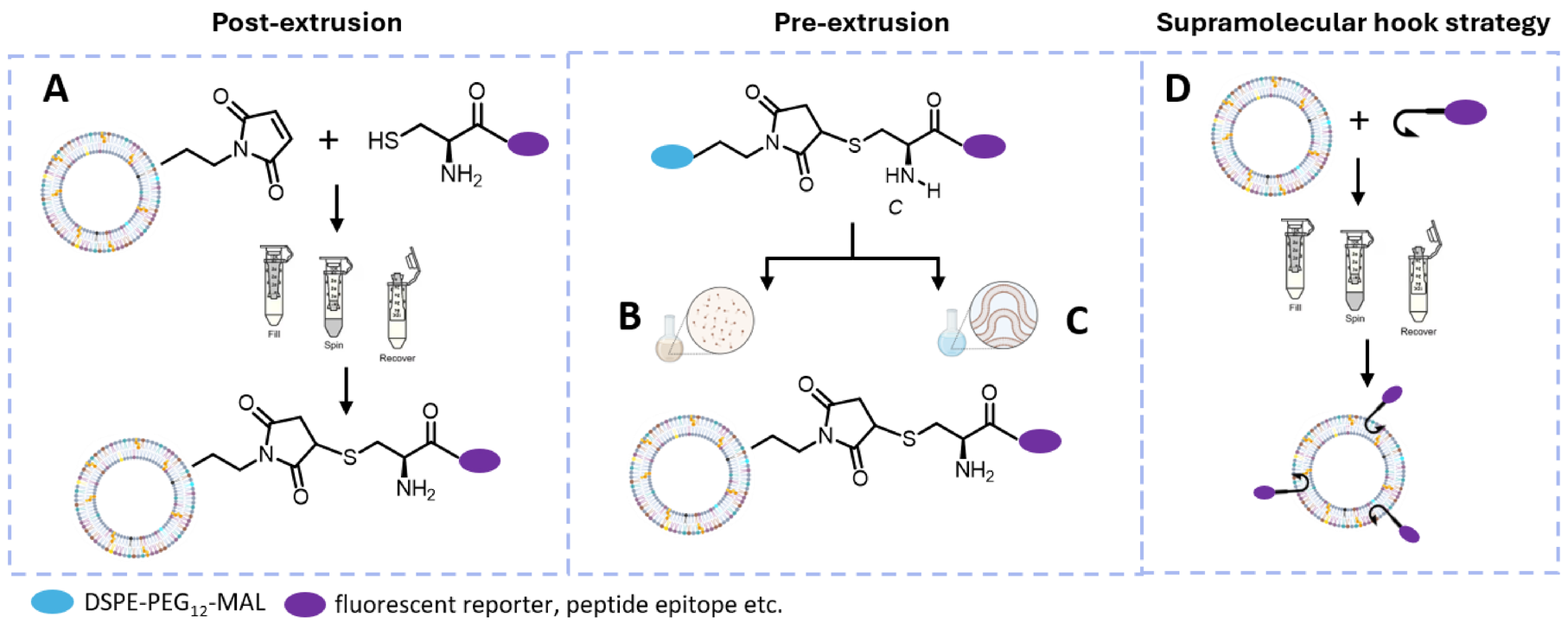
https://doi.org/10.17952/38EPS.2026.P411

Peptides for liposome surface functionalization

Efficient and selective targeting remains a major challenge in liposome-based therapies. Surface functionalization with peptides offers a versatile strategy to enhance receptor-mediated uptake, combining small size, low steric hindrance, chemical versatility, and precise control over sequence and surface density.

In this study, we investigated different peptide conjugation strategies for our biomimetic **Lipo-EV platform**, comparing **covalent maleimide–thiol coupling** and a non-covalent **"hook peptide" approach** enabling spontaneous membrane insertion. Different peptide-to-lipid ratios were evaluated in terms of **conjugation efficiency, stability, and peptide accessibility** using complementary analytical techniques. Peptide epitope exposure and functionality were further assessed by **peptide microarray immunoassays** and **fluorescence-based nanoparticle tracking analysis (NTA)**.



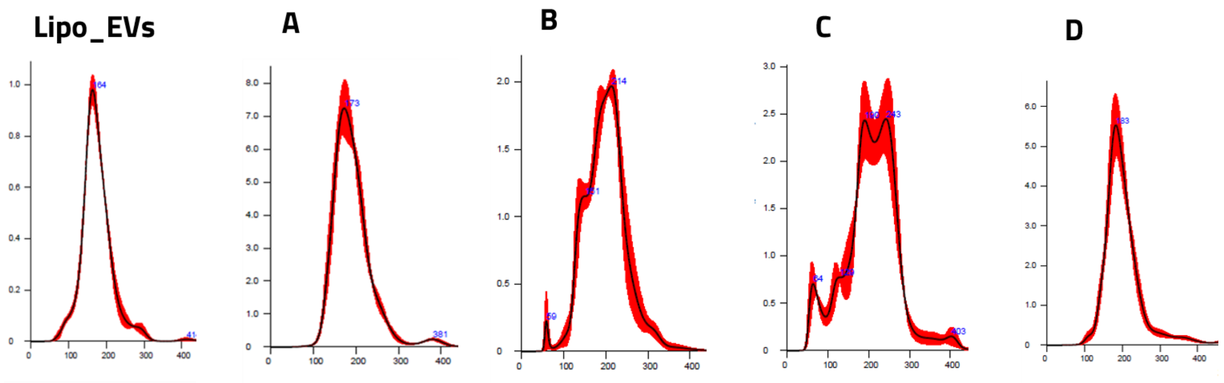


(A) Covalent peptide conjugation to maleimide-functionalized liposomes, followed by purification. **(B–C)** Peptide–lipid incorporation during liposome preparation by hydration and extrusion.

(D) Post-assembly insertion of hook peptides into preformed liposomes, followed by purification, enabling stable peptide insertion into the lipid bilayer.

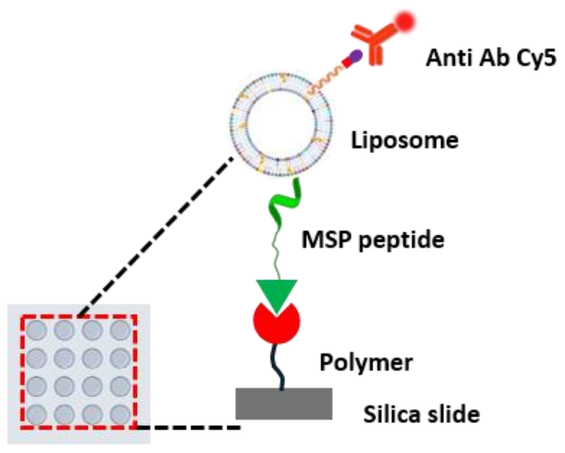
Assessing functionalization

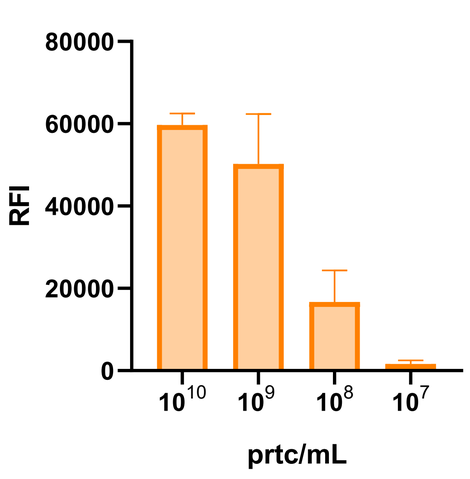
NTA



NTA analysis showed comparable particle size distributions for most functionalization strategies, while **Strategy C** displayed increased polydispersity, likely due to peptide–lipid micelle formation during hydration.

Microarray immunoassay

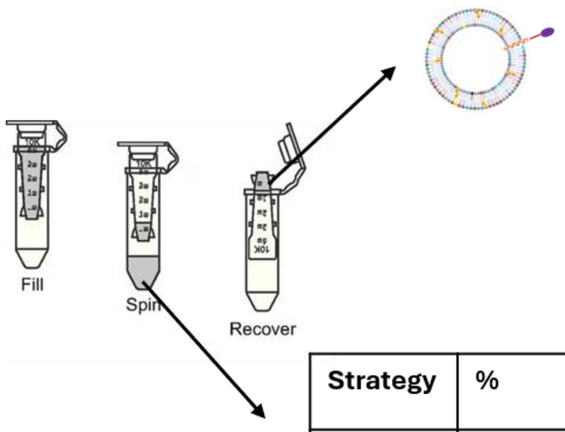




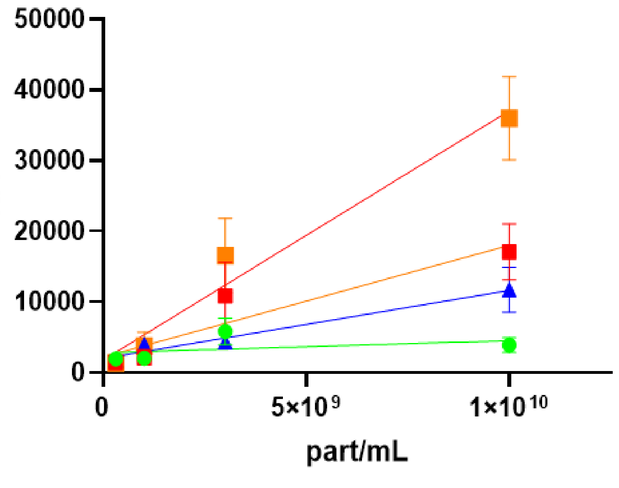
Epitope exposure was assessed using V5-tagged liposomes (5% peptide/lipid) captured on a silica MSP4 slides and detected by Cy5-labelled antibody. DiI Lipo_Evs were captured on MSP silica slide and detected through fluorescence to verify the capturing efficiency using this approach.

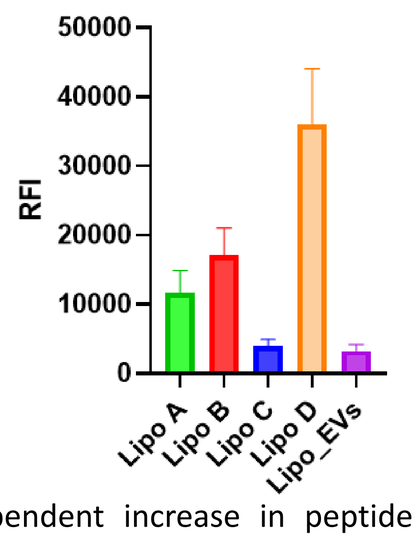
HPLC

HPLC was used to assess functionalization efficiency by monitoring peptide consumption. For Strategies A and B, Amicon wash fractions were analyzed, while for Strategies B and C, peptide–lipid conjugation was monitored directly.



Strategy	%
A	80%
B*	100%
C*	100%
D	65 %





Lipo A, B, and D showed a clear concentration-dependent increase in peptide functionalization, with Lipo D exhibiting the highest efficiency (~12-fold signal vs. unfunctionalized Lipo-EVs).

Conclusion

This study systematically compared different peptide functionalization strategies for EV-inspired liposomal nanoplatforms, highlighting the key role of functionalization approach in peptide display and accessibility. Strategy B emerged as the most effective conventional approach, providing efficient functionalization and favorable peptide exposure. Notably, Strategy D, based on a supramolecular hook peptide, offers greater versatility and modularity while avoiding extensive membrane chemical modification. Its simple, rapid, and adaptable design makes Strategy D particularly promising for future biomedical and clinical translation.

[1] Liu, Y., et al. (2021). **Nanoscale Horizons, 6**, 78–94. **[2]** Aronson, M. R., et al. (2021). **APL Bioengineering, 5**(1), 011501. **[3]** Sonju, J. N., et al. (2021). **Journal of Controlled Release, 329**, 624–644. **[4]** A. Gori, A. et al. **Journal of extracellular vesicles**, 2020, 9, 1751428.

SEQUENCE-PROGRAMMED CONTROL OF COACERVATE STABILISATION MECHANISMS USING MODULAR PEPTIDES

Roi Lopez-Blanco, Willem van den Hout, Sander Huisman, Jan C. M. van Hest

Institute for Complex Molecular Systems, Department of Chemical Engineering and Chemistry
Eindhoven University of Technology, Eindhoven, The Netherlands

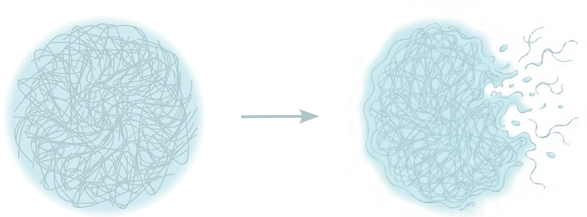
https://doi.org/10.17952/38EPS.2026.P532



r.lopez.blanco@tue.nl

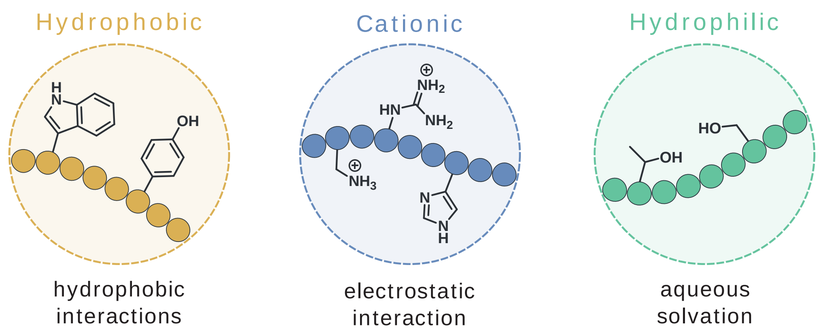
Background and objectives

- Coacervates are dynamic, crowded compartments with potential as artificial cell models.
- Their liquid nature promotes fusion and coalescence, limiting long-term stability.
- Current interfacial stabilisers improve robustness but offer limited programmability.

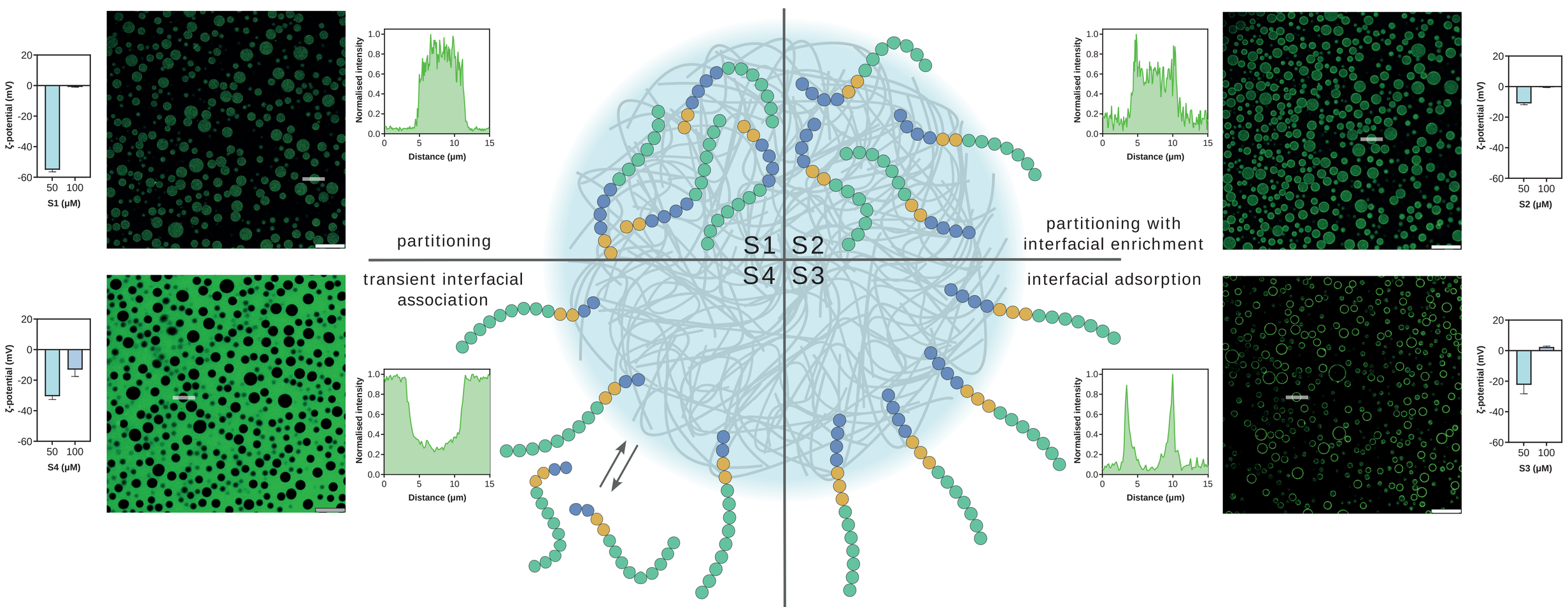


Can short, sequence-defined peptides provide programmable coacervate stabilisation?

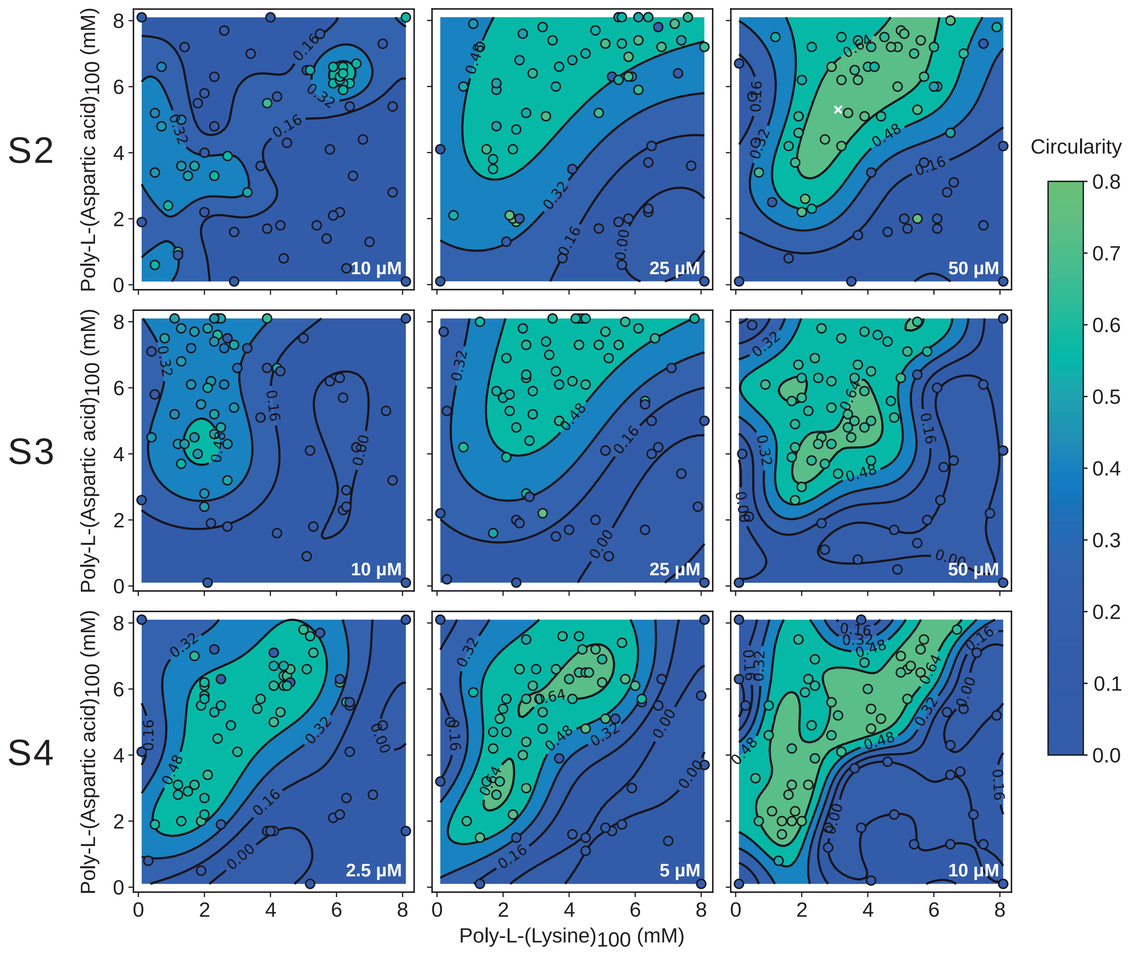
Peptide design



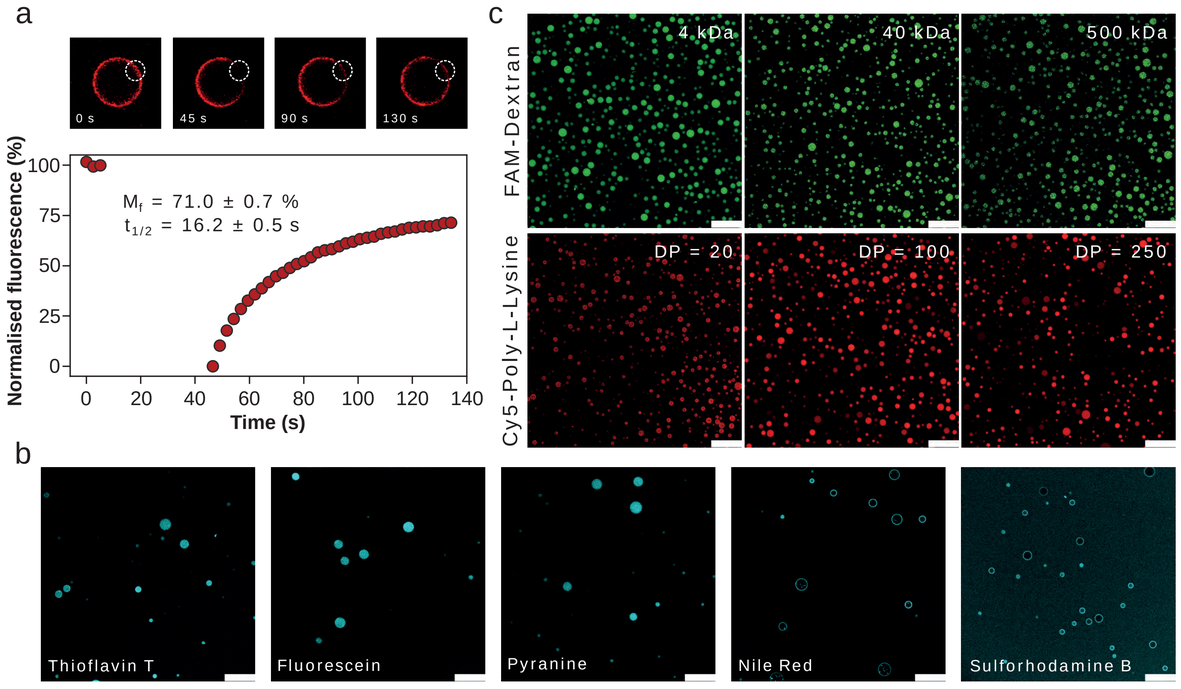
Domain position and composition rationalise peptide stabilisation modes



Sequence-dependent stabilisation landscapes



A dynamic peptide-enriched interface



FRAP of S3-enriched interface (a). Confocal microscopy micrographs of small-molecule (b) and macromolecular (c) fluorescent probes. Scale bars, 20 μm

Take-home messages

Domain order and composition
Domain order and composition dictates the stabilisation mechanism.

Single modular peptide scaffold, four stabilisation modes
A single modular scaffold spans a full mechanistic continuum: partitioning, interfacial enrichment, adsorption, or dynamic association.

Stabilised, not sealed
The interfacial layer stays dynamic and permeable.

A peptide code for programmable coacervate stabilisation
A modular peptide code for programming coacervate and protocell stabilisation modes on demand.

References

1. Banani, S. F., Lee, H. O., Hyman, A. A. & Rosen, M. K. Nat. Rev. Mol. Cell Biol. 18, 285–298 (2017).
2. Nikroo, A. H., Das, A., Verwiel, M. A. M. & van Hest, J. C. M. Angew. Chem. Int. Ed. Engl. 65, e00002 (2026).
3. Tang, D., Zhu, J., Wang, H., Chen, H., Wang, H., Huang, Y. & Jiang, L. Nat. Chem. 17, 911–923 (2025).
4. Schneider, T. N., Gil-Garcia, M., Bühler, M. A., Santos, L. F., Faltova, L., Guillén-Gosálbez, G. & Arosio, P. Nat. Commun. 17, 6497 (2026).
5. Leurs, Y. H. A., Giezen, S. N., van den Hout, W., Beeren, J., van den Aker, L. J. M., Voets, I. K., van Hest, J. C. M. & Brunsveld, L. J. Am. Chem. Soc. 147, 18412–18418 (2025).
6. Mason, A. F., Buddingh', B. C., Williams, D. S. & van Hest, J. C. M. J. Am. Chem. Soc. 139, 17309–17312 (2017).

38th European Peptide Symposium

TU/e EINDHOVEN UNIVERSITY OF TECHNOLOGY

vanHestLab

USC UNIVERSIDADE DE SANTIAGO DE COMPOSTELA

CiQUS Centro Singular de Investigación en Química Biolóxica e Materiais Moleculares

XUNTA DE GALICIA

This work was supported by Xunta de Galicia under the postdoctoral grant ED481B-2025/041

Azapeptide Assembly Using Resonant Acoustic Mixing

William D. Lubell[1], Michael Quagliata[1], Justin Desjardins-Michaud[1], Nassim Maarouf-Mesli[1], Ida Boccino[1], Zahra Bigdeli[1] and Felix Polyak[1,2]

[1]*Département de Chimie, Université de Montréal, Complexe des Sciences, 1375 Avenue Thérèse-Lavoie-Roux, Montréal, Québec, H2V 0B3, Canada.*
[2]*Studio Bioscience Inc., 111 Rue Terry Fox, Verdun, Québec, H3E 1L4, Canada.*

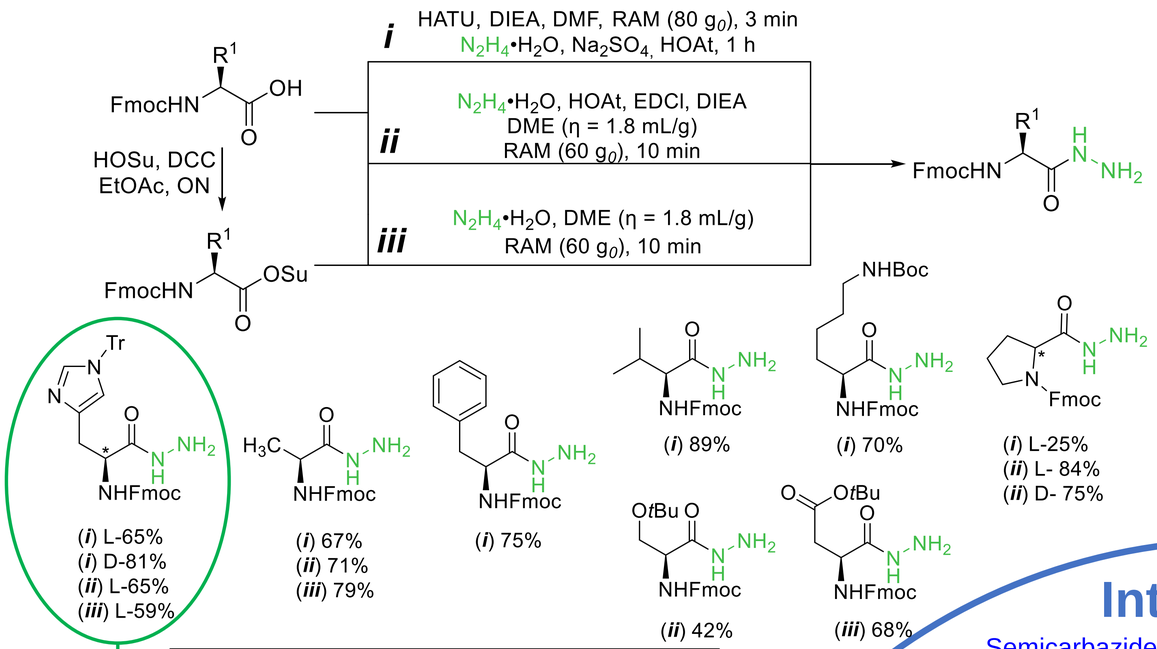
https://doi.org/10.17952/38EPS.2026.P132

Abstract

Azapeptide assembly amenable for Fmoc based peptide synthesis can be challenging because hydrazine differentiation requires selectivity. A greener solution-phase method is presented for making azapeptide by assembling *N*-(Fmoc)amino hydrazide and (Suoc)amino [*N*-succinyl carbamate] ester components at high concentration using resonant acoustic mixing (RAM). Hydrazinolysis was achieved without Fmoc cleavage, diacylation, and epimerization, eliminating chromatographic purification. Without hydantoin side products, (Suoc)amino acid analogs were effectively prepared and used in RAM-assisted semicarbazide synthesis. Aza-di-, tri-, and tetrapeptide building blocks were assembled using RAM with *N*-hydroxy-7-azabenzotriazole (HOAt) as catalyst and *N*-methylmorpholine (NMM) as solvent at high concentration. Aza-tripeptide building blocks proved useful in solid-phase synthesis of challenging bioactive targets. This sustainable, scalable approach minimizes hazardous reagents and solvents, facilitating azapeptides access for drug discovery.

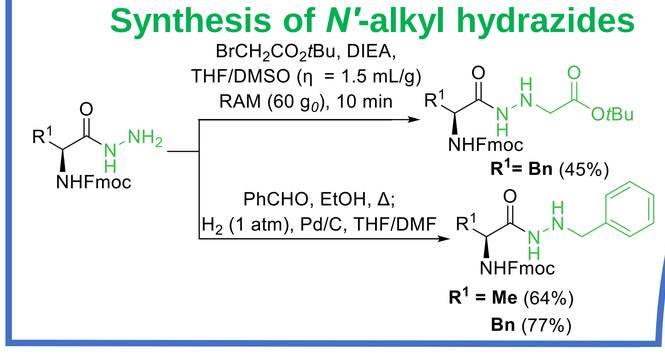
Synthesis of Fmoc-amino hydrazides

Hydrazine monohydrate was reported to cleave the Fmoc protecting group and liberate the amine in peptide synthesis [4]. The exothermic acylation of hydrazine hydrate using *N*-Fmoc-amino active esters was studied to minimize the generation of dibenzofulvene from Fmoc deprotection and diacyl-hydrazide byproduct [5]. Three strategies were successful employing *in-situ* generation of active ester (***i*** and ***ii***) and the direct acylation with succinimidyl esters (***iii***), all using RAM to expedite conversion.



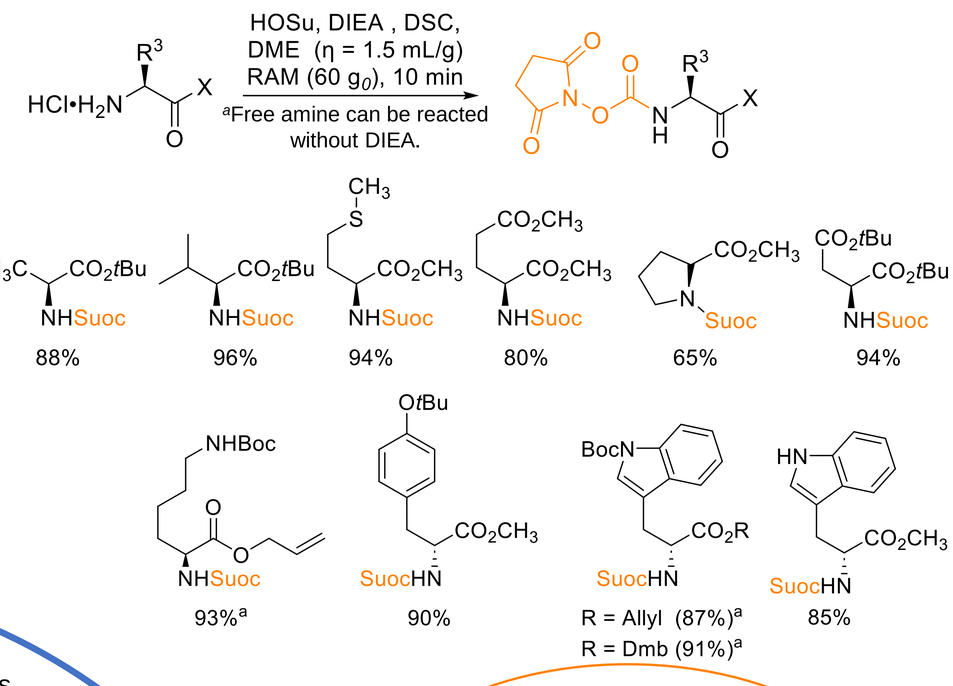
Condition	% diacyl-hydrazide	% dibenzofulvene	% D-epimer
i	<3	<2	9
ii	3	<2	<1
iii	<2	<2	<2

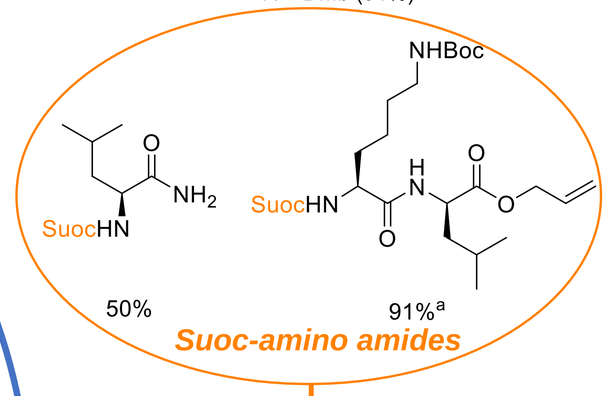
Synthesis of *N'*-alkyl hydrazides



Synthesis of Suoc-amino derivatives

Succinimidyl carbamates (Suoc) offer balanced stability and reactivity. They are readily prepared by RAM of amino ester/amide hydrochlorides with *N,N'*-disuccinimidyl carbonate (DSC), DIEA, and HOSu [6]. The HOSu (pKa 6.0) serves as buffer and reduces urea byproduct (0.4%).

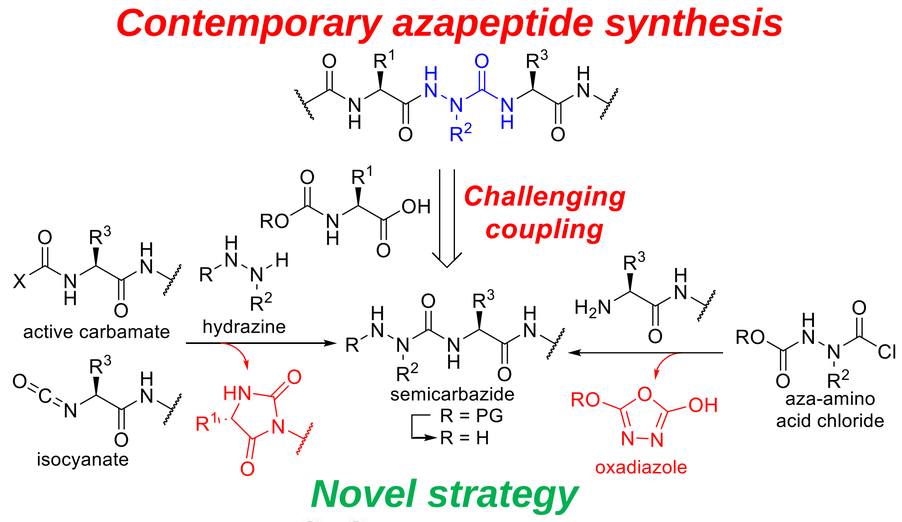




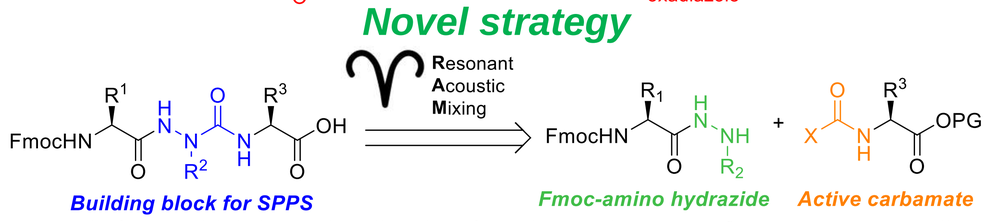
Introduction

Semicarbazides are amino amide surrogates. In azapeptides, semicarbazides can improve metabolic stability and enhance efficacy to achieve clinical success. The synthesis of semicarbazide peptidomimetics can be challenging [1].

Contemporary azapeptide synthesis

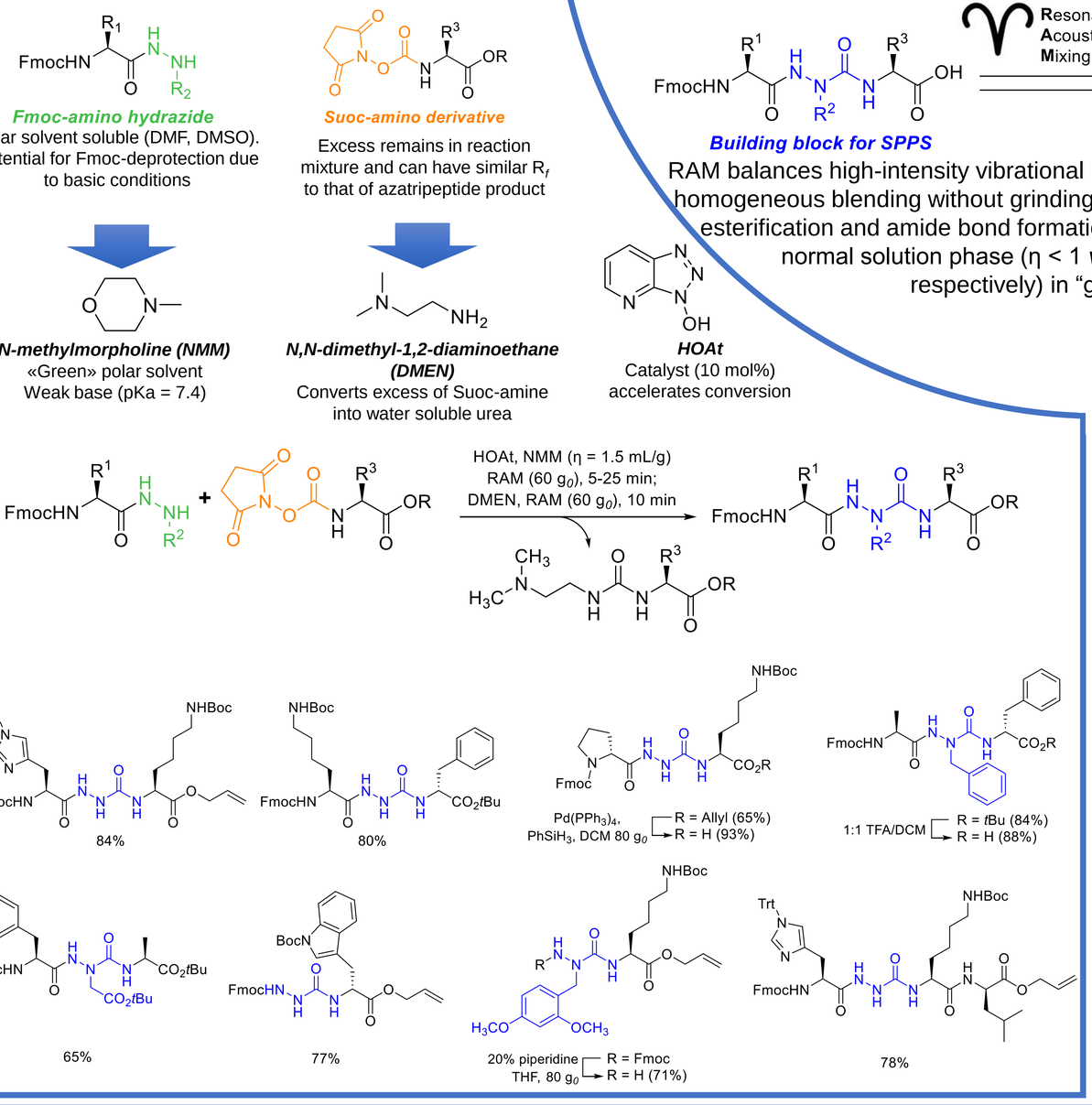


Novel strategy



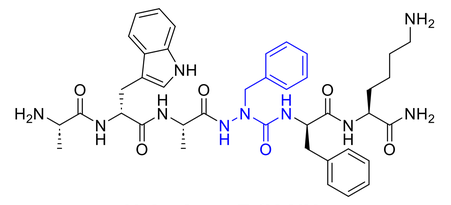
RAM balances high-intensity vibrational motion and acoustic frequency to expedite homogeneous blending without grinding. For peptide chemistry, RAM accelerated esterification and amide bond formation at higher concentration compared to normal solution phase (η < 1 *vs.* 10-20 mL/g of total reactant, respectively) in "green" solvent [2,3].

Synthesis of Fmoc protected azatripeptide



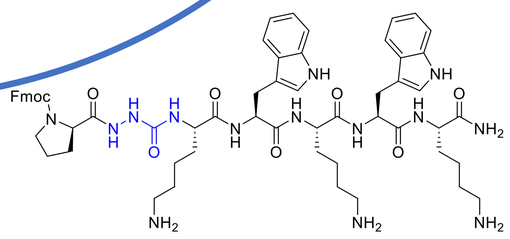
Building block incorporation into azapeptides

Biologically active peptide synthesis with aza-tripeptide building block was expedited by ultrasound-assisted SPPS (US-SPPS) [7].



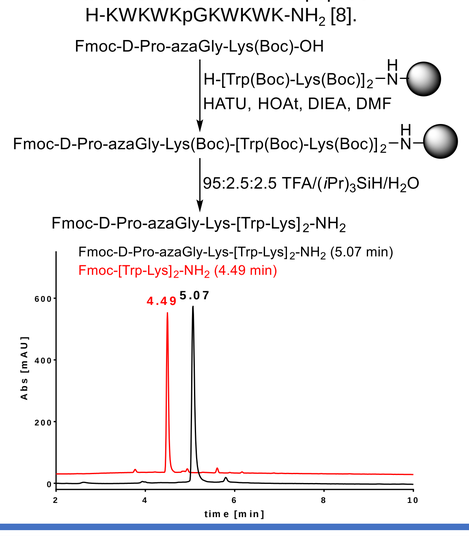
H-AwA-azaF-fK-NH$_2$

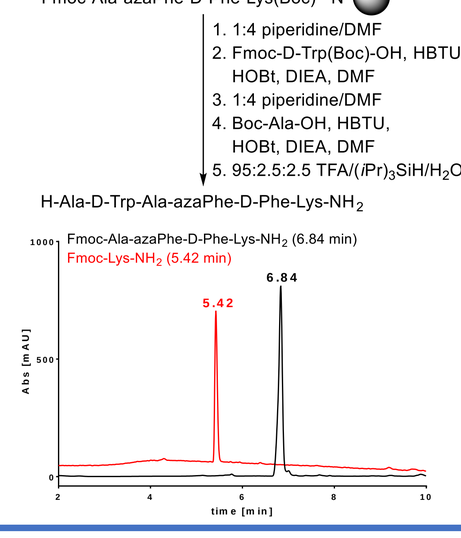
An aza-analogue of growth hormone releasing peptide-6 (GHRP-6) modulates the cluster of differentiation-36 receptor (CD36) exerting cardio protective activity against myocardial ischemia and reperfusion injury and dysfunction [9].



Fmoc-p-azaG-KWKWK-NH$_2$

Half sequence of aza-glycine variant of the antimicrobial peptide H-KWKWKpGKWKWK-NH$_2$ [8].





Conclusions

Azapeptides are promising therapeutic candidates. Their synthesis is challenging due to semicarbazide installation. An aza-tripeptide building block strategy has been developed and overcomes issues for scalable azapeptide synthesis by enabling efficient one-step coupling. Using RAM to prepare and couple *N*-(Fmoc)amino hydrazides with Suoc-amino esters, aza-tripeptide building blocks were effectively obtained and subsequently coupled onto peptide sequences linked to solid phase. Production methods for hydrazides, carbamates, ureas, and semicarbazides were all facilitated for the development of azapeptide therapeutics [10].

References

[1] C. Proulx *et* al., *Future Med. Chem.* **2011**, 3, 9, 1139–1164. https://doi.org/10.4155/fmc.11.74
[2] N. Maarouf-Mesli *et* al., *Green Chem*. **2026**, 28, 264−276. https://doi.org/10.1039/d5gc04619j
[3] N. Maarouf-Mesli *et* al., *J. Org. Chem.* **2026**, 91, 18, 6495–6501. https://doi.org/10.1021/acs.joc.6c00445
[4] V. Rodríguez *et* al., *Tetrahedron Lett*. **2019**, 60, 1, 48−51. https://doi.org/10.1016/j.tetlet.2018.11.054
[5] M. Quibell *et* al., *J. Chem. Soc. Perkin,* **1993**, 1, 22, 2843. https://doi.org/10.1039/P19930002843
[6] K. Takeda *et* al., *Tetrahedron Lett.*, **1983**, 24, 42, 4569-4572. https://doi.org/10.1016/S0040-4039(00)85958-4
[7] F. Merlino *et* al., *Org. Lett.* **2019**, 21, 16, 6378−6382. https://doi.org/10.1021/acs.orglett.9b02283
[8] L. Xu *et* al., *Amino Acids*, **2015**, 47, 11, 2385−2397. https://doi.org/10.1007/s00726-015-2029-7
[9] D. Huynh *et* al., *FASEB J.Off. Publ. Fed. Am. Soc. Exp. Biol.* **2018**, 32, 2, 807−818. https://doi.org/10.1096/fj.201700505R
[10] M. Quagliata *et* al., *Org. Lett*. **2026**. 28, 11, 3510-3516. https://doi.org/ 10.1021/acs.orglett.6c00458

Acknowledgements

For support of the Centre in Green Chemistry and Catalysis (CGCC, FRQNT 2020-RS4-265155-CCVC) and MQ Postdoctoral fellowship (https://doi.org/10.69777/370615)

For funding a Discovery Research Projects (RGPIN-2019-04079 and RGPIN-2025-04423)

For the project PJT-186296

https://doi.org/10.17952/38EPS.2026.P152

Scalable Cyclic Peptide Synthesis Featuring Copper-Catalyzed Aldehyde–Alkyne–Amine Chemistry

Nassim Maarouf-Mesli,[1] Felix Polyak,[1,2] William D. Lubell[1]

[1]Département de Chimie, Université de Montréal, and [2]Studio Bioscience Inc., Québec, Canada.

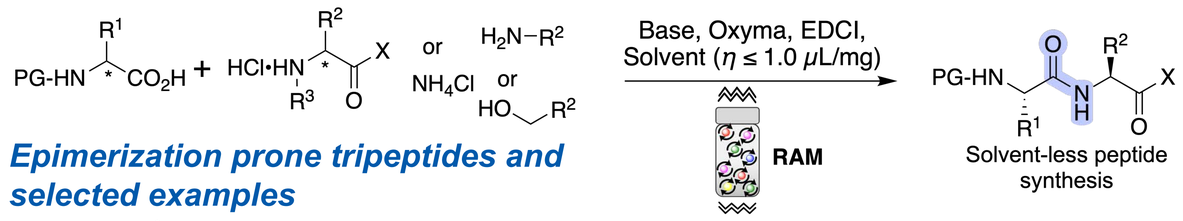
Groupe de recherche William D. Lubell Research Group

Abstract

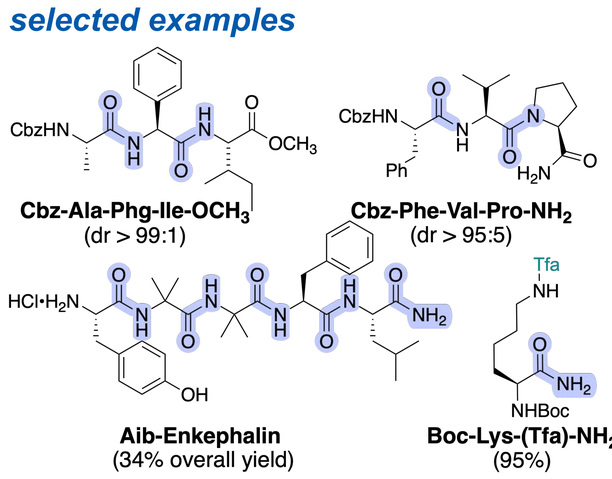
The solution-phase synthesis and applications of a macrocyclic peptidomimetic are presented. Solvent-less syntheses are demonstrated using environmentally benign, high-concentration methods enabled by resonant acoustic mixing (RAM). For example, RAM-assisted azapeptide synthesis was achieved through solvent-less peptide synthesis and phosgene-free semicarbazide construction. Using inter- and intramolecular copper-catalyzed aldehyde–alkyne–amine reactions, convergent solution-phase routes to the antiatherosclerotic agent cyclic azapeptide **298** were developed, with RAM employed for peptide and semicarbazide construction.

Green Aolvent-less Peptide Synthesis

First, we introduced the use of RAM for solution-phase peptide synthesis, successfully preparing amides, dipeptides, epimerization-prone tripeptides, and Aib-enkephalin [4].



Epimerization prone tripeptides and selected examples



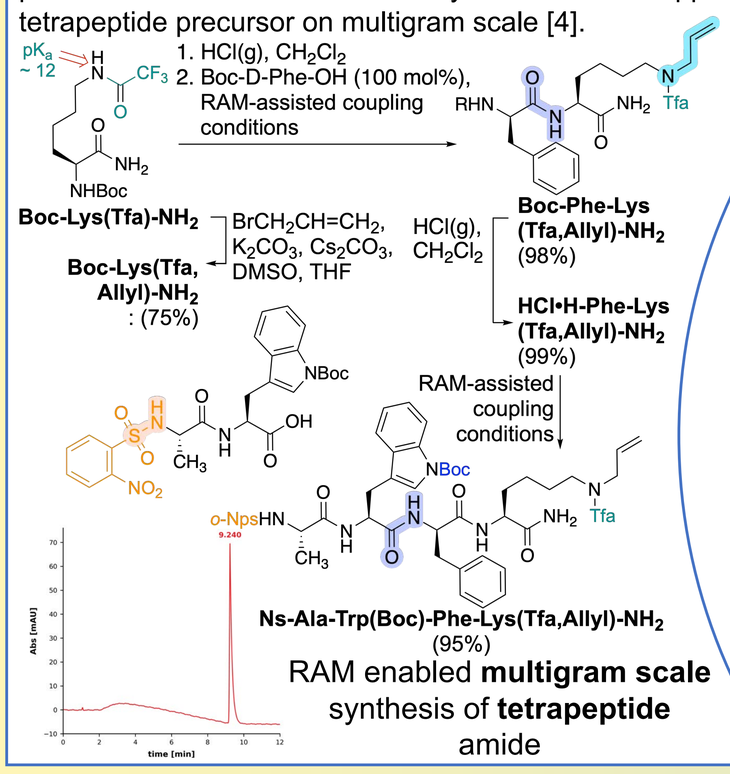
Resonant acoustic mixing (RAM)



20-gram slurry — Exceptional blending by vibrational and acoustic mixing energies — >99% conversion

Dipeptides, esters and amide

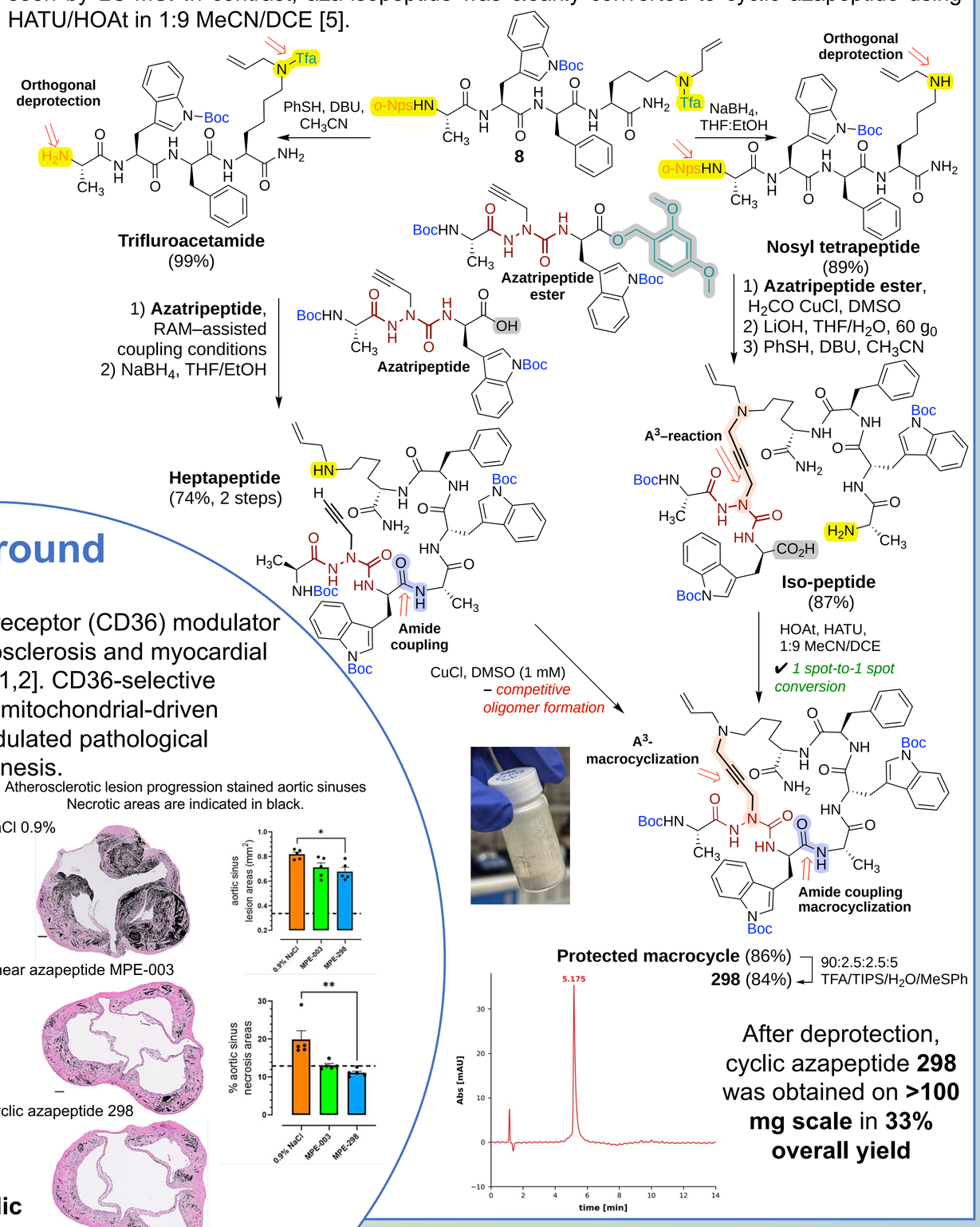
Orthogonal *o*-nitrophenylsulfonamide - trifluoroacetamide protection enabled effective synthesis and application of tetrapeptide precursor on multigram scale [4].



RAM enabled **multigram scale** synthesis of **tetrapeptide** amide

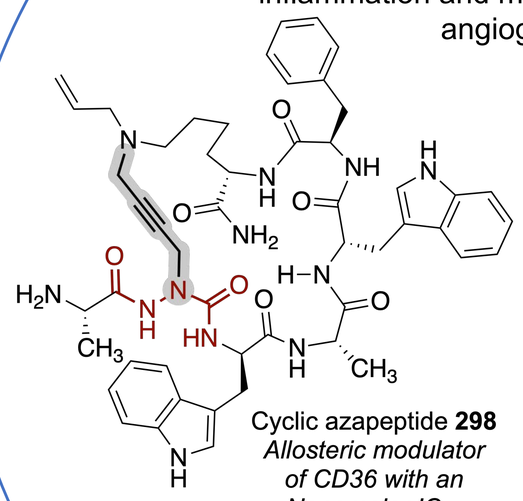
Macrocyclization Pathways

RAM [3+4] amide coupling to linear azapeptide and inter A^3-reaction to linear iso-peptide proceeded smoothly. In contrast, A^3-macrocyclization gave dimer and oligomer formation as seen by LC-MS. In contrast, aza-isopeptide was cleanly converted to cyclic azapeptide using HATU/HOAt in 1:9 MeCN/DCE [5].



Background

Cluster of differentiation 36 receptor (CD36) modulator **298** protects against atherosclerosis and myocardial ischemia reperfusion [1,2]. CD36-selective azapeptides mitigated mitochondrial-driven inflammation and modulated pathological angiogenesis.



Cyclic azapeptide **298**
Allosteric modulator of CD36 with an Nanomolar IC_{50}

Atherosclerotic lesion progression stained aortic sinuses
Necrotic areas are indicated in black.

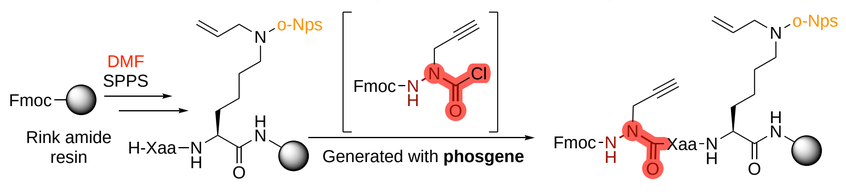
Previously [3], cyclic azapeptide 298 was made by a diversity oriented solid-phase synthesis with issues. A greener more scalable synthesis is needed.

✗ DMF
✗ Phosgene
✗ mg scale
✗ 1% overall yield

Solvent-less Azapeptide Aynthesis

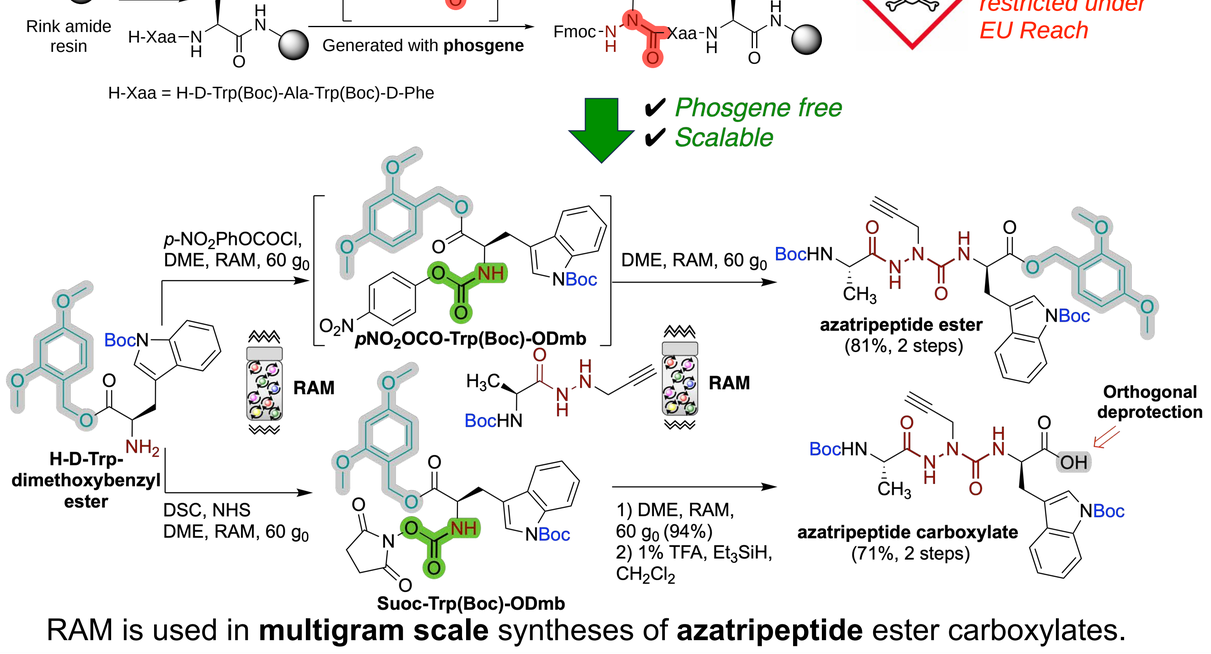
Second, a scalable phosgene-free approach to azatripeptide was developed using RAM-based strategies featuring amine activation nitrophenyl carbamate and succcinyloxy carbamate [5,6].

Previously semicarbazide assembly was performed using phosgene and DMF.



– *Phosgene is deadly*
– *DMF is toxic and restricted under EU Reach*

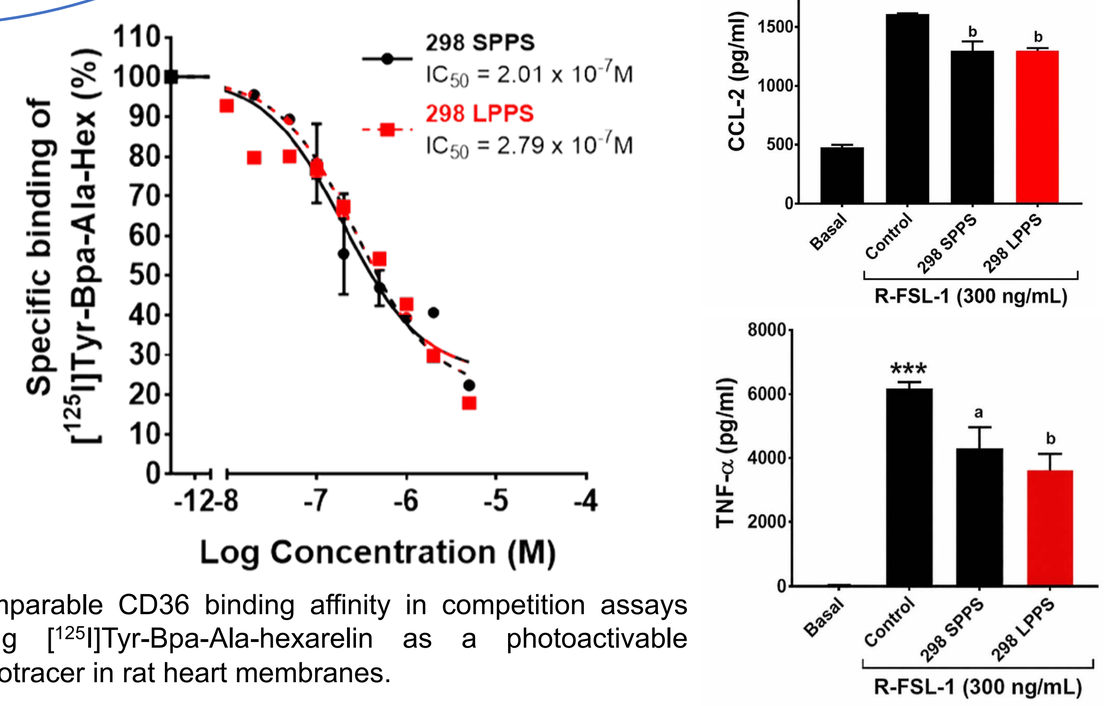
✔ *Phosgene free*
✔ *Scalable*



RAM is used in **multigram scale** syntheses of **azatripeptide** ester carboxylates.

Biological Application

Effects of **298** (0.1 μM) on RFSL-1-induced proinflammatory cytokine (TNF-α) and chemokine (CCL2) secretion on murine RAW264.7 macrophages.



Comparable CD36 binding affinity in competition assays using [^{125}I]Tyr-Bpa-Ala-hexarelin as a photoactivable radiotracer in rat heart membranes.

Batches made in solution **exhibit identical properties** as that made on solid-phase [5,7], expediting the batch for broader preclinical evaluation.

Conclusions

A 33-fold increase in overall yield was achieved using RAM-assisted peptide and azapeptide synthesis, intermolecular A³ chemistry, and lactam macrocyclization. RAM enabled the rapid, high-concentration synthesis of amides and structurally diverse peptides, including epimerization-prone sequences and azapeptides, in environmentally preferred solvents. These advances culminated in a scalable, optimized synthetic route to cyclic azapeptide 298, providing sufficient material for broader preclinical applications.

References

[1] Gauvin, J.; et al. Front. Pharmacol., **2023**, 14, 1204905
[2] Gauvin, J., et al. FEBS Open Bio. DOI: 10.1002/2211-5463.70265
[3] Zhang, J.; Mulumba, M.; Ong, H. and Lubell, W. D. *Angew. Chem. Int. Ed.* **2017**, *56*(22), 6284-6288.
[4] Maarouf-Mesli, N.; et al. *Green. Chem*, **2026**, *28*(1), 264-276.
[5] Maarouf-Mesli, N.; et al. *J. Org. Chem.* **2026**, *91*(18), 6495-6501.
[6] Quagliata, M.; Maarouf-Mesli, N.; et al. Org. Lett. **2026**, *28*(11), 3510-3516.
[7] Maarouf-Mesli, N.; Yongo-Luwawa, C.D. et al. D. *J. Org. Chem.,* **2026**, DOI:10.1021/acs.joc.6c00686

Contact

Groupe de recherche William D. Lubell Research Group
https://www.wdlubellgroup.com/
nassim.maarouf@umontreal.ca
linkedin.com/in/nassim-maarouf-66742a195

Scan for link to publications and media ..!

Acknowledgements

NSERC CRSNG
Fonds de recherche Nature et technologies Québec
CIHR IRSC
FIGHTING BLINDNESS CANADA

Turning Peptides with Cyrene-Derived Amino Acid Residues

Kajumee Bora Bhowal,[1] and William D. Lubell[1]*

[1]Department of Chemistry, Montréal, QC, Canada

https://doi.org/10.17952/38EPS.2026.P479

Abstract

α,α-Disubstituted amino acids rigidify conformation and improve pharmacokinetic properties of peptides. A novel Cyrene-derived residue (Cyr) is made using the Ugi reaction and incorporated into peptides. The Cyr residue shows promise for favoring different turn conformers contingent on environment as observed in X-ray crystallographic and NMR spectroscopic analyses.

Introduction

α,α-Disubstituted residues restrain conformation in peptides through the Thorpe–Ingold effect,[1] stabilizing backbone torsion angles characteristic of 3_{10}-helices (ϕ ≈ ±60°, ψ ≈ ±30°) and α-helices (ϕ ≈ ±55°, ψ ≈ ±45°).[2–4]

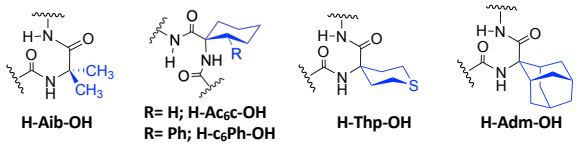


Figure 1: Representative α,α-disubstituted amino acid residues in peptides.

α,α-Disubstituted residues (**Figure 1**) alter peptide conformational preferences from extended C5 to turn and helical conformers contingent on β-substituents.[1] For example, 2-aminoadamantane- 2-carboxylic acid (H-Adm-OH)residues have been used to synthesize the first example of a single α-helical turn as well as an incipient γ-helix contingent on the C-terminal amide (**Figure 2**).[5]

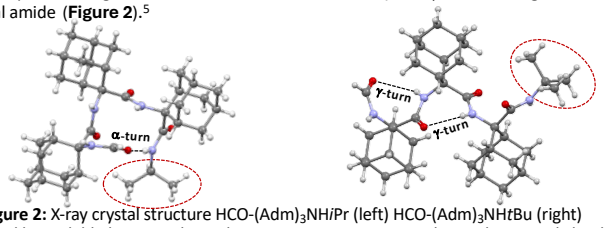
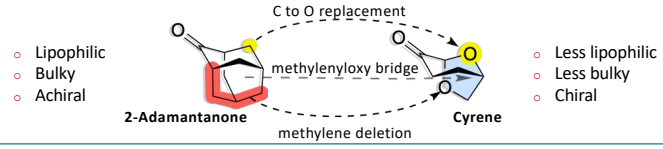


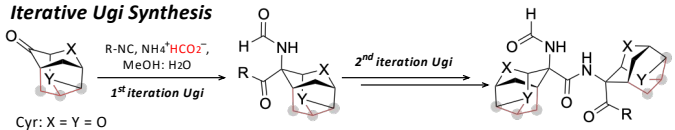
Figure 2: X-ray crystal structure HCO-(Adm)$_3$NH*i*Pr (left) HCO-(Adm)$_3$NH*t*Bu (right)

A readily available biomass-derived precursor, Cyrene was used to make a novel chiral α,α-disubstituted amino acid, Cyr, which offers complementary properties to Adm (from 2-adamantanone) for peptide conformational analysis.[6]



Result

Iterative Ugi Synthesis



Cyr: X = Y = O
Adm: X = Y = CH_2 + 'CH and 2 x CH_2'

Cyr: R = NHPhOMe
Adm: R = NH*i*Pr; NH*t*Bu

X-ray Crystallographic Analysis

In the solid state, both (4*R*)- and (4*S*)-Cyr favor α-helical conformations (**Figure 3**) in contrast to Aib and Thp, which favor 3_{10}-helices, and Adm, which favors a γ-turn (**Table 1**).[6]

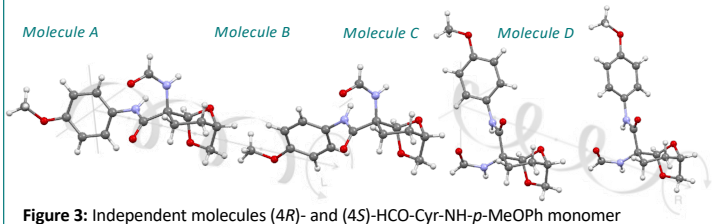


Figure 3: Independent molecules (4*R*)- and (4*S*)-HCO-Cyr-NH-*p*-MeOPh monomer

Table 1. Backbone ϕ and ψ torsion angle values in degrees

	ϕ	ψ	Type
Ideal α-helix	−55	−45	right-handed
Ideal 3_{10}-helix	−60	−30	right-handed
Ideal β-turn	60	−120	type II′
Ideal β-sheet	−154.3	154.4	parallel sheet
γ-turn	−76	83	regular
(4*R*)-HCO-**Cyr**-*p*-MeOPh (Molecule A)	52.0 (3)	48.8 (3)	left-handed
(4*R*)-HCO-**Cyr**-*p*-MeOPh (Molecule B)	58.9 (3)	45.8 (3)	left-handed
(4*S*)-HCO-**Cyr**-*p*-MeOPh (Molecule C)	−51.6 (3)	−51.6 (3)	right-handed
(4*S*)-HCO-**Cyr**-*p*-MeOPh (Molecule D)	−53.6 (3)	−48.7 (3)	right-handed
Ac-**Ac6c**-NHMe	−52	−46	α-helical
Ac-**Aib**-NHMe	−55.5 −53.8	−40.3 −46.4	3_{10}-helices
HCO-**Thp**-Ac$_6$c-Phe-OMe	−61.3	−33.9	3_{10}-helices
Cbz-**Adm**-NH*i*Pr	−72.22(15)	91.66 (14)	γ-turn

In the solid state, (4*S*, 4′*S*)-HCO-(Cyr)$_2$-NHPhOMe adopts a distorted type III β-turn,[6] distinct from the type II β-turn of HCO-(Adm)$_2$-Aib-OMe (**Table 2**),[5] with an intramolecular hydrogen bond between the formamide carbonyl oxygen and C-terminal amide NH (N···O = 3.03(16) Å; H···O = 2.30(2) Å) (**Figure 4**, left).[6]

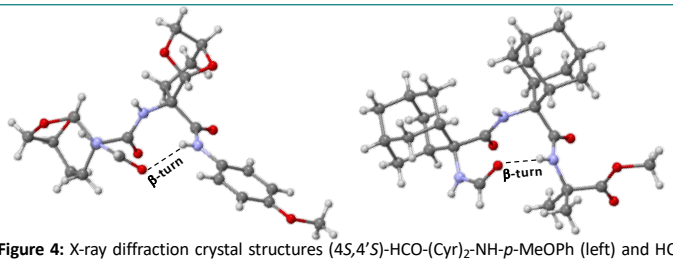


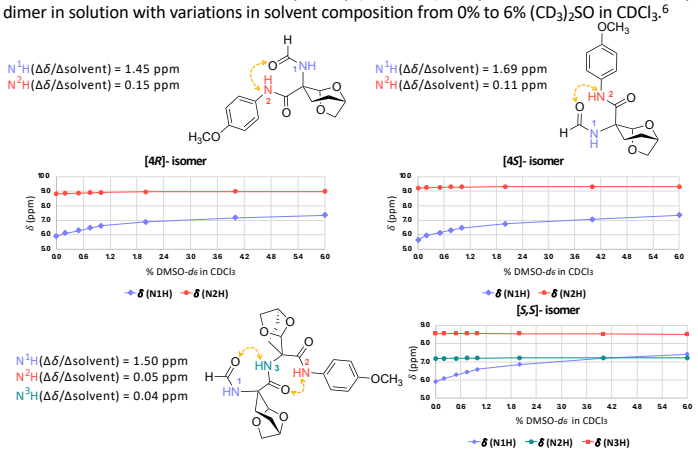
Figure 4: X-ray diffraction crystal structures (4*S*,4′*S*)-HCO-(Cyr)$_2$-NH-*p*-MeOPh (left) and HCO-(Adm)$_2$-Aib-OMe (right)

Table 2. Backbone ϕ and ψ torsion angle values in degrees

	ϕ	ψ	Type
(4*S*, 4*S*)-HCO-**Cyr**-Cyr-NH-*p*-MeOPh (4*S*, 4*S*)-HCO-Cyr-**Cyr**-NH-*p*-MeOPh	−44.41 (16) −54.98 (15)	−47.91 (15) −42.48 (15)	right-handed α-turn
HCO-**Adm**-Adm-Aib-OMe HCO-Adm-**Adm**-Aib-OMe HCO-Adm-Adm-**Aib**-OMe	63.1 (5) −51.4 (5) 56.2 (5)	−96.9(4) −49.6 (5) 43.9 (5)	type II′ β-turn

NMR Spectroscopic Analysis

The C7$^{\gamma}$-turn conformation was adapted by (4*R*)- and (4*S*)-Cyr monomer, and (4*S*,4′*S*)-Cyr dimer in solution with variations in solvent composition from 0% to 6% $(CD_3)_2SO$ in $CDCl_3$.[6]



Conclusion

The Cyr residue is a novel bio-sourced chiral α,α-disubstituted scaffold which can be readily introduced into peptides by the Ugi reaction on cyrene. In the solid state, (*R*)- and (*S*)-Cyr induced left- and right-handed helices, respectively, and Cyr dimers adopted type III β-turn. In solution, Cyr exhibited hydrogen bonding patterns characteristic of single and consecutive γ-turn conformers. In peptide design, Cyr offers interesting promise and merits further investigation in longer assemblies.

References

1. C. Toniolo, M. Crisma, F. Formaggio, and C. Peggion *Biopolymers* **60**, no. 6 (2001): 396–419.
2. G. R. Marshall, E. E. Hodgkin, D. A. Langs, D. Smith, J. Zabrocki, and M. T. Leplaw *Proc. Natl. Acad. Sci.* **87**, (1990): 487–491.
3. Y. Paterson, S. M. Rumsey, E. Benedetti, G. Némethy, and H. A. Scheraga, *J. Am. Chem. Soc.* **103**, no. 11 (1981): 2947–2955.
4. C. Toniolo and E. Benedetti *Macromolecules* **24**, no. 14 (1991): 4004–4009.
5. F. M. Mir, M. Crisma, C. Toniolo, and W. D. Lubell *Pept. Sci.* **112**, no. 1 (2020): e24121.
6. K. Bora Bhowal, R. Hitti, and W. D. Lubell *J. Pept. Sci.* **32**, no. 3 (2025):e70084.

Acknowledgement

We are grateful for NSERC (RGPIN-2025-04423), FRQNT (FRQNT-2020-RS4-265155-CCVC) and the Institute Courtois support, and for U. Montréal facility assistance from Dr. A. Fürtös and K. Gilbert (mass spectrometry), Drs. T. Maris and D. Chartrand (X-ray), and Dr. P. Aguiar (NMR spectroscopy).

Scalable PEC Purification Enables API-Grade Semaglutide with Minimal HPLC Intervention

PurePep®

Stephan Lüdtke[1], Lucrezia Sforza[2], Manoj Muthyala[1], Robert Zitterbart[1], Dominik Sarma[1], Paolo Rovero[2], Anna Maria Papini[2]

[1] Gyros Protein Technologies, Teltow, Germany

[2] Interdepartmental Research Unit of Peptide and Protein Chemistry and Biology, Departments of Chemistry "Ugo Schiff" and NeuroFarBa, University of Florence, Florence, Italy

https://doi.org/10.17952/38EPS.2026.P013

Introduction

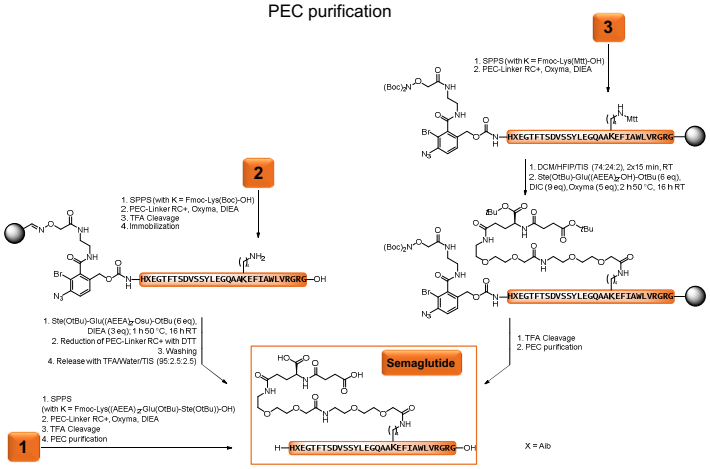
Rising demand for GLP-1 receptor agonists such as Semaglutide requires scalable workflows that connect method development, synthesis scale-up and efficient downstream purification. Here, three SPPS strategies were developed on PurePep® Chorus, upscaling the synthesis from 100 µmol to 1 mmol while reducing amino-acid excess. These strategies were evaluated as a basis for further scale-up to 8 mmol on PurePep® Sonata+. As processing crude material is difficult and chromatographic purification requires multiple runs, the catch-and-release based PurePep® EasyClean (PEC™)[1] technology was integrated as an orthogonal purification step to reduce the impurity burden between SPPS and a final preparative chromatography. The overall objective was not to eliminate HPLC, but to simplify final polishing to a single RP-HPLC run while maintaining high recovery and achieving >99% UV purity.

Three Routes – one Goal

Route 1
Pre-assembled building block
SPPS using Fmoc-L-Lys[(AEEA)$_2$-Glu(OtBu)-Ste(OtBu)]-OH followed by PEC purification

Route 2
Lys modification on PEC resin
SPPS using Fmoc-L-Lys(Boc)-OH followed by PEC purification and side-chain modification with the lipid moiety on PMA beads

Route 3
Lys modification on SPPS resin
SPPS using Fmoc-L-Lys(Mtt)-OH followed by side-chain modification with the lipid moiety on SPPS resin and PEC purification



Scheme 1. SPPS and PEC purification of Semaglutide, following the 3 different Routes

SPPS development and upscaling

The three Routes were first screened on PurePep Chorus in 100 µmol scale using 5 eq of amino acid per coupling at room temperature. Preloaded Fmoc-Gly-Trt-PS resin was used for routes 1 and 2 and Fmoc-Gly-Wang-PS resin for Route 3. Each SPPS cycle comprises of:

- Fmoc deprotection with DMF/piperidine (80:20), 2 × 5 min at RT;
- Single coupling with 5 eq AA, 5 eq Oxyma, and 7.5 eq DIC, 1 h at RT;
- Capping with DMF/acetic anhydride/pyridine (65:19:16), 1 × 5 min at RT.

After Fmoc deprotection and after capping, the SPPS resin was washed 4 and 3 times with EtOAc/DMSO (8:2) respectively.

Difficult coupling steps identified during this exploratory run were subsequently optimized using induction heating at 50 °C. More precisely, induction heating was used for the coupling of the following residues (from C- to N-Terminus): **8-16**, **20-31**.

The optimized methods were then upscaled to 1 mmol, while reducing the amino-acid, Oxyma and DIC excess to 3, 3 and 4 eq per coupling respectively to improve material efficiency. Crude UV-purity and SPPS recovery were used to assess whether and how synthesis performance would be affected by this adaptation.

Table 1. UV-purities and SPPS recoveries of the optimized and upscaled SPPS' of Semaglutide

	Optimized SPPS (5 eq AA)		1 mmol upscaled SPPS (3 eq AA)	
Route	Crude UV-purity (@210 nm)	SPPS recovery*	Crude UV-purity (@210 nm)	SPPS recovery*
1	67%	43%	49%	35%
2	63%	40%	47%	36%
3	61%	44%	48% ‖ 52%§	40%

* SPPS recovery calculated by dividing the obtained crude amount by the SPPS scale
§ Crude purity determined after modification of the lysine side-chain with the lipid moiety

PurePep EasyClean (PEC™) in 1 mmol scale

Semaglutide or its precursor was N-terminally modified with PEC-Linker RC+ and cleaved from SPPS resin using TFA/thioanisole/water/TIS (85:10:2.5:2.5) for 2 h at RT. With PEC2.0, the peptide was directly immobilized on aldehyde-functionalized PMA solid support from the cleavage mixture after addition of 35 vol% MeCN/pyridine (7:3). Non-immobilized impurities (i.e. capped truncations from SPPS) were removed by washing the PMA beads with water and DMSO. Subsequent DTT-mediated reduction and cleavage of the PEC-Linker RC+ with TFA/water/TIS (95:2.5:2.5) released the N-terminal free Semaglutide.

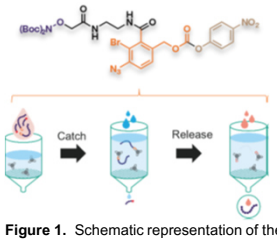


Figure 1. Schematic representation of the PEC purification with PEC-Linker RC+

Lysine Side-chain Modification

Routes 2 and 3 require orthogonal functionalization of the lysine side-chain on the PMA beads and SPPS resin, respectively (as shown in Scheme 1).

For Route 2, the lipid moiety was introduced during PEC purification while the peptide was immobilized on the PMA solid support. A freshly prepared NHS ester (6 eq) in NMP was reacted in the presence of DIEA (3 eq) for 1 h at 50 °C, followed by 16 h at RT.

For Route 3, the lipid moiety was introduced directly on the SPPS resin after coupling of PEC-Linker RC+. The Mtt protecting group was selectively removed by 2x treatment for 15 min with DCM/HFIP/TIS (74:24:2), followed by coupling of the lipid moiety (6 eq) with DIC (9 eq) and Oxyma (5 eq) in NMP for 2 h at 50 °C and 16 h at RT.

Purification Results

Route 3 provided the best overall balance of UV-purity and recovery. Following lysine side-chain modification on the SPPS resin and subsequent PEC purification, Semaglutide was obtained with **78% UV purity** and a **total recovery of 26%** relative to the 1 mmol synthesis scale.

An aliquot of the PEC-purified material was subjected to a single RP-HPLC polishing run, increasing the UV purity to **>99%** (Figure 2)**.** This demonstrates the potential of PEC to reduce downstream chromatographic burden while retaining HPLC as a single final polishing step.

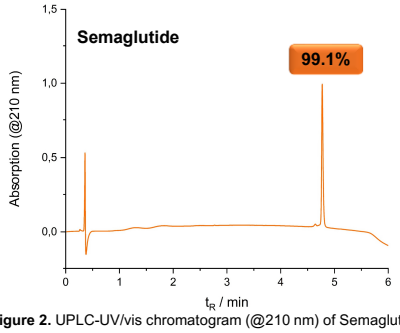


Figure 2. UPLC-UV/vis chromatogram (@210 nm) of Semaglutide after PEC purification and a single HPLC purification

Conclusion & Perspectives

Reducing the amino-acid excess from 5 to 3 eq during scale-up maintained comparable SPPS recoveries across all three strategies. At 1 mmol, Route 3 provided the highest crude UV-purity (52%) and SPPS recovery (40%) and enabled purification with PEC and a single HPLC run to achieve >99% UV-purity.

This route was therefore selected for further upscaling to 8 mmol on pilot scale synthesizer PurePep Sonata+ with additionally decreasing the amount of the lipid moiety needed for coupling on SPPS resin to 2 eq.

Access the live collection to receive the poster, the original papers, the recording of our presentation and additional synthesis resources.

SCAN ME

We greatly acknowledge the PeptLab Interdepartmental Research Unit of the University of Florence for their collaboration, especially Lucrezia Sforzi's contribution to the experimental work, analysis and interpretation of the results. L.S. is the recipient of the PhD fellowship D.M. 118/2023, Ricerca PNRR "SVILUPPO DI PEPTIDI BIOATTIVI DI INTERESSE COSMETICO TRAMITE PROCESSI ECOSOSTENIBILI", XXXIX Cycle, in Area del Farmaco e Trattamenti Innovativi (2023-2026).

References

[1] R. Zitterbart, et. al., Chemical Science, 2021

GYROS PROTEIN Technologies

www.gyrosproteintechnologies.com/peptides peptides@gyrosproteintech.com

Gyros Protein Technologies logo, Intellisynth, Prelude, PS3, PurePep, Single-Shot, Sonata, Symphony, PEC, and Tribute are trademarks of Gyros Protein Technologies Group. COMU, OxymaPure, PyOtbok, K-Oxyma and Py-Oxim are trademarks owned by Luxembourg Bio Technologies Ltd. All other trademarks are the property of their respective owners. © Gyros Protein Technologies 2026

Tag-Assisted Peptide Synthesis (TAPS)

Enabling Efficient and Sustainable Peptide Synthesis and Purification

Raimund Maier[1], Karin Rustler[1], Haixiang Zhang[1], Thomas Bruckdorfer[1], Kai Holland-Nell[2], Jacqueline Dalski[2], Stephan Pritz[2]

[1] Iris Biotech GmbH, Adalbert-Zoellner-Str. 1, 95615 Marktredwitz, Germany; [2] Biosyntan Gesellschaft für bioorganische Synthese mbH, Robert-Roessle-Straße 10, 13125 Berlin, Germany

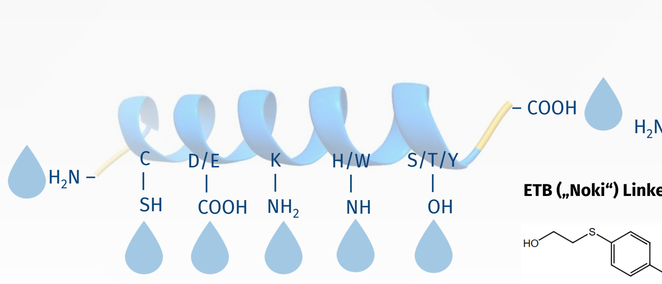
https://doi.org/10.17952/38EPS.2026.P005

Abstract

Discovery and production of synthetic peptides significantly progressed in the last years resulting in the fact that complex peptides like GLP-1 analogues are produced in large quantities for commercial consumption. However, peptide length, solubility, secondary structure and modifications challenge to develop robust synthesis processes. Especially aggregation-prone sequences can be handled more efficiently when adding semi-permanent solubilizing tags during synthesis and purification.

Herein we demonstrate how tags placed at the C-terminus of a peptide can help to manufacture a difficult peptide sequence in high yield and how such tags can be removed. Different tag linkers enable peptide acids or amides, and the choice of the linker may affect coupling efficiency, resin cleavage, purification, and tag removal.

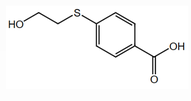
Potential Tag and Linker Positioning



Concept of C-Terminal Arg_6-Tagging with Cleavable Linkers

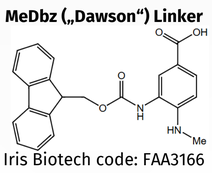


ETB („Noki“) Linker



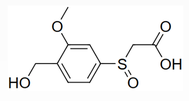
Iris Biotech code: RL-8715
Oxidative activation by mCBPA
Cleavage with DEA and piperidine

MeDbz („Dawson“) Linker



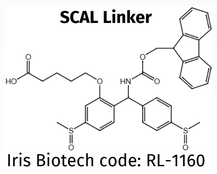
Iris Biotech code: FAA3166
Activation by acylation
Cleavage by hydrolysis

Mmsb Linker



Iris Biotech code: RL-3895
Reductive activation by NMe_4I
Cleavage with TFA

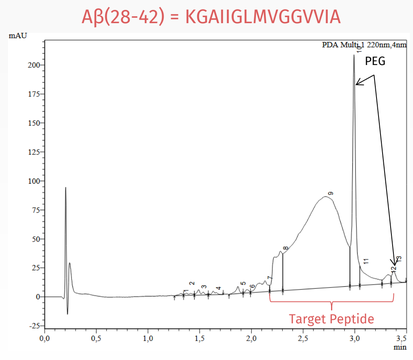
SCAL Linker



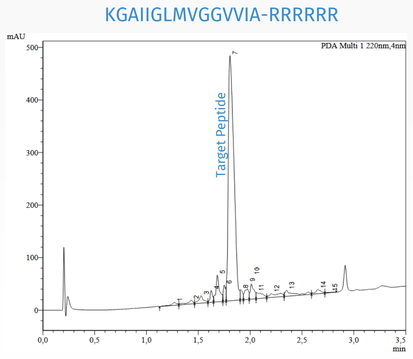
Iris Biotech code: RL-1160
Reductive activation by NMe_4I
Cleavage with TFA

Aggregation Suppression

Aβ(28-42) = KGAIIGLMVGGVVIA



KGAIIGLMVGGVVIA-RRRRRR



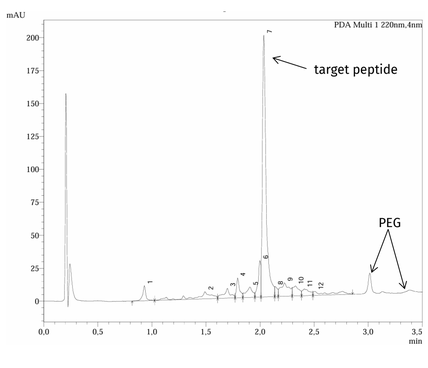
KGAIIGL-Nle-VGGVVIA-ETB(O_2)-R_6-NH_2 KGAIIGL-M-VGGVVIA-MeDbz-R_6-NH_2 KGAIIGL-M(O)-VGGVVIA-Mmsb-R_6-NH_2 KGAIIGL-M(O)-VGGVVIA-SCAL-R_6-NH_2

C-terminal Arg_6-tagging can convert the hydrophobic and aggregation-prone amyloid beta sequence 28-42 into a well synthesizable and separatable peptide.

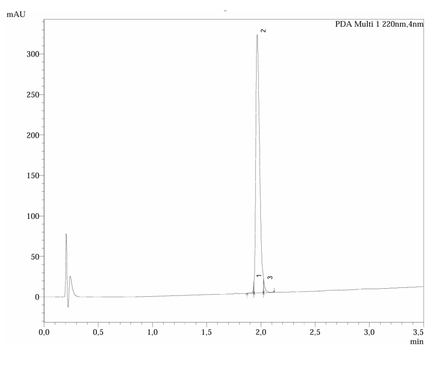
Results for Arg_6-Tagging with Different Cleavable Linkers

- **ETB (“Noki”) Linker** yielding peptide acids

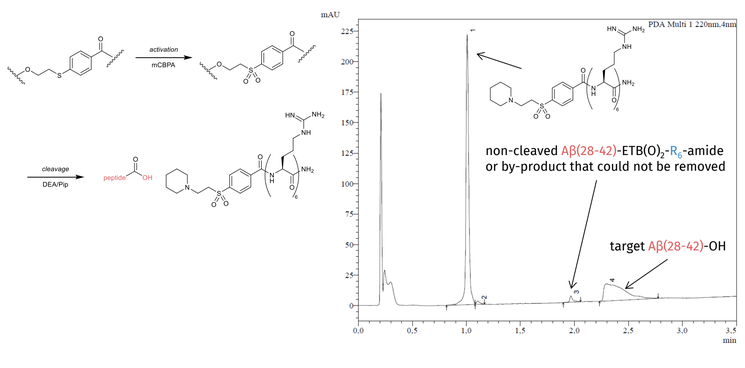
crude KGAIIGL-Nle-VGGVVIA-ETB(O_2)-RRRRRR-NH_2



purified KGAIIGL-Nle-VGGVVIA-ETB(O_2)-RRRRRR-NH_2



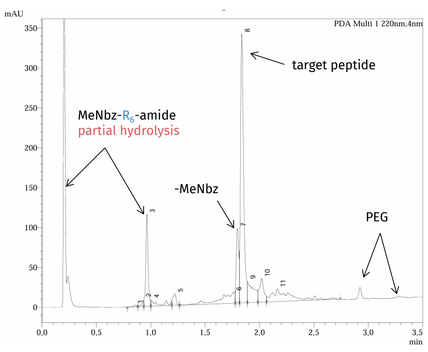
Tag removal by ETB cleavage to yield KGAIIGL-Nle-VGGVVIA-OH



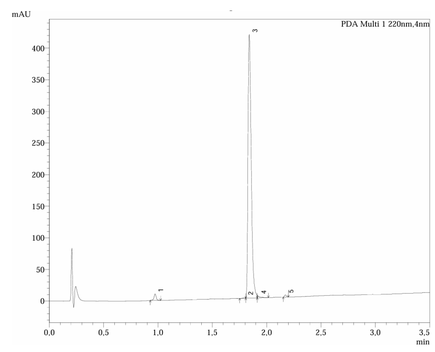
Linker and first amino acid coupling were difficult; slight tendency for diketopiperazine formation; linker activation on the resin and cleavage from the resin worked nicely; purification of the tagged peptide worked well with a little bit of sticking to the column; linker cleavage by piperidine released the desired peptide as a peptide acid.

- **MeDbz (“Dawson”) Linker** yielding peptide acids

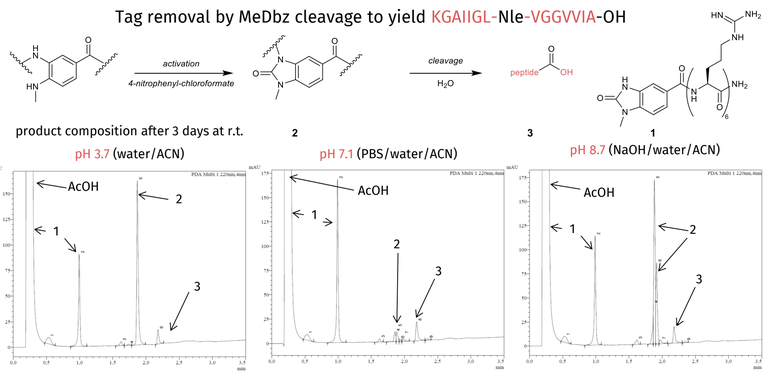
crude KGAIIGL-Nle-VGGVVIA-MeDbz-RRRRRR-NH_2



purified KGAIIGL-Nle-VGGVVIA-MeDbz-RRRRRR-NH_2



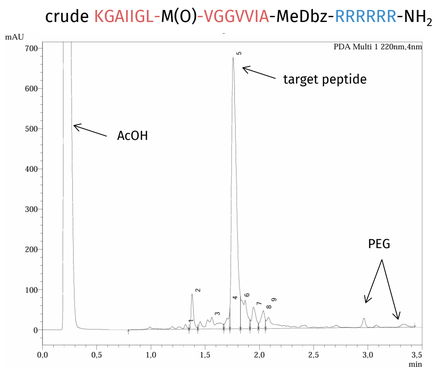
Tag removal by MeDbz cleavage to yield KGAIIGL-Nle-VGGVVIA-OH



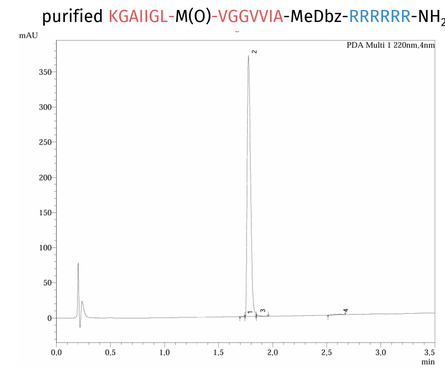
Linker activation on resin did not perform well – taking several repeats; premature cleavage and linker fragmentation reduced the yield of crude peptide; purification of tagged peptide worked fine; finally, the linker did not hydrolyze completely at any pH - even after days; in this prolonged time frame, the linker was rather decomposing than hydrolyzing, resulting in numerous undesired side products and low yield of desired peptide acid.

- **Mmsb Linker** yielding peptide acids

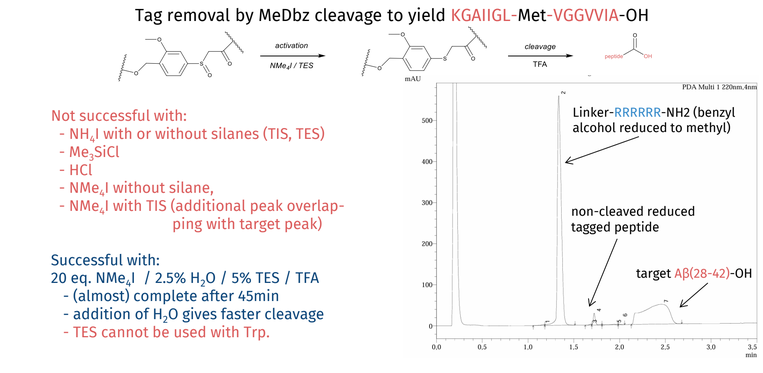
crude KGAIIGL-M(O)-VGGVVIA-MeDbz-RRRRRR-NH_2



purified KGAIIGL-M(O)-VGGVVIA-MeDbz-RRRRRR-NH_2



Tag removal by MeDbz cleavage to yield KGAIIGL-Met-VGGVVIA-OH



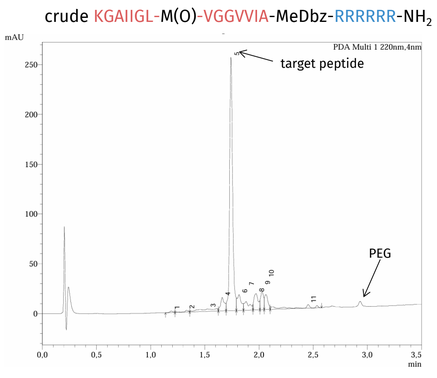
Not successful with:
- NH_4I with or without silanes (TIS, TES)
- Me_3SiCl
- HCl
- NMe_4I without silane,
- NMe_4I with TIS (additional peak overlapping with target peak)

Successful with:
20 eq. NMe_4I / 2.5% H_2O / 5% TES / TFA
- (almost) complete after 45min
- addition of H_2O gives faster cleavage
- TES cannot be used with Trp.

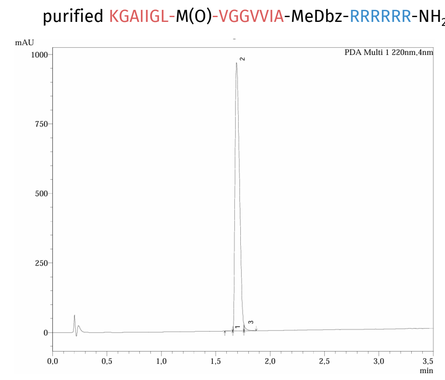
Mmsb linker coupling and peptide synthesis worked well; yield of crude tagged peptide and purification were satisfying; first standard protocols for linker cleavage did not work at all; finally, linker reduction worked with tetramethylammoniumiodide plus a silane (TIS), however producing an adduct peak overlapping with the target peak; this could be overcome using triethylsilane (TES) with tetramethylammoniumiodide, TFA, and some water;
note: TES is incompatible with tryptophan!

- **SCAL Linker** yielding peptide amides

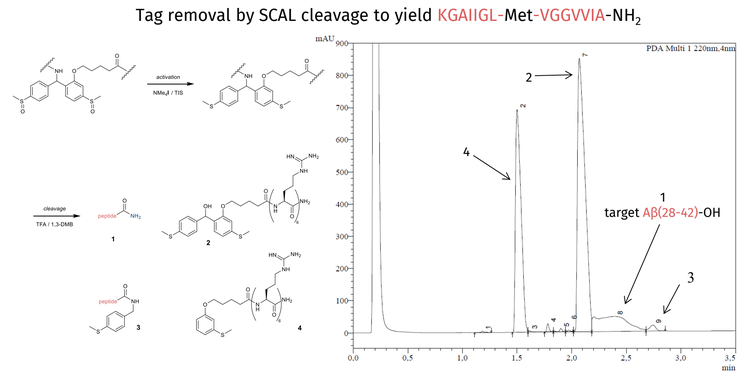
crude KGAIIGL-M(O)-VGGVVIA-MeDbz-RRRRRR-NH_2



purified KGAIIGL-M(O)-VGGVVIA-MeDbz-RRRRRR-NH_2



Tag removal by SCAL cleavage to yield KGAIIGL-Met-VGGVVIA-NH_2



SCAL linker coupling and peptide synthesis worked smoothly, yielding the largest quantities of crude and purified tagged peptide of the four linker variants; during linker reduction, Met(O) is reduced to Met; cleaving the linker, we found fragmentation behavior that is known also from other benzhydryl systems, yielding also a peptide still having “one half” of the former benzhydryl group attached (3); could be minimized by adding 1,3-dimethoxybenzene.

Summary

C-terminal Arg_6-tagging can strongly improve peptide yield and purity. However, removing the tag by cleavable linkers is not trivial and conditions have to be optimized case by case.

References:

- Safety-Catch Linkers for Solid-Phase Peptide Synthesis; S. Noki, B. G. de la Torre, F. Albericio; *Molecules* 2024; **29(7):** 1429-1442. https://doi.org/10.3390/molecules29071429
- An efficient Fmoc-SPPS approach for the generation of thioester peptide precursors for use in native chemical ligation; J. B. Blanco-Canosa, P. E. Dawson; *Angew. Chem. Int. Ed. Engl.* 2008; **47(36):** 6851-6855. https://doi.org/10.1002/anie.200705471
- A safety-catch type of amide protecting group; M. Pátek, M. Lebl; *Tetrahedron Lett.* 1990; **31**: 5209-5212. http://doi.org/10.1016/S0040-4039(00)97844-4

Characterizing the cell-permeability, stability and toxicity of high affinity foldamer targeting the histone chaperone ASF1

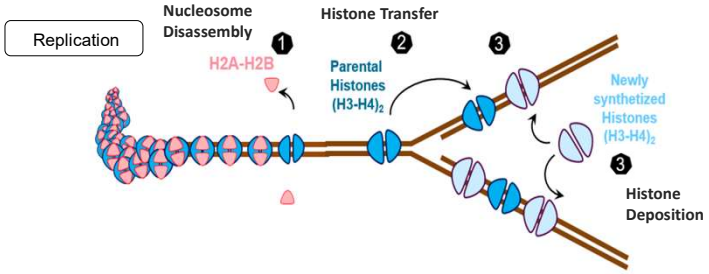
EMMA MAILLARD[1], BO LI[2], MARIE PERRIN[1], ARTHUR VITARD[1], GWENAELLE MOAL[1], JOHANNE MBIANDA[2], CHRISTOPHE ANDRÉ[2], MAGDA TEIXERIRA-NUNES[3], MARIE VANDAMME[4], GUILLAUME PINNA[4], CÉLINE DOUAT[5], EMMANUELLE THINON[2], RAPHAEL GUEROIS[1], PIERRE LEGRAND[3], FRANCOISE OCHSENBEIN[1]

https://doi.org/10.17952/38EPS.2026.P076

[1]Institute for Integrative Biology of the Cell (I2BC), CEA, CNRS, Université Paris Saclay,Gif-sur-Yvette, France. [2]Univ. Bordeaux, CNRS, Bordeaux INP, CBMN, IECB, Pessac, France. [3]Synchrotron SOLEIL, l'Orme des Merisiers, Saint-Aubin, France. [4]Université Paris Cité, Université Paris-Saclay, Inserm, CEA, PARi facility, iRCM/IBFJ, Stabilité Génétique Cellules Souches et Radiations, Fontenay-aux-Roses, France. [5]Department Pharmazie, Ludwig-Maximilians-Universität München, München Germany

Nucleosome, the elementary unit of chromatin

In eukaryotic cells, histones are a key component of the chromatin, regulating gene expression and DNA accessibility. During DNA replication, nucleosome undergoes dynamic changes to allow transfer of genetic information. This process can lead to genetic and epigenetic modifications that can cause important diseases such as cancers. Histones buffering, transportation and deposition is facilitated by histones chaperones.

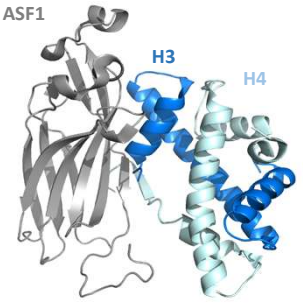


Histone chaperone ASF1 (Anti Silencing Function 1)

ASF1 associate with the histone dimer H3-H4.

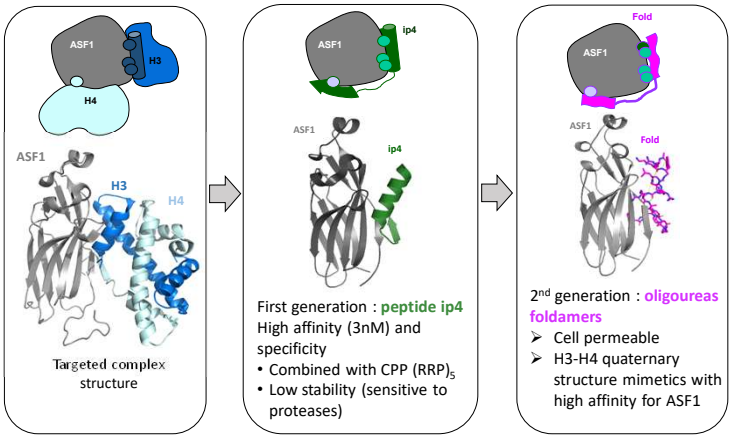
ASF1 plays an essential role in cell growth and proliferation because it is involved in nucleosome assembly/disassembly and regulation of gene expression.

Its overexpression is correlated to tumor proliferation, in particular in triple-negative breast cancer. In contrast, its knockdown makes cancer cells more sensitive to chemo- and radiotherapy, making it an interesting therapeutic target.



X-ray structure of ASF1 in interaction with H3-H4 (1,7A). PDB 2HUE

Inhibitors design



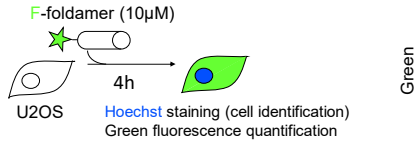
Bakail et al. Cell Chem Biol 2019

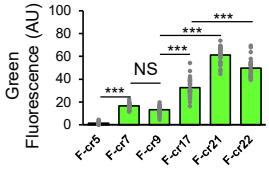
	Optimization	K_D (nM)
cr5	*Formal charge 0*	135 ± 29
cr7	*Formal charge +4*	38 ± 3.1
cr9	L14 + Dap^U + Gly deletion	33 ± 6
cr17	T14 + Dap^U + 3-F + Gly deletion	6 ± 1
cr21	*cr9 analogue + N-methylation*	38 ± 6
cr22	*cr17 analogue + N-methylation*	27 ± 3

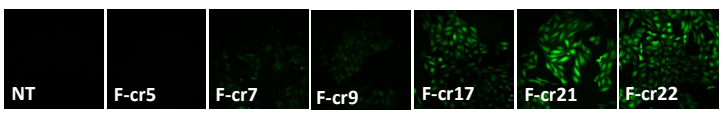
For peptide design and optimization see Poster 331

For foldamers design and synthesis see Poster 136

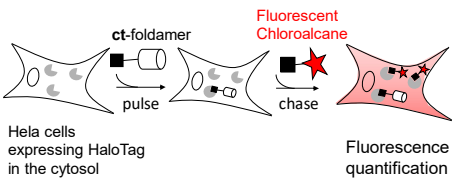
Foldamer cytosolic internalization

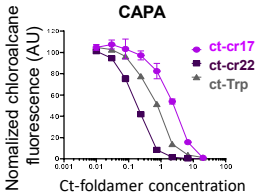






➢ **Positive global charge and N-methylation improves cellular uptake**

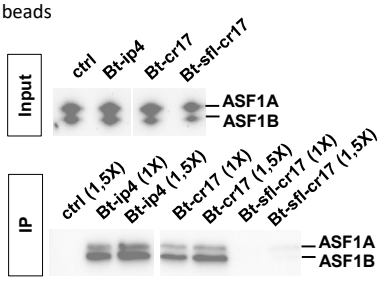


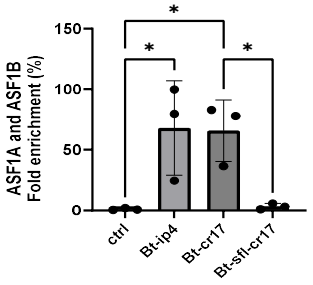


➢ **Foldamers are present in the cytosol of Hela cells**

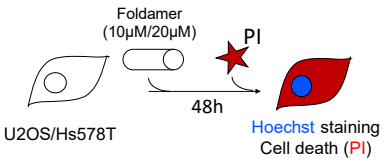
Functional assessment of foldamers

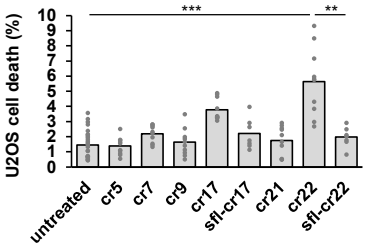
Pull down of biotinylated peptide **Bt-ip4** and foldamers **Bt-cr17** and negative control **Bt-sfl-cr17** from U2OS total cell extracts on streptavidin-functionalized sepharose beads

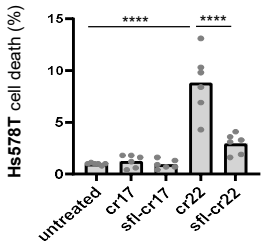




Toxicity of foldamers measurment after 48h incubation in U2OS and Hs578T cell lines.







➢ **Best foldamer is able to bind ASF1 in a cellular context and shows slight toxicity in both U2OS and Hs578T cells, compared to negative control**

Conclusion & Perspectives

Structural analysis enabled the design of a medium-sized, high affinity binder for the histone chaperone ASF1 that recapitulates the quaternary structure of its interaction with H3-H4. These peptide-oligourea foldamers were optimized by formal charge optimization and backbone N-methylation to improve their cellular uptake. Both cr17 and cr22 demonstrate significant cell permeability and cytosolic localization.

Furthermore, cr17 engage ASF1 similarly to the previously designed high-affinity peptide ip4 in a cellular context.

Finally, only cr22 exhibits a significant, although modest cellular toxicity in two cancer cell lines. Ongoing experiments in our laboratory, suggest that this inhibitor and second-generation ASF1 foldamer inhibitors (to be reported) may act synergistically with established anticancer drugs. Preliminary data indicate that, at suboptimal doses, where neither the foldamer nor the cytotoxic agent alone is active, their combination leads to high levels of cell death.

September 2026

38th EPS European Peptide Symposium

P330

https://doi.org/10.17952/38EPS.2026.P330

38TH EUROPEAN PEPTIDE SYMPOSIUM • VIENNA, AUSTRIA • 6–11 SEPTEMBER 2026

NOVLTEX: A New Class of Antibiotics with Potent Activity against Multidrug-Resistant Bacterial Pathogens

Esra Malkawi* **Anish Parmar** **Ishwar Singh**

College of Pharmacy, Amman Arab University (AAU), Jordan

Antimicrobial Pharmacodynamics & Therapeutics and Department of Chemistry, University of Liverpool, United Kingdom

Presenting author — e.malkawi@aau.edu.jo

https://doi.org/10.17952/38EPS.2026.P330

1 THE PROBLEM

Antimicrobial resistance (AMR) **is one of the defining health threats of our time**. Resistance keeps rising while the discovery of **new classes of antibiotics has all but stopped,** and the burden falls hardest on low and middle income countries.





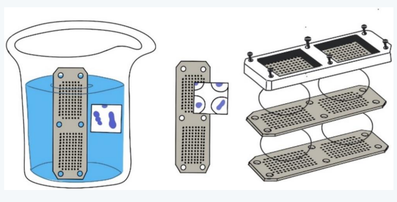
≈5 M
deaths associated with bacterial AMR worldwide (2019)

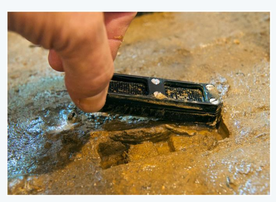
2
WHO-priority Gram-positive targets: MRSA and *E. faecium*

LMICs
carry a disproportionate share of the AMR burden

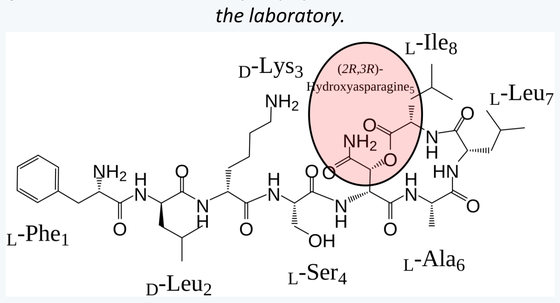
2 THE STARTING POINT: NOVO29

Clovibactin (Novo29):
A groundbreaking discovery of a highly effective Novel Antibiotic with lower risk of Bacterial Resistance





The iChip gives access to the vast majority of soil bacteria that cannot be grown in the laboratory.

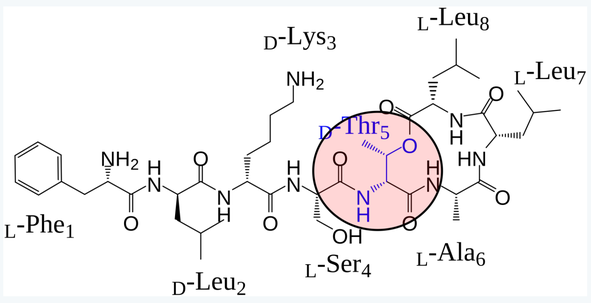


Novo29 / clovibactin: the unnatural D-hydroxy-asparagine$_5$ (D-Hyn$_5$, circled) links macrocycle and tail.

- ✕ Overall synthetic yield of only ≈1 %
- ✕ D-Hyn$_5$ is not commercially available
- ✕ Long, multistep and repetitive coupling route

3 THE DESIGN: NOVLTEX

Novltex fuses the **Leu^{10}-teixobactin macrocycle** to the **Novo29 N-terminal tail**, replacing the costly D-Hyn$_5$ with inexpensive, commercially available threonine.



Novltex analogue 4 — D-Hyn$_5$ replaced by D-Thr$_5$ (circled).

- ✓ D-Hyn$_5$ is not essential for antibacterial activity
- ✓ Rapid, simple and inexpensive synthesis
- ✓ High-yielding and ready for low-cost scale-up

4 SYNTHESIS

Fmoc-SPPS on 2-chlorotrityl resin: DIC/DMAP esterification, orthogonal Alloc/Trt protection, microwave DIC–Oxyma couplings and on-resin HATU cyclisation, **with a single purification after final cleavage.**

30 %
isolated yield, vs ≈1 % for Novo29

10 min
microwave coupling cycles

> 95 %
purity by HPLC

16
analogues in the library

5 STEREOCHEMISTRY DRIVES ACTIVITY

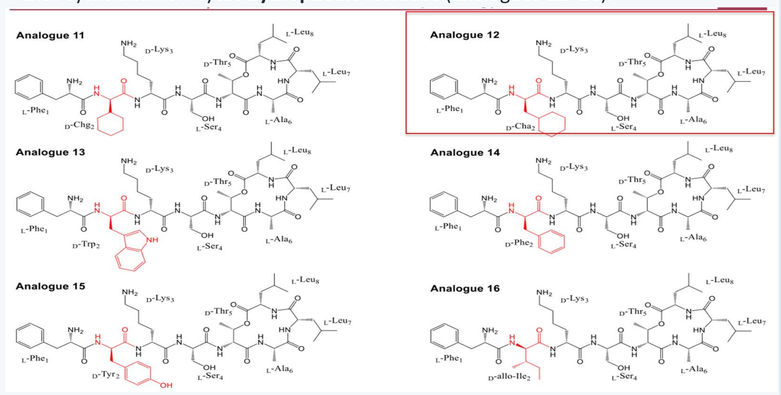
A systematic configuration scan of the tail and the macrocycle (analogues 1–10) against MRSA ATCC 33591:

#	Phe$_1$	Leu$_2$	Lys$_3$	Ser$_4$	Thr$_5$	Ala$_6$	Leu$_7$	Leu$_8$	MIC (µg/mL)
1	L	D	D	L	L	L	D	L	8
2	L	D	D	L	D	L	D	L	32
3	D	L	L	D	D	L	L	L	32
4	**L**	**D**	**D**	**L**	**D**	**L**	**L**	**L**	**2–4**
5	D	L	D	L	D	L	L	L	> 32
6	L	D	L	D	D	L	L	L	> 32
7	D	D	L	L	D	L	L	L	32
8	L	L	L	L	D	L	L	L	> 32
9	D	D	D	D	D	L	L	L	16
10	L	D	D	L	D	L	L	L[a]	8
Vancomycin	–	–	–	–	–	–	–	–	0.5–1

Analogue 4 (L$_1$DDL$_4$ tail + Leu^{10}-teixobactin macrocycle) is the initial lead — MIC 2–4 µg/mL, comparable to vancomycin. [a] Analogue 10 carries L-Ile$_8$.

6 POSITION-2 SCAN → THE HIT

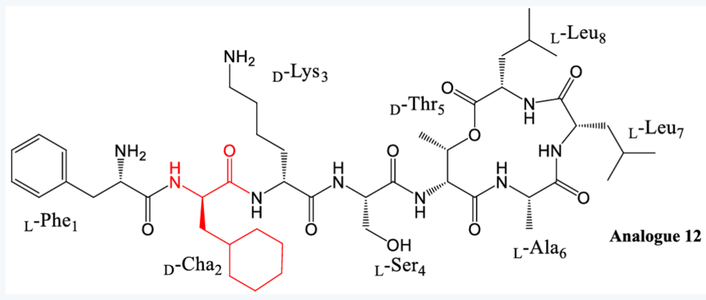
The Leu$_2$ side chain contacts the bacterial membrane, so position 2 was replaced with cyclic and non-cyclic **hydrophobic residues** (analogues 11–16).



Analogues 11–16 — built on the configuration of analogue 4; the residue replacing Leu$_2$ is red.

#	Residue at position 2	MIC vs MRSA (µg/mL)
11	D-Cyclohexylglycine (Chg)	8
12	**D-Cyclohexylalanine (Cha)**	**0.25**
13	D-Tryptophan (Trp)	> 32
14	D-Phenylalanine (Phe)	8
15	D-Tyrosine (Tyr)	> 32
16	D-allo-Isoleucine	16

Analogue 12 (D-Cha$_2$): MIC 0.25 µg/mL — 16× more potent than analogue 4 and 32× more potent than the one-carbon-shorter Chg analogue 11. Bulky, polar or aromatic side chains are not tolerated.



Novltex analogue 12 — the lead compound.

7 POTENT AGAINST MDR ISOLATES

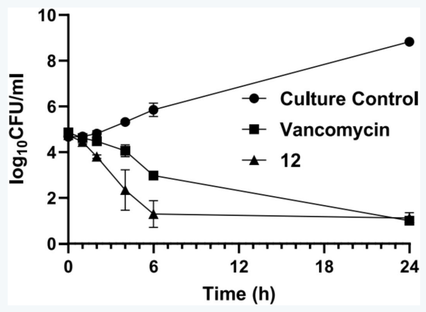
Analogue 12 was tested against MDR clinical isolates of *S. aureus* (NARSA) and *E. faecium* (IHMA), alongside licensed antibiotics and synthetic clovibactin.

MIC (µg/mL)	*Staphylococcus aureus*				*Enterococcus faecium*		
	NR 45914	NR 45926	NR 45930	NR 46062	1581582	1766686	1563254
Analogue 12	**0.125**	**0.125**	**0.125**	**0.063**	**0.5**	**0.125**	**0.25**
Clovibactin	0.063	0.063	0.25	0.063	0.25	0.25	0.063
Vancomycin	1	0.5	1	2	> 32	> 32	> 32
Linezolid	2	32	4	16	1	1	16
Cefotaxime	4	16	8	16	> 32	> 32	> 32
Levofloxacin	1	4	> 32	32	32	32	32
Ampicillin	2	32	8	8	> 32	> 32	> 32
Daptomycin	2	4	2	2	> 32	> 32	> 32

≤ 1 potent 2–4 moderate ≥ 8 poor

Analogue 12 matches clovibactin and outperforms vancomycin, linezolid, cefotaxime, levofloxacin, ampicillin and daptomycin across both WHO-priority species.

8 RAPID KILLING — NO RESISTANCE



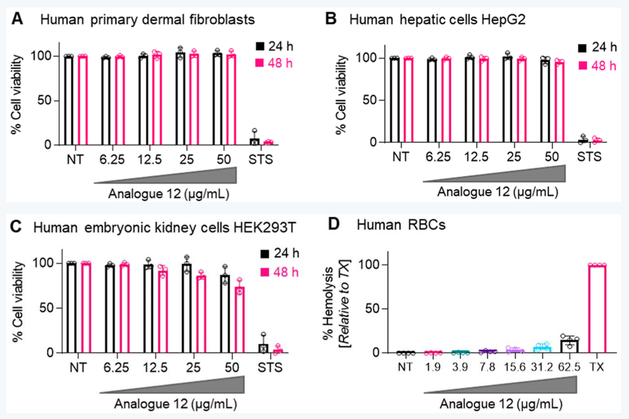
Time-kill kinetics of analogue 12 and vancomycin against MRSA ATCC 33591 (mean ± SD of two independent experiments in duplicate).

At 2.5 µg/mL (10× MIC), analogue 12 produced **significant killing of MRSA within 6 h**; vancomycin needed 24 h at twice that concentration.

- ✓ No resistant MRSA mutants after 24 h at 10× MIC

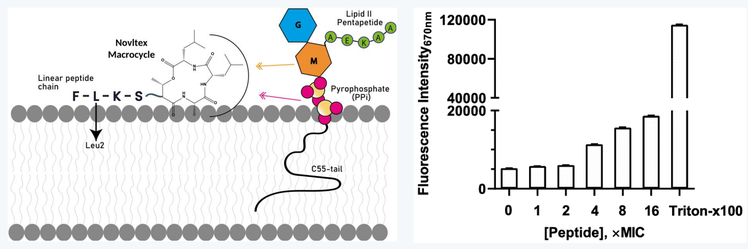
9 EXCELLENT SAFETY PROFILE

No major cytotoxicity up to 50 µg/mL at 24 and 48 h — **≈100× the average MIC** — in human primary dermal fibroblasts, HepG2 and HEK293T cells, and no detectable haemolysis up to 31.2 µg/mL (> 60× MIC).



Viability of human cells (MTS assay) and haemolysis of human red blood cells after exposure to analogue 12. NT = no treatment, STS = staurosporine, TX = Triton X-100.

10 MECHANISM RETAINED



Left: Novltex macrocycle binding the pyrophosphate of lipid II. Right: DiSC$_3$(5) fluorescence rises with analogue 12 — membrane depolarisation of intact MRSA.

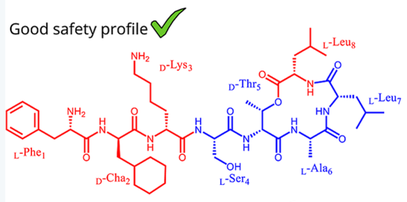
- ✓ Lipid II abolishes activity in spot-on-lawn assays
- ✓ Cytoplasmic membrane depolarisation, pronounced at 4× MIC

11 CONCLUSIONS • OUTLOOK • REFERENCES

- Novltex is a new hybrid antibiotic class, potent, inexpensive to make and scalable.
- Analogue 12 reaches MIC 0.063–0.5 µg/mL against MDR MRSA and *E. faecium*, surpassing several licensed antibiotics.
- It kills rapidly, selects no resistance *in vitro*, and spares human cells.
- The parent lipid II mechanism is fully preserved.

The lead at a glance

Potent activity: ✓
MRSA & *Enterococcus faecium* (MIC: 0.063 - 0.5 µg/mL)
Good safety profile ✓



High yielding novel synthesis 30% ✓

What's next — towards the clinic



References

1. Malkawi E, Parmar A, Das S, et al. J Med Chem 2025;68:19143–52.
2. IHME Pathogen Core Group. Lancet Infect Dis 2024;24(8):868–95.
3. Butler MS, et al. Antimicrob Agents Chemother 2022;66(3):e01991-21.
4. Iyer A, Madder A, Singh I. Future Microbiol 2019;14(6):457–60.
5. Shukla R, et al. Cell 2023;186(19):4059–73.
6. Parmar A, et al. Chem Sci 2017;8(12):8183–92.
7. Dallas H, et al. US Patent 11,203,616 B2, 2020.

Acknowledgements: Innovate UK & DHSC (SBRI 106368–623146), Rosetrees Trust (CF-2021-2\102) and EPSRC. MDR strains were provided by NARSA / BEI Resources, NIAID, NIH; synthetic clovibactin by J. S. Nowick (University of California, Irvine).

Amman Arab University • University of Liverpool
e.malkawi@aau.edu.jo • 38th EPS, Vienna 2026

The antimicrobial peptide Esc(1–21) potentiates CFTR channel via direct targeting of the nucleotide binding domains

https://doi.org/10.17952/38EPS.2026.P564

Maria Luisa Mangoni[1], Loretta Ferrera[2], Giacomo Cappella[1], Mario Passalacqua[3], Mattia Mori[4], Debora Baroni[5]

[1]Department of Biochemical Sciences, Sapienza University of Rome, Laboratory affiliated to Pasteur-Italia Fondazione Cenci Bolognetti; [2]U.O.C. Genetica Medica, Istituto Di Ricovero e Cura a Carattere Scientifico, Istituto Giannina Gaslini, Genova; [3]Department of Experimental Medicine, University of Genova, 16132, Genova ; [4]Department of Biotechnology, Chemistry and Pharmacy, University of Siena; [5]Istitute Institute of Biophysics, National Research Council, Genoa

BACKGROUND

Cystic fibrosis (CF) is caused by mutations in the CFTR ion channel, leading to impaired chloride transport, chronic lung infections, and progressive respiratory damage[1]. The most common mutation is the loss of Phe 508 (F508del-CFTR). Although CFTR modulators have improved patient outcomes, a subset of individuals remains unresponsive or continues to suffer from persistent infections [2], highlighting the need for alternative therapeutic strategies. We identified frog skin–derived antimicrobial peptides (Esc peptides) that reduce bacterial burden in murine models of *Pseudomonas aeruginosa* lung infection. Notably, Esc(1-21) also acts as a potentiator of F508del-CFTR, enhancing chloride transport in both cell lines and primary bronchial epithelial cells [3] **(Figure 1).**

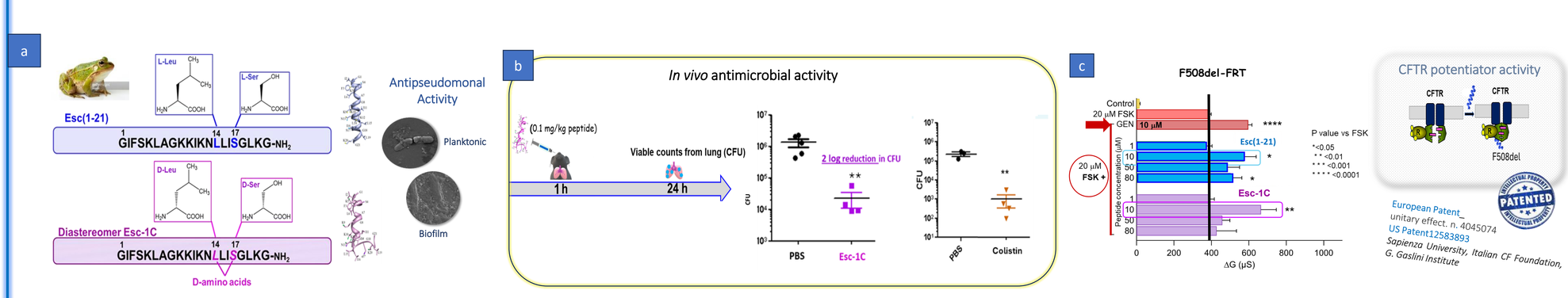


Figure 1. Schematic representation of biological properties of Esc peptides. **a,** *Esc peptides* primary structure. **b,** *In vivo* efficacy of Esc-1C upon intratracheal administration in mice with *P. aeruginosa* lung infection. The number of viable bacterial cells was evaluated after 24 h treatment and compared to that of colistin. **, p < 0.01; ***c***, Transepithelial-electrical-conductance, experiments showing the CFTR potentiator activity of Esc peptides in the presence of forskolin (FSK) on Fisher Rat Thyroid (FRT) cells expressing F508del-CFTR, compared to genistein (GEN)

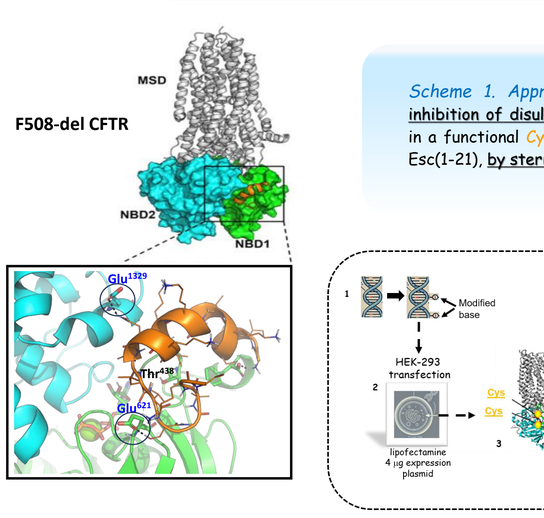
AIMS

1. Identify the binding site of Esc(1-21) on CFTR
2. Validate the peptide interaction by disulfide cross-linking experiments
3. Determine whether Esc(1-21) enters the cells and reaches CFTR

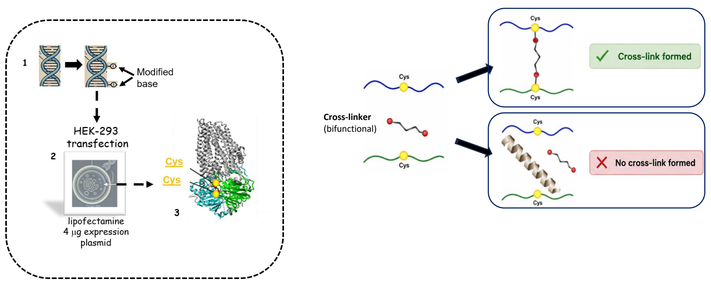
RESULTS

By combining molecular dynamics, mutagenesis, and disulfide cross-linking assays **(See Scheme 1, Figures 2 and 3**), we show that Esc(1-21) directly interacts with the CFTR nucleotide-binding domain interface. Confocal imaging confirms peptide internalization and co-localization with CFTR **(Figure 4).** These findings identify Esc peptides as multifunctional molecules with antimicrobial and CFTR-modulating activities, supporting their development as novel therapeutic candidates for CF [4] .

Computational studies & Cross-linking



Scheme 1. Approach to verify peptides' binding region to CFTR: inhibition of disulfide cross-linking between 2 cysteines (Cys) introduced in a functional Cys less CFTR mutant, at the predicted binding region of Esc(1-21), by sterically hindering the access of the cross-linker



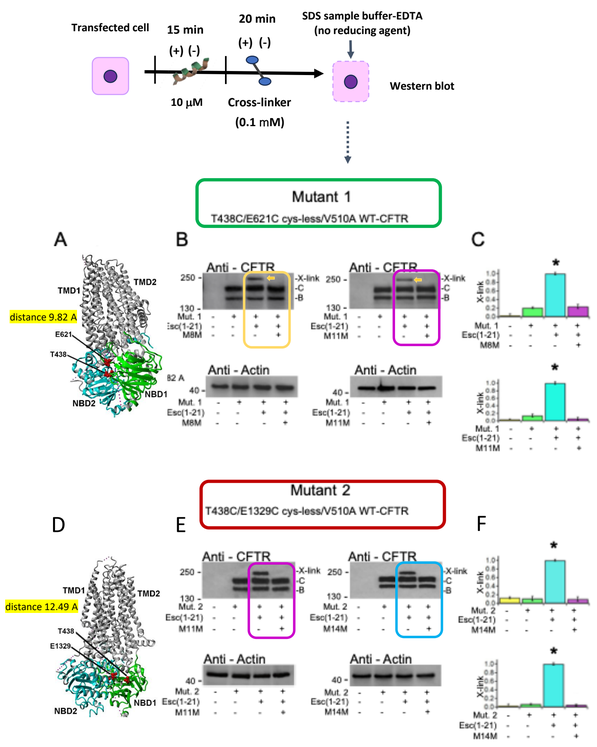


Figure 2. Effect of Esc(1-21) on disulfide cross-linking of CFTR double-cys mutants at the NBD1-NBD2 interface. **Panels A, D**: MD-based structural models of the cys-less/V510A WT-CFTR scaffold showing positions of reintroduced cys residues in mutant 1 (T438C/E621C), mutant 2 (T438C/E1329C); cys residues are in red, with median inter-residue distance indicated. **Panels B, E:** HEK-t cells expressing mutants were incubated with (+) or without (–) 10 μM Esc(1-21) for 15 min and treated (+) or not (–) with 0.1 mM M8M, M11M, M14M cross-linkers, as indicated for 20 min. Lysates were analysed by immunoblotting with anti-CFTR (upper blots) and anti-actin (lower blots) antibodies. Immature (B), mature (C) and cross-linked CFTR species (X-link) are indicated. **Panels C, F**: Bar graphs showing relative X-link abundance, normalized to the X-link signal detected in lysates treated with the cross-linker alone. Data are expressed as mean ± SD.

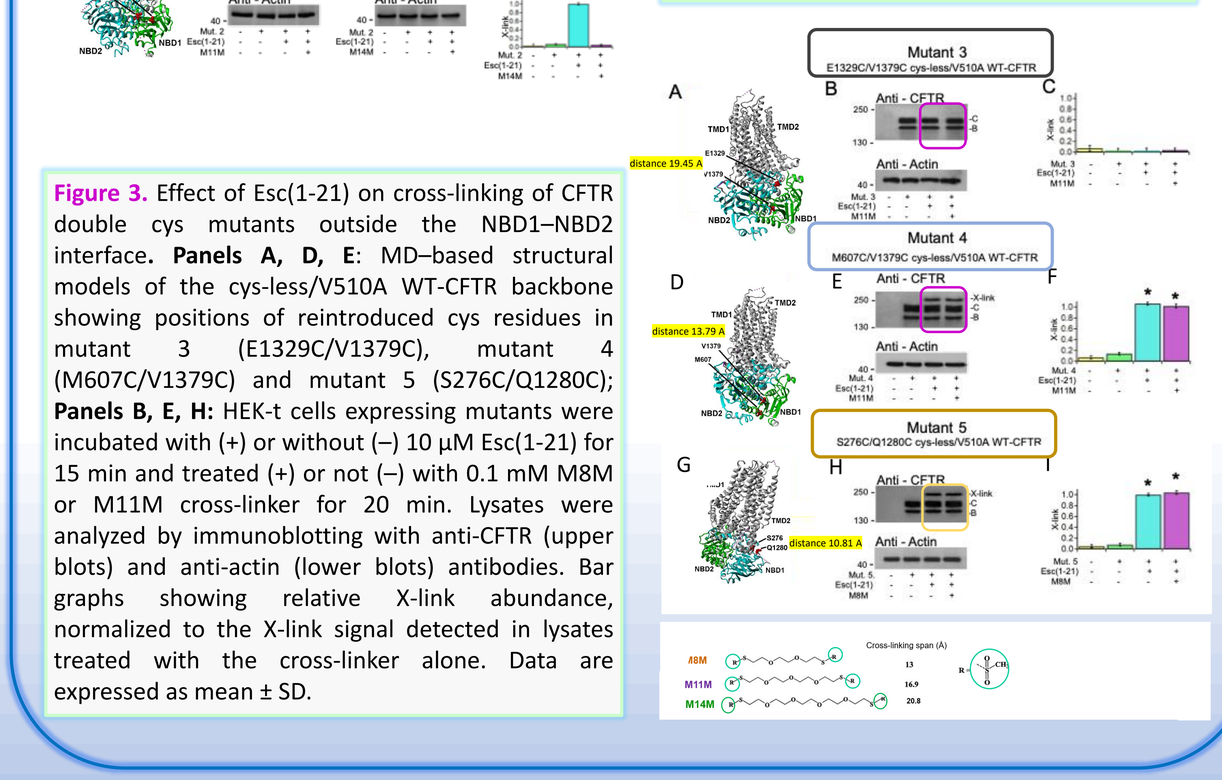
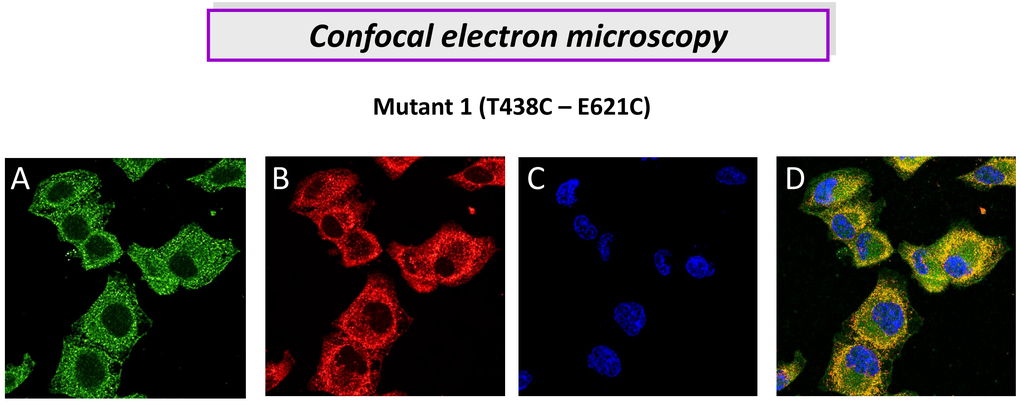


Figure 3. Effect of Esc(1-21) on cross-linking of CFTR double cys mutants outside the NBD1–NBD2 interface**. Panels A, D, E**: MD–based structural models of the cys-less/V510A WT-CFTR backbone showing positions of reintroduced cys residues in mutant 3 (E1329C/V1379C), mutant 4 (M607C/V1379C) and mutant 5 (S276C/Q1280C); **Panels B, E, H:** HEK-t cells expressing mutants were incubated with (+) or without (–) 10 μM Esc(1-21) for 15 min and treated (+) or not (–) with 0.1 mM M8M or M11M cross-linker for 20 min. Lysates were analyzed by immunoblotting with anti-CFTR (upper blots) and anti-actin (lower blots) antibodies. Bar graphs showing relative X-link abundance, normalized to the X-link signal detected in lysates treated with the cross-linker alone. Data are expressed as mean ± SD.

Confocal electron microscopy

Mutant 1 (T438C – E621C)



Rabbit anti-Esc(1-21) Secondary Ab: Anti-rabbit IgG, conjugated to Alexa Fluor 594	Mouse anti-CFTR Secondary Ab: Anti-mouse IgG conjugated to Alexa Fluor® 488	DAPI for nuclei detection	Merge image: co-localization CFTR/Esc(1-21)

Esc(1-21) interferes with cross-linking at the predicted binding site and colocalizes with CFTR

Figure 4. Confocal immunofluorescence analysis of co-localization between cys-less CFTR and the Esc(1-21) peptide. Representative confocal images of highly transfectable embryonic kidney 293 (HEK-t) cells expressing the T438C/E621C cys-less/V510A WT-CFTR construct following incubation with Esc(1-21). **(A)** CFTR cys-less mutant immunostaining (green) detected using a monoclonal anti-CFTR antibody and an Alexa Fluor 488-conjugated secondary antibody. **(B)** Esc(1-21) peptide localization (red), revealed using a rabbit polyclonal anti-peptide primary antibody and an Alexa Fluor 568-conjugated secondary antibody. **(C)** Nuclear counterstaining with 4',6-diamidino-2-phenylindole (DAPI, blue). **(D)** Merged image highlighting CFTR cys-less-peptide co-localization (yellow).

CONCLUSIONS

These results support:

- *Direct interaction of Esc(1-21) with the NBDs interface*
- *Intracellular localization of Esc(1-21) and colocalization with CFTR*

→ Esc(1-21) as potential candidate for the development of new as dual-function candidates for CF therapy

References

1. Veit G, et al. Mol Biol Cell 27: 424-433. 10.1091/mbc.E14-04-0935
2. Almughem FA, et al. Pharmaceutics 12: 10.3390/pharmaceutics12070616
3. Ferrera L et al. Cell Mol Life Sci 82: 121. 10.1007/s00018-025-05633-9
4. Baroni D. et al. ACS Omega in press

Acknowledgments:

Fondazione per la Ricerca sulla Fibrosi Cistica - ETS
italian cystic fibrosis research foundation

FFC Project 6/2025 adopted by:
-GRUPPO DI SOSTEGNO FFC RICERCA DI SCAURI – MINTURNO
-DELEGAZIONE FFC RICERCA DI MONCALVO – ASTI
-DELEGAZIONE FFC RICERCA DI DONGO - COMO

https://doi.org/10.17952/38EPS.2026.P502

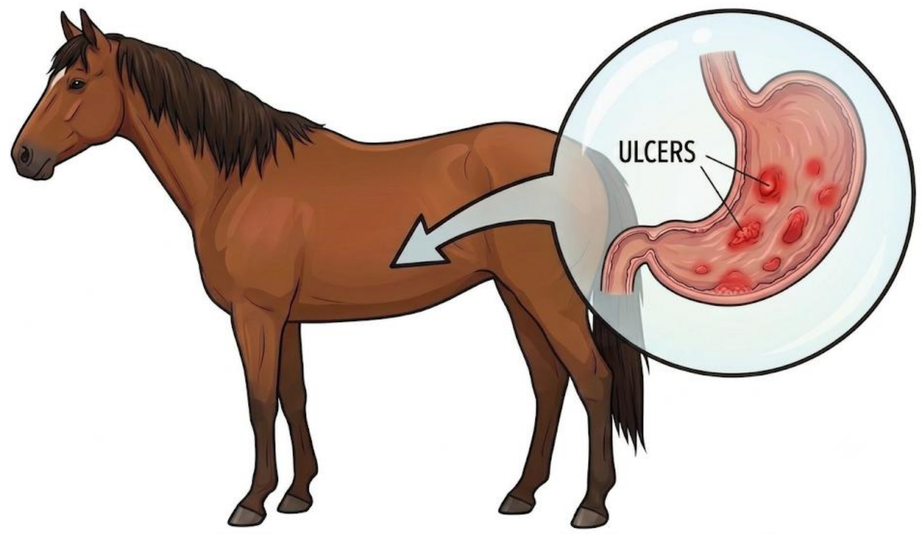
Design and synthesis of therapeutic peptides with anti-inflammatory and regenerative properties for use in the treatment of equine gastric ulcer syndrome (EGUS)

Kinga Marszałek[1], Ewa Wieczerzak[1], Krzysztof Marycz[2] & Sylwia Rodziewicz-Motowidło[1]

[1]*Department of Biomedical Chemistry, Faculty of Chemistry, University of Gdańsk*
[2] *International Institute of Translational Medicine (MIMT), Wrocław, Poland*

1. Introduction

Gastric ulcers are a common and serious clinical problem in veterinary medicine. In sport horses, Equine Gastric Ulcer Syndrome (EGUS) occurs with very high prevalence, reaching 50–90%, especially those subjected to intense training and transport stress[1]. Currently, two drugs are primarily used: omeprazole (a proton pump inhibitor, PPI) and sucralfate, which acts as a protective coating by forming a barrier on the gastric mucosa. Both have significant limitations and side effects with long-term use[2,3].



2. The aim of study

The project aims to develop bioactive peptides targeting molecular mechanisms involved in mucosal regeneration and regulation of the local inflammatory response. The design of bioactive peptide sequences was carried out based on the current state of knowledge described in the scientific literature, with particular emphasis on peptides involved in gastrointestinal epithelial regeneration and modulation of the inflammatory response.

3. Methods

Peptide Stability

- **Incubation:** Aqueous solutions and simulated gastric fluid (pH 1.2) at 37°C.
- **Sampling & Analysis:** Samples collected at specified time points and evaluated using HPLC.

Cytotoxicity Assay

- **Cell seeding:** L929 cells (2 × 10^4 cells/well) incubated overnight in 96-well plates.
- **Treatment:** 24 h exposure to peptides (0.78–1600 µg/mL).
- **Viability assessment:** MTT assay (0.5 mg/mL). Results expressed as % metabolic activity vs. non-treated control (100%). Toxicity control included.

4.Results

Peptide Stability

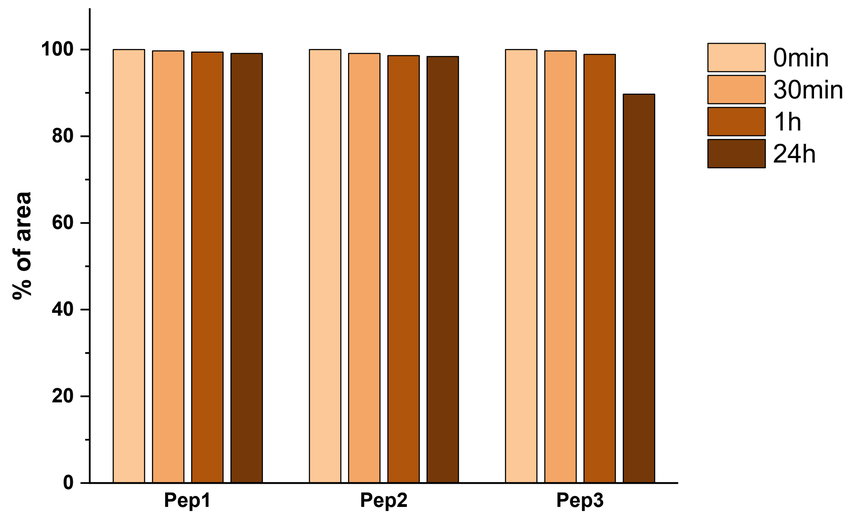


Fig 1: Stability of selected peptides in water over time

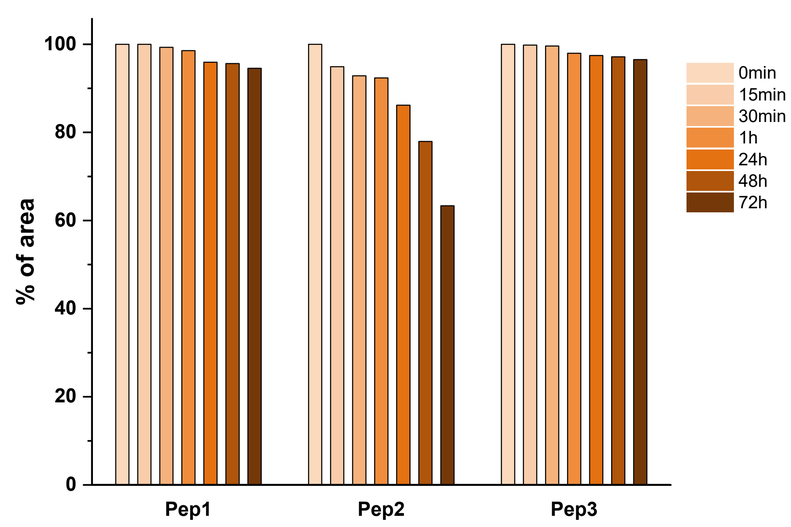


Fig 2: Stability of selected peptides in a solution simulating gastric fluid over time

Cytotoxicity Assay

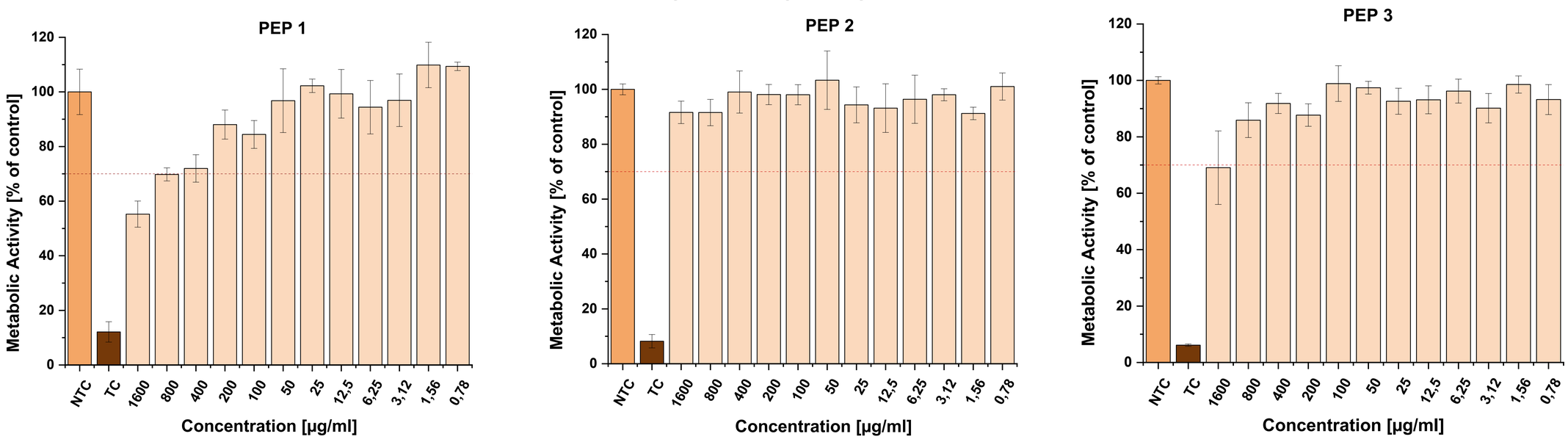


Fig 3: Effect of tested peptides on L929 cell viability. Metabolic activity assessed by MTT assay after 24 h exposure. NTC – non-treated control, TC – toxicity control. *Data expressed as mean ± SD.*

5.Conclusion

The comprehensive evaluation of peptide stability and cytotoxicity presented in this study serves as a critical first step in their preclinical assessment. The obtained baseline data will directly guide our subsequent research efforts, which will focus on structural optimization of the peptides and evaluating their therapeutic efficacy in more complex biological models.

References: [1] Murray, M. J., Schusser, G. F., Pipers, F. S., & Gross, S. J. (1996). Factors associated with gastric lesions in thoroughbred racehorses. *Equine Veterinary Journal*, 28(5), 368–374.

[2]Sykes, B. W., Hewetson, M., Hepburn, R. J., Luthersson, N., & Tamzali, Y. (2015). European College of Equine Internal Medicine Consensus Statement—Equine Gastric Ulcer Syndrome in Adult Horses. *Journal of Veterinary Internal Medicine*, 29(5), 1288–1299.

[3]Szabo, S., & Hollander, D. (1989). Pathways of gastrointestinal protection and repair: mechanisms of action of sucralfate. *The American Journal of Medicine*, 86(6), 23-31.

Acknowledgements: This work was supported by NAWA under grant FERS.01.05-IP.08-0218/23

Multifunctional Bone-Targeting Peptides for Inhibition of the RANK-TRAF6 Interaction

P2.373

https://doi.org/10.17952/38EPS.2026.P373

Sofia A. Martins[1], Cátia Rosa[1], Marco Cavaco[2], Rita Melo[1], David Andreu[3], Javier Valle[3], Vera Neves[2], Miguel A. R. B. Castanho[2], Sandra Casimiro[2], João D.G. Correia[1,4]

[1] Center for Nuclear Sciences and Technologies, Instituto Superior Técnico, Universidade de Lisboa, Estrada Nacional 10, ao km 139,7; 2695-066 Bobadela LRS, Portugal;

[2] Gulbenkian Institute of Molecular Medicine, Professor Egas Moniz 1649-028 Lisboa, Portugal;

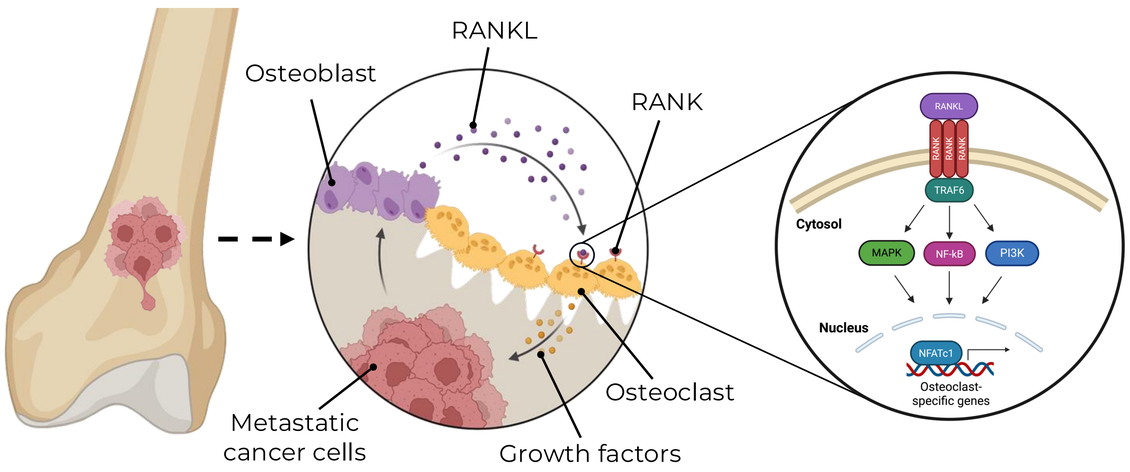
[3] Department of Medicine and Life Sciences, Pompeu Fabra University, Dr. Aiguader 88, Barcelona Biomedical Research Park, 08003 Barcelona, Spain;

[4] Department of Nuclear Sciences and Engineering, Instituto Superior Técnico, Universidade de Lisboa, Estrada Nacional 10, ao km 139,7; 2695-066 Bobadela LRS, Portugal

1. Background

Bone metastases remain a major cause of **cancer-related mortality**[1].

The bone undergoes **constant remodelling** during an individual's lifetime. This **remodelling** is **disrupted** in **metastasis**[1].



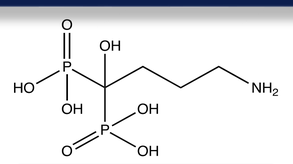
The vicious cycle of bone metastasis and its signalling pathways

Cancer cells induce **osteoblasts** to secrete receptor activator of nuclear factor kappa B ligand (**RANKL**), which binds to its receptor, **RANK**, in **osteoclasts**[1].

Through tumour necrosis factor receptor associated factor 6 (**TRAF6**), this interaction increases **osteoclast activity**, promotes **bone resorption** and **secretion of growth factors**[1].

2. Aim

Develop **multifunctional peptide conjugates** that **disrupt** the **RANK/TRAF6** axis and thus **hinder osteoclastogenesis** and **metastatic potential**



\+ Fragment A +

① **Bone-targeting unit**

A bisphosphonate **(alendronate)** with **high affinity** for **bone mineral**[2]

② **Cathepsin K-sensitive linkers**

Cathepsin K is an abundant **protease** in the **bone microenvironment**[3]

Fragment B + Fragment C

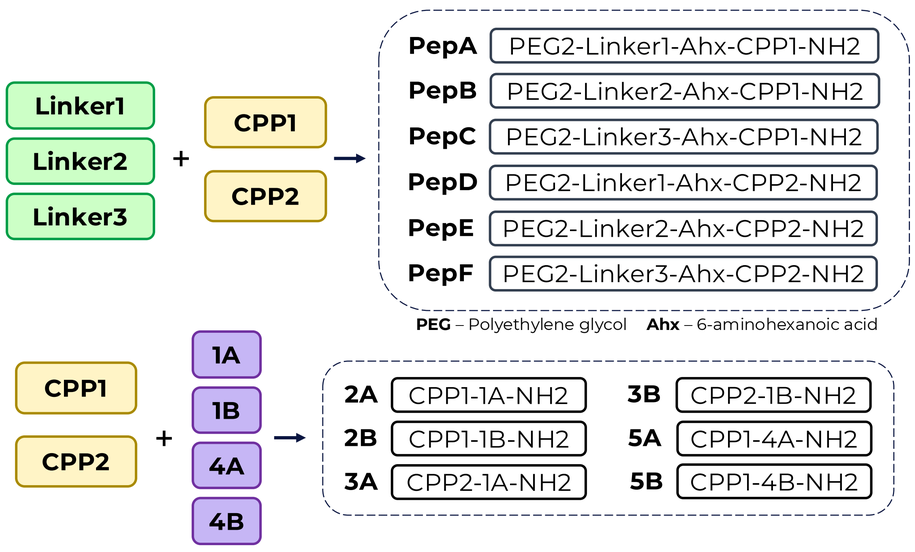
③ **Cell-penetrating peptides (CPPs)**

Peptide sequences able to promote **cell entry** of different cargoes[4]

④ **RANK-derived sequences**

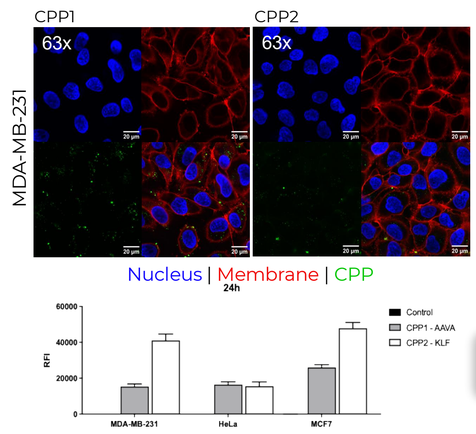
Bind to **TRAF6** and **disrupt** the **RANK/TRAF6 interface**[5]

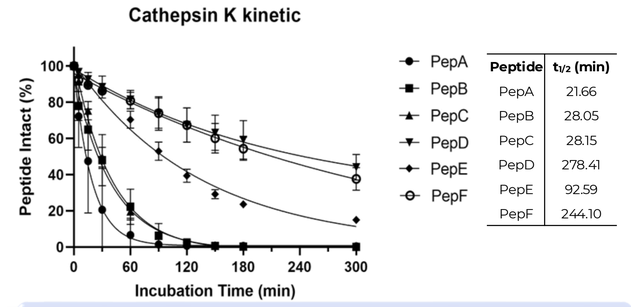
3. Approach



4. Results

Cell Internalization and Cathepsin K Cleavage

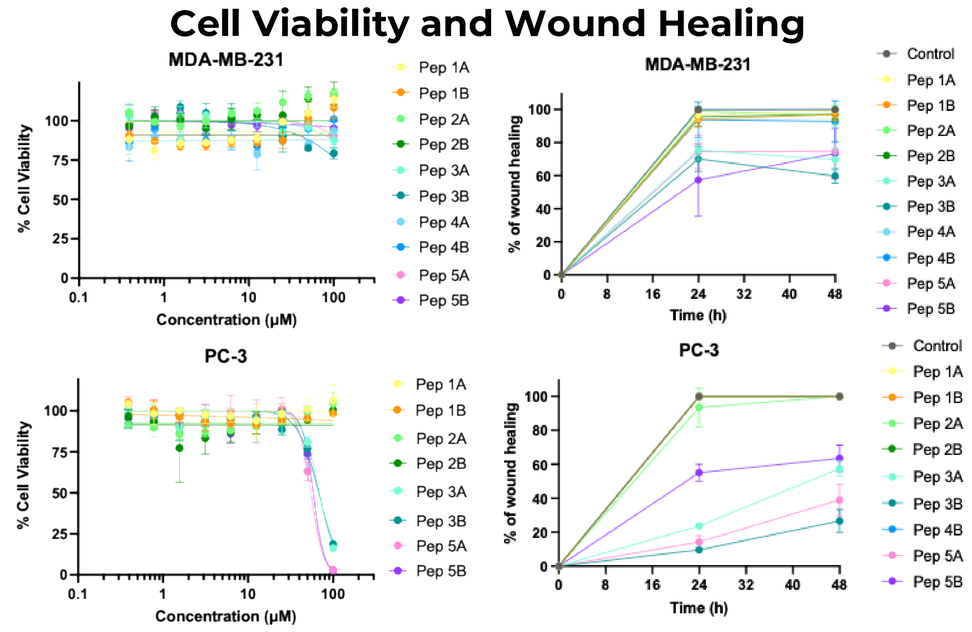




Peptide	$t_{1/2}$ (min)
PepA	21.66
PepB	28.05
PepC	28.15
PepD	278.41
PepE	92.59
PepF	244.10

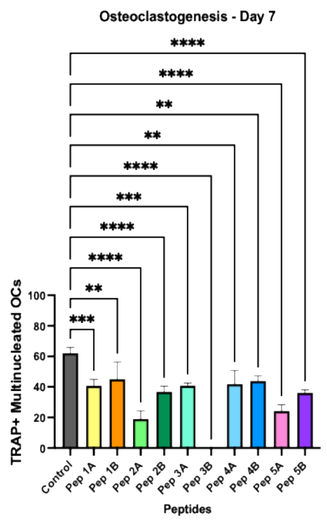
Both CPPs are **internalized; peptides A, B and C** show **faster cleavage kinetics** than D, E and F.

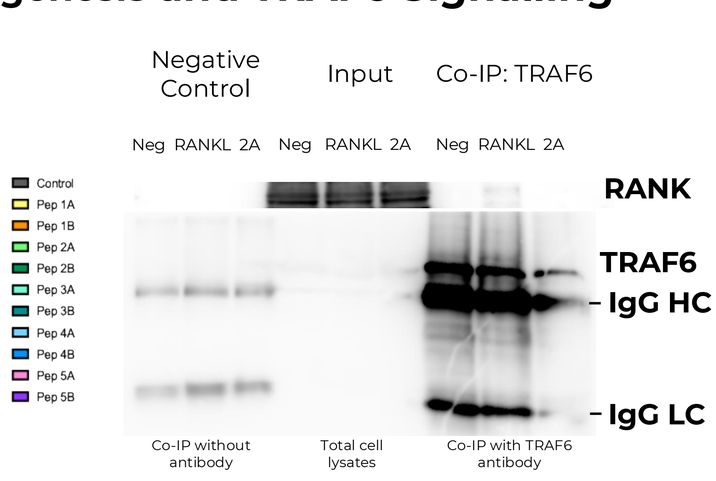
Cell Viability and Wound Healing

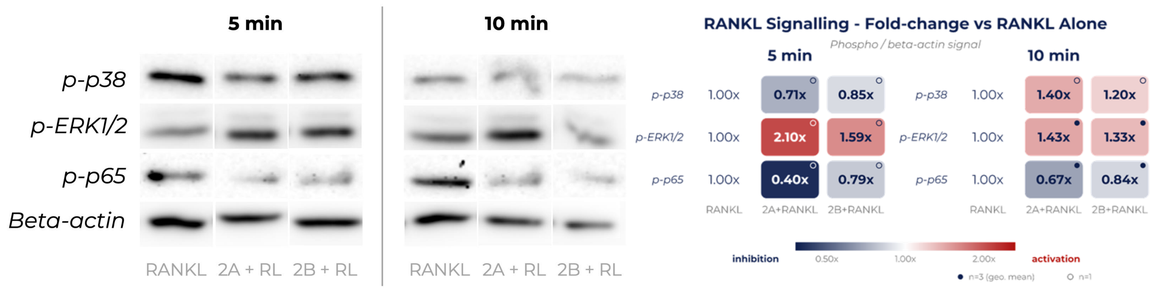


Only **3A, 3B, 5A and 5B** show **slight cytotoxicity** and also **impair wound healing** in **prostate cancer cells** – likely **reflecting cytotoxicity, not an anti-migratory effect**.

Osteoclastogenesis and TRAF6 Signalling







2A and 5A show the **strongest inhibition of osteoclastogenesis**; **3B** is **cytotoxic** to **monocytes. 2A disrupts RANK/TRAF6,** and seems to **modulate downstream signalling**.

5. Conclusions

- **Both CPPs display internalization** and **cleavage kinetics** seems to strongly depend on the **CPP sequence** rather than on the **type of cathepsin K-sensitive linker** – supporting **CPP selection** as **key for cargo release**.
- Peptides **3A, 3B, 5A and 5B** exhibit **slight cytotoxicity** and **impair wound healing**, but **re-evaluation** at **sub-cytotoxic concentrations** is **warranted**.
- Peptides **2A** and **5A** show the **highest inhibitory effect in osteoclastogenesis,** highlighting their **potential** as the **most promising anti-resorptive candidates.**
- Peptide **2A** can **disrupt the RANK/TRAF6 interface; both 2A and 2B** appear to **modulate downstream signalling**.
- Taken together, these results support the **selection of Linker 1 and 2A** as the **lead candidates** for the **development** of the **full peptide**.

REFERENCES

1. Kottmann, V. *et al.* Biochim. Biophys. Acta – Rev. Cancer. 189551 (2026).
2. Bruschi, A. *et al.* Cancer Med. 14(9), e70901 (2025).
3. Dey, G. *et al.* Jacs Au. 5(3), 1104 (2025).
4. Jankowski, A. M. *et al.* Nanoscale. 17(35), 20006-20019 (2025).
5. Anzai, M. *et al.* Commun. Biol. 8(1), 643 (2025).

ACKNOWLEDGEMENTS

This work was supported by FCT through PTDC/QUI-OUT/3854/2021, UI/BD/154474/2022 and UID/Multi/04349/2020.

Diagnostic 7-Mer Model Peptide for Rapid Evaluation of Cysteine Racemization in Solid-Phase Peptide Synthesis

Saundra Mason, Wesley Grenier, Dario Slavazza, Hanson Chang
CSBio Instrumentation, Mountain View, CA, 94043

https://doi.org/10.17952/38EPS.2026.P002

Introduction

- High-temperature synthesis reduces reaction time and can improve crude purity and yield.
- Elevated temperatures increase the risk of racemization in sensitive residues like Cysteine (Cys).
- Racemization is difficult to detect as L and D forms may co-elute.
- Epimerization can change peptide 3-D structure, affecting biological activity and safety.
- Regulatory bodies expect impurities to be appropriately characterized and controlled.
- We developed a diagnostic 7-mer (KGP**X**GEG) that can be used to screen synthesis conditions that cause racemization. This sequence can be used to identify Cysteine racemization on a standard RPHPLC C18 column without pre-column derivatization.

Method

Syntheses were carried out on a CSBio II utilizing conduction heating with preheated solvents.



Coupling and deprotection times are specified in the figure legends. Synthesis methodology and analytical methods are summarized below.

Parameter	Specification/Condition
Model Sequence	KGP**X**GEG-NH_2 (X = L-Cys or D-Cys)
Resin	Rink-Amide Resin
Coupling Conditions	DIC/Oxyma: 90 °C, 110 °C HBTU/DIEA: 30 °C, 45 °C, 60 °C, 90 °C
HPLC	Stationary Phase: C18 Buffer A: 0.1 % TFA:H_2O Buffer B: 0.1 % TFA:ACN Phenomenex Luna C18 (250 x 4.6 mm) 214 nm Flow rate: 1 mL/min 0 to 30 % B in 20 min Column temperature: 25 °C
MS	ITMS ESI+ (Identity Confirmation Only)
Chiral AA Analysis of DIC/Oxyma 90 °C L-Cys and D-Cys Peptides by GC-MS	C.A.T. Labs method A.0.3 Enantiomeric Purity

Table 1. Synthesis parameters and analytical methods.

DIC/Oxyma Synthesis

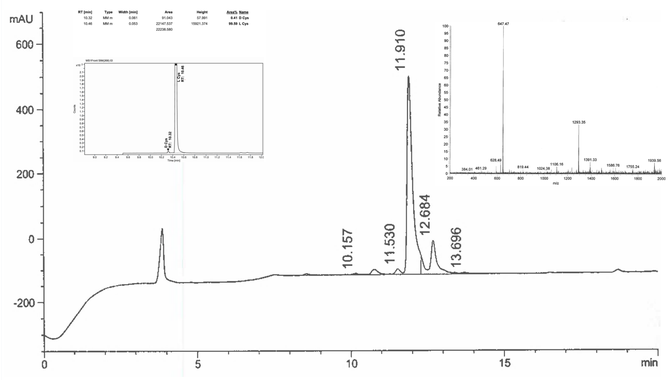


Figure 1. HPLC of peptide synthesized with **L-Cys in sequence position X using DIC/Oxyma at 90 °C**, 1 min deprotection and 5 min coupling. L-Cys variant elutes at ~11. 9 min. MS shows m/z 647. Enantiomeric purity 99.59% L-Cys (C.A.T. Lab Method A.03).

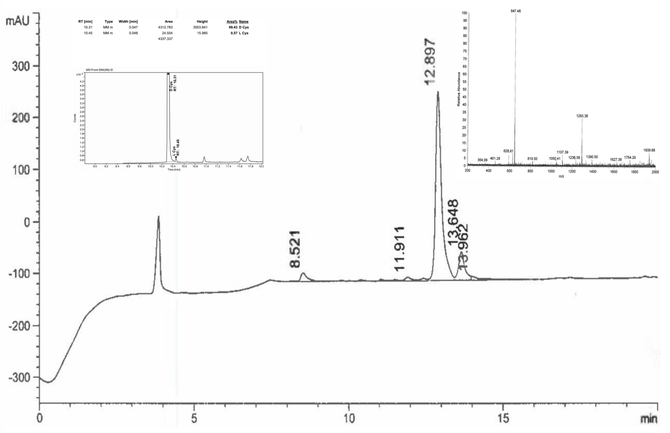


Figure 2. HPLC of peptide synthesized with **D-Cys in position X using DIC/Oxyma at 90 °C**, 1 min deprotection and 5 min coupling. D-Cys variant elutes at ~12.9 min. MS shows m/z 647. Enantiomeric purity 99.43% D-Cys (C.A.T. Lab Method A.03).

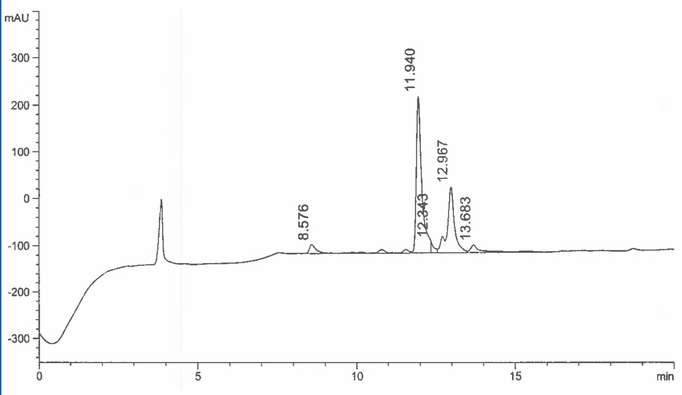


Figure 3. Co-injection HPLC of L-Cys and D-Cys enantiomerically pure peptides synthesized with DIC/Oxyma at 90 °C, 1 min deprotection and 5 min coupling. The L-Cys and D-Cys variants elute at ~11.9 min and ~12.9 min, respectively.

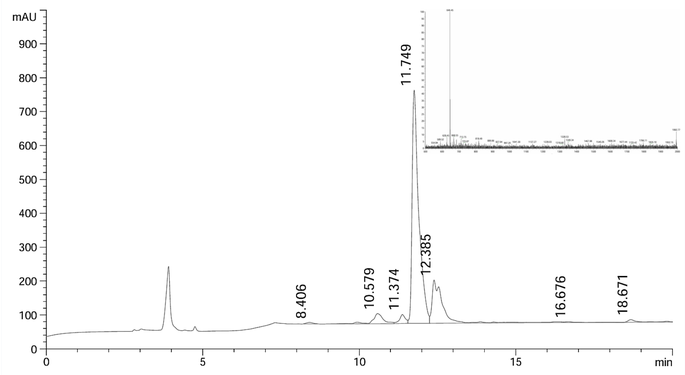


Figure 4. HPLC of peptide synthesized with **L-Cys in position X using DIC/Oxyma at 110 °C**, 1 min deprotection and 5 min coupling. MS shows m/z 646.

HBTU/DIEA Synthesis

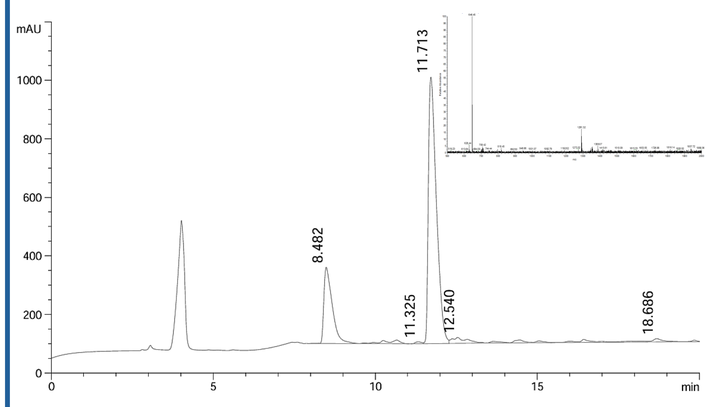


Figure 5. HPLC of peptide synthesized with **L-Cys in position X using HBTU/DIEA at 30 °C**, 2 x 5 min deprotection and 60 min coupling. MS shows m/z 646.

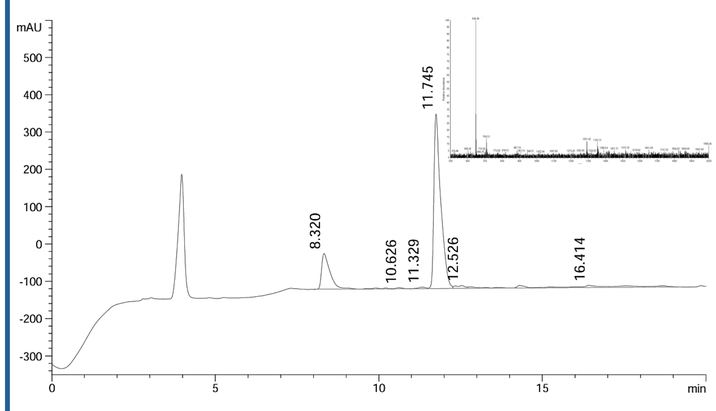


Figure 6. HPLC of peptide synthesized with **L-Cys in position X using HBTU/DIEA at 45 °C**, 2 x 5 min deprotection and 30 min coupling. MS shows m/z 646.

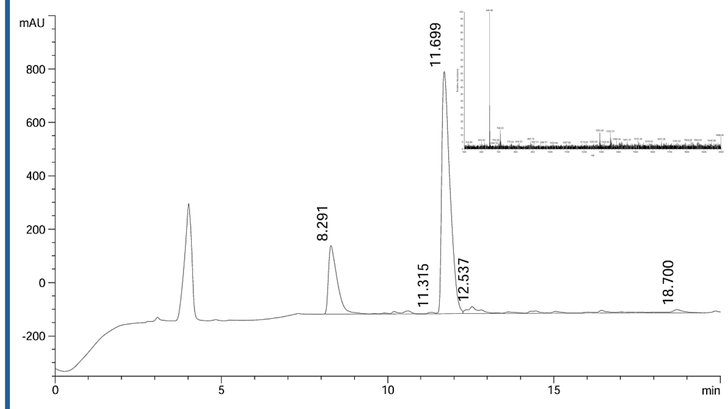


Figure 7. HPLC of peptide synthesized with **L-Cys in position X using HBTU/DIEA at 60 °C**, 2 x 5 min deprotection and 5 min coupling. MS shows m/z 646.

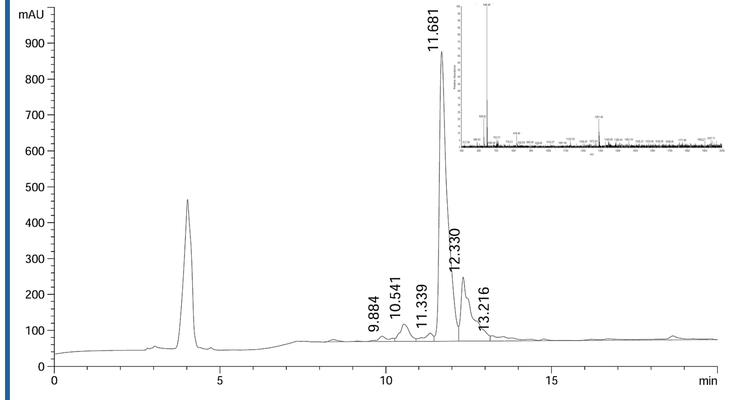


Figure 8. HPLC of peptide synthesized with **L-Cys in position X using HBTU/DIEA at 90 °C**, 1 min deprotection and 5 min coupling. MS shows m/z 646.

Process Workflow Impact and Conclusions

- We designed a sequence that resolves Cysteine racemization on standard RPHPLC. This method is accessible, with no pre-column derivatization or chiral column required.
- DIC/Oxyma coupling chemistry maintains stereochemical integrity of Cysteine at 90 °C using conduction heating as confirmed by chiral amino acid analysis using GC-MS.
- Bypassing the recommended high temperature for each coupling chemistry causes racemization; tight temperature control, like that conferred by conduction heating, is critical for maintaining stereochemistry at chiral centers.
- Easy screening tool for identifying conditions that minimize racemization in a target peptide sequence. However, racemization may be sequence-dependent and temperature is the critical synthesis condition to control. Uniform heating may be difficult to control with other heating methods when changing reaction volume, resin loading, and peptide mass.

References

[1] Duengo, S., Muhajir, M.I., Hidayat, A.T., Musa, W.J.A., Maharani, R. (2023) Epimerisation in Peptide Synthesis. Molecules, 28, 8017. https://doi.org/10.3390/ molecules28248017

[2] Huang, Y.; Pan, L.; Zhao, L.; Mant, C.T., Hodges, R.S.; Chen, Y. (2014). Structured Guided RP-HPLC Chromatography of Diastereomeric Alpha-Helical Peptide Analogs Substituted with Single Amino Acid Stereoisomers, Biomedical Chromatography, 28(4), 511-517. doi:10.1002/bmc.3061

CSBio INSTRUMENTATION

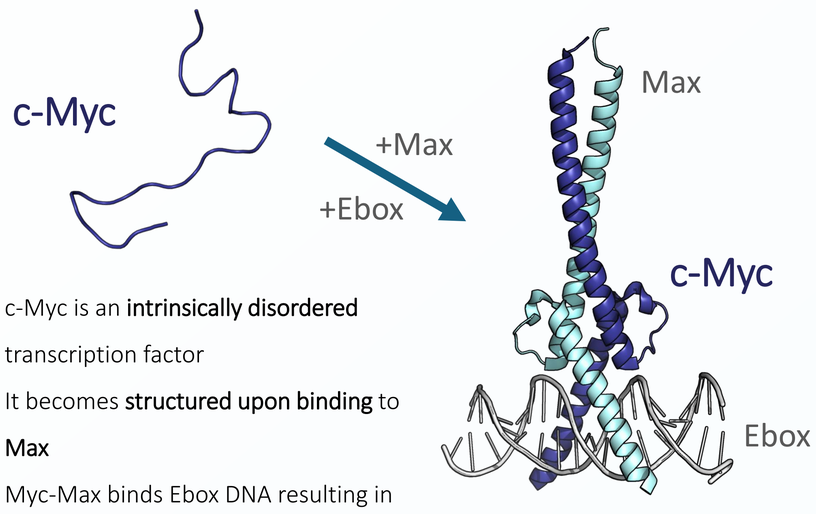
Conformational reprogramming of c-Myc via intracellular cyclisation

Rachel A. Johnson, Jody M. Mason

Department of Life Sciences, University of Bath, UK

https://doi.org/10.17952/38EPS.2026.P111

c-Myc in Cancer



Structure of the c-Myc-Max heterodimer bound to Ebox DNA (PDB: 1NKP).[1]

- c-Myc is an **intrinsically disordered** transcription factor
- It becomes **structured upon binding** to **Max**
- Myc-Max binds Ebox DNA resulting in **transcriptional activation**[2]

Loss of regulation:

- c-Myc is oncogenic and **upregulated in 70% of cancers**
- Myc-Max binds weaker Ebox sequences
- Results in aberrant gene expression[3]

Targeting Myc:

- Key target for anti-cancer therapeutics
- No c-Myc antagonists have been clinically approved
- Considered '**undruggable**' due to its **lack of secondary structure** and its broad, shallow interaction with Max

Aims & Approach

Aim:

- To induce helicity in c-Myc using bis-alkylating agents, thereby **structurally stabilising an IDP**

Approach:

- Express and purify a series of double cysteine c-Myc mutants that have been **chemically stapled *in vivo***
- **Characterise** their interaction with both Max and Ebox DNA using circular dichroism (**CD**) and electromobility shift assays (**EMSA**)

Impact:

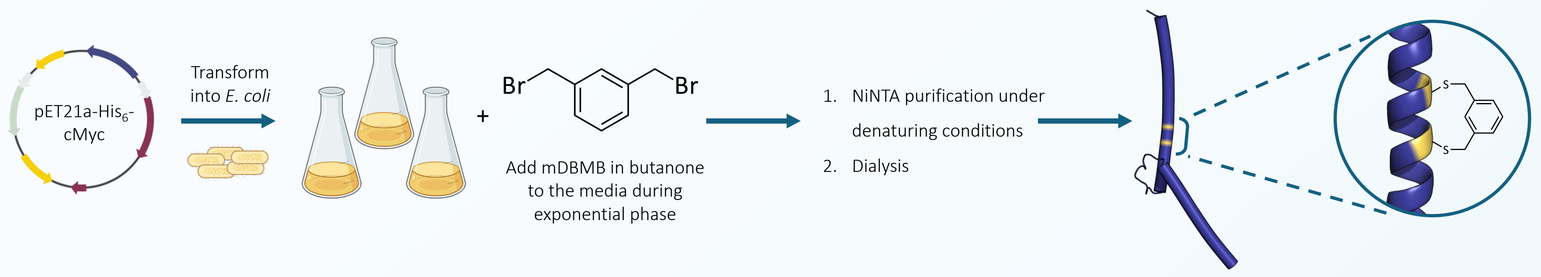
- Generating a structured c-Myc construct has the potential to **enable discovery of improved antagonists**
- Raises implications for structurally reprogramming other previously undruggable IDPs in a similar manner

Construct Design

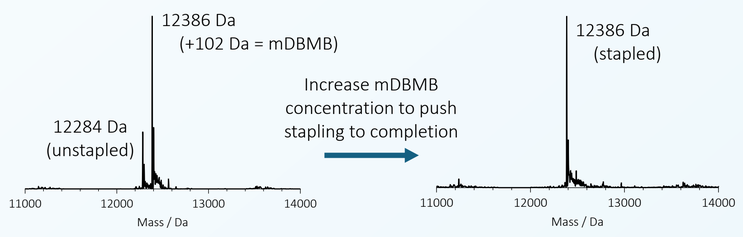
- Native c-terminal Cys mutated to Ser, creating **unstapled control construct**, MycSSA
- Generated a series of ***i* to *i+4* double cysteine mutants** at solvent-facing positions in c-Myc
- Sampled across the basic helix-loop-helix leucine zipper (bHLHZip) to assess the effect of staple position

```
Domain:        Loop       Helix 2            Leucine Zipper
Heptad:                 defgabcdefgab cdefgabcdefgabcdefgabcdefgabc def
>WT cMyc … PELENNEKAP KVVILKKATAYIL SVQAEEQKLISEEDLLRKRREQLKHKLEQ LRNSCA
>MycSSA … PELENNEKAP KVVILKKATAYIL SVQAEEQKLISEEDLLRKRREQLKHKLEQ LRNSSA
>MycH2  … PELENNEKAP KVCILKCATAYIL SVQAEEQKLISEEDLLRKRREQLKHKLEQ LRNSSA
>MycZ1  … PELENNEKAP KVVILKKATAYIC SVQCEEQKLISEEDLLRKRREQLKHKLEQ LRNSSA
>MycZ2  … PELENNEKAP KVVILKKATAYIL SVQAEEQKLISEECLLRCRREQLKHKLEQ LRNSSA
>MycZ3  … PELENNEKAP KVVILKKATAYIL SVQAEEQKLISEEDLLRKRREQLKHKLCQ LRCSSA
```

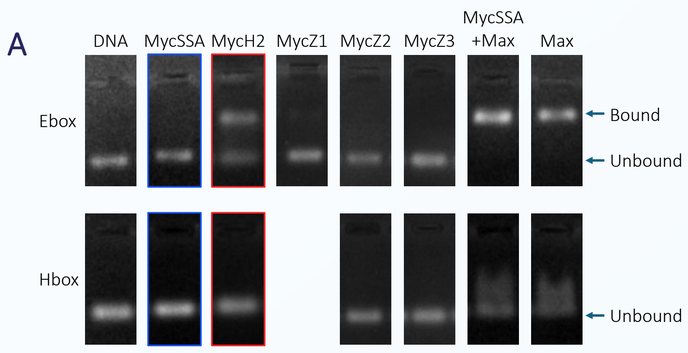
Expression & Purification



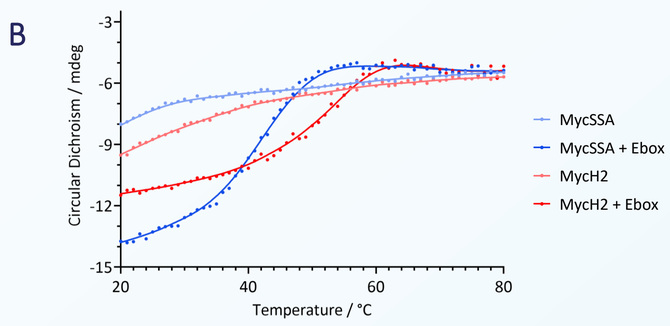
- The addition of mDBMB to the media during expression in *E. coli* results in the generation of stapled c-Myc constructs *in vivo*[4]
- This is despite c-Myc expression being insoluble, necessitating NiNTA purification under denaturing conditions
- Mass spectrometry analysis of each construct following dialysis demonstrates the +102 Da mass increase from mDBMB addition



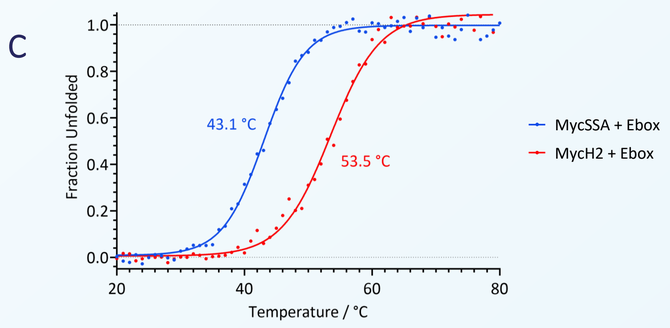
CD & EMSA Characterisation

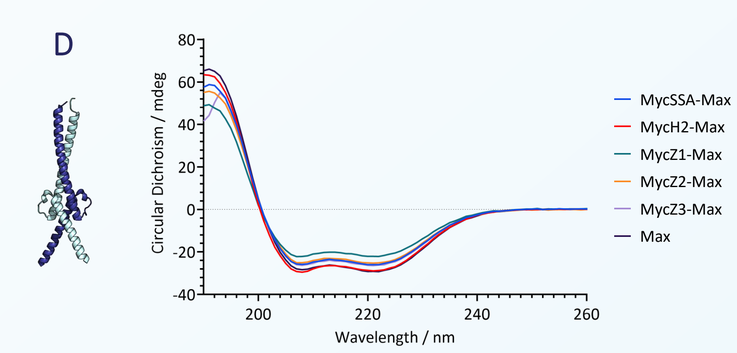


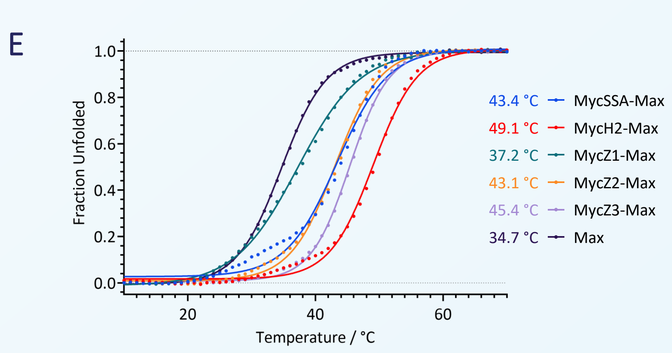
- EMSA data showed the expected shifts for the MycSSA-Max heterodimer and the Max homodimer in complex with Ebox DNA.
- However, a partial, **sequence specific shift** was **also observed for MycH2** in the **absence of Max** (Fig. A).

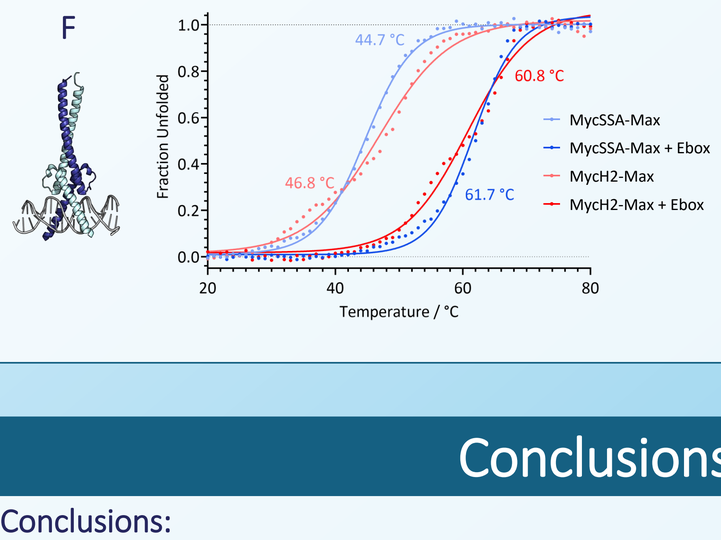


- A T_m could not be determined for MycSSA or MycH2 by CD (Fig. B) - either alone or with Hbox (data not shown).
- **Transitions were observed** for both MycSSA and MycH2 in the **presence of Ebox DNA** (Fig. C), with a significant **10°C rightward shift** for the **stapled construct**.









- All five Myc-Max heterodimers adopt a typical **alpha helical, coiled coil structure** (Fig. D) and show **higher melting temperatures** compared to the Max homodimer (Fig. E).
- A **~15°C rightward shift** was seen upon **addition of Ebox** DNA (Fig. F), corroborating the EMSA observations.
- Collectively, this shows that **stapling c-Myc has not adversely affected its ability to bind Max and Ebox**.

Conclusions & Future Work

Conclusions:

- Bis-alkylating agents can be added to media during expression in E. coli to generate stapled proteins *in vivo*.
- EMSA and CD data shows that stapling in helix two uniquely enables Ebox DNA binding in the absence of Max.
- Gain of function does not recapitulate the coiled coil conformation of Myc-Max, instead adopting a non-native yet functional conformation.
- Stapling does not perturb native heterodimerisation or ternary complex formation.

Future Work:

- Structurally characterise the interaction of stapled MycH2 with Ebox.
- Investigate the potential benefits of screening against a stapled c-Myc construct to elucidate more potent inhibitors.

Selected References:

1. Nair S. K. and Burley S. K. *Cell*, **2003**, *112* (2), 193-205, DOI: 0.1016/s0092-8674(02)01284-9
2. Whitfield J. R. and Soucek L. *Nat. Rev. Drug Discov.* **2025**, *24* (6), 445-457, DOI: 10.1038/s41573-025-01143-2
3. Madden S. K., Dantas de Araujo A., Gerhardt M., Fairlie D. P. and Mason J. M. *Mol. Cancer*, **2021**, *20* (1), DOI: 10.1186/s12943-020-01291-6
4. Brennan A., Vance K. W. and Mason J. M. *Cell Chem. Biol.* **2026**, *33* (3), 409-423, DOI: 10.1016/j.chembiol.2026.02.002

Development of pH-Responsive Peptide Systems for mRNA-Mediated Antimicrobial Peptide Delivery

Hala Alnasif Alhadi[1], Tam T. Bui[2], Jenny Lam[3], Vincenzo Abbate[1] & A. James Mason[1]

[1] Institute of Pharmaceutical Sciences, King's College London, London, United Kingdom
[2] Centre for Biomolecular Spectroscopy and Randall Division of Cell and Molecular Biophysics, King's College London
[3] School of Pharmacy, University College London, London, United Kingdom
Contact: hala.alhadi@kcl.ac.uk
https://doi.org/10.17952/38EPS.2026.P403

Background and Challenge

- mRNA therapeutics offer a promising strategy for treating infectious diseases, cancer, and genetic disorders through transient protein expression without genomic integration.
- Clinical application is limited by delivery challenges, including mRNA instability, poor cellular uptake, and inefficient endosomal escape.
- Current lipid nanoparticle delivery systems have limitations such as immunogenicity, limited tissue specificity, and restricted design flexibility.
- The pH responsive peptide – LAH4-L1 or its analogues – is very effective at delivering a wide range of cargoes *in vitro* including mRNA and could be used to produce therapeutics *in vivo* with PEGylation[1-5].

Research questions

- Can we use pH responsive cationic amphipathic peptides as a vector to help deliver cargo mRNA, encoding for HDPs (defensin) to achieve continuous production at the site of infection?
- How can the pH responsive peptide LAH4-L1 be modified to effectively deliver mRNA both *in vitro* and *in vivo*?
- What is the effect of PEGylation on uptake and endosomal escape? How can any effect of PEGylation be mitigated?

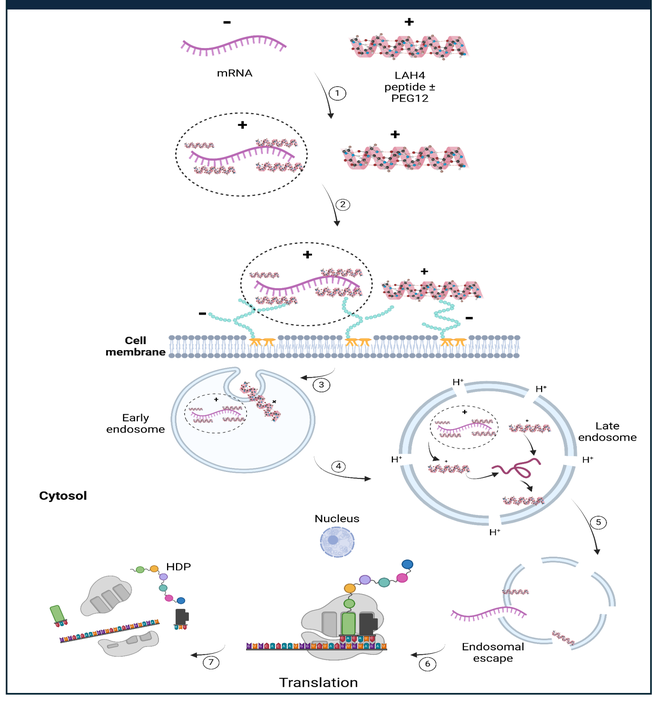
Aim and Objectives

Develop, design and characterise pH-responsive cationic amphipathic peptide vectors for efficient delivery of mRNA encoding HDPs to achieve continuous production at the site of infection.

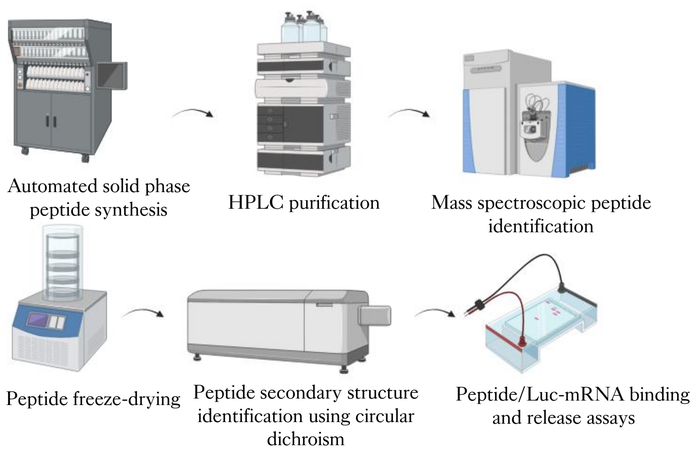
Objectives:

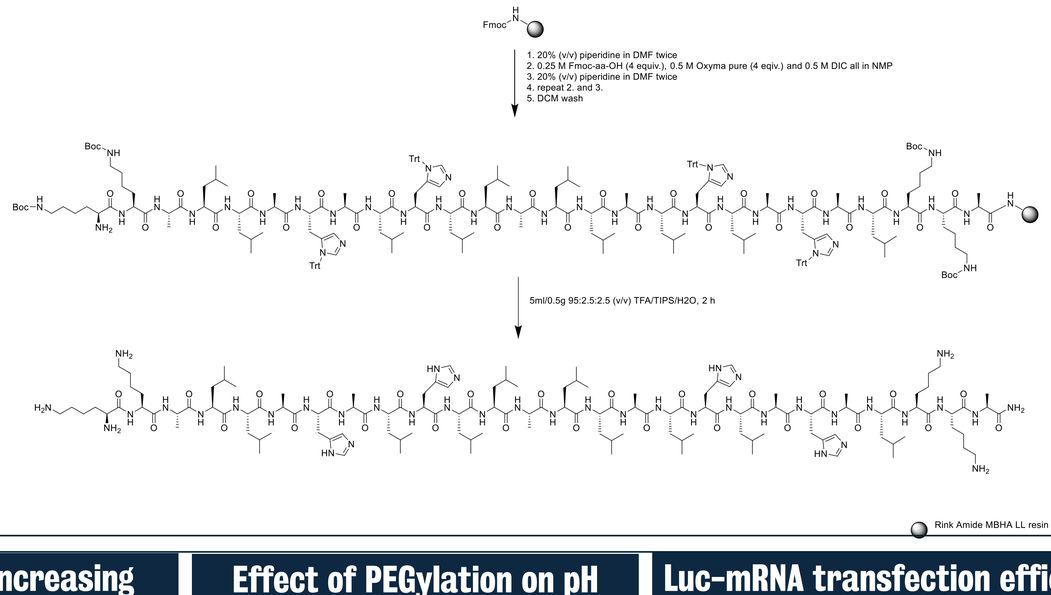
- Investigate the effect of PEGylation on the peptides' pH dependent conformational change.
- Design and modify peptide vectors to fine tune pH-triggered conformational switching.

Delivery Concept: key steps of LAH4 mediated mRNA transfection of human cells



LAH4-L1 Solid Phase Peptide Synthesis , characterisation and testing

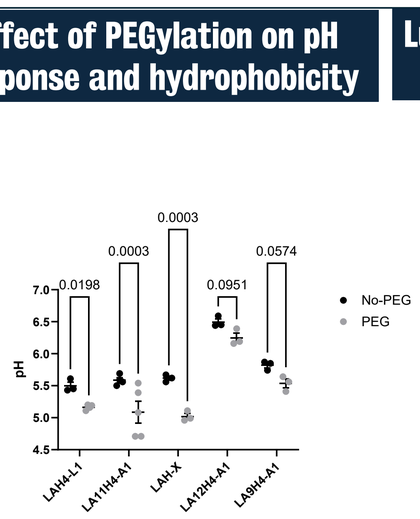


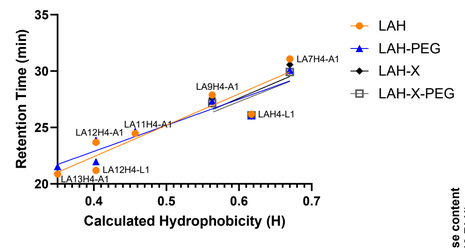




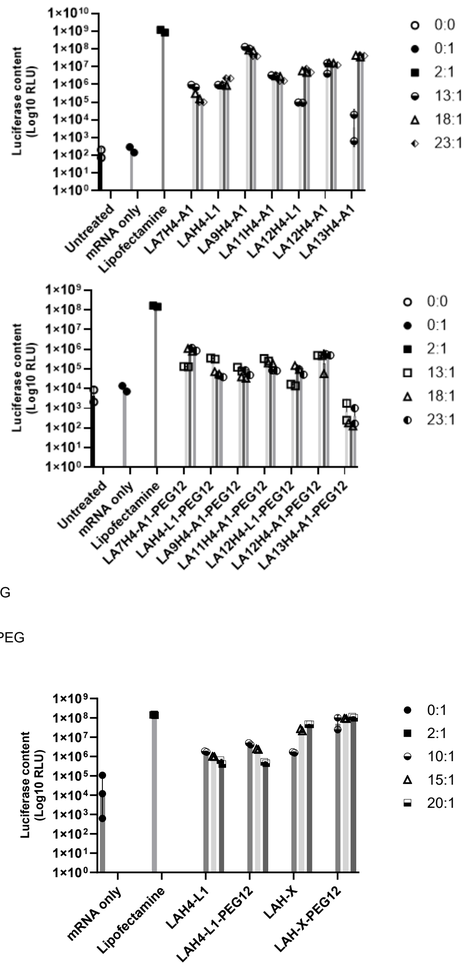
Restoring lost hydrophilic peptide α-helicity by increasing amphipathicity

Effect of PEGylation on pH response and hydrophobicity

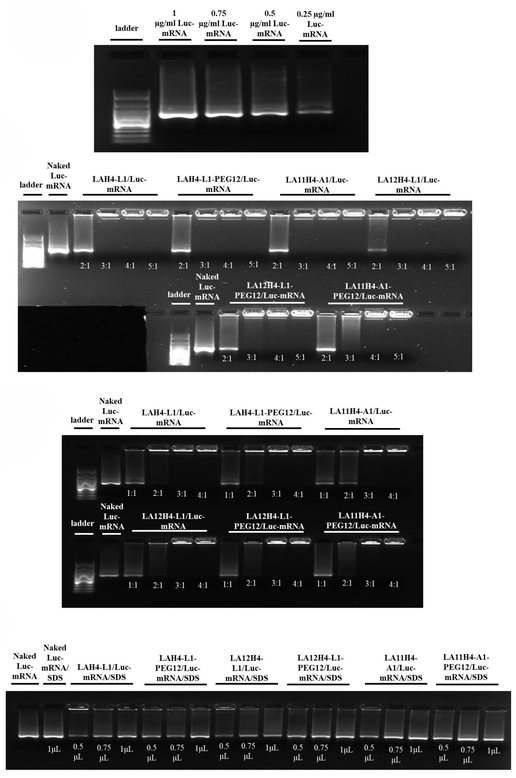




Luc-mRNA transfection efficiencies of LAH4-L1 derivatives



Luc-mRNA/peptide complexes binding and release



Conclusions

- Amphipathicity and structured partitioning of hydrophobic and hydrophilic residues within a peptide is important for folding in solution.
- PEGylation does not affect the ability of LAH4-L1 or its analogues to bind mRNA.
- Amino acid residues position within the peptide sequence affects the peptide behaviour.
- α-helicity of peptide is however poorly related to transfection efficiency.

Future Work

- Characterisation and sizing studies of mRNA/peptide nanocomplexes
- *In vitro* toxicity and characterisation of nanocomplexes.
- Selected lead pH responsive mRNA vector system will be advanced to *in vivo* pulmonary delivery studies.

References

1. Yingying Xu, et al, PEGylated pH-responsive peptide-mRNA nano self-assemblies enhance the pulmonary delivery efficiency and safety of aerosolized mRNA, Drug Delivery, 30 (2023) 2219870
2. A. Kichler, et al, Histidine-rich amphipathic peptide antibiotics promote efficient delivery of DNA into mammalian cells, Proc. Natl. Acad. Sci. USA 96 (2003) 1564-1568.
3. B. Langlet-Bertin, et al, Design and evaluation of histidine-rich amphipathic peptides for siRNA delivery, Pharm. Res. 27 (2010) 1426-1436
4. T.T. Zhang, et al, T-C. Wu, LAH4 enhances CD8+ T cell immunity of protein/peptide-based vaccines. Vaccine 30 (2012) 784-793
5. Kichler A, et al, Cationic amphipathic histidine-rich peptides for gene delivery. Biochimica et Biophysica Acta (BBA) - Biomembranes. 1758 (2006) 301-7.

Transfer Learning for Prediction of Liquid-Liquid Phase Separation

Karlo Barjaktarić[1], Patrik Paunović[1], Leonard Lečić[1], Erik Otović[1], Joana Calvário[2], Ana Sofia Pina[2], Yoshimasa Kawaguchi[3], Daniela Kalafatovic[1], Goran Mauša*[1]

DOI: https://doi.org/10.17952/38EPS.2026.P250

*Contact email: goran.mausa@uniri.hr

[1] University of Rijeka, Faculty of Engineering, Rijeka, Croatia
[2] Institute of Chemical and Biological Technology, NOVA University of Lisbon, Oeiras, Portugal
[3] Institute for Chemical Research, Kyoto University, Kyoto, Japan

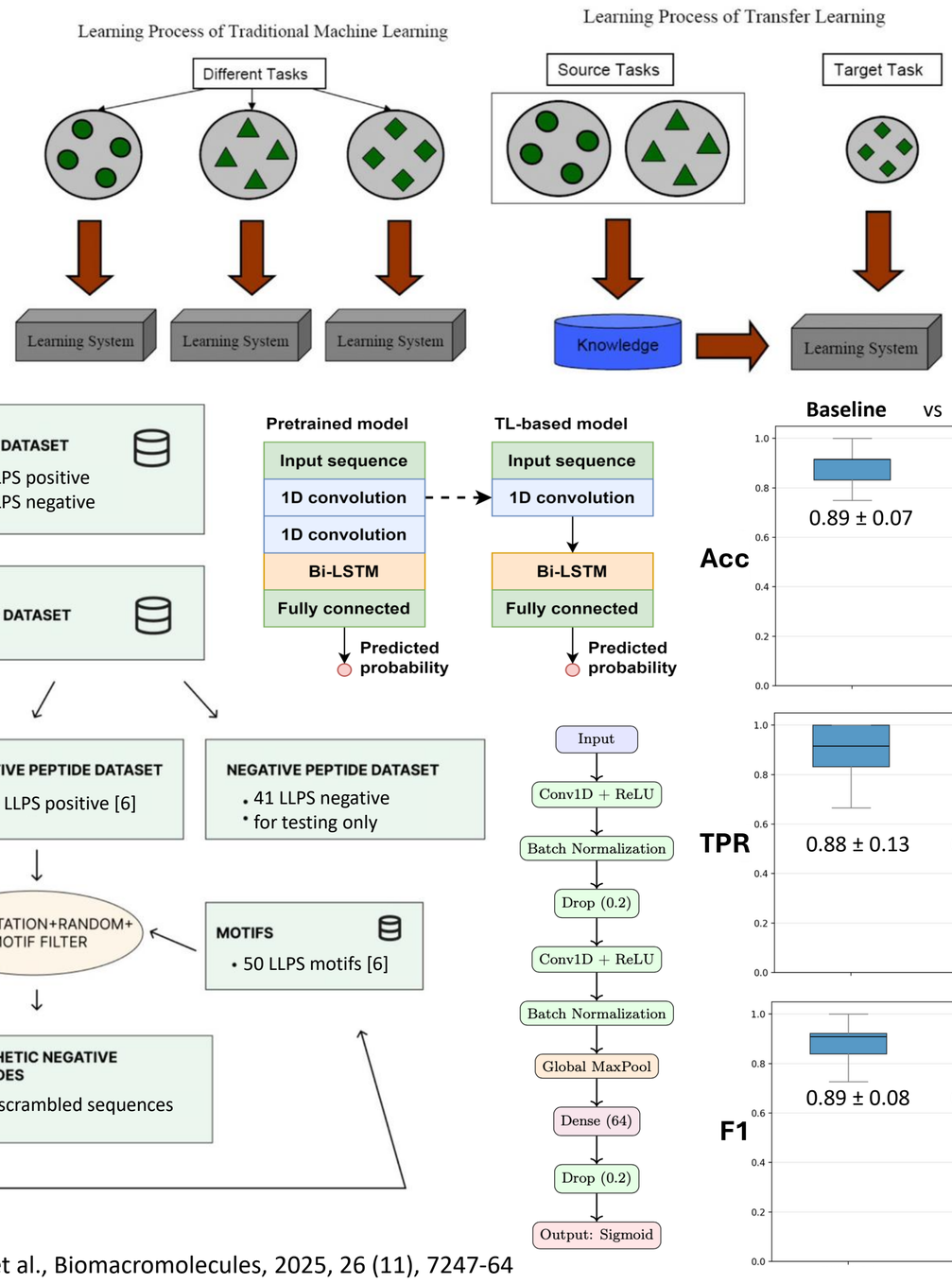
1. Amount of Data Required to Train a Peptide Classifier



	Catalytic [1]	Self-assembly [2]	AVP [3]	Permeability [4]	AMP [3, 5]
Size:	~100	~400	~1,000	~7,000	~10,000
Ratio:	68 : 31	67 : 33	61 : 39	69: 31	56 : 44
Acc:	95%	82%	85%	82 %	92%
AUC:	0.95	0.86	0.88	0.78	0.97

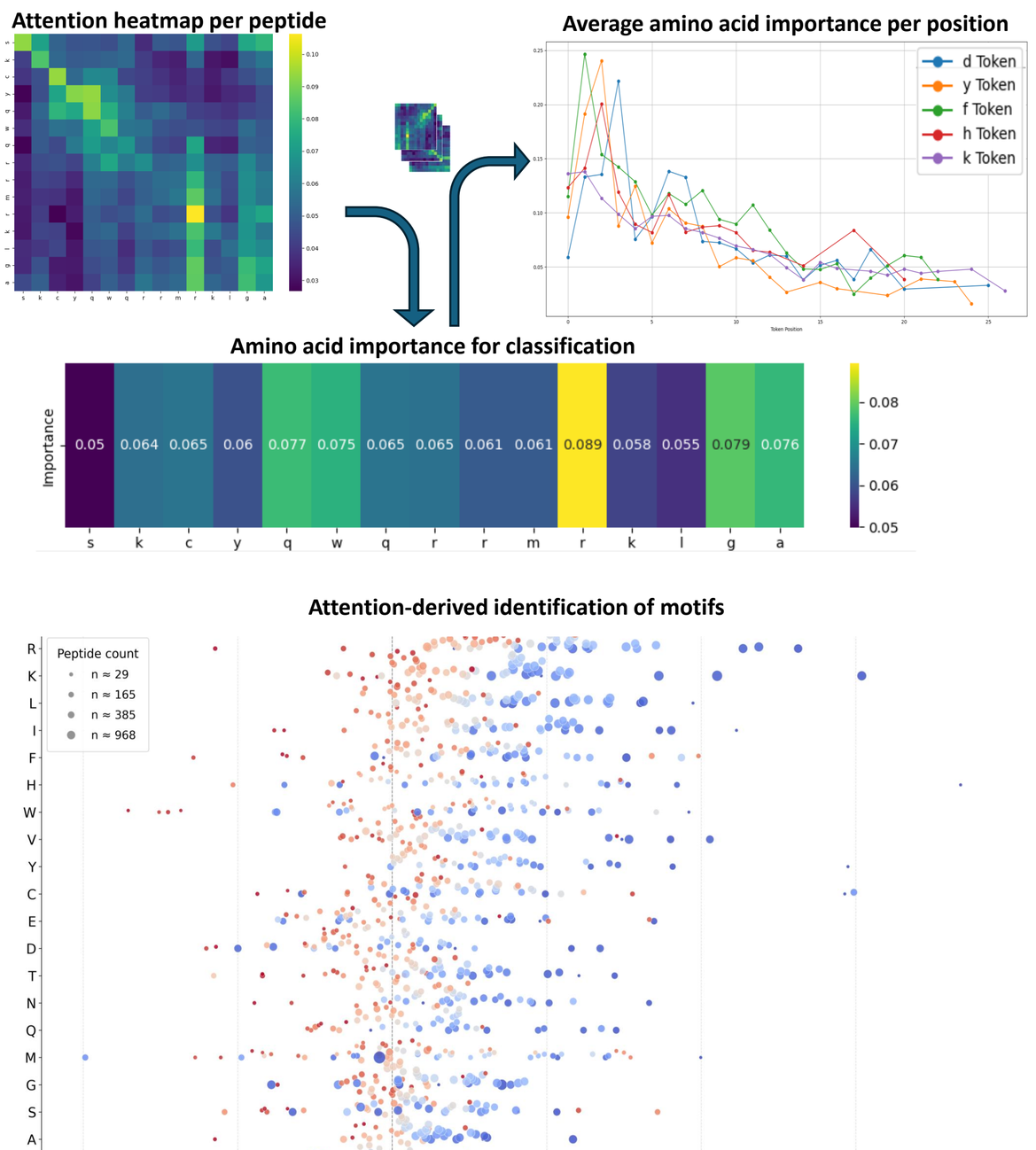
[1] Mauša et al., MRS Advances, 2023, 8, 1068–1074
[2] Njirjak et al., Nature Machine Intelligence, 2024, 6, 1487–1500
[3] Otović et al., Journal of Chemical Information and Modeling, 2022, 62 (12), 2961-2972
[4] Cabezón Vizoso et al., Digital Discovery, 2025, 4, 1259-1275
[5] Negovetić et al., Digital Discovery, 2024, 3, 1182

2. Protein – to – Peptide Transfer Learning for LLPS Prediction



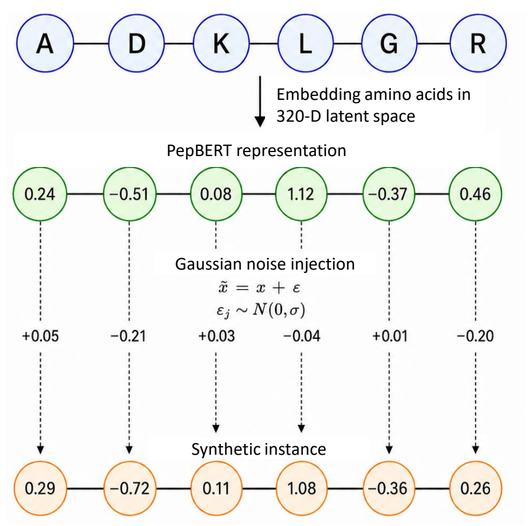
[6] Calvário et al., Biomacromolecules, 2025, 26 (11), 7247-64

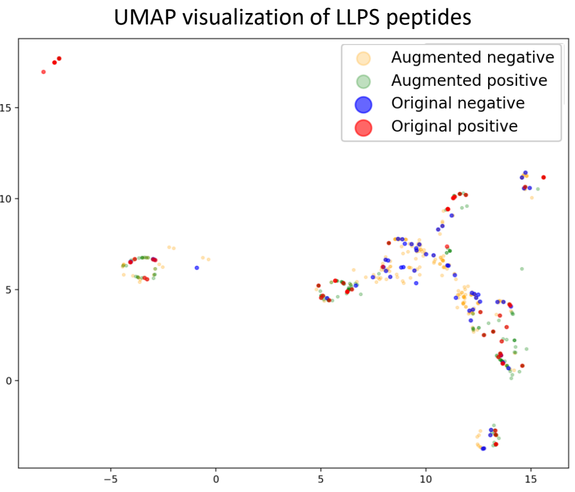
3. Position-specific Sequence Determinants for Peptide Classification Derived from Token Importance



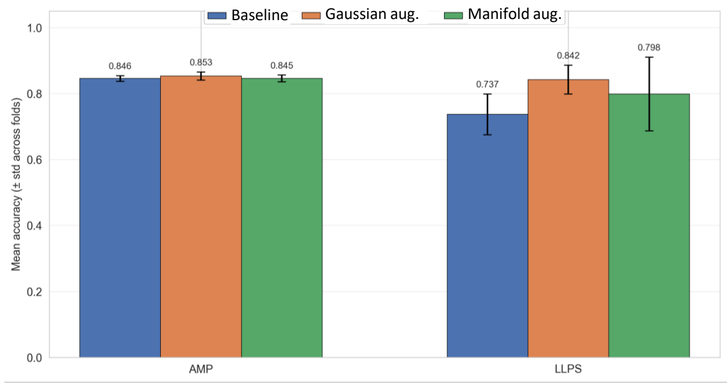
[7] Du et al., Future Foods, 2026, 13, 2961-2972
[8] Devlin et al., Proceedings of NAACL-HLT 2019, 4171--4186

4. Noise Injection-based Augmentation Strategy





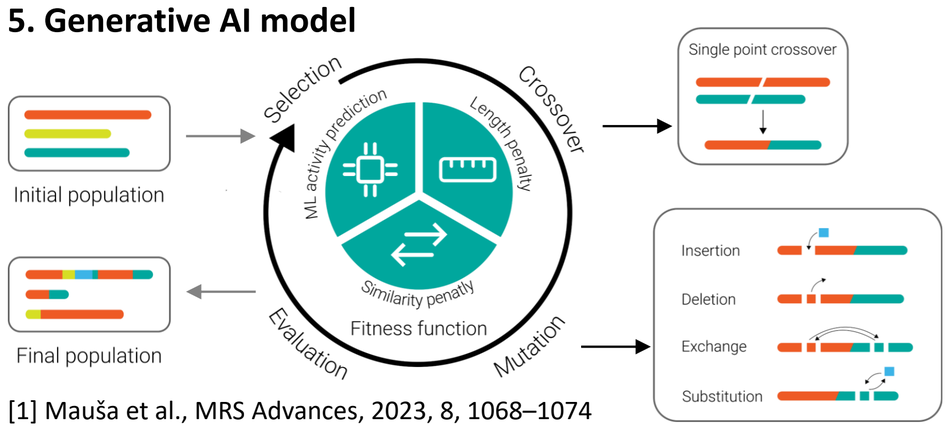
Data	Representation	Acc	F1	MCC
AMP	PepBERT (320-D) [7]	**84.6**	**0.80**	**0.68**
AMP	SeqProps (28-D) [3]	79.6	0.73	0.57
LLPS	PepBERT (320-D) [7]	73.7	0.74	0.48
LLPS	SeqProps (28-D) [3]	**84.2**	**0.84**	**0.69**

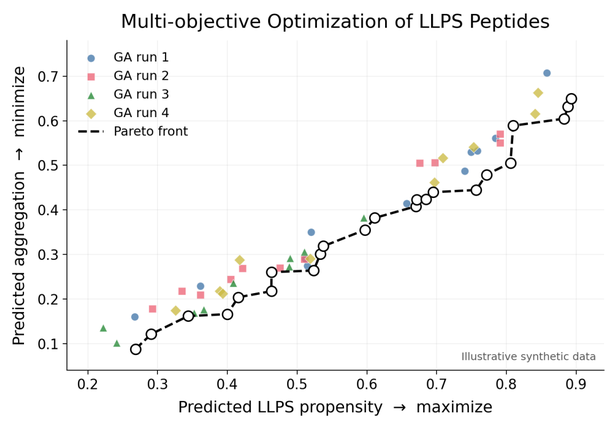


Settings	Acc	F1	MCC
PepBERT + Gaussian injection (noise =0.5, fraction = 100)	84.2	0.85	0.70
SeqProps + Gaussian injection (noise =0.1, fraction = 100)	86.0	0.86	0.72

[3] Otović et al., Journal of Chemical Information and Modeling, 2022, 62 (12), 2961-2972
[7] Du et al., Future Foods, 2026, 13, 2961-2972

5. Generative AI model





[1] Mauša et al., MRS Advances, 2023, 8, 1068–1074

Acknowledgment

NextGenerationEU project: SCI-PHI (uniri-mzi-25-25)

Funded by the European Union NextGenerationEU

Croatian Science Foundation projects: Super Deshpet 2.0 (IP-2025-02-3357) MOPED (IP-2026-4962)

HrZZ

COST action: SNOOPY (CA23111)

cost EUROPEAN COOPERATION IN SCIENCE & TECHNOLOGY

SNOOPY

Active Learning-Driven Surrogate Modeling for the Generative Discovery of Self-Assembling Peptides

Denis Ibiši[1] · Daniela Kalafatović[1] · Goran Mauša[1]
[1]University of Rijeka, Faculty of Engineering, Rijeka, Croatia
https://doi.org/10.17952/38EPS.2026.P264
e-mail: denis.ibisi123@gmail.com

ACKNOWLEDGEMENTS

SNOOPY COST Action – CA23111
SCI-PHI – uniri-mzi-25-25
Super DeShPet 2.0 – IP-2025-02-3357

Funded by the European Union
NextGenerationEU

Croatian Science Foundation

Motivation

Self-assembling peptides are versatile building blocks that spontaneously organise through non-covalent interactions into functional nanostructures such as fibrils, micelles and hydrogels. Their assembly depends strongly on amino acid sequence and experimental conditions, while the number of possible sequences grows exponentially with peptide length.

Conventional discovery relies on experimental screening, molecular simulations and expert-designed rules, which are costly, time-consuming, or may restrict exploration to familiar sequence motifs. Machine learning (ML) can broaden the search space and reduce screening costs by prioritising promising and non-intuitive peptide candidates for simulation and experimental validation.

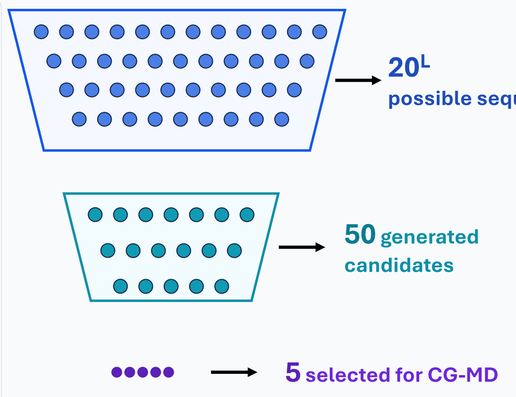
An ML surrogate model can rapidly estimate self-assembly probability, while a generative algorithm explores sequence space to propose new peptide candidates [1].

[1] Njirjak et al., Nature Machine Intelligence, 2024, 6, 1487–1500

GOAL:

Design and compare active learning / Bayesian optimisation acquisition functions for efficiently prioritising generated peptide candidates under limited labelled data and evaluation budgets

Search space challenge



AP-SP model performance

0.8686 ± 0.0253 F_1 (mean ± SD)	**0.8431 – 0.9072** F_1 (fold range)
0.9356 PR-AUC	**0.8673** ROC-AUC
0.1481 Brier score	**0.1232** ECE-10

Designed acquisition functions

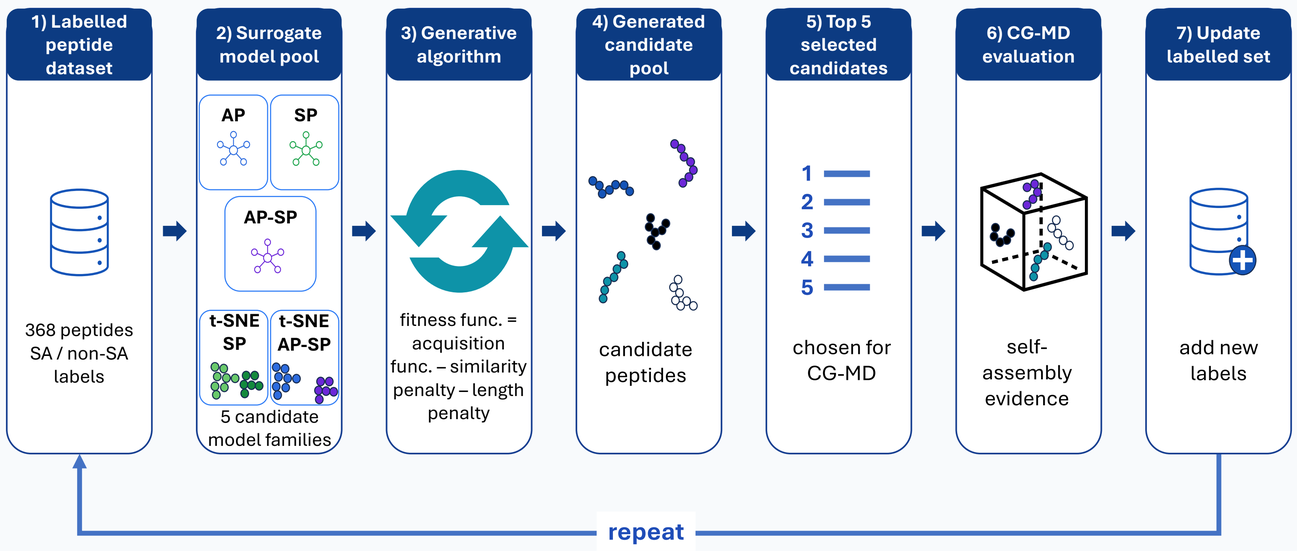
Active learning

Function	Principle(s)	Scoring method
Predictive entropy	Informativeness	Uncertainty of the mean prediction: $H(\bar{p}(x))$.
Ensemble mutual information (MI)	Informativeness	Epistemic uncertainty: $H(\bar{p}(x)) - \frac{1}{M}\sum_{m=1}^{M} H(p_m(x))$.
Family QBC	Informativeness	Vote entropy across 5 model families.
Cluster-diverse representative	Representativeness Diversity	Centroid-nearest representatives from clusters prioritised by novelty to labels.
OED logdet	Representativeness Diversity	Greedy log-determinant information gain.
Hybrid MI-diverse	Informativeness Diversity	MI selection followed by farthest-first embedding selection.
Static easy entropy	Informativeness Representativeness	Entropy ranking within the 30% most familiar candidates.
Self-paced entropy	Informativeness Representativeness	Entropy ranking within a familiar pool expanding from 30% to 100%.

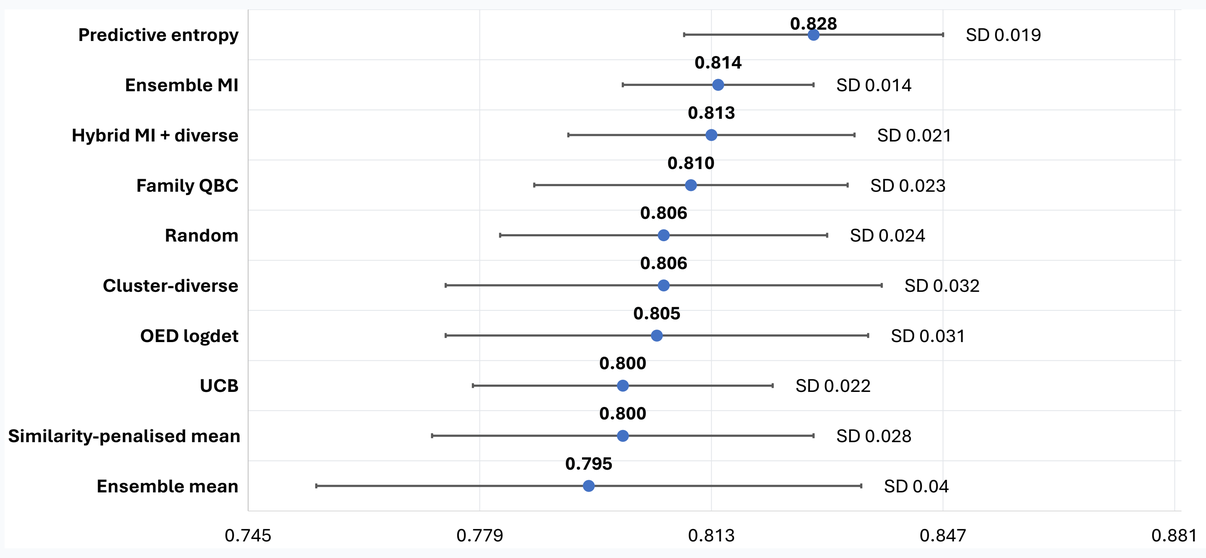
Bayesian optimisation

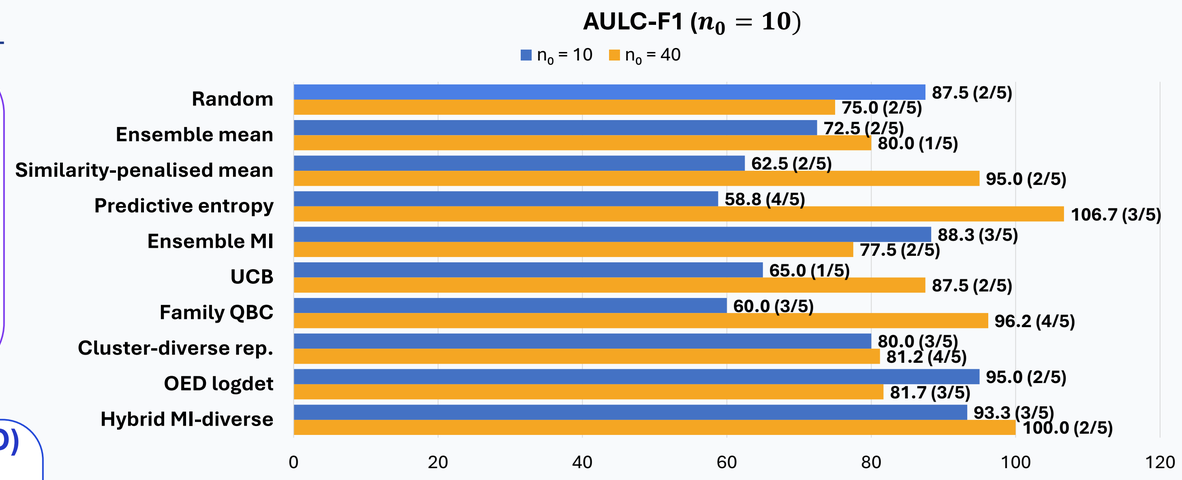
Function	Principle(s)	Scoring method
Ensemble mean / Greedy	Exploitation	Rank by mean ensemble SA probability $\bar{p}(x)$.
Similarity-penalised mean	Exploitation Exploration	$Score = \bar{p}(x) - composition\ similarity\ penalty$.
Upper Confidence Bound (UCB)	Exploitation Exploration	$Score = \bar{p}(x) + \sigma_p(x)$.
Probability of Improvement (PI)	Exploitation	Probability of improvement over incumbent f^*.
Expected Improvement (EI)	Exploitation Exploration	Expected improvement over incumbent f^*.
Maximum Entropy Search (MES)	Exploitation Exploration	Expected information gain about the optimum.

Project workflow

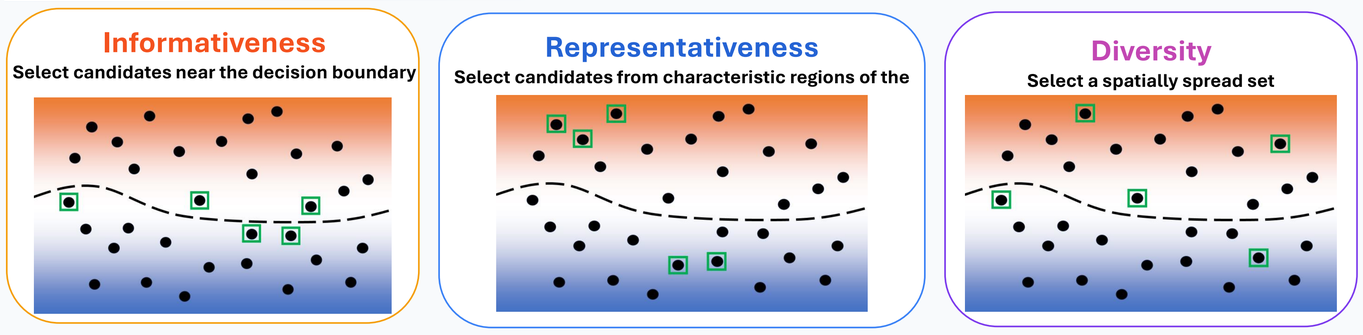


Results – AULC, Labels to F1 ≥ 0.86, Diversity gain





Candidate-selection principles: Active Learning and Bayesian Optimisation



Active learning (AL)

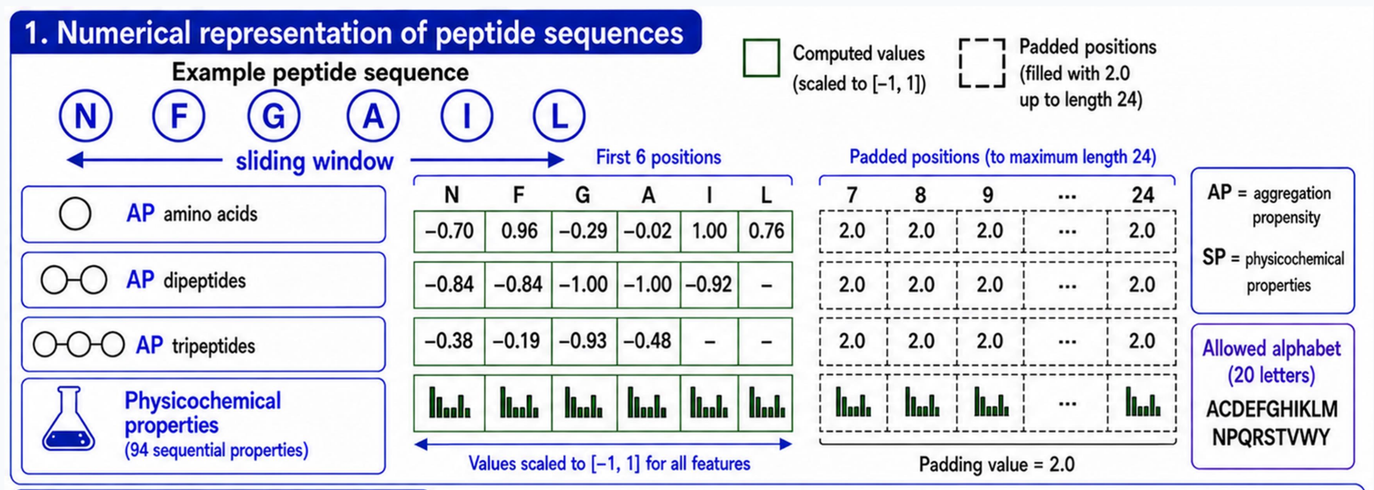
- Improve the predictive model under a limited labelling budget.
- Use informativeness, representativeness, or diversity to guide candidate selection.

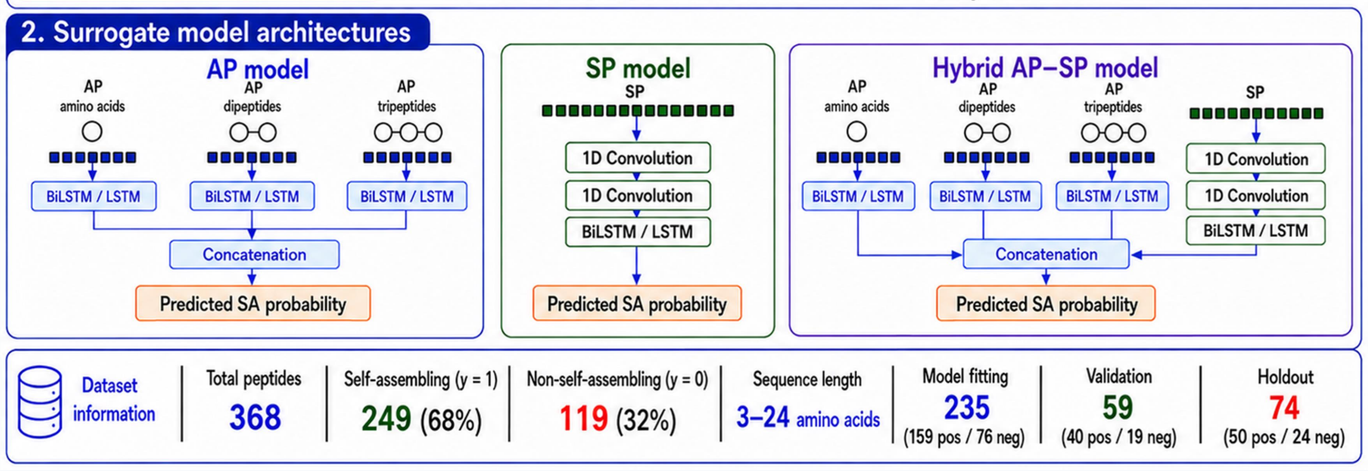
Informativeness ⟷ Exploitation
Representativeness ⟷ Exploration
Diversity ⟷ Exploration

Bayesian optimisation (BO)

- Prioritise promising candidates for expensive evaluation.
- Balance exploitation and exploration to find the best solution.

Peptide representation / Surrogate model architectures / Dataset





Dataset information	Total peptides	Self-assembling (y = 1)	Non-self-assembling (y = 0)	Sequence length	Model fitting	Validation	Holdout
	368	**249** (68%)	**119** (32%)	**3–24** amino acids	**235** (159 pos / 76 neg)	**59** (40 pos / 19 neg)	**74** (50 pos / 24 neg)

Self-paced active-learning replay

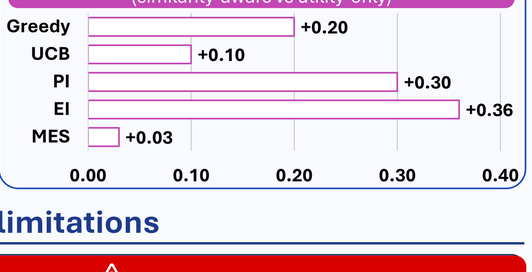
Strategy	AULC (10-235)*	Labels to F1 ≥ 0.86 **
Predictive entropy	**0.8223**	105.0 (3/3)
Random	0.8171	112.5 (2/3)
Self-paced entropy	0.8147	**71.7 (3/3)**
Static easy entropy	0.8016	102.5 (2/3)

* Normalised area under the F1 learning curve (10-235 labels); higher is better.
** Conditional mean labels revealed to first reach F1 ≥ 0.86; parentheses show folds reaching the target.

Fixed-surrogate proposal policies

Strategy	Positive	Yield	Diversity	Mean length
Random	3/5	0.600	**0.860**	**5.0 aa**
Greedy	2/5	0.400	0.480	**10.0 aa**
UCB	1/5	0.200	0.610	**10.0 aa**
PI	**5/5**	**1.000**	0.081	20.8 aa
EI	3/5	0.600	0.769	**6.2 aa**
MES	1/4	0.250	0.083	23.6 aa

Diversity gain
(similarity-aware vs utility-only)



Conclusions and limitations

☑ CONCLUSIONS

1. AULC gains were small, but some strategies reached $F1 \geq 0.86$ with fewer labels.
2. Uncertainty- and disagreement-based methods were best for model improvement.
3. Different acquisition objectives explored complementary regions of peptide space.
4. Higher utility often reduced diversity; explicit diversity control broadened coverage.
5. CG-MD simulations provided an effective way to obtain labels for iterative peptide discovery.

⚠ LIMITATIONS

1. Martini 2.2P was used; Martini 2.1P may be better for short peptides.
2. No statistical significance tests were performed.
3. CG-MD strategy selection was post hoc.
4. Fixed-surrogate evaluation used only one round with five candidates per policy.

Match the acquisition strategy to the scientific goal

Photocatalytic Proximity Labelling to Probe Cell Surface Glycan Interactomes

Lucy McCormack[a], Jerrard Hayes[a], Mia L. Huang[b], Eoin M. Scanlan[a]

[a]Trinity Biomedical Sciences Institute (TBSI), Trinity College Dublin, 152-160 Pearse St., Dublin, Ireland

[b]Scripps Research, 10550 North Torrey Pines Road, La Jolla, CA 92037, United States

Contact: mccormlu@tcd.ie, scanlae@tcd.ie

Introduction

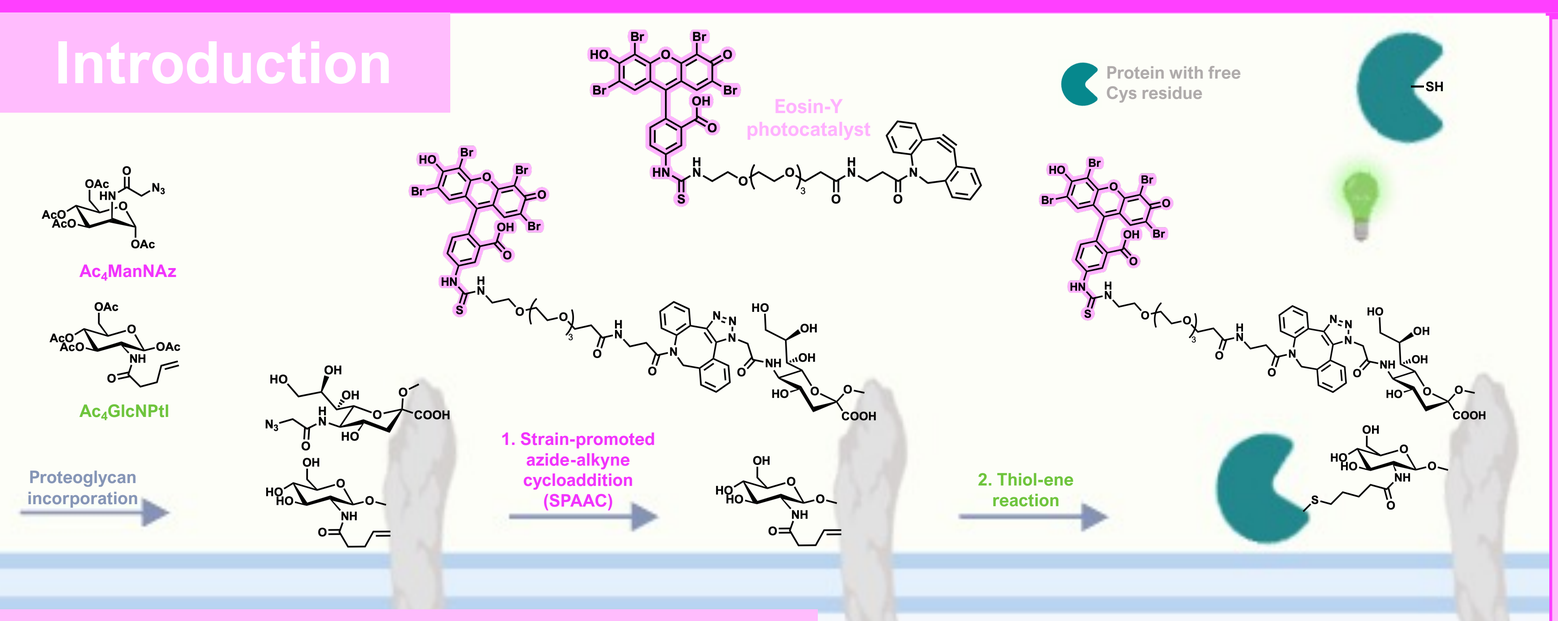


Fig. 2 Photocatalytic proximity labelling approach involving the installation of a cell surface catalyst, Eosin-Y, via SPAAC, followed by the thiol-ene trapping of Cys-containing proteins of interest.

Metabolic glycome labelling (MGL) is a powerful approach for investigating glycan dynamics during biological processes, including embryonic development and disease progression. The technique relies on the incorporation of chemically modified monosaccharide analogues into cellular glycans through endogenous biosynthetic pathways, followed by selective labelling using bioorthogonal reactions.[1]

This work presents the first application of thiol-ene chemistry in combination with strain-promoted azide alkyne cycloaddition (SPAAC) for the dual labelling of metabolically incorporated sugars. Thiol-ene reactions possess key bioorthogonal characteristics, including high selectivity, rapid kinetics, physiological stability, aqueous compatibility, and orthogonality to established click chemistry, yet remain underexplored in the context of MGL (fig. 1).[2]

Furthermore, incorporation of a covalently linked Eosin-Y photocatalyst enables spatially resolved cysteine interactome profiling through thiol-ene covalent trapping, followed by proteomic analysis (fig. 2).

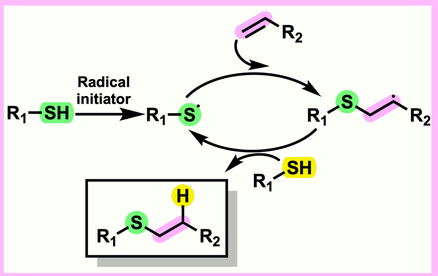


Fig. 1 The thiol-ene reaction mechanism

Thiol-ene Reaction In Vitro

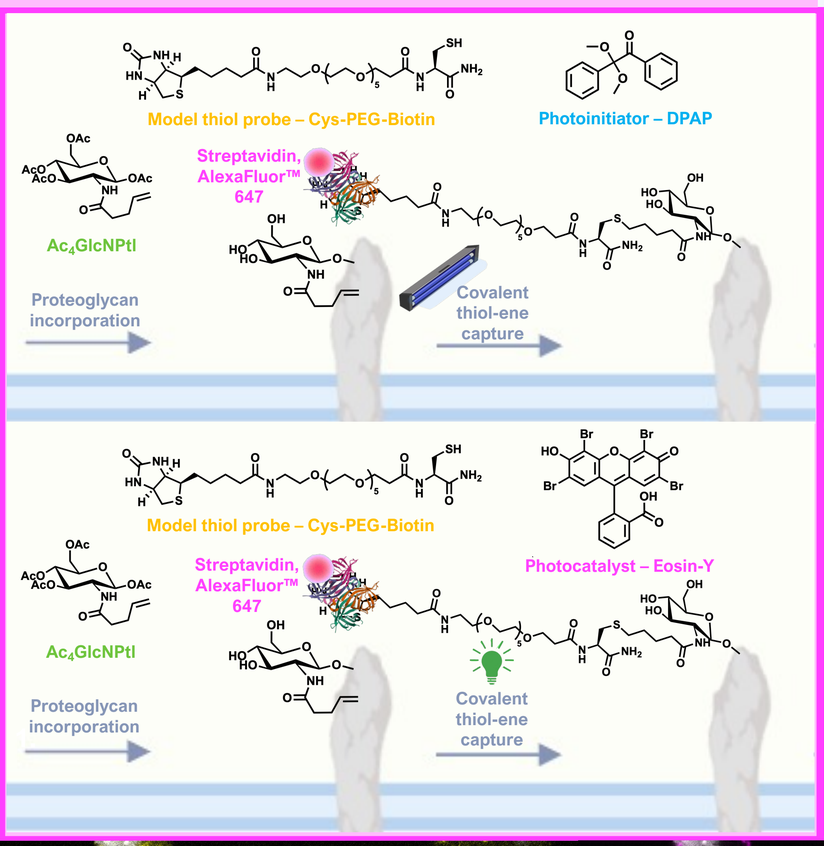


Fig. 3 HeLa cells were cultivated in the presence of $Ac_4GlcNPtl$ (50 μM) and incubated overnight at 37 °C and 5% CO_2. After washing with PBS, cells were treated with a thiol-ene cocktail (Cys-PEG-biotin (5 mM) and **DPAP (1 mM)** in 1% DMSO:PBS), irradiated at **354 nm** for 5 min, and then stained with streptavidin–AlexaFluor™ 647 prior to fixation, mounting, and imaging by confocal or STED microscopy.

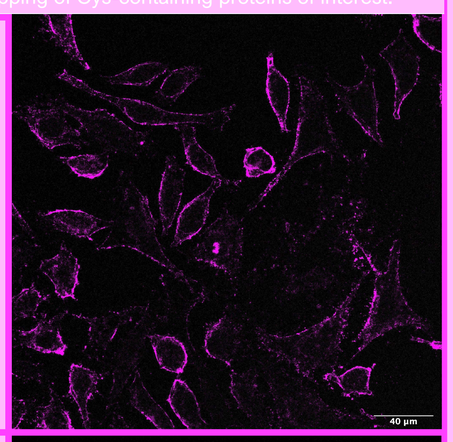
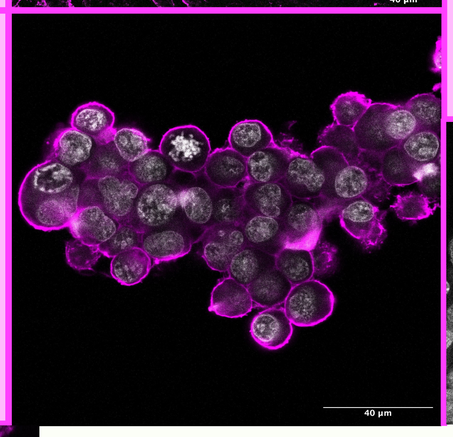


Fig. 4 HEK-293 cells were cultivated in the presence of $Ac_4GlcNPtl$ (50 μM) and incubated overnight at 37 °C and 5% CO_2. After washing with PBS, cells were treated with a thiol-ene cocktail (Cys-PEG-biotin (5 mM) and **Eosin-Y (7 μM)** in 1% DMSO:PBS), irradiated at **525 nm** for 10 min, and then stained with streptavidin–AlexaFluor™ 647 prior to fixation, mounting, and imaging by confocal or STED microscopy.



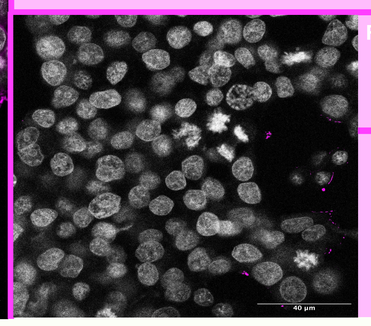


Fig. 5 Control HEK-293 cells incubated in the absence of $Ac_4GlcNPtl$

Dual Labelling via SPAAC and Thiol-ene

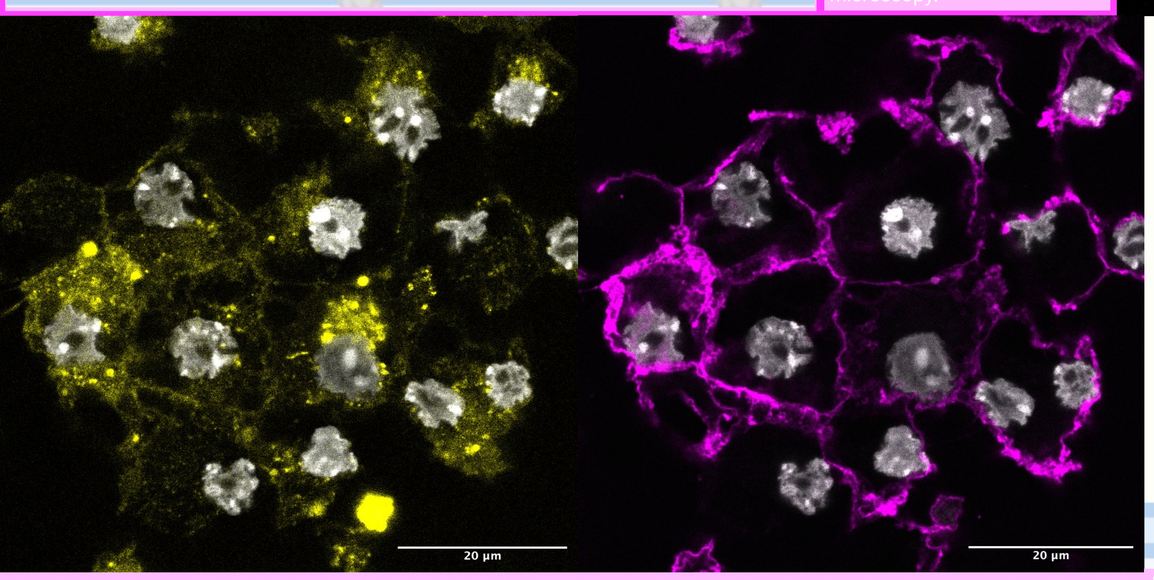


Fig. 5 Confocal images of dual labelled HEK-293 cells. Left: EY-PEG-DBCO photocatalyst installed on the cell surface, fluorescence detection ~ 550 nm. Right: Cys-PEG-Biotin probe installed on the cell surface, labelled with streptavidin, AlexaFluor ™ 647 for fluorescence detection, ~ 650 nm.

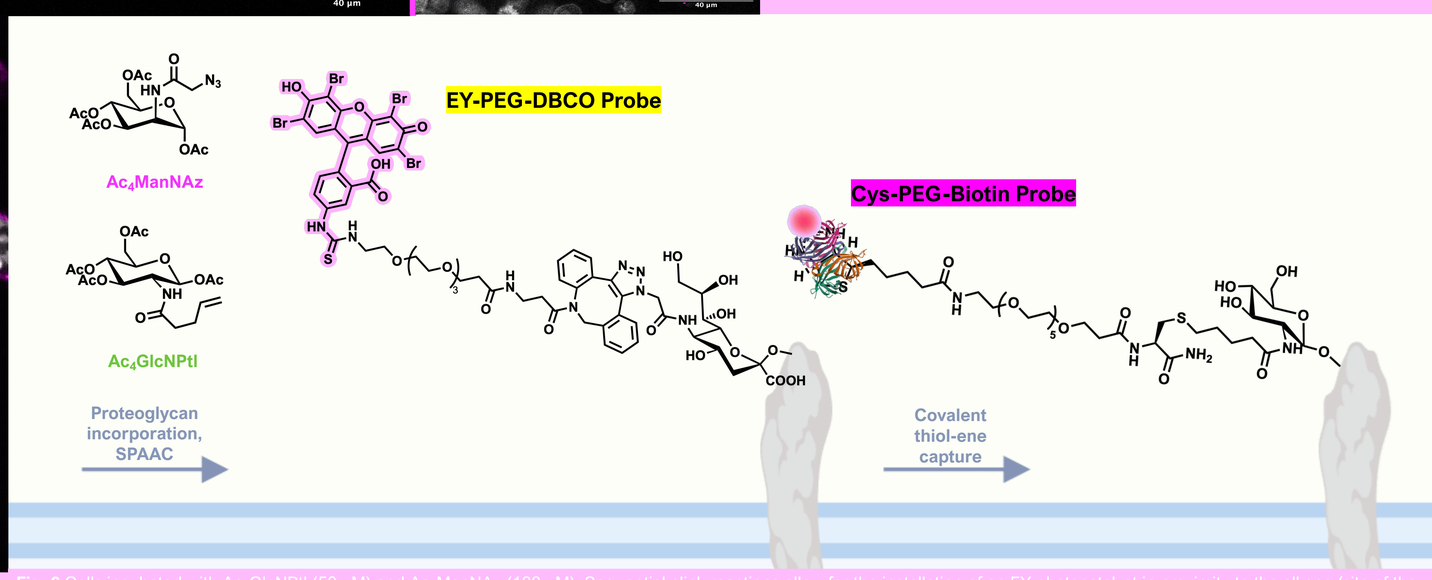


Fig. 6 Cells incubated with $Ac_4GlcNPtl$ (50 μM) and $Ac_4ManNAz$ (100 μM). Sequential click reactions allow for the installation of an EY photocatalyst in proximity to the alkene (site of the thiol-ene reaction, followed by the EY-mediated thiol-ene reaction to trap biomolecules/proteins containing a cysteine residue.

To expand the utility of the optimised thiol-ene approach, using Eosin-Y (EY) as a more biocompatible photocatalyst, a dual-labelling strategy was developed. This approached was inspired by the proximity labelling proteomics work developed by MacMillan and Wells, which involves the covalent linkage of a photocatalyst in proximity to a reaction site of interest.[3,4] An azide-functionalised sialic acid precursor ($Ac_4ManNAz$) was metabolically incorporated into cell surface glycans and subsequently labelled using an EY-PEG-DBCO probe via SPAAC. Following probe installation, the surface-bound EY catalysed the thiol-ene reaction, between a Cys-containing probe and the reactive alkene handle introduced through $Ac_4GlcNPtl$ incubation. This enables selective labelling of a second glycan population, and future iterations of this method would include Cys-containing proteins such as galectins and mucins. Dual fluorescence imaging successfully demonstrated simultaneous visualisation of both labelled glycan populations on HEK-293 cells (fig. 5), highlighting the potential of photocatalytic proximity labelling for multiplexed glycome analysis.

Conclusions and Future Work

Following the successful optimisation of the SPAAC, thiol-ene dual labelling strategy, future work will involve collaboration with Prof. Mia Huang, Scripps Research Institute, to elucidate cell surface glycan interactomes. Thiol-ene ligation will be used as a capture method to give a greater insight complex glycan-protein networks by overcoming the technical challenges associated with the inherently transient nature and low binding affinities of these interactions. Thiol-ene ligation offers superior temporal resolution in comparison to traditional analytical methods, and, as such, will be the current best-in-class method for mapping glycome landscapes.



LinkedIn

ORCiD

Taighde Éireann Research Ireland

Scripps Research

References

1. L. K. Mahal, K. J. Yarema and C. R. Bertozzi, *Science*, 1997, **276**, 1125–1128.
2. Y. Iwasaki, Y. Tabe, R. Tanaka and Y. Okuno, *Org. Biomol. Chem.*, 2025, **23**, 4893–4896.
3. J. B. Geri, J. V. Oakley, T. Reyes-Robles, T. Wang, S. J. McCarver, C. H. White, F. P. Rodriguez-Rivera, D. L. Parker, E. C. Hett, O. O. Fadeyi, R. C. Oslund and D. W. C. MacMillan, *Science*, 2020, **367**, 1091–1097.
4. Z. Lin, K. Schaefer, I. Lui, Z. Yao, A. Fossati, D. L. Swaney, A. Palar, A. Sali and J. A. Wells, *Science*, 2024, **385**, eadl5763.

10.17952/38EPS.2026.P457

A Novel Metal Catalyzed Peptide Ligation Method

Nathalie Ollivier[a], Remi Desmet[a], and Oleg Melnyk[a]

[a] Univ. Lille, CNRS, Inserm, CHU Lille, Institut Pasteur de Lille, U1019 - UMR 9017 - CIIL - Center for Infection and Immunity of Lille, F-59000 Lille, France

https://doi.org/10.17952/38EPS.2026.P028

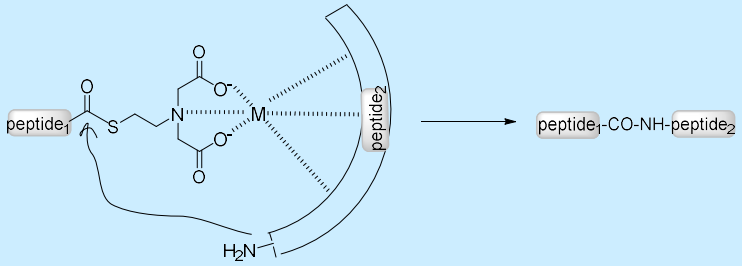
Introduction.

Native Chemical Ligation (NCL[1]) is a widely used chemoselective peptide ligation method for the semi-synthesis or total chemical synthesis of proteins. NCL involves the condensation of a peptide thioester with a cysteinyl (Cys) peptide, forming a larger peptide linked via a native amide bond at the cysteine residue. However, the low natural abundance of Cys in proteins significantly limits the applicability of NCL.[2]

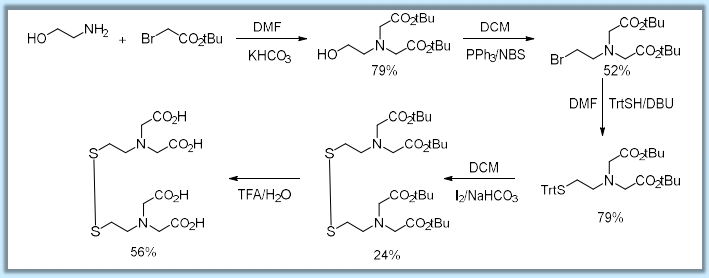
Peptide thioesters are valuable acyl donors for developing novel ligation strategies, as they can be readily synthesized through chemical, biochemical, or biological methods. Motivated by their unique reactivity, we aimed to design new peptide ligation methods that expand beyond the constraints of NCL.

Here we present our preliminary investigations of the use of metal catalysis for promoting the condensation of peptide thioesters derived from iminodiacetic acid (IDA) with peptide amine nucleophiles.

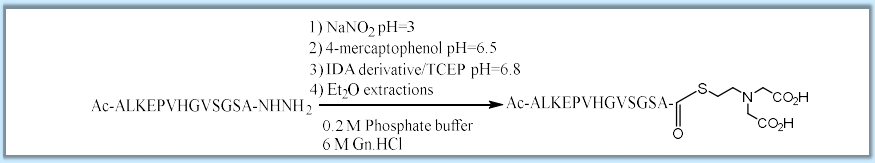
Principle of the metal catalyzed peptide ligation method



Synthesis of IDA derivative (n=2)

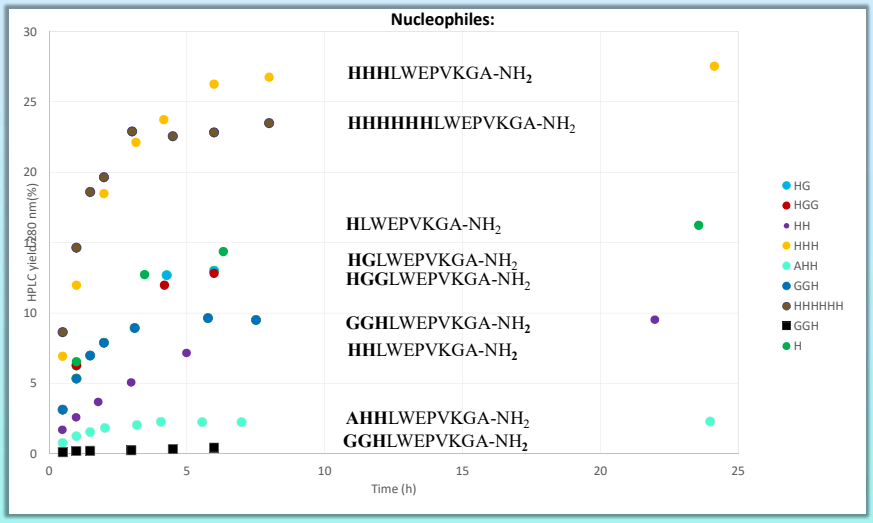


Synthesis of IDA thioester peptide (n=2)

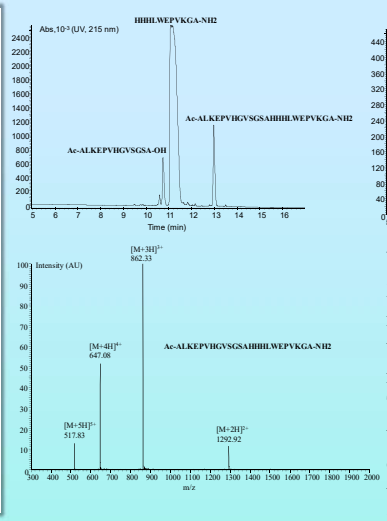


We used here an adapted procedure that significantly enhances thioester production with just a minimal thiol excess, facilitating the use of advanced thiol nucleophiles.[3]

Cu^{2+} catalyzed peptide ligation between IDA thioester peptide (n = 2 or n = 3) and various nucleophiles at pH = 5.5



Histidyl peptide (5 mM) was dissolved in 50 mM acetate buffer pH = 5.5 and added to IDA thioester (n = 2 circle, n = 3 square, 1 mM). pH was adjusted to 5.5. A solution of copper sulfate (1 mM) was then added to the reaction mixture, which was then placed at 25 °C.



UPLC-MS profiles (at 215 or 280 nm) of the final reaction mixture between IDA (n = 2) thioester peptide and HHH nucleophile peptide at pH = 5.5. The presence of tryptophan in the sequence enables quantification of the progress of the reaction by monitoring at 280 nm.

Conclusion.

Several parameters were systematically investigated. Two IDA thioesters were synthesized, with the variant containing n = 2 yielding the best results. Chemoselective ligation was achieved at pH 5.5, whereas no selectivity was observed at pH 7.

A range of metal ions (Co^{2+}, Ni^{2+}, Zn^{2+}, Cu^{2+}, Fe^{2+}, Mn^{2+}, and Mg^{2+}) were screened as potential catalysts. Among them, Cu^{2+} provided the highest efficiency. Various histidine-containing peptides were evaluated, and the best ligation yield was obtained with the peptide bearing three histidine residues at the N-terminus.

Although the crude product profile was satisfactory, the overall yield was limited by competing hydrolysis of the thioester.

References.

(1) Dawson, P.E.; Muir, T.W.; Clark-Lewis, I.; Kent, S.B.H. *Science* 1994, 266, 776-779.

(2) a) Agouridas, V., El Mahdi, O., Cargoet, M., Melnyk, O. *Bioorg Med Chem* 2017, 25, 4938-4945.

b) Agouridas, V., El Mahdi, O., Diemer, V., Cargoet, M., Monbaliu, J.C., Melnyk, O. *Chem. Rev.* 2019, 119, 12, 7328–7443.

c) Agouridas, V., El Mahdi, O., Melnyk, O. *J. Med. Chem.* 2020, 63, 24, 15140–15152.

(3) Di Adamo, J.; Ollivier, N.; Cantel, S.; Diemer, V.; Melnyk, O. *J.Org. Chem.* 2024, 89, 18, 13719–13724.

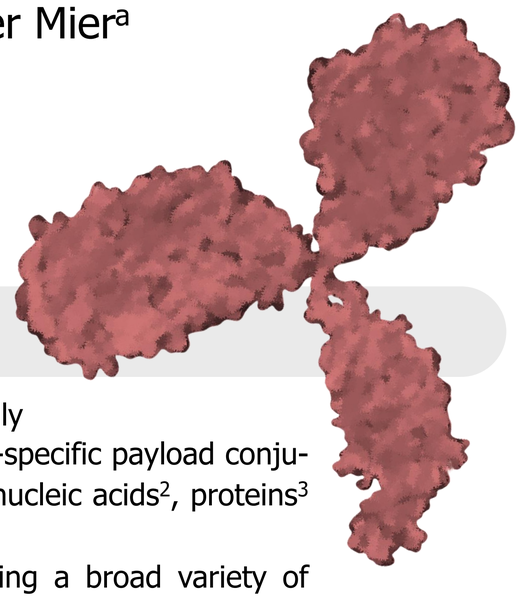
Comprehensive Chromatographic and Mass Spectrometric Approaches for in Vitro Analysis of Site-Specific Antibody–Peptide Conjugates

Niklas van den Bergh[a], Eric Mühlberg[b], Barbara Roether[a] and Walter Mier[a]

[a] Department of Nuclear Medicine, Heidelberg University Hospital, Germany
[b] Institute of Pharmacy and Molecular Biotechnology, Heidelberg University, Germany

niklas.vandenbergh@med.uni-heidelberg.de
http://doi.org/10.17952/38EPS.2026.P247

HEIDELBERG FACULTY OF MEDICINE



Background

Biologics are indispensable compounds in today's pharmaceutical landscape. Since the field of antibody–drug conjugates (ADCs) is rapidly expanding and in continuous development, new technologies and concepts evolve day by day. While many recent studies focus on site-specific payload conjugation[1], the spectrum of cargos used in research expands as well. Given this gaining significance of more complex payloads, such as nucleic acids[2], proteins[3] or peptides[4], universal strategies for a thorough analysis are strongly required.

Here, we synthesized 15 site-specific Trastuzumab–peptide conjugates with a peptide-to-antibody ratio (PAR) of two, while covering a broad variety of structural features and therefore divers chemical properties of the payload. As part of that, we validated comprehensive yet readily adjustable mass spectrometric and chromatographic methods towards systematic *in vitro* characterization of antibody–peptide conjugates and re-evaluated existing methods for their reliability in this field.

Scope and Results

Conjugate Synthesis

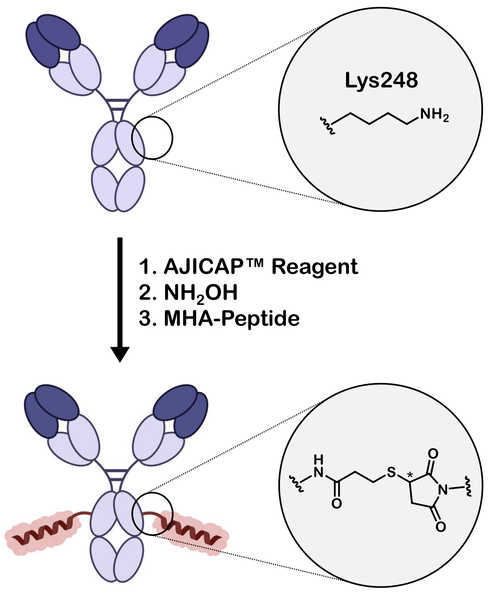


Table 1. Sequences of MHA-peptides used for protocol validation. Unless *N*-terminally attached, brackets indicate the coupling of maleimidohexanoic acid (MHA) to the ε-amino group of the lysine side chain.

Peptide	Class	Sequence
NLS	Hydrophilic	PKKKRKVK(MHA)
TAT		MHA-GRKKRRQRRRPPQ
R_9		MHA-RRRRRRRRR
D_6		MHA-DDDDDD
iRGD		MHA-CRGDKGPDC (cyclic disulfide)
$SynB_1$		MHA-RGGRLSYSRRRFSTSTGR
Ang-2		MHA-TFFYGGSRGKRNNFKTEEY
LPETG		MHA-GGGGSGGGGSGGGGSLPETGG
Pen		MHA-RQIKIWFQNRRMKWKK
MAP	Amphipathic	MHA-KLALKLALKALKAALKLA
TP_{10}		AGYLLGK(MHA)INLKALAALAKKIL
L17E		IWLTALKFLGKHAAKHDAKQQLSKLK(MHA)
pVEC		MHA-LLIILRRRIRKQAHAHSK
$PreS_2$		MHA-PLSSIFSRIGDP
MTS	Hydrophobic	AAVALLPAVLLALLAPK(MHA)

Scheme 1. Synthesis of site-specific Trastuzumab–peptide conjugates *via* the second generation AJICAP™ method. Using hydroxylamine the covalently bound AJICAP™ affinity peptide is cleaved resulting in 3-mercaptopropionyl modified Lys248 followed by maleimide–thiol conjugation.[5]

Hydrophobic Interaction Chromatography (HIC)

While HIC is a common tool used for drug-to-antibody ratio determination in ADCs, its utility in antibody–peptide conjugates is hardly elucidated yet. Here, the examined intact conjugates showed distinct retention time shifts strongly correlating with the hydrophilic properties of their amino acid sequences (Fig. 1, top).

Notably, for some of the conjugates significant peak broadening occurred. In particular, late-eluting conjugates (Fig. 1, bottom) were prone to this phenomenon. The presence of more than one signal opens up the thought of conformational heterogeneity of the payload. This may lead to structurally varying conjugate species restricting reliable PAR analysis.

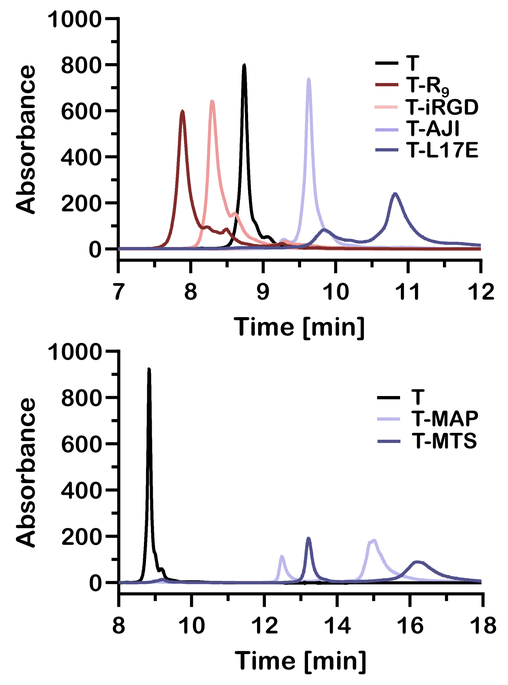
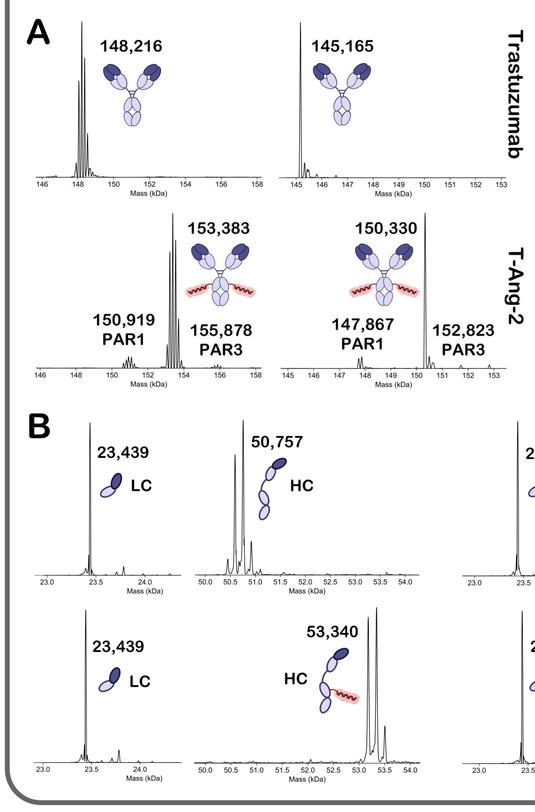


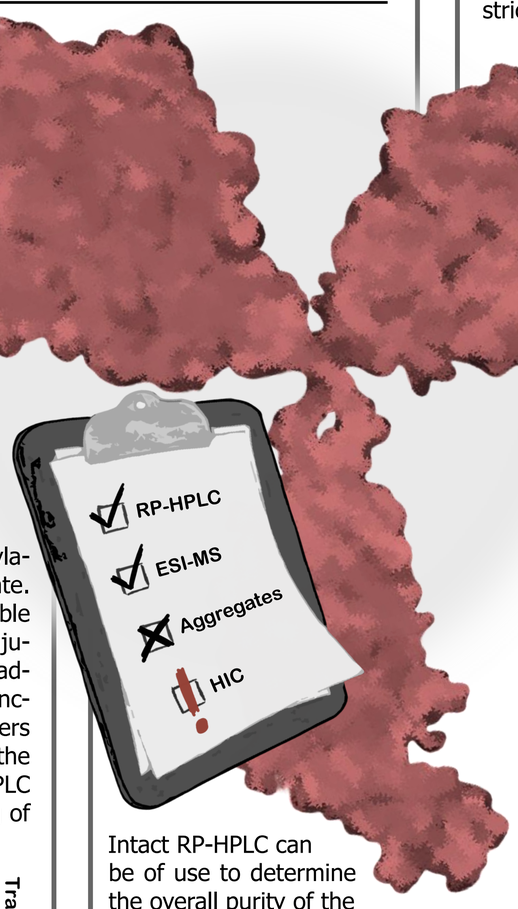
Figure 1. HIC chromatograms of early- (top) and late-eluting (bottom) antibody–peptide conjugates. T-AJI: Synthetic intermediate comprised of two AJICAP™ affinity peptides covalently attached to Trastuzumab.

ESI-Mass Spectrometry (ESI-MS)

Figure 4. Deconvoluted ESI-MS spectra of (A) intact and (B) TCEP-reduced antibody samples in the glycosylated (left) and deglycosylated (right) forms.



Mass spectrometric analysis of antibody conjugates was performed both for intact (Fig. 4A) and reduced (Fig. 4B) samples. Maximum mass accuracy was achieved through deglycosylation of the reduced conjugate. Sample preparation was feasible for all antibody–peptide conjugates (Tab. 1) and readily adjustable for more sensitive functional groups, such as thioesters found in T-AJI. Supporting the findings from reduced RP-HPLC analysis, site-specific labelling of the heavy chain was verified.



Intact RP-HPLC can be of use to determine the overall purity of the conjugate sample. Highly hydrophobic peptide payloads even showed baseline separation of PAR species (Fig. 3, top). Upon sample reduction retention time shifts of the modified heavy chain (HC) changed significantly whereas light chain (LC) signals remained identical (Fig. 3, bottom). While reduction can be performed using both DTT and TCEP, the latter resulted in broadened signals.

RP-HPLC

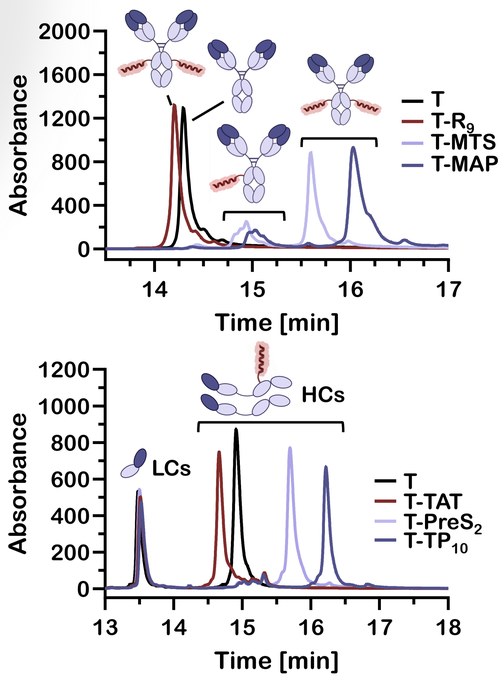


Figure 3. RP-HPLC chromatograms of intact (top) and DTT-reduced (bottom) Trastuzumab–peptide conjugates. Both intact samples and reduced heavy chains show distinct hydrophilic or hydrophobic retention time shifts depending on the peptide payload.

DLS

Particle size measurements did not show formation of aggregates but suggest monomeric species with a diameter of around 10 nm, which is typical for mAbs.[6]

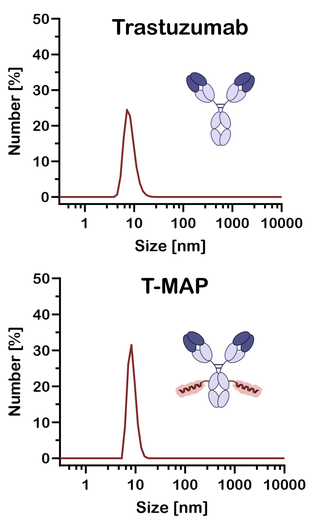


Figure 2. Particle size distribution measured in PBS (0.3 g/L) after storage in PBS (10 g/L) at 4 °C for 14 days.

Contact me

Summary and Outlook

We validated and standardized mass spectrometric and chromatographic approaches towards a more systematic analysis of site-specific antibody–peptide conjugates. We found that by a combination of both ESI-MS and RP-HPLC, a reasonable and thorough quality control of such conjugates can be achieved. Moreover, we performed HIC for all of the prepared conjugates and would like to put forward that it does not seem to generally qualify for a reliable PAR determination tool without the support of other aforementioned methods.

References

1. Q. Fan *et al.*, *Antibody Therapeutics* **2025**, *8* (2), 157-170.
2. M. Li *et al.*, *Eur. J. Pharm. Sci.* **2025**, *215*, 107292.
3. J. Park *et al.*, *Bioorg. Med. Chem.* **2021**, *30*, 115946.
4. A. Petruzzella *et al.*, *Nat. Chem. Biol.* **2024**, *20* (9), 1188-1198.
5. T. Fujii *et al.*, *Bioconjug. Chem.* **2023**, *34* (4), 728-738.
6. H. B. Nguyen *et al.*, *J. Med. Chem.* **2025**, *68* (1), 555-565.

Enhancer-driven changes in Peptide Permeability on *In Vitro* models

Mihalac Josip [1,2], Milić Astrid [1], Kalafatović Daniela [3]

[1] Selvita d.o.o., Zagreb, Croatia; [2] Faculty of Biotechnology and Drug Development, University of Rijeka, Rijeka, Croatia; [3] Faculty of Engineering, University of Rijeka, Croatia; https://doi.org/10.17952/38EPS.2026.P521

Contact email: josip.mihalac@selvita.com

Introduction

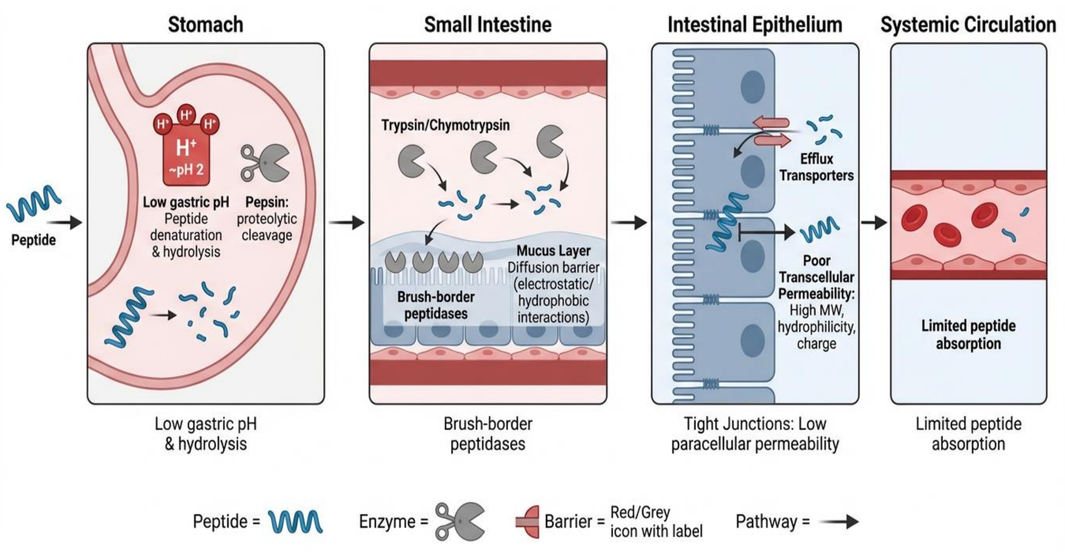
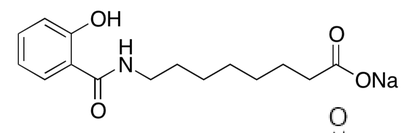
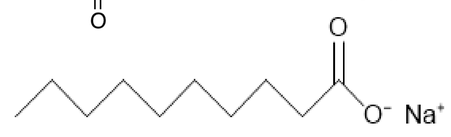


Figure 1. Overview of physicochemical barriers affecting the oral absorption of peptide therapeutics in the human GI tract

- The development of oral peptide therapeutics is significantly impacted by poor permeability through the gastrointestinal (GI) epithelium, as well as by enzymatic degradation - finally resulting in low peptide absorption and low bioavailability
- Permeation enhancers SNAC (salcaprozate sodium) and C10 (sodium caprate) are used in advanced oral peptide formulations to fix low peptide's GI absoption
- SNAC



- C10



- Accurate assessment of peptide's *in vitro* apparent permeability considered essential for identifying viable drug candidates

Key challenges

- **Low intestinal permeability**
  large size and high polarity of peptides results in poor oral absorption
- **Poor recovery and non-specific binding**
  Adsorption to assay components can lead to significant loss and inaccurate estimates (poor *in vitro to in vivo* correlation)
- **Enzymatic instability**
  Rapid degradation by intestinal and cellular proteases complicates interpretation of transport data

Aim

Systematically evaluate how C10 and SNAC modulate permeability and recovery of a panel of linear and cyclic peptides across *in vitro* epithelial cell models

Methods

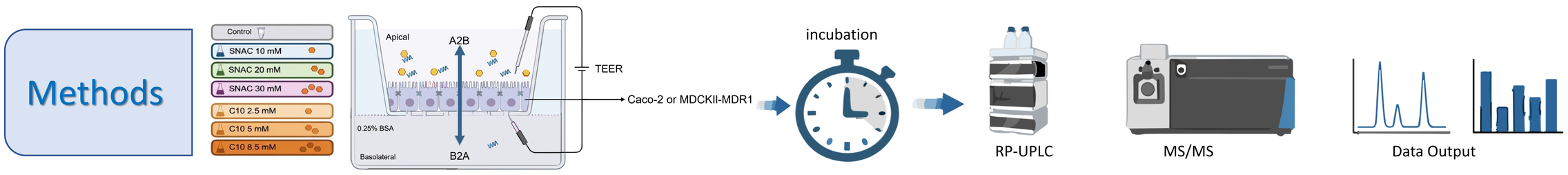


Figure 2. Schematic representation of the *in vitro* epithelial barrier model and experimental workflow

Results

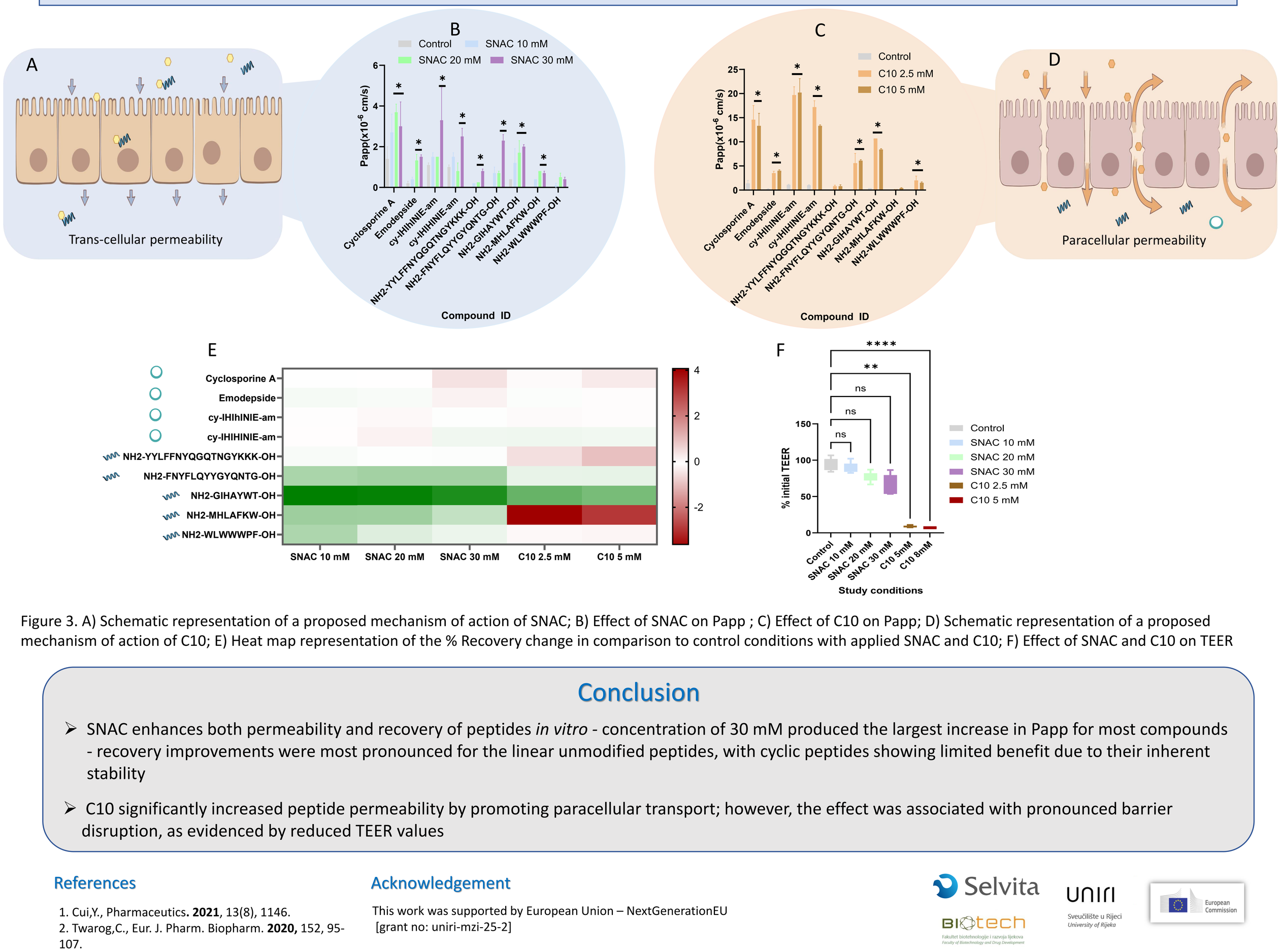


Figure 3. A) Schematic representation of a proposed mechanism of action of SNAC; B) Effect of SNAC on Papp ; C) Effect of C10 on Papp; D) Schematic representation of a proposed mechanism of action of C10; E) Heat map representation of the % Recovery change in comparison to control conditions with applied SNAC and C10; F) Effect of SNAC and C10 on TEER

Conclusion

- SNAC enhances both permeability and recovery of peptides *in vitro* - concentration of 30 mM produced the largest increase in Papp for most compounds - recovery improvements were most pronounced for the linear unmodified peptides, with cyclic peptides showing limited benefit due to their inherent stability
- C10 significantly increased peptide permeability by promoting paracellular transport; however, the effect was associated with pronounced barrier disruption, as evidenced by reduced TEER values

References

1. Cui,Y., Pharmaceutics**. 2021**, 13(8), 1146.
2. Twarog,C., Eur. J. Pharm. Biopharm. **2020,** 152, 95-107.

Acknowledgement

This work was supported by European Union – NextGenerationEU
[grant no: uniri-mzi-25-2]

Development of new peptide-based antimicrobial agents targeting *trans*-translation in bacteria

Flore Miomandre[1,2], Andrés Corral Lugo[2], Olivier Delalande[2], Emmanuel Guidice[2], Sophie Chat[2], François-Hugues Porée[1], Charlène Gadais[1], Reynald Gillet[2]

[1]ISCR (Institut des Sciences Chimiques de Rennes) – UMR 6226, Univ Rennes, CNRS, F-35000 Rennes, France

[2]IGDR (Institut de Génétique & Développement de Rennes) – UMR 6290 CNRS /UR – ERL U1305 Inserm, F-35000 Rennes, France

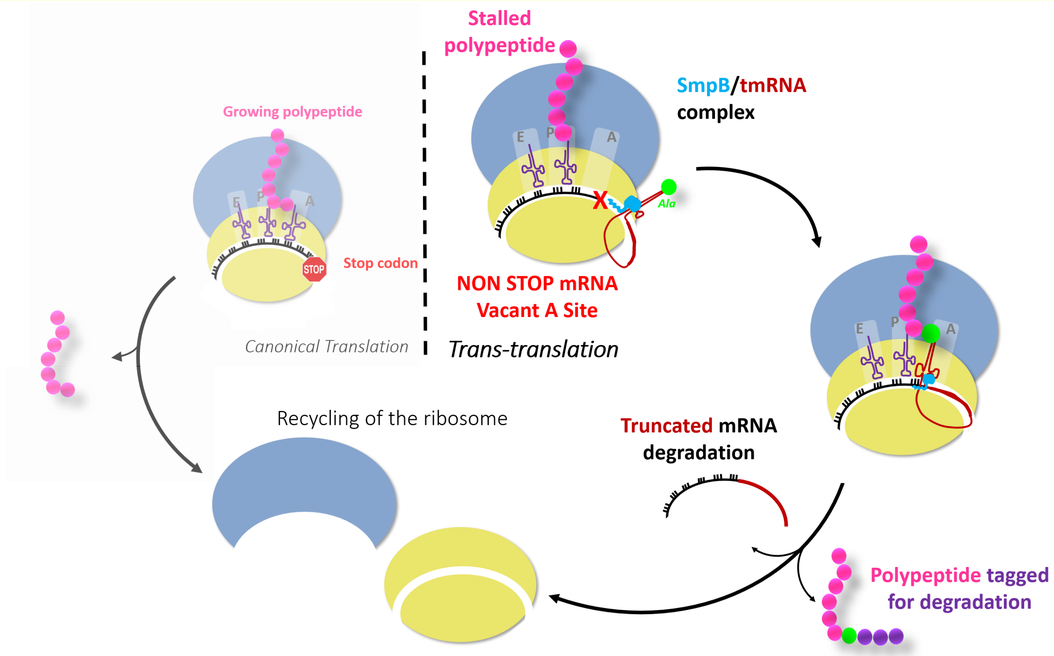
https://doi.org/10.17952/38EPS.2026.P230

Trans-translation is the main recue system in bacteria. It is required for bacteria stress tolerance, growth and virulence, and permits resuming stalled translation when errors occur, hence ensuring bacterial survival. In this bacteria specific process, a small protein called SmpB recognizes stalled ribosomes by inserting its helical C-terminal tail in the vacant ribosomal mRNA path and allows the correct positioning of its partner, transfer-messenger RNA. In the search for **alternative antibiotic strategies**, the **rational design of SmpB C-ter tail peptide decoy** would provide a **highly specific *trans*-translation inhibitor** with potentially **broad-spectrum antimicrobial activity** and **limited side-effects on host cells**.

1 - *Trans*-translation, an appealing target in the fight against antibioresistance[1]

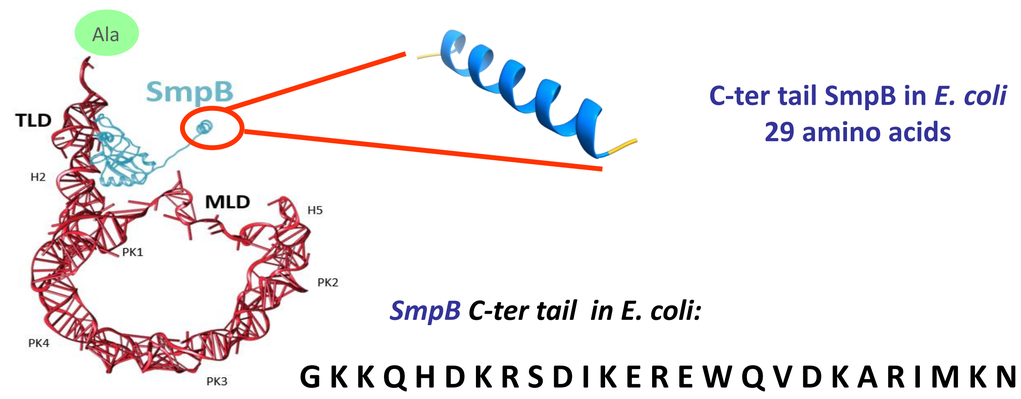
What is ***trans*-translation ?**

- Under stress, ribosome can get stalled during translation due to non-Stop mRNA
- SmpB/tmRNA complex identifies and initiates **rescue** of the stalled ribosome
- Release of the stalled ribosome and degradation of the faulty mRNA and incomplete peptide



Trans-translation is an **appealing target** because:

- It is absent in eukaryotes
- It is necessary for bacterial **survival**
- It is required for the **virulence** of some species
- When deletion is not lethal (due to backup systems), it induces **hypersensitive** phenotypes



C-ter tail SmpB in *E. coli*
29 amino acids

***SmpB* C-ter tail in *E. coli*:**

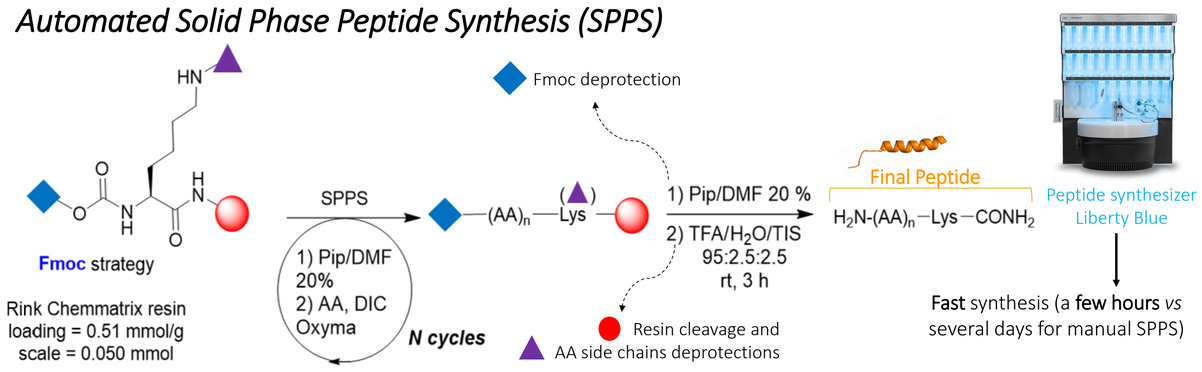
G K K Q H D K R S D I K E R E W Q V D K A R I M K N A H R

Goal:

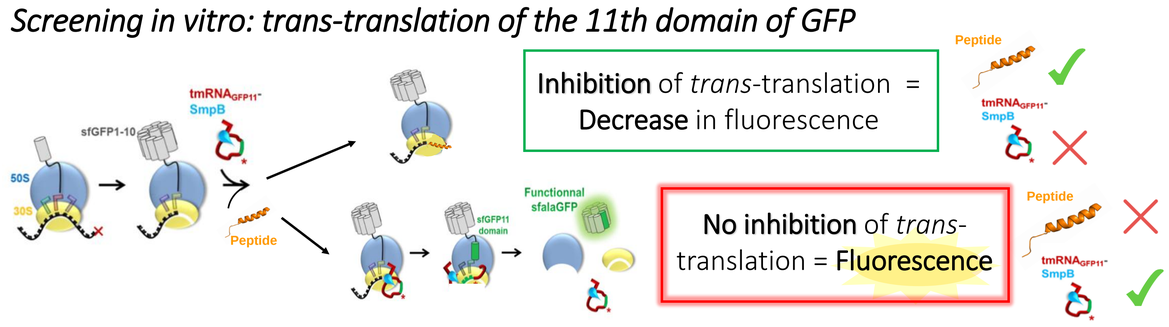
Design of the shortest **mimetic** of the SmpB C-ter tail that **selectively** inhibits *trans*-translation

2 - Synthesis and *in vitro* screening[3] of the peptides

Automated Solid Phase Peptide Synthesis (SPPS)



Screening in vitro: trans-translation of the 11th domain of GFP



In vitro experiments are implemented to determine the **inhibition capacity** of a designed peptide over the ***trans*-translation** using GFP fluorescence[3].

3 - Results on the mimic SmpB_29 (*E. coli*)

The 29 amino acids peptide corresponding to the C-ter tail of the protein SmpB (SmpB_29) was tested with the *in vitro* system.



In the system :

- $C_{estimated\ ribosome}$ = 1,5 µM
- C_{SmpB} = 2,5 µM
- C_{tmRNA} = 1,25 µM

Ratio protein SmpB/peptide:

- 100x (250 µM)
- 50x (125 µM)
- 10x (25 µM)
- 1x (2,5 µM)

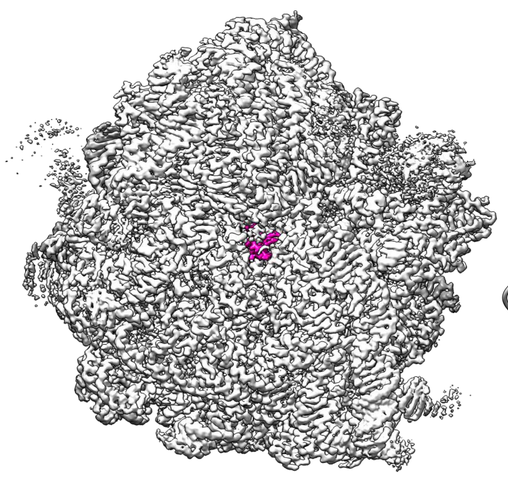
The peptide SmpB_29 showed great efficiency toward the inhibition of *trans*-translation : **still 88% of inhibition of *trans*-translation at 10x (25 µM)**

Comparatively, **only 20% of inhibition of translation at 10x (25 µM)**

A **peptide** mimicking the C-ter tail of SmpB can **selectively** inhibit *trans*-translation over translation at low concentration, and **in a competitive manner** in regard with the SmpB/tmRNA complex.

4 - Cryo-electron microscopy of SmpB_29 bound to a stalled ribosome

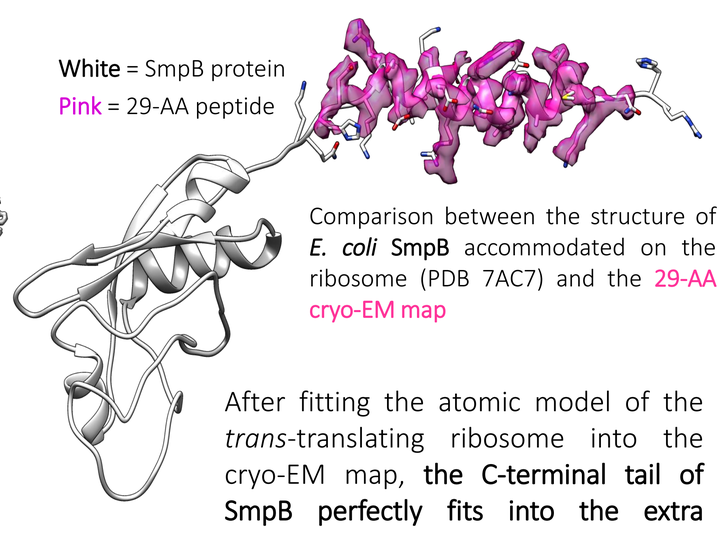
To precisely confirm the target of the peptide SmpB_29, we obtained a Cryo-EM density map of the peptide into a stalled *E. coli* ribosome.



Resolution : **1.84Å**

Extra density corresponding to the peptide

Huge excess of peptide (SmpB_29 / ribosome = 250)



White = SmpB protein

Pink = 29-AA peptide

Comparison between the structure of ***E. coli* SmpB** accommodated on the ribosome (PDB 7AC7) and the 29-AA cryo-EM map

After fitting the atomic model of the *trans*-translating ribosome into the cryo-EM map, **the C-terminal tail of SmpB perfectly fits into the extra density**

The 29-AA peptide occupies the **same binding site** as SmpB C-ter tail, and can therefore **compete** with the *trans*-translation machinery

5 - Conclusion and perspectives

- **Selective inhibition** of *trans*-translation by a **decoy peptide** is possible
- Inhibition of *trans*-translation without inhibiting translation is possible even
- Truncated versions showed inhibition too, allowing the design of a **shorter peptide**

→*Perspectives:*

- **Strengthen the interactions** with the ribosome and improve the **metabolic stability: chemical modifications** on strategic positions of the peptide chain identified through *in silico* studies
- ***In vivo* activity** of the "hit" peptide to be determined: introduction of a **cell-penetrating peptide** (CPP)
- Extrapolation of the *E. coli* results on other pathogenic bacteria (**ESKAPEE**)

References

1. Campos-Silva, R.; D'Urso, G.; Delalande, O.; Giudice, E.; Macedo, A. J.; Gillet, R. Trans-Translation Is an Appealing Target for the Development of New Antimicrobial Compounds. *Microorganisms* **2022**, *10* (1), 3. https://doi.org/10.3390/microorganisms10010003.
2. Guyomar, C.; D'Urso, G.; Chat, S.; Giudice, E.; Gillet, R. Structures of TmRNA and SmpB as They Transit through the Ribosome. *Nature Communications* **2021**, 12, 4909. https://doi.org/10.1038/s41467-021-24881-4.
3. Thépaut, M.; Campos-Silva, R.; Renard, E.; Barloy-Hubler, F.; Ennifar, E.; Boujard, D.; Gillet, R. Safe and Easy in Vitro Evaluation of TmRNA-SmpB-Mediated Trans-Translation from ESKAPE Pathogenic Bacteria. *RNA* **2021**, *27* (11), 1390–1399. https://doi.org/10.1261/rna.078773.121.

Engineered Peptide-Based Nanosystems for Improving Therapeutic and Diagnostic Potential of Anticancer agents

Prashant Mishra • Ritu Bhardwaj
Department of Biochemical Engineering and Biotechnology, Indian Institute of Technology Delhi, India

https://doi.org/10.17952/38EPS.2026.P394



38th EPS
European Peptide Symposium
Vienna. Austria

PEPTIDES : • *High specificity* • *Low toxicity* • *Low immunogenicity*

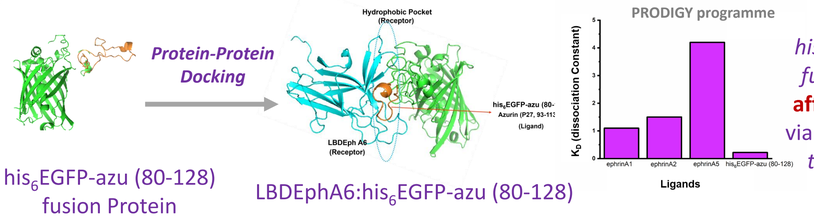
ENGINEERED PROTEINS & PEPTIDES TRANSFORMED INTO MULTIFUNCTIONAL NANOMEDICINES

FROM MOLECULAR DESIGN TO CANCER RESPONSE

DESIGN → SELF-ASSEMBLE → TARGET → IMAGE → TREAT

NANOSYSTEM : his$_6$EGFP-azu (80-128 aa)

(A). BIOMARKER CELL SURFACE RECEPTOR, EPHA6 RECOGNITION BY ENGINEERED his$_6$EGFP-AZU(80–128): AN *IN-SILICO* TARGETING STRATEGY

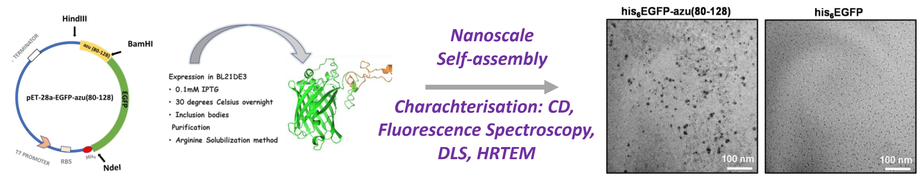


his$_6$EGFP-azu (80-128) fusion Protein

LBDEphA6:his$_6$EGFP-azu (80-128)

his$_6$EGFP-azu(80–128) fusion, showed **high-affinity** EphA6 binding via azu(80–128) *than its traditional ephrin A ligands.*

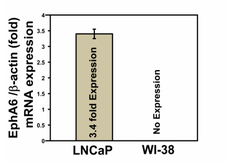
(B). his$_6$EGFP-azu(80–128) NANOSYSTEM ENGINEERING



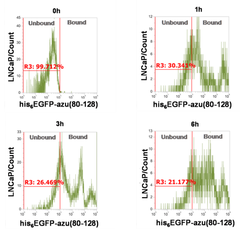
his$_6$EGFP-azu(80–128) engineered and purified as a recombinant fusion protein

HRTEM Characterisation :**~20–25 nm Spherical Nanoparticles**

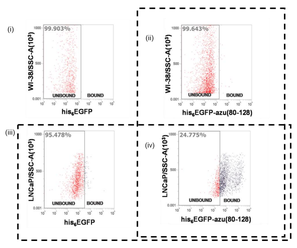
(C). SELECTIVE CANCER TARGETING (EphA6-DEPENDENT CELLULAR BINDING)



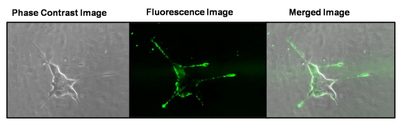
LNCaP: **~3.4-fold** EphA6 mRNA expression
WI-38: No detectable EphA6 expression



his$_6$EGFP-azu(80-128) binds **~70%** cell population within 1 hour

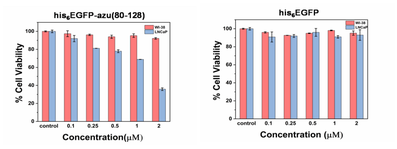


his$_6$EGFP-azu(80-128) drives selective EphA6$^+$ cancer-cell targeting
EphA6$^-$ → ~0.4%
EphA6$^+$ → ~76%

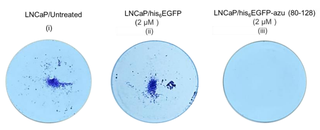


Fluorescent his$_6$EGFP-azu(80-128) Nanosystem enables **Cancer-cell Imaging**

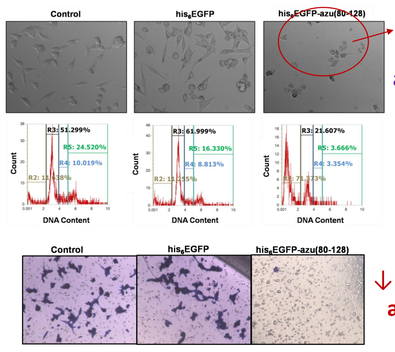
D). CYTOTOXICITY, ANTI-METASTATIC, ANTI-PROLIFERATIVE ACTIVITY AGAINST LNCaP CELLS.



MTT/Overnight: >50% Cancer-cell Killing at **2 μM** his$_6$EGFP-azu(80–128)



15-day **COLONY FORMATION ASSAY**: **Complete suppression** of clonogenic growth



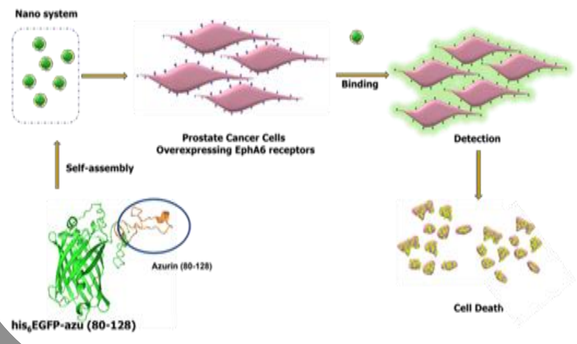
Loss of normal cell morphology and reduced cell density

CELL-CYCLE ANALYSIS
↓ S-phase population
↓ G_2/M population
altered cell-cycle progression

TRANS-WELL ASSAY: reduced cell migration, reduced cell invasion

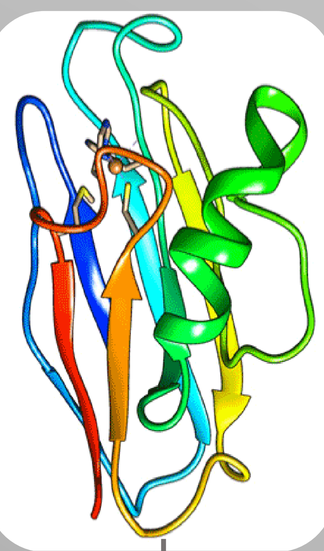
KEY FINDINGS

✓ *Engineered azurin converts a naturally bioactive protein into a multifunctional* ***theranostic nanosystem*** *for selective cancer targeting and therapy.*



✓ **SELF-ASSEMBLES** → *~20–25 nm nanosystem*
✓ **TARGETS** → *EphA6$^+$ prostate cancer cells*
✓ **IMAGES** → *EGFP-enabled cancer-cell visualization*
✓ **KILLS** → *>50% cancer-cell killing at 2 μM*
✓ **SUPPRESSES** → *Migration, invasion & clonogenic growth*

AZURIN



WHY AZURIN?

NATURAL ANTICANCER PROTEIN
128 aa • ~14 kDa • Cu-containing redox protein
From Pseudomonas aeruginosa

CANCER-SELECTIVE ACTIVITY
Preferential cancer-cell entry → selective cytotoxicity

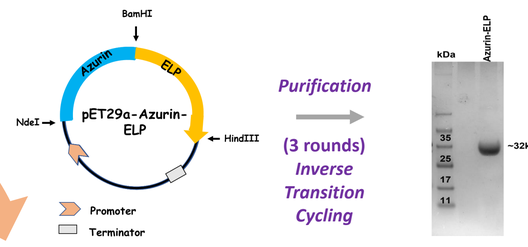
ANTICANCER HOTSPOTS
P28 (azu 50–77 aa) + C-terminal region
→ Key regions linked to anticancer activity

MULTIPLE CANCER PATHWAYS
Azurin interacts with cancer-associated signaling pathways
→ Growth • migration • invasion

TARGETING BEHAVIOUR
C-terminal region
Eph receptors → cancer progression & metastasis
→ A rationale for EphA6-targeted nanomedicine

NANOSYSTEM : Azurin-(Elastin-like Polypeptide)

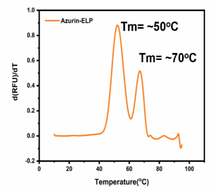
(A). CLONING, EXPRESSION, AND PURIFICATION OF RECOMBINANT FUSION PROTEIN AZURIN-ELP DI-BLOCK COPOLYMER



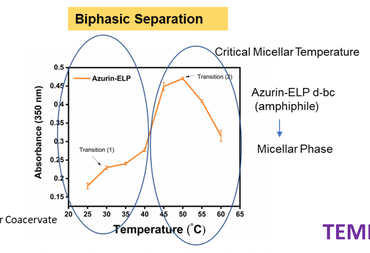
Recombinant Plasmid vector containing fused genes, *AZURIN* and *ELP*

STRUCTURE RETAINED → *Azurin maintains its structural integrity post-ELP fusion.*
CYTOTOXICITY PRESERVED → *Anticancer activity remains intact in the conjugate.*
CELLULAR UPTAKE MAINTAINED → *Efficient cancer-cell internalization is retained.*

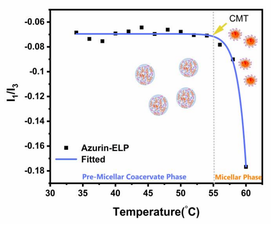
(B). TEMPERATURE-TRIGGERED SELF-ASSEMBLY OF AZURIN-ELP D-BC



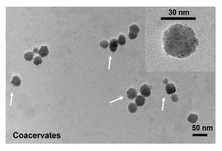
THERMAL SHIFT ASSAY : Phase Transition temperatures



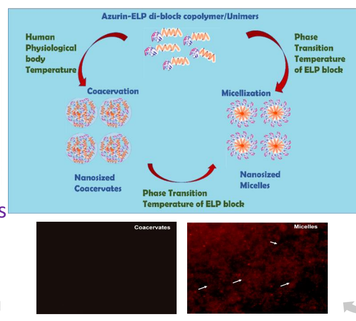
UV-VISIBLE SPECTROSCOPY: showing Biphasic Separation

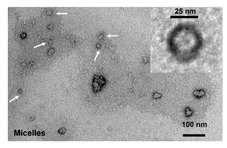


TEMPERATURE-TRIGGERED MICELLIZATION
Pyrene fluorescence (I_1/I_3) → Critical micellization temperature → MICELLE FORMATION

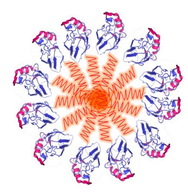


HRTEM :Coacervates (Size: ~ 30 nm)





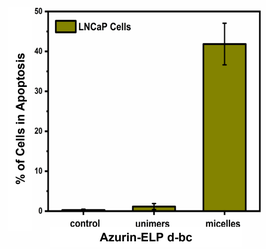
HRTEM :Micelles (~ Size: 25 nm)



THERMORESPONSIVE TRANSFORMATION
Coacervates (~37-40 °C) → Micelles (~50-55 °C)
Potential platform for controlled drug & contrast-agent delivery

SYPRO ORANGE FLUORESCENCE visualizes temperature-driven morphological transformation

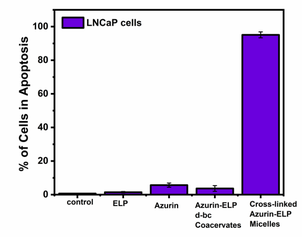
(C). EVALUATION OF CYTOTOXICITY OF THE MICELLAR NANOSTRUCTURES OF AZURIN-ELP D-BC



UNIMERS VS MICELLES : **~ 38%** Cancer cells in Apototic Phase at 5 μM concentration

THERAPEUTIC EFFICACY ?

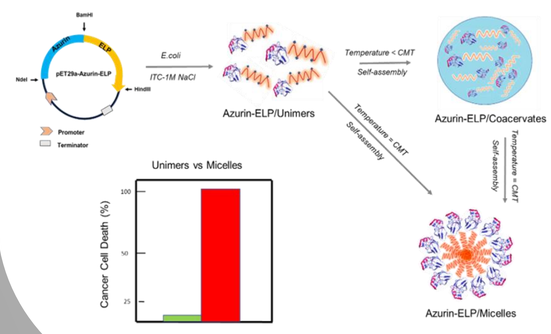
The crosslinked azurin-ELP micelles were more effective.



COMPARATIVE CYTOTOXICITY: **~ 97%** Cancer cells in Apototic Phase at 20 μM concentration

KEY FINDINGS

✓ *First study to examine utility of ELP based nano-delivery of azurin.*



✓ **THERMORESPONSIVE SELF-ASSEMBLY**
→ *Programmable temperature-triggered nanostructure formation*
✓ **NANOSCALE ORGANIZATION**
→ *~25–30 nm micelles*
✓ **ENHANCED CYTOTOXICITY**
→ *Improved anticancer activity against cancer cells by micelles*
✓ **THERAPEUTIC DELIVERY**
→ *A modular platform for cargo encapsulation and delivery*

TAKE-AWAYS

Engineering **peptides** into **multifunctional nanosystems** established a modular platform for precision oncology, integrating:

CANCER-CELL TARGETING

FLUORESCENCE IMAGING

THERMORESPONSIVE SELF-ASSEMBLY

THERAPEUTIC DELIVER

PRECISION NANOMEDICINE

References:
1. R. Bhardwaj and P Mishra, *Molecular Pharmaceutics* **2023**, *20*, 6066–6078.
2. R. Bhardwaj and P Mishra, *Biomacromolecules* **2024,** *25*, 508-521.

Cyclo-(His-Phe) Complexes with Copper and Zinc Nanoparticles Have Targeted Anticancer Potential Against Osteosarcoma Cells

Anna Mitraki[1,2*] Chrysanthi Pinelopi Apostolidou[1,2] · Georgios Charalambidis[3,4] · Aikaterini Gialouri[1,5] · Maria Chatzinikolaidou[1,2]

[1] Department of Materials Science and Engineering, University of Crete · [2] IESL, FORTH · [3] Laboratory of Bioinorganic Chemistry, University of Crete · [4] Theoretical and Physical Chemistry Institute, National Hellenic Research Foundation · [5] School of Medicine, University of Crete

https://doi.org/10.17952/38EPS.2026.P165

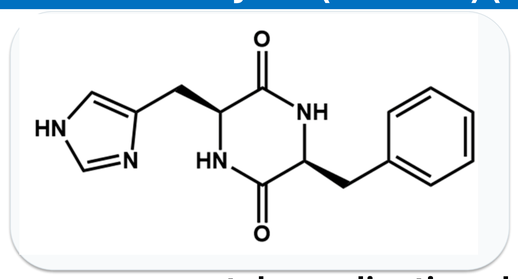
38th European Peptide Symposium · Vienna, Austria · 6–11 September 2026

POSTER No. 165

OUTLINE

- The development of chemotherapy agents that exploit molecular carriers for controlled and targeted delivery in cancer cells is a crucial area in modern molecular medicine.
- Herein, we examined the potential of the cyclic peptide cyclo-(His-Phe) to chelate copper and zinc ions that have been recently proposed as therapeutic agents against osteosarcoma cells.
- The peptide self-assembled into amyloid-type fibrils; morphological and structural characterization following metal ion addition confirmed the formation of cHF–CuNPs and cHF–ZnNPs.
- We evaluated the optimal concentration of cHF–metalNP complexes with antimicrobial activity against *E.coli* and *S.aureus,* limited cytotoxicity to L929 fibroblasts and high cytotoxic effects against MG-63 osteosarcoma cells.

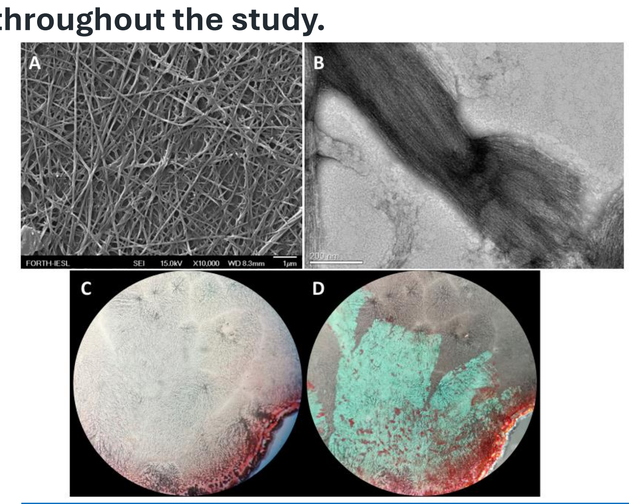
PEPTIDE DESIGN cyclo-(His-Phe) (cHF)



Histidine conveys metal coordination ability; the cyclic peptide backbone and the phenylalanine rin support self-assembly.

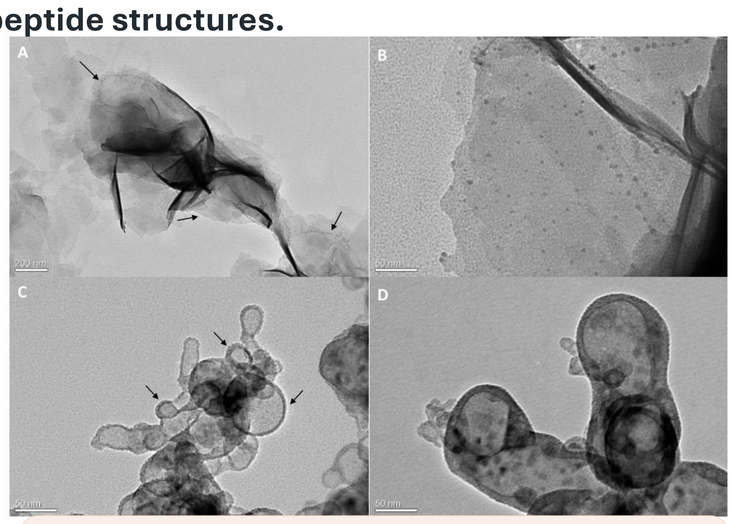
SELF-ASSEMBLY OF cHF in PBS

FESEM/TEM and CongoRed staining show fibrillar, amyloid-like cHF assemblies. The peptide concentration used was 5 mM throughout the study.



METAL ION COORDINATION

At 1 mM metal ion concentration, cHF-copper complexes form petal/flower-like structures, while cHF-zinc complexes form bubble-like spherical assemblies. TEM shows electron-dense nanoparticle dots templated on or within peptide structures.

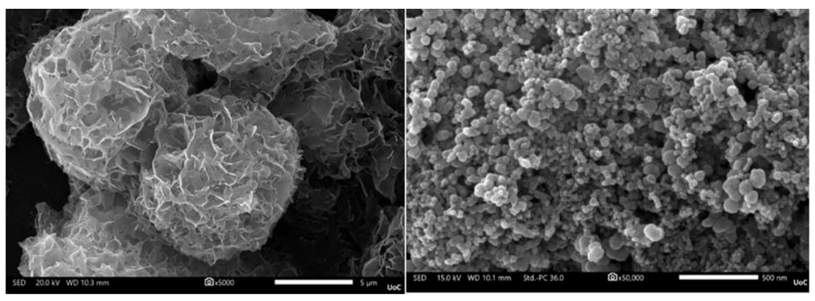


A,B =Cu^{2+} → flower-like / nanosheet-rich assemblies

C,D = Zn^{2+} → spherical / bubble-like assemblies

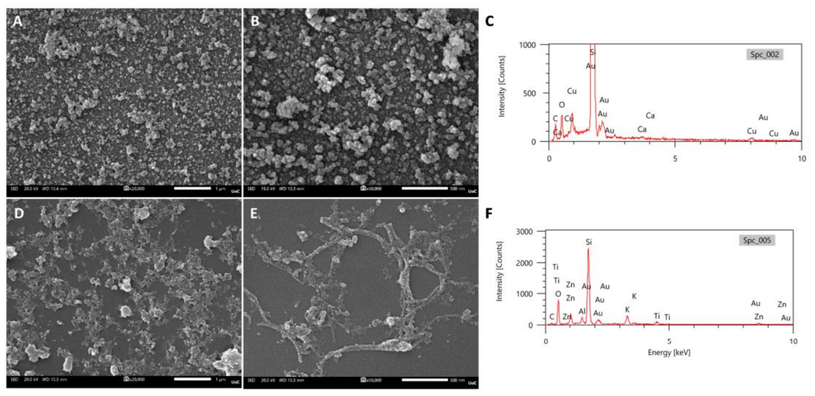
CHF ASSEMBLIES WITH COPPER and ZINC

Following **$NaBH_4$ reduction,** cHF in the presence of copper chloride forms flower-like spherical assemblies with diameters in the range of 10 μM (left), while in the presence of zinc chloride forms quasi-spherical assemblies at the nanoscale range (right).



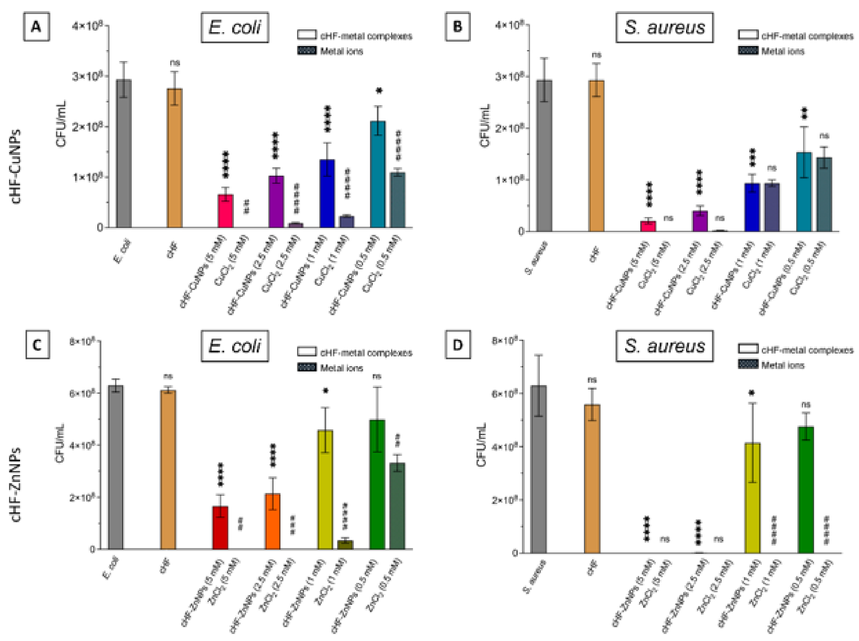
PH-RESPONSIVE STRUCTURAL CHANGE

At pH 6.4, the ordered peptide assemblies with Cu/Zn become smaller and more amorphous, with peptide fibrils reappearing—consistent with complex dissociation and metal ion release
A, B, C =copper, D, E,F =zinc.



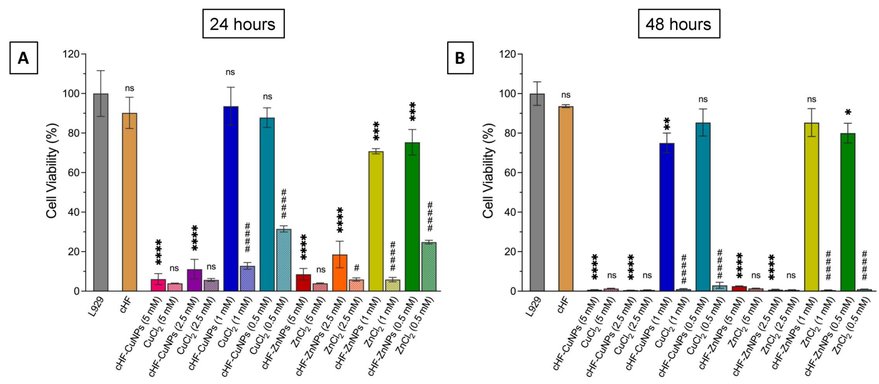
ANTIBACTERIAL ACTIVITY

- cHF alone (5 mM) showed no notable antimicrobial activity.
- Both complexes (cHF–CuNPs and cHF–ZnNPs) retained antimicrobial activity at 1 mM, with increasing effect at 2.5 and 5 mM, however, higher concentrations were more cytotoxic to mammalian cells (see “Fibroblast compatibility” graphs).



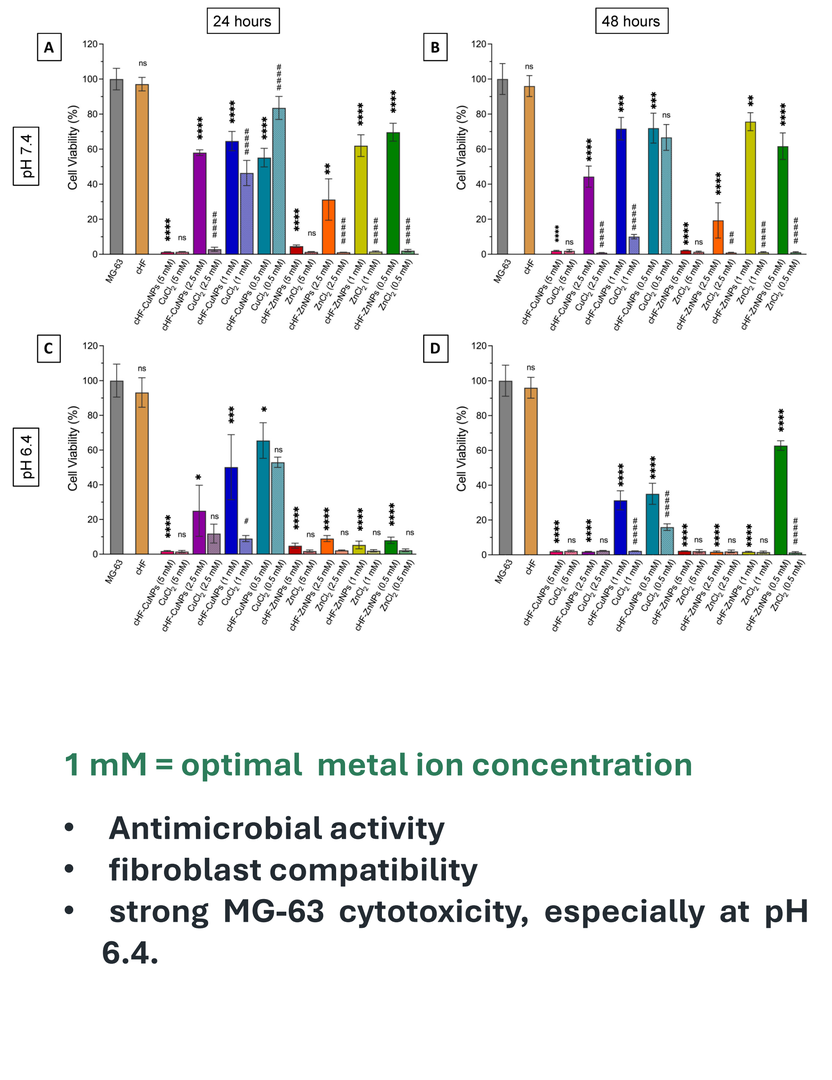
FIBROBLAST COMPATIBILITY

Peptide – metal ion complexes at metal concentrations 2.5–5 mM caused pronounced L929 fibroblast toxicity. Lower concentrations were substantially better tolerated.



ANTI-OSTEOSARCOMA ACTIVITY IS ENHANCED AT ACIDIC pH

- cHF alone (5 mM) remained essentially non-cytotoxic to osteosarcoma MG-63 cells.
- Both cHF–CuNPs and cHF–ZnNPs reduced MG-63 viability, with stronger effects at pH 6.4.
- At 1 mM, lowering pH from 7.4 to 6.4 produced an additional ~15% reduction in survival for cHF–CuNPs and ~50% for cHF–ZnNPs.



1 mM = optimal metal ion concentration

- Antimicrobial activity
- fibroblast compatibility
- strong MG-63 cytotoxicity, especially at pH 6.4.

CONCLUSIONS and OUTLOOK

- cHF fibrils efficiently chelates Cu^{2+} and Zn^{2+} and act as a structural/templating scaffold.
- Both complexes show concentration-dependent antibacterial activity against *E. coli* and *S. aureus*.
- Above 1 mM, mammalian-cell toxicity becomes a major limitation.
- At 1 mM, both complexes show the most attractive balance for further study, with stronger MG-63 effects under acidic pH.
- This work highlights the potential of cyclic peptides containing histidine as versatile carriers for the targeted delivery of metal ions against osteosarcoma treatment.
- Further optimization and combination with conventional anticancer drugs can be foreseen.

Reference

Apostolidou et al., Biomolecules 2026, 16, 284
doi:10.3390/biom16020284

Acknowledgements

This work was supported by the Hellenic Foundation for Research and Innovation (H.F.R.I.) under grant # 9578.

Target-Directed Stapled Peptides through Dynamic Combinatorial Chemistry

Ashmi Rodrigues, Jose Garcia Coll, Delphine Ravault, Benjamin Zagiel, Ludovic Carlier, Lou Rocard, and Roba Moumné*
Sorbonne Université, École Normale Supérieure, PSL University, CNRS, Chimie Physique et Chimie du Vivant (CPCV), 75005 Paris, France
https://doi.org/10.17952/38EPS.2026.P138
*roba.moumne@sorbonne-universite.fr

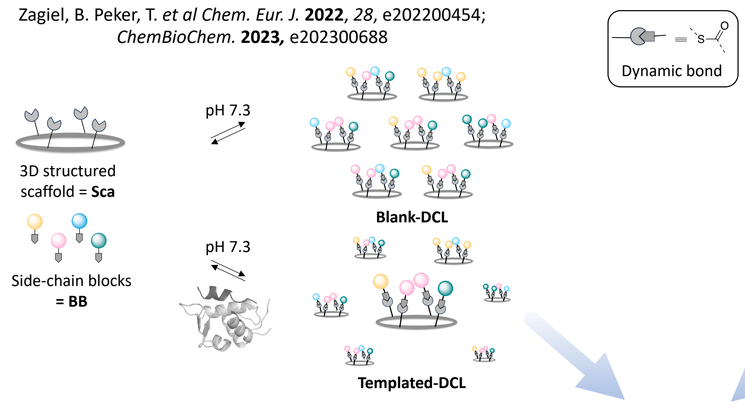
Introduction

Protein–protein interactions (PPIs) are challenging targets for conventional small-molecule drug discovery. Peptides offer a promising alternative, but short linear peptides are highly flexible and susceptible to proteolytic degradation, limiting their pharmacological potential. Conformational constraint can overcome these limitations by stabilizing the bioactive conformation. Two complementary strategies can be considered: (i) constraining the native peptide framework, or (ii) grafting key residues onto a rigid scaffold to reproduce their optimal spatial arrangement. Both aim to recapitulate protein interaction hotspots, but their optimization remains challenging.

Dynamic Combinatorial Chemistry (DCC) enables the rapid exploration of chemical space through reversible library formation and target-driven selection and amplification of high-affinity ligands.[1] DCC has recently been extended to peptide discovery.[2] Building on this concept, we developed target-directed DCC (tdDCC) for both strategies: (i) side-chain selection on defined peptidic scaffolds,[3,4] and (ii) selection of conformational constraints (“staples”) on flexible peptide sequences.[5] Thiol–thioester exchange enables reversible library formation under biologically compatible conditions. The p53–hDM2 interaction was used as a model PPI.[6] Here, we focused on the target-directed optimization of stapled peptides.

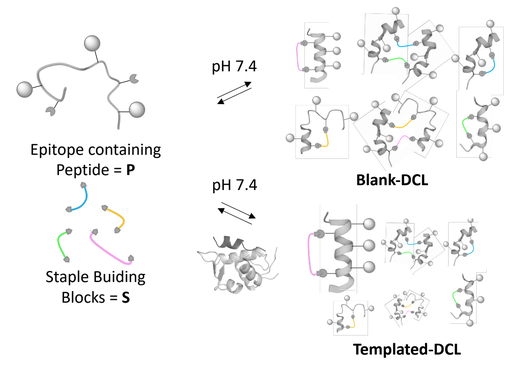
Target-Directed Side-Chain Grafting

Zagiel, B. Peker, T. *et al Chem. Eur. J.* **2022**, *28*, e202200454; *ChemBioChem.* **2023,** e202300688

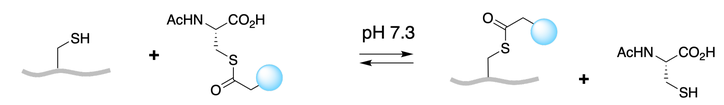


Target-Directed Peptide Stapling

Rodrigues *et al submitted* (Preprint on ChemRxiv)



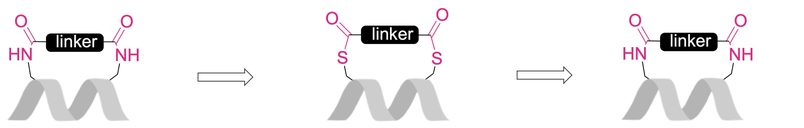
Reversible Chemistry: Thiol to thioester Exchange



- ✓ Reversible in physiological conditions
- ✓ Biocompatible
- ✓ Freezable at acidic pH

tdDCC for Peptide Stapling

Concept

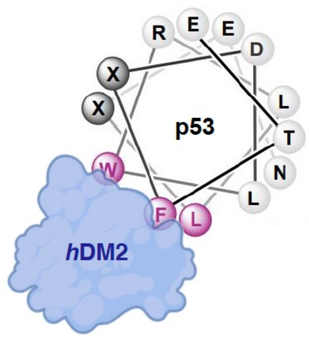


Bis-amide stapled peptides
Inouye and coworkers
Chem. Eur. J. **2008**, *14*, 857–863

Reversible bis-thioester stapled peptide
This work

Transposition into a stable bis-amide stapled peptide surrogate

Peptide Design

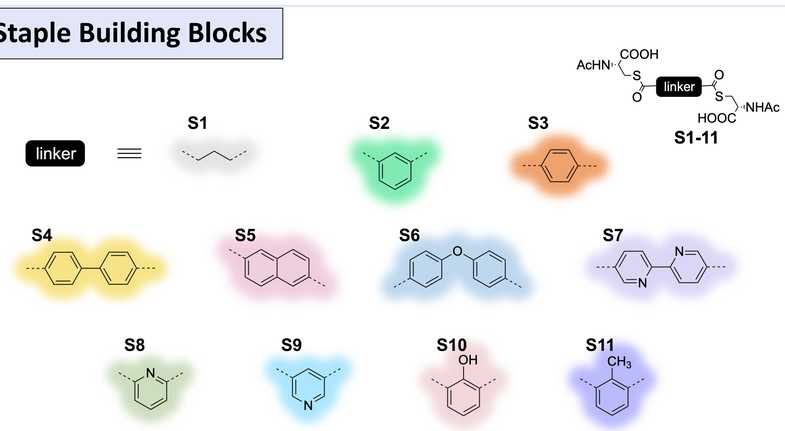


p53$^{17-29}$: ETFSDLWKLLPEN

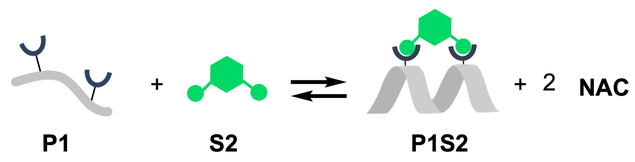
P1-2: Ac-ETF**X**DLWRLL**X**EN-NH_2

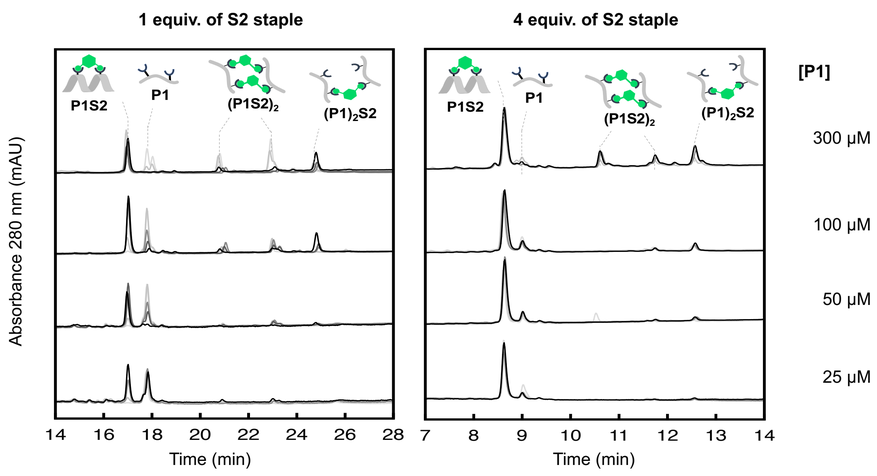
P1: X=Cys and **P2**: X=hCys

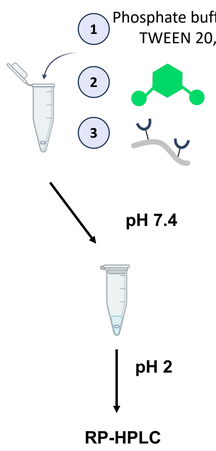
Staple Building Blocks



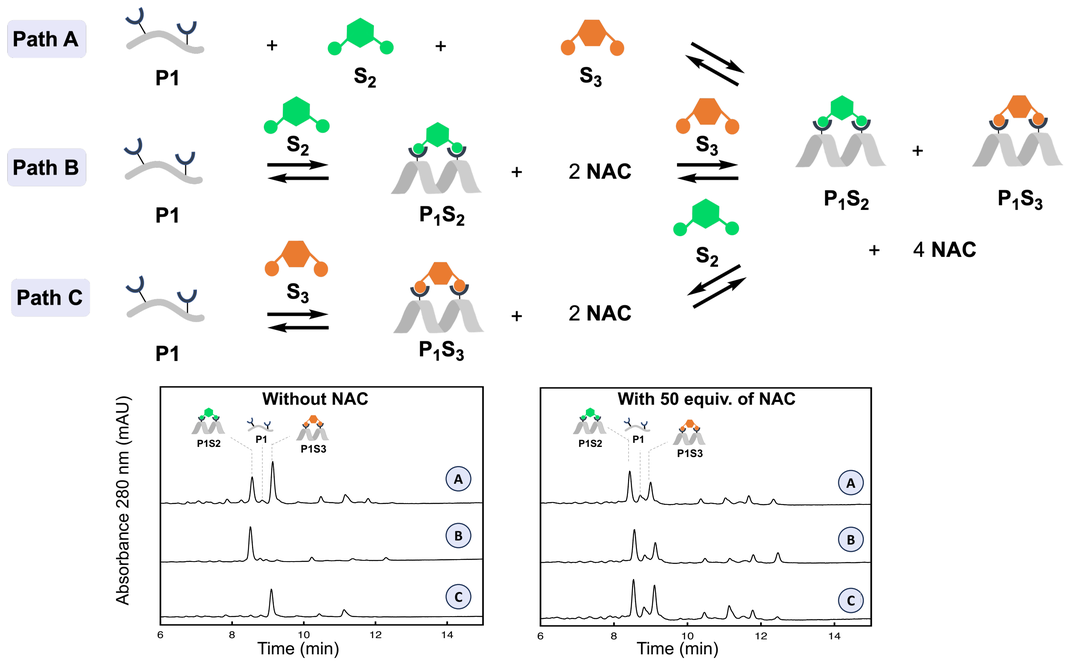
Reaction Optimization







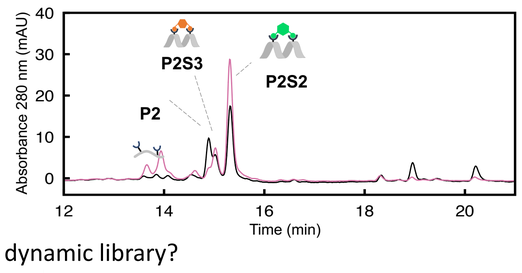
Reversibility



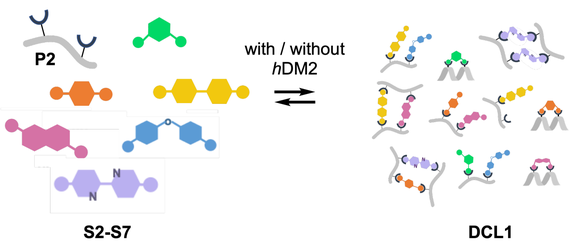
Target-Directed DCC Screening

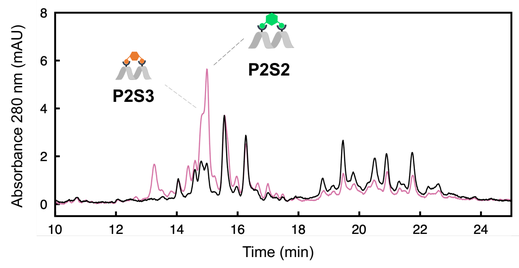
❖ Can tdDCC identify target-stabilized stapled peptides?



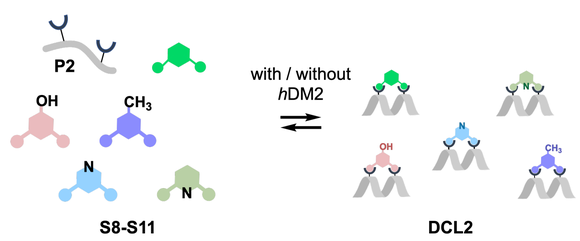


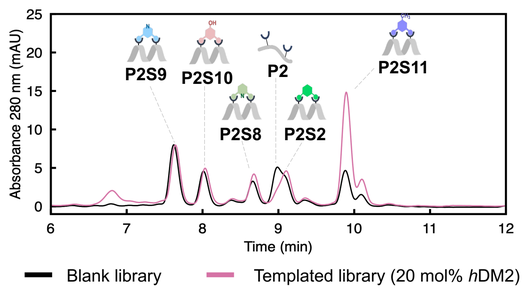
❖ Can tdDCC select the preferred stapling geometry from a larger dynamic library?





❖ Can tdDCC reveal target-dependent chemical preferences within the selected m-phenylene stapling scaffold?





DCC Hit Validation

Competition fluorescence polarization binding curves: tdDCC hit translate into tighter binder

Circular dichroism analysis

Hit Translation

P3: Ac-ETF**Dab**DLWRLL**Dab**EN-NH_2

Acknowledgements

We thank **Prof. Andrew Wilson** for providing the fluorescent probe and for helpful advice on the FP assay. We also thank the **MS^{3}U Platform, SPPS Platforms, and Fédération de Chimie Moléculaire de Paris Centre (FR2769, Sorbonne Université)** for technical support.

Funding: French Ministry of Higher Education and Research (PhD funding, AR and BZ); **ANR** (postdoctoral funding, JGC).

Key Takeaways

We demonstrate target-directed dynamic combinatorial chemistry (tdDCC) as an adaptive strategy for the discovery and optimization of stapled peptides with target-dependent recognition properties. By enabling peptides to dynamically sample multiple staple architectures, tdDCC first identifies the preferred stapling geometry and subsequently reveals target-dependent chemical preferences within the selected scaffold. This hierarchical selection provides a streamlined strategy for staple optimization from a single peptide sequence.

References:

[1] P. Frei, R. Hevey, B. Ernst, *Chem. Eur. J.* **2019**, *25*, 60–73; [2] A. Rodrigues, L. Rocard, R. Moumné, *ChemSystemsChem* **2023**, e202300011 [3] B. Zagiel, T. Peker, R. Marquant, G. Cazals, G. Webb, E. Miclet, C. Bich, E. Sachon, R. Moumné, *Chem. – Eur. J.* **2022**, *28*, e202200454, [4] T. Peker, B. Zagiel, L. Rocard, C. Bich, E. Sachon, R. Moumné, *ChemBioChem* **2023**, *24*, e202300688; [5] A. Rodrigues, J. G. Coll, D. Ravault, B. Zagiel, L. Carlier, L. Rocard, R. Moumné, **2026**, ChemRxiv; [6] L. Rocard, S. Mehdi, M. Dogrusoz, A. Rodrigues, R. Moumné, “Peptide Constraining and Scaffold Grafting for Protein Mimetics Design: Lessons from the p53–hDM2 Interaction.” *RSC Medicinal Chemistry* **2026**, *accepted*.

Structure-Guided Synthesis of Triazole-Stabilized Peptidomimetics as Inhibitors of New Delhi Metallo-β-Lactamase-1

[1,2]Msanif Msanif*, [1]M. Jewgiński, [2]F. Nuti, [3]P. Rovero, [2]A. M. Papini, [1]R. Latajka

[1]Department of Bioorganic Chemistry, Wrocław University of Science and Technology, 50-370 Wrocław, Poland
[2]Interdepartmental Laboratory of Peptide and Protein Chemistry and Biology, Department of Chemistry "Ugo Schiff", University of Florence, 50019 Sesto Fiorentino (FI), Italy
[3]Interdepartmental Laboratory of Peptide and Protein Chemistry and Biology, Department of Neurosciences, Psychology, Drug Research and Child Health, University of Florence, 50019 Sesto Fiorentino (FI), Italy
msanif.msanif@pwr.edu.pl
https://doi.org/10.17952/38EPS.2026.P154

1. Introduction

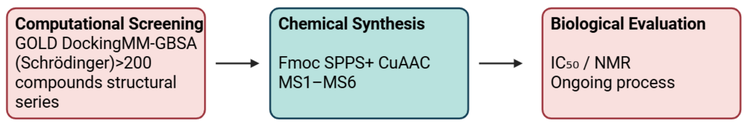
The global emergence of New Delhi metallo-β-lactamase-1 (NDM-1) has critically undermined the efficacy of β-lactam antibiotics, including last-resort carbapenems. As a zinc-dependent enzyme operating via a bimetallic Zn(II) center, NDM-1 hydrolyzes the β-lactam ring through a mechanism that renders all currently approved β-lactamase inhibitors ineffective [1,2]. Its flexible L3 loop and broad substrate-binding groove present a compelling multi-contact surface for peptidomimetic inhibitor design [3]. Triazole-constrained cyclic peptides formed via intramolecular CuAAC offer conformational rigidity, proteolytic stability, and direct zinc coordination as a structurally innovative inhibitor strategy [4,5]. No clinically approved NDM-1 inhibitor exists, making it one of the most urgent unmet targets in antimicrobial therapy and lead the urgency of structurally innovative inhibition strategies.

2. Aim of study

To design, synthesize, and biochemically evaluate triazole-constrained peptidomimetics as structurally innovative inhibitors of NDM-1 metallo-β-lactamase, guided by computational modeling and targeting the bimetallic Zn(II) active site.

3. Methods

Rational Design Strategy



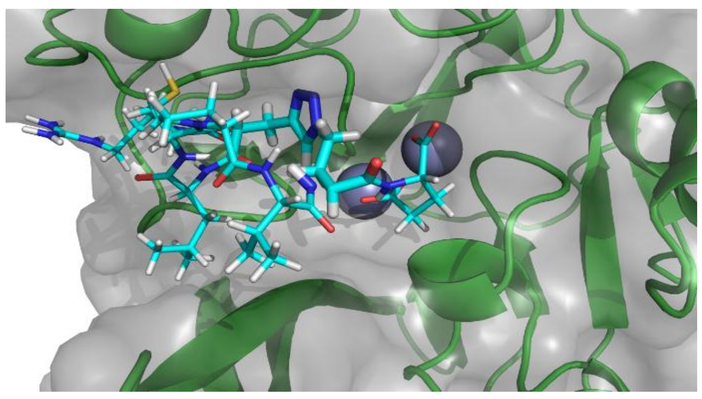


***Figure 1**. Molecular docking pose of lead compound 6xbe-pept1 within NDM-1 active site (PDB: 6XBE). The compound is accommodated in the groove formed by L1, L2, and L3 loops with docking score −9.185 and MM-GBSA ΔGbind(NS) = −116.94 kcal/mol.]*

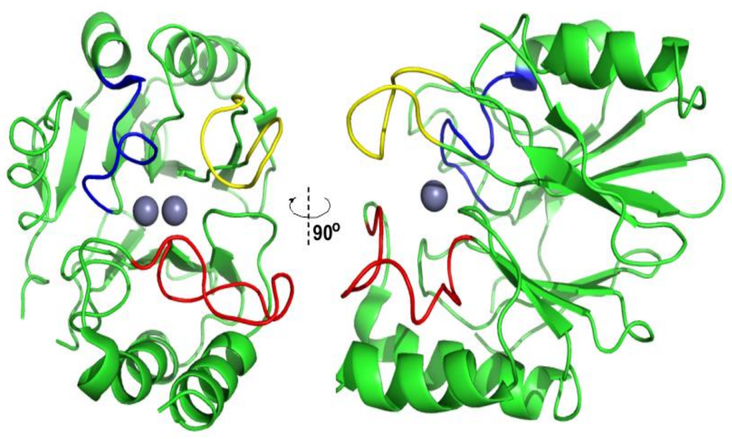


Figure 2: *Overall structure of NDM-1 (PDB: 5ZGE) shown in cartoon representation with active site loops highlighted: loop L3 (red), loop L10 (blue), and loop L7 (yellow). Zinc ions at the catalytic center are shown as grey spheres. Right panel shows a 90° rotated view.*

Table 1. **Summary of Best-Performing Compounds Across Stapled Peptidomimetic Series I–VIII**

Series	Best Compound	Staple/Linker	Docking Score	MM-GBSA ΔGbind (kcal/mol)	MM-GBSA ΔGbind(NS) (kcal/mol)
I	6xbe-peptyd_1	Direct triazole (i→i+3, C→N)	−9.932	−81.75	−102.69
II	6xbe-peptyd_2	Alkyl -$(CH_2)_5$-	−8.419	−87.46	−118.52
III	**6xbe-peptyd_3**	**Pra/Lys(N_3) direct triazole**	**−9.185**	**−76.16**	**−116.94**
IV	6xbe-peptyd_4	PEG-like -$(CH_2)_2$-O-$(CH_2)_2$-	−10.403	−67.58	−107.43
V	6xbe-2-5	Direct triazole (shortened chain)	−7.680	−53.39	−67.29
VI	6xbe-2-6	1,3-Phenyl linker	−7.310	−63.16	−75.65
VII	6xbe-peptide_2_7	N-N allyl staple	−11.104	−61.81	−86.68
VIII	6xbe-peptide_2_8	S-Ph-S thioether-phenyl	−13.78	−73.99	−114.05

ΔGbind = MM-GBSA binding free energy

4. Result

Docking, Chemical Synthesis and characterization - Compounds MS1- MS6

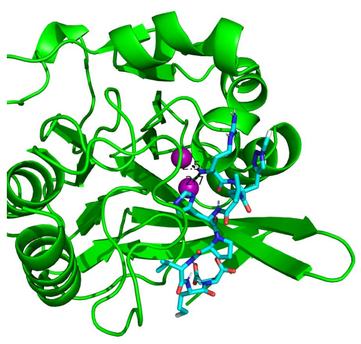


***Figure 3.** Best-scoring AutoDock Vina pose of MS5 docked into the NDM-1 active site (PDB 6XBE). The ligand (cyan sticks) engages both catalytic Zn^{2+} ions (magenta spheres) directly, with contact distances of 2.5 Å and 2.7 Å. Rendered in PyMOL.*

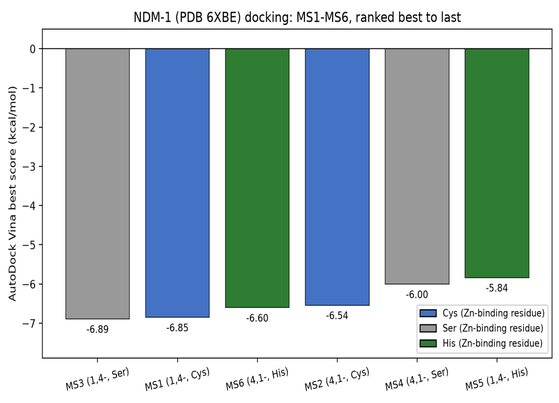


***Figure 4.** Vina predicted binding affinity by compound, grouped by position-4 zinc-binding residue (blue = Cys, grey = Ser, green = His).*

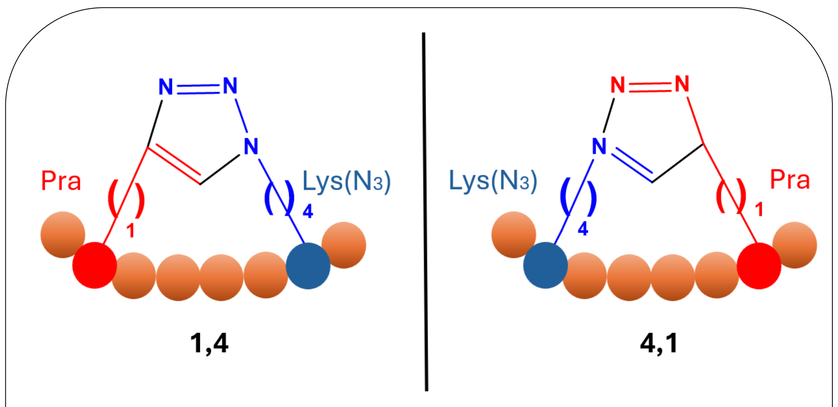


Figure 5. The triazole staple - 1,4- and 4,1- regiochemistry. Intramolecular CuAAC joins the propargylglycine (Pra) alkyne and the Nε-azido-lysine [Lys(N_3)] side chain: Pra → triazole C4 (–CH_2–, red), Lys(N_3) → triazole N1 (–$(CH_2)_4$–, blue). Both series carry the same 1,4-disubstituted 1,2,3-triazole; "1,4-" (MS1/MS3/MS5) and "4,1-" (MS2/MS4/MS6) denote the N→C order of the two handles along the backbone, set by residue placement.

Table 2 **Summary of characterized and synthesized Compounds MS1–MS6**

Compound	Triazole	Zn-Binding Residue	Purity	Yield
MS1	1,4-	Cys (-SH)	90%	8 mg
MS2	4,1-	Cys (-SH)	90%	34 mg
MS3	1,4-	Ser (-OH)	95%	35 mg
MS4	4,1-	Ser (-OH)	95%	45.8 mg
MS5	1,4-	His	95%	42 mg
MS6	4,1-	His	95%	34.9 mg

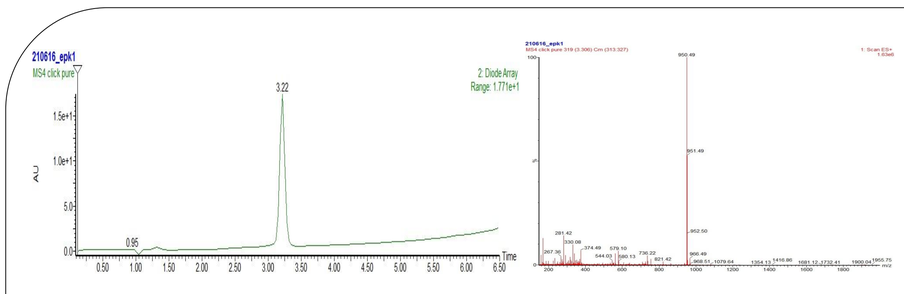


***Figure 6**. HPLC chromatogram (left) and ESI-MS (right) of peptide MS4*

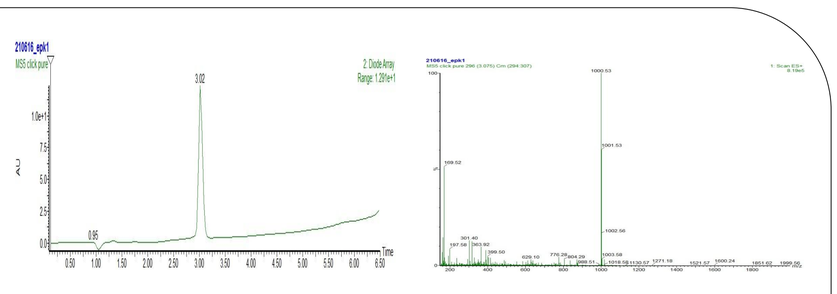


***Figure 7.** HPLC chromatogram (Left) and ESI-MS (right) of peptide MS5*

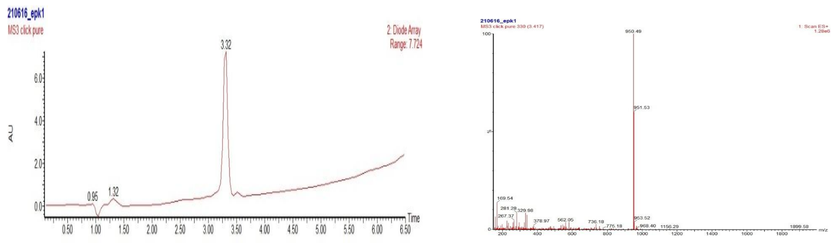


***Figure 8**. HPLC chromatogram (left) and ESI-MS (right) of peptide MS3*

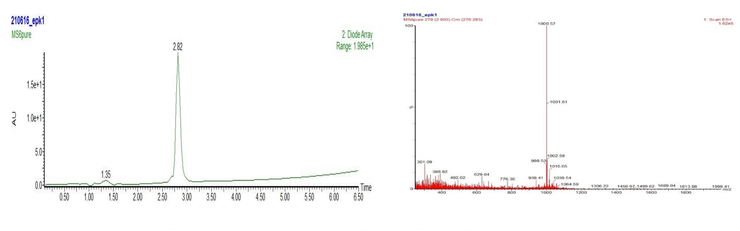


***Figure 9.** HPLC chromatogram (Left) and ESI-MS (right) of peptide MS6*

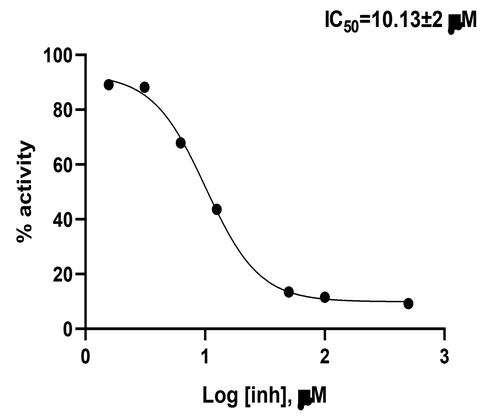


***Figure 10.** Preliminary results showing of Dose-response inhibition curve against NDM-1*

5. Conclusion

▶ A library of >200 stapled peptidomimetics across 8 structural series was computationally evaluated by GOLD docking and MM-GBSA against NDM-1 (PDB: 6XBE)
▶ Six triazole-constrained cyclic peptidomimetics (MS1-MS6) were successfully designed, synthesized, and characterized via Fmoc SPPS and on-resin CuAAC click chemistry
▶ Systematic variation of zinc-binding residue (Cys, Ser, His) and triazole orientation (1,4- vs. 4,1-) provides a structured SAR framework for NDM-1 inhibitor optimization
▶ Preliminary resazurin screening of Minimum inhibitory concentration and Inhibitory concentration of 50% identified as there are promising candidate for potentiating meropenem activity against NDM-1-producing bacteria. Further optimization and biological replicates of experiments are ongoing

6. Future direction

▶ Full IC_{50}/MIC profiling against VIM-2 and IMP-1, and replicate NDM-1 assays
▶ NMR analysis
▶ Second-generation synthesis - MM-GBSA-guided design and synthesis of optimized analogs at PeptLab, University of Florence

References

[1] Yong, D. et al. *Antimicrob. Agents Chemother.* **2009**, *53*, 5046–5054.
[2] Bush, K.; Bradford, P.A. *Clin. Microbiol. Rev.* **2020**, *33*, e00047-19.
[3] King, D.T. et al. *J. Am. Chem. Soc.* **2012**, *134*, 11362–11365.
[4] Meldal, M.; Tornøe, C.W. *Chem. Rev.* **2008**, *108*, 2952–3015.
[5] Moses, J.E.; Moorhouse, A.D. *Chem. Soc. Rev.* **2007**, *36*, 1249–126

Acknowledgements
The work was supported by the project Minigrants for doctoral students of the Wroclaw University of Science and Peptide infrastructure of the University of Florence (PeptLab) for synthetic work under the Erasmus programme

A MULTIMODAL MOLECULAR TOOLBOX FOR IN VITRO AND IN VIVO STUDIES OF THE OXYTOCIN RECEPTOR



monika.perisic.boehm@univie.ac.at
PhD candidate
Neuropeptide Research Lab

Monika Perisic Böhm[1,2], Predrag Kalaba[2], Erik Keimpema[3], Rachel S. Gormal[4], Frédéric A. Meunier[4,5], Thierry Langer[6], Karine Mardon[7], Christian W. Gruber[8], Markus Muttenthaler[2,9]

[1]University of Vienna, Vienna Doctoral School in Chemistry (DoSChem), 1090 Vienna, Austria
[2]University of Vienna, Institute of Biological Chemistry, 1090 Vienna, Austria
[3]Medical University of Vienna, Center for Brain Research, 1090 Vienna, Austria
[4]The University of Queensland, Queensland Brain Institute, 4072 Brisbane, Australia
[5]The University of Queensland, School of Biomedical Sciences, 4072 Brisbane, Australia
[6]University of Vienna, Department of Pharmaceutical Sciences, 1090 Vienna, Austria
[7]The University of Queensland, ARC Training Centre for Innovation in Biomedical Imaging Technology, 4072 Brisbane, Australia
[8]Medical University of Vienna, Center for Physiology and Pharmacology, 1090 Vienna, Austria
[9]The University of Queensland, Institute for Molecular Bioscience, 4072 Brisbane, Australia

https://doi.org/10.17952/38EPS.2026.P522

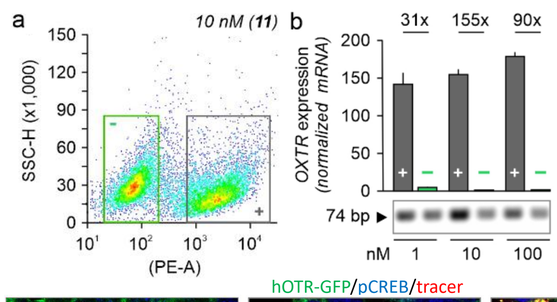
Significance & Aims

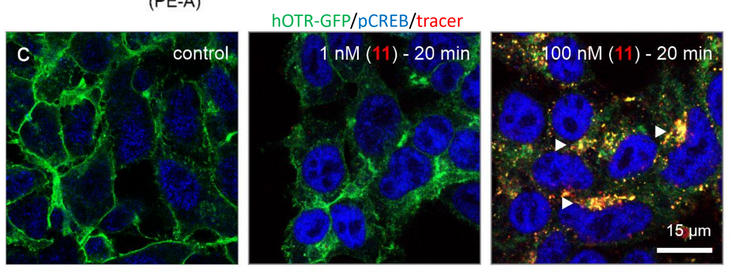
The oxytocin receptor (OTR) is a G protein-coupled receptor (GPCR) central to reproduction and social behavior and a promising target for studying neuropsychiatric disorders and cancer.[1] However, progress has been limited by an incomplete understanding of OTR expression and function across tissues, creating a need for tools that can probe the receptor at multiple biological scales.[2,3] To address this gap, we are developing a **multimodal molecular imaging platform** based on peptide-derived tracers for both fluorescence and positron emission tomography (PET) applications. Together, **these tools aim to provide a comprehensive framework for characterizing OTR biology and accelerating the development of next-generation OTR-targeted theranostics**.

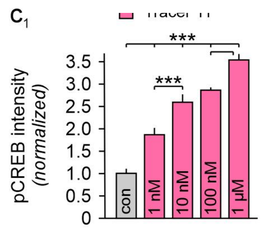
Fluorescent Tracers

Fluorescent agonist tracers were tested in various experimental set-ups,[4] such as **fluorescence-activated cell sorting (FACS) and *in vitro* OTR detection and activation**.

Tracer application to a mix of hOTR- and $hV_{1a}R$-expressing HEK293 cells resulted in successful sorting as confirmed by RT-qPCR (***a,b***). Incubation of HEK293 cells expressing hOTR-GFP with tracer resulted in receptor internalization (*arrowheads*) and dose-dependent phosphorylation of cAMP-responsive element binding protein (pCREB) (***c-c₁***).

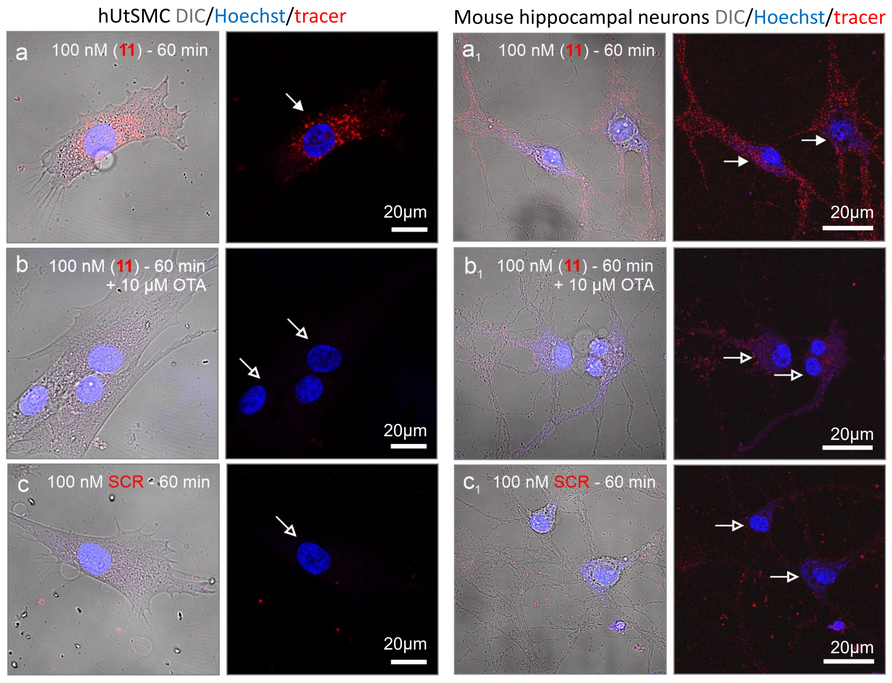






hUtSMC DIC/Hoechst/tracer

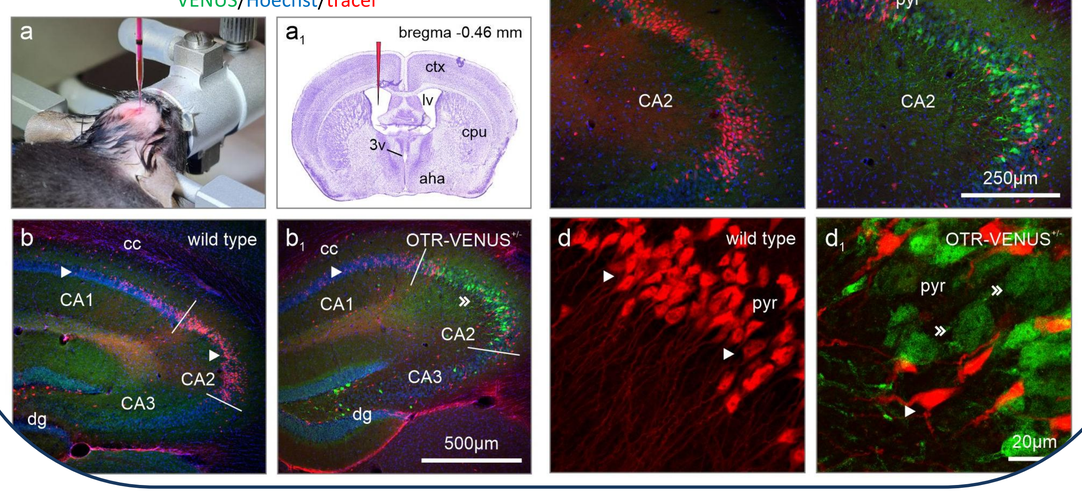
Mouse hippocampal neurons DIC/Hoechst/tracer



In human uterine smooth muscle cells (hUtSMC) and mouse neurons, the tracer **labeled endogenous OTR expression sites** (*arrows* in ***a, a₁***). Labeling was blocked by peptide antagonist OTA, and a tracer with **scrambled amino acid sequence SCR** did not label OTR (*empty arrows* in ***b-c₁***).

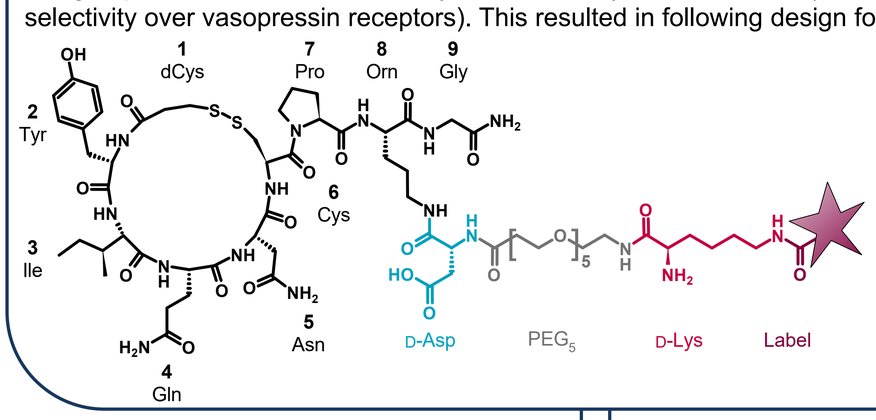
Intracerebroventricular injection of tracer into the mouse brain resulted in labeling of OTR-expressing neurons (***a,a₁***). After 2 hours, tracer was detectable in the CA1, CA2, and dg of the hippocampus (*arrowheads*, ***b,c,d***). In the OTR hypomutant, tracer signal was reduced significantly, indicating OTR specificity (*double arrows*, ***b₁,c₁,d₁***).

VENUS/Hoechst/tracer



Approach

Tracers consisting of **peptide backbone, functional linker, and labeling group** were prepared *via* manual Fmoc-solid phase peptide synthesis (Fmoc-SPPS) and solution phase labeling group attachment. Compound pharmacology was determined in radioligand binding assays and the design optimized until desired affinity and selectivity were achieved (~1 nM OTR affinity, >100-fold selectivity over vasopressin receptors). This resulted in following design for fluorescent tracers:



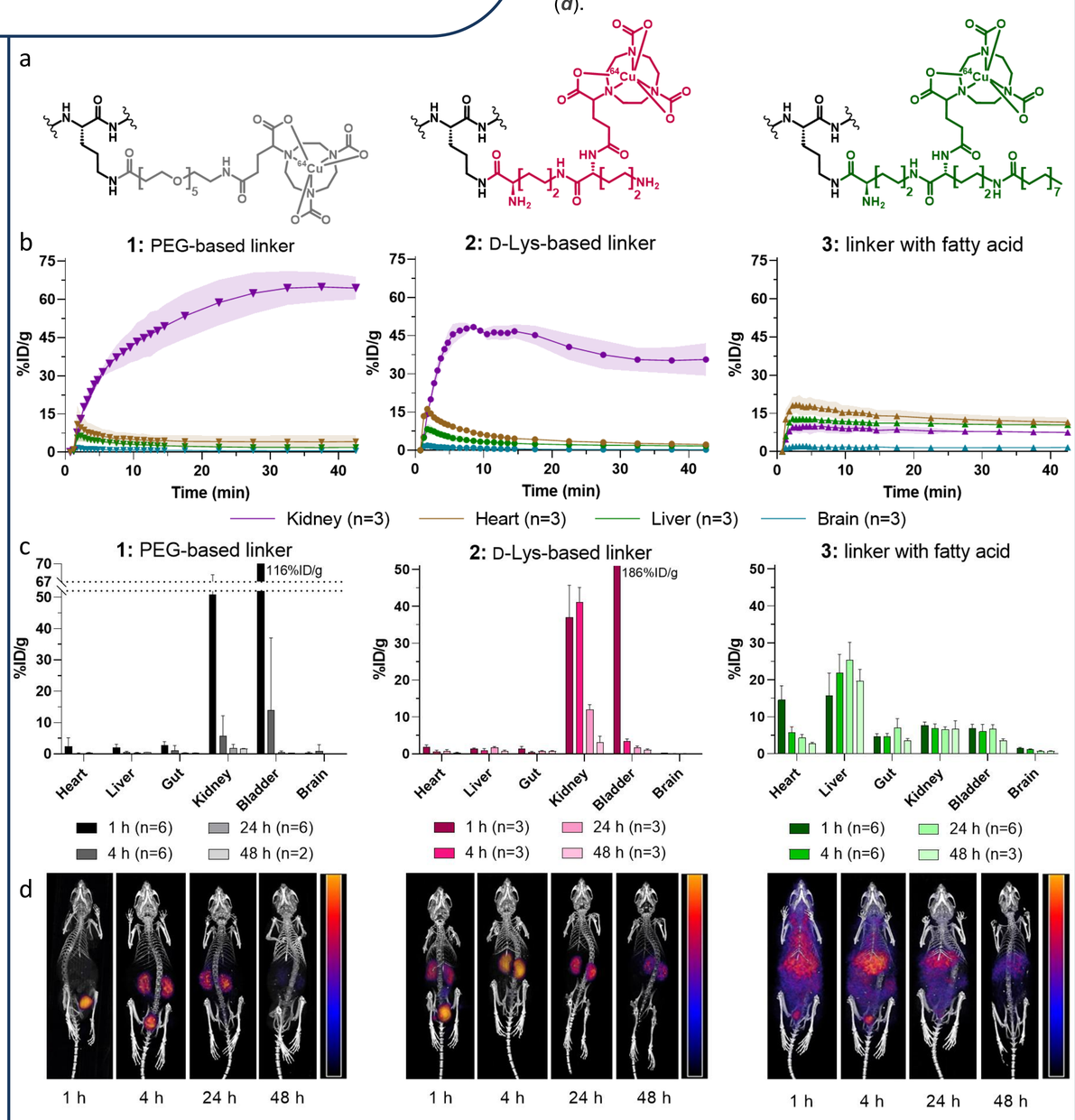
Patented functional linker fulfils multiple tasks *via* modular design:

i) 100-fold selectivity
ii) Distance from binding pocket
iii) Tracer fixability
iv) Handle for labeling group attachment

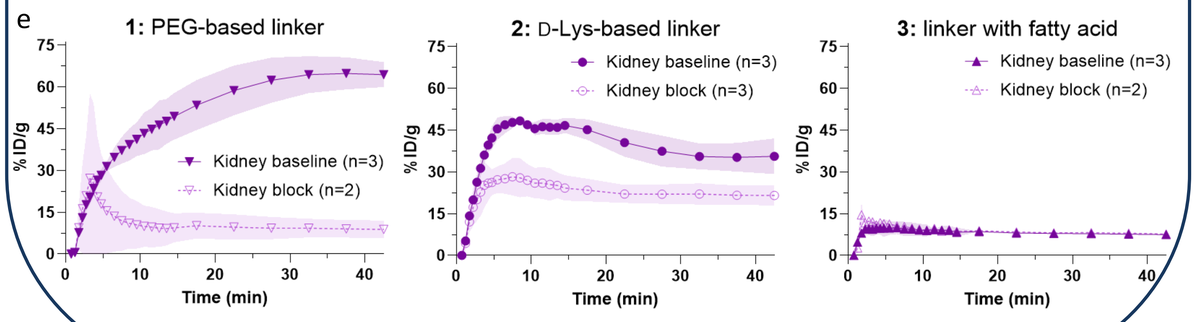
PET Tracers

Compared to fluorescent tracers, PET tracers additionally require the optimization of **pharmacokinetic properties** (proteolytic stability, clearance rates, tissue distribution and retention, etc). We are currently in the process of optimizing PET tracer design by testing the impact of different linker components on tracer performance in healthy mice *in vivo*.

Three PET tracers with different linkers (***a***) were labeled with copper-64, injected into the tail vein of healthy mice, and their distribution followed on a PET/CT scanner (***b-d***). **Clear differences in biodistribution are observable depending on the type of linker** both within the first hour of injection (***b***) as well as after up to 48 h (***c***), with lipidated tracers having prolonged circulation half-lives. Representative PET/CT images of mice for are depicted in (***d***).



Additionally, the impact of **receptor blocking** by preinjection of cold OT (2 mg/kg) 30 min prior tracer injection was tested with signal reduction across all observed tissues. Most significant differences were obtained for the kidneys (***e***), likely due to saturation of kidney-expressed transporters.



Conclusions & Outlook

Our selective fluorescent tracers enable high-resolution OTR detection through confocal microscopy and flow cytometry and support real-time visualization of receptor dynamics using live-cell single-molecule imaging. They are highly useful for **receptor localization, activation, and trafficking** studies as well as **FACS**.[4] Future experiments encompass mapping of OTR at high resolution in different tissues as well as the design of antagonistic and hyperfluorescent tracers. For non-invasive imaging, PET tracers are being developed to **study OTR expression *in vivo*.** Initial biodistribution studies were performed in healthy mice, and ongoing efforts focus on optimizing linker design to enhance pharmacokinetics, target tissue uptake, and specificity. PET tracers will also be applied in cancer models. Overall, our multidisciplinary approach holds promise of shedding light on the intricate role of OTR in various diseases, potentially paving the way for new therapies.

1 C.S. Carter et al. Pharmacol Rev, 2020, 72, 829-861.
2 M. Perisic et al. Trends Biochem Sci, 2024, 49, 361-377.
3 P. Kalaba et al. J Med Chem, 2024, 67 (3), 1625-1640.
4 M. Perisic Böhm et al. Angew Chem Int Ed Engl, 2025, e202515180.

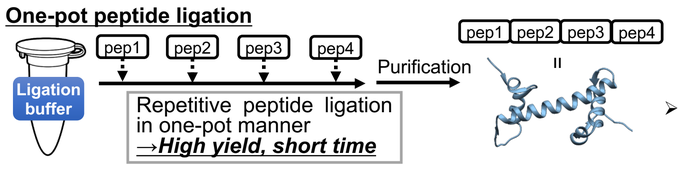
ÖAW Österreichische Akademie der Wissenschaften
Institut für Biologische Chemie
universität wien
The University Of Queensland Australia CREATE CHANGE
Center for Physiology and Pharmacology Medical University of Vienna Institute of Pharmacology

Direction-Switching One-Pot Peptide Ligation with Orthogonal Cysteinyl Protection

Koki Nakatsu[1]; Fumika Yoshitomi[2]; Hiroki Onoda[3]; Reia Shikimachi[3]; Kyohei Arita[3]; Akimitsu Okamoto[4]; Hiroshi Murakami[2]; Gosuke Hayashi[2]
([1]*University of Cambridge,* [2]*Nagoya University,* [3]*Yokohama City University,* [4]*The University of Tokyo*)
https://doi.org/10.17952/38EPS.2026.P042

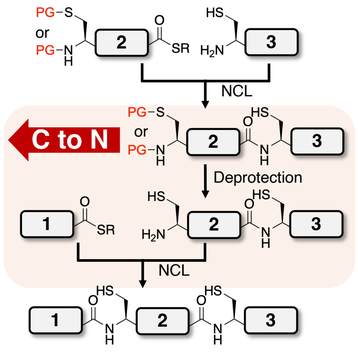
Introduction / Background

One-pot peptide ligation



C-to-N peptide ligation

➢ **N-terminal cysteine** is protected by a protecting group

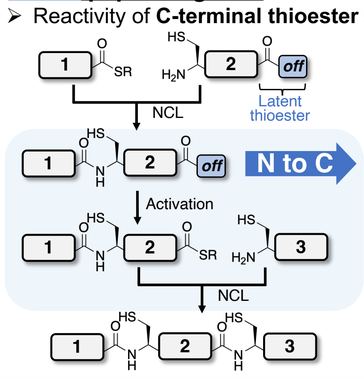


N-terminal cysteinyl protecting groups used in one-pot peptide ligation.

Thz … D. Bang, et al. *Angew. Chem. Int. Ed.* **2004**
Acm … S. K. Maity, et al. *Angew. Chem. Int. Ed.* 2016.
Tfacm … S. Tang, et al. *Angew. Chem. Int. Ed.* 2015.
PPQZ … S. Wang, et al. *J. Am. Chem. Soc.* 2022.
Dobz … J. Li, et al. *Org. Biomol. Chem.* 2014.
Fmoc … A. Kar, et al. *Angew. Chem. Int. Ed.* 2020.

N-to-C peptide ligation

➢ Reactivity of **C-terminal thioester surrogate** is controlled.

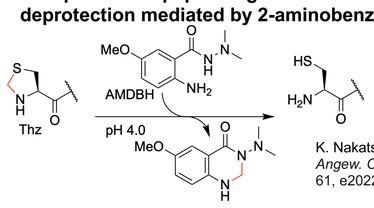


1. Kinetically Controlled Ligation
e.g.) Alkyl & Phenyl Thioester
D. Bang et al. *Angew. Chem. Int. Ed.* **2006**.

2. Activatable Thioester
e.g.) hydrazide → pyrazole
Flood, D. T et al. *Angew. Chem. Int. Ed.* **2018**.

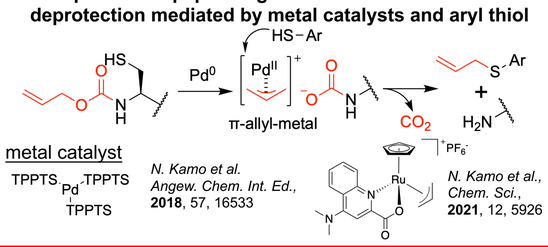
3. Caged Thioester
eg) SEAlide+NV
Aihara, K. et al. *Org. Lett.* **2016**.

➢ **One-pot C-to-N peptide ligation with thiazolidine (Thz) deprotection mediated by 2-aminobenzamide derivative**



K. Nakatsu et al. *Angew. Chem. Int. Ed.* **2022**, 61, e202206240

➢ **One-pot C-to-N peptide ligation with N-terminal Alloc deprotection mediated by metal catalysts and aryl thiol**

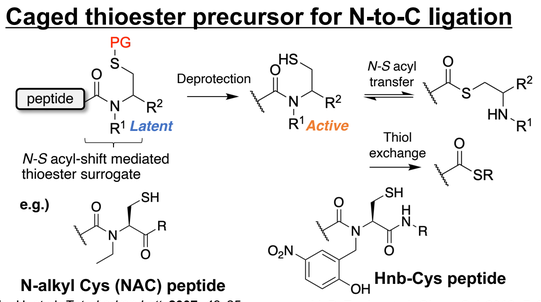


N. Kamo et al. Angew. Chem. Int. Ed., **2018**, 57, 16533

N. Kamo et al., Chem. Sci., **2021**, 12, 5926

These orthogonal methods enable only C-to-N ligation, not N-to-C ligation.

Caged thioester precursor for N-to-C ligation



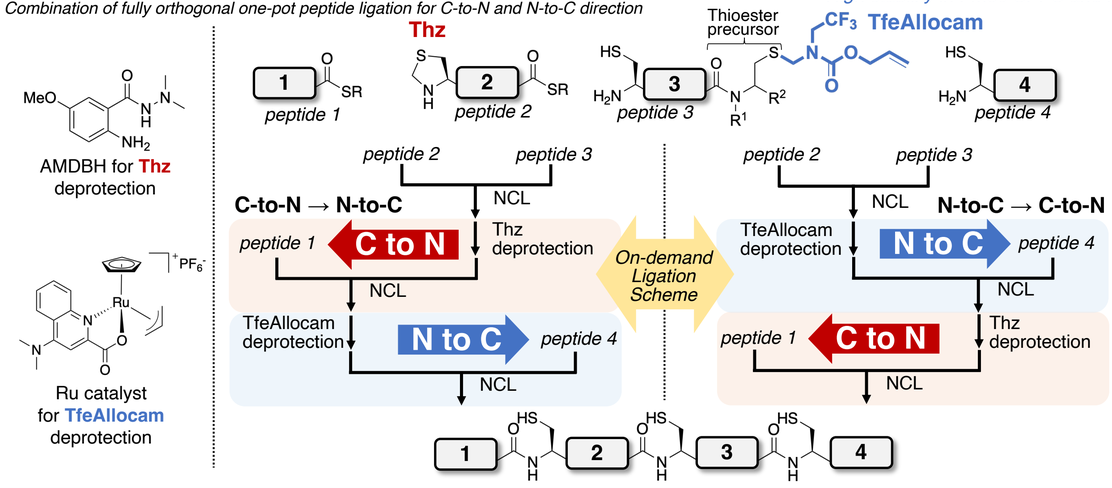
Hojo, H. et al. *Tetrahedron Lett.* **2007**, *48*, 25.

V. P. Terrier et al. *Chem. Sci.* **2016**, *7*, 339.

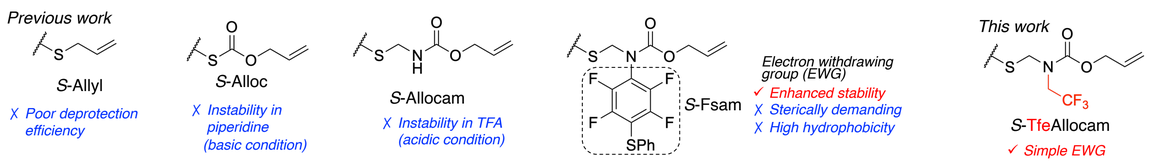
Concept

This work … Direction-Switching One-pot Peptide Ligation

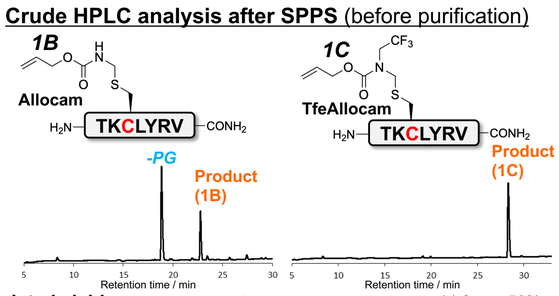
- ✓ *A new S-allylic protecting group compatible with chemical protein synthesis*
- ✓ *Combination of fully orthogonal one-pot peptide ligation for C-to-N and N-to-C direction*



Results: Design of A New Allylic Thiol Protecting Group



Crude HPLC analysis after SPPS (before purification)



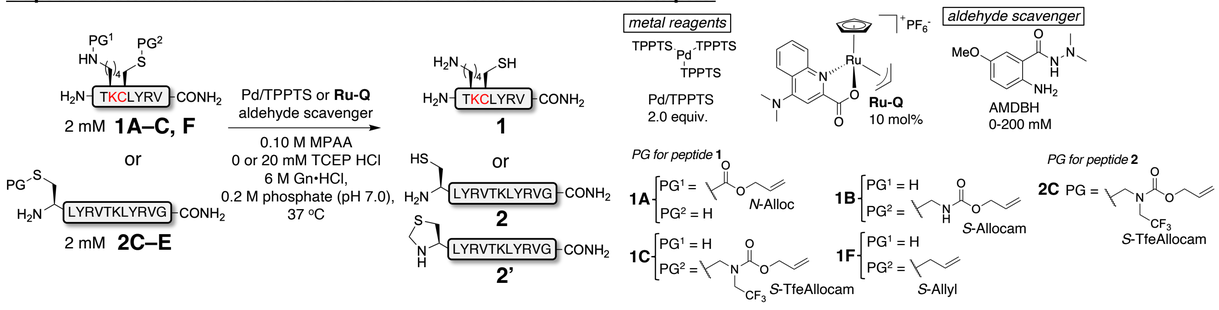
Isolated yields 4.7 mg, 18% 14.6 mg, 52%

Stability of S-Allylic Cysteinyl Protecting Groups of Peptides

	remaining yield/%		
peptide	**TFA cocktail[a] (4 h)**	**20% piperidine[b] (24 h)**	**NCL buffer (24 h)[c]**
1B (*S*-Allocam)	15%	<2%	46%
1C (*S*-TfeAllocam)	>98%	83%	>98%

[a] TFA cocktail: TFA/TIPS/H_2O = 95/2.5/2.5 at r.t.
[b] 20% piperidine: piperidine/DMF = 20/80 (v/v) at r.t.
[c] NCL buffer: 6 M Gn·HCl, 0.2 M phosphate (pH 7.0), 100 mM MPAA, 20 mM TCEP·HCl at 37 ° C.

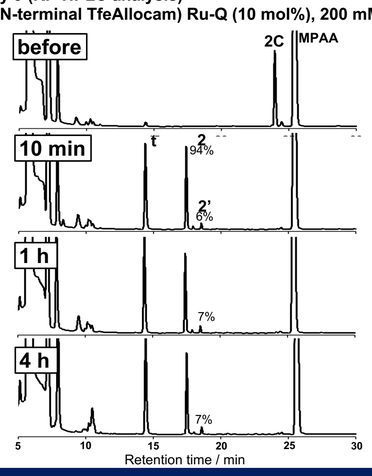
Deprotection Studies of Allocam Derivatives with a Pd or Ru Complex



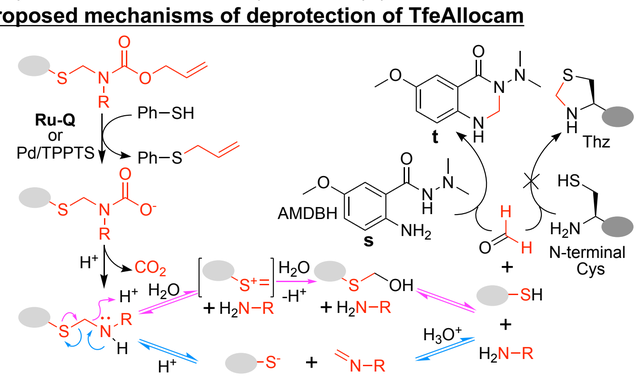
			conversion yields/% (Thz 2' formation yield/%)[a]		
entry	**peptide**	**additional deprotection conditions[a]**	**10 min**	**1 h**	**4 h**
1	**1A** (*N*-Alloc)	2.0 equiv. Pd/TPPTS, 20 mM TCEP·HCl	>98%		
2	**1B** (*S*-Allocam)	2.0 equiv. Pd/TPPTS, 20 mM TCEP·HCl	>98%		
3	**1C** (*S*-TfeAllocam)	2.0 equiv. Pd/TPPTS, 20 mM TCEP·HCl	>98%		
4	**1F** (*S*-Allyl)	2.0 equiv. Pd/TPPTS, 20 mM TCEP·HCl	N/D	N/D	
5	**1C** (*S*-TfeAllocam)	10 mol % **Ru-Q** b	96% (4%d)		
6	**2C** (*S*-TfeAllocam)	2.0 equiv. Pd/TPPTS, 20 mM TCEP·HCl	97% (3%)	84% (16%)	27% (73%)
7	**2C** (*S*-TfeAllocam)	10 mol % **Ru-Q** b	61% (39%)	9% (91%)	2% (98%)
8	**2C** (*S*-TfeAllocam)	2.0 equiv. Pd/TPPTS, 20 mM TCEP·HCl, AMDBH 200 mM	>98%	96% (4%)	95% (5%)
9	**2C** (*S*-TfeAllocam)	10 mol % **Ru-Q** b, AMDBH 200 mM	94% (6%)	93% (7%)	93% (7%)

[a] A standard deprotection condition is an aqueous buffer containing 0.10 M MPAA, 6 M Gn·HCl, and 0.2 M phosphate (pH 7.0) at 37 ° C.
[b] **Ru-Q** is [CpRu(QANMe$_2$)allyl]PF_6.
[c] Conversion yields calculated from the ratio of peak area of RP-HPLC analysis (220 nm).
[d] The yield is derived from a formaldehyde adduct of peptide **1**.

entry 9 (RP-HPLC analysis)
2C (N-terminal TfeAllocam) Ru-Q (10 mol%), 200 mM AMDBH

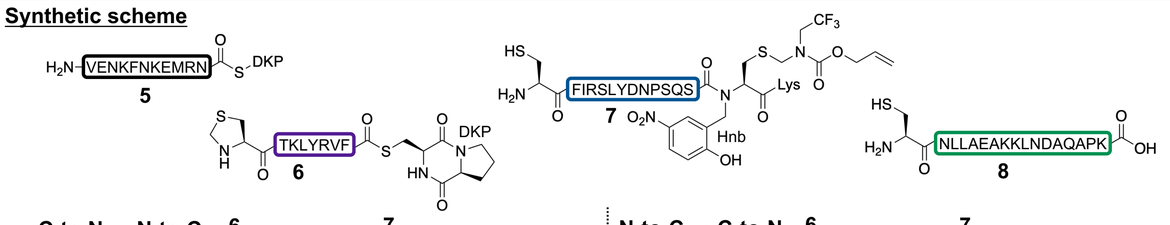


Proposed mechanisms of deprotection of TfeAllocam

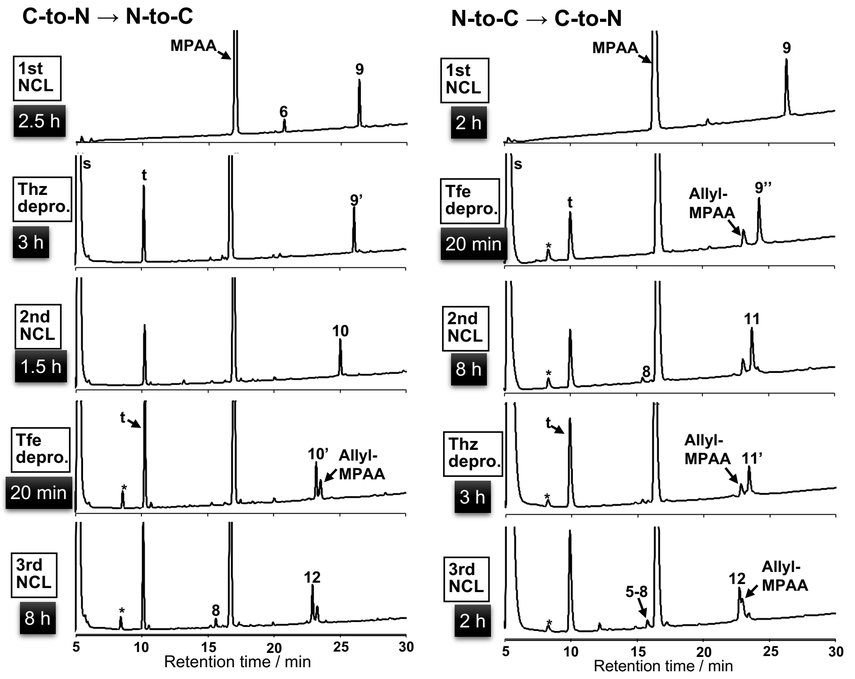


Results: Direction-Switching One-Pot Peptide Ligation

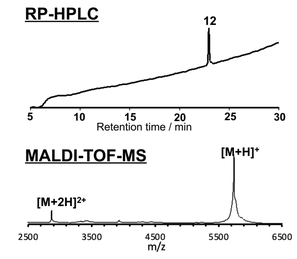
Synthetic scheme



RP-HPLC analysis of ligation reactions

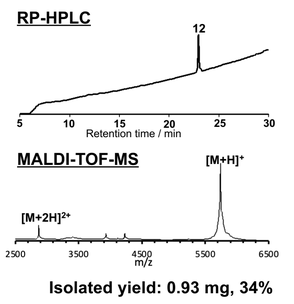


Ligation product 12 (C-to-N → N-to-C)



Isolated yield: 1.16 mg, 41%

Ligation product 12 (N-to-C → C-to-N)



Isolated yield: 0.93 mg, 34%

Both C-to-N → N-to-C and N-to-C → C-to-N assembly routes are possible using the same peptide segments, expanding flexibility in ligation-route design.

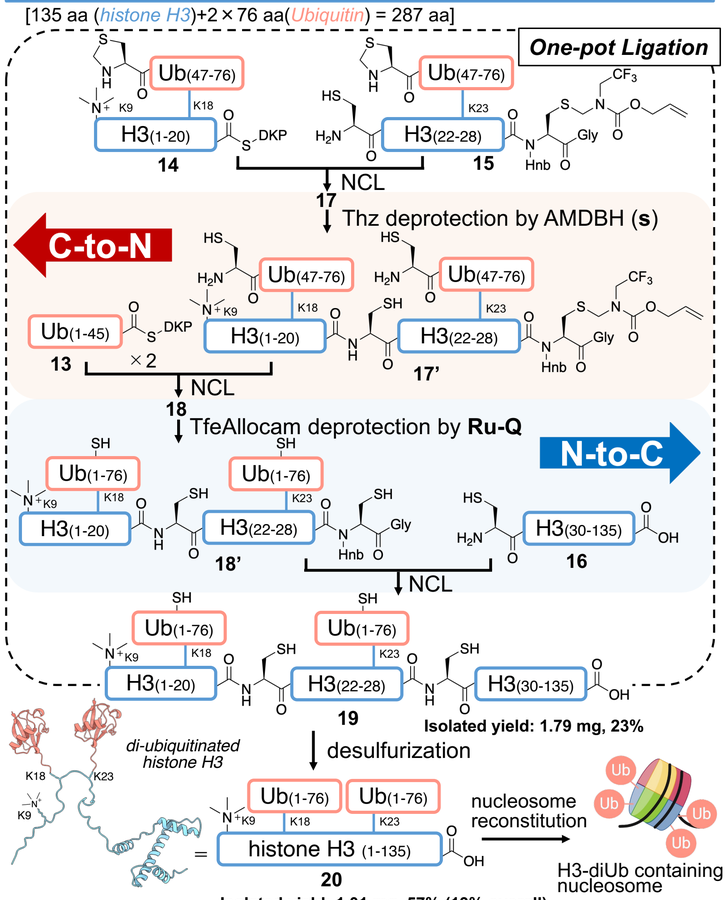
Results: Chemical Synthesis of Diubiquitinated Histone H3

Synthetic scheme

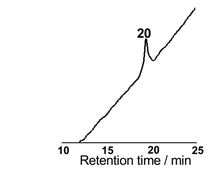
Ubiquitin: H-MQIFVKTLTGKTITLEVEPSDTIENVKAKIQDKEGIPPDQQRLIF$_{45}$ / AGKQLEDGRTLSDYNIQKESTLHLVLRLRGG$_{76}$-*(linked to histone H3)*

histone H3: H-ARTKQTARK(Me$_3$)STGGKAPRK*(Ubiquitin)*QL$_{20}$ / ATK*(Ubiquitin)*AARKS$_{28}$ / APATGGVKKPHRYRPGTVALREIRRYQKSTELLIRKLPFQRLVREIAQDFKTDLRF QSSAVMALQEASEAYLVGLFEDTNLAAIHAKRVTIMPKDIQLARRIRGERA$_{135}$-OH

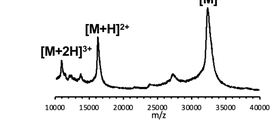
[135 aa (*histone H3*)+2 × 76 aa(*Ubiquitin*) = 287 aa]



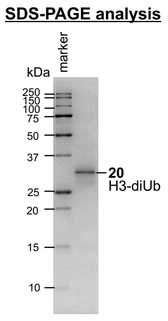
RP-HPLC profile after purification



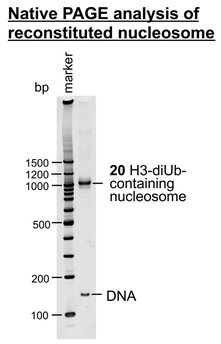
MALDI-TOF-MS spectrum



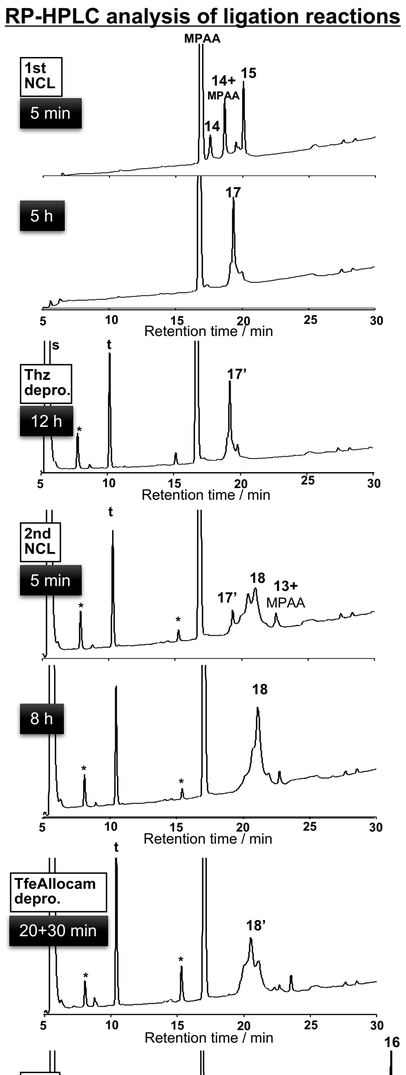
SDS-PAGE analysis



Native PAGE analysis of reconstituted nucleosome



RP-HPLC analysis of ligation reactions



Conclusions / Perspectives

- TfeAllocam provides robust cysteine protection and can be selectively removed under NCL-compatible conditions.
- Orthogonal Thz and TfeAllocam protection enables programmable direction-switching one-pot NCL.
- Alternative orthogonal systems may enable more efficient and versatile direction-switching ligation strategies.
- Final-product HPLC purification and byproduct accumulation remain challenges for further iterative ligation.

View the paper

Publication: Koki Nakatsu et al. Chemical Protein Synthesis via Direction-Switching One-Pot Peptide Ligation Enabled by Orthogonal Cysteinyl Protection. *J. Am. Chem. Soc.* 2026; 148 (4): 4622–4634. DOI: 10.1021/jacs.5c20510

FUNCTIONAL AND BIOINFORMATIC ANALYSIS OF ANTIMICROBIAL PEPTIDE DERIVED FROM LACTIC ACID BACTERIA

Sylwia Nawrot (**1**), N. Czarnecka (**1,2**), M. Jankowska (**2**), A. Jabłońska-Wawrzycka (**3**), P. Rogala (**3**), G. Czerwonka (**1**)
(**1**) Institute of Biology, Jan Kochanowski University, 7 Uniwersytecka Str., 25-406 Kielce, Poland,
(**2**) Regeneris Sp. z o.o., Podzamcze 45, Poland,
(**3**) Institute of Chemistry, Jan Kochanowski University, 7 Uniwersytecka Str., 25-406 Kielce, Poland
contact email: sylwianawrot18@gmail.com

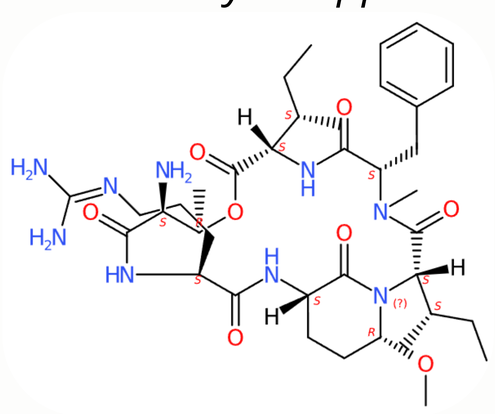
https://doi.org/10.17952/38EPS.2026.P207

Introduction

Lactic acid bacteria (LAB), such as ***Lacticaseibacillus rhamnosus***, are producers of various bioactive compounds. Among them are **antimicrobial peptides (AMPs)**. These natural bioactive molecules play a crucial role in microbial competition and have been widely applied in the food industry as natural preservatives. Due to their broad-spectrum antimicrobial activity, they represent promising tools in the fight against pathogenic microorganisms.

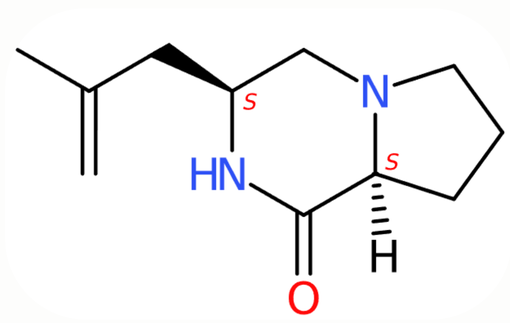
Preliminary analyses of the newly identified *L. rhamnosus* 72 strain (POIR.01.01.01-00-0632/19) demonstrated its antibacterial properties, and cyclic dipeptides were identified within its excretome, suggesting potential application against pathogens.

Microcystis spp.



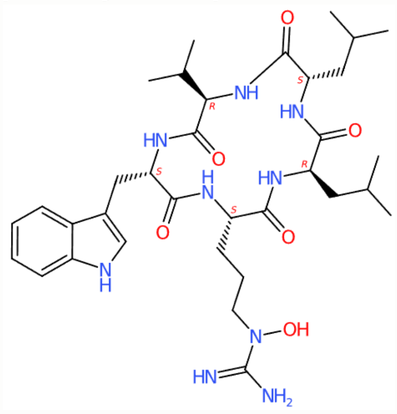
Micropeptin MZ771 ($C_{38}H_{61}N_9O_8$)

Penicillium purpurogenum G59



Penicimutide ($C_{11}H_{18}N_2O$)

Streptomyces sp. RK88-1441



Pentaminomycin B ($C_{34}H_{53}N_9O_6$)

Lacticaseibacillus rhamnosus 72

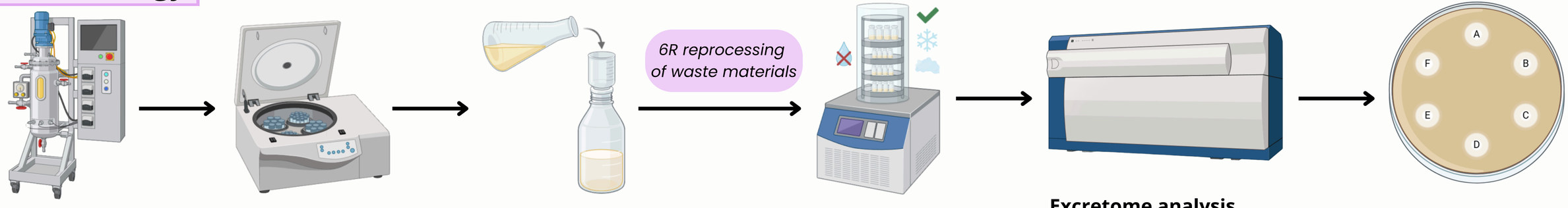
Aim

This study aimed to evaluate the antibacterial activity of the cell-free culture supernatant using culture-based methods and to assess the therapeutic potential of the main peptide using bioinformatic tools.

Convergence

the process by which unrelated organisms living in similar environments develop similar morphological and functional characteristics.

Methodology



Bacterial culture → **Centrifugation** → **Filtration** → **Freeze-drying** → **Excretome analysis at IBB in Warsaw** → **Disk-diffusion testing**

Results

PATHOGEN	A postbiotic obtained from the result of culturing probiotic bacteria carried out by: 24 h	48 h	72 h	7 days
	A	**B**	**C**	**D**
Candida albicans (Robin) Berkhout ATCC 10231			L P	G
Streptococcus agalactiae PCM2683		L P	L P	G
Proteus mirabilis ATCC 29906		P	G P	
Staphylococcus epidermidis			G P	
Streptococcus pyogenes		L	G P	
Staphylococcus aureus 6538P			G	G
Escherichia coli ATCC 8739		G L P	G L P	
Pseudomonas aeruginosa PAO1		L	L G	G

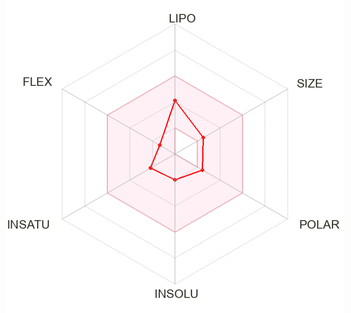
Legend: ***L -*** *laboratory medium MRS* ***P*** *- production medium (5% whey + 2% yeast)*
G *- production medium supplemented with 2% glucose*

MIC
7.82 mg/mL

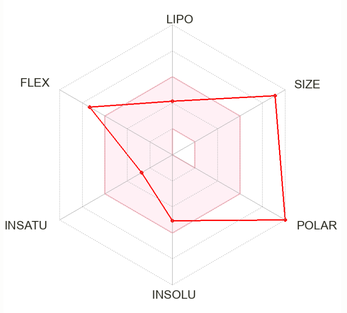
MBC
15.63 mg/mL

MBC
15.63 mg/mL

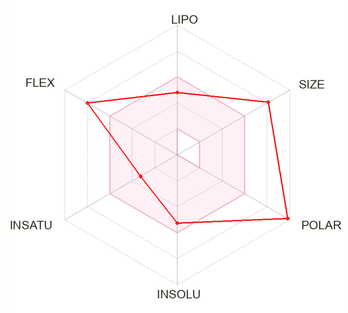
Penicimutide



Micropeptin MZ771



Pentaminomycin B



Legend:
LIPO (LIPOPHILITY): *-0.7 < XLOGP3 < +5.0*
SIZE: *150G/MOL < MW < 500G/MOL*
POLAR (POLARITY): *20Å² < TPSA < 130Å²*
INSOLU (INSOLUBILITY): *-6 < LOG S (ESOL) < 0*
INSATU (INSATURATION): *0.25 < FRACTION CSP3 < 1*
FLEX (Flexibility): *0 < Num. rotatable bonds < 9*

Data derived from:

SwissDrugDesign

Feature	Micropeptin MZ771	Penicimutide	Pentaminomycin B
Water Solubility Class	*Moderately soluble*	*Very soluble*	*Moderately soluble*
GI absorption	*Low*	*High*	*Low*
BBB permeant	*No*	*No*	*No*
Log Kp (skin permeation)	*-9.79 cm/s*	*-6.28 cm/s*	*-8.39 cm/s*
Druglikeness (Lipinski)	*No; 3 violations*	*Yes; 0 violation*	*No; 3 violations*
Bioavailability Score	*0.17*	*0.55*	*0.17*

Legend: ***GI*** *- gastrointestinal absorption,* ***BBB*** *- Blood-brain barrier permeant*

Conclusions

- Biofilm inhibition was additionally confirmed by a reduction in pyoverdine production by *Pseudomonas aeruginosa* PAO1 , which is regulated by the quorum-sensing system. This observation suggests that the mechanism of action of the investigated AMPs may involve membrane interaction or inhibition of pyoverdine recycling.
- The predicted profiles of the AMPs indicated high water solubility, high absorption, good membrane permeability, and gastrointestinal uptake, without the ability to cross the blood–brain barrier.
- The results indicate the investigated peptide's potential therapeutic application.

This work was supported by Medical Research Agency under grant 2024/ABM/03/KPO/KPOD.07.07-IW.07-0227/24-00

Schemes created in BioRender.com

Accelerating peptide discovery via high throughput plate-based synthesis

An Nguyen[1], Siddique Amin[1], Caroline Morris[1], Christina Dumitriu Jackson[1], Hannah Bolt[1], Jefferson Revell[1]

[1] Hit Discovery, Discovery Sciences, BioPharmaceuticals R&D, AstraZeneca, Cambridge, UK.

https://doi.org/10.17952/38EPS.2026.P027

Introduction

In early peptide discovery, peptides are often synthesised, purified and characterised one at a time, creating a bottleneck that limits throughput and slows hit validation. To address this, we established a high-throughput, plate-based synthesis workflow that enables parallel production of diverse linear and cyclic peptides in a 96-well format. The workflow is fully optimised for the synthesis of both linear and disulfide-containing peptides. This miniaturised approach increases throughput, reduces solvent and reagent consumption, and supports broader sequence exploration. Plate-based peptide samples can be tested directly in multiple assay formats, accelerating progression through the hit-to-lead stage. Benchmarking against individually purified peptides showed strong concordance in activity, supporting the suitability of this workflow for direct-to-biology evaluation.

Methods

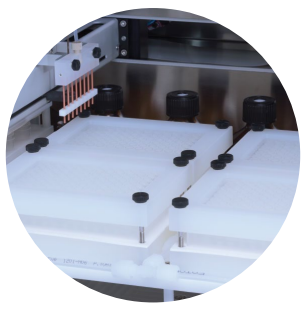
Synthesis → **Analysis** → **Purification** → **Concentration determination** → **Direct to Biology assays**



Results

Capacity

Parallel synthesis capacity increased by **16 times** from **6** to **96-384 compounds** per run

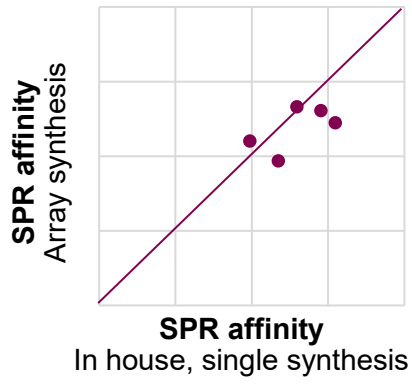


Workflow validation

Productivity

Validating and optimising hits faster to accelerate targeting projects

Figure 2. SPR affinity trends were concordant between array-derived and individually synthesised reference compounds



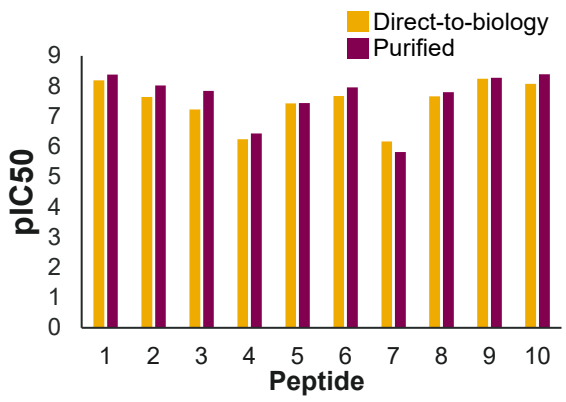




Sustainability

Reaction scale decreased from **10-100 mg** to **1-10 mg**, reducing reagent consumption and solvent use by approximately **10 L per plate**.

Figure 1. 96 disulfide-cyclised peptides were tested by HTRF, showing nanomolar binding for project A. Strong data correlation shown for HT workflow and direct-to-biology profiling of the same peptide sequences individually synthesised & purified to >95% purity.



Project impact

Hit Validation Stage

Typical Workflow — 6 months

Project B — 6 weeks → Progressed to patent filing

In project B, hit-validation timeline was reduced from a typical 6 months to 6 weeks, supporting rapid project progression.

Conclusions

- In-house array synthesis increased hit-validation capacity, expanding parallel synthesis from 6 to 96-384 compounds per run.
- The workflow improved project productivity and sustainability, reducing one hit-validation timeline from 6 months to 6 weeks and decreasing reaction scale from 10-100 mg to 1-10 mg, with approximately 10 L less solvent used per plate.
- Workflow validity was supported by concordant SPR and HTRF affinity trends versus reference compounds, indicating that higher-throughput, lower-scale synthesis was suitable for hit validation.
- This platform is now routinely applied to all AZ peptide projects.

Future work

- Expand throughput to 384-peptide parallel synthesis, targeting a 64-fold increase in capacity.
- Broaden chemistry scope by exploring cyclisation chemistries and conjugation to oligonucleotides and radioligands.
- Develop an AI/ML workflow to enable concentration measurement of peptides containing non-natural amino acids.
- Implement the HT workflow routinely across all peptide projects.
- Evaluate alternative green solvents systematically within the HT workflow to improve sustainability and enable process optimisation.

References

1. Wang et al., Sig. Transduct. Target Ther., **2022**, 7, 48.

Supported by AstraZeneca

Presented at the 38th European Peptide Symposium, Vienna, Austria,6-11th September 2026

THE DEVELOPMENT OF TOPICAL FORMULATIONS OF LIPOSOMAL MICROCOCCIN P1 FOR WOUND INFECTIONS

OSLO METROPOLITAN UNIVERSITY
STORBYUNIVERSITETET

B. F. Gurmessa[1], C. Charnock[1], K.V. Ovchinnikov[2], T. Thorstensen[2] & S. Nguyen[1]

[1] Department of Pharmacy, Faculty of Health Sciences, Oslo Metropolitan University, Oslo, Norway

https://doi.org/10.17952/38EPS.2026.P412

[2] Agribiotix AS, Ås, Norway

Contact information: sankon@oslomet.no

BACKGROUND

The antimicrobial peptide micrococcin P1 (MP1, fig. 1) has previously demonstrated antimicrobial activity against several clinically important gram-positive bacteria, such as methicillin-resistant *Staphylococcus aureus* (MRSA), even on *S. aureus* biofilm, and showed no toxic effects against several human cell lines including skin keratinocytes[1-3]. As such, MP1 is a highly promising candidate for drug development, particularly targeting wound infections. However, MP1 is challenging to formulate due to its hydrophobic structure (fig.1) and poor water solubility. In this study, we develop topical formulations of MP1 entrapped in liposomes (fig. 2) and evaluated the antimicrobial effect of the formulations *in vitro*.

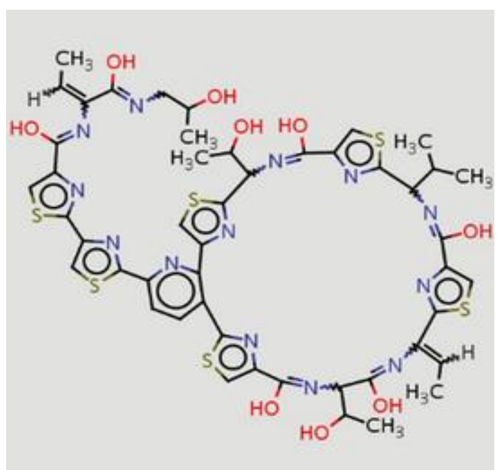


Fig. 1: The chemical structure of MP1.

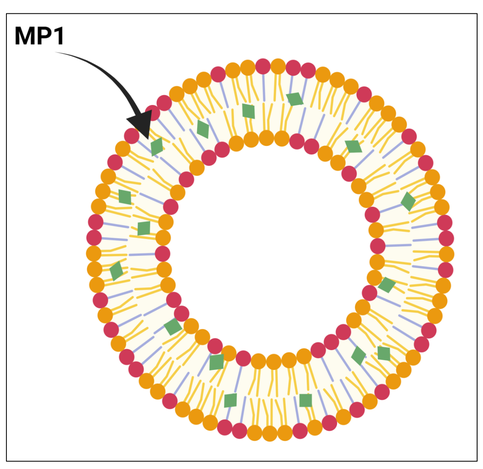


Fig. 2: MP1 (green squares) entrapped in the liposomal bilayer.

MATERIALS AND METHODS

MP1 (isolated from *S. equorum*, Agribiotix AS, Norway) was entrapped in conventional and fusogenic liposomes (phospholipids from Avanti Polar Lipids, AL, USA) by thin film-extrusion method and characterized by particle size, size distribution (polydispersity index, PDI), and zetapotential by dynamic light scattering (DLS), and MP1 entrapment efficiency (%EE) by high-performance liquid chromatography (HPLC). Unentrapped MP1 was separated by gel filtration (Sephadex G-25) before quantification and before incorporation into three semi-solid formulations; ointment, gel and cream, respectively. The ointment contained 60% vaseline, 20% liquid paraffin, 15% wool fat, and 5% cetyl alcohol (w/w, Apotekproduksjonen AS, Norway) and prepared by melting the solid/semi-solid components before adding liquid paraffin. The mixture was cooled down to room temperature under continuous stirring. The gel was prepared by gradually suspending 5% (w/w) hydroxypropylmethylcellulose (HPMC, Apotekproduksjonen AS, Norway) in water at room temperature under magnetic stirring (1000 rpm). The gel was left overnight to ensure complete swelling before use. Commercially available cream base was used (Apobase®, Karo Pharma, Sweden) for mixing with liposomes. The final topical formulations were prepared by adding 100 µl liposomal suspension to a gram semi-solid base and carefully mixed with an inoculating needle. The antimicrobial activity of the topical formulations was evaluated by disc diffusion method using *S. aureus* Xen29 (ATCC 112600, Revvity, MA, USA) as test organism. A commercially available antibiotic product containing fucidic acid (Fucidin® 2% ointment) was used as the positive control.

CONCLUSIONS

This study shows that liposomal entrapment and incorporation into semisolid systems did not impair MP1's antibacterial activity. However, the degree of activity is affected by the type of liposomes and semisolid base selected. For further pharmaceutical development of MP1, the most optimal formulation combination for the delivery to wound infections seems to be MP1 in fusogenic liposomes incorporated in gels.

RESULTS

Physicochemical characterization

Table 1 shows that both types of liposomes were positively charged and very similar in size and size distribution (both monodisperse), however, fusogenic liposomes could entrap more MP1 (35% corresponding to 0.175 mg/ml). Minimum inhibition concentration (MIC) of MP1 for *S. aureus* Xen29 has previously been shown to be 1-2 µg/ml[2] indicating 20-35% of MP1 entrapment in liposomes is sufficient to exert antibacterial activity. In addition, both types of liposomes demonstrated minimal changes in terms of particle size, size distribution and zeta potential when stored at 4° for 23 days (data not shown) indicating formation of stable nanoparticulate structures. Based on these results, both types of liposomes appears to be suitable nanocarrier systems for MP1 with fusogenic liposomes having higher entrapment of MP1.

Liposomal formulation	Particle size (nm in dm) ± S.D.	PDI	Zetapotential (mV) ± S.D.	% EE
MP1 in conventional liposomes (70% egg-PC/ 30% DOTAP)	90.7 ± 1.1	0.1	28.9 ± 0.3	20.0 ± 0.4
MP1 in fusogenic liposomes (50% DOTAP/25% DOPE/ 25% DAPC)	91.3 ± 0.6	0.1	35.4 ± 0.5	35.0 ± 0.4

Table 1: Physicochemical characterization of MP1-loaded liposomes. Egg-PC: L-α-phosphatidylcholine from egg (chicken), DOTAP: 1,2-dioleoyl-3-trimethylammonium-propane, DOPE: 1,2-dioleoyl-sn-glycero-3-phosphoethanolamine, DAPC: 1,2-diarachidoyl-sn-glycero-3-phosphocholine.

Evaluation of antimicrobial activity

The results from disc diffusion (Table 2) revealed that all formulations tested (MP1-loaded liposomes in semisolid formulations, MP1 alone in semisolid formulations, and MP1-loaded liposomes) showed measurable antibacterial activity compared to the negative control (no MP1 present) indicating that the topical formulations did not obstruct the MP1 release and activity. The zones of inhibition were higher for the gel-based formulations and significantly highest ($p < 0.05$) when MP1 was entrapped in fusogenic liposomes.

Topical formulation		Zones of inhibition (dm in mm) avg. ± S.D. n = 3
MP1-loaded conventional liposomes in:	ointment	9.33 ± 0.58
	cream	11.33 ± 0.58
	gel	12.33 ± 0.58
MP1-loaded fusogenic liposomes in:	ointment	10.67 ± 0.58
	cream	12.67 ± 0.58
	gel	**16.00 ± 1.00***
MP1 (without liposomes) in:	ointment	9.00 ± 1.00
	cream	11.00 ± 1.00
	gel	13.33 ± 0.58
MP1-loaded fusogenic liposomes	(alone)	15.67 ± 1.15
MP1-loaded conventional liposomes	(alone)	14.33 ± 0.58
Positive control (fucidic acid)	Fucidin® 2% ointment	27.0 ± 1.00
Negative controls (no MP1 present)	Ointment base	0
	Cream base	0
	Gel base	0

Table 2: Zones of inhibition for different formulations with and without MP1 against the test organism *S. aureus* Xen29 determined by disc diffusion. * indicate statistically significant difference between MP1-loaded conventional liposomes and MP1 without liposomes within the same type of semisolid formulation (one-way ANOVA, $p > 0.05$).

References

1. K. V. Ovchinnikov et al., Antimicrob. Agents Chemother. 2020, 64, 10-1128.
2. A. M. Amer et a., Eur. J. Pharm. Sci. 2025, 211, 107149.
3. Y. Liu et al., Microbiome 2020, 8, 85.

Acknowledgements

This work was supported under grant # 341669 by Research Council of Norway

Engineering a snake toxin as a positron emission tomography agent for diagnosing metastatic renal carcinoma

Goran Stanajic-Petrovic1,2, Khawla Chmeis1, Benoit Jego2, Dimitri Kereselidze2, Pascal Kessler1, Denis Servent1, Charles Truillet2, Nicolas Gilles1

1 Université Paris Saclay, CEA, Département Médicaments et Technologies pour la Santé, SIMoS, 91191 Gif-sur-Yvette, France 2 Université Paris-Saclay, CEA, CNRS, Inserm, BioMaps, Orsay, 91401, France Nicolas.gilles@cea.fr

https://doi.org/10.17952/38EPS.2026.P052

=> Mambaquaretin has been identified for its capacity to bind the vasopressin type 2 receptor (V2R, Ciolek, PNAS, 2017)

=> The V2R is expressed in the kidney where it regulates water homeostasis

=> V2R is also ectopically expressed in several cancer cells like the metastatatic form of clear cell renal carcinoma (mccRCC)

=> The MQ232, an optimized form of the mambaquaretin detects mccRCC at early stage (Stanajic, theranostics, 2025)

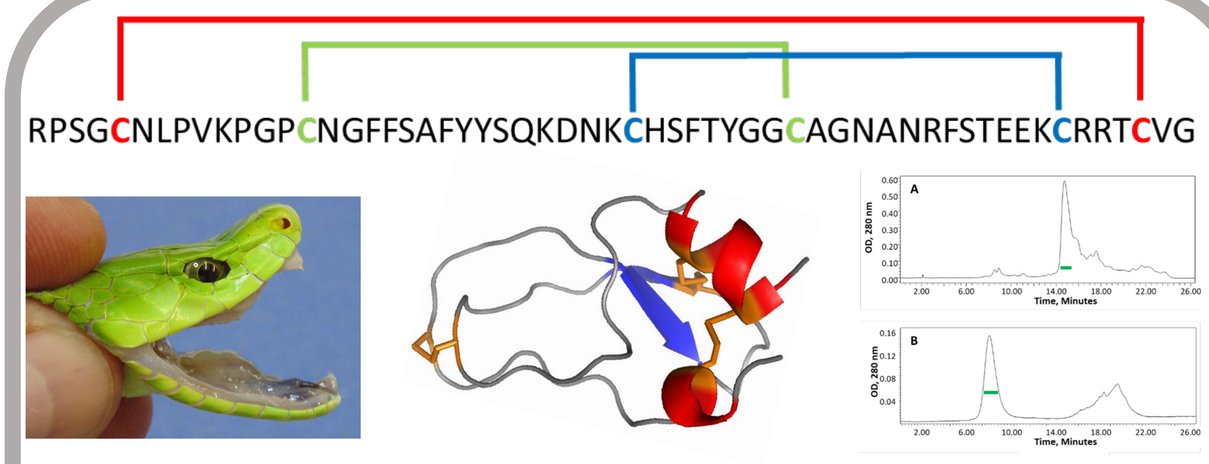
The earlier, The better

Early diagnosis of metastatic clear cell renal cell carcinoma (mccRCC) is of vital importance for patient survival.

Early diagnosis is not possible by lack of specific diagnostic tools.

As snake derived toxin detects early form of mccRCC.

The mambaquaretin



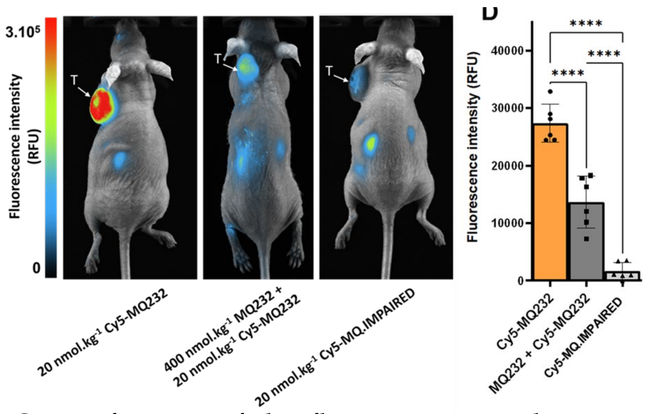
Sequence of the mambaquaretin, 57 residues, 3 disulfide bridges. The African green mamba snake *Dendroaspis angusticeps*. X-ray structure of the mambaquaretin, a Kunitz peptide. The mambaquaretin is produce by one step SPPS. HPLC of the crude peptide before (top) and after (down) of the oxidation of the 3 disulfide bridges.

In vivo selectivity of Cy5-MQ232 probe

The CHO-304 genetically modified cell line express the hV2R (Droctové et al. Theranostics. 2020. PMID: 33052234). 5 millions of cell implanted in NMRI-*Foxn1*$^{nu/nu}$ mice.



The Vilber camera to image live mice



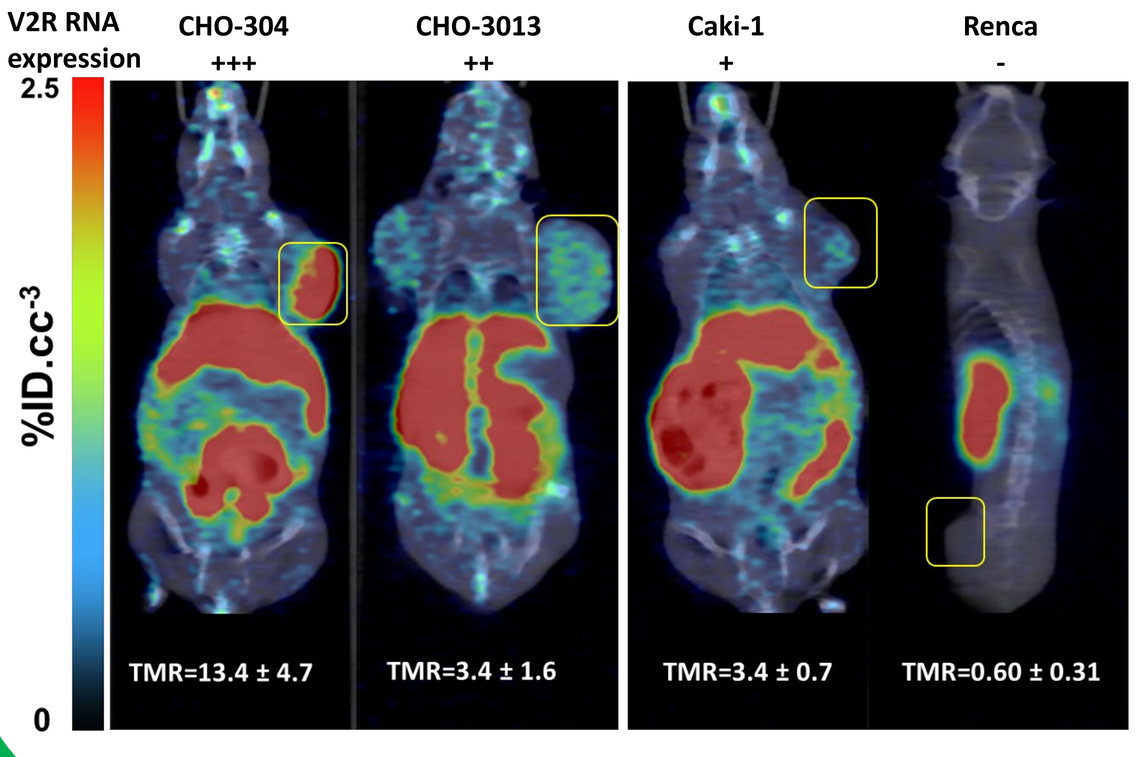
Quantification of the fluorescence in the organs of interest obtained from CHO-304 xenografted NMRI-Foxn1nu/nu mice euthanized at t+4 h after i.v. injection

In vivo visualization of V2R^{+} tumors in mccRCC representative mice model using [^{18}F]F-MQ232

The Caki-1 cell line, derived from human mccRCC express the V2R (Brodaczewska, et al . *Molecular Cancer* 2016). The Renca cell line, derived from a mice renal cancer, neither expressed the V2R.
5 millions of cell implanted in NMRI-*Foxn1*$^{nu/nu}$ mice for 3-4 weeks before imaging
PET imaging 4h after i.v. injection of [^{18}F]F-MQ232 (3.0 ± 0.7 MBq) per mice.



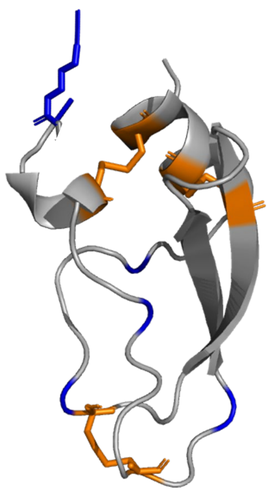
Micro-PET apparatus



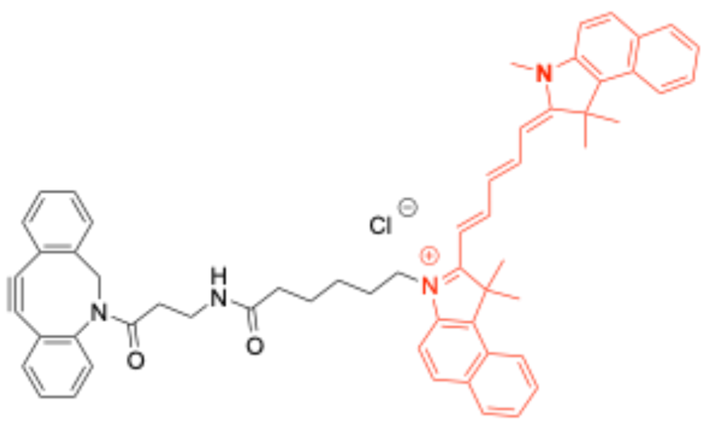
MQ232-derived probes are able to image the V2R ectopically expressed in tumors.

[^{18}F]F-MQ232 is the starting point for the development of a diagnostic tool that could enable early detection of mccRCC.

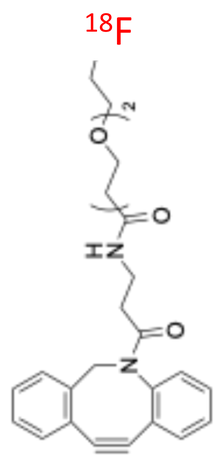
MQ232 derived in diagnostic tools



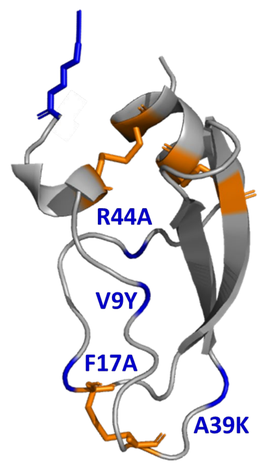
MQ232 with an azido moiety



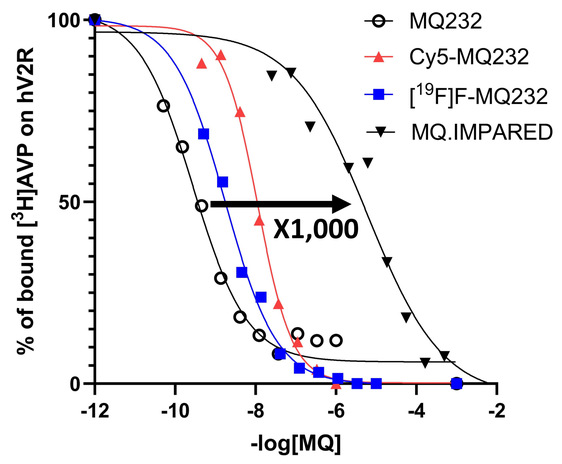
Cy5-dibenzocyclooctyne molecule for fluorescence imaging



[^{18}F]F-dibenzocyclooctyne molecule for PET imaging



The MQ-IMPAIRED, an inactive form of the MQ232



MQ232 and derivate display nM affinities. MQ-IMPAIRED displays µM affinity

Green Liquid-Phase Peptide Synthesis (LPPS) Methodology for the Sustainable Production of Therapeutic Peptides

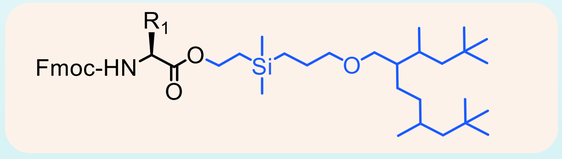
Naoki Nishizawa, Haruka Machida, Ryo Hatakochi, Yuji Mimori, Akihiro Nagaya, Michiharu Handa, Nissan Chemical Corporation, Chiba, Japan

https://doi.org/10.17952/38EPS.2026.P277

Introduction

Solid-phase peptide synthesis (SPPS) remains the dominant approach for peptide production, but its very high process mass intensity (PMI, ~13,000) poses a significant challenge to sustainable manufacturing. In addition, the extensive use of N,N-dimethylformamide (DMF), a key solvent in SPPS, is now subject to increasingly strict regulatory restrictions in Europe. Tag-assisted liquid-phase peptide synthesis (LPPS) has therefore attracted attention as a low-PMI, DMF-free, and more sustainable alternative to SPPS. However, the linker moieties of most existing LPPS tags were originally designed for solid-phase synthesis, resulting in limitations such as acid instability and difficulties in chemoselective deprotection without side reactions. Consequently, these tags are not well suited for the preparation of fully protected peptide fragments for convergent synthesis or C-terminal modification. To address these challenges, we developed a new liquid-phase synthesis tag, FMSE, featuring a linker architecture specifically optimized for LPPS.

FMSE: Alkyl silane-based solubilizing tag



Stable under both acidic and basic conditions

- Compatible with Boc / Fmoc / Cbz chemistries
- Diketopiperazine (DKP) formation is effectively suppressed under Boc / Cbz conditions

Selectively cleavable

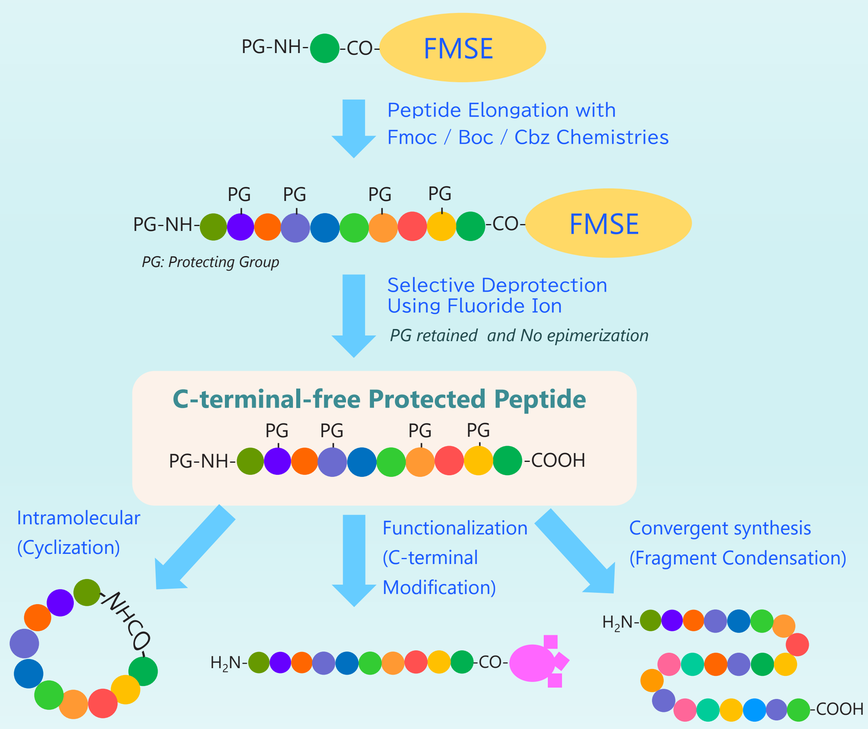
- Selective deprotection by TBAF treatment without loss of other protecting groups (except Fmoc) or C-terminal epimerization

*TBAF: tetrabutylammonium fluoride (fluoride ion source)

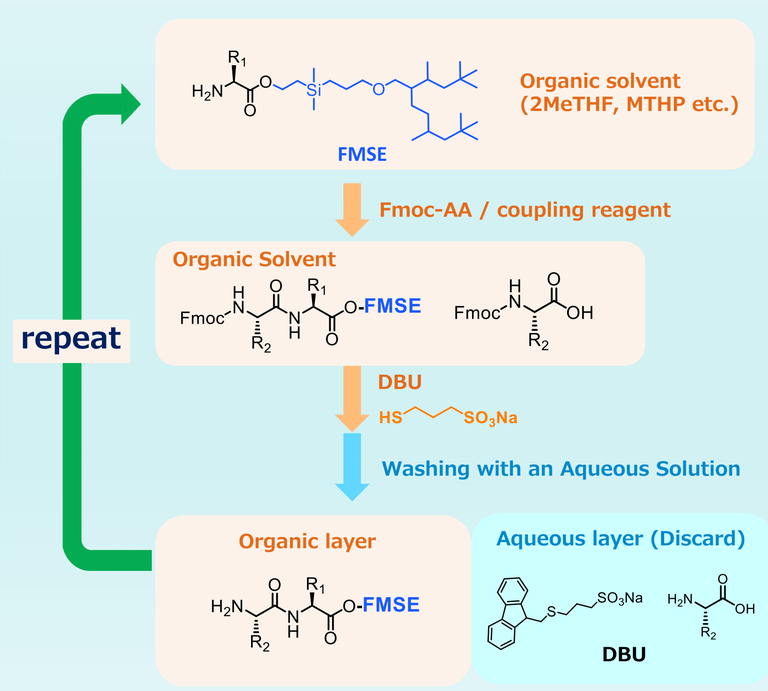
Effective solubilizing capability in green solvents

- Enables peptide elongation without regulated solvents such as DMF or NMP

General Scheme for Protected Peptide Synthesis and Utilization

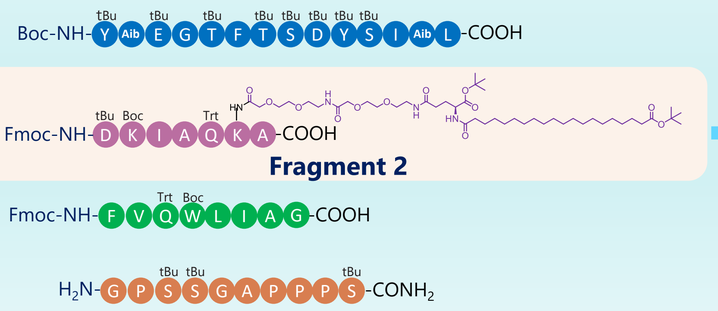


DMF/NMP-Free LPPS Synthetic Cycle Using the FMSE Tag

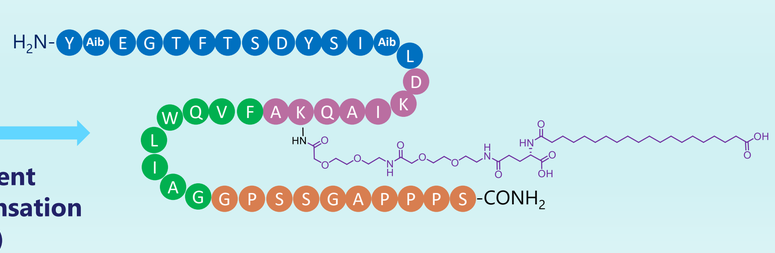


SPPS/LPPS Hybrid Strategy for Tirzepatide Manufacturing

Tirzepatide Fragments (SPPS synthesis)



Fragment condensation (LPPS)

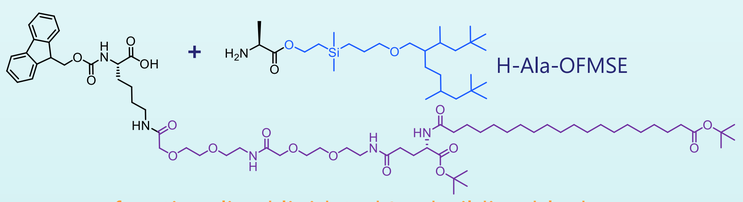


Key Challenges

- High PMI in SPPS-based fragment manufacturing
- Expensive pre-assembled lipidated Lys building blocks
- Large consumption of regulated solvents (DMF/NMP)

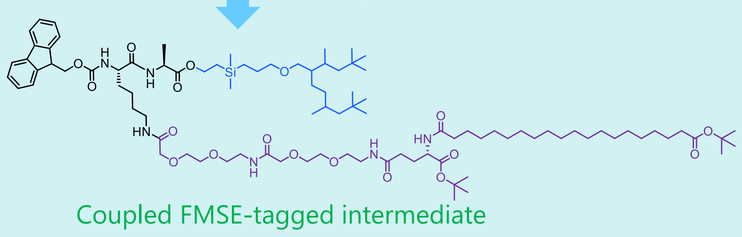
Org. Process Res. Dev. (2021) 25 (7): 1628–1636.

Issues in LPPS Coupling with Lipidated Lys Building Blocks



pre-functionalized lipidated Lys building block

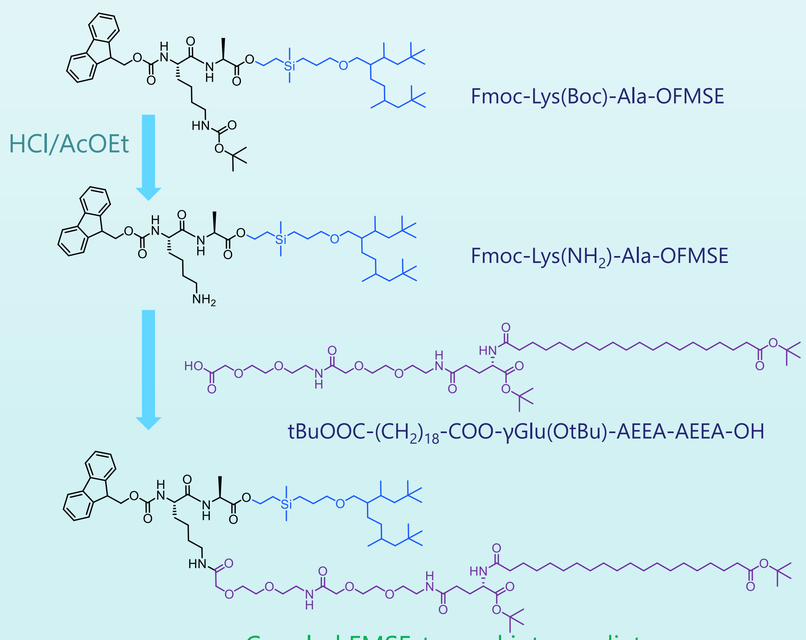
Coupling



Coupled FMSE-tagged intermediate

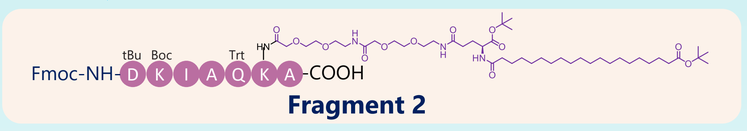
- Costly, pre-functionalized lipidated Lys building block
- Slow coupling of bulky Fmoc-Lys(Alkyl)-OH derivatives
- Poor separation of Fmoc-Lys(Alkyl)-Ala-O-FMSE from unreacted/excess Fmoc-Lys(Alkyl)-OH
- Separation remained difficult even after Fmoc deprotection to H-Lys(Alkyl)-Ala-O-FMSE and H-Lys(Alkyl)-OH

Alternative Strategy for Fragment 2 Synthesis



Coupled FMSE-tagged intermediate

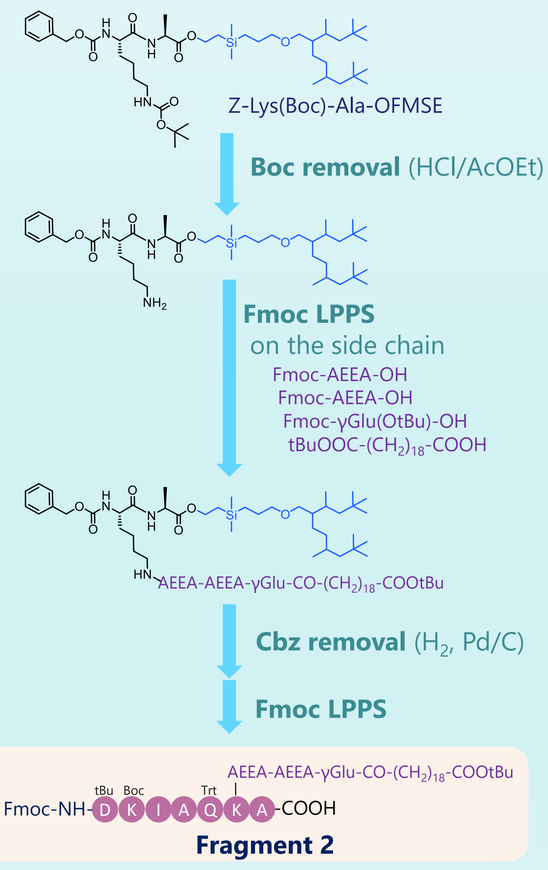
Stepwise LPPS and FMSE deprotection



FMSE-based stepwise side-chain construction

- Avoids costly pre-functionalized PEG–alkyl Lys building blocks
- Efficient coupling from less hindered Lys intermediates
- Enables clean aqueous workup with favorable phase separation
- Improves robustness in downstream peptide elongation

Bidirectional Extension for Lipidated Peptide Manufacturing



- Bidirectional elongation via Fmoc/Boc/Cbz chemistry
- Cbz removal after side-chain extension enables N-terminal LPPS
- Customized PEG–alkyl side chains without pre-assembled building blocks

Take-home Message

- FMSE enables DMF/NMP-free LPPS with low-PMI potential
- Fluoride-mediated FMSE removal provides protected peptide fragments without C-terminal epimerization
- Stepwise Lys side-chain construction expands access to lipidated peptide intermediates

SYNCSOL Company website

Contact: Naoki Nishizawa (Nissan Chemical Corporation) — nishizawan@nissanchem.co.jp | Scan to email

Phage display validation of lysosomal targeting receptors for the treatment of lung cancer

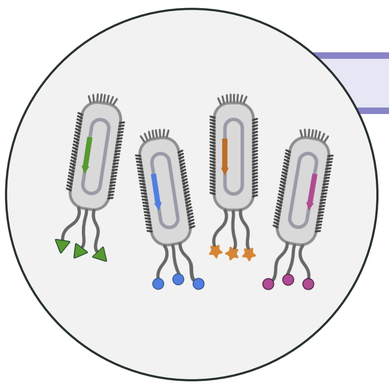
Vanesa Nozal[1], Petar Petrov[2], Juan Sebastián Ruiz[2], Benjamí Oller-Salvia[1], Cristina Díaz-Perlas[1]

[1]Institut Químic de Sarrià - Universitat Ramon Llull (IQS-URL), Barcelona, Spain

[2]Aptadegrad, Santiago de Compostela (A Coruña), Spain

vanesa.nozal@iqs.url.edu, chemsynbio@iqs.edu

https://doi.org/10.17952/38EPS.2026.P422

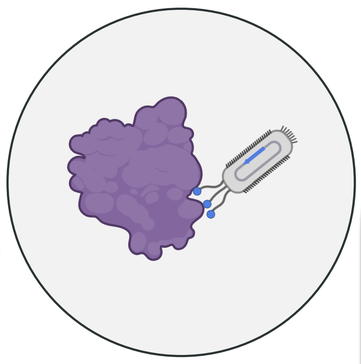


INTRODUCTION

Phage display libraries have been used to identify new peptide-binders for the treatment of non-small cell lung cancer (NSCLC). This type of cancer is one of the leading causes of cancer-related mortality and the second most frequently diagnosed cancer worldwide. With the current frontline therapies relying on tyrosine kinase inhibitors emergence of resistance after 12 to 24 months alternative therapeutic strategies such as targeted protein degradation offer a promising approach[1]. In this work, we are developing new lysosomal targeting chimeras (LYTACS)[2,3] exploiting the well-characterized anti VEGF antibody bevacizumab combined with a lysosome-targeting moiety which will be a novel peptide. Two different workflows have been applied to maximise the success in the identification of novel peptides with the potential to direct our protein of interest to the lysosome.

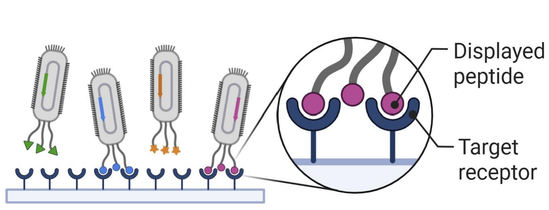
TARGET DIRECTED

With the aim to treat NSCLC we have identified two relevant receptors with the potential to direct the target to the lysosome. These two receptors have been immobilised and presented to a peptide phage display library with 12 amino acids in the protein III of the M13 phage:

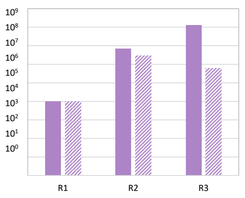


PHAGE LIBRARY

- M-13 phage
- 12-mer linear peptide library
- Diversity 10^{12}
- Fused to pIII: 3-5 copies per phage
- Leucine-Arginine sequence: trypsin sensitive for elution
- Amp resistance



1 PANNING



3 rounds of panning with increasing stringency and decreasing concentrations of immobilised protein were performed to obtain promising peptide candidates.

Figure 1. Library enrichment after each panning cycle for Receptor 1 (plain purple) and Receptor 2 (striped purple).

2 PHAGE ELISA

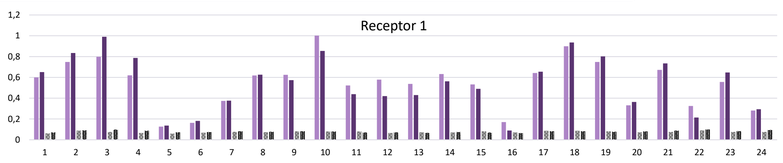


Figure 2. Screening of positive clones by phage ELISA from competitive elution at two concentrations (purple bars) for Receptor 1, non receptor coated wells (dotted bars) were used as negative control.

3 SANGER SEQUENCING AND PEPTIDE SYNTHESIS

Two new peptides were identified for receptor 1 and four for receptor 2. These peptides were synthesized including a GGG-motif for sortA conjugation to the mAb. Their biotinylated versions were also synthesized in order to determine their Kd.

RECEPTOR 1 — 2 PEPTIDES

RECEPTOR 2 — 4 PEPTIDES

Kd peptide B: 1.2 µM Kd peptide D: 2.6 µM

4 CELLULAR EXPERIMENTS

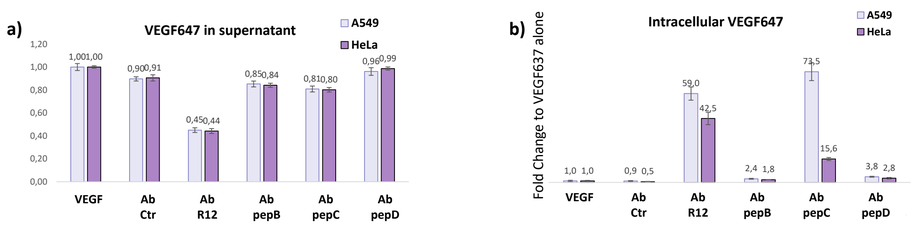


Figure 3. a) Quantification of VEGF647 supernatant and b) intracellular levels in A549 and HeLa treated for 6h with 50nM VEGF647 and 100nM Beva Enzymatic Sortase Conjugates.

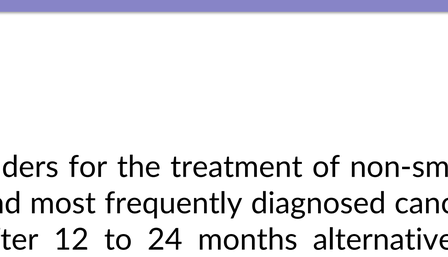
Further experiments did not conclusively confirm the receptor-dependent uptake of the Ab-peptide conjugates. The observed decrease in VEGF levels may be related to internalization processes, potentially involving non-specific precipitate engulfment, and additional studies will be required to clarify this mechanism.



TARGET AGNOSTIC

We tested lung carcinoma cells against the MIM-12 library in order to identify peptides which would bind selectively to the disease. We also introduced two rounds of negative selection to increase the selectivity of the process.

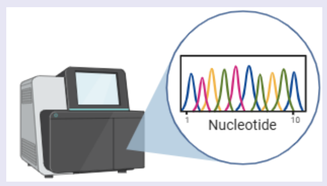
1 PANNING



Four rounds of panning using the MIM-12 library have been performed. Two negative selection steps using BEAS-2B bronquial epitelial cell lines were performed in R1 and R3 to guide the panning towards increased cellular selectivity. A round of degradation was also performed, using degradation inhibitors.

Figure 4. Library enrichment after each panning cycle for whole cell panning.

2 NGS SEQUENCING



We analysed R3 and R4 and observed an enrichment of two different peptide sequences. When the library was tested for cellular degradation, the two lead peptides were not among the most abundant examples, suggesting a that those peptides get degraded via lysosomal pathway.

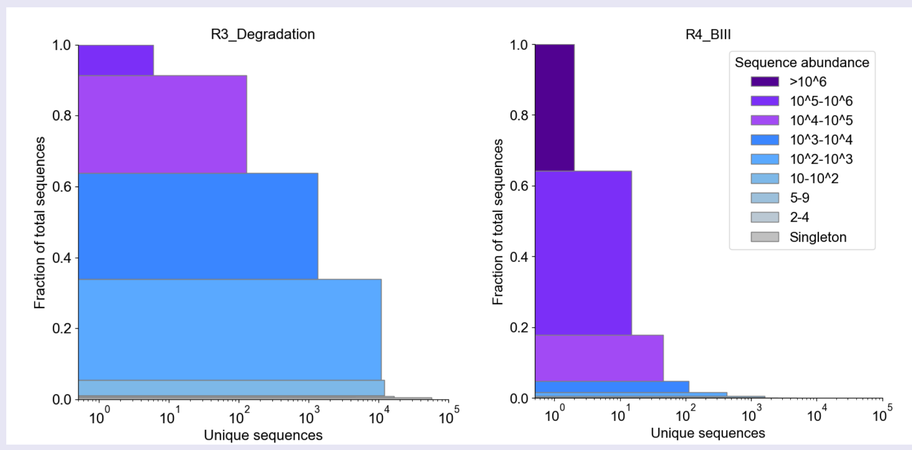


Figure 5. Diversity plots to visualize selection effects on sequence abundances per panning round as revealed by complete library sequencing by NGS. Each colored segment contains all sequences with the specific abundance. The segment height is equal to the fraction of total library, and the width corresponds to the number of unique sequences per segment.

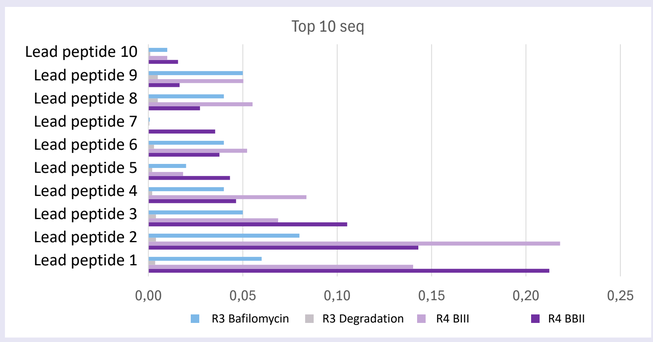


Figure 6. Relative abundance of the top 10 lead peptides in the four NGS-analysed rounds. R3 bafilomycin cells were evaluated under lysosomal inhibition, while R3 degradation assays were conducted in the absence of the inhibitor.

3 PEPTIDE SYNTHESIS AND CELLULAR VALIDATION

The next steps include the synthesis of a peptide series and their conjugation to fluorescent markers to evaluate lysosomal colocalization. Follow-up antibody conjugation and detailed cellular experiments will then assess the potential of these peptides to promote degradation of the protein of interest.

CONCLUSION

New peptide-binders have been identified for the selected lysosomal targeting receptors, the affinity of two of them has been successfully reported. However, their ligation to therapeutic antibodies suggests that the protein of interest may undergo non-specific internalization, and additional experiments will be required to confirm this possibility. Whole cell-panning experiments have highlighted two lead peptides which could potentially selectively degrade the target of interest in the desired cell lines. Subsequent chemical synthesis and fluorescent labelling will confirm the potential of the newly discovered peptides.

REFERENCES

1. Du, et. al. *Pharmacol. Rev.* **2025**, 77, 100076
2. Banik, et al. *Nature*, **2020**, 584, 291
3. Yang, et. al. *J. Med. Chem.* **2025**, 68, 18040

This work has been suported by proyectos en colaboración público-privada 2023 from MICI: CPP2023-010665 and PID2023-151988OB-I00 from MICIU. Some images in this poster have been created with BioRender.com

P312

Discovery of Potent RSV Peptides Antivirals

https://doi.org/10.17952/38EPS.2026.P312

Origène Nyanguile[a], Nadège Pidoux[a], Stéphane Duquerroy[b], Mathilde Keck[c], Thibaut Larcher[d], Marie Galloux[e]

[a]HES-SO Valais-Wallis, Institute of Life Sciences, HES-SO University of Applied Sciences Western and Arts Switzerland, Sion 1950, Switzerland, [b]Université Paris Saclay, Structural Virology Unit, Institut Pasteur, Paris 75015, France , [c]Université Paris-Saclay, CEA, INRAE, Département Médicaments et Technologies pour la Santé (DMTS), SIMoS, Gif-sur-Yvette 91191, France Paris 75015, [d]INRAE, Oniris, UMR 703 Apex, Nantes 44307, France, [e]VIM, INRAE, Domaine de Vilvert, Jouy-en-Josas 78350, France.

INTRODUCTION

Respiratory Syncytial Virus (RSV) is very contagious and represents the main cause of severe acute respiratory tract illness in young children worldwide and in adults over the age of 65.

RSV F is a fusion protein located on the surface of the virion that mediates RSV entry into the respiratory tract epithelial cells. RSV F is activated upon cell entry into a metastable prefusion form named “preF”, which contains a hydrophobic fusion peptide, two heptad repeats (HR1 and HR2), and a viral transmembrane domain. Following the insertion of the fusion peptide into the target cell membrane, preF undergoes a dramatic conformational rearrangement to yield a postfusion six-helix bundle hairpin structure named “postF”, whereby 3 HR2 sequences bind in an antiparallel manner to a trimeric HR1 coiled coil. This hairpin structure brings the viral and cell membranes into close apposition, thereby facilitating membrane fusion and subsequent viral entry.

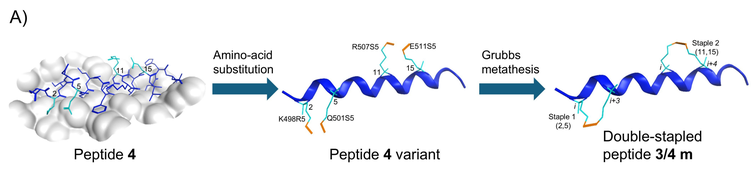
Previously, we reported antiviral peptides inhibiting RSV fusion, named 4bb and 4ca (1). These peptides are derived from the HR2 domain of RSV F, and function as dominant negative inhibitors by binding to the transiently exposed HR1 coiled coil in the pre-hairpin fusion intermediate. Through performing a stapled peptide walk across the HR2 sequence, we identified a minimal domain named peptide 4 ((RSV F (485-515)).

Here, we have expanded our screen and identified 3 potent RSV peptides leads.

DISCOVERY OF POTENT DOUBLE STAPLED PEPTIDES, FUSION INHIBITORS OF RSV

We performed an extended double staple scan across peptide 4. Four amino acids of peptide 4 were substituted with crosslinking unnatural residues (Scheme 1B) with the aim to yield a peptide containing two staples cross-linking one α-helical turn each (Scheme 1A). Only the amino acids that are not in hydrophobic contact with trimeric HR1 (color coded in black in Scheme 1D) were substituted. Of all peptides that were tested only peptide 4/4g, 3/4i and 3/4m were significantly more potent than peptides 4bb and 4ca, displaying EC_{50} values of 120, 83 and 53 nM, respectively (Scheme 1C).

Interestingly, these 3 lead peptides appear to use only two staple combinations, that is, staple 1 (2,5) or (4,8) combined with staple 2 (11,15) or (12,16).



Peptide	Staple 1	Staple 2	EC_{50}(μM)	Peptide	Staple 1	Staple 2	EC_{50}(μM)
4bb	4,8	11,15	0.74±0.27	**4ca**	2,5	8,12	0.59±0.13
4/4a	1,5	15,19	> 33	**3/4a**	2,5	15,19	8.89±3.21
4/4b	8,12	14,18	186.69±117	**3/4b**	9,12	14,18	4.94±1.88
4/4c	7,11	14,18	6.52±0.58	**3/4c**	8,11	14,18	33.95±10.6
4/4d	4,8	14,18	5.68±0.65	**3/4d**	5,8	14,18	17.15±1.86
4/4e	1,5	14,18	6.77±6.51	**3/4e**	4,7	14,18	5.87±0.83
4/4f	5,9	12,16	0.95±0.66	**3/4f**	2,5	14,18	73.42±53.3
4/4g	4,8	12,16	0.12±0.14	**3/4g**	5,8	12,16	19.69±10.2
4/4h	2,6	12,16	0.53±0.04	**3/4h**	4,7	12,16	4.48±3.52
4/4i	1,5	12,16	0.36±0.21	**3/4i**	2,5	12,16	0.083±0.078
4/4j	5,9	11,15	34.32±8.89	**3/4j**	1,4	12,16	>33
4/4k	2,6	11,15	54.63±68.70	**3/4k**	5,8	11,15	3.95±5.19
4/4l	1,5	11,15	2.61±2.35	**3/4l**	4,7	12,15	10.92±5.19
4/4m	1,5	8,12	9.13±6.94	**3/4m**	2,5	11,15	0.053±0.041
4/4n	1,5	7,11	>33	**3/4n**	1,4	11,15	2.61±1.79
Reference				**3/4o**	1,4	8,12	66.50±47.38
Ziresovir			0.0003±0.0002	**3/4p**	2,5	7,11	1.88±0.46
				3/4q	1,4	7,11	2.42±0.20

Peptide	497			500					505					510						515	
4	E	K	**I**	N	Q	**S**	L	A	F	**I**	R	K	**S**	D	E	L	**L**	H	N	**V**
Residue #	1	2	3	4	5	6	7	8	9	10	11	12	13	14	15	16	17	18	19	20

Scheme 1. Double stapled peptide walk across peptide 4 and identification of lead peptides inhibitors (Reproduced from Pidoux et al., J. Med. Chem. 2026, 69, 12910–12924. DOI: 10.1021/acs.jmedchem.5c02932, under CC BY 4.0, (2)).

X-RAY STRUCTURE OF PEPTIDE 3/4m AND 4/4g IN COMPLEX WITH TRIMERIC HR1

HR1 (RSV F (159-209)) was synthesized by SPPS using pseudoproline analogs and mixed with an equimolar amount of peptide 3/4m or 4/4g. The complexes were purified to homogeneity by size exclusion chromatography, and crystals diffracting to 1.6 Å and 1.3 Å were obtained using the vapor diffusion method for HR1−3/4m and HR1−4/4g complexes, respectively.

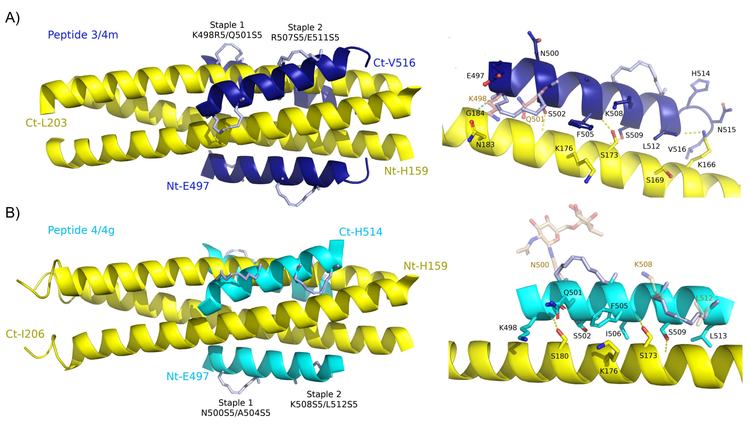


Figure 1. Crystal structure of HR1-3/4m and HR1-4/4g complexes. Left panel, ribbon diagram of the HR1−3/4m complex, top, and of the HR1−4/4g complex, bottom. The HR1 helices are shown in yellow, and the 3/4m and 4/4g peptides are depicted in dark blue and cyan, respectively. Staples 1 and 2 are shown in tubular structures in light blue. Top right panel, view of the 3/4m staple 1 binding site. Bottom right, view of the 4/4g staple 2 binding site. (Reproduced from Pidoux et al., J. Med. Chem. 2026, 69, 12910–12924. DOI: 10.1021/acs.jmedchem.5c02932, under CC BY 4.0).

As expected, the peptides pack with trimeric HR1 into a six helix bundle (Figure 1 left). **The peptides are totally helical although the 3 last residues 514-HNV-516 adopt a 3_{10} helix structure in 3/4m, allowing Val516 to deeply insert into HR1**. This Cterm region is not resolved in 4/4g, which ends at H514. The two peptides make a very tight interaction with the two helices making the groove of the HR1 trimeric coiled coil. **For 3/4m, the interaction of staple 1 with trimeric HR1 contributes significantly to the enhancement of inhibitory activity of peptide 3/4m** (Figure 1, top right panel).

In contrast to peptide 3/4m, staple 1 of 4/4g remains exposed and does not contribute to interactions with HR1 (Figure 1, bottom left panel), whereas staple 2 engages in hydrophobic contacts with residues of trimeric HR1 (Figure 1, bottom right panel).

Although crystallization trials with peptide 3/4i were unsuccessful, this peptide incorporates staple 1 from 3/4m and staple 2 from 4/4g, enabling the construction of a structural model for this third potent peptide (Figure 2). In this model, both staples participate in hydrophobic interactions with residues of the trimeric HR1, consistent with observations from the X-ray structures of the 3/4m and 4/4g complexes.

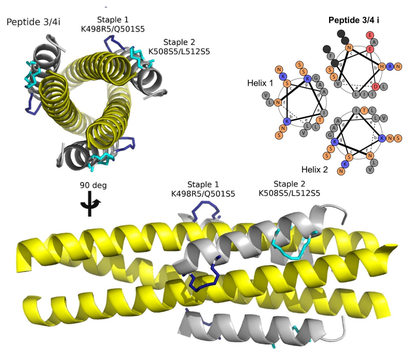


Figure 2. Ribbon diagram of the HR1-3/4i complex. Left panel, rotated 90deg. relative to the view shown in Figure 1. The HR1 helices are shown in yellow, and the 3/4i peptides in gray. Staples 1 and 2 are shown in a tubular structure in dark blue and cyan for 3/4i peptide. Right panel, α-helical wheel representations depicting the interactions of peptide 3/4i with helix 1 and helix 2 of trimeric HR1. Bottom panel, model of the HR1-3/4i complex.(Adapted from Pidoux et al., J. Med. Chem. 2026, 69, 12910–12924. DOI: 10.1021/acs.jmedchem.5c02932, under CC BY 4.0).

DOUBLE STAPLED PEPTIDE LEAD INHIBIT SMALL-MOLECULE ESCAPE MUTANTS

Small molecules fusion inhibitors bind to a 3-fold symmetry cavity in trimeric preF (3), and will yield the same viral escape mutants. Peptide 3/4m was capable of inhibiting infection by RSV mCherry S398L/K394R double mutant (Figure 3). The S398L small-molecule escape mutant was observed in a phase 2a human challenge study against presatovir (Gilead) and the K394R mutation was identified in an *in vitro* cellular resistance study against BMS-433771 (Bristol-Myers).

In contrary the inhibition of presatovir (GS-5806) was completely abrogated against the double resistant mutant (> 38’000-fold change relative to wild type rRSV-mCherry).

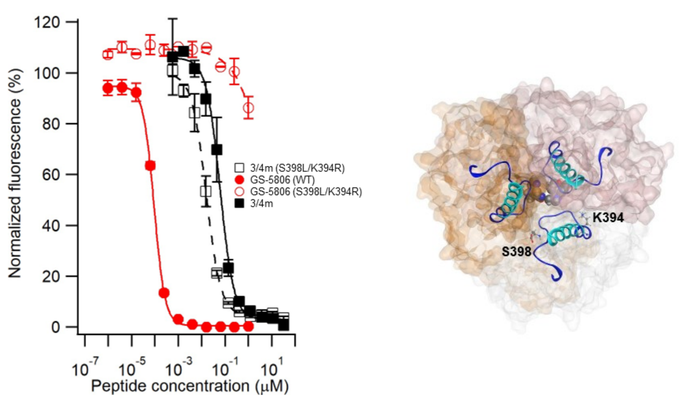


Figure 3. Inhibition of RSV F small-molecule escape mutant. A) Inhibition of rRSV-mCherry WT and S398L/K394R variant infection by lead double stapled peptide 3/4m and GS-5806 in HEp-2 cells. B) Top view of X-ray structure of BSM -433771 bound to preF (PDB code 5EA7). The 3 RSV F protomers are shown as surface representation in grey, gold and pink. The 3 HR2 domains are shown in a ribbon representation with peptide 4 color coded in cyan. BMS-433771 is shown in a sphere model, K394 and S398 in ball and stick.

IN VITRO STABILITY OF PEPTIDE LEADS

Lead peptides were incubated with trypsin, chymotrypsin and mice serum, and the amount of remaining peptide was quantified at different time points by LC/MS-MS.

Wild-type peptide 4 was rapidly degraded by trypsin and chymotrypsin (Fig. 4A-B) with a half-life of 4.91 min and 4.25 min, respectively. In contrast, the stapled peptides were much less susceptible to trypsin and chymotrypsin than peptide 4.

The resistance of stapled peptides to degradation by trypsin decreased in the order of 4/4g, 3/4i and 3/4m ($t_{1/2}$ of 91.98, 40.91 and 18.15 min, respectively, Fig. 4A).

The resistance of stapled peptides to degradation against chymotrypsin was of 36.36, 20.13 and 108.3 minutes for peptides 4/4g, 3/4i and 3/4m, respectively (Fig. 4B).

Stapled peptides did not show any degradation over the entire time course (>24 hours; Fig. 4C), when they were incubated in the presence of mouse plasma at 37°C.

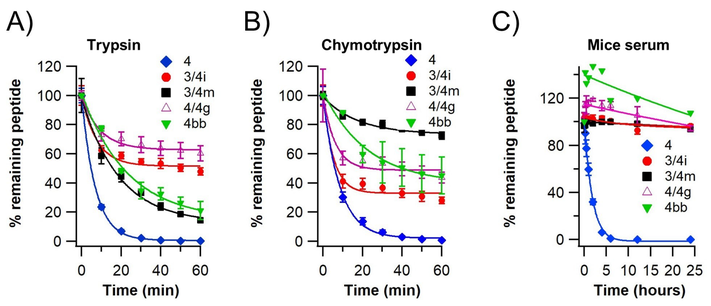


Figure 4. Proteolytic stability assay. Susceptibility of double-stapled peptides 3/4i, 3/4m, and 4/4g in comparison to peptides 4bb and 4 toward degradation by A) trypsin, B) chymotrypsin, and C) mouse serum, in comparison to peptide 4, i.e., RSV F (497−516). (Reproduced from Pidoux et al., J. Med. Chem. 2026, 69, 12910–12924. DOI: 10.1021/acs.jmedchem.5c02932, under CC BY 4.0).

FEASIBILITY STUDY IN BALB/c MOUSE MODEL

Balb/c mice were treated by intranasal (IN) administration of peptide 3/4i or vehicle, followed by IN inoculation of a recombinant human RSV encoding the gene for firefly luciferase, rHRSV-Luc. The mice were treated once daily and were anesthetized at 2- and 4-days post infection (dpi) to quantify viral replication using an *in vivo* imaging system (IVIS). As shown in Fig. 5, a significant reduction of bioluminescence signal was detected at both 2 and 4 dpi in mice treated with peptide 3/4i in comparison of the untreated control group

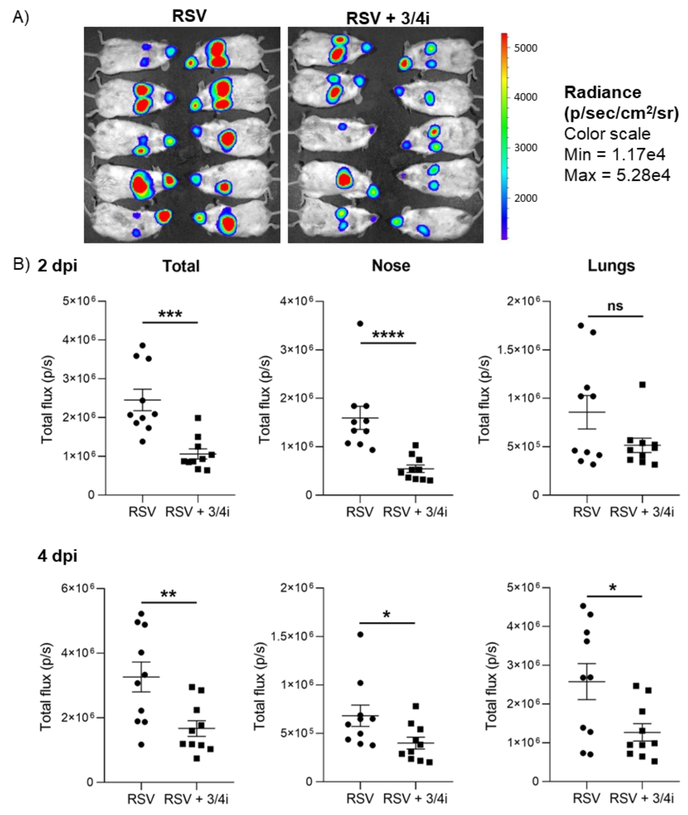


Figure 5. **Protective effect of peptide 3/4i on RSV infection in mice.** 8 weeks-old female Balb/c mice were treated intranasally with 1.17 mg/kg peptide 3/4i or vehicle. Groups of 10 mice were treated at day 0 individually with either 50 µL PBS or 50 µL peptide 3/4i (200 µM) in PBS containing 0.8% DMSO and infected 10 min later by 60 µL rHRSV-Luc (8 x 10^4 PFU per mouse). The administration of peptide 3/4i was repeated daily until day 3. A) Bioluminescence was measured at day 4 post inhalation (dpi) by intranasal administration of 50 µL of D-luciferin. Luciferase activities were quantified for each mouse using Living Image software. Luciferase activity is expressed as photons per second (p s^{-1}); B) Total bioluminescence, or bioluminescence in the nose and lungs was quantified for each animal at 2 and 4 dpi. Each dot represents one animal.*(Adapted from Pidoux et al., J. Med. Chem. 2026, 69, 12910–12924. DOI: 10.1021/acs.jmedchem.5c02932, under CC BY 4.0).*

CONCLUSION

Novel double stapled peptides capable of inhibiting RSV fusion in cellular antiviral assays were discovered. Intranasal administration of 3/4i to Balb/c RSV infected mice resulted in approximately one log decrease of viral load. Recent SAR studies resulted in the identification of highly potent peptides displaying single digit nanomolar EC_{50} values in Hep-2 cellular inhibition assay. To identify the most appropriate route of administration for optimal targeted delivery of these peptides to the lungs, their ability to penetrate the mucus layer is currently being evaluated in Calu-3D cells. The most suitable administration route will subsequently be selected and validated using the Epithelix MucilAir™ and SmallAir™ epithelial tissue models.

REFERENCES

(1) Gaillard, V.; Galloux, M.; Garcin, D.; Eleouet, J. F.; Le Goffic, R.; Larcher, T.; Rameix-Welti, M. A.; Boukadiri, A.; Heritier, J.; Segura, J. M.; Baechler, E.; Arrell, M.; Mottet-Osman, G.; Nyanguile, O., A Short Double-Stapled Peptide Inhibits Respiratory Syncytial Virus Entry and Spreading. *Antimicrob Agents Chemother* **2017,** *61* (4).

(2) Pidoux, N.; Roh, L; Nicolet, N;, Marti, R.; Le Rouzic, A.; Prompt, C.; Fix, J.; Duquerroy, S.; Rey, R.; Rameix-Welti, M-A.; Keck, M.; Barbe, P.; Garcin, D.; Mottet-Osman, G.; Larcher, T.; Galloux, M.; Nyanguile, O., Double-Stapled Peptide Scan Yields Potent Fusion Inhibitors of Respiratory Syncytial Virus, *J. Med. Chem.* **2026**, *69*, 12910–12924.

(3) Battles, M. B.; Langedijk, J. P.; Furmanova-Hollenstein, P.; Chaiwatpongsakorn, S.; Costello, H. M.; Kwanten, L.; Vranckx, L.; Vink, P.; Jaensch, S.; Jonckers, T. H.; Koul, A.; Arnoult, E.; Peeples, M. E.; Roymans, D.; McLellan, J. S. Molecular mechanism of respiratory syncytial virus fusion inhibitors. *Nat. Chem. Biol.* **2016**, *12* (2), 87−93.

ACKNOWLEDGMENTS

This work was partly funded by the HES-SO and domaine Ingénierie et Architecture (HES-SO 78166/IA-INTERDISC17-2, 135271/IA RECHERCHE24-14). We thank Dr. Jean-François Eleouet for sharing recombinant RSV. We thank the animal facilities of Infectiology of Fishes and Rodents (IERP, INRAE, doi: 10.15454/1.5572427140471238E12) and the Emerg’in platform for access to IVIS200 that was financed by the Region Ile De France (SESAME). This work has benefited from the facilities and expertise of @BRIDGe (Universite Paris-Saclay, INRAE, AgroParisTech, GABI, Jouy-en-Josas, France).

CONTACT

Address correspondence to Origène Nyanguile, origene.nyanguile@hevs.ch and Marie Galloux, marie.galloux@inrae.fr

Computational approaches for analysis and design of peptides containing non-canonical amino acids

Rodrigo Ochoa, and many other collaborators*

Novo Nordisk A/S, Novo Nordisk Park, Måløv, DK-2760, Denmark (https://doi.org/10.17952/38EPS.2026.P251)

*See acknowledgements

Motivation

Computational methods are required to study peptides and to gain insights into rational design strategies. In the special case of peptides containing non-canonical amino acids, additional strategies and data are necessary to overcome computational challenges.

This work aims to summarize a set of tools and benchmark studies for modified peptides, using both ligand- and structure-based approaches.

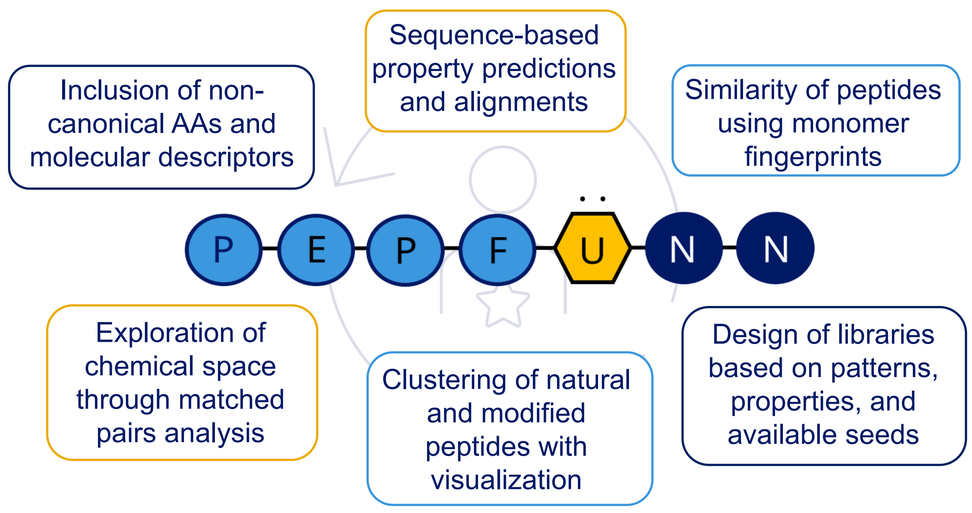
How to represent modified peptides?

Simple linear peptides can be represented using FASTA format. For non-canonical elements, line notations to allow the representation of complex peptides are suggested (i.e., BILN format).

Description	FASTA	BILN
Simple linear peptide	PEPTIDE	P-E-P-T-I-D-E
Peptide with internal C-C disulfide bridge and amidation at the C-terminus	ACGAGCD	A-C(1,3)-G-Aib-G-C(1,3)-D-NH2
C-term to N-term cyclic peptide	CYCLIC	C(1,1)-Y-C-L-I-C(1,2)

Fox, Bieler, Haebel, Ochoa, Peters, Weber. *J. Chem. Inf. Model.* 2022

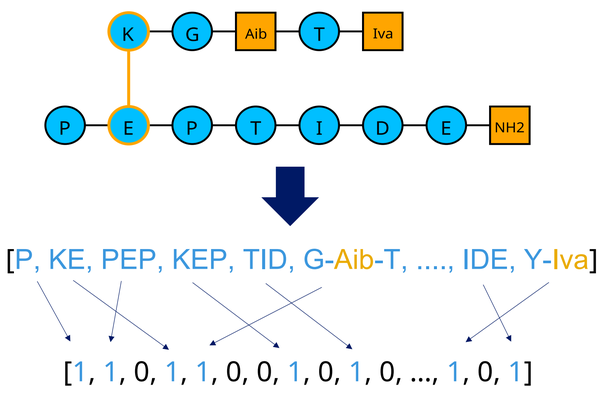
1. PepFuNN – peptide analysis toolkit from Novo Nordisk



PepFuNN modules contain multiple functions to support the analysis and design of peptides, including those modified with non-canonical components.

Special fingerprints and properties can be estimated for modified peptides, for example, to create customized machine learning models

Monomer-based fingerprints:



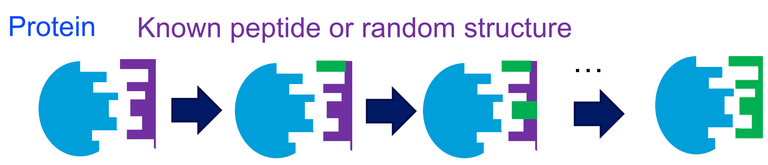
Fixed length fingerprint **(e.g., 1024 bits)**

https://github.com/novonordisk-research/pepfunn

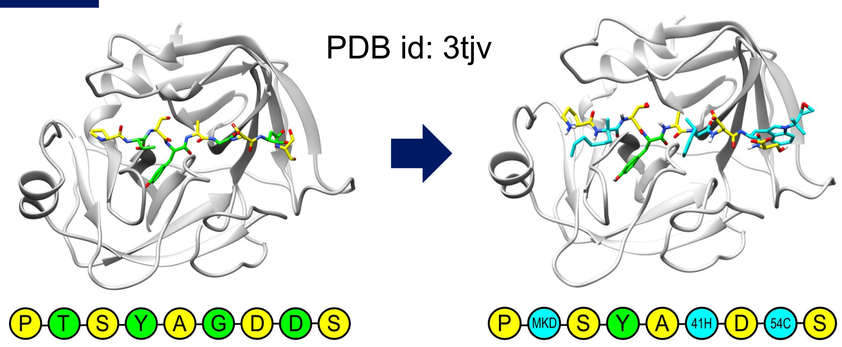
Ochoa & Deibler. *J. Pept. Sci.* 2025

2. mPARCE – protocol for the optimization of bound modified peptides

mPARCE allows adding non-canonical amino acids into peptide binders while improving their binding affinity. The workflow makes single point mutations on the peptide sequence based on a Monte Carlo approach



Non-canonical amino acids from the PDB can be incorporated

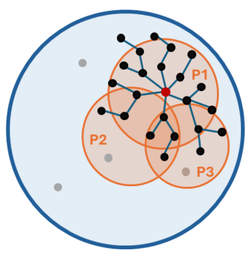


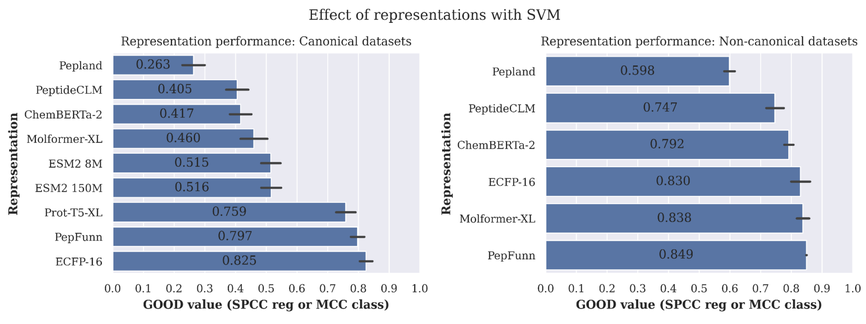
Ochoa, Cossio, Fox. *J. Comput.-Aided Mol. Des.* 2022

3. Machine learning (ML) representation for modified peptides

Traditional sequence-based approaches are often inadequate for modelling non-canonical peptides, and there is a critical need for advanced ML techniques that can effectively represent modified peptides, addressing challenges related to molecular representation and dataset partitioning.

- Molecular similarity functions can be effective for guiding dataset partitioning for both canonical and non-canonical peptides
- The findings inform the best configurations (model and representations) for enabling the routine modeling of peptides with or without chemical modifications. Example using a SVM architecture:



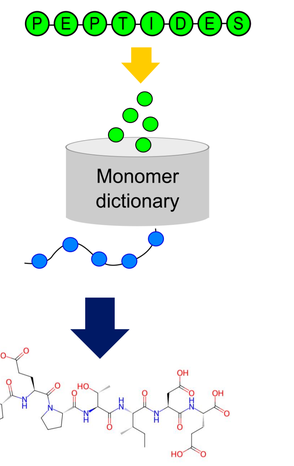


Fernandez-Diaz, Ochoa, Hoang, Lopez, Shields. *J. Cheminformatics.* 2025

4. pyPept – peptide format conversion

Python package to connect natural and non canonical residues through defined R-groups, and translate BILN and FASTA format to all-atom formats (i.e. SMILES)

- **Input:** peptide (BILN format) + Monomer dictionary with non-canonical components
- **Output:** RDKit molecular object that can be transformed to 2D and 3D formats

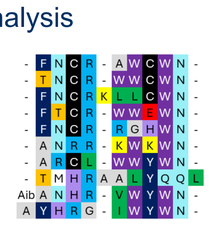


Ochoa, Brown, Fox. *J. Cheminformatics.* 2023

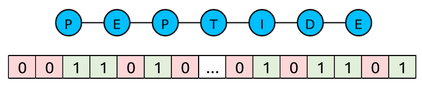
Summary

These open-source tools allow users to incorporate chemical modifications for in silico peptide drug discovery purposes

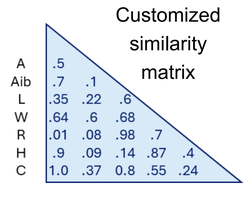
Structure activity relationship (SAR) analysis



Similarity calculations



Property prediction



Sequence design



Erckes, Abderrahmane, Jusot, Steuer, Ochoa. *Drug Discov. Today.* 2026

Acknowledgements

- Kristine Deibler (Molecular AI team, Novo Nordisk, USA)
- Jovan Damjanovic & David Rodriguez (Digital Chemistry & Design, Novo Nordisk, Denmark)
- Thomas Fox (Computational Chemistry, Boehringer Ingelheim, Germany)
- Denis Shields & Raul Fernandez (University College Dublin & IBM Research, Ireland)
- Vanessa Erckes & Christian Steuer (ETH Zurich, Switzerland)
- Maud Jusot & Massina Abderrahmane (Isomorphic Labs, UK & Iktos, France)
- Pilar Cossio (Flatiron Institute, USA)

https://doi.org/10.17952/38EPS.2026.P331

Optimization and Selection of ASF1-Binding Peptides with optimized quantitative bacterial two-hybrid Using qB2H

Francoise Ochsenbein[1], Antoine Guyot[2,3], Emma Maillard[1], Kelly Ferreira-Pinto[3], Laure Plançon-Arnould[1], Aravindan A. Nadaradjane[1], Raphaël Guérois[1], Loïc Martin[3], and Oscar H.P. Ramos[3]

[1]Université Paris-Saclay, CEA, CNRS, Institute for Integrative Biology of the Cell (I2BC), 91198, Gif-sur-Yvette, France. [2]Sanofi Large Molecule Research, Vitry-sur-Seine, France. [3]CEA, Département Médicaments et Technologies pour la Santé (DMTS), SIMoS. Université Paris-Saclay, 91191 Gif-sur-Yvette, France.

ASF1-binding peptides: a model system for qB2H development and binder optimization

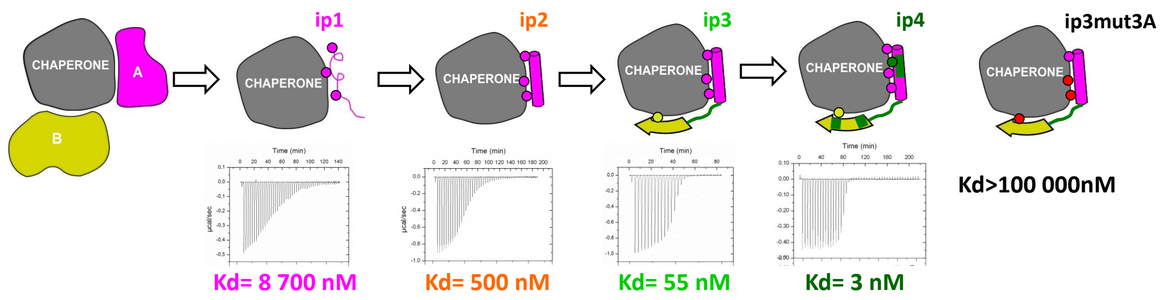
Peptides are powerful tools to perturb protein–protein interactions (PPIs), but their optimization requires detailed knowledge of interaction interfaces and efficient strategies to generate high-affinity binders.

We previously developed synthetic peptides targeting the histone chaperone ASF1 with a broad range of binding affinities.[1] This well-characterized peptide series provided a model system to develop and optimize a quantitative bacterial two-hybrid (qB2H) assay. We then used qB2H to map interaction interfaces and to identify improved ASF1-binding peptides by screening a peptide library. [2]

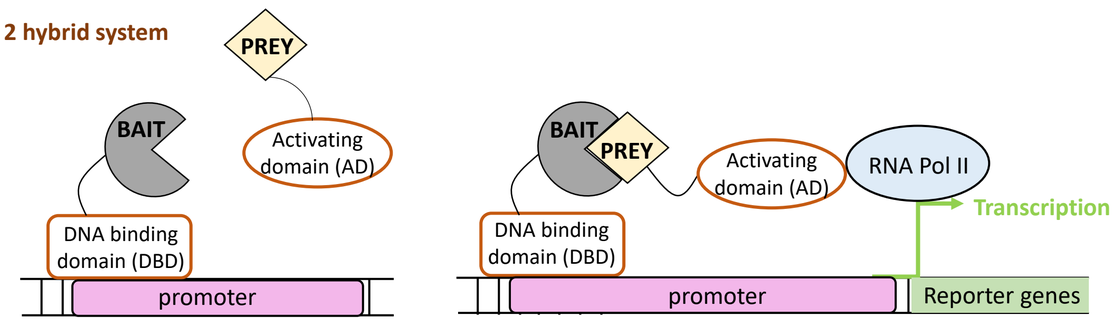
Optimized peptides can further provide molecular templates for the development of foldamer-based binders with enhanced drug-like properties, as illustrated for ASF1-targeting ligands in previous studies[3-5] and **Posters 106 and 76**.

[1] M. Bakail, et al. *Cell Chem Biol* **2019**, 26, 1573–1585 e1510.
[2] A. Guyot, et al. Comput Struct Biotechnol J. 2026 May 25;35(1):0098.
[3] M. Bakail, et al. *Chembiochem* **2019**, 20, 891–895.
[4] J. Mbianda, et al. *Sci Adv* **2021**, 7, eabd9153.
[5] M. E. Perrin, et al. *Chem Commun (Camb)* **2023**, 59, 8696–8699

❖ **Synthetic peptides targeting ASF1**

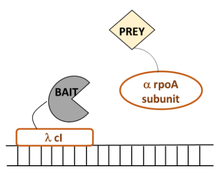


❖ **2 hybrid system**



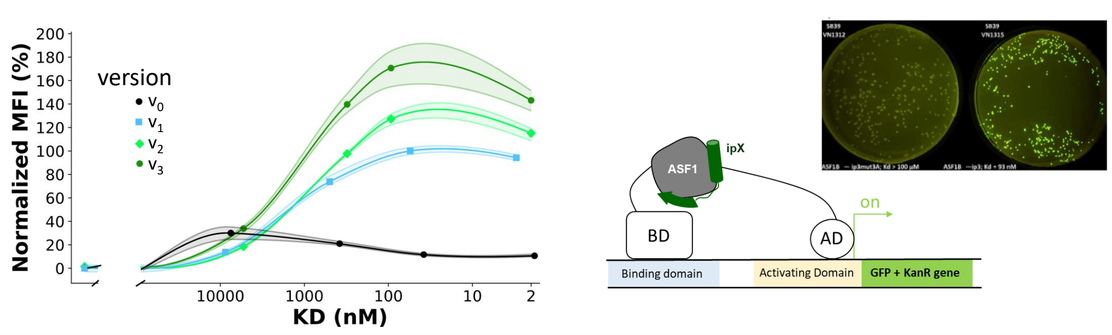
1. qB2H ingeneering

Bacterial two hybrid : Easy manipulation, fast screening, resilient to false results, good for large librairies



Is the fluorescence linear with the affinity between the bait and the prey ?

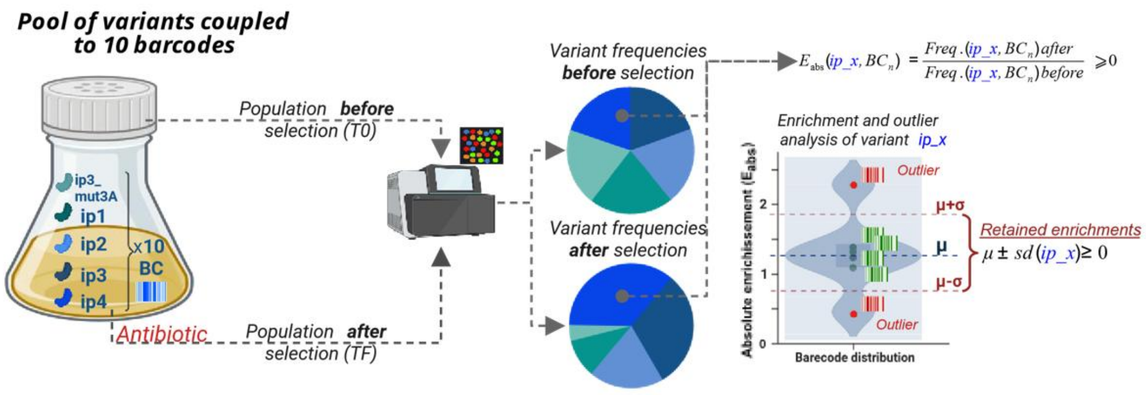
➔ **Test and optimization of reproducibility, signal-to-noise ratio, and correlation between qB2H signal and binding affinity using our series of ASF1-binding peptides spanning a wide range of affinities**

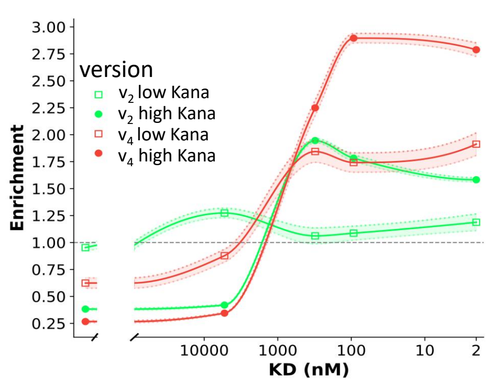


Version	V0 *	V1	V2	V3	V4
Number of Plasmids	3	2	**1**	1	1
cI expression	pZS22	lac_UV5	lac_UV5	**L_tetO**	L_tetO
cI RBS	—	strong	strong	**weaker**	**very weak**
qB2H promoter	Two cI binding sites	Single cI binding site	single cI binding site	Optimized single cI binding site	Optimized single cI binding site
Reporter	eGFP	eGFP + KanR	eGFP + KanR	weak eGFP + KanR	**KanR only**
Main step	**Initial system**	promoter optimization	single plasmid	quantitative optimization	library selection / NGS

** McLaughlin RN et al. Nature. 2012;491:138–142.*

Does fitness correlate linearly with bait–prey affinity?



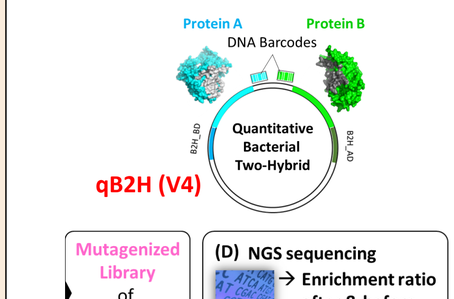


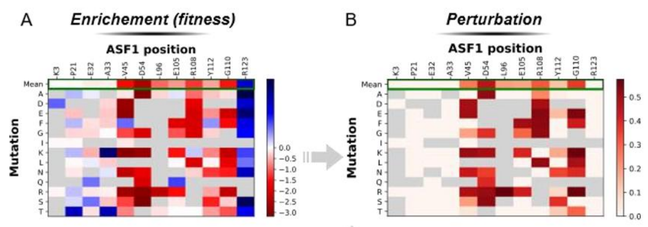
✓ **Optimized version (V4) qB2H response is linear from 5µM to 50nM**

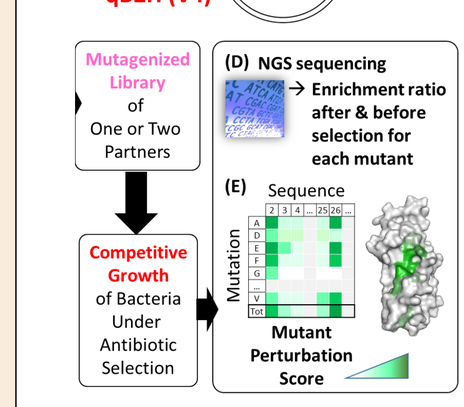
- **Bacterial strain** → **SB39**
  Best Kd- fluorescence correlation, lowest variability
- **Plasmid number** → **1 plasmid**
  Simpler, robust quantitative readout
- **qB2H promoter** → **Single λ cI-binding site**
  Best Kd and signal correlation
- **cI expression** → **L_tetO + weak RBS**
  Tight and reduced expression of the cI fusion ↑signal-to-noise, ↓ stochasticity
- **Reporter** → **Weak KanR only** (v4)
  ↓ metabolic burden, improved quantification

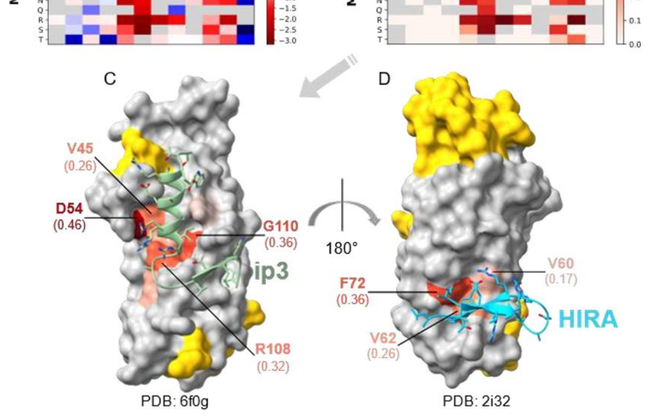
2. interface mapping application

Can qB2H map PPIs using a mutant library?







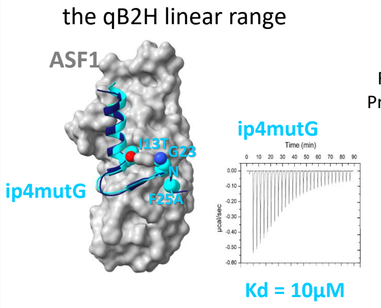


✓ **qB2H (v4) enables PPI interface mapping**

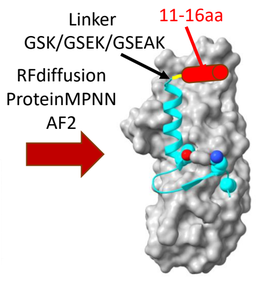
3. Screening for improved variants

Can qB2H identify improved variants from AI-designed libraries?

1) Rational mutant design to start at the lower end of the qB2H linear range



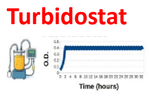
2) Peptide lengthening using generative AI tools



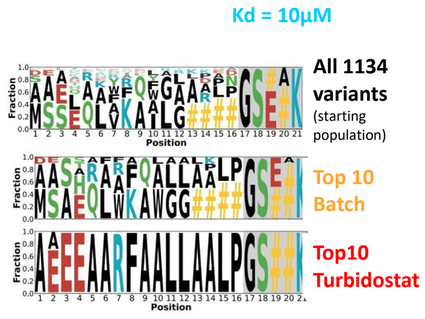
3) Test different selection pressure

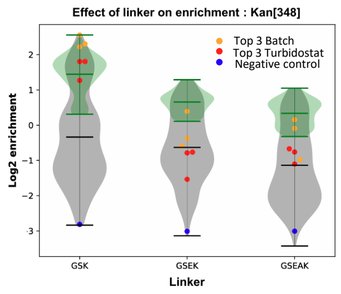


short term (4-5h) batch selection, increasing kanamycin concentration



long term (24-32h) selection using turbidostat, fixed kanamycin concentration

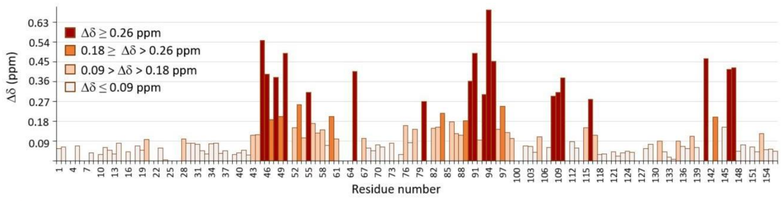


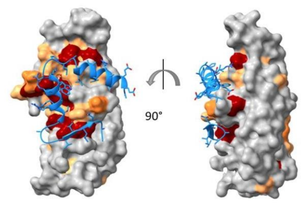


3) Affinity measurement of the two Top1

ip4mutG	10 000nM
Top 1 Batch	209nM
Top 1 Turbidostat	135nM

4) Mapping the interacting surface by NMR of the best binder selected





✓ **qB2H (v4) can identify binders with improved affinity from AI-designed libraries**

Conclusion & Perspectives

Guyot, et al. Comput Struct Biotechnol J. 2026 May 25;35(1):0098

- ASF1-binding peptides enabled the development of an optimized quantitative B2H assay (qB2H v4).
- qB2H v4 enables quantitative PPI analysis, interface mapping, and selection of improved binders from large libraries.
- Coupling qB2H selection with generative AI provides an efficient strategy to identify higher-affinity ASF1-binding peptides.

➔ Selected peptides provide promising templates for the development of foldamer-based ASF1 binders

Contact : francoise.ochsenbein@cea.fr

Uncovering the structural logic of Cnn autoinhibition: an integrative NMR, SAXS, and AlphaFold approach

A. Vitard[2†], A. Elfarkouchi[1†], N. Joly[1], L. Mammri[1], Sébastien Brier[3], L. Tanneur[1], Cécile Hu[1], Aurélien Thureau[4], Nicolas Joly[1], F. Ochsenbein[2*], P. Conduit[1*]

[1]Université Paris Cité, CNRS, Institut Jacques Monod, F-75013 Paris, France.

[2]Institute for Integrative Biology of the Cell (I2BC), CEA, CNRS, Univ. Paris-Sud, Université Paris-Saclay, F–91198, Gif-sur-Yvette, cedex, France

[3]Biological NMR and HDX-MS Platform, Institut Pasteur, Université Paris Cité, CNRS UMR 3528, 75015 Paris, France

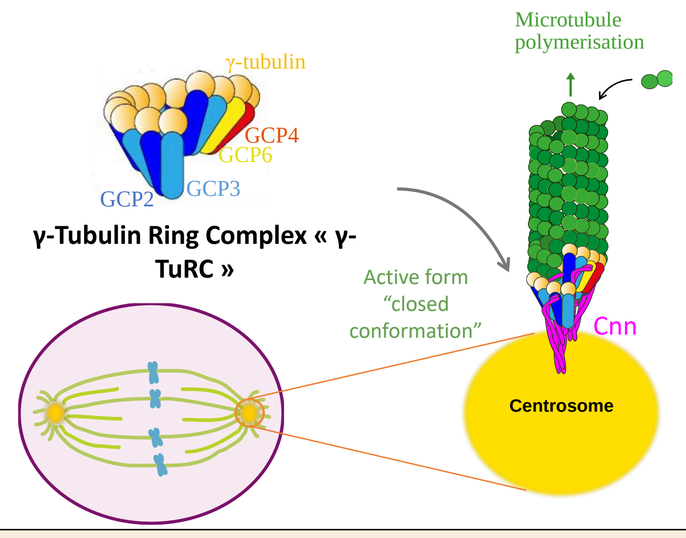
[4]Swing Beamline, Synchrotron SOLEIL, Gif sur Yvette, France

[†]Co-first authors, [*]Co-corresponding authors

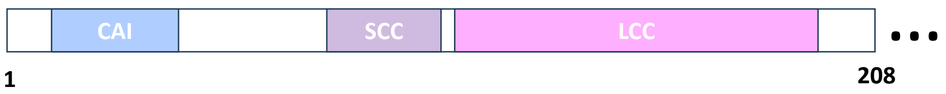
https://doi.org/10.17952/38EPS.2026.P466

Cnn: a modular centrosomal scaffold with unresolved structural regulation

Centrosomin (Cnn) is a key component of the *Drosophila melanogaster* centrosome, involved in microtubule nucleation. During cell division, Cnn is recruited to the centrosomes to form a scaffold essential for recruiting centrosomal factors. Among those factors, g-TuRC complex is recruited by Cnn N-ter region to template microtubules nucleation during mitosis.



Microtubule nucleation is tightly regulated, with Cnn maintained in an autoinhibited state in the cytosol to prevent ectopic γ-TuRC activation. The N-terminal region (residues 1–208) comprises three main sub-regions: an N-terminal autoinhibitory segment (CAI) present only in species close with drosophilae, a short α-helical motif (SCC), and a long coiled-coil domain (LCC).



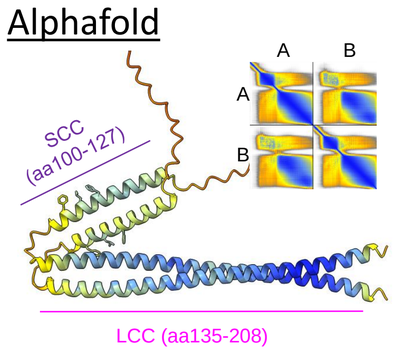
In *Drosophila*, autoinhibition is mediated exclusively by the CAI domain, whereas both the SCC and LCC are required for activation. In humans, by contrast, the SCC-equivalent alone is sufficient to activate γ-TuRC, while the LCC-equivalent negatively regulates SCC activity.

	Activation	inhibition
CDK5RAP2 (human)	Y-TuNA (equivalent of SCC)	γ-TuNA-In (equivalent of LCC)
Cnn (drosophilae)	**CM1 (SCC+LCC)**	**CAI**

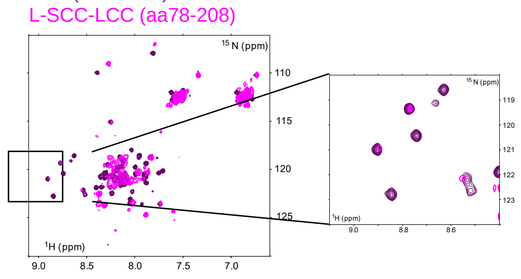
Key question : How does the CAI domain structurally inhibit the CM1 domain?

1. SCC+LCC: a necessary hairpin structure

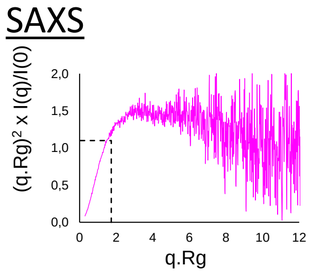
Alphafold



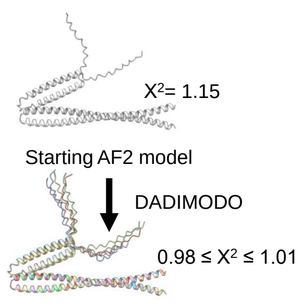
NMR



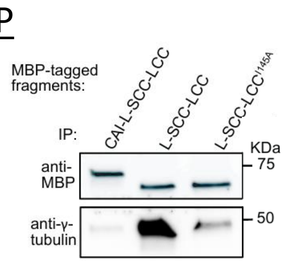
SAXS



Kratky plot shows an extended structure and some disordered region



Co-IP

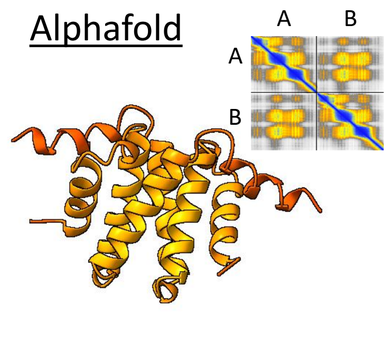


I145 is a key in the hairpin structure model

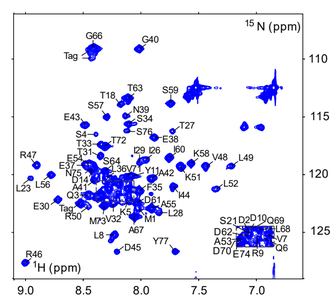
Validation of the hairpin structure

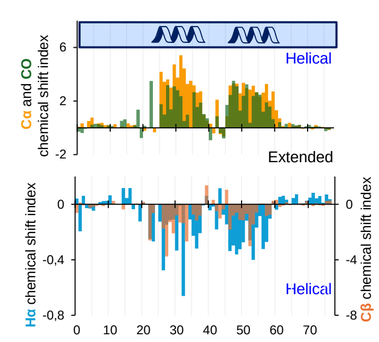
2. CAI: a domain hard to predict

Alphafold

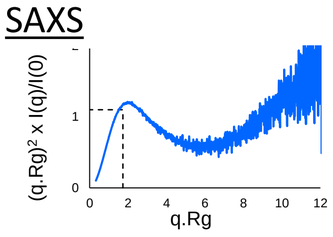


NMR

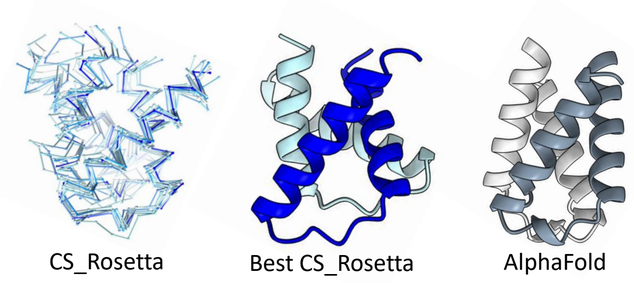




SAXS



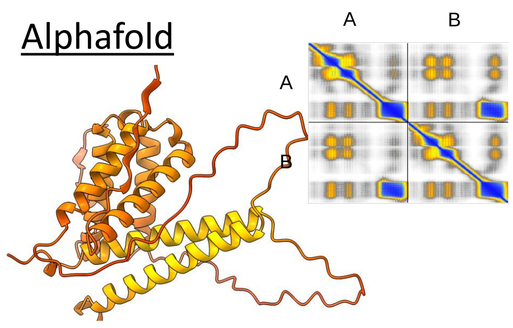
Kratky plot shows a globular structure with some disordered region



CAI adopts a double helix conformation

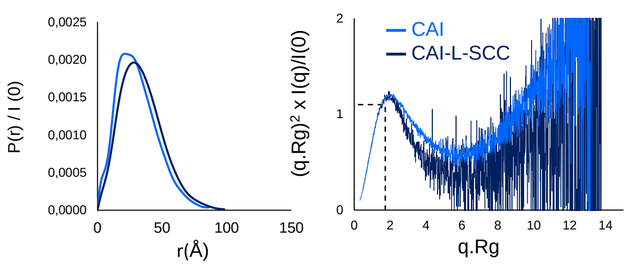
3. CAI in interaction with SCC

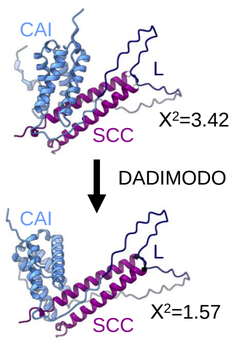
Alphafold



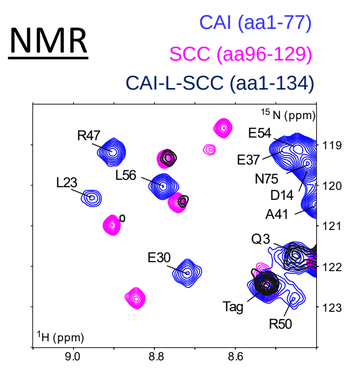
AF2 converges with a low confidence score on the interaction

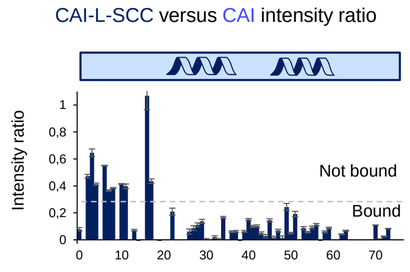
SAXS





NMR

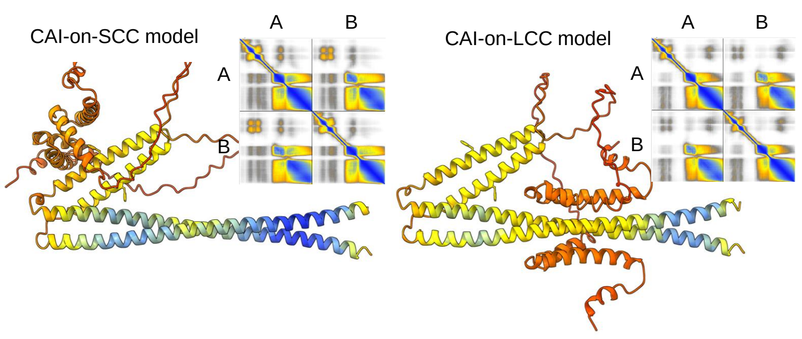




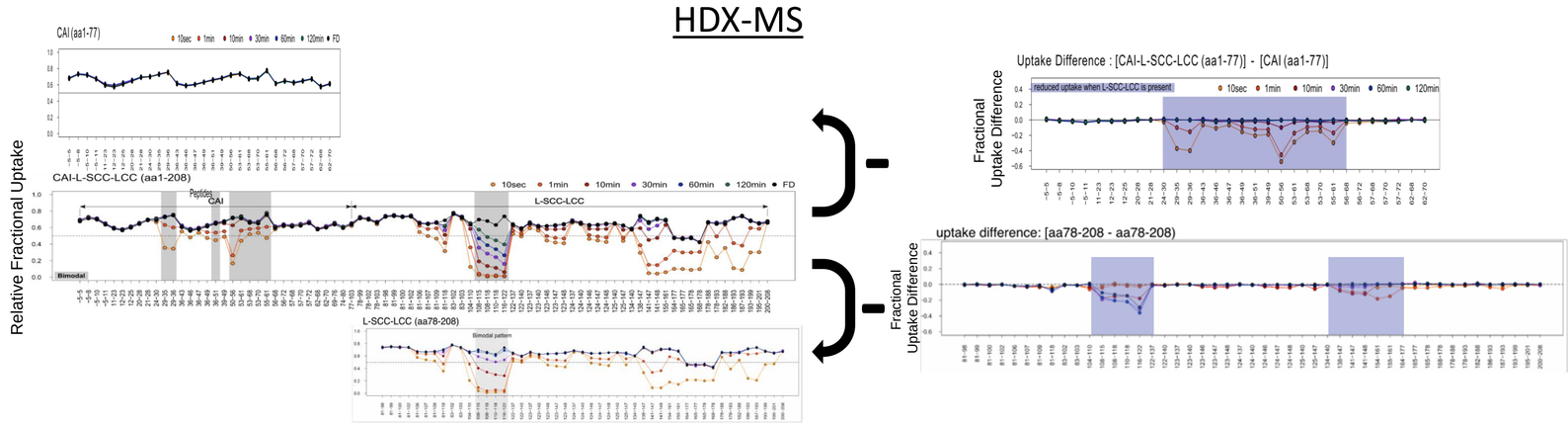
CAI interacts with SCC

4. CAI in interaction with SCC or LCC?

Alphafold



HDX-MS



CAI interacts with SCC even in the full construct

Conclusion & Perspectives

By combining HDX-MS, AlphaFold, SAXS, and NMR, we show that the CAI domain adopts a structured conformation and folds back onto the SCC motif, masking the γ-TuRC-binding interface and providing a structural basis for Cnn autoinhibition in *Drosophila*.

Future studies will focus on capturing the transition from the autoinhibited to the active state and elucidating how centrosomal cues, including phosphorylation, trigger SCC/LCC exposure and γ-TuRC activation.

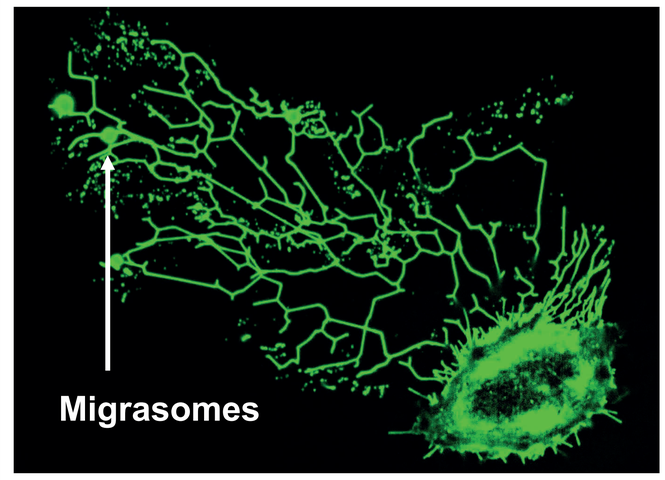
A peptide interface for collection and functional analysis of migrasomes

ᵒ Mina Okochi, Shogo Saito (Institute of Science Tokyo, Japan)

Abstract

https://doi.org/10.17952/38EPS.2026.P535

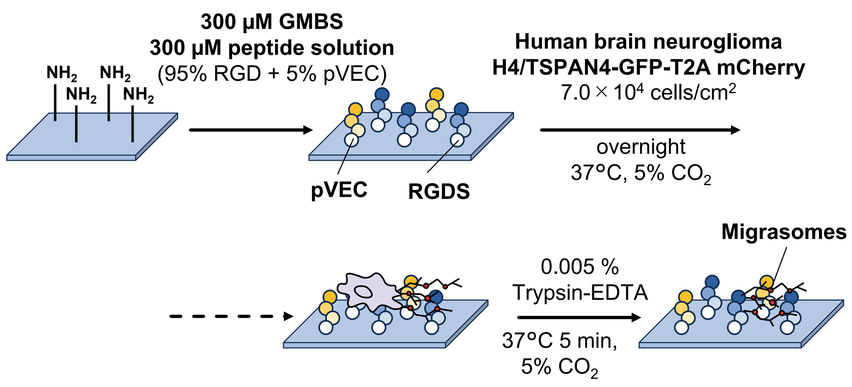
Migrasomes are a specific type of extracellular vesicle that form onto filamentous structures, called retraction fibers, left behind by migrating cells [1]. Recently, we developed a method to collect migrasomes using the peptide-modified substrates while detaching the cells [2]. Capturing migrasomes in an intact manner is crucial for evaluating their function, as they exhibit a multivesicular structure and contain mechanisms for the release of internal molecules. Moreover, because migrasome formation on retraction fiber is closely linked to cell migration, the number of migrasomes produced is generally lower than that of other secreted vesicles. Therefore, the use of peptide-modified substrates for selective fractionation allows for the functional assessment of small quantities of intact migrasomes generated by migrating cells and their effects on recipient cells. Consequently, this method holds promise for elucidating migrasome-mediated communication in cell-cell interactions, such as those involving the IL-6 amplifier.



[1] L. Ma *et al.*, *Cell Res.*, 25, 24-38 (2015), [2] S. Saito *et al.*, *Mater. Sci. Eng. C*, 131, 112495 (2021).

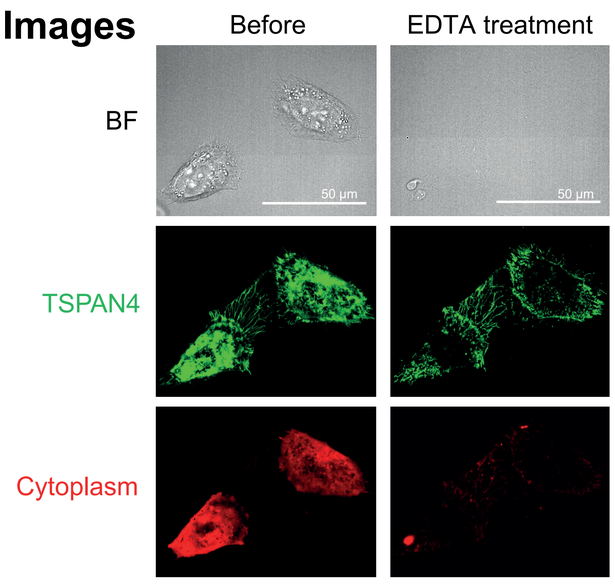
1 Capture of H4 cell-derived migrasomes using the peptide-modified substrate

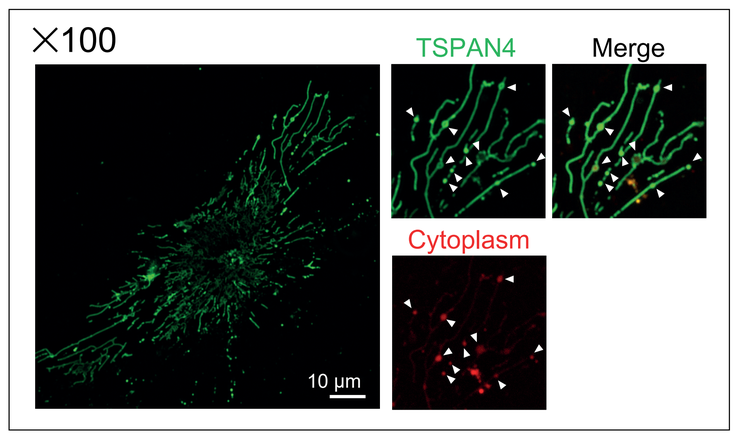
Peptide modification of NH_2-surface



RGD: Integrin ligand, GRGDSGGGC
pVEC: Cell-penetrating peptide, LLIILRRRIRKQAHAHSKGGGC

Images

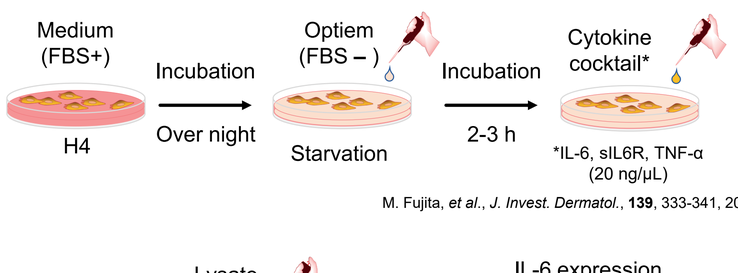




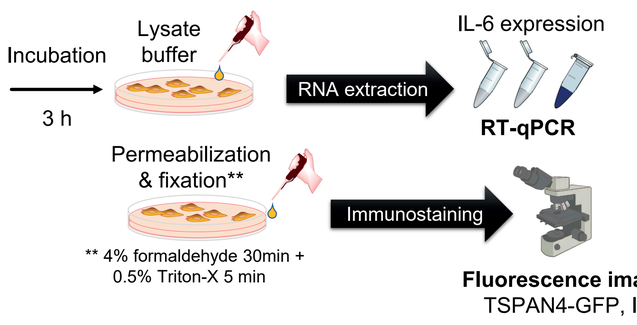
Cytoplasmic component observed inside of migrasomes
→ **Migrasomes were captured on the peptide-immobilized substrate without damages.**

2 Induction of IL-6 amplifier

Cell treatment



M. Fujita, *et al.*, *J. Invest. Dermatol.*, **139**, 333-341, 2019



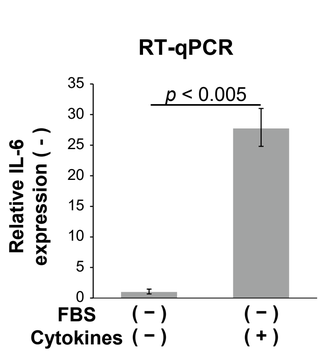


Fig. Evaluation of IL-6 expression level by RT-qPCR.

IL-6 expression increased by 25-fold.

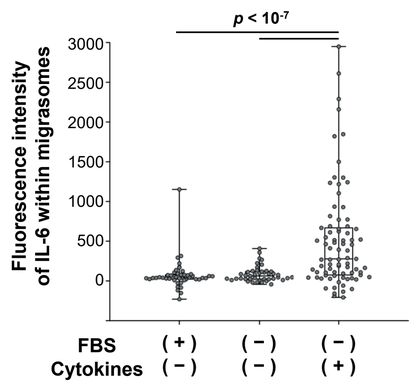
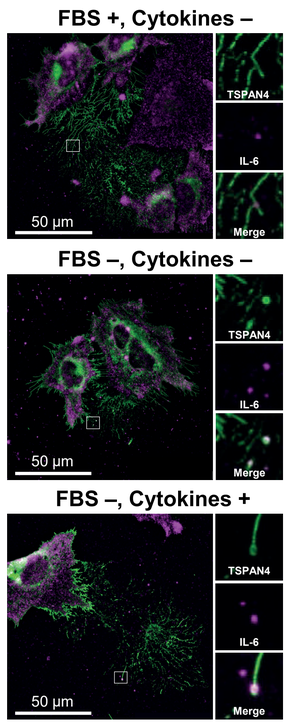


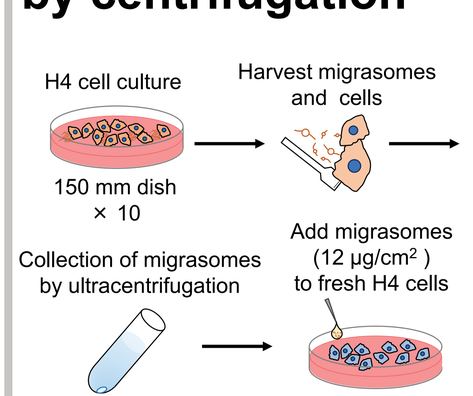
Fig. Evaluation of fluorescence intensity in the migrasome region by immunostaining.

The amount of IL-6 expression increased in migrasomes.

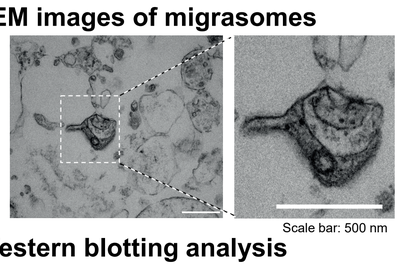
IL-6 were concentrated in migrasomes compared to the cell body upon IL-6 amplification.



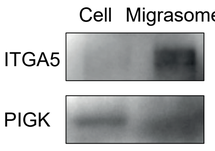
3 IL-6 amplifier induction using migrasome collected by centrifugation



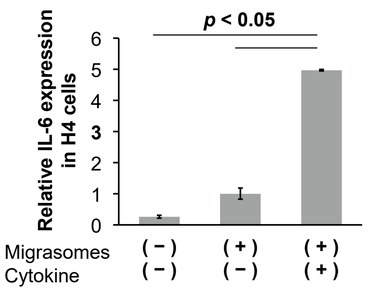
TEM images of migrasomes



Western blotting analysis

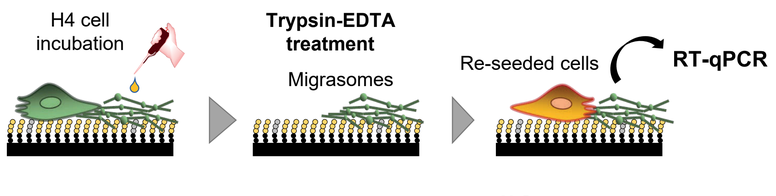


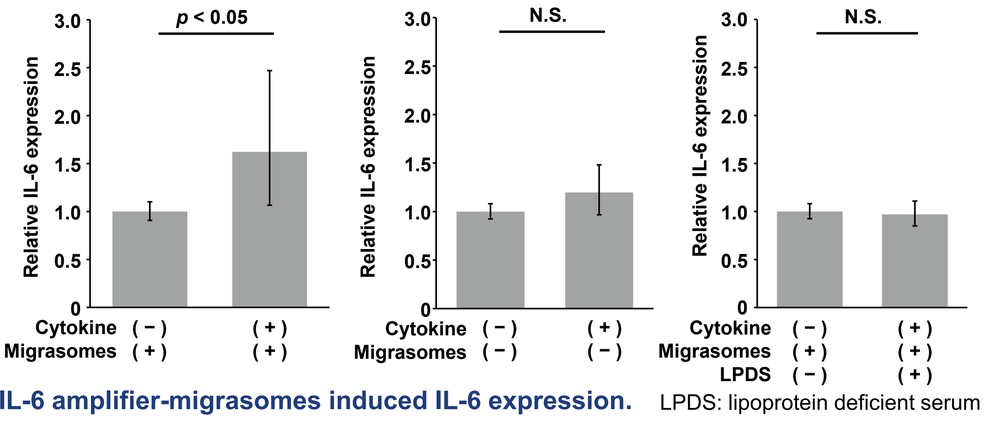
Migrasome marker proteins
ITGA5: Integrin α5
PIGK: Phosphatidylinositol glycan anchor biosynthesis class K



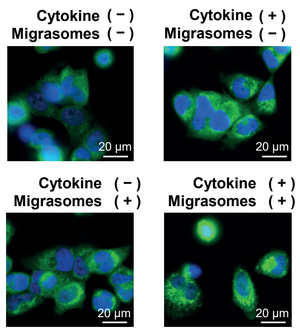
Addition of migrasomes increased IL-6 expression by 5-fold.

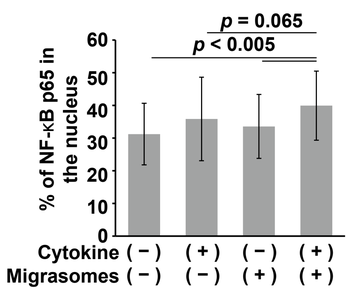
4 IL-6 amplifier-induced cell derived migrasomes promote IL-6 expression in the recipient cells



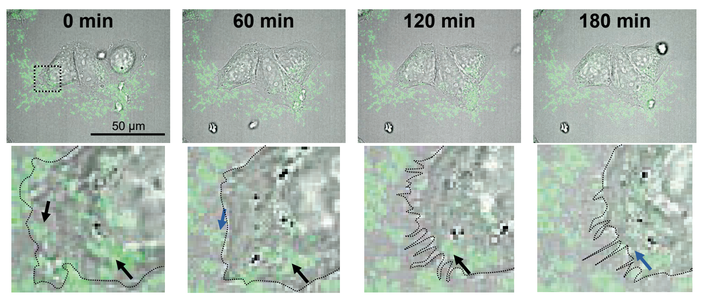


IL-6 amplifier-migrasomes induced IL-6 expression. LPDS: lipoprotein deficient serum





IL-6 amplifier-migrasomes induced NF-κB activation.



Cellular uptake of migrasomes (green, black arrow) **captured on the surface.** The photos below are a time course of an enlarged view of the area within the dashed-line square.

Conclusions

Migrasomes derived from IL-6 amplifier-induced human neuroglioma were shown to promote inflammatory responses in the recipient cells. When migrasomes from the IL-6-amplifier-induced cells captured on a peptide-modified substrate were used to stimulate cells, even a small number of migrasomes was sufficient to induce IL-6 expression [3,4]. These findings suggest that migrasomes contribute to inflammatory signaling via cell-to-cell communication, highlighting their potential roles in cytokine transduction and offering insights into therapeutic strategies targeting intercellular communication in inflammatory diseases.

[3] S. Saito et al. Inflammation-induced cell-secreted migrasome promotes IL-6 expression in the recipient cells. *Biomater. Adv.*, 184, 214793 (2026) . [4] A. B. R. D. Putra et al. *J. Biosci. Bioneg.* (in press)

https://doi.org/10.17952/38EPS.2026.P268

Machine Learning–driven Prediction of Circular Dichroism Spectra for Peptides through Multi-scale Structural Descriptors

Michele Casoria[1,2,4], Marina Macchiagodena[1,3], Paolo Rovero[2,3], Claudia Andreini[1,4], Anna Maria Papini[2,3], Marco Pagliai[1,3]

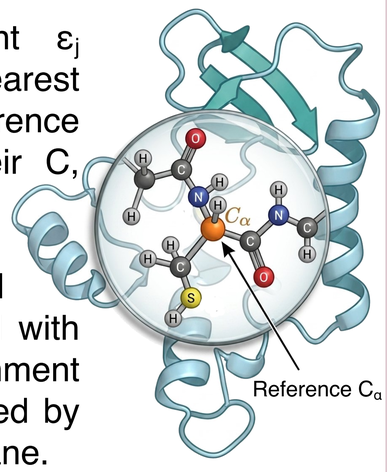
1 Research Unit of Computational Chemistry, University of Florence, 50019 Sesto Fiorentino, Italy
2 Interdepartmental Research Unit of Peptide and Protein Chemistry and Biology, University of Florence, 50019 Sesto Fiorentino, Italy
3 Department of Chemistry “Ugo Schiff”, University of Florence, 50019 Sesto Fiorentino, Italy
4 Magnetic Resonance Center - University of Florence, 50019 Sesto Fiorentino, Italy
e-mail: michele.casoria@unifi.it

Introduction

Circular dichroism (CD) spectroscopy provides rapid characterization of protein secondary structure, but limited scalability and high-purity requirements hinder high-throughput applications. Experimental CD spectra were retrieved from the Protein Circular Dichroism Data Bank (PCDDB), curated by removing duplicates and retaining room-temperature measurements associated with experimentally determined structures. Here, we develop a structure-based machine learning framework using a rotationally invariant Smooth Overlap of Atomic Positions (SOAP) representation and tensor neural network to predict CD spectra from 3D structures.

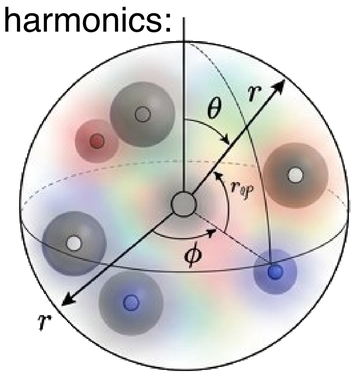
Local Environment in Reference Frame

Each local environment ε_j comprises the six nearest residues around the reference Cα, represented by their C, Cα, N, and O atoms.
A canonical frame is then constructed from the local geometry, with z aligned with the mean environment direction and x determined by PCA in the orthogonal plane.



Atom-Type Resolved Spherical Expansion

The local atomic density is expanded over Gaussian radial functions and complex spherical harmonics:



$$\rho_a(r) \rightarrow C_{nlm}^{(a)}$$

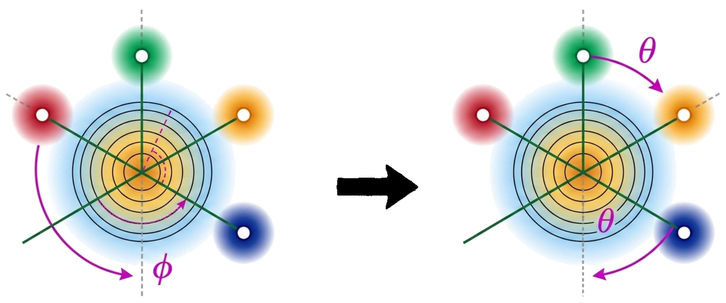
Radial + Angular chemical information

$$C_{anlm}^{(i)} = \sum_{j \in \mathcal{E}_i} \delta_{a,a_j}\, g_n(r_j)\, Y_l^m(\theta_j, \phi_j)$$

Rotationally Invariant Power Spectrum

Rotational invariance is obtained by contracting over m: for four atom types, the 10 unique atom-type pairs are retained.

$$P_{abnn'l}^{(i)} = \sum_{m=-l}^{l} C_{anlm}^{(i)} C_{bn'lm}^{(i)*}$$



Residue-level descriptors are averaged over the protein:

$$\langle P \rangle = \frac{1}{N_{\text{res}}} \sum_{i=1}^{N_{\text{res}}} P^{(i)} \in \mathbb{R}^{10\times13\times13\times9}$$



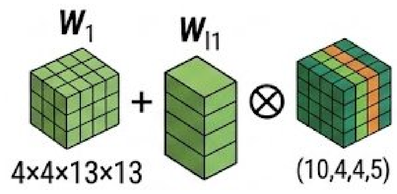
Spectral Target Compression

Experimental CD spectra over the selected wavelength range are compressed using PCA.
The first five principal components are retained as regression targets.

$$\mathbf{y}_{\text{CD}} \in \mathbb{R}^{N_\lambda} \xrightarrow{\text{PCA}} \mathbf{y}_{\text{PCA}} \in \mathbb{R}^5$$

Tensor Neural Network

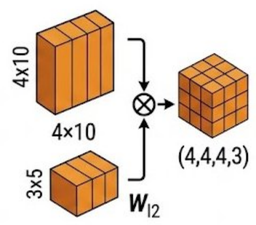
The protein-level descriptor $\langle P \rangle$ retains the structure of atom-type, radial (n, n′), and angular (l) correlations.
Instead of flattening the descriptor, the network performs learnable tensor contractions along the physical dimensions.
The first layer simultaneously contracts the two radial dimensions and mixes the angular components using:



$$W_1 \in \mathbb{R}^{4\times4\times13\times13}$$

$$W_{l1} \in \mathbb{R}^{5\times9}$$

The second layer contracts the atom-type and angular dimensions while preserving the two learned radial dimensionss:

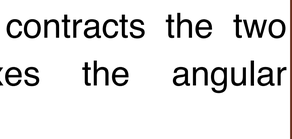


$$W_2 \in \mathbb{R}^{4\times10}$$

$$W_{l2} \in \mathbb{R}^{3\times5}$$

The resulting latent tensor is contracted with a learnable readout tensor to predict the five principal components of the CD spectrum.

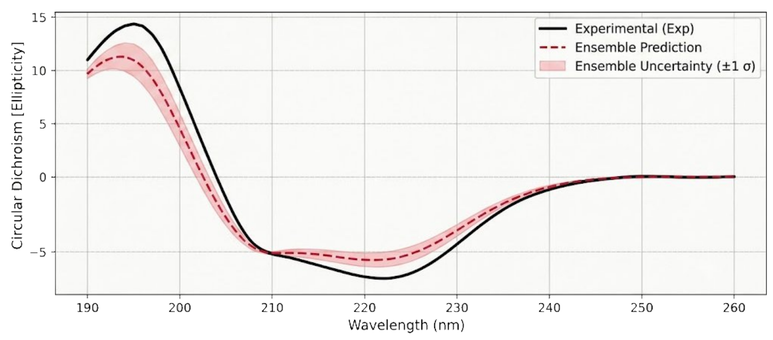
$$W_3 \in \mathbb{R}^{5\times4\times4\times4\times3}$$



The training loss is computed as the mean squared error (MSE) between the five predicted PCA components and the corresponding target components. The architecture preserves the physical organization of the descriptor while learning separate transformations along atom-type, radial, and angular dimensions.

Model Training & Validation

The dataset was randomly partitioned into five folds, using four folds for training and one for validation in each iteration. The network was optimized by minimizing the mean squared error (MSE) between the predicted and target five-dimensional PCA representations.
For validation, the predicted PCA components were transformed back into the original CD spectral space using the inverse PCA transformation. The coefficient of determination R^2 was then computed between the reconstructed and experimental CD spectra.
The model parameters yielding the highest validation R^2 were retained for each fold, resulting in a five-fold ensemble.



Metric	Value
Mean R^2	0.85
Mean RMSD	0.66
Pearson Correlation	0.96
Sign Accuracy	87.8%
Ensamble Uncertainty	0.42
Spectral Diversity	0.85

Conclusions

The proposed tensor-based neural network accurately reproduces experimental CD spectra while preserving most of their spectral diversity, with low ensemble uncertainty, and will be further validated on independent experimental peptide spectra to assess its generalizability and robustness.

Acknowledgments

European Peptide Society is kindly acknowledged for the awarded registration grant to Dr. Michele Casoria.

Stability and Antimicrobial Activity of Synthetic Peptides Derived from Lactoferricin B20-30

T.I. Pajpanova[1], I.P. Bogdanov[1], M. Lambev[2], G.I. Ivanov[1], S. Mihaylova[2], V. Sándor[3], K. Kaliková[4], N.T. Tzvetkov[1] & F. Kilar[3]

[1]Institute of Molecular Biology "Roumen Tsanev", Bulgarian Academy of Sciences, Acad. G. Bonchev str.Bl. 21, Sofia 1113, Bulgaria; [2]Medical College, Medical University "Prof. Dr. Paraskev Stoyanov", 55 Marin Drinov str., Varna 9002, Bulgaria; [3]Institute of Bioanalysis, Faculty of Medicine, University of Pécs, Honvéd str 1, 7624 Pécs, Hungary; [4]Department of Physical and Macromolecular Chemistry, Faculty of Science, Charles University, Hlavova 8, 12800 Prague, Czech Republic

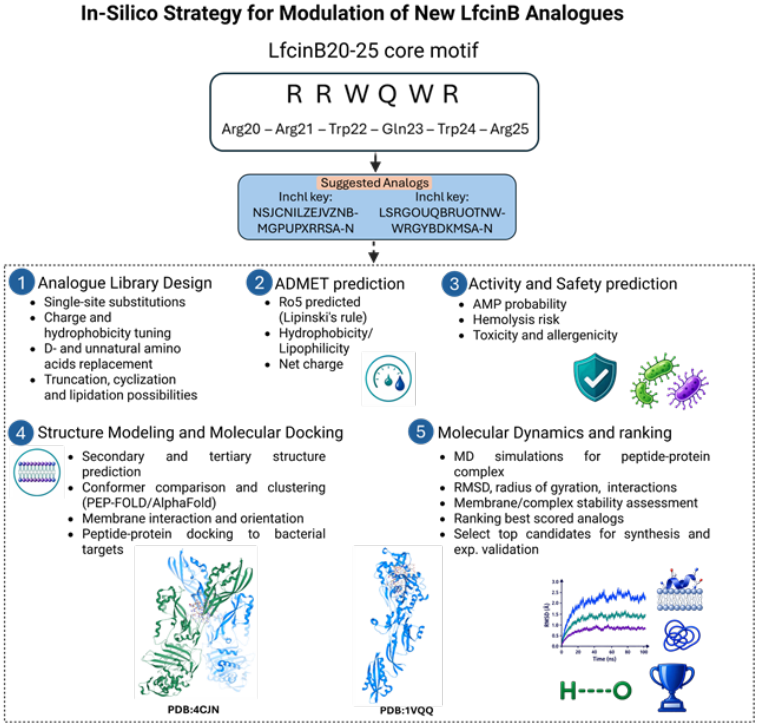
***Corresponding author:** tamara@bio21.bas.bg
https://doi.org/10.17952/38EPS.2026.P191

With the increasing prevalence of multidrug-resistant (MDR) bacteria, the design of new types of drugs, including synthetic antimicrobial peptides (AMPs), is highly urgent. Antimicrobial peptides are effective and selective for bacteria, i.e., are not toxic to mammalian cells.

Numerous natural AMPs, such as lactoferricin B (LfcinB) exhibit a cationic amphipathic helical conformation, wherein cationic amino acids such as lysine and arginine play pivotal role in antimicrobial activity due to their capacity to electrostatically interact with negatively charged bacterial membranes. However, these residues also constitute the vulnerable spot of many cationic AMPs, rendering them susceptible to proteolytic digestion.

In our previous studies, we developed and reported a series of short non-toxic LfcnB20-25 hexapeptides composed of various natural and unnatural amino acid residues, demonstrating promising antibacterial activity, as well as high hydrolytic stability [1,2].

Recently, we have created a new series of 12 hexapeptide analogues of ^{20}**RRWQWR**^{25} and 1 heptapeptide analogue of ^{20}**RRWQWRM**^{26}, based on the concept that cationic charge and lipophilicity are major factors determining the antibacterial activity of short cationic peptides, and modifications with unnatural and D-isomeric acids will potentiate their activity and stability. In-silico drug design was applied also.



Acknowledgements

This work is financially supported by the Bulgarian National Science Fund project KP-06- N93/10 (КП-06-Н93/10).

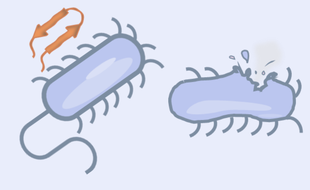
References

1. T. Pajpanova, D. Dimitrova, I. Bogdanov, V. Sandor, S. Mihaylova, T. Dzimbova, F. Kilar. J. Pept Sci. 2024, 30(S2), 636.
2. D. Dimitrovaq A. Tzvetkova, S. Mihaylova, M. Lambev, S. Ualcheva-Kuzmanova, T. Paypanova. Pharmacia, 2026, 73, 1-6.

SAR Study of Antimicrobial Peptide with Cross-Kingdom Activity

Aparna Palakkurussi Rathessan [1], Fereshteh Ghazisaeedi [2,3], Krithika Unmesh [5], Pascal-Kolja Bingül [6], Johannes Kupke [2], Suvrat Chowdhary [1], Dennis Hanke[2,3], Maria Andrea Mroginski [5], Marcus Fulde [2,3,4] and Beate Koksch [1]

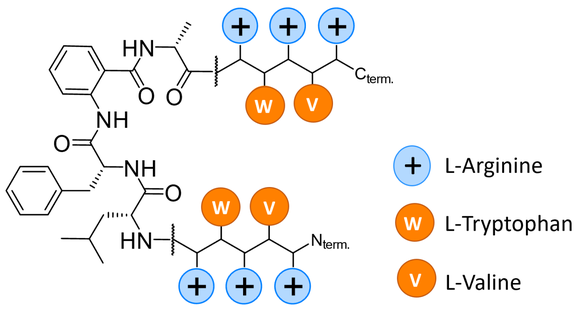
[1] Institute of Chemistry and Biochemistry, Freie Universität Berlin, Berlin, Germany
[2] Institute of Microbiology and Epizootics, Center of Infection Medicine, Freie Universität Berlin, Berlin, Germany
[3] Institute of Microbiology, University of Veterinary Medicine Hannover, Hannover, Germany
[4] Veterinary Center for Resistance Research (TZR), Freie Universität Berlin, Berlin, Germany
[5] Department of Chemistry, Technische Universität Berlin, Berlin, Germany
[6] School of Veterinary Medicine, Institute of Veterinary Anatomy, Freie Universität Berlin, Berlin, Germany
https://doi.org/10.17952/38EPS.2026.P166



Research Aim

Antimicrobial resistance (AMR) is a critical global health concern that threatens the effective prevention and treatment of an ever-increasing range of infections caused by microbial pathogens. Antimicrobial peptides (AMPs) are recognized as potential lead structures for developing next-generation therapeutics. We aim to enhance the immense potential of AMPs through conformational tuning and differential fluorination on two different turn-like peptide architectures, SAJO and C7.

SAJO System



SAJO-2 [1,2,3]

N-	*N-terminal strand*	*β-turn motif*	*C-terminal strand*	*-C*

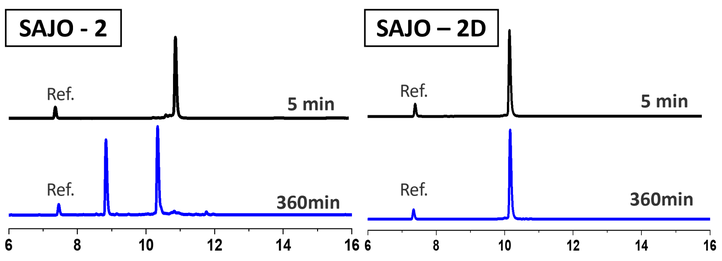
N_{term}-Arg-Val-Arg-Trp-Arg---[D-Leu-D-Phe-[2]Abz-D-Ala]---Arg-Trp-Arg-Val-Arg-C_{term}

Arg-Val-Arg-Trp-Arg	SAJO-2	Arg-Trp-Arg-Val-Arg
D-Arg-Val-D-Arg-Trp-D-Arg	SAJO-D	D-Arg-Trp-D-Arg-Val-D-Arg
Arg-Val-D-Arg-Trp-Arg	SAJO-1D	Arg-Trp-D-Arg-Val-Arg
D-Arg-Val-D-Arg-Trp-Arg	SAJO-2D	Arg-Trp-D-Arg-Val-D-Arg
Arg-Pfp-D-Arg-Trp-Arg	SAJO-PfpGly-1D	Arg-Trp-D-Arg-Pfp-Arg

peptides (serial dilutions, start: 1024 µg/mL) *incubated with bacteria culture (2 × 10^6 CFU/mL), pH 7.4; 37 °C (24 h).*

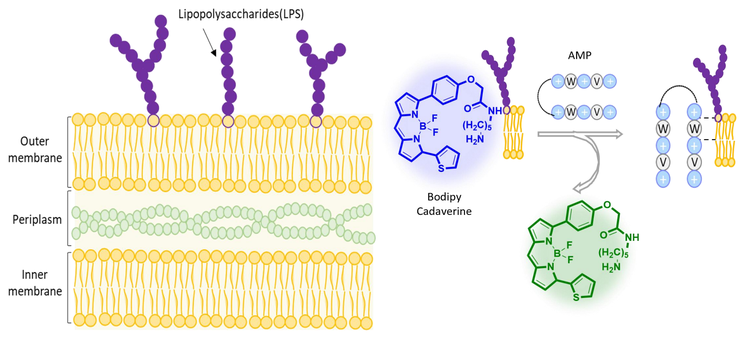
Antimicrobial Peptide	*S.* Typhimurium ATCC 14028	*E. coli* ATCC 25922	*S. aureus* ATCC 29213	*P. aeruginosa* ATCC 27853	*C. albicans* IMT 9655
SAJO - 2	32	**16**	64	64	**32**
SAJO - D	32	**16**	256	512	**32**
SAJO - 1D	32	32	128	1024	**32**
SAJO - 2D	**16**	32	256	1024	**32**
SAJO - PfpGly-1D	32	32	64	512	**32**

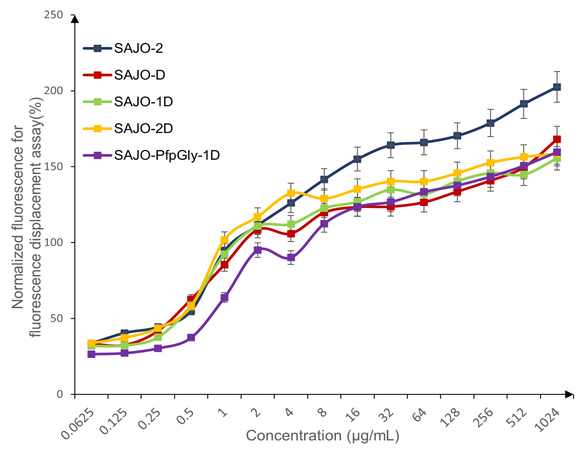
Enzymatic digestion



Digestion profile of SAJO-2 and SAJO-2D by *α-chymotrypsin*

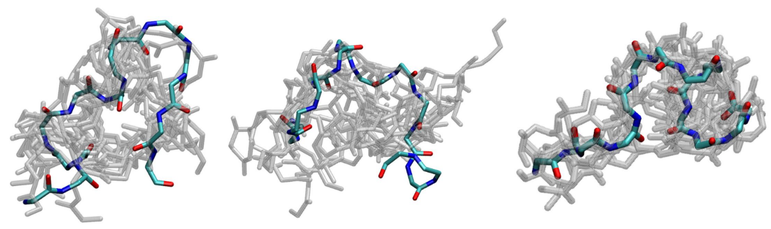
LPS Binding Affinity Studies





The peptides displace Bodipy Cadaverine dye from the lipid A, which dequenches the dye and enhances the fluorescence signal

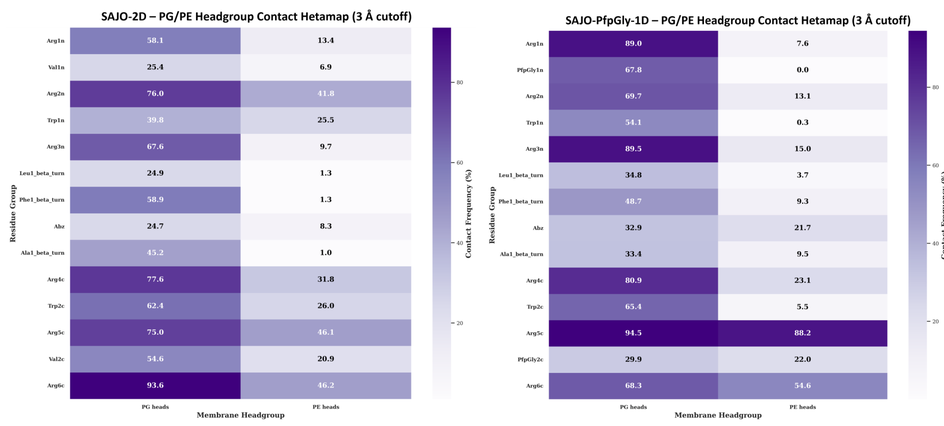
Molecular Dynamics Simulations: In Solution



SAJO-2D **SAJO-PfpGly-1D** **SAJO-PfpGly**

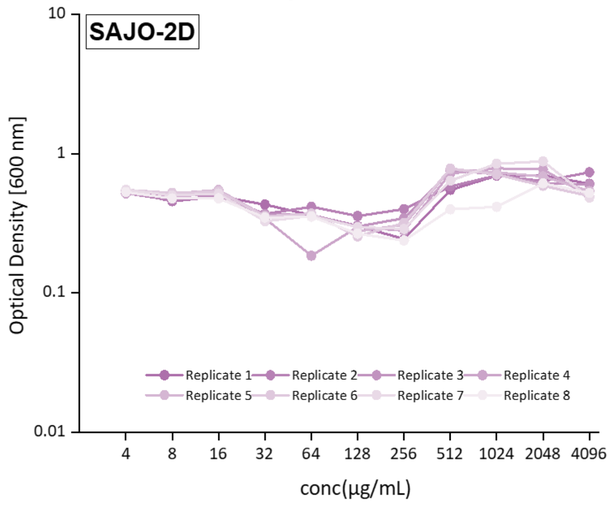
Simulations performed in aqueous solution reveals D-modified fluorinated analogue leads to a more open structure and a markedly broader conformational ensemble

Molecular Dynamics Simulations: POPG/POPE Bilayers



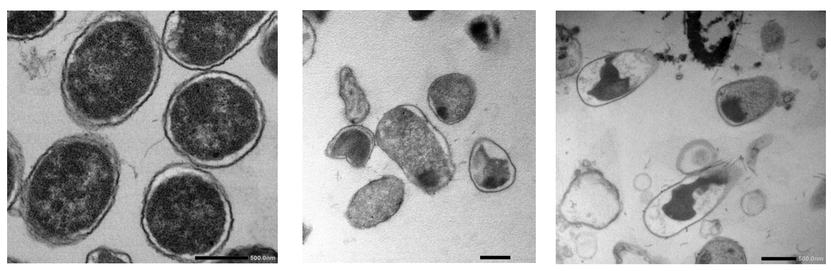
SAJO-2D shows stronger membrane contacts, through its C-terminal residues, and displays enhanced POPG selectivity. SAJO-PfpGly-1D displays the strongest minimal POPE interaction profile, followed by tryptophan and the PfpGly unit.

Adaptive Laboratory Evolution with *E. coli*



Rapid bacterial adaptation to AMPs

Transmission Electron Microscopy

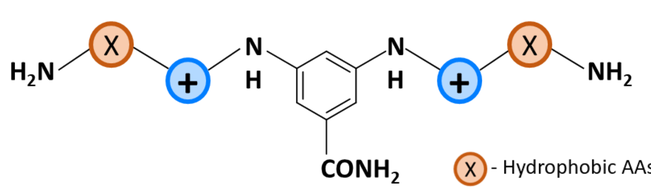


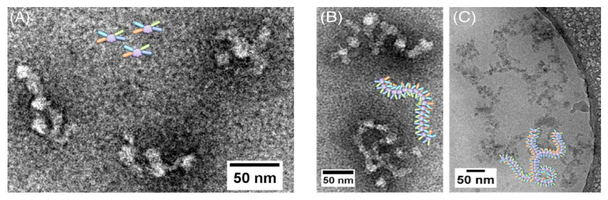
E. Coli (Control) | SAJO-2D 2 x MIC (24h) | SAJO-PfpGly-1D 2 x MIC (24h)

Extensive disruption to cells by SAJO analogues

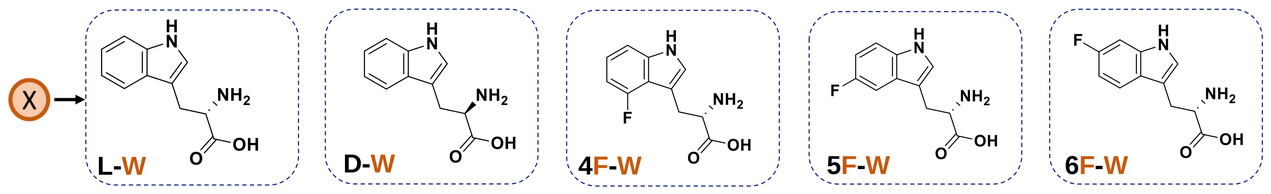
Read full publication [4]

C7 System

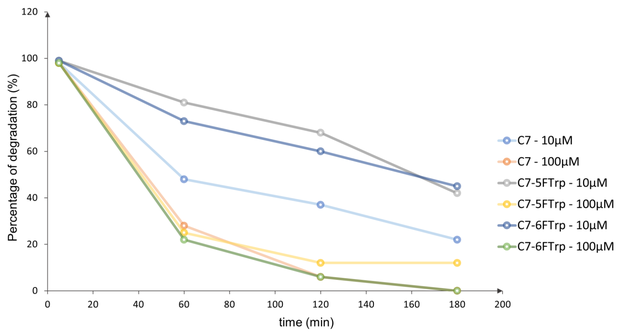




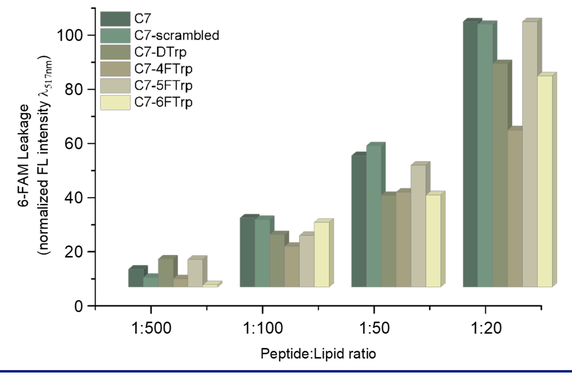
(A) monomers, (B) oligomers and (C) multimers [5]



Enzymatic Digestion



POPE/POPG Liposome Leakage Assay



Outlook

- SAJO peptides will be investigated for their efficiency in targeting yeast and hyphal forms of *Candida* species.
- Further antimicrobial and toxicity studies will be performed on the C7 peptidomimetic system

Acknowledgements

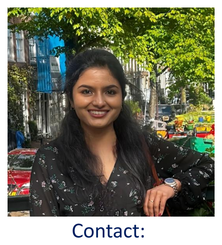
We gratefully acknowledge financial support from the RTG2473 ‘’ Bioactive Peptides’’, and the assistance provided by the Core Facility *BioSupraMol* supported by the Deutsche Forschungsgemeinschaft (DFG).

References

[1] A.J Cameron, K.G Varnava, P.J.B Edwards, R. Harjes, and V. Sarojini, *Journal of Peptide Science*, 2018, 24, e3094
[2] S. Chowdhary, T. Pelzer, M. Saathoff, E. Quaas, J. Pendl, M. Fulde, B. Koksch, *Peptide Science*, e24306, 2023
[3] S. Chowdhary, A. P. Rathessan, T. Pelzer, M. Fulde, B. Koksch, “Peptide With Antimicrobial Activity”, int. patent, EP4375289A1
[4] A. P. Rathessan, F. Ghazisaeedi, K. Unmesh, P. Bingul, J. Kupke, S. Chowdhary, D. Hanke, M. A. Mroginski, M. Fulde, B. Koksch, *Biochemistry*, 2026, 65 (12): 1944-1956
[5] C. K. Thota, A. A. Berger, B. Harms, M. Seidel, C. Botcher, H. V. Berlepsch, C. Xie, R. Sussmuth, C. Roth, B. Koksch, Peptide Science, 2019, e24130

Collaborators and funding:

LinkedIn: Aparna Palakkurussi Rathessan



Contact: a.palakkurussi.rathessan @fu-berlin.de

https://doi.org/10.17952/38EPS.2026.P239

RATIONAL DESIGN AND SYNTHESIS OF BIOACTIVE MIPEP205-DERIVED FRAGMENTS AS MODULATORS OF WNT/B-CATENIN SIGNALING IN TRIPLE-NEGATIVE BREAST CANCER

F. Tammaro [1], C. Irace [1], M.G. Ferraro [1,2], M. Piccolo [1], S. Galdiero [1], R. Bellavita [1], P. Grieco [1]

[1] *Department of Pharmacy, University of Naples Federico II, Naples (80131), Italy.*

[2] *Department of Molecular Medicine and Medical Biotechnology, University of Naples Federico II, Naples (80131), Italy*

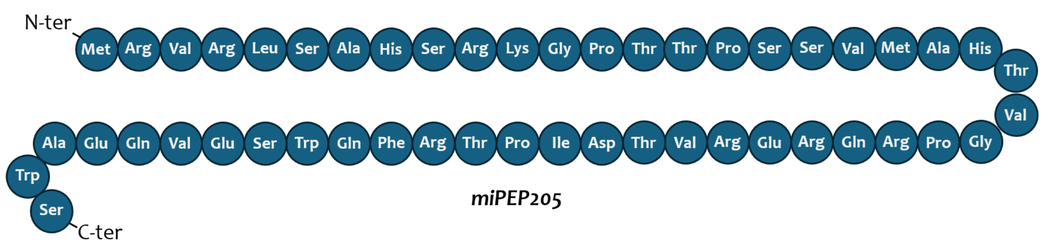
38th EPS
European Peptide Symposium
Vienna, 6.-11.9.2026

ABSTRACT

Triple-Negative Breast Cancer (TNBC) is the most aggressive breast cancer subtype, accounting for 15 to 20% of cases and showing poor survival outcomes despite chemotherapy, largely due to tumor relapse and an immunosuppressive microenvironment [1]. These limitations highlight the necessity for new molecular targets. **miPEP205**, a 49-aminoacid micropeptide encoded by MIR205HG, acts as a negative regulator of the canonical **Wnt/β-catenin** pathway, a key driver of TNBC progression. By interacting with **GSK-3β,** miPEP205 promotes β-catenin phosphorylation and degradation, ultimately reducing tumor cell proliferation [2].

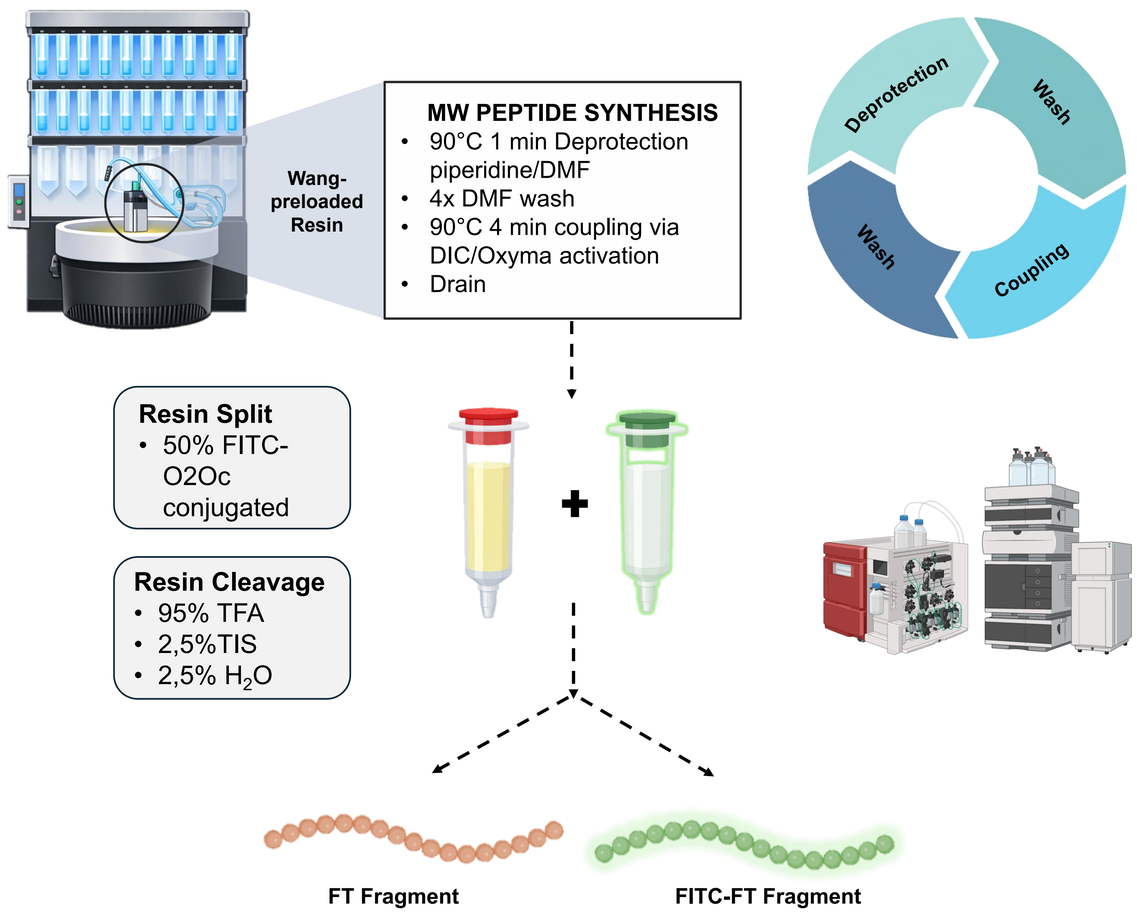
SCAN ME FOR 3D MODEL

RATIONALE & DESIGN



Representation of rationale design of FT-fragments deriving from miPEP205: **overlapping peptide mapping** consists in maintaining for each fragment a certain number of amminoacidic residues from the previous & the successive peptide fragment

SYNTHETIC PROCEDURES

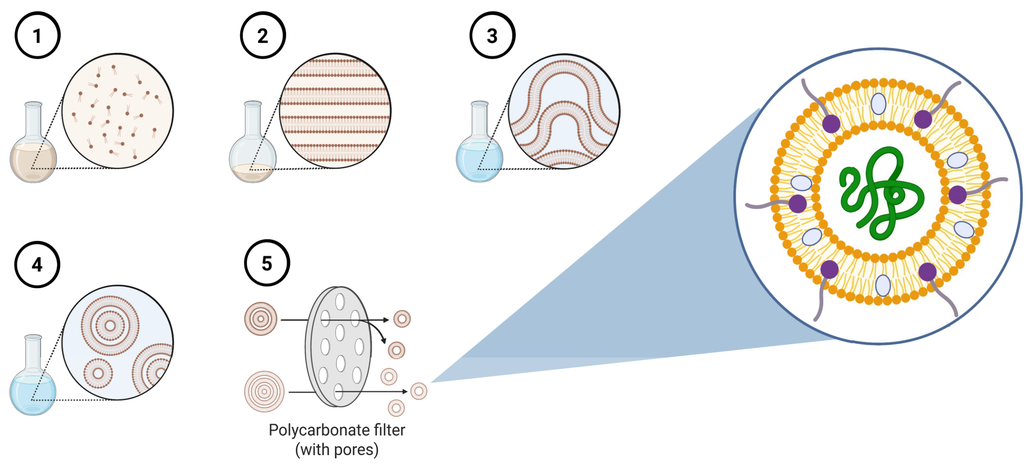


miPEP205-derived fragments were synthesized by automated microwave-assisted Fmoc-SPPS using **a Liberty Blue™ 2.0 peptide synthesizer**, followed by cleavage in acid condition, purification and analytical characterization via analytical & preparative HPLC.

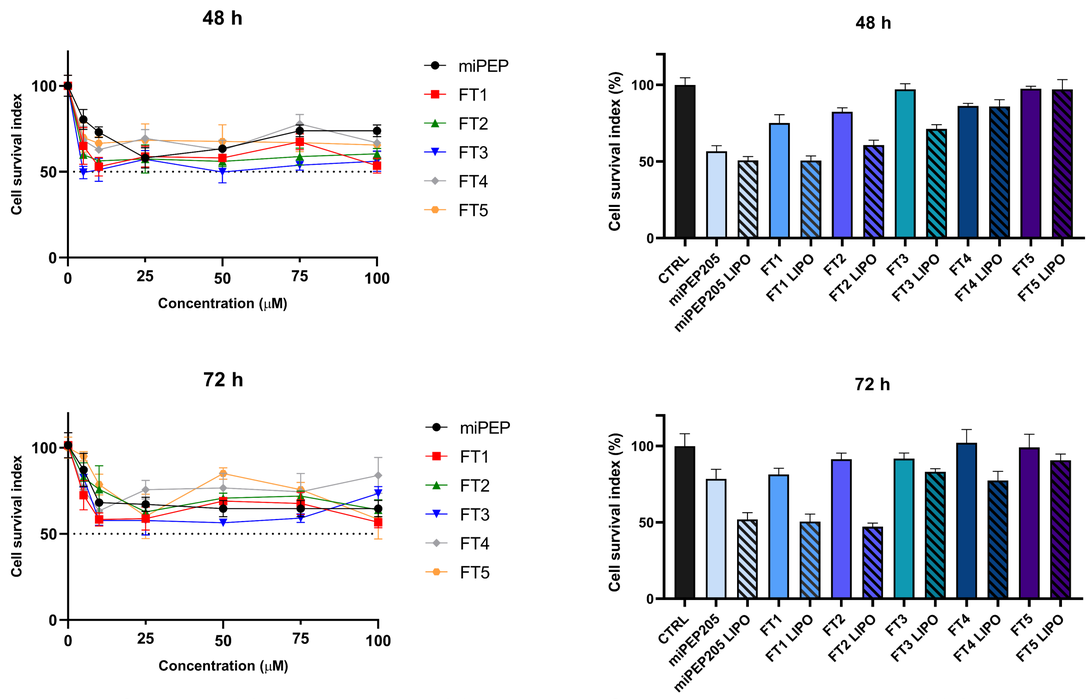
CONCLUSIONS

- Five overlapping fragments (FT1-5) were rationally designed from miPEP205 and synthesized
- In vitro testing on **MDA-MB-231** TNBC cells→ **FT1** and **FT2** most promising candidates
- Liposome-formulated FT1-FT2 cytotoxicity ≈ liposome miPEP205 citotoxicity
- Focus on FT1 & FT2 for future therapeutical optimizations

RESULTS



Liposome composition	Molar ratio (%)	Lipid concentration	Peptide concentration	Reference
DSPC/Cholesterol/DSPEPEG2000	32:60:8	1 mg/mL	0,08 mg/mL	[3]



Bioscreening of miPEP205 and miPEP205-derived fragments in **MDA-MB-231 cells**. **[A]** Cell survival index was assessed after treatment with miPEP205 and its fragments at concentrations ranging from 0 to 100 μM for 48 h and 72 h. **[B]** miPEP205 and the most active fragments, FT1, FT2, and FT3, were further evaluated at the selected concentration of 20 μM, either as free/naked peptides or in liposome formulation, after 48 h and 72 h of treatment.

	48H	72H
MIPEP205	56,6 %	78,5 %
MIPEP205-LIPO	50,7 %	51,9 %
FT1	75,1 %	81,3 %
FT1-LIPO	50,6 %	50,5 %
FT2	82,4 %	91,3 %
FT2-LIPO	60,7%	47,1 %
FT3	97,1 %	91,7 %
FT3-LIPO	71,2 %	83,1 %

Summary table showing cell survival index values in MDA-MB-231 cells, expressed as percentages relative to untreated control cells, after 48 h and 72 h of treatment with the selected free/naked and liposome-formulated peptides at 20 μM.

[1] Vagia E, Mahalingam D, Cristofanilli M. The Landscape of Targeted Therapies in TNBC. *Cancers (Basel)*. **2020**;12(4):916.

[2] Zhang Z, Li F, Dai X, Deng J, Wang Y, Zhang S, Liu W, Xie Y, Pan Y, Wang J, Zhao T, Wang S, Li W, Jin C, Zhang H, Lu J, Guo B, Zhou Y. A novel micropeptide miPEP205 suppresses the growth and metastasis of TNBC. *Oncogene*. **2025**;44(8):513-529.

[3] Jaradat E, Weaver E, Meziane A, Lamprou DA. Synthesis and Characterization of Paclitaxel-Loaded PEGylated Liposomes by the Microfluidics Method. *Mol Pharm*. **2023**;20(12):6184-6196.

E-mail: francesco.tammaro@unina.it

https://doi.org/10.17952/38EPS.2026.P303

Selective peptide bond formation via side chain reactivity and self-assembly of abiotic phosphates

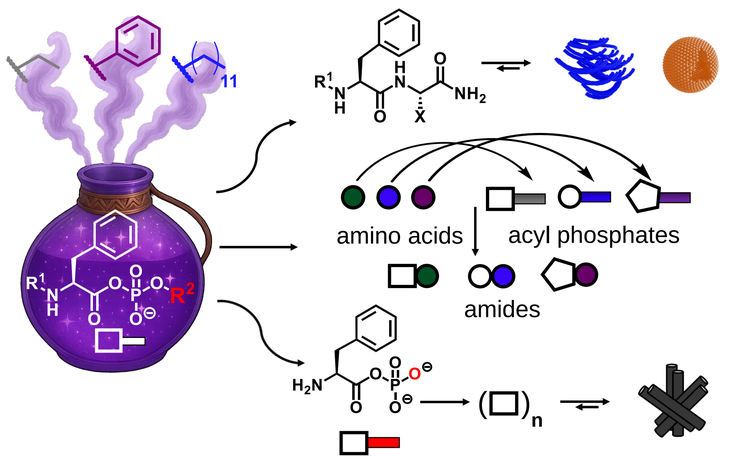
universität-freiburg

Arti Sharma[1,4] , Kun Dai[2] , Charlampos G. Pappas[1,3,4]

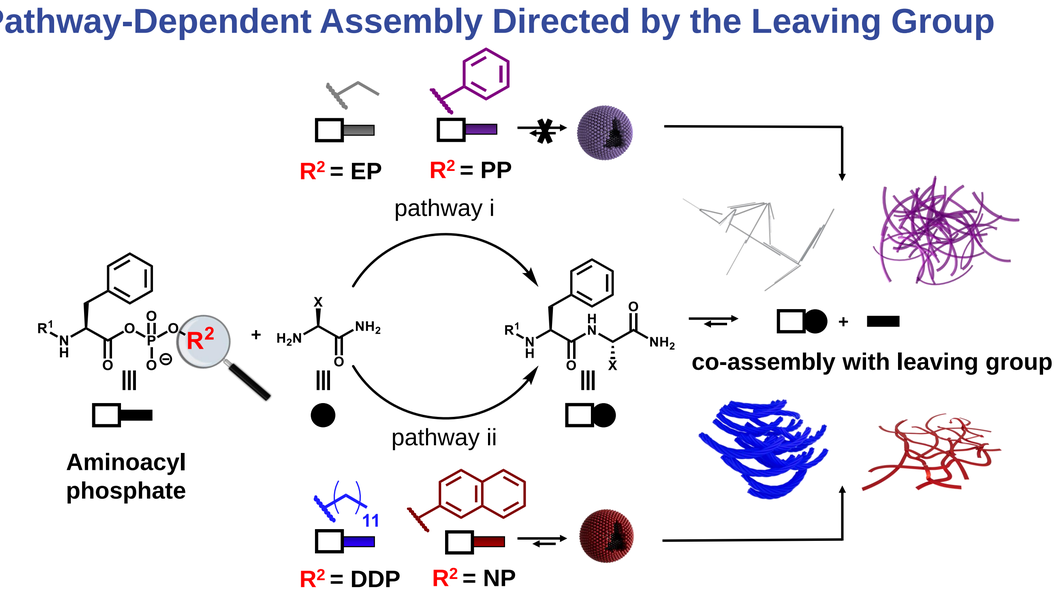
[1]Freiburg Center for Interactive Materials and Bioinspired Technologies (FIT), [2]Freiburg Institute for Advanced Studies, [3]Cluster of Excellence *liv*MatS, [4]Institute of Organic Chemistry, University of Freiburg, Germany

Introduction

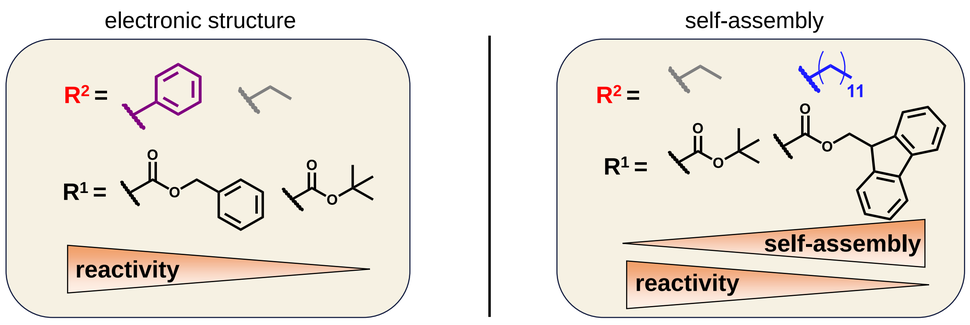
Phosphate esters and anhydrides are central to biology, storing and transferring chemical energy to sustain processes from metabolism to translation. Among them, acyl phosphates are highly reactive, yet biology channels their activation chemistry almost exclusively through aminoacyl adenylates. This conserved design leaves unexplored how alternative phosphate leaving groups might influence reactivity and structure. Here we show that aminoacyl phosphate esters with varied leaving groups (ethyl, phenyl, naphthyl, dodecyl) direct peptide bond formation and self-assembly through distinct pathways in water.



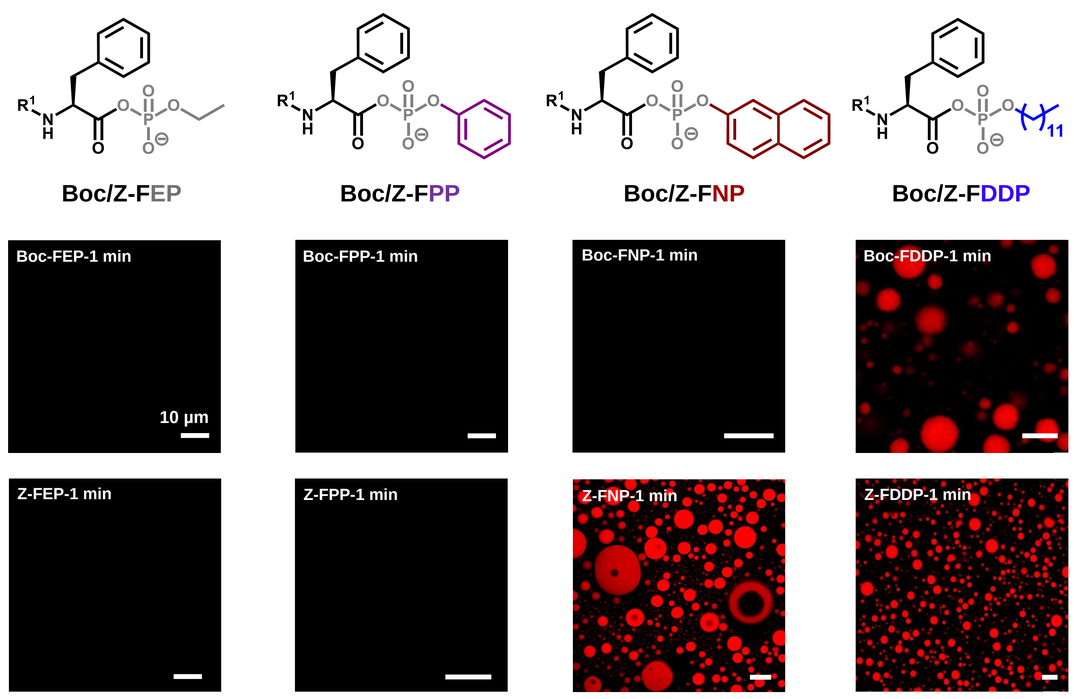
Pathway-Dependent Assembly Directed by the Leaving Group



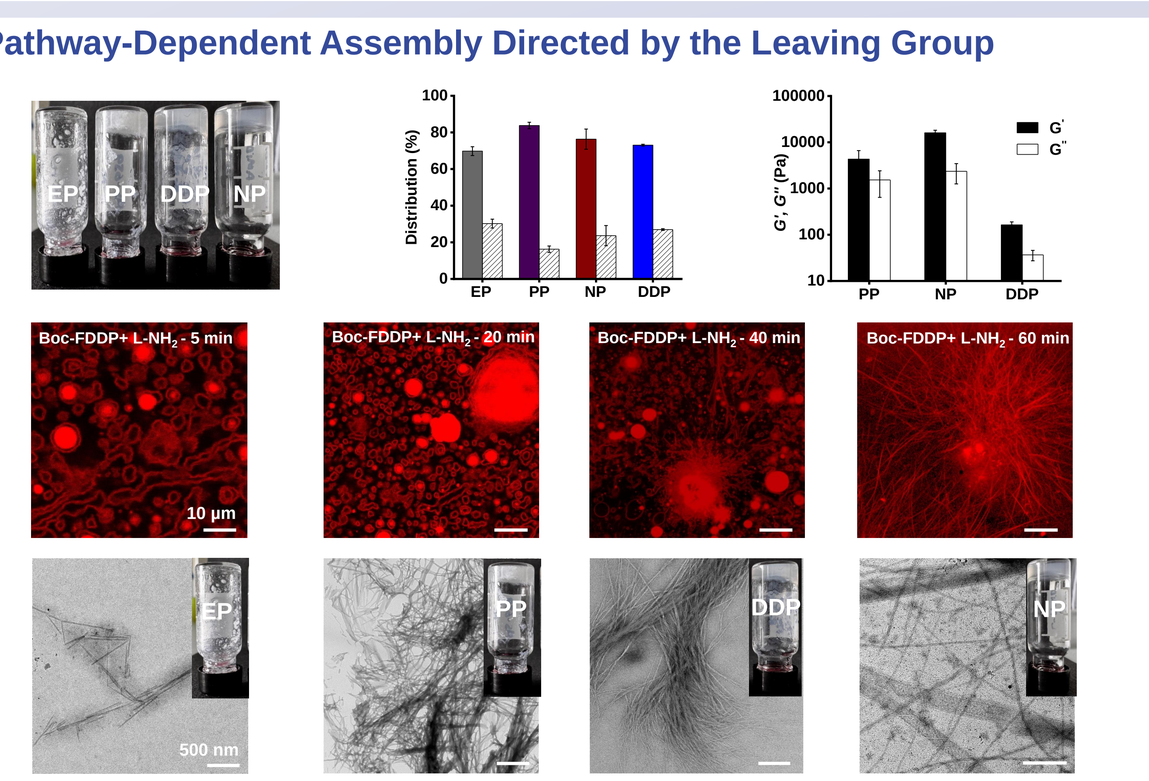
Effect of electronic structure and self-assembly on the reactivity of phosphate esters



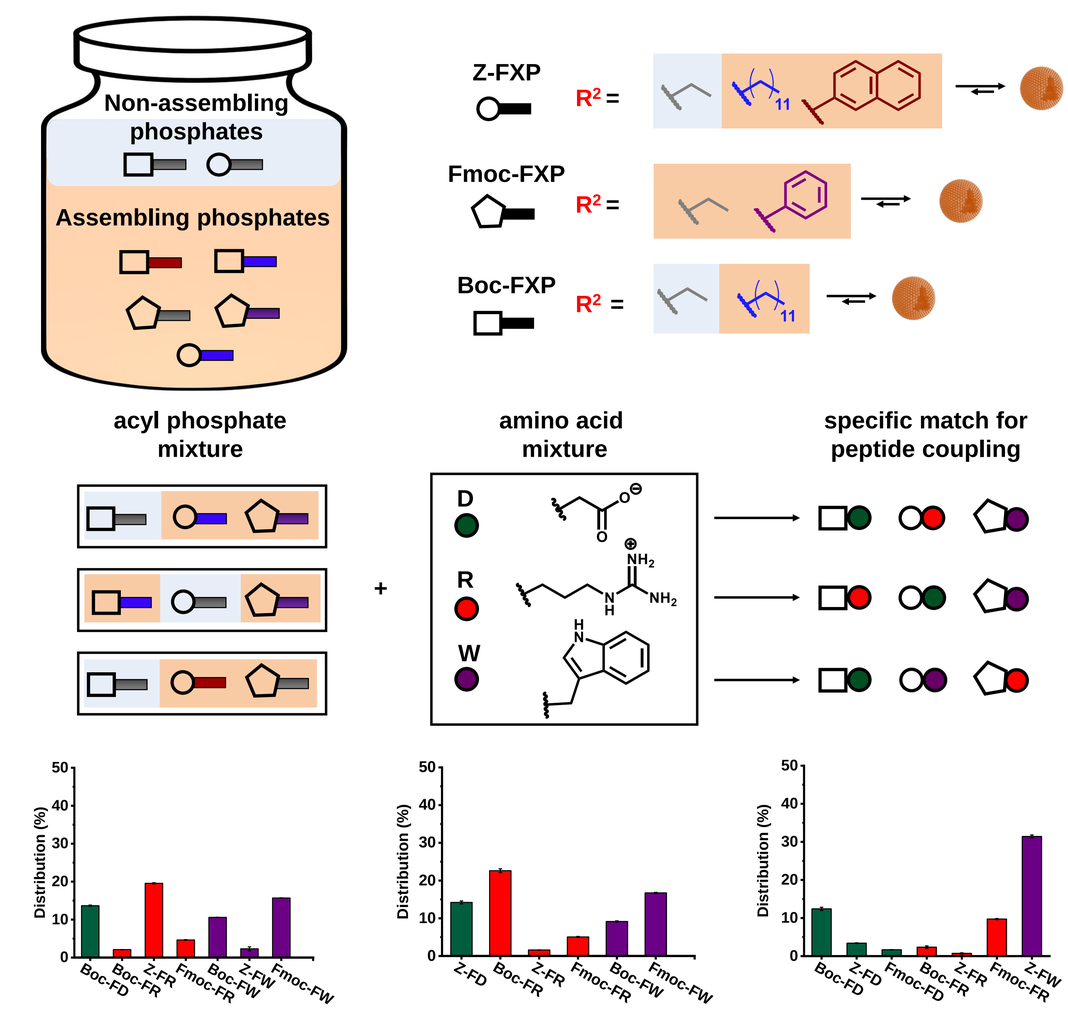
Designing Phosphate Leaving Groups



Pathway-Dependent Assembly Directed by the Leaving Group



Sequence Selection from Acyl Phosphate-Nucleophile Matching



Conclusion

- ❑ Aminoacyl phosphates bearing aromatic or hydrophobic aliphatic groups in the “phosphate tail” self-assembled into compartments that controlled reactivity and redirected covalent transformation pathways.
- ❑ Embedding structural features directly within the activating group offers a previously overlooked strategy to control aqueous amide bond formation and supramolecular assembly in peptide systems chemistry.

References

1. Sharma, A.; Pappas, C. G. et. al. *Nat.comm.* **2025**, *16* (1), 1306
2. Sharma, A.; Pappas, C. G. et. al. *J. Am. Chem. Soc.* **2026**, *148* (8), 8200-8212

Acknowledgements

Deutsche Forschungsgemeinschaft (DFG, German Research Foundation) (project PA 3783/2-1) and European Union (ERC-2023-StG grant, PhosphotoSupraChem, 101117240).



Contact
Arti Sharma
Doctoral Researcher
FIT Freiburg Center for Interactive Materials and Bioinspired Technologies, University of Freiburg
Email- arti.sharma@mail.fit.uni-freiburg.de
Mo.No.- 015736246726

@sharmaarti796

Pappas Group

GDCh Gesellschaft Deutscher Chemiker

DFG Deutsche Forschungsgemeinschaft

Boehringer Ingelheim Stiftung

erc

Identification of novel peptide binders targeting TPP riboswitch in *E. coli*

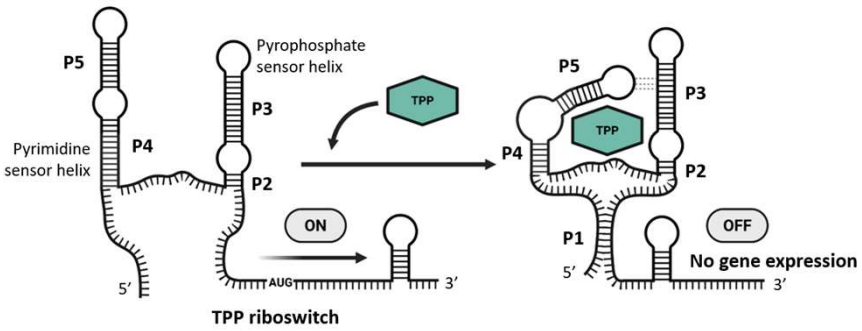
Jinseo Park[1, 2], Yujin Jung[1]. Dasom Song[1], Jung Kim[1] & Hong Gi Kim[1, 2]

[1]*Department of center for infectious disease vaccine and diagnosis innovation, Korea Research Institute of Chemical Technology (KRICT), Daejeon, Republic of Korea*
[2]*Institute of Pharmacology, Department of Medicinal Chemistry and Pharmacology, University of Science and Technology (UST), Daejeon, Republic of Korea*
Email: tenork@krict.re.kr
https://doi.org/10.17952/38EPS.2026.P180

Abstract

Antimicrobial resistance (AMR) strains has been directly emerged by the improper use of antibiotics. Gram-negative pathogens, including *Pseudomonas aeruginosa*, *Klebsiella*, and *Escherichia coli*, are four-times more likely to cause Healthcare-associated Infections (HAI) compare to Gram-positive pathogens. Development of antibiotics for Gram-negative bacteria is difficult because their additional membrane, name as LPS, restricts the intracellular penetration of antibiotics. The presence of efflux pumps within bacteria makes it harder to develop the antibiotics.[1] The previous studies of antibiotics have mainly focused on bacterial proteins such as efflux pumps, ribosomal subunits, and RNA polymerases. Targeting the bacterial proteins has the disadvantage that easily proceeds bacterial mutation. Constantly, targeting RNA structure for novel antimicrobial therapy might be one of the promising strategies to overcome the limitation of current treatments. Among these, riboswitches, highly conserved tertiary RNA structures located in the untranslated regions (UTRs) of mRNA, regulate approximately 4% of the bacterial genome by sensing specific ligands.[2] Riboswitches have the unique tertiary structure that comprises the aptamer region and expression platform. When the specific ligand binds the aptamer region of riboswitch, expression platform regulates the gene of bacterial metabolism through structure change. The thiamine pyrophosphate (TPP) riboswitch is particularly significant as it is widely conserved in pathogenic bacteria and strictly regulates the synthesis of TPP, the active form of thiamine. The regulation of TPP supplement through TPP riboswitch plays a key role in bacterial survival. In this study, novel peptide binders targeting TPP riboswitch of *E. coli* were investigated by a modified fluorescent indicator displacement with the peptide library. Identified peptide binders demonstrated significant binding affinities as well as potent antibacterial activities. Therefore, peptide binders suggest a potent candidate of antibiotics via the regulation of TPP riboswitch in *E. coli*.

Introduction



The **TPP riboswitch** forms tertiary interactions with its specific ligand, TPP, and is divided into the pyrimidine sensor helix and pyrophosphate sensor helix according to the ligand-binding sites. Upon TPP binding to the bulges of the two sensor helices, the loop of the pyrimidine sensor helix forms hydrogen bonds, resulting in clamp closure. Simultaneously, hydrogen bonds form between the terminal regions, leading to repression of gene expression.

Results

1. Screening hit binders against TPP riboswitch

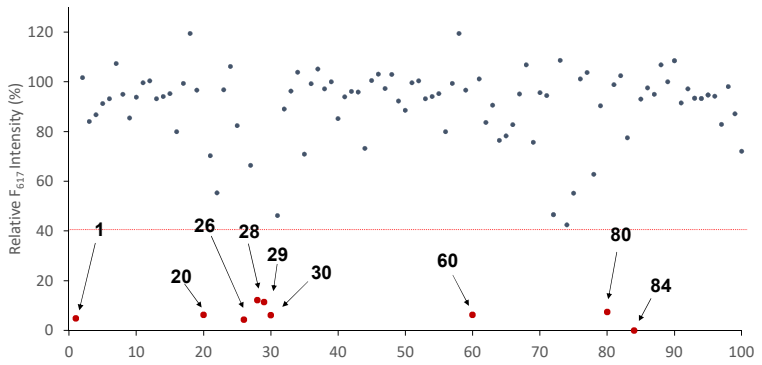
- **A Modified Fluorescent Indicator Displacement (FID) Assay**



Peptide binders targeting the TPP riboswitch were identified by utilizing the competitive binding between ligands and fluorophores via the FID principle.

100 peptides

Selection criteria : < 60% inhibition of relative fluorescence intensity

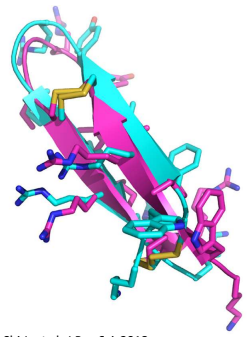


9 hit peptides

2. Peptide sequences of peptide binders

	Sequences
CTPep-1	RSVCRQIKICRRRGGCYYKCTNRPY
CTPep-20	RKIKKRRKKWR
CTPep-26	FKCRRWQWRMKKLG
CTPep-28	FKCRRWQWRMKKLGAPSITCVRRAF
CTPep-29	CRRWQWRMKKLGAPSITCV
CTPep-30	CFQWQRNMRKVRGPPVSCI
CTPep-60	RLCRIVVIRVCR
CTPep-80	KWCFRVCYRGICYRRCRG
CTPep-84	RGGRLCYCRRRFCVCVGR

3. Structural Feature of Tachyplesin-1 (CTPep-80)



CTPep-80 KWCFRVCYRGICYRRCRG

Shi J. et al. *J Pep Sci.* 2018

- CTPep-80 is naturally formed a **β-sheet structure** containing two cysteine bridges.
- Disulfide-bridged form of CTPep-80 binds to the bacterial membrane and forms pores to induce cellular leakage.
- The linear form of CTPep-80 also exhibited **similar antimicrobial activity** compared to the intra disulfide-bridged form of CTPep-80.

4. Antimicrobial activities of CTPep-80

Number		MIC_{50} of *E. coli* ATCC 25922 (μM)		
		Muller-Hinton Broth (MH)	LB	M9 glucose
CTPep-80	Intra S-S bridge	2.863	2.529	2.452
	Linear*	5.262	2.691	8.354
Colistin (Control)		2.277	0.485	1.173

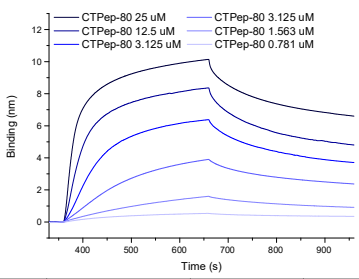
*Treated with 0.5 mM Tris(2-carboxyethyl)phosphine (TCEP).

Abbreviations : Abs. : Absorbance, PS : Polystyrene, TC : Tissue-culture surface treatment

5. Binding Affinity between CTPep-80 and TPP riboswitch

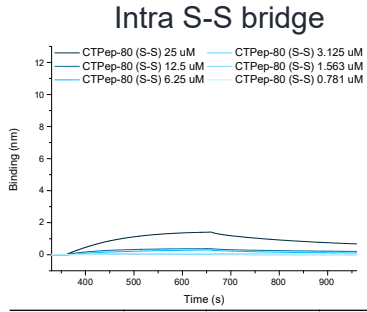
- **Bio-layer Interferometry (BLI) Assay**

Linear



KD (μM)	1.741	kd (1/s)	2.461×10^{-3}
ka (1/Ms)	1.413×10^{3}	R-square	0.994

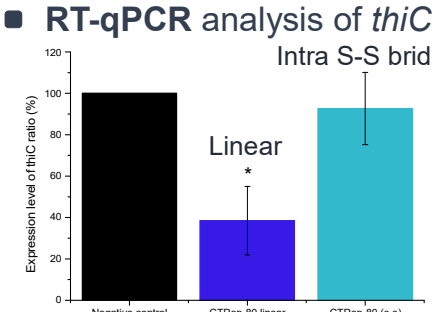
Intra S-S bridge



KD (μM)	42.35	kd (1/s)	3.705×10^{-3}
ka (1/Ms)	87.47	R-square	0.998

6. mRNA Expression of *thiC* in *E. coli*

- **RT-qPCR** analysis of *thiC* mRNA with CTPep-80 for 3 hours



*p-value < 0.005 vs. negative control

- Structure-dependent effects of peptide binders on **mRNA expression** of *thiC* in *E. coli*

Conclusion

- Among the 9 hit peptide binders, CTPep-80 exhibited antimicrobial activity regardless of its structures, with intra disulfide bridges or not.
- The higher binding affinity of the linear form CTPep-80 was investigated than the intra disulfide-bridged form.
- The downstream gene *thiC*, regulated by the TPP riboswitch, was also downregulated by the linear form of CTPep-80.

Therefore, the linear form of CTPep-80 suggest a potent candidate of antibiotics via the regulation of TPP riboswitch in *E. coli*.

[1]D. Terefinko, M. Caban, A. Motyka, et al. *Chem. Eng. J.* **2023**, 452, 139415.
[2]A. Hübenthal, V. Panchal, R. Brenk, M. Mack. *J. Bacteriol.* **2025**, 207.

38th EPS
European Peptide Symposium
Vienna, 6.-11.9.2026

SHORTENED AURELIN-DERIVED PEPTIDES

The Role of Derivatization in Modulating Antimicrobial Efficacy

L. Pašalić[1], Anna Marin[2], J. Tuzlak[2], N. Malanović[2] & A. Jakas[1]

[1] Rudjer Bošković Institute, Division of Organic Chemistry and Biochemistry, Zagreb, Croatia
[2] University of Graz, Institute of Molecular Bioscience, Graz, Austria
https://doi.org/10.17952/38EPS.2026.P232
lea.pasalic@irb.hr

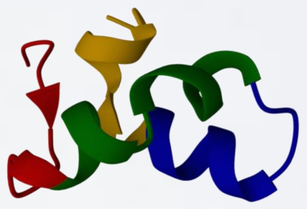
01 FROM AURELIN TO SHORTENED FRAGMENTS

Aurelin is 40 aa **cationic antimicrobial peptide** isolated **from jellyfish *Aurelia Aurita*** that exhibits activity against both Gram-positive and Gram-negative bacteria.
Four distinct fragments were selected as promising scaffolds for further optimization.

Full length sequence:
AACSDRAHGHICESFKSFCKDSGRNGVKLRANCKKTCGLC



Aurelia Aurita



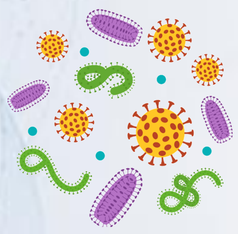
Aurelin 40 aa

Selected shortened fragments

AACSDRAHGH
ICESFKSFCK
DSGRNGVKLR
ANCKKTCGLC

02 WHY REDISIGN THEM?

Initial antimicrobial screening

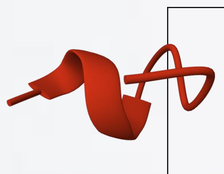
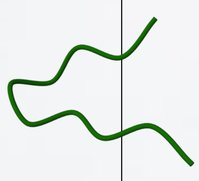
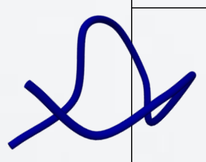


NO DETECTABLE ACTIVITY against *E.coli* and *S.epidermidis (>1.2 mM)*
-for all parent fragments - most likely due to low cationicity



RATIONAL REDESIGN to enhance cationic character and modulate activity

03 DESIGN STRATEGY

	PARENT FRAGMENTS	MODIFIED FRAGMENTS Cys to Arg	CYCLIC ANALOGUES
	AACSDRAHGH ~ 0	AARSDRAHGH +2	
	ICESFKSFCK +1	IRESFKSFRK +4	ICESFKSFCK +1
	DSGRNGVKLR +1		
	ANCKKTCGLC +1	ANRKKTRGLR +7	ANCKKTCGLR +3

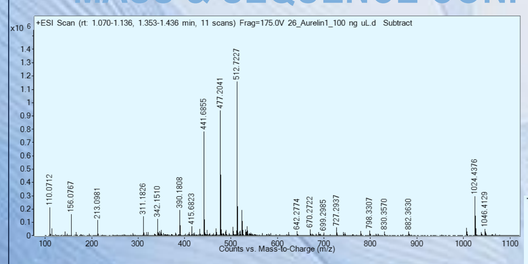
04 SYNTHESIS & CHARACTERIZATION

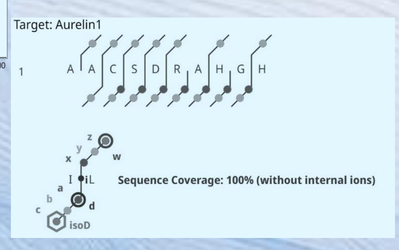


Automated SPPS — SYNTHESIS → **Preparative RP-HPLC** — PURIFICATION → **Analytical RP-HPLC** — PURITY CHECK

HR MS

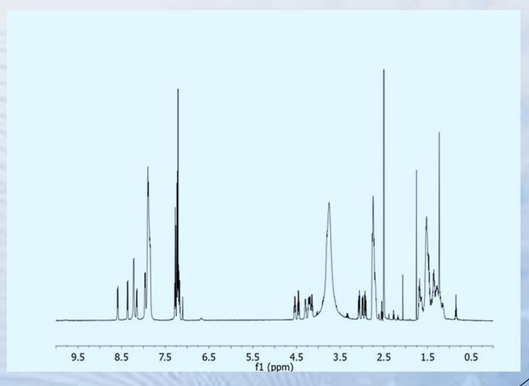
MASS & SEQUENCE CONFIRMATION





NMR

STRUCTURAL CHARACTERIZATION



05 DOES REDISIGN CHANGE ACTIVITY?

Antimicrobial activity, MIC

PARENT FRAGMENTS
NO DETECTABLE ACTIVITY

MODIFIED & CYCLIC FRAGMENTS
?

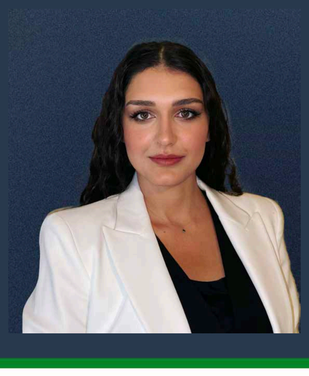
REFERENCES

1.Ovchinnikova T., et al. (2006) Aurelin, a novel antimicrobial peptide from jellyfish Aurelia aurita with structural features of defensins and channel-blocking toxins, *Biochem. Biophys. Res. Commun*. 348 (2): 514-523
2. Berger, I.; Loewy, Z.G. (2024) Antimicrobial Resistance and Novel Alternative Approaches to Conventional Antibiotics. *Bacteria* , 3, 171-182.
3. Poluri, K.M., Gulati, K., Sarkar, S. (2021). Structural and Functional Properties of Proteins. In: Protein-Protein Interactions. Springer, Singapore. 1-60.

TAKE-HOME MESSAGE: Loss of activity upon aurelin shortening guided the rational design of new derivatized and cyclic peptide candidates.

This work was supported by Croatian Science Foundation under grant HRZZ IP-2024-05-1216 and Croatian Government and the European Union, Program (KK.01.1.1.01), under the project Sustainable Bioprospecting of Organisms from the Adriatic Sea for Innovative Natural Products (KK.1.1.10.0001)— BioProCro, granted to the Center of Research Excellence for Marine Bioprospecting.

https://doi.org/10.17952/38EPS.2026.P252



AI-driven generative peptide design targeting the GC-C dimer for Parkinson's

Generative design and MD screening of cyclic & linear peptides that stabilise the GC-C dimer

POSTER
No. 252
Session 1
EPS 2026

Elpiniki PASPALI, Lars van der Heide, Ioana M. ILIE • University of Amsterdam • **e.paspali@uva.nl** • **BioSim-Lab.com**

❶ WHY TARGET GC-C? — Parkinson's disease

The fastest-growing neurodegenerative disease in the world

11.8 M people living with Parkinson's (2021)

25.2 M projected cases by 2050

0 No therapy

Neurons die
Progressive loss of dopaminergic neurons in the substantia nigra.

GC-C is expressed there
Guanylyl cyclase C (GC-C) is present in dopaminergic neurons.

GC-C activation protects
Receptor activation raises cGMP and is neuroprotective in PD models.

GOAL

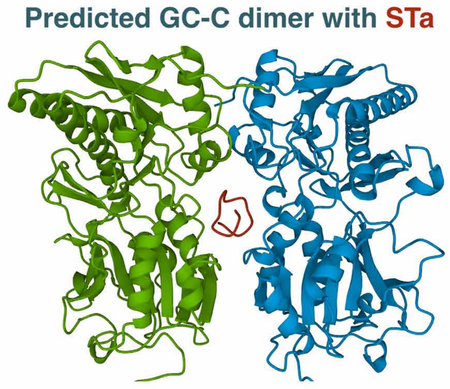
Design peptides that activate GC-C to enhance neuroprotection

GBD Study 2021 · BMJ modelling study 2025 · Cheslow et al., npj Parkinsons Dis 2024 · GUCY2C: Cell Biosci 2024

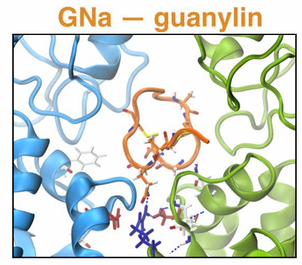
❷ THE TARGET — GC-C dimer interface

GC-C is activated by the endogenous hormones **guanylin** and **uroguanylin,** and by the bacterial **heat-stable enterotoxin** STa.

Predicted GC-C dimer with STa

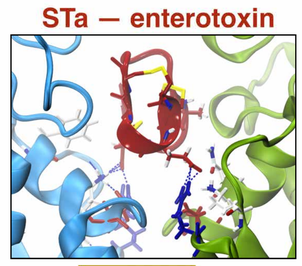


GNa — guanylin

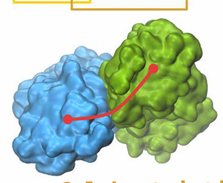


PGTCEICAYAACTGC

STa — enterotoxin



CCELCCNPACAGCY

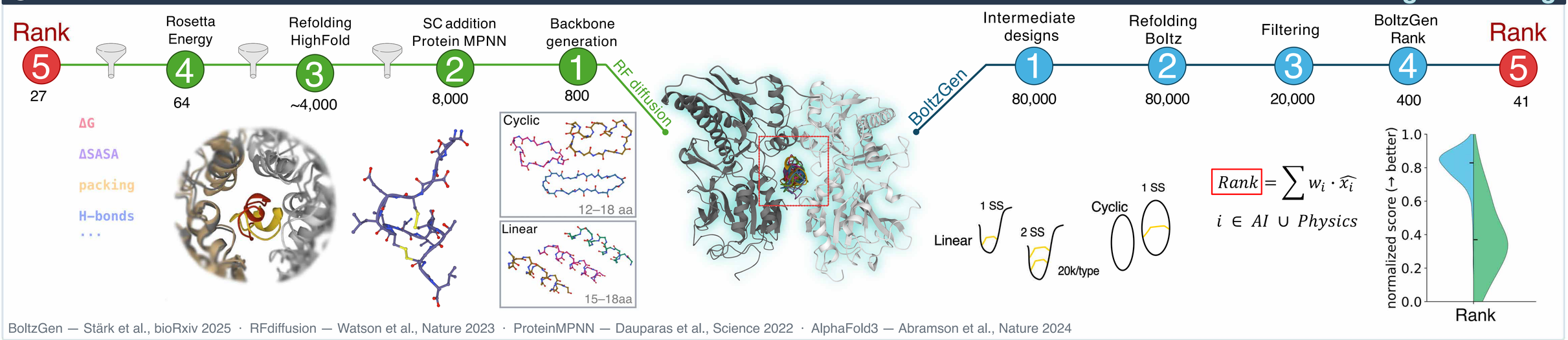


C-lobe twisting

HYPOTHESIS

A peptide that locks the two protomers together should stabilise the active dimer → sustained cGMP signalling.

❸ TWO GENERATIVE TRACKS → 68 CANDIDATES — in silico design & ranking



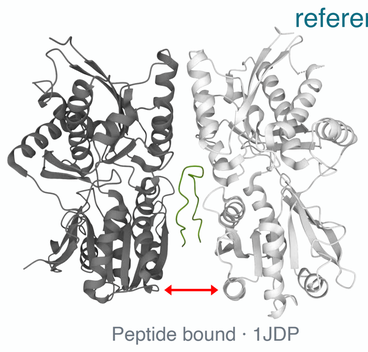
BoltzGen — Stärk et al., bioRxiv 2025 · RFdiffusion — Watson et al., Nature 2023 · ProteinMPNN — Dauparas et al., Science 2022 · AlphaFold3 — Abramson et al., Nature 2024

❹ MD SCREENING — 68 peptides · 100 ns each

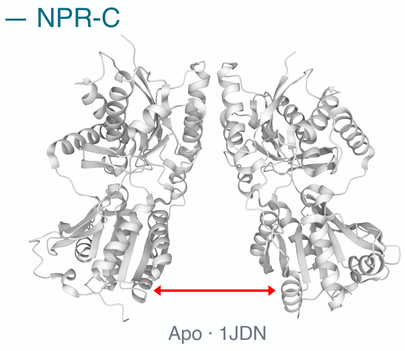
MD → Stability filter → Reject / Accept → Binding free energy

CHARMM36m | TIP3P | 150 mM NaCL | 100 nsl

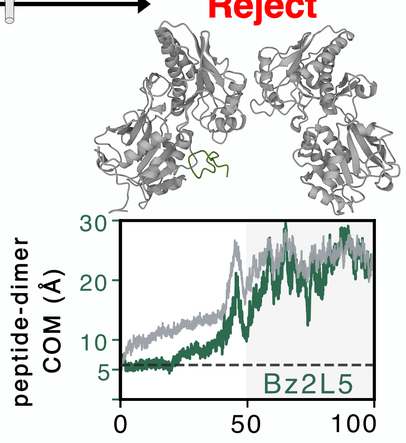
reference — NPR-C

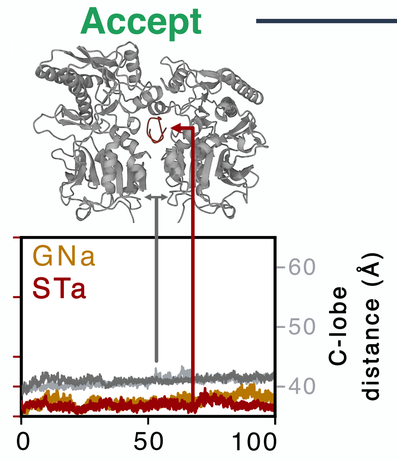


Peptide bound · 1JDP



Apo · 1JDN





Binding free energy

MM-PBSA over the last 50 ns

$$\Delta G_{bind} = \Delta G_{gas} + \Delta G_{solv}^{cpx} - \Delta G_{solv}^{rec} - \Delta G_{solv}^{lig}$$

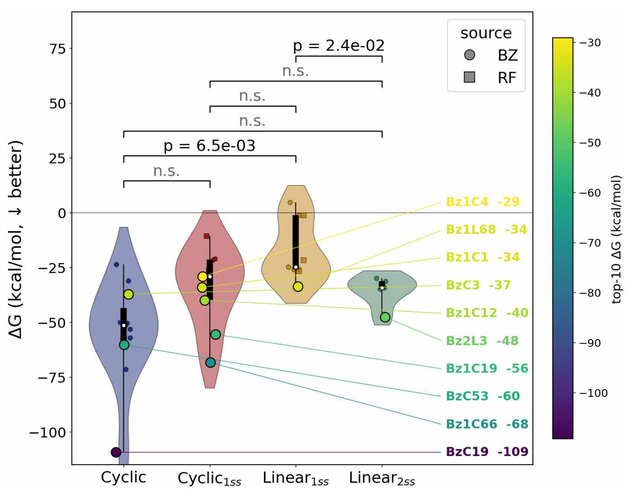
Select & advance

lowest energy + sequence diversity → toxicity, synthesisability

❺ RESULTS — MD-validated designs

Architecture matters

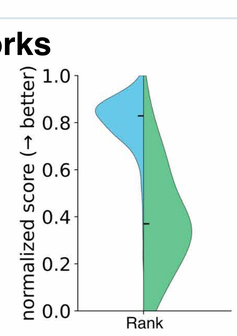
Cyclic peptides bind most favourably



The ranking method works

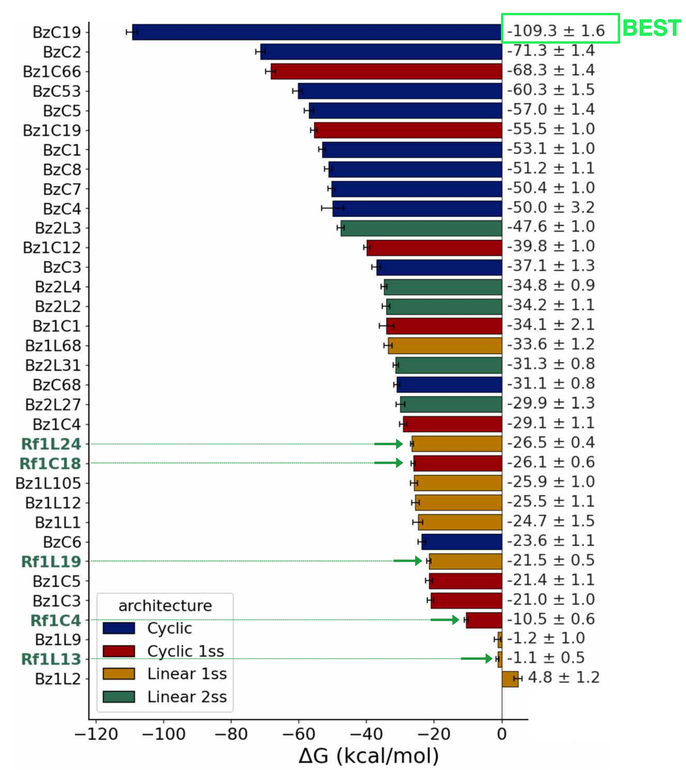
It correctly predicted

BoltzGen > RF diffusion before MD



BoltzGen outperforms RF diffusion

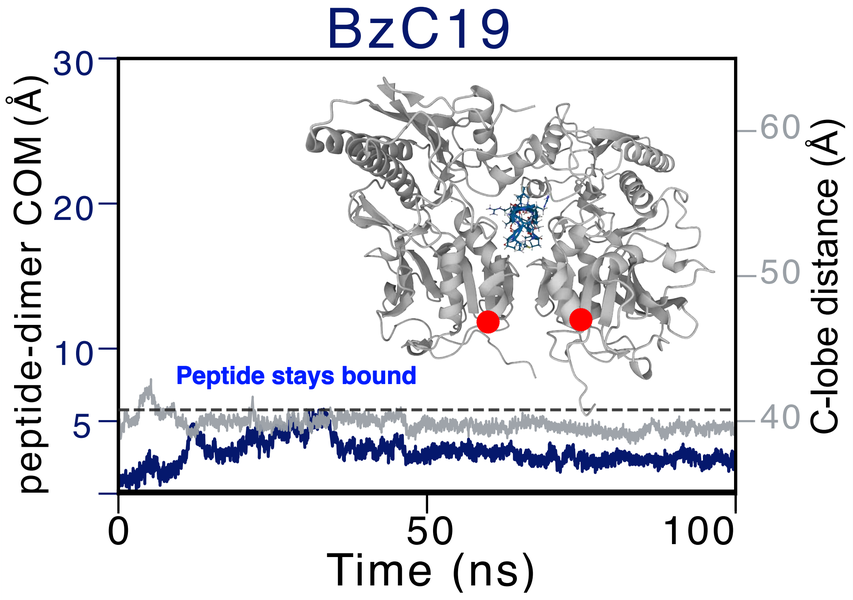
Binding free energy of the 34 designs that kept the dimer intact. BoltzGen (Bz) peptides dominate over RFdiffusion (Rf)



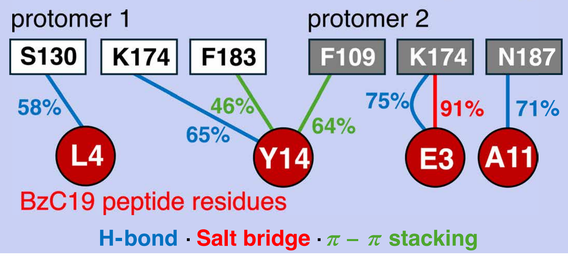
Only 5 RF diffusion peptides were able to hold protomers close & have weaker binding than Boltzgen peptides

Peptides stabilise the dimer interface

BzC19



Persistent contacts over the trajectory



CONCLUSIONS

- First generative peptide-design campaign against the GC-C dimer interface.
- Two complementary generators (BoltzGen + RFdiffusion) gave a large, chemically diverse pool.
- Our ranking predicted BoltzGen > RFdiffusion — confirmed by MD.
- Multi-stage screening: MD dimer-stability → binding free energy → developability.

OUTLOOK

Synthesis

Assay function

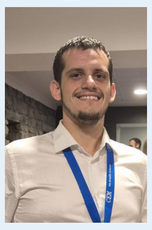
Neuroprotection

CONTACT

Happy to discuss collaborations.

BioSim-Lab.com

TBDCs: ADVANCED COUPLING REAGENTS FOR LIQUID PHASE PEPTIDE SYNTHESIS (LPPS)



N. Patrian[1] , D. Corbisiero[1], R. Grigolato[1], A. Tiberti[1], L. Rapisarda[1], L. Ferrazzano[1], A. Tolomelli[1], W. Cabri[1]

[1]Department of Chemistry "G. Ciamician" Alma Mater Studiorum – University of Bologna, Via P. Gobbetti 85, 40126, Bologna
nicola.patrian2@unibo.it
https://doi.org/10.17952/38EPS.2026.P284

Abstract

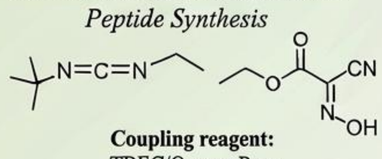
The growing market demand for oligopeptides has led to increased efforts toward the development of sustainable and more efficient synthetic processes for these significant bioactive molecules. In 2024, our group demonstrated that amino acids without side-chain protecting groups could be employed in Solid Phase Peptide Synthesis (SPPS), increasing the Atom Economy (AE) of the process.[1] In this work, we introduce a novel carbodiimide, N-(3-dimethylaminopropyl)-N′-tert butylcarbo diimide (TBDC), as the p-toluenesulfonic acid salt, for Liquid Phase Peptide Synthesis (LPPS). We successfully applied it to the synthesis of peptides containing arginine, histidine, tyrosine, and tryptophan without side-chain protecting groups, using a green solvent, thereby increasing both AE and Process Mass Intensity (PMI) for LPPS. In line with a PFAS-free approach, we also removed trifluoroacetic acid (TFA) from the final cleavage step, which was performed using a commercially available 1 M HCl solution in acetic acid. Overall, these results further improve the sustainability of TAG-assisted peptide chemistry.



Minimal Protection Peptide Synthesis : From SPPS to LPPS

MP-SPPS(2024)[1]

Minimal-Protection Solid-Phase Peptide Synthesis



Coupling reagent: TBEC/Oxyma Pure

Side-chain protections eliminated for Arg, His, Tyr, Trp, Ser, Thr

Reduced impurity generation during cleavage

Improved atom economy (+10–15%)

Compatible with standard Fmoc-SPPS workflows

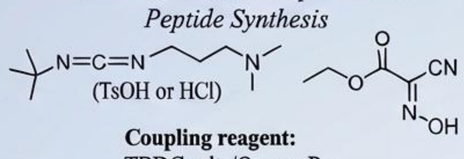
Demonstrating with challenging peptide sequence:
- Linear vasapressin
- Etecalcetide
- Histidine terminal liraglutide
- Histidine terminal semaglutide

Evolution of Minimal-Protection Peptide Synthesis

increasing atom economy

MP-LPPS(2026)[2]

Minimal-Protection Liquid-Phase Peptide Synthesis



Coupling reagent: TBDC salts/Oxyma Pure

Side-chain protections eliminated for Arg, His, Tyr, Trp, Ser, Thr

Improved atom economy and reduced PMI

TAG-assisted LPPS in 2-MeTHF

One-pot coupling-Fmoc removal-precipitation

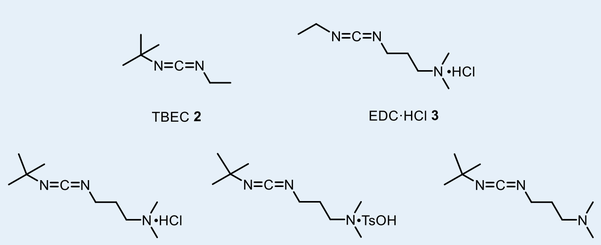
1 M HCl in AcOH cleavage (PFAS-free)

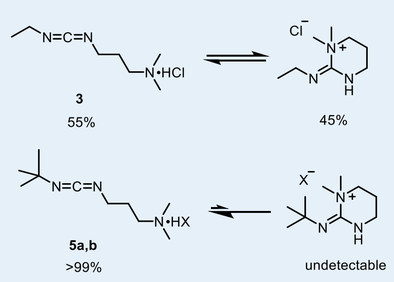
Demonstrated on challenging peptide sequences

The coupling reagent

Green = Complete solubility; **Yellow** = Partial solubility ; **Red** = Complete insolubility

Solvent	TBEC 2	EDC·HCl 3	TBDC·HCl 5a	TBDC·TsOH 5b
DMF				
DCM				
Anisole				
DMC				
DEC				
NOP				
NBP				
NBP:DMC 8:2				
EtOAc				
DMSO				
EtOAc:DMSO 7:3				
ACN				
ACN:DMSO 7:3				
PrOAc				
^{i}PrOAc				
^{t}BuOAc				
CPME				
2-MeTHF				
2-MeTHF:DMSO 9:1				
GVL				
DOS				
TEP				
Water				



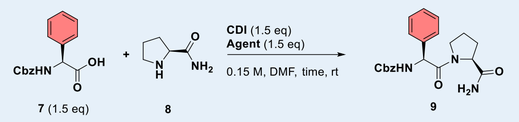


DMF: dimethyl formamide; **DCM**: dichloromethane; **DEC**: diethyl carbonate; **NOP**: *N*-octyl pyrrolidone; **NBP**: *N*-butyl pyrrolidone, **DMC**: dimethyl carbonate; **EtOAc**: ethyl acetate; **DMSO**: dimethylsulphoxide; **PrOAc**: propyl acetate; **^{i}PrOAc**: isopropyl acetate; **^{t}BuOAc**: tertbutyl acetate; **CPME**: cyclopentyl methyl ether; **2-MeTHF**: 2-methyl tetrahydrofuran; **GVL**: gamma Valero lactone; **DOS**: 1,3-diossolane; **TEP**: triethyl phosphate.

TBDC is less prone to intramolecular cyclization than EDC !

Evaluation of ability to avoid racemization

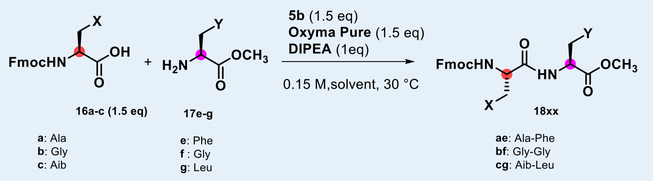
Entry	CDI	Acid	Acid pKa[a]	Agent (eq)	C_{max} %[b]	Time (min)	LL/DL[b]
1	**2**	-	-	Oxyma Pure	95.7	15[c]	98:2
2	**5**	CH_3SO_3H	-1.9	Oxyma Pure	77.6	60	96:4
3	**5**	p-TolSO$_3$H	-2.8	Oxyma Pure	86.8	60	96:4
4	**5**	TCA	0.6	Oxyma Pure	91.0	60	69:31
5	**5**	TFA	0.2	Oxyma Pure	89.1	60	91:9
6	**3**	-	-	OxymaPure	100	15	93:7
7	**5a**[d]	-	-	OxymaPure	100	30	97:3
8	**5b**[d]	-	-	OxymaPure	100	30	97:3
9	**3**	-	-	HOBt	100	15	75:25
10	**5a**[d]	-	-	HOBt	100	15	81:19
11	**5a**[d]	-	-	HOAt	100	15	87:13
12	**5a**[d]	-	-	Oxyma B	100	60	96:4



a. Values retrieved from Handbook of Chemistry and Physics (D.R. Lide), Internet Version 2005, CRC Press, Boca Raton, FL, 2004.
b. Data determined by HPLC chromatograms.
c. Value unchanged at 1h.
d. CDI was added as 1M solution in DMF.

Coupling conditions for lyphophilic residues in green solvents (Tirzepatide)

Entry	AA[b]	Solvent	C_{max}%[a]	Time (h)
1	**18ae**	DMF	97.9 (91.3)	1.5
2		ACN:DMSO 7:3	86.6 (84.6)	3.0
3		MeTHF:DMSO 9:1	93.1 (91.2)	1.5
4	**18bf**[c]	DMF	100 (92.4)	3.0
5		ACN:DMSO 7:3	80.2 (69.6)	5.0
6		MeTHF:DMSO 9:1	76.9 (75.6)	6.0
7	**18cg**[c]	DMF	100	0.5
8		ACN:DMSO 7:3	100 (95.2)	2.0
9		MeTHF:DMSO 9:1	100 (99.3)	2.0



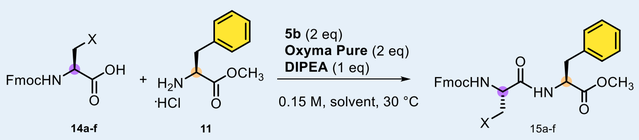
a: Ala
b: Gly
c: Aib

e: Phe
f : Gly
g: Leu

ae: Ala-Phe
bf: Gly-Gly
cg: Aib-Leu

a. Data reported when conversion is complete, or the highest.
b. Residues selected according to coupling of fragments reported in OPRD 2021, 25, 7, 1628-1636
c. Benzyl ester used instead methyl ester to make limiting reagent detectable with HPLC-MS

Coupling conditions for sidechain unprotected residues in green solvents

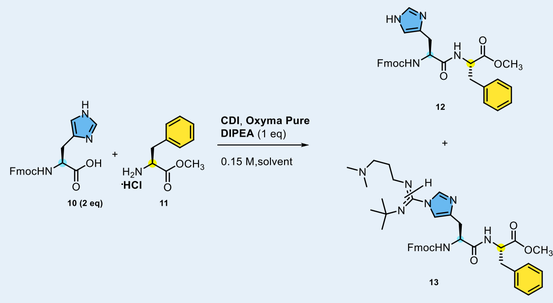


a: Trp=2-indole
b: Ser=OH
c: Thr=CH(OH)CH$_3$
d: Tyr=4-OH-Ph
e: Arg=CH$_2$CH$_2$C(=NH)NH$_2$

a: Trp=2-indole
b: Ser=OH
c: Thr=CH(OH)CH$_3$
d: Tyr=4-OH-Ph
e: Arg=CH$_2$CH$_2$C(=NH)NH$_2$

Entry	AA	Solvent	C_{max}%[a]	Time (h)
1	**14a**	DMF	100	1h
2		MeTHF	100	1h
3		MeTHF:DMSO 9:1	100	1h
4	**14b**	DMF	100	1h
5		MeTHF	100	1h
6		MeTHF:DMSO 9:1	100	1.5h
7	**14c**	DMF	100	1h
8		MeTHF	100	0.5h
9		MeTHF:DMSO 9:1	100	1h
10	**14d**	DMF	100	0.5h
11		MeTHF	100	0.5h
12		MeTHF:DMSO 9:1	100	1h
13	**14e**[b]	DMF	100	0.5h
14		MeTHF	100	0.5h
15		MeTHF:DMSO 9:1	100	0.5h

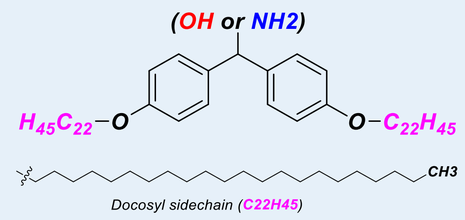
a. Data reported when conversion is complete, or the highest.
b. OxymaPure **6** was used in 5 eq, according to Green Chem. 2024, **26**, 10929-10939.

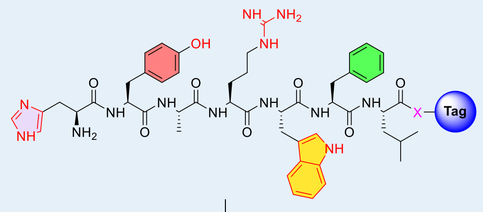


Entry	CDI	CDI (eq)	Oxyma Pure (eq)	Solvent	C_{max}%[b]	Time (h)	T (°C)	LL/DL[b]	12/13[b]
1	**3**	2	2	DMF	90.8[a]	2.0	30	97:3	85.6:14.4
2	**5a**	2	2	DMF	100	2.0	30	97:3	99.7:0.2
3	**5b**	2	2	DMF	100	1.5	30	98:2	99.4:0.6
4	**5a**	2	4	DMF	100	1.5	30	98:2	98.8:1.2
5	**5b**	2	4	DMF	100	1.5	30	99:1	100:0
6	**5a**	2	4	MeTHF:DMSO 9:1	100	1.0	30	97:3	99:1
7	**5b**	2	4	MeTHF:DMSO 9:1	100	1.0	30	97:3	98.8:1.2
8[a]	**5a**[c]	1+1	3	DMF	100 (65.0)	3.0	30	97:3 (98:2)	100:0
9[a]	**5b**	1+1	3	DMF	100 (72.1)	3.0	30	98:2 (98:2)	100:0
10[a]	**5a**[c]	1+1	3	MeTHF:DMSO 9:1	100 (82.8)	1.5	30	97:3 (98:2)	100:0
11[a]	**5b**	1+1	3	MeTHF:DMSO 9:1	100[d] (64.6)	4.0	30	96:4 (98:2)	100:0
12[a]	**5a**[c]	1+1	4	MeTHF:DMSO 9:1	100 (78.1)	1.5	30	97:3 (98.2)	100:0
13[a]	**5b**	1+1	4	MeTHF:DMSO 9:1	100 (81.6)	1.5	30	97:3 (98:2)	100:0

a. Portionwise addition of CDI, second portion of CDI (1eq) added after 1h
b. Data reported when conversion is complete, or the highest. In brackets, the values after 1h.
c. Addition of **5a** was performed by direct addition of solid carbodiimide to ensure complete solubilization in solvent mixture, while in all the other experiments a preformed 1M solution of carbodiimide was preferred.
d. Conversion reached 99.2% at 3h (previous point in the kinetic study).

LPPS of a challenging sequence





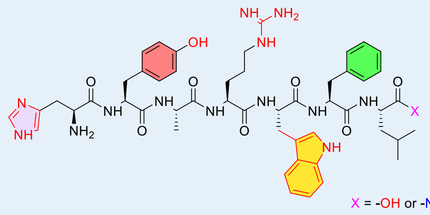
1st generation Ajinomoto tags

Cleavage
1M HCl in AcOH

Synthesis in MeTHF and in MeTHF:DMSO 9:1

Precipitation with ACN after Fmoc-deprotection

Precipitation after cleavage performed in DIPE, CPME or MTBE



Entry	Sequence	Purity[a](%)	Yield (%)
1	H-HYARWFL-OH	100	81
2	H-HYARWFL-NH_2	>98	80

[a] Determined via HPLC on crude product obtained after precipitation

References: [1] T. Fantoni et al., Green Chem, **2024**, 26, 10929-10939; [2] D. Corbisiero, N. Patrian et al., ACS Sustainable Chem. Eng., **2026**, 14, 26, 11707-11721

Aknowledgements: All coupling reagents were provided by Luxembourg Bio Technologies (www.luxembourg-bio.com/products/)

P4i PEPTIDE & PEPTIDOMIMETICS for green innovation — Cabri-Tolomelli-Ferrazzano research group

Cabri–Tolomelli–Ferrazzano Research Group

Luxembourg Bio Technologies

Italiadomani — PIANO NAZIONALE DI RIPRESA E RESILIENZA

Electronic Reprogramming of Amylin Self-Assembly via Single-Residue Aromatic Tuning

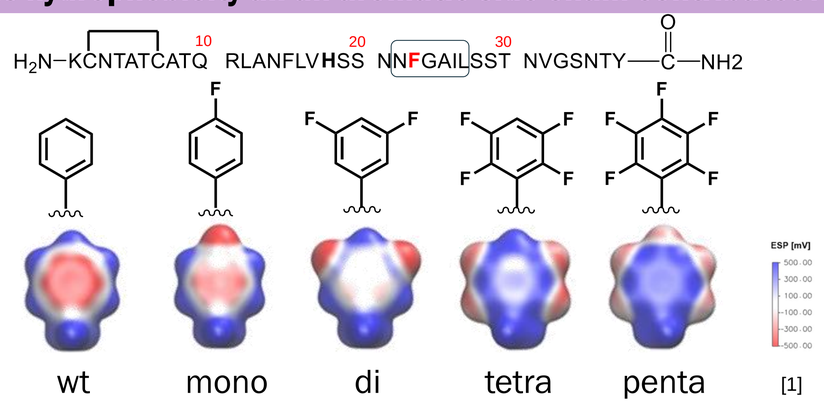
FULL PAPER

Artem Pavlov, H. Batebi , N. Österlund, K. Pagel, M. Schubert, R. Netz, Beate Koksch*
Presenting author: artem.pavlov@fu-berlin.de; Corresponding author: beate.koksch@fu-berlin.de
Department of Biology, Chemistry, and Pharmacy, Freie Universität Berlin, Arnimallee 20, 14195 Berlin, Germany
https://doi.org/10.17952/38EPS.2026.P122

SFB 1114

Rationale

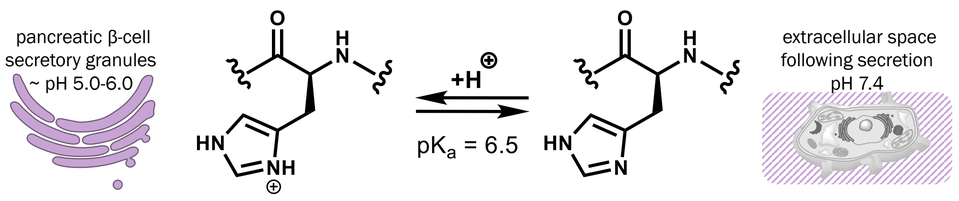
1. Is hydrophobicity all an aromatic side chain contributes?



[1]

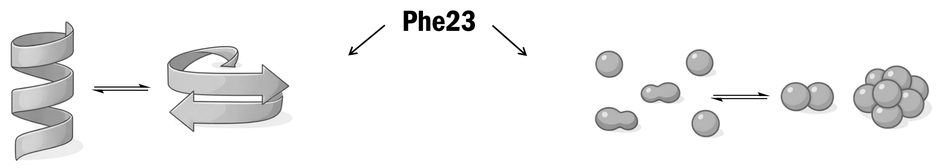
Most properties change **linearly**; only the dipole moment groups **wt** with **tetra**. If any single property governs aggregation, the **kinetics should follow**.

2. Do fragment models like NFGAIL transfer to the full-length peptide?



NFGAIL contains Phe23 but not His18. If the two are uncoupled, fragment trends should transfer directly.

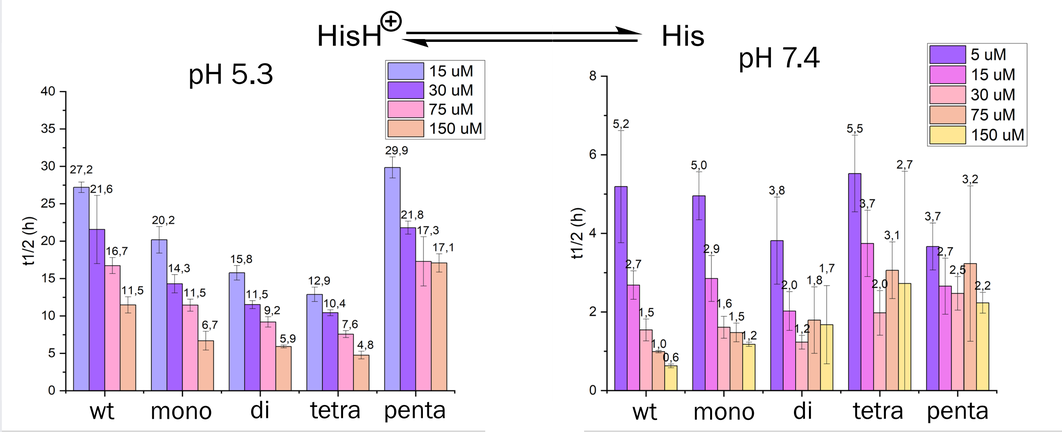
3. Does β-conformation and higher oligomerization assist aggregation?



If β-structure and oligomers were productive, the variants that form them soonest should fibrillate fastest.

Results

R1. Fluorination accelerates, but reverses twice — once on Phe23, once on His18

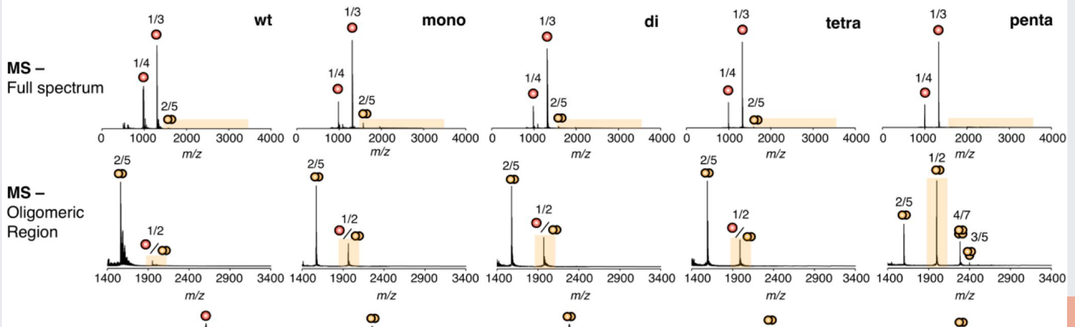


Each fluorine accelerates, 27.2 → 12.9 h; **wt → tetra**, 15 μM. **Penta** reverses it, slower than **wt.**

The order inverts; **tetra** is now slowest. Neutral His18. Above 30 μM only **wt** keeps accelerating.

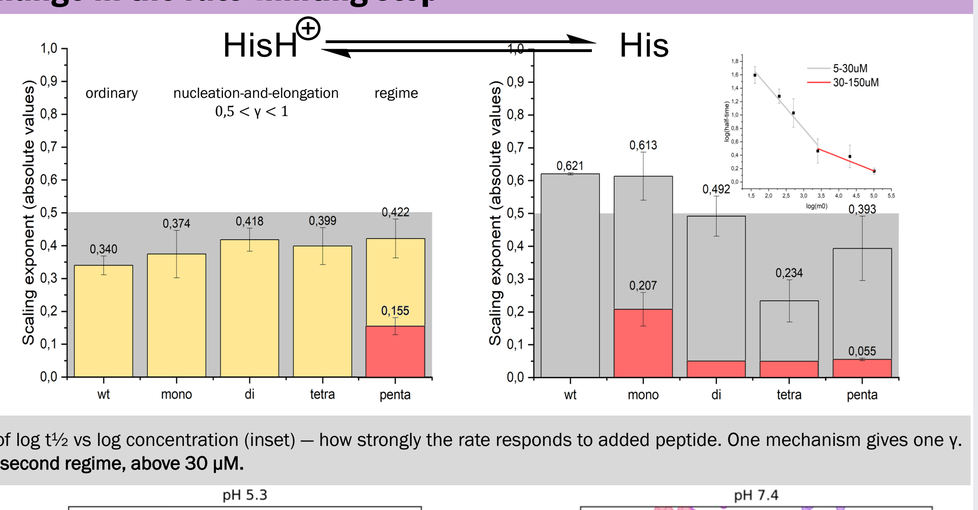
PROPERTIES	wt	mono	di	tetra	penta
Hydrophobicity	increasing				
Quadrupole	negative face			positive face	
Dipole	0	~1.5		0	~1.5
KINETICS					
ThT, pH 5.3	accelerating				reversed
ThT, pH 7.4	canonical	all self-limited			

The properties break between di and tetra, or group wt with tetra. **The kinetics break somewhere else** — after tetra at pH 5.3, after wt at pH 7.4. No property boundary coincides with a kinetic one, so **no single property sets the rate.**

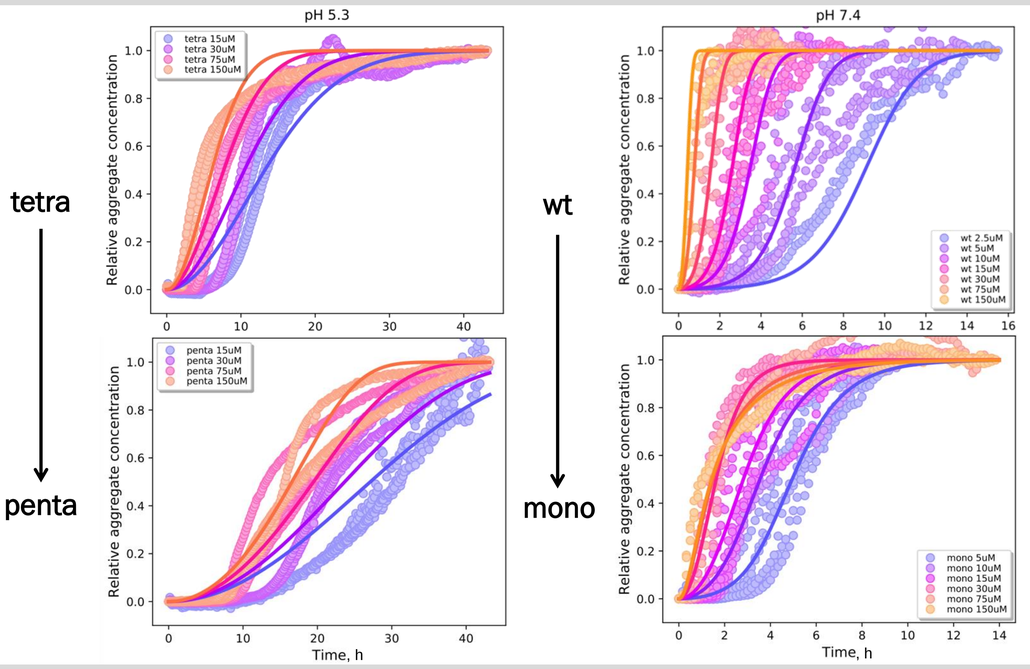


Native IM-MS, 15 μM, pH 7.4 — **wt** is mainly monomer with some dimer; **mono, di and tetra** dimerise more. **Penta** alone populates a discrete tetramer. Acidifying returns it to a wt-like distribution, so the species belongs to the neutral-pH regime. Such assemblies could either withdraw monomer from the productive pool or interfere with surface-catalysed secondary nucleation.

R2. Change in the rate-limiting step

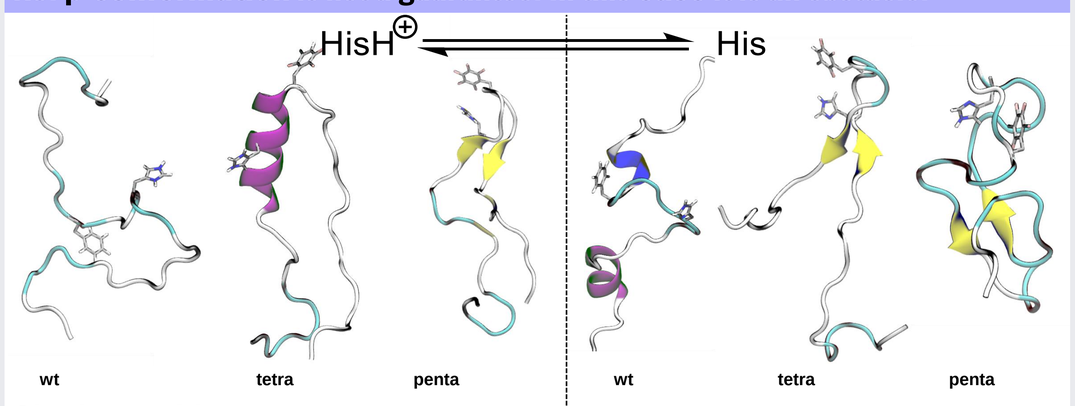


γ = slope of log t½ vs log concentration (inset) — how strongly the rate responds to added peptide. One mechanism gives one γ. **Red = the second regime, above 30 μM.**



wt shows canonical concentration-dependent sigmoids; fluorination progressively distorts kinetics

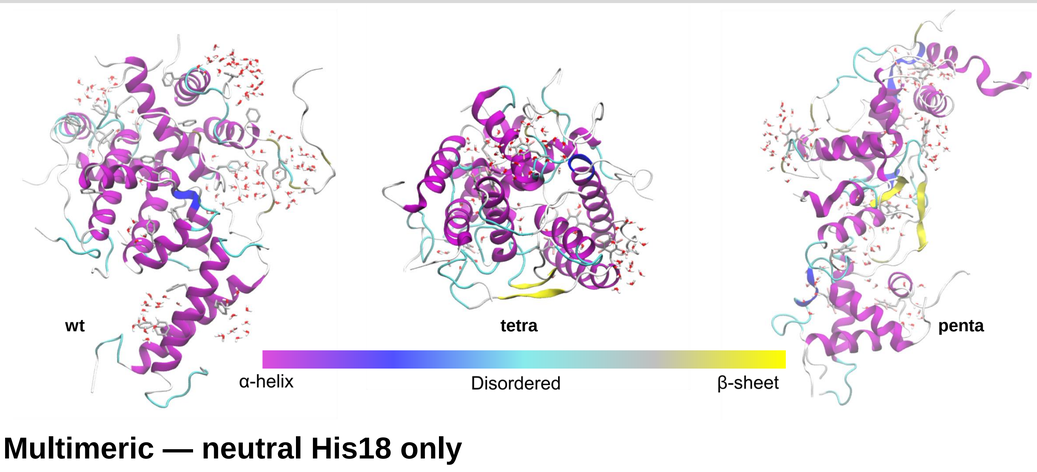
R3. β-conformation is not a guarantee. In this case it is an obstacle.



Single peptide MD

Variant	Protonated His18 — "acidic" α-helix	Protonated His18 — "acidic" β-sheet	Neutral His18 — "pH 7.4" α-helix	Neutral His18 — "pH 7.4" β-sheet
wt	11 %	2.5 %	22.7 %	2.6 %
tetra	34.1 %	**0.8 %**	13.2 %	5.5 %
penta	13.7 %	**11.8 %**	7.5 %	5.9 %

Tetra and **penta** variants differ in behaviour only when His18 is protonated. At neutral His18 they converge.



Multimeric — neutral His18 only

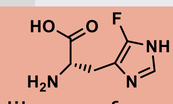
Variant	α-helix	β-sheet
wt	44 ± 2.4 %	1.1 ± 0.7 %
tetra	41.8 ± 2.7 %	2.9 ± 1.2 %
penta	35.6 ± 2.9 %	3.5 ± 1.6 %

Helix falls and β rises with fluorine count, which correlates with the aggregation kinetics.

Conclusions:

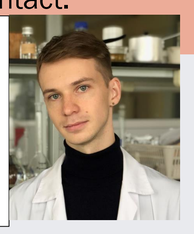
- Hydrophobicity is not the whole story. At pH 5.3 **penta,** the most hydrophobic variant, is the slowest.
- Fragment trends do not transfer. Phe23 electronics and His18 protonation are coupled; NFGAIL predicted **penta** as fastest.
- β-structure and oligomers mark the slow variants. Retained α-helical access speeds up the aggregation at both pH values.

Outlook:



Ongoing. A focused library of multi-substituted fluorinated aromatics including **4-fluorohistidine** as ^{19}F probes of intermolecular contact.

MY LINKEDIN



References

[1] S. Chowdhary, et al., *ChemBioChem*, **2020**, 21, 3544-3554
[2] A. Pavlov, et al., *ACS BioMedChem Au*, **2026,** 6, 381–392
[3] Ling-Hsien Tu, D.P. Raleigh, *Biochemistry*, **2013**, 52, 2, 333–342

Acknowledgments:
We gratefully acknowledge financial support from grant CRC 1114 "Scaling Cascades in Complex Systems" (Project-ID 235221301), Project B03, and thank GDCh Biochemie for a travel grant.

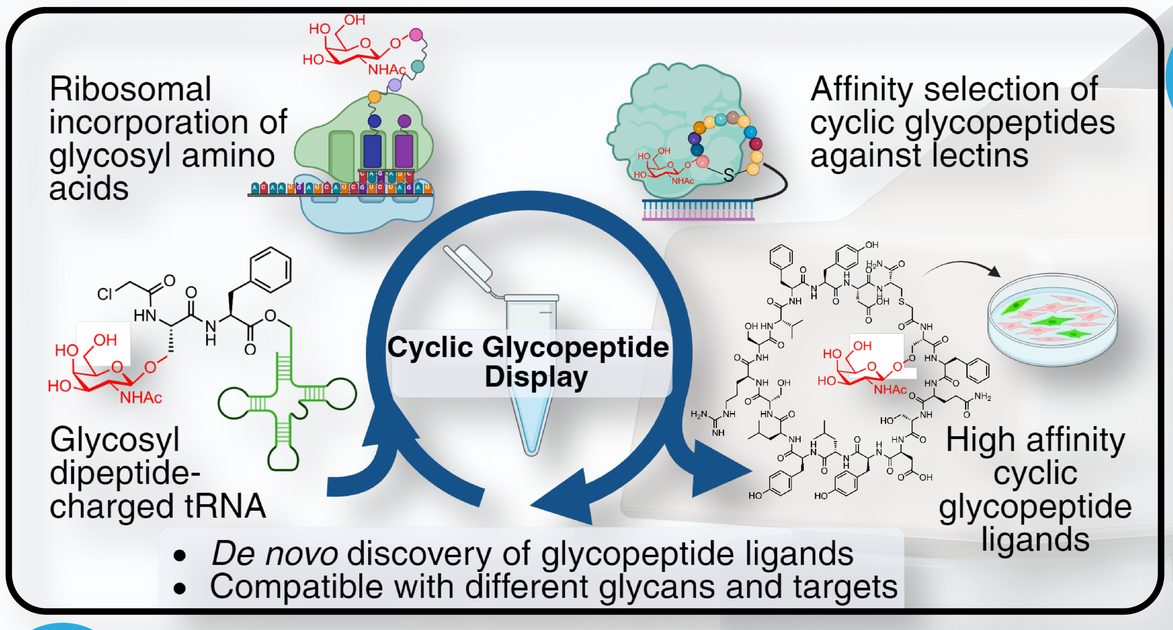
https://doi.org/10.17952/38EPS.2026.P407

Ribosomal Translation and Display Selection of Cyclic Glycopeptides Through Genetic Reprogramming

Jason Johansen-Leete[1,2], Yichen Zhong[1,2], **Beiyuan Cui**[1,2], Bernardo Cavallazzi Sebold[1,2], Lucas Kambanis[1,2], Caitlin E. Clarke-Shepperson[1,2], Christopher Lehmann[1,2], Ka Hin Toby Mak[1,2], Arthur H. Tang[1,2], James Burchfield[1,2], Walter Becker[1,2], Jose Perdomo[3], David M. McDonald[1,4], Leo Corcilius[1,2], Toby Passioura[1,2], Freda H. Passam[1,2], Daniel J. Ford[1,2], Richard J. Payne[1,2]

Affiliations:

1. School of Chemistry, The University of Sydney, NSW, 2006, Australia; 2. Council Centre of Excellence for Innovations in Peptide and Protein Science; 3. Charles Perkins Centre, The University of Sydney, NSW, 2006, Australia; 4. Department of Chemistry, Yale University, New Haven, Connecticut 06520, United States.

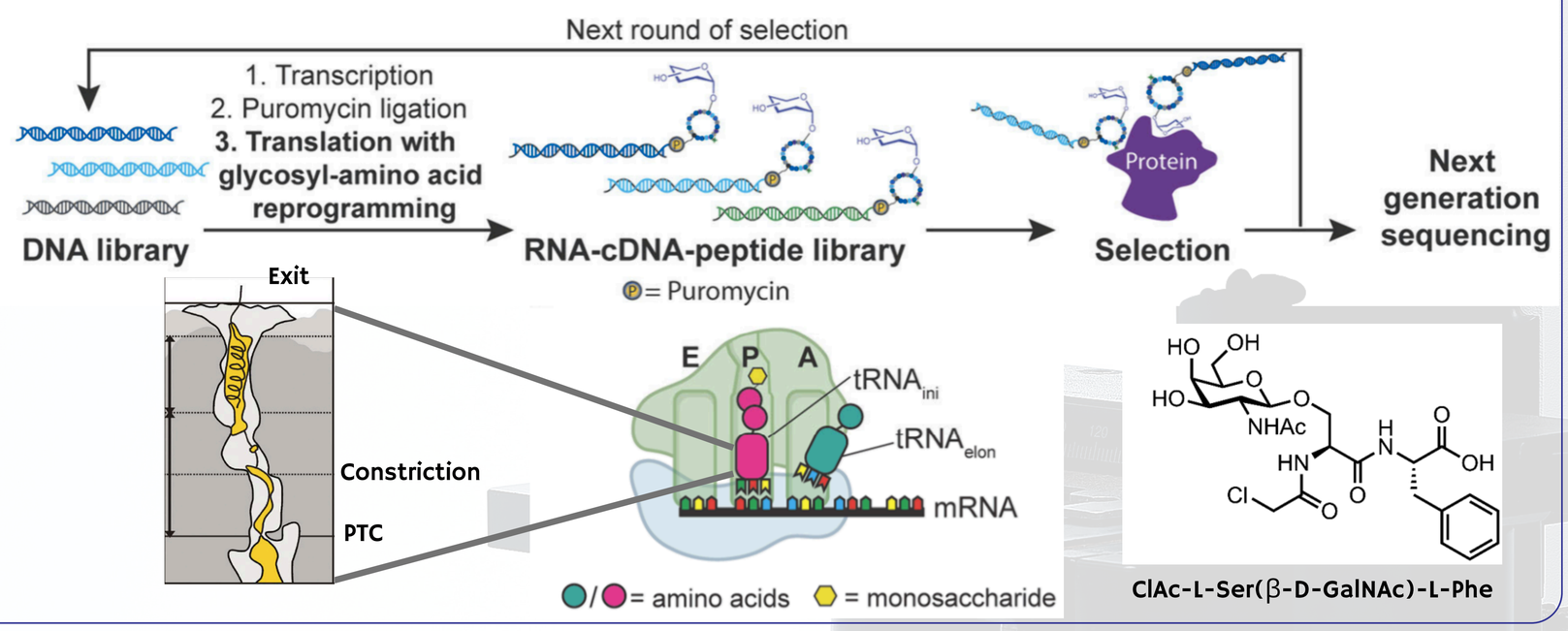


Background

Macrocyclic peptides are attractive therapeutic molecules because they can bind protein targets with high affinity and specificity, including targets that are difficult for small molecules to engage. mRNA display enables the screening of numerous peptide libraries (>10^{12} sequences).

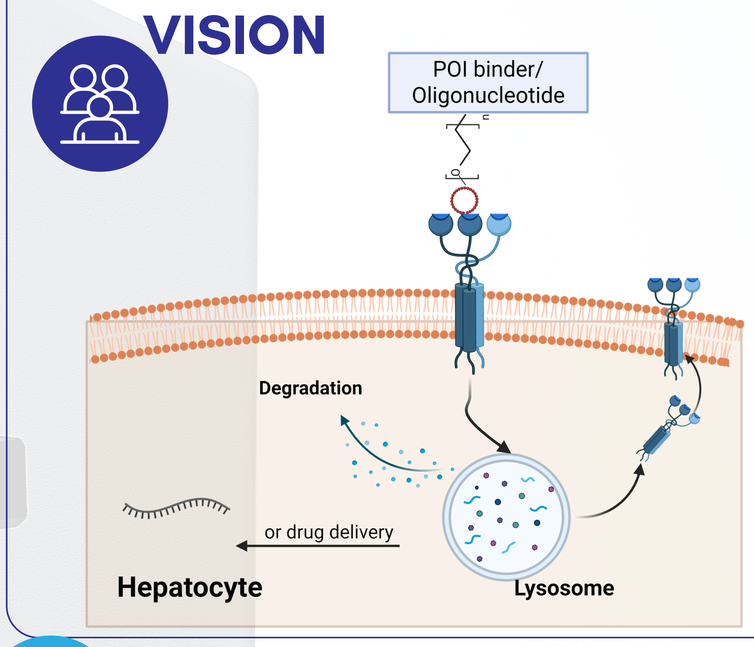
Although mRNA display and genetic code reprogramming provide powerful platforms for discovering macrocyclic peptides, inefficient ribosomal incorporation of glycosyl-amino acids has prevented the *de novo* discovery of glycopeptides with native glycosidic linkages. This paper aims to overcome that limitation through glycosyl-dipeptide-mediated genetic reprogramming

mRNA Display Screening with Glyco-cyclic Peptides

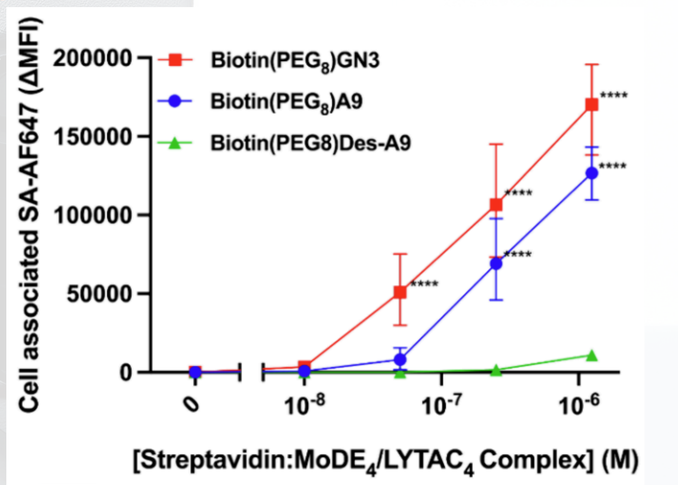


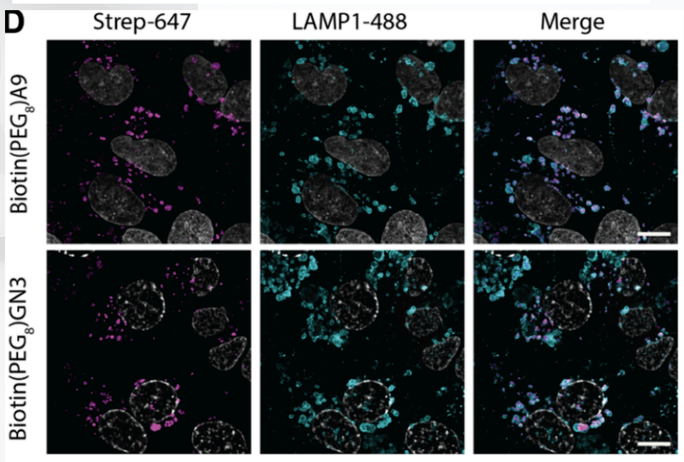
- After seven rounds of selection, the resulting peptides were identified by next-generation sequencing, and the **top 10 most enriched** peptides were selected for synthesis and further evaluation;
- Initiating with a dipeptide bearing an N-terminal ClAc-L-Ser(β-D-GalNAc)-L-Phe may alleviate the **steric clashes** of the sugar moiety within the ribosomal P-site.

Lysosomal Degradation



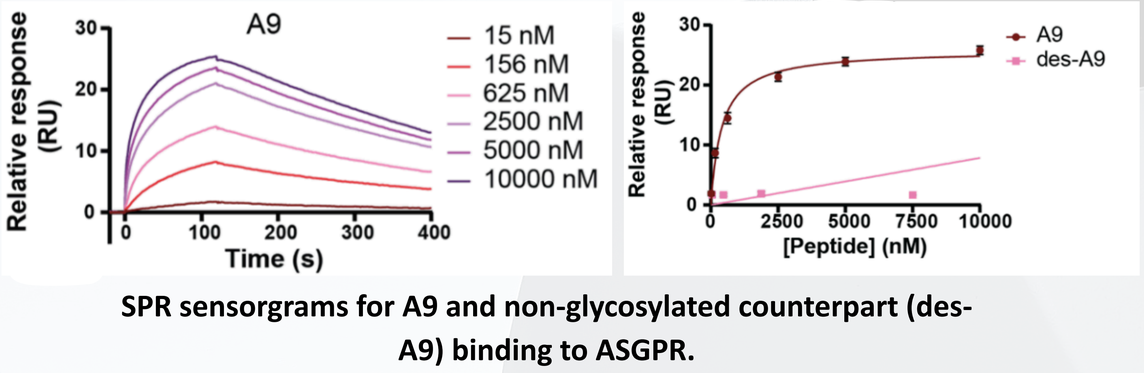
Lysosomal Trafficking of A9





A9 could traffic extracellular protein into lysosomes.

High-affinity Hits Screened by SPR



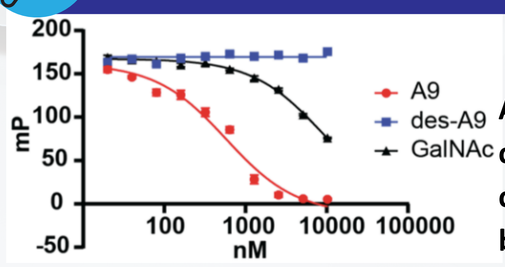
SPR sensorgrams for A9 and non-glycosylated counterpart (des-A9) binding to ASGPR.

- **The binding affinity of A9 significantly decreased by removing the glycan;**
- **This indicates that the GalNAc moiety was critical for ASGPR binding, and may play a role in stabilising the binding conformation within the peptide.**

Conclusion

In summary, we have developed a robust genetic reprogramming methodology for the ribosomal translation of glycosyl-amino acids into in vitro translated cyclic glycopeptides compatible with mRNA display selection. The hits now serve as attractive alternatives to the Tri-GalNAc (GN3) for the development of next-generation LYTACs.

Top Hits Compete CRD



	K_D by SPR (μM)	IC_{50} by FP (μM)
GalNAc	~40 *	~14
A9	0.41 ± 0.07	0.58 ± 0.08
des-A9	>100	>40

A9 could compete carbohydrate binding domain(CRD) of ASGPR with tri-GalNAc.

References

- Passioura, T. et al., *Chem. Commun.* **2017**, 53 (12), 1931-1940.
- Passioura, T.et al.. *Annu. Rev. Biochem.* **2014**, 83, 727-752.
- Goto, Y.; Katoh, T.; Suga, H. Flexizymes for genetic code reprogramming. *Nat. Protoc.* **2011**, 6 (6), 779-790.
- Bhushan, S. et al., *Nat Struct Mol Biol*, **2010**, 17, 313-317.
- Ahn, G.; Bertozzi, C. R. et al., *Nat. Chem. Biol.* **2021**, 17 (9), 937-946.

Scan For Full paper

Self-Assembled Peptide-Au Nanoparticle Hybrid Systems for Catalytic Applications

CICA | INTERDISCIPLINARY CENTER FOR CHEMISTRY AND BIOLOGY

Vanessa Quattrociocchi[1], Claudia Pigliacelli[2], and Elena Pazos[1,3]

UNIVERSIDADE DA CORUÑA

vanessa.quattrociocchi@udc.es

[1]CICA – Centro Interdisciplinar de Química e Bioloxía and Departamento de Química, Facultade de Ciencias, Universidade da Coruña, Campus de Elviña, 15071 A Coruña (Spain).

[2]Laboratory of Supramolecular and Bio-Nanomaterials (SupraBioNano Lab), Department of Chemistry, Materials, and Chemical Engineering "Giulio Natta", Politecnico di Milano, Via Luigi Mancinelli 7, 20131 Milan, Italy.

https://doi.org/10.17952/38EPS.2026.P559

[3]Oportunius, Axencia Galega de Innovación, 15702 Santiago de Compostela, Spain.

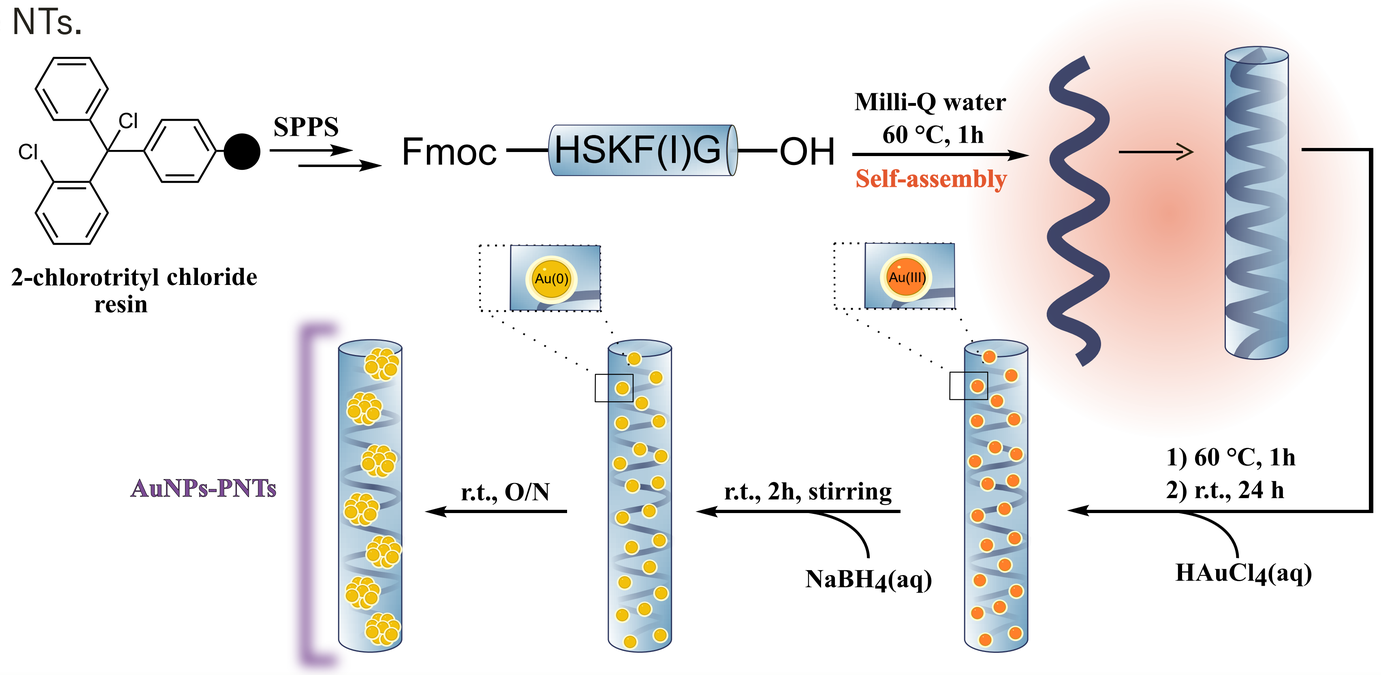
Background

Peptide-inorganic nanoparticle **hybrid structures** have attracted considerable attention due to their potential applications in biomedicine, electronics, or catalysis. The challenging aspect is the controlled design of **metal nanoparticles** (NPs), whose properties are highly dependent on their size, shape, composition, and spatial distribution.[1] To address this, **peptides** have emerged among various scaffolds for the controlled assembly and growth of NPs, owing to their self-assembly, binding capabilities, and sequence tunability.[2,3]

In this work, we exploit a short peptide's ability to self-assemble and, through physicochemical characterization, confirm the formation of **ordered and homogeneous supramolecular architectures, with preliminary investigations also suggesting catalytic activity in the reduction of 4-nitrophenol to 4-aminophenol.**

Synthesis

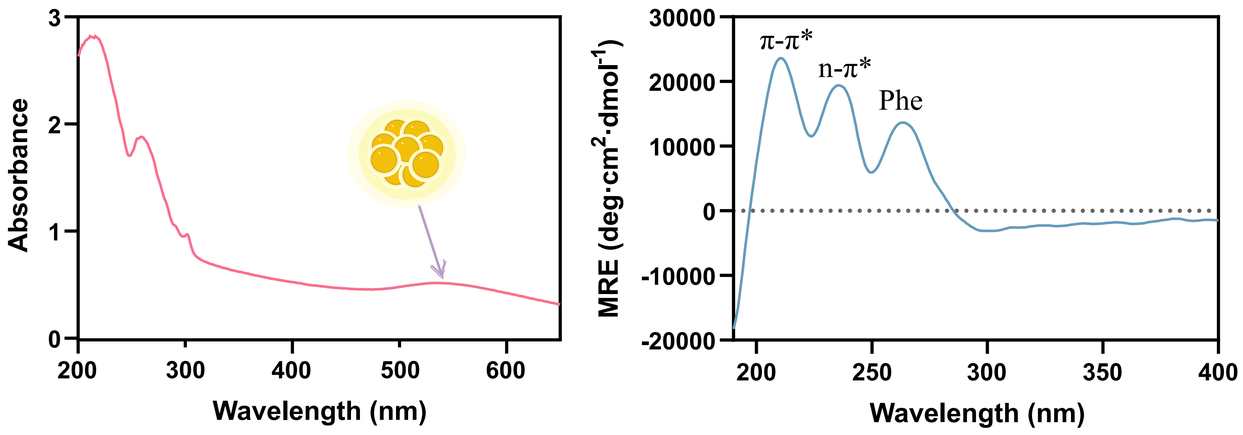
Herein we present the synthesis of hybrid peptide-gold nanostructures, harnessing a **Fmoc-pentapeptide's self-assembly into nanotubes** (NTs) as a supramolecular template able to **direct the nucleation and growth of gold NPs** evenly spaced over the surface of the NTs.



Characterization

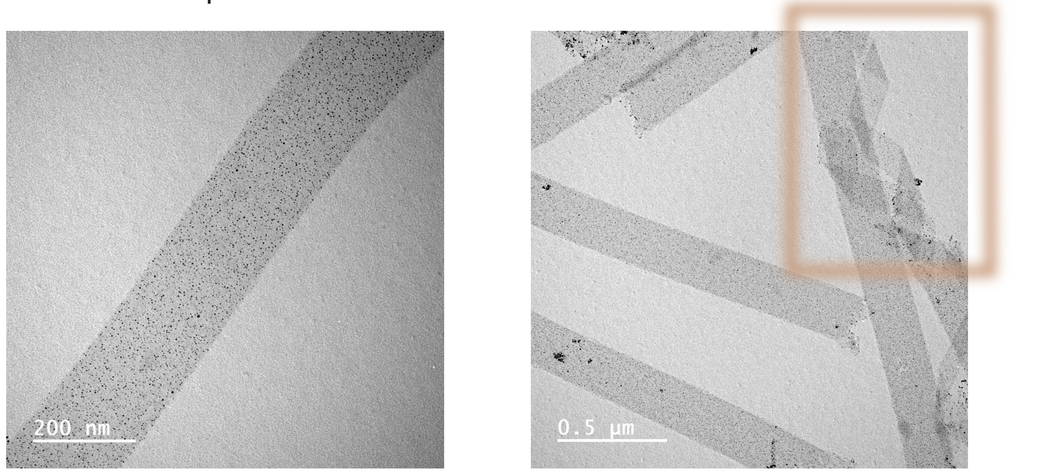
The **UV-vis** spectrum showed a distinct **plasmonic band around 530 nm**, indicating the presence of **Au-NPs**. Fluorescence spectra were also acquired, and the absence of a clear emission band upon excitation at different wavelengths further corroborated the presence of NPs rather than smaller NCs.

The **CD signal** contains **contributions from peptide conformation and interactions between Phe residues** which provide insights into the supramolecular arrangement of the system.



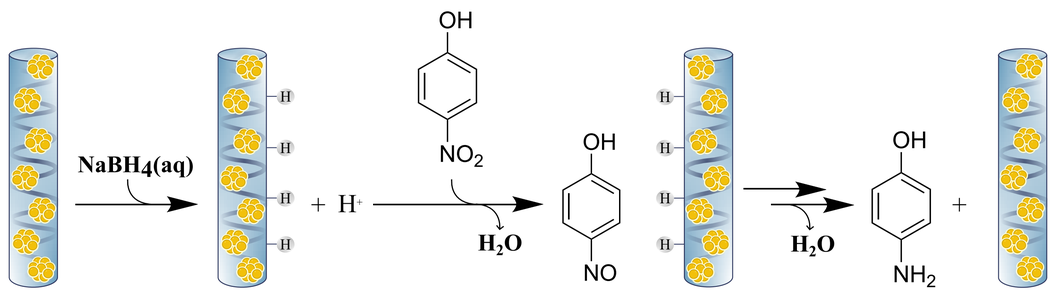
Left. UV-vis spectrum of 250 µM AuNPs-PNTs hybrid architectures ([P]:[Au] = 1:1) solution in Milli-Q water, T= 25 °C . Absorption bands at 214 and 258 nm correspond to peptide bonds and Phe respectively. Plasmonic band around 530 nm. **Right.** CD Spectrum of 250 µM AuNPs-PNTs hybrid system solution in Milli-Q water.

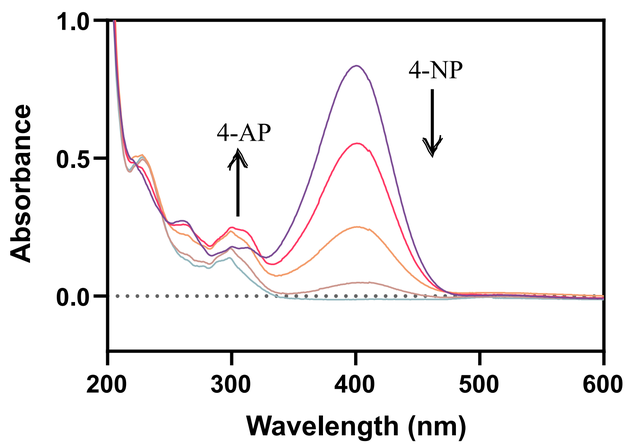
TEM images showed a population of **nanotubes with homogeneous diameter of ~ 200 nm, uniformly decorated with Au-NPs** with an **average diameter of around 2 nm**. Notably, intermediate stages of the nanotubes formation were captured.



Above. TEM images of 50 µM AuNPs-PNTs hybrid nanostructures in Milli-Q water.

Catalysis





Above. The reaction was monitored acquiring UV-vis spectra after 3 min (—), 15 min (—), 35 min (—), 55 min (—), 15 h (—). The decreasing intensity of the peak at 400 nm corresponds to 4-nitrophenol conversion over time. Reaction conditions: reaction temperature, 20 °C; 4-nitrophenol concentration, 50 µM; AuNPs-PNTs concentration, 22.2 µM; $NaBH_4$ concentration, 5 mM.

Conclusion

Harnessing peptide self-assembly enables the rational design of hybrid peptide-nanoparticle systems with controlled nanoparticle size and morphology, opening new opportunities for advanced catalytic applications.

References

1. Tang, Z.; Kotov, N. A. One-Dimensional Assemblies of Nanoparticles: Preparation, Properties, and Promise. Adv. Mater. **2005**, 17 (8), 951–962.
2. Pigliacelli, C., et al. - Self-assembled peptide-inorganic nanoparticle superstructures: from component disgn to applications. Chem. Commun. **2020**, 56, 8000–8014.
3. Yang S., et al. - Self-assembled short peptides: recent advances and strategies for potential pharmaceutical applications. Materials Today Bio **2023**, 20, 100644.

Acknowledgements

CICA, as a center accredited for excellence within the Galician University System and a member of the CIGUS Network, receives subsidies from the Department of Education, Science, Universities, and Vocational Training of the Xunta de Galicia. Additionally, it is co-financed by the EU through the FEDER Galicia 2021-27.

Cofinanciado por la Unión Europea
Cofinanciado pola Unión Europea
Fondos Europeos
CIGUS Network Research Centres of the Galician University System
Project PID2022-142374NBI00 financed by MINISTERIO DE CIENCIA, INNOVACION Y UNIVERSIDADES
Cofinanciado por la Unión Europea
AGENCIA ESTATAL DE INVESTIGACIÓN

https://doi.org/10.17952/38EPS.2026.P313

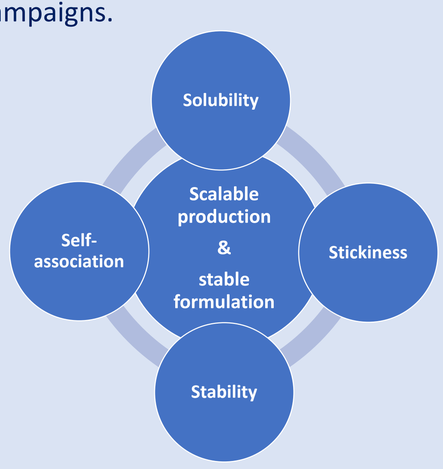


Developability Screening of Pharmaceutical Peptides

Marie Pedersen, Rodrigo Ochoa, Mathias Norrman, Christian Tornøe, Sebastian Swanson (Novo Nordisk A/S)
Jacob Larsen, Stephanie Hansen, Alexander Büll (Danish Technical University)

DEVELOPABILITY

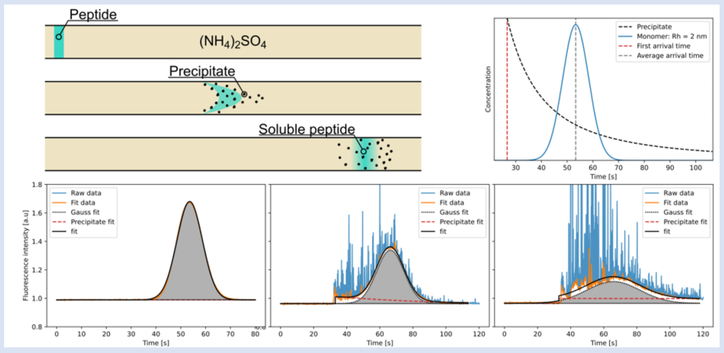
To transform peptides into safe bio-pharmaceutical, they must be soluble, stable and manufacturable in addition to having suitable biological properties.
Fast developability screens addressing key biophysical properties increase chances of success during design-make-test-analyze campaigns.



SCREENING PLATFORM

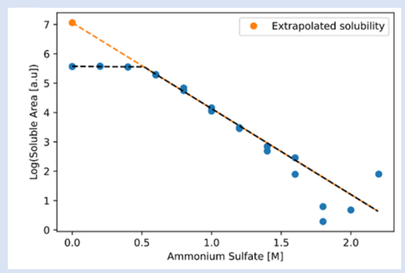
Precipitation of peptides injected in nL volumes by Taylor Dispersion Analysis in Fida1 / FidaNEO (FidaBio)

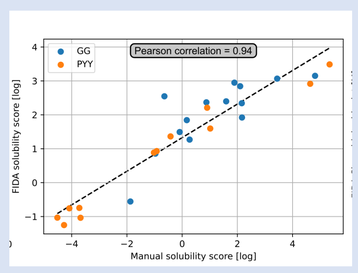




0 M Ammonium Sulfate | 1 M Ammonium Sulfate | 1.3 M Ammonium Sulfate

A 42 nL peptide plug is injected into a capillary and mixed with running buffer containing increasing ammonium sulfate. As solubility decreases, soluble peptide and precipitate separate according to Taylor-Aris theory of transient incomplete separation(Aris 1956). Fitting the signals yields a typical precipitation profile as seen in traditional forced precipitation methods from which we derive a solubility score. We compared peptide solubility quantified using the Fida platform with solubility scores obtained with manual equilibration experiment and find good correlation (Pearson corr = 0.94).





Solubility Profiling of Therapeutic Peptides by Taylor Dispersion Induced Precipitation using Nanoliter Sample Volumes
Larsen JA, Ochoa R, Norrman M, Büll A, Pedersen MØ
2026 Preprint ChemRxiv

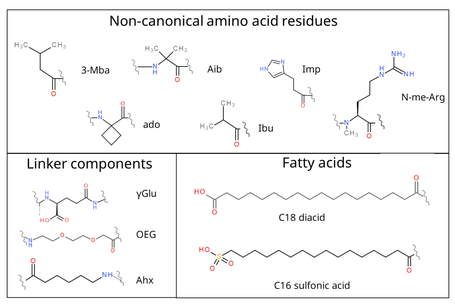
R. Aris, On the dispersion of a solute in a fluid flowing through a tube, *Proceedings of the Royal Society of London. A. Mathematical and Physical Sciences* **1956**, *235*, 67-77

LEARNINGS FROM TWO PEPTIDE FAMILIES: Y2 agonists (PYY) & GLP1/glucagon receptor dual agonists

PEPTIDE LIBRARY

Name	1	2	3	4	5	6	7	8	9	10	11	12	13	14	15	16	17	18	19	20	21	22	23	24	25	26	27	28	29	30	31	Linker	Fatty acid
GG-1151	H	Acb	Q	G	T	F	T	S	D	L	S	K	Y	L	D	L	R	R	A	R	D	F	V	Q	W	L	L	K*	T	-	-	2·γGlu-2·OEG-2·γGlu	C18 diacid
GG-1177	H	Aib	Q	G	T	F	T	S	D	L	S	K	Y	L	E	S	K	R	A	R	E	F	V	Q	W	L	L	K*	T	-	-	2·γGlu-Ser-Glu-Ser-2·γGlu	C18 diacid
GG-1359	Imp	Aib	H	G	T	F	T	S	D	V	S	K	Y	L	E	E	Q	A	A	R	E	F	I	A	W	L	L	K*	T	-	-	2·γGlu-2·OEG	C18 diacid
GG-1139	H	Acb	Q	G	T	F	T	S	D	L	S	K	Y	L	E	S	R	R	A	R	E	F	V	Q	W	L	L	K*	T	-	-	γ·Glu-2·OEG-2·γGlu	C18 diacid
GG-1155	H	Acb	Q	G	T	F	T	S	D	L	S	K	Y	L	D	L	K	R	A	R	E	F	V	Q	W	L	L	K*	T	-	-	2·γGlu-Ser-Gly-Glu-Ser-Gly	C18 diacid
GG-1166	H	Aib	Q	G	T	F	T	S	D	L	S	K	Y	L	D	L	R	R	A	Q	D	F	V	Q	W	L	L	K*	T	-	-	2·γGlu-Ser-Glu-Ser-2·γGlu	C18 diacid
GG-1197	H	Aib	Q	G	T	F	T	S	D	L	S	K	Y	L	D	A	R	R	A	R	D	F	V	Q	W	L	L	K*	T	-	-	3·γGlu-2·OEG	C18 diacid
GG-1223	H	Aib	Q	G	T	F	T	S	D	Y	S	K	Y	L	E	S	R	R	A	R	D	F	V	K*	W	L	I	S	T	-	-	3·γGlu-2·OEG	C18 diacid
GG-1305	Imp	Acb	H	G	T	F	T	S	D	V	S	K	Y	L	E	E	Q	A	A	R	E	F	I	A	W	L	L	K	K*	-	-	2·γGlu-Ser-Gly-Glu-Ser-Gly	C18 diacid
GG-1380	Imp	Aib	H	G	T	F	T	S	D	V	S	R	Y	L	E	G	Q	A	A	R	E	F	I	A	W	L	L	K*	T	-	-	2·γGlu-Ser-Gly-Glu-Ser-Gly	C18 diacid
GG-1383	H	Acb	Q	G	T	F	T	S	D	V	S	K	Y	L	E	S	R	R	A	R	E	F	V	Q	W	L	I	K*	T	-	-	2·γGlu-2·OEG-2·γGlu	C18 diacid
GG-1385	H	Aib	Q	G	T	F	T	S	D	L	S	K	Y	L	D	A	R	R	A	R	D	F	V	Q	W	L	I	N	K*	-	-	gGlu-2·OEG-2·γGlu	C18 diacid
GG-1387	H	Aib	Q	G	T	F	T	S	D	L	S	K	Y	L	D	L	R	R	A	R	E	F	V	Q	W	L	I	N	K*	-	-	gGlu-2·OEG-2·γGlu	C18 diacid
GG-1400	Imp	A	H	G	T	F	T	S	D	V	S	K	Y	L	E	G	R	A	A	R	E	F	I	A	W	L	L	K*	G	G	G	3·γGlu-2·OEG	C18 diacid

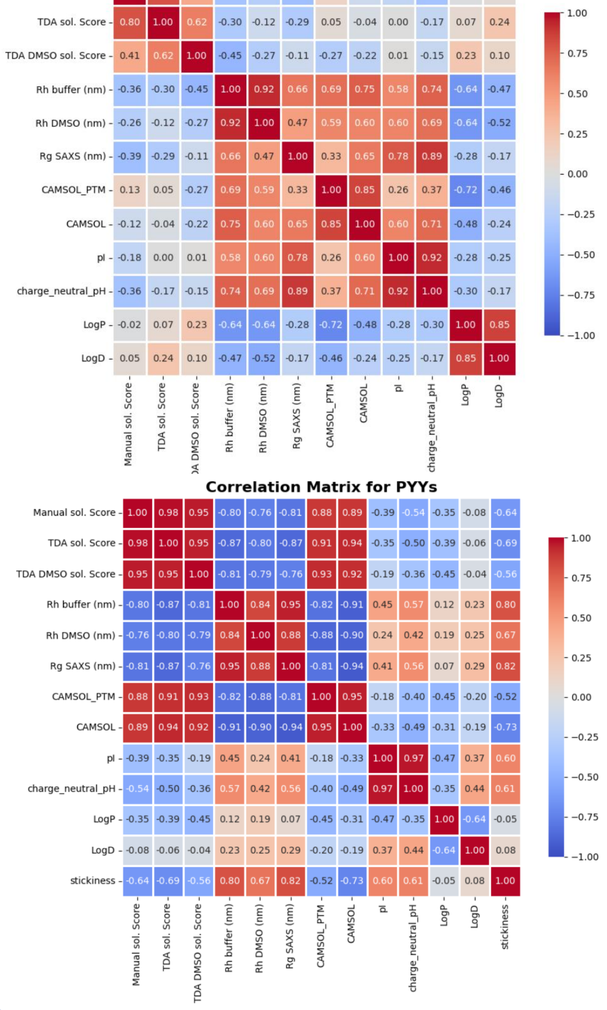
Name	3	4	5	6	7	8	9	10	11	12	13	14	15	16	17	18	19	20	21	22	23	24	25	26	27	28	29	30	31	32	33	34	35	36	Linker	Fatty acid
PYY-1562	3-Mba	R	P	E	K*	P	G	E	D	A	S	P	E	E	L	Q	R	Y	Y	A	S	L	R	H	Y	L	N	W	V	T	R	Q	N-Me-Arg	Y	γ·Glu-2·OEG	C16 Sulfonic acid
PYY-1875	3-Mba	R	P	E	K*	P	P	E	D	A	S	P	E	E	L	Q	R	Y	Y	A	S	L	R	H	Y	Y	N	W	L	T	R	Q	R	Y	γGlu-Ahx	C18 diacid
PYY-1679	3-Mba	R	P	E	A	P	G	K*	D	A	S	P	E	E	L	Q	R	Y	Y	A	S	L	R	H	Y	L	N	W	V	T	R	Q	N-Me-Arg	Y	γGlu	C16 Sulfonic acid
PYY-1686	3-Mba	R	P	E	K*	P	G	E	D	A	S	P	E	E	L	Q	R	Y	Y	I	S	L	R	H	Y	L	N	W	V	T	R	Q	R	Y	γGlu-3·OEG	C18 diacid
PYY-1688	3-Mba	R	P	E	A	P	G	K*	D	A	S	P	E	E	L	Q	R	Y	Y	I	S	L	R	H	Y	L	N	W	V	T	R	Q	R	Y	γGlu-2·OEG	C18 diacid
PYY-1696	3-Mba	R	P	E	K*	P	G	E	D	A	S	P	E	E	L	S	R	Y	Y	I	S	L	R	H	Y	L	N	W	V	T	R	Q	N-Me-Arg	Y	γGlu-2·OEG	C18 diacid
PYY-1698	3-Mba	R	P	E	A	P	G	K*	D	A	S	P	E	E	L	S	R	Y	Y	I	S	L	R	H	Y	L	N	W	V	T	R	Q	N-Me-Arg	Y	γGlu-2·OEG	C18 diacid
PYY-1699	3-Mba	R	P	E	A	P	G	K*	D	A	S	P	E	E	L	S	R	Y	Y	I	S	L	R	H	Y	L	N	W	V	T	R	Q	R	Y	γGlu-2·OEG	C18 diacid
PYY-1700	3-Mba	R	P	E	A	P	G	K*	D	A	S	P	E	E	L	S	R	Y	Y	I	S	L	R	H	Y	L	N	W	V	T	R	Q	N-Me-Arg	Y	γGlu-2·OEG	C16 Sulfonic acid
PYY-1709	Aib	E	P	E	K*	P	G	E	D	A	S	P	E	E	L	Q	R	Y	Y	A	S	L	R	H	Y	L	N	W	V	T	R	Q	N-Me-Arg	Y	γGlu-2·OEG	C18 diacid
PYY-1710	Ibu	R	P	E	K*	P	G	E	D	A	S	P	E	E	L	Q	R	Y	Y	A	S	L	R	H	Y	L	N	W	V	T	R	Q	N-Me-Arg	Y	γGlu-2·OEG	C18 diacid
PYY-1713	Y	E	P	E	K*	P	G	E	D	A	S	P	E	E	L	Q	R	Y	Y	A	S	L	R	H	Y	L	N	W	V	T	R	Q	N-Me-Arg	Y	γGlu-2·OEG	C18 diacid



We selected a library of 26 lipidated therapeutic peptides from two discontinued discovery programs targeting obesity. The first group comprised 14 GLP-1/glucagon co-agonists (GG). The second group contained 12 selective Y2 receptor agonists derived from peptide YY (PYY). The library included a broad range of peptides, from early research to preclinical and clinical-stage molecules, providing a relevant test set for comparing solubility and assembly behavior.

Correlations

GG and PYY families showed different correlation patterns linking solubility and oligomer size with calculated properties demonstrating the importance for experimental solubility profiling for new peptide classes

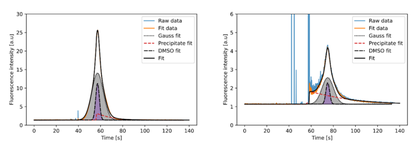


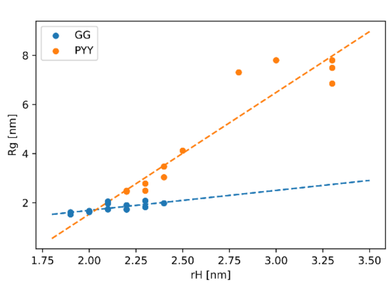
Solubility, Size & Stickiness – all in one assay consuming < 1 µg

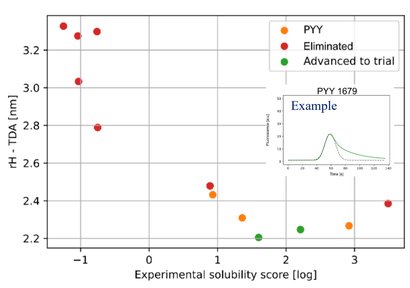
Size
Taylor Dispersion Analysis estimates peptide size from diffusion-driven peak broadening (Taylor 1953). Applying the Stokes–Einstein relation gives an apparent hydrodynamic radius (rH), a readout of oligomerization. We compared rH with SAXS-derived radius of gyration (Rg) to validate the measurements.

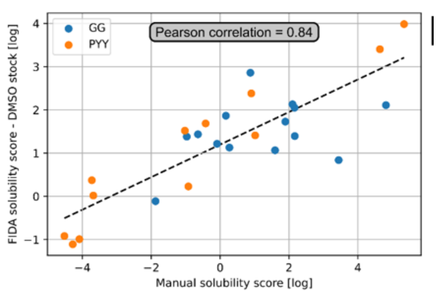
Stickiness
Peptide stickiness appears as tailing in the trace at 0 M ammonium sulfate, indicating interaction with the glass capillary. Combining stickiness, solubility, oligomer size and salt sensitivity flagged 7 of 12 PYY candidates as potentially unsuitable. The two clinical-stage peptides showed favorable profiles.

Compatible with DMSO stocks
DMSO plugs required a modified fitting model to account for DMSO fluorescence and delayed precipitation. Despite this complexity, solubility scores correlated well with aqueous and manual measurements.



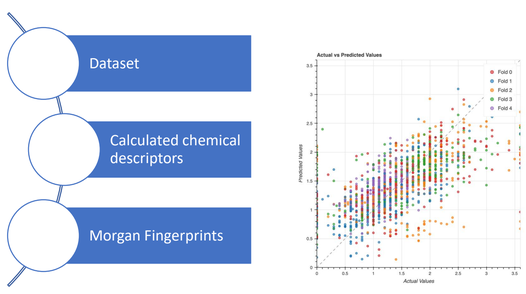






OUTLOOK: ML model

We have demonstrated that we can train a predictive model on in-house solubility data (Sebastian Swanson). For more about chemical descriptors, see Rodrigo Ochoa (poster 251)



G. I. Taylor, Dispersion of soluble matter in solvent flowing slowly through a tube, *Proceedings of the Royal Society of London. A. Mathematical and Physical Sciences* **1953**, *219*, 186-203.

Multifunctional Bioactive Cotton: Synergistic Antimicrobial and Regenerative Properties through Chemoselective Peptide Conjugation

F. Albini[1], A. Di Stasi[2], M. Mardirossian[2], B. Biondi[3] & C. Peggion[1,3]

[1] Department of Chemical Sciences, University of Padova, Padova, Italy
[2] Department of Life Sciences, University of Trieste, Trieste, Italy
[3] Institute of Biomolecular Chemistry, CNR, Padova, Italy

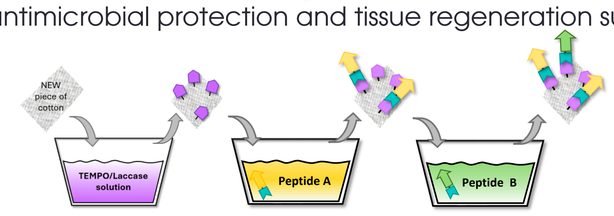
10.17952/38EPS.2026.P399
Email: cristina.peggion@unipd.it

SUMMARY

Skin wounds represent a significant public health challenge, requiring the development of active dressings that can prevent infections and support the healing process.

While cotton is the most widely used material for wound bandages, it lacks intrinsic bioactivity. In this work, we present chemoselective strategies to transform cotton into a versatile multifunctional platform by functionalizing it with bioactive peptides using 'click chemistry' approaches.

By conjugating two biological active peptides we developed a dressing that offers simultaneous antimicrobial protection and tissue regeneration support.



ACTIVE PEPTIDES

Antibacterial ①

from PMAP36(12-24) H-KRLKKIGKVLKWIH-NH_2

- Broad spectrum antibacterial properties and low cytotoxicity
- Membranolytic mechanism of action
- Its D-enantiomer is resistant to proteases
- High solubility in water

2a

H-**Cys**-KRLKKIGKVLKWI-NH_2

PMAP36(12-24)
Maintains the helicity and **antimicrobial activity** of the natural PMAP36(1-36)

MIC (μM)*					
E.coli ATCC 25922	*S.aureus* ATCC 25923	*A.baumanni* ATCC 19606	*K.pneumoniae* ATCC 700603	*P.aeruginosa* ATCC 27853	*S.epidermidis* ATCC 12228
4	>64	2	8	8	4

- Not cytotoxic against HaCaT
- Not hemolitic against red blood cells

Collagen Boosting ②

from pentapeptide 4 H-KTTKS-OH

- Fragment of procollagen sequence
- Collagen regenerative properties by inhibiting the collagenase activity and promote the ECM.
- Palmitic chain at the N-terminus is reported to give better stability and higher permeability through the skin.

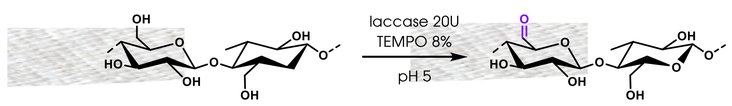
4d

H-**Cys**-WKTTKS-NH_2

THE METHOD

The cellulose backbone is modified with aldehyde groups through mild TEMPO/laccase/O_2 catalysed oxidation, which preserves the fibres' structural integrity. Then, thiazolidine was employed to covalently graft bioactive peptides.

This strategy was employed to produce dual-functional materials through consecutive ligations.

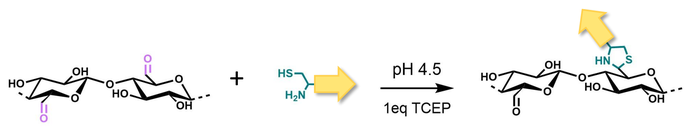


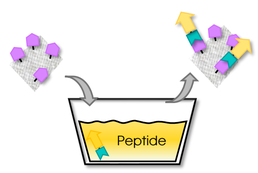


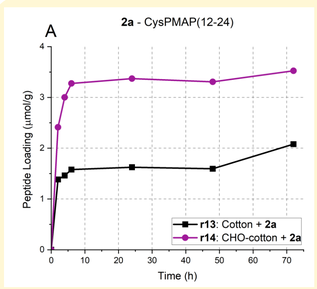
Colorimetric Schiff test to evaluate the presence of the aldehyde. From left to right cotton, 1st , 2nd and 3rd use of the oxidizing solution.

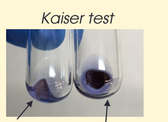
Titration with NaOH 0.01M to quantify the grafting

- Selective for primary OH
- Aqueous solution
- Room temperature
- Oxidizing solution can be re-used



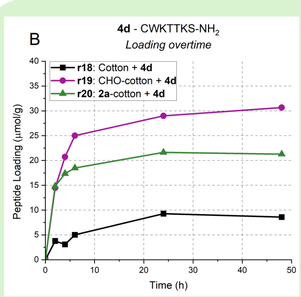


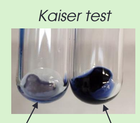




Peptide loading overtime (monitored by absorbance at 280nm) for the reaction with cotton.

	Sample	2a loading (μmol/g_{cot})	4d loading (μmol/g_{cot})	Time of Reaction
r13	Cotton + 2a	1.5	-	3 days
r14	CHO-Cotton + 2a	3.5	-	3 days

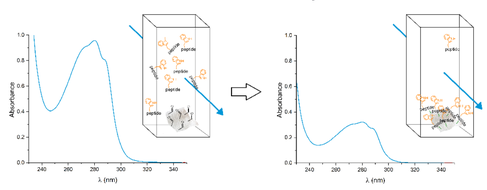




Peptide loading overtime (monitored by absorbance at 280nm) for the reaction with cotton.

	Sample	2a loading (μmol/g_{cot})	4d loading (μmol/g_{cot})	Time of Reaction
r18	Cotton + 4d	-	8.6	2 days
r19	CHO-cotton + 4d	-	30.7	2 days
r20	r14 (CHO-cotton+2a)+ 4d	3.5	21.3	2 days

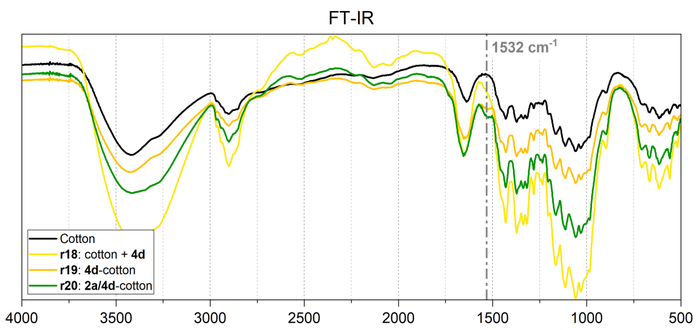
- One-pot reactions monitored by the decrease of the peptide from the reaction solution by UV-vis



- TCEP to avoid formation of dimers through disulfide bonds

RESULTS

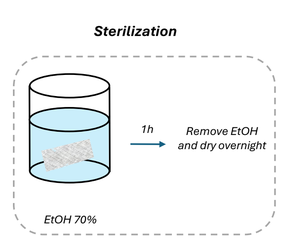
Successful conjugation was confirmed via FT-IR, amino acid analysis, and XPS spectroscopy.

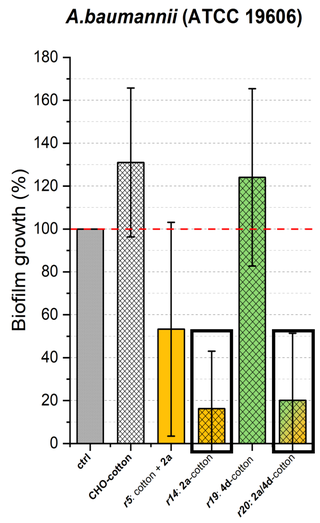


1532 cm-1, that can be attributed to the amide II stretching signal of the amides present in the peptide backbone

Bioactivity was assessed by biological assays against *Acinetobacter baumannii*.

The results demonstrate that chemoselective functionalization can effectively turn simple cotton into a high-performance, biocompatible medical textile with tailored multifunctional properties.





CONCLUSIONS

- With this approach all **reactions are performed in water**.
- In a **one-pot** reaction vessel
- All reaction steps can be followed by simple **colorimetric tests**.
- FT-IR and XPS (not shown) confirmed the **presence of peptides** on cotton.
- Varying the reaction time, peptide concentration and peptide excess, we can **modulate the cotton loading**: from 0.02-0.20 mmol/g cotton, quantified by UV.
- Thiazolidine bond allowed to bind **multiple peptides.**
- The **antibacterial** properties of PMAP(12-24) are maintained in the conjugate with CHO-cotton.
- Tests are undergoing to evaluate the **collagen regenerative properties** of 2a+4d-cotton.

REFERENCES

- A. Orlandin, et al., *Coatings*, **2019**, 9, 2079.
- S. Scapin, et al., *Macromol. Biosci.* **2020**, 20, 2000199.
- B. Biondi, et al., *Sci. Rep.* **2023**, 13, 5132.
- F. Albini, et al., *Cellulose*, **2023**, 30, 5573.
- F. Albini, et al., *Bioorg. Chem*, **2025**, 163, 108715.

UNI IMPRESA

Co-funded by the European Union



Evolution Did Not Eliminate Aggregation: Functional Amyloids Enable Hormone Storage and Signaling

Dániel Horváth[a,b]*, Zsolt Dürvanger[a,b], Szebasztián Szaniszló[a,b], Anna Kiss-Szemán[b], Duong Kim Hoang Yen[b], Michael Hons[c], Meytal Landau[c], **András Perczel[a,b]**



ELTE FACULTY OF SCIENCE | INSTITUTE OF CHEMISTRY

HUN-REN Hungarian Research Network

ELTE Eötvös Loránd University, Budapest, Hungary
[a] HUN-REN-ELTE Protein Modeling Research Group
[b] Laboratory of Structural Chemistry and Biology
[c] CSSB Centre for Structural Systems Biology, Deutsches Elektronen-Synchrotron DESY, 22603 Hamburg, Germany

https://doi.org/10.17952/38EPS.2026.P493

A functional reservoir with a molecular cost

Members of the PACAP–glucagon hormone family play pleiotropic roles in human physiology, regulating metabolic, nervous system, endocrine, and developmental processes. Their synthetic derivatives, including today's **blockbuster GLP-1 receptor agonists**, have consequently become highly **important pharmaceutical agents**.

These peptides, however, share an **intrinsic propensity** to self-assemble and **form amyloid structures**. This property presents a particular challenge for the production and formulation of peptide-based active ingredients, where aggregation is generally regarded as undesirable.

From a biological perspective, however, aggregation is not necessarily pathological. Following post-translational maturation, peptide hormones awaiting secretion can exist in a self-assembled state within acidic secretory granules. This transient amyloid state is thought to provide a compartmentalized reservoir, allowing large amounts of peptide to be stored in a dense, stabilized form and released when required. This raises a fundamental question: **why do** peptide **hormones possess a molecular architecture** that **simultaneously supports biological recognition and amyloid assembly?**

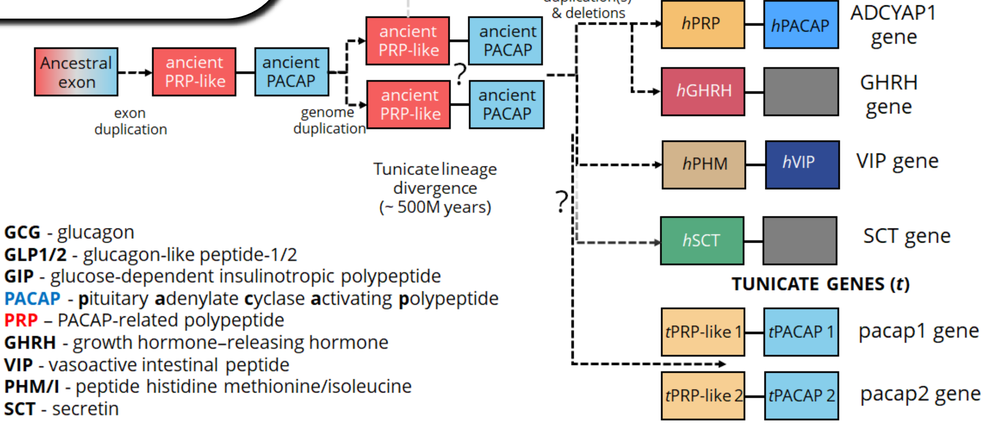
An evolutionary perspective

If this relationship is intrinsic to peptide architecture, it raises a further question: **how has the balance** between **biological function** and **aggregation** been shaped during evolution?

The PACAP–glucagon family provides an unusually informative system in which to address this question. Its members have been **conserved throughout hundreds of millions of years of** vertebrate **evolution**, while their individual receptor specificities and biological functions have diversified substantially.

We therefore asked whether the intrinsic propensity of these hormones to aggregate has remained conserved alongside their biological functions, and which structural features determine this propensity.





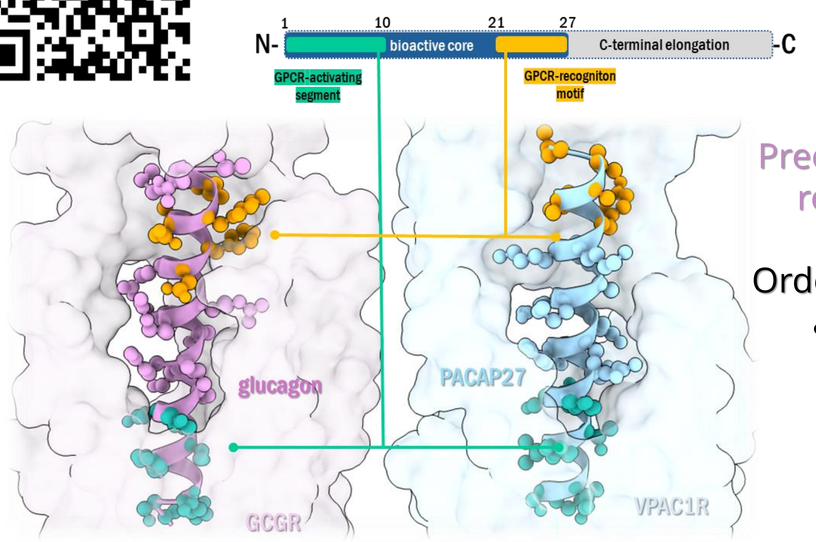
GCG - glucagon
GLP1/2 - glucagon-like peptide-1/2
GIP - glucose-dependent insulinotropic polypeptide
PACAP - **p**ituitary **a**denylate **c**yclase **a**ctivating **p**olypeptide
PRP – PACAP-related polypeptide
GHRH - growth hormone–releasing hormone
VIP - vasoactive intestinal peptide
PHM/I - peptide histidine methionine/isoleucine
SCT - secretin

From receptor recognition to amyloid assembly

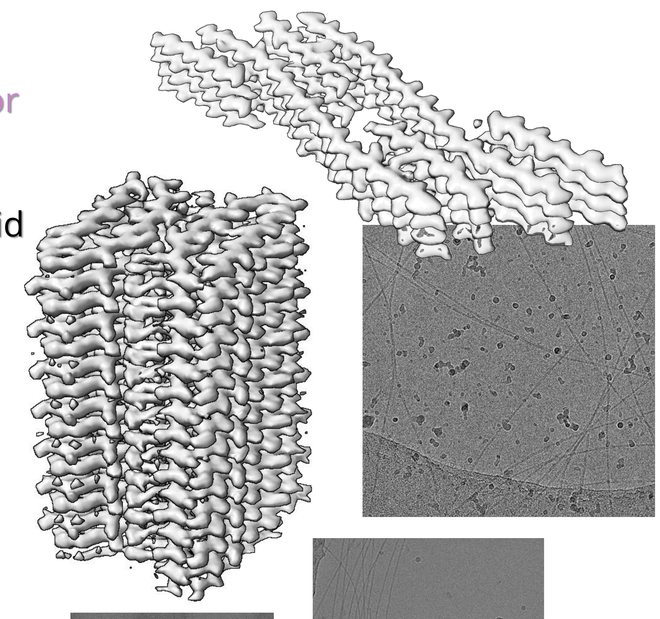
Peptide hormones of the PACAP–glucagon family recognize their cognate G-protein-coupled receptors (GPCRs) through highly specific molecular interactions. Their biological activity therefore depends on **precise recognition of receptor surfaces**, involving complementary shapes, electrostatic interactions, hydrogen bonds, and hydrophobic contacts.

Remarkably, many of the same molecular features can also promote self-association. The side chains required for specific intermolecular recognition can establish complementary interfaces between peptide molecules, **enabling ordered assembly into amyloid structures**.

Thus, receptor recognition and amyloid aggregation may represent two different structural manifestations of the same molecular interaction landscape.



Precise receptor recognition
↔
Ordered amyloid assembly

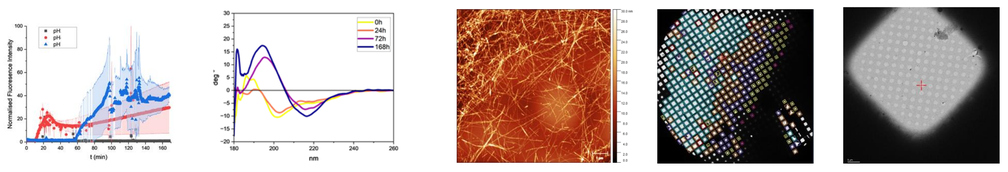


The role of molecular environment

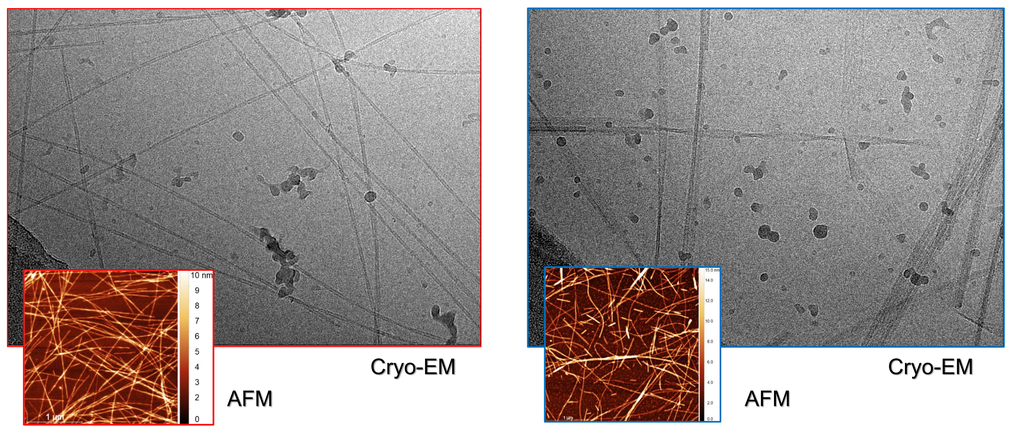
Amyloid formation is not determined **by sequence alone**. The conformational landscape of a peptide and the interactions between assembling molecules are strongly **influenced** by their **molecular environment**. In secretory granules, for example, pH, ionic strength, and macromolecular components create conditions that can profoundly alter the balance between soluble and assembled states.

Understanding this environment-dependent structural landscape is **essential for distinguishing** functional and regulated self-assembly from uncontrolled aggregation.

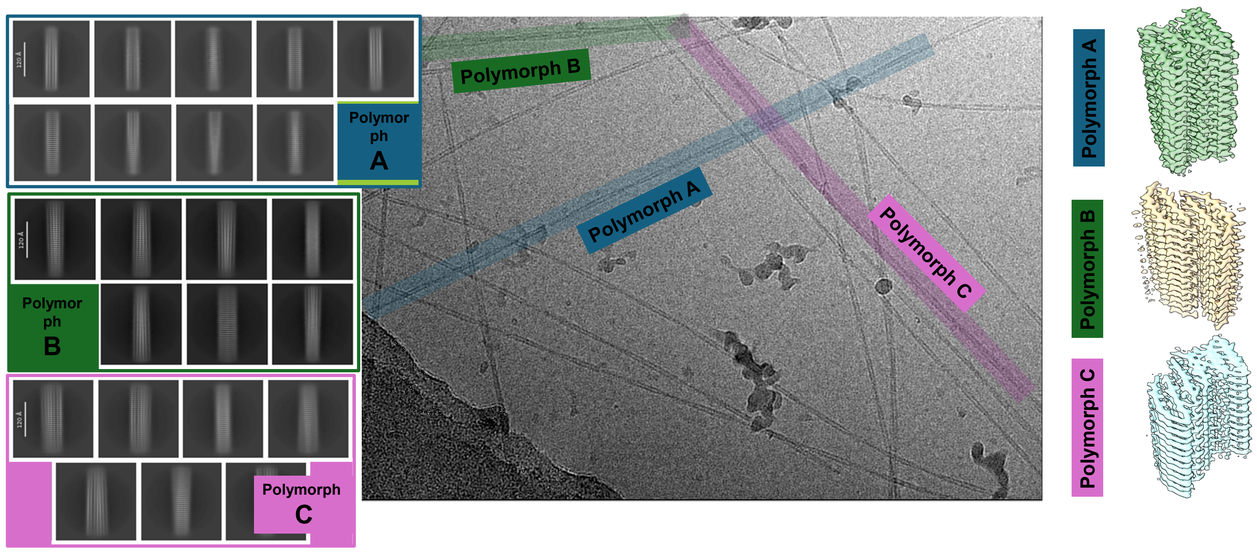
peptide	pH	c_{NaCl}	Agitation-period	dilution
GLP-1	A or B	0mM	168h	1x



Sample A (pH A) ⟷ **Sample B (pH B)**

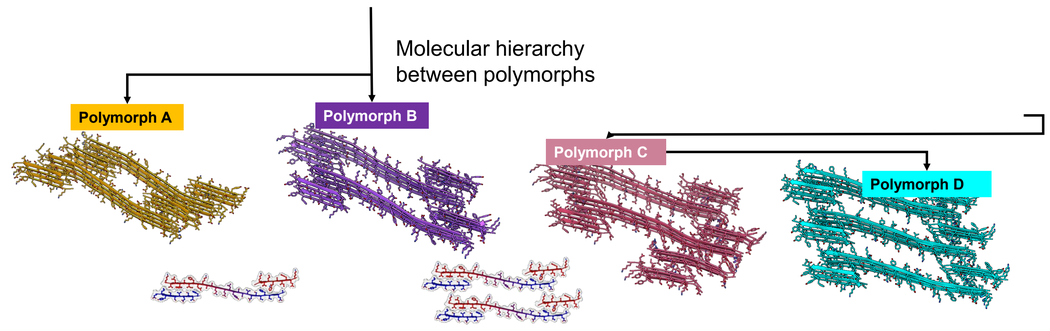






From Aggregation to Function

Amyloid architecture can be both stable and reversible. Our results show that this apparent paradox is resolved at the level of higher-order interface organization. Functional amyloids are therefore not failed soluble proteins, but programmable molecular reservoirs



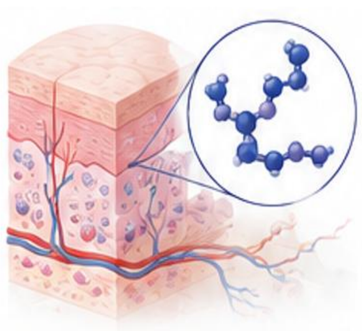
https://doi.org/10.17952/38EPS.2026.P233

Multifunctional Short Chimeric Peptides: Potential Antimicrobial Activity and Enhanced Cell Proliferation for Tissue Healing

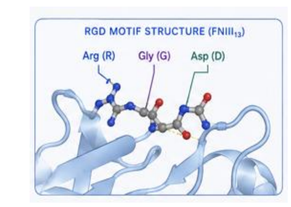
Naiara Maia Pereira, **Reinaldo Marchetto**

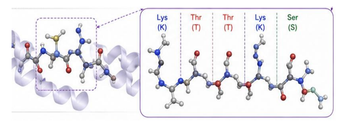
UNESP – Institute of Chemistry – Department of Biochemistry and Organic Chemistry, Araraquara, São Paulo, Brazil

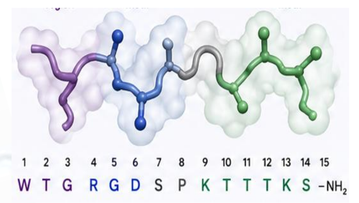
INTRODUCTION



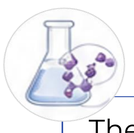
Tissue healing is a complex biological process that can be impaired or delayed by several factors, such as hypoxia, ischemia, altered cellular response, bacterial colonization and defects in collagen synthesis, extending the healing period from a few weeks to many years[1]. There are four phases of healing, each playing a crucial role in restoring tissue function: hemostasis, inflammation, proliferation, and maturation. Short peptides can be combined to control and enhance some of these phases, resulting in faster healing processes in a more controlled environment[1,2]. Studies have shown that short sequences of peptides can inhibit the microbial growth of some species and stimulate the Extracellular Matrix to increase the cell proliferation, supporting some events of the healing processes and making them more effective[2,3,4]. In this context, we designed and synthesized a series of novel chimeric peptides with structures that combines fibronectin fragments and a sub-fragment of type I collagen propeptide, to achieve enhanced cell proliferation, collagen synthesis and microbial control. The peptides were chemically synthesized by Solid Phase methodology, purified by RP-HPLC and characterized by mass spectrometry (ESI-MS). Cytotoxicity analysis was performed by Hemolytic Assay against human blood cells and by MTT assay against MRC-5 (ATCC CCL-171) and keratinocyte (BCRJ 0341) cell lines. Microbial growth inhibition was evaluated by the minimum inhibitory concentration (MIC) assay against Staphylococcus aureus (ATCC 14458) and Escherichia coli (ATCC 43895). The NMB peptide showed no significant cytotoxicity in fibroblasts or keratinocytes. In addition, low hemolytic activity was observed indicating a safety profile that is favorable in the context of wound healing. Finally, NMB peptide significantly reduced microbial growth for both strains analyzed, by approximately 50% at all tested concentrations. Our findings indicate that the NMB peptide combines antimicrobial activity with low cytotoxicity and hemolytic effect, making it a promising candidate for future research as a wound-healing compound for the treatment of wounds





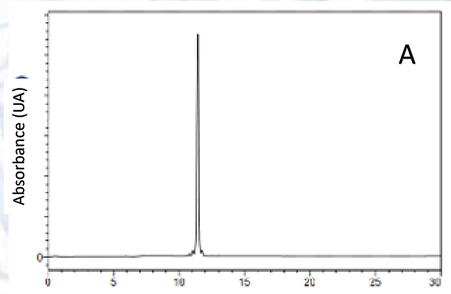


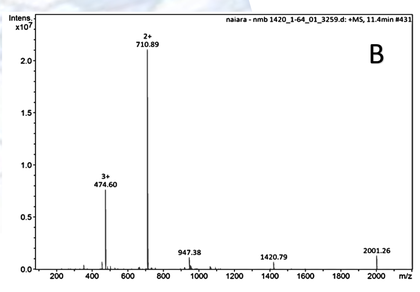
MATERIAL, METHODS AND RESULTS



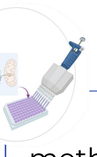
The peptide NMB, WTGRGDSPKTTKS, was synthesized by solid-phase methodology, using Fmoc/tBu Chemistry with a Fmoc-Ser(tBu)-Wang resin (0.33 mmol g^{-1}) and DIC/HOBt activation. After deprotection and cleavage with TFA/water/TIS (95:2.5:2.5) for 120min at RT, the peptide was precipitated, solubilized and dried under vacuum. Analysis and purification was performed by RP-HPLC and the identity confirmed by ESI-MS.

Calculated MW (g.mol-1)	ES+	ES m/z (g.mol-1)	Obtained MW (g.mol-1)
1.420,53	+2	710,89	1420,46
	+3	474,6	

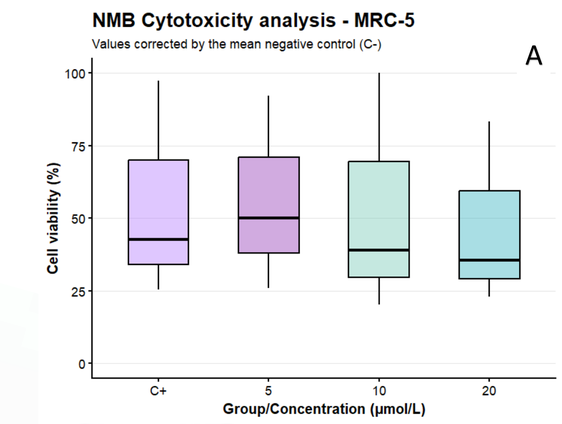


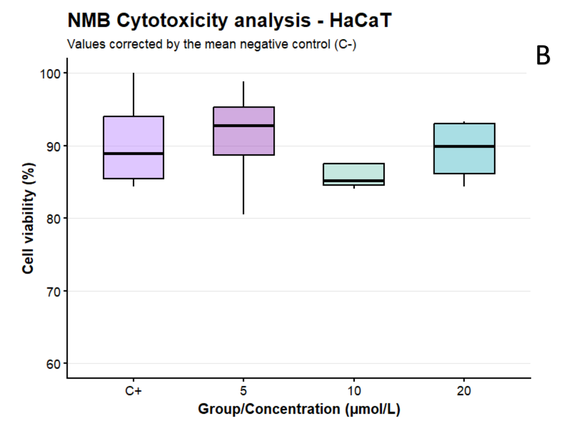


Analytical-scale chromatographic profiles of the NMB peptide obtained after purification (A). Separation was performed on a Jupiter C18 reverse-phase column (250 × 4.6 mm, 5 µm, 300 Å; Phenomenex). A linear gradient from 5 to 95% solvent B (A: water containing 0.045% TFA; B: acetonitrile containing 0.036% TFA) was applied over 30 min at a flow rate of 1.0 mL min^{-1}, with UV detection at 220 nm. (B) Mass spectra obtained via ESI-MS confirming the pureness of the peptide obtained



Cytotoxicity analysis was performed using the MTT colorimetric method for 24h, using fibroblasts MRC-5 (ATCC CCL-171) and HaCaT cells, immortalized human keratinocytes (BCRJ 0341). To perform the MTT assay, the supernatants were removed and discarded. So, 100 µl of sterile PBS buffer was added to the wells to remove dead cells and other metabolic residues present. Next, 180 µL of DMEM and PBS (1:4) solution were added, followed by the addition of 20 µL of MTT solution at 1.0 $mg.mL^{-1}$. The plates were kept in incubation for 4 hours at 37°C and 5% CO_2. Finally, the supernatants were discarded and 100 µL of a mixture 1:1 of isopropyl alcohol and dimethyl sulfoxide was added to each well to dissolve the formed crystals, keeping the set protected from light and under agitation for 1 hour. The absorbance was read using a microplate reader spectrophotometer at 540 nm.

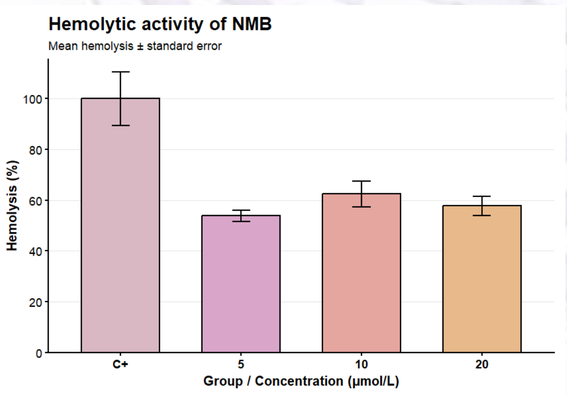




Cell viability of fibroblasts (A) and keratinocytes (B) treated with NMB at different concentrations. Cell viability was evaluated by the MTT assay after treatment with NMB at 5, 10, and 20 µmol/L, compared with the untreated control (C+). Values were corrected using the cytotoxicity control (C−) and normalized to the highest value obtained, which was set as 100% viability. Data are presented as boxplots from three independent experimental replicates, with technical duplicates averaged within each replicate. No statistically significant differences were observed among the groups for either cell line (one-way ANOVA followed by Tukey's multiple comparisons test, $p > 0.05$).



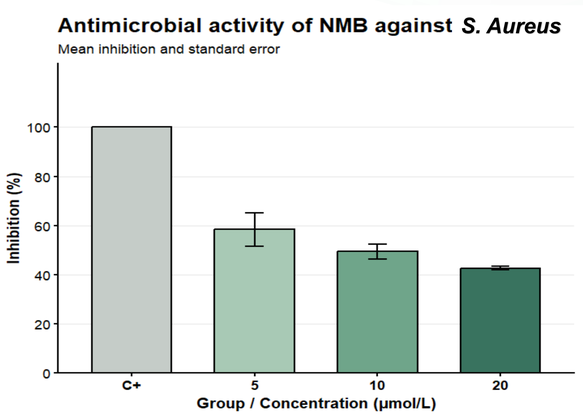
Hemolytic analysis were performed using washed erythrocytes isolated from human blood cells. To perform the assay, 100 µL of washed erythrocytes solution were added to a microtube with 100 µL of the peptide solution and incubated under 37°C for 1 hour. After that, the microtubes were centrifuged for 3 minutes at 3000 rpm and 100 µL of the supernatant were transferred to a 96 well plate and placed in a microplate reader to measure absorbance at 540 nm. The positive control was washed erythrocytes solution with an 1% triton solution and negative control was the equivalent number of cells with PBS, pH 7,4.



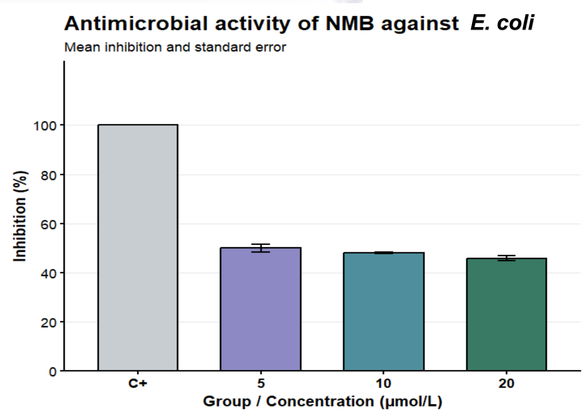
Hemolytic activity of NMB at 5, 10, and 20 µmol/L compared with the positive control (C+). Hemolysis was normalized to the positive control, which was defined as 100% hemolysis. Data represent three independent experiments. NMB exhibited significantly lower hemolysis than the positive control at all concentrations tested, respectively for 5 µmol/L, 10 µmol/L and 20 µmol/L, $p = 0{,}0037$; $p = 0{,}0123$ and $p = 0{,}0062$, although one-way ANOVA ($F_{3,8} = 11.48$, $p = 0.00286$) and Tukey's multiple comparisons test ($p < 0.05$), have shown no significant differences among NMB concentrations ($p > 0.05$).



Antimicrobial activity was performed using the plate microdilution method with modifications described by the Clinical and Laboratory Standards Institute (CLSI – M7-A10, 2015 and M27-A3, 2017). After initial growth, a cellular suspension was adjusted to McFarland scale 0.5 (10^8 CFU/mL) and diluted to 10^7 CFU/mL. For peptide analysis, 80 µL of culture media and 100 µL of peptide solution were added to each well, followed by 20 µL of microbial suspension, and incubated for 24 hours at 37°C. Positive controls were prepared similarly, using microorganisms and culture media, while negative controls included media-only. After the incubation period, bacterial growth was assessed by measuring the optical density at 595 nm using a microplate reader spectrophotometer.



NMB reduced *S. aureus* growth by approximately 42–57% relative to the positive control across all concentrations tested (5, 10, and 20 µmol/L). All NMB concentrations differed significantly from the positive control (one-way ANOVA, $F(3,8) = 48.73$, $p < 0.001$; Tukey's multiple comparisons test, all $p < 0.001$). No significant differences were observed among NMB concentrations (all $p > 0.05$).



NMB reduced *E. coli* growth by approximately 50–54% relative to the positive control at the concentrations tested (5, 10, and 20 µmol/L). All NMB concentrations differed significantly from the positive control (one-way ANOVA, $F(3,8) = 739.4$, $p < 0.001$; Tukey's multiple comparisons test, all $p < 0.001$), whereas no significant differences were observed among NMB concentrations (all $p > 0.05$).

CONCLUSION

The fibronectin- and collagen-derived peptides were successfully obtained, containing the RGD and KTTKS sequences, and showed no significant cytotoxicity in fibroblasts or keratinocytes at any of the tested concentrations (5–20 µmol/L). In addition, low hemolytic activity was observed compared to the control, indicating a safety profile that is favorable in the context of wound healing, as it helps control bleeding from an acute wound and promotes the initiation of the healing process, possibly triggering the homeostasis. Finally, the peptide significantly reduced microbial growth for both strains analyzed, by approximately 50% at all tested concentrations. Thus, the findings indicate that the NMB peptide combines promising antimicrobial activity with low cytotoxicity and hemolytic effect, making it a promising candidate for future research as a wound-healing compound for the treatment of wounds.

REFERENCES

1. N. H. Abu Samah, C. M. Heard, Int. J. Cosmet. Sci. 2011, 33, 483–490.
2. C. Zhang, L. Meng, G. Sethi, J. Wang, B. Li, Drug Discovery Today 2025,30, 104440.
3. N.I. Md Fadilah, N.A. Shahabudin, R.A. Mohd Razif, A. Sanyal, et al. J. Tissue Engineering 2024, 15, 1-31.
4. M. Alipour, M. Baneshi, S. Hosseinkhani, R. Mahmoudi, et al. J. Biomed. Mater. Res. A 2020, 108, 839–850.

FINANCIAL SUPPORT

CAPES
CNPq Conselho Nacional de Desenvolvimento Científico e Tecnológico
FAPESP

Tag-Assisted Peptide Synthesis (TAPS) – Development of a continuous liquid-phase process

Stefan Peters[1], Tim Kramer[1], Mareike Helmdach[1], Fabian Hogenkamp[1], Andreas Heindl[1]
[1] Corden Pharma International GmbH, Frankfurt am Main, Germany

https://doi.org/10.17952/38EPS.2026.P278

TAPS vs. SPPS

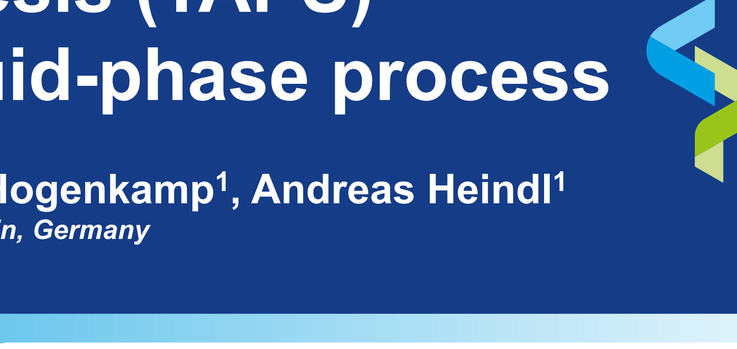
Advantages:

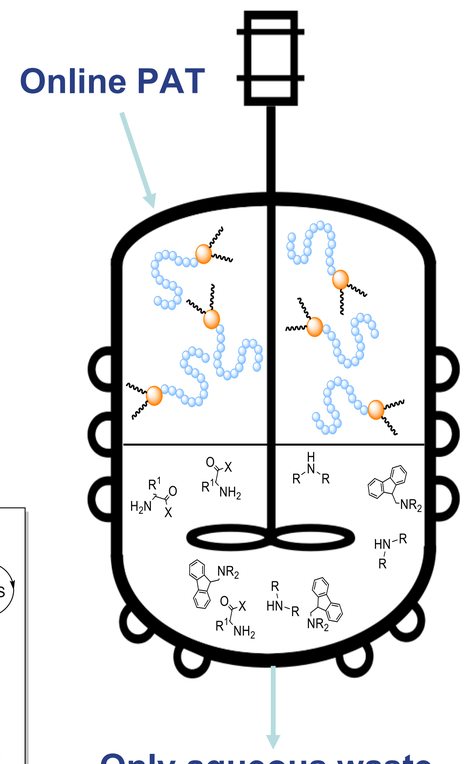
- Green solvents (TAPS) compared to DMF (SPPS)
- Excess of amino acids up to 99% reduced
- Replacement of piperidine by low toxic to non-toxic amines
- Direct IPC and online PAT monitoring
- Aqueous washing compared to very large DMF volumes in SPPS
- Drastic reduction of PMI (~90% lower solvent amount)
- Cost savings due to lower solvent / RM consumption / better quality
- TAPS can better handle difficult sequences

TAPS Principle

Synthesis Cycle:

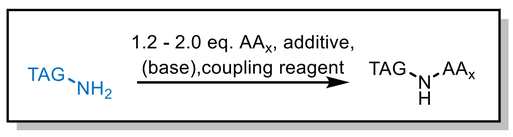
- Fmoc-Amino Acid coupling
- *In Situ* Fmoc deprotection
- Aqueous wash, to waste
- Organic solution retained
- Ready for next cycle

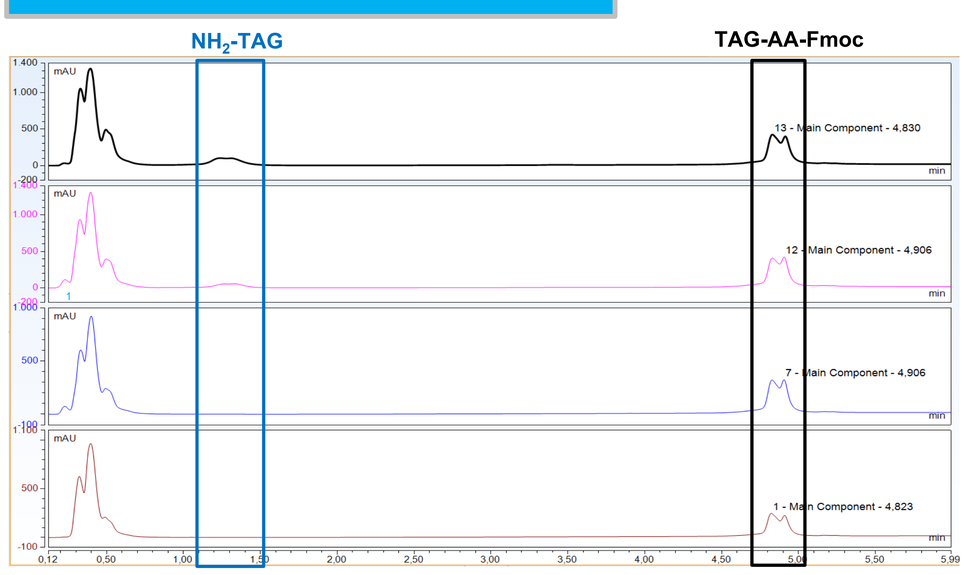




Development History - Coupling Chemistry

- **Coupling reagent choice**
  - By-products water soluble
  - Very fast reaction kinetics
  - No pre-activation necessary

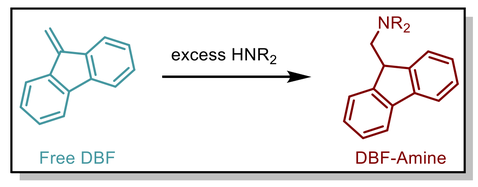


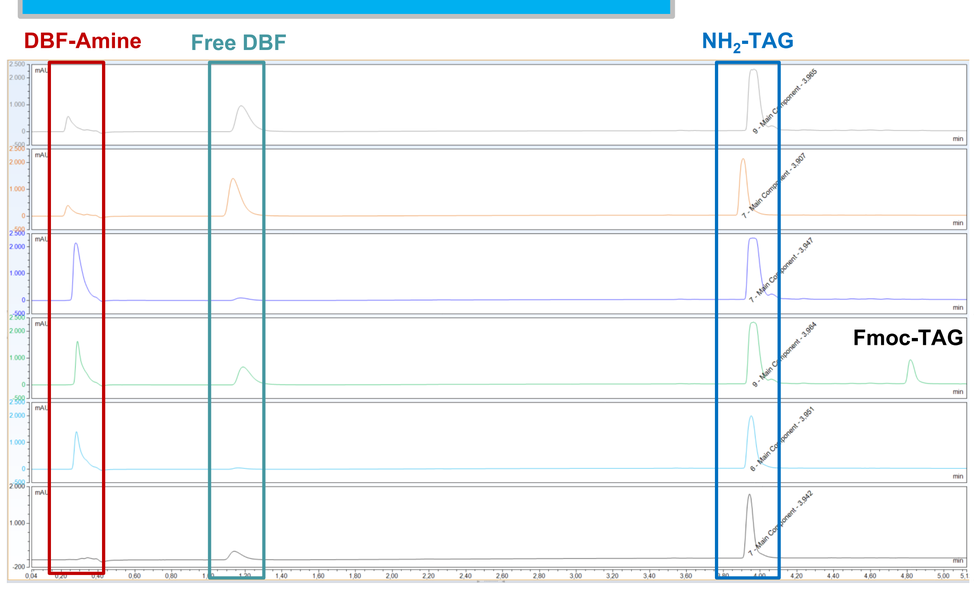


Note: TAG features stereocenter. Forms diastereomers after loading with amino acids

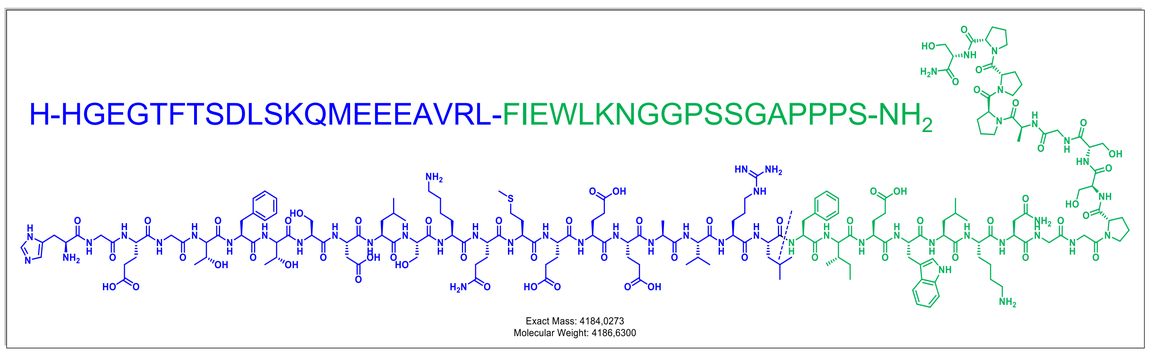
Development History - Fmoc Deprotection

- **Amines with three main features:**
  - Fast deprotection (high basicity)
  - DBF scavenging (high nucleophilicity)
  - Water soluble (efficient work-up)





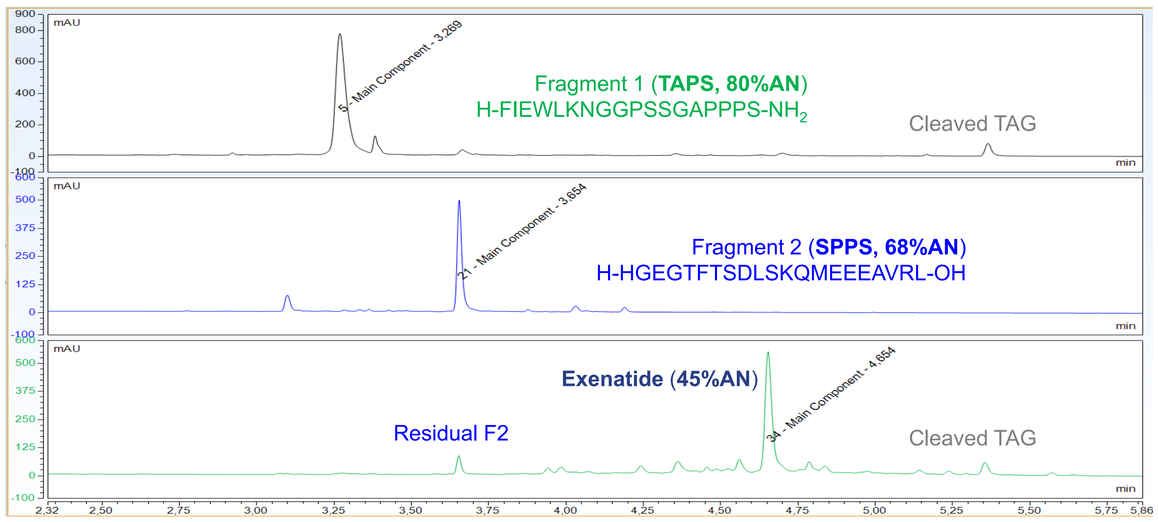
Case Study - Exenatide



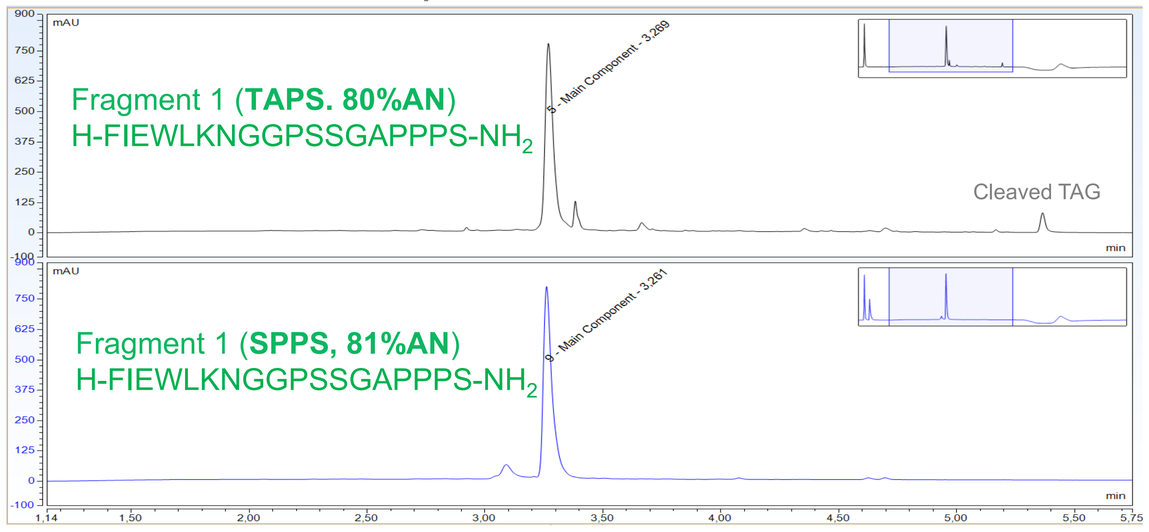
Major Achievements:

- Comparison TAPS fragment vs SPPS fragment synthesis
- → Same quality achieved
- Fragment condensation using **Peptidyl-TAG** fragment and **SPPS-fragment** to Exenatide „on-TAG“

Condensation of Exenatide



Comparison of TAPS vs. SPPS



Contact Details

StefanLukas.Peters@cordenpharma.com Tim.Kramer@cordenpharma.com Andreas.Heindl@cordenpharma.com

Investigating the Synergistic Effect of Acetylation and Phosphorylation on Alpha-Synuclein Function Using Bioorthogonal Chemistry

Bernard Abakah,[1] Marie Shimogawa,[1] Grace Shin Hye Park,[2] Elizabeth Rhoades,[1,2] E. James Petersson[1,2]

[1]Department of Chemistry; School of Arts and Sciences, University of Pennsylvania

[2]Biochemistry, Biophysics, and Chemical Biology Graduate Group; Perelman School of Medicine, University of Pennsylvania

https://doi.org/10.17952/38EPS.2026.P116

Abstract

Alpha-synuclein (αS) is a 14 kDa neuronal protein found at synaptic termini. Its physiological roles are synaptic vesicle trafficking and managing neurotransmitters. Aggregates of αS are commonly found in Parkinson's Disease (PD), Multiple System Atrophy (MSA), and Dementia with Lewy Bodies (DLB). Recent results show that αS fibrils formed under different disease environments behave differently, but the mechanism of this is not fully understood.

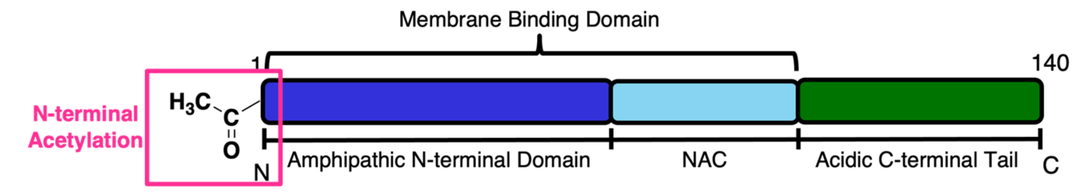
It has been suggested that various post-translational modifications (PTMs) contribute to these differences. Prior works have investigated how a single modification of αS affects its function, structure, and aggregation kinetics. It is important to know how combinations of PTMs on αS affect its native function, structure, and aggregation kinetics. Our ability to understand how combinatorial PTMs regulate αS functions in health and disease has been hindered by the absence of tools for generating site-specific PTMs.

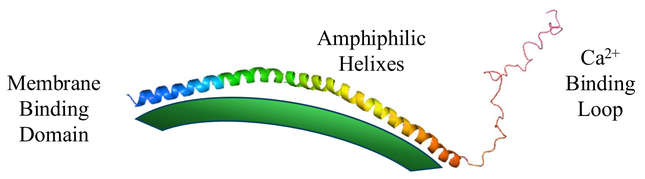
Herein, we present a novel approach to the study of αS. By utilizing genetic code expansion, enzymatic modification, click chemistry and other biochemical approaches, we have synthesized triple PTM αS and labeled the C-terminus with a fluorophore. This innovative method has allowed us to further characterize PTM effects, providing new insights into the behavior of αS.

Background

αS Background:

αS is a 140 amino acid, intrinsically disordered, and physiologically monomeric protein.

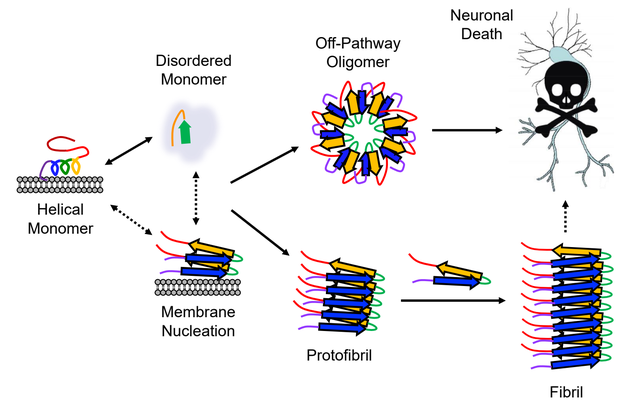


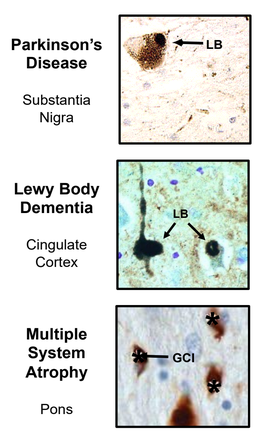


When bound to membranes, αS adopts an α-helical secondary structure. It is involved in neurotransmitter release, SNARE complex assembly, and vesicle trafficking.

αS Misfolding Diseases:

αS can oligomerize and form aggregates that are associated with Parkinson's Disease.

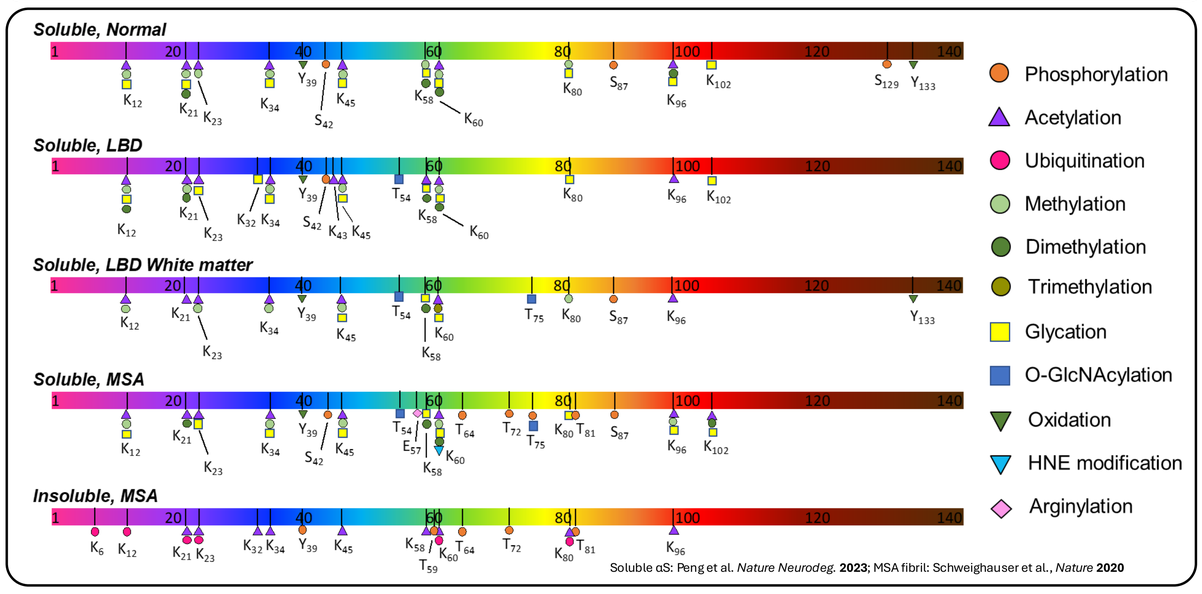




In different pathological contexts, αS can have different activities and conformations. This may be due to various combinations of PTMs.

Lindquist et. al., *Annu. Rev. Cell. Dev. Biol.* **2010;** Spillantini et al., *Nature* **1997**

αS PTMs in LB Disease/MSA Patients



Soluble αS: Peng et al. *Nature Neurodeg.* **2023;** MSA fibril: Schweighauser et al., *Nature* **2020**

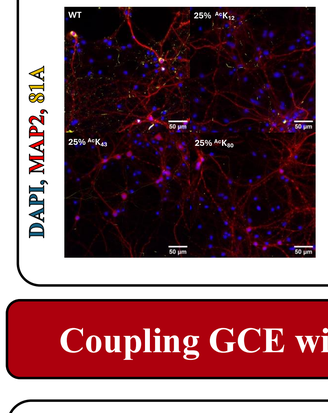
Acetylation has Differential, Site-Specific Effects on αS Aggregation

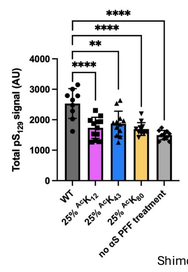
Sites of Interest:

Acetylation of αS has been demonstrated to affect both its aggregation kinetics and seeding.

GCE can be used to authentically and site-specifically scan through different acetylation sites and determine their effects.

Aggregation Seeding in Primary Neurons:

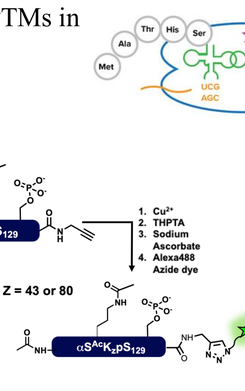




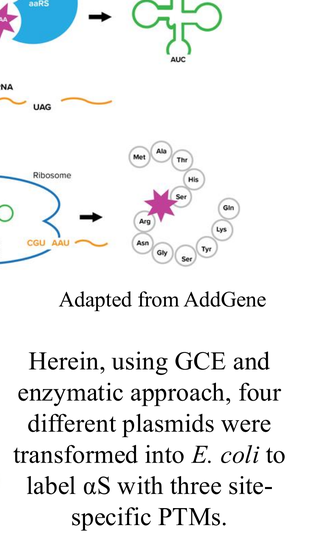
Shimogawa et al; ***2025***

Methods:

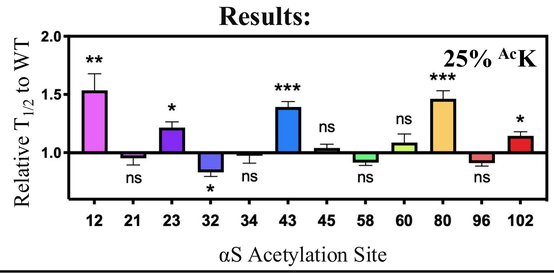
As αS begins to form aggregates, ThT binds to the beta-sheets and the fluorescent signal increases.



Thioflavin T (ThT)



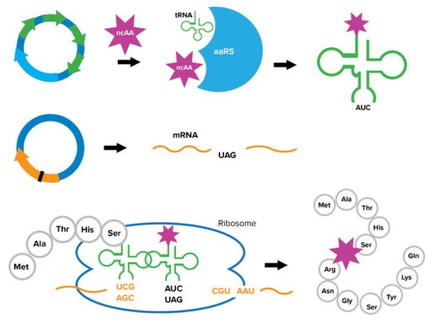
Results:



Coupling GCE with Enzymatic Methods Allows for Triple Labeling of αS

PTM studies often use protein fragments, non-specific overall modification, PTM mimics, or native chemical ligation (NCL).

Genetic code expansion (GCE) integrates modified amino acids into proteins.
Therefore, GCE can be utilized to study the role of PTMs in the function and pathology of αS.

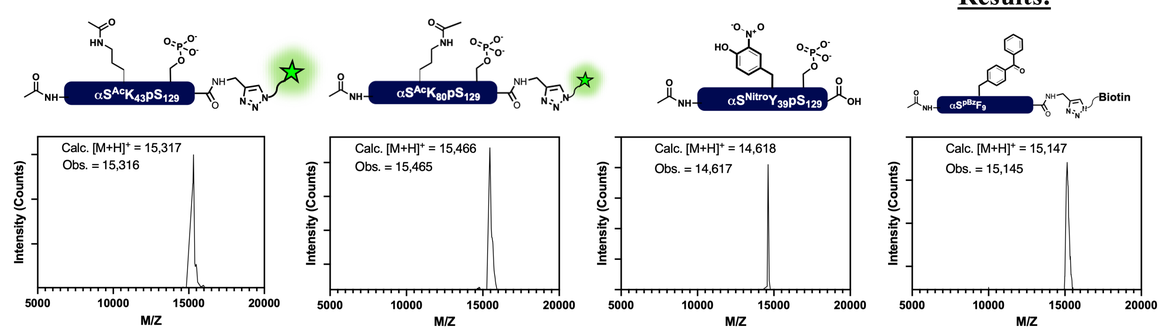


Adapted from AddGene

Herein, using GCE and enzymatic approach, four different plasmids were transformed into *E. coli* to label αS with three site-specific PTMs.

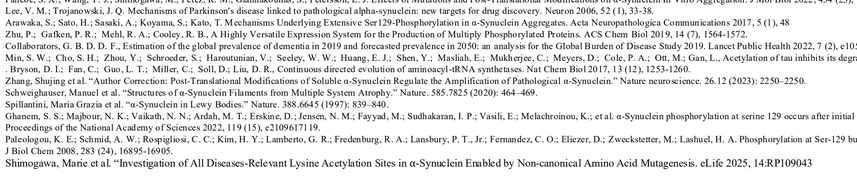
Multiply Modified αS Generated by Combing GCE with Enzymatic Approach

Results:



^{Ac}K80 has an Aggregation Rescuing Effect on αS

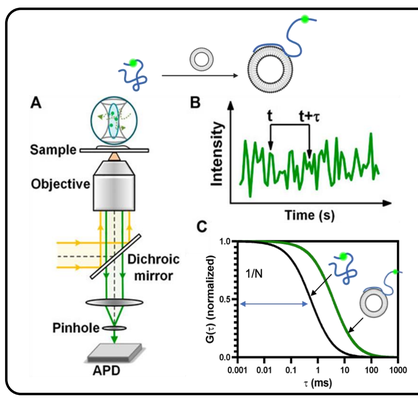
***In Vitro* Aggregation Kinetics**



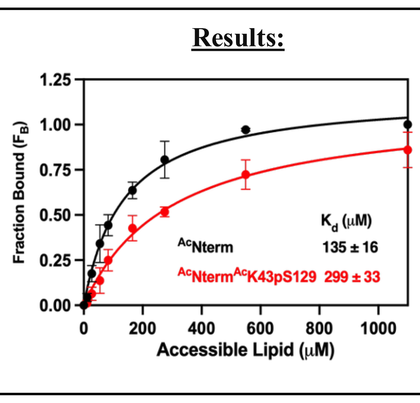
Results:

Incorporated acetylation at N-terminal, K80, and phosphorylation of S129 successfully. Using ThT as a fluorescence readout, preliminary seeded aggregation in vitro show that acetylation at K80 rescues aggregation.

^{Ac}Nterm^{Ac}K43pS129 αS Binds Less to Membranes



Results:



- Fluorescence Correlation Spectroscopy was used to determine the effect of multiple αS PTMs on vesicle (60:25:15 POPC:POPE:POPS) binding.
- ^{Ac}Nterm^{Ac}K43pS129αS binds with less affinity to the membranes compared to ^{Ac}NtermαS.

Acknowledgements

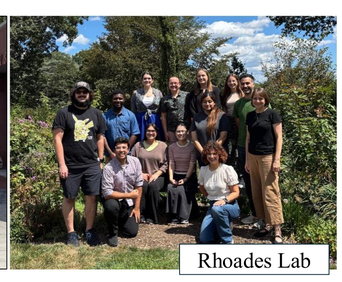
Thank you to **Prof. E. James Petersson** and **Prof. Elizabeth Rhoades**, as well as all EJP and Rhoades lab members. Special thanks to our collaborators at OSU, **Prof. Ryan Mehl** and **Prof. Rick Cooley,** for their guidance and for providing the GCE plasmids. Thank you to the **UPenn Chemistry Department**.
This project was supported by NIH RF1 NS125770.

Part of the data included in this poster was collected by:



Dr. Marie Shimogawa





References

1. Dumas, A.; Lercher, L.; Spicer, C. D.; Davis, B. G., Designing logical codon reassignment - Expanding the chemistry in biology. Chem Sci 2015, 6 (1), 50-69.
2. Pan, B.; Shimogawa, M.; Zhao, J.; Rhoades, E.; Kashina, A.; Petersson, E. J. Cysteine-Based Mimic of Arginylation Reproduces Neuroprotective Effects of the Authentic Post-Translational Modification on α-Synuclein. Journal of the American Chemical Society 2022, 144 (17), 7911-7918.
3. Zhang, S.; Zhu, R.; Pan, B.; Xu, H.; Olufemi, M. F.; Gathagan, R. J.; Li, Y.; Zhang, L.; Zhang, J.; Xiang, W. Post-translational modifications of soluble α-synuclein regulate the amplification of pathological α-synuclein. Nature neuroscience 2023, 26 (2), 213-225.
4. Pancoe, S. X.; Wang, Y. J.; Shimogawa, M.; Perez, R. M.; Giannakoulias, S.; Petersson, E. J. Effects of Mutations and Post-Translational Modifications on α-Synuclein In Vitro Aggregation. J Mol Biol 2022, 434 (23), 167859.
5. Lee, V. M.; Trojanowski, J. Q. Mechanisms of Parkinson's disease linked to pathological alpha-synuclein: new targets for drug discovery. Neuron 2006, 52 (1), 33-38.
6. Arawaka, S.; Sato, H.; Sasaki, A.; Koyama, S.; Kato, T. Mechanisms Underlying Extensive Ser129-Phosphorylation in α-Synuclein Aggregates. Acta Neuropathologica Communications 2017, 5 (1), 48
7. Zhu, P.; Gafken, P. R.; Mehl, R. A.; Cooley, R. B., A Highly Versatile Expression System for the Production of Multiply Phosphorylated Proteins. ACS Chem Biol 2019, 14 (7), 1564-1572.
8. Collaborators, G. B. D. D. F., Estimation of the global prevalence of dementia in 2019 and forecasted prevalence in 2050: an analysis for the Global Burden of Disease Study 2019. Lancet Public Health 2022, 7 (2), e105-e125.
9. Min, S. W.; Cho, S. H.; Zhou, Y.; Schroeder, S.; Haroutunian, V.; Seeley, W. W.; Huang, E. J.; Shen, Y.; Masliah, E.; Mukherjee, C.; Meyers, D.; Cole, P. A.; Ott, M.; Gan, L., Acetylation of tau inhibits its degradation and contributes to tauopathy. Neuron 2010, 67 (6), 953-66.
10. . Bryson, D. I.; Fan, C.; Guo, L. T.; Miller, C.; Soll, D.; Liu, D. R., Continuous directed evolution of aminoacyl-tRNA synthetases. Nat Chem Biol 2017, 13 (12), 1253-1260.
11. Zhang, Shujing et al. "Author Correction: Post-Translational Modifications of Soluble α-Synuclein Regulate the Amplification of Pathological α-Synuclein." Nature neuroscience. 26.12 (2023): 2250–2250.
12. Schweighauser, Manuel et al. "Structures of α-Synuclein Filaments from Multiple System Atrophy." Nature. 585.7825 (2020): 464–469.
13. Spillantini, Maria Grazia et al. "α-Synuclein in Lewy Bodies." Nature. 388.6645 (1997): 839–840.
14. Ghanem, S. S.; Majbour, N. K.; Vaikath, N. N.; Ardah, M. T.; Erskine, D.; Jensen, N. M.; Fayyad, M.; Sudhakaran, I. P.; Vasili, E.; Melachroinou, K.; et al. α-Synuclein phosphorylation at serine 129 occurs after initial protein deposition and inhibits seeded fibril formation and toxicity. Proceedings of the National Academy of Sciences 2022, 119 (15), e2109617119.
15. Paleologou, K. E.; Schmid, A. W.; Rospigliosi, C. C.; Kim, H. Y.; Lamberto, G. R.; Fredenburg, R. A.; Lansbury, P. T., Jr.; Fernandez, C. O.; Eliezer, D.; Zweckstetter, M.; Lashuel, H. A. Phosphorylation at Ser-129 but not the phosphomimics S129E/D inhibits the fibrillation of alpha-synuclein. J Biol Chem 2008, 283 (24), 16895-16905.
16. Shimogawa, Marie et al. "Investigation of All Diseases-Relevant Lysine Acetylation Sites in α-Synuclein Enabled by Non-canonical Amino Acid Mutagenesis. eLife 2025, 14:RP109043

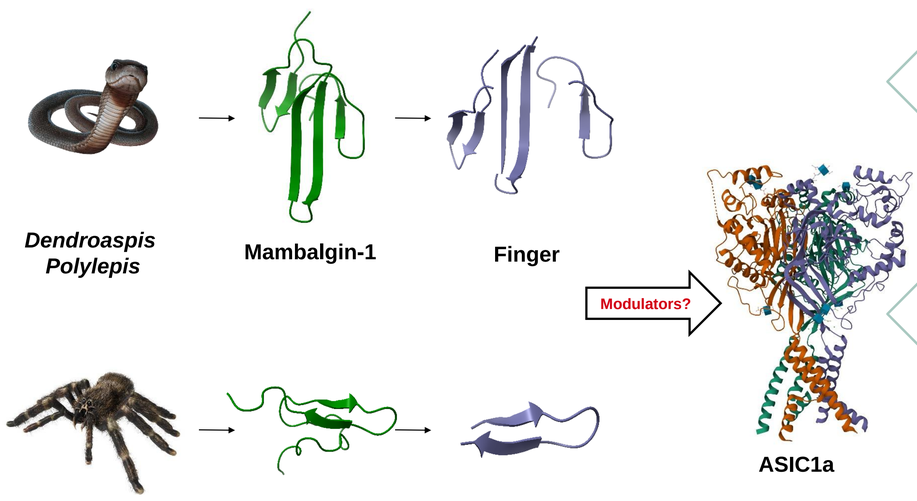
https://doi.org/10.17952/38EPS.2026.P516

1-Karlsruhe Institute of Technology, Institute of Biological Interfaces 2, Karlsruhe, Germany
2-Nonprofit Organization “National Cancer Institute,” Kyiv, Ukraine
3-Taras Shevchenko National University of Kyiv, Kyiv, Ukraine.
4-Karlsruhe Institute of Technology, Institute of Organic Chemistry, Karlsruhe, Germany
5-Katholieke Universiteit Leuven, Faculty of Pharmaceutical Sciences, Leuven, Belgium

Rational Design and Structure–Activity Relationship of Spider- and Snake-Venom-Derived Peptides Targeting Acid-Sensing Ion Channels

N. Petlovana[1], S. Kharchenko[1], T. Sussek[1], V. Hryhorieva[2,3], F. Hoffmann[1], I. Hutskalov[1], I. Semchuk[2,3], S. Afonin[1], J. Tytgat[5], Anne S. Ulrich[1,4]

Graphical abstract and Background



ASIC1a

- CNS/PNS-expressed, DEG/ENaC channel
- Homotrimeric, proton-activated channel
- Na^+/Ca^{2+} permeable; $pH_{50} \approx 6.4\text{-}6.7$
- Roles in pain, plasticity and neuronal injury

Mambalgin-1

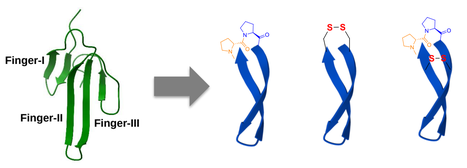
- Isolated from the venoms of *Dendroaspis polylepis*
- 57-mer, disulfide-rich
- Three-finger toxin fold
- Inhibits ASIC1-containing channels
- IC_{50} = 55 nM (rASIC1a)

Psalmotoxin-1

- Isolated from the venom of *Psalmopoeus cambridgei*
- Disulfide-rich, 40-mer
- Knottin fold
- Selective inhibitor of ASIC1a
- IC_{50} = 1,17 nM (rASIC1a)

Experimental design

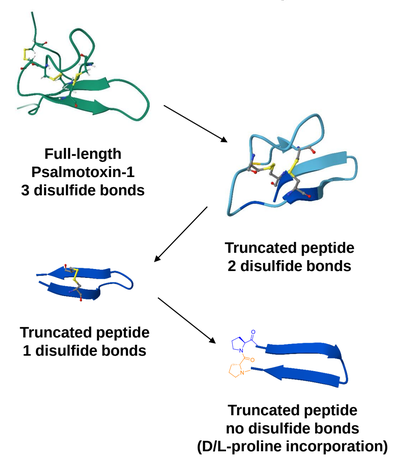
Mambalgin-1 library:



Mambalgin-1 — Strategies of cyclization for Finger I and II

No.	Sequence	linear	Back-bone / SH	Back-bone + S-S	S-S	Ac-NH + S-S
	Finger I					
Md-1	PKCYQHGKVVTCHRDp	1.1a			1d	
	AcNH-PKCYQHGKVVTCHRDp	1.2a				1e
	KCYQHGKVVTCHRDpP	1.3a				
	KVVTCHRDpPKCYQHG	1.4a	1b	1c		
Md-2	LKCYQHGVVTCHRDM	2.1a			2d	
	AcNH-LKCYQHGVVTCHRDM	2.2a				2e
	Finger II					
Md-3	LQGpPYHNTGMPFRNLKLI	3a	3b			
Md-4	LQpPHNTGMPFRNLKLI	4a	4b			
Md-5	LpPNTGMPFRNLKLI	5a	5b			
Md-6	QpPNTGMPFRNLKLI	6a	6b			
Md-7	AcNH-CYHNTGMPFRNLKLILQGC	7a				7e
Md-8	AcNH-CHNTGMPFRNLKLILQC	8a				8e
Md-9	AcNH-CNTGMPFRNLKLILC	9a				9e
Md-10	pPFCYHNTG-Nle-PFRNLKLILQGCA	_		10c		
Md-11	pPFVYHNTG-Nle-PFRNLKLILQGLA	_	11b			
Md-12	pPYHNTG-Nle-PFRNLKLILQG	_	12b			
	Finger III					
Md-13	HSSCSETENNKCCSTDRCNK	_			13d	

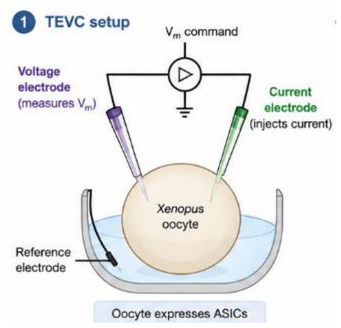
Psalmotoxin-1 library:



No.	Sequence	linear	Back-bone	S-S, $CONH_2$
Pd-1	LECWKRRRSFEVCVP	1a		1c
Pd-2	LpPVWKRRRSFEV	2a	2b	
Pd-3	pPLEAWKRRRSFEVAV	3a	3b	
Pd-4	KWKGCVNRHGD**(Acm)**CSEGLE CWKRRRSFEV**(Acm)**CV	4.1a		4.1c
	KWKGCVNRHGDCSEGLECWKR RRSFEVCV	4.2a		4.2c
	Full Psalmotoxin-1:			
PcTx-1	SEDCIPKWKGCVNRHGDCCEGL ECWKRRRSFEVCVPKTPKT	Lin PcTx-1		PcTx-1

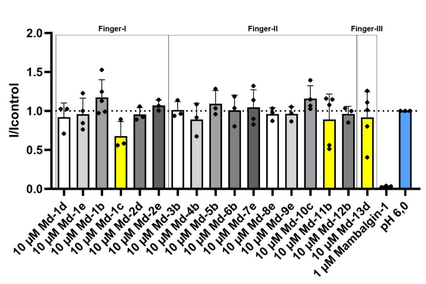
Key findings

TEVC



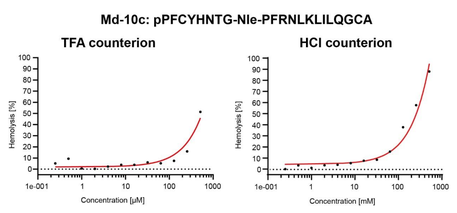
- The libraries were screened by manual two-electrode voltage clamp (TEVC) at 10 µM using *Xenopus oocytes* expressing human ASIC1a.
- Native Mambalgin-1 (Alomone Labs) and synthetic Psalmotoxin-1 were used as controls.

Screening of Mambalgin-1 library



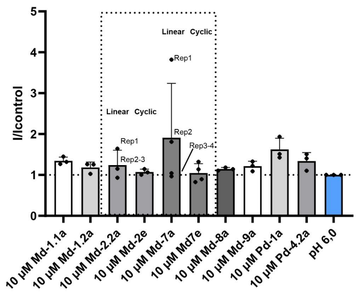
- Finger I: only the bicyclic variant **Md-1c** showed inhibitory activity under the conditions tested.
- Finger II: peptide **Md-11b** showed inconsistent responses between replicates, potentially due to lytic activity (to be confirmed).
- Finger III: **Md-13d** showed inconsistent responses across five replicates, potentially due to lytic activity (to be confirmed).

Peptide counterion affects hemolytic activity



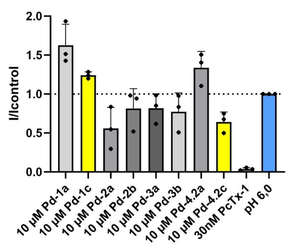
- A possible shielding effect of arginine residues was considered, given the high affinity of guanidinium groups for TFA.
- To minimize potential confounding effects of the counterion on oocyte viability and peptide activity, subsequent experiments were performed using the HCl salt forms.

Free cysteines: time-dependent ASIC1a potentiation



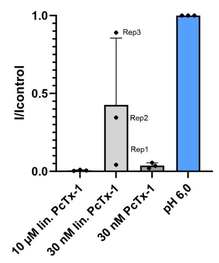
- Fresh linear peptides with free cysteines potentiated ASIC1a.
- Potentiation decreased with sample age, with later replicates increasingly resembling the corresponding cyclic peptides.
- Physiological pH and exposure to air may promote gradual cysteine oxidation and disulfide-bond formation.

Screening of Psalmotoxin-1 library



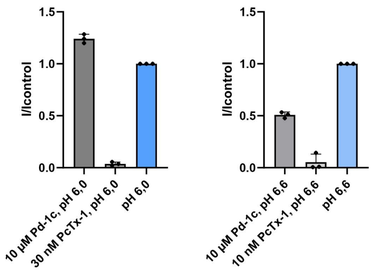
- **Pd-1c** was the only cyclic peptide showing potentiation (~25%).
- **Pd-4.2c** showed a consistent tendency toward inhibition. However, the native-like folding of the peptide remains to be confirmed.
- **Pd-3b** (30 µM) caused loss of oocyte viability. This concentration corresponds to a range previously associated with >30% hemolysis in the project.

Linear PcTx-1 showed unexpected behavior related to folding



- Linear PcTx-1 unexpectedly inhibited ASIC1a at 10 µM, consistent with formation of an active conformation in ND96.
- At 30 nM, inhibition declined from near-complete to ~20% across replicates, potentially reflecting time-dependent loss of the active conformation.

pH-dependent modulation of ASIC1a by Pd-1c



- **Pd-1c** modulates ASIC1a in a pH-dependent manner, switching from potentiation to inhibition at pH 6.6 (~50% inhibition).
- Similar pH-dependent modulation has also been reported for Mambalgin-1 and Psalmotoxin-1. However, further studies are required to elucidate the underlying mechanism and enable a proper interpretation of the observed effects.

Conclusions and outlook

Conclusions

- Both peptide libraries were successfully synthesized, characterized, and screened against ASIC1a by TEVC.
- Potential lead compounds were identified.
- Peptides containing free cysteine residues induced time-dependent ASIC1a potentiation, consistent with disulfide bond formation in ND96.
- Linear PcTx-1 exhibited ASIC1a activity consistent with formation of an active conformation in ND96.
- Counterion-dependent differences in hemolytic activity were observed.

Outlook

- Determine the hemolytic activity of lead compounds in the HCl salt form and of the native toxins.
- Characterize **Pd-4.1c** and assess its ASIC1a activity to validate the activity observed for **Pd-4.2c**.
- Determine the concentration and pH dependence of lead-compounds activity at ASIC1a.

Screening of the library by TEVC was done in collaboration with Prof. Jan Tytgat at KU Leuven

This work was supported by a scholarship from the Deutscher Akademischer Austauschdienst (DAAD, German Academic Exchange Service) under “Forschungsstipendien - Promotionen in Deutschland, 2024/25 (57693453)”

References:
- Sikora et al., Pharmaceuticals (2020).
- Sherwood et al., Am. J. Physiol. Cell Physiol. 303 (2012).
- Salinas et al., J. Biol. Chem. 289 (2014).
- Diochot et al., Nature 490 (2012).
- Sun et al., Biomolecules 13 (2023).
- Pettersen et al., Protein Sci. 30 (2021).
- Noisier et al., J. Med. Chem. (2025).
- Mourier et al., J. Biol. Chem. (2016).
- Salinas et al., Neuropharmacology (2021).
- Abramson et al., Nature (2024).
- Liu et al., Biomolecules (2025).
- Cristofori-Armstrong et al., PNAS 118 (2021).
- Chen et al., J. Gen. Physiol. 126 (2005).

Image / Structure Sources:
- Black mamba image: PNGAll, Black Mamba PNG
- Psalmopoeus cambridgei image: RenderHub, Jaka Ardian
- TEVC setup illustration: ChatGPT 5.0
- Graphics: GraphPad Prism 9.0

https://doi.org/10.17952/38EPS.2026.P516

Contact:
nataliia.petlovana@student.kit.edu

Rapid Assessment of Size, Shape, and Chemical Complementarity of Ligands for Computational Protein Design

Rokas Petrenas[1*], Katarzyna Ożga[1], Joel J. Chubb[1], Andrey V. Romanyuk[1], Jennifer J. McManus[1], Graham J. Leggett[2], Nigel S. Scrutton[3], Thomas A. A. Oliver[1], Derek N. Woolfson[1]

[1]University of Bristol, [2]University of Sheffield, [3]University of Manchester
*rokas.petrenas@bristol.ac.uk https://doi.org/10.17952/38EPS.2026.P081

Overview

Driven by deep-learning approaches, computational protein design is advancing rapidly, and it is now possible to generate many *de novo* protein structures quickly and robustly.[1] This sets new frontiers for the field, including designing proteins that bind small molecules tightly and specifically, and understanding the non-covalent interactions that underpin such designs to make binding predictable and tunable. Here we address these challenges with a rapid physics-based computational method to generate isosteric and chemically complementary binding pockets for small-molecules in de novo designed coiled-coil peptides and proteins. We test this experimentally by constructing and characterising binding proteins for several synthetic and natural chromophores. For each ligand tested, the pipeline delivers stable proteins with pre-organised binding sites confirmed by X-ray crystallography, and micromolar binding affinities.

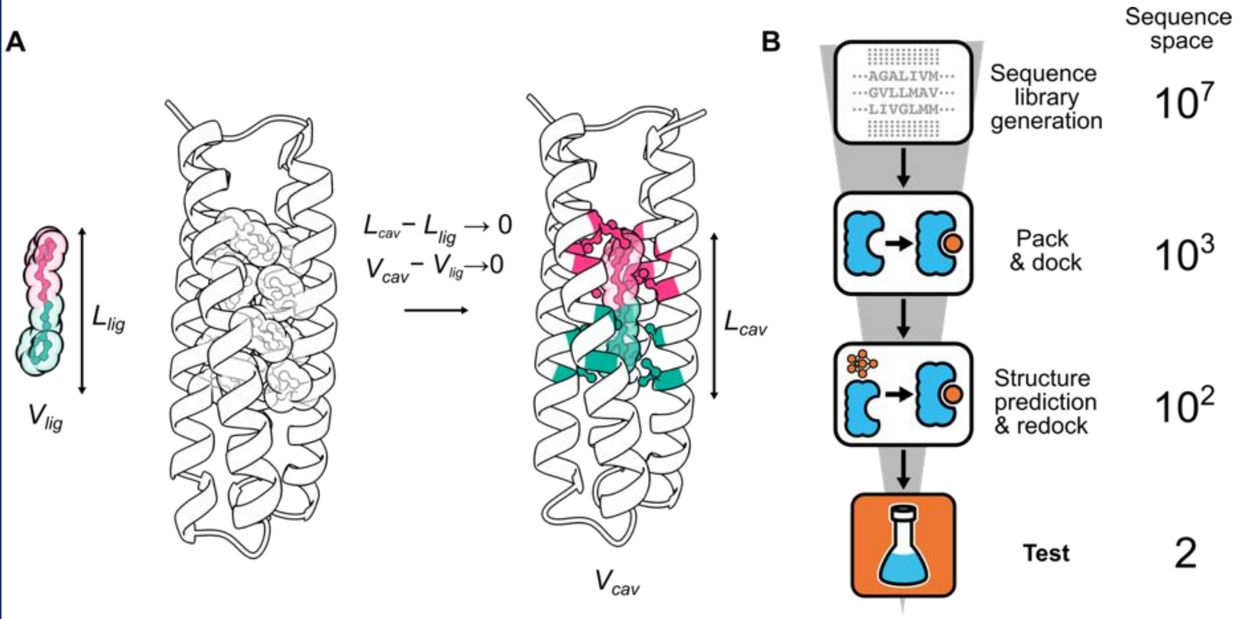


Figure 1. Design pipeline. (A) A binding site (L_{cav}) is identified based on the ligand length (L_{lig}). To match the ligand's shape, the protein scaffold is segmented (magenta and green). A volume constraint is used to minimise the difference between the binding cavity (V_{cav}) and the ligand (V_{lig}) in each segment; effectively, replacing atoms of the side chains with those of the ligand. (B) Sequences passing the volume constraint are packed onto the scaffold for evaluation using ligand docking, followed by modelling with AlphaFold2.

Delivering tight binding with sub-Å accuracy

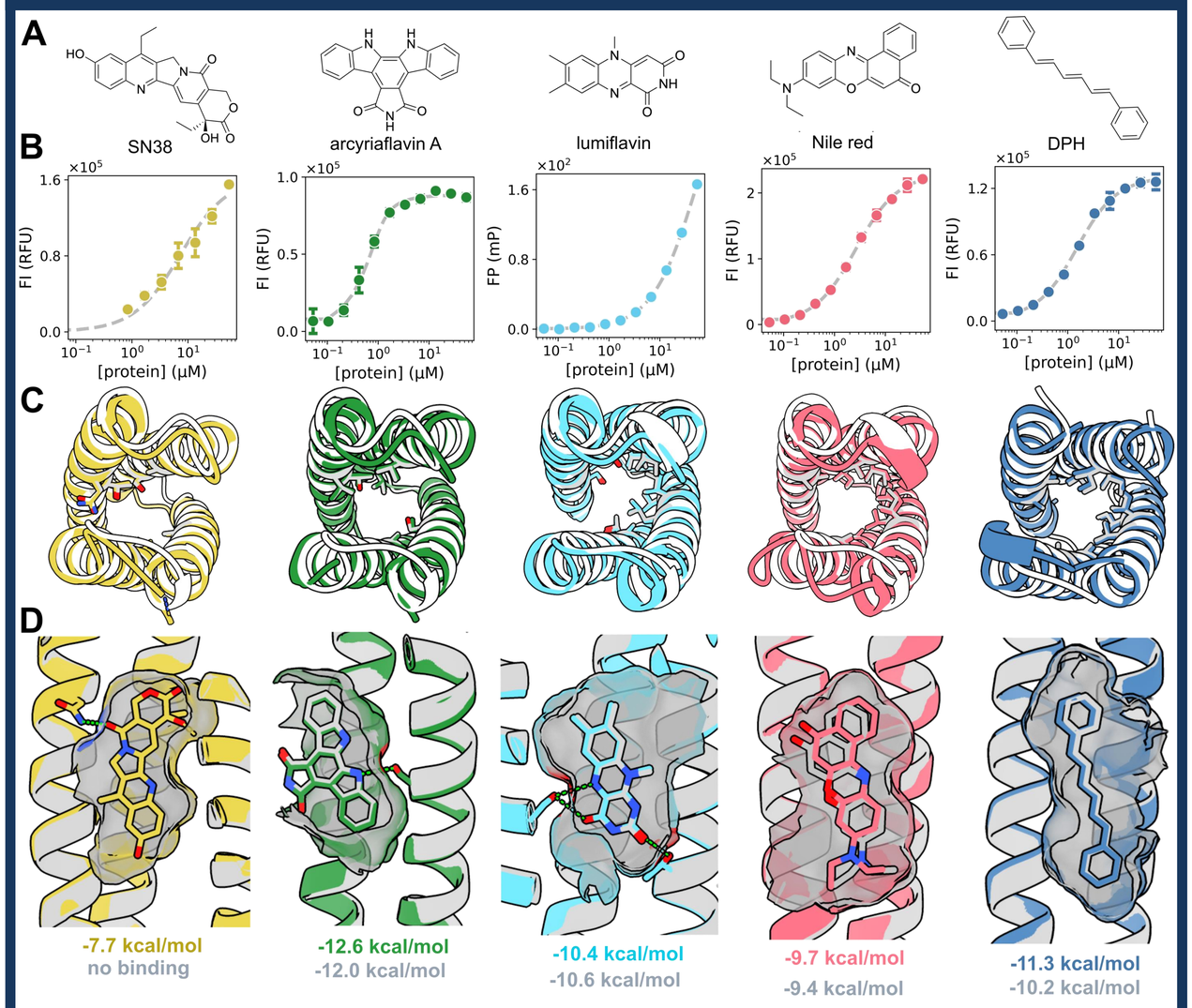


Figure 2. *De novo* designed binders for a wide range of ligands. (A) Ligands tested for binding. (B) Saturation-binding data measured by fluorescence intensity (FI) or fluorescence polarisation (FP) . Fitted dissociation constants, top to bottom: $K_{D(DPH)}$ = 1.25 ± 0.07 μM; $K_{D(Nile\ red)}$ = 2.4 ± 0.06 μM; $K_{D(lumiflavin)}$ = 51.64 ± 1.23 μM; $K_{D(arcyriaflavin\ A)}$ = 0.11 ± 0.02 μM; $K_{D(SN38)}$ = 6.92 ± 1.55 μM. (C) Binding-site heavy atom alignments between AF2 models (grey) and the ligand-free X-ray crystal structures. RMSD < 0.4 Å for all designs. (D) Docked poses and AutoDock Vina scores for the target ligands within the crystal structures, overlaid with the docked poses within the AF2 models (grey). Binding-site residues are highlighted and shown as sticks, with oxygen atoms in red and nitrogen atoms in blue. Hydrogen bonds are shown as dashed green lines.

Designs for *in vitro* and cellular applications

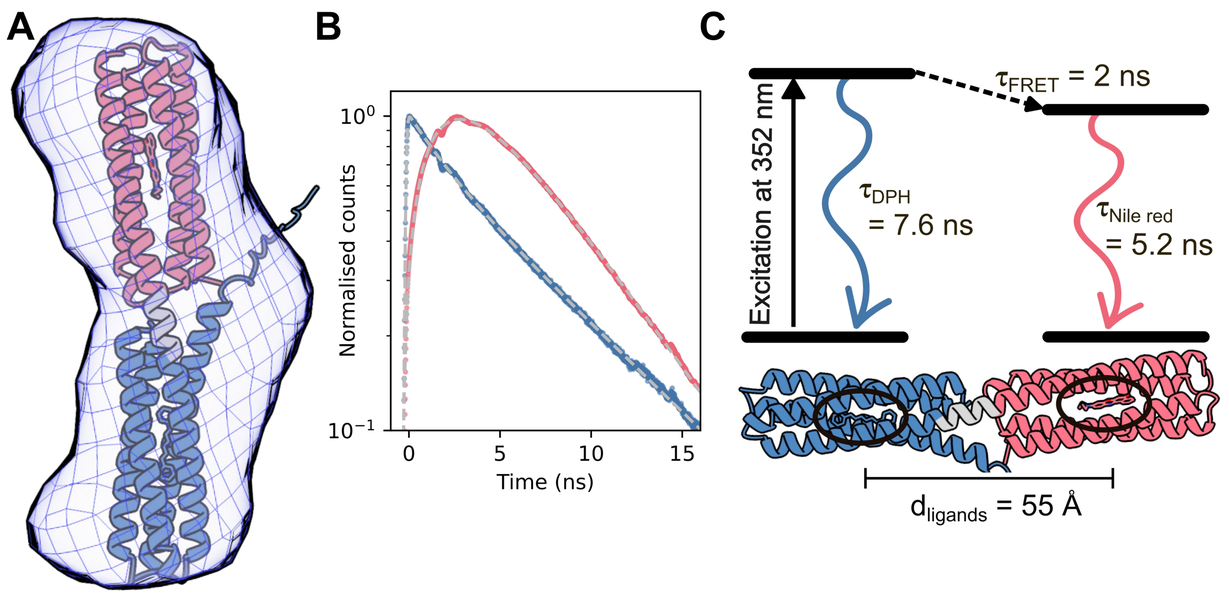


Figure 3. Dual binder promotes FRET between DPH and Nile red on a nanosecond scale. (A) AF2 model of the double-binder that combines DPH and Nile red binders, superposed to the averaged *ab initio* model from small angle X-ray scattering data. (B) Fluorescence lifetime decay measurements for DPH (blue, < 450 nm) and Nile red (red, >600 nm) after selective excitation of DPH at 352 nm. The delayed rise in Nile red emission over the first few nanoseconds originates from Förster resonance energy transfer between DPH and Nile red. (C) Kinetic model for energy transfer between DPH and Nile red, derived from (B).

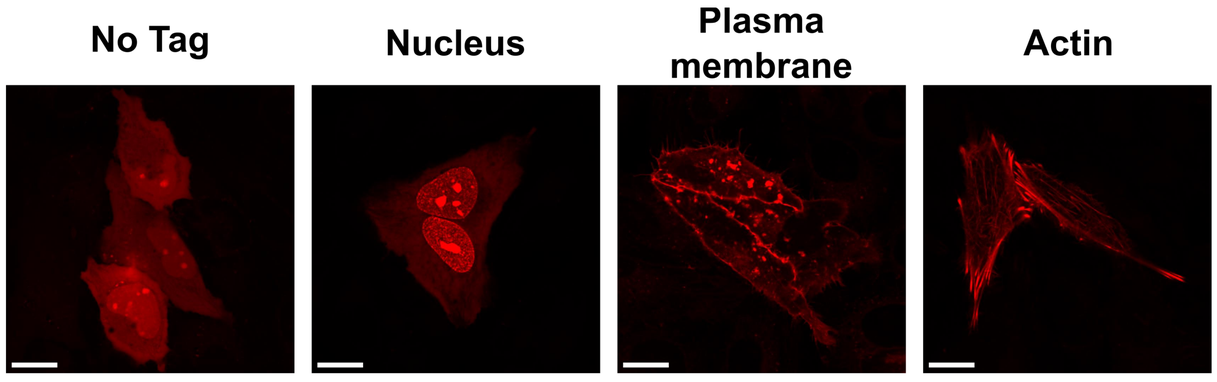


Figure 4. Nile red binder functions as a fluorescent reporter in mammalian cells. Fluorescence confocal microphotographs of live HeLa cells expressing the binder with N-terminal tags targeting the nucleus, plasma membrane and actin. Scalebar = 20 μm. Stained with 0.1 μM Nile red.

Controlling ligand specificity

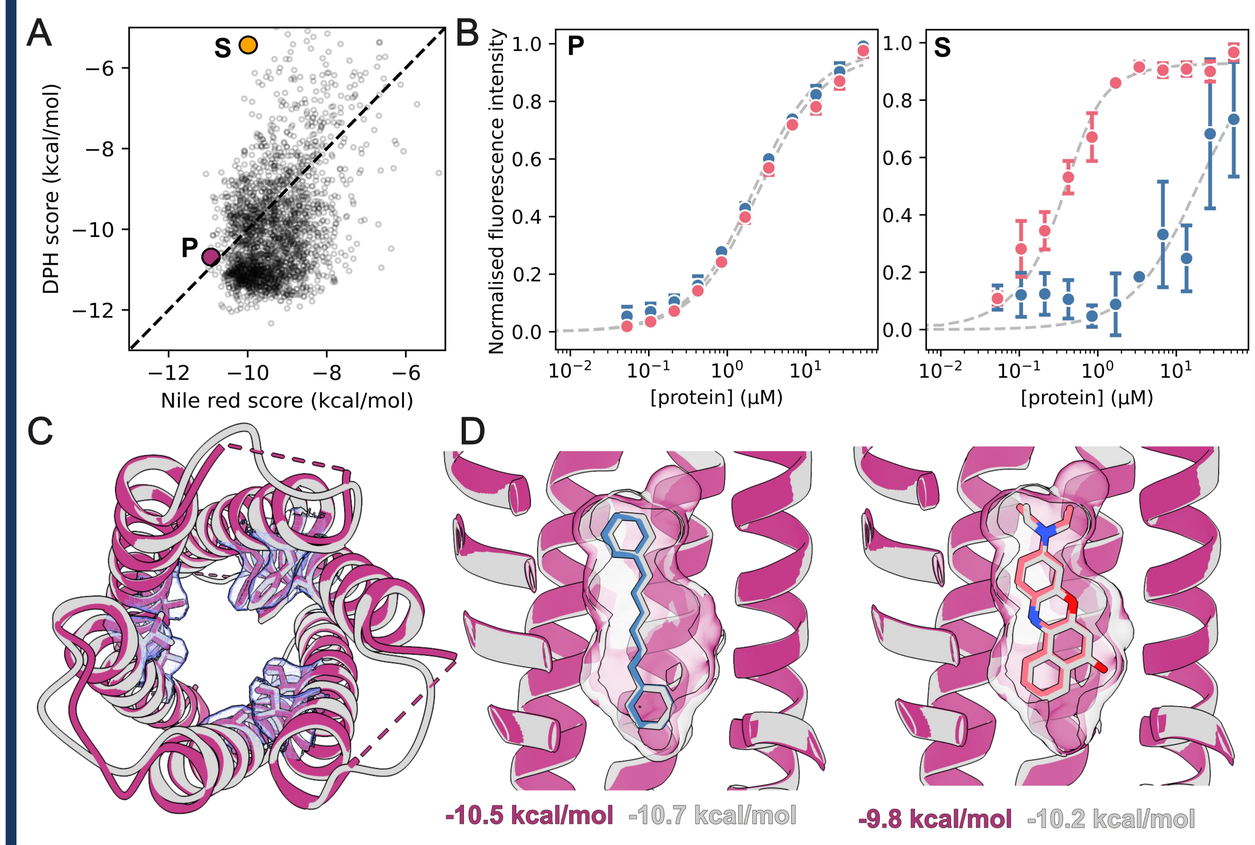


Figure 5. Designed promiscuous (P) and selective (S) binders for DPH and Nile red. (A) AutoDock Vina scores for DPH and Nile red docked into AF2 models. (B) Saturation binding curves and fits for Nile red (red) and DPH (blue) to the proteins. Promiscuous binder, $K_{D(DPH)}$ = 1.9 ± 0.17 μM; $K_{D(Nile\ red)}$ = 2.20 ± 0.17 μM. Specific binder, $K_{D(DPH)}$ > 20 μM; $K_{D(Nile\ red)}$ = 0.11 ± 0.04 μM. (C) Structural alignment between the AF2 model (grey) and the ligand-free X-ray crystal structure of the promiscuous binder. RMSD < 0.3 Å. (D) Docked poses of DPH and Nile red in the crystal structure of the promiscuous binder, overlaid with the docked poses within the AF2 models (grey).

SWBio DTP
UKRI Biotechnology and Biological Sciences Research Council
rosa biotech

References: [1] [a] E. A. Naudin, K. I. Albanese, A. J. Smith, B. Mylemans, E. G. Baker, O. D. Weiner, D. M. Andrews, N. Tigue, N. J. Savery, D. N. Woolfson, *Chem. Sci.*, **2022**, 13, 11330–11340. [b] K. I. Albanese, R. Petrenas, F. Pirro, E. A. Naudin, U. Borucu, W. M. Dawson, D. A. Scott, G. J. Leggett, O. D. Weiner, T. A. A. Oliver, D. N. Woolfson, *Nat. Chem. Biol.*, **2024**, 20, 991–999. [c] R. Petrenas, K. Ożga, J. J. Chubb, A. V. Romanyuk, J. J. McManus, G. J. Leggett, N. S. Scrutton, T. A. A. Oliver, D. N. Woolfson, *bioRxiv*, **2025**, 2025.06.30.662286.

38th EPS
European Peptide Symposium
6 - 11th of September 2026
Vienna, Austria

DESIGN AND SYNTHESIS OF NOVEL DESMURAMYL PEPTIDE GLYCOCONJUGATES

Vesna Petrović Peroković,[a]* Željka Car,[a] Jelena Pavić, [a] Luka Sumić,[a] Rosana Ribić[b]

[a]Department of Chemistry, Faculty of Science, University of Zagreb, Horvatovac 102a, 10000 Zagreb, Croatia

[b]University North, University Center Varaždin, Jurja Križanića 31b, 42000 Varaždin, Croatia

*E-mail: vpetrovi@chem.pmf.hr

Poster DOI: https://doi.org/10.17952/38EPS.2026.P346

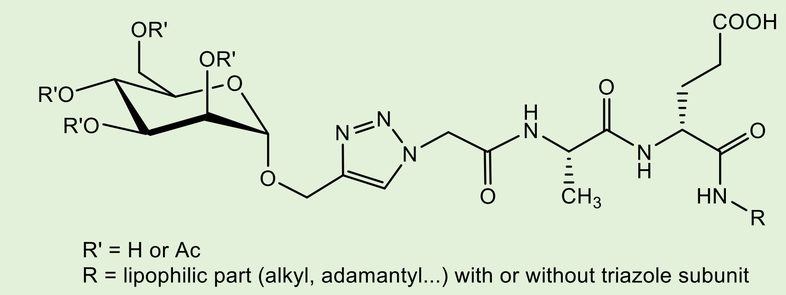
INTRODUCTION

Muramyl dipeptide (MDP, Mur*N*Ac-L-Ala-D-*iso*Gln) is the minimal structural motif of peptidoglycan with adjuvant properties. Since the muramyl group isn't essential for inducing this response, various structurally simplified desmuramyl peptide analogues (DMP, L-Ala-D-*iso*Gln) lacking the hydrophilic *N*-acetylmuramyl moiety were, so far, designed and synthesized by our group.[1,2] Successful structural modifications of DMP were carried out by introducing a mannose subunit to the amino-group of L-Ala via a glycolyl linker and/or incorporation of various lipophilic subunits through an amide bond to the α- or γ-position of D-*iso*Gln.

[1] V. Petrović Peroković, Ž. Car, J. Draženović, R. Stojković, L. Milković, M. Antica, Đ. Škalamera, S. Tomić, R. Ribić, *Molecules* **2021**, 26, 6352.
[2] V. Petrović Peroković, Ž. Car, M. Bušljeta, D. Mihelec, M. Paurević, S. Ivanković, R. Stojković, R. Ribić, *Int. J. Mol. Sci.* **2022**, 23, 8628-8648.

SYNTHESIS

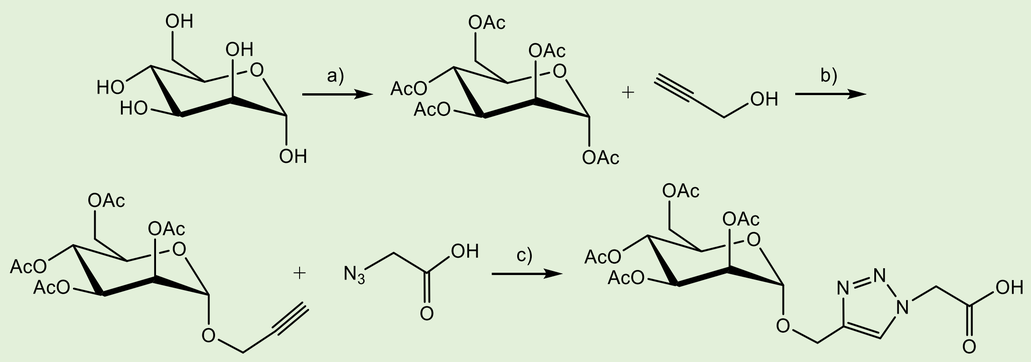
In the continuation of our research, new DMP derivatives were designed in which the mannose subunit is attached via triazole linkers to the peptide part (Fig. 1). In the synthesis of novel DMP derivatives two steps are crucial: a) preparation of a mannose-triazole precursor (Scheme 1) and b) preparation of an appropriately protected DMP precursor for binding lipophilic substituents by an amide bond (Scheme 2). In addition to the classical solution-phase peptide synthesis, a new approach under microwave conditions is currently being investigated in the preparation of DMP.



R' = H or Ac
R = lipophilic part (alkyl, adamantyl...) with or without triazole subunit

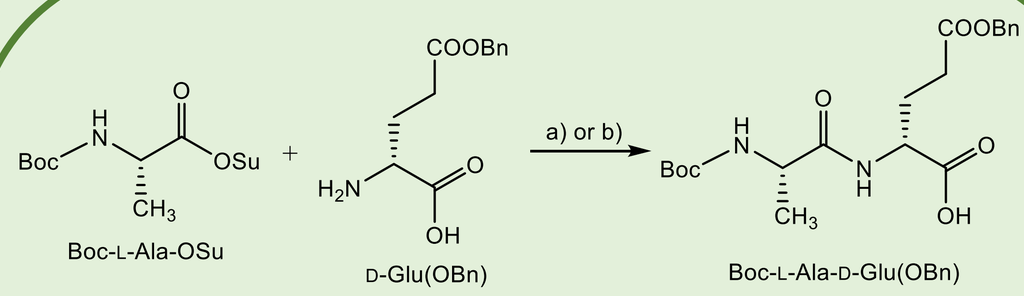
Figure 1. General structure of novel desmuramyl peptide mannoconjugates

SYNTHESIS OF MANNOSE-TRIAZOLE PRECURSOR



Scheme 1. Reagents and conditions: a) Ac_2O, I_2, rt, 45 min, Ar, 95%; b) $BF_3 \times OEt_2$, dry DCM, 0 °C to rt 30 min, 24 h, Ar 80%; c) $CuSO_4 \times 5\ H_2O$, Na-ascorbate, dioxane/H_2O = 4:3, 35 °C, 24 h, Ar, 63%.

SYNTHESIS OF PROTECTED DIPEPTIDE UNIT



Scheme 2. Reagents and conditions: a) TEA, THF, Ar(g), 0 °C to rt, 24 h, 95%; b) MW assisted synthesis (Table 1).

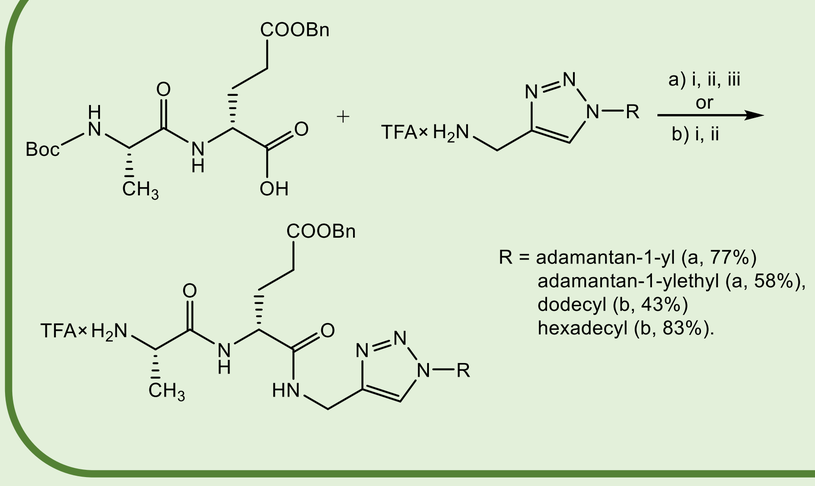
Table 1. Optimized conditions and results for MW assisted synthesis of Boc-L-Ala-D-Glu(OBn)

m (D-Glu(OBn)) / mg	*n* (D-Glu(OBn)) / mmol	*n* (Boc-L-Ala-OSu) / mmol	*V* (TEA) / mL	*V* (THF) / mL	Yield / %
50	0.21	0.21	0.059	1	88
200	0.84	0.84	0.235	4	80
500	2.10	2.10	0.585	10	82

All reactions were performed using CEM Discover SP Microwave Reaction System at the same conditions:

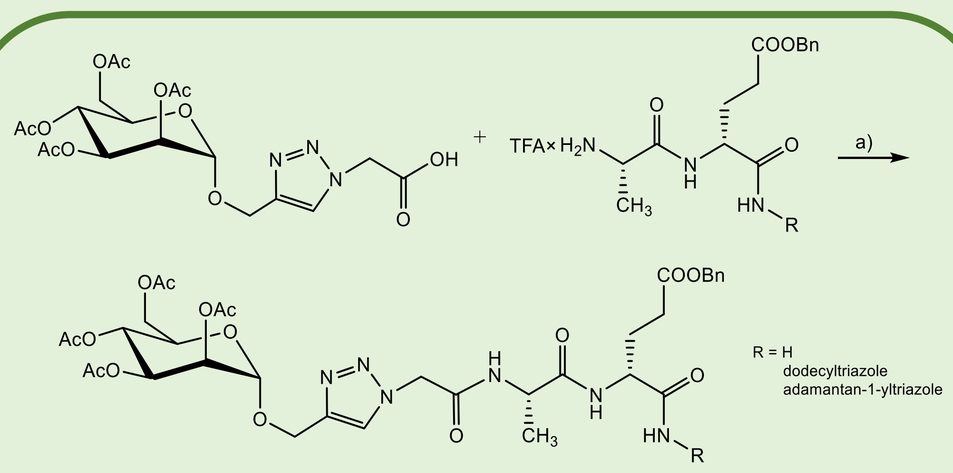
t / min	75
T / °C	50
p / psi	250
power / W	150

SYNTHESIS OF LIPOPHILIC DERIVATIVES OF DMP



Scheme 3. Reagents and conditions: (a) (i): NMM, *n*-buthyl chloroformate, THF, Ar, -10 °C, 2 h, (ii) NaHCO3, rt, 2 h; (iii) TFA, dry DCM, rt, 4h. b) (i) HBTU, TEA, dry THF/DCM (1:1), Ag, rt, 24 h; (ii) TFA, dry DCM, rt, 4h.

SYNTHESIS OF MANNOSYLATED DERIVATIVES OF DMP



Scheme 4. Reagents and preliminary conditions: EDC×HCl, HOBt, TEA, dry DCM, Ar, 0 °C to rt, 24 h.

CONCLUSIONS

- novel mannose-triazole subunit was successfully prepared from propargylated mannose subunit and azidoacetic acid by Cu(I) catalysed click reaction (CuAAC, Scheme 1)
- the protected dipeptide Boc-L-Ala-D-Glu(OBn) was prepared by conventional synthesis (Scheme 2) and microwave-assisted synthesis (Table 1) which significantly shortened the reaction time
- lipophilic derivatives of DMP were prepared using activated ester method (adamantan-1-yl, adamantan-1-ylethyl) or HATU condensation reagent (dodecyl, hexadecyl) for amide bond formation on α-position of DMP (Scheme 3)
- preliminary condensation of mannose-triazole precursor with DMP and lipophilic derivatives of DMP using EDC/HOBt method was successfully carried out, and the optimization of the reaction conditions is in progress
- the immunological activity of fully deprotected DMPP mannoconjugates will be evaluated in future studies.

ACKNOWLEDGEMENTS:

This work has been fully supported by Croatian Science Foundation under the project IP 2025-02-5568.

38th EPS
European Peptide Symposium
6 - 11th of September 2026
Vienna, Austria

An N-capping asparagine–lysine–proline (NKP) motif contributes to a hybrid flexible/stable multifunctional peptide scaffold

João P. F. Pimentel[1], Lai Y. Chan[2], Elizabete S. Cândido[1,3], Danieli F. Buccini[1], Samilla B. Rezende[1], Marcelo D. T. Torres[4], Karen G. N. Oshiro[1], Ítala C. Silva[5], Sónia Gonçalves[5], Timothy K. Lu[6], Nuno C. Santos[5], Cesar de la Fuente-Nunez[4], David J. Craik[2], Octávio L. Franco[1,3*] & Marlon H. Cardoso[1,7*]

[1]S-Inova Biotech, Programa de Pós-graduação em Biotecnologia, Universidade Católica Dom Bosco, Avenida Tamandaré 6000, Campo Grande – MS, 79117900, Brazil; [2]Institute for Molecular Bioscience, Australian Research Council Centre of Excellence for Innovations in Peptide and Protein Science, The University of Queensland, Brisbane, QLD, 4072, Australia; [3]Centro de Análises Proteômicas e Bioquímicas, Programa de Pós-graduação em Ciências Genômicas e Biotecnologia, Universidade Católica de Brasília, SGAN 916 Módulo B, Asa Norte, Brasília – DF, 70790160, Brazil; [4]Machine Biology Group, Departments of Psychiatry and Microbiology, Institute for Biomedical Informatics, Institute for Translational Medicine and Therapeutics, Perelman School of Medicine, Departments of Bioengineering and Chemical and Biomolecular Engineering, School of Engineering and Applied Science, Penn Institute for Computational Science, University of Pennsylvania, Philadelphia, Pennsylvania, USA; [5]Instituto de Medicina Molecular, Faculdade de Medicina, Universidade de Lisboa, Lisbon, Portugal; [6]Synthetic Biology Group, MIT Synthetic Biology Center, The Center for Microbiome Informatics and Therapeutics, Research Laboratory of Electronics, Department of Biological Engineering, Department of Electrical Engineering and Computer Science, Massachusetts Institute of Technology, Cambridge – MA, 02139, USA; [7]Programa de Pós-graduação em Ciências Ambientais e Sustentabilidade Agropecuária, Universidade Católica Dom Bosco, Avenida Tamandaré 6000, Campo Grande – MS, 79117900, Brazil; *Corresponding authors.

DOI: 10.17952/38EPS.2026.P202

INTRODUCTION

Structural diversity drives multiple biological activities and mechanisms of action in linear peptides. Here we describe an unusual N-capping asparagine-lysine-proline (NKP) motif that confers a hybrid multifunctional scaffold to a computationally designed peptide (PaDBS1R7). This peptide was characterized for its antibacterial, antibiofilm, anticancer, anti-infective and wound healing properties.

MATERIAL AND METHODS

Structural studies
- Peptide design (flexibility inducer residues)
- Circular dichroism (CD)
- Nuclear magnetic resonance (NMR)
- Molecular dynamics (MD) simulations

Biological studies
- Antibacterial, antibiofilm, anti-infective
- Anticancer
- NO and cytokines modulation
- Wound healing

Mechanisms of action
- CD with different mimetic vesicles
- Leakage assays
- MD simulations

RESULTS AND DISCUSSION

PaDBS1R7 has a shorter α-helix segment than other computationally designed peptides of similar sequence but with key residue substitutions (Fig. 1A – J). Although this motif acts as an α-helix breaker in PaDBS1R7, the Asn5 presents exclusive N-capping effects, forming a belt to establish hydrogen bonds for an amphipathic α-helix stabilization. The combination of these different structural profiles was described as a coil/N-cap/α-helix scaffold, which was also observed in diverse computational peptide mutants. Biological studies revealed that all peptides displayed antibacterial activities (Fig. 3 A – J). However, only PaDBS1R7 displayed anticancer properties, eradicated *Pseudomonas aeruginosa* biofilms, decreased bacterial counts by 100-1,000-fold *in vivo* (Fig. 4C), reduced lipopolysaccharide-induced macrophages stress (Fig. 4D), and stimulated fibroblast migration for wound healing (Fig 5A – H). This study extends our understanding of an N-capping NKP motif to engineering hybrid multifunctional peptide drug candidates with potent anti-infective and immunomodulatory properties.

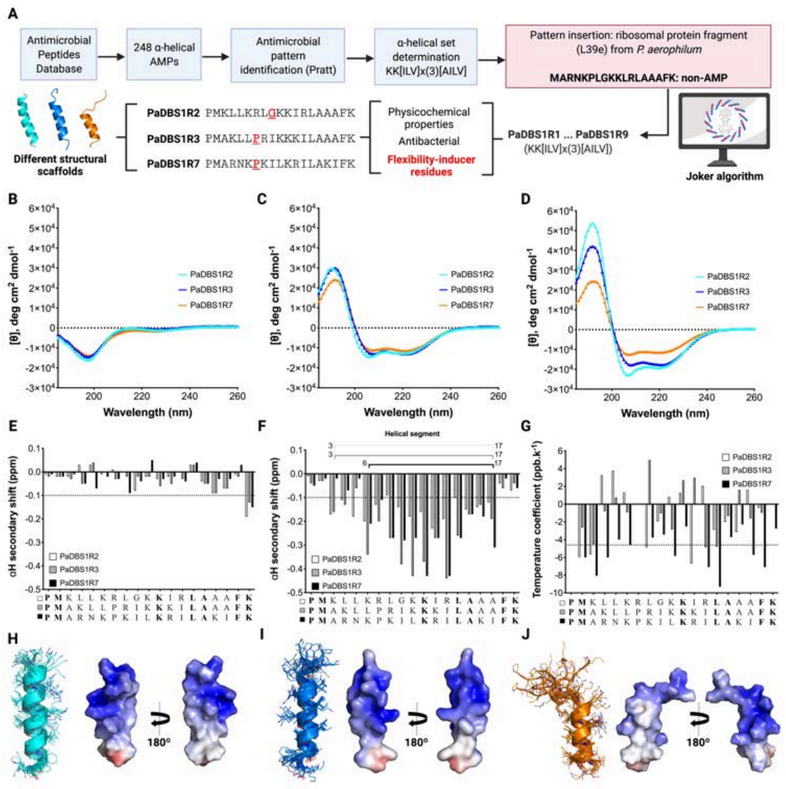


Fig. 1. Computer-aided design of PaDBS1 peptides and selection of PaDBS1R2, R3 and R7 for structural analysis. (A) For the computer-aided design of PaDBS1 peptides, 248 α-helical AMP sequences were retrieved from the Antimicrobial Peptide Database (APD). CD spectra were obtained in ultrapure water (B), 30% TFE in water (v/v) (C) and 50 mmol L^{-1} SDS (D). αH secondary chemical shifts in 90% H_2O (v/v) and 10% D_2O (v/v) (E), 60% H_2O (v/v) 30% TFE-d3 (v/v) and 10% D2O (v/v) (F) and amide proton (NH) temperature coefficients (G), of PaDBS1R2, R3 and R7 are also shown. Values more negative than -0.1 ppm (dashed lines in (E) and (F)) were interpreted as α-helix formation. Hydrogen bonds were considered for amide temperature coefficient values more positive than -4.6 ppb K_{-1} (dashed line in (G)). Conserved residues between all the peptides listed are in bold type. The superposition of the ten lowest energy NMR structures for PaDBS1R2 (PDB: 6CSK) (H), R3 (PDB: 6CSZ) (I) and R7 (PDB: 6CTI) (J) are also shown (H-J).

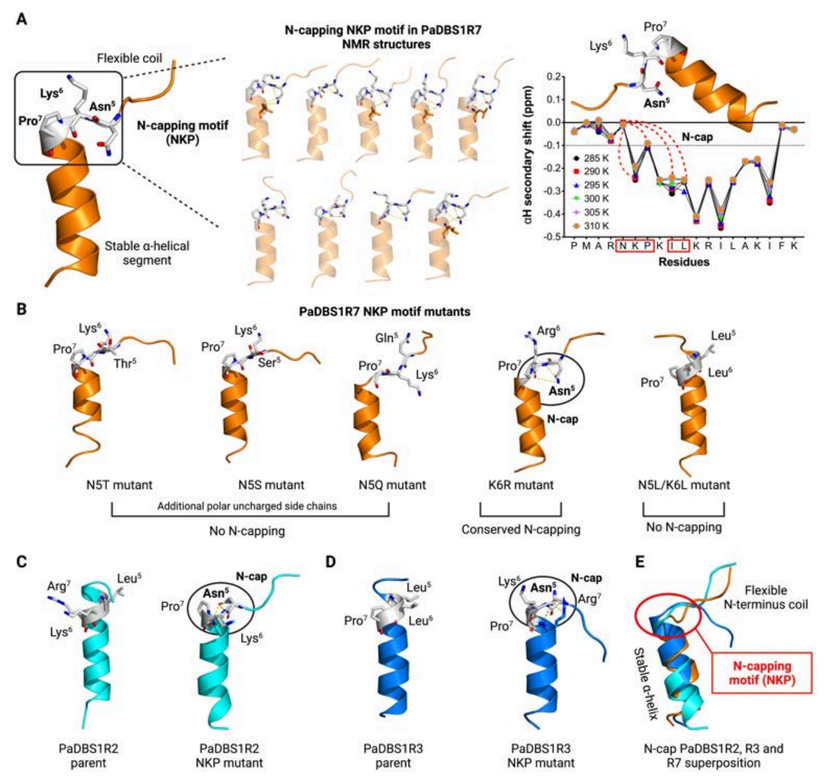


Fig. 2. An NKP motif in PaDBS1R7 triggers the coil/N-cap/α-helix structural scaffold. (A) The lowest energy NMR structure for PaDBS1R7 presents an NKP motif that influences on the peptide's scaffold by interrupting the α-helical segment at Pro7. This coil/N-cap/α-helix structural scaffold was observed for all ten lowest energy PaDBS1R7 NMR structures. The αH secondary shifts at different temperatures are also shown, revealing that the coil/N-cap/α-helix scaffold is conserved from 285 to 310 K, with primary N-capping involving Asn5 side chain atoms and Lys6, Pro7, Ile9 and Leu10 backbone atoms (red dashes). (B) Computational PaDBS1R7 mutants at position 5 replacing asparagine by other polar uncharged residues were also generated, leading to N-cap effect loss (C – E).

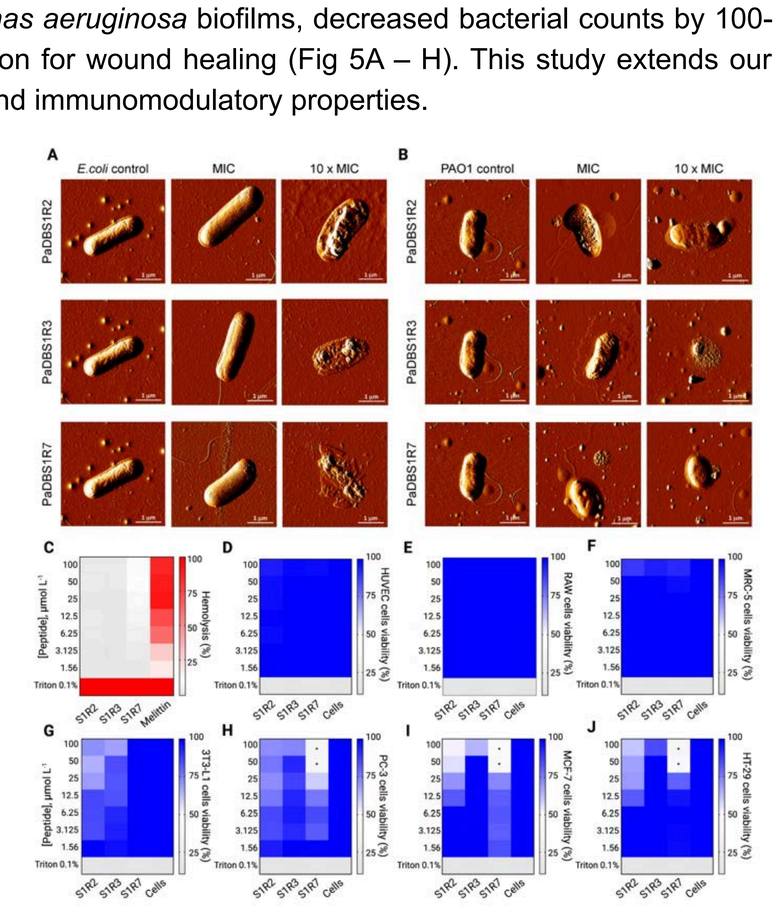


Fig. 3. *Escherichia coli* cells (A) treated with PaDBS1R2, R3 and R7 at their MIC and 10-fold MIC. The same conditions were used for *P. aeruginosa* cells (B) treated with PaDBS1R2, R3 and R7. Total scanning area of 5 × 5 μm; scale bar: 1 μm. The hemolytic activity of PaDBS1R2 (S1R2), R3 (S1R3) and R7 (S1R7) was evaluated using fresh human erythrocytes (C). Cell viability assays were performed using healthy mammalian cells, including HUVEC (D), RAW 267.4 (E), MRC-5 (F) and 3T3-L1 cells (G); and cancer cells, including PC-3 (H), MCF-7 (I) and HT-29 cells (J). All cell lines were treated with PaDBS1R2, R3 and R7 from 1.56 to 100 μmol L^{-1}. *Indicate peptide concentrations at which halfmaximal inhibitory concentrations (IC50) were determined.

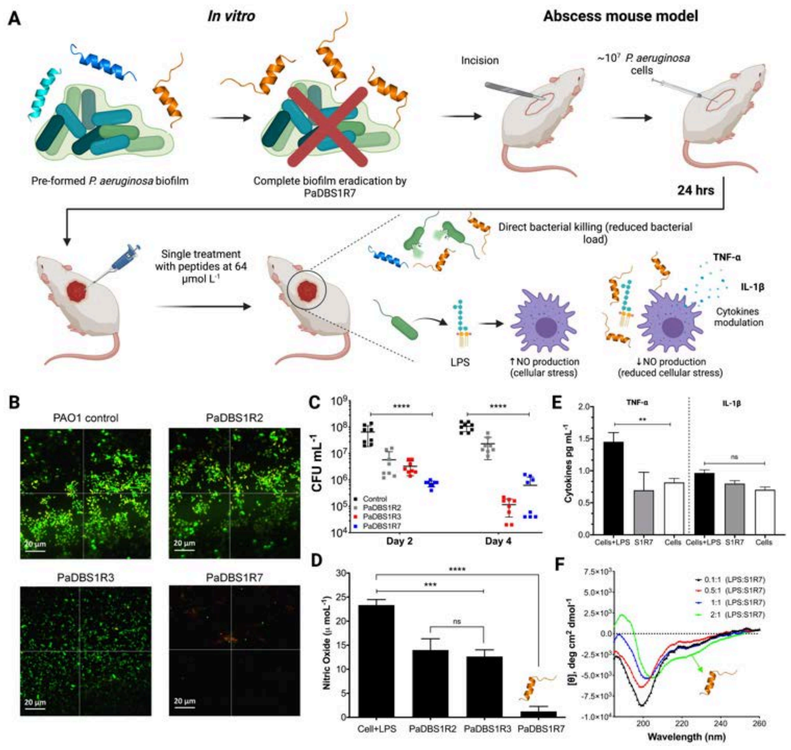


Fig. 4. Flow cell analysis of two-day-old *P. aeruginosa* biofilms (A and B), skin abscess mouse model with *P. aeruginosa* (C), nitric oxide (NO) (D) and cytokines production by macrophages in the presence of LPS (E), and LPS titration using CD experiments (F). Statistical significance was assessed using one-way analysis of variance (ANOVA), followed by Dunnett's multiple comparison tests. ** $p < 0.05$; *** $p < 0.001$ **** $p < 0.0001$. The error bars represent standard deviation values. ns: not significant.

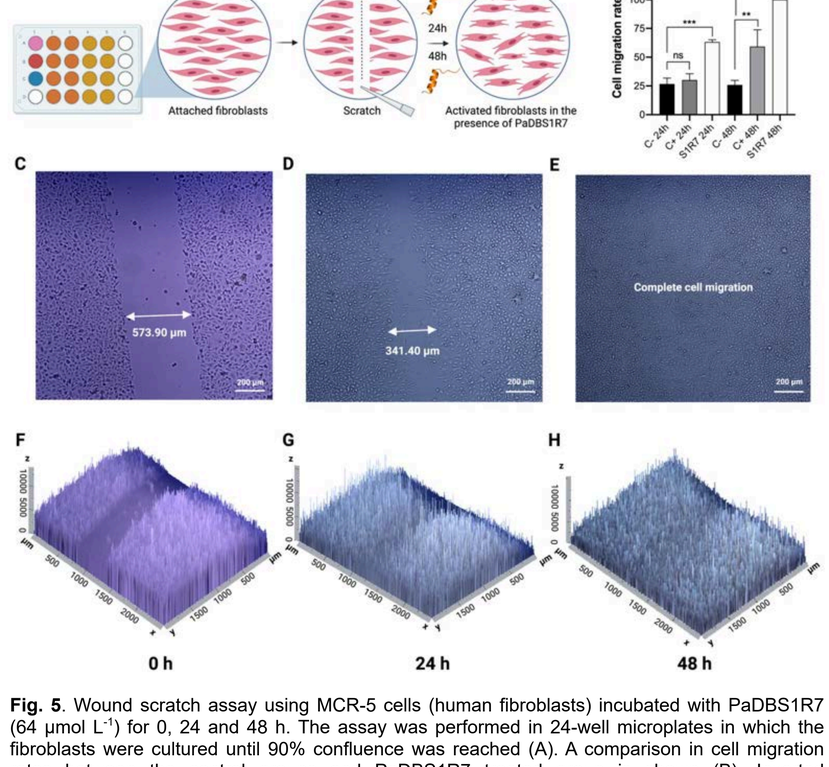


Fig. 5. Wound scratch assay using MCR-5 cells (human fibroblasts) incubated with PaDBS1R7 (64 μmol L^{-1}) for 0, 24 and 48 h. The assay was performed in 24-well microplates in which the fibroblasts were cultured until 90% confluence was reached (A). A comparison in cell migration rates between the control groups and PaDBS1R7 treated group is shown (B). Inverted microscopy images were captured to measure the gap distances in the scratches at 0 (C), 24 (D) and 48 h (E). 2.5D images were also obtained to visualize the gap distances and cell density at the incubation times 0 (F), 24 (G) and 48 h (H).

CONCLUSION

This study extends our understanding of the rules governing AMPs with N-cap motifs. In the peptides studied here, this unusual structural scaffold is triggered by an N-cap NKP motif, which resulted in a multifunctional AMP selective for anionic surfaces and capable of exerting antibacterial, antibiofilm, anticancer and anti-infective (skin infection) effects, also reducing LPS-induced macrophage stress and recruiting fibroblasts to assist wound healing. The biological multifunctionality associated with the N-cap NKP motif makes PaDBS1R7 a highly attractive coil/N-cap/α-helix scaffold for peptide-based drug design.

REFERENCE

Cardoso, *et al*. **Chem. Sci**., 2022. DOI: 10.1039/D1SC06998E

ACKNOWLEDGMENTS

This work was supported by CAPES, CNPq, Finep and FUNDECT.

Two New Orbitides, [1–10-NαC]-croheorbs A1 and A2, Isolated from the Latex of *Croton heliotropiifolius*

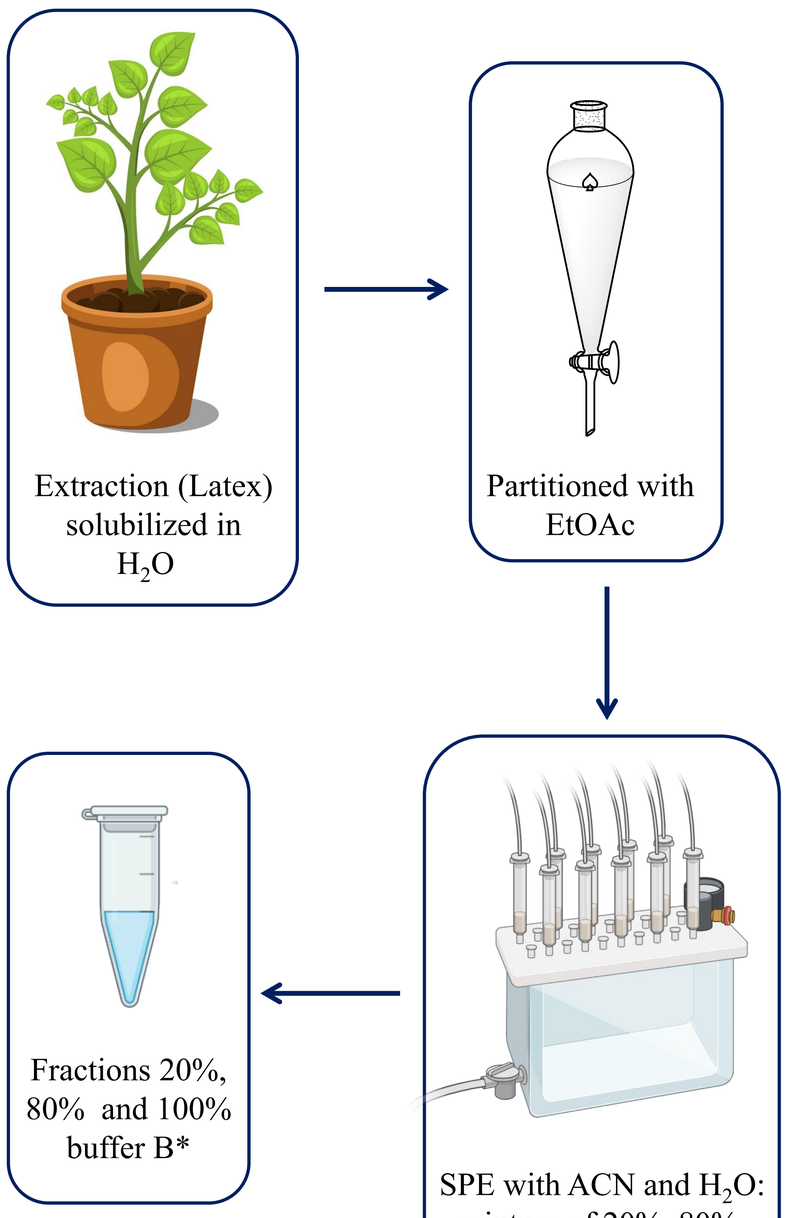
Suzana A. S. Queiroz[1], Ana Letícia P. Dos Santos[1], Paula Rezende-Teixeira [2,3], Letícia Costa-Lotufo [2] & Vanderlan S. Bolzani[1]
[1]*São Paulo State University – UNESP-IQ, Araraquara, SP, Brazil.*
[2] *University of São Paulo- USP - USP, São Paulo, SP, Brazil*
[3] *Santo Amaro University - UNISA, São Paulo, SP, Brazil*
**alp.santos*@unesp.br **vanderlan.bolzani*@unesp.br

https://doi.org/10.17952/38EPS.2026.P314

INTRODUCTION

Peptides are an important class of natural products with significant therapeutic potential, due to their structural properties[1]. Among plants, there are three classes of ribosomal-synthesized cyclic peptides (RiPPs): cyclotides, PawS-derived peptides (PDPs), and orbitides. Among these, orbitides are ribosomally synthesized, head-to-tail cyclized plant peptides typically comprising 5 to 11 amino acid residues.[2] Although Brazil has the largest biodiversity in the world there are still few studies describing the isolation of orbitides from Brazilian plants.

EXPERIMENTAL PROCEDURES

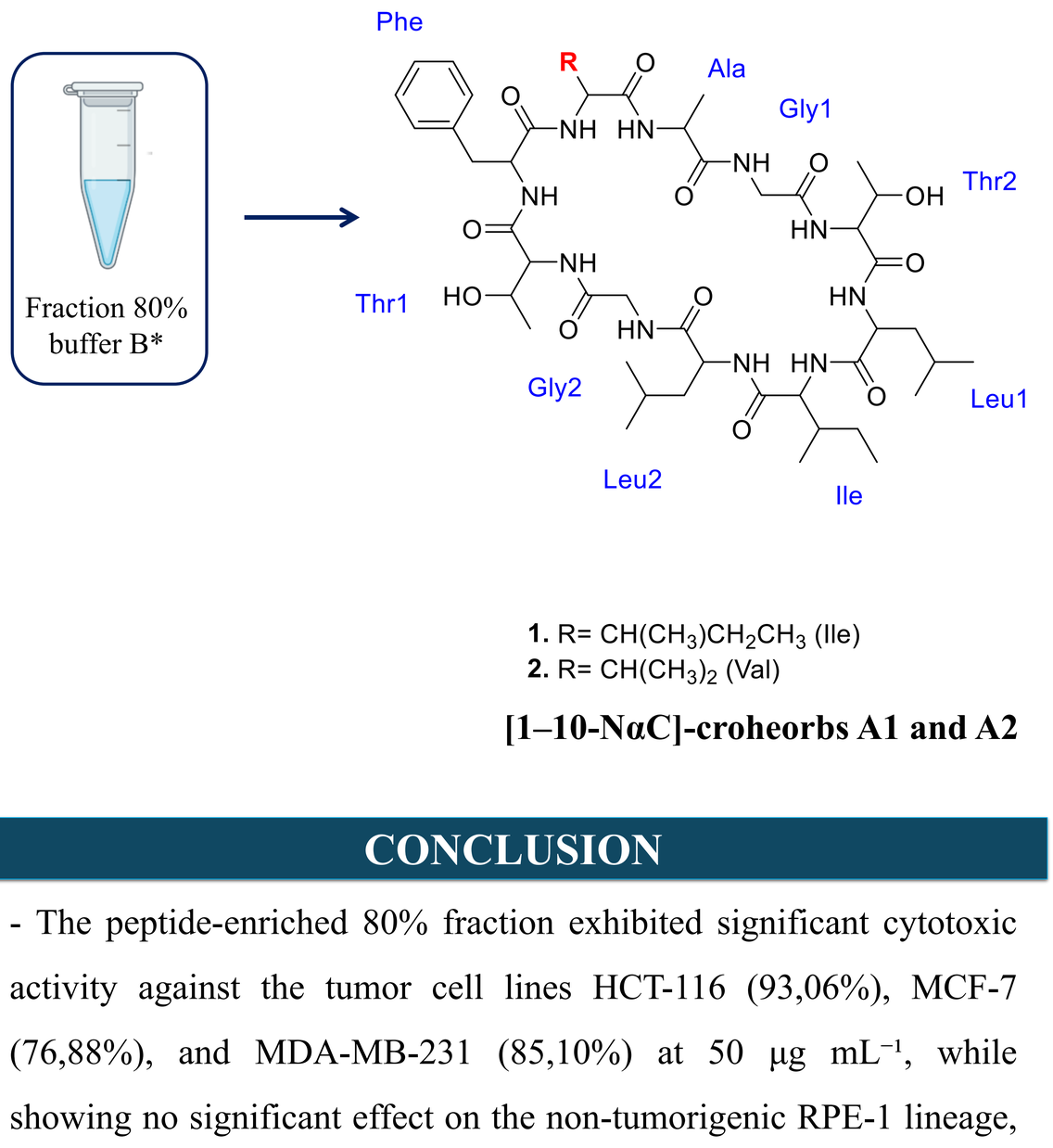


Solvent A: H_2O + 0.1% CF_3COOH
Solvent B: ACN + 0.1% CF_3COOH

RESULTS AND DISCUSSION

Table 1. Cytotoxic activity with fraction 80% from latex of *Croton heliotropiifolius*

Cell lines	Fraction 80%	
	50 µg mL^{-1}	**5 µg mL^{-1}**
HCT-116	93.06%	15.46%
MCF-7	76.88%	16.30%
MDAMB-231	85.10%	0%
RPE-1	4.67%	0%



1. R= $CH(CH_3)CH_2CH_3$ (Ile)
2. R= $CH(CH_3)_2$ (Val)

[1–10-NαC]-croheorbs A1 and A2

CONCLUSION

- The peptide-enriched 80% fraction exhibited significant cytotoxic activity against the tumor cell lines HCT-116 (93,06%), MCF-7 (76,88%), and MDA-MB-231 (85,10%) at 50 µg mL^{-1}, while showing no significant effect on the non-tumorigenic RPE-1 lineage, suggesting selective activity.

- This study expands the structural diversity known for orbitides and represents the first phytochemical investigation of *C. heliotropiifolius*

REFERENCES

1. Buchanan, D. et al. *Biomedicines*. **2025**,13, 240.
2. Shim, Y. Y., Young, L. W., et al. *J. Nat. Prod.* **2015**, 78, 645.
3. Icons were obtained from BioRender.com.

ACKNOWLEDGMENTS

FAPESP Nº 2025/08311-2.

PDGF-Derived Peptides: From Receptor Binding to Cellular Signaling in Wound Healing

Krzysztof Polaczek[1], Przemysław Karpowicz[1], Małgorzata Zawrzykraj[2], Milena Deptuła[2], Michał Pikuła[2], Emilia Iłowska[3], Rafał Ślusarz[3], Emilia Sikorska[3],

[1]Department of Biomedical Chemistry, Faculty of Chemistry, University of Gdańsk, Wita Stwosza 63 st. 80-308 Gdańsk, Poland, [2]Laboratory of Tissue Engineering and Regenerative Medicine, Medical University of Gdańsk, Dębinki 1 st. 80-211 Gdańsk, [3]Department of Organic Chemistry, Faculty of Chemistry, University of Gdańsk, Wita Stwosza 63 st. 80-308 Gdańsk, Poland

krzysztof.polaczek@phdstud.ug.edu.pl

https://doi.org/10.17952/38EPS.2026.P347

Introduction

Clinical background

Chronic wounds affect 1-2% of Europeans annually with, treatment costs reaching 2-3% of healthcare budgets.

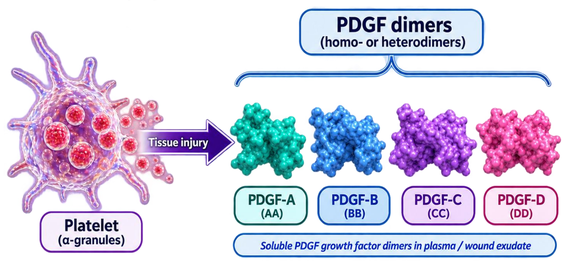


Patients with diabetes are particularly vunlnerable to diabetic foot ulcers and other chronić wounds.

The underlying pathophysiology involves i.e. impaired tissue repair, neuropathy and deficiency of growth factors, notably PDGF (Platelet-Derived Growth Factor) and VEGF (Vascular Endothelial Growth Factor) [1].

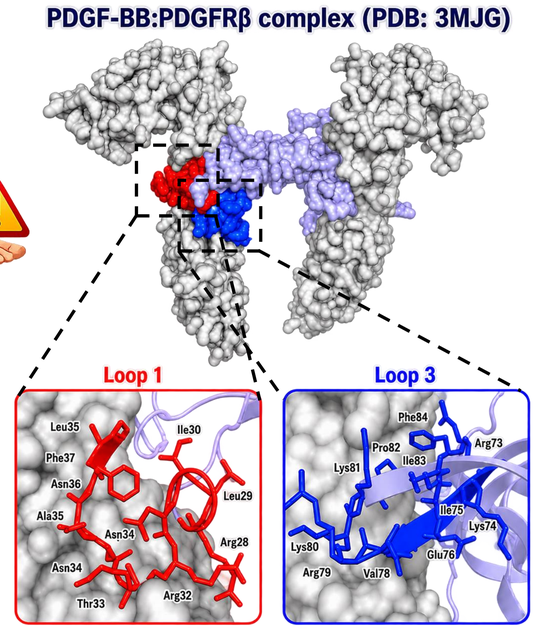
PDGF biology

PDGF proteins are stored in platelet α-granules and released after tissue injury as homo- or heterodimers.



Among these isoforms, PDGF-BB plays a central role in wound healing from injury to scar formation.

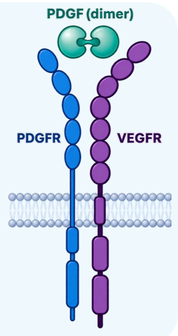
PDGF-BB:PDGFRβ complex (PDB: 3MJG)



- Activation of PDGFR and VEGFR receptors requires the binding of the protein in dimeric form, which induces autophosphorylation and the initiation of signalling cascades [2].
- The binding of PDGF and VEGF proteins to the receptor is mediated by so-called binding loops.

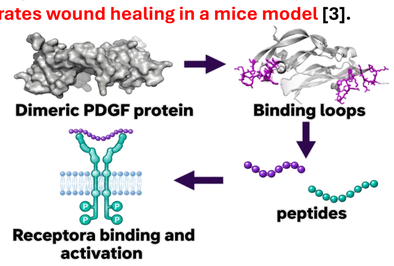
PDGF cross-activity

- PDGF and VEGF proteins show structural similarity, resulting in partial cross-activity between their receptors.
- Several PDGF (PDGF-AA, PDGF-BB, PDGF-CC) isoforms have been shown to bind VEGFR2. This structural and functional overlap suggests that PDGF-derived peptides may retain or acquire a broader receptor-binding profile.



Our research

Our team's research on the PDGF-BB protein has led to the identification of a fragment (the L1 loop region) that effectively stimulates skin cell proliferation and accelerates wound healing in a mice model [3].



Encouraged by our previous studies on the pro-regenerative potential of binding loops derived from the PDGF-BB protein, we decided to investigate the remaining isoforms of this protein, namely PDGF-A, PDGF-C, and PDGF-D.

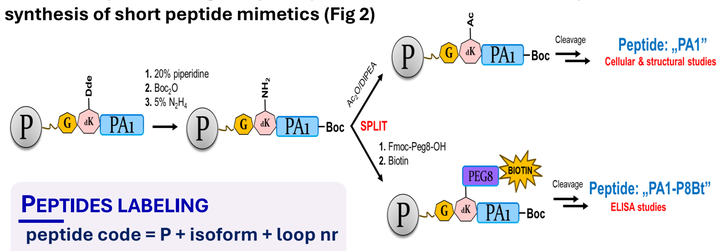
Peptide design and synthesis

Based on the amino acid sequences of the binding loop regions, aligned according to the conserved cystine knot motif, we designed (*Fig. 1*) a series of novel peptides.

Protein:	Peptide:		Sequence		Loop
hPDGF-A	PA1	94	:AVCK-TRTVIYEIPRSQVDPTSANFLIWPPCVEVKRCT---GCC-----NT:	135	Loop„L1"
hPDGF-B	PB1	95	:AECK-TRTEVFEISHRLIDRTNANFLIWPPCVEVQRCS---GCC-----NN:	136	
hPDGF-C	PC1	248	:YSCT-PRNFSVSIRELK---RTDTIFWPPCLLVKRCG---GNCACCLHNC:	291	
hPDGF-D	PD1	270	:YSCT-PRNYSVNIRELK---LANVVFFPRCLLVQRCG---GNCGCGTVNW:	313	
hPDGF-A	PA3	136	:SSVKCQPSRVHHRSVKVAKVEYVRKKPKLK-----EVQVRLEEHLECACAT:	181	Loop„L3"
hPDGF-B	PB3	137	:RNVQCRPTQVQLRPVQVRKIEIVRKKPIFK-----KATVTLEDHLACKCET:	182	
hPDGF-C	PC3	292	:NECQCVPSKVTKKYHEVLQLRP---KTGVRGLHKSLTDVALEHHEECDCVC:	339	
hPDGF-D	PD3	314	:RSCTCNSGKTVKKYHEVLQFEPGHIKRRGRAKTMALVDIQLDHHERCDCTC:	364	

Fig. 1 Sequences of peptides derived from L1 and L3 loops of PDGFs.

PDGF receptor-binding loop sequences were used as templates for the synthesis of short peptide mimetics (Fig 2)



Peptides labeling

peptide code = P + isoform + loop nr

P = PDGF	Loops:
isoforms A-D	Loop 1 & Loop 3

PA1 = P A 1
e.g. label PDGF isoform loop

Fig. 2 Schematic flow of peptides' synthesis.

Methodology

1. Screening and initial characterization

ELISA-based affinity screening: lack 96-well plates were Ni^{2+}-functionalized to immobilize 6×His-tagged **PDGFRα, PDGFRβ, VEGFR1 and VEGFR2**. **Biotinylated peptides** were added, and receptor binding was detected using **streptavidin–alkaline phosphatase** and **AttoPhos** substrate. Fluorescence was measured kinetically using a Tecan Infinite 200 plate reader.

Cell-based assays: Human **HaCaT keratinocytes, 46BR.1N and BJ fibroblasts** were cultured in DMEM supplemented with 10% FBS at 37°C and 5% CO_2. Cells were serum-starved for 24 h prior to peptide treatment. **Proliferation** was assessed using the XTT assay after 48 and 72 h of stimulation, while **cytotoxicity** was evaluated by measuring LDH release into supernatants after 48 h.

2.Detailed characterization of selected peptides

Microscale thermophoresis: Receptor proteins were fluorescently labeled using the **RED-NHS 2nd Generation** labeling kit (NanoTemper). Peptides were dissolved in water and serially diluted in **50 mM Tris buffer, pH 8.0, containing 0.05% Pluronic**. Measurements were performed in **spectral shift mode at 650 and 670 nm** using a Monolith instrument (NanoTemper).

Serum stability: Peptides at a concentration of **1 mM** were incubated with human serum in a **1:1 ratio**. Samples were collected at defined time points, and serum proteins were precipitated with **15% TCA** followed by centrifugation. Peptide degradation was monitored chromatographically based on changes in peak area. **Mass spectra were recorded for samples containing approximately 50% of the initial peptide amount** to identify degradation products

Circular Dichroism: Peptide structure was analyzed in the **190–260 nm range** using a Jasco J-815 spectropolarimeter, with **buffer-subtracted** spectra reported as mean residue ellipticity.

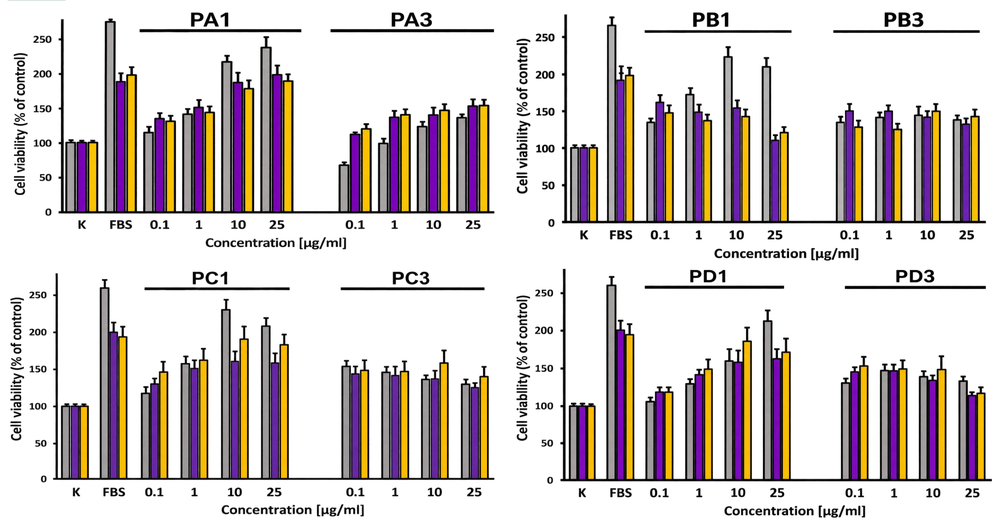
Screening Phase

One peptide library • two complementary biological readouts

8 PDGF-Derived peptides

PDGF-A •PDGF-B • PDGF-C • PDGF-D | Loop 1 + Loop 3

Cellular studies of PDGF peptides



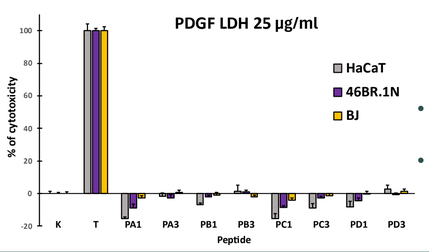
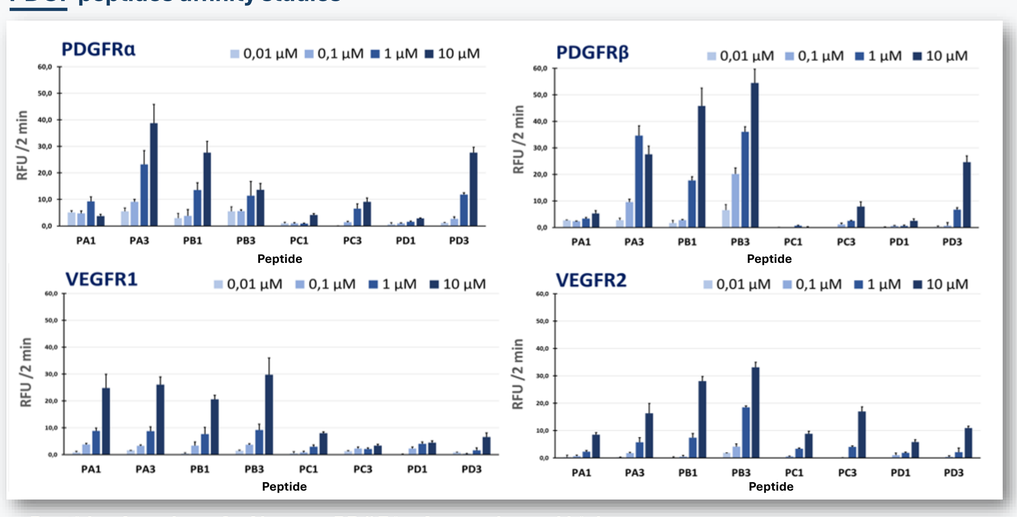


Fig. 3 Proliferation of HaCaT, 46Br.1N and BJ cells after 72h incubation with PDGF-derrived peptides.

- All PDGF peptides stimulated cel proliferation, whereas peptides designed from the L1 loop show stronger effects.
- The pro-proliferative effect is most strongly visible in keratinocytes.

Fig. 4 Cytotoxicity of PDGF-derrived peptides

PDGF peptides affinity studies



- Peptides from loop 3 of human PDGF isoforms showed higher affinity for receptors,
- Peptides from isoforms A and B exhibiting the strongest affinity.

Fig. 5 Affinity of the PDGF peptides to receptors from PDGFR and VEGFR groups

KEY SCREENING CONTRAST

LOOP 1 stronger cellular response

LOOP 3 stronger receptor binding

Selected for detailed characterization

Integrating cellular activity + receptor binding behavior

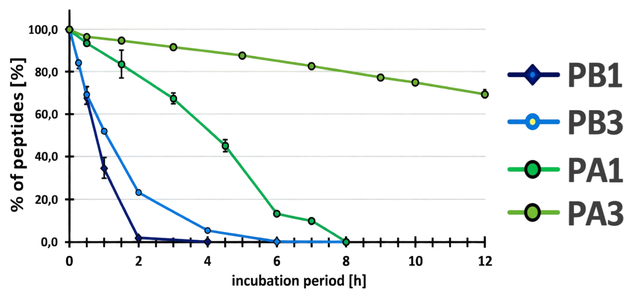
PA1 PA3 PB1 PB3

Detailed Characterization

A focused „deep dive" into four lead peptides selected from the screening phase

Serum stability

Percentage change in the quantity of PDGF peptides over time



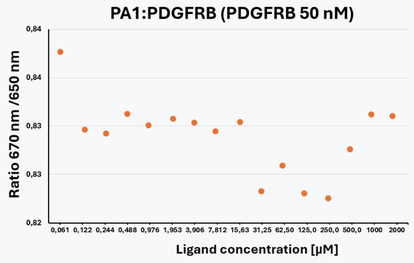
Identified cleavage sites and peptide half-lives:

		$t_{1/2}$
PB1	R-L-I-DRTNANFLk(Ac)G-NH_2	40 min
PB3	R-K-I-EIVRKKPIFk(Ac)G-NH_2	1 h
PA1	S-Q-V-D-PTSANFLk(Ac)G-NH_2	4,5 h
PA3	A-K-VEYVRKKPKLk(Ac)G-NH_2	-

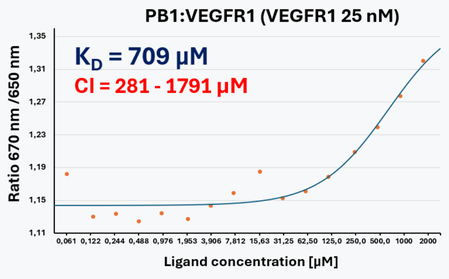
Microscale thermophoresis

Types of curves recorded during MST analysis:

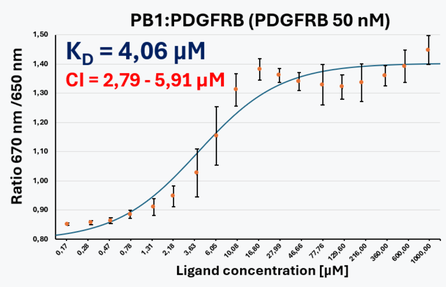
a) No binding



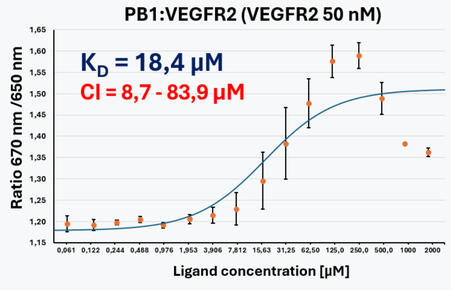
b) No plateau



c) A correct curve with the K_D value plotted



d) Non-standard curve shape



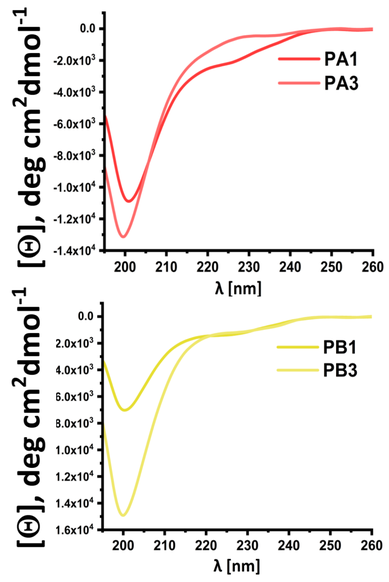
Dissociation constants K_D:

	PDGFRα	PDGFRβ
PA1	2,09 mM (1,64-2,67)	-
PA3	28,5 µM (22,2-36,4)	8,22 µM (5,61-12,02)
PB1	20,8 µM (15-28,8)	4,06 µM (2,79-5,91)
PB3	39,3 µM (31,3-49,4)	9,12 µM (7,01-11,86)

	VEGFR1	VEGFR2
PA1	-	-
PA3	-	1,55 µM (0,87-2,79)
PB1	709 µM (281-1791)	18,4 µM (8,7-83,9)
PB3	354 nM (86-1464)	1,39 µM (0,99-1,95)

Circular dichroism spectra

Peptides have a disordered structure typical of short peptides;



Conclusions

- PDGF-derived peptides were non-cytoxic and stimulated proliferation of skin-derived cells, with Loop 1 peptides showing stronger pro-proliferative effects.
- ELISA and MST confirmed interactions of selected peptides; however, stronger receptor binding did not directly translate into higer cellular activity.
- MST reveald non-classical binding profiles for some peptide-receptor pairs, suggesting more complex interaction modes.
- Serum stability was strongly sequence-dependent, while MS analysis indicated predominantly N-terminal peptide degradation.

Literature:

[1] K. Järbrink, G. Ni, H. Sönnergren *et al.*, *Syst. Rev.*, 2016, vol. 5, no. 1, pp. 1–6,
[2] Evrova, Olivera & Buschmann, Johanna. *European Cells and Materials.* 2017, 34. 15-39. 10.22203/eCM.v034a02.
[3] M. Deptuła, P. Karpowicz, A.Wardowska et al., *Adv. Wound Care*, 2020, vol. 9, no. 12, pp. 657-675

National Science Centre

Founding: *this work was supported by the National Science Centre* ***(UMO-2023/51/D/NZ7/02791)***

Rational Design of Fc-Binding Peptide Ligands as Next-Generation Alternatives to Protein A for Antibody Purification

Tuba Polat[1], Alp Ertunga Eyupoglu[2], Ahmet Can Timucin[3], Batu Erman[3], Tanil Kocagoz[4], Ozge Can[5]

[1]Institute of Health Sciences, Department of Medical Biotechnology, Acibadem Mehmet Ali Aydinlar University, Istanbul, Turkiye

[2]Institute of Science and Engineering, Department of Molecular Biology and Genetics, Bogazici University, Istanbul, Turkiye

[3]Faculty of Engineering and Natural Sciences, Department of Molecular Biology and Genetics, Acibadem Mehmet Ali Aydinlar University, Istanbul, Turkiye

[4]Faculty of Medicine, Department of Basic Medical Sciences, Department of Medical Microbiology, Acibadem Mehmet Ali Aydinlar University, Istanbul, Turkiye

[5]Faculty of Engineering and Natural Sciences, Department of Biomedical Engineering, Acibadem Mehmet Ali Aydinlar University, Istanbul, Turkiye

https://doi.org/10.17952/38EPS.2026.P429

INTRODUCTION

Staphylococcal Protein A (SpA) is a 42 kDa cell wall-associated virulence factor that contributes to bacterial immune evasion by binding to human IgG1[1,2]. Owing to its high affinity and specific interaction with the Fc region of IgG, SpA is widely used as an affinity ligand for antibody purification[3]. However, its high cost and limited stability under harsh purification and regeneration conditions have created a need for alternative affinity ligands. In this study, a computational peptide engineering strategy was employed to design novel Fc-binding peptide ligands derived from the Protein A–IgG interaction interface.

MATERIAL & METHODS

Peptide Ligands Prediction

Novel peptide ligand candidates were predicted using Rosetta PeptiDerive[4] based on the Protein A–human IgG1 Fc complex (PDB ID: 4WWI), with chains A and D selected for peptide prediction. Each amino acid in the original peptide sequence was screened against all 20 possible amino acids using FoldX[5], and substitutions predicted to improve stability (ΔΔG < −0.5 kcal/mol) were selected, resulting in 15 novel peptide ligand candidates.

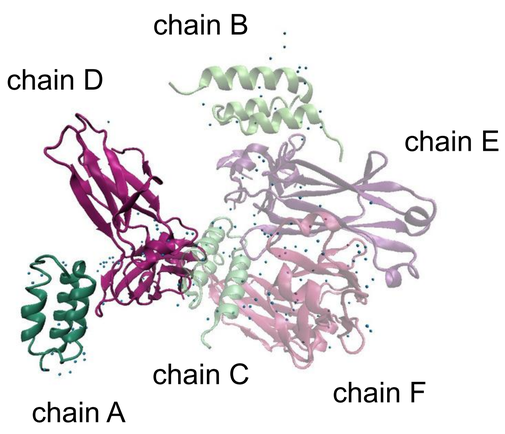


Figure 1. The crystal structure of the C domain of staphylococcal protein A in complex with the Fc fragment of human IgG (PDB ID: 4WWI).

Together with pep0, all 16 peptides were modeled using PEP-FOLD 4.0 and evaluated by molecular docking, interaction analysis, and MD simulations. Based on their similarity to the Protein A–IgG1 interaction, pep9, pep15, and pep16, along with pep0, were selected and synthesized by solid-phase peptide synthesis (SPPS).

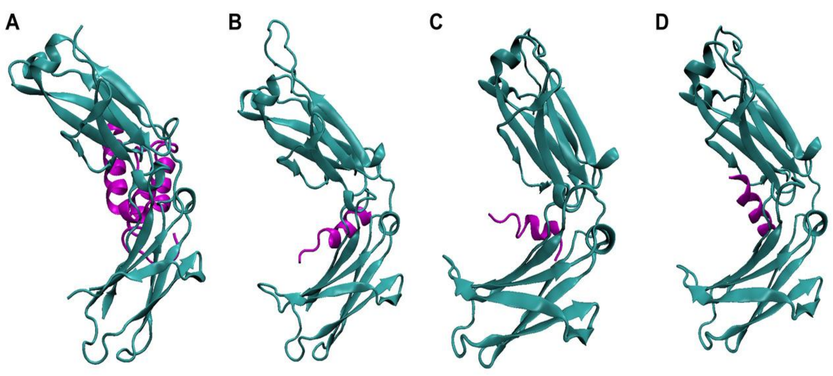


Figure 2. HADDOCK based local docking showing the interaction between the Fc fragment of human IgG1 and **A.** the C domain of protein A (positive control) **B.** pep9, **C.** pep15, and **D.** pep16.

Peptide - Human IgG Interaction

The binding affinities of the synthesized peptide candidates were experimentally evaluated by Microscale Thermophoresis (MST; NanoTemper). Humira® (adalimumab) and Herzuma® (trastuzumab), both human IgG1 monoclonal antibodies, were used as target molecules. Eculizumab, a humanized IgG2/IgG4κ hybrid monoclonal antibody, was included as a non-IgG1 control to assess potential IgG subclass-dependent binding.

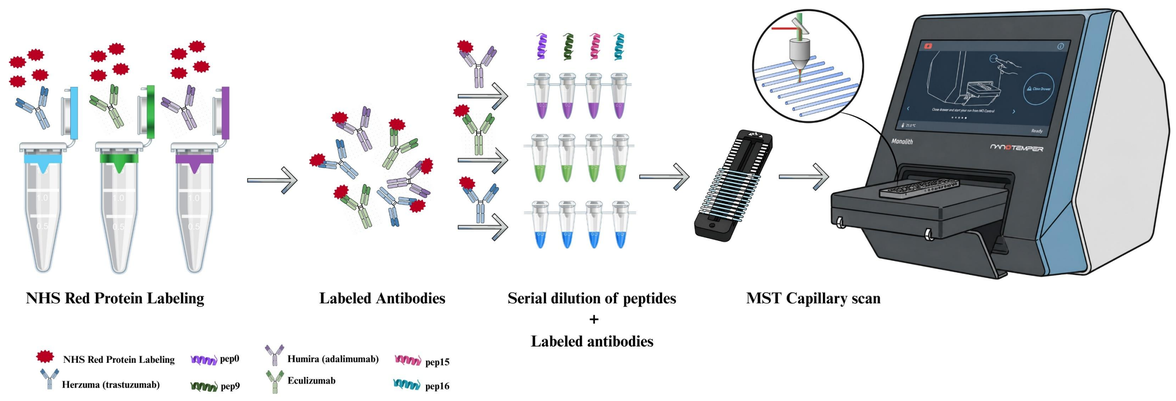


Figure 3. Schematic representation of the MST workflow.

RESULTS

The MST results demonstrated that the rationally optimized peptide candidates exhibited improved binding to human IgG1 compared with the original peptide sequence, pep0, which was directly derived from the Protein A–human IgG1 interaction interface. In particular, pep9, pep15, and pep16 showed higher binding affinities than pep0. In contrast, no detectable binding was observed between the peptide ligands and eculizumab, a humanized IgG2/IgG4κ hybrid monoclonal antibody used as a non-IgG1 control, suggesting preferential binding of the designed peptides toward IgG1.

The dose–response curves obtained from MST measurements are presented in Figure 4, and the corresponding KD values are summarized in Table 1. Overall, pep15 exhibited the lowest KD value and therefore the highest binding affinity toward human IgG1, followed by pep9 and pep16. These findings indicate that the computationally guided sequence modifications successfully enhanced the IgG1-binding properties of the parent peptide and support the effectiveness of the rational peptide optimization strategy in identifying improved Protein A-mimetic affinity ligands.

Table 1. KD values of peptide ligands for Humira and Herzuma determined by MST analysis.

Peptide	KD value (µM)	
	Humira (adalimumab)	Herzuma (trastuzumab)
Pep0	98	45.46
Pep9	0.027	1.47
Pep15	0.009	0.008
Pep16	41.72	1.16

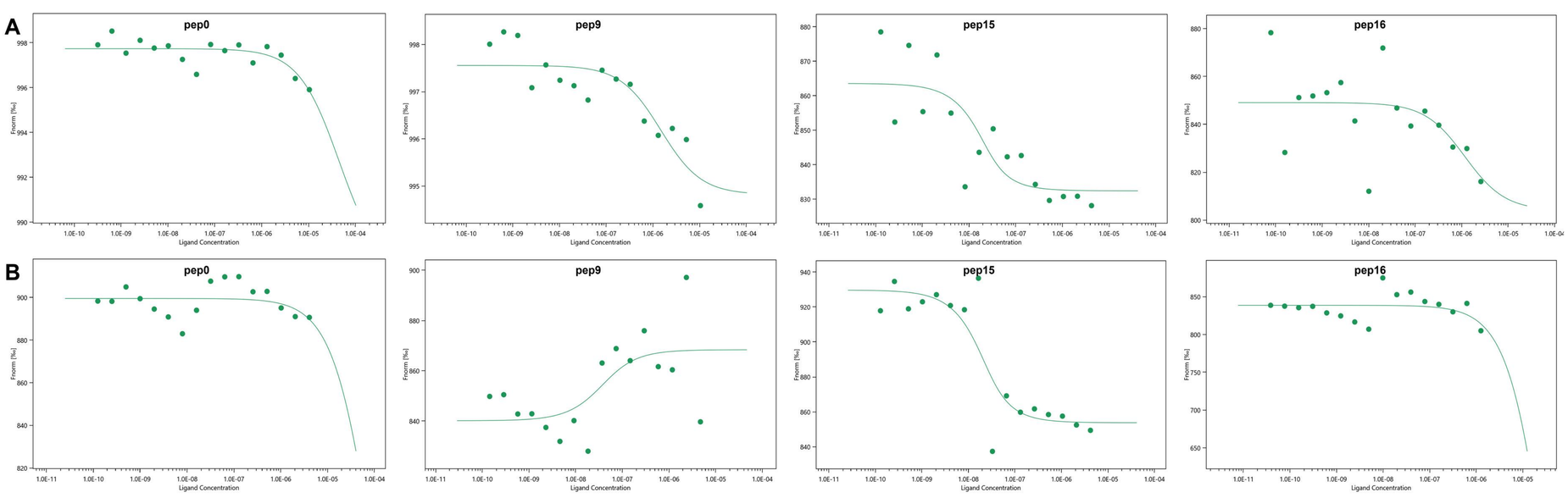


Figure 4. MST dose–response curves showing the binding interactions of the peptide ligands (pep0, pep9, pep15, and pep16) with human IgG1 monoclonal antibodies: **A.** Herzuma and **B.** Humira.

REFERENCES

This work was supported by the TUBITAK 1507 Project (No. 7240199), titled “Development of an Innovative Peptide-Based Antibody Purification Technology”.

Hybrid Peptide Functionalized Nanoparticles For Breast Cancer Therapeutics

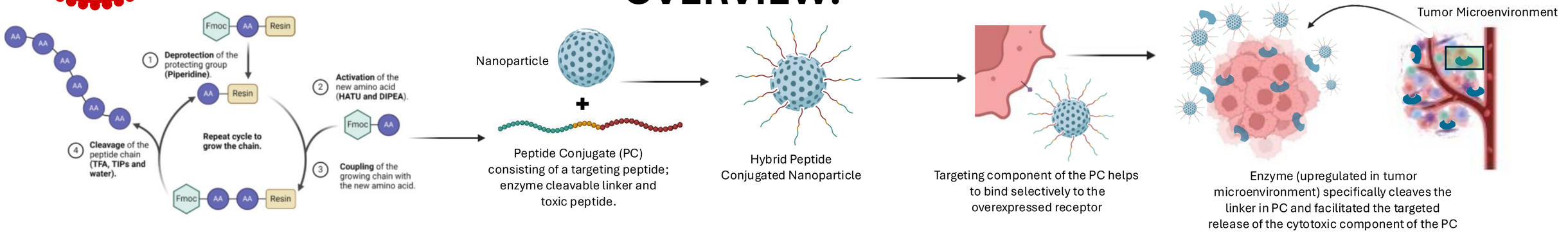
Priyanshu Priya[1,2,4], Peter M Moyle[2,4] ,Zyta M Ziora[3,4], Prashant Mishra[1,4]

1. *Department of Biochemical Engineering and Biotechnology, Indian Institute of Technology Delhi, India*
2. *School of Pharmacy and Pharmaceutical Sciences (SPPS), University of Queensland, Australia*
3. *Institute for Molecular Bioscience (IMB), University of Queensland, Australia*
4. *University of Queensland and Indian Institute of Technology Delhi Research Academy (UQ-IITD)*

https://doi.org/10. 17952/38EPS.2026.P400

38th EPS European Peptide Symposium

OVERVIEW:



INTRODUCTION

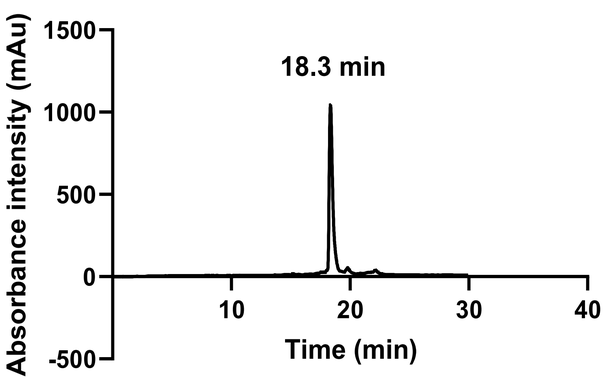
- **Clinical challenge:** Limited tumor penetration and toxicity of ADCs
- **Therapeutic strategy:** Targeting peptide + cleavable linker + cytotoxic peptide
- **Goal:** Peptide-functionalized nanoparticles for selective drug delivery
- **Benefit:** Better tumor targeting with reduced off-target toxicity

METHODOLOGY

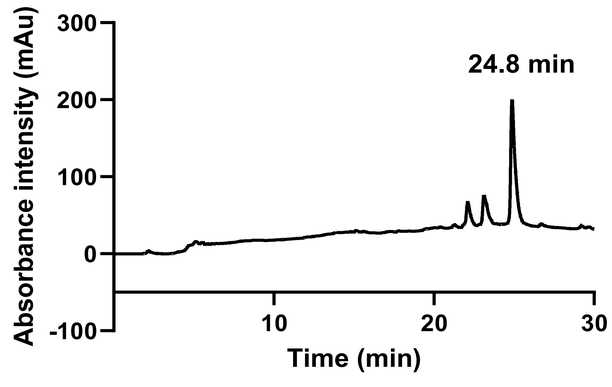
- **Synthesis:** Fmoc solid-phase synthesis, HPLC purification, and LC-MS confirmation.
- **Conjugation:** Attach to nanoparticles; test size, charge, morphology, and efficiency.
- **Selective Release:** Evaluate linker cleavage in acidic/enzymatic tumor conditions.
- **Uptake study:** Assess cellular uptake via flow cytometry and microscopy.
- **Validation:** Run cytotoxicity, selectivity, and viability assays on breast cancer cells.

RESULTS

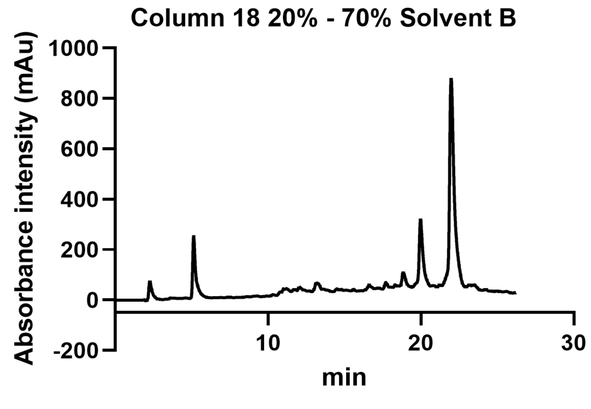
HPLC spectrum of the synthesized targeting peptide



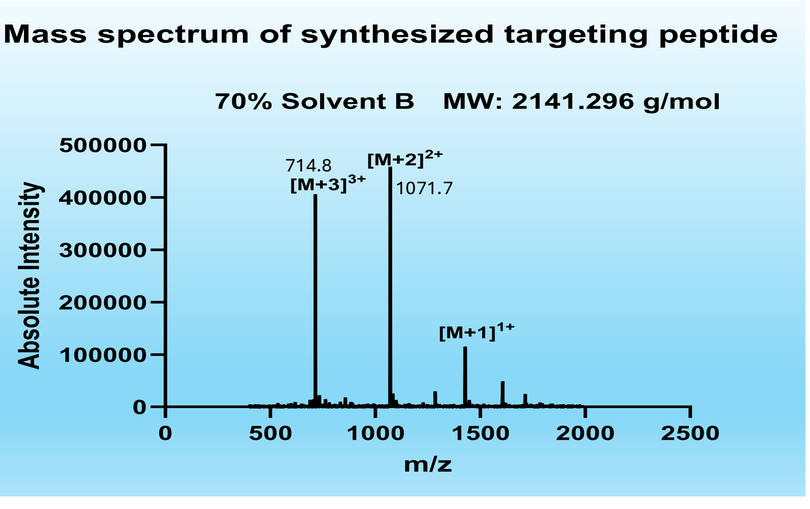
HPLC spectrum of the synthesized Cytotoxic peptide



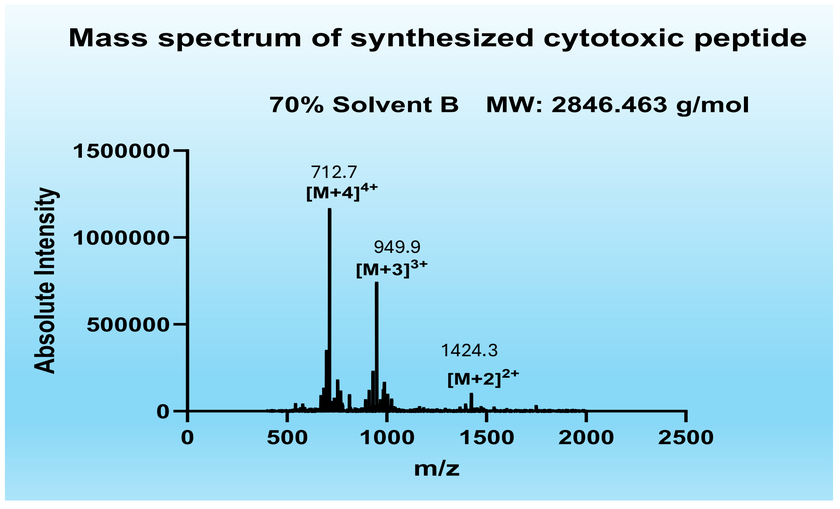
HPLC spectrum of the synthesized peptide conjugate



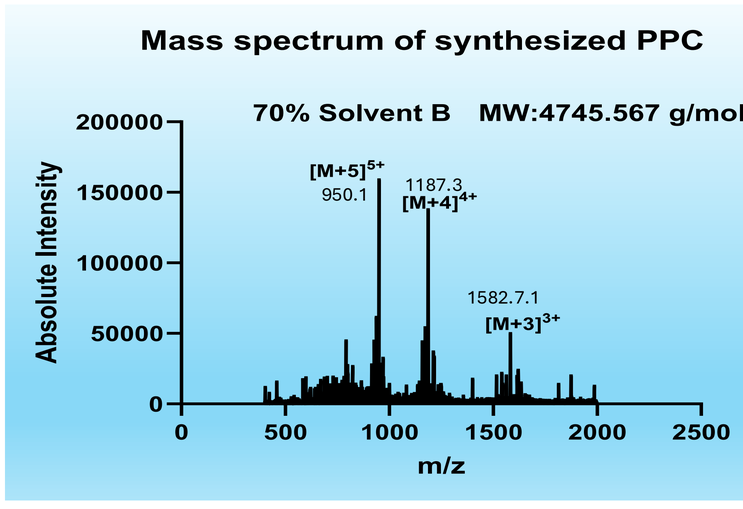
Mass spectrum of synthesized targeting peptide

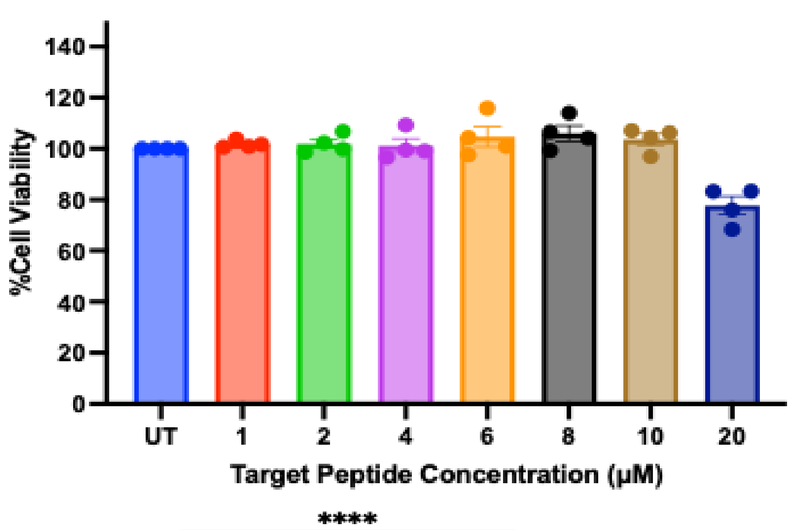


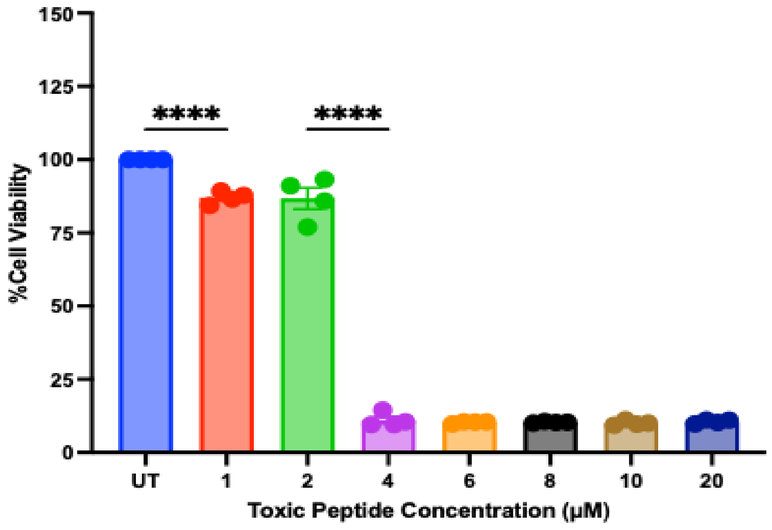
Mass spectrum of synthesized cytotoxic peptide

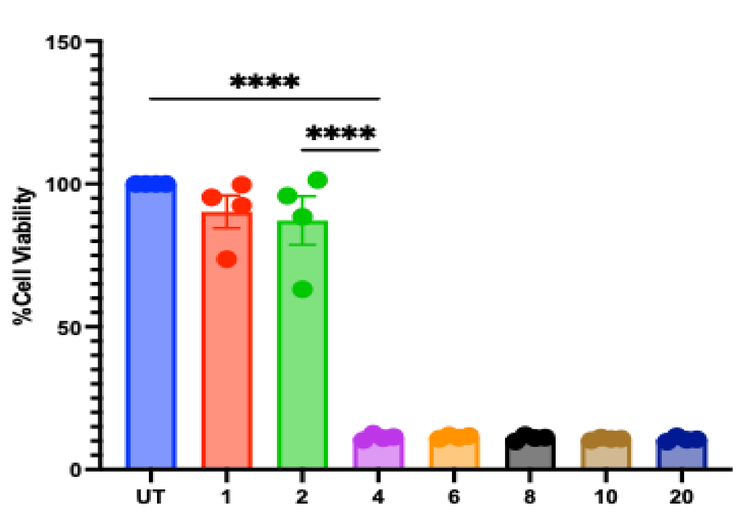


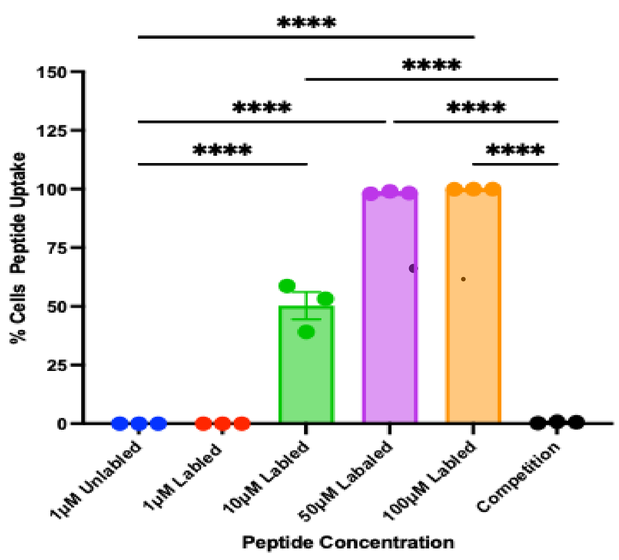
Mass spectrum of synthesized PPC











CONCLUSIONS

- The peptide nanoparticle construct offers a fully synthetic, stable, and tumor-penetrating alternative to traditional ADCs.
- By combining targeted peptides, cleavable linkers, and cytotoxic moieties, it aims to achieve highly selective and efficient cancer cell killing
- This platform has strong potential to advance next-generation targeted breast cancer therapeutics.

ACKNOWLEDGEMENTS

- The Indian Institute of Technology, Delhi, India
- The University of Queensland, Brisbane Australia
- Department of Biotechnology, Govt. of India

38th EPS
European Peptide Symposium
6 - 11th of September 2026
Vienna, Austria
https://doi.org/10.17952/38EPS.2026.P266

Peptides involved in interaction with heavy metals for environmental remediation, an *in silico* approach.

X. C. Pulido[1], H. F. Cortes Hernandez[1] & C. Jaramillo-Páez[1]

[1] Grupo de Investigación en Química Aplicada a Procesos Ecológicos, Departamento de Química, Facultad de Ciencias, Universidad del Tolima, Ibagué, Colombia

xpulido@ut.edu.co

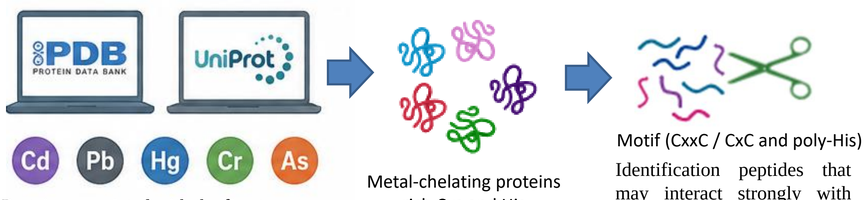
1. INTRODUCTION



Heavy metal (HM) pollution is an increasingly critical global concern with significant environmental and public-health implications. HM are non-biodegradable, accumulate along trophic chains, and remain in soils and water bodies for decades.



***In silico* approach for environmental remediation**



Proteins associated with the five target metals

Metal-chelating proteins rich Cys and His

Motif (CxxC / CxC and poly-His)

Identification peptides that may interact strongly with HM

The aim was to perform an *in silico* analysis of proteins associated with Cd, Pb, Hg, Cr and As deposited in the PDB (through its wwPDB portals) and in UniProt, and to derive, through controlled *in silico* digestion, a non-redundant catalogue of peptides with putative metal-binding properties, characterized by mass and absorption coefficient.

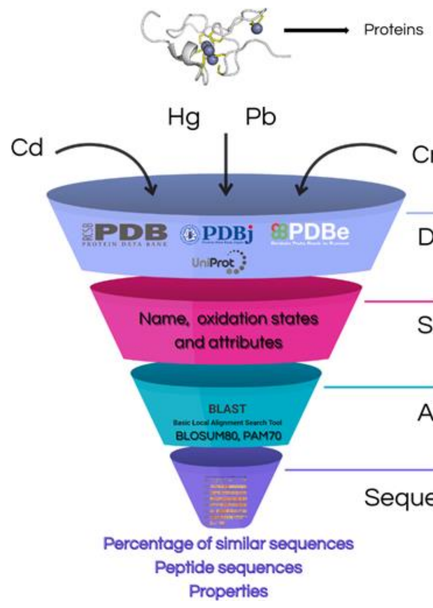


FIGURE 1. Flowchart of the *in silico* process: metal-based database queries feed structural and sequence retrieval, local alignment, and the selection of non-redundant sequences and candidate peptides.

2. MATERIALS AND METHODS

1. **Database search and data collection/** Worldwide Protein Data Bank (wwPDB), consulted through its PDB, PDBe and PDBj portals, for three-dimensional structures[8], and UniProtKB
2. **Sequence similarity and redundancy reduction/** local alignment using the BLAST algorithm[10], with BLOSUM and PAM substitution matrices
3. ***In silico* digestion/** PeptideCutter (ExPASy)[13] and the Protein Sequence Digestion Calculator
4. **Peptide analysis /** PeptideCutter (ExPASy)[13] and the Protein Sequence Digestion Calculator
5. **Mass and absorption coefficient determination/** Prot pi | Peptide Tool
6. **Motif and binding-site identification /** cysteine- and histidine-rich patterns (CxxC, CxC, HxH and poly-His) Si se encontraron péptidos con HxH y poli-His
7. **Gene Ontology (GO) Analysis /** UniProt database
8. **Statistical analysis**

3. RESULTS AND DISCUSSION

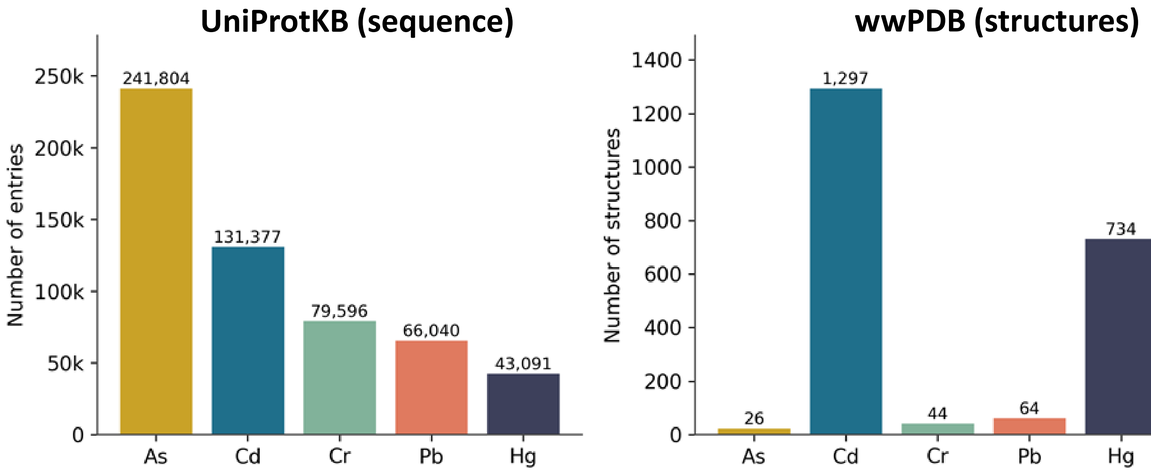


FIGURE 2. Number of macrostructures retrieved per metal in the sequence resource (UniProtKB, left, all entries) and the structural archive (wwPDB, right). wwPDB structures are counted once against the shared archive.

The raw retrieval returned 561,908 UniProtKB entries and 2,165 wwPDB structures across the five metals (Figure 2). In UniProt, the abundance order was As > Cd > Cr > Pb > Hg, with arsenic alone accounting for 241,804 sequence entries, reflecting the broad annotation of arsenate/arsenite resistance and metabolism systems in prokaryotic genomes. In the structural archive, the order was reversed toward cadmium (1,297 structures), consistent with the extensive crystallographic characterization of Cd-substituted metalloproteins. Reporting sequence and structural counts separately, and counting the shared wwPDB archive only once, avoids the portal-by-portal overcounting that would otherwise inflate the totals several-fold.

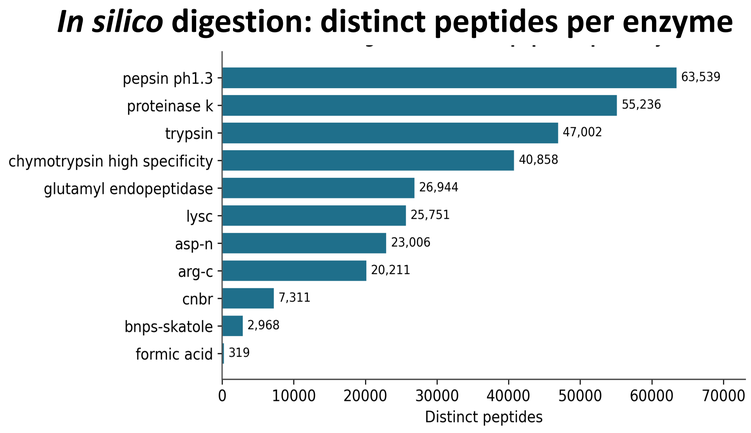


FIGURE 3. Distinct peptides produced by each enzyme or chemical agent during *in silico* digestion of the non-redundant protein set.

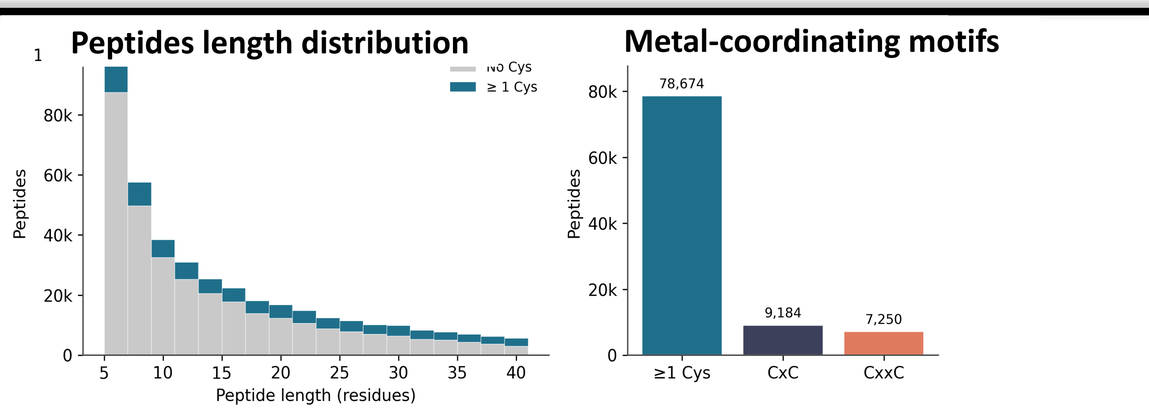


FIGURE 4. Peptide length distribution stratified by cysteine content (left) and abundance of metal-coordinating cysteine motifs (right).

Table 1. Top ten candidate peptides ranked by metal-coordination potential. Cysteine residues (thiolate donors) are highlighted in red; masses are monoisotopic.

Peptide (Cys highlighted)	UniProt	Len	Cys	CxxC / CxC	Mass (Da)	pI
LCCCFCCYETCEHCLECFCCCCKKDN	A3A4E0	26	12	6 / 5	3047.98	4.83
GCLYACLFTLCCCFCCYETCECCLECLCCC	Q5VRD7	30	14	5 / 5	3363.10	4.05
SCKCSNCQCACCKKSCCSCCPSGCSKCA	O93571	28	12	5 / 4	2826.94	8.50
CCYETCECCLDCLCCCCN	Q5VSB5	18	10	4 / 4	2025.54	4.05
CTNCSCKCCKKSCCSCCPSGCSKCA	Q92044	25	11	5 / 3	2538.85	8.56
PNCSACCAGSCCSPDCCSCCKPNCSCCK	Q67UU9	28	12	4 / 2	2778.84	7.83
GSCKCKNCRCQSCRKSCCSCCPASCSNCA	P15787	29	11	5 / 3	3022.08	8.74
DSCKCEGCKCTSCKKSCCSCCPAECEKCAK	P25713	30	11	5 / 3	3167.16	8.07
DKCKCKGCKCTNCKKSCCSCCPAGCEKCAK	P28184	30	11	5 / 3	3162.27	8.84
GDSCSCAGSCKCKNCRCQSCRKSCCSCCPA	P15787	30	11	4 / 4	3080.09	8.57

Motif counts (CxxC / CxC) include overlapping occurrences. Source proteins (UniProt accessions) correspond to metallothioneins and metallothionein-like sequences.

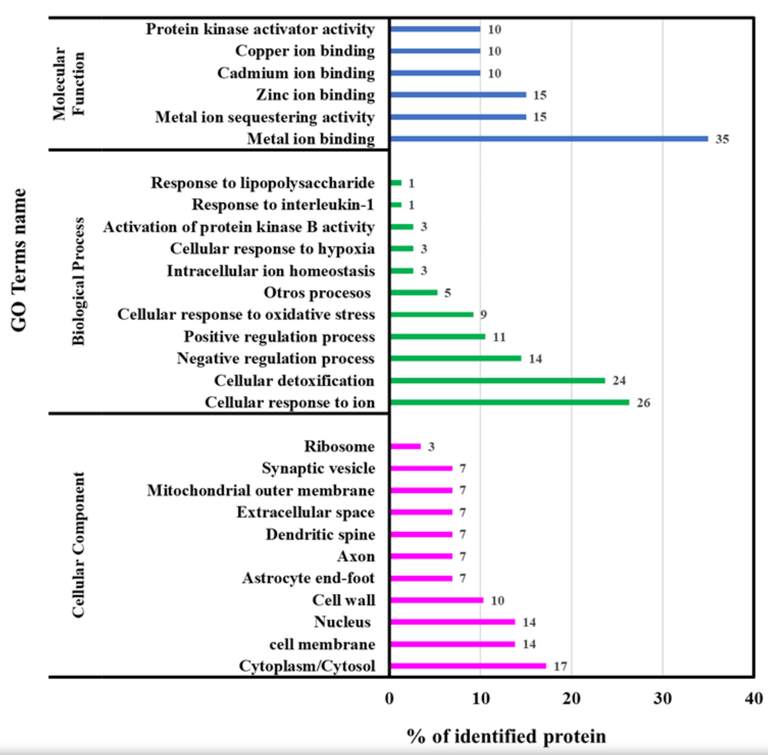


FIGURE 5. Gene Ontology (GO) classification of the nine proteins from which the candidate peptides were selected. This functional analysis divided proteins into three groups: Molecular Function, Biological Process and Cellular Component.

CONCLUSION

An *in silico* pipeline combining database mining, curation, enzymatic fragmentation, and physicochemical characterization reduced a raw retrieval of 561,908 UniProtKB entries to a non-redundant, high-confidence set of 5,156 metal-associated proteins, from which it derived 275,933 distinct candidate peptides using eleven cleavage specificities. Nearly one in five peptides carried a cysteine, and thousands reproduced the CxxC/CxC motifs that coordinate soft divalent ions, providing a well-defined priority pool of Cd-, Pb-, and Hg-binding candidates. Future work will validate the prioritized cysteine- and histidine-rich peptides experimentally and quantify their metal-binding affinity, advancing the design of peptide-based biosorbents for environmental remediation.

ACKNOWLEDGMENTS

We thank to the University of Tolima for its financial support under the research project, code: 470121.

REFERENCE

1. M. Balali-Mood, K. Naseri, Z. Tahergorabi,M. R. Khazdair, & M. Sadeghi. Frontiers in pharmacology, **2021**, 12, 643972. 1-19.
2.The Protein Data Bank (2000) Nucleic Acids Research, **2000**, 28, 235-242.
3. R. Ochoa and K. Deibler, J Pept Sci, **2025**, 31, e3666, 1-9.

AI-Guided Discovery of Anti-Inflammatory Peptides from Edible Rhizomes and Root Vegetables

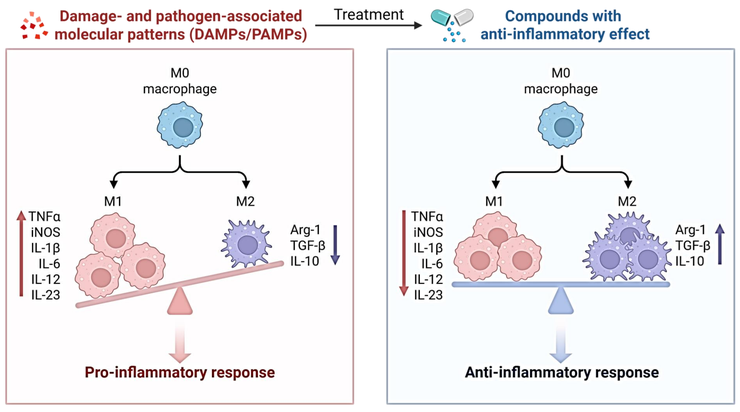
https://doi.org/10.17952/38EPS.2026.P523

Kruttika Purohit [1,2] · Mitchell Low [2,3] · Fabien Plisson [1,4] · Evan Hayes [5] · Anwar Sunna [1,2]

[1]School of Natural Sciences, Macquarie University | [2]ARC Training Centre for Facilitated Advancement of Australia's Bioactives (FAAB) | [3]NICM Health Research Institute, Western Sydney University | [4]Ingenie Bio | [5]Factors Group Australia

CONNECT WITH ME

Chronic Inflammation a central driver of metabolic dysregulation & lifestyle-associated disorders [1]



Why Edible Rhizomes & Root Vegetables ?

- Underexplored as sources of bioactive peptides [2,3]
- Recognised in Traditional Medicinal Systems [2,3]

Objectives

- Mine hydrolysates by AI-guided QSAR/QSPR triage (sequence + structure based predictors).
- Validate predicted lead candidate at the bench.
- Resolve bioactivity mechanism across metabolic & proteomic endpoints.

Discovery pipeline — AI as the triage step prioritizes candidates & shrinks the search space

EXTRACT
4 root-vegetable protein matrices
Ginger . Sweet Potato. Red Radish . Purple Carrot

→

HYDROLYSE
15 food-grade protease Configurations
Individual/ Sequential/ Concurrent

→

SEQUENCE
10,049
unique peptides identified by LC-MS/MS

→

AI TRIAGE
36
5 Sequence-based bioactivity predictors + Molecular Docking + Toxicity Predictor

→

VALIDATE
7
Biochemical and cell-based In vitro assays

Nitric oxide Inhibition

Griess assay · LPS-stimulated RAW 264.7 (murine) macrophages

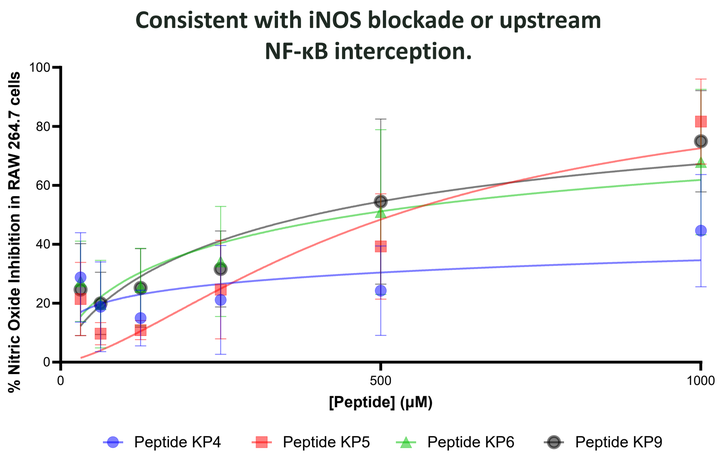


Figure 1. NO inhibition (%) relative to LPS-positive control. Mean ± SEM, n = 9.

Cyclooxygenase-2 Inhibition

Cell-free COX-2 enzyme inhibition quantified via PGE_2 product formation (LC-MS/MS)

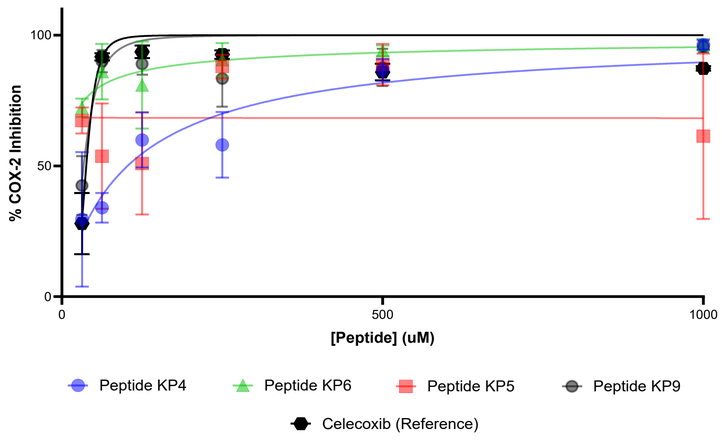


Figure 2. COX-2 inhibition (%) relative to Celecoxib reference. Mean ± SEM, n = 3.

Pro-Inflammatory Cytokine Release

IL-6 and TNF-α ELISA · RAW 264.7 (murine) macrophages

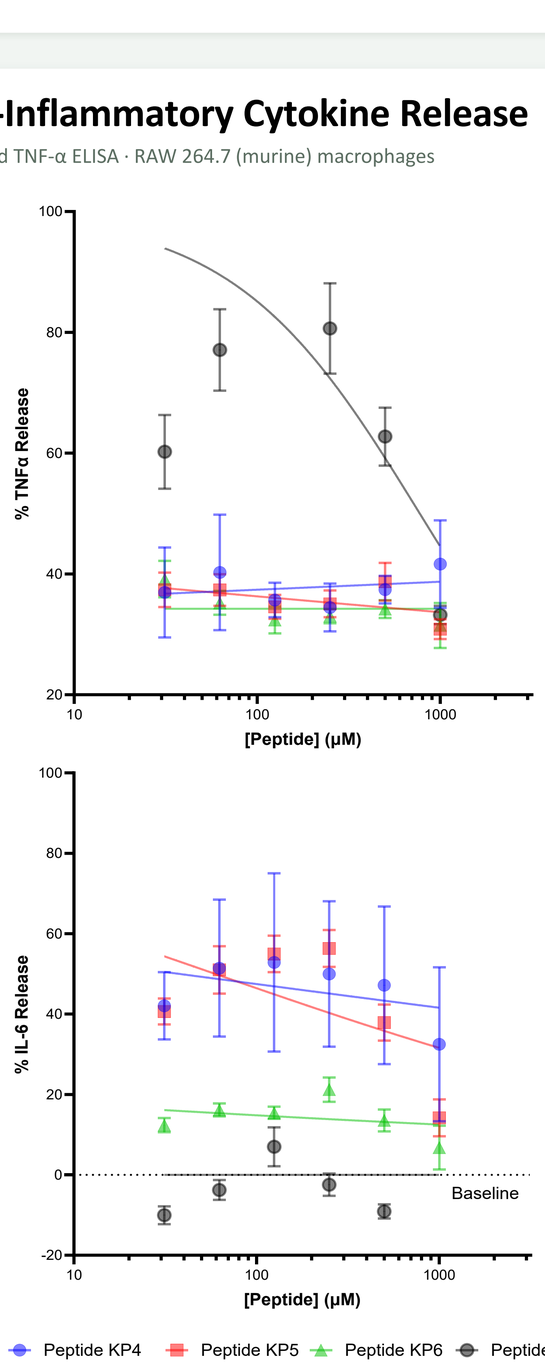


Figure 3. Pro-inflammatory cytokine release in LPS-stimulated macrophages. Mean ± SEM, n = 9.

Dual suppressors: Peptides **KP4**, **KP5** & **KP6** lowered both IL-6 and TNF-α pro-inflammatory cytokines.

Divergent responder: Peptide **KP9** suppressed IL-6 below baseline, while inducing TNF-α

Metabolic reprogramming of inflamed macrophage

LPS-stimulated RAW 264.7 (murine) macrophages

Figure 4. Untargeted metabolomics of peptide-treated versus LPS-stimulated macrophages. (A) PCA scores. (B) Profiling for NO-pathway metabolite changes (top 25 abundant metabolites).

Peptide KP4 Anti-inflammatory pathway enrichment

Peptide KP9 Pro-inflammatory pathway blockade

Peptide KP6 Distinct reprogramming, unrelated to LPS reversal

Mechanistic Evaluation

Tail MM/GBSA binding free energies across inflammatory targets· Orthosteric vs interfacial binding sites

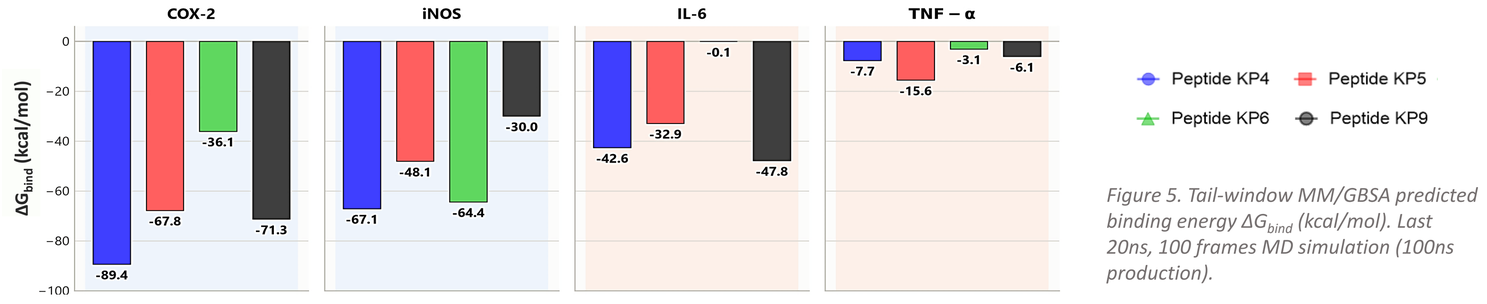


Figure 5. Tail-window MM/GBSA predicted binding energy ΔG_{bind} (kcal/mol). Last 20ns, 100 frames MD simulation (100ns production).

Peptide KP4 is the strongest overall anti-inflammatory lead — dual IL-6/TNF-α suppression, NO inhibition, and dose-dependent COX inhibition — consistent with its most favourable predicted binding across targets.

Peptide KP6 binds the studied targets weakly yet is potently active, suggesting its anti-inflammatory effect is driven through an off-target/alternative mechanism.

Conclusions

- AI triage compressed 10,049 sequences to 36 candidates, 7 of which entered lab validation.
- **4 of 7 leads were active in LPS-stimulated macrophages across Nitric Oxide Pathway, Pro-inflammatory cytokines and Cyclooxygenase endpoints.**
- Root vegetables are a credible, sustainable source of anti-inflammatory bioactive peptide with further implications for metabolic syndrome management.

Next Steps

- Proteomic profiling of peptide-treated inflamed murine RAW 264.7 macrophages (ongoing).
- Replicate metabolic and proteomic analysis in differentiated human THP-1 monocytes (ongoing).
- Antidiabetic and antihypertensive bioactivity profiling – metabolic syndrome.
- Deep mutational scanning to optimise affinity, potency and stability.

SUSTAINABLE DEVELOPMENT GOALS

Acknowledgements

APAF australian proteome analysis facility · Macquarie University Sydney-Australia · Western Sydney University NICM Health Research Institute · factorsgroup Australia Pty Ltd. · FAAB Facilitated Advancement of Australia's Bioactives ARC Training Centre

Funding The work is funded by **International Macquarie Research Excellence Scholarship (iMQRES)** and **the ARC Industrial Transformation Training Centre for Facilitated Advancement of Australia's Bioactives (Grant IC210100040)**.

References [1] Furman D et al. *Nat Med* 2019; 25:1822–1832. [2] Purohit K et al. *Food Chem* 2025; 484:144432. [3] Purohit K et al. *IJMS* 2024; 25(3):1391.

Targeting the SARS-CoV-2 fusion mechanism: potent peptide inhibitors of the IFP-MPER interaction

M. Quagliata[1,2], M.A. Stincarelli[3], A. Di Santo[1,2], R. Arvia[3], S. Siadohoni[1,4], S. Bazhenova[5], F. Real-Fernandez[6], D. Friedrich[5], S. Giannecchini[3], A.M. Papini[1,4] and P. Rovero[1,2]

[1]*Interdepartmental Laboratory of Peptide and Protein Chemistry and Biology, University of Florence, 50019-Sesto Fiorentino, (FI), Italy.*
[2]*Department of Neurosciences, Psychology, Drug Research and Child Health, University of Florence, 50019-Sesto Fiorentino, (FI), Italy*
[3]*Department of Experimental and Clinical Medicine, University of Florence, 50134-Florence, Italy.*
[4]*Department of Chemistry "Ugo Schiff", University of Florence, 50019-Sesto Fiorentino, (FI), Italy*
[5]*Department of Chemistry and Biochemistry, University of Cologne, 50939-Cologne, Germany*
[6]*CNR - Istituto di Chimica Dei Composti Organometallici (CNR-ICCOM), 50019-Sesto Fiorentino, (FI), Italy*

https://doi.org/10.17952/38EPS.2026.P235

MPER peptides exhibit strong antiviral activity with nanomolar IC_{50}

The MPER-derived peptide Spike(1196-1220), rich in aromatic residues (Phe, Tyr, Trp), was synthesized via Induction-Assisted SPPS (IA-SPPS). To identify the minimal active sequence, we progressively shortened it from the N-terminus.

Peptide	Sequence	IC_{50} μM	CC_{50} μM	R (%)
Spike(1196-1220)	Ac-SLIDLQELGKYEQYIKWPWYIWLGF-NH_2	1.92 ± 0.67	>100	67
Spike(1198-1220)	Ac-IDLQELGKYEQYIKWPWYIWLGF-NH_2	1.10 ± 0.21	>100	68
Spike(1200-1220)	Ac-LQELGKYEQYIKWPWYIWLGF-NH_2	0.99 ± 0.71	>100	59
Spike(1202-1220)	Ac-ELGKYEQYIKWPWYIWLGF-NH_2	0.40 ± 0.31	52 ± 8	58
Spike(1204-1220)	Ac-GKYEQYIKWPWYIWLGF-NH_2	0.08 ± 0.07	>100	53
Spike(1206-1220)	Ac-YEQYIKWPWYIWLGF-NH_2	0.11 ± 0.05	84 ± 11	51
Spike(1208-1220)	Ac-QYIKWPWYIWLGF-NH_2	0.94 ± 0.48	>100	48
Spike(1210-1220)	Ac-IKWPWYIWLGF-NH_2	0.40 ± 0.13	>100	48
Spike(1212-1220)	Ac-WPWYIWLGF-NH_2	0.03 ± 0.02	>100	>100
Spike(1214-1220)	Ac-WYIWLGF-NH_2	5.47 ± 1.02	>100	38

Shortening the C-terminus boosts antiviral activity, with Spike(1212-1220) being most potent, while removing Trp1212 drastically reduces antiviral activity, underscoring the importance of aromatic residues.

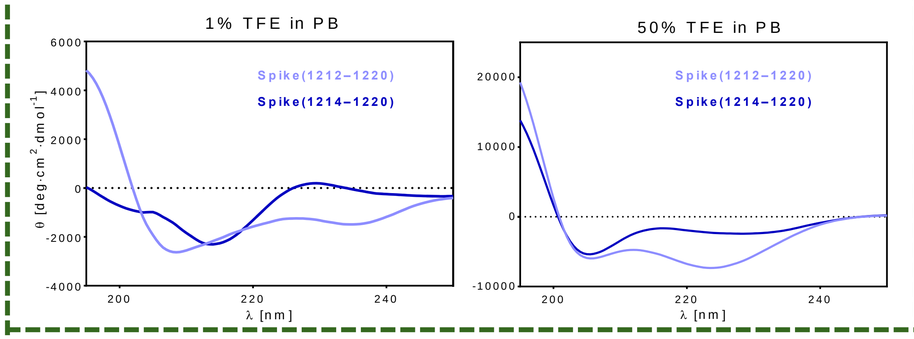
Aromatic residues and sequence specificity are crucial for biological activity

Peptide	Sequence	IC_{50} μM	CC_{50} μM	R (%)
Spike(1212-1218)	Ac-WPWYIWL-NH_2	4.68 ± 1.34	82 ± 10	-
Spike(1196-1211)	Ac-SLIDLQELGKYEQYIK-NH_2	20.08 ± 9.01	>100	76
Spike(1204-1220) scramble	Ac-WKFQYGPWGIIWLYKEY-NH_2	45.92 ± 7.56	>100	-
[Ala[1212,1214,1217]]Spike(1212-1220)	Ac-APAYIALGF-NH_2	40.90 ± 7.40	>100	75

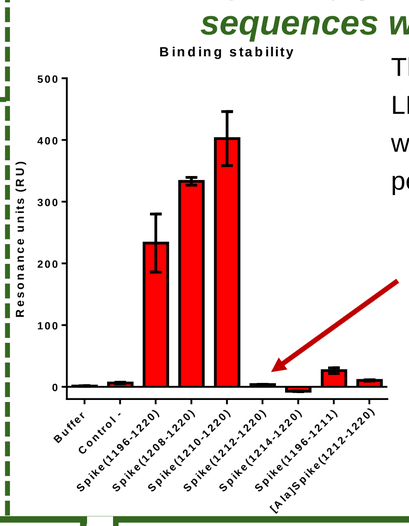
CD analysis revealed α-helical conformation propensity with aromatic side-chains interactions

1% TFE in PB: All peptides showed spectra of random-coil conformation.
50% TFE in PB: All peptides adopted an α-helical secondary structure, except for Spike(1212-1218) and Spike(1204-1220) scramble.

N-terminal truncation lowered the R-value, confirming the α-helix is mainly in the N-terminus. Indeed, Spike(1196–1211) had strong helicity (R = 75%); alanine substitution gave R-value = 65% (Ala penalty = 0 kcal/mol) [2].



SPR binding assay proves the interaction of MPER sequences with Fusion peptide



The fusion peptide [Cys[891]]Spike(861-891), LPPLLTDEMIAQYTSALLAGTITSGWTFGAC was immobilized onto the chip, while MPER peptides were used as analytes.

Spike(1212-1220) did not yield any signal, probably due to peptide aggregation

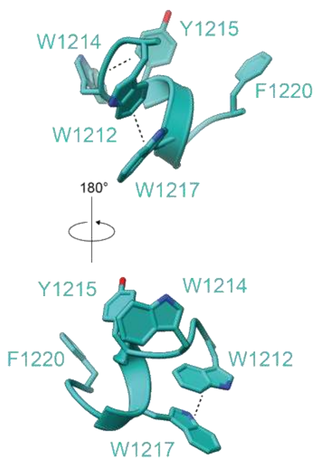
PB: 10 mM phosphate buffer, pH 7.4

π - π Stacking interactions were confirmed by high-resolution structure NMR

The high resolution structures of Spike(1212-1220) and Spike(1214-1220) were determined by NMR in both DMSO/H_2O and *n*-dodecylphosphocholine (DPC) [3,4].

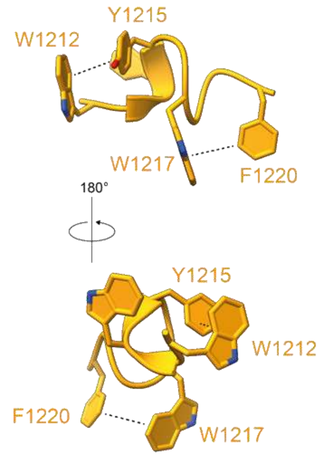
Spike(1212-1220)

π-π: W1212-W1217 parallel, W1214-Y1215 perpendicular

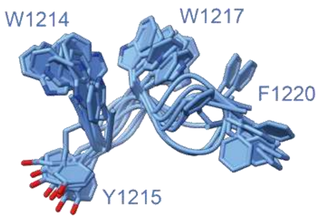


Spike(1212-1220) with DPC

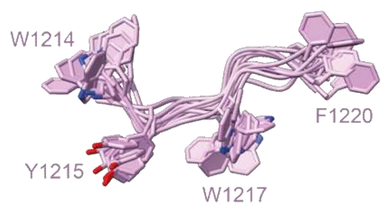
π-π: W1212-Y1215 parallel, W1217-F1220 perpendicular

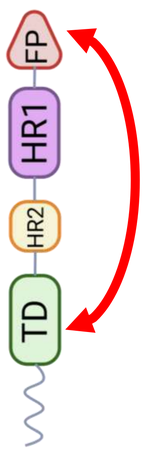


Spike(1214-1220)

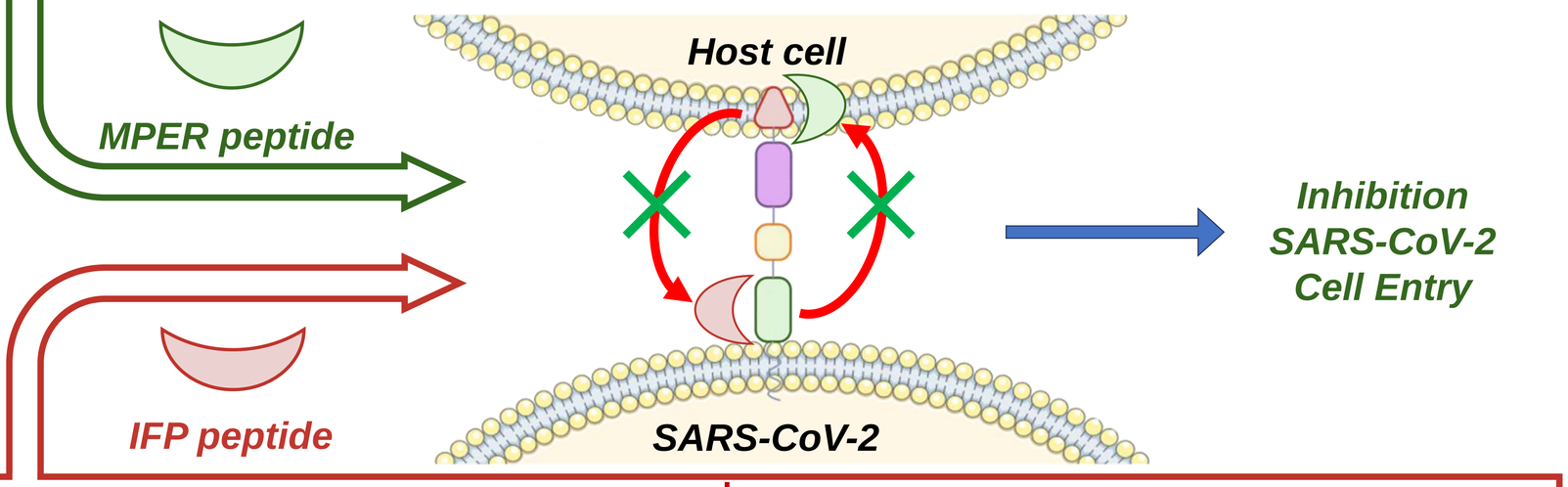


Spike(1214-1220) with DPC



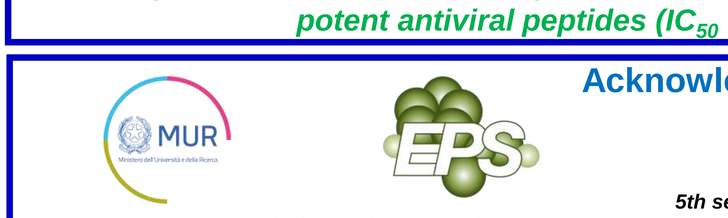


The spike protein is a trimeric surface protein anchored by its Transmembrane Domain (TD) and split into S1 and S2 subunits. S1 carries the Signal Peptide and Receptor Binding Domain for host cell recognition. After protease priming of S1, the Fusion Peptide (FP) inserts into the host membrane. Then, Heptad Repeats 1 and 2 (HR1, HR2) form a 6-Helix Bundle (6-HB), drawing the membranes together to create a pore for viral RNA entry. The formation of this bundle is mediated by the interaction between the Membrane Proximity External Region (contained in TD) and Internal Fusion Peptide (contained in FP) [1].



Enhancing antiviral activity by targeting lipid rafts via cholesterol functionalization

The IFP peptide Spike(888–906), designated PN19, exhibits potent antiviral activity against SARS-CoV-2 (IC_{50} = 0.49 μM) [5]. To target the lipid rafts present on the viral membrane, cholesteryl analogs of PN19 were synthesized [6].



Chemoselective and quantitative [7]

C-terminal cholesterol modification resulted in superior antiviral activity compared to N-terminal modification.

Peptide	Sequence	IC_{50} μM	CC_{50} μM
PN19	Ac-FGAGAALQIPFAMQMAYRF-NH_2	0.49 ± 0.15	>100
[C[1](chol)]PN19	Ac-C(chol)FGAGAALQIPFAMQMAYRF-NH_2	0.38 ± 0.11	>100
[C[20](chol)]PN19	Ac-FGAGAALQIPFAMQMAYRFC(chol)-NH_2	0.08 ± 0.04	>100

The linker length between PN19 and the cholesterol moiety plays a secondary role in antiviral activity

Several PN19 analogs bearing different linkers were synthesized. In particular, the pentapeptide spacer GSGSG and the PEG_6 linker were employed, either singularly or in combination. Both N- and C-terminal modifications were explored.

Peptide	Sequence	IC_{50} μM	CC_{50} μM
[C[1](chol)]PN19-spacer	Ac-C(chol)-GSGSG-FGAGAALQIPFAMQMAYRF-NH_2	0.98 ± 0.12	>100
[C[25](chol)]PN19-spacer	Ac-FGAGAALQIPFAMQMAYRF-GSGSG-C(chol)-NH_2	0.74 ± 0.34	>100
[C[1](chol)]PN19-PEG_6	Ac-C(chol)-PEG_6-FGAGAALQIPFAMQMAYRF-NH_2	3.70 ± 1.01	>100
[C[20](chol)]PN19-PEG_6	Ac-FGAGAALQIPFAMQMAYRF-PEG_6-C(chol)-NH_2	0.14 ± 0.12	>100
[C[1](chol)]PN19-spacer-PEG_6	Ac-C(chol)-PEG_6-GSGSG-FGAGAALQIPFAMQMAYRF-NH_2	1.75 ± 0.71	>100
[C[25](chol)]PN19-spacer-PEG_6	Ac-FGAGAALQIPFAMQMAYRF-GSGSG-PEG_6-C(chol)-NH_2	0.04 ± 0.02	>100

Amino acid sequence is crucial for biological activity

Peptide	Sequence	IC_{50} μM	CC_{50} μM
[C[10](chol)]PN9 scramble	Ac-RFQAYMFMAC(chol)-NH_2	>100	>100
[C[15](chol)]PN9-spacer-PEG_6 scramble	Ac-RFQAYMFMA-GSGSG-PEG_6-C(chol)-NH_2	>100	>100

N-terminal truncation confirms that the active region of PN19 is the aromatic-rich C-terminal

The shorter sequences were selected from a previous study based on their length and retention of biological activity [5]. In particular, PN13 and PN9 were selected, along with PN8, which served as the first inactive peptide.

Peptide	Sequence	IC_{50} μM	CC_{50} μM
PN13	Ac-LQIPFAMQMAYRF-NH_2	1.70 ± 0.52	>100
PN9	Ac-FAMQMAYRF-NH_2	5.93 ± 9.74	>100
[C[1](chol)]PN13	Ac-C(chol)-LQIPFAMQMAYRF-NH_2	1.20 ± 1.04	>100
[C[14](chol)]PN13	Ac-LQIPFAMQMAYRF-C(chol)-NH_2	0.28 ± 0.31	>100
[C[1](chol)]PN9	Ac-C(chol)-FAMQMAYRF-NH_2	3.44 ± 0.90	>100
[C[10](chol)]PN9	Ac-FAMQMAYRF-C(chol)-NH_2	0.27 ± 0.31	>100
[C[9](chol)]PN8	Ac-AMQMAYRFC(chol)-NH_2	15.02 ± 3.04	>100
[C[1](chol)]PN13-spacer-PEG_6	Ac-C(chol)-PEG_6-GSGSG-LQIPFAMQMAYRF-NH_2	21.14 ± 10.12	>100
[C[19](chol)]PN13-spacer-PEG_6	Ac-LQIPFAMQMAYRF-GSGSG-PEG_6-C(chol)-NH_2	0.37 ± 0.31	>100
[C[1](chol)]PN9-spacer-PEG_6	Ac-C(chol)-PEG_6-GSGSG-FAMQMAYRF-NH_2	16.08 ± 8.04	>100
[C[15](chol)]PN9-spacer-PEG_6	Ac-FAMQMAYRF-GSGSG-PEG_6-C(chol)-NH_2	0.14 ± 0.11	>100
[C[14](chol)]PN8-spacer-PEG_6	Ac-AMQMAYRF-GSGSG-PEG_6-C(chol)-NH_2	6.03 ± 3.05	>100

Conclusions

- ***IFP-MPER interaction is key for membrane fusion and a therapeutic target.***
- ***MPER truncation identified Spike(1212-1220) as potent inhibitor, stabilized by π - π stacking.***
- ***Cholesterol conjugation to IFP peptide (PN19) boosts antiviral activity, with C-terminal lipidation superior to N-terminal.***
- ***Linker length has minimal effect, but both amino acid sequence and aromatic C-terminus are crucial for antiviral activity.***

Our study led to two novel cell-entry inhibitors, Spike(1212-1220) and [C[25](chol)]PN19-spacer-PEG_6 as potent antiviral peptides (IC_{50} = 0.03, 0.04 μM, respectively) [8,9].

Perspectives

WORK IN PROGRESS

Studies are ongoing in order to increase the antiviral activity further into the nanomolar range

STAY TUNED

Acknowledgments

For Michael Quagliata's PhD scholarship

For travel grant to Michael Quagliata

5th seed funding call for the TTPep project and 3rd Well-Being Research Incubator Call for the project "Sustainable and green upscaling processes for peptide(-based) in vitro diagnostics and cosmeceuticals" and the Champion program "Peptides4Wellness"

References

[1] Y. Liao *et* al., *Biochemistry*, **2015**, 54, 1819–1830. https://doi.org/10.1021/bi501352u
[2] L. Zhang *et* al., *J. Am. Chem. Soc*. **1994**, 116, 26, 11915-11921. https://doi.org/10.1021/ja00105a034.
[3] D.A. Kallick *et* al., *J. Magn. Reson. B*, **1995**, 109, 1, 60-65. https://doi. org/10.1006/jmrb.1995.1146.
[4] P. Klukowski *et* al., *Sci. Data*, **2024**, 11, 30. https://doi.org/10.1038/s41597-023-02879-5.
[5] M.A. Stincarelli *et* al., *Virus Research*, **2023**, 334, 199170. https://doi.org/10.1016/j.virusres.2023.199170
[6] M. Quagliata *et* al., *J. Pept. Sci.*, **2024**, 30, 2, e3541. https://doi.org/10.1002/psc.3541
[7] P. Ingallinella *et* al., *Proc. Natl. Acad. Sci.* **2009**, 106, 14, 5801-5806. https://doi.org/10.1073/pnas.0901007106
[8] M. Quagliata *et* al., *Eur. J. Med. Chem*. **2026**, 317, 119122. https://doi.org/10.1016/j.ejmech.2026.119122
[9] A. Rosaria *et* al., *Viruses,* **2026**, 18, 6, 682. https://doi.org/10.3390/v18060682

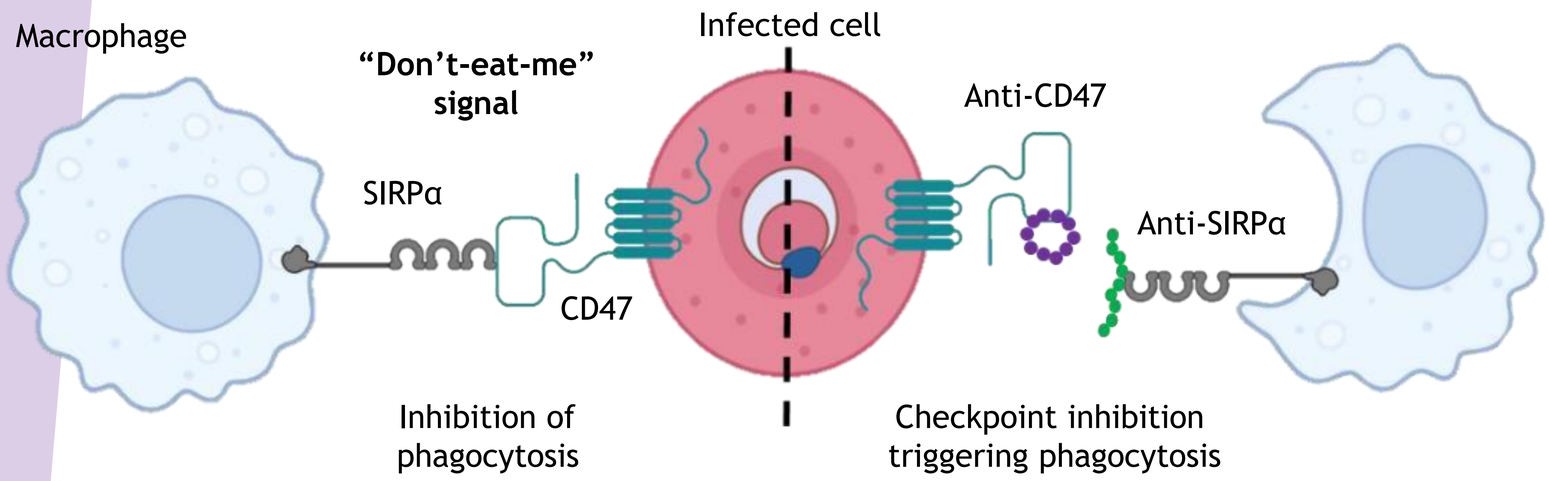
OBOC LIBRARIES TARGETING THE SIRPα/CD47 AXIS: FROM COMBINATORIAL DIVERSITY TO CHECKPOINT MODULATION

P. Quesada-Martínez,[a] M. Sánchez-Navarro [a]

[a] *Instituto de Parasitología y Biomedicina "López-Neyra"- CSIC, Avda. Conocimiento 17,18016, Granada, Spain*
e-mail: paula.quesada@ipb.csic.es

https://doi.org/10.17952/38EPS.2026.P236

Abstract



We propose the use of new protease-resistant peptides with affinity for the **SIRPα/CD47** axis to **inhibit** this **interaction** and **enhance phagocytosis.**
Large linear and cyclic **OBOC libraries** containing non-proteinogenic amino acids have been prepared, and they were evaluated againts these proteins using affinity selection coupled to mass espectrometry (**AS-MS**) assays to identify binders of this axis.

Discovery of peptides blocking CD47/SIRPα interaction using OBOC libraries

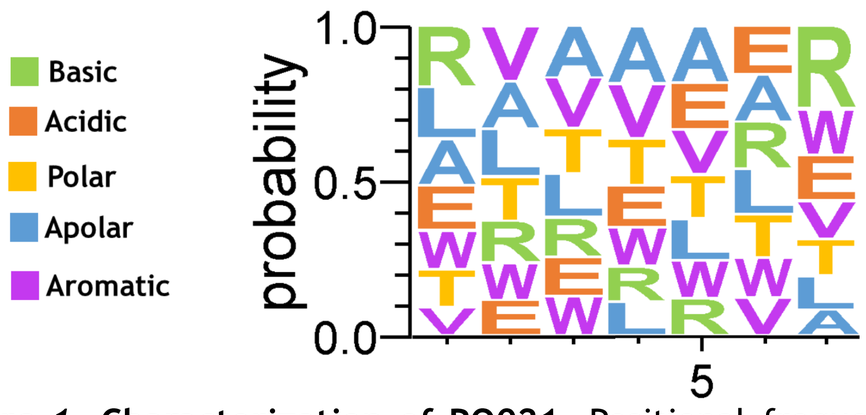


***Figure 1*. Characterization of PQ021**. Positional frequency plot shows theoretical possibilities of finding every amino acid in each position equally. More than 10000 sequences identified in a representative sample.

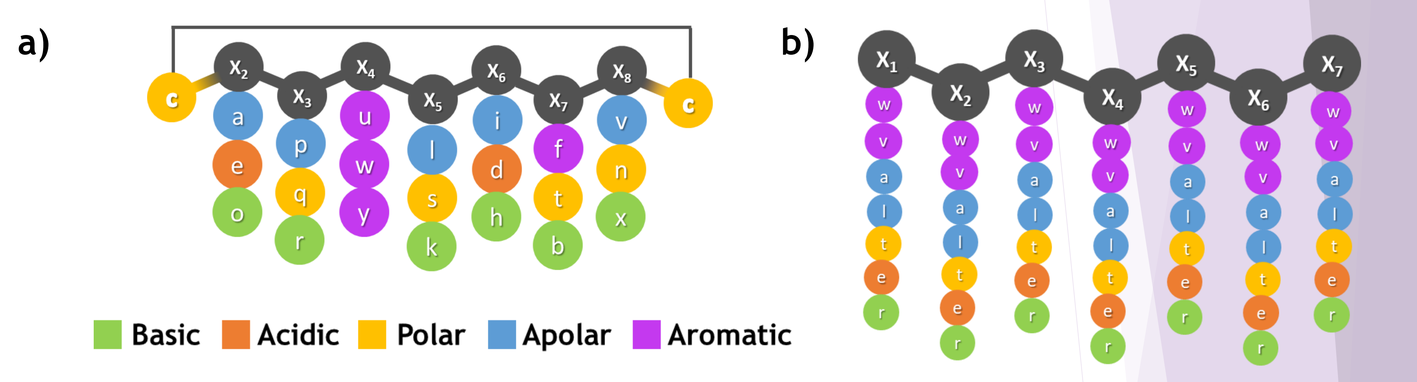
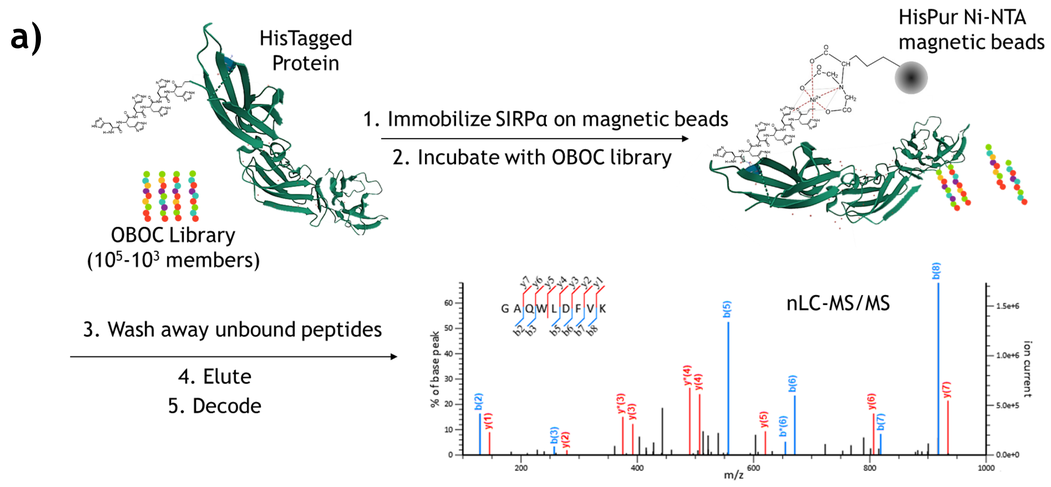
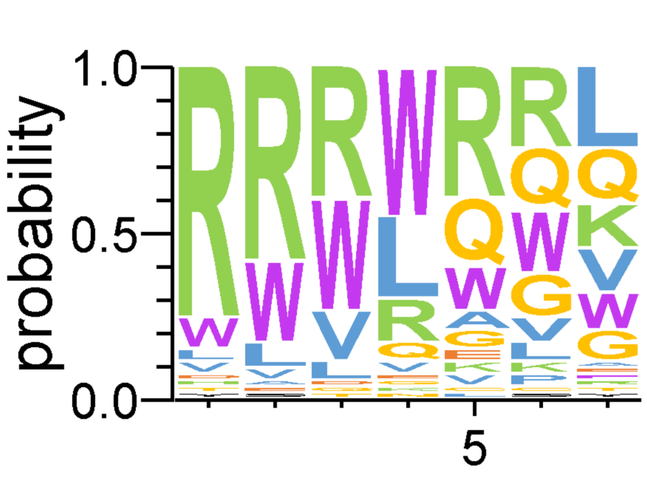


***Figure 2*. OBOC Libraries. a) Cyclic PQ020** Library. D-Amino acids have been introduced in seven positions of the sequence. 2187 possible peptides. **b) Linear PQ021** Library. Seven D-amino acids are used in each position. 823543 possible peptides. Characterization was performed after analysis via nLC-MS/MS.

Affinity Selection-Mass Spectrometry (AS-MS) assay





PQ021 Hits for specific union		
Sequence	**ALC (%)**	**Interaction**
RRVWRVT	94.96	SIRPα
RRWVRTV	74.85	SIRPα
RLWLRTL	71.78	SIRPα
RVRVRTW	71.63	SIRPα
WRRVRLV	66.35	CD47
LWLRLEE	59.43	SIRPα
RLRLWLL	53.71	SIRPα

***Figure 3*. a) Workflow of AS-MS assay.** OBOC libraries are incubated with immobilized SIRPα/CD47 proteins. After incubation and wash, hits are decoded by MS analysis. **b) Analysis results** revealed some possible hits sequences. **Positional frequency plot** shows peptides with an ALC >90% for PQ021. **Table** shows sequences that might interact with SIRPα/CD47 in a specific way, inhibiting their interaction.

Conclusion

· OBOC libraries with different size and structure have been designed, synthesized by SPPS and successfully characterised by nLC/MS-MS.
· AS-MS assays were performed using SIRPα and CD47 against prepared OBOC libraries and results show posible peptide binder candidates, inhibiting their interaction.

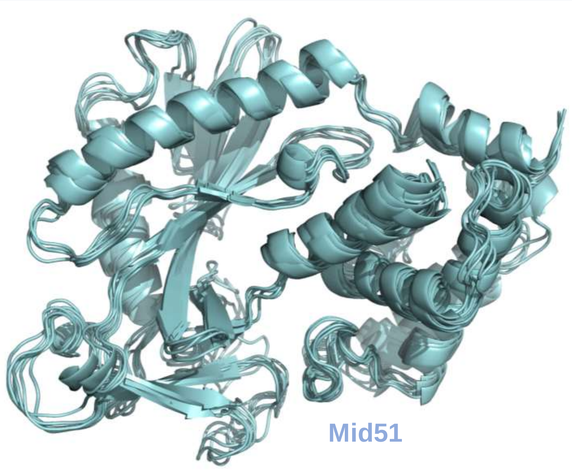
Future Perspectives

· Optimization of analysis pipeline to process data obtained in the nLC-MS/MS are being performed to check reproducibility and sturdiness of the experiments.
· Possible sequences found as inhibitors of the interaction are being synthesized to validate their affinity and specifity with proteins CD47 and SIRPα. Competition assays will be perfomed.

PID2023-153380B-I00 funded by MICIU/AEI/10.13039/501100011033 and by FEDER, EU

References

[1] *Amino Acids*, 2020, 52, 1207-1226.
[2] *Antibodies*, 2020, 9(3), 44.
[3] *Nat. Commun.*, 2020, 11, 3183.
[4] *Chemical Science*, 2021, 12(32), 10817-10824.



Peptide Therapeutics Targeting Drp1-Mid51 Protein-Protein Interactions to Preserve Mitochondrial Dynamics in Cardiovascular Disease

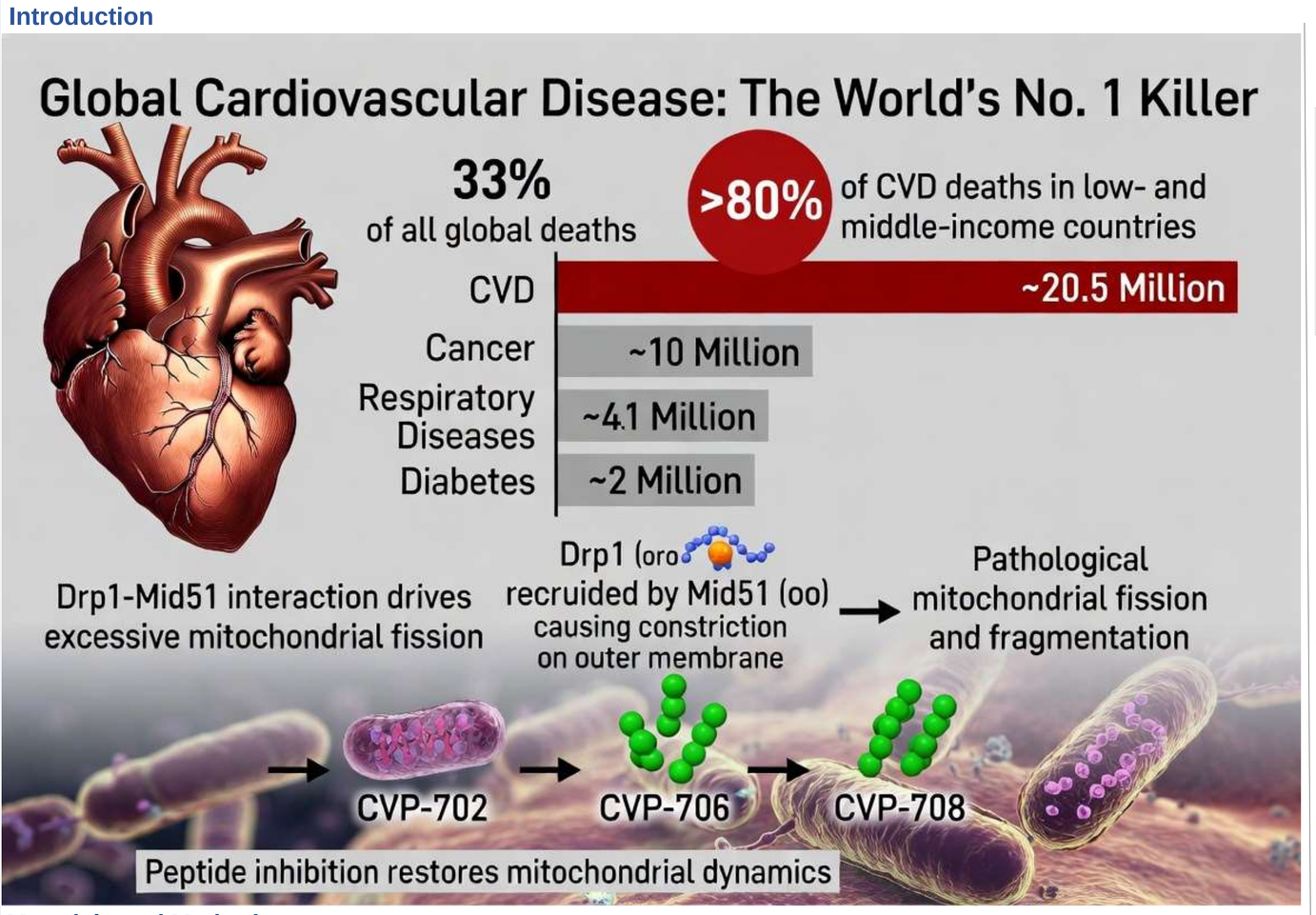
Rajkumar Khubiram, Liron Davis, Nir Qvit
The Azrieli Faculty of Medicine in the Galilee, Bar-Ilan University, Safed 1311502, Israel
Email: raj.kumar1@biu.ac.il



QVIT LAB

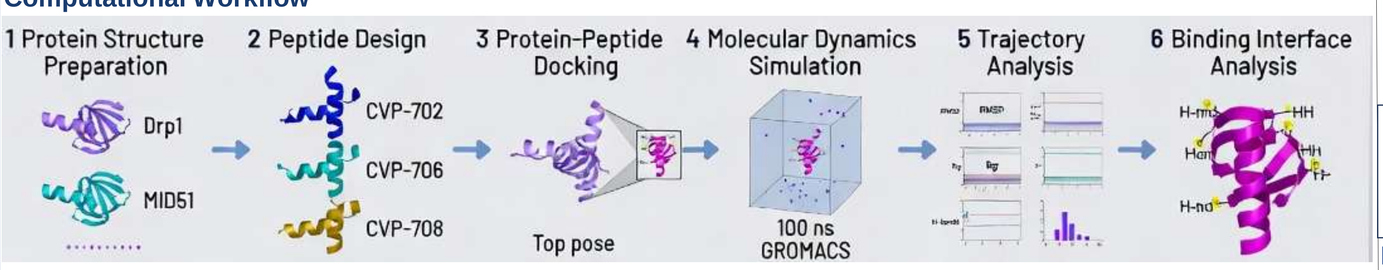
https://doi.org/10.17952/38EPS.2026.P121

Introduction



Materials and Methods

Computational Workflow



Experimental Methods and Instrumentation

Peptide designing

CVP-702	CH_3-C(O)-XXXXXXX-NH_2
CVP-706	CH_3-C(O)-XXXXXXXX-NH_2
CVP-708	CH_3-C(O)-XXXXXXXX-NH_2



Syro Peptide Synthesisers



Analytical and Preparative HPLC



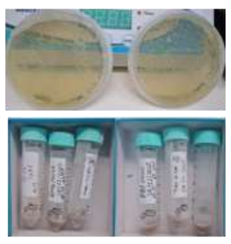
MALDI-TOF - Mass

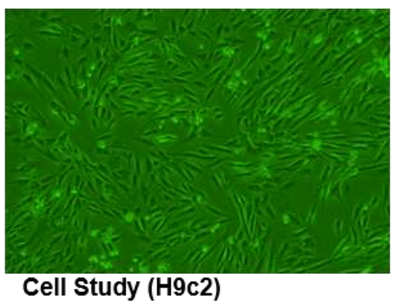


Field effect biosensing (R100)



Akta for proteins purification





Cell Study (H9c2)



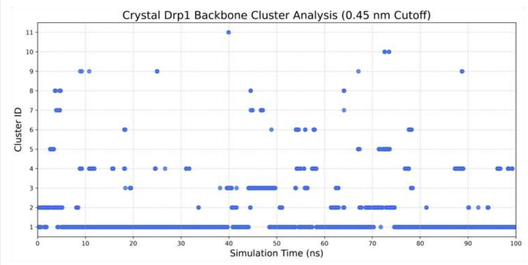
Rat model (*in Vivo*)

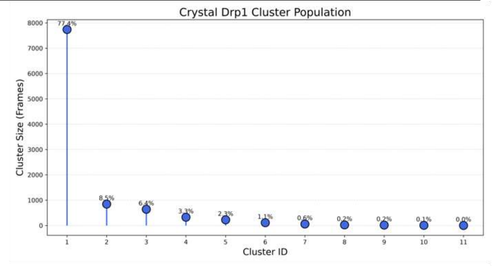
Results

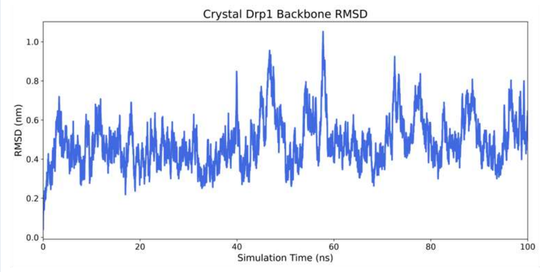
Computational Analysis

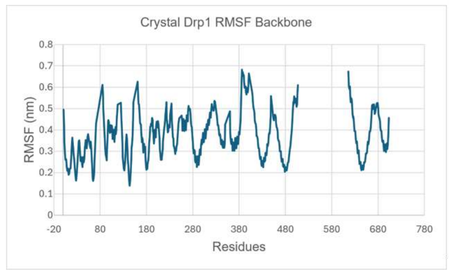
Structural Stability and Conformational Analysis of Drp1 (PDB ID: 4BEJ)

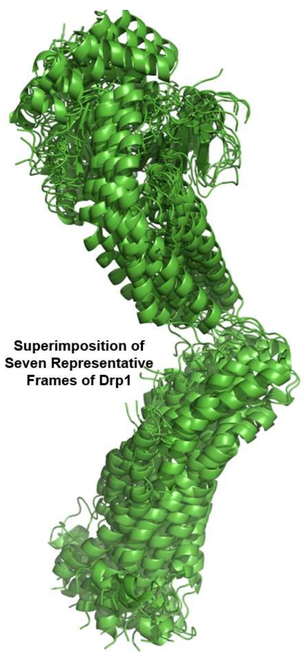
Clusters	1	2	3	4	5	6	7	8	9	10	11
Frames	7739	846	641	327	228	111	59	25	16	7	2
Size %	77	8	6	3	2	1	1	0	0	0	0







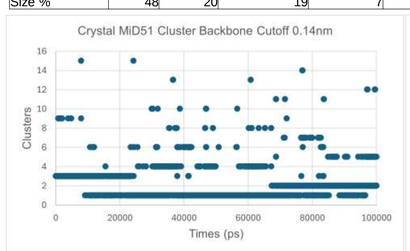


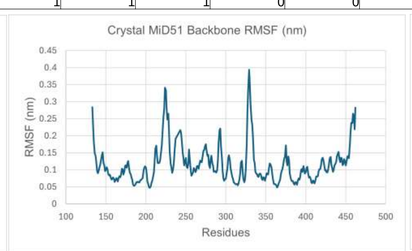


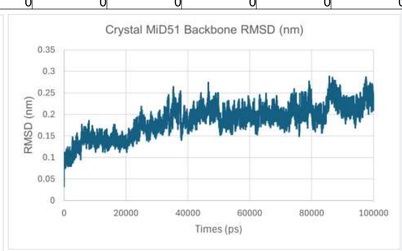
100 ns molecular dynamics simulations reveal a dynamic Crystal Drp1 framework, with backbone RMSD fluctuating between 0.2 and 0.8 nm due to localised loop and domain flexibility. Cluster analysis (0.45 nm cutoff) further shows that, despite this conformational mobility, Crystal Drp1 predominantly adopts a single dominant structural state, representing 77% of the simulation.

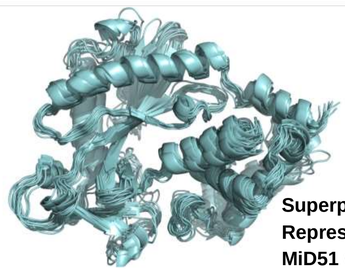
Structural and Molecular Dynamics Analysis of Crystal MiD51

Clusters	1	2	3	4	5	6	7	8	9	10	11	12	13	14	15
Frames	4851	2036	1960	747	147	125	70	19	17	10	6	5	4	2	2
Size %	48	20	19	7	1	1	1	0	0	0	0	0	0	0	0





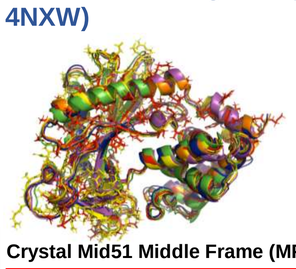




100 ns molecular dynamics simulations reveal a stable Mid51 crystal structure (RMSD: 0.15–0.25 nm), with localised loop dynamics that identify potential protein-interaction and therapeutic-target regions.

Superposition of Representative MiD51 Clusters

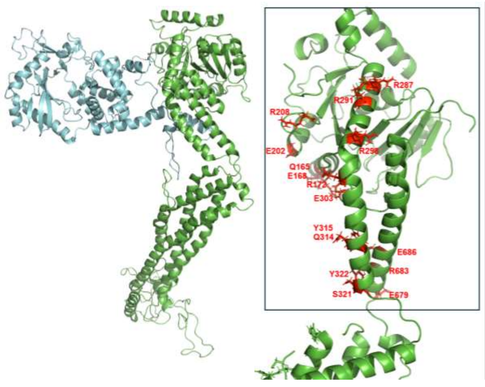
ClusPro Docking Analysis of the Interaction Between Drp1 (PDB: 4BEJ) and Mid51 (PDB: 4NXW)



Crystal Mid51 Middle Frame (MF1-MF6) Superimposition

Complexes	Docking Results
Drp1_Mid51_MF1	30
Drp1_Mid51_MF2	30
Drp1_Mid51_MF3	30
Drp1_Mid51_MF4	30
Drp1_Mid51_MF5	30
Drp1_Mid51_MF6	30
Sum	180

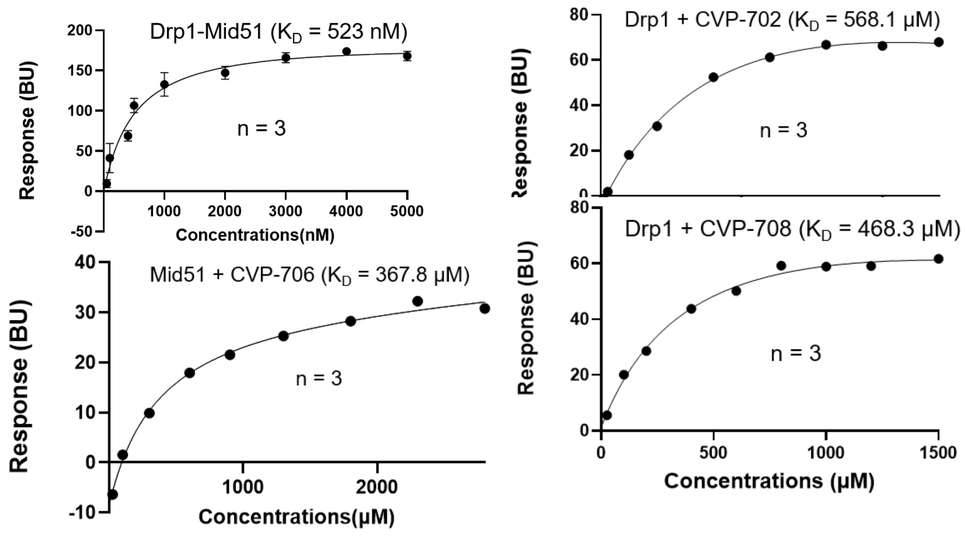
Crystal_MiD51_1MF	RMSD =	0	(4445 atoms)
Crystal_MiD51_2MF	RMSD =	1.551	(4445 atoms)
Crystal_MiD51_3MF	RMSD =	1.415	(4347 atoms)
Crystal_Mid51_4MF	RMSD =	1.530	(4616 atoms)
Crystal_Mid51_5MF	RMSD =	1.702	(4545 atoms)
Crystal_Mid51_6MF	RMSD =	1.635	(4611 atoms)



Crystal (Drp1&Mid51)	
DRP1 Count	
N448	87
R172	84
R365	82
Q314	72
Y322	65
Y315	63
R683	54
E168	52
R441	50
E202	43
D679	42
Y449	40
Q165	39
E686	39
C361	36
D21	36
R291	35
E303	33
L287	32

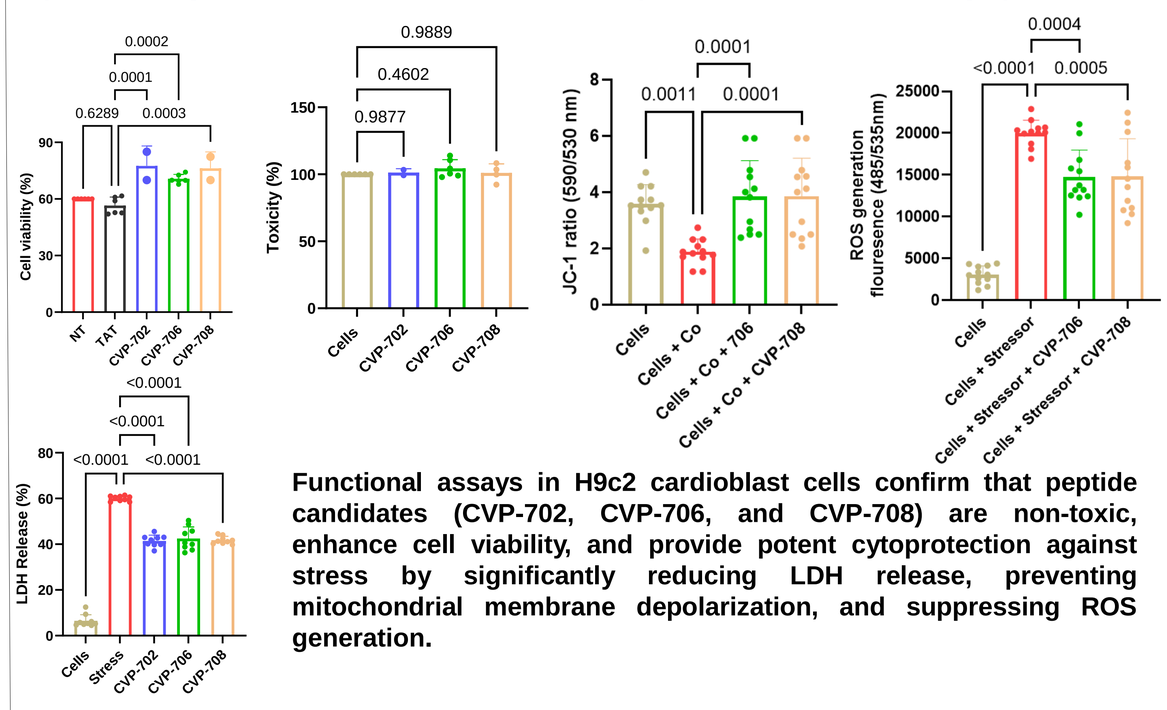
Docking representative Mid51 middle frame ensembles (RMSD range: 1.415–1.702 nm) against Drp1 identified primary interface hotspots (led by N448, R365, and Y322), revealing the core residues driving dynamic protein-protein binding across 180 total predicted complexes.

R100 Binding Affinity Analysis of CVP-702, CVP-706, and CVP-708 Peptides with Drp1, Mid51, and the Drp1-Mid51 Interaction



Using an R100 Field-Effect Biosensor (n= 3), the Drp1-Mid51 complex demonstrated strong nanomolar affinity ($K_D = 523$ nM), while individual peptide interactions displayed dose-dependent micromolar binding affinities ranging from $568.1\ \mu$M (Drp1 + CVP-702), to $367.8\ \mu$M (Mid51 + CVP-706) with Drp1 + CVP-708 exhibiting intermediate affinity ($K_D = 468.3\ \mu$M).

Peptide Activity Assessment in H9c2 Cardioblasts (XTT, JC-1, ROS, LDH Assays)



Functional assays in H9c2 cardioblast cells confirm that peptide candidates (CVP-702, CVP-706, and CVP-708) are non-toxic, enhance cell viability, and provide potent cytoprotection against stress by significantly reducing LDH release, preventing mitochondrial membrane depolarization, and suppressing ROS generation.

Conclusion

Computational protein-protein docking and molecular dynamics simulations defined the Drp1-Mid51 interaction interface and identified key interaction hotspots that provide a structural basis for peptide-mediated disruption of this protein-protein interaction. R100 binding assays validated the binding of **CVP-706 to Mid51** and **CVP-702 and CVP-708 to Drp1**, while cellular studies confirmed their cytoprotective activity. Collectively, these findings support peptide-mediated modulation of the Drp1-Mid51 interaction as a promising therapeutic strategy for preserving mitochondrial dynamics in cardiovascular disease.

PI: Prof. Nir Qvit (Email: nir.qvit@biu.ac.il)

Evaluation of Different Photocaging Strategies to Develop Next-Generation Photoprobes

https://doi.org/10.17952/38EPS.2026.P524

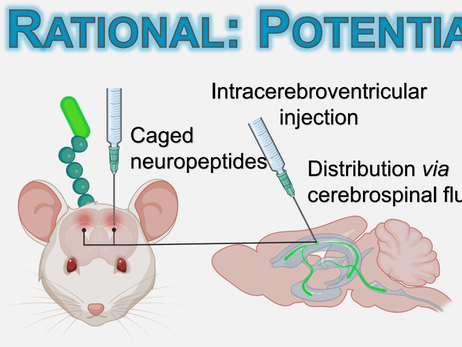
Konstantin Raabe,[A,B] Predrag Kalaba,[A] Hilary Yong,[C] Greta Crudeli,[D] Sarah Melzer,[D] Victor Anggono,[C] Erik Keimpema,[E] Markus Muttenthaler[A,F*]

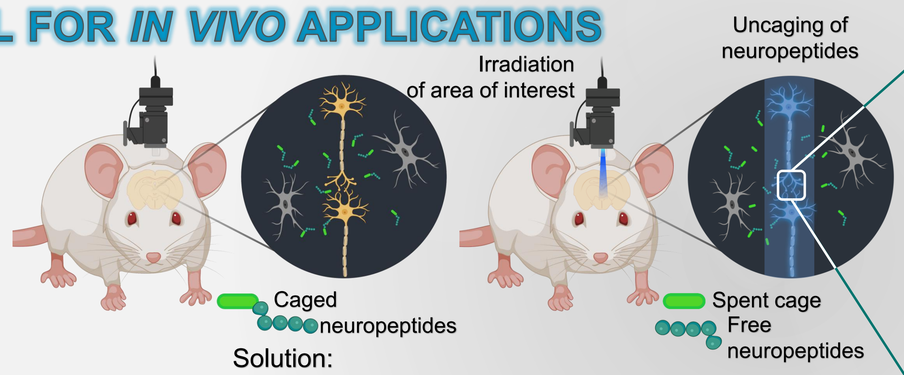
A) University of Vienna, Institute of Biological Chemistry, Austria
B) University of Vienna, Vienna Doctoral School in Chemistry (DoSChem), Vienna, Austria
C) The University of Queensland, Clem Jones Centre for Ageing Dementia Research, Brisbane, Australia
D) Medical University of Vienna, Department of Molecular Neurosciences, Vienna, Austria
E) Medical University of Vienna, Department of Neuronal Cell Biology, Vienna, Austria
F) Institute for Molecular Bioscience, The University of Queensland, Brisbane, Australia

Neuropeptides and Photopharmacology

Peptide signalling pathways govern diverse physiological and behavioural processes, yet their complex spatial and temporal dynamics remain difficult to study due to widespread receptor expression, long peptide half-lives, and extensive diffusion in neuronal tissue. To address these limitations and to enable precise control over neuropeptide activity, we systematically evaluated three classes of photolabile protecting groups – coumarin, nitrophenylpropyl, and boron-dipyrromethene – to establish a broadly applicable photocaging strategy for peptides. These cages support controlled one-photon (365-527 nm) and two-photon (730-780 nm) activation while avoiding cytotoxic by-products. Using the neuropeptides oxytocin and vasopressin as a proof-of-concept model system, we synthesised and characterised the photopharmacological profiles of these photocaged neuropeptide probes at their neuronal receptors (OTR, $V_{1a}R$, $V_{1b}R$) and in acute mouse cortical slices. The experiments identified the coumarin derivative DCMAC as the most effective photocage, providing robust bioactivity masking while maintaining biocompatibility. Rapid release of the native peptides and receptor activation could be achieved upon irradiation with both low-cost LED setups and high-precision two-photon lasers. Guided by these findings, we extended the DCMAC-based strategy to somatostatin and vasoactive intestinal peptide, demonstrating its broad applicability to other peptide families. Together, this generalised photocaging platform enables on-demand modulation of peptide signalling with high spatiotemporal precision, opening new avenues for mechanistic studies across diverse peptide systems in health and disease.

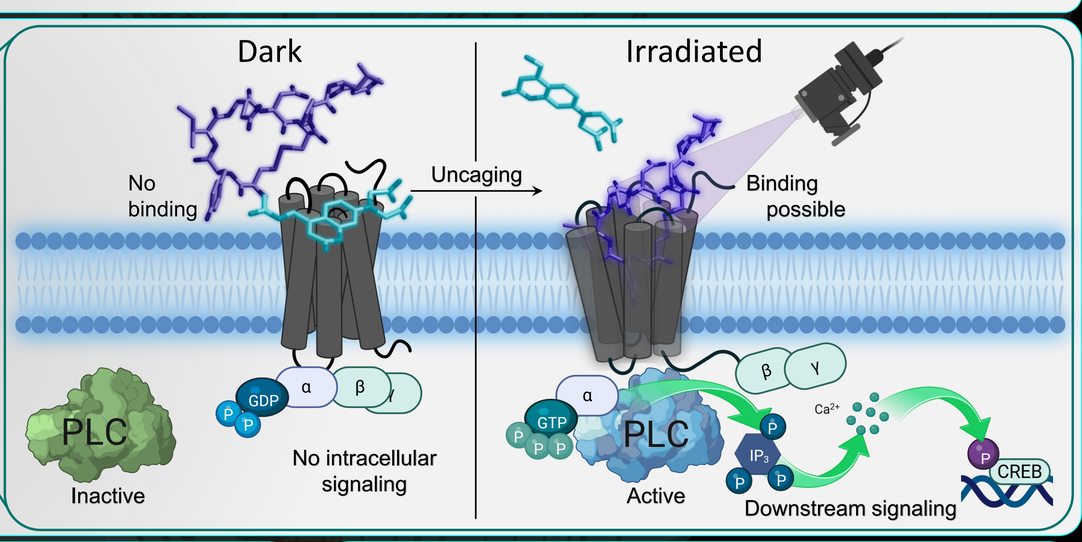
Rational: Potential for *in vivo* Applications



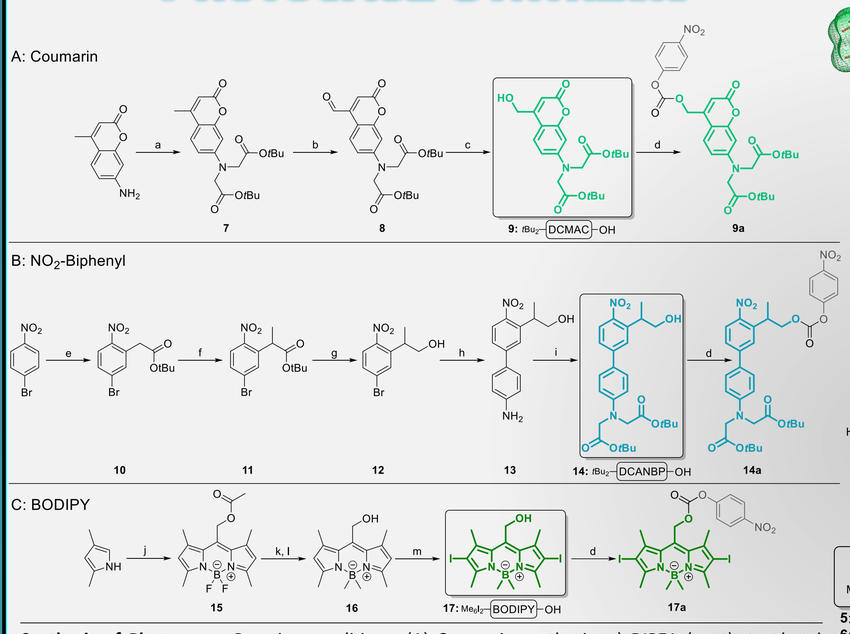


Problem:
- Injection stressful for the animal
- Limited time window for behavioural experiments
- Diffusion away from original point of injection
- Interactions in non-targeted areas

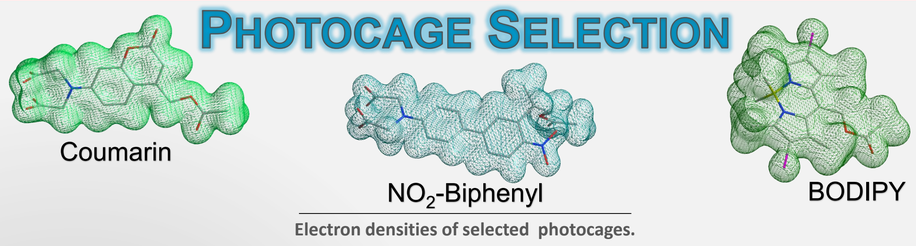
Solution:
- Combination with Photopharmacology
- Caged neuropeptides biologically inert
- Uncaging releases high concentration of native peptides
- High spatiotemporal control of receptor activation



Photocage Synthesis

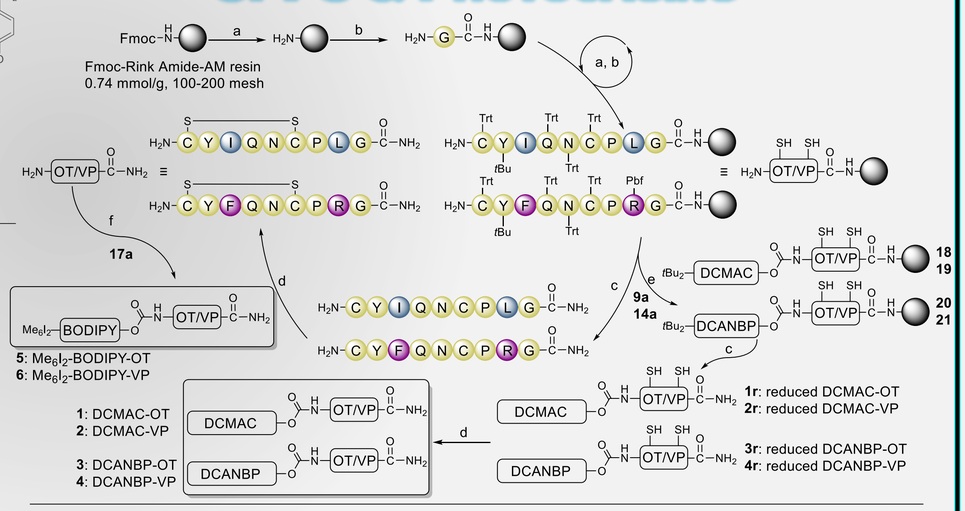


Photocage Selection



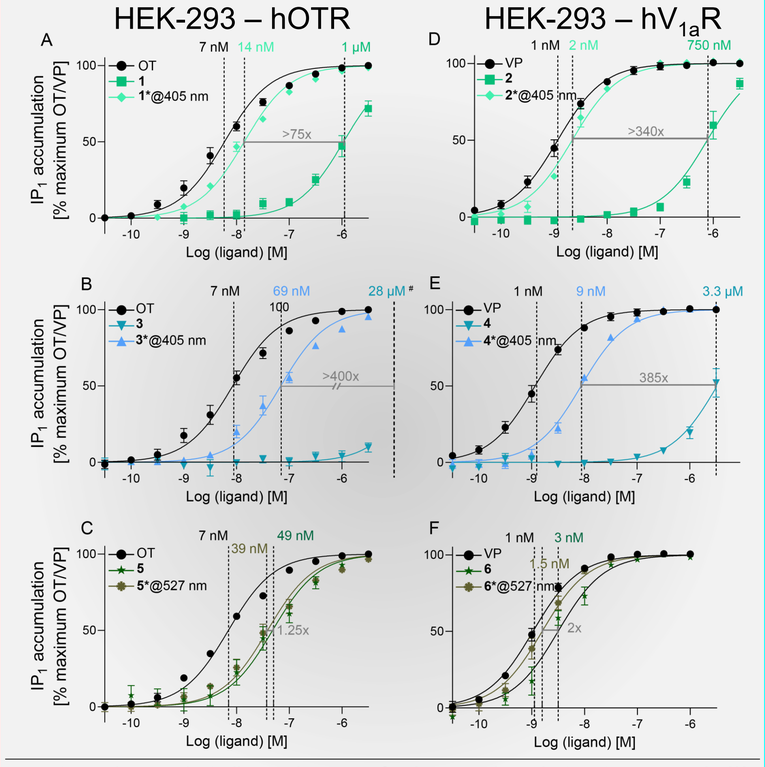
Electron densities of selected photocages.

SPPS & Photocaging



SPPS and caging of OT and VP. Reaction conditions: a) 1) 1 min DMF flow-wash, 2) 2x 1 min piperidine/DMF (1:1), 3) 1 min DMF flow-wash; b) HATU (0.5 M in DMF)/amino acid/DIPEA (3.95/4/4 with respect to resin loading), RT, 15 min; c) 1) 1 min DCM flow-wash, 2) TFA/ddH_2O/TIPS (90/5/5), RT, 2 h, 3) N_2-stream, Et_2O, 0 °C; d) 1) 0.1 M NH_4HCO_3 buffer (pH=8.2), RT, 24 h, 2) TFA; Yields after folding and RP-HPLC: 18% **1**, 17% **2**, 28% **3**, 12% **4**; e) DMF, pyridine, **9a** or **14a**; f) THF, DMF, pyridine, **17a**; Yields after photocaging and RP-HPLC: 56% **5**, 24% **6**; HATU: 1-[bis(dimethylamino)methylene]-1*H*-1,2,3-triazolo[4,5-b]pyridinium 3-oxide hexafluorophosphate, TIPS: triisopropylsilane.

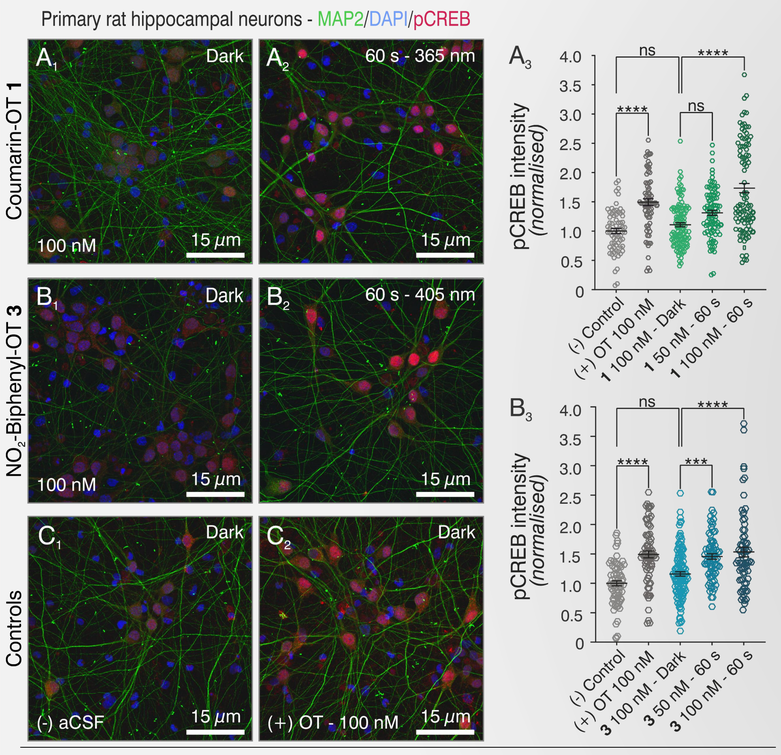
Pharmacology



***In vitro* pharmacologically evaluation of photocaged and *in situ* uncaged (*) neuropeptides**. Cellular functional IP_1-assay performed on stable HEK-293 cells, overexpressing hOTR and $hV_{1a}R$ (N≥3, n=3). Results normalised to OT/VP (100%) and negative control (buffer; 0%) activity. Error bars indicate standard error of the mean. (A-C) hOTR, (D-F) $hV_{1a}R$. EC_{50} values shown above with same color coding for the corresponding compounds, asterisks indicate 60 s *in situ* uncaging, # indicate extrapolated values values, grey numbers and lines indicate x-fold difference of EC_{50} values before and after uncaging.

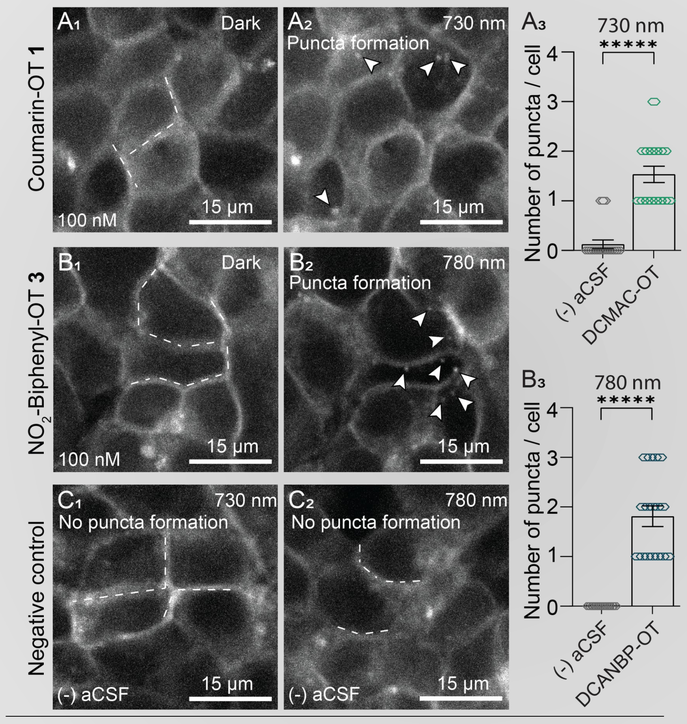
Biological Evaluation

1PE Uncaging – Neurons



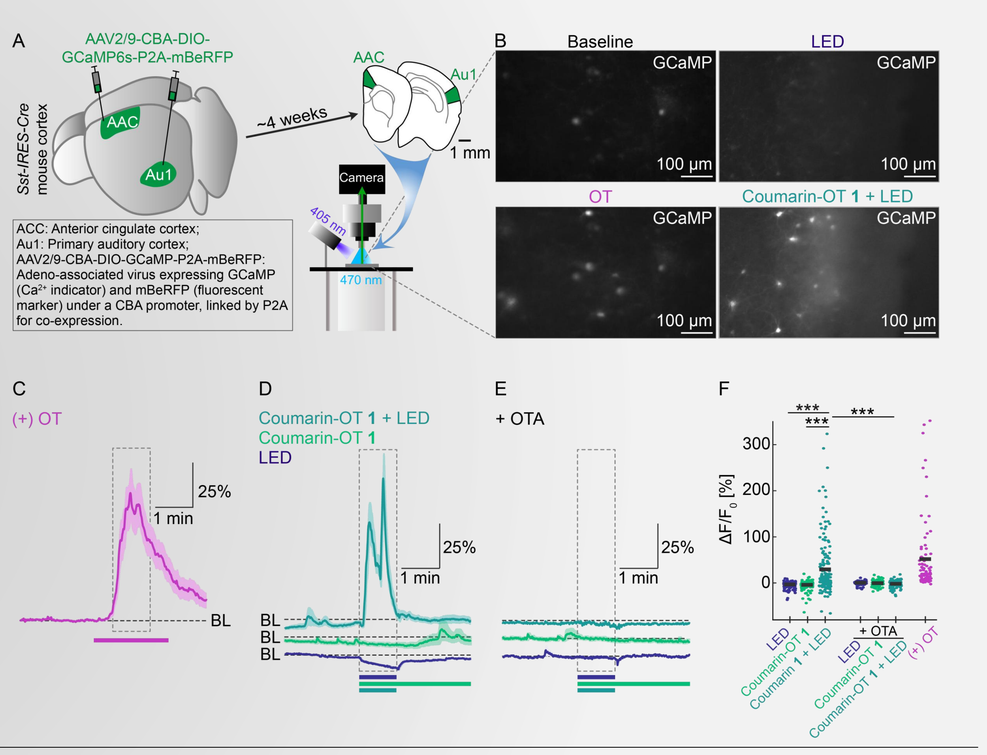
***In vitro* evaluation of the bioactivity of OT photoprobes, caged and uncaged**. Right on primary rat hippocampal neurons. Nuclei were stained with DAPI (blue), and dendrites with antibodies for MAP2 (green). Phosphorylation of CREB (red) was quantified after immunocytochemistry of n=~100 cells over two coverslips and normalised to the negative control (aCSF). (A_{1-3}) Coumarin-OT **1**, 100 nM, dark and irradiated at 365 nm for 60 s. (B_{1-3}) NO_2-Biphenyl-OT **3**, 100 nM, dark and irradiated at 405 nm for 60 s. (C_{1-2}) Negative control (aCSF) and positive control (OT, 100 nM) dark; ns, non-significant; *=p<0.05; ***=p<0.001; ****=p<0.0005; *****=p<0.0001

2PE Uncaging – HEK-293



2PE OT photoprobe uncaging during live-cell imaging. HEK-293 cells stably overexpressing hOTR-GFP, Ti:Sapphire laser tuned to 730 nm or 780 nm. (A_{1-3}) Coumarin-OT **1** 100 nM in the dark and 10 min after local irradiation (dashed lines) at 730 nm. (B_{1-3}) NO_2-Biphenyl-OT **3** 100 nM in the dark and 10 min after local irradiation (dashed lines) at 780 nm. (C_{1-2}) aCSF 10 min after local irradiation (dashed lines) at 730/780 nm. Arrowheads indicate puncta; puncta formation was quantified for n=15 cells; *****=p<0.0001

1PE Uncaging – Acute Cortical Slices



***Ex vivo* evaluation of Coumarin-OT 1 *via* epifluorescence GCaMP imaging**. (A) Schematic of cortical injection sites. (B) Example images of *ex vivo* epifluorescence GCaMP imaging. (C-E) Normalised GCaMP fluorescence changes ($\Delta F/F_0$) shown as solid lines with ± SEM as translucent areas: (C) Pink: 1 µM OT, N=3 mice, n=4 slices; (D) Blue: 405 nm LED control; green: 1-5 µM Coumarin-OT **1** in the dark; turquoise: 1-5 µM Coumarin-OT **1** and 60 s uncaging with 405 nm LED, N=3 mice, n=5 slices; (E) In the presence of 10 µM OTR antagonist (OTA: $d(CH_2)_5[yITNCP(Orn)]$-COOH). Blue: 405 nm LED control; green: 1 µM Coumarin-OT **1** in the dark; turquoise: 1 µM Coumarin-OT **1** and 60 s uncaging with 405 nm LED, N=2 mice, n=4 slices. (F) Quantification of normalised GCaMP fluorescence changes ($\Delta F/F_0$). Coloured bars indicate application times of the compounds or LED irradiation times; dashed lines indicate baseline fluorescence (BL); dashed boxes indicate time windows used for GCaMP $\Delta F/F_0$ quantification; ***=p<0.001.

Figures created in BioRender.com

K. Raabe *et al.*, Angew. Chem. Int. Ed. 2026, 65, e13373
doi.org/10.1002/anie.202513373
doi.org/10.1002/ange.202513373

1PE: one-photon excitation; 2PE: two-photon excitation; aCSF: artificial cerebrospinal fluid
MAP2: Microtubule-associated protein 2; pCREB: phosphorylated cAMP response binding protein; GFP: Green fluorescent protein

Konstantin Raabe
konstantin.raabe@univie.ac.at
www.neuropeptidelab.com

universität wien
Vienna Doctoral School in Chemistry
The University Of Queensland
AUSTRALIA
erc European Research Council
Institute of Biological Chemistry
Center for Brain Research
Medizinische Universität Wien

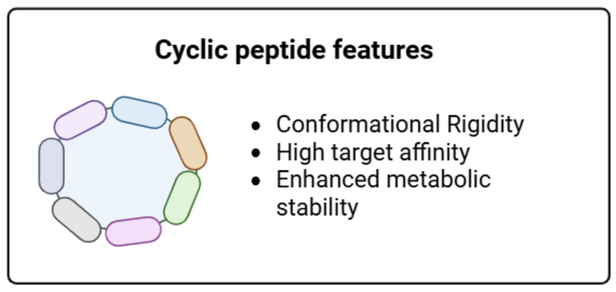
Enantioselective synthesis of antiplasmodial cyclic tetrapeptide Koshidacin A

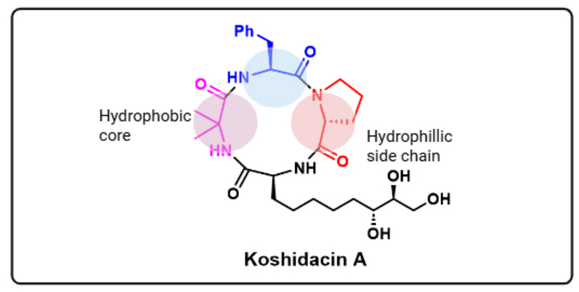
Preeti Kapri, Devki Nandan, Ramesh Ramapanicker*
Department of Chemistry, Indian Institute of Technology Kanpur, Kanpur- 208016, India
Email: preetik21@iitk.ac.in, rameshr@iitk.ac.in
https://doi.org/10.17952/38EPS.2026.P293

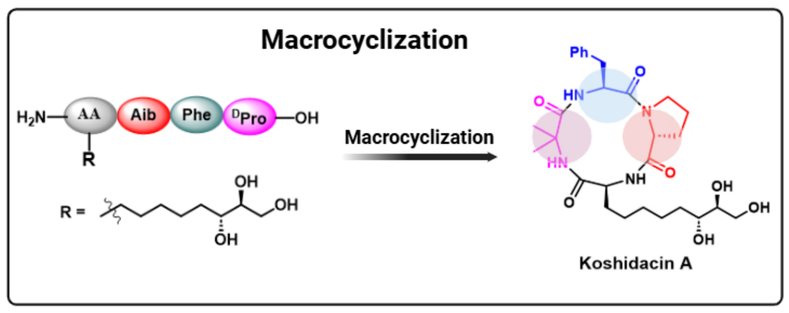
38th EPS
European Peptide Symposium

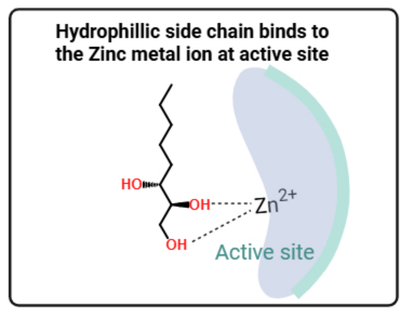
Introduction

- Cyclic peptides offer promising therapeutic scaffolds owing to their conformational rigidity, high target affinity, and enhanced metabolic stability.
- Natural cyclic tetrapeptides often feature a hydrophobic core and a hydroxyl-rich side chain capable of coordinating Zn^{2+} at the HDAC active site.
- Iwatsuki et al. isolated two cyclic tetrapeptides, Koshidacins A and B, from *Pochonia boninensis* FKR-0564, both showing antiplasmodial activity against the *Plasmodium falciparum* FCR3 strain (IC_{50}: 17.1–0.89 μM).
- The synthesis of Koshidacin A features a stereoselective approach to the side-chain triol unit via Sharpless asymmetric epoxidation followed by Payne rearrangement.
- Herein, we developed the synthesis of the antiplasmodial cyclic tetrapeptide Koshidacin A from Homo-Garner aldehyde as the key starting material.



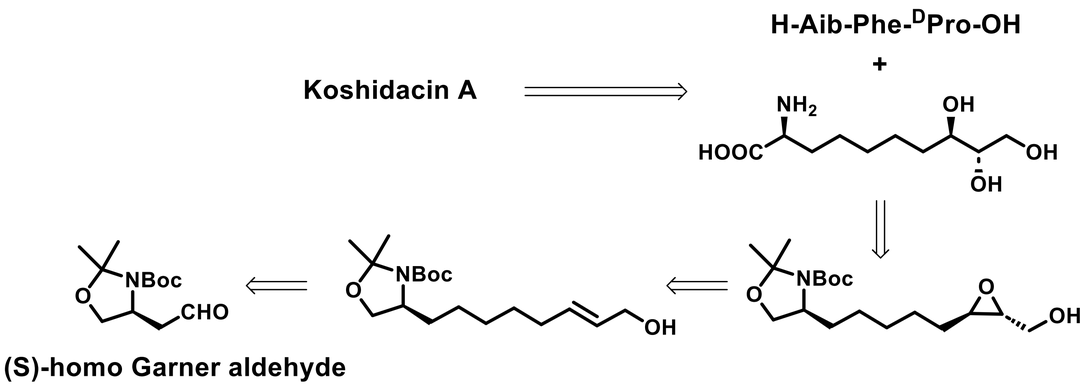




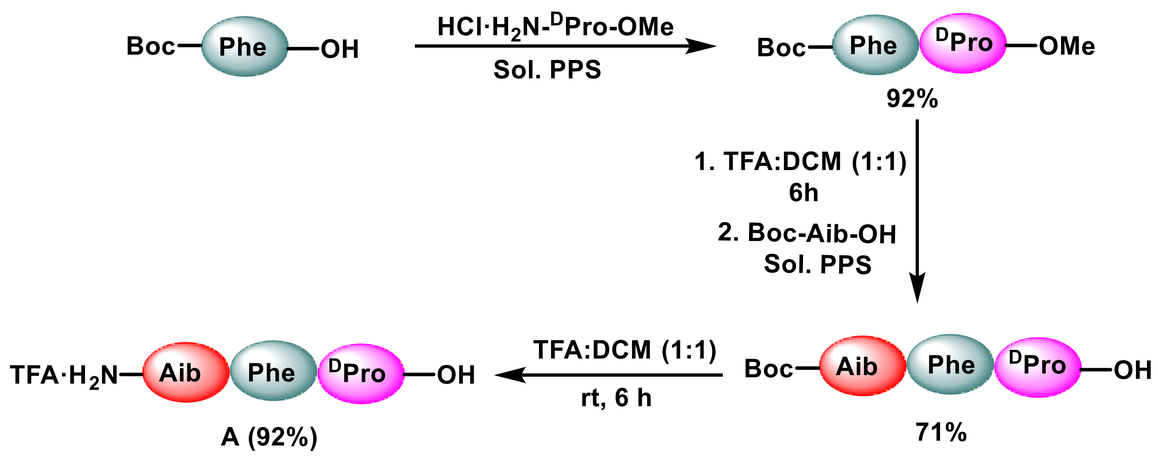


Retrosynthetic Approach

The synthetic route involves Sharpless asymmetric epoxidation followed by a Payne rearrangement, enabling the introduction of a trihydroxy-substituted lipophilic side chain within a specific amino acid fragment.

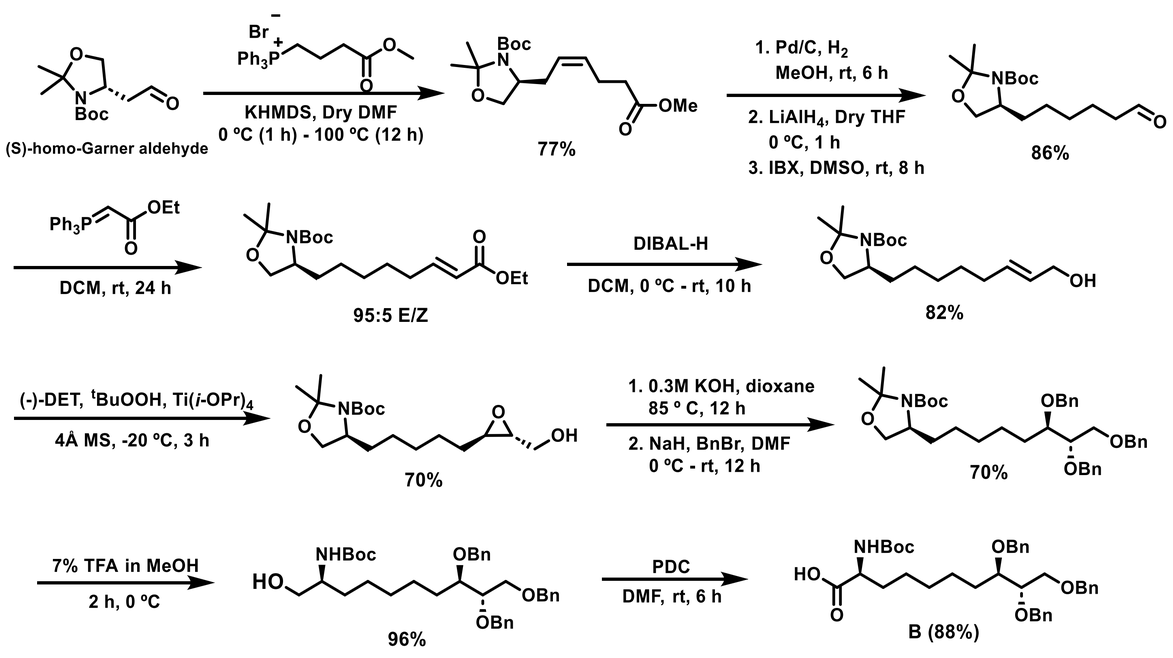


Synthesis of tripeptide fragment A

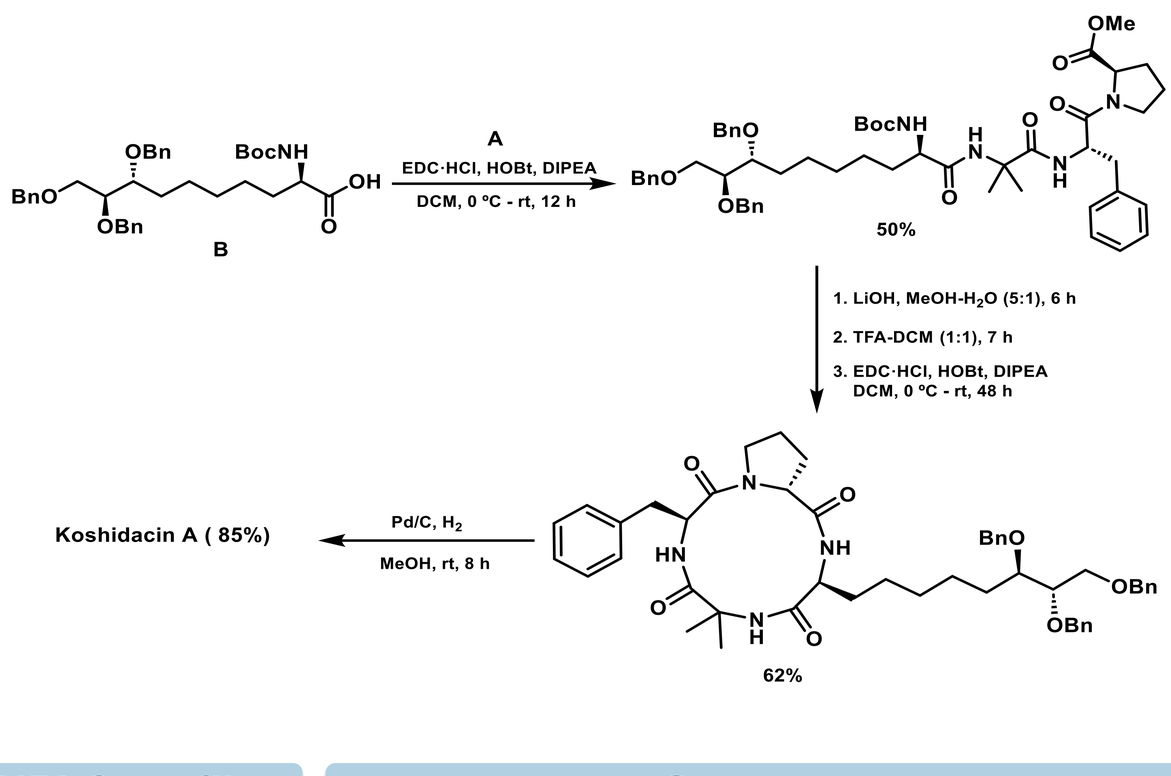


Synthesis of lipophilic amino acid fragment B

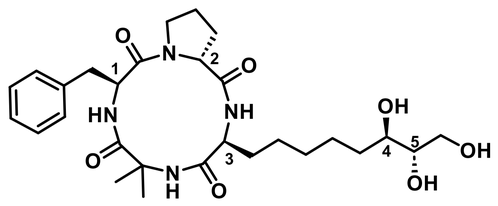
Using (S)-homo-Garner aldehyde as the key starting material to enantioselectively construct the side chain.



Synthesis of Koshidacin A



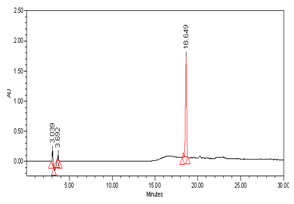
NMR comparison: Natural vs Synthetic Koshidacin A and HPLC profile



	^{1}H NMR data of Koshidacin A	^{1}H NMR data of Synthetic 1	^{13}C NMR data of Koshidacin A	^{13}C NMR data of Synthetic 1
1	5.14 (ddd, 10.0, 10.0, 5.8)	5.12 (td, 10.0, 5.8)	53.4	53.4
2	4.67 (d, 6.3)	4.65 (d, 7.1)	57.8	57.8
3	4.20 (ddd, 10.0, 7.5, 7.4)	4.20 (ddd, 10.0, 7.5, 7.6)	54.5	54.5
4	3.75 (m)	3.75 (m)	73.6	73.6
5	3.61 (m)	3.66-3.57 (m)	73.8	73.9

HPLC Analysis

- **Column:** XTerra® RP-C18 (250 × 4.6 mm, 3.5 μm)
- **Mobile phase:** ACN/H_2O + 0.1% TFA
- **Flow rate:** 1.0 mL min^{-1}
- **Detection:** UV 215 nm
- **tR:** 18.649 min
- **Purity:** 86.14%



Summary

- Developed a concise, efficient method for synthesizing the cyclic tetrapeptide Koshidacin A.
- Established a stereoselective route to the unusual trihydroxy side chain through Sharpless asymmetric epoxidation followed by Payne rearrangement.
- Achieved good yield and reproducibility with the current synthetic strategy.
- The modular synthetic strategy provides a promising platform for the synthesis of Koshidacin A analogues and related cyclic tetrapeptides, enabling future studies of their biological and supramolecular properties.

Acknowledgement

I gratefully acknowledge Prof. Ramesh Ramapanicker for his guidance and Dr. Devki Nandan for valuable discussions. I thank CSIR-UGC for the fellowship and IIT Kanpur for the research facilities.

Reference

Kapri *et al.*, *Eur. J. Org. Chem.* **2026**, *29*, e202500975.

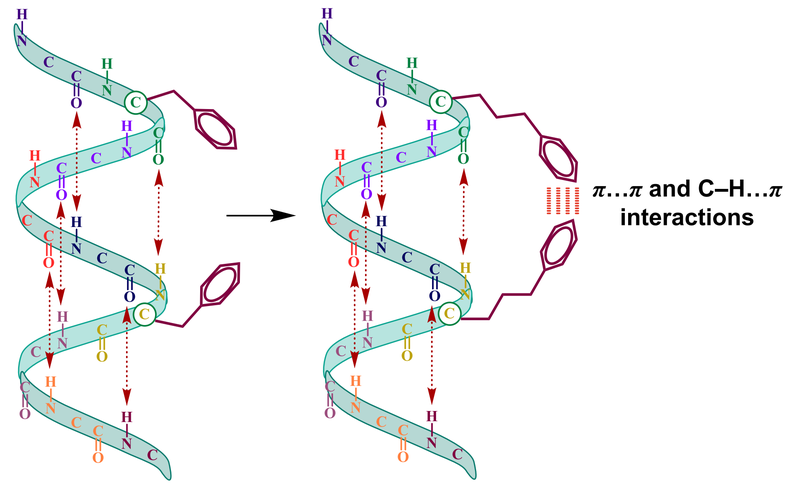
Stabilization of Helical Structures in Oligopeptides through Modification of Phenylalanine Residues

Vikrant Vini[1], Jisna T.[2], Ramesh Ramapanicker[1]* and Prema G. Vasudev[2]*
[1]Department of Chemistry, Indian Institute of Technology Kanpur, Kanpur, UP – 208016, India.
[2]Plant Biotechnology Division, CSIR – Central Institute of Medicinal and Aromatic Plants, Lucknow, UP – 226015, India.
Email: vikrantv21@iitk.ac.in
https://doi.org/10.17952/38EPS.2026.P475

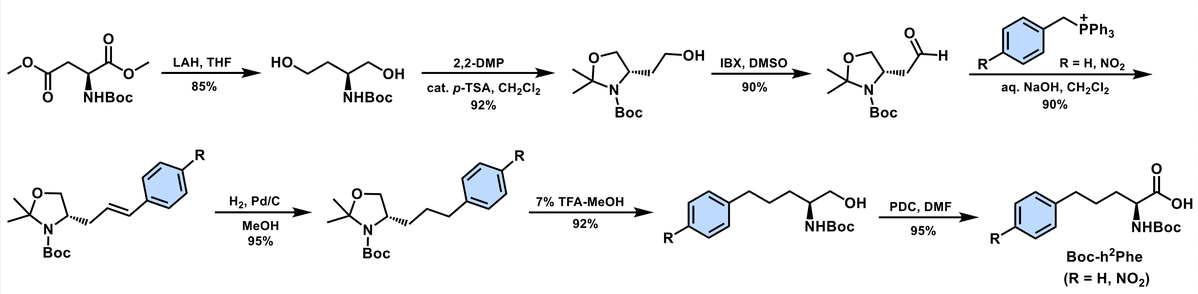


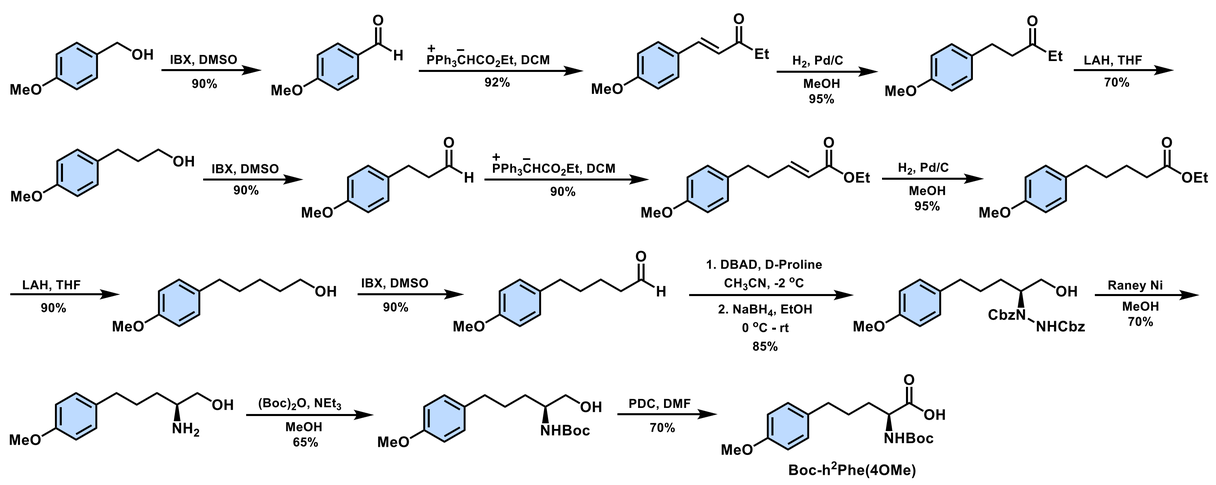
Introduction

- Non-covalent interactions between aromatic side chains of amino acids play a crucial role in directing peptide folding and stabilizing secondary structures in oligopeptides.
- In helical peptides, canonical phenylalanine (Phe) residues placed at the *i* and *i*+4 positions are too distant to have effective, stabilizing intramolecular aromatic interactions.
- Modification of Phe side-chains can tune both the spatial and electronic properties of aromatic residues, thereby influencing aromatic interactions and peptide folding.
- This study explores a library of Phe-modified oligopeptides to elucidate how aromatic side-chain engineering promotes intramolecular aromatic interactions and stabilizes helical conformations.

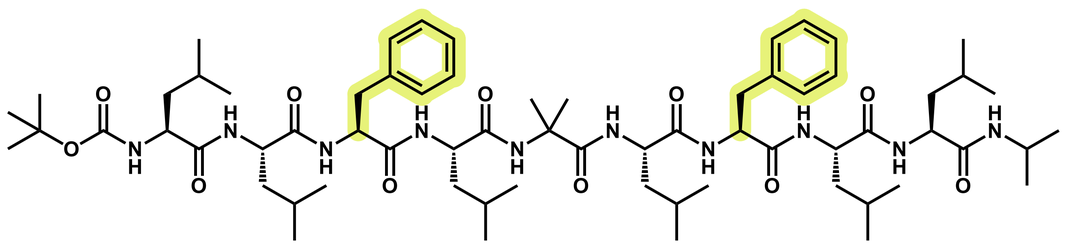


Synthetic Scheme of Modified Phenylalanine Residues

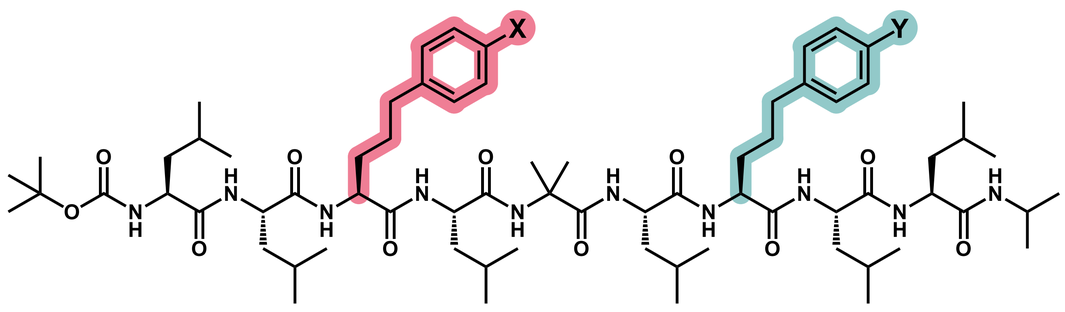




Design of Peptides Containing Modified Phe Residues



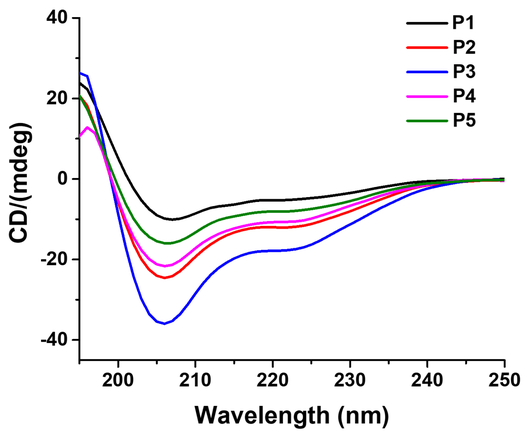
Boc-Leu-Leu-Phe-Leu-Aib-Leu-Phe-Leu-Leu-NH*i*Pr
P1



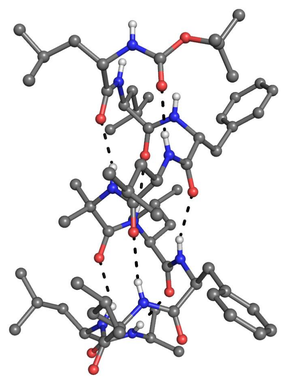
Boc-Leu-Leu-Phe*-Leu-Aib-Leu-Phe*-Leu-Leu-NH*i*Pr
Phe* = Modified Phe

P2 : X = Y = H
P3 : X = NO_2 ; Y = H
P4 : X = NO_2 ; Y = OMe
P5 : X = OMe ; Y = H

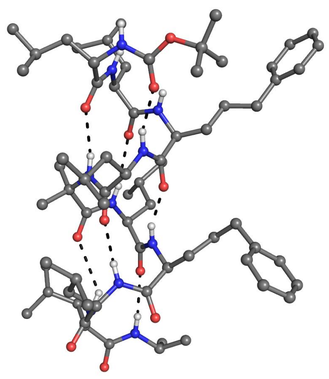
Conformational Analysis of Designed Peptides



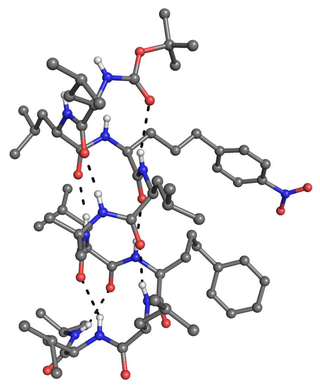
CD spectra of 1 mM peptides P1-P5 in MeOH



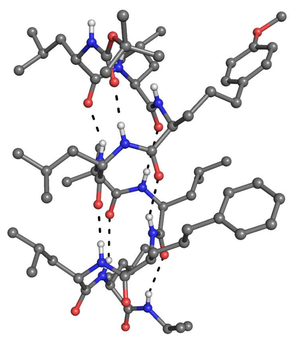
P1



P2 (X and Y = H)

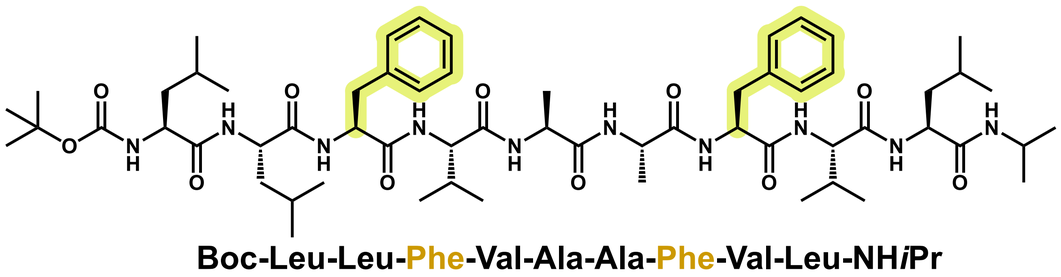


P3 (X = NO_2 ; Y = H)

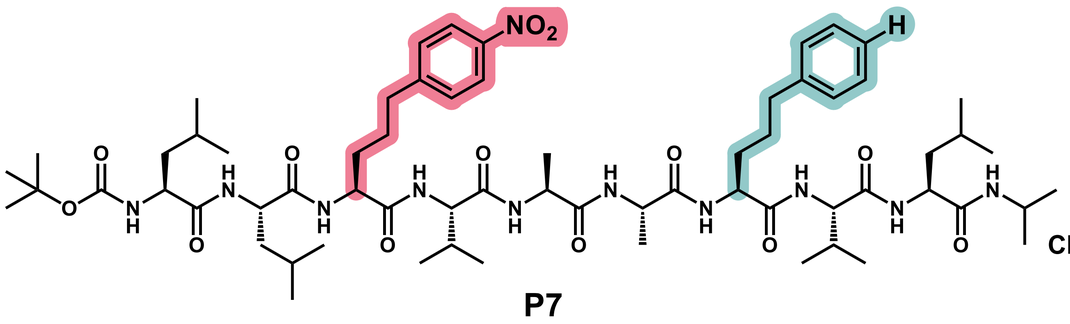


P5 (X = OMe ; Y = H)

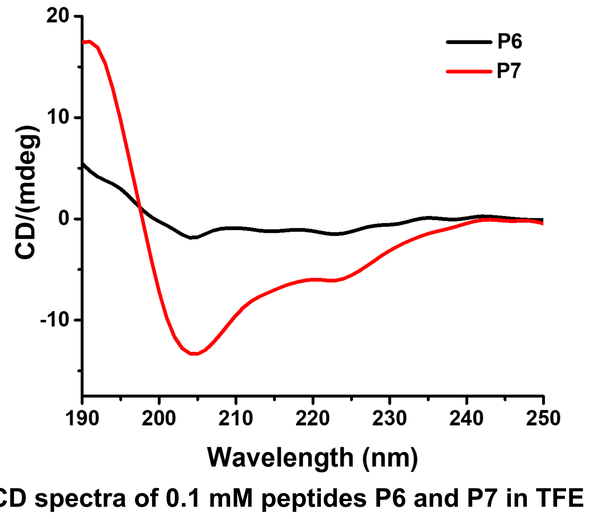
Modified Phe Residues as Non-Covalent Staples



Boc-Leu-Leu-Phe-Val-Ala-Ala-Phe-Val-Leu-NH*i*Pr
P6



P7



CD spectra of 0.1 mM peptides P6 and P7 in TFE

Summary

- Side-chain homologation of Phe residues at the i^{th} and i+4th position enables favourable intramolecular aromatic interactions that promote helix formation.
- Non-covalent stapling through modified Phe residues demonstrates an effective method to stabilize helical conformations in peptides with low intrinsic helical propensity.

Acknowledgement

- Department of Chemistry, IIT Kanpur

References

- Ramapanicker *et al*., *J. Pept. Sci.* **2025**, *31*, e3667.
- Ramapanicker *et al*., *Pept. Sci.* **2026**, *118*, e70032.

Multifunctional amphicharged and bolaamphiphilic surfactants derived from amino acids: The effect of pH and temperature on their interactions with bovine serum albumin (BSA) and lysozyme (LYZ)

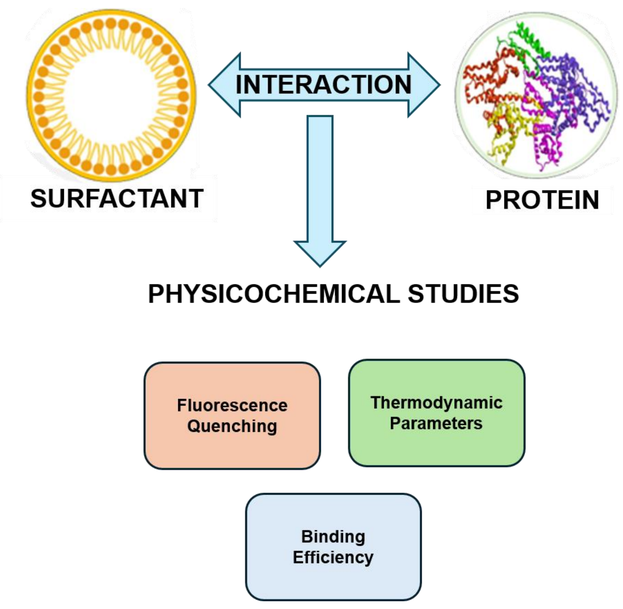
*Sumedha Gupta, Neelakshi, Nikita Jain, Ramesh Ramapanicker**

Department of Chemistry, Indian Institute of Technology Kanpur
Kanpur - 208016
Email: sumedhag21@iitk.ac.in, rameshr@iitk.ac.in
https://doi.org/10.17952/38EPS.2026.P550



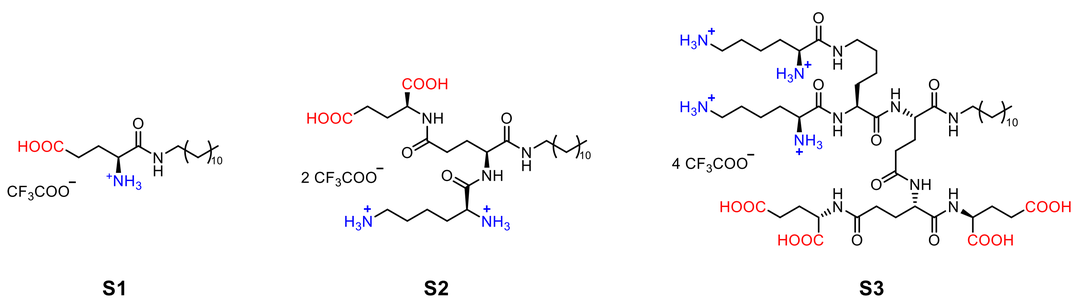
Introduction

- Surfactants, on binding with proteins, are known to exhibit certain structural and functional modifications in the protein structure which can be exploited for their applications in cosmetics and pharmaceutical industries.
- Traditionally, amino acid-based surfactants containing only one functionality in the head group have been studied.
- To explore the applications of surfactants derived from amino acids and peptides, we have designed amphicharged and bolaamphiphilic surfactants for the first time.
- These surfactants exist in different ionic forms at different environmental conditions. We have studied their varied interactions with BSA and LYZ at different pH and temperatures.



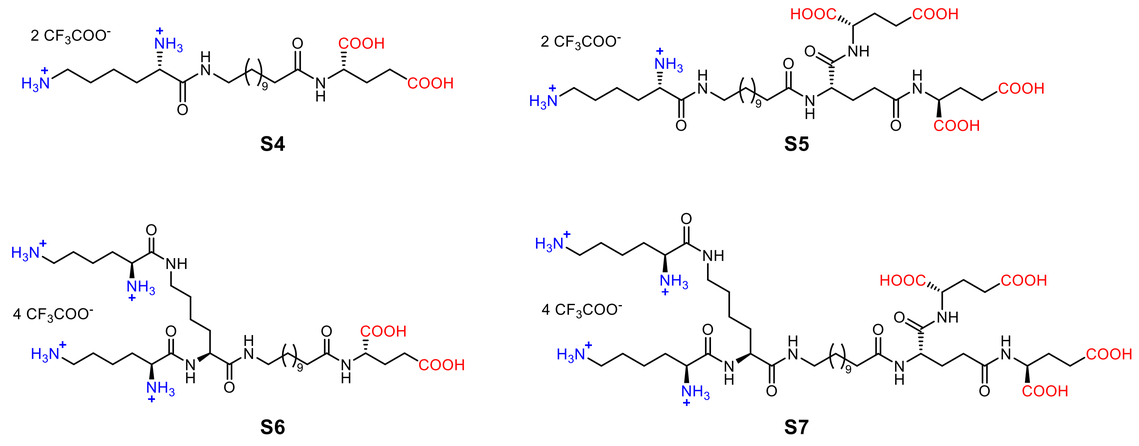
Structure of the surfactants

Structure of amphicharged surfactants

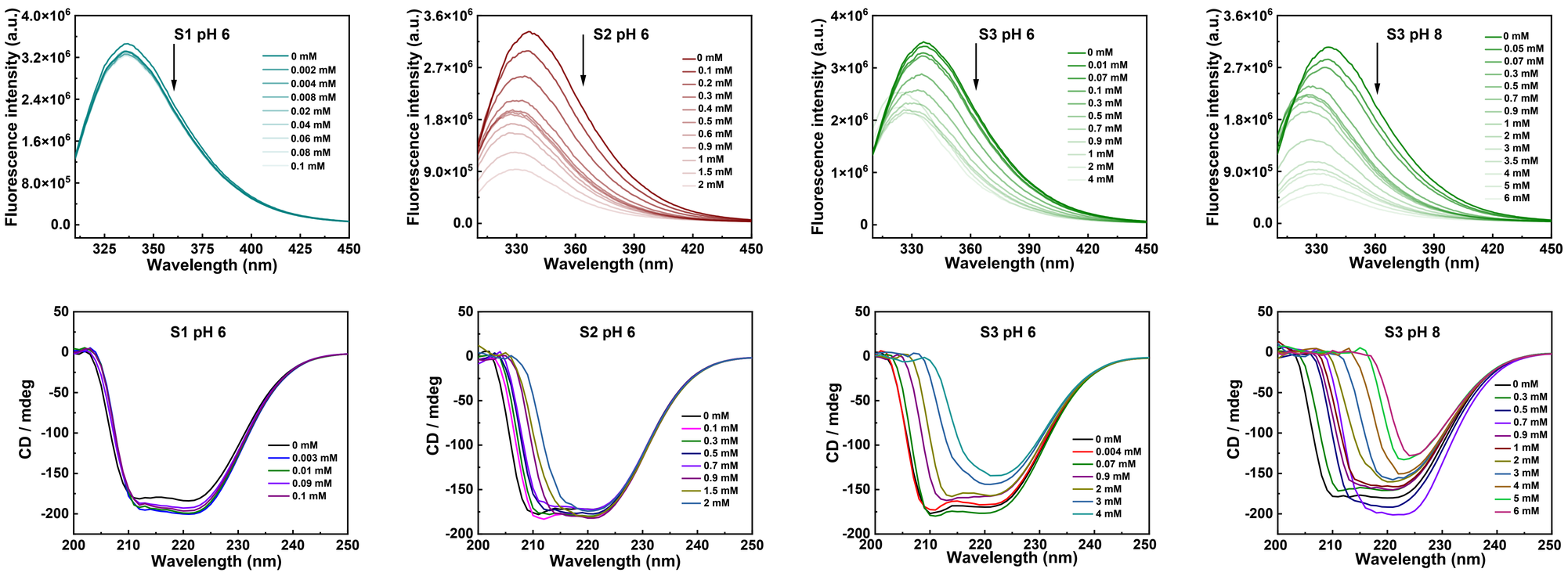


Surfactants **S1-S7** were synthesized using conventional solution phase peptide coupling strategy employing carbodiimide-mediated activation of the carboxylic acid (EDC·HCl) in the presence of HOBt and DIPEA.

Structure of bolaamphiphilic surfactants



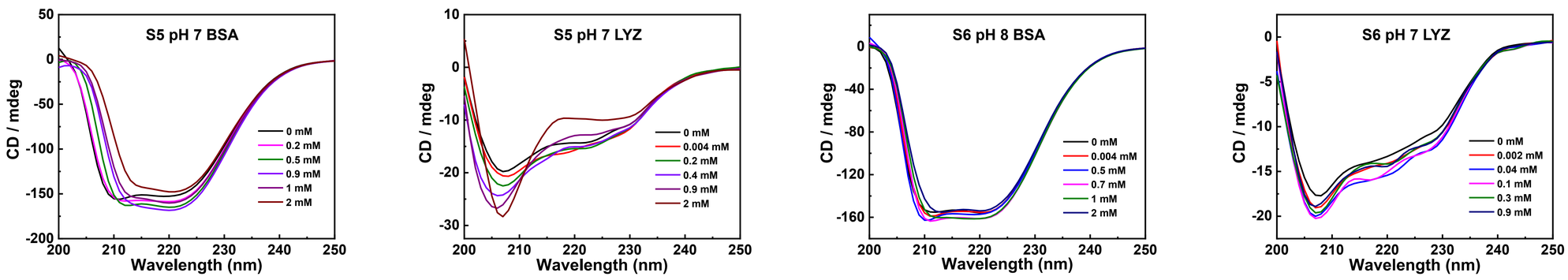
Studies showing quenching of fluorescence intensity of BSA and conformational changes in its secondary structure in the presence of amphicharged surfactants (S1-S3)



S2 exhibits maximum BSA binding affinity at pH 6, whereas **S3** shows increasing binding affinity with increasing pH from 6 to 8

S2 and **S3** stabilize the α-helical structure of BSA at low concentrations, which transitions to a β-sheet-rich conformation at higher concentrations

Circular Dichroism studies showing conformational changes in the secondary structure of BSA and LYZ in the presence of bolaamphiphilic surfactants S5 and S6 at different pH



The surfactants destabilize the secondary structure of BSA but enhance the % α-helicity of LYZ

Summary

- Temperature- and pH-dependent surfactant-protein interactions with BSA and LYZ were studied spectroscopically. Amphicharged surfactants bind strongly under optimized conditions, whereas bolaamphiphilic surfactants maintain efficient interactions across broader conditions.

Acknowledgement

- Department of Chemistry, IIT Kanpur

References

- Gupta *et al.*, *J. Surfact. Deterg.* **2025**, *28*, 501.
- Gupta *et al.*, *Langmuir* **2026**, *42*, 12108.

https://doi.org/10.17952/38EPS.2026.P062

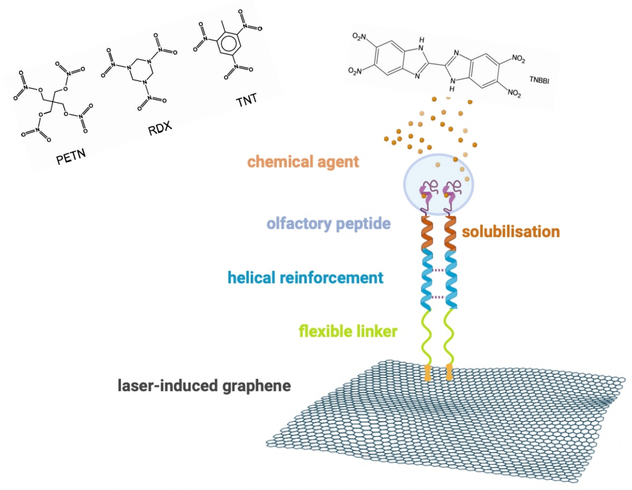
Olfactory Inspired Peptides as Tunable Platforms for Selective Detection of Explosives

Adriana Rathner[1], Prabhat Prakash[2], Julian Widhalm[1], Malina Mairhofer[1], Vera Podrabska[1], William III Goddard[2]

[1]Institute of Biochemistry, Johannes Kepler University Linz, Linz, Austria
[2]California Institute of Technology, Pasadena, California, United States of America

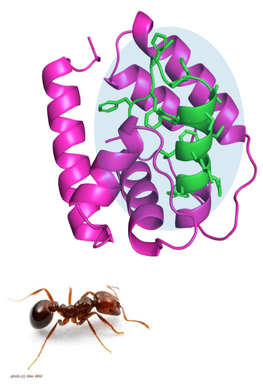
Motivation

Olfactory systems have inspired **biosensor** design due to their ability to fine-tune interactions between amino acid sequences and target volatile compounds for selectivity and sensitivity[1]. In this project's first phase, **insect-derived** olfactory receptors and odorant-binding proteins were used to design **artificial peptides** sensitive to **TNT** and **DNT.** These peptides were synthesized using solid-phase peptide synthesis and characterized by solution NMR spectroscopy. MD simulations assessed their interactions with TNT/DNT, aiding peptide optimization. Future work includes chemical shift mapping of these interactions and immobilizing peptides on **laser-induced graphene** substrates for cost-effective electrochemical sensors targeting **chemical warfare** agents.



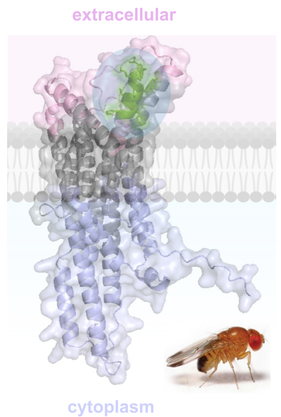
Architecture of the peptide portion of the biosensor. Individual functional parts are highlighted.

siOBP5 from *Solenopsis invicta*



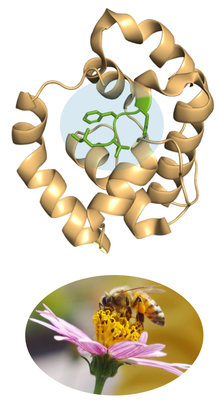
C-terminus from Odorant-binding protein (OBP)
TYQFSKGSYSTDPDHFF
binds alarm pheromone[2]

Or67a from *Drosophila melanogaster*



Soluble helix from Odorant receptor (OR)
SWLFYPSYFH
general activity towards aromatic compounds[3]

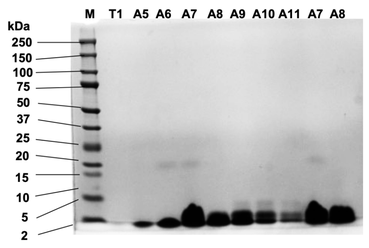
ASP1 from *Apis mellifera*



Pheromone-binding site of Odorant-binding protein (OBP)
WFVI
TNT-reactive[4]

Name	Sequence	No. of AA
P4	GGGGLQELNQKLGYFVIG	18
P5	GGGGLQELTSKLGWFVIG	18
P6	CGGGGLQELTSKLGWFVIG	19
P8	GGGGLQELTSKLHANFSKYILHQRG	25
P9	GGGGLQELTSKLKARGSAEGWFVIG	25
P10	GGGGLQELTSKLKARGSAEGSWLKYPSYFHG	31
P11	GGGGLQELTSKLKARGSAEGSWLKPSFHG	29
P12	GGGGKARGSAEGTYQFSKGSYSTDPDHFFG	30
P13	GGGGKARGSAEGTYQFSKGSYSTHFG	26
P14	GGGGKARGSAEGWHSAMAKGVYG	23

Polyglycine…flexibility
Solubilisation insert
Helicity-inducing region
Sensing region



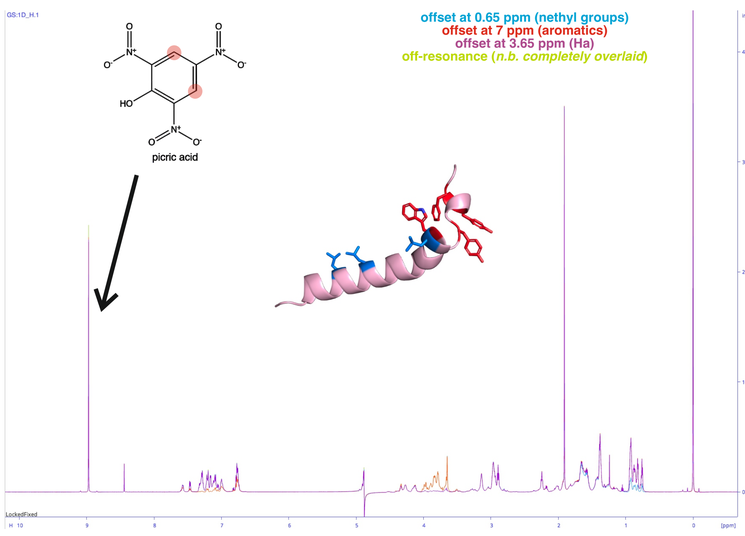
Tris-Tricine SDS-PAGE

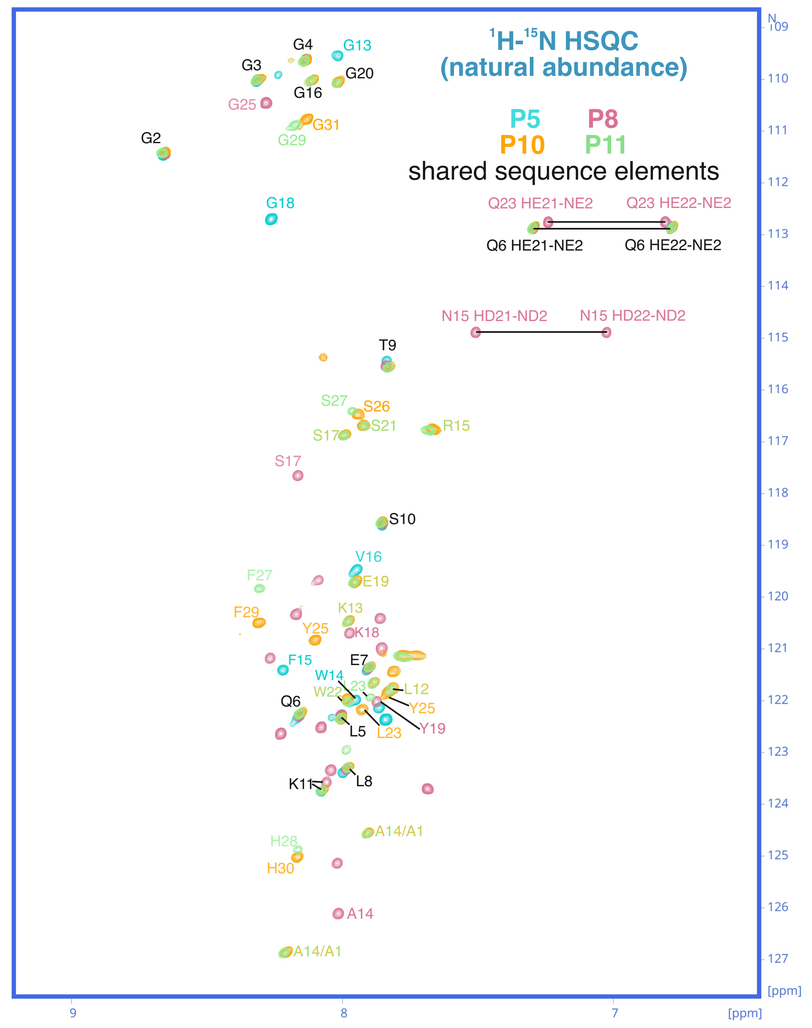
Solid-phase peptide synthesis

Peptides were synthesized on a 0.1 mmol scale using Wang resin and an automated microwave-assisted SPPS synthesizer (Liberty Blue 1.0, CEM). Fmoc-protected amino acids with appropriate side-chain protection were used. Cleavage from resin was performed via TFA, and products were precipitated with diethyl ether. Yields ranged from 55–91% (100–350 mg crude product, depending on peptide size). Peptides were purified alternatively by ion-exchange chromatography (HiTrap CaptoS/Q, Cytiva) or HPLC (70% acetonitrile gradient) and analyzed by Tris-Tricine SDS-PAGE. Final product quality was confirmed by HPLC ESI-MS (0.1% formic acid/acetonitrile gradient; Agilent TOF/Q-TOF).

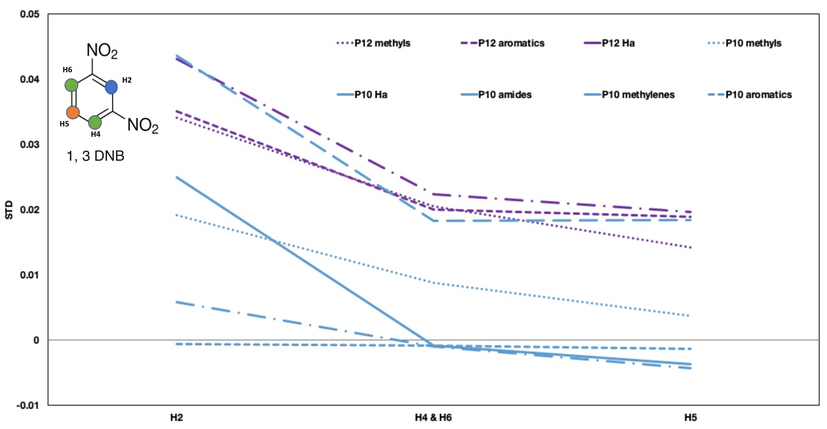
NMR spectroscopy

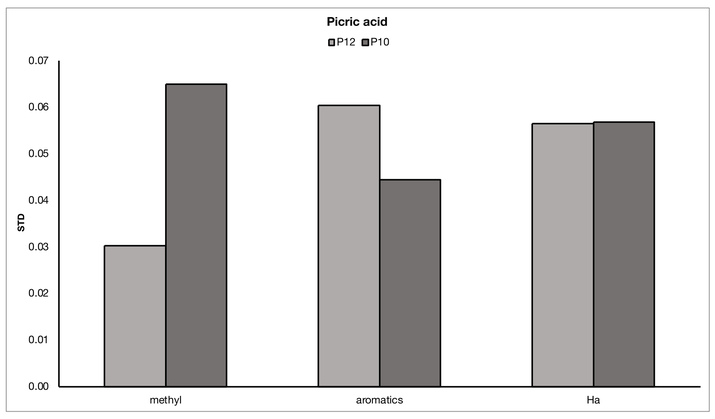
Peptides were analyzed as crude products in **DMSO-d$_6$** at 298 K on a Bruker Ascend **700 MHz** with TCI cryoprobe, at 30–40 mM concentration and **natural isotope abundance**. Due to sequence repetition and DMSO-induced unfolding, standard 2D methods (TOCSY, COSY, HMBC/HMQC) were ineffective. Instead, a strategy using ^{1}H-^{15}N HSQC, ^{1}H-^{13}C HSQC, ^{1}H-^{15}H SQC-TOCSY, and ROESY was employed. Full **assignment spectra** for one peptide required **16–20 hours**; 2D HSQC-TOCSY was acquired with **50% non-uniform sampling** (NUS). **Saturation transfer difference** NMR was probed to observe interactions between surrogate ligands (1, 3 dinitrobenze, picric acid) and peptides in D_2O.



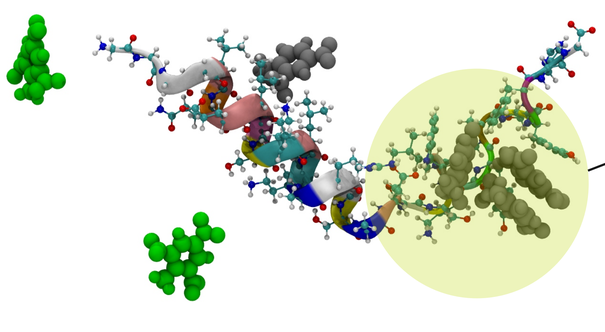


STD shows selectivity of P10 and P12 towards picric acid and 1,3 DNB



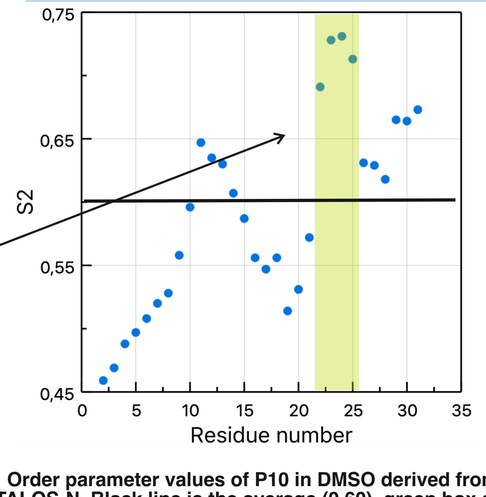


DNT binding to P10 obtained by MD simulations



Result of P10 interaction (AF^2 model) with 4 DNT and 4 TNT molecules W22 and Y25/Y28 in detail with 3 DNT molecules

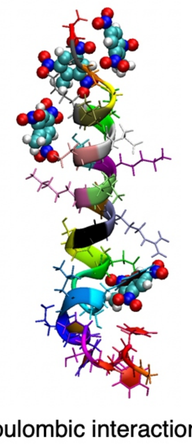
Predicted binding site most rigid in DMSO



Order parameter values of P10 in DMSO derived from TALOS-N. Black line is the average (0.60), green box are residues W22-Y25

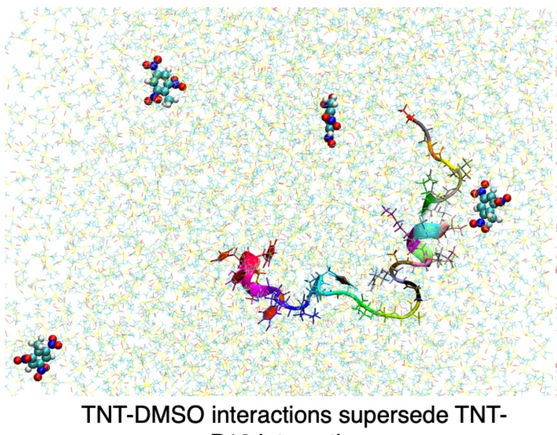
Role of a polar-solvent essential for TNT and DNT interactions with peptides

Gas-phase



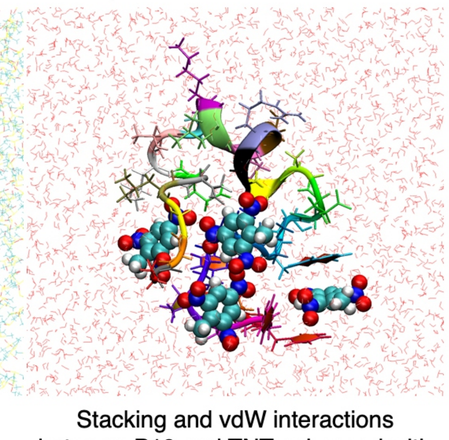
Coulombic interactions

Gas-phase structure solvated in DMSO



TNT-DMSO interactions supersede TNT-P10 interactions

Gas-phase structure solvated in water



Stacking and vdW interactions between P10 and TNT enhanced with water environment

References:

1. A.J.M. Barbosa, A.R. Oliveira, A.C.A. Roque, Trends Biotechnol. 36 (2018) 1244–1258
2. Du, Y.; Chen, J. Biomolecules (2021), 11, 1595
3. R. Benton, Proc. R. Soc. B Biol. Sci. 289 (2022) 20222054
4. Z. Kuang, S.N. Kim, W.J. Crookes-Goodson, B.L. Farmer, R.R. Naik, ACS Nano 4 (2010) 452–458
5. Jumper, J. et al. Nature (2021), 596, 583–589

Acknowledgement:
ESI-MS measurements were conducted under supervision of Prof. Markus Himmelsbach (Inst. of Analytical Chemistry, JKU Linz). NMR experiments were performed at 700 MHz Bruker AVANCE III (cryogenically cooled probe) at the NMR laboratory of the Upper Austrian - South Bohemian Research Infrastructure Center in Linz, co-financed by the European Union in the context of the project "RERI-uasb", EFRE RU2-EU-124/100-2010 (ETC Austria-Czech Republic 2007-2013, project M00146). This project „Laser-printed Early Warning Sensors: Quantum Detection of Chemical and Biological Agents (LiGAlert)" is supported from the Science for Peace and Security Program of NATO (project number SPS MYP G6112)

Design of biased GPCR modulators by combining artificial intelligence and molecular simulation

Alaa Reguei[1], Samuel Murail[1], Serge Luquet[2], Franck Oury[3], Pierre Tuffery[1]

[1]Unité de Biologie Fonctionnelle et Adaptative, INSERM ERL 1133, CNRS UMR 8251, Université Paris Cité, Paris, France

[2]Unité de Biologie Fonctionnelle et Adaptative, CNRS UMR 8251, Université Paris Cité, Paris, France

[3]Institut Necker Enfants Malades, INSERM UMR-U1151, CNRS UMR-8253, Université Paris Cité Paris, France

https://doi.org/10.17952/38EPS.2026.P517

1. Context of the study

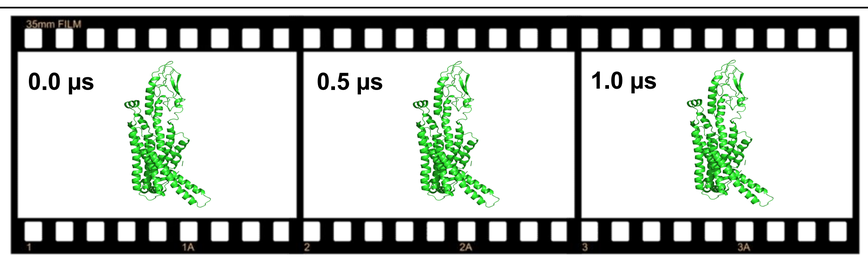
- G-protein coupled receptors (GPCR) are major drug targets involved in key physiological pathways.
- GPCRs Ligand bias: different ligands acting on the same receptor can selectively activate distinct intracellular signaling pathways.
- Parathyroid hormone receptor (PTH1R), a class B GPCR, is activated by two endogenous ligands PTH (parathyroid hormone) and PTHrP (parathyroid hormone-related peptide) **[1]**.

```
                        10        20        30
PTHrP/1-34   1 AVSEHQLLHDKGKSIQDLRRRFFLHHLIAEIHTA
PTH/1-34     1 SVSEIQLMHNLGKHLNSMERVEWLRKKLQDVHNF
```

Identity 32.35 %

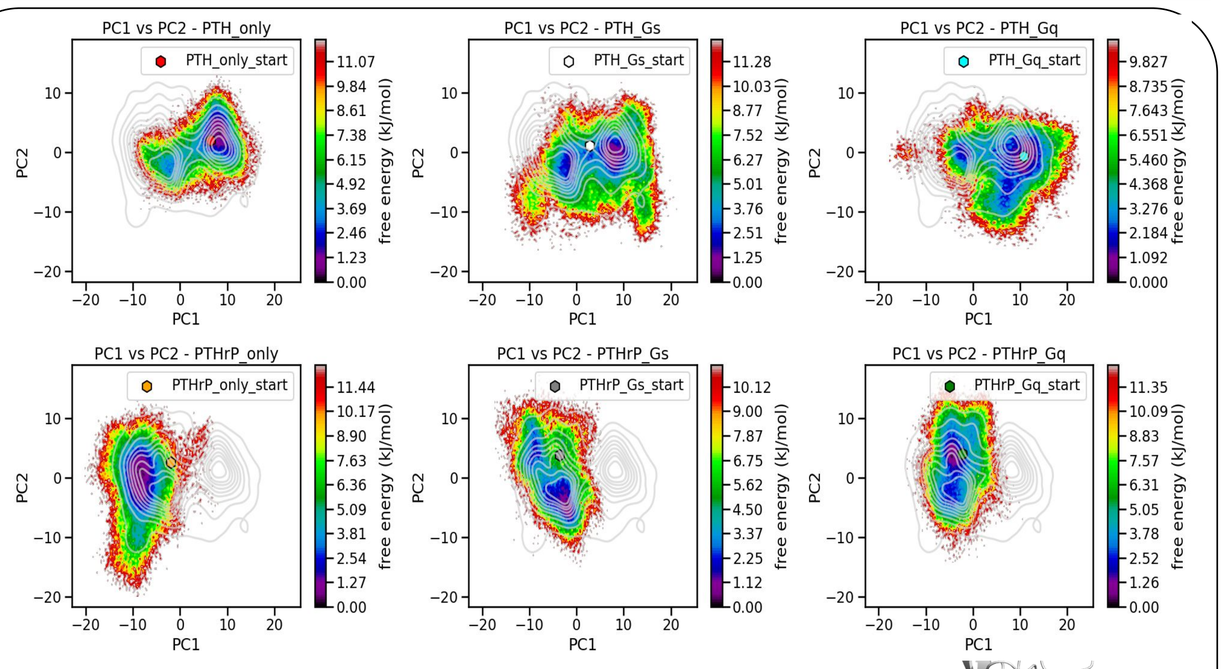
- They trigger distinct cellular responses , displaying distinct signaling profiles:
  - PTH → Gαs–cAMP–PKA
  - PTHrP → Gαq–PLCβ–PKC
- PTH1R is our study system as it showed evidences for ligand-biased signaling in the central nervous system **[2]**.
- **Objective**: To understand the molecular basis of PTH1R ligand bias using molecular dynamics simulations and identify strategies for designing biased GPCR modulators for potential therapeutic applications in metabolic disorders.

2. Molecular Dynamics: A Computational Microscope

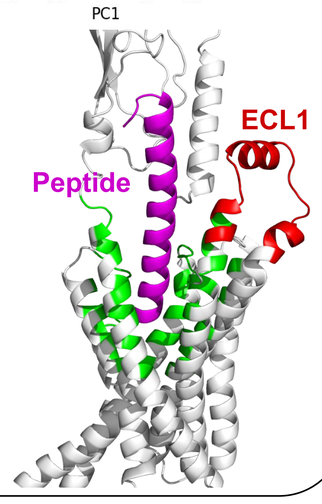


- Molecular dynamics (MD) is a computational technique that document the protein dynamics.
- The main output of MD simulation is a trajectory, which can be seen as a movie describing the evolution in time of a molecular system.
- This movie can capture every atomic movements and interactions in detail.
- These movie scenes can then be analysed using various techniques, including Principal Component Analysis (PCA), which captures the largest structural movements, or Time-lagged Independent Component Analysis (tICA), which identifies the slowest conformational transitions.
- For our simulated systems, these techniques are used to study the effect of ligands on receptor conformations, helping us understand the molecular basis of PTH1R ligand bias.

4. Peptide Binding Pocket Conformational Analysis



- PCA on binding pocket Cα residues (< 5 Å from ligand N-terminus; PC1 27%, PC2 10%) clearly separates PTH and PTHrP trajectories.
- PC1 loading analysis identifies Extracellular Loop 1 (ECL1) structural rearrangements as the primary driver of this conformational divergence.
- This dynamical divergence is strongly supported by recent literature **[4]**, showing that the long ECL1 acts as an electrostatic filter. Negatively charged ECL1 residues (E258–E260) repel acidic residues (E19, E22) in PTH while stabilizing the basic C-terminus of PTHrP, modulating peptide insertion and biasing downstream Gs *vs* Gq signaling.



3. Materials and Methods

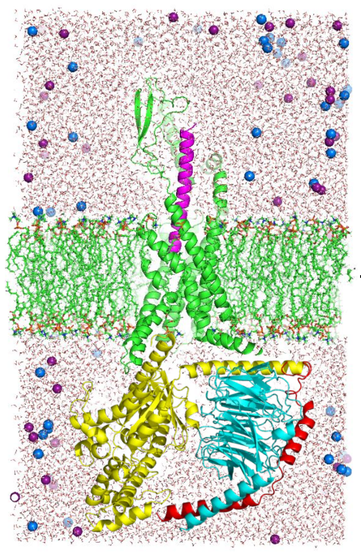
Structure Modelling (AlphaFold3)

↓

Membrane embedding POPC bilayer (CHARMM-GUI)

↓

All Atoms Molecular dynamics (OpenMM Program)



➔ AMBER14SB; PME, 1.0 nm cutoff; H-bond constraints; 4 fs timestep with HMR; Langevin thermostat, 300 K; semi-isotropic Monte Carlo barostat, 1bar

➔ Minimization (10,000 steps) + equilibration (2 NVT + 4 NPT) with 2.4 ns in total

↓

Conformational Analysis (PCA, tICA, Clustering, …)

↓

Peptide Design

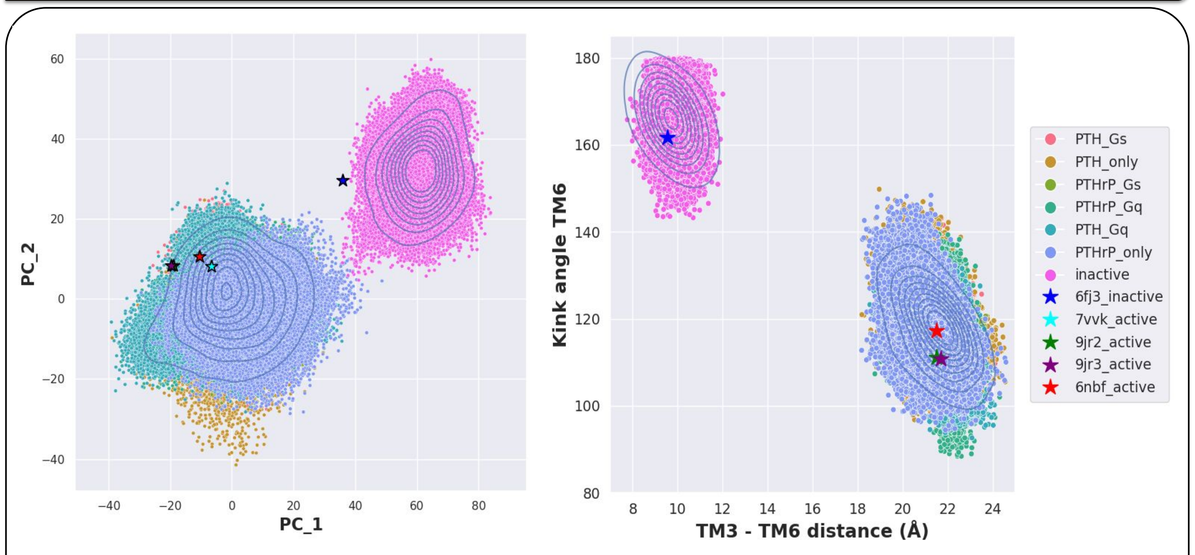
Simulated Systems

- PTH1R - **PTH** (10 rep *3 µs)
- PTH1R - **PTHrP** (10*3 µs)
- PTH1R - **PTH - Gs** (10*3 µs)
- PTH1R - **PTHrP - Gq :** (10*3 µs)
- PTH1R - **PTH - Gq** (10*2 µs)
- PTH1R - **PTHrP - Gs :** (10*2 µs)

[135,000 - 194,000 atoms]

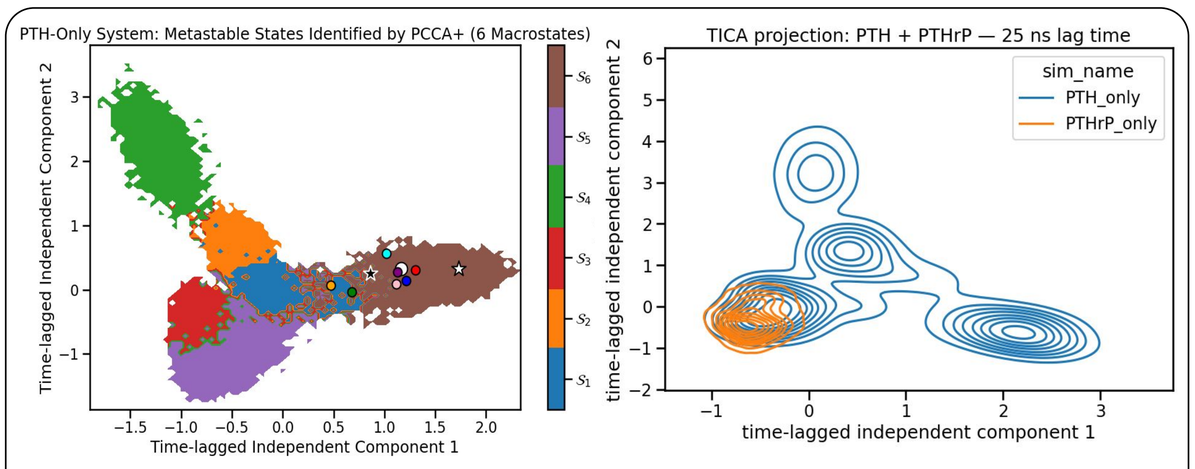
Total simulated time 160 µs

5. TMD Cα Backbone Conformational Analysis



- Key activation collective variables and PCA of the TMD Cα backbone confirm all simulated systems remain in an active conformation, separated from inactive (pink) **[3]**.
- No significant structural divergence between ligands, nor between Gs and Gq coupling.
- This suggests that signaling selectivity arises from subtler structural differences.

6. TMD tICA-Based Conformational Analysis



- Time-lagged Independent Component Analysis (tICA) based on TMD Residue-Residue Contact Scores (RRCS) was performed using a 25 ns lag time (validated via ITS plots), following the strategy of Zhou et al. **[5]**.
- PTH induces higher conformational flexibility, exploring multiple energy basins, whereas PTHrP remains confined to a single energy basin (also sampled by PTH).
- Preliminary results show that TIC1 is dominated by Arg2.60–Tyr6.53 interactions, and TIC2 by interactions between Phe5.51–Phe6.49 and His6.52–Phe6.56.
- Metastable Macrostates: PCCA + clustering performed on the PTH trajectory ensemble identified 6 metastable macrostates (validated by Chapman-Kolmogorov tests).
- Structural characterization of these macrostates is currently ongoing.

7. Conclusion

- Our findings highlight distinct pocket dynamics and conformational flexibility across ligands, resolving multiple metastable molecular states.
- These encouraging results pave the way for in-depth structural characterization to guide the rational design of biased PTH1R peptides.

References

1. Zhao LH, et al. Acta Pharmacol Sin. 2023.
2. Galerne M. PhD dissertation,. 2024.
3. Bansal P, et al. bioRxiv. 2026.
4. McArthur ES, et al. Biochemistry. 2026.
5. Zhou Q, et al. eLife. 2019.

Acknowledgements

- This research was funded by the MSD Avenir foundation, MSD being a trade name of Merck & Co., Université Paris Cité, and Inserm.
- This work was supported by a PhD grant from the MTCI Doctoral school (ED563) - IdEx program.

Radiolabelling in the New Age of Peptide Therapeutics

Cian Reid[1], Roger Glanville[1], Yukuang Guo[2], Eric Ballard[2] & Sean Zhu[2]

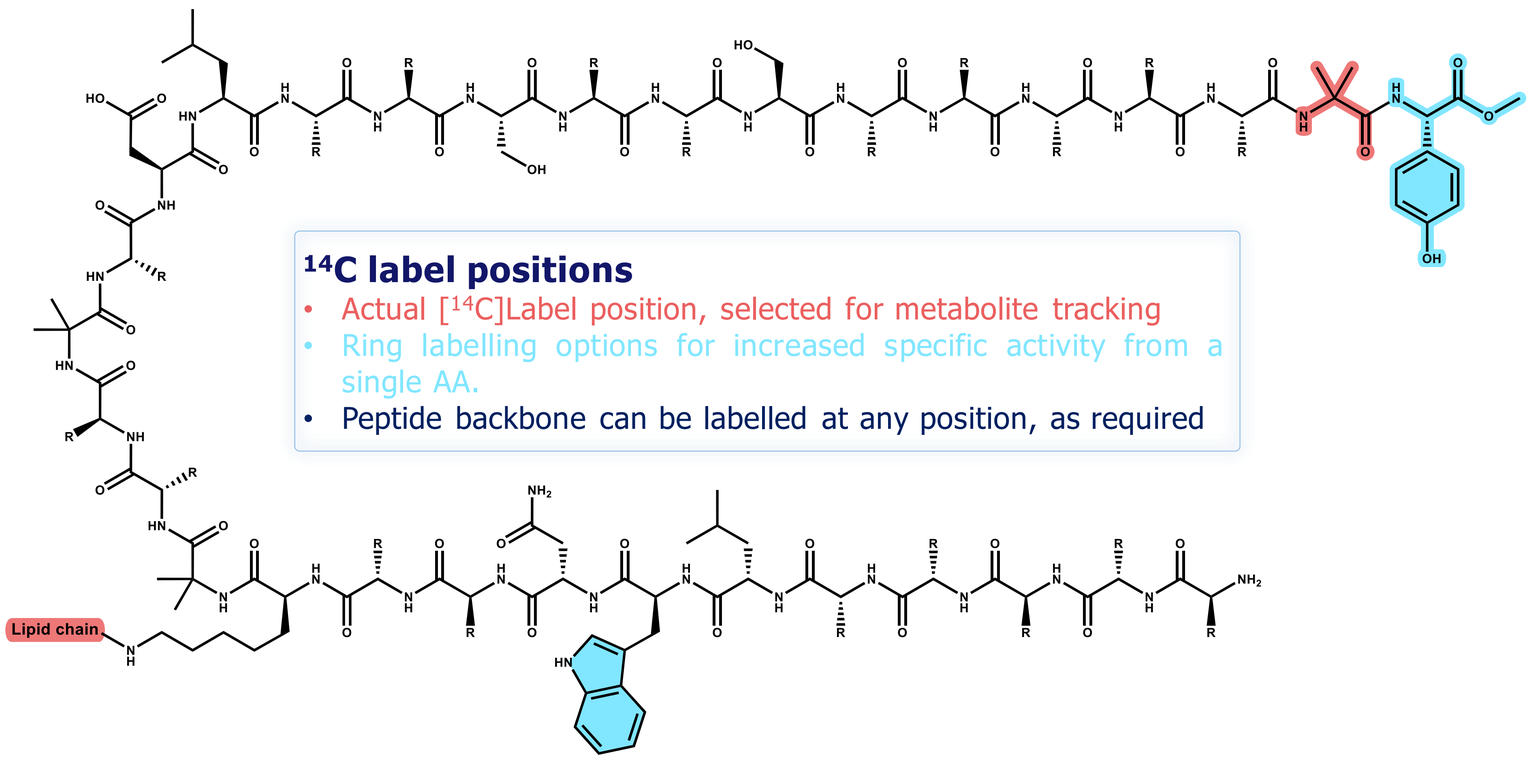
https://doi.org/10.17952/38EPS.2026.P449

[1]Pharmaron UK Ltd, Cardiff, UK
[2]Takeda Development Center Americas, Inc., Cambridge, MA. All authors are employees of Takeda and own stock and/or stock options in the company

bd@pharmaron.com | www.pharmaron.com

[^{14}C]TAK-510

[^{14}C]TAK-510 is a dual-radiolabelled, lipidated 31-amino acid peptide developed as a glucose-dependent insulinotropic polypeptide receptor (GIPR) agonist for the treatment of cyclic vomiting syndrome (CVS). The molecule is presented here as a case study demonstrating contemporary radiolabelling approaches for peptide therapeutics used in preclinical and early clinical development, including quantitative whole-body autoradiography (QWBA), mass balance, ADME, and human ADME (hADME) studies. Developed in partnership with Takeda to support a mass balance study, [^{14}C]TAK-510 incorporates two strategically positioned radiolabels: one within the peptide backbone at aminoisobutyric acid (AIB^{2}) and a second within the lipid moiety attached to Lys^{21}. This dual-labelling strategy enabled comprehensive profiling of metabolites and confirmed the presence of parent TAK-510 as the sole circulating drug-related component in plasma.



^{14}C label positions

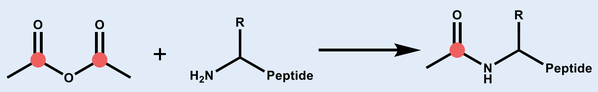
- Actual [^{14}C]Label position, selected for metabolite tracking
- Ring labelling options for increased specific activity from a single AA.
- Peptide backbone can be labelled at any position, as required

Peptide backbone

The traditional [^{14}C] labelling strategy for linear unmodified peptides is to position the label near the N-terminus or in an n-terminus acetylation, for convenience of synthesis. However, metabolic data may require labels to be incorporated towards the middle of the chain or in multiple locations in the sequence. If a high specific activity is required, more than one label could be required. Ring labelled amino acids such as phenylalanine and tyrosine can provide high specific activity by incorporating universally labelled aromatic rings which can be tuned to >120 mCi/mmol if required.

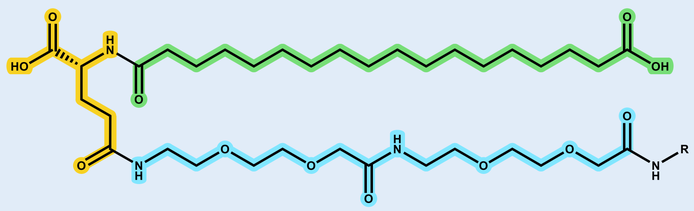
The high specific activity achieved with ring labelled compounds can prove suitable for tests that usually require high radioactivity/weight ratios, such as QWBA studies, which usually rely on the relatively high specific activity associated with tritiated compounds instead.

End capping the *N*-terminus with [^{14}C]acetic anhydride is one of the simplest ways to introduce a label into a peptide backbone



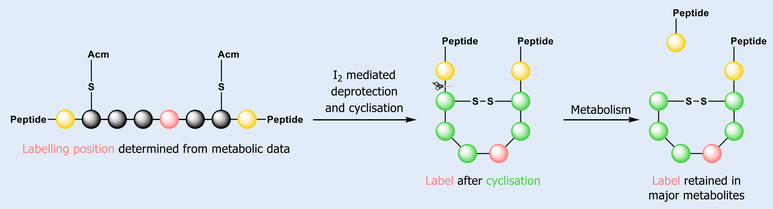
Lipidation

Lipidation is an increasingly common technique for extending peptide half-life and circulation time in the body. It has also provided additional convenient radiolabelling options. The spacers, γ-glutamic acid and lipids themselves can all be labelled. It is common for the lipid to be built on the resin after the completion of the main peptide chain. This is convenient for radiolabelling as it minimises the number of radioactive steps required. Below we've illustrated the lipid side chain of Semaglutide with the potential label sites highlighted. Most lipidation strategies use the similar functionalities which has prompted the development of synthetic strategies for [^{14}C] label incorporation into any length lipid, suitably protected γ-glutamic acid and 2-aminoethoxy-2-ethoxyacetic acid (AEEA).



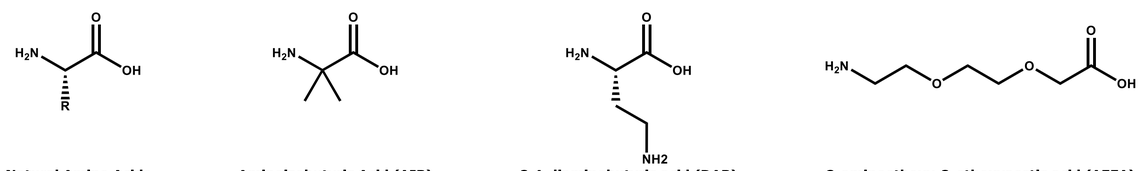
Cyclisation

Although not a consideration for TAK-510, the increase in cyclic therapeutic peptides with improved circulating half-life, target specificity, and conformational stability has required a shift in labelling strategy. From a preclinical study perspective, these metabolically robust cyclic structures can persist in vivo for extended periods and are often present in most identifiable metabolites. Therefore, they require appropriate radiolabelling to enable comprehensive metabolite identification and profiling during preclinical development. This frequently necessitates incorporation of the radiolabel at positions located deep within the loop/s to ensure retention of the label.



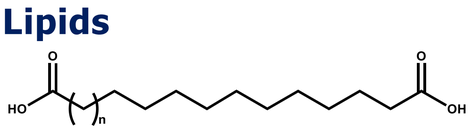
Library of available labelling locations

Natural and non-natural amino acids



We have the capability to label at multiple sites in all natural amino acids as well as a host of non-natural amino acids. Our library of non-natural amino acids is continuously being expanded.

Lipids



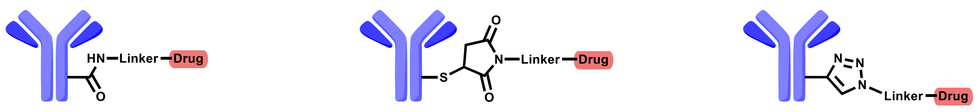
As lipid side chains have become an important part of increasing the bioavailability and reducing degradation of peptide-based drugs radiolabelling at various sites on the lipid has become more important. With the capacity to label throughout the chain and at either of the carbonyl groups, the entire lipid can be labelled based on customer needs or convenience.

PEGs



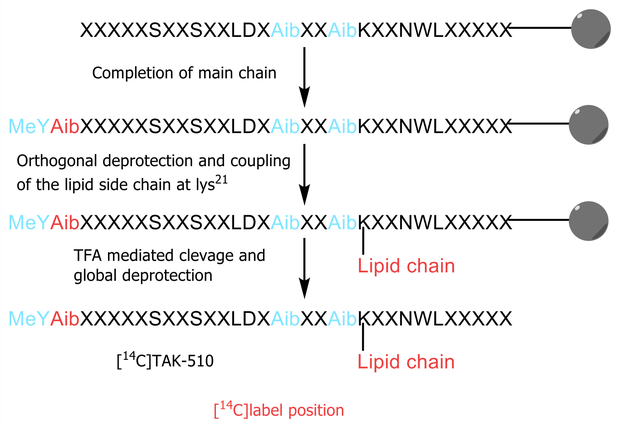
PEGylation is another common technique of adjusting the target specificity or circulating half-life of peptides in vivo. We've developed highly flexible labelling strategies that can accommodate linear or branched PEGs of any size. Labelling sites include the main chain, terminal residues and branched linkers.

Antibody Drug Conjugates (ADCs)



We can label ADC drug payloads using lysine-peptide ligation, thiomaleimide chemistry, or (2+3) cycloaddition. ADCs are purified using diafiltration, tangential flow filtration (TFF), and size exclusion chromatography (SEC). We determine ^{14}C-labelled drug-to-antibody ratios (DAR) and provide SEC-HPLC, RP-HPLC, and mass spectrometry analysis. We also operate with OEB 5 containment capability.

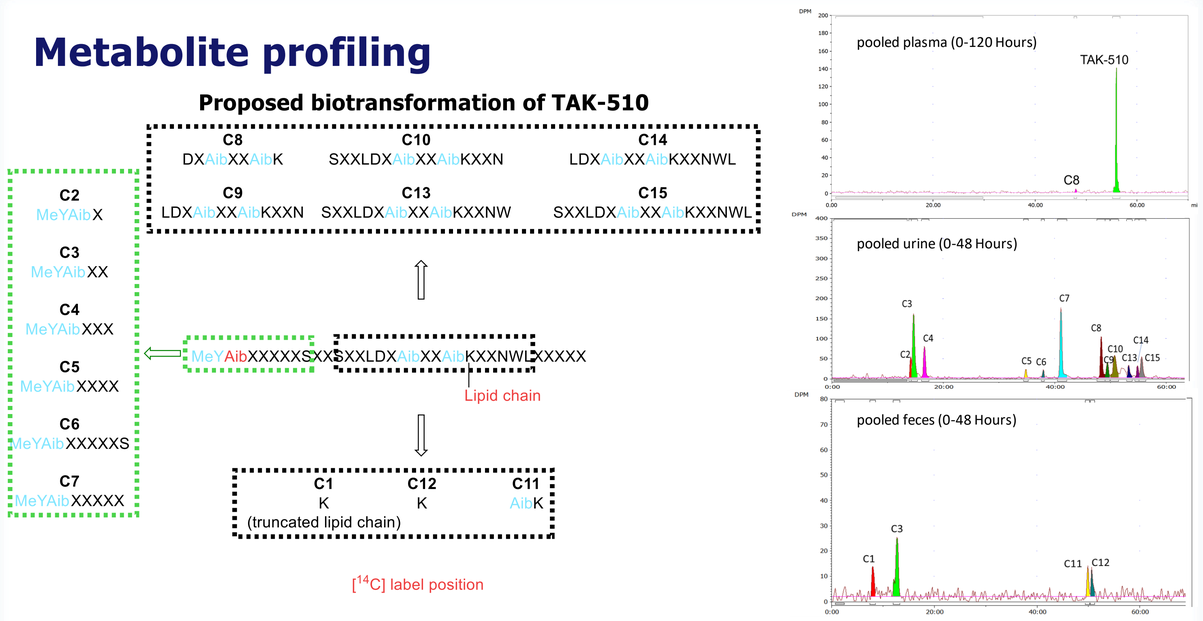
Synthesis



[^{14}C]TAK-510 was synthesised on resin using orthogonal protection on lys^{21} to build the peptide backbone, coupling the [^{14}C]aib^{2} and MeY^{1} to complete the main chain. Once complete, lys^{21} was deprotected and the lipid side chain was built up using standard Fmoc chemistry. Global cleavage and deprotection under TFA conditions yielded crude TAK-510 which was purified by preparative HPLC.

While this was a convenient strategy for obtaining the desired label positions it was noted that there was significant wastage of labelled material when coupling onto the side chain due to its proximity to the C-terminus. This required more lipid-labelled material than anticipated to achieve complete coupling of the exposed lysine side chain.

Metabolite profiling



The above data was first published at ISSX 2024 by Yukuang Guo, Eric Ballard, Sean Zhu: **Takeda Development Center Americas, Inc., Cambridge, MA**

https://doi.org/10.17952/38EPS.2026.P449

Catalytic peptide-based coacervates for enhanced function through structural organization and substrate specificity

David Reis[1], Sara Pereira[1], Ana P. Ramos[1], Pedro M. Pereira[1], Leonor Morgado[2], Joana Calvário[1] and Ana S. Pina[1]

Drq.reis@itqb.unl.pt

[1] Instituto de Tecnologia Química e Biológica António Xavier, Universidade Nova de Lisboa, Av. da República,, 2780-157 Oeiras, Portugal

[2] Associate Laboratory i4HB – Institute for Health and Bioeconomy and UCIBIO – Applied Molecular Biosciences Unit, NOVA School of Science and Technology, Universidade NOVA de Lisboa, 2829-516 Caparica, Portugal

https://doi.org/10.17952/38EPS.2026.P029

INSTITUTO DE TECNOLOGIA QUÍMICA E BIOLÓGICA ANTÓNIO XAVIER | ITQB.UNL.PT

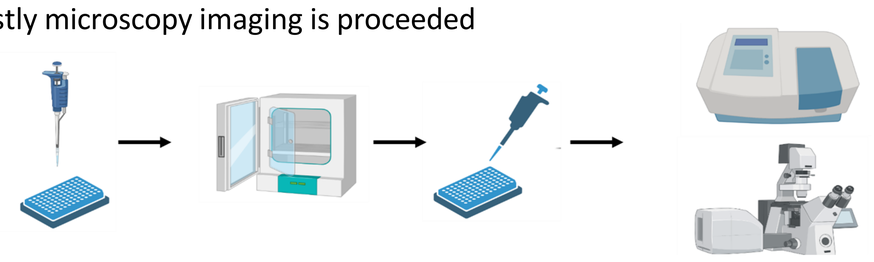
Bioinspired Peptide Systems Laboratory

Introduction

Cells use membrane-less organelles formed by liquid–liquid phase separation (LLPS) to spatially regulate biochemical reactions[1]. In polymer and colloid science, this process is known as coacervation and provides a framework for understanding biomolecular condensates. Nature exploits LLPS-driven coacervation in diverse contexts, such as β-carboxysome biogenesis[2]. Although coacervation has been widely explored to enhance enzyme activity, its application to catalytic peptides remains limited. Here, we show that LLPS-driven coacervation modulates P7, a 12-residue β-hairpin peptide with modest phosphatase activity and affinity for phosphorylated assemblies[3]. P7 coacervates adopt a fully folded β-hairpin conformation, forming densely packed internal domains, and compartmentalize guest molecules depending on charge and hydrophobicity, showing high affinity towards phosphorylated assemblies[4]. Remarkably, P7 coacervates yield a 15,000-fold increase in catalytic efficiency toward pNPP hydrolysis, underscoring their potential for advancing enzymatic applications.

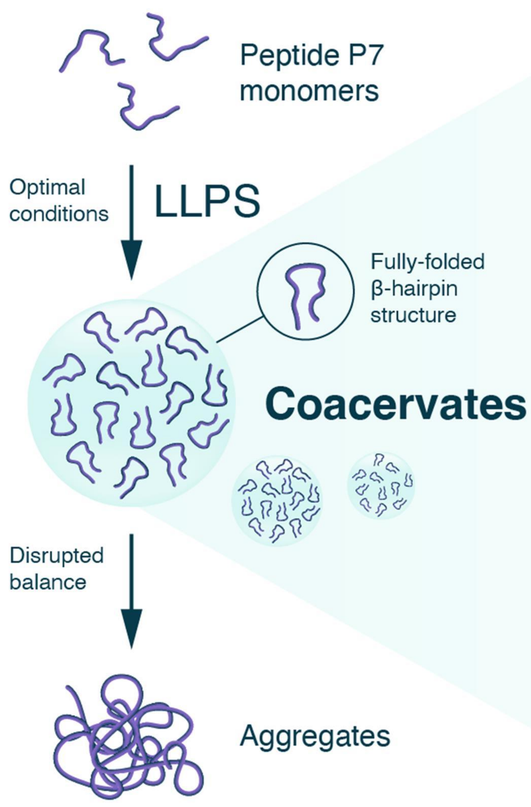
Methodology

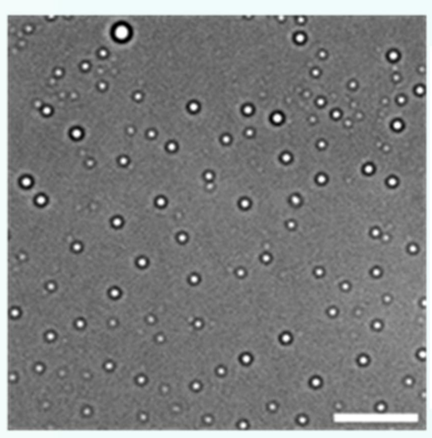
- Coacervation was achieved by mixing 5 mg/mL of P7 peptide[4] in 100mM of sodium phosphate buffer, containing 1M NaCl, at pH 8.0, to final peptide concentration of 1mg/mL
- This is followed by 1h of incubation at 27°C, leading to the formation of a milky-like state
- Lastly microscopy imaging is proceeded

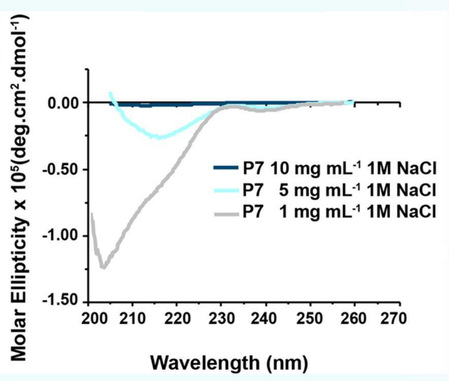


Results and Discussion

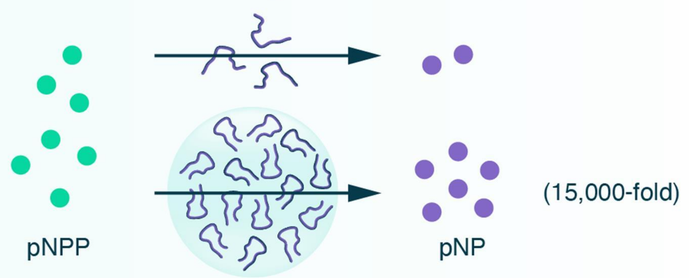
LLPS Propensity



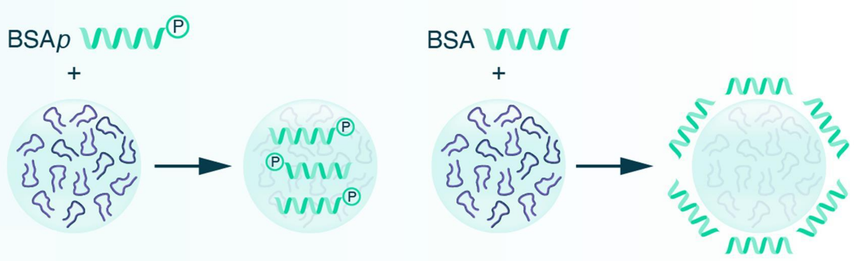




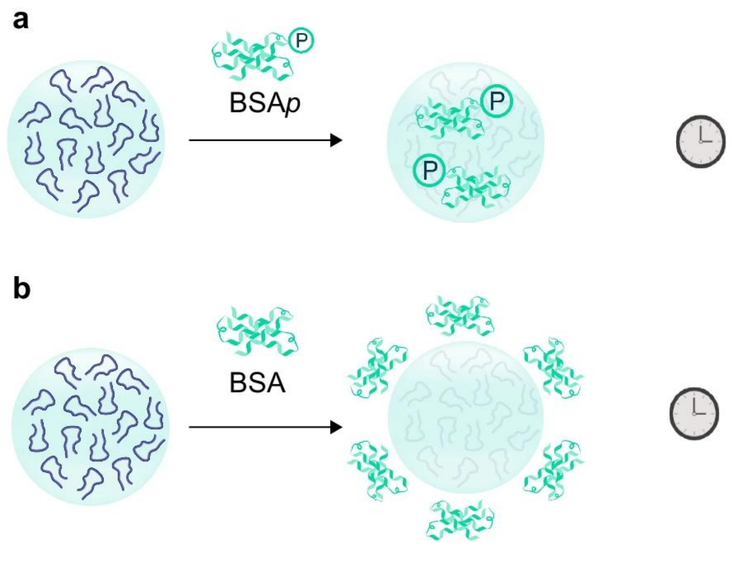
① Increased catalytic efficiency

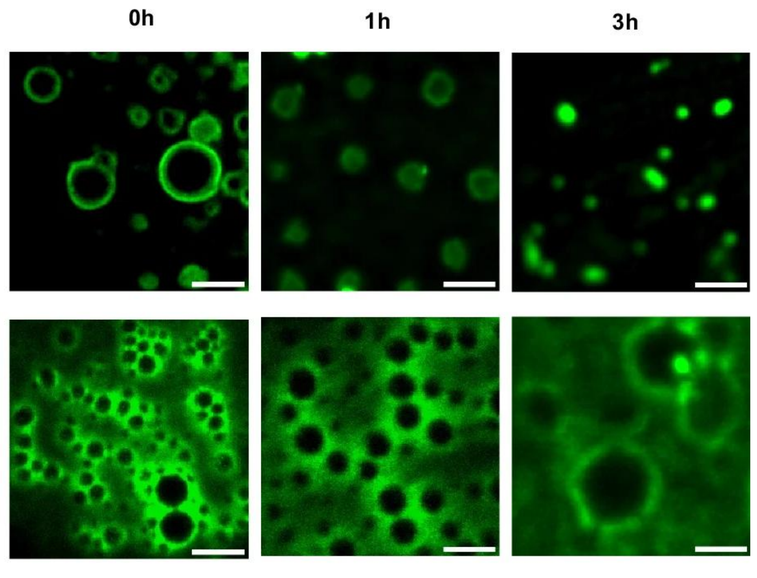


② Affinity-mediated molecular uptake



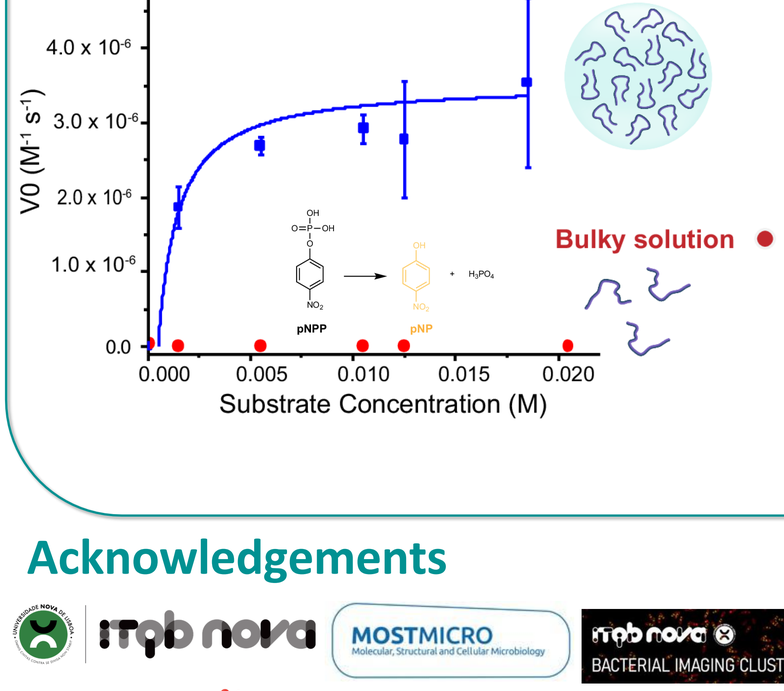
Affinity-mediated Sequestration





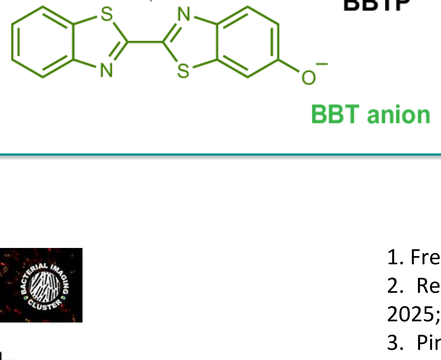
- Upon coacervate formation, P7's affinity for phosphorylated assemblies facilitates the sequestration of phosphorylated supramolecules (BSAp).
- P7 coacervates demonstrate a faster sequestration of phosphorylated BSAp compared to non-phosphorylated BSA.

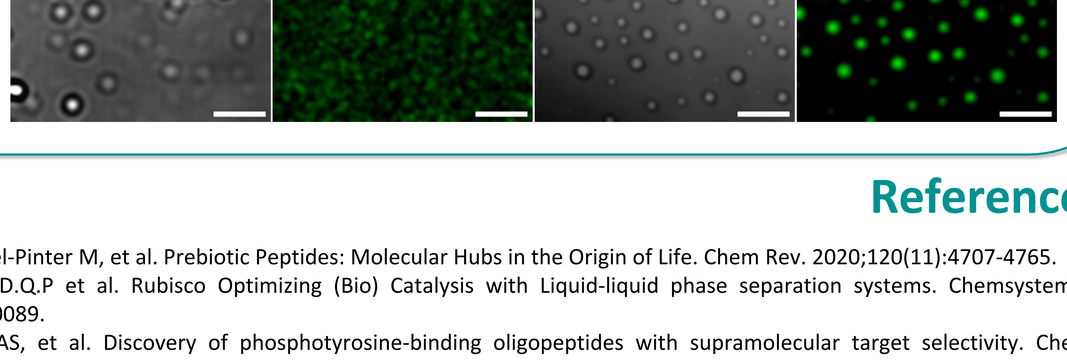
Catalytic Microreactors



Catalyst	k_{cat} (s^{-1})	K_M (M)	k_{cat}/K_M ($M^{-1}\ s^{-1}$)
P7-based Peptide Coacervates	(4.9 ± 0.6) x10^{-3}	(8.2 ± 3.2) x 10^{-4}	5.9 ± 0.2
P7 Peptide in solution	(1.0 ± 0.0) x10^{-5}	(1.4 ± 3.2) x 10^{-2}	(4.0 ± 0.3) x 10^{-4}

- 15,000-fold increase when P7 peptide coacervates are formed
- The catalytic reaction takes place within P7 coacervates





Acknowledgements

MOSTMICRO Molecular, Structural and Cellular Microbiology

BACTERIAL IMAGING CLUSTER

ROYAL SOCIETY OF CHEMISTRY | UCIBIO Applied Molecular Biosciences Unit | NOVA SCHOOL OF SCIENCE & TECHNOLOGY | i4HB Institute for Health and Bioeconomy | fct Fundação para a Ciência e a Tecnologia

References

1. Frenkel-Pinter M, et al. Prebiotic Peptides: Molecular Hubs in the Origin of Life. Chem Rev. 2020;120(11):4707-4765.
2. Reis, D.Q.P et al. Rubisco Optimizing (Bio) Catalysis with Liquid-liquid phase separation systems. Chemsystemschem 2025;e00089.
3. Pina AS, et al. Discovery of phosphotyrosine-binding oligopeptides with supramolecular target selectivity. Chem Sci. 2022;13(1):210-217.
4. Reis, D.Q.P, et al. Catalytic peptide-based coacervates for enhanced function through structural organization and substrate specificity. Nat Commun. 2024 ;15,9368.

Funded by
Deutsche Forschungsgemeinschaft
German Research Foundation

Deciphering the Fluorous Effect in Protein Quaternary Assembly

David Reiter,[1] Jacob S. Jordan,[1] Javier Camargo Díaz,[1] Malkeet Singh,[2] Moritz Engl,[1] Kevin Pagel,[1] Beate Paulus,[1] Mario Schubert,[1] Christian Roth,[2] and Beate Koksch[1]

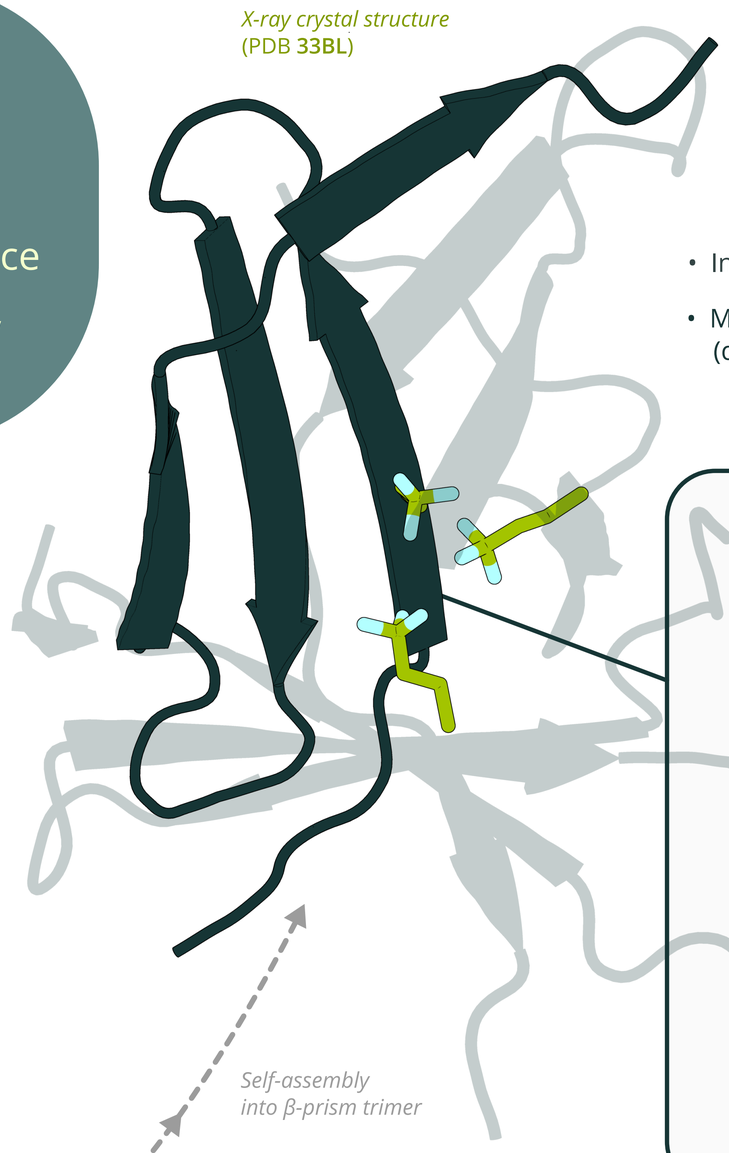
[1] Institute of Chemistry and Biochemistry, Freie Universität Berlin, Germany, [2] Max Planck Institute of Colloids and Interfaces, Potsdam, Germany
david.reiter@fu-berlin.de | orcid.org/0009-0009-9136-0717 | https://doi.org/10.17952/38EPS.2026.P461

Summary

- β-Sheet protein trimer, accessible by chemical synthesis
- Fluorine-substitution at trimer interface
- Structure/stability investigation (X-ray crystallography, NMR, native MS, CD)

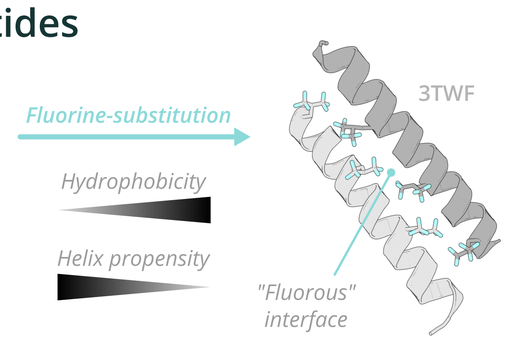
Highlights

- Defined quaternary strucuture with **fluorine cluster**
- Noncovalent, electrostatic **R–CF₃···F interaction**

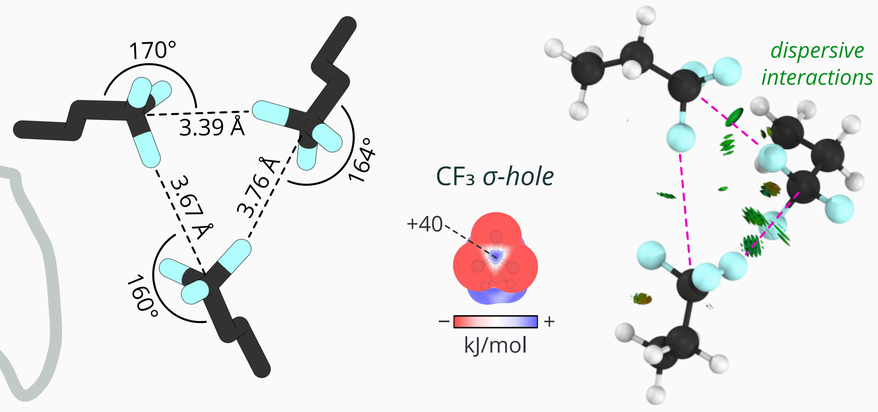


Previous studies focused mainly on coiled-coil peptides

- Increased coiled-coil stability[1 2]
- Modulation of cc oligomerization (dimer, trimer, etc.)[3]



Noncovalent R–CF₃···F Interaction

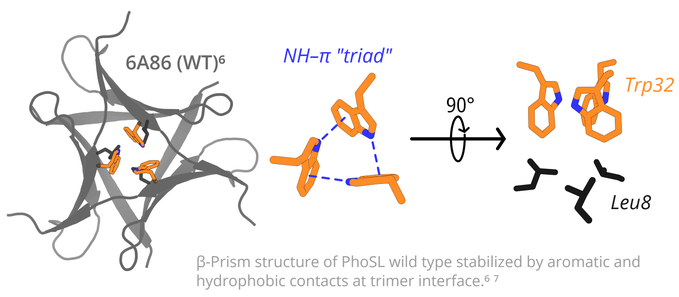


$$E_{int} = E_{ABC} - [E_A + E_B + E_C] = -3.4 \text{ kJ/mol}$$

Near-linear, σ-hole directed R–CF₃···F arrangement resembles tetrel bond.[4 5] Quantum chemical analysis (TPSSh-D3BJ/def2-TZVP) of truncated side chain model using crystal structure coordinates: Non-covalent, dispersive interactions characterized by NCI analysis are shown as green discs. Interaction energy of the trimer calculated at RI-MP2/def2-TZVP level.

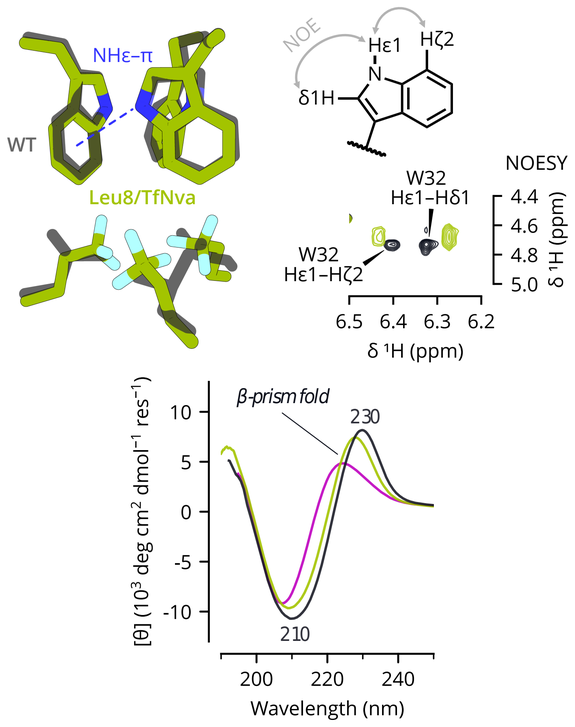
*A modular **β-strand scaffold** to investigate noncovalent **side chain interactions** in **protein self-assembly***

Pholiota squarrosa lectin (PhoSL)



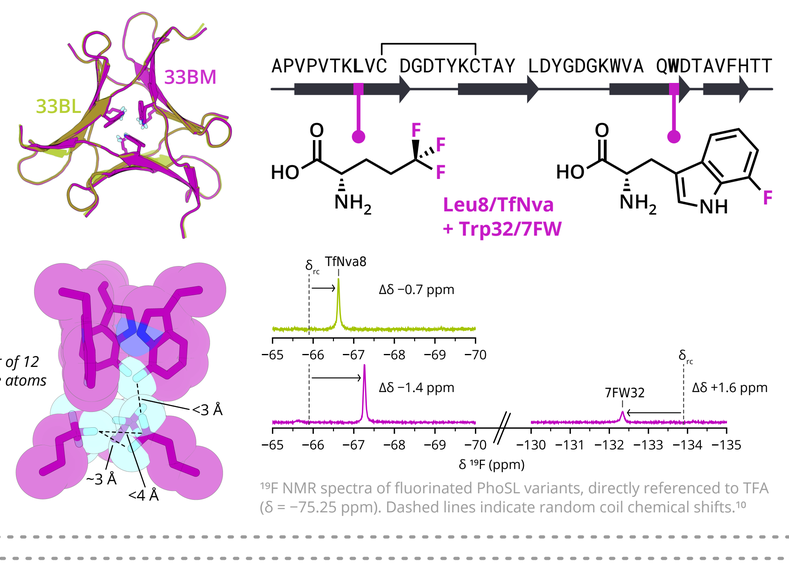
β-Prism structure of PhoSL wild type stabilized by aromatic and hydrophobic contacts at trimer interface.[6 7]

Interactions at trimer interface



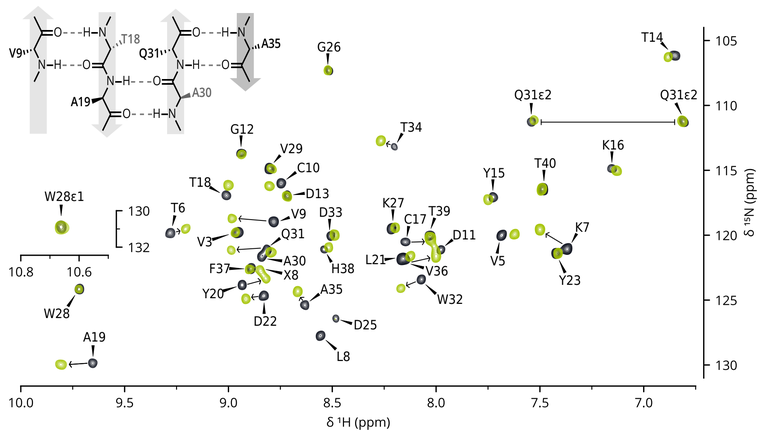
CD spectra of PhoSL variants (50 µM, pH 7.5, 20 °C)

High degree of fluorination tolerated



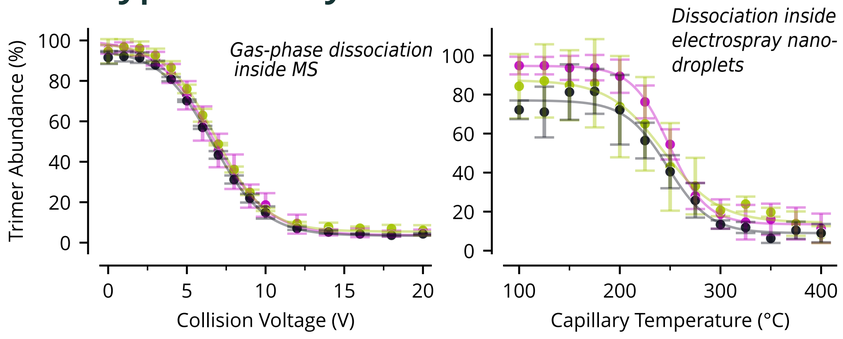
¹⁹F NMR spectra of fluorinated PhoSL variants, directly referenced to TFA (δ = −75.25 ppm). Dashed lines indicate random coil chemical shifts.[10]

Global protein structure conserved



¹H-¹⁵N HSQC spectra of wild type (gray) and Leu8/TfNva substituted PhoSL (lime) with scheme representing cross-strand hydrogen bond network.

Wild-type stability retained



Dissociation of PhoSL trimers in the gas-phase and in quasi-solution monitored by native MS.[8 9]

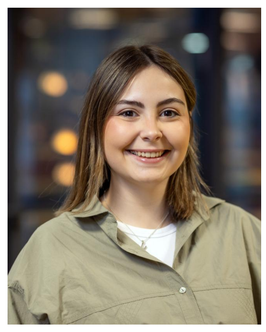
References

This work: Reiter, D., et. al. *Manscript submitted for publication*.
1. Berger, A. A., Völler, J.-S., Budisa, N. & Koksch, B. *Acc. Chem. Res.* **50**, 2093–2103 (2017).
2. Buer, B. C., Meagher, J. L., Stuckey, J. A. & Marsh, E. N. G. *Proc. Natl. Acad. Sci. U.S.A.* **109**, 4810–4815 (2012).
3. Hohmann, T., Dubatouka, P., Pfeifer, K. & Koksch, B. *Biomacromolecules* **24**, 3357–3369 (2023).
4. García-LLinás, X., Bauzá, A., Seth, S. K. & Frontera, A. *J. Phys. Chem. A* **121**, 5371–5376 (2017).
5. Varadwaj, P. R., Varadwaj, A., Marques, H. M. & Yamashita, K. *CrystEngComm* **25**, 1411–1423 (2023).
6. Yamasaki, K. et al. *Glycobiology* **29**, 576–587 (2019).
7. Yamasaki, K., Tsuzuki, S. & Tateno, H. *J. Phys. Chem. B* **128**, 7401–7406 (2024).
8. Jordan, J. S. & Williams, E. R. *Anal. Chem.* **94**, 16894–16900 (2022).
9. Jordan, J. S., Chen, C. J., Lee, K. J. & Williams, E. R. *J. Am. Chem. Soc.* **147**, 3412–3420 (2025).
10. Reiter, D., Türk, S., Schubert, M. & Koksch, B. *J. Fluorine Chem.* **291**, 110567 (2026).

Acknowledgements

DR and BK gratefully acknowledge financial support by the Deutsche Forschungsgemeinschaft (DFG) through the collaborative research center (CRC) 1349 "Fluorine-Specific Interactions", project-no. 387284271. We thank the DFG-funded CoreFacility BioSupraMol, project-no. 213868804, for providing access to advanced analytical instruments.

CYTOSKELETON STABILIZED ARTIFICIAL CELLS AND THEIR DYNAMIC BEHAVIOUR



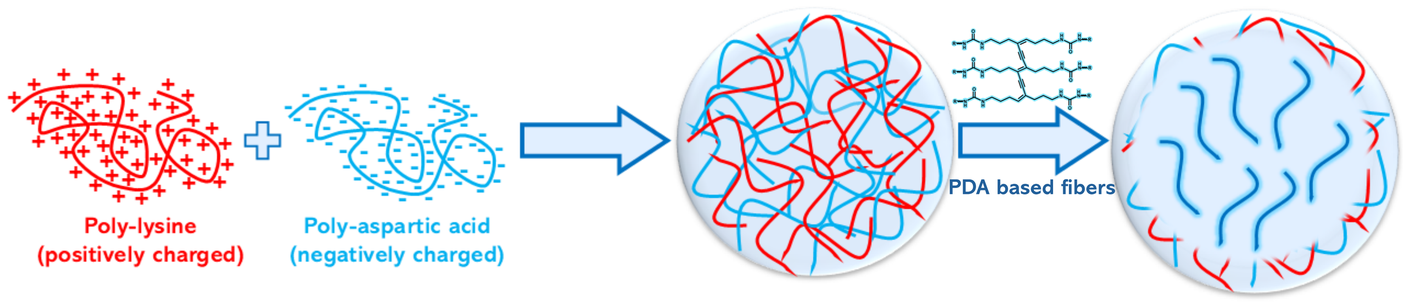
Victoria Remacha[1], Lars Paffen[1], Andoni Rodríguez[1], Angshuman Das[1], Roi Lopez[1], Jan van Hest[1].

[1]Eindhoven University of Technology, department of Chemical Engineering and Chemistry, Bio-Organic Chemistry Group, De Groene Loper 3, 5612 AE Eindhoven/Netherlands, m.v.remacha.goni@tue.nl

https://doi.org/10.17952/38EPS.2026.P545

INTRODUCTION

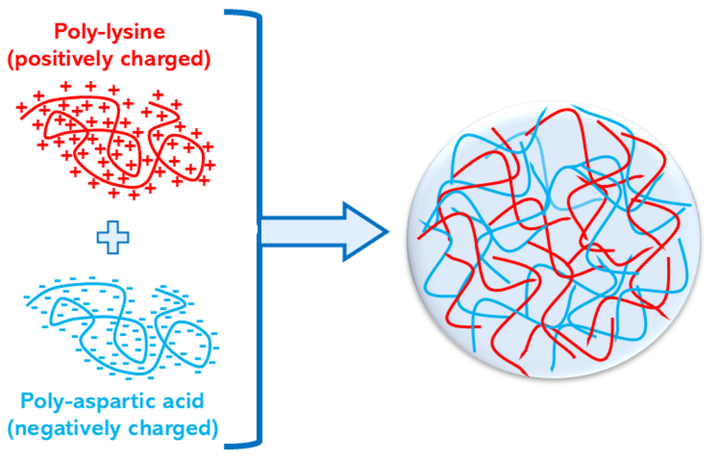
The development and characterization of **artificial cells** is a research field of high potential because these artificial systems can **mimic features and functions of life**, being able to exchange biomolecules with each other or respond to changes in their environment as pH or temperature, which makes them suitable for **biomedical applications.**[1]



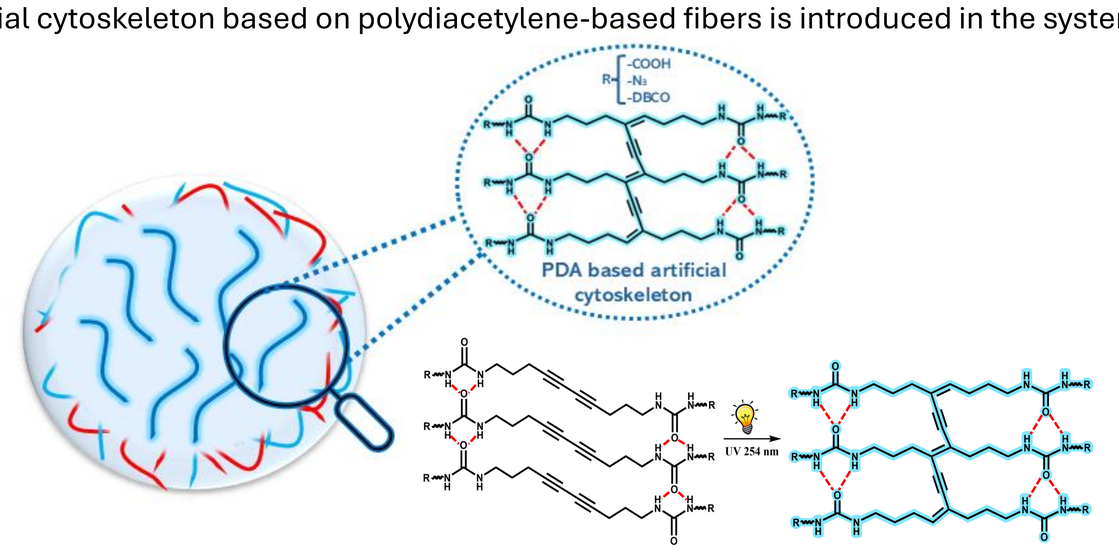
The **objective** of this project is to develop an artificial cell system based on **phase-separated polypeptides** and introduce inside it an **artificial cytoskeleton** based on **polydiacetylene fibers.**[3]

METHODOLOGY

Our artificial cells are originated by mixing of two opposite charged polypeptides: poly-lysine and poly-aspartic acid, leading to micron-sized droplets.

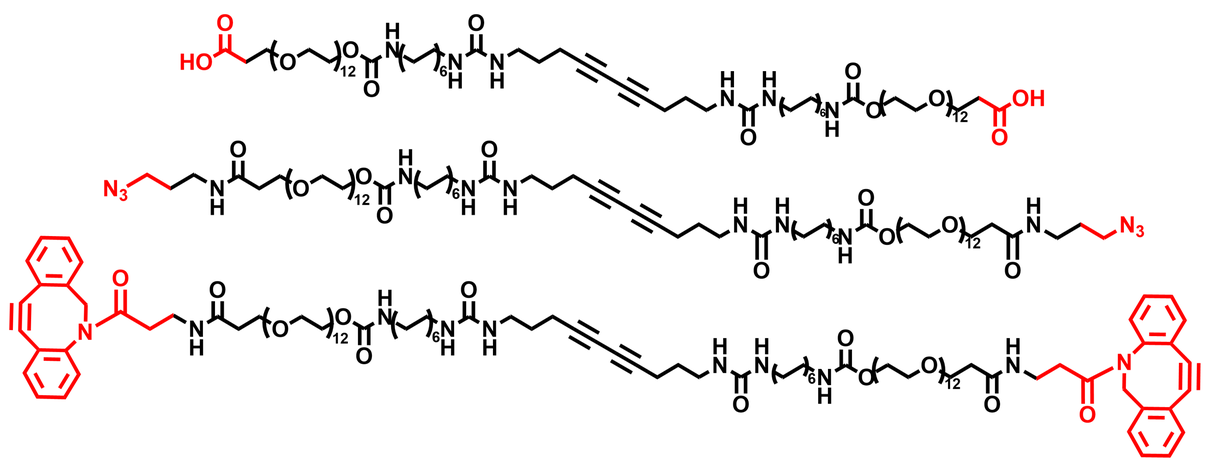


An artificial cytoskeleton based on polydiacetylene-based fibers is introduced in the system.[3,4]



The self assembly of the fibers is possible due to the hydrogen bonds between the bis-urea and the carbonyl groups, and the π-π stacking of the diacetylene backbone.[3,4]

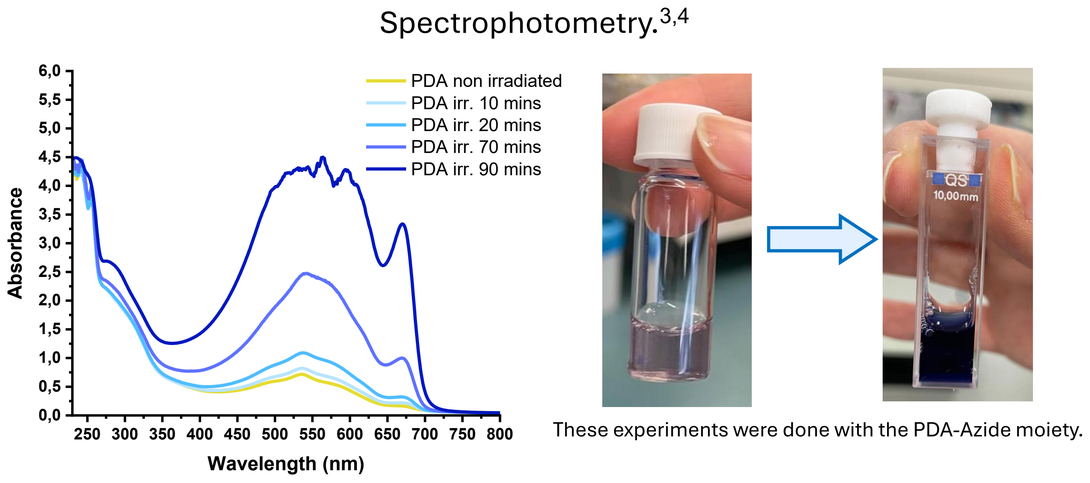
The photopolymerization induces a conjugated system, which stabilizes the fibers self-assembly and presents self-fluorescence.[3,4]



The terminal groups of these molecules allow them to be functionalized with peptides and small biomolecules such as DNA, which will be explored in the future.[3]

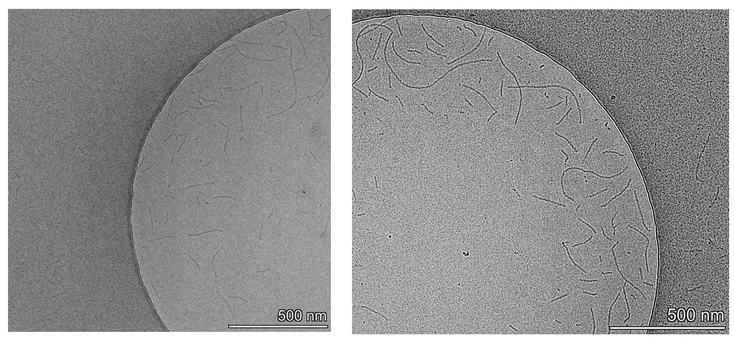
RESULTS

The photopolymerization of the fibers was achieved, showing a color change from transparent to blue, which was also analyzed by UV-Vis Absorbance Spectrophotometry.[3,4]

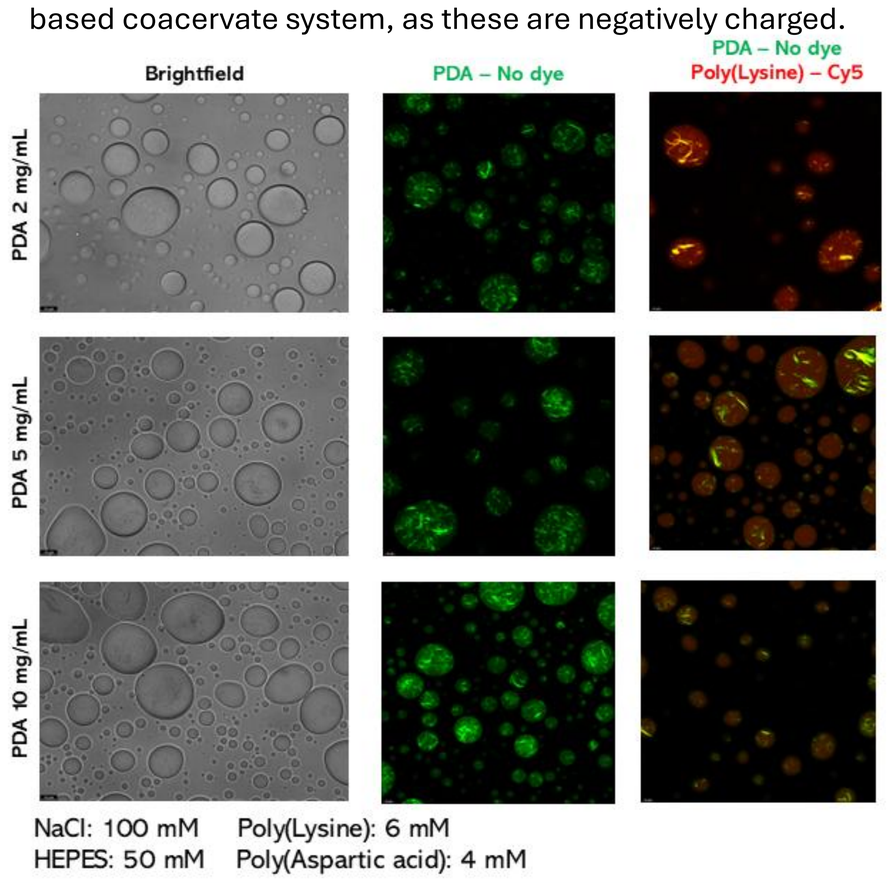


These experiments were done with the PDA-Azide moiety.

The obtained morphology was characterized by **Cryo-TEM**. PDA-COOH fibers are approximately 6 nm thick and 100-400 nm long.[3]



PDA-Azide fibers were successfully introduced into the positive polypeptide-based coacervate system, as these are negatively charged.



CONCLUSIONS AND OUTLOOK

- ✓ **Polydiacetylene-backboned molecules self-assemble** into **fibers** by hydrogen bonding and π-π stacking , followed by stabilization by photopolymerization.
- ✓ The **photopolymerization** of the **polydiacetylene-based molecules** leads to a color change and autofluorescence of the fibers.
- ✓ **Polydiacetylene fibers** have been successfully introduced in the **polypeptide-based coacervate system.**
- ✓ Introduction of biomolecules into the artificial cell system will be performed in the future by linking them to the PDA fibers.

REFERENCES

1.Cook AB, Novosedlik S, van Hest J. Complex Coacervate Materials as Artificial Cells. Accounts of Materials Research. 2023 Feb 13;4(3):287–98.
2.Cook AB, Schlich M, Manghnani PN, Moore TL, Paolo Decuzzi, Palange AL. Size effects of discoidal PLGA nanoconstructs in Pickering emulsion stabilization. Journal of Polymer Science. 2022 Jan 20;60(9):1480–91.
3.Novosedlik S, Reichel F, Thijs van Veldhuisen, Li Y, Wu H, Janssen H, et al. Cytoskeleton-functionalized synthetic cells with life-like mechanical features and regulated membrane dynamicity. Nature Chemistry [Internet]. 2025 Jan 3; Available from: https://www.nature.com/articles/s41557-024-01697-5
4.Pal A, Panayiotis Voudouris, Marcel, Pol Besenius, Wyss HM, Volkan Degirmenci, et al. Topochemical polymerization in self-assembled rodlike micelles of bisurea bolaamphiphiles. Soft Matter. 2013 Dec 2;10(7):952–2.

This project has been founded by ERC with the grant PRO-ARTIS-ERC-2023-ADG-ST-101141866-ST

Investigation of the interactions between mannosylated desmuramyl peptides and mannose-binding proteins

Marija Paurević[1], Vesna Petrović Peroković,[2] Željka Car,[2] Rosana Ribić[3]

[1]Department of Chemistry, Josip Juraj Strossmayer University of Osijek, Ulica cara Hadrijana 8/A, HR-31000 Osijek, Croatia
[2]Department of Chemistry, Faculty of Science, University of Zagreb, Horvatovac 102a, HR-10000 Zagreb, Croatia
[3]University North, University Center Varaždin, Jurja Križanića 31b, HR-42000 Varaždin, Croatia
Email: rribic@unin.hr
https://doi.org/10.17952/38EPS.2026.P454

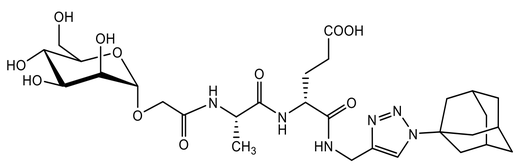
INTRODUCTION

N-acetylmuramyl-L-alanyl-D-isoglutamine, known as muramyl dipeptide (MDP) represents the minimal peptidoglycan fragment showing immunostimulatory activity. Introduction of lipophilic groups to desmuramyl peptide core (L-alanyl-D-isoglutamine, DMP) of MDP leads the derivatives with improved pharmacological properties. We have prepared mannosylated adamantane-containing DMPs with immunostimulatory properties in vivo.[1,2] It has been demonstrated that conjugation of mannose to DMP plays a significant role in enhancing immune stimulation. However, the specific pattern-recognition receptors activated by these mannosylated DMPs remain undefined, and a contribution of mannose-mediated binding to mannose receptors cannot be excluded.

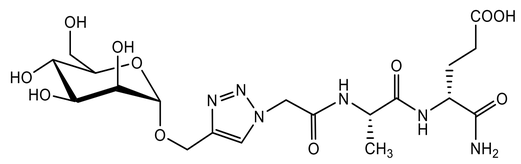
To address this question, we investigated the binding of a representative mannosylated DMP to mannose-binding protein: concanavalin A (ConA) and the macrophage mannose receptor (MR). ConA is a plant lectin that selectively recognizes α-D-mannose and mannose-rich N-linked oligosaccharides through a well-defined carbohydrate-binding site stabilized by Ca^{2+} and Mn^{2+} ions.[3] It is frequently used as an experimental model system for studying interactions relevant to immunologically important mannose-recognizing receptors (e.g., C-type lectin receptors) involved in pathogen recognition and antigen uptake. In contrast, the macrophage mannose receptor (MR, CD206) is a transmembrane C-type lectin that binds terminal mannose, fucose, and N-acetylglucosamine residues on glycoconjugates. Its carbohydrate recognition domain 4 (CRD4) mediates Ca^{2+}-dependent binding to sugars in a manner mechanistically analogous to other C-type lectins.[4]

[1] V. Petrović Peroković *et al. Molecules* 2021, *26,* 6352. [2] M. Paurević *et al. Org. Biomol. Chem.,* 2024, *22, 6506*. [3] P. Pavashe *et al. J. Org. Chem.* 2016, 21, 10106. [4] H. Feinberg *et al. J. Biol. Chem.* 2021, *296,* 100368.

Structures of investigated mannosylated desmuramyl peptides

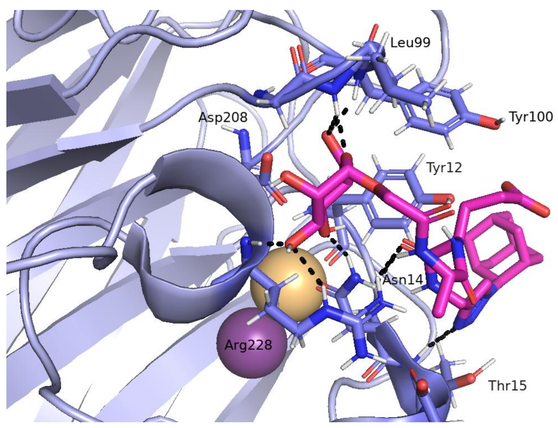


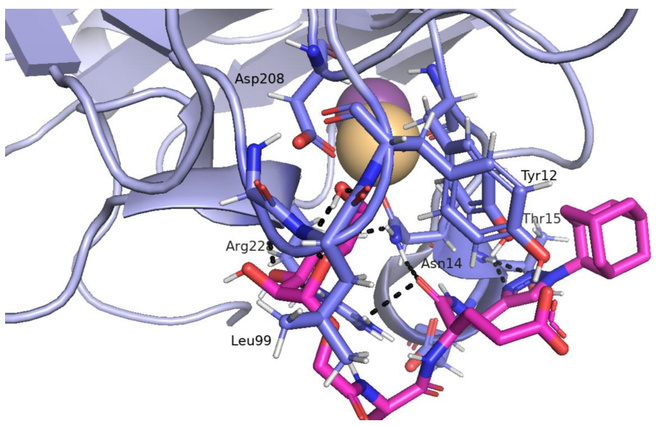
I



II

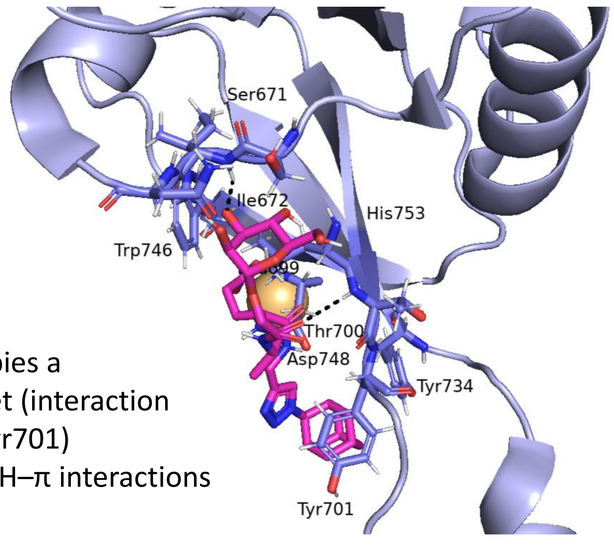
Molecular interactions between compound I and ConA (PBD ID: 9J1A)





- key ConA residues for Man recognition: Asp208, Asn14, Arg228, Gly98, Leu99, Tyr100, Tyr12
- docking score: −7.6 kcal/mol
- 10 H-bonds in the protein–ligand complex; Man formed six H-bonds with ConA: Arg228 (2), Leu99 (2), Asn14 (1), and Tyr100 (1) → results support a canonical Man-binding mode
- Asn14, a residue important for ligand positioning in the binding site
- triazole ring formed two hydrogen bonds with Thr15
- isoGln carbonyl group (C=O) formed H-bonds with Arg228 and Asn14

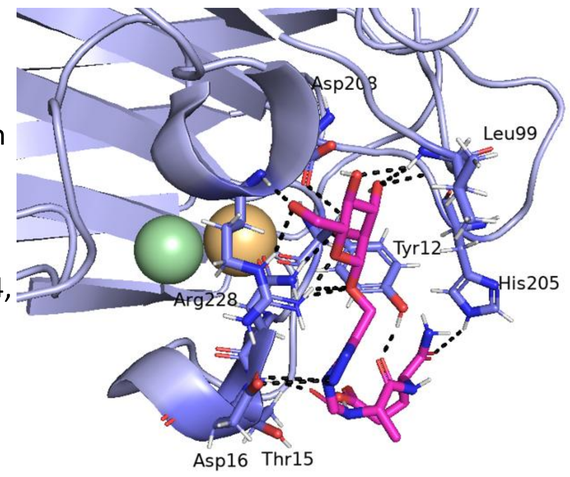
Interactions between I and CRD4 domain of macrophage mannose receptor (PDB ID: 1EG1)



- docking score: −7.4 kcal/mol
- adamantane occupies a hydrophobic pocket (interaction with Tyr734 and Tyr701)
- mannose formes CH–π interactions with Trp74

Interactions between compound II and ConA

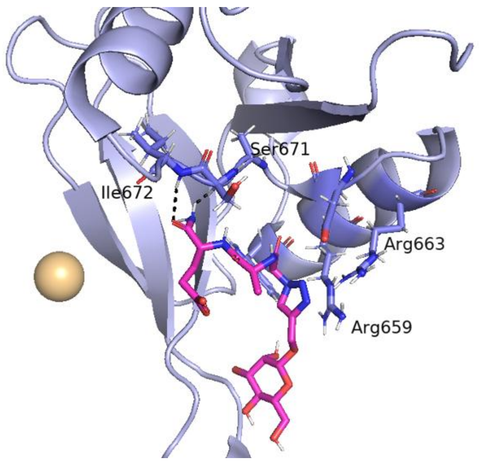
- docking score: −6.8 kcal/mol
- favorable ligand orientation within the binding site
- compound **II** interacts with key residues for Man recognition; Asp208, Asn14, Arg228, Leu99, Tyr100, Tyr12, and with His205, Asp16, Thr15



- experimental investigation using isothermal titration calorimetry confirmed that the tested mannosylated DMPs bind Con A with moderate affinity (log *K* = 3.71–4.22)
- binding is enthalpically driven with an unfavourable entropic contribution ($\Delta S° < 0$) — a characteristic of lectin–carbohydrate interactions
- compared to the reference ligand methyl α-D-mannopyranoside (MeαMan, log *K* ≈ 3.5–3.7, $\Delta H° \approx -28$ kJ mol^{-1}), compounds display comparable or enhanced affinities with more negative binding enthalpies, suggesting additional favourable contacts within the Con A binding site

Interactions between II and CRD4 domain

- docking score: −5.8 kcal/mol



CONCLUSIONS

Molecular docking of compounds **I** and **II** into the Con A binding site revealed a canonical mannose-binding mode, characterized by hydrogen bonds with key residues and additional interactions involving the triazole ring, suggesting that the structural modifications enhance complementarity with the lectin binding site. The computational data consistently identify compound **I** as the more promising mannose-mimetic ligand, with favorable binding to both Con A and the macrophage mannose receptor, highlighting the importance of the lipophilic substituent introduced at the D-isoGln moiety.

Acknowledgements: This work has been fully supported by Croatian Science Foundation under the project IP-2025-02-5568.

38th EPS
European Peptide Symposium
6 - 11th of September 2026
Vienna, Austria

Peptide Evolution

Molecular Mimicry by Venom Peptides

Samuel D. Robinson

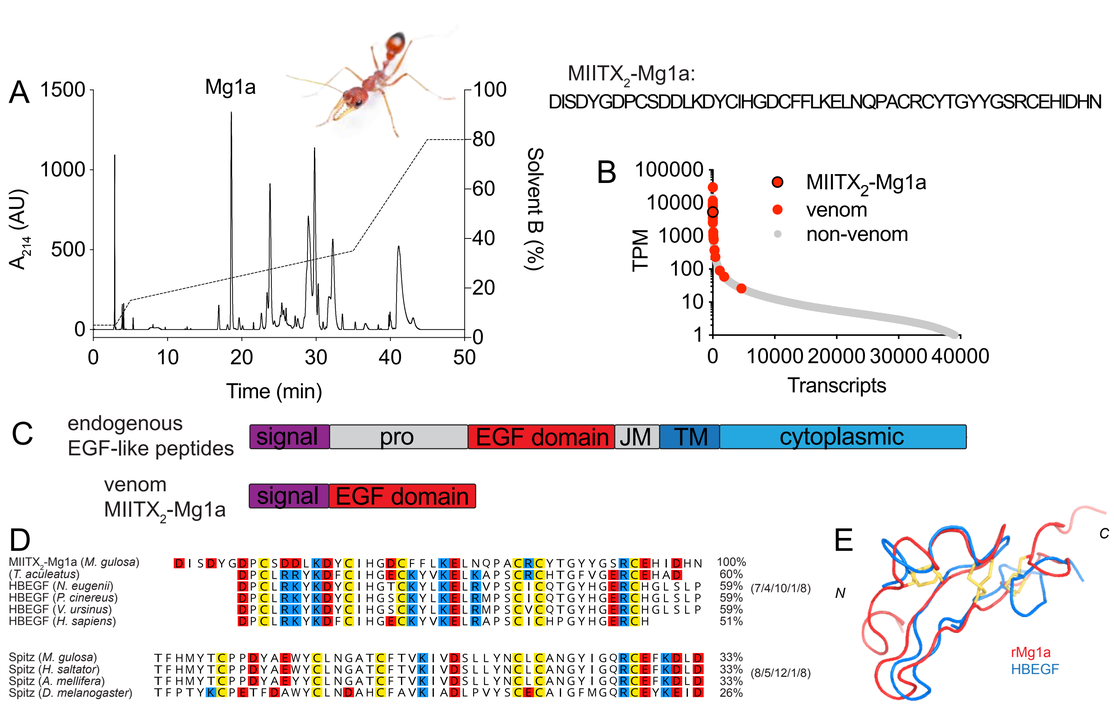
Institute for Molecular Bioscience, University of Queensland; QLD 4072, Australia.
https://doi.org/10.17952/38EPS.2026.P494

@StingScience
sam.robinson@uq.edu.au

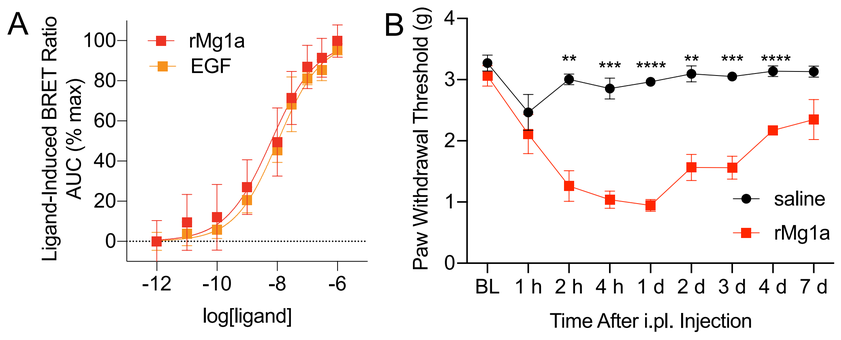


Natural selection can drive the evolution of similar traits through convergent evolution. Peptides identical to certain vertebrate hormones are present as toxins in the venoms of species of ants and wasps (hymenopterans) and the defensive skin secretions of frogs. The genes encoding the hymenopteran and frog peptide toxins do not share common ancestry with those of the vertebrate hormones but instead independently evolved, sometimes multiple times, from other peptide toxin genes.

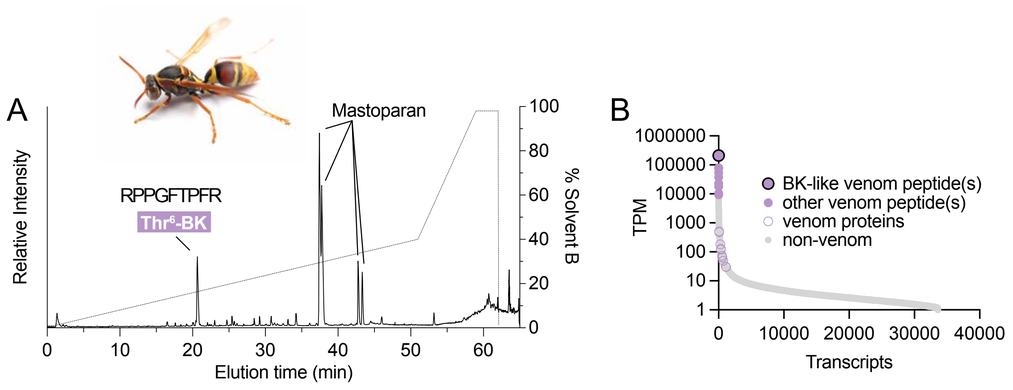
These peptides serve a defensive function against vertebrate predators and their resemblance to vertebrate hormones was driven by selection for efficacy at the predators' receptors. These studies highlight how with a suitable genetic substrate and shared environmental pressure, natural selection can result in repeated convergent evolution of identical peptides even across distantly related species.[1,2]



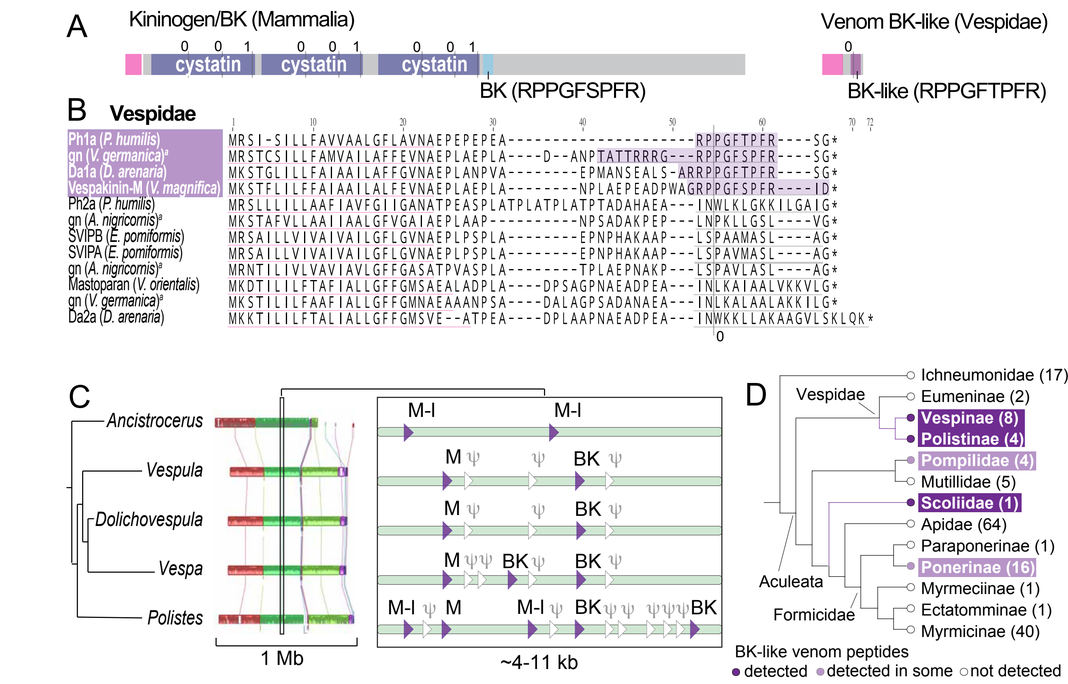
1 Mg1a, a major component of the venom of the Giant red bull ant (*Myrmecia gulosa*), is an analog of vertebrate EGF-like peptide hormones. (A) An RP-HPLC chromatogram of *M. gulosa* venom. The peak corresponding to Mg1a is labeled. (B) The Mg1a-encoding transcript is found in the highly expressed portion of the venom-apparatus transcriptome (highlighted in red). TPM, transcripts per million. (C) The precursor structures of endogenous EGF-like peptide hormones and Mg1a. JM, juxtamembrane domain; pro, propeptide; TM, transmembrane domain. (D) Sequence alignment of Mg1a (mature peptide) with the EGF-like domain of the short-beaked echidna (*T. aculeatus*) peptide and HBEGF of other mammals. Alignment of Spitz sequences from *M. gulosa* and other insects. Percentage sequence identity with Mg1a is indicated (Right). The intercysteine loop length of each group is indicated (Far Right). (E) Alignment of the closest-to-average structures of Mg1a (red) and HBEGF (blue).



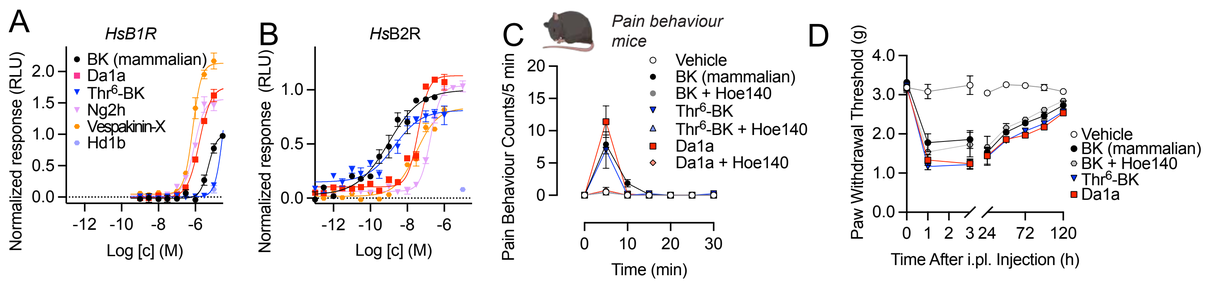
2 Mg1a is a potent ligand of mammalian ErbB1 and intraplantar injection of Mg1a in mice caused long-lasting hypersensitivity. (A) Concentration–response curves of ligand-induced BRET ratio for HEK293T cells transiently expressing hErbB1/Rluc8 and Grb2/Venus following stimulation with rMg1a or hEGF. Data are mean ± SEM (n = 3). (B) Paw-withdrawal threshold to mechanical stimulus. Data are mean ± SEM (n = 6 per group). **P < 0.01, ***P < 0.001, ****P < 0.0001, two-way ANOVA, Sıdak's multiple comparisons. Note: The x axis is nonlinear.



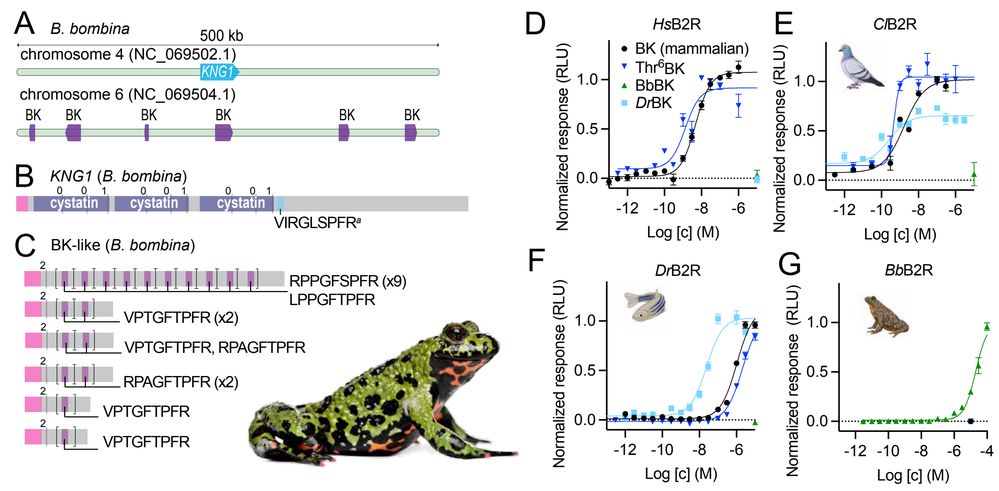
3 Bradykinin (BK) is a vertebrate hormone but is present in wasp venoms. (A) Total ion chromatogram from liquid chromatography–tandem mass spectrometry analysis of Australian paper wasp (*P. humilis*) venom, with peaks corresponding to major venom peptides labeled and that corresponding to Thr^6-BK highlighted. (B) The Thr^6-BK–encoding transcript was the single most highly expressed transcript in the *P. humilis* venom gland transcriptome. Bradykinin-like peptides are major components of the venoms of diverse hymenopteran species.



4 Wasp venom BK-like peptides evolved multiple times from ancestral venom peptide precursors, independently of vertebrate BK. (A) Transcript structure of mammalian BK and, at the same scale for comparison, that of a representative vespid venom BK- like peptide (Ph1a). Signal peptides are colored pink. Exon/intron boundaries are indicated by a dashed line and labeled with phase. (B) Alignment of the precursor sequences of BK-like peptide precursors of Vespidae with related wasp venom peptide precursors. Signal peptides and mature peptides are underlined in pink and gray, respectively. BK-like peptides are highlighted in purple. (C) Alignment of 1-Mb genomic region containing BK-like peptide genes of representative Vespidae. (Inset) Alignment of local genomic region. M- I, mastoparan-like genes; M, mastoparan genes; BK, BK genes; ψ, pseudogenes. (D) Cladogram of selected hymenopteran families and subfamilies showing presence or absence of BK- like venom peptides. The number of genomic or transcriptomic datasets used for each lineage is indicated in parentheses.



5 Wasp venom BK-like peptides functionally mimic mammalian BK. Venom BK-like peptides are agonists of mammalian BK receptors. Concentration-response relationships for venom BK-like peptides at (A) *Hs*B1R and (B) *Hs*B2R. (C) Spontaneous pain behaviors in mice after shallow intraplantar injection of BK (200 pmol), Thr^6-BK (200 pmol), or Da1a (200 pmol) with and without coapplication of Hoe140 (400 pmol). P values are derived from a one-way ANOVA with Dunnett's multiple comparison test (n = 4 to 8 mice per group). (D) Shallow intraplantar injection of Thr^6-BK (20 pmol) or Da1a (20 pmol) caused mechanical allodynia in mice equivalent to BK (20 pmol). The effect of BK was not inhibited by coapplication with Hoe140 (200 pmol).



6 Frog skin BK-like peptides do not share common ancestry with the endogenous frog BK but evolved independently to mimic specific vertebrate BKs. (A) Fire-bellied toad (*B. bombina*) KNG1 ortholog and BK-like peptide genes are present at distinct genetic loci. (B) Transcript structure of *B. bombina* kininogen. (C) Transcript structure of *B. bombina* BK-like peptides (at the same scale). (D) Concentration-response relationships for BKs at *Hs*B2R andequivalent data for (E) *Cf*B2R, (F) *Dr*B2R, and (G) *Bb*B2R.

These studies highlight the importance of EGF and BK receptor signalling in vertebrate physiology (including in pain) and the importance of vertebrate predation in Hyemnoptera and frog evolution. They illustrate how natural selection can mold the gene product of one organism to resemble that of another (in this case, the gene product of the prey resembles that of the predator). They are examples of both convergent evolution and molecular mimicry that brings to mind the ancient proverb "To know your enemy, you must become your enemy."

[1]Eagles, D. A., ... S. D. Robinson (2022). A peptide toxin in ant venom mimics vertebrate EGF-like hormones to cause long-lasting hypersensitivity in mammals. *Proceedings of the National Academy of Sciences of the United States of America* 119(7).
[2]Shi, N., ... S. D. Robinson (2026). Repeated convergent evolution of bradykinin mimics as defensive toxins. *Science* 391(6789): 1046-1052.

THE UNIVERSITY OF QUEENSLAND
AUSTRALIA

Identification of SPINK1 from CytoSorb Desorbate as a Novel Antiviral TMPRSS2 Inhibitor

Armando A. Rodríguez Alfonso[1,2], Jan Lawrenz[3], Nico Preising[1], Ludger Ständker[1], Sebastian Wiese[2], Eberhard Barth[4], Frank Kirchhoff[3], Jan Münch[3]

armando.rodriguez-alfonso@uni-ulm.de
https://doi.org/10.17952/38EPS.2026.P192
[1]ULMTeC Core Facility Functional Peptidomics, Ulm University Medical Center, Germany. [2]ULMTeC Core Facility Mass Spectrometry and Proteomics, Ulm University Medical Center, Germany. [3]Institute of Molecular Virology, Ulm University Medical Center, Ulm, Germany. [4]Anesthesiology and Intensive Medicine Clinic, Ulm University Medical Center, Ulm, Germany

CRC 1279

Abstract

TMPRSS2, a host serine protease, activates the SARS-CoV-2 Spike and is a validated antiviral target. We asked whether the desorbate of used CytoSorb hemoadsorption cartridges, an underexplored clinical matrix, is a source of protease inhibitors. Desorbed material was enriched by trypsin-affinity chromatography (trypsin as a TMPRSS2 surrogate), fractionated by RP-HPLC, and screened for antiviral activity against SARS-CoV-2 Spike pseudoparticles. The active fraction was identified as full-length SPINK1 by MALDI-TOF/PSD. Recombinant SPINK1 inhibited TMPRSS2 (IC_{50} ≈ 134 nM) and blocked XBB.1.5 Spike-mediated entry (IC_{50} ≈ 562 nM) dose-dependently, establishing hemoadsorption desorbates as a viable discovery matrix for bioactive protease inhibitors.

Reference

1 Lawrenz J, Wettstein L, Rodríguez Alfonso A, Nchioua R, von Maltitz P, Albers DPJ, Zech F, Vandeput J, Naesens L, Fois G, Neubauer V, Preising N, Schmierer E, Almeida-Hernandez Y, Petersen M, Ständker L, Wiese S, Braubach P, Frick M, Barth E, Sauter D, Kirchhoff F, Sanchez-Garcia E, Stevaert A, Münch J. Trypstatin as a Novel TMPRSS2 Inhibitor with Broad-Spectrum Efficacy against Corona and Influenza Viruses. Adv Sci (Weinh). 2025 Jul;12(25):e2506430. doi: 10.1002/advs.202506430. Epub 2025 May 14. PMID: 40365759; PMCID: PMC12224939.

General strategy

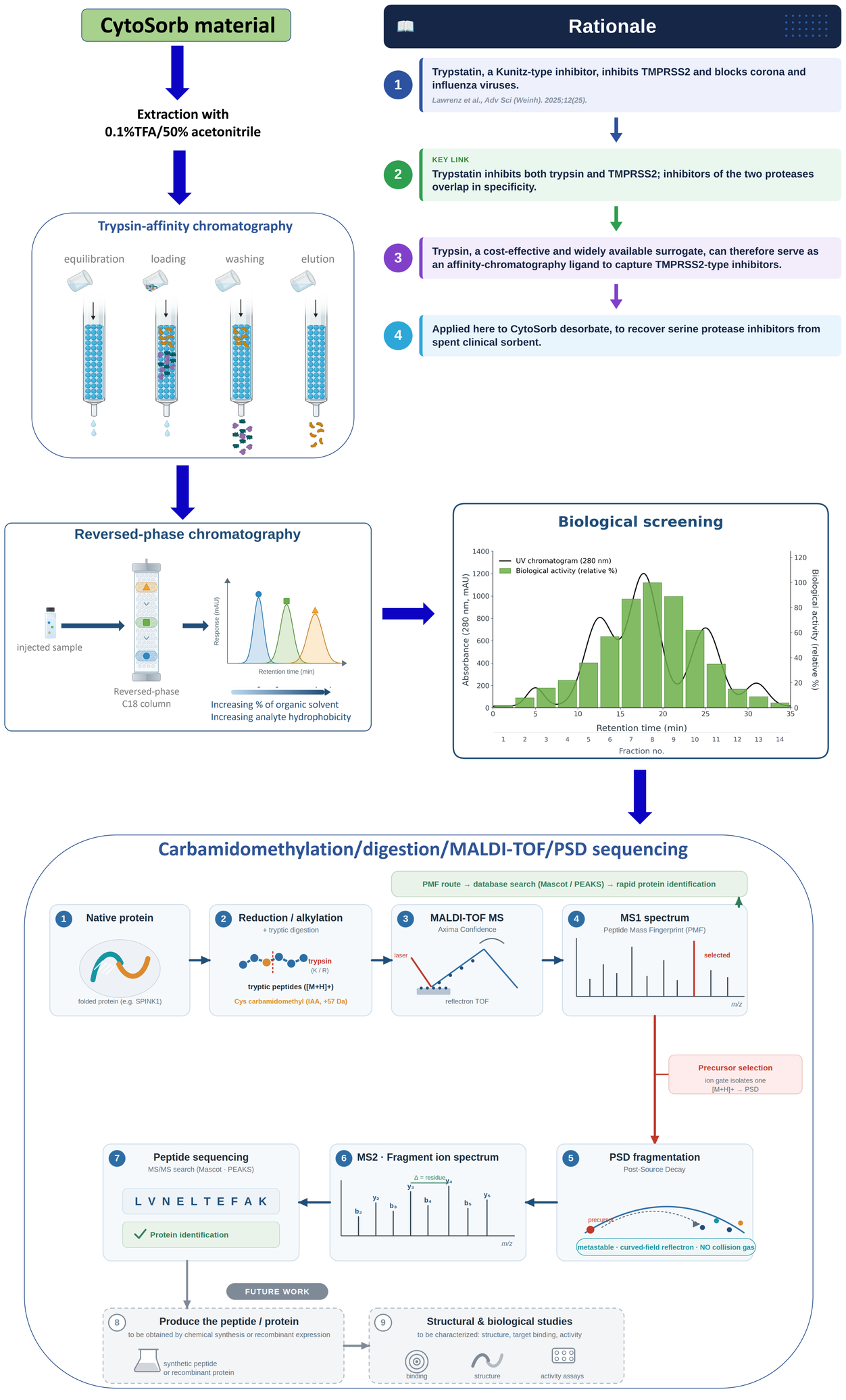


Figure 1. Chromatographic and MS workflow to isolate and sequence serine protease inhibitors with antiviral activity against SARS-CoV2. CytoSorb material was extracted with 0.1% TFA/50% acetonitrile and then subjected to affinity chromatography. The eluate was subjected to RP-HPLC fractionation, and the chromatographic fractions were evaluated for their activity against SARS-CoV-2. The active fraction was carbamidomethylated, digested, and analyzed by MALDI-TOF-PSD, and the raw data were processed by MASCOT.

Results

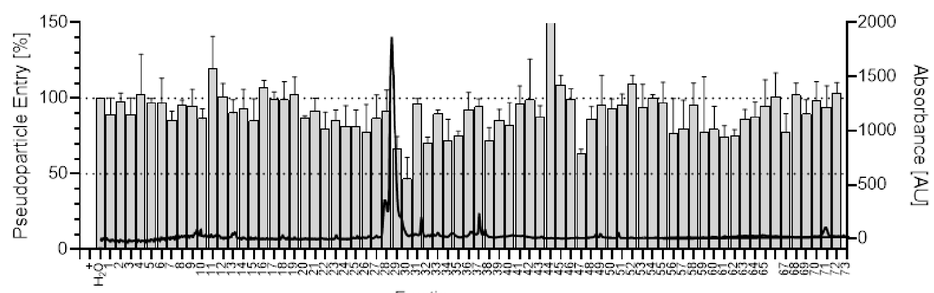


Figure 2. Biological screening of RP-C18 fractions (1–73) from the affinity eluate against SARS-CoV-2 Spike pseudoparticles. Bars: pseudoparticle entry (mean ± SEM, n = 3); black trace: UV absorbance (280 nm). Fractions 29–30 showed the lowest entry (highest antiviral activity) and matched a dominant chromatographic peak.

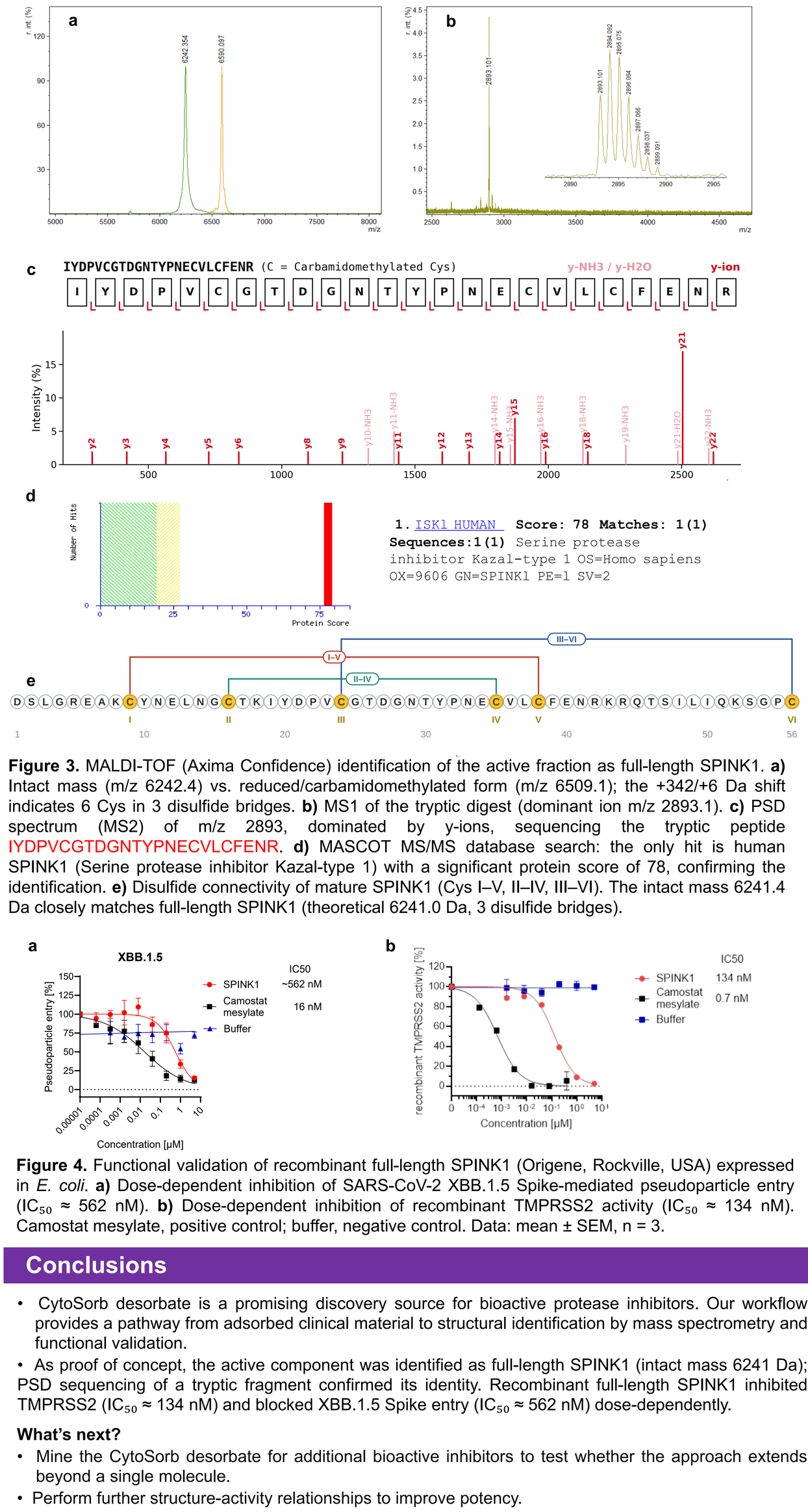


Figure 3. MALDI-TOF (Axima Confidence) identification of the active fraction as full-length SPINK1. **a)** Intact mass (m/z 6242.4) vs. reduced/carbamidomethylated form (m/z 6509.1); the +342/+6 Da shift indicates 6 Cys in 3 disulfide bridges. **b)** MS1 of the tryptic digest (dominant ion m/z 2893.1). **c)** PSD spectrum (MS2) of m/z 2893, dominated by y-ions, sequencing the tryptic peptide IYDPVCGTDGNTYPNECVLCFENR. **d)** MASCOT MS/MS database search: the only hit is human SPINK1 (Serine protease inhibitor Kazal-type 1) with a significant protein score of 78, confirming the identification. **e)** Disulfide connectivity of mature SPINK1 (Cys I–V, II–IV, III–VI). The intact mass 6241.4 Da closely matches full-length SPINK1 (theoretical 6241.0 Da, 3 disulfide bridges).

Figure 4. Functional validation of recombinant full-length SPINK1 (Origene, Rockville, USA) expressed in *E. coli*. **a)** Dose-dependent inhibition of SARS-CoV-2 XBB.1.5 Spike-mediated pseudoparticle entry (IC_{50} ≈ 562 nM). **b)** Dose-dependent inhibition of recombinant TMPRSS2 activity (IC_{50} ≈ 134 nM). Camostat mesylate, positive control; buffer, negative control. Data: mean ± SEM, n = 3.

Conclusions

- CytoSorb desorbate is a promising discovery source for bioactive protease inhibitors. Our workflow provides a pathway from adsorbed clinical material to structural identification by mass spectrometry and functional validation.
- As proof of concept, the active component was identified as full-length SPINK1 (intact mass 6241 Da); PSD sequencing of a tryptic fragment confirmed its identity. Recombinant full-length SPINK1 inhibited TMPRSS2 (IC_{50} ≈ 134 nM) and blocked XBB.1.5 Spike entry (IC_{50} ≈ 562 nM) dose-dependently.

What's next?

- Mine the CytoSorb desorbate for additional bioactive inhibitors to test whether the approach extends beyond a single molecule.
- Perform further structure-activity relationships to improve potency.
- Establish physiological relevance in SARS-CoV-2, test other TMPRSS2-dependent viruses (e.g., influenza), and profile protease specificity.

Acknowledgements

The authors gratefully acknowledge the German Research Foundation (DFG) for funding this study under CRC1279. Anthropic Claude (Opus 4.8) and BioRender were used for figure preparation and text editing.

Beyond SMCC: Uniform Isothiocyanate-Peptide Bioconjugates

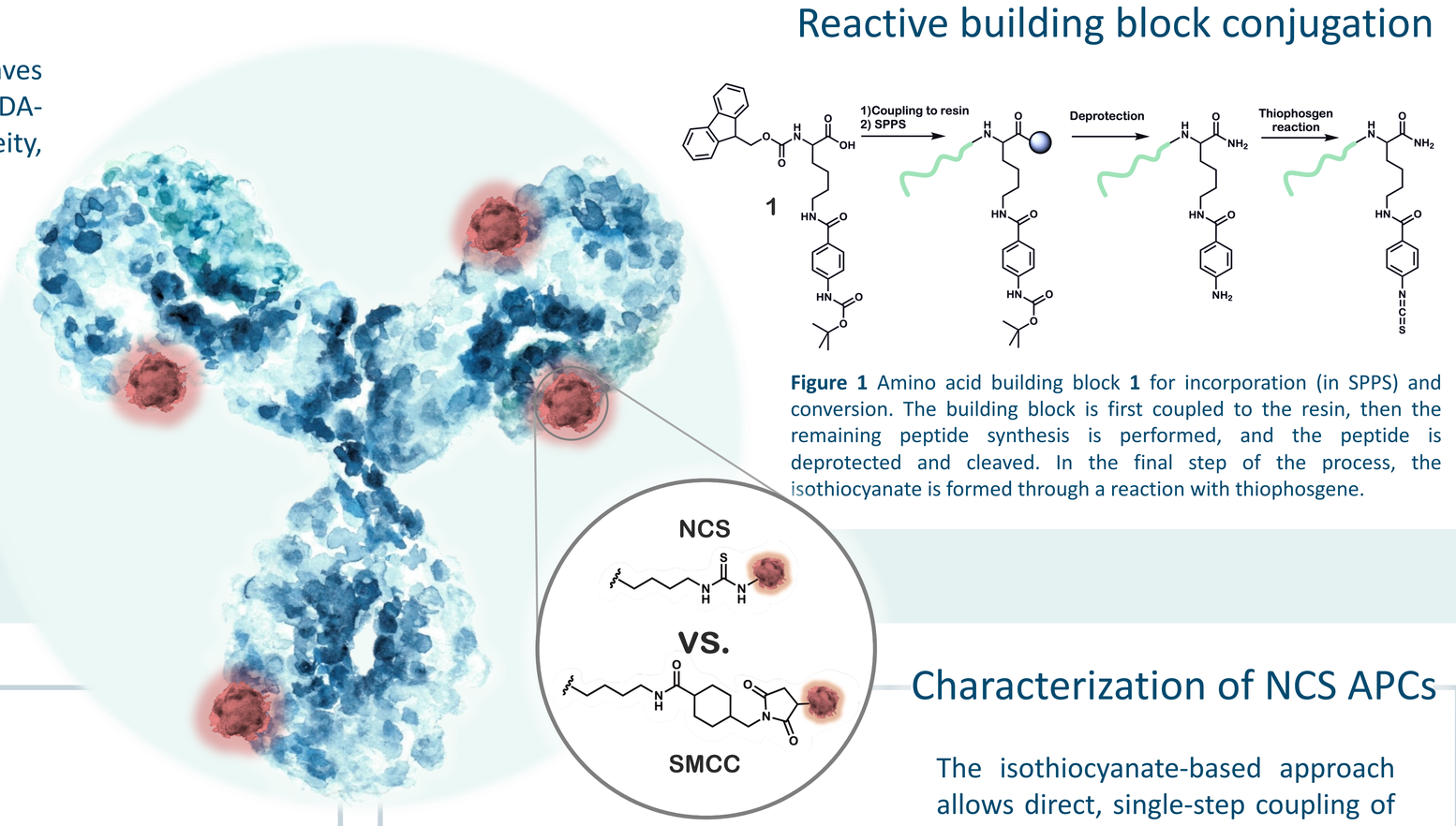
HEIDELBERG UNIVERSITY HOSPITAL

Barbara Roether[1], Eric Mühlberg[2], Niklas van den Bergh[1], Uwe Haberkorn[1] and Walter Mier[1]

[1]Department of Nuclear Medicine, Heidelberg University Hospital, Heidelberg, Germany
[2]Department of Pharmaceutical Technology and Biopharmacy, Heidelberg University, Heidelberg, Germany
barbara.roether@med.uni-heidelberg.de
https://doi.org/10.17952/38EPS.2026.P297

Motivation and Objective

Conventional SMCC-based antibody conjugation often leaves unreacted or crosslinked linker residues, as seen in the FDA-approved ADC Kadcyla®, leading to structural heterogeneity, incomplete reactions, and reduced reproducibility.[1,2]
To address these challenges, we developed a direct, single-step isothiocyanate-based conjugation approach that allows stochastic attachment of peptides or chelator-peptides to antibodies. This streamlined. method enhances uniformity and stability while minimizing structural alterations and simplifying radioimmunoconjugate synthesis.

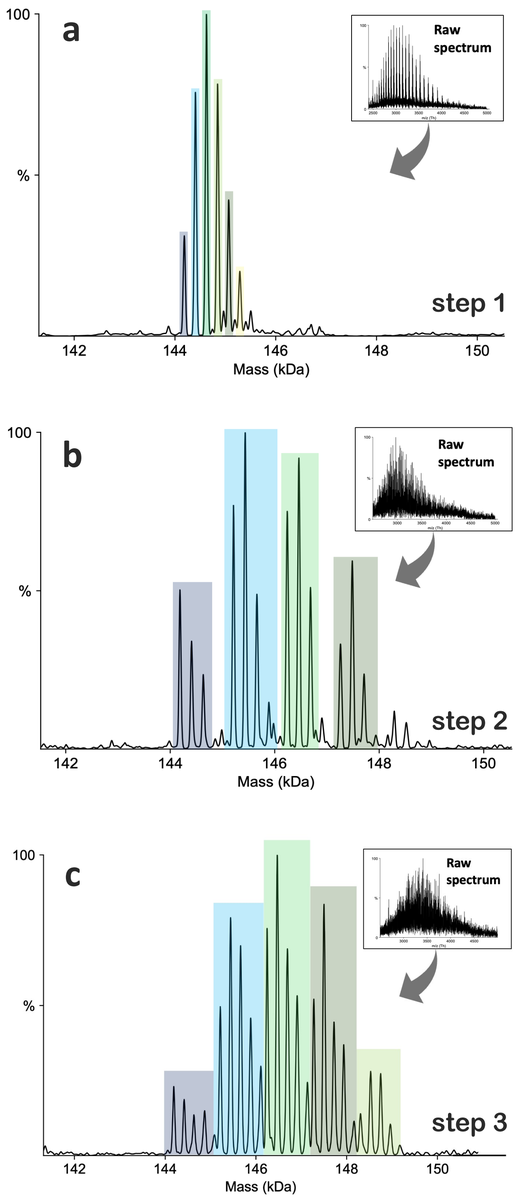


Reactive building block conjugation

Figure 1 Amino acid building block **1** for incorporation (in SPPS) and conversion. The building block is first coupled to the resin, then the remaining peptide synthesis is performed, and the peptide is deprotected and cleaved. In the final step of the process, the isothiocyanate is formed through a reaction with thiophosgene.

Results

Characterization of SMCC APCs



Mass spectrometric characterization of SMCC-based antibody-peptide conjugates (APCs) revealed incomplete coupling and significant product heterogeneity. Despite the use of an excess of thiol-peptide after the initial SMCC conjugation (**Figure 2a**), unreacted or crosslinked maleimidocaproyl (MCC) residues persisted, leading to several minor peaks observed in the deconvoluted spectra (**Figure 2b**). Optimization of reaction parameters, including incubation time and purification, resulted in only slight improvements in peptide-antibody ratio and reproducibility. Additional experiments with N-acetylcysteine confirmed that most MCC groups became chemically inactive, likely through intra- and inter-molecular crosslinking rather than hydrolysis.[1,2] The subsequent DOTA coupling step (**Figure 2c**) further increased conjugate complexity, generating mixed species with varying degrees of peptide and chelator substitution.

Figure 2 (a) Multi-charged *m/z* profiles (right corner) and deconvoluted spectrum of conjugation step 1 (SMCC conjugation) after deglycosylation using Rapid PNGase F. Colors represent the different MCC species. (b) Multi-charged *m/z* profiles (right corner) and deconvoluted spectrum of conjugation step 2 (coupling of SH-peptide to the MCC-antibody) after deglycosylation using Rapid PNGase F. Colors indicates the same number of coupled peptides. (c) Multi-charged *m/z* profiles (right corner) and deconvoluted spectrum of conjugation step 3 (DOTA conjugation to the peptide-MCC-antibody) after deglycosylation using Rapid PNGase F. Colors indicate the same number of coupled peptides.

Characterization of NCS APCs

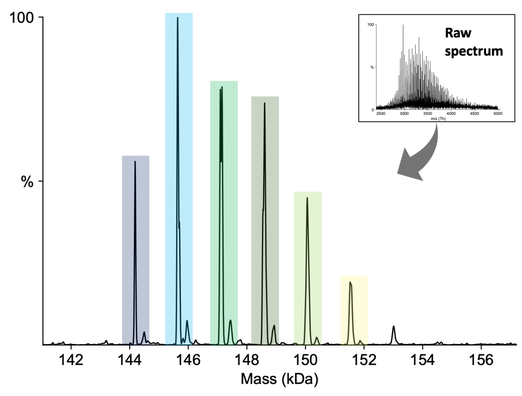


Figure 4 Multi-charged *m/z* profiles (right corner) and deconvoluted spectrum of NCS-peptide-mAb conjugate following deglycosylation with Rapid PNGase F. Colors indicate the different PAR assignment (0-5).

The isothiocyanate-based approach allows direct, single-step coupling of DOTA-NCS-peptides to antibodies under mild basic conditions (pH 9, 24 h). In contrast to the multi-step SMCC method, purification involves only one ultrafiltration step, resulting in reproducible conjugation efficiency across experiments. Mass showed distinct and well-resolved peaks for each peptide-to-antibody ratio, confirming uniform conjugation without side reactions or residual linker species (**Figure 4**). The resulting conjugates displayed high structural integrity and uniform modification, providing a reliable platform for subsequent radiolabelling.[3,4]

Conjugation steps

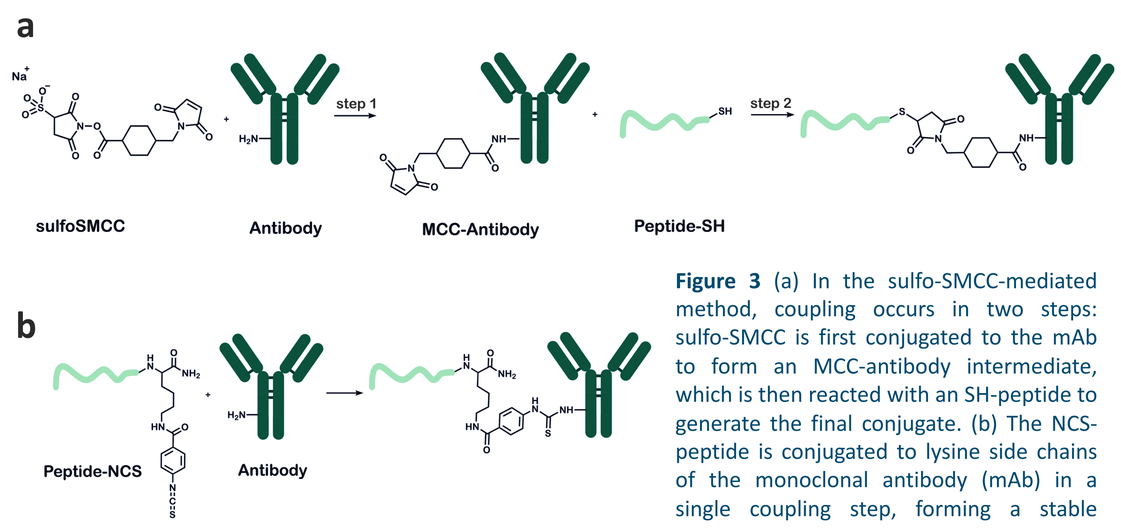


Figure 3 (a) In the sulfo-SMCC-mediated method, coupling occurs in two steps: sulfo-SMCC is first conjugated to the mAb to form an MCC-antibody intermediate, which is then reacted with an SH-peptide to generate the final conjugate. (b) The NCS-peptide is conjugated to lysine side chains of the monoclonal antibody (mAb) in a single coupling step, forming a stable thiourea bond.

Summary

Isothiocyanate-mediated peptide conjugation using our amino acid building block offers an efficient, one-step alternative to SMCC-based methods. This approach enables non-site-specific antibody attachment while preserving structural integrity and producing uniform, stable conjugates suitable for diverse applications.

CONTACT

References

(1) Wu, G. *et al*. *ACS Omega* **2019**, *4* (5), 8834-8845. DOI: 10.1021/acsomega.9b00430
(2) Chen, L. *et al*. *mAbs* **2016**, *8* (7), 1210-1223. DOI: 10.1080/19420862.2016.1204502.
(3) Johnston, P. B. *et al. Expert Review of Anticancer Therapy* **2006**, *6* (6), 861-869. DOI: 10.1586/14737140.6.6.861.
(4) Perk, L. R. *et al. European Journal of Nuclear Medicine and Molecular Imaging* **2006**, *33* (11), 1337-1345. DOI: 10.1007/s00259-006-0160-0.

https://doi.org/10.17952/38EPS.2026.P458

Engineering antimicrobial peptides through nanocarrier surface design and intracellular targeting for tuberculosis therapy

cesar.roque@unesp.br

Cesar Augusto Roque-Borda[1,2], Laura MDG Primo[1], Christian S.C. Canales[1], Eduardo F. Vicente[1], João Perdigão[2], Beatriz G. de la Torre[3,4]; Fernando Albericio[3,5]; Henrik Franzyk[6], Paul Robert Hansen[6], Fernando R. Pavan[1].

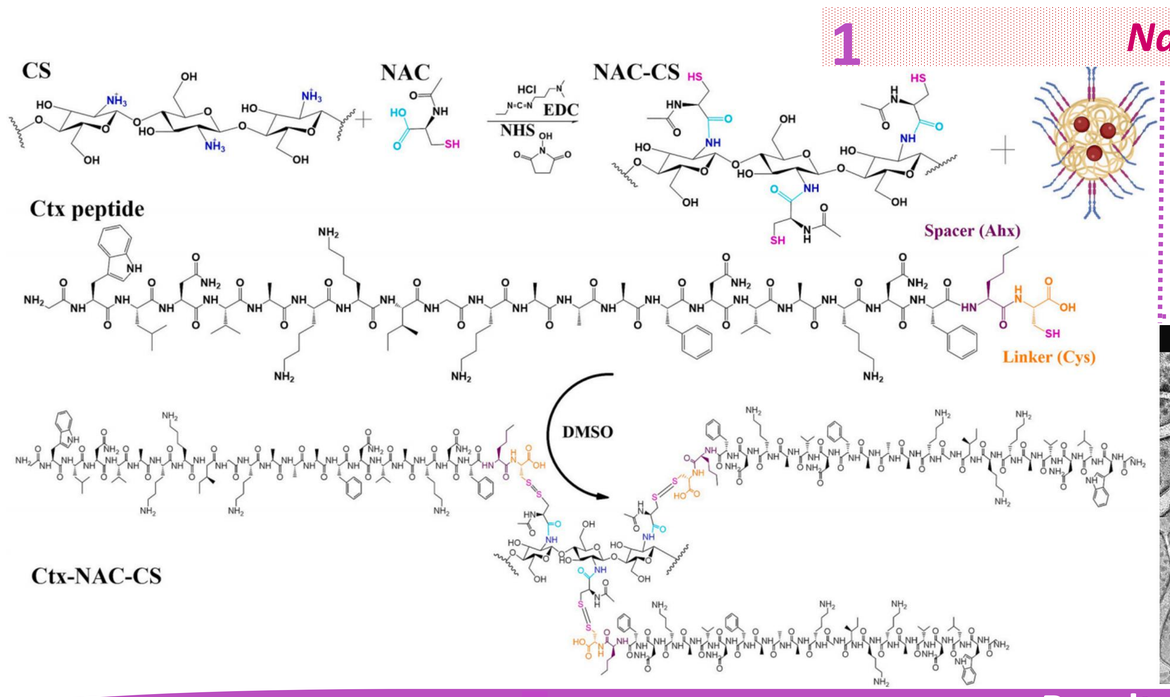
[1]São Paulo State University (UNESP), School of Pharmaceutical Sciences, Araraquara, São Paulo – Brazil. [2]iMed.ULisboa–Institute for Medicines Research, Faculty of Pharmacy, University of Lisbon, Portugal. [3]Peptide Science Laboratory, School of Chemistry and Physics, University of KwaZulu-Natal, South Africa. [4]School of Laboratory Medicine and Medical Sciences, College of Health Sciences, University of KwaZulu-Natal, South Africa. [5]Department of Inorganic and Organic Chemistry, University of Barcelona, Spain. [6]University of Copenhagen, Faculty of Health and Medical Sciences, Department of Drug Design and Pharmacology, Denmark.



Introduction

The emergence of multidrug-resistant *Mycobacterium tuberculosis* highlights the urgent need for therapeutic strategies capable of overcoming intracellular persistence and antibiotic failure. Although antimicrobial peptides exhibit potent antibacterial activity, their clinical translation remains limited by instability, rapid degradation, and inefficient delivery to infected macrophages. A nanotechnology-centered strategy is presented to examine how nanocarrier architecture can modulate and enhance antimicrobial peptide performance against tuberculosis.

Materials and Methods



Results and Discussions

Biological properties

Table 1. MIC values of antibiotics and NP formulations by the REMA method after 7 days of exposure.

Code	Formulation	H37RV (µg/mL)	CF 169 (µg/mL)	CF 110 (µg/mL)
INH	Isoniazid	0.5–1.0	>50	>50
RIF	Rifampicin	0.5	>25	16.29
GAT	Gatifloxacin	0.03–0.25	1.2	<0.05
MOX	Moxifloxacin	0.03–0.5	1.6	<0.05
OFL	Ofloxacin	0.71	11.5	0.3
AMK	Amicacin	0.5–1.0	0.6	0.5
CAP	Capreomycin	2.0	1.4	3.0
KAN	Kanamycin	2.0	1.5	2.8
NP1	NAC-CS	NA	NA	NA
NP2	CS@RIF[a]	<0.977	NA	NA
NP3	Ctx-NAC-CS	NA	NA	NA
NP4	NAC-CS@RIF[a]	1.47	199.05	NA
NP5	CS	NA	NA	NA
NP6	Ctx-CS	NA	NA	NA
NP7	Ctx-CS@RIF[a]	<0.977	104.34	NA
NP8	Ctx-NAC-CS@RIF[a]	<0.977	0.977	<0.977
Ctx	Ctx(Ile^{21})-Ha-Ahx-Cys	7.57	12.24	>250
Ctx wild-type	Ctx(Ile^{21})-Ha	14.0	NT	NT
NAC	*N*-acetylcysteine	NA	NA	NA

NA: no activity. NT: not tested.
CF169 strain: XDR MTB. CF110 strain: MDR MTB.
[a] MIC values based on RIF concentration. All NPs were tested based on their weight.

Table 2. Antitubercular activity, cytotoxicity in mammalian cells, and selectivity indices for peptides. All values are expressed in micromolar (µm).

AMPs	$H_{37}Rv$	IC_{50} MRC-5	IC_{50} J774A.1	SI MRC-5	SI J774A.1
DC05	12.46 ± 0.06	>250	115.18 ± 8.49	>20.05	9.24 ± 0.68
DC08	37 ± 2.07	>250	229.78 ± 4.08	>6.76	6.21 ± 0.36
DC09	49 ± 2.89	>250	236.77 ± 4.57	>5.10	4.83 ± 0.30
DC10	24 ± 1.72	>250	211.08 ± 3.63	>10.41	8.79 ± 0.65
CPP	>50	>250	205.9 ± 6.5	n.d	≤ 4.12

Table 3. Antimycobacterial activity of MSN-based nanoplatforms.

MIC of MSN formulations		
Nanoplatform	MIC values (Mtb $H_{37}Rv$)[a]	MIC values (Mtb $H_{37}Rv$)[b]
MSN	N.A.	–
MSN-CPP	N.A.	–
MSN@DC05	205 µg/mL	7.74 µg/mL
MSN-CPP@DC05	284.66 µg/mL	10.75 µg/mL

a MIC values calculated based on the total nanoparticle mass required to inhibit *M. tuberculosis* H37Rv. **b** MIC values calculated based on the effective peptide content encapsulated within each formulation. **N.A.** not active under the tested conditions.

Figure 1. Confocal analysis of internalization of FITC-NPs in macrophages after incubation for 24 h.

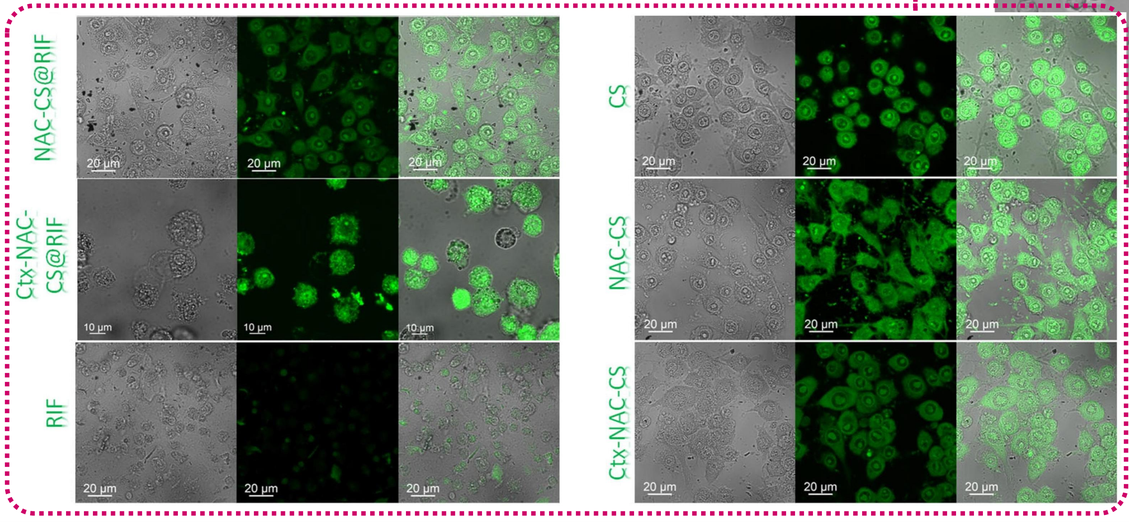


Figure 2. Confocal analysis of internalization of FITC-NPs in macrophages after incubation for 24 h.

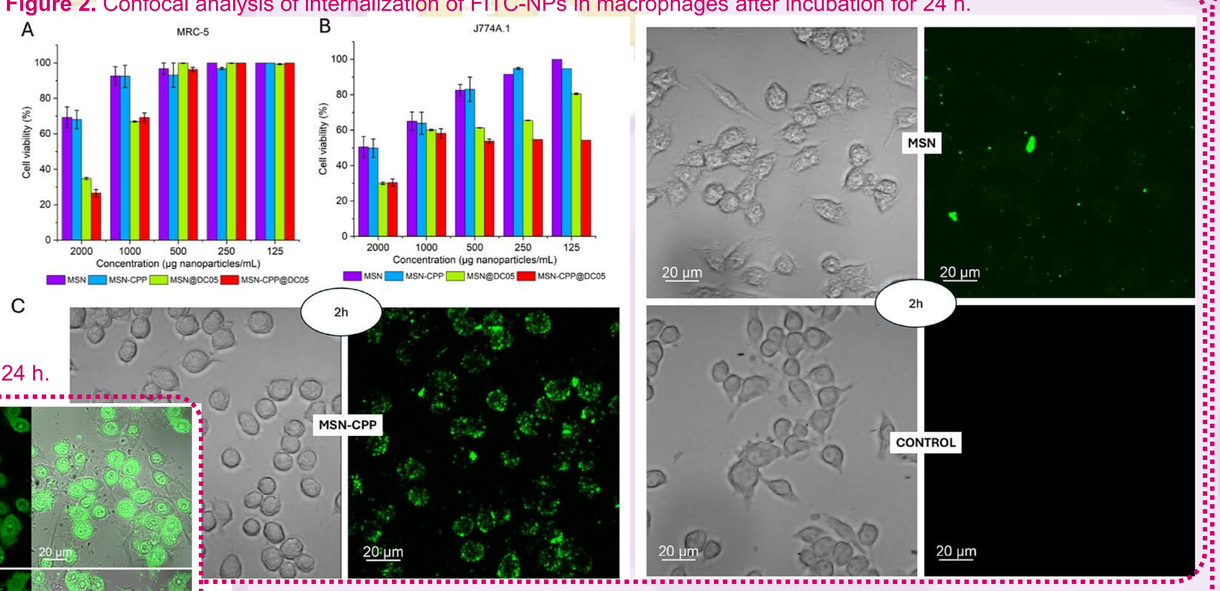
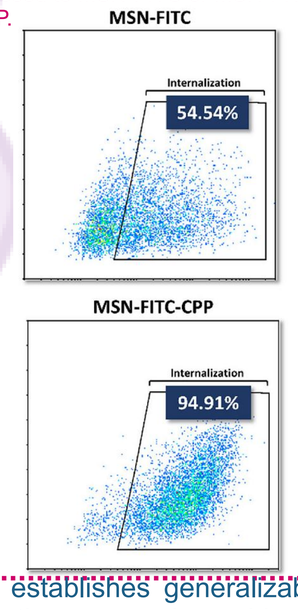


Figure 3. Representative flow cytometry dot plots showing untreated cells (control) and cells exposed to MSN-FITC or MSN-FITC-CPP.



Conclusions

By integrating peptide engineering with advanced nanomaterial design, this work establishes generalizable principles for next-generation peptide-based therapeutics targeting intracellular pathogens and provides a strategic foundation for precision antimicrobial interventions against resistant tuberculosis.

Acknowledgments

This study was supported by the São Paulo Research Foundation (FAPESP): Research Grant: 2023/01664-1 and Fellowships: 2025/06167-1, 2024/23710-8, 2020/16573-3, 2021/14603-5. This study was financed in part by the Coordenação de Aperfeiçoamento de Pessoal de Nível Superior – Brasil (CAPES) - Finance Code 001.

References

1. Primo, L. M. D. G., Roque-Borda, C. A., Canales, C. S. C., Caruso, I. P., de Lourenço, I. O., Colturato, V. M. M., ... & Pavan, F. R. (2024). Antimicrobial peptides grafted onto the surface of N-acetylcysteine-chitosan nanoparticles can revitalize drugs against clinical isolates of Mycobacterium tuberculosis. Carbohydrate Polymers, 323, 121449.2. Roque-Borda, C.A. et al. Chitosan and HPMCAS double-coating as protective systems for alginate microparticles loaded with Ctx(Ile21)-Ha antimicrobial peptide to prevent intestinal infections. Biomaterials 2023, 293, 121978.
2. Carnero Canales, C. S., Roque-Borda, C. A., Negri, A. C. C., Delgado, O. R., Catarin Nunes, L. O., Resende, F. A., ... & Pavan, F. R. (2026). Dual-Peptide Nanoplatform: Mesoporous Silica Nanoparticles Functionalized With a Cell-Penetrating Peptide and Loaded With Rationally Designed Antimicrobial Peptides for Tuberculosis Therapy. Advanced Healthcare Materials, 15(21), e04285.

Development of PNA-Peptide Chimeras targeting G-quadruplex structures

Matilde Rossi[a,b,c], Paola Gratteri[c], Ines Neundorf[d], Carla Bazzicalupi[a], Daniel Friedrich[e] and Anna Maria Papini[a,b]

[a] *Department of Chemistry "Ugo Schiff", University of Florence, Via della Lastruccia 3, 50019 Sesto F.no, Italy*
[b] *Interdepartmental Research Unit of Peptide and Protein Chemistry and Biology, University of Florence, 50019 Sesto F.no, Italy*
[c] *Department of NeuroFarBa, University of Florence, Via Ugo Schiff 6, 50019 Sesto F.no, Italy*
[d] *Institute for Biochemistry, University of Cologne, Zülpicher Str. 47, 50674 ,Cologne, Germany*
[e] *Department of Chemistry and Biochemistry, University of Cologne, Greinstraße 4, 50939, Cologne, Germany*

https://doi.org/10.17952/38EPS.2026.P376

matilde.rossi@unifi.it

38th EPS
European Peptide Symposium



Introduction and Project Overview

The growing demand for peptide-based solutions for "well-being" highlights a critical gap in Europe, where an integrated and coordinated network covering the entire peptide life cycle is still lacking. This work contributes to the broader EUniWell effort to establish a European "infrastructure without walls", bringing together complementary expertise across the entire peptide life cycle, from design and green synthesis to structural characterization and biological evaluation. Within this framework, the present study focuses on peptide-based strategies for selective G-quadruplex recognition.

G-quadruplexes (G4s) are non-canonical structures formed in G-rich sequences by stacked G-tetrads. Their enrichment at telomeres and proto-oncogene promoters makes them attractive anticancer targets, although selective recognition remains challenging because G4 ligands often poorly discriminate among different G4s.[1] Peptide nucleic acids (PNAs), characterized by an achiral, uncharged polyamide backbone, offer high-affinity and sequence-specific nucleic-acid recognition.[2] As a complementary G4-recognition module, we focused on peptides derived from DHX36/RHAU, a helicase with high specificity for G4 structures. Rhau16 (HPGHLKGREIGMWYAK) is the shortest construct showing detectable G4 binding. Structural analysis of the Rhau18-G4 complex revealed an L-shaped conformation containing an α-helix spanning G5-A17. G9, I12, G13 and A17 directly engage the terminal G-tetrad, whereas P4, L7 and W15 mainly support the peptide conformation.[3]

Sequence minimization of RHAU16

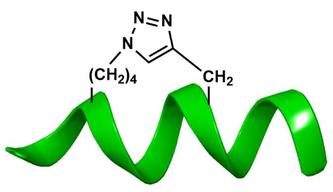
Rhau16 HPGHLKGREIGMWYAK

Rhau11 KGREIGMWYAK

N-terminal segment removed

Key G4-interacting residues retained

i,i+4 triazole stapling to favor α-helicity and retain G4 binding

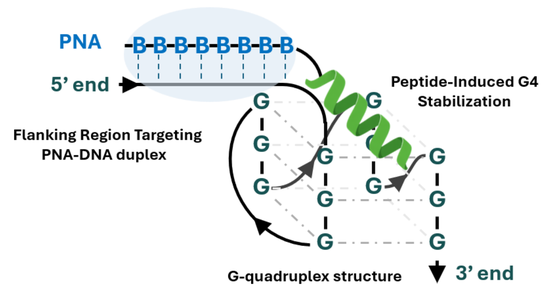


Dual sequence/structure recognition for enhanced G4 selectivity

PNA → *sequence-specific recognition of the G4 flanking region*

+

Rhau11-derived peptide → *G4 recognition and stabilization*



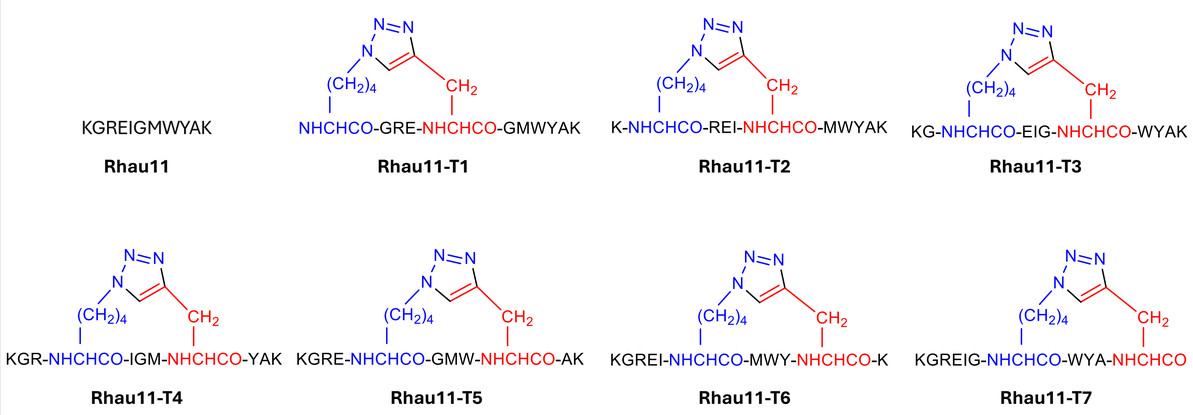
Design and Synthesis

Peptides

A systematic positional scan was performed by shifting the $i, i+4$Lys(N_3)/Pra pair along the Rhau11 sequence, generating seven triazole-stapled analogues (T1-T7).

Fmoc/t-Bu SPPS
Deprotection: 20% piperidine in DMF, 90 °C, 2 min.
Coupling: AA/DIC/OxymaPure (5/5/5 eq) DMF, 90 °C, 3 min.

→ **Microwave-Assisted On-Resin CuAAC:**
CuBr/DIPEA/2,6-lutidine = 1.5/5/5 equiv.
DMSO/DMF 1:2 (v/v), 55 °C, 10 min.



PNA

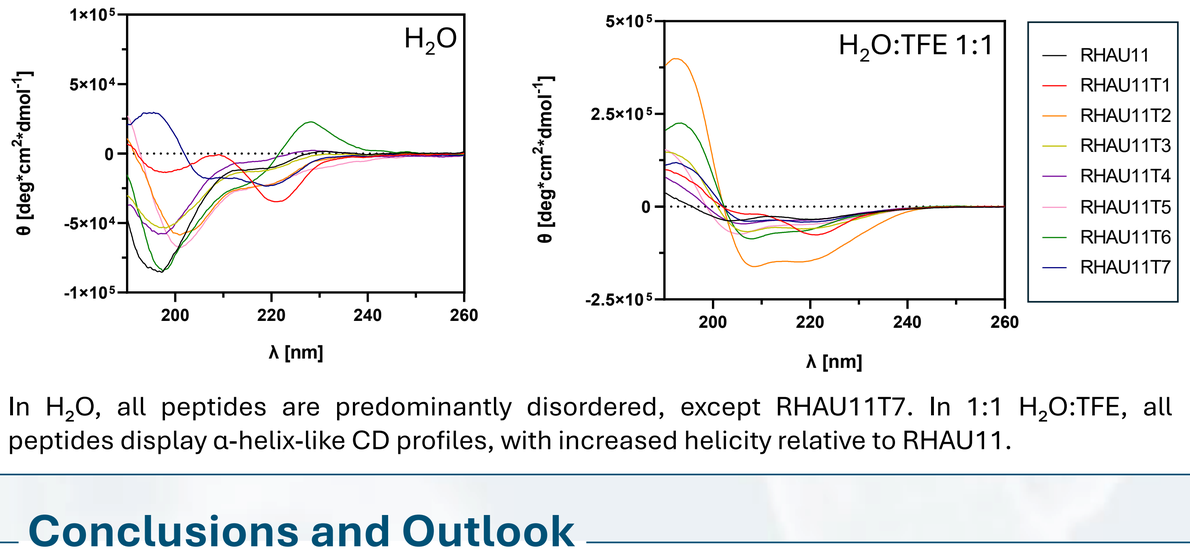
Note: *here the letters A, T, C, and G are used to denote both DNA nucleotides and the corresponding PNA building blocks.*

DNA G4 (Myc27): 5'- T A T G T T G A G G G T G G G T A G G G T G G G T A A -3'
5' flanking region — *G4-forming region*

PNA sequence (PNA_{myc}): N_{ter}- Lys - TCAACATA - C_{ter}

Fmoc/t-Bu SPPS
Deprotection: 20% piperidine in DMF, rt, 10 min + 5 min.
Coupling: Building Block/DIC/OxymaPure = 4/4/4 equiv, DMF, 70 °C, 8 min.

CD experiments



In H_2O, all peptides are predominantly disordered, except RHAU11T7. In 1:1 H_2O:TFE, all peptides display α-helix-like CD profiles, with increased helicity relative to RHAU11.

Effect of Peptide Stapling on MYC G4 Stability

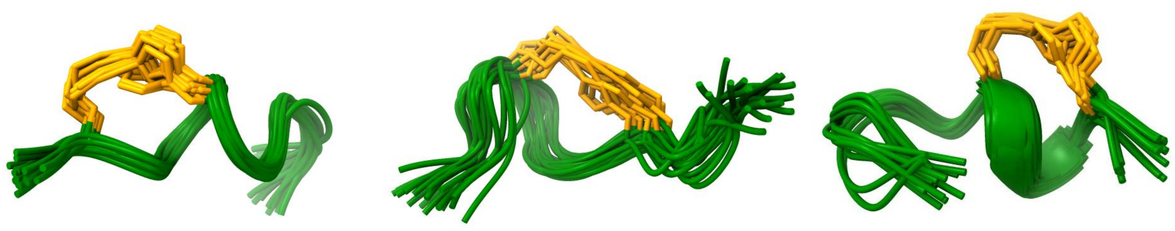
Three peptides were selected based on the increase in MYC G4 (5'- AGG GTG GGG AGG GTG GGG -3') melting temperature (ΔT_m) induced by peptide addition: **RHAU11T2**, **RHAU11T4**, and **RHAU11T6**.

Complex	T_m (°C)	ΔT_m (°C)
DNA Myc Pu18	66.0 ± 0,8	-
DNA/**RHAU11**	74.0 ± 0,9	8.0 ± 1.2
DNA/**RHAU11T1**	74.7 ± 0,3	8.7 ± 0.9
DNA/**RHAU11T2**	78.0 ± 1,1	12.0 ± 1.4
DNA/**RHAU11T3**	73.3 ± 0,3	7.3 ± 0.9
DNA/**RHAU11T4**	81.6 ± 0,2	15.6 ± 0.8
DNA/**RHAU11T5**	75.6 ± 2.0	9.6 ± 2.1
DNA/**RHAU11T6**	78.6 ± 1,1	12.7 ± 1.1
DNA/**RHAU11T7**	70.9 ± 0,2	4.9 ± 0.8

NMR Structural Characterization

NMR Structural Characterization of Selected Peptides

Peptides concentration 3.5 mM. Buffer 5 mM potassium phosphate, 50 mM KCl, 10% D_2O, pH 7.0



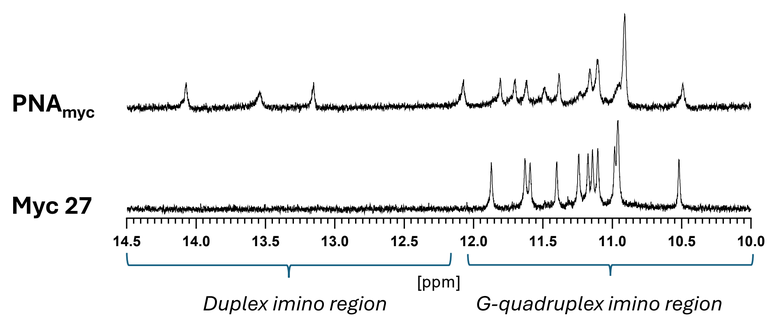
Rhau11-T2 **Rhau11-T4** **Rhau11-T6**

NMR-derived structures reveal different degrees of conformational organization among the selected peptides. T6 displays partial α-helical character, whereas T4 appears the least ordered despite its G4-stabilizing effect.

PNA–DNA Interaction

PNA and DNA concentration 0.1 mM. Buffer 10 mM Tris-HCl buffer, 60 mM KCl, pH 7.0

PNA addition produced Watson–Crick imino signals and perturbed the G4 imino resonances, indicating an effect of flanking-region duplex formation on the G4 environment.



Conclusions and Outlook

Systematic *i,i+4* triazole stapling of Rhau11 yielded analogues able to enhance the thermal stability of the MYC G4. NMR-derived structures in aqueous buffer revealed a recurrent bent backbone organization with limited secondary structure, except for T6, which showed partial α-helical character. CD analysis showed no stable α-helical structure in aqueous solution, whereas in the presence of TFE all stapled peptides displayed a higher α-helical propensity than linear Rhau11, suggesting that stapling facilitates access to helical conformations. Qualitative 1D NMR analysis of the PNA-DNA system was consistent with PNA association with the MYC flanking sequence and probable heteroduplex formation.
Future perspectives include the conjugation of the selected G4-stabilizing peptides to the PNA module to generate PNA-peptide chimeras combining sequence-specific recognition of the MYC flanking region with stabilization of the adjacent G4.

Acknowledgments

This project was funded in part by EUniWell: 5th seed funding call for the TTPep project and 3rd Well-Being Research Incubator Call for the project "Sustainable and green upscaling processes for peptide(-based) in vitro diagnostics and cosmeceuticals" and the Champion program "Peptides4Wellness".

References

1. Chen L, Dickerhoff J, Sakai S, Yang D. *Acc Chem Res.* **2022,** 55, 2628-2646
2. Cadoni E, De Paepe L, Manicardi A, Madder A. *Nucleic Acids Res*. **2021**, 49, 6638-6659.
3. Heddi B, Cheong VV, Martadinata H, Phan AT *Proc Natl Acad Sci U S A*. **2015**,112, 9608-9613.

Mapping the G-Quadruplex Binding Determinants of a Vimentin-Derived Peptide by Alanine Scanning

M. Rotondo,[1] N. Dal Ponte,[2] M. Cozzaglio,[2] R. Rigo,[2] B. Biondi[3] and C. Sissi[2]

[1]*Department of Chemical Sciences, University of Padova*

https://doi.org/10.17952/38EPS.2026.P208

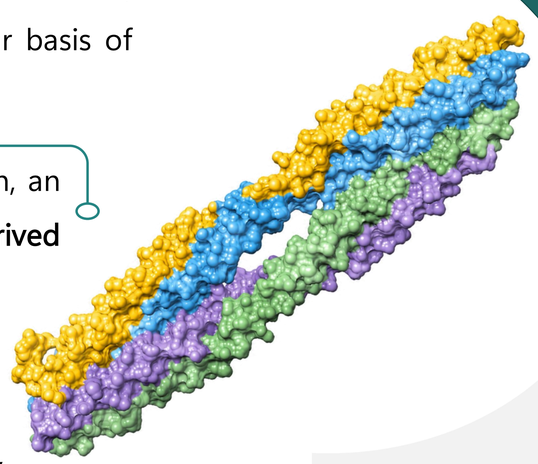
[2]*Department of Pharmaceutical and Pharmacological Sciences, University of Padova*

[3]*CNR, Institute of Biomolecular Chemistry, Padova Unit*

VIMENTIN AND G4-RECOGNITION

Vimentin is a type III intermediate filament protein involved in the epithelial-mesenchymal transition (EMT) process and cancer progression. Soluble tetrameric Vimentin **selectively recognises G-quadruplex (G4) DNA structures**, suggesting a potential in gene regulation, although the molecular basis of this interaction remains unclear.

In this study, to investigate the residues involved in G4 recognition, an **alanine-scanning approach was applied to the Vimentin-derived peptide 11-30.**



CONVERGENT SYNTHESIS AND ALA-SCAN

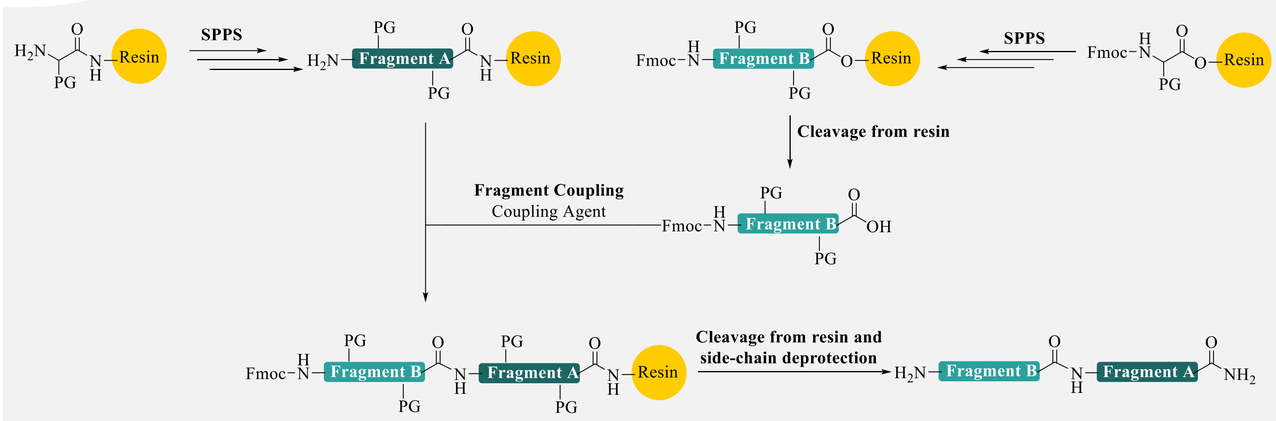
The Vimentin-derived peptide and its analogue were prepared by Fmoc-based solid-phase peptide synthesis using a **convergent synthetic strategy**.

Independent peptide fragments were assembled separately and subsequently combined, reducing the number of sequential coupling steps and improving the overall efficiency of the synthesis. This approach proved particularly advantageous for the preparation of a relatively long sequence such as Vimentin 11-30 fragment.

EXPERIMENTAL APPROACH

1. **Peptide Synthesis.** The reference peptide and a series of alanine-substituted analogues were synthesized by fragment-based and convergent peptide synthesis.
2. **Biophysical Characterization.** Peptide-G4 interactions were evaluated through fluorescence melting assays (FM) and surface plasmon resonance (SPR).
3. **Structure-activity Relationship Analysis.** Assessment of the contribution of individual residues to G4 recognition.

Schematic representation of fragment based and convergent peptide synthesis



PEPTIDES SYNTHESISED

Reference sequence:

^{11}Y R R M F G G P G^{20}T A S R P S S S R S^{30}Y

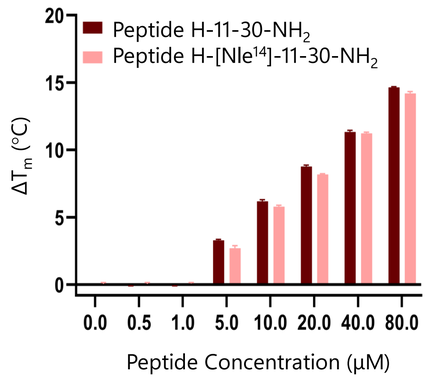
Met^{14} → Nle^{14}

Targeted alanine substitutions:

Aromatic residues Basic residues

A focused library of single-point mutants was generated through systematic **alanine substitution**. This approach preserves the peptide backbone while enabling the evaluation of the contribution of individual side chains to peptide activity.

The Vimentin 11-30 sequence (**YRRMFGGPGTASRPSSSRSY**) was used as the reference peptide. To improve oxidative stability, methionine was replaced by norleucine (**Nle^{14}**) without significantly affecting G4 recognition, as confirmed by fluorescence melting experiments. Aromatic (**Tyr, Phe**) and basic (**Arg**) residue were systematically replaced by alanine to assess their contribution to G4 binding.

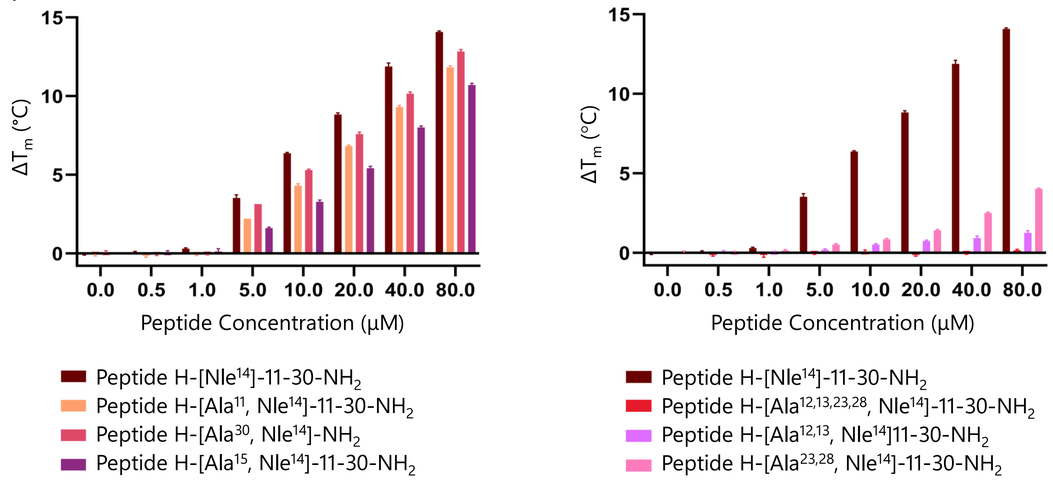


Fluorescence melting analysis of the interaction between H-11-30-NH_2 peptide and its Nle substituted analogue H-[Nle^{14}]-11-30-NH_2 peptide with the G4-forming sequence Tel23.

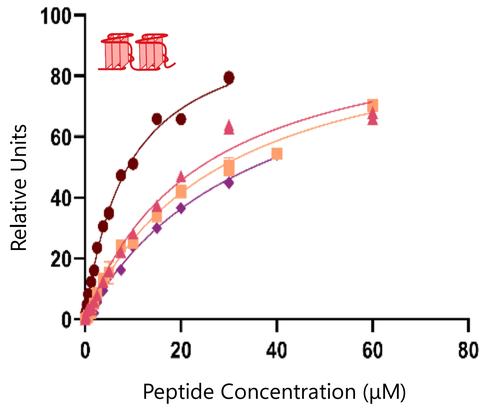
Peptide	Retention Time (min)	Purity (%)	MW_{calc} (g/mol)	$[M+H]^+$
H-11-30-NH_2	10.20	98	2219.1	2218.9
H-[Nle^{14}]-11-30-NH_2	10.10	99	2201.4	2201.0
H-[Ala^{11}, Nle^{14}]-11-30-NH_2	9.38	99	2108.1	2108.8
H-[Ala^{30}, Nle^{14}]-NH_2	10.22	98	2109.3	2108.9
H-[Ala^{15}, Nle^{14}]-11-30-NH_2	9.03	99	2125.2	2124.9
H-[Ala^{12,13,23,28}, Nle^{14}]-11-30-NH_2	11.94	99	1861.0	1860.3
H-[Ala^{12,13}, Nle^{14}]-11-30-NH_2	10.94	98	2031.2	2030.8
H-[Ala^{23,28}, Nle^{14}]-11-30-NH_2	10.94	99	2031.2	2030.8

BIOPHYSICAL CHARACTERIZATION

Peptide-G4 interactions were characterized by **fluorescence melting** and **surface plasmon resonance** experiments to evaluate G4 stabilization, binding affinity and kinetic parameters



Fluorescence melting analysis of the interaction between H-[Nle^{14}]-11-30-NH_2 peptide and its aromatic (left) and basic (right) substituted analogue peptides with G4 forming sequence Tel23.



Peptide	K_D
H-11-30-NH_2	8.9 ± 1.6μM
H-[Ala^{11}, Nle^{14}]-11-30-NH_2	28.1 ± 3.9μM
H-[Ala^{30}, Nle^{14}]-NH_2	23.8 ± 5.0μM
H-[Ala^{15}, Nle^{14}]-11-30-NH_2	35.0 ± 7.7μM

SPR analysis of the interaction between H-11-30-NH_2 peptide and its aromatic substituted analogue peptides with G4-repeat forming sequence.

CONCLUSION AND FUTURE PERSPECTIVES

The Vimentin-derived peptide 11-30 was identified as the minimal region responsible for selective G4 recognition with micromolar affinity. Alanine-scanning studies revealed that arginine residues are the main determinants of the binding and G4 stabilization, while aromatic residues provide an additional contribution to molecular recognition. The identified binding determinants will guide the design of optimized peptide ligands for investigating and modulating Vimentin–G4 interactions in cancer-related pathways.

REFERENCES

[1] Danielsson F., Peterson M.K., Caldeira Araújo H., Lautenschläger F., Gad A.K.B. *Cells*, **2018**, *7*, 147.

[2] Cozzaglio M., Ceschi S., Groaz E., Sturlese M., Sissi C. *Frontiers in Chemistry*, **2022**, *10*, 1-10.

[3] Ceschi S., Berselli M., Cozzaglio M., Giantin M., Toppo S., Spolaore B., Sissi C. *Nucleic Acids Res.*, **2022**, *50*(3), 1370-1381.

[4] Cozzaglio M., Dal Ponte N., Rotondo M., Biondi B., Rigo R., Spolaore B., Sissi C. *Nucleic Acid Res.*, **2026**, *54*(6), gkag247.

AKNOWLEDGEMENT

This research was supported by EU funding within the MUR PNRR "National Center for Gene Therapy and Drugs based on RNA Technology". (Project no. CN00000041 CN3 RNA) and AIRC under IG 2021 - ID. 26474 project – P.I. Sissi Claudia.

Conformational Effects of Fluorinated Aminocyclopropane Carboxylic Acids Incorporation in Peptides

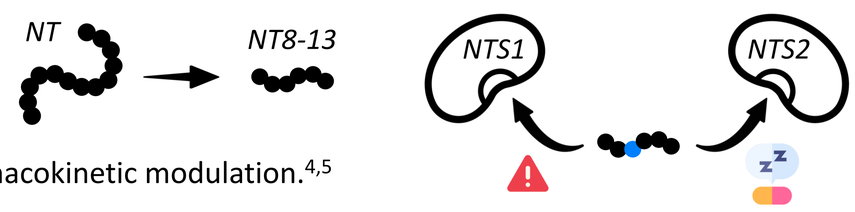
Eliott ROY,[1] Zoé WEBER,[2] Baptiste LEGRAND,[1] Thomas POISSON,[2] Ludovic MAILLARD,[1] Philippe JUBAULT[2] & Florine CAVELIER[1]

[1]*Institut des Biomolécules Max Mousseron, IBMM, UMR 5247, CNRS, Université de Montpellier, ENSCM, Montpellier, France*
[2]*INSA Rouen Normandie, Univ. Rouen Normandie, CNRS, Institut CARMeN UMR 6064, Rouen, France*

https://doi.org/10.17952/38EPS.2026.P478

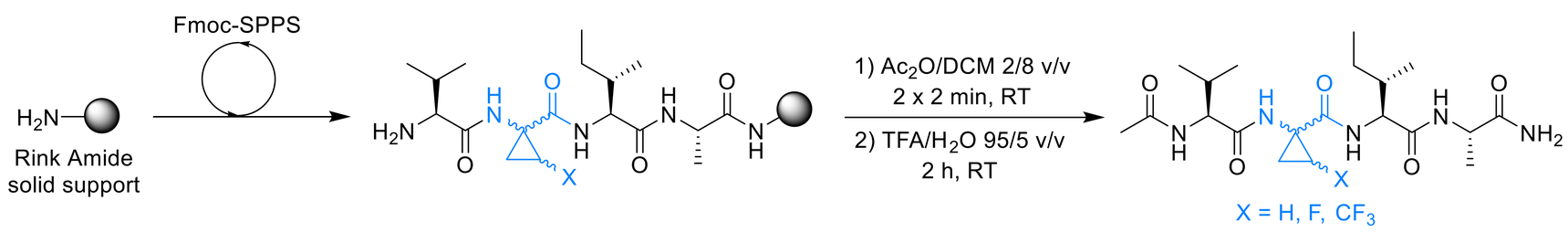
Context of the study

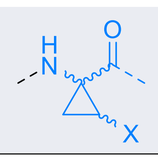
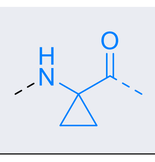
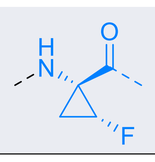
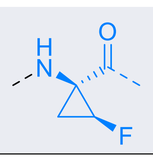
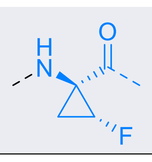
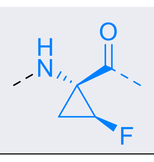
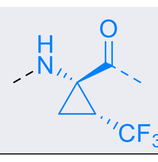
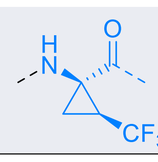
- **Neurotensin** (**NT**), a tridecapeptide with analgesic properties, acts through binding to the NTS2 receptor.[1,2,3]
- NT's poor NTS2/NTS1 receptor selectivity causes undesirable side effects.
- Constrained amino acids, such as α,α-dialkylamino acids, promote specific peptide conformations, aiding pharmacokinetic modulation.[4,5]
- Previous work showed that replacing Pro in the NT8-13 sequence with a fluorinated aminocyclopropane carboxylic acid (**FACC**) improves NTS2/NTS1 selectivity.



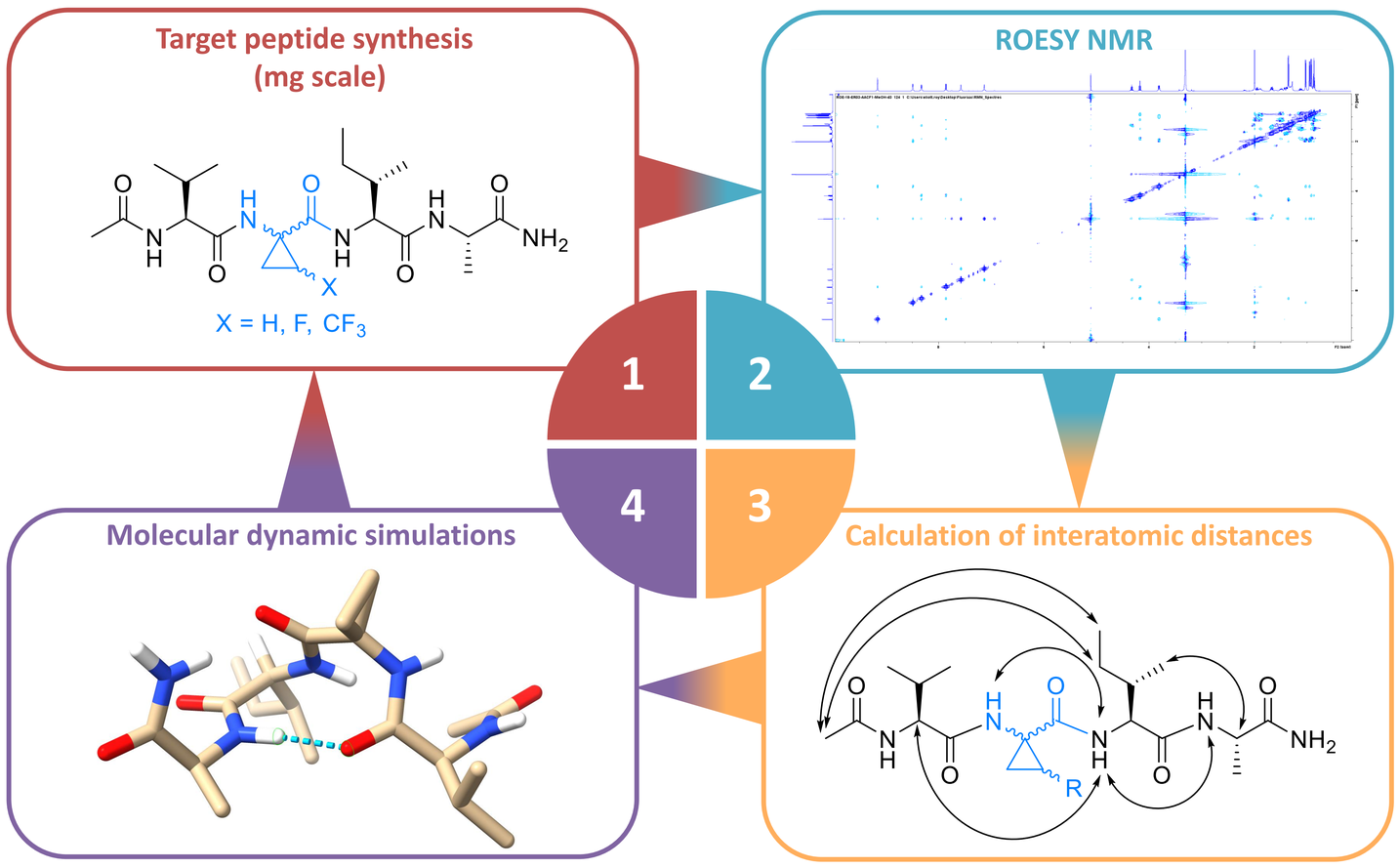
Objectif: Investigate how **FACCs** influence peptide conformation to gain new insights into their **structure-activity relationship** for medicinal applications.

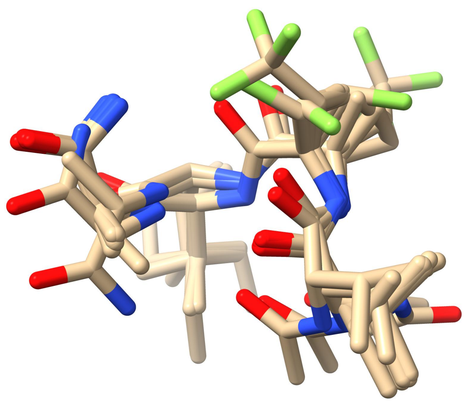
1) Synthesis of model peptides



							
Isolated yield (%)	28	15	42	3	4	5	6

2) Structural analysis





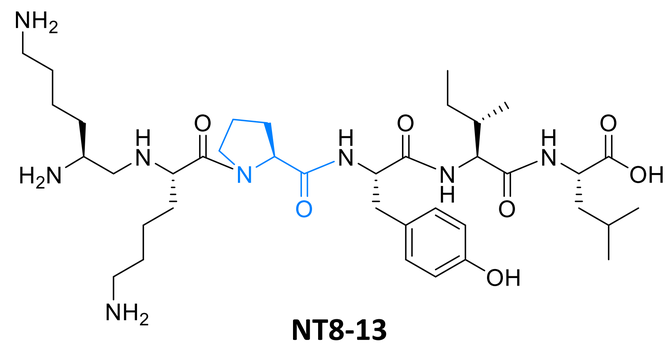
Superimposition of the lowest energy structures of model peptides.

Observations:

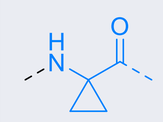
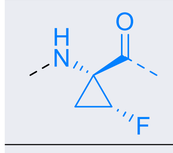
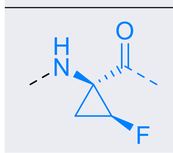
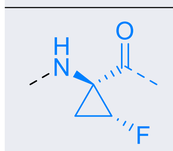
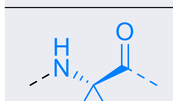
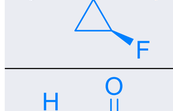
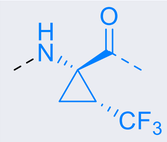
- Cyclopropane substituents seem not to influence peptide conformations.
- Peptide conformations seem only guided by the cyclopropane in a C10 turn.

3) Affinity of NT8-13 analogues

After the synthesis of **Pro[10]FACC NT8-13 analogues**, compounds' affinities toward NTS1 and NTS2 were tested by dose-response displacement of radiolabeled NT.



NT8-13

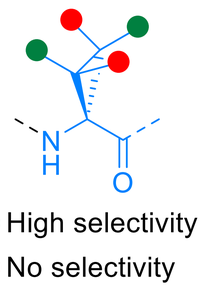
	Isolated yield (%)	Ki ± SEM (nM) hNTS1	Ki ± SEM (nM) rNTS2
	96	786 ± 226	340 ± 191
	65	> 10 000	303 ± 190
	10	2836 ± 986	457 ± 219
	17	> 10 000	226 ± 141
	15	509 ± 103	101 ± 18
	57	1598 ± 450	786 ± 496
	22	> 10 000	117 ± 52

Observations:

- Unsubstituted cyclopropane gives no selectivity.
- Presence of –F or –CF3 substituents on specific positions seems to confer high NTS2/NTS1 selectivity.

Conclusion & Perspectives

- Incorporation of the aminocyclopropane carboxylic acid motif into peptide sequences induces a C10 turn conformation, regardless of cyclopropane substitution.
- However, substitution at only 2 out of the 4 positions on the cyclopropane with hydrophobic substituents confers high NTS2/NTS1 selectivity.
- New FACCs will be tested soon to further decipher the SAR of these residues.



Acknowledgements: We gratefully acknowledge the support of the Agence Nationale de la Recherche (ANR) under grant FLUORAAC.
We also thank Prof. Philippe SARRET (University of Sherbrooke) for performing the NT analogue binding assays.

References:

[1] St-Gelais, F. et al. *Psychiatry Neurosci*. **2006**, *31*, 229.
[2] Sarret, P. et al. *Neurosc. Biobehav. Psychol*. **2018**, hal-03150277.
[3] Previti, S. et al. *J. Pept. Sci.* **2023**, *29*, e3471.
[4] Yokum, T. S. et al. *J. Med. Chem.* **1996**, *39*, 3603.
[5] De Zotti, M. et al. *Amino Acids* **2012**, *43*, 1761.

https://doi.org/10.17952/38EPS.2026.P552

Self-Assembled Biomaterials Lab

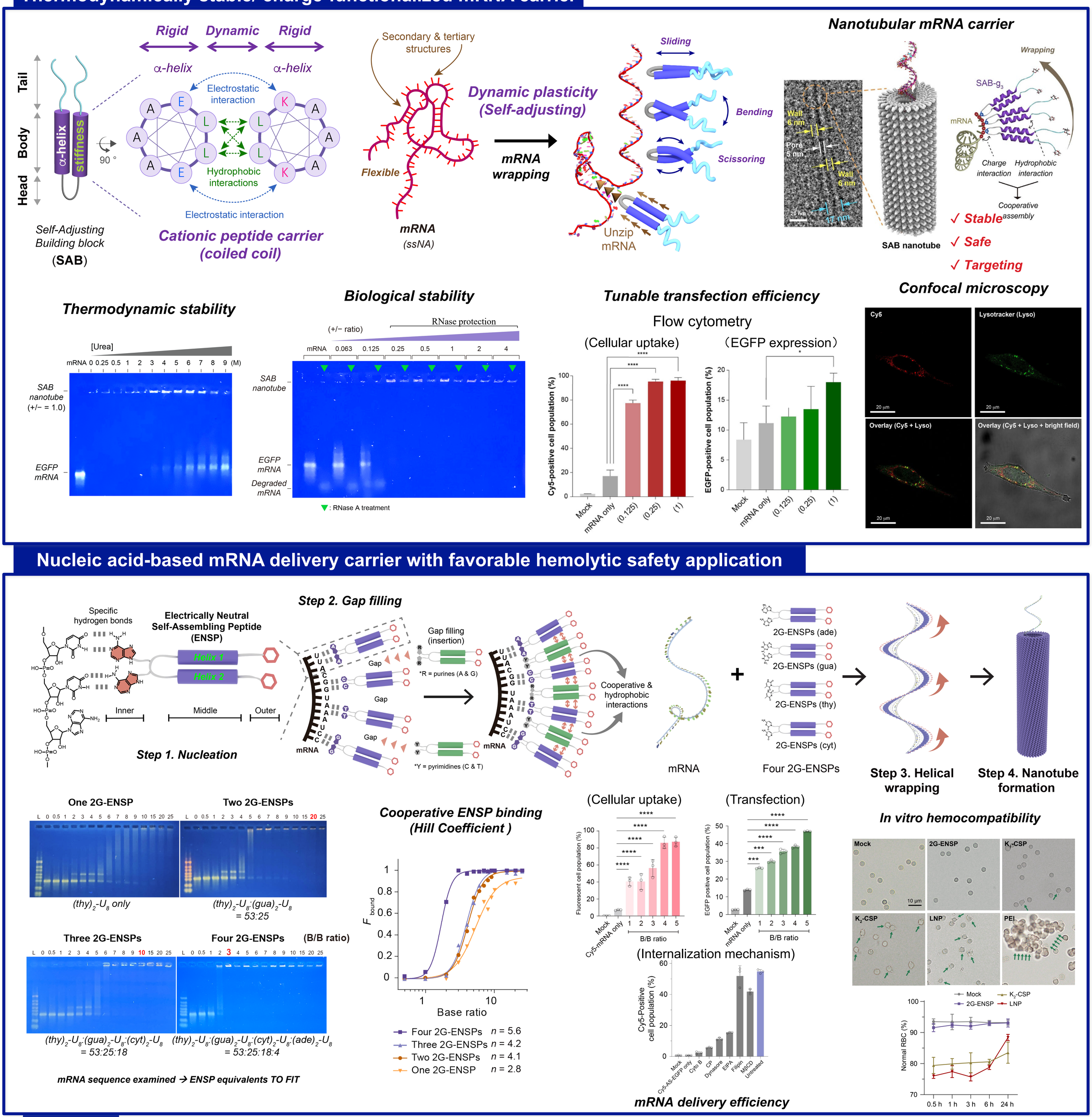
From Thermodynamic Stability to Hemocompatibility: Self-Assembling Peptide Nanotubes for mRNA Delivery

JY.Ryu, HS.Hwang, KW.Hwang, TH.Kim, and YB.Lim

Introduction

While mRNA delivery technology holds significant potential for vaccines and therapeutics, the development of carriers with sufficient stability and safety remains a major challenge. Conventional mRNA carriers are predominantly based on cationic or amphiphilic materials, which efficiently condense mRNA but may cause cyt otoxicity and undesirable membrane interactions. Recent studies have demonstrated that electrically neutral self-assembling peptides can provide an alternative strategy by organizing mRNA through cooperative hydrogen-bonding and hydrophobic interactions while minimizing cytotoxic effects. Moreover, considering the i ntrinsically filamentous nature of mRNA, the formation of nanotubular assemblies may offer greater structural and thermodynamic stability than conventional sphe rical architectures. Peptide–mRNA nanotubes can thus generate virus-like structures in which peptide building blocks cooperatively assemble along the mRNA str and, providing a stable and well-defined supramolecular architecture. Together, these findings highlight the potential of neutral peptide-based nanotubes as a safe r and more durable platform for mRNA delivery.

Thermodynamically stable/ charge-functionalized mRNA carrier



Nucleic acid-based mRNA delivery carrier with favorable hemolytic safety application

Reference

- Zihao Zhang *et al.* "Nontoxic mRNA Vehicles based on Electrically Neutral Self-assembling Peptides." ***Nature Communications,*** In press
- You-jin Jung *et al.* "Cooperative Assembly of Self-Adjusting α-Helical Coiled Coils along the Length of an mRNA Chain to Form a Thermodynamically Stable Nanotube Carrier." ***Journal of the American Chemical Society,*** In press

Amino-acid based amphiphiles as chemical permeation enhancers, for transdermal drug delivery: Synthesis and *In vitro* permeation activity

Bárbara Sampaio, Luísa do Vale

LAQV-REQUIMTE, Department of Chemistry and Biochemistry, Faculty of Sciences, University of Porto, Porto, Portugal

https://doi.org/10.17952/38EPS.2026.P144

Background

Transdermal drug delivery (TDD) is the direct delivery of drugs through the skin so that they can reach systemic circulation. This methodology offers numerous **advantages** over the most conventional routes of administration, such as oral and parenteral drug delivery. In fact, it avoids liver and gastrointestinal first pass effects, it is painless, non-invasive and easy-to-use, presenting this way enhanced patient compliance [1]. Nevertheless, TDD has not yet reached its full potential, and it is still **limited** to a small number of drugs with favorable lipophilic behavior and low molecular mass. The *stratum corneum (SC),* the uppermost layer of the skin, constitutes the biggest barrier to drug penetration, mostly because of its unique lipidic composition and lipid structural organization. To circumvent this difficulty, one of the most studied strategies consists in the use of **chemical permeation enhancers** (CPEs). Particularly, amino acid-based amphiphiles represent an important class of biocompatible, biodegradable and reversible CPEs, showing enhanced activity [2,3].

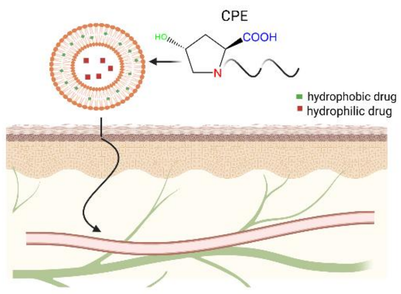


Figure 1. Schematic representation of TDD (made using biorender).

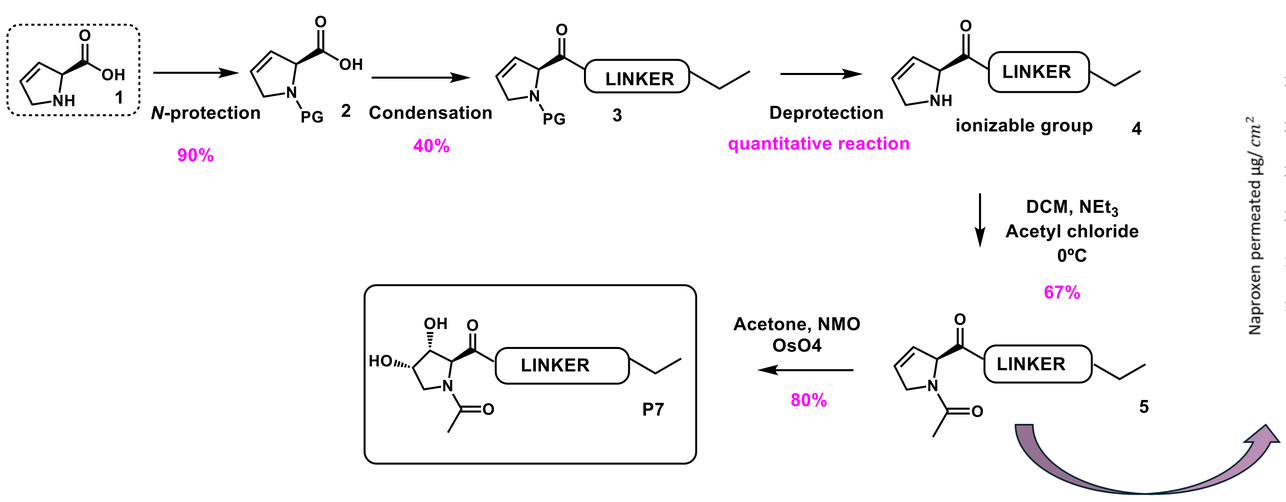
In this regard and to contribute to this field, this work aims at:

- Synthesis of amphiphilic proline and proline mimetic-derived surfactants (monomeric and dimeric) and development of DES thereof;
- Permeation enhancement evaluation using Franz diffusion cells;
- Study of the thermodynamic properties of the amphiphiles;
- Cytotoxicity evaluation in fibroblasts and keratinocytes using the MTS assay.

Results

Monomeric proline and proline mimetic amphiphilic derivatives

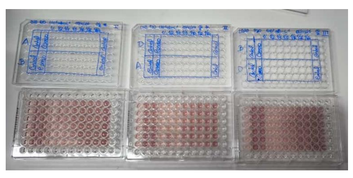
- **Synthesis of monomeric derivatives**



Scheme 1. Synthesis of P7

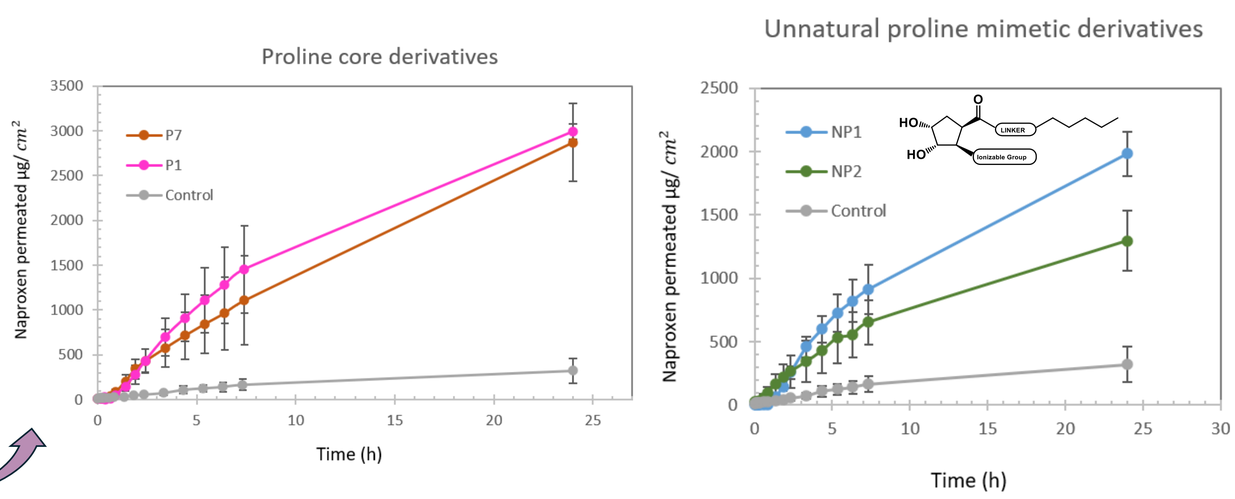
The major difficulties encountered in the represented chemical synthesis (**scheme 1**) included the condensation reaction for obtention of **3** and the amide bond formation reaction for obtention of **5**. These reactions provided lower yields due to the harsh purification of the target crudes.

- **Cytotoxicity evaluation (on-going work)**



Preliminary cytotoxicity studies conducted in L929 cells with the monomeric derivatives indicate that the compounds are non-toxic. These experiments are still on-going.

- **Permeation enhancement potential evaluation with Franz diffusion cells**



Graphs 1 and 2. Permeation enhancement profiles of the monomeric amphiphilic compounds.

Table 1. Permeation enhancement parameters obtained for the monomeric family.

Compound	Naproxen (10mg/mL)		
	Jss (µg/cm²/h)	ER	Q 24h (µg/cm²)
Control	21±8	-	321±137
NP1	183.±12	8	1982±174
NP2	95±14	4	1296±236
P1	201± 74	9	2994 ±86
P7	134 ± 71	6	2868±436



Double-chained proline derived surfactants

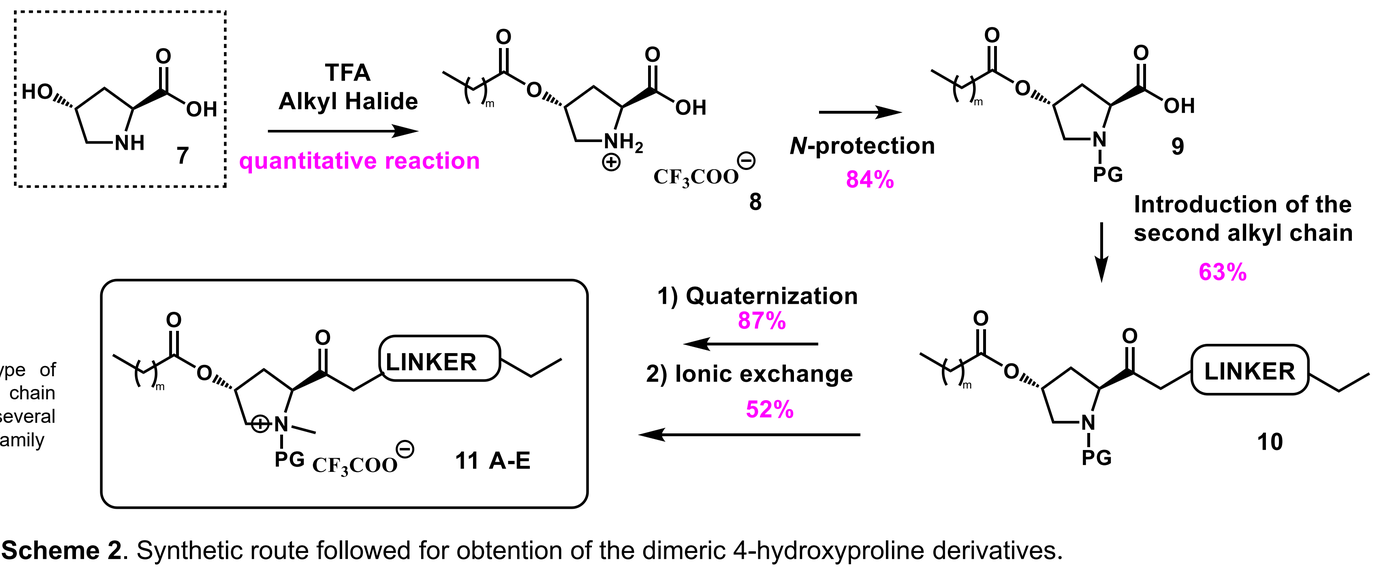
- **Thermodynamic studies with DSC and TG.**

Table 2. Melting points and degradation temperatures of the double-chained compounds.

Compound 11	T_m / ºC	ΔH_f / kJ· mol^{-1}	T_{deg} / ºC
A	61.4	60.6	299
B	70.6	74.9	305
C	66.2	64.9	306
D	61.6	74.0	302
E	62.2	57.6	314

The target structures of the designed dimeric family presented low melting points and high thermal stability.

- **Synthesis of double-chained derivatives**



Scheme 2. Synthetic route followed for obtention of the dimeric 4-hydroxyproline derivatives.

All the reactions presented good to high yields, after optimization.

Conclusions:

In this work, **several families** of target structures were synthesized to be tested for their potential as chemical permeation enhances. All the synthetic steps were optimized and the reactions provided high yields. The final compounds were characterized by ^{1}H-NMR, ^{13}C-NMR, DEPT and ESI-MS.

The monomeric derivatives **highly enhanced naproxen´s permeation** with ER values between 4-9; preliminary cytotoxicity assessments using the MTS assay indicate that the compounds are non-toxic for L929 cells.

Dimeric derivatives presented melting temperatures bellow 100° C, which is favourable for permeation enhancement, and high thermal stability.

Future prospects include the study of the **aggregation behaviour** and **self-assembly** properties of the amphiphiles as well as the development of **Deep Eutectic Systems** thereof for the transdermal delivery of a wide variety of drugs.

References:

[1] Pereira R, Silva SG, Pinheiro M, Reis S, Do Vale M.L., *Membranes (Basel)*. 2021;11(5). doi:10.3390/membranes11050343.
[2] Kopečná M, Macháček M, Roh J, Vávrová K., *Sci Rep*. Published online 2022:1-10. doi:10.1038/s41598-022-24108-6.
[3] Janůšová B, Školová B, Tükörová K, et al., *J Control Release*. 2013;165(2):91-100. doi:10.1016/j.jconrel.2012.11.003.
[4] Kopciuch, E., et al., *Eur J Pharm Biopharm*, 2024. **204**: p. 114505.

Acknowledgements: This work received financial support from PT national funds (FCT/MECI, Fundação para a Ciência e Tecnologia and Ministério da Educação, Ciência e Inovação) through project UID/50006/2025 DOI 10.54499/UID/50006/2025 - Laboratório Associado para a Química Verde - Tecnologias e Processos Limpos. Bárbara Sampaio ackwoledges FCT for PhD grant 2024.04857.BD, DOI: https://doi.org/10.54499/2024.04857.BD. Special thanks are due to Dr. Isabel Olivera from CIQUP for all the help with the transdermal and thermodynamic studies.

ARHLFW: More than a cosmetic peptide

Y. Sarigiannis[1], A. Miliotou[2], T. Panayi[2], Ch. Petrou[2], P. Rodosthenous[2], P. Kaloumenos[2], C.M. Samiotou[2], M.V. Fronimou[3], C.M. Mikelis[3]

[1] Department of Health Sciences, University of Nicosia, UNIC Athens, GR-16777 Athens, Greece
[2] Department of Health Sciences, University of Nicosia, CY-2417 Nicosia, Cyprus
[3] Department of Pharmacy, University of Patras, GR-26504 Patras, Greece
Contact: sarigiannis.i@unic.ac.cy

https://doi.org/10.17952/38EPS.2026.P193

Introduction

Ultra-short synthetic peptides are emerging as multifunctional bioactives for skin applications. The ARHLFW motif is known from its N-acetylated cosmetic analogue (Ac-ARHLFW-NH_2; marketed as Acetyl Hexapeptide-1), while the broader properties of the free-N-terminus H-ARHLFW-NH_2 remain poorly explored. Here, we investigate its physicochemical stability, cytocompatibility, wound-healing-associated gene modulation and antibacterial activity.

Peptide synthesis and Physicochemical Stability

An ultra fast method developed in-house applying MW-SPPS and employing green solvents was used for the synthesis of the peptide, reducing total synthesis time and solvent consumption in comparison with the conventional methods [1]. Identity and purity was confirmed by HPLC and LC-MS. A single dominant HPLC peak (R_t ≈ 13.3 min) and the intact LC-MS ion (m/z 828.7 $[M+H]^+$; 414.9 $[M+2H]^{2+}$) remain detectable from Day 1 to Day 6 in water and PBS — no new degradation peaks.

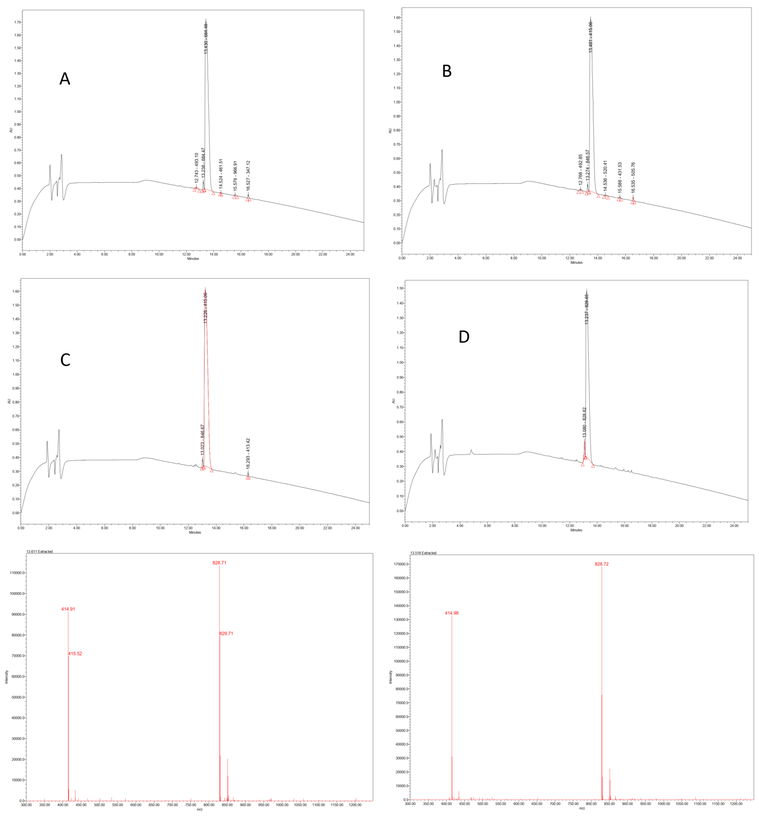


Fig 1. HPLC (220 nm) chromatograms and mass spectra of H-ARHLFW-NH_2 in water (A, C) and PBS (B, D) at Day 1 (up) and Day 6 (down). Day-6 chromatograms retain a dominant peak at approximately 13.0–13.2 min, while peptide-related MS signals remain detectable. HPLC Conditions: XBridge Peptide BEH C18 (4.6 × 150 mm, 2.5 µm, 300 Å); 0.1% formic acid in H_2O/ACN, 5–65% B over 25 min, 0.8 mL min^{-1}, 5 µL injection, detection at 220/280 nm. MS was used for molecular-ion confirmation.

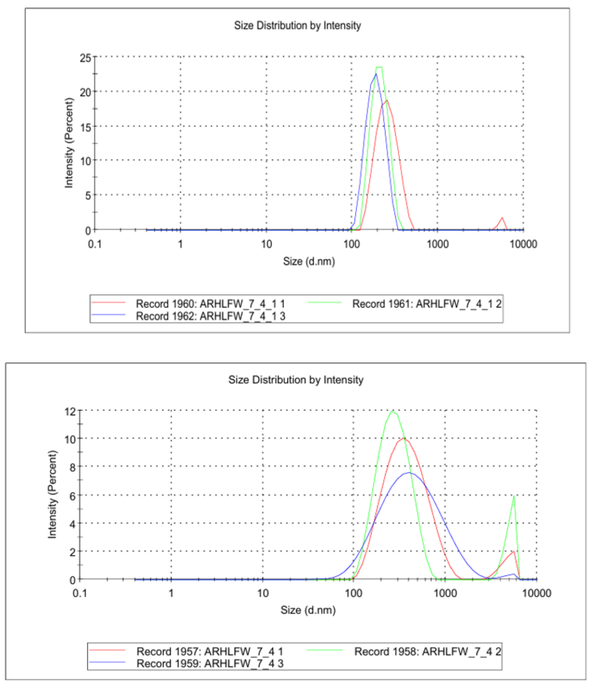


Fig 2. Dynamic Light Scattering (DLS) of ARHLFW at 25°C in Water (up) and PBS pH 7.4 (down). At 25°C, ARHLFW forms larger and more heterogeneous assemblies in PBS than in water (324.7 vs 260.5 nm; PDI 0.338 vs 0.285), highlighting the influence of ionic environment on self-assembly.

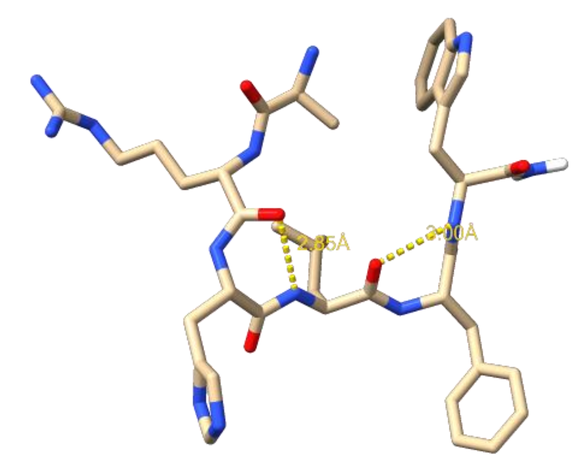


Fig 3. AlphaFold 3-predicted conformation of H-ARHLFW-NH_2, visualised in ChimeraX 1.11.1 after post-prediction C-terminal amidation. Short intramolecular backbone O···N contacts (2.85 and 3.00 Å) are consistent with a compact turn-like arrangement.

Biocompatibility — HaCaT & MDA-MB-231 cells

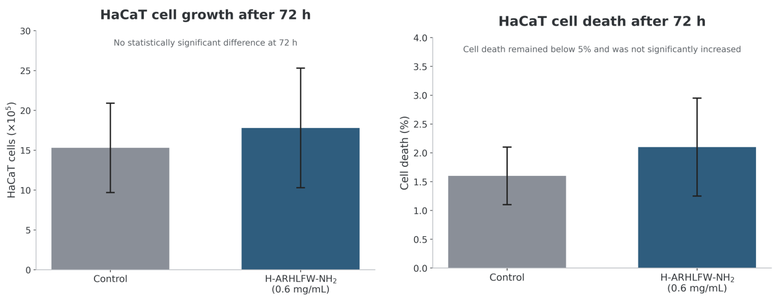


Fig 4. HaCaT response to H-ARHLFW-NH_2 (0.6 mg/mL, 72 h): cell growth was maintained and cell death remained low, with no statistically significant difference versus control (n=3).

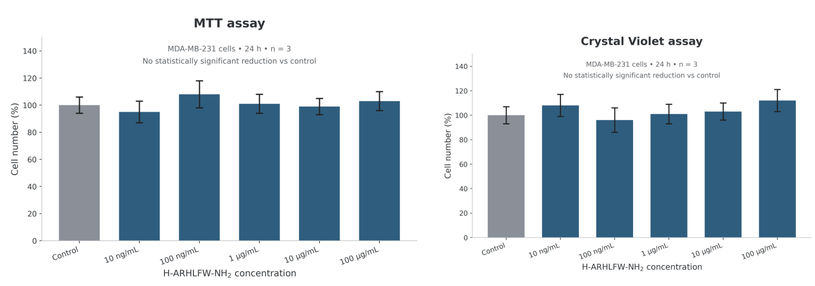


Fig 5. MDA-MB-231 cells exposed to H-ARHLFW-NH_2 for 24 h showed no statistically significant reduction in proliferation or survival across 10 ng/mL–100 µg/mL by either MTT or Crystal Violet assays (n=3).

Wound-healing associated transcriptional activity

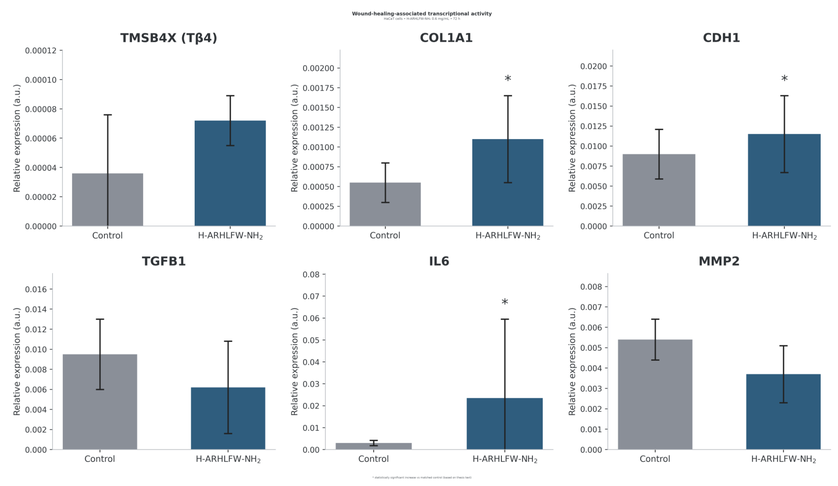


Fig 6. H-ARHLFW-NH_2 induced a distinct repair-associated transcriptional profile in HaCaT cells, characterised by increases in COL1A1, IL6 and CDH1, together with an upward trend in TMSB4X expression, without parallel upregulation of TGFB1 or MMP2 (n=3) (*P<0.05).

Proposed wound-healing-associated transcriptional programme

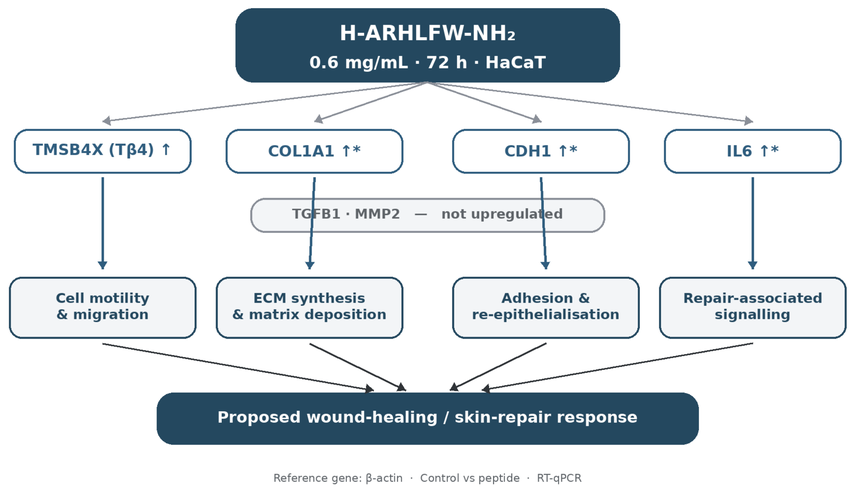


Fig 7. Schematic interpretation of the H-ARHLFW-NH_2-associated transcriptional response, integrating ECM support, epithelial cohesion and repair-related signaling.

Antimicrobial activity

H-ARHLFW-NH_2 was evaluated at 2% (w/v) against *E. coli* (ATCC-700926) , *S. Epidermidis* (ATCC-14990) and *N. Subflava* (ATCC-49275) using solid-lawn and 24 h liquid-culture assays. Ampicillin and WFI were used as positive and negative controls, respectively.

Liquid cultures: 4-log_{10} CFU/mL reduction was observed for both *E. Coli* and *S. Epidermidis* (~99.99% reduction), whereas *N. Subflava* showed little or no response.

Solid bacterial lawns: Visible growth inhibition was observed against all three tested species, indicating that the apparent activity of H-ARHLFW-NH_2 depends on the assay environment.

H-ARHLFW-NH_2 displayed marked antibacterial activity against *E. coli* and *S. epidermidis* in liquid culture, while the solid/lawn assays revealed broader but assay-dependent inhibition.

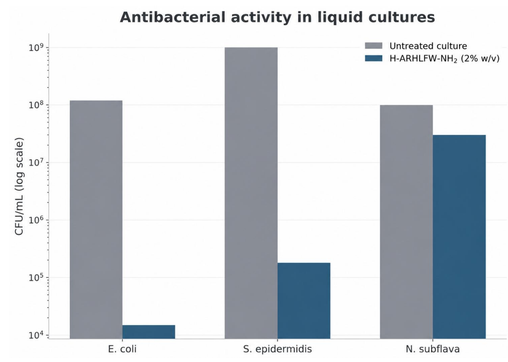


Fig 8. H-ARHLFW-NH_2 (2% w/v) produced an approximately 4-log_{10} reduction in viable E. coli and S. epidermidis after 24 h, while N. subflava showed little response.

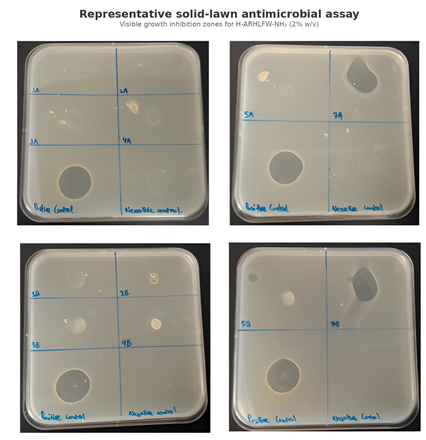


Fig 9. Solid-lawn assays, H-ARHLFW-NH_2 (2% w/v) produced visible growth-inhibition zones against all three tested bacterial species, indicating broader but assay-dependent antibacterial activity.

Take Home Message: H-ARHLFW-NH_2 emerges as more than a cosmetic peptide, combining physicochemical stability, cellular compatibility, repair-associated transcriptional activity and antibacterial effects that support its further investigation for skin-repair and topical applications.

References

[1]. Topouzidou, N et al., Unraveling the Molecular Mechanisms of Synthetic Acetyl Hexapeptide in E-Cadherin Activation for Tissue Rejuvenation. *Cosmetics* **2025**, *12*, 48. https://doi.org/10.3390/cosmetics12020048.

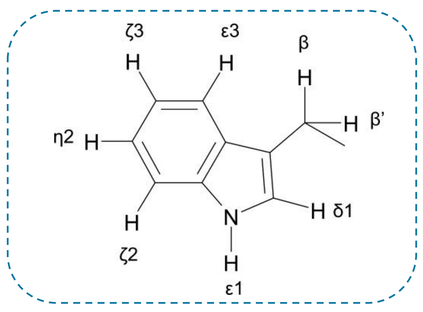
Engineering Robust and Photoswitchable β-turns Through Hydrazide Incorporation

Samprete Bhattacharyya, Kalpita Baruah & Bani Kanta Sarma*
Peptidomimetics Laboratory, New Chemistry Unit
https://doi.org/10.17952/38EPS.2026.P148
Email: samprete@jncasr.ac.in, bksarma@jncasr.ac.in

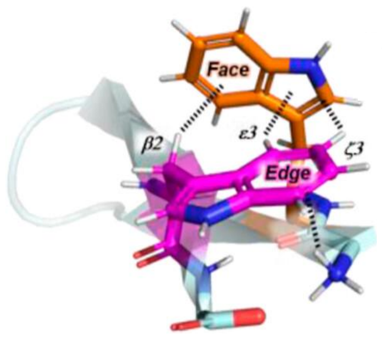
Abstract:

The Tryptophan Zipper (TrpZip) is an iconic folding motif of β-hairpin peptides stabilized by cross-strand tryptophan–tryptophan interactions, each stabilized by an aromatic–aromatic stacking in an edge-to-face geometry. They serve as minimal model systems for understanding protein folding, stability, and hydrophobic interactions. Herein, we report one promising strategy for specifying the conformation of glycine by substituting the alpha carbon with nitrogen, thereby creating an azapeptide which would therefore restrict the conformational landscape as compared to glycine. Further, we set out to enable spatiotemporal control over β-hairpin formation by the introduction of a photosensitive β-turn mimic in the TrpZip backbone. Finally, we anticipate that this mimic will be useful in better deciphering of the roles of β-hairpin structures in protein folding processes, development of peptidomimetic systems, and chemical biology more generally.

Tryptophan as a unique residue



- Tryptophan as a residue has the lowest abundance (~1.4%) amongst all naturally occurring amino acids.



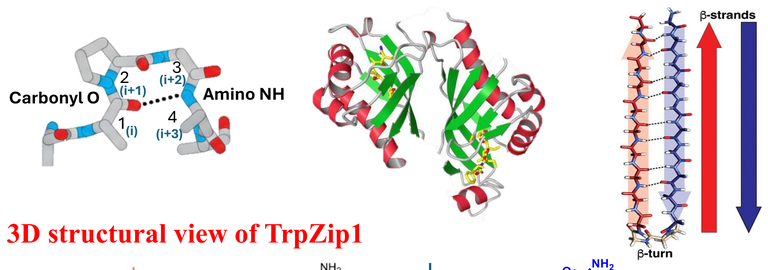
Trp/Trp
Edge-to-Face stacking

- This stacking preference arises from Coulombic interactions between electron-deficient hydrogens and the electron-rich π-cloud.

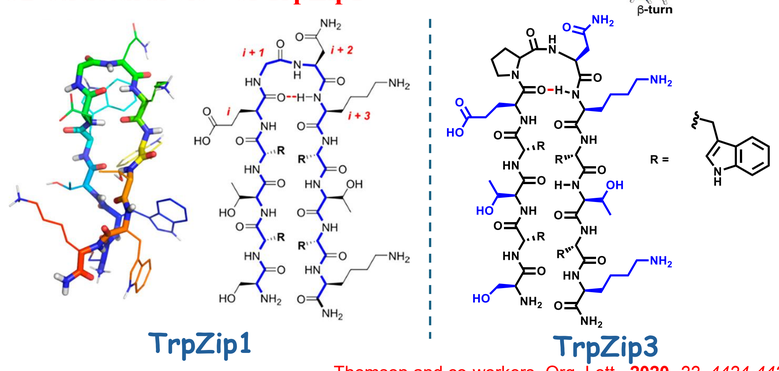
Roche and co-workers, ACS Chem. Biol., **2023**, *18*, 2555-2563

β-turn & β-hairpin

β-turn | β-turn in globular protein | β-hairpin



3D structural view of TrpZip1

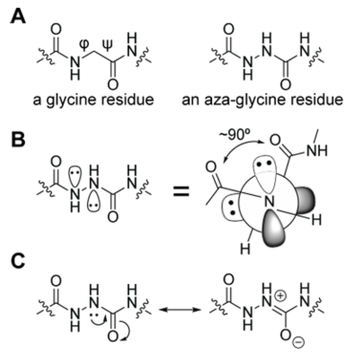


TrpZip1 | TrpZip3

Thomson and co-workers, Org. Lett., **2020**, *22*, 4424-4428

Azapeptide incorporation in TrpZip3

- Aza-glycine restricts the backbone dihedral angles φ and ψ.
- Aza-glycine might stabilize the type I′ turn in Trpzip3, where glycine is present at the i+2 position.



TrpZip3-azGly

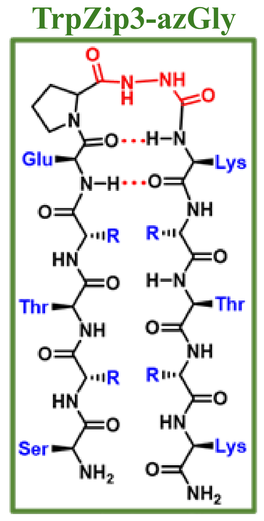


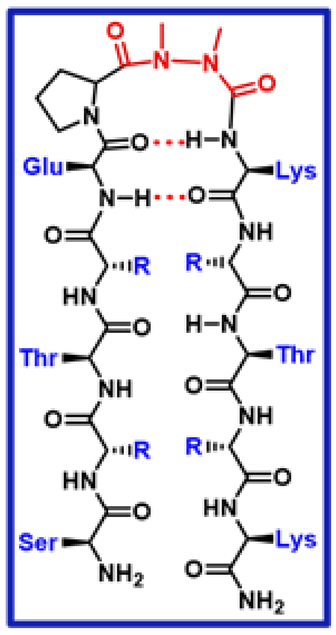
Table 1. Preferred approximate dihedral angles of glycine residues in β-turns

	φ (C′i–1–Ni–Cαi–C′i)	ψ (Ni–Cαi–C′i–Ni+1)
Type I′ β-turn, i+2 position	90°	0°
Aza-glycine conformational minima	±90°	0°/180°

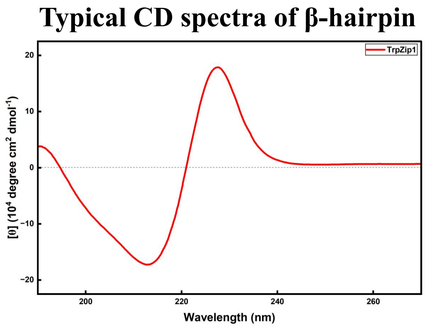
Newberry and co-workers, Chem. Rxiv., **2024**

Can Aza substitution enhance stability?

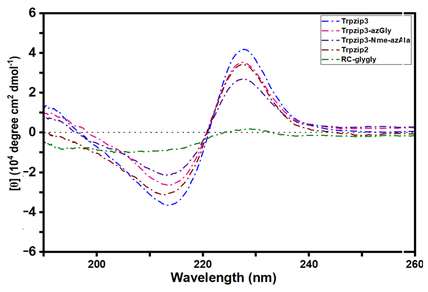
TrpZip3-NMeNme



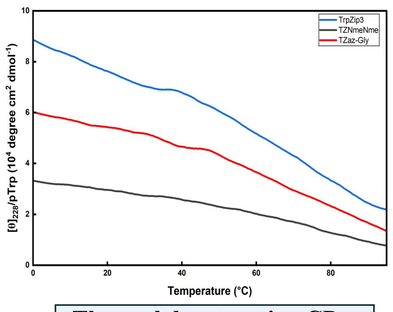
Typical CD spectra of β-hairpin



CD spectra of TrpZip1 (1mg/ml) in 20mM sodium phosphate buffer (at 4°C)



CD spectra in 20mM sodium phosphate buffer (at 4°C)



Thermal denaturation CD monitored at 228nm

Tm (°C)

TrpZip3	65
Tz3aza-Gly	70
Tz3NMeNme	40

Photocontrol of β-hairpin peptide via Hydrazide incorporation

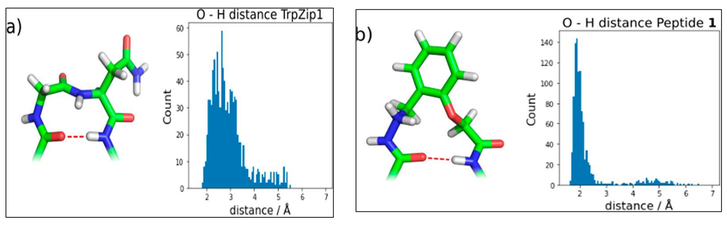


Fig: MD Analysis showing the MD trajectory and a Histogram of the O–H distance for the β-turn hydrogen bond. (a) TrpZip1. (b) Peptide 1.

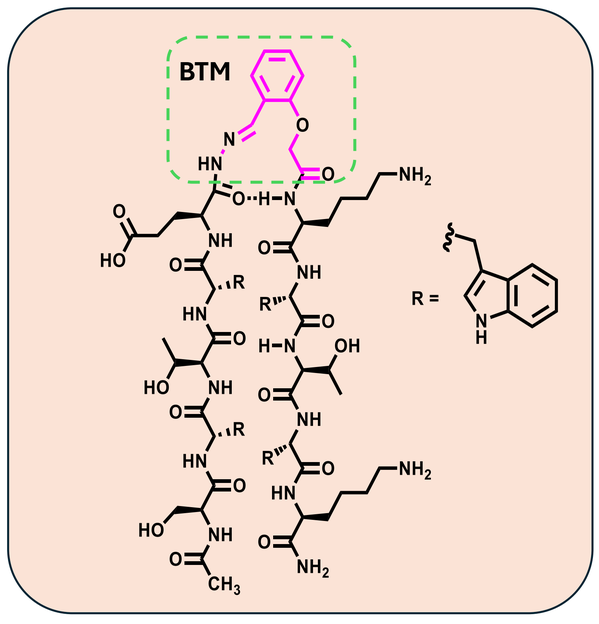
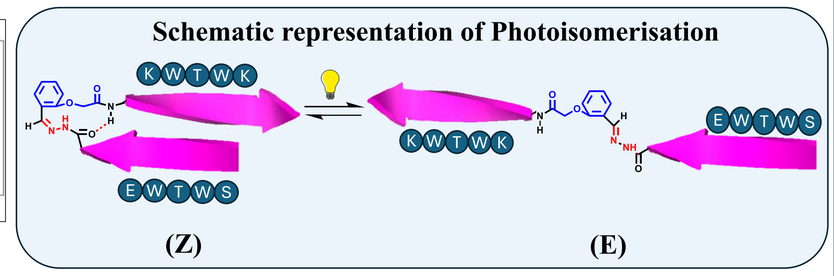
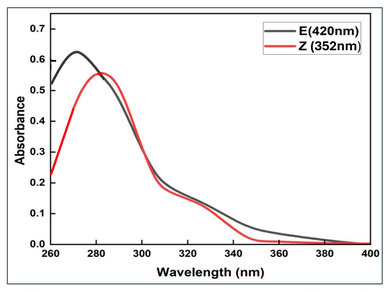
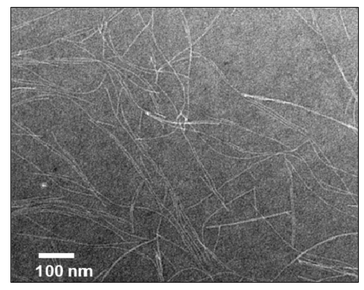


Fig: Introduction of β-turn peptidomimetic in a β-hairpin Tryptophan Zipper 1 (Peptide 1).

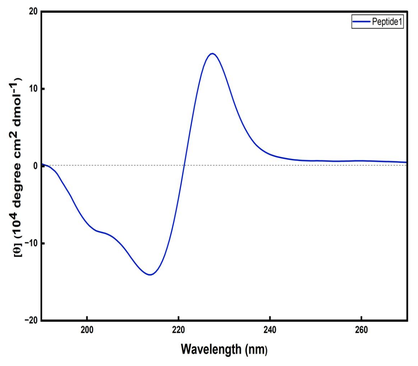




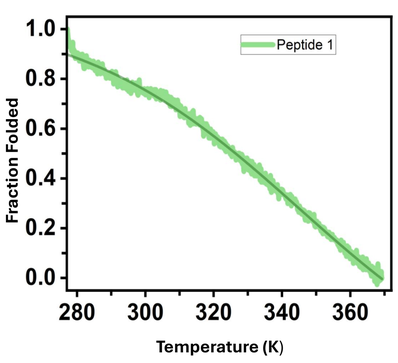
UV-vis absorption spectra of Peptide 1 In DMSO (1×10^{-5} M); $\Delta\lambda_{max}$ 16nm



TEM image of fibrils



CD spectra of Peptide 1 in 20mM Sodium phosphate buffer (at 4°C)



Thermal denaturation CD of Peptide1 monitored at 228nm

Summary and Outlook

1. Aza substitution moderately enhances TrpZip3 stability and may help reduce aggregation in glycine-rich sequences.
2. We successfully incorporated BTM into TrpZip1 to create a photoresponsive peptide and further plan to study its photoisomerization via NMR.

Acknowledgement

JNCASR | SERB INDIA | ज्ञान-विज्ञान विमुक्तये | सत्यमेव जयते Department of Science and Technology (DST) DST



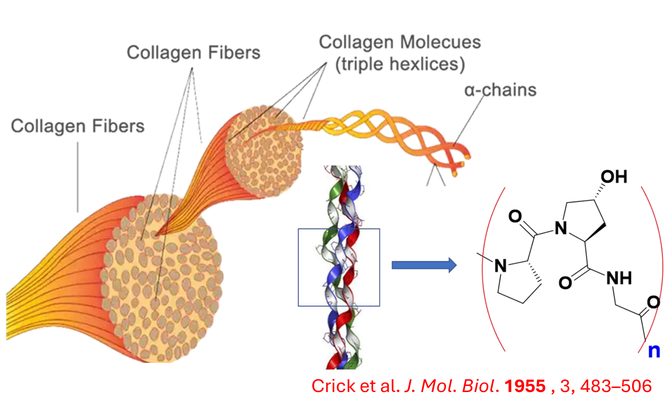
Twist in the Tail: Capping Turns Modulates Collagen Thermal Stability

Aritra Naha, Dr. Amar Ghosh, Prof. Bani Kanta Sarma
Peptidomimetics Laboratory, NCU, Jawaharlal Nehru Centre for Advanced Scientific Research (JNCASR), Bangalore,India-560064
aritranaha@jncasr.ac.in

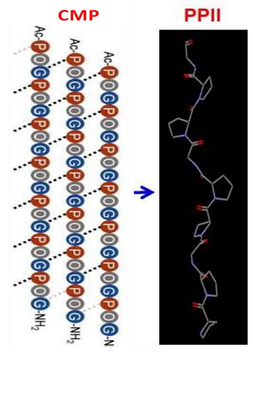
EPS-2026

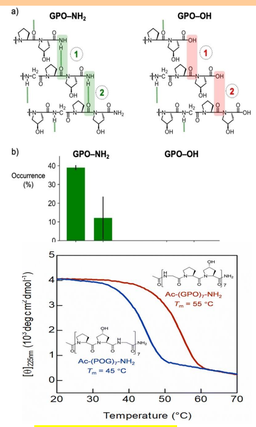
P470

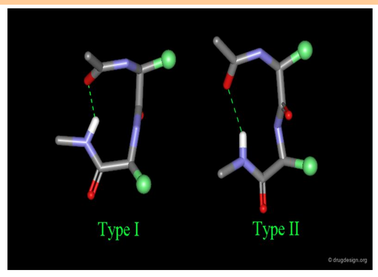
Frame-dependent differences in collagen triple-helix stability are well recognized, yet their structural basis remains unclear. Here, we investigate the role of a C-terminal β-turn as a potential competing structural motif governing this dependence. In collagen mimetic peptides adopting the POG frame, a C-terminal amide can promote intramolecular hydrogen bonding that may sequester the Pro carbonyl and interfere with interstrand hydrogen bonds required for triple-helix assembly. By contrast, in the GPO frame, such competition is reduced, allowing the terminal amide to participate in stabilizing interstrand interactions.



Crick et al. *J. Mol. Biol.* **1955** , 3, 483–506

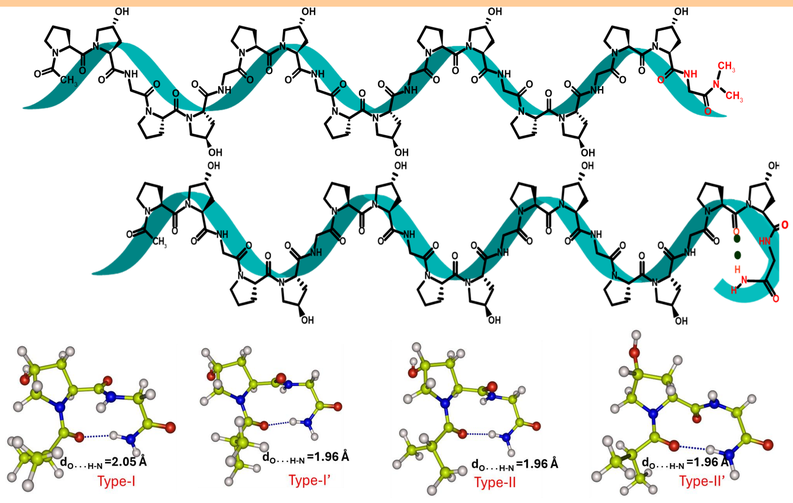






Does Proline(Hyp) and Glycine diad facilitate the formation of any competing intra strand interaction ?

Can we have a terminal cap at C terminal which is neutral to any inter or intra-strand interaction ?



OGP Frame

Ac-(OGP)9-NH2
Ac-(OGP)9-NH2
Ac-(OGP)9-NH2

T_m = 42.3 °C

POG Frame

Ac-(POG)9-NH2
Ac-(POG)9-NH2
Ac-(POG)9-NH2

T_m = 43.7 °C

GPO Frame

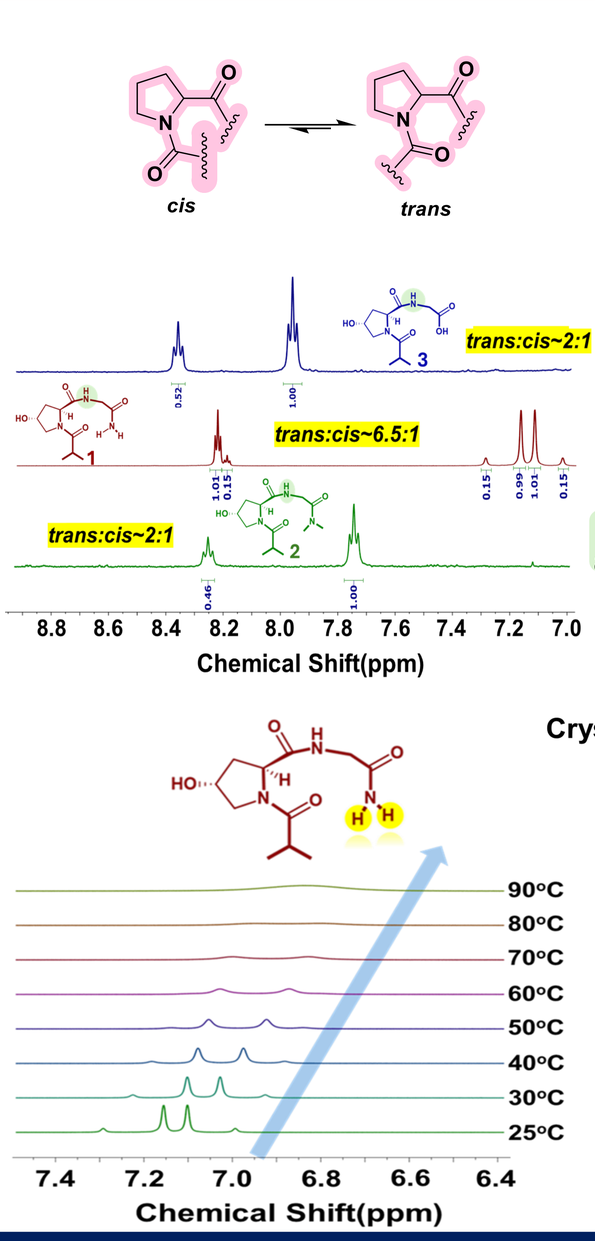
Ac-(GPO)9-NH2
Ac-(GPO)9-NH2
Ac-(GPO)9-NH2

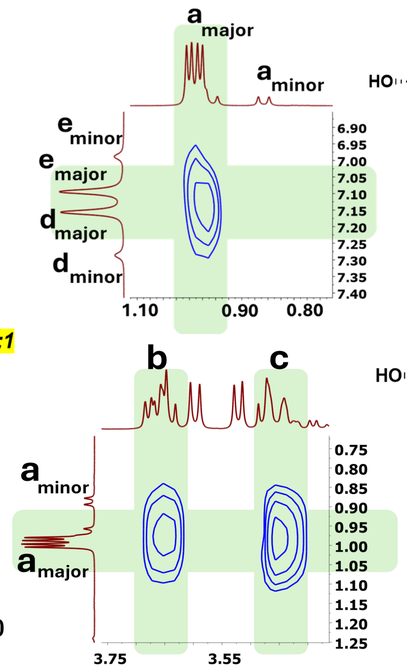
T_m = 53.2 °C

^{t}BU-Hyp-Gly-NH$_2$(1)	Type-I	Type-I'	Type-II	Type-II'	PPII
Δ(ΔE+ZPE) [kcal/mol]	3.03	0.17	0.00	-0.05	3.53

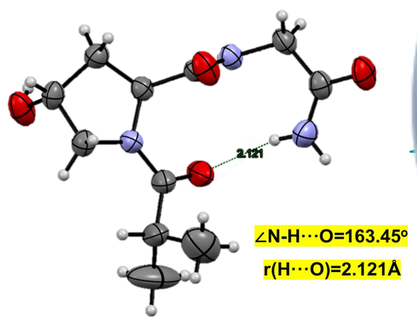
Formation of β Turns : Systematic Studies on Small Molecules and Collagen Mimetic Peptides

Probing formation of β turns through NMR & SC-XRD



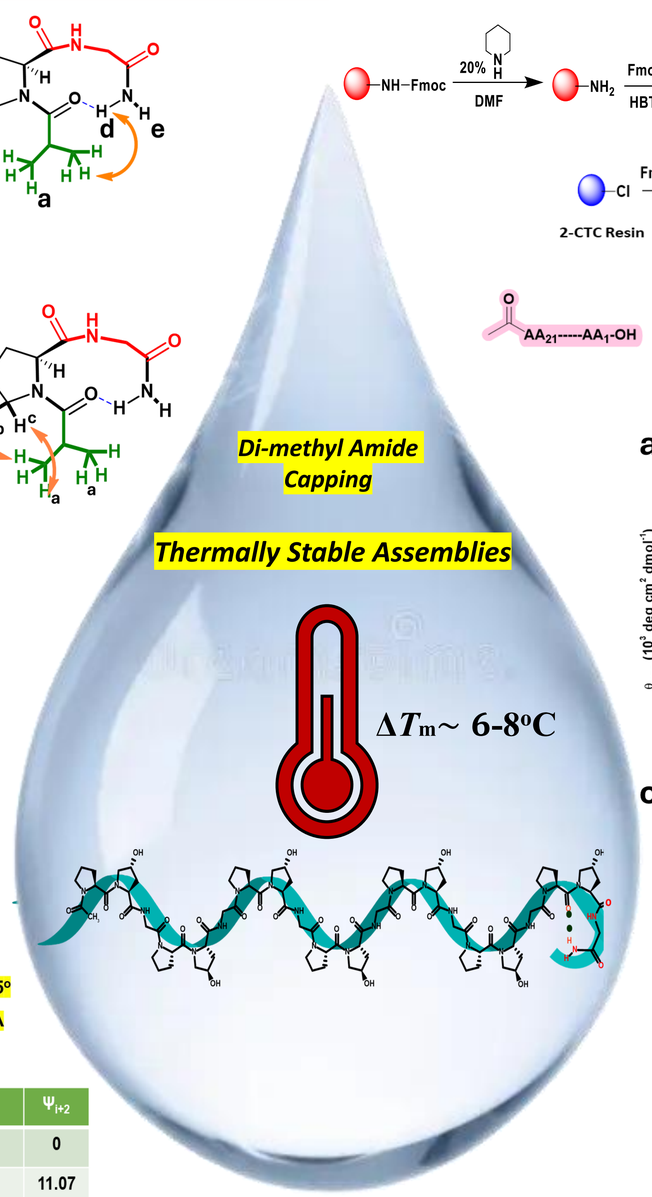


Crystal Structure of Compound 1

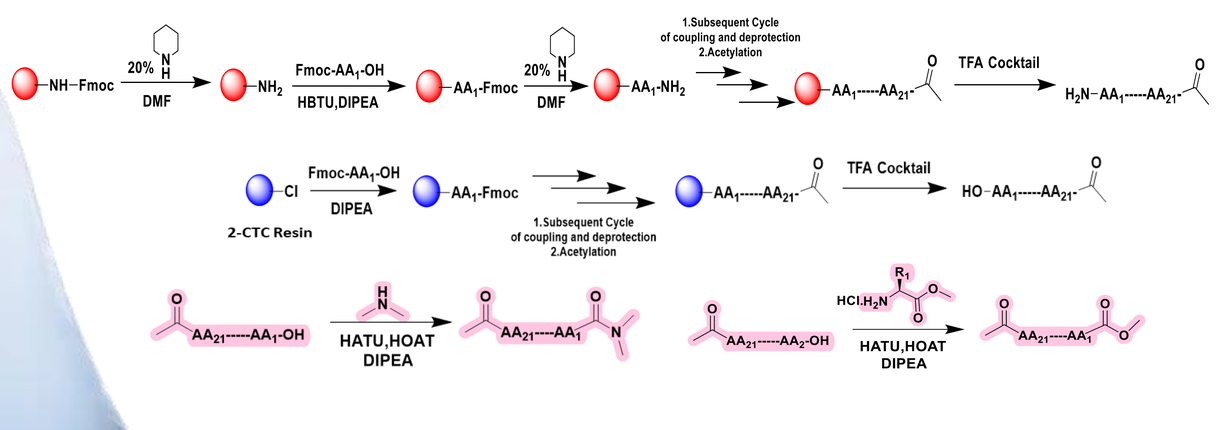


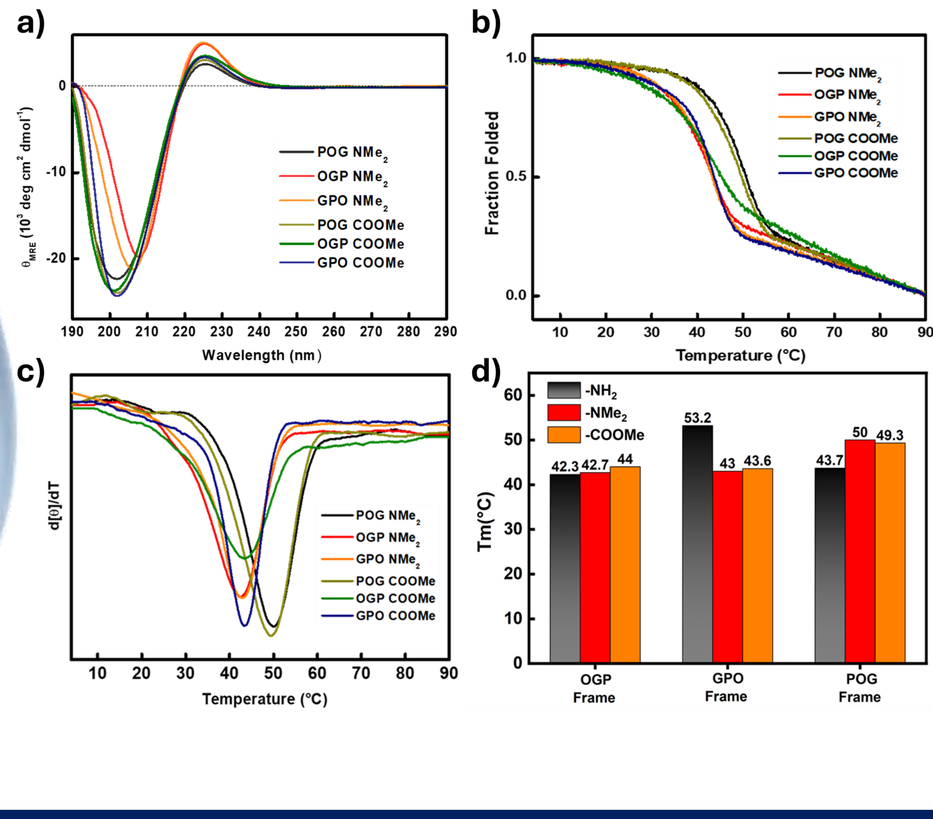
∠N-H···O=163.45°
r(H···O)=2.121Å

Type	φ_{i+1}	Ψ_{i+1}	φ_{i+2}	Ψ_{i+2}
Type-II β turn	-60	120	80	0
^{t}Bu-OG-NH$_2$(1)	-61.17	122.72	74.18	11.07



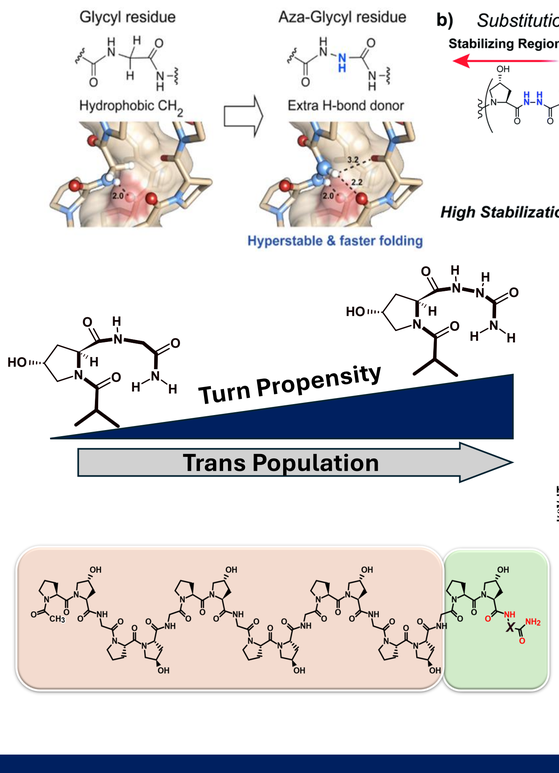
CD studies of CMPs





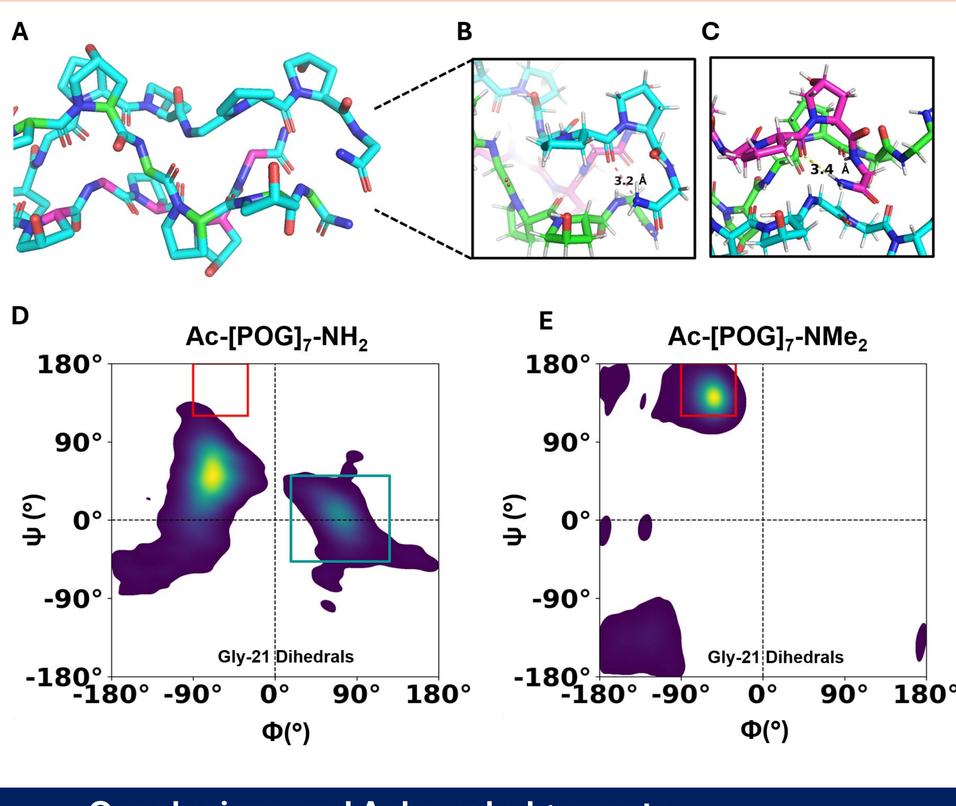
Effect of Competitive β Turns : From Cap to Core

Azaglycine incorporation in CMPs

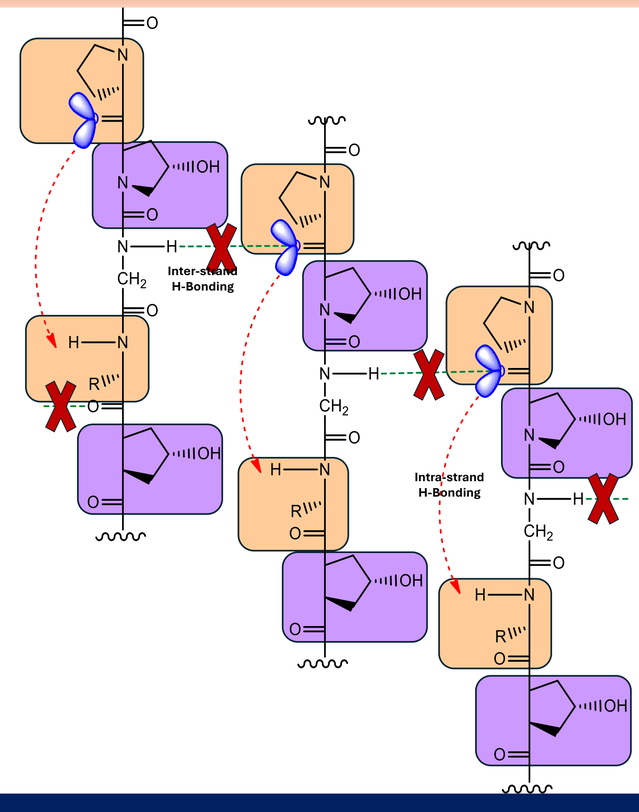


Chenoweth et al. *J. Am. Chem. Soc.* **2015**, 137, 12422−12425

MD simulations



Effect on core substitution



Conclusions and Acknowledgements

This study reveals that β-turn formation at Pro/Hyp–Gly diads competitively disrupts collagen triple-helix stability, with C-terminal caps modulating this effect through their hydrogen-bonding capacity. Frame-dependent analyses of GPO, POG, and OGP systems uncover distinct terminal interactions, establishing design rules for tuning collagen mimetic peptide stability. https://doi.org/10.17952/38EPS.2026.P470

Department of Science and Technology (DST)
DST
iNSERB DIA
JNCASR
PEPTIDOMIMETICS LABORATORY

Toward True αvβ8 Selectivity: Cyclopeptide Ligands that Discriminate Homologous Integrins

C. Savian[1], M. Spirelli[1], A. Sartori[1], P. Delcanale[2], C. Viappiani[2], M. Civera[3], F. Vasile[3], L. Belvisi[3], F. Zanardi[1] & L. Battistini[1]

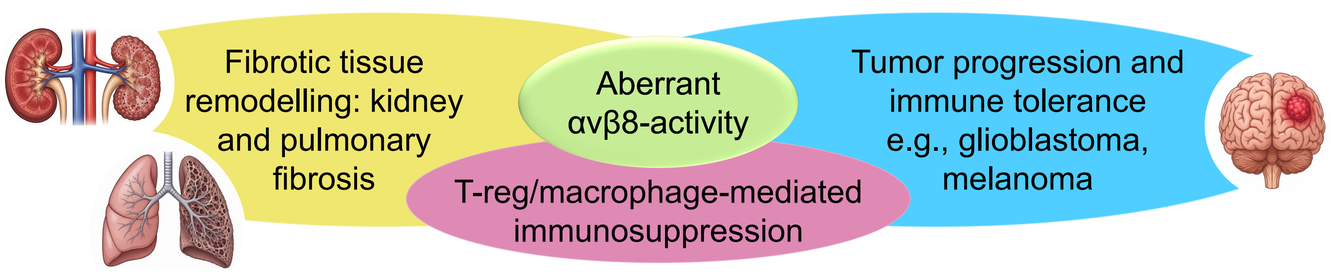
[1]*Department of Food and Drug, University of Parma, Parma, Italy*; [2]*Department of Mathematical, Physical and Computer Sciences, University of Parma, Parma, Italy;* [3]*Department of Chemistry, University of Milan, Milan, Italy*.

Email: chiara.savian@unipr.it **https://doi.org/10.17952/38EPS.2026.P139**

38th EPS European Peptide Symposium

αvβ8 Integrin: latent TGF-β activator

Together with αvβ6, αvβ8 integrin is a key activator of TGF-β, regulating its bioavailability and downstream signalling, and thereby influencing its pathophysiological roles.[1,2]



Challenge: αvβ8 and αvβ6 homology

The high structural homology between integrins αvβ8 and αvβ6 represents a major challenge for the development of truly αvβ8-selective ligands. Both integrins bind the RGDLXX(L/I) motif in TGF-β1/β3 with nanomolar affinity. To date, no high-affinity, αvβ8-selective small molecules have been reported, except for miniproteins described in 2023.[3]



Integrin heterodimers αv (green), β6 (blue), and β8 (violet) with RGDLXX(L/I) (yellow). Image adapted from ref. 3.

Dual c-AmpRGD ligands: starting point

The affinity of the Amp-RGD cyclopeptides was assessed by competitive solid-phase binding assays using immobilized LAP (pro-TGF-β) and soluble αvβ8 or αvβ6 integrins, revealing dual integrin-binding activity.

Structure	IC_{50} (nM) for αvβ8	IC_{50} (nM) for αvβ6
c(Amp[BuN_3]LRGDL)	**2.28** ± 0.12	4.52 ± 1.02
c(Amp[$HexN_3$]LRGDL)	**1.09** ± 0.05	30.3 ± 5.1
c(Amp[$HexN_3$]FRGDL)	**1.29** ± 0.03	43.6 ± 4.9
c(Amp[$HexN_3$]RLD)	**> 10000**	**> 10000**

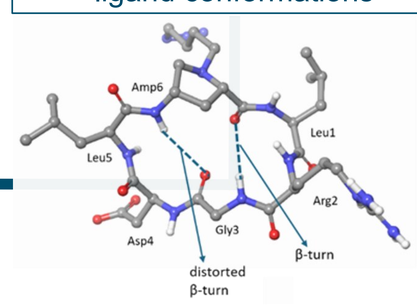
NMR and computational studies

Molecular dynamic simulation (500 ns, 320K) → 5000 frames → Filters from experimental studies (NMR, X-ray structure)
- d(Amp C=O - Gly3 NH) ≤ 4.5 Å
- d(Leu1/Phe1 NH – Arg2 NH) ≤ 3 Å
- d(Cβ-Arg2 and Cβ-Asp4) > 8.25 Å

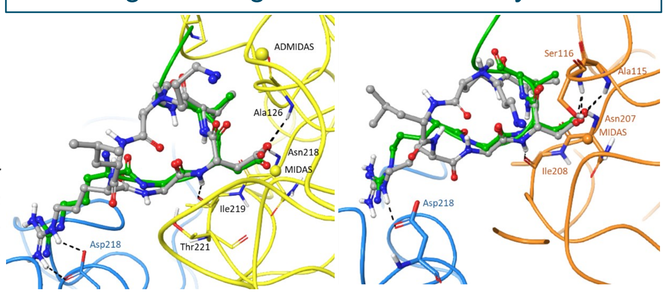
→ MD-NMR-derived ligand conformations

A molecular dynamic-driven docking protocol was implemented to identify the crucial structural determinants and bioactive conformations of dual c-AmpRGD ligands.

Glide SP peptide docking in αvβ8 and αvβ6 → Binding mode selection → Redocking of one selected pose for each ligand → Ligand integrin interaction analysis



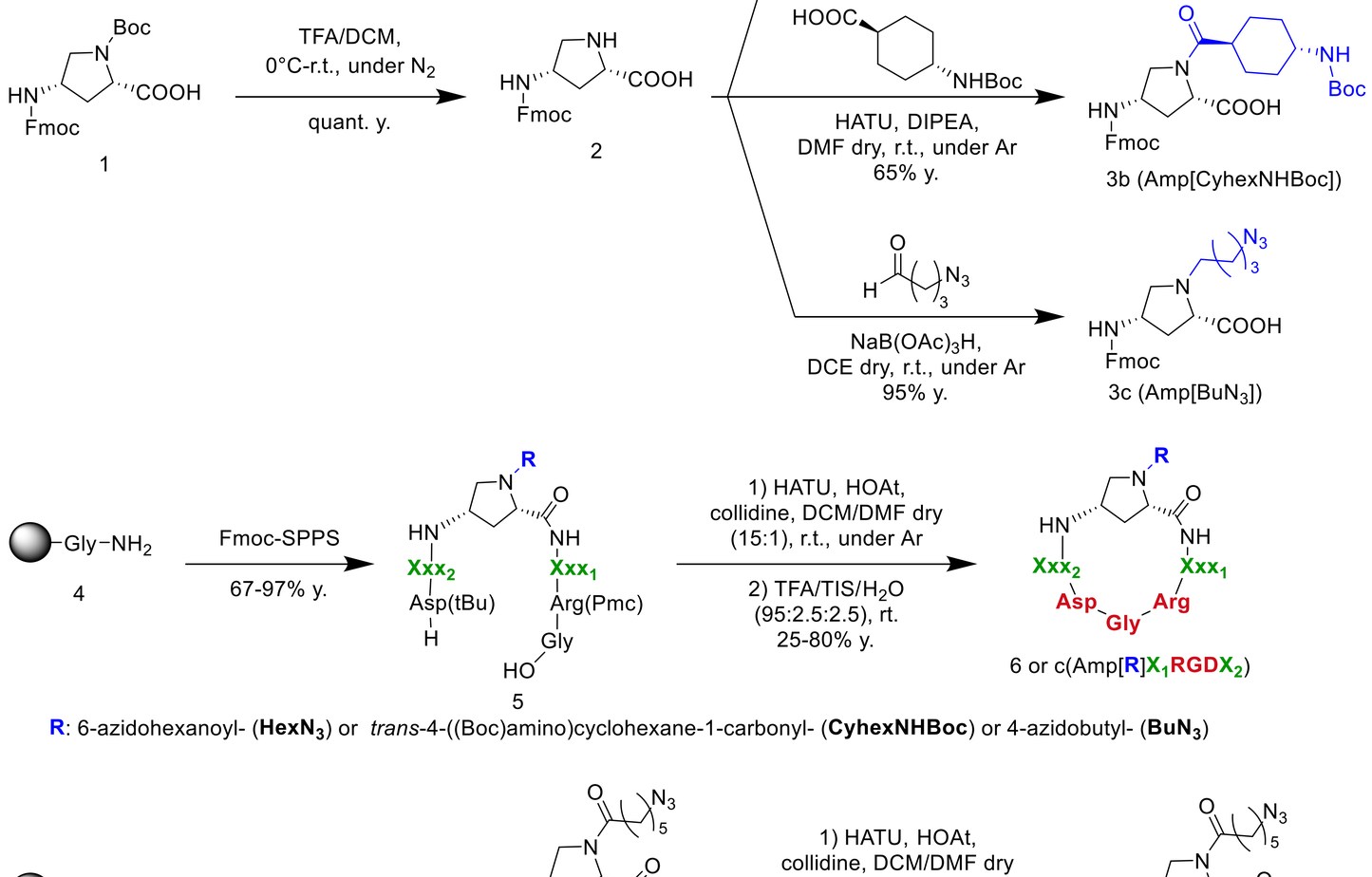
Representative MD-NMR-derived conformation of c(Amp[$HexN_3$]LRGDL).



Docking best poses of c(Amp[$HexN_3$]LRGDL) (grey) in αvβ6 (left) and αvβ8 (right) integrins overlaid to the X-ray structure of the TGF-β3/ β1 (green).

Synthesis of FITC-probe and cAmpRGD ligands

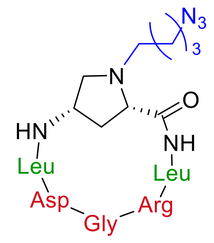
The Amp-RGD cyclopeptides[4] and a FITC-labelled decapeptide probe[5] have been synthesized via standard solid- and solution-phase procedures, purified by flash chromatography or preparative HPLC, and characterized using LC/MS and NMR.



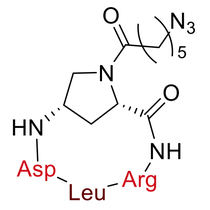
Fmoc-SPPS: (*i) Coupling*: Fmoc-Arg(Pmc)-OH, **Fmoc-$Xxx_{1/2}$-OH** (**$Xxx_{1/2}$**: **none**, **Phe**, **Leu**), **3a** or **3b** or **3c**, Fmoc-Asp(tBu)-OH, Fmoc-Lys(Boc)-OH; HATU, HOAt, collidine, DMF, r.t. *(ii) Fmoc-deprotection*: piperidine, DMF, r.t. *(iii) Resin cleavage*: AcOH, TFE, DCM, r.t.

Fluorescence anisotropy displacement binding assays

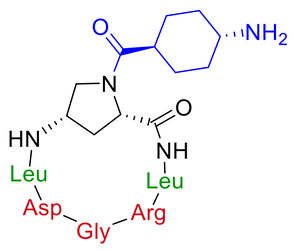
The FITC-labelled probe and an in-house focused library of cyclopeptides with known αvβ6/αvβ8 affinity were used to establish a rapid and reliable cell-free displacement binding assay based on fluorescence anisotropy.



c(Amp[BuN_3]LRGDL)
αvβ6/αvβ8 dual affinity

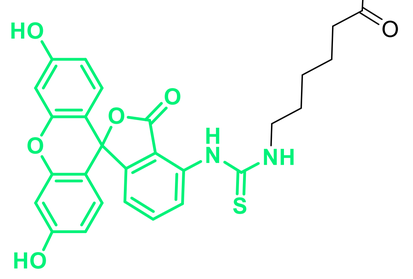


c(Amp[$HexN_3$]RLD)
negative control

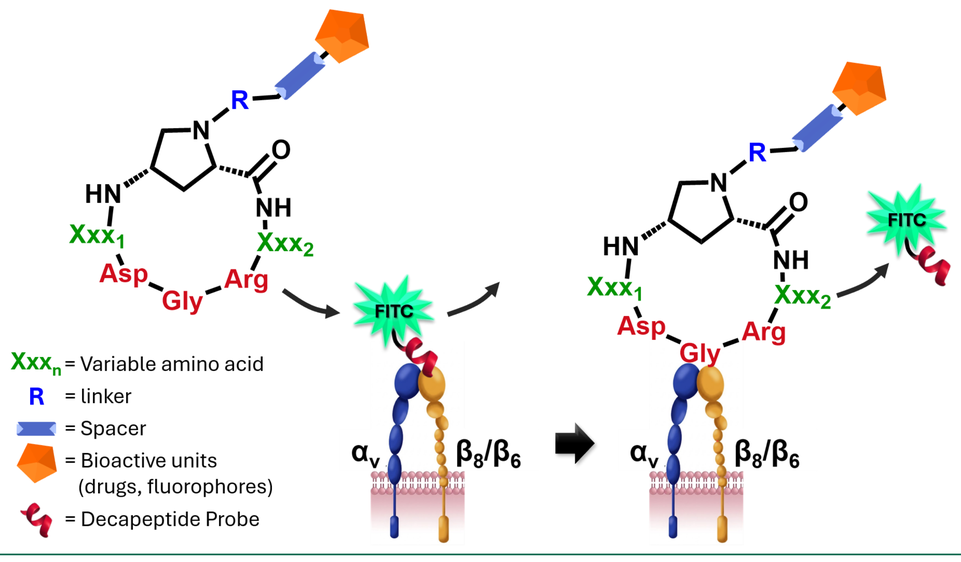


c(Amp[$CyhexNH_2$]LRGDL)

HO—Lys-Lys-Leu-Arg-Gly-Leu-Asp-Gly-Arg-Gly-NH



The setup of the biophysical binding assay has enabled the affinity evaluation of the newly synthesized Amp-RGD cyclopeptides (*experiment ongoing*).



Conclusions and future perspectives

Once the affinity and selectivity of the newly developed ligands have been established, the most promising ones will be optimized to improve their binding profiles and subsequently functionalized with fluorescent or therapeutic payload through suitable linker/spacer moieties.

By integrating structure-guided design, chemical synthesis, and biophysical screening, this approach aims to generate αvβ8-selective Amp-cyclopeptides as innovative platforms for αvβ8-targeted biomedical and pharmacological applications.

References

1. J. H. McCarty, *J. Cell Sci.*, **2020**, *133*, jcs239434.
2. N. F. Brown, J. F. Marshall, *Cancers*, ***2019***, *11*, 1221.
3. A. Roy, T. Springer, D. Baker et al., *Nat. Commun.*, **2023**, *14*, 5660.
4. K. Bugatti, A. Bruno, D. Arosio et al., *Chem. – Eur. J.*, **2020**, *26*, 13468–13475.
5. J. Wang, X. Dong, T.A. Springer et al., *Proc. Natl. Acad. Sci. U.S.A.*, **2017**, *114 (21)*, E4168-E4174.

https://doi.org/10.17952/38EPS.2026.P001

Maastricht University

Diastereoselective Ugi Reactions via Biocatalytic Desymmetrization: A Modular Route to Collagen Mimetic peptides

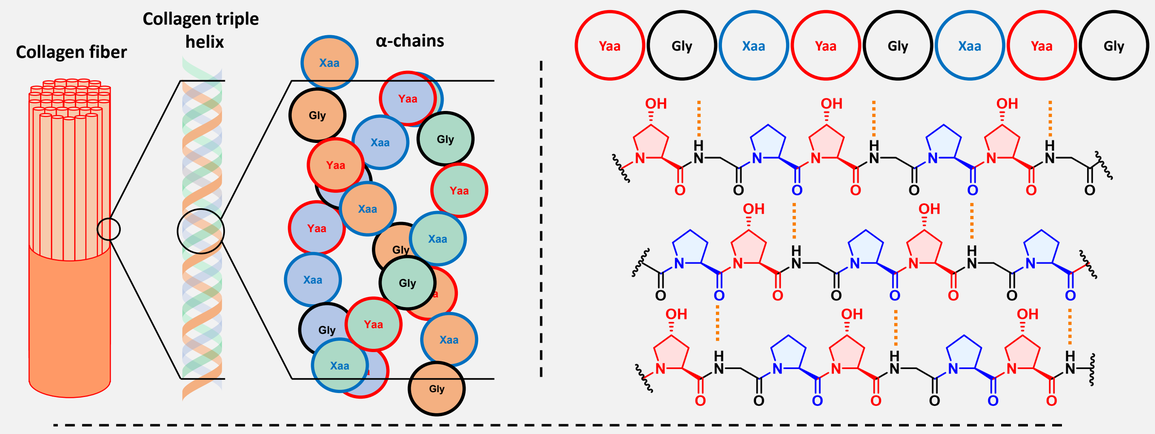
Felix M.J. Boerman[1], Jannes Wagemakers[1], Alessia Bubula[1], Daniele Castagnolo[2], Romano V.A. Orrù[1], Jordy M. Saya*[1]

[1]*Biobased Organic Chemistry, Aachen-Maastricht Institute for Biobased Materials, Maastricht University, Urmonderbaan 22, 6167RD Geleen, The Netherlands*

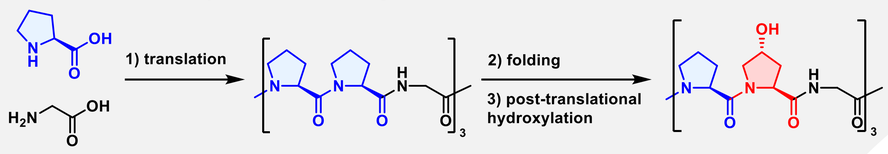
[2]*University College London, Gower St, London WC1E 6BT, United Kingdom.*

A Synthetic Approach to Collagen

Collagen's unique triple-helix structure makes it highly valuable for medical and material applications. However, relying on animal-derived sources introduces disease risks and inconsistent yields. Synthesizing collagen is difficult, but our research offers a novel solution. By combining biocatalytic desymmetrization with diastereoselective Ugi reactions, we efficiently construct collagen's core tripeptide units. Using solid-phase synthesis, we assemble these into collagen-mimetic peptides (CMPs) that accurately replicate natural structural features. This stereo-controlled, modular approach enables detailed studies of triple-helix folding and thermal stability, laying the essential groundwork for scalable, fully synthetic collagen.



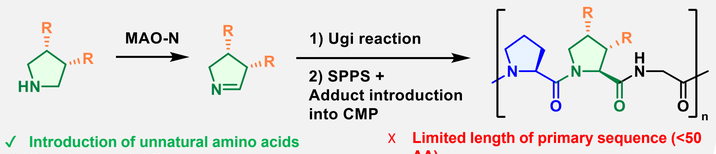
A) Recombinant synthesis of collagens



✓ Primary sequence 1000 amino acids
✓ Folding during translation

X Only natural amino acids
X Difficult Post-translational hydroxylation
X Expensive and difficult to scale up

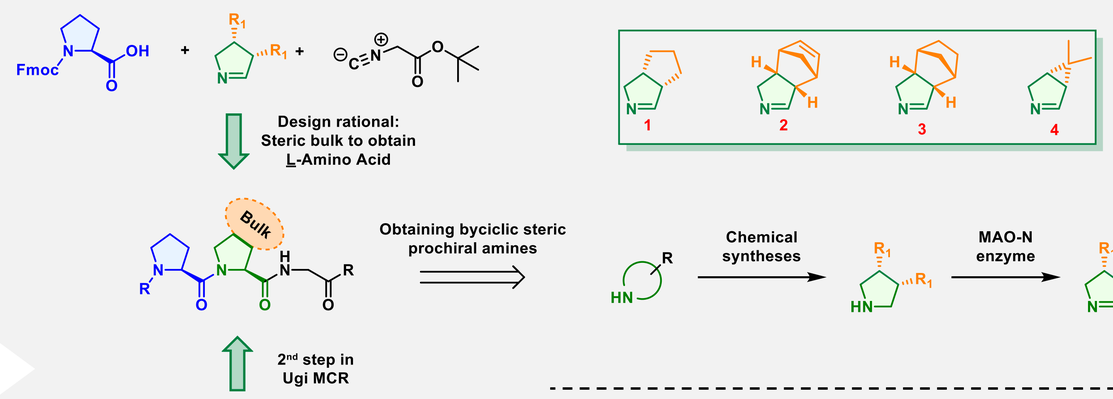
B) Diastereoselective Ugi reactions to synthesize proline-rich peptides



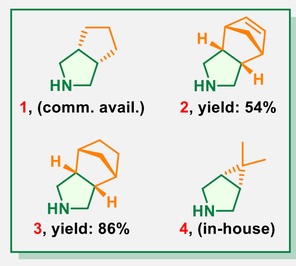
✓ Introduction of unnatural amino acids
✓ Spontaneous folding
✓ Foundation for scalable synthetic collagen
✓ Introducing tripeptide via single step

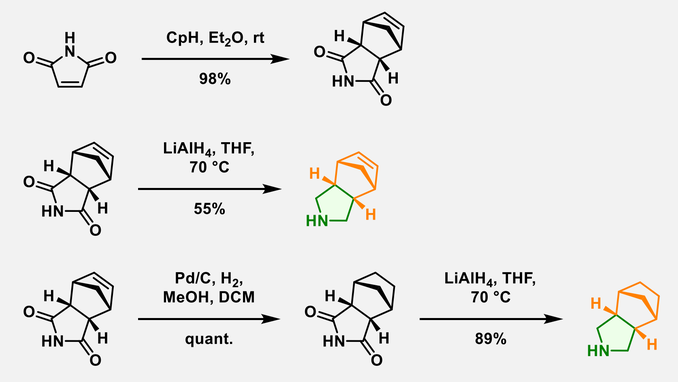
X Limited length of primary sequence (<50 AA)

Design & Synthesis of Prochiral Amines

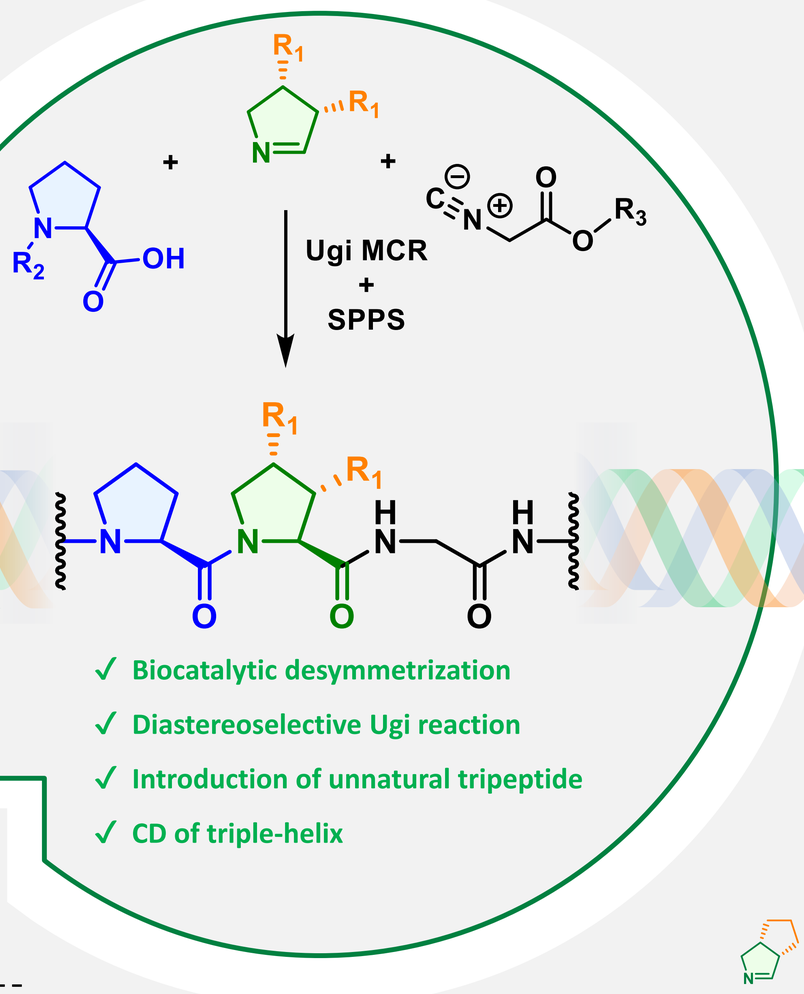


Prochiral Cyclic Amine syntheses



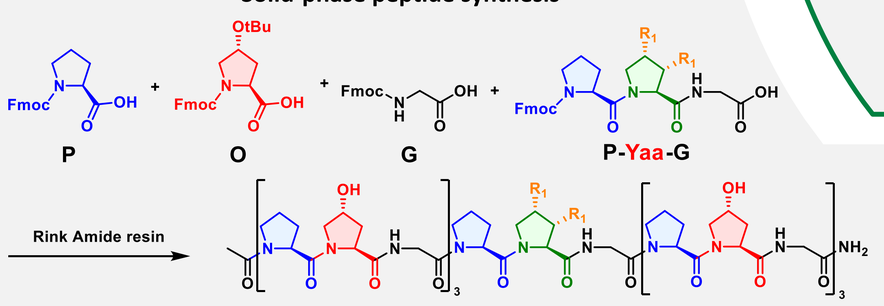


[1] CpH = Cyclopentadiene, THF = Tetrahydrofuran, DCM = Dichloromethane



CD Analysis Protocol: Assessing Triple Helix Stability

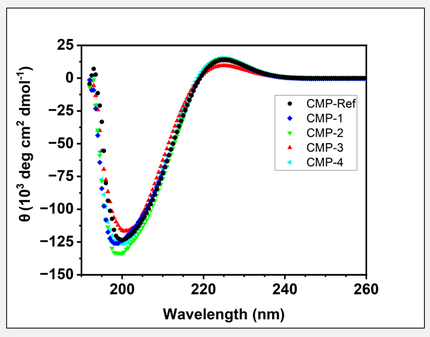
Solid-phase peptide synthesis



Circular Dichroism Analyses Results

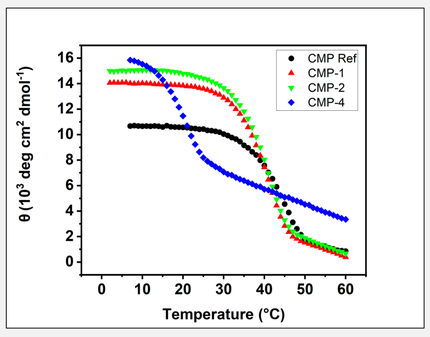
Waves scan:

Determining **secondary structure** and **folding quality** of CMPs in solution (200 µM in phosphate-buffered saline (PBS), pH 7.4)



Thermal denaturation study:

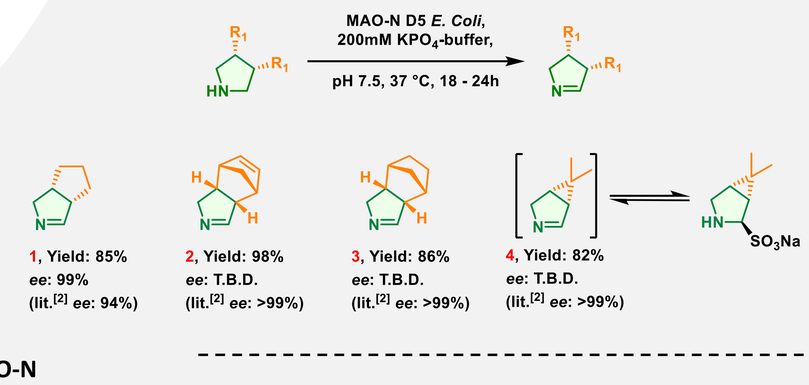
Determining when 50% of triple-helix's have **denatured** and **temperature stability** of CMPs in solution (200 µM in phosphate-buffered saline (PBS), pH 7.4).



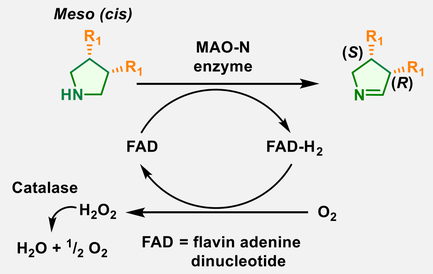
Entry	Imine	CMP	T_m (°C)	ΔT_m (°C)
Ref.	-	Ac-(POG)$_7$-NH$_2$	42.6	-
1		Ac-(POG)$_3$-P-1-G-(POG)$_3$-NH$_2$	39.3	- 3.3
2		Ac-(POG)$_3$-P-2-G-(POG)$_3$-NH$_2$	39.1	-3.5
3		Ac-(POG)$_3$-P-3-G-(POG)$_3$-NH$_2$	T.B.D.	-
4		Ac-(POG)$_3$-P-4-G-(POG)$_3$-NH$_2$	18.5	-24.1

Generating optically pure chiral imines as Ugi partners

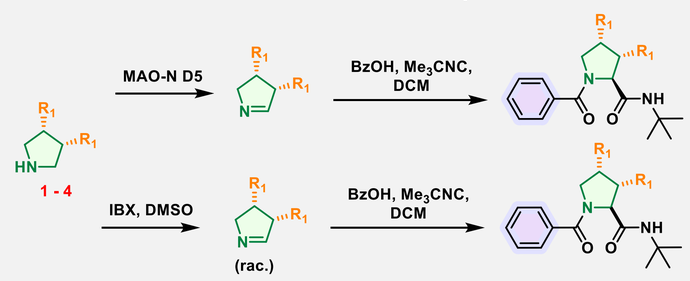
Biocatalytic Desymmetrization using MAO-N



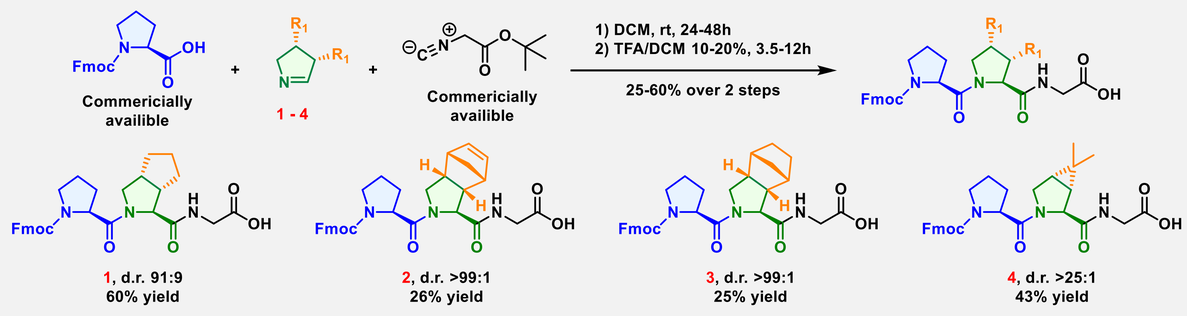
Biocatalytic Cycle of MAO-N



Derivatization for Enantioselectivity Determination



Diastereoselective Ugi MCR and Deprotection



Correspondence to:
Felix Boerman, Organic Chemistry

felix.boerman@maastrichtuniversity.nl T +31642570282

Biobased Organic Chemistry
biobasedorgchem.com

Maastricht University

Urmonderbaan 22, 6167RD,
Geleen, The Netherlands

[1] De Graaff, C., Bensch, L., Van Lint, M. J., Ruijter, E. and Orru. R. V. A. Org. Biomol. Chem., 2015, 13, 10108–10112 [2] Znabet, A., Raftery, J., Helliwell, M. and Turner, N. Angew. Chem. Int. Ed. 2010, 49, 2182 –2184. [3] Chen, W., Ma, L., Paul, A., D. Seidel. Nature Chem, 2018, 10, 165–169. [4] Liu, L., Wang, F., Tian, F., Peng, l., and Wang. L. Org. Process Res. Dev. 2016, 20, 320–324. [5] Fiala, T., Barros, E. P., Ebert, M. O., Ruijsenaars, E., Riniker, S. and Wennemers, H. J. Am. Chem. Soc. 2022, 144, 18642–18649.

38th EPS
European Peptide Symposium

γ-Valerolactone–sulfuric acid: a sustainable alternative to TFA for efficient peptide cleavage and global deprotection

Maria Carmina Scala, [a] Miriana Rega,[a] Pietro Campiglia[a] and Marina Sala[a]

[a] Department of Pharmacy, University of Salerno, Fisciano, SA, Italy; https://doi.org/10.17952/38EPS.2026.P286

Solid-phase peptide synthesis (SPPS) is a powerful and widely adopted methodology for peptide preparation, enabling the rapid and reproducible assembly of complex sequences.[1,2] Despite these advantages, SPPS still relies heavily on hazardous solvents and reagents, limiting the overall sustainability of the process.[3,4] In particular, the final cleavage and global deprotection step typically relies on trifluoroacetic acid (TFA)-based cocktails, which remain among the least sustainable aspects of peptide manufacturing. Besides being highly corrosive and volatile, TFA is increasingly recognized as a problematic PFAS-related chemical because of its environmental persistence and associated ecological concerns.[5] In this context, the objective of the present study is to develop a sustainable alternative to conventional TFA-based cleavage systems with alternative solvents or solvent systems characterized by high sustainability scores according to the GSK Green Solvents Selection Guide, without compromising the efficiency of peptide release and side-chain deprotection. [6]

RATIONALE AND STRATEGY

Among the different alternatives considered, dilute sulfuric acid (H_2SO_4) in combination with γ-valerolactone (GVL) was selected as a sustainable alternative to conventional TFA-based cleavage systems. H_2SO_4 was chosen as the acidic component because its strong Brønsted acidity can provide the proton activity required for efficient peptide–resin cleavage and global deprotection. In contrast to TFA, H_2SO_4 is non-volatile and non-halogenated, while its widespread use in industrial and biomass-processing applications and favourable economic profile make it an attractive candidate for scalable applications in peptide synthesis.

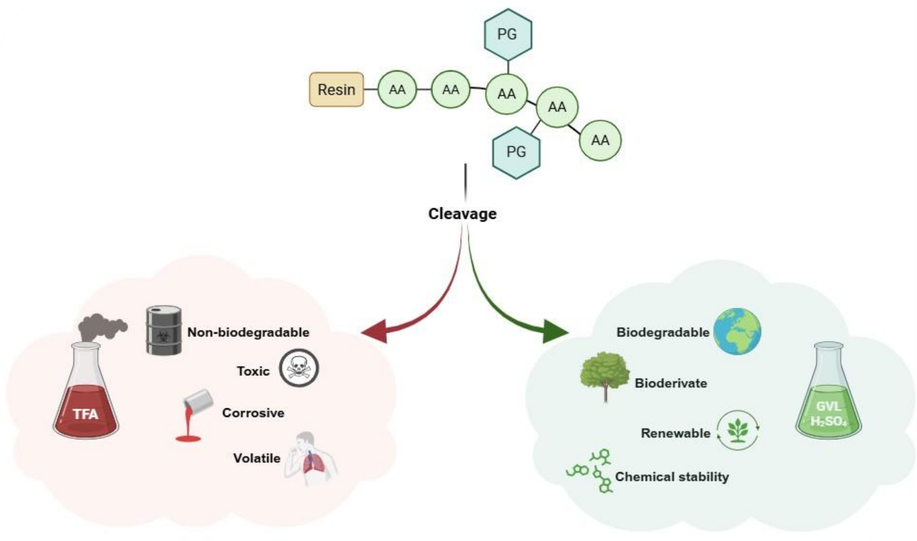


Figure 1: Green H_2SO_4/GVL system as a sustainable alternative to TFA for peptide cleavage and global deprotection in SPPS of model and complex peptides.

GVL was selected as the reaction medium because of its favourable sustainability and physicochemical properties. Derived from lignocellulosic biomass, GVL is a renewable, biodegradable and low-toxicity solvent with low vapour pressure, high boiling point and good solvating ability. Beyond serving as a sustainable reaction medium, GVL may also influence the behaviour of the acidic system: under strongly acidic conditions, it can undergo reversible ring opening, potentially modifying the polarity, solvation and proton-transfer properties of the medium.

Based on these considerations, we hypothesized that H_2SO_4 and GVL could act synergistically to generate a strongly acidic, polar and PFAS-free cleavage environment (Fig. 1).

RESULTS and DISCUSSION

A series of Leu-enkephalin analogues was synthesized by standard Fmoc-SPPS on Rink amide resin to evaluate the efficiency of the proposed H_2SO_4/GVL cleavage system. The effects of H_2SO_4 concentration (1 or 2 M) and scavenger identity were investigated and compared with the conventional TFA/TIS/H_2O (95:2.5:2.5) protocol (Table 1). H_2SO_4/ACN control experiments were also performed to elucidate the specific contribution of GVL to cleavage efficiency (data not shown). Overall cleavage efficiency was determined by subsequent TFA/TIS/H_2O treatment of the residual resin, while crude peptide purity and yield were assessed by RP-HPLC.

The parent peptide YGGFL-NH_2 showed excellent compatibility with H_2SO_4/GVL, affording 98–99% conversion, compared with 86% using the conventional TFA-based protocol (Fig. 2). In contrast, H_2SO_4/ACN resulted in lower conversion and increased sulfonation, particularly at 2 M H_2SO_4. These results highlight the key role of GVL in modulating the acidic reaction medium and suppressing undesired side reactions.

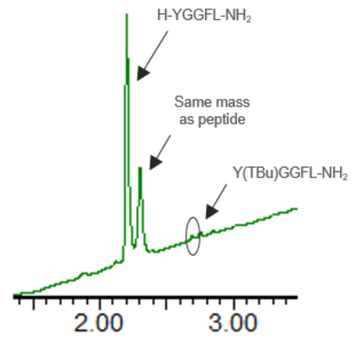


Figure 2. RP-HPLC chromatogram of crude YGGFL-NH_2 obtained after cleavage using the H_2SO_4 (1 M)/GVL system.

The optimized H_2SO_4/GVL conditions were successfully applied to Tyr-, Ser- and Thr-containing peptides, providing efficient cleavage and global deprotection (Fig 3). For YSSFL-NH_2, milder conditions (1M H_2SO_4) suppressed N→O acyl migration, while higher acid concentration led to minor reversible side reactions.

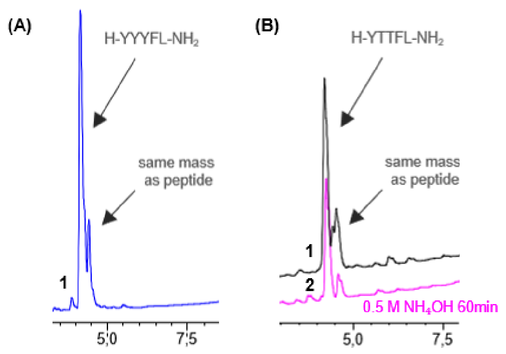


Figure 3. Purity of YYYFL-NH_2 and YTTFL-NH_2 under different cleavage conditions, 2h, rt.

Amino acid	Model peptide (sequence)	Protecting group (side chian)	Crude peptide purity (%)				Overall compatibility with H_2SO_4/GVL	Key observations
			TFA/TIS/H_2O (reference)	H_2SO_4/GVL/TIS		H_2SO_4/GVL/ scavenger		
				1M	2M			
Glycine	YGGFL-NH_2	-	86	99	98	-	★★★★★ Excellent	Quantitative cleavage, minimal by-product.
Tyrosine	YYYFL-NH_2	tBu	97	>99	>99	-	★★★★★ Excellent	Quantitative cleavage, minimal by-product.
Tryptophan	YWWFL-NH_2	Boc	43	>99	>99	-	★★★★★ Excellent	Complete conversion under H_2SO_4/GVL, strong reduction of Trp modifications.
Serine	YSSFL-NH_2	tBu	82	>99	>99	-	★★★★★ Excellent	High compatibility, clean cleavage.
Threonine	YTTFL-NH_2	tBu	93	>99	>99	-	★★★★★ Excellent	Excellent tolerance, minimal by-products.
Lysine	YKKFL-NH_2	Boc	85	93		-	★★★★★ Excellent	Boc removal efficient under mild conditions.
Arginine	YRRFL-NH_2	Pbf	73	0.5	18	6.5 (DODT)	★★★★★ Poor	Pbf removal is rate-limiting. Stronger acid/longer time required.
Aspartic acid	YDDFL-NH_2	OtBu	49	68	41	-	★★★★★ Good	Excellent at 1M; slight decrease at higher acidity.
Glutamic acid	YEEFL-NH_2	OtBu	>99	77	73	-	★★★★★ Moderate	Strong acid improves deprotection but increases by- products.
Cysteine	YCCFL-NH_2	Trt	41	3	15	92 (DODT)	★★★★★ Excellent *(only with DODT)	Scavenger essential to suppress sulfur-mediated side reactions.
Methionine	YMMFL-NH_2	-	81	82	90	-	★★★★★ Good	Good compatibility; slight increase of by-products at higher acidity.
Histidine	YHHFL-NH_2	Trt	>99	22	37	-	★★★★★ Poor	Low crude purity due to side reactions, not to incomplete Trt removal.

Compatibility scale	
★★★★★	Excellent (>90%)
★★★★☆	Good (70-89%)
★★★☆☆	Moderate (40-69%)
★★☆☆☆	Poor (10-39%)
★☆☆☆☆	Very poor (<10%)

	>90%
	70-89%
	40-69%
	10-39%
	<10%

All purities refer to crude peptide after cleavage and LC-MS analysis.

TIS= triisopropylsilane
DODT= 1,4-dimercaptobutane

Table 1. Compatibility of H_2SO_4/GVL with different amino acid side-chain protecting groups. Crude peptide purities and overall compatibility are compared with conventional TFA/TIS/H_2O cleavage.

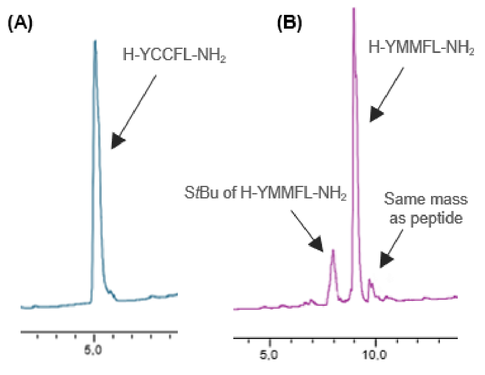


Figure 4. Purity of YYYFL-NH_2 under different cleavage conditions, 2h, rt.

The scope was extended to a broader range of amino acid side chains. Trp, Lys and Met showed good-to-excellent compatibility with H_2SO_4/GVL, with crude purities up to >99% (Fig. 4). Asp and Glu displayed moderate, concentration-dependent performance, reflecting a balance between deprotection and side-product formation (Fig. 5). Arg and His represented the main limitations, with poor cleavage of the Pbf- and Trt-protected derivatives. Notably, DODT significantly improved the cleavage of the Cys-containing peptide, affording 92% crude purity.
Finally, the methodology was applied to the more demanding ACP decapeptide, synthesized on Wang–Gly resin. H_2SO_4/GVL provided 77–82% crude purity, with no additional peptide released from the residual resin after subsequent TFA treatment, confirming efficient peptide–resin cleavage. Thus, the lower purity was attributed to side-product formation rather than incomplete cleavage, demonstrating that the methodology can be extended beyond short model peptides while maintaining sequence integrity.

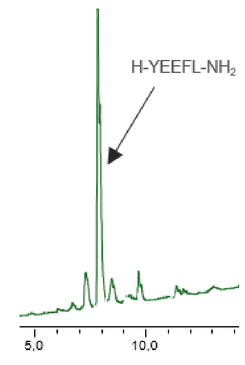


Figure 5. Purity of YYYFL-NH_2 under different cleavage conditions, 2h, rt.

CONCLUSION

GVL/H_2SO_4-based cleavage systems demonstrated high efficiency and strong cleavage performance across various peptide sequences, often surpassing TFA-based methods in both yield and purity. They also enable effective removal of acid-labile protecting groups, even in challenging sequences, while limiting side reactions. In contrast, H_2SO_4/ACN systems without GVL led to increased undesired reactions, particularly sulfonation, emphasizing the important role of GVL in improving chemoselectivity. Overall, GVL-based systems emerge as effective and more sustainable alternatives for peptide cleavage, although further optimization may be needed for highly sensitive residues.

REFERENCES

1. Merrifield, R.B. et al. (1963) *J. Am. Chem.*, **85**, 2149–2154.
2. Albericio, F. et al. (2012) *Future Med. Chem.*, **4**, 1527–1531.
3. Jad, Y. E., et al. (2019) *ACS Sustainable Chemistry & Engineering*, **7**, 3671-3683.
4. Pawlas, J. et al. (2024) Sustainability in Tides Chemistry, 424, 50-84.
5. Arp, H.P.H. et al. (2024) *Environ Sci Technol,* **58**, 19925-19935.
6. Henderson, R.K. et al. (2015) *Green Chem.*, **17**, 945.

mscala@unisa.it

UNIVERSITÄT LEIPZIG

Medizinische Fakultät

Transcending Amino Acid Limitations: Enzymatic Halogenation for Phage Display Diversification

Richard Schreiter[1], Prof. Dr. Leonard Kaysser[1], Jun. Prof. Dr. Christina Lamers[2]

[1] Department of Pharmaceutical Biology, Institute for Drug Discovery, Leipzig; [2] Department of Pharmaceutical Chemistry, Institute for Drug Discovery, Leipzig

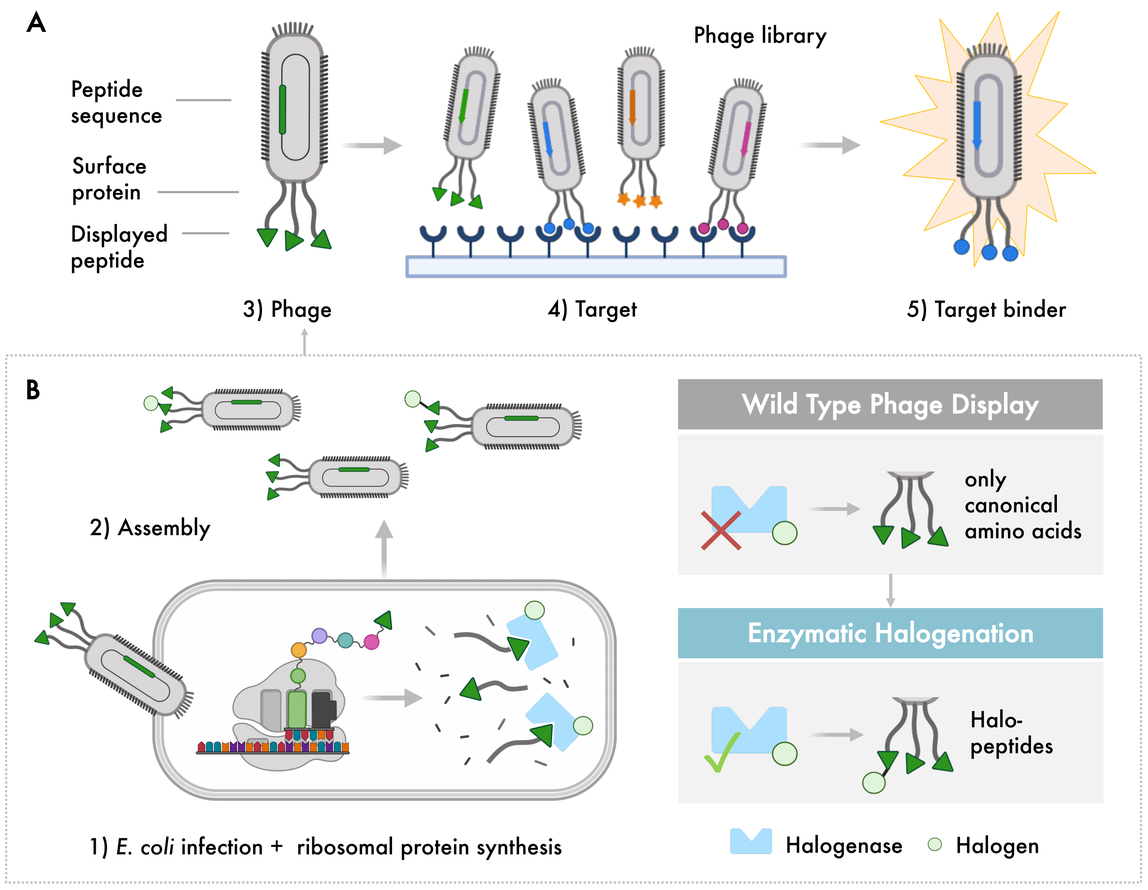
https://doi.org/10.17952/38EPS.2026.P425

Towards more drug-like peptides via enzymatic halogenation

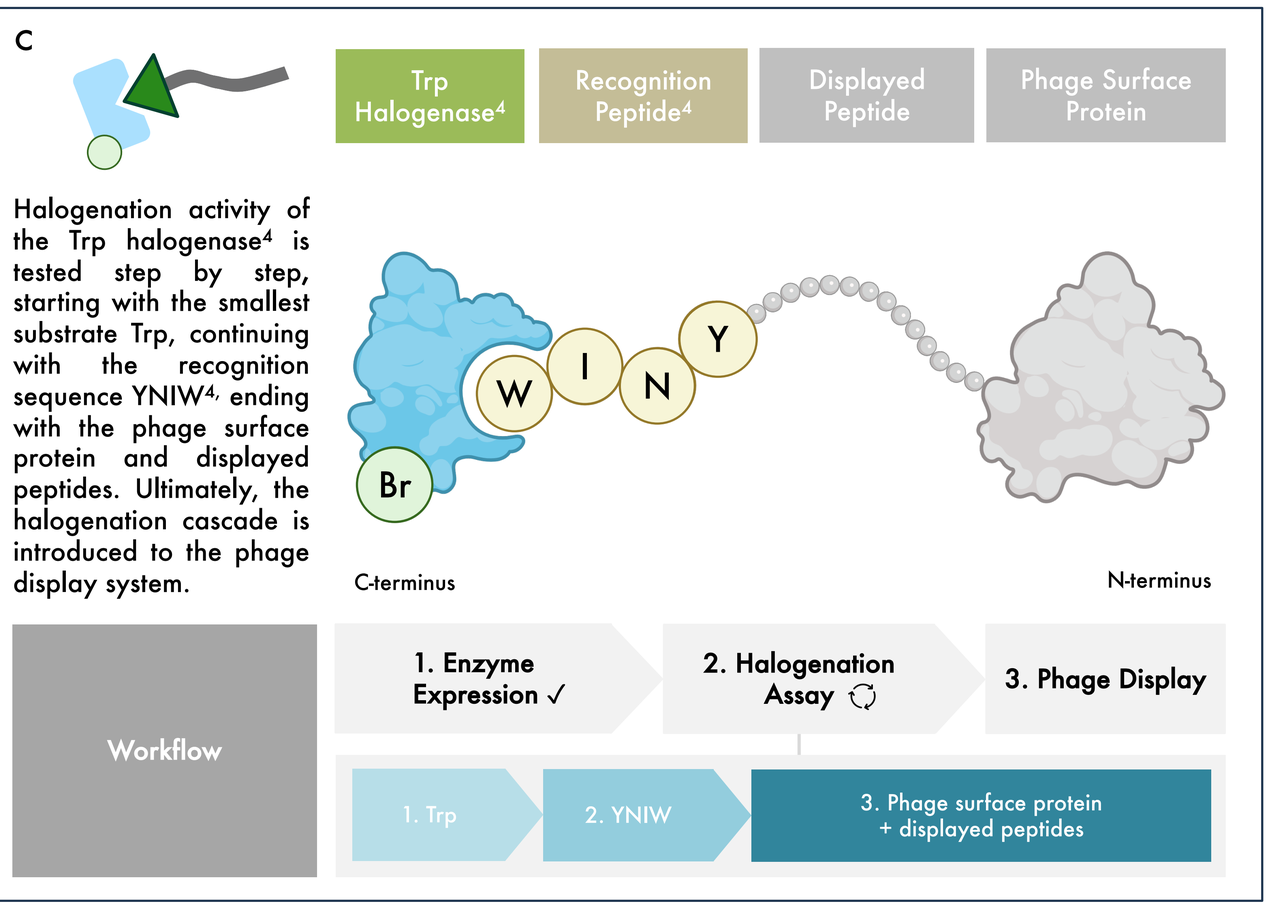
Over the past decades, peptides have gained significant attention in drug discovery due to their favorable pharmacological properties, including high potency, target selectivity, and low toxicity.[1] In this context, phage display has become a pivotal technology, capable of screening huge peptide libraries for target binders.[2] However, phage libraries are restricted to the 20 canonical amino acids, as displayed peptides are synthesized ribosomally.[3] Our study aims to address this challenge via enzymatic halogenation: as recent publications have demonstrated that several halogenases are capable of peptide or protein halogenation,[4] we hypothesize that selective halogenation of peptides displayed on phages is achievable.

Once established, this method could offer significant advantages over existing approaches: (1) site-selective halogenation without altering phage particles and (2) halogenated peptides as valuable intermediates for further modifications of phage display.

Ribosomal synthesis limits phage libraries to canonical amino acids

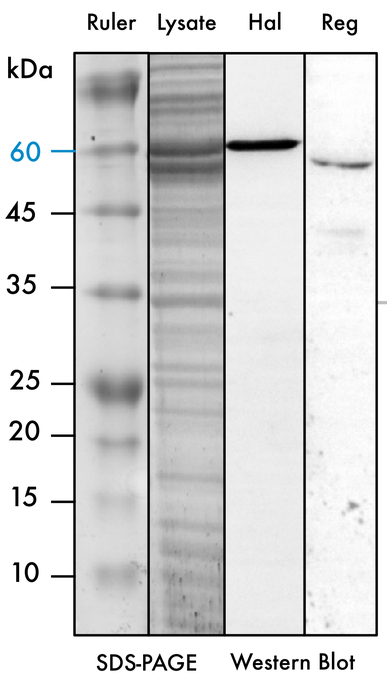


Enzymatic halogenation is assumed to make bromopeptides available

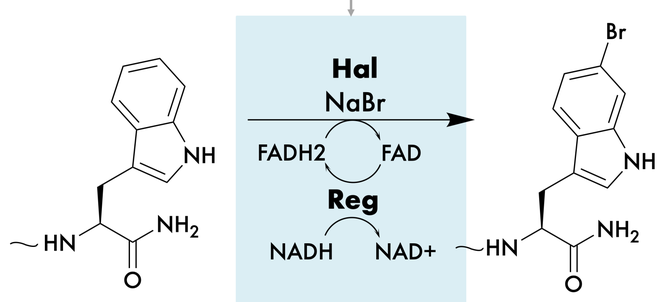


Halogenation assays show halogenation of Trp & recognition peptide

1. Enzyme Expression ✓ → 2. Halogenation Assay



Coexpression Lysate[5]
No purified proteins, contains proteases



Hal	Halogenation[4]	62 kDa
Reg	Cofactor Regeneration[4]	59 kDa

Halogenase & cofactor regeneration enzymes are co-expressed in *E. coli*. The cell lysate is directly used for the halogenation assay, therefore containing e.g. proteases as byproduct.[5]

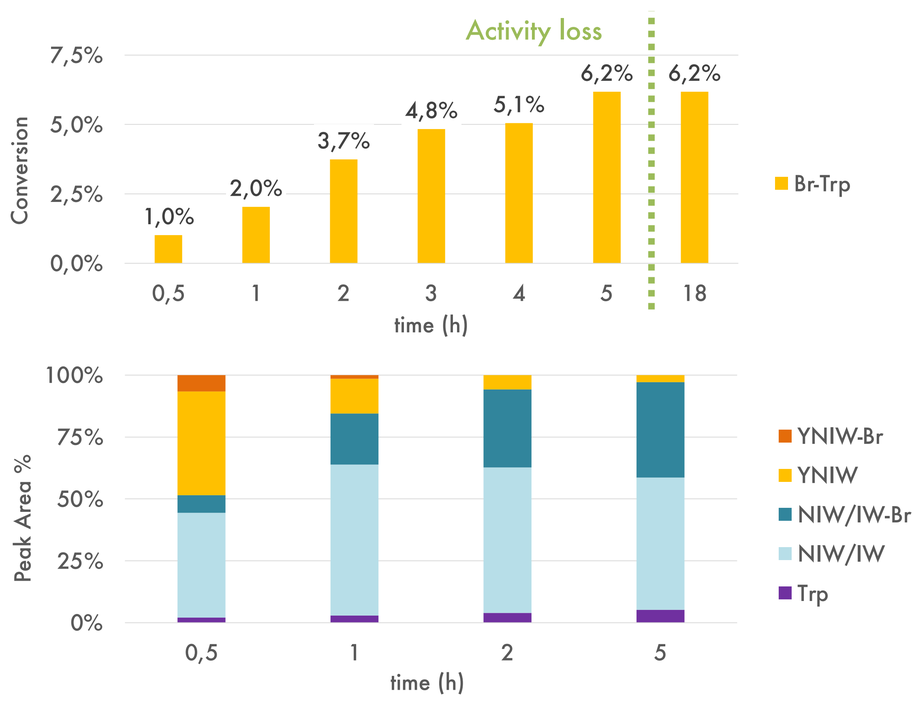
1. Trp

Halogenation ✓
Low conversion
Activity loss after 5h

2. YNIW

Halogenation ✓
Lysate proteases degrade peptides

Phage surface protein



Trp and YNIW are succesfully halogenated. Activity loss after 5h is in line with reported low total turnover number of halogenase family. WT Trp Halogenase was mutated in favor of YNIW, explaining low Trp halogenation. Protease degradation is assumed to not be a limitation in phage surface protein halogenation assays.

References
[1] Muttenthaler et al. Nat. Rev. Drug Discov. 2021, 20, 309.
[2] Jaroszewicz et al. FEMS Microbiol. Rev. 2022, 46, 1.
[3] Hampton & Liu. Chem. Rev. 2024, 124, 6051.
[4] Montua et al. Angew. Chem. Int. Ed. 2024, 63, e202314961.
[5] Montua & Sewald, ChemBioChem 2023, 24, e202300478.

Figures created with BioRender.com

Kaysser Lab

IDD

LAMERS LAB

Contact
Richard Schreiter
Leipzig University
Medicinal Faculty
Institute for Drug Discovery
Pharmaceutical Biology
richard.schreiter@medizin.uni-leipzig.de

Insulin Analogues Derived from Venom Insulins are Potential Treatments for Type 1 Diabetes

Chemical synthesis and evaluation of insulins derived from a venom insulin of the cone snail *Conus geographus*

Connect with me!

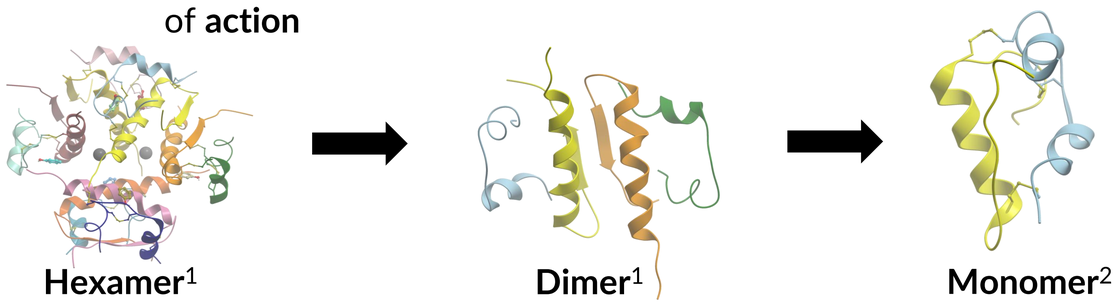
Nicholas Schumann, Amber Vogel, Reza Moosavi, Zildjian Acyatan, Christopher Hill and Helena Safavi-Hemami

https://doi.org/10.17952/38EPS.2026.P315

Introduction

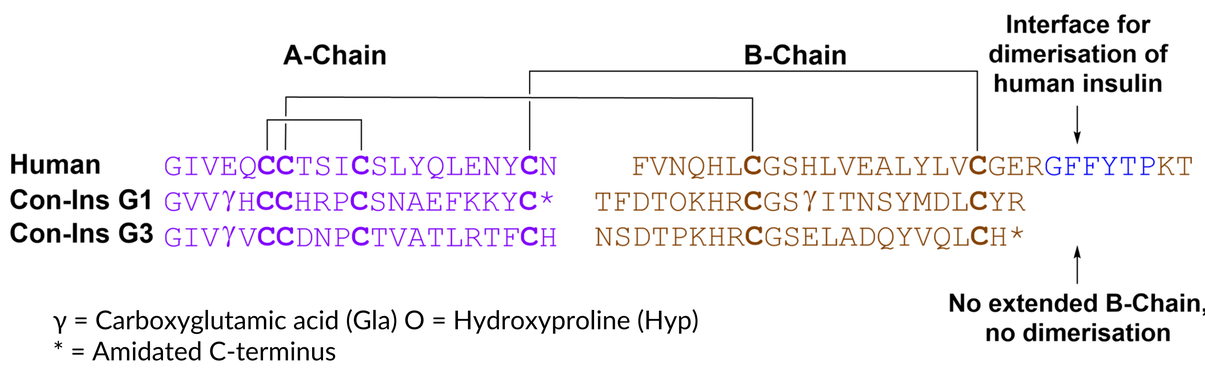
- **Human insulin**, and **analogues** thereof:
  - **Essential** for **managing type 1 diabetes** (**T1D**)
- **Major limitation** of insulin therapy:
  - **Delayed onset** and **prolonged action leading** to **increased risk** of **hyper-** and **hypoglycemia**, respectively, because:
    - **All insulin formulations** (human and analogues) are **hexameric**
    - **Hexamer** to **dimer** to **monomer** dissociation at the injection site is **slow**
    - **Monomer formation** is required for **activation** of **the human insulin receptor (hIR)**

  → Overall kinetics result in **slow onset** and **offset** (clearance) of **action**



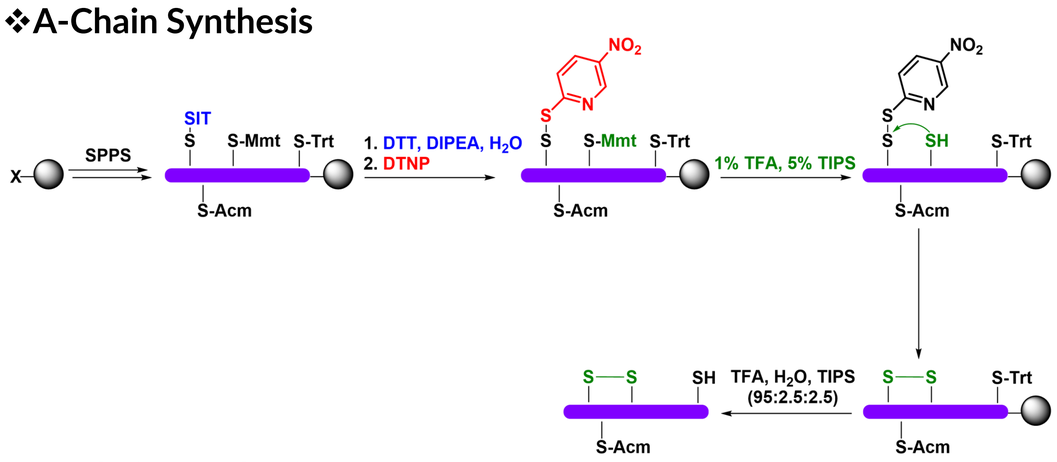
- **Novel insulins**, **Con-Ins G1** and **G3**,[3,4] found in the **venom** of ***Conus geographus*** (**pictured**), a fish-hunting cone snail:
  - **Rapidly lower blood glucose** in fish prey
  - **Monomeric**
  - **Potent agonists** of the **hIR**
  - **Scaffolds** for the **development** of **ultra-fast acting insulins**



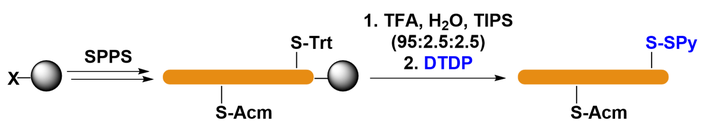


Insulin Synthesis

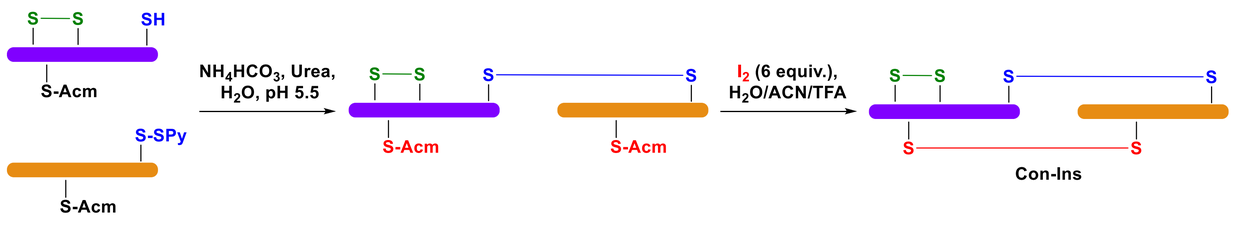
❖A-Chain Synthesis

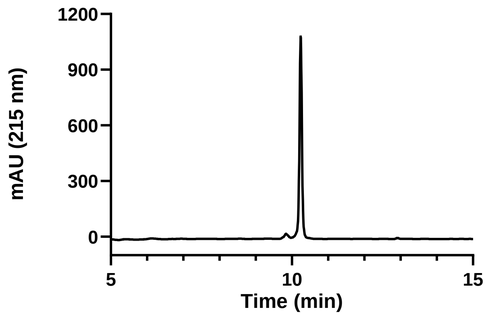


❖B-Chain Synthesis

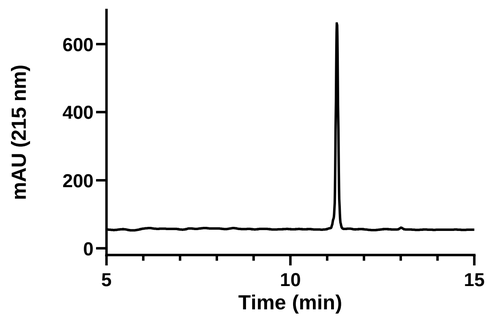


❖A-B Conjugation and Oxidation (One Pot Reaction)





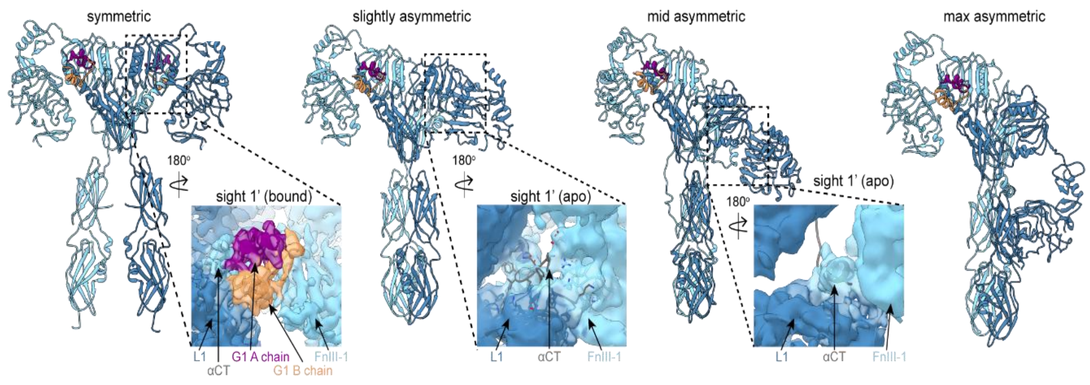
Con-Ins G1
Purity: 96.0%
Overall yield: 0.5%
83-fold yield improvement
compared to literature synthesis[3]



Con-Ins G3
Purity: 97.3%
Overall yield: 4.7%
684-fold yield improvement
compared to literature synthesis[4]

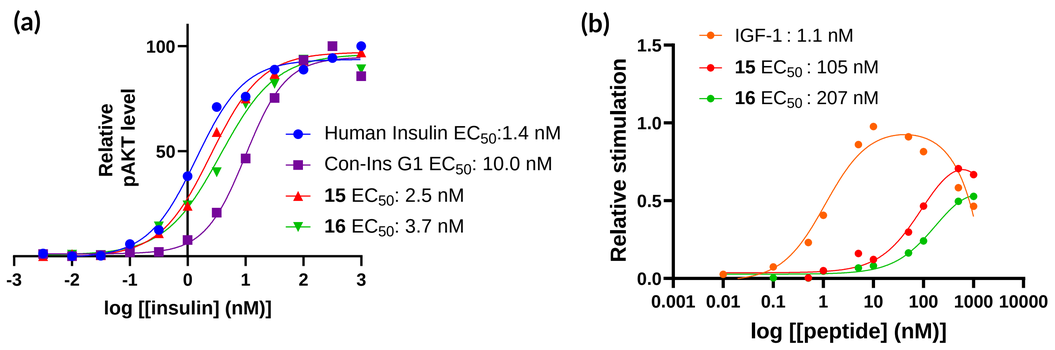
Structural Studies

- A **cryo-EM** structure of **Con-Ins G1** bound to the **hIR** was obtained
- The **hIR** has **two binding sites**: **site-1** and **site-2** as a dimer of αβ-protomers $(\alpha\beta)_2$, thereby having **four total binding sites**
  - **Con-Ins G1** binds to **only site-1**, even under **saturating conditions**. From the **ensemble** of the **ligand-receptor complex conformations**, Con-Ins G1 binds in both a **symmetric** and **asymmetric fashion** (**multiple hybrid states**) to **site-1**
  - **Human insulin**, however, binds to all **four binding sites** in **symmetric fashion** under **saturating conditions**



Biochemical Evaluation of 15 & 16

- The **cryo-EM** data provides **valuable** insight into **critical binding interactions** between **Con-Ins G1** and the **hIR**
  - **Seventeen** Con-Ins G1 **analogues** were **designed and synthesized**
  - The potencies of analogues were assessed in an **IR pAKT assay**
  - Two analogues, **15** and **16**, were identified with **potencies approaching human insulin**
  - **15** and **16 do not** strongly activate the **IGF-1R**, a **receptor** associated with **mitogenicity**
  - **15** and **16** retain the **monomeric** character of Con-Ins G1



(a) Activity of human Insulin, Con-Ins G1, **15** and **16** in a pAKT signaling assay at IR-B, **(b)** Activity of human Insulin, Con-Ins G1, **15** and **16** in a pAKT signaling assay at IGF-1R, **(c)** SV-AUC data for human Insulin, **15** and **16**

Future Directions

- **Additional biochemical and in vivo evaluation of 15 and 16:**
  - **Activation** of **Akt** versus **ERK** (biased signaling)
  - **Aggregation propensities** (monomeric insulins have a higher propensity to aggregate)
  - **Insulin tolerance test** (blood glucose lowering capacity) in a T1D model of:
    - **Mice**
    - **Minipig** (better model for subcutaneous injection)

References

1. PDB: 1AIO, **2.** PDB: 3I40, **3.** Safavi-Hemami, H., et al., Specialized insulin is used for chemical warfare by fish-hunting cone snails. *PNAS* **2015**, *112* (6), 1743-8. **4.** Ahorukomeye, P., et al., Fish-hunting cone snail venoms are a rich source of minimized ligands of the vertebrate insulin receptor. *eLife* **2019**, *8*, e41574.

From inhibitor to affinity probe: Pepstatin A derivates enable AfBPP of plant aspartic proteases



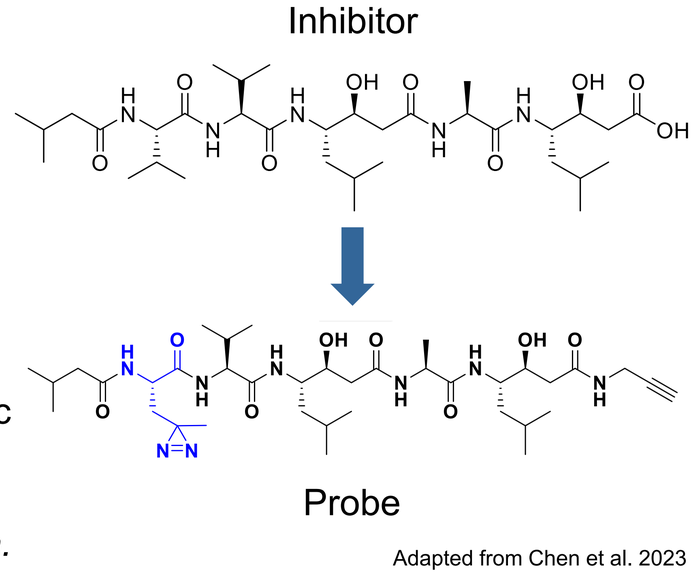
Pierre Bena[1], Paula Dewes[2], Alexander Ciattoni[1], Leonardo González Ceballos[3], Bernhard Westermann[3], Pitter Huesgen[2], Mariana Schuster[1]

[1]Receptor Biochemistry, Leibniz Institute of Plant Biochemistry, Halle (Saale), Germany
[2]Biochemistry and Functional Proteomics, University of Freiburg, Germany
[3]Biofunctional Synthesis Group, Leibniz Institute of Plant Biochemistry, Halle (Saale), Germany

https://doi.org/10.17952/38EPS.2026.P108

Introduction

- Plant proteases regulate diverse biological processes, including growth, development, and immunity.
- Five major mechanistic classes of proteases.
- Aspartic proteases are more numerous and diverse in plants than in humans.
- Pepstatin A is a natural inhibitor of aspartic proteases.
- Pepstatin A-based probes were developed for affinity-based profiling (AfBPP) of human aspartic proteases.
- Aspartic protease 1 (APA1) confers drought tolerance in the model plant *Arabidopsis thaliana.*



Adapted from Chen et al. 2023

Aim

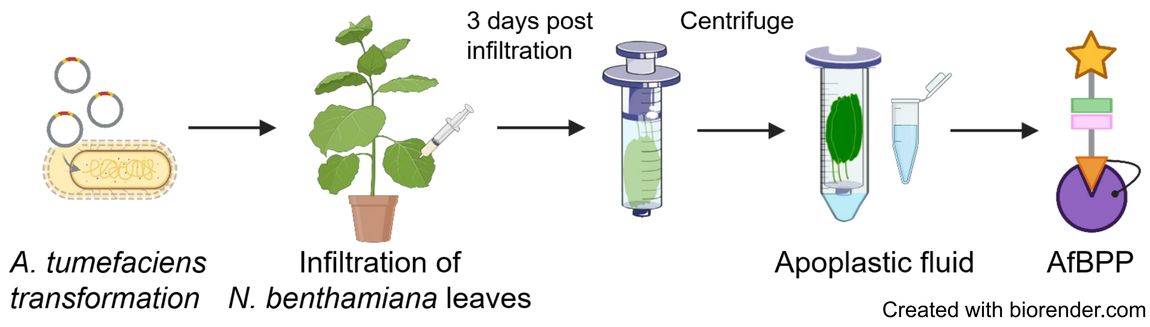
Adapt existing Pepstatin A-based probes for AfBPP of plant aspartic proteases.

→ Elucidate their roles in plant physiology.

Mechanistic class	Year of development for plant ABPP
Cysteine	van der Hoorn et al. 2004
Serine	Kaschani et al. 2009
Threonine	Kolodziejek et al. 2011
Metalloproteases	Lenger et al. 2012
Aspartic	**Bena et al. in preparation**

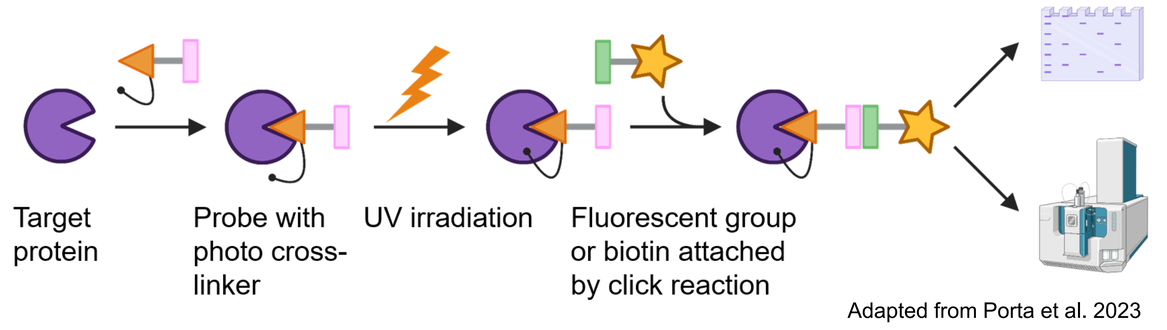
Key methods

Transient expression of plant aspartic protease APA1



Created with biorender.com

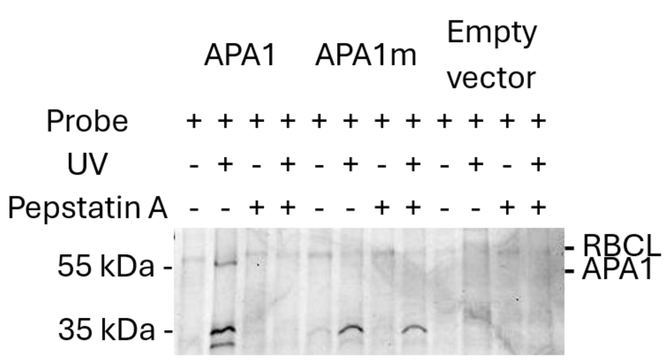
Principle of AfBPP

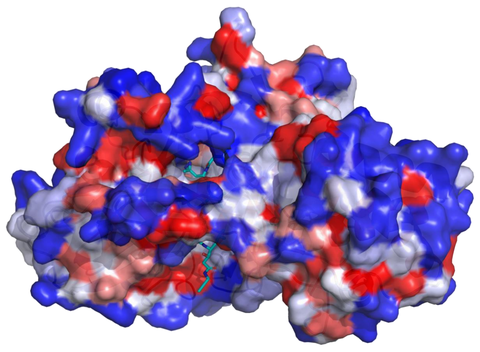


Adapted from Porta et al. 2023

Results

Probe binds specifically active APA1

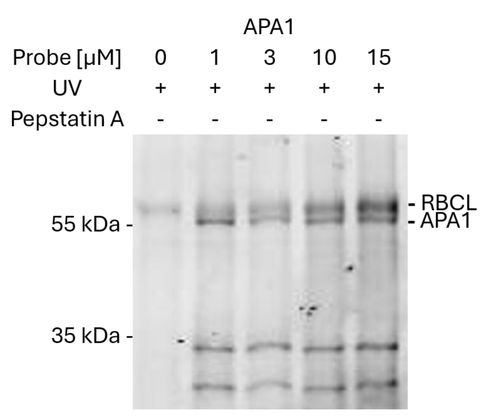


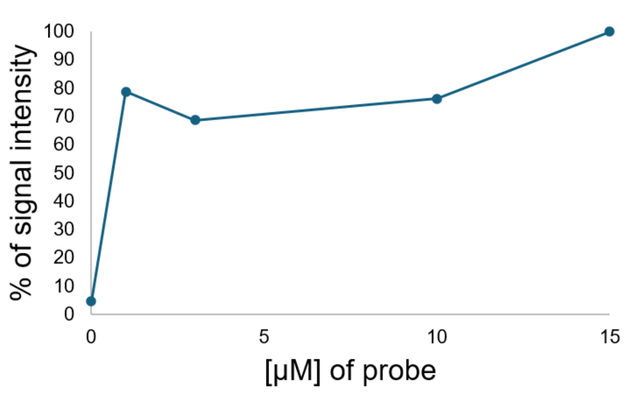


Boltz-2 (AlphaFold3) model of APA1 with probe

- No UV irradiation → no binding
- Pepstatin A → blockage of the binding pocket
- APA1m → catalytically dead version
- RBCL → rubisco, enzyme responsible for photosynthesis

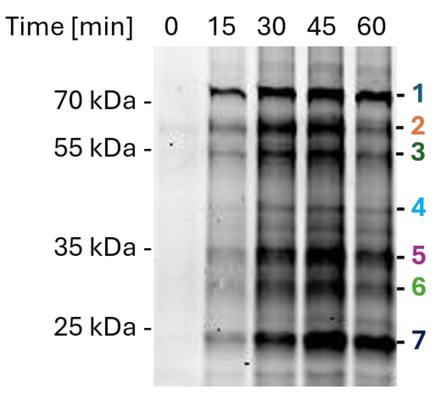
1 µM of probe is sufficient for efficient labelling

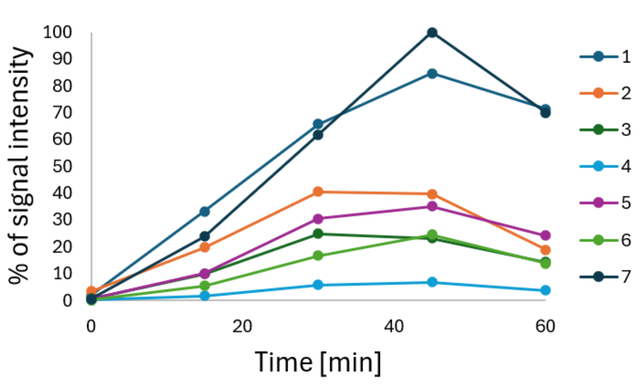




- Highest signal intensity set at 100%

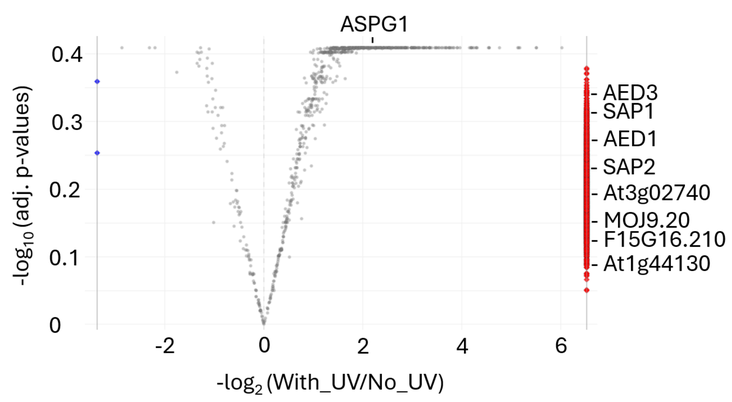
Efficient labeling is achieved after 30 min of UV irradiation





- Labelling of apoplastic fluid of *N. benthamiana* leaves

AfBPP-MS enriches eight plant aspartic proteases



- Labelling of total extract of *A. thaliana* leaves

Conclusion

- Pepstatin-based AfBPP probes selectively label APA1, with efficient labeling achieved using 1 µM probe and 30 min of UV irradiation and enabled the enrichment of eight aspartic proteases from plant leaves.

Outlook

- Apply the probe to investigate the biological roles of plant aspartic proteases.
- Use computational modelling and docking to design subgroup-selective probes for plant aspartic proteases.

Funded by
Deutsche Forschungsgemeinschaft
German Research Foundation
GRK 2670 BEAM PHIPHILICITY YOND

References

1. Duan et al., 2023, doi:10.3389/fpls.2023.1072168
2. Chen et al., 2023, doi:10.1021/acschembio.2c00946
3. Sebastiánet al., 2020, doi:10.1016/j.plantsci.2020.110406
4. van der Hoorn et al., 2004, doi:10.1104/pp.104.041467
5. Kaschaniet al., 2009, doi:10.1074/mcp.M800494-MCP200
6. Kolodziejek et al., 2011,doi:10.1104/pp.110.163733
7. Lengeret al., 2012, doi:10.1016/j.bmc.2011.06.068
8. Porta et al., 2023, doi:10.1016/j.crphar.2023.100164

Contact information

pbena@ipb-halle.de
https://tinyurl.com/RBI-Group

Unlocking Macrocycles at Scale with ⁿGen: Integrated High-Throughput Synthesis and Generative AI

Herve Siendt, Mischa Schüttel, Zander Harteveld, Sevan Habeshian, Chiara Toniolo & Sara Cristinelli

Orbis Medicines Aps, Copenhagen, Denmark ; Orbis Medicines SA, Lausanne, Switzerland

orbismedicines.com
rvs@orbismedicines.com

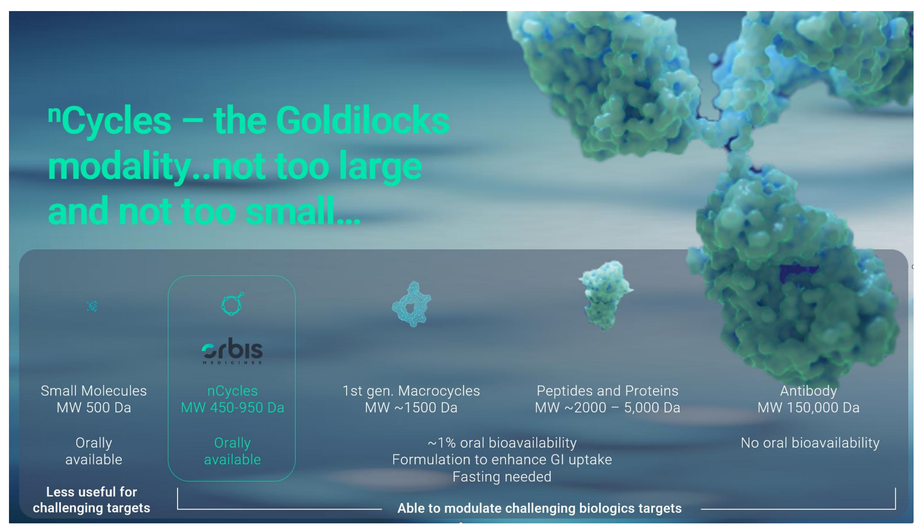
https://doi.org/10.17952/38EPS.2026.P333

Abstract

Small macrocycles represent a promising therapeutic modality against challenging proteins and protein-protein interactions (PPIs) often inaccessible to traditional small molecules, particularly in immunology, inflammatory- and cardiometabolic disease. However, their broader application has been hampered by synthetically complex, low-throughput production methods, limiting efficient exploration of chemical space, systematic SAR development, and the simultaneous optimization of key properties such as potency and permeability.

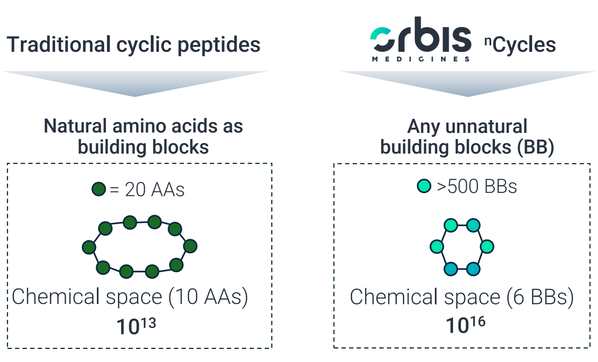
The ⁿGen platform developed by Orbis Medicines, based on seminal work at EPFL, addresses these limitations by enabling automated parallel synthesis of tens of thousands of drug-like macrocycles (ⁿCycles) within a few weeks. The platform supports large target-agnostic libraries, systematic chemical space exploration, and computationally *de novo*-designed target-focused libraries - all screened in parallel and high-throughput for activity and cellular function alongside biophysical characterization. The resulting proprietary datasets continuously fuel internally developed computational models that prioritize compounds for the next round of optimization.

Here, we illustrate the strength and versatility of the platform across three target classes: (1) an enzyme target, Thrombin, for which we computationally designed novel inhibitors from scratch [1]; (2) a PPI, where first-in-class, potent, orally active cytokine receptor antagonists were obtained within months; and (3) a GPCR relevant to obesity, for which - starting from a native linear ligand - we forged functionally active, low-nanomolar agonists with exquisite selectivity over closely related GPCRs and improved physicochemical properties while demonstrating in-vo permeability for key representatives. Together, these examples highlight the potential of Orbis Medicines' platform to unlock difficult target classes and enable the efficient discovery of novel, potent, selective, and orally available macrocyclic therapeutics.

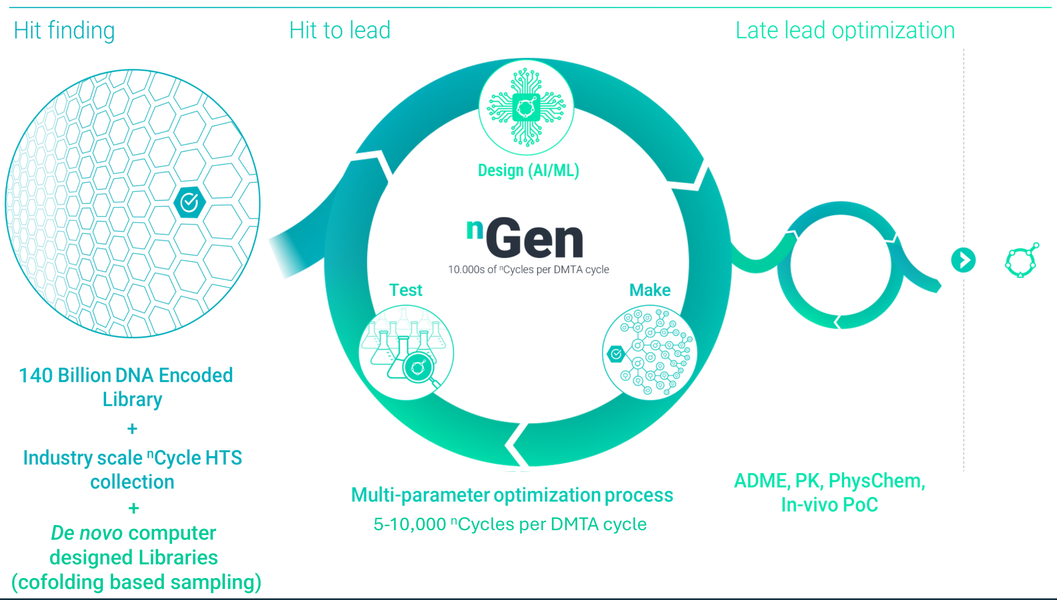


Orbis macrocycle "ⁿGen" platform

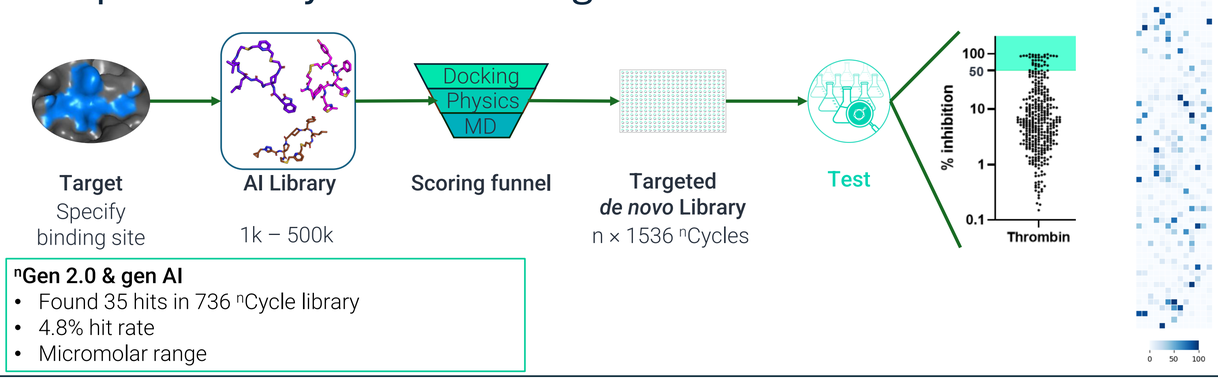
- Hits are identified by screening of either general (DEL and HTS) or target-specific *de novo* designed libraries (ligand-based and structure-based cofolding technologies)
- The Orbis ⁿGen platform – with its massive productivity of thousands of ⁿCycles (<1000 Da) monthly – is then applied for the rapid optimization of the macrocycle Hits



- Access to much larger chemical space
- High affinity despite smaller size
- Rapid optimization process
- More resistant to proteolytic degradation
- Oral bioavailability and cell permeability

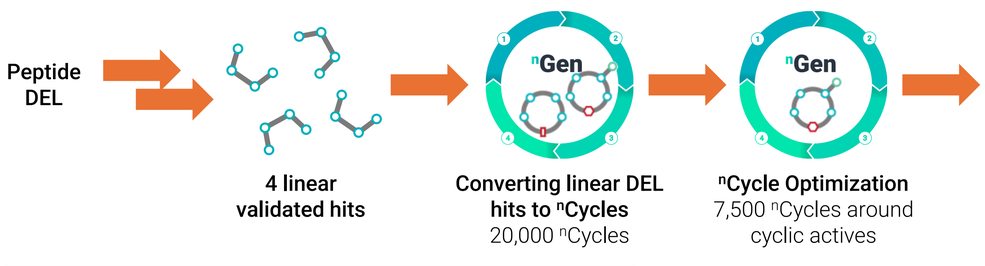


Computationally *de novo* designed Thrombin inhibitors



ⁿGen 2.0 & gen AI
- Found 35 hits in 736 ⁿCycle library
- 4.8% hit rate
- Micromolar range

Hit finding : First-in-class oral cytokine receptor antagonist



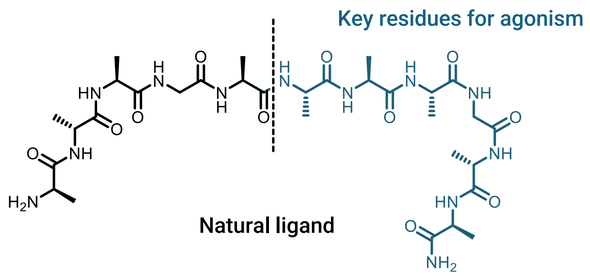
- Potent ⁿCycles with decent properties rapidly obtained
- A vast amount of SAR data generated for further optimization
- Numerous D-M-T-A cycles completed in 6 months

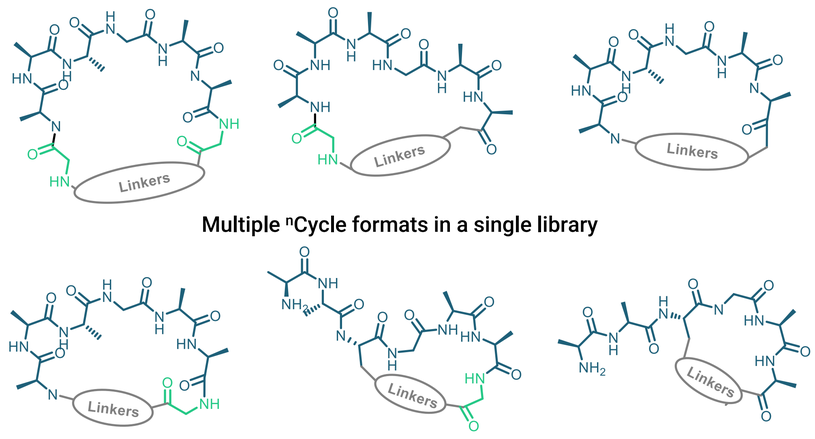
Case study: discovery of novel macrocyclic GPCR agonists (undisclosed target)

- We are targeting a GPCR relevant in treatment of obesity
- No orally available candidates in development

- A cyclic library was designed around the natural linear ligand
  - Cut down to **key residues** required for agonism
  - Introduce **unnatural amino acids**
  - Cyclize with **diverse linkers**

⇨ 10,680 ⁿCycles synthesized in the first library





Library 1 - 11,000 ⁿCycles
From linear to cyclic
ⁿGen
Potent (3 nM)
Selective (~20x)
Partial agonism

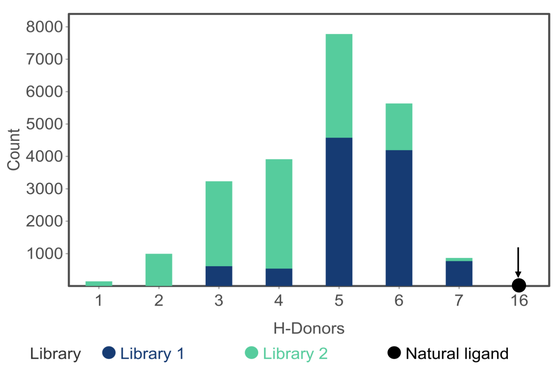
Library 2 - 12,000 ⁿCycles
Optimize potency & properties
ⁿGen
Potent (<1 nM)
Selective (~80x)
Full agonism

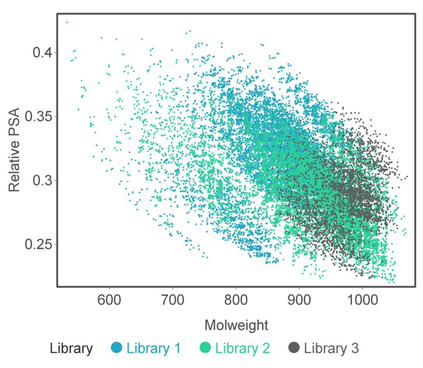
Library 3 - 3,000 ⁿCycles
Optimize stability
ⁿGen
Fine-tuning activity, permeability, selectivity
Addressing metabolic liabilities

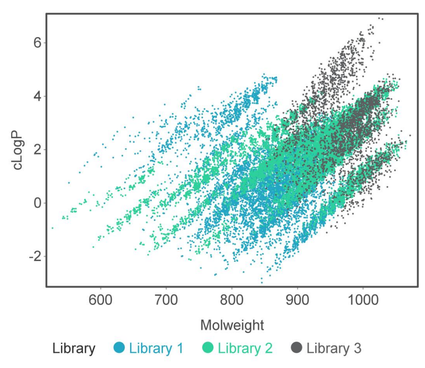
ⁿCycle	Target GPCR EC_{50} (nM)	x selective over GPCR 1	x selective over GPCR 2
ORB-xxxxx102	13	33	402
ORB-xxxxx291	3	83	1549
ORB-xxxxx023	93	271	583

Some key-representative ⁿCycles

- Several potent and selective ⁿCycles were identified. Minimal permeability was observed from library 1 hits in PAMPA and MDCK assays
- N-methylated and non-methylated amino acids were used in a combinatorial fashion to determine the optimal N-methylation pattern for activity, selectivity, and permeability
- Following libraries were constructed to improve potency, stability and physicochemical properties: reduction of polar surface area and number of hydrogen bond donors







Properties of focused libraries. They show vast improvements compared to the natural ligand with stepwise improvement in PSA/MW – a key metric for developing membrane permeable bRo5 compounds. 8,400 of 11,900 macrocycles have values between 0.2 and 0.3 A^2/Da and are thus in an optimal space ("Rule of 1/5": Möbitz H. , ChemMedChem. 2024 Mar 1;19(5): Design Principles for Balancing Lipophilicity and Permeability in beyond Rule of 5 Space).

In less than 6 months, we identified potent and selective GPCR agonists. This program is now available for partnering. Next steps focus on improving further permeability and advancing in vivo characterization. In parallel, the vast amount of proprietary data generated throughout the project feeds and strengthens our Data Science platforms and algorithms, accelerating future DMTA cycles and supporting every discovery programs at all stages (from Hit Finding up to Lead Optimization).

Acknowledgements

We would like to thank the entire Orbis Medicines team for their contributions to the projects depicted in this poster and to the macrocycle synthesis & screening platform. Physicochemical properties were calculated and plotted using DataWarrior. [1] : Manuscript in preparation.

Impact of glycoclustering on the structure of mucin peptides

Oliver Seitz[a]*, Arseniy Galashov[a], Elisabetta di Gregorio[b], Polina Ponomareva[b], Marc Safferthal[b], Ekaterina Kazakova[a], Leïla Bechtella[b], Kevin Pagel[b], Marina Pigaleva[b], Benesh Joseph[b], Kim Greis[c], Lyna Bourehil[c], Renato Zenobi[c]

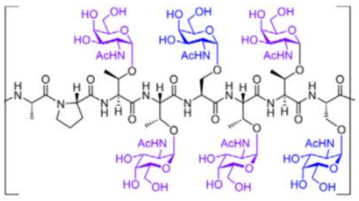
[a] Humboldt-Universität zu Berlin, Germany, [b] Freie Universität Berlin, Germany, [c] ETH Zürich, Switzerland

https://doi.org/10.17952/38EPS.2026.P422

*oliver.seitz@chemie.hu-berlin.de

Introduction

Glycosylation is thought to play a key role in rigidifying the peptide backbone of secreted mucins such as MUC5AC. However, its is not known how many of the potential O-glycosylation sites need to be occupied in order to impart rigid rod character. In MUC5AC, each of the Ser/Thr residues of the PTTSTTSX consensus octad (X: Ala, Thr) can carry α-O-GalNAc or larger glycans. Challenges in the synthesis of glyco-clustered peptides made it difficult to elucidate the impact of O-GalNAcylation on the length and flexibility of peptides. Here, we report glyco-economic syntheses of peptides featuring a previously unattained degree of glycoclustering. Circular dichroism (CD) spectroscopy and Electron Spin Resonance (EPR) and gas phase FRET measurement revealed that peptide stiffening depends on GalNAc clustering. Interestingly, GalNAcylation induces compaction upon desolvation.

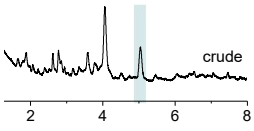


Fully GalNAcylated tandem repeat of MUC5AC

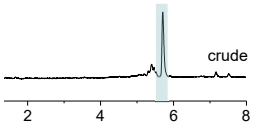
Replacing DMF by DOL + 1% Tween-20 improves efficiency of SPPS of MUC5AC tandem repeats

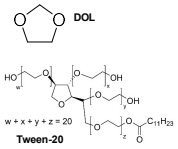
Ac-C-(APTTSTTS)$_5$-C-NH$_2$

20% Piperidine in **DMF**
5 eq AA/DIC/Oxyma, **DMF**, 75°C, 5 min
Ac_2O/DIPEA, **DMF**



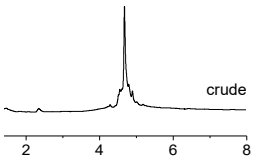
20% Pyrrolidine in **1% Tween-20/DOL**
5 eq AA/ DIC/Oxyma, **1% Tween-20/DOL**, 20 °C, 5 min
Ac_2O/DIPEA, **DOL**

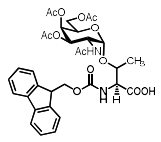




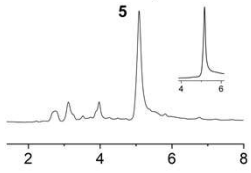
H_2N-CO-**PTTSTTS-(APTTSTTS)$_2$-NH$_2$**
HSe

Coupling glyco AA: 60 mM (Fmoc-Ser/Thr(Ac_3GalNAc) + Oxyma), 430 mM DIC in **1% Tween-20/DOL**, 10 min





Ac-C-(APTTSTTS)$_2$-N_2H_3



Ligation techniques to obtain long mucin glycopeptides

✓ C-terminal glycoserine does not interfere with neither ligation nor dechalcogenation methods

Native Chemical Ligation with C-terminal glycoamino acid[1]

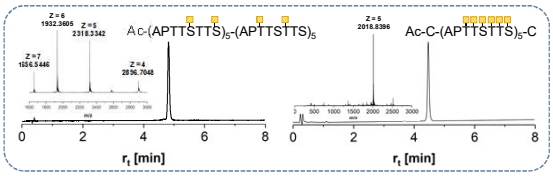
Ac-(APTTSTTS)$_5$-NH-NH$_2$ → 1. MPAA, acac, Gd-HCl buffer; 2. MPAA extraction with EtOAc, then $NaBEt_4$/TCEP → CPTTSTTS-(APTTSTTS)$_4$

Ac-C-(APTTSTTS)$_5$-(APTTSTTS)$_5$
with 80 aa, 20 GalNAc, yield 17%

Diselenide-Selenoester Ligation with C-terminal glycoamino acid

Ac-C-(APTTSTTS)$_2$-NH-NH$_2$ → 1. Ph_2Se_2, TCEP, acac, buffer A, pH 3, 37°C; 2. Buffer A, pH 7, RT; 3. Ph_2Se_2 extraction with hexane, then TCEP/DTT → (UPTTSTTS-(APTTSTTS)$_2$-C)$_2$

Ac-C-(APTTSTTS)$_5$-C
with 42 aa, 30 GalNAc, yield 22%

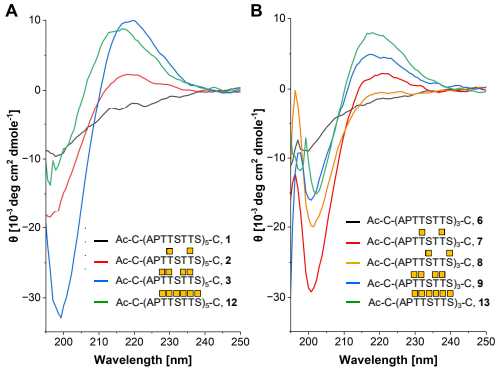


Conformational effect of clustered GalNAcylation – CD

GalNAcylation of two out of six Ser/Thr residues sufficient to induce PPII helix
→ Compare **2** with **1** or **7** with **6**

GalNAcylation of Thr more potent in inducing PPII helix than GalNAcylation of Ser
→ Compare **7** with **8**

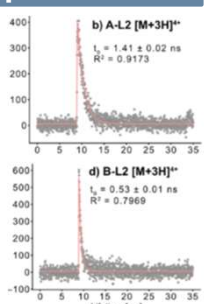
PPII conformation progressively stabilized with increasing degree of GalNAcylation



CD spectra of peptides containing A) five tandem repeats (**1**-**3**,**12**) or B) three tandem repeats (**6**-**9**, **13**). Conditions: 50 µM peptide, 150 mM NaCl, 25 mM Tris-HCl, pH 6.9. Spectra are corrected with calibration to pure GalNAc.

Compaction upon desolvation – Gas-phase FRET

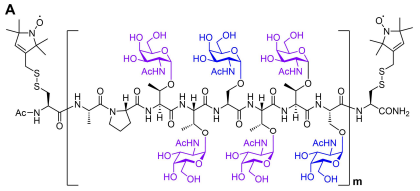
	FRET efficiency	
	gas phase ([M+3H]$^{3+}$)	solution phase H_2O, 50 mM NH_4OAc
CR6G QSY7 Ac-K-(APTTSTTS)$_3$-C, **A-L2**	77.5 %	40.3 %
CR6G QSY7 Ac-K-(APTTSTTS)$_3$-C, **B-L2**	92.4 %	21.3 %
CR6G QSY7 Ac-K-(APTTSTTS)$_3$-C, **C-L2**	93.1 %	2.7 %



Gas-phase fluorescence decay curves in the charge state [M + 3H]$^{3+}$ and [M + 3H]$^{4+}$. Gray circles represent single data points and the fit through these data points is represented by a red curve. The fluorescence lifetime is obtained through the fit. The error is the statistical error of the fit.

Stiffening effect of clustered GalNAcylation – PELDOR

A) Representative example of MTSL-labelled, multi-GalNAcylated MUC5AC tandem repeats. B-K) Primary 4-pulse and/or 5-pulse PELDOR data (left) and the corresponding distance distributions (right) determined using the DeerLab program. The error bounds indicate a 95% confidence interval. Conditions: 15 - 25 µM peptide, 150 mM NaCl, 25 mM Tris-HCl + 15% deuterated glycerol (v/v).



Ac-C*-(APTTSTTS)$_n$-C*, n=5 (**1'**), 3 (**6'**)

→ non-glycosylated peptides sample large conformational space

Ac-C*-(APTTSTTS)$_n$-C*, n=5 (**2'**), 3 (**7'**)

→ shift towards longer distances with two GalNAcs on Thr, particularly for longer peptide
→ broad distribution indicates backbone flexibility

Ac-C*-(APTTSTTS)$_n$-C*, n=3 (**8'**)

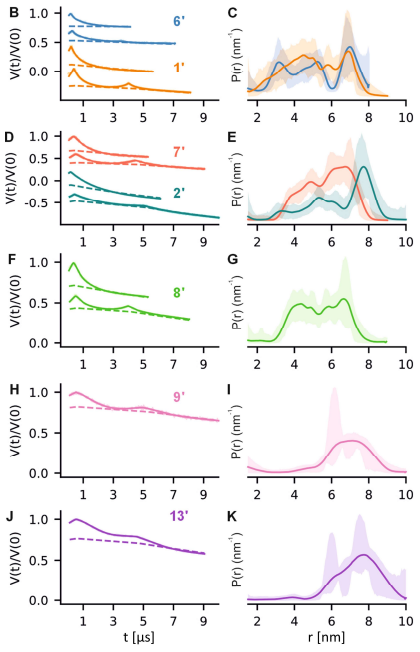
→ broad distance distribution with two GalNAcs on Ser

Ac-C*-(APTTSTTS)$_n$-C*, n=3 (**9'**)

→ significant stiffening of peptide backbone with four GalNAcs on Thr

Ac-C*-(APTTSTTS)$_n$-C*, n=3 (**13'**)

→ significant stiffening of peptide backbone at 100 % occupancy of glycosylation sites
→ technical limitations prevent accurate measurement of end-to-end distance



Conclusions

- ✓ 1% Tween-20 in DOL is an excellent solvent for SPPS of GalNAcylated MUC5AC tandem repeats.
- ✓ NCL proceeds smoothly when C-terminl amino acid is GalNAcylated.
- ✓ Two GalNAcs on Thr (but not Ser) induce PPII helix conformation, but this is not sufficient for stiffening.
- ✓ Four GalNAcs on Thr (50% of all amino acids glycosylated) required for stiffening of peptide backbone.
- ✓ GalNAcylation induces compaction after desolvation (perhaps due to intramolecular interactions between glycans), in contrast to stiffening in solution.

References

Galashov, A., Kazakova, E., Stieger, C. E., Hackenberger, C. P. R., Seitz, O. (2024). Rapid building block-economic synthesis of long, multi-O-GalNAcylated MUC5AC tandem repeat peptides. *Chem. Sci, 15*(4), 1297-1305.

Galashov, A., di Gregorio, E., Ponomareva, P., Safferthal, M., Kazakova, E., Bechtell, L., Pagel, K., Pigaleva, M., Joseph, B. Seitz, O. (2025). Impact of glycoclustering on stiffening of MUC5AC peptides revealed by high efficiency synthesis. *Angew. Chem. Int. Ed., 64*, e202508278.

Greis, K., Galashov, A., Bourehil, L., Kazakova, E., Seitz, O., Zenobi, K. (2026). Studying mucin-derived O-glycopeptides with gas-phase FRET. *Anal. Chem.*, DOI: 10.1021/acs.analchem.6c01957.

Acknowledgements

Funded by the Deutsche Forschungsgemeinschaft (DFG, German Research Foundation) – Project ID 431232613 – SFB 1449.

CRC 1449
HUMBOLDT-UNIVERSITÄT ZU BERLIN

https://doi.org/10.17952/38EPS.2026.P025

Driving the innovation SUNRESIN

High-Loading Seplife Fmoc-RinkAmide-PS-PEG Resin: A Robust Solid Support for the Synthesis of Complex Peptides and Tirzepatide

Simona Serban[1], Ashish Kumar[2], Chaoyang Wang[1], Cheng Zhang[1], Alessandra Basso[1], Peter K. Kabwe[2], Mahama Alhassan[2], Anamika Sharma[2], Beatriz de la Torre[2], Fernando Albericio[2]
[1]Sunresin New Materials, Sunresin Park, No. 135 Jinye Rd, Xi'an Hi-tech Industrial Development Zone, Shaanxi, China.
[2]University of KwaZulu-Natal, School of Chemistry and Physics, Westville Campus, Durban, 4001, South Africa

Contact email: simona.serban@sunresin-international.com
www.sunresinlifesciences.com

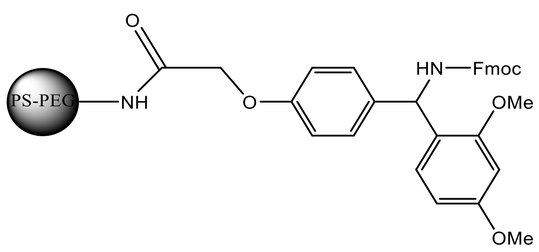
Reference: A. Kumar, P.K. Kabwe, M. Alhassan, W. Hou, C. Wang, C. Zhang, Y. Li, XK. Kou, S. Serban, A. Basso, A. Sharma, BG. De La Torre, F. Albericio. "An Original PEG-Functionalized PS Resin Enables Synthesis of Difficult Peptides: Application to Tirzepatide." ChemistrySelect11, no. 6 (2026): e06541

01 Introduction

- **The Problem**: Standard Polystyrene (PS) is hydrophobic, causing poor swelling in solvents like DMF. This leads to peptide aggregation, incomplete reactions, and low purity, especially in complex sequences.
- **The Trade-off:** While existing PEG-modified resins improve solvation, they typically suffer from significantly reduced loading capacity.
- **Solution**: Seplife® Fmoc-RinkAmide-PS-PEG resin uses a PS matrix cross-linked with 1% divinylbenzene. A proprietary PEG grafting process achieves high loading while maintaining excellent swelling in polar and non-polar solvents.
- **Validation**: Performance was confirmed via successful synthesis of a diverse library, including small pentapeptides, the ACP decapeptide, Afamelanotide (13-mer) and Tirzepatide (39-mer).

02 Seplife® Fmoc-RinkAmide-PS-PEG Resin general characteristics

Product	Seplife® Fmoc-RinkAmide-PS-PEG Resin
Matrix	Crosslinked polystyrene grafted with polyethylene glycol
Substitution (mmol/g)	<0.2; 0.2-0.3; 0.3-0.4; 0.4-0.5
Particle size range (micron)	100-250



Properties

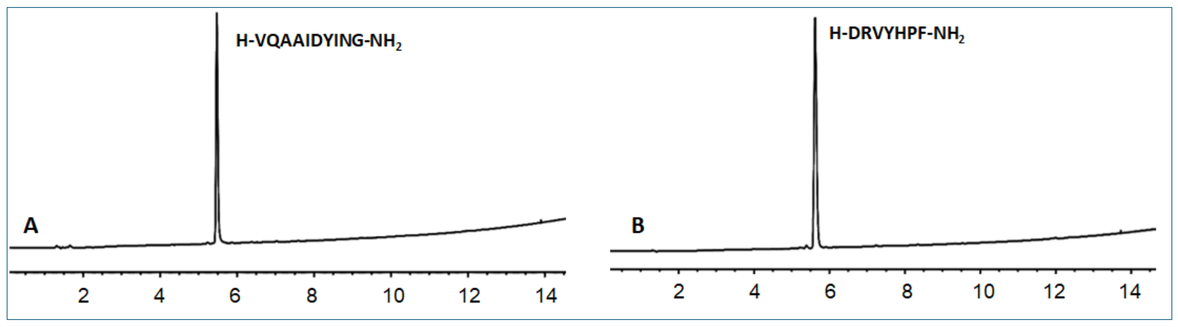
- **Enhanced Stability**: PEG is grafted onto a low crosslinked polystyrene (PS) matrix via an ethyl ether group, which increases acid treatment stability and minimizes PEG leaching.
- The grafted copolymer shows modified physicochemical properties driven by the PEG moiety, combining hydrophobic and hydrophilic characteristics.
- **Fmoc SPPS Ready**: Functionalized with a modified Rink Amide linker, ideal for the Fmoc SPPS of peptide amides. Cleavage from this support is achieved by 95% TFA.

03 Short peptide synthesis using Seplife® Fmoc-RinkAmide-PS-PEG Resin

Short Peptide Synthesis Performance, using a standard Fmoc strategy with DMF as a solvent

- **High Efficiency**: Successfully synthesized a library of 5 to 20-mer peptides with crude purities up to 98%.
- **Performance Parity**: Demonstrated results equivalent or superior to leading commercial PEG-resins across various sequences.
- **Consistency**: Maintains high purity, proving the robustness of the Seplife® PS-PEG matrix.

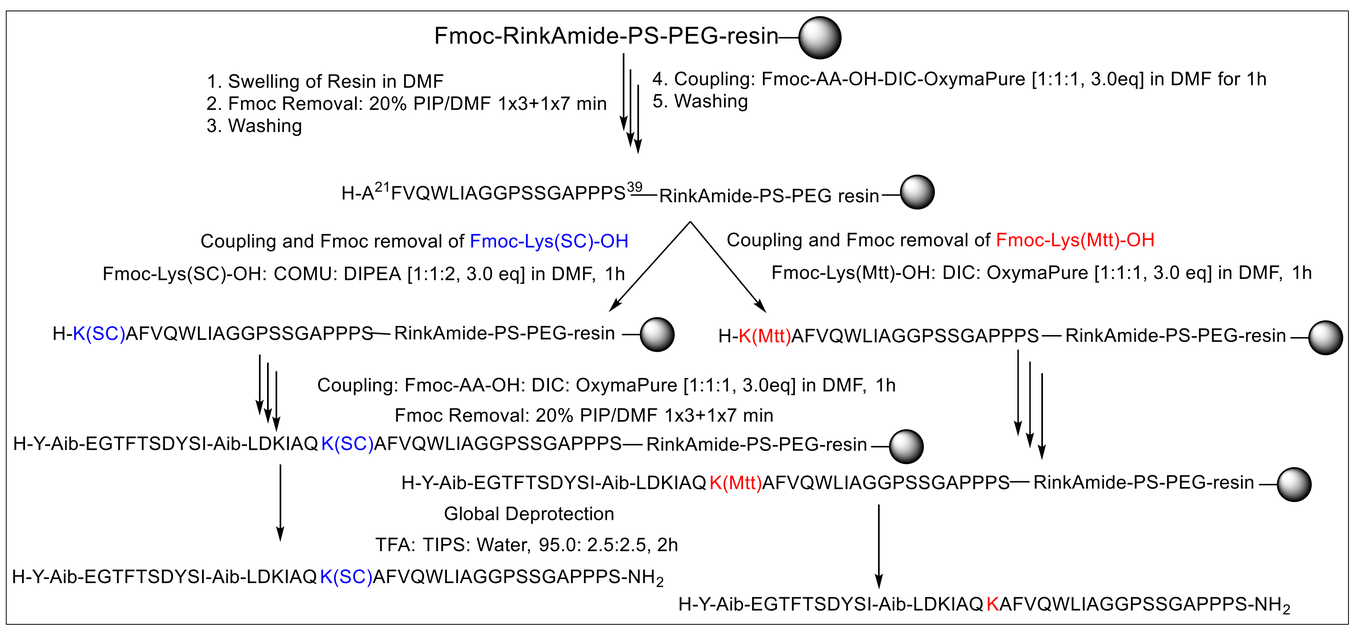
Peptide Sequence	Crude purity of peptides (%)	
	Seplife® Fmoc-RinkAmide-PS-PEG	Competitor PEG-resin
H-Tyr-Sar-Sar-Phe-Leu-NH2	98%	98%
H-Tyr-Ser-Ser-Phe-Leu-NH2	95%	NA
H-Asp-Arg-Val-Tyr-His-Pro-Phe-NH2	97%	97%
H-Val-Gln-Ala-Ala-Ile-Asp-Tyr-Ile-Asn-Gly-NH2	97%	97%
Ac-Ser-Tyr-Ser-Leu-Glu-His-Phe-Lys-Trp-Gly-Lys-Pro-Val-NH2	95%	97%

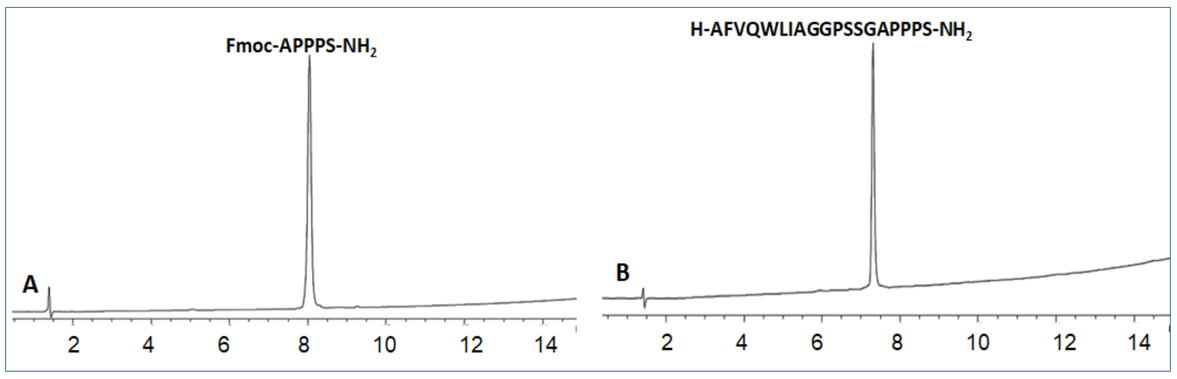


Representative analytical HPLC chromatograms of crude peptides,
A) ACP Decapeptide (H-VQAAIDYING-NH2), **(B)** H-DRVYHPF-NH2,
Method: (5-95 % B into A) in 15 min; flow rate: 1 mL/min; detection at 220 nm.

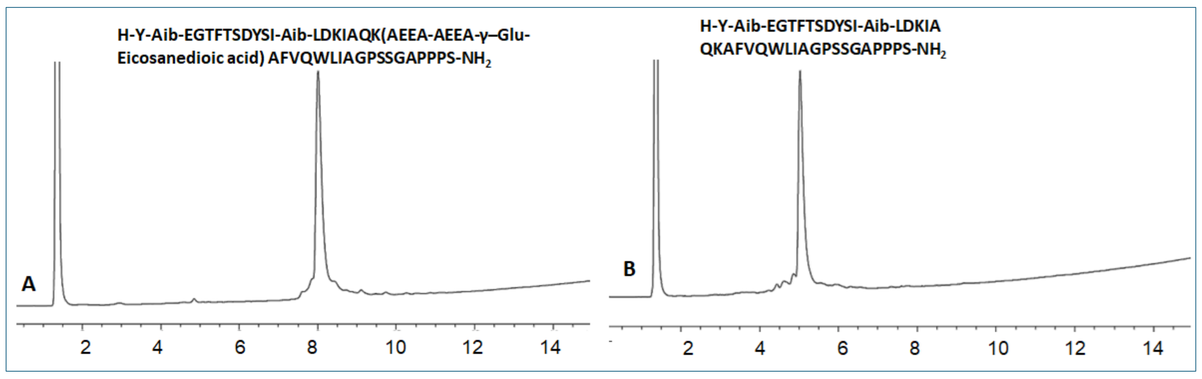
04 Tirzepatide SPPS synthesis using Seplife® Fmoc-RinkAmide-PS-PEG Resin

- **Objective**: Benchmark resin performance using a complex 39-amino acid therapeutic peptide.
- **Scale & Loading:** Synthesized at a 0.05 mmol scale using a loading of 0.37 mmol/g.
- **Dual-Route Strategy:** Validated success through both direct side-chain incorporation and on-resin modification (Fmoc-Lys(Mtt)-OH) at position 20.
- **In-Process Monitoring**: HPLC analysis of 5-mer and 19-mer fragments confirmed excellent purity throughout the assembly.
- **Final Result**: Both synthetic routes achieved a final product with 84% crude purity, demonstrating superior efficiency for long, complex sequence





HPLC analytical characterization of crude peptide 5-mer and 19-mer of Tirzepatide.
(A) Fmoc-APPPS-NH_2, Fmoc-35-39-NH_2, **(B)** H-AFVQWLIAGGPSSGAPPPS-NH_2
Method: (5-95 % B into A) in 15 min; flow rate: 1 mL/min; detection at 220 nm.



HPLC analytical characterization of crude peptide Tirzepatide
(A) H-Y-Aib-EGTFTSDYSI-Aib-LDKIAQK(AEEA-AEEA-γ–Glu-Eicosanedioic acid) AFVQWLIAGPSSGAPPPS-NH2
(B) H-Y-Aib-EGTFTSDYSI-Aib-LDKIAQKAFVQWLIAGPSSGAPPPS-NH2
Method: (30-95 % B into A) in 15 min; flow rate: 1 mL/min; detection at 220 nm

Conclusion

- **Versatile Performance**: Seplife® Fmoc-RinkAmide-PS-PEG resin where PEG is grafted onto PS is highly effective for the synthesis of long and challenging sequences, successfully producing peptides ranging from small pentapeptides to the 39-mer Tirzepatide.
- **Optimal Solvation**: The resin demonstrated excellent swelling in both DMF and DCM, ensuring efficient coupling and minimizing peptide aggregation.
- **Superior Productivity:** By modulating the PEG content, the resin achieves high loading capacities without sacrificing solvation or synthesis performance, with similar performance of other PEG-based PS resins containing more PEG and therefore inferior loading
- **High Purity Results**: Seplife® Fmoc-RinkAmide-PS-PEG-resin delivers high crude purity, proving to be a promising tool to produce complex therapeutic peptides.

Eco-Friendly SPPS: overcoming challenges in cosmetic Argireline production

Lucrezia Sforzi [1,2,4], Fosca Errante [1,2], Robert Zitterbart [4], Manoj Kumar Muthyala [4], Stephan Lüdtke [4], Dominik Sarma [4], Anna Maria Papini [1,3] & Paolo Rovero [1,2].

[1] Interdepartmental Research Unit of Peptide and Protein Chemistry and Biology, University of Florence, 50019-Sesto Fiorentino (Fl), Italy.
[2] Department of Neurosciences, Psychology, Drug Research and Child Health, University of Florence, 50019-Sesto Fiorentino (Fl), Italy.
[3] Department of Chemistry "Ugo Schiff", University of Florence, 50019-Sesto Fiorentino (Fl), Italy.
[4] Gyros Protein Technologies Inc., 4675 South Coach Drive, Tucson, AZ 85714, USA.

https://doi.org/10.17952/38EPS.2026.P302

Introduction

The growing demand of peptide based active ingredients has highlighted the need to the reduce the environmental impact of cosmetic products. TFA which is currently used in SPPS to both detach the peptide form the resin and remove the protecting groups present on the amino acids side chain, is a highly volatile and corrosive ultra-short-chain per- and polyfluoroalkyl substance (PFAS), a class of persistent "forever chemicals". PFAS are characterized by exceptionally stable C–F bonds and increasing environmental and health concerns, therefore, the development of fluorine-free and more sustainable alternatives to TFA represents an important challenge for the future production of cosmetic-grade peptides.

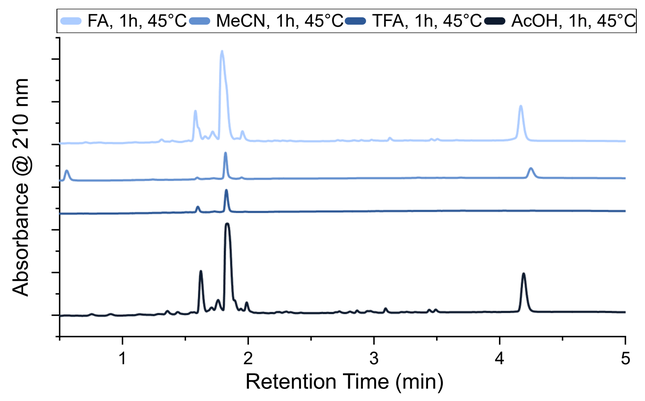
In this work, greener SPPS strategies are investigated using as proof-of-concept a commercially relevant cosmetic peptide Argireline (**Ac-EEMQRR-NH_2**). Ultimately, the study aims to develop scalable, environmentally compatible SPPS protocols that reduce PFAS-related impacts while maintaining the quality and performance required for cosmetic applications.

The rapid rise in demand for peptides for "well-being" is facing a critical gap: Europe lacks an integrated and organized network for the entire peptide life cycle from design and green synthesis to characterization, biological evaluation, and sustainable manufacturing. EUniWell institutions hold complementary, world-class technologies, but their potential remains underutilized without a structured framework to share an European "infrastructure without walls" with specialized scientific know-how and skills. Overcoming this fragmentation will contribute to support the development of the next generation of scientists, equipping them with the advanced skills including entrepreneurial drive needed to successfully translate lab discoveries into market-ready peptide innovation for wellness.

Results: green cleavage "cocktail"

The influence of solvent

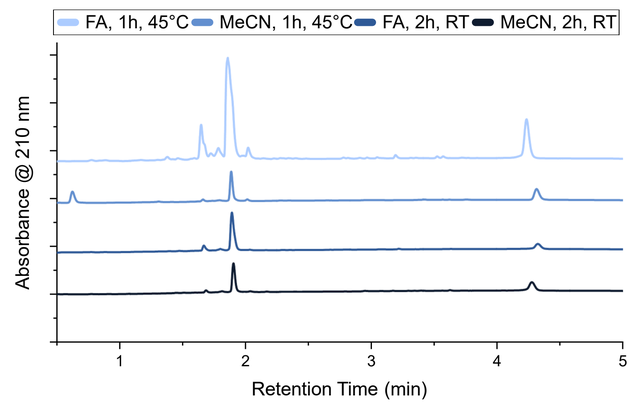
Sample	Conditions	Time; T °C	Argireline t_R= 1.8 min HPLC crude Purity (%)	t-Butylated Argireline HPLC crude Purity (%)	Glutarimide HPLC crude Purity (%)
A	30% MSA, 4% HCl (37%), 10% Thioanisole, 2.5% TIS, 53.5% Formic Acid.	1h; 45°C	72.30	13.73	3.59
B	30% MSA, 4% HCl (37%), 10% Thioanisole, 2.5% TIS, 53.5% Acetonitrile.	1h; 45°C	74.97	6.21	5.54
C	95% TFA, 2.5% TIS, 2.5% H_2O.	1h; 45°C	72.48	18.21	1.14
D	30% MSA, 4% HCl (37%), 10% Thioanisole, 2.5% TIS, 53.5% Acetic Acid.	1h; 45°C	65.81	12.44	2.78



RP-UHPLC/MS analysis carried out on H Class Acquity UPLC from Waters, with an Acquity PDA detector and a Acquity QDa MS detector using Accura Triart C18 (50x2.1 mm, 1.9 µm, 12 nm) column; temperature 40 °C; flow, 0.5 mL/min; eluent, 0.1% (v/v) TFA in H_2O (A) and 0.1% (v/v) TFA in CH3CN (B); λ, 210 nm, gradient, 00–70% B in 5 min.

The influence of time and temperature

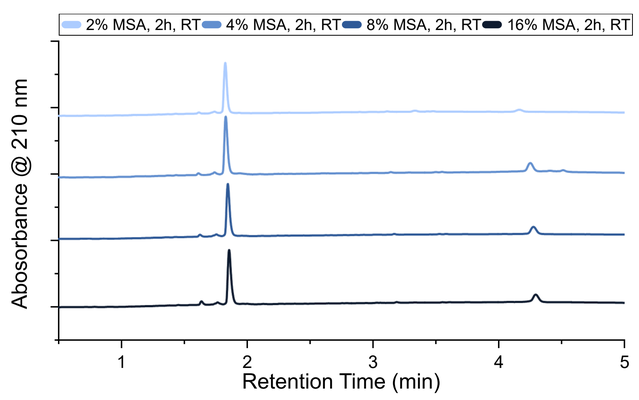
Sample	Conditions	Time; T	Argireline t_R= 1.8 min HPLC crude Purity (%)	t-Butylated Argireline HPLC crude Purity (%)	Glutarimide HPLC crude Purity (%)
A	30% MSA, 4% HCl (37%), 10% Thioanisole, 2.5% TIS, 53.5% Formic Acid.	1h; 45°C	72.30	13.73	3.59
B	30% MSA, 4% HCl (37%), 10% Thioanisole, 2.5% TIS, 53.5% Acetonitrile.	1h; 45°C	74.97	6.21	5.54
E	30% MSA, 4% HCl (37%), 10% Thioanisole, 2.5% TIS, 53.5% Formic Acid.	2h; r.t.	78.83	10.30	1.44
F	30% MSA, 4% HCl (37%), 10% Thioanisole, 2.5% TIS, 53.5% Acetonitrile.	2h; r.t.	77.59	5.25	3.43



RP-UHPLC/MS analysis carried out on H Class Acquity UPLC from Waters, with an Acquity PDA detector and a Acquity QDa MS detector using Accura Triart C18 (50x2.1 mm, 1.9 µm, 12 nm) column; temperature 40 °C; flow, 0.5 mL/min; eluent, 0.1% (v/v) TFA in H_2O (A) and 0.1% (v/v) TFA in CH3CN (B); λ, 210 nm, gradient, 00–70% B in 5 min.

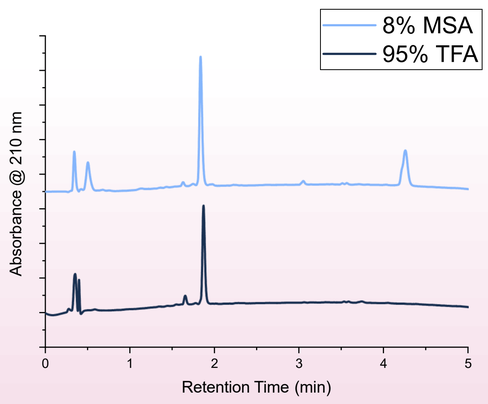
The influence of Methanesulfonic acid (MSA) quantity

Sample	Conditions	Time; T	Argireline t_R= 1.8 min HPLC crude Purity (%)	t-Butylated Argireline HPLC crude Purity (%)	Glutarimide HPLC crude Purity (%)
G	2% MSA, 4% HCl (37%), 10% Thioanisole, 2.5% TIS, 81.5% Formic Acid.	2h; r.t.	86.54	1.77	-
H	4% MSA, 4% HCl (37%), 10% Thioanisole, 2.5% TIS, 79.5% Formic Acid.	2h; r.t.	85.10	2.13	-
I	8% MSA, 4% HCl (37%), 10% Thioanisole, 2.5% TIS, 75.5% Formic Acid.	2h; r.t.	87.72	3.03	-
J	16% MSA, 4% HCl (37%), 10% Thioanisole, 2.5% TIS, 67.5% Formic Acid.	2h; r.t.	83.37	5.19	1.46



RP-UHPLC/MS analysis carried out on H Class Acquity UPLC from Waters, with an Acquity PDA detector and a Acquity QDa MS detector using Accura Triart C18 (50x2.1 mm, 1.9 µm, 12 nm) column; temperature 40 °C; flow, 0.5 mL/min; eluent, 0.1% (v/v) TFA in H_2O (A) and 0.1% (v/v) TFA in CH3CN (B); λ, 210 nm, gradient, 00–70% B in 5 min.

Results: full green synthesis and green cleavage



Instrument: PurePep® Chorus. Scale: 50 µmol. Synthesis: 3 eq. of AAs + 3 eq. of Oxyma dissolved in BuOAc/DMSO (7:3) at 0.5 M concentration; 4 eq. of TBEC in BuOAc at 1.33 M concentration. Washing Solvent: EtOAc/DMSO (8:2). Capping Mixture: Ac_2O/NMM/EtOAc (25:25:50). Deprotection: 20% 4-Methylpiperidine in EtOAc/DMSO (4:6).

Sample	Conditions	Time; T	HPLC crude Purity (%)	Crude Yields (%)
L	8% MSA, 4% HCl (37%), 10% Thioanisole, 2.5% TIS, 75.5% Formic Acid	2h; r.t.	88.30	84.70
M	95% TFA, 2.5% TIS, 2.5 % H_2O	2h; r.t.	85.70	48.50

RP-UHPLC/MS analysis carried out on H Class Acquity UPLC from Waters, with an Acquity PDA detector and a Acquity QDa MS detector using Accura Triart C18 (50x2.1 mm, 1.9 µm, 12 nm) column; temperature 40 °C; flow, 0.5 mL/min; eluent, 0.1% (v/v) TFA in H_2O (A) and 0.1% (v/v) TFA in CH3CN (B); λ, 210 nm, gradient, 00–70% B in 5 min.

Conclusion

- A greener SPPS strategy for Argireline has been successfully developed using alternative solvents and reagents.
- MSA-based cleavage proved to be a promising PFAS-free alternative to conventional TFA, providing high crude purity while minimizing side products.
- These results demonstrate the feasibility of more sustainable SPPS approaches for cosmetic-grade peptides that can be translated into market-ready peptide for wellness.

Acknowledgments

This project was funded in part by EUniWell: 5th seed funding call for the TTPep project and 3rd Well-Being Research Incubator Call for the project "Sustainable and green upscaling processes for peptide(-based) in vitro diagnostics and cosmeceuticals" and the Champion program "Peptides4Wellness".
Thanks to Luxembourg BioTechnolgies for supporting L. Sforzi's partecipation at 38th EPS.

References

[1] G. Vivenzio, S. Noki, A. Chakraborty, J. Lopez, B.G. De La Torre, F. Albericio, ChemSusChem 18 (2025) e202402752.
[2] L. Pacini, M.K. Muthyala, R. Zitterbart, O. Marder, P. Rovero, A.M. Papini, Int. J. Pept. Res. Ther. 31 (2025) 43.
[3] L. Pacini, M. Muthyala, L. Aguiar, R. Zitterbart, P. Rovero, A.M. Papini, J. Pept. Sci. 30 (2024) e3605.
[4] F. Fidha, A. Kumar, M. Leko, O. Marder, S. Burov, A. Sharma, B.G. De La Torre, F. Albericio, Green Chem. 27 (2025) 14911–14918.

38th EPS

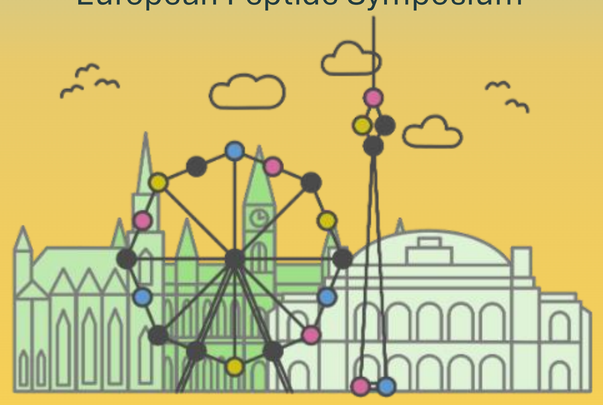
Design, Synthesis, and Biological Evaluation of Triazolyl-Bridged Antiviral Peptides Against Arboviruses

S. Siadohoni[1,2], M. Quagliata[1,2], S. Bracci[1,2], R. Arvia[3], S. Giannecchini[3], A.M. Papini[1,2] & P. Rovero[1,4]

[1] *Interdepartmental Research Unit of Peptide and Protein Chemistry and Biology, University of Florence, 50019 Sesto Fiorentino, Italy*
[2] *Department of Chemistry "Ugo Schiff", University of Florence, Sesto Fiorentino 50019, Italy*
[3] *Department of Experimental and Clinical Medicine, University of Florence, 50134 Firenze, Italy*
[4] *Department of Neurosciences, Psychology, Drug Research and Child Health, University of Florence, 50019 Sesto Fiorentino, Italy*

Email: shima.siadohoni@unifi.it https://doi.org/10.17952/38EPS.2026.P209

38th EPS
European Peptide Symposium



Introduction

Global Threat: Arboviruses (DENV, WNV, ZIKV) cause severe neurotropic and visceral epidemics worldwide; no approved specific antiviral drugs exist.

Fusion Target: Entry is driven by the Envelope (E) glycoprotein. Endosomal low pH triggers a dimer-to-trimer transition, exposing the conserved hydrophobic fusion loop (FL) to initiate membrane fusion (Figures 1 & 2).[1]

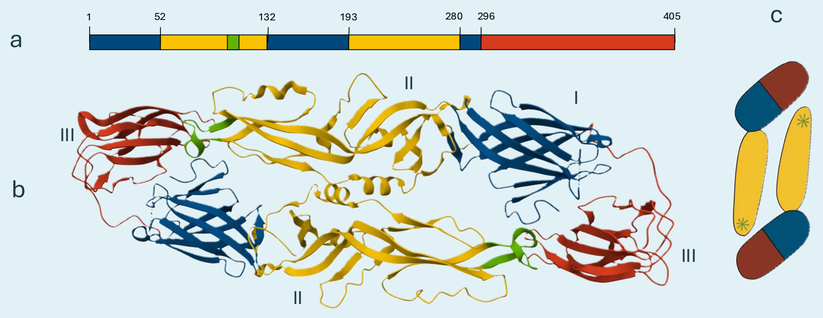


Figure 1. Structure of the dimer of the E protein.
(a) The three domains of E: Domain I is blue, Domain II is orange, Domain III is red, and FL is green.[2] (b) The conformation of E in solution above the fusion pH. (c) Neutral Prefusion Dimer (RCSB Protein Data Bank: 5JHM).

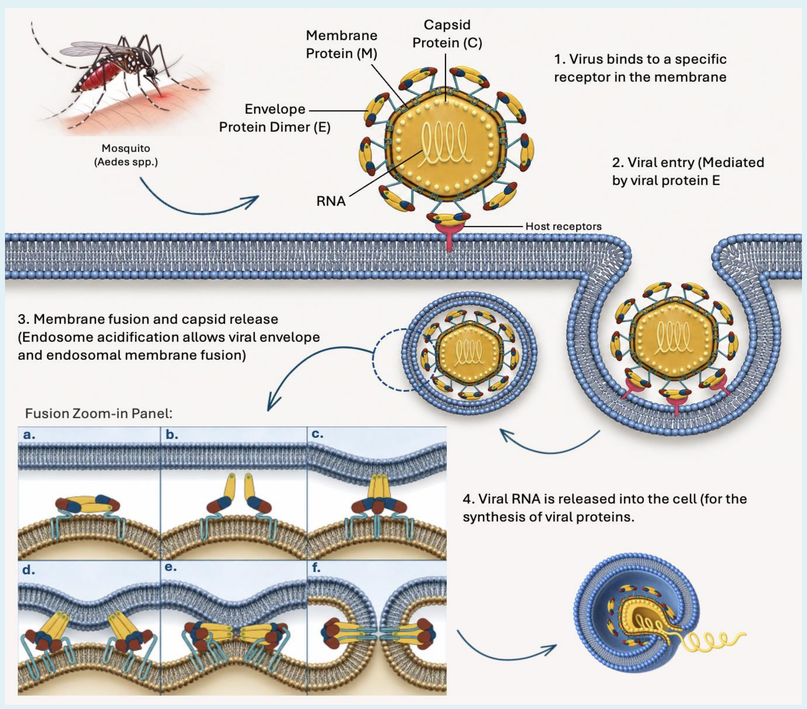
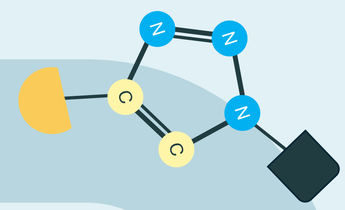


Figure 2. Schematic Model of the Flavivirus Lifecycle and Class II Membrane Fusion Cascade
Receptor-mediated entry is followed by E-dimer dissociation, fusion loop insertion (a–c), and Domain III fold-back (d), driving membrane hemifusion (e) and pore opening (f) for genome release. (Adapted from Modis Y, et al. Nature, 2004).[2]

Aim of the work

This project aims to:



1 Design and Synthesis of Linear Precursor

Microwave-Assisted Solid-Phase Peptide Synthesis (SPPS) using Fmoc/tBu chemistry for the preparation of peptides derived from the Envelope (E) glycoprotein.

2 Copper(I)-catalyzed Azide-Alkyne Cycloaddition (CuAAC)

Microwave-assisted intramolecular CuAAC click reaction using lysine azide and propargylglycine (Pra) to form a triazole bridge, stabilizing and mimicking the β-turn.

3 Biological Evaluation

Antiviral Activity: Plaque Reduction Assay (PRA) against ZIKV, WNV, and DENV in Vero E6 cells.
Cytotoxicity: MTT cell viability assay in Vero E6 cells.

Purification characterization

We initially selected a 13-mer E-protein fragment (PepE13), whose sequence cannot be disclosed for confidentiality reasons, and we performed Cu(I) catalyzed Azide-Alkyne Cycloaddition (CuAAC) to obtain progressively shortened cyclic and conformationally stable analogs.[3,4]

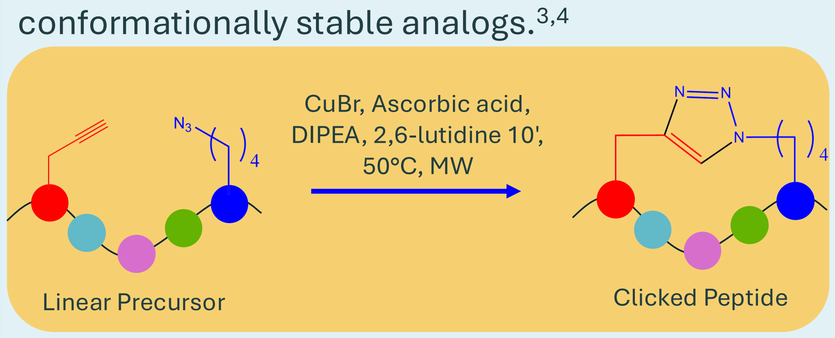


Figure 3. Schematic of the CuAAC

Table 1. List of selected peptides

Peptide	Sequence	LC gradient (% B)[a] Rt (min)	*HPLC purity (%)*
PepE13	Linear, 13 mer	10-90 3.62 min	>96
CycloPepE13	Cyclo(1-13), 13 mer	10-90 3.78 min	>96
CycloPepE11	Cyclo(1-11), 11 mer	10.90 3.88 min	>97
CycloPepE9	Cyclo(1-9), 9 mer	10.90 3.48 min	>97
CycloPepE7	Cyclo(1-7), 7 mer	10-90 2.90 min	>95

[a] *Eluents: 0.1% (v/v) TFA in H_2O (A) and 0.1% (v/v) TFA in ACN (B)*

Synthesis and Characterization

To analyze secondary structure, chirality, and conformational changes in different environments, CD spectra were recorded at 25 °C in phosphate buffer (PB) and increasing concentrations of trifluoroethanol (TFE), up to 50% (v/v).

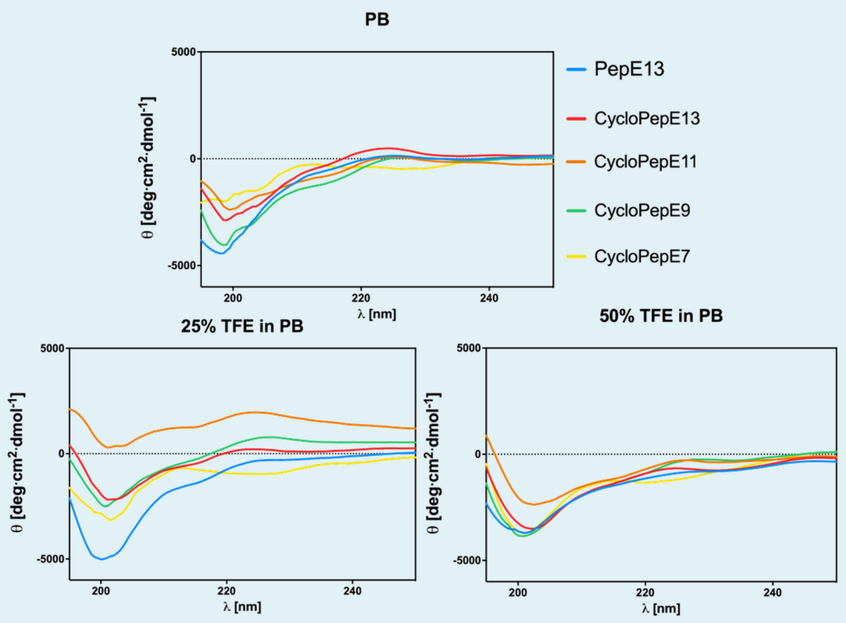


Figure 4. CD spectra of novel antiviral peptides in 10mM phosphate buffer (PB), pH 7.4

CD analysis shows that the linear E-protein mimic (PepE13) adopts a random-coil conformation, characterized by a prominent minimum at ~200 nm. In contrast, a red shift of the negative minimum and the appearance of characteristic features around 205 and 218 nm are observed, most clearly in the final peptide variant (CycloPepE7), indicating the stabilization of a β-turn conformation.[5]

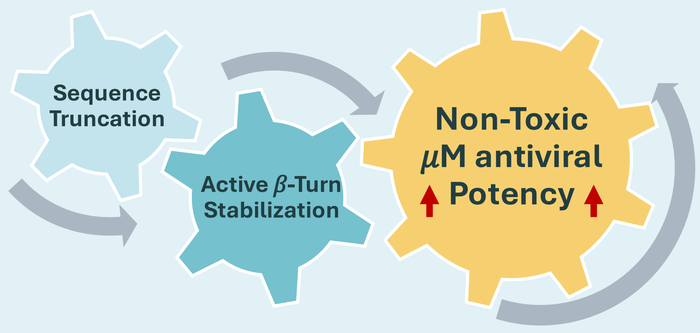
Circular Dichroism (CD)

Table 2. Inhibitory and cytotoxic activity of novel peptides

Peptide	ZIKA		WNV		DENV	
	IC50 μM	CC50 μM	IC50 μM	CC50 μM	IC50 μM	CC50 μM
PepE13	4.93 ± 2.20	>100	1.96 ± 1.60	>100	0.78 ± 0.31	>100
CycloPepE13	0.64 ± 0.60	>100	0.37 ± 0.30	>100	0.28 ± 0.13	>100
CycloPepE11	0.45 ± 0.40	>100	0.21 ± 0.2	>100	0.08 ± 0.03	>100
CycloPepE9	0.17 ± 0.10	>100	0.17 ± 0.05	>100	0.11 ± 0.02	>100
CycloPepE7	0.14 ± 0.04	>100	0.08 ± 0.02	>100	0.21 ± 0.30	>100

Triazole Safety: Triazole stapling showed an excellent safety profile (CC_{50} > 100 μM).
Enhanced Potency: Truncation to a 7-mer maximized activity, achieving micromolar potency against WNV (0.08 μM) and ZIKV (0.14 μM).

Antiviral activity



Conclusion

References:

1. Zhang X, et al. Viruses. 2017;9:338
2. Modis Y, et al. Nature. 2004;427:313
3. Quagliata M, et al. ACS Omega. 2023;8:22665
4. Stincarelli MA, et al. Virus Res. 2023;334:199170
5. Nazeer N, et al. J. Med. Chem. 2024;67:8693

Acknowledgments:

The author, Shima Siadohoni, gratefully acknowledges the Italian Ministry of Health for funding the Ph.D. project under project code RF-2021-12374177.

Thanks to the European Peptide Society for the travel grant to attend the 38th European Peptide Symposium. (6 - 11th of September 2026, Vienna, Austria).

38th EPS
European Peptide Symposium
6 - 11th of September 2026
Vienna, Austria

Antidiabetic Effects of Cyclotide-Rich Extracts from Selected Nigerian Medicinal Plants: An Ethnopharmacological Approach

Latifat. O. SIDIQ[1,2,] Abraham.O. NKUMAH[2] & Omonike.O OGBOLE[2]*

[1] Faculty of Pure and Applied Sciences, Department of Plant and Environmental Biology, Kwara State University, Malete. Nigeria
[2] Faculty of Pharmacy, Department of Pharmacognosy, University of Ibadan, Ibadan. Nigeria
https://doi.org/10.17952/38EPS.2026.P377

*Author for Correspondence (Email: nikeoa@yahoo.com)

Introduction

Cyclotide has attracted great interest from both pharmaceutical industry and academia as potential scaffolds in drug design, due to exceptional properties of circular topology (Wang *et al*., 2024). They have been identified with versatile biological activities, including hypoglycemic properties (Tran *et al*., 2023; Gattringer *et al*., 2012). Diabetes mellitus is a metabolic disorder characterized by high level of sugar in the blood due to insufficient insulin production or insulin resistance (Nyakudya *et al*., 2020). The various undesirable effects associated with synthetic anti-diabetic drugs have necessitated search for safer treatment agents from plants. Therefore, this study investigated antidiabetic properties of cyclotide-rich extracts of selected plants using invitro and in-vitro assays.



Results

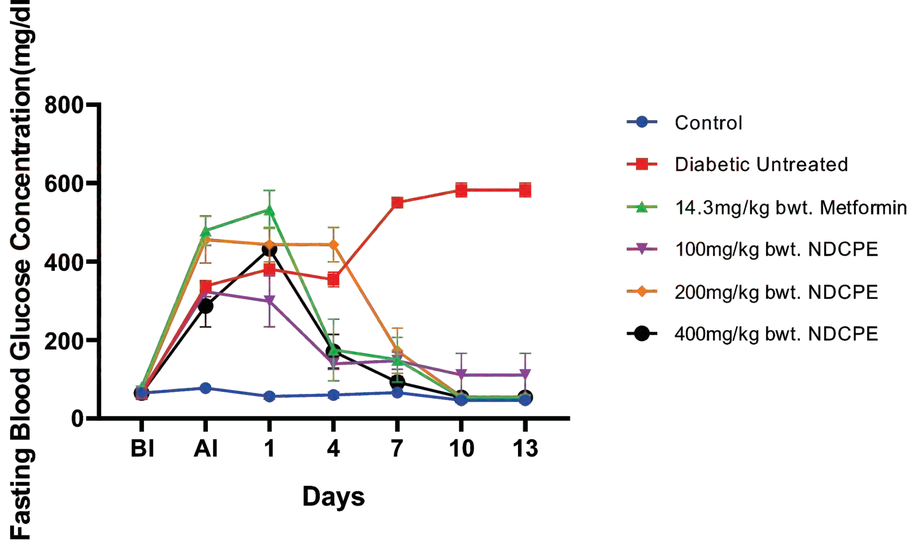


Figure 1: Effect of cyclotide-rich leaf extract of *Nauclea diderichii* on Fasting Blood Glucose (mg/dL) in streptozotocin (STZ) -induced diabetic rats

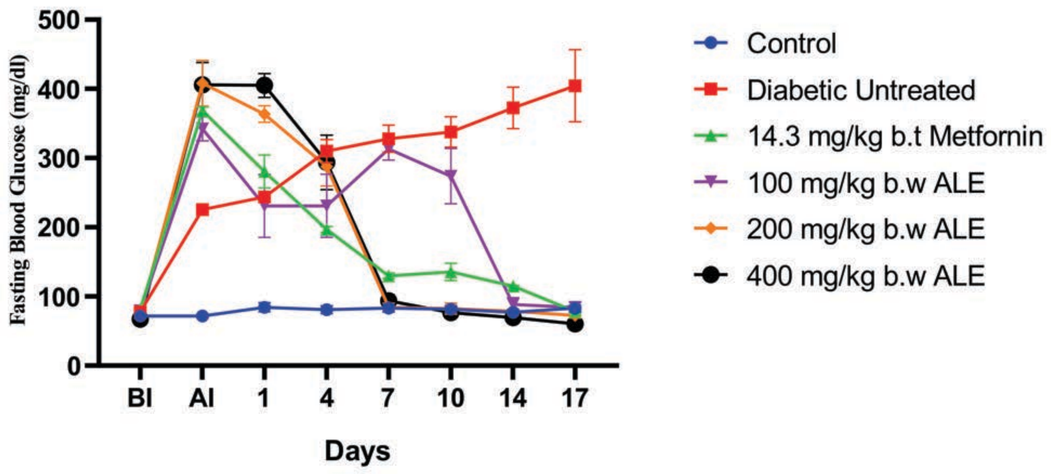


Figure 2: Effect of cyclotide-rich leaf extract of *Alchornea laxiflora* on Fasting Blood Glucose (mg/dL) in streptozotocin (STZ) -induced diabetic rats

Take-home message and Outlook

- *N. diderrichii* extract at 400 mg/kg b.wt. significantly ($P<0.05$) lowered blood glucose level from 7th day onwards till the end of the experiment which compared favourably with metformin at 14.3 mg/kg b.wt. *A. laxiflora* extract at 200 and 400 mg/kg b.wt. significantly ($P<0.05$) lowered blood glucose level and significantly performed better than metformin (14.3 mg/kg b.wt.) at 400 mg/kg b.wt.
- Cyclotide-rich extracts of both plants significant possessed antidiabetic properties.
- Extracts will be subjected to further peptide purification to obtain pure peptide which shall be evaluated for antidiabetic properties.

Acknowledgement

We specially thank Kwara State University (KWASU), Malete, Nigeria for the partial funding of the conference participation.

Selected References

1. Koehbach, J., O'Brien, M., Muttenthaler, M., Miazzo, M., Akcan, M., Elliott, A.G., Daly, N.L., Harvey, P.J., Arrowsmith, S., Gunasekera, S., Smith, T.J., Wray, S., Göransson, U., Dawson, P.E., Craik, D.J., Freissmuth, M. and Gruber, C.W. 2013b. Oxytocic plant cyclotides as templates for peptide G protein-coupled receptor ligand design. Proc Natl Acad Sci U S A, 110: 21183–8.

NMR - Restrained Structural Elucidation of Mitoxantrone Conjugates with GnRH Peptide Analogues

Carmen Simal[1], Georgia Biniari[1], Haralambos Tzoupis[1,2], Nikitas Georgiou[3,4], Thomas Mavromoustakos[3], Theodore Tselios[1]

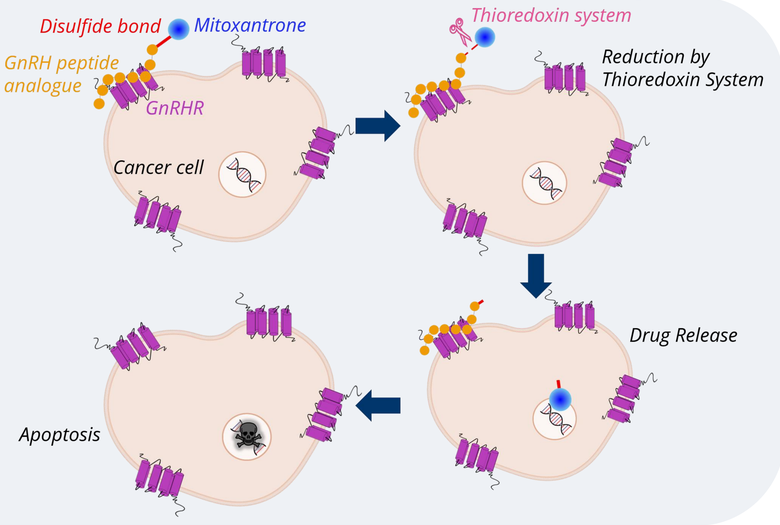
[1]Department of Chemistry, University of Patras, 26504, Rion Patras, Greece
[2]Department of ChemoInformatics, NovaMechanics Ltd., 1070, Nicosia, Cyprus
[3]Department of Chemistry, National and Kapodistrian University of Athens, 10679, Athens, Greece
[4]Center for Interdisciplinary Biosciences, Technology and Innovation Park, P.J. Safarik University in Kosice, Jesenna 5, 04001 Kosice, Slovakia

https://doi.org/10.17952/38EPS.2026.P474

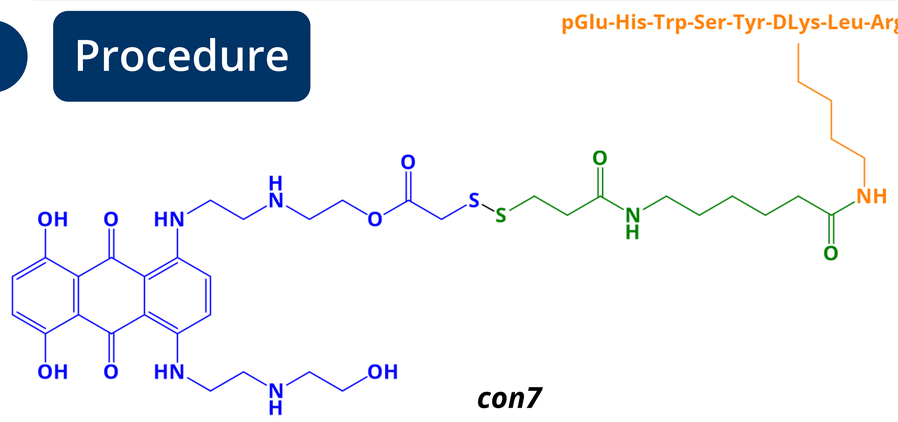
Scan for the paper

Introduction

Gonadotropin-releasing hormone receptors (GnRHRs) are overexpressed in several hormone-dependent cancers, making them promising targets for selective drug delivery[1,2]. GnRH peptide–drug conjugates exploit GnRHR-mediated targeting to preferentially deliver cytotoxic agents to cancer cells[2]. **GnRH–mitoxantrone conjugates** have demonstrated selective **anticancer activity** against endometrial and ovarian cancer cells[3-5]. The cytotoxic molecule is linked to the peptide through a disulfide bond, enabling thioredoxin-mediated cleavage and drug release. However, their **structural features** and peptide–drug interactions involved in receptor recognition remain insufficiently understood. Therefore, these GnRH–mitoxantrone conjugates incorporating peptide analogues derived from the GnRH agonist Leuprolide were structurally characterized to elucidate their conformational properties, drug orientation, disulfide-bond accessibility, and implications for GnRHR recognition[6].



1 Procedure



Study Overview

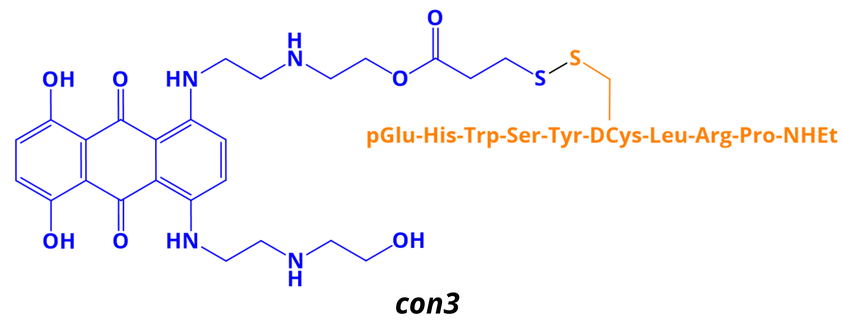
A) Synthesis of conjugates

B) ^{1}H and ^{13}C Assignment

C) NOESY spatial proximities estimation

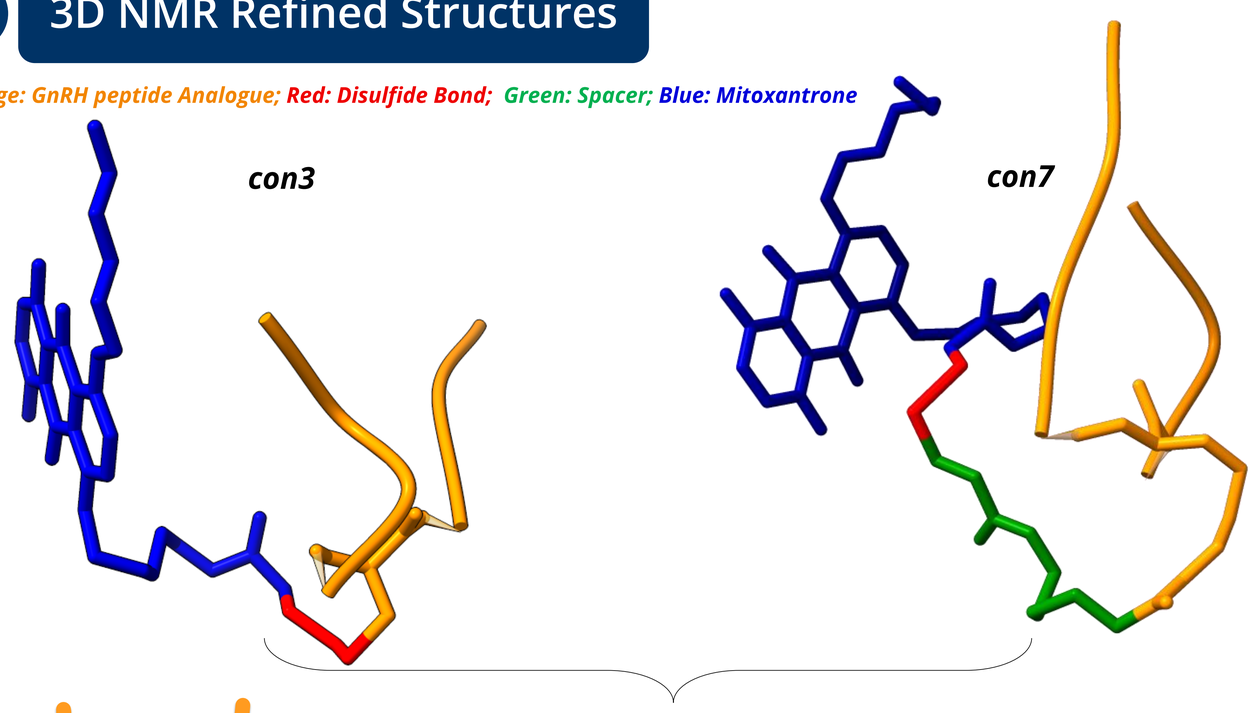
D) NMR-restrained MD refinement

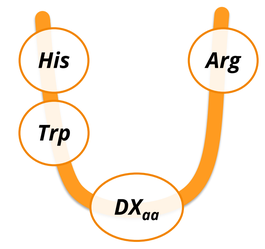
E) Docking studies



2 3D NMR Refined Structures

Orange: GnRH peptide Analogue; Red: Disulfide Bond; Green: Spacer; Blue: Mitoxantrone



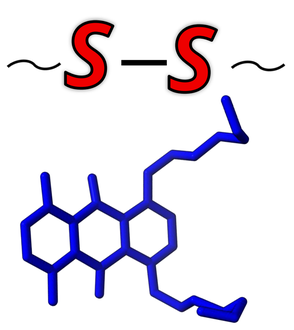


U-shaped peptide backbone

DX_{aa}: DCys[6] or DLys[6], maintain a compact bend conformation

Receptor recognition and binding residues exposed

His[2], Trp[3] and Arg[8] remain solvent-exposed



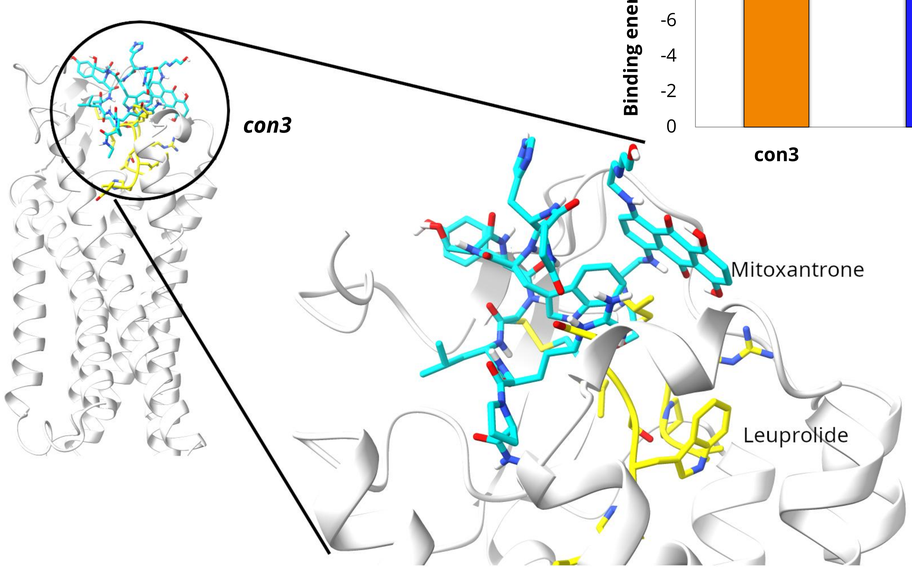
Accessible disulfide bond

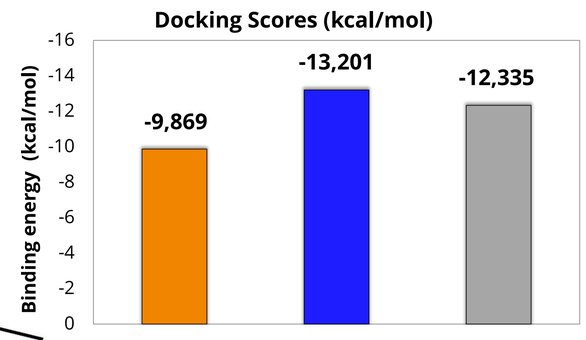
Disulfide bond is solvent-exposed and available for reduction

Mitoxantrone analogue away from the peptide backbone

The mitoxantrone moiety adopts an extended orientation away from the peptide backbone.

3 Docking Studies





Con7 showed a more favorable docking score than Leuprolide, while con3 displayed a less favorable score. The mitoxantrone analogue did not show interactions with GnRHR.

Both conjugates adopted **binding modes** compatible with **GnRHR recognition and binding**, indicating that receptor interactions are primarily mediated by the **peptide moiety**.

4 Conclusions

- ✓ *Con3* and *con7* adopt compact, bent conformations characterized by a U-shaped peptide backbone, consistently supported by NMR spectroscopy and MD simulations.
- ✓ The different substitution at position 6, DCys in *con3* and DLys in *con7*, has a limited influence on the peptide conformation.
- ✓ Key GnRHR recognition residues (His[2], Trp[3] and Arg[8]) remain solvent-exposed and accessible for receptor recognition in both conjugates.
- ✓ The disulfide bond is solvent-exposed and accessible for reduction by thioredoxin system.
- ✓ Docking of the NMR-refined structures supports their compatibility with GnRHR recognition and provides a structural basis for the previously reported biological activity[3].

Contact details: Carmen Simal, Department of Chemistry, University of Patras, Rion, Greece. **csimal@upatras.gr**

References

1. Tzoupis, H., et al., (**2020**), *Curr Med Chem*, 27(36), 6136–6158, doi: 10.2174/0929867326666190712165444.
2. Chavda, V.P., et al., (**2022**), *Molecules*, 27(21), 7232–7260, doi: 10.3390/molecules27217232.
3. Biniari, G., et al., (**2023**), *Int J Mol Sci*, 24(20), 15232–15250, doi: 10.3390/ijms242015232.
4. Markatos, C., et al., (**2024**), *Curr Mol Pharm*, 17, 1–16, doi: 10.2174/0118761429343090250121052955.
5. Markatos, C., et al., (**2024**), *Molecules*, 29(17), 4127–4146. doi: 10.3390/molecules29174127.
6. Biniari, G., et al., (**2026**), *Int J Mol Sci,* 27(16), 7437, doi: 10.3390/ijms27167437.

Acknowledgments

The research project has been partially funded by the **Research Council of the University of Patras** (ELKE PATRAS) under the **MEDICUS** call. The authors acknowledge **the CERIC-ERIC Consortium** (Project Numbers: **20227133**; **20237078**) for providing access to experimental facilities to accomplish NMR experiments.

Full Circle Chemistry: Expanding Macrocyclic Peptidomimetics

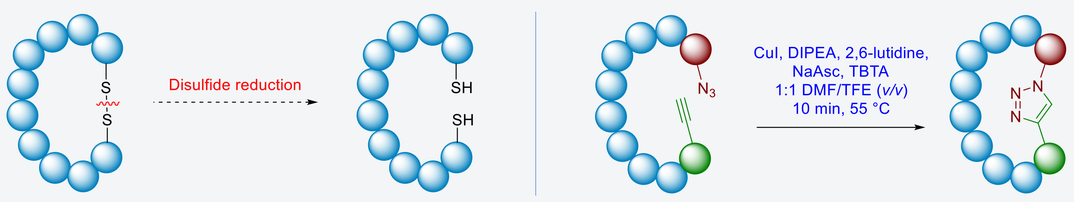
Jacob E. Simms[a], Oscar A. Shepperson[a], Michael A. Malone[a], Andrew J. Reid[a], Maxime Rouah[b], David J. Battersby[b] and Andrew G. Jamieson[a].

[a]*Advanced Research Centre, School of Chemistry, University of Glasgow, Glasgow, G11 6EW, UK.*
[b]*GSK Medicines Research Centre, Gunnels Wood Road, Stevenage, Hertfordshire, SG1 2NY, UK.*

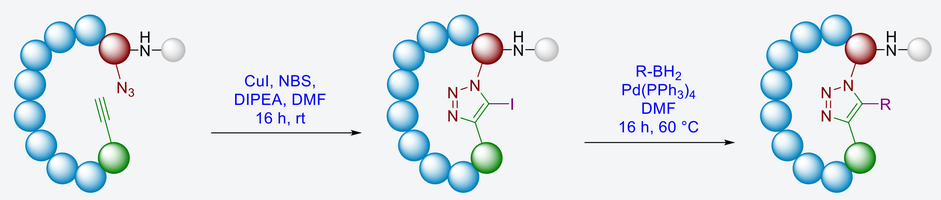
https://doi.org/10.17952/38EPS.2026.P156 j.simms.1@research.gla.ac.uk Jacob Simms

1. Background and Aims

- **Disulfide bridge mimetics** are synthetic replacements of native disulfide bridges which **preserve peptide structure** and **biological activity** while **enhancing stability**. Previously, the Jamieson group has focused on developing **triazole-based** disulfide bridge mimetics.
- This approach has been successfully applied to **α-Conotoxins**, **Urotensin-II**, **Oxytocin**, and **RGD** peptides.[1,2]



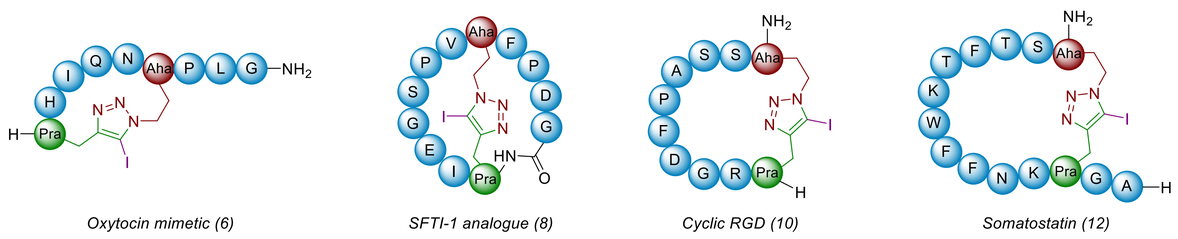
- Recent work in the Jamieson group has developed **novel on-resin chemistry** to access **5-iodo-1,4-triazole** cyclised peptides.[3]
- The 5-iodo-1,4-triazole is a **bifunctional** mimetic, as it acts as a **conformational constraint**, while also providing a **reactive handle** for further functionalisation.



- This work aims to expand the **scope** of this novel on-resin chemistry.

2. Variable Ring Size Investigations

- To probe the **versatility** of the 5-iodo-1,4-triazole chemistry, four **diverse** model peptides were selected, encompassing a range of amino acid functionalities and macrocyclic ring sizes.
- 5-iodo-1,4-triazole analogues of all model peptides were **efficiently** formed **on-resin** with good conversion from their linear precursors.

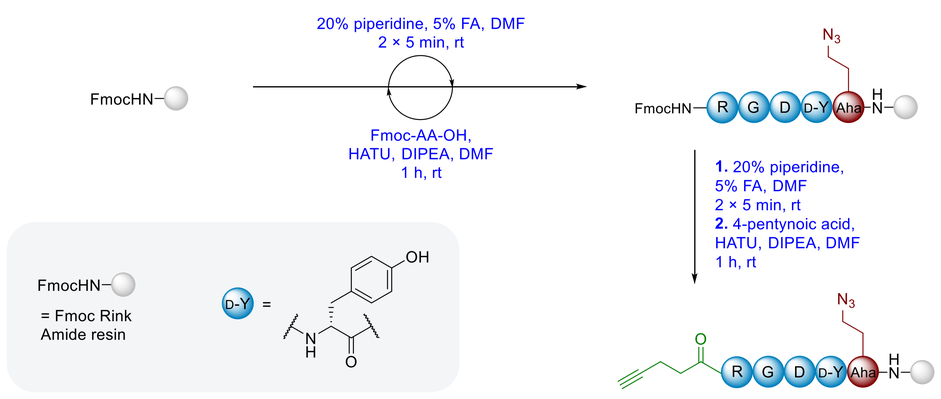


Oxytocin mimetic (6) | *SFTI-1 analogue (8)* | *Cyclic RGD (10)* | *Somatostatin (12)*

- Subsequent **Suzuki-Miyaura** and **Sonogashira** cross-coupling reactions were successful on all 5-iodo-1,4-triazole substrates, except for the histidine-containing oxytocin mimetic (suspected palladium poisoning).[4]

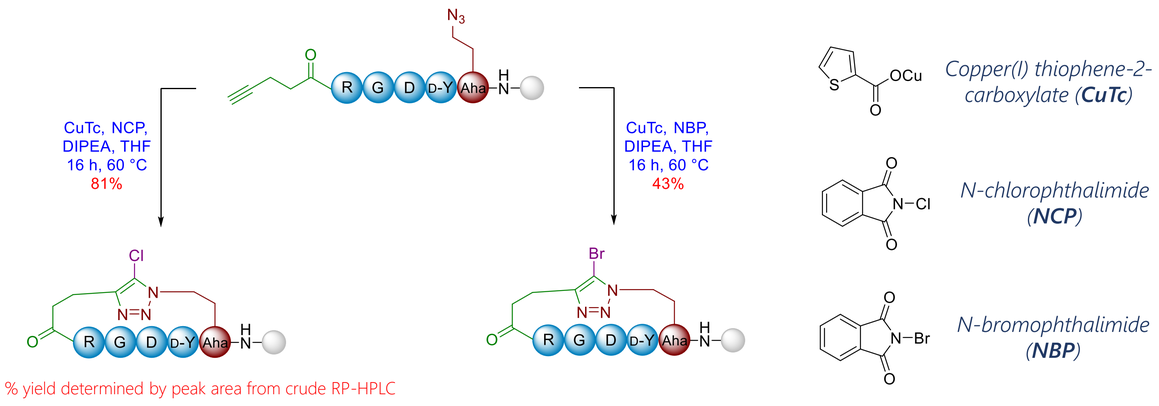
3. Peptide Synthesis

- Reaction scope studies were performed on a model peptide containing the biologically relevant **RGD** motif, synthesised by Fmoc solid-phase peptide synthesis.



4. Development of 5-Halo-1,4-Triazoles

- Optimised conditions were developed to efficiently access **5-chloro-1,4-triazole** and **5-bromo-1,4-triazole** cyclised peptides **on-resin**.



*Copper(I) thiophene-2-carboxylate (**CuTc**)*

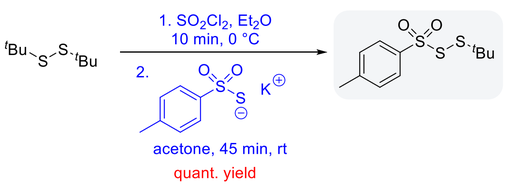
*N-chlorophthalimide (**NCP**)*

*N-bromophthalimide (**NBP**)*

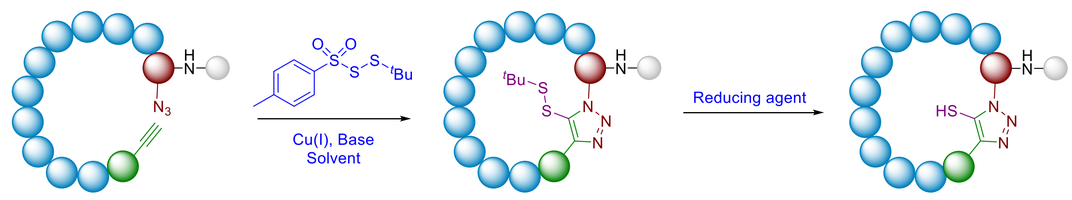
% yield determined by peak area from crude RP-HPLC

5. 5-Thio-1,4-Triazole

- The scope of 5-substituted triazoles amenable to on-resin peptides was expanded by developing a **5-thio-1,4-triazole**.
- Facile synthesis under mild conditions gave an **electrophilic persulfur reagent**, with previous literature precedent in modified CuAAC reactions.[5]

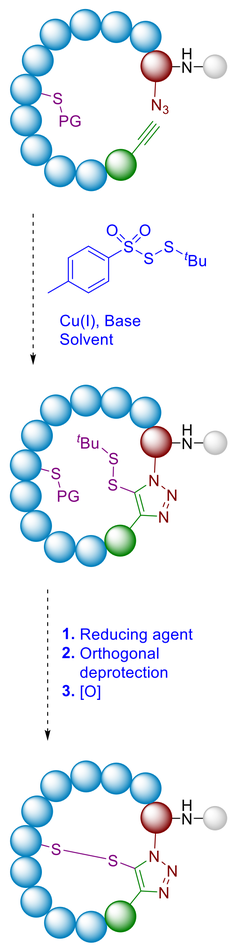


- This reagent enabled formation of a **triazole disulfide**, which could be reduced **on-resin** to access the free thiol.



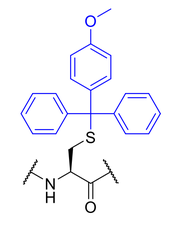
Current Work:

- This chemistry may be used to access **bicyclic** peptides.
- Bicyclic peptides are **privileged medicinal chemistry scaffolds** due to their advantageous **stability** and **specificity** profiles over monocyclic peptides.

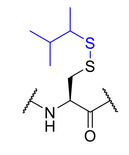


- Inclusion of an **orthogonally protected cysteine** in the peptide sequence allows for a short route to the desired bicycle.
- The proposed synthesis route involves an **interrupted CuAAC** to yield the monocyclic peptide, followed by **disulfide cleavage**, **orthogonal deprotection**, and **thiol oxidation**.
- The choice of a suitable orthogonal protecting group for the cysteine residue could shorten the synthesis *via* **simultaneous** disulfide cleavage and thiol deprotection:

***S-PG**:*



Cys(Mmt)
Deprotected with weak acid (1-5% TFA in DCM)



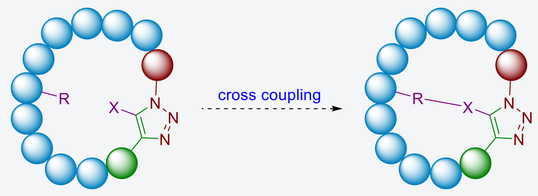
Cys(SIT)
Deprotected under reducing conditions (3 equiv. Dithiothreitol in DMF)

6. Conclusions and Future Work

- A **5-chloro-1,4-triazole** bridged peptide was successfully utilised in an **on-resin** Suzuki-Miyaura cross-coupling reaction.
- Further optimisation is required for the **5-bromo-1,4-triazole**, to enhance conversion.



- The feasibility of the 5-thio-1,4-triazole chemistry will be assessed in a **bioactive** model peptide as an alternative methodology for macrocyclization, incorporating the **redox stable** triazole chemistry.
- Metal-catalysed cross couplings with **halo-triazoles** and **non-natural amino acids** could afford increased stability in the bicycles, removing disulfide bridges.



References

1. S. Pacifico, A. Kerckhoffs, A. J. Fallow, R. E. Foreman, R. Guerrini, J. McDonald, D. G. Lambert and A. G. Jamieson, *Org. Biomol. Chem.*, 2017, **15**, 4704–4710.
2. A. Knuhtsen, C. Whitmore, F. S. McWhinnie, L. McDougall, R. Whiting, B. O. Smith, C. M. Timperley, A. C. Green, K. I. Kinnear and A. G. Jamieson, *Chem. Sci.*, 2019, **10**, 1671–1676.
3. O. A. Shepperson, M. A. Malone, K. I. M. Arnott, R. J. Brown and A. G. Jamieson, *Org. Lett.*, 2025, **27**, 11249–11253.
4. M. A. Malone, O. A. Shepperson, J. E. Simms, A. J. Reid and A. G. Jamieson, *J. Org. Chem.*, 2026, **91**, 22, 7416–7422.
5. W. Wang, Y. Lin, Y. Ma, C-H. Tung and Z. Xu, *Org. Lett.*, 2018, **20**, 10, 2956–2959.

Acknowledgements

Financial support from the JMS PhD scholarship and GSK is gratefully acknowledged.

Jamieson Lab

Targeting GLP-1 Receptor and DPP-4 Enzyme for Diabetes Drug Discovery

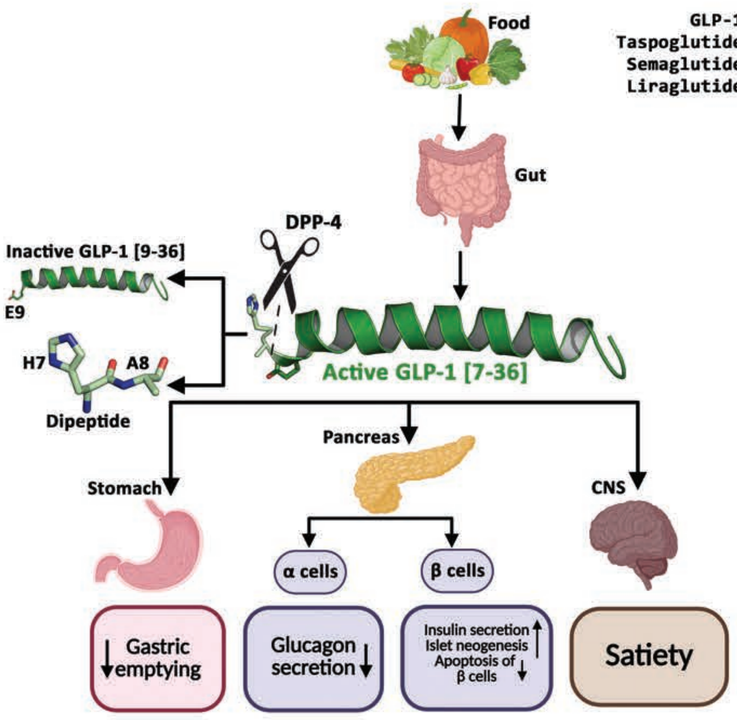
Aditi Singh[1], Soumendra Rana*[1]
a22bs09004@iitbbs.ac.in, *soumendra@iitbbs.ac.in
[1]Chemical Biology Laboratory, School of Basic Sciences
Indian Institute of Technology Bhubaneswar, Odisha, India
https://doi.org/10.17952/38EPS.2026.P378

P378

Abstract

Type 2 Diabetes Mellitus (T2DM) accounts for around 90% of global diabetes cases and remains a leading cause of morbidity and mortality worldwide. This systemic condition arises predominantly due to the interplay of two key components: (a) compromised insulin production by the pancreatic β-cells, and (b) the failure of insulin-sensitive tissues to react to insulin. Notably, it is well established that incretin hormones, such as glucagon-like peptide-1 (GLP-1) and glucose-dependent insulinotropic peptide (GIP), which belong to the glucagon superfamily, are involved in intestinal insulin secretion. The insulinotropic impacts of secreted GLP-1 are facilitated by its interaction with GLP-1 receptor (GLP-1R), a class B G-protein-coupled receptor (GPCR). However, the therapeutic potential of endogenous GLP-1 is limited due to rapid proteolytic degradation by dipeptidyl peptidase-4 (DPP-4), resulting in a plasma half-life of ~2 minutes. Current therapeutic strategies address this limitation either by administering GLP-1 analogs resistant to DPP-4 cleavage or by inhibiting DPP-4. In this context, the current study describes the computational design and in silico evaluation of a DPP-4-resistant, potent designer helical peptide agonist (SR18; ≤18 aa) of the GLP-1R comprised of both coded and noncoded amino acids necessary for effective interactions with the GLP-1R, similar to those found in GLP-1, liraglutide, and semaglutide. The biophysical studies confirm that synthetically prepared SR18 maintains an ordered, alpha-helical conformation under various solvent conditions. Interestingly, the binding of SR18 mimics that of a small-molecule agonist (Orforglipron) of GLP-1R. Furthermore, in reference to GLP-1, SR18 exhibits stable interactions with GLP-1R over 1 μs of molecular dynamics (MD) simulations, with appreciable binding affinity and energy, supporting its immense potential as an alternative to current long-chain GLP-1R peptide agonists. In parallel, a drug repurposing approach was employed to identify potential new chemical entities targeting DPP-4. Computational biological techniques were further utilized to investigate the structure-activity relationships (SARs) of gliptins and characterize their interactions within the DPP-4 active site. The designer GLP-1R agonist peptide and the selected DPP-4-targeting small molecule represent promising therapeutic candidates and will be advanced for further experimental validation in relevant biological systems.

1. Introduction



2. Rational Design of SR18

GLP-1	HAEGTFTSDVSSYLEGQAAKEFIAWLVKGRG 31
Taspoglutide	HXEGTFTSDVSSYLEGQAAKEFIAWLVKXR- 30
Semaglutide	HXEGTFTSDVSSYLEGQAAKEFIAWLVRGRG 31
Liraglutide	HAEGTFTSDVSSYLEGQAAKEFIAWLVRGRG 31

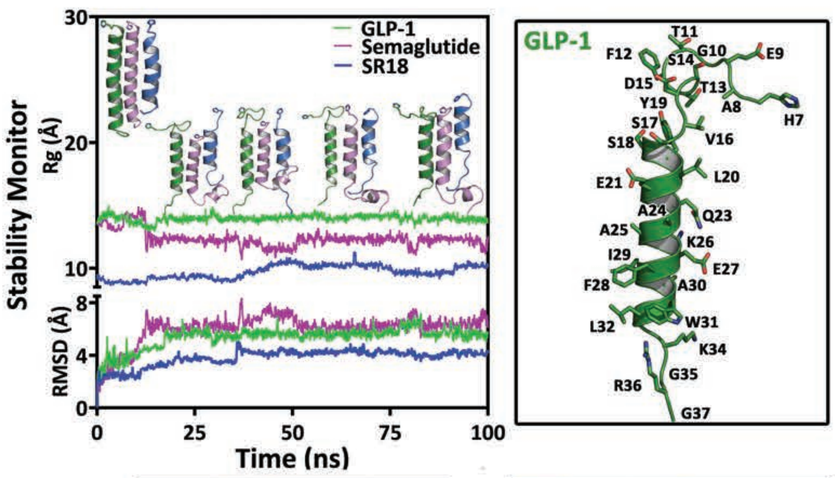
Hed3 NH_3^+-YGKAAAAKIglAAAKAAAAK-COO^-
Hed6 HIglEAibAAAKAAAAKAAAKA-NH_2

Peptide Screening through Docking and MD

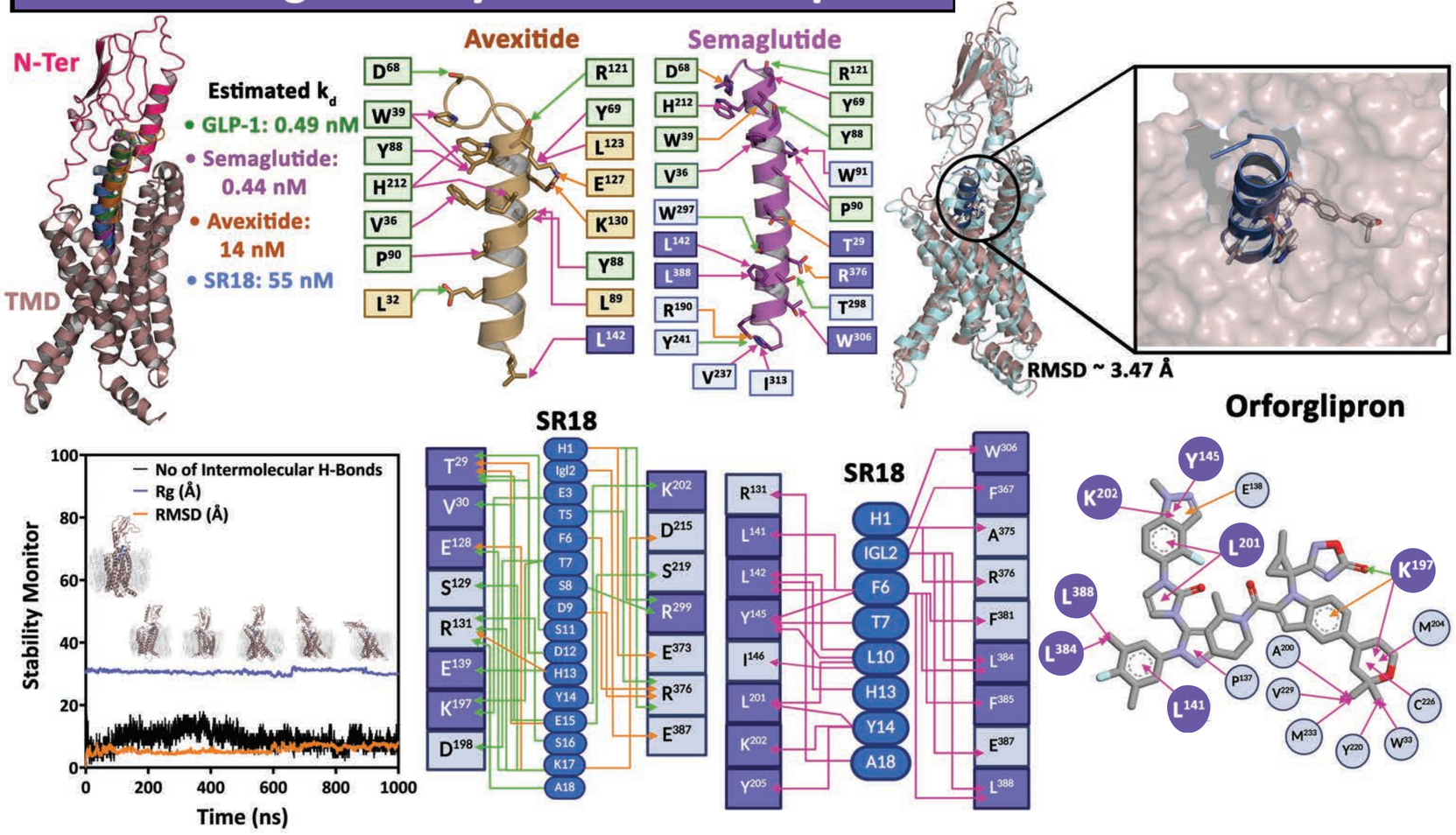
HIglEAibTFTSDLSDHYESKA-NH_2



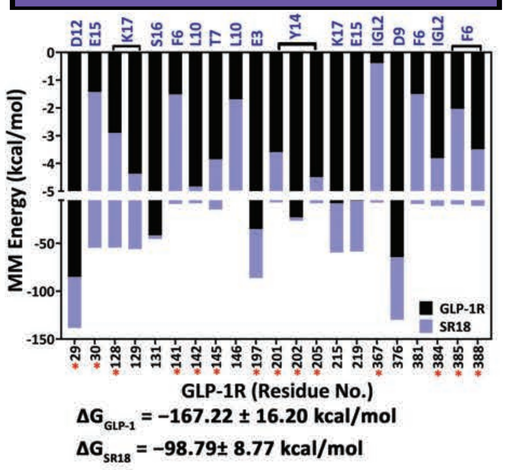
3. Monitoring Stability of Peptides



4. Monitoring Stability of GLP-1R Complexes

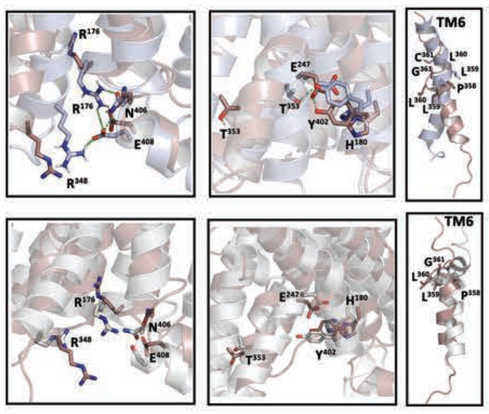


5.MMPBSA Studies

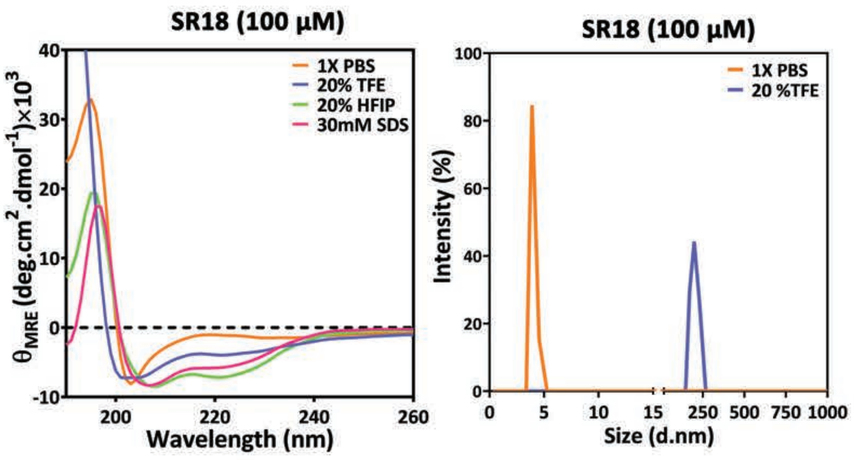


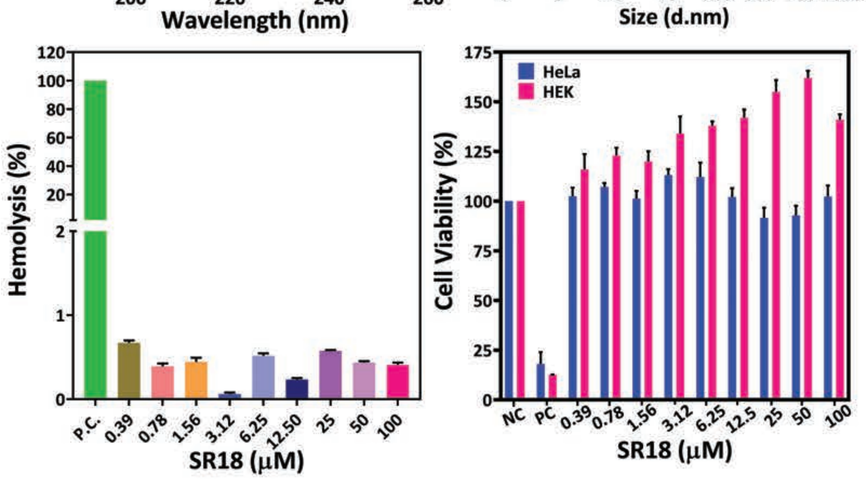
ΔG_{GLP-1} = −167.22 ± 16.20 kcal/mol
ΔG_{SR18} = −98.79± 8.77 kcal/mol

6. Motif Dynamics

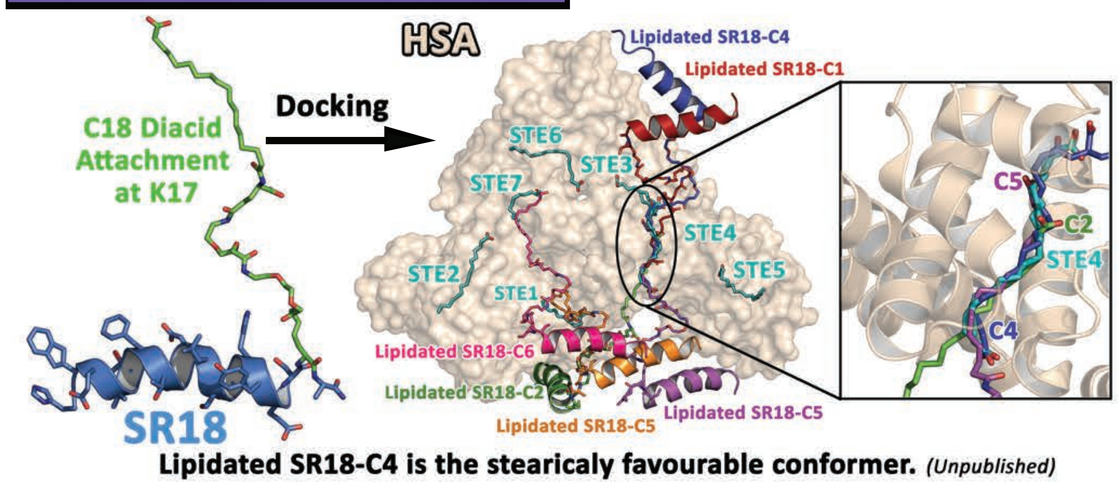


7. Pharmacological Studies





8. SR18 Modification



Lipidated SR18-C4 is the stearicaly favourable conformer. *(Unpublished)*

9. Proteolytic Study

SR18 (Mol. Wt. 2124)

^{1}HIglEAibTFTSDLSDHYESKA^{18}

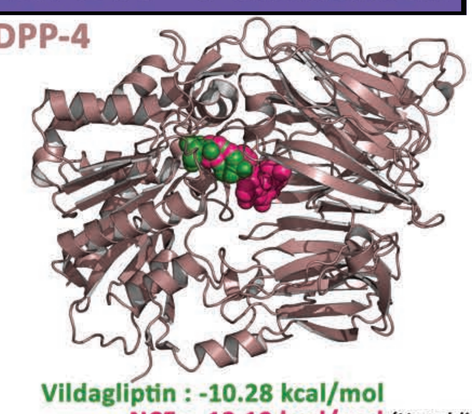
Trypsin treatment

^{1}HIglEAibTFTSDLSDHYESK^{17} | A^{18}

(Mol. Wt. 2057)

N-terminal 17 amino acids remains intact.

10. DPP-4 Inhibiton



Vildagliptin : -10.28 kcal/mol
NCE : -12.19 kcal/mol *(Unpublished)*

Conclusions

SR18 shows:

1. **Stable Binding:** Maintains consistent interactions with GLP-1R throughout MD.
2. **Target Precision:** Shares binding pocket with GLP-1,semaglutide and orforglipron.
3. **Structural Stability:** CD spectra reveal a stable α-helical conformation.
4. **Protease Resilence:** Core 17 residues remain intact after trypsin exposure.
5. **Biocompatible:** Confirmed non-toxic to mammalian cells.
6. **Blood Compatible:**Non-hemolytic to human RBCs.
7. **Predicted BBB Permeability.**
8. **DPP-4 Inhibition:** Vildaglitpin and NCE shares similar binding pocket.

References

1.Singh, A., Shadangi, S., & Rana, S. (2026). A rationally designed 18-amino acid peptide with potential as GLP-1 receptor agonist. Frontiers in Pharmacology, 17, 1789257.

2.Singh, A., Shadangi, S., Gupta, P. K., & Rana, S. (2025). Type 2 diabetes mellitus: a comprehensive review of pathophysiology, comorbidities, and emerging therapies. *Comprehensive Physiology*, 15(1), e70003.

Acknowledgments

Scan here

https://doi.org/10.17952/38EPS.2026.P238

Rational Design of Melittin-Derived Peptides for Enhanced Biological Activity

M. Śleziak[1], J.J. Panek[1], T. Janek[2], A. Jezierska[1], K. Cieślik-Boczula[1], M. Kijewska[1]

[1] Faculty of Chemistry, University of Wrocław, Wrocław, Poland **Email:** mikolaj.sleziak@uwr.edu.pl

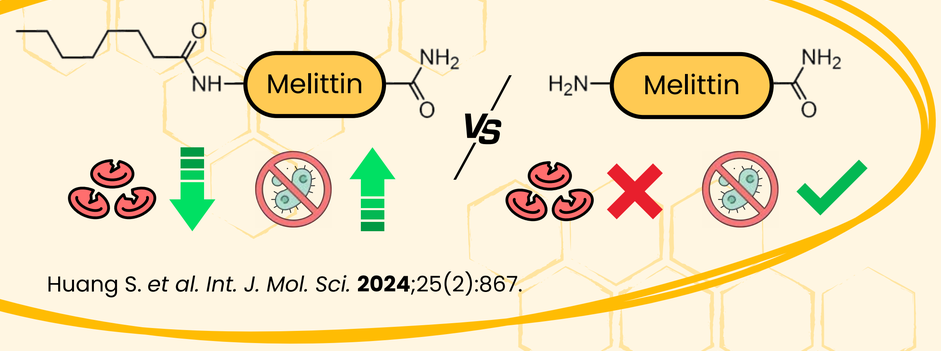
[2] Faculty of Biotechnology and Food Science, Wrocław University of Environmental and Life Sciences, Wrocław, Poland

Introduction

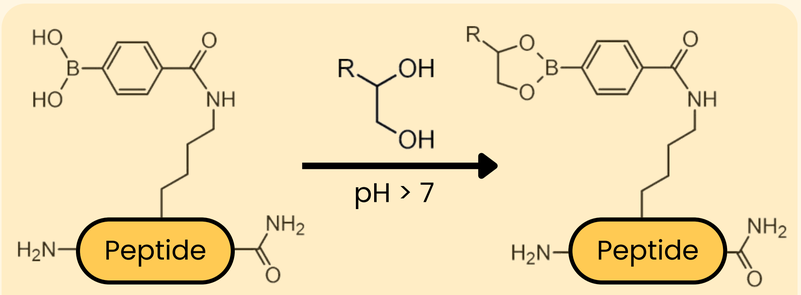
Melittin: H-G I G A V L K V L T T G L P A L I S W I K R K R Q Q -NH_2

MCFA: H-G L K K L I S W I K R A A Q Q G -NH_2

Subbalakshmi C. *et al. FEBS Lett.* **1999**;448(1):62.



Huang S. *et al. Int. J. Mol. Sci.* **2024**;25(2):867.



Kijewska M. *et al. Chem. Eur. J.* **2023**;29(40):e202301370.

Objectives

Synthesis of more selective MCFA analogs with lower cytotoxicity and enhanced proteolitic stability.

- Synthesis of 6 MCFA analogs modified with 4-carboxyphenylboronic acid and/or caprylic acid.
- Purification of all synthesized compounds by preparative HPLC.
- Evaluation of antimicrobial activity against Gram+ and Gram- bacteria.
- Evaluation of proteolytic stability against trypsin.

Results

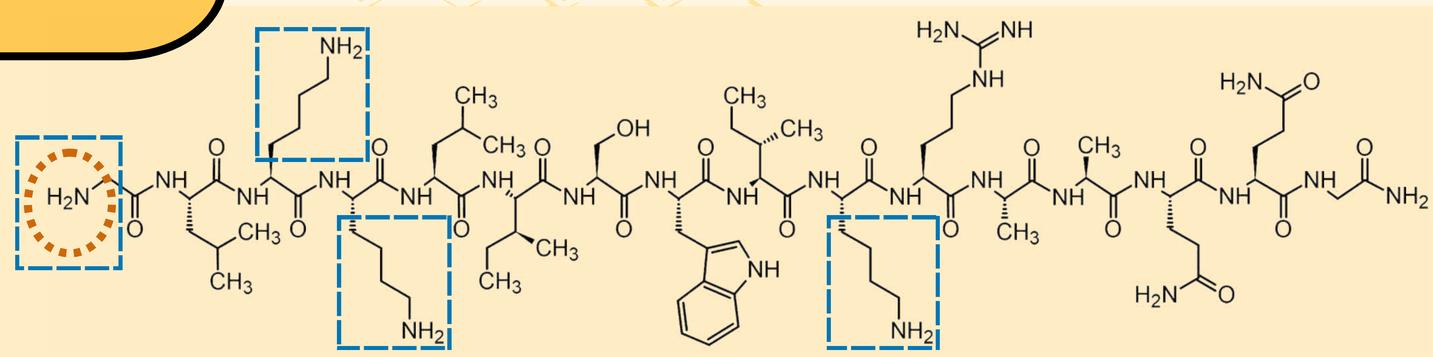
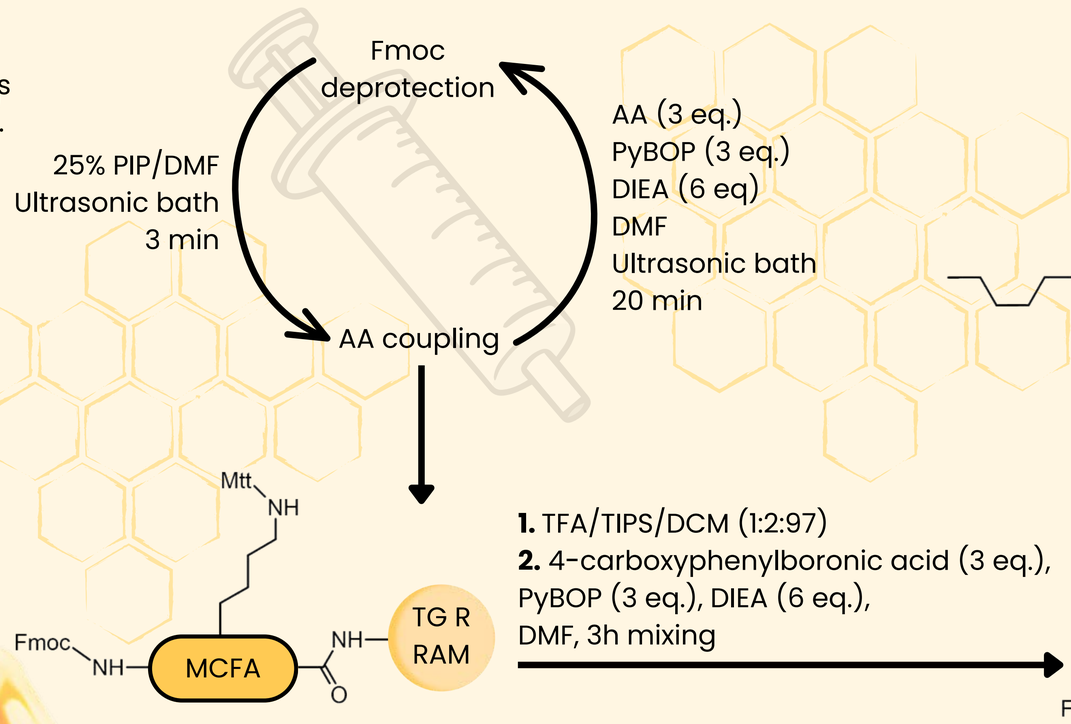


Fig. 1. Structure of MCFA with marked sites of post-synthetic modifications with 4-carboxyphenylboronic acid and caprylic acid.

Tab. 1. *In vitro* hemolytic activity of peptides determined as 50% hemolytic concentration.

Compound	HC_{50} [µg/mL]
MCFA	16
MCFA-C8	128
MCFA-PBA(2.Lys)	n/d
MCFA-PBA(2.Lys)-C8	64
MCFA-2PBA(1.3.Lys)-C8	32
MCFA-2PBA(1.2.Lys)-C8	Not tested yet
MCFA-2PBA(1.2.Lys)-PBA	Not tested yet



Tab. 2. *In vitro* antibacterial activity determined as a minimal inhibitory concentration (MIC). MCFA-2PBA(1.2.Lys)-C8 and MCFA-2PBA(1.2.Lys)-PBA have not yet been tested.

Strain	MIC [µg/mL]				
	MCFA	MCFA-C8	MCFA-PBA(2.Lys)	MCFA-PBA(2.Lys)-C8	MCFA-2PBA(1.3.Lys)-C8
S. aureus	8	4	4	16	8
S. epidermidis	32	16	8	32	16
E. coli	16	8	32	4	8
K. pneumoniae	4	4	16	4	4
K. rhinoscleromatis	4	2	2	8	2

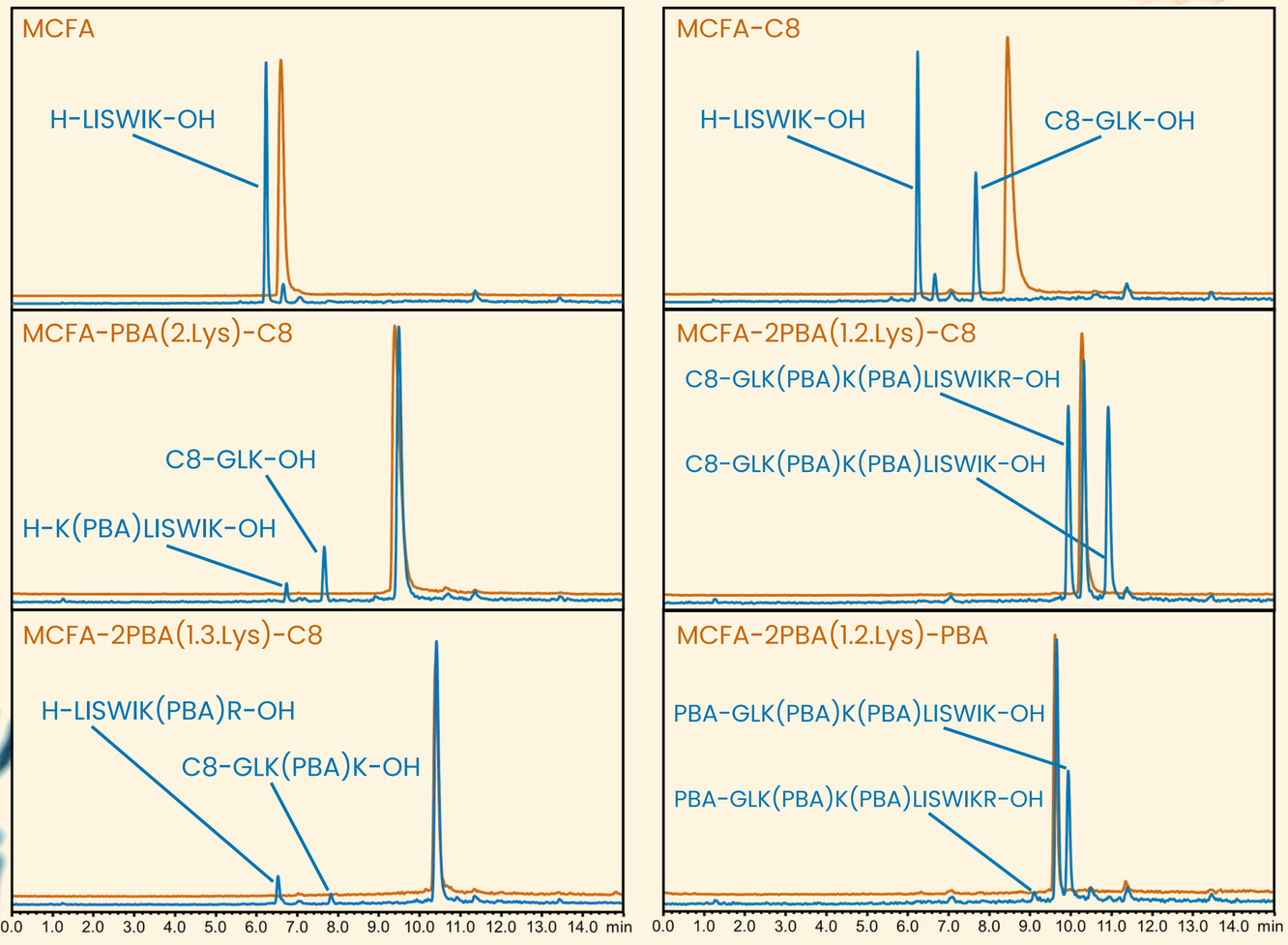


Fig. 2. LC-MS (TIC) of peptides before and after trypsin digestion. MCFA-PBA(2.Lys) has not yet been tested.

Conclusions

- PBA improved MCFA selectivity, with MCFA-PBA(2.Lys) showing no hemolysis.
- The strain-dependent activity of PBA-modified analogs suggests that differences in bacterial surface glycoconjugates may contribute to peptide recognition and selectivity.
- C8 lipidation maintained or enhanced antibacterial activity while substantially reducing hemolytic activity, consistent with previous reports on lipidated melittin analogs.
- Post-synthetic modifications altered the proteolytic degradation patterns of MCFA analogs, highlighting their potential to modulate peptide stability.

Acknowledgements

We gratefully acknowledge computer facilities and support provided by the Wrocław Centre for Networking and Supercomputing (WCSS) - grant no. 206 as well as the Polish high-performance computing infrastructure PLGrid (HPC Center: ACK Cyfronet AGH) - computational grant no. PLG/2025/018939.

Efficient TEV tag-assisted one-pot protein semisynthesis

Benoît Snella,[a] Magalie Sénéchal,[a] Jérôme Vicogne,[a] Vangelis Agouridas,[a,b] Oleg Melnyk[a]

[a] Univ. Lille, CNRS, Inserm, CHU Lille, Institut Pasteur de Lille, U1019 -UMR 9017 - CIIL -Center for Infection and Immunity of Lille, F-59000, Lille, France
[b] Centrale Lille, F-59000, Lille, France

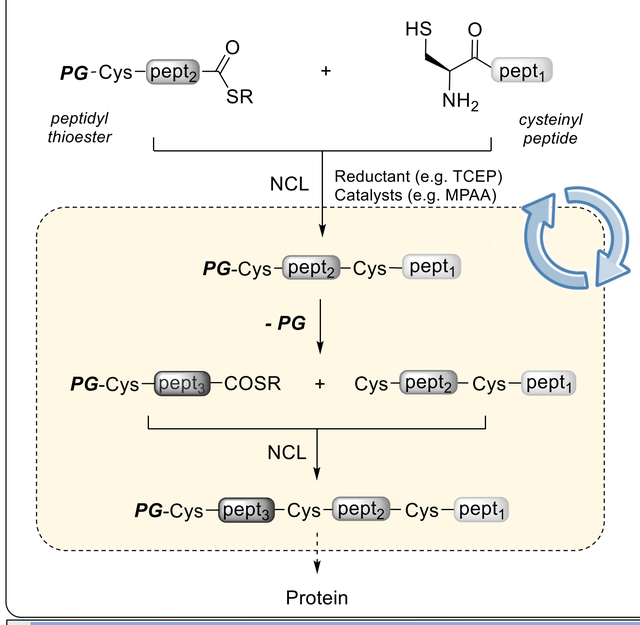
https://doi.org/10.17952/38EPS.2026.P296

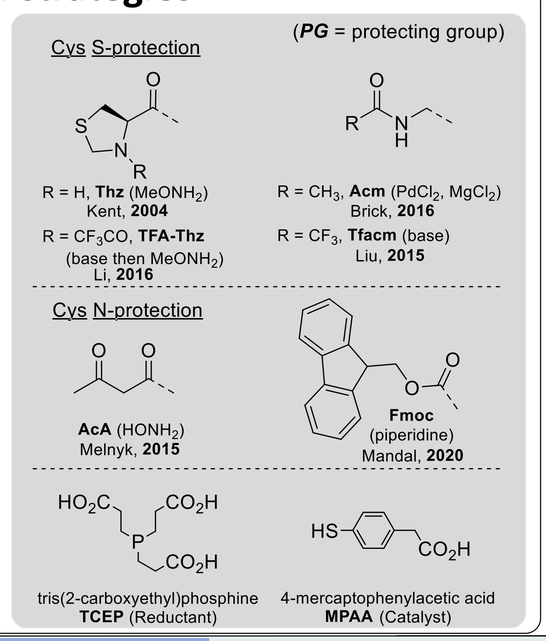
Introduction

Peptide and protein drugs are attracting significant interest due to their high specificity and efficacy.[1] Significant efforts have been made to develop efficient chemical and biochemical processes for the synthesis of these biomolecules, with the repurposing of enzymes for synthetic applications representing an attractive approach.[2,3]

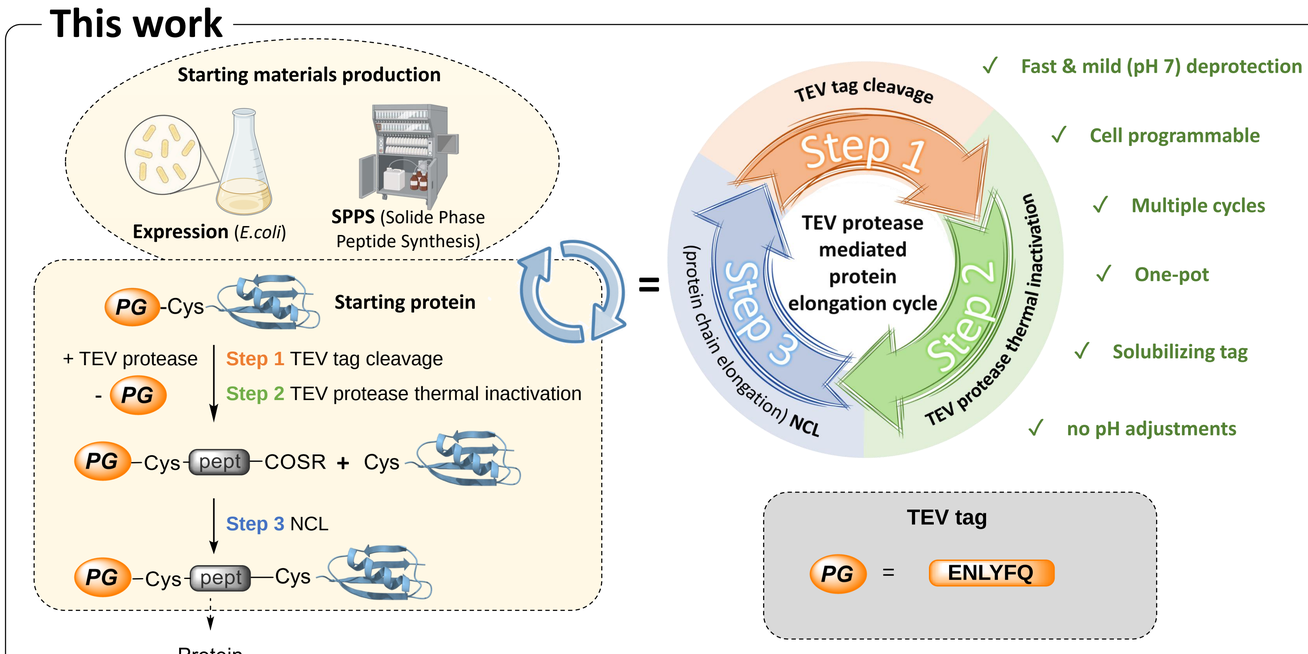
In this work, we designed an innovative and efficient method for protein semisynthesis. This protein elongation strategy exploits the Native Chemical Ligation (NCL) to form the peptide bonds and the Tobacco Etch Virus (TEV) tag as a protecting group (*PG*) for cysteine (Cys) to control the sequential concatenation of synthetic or recombinant peptide segments in water.[4,5] The TEV tag is removed under mild conditions by the addition of TEV protease, an enzyme with high specificity and cleavage efficiency, thereby minimizing the formation of by-products. After cleavage, the enzyme is thermally inactivated in a few minutes, allowing the elongation process to continue in one pot with a new TEV-protected peptide.[6] Iterative cycles afford long polypeptides with high purity and isolated yields.

Existing C to N peptide elongation strategies





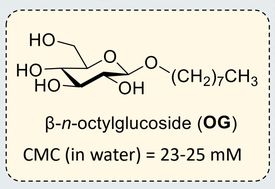
This work

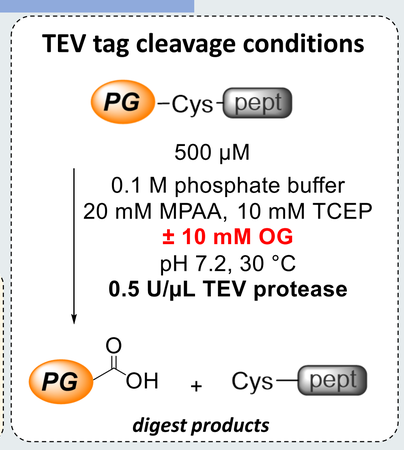


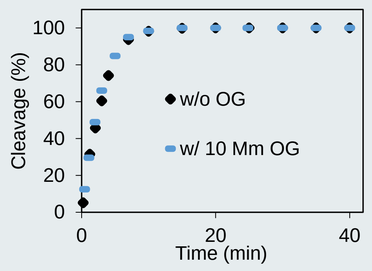
1. NCL and TEV protease buffer conditions

We used OG (10 mM) in the NCL reaction buffer to improve peptide solubility. OG is a non-ionic detergent with a critical micelle concentration (CMC) of 23–25 mM in water. However, several studies have shown that TEV protease activity can be affected by detergents.[6]

We therefore investigated the impact of OG on TEV protease activity.



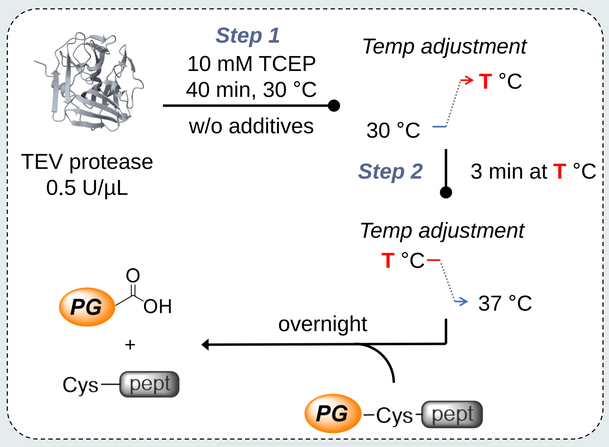




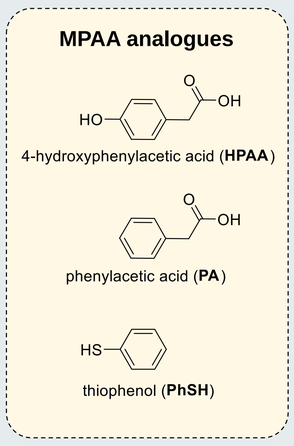
No effect of 10 mM OG on TEV protease activity

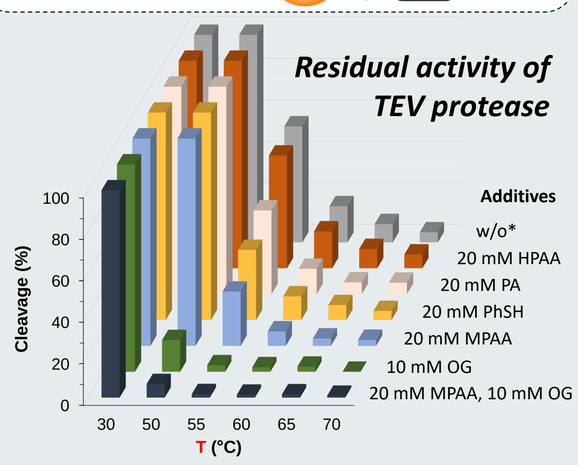
2. Irreversible thermal inactivation and TEV protease melting temperature (T_m): the impact of OG and MPAA

Heat-induced TEV protease inactivation was assessed after 3 min in 10 mM TCEP buffer in the presence of different additives.[7] Interestingly, we observed a significant reduction in residual enzyme activity when MPAA and OG were used, with a pronounced effect when used in combination. MPAA analogues were also tested, revealing the importance of the thiophenol group in MPAA in promoting TEV protease inactivation. We performed complementary studies using nano differential scanning fluorimetry (NanoDSF) that showed a significant reduction of the melting temperature (T_m) of TEV protease when OG and MPAA were used in combination.



MPAA analogues





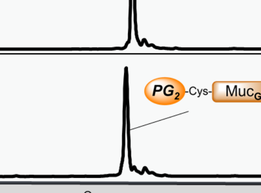
Buffer	TEV protease T_m (°C)
w/o*	54.3
20 mM MPAA	51.2
10 mM OG	49.0
20 mM MPAA, 10 mM OG	40.9

Best inactivation condition: 20 mM MPAA, 10 mM OG, 55 °C

* 10 mM TCEP, 0.1 M phosphate buffer, pH 7.2

3. TEV-assisted elongation cycle

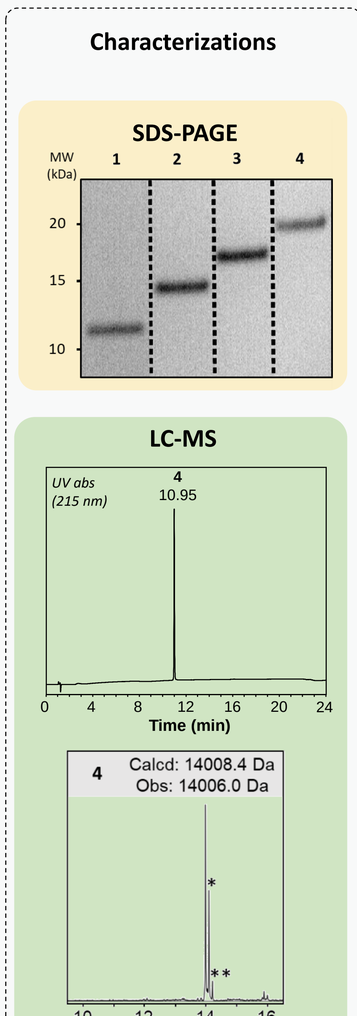
Thus, we designed a TEV-assisted elongation cycle in a buffer containing 10 mM TCEP, 20 mM MPAA, 10 mM OG in 0.1 M phosphate buffer, pH 7.2 as follows:



- Step 1: **TEV tag cleavage** (30 °C, 40 min)
  in situ production of cysteinyl protein
- Step 2: **TEV protease inactivation**
  (55 °C, 3 min)
- Step 3: **NCL**, addition of peptide thioester
  (1 equivalent, 37 °C, overnight)

4. Application of TEV-assisted elongation cycle to protein semisynthesis

The elongation cycle was repeated three times in one pot. We used this method to elongate a recombinant TEV-tagged protein (PG_1-Cys-GB1, 30 nmol, produced in *Escherichia coli* cells) using different mucin1-derived (PG_2-Cys-Muc) peptide thioesters.[8] *PG*s differ by the amino acid sequence preceding the tag and can incorporate charged residues to enhance the solubility of the segments.



Isolated yields: 27% (2), 31% (3), and 31% (4)

Conclusion

The TEV protease-mediated one-pot elongation cycle was successfully demonstrated over three consecutive steps, yielding a 14 kDa polyMuc-GB1 protein.

The combination of OG and MPAA enabled a fast and efficient TEV protease inactivation at a mild temperature of 55 °C, providing suitable conditions for iterative protein elongation.

Acknowledgment We gratefully acknowledge the EPS for funding my conference registration.

References

(1) Agouridas, V.; El Mahdi, O.; Melnyk, O. *J. Med. Chem.* **2020**, *63*, 15140–15152.
(2) C. Wang, R. Desmet, B. Snella, J. Vicogne, O. Melnyk, V. Agouridas, *Org. Lett.*, **2025**, *27*, 11845-11858.
(3) C. Wang, R. Desmet, B. Snella, O. Melnyk, V. Agouridas, *Angew. Chem. Int. Ed.*, **2025**, *64*, e202507236.
(4) Dawson, P. E.; Muir, T. W.; Clark-Lewis, I.; Kent, S. B. *Science* **1994**, *266*, 776–779.
(5) Agouridas, V.; El Mahdi, O.; Diemer, V.; Cargoët, M.; Monbaliu, J.-C.; M.; Melnyk, O. *Chem. Rev.* **2019**, *119*, 7328–7443.
(6) Mohanty, A. K.; Simmons, C. R.; Wiener, M. C. *Protein Expr. Purif.* **2003**, *27*, 109–114.
(7) Raran-Kurussi, S.; Tőzsér, J.; Cherry, S.; Tropea, J. E.; Waugh, D. S. *Anal. Biochem.* **2013**, *436*, 142-144.
(8) F. Terzani, C. Wang, S. Rostami, R. Desmet, B. Snella, M. Sénéchal, B. Wiltschi, J. Vicogne, O. Melnyk, V. Agouridas, *STAR Protocols* **2024**, *5*, 103390.

https://unicorn-prizma.rs/

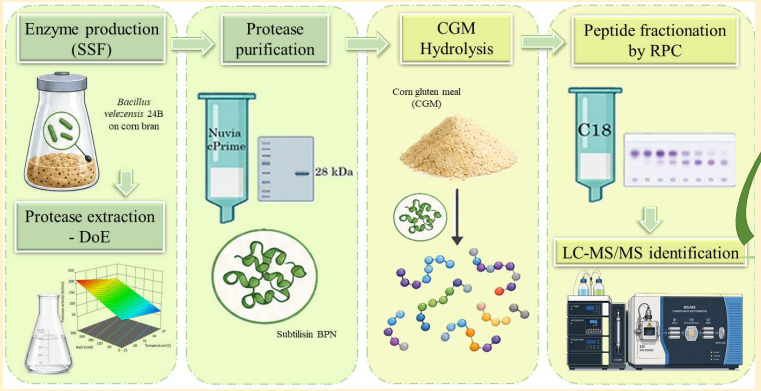
Bioassay-guided peptidomic characterization of antioxidant peptides generated from corn gluten meal using SSF-produced subtilisin BPN

N. Drulović[1], M. Pavlović[1], M. Ristović[1], A. Leonardi[2], I. Križaj[2], S. Orhanović[3], B. Dojnov[1] & M. Šokarda Slavić[1,*]

1 University of Belgrade, Institute of Chemistry, Technology and Metallurgy – National Institute of the Republic of Serbia, Department of Chemistry, Belgrade, Serbia
2 Department of Molecular and Biomedical Sciences, Jožef Stefan Institute, Ljubljana, Slovenia
3 Department of Chemistry, Faculty of Science, University of Split, Croatia
** marinela.sokarda@ihtm.bg.ac.rs*
https://doi.org/10.17952/38EPS.2026.P246

Background

- Corn wet milling produces two underused coproducts: corn bran (fibre-rich) and corn gluten meal, CGM (60–70% protein, mostly zein).
- Zein's hydrophobicity and structural recalcitrance limit CGM's use in food/nutraceutical applications.
- Zein-derived peptides show promise as antioxidants, but efficient release requires targeted enzymatic hydrolysis.
- Sustainable protease production (e.g., solid-state fermentation on agro-residues) enables low-cost valorisation within a circular bioeconomy.



Objective

To valorise CGM into structurally defined antioxidant peptides via enzymatic hydrolysis, ultrafiltration and C18 fractionation — guided at every step by antioxidant bioassay screening.

~70%
zein content in corn gluten meal

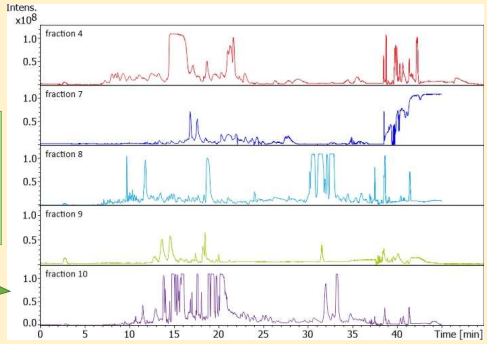
<3 kDa
peptide fraction selected by ultrafiltration

Why This Approach

- **Low-cost substrate**
  Corn bran and CGM are cheap, abundant agro-industrial residues.
- **Circular valorisation**
  Converts a low-value by-product into a high-value bioactive ingredient.
- **Bioassay-guided selection**
  Only fractions with confirmed antioxidant activity advance to peptidomics.

Results

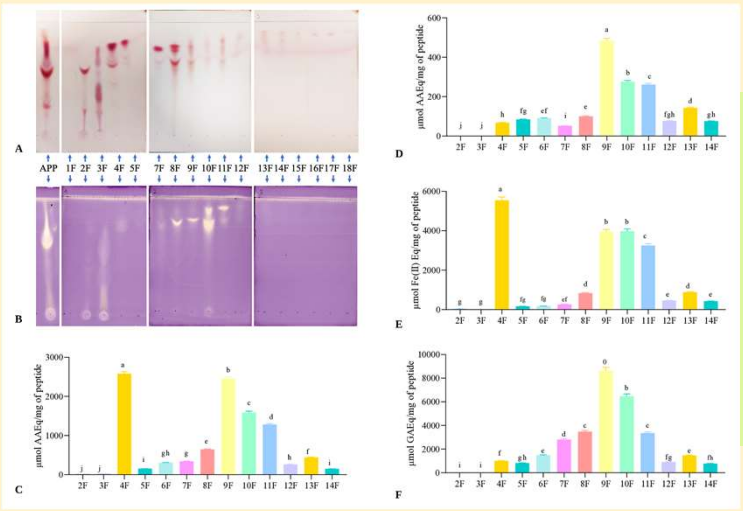
High-resolution LC–MS/MS peptidomics of the most antioxidant-active fractions revealed



Methods

1. **SSF enzyme production**
   Subtilisin BPN' from *Bacillus velezensis* 24B via SSF on corn bran.
2. **Enzymatic hydrolysis**
   CGM zein hydrolysed to release low-MW peptides.
3. **Ultrafiltration**
   3 kDa cut-off isolates the low-MW peptide fraction.
4. **C18 fractionation**
   Stepwise MeOH/MeCN elution yields discrete fractions.
5. **Bioassay-guided screening**
   Fractions ranked by antioxidant activity.
6. **LC–MS/MS peptidomics**
   Peptide sequencing in the most active fractions.

Antioxidant Activity by Fraction



Characterisation of RP-C18 peptide fractions.
(A) Ninhydrin-stained TLC plate of applied sample (APP) and fractions 1F–18F.
(B) DPPH bioautographic assay of the same fractions.
(C) ABTS radical-scavenging activity (n = 3, mean ± SD).
(D) DPPH radical-scavenging activity (n = 3, mean ± SD).
(E) FRAP (n = 3, mean ± SD).
(F) Folin–Ciocalteu total phenolic content (n = 3, mean ± SD).
Different letters indicate statistically significant differences (Tukey post hoc test, $p < 0.05$).

Conclusion

This integrative ultrafiltration–chromatographic–peptidomic approach shows that SSF-derived subtilisin BPN' efficiently converts corn gluten meal into structurally defined antioxidant peptides — supporting sustainable valorisation of corn-processing waste into high-value bioactive molecules.

Acknowledgements

Supported by the Science Fund of the Republic of Serbia, #7347, "Unique enzyme solutions for obtaining added value products from corn – UniCorn", and by the Ministry of Science, Technological Development and Innovation of the Republic of Serbia (Contract No. 451-03-136/2025-03/200026).

P413*

38th EPS 2026

Preliminary Evaluation of the Stability of a Liposomal Formulation of OmegaCalm Based on Active Peptides for Cosmetic Applications

Y. Solís[1], **Y. Campos**[1], **J.C. Aguilar**[1], **G. Esteruelas**[1], **E. Sánchez**[1] & **L.J. Cruz**[2]

[1] Dept. of Pharmacy, Pharmaceutical Technology and Physical Chemistry, Faculty of Pharmacy and Food Sciences, University of Barcelona, Spain

[2] Peptidepharma Nova S.L., Gavà, Barcelona, Spain

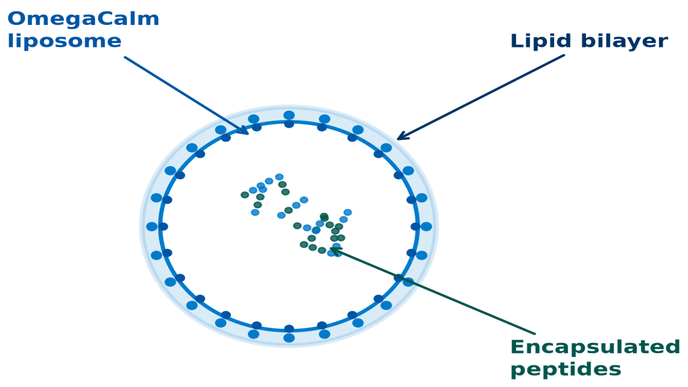
* https://doi.org/10.17952/38EPS.2026.P413

Introduction

The stability of liposomal systems is a **critical aspect** to guarantee their performance as vehicles for bioactive peptides in cosmetic applications.

Stability testing determines the **shelf life** of a finished product under specified storage conditions.

Liposome Structure



Preparation Method

Liposome Preparation Scheme

1. **Lipid Dissolution** — Phospholipids dissolved in organic solvent (CHCl3/MeOH)
2. **Thin-Film Formation** — Solvent evaporation under reduced pressure
3. **Hydration** — Aqueous phase with OmegaCalm peptides added
4. **Sonication / Extrusion** — Size reduction and homogenization
5. **Liposomal Dispersion** — Characterization: size, PDI, zeta potential
6. **Stability Evaluation** — Storage under controlled conditions (6 months)

Study Instruments

Stability Study Instruments

Storage Conditions: 25 C | 40 C | 4-10 C

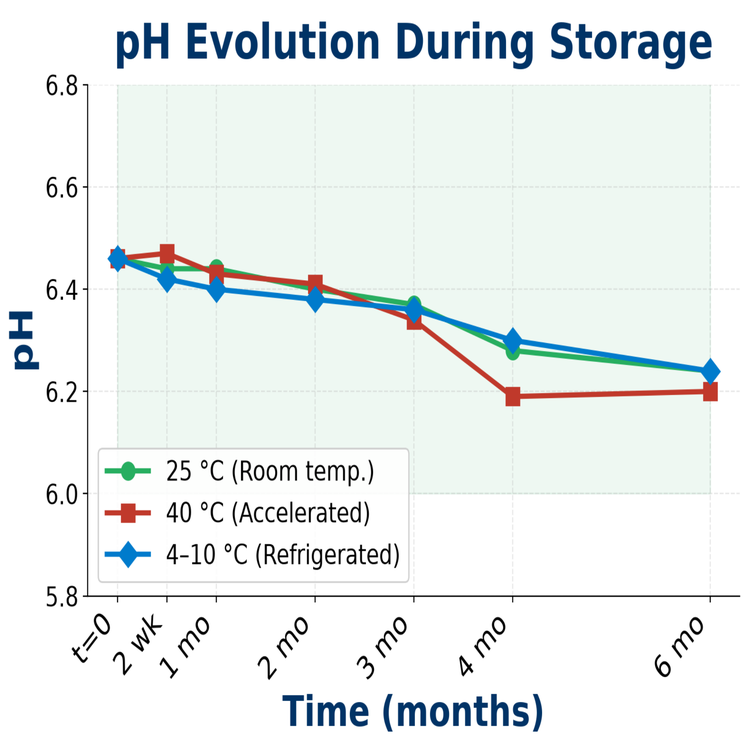
Analytical Instruments:

- **pH Meter** — pH measurement (6.0 - 7.0 range)
- **Viscometer** — Viscosity measurement (450-1300 cP range)

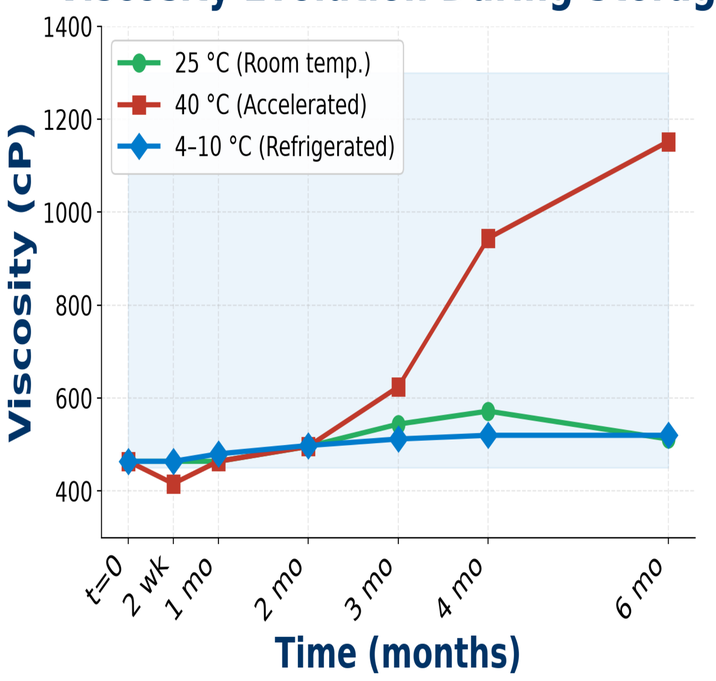
Timeline: t=0 | 2 wk | 1, 2, 3, 4, 6 months | Total: 18 samples

Results

pH Evolution During Storage



Viscosity Evolution During Storage





OmegaCalm liposomal formulation samples

KEY RESULTS & CONCLUSIONS

24

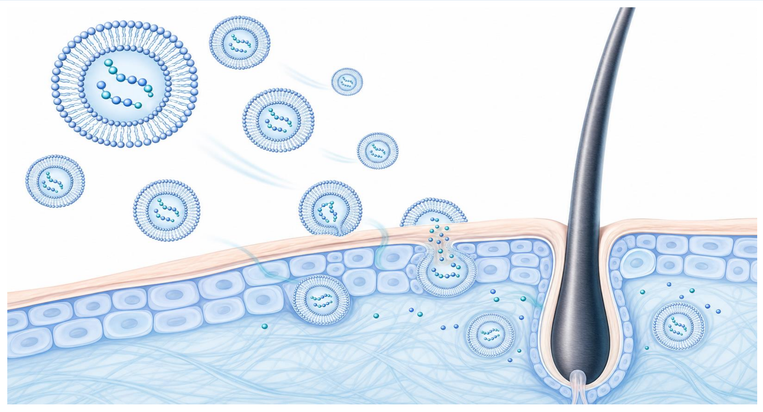
months

pH: 6.0 - 7.0

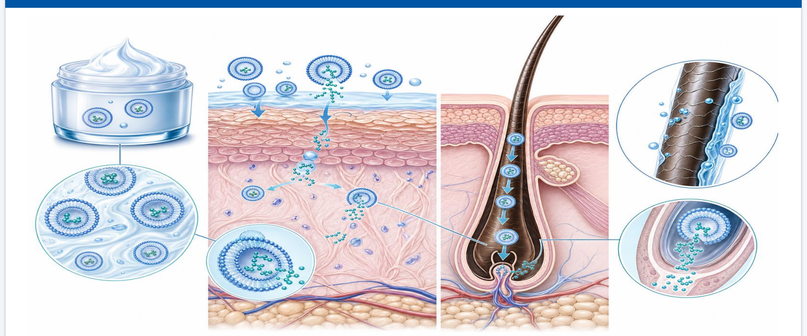
Viscosity: 450 - 1300 cP

Normal storage: room temperature, protected from light

Cosmetic Application



Multiple Applications



Skin care: anti-aging, hydration
Hair care: follicle delivery, protection
Topical formulations: creams, serums

pH Stability

✓ **6.0 - 7.0**

Stable across all conditions

Viscosity at 40 C

! **1152 cP**

Increase from month 3 (accelerated)

Shelf Life

★ **24 months**

Under normal storage conditions

Acknowledgements

Supported by **University of Barcelona** via **AGAUR** grant **2024 DI 00074**

References

1. *P. Jingyan, et al., Curr. Res. Food Sci.*. 2022, 5, 2162-2170.

2. *M. Lens, Int. J. Mol. Sci.*. 2025, 26, 2484.

3. *M. Dymek, et al., Int. J. Mol. Sci.*. 2025, 26, 5321.

4. *Y.K. Lin, et al., J. Cosmet. Dermatol.*. 2026, 25, e70834.

5. *H. Bao, et al., Sci. Rep.*. 2025, 15, 42260.

Contact: **yaimaras@gmail.com**

P413*

38th EPS 2026

Preliminary Evaluation of the Stability of a Liposomal Formulation of OmegaCalm Based on Active Peptides for Cosmetic Applications

Y. Solís[1], **Y. Campos**[1], **J.C. Aguilar**[1], **G. Esteruelas**[1], **E. Sánchez**[1] & **L.J. Cruz**[2]

[1] Dept. of Pharmacy, Pharmaceutical Technology and Physical Chemistry, Faculty of Pharmacy and Food Sciences, University of Barcelona, Spain

[2] Peptidepharma Nova S.L., Gavà, Barcelona, Spain

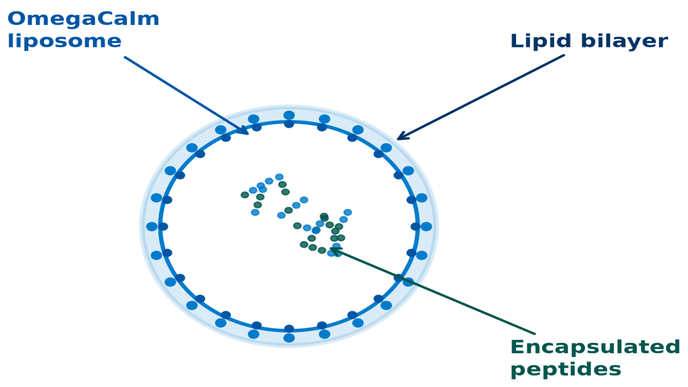
* https://doi.org/10.17952/38EPS.2026.P413

Introduction

The stability of liposomal systems is a **critical aspect** to guarantee their performance as vehicles for bioactive peptides in cosmetic applications.

Stability testing determines the **shelf life** of a finished product under specified storage conditions.

Liposome Structure



Preparation Method

Liposome Preparation Scheme

1. **Lipid Dissolution** — Phospholipids dissolved in organic solvent (CHCl3/MeOH)
2. **Thin-Film Formation** — Solvent evaporation under reduced pressure
3. **Hydration** — Aqueous phase with OmegaCalm peptides added
4. **Sonication / Extrusion** — Size reduction and homogenization
5. **Liposomal Dispersion** — Characterization: size, PDI, zeta potential
6. **Stability Evaluation** — Storage under controlled conditions (6 months)

Study Instruments

Stability Study Instruments

Storage Conditions: 25 C | 40 C | 4-10 C

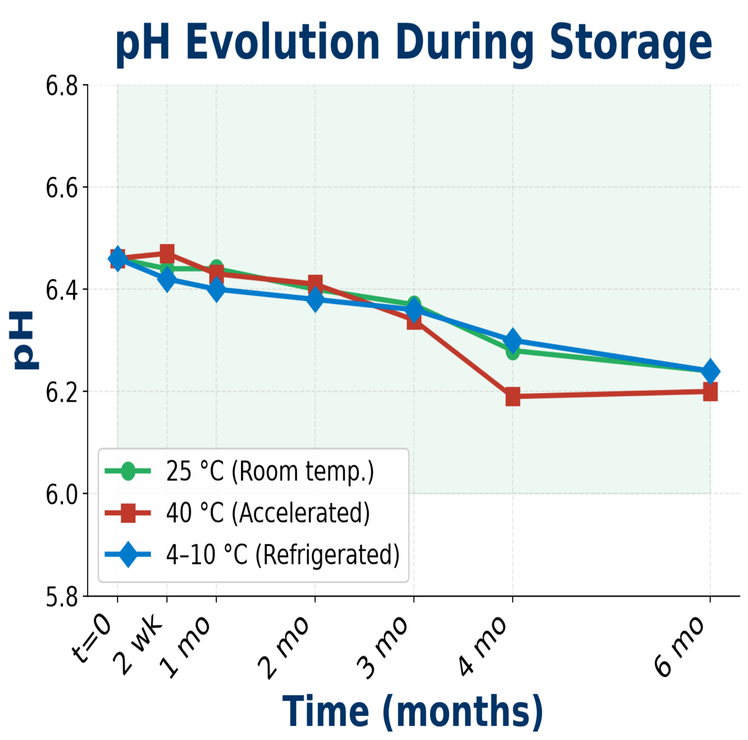
Analytical Instruments:

- **pH Meter** — pH measurement (6.0 - 7.0 range)
- **Viscometer** — Viscosity measurement (450-1300 cP range)

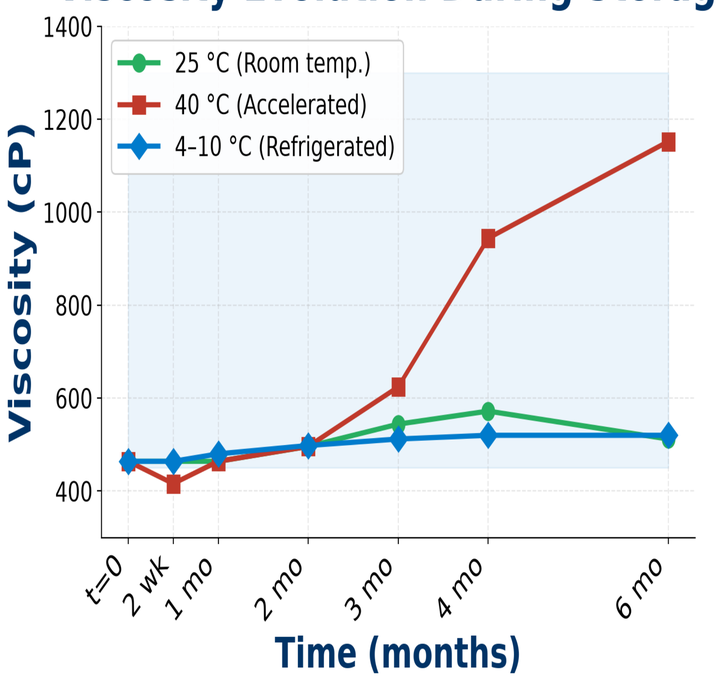
Timeline: t=0 | 2 wk | 1, 2, 3, 4, 6 months | Total: 18 samples

Results

pH Evolution During Storage



Viscosity Evolution During Storage





OmegaCalm liposomal formulation samples

KEY RESULTS & CONCLUSIONS

24

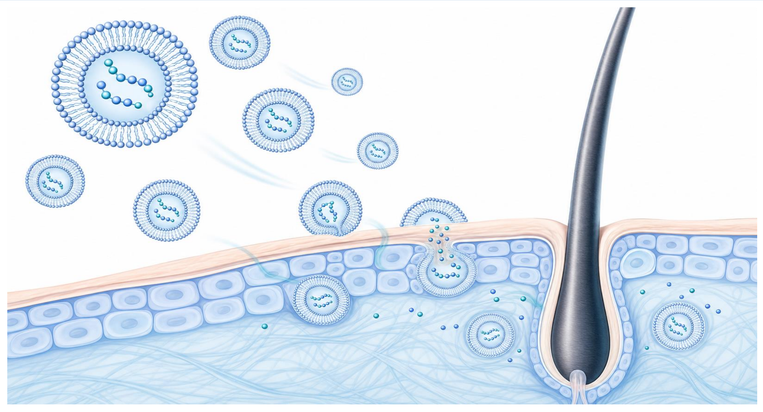
months

pH: 6.0 - 7.0

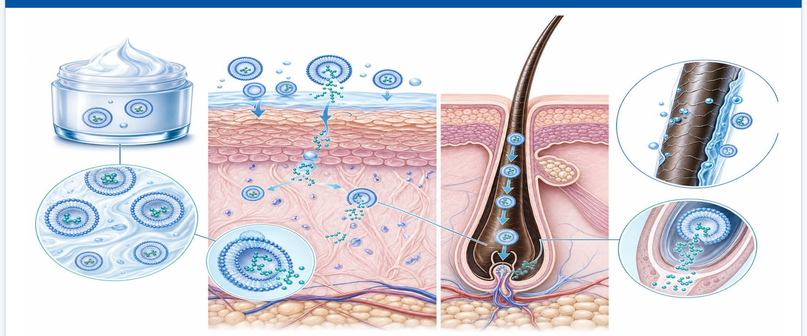
Viscosity: 450 - 1300 cP

Normal storage: room temperature, protected from light

Cosmetic Application



Multiple Applications



Skin care: anti-aging, hydration
Hair care: follicle delivery, protection
Topical formulations: creams, serums

pH Stability

✓ **6.0 - 7.0**

Stable across all conditions

Viscosity at 40 C

! **1152 cP**

Increase from month 3 (accelerated)

Shelf Life

★ **24 months**

Under normal storage conditions

Acknowledgements

Supported by **University of Barcelona** via **AGAUR** grant **2024 DI 00074**

References

1. *P. Jingyan, et al., Curr. Res. Food Sci.*. 2022, 5, 2162-2170.

2. *M. Lens, Int. J. Mol. Sci.*. 2025, 26, 2484.

3. *M. Dymek, et al., Int. J. Mol. Sci.*. 2025, 26, 5321.

4. *Y.K. Lin, et al., J. Cosmet. Dermatol.*. 2026, 25, e70834.

5. *H. Bao, et al., Sci. Rep.*. 2025, 15, 42260.

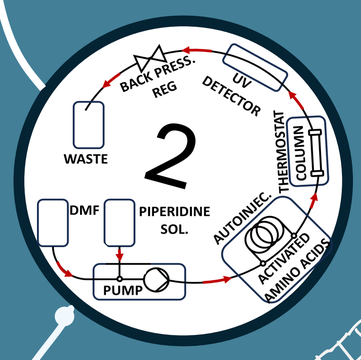
Contact: **yaimaras@gmail.com**

Methionine Oxidation Effect on GLP-2 Synthesis and Amyloid Kinetics

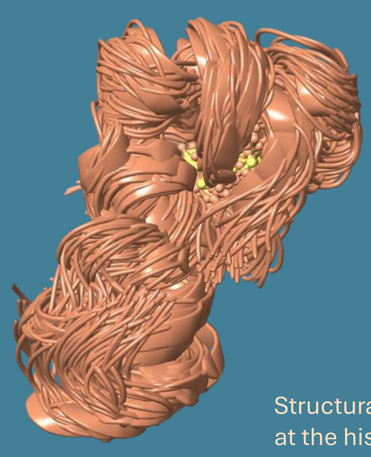
https://doi.org/10.17952/38EPS.2026.P044

Szebasztián Szaniszló; Dániel Horváth; Kata Geszti; Anna J. Kiss-Szemán; Dóra K. Menyhárd and András Perczel
HUN-REN – ELTE Protein Modeling Research Group, ELTE Eötvös Loránd University
szaniszlo.szebasztian@ttk.elte.hu

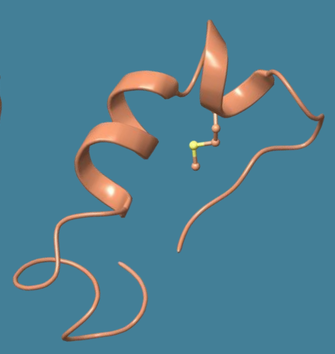
Glucagon-like peptide-2 (GLP-2) might just be the "second most important" peptide after GLP-1
It exerts key physiological functions, including stimulating intestinal epithelial growth, enhancing nutrient absorption, and reducing intestinal inflammation. However, it's one of those "difficult peptides," which makes solid-phase peptide synthesis (SPPS) challenging.
To overcome this, we set out to improve the synthesis by testing different amino acid protecting groups and structural tricks, including pseudoproline derivatives and Asp(Bno). Ultimately, the best effect came from using methionine sulfoxide.
Beyond improving yield, we were also curious to see what happens if we leave the sulfoxide derivatives in after synthesis to observe how they influence the peptide's behavior.
Below are the results of our synthesis trials, along with CD spectra, ThT tests, molecular dynamics (MD) simulations, and AFM images.

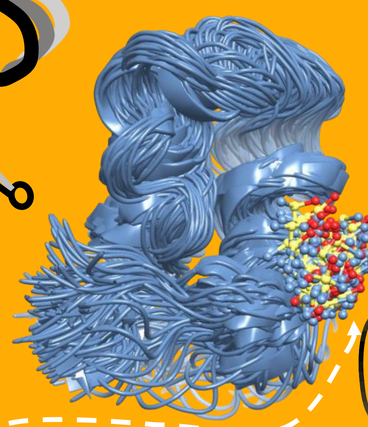


FLOW PEPTIDE SYNTHESIS



Structural alignment of GLP-2 variants protonated at the histidine side chain (162 structures)





Structural alignment of protonated oxidized variant GLP-2-M(O^R) (157 structures) and its representative.

5 CONCLUSION

Synthetic Handle: Reversible Fmoc-Met(O)-OH incorporation overcomes SPPS aggregation bottlenecks to deliver high crude GLP-2 purity, with post-purification reduction restoring the authentic native peptide.

Pathway Selector: Rather than acting as a simple aggregation inhibitor, methionine sulfoxidation functions as a pH-dependent pathway selector—bypassing off-pathway amorphous collapse near the pI (pH 4) to promote ordered fibril assembly (like a zipper).

Molecular Mechanism: Molecular dynamics simulations reveal that sulfoxidation disrupts the buried, hydrophobic "methionine cage" around Met10, exposing the polar sidechain to act cooperatively with His1 protonation to preserve N-terminal helicity.

Native GLP-2: Remains practically unchanged in overall helical content, as the hydrophobic "methionine cage" keeps Met buried **(SASA = 32.3 Å²).**

Met(O) Variants: Triggers a notable **increase in helicity** (rising to 30.5% for the *R*-epimer). **(SASA = 110.2 Å²)**

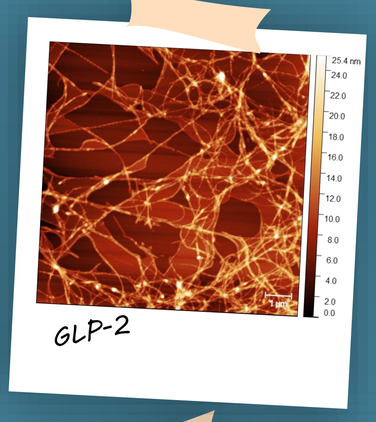
Mechanism: Because His1 interacts more heavily with nearby residues or hydrophobic regions in the oxidized states, its protonation destabilizes off-pathway contacts and exposes the polar Met(O) sidechain further to the solvent (SASA increases up to 110.2 AA^2). This stabilizes the helical fold and boosts resistance to aggregation.

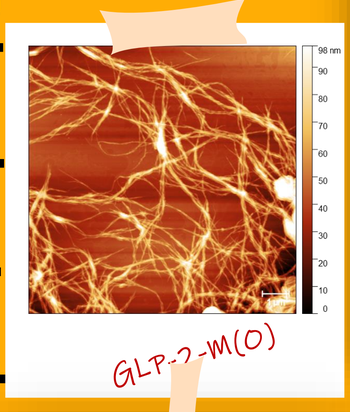
Protonating His1 (modeling pH < 6.5) affects the variants in the following ways:

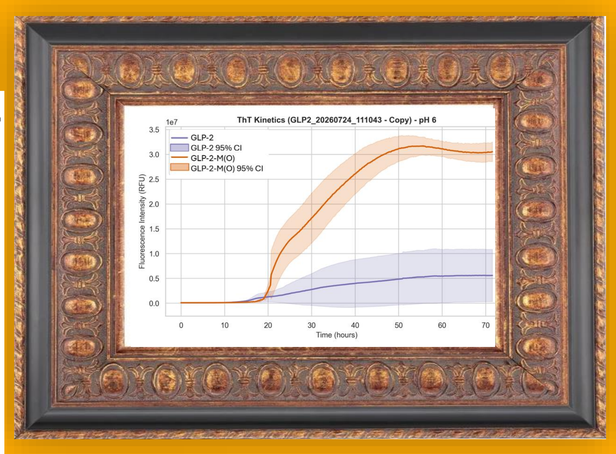
4 MOLECULAR DYNAMICS SIMULATIONS

pH 6

At pH 6 (~50% His protonation), GLP-2-Met(O) accelerates elongation ($k_{app} = 0.04\ h^{-1}$) and exhibits a ~4-fold higher ThT peak ($F_{max} = 3.19 \times 10^7$ vs. 8.32×10^6 RFU) than native GLP-2.
While native GLP-2 retains higher total β-sheet content (43% vs. 32%), AFM confirms that GLP-2-Met(O) uniquely assembles into thick, multi-filament hierarchical cables (10–28 nm).



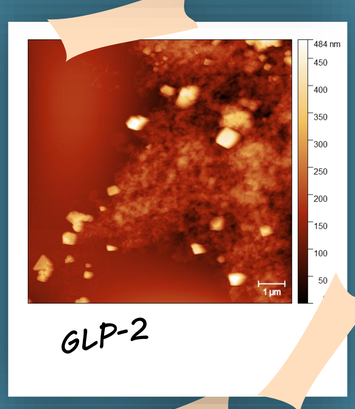


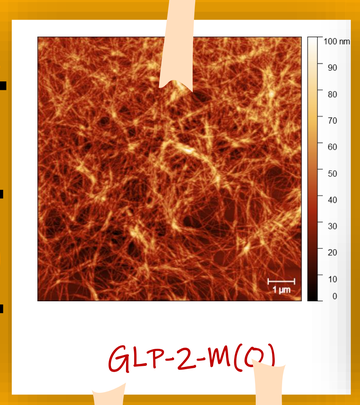


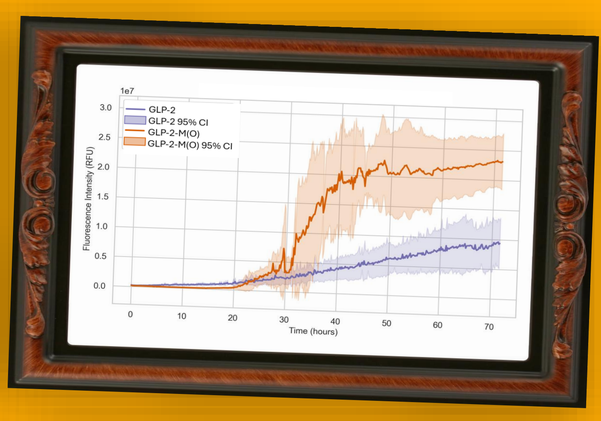
pH 4

At pH 4 (near pI = 3.9), native **GLP-2** undergoes immediate amorphous collapse into static, high β-sheet character (64% at $t = 0$ h → 68% at 72 h), trapping it in unorganized aggregates (~2 nm).

In stark contrast, GLP-2-Met(O) avoids kinetic trapping, navigating a progressive structural evolution from 52% to 76% β-sheet.



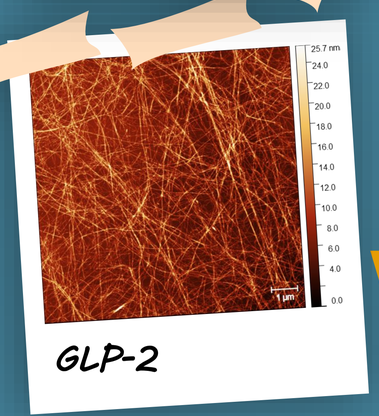


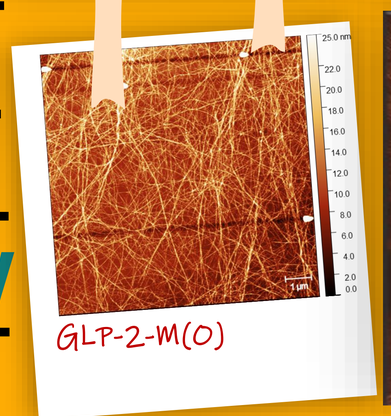


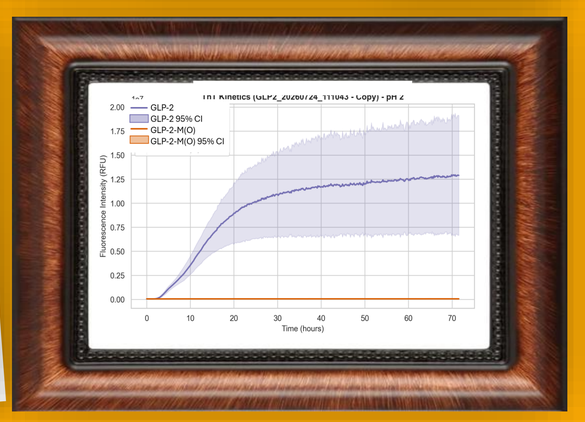
Data for pH 3, 5, and 7 are not presented on the poster.

pH 2

At pH 2, both variants assemble rapidly ($t_{lag} = 0$ h) into β-sheet-rich mature fibrillar networks over 72 h (60% β-sheet, 2.5–10 nm for GLP-2; 52% β-sheet, 3–6 nm for GLP-2-Met(O)). Notably, GLP-2-Met(O) exhibits a ~200-fold quenching in peak ThT fluorescence relative to native GLP-2.



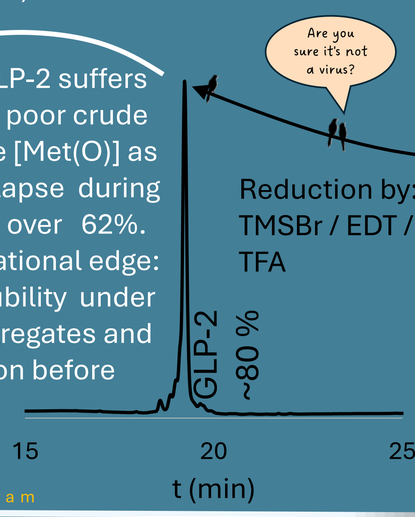


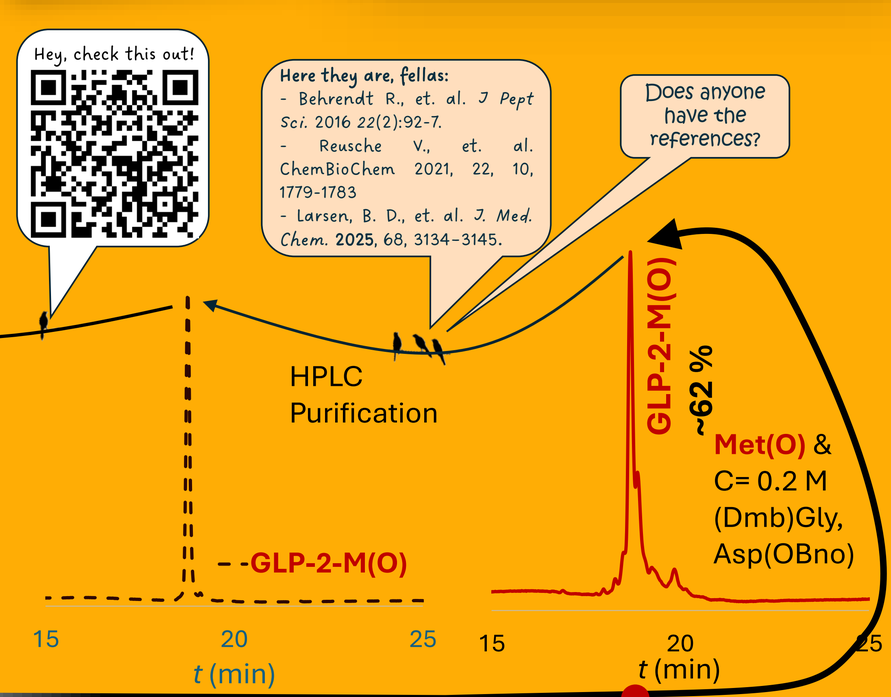


3

To compare native GLP-2 and its **methionine sulfoxide** variant [**GLP-2-Met(O)**], we integrated a multi-technique biophysical platform combining Far-UV circular dichroism (CD), Thioflavin T (ThT) fluorescence kinetics, and atomic force microscopy (AFM) across a broad pH gradient (pH 2–7):

Automated solid-phase peptide synthesis of GLP-2 suffers from severe interchain aggregation, resulting in poor crude purity (~19%). Introducing methionine sulfoxide [Met(O)] as a reversible handle disrupts hydrophobic collapse during chain elongation, boosting crude purity to over 62%. Beyond purity, Met(O) provides a decisive operational edge: it dramatically improves crude peptide solubility under identical conditions, eliminating insoluble aggregates and enabling seamless preparative HPLC purification before reduction back to native GLP-2.





methionine sulfoxide improves crude purity, as seen in the red chromatogram

HAARDFINWILLIQTKITD

Integrating semiconducting organic polymers with biological systems

Chao Lyu[1], Bob Schroeder[1*], Alethea Tabor[1*]

[1]Department of Chemistry, University College London, London, WC1H 0AJ, UK

https://doi.org/10.17952/38EPS.2026.P557

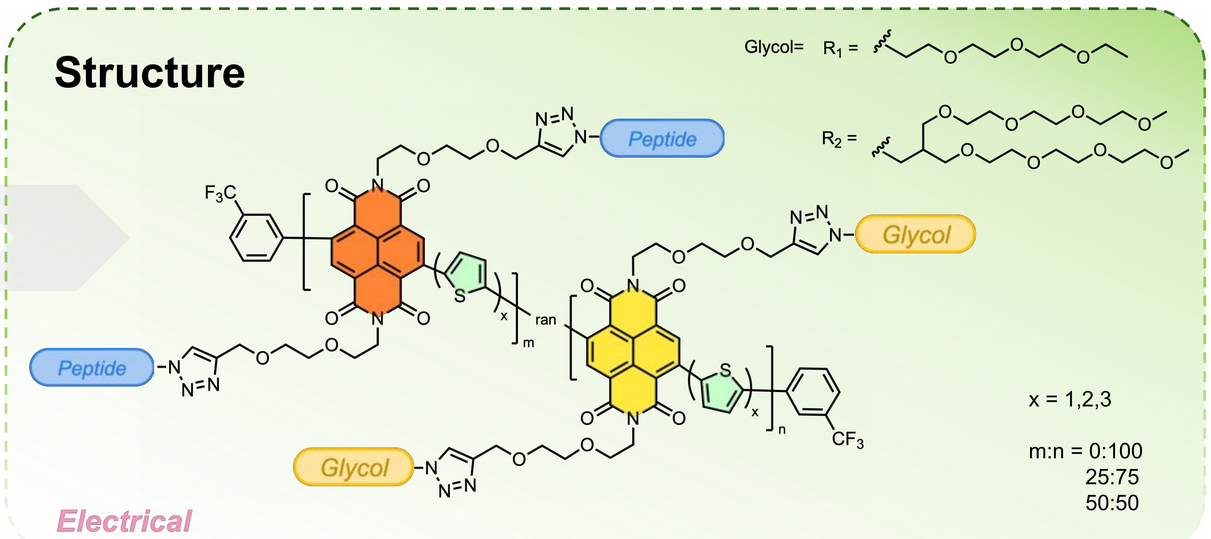
Introduction

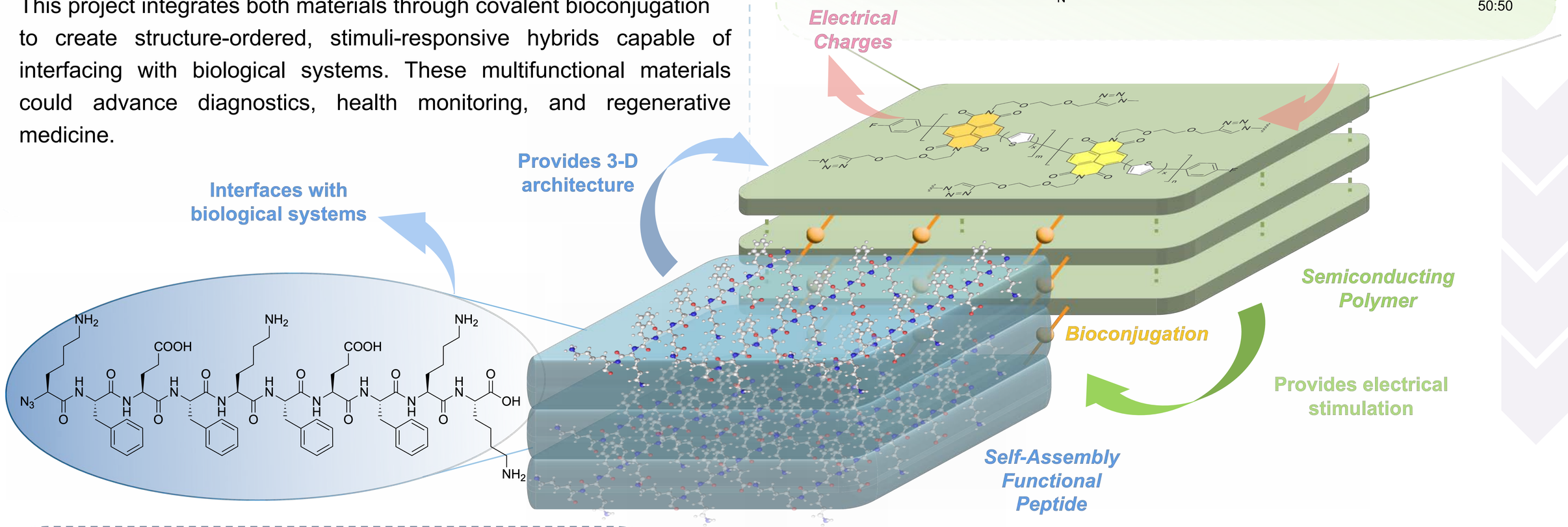
Semiconducting organic polymers

- ***Advantages****:* Good electronic performance, flexibility, tunability, and solution-processability
- ***Problems****:* Hydrophobicity, biological incompatibility, lack of control over 3-D architecture.
- ***Solutions:*** Introduce biocompatible components – peptides, which provide structural support for the polymer chains to optimise the charge-transport properties and give the option for the introduction of additional functionalities.

This project integrates both materials through covalent bioconjugation to create structure-ordered, stimuli-responsive hybrids capable of interfacing with biological systems. These multifunctional materials could advance diagnostics, health monitoring, and regenerative medicine.

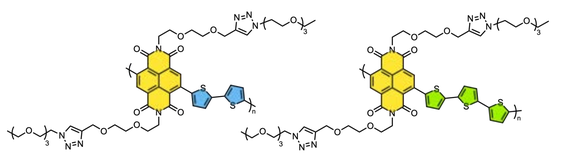
Structure

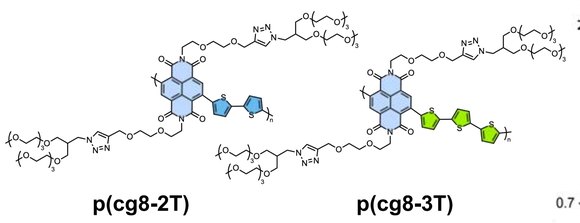




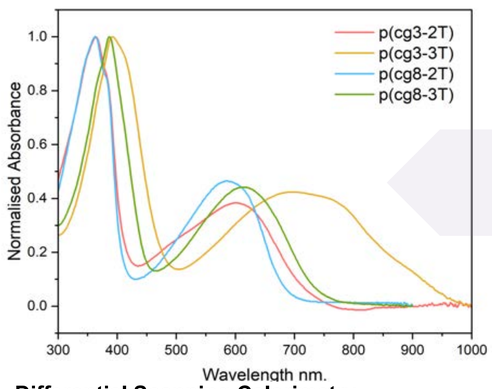
Reference Polymer Characterisation

Reference Polymer Structures

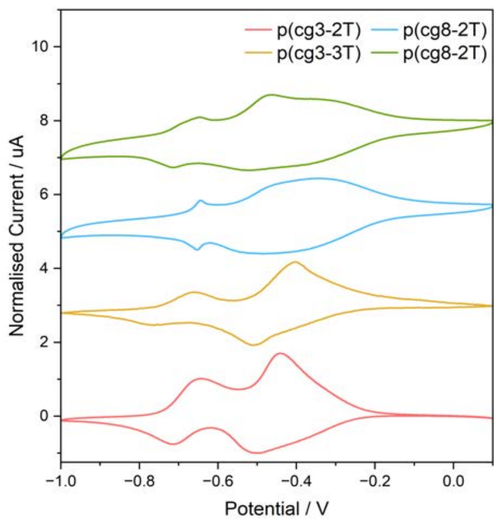




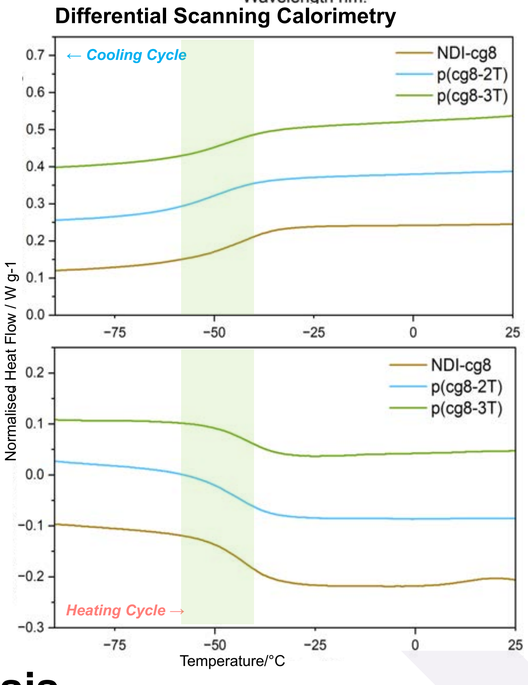
UV-Vis



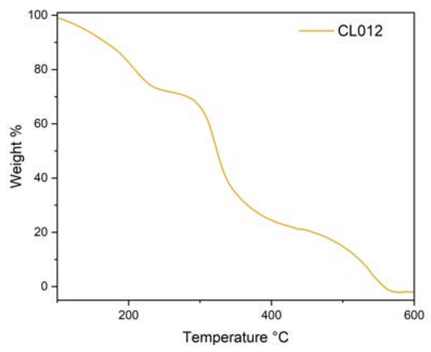
Cyclic Voltammetry



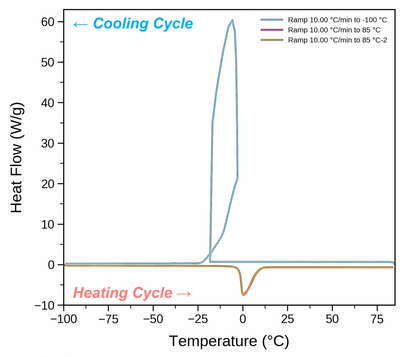
Differential Scanning Calorimetry



Peptide Thermal Analysis



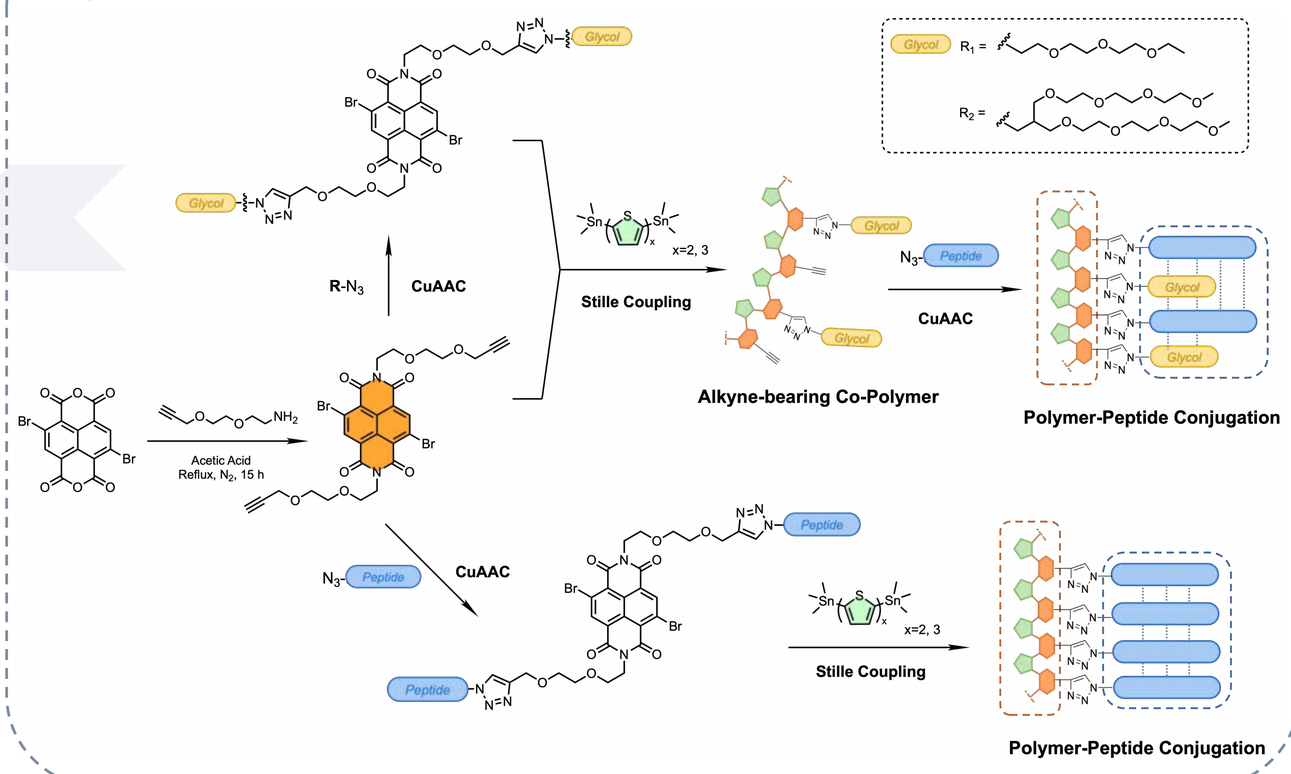
Thermogravimetric Analysis of Peptide Powder



Differential scanning calorimetry of Peptide Hydrogel



Synthesis Scheme



Conclusion

NDI-based reference polymers and copolymers were successfully synthesised and characterised, establishing a versatile synthetic platform for subsequent peptide conjugation. The use of different side-chain architectures also provides a basis for tuning polymer solubility, aggregation, and intermolecular interactions.

Ongoing peptide functionalisation will enable the influence of peptide incorporation on polymer organisation, self-assembly, and charge-transport properties to be investigated. This work therefore provides a foundation for developing peptide–polymer hybrid materials that combine the electronic properties of conjugated polymers with the structural and functional versatility of peptides, with potential applications in bioelectronics.

Reference

1. M. Al Kobaisi, S. V. Bhosale, K. Latham, A. M. Raynor, and S. V. Bhosale, *Chem. Rev.,* 2016, **116**, 11685-11796
2. J. K. Wychowaniec, A. M. Smith, C. Ligorio, O. O. Mykhaylyk, A. F. Miller, A. Saiani, *Biomacromolecules*, 2020, **21**, 2285-2297

chao.lyu.20@ucl.ac.uk

P-344 New Positive Allosteric Modulators for μ Opioid Receptor from Oxytocin

Takaaki Mizuguchi[1], Kanako Miyano[2,3], Ami Yamazaki[1,3], Hideki Takahashi[1,3], Risa Yamauchi[1], Yuki Yoshida[3,4], Haruka Ono[1,3], Miku Inagaki[1,3], Miki Nonaka[3,5], Yasuhito Uezono[3,5], Hideaki Fujii[1]

[1]Laboratory of Medicinal Chemistry, School of Pharmacy, Kitasato University, Tokyo, Japan.
[2]Laboratory of Pharmacotherapeutics, Faculty of Pharmacy, Juntendo University, Chiba, Japan.
[3]Division of Cancer Pathophysiology, National Cancer Center Research Institute, Tokyo, Japan.
[4]Laboratory of Molecular Pathology and Metabolic Disease, Faculty of Pharmaceutical Sciences, Tokyo University of Science, Tokyo, Japan.
[5]Department of Pain Control Research, The Jikei University School of Medicine, Tokyo, Japan.

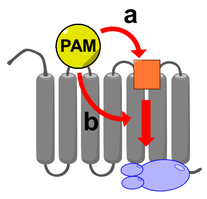
https://doi.org/10.17952/38EPS.2026.P344

Introduction

Positive allosteric modulators (PAMs) of G protein-coupled receptors (GPCRs) can increase the receptor signaling, the affinity of their orthosteric agonists, or both. Because PAMs can enhance the activity of an endogenous agonist which is not only secreted at an appropriate time and at a required part in our body but is also immediately metabolized, this class of modulators is expected to have fewer side effects than exogeneous orthosteric agonists. Therefore, PAMs are expected to have therapeutic advantages for the development of novel drug candidates. To date, **our group reported the first direct evidence that oxytocin (OT) functions as a PAM, but not an ago-PAM, toward the μ opioid receptor (MOR)**, which was a member of GPCR superfamily and a main target molecule of clinically used opioid analgesics. We also reported that **OT functions as a PAM at the κ opioid receptor** but not δ opioid receptor in the G protein signaling pathway[1]. Therefore, OT is expected to be a useful peptide to develop novel analgesic adjuvants. Our structure-activity relationship study of OT disclosed that the cyclic structure with an intramolecular disulfide bridge of OT was essential to exhibit the MOR-PAM activity as shown below. In addition, we found that the small Gly residue at the *C*-terminal would be a particularly critical structure for the MOR-PAM activity. **In this study, we attempted to identify side-chains of OT responsible for the MOR-PAM activity by using various OT mono-substituted analogs**. Their PAM activities for MOR agonistic activity induced by endmorphin-1 (EM-1) was evaluated by an electrical impedance-based receptor biosensor assay with CellKey™ system (label-free assay) using cells stably expressing human MOR[2].

1) Miyano, K., Uezono, Y. *et al. Cells* **2021**, *10*, 2651.
2) Miyano, K., Uezono, Y. *et al. J. Pharmacol. Sci.* **2014**, *126*, 302–309.

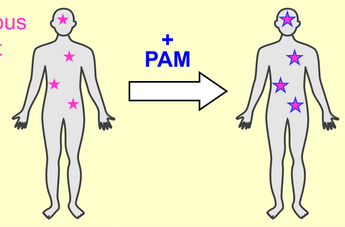
Positive allosteric modulator (PAM) of GPCRs[3]



Orthosteric agonist
a) **Binding affinity** ↑
b) **Efficacy** ↑

Signaling↑

【Merits of PAM versus synthetic agonist】

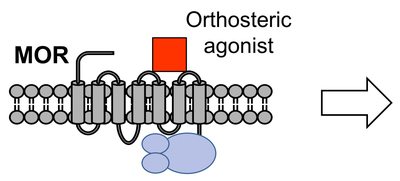


	Site of Action	During of Action
Endogenous Agonist	Localized	Transient
Exogenous Agonist	Widespread	Sustained
Endogenous Agonist + PAM	Localized	Transient

3) Burford, N. T., Alt, A. *et al.*, *Br. J. Pharmacol.*, **2015**, *172*, 277–286.

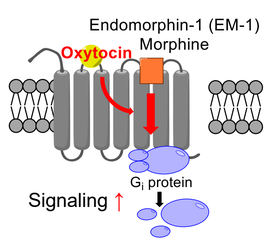
Oxytocin (OT) acts at μ opioid receptor (MOR) as a PAM[4].

μ opioid receptor (MOR) is the main target of clinically used opioid analgesics.

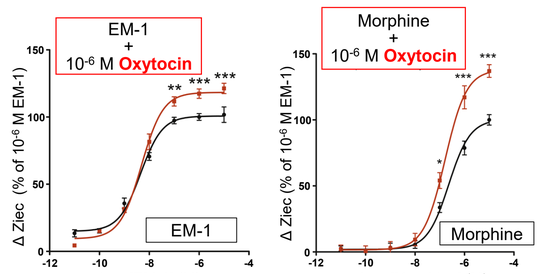


【Therapeutic efficacy】
✓ **Analgesia**

【Adverse effects】
✓ Constipation
✓ Nausea and Vomiting
✓ Respiratory depression
✓ Dependence



Oxytocin is expected to be a promising lead compound to develop novel analgesic adjuvants.



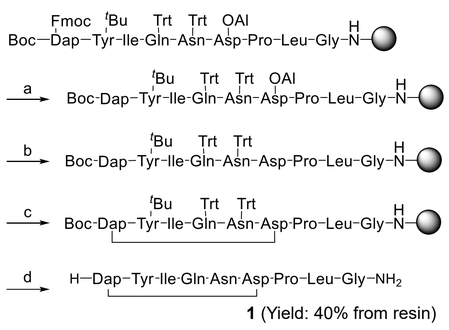
Concentration-response curves for opioid-induced ΔZiec in the absence and presence of 10^{-6} M oxytocin. All data are presented as means ± S.E.M. of 3–7 independent experiments (n = 9–21), *P < 0.05, **P < 0.01, ***P < 0.001, compared to each opioid treatment alone.

4) Meguro, Y., Uezono, Y. *et al.*, *J. Pharmacol. Sci.*, **2018**, *137*, 67–75.

Our previous SAR study[5]

Analog 1 having an amide bridge instead of the disulfide linkage

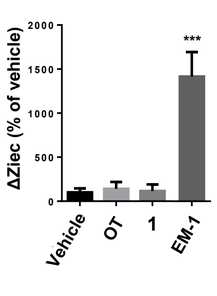
Synthesis of analog 1



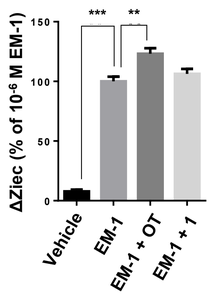
1 (Yield: 40% from resin)

Reagents and Conditions: a) 20% Piperidine/DMF, b) $Pd[P(C_6H_5)_3]_4$ (0.25 eq.), Phenylsilane (48 eq.), DCM, c) HATU (4 eq.), HOAt (4 eq.), DIPEA (8 eq.), DMF, d) TFA/TIS/H_2O (40:1:1, v/v)

MOR agonistic activity



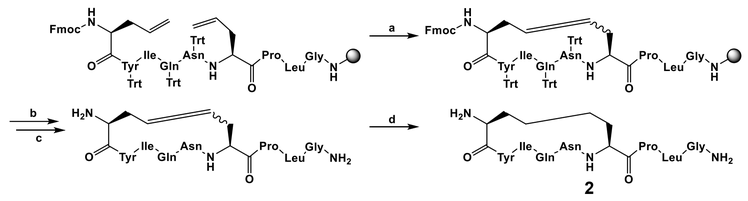
MOR-PAM activity



Flag-MOR-expressing HEK293 cells were treated with EM-1 and analog **1** at the concentration of 10^{-6} M. The data are presented as means ± S.E.M. of three to five independent experiments (n = 9–15). One-way ANOVA followed by Tukey's post hoc test. **, *** indicated $p < 0.01$, 0.001, respectively.

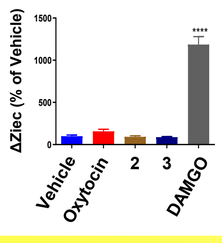
The intramolecular disulfide bridge of OT was a key structure to exert the MOR-PAM activity.

Analog 2 having an ethylene tether

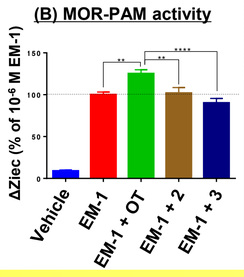


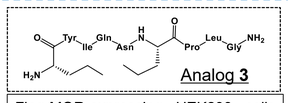
Reagents and Conditions: a) Hoveyda-Grubbs Catalyst® 2nd Generation, CH_2Cl_2, 40 °C, Ar, 12 h; b) 20% Piperidine/DMF; c) TFA, H_2O, TIS, 3 h; d) 10% Pd/C, H_2, MeOH, 20 h

(A) MOR agonistic activity



(B) MOR-PAM activity



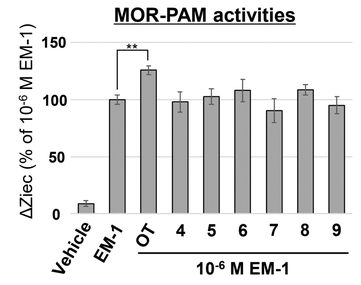


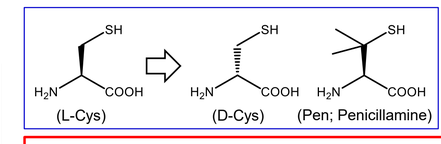
Flag-MOR-expressing HEK293 cells were treated with test analogs at the concentration of 10^{-6} M. The data are presented as means ± S.E.M. of three independent experiments (n = 6–10 and n = 12–15 in A and B, respectively). One-way ANOVA followed by Tukey's post hoc test. **, **** indicated $p < 0.01$, 0.001, respectively.

Configurational and sterical effects of cysteines

Analog	Amino-acid sequence	Yield
4	H-Cys-Gly-Ile-Gln-Asn-D-Cys-Pro-Leu-Gly-NH_2	25%
5	H-D-Cys-Tyr-Gly-Gln-Asn-Cys-Pro-Leu-Gly-NH_2	19%
6	H-D-Cys-Tyr-Ile-Gly-Asn-D-Cys-Pro-Leu-Gly-NH_2	16%
7	H-Pen-Tyr-Ile-Gln-Gly-Cys-Pro-Leu-Gly-NH_2	30%
8	H-Cys-Tyr-Ile-Gln-Asn-Pen-Gly-Leu-Gly-NH_2	25%
9	H-Pen-Tyr-Ile-Gln-Asn-Pro-Gly-Gly-NH_2	22%

MOR-PAM activities





Flag-MOR-expressing HEK293 cells were treated with test analogs at the concentration of 10^{-6} M. The data are presented as means ± S.E.M. of two independent experiments (n = 5), one-way ANOVA, followed by Tukey's post hoc test. ** indicated $p < 0.01$.

The configurations of two cysteine residues in OT presumably affect its PAM activity at the MOR. The sterically unhindered linker containing the disulfide bond would be necessary for exerting the MOR-PAM activity of OT.

5) Mizuguchi, T., Fujii, H. *et al.*, *Peptides* **2023**, *159*, 302–309.

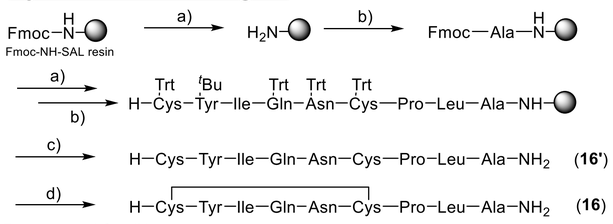
Results and Discussion

1. Investigation of responsible side-chains of oxytocin for MOR-PAM activity

List of analogs 10–24

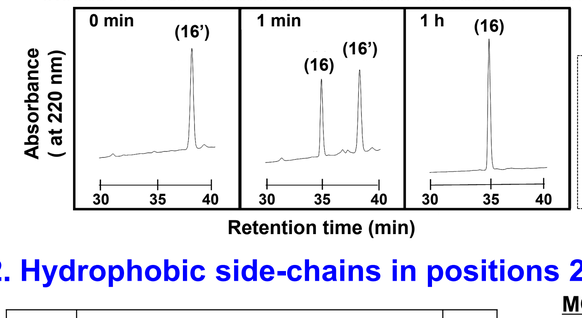
Analog	Amino-acid sequence	Yield
OT	H-Cys[1]-Tyr[2]-Ile[3]-Gln[4]-Asn[5]-Cys[6]-Pro[7]-Leu[8]-Gly[9]-NH_2	38%
10	H-Cys-Ala-Ile-Gln-Asn-Cys-Pro-Leu-Gly-NH_2	26%
11	H-Cys-Tyr-Ala-Gln-Asn-Cys-Pro-Leu-Gly-NH_2	37%
12	H-Cys-Tyr-Ile-Ala-Asn-Cys-Pro-Leu-Gly-NH_2	37%
13	H-Cys-Tyr-Ile-Gln-Ala-Cys-Pro-Leu-Gly-NH_2	25%
14	H-Cys-Tyr-Ile-Gln-Asn-Cys-Ala-Leu-Gly-NH_2	50%
15	H-Cys-Tyr-Ile-Gln-Asn-Cys-Pro-Ala-Gly-NH_2	36%
16	H-Cys-Tyr-Ile-Gln-Asn-Cys-Pro-Leu-Ala-NH_2	34%
17	H-Cys-Tyr-Ile-Gln-Asn-Cys-Pro-Leu-Gly-OH	30%
18	Ac-Cys-Tyr-Ile-Gln-Asn-Cys-Pro-Leu-Ala-NH_2	23%
19	H-Cys-Gly-Ile-Gln-Asn-Cys-Pro-Leu-Gly-NH_2	17%
20	H-Cys-Tyr-Gly-Gln-Asn-Cys-Pro-Leu-Gly-NH_2	39%
21	H-Cys-Tyr-Ile-Gly-Asn-Cys-Pro-Leu-Gly-NH_2	27%
22	H-Cys-Tyr-Ile-Gln-Gly-Cys-Pro-Leu-Gly-NH_2	54%
23	H-Cys-Tyr-Ile-Gln-Asn-Cys-Gly-Leu-Gly-NH_2	31%
24	H-Cys-Tyr-Ile-Gln-Asn-Cys-Pro-Gly-Gly-NH_2	38%

Synthesis of analog 16



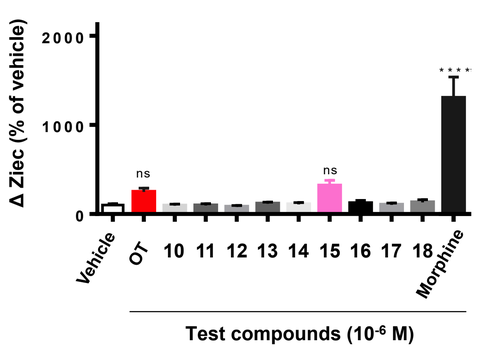
Reagents and Conditions:
a) 20% piperidine/DMF, b) Fmoc-AA-OH (3 eq.), DIPCDI (3 eq.), HOBt·H_2O (3 eq.), DMF, c) TFA/TIS/EDT/H_2O (40:1:1:1, v/v) , d) 0.1 M NH_4HCO_3 aq. (pH ~8.0)

*<Oxidative intramolecular disulfide bond formation in analog **16**>*



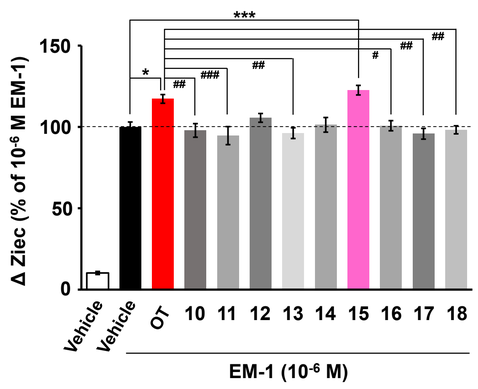
The cyclization reaction was monitored by analytical HPLC [$5C_{18}$-AR-II (4.6 mm I.D. × 150 mm); solvent, 0.1% TFA/CH_3CN-H_2O (gradient from 5:95 to 25:75 over a period of 40 min) at a flow rate of 1.0 mL/min, detected at 220 nm].

MOR agonistic activities of 10–18



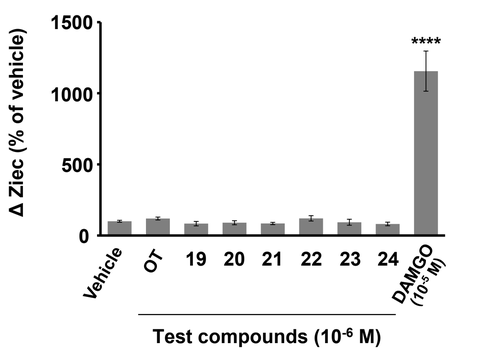
Flag-MOR-expressing HEK293 cells were treated with test analogs at the concentration of 10^{-6} M. The data are presented as means ± S.E.M. of three independent experiments (n = 9), One-way ANOVA followed by Tukey's multiple-comparison test. ****$p < 0.0001$ vs. vehicle alone. ns: not significant.

MOR-PAM activities of 10–18



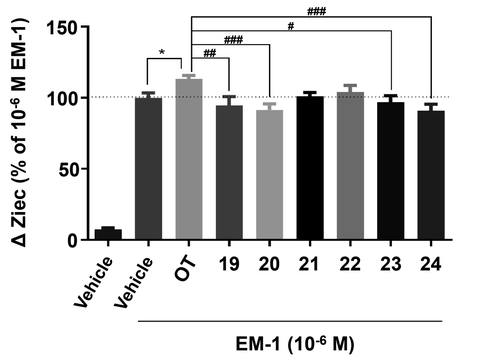
The data are presented as the means ± S.E.M. of three independent experiments (n = 9). One-way ANOVA followed by Tukey's multiple-comparison test. *$p < 0.05$, ***$p < 0.001$ vs. EM-1; #$p < 0.05$, ##$p < 0.01$, ###$p < 0.001$ vs. EM-1 + OT.

MOR agonistic activities of 19–24



The data are presented as means ± S.E.M. of three independent experiments (n = 9–13), One-way ANOVA followed by Bonferroni's multiple comparison test, ****$p < 0.0001$ vs. vehicle alone.

MOR-PAM activities of 19–24



The data are presented as means ± S.E.M. of three independent experiments (n = 6–7), One-way ANOVA followed by Bonferroni's multiple comparison test. *$p < 0.05$ vs. EM-1; #$p < 0.05$, ##$p < 0.01$, ###$p < 0.001$ vs. EM-1 + OT.

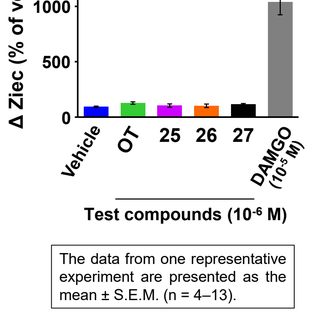
The assay results of analogs **10**–**15** and **19**–**24** indicated that side-chains of Tyr^2, Ile^3, Gln^4, Asn^5, and Pro^7 would be necessary for the MOR-PAM effect of OT. The results of analogs **17** and **18** suggested that the charge states of both termini of OT may contribute to its MOR-PAM effect. The results of analogs **16** supported the importance of Gly in position 9 for the MOR-PAM activity of OT.

2. Hydrophobic side-chains in positions 2 and 8

Analog	Amino-acid sequence	Yield
25	H-Cys-Phe-Ile-Gln-Asn-Cys-Pro-Leu-Gly-NH_2	17%
26	H-Cys-Tyr-Ile-Gln-Asn-Cys-Pro-Phe-Gly-NH_2	39%
27	H-Cys-Tyr-Ile-Gln-Asn-Cys-Pro-Cha-Gly-NH_2	27%

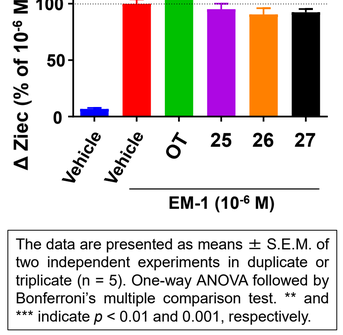
Small-sized hydrophobic amino acids in the range from Ala to Leu would be suitable for position 8 of OT. In addition, the phenolic hydroxy group of Tyr in position 2 may play a role in exerting the MOR-PAM activity.

MOR agonistic activities



The data from one representative experiment are presented as the mean ± S.E.M. (n = 4–13).

MOR-PAM activities

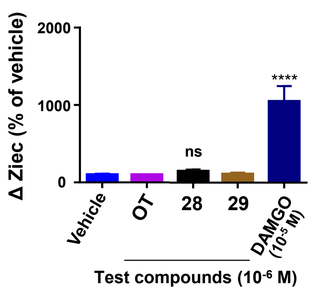


The data are presented as means ± S.E.M. of two independent experiments in duplicate or triplicate (n = 5). One-way ANOVA followed by Bonferroni's multiple comparison test. ** and *** indicate $p < 0.01$ and 0.001, respectively.

3. MOR-PAM activities of oxypressin and vasotocin

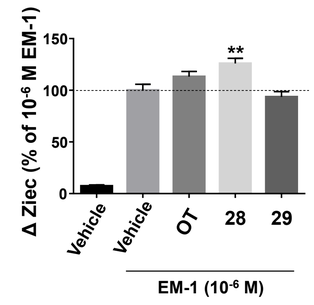
Analog	Amino-acid sequence	Yield
28 (Oxypressin)	H-Cys-Tyr-Phe-Gln-Asn-Cys-Pro-Leu-Gly-NH_2	43%
29 (Vasotocin)	H-Cys-Tyr-Ile-Gln-Asn-Cys-Pro-Arg-Gly-NH_2	39%

MOR agonistic activities



The data are presented as means ± S.E.M. of three independent experiments (n = 8–9), One-way ANOVA followed by Tukey's test. ****$p < 0.0001$ vs. vehicle. ns: not significant.

MOR-PAM activities



The data are presented as means ± S.E.M. of three independent experiments (n = 9), One-way ANOVA followed by Tukey's test. **$p < 0.01$ vs. vehicle + EM-1.

These findings suggest that the size of the hydrophobic moiety at position 3 of OT would be a critical determinant of MOR-PAM activity.

4. Concentration-dependent MOR-PAM activity

The data are presented as means ± S.E.M. of three independent experiments (n = 6–15). One-way ANOVA followed by Dunnet's test. ***P < 0.005 vs. EM-1.

Analog **15** possessing Ala instead of Leu in the position 8 concentration-dependently showed almost comparable MOR-PAM activity to OT.

Conclusion

In this study, we synthesized and evaluated various OT analogs to identify side-chains of OT responsible for the MOR-PAM activity. Among analogs **10**–**16** and **19**–**24**, only analog **15** containing Ala instead of Leu in position 8 exhibited the MOR-PAM activity. These results suggested that other side-chains of Tyr^2, Ile^3, Gln^4, Asn^5, and Pro^7 would be necessary for the PAM effect of OT. On the other hand, analogs **24**, **26** and **27** containing Gly, Phe and Cha, respectively, in the position 8 did not enhance the agonistic activity of EM-1 for the MOR. Therefore, small-sized hydrophobic amino acids in the range from Ala to Leu would be suitable for the position 8. In addition, the results of analogs **17** and **18** indicated that the uncharged *C*-terminal amide and the positively charged *N*-terminal primary amine of OT under physiological conditions are likely to contribute to the MOR-PAM activity. Furthermore, we found that analog **28** having Phe instead of Ile in position 3 exerted the MOR-PAM activity approximately at the same level as OT. This result indicated that hydrophobicity in position 3 of OT would also play an important role in the MOR-PAM activity. Analogs **15** and **28** are clearly new peptide MOR-PAMs identified following OT.

Acknowledgement

This work was supported by JSPS KAKENHI Grant Numbers JP21K06460 (T.M.), JP20K07750 (K.M.) and JP21K06584 (Y.U.).

We have no conflicts of interest with regard to the presentation.

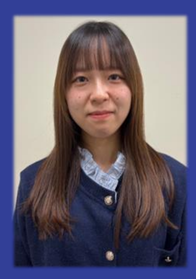
334

https://doi.org/10.17952/38EPS.2026.P334

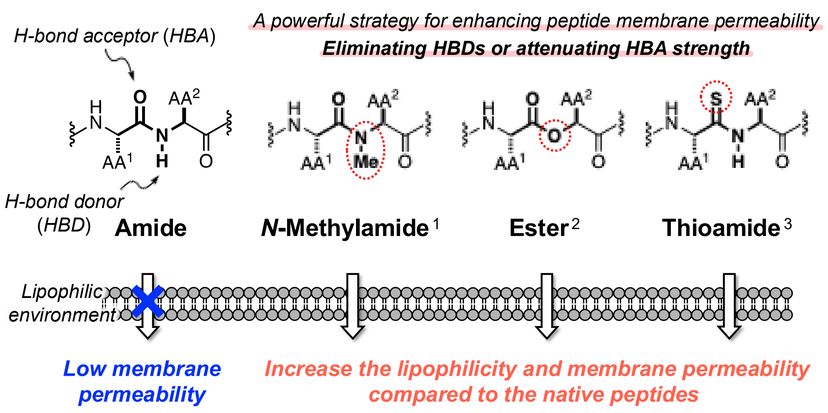
Amide-to-Chloroalkene Substitution as Peptide Backbone Modification for Enhancement of Membrane Permeability

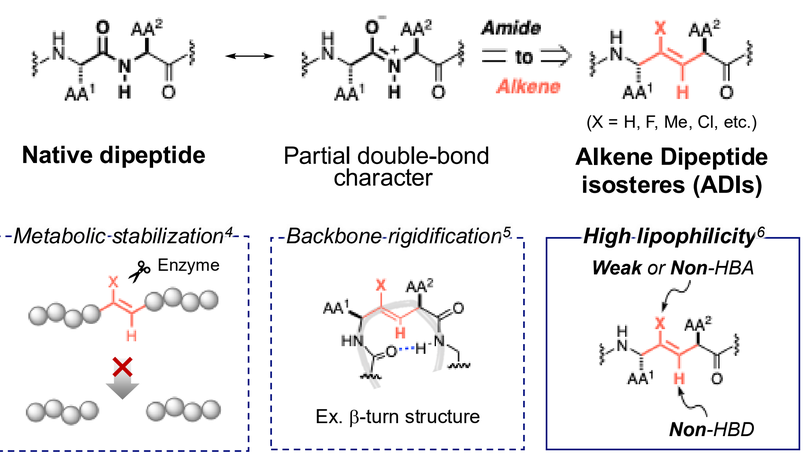
Sayuri Takeo[1†], Mio Takeda[2], Chihiro Iio[1], Ai Sakakibara[2], Showmitra Saha[3], Natsuki Shibata[3], Yuki Yamazaki[4], Takahiro Fujii[5], Ryuhei Harada[6], Kohei Sato[2,7,8], Nobuyuki Mase[2,7,8], Mizuki Watanabe[4], Takanori Oyoshi[3,8], Tetsuo Narumi [1,2,7,8]

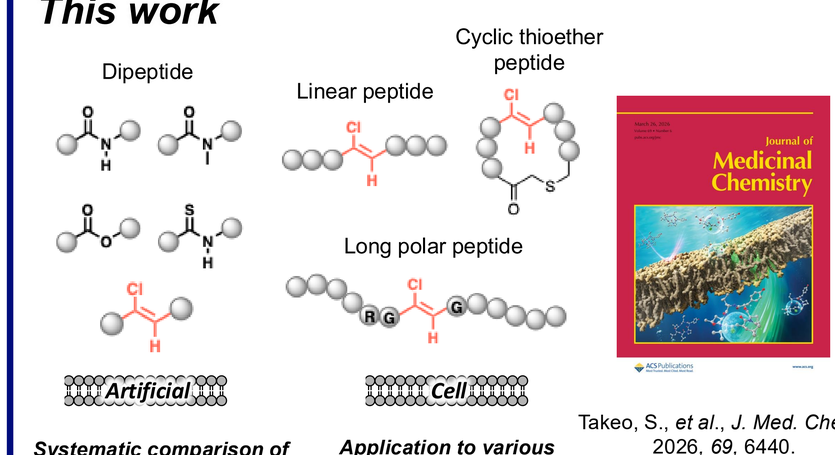
[1]Graduate School of Medical Photonics, Shizuoka University, [2]Department of Engineering, Graduate School of Integrated Science and Technology, Shizuoka University, [3]Department of Science, Graduate School of Integrated Science and Technology, Shizuoka University, [4]Faculty of Pharmaceutical Sciences, Hokkaido University, [5]College of Biological Sciences, University of Tsukuba, [6]Center for Computational Sciences, University of Tsukuba, [7]Department of Applied Chemistry and Biochemical Engineering, Faculty of Engineering, Shizuoka University, [8]Research Institute of Green Science and Technology, Shizuoka University, [†]Current address: Faculty of Pharmaceutical Sciences, Kobe Gakuin University



Introduction







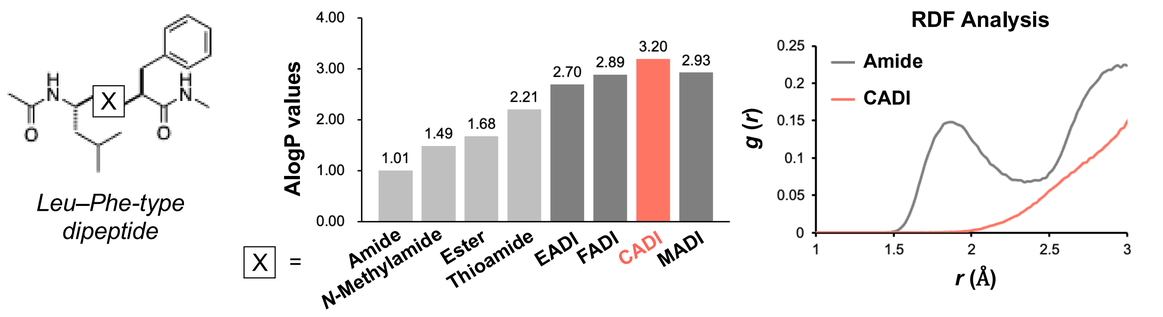
Takeo, S., *et al.*, *J. Med. Chem.* 2026, *69*, 6440.

[1] White T. R., *et al.*, *Nat. Chem. Biol.* **2011**, *7*, 810. [2] Hosono, Y., *et al.*, *Nat. Commun.* **2023**, *14*, 1416. [3] Ghosh, P., *et al.*, *Nat. Commun.* **2023**, *14*, 6050.

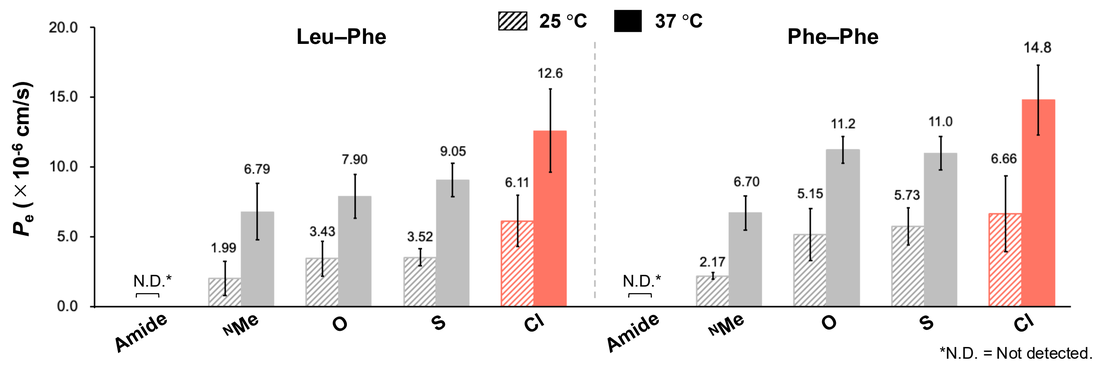
[4] Altman, R. A., *et al.*, *ACS Chem. Neurosci.* **2018**, *9*, 1735. [5] (a) Wipf, P., *et al.*, *J. Org. Chem.* **1998**, *63*, 6088. (b) Kodama, Y., *et al.*, *J. Org. Chem.* **2022**, *87*, 2167. (c) Takeo, S., *et al.*, *J. Org. Chem.* **2026**, *91*, 8588. [6] Takeo, S., *et al.*, *J. Med. Chem.* 2026, *69*, 6440.

■ *Artificial membrane permeability of dipeptide mimics*

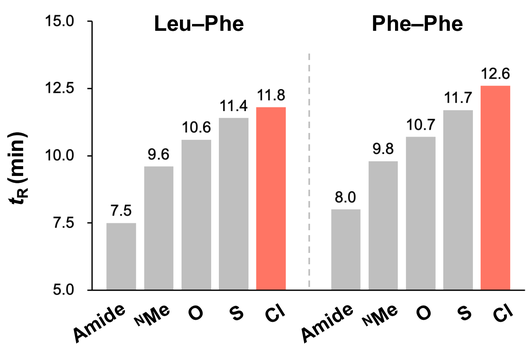
Mechanistic analyses combining AlogP calculations and molecular dynamics simulations



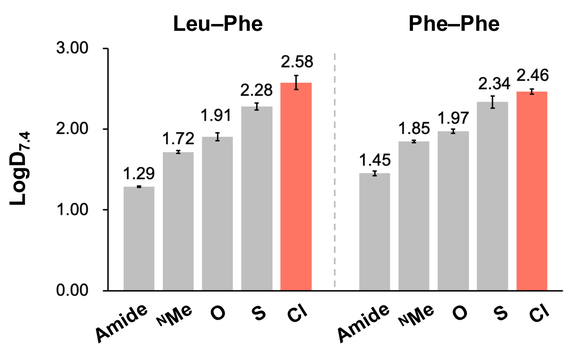
Passive permeability using PAMPA[7]



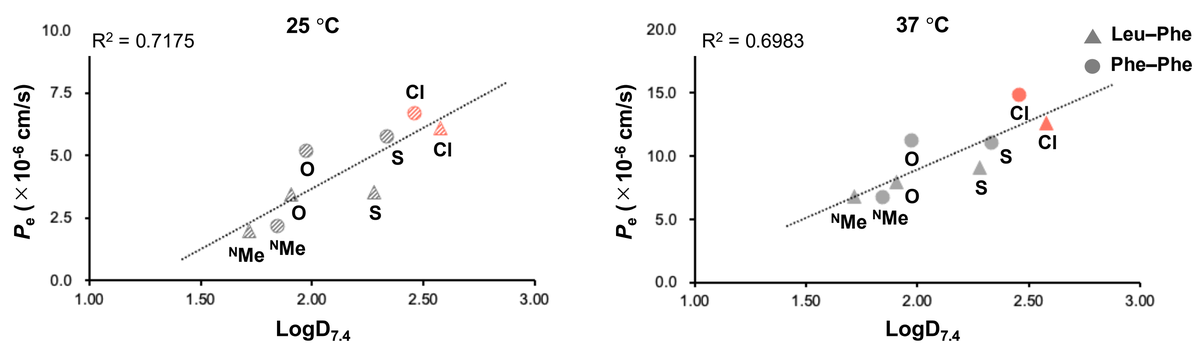
HPLC retention time in C18 column



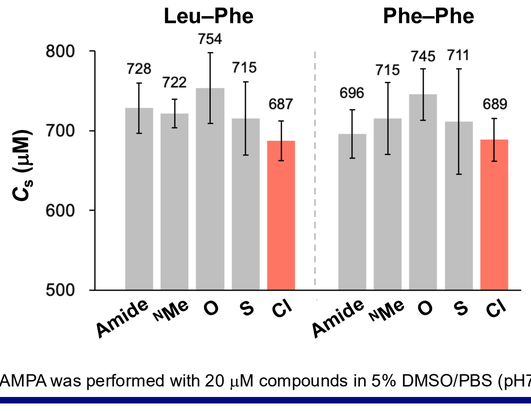
$LogD_{7.4}$ values



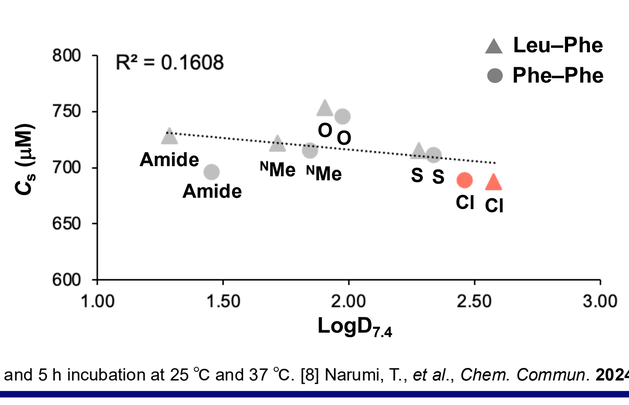
Linear correlation plot of P_e (PAMPA) vs.$logD_{7.4}$



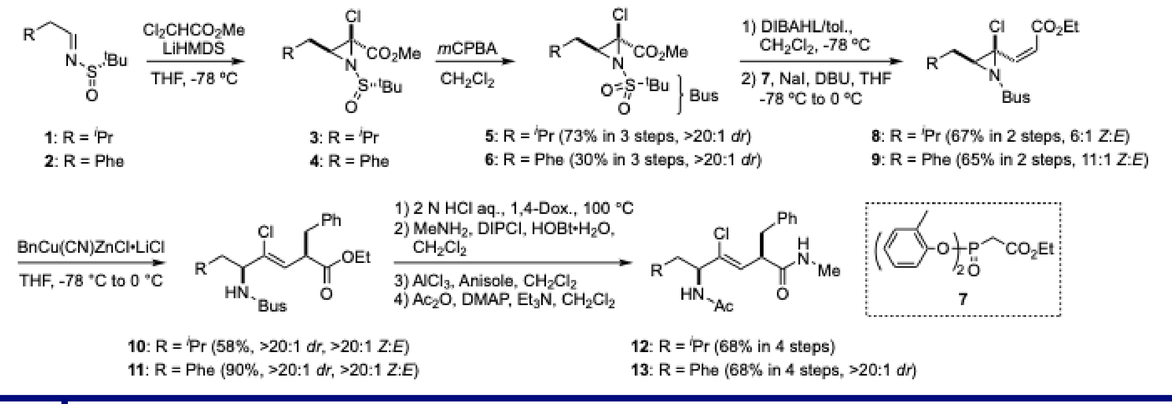
Aqueous solubility of dipeptide mimics



Linear correlation of solubility vs. $logD_{7.4}$



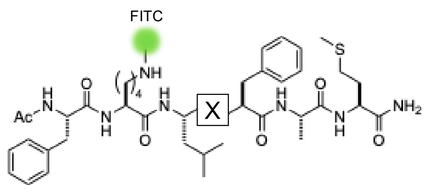
Synthesis of the CADI mimic of Ac-L-Leu-L-Phe-NHMe and Ac-L-Phe-L-Phe-NHMe[8]



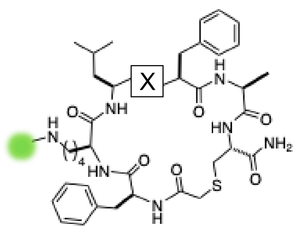
[7] PAMPA was performed with 20 μM compounds in 5% DMSO/PBS (pH7.4) and 5 h incubation at 25 ℃ and 37 ℃. [8] Narumi, T., *et al.*, *Chem. Commun.* **2024**, *60*, 3563.

■ *Cell membrane permeability of the hexapeptide mimics*[9]

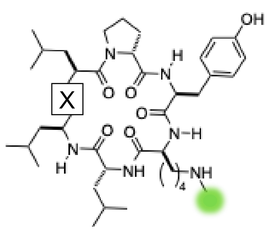
Linear hexapeptide **14**

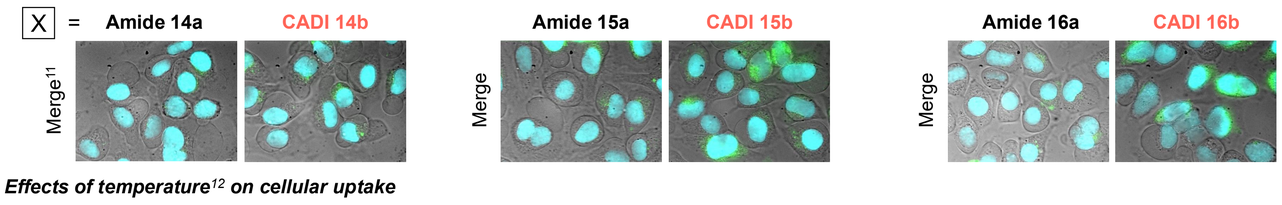


Cyclic thioether hexapeptide **15**

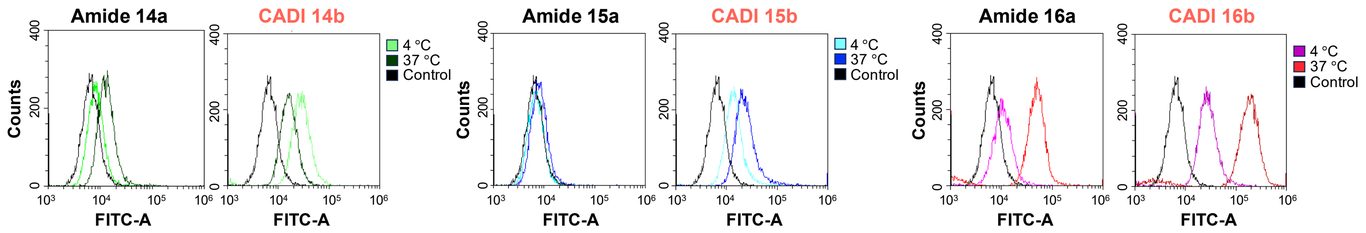


Cyclic hexapeptide[10] **16**

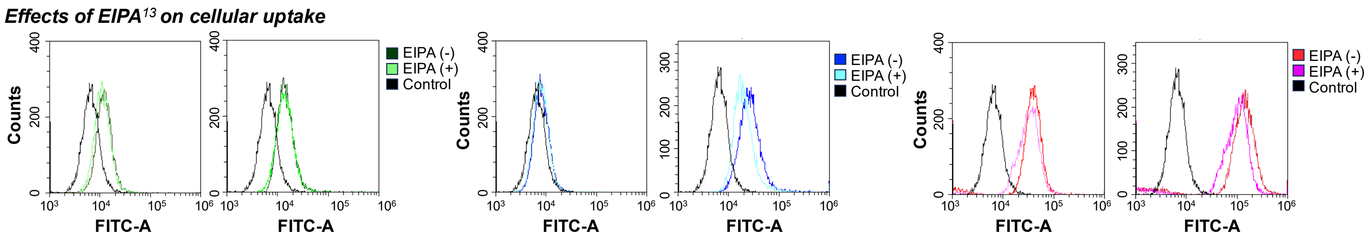




Effects of temperature[12] on cellular uptake

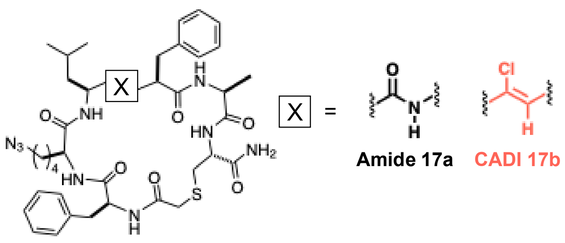


Effects of EIPA[13] on cellular uptake

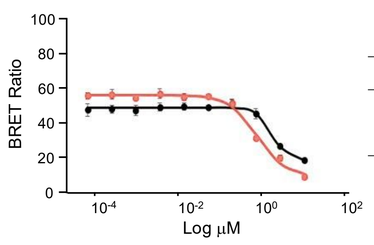


CADI-enhanced uptake mainly occurs via an energy-dependent endocytic pathway.

Quantitatively compare the membrane permeability



Concentration response curves obtained from the NanoClick assay

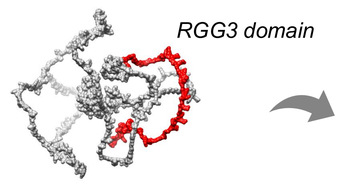


Comp.	EC_{50}
Amide 17a	1.85 ± 0.21 μM
CADI 17b	0.67 ± 0.04 μM

CADI enhances cytosolic delivery by 2.8-fold.

[9] Cell: Hela, Hoechst 0.5 μg/ml for 5 min at 37 °C. [10] Rezai, T., *et al.*, *J. Am. Chem. Soc.* **2006**, *128*, 2510. [11] sample: 5 μM for 3 h at 37 °C. [12] sample: 5 μM for 1 h at 4 °C or 3 h at 37 °C. [13] Nakase, I., *et al.*, *Molecular Therapy* **2004**, *10*, 1011. EIPA: 100 μM for 30 min at 37 °C, sample: 5 μM for 30 min at 37 °C.

■ *Application of ADIs to G4-binding RGG peptides*[14]



STK5-1[15] (Amide-type) K_d = 1.47 μM

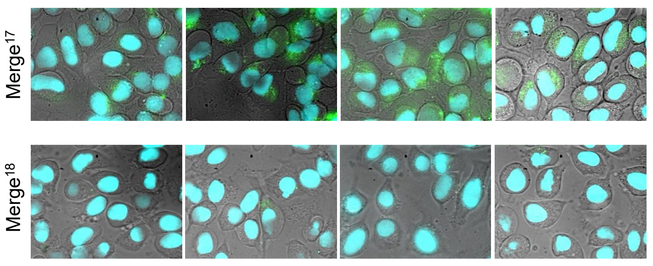
H-GDDRRGGRGGYDR-G-X-G-YRGRGGK

YTK-11 (CADI-type) K_d = 14.6 μM

RGG peptide **18**



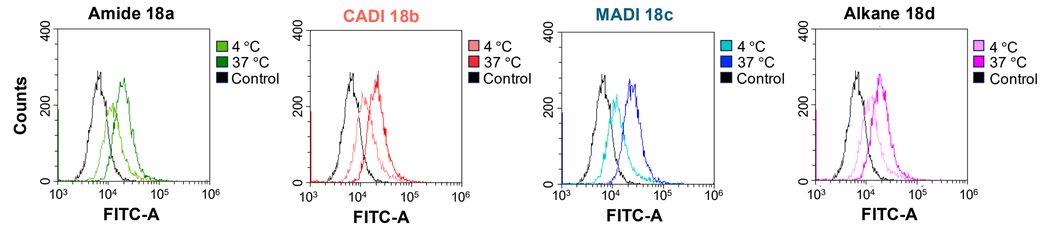
X = Amide 18a, CADI 18b, MADI 18c, Alkane 18d



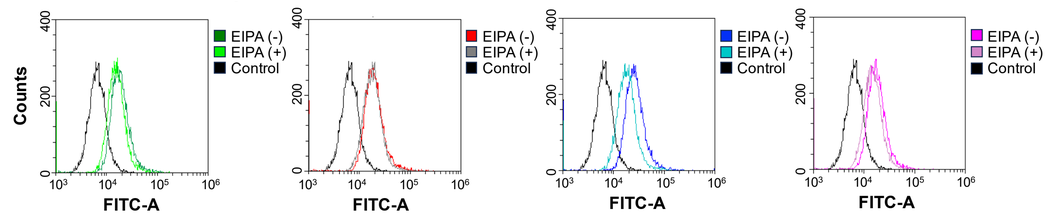
G4-binding affinity of RGG peptide mimics

	Binding constants: K_d (μM)		Selectivity Index (SI)
	G4 (TERRA)	Single strand	
18a	33 ± 2.7	52 ± 5.1	1.6
18b	36 ± 8.3	174 ± 41	**4.8**
18c	21 ± 2.0	133 ± 25	**6.3**
18d	> 500	162 ± 7.8	-

Effects of temperature[19] on cellular uptake



Effects of EIPA[20] on cellular uptake



Amide-to-alkene substitution in RGG peptides can enhance not only membrane permeability but also biologically relevant properties.

[14] Cell: Hela, Hoechst 0.5 μg/ml for 5 min at 37 °C. [15] Takeo, S., *et al.*, *Chem. Pharm. Bull.* **2025**, *73*, 938. [16] Nakase, I., *et al.*, *Molecular Therapy* **2004**, *10*, 1011. [17] sample: 5 μM for 3 h at 37 °C. [18] Cytochalasin D: 10 mM for 30 min, sample: 5 μM for 3 h at 37 °C. [19] sample: 5 μM for 1 h at 4 °C or for 3 h at 37 °C. [20] EIPA: 100 μM for 30 min at 37 °C, sample: 5 μM for 30 min at 37 °C.

Making new PALs: A Directed Evolution Platform for Rapid Peptide Asparaginyl Ligase Engineering

T. M. Simon Tang,*[a] James Leech,[a] Zihao Song,[b] Louis Y. P. Luk,[b] Jody M. Mason*[a]

[a] Department of Life Sciences, University of Bath, Claverton Down, Bath, BA2 7AY, United Kingdom

[b] School of Chemistry, Cardiff University, Park Place, Cardiff, CF10 3AT, United Kingdom

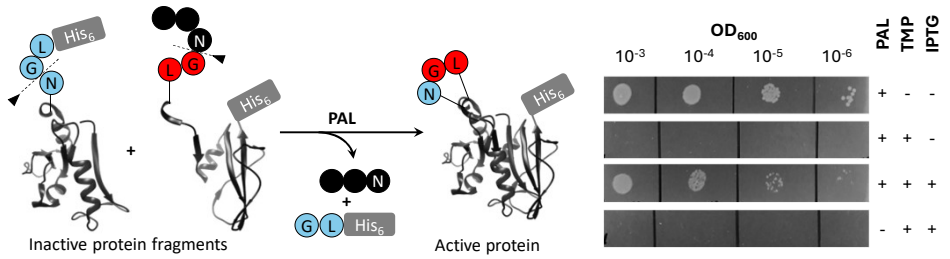
https://doi.org/10.17952/38EPS.2026.P401

Biotechnology and Biological Sciences Research Council

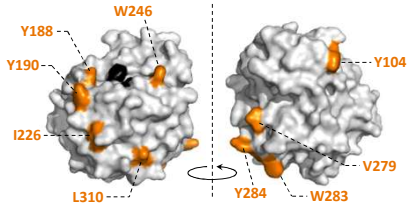
Introduction

- Peptide asaparaginyl ligases (PALs) are ultra-fast transpeptidases that catalyse peptide ligation and head-to-tail cyclisation.[1,2]
- Recombinant OaAEP1b and its engineered derivatives have been increasingly employed for protein and peptide conjugations across various applications.[3,4]
- Protein engineering is central to the development of enzymes into robust biocatalysts, but low mutant screening throughput present a major bottleneck.[5,6]

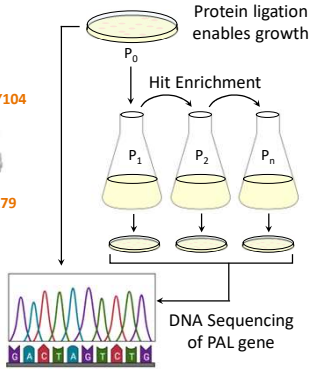
Split-protein reporter links ligase activity to bacterial growth



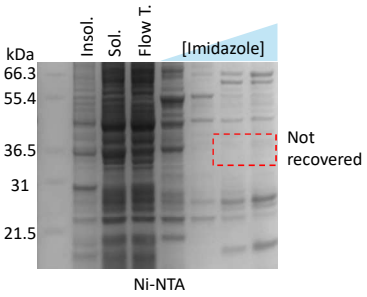
Growth-linked selection identifies s-PAL



Library Size: 589,824 variants

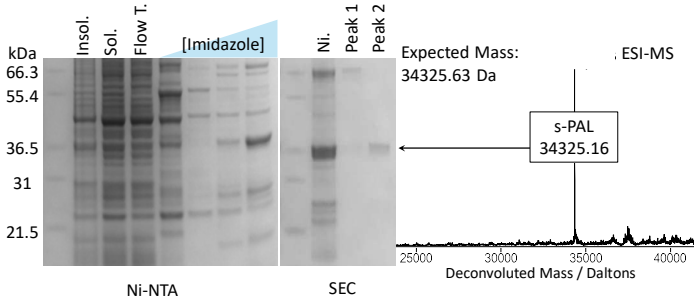


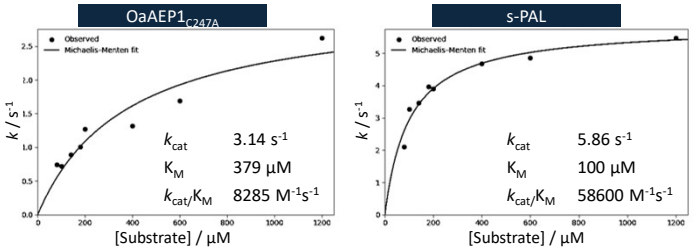
OaAEP1$_{C247A}$



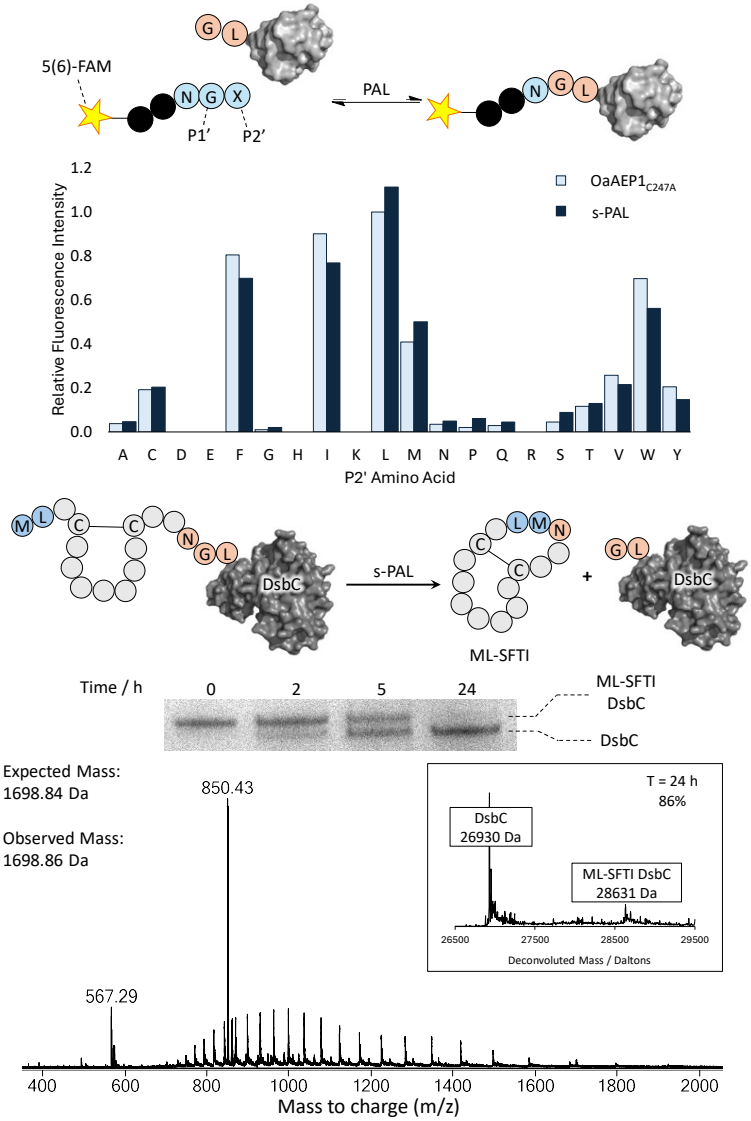
Pos	Amino Acid Options	OaAEP1$_{C247A}$	s-PAL
104	Y H N D	Y	N
188	Y H N D	Y	N
190	Y H N D	Y	N
226	I T N S	I	N
246	W S T R K *	W	W
279	V E K I	V	E
283	W S T R K *	W	K
284	Y H N D	Y	D
310	L Q E V	L	L

s-PAL





Applications to peptide ligation and cyclisation



Conclusion and next steps

- A growth-linked selection platform for rapid PAL engineering was established.
- s-PAL showed improved soluble recombinant protein purification, enhanced kinetics at pH 7.0 and comparable P2' substrate specificity to the parental OaAEP1$_{C247A}$.
- Semi-biosynthetic SFTI-1 analogue demonstrated application.
- Next-generation sequencing will be employed to further elucidate selection dynamics.
- Apply selection system to engineer PAL substrate specificity.

References

1. Nguyen, G. K. T.; Wang, S. J.; Qiu, Y. B.; Hemu, X.; Lian, Y. L. *et al.*, Butelase 1 is an Asx-specific ligase enabling peptide macrocyclization and synthesis. *Nat. Chem. Biol.* **2014**, 10, 732.
2. Tang, T. M. S.; Luk, L. Y. P. Asparaginyl endopeptidases: enzymology, applications and limitations. *Org. Biomol. Chem.* **2021**, 19, 5048
3. Tang, T. M. S.; Cardella, D.; Lander, A. J.; Li, X.; Escudero, J. S. *et al.*, Use of an asparaginyl endopeptidase for chemo-enzymatic peptide and protein labeling. *Chem. Sci.* **2020,** 11, 5881.
4. F. B. H. Rehm, T. J. Tyler, Y. Zhou, Y.-H. Huang, C. K. Wang, N. Lawrence, et al. Repurposing a plant peptide cyclase for targeted lysine acylation. *Nat. Chem.* **2024**, 16, 1481
5. X. Hemu, X. Zhang, H. Y. Chang, J. E. Poh and J. P. Tam, Consensus design and engineering of an efficient and high-yield peptide asparaginyl ligase for protein cyclization and ligation. *J. Biol. Chem.*, **2023,** 299, 102997
6. Y. Zhou, S. J. de Veer, T. J. Tyler, Y. Chen, T. Durek, D. J. Craik, et al. Asparaginyl Ligases with Engineered Substrate Specificity for Controlled, Sequential Transpeptidation Reactions. *J. Am. Chem. Soc.*, **2025,** 147, 21824

Self-assembly control with hydrophobicity gradients in short peptide sequences

Irene Toledo Alday[1,2], Natalia S. Baranova[2,3], Ivan R. Sasselli[1]

irene.toledo@csic.es

[1] *Materials Physics Center (CFM), CSIC-UPV/EHU, Donostia-San Sebastian, Spain*

[2] *Centro de Investigación Cooperativa en Biomateriales CICbiomaGUNE, Parque Científico y Tecnológico de Gipuzkoa, Donostia-San Sebastián, Spain*

[3] *Ikerbasque, Basque Foundation for Science, 48009 Bilbao, Spain*

Funded by the European Union

https://doi.org/10.17952/38EPS.2026.P438

MOTIVATION

We develop tunable biomaterials based on amphiphilic peptides that self-assemble into supramolecular peptide assemblies (**SPAs**) with potential applications in **tissue regeneration** and **drug delivery**[1,2]. However, the molecular mechanisms governing early aggregation events and their impact on final material properties remain poorly understood, limiting rational design. Here, we combine **fluorescence spectroscopy**, circular dichroism (**CD**), Fourier transform Infrared Spectroscopy (**FTIR)**, Atomic Force Microscopy (**AFM)**, and coarse-grained molecular dynamics (**CG-MD**) **simulations** to resolve self-assembly with enhanced molecular detail. We show that analyzed SPAs with different hydrophobic gradients form predominantly fibrous structures alongside other morphologies. Finally, we aim to incorporate positively charged peptides to provide antibacterial activity against pathogens such as *Pseudomonas aeruginosa* infection.

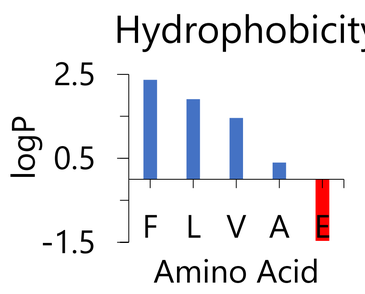
EXPERIMENTAL DEVELOPMENT

DESIGN

Hydrophobic Charged

$A_1\ A_2\ B_1\ B_2\ C_1\ C_2$ E E

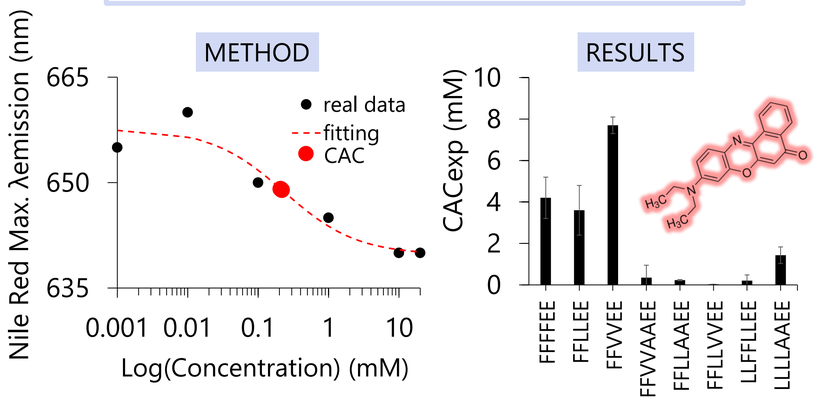
$A_1\ A_2\ B_1\ B_2$ E E



Design of the peptide amphiphiles analyzed with a hydrophobic gradient based on logP values

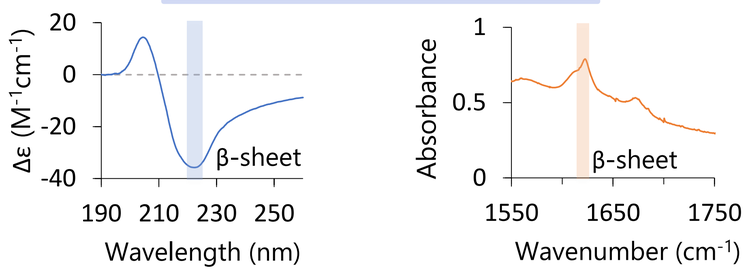
CHARACTERIZATION

Calculation of Critical Concentrations

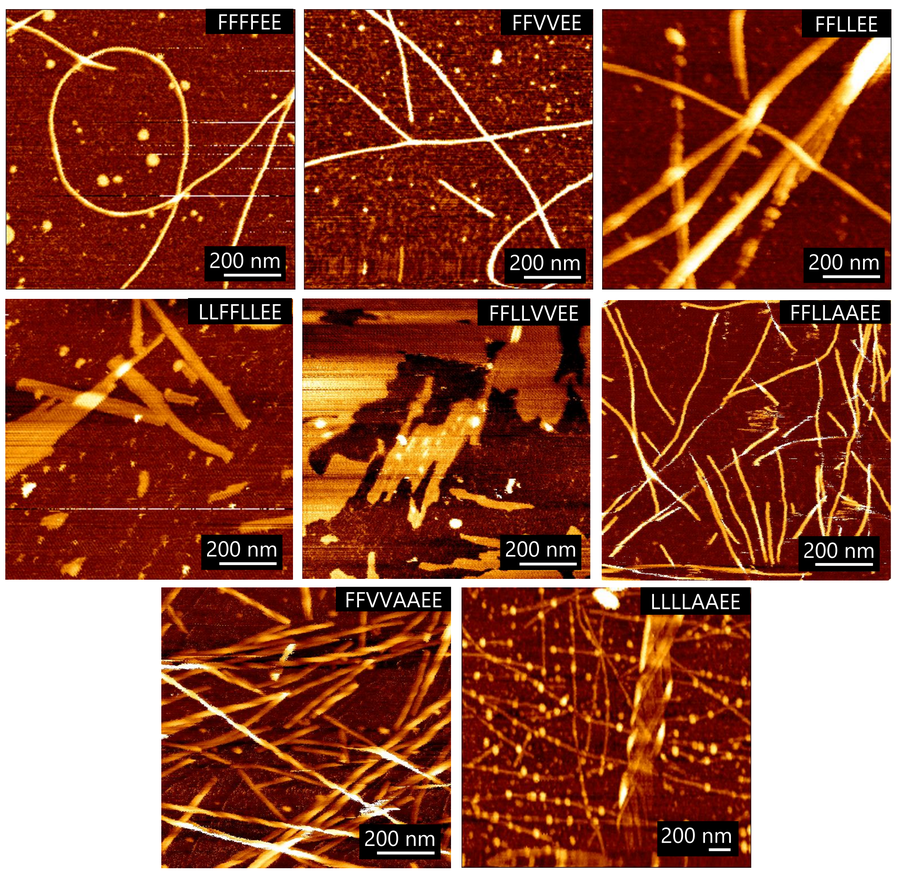


Critical Aggregation Concentrations (CAC) are extracted from the inflexion point (x_0) of sigmoidal fittings

Spectroscopy: CD & FTIR



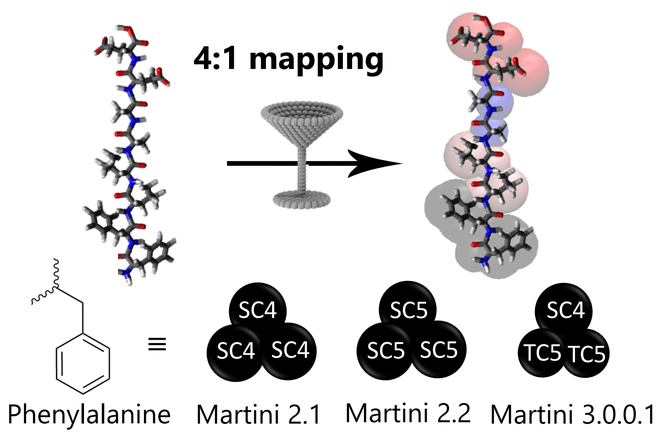
Microscopy: AFM at 10 mM



COMPUTATIONAL TOOL

CG-MD SIMULATIONS

Martini Force Field



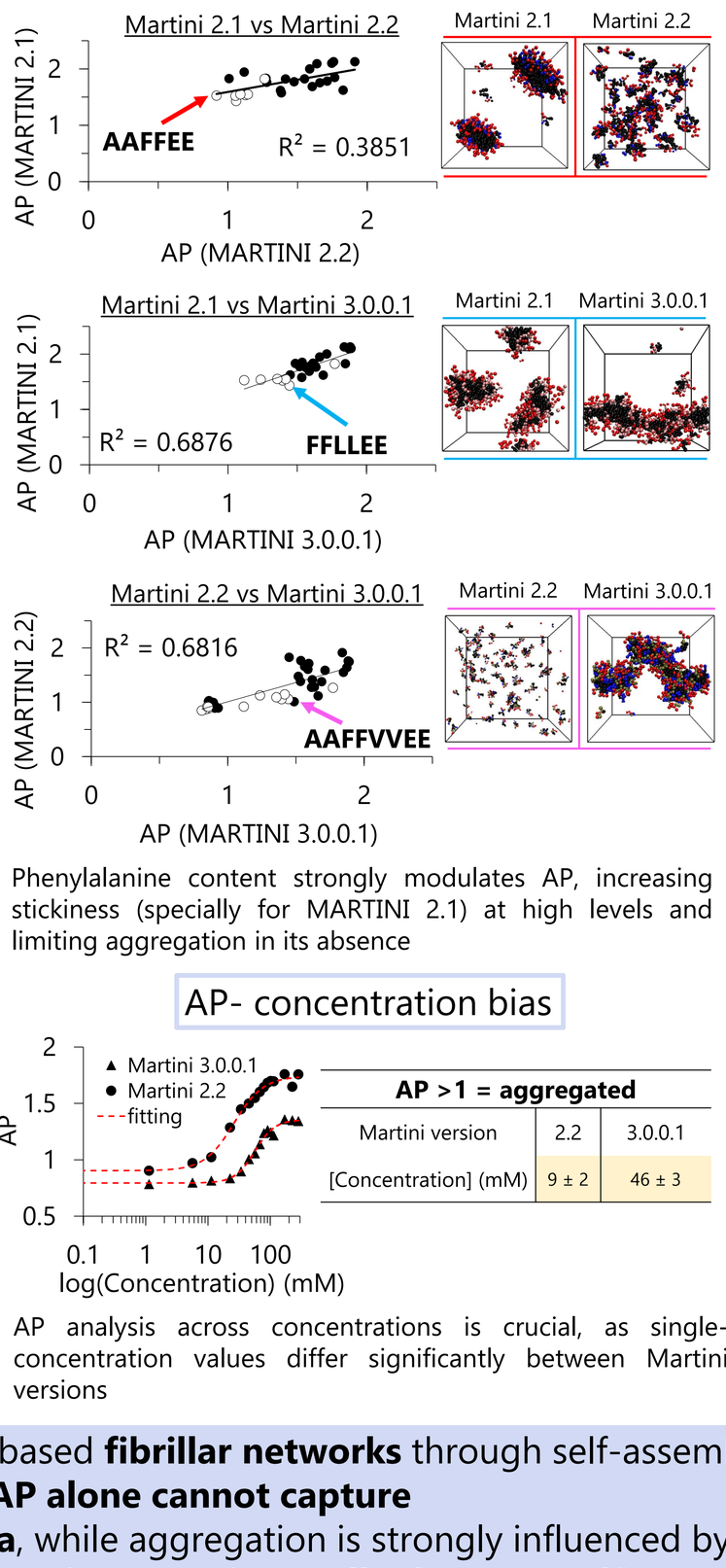
- Martini Force Field → Structure simplification
- Successive versions → Changes in bead types → impact on self-assembly [3]

SCREENING

AP across versions (11.3 mM)

8 AA
6 AA

AP = Aggregation Propensity



Phenylalanine content strongly modulates AP, increasing stickiness (specially for MARTINI 2.1) at high levels and limiting aggregation in its absence

AP- concentration bias

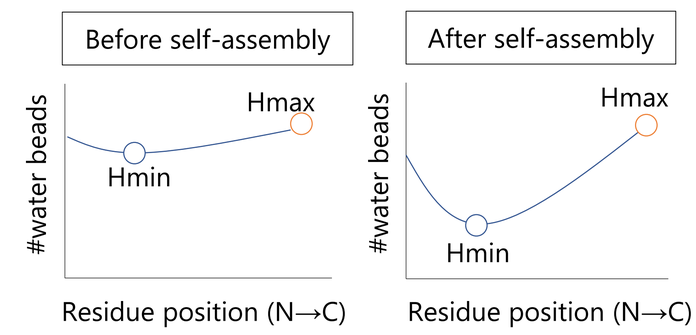
AP >1 = aggregated		
Martini version	2.2	3.0.0.1
[Concentration] (mM)	9 ± 2	46 ± 3

AP analysis across concentrations is crucial, as single-concentration values differ significantly between Martini versions

EXP/COMP COMBINED APPROACH

FRAMEWORK

AP quantifies molecular association and does not directly capture molecular organization → **Hydration as a molecular descriptor of self-assembly**

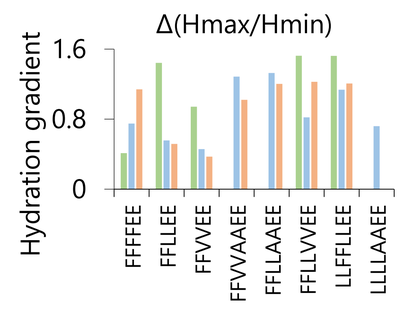


Hydration captures changes in the exposed surface of the peptides before and after self-assembly

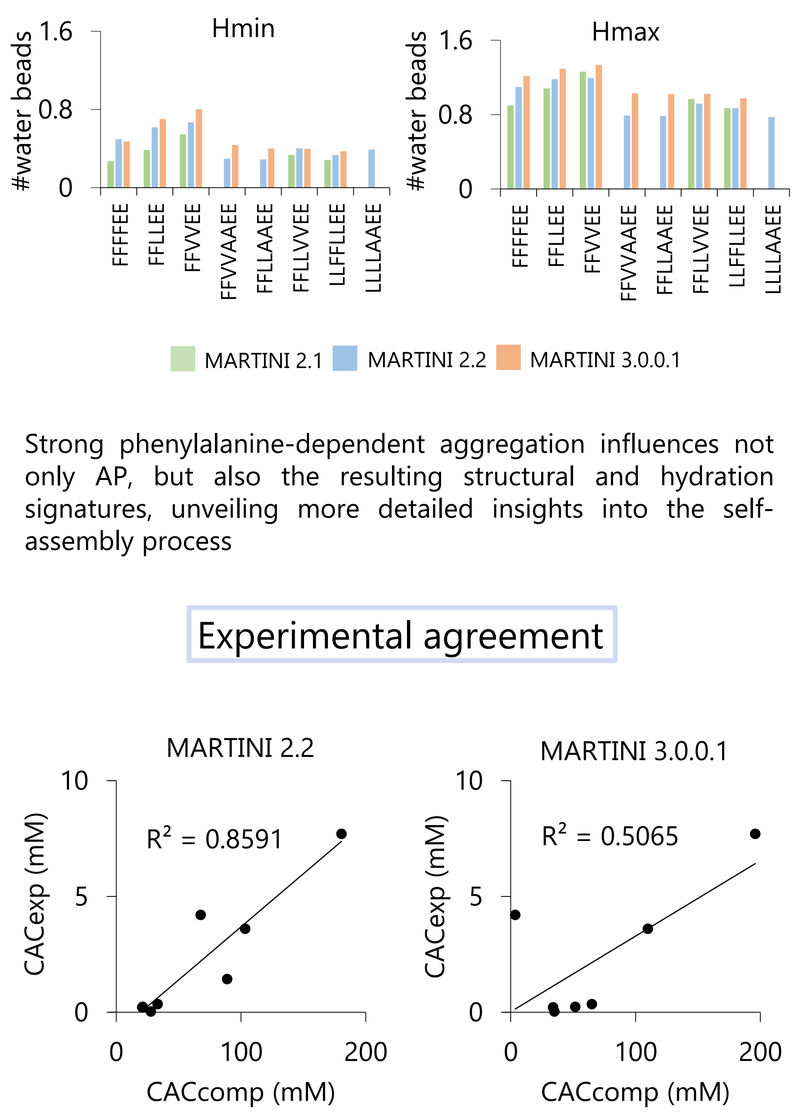
Δ(Hmax/Hmin)

$$\left(\frac{Hmax}{Hmin}\right)_A - \left(\frac{Hmax}{Hmin}\right)_B$$

A: After self-assembly
B: Before self-assembly



MOLECULAR RESOLUTION



Strong phenylalanine-dependent aggregation influences not only AP, but also the resulting structural and hydration signatures, unveiling more detailed insights into the self-assembly process

CORRLEATION

Experimental agreement

Martini 2.2 shows the best correlation with experimental data regarding aggregation onset, making it the most suitable model for an in-depth investigation of self-assembly in the systems analyzed

- Designed peptide amphiphiles form β-sheet–based **fibrillar networks** through self-assembly
- **Hydration reveals structural changes that AP alone cannot capture**
- **Martini 2.2 best matches experimental data**, while aggregation is strongly influenced by F-content and concentration:
  → **force-field shows a bias towards F-content**, but **experimentally there are self-assembling F-free sequences**
- Morphological analysis reveals nanofibers and nanosheet-like structures, with **hexapeptides displaying the smallest widths**

REFERENCES

1. Álvarez, Z., et al., Science 2021, 374, 848-856
2. Álvarez, Z., et al., Cell Stem Cell 2022, 30, 1-20
3. Marrink, S. J., et al., WIREs Comput. Mol. Sci. 2023, 13, e1620

ACKNOWLEDGEMENTS

- JAE-PRE predoctoral fellowship (JAEPRE23-45), CSIC
- Ramon y Cajal (RYC2021-033294-I), AEI
- Spanish State Research Agency (PID2022-136392NA-I00), AEI

Synthesis of PLGA Nanoparticles Encapsulated with Immunodominant $MOG_{35–55}$ Peptide Analogues for the Treatment of Multiple Sclerosis

Georgia Biniari ‡, Iro Triantafyllakou ‡, Carmen Simal, Spyridon Mourtas, Theodore Tselios

Department of Chemistry, University of Patras, 26504 Rion, Greece

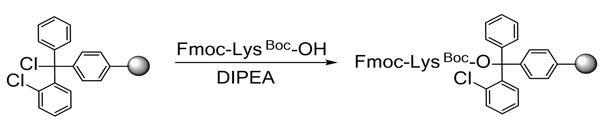
‡ These authors contributed equally to this work.

https://doi.org/10.17952/38EPS.2026.P357

Introduction

Multiple sclerosis (MS) is a chronic autoimmune disease of the central nervous system (CNS), characterized by inflammation and demyelination[1]. $MOG_{35–55}$ is an immunodominant myelin epitope widely used in experimental autoimmune encephalomyelitis (EAE), a principal animal model of MS[1, 2]. In this study, our aim was to modulate the pathogenic T-cell response, the TCR-interacting residues **Arg^{41} and Arg^{46} of $MOG_{35–55}$ were replaced with Ala**, generating **$[Ala^{41}]MOG_{35–55}$** and **$[Ala^{41,46}]MOG_{35–55}$**, respectively[3]. The peptide analogues were **encapsulated in PLGA nanoparticles** to protect the peptides from degradation and enable their sustained and controlled release, providing a suitable delivery strategy for subsequent *in vivo* evaluation in the EAE model[4].

1 Solid Phase Peptide Synthesis on 2-CLTR-Cl



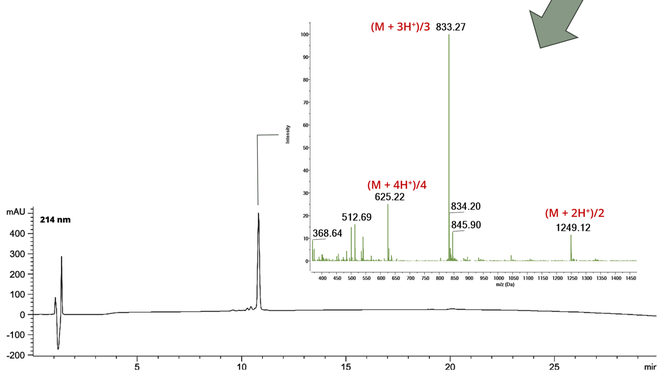
1) 25% 4-Methylpiperidine/DMF ⟲ 2) Fmoc-AA-OH, HOBt, DIC

Met-Glu tBu-Val-Gly-Trp Boc-Tyr tBu-X_{AA}-Ser tBu-Pro-Phe-Ser tBu-Y_{AA}-Val-Val-His Trt-Leu-Tyr tBu-Arg Pbf-Asn Trt-Gly-Lys Boc-O-

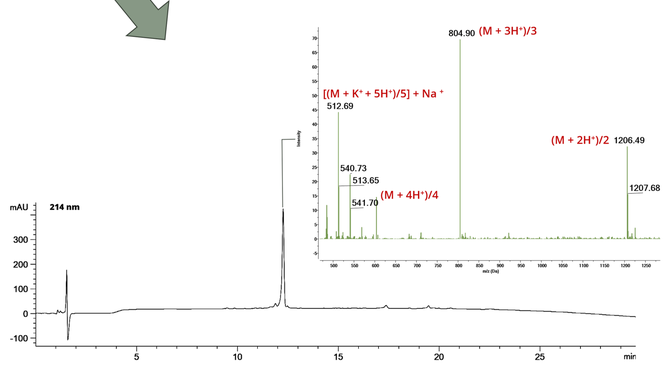
1) DCM/TFE, (7: 3), 1 h
2) TFA/DCM/EDT, (95: 4: 1), 5 h

H_2N-Met-Glu-Val-Gly-Trp-Tyr- X_{AA}-Ser-Pro-Phe-Ser- Y_{AA}-Val-Val-His-Leu-Tyr-Arg-Asn-Gly-Lys-COOH

X_{AA}: Ala , Y_{AA}: Arg

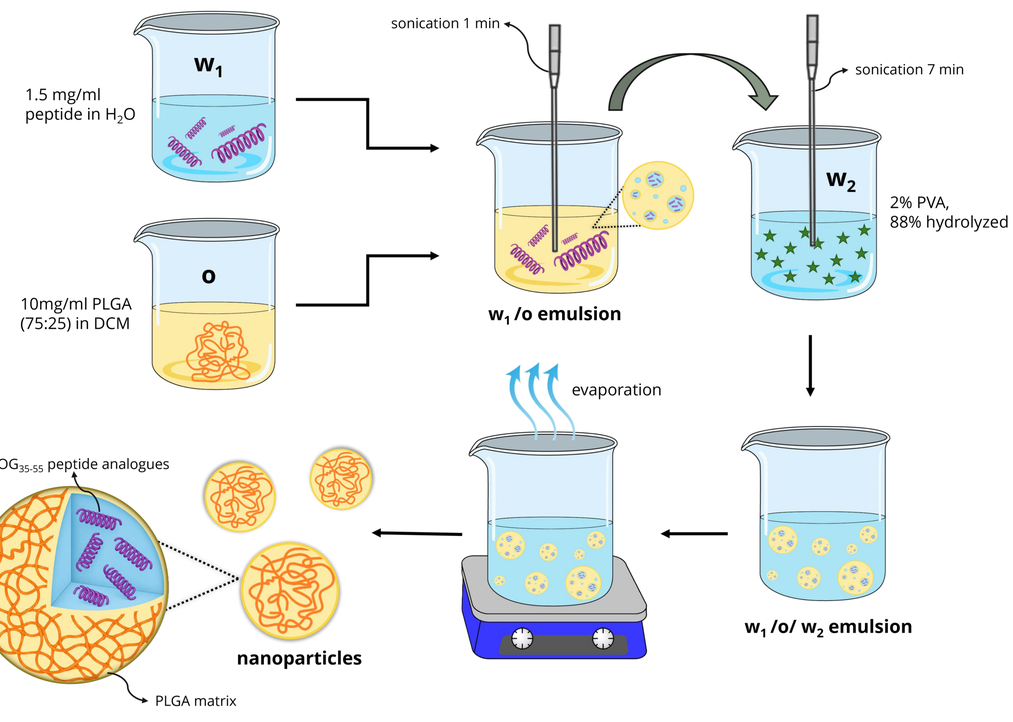


X_{AA}: Ala , Y_{AA}: Ala



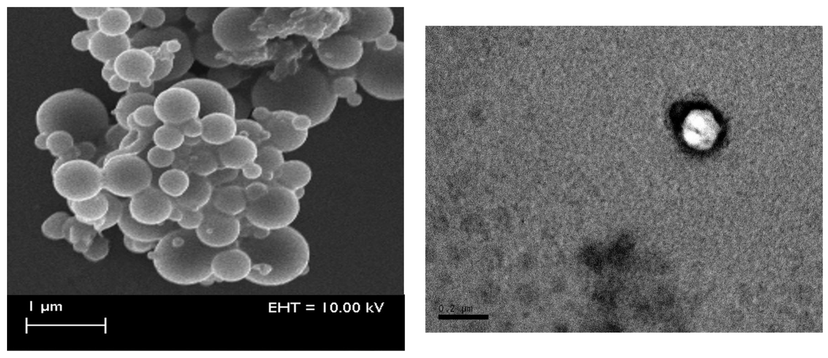
2 Preparation of PLGA Nanoparticles

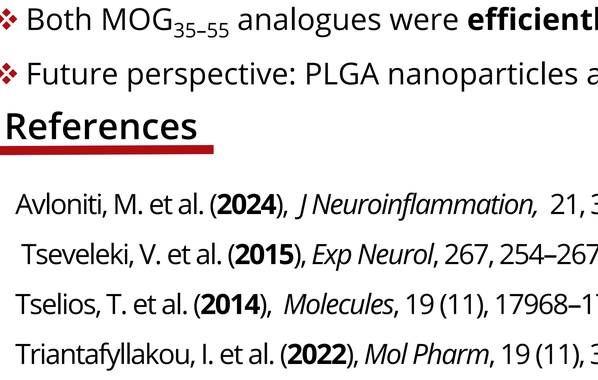
❖ Double emulsion technique: water - in – oil - in - water



3 Characterization of PLGA Nanoparticles

$[Ala^{41}]MOG_{35-55}$





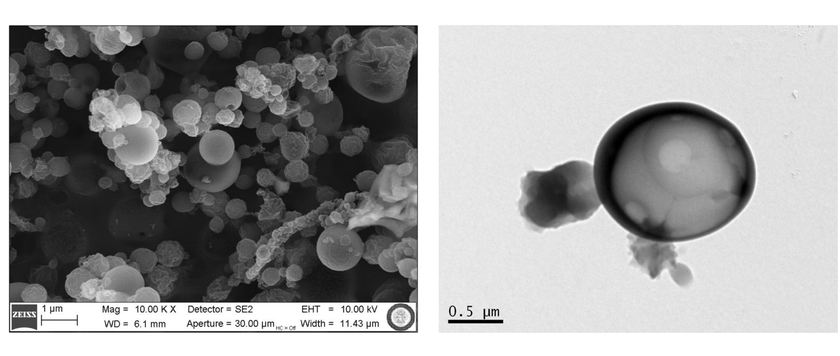
Particle size (average): **378.4 nm**

PDI: **0.4**

ζ-potential: **-34.8V**

Encapsulation efficiency: **84%**

$[Ala^{41, 46}]MOG_{35-55}$

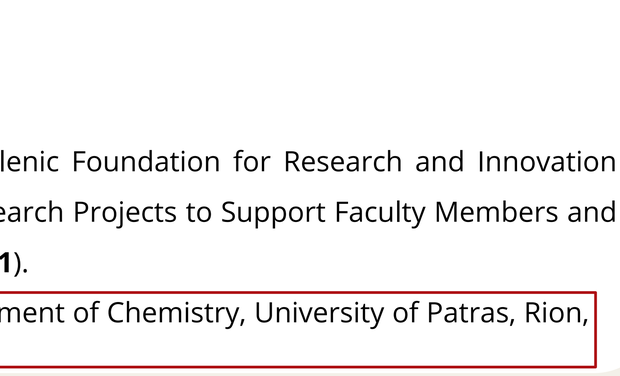


Particle size (average): **442.9 nm**

PDI: **0.45**

ζ-potential: **-33.5V**

Encapsulation efficiency: **79%**



Both nanoparticle formulations showed heterogeneous particle size distributions within the **300–500 nm range**, with a minor population of larger particles.

Conclusions

❖ Successful synthesis of **$[Ala^{41}]MOG_{35–55}$** and **$[Ala^{41,46}]MOG_{35–55}$** peptide analogues

❖ **PLGA nanoparticles** were successfully prepared using a **W/O/W double-emulsion** approach, although further optimization of the particle size is required.

❖ Both $MOG_{35–55}$ analogues were **efficiently encapsulated** within PLGA nanoparticles

❖ Future perspective: PLGA nanoparticles are a **promising delivery strategy** for *in vivo* evaluation in the EAE model

References

1. Avloniti, M. et al. (**2024**), *J Neuroinflammation,* 21, 34–62, doi: 10.1186/s12974-024-03023-9.
2. Tseveleki, V. et al. (**2015**), *Exp Neurol*, 267, 254–267, doi: 10.1016/j.expneurol.2014.10.019.
3. Tselios, T. et al. (**2014**), *Molecules*, 19 (11), 17968–17984, doi: 10.3390/molecules191117968.
4. Triantafyllakou, I. et al. (**2022**), *Mol Pharm*, 19 (11), 3795–3805, doi: 10.1021/acs.molpharmaceut.2c00277.

Acknowledgments

The research project is funded by the Hellenic Foundation for Research and Innovation (H.F.R.I.) under the "3rd Call for H.F.R.I. Research Projects to Support Faculty Members and Researchers" (H.F.R.I. Project Number: **25251**).

Contact details: Theodore Tselios, Department of Chemistry, University of Patras, Rion, Greece. **ttselios@upatras.gr**

Inverse folding improves structure prediction for confidence-aware peptide deorphanization

A.Dougha[1], S. Murail[1], J. Leprince[2,3], P. Tufféry[1]

[1]BFA, INSERM ERL 1133, CNRS UMR 8251, Université Paris Cité, F-75013 Paris, France
[2]Univ Rouen Normandie, Inserm, NorDiC UMR 1239, Rouen, France
[3]Univ Rouen Normandie, Inserm, CNRS, HeRacLeS US 51 UAR 2026, PRIMACEN, Rouen, France
Contact: pierre.tuffery@u-paris.fr, alexis.dougha@u-paris.fr

https://doi.org/10.17952/38EPS.2026.P269

1. Background and objectives

- Peptide hormones are involved in the regulation of a wide range of physiological processes, including but not limited to homeostasis, immunity and growth. They bind to their cognate receptors to trigger downstream signaling pathways (see **Figure 1**), but the identity of the receptors is not always known. In some cases, experimental evidence suggests that the peptide of interest binds to a G protein-coupled receptor (GPCR) which remains to be identified.

- Structure prediction-based confidence metrics like the interface predicted Template Modeling (ipTM) score have been applied to solve this issue[1]. While promising, the protocol suffers from the imperfection of the ipTM, which makes its use limited under a realistic peptide deorphanization scenario where only a small number of candidates can be tested.

- We aim to identify the best protocol to deorphanize peptides, benchmarking structure prediction (AlphaFold-Multimer[2], AlphaFold 3[3], Boltz-2[4]) and scoring functions including popular ones (ipTM, ipSAE[5], LIS[6], pDockQ[7], pDockQ2[8], peptide pLDDT) and others based on inverse folding used in this context for the first time (peptide perplexity computed with ESM-IF1[9] and ProteinMPNN[10]).

- Specifically, we address the deorphanization process by considering the value of the proposed protocol in a real-world scenario where, beyond ranking candidate pairs, our protocol enables evaluation of the probability of success when testing only a small number of top predictions (i.e., confidence-aware peptide deorphanization).

- First, all the combinations of structure prediction models and scoring functions are benchmarked on a rat dataset (17 peptides, 359 GPCRs, 29 interacting pairs). Then, the best protocol was applied to a larger human dataset (122 peptides, 393 GPCRs, 244 interacting pairs) assembled from IUPHAR[11].

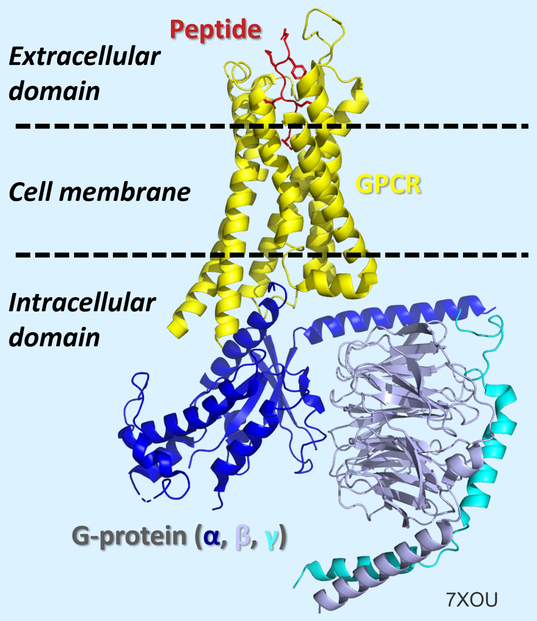


Figure 1. A peptide–GPCR–G protein complex resolved by cryo-EM. Cholecystokinin (CCK) binds to the CCK receptor type A, promoting G protein recruitment. CCK is known to regulate digestion.

2. Computational workflow

- For each peptide (**Figure 2**), we predict its structure in interaction with all the GPCRs to be tested *in silico*. We generated 25 structures per peptide-GPCR pair for each model evaluated.

- All the scores are evaluated with all the structure prediction models on the rat dataset, so that we keep only the best combinations for the large-scale prediction of the human dataset (2 * 25 models * 122 peptides * 393 GPCRs = 2,397,300 predicted structures). In **Figure 2**, only the best scoring function associated with AFmm (ProteinMPNN perplexity) and AF3 (ipSAE) is shown.

- We employed the ColabFold[12] implementation of AFmm (MMSeqs2 MSA and dropout enabled), and AF3 with default parameters (data pipeline using JackHMMER MSA).

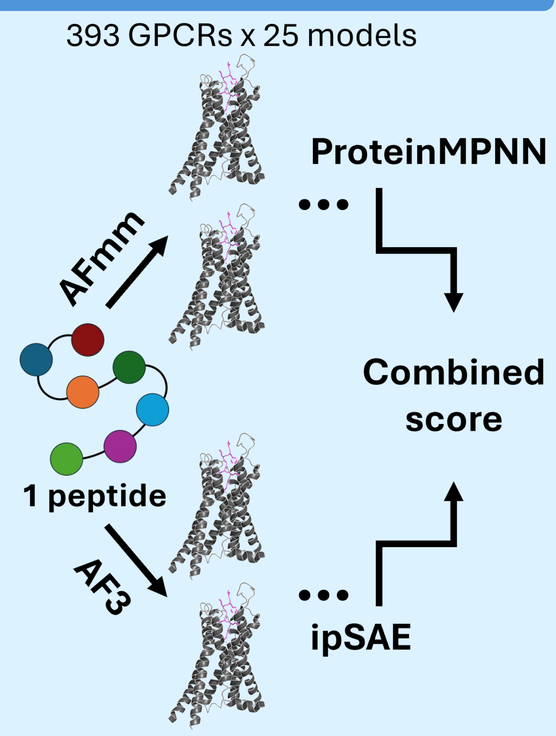


Figure 2. Computational workflow applied for each case study. All the structures are scored with a range of scoring functions benchmarked. Boltz-2 was also employed for the rat dataset.

3. Benchmark with rat interactions

- Interestingly, ipSAE is the best score (in term of average precision AP) when employed with AF3, while for AFmm and Boltz-2, rescoring with the peptide perplexity computed with ProteinMPNN is beneficial (**Figure 3**).

- Although Boltz-2 was trained on a larger dataset, AF3 and AFmm achieve better performance.

- Even if AFmm achieves a higher AP than AF3, we speculate that the combination of both protocols could improve the results since AF3 performs better than AFmm in the high-recall region of the curve.

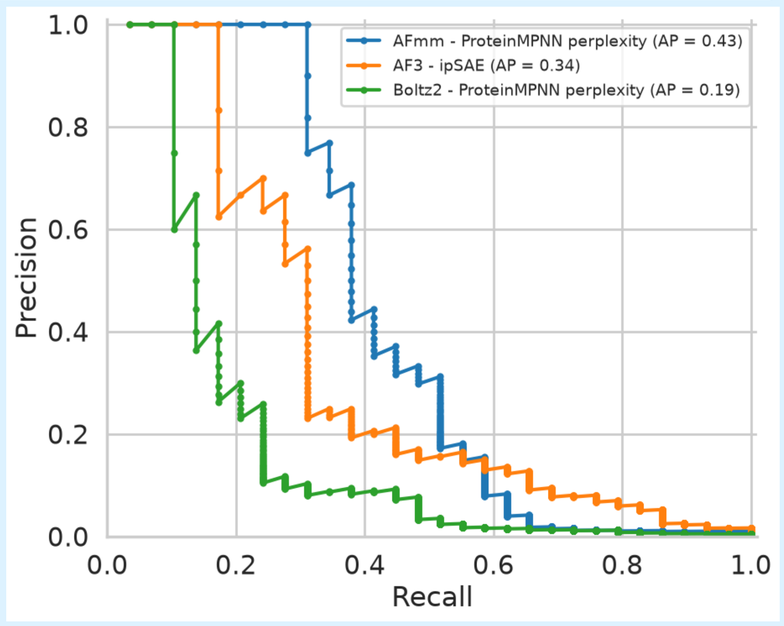


Figure 3. Precision-recall curves showing only the best scoring function associated with each structure prediction model tested (rat dataset). The average precision (AP) values summarize the overall performance of each method. While AFmm has the highest AP, AF3 performs better in the high-recall region (above 0.6). Boltz-2 performs poorly compared with the two other protocols, so it was not employed for the human dataset.

4. Validation on human interactions

- The final protocol considers both AFmm and AF3-derived scores in a new combined one. For each score threshold, both precisions were calculated as the proportion of correct pairs among all GPCR-peptide pairs with a score exceeding the corresponding threshold. The combined score was then obtained by averaging the precision values of the two scores.

- The protocols based on AFmm + ProteinMPNN and AF3 + ipSAE achieve similar performance when considering only the top *N* predictions where $N \leq 7$, which is the most important region of the curve (**Figure 4**) for the peptide deorphanization problem (we want to experimentally test a small number of GPCRs for a given peptide of interest).

- The combined score outperforms the two separate ones (based on AFmm only or AF3 only) to identify a larger number of peptide-GPCR pairs when only considering a small number of potential GPCRs for each peptide.

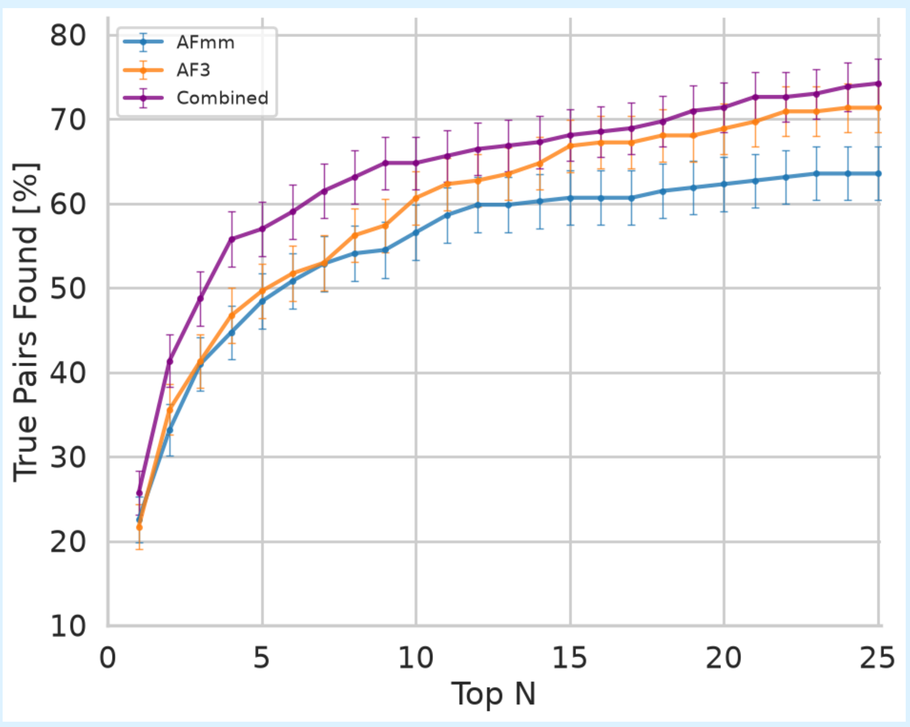


Figure 4. Enrichment curves showing the percentage of true pairs recovered within the top *N* predictions (human dataset). For each value of *N*, the percentage of true pairs recovered was calculated across 1,000 bootstrap resamples. Points represent the mean across bootstrap replicates, with error bars indicating the corresponding standard deviation.

5. Conclusion

1. Inverse folding can be used in combination with structure prediction to prioritize potential GPCRs that can interact with a peptide of interest.
2. Combining "orthogonal" protocols (AFmm/ProteinMPNN + AF3/ipSAE) improves the performance.
3. The combined protocol was employed to deorphanize four peptides of known activity but unknown target. For each one, at least one GPCR was predicted with a confidence score over 53%.
4. 133 potential secondary peptide–GPCR interactions were identified with high confidence in humans (defined as not annotated as interacting in IUPHAR, predicted rank = 1 or confidence score over 50%).
5. *In vitro* validation is ongoing to validate the predictions of points 3 and 4.

References

[1] Teufel, F. et al, *J. Chem. Inf. Model.* **2023**, *63(9)*, 2651-2655.
[2] Evans, R. et al, *biorxiv* **2021**.
[3] Abramson, J. et al, *Nature* **2024**, *630(8016)*, 493-500.
[4] Passaro, S. et al, *biorxiv* **2025**.
[5] Dunbrack Jr, R. L., *biorxiv* **2025**.
[6] Kim, A. R., *biorxiv* **2024**.
[7] Bryant, P. et al, *Nat. Commun.* **2022**, *13(1)*, 1265.
[8] Zhu, W. et al, *Bioinformatics* **2023**, *39(7)*, btad424.
[9] Hsu, C. et al, *ICML* **2022**.
[10] Dauparas, J. et al, *Science* **2022**, *378(6615)*, 49-56.
[11] Harding, S. D. et al, *Nucleic Acids Res.* **2026**, *54(D1)*, D1446-D1456.
[12] Mirdita, M. et al, *Nat. Methods* **2022**, *19(6)*, 679-682.
[13] Alland, C. et al, *Nucleic Acids Res.* **2026**, *33(suppl_2)*, W44-W49.

Acknowledgements

This work was supported by Université Paris Cité. Computational resources were partly provided by RPBS[13]. This project was provided with computing HPC and storage resources by GENCI at IDRIS thanks to the grant 2026-AD010717472 on the supercomputer Jean Zay's CSL, V100, A100, H100 partitions.

From small molecules investigated as Factor XIIIa Inhibitors to biological target diversity

I.P. Bogdanov[1] and N.T. Tzvetkov[1,*]

[1]*Institute of Molecular Biology "Roumen Tsanev", Bulgarian Academy of Sciences, Acad. G. Bonchev str. Bl. 21, Sofia 1113, Bulgaria*

Email: ntzvetkov@bio21.bas.bg

https://doi.org/10.17952/38EPS.2026.P368

Activated Factor XIIIa (FXIIIa) is a key enzyme in the final stage of the blood coagulation cascade. It catalyses the crosslinking of γ-glutamyl and ε-lysyl residues on adjacent fibrin strands and as a result the formed fibrin mesh becomes more stable and resistant to fibrinolytic degradation. While physiological hemostasis is essential to prevent bleeding, excessive or inappropriate clot formation can lead to vascular obstruction, and in some cases can cause life-threatening situations such as heart attack or stroke. Inhibition of FXIIIa represents an interesting anticoagulant strategy, as reduced fibrin crosslinking is expected to produce mechanically weaker clots that are more susceptible to fibrinolysis and also having lower risk of side-effect bleeding.[1] Despite reported FXIIIa inhibitors, to date, there is no medically approved drug specifically targeting this enzyme. The main focus of this study is on the computational identification and characterization of small-molecule compounds with peptide-mimicking structure as virtually active towards diverse biological targets, initially investigated for their inhibitory potential against FXIIIa (Figure 1). Structure-based molecular docking was combined with ligand-based target prediction approaches to evaluate reference and query drug sets against selected biological target.

Ligand-based target prediction tools were employed to investigate potential secondary biological targets and off-target activities based on chemical similarity principles. The investigated compounds are comprised of two sets: (i) a reference set of molecules with documented physicochemical and biological relevance, including the approved drugs **donepezil**, **safinamide**, **galantamine**, and the investigational drugs **NTZ-1091**, and (ii) a drug test set derived from novel scaffolds as well as previously synthesized and characterized by our group.[2, 3] Based on target prediction results obtained from target-prediction sources, additional docking experiments were performed against biologically relevant enzymes, including human monoamine oxidase A and B (MAO-A/B) as a starting point of our investigations. The identification of MAO as a potential secondary target (off-target) is supported further by literature evidence demonstrating that structurally optimized small molecules can achieve high potency and selectivity toward MAO-B. In particular, indazole-5-carboxamide inhibitors with slight modifications enhance MAO-B affinity, selectivity, and drug-like properties.[2, 3] These findings reinforce the applicability of structure and ligand-based target prediction approaches, having higher score rates when investigating structurally related analogues, and providing a good starting point for subsequent compound optimization and experimental validation.

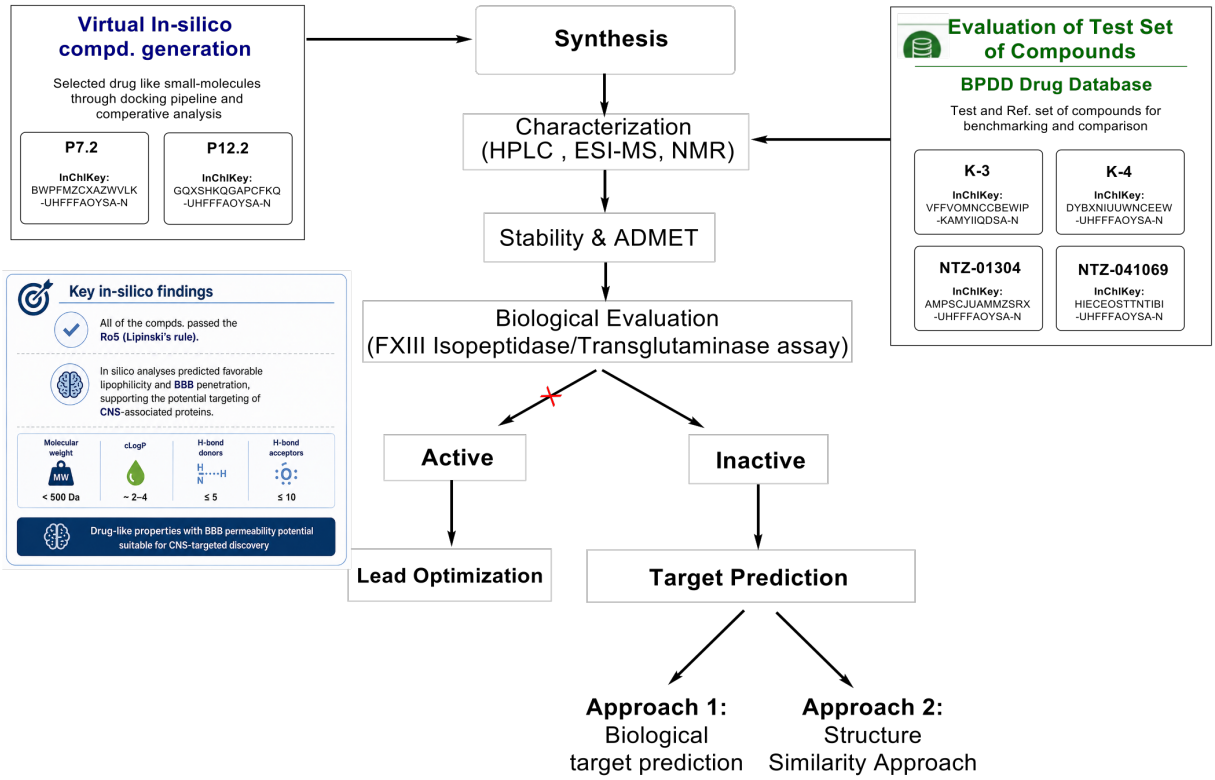


Figure 1. Workflow for generating small molecules as FXIIIa inhibitors and their further evaluation development as biologically active compounds.

Acknowledgements

This work is financially supported by the Bulgarian National Science Fund project KP-06-N93/10 (КП-06-Н93/10).

References

1. T. Schmitz, C. A. Bäuml, D. Imhof, *Anal. Biochem.* **2020,** *605*,113708.
2. N. T. Tzvetkov; H.-G. Stammler, B. Neuman, S. Hristova, L. Antonov, M. Gastreich, *Eur. J. Med. Chem.* **2017**, *127*, 470-492.
3. N. T. Tzvetkov and L. Antonov, *J. Enzyme Inhib. Med. Chem.,* **2017**, *32*, 1, 960–967.

DESIGN AND DEVELOPMENT OF NOVEL LOW-MOLECULAR-WEIGHT CARBOXAMIDES AS DUAL MODULATORS OF MAO-B AND α-SYNUCLEIN

Georgi I. Ivanov[1] and Nikolay T. Tzvetkov[1,*]

[1]*Institute of Molecular Biology, Department of Biochemical Pharmacology and Drug Design, Bulgarian Academy of Sciences, Acad. G. Bonchev str. Bl. 21, Sofia 1113, Bulgaria*

Email: ntzvetkov@bio21.bas.bg

https://doi.org/10.17952/38EPS.2026.P370

Neurodegenerative disorders such as Parkinson's disease (PD) are characterized by progressive dopaminergic neuronal loss and the pathological aggregation of α-synuclein (α-syn), accompanied by dysregulation of monoaminergic neurotransmission. Monoamine oxidase B (MAO-B) represents a validated enzymatic target involved in dopamine metabolism and oxidative stress[1–4], while α-syn constitutes a central disease-modifying target associated with protein misfolding, aggregation, and neurotoxicity[4]. Simultaneous modulation of both targets represents a rational multitarget strategy for the development of small-molecule therapeutics, as for example, indazole-5-carboxamide derivatives.[2,3]

Inhibition of MAO-B reduces dopamine degradation and limits the formation of reactive oxygen species[1], thereby attenuating oxidative stress–mediated neuronal damage, while modulation of α-Syn–related processes interfere with protein aggregation, toxicity, and pathological spreading. Targeting both mechanisms within a single low-molecular-weight framework is expected to address complementary pathological pathways implicated in neurodegeneration and may contribute to slowing disease progression through combined symptomatic and disease-modifying effects.[4]

This work is focused on the design of novel low-molecular-weight compounds acting as dual MAO-B/α-syn inhibitors, employing an integrated strategy based on molecular docking, molecular dynamics simulations, virtual screening, synthesis, and *in vitro* physicochemical and biological evaluation using the approved drug safinamide (Figure 1). The combined application of these approaches provides a systematic framework for the identification and optimization of small molecules with potential relevance for neurodegenerative disease research.

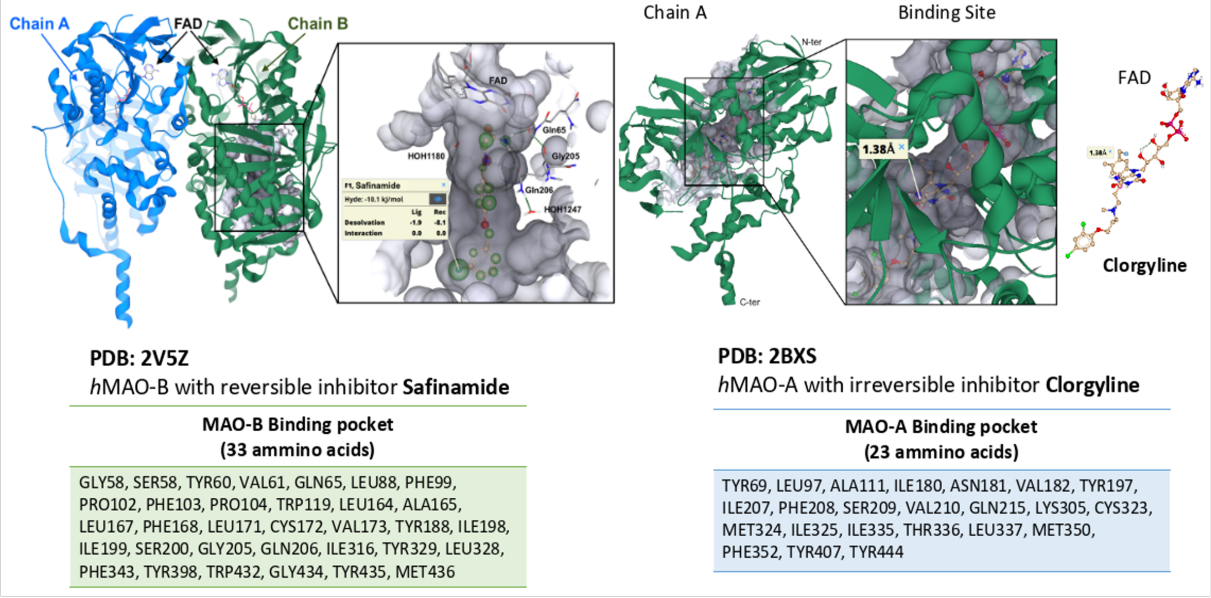


Figure 1. Structural comparison of human MAO-B and MAO-A active sites using safinamide and clorgyline as reference inhibitors.[1,3]

Acknowledgements

This work is financially supported by the Bulgarian National Science Fund project KP-06-N93/10 (КП-06-Н93/10).

References

1. A. W. K. Yeung, N. T. Tzvetkov, M. G. Georgieva, I. V. Ognyanov, K. Kordos, A. Jozwik, T. Kühl, G. Perry, M. C. Petralia, E: Mazzon, A. G. Atanasov, *Antioxid. Redox. Signal.* **2021**, 34, 5, 402–420.
2. N. T. Tzvetkov, S: Hinz, P. Küppers, M. Gastreich, C. E. Müller, *J. Med. Chem.* **2014**, *57*, 6679–6696.
3. N. T. Tzvetkov, H.-G. Stammler, B. Neumann, S. Hristova, L. Antonov, M. Gastreich, *Eur. J. Med. Chem.* **2017**, 127, 470–492.
4. P. Calabresi, A. Mechelli, G. Natale, L. Volpicelli-Daley, G. Di Lazzaro, V. Ghiglieri, *Cell Death & Dis.* **2023**, 14, 173.

A MODULAR NEUROPILIN–HSV DERIVED RF–TUFTSIN PLATFORM FOR TARGETED DELIVERY: VALIDATED IN SPHEROIDS AND EPITHELIAL BARRIER MODELS

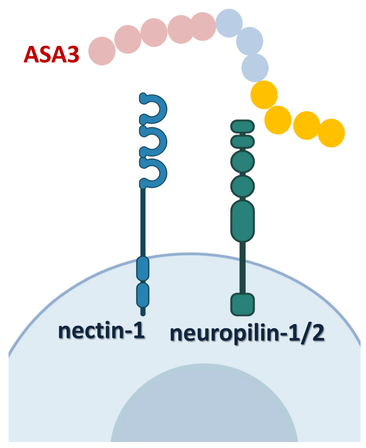
K. URAY[1], M. KRÁTKÝ[2], E.L. MÉHES[3,4], F. SEBÁK[5], A. BODOR[5], F. ZSILA[6], T. VISNOVITZ[7,8], T. BÁRKAI[7], F.K. GRÉBECZ[7], K. FODOR[9], L. LAKATOS[1,10], R. OLÁHNÉ SZABÓ[7], J. HORČIC[2], J. VINŠOVÁ[2], S.E. BŐSZE[1,7]

[1]HUN-REN–ELTE Research Group of Peptide Chemistry, Hungarian Research Network, Eötvös Loránd University (ELTE), Budapest, Hungary; [2]Department of Organic and Bioorganic Chemistry, Faculty of Pharmacy, Charles University, Hradec Králové, Czech Republic; [3]Institute of Chemistry, ELTE; [4]Department of Biological Physics, ELTE; [5]Analytical and BioNMR Laboratory, Institute of Chemistry, ELTE; [6]H-2092, Rózsa Street 18, Budakeszi; [7]Department of Genetics, Cell- and Immunobiology, Semmelweis University, Budapest; [8]Department of Plant Physiology and Molecular Plant Biology, ELTE; [9]Department of Laboratory Animal Science and Animal Welfare, University of Veterinary Medicine, Budapest; [10]Doctoral School of Biology, Institute of Biology, Faculty of Science, ELTE

Email: katalin.uray@ttk.elte.hu; szilvia.bosze@ttk.elte.hu, bosze.szilvia@semmelweis.hu **https://doi.org/10.17952/38EPS.2026.P506**

MODULAR TANDEM DESIGN

QRTVAVYSLRIAGFHG [1]	LINKER [5,6]	TUFTSIN [2-4]



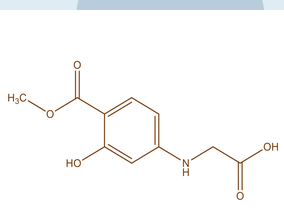
TANDEM ARCHITECTURE/RECEPTOR PROXIMITY MODEL

HSV-gD-RF — **BASED ON HSV-1 gD SERVING AS DERIVED PRIMARY ENTRY SEQUENCE[1]**

TUFTSIN — **NEUROPILIN-ASSOCIATED TARGETING**

SGSG/H12 LINKER — **TUNABLE DISTANCE, NET CHARGE, HYDROPHILICITY/logP VALUES PHYSICOCHEMICAL VERSATILITY**

Cf/ASA3 CARGO — **FOR UPTAKE AND DELIVERY EVALUATION**



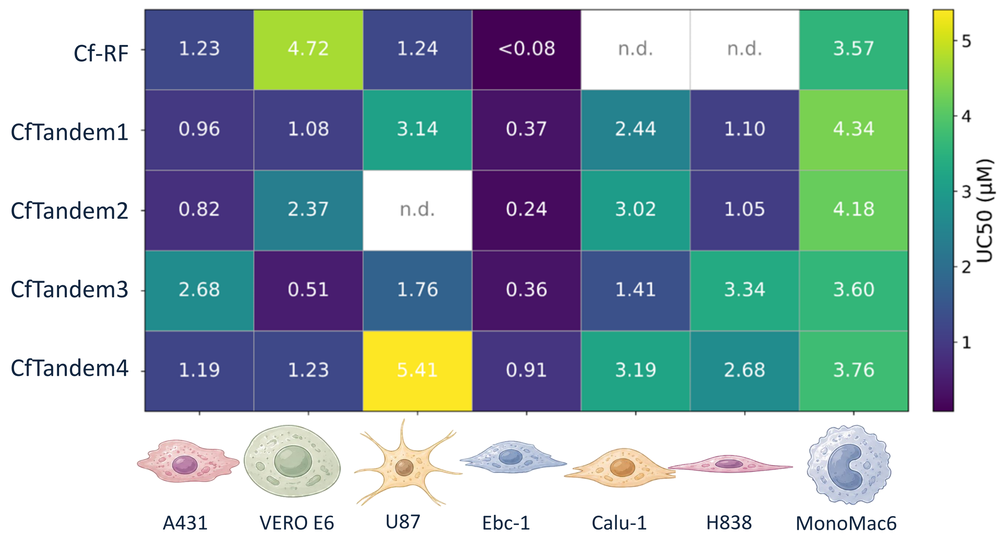
ASA3[2] : (3-hydroxy-4-(methoxycarbonyl)phenyl)glycine

	Code	Mw. calc.	Mw. meas.	Net charge	logP
Cf-RF	Cf-RF *	2132.36	2132.17	2.52	-5.847
Cf-RF-OT5(P)	Cf-RF-OT5(P) *	2712.10	2710.81	4.52	-9.718
CfTandem1	Cf-RF-H12-OT5(P) *	3859.31	3857.33	4.54	-19.552
CfTandem2	Cf-RF-H12-OT5 *	3791.23	3790.98	4.54	-20.159
CfTandem3	Ac-RF-K(Cf)-SGSG-OT5(P) *	3170.49	3169.44	4.52	-15.945
CfTandem4	Ac-RF-K(Cf)-SGSG-OT5 *	3102.41	3101.13	4.52	-16.552
Tandem1	Ac-RF-H12-OT5(P) #	3543.01	3542.65	4.11	-22.863
Tandem2	Ac-RF-H12-OT5 #	3474.93	3474.58	4.11	-22.848
Tandem3	Ac-RF-K(Ac)-SGSG-OT5(P) #	2854.24	2852.51	4.11	-19.256
Tandem4	Ac-RF-K(Ac)-SGSG-OT5 #	2786.16	2786.11	4.11	-19.241
Cf-M3	ASA3-RF-K(Cf)-SGSG-OT5(P) §	3335.65	3335.17	4.03	-14.345
Cf-M4	ASA3-RF-K(Cf)-SGSG-OT5 §	3266.71	3267.57	4.02	-14.947
M2	ASA3-RF-H12-OT5 ‡	3640.07	3639.60	4.35	-21.954
M3	ASA3-RF-K(Ac)-SGSG-OT5(P) #‡	3019.38	3019.01	4.03	-18.061
M4	ASA3-RF-K(Ac)-SGSG-OT5 #‡	2951.31	2950.15	4.10	-17.917

OT5(P): TKPPR, OT5: TKPKG. Mw: Bruker Amazon SL ESI MS, Net charge (pH: 7.4) and logP calculated by www.chemicalize.com/ChemAxon.[4,7,8].
* Fluorescently labeled carriers for uptake and penetration studies # Acetylated carriers for NMR ‡ Drug conjugates for therapeutic evaluation, § Fluorescently labeled drug conjugates for uptake and penetration

CELLULAR AND MECHANISTIC PROFILING & THERAPEUTIC PROOF OF CONCEPT

Figure 1. *In vitro* cellular internalization of Cf-peptides represented by UC_{50} value [1] (concentration value Cf positivity in 50 % of live cells). Treatment: 3h. Quantified by flow cytometry.



EBC-1: **HIGHEST UPTAKE**
H838: **FAVORABLE UPTAKE FOR H12 TANDEMS**
A431 / VERO E6: **LINKER-DEPENDENT DIFFERENCES**
MM6: **GOOD DETECTOR CELLS IN TRANSWELL SYSTEM**

ENERGY-DEPENDENT UPTAKE AND LYSOSOMAL LOCALIZATION

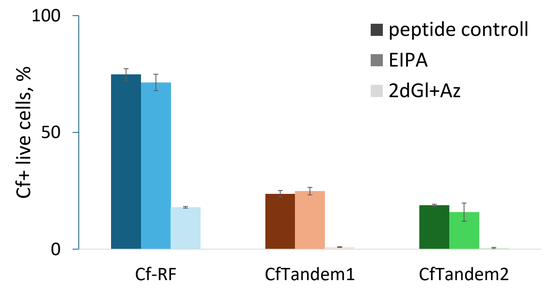
ANTIPROLIFERATIVE ASA3-CONJUGATES

TANDEM DIMINISHED ASA3'S HEMOLYTIC ACTIVITY

BASED ON NMR
TANDEMS MAINLY DISORDERED

ASA3 HAS NO INFLUENCE ON STRUCTURE

Figure 2. Inhibition of internalization[9] with EIPA and ATP depletion, A431 cells

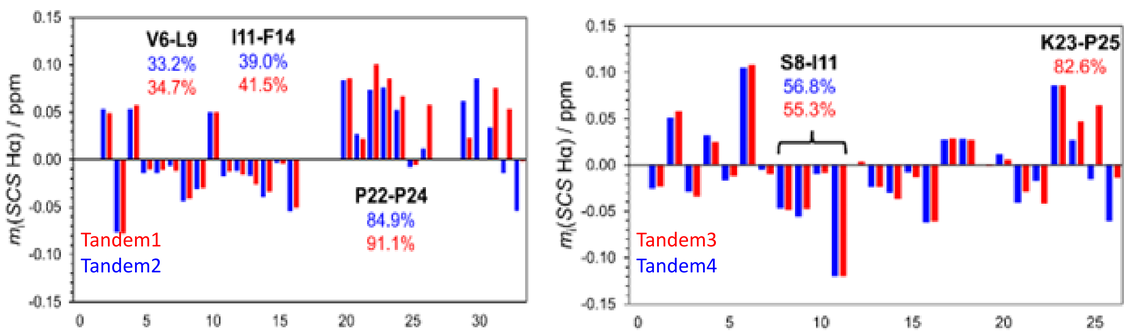


Antiproliferative and hemolytic activity of tamdem conjugates *vs* free ASA3

code	IC_{50} (μM)		HC_{50} (μM)
	U87	Ebc-1	RBC
ASA3	> 100	> 100	3.8
M2	73.0	6.1	> 100
M3	>100	18.6	> 100
M4	>100	23.8	> 100

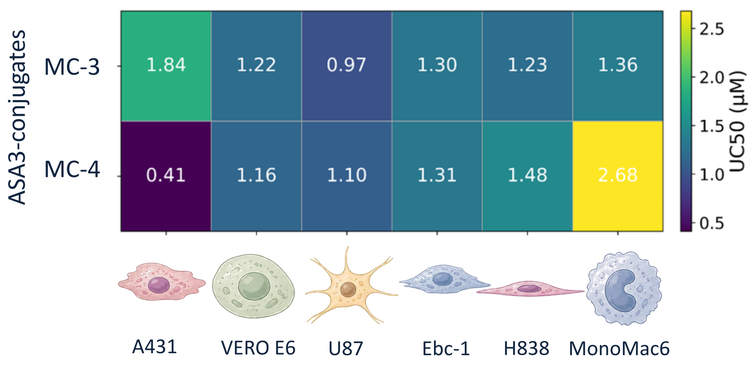
Cytostatic activity was determined by end-point MTT
Hemolytic activity, 1 v/v % RBC: red blood cells, 4 h, 37 °C

Figure 3. Average $^1H^{\alpha}$ secondary chemical shifts (SCS $\delta=\delta_{measured}$ – RCCS of a given atom), ^1H,^{15}N SOFAST-HMQC spectra, 298K, 700MHz. Structural Propensity Identification [10] >95% (– helical, + extended).



VALIDATION IN TISSUE MODELING BARRIER SYSTEMS AND SPHEROIDS

Figure 4. *In vitro* cellular internalization of ASA3-Cf-conjugates represented by UC_{50} value (concentration value Cf positivity in 50 % of live cells). Treatment: 3h. Quantified by flow cytometry.



HIGH TANDEM TRANSPORT ACROSS BRONCHIAL AND ALVEOLAR BARRIER MODELS

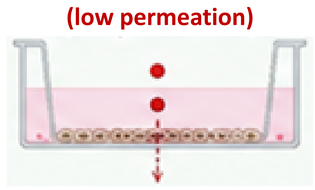
HIGHEST ACCUMULATION IN EBC-1 SPHEROIDS AS LUNG TISSUE MODEL

H12-TANDEMS PROMOTED DEEPER, MORE EFFICIENT PENETRATION

ASA3-CONJUGATES RETAINED UPTAKE AND SPHEROID PENETRATION

Figure 5. Transwell permeation[2-4], comparison on Caco-2, Calu-1 and H838

Caco-2 / MM6 (low permeation)



Calu-1, H838 / MM6 (high permeation)

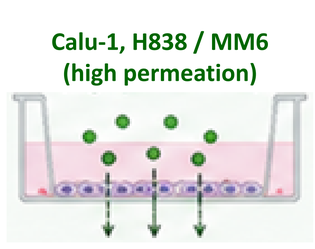
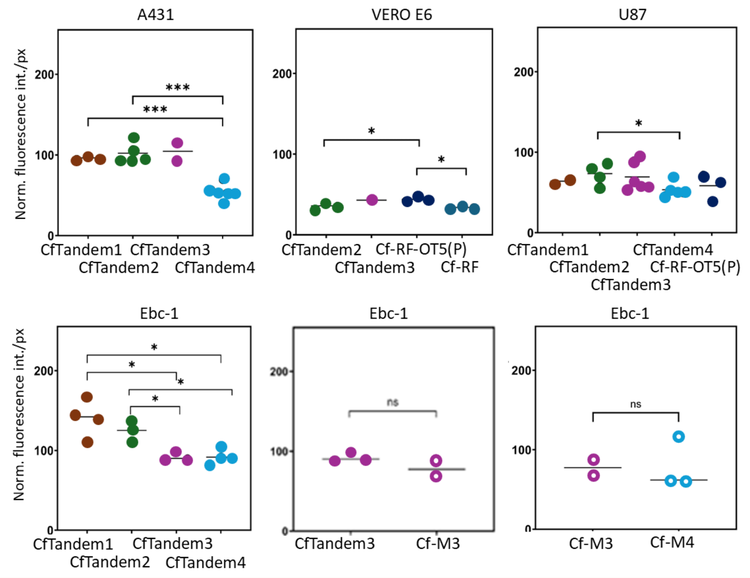
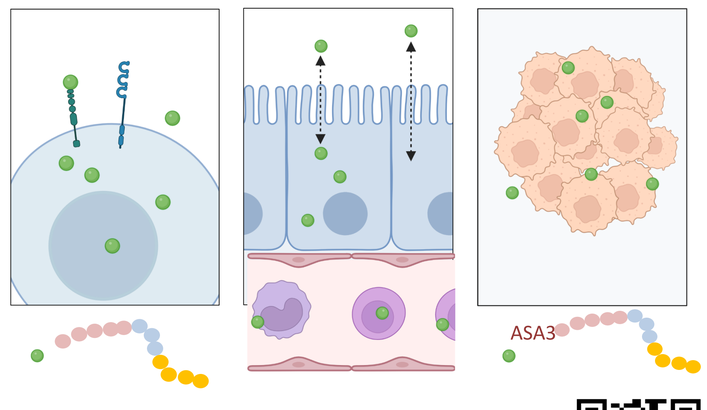


Figure 6. Penetration profile of tamdem derivatives on spheroids [2-4,11]



KEY FINDINGS AND CONCLUSION

1. **TANDEMS SHOWED ROBUST, CELL-DEPENDENT UPTAKE FAVORING EBC-1 AND H838 CELLS**
2. **EMPLOYING LINKER TUNED UPTAKE AND INTRACELLULAR TRAFFICKING**
3. **TANDEMS EXHIBITED ENERGY-DEPENDENT INTERNALIZATION UNLIKE CYTOPLASMIC PARENT RF**
4. **OT5(P)-TANDEMS PERFORMED BEST IN CALU-1 BARRIERS**
5. **H12-TANDEMS SHOWED DEEPER SPHEROID PENETRATION**
6. **TANDEMS DELIVERED ASA3 INTO TUMOR CELLS AND MADE THE CARGO EFFECTIVE**
7. **ASA3-CONJUGATES PRESERVED UPTAKE, PENETRATION AND CONFORMATIONAL FEATURES**



Acknowledgements: NNKFIH K142904, K137940, PD146764, 150838; VEKOP-2.3.3-15-2017-00020, 2.3.3-15-2017-00016; ELTE Excellence Fund EKA 2023/071-P085-1, National Cardiovascular Laboratory Program RRF-2.3.121-2022-00003, Therapeutic Thematic Programme TKP2021-EGA-23, EU HORIZON WIDERA 2023 IDP2Biomed 101160233.

Scan for full References

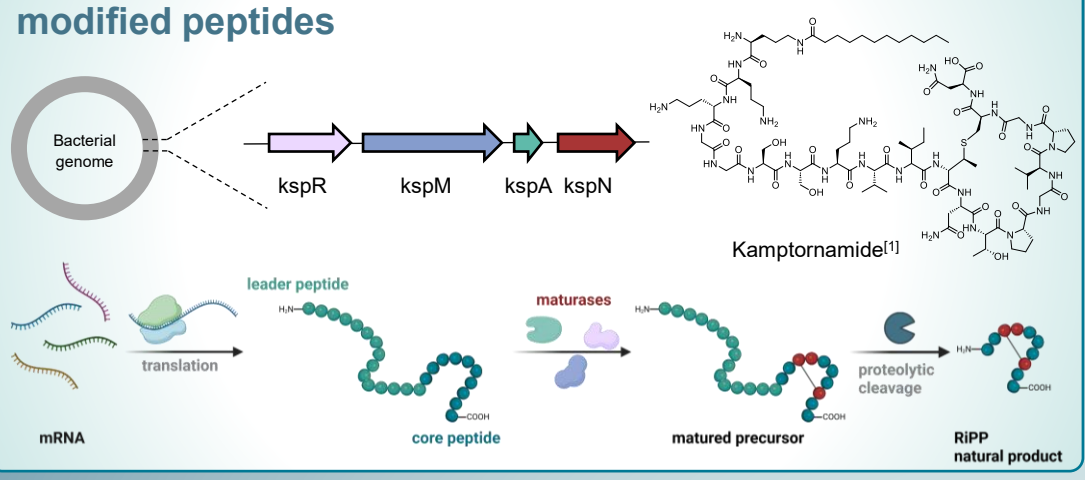
Structural characterization of fatty acid modifications in ribosomally encoded *N*-acylated lipopeptides

Julien A. König[1], Johannes A. Eckert[1], Ian S. Yunus[1], Gabriel Cervera Arriaga [1], Anna L. Vagstad*[1]
[1]Institute of Microbiology, Department of Biology, ETH Zürich

https://doi.org/10.17952/38EPS.2026.P447



RiPPs: ribosomally synthesized and posttranslationally modified peptides

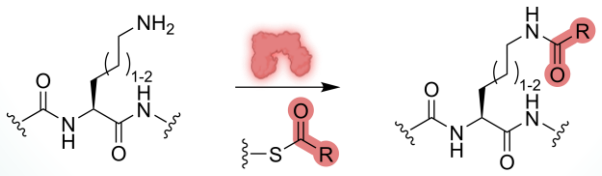


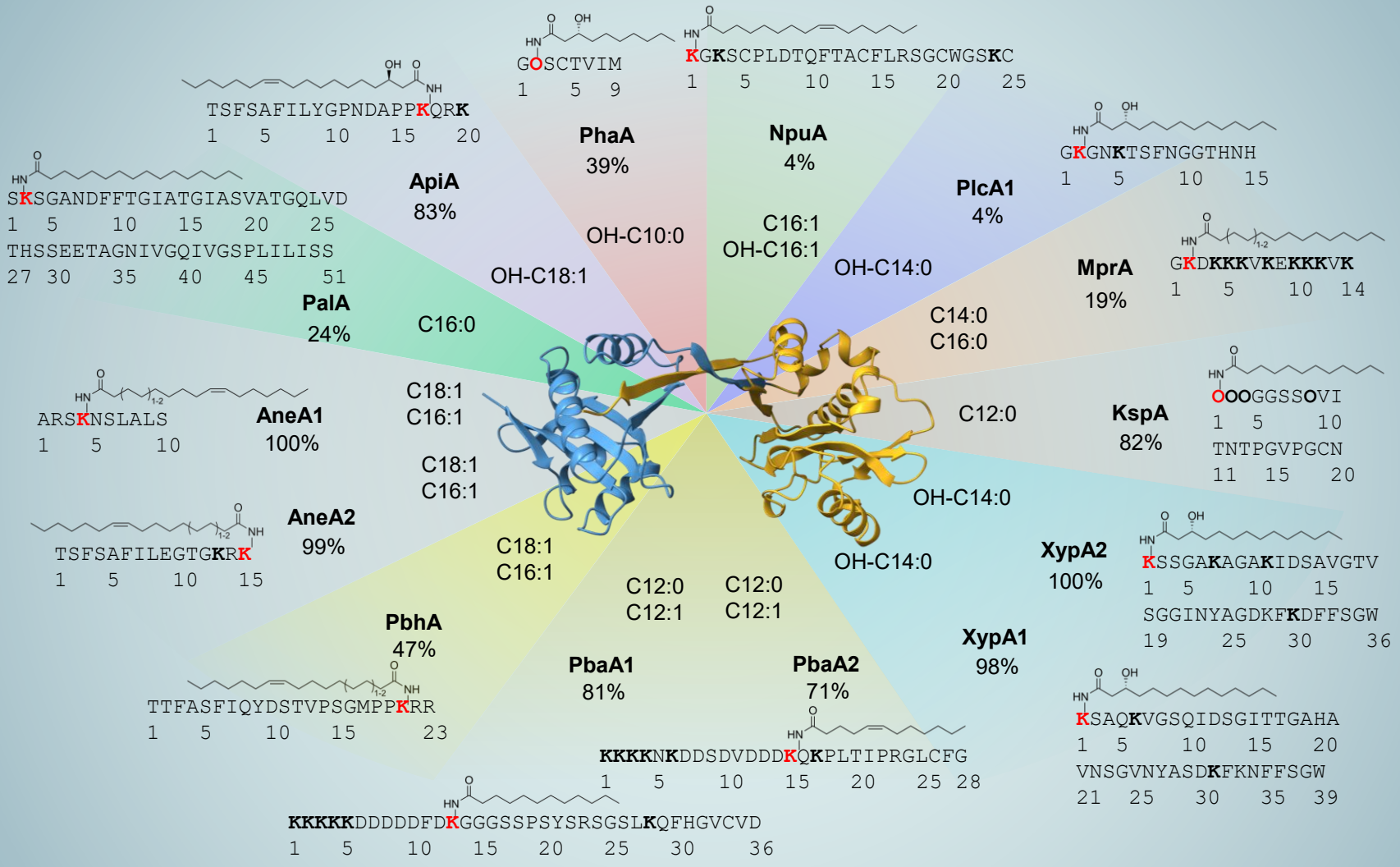
Lipopeptides

- Antimicrobial, antitumor, immunosuppressant and biosurfactant activities, as well as drug-delivery and vaccine agent applications.

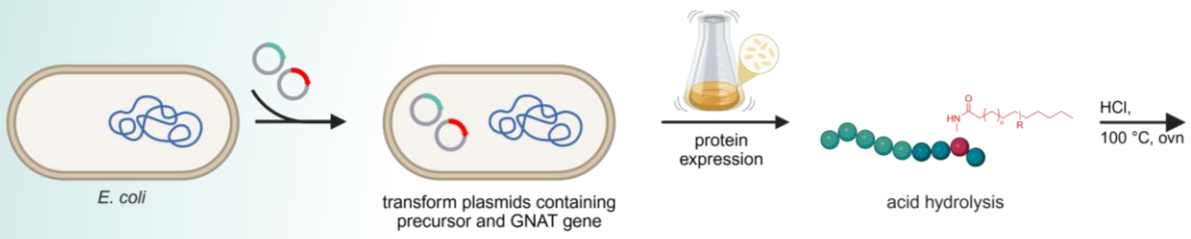
GNATs

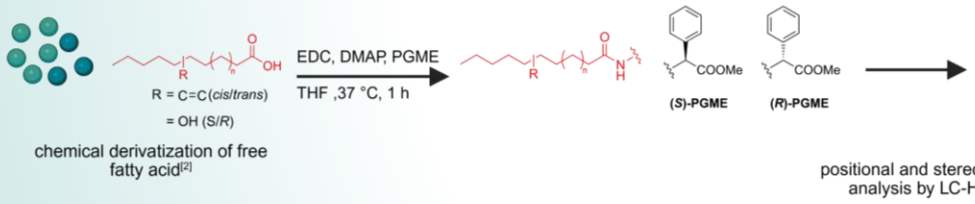
- GCN5-related *N*-acetyltransferases (GNATs) in RiPP biosynthetic pathways install defined fatty acid moieties regiospecifically onto the side chains of (hydroxy)ornithines and lysines.

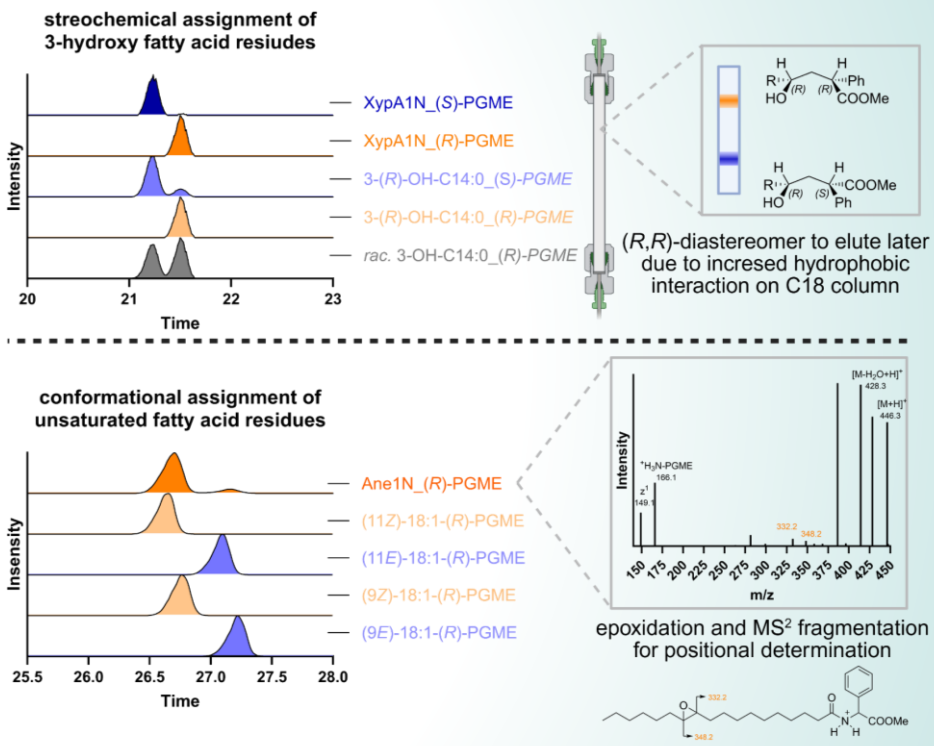




Workflow







References [1] F. Hubrich, N. M. Bösch *et al. Proc. Natl. Acad. Sci.* **2022**, *119*, e2113120119. [2] S. Um *et al. Anal. Chem.* **2025**, *97*, 12947–12952.

ETH piellab
Swiss National Science Foundation
NOVARTIS
LinkedIn

P305

Decoding Heme-Gαi Protein Crosstalk with Peptide Tools

Sabriye Aydogdu[1], Sonali M. Vaidya[1], and Diana Imhof[1]

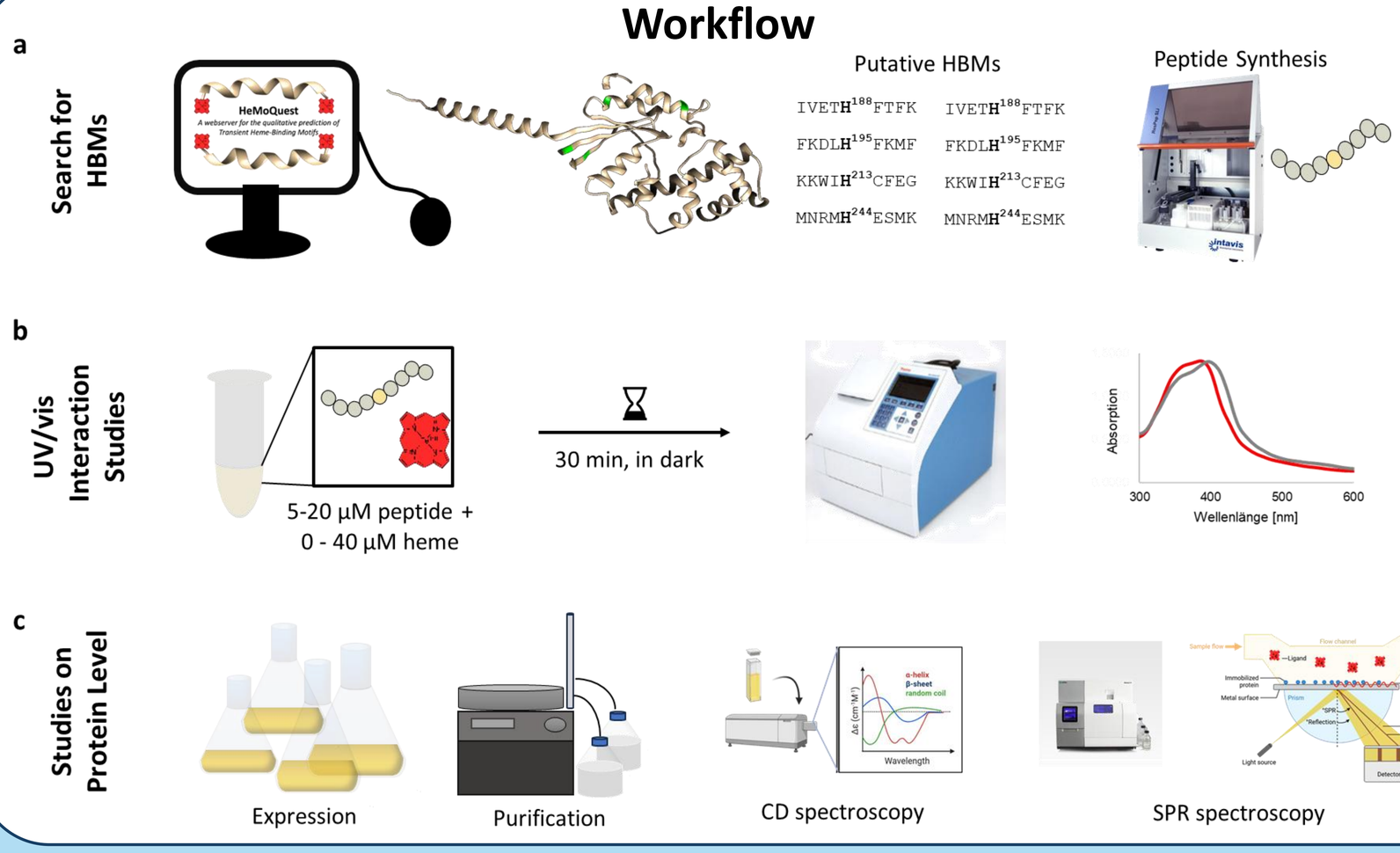
[1] Pharmaceutical Biochemistry and Bioanalytics, Pharmaceutical Institute, University of Bonn, Bonn, Germany
https://doi.org/10.17952/38EPS.2026.P305

UNIVERSITÄT BONN

Background

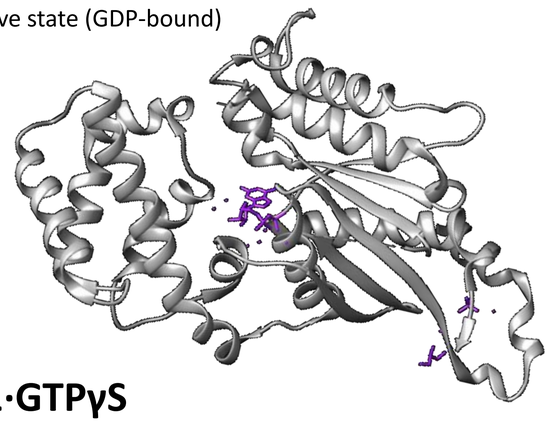
Heme is an iron-containing porphyrin that serves as an essential prosthetic group in proteins involved in oxygen transport, electron transfer, and catalysis. Beyond these classical functions, **heme can also act as a signaling molecule**. Recent evidence suggests that extracellular heme influences **G protein-coupled receptor (GPCR) signaling** in mouse models of sickle cell disease and intravascular hemolysis.[1] However, whether heme can **interact directly with G proteins** and modulate their signaling remains poorly understood. Gα proteins contain functional heme-binding motifs (HBMs) that allow direct heme binding and influence G-protein structure and activity. The aim is to characterize **heme binding to Gα proteins** and its consequences for **G-protein activity and function**.

Workflow



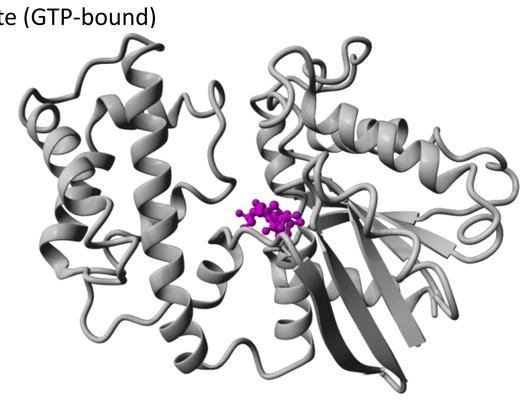
Gαi · GDP

inactive state (GDP-bound)



Gαi1·GTPγS

active state (GTP-bound)



PDB: 3UMR[6]. (purple: nucleotide)

Results & Discussion

HeMoQuest and *in silico* investigations identified potential heme-binding sites in Gαi. The corresponding motifs were synthesized by solid-phase peptide synthesis (SPPS) and analyzed for heme binding by UV/vis spectroscopy (Fig. 3, Tab. 1).

Sequence	Binding Affinity (K_D)
IVETH188FTFK	n.b
FKDLH195FKMF	12.5 µM
KKWIH213CFEG	5.2 µM
MNRMH244ESMK	36.5 µM

Table 1. UV/vis data for heme-binding to HBMs within Gαi.

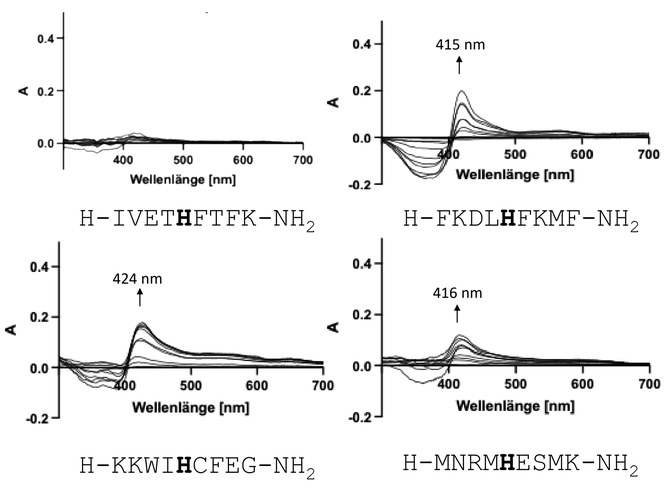


Figure 3. UV/vis difference spectra of HBMs in Gαi.

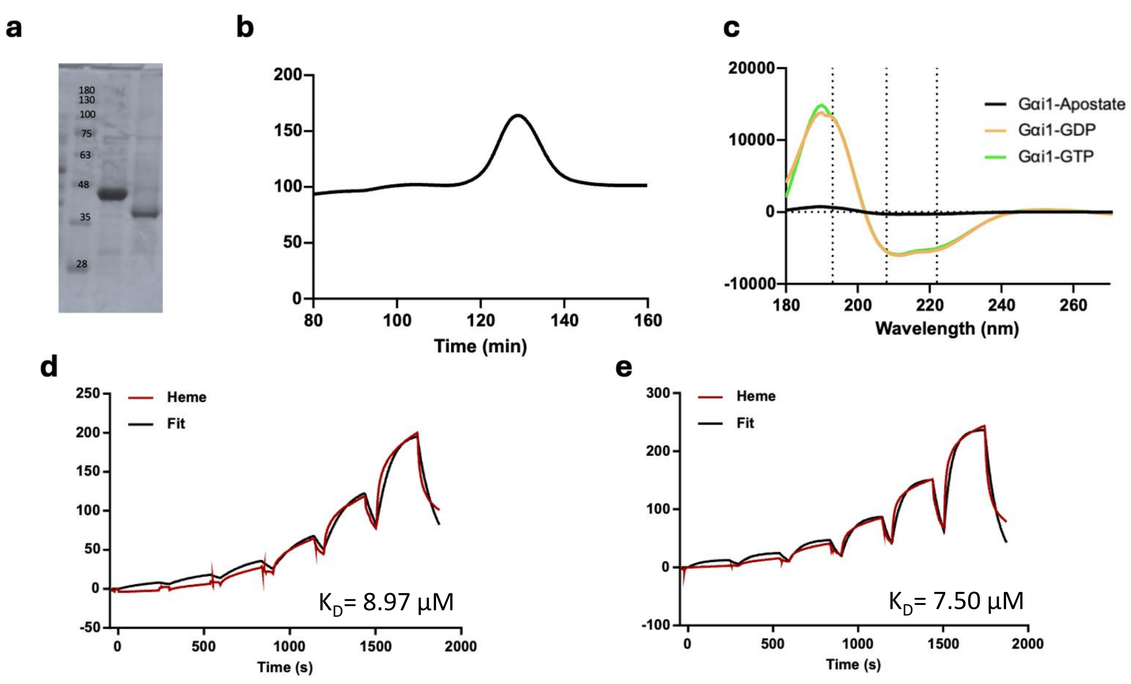


Figure 4. Overview of protein level studies. (a) 10%-SDS-Gel of Gαi before and after His_6-tag cleavage. (b) Chromatogram of size-exclusion chromatography of Gαi purification. (c) CD spectroscopy results of His_6-tag cleaved Gαi. (d,e) SPR sensograms of heme binding to Gαi-GDP and Gαi-GMPPNP, respectively.

References

1. Gavard J, Gutkind JS. Protein kinase C-related kinase and ROCK are required for thrombin-induced endothelial cell permeability downstream from Galpha12/13 and Galpha11/q.. J. Biol. Chem. 2008; 283.
2. Aydoğdu S, Pepanian A, Rathod DC, Schulz F, Imhof D. Physiological functions and structural features of Gα12/13 proteins. Biomed. Pharmacother.; 2025; 191.
3. Yang YM, Kuen DS, Chung Y, Kurose H, Kim SG. Gα12/13 signaling in metabolic diseases. Exp. Mol. Med.; 2020; 52.
4. Grunenwald A, Peliconi J, Zarantonello A, Dimitrov JD, Roumenina LT, Merle NS . HCAR2 is a novel receptor for heme. Blood Adv.; 2025; 9.
5. Paul George AA, Lacerda M, Syllwasschy BF, Hopp MT, Wißbrock A, Imhof D.. HeMoQuest: a webserver for qualitative prediction of transient heme binding to protein motifs. BMC Bioinformatics; 2020; 21
6. Pepanian A, Binbay FA, Pei D, Imhof D. Design, synthesis, and analysis of macrobicyclic peptides for targeting the Gαi protein. JPS 2024:30.

Conclusions & Outlook

- Gαi1 contains specific, surface-exposed HBMs.
- Predicted interactions were validated at the peptide and the protein level.
- Heme-G protein complex formation can affect Gαi catalytic activity.
- Further studies will explore the underexplored mechanisms by which heme may modulate GPCR/G-protein signaling in blood cells.

Acknowledgements

We gratefully acknowledge financial support from the DFG (to D.I.) and the University of Bonn.

Check Imhof Lab

Smart Amino Acid-based Nanovectors For RNA Anti-viral Therapeutics: Design, Synthesis And Physicochemical / Biological Characterization

M. Luísa C. do Vale[a]; Sandra G. Silva[a]; Pedro C. Cardoso[a], Isabel S. Oliveira[b], Eduardo F. Marques[b]

a) LAQV@REQUIMTE, Department of Chemistry and Biochemistry, Faculty of Sciences, University of Porto, Porto, Portugal
b) CIQUP@IMS, Department of Chemistry and Biochemistry, Faculty of Sciences, University of Porto, Porto, Portugal
https://doi.org/10.17952/38EPS.2026.P133

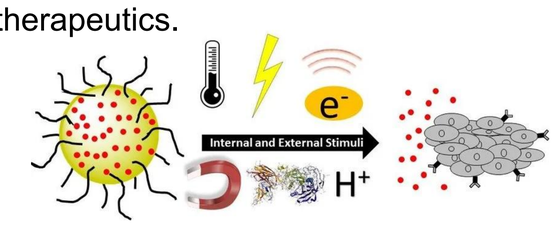
mcvale@fc.up.pt

1. Introduction

The development of effective therapeutics against viral diseases remains a major global health challenge. RNA-based strategies offer promising solutions by enabling the expression of therapeutic proteins or the silencing of pathological genes[1,2]. Their success, however, depends on nanocarriers capable of delivering RNA safely and efficiently. Gemini surfactants have emerged as versatile candidates for this purpose. When derived from natural building blocks, such as amino acids, peptides, or sugars, they also exhibit improved safety profiles, reinforcing their potential for biomedical applications[3].

2. Aim and Scope

Herein we present the work carried out at our laboratories, regarding the design and synthesis of versatile, stimuli-responsive, hence smart, amino acid and peptide-based gemini surfactants for RNA anti-viral therapeutics.

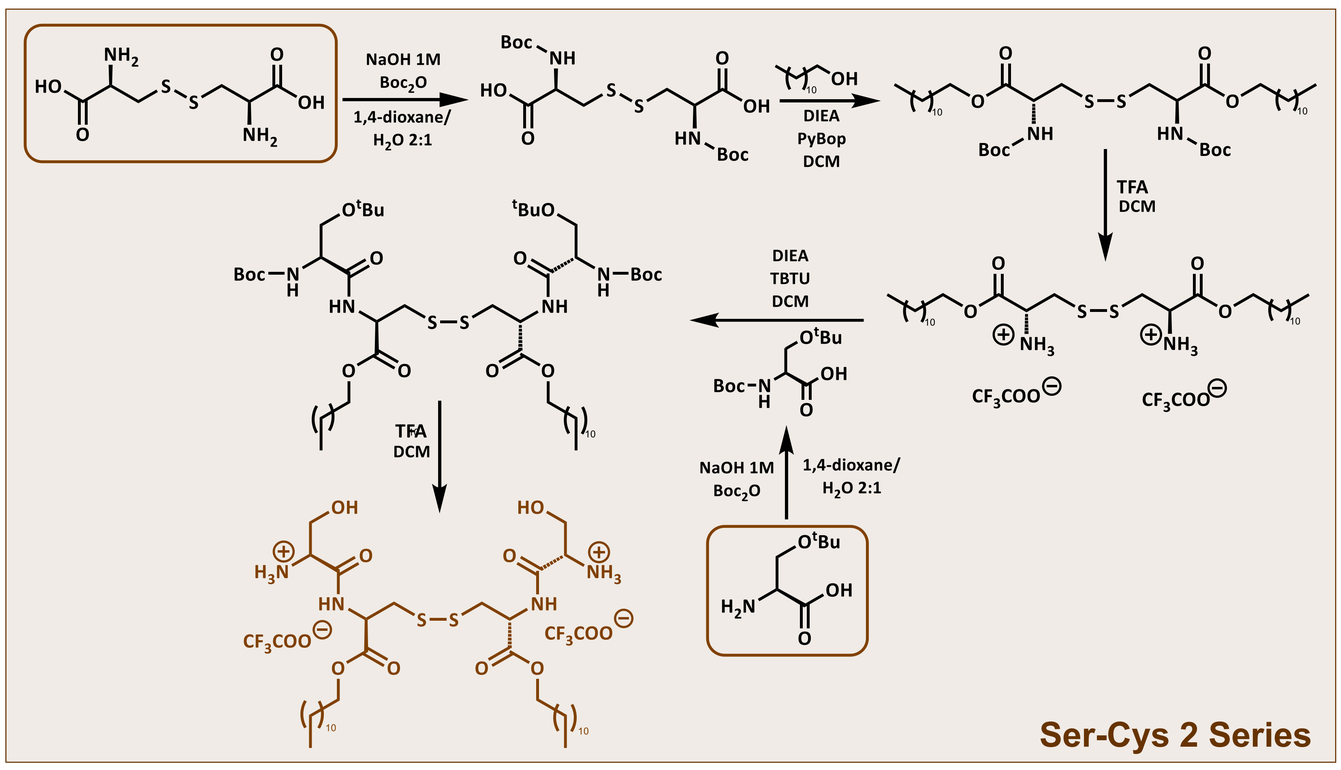


3. Results

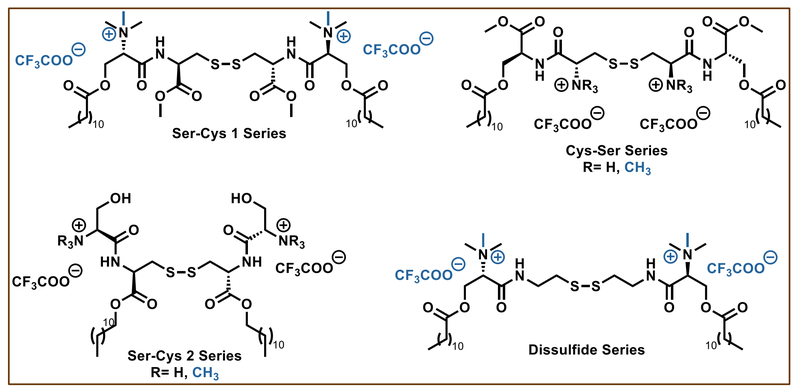
Design of amino acid-based gemini surfactants, **responsive to local pH and redox environment**, as nanovectors for viral infections – **Project SMART4VIR**.

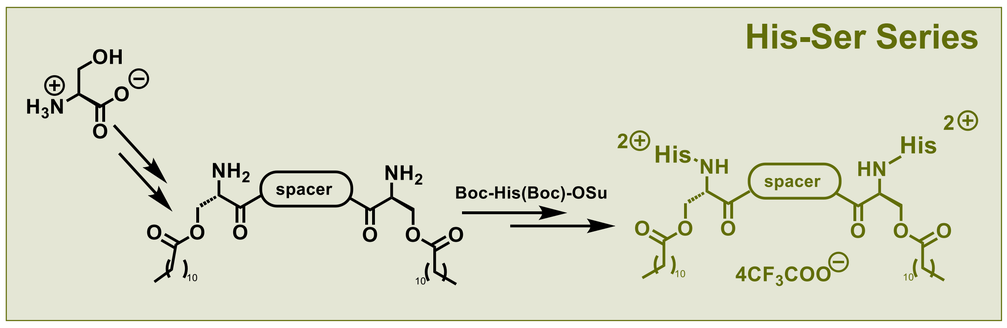
Surfactant-based RNA nanocarriers will change their properties along the delivery path to be effective in the different critical steps.

Design and Synthesis



Surfactants based on **serine** and **cystine** synthesized





Physical Chemistry

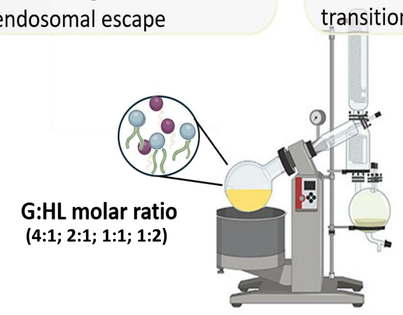
Development of surfactant / lipid vesicles

Novel Serine-derived gemini surfactants (G)

Positive charge
Ester linkages to facilitate endosomal escape

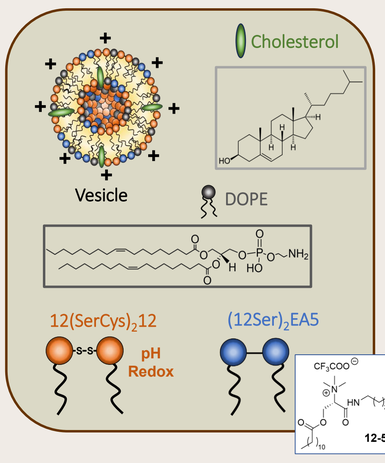
Helper lipid (HL)

Enhances bilayer fluidity and Promotes inverted phase transitions

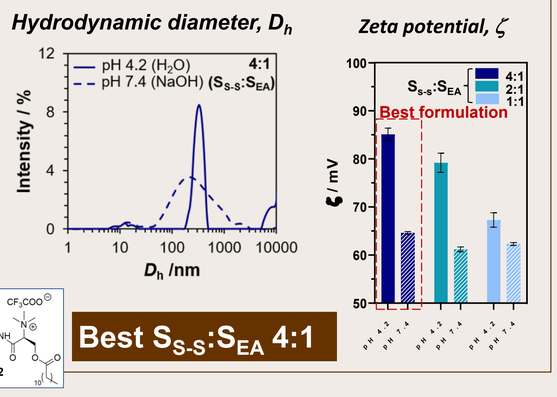


Developed systems show potential for stimuli-responsive intracellular gene delivery.

Ser-Cys 2 Series

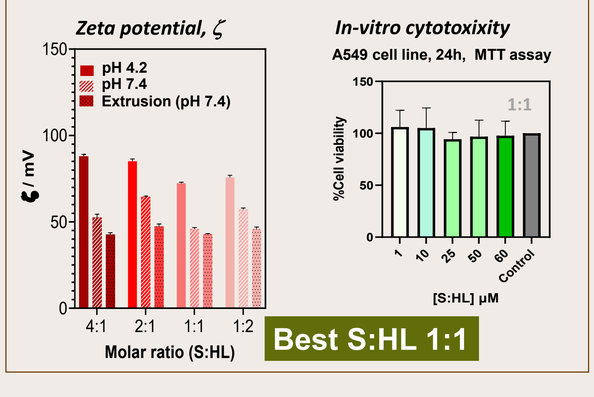


Optimization of the $S_{S\text{-}S}$:S_{EA} ratio



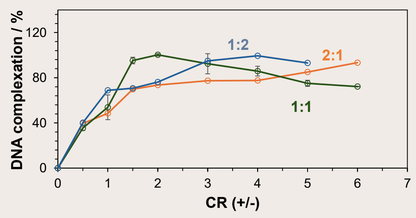
Best $S_{S\text{-}S}$:S_{EA} 4:1

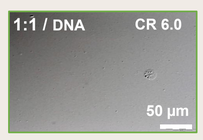
Optimization of the S:HL ratio, $S_{S\text{-}S}$:S_{EA} fixed (4:1)



Best S:HL 1:1

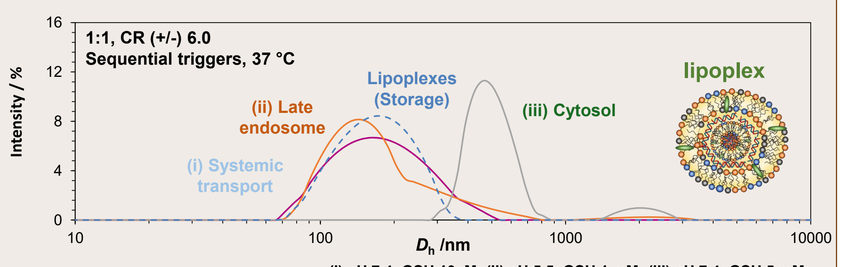
DNA complexation → lipoplexes





Light micrography of vesicles / DNA interactions

DNA release under cytosol mimicking conditions



(i) pH 7.4; GSH 10µM; (ii) pH 5.5; GSH 1 mM; (iii) pH 7.4; GSH 5 mM.

From D_h determinations

Mix 1:1(S:HL) successfully generates small, monodisperse lipoplexes

4. Conclusions

Amongst the surfactants based on serine and cystine/disulfide, the **Ser-Cys 2** derivative presented the best profile:

- The 1:1 (S:HL) formulation was identified as the optimal composition, combining efficient DNA complexation, high surface charge, and favourable size distribution.
- Lipoplexes exhibit high sequential stimuli-triggered destabilization, releasing the DNA under cytosol-mimicking conditions.

Preliminary studies highlight the promising profile of the **His-Ser** derivative. This surfactant exhibits pH- and temperature-dependent self-assembly, spontaneously forming vesicles at near-natural pH. Upon acidification, a transition to tubular aggregates occurs, leading to solution gelation. Moreover, it is non-cytotoxic up to 100 µM and promotes cell proliferation.

References

1. R.M. Meganck, R.S. Baric, *Nat. Med.,* **2021**, *27*, 401-410.
2. C. Wang, Y. Zhang, Y. Dong, *Acc. Chem. Res.*, **2021**, *54*, 4283-4293.
3. C. Costa, I.S. Oliveira, J.P.N. Silva, S.G. Silva, C. Botelho, M.L.C. do Vale, M. Oliveira, A.C. Gomes, E.F. Marques, *J. Colloid Interface Sci.*, **2021**, *584*, 34-44.

Funding / Acknowledgments

This work received **financial support** from PT national funds (FCT/MECI, Fundação para a Ciência e Tecnologia and Ministério da Educação, Ciência e Inovação) through project UID/50006/2025 DOI 10.54499/UID/50006/2025 – Laboratório Associado para a Química Verde – Tecnologias e Processos Limpos.
Thanks are due to project 20022.05543.PTDC – Smart4Vir. SGS acknowledges FCT for researcher employment contract through the Individual Call to Scientific Employment Stimulus, CEEIND/01932/2017/CP1427/CT0003. P.C. thanks FCT for BI-research grant REQUIMTE 2023-54.

https://doi.org/10.17952/38EPS.2026.P123

Macrocyclic Molecular Glues for the 14-3-3/ChREBP Interaction; Affinity and Cooperativity in an Inverse Relationship

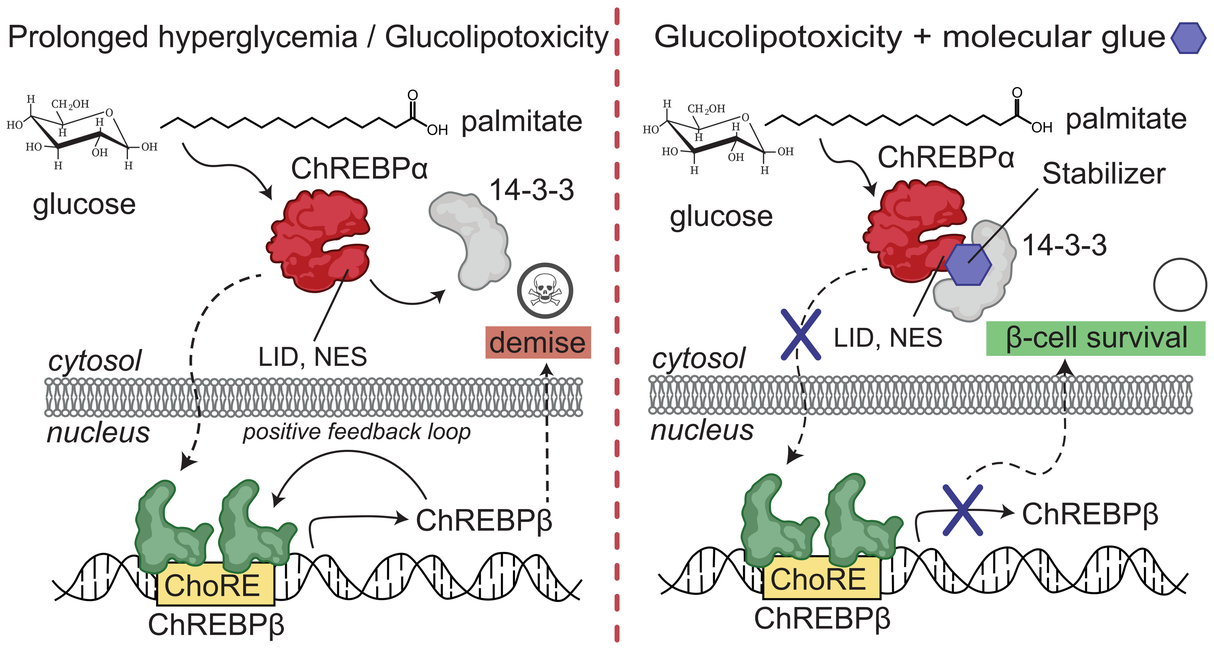
Merel A.W. van den Bosch,[a] Marloes A.M. Pennings,[a] Ansgar Oberheide,[a] Carlo J.A. Verhoef,[a] Christian Ottmann,[a] Albert J. Markvoort,[b] Galen P. Miley,[a] Luc Brunsveld*[a]



M.a.w.v.d.bosch@tue.nl

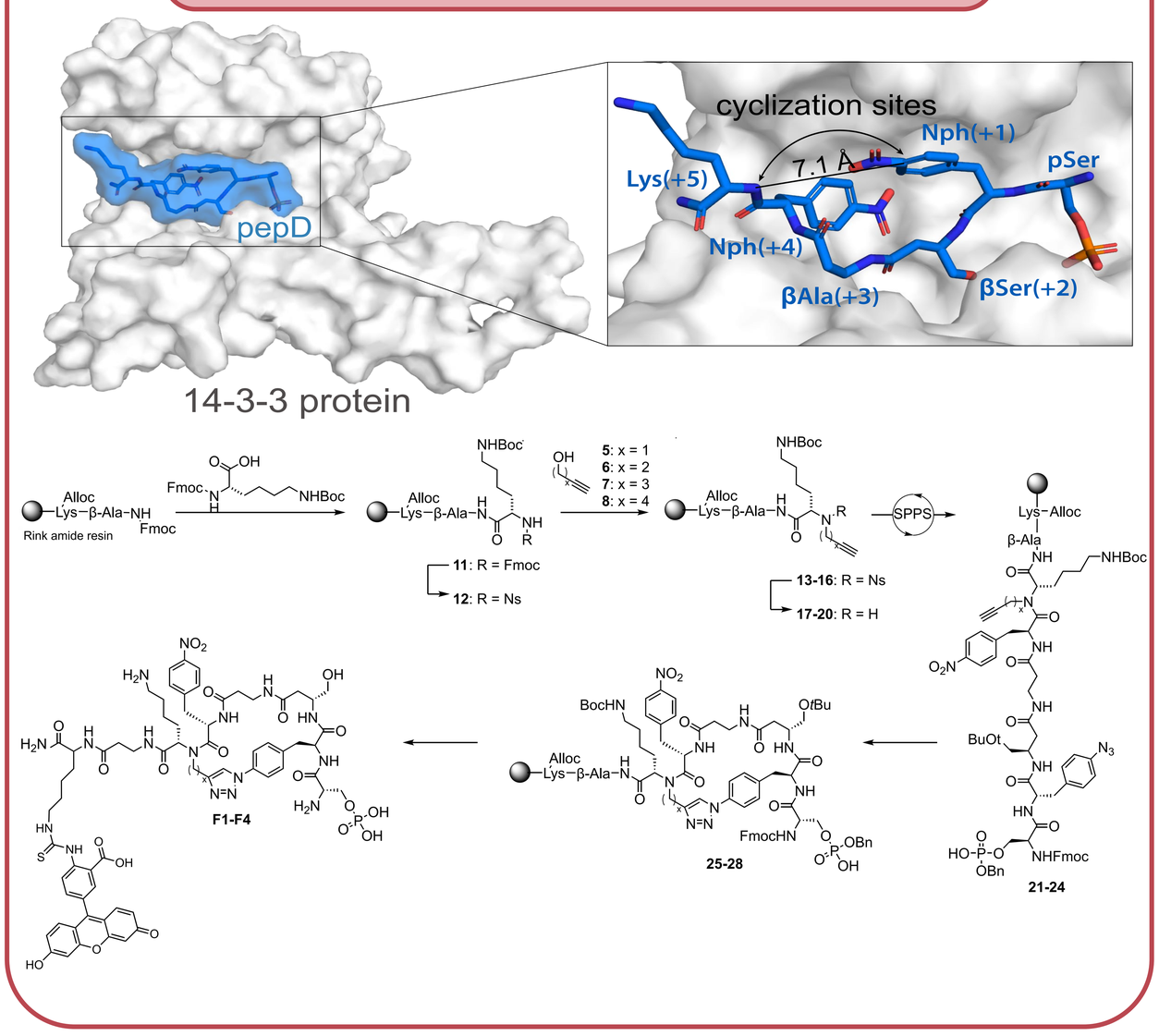
[a] Laboratory of Chemical Biology, Department of Biomedical Engineering and Institute for Complex Molecular Systems (ICMS), Eindhoven University of Technology, 5600MB, Eindhoven, The Netherlands
[b] Synthetic Biology Group, Department of Biomedical Engineering and Institute for Complex Molecular Systems (ICMS) Eindhoven University of Technology, 5600MB, Eindhoven, The Netherlands

1. The 14-3-3/ChREBPα interaction regulates β-cell fate

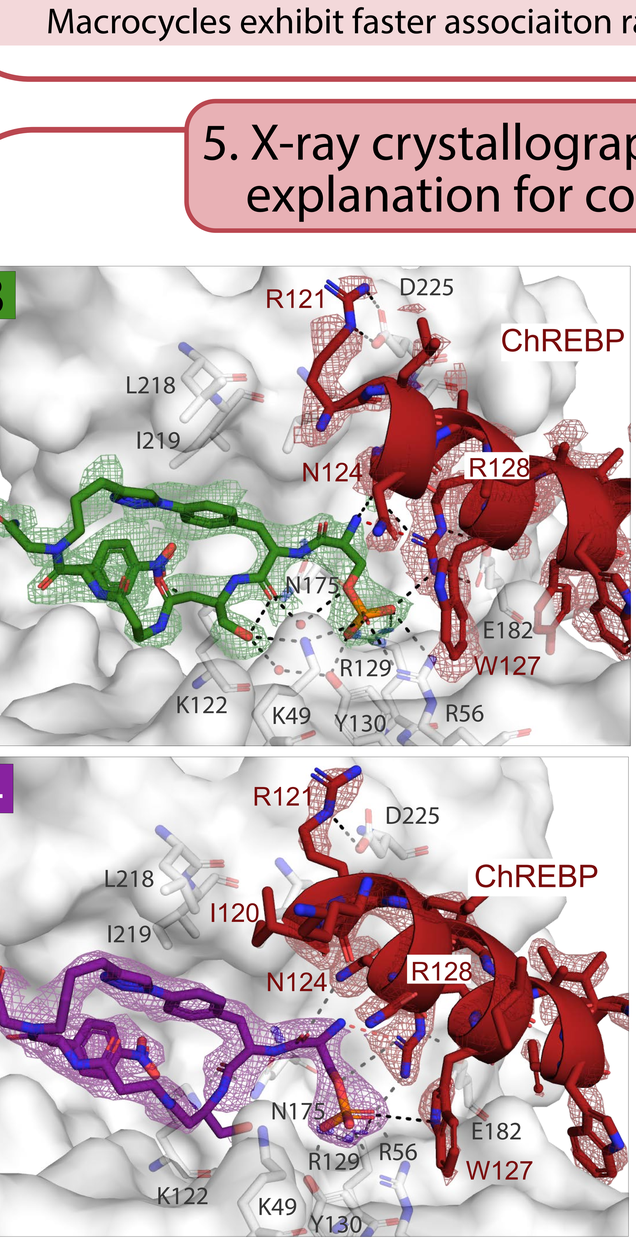


ChREBP as a glucose responsive transcription factor
Overexpression of ChREBPα leads to β-cell death
Stabilization of the 14-3-3/ChREBPα PPI rescues β-cells

2. Cyclization of previously discovered 14-3-3 peptidic molecular glue

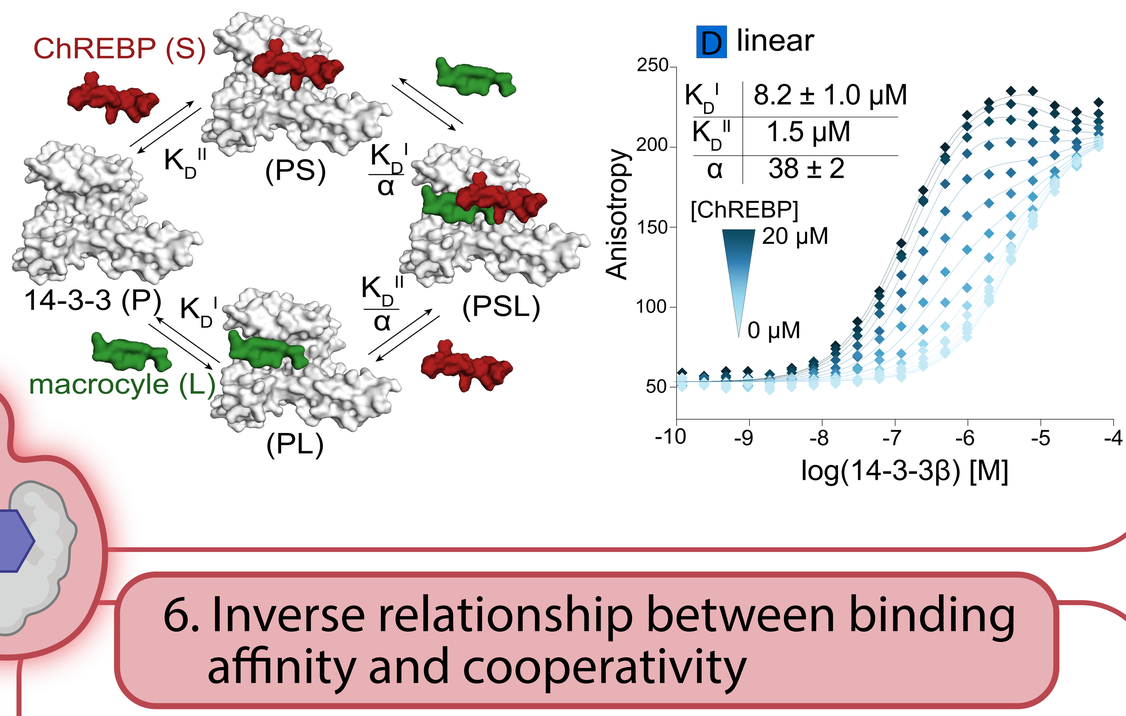


3. Cyclization leads to more favorable binding properties



Cyclization leads to more favorable entropy, leading to higher binding affinities
Macrocycles exhibit faster associaiton rates compared to linear peptide

4. Cooperativity as a measure for ternary complex formation

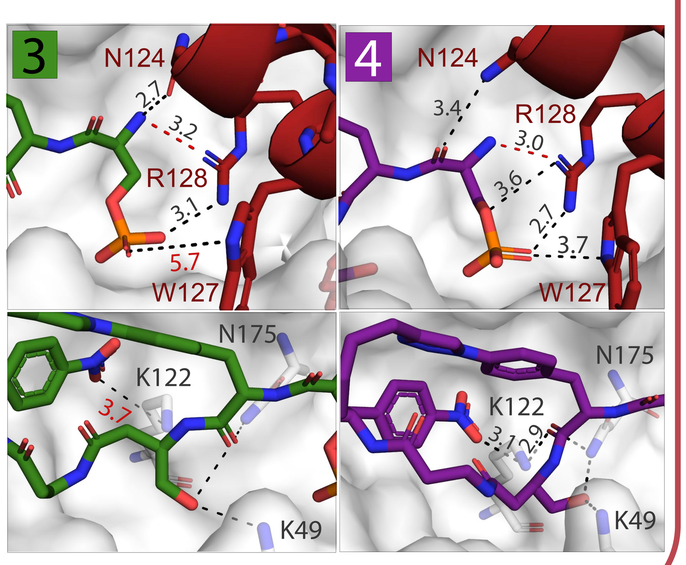


K_D^I	8.2 ± 1.0 μM
K_D^{II}	1.5 μM
α	38 ± 2

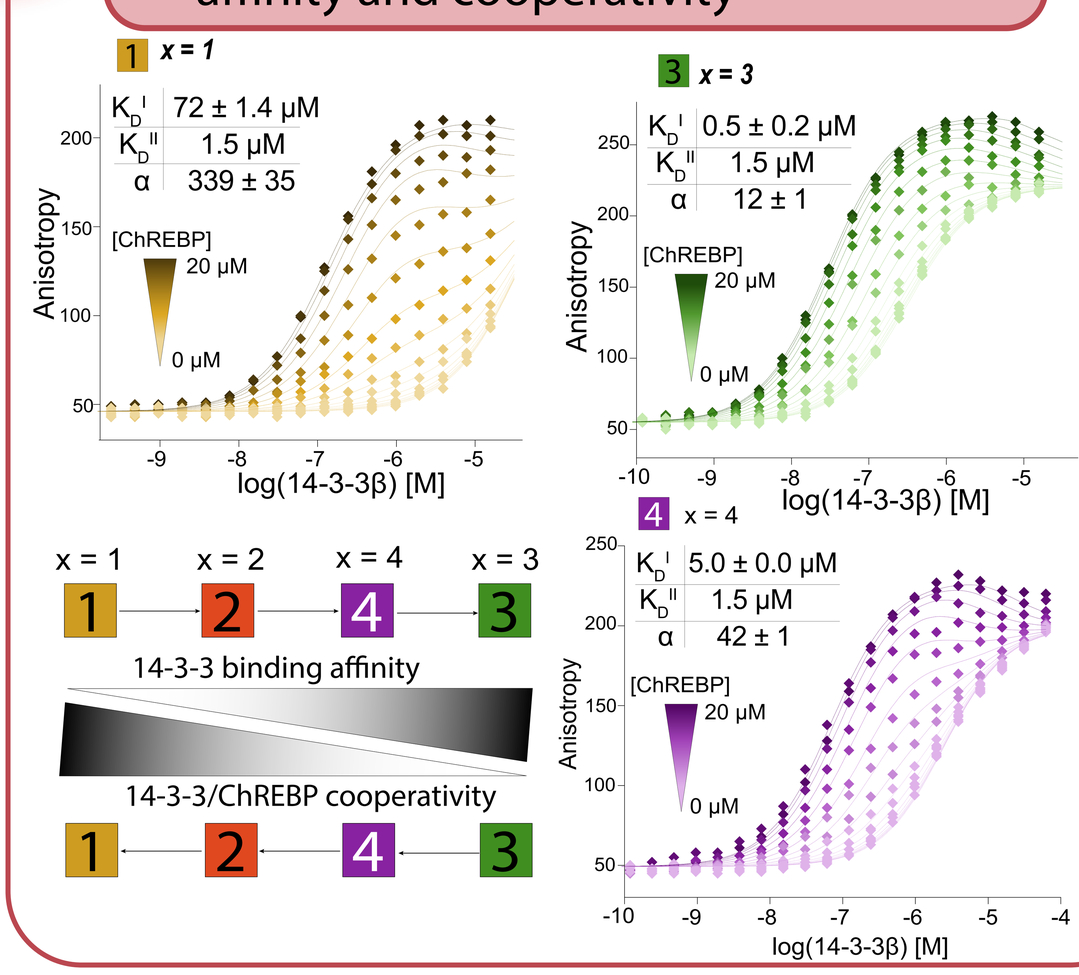
5. X-ray crystallography gives molecular explanation for cooperativity

Interactions at the macrocycle/ChREBP interface are the basis of cooperativity

Loss of hydrogen bonds in ternary complex gives structural explanation for higher cooperativity of macrocycle 4 compared to 3



6. Inverse relationship between binding affinity and cooperativity



K_D^I	72 ± 1.4 μM
K_D^{II}	1.5 μM
α	339 ± 35

K_D^I	0.5 ± 0.2 μM
K_D^{II}	1.5 μM
α	12 ± 1

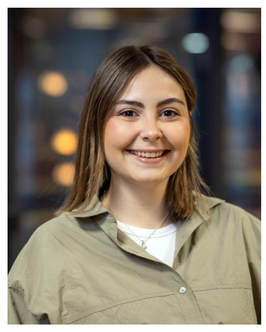
K_D^I	5.0 ± 0.0 μM
K_D^{II}	1.5 μM
α	42 ± 1

B.A. Somsen, F.W.B. Craenmehr, W.-H.W. Liu, A.A. Koops, M.A.M. Pennings, E.J. Visser, C. Ottmann, P.J. Cossar, L. Brunsveld, Functional Mapping of the 14-3-3 Hub Protein as a Guide to Design 14-3-3 Molecular Glues. Chem. Sci. 2022.

N.H.J. Geertjens, P.J. de Vink, T. Wezeman, A.J. Markvoort, L. Brunsveld, Straightforward Model Construction and Analysis of Multicomponent Biomolecular Systems in Equilibrium. RSC Chem Biol 2023, 4 (4), 252 – 260.

L.S. Katz, E.J. Visser, K.F. Plitzko, M.A.M. Pennings, P.J. Cossar, I.L. Tse, M. Kaiser, L. Brunsveld, C. Ottmann, D.K. Scott, Molecular Glues of the Regulatory ChREBP/14-3-3 Complex Protect Beta Cells from Glucolipotoxicity. Nat Commun 2025, 16 (1), 2110.

CYTOSKELETON STABILIZED ARTIFICIAL CELLS AND THEIR DYNAMIC BEHAVIOUR



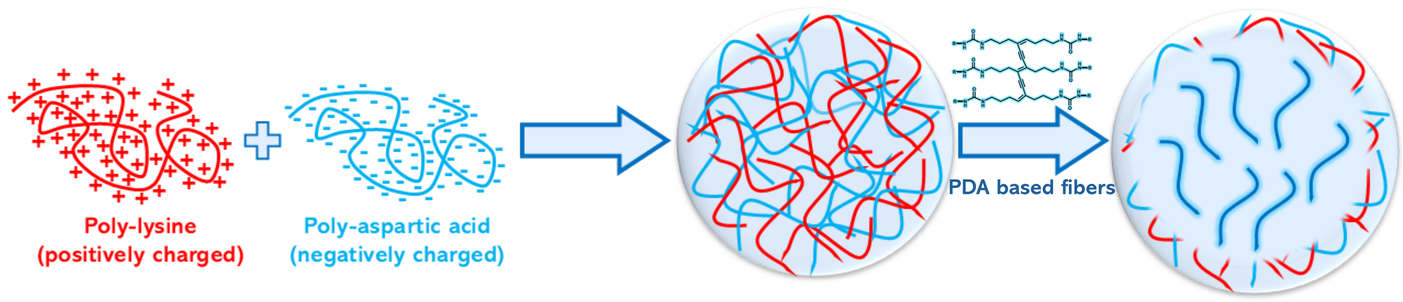
Victoria Remacha[1], Lars Paffen[1], Andoni Rodríguez[1], Angshuman Das[1], Roi Lopez[1], Jan van Hest[1].

[1]Eindhoven University of Technology, department of Chemical Engineering and Chemistry, Bio-Organic Chemistry Group, De Groene Loper 3, 5612 AE Eindhoven/Netherlands, m.v.remacha.goni@tue.nl

https://doi.org/10.17952/38EPS.2026.P545

INTRODUCTION

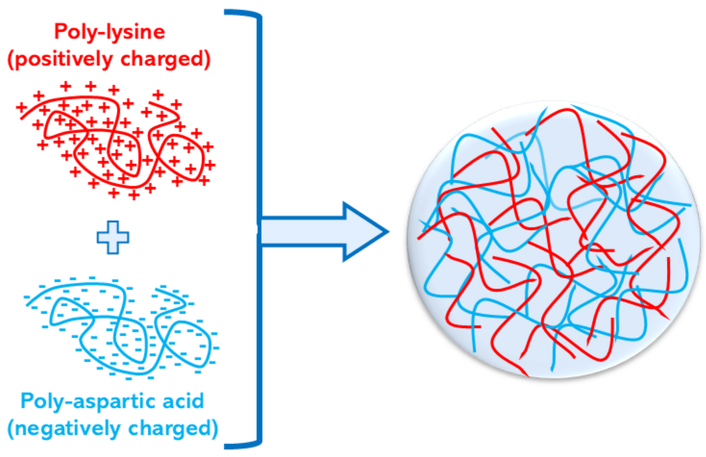
The development and characterization of **artificial cells** is a research field of high potential because these artificial systems can **mimic features and functions of life**, being able to exchange biomolecules with each other or respond to changes in their environment as pH or temperature, which makes them suitable for **biomedical applications.**[1]



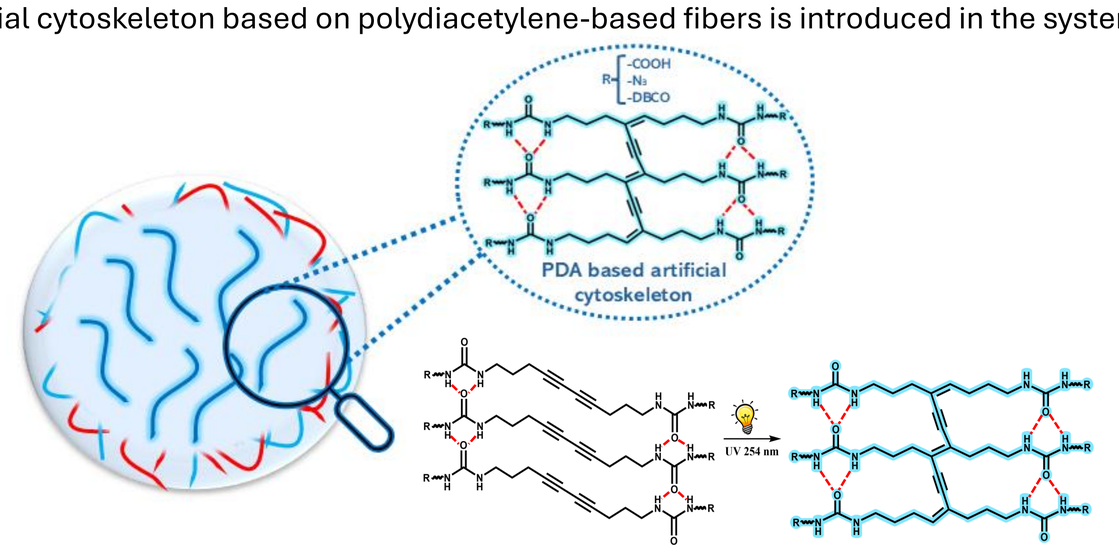
The **objective** of this project is to develop an artificial cell system based on **phase-separated polypeptides** and introduce inside it an **artificial cytoskeleton** based on **polydiacetylene fibers.**[3]

METHODOLOGY

Our artificial cells are originated by mixing of two opposite charged polypeptides: poly-lysine and poly-aspartic acid, leading to micron-sized droplets.

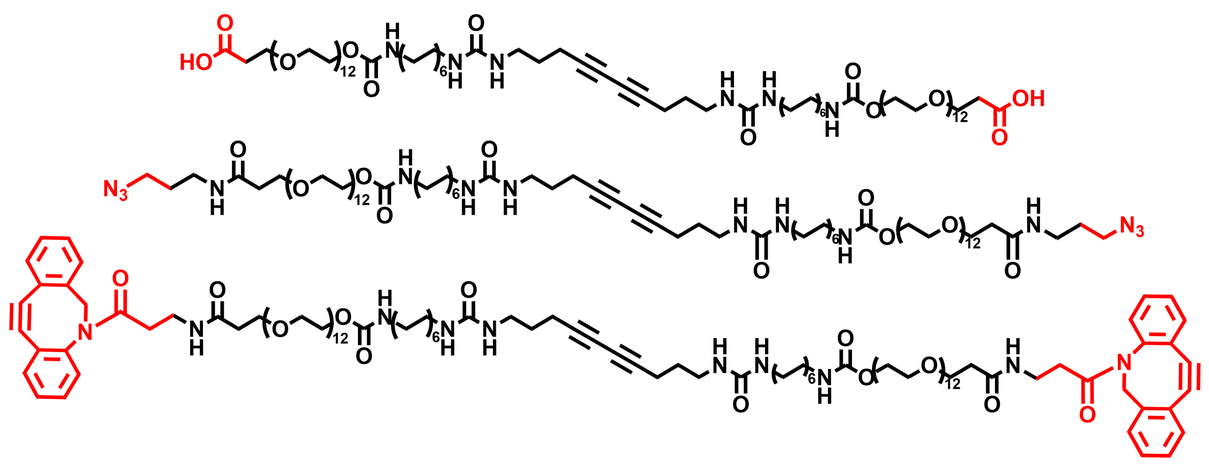


An artificial cytoskeleton based on polydiacetylene-based fibers is introduced in the system.[3,4]



The self assembly of the fibers is possible due to the hydrogen bonds between the bis-urea and the carbonyl groups, and the π-π stacking of the diacetylene backbone.[3,4]

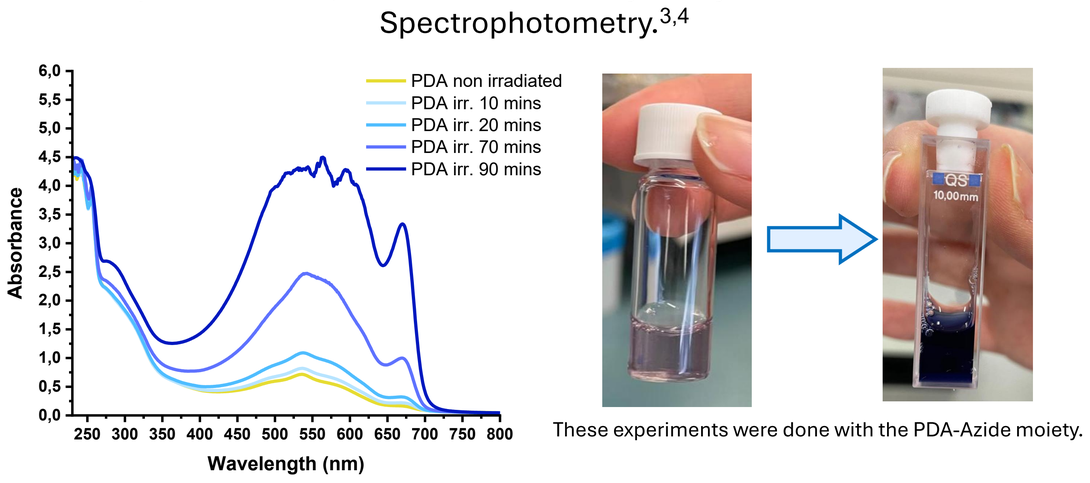
The photopolymerization induces a conjugated system, which stabilizes the fibers self-assembly and presents self-fluorescence.[3,4]



The terminal groups of these molecules allow them to be functionalized with peptides and small biomolecules such as DNA, which will be explored in the future.[3]

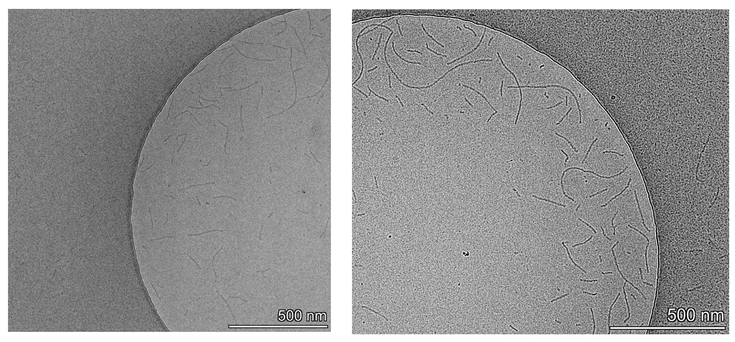
RESULTS

The photopolymerization of the fibers was achieved, showing a color change from transparent to blue, which was also analyzed by UV-Vis Absorbance Spectrophotometry.[3,4]

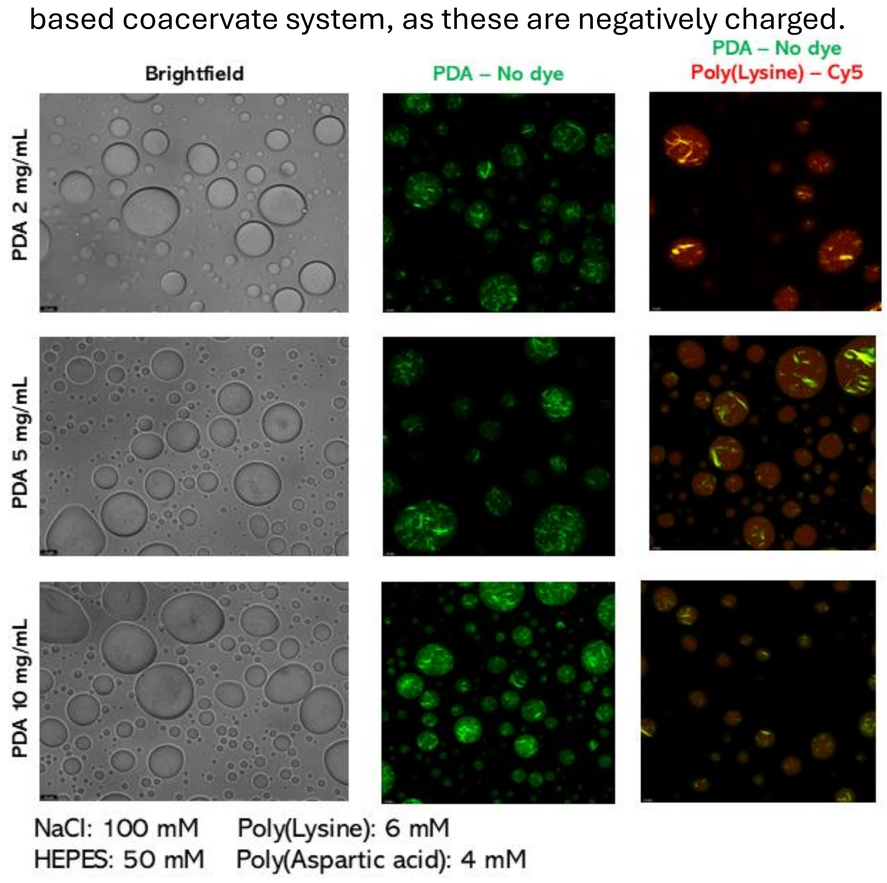


These experiments were done with the PDA-Azide moiety.

The obtained morphology was characterized by **Cryo-TEM**. PDA-COOH fibers are approximately 6 nm thick and 100-400 nm long.[3]



PDA-Azide fibers were successfully introduced into the positive polypeptide-based coacervate system, as these are negatively charged.



CONCLUSIONS AND OUTLOOK

- ✓ **Polydiacetylene-backboned molecules self-assemble** into **fibers** by hydrogen bonding and π-π stacking , followed by stabilization by photopolymerization.
- ✓ The **photopolymerization** of the **polydiacetylene-based molecules** leads to a color change and autofluorescence of the fibers.
- ✓ **Polydiacetylene fibers** have been successfully introduced in the **polypeptide-based coacervate system.**
- ✓ Introduction of biomolecules into the artificial cell system will be performed in the future by linking them to the PDA fibers.

REFERENCES

1.Cook AB, Novosedlik S, van Hest J. Complex Coacervate Materials as Artificial Cells. Accounts of Materials Research. 2023 Feb 13;4(3):287–98.
2.Cook AB, Schlich M, Manghnani PN, Moore TL, Paolo Decuzzi, Palange AL. Size effects of discoidal PLGA nanoconstructs in Pickering emulsion stabilization. Journal of Polymer Science. 2022 Jan 20;60(9):1480–91.
3.Novosedlik S, Reichel F, Thijs van Veldhuisen, Li Y, Wu H, Janssen H, et al. Cytoskeleton-functionalized synthetic cells with life-like mechanical features and regulated membrane dynamicity. Nature Chemistry [Internet]. 2025 Jan 3; Available from: https://www.nature.com/articles/s41557-024-01697-5
4.Pal A, Panayiotis Voudouris, Marcel, Pol Besenius, Wyss HM, Volkan Degirmenci, et al. Topochemical polymerization in self-assembled rodlike micelles of bisurea bolaamphiphiles. Soft Matter. 2013 Dec 2;10(7):952–2.

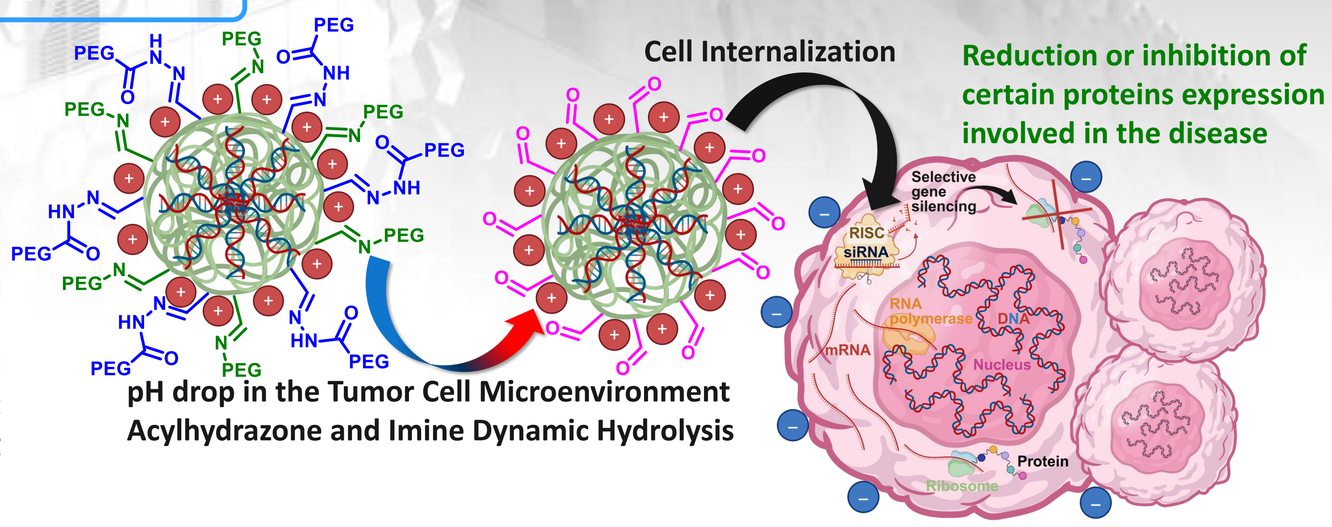
This project has been founded by ERC with the grant PRO-ARTIS-ERC-2023-ADG-ST-101141866-ST

Dynamic PEGylation of Peptide-based Nanoparticles for siRNA Delivery

Jules Vastra[a], **Thania Hammoum**[b], **Prisca Boisguérin**[b], **Sébastien Ulrich**[a]
[a] *IBMM, Université de Montpellier, CNRS, ENSCM, Montpellier, France*
[b] *PhyMedExp, Université de Montpellier, INSERM, CNRS, Montpellier, France*
E-mail : jules.vastra@etu.umontpellier.fr
https://doi.org/10.17952/38EPS.2026.P526

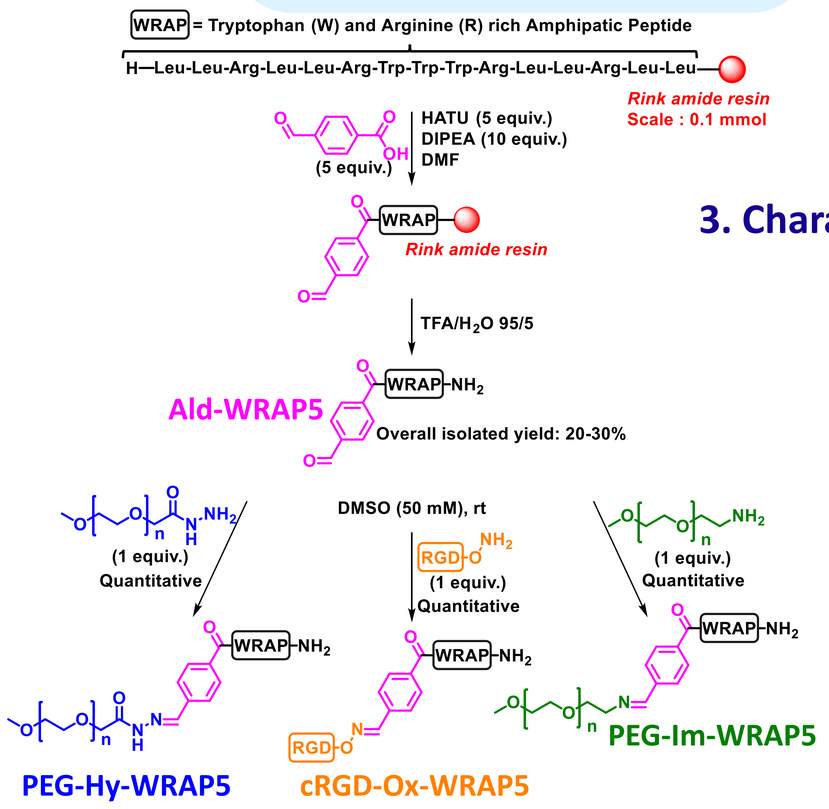
Project Motivation

Despite recent successes in the design of effective nucleic acid vectors enabling to reach therapeutic applications,[1,2] there are still huge opportunities for improvement since only less than 5% of the RNA payload actually ends up being released by the nanoparticles.[3] Although PEGylation of nanoparticles is a general strategy to improve the circulation time *in vivo*, this shielding is often detrimental to cell uptake and nucleic acid release, which calls for a dynamic PEGylation approach.[4] In this context, we recently reported on a Tryptophan and Arginine rich Amphipatic Peptide (WRAP), previously shown to effectively complex and deliver siRNA,[5] coupled to a PEG 2000 via an acylhydrazone linkage, and undergoing a pH-controlled dePEGylation.[6] Although this work set a nice proof-of-concept, the kinetics and efficacy of dePEGylation were unfortunately not fitted for a real application, with half-lives at pH 4 of 2 to 8 hours. In this presentation, we will describe a **new approach combining multiple dynamic linkages in order to better tune the dePEGylation process**.

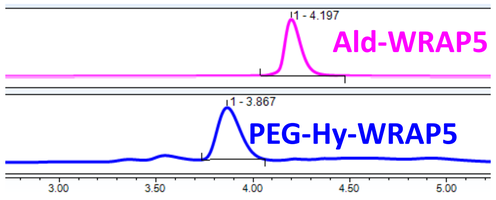


Design, Synthesis and Characterization of Acylhydrazone and Imine PEG-WRAP5 Conjugates

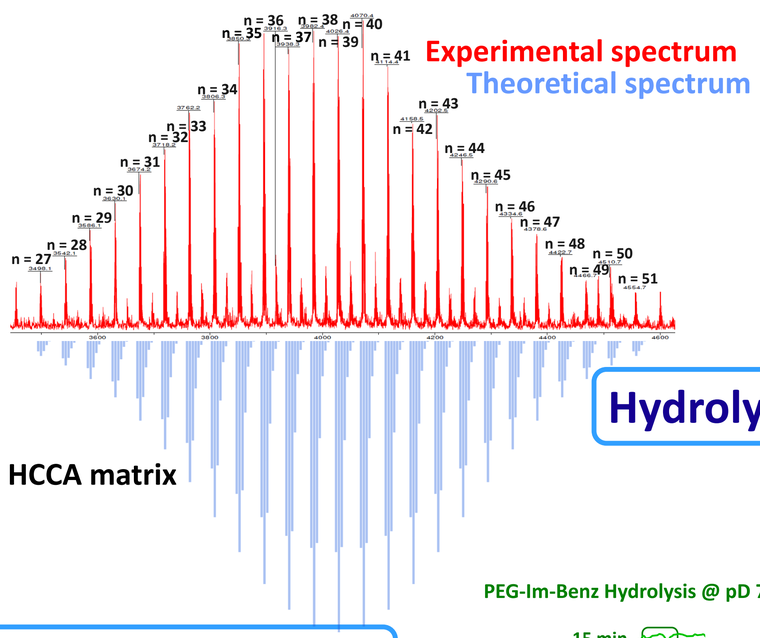
1. Design and Synthesis



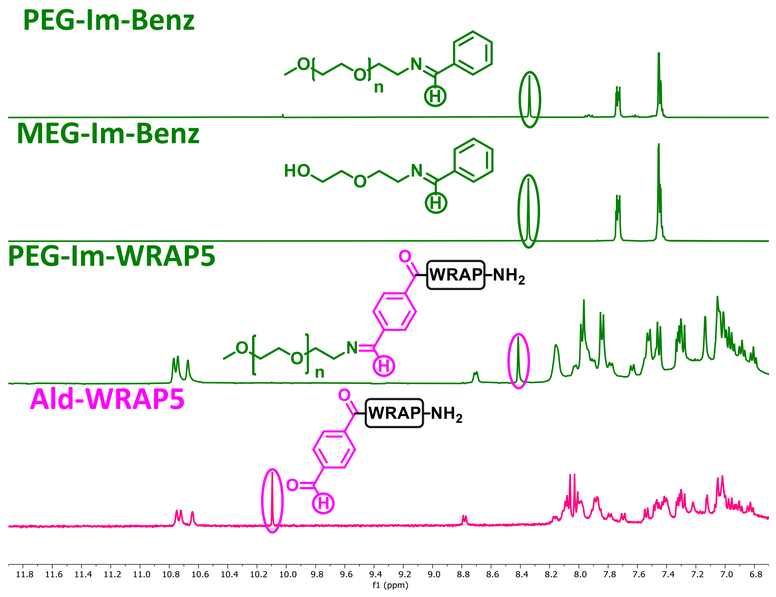
2. HPLC Reaction Monitoring



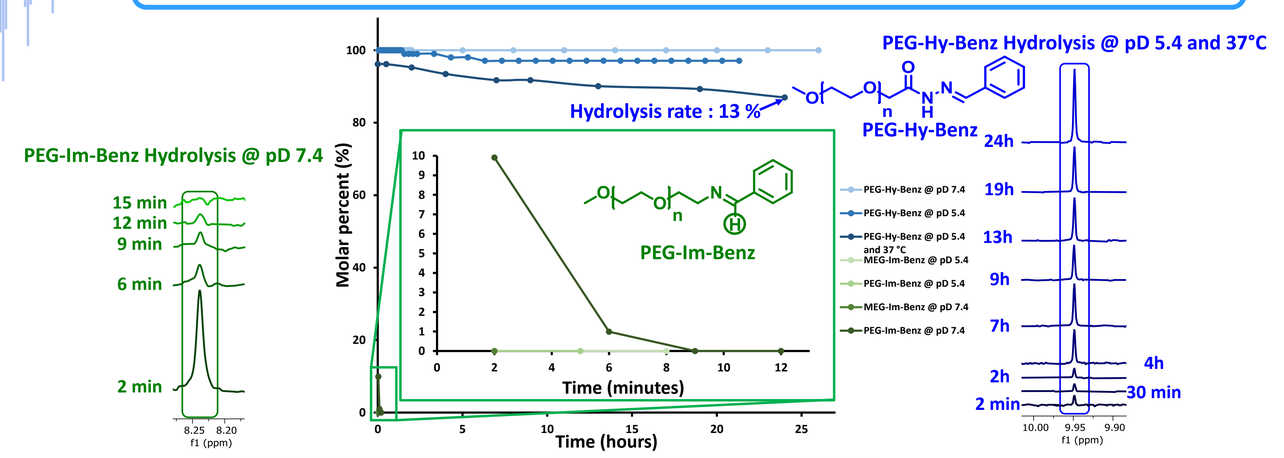
3. Characterization of PEG-Hy-WRAP5 by MALDI-MS



4. ^{1}H NMR of Imine Conjugates



Hydrolysis Kinetics of Acylhydrazone and Imine Bonds

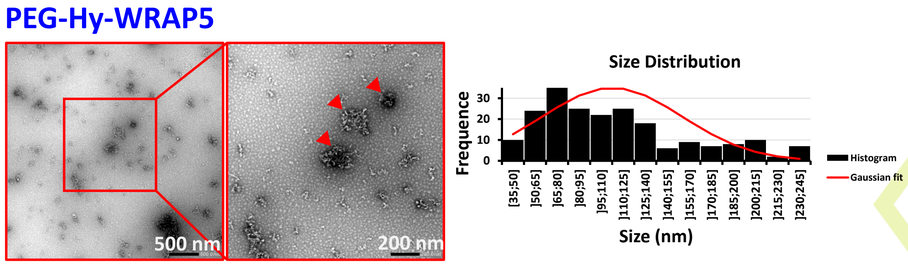


Nanoparticle Characterization by TEM, DLS and ζ Potential

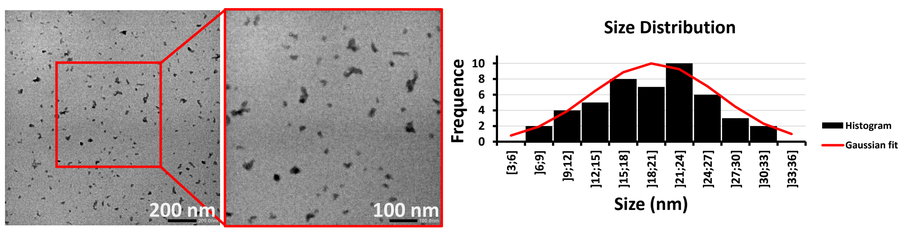
Formulation conditions:
Conjugate/siRNA 20/1 in H_2O/EtOH 80/20
5% glucose (m/V) for DLS and ζ potential and NaCl 1 mM for ζ potential

Nanoparticles	Ald-WRAP5	PEG-Hy-WRAP5	PEG-Im-WRAP5
Size Intensity (nm)	124.9 ± 1.3	162.1 ± 2.3	164.5 ± 4.4
PdI	0.244 ± 0.012	0.303 ± 0.038	0.179 ± 0.010
Size Number (nm)	44.2 ± 22.6	80.9 ± 12.6	29.3 ± 5.5
ζ potential (mV)	+ 20.8 ± 2.1	+ 25.1 ± 5.7	+ 43.3 ± 2.5

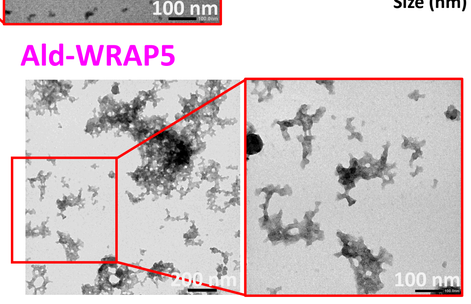
PEG-Hy-WRAP5



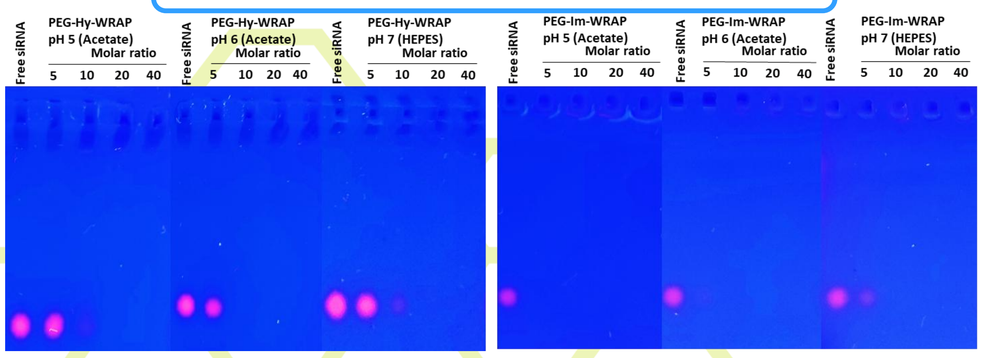
PEG-Im-WRAP5



Ald-WRAP5

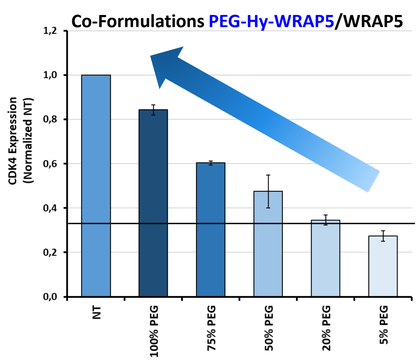


Evidence of siRNA Complexation

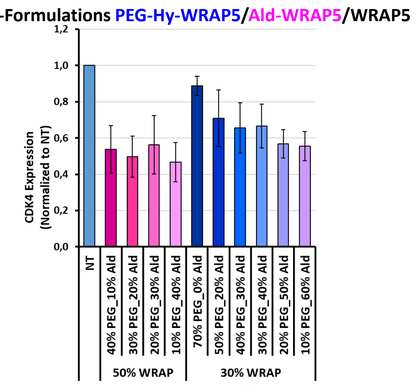


Biological Activity in GIST-T1 Cells

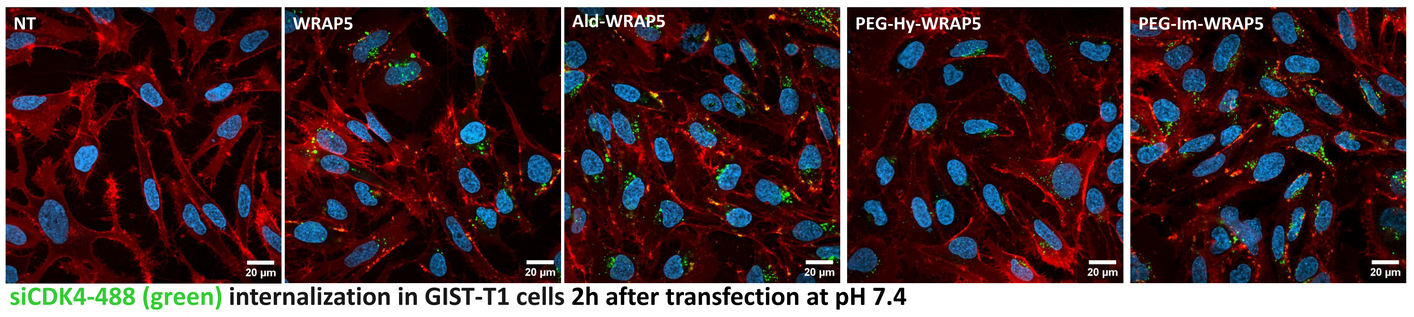
Shielding Effect of PEGylation



Potential of dePEGylation



Retention of activity when WRAP5 and Ald-WRAP5 are co-formulated



siCDK4-488 (green) internalization in GIST-T1 cells 2h after transfection at pH 7.4
Nuclei Hoechst (cyan)
Cytoskeletons phalloidin (red)

Conclusions and Outlook

- Effective **diversification** of Ald-WRAP5 using unique conditions to synthesize conjugates featuring distinct **acylhydrazone**, **imine** and **oxime** linkages, exhibiting **different hydrolysis stabilities**
- Significant **shielding effect** observed when nanoparticles are PEGylated and **retention of activity** when **WRAP5** and Ald-WRAP5 are **co-formulated**

Perspectives:

- New co-formulations containing **PEG-Hy-WRAP5** and **PEG-Im-WRAP5**

References

1. Egli, M., Manoharan, M. *Nucleic Acids Res.* **2023**, *51*, 2529-2573
2. Kulkarni, J. A., Witzigmann, D., Thomson, S. B., Chen, S., Leavitt, B. R., Cullis, P. R., Van der Meel, R. *Nat. Nanotechnol.* **2021**, *16*, 630-643
3. Mrksich, K., Padilla, M. S., Mitchell M. J. *Adv. Drug Deliv. Rev.* **2024**, *214*, 115446
4. Gao, Y., Joshi, M., Zhao, Z., Mitragotri, S. *Bioeng. Transl. Med.* **2024**, *9*, e10600
5. Konate, K., Dussot, M., Aldrian, G., Vaissière, A., Viguier, V., Ferreiri Neira, I., Couillaud, F., Vivès, E., Boisguérin, P., Deshayes, S. *Bioconjugate Chem.* **2019**, *30*, 592-603
6. Di Gregorio, G., Vallée, C., Konate, K., Teko-Agbo, C. A., Hammoum, T., Faure-Gautron, H., Bessin, Y., Deshayes, S., Vivès, E., Meli, A. C., De Santa Barbara, P., Faure, S., Barrère-Lemaire, S., Ulrich, S., Boisguérin, P. *ChemMedChem* **2025**, *20*, e202400885

Synthesis, Characterization and Microencapsulation of the Antimicrobial Peptide Ctx(Ile^{21})-Ha for Necrotic Enteritis Control in Broiler Chickens

Rayssa Piton Rijo Costa[1]; Andrea B. Meneguin[2]; Mariana Q. Nascimento[3]; Cesar A. Roque-Borda[2]; Silvio R. Teixeira[4]; Marcus Chorilli[2] and Eduardo Festozo Vicente[1]

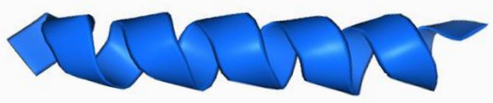
[1]*São Paulo State University (Unesp), School of Agricultural and Veterinary Sciences, Jaboticabal, 14884-900, São Paulo, Brazil.*
[2]*São Paulo State University (Unesp), School of Pharmaceutical Sciences, Araraquara, 14801-902, São Paulo, Brazil.*
[3]*Sapiens Artificial Intelligence in Microbiome Ltda., Jundiaí, 13212-321, São Paulo, Brazil.*
[4]*São Paulo State University (Unesp), School of Science and Technology, Presidente Prudente, 19060-900, São Paulo, Brazil.*
[5]*São Paulo State University (Unesp), School of Science and Engineering, Tupã, 17602-496, São Paulo, Brazil.*

eduardo.vicente@unesp.br
https://doi.org/10.17952/38EPS.2026.P234

INTRODUCTION

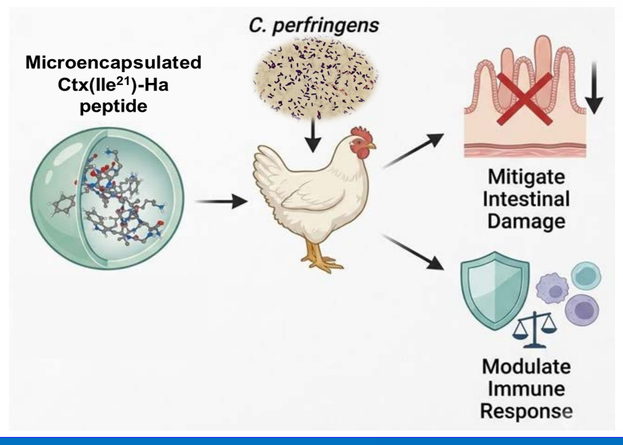
Necrotic enteritis, primarily caused by *Clostridium perfringens*, is an important challenge in poultry production and has become increasingly relevant following restrictions on the use of antibiotic growth promoters [1]. Antimicrobial peptides (AMPs) have emerged as promising alternatives due to their broad-spectrum antimicrobial activity and multiple mechanisms of action. Microencapsulation represents a promising strategy to protect AMPs during gastrointestinal transit and promote their controlled release at the intestinal site of action [2].





Antimicrobial Peptide Ctx(Ile^{21})-Ha
(*secondary structure predicted by AlphaFold3*)

OBJETIVES



Evaluate the potential of microencapsulated Ctx(Ile^{21})-Ha as a peptide-based strategy to mitigate intestinal damage and modulate immune responses in broiler chickens experimentally challenged with *Clostridium perfringens.*

METHODOLOGY

The antimicrobial peptide Ctx(Ile^{21})-Ha was synthesized by solid-phase peptide synthesis (SPPS), purified by reverse-phase high-performance liquid chromatography (RP-HPLC), and characterized by mass spectrometry. The peptide was microencapsulated using sodium alginate and subsequently coated with hydroxypropyl methylcellulose phthalate (HPMCP) to improve gastrointestinal stability and promote intestinal release. Encapsulation efficiency was determined by an indirect fluorescence method, while Fourier-transform infrared spectroscopy (FT-IR), X-ray diffraction (XRD), and thermal analysis were used to characterize the polymeric system and evaluate peptide incorporation and structural integrity. *In vitro* release assays were performed under simulated gastrointestinal conditions. Subsequently, an *in vivo* experiment was conducted in broiler chickens experimentally challenged with *C. perfringens*, in which the effects of dietary supplementation with microencapsulated Ctx(Ile^{21})-Ha antimicrobial peptide were evaluated through intestinal morphometry and serum protein profiling.

RESULTS

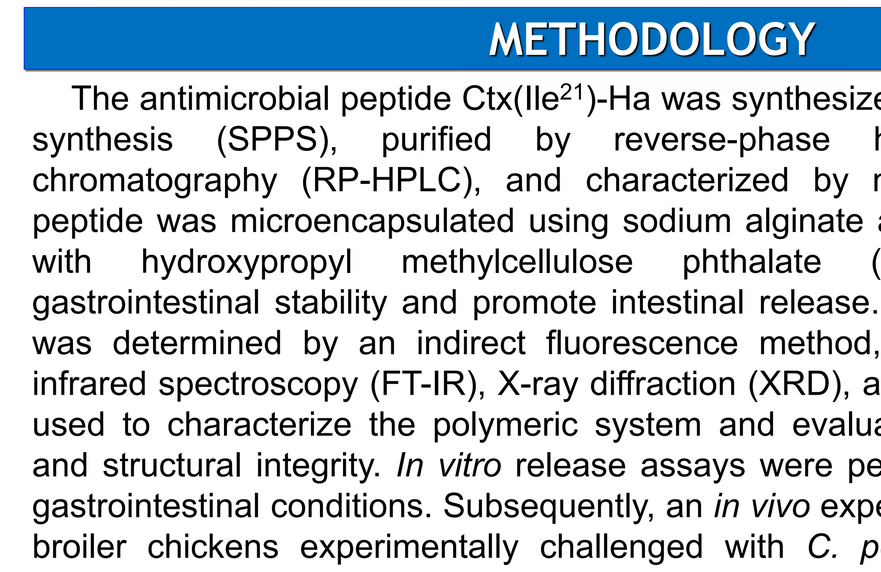


Figure 2. (A) Chromatogram profile of the synthesized Ctx(Ile^{21})-Ha antimicrobial peptide and **(B)** Mass spectrometry spectra. Retention time at approximately 18,5 min and purity greater than 95%. From the analysis of the LC-MS spectrum, it was able to detect the peaks of the [M+2H$^+$], [M+3H$^+$], [M+4H$^+$] and [M+5H$^+$] which confirm the material obtaining.

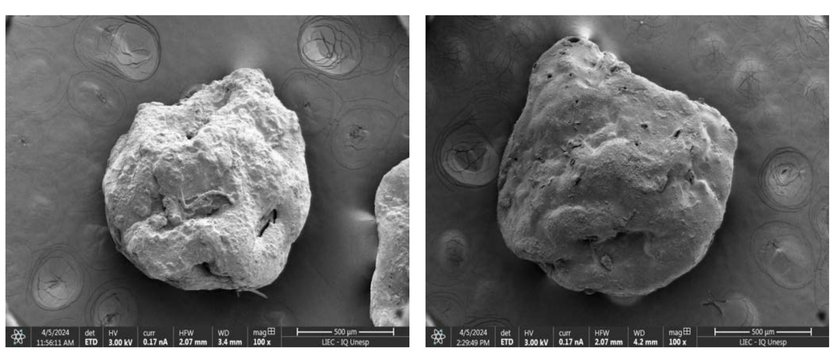


Figure 3. Scanning electron microscopy of coated microcapsules produced from microencapsulation solutions containing 100 mg (A) and 200 mg (B) of Ctx(Ile^{21})-Ha peptide.

RESULTS

Table 1. Release profile of coated microcapsules containing the antimicrobial peptide Ctx(Ile^{21})-Ha in simulated gastric solution (SGS) and simulated intestinal solution (SIS), according to the peptide loading.

Type of simulated solution	Mass	Measurement time (min–h)								
		0'	3'	5'	10'	15'	20'	30'	1h	2h
SGS (%)	100 mg	0%	0%	0%	0%	1%	0%	1%	2%	-
	200 mg	0%	0%	0%	1%	0%	0%	0%	1%	-
SIS (%)	100 mg	2%	9%	16%	25%	38%	52%	49%	77%	53%
	200 mg	1%	1%	23%	12%	8%	8%	12%	18%	20%

Table 2. Analysis of intestinal morphometry of the duodenum, jejunum, and ileum.

Intestinal segment	Treatments	Variables			*P*-value		
		Villus height (V)	Crypt depth (C)	Villus:crypt ratio (V:C)	V	C	V:C
Duodenum	T1	1.612^{a} ± 0.178	0.150^{c} ± 0.018	10.920^{a} ± 2.06	0.023	< 0.001	< 0.001
	T2	1.229^{b} ± 0.158	0.196^{bc} ± 0.030	6.345^{bc} ± 0.73			
	T3	1.310^{ab} ± 0.268	0.252^{a} ± 0.049	5.281^{c} ± 1.07			
	T4	1.204^{b} ± 0.276	0.219^{ab} ± 0.025	5.555^{c} ± 1.32			
	T5	1.385^{ab} ± 0.279	0.176^{bc} ± 0.049	8.121^{b} ± 1.63			
Jejunum	T1	0.764 ± 0.101	0.125^{b} ± 0.038	6.447^{a} ± 1.51	0.159	0.036	< 0.001
	T2	0.708 ± 0.101	0.188^{a} ± 0.054	3.934^{b} ± 0.79			
	T3	0.696 ± 0.139	0.176^{ab} ± 0.028	3.945^{b} ± 0.44			
	T4	0.627 ± 0.058	0.139^{ab} ± 0.030	4.628^{b} ± 0.81			
	T5	0.702 ± 0.061	0.147^{ab} ± 0.045	5.111^{ab} ± 1.44			
Ileum	T1	0.623 ± 0.120	0.096 ± 0.014	6.562^{a} ± 1.06	0.342	0.061	< 0.001
	T2	0.514 ± 0.075	0.133 ± 0.040	4.102^{b} ± 0.98			
	T3	0.548± 0.155	0.150 ± 0.050	3.835^{b} ± 0.93			
	T4	0.504 ± 0.102	0.138 ± 0.027	3.767^{b} ± 0.91			
	T5	0.562 ± 0.111	0.129 ± 0.024	4.417^{b} ± 0.90			

Data are presented as mean ± SD (standard deviation). Different letters among treatments within each intestinal segment indicate significant differences by Tukey's test at the 5% significance level (P < 0.05).

Table 3. Electrophoretic profile of total serum proteins* of broiler chickens subjected to the experimental treatments.

Variables	Treatments					SEM	*P*-value
	T1	T2	T3	T4	T5		
ProT (g/dL)	3.227	3.347	3.126	3.226	3.274	0.041	0.554
IgA (%)	0.067	0.085	0.076	0.087	0.079	0.002	0.106
CER (%)	0.049^{b}	0.080^{a}	0.0662^{ab}	0.069^{ab}	0.059^{ab}	0.003	0.008
TRANS (%)	0.114^{b}	0.174^{a}	0.170^{a}	0.189^{a}	0.170^{a}	0.007	0.004
ALB (%)	2.396	2.469	2.248	2.299	2.386	0.033	0.230
IgG (h.c.) (%)	0.067^{b}	0.084^{ab}	0.085^{ab}	0.111^{a}	0.085^{ab}	0.004	0.003
HAPTO (%)	0.012^{ab}	0.014^{ab}	0.017^{ab}	0.011^{b}	0.018^{a}	< 0.001	0.023
A1GA (%)	0.002	0.001	0.001	0.001	0.001	< 0.001	0.646
IgG (l.c.) (%)	0.020	0.023	0.022	0.029	0.041	< 0.001	0.152
PM (%)	0.377^{a}	0.245^{b}	0.256^{b}	0.273^{b}	0.287^{b}	0.010	< 0.001

** ProT – total proteins (g/dL); IgA – immunoglobulin A (%); CER – ceruloplasmin (%); TRANS – transferrin (%); ALB – albumin (%); IgG (heavy c.) – immunoglobulin G heavy chain (%); HAPTO – haptoglobin (%); A1GA – alpha-1-acid glycoprotein (%); IgG (light c.) – immunoglobulin G light chain (%); PM – molecular weight (%). Data are presented as mean, and SEM (standard error of the mean). Different letters among treatments for each protein indicate significant differences by Tukey's test at the 5% significance level (P < 0.05).*

- Ctx(Ile^{21})-Ha attenuated intestinal lesions resulting from the enteric challenge, optimizing the integrity and absorptive capacity of duodenal mucosa.
- Changes in serum markers (IgG, HAPTO, CER, TRANS) indicate a possible systemic immune control complementing the peptide antimicrobial activity.

CONCLUSIONS

Microencapsulated Ctx(Ile^{21})-Ha showed promising physicochemical stability, gastrointestinal protection, and controlled intestinal release, together with protective and immunomodulatory effects in broiler chickens challenged with *C. perfringens*. These findings support the potential of microencapsulated Ctx(Ile^{21})-Ha as a peptide-based alternative for the control of necrotic enteritis and as a promising strategy for reducing the reliance on antibiotic growth promoters in poultry production.

REFERENCES

[1] Brown K, Uwiera RRE, Kalmokoff ML, et al (2017) Antimicrobial growth promoter use in livestock : a requirement to understand their modes of action to develop effective alternatives. *Int J Antimicrob Agents* 49:12–24.

[2] Roque-Borda CA, Silva HRL, Crusca Junior E, et al (2021) Alginate-based microparticles coated with HPMCP/AS cellulose-derivatives enable the Ctx(Ile^{21})-Ha antimicrobial peptide application as a feed additive. *Int J Biol Macromol* 183:1236–1247.

ACKNOWLEDGEMENTS

FAPESP FUNDAÇÃO DE AMPARO À PESQUISA DO ESTADO DE SÃO PAULO
FAPESP Grant process numbers 2021/06706-9 and 2022/09379-1

CNPq Conselho Nacional de Desenvolvimento Científico e Tecnológico
Grant process number 311935/2022-2

unesp UNIVERSIDADE ESTADUAL PAULISTA "JÚLIO DE MESQUITA FILHO"

Mapping and Linking Druggable Sites on Rad6 Using Proteomimetic Fragments and AI-assisted Design

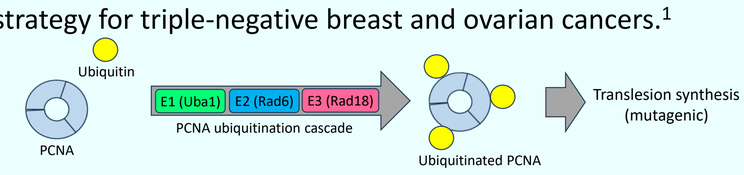
E. Wéber[1,2], F. Bogár[1,2], B. Nagymihály[1], M. R. F. Mohamed[1,3], É. Bartus[1], A. Tököli[4], Z. Kupihár[1], G. M. Keserű[5] & T.A. Martinek[1,2]

[1]*Department of Medical Chemistry, University of Szeged, Szeged, Hungary*
[2]*HUN-REN-SZTE Biomimetic Systems Research Group, University of Szeged, Szeged, Hungary*
[3]*Department of Medicinal Chemistry, Faculty of Pharmacy, Minia University, Minia, Egypt*
[4]*Department of Biochemistry, University of Cambridge, Cambridge, UK*
[5]*Medicinal Chemistry Research Group, HUN-REN Research Centre For Natural Sciences, Budapest, Hungary*
Email: weber.edit@med.u-szeged.hu
https://doi.org/10.17952/38EPS.2026.P336

Identifying druggable sites and modulating interactions on protein surfaces that lack well-defined cavities remain challenging for traditional drug-like small molecules. Our target, Rad6, containes a shallow, solvent-exposed catalytic region and broad protein–protein interaction (PPI) surfaces. These features make the development of Rad6 inhibitors difficult.

We present a **modular proteomimetic strategy** to disrupt Rad6-mediated PPIs and covalently engage the active-site Cys88. After screening for fragments capable of binding Rad6, we linked proteomimetic building blocks and warheads using dynamic covalent library (DCL) experiments and an AI-assisted linker optimization strategy.

Rad6 plays an essential role in the PCNA ubiquitination cascade and the DNA damage tolerance pathway translesion synthesis (TLS). TLS is error-prone, and promotes tumor cell survival and chemoresistance. Rad6 inhibition is a promising therapeutic strategy for triple-negative breast and ovarian cancers.[1]

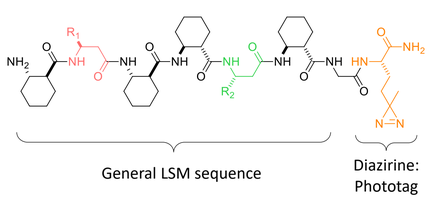


Mapping druggable sites – identifying potential building blocks

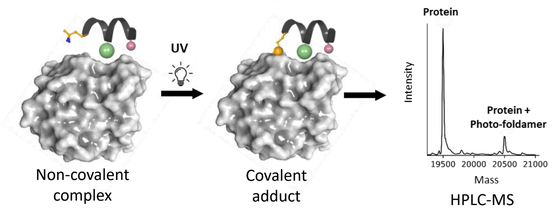
Druggable PPI sites on Rad6: Screen proteomimetic foldamer fragment library

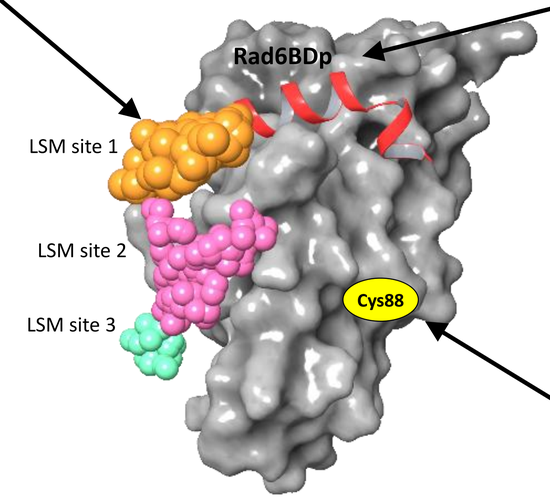
We screened a 100-membered local surface mimetic (LSM) foldamer library[2,3] using a photoscreening assay. Best Rad6-binders contained positively charged side chains, e.g. **RW**, **RF**, **RR**, **RL**, **WR**, **QR** (LSM names correspond to R_1 and R_2 side chains).

LSM foldamer library



Screening against Rad6





Helical peptide segment from the native interacting partner

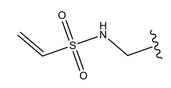
Mimicking a native binding partner is a straightforward strategy in peptidomimetics design. The 21mer helical peptide segment of the Rad6-binding domain of the Rad18 protein (**Rad6BDp)** binds to Rad6 relatively weakly (K_d~ 60 µM).

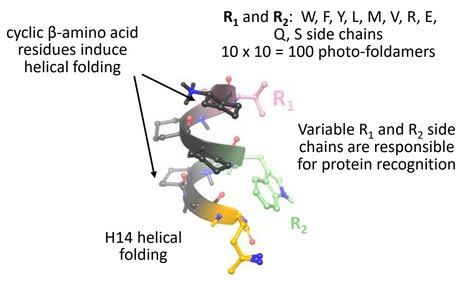
Rad6BDp KYRKKHKSEFQLLVDQARKGY

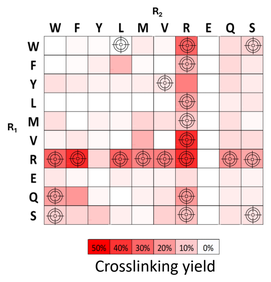
We exploited **Rad6BDp** as a building block of larger Rad6-binding constructs.

Covalent targeting of Cys88 with warheads

Rad6 accepts ubiquitin at its active-site Cys88. Targeting Cys88 with covalent inhibitors (warheads) can therefore inactivate Rad6. After screening a library of cysteine-selective covalent inhibitors by HPLC-MS, we selected vinylsulfonamide (VSA) for incorporating into Rad6 ligands.

VSA 





Localization of LSM hits

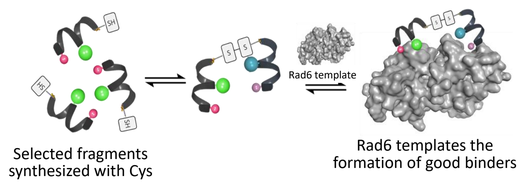
Three main LSM sites were determined (spheres represent the center of mass of the docked foldamer structures).

- **Proteomics**: covalent Rad6-LSM adducts were digested by trypsin/chymotrypsin and analysed by HPLC-MS
- **NMR**: ^{15}N HSQC NMR titrations
- **Docking** with the ab initio mode of the HADDOCK program.[4,5]

Connecting Rad6-binding peptide fragments and warheads

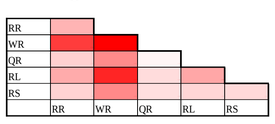
Linking nearby sites – templated DCL experiments

LSM hits (**RR, WR, QR, RS, RL**) and **Rad6BDp** bind to adjacent and partially overlapping sites on Rad6. To obtain higher-affinity compounds by linking two LSM hits or an LSM and **Rad6BDp,** and to identify the best combination of building blocks, we used protein-templated dynamic covalent library (DCL) experiments that enable selective enrichment of fragment combinations with enhanced target binding.

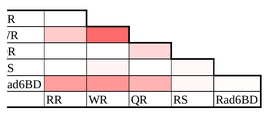


60 µM for each fragment in the DCL
60 µM Rad6 template
20 mM borate buffer (pH 8.2), 50 mM NaCl,
glutathione redox buffer: 500 µM GSH, 125 µM GSSG
incubation for 3 days at 37 °C
HPLC-MS analysis

Linking two LSM hits



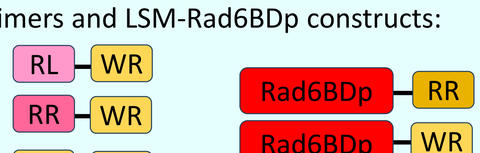
Linking LSMs with **Rad6BDp**



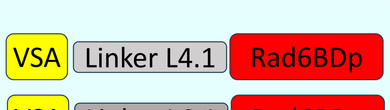


$$\text{Amplification factor (AF)} = \frac{\text{AUC (Rad6-templated)}}{\text{AUC (control without Rad6)}}$$

LSM dimers and LSM-Rad6BDp constructs:

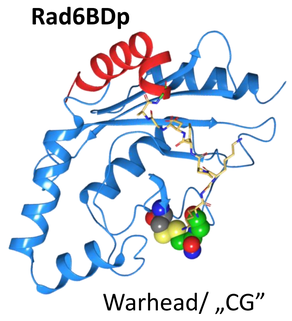


Proteomimetic warhead constructs:



Linking distant sites – linker optimization by AI tools

Rad6BDp

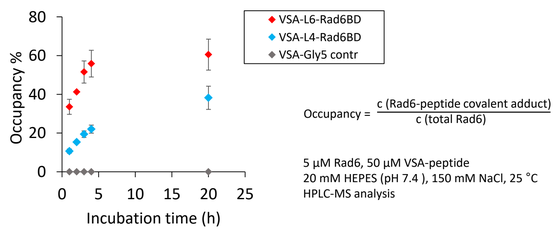


The linker between the Rad6BDp and the warhead moiety was designed using recently developed AI tools:

1. The backbone structure of the linker was generated using the RFDiffusion code.[6]
2. The sequence and 3D structure of the side chains were designed using the full-atom MPNN.[7]
3. The structures were then refined and ranked using Rosetta tools from Baker's lab.[8]

Selected linker sequences:
L4.1 sequence: PYTKAGDGQ
L6.1 sequence: KGKPIDGA

While the VSA-Gly_5 control did not label Rad6, VSA-linker-Rad6BDp constructs were effective



Summary and outlook

The identified LSM hits, acting as proteomimetic fragments, recognize PPI sites on Rad6. However, they do not fully cover the Rad6 surface interacting with Rad6BDp and did not engage the catalytic site around Cys88. Therefore, we used not only LSM hits, but also the native binding partner Rad6BDp and the cysteine-selective warhead VSA as building blocks to engineer a range of Rad6-binding constructs. Compound characterization is ongoing, but the initial results indicate that combining distinct chemical modalities is a worthwhile modular strategy for inhibitor development.

References

[1] Haynes *et al.*, *BBA Mol. Basis Dis.* **2020**, 1866, 165561.
[2] Tököli *et al., Chem. Sci.* **2020**, 11, 10390–10398
[3] Wéber *et al., Angew. Chem. Int. Ed.* **2024**, e202410435
[4] Dominguez *et al., JACS* **2003**, 125, 1731.
[5] Honorato *et al.*, *Nat. Protoc.* **2024**, 19, 3219.
[6] Watson *et al.*, *Nature* **2023**, 620, 1089.
[7] Di Geronimo *et al.*, *bioRxiv* **2026**, 2026.04.20., 719482.
[8] Leman *et al.*, *Nat. Methods* **2020**, 17, 665.

Acknowledgement
This research was supported by the Ministry of Culture and Innovation of Hungary through the National Research, Development and Innovation Office under the ADVANCED_25 funding programme (project No. 152867).

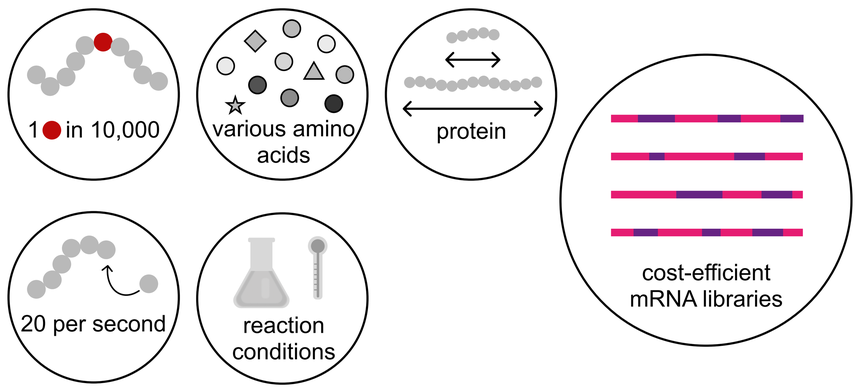
National Research, Development and Innovation Office Hungary
PROGRAM FINANCED FROM THE NRDI FUND

Towards the improvement of non-canonical amino acid incorporation via Decoupled Synthesis of Ribosomes (DeSyR)

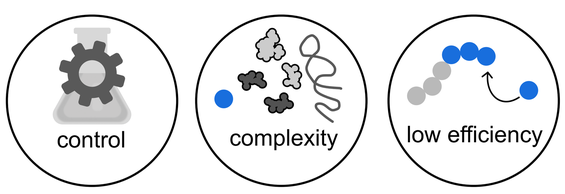
*Benedikt Golisch**†, *Anton Meier*†, *Martin J. Weissenborn*†



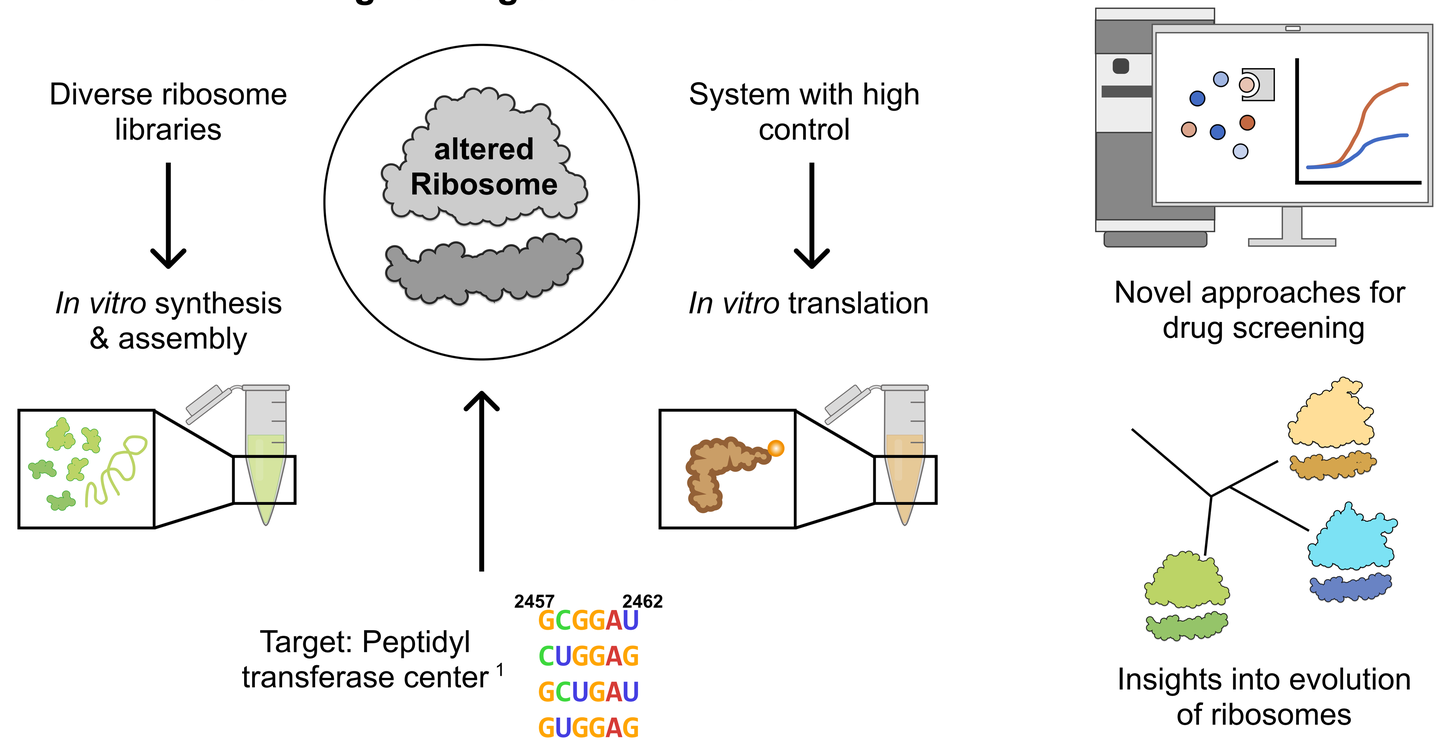
Advantage of ribosomal peptide synthesis



Disadvantage of ribosomal peptide synthesis

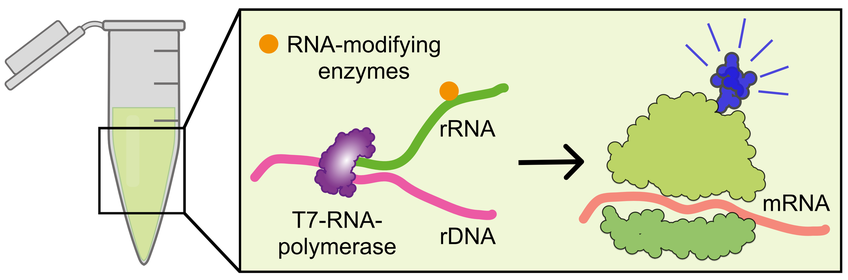


Goal: Engineering of ribosomes



Decoupled Synthesis of Ribosomes (DeSyR)

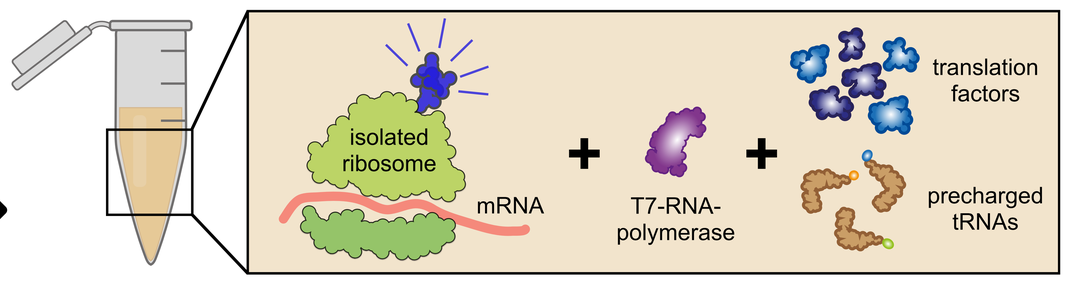
In vitro synthesis of active ribosomes



Cell extract based iSAT (integrated synthesis, assembly & translation)[2]

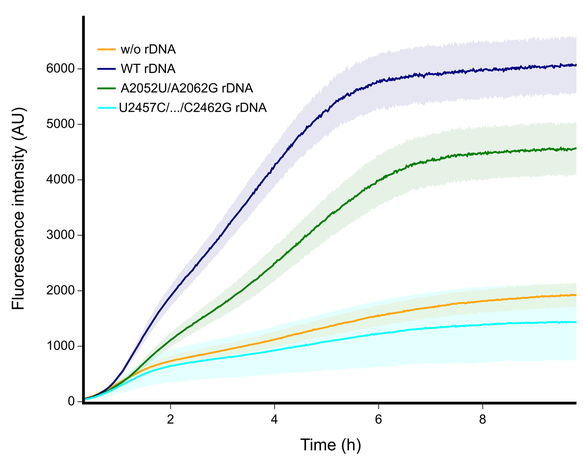
Ribosome isolation via ultracentrifugation

In vitro translation

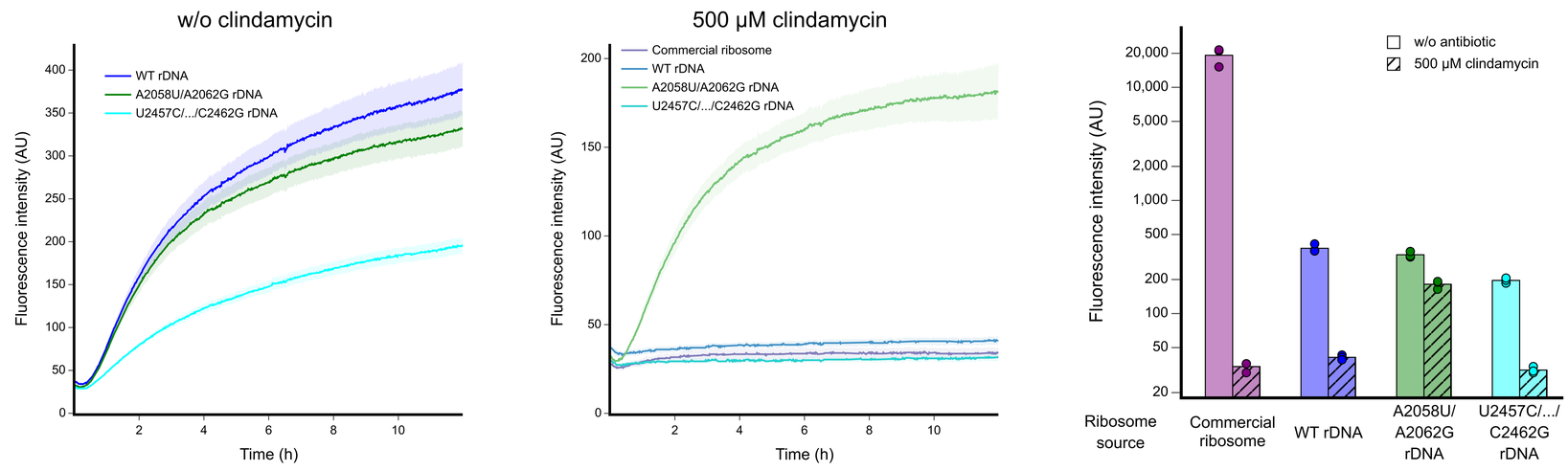


PURE system (Protein synthesis Using Recominant Elements)[3]

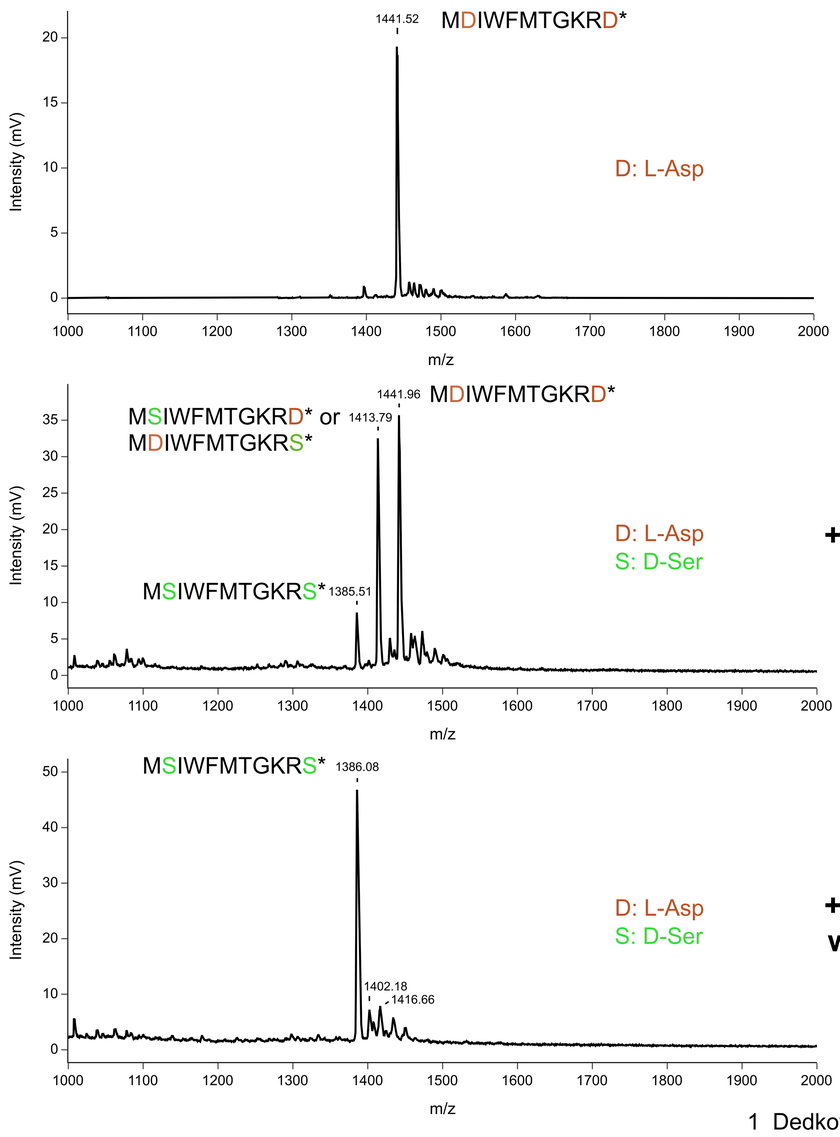
Successful synthesis of WT ribosome and a double mutant monitored via GFP-translation



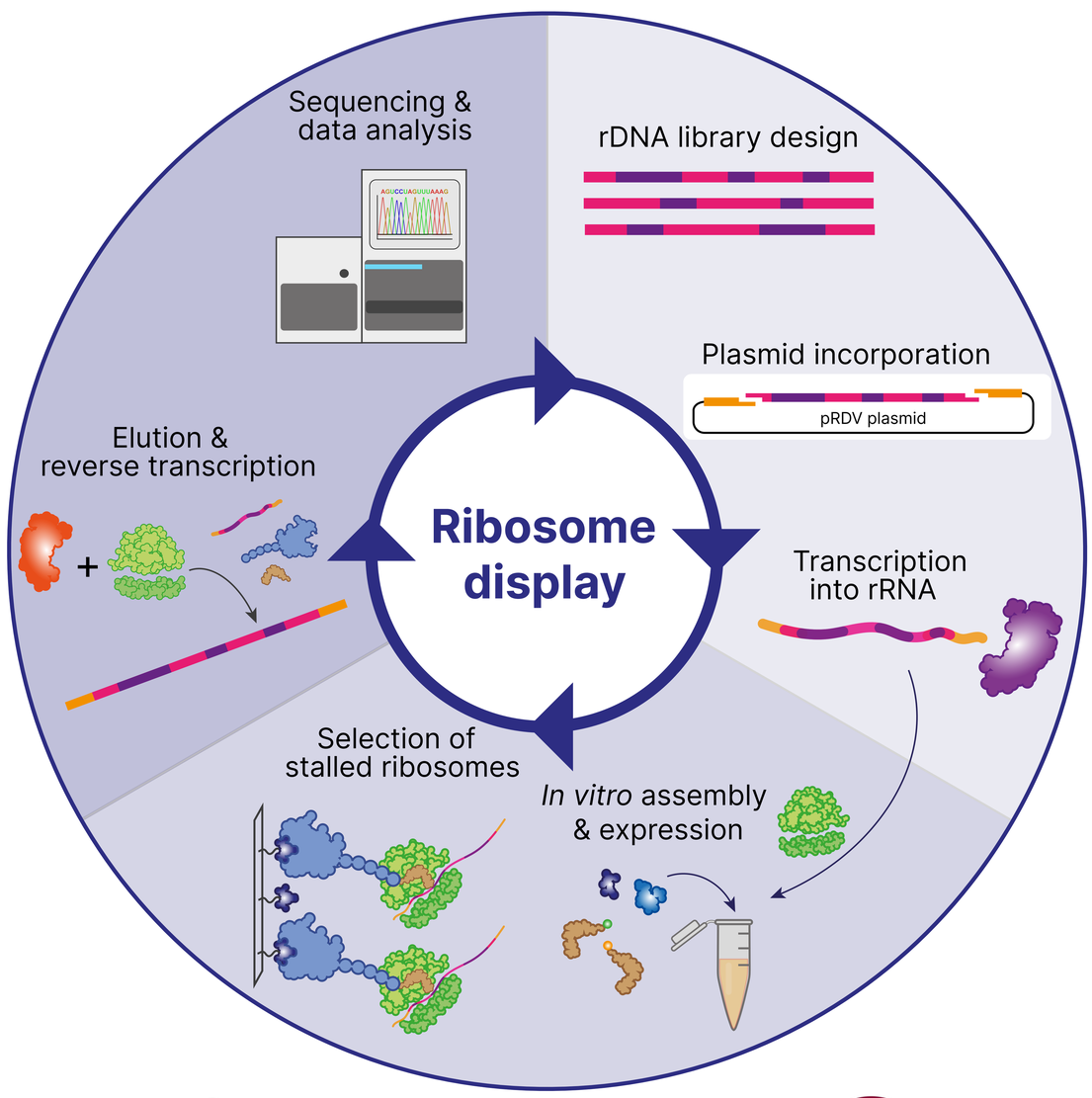
Activity of 1.5 µM isolated ribosomes using PURExpress



Incorporation of D-amino acids



Outlook: Ribosome engineering[4]



Available under https://doi.org/10.17952/38EPS.2026.P300

* presenting author

† Department of Chemistry, Martin-Luther-Universität Halle-Wittenberg

1 Dedkova *et al.*, JACS, 2013.

2 Jewett *et al.*, Molecular systems biology, 2013.

3 Shimizu *et al.*, Nature biotechnology, 2001.

4 Hammerling *et al.*, Nature Communications, 2020.

MARTIN-LUTHER-UNIVERSITÄT HALLE-WITTENBERG

Cusanuswerk Bischöfliche Studienförderung

Targeting Neurodegenerative Diseases with Priavoid's Peptide Drug Development Platform

https://doi.org/10.17952/38EPS.2026.P317

Mathias Wendt[1], Marc Sevenich[1], Kira Allmeroth[1], Gina Hartmann[1], Karolina Korostov[1], Antje Willuweit[1,2] and Dieter Willbold[1,3]

[1] Priavoid GmbH, Düsseldorf, Germany
[2] Institute for Neuroscience and Medicine (INM-4), Forschungszentrum Jülich, Jülich, Germany
[3] Institut für Physikalische Biologie, Heinrich-Heine-Universität Düsseldorf, Düsseldorf, Germany

Publication on α-syn targeting all-D- npj | parkinson's disease

Priavoid @ LinkedIn

Objectives and Introduction

Priavoid GmbH advances clinical and preclinical drug development programs for neurodegenerative diseases by developing **oral all-D-peptides** designed to **detangle toxic oligomers**. Our mission is to deliver disease-modifying therapies that target the root causes of **neurodegeneration**.

Our **Peptide Drug Development Platform** consistently yields active D-enantiomeric peptides **acting as pharmacological chaperones** and detangle protein aggregates into native monomers.

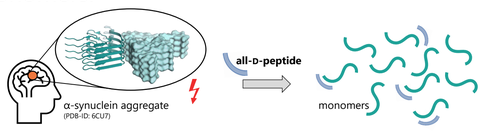


Figure 1: Priavoid develops orally available all-D-peptides that detangle neurotoxic oligomer species to inhibit and reverse disease-specific protein aggregation in neurodegenerative disorders.

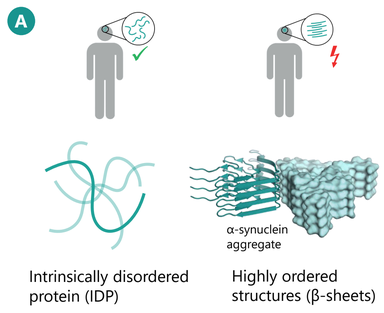
Here, we present our **platform with focus on cell permeability studies** expanding our scope to intracellular drug targets and show case the identification of a cell permeable all-D-peptide ligand that addresses **intracellular α-synuclein**, the disease-driving protein in **Parkinson's Disease** (PD).

About Priavoid

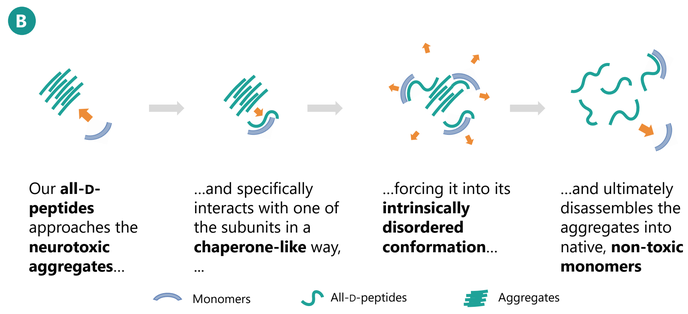
- Founded in 2017 and located in Düsseldorf
- Thirty-two highly skilled employees
- One phase II clinical trial against Alzheimer's
- One partnership ready drug development program
- Six preclinical programs - four addressing high-burden neurodegenerative disorders

PRImus-AD

Peptide Drug Platform Technology



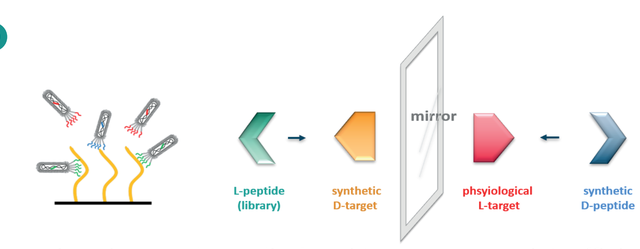
Protein aggregation is a hallmark of various neurodegenerative disorders.



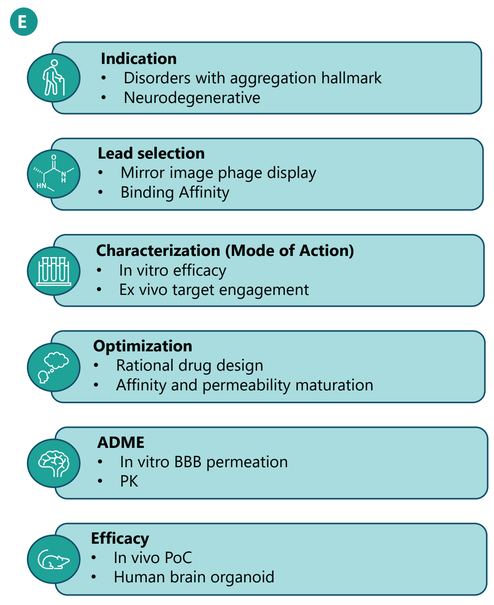
Our compounds act as chaperone-like detanglers and effectively disassemble neurotoxic aggregates.



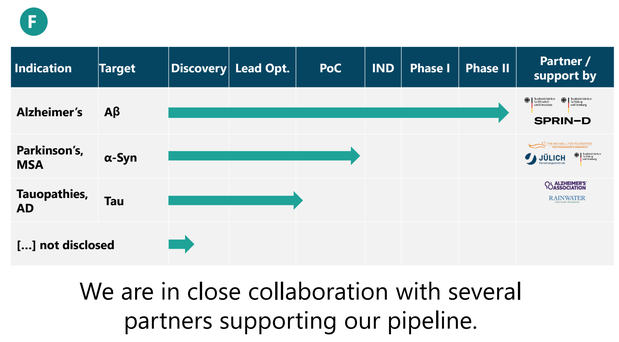
Peptide and target form a stable intrinsically disordered complex.



Mirror image phage display aids to generate high affinity initial screening hits – peptides that consist of D-amino acids.



We advance our peptide platform through the complete preclinical development.



We are in close collaboration with several partners supporting our pipeline.

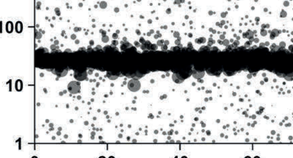
All-D-peptides

- Proteolytically stable and orally available
- Metabolic stability
- Very good safety profile
- No demand for modified building blocks
- Low immunogenic risk
- Extra- and intracellular application

Advancing Parkinson's Therapy with PRI-101

Indication

α-Synuclein forms aggregates



PD Patients

- 8.5 million worldwide and rising every year.
- Many live 15–30 years after diagnosis.
- Dopaminergic neuron loss in the substantia nigra.

Patients suffer major disability

- Motor symptoms (muscle rigidity, tremor, twitching movements etc.)
- Non-motor symptoms (cognitive decline, mood disorders etc.)

Standard of care

- Symptomatic treatment (dopamine)
- Deep brain stimulation (surgery)

Lead selection

PRI-101 binds α-synuclein target

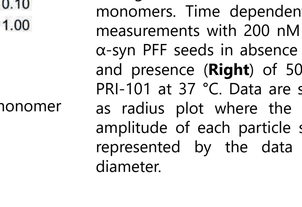


Figure 2: SPR with immobilized PRI-101. α-Syn was injected for 100 s at 30 µl/min ranging from 30 to 500 nM. The interaction was fitted with a 1:1 kinetic interaction model.

Characterization (mode of action)

PRI-101 inhibits seeded aggregation

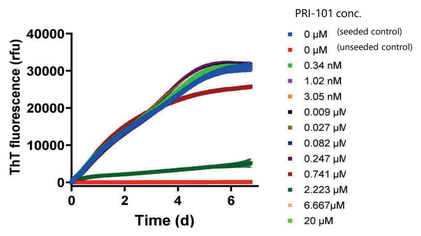


Figure 3: PRI-101 eliminates seeding activity of small α-syn PFFs (50 nM monomer eq.). Before addition of α-syn (20 µM) monomers, fibrils and peptide (up to 20 µM) were incubated for 20 h (n = 4, Read-out: Tht fluorescence).

Seeded aggregation in α-synA53T-YFP cells stopped

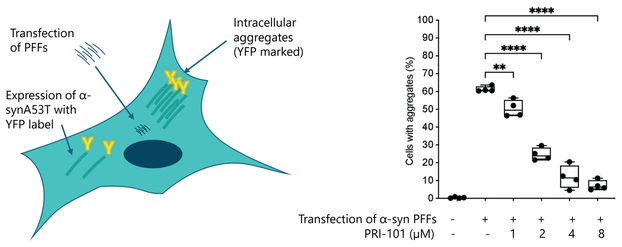


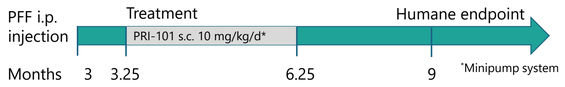
Figure 4: Left: HEK293T cells expressing α-syn monomer are transfected with α-syn PFFs to induce intracellular aggregation. **Right:** Addition of PRI-101 to cell culture medium at low µM concentration is inhibiting seeding capacities of PFFs.

DLS measurement with pre-formed α-syn fibrils (PFFs) reveals disintegration of seeds by PRI-101

Figure 5: PRI-101 reduces the particle size of α-syn small PFFs through stabilization of monomers. Time dependent DLS measurements with 200 nM small α-syn PFF seeds in absence (**Left**) and presence (**Right**) of 500 nM PRI-101 at 37 °C. Data are shown as radius plot where the signal amplitude of each particle size is represented by the data point diameter.

Efficacy

Survival prolonged in TgM83+ (α-synA53T) mice



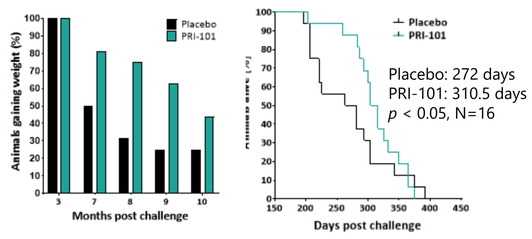


Figure 6: TgM83+ mice carrying a A53T α-syn mutation were injected with α-syn fibrils (PFFs) to induce protein aggregation at 3 months. After short time PRI-101 at 10 mg/kg daily was dosed s.c. using implanted mini-pumps for 3 month. PRI-101 treatment delays weight loss and prolongs the survival of TgM83+ mice.

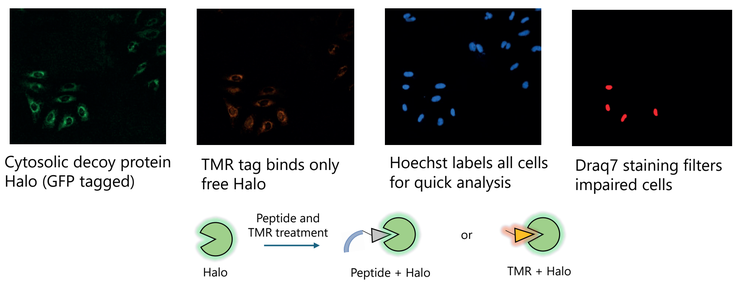
Highlights of PRI-101

	Property	Parameter	PRI-101
In vitro	Binding affinity	SPR (kinetic fit) [K_d]	1 nM
	Seeded aggregation	Inactivation of seeds [EC_{50}]	1.4 µM
	Intracellular aggregation	Reduction of aggregation [IC_{50}]	1.6 µM
ADME	Cell permeability	CAPA assay [EC_{50}]	4.3 µM
	Mouse PK	Brain uptake	Sufficient
PD	Ex vivo target engagement	Reduction of aggregates (human PD brain)	72%
	In vivo seeding/spreading	Prolongation of survival	38 d
Safety	Safety panel	Off-target binding assay	No off-target hits

Cellular Permeability

Optimization

Chloroalkane Penetration Assay (CAPA) analyzed by fluorescence microscopy



Cytosolic localization of PRI-101

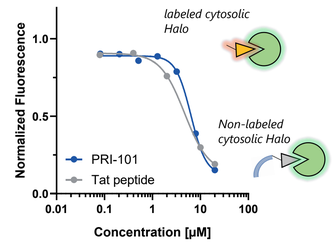


Figure 7: Left: Principle of CAPA. Cells producing cytosol localized Halo protein (green) are treated with tagged Peptide (grey) and TMR-tagged Halo protein ligand. Only free Halo protein reacts with TMR and shows orange signal. TMR fluorescence intensity is anti-proportional to cytosolic localized peptide concentration. Hoechst labels all nuclei and Draq7 staining is used to analyze and filter membrane disturbing peptides. **Right:** Halo ligand tagged PRI-101 is tested in HeLa cells using the CAPA system. Peptides were incubated with cells in OptiMEM for 24 h.

Focus screening library changing amino acid residues to improve permeability

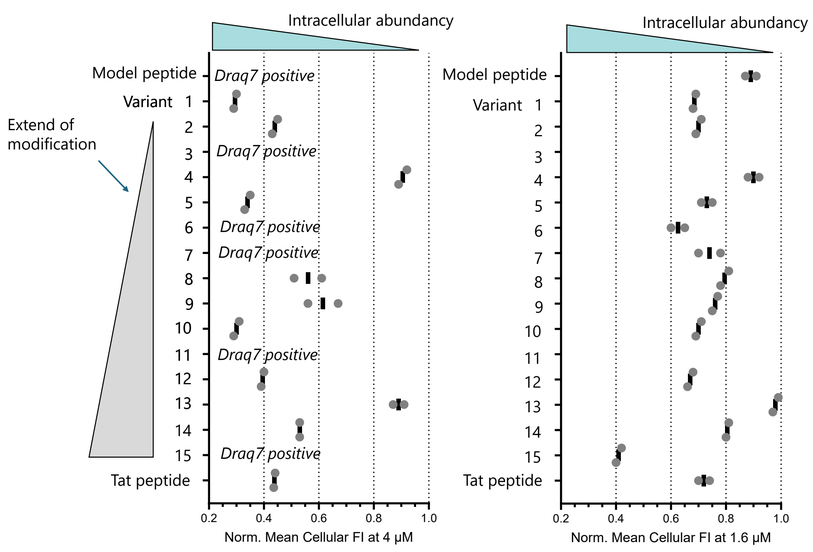


Figure 8: Example data of a small peptide library, synthesized with single, double and triple aa mutations. CAPA can be used to determine quickly their intracellular localization rates. Halo expression levels are accounted for by GFP signal and TMR fluorescence intensity is normalized to maximum and minimal TMR signal. Draq7 positive conditions with impaired cells can be excluded (example data with n = 2).

mathias.wendt@priavoid.com
Senior Peptide Scientist

ETH zürich

Laboratory of Organic Chemistry

An Artificial Light-Harvesting System Built from a Peptide-Based Triaxial Weave

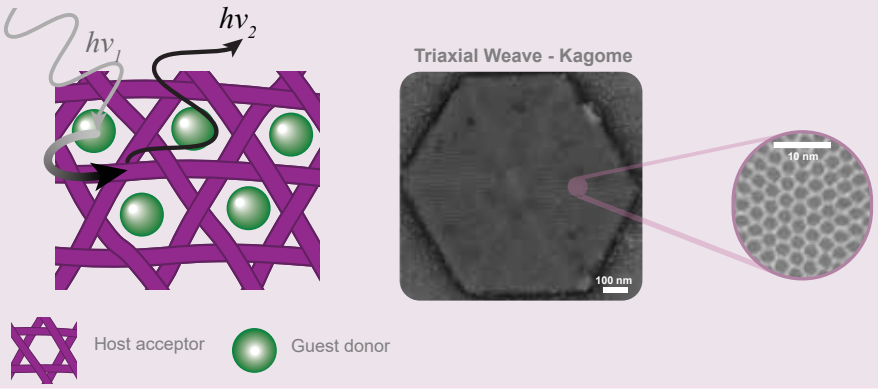
Tatiana Da Silva-Ferreira, Helma Wennemers*
Laboratory of Organic Chemistry, D-CHAB, ETH Zurich

https://doi.org/10.17952/38EPS.2026.P540

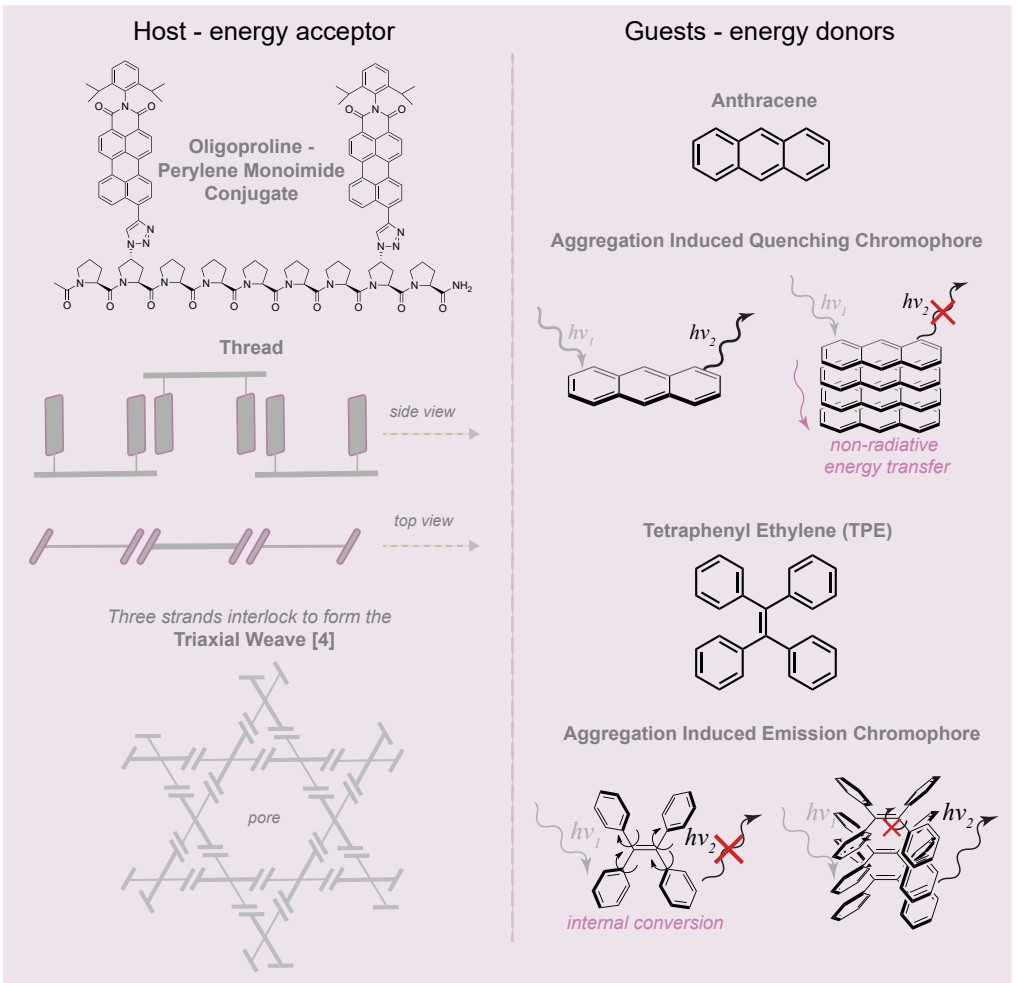
1 Introduction

Artificial light-harvesting systems (ALHS), which take inspiration from the principles of natural photosynthesis, have garnered significant attention for their potential in photocatalysis, bioimaging, and related photonic applications [1,2]. Typically, ALHSs rely on Förster resonance energy transfer (FRET) between a supramolecular host acting as the energy donor and an encapsulated fluorescent guest serving as the acceptor [3].

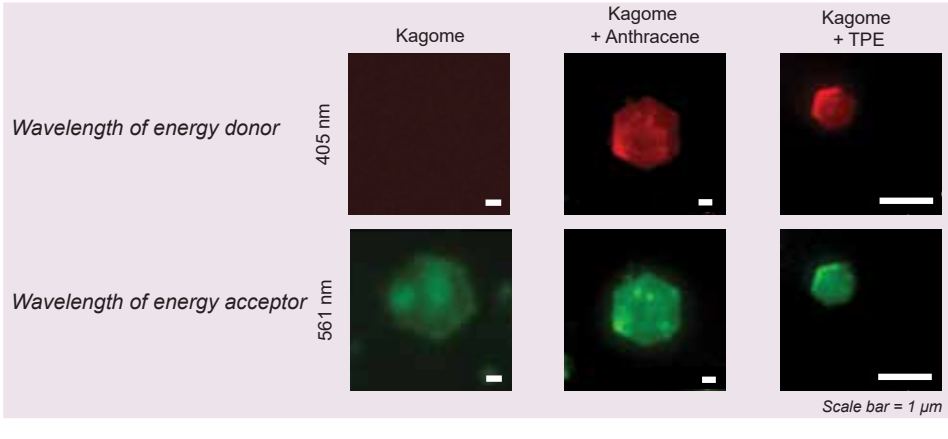
In this work, we introduce an inverted ALHS with reversed roles of the donor and acceptor. This work builds on our previously developed triaxial supramolecular weave, which is formed by the self-assembly of a rigid oligoproline scaffold bearing two perylene monoimide chromophores [4].



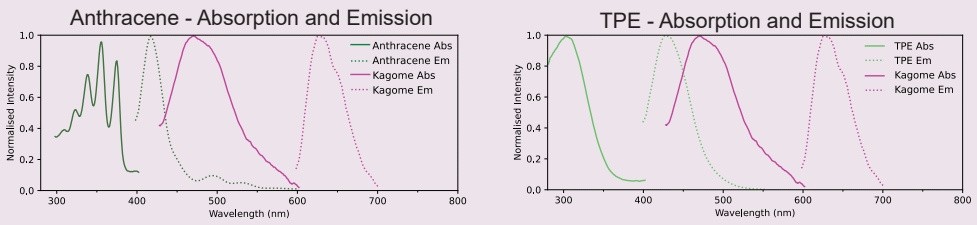
2 Our System



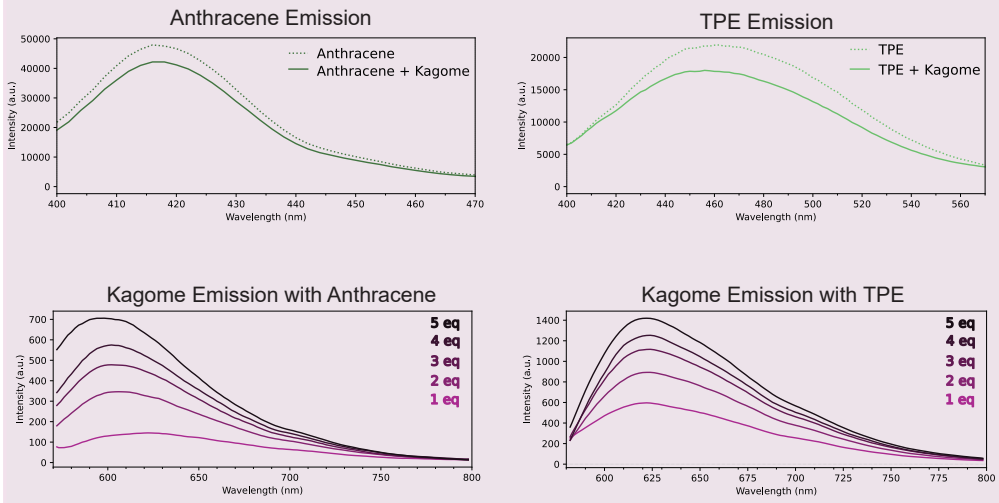
3 Fluorescence Microscopy



4 Förster Resonance Energy Transfer



The weave was incubated with increasing equivalents of anthracene or TPE, and the fluorescence spectra of the host - guest systems were measured at an excitation wavelength of 350 nm.



5 Further Characterisation

Fluorescence lifetimes and energy transfer efficiencies of the donor - acceptor systems

Sample		τ_1	τ_2	Φ_{ET}
Anthracene	–	3.59	11.99	/
	+	3.36	10.94	13%
TPE	–	3.66	7.06	/
	+	2.74	5.81	19%

6 Conclusion

- Fluorescence microscopy showed encapsulation of anthracene and TPE inside the triaxial supramolecular weave.
- Fluorescence spectroscopy revealed that the emission of anthracene or TPE was quenched upon their addition, relative to the emission of the free guest, further indicating encapsulation.
- At constant concentration of the weave, increasing amount of the donor enhanced fluorescence at 650 nm, the wavelength characteristic of perylene monoimide.
- The reduced fluorescence lifetime of both TPE and anthracene, in the presence of the weave, shows that both energy donors engage in energy transfer with the weave.

➢ The results demonstrate that both systems operate as reversed ALHSs.

➢ The ALHS with the energy donor TPE performed better than the ALHS with anthracene. This finding is consistent with the better spectral overlap between TPE and the weave, and with the aggregation induced emission property of TPE.

References

1. M. Hao, G. Sun, M. Zuo, Z. Xu, Y. Chen, X. Y. Hu, L. Wang, *Angew. Chem. Int. Ed.*, **2020**, *59*, 10095-10100
2. X. M. Chen, Q. Cao, H. K. Bisoyi, M. Wang, H. Yang, Q. Li, *Angew. Chem. Int. Ed.*, **2020**, *59*, 10493-10497
3. Y. Wang, N. Han, X. Li, S. Yu, L. Xing, *Chem. Phys. Mater.*, **2022**, *1*, 281-293
4. U. Lewandowska, W. Zajaczkowski, S. Corra, J. Tanabe, R. Borrmann, E. M. Benetti, S. Stappert, K. Watanabe, N. A. K. Ochs, R. Schaeublin, C. Li, E. Yashima, W. Pisula, K. Müllen, H. Wennemers, *Nat. Chem.*, **2017**, *9*, 1068-1072

WENNEMERS GROUP

Let's connect!

Wennemers group Tatiana Da Silva-F.

D CHAB

Target, Capture, Treat

Peptide Nucleic Acid (PNA)-Guided Pretargeting for HER2-Targeted Antibody-Mediated Radionuclide Therapy

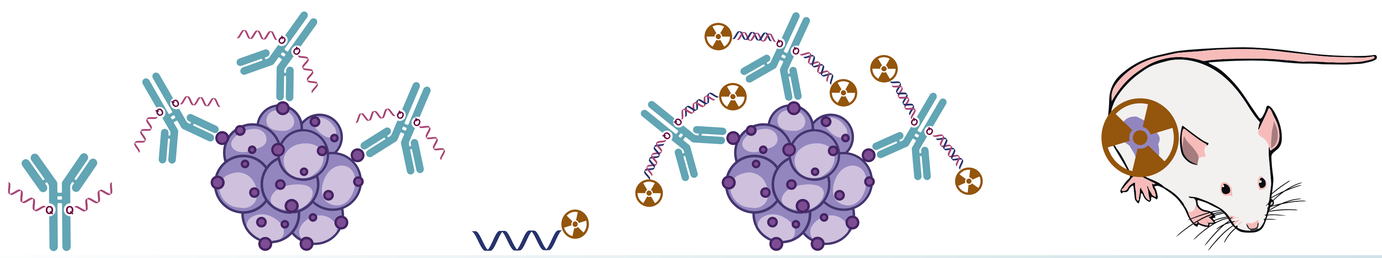
Westerlund K[1]., Altai M[2]., Zedan W[2]., Clinton J[1]., Geres S[2]., Ulmert D[2]., and Eriksson Karlström A[1].

1. KTH Royal Institute of Technology, Stockholm, Sweden
2. Lund University, Lund, Sweden

https://doi.org/10.17952/38EPS.2026.P443

In conventional radioimmunotherapy, directly radiolabeled antibodies deliver radiation to tumors but circulate in blood for extended periods, exposing healthy tissue, including the radiosensitive bone marrow, to radiation.

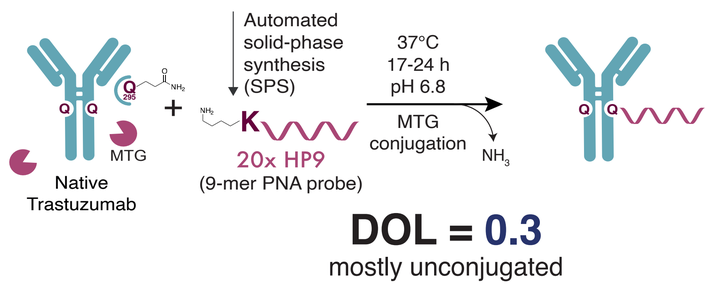
Pretargeted radioimmunotherapy (PRIT) addresses this limitation by administering the antibody and radiolabel separately, allowing the antibody to accumulate at the tumor before the radiolabel is introduced, reducing systemic radiation exposure while maintaining tumor-specific delivery.



Target

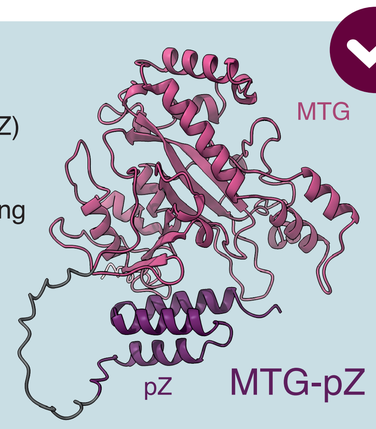
Arming Trastuzumab with PNA for HER2 Targeting

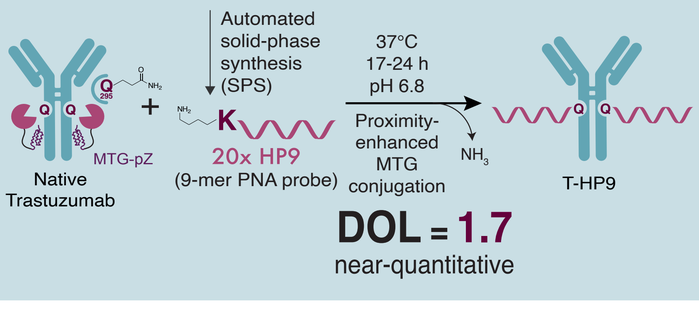
The primary PNA probe HP9 was conjugated to the native anti-HER2 antibody trastuzumab in a site-specific, single-step reaction using the enzyme microbial transglutaminase (MTG). MTG catalyzes an acyl transfer between Q295 in the IgG heavy chain (HC) and a lysine residue on the incoming PNA probe, forming a stable isopeptide bond. Although efficient for small substrates[1,2], soluble MTG achieves only 15% HC labeling (DOL = 0.3) when used for PNA conjugation.



DOL = 0.3
mostly unconjugated

Fusion of MTG with an Fc-binding Z-domain (MTG-pZ) enables proximity-enhanced conjugation at Q295, increasing PNA labeling to the HC from 15% to 85% (DOL = 1.7). No PNA purification is required prior to conjugation.





DOL = 1.7
near-quantitative

K_D = 30 pM (SPR)

HER2 binding is retained after conjugation (Trastuzumab K_D = 20 pM)

Single-step, site-specific PNA conjugation yields a well-defined antibody-PNA conjugate ready to target HER2-expressing tumors.

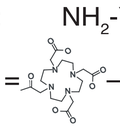
Capture

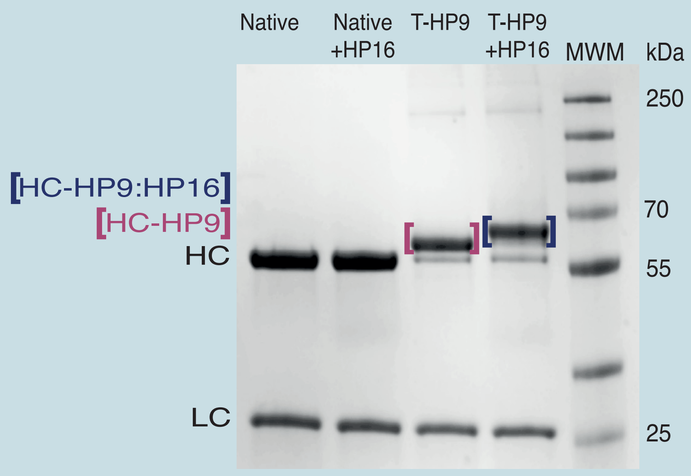
High-Affinity PNA:PNA Hybridization Enables Selective Probe Capture

Peptide nucleic acid (PNA) is a synthetic DNA analogue with a neutral peptide-like backbone, conferring higher binding affinity and specificity toward complementary sequences than natural nucleic acids. PNA-peptide chimeras are readily synthesized using commercially available building blocks and standard automated solid-phase synthesis (SPS).

Here, two complementary 9-mer PNA strands, HP9 and HP16[3,4], were employed as the primary and secondary probes, respectively: HP9 is conjugated to trastuzumab for tumor targeting, while HP16 serves as the radiolabeled secondary probe.

HP9: RA**K**GGGSS-**cct ggt gtt**-EK(DOTA)-(PEG_2)-E-NH_2
HP16: NH_2-YEE-**gga cca caa**-SS-(PEG_2)-DOTA

DOTA =  – a highly versatile radiometal chelator



Reducing SDS-PAGE of T-HP9 pre-hybridized with HP16 shows a distinct band shift to HC-HP9:HP16, confirming stable PNA-PNA dimer formation.
No shift is observed for native trastuzumab + HP16.

K_D = 90 pM (SPR)

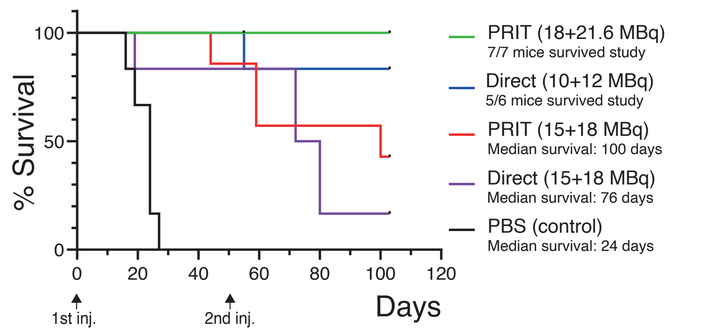
HP16 binds to T-HP9 with high-affinity

HP9:HP16 hybridization is specific, stable even under denaturing conditions, and enables selective capture of ^{161}Tb-HP16 at the tumor.

Treat

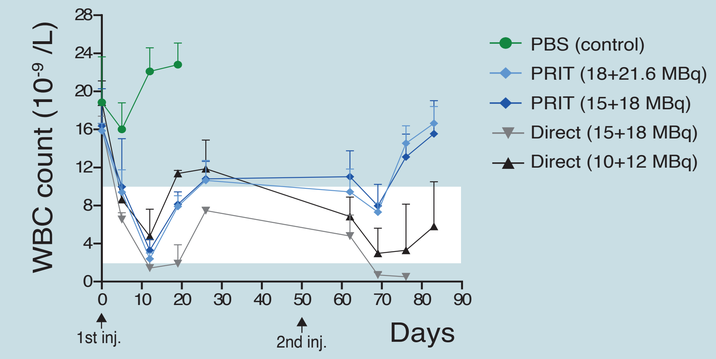
Delivering Localized ^{161}Tb Radiation to HER2+ Tumors

The therapeutic efficacy of T-HP9/^{161}Tb-HP16 pretargeting was evaluated in SKOV3 HER2+ xenograft-bearing mice and compared to directly ^{161}Tb-labeled trastuzumab. Two treatment cycles were initiated at day 0 and day 50.



PRIT at 18+21.6 Mbq achieved comparable survival to direct targeting at the lower dose of 10+12 MBq. Direct targeting at a higher dose of 15+18 MBq proved toxic to the mice.

Despite comparable survival, hematological recovery differed markedly. Total white blood cell (WBC) counts recovered toward normal range in PRIT-treated mice following repeated injections, whereas direct targeting groups showed prolonged WBC suppression, even at the lower dose, indicating increased bone marrow toxicity.



7/7 of pretargeted mice survived the end of the therapy study

PRIT (18+21.6 MBq)

Pretargeting achieves tumor-selective ^{161}Tb delivery with 7/7 survival (18+21.6 MBq), while sparing the radiosensitive bone marrow.

Conclusions

- **MTG-pZ achieves near-quantitative, site-specific PNA conjugation to native trastuzumab in a single step.**
- **Picomolar HP9:HP16 hybridization confirmed by SPR.**
- **Pretargeting achieves 7/7 survival (18+21.6 MBq) with improved hematological recovery in mice with HER2+ xenografts.**

Acknowledgements

CANCERFONDEN

References

1. Dickgiesser et al. *Bioconjug Chem.* 2020
2. Wehrmüller et al. *Chembiochem.* 2025
3. Westerlund et al. *ACS Pharmacol Transl Sci.* 2024
4. Altai et al. *J Control Release.* 2025

Scan to follow our research

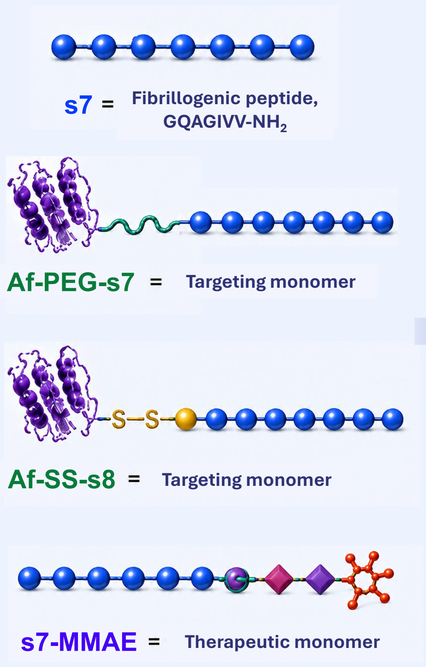
Targeting HER2-Positive Breast Cancer With a New Affibody-Nanodrug System

Ewa Wieczerzak[1], Milena Czeszejko[1], Patrycja Rachubik[2], Daria Sowik[1], Justyna Sawicka[1], Kamila Kitowska[3], Rafał Sądej[3] & Sylwia Rodziewicz-Motowidło[1]

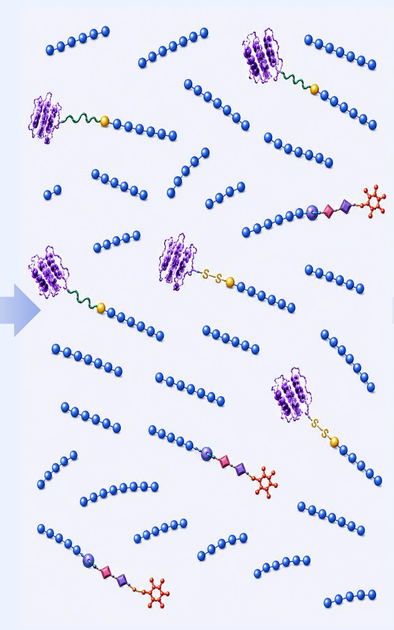
[1] *Department of Biomedical Chemistry, Faculty of Chemistry, University of Gdańsk, Poland*
[2] *Laboratory of Molecular and Cellular Nephrology, Mossakowski Medical Research Institute, Polish Academy of Sciences, Gdańsk, Poland*
[3] *Laboratory of Molecular Enzymology and Oncology, Institute of Medical Biotechnology and Experimental Oncology, Intercollegiate Faculty of Biotechnology of University of Gdańsk and the Medical University of Gdańsk, Poland*
doi.org/10.17952/38EPS.2026.P354

1 Concept of the designed nanocarrier

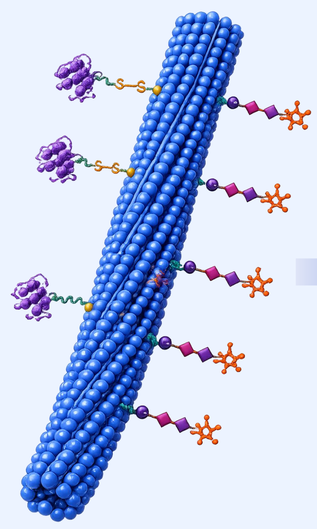
1 Modular building blocks



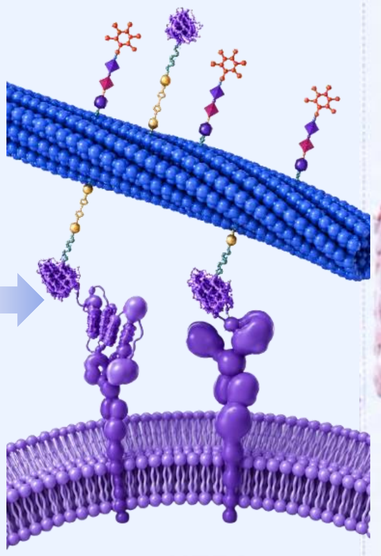
2 Fibrillization of the components at the desired ratio



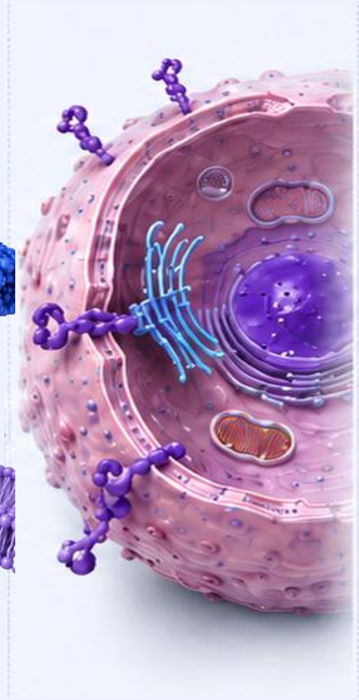
3 Hybrid peptide fibril



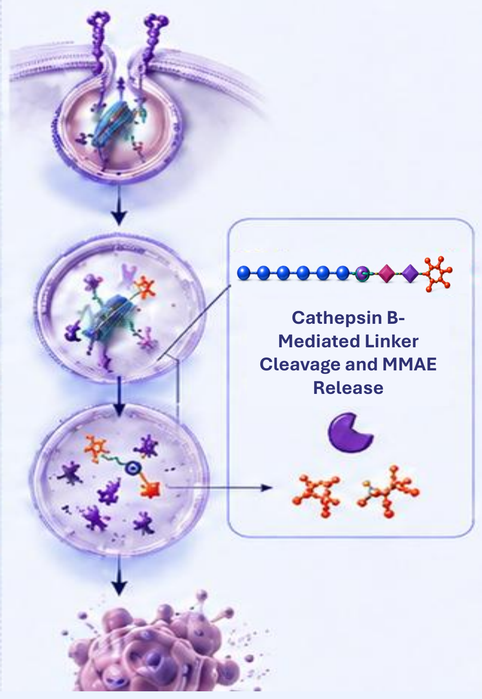
4 Targeting the HER2 receptor



5 HER2-positive cell



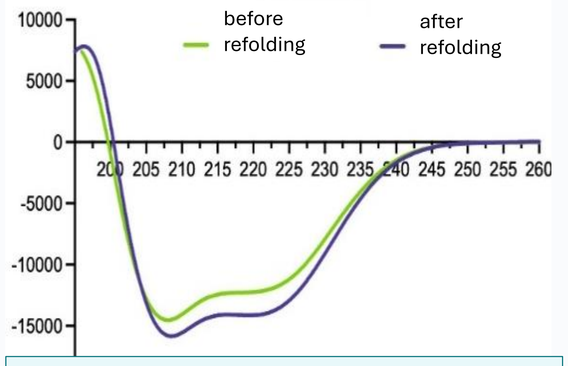
6 MMAE delivery and anticancer effect



2 Validation of the HER2-targeting module

Structural and functional evaluation of free affibody prior to incorporation into the fibrillar platform

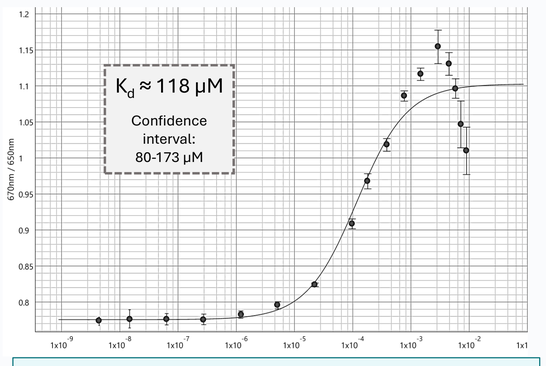
A. Circular Dichroism Spectroscopy: affibody before and after refolding



The CD spectra recorded before and after refolding were highly similar and displayed features consistent with a predominantly α-helical structure

✓ As the refolding procedure did not substantially alter the secondary-structure profile, the affibody without additional refolding was used in the HER2-binding assay

B. MST: interaction with HER2



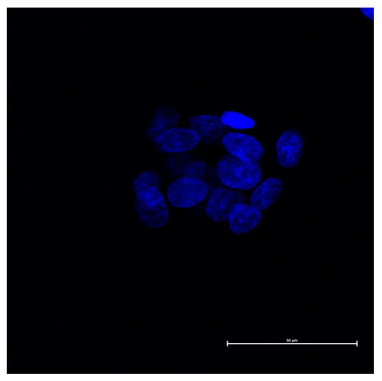
MST measurements were performed using 20 nM recombinant human HER2 and a concentration series of the affibody

✓ A concentration-dependent response was observed, supporting an interaction between the affibody and HER2. At the highest affibody concentration, the signal deviated from the expected binding profile, potentially due to self-association, aggregation, or cysteine-mediated dimerization

3 Confocal validation at the cellular interface

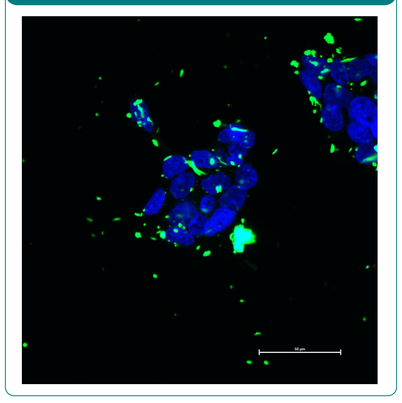
Localization of fluorescently labelled fibrils and free HER2-binding affibody relative to BT-474 cells

Control (DAPI)



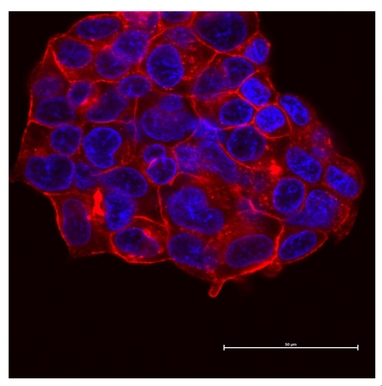
- DAPI - nuclei (blue)

Fibrils (BODIPY)



- BODIPY-labelled fibrils (green)

Affibody (Alexa Fluor 546)



- Alexa Fluor-labelled affibody (red)

BT-474 cells were cultured as a 2D monolayer in RPMI medium, allowed to adhere for 24 h, and subsequently incubated with the tested systems for 48 h. The cells were then fixed with methanol, stained with DAPI, and analysed by confocal microscopy. BODIPY-labelled fibrils and Alexa Fluor-labelled affibody were detectable in the vicinity of BT-474 cells

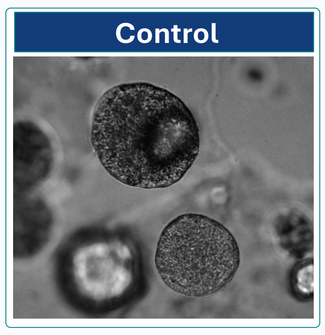
✓ Alexa Fluor-labelled affibody signal was concentrated along the cell outline, consistent with predominantly surface-associated localization

4 Biological readout

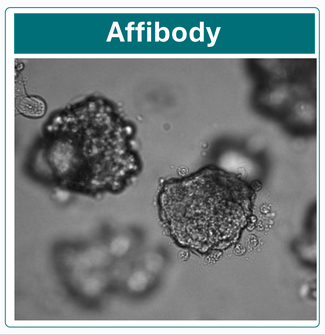
Effect of the investigated systems on BT-474 spheroids

A. Morphology

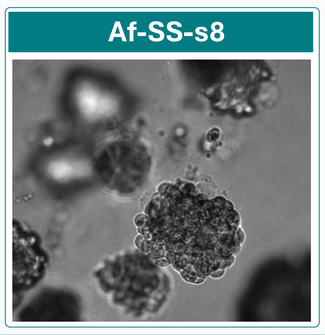
Control



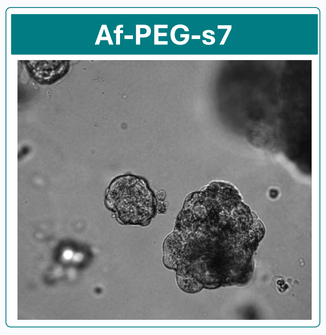
Affibody



Af-SS-s8



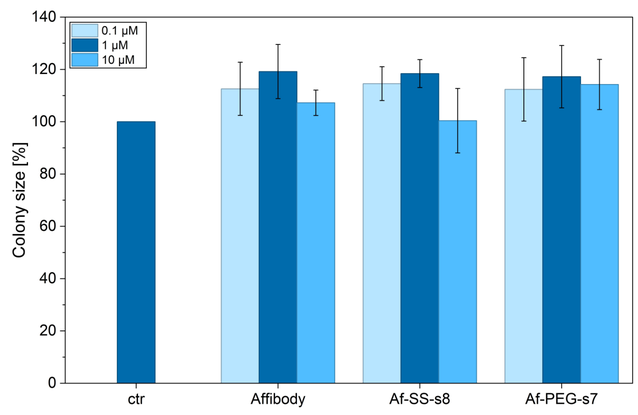
Af-PEG-s7



BT-474 spheroids were cultured in Matrigel and treated with the investigated systems (10 µM) for 19 days. Spheroid morphology was assessed by bright-field microscopy

✓ Affibody-containing systems induced visible morphological changes in BT-474 spheroids, characterized by reduced compactness and irregular borders

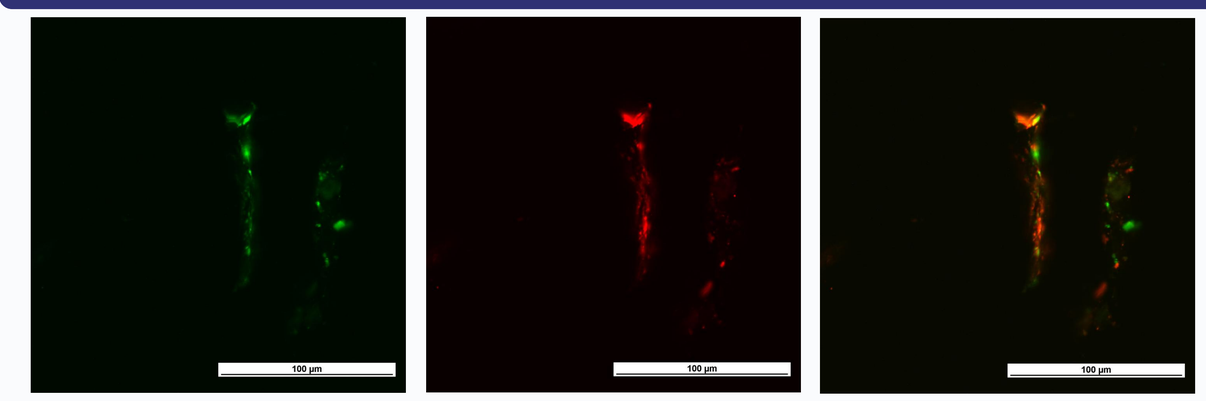
B. Colony size



BT-474 spheroids were cultured in Matrigel and treated with the investigated systems (0.1–10 µM) for 19 days. Colony size was quantified from bright-field images and expressed relative to untreated controls

✓ No reduction in BT-474 colony size was observed following treatment with affibody or affibody conjugates. Colony size remained comparable to or slightly higher than that of untreated controls across all tested concentrations

5 Affibody incorporation into fibrils



Mixed fibrillar systems composed of Alexa Fluor-labelled affibody, PyTAP-labelled s7, and unlabelled s7 (1:10:1000 ratio) were analysed by confocal microscope after 7 days of fibrillization. Numerous well-defined fibrils were visible in both fluorescence channels. The signal pattern was consistent with the co-presence of both labelled affibody and s7 within the fibrillar network

6 Conclusions

1. CD spectra demonstrated that the chemically synthesized $Z_{HER2:2891}$ affibody adopted a predominantly α-helical structure both before and after refolding
2. MST indicated a concentration-dependent interaction between the affibody and HER2, although quantitative affinity determination was limited by nonspecific effects at higher affibody concentrations
3. Confocal imaging showed fibril-associated fluorescence near BT-474 cells and predominantly surface-associated localization of the fluorescently labelled affibody
4. Affibody-containing systems altered BT-474 spheroid morphology without reducing colony size, indicating disruption of spheroid architecture rather than clear growth inhibition
5. Confocal microscopy confirmed the formation of mixed fibrils and demonstrated the incorporation of affibody and s7 within the fibrillar network

This work was supported by NCN under grant 2022/45/B/NZ7/03889

Thiol-yne Mediated Peptide Macrocyclisation and Derivatisation Strategies

Conor Williams[1], Dearbhla Tully[1], Konstantin Raabe[2], Dominik Windisch[2], James O'Brien[3], Cristina Trujillo[3], Joanna F. McGouran[1], Markus Muttenthaler[2,4] and Eoin M. Scanlan[1]

[1] Trinity Biomedical Sciences Institute, Trinity College Dublin, 152-160 Pearse St., Dublin 2, Ireland
[2] Faculty of Chemistry, Institute of Biological Chemistry, University of Vienna, Währinger Straße 38, 1090 Vienna, Austria
[3] Department of Chemistry, The University of Manchester, Oxford Road, Manchester, M13 9PL United Kingdom
[4] Institute for Molecular Bioscience, The University of Queensland, 4072 Brisbane, Queensland, Australia

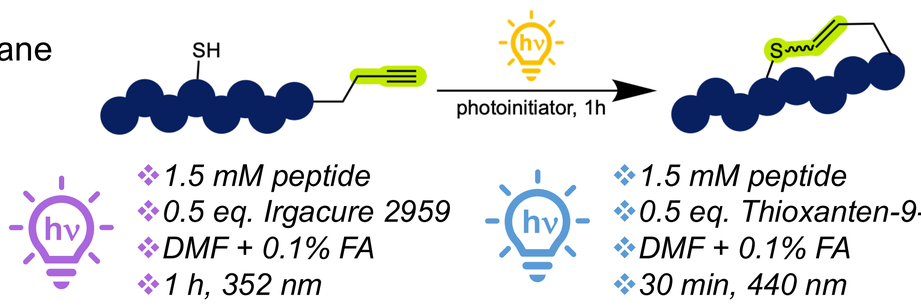
Contact: cowillia@tcd.ie, eoin.scanlan@tcd.ie

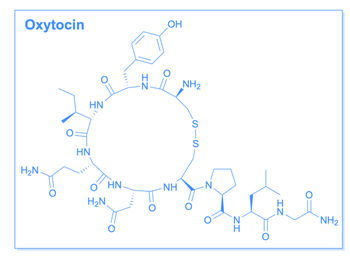
Taighde Éireann Research Ireland

https://doi.org/10.17952/38EPS.2026.P045

Introduction

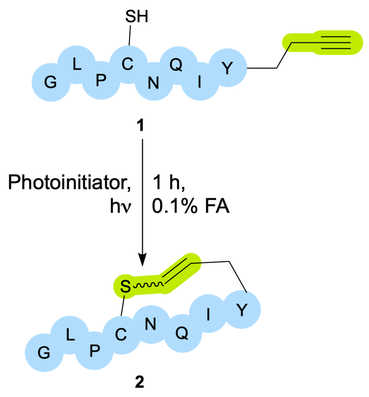
- Peptides offer significant potential as therapeutics. However, poor membrane permeability and susceptibility to peptidases are of concern [1]
- Replacement of disulfide bonds offers a solution to increase stability [2,3]
- Thiol-yne 'click' cyclisation has been poorly explored [4]
  - Mild, metal free, selective and light mediated solution
  - Vinyl sulfide adds rigidity with minimal perturbation of native sequence





Thiol-yne Optimisation

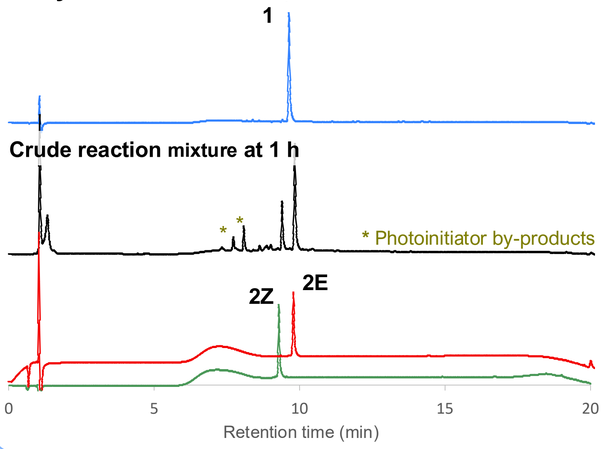
- Alkyne containing peptides synthesised through incorporation of an alkyne amino acid or carboxylic acid during SPPS
- Optimisation carried out exploring photoinitiator, pH, concentration and solvent effects



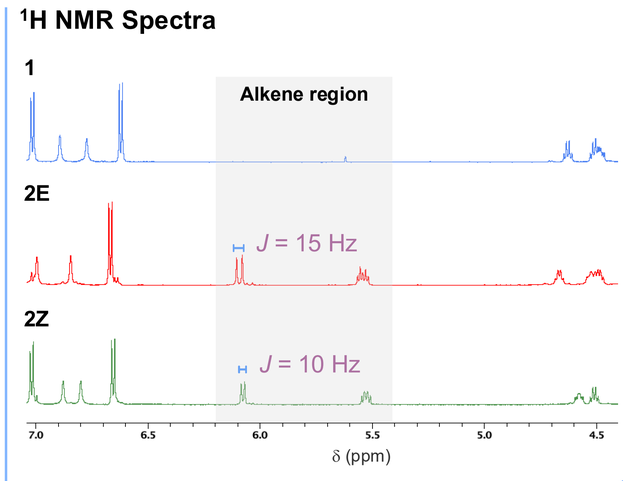
Photoinitiator	eq.	Conc.	Solvent	Additive	Conversion
DPAP	1.0	1.7 mM	H_2O : AcN	0.1% TFA, MAP	N.R.
DPAP	0.5	0.5 mM	DMF	–	26%
Irgacure 2959	0.5	0.5 mM	DMF	–	31%
Irgacure 2959	0.5	0.5 mM	DMF	0.1% TFA	16%
Irgacure 2959	0.5	0.5 mM	DMF	0.1% FA	60%
Irgacure 2959	0.5	1.0 mM	DMF	0.1% FA	81%
Irgacure 2959	**0.5**	**1.5 mM**	**DMF**	**0.1% FA**	**>95%**
Irgacure 2959	0.5	2.5 mM	DMF	0.1% FA	89%

- Reaction can be modified for use in aqueous conditions or with Blue LED initiation, for compatibility with biological applications

Analytical HPLC traces, 214 nm

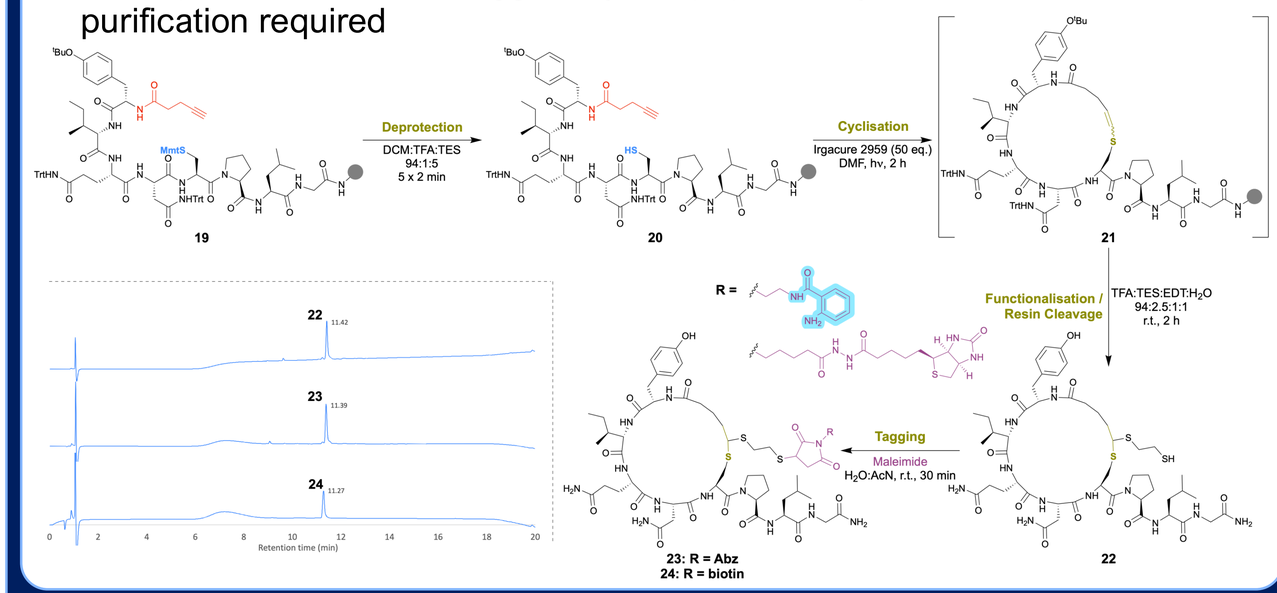


^{1}H NMR Spectra



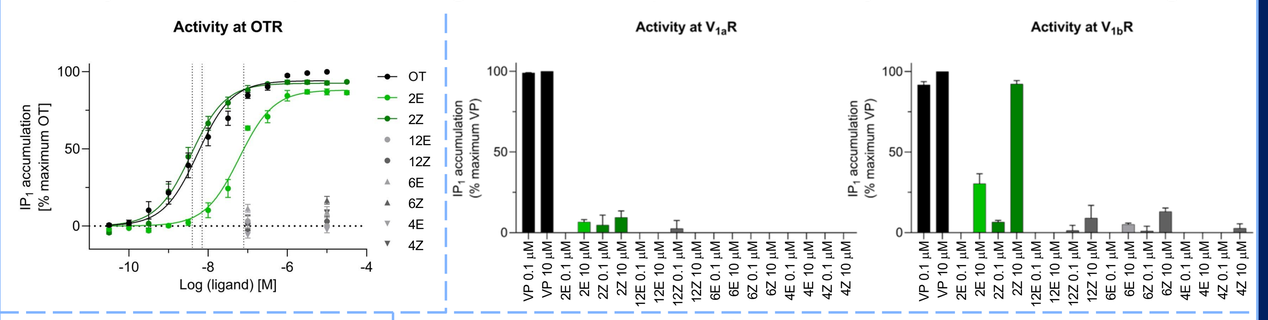
On-resin Cyclisation & Modification

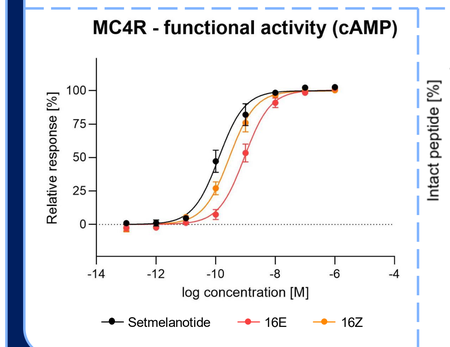
- On-resin thiol-yne reaction, followed by concomitant ionic hydrothiolation during peptide cleavage yields a cyclic peptide with a free thiol handle
- Suitable for functionalisation with maleimide tags
- Fluorophore and biotin tagged cyclic peptides synthesised with minimal purification required

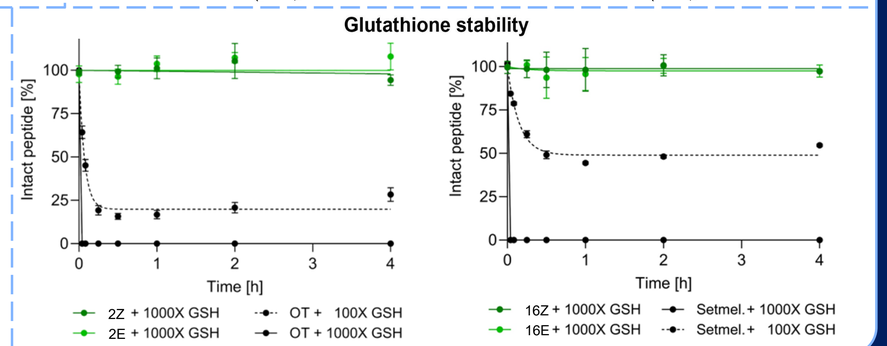


Biological Assays

- Biological activity assays of isolated neuropeptide analogues were obtained [5]
- Peptides analogues **2Z** and **16Z** demonstrate EC_{50} values with equivalent or improved activity relative to their respective parent compounds
- Oxytocin analogues do not show crossover activity at vasopressin receptors
- Vinyl sulfide stapled analogues have improved stability over disulfide bridges



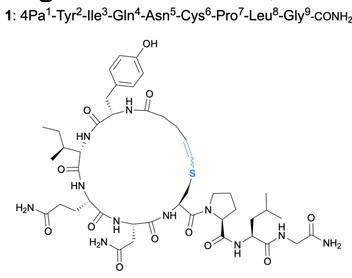




Cyclic Neuropeptide Analogues

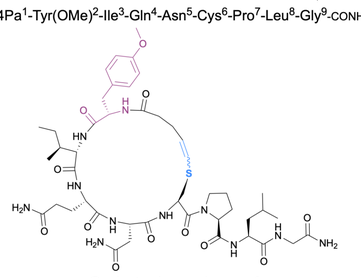
- Analogues synthesised by SPPS and solution phase thiol-yne cyclisation
- *(E)* and *(Z)* isomers typically separable by HPLC
- High conversions, all 20 canonical amino acids, 21-39 membered macrocycles

1: 4Pa[1]-Tyr[2]-Ile[3]-Gln[4]-Asn[5]-Cys[6]-Pro[7]-Leu[8]-Gly[9]-$CONH_2$



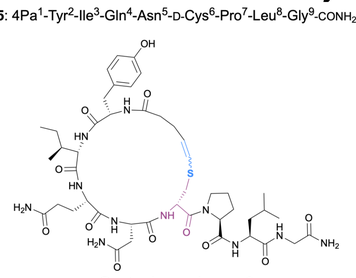
Oxytocin analogue **2**
(>95% conversion)
3 : 1 *(E)* : *(Z)*

3: 4Pa[1]-Tyr(OMe)[2]-Ile[3]-Gln[4]-Asn[5]-Cys[6]-Pro[7]-Leu[8]-Gly[9]-$CONH_2$



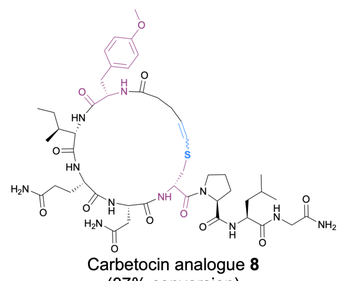
Carbetocin analogue **4**
(90% conversion)
5 : 2 *(E)* : *(Z)*

5: 4Pa[1]-Tyr[2]-Ile[3]-Gln[4]-Asn[5]-D-Cys[6]-Pro[7]-Leu[8]-Gly[9]-$CONH_2$



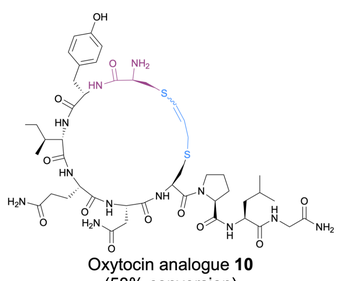
Oxytocin analogue **6**
(89% conversion)
3 : 2 *(E)* : *(Z)*

7: 4Pa[1]-Tyr(OMe)[2]-Ile[3]-Gln[4]-Asn[5]-D-Cys[6]-Pro[7]-Leu[8]-Gly[9]-$CONH_2$



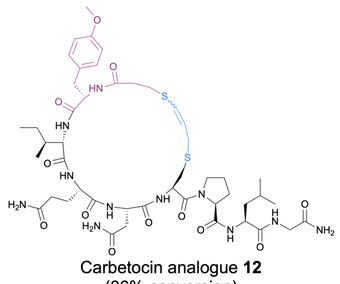
Carbetocin analogue **8**
(87% conversion)
3 : 2 *(E)* : *(Z)**

9: H_2N-Cys[1]-Tyr[2]-Ile[3]-Gln[4]-Asn[5]-Pcy[6]-Pro[7]-Leu[8]-Gly[9]-$CONH_2$



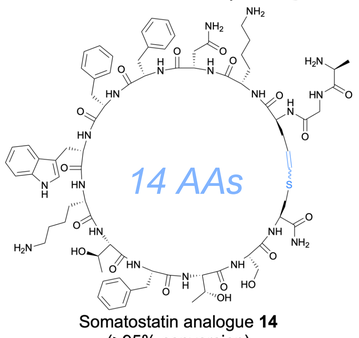
Oxytocin analogue **10**
(58% conversion)
1 : 1 *(E)* : *(Z)*

11: 3Ma[1]-Tyr(OMe)[2]-Ile[3]-Gln[4]-Asn[5]-Pcy[6]-Pro[7]-Leu[8]-Gly[9]-$CONH_2$



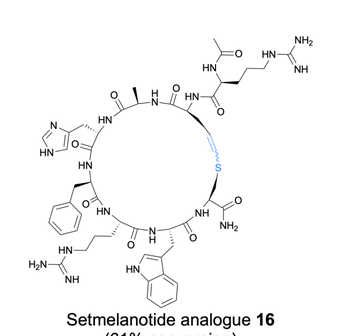
Carbetocin analogue **12**
(86% conversion)
1 : 1 *(E)* : *(Z)*

13: H_2N-Ala[1]-Gly[2]-Pra[3]-Lys[4]-Asn[5]-Phe[6]-Phe[7]-Trp[8]-Lys[9]-Thr[10]-Phe[11]-Thr[12]-Ser[13]-Cys[14]-$CONH_2$



Somatostatin analogue **14**
(>95% conversion)
1 : 1 *(E)* : *(Z)**

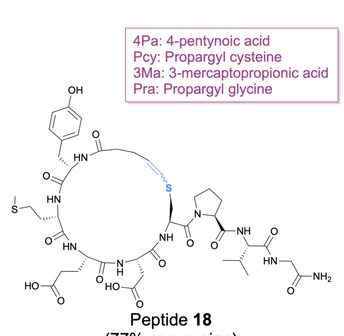
15: Ac-Arg[1]-Pra[2]-D-Ala[3]-His[4]-D-Phe[5]-Arg[6]-Trp[7]-Cys[8]-$CONH_2$



Setmelanotide analogue **16**
(61% conversion)
3 : 2 *(E)* : *(Z)*

17: 4Pa[1]-Tyr[2]-Met[3]-Glu[4]-Asp[5]-Cys[6]-Pro[7]-Val[8]-Gly[9]-$CONH_2$

4Pa: 4-pentynoic acid
Pcy: Propargyl cysteine
3Ma: 3-mercaptopropionic acid
Pra: Propargyl glycine

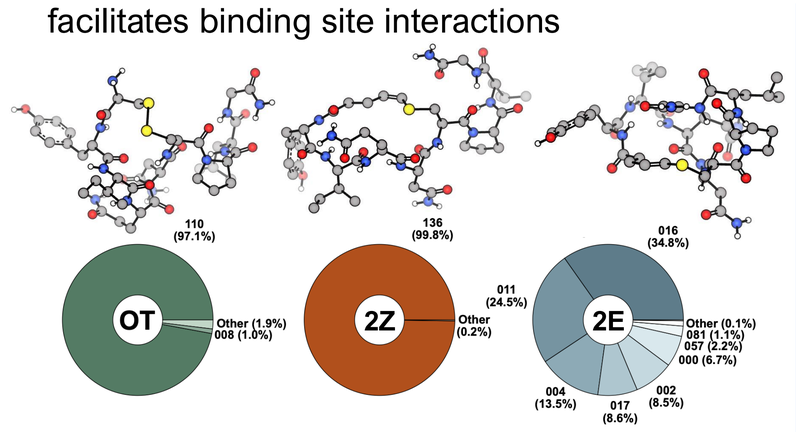


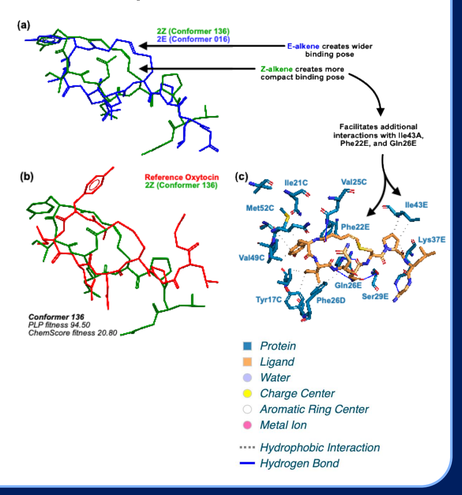
Peptide **18**
(77% conversion)
1 : 1 *(E)* : *(Z)*

* Analogues inseparable by RP-HPLC, isomeric ratio determined by ^{1}H NMR

Conformational Analysis

- Analysis of **2Z** and **2E** shows *(Z)* vinyl sulfide has a single dominant conformer while *(E)* has 8 major conformers
- *(E)* vinyl sulfide has a wider ring size, *(Z)* more compact which better facilitates binding site interactions





Conclusions

- ✓ 'Click' type reaction
- ✓ Mild, rapid, photo-radical conditions
- ✓ Late stage on-resin modification
- ✓ Increased rigidity & stability
- ✓ Promising biological activity
- ✓ *(E)* and *(Z)* isomers available
- Investigating methodology for medium sized ring synthesis

https://doi.org/10.1021/jacs.6c08113

References

1. L. Wang, N. Wang, W. Zhang, X. Cheng, Z. Yan, G. Shao, X. Wang, R. Wang and C. Fu, *Sig. Transduct. Target Ther.*, 2022, **7**, 48.
2. S. Tomassi, A. M. Trotta, C. Ieranò, F. Merlino, A. Messere, G. Rea, F. Santoro, D. Brancaccio, A. Carotenuto, V. M. D'Amore, F. S. Di Leva, E. Novellino, S. Cosconati, L. Marinelli, S. Scala and S. Di Maro, *Chem. Eur. J.*, 2020, **26**, 10113–10125.
3. M.D. Nolan, C. Shine, E.M. Scanlan and R. Petracca, *Org. Bimol. Chem.*, 2022, **20**, 8192-8196
4. Y. Tian, J. Li, H. Zhao, X. Zeng, D. Wang, Q. Liu, X. Niu, X. Huang, N. Xu and Z. Li, *Chem. Sci.*, 2016, **7**, 3325–3330.
5. A. D. De Araujo, M. Mobli, J. Castro, A. M. Harrington, I. Vetter, Z. Dekan, M. Muttenthaler, J. Wan, R. J. Lewis, G. F. King, S. M. Brierley and P. F. Alewood, *Nat. Commun.*, 2014, **5**, 3165.

CIC biomaGUNE
MEMBER OF BASQUE RESEARCH & TECHNOLOGY ALLIANCE

BECKER LAB VIENNA

universität wien

Small Molecules, Big Impact: Quantifying the Influence of Molecular Influencers on Protein Interactions

Pamina M. Winkler[a,b], **Christian F.W. Becker**[a]

[a] Institute of Biological Chemistry, Faculty of Chemistry, University of Vienna, Währinger Str. 38, 1090 Vienna, Austria

[b] Center for Cooperative Research in Biomaterials (CIC biomaGUNE), Paseo de Miramon 194, 20014, Donostia-San Sebastián, Spain

Email address: pamina.winkler@univie.ac.at; pwinkler@cicbiomagune.es

https://doi.org/10.17952/38EPS.2026.P067

Motivation

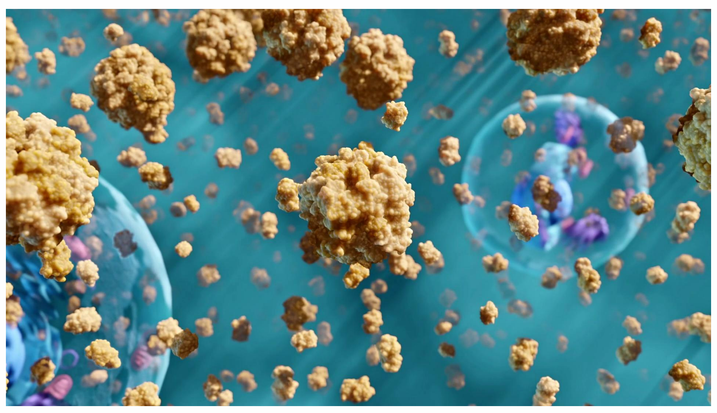
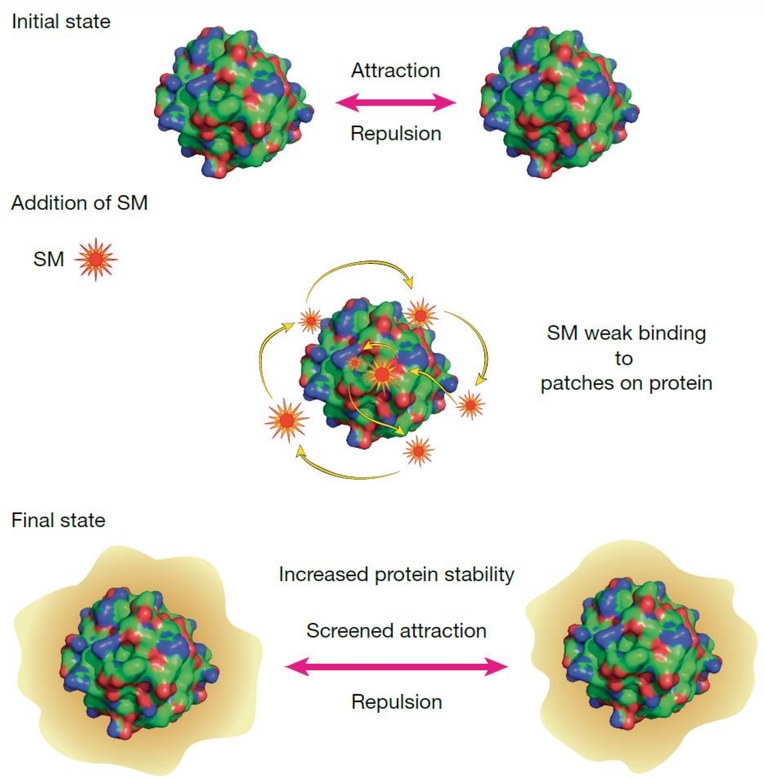


Illustration of protein interactions and aggregation (beige) in solution against the backdrop of living cells.

Protein dynamics determine biological function and understanding how protein interactions are influenced by other proteins and small molecules, such as amino acids, is key to connecting dynamics with function. There is growing evidence that the dynamics of proteins are a function of the cellular environment.

Amino acids stabilize protein dispersions.

To precisely measure the stability in solution and the interactions of proteins, we measured the second osmotic virial coefficient (B_{22}) and the binding affinity (K_D), both proxies for interaction strength by applying self-interaction chromatography and surface plasmon resonance studies. We have developed a theory that explains all the experimental observations and agrees quantitatively with the measurements we performed. It postulates that the **effect is due to weak amino acid-protein screening interactions that in turn modulate the protein self- and cross-interactions** (*1,2*).



Schematic of the proposed theoretical framework for colloidal stability caused by small molecules *(1)*.

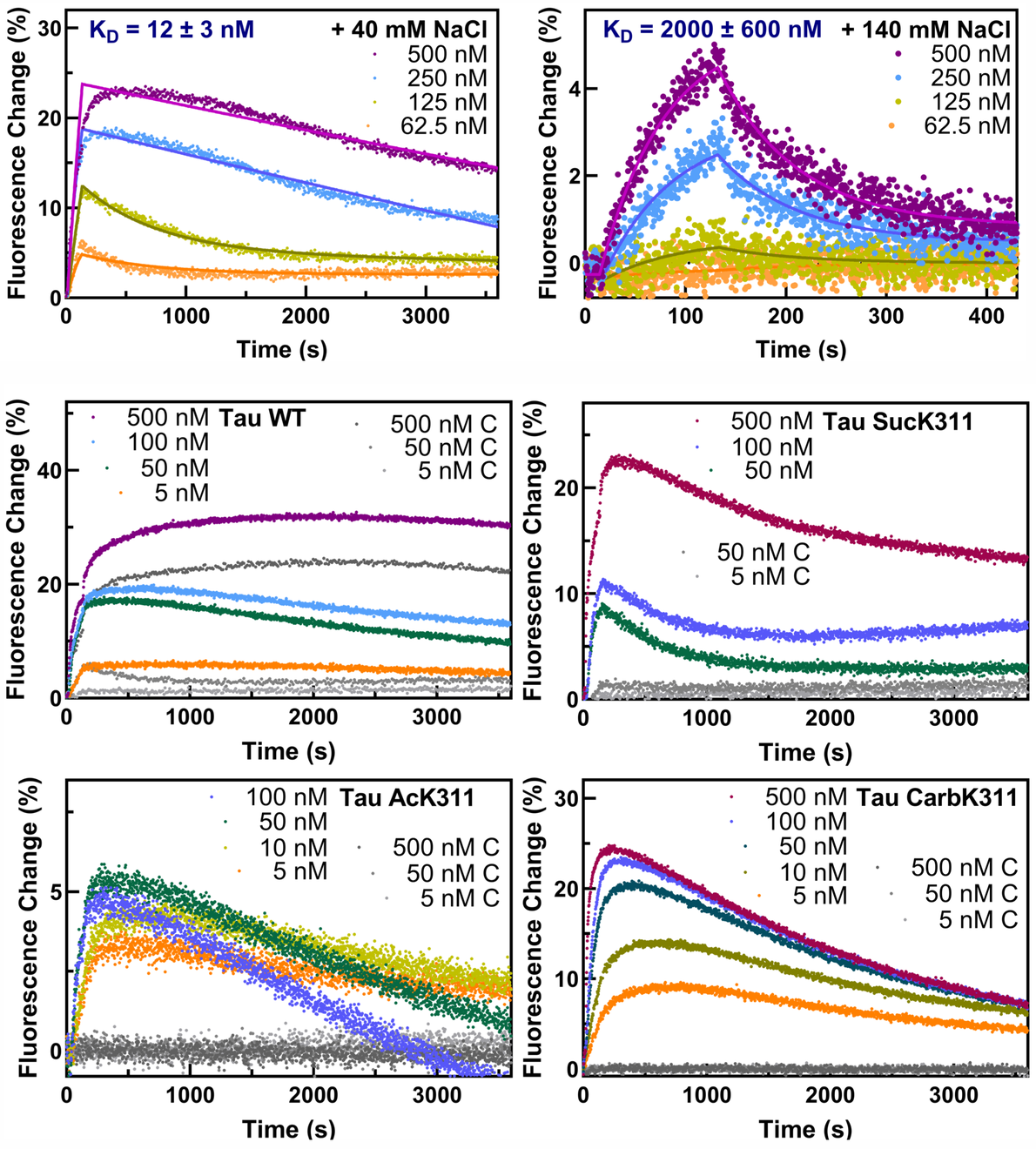
How do molecular influencers shape protein interaction dynamics?

For protein cross-interactions between lysozyme and whey protein isolates, we showed that millimolar concentrations of glutamine, proline, and arginine can stabilize interactions and shift binding affinity by orders of magnitude *(2)*. This has physiological relevance, as intracellular free amino acid concentrations range from a few to ~100 mM *(3)*. We propose that amino acids represent one manifestation of a broader principle: **the molecular environment regulates protein interaction dynamics.** This local cellular environment is **defined by ionic composition, small molecules, post-translational modifications (PTMs), molecular crowding, and condensates**—collectively termed **molecular influencers**.

We recently found that **changing NaCl concentration from 40 to 140 mM** in phosphate buffer shifts the K_D of tau by two orders of magnitude. These preliminary results suggest that **salt ions can substantially alter the molecular environment of intrinsically disordered proteins** such as tau, markedly more strongly than in proteins with defined structures.

PTMs alter protein charge distribution. Preliminary results with **tau variants carrying a single PTM** at K311—succinylation (SucK311), acetylation (AcK311), or carbamylation (CarbK311)—**show distinct binding kinetics** with wildtype (WT) tau and **altered interactions with polyanions e.g. DNA** (grey curves).

We hypothesize that **neighboring amino acid residues in tau compete for interaction partners**—including salt ions, polyanions, metabolites, and other tau monomers—as a function of their concentration and protein charge distribution modulated by PTMs. **Understanding these dynamics requires deciphering how molecular "influencers" act across spatial and temporal scales in model and native living systems**. The currently existing large gap between *in vitro* and *in vivo* results reflects differences in molecular conditions, forces, and drivers, preventing quantitative and predictive models of protein interactions in cells. **Correlative multidisciplinary approaches are key to advance on bridging this gap**.



(1) T. Mao, X. Xu, P.M. Winkler *et al.*, *Nature*. (2025). (2) P. M. Winkler *et al.*, *J. Phys. Chem. B*. (2024).
(3) R. Rollin, J.-F. Joanny, P. Sens, *eLife*. (2023).

Mining bacteriophage endolysin structures for novel membrane-active antibacterial peptides

M. Wojciechowska, M. Wdowiak, E. Stefańczyk, J. Trylska

University of Warsaw, Centre of New Technologies, Warsaw, Poland | m.wojciechowska@cent.uw.edu.pl

https://doi.org/10.17952/38EPS.2026.P169

CENTRAL IDEA

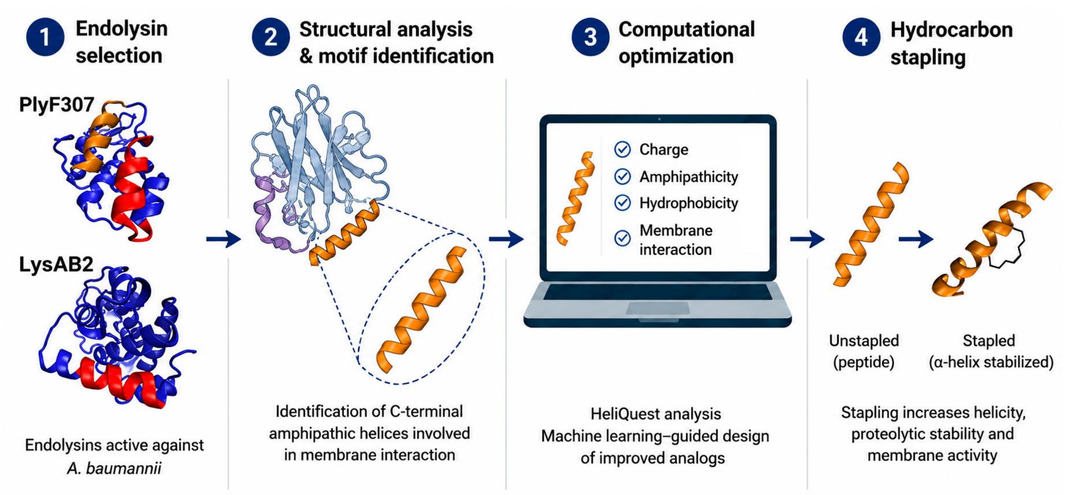
Can bacteriophage endolysins serve as blueprints for novel antimicrobial peptides?

We hypothesized that hidden amphipathic motifs within endolysin structures can be identified, rationally optimized and structurally stabilized to generate potent membrane-active antibacterial peptides.

RESULTS

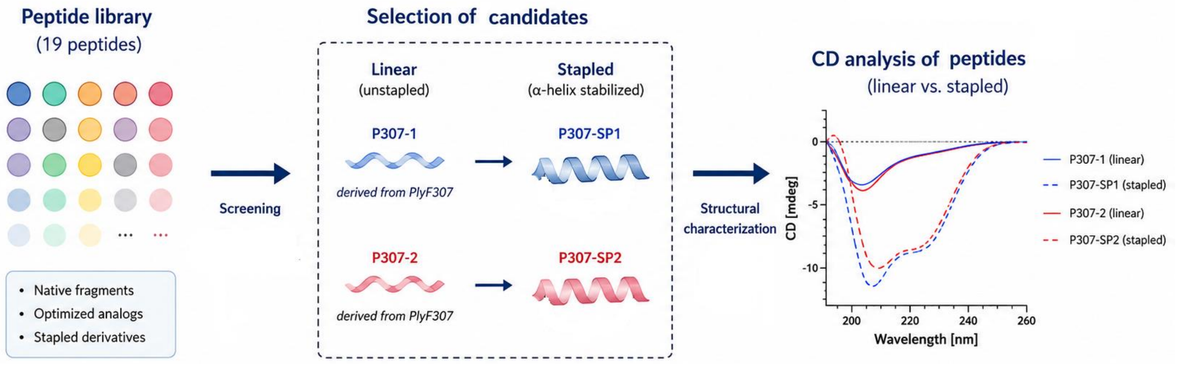
1. RATIONAL AND ML-GUIDED DESIGN

Structural analysis of PlyF307 and LysAB2 revealed amphipathic, positively charged motifs as potential templates for membrane-active peptides. ML-assisted design was then used to optimize their physicochemical properties.



2. FROM PEPTIDE LIBRARY TO LEAD CANDIDATES

Selected sequences were further optimized by hydrocarbon stapling to stabilize their α-helical conformation. This strategy yielded the most promising antibacterial candidates.



3. POTENT ANTIBACTERIAL ACTIVITY

The lead stapled peptides P307-SP1 and P307-SP2 displayed broad antibacterial activity (**MIC = 1–4 µM**), including potent activity against resistant *A. baumannii* and clinically relevant UPEC strains.

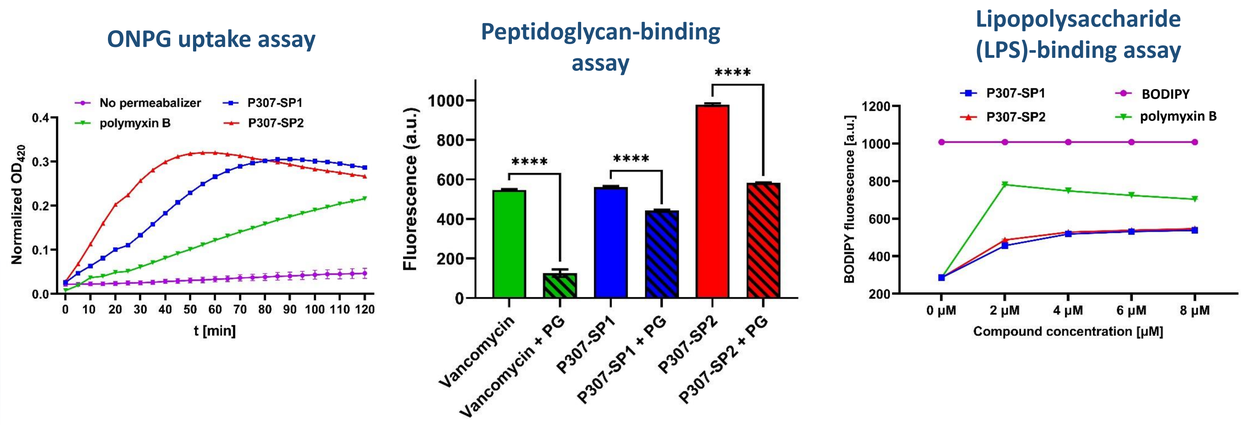
	Minimum inhibitory concentration (MIC) [µM]		
Bacterial strain	**P307-SP1**	**P307-SP2**	**Polymyxin B**
E. coli K-12 MG1655	2	4	0.25
E. coli AS19	2	2	1
E. coli O6:K15:H31 536 (UPEC)	2	4	-
E. coli ATCC 700928 (UPEC)	2	4	-
A. baumannii ATCC 19606	1	2	0.5
A. baumannii ATCC BAA-1605	2	2	0.5
A. baumannii ATCC 19606R	1	1	32
S. aureus ATCC 29213	2	2	>32
M. catarrhalis PCM 1902	2	2	0.5

1 µM (very potent)

2 µM (potent)

4 µM (moderate)

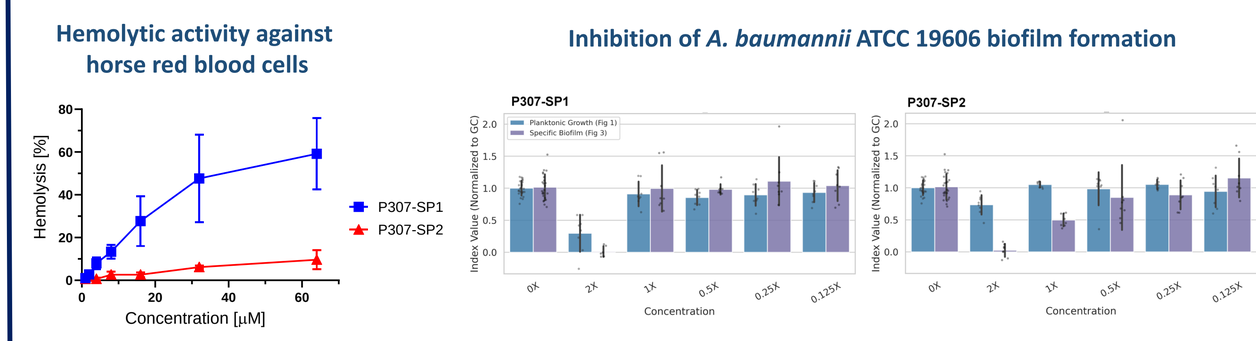
4. MEMBRANE-TARGETING MECHANISM



The lead peptides interact with bacterial envelope components and permeabilize the bacterial membrane. These results support a membrane-targeting mechanism underlying their antibacterial activity.

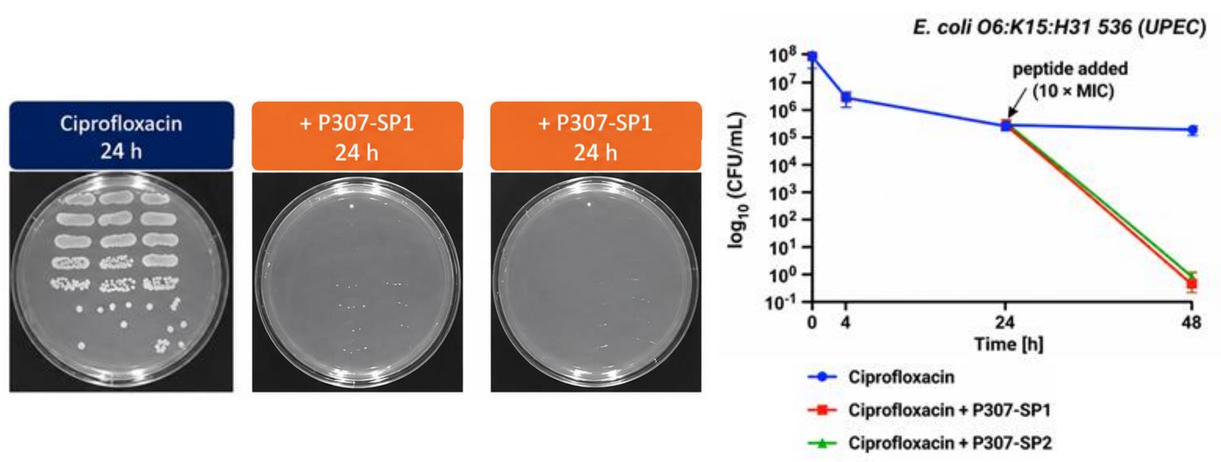
5. SELECTIVITY AND ANTIBIOFILM EFFECT

Despite their potent antibacterial activity, the lead peptides showed low hemolytic activity. Both peptides also reduced *A. baumannii* biofilm formation.



6. TOWARD DIFFICULT-TO-ELIMINATE POPULATIONS

The lead peptides retained antibacterial activity against persister cells, demonstrating their potential against difficult-to-eradicate bacterial populations.



TAKE-HOME MESSAGE

- Bacteriophage endolysins are a promising and underexplored source of membrane-active peptide sequences.
- Structure-guided and ML-assisted design enabled the identification and optimization of antibacterial peptides derived from endolysin motifs.
- Hydrocarbon stapling promoted α-helical structure and generated highly active peptide variants.
- The lead stapled peptides showed broad antibacterial activity, **with MIC values of 1–4 µM**, including activity against resistant *A. baumannii*.
- Their antibacterial activity is associated with membrane disruption, while maintaining low hemolytic activity.
- Beyond planktonic bacteria, the lead peptides retained activity against clinically relevant UPEC strains and difficult-to-eradicate bacterial populations, including persisters, and reduced *A. baumannii* biofilm formation.

From hidden endolysin motifs to potent antibacterial peptides active against planktonic cells, biofilms and persisters.

REFERENCES

Wojciechowska M. et al. *Frontiers in Microbiology* DOI: 10.3389/fmicb.2021.772038

Macyszyn J. et al. *Scientific Reports* DOI: 10.1038/s41598-023-38745-y

Wojciechowska M. *Frontiers in Microbiology* DOI: 10.3389/fmicb.2025.1603380

Acknowledgements: This work was supported by National Science Centre (2023/50/E/NZ1/00346)

Hydrophilic-Interaction-Chromatography (HILIC) as a Go-To Alternative for Synthetic Peptide Analysis and Purification

Yiping Wu[1], Daniel Tietze[1], Annika L. Weinmann[1] & Linda Thunberg[1]

Separation Science Laboratory, Discovery Sciences, BioPharmaceuticals R&D, AstraZeneca, Gothenburg, Sweden[1]

https://doi.org/10.17952/38EPS.2026.P245

Abstract

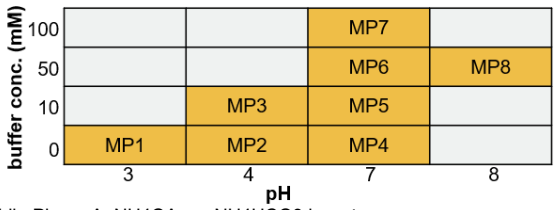
We conducted a multifactor study encompassing: (a) HILIC stationary phases with distinct surface chemistries, (b) TFA-free mobile phases varying in buffer strength and pH, (c) a representative panel of peptides spanning a wide range of length, charge, hydrophobicity, and sequence composition. Compared with C18 reversed-phase liquid chromatography (RP-LC), HILIC covers a comparable chemical space while providing different retention, selectivity, and resolution. HILIC also enhanced separation of structurally subtle and process-relevant impurities. Moreover, we established one-step HILIC purifications of peptide crudes, beneficial for process sustainability and sample in vivo readiness.

Methods

Initial Screening

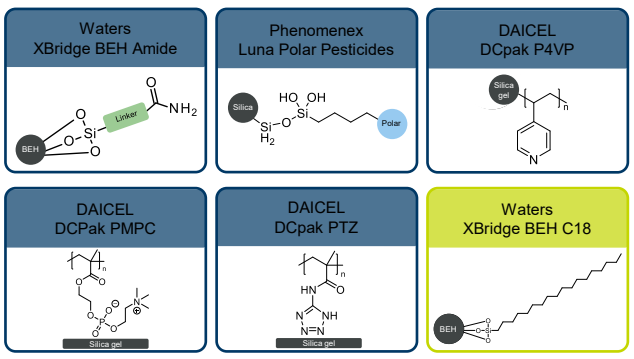
8 mobile phase pairs × (5 HILIC columns + 1 RP C18 column)

Mobile Phase Conditions



Mobile Phase A: NH4OAc or NH4HCO3 in water
Mobile Phase B: +/- 0.5% AcOH in acetonitrile/water 95/5

Column Chemistry



2.1 × 100 mm, 2.5 µm (C18, Amide) or 3.0 µm (Luna, P4VP, PMPC, PTZ)

Table 1 The peptide test-set for screening

Peptide Name	Molecular Weight (g/mol)	pI	Structure Class
Leucine Enkephaline	555.6	6.0	linear
Angiotensin II	1046.2	7.7	linear
Carbetocin	988.2	N.A.	cyclic, thioether
Desmopressin	1069.2	8.7	cyclic, disulfide
Leuprolide	1209.4	9.7	linear
Triptorelin	1311.4	7.7	linear
Somatostatin	1637.9	8.9	cyclic, disulfide
Liraglutide analogue*	3512.8	4.6	linear
ACTH (Porcine)	4541.1	9.4	linear

(*) Liraglutide analogue refers to the parental peptide minus the lipid moiety
The peptides were mixed and dissolved in ACN/water (1/1, v/v) to a final concentration of 0.5 mg/mL each.

Real sample testing

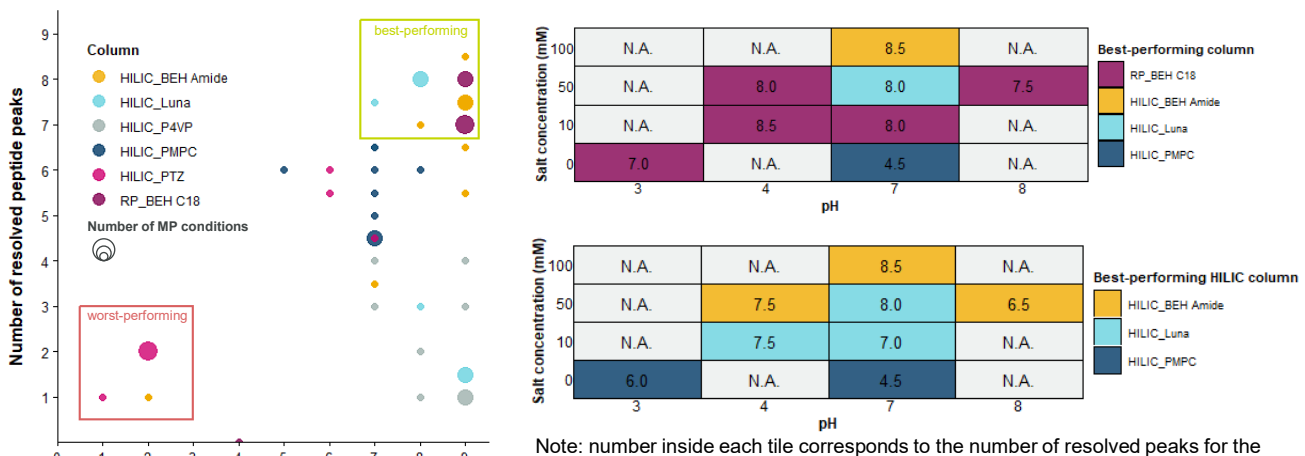
The peptide crudes were analyzed on Waters XBridge BEH C18 and XBridge BEH Amide for comparison.

Table 2 The peptide crudes with challenging impurities

Peptide	Molecular Weight (g/mol)	Structure Class
P1	4310.8	linear
P2	1993.1	maleimide-bridged monocyclic
P3	1526.8	bicyclic
P4	2645.0	peptide-small molecule conjugate

Results

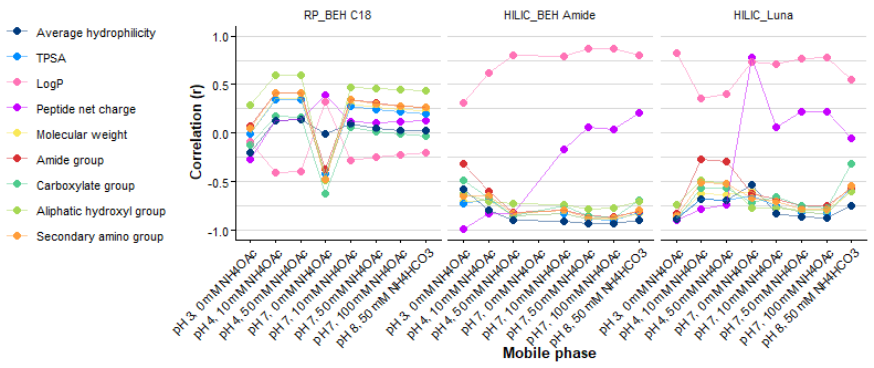
HILIC Column Screening for Generic Peptide Separation Method



Note: number inside each tile corresponds to the number of resolved peaks for the best-performing column at a specific mobile phase composition.

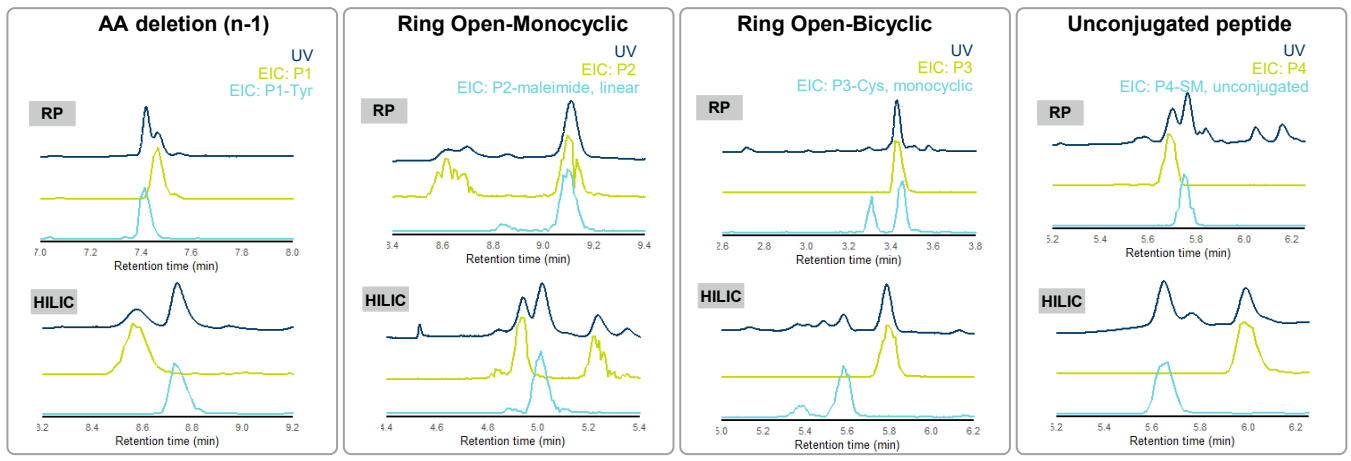
- **Selection criteria for initial screening:** Peptide coverage and chromatographic resolving power
- **Benchmarked by RP**: HILIC can provide comparable performance per selection criteria
- **Best-performing HILIC columns:** XBridge BEH Amide and Luna Polar Pesticides
- **Salt concentration impact:**
  - **DCPak PMPC:** Best under low- or no-salt conditions
  - **Luna Polar Pesticides:** Optimal at low-to-medium salt concentrations
  - **XBridge BEH Amide:** Optimal at medium-to-high salt concentrations
- **pH compatibility:** XBridge BEH Amide provided the broadest pH operating range

Correlation of peptide properties with retention on HILIC columns



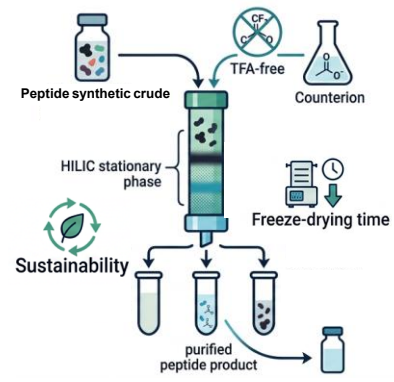
- **Charged HILIC columns**: No consistent relationship between peptide properties and retention (data not shown)
- **Neutral HILIC columns** (BEH Amide, Luna):
  - **LogP**: Strong positive correlation with retention
  - **Average hydrophilicity**: Inverse correlation with retention

New chance for resolving challenging synthetic peptide impurities



Mobile phase A: 50 mM NH4OAc + 0.5% AcOH in water; mobile phase B: 0.5% AcOH in ACN/water 95/5.
RP gradient: 10-50 % B in 10 min; HILIC gradient: 100-60% B in 10 min

One-step TFA-free purification on HILIC



- **One-step purification**: HILIC enables single-step peptide processing without compromising purity
- **Workflow flexibility**: Applicable as a standalone method or complementary dimension in RP-based 2D-LC workflows
- **Hydrophobic peptide compatibility**: High-organic mobile phase supports dissolution and purification of highly hydrophobic peptides
- **In vivo readiness**: Acetate counterion in purified peptide products
- **Sustainability**: TFA-free mobile phase
- **Process efficiency**: Reduced freeze-drying time for HILIC fractions

Conclusions

We have evaluated HILIC as a versatile, TFA-free platform for efficient peptide analysis and purification. HILIC can be particularly advantageous for hydrophobic therapeutic peptides that require high organic content for dissolution, as well as for method development focused on challenging impurity profiles.

Supported by AstraZeneca

Presented at the European Peptide Symposium 2026, Vienna, September, 2026

P439 Nuclear Delivery of Antibodies for the Modulation of TDP-43 Liquid-Liquid Phase Separation

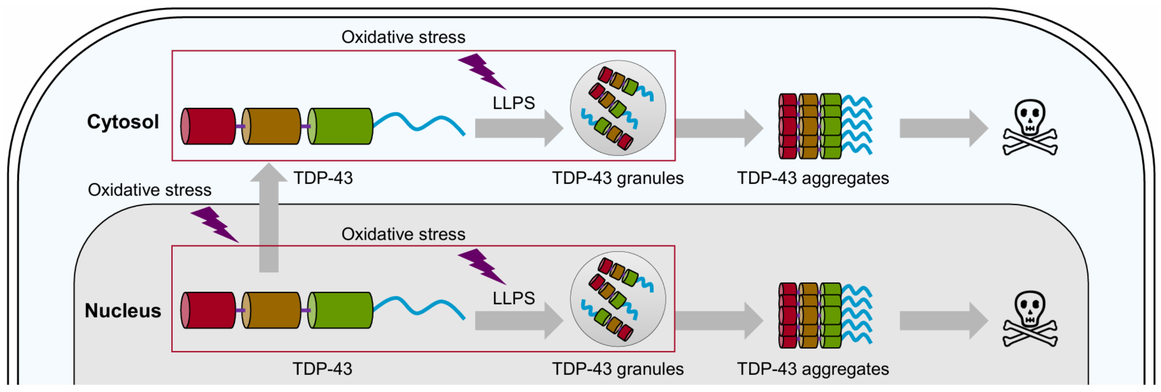
○Daisuke Yamasaki[1], Yoshimasa Kawaguchi[1], Miki Imanishi[1], and Shiroh Futaki[2]
([1]Institute for Chemical Research, Kyoto University, [2]Graduate School of Pharmaceutical Sciences, Kyoto University)
https://doi.org/10.17952/38EPS.2026.P439

Introduction: TDP-43 and ALS

- ✓ TDP-43 translocates from the nucleus to the cytoplasm in response to oxidative stress.
- ✓ TDP-43 forms granules through liquid–liquid phase separation (LLPS).
- ✓ TDP-43 granules can transition into aggregates, leading to cytotoxicity associated with amyotrophic lateral sclerosis (ALS).

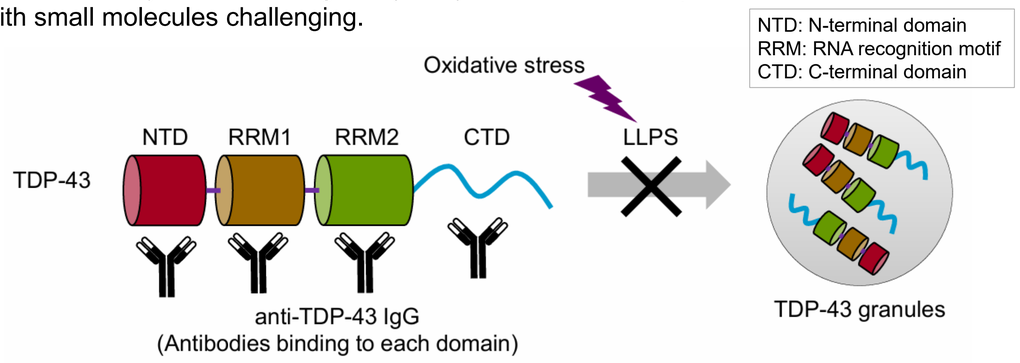
Huang, WP. *et al, Cell Reports*, 2024, 43, 114421.

- ✓ TDP-43 also forms aggregates in the nucleus, which are associated with ALS.



Object: Development of an Intracellular LLPS Regulatory Tool

- ✓ Each domain of TDP-43 contributes to LLPS in cells.
- ✓ The intrinsically disordered regions (IDRs) of TDP-43 make specific LLPS modulation with small molecules challenging.



Nitch, R. *et al.*, TDP-43 Specific Binding Molecules. US9,587,014 B2, **2017**.

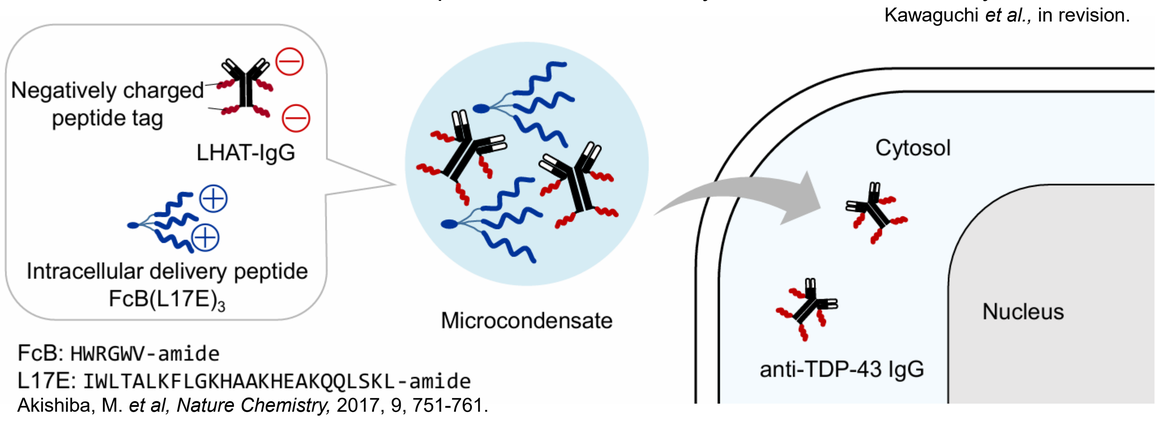
We aimed to develop an antibody-based tool for spatial control of LLPS in the cytosol and nucleus.

Strategy: Method for Intracellular Antibody Delivery

- ✓ A negatively charged peptide tag composed of glutamate and tyrosine was genetically fused to the C-termini of the antibody heavy and light chains.
- ✓ The antibodies formed microcondensates through electrostatic interactions.

→The microcondensates enabled rapid and efficient delivery of antibodies into the cytosol.

Kawaguchi *et al.,* in revision.

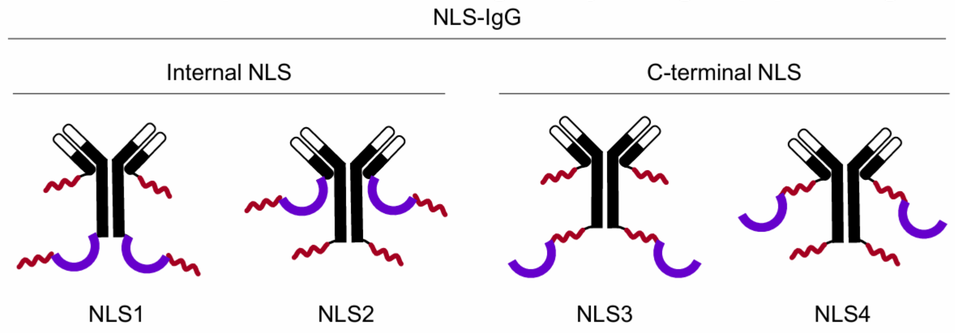


FcB: HWRGWV-amide
L17E: IWLTALKFLGKHAAKHEAKQQLSKL-amide
Akishiba, M. *et al, Nature Chemistry,* 2017, 9, 751-761.

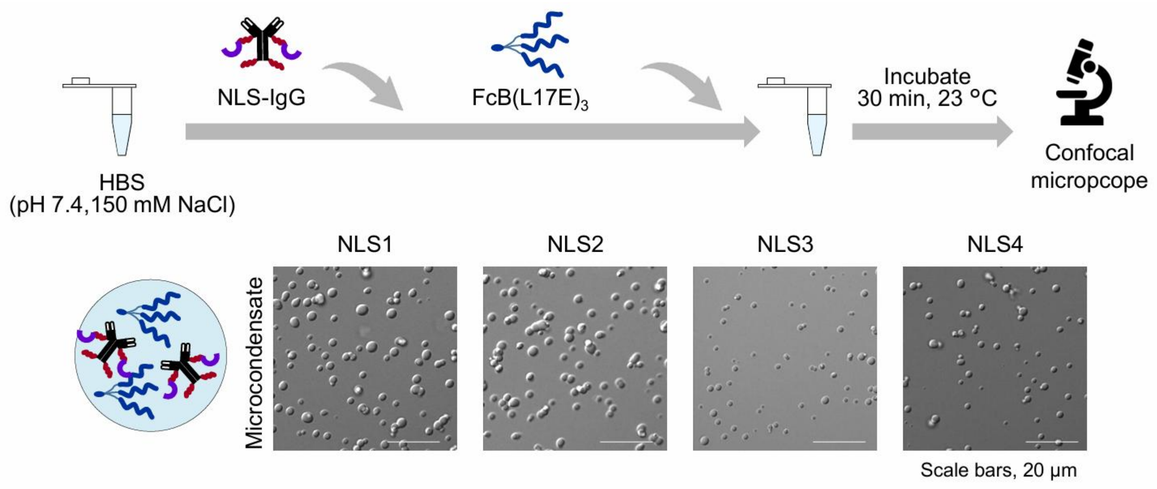
Results & Discussion

Design of Nuclear-Translocating Antibodies

■Optimization of the positions of the negatively charged peptide tag and NLS

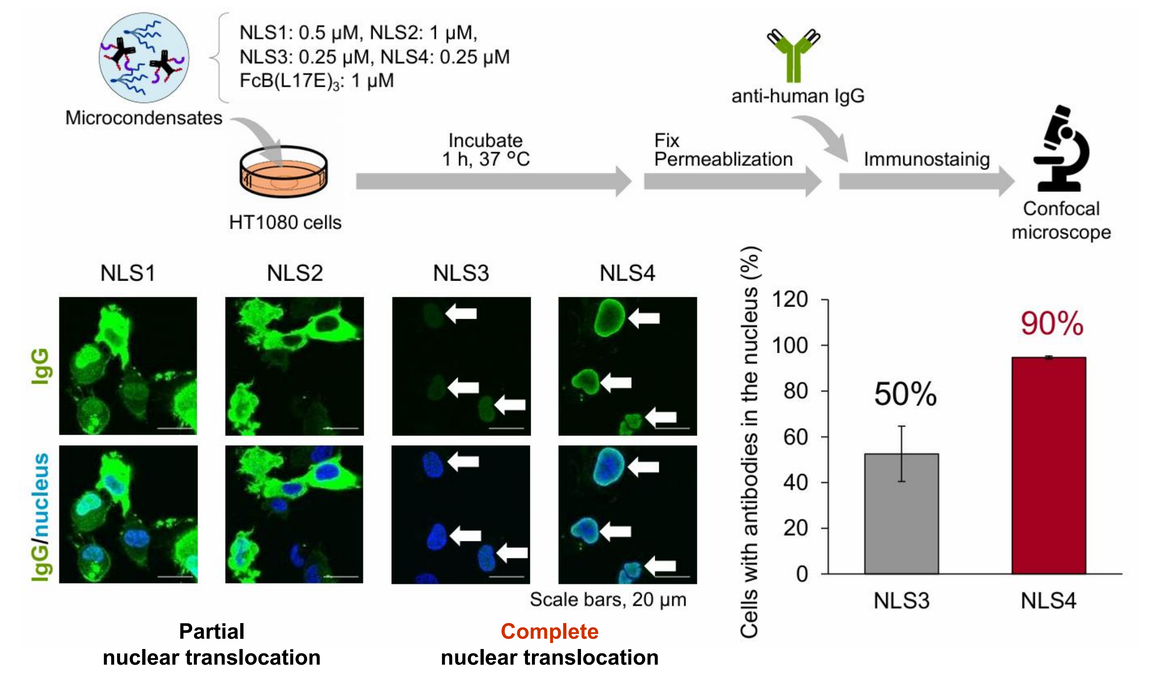


■Confirmation of microcondensate formation



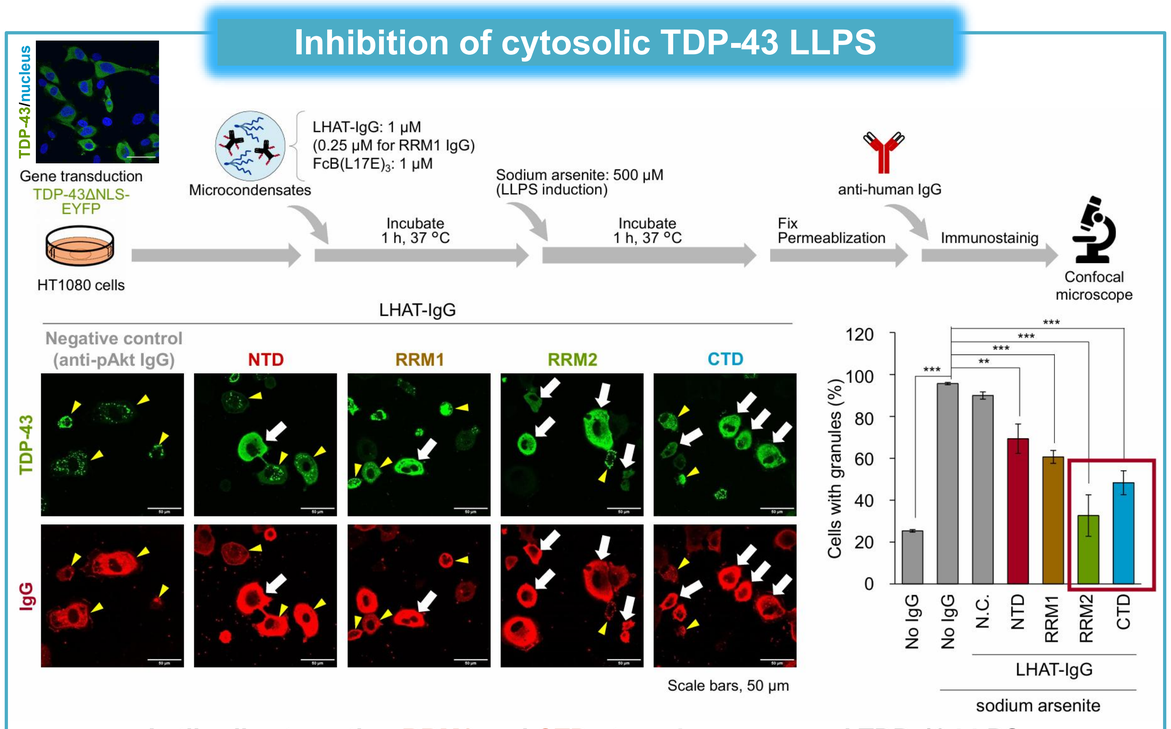
Nuclear-translocating antibodies formed microcondensates.

■Evaluation of nuclear translocation



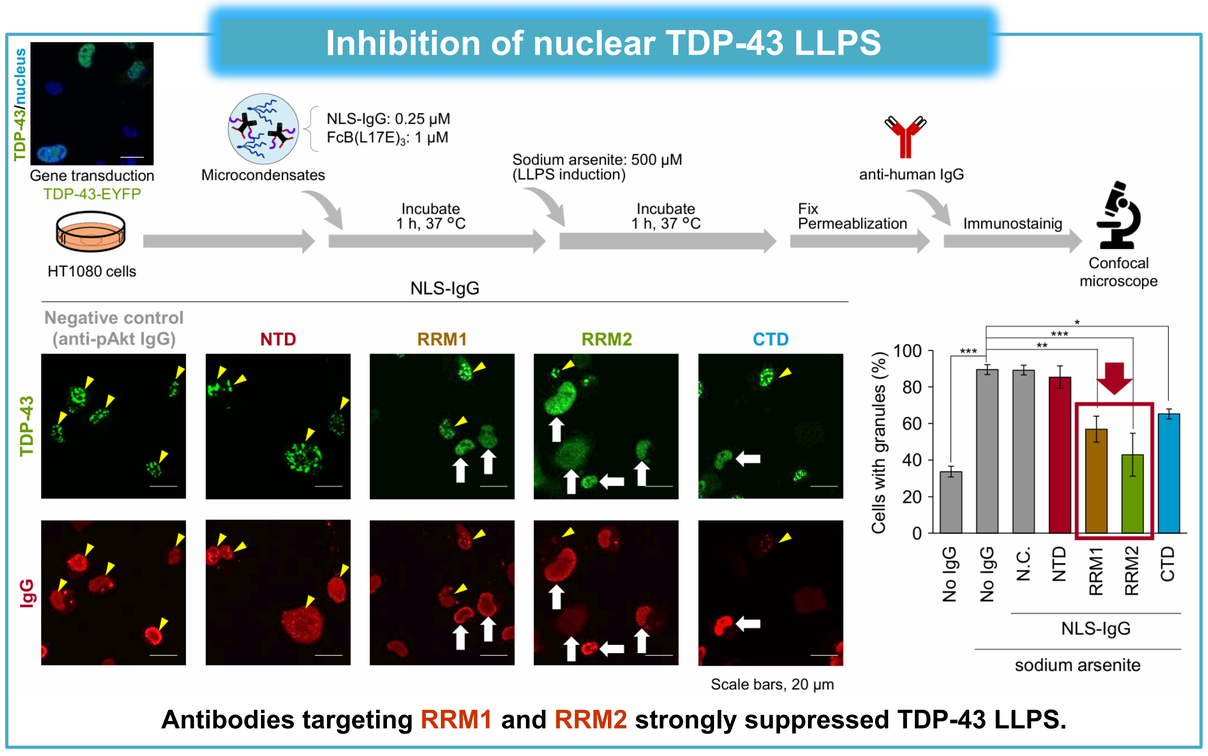
NLS4 showed the highest nuclear delivery efficiency.

Inhibition of cytosolic TDP-43 LLPS



Antibodies targeting RRM2 and CTD strongly suppressed TDP-43 LLPS.

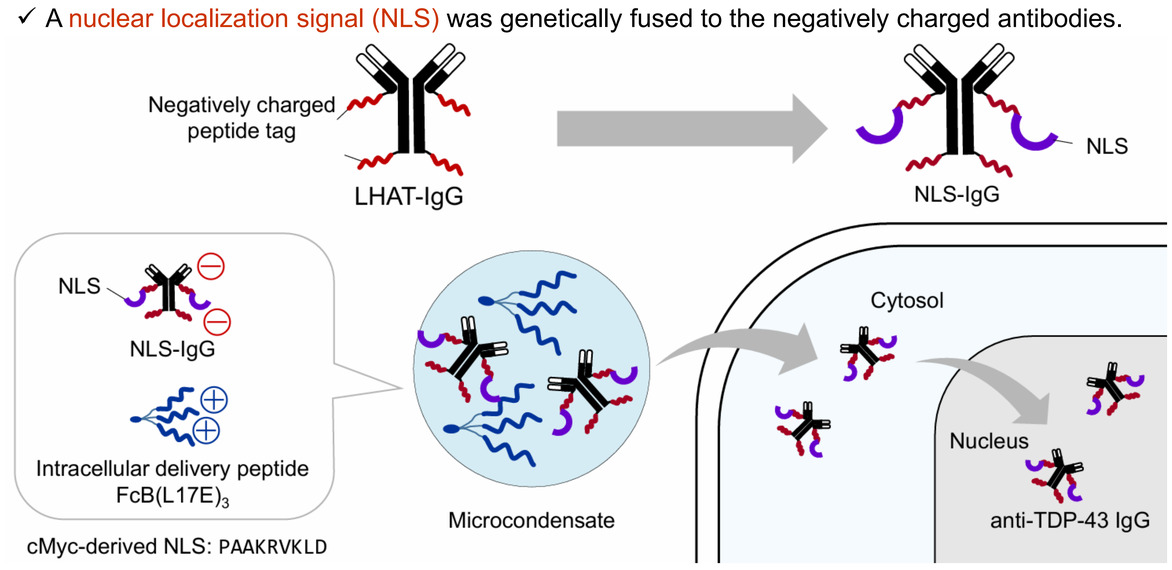
Inhibition of nuclear TDP-43 LLPS



Antibodies targeting RRM1 and RRM2 strongly suppressed TDP-43 LLPS.

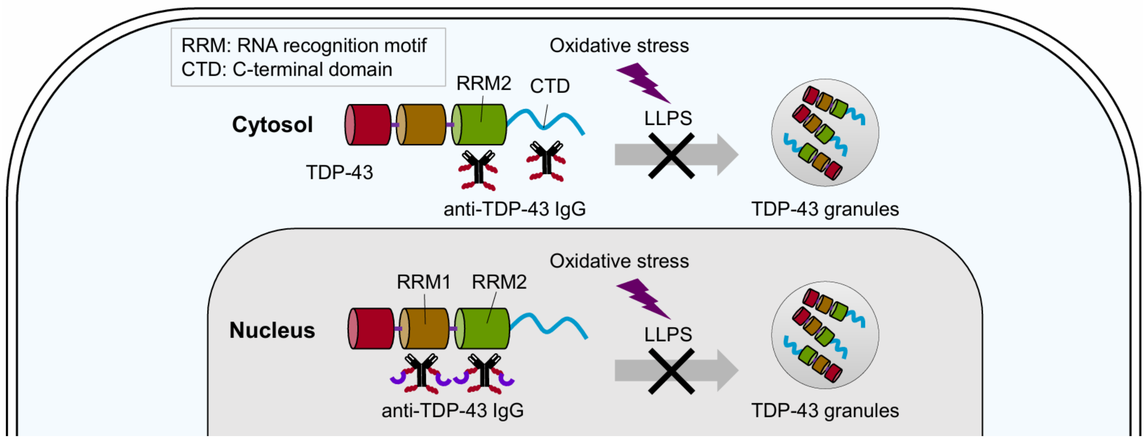
Strategy: Method for Nuclear Delivery of Antibodies

- ✓ A nuclear localization signal (NLS) was genetically fused to the negatively charged antibodies.



Summary

- ✓ TDP-43-binding antibodies suppressed TDP-43 LLPS in the cytosol.
- ✓ We successfully developed nuclear-translocating antibodies.
- ✓ TDP-43-binding antibodies suppressed TDP-43 LLPS in the nucleus.
- ✓ The domains involved in LLPS differed depending on the intracellular localization of TDP-43.



426

https://doi.org/10.17952/38EPS.2026.P426

ADMET of peptides: Are we there yet?

C. Yildiz, N. Köhler, A. Park, T. Kühl, D. Imhof

Department of Pharmaceutical Biochemistry and Bioanalytics, Pharmaceutical Institute, University of Bonn, 53121 Bonn, Germany

Introduction and Objectives

The **development of new pharmaceuticals** requires a preliminary evaluation of efficacy and safety, in which ***in-vitro*** **ADMET-studies** play a central role**. Peptide-based therapeutics** have emerged as a rapidly expanding drug class. However, the establishment of predictive, and standardized ADMET-assessment strategies for peptides remain an ongoing challenge.

This raises a critical question for the field: are current ADMET methodologies sufficient to support the **development of peptide-based drugs**?

Investigate

1. solubility
2. lipophilicity
3. plasma stability (PS)
4. plasma protein binding (PPB)
5. hepatic microsomal stability (HLM)
6. cytotoxicity

Identify

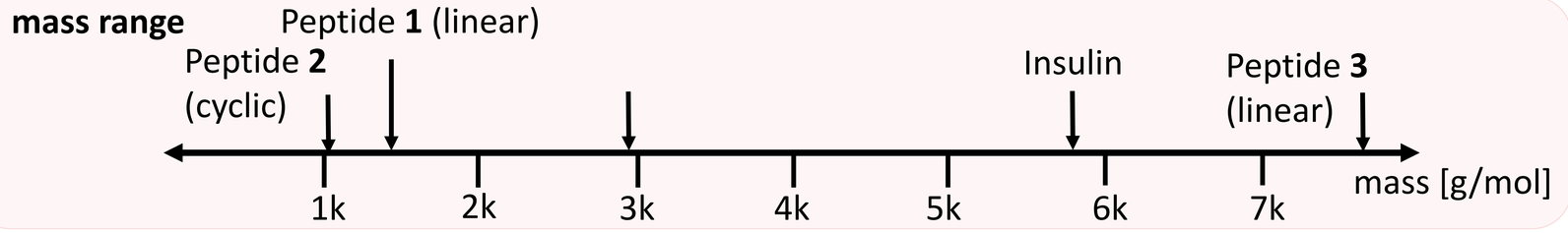
methodological challenges

peptide-specific limitations

Establish

adaptations

standardized *in-vitro* workflow

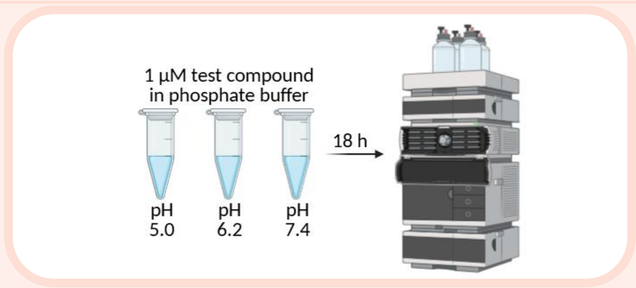


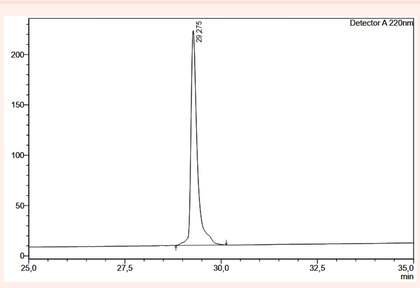
Methods

Results

Modifications

1 solubility



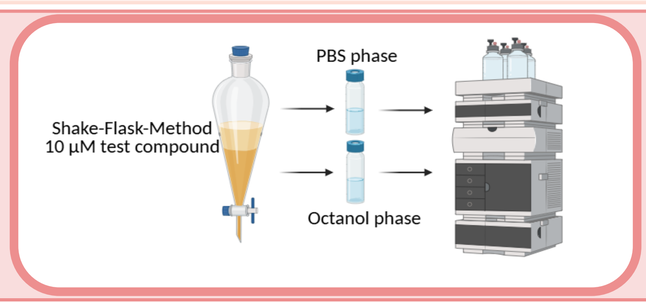


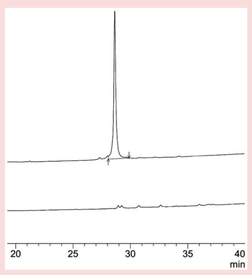
P	pH 5.0	pH 6.2	pH 7.4
Insulin	0	0	72.9
1	91.1	87.7	91.8
2	>100	>100	87.7
3	90.4	93.3	89.5

- HPLC-based peptide quantification

☑ Confirms previously published values for insulin

2 lipophilicity



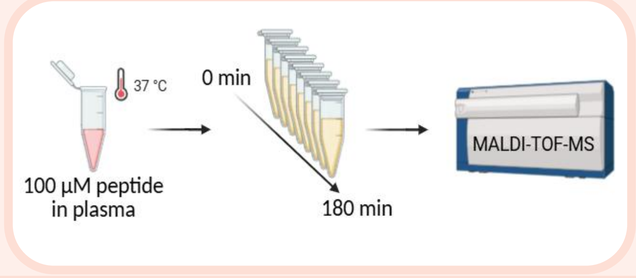


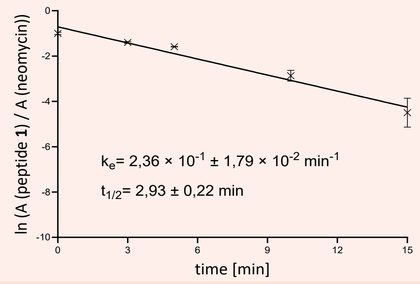
P	$logD_{7.4}$
Insulin	-2.08 ± 0.07
1	< 0
2	-2.20 ± 0.03
3	-2.10 ± 0.05

- HPLC-based peptide quantification

☑ Consistent with hydrophilic character of peptides

3 PS



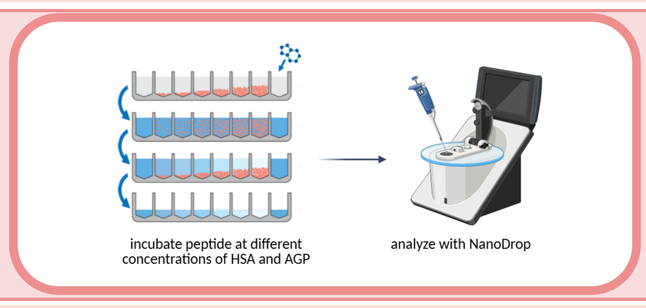


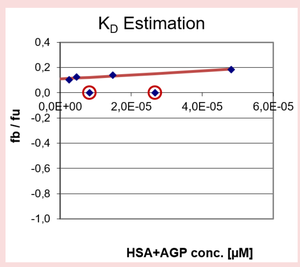
P	$t_{1/2}$ [min]
Insulin	> 180
1	2.93 ± 0.22
2	> 180
3	> 180

- 3 % TCA as precipitation solution
- Shorter incubation and centrifugation times

☑ Reliable detection of enzymatic degradation

4 PPB



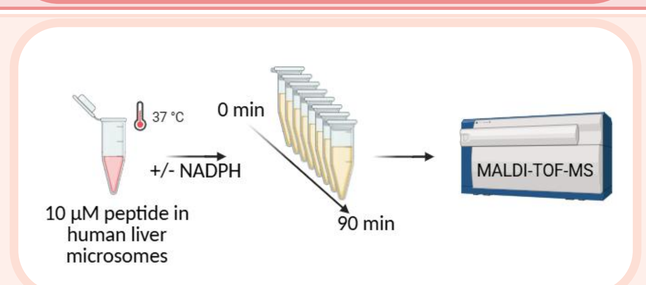


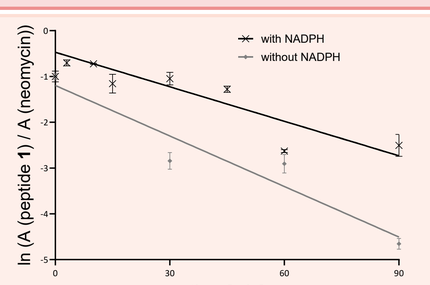
P	PPB [%]
Insulin	49.3 ± 6.11
1	82.4 ± 9.37
2	ongoing
3	ongoing

- Evaluation of a peptide-compatible PPB assay kit

☐ Validation ongoing

5 HLM



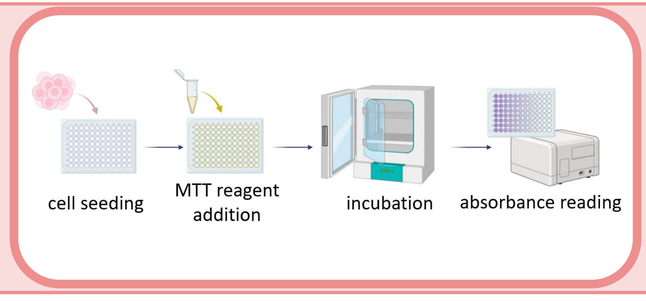


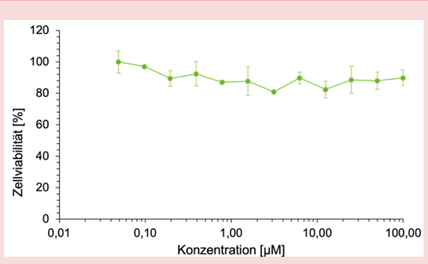
P	Cl_{int} [µl/min/mg]
Insulin	4.13 ± 1.15
1	25.11 ± 2.97
2	0
3	2.10 ± 0.26

- 3 % TCA as precipitation solution
- Shorter incubation and centrifugation times

☑ Reliable detection of metabolic stability

6 cytotoxicity





P	LD_{50} (HepG2) [µM]
Insulin	> 50
1	> 100
2	> 100
3	> 100

- No specific adaptation of the assay for peptides was required

☑ Reliable detection of cytotoxicity

Conclusion and Outlook

Established ADMET assessment strategies are designed for small molecules. We identified key methodological challenges and implemented peptide-specific adaptations. An optimized and standardized *in-vitro* workflow was successfully established for the assessment of solubility, lipophilicity, plasma stability hepatic microsome stability and cytotoxicity of peptides across a broad range of molecular weights. Further peptide-specific ADMET assays remain to be established and optimized to enable a more comprehensive assessment of peptide pharmacokinetics.

References

1. Y. Y. Elsayed, T. Kühl, D. Imhof, *J. Pep Sci*. **2025**, 31, e70001.
2. D. Sun, W. Gao, H. Hu, S. Zhou, *Acta. Pharm. Sin. B.* **2022**, 12, 3049-3062.
3. B. Zheng, X. Wang, M. Guo, C. M. Tzeng, *Int. J. Mol. Sci.* **2025**, 26, 5131.
4. T. D. Y. Chung et al., *Assay Guidance Manual*; Eli Lilly & Company and the National Center for Advancing Translational Sciences: Bethesda, MD, **2015**, 2004.

Check Imhof lab

Acknowledgments

University of Bonn
The German Heart Research Foundation
Dr. Laura Orsatti (IRBM Science Park, Pomezia, Italy)
Prof. Dr. Marianne Engeser for access to the MALDI-TOF/TOF MS (Uni Bonn)

38th EPS European Peptide Symposium — 6 - 11th of September 2026 — Vienna, Austria

Non-destructive quantification of peptide trifluoroacetates[1]

Charity D. Yongo-Luwawa[1], Nassim Maarouf-Mesli[1], Ida Boccino[1], Karen C. Waldron[1] and William D. Lubell[1]

Department of chemistry, Université de Montréal, Montreal, Canada

https://doi.org/10.17952/38EPS.2026.P381

Université de Montréal

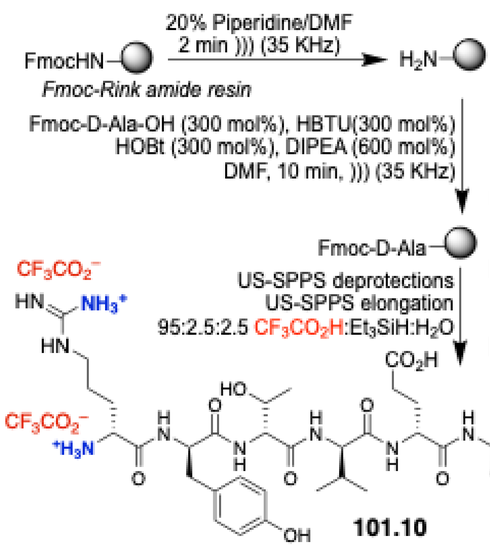
Groupe de recherche William D. Lubell Research Group

Abstract

Trifluoroacetic acid (TFA) is widely used in peptide science but can influence conformation, cytotoxicity, and IR spectroscopic analysis. Quantification of TFA often relies on accurate weighing of peptide salts. A rapid, non-destructive NMR method for quantifying TFA in peptides without weighing is now described using correlation of ^{1}H and ^{19}F integrations with fluorinated alcohols as internal standards in D_2O.

TFA in peptide science and medicine

Trifluoroacetic acid (TFA) is central in peptide synthesis, purification and biological analysis.[2]

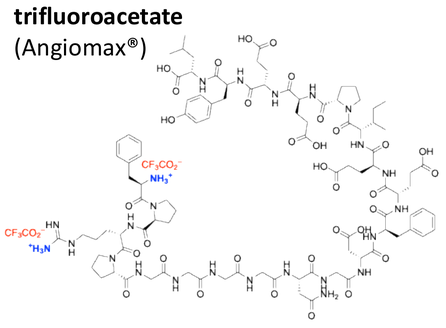


Versatile and volatile, TFA is key to Fmoc/*t*-Bu peptide synthesis,[2] as illustrated by the synthesis of allosteric interleukin-1 receptor modulator **101.10** (H-D-Arg-D-Tyr-D-Thr-D-Val-D-Glu-D-Leu-D-Ala-NH_2) using ultra-sound solid phase peptide synthesis (US-SPPS).[3-4]

A per- and polyfluoroalkyl substance (PFAS), TFA is a regulated environmental toxin,[5] and in trace amounts, may alter peptide conformation, cytotoxicity, and pharmacological profile.[6]

Common in biological studies,[7] two peptide trifluoroacetates are U.S. Food and Drug Administration (FDA) approved: Bivalirudin TFA (Angiomax®) for treating thrombotic disorders;[8] Corticorelin ovine TFA (Acthrel®) for pituitary–adrenal function evaluation.[9]

Bivlirudin trifluoroacetate (Angiomax®)

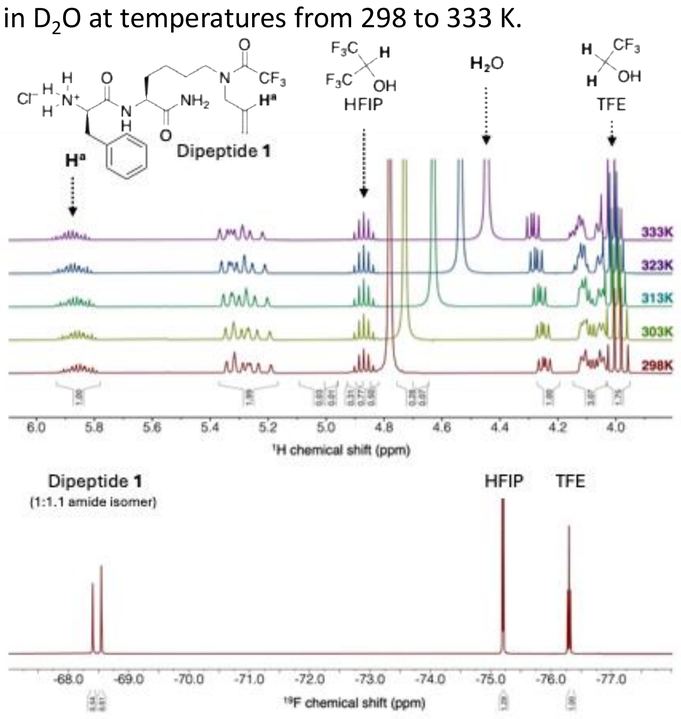


Issues in peptide TFA quantification

Commonly used methods for TFA quantification are often destructive and require accurate sample weighing: e.g., FT-IR,[10] liquid-phase chromatography,[11] gas chromatography,[12] ion chromatography,[13] and capillary electrophoresis (CE).[14]

Benchmarking HFIP and TFE as NMR probes

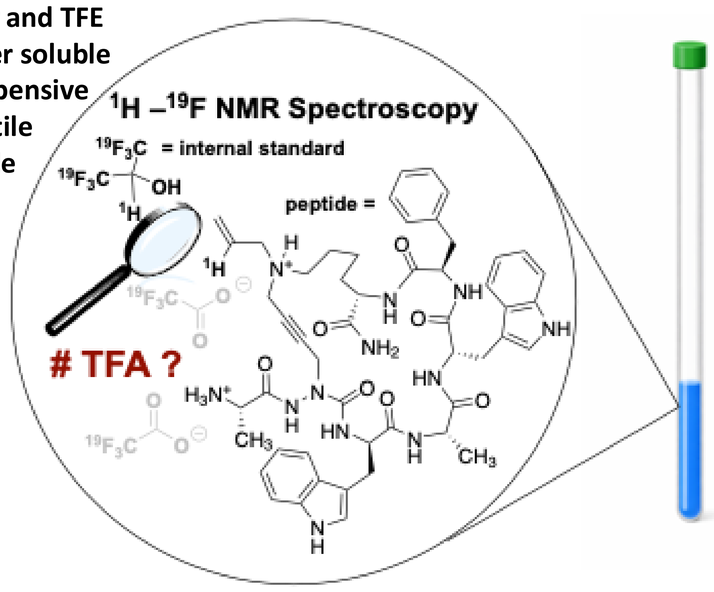
Dipeptide **1** [HCl•H-D-Phe-Lys(Tfa,allyl)-NH_2] is used to benchmark hexafluoroisopropanol (HFIP) and trifluoroethanol (TFE) in D_2O at temperatures from 298 to 333 K.



TFA quantification by NMR Correlation

Solution : Peptide to TFA ratios are quantified using nuclear resonance magnetic (NMR) spectroscopy and correlation of ^{1}H and ^{19}F signal integrations employing internal standards: hexafluoroisopropanol (HFIP) and trifluoroethanol (TFE). Without signal overlap, TFA equivalents are calculated from $^{1}H/^{19}F$ integration ratios (Eq. 1, Method A).

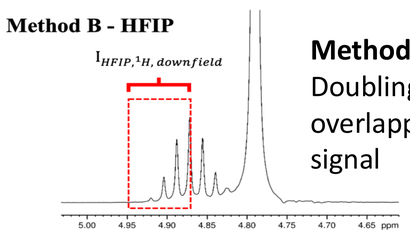
HFIP and TFE
- ✓ water soluble
- ✓ inexpensive
- ✓ volatile
- ✓ stable



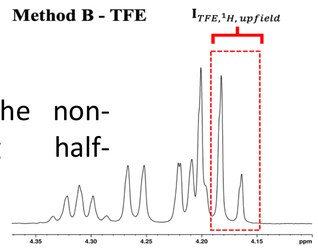
$$Eq.\,1:\ TFA\ equivalents = \frac{^{1}H\ probe}{^{1}H\ peptide} \Big/ \frac{^{19}F\ probe}{^{19}F\ peptide}$$

Integration correction strategies

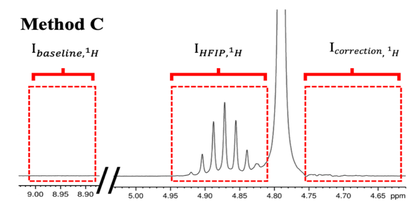
^{19}F signals are readily integrated.
^{1}H quantification is affected by temperature and peak overlap.
Correction methods can overcome signal overlap.



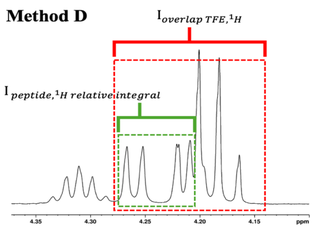
Method B: Doubling the non-overlapping half-signal



Method C: HFIP integral correction using H_2O symmetry

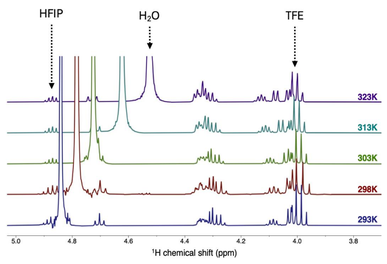


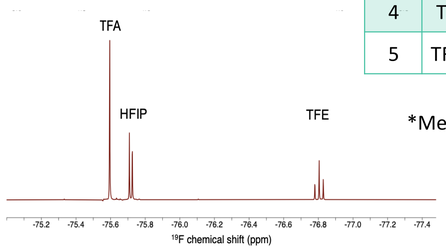
Method D: TFE integral correction by peptide integral subtraction



Studies of temperature and equiv. of standard

Influences of temperature (293–323 K) and internal standard equivalents on TFA/peptide ratio were studied using the TFA salt of **101.10** (**1**, H-rytvela-NH_2).





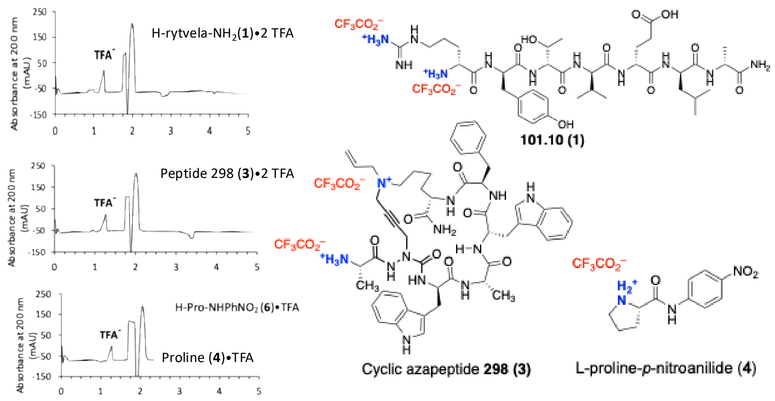
Entry	Standard (equiv.)	Temp. (K)	Method		
			A	B	C/D*
1	HFIP (1)	298	1.86	1.87	**1.96**
2	HFIP (5)		1.90	1.91	**2.04**
3	HFIP (1)	323	**1.97**	1.96	1.33
4	TFE (3)	298	2.45	2.15	**2.02**
5	TFE (14)		2.23	2.11	**2.05**

*Methods C and D were respectively used with HFIP and TFE

Higher internal standard equivalents (5 equiv. for HFIP and 14 equiv. for TFE) improved quantification accuracy.
For HFIP, Method A at **323 K provided the highest accuracy**, likely due to the displacement of the H_2O peak in D_2O.

Comparable accuracy vs CE method

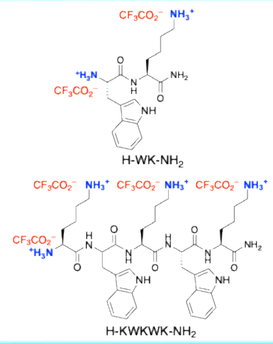
Benchmarked against the previously reported capillary electrophoresis (CE) method, NMR correlation spectroscopy shows comparable accuracy with differences arising from relative signal-based quantification versus weight-based absolute quantification.[14]



TFA Salt	Expected # TFA	TFA # by CE	TFA # by NMR (HFIP) Method C at 298 K	TFA # by NMR (TFE) Method A/D at 298 K
101.10•2 TFA	2	1.48	1.96	2.02 (D)
298 •2 TFA	2	1.43	2.04	2.04 (A)
Proline **4**•TFA	1	**0.99**	**0.99**	**0.94 (A)**

Quantification of peptides with multiple TFAs

Positive charge is abundant in antimicrobial peptides.[11] Model Lys/Trp peptides H-WK-NH_2 and H-KWKWK-NH_2 were made by US-SPPS and assessed using Method B with HFIP at 313 K to have 2.19 and 4.20 TFA equivalents, respectively.



Conclusions and Perspectives

- ✓ Non-destructive NMR correlation quantifies TFA in peptides effectively.
- ✓ HFIP and TFE proved reliable internal standards.
- ✓ Accuracy is contingent on equivalents of internal standards, temperature, and integration method.
- ➢ Applicable to diverse therapeutic peptides without sample destruction.

References

1. Maarouf–Mesli, N.; Yongo–Luwawa, C. D.; Boccino, I.; Waldron, K. C.; Lubell, W. D., Method for Quantifying Trifluoroacetic Acid in Peptides by 1H–19F NMR Spectral Correlation. *J. Org. Chem.* **2026**, ASAP.
2. Amblard, M.; Fehrentz, J.-A.; Martinez, J.; Subra, G., Methods and protocols of modern solid phase peptide synthesis. *Mol. Biotechnol.* **2006,** *33* (3), 239–254.
3. Merlino, F.; Tomassi, S.; Yousif, A.M.; Messere, A.; Marinelli, L.; Grieco, P.; Novellino, E.; Cosconati, S.; Di Maro, S. Boosting Fmoc Solid-Phase Peptide Synthesis by Ultrasonication. *Org. Lett.* **2019**, *16*, 6378–6382.
4. Quiniou, C.; Sapieha, P.; Lahaie, I.; Hou, X.; Brault, S.; Beauchamp, M.; Leduc, M.; Rihakova, L.; Joyal, J.-S.; Nadeau, S., Development of a novel noncompetitive antagonist of IL-1 receptor. *J. Immunol.* **2008,** *180* (10), 6977–6987.
5. Wang, Y.; Liu, M.; Duy, S. V.; Munoz, G.; Sauvé, S.; Liu, J., Fast analysis of short-chain and ultra-short-chain fluorinated organics in water by on-line extraction coupled to HPLC-HRMS. *Sci. Total Environ.* **2024,** *943*, 173682.
6. Gaussier, H.; Morency, H.; Lavoie, M. C.; Subirade, M., Replacement of TFA with HCl in the hydrophobic purification steps of pediocin PA-1: a structural effect. *Appl. Environ. Microbiol.* **2002,** *68* (10), 4803–4808.
7. Yanamandra, N.; Buzzeo, R. W.; Gabriel, M.; Hazlehurst, L. A.; Mari, Y.; Beaupre, D. M.; Cuevas, J., Tipifarnib-induced apoptosis in acute myeloid leukemia and multiple myeloma cells depends on Ca2+ influx through plasma membrane Ca2+ channels. *J. Pharmacol. Exp. Ther.* **2011,** *337* (3), 636–643.
8. Zupančič, O.; Grießinger, J. A.; Lam, H. T.; Bernkop-Schnürch, A., Storage stability of bivalirudin: hydrophilic versus lipophilic solutions. *J. Pharm. Sci.* **2017,** *106* (5), 1322–1330.
9. Pillay, V.; Hibbins, A. R.; Choonara, Y. E.; Du Toit, L. C.; Kumar, P.; Ndesendo, V. M., Orally administered therapeutic peptide delivery: enhanced absorption through the small intestine using permeation enhancers. *Int. J. Pept. Res. Ther.* **2012,** *18* (3), 259–280.
10. Valenti, L. E.; Paci, M. B.; De Pauli, C. P.; Giacomelli, C. E., Infrared study of TFA unpurified synthetic peptides in aqueous solution: Trifluoroacetic acid removal and band assignment. *Anal. Biochem.* **2011,** *410* (1), 118–123.
11. Streuli, A.; Coxon, C. R.; Steuer, C., Simultaneous quantification of commonly used counter ions in peptides and active pharmaceutical ingredients by mixed mode chromatography and evaporative light scattering detection. *J. Pharm. Sci.* **2021,** *110* (8), 2997–3003.
12. Ardino, C.; Sannio, F.; Pasero, C.; Botta, L.; Dreassi, E.; Docquier, J. D.; D'Agostino, I., The impact of counterions in biological activity: case study of antibacterial alkylguanidino ureas. *Mol Divers* **2023,** *27* (3), 1489–1499.
13. Moore, J. V.; Cross, E. R.; An, Y.; Pentlavalli, S.; Coulter, S. M.; Sun, H.; Laverty, G., Impact of counterion and salt form on the properties of long-acting injectable peptide hydrogels for drug delivery. *Faraday Discuss.* **2025,** *260*, 215-234.
14. Little, M. J.; Aubry, N.; Beaudoin, M.-E.; Goudreau, N.; LaPlante, S. R., Quantifying trifluoroacetic acid as a counterion in drug discovery by 19F NMR and capillary electrophoresis. *J. Pharm. Biomed. Anal.* **2007,** *43* (4), 1324–1330.

Acknowledgements

We thank Drs. A. Furtos and P. Aguiar of the regional centers of mass spectrometry and NMR spectroscopy (UdeM) for help with analyses. We are grateful for financial support from Institut Courtois, NSERC, CIHR, FRQNT and CGCC. We are grateful for the registration waiver offered by the EPS. CDYL thanks FRQNT for a doctoral fellowship.

NSERC CRSNG · CIHR IRSC · Institut Courtois · Fonds de recherche Nature et technologies Québec · EPS

Toward Next-Generation ADC Platform tCAP for Site-Specific IgG Modification

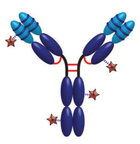
Hiroko Kawakami[1,2], Abdur Rafique[1], Shugo Tsuda[2], Taku Yoshiya[2,3] and Yuji Ito[1]

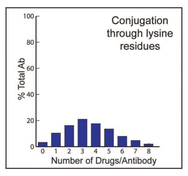
[1]Graduate School of Science and Engineering, Kagoshima University, Kagoshima, Japan.,
[2]Peptide Institute, Inc., Osaka, Japan., [3]Institute for Protein Research, The University of Osaka, Osaka, Japan

https://doi.org/10.17952/38EPS.2026.P561

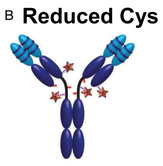
Traditional antibody conjugation

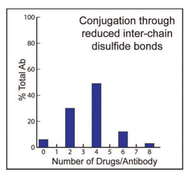
A **Amine**

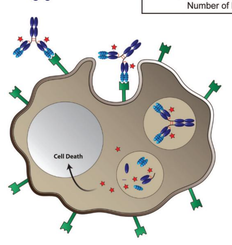




B **Reduced Cys**





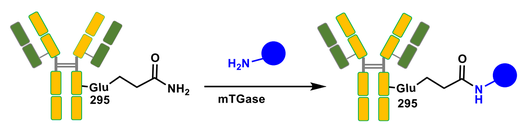


ADC

Product Name	Target Molecule	Average DAR	Modification Site	Indications / Remarks
Adcetris	CD30	4	Cys (Hinge region)	Hodgkin lymphoma, malignant lymphoma, etc.
Kadcyla	HER2	3.5	Lys residue (Random method)	HER2-positive breast cancer
Enhertu	HER2	8	Cys (Hinge region)	HER2-positive/low breast cancer, gastric cancer, etc.
Elahere	FRα	3.5	Lys residue (Random method)	Ovarian cancer
Datroway	TROP2	4	Cys (Hinge region)	Breast cancer, non-small cell lung cancer, etc.

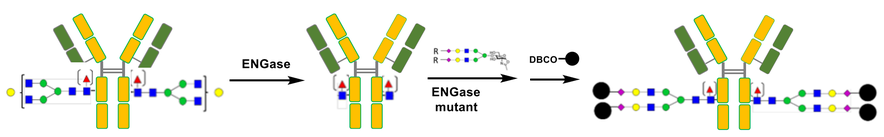
Site-specific IgG modification

Enzymatic modification



Glycans need to be trimmed by endoglycosidase (EndoS2)

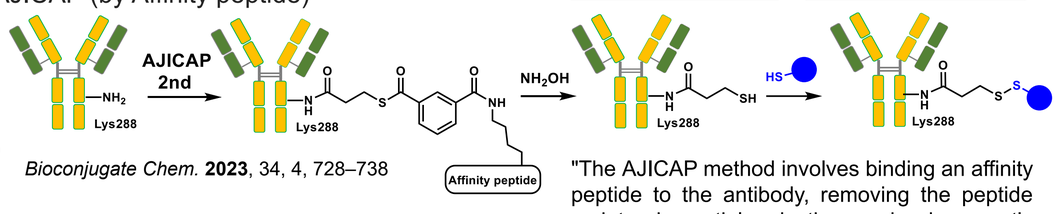
Bioconjugate Chem. **2024**, 35, 4, 465–471



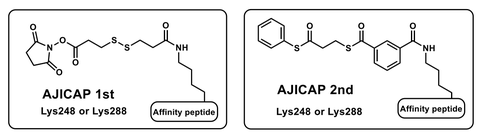
Bioconjugate Chem. **2019**, 30, 5, 1343–1355

Chemical modification

AJICAP (by Affinity peptide)



Bioconjugate Chem. **2023**, 34, 4, 728–738



"The AJICAP method involves binding an affinity peptide to the antibody, removing the peptide moiety via partial reduction, and subsequently introducing the payload in two steps."

Manabe *et al.* succeeded in producing homogeneous ADCs by trimming N-linked glycans with ENGase and attaching small molecules to the glycan moiety using an engineered variant of ENGase.

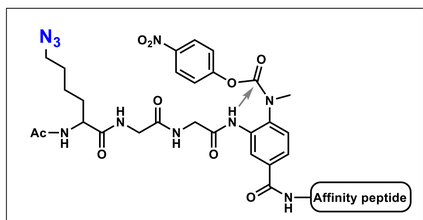
Mechanism of site-specific IgG modification " tCAP(N3)"

✓**Fmoc solid-phase peptide synthesis**

Affinity peptide

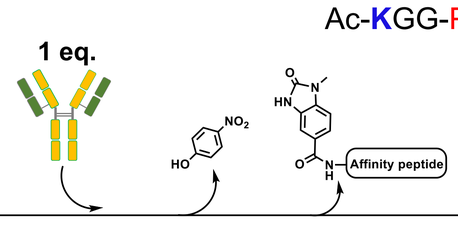
Ac-**K**GG-PMD(NO_2)-Gaba - NMQCQRRFYEALHDPNLNEEQRNAR**I**R**I**RSIRDDC-NH_2

The tCAP(N3) reagent, featuring a stable and self-activating precursor, enables site-specific conjugation of native IgGs.
This Fc-affinity peptide approach selectively transfers an Ac-Lys(N_3)-Gly-Gly payload to Lys248, producing divalently azidated antibody while preserving its biological function.

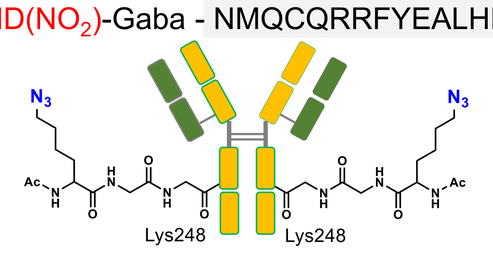


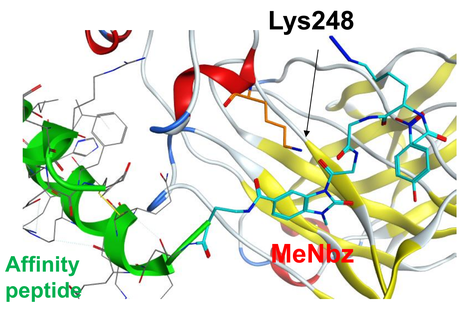
tCAP(N3) **5 eq.**

1 eq.



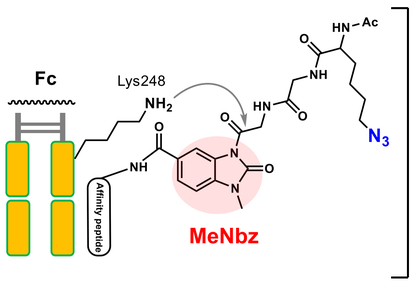
Site selective modification
rt., 2 h





Model of human IgG_1 complexed with the tCAP intermediate, highlighting the ε-amino group of Lys 248 in the Fc region.

Self-activation under neutral conditions

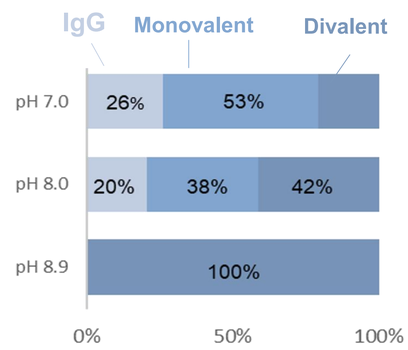


Active compound generated *in situ*

You can find modification protocol on our web site!!

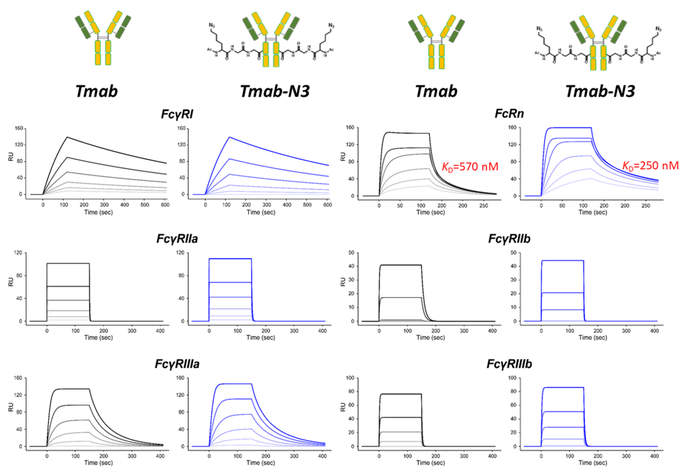
1) Pala-Pujadas,J. *et al.*, *Angew.Chem.Int.Ed.*, **2018**, 57,16120
2) Tsuda,S. *et al.*, *Chem.Commun.*, **2018**, 54,. 8861.

Effect of pH on IgG modification



The reaction was incomplete at pH 8.0 but proceeded to completion under more basic conditions (pH8.9), yielding divalently Tmab-N3.

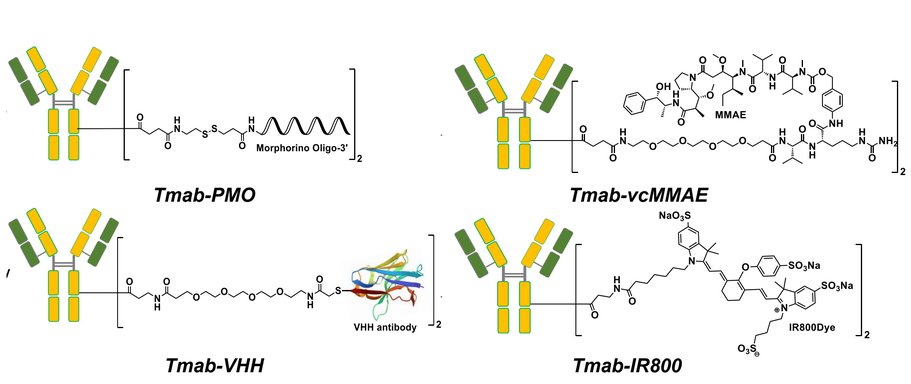
SPR analyses with Fc receptors



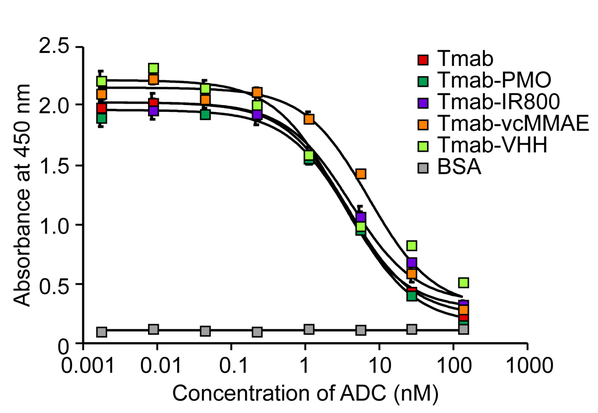
Surface plasmon resonance (SPR) analyses were performed to compare the binding affinities of Tmab with Tmab-N3 toward Fc receptors.

Several antibody conjugates

ADCs



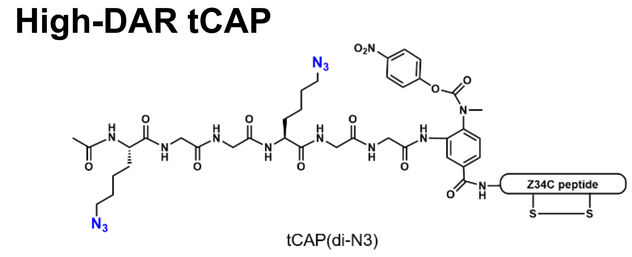
HER2 recognition of Tmab-based ADCs evaluated by competitive ELISA



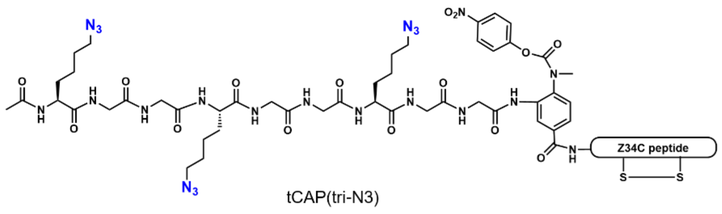
Several antibody conjugates were prepared from Tmab-N3 using strain-promoted alkyne azide–cycloaddition with a fivefold molar excess of DBCO-functionalized payloads.

Next-Generation ADC Platform tCAP

High-DAR tCAP

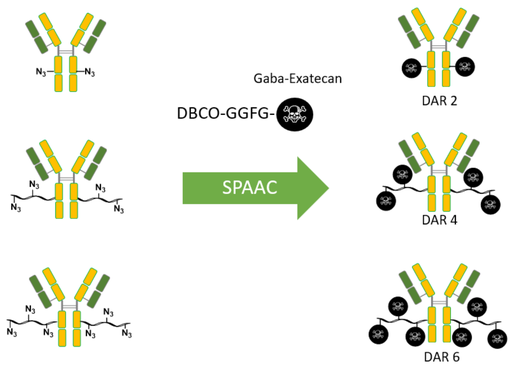


tCAP(di-N3)



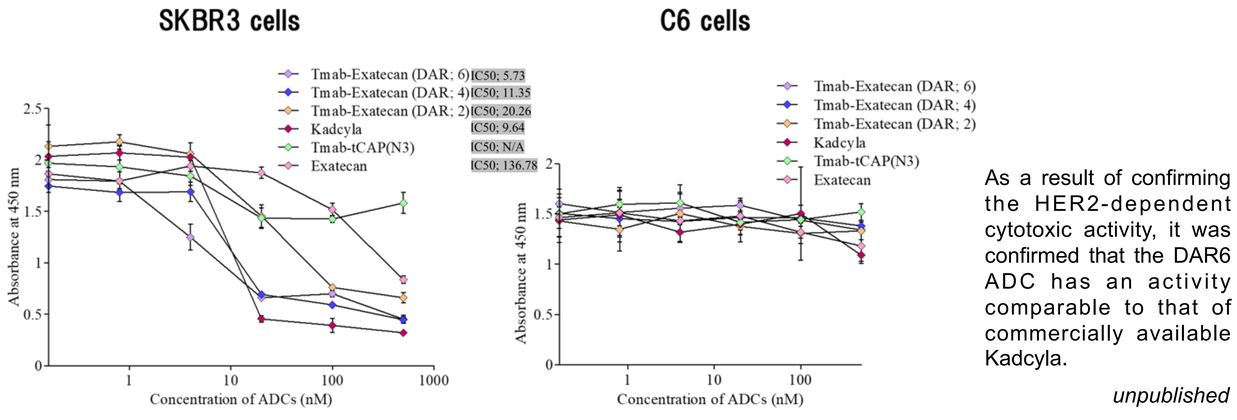
tCAP(tri-N3)

High-DAR ADC



ADCs prepared using tCAP(tri-N3) or tCAP(di-N3) easily achieved the preparation of DAR4 or DAR6 ADCs using multiple N3 groups as a foothold.

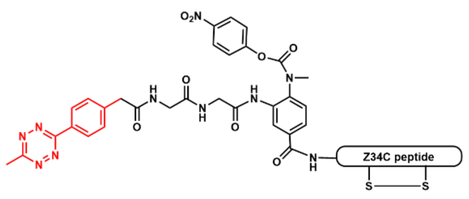
Cytotoxicities of the ADCs



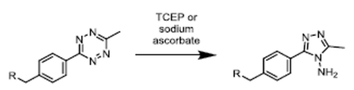
As a result of confirming the HER2-dependent cytotoxic activity, it was confirmed that the DAR6 ADC has an activity comparable to that of commercially available Kadcyla.

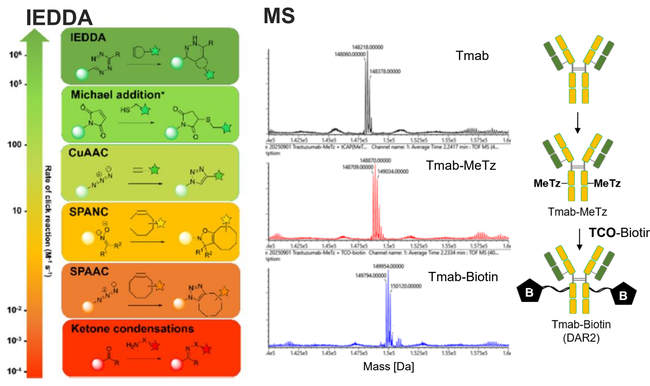
unpublished

tCAP(MeTz)



tCAP(MeTz)



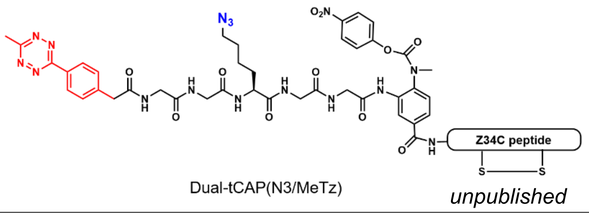


Bioconjugate Chem. **2025**, 36, 1054–1065

The conjugation reaction between MeTetrazine (MeTz) and trans-cyclooctenes (TCO) are faster than that between azide and DBCO; therefore, we also prepared tCAP(MeTz) for future challenging antibody modifications.

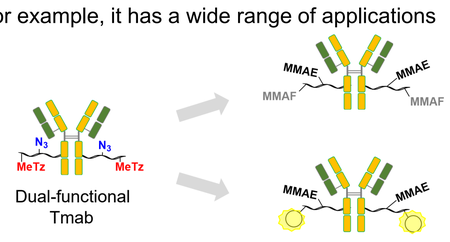
unpublished

Dual-functional tCAP



Dual-tCAP(N3/MeTz)

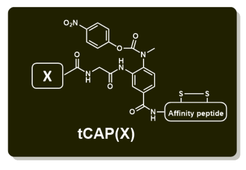
For example, it has a wide range of applications



unpublished

Summary

tCAP technology is expected to advance as a core platform for next-generation antibody drugs, enabling optimal DAR, linker, and payload design, along with multi-payload complex modalities.



Welcome collaboration!!
(kawakami@peptide.co.jp)

Patent filed (WO 2023/038082 A1).

[1] H. Kawakami, A. Rafique, S. Tsuda, A. Nagashima, Y. Nohara, N. Dozono, K. Sakamoto, S. Masuda, M. Kiyoshi, H. Shibata, A. Ishii-Watabe, T. Yoshiya, and Y. Ito, *Chem.Eur.J.*, **32**, e03144 (2026). DOI: 10.1002/chem.202503144
[2] K. Tsuji, Y. Miura, T. Kuwata, R. Matsuzaki, T. Kobayakawa, K. Matsumoto, Y. Ito, T. Yoshiya, S. Matsushita, and H. Tamamura, *ChemMedChem*, **21**, 500820 (2026). DOI: 10.1002/cmdc.202500820

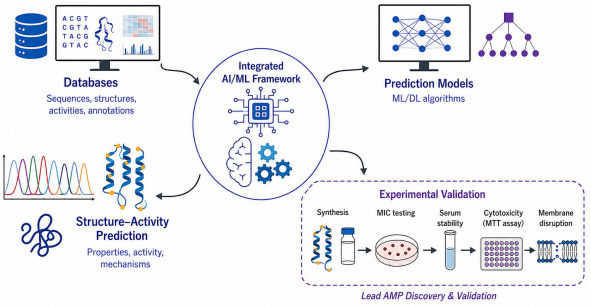
*Presenting Author

AN INTEGRATED AI-GUIDED PIPELINE FOR ANTIMICROBIAL PEPTIDE DISCOVERY AND OPTIMIZATION

Maryam Nawaz[1*], Ma Tianyue[1], Fahad Akhtar, Liu Hongyu[1], Amna Farooq, Heng Zheng[1#],
[1] *School of Life Science and Technology, China Pharmaceutical University, Nanjing 211100, PR China*
https://doi.org/10.17952/38EPS.2026.P261

Introduction

- Antimicrobial peptides represent a promising therapeutic space for addressing drug-resistant infections, yet their translation is constrained by the complex relationship between sequence, physicochemical properties, potency and host compatibility.
- Bridging computational prediction with experimentally validated function remains a key challenge in antimicrobial peptide discovery.



Our Laboratory Peptide Databases

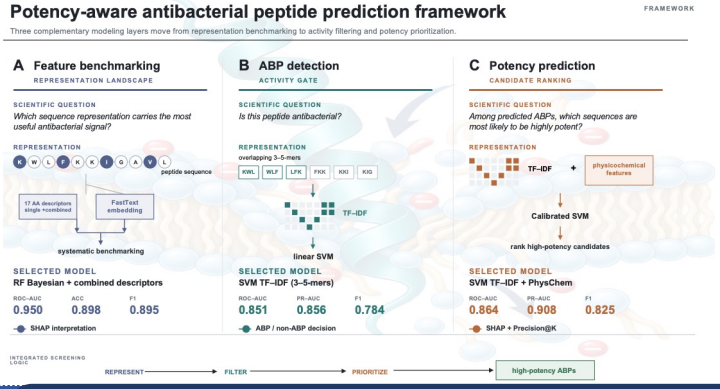
- To address these challenges, our lab integrates artificial intelligence (AI) with peptide biology to accelerate discovery, design, and validation.
- By leveraging AI-driven analyses of curated peptide datasets, we enable predictive modeling, hypothesis generation, and data-informed experimentation, advancing the development of next-generation peptide therapeutics.

DRAMP DRAVP DCTPep HORDB

Multi-Stage Computational Framework for Antibacterial Peptide Discovery

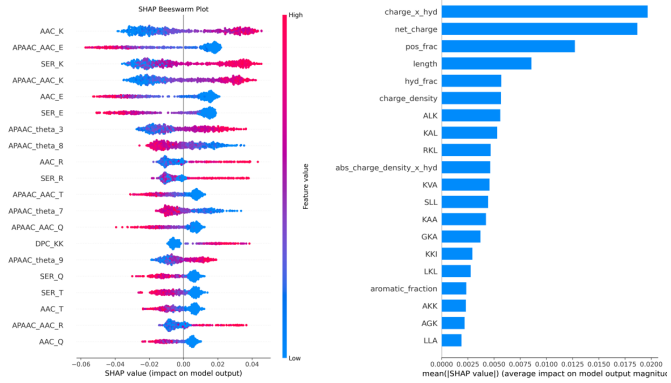
Computational prediction framework

- A multi-stage machine-learning pipeline was developed to benchmark peptide representations, classify antibacterial peptides, and predict antibacterial potency for candidate prioritization.



Model interpretation

- SHAP analysis identified the sequence and physicochemical features that contributed most strongly to antibacterial activity and potency predictions, highlighting the importance of charge, hydrophobicity, and amino-acid composition.

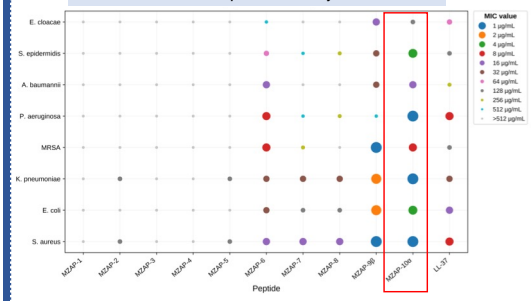


Computationally Guided Physicochemical Optimization of LL-37–Derived Novel Peptides

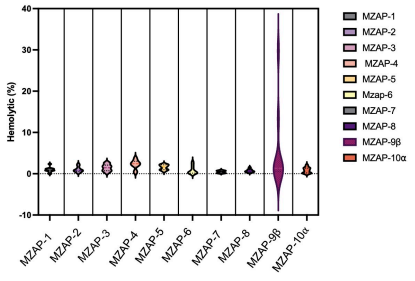
Experimental Validation

- Antibacterial activity was evaluated by MIC/MBC profiling across Gram-positive and Gram-negative pathogens.
- Lead candidates were further assessed for hemolysis, mammalian-cell compatibility, serum stability, and bacterial morphology.

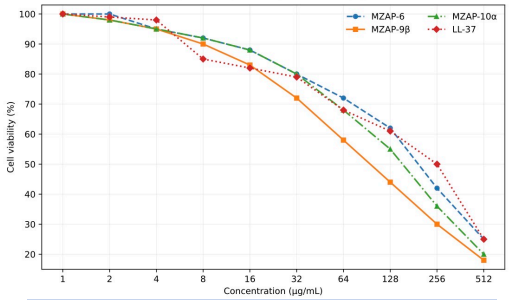
MZAP peptides Display Broad-Spectrum Antibacterial Activity with Strain-Dependent Variability



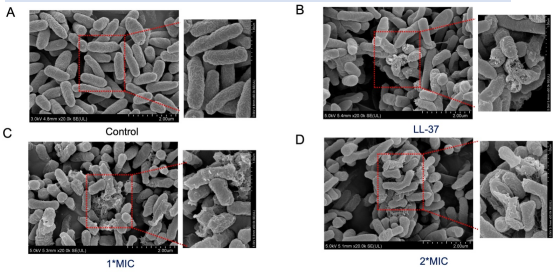
MZAP Peptides Exhibit Minimal Hemolytic Activity at Therapeutically Relevant Concentrations



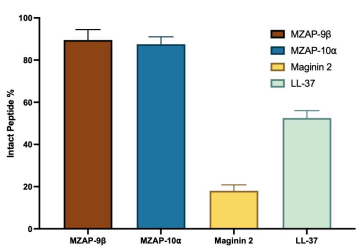
Selected MZAP peptides Maintain High Mammalian Cell (HEK-293T) Viability at Active Concentrations



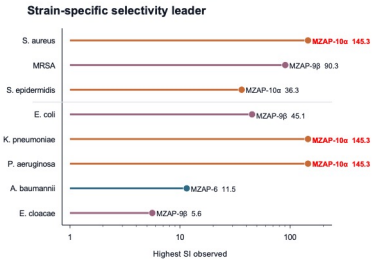
MZAP-10α Induces Concentration-Dependent Morphological Disruption of P.Aeruginosa cells



MZAP Peptides Show Enhanced Serum Stability Compared to LL-37



Selectivity Index Analysis Identifies MZAP-10α as the Most Balanced Antimicrobial Candidate



- ***MZAP-10α showed the most favorable overall balance of potency, stability, and host-cell compatibility.***

Conclusion

- Interpretable ML identified sequence and physicochemical features predictive of antibacterial potency.
- ML-guided prioritization coupled with experimental validation enabled efficient identification of active LL-37-derived peptides.
- MZAP-10α emerged as a lead candidate for further preclinical evaluation.
- The integrated computational–experimental workflow provides a data-informed framework for antimicrobial peptide discovery and optimization

Future Directions

- In vivo validation
- Mechanistic characterization
- Sequence optimization

References

- Nawaz M, Yao H, et al. DRAVP 2.0: A Curated and Genomically Annotated Database of Antiviral Peptides and Proteins. *J Mol Biol*. 2026;438(18):169628.
- Nawaz, M., et al., Deep learning in the discovery of antiviral peptides and peptidomimetics: databases and prediction tools. Mol Divers, 2025. 29(4): p. 3753-3788.
- Ma, T., et al., DRAMP 4.0: an open-access data repository dedicated to the clinical translation of antimicrobial peptides. Nucleic Acids Research, 2024.53(D1): p. D403-D410

Acknowledgements

We sincerely thank the members of the Prof. Zheng's Lab for their valuable contributions and support throughout this study.

Development of a Generalized Platform for Hydrophobic Peptide Synthesis by Utilizing WuXi TIDES-Solubilizing Tag

QINGQING ZHOU, XIAOSHENG LUO, YAZHOU LI, XIAO ZHANG, YVONNE ANGELL, LI WANG & HAIYING HE
WuXi TIDES, an integral part of WuXi AppTec

https://doi.org/10.17952/38EPS.2026.P020

Introduction

In 2025, WuXi TIDES Peptide Discovery team had synthesized over 50,000 peptides, with ~20% classified as highly hydrophobic. Such peptides with **poor aqueous solubility** impede SPPS due to resin-bound aggregation, resulting in poor solvation and inefficient coupling. This necessitates excessive reagents, prolonged reaction time, and risk of truncated products, thus results in the challenge of synthesis, purification and scale-up.[1]

To address this issue, we have developed a novel solubilizing platform via screening of 20 solubilizing tags.[2-5] Our optimized **WuXi TIDES- Solubilizing Tag** enables high-yield synthesis of challenging highly hydrophobic peptides to support fast SAR studies and potential future scale-up.

Strategy

Our innovation involves pre-installing solubilizing tags on resin before peptide elongation, enhancing solubility and coupling efficiency while enabling mild tag removal. As shown in Figure 1, the solubility tag is immobilized via SPPS, followed by affinity tag/linker addition and peptide chain elongation. Post-cleavage yields a hydrophilic peptide with tag (HPLC-purified).

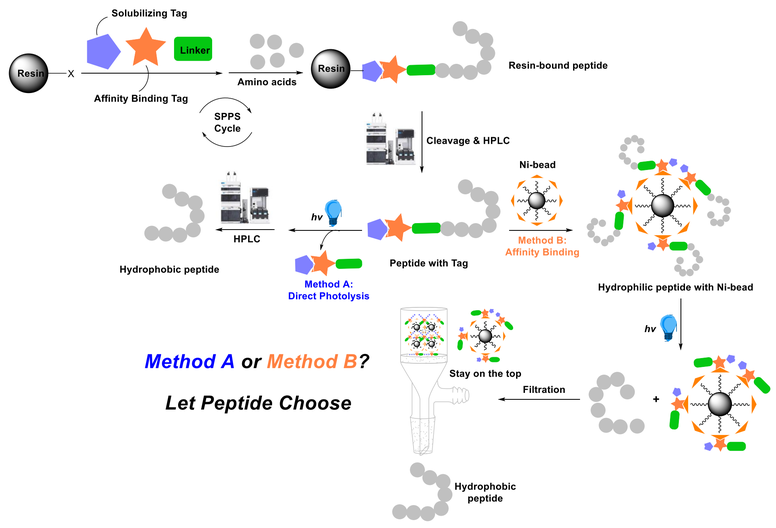


Figure 1. Strategy design for the synthesis of hydrophobic peptides with Solubilizing Tags.

For final peptide isolation, two methodologies were employed: **Method A:** The peptide with tag undergoes UV photolysis, followed by additional HPLC purification to generate the pure target peptide. **Method B:** The peptide with tag is subjected to Ni-NTA affinity bead, followed by photolytic release, to directly yield the target hydrophobic peptide without requiring additional HPLC purification.

Result

1. Screening of Solubilizing Tags: Performance Evaluation

To screen solubilizing tags, we tested eight variants on a model peptide. Tags 1-8 were linked to resin via SPPS, followed by linker addition, peptide elongation, cleavage, and purification. Solubility was assessed by precipitation/Tyndall effect observation (Figure 2 and Table 1). After photolysis/HPLC purification, model peptide yields were calculated.

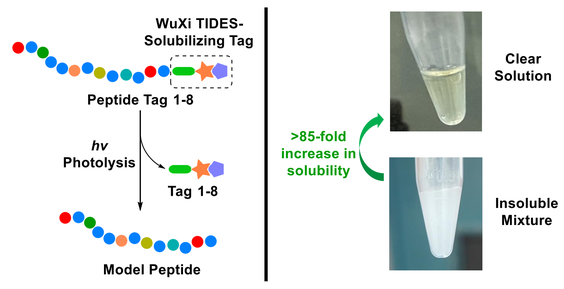


Figure 2. Solubilizing tag screening.

Table 1. The result comparison of the model peptide with/without solubilizing tag.

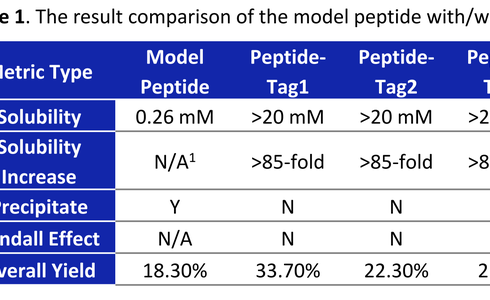
Metric Type	Model Peptide	Peptide-Tag1	Peptide-Tag2	Peptide-Tag3	Peptide-Tag4	Peptide-Tag5	Peptide-Tag6	Peptide-Tag7	Peptide-Tag8
Solubility	0.26 mM	>20 mM	>20 mM	>20 mM	17 mM	19 mM	0.05 mM	14 mM	0[2]
Solubility Increase	N/A[1]	>85-fold	>85-fold	>85-fold	68-fold	75-fold	N/A	27-fold	N/A
Precipitate	Y	N	N	N	N	N	Y	N	N
Tyndall Effect	N/A	N	N	N	Y	Y	N/A	Y	Y
Overall Yield	18.30%	33.70%	22.30%	2.90%	8.90%	17.70%	13.20%	14.40%	12.50%

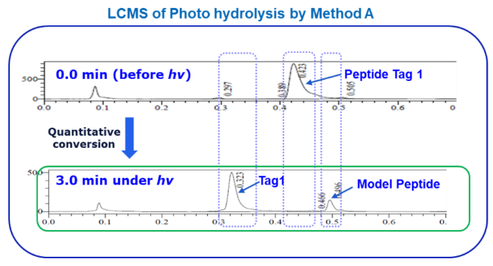
Key results: Tags 1-3 were advanced to secondary screening, identifying 10 effective tags (not shown here).

2. Efficient Photolytic Cleavage Evaluation

Using optimized WuXi TIDES-Solubilizing Tag, we assessed two cleavage methods (Figure 3):

Method A: Photolysis quantitatively converted tagged peptide to target in 3 min (LCMS-confirmed), yielding 33.7% pure product with the purity of 97.2% after HPLC purification.
Method B: Immobilization on Ni-beads enabled photolytic release in 15 min; filtration directly isolated target peptide (42.2% yield, 94.3% purity) with simultaneous tag-resin retention (reusable). Method A offers speed but requires HPLC, while Method B integrates tag absorption/isolation. Both provide complementary production strategies.





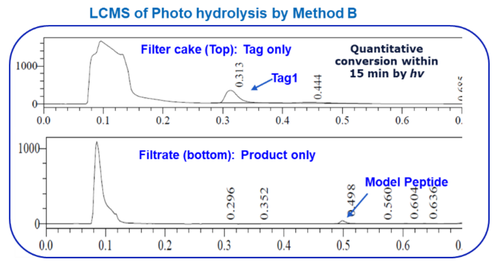


Figure 3. Efficiency evaluation for model peptide with Method A and B.

Case Studies

This strategy was applied to troubleshoot difficulties encountered in real cases. Comparative experiments were employed to synthesize cyclic peptides 1-5, both with and without the **WuXi TIDES-Solubilizing Tag**. Comparative analysis revealed that tagged peptides consistently achieved (see table below): 1) >10-fold higher yields; 2) Elevated purity; 3) Reduced purification rounds. This comparison clearly indicates that the **WuXi TIDES-Solubilizing Tag** strategy offers significant advantages.

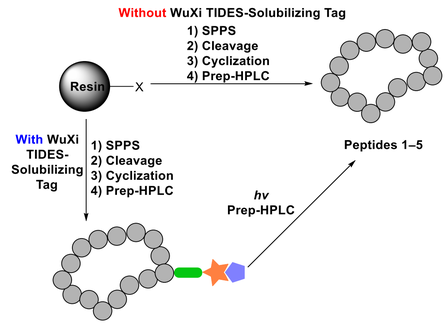


Figure 4. Comparative synthesis of peptides with/without **WuXi TIDES-Solubilizing Tag.**

Table 2. The results of Peptides 1-5 with/without **WuXi TIDES-Solubilizing Tag**

Compound ID	Strategy	Overall Yield	Purity	Number of HPLC Purifications
Peptide 1	Without Tag	1.5%	95%	5
	With Tag	8.8%	99%	2
Peptide 2	Without Tag	1.8%	97%	3
	With Tag	21.2%	95%	2
Peptide 3	Without Tag	0.9%	80%	2
	With Tag	3.0%	98%	2
Peptide 4	Without Tag	0.7%	70%	2
	With Tag	4.2%	97%	2
Peptide 5	Without Tag	0.7%	69%	2
	With Tag	2.5%	92%	2

Conclusion

WuXi TIDES has developed a generalized solubilizing tag strategy to address the synthesis and purification of poorly aqueous soluble peptides. We have identified 10 highly effective solubilizing candidates. Application of this strategy to challenging peptides significantly improved yields and purity while reduced the number of purification cycles. Moving forward, we will further optimize the solubilizing tags along with the affinity purification process and cleavable linkers to broaden applicability, ultimately enabling scale-up and manufacturing implementation.

Reference

1. M. T. Jacobsen, M. E. Petersen, X. Ye, M. Galibert, G. H. Lorimer, V. Aucagne and M. S. Kay, *J. Am. Chem. Soc.* **2016**, *138*, 11775-11782.
2. X. Wang and K. Jin, *J. Org. Chem.* **2024**, *89*, 3143-3149.
3. H. Bürgisser, E. T. Williams, A. Jeandin, R. Lescure, A. Premanand, S. Wang and N. Hartrampf, *J. Am. Chem. Soc.* **2024**, *146*, 34887-34899.
4. M. Paradís-Bas, J. Tulla-Puche, F. Albericio. *Chem. Soc. Rev.* **2016**, *45* (3), 631–654.
5. V. Freiburghaus, A. Jeandin, Ł. Frankiewicz, J. Yang, N. Hartrampf. *ACS Chem. Biol.* **2025**, *20* (11), 2733–2740.

https://doi.org/10.17952/38EPS.2026.P476

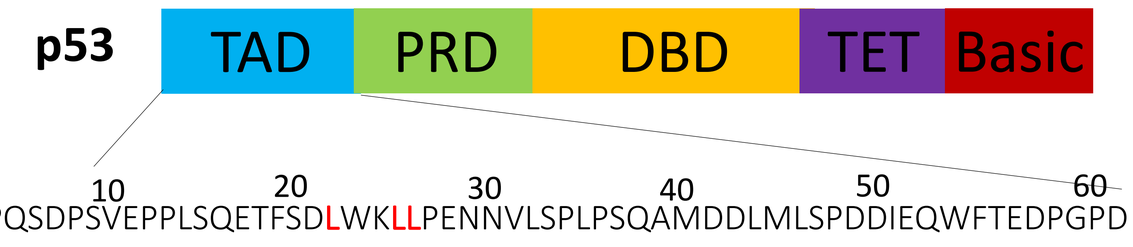
Conformational complexity of the disordered N-terminal region in biological function of tumor suppressor p53 protein

Elena Zindovic, Mo'ath Yousef, Edwige Voisset*, Vladimir Torbeev*

Laboratory of Biosystems Chemistry, École supérieure de biotechnologie de Strasbourg, UMR7242, CNRS and Université de Strasbourg

P53 and TAD

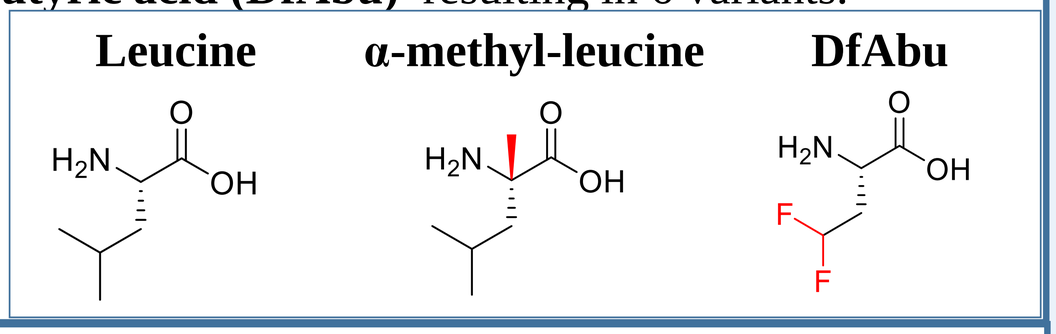
p53 is a **transcriptional activator**, involved in a majority of cancers. It's sequence contains several domains **Transactivation domain (TAD) is an intrinsically disordered region** and binds with various proteins like **CREB-binding protein** (CBP/p300), Double minute 2 protein (HDM2) and many others.[1]
To modify its interactions, TAD variants were synthesized with α-methylated leucine and fluorinated amino acids.



6 variants of TAD with modified LXXLL motif (residues 22-26)

The **LXXLL motif of TAD** was targeted because it is known to **mediate many protein-protein interactions**. This conserved modification sequence mediates **particular interactions with nuclear receptors and their coactivators**, making it a reliable choice for motif to target.[2] Here, only one leucine residue of the LXXLL motif was modified per variant, being individually replaced either by an **α-methylated leucine or by 4,4-difluoro-2-aminobutyric acid (DfAbu)** resulting in 6 variants.

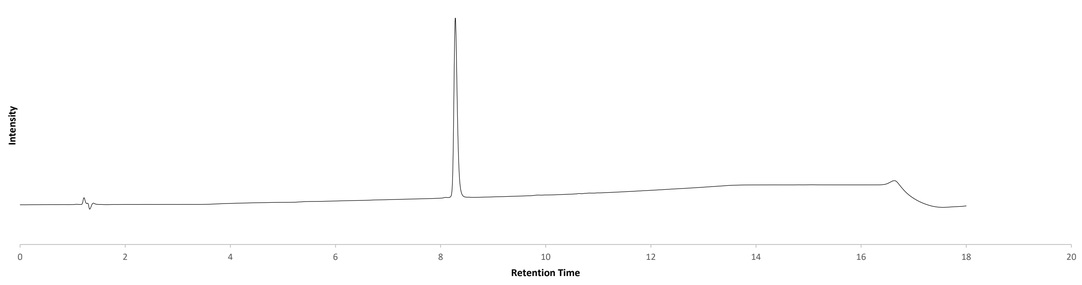
We used **α-methylated leucine** to conformationally **constrain the backbone** and **stabilize helical conformations**.[3] **DfAbu** was chosen as a nearly **isosteric fluorinated analogue** of leucine, while its fluorine atoms also make it as a valuable ^{19}F NMR probe.[4]

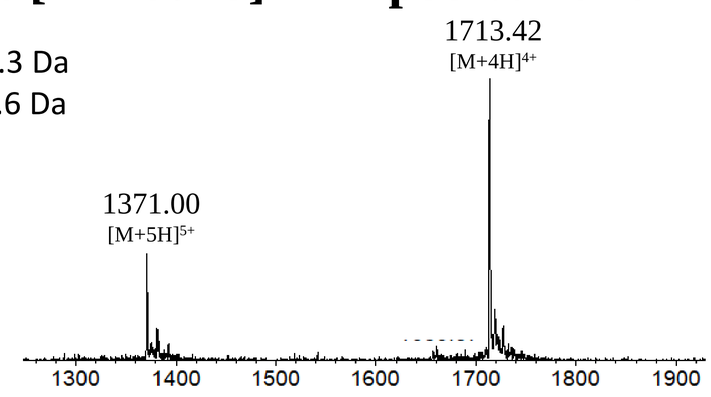


HPLC and mass-spectrometry analysis of the [DfAbu25]TAD-p53 variant

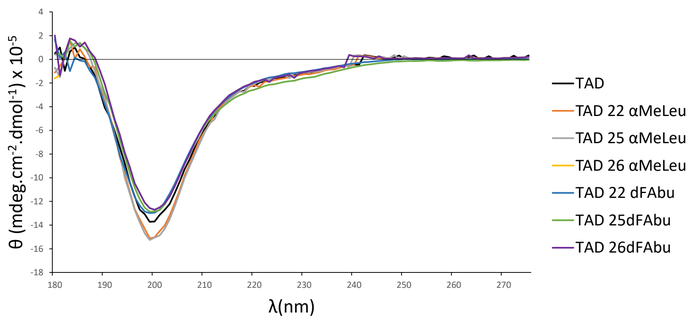
TAD-1-61NH2-25DfAbu
Nle-EEPQSDPSVEPPLSQETFSDLWKL(dFAbu)LPENNVLSPLPSQA-Nle-DDL-Nle-LSPDDIEQWFTEDPGPD-NH2

Mass calculated : 6852.3 Da
Mass measured : 6849.6 Da

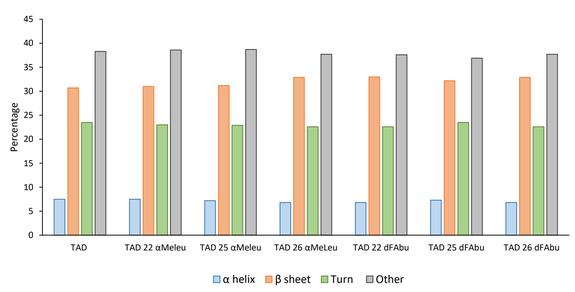




Circular Dichroism of TAD and its variants alone and in complex with NCBD

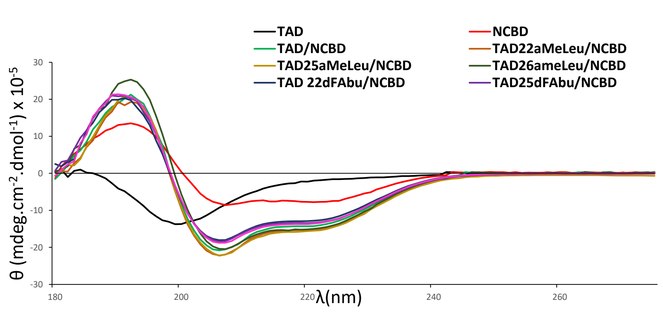


(CD) spectra of TAD and variants in 25 mM phosphate buffer at pH 7 at 25 °C (concentration of protein = 25µM)

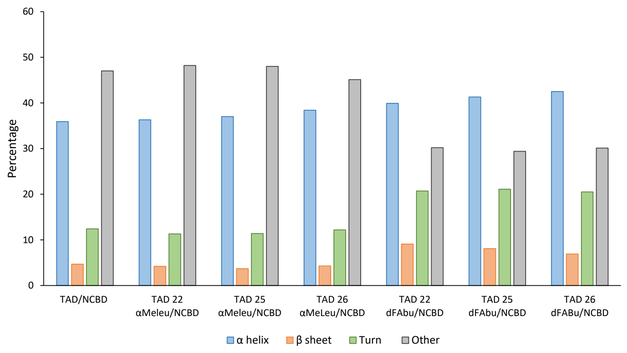


Graphic representation of percentage of α helix, β sheets, turns and others for each variants of TAD estimated using CDPro software (CONTINILL method)

TAD analogs do not alter the overall secondary structure of the transactivation domain, preserving its native conformation.



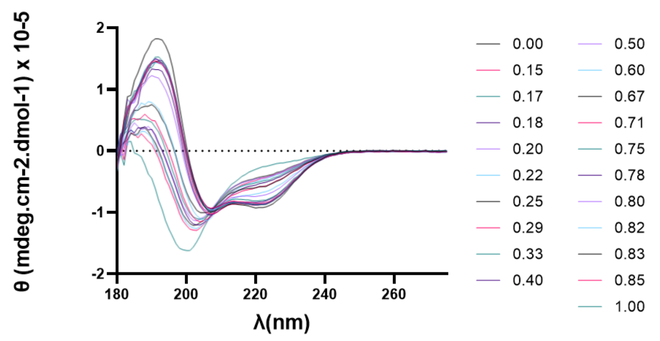
(CD) spectra of TAD and its α methyleucine variant, NCBD and their 1:1 complex in 25 mM phosphate buffer at pH 7 at 25 °C (concentration of protein = 25µM)



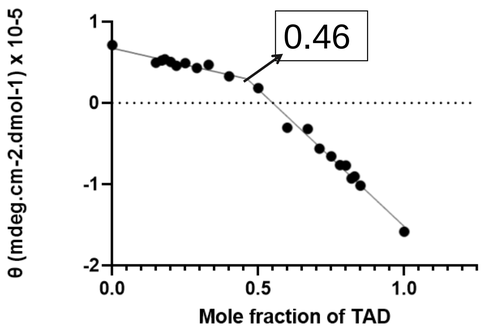
Graphic representation of percentage of α helix, β sheets, turns and others for each variants of TAD, NCBD and their 1:1 complexe estimated using CDPro software (CONTINILL method)

TAD and α-methylated analogs exhibit similar proportions of α-helices, β-sheets, turns, and other secondary structures. In contrast**, the fluorinated analog shows an increase in turns** and a decrease in other structures.

Stoichiometric Analysis of the TAD–NCBD Complex by Job Plot



Graphic representation of TAD–NCBD binding at different concentrations in 25 mM phosphate buffer, pH 7, 25 °C (protein concentration = 25 µM), proportions of TAD are indicated



Since the plot exhibits a maximum at a **TAD mole fraction of 0.5, it** indicates the formation of a **1:1 complex between TAD and NCBD.**

Graphic representation at **198 nm** of TAD–NCBD binding at different concentrations with proportions of TAD indicated

Conclusions:

- **Six new TAD-p53 variants** were **synthesized** incorporating either **α-methylated leucine or DfAbu substitutions.**
- CD spectra indicate that **TAD and its analogues adopt similar secondary structures** in the free state. Upon binding to NCBD, α-methylated variants display behavior comparable to the wild type, whereas **fluorinated analogues show altered secondary structure** profiles. These results suggest that **fluorination affects the folding-upon-binding mechanism**, while **α-methylation largely preserves** it.
- The Job plot exhibits a maximum at a TAD mole fraction of 0.5, confirming the **formation of a 1:1 complex between TAD and NCBD.**

References:

[1] Raj, N.; Attardi, L. D. The Transactivation Domains of the P53 Protein. *Cold Spring Harb. Perspect. Med.* **2017**, *7* (1), a026047.
[2] Plevin, Michael J., Morgon M. Mills, et Mitsuhiko Ikura. « The LxxLL motif: a multifunctional binding sequence in transcriptional regulation ». *Trends in Biochemical Sciences* 30, nº 2 (2005): 66-69.
[3] M. Crisma and C. Toniolo , *Biopolymers*, 2014, **104** , 46
[4] Marsh, E. Neil G., et Yuta Suzuki. « Using 19F NMR to Probe Biological Interactions of Proteins and Peptides ». ACS Chemical Biology 9, no 6 (2014): 1242-50.

Chemo-Selective Catch-and-Release Purification: An Orthogonal Alternative When Chromatography Fails

PurePep®

Robert Zitterbart[1] & Dominik Sarma[1]

[1] Gyros Protein Technologies, Teltow, Germany

https://doi.org/10.17952/38EPS.2026.P289

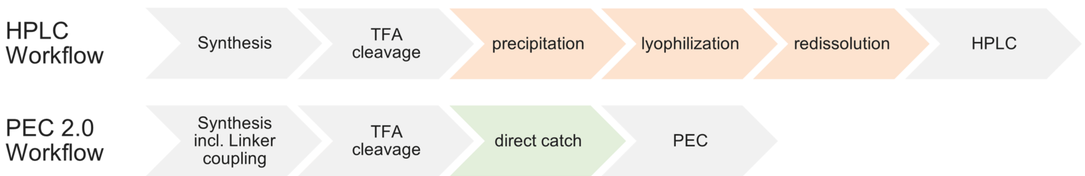
Introduction

The problem it solves: Reversed Phase High-Pressure Liquid Chromatography (RP-HPLC) fails on peptides that won't redissolve, flush through without retention, or co-elute with impurities; PurePep EasyClean (PEC™) captures peptides by chemical reactivity instead of hydrophobic interaction

What's new in 2.0: TFA-stable polymethacrylate (PMA) beads allow direct capture straight from the cleavage cocktail, eliminating ether precipitation and redissolution, and with them the oxime side products and solubility failures that plagued PEC 1.0's agarose workflow.

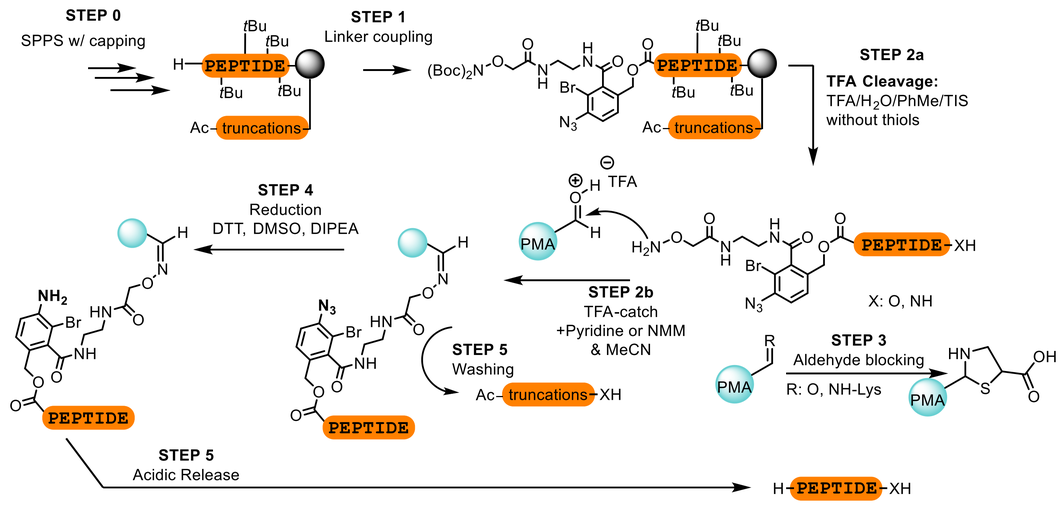
Demonstrated results: Validation across many peptides, 32 peptides in High-Throughput (including known-difficult, very hydrophilic, and very hydrophobic sequences) with mean purity jumping from 50% to 84% with up to **96 purifications/day**, and roughly 20x less solvent than HPLC.

Enabling a redissolution free workflow



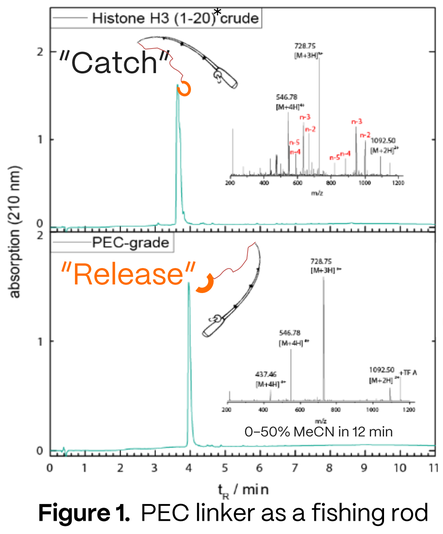
- The first generation of PEC (1.0)[1] wash using crosslinked agarose beads and relied on ether precipitation and redissolution in DMSO/citrate buffer 9:1 or neat HFIP.
- This method suffered from ketone impurities in the ether or in the solvents used for redissolution.
- Additionally, the mentioned solvents weren't always able to solubilize aggregating and hydrophobic peptides.
- To address these pitfalls, we established a TFA-catch method that uses the TFA cleavage cocktail as the medium for the catch step, thus enabling:
  - ✓ No ether precipitation, meaning no risks of unwanted oxime side products
  - ✓ Redissolution-free workflow, thus no problems with solubilizing aggregating and/or hydrophobic peptides

PurePep EasyClean (PEC2.0) mechanism



Scheme 1. Mechanism of PEC purification[2]

Benefit of Catch-And-Release purification



91% UV purity
28% peak purity
(ESI-MS)

96% UV purity
95% peak purity
(ESI-MS)

Figure 1. PEC linker as a fishing rod

- We have developed PEC to ease up peptide purification.
- The PEC-Linker RC+ is a fishing rod for peptides – installed on the N-terminus or amino side chain, fishing out the desired peptide from even the most complex mixtures!

*H3(1-20): H-ARTKQTARKSTGGKAPRKQL-NH_2, X: hydrophobic (L, I, V, W, M, F), Z: intermediate (H, S, T, P, Y, C, G, A), B: hydrophilic (R, K, E, D, N, Q)

Table 1. Comparison of HPLC, PEC1.0 and PEC 2.0 purification of peptides.

	RP-HPLC	PEC 1.0	PEC 2.0
Capture Media	C4-C18 coated silica	Agarose beads	TFA-stable PMA beads
Ether precipitation	Required	Required	Eliminated
Peptide redissolution	Required	Required	Eliminated
Ease of use	Automated; Needs development for each peptide	Multiple critical manual steps	Streamlined workflow
Robustness	Sequence-dependent	More user-dependent	Significantly more robust
Purity	Very high: Dependent on type and amount of impurities	Good purification performance	Improved purity in validation and beta tests
Yield / Recovery	0-80%	10-90%	50-90%
Hydrophilic peptides	Tendency to elute too quickly	Working well	
Hydrophobic peptides	Difficulty to solubilize and to isolate	More challenging	Working well
Aggregating peptides	Difficult to solubilize and to isolate	More challenging	Working well
Scalability	Each new scale demands a new column or device	Easily scalable	
Throughput/day	2-6 runs	16 (Starter Kits) 96 (2-days HT-Kit)	16 (Starter Kits) 96 (HT-Kit)
Solvent per peptide	500-1'000 mL	50 mL (Starter-Kit) 20 mL (HT-Kit)	30 mL (Starter-Kit) 12 mL (HT-Kit)
Applicability	Almost all peptides	Not compatible w/ N-term acetylation or azides	

Purification Results

- Purification of the peptide hormone Met-Somatostatin by PEC-cartridge (Figure 2)
- Purification of a library of 32 peptides with the PEC high-throughput kit (Figure 3)
  - ✓ 12 validation peptides (10-20 res.), including Aß 1-20, Barstar (75-90), JR10, ACP65-74 & Poly Ala)
  - ✓ 10 very hydrophilic (15-18 res.)
  - ✓ 10 very hydrophobic (15-20 res.)

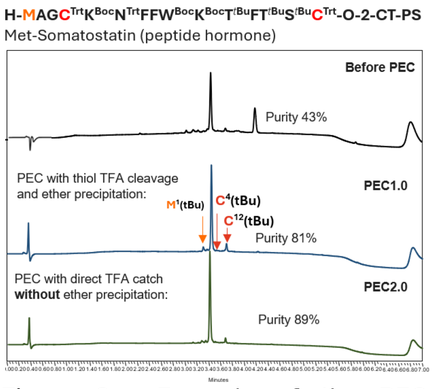


Figure 2. Example of the PEC purification of the peptide hormone Met-Somatostatin by PEC-cartridge.

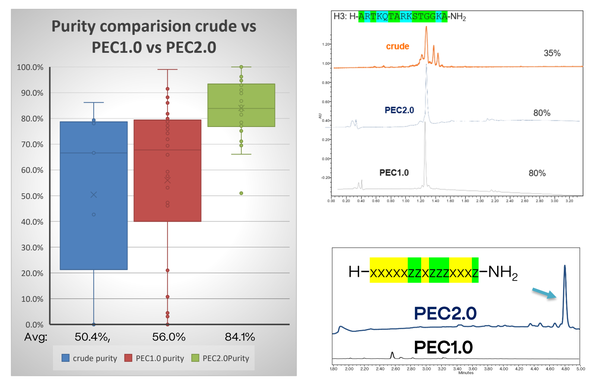


Figure 3. Example of the PEC purification in plate format.

Summary

PEC 2.0 delivers orthogonal peptide purification:

- Handles peptides that chromatography struggles with, including hydrophilic, hydrophobic and aggregating sequences;
- Eliminates ether precipitation and peptide redissolution through direct capture from the TFA cleavage cocktail;
- Supports **flexible scales** and **high-throughput demands**, with up to **96 purifications/day**
- Reduces solvent use to **12 mL per peptide** with the HT kit and saves processing time
- Delivers **84.1% mean purity** across a 32-peptide panel
- Simplifies purification with a streamlined workflow and no gradient development

Access the live collection to receive the poster, the original papers, the recording of our presentation and additional synthesis resources.

SCAN ME

References

[1] R. Zitterbart, et. al., Chemical Science, 2021
[2] R. Zitterbart, S. Lüdtke, M. Muthyala, manuscript in prepartion

GYROS PROTEIN Technologies

www.gyrosproteintechnologies.com/peptides peptides@gyrosproteintech.com

Gyros Protein Technologies logo, Intellisynth, Prelude, PS3, PurePep, Single-Shot, Sonata, Symphony, PEC, and Tribute are trademarks of Gyros Protein Technologies Group. COMU, OxymaPure, PyClock, K-Oxyma and Py-Oxim are trademarks owned by Luxembourg Bio Technologies Ltd. All other trademarks are the property of their respective owners. © Gyros Protein Technologies 2025